Please note: The buttons have no imbedded links

EUROPEAN AEROSOL CONFERENCE 2009

SEPTEMBER 6 – 11, 2009
KARLSRUHE, GERMANY

| Preface | Program | List of Authors | List of Keywords |

Print files for all abstracts:

T01 Aerosol-based nanotechnology	78 abs.	T07 Fundamentals	49 abs.
T02 Aerosol chemistry	73 abs.	T08 High temperature aerosols	47 abs.
T03 Aerosol modelling	53 abs.	T09 Instrumentation	61 abs.
T04 AA aerosol processes and properties	108 abs.	T10 Particle-lung-interaction	68 abs.
T05 AA specific aerosol types	126 abs.	T11 PMx	27 abs.
T06 Electrical effects	31 abs.	T12 Radioactive aerosols	14 abs.

T13 Special Session 1	11 abs.
T15 Special Session 3	27 abs.
T16 Special Session 4	17 abs.
T17 Special Session 5	23 abs.
T19 Special Session 7	11 abs.
T20 Special Session 8	9 abs.

EAA
European Aerosol Assembly

Gesellschaft für
Aerosolforschung
(GAeF)

European Aerosol Conference 2009

Karlsruhe Germany, September 6 to 11, 2009

Organized by Gesellschaft für Aerosolforschung, Conference Chair: Prof. Gerhard Kasper

Table of contents

Remark: Special sessions 3 (T13) and 6(T18) did not take place.

Foreword

PREFACE

The European Aerosol Conference is the meeting place in Europe for the international research community working in the field of aerosol science and technology. These conferences are organized annually under the auspices of the European Aerosol Assembly (EAA), which decides on the date and venue. The 2009 conference takes place in Karlsruhe, Germany. It is jointly organized by the Gesellschaft für Aerosolforschung (GAeF) and the University of Karlsruhe as the host institution.

In terms of submitted abstracts – all in all 840 – the EAC 2009 in Karlsruhe is once again the largest in its history. The format of the conference follows a well established and tested format, with 45 oral sessions, preceded by a daily plenary lecture in one of the key areas of active aerosol research. Wednesday afternoon leaves ample room for individual discussion, working group meetings etc. A total of 270 oral papers will be given, along with a maximum of 284 posters in each of 2 poster sessions. Following numerous requests, it was also possible to accommodate 6 special session topics. It should also be mentioned that the EAC 2009 is preceded by a Workshop on the Health Effects of Aerosols, thereby taking advantage of the presence of numerous international experts in this field.

One conference highlight will be the lecture by Prof. Rolf Müller on climate and geo-engineering, which will be held on Tuesday evening. The event will be open to the general public.

The organizers of the EAC 2009 gratefully acknowledge the efforts of the EAA Working Groups who played a major role in the process of reviewing and selecting the abstracts, and of the members of Committee responsible for the scientific program who suggested plenary speakers and helped in setting up the various special sessions. A very special Thank-You goes to all sponsors and exhibitors for their financial support. We wish to mention in particular, that the student registration fees could be reduced substantially with the generous help of BASF SE.

Gerhard Kasper
Universität Karlsruhe (TH)
Conference Chairman

Program

We have received in total 830 abstracts, 499 of them were submitted for oral presentation. At least we have in the five parallel sessions 270 slots for an oral presentation. (Last change 14 July 2009)

Sunday 6 September 2009

Sunday 6 September 2009	17:00 - 19:00	Pre-Registration

Sunday 6 September 2009	18:00 - 21:00	Welcome Party

Monday 7 September 2009

Monday 7 September 2009	08:00 - 16:15	Registration

Monday 7 September 2009	08:30 - 09:00	Audimax
Opening Ceremony		
08:30	**Aladar Czitrovski** President of the European Aerosol Assembly (EAA)	
	Margret Mergen Mayor of the City of Karlsruhe	
	Detlef Löhe Prorektor for Research, University of Karlsruhe (TH) Board member of the Forschungszentrum Karlsruhe GmbH	
	Gerhard Kasper President of the Gesellschaft für Aerosolforschung (GAeF)	

Monday 7 September 2009	09:00 - 10:00	Audimax
Plenary Lecture I		
Chair:	**Aladar Czitrovski**	
09:00	Plenary Lecture	**Particulate matter in the atmosphere: from measurements to models to policy** *Spyros Pandis*

Monday 7 September 2009	10:00 - 10:15	Coffee Break

Monday 7 September 2009	10:15 - 12:15	Audimax

Atmospheric Aerosols - New Particle Formation

Chairs: Otto Klemm and Tuukka Petäjä

10:15	T041A17	**Modelling of aerosol dynamics and particle chemistry using a new nucleation theory**
		P. Roldin, G. Schurgers, B. Svenningson, E. Swietlicki, A. Eriksson, J. Pagels, E. Nilsson, M. Ketzel, and S. Gustafson
10:35	T041A08	**On the connection between new particle formation rate, sulphuric acid concentration and organic compounds: field measurements in Hohenpeissenberg (Germany)**
		P. Paasonen, S.-L. Sihto, T. Nieminen, H. Vuollekoski, I. Riipinen, E.Asmi, C. Plass-Dülmer, H. Berresheim, W. Birmili, and M. Kulmala
10:55	T041A09	**Nucleation in boreal forest environments: How biogenic terpenes govern the correlation of formation rates with sulphuric acid**
		B. Bonn, M. Boy, M. Kulmala, I. Riipinen, and S.-L. Sihto
11:15	T041A12	**Aerosol particle characteristics in a semi-clean savannah environment**
		V. Vakkari, H. Laakso, D. Mabaso, M. Molefe, N. Kgabi, M. Kulmala, and L. Laakso
11:35	T041A14	**Ambient measurements of sulfuric acid, ammonia and aerosol size in Kent, Ohio**
		J. Li, D. Benson, V. Cunningham, F. Frimpong, W. Montanaro, B. Dailey, and S.-H. Lee
11:55	T041A03	**Simulation experiments studying the influence of plant VOC emission patterns on the formation of new particles**
		A. Kiendler-Scharr, J. Wildt, M. Dal Maso, T. Hohaus, E. Kleist, T.F. Mentel, R. Tillmann, R. Uerlings, U. Schurr, and A. Wahner
Back-up Paper	T041A07	**Why does high relative humidity suppress continental nucleation events?**
		A. Hamed, H. Korhonen, S. L. Sihto, J. Joutsensaari, H. Järvinen, K.E.J. Lehtinen, M. Kulmala, and A. Laaksonen

Monday 7 September 2009	10:15 - 12:15	Neuer Chemie Hörsaal

Aerosol Chemistry - Chemical Characterization of Aerosols: Composition, Identification, and Sources I

Chairs: Johanna Gietl and Krystal Godri

10:15	T150A28	**Polar organic compounds in PM2.5 aerosols from Brasschaat, Belgium, during a 2007 summer campaign: Sources and diel variations**
		Y. Gómez-González, R. Vermeylen, W. Maenhaut, and M. Claeys
10:35	T022A26	**On-line measurements of fine organic aerosols in the region of Paris (France): Evidence of a major source of domestic wood burning**
		O. d'Argouges, J. Sciare, and R. Sarda-Estève
10:55	T022A08	**High-time-resolution chemistry measurements of fine particles at an urban site in Helsinki, Finland**
		M. Aurela, S. Carbone, S. Saarikoski, K. Saarnio, T. Mäkelä, P. Keronen, M. Kulmala, D. Worsnop, and R. Hillamo
11:15	T022A07	**An AMS/TDMA study of organic aerosol properties at a Finnish background site**
		T. Raatikainen, P. Vaattovaara, P. Tiitta, J. Rautiainen, M. Ehn, M. Kulmala, A. Laaksonen, and D.R. Worsnop
11:35	T022A01	**Chemical characterisation of PM2.5 aerosols collected during a 2007 summer campaign at a forested site in Brasschaat, Belgium**
		W. Wang, X. Chi, and W. Maenhaut
11:55	T024A02	**Formation of secondary organic particles in elementary school classrooms**
		C. He, L. Morawska, G. Johnson, H. Guo, E. Uhde, and Godwin Ayoko
Back-up Paper	T022A06	**Characteristics of dicarboxylic acids in Pearl River Delta Region**
		S.C. Lee, K F. Ho, K. Kawamura, and J.J. Cao

Monday 7 September 2009	10:15 - 12:15	HSI-Hörsaal

PM - Composition and Sources

Chairs: Willy Maenhaut and Roberta Vecchi

10:15	T112A02	CHEMKAR PM10: The extended results of a yearlong chemical characterisation of PM10 at six sites in Flanders (Belgium)
		J. Vercauteren, C. Matheeussen, E. Roekens, B. Geypens, R. Van Grieken, and W. Maenhaut
10:35	T113A03	Approaches to determine the contribution of natural sources to PM10 concentrations in North-West Germany
		U. Quass, O. Sperber, O. Romazanowa, F. Luther, A. Caspari, M. Beyer, U. Pfeffer, T. Zang, P. Bruckmann, and T.A.J. Kuhlbusch
10:55	T113A02	Week daily variation of PM10 depending on air mass origin at German lowlands (Melpitz site) – a four year study
		G. Spindler, E. Brüggemann, Th. Gnauk, A. Grüner, H. Herrmann, K. Müller, and M. Wallasch
11:15	T113A05	Sea salt concentrations in the Netherlands from a European perspective
		A.M.M. Manders, M. Jozwiecka, and M. Schaap
11:35	T112A06	Analysis of ROS generated by PM10 sampled at a rural and urban location in North Rhine Westphalia
		B. Hellack, U. Quass, T.A.J. Kuhlbusch , C. Albrecht, and R.P.F. Schins
11:55	T113A04	Is PM2.5 the best descriptor of the atmospheric fine fraction aerosol?
		M. Manigrasso, A. Febo, F. Guglielmi, V. Ciambottini, and P. Avino
Back-up Paper	T112A04	Indoor versus outdoor air quality measurements: number, mass concentrations and chemical composition of PM at the University of Perugia, Italy
		S. Ortu, L. Barcherini, D. Cappelletti, F. Marmottini, F. Scardazza, B. Moroni, and B. Sebastiani

Monday 7 September 2009	10:15 - 12:15	Hörsaal 3

Fundamentals - Aerosol Dynamics

Chairs: Charles F. Clement and Pedro L. Garcia-Ybarra

10:15	T074A01	An acoustic trap for submicron aerosol particles
		P. Vainshtein and M. Shapiro
10:35	T078A01	Dust cloud manipulation in microgravity: positioning, squeezing and trapping
		A.A. Vedernikov
10:55	T072A01	Size dependent nanoparticle transport in rising bubbles
		M. Hermeling and A.P. Weber
11:15	T074A06	Calculation of aggregate friction coefficient from active surface
		L. Isella and Y. Drossinos
11:35	T074A02	Modeling source strength modification due to coagulation in a diffusing aerosol puff
		Y. S. Mayya and S. Anand
11:55	T074A03	Dynamics of aerosols at nonlinear oscillations in tubes. The theory and experiment
		D.A. Gubaidullin, R.G. Zaripov, A.L. Tukmakov, and L.A. Tkachenko
Back-up Paper	T074A04	Aerosol Clustering Patterns in Oscillating Flows
		D. Katoshevski

Monday 7 September 2009	10:15 - 12:15	Hörsaal 1

Radioactive Aerosols

Chairs: Denis Boulaud and Constantin Papastefanou

10:15	T121A06 invited 40min	Key issues in radionuclide labeled aerosol monitoring for resuspension studies and short to long-term post-accident characterizations
		O. Masson, D. Piga, and L. Bourcier

10:55	T121A01	**Ten-year measurements of Radon's decay products to study the role of atmospheric dispersion on PM levels**
		*R. Vecchi, G. Valli, **V. Bernardoni**, and A. Franchin*
11:15	T122A03	**Parametric study of the ionizer induced Thoron progeny concentration depletion**
		***M. Joshi**, P. Kothalkar, A. Khan, R. Mishra, B.K. Sapra, and Y.S. Mayya*
11:35	T123A01	**Determination of loss factors of aerosol particles in the sampling systems of nuclear power plants**
		***R.F.W.Jonas** and G.F.Lindenthal*
11:55	T123A03	**Aerosol release from Silver Indium Cadmium control rod**
		***T. Lind**, A. Pintér Csordás, and J. Stuckert*
Back-up Paper	T122A02	**Airway deposition and health effects of inhaled radon progenies**
		***I. Balásházy**, Á. Farkas, and I. Szokez*

Monday 7 September 2009	12:15 - 13:45	Lunch Break
Monday 7 September 2009	12:15 - 13:45 (Meeting Room)	EAA Board Meeting

Monday 7 September 2009	13:45 - 15:45	Audimax

Atmospheric Aerosols - Bioaerosols

Chairs: Ruprecht Jaenicke and Viviane Després

13:45	T058A01	**Primary biological aerosol particles: Detection and identification of characteristic compounds by aerosol mass spectrometry**
		***F. Freutel**, J. Schneider, S.R. Zorn, F. Drewnick, S. Borrmann, and T. Hoffmann*
14:05	T058A07	**Collection of airborne spores from combustion environments**
		***S.A. Grinshpun**, A.Adhikari, C. Li, T. Reponen, M. Schoenitz, E.L. Dreizin, and M. Trunov*
14:25	T058A17	**Modelling mineral dust and airborne micro-organisms with the Danish Eulerian Hemispheric Model**
		***L.M. Frohn**, C. Geels, C.A. Skjøth, K.M. Hansen, J.H.Christensen, J. Brandt, G.B. Hedegaard, A.B. Hansen, and O.Hertele*
14:45	T058A13	**Characteristics of biological particles in indoor environment**
		M. Moustafa, M. Abd El-Hady, and A. Mohamed
15:05	T058A04	**Antibiotic-resistant microorganisms in atmospheric aerosol of Southwestern Siberia**
		***A.S. Safatov**, L.I. Puchkova, G.A. Buryak, and I.S. Andreeva*
15:25	T058A03	**High diversity of fungi in air particulate matter**
		***J. Fröhlich-Nowoisky**, V.R. Després, and U. Pöschl*
Back-up Paper	T058A16	**DEHM-Pollen: A regional scale pollen dispersion model**
		***C.A.Skjøt**h, J.Brandt, J.Christensen, L. M. Frohn, C. Geels, A.B.Hansen, K.M.Hansen, G.B.Hedegaard, and J. Sommer*

Monday 7 September 2009	13:45 - 15:45	Neuer Chemie Hörsaal

Aerosol Chemistry - Chemical Characterization of Aerosols: Composition, Identification, and Sources II

Chairs: Magda Claeys and Manuel Dall'Osto

13:45	T026A01	**Characterisation of particle-phase wood smoke tracer compounds in ambient air of a residential area**
		***M.A. Bari**, G. Baumbach, G. Scheffknecht, and B. Kuch*
14:05	T022A17	**Towards single particle surface analysis using fluorescence labelling**
		***M. Putkiranta**, M. Seipenbusch, M. Marjamäki, and J. Keskinen*
14:25	T022A24	**Results of the first EC/OC intercomparison exercise for National Air Quality Reference Laboratories**

		L. Emblico and *A. Borowiak*
14:45	T022A25	**Identification of homologous series as organic tracers in PM samples: a signal processing method for studying complex GC-MS signals**
		M.C. Pietrogrande, *M. Mercuriali, L. Pasti, D. Bacco,and F. Dondi*
15:05	T022A14	**OC and EC determination in aerosol samples collected on Teflon filters by Particle Elastic Scattering Analysis (PESA) and Ion Chromatography (IC)**
		*L. Bonanni, G. Calzolai, M. Chiari, **F. Lucarelli**, S. Nava, S. Becagli, and R. Udisti*
15:25	T024A01	**Cluster analysis on mass spectra of biogenic secondary organic aerosol**
		C. Spindler, A. Kiendler-Scharr, E. Kleist, A. Mensah, Th. F. Mentel, R. Tillmann, and J. Wildt
Back-up Paper	T025A01	**Sources of fine particulate organic matter in a Mediterranean urban area: Marseilles**
		***I. El Haddad**, N. Marchand, B. Temime-Roussel, H. Wortham, C. Piot, A. Albinet, J.L. Besombes, and J.L. Jaffrezo*

Monday 7 September 2009	**13:45 - 15:45**	**HSI-Hörsaal**

Aerosol-based Nanotechnology - Health Effects, Worker Protection and Gas Phase Synthesis

Chairs:	**Sylvia Diabaté and Michel B. Attoui**	
13:45	T013A01	**Tailor-made nanoparticles as testing materials with changing chemical composition and similar physical properties**
		***L.K. Limbach**, N.A. Luechinger, R.N. Grass, and W.J. Stark*
14:05	T013A04	**Nanoparticles: Synthesis, characterisation and cellular effects-The NANO-SYNCC- Project**
		***H.-R. Paur**, W. Baumann, H. Bockhorn, A. Comouth, S. Diabate, H.Mätzing, S. Mülhopt, O. Nalcaci, A. Panas, E. Ruzin, H. Saathoff, H. Seifert, and C. Weiss*
14:25	T013A05	**Integration of two mathematical models for monitoring of biological doses from inhalation exposure to nano and fine particles in industrial workplace**
		*A. Nikolopoulou, **P. Neofytou**, C. Housiadas, P. Papazafiri, K. Eleftheriadis, and L. Tran*
14:45	T013A06	**NanoImpactNet – building a multi-stakeholder dialogue on the health and environmental impact of nanomaterials**
		*N. Boschung, D. Hart, and **M. Riediker***
15:05	T015A33	**Production of equally sized atomic clusters by a glowing wire**
		*C. Peineke, M. Attoui, R. Robles, A.C. Reber, S.N. Khanna, and **A. Schmidt-Ott***
15:25	T015A31	**Analysing the electrical behaviour of the Spark Generator in view of novel applications**
		***V.A. Vons**, A. Evirgen, and A. Schmidt-Ott*
Back-up Paper	T018A02	**Modelling of accidental nanoparticle release into a workplace**
		***C. Asbach**, U. Rating, T. van der Zwaag, H. Fissan, T.A.J. Kuhlbusch*

Monday 7 September 2009	**13:45 - 15:45**	**Hörsaal 3**

Special Session 8: Artifacts in Measuring PM

Chairs:	**Janja Tursic and Harry ten Brink**	
13:45	T200A07	**What's up with the European PM reference methods?**
		J. Vercauteren, C. Matheeussen, R. De Lathouwer, V. Keppens, and E. Roekens
14:05	T200A01	**PM gravimetric measurements and blank filters**
		***D. de Jonge** and J.H. Visser*
14:25	T200A09	**Water uptake and retention by filter material used for PM sampling**
		*T. Torzicky and **R. Hitzenberger***
14:45	T200A05	**Novel approach to identifying size dependent losses of semivolatile compounds during room temperature storage of sampled aerosol matter**
		K. Wittmaack
15:05	T200A04	**The effect of season and microenvironment type on measurement bias of a photometer DustTrak**

		M. Braniš
15:25	T200A02	**Semivolatile behaviour of dicarboxylic acids during summer campaigns at K-puszta**
		W. Maenhaut, W. Wang, L. Copolovici, and X. Chi
Back-up Paper	T200A08	**Organic carbon in Whatman-QMA field-blanks**
		H.M. ten Brink and F. van Arkel

Monday 7 September 2009	**13:45 - 15:45**	**Hörsaal 1**

High Temperature Aerosols

Chairs: Jorma Jokiniemi and Alfred Weber

13:45	~~T082A03~~	~~**Rapid characterization of agglomerate aerosols by in situ mass-mobility measurements**~~
		*J.H. Scheckman, **S.E. Pratsinis**, and P.H. McMurry*
14:05	T083A19	**Evaluation of a high temperature aerosol sampling probe**
		*O. Sippula and **J.K. Jokiniemi***
14:25	T083A29	**Raman study of nanostructure evolution of diesel soot during oxidation**
		***A. Zygogianni**, V. Polatidis, and A. Konstandopoulos*
14:45	T081A03	**Temperature-induced reduction of the work function of submicron aerosol particles and its implication on thermionic particle charging**
		*K. Reuter-Hack, G. Kasper, and **A.P. Weber***
15:05	T081A02	**Gas phase synthesis of zinc sulfide nanoparticles**
		***E.K. Athanassiou**, R.N. Grass, and W.J. Stark*
15:25	T083A04	**Measurement of soot in atmospheric and low pressure flames with a novel particle mass spectrometer**
		***H. Mätzing**, W. Baumann, O. Bayode, T. Felleisen, H.-R. Paur, and H. Seifert*
Back-up Paper	T083A31	**Fast evaluation method of the ash aging effect on catalyzed Diesel Particulate Filters**
		***D. Zarvalis**, S. Lorentzou, and A.G. Konstandopoulos*

Monday 7 September 2009	**15:45 - 16:15**	**Coffee Break and Exhibition**

Monday 7 September 2009	**16:15 - 18:15**	**Audimax**

Atmospheric Aerosols - Urban Aerosols I

Chairs: Sergey Grinshpun and Thomas Mentel

16:15	T051A14	**Improvement in ambient air quality in East Germany after the German reunification: Analysis of the trends in exposure and their implications**
		***J.Cyrys**, M. Pitz, S. Breitner, M. Stölzel, W. Kreyling, J. Heinrich, H-Erich Wichmann, and A. Peters*
16:35	T051A26	**Chemically-resolved aerosol volatility measurements from two megacity field studies**
		***J.A. Huffman**, K.S. Docherty, A.C. Aiken, M.J. Cubison, I.M. Ulbrich, P.F. DeCarlo, D. Sueper, J.T. Jayne, D.R. Worsnop, P.J. Ziemann, and J.L. Jimenez*
16:55	T051A31	**Influence of petrochemical activities on fine particles and VOC observed in a Mediterranean urban area**
		***N. Marchand**, B. d'Anna, J.L. Jaffrezo, Sellegri K., J.L. Besombes, I. El Haddad, V. Michaud, C. Piot, B. Temime-Roussel, C. George, P. Laj, H. Wortham, D. Voisin, A. Armengaud, G. Gille, and D. Robin*
17:15	T051A25	**Spatial and temporal variability of ultrafine particles within an urban agglomeration, the Ruhr-Area, Germany**
		***C. Nickel**, S. Weber, H. Kaminski, U. Pfeffer, P. Bruckmann, and T.A.J. Kuhlbusch*
17:35	T051A16	**First measurements of aerosols on a ZEPPELIN airship**
		***R. Tillmann**, Th..F. Mentel, A. Kiendler-Scharr, and A. Wahner*
17:55	T051A02	**The particle size distribution variation in fine particle to the inland area of South Kanto from the coastal line of Tokyo bay**
		***H. Minoura** and N. Shimo*

Back-up Paper	T051A37	**Reduction of PM industrial ceramic emissions reflected on key components concentrations of ambient PM10**
		M.C. Minguillón, X. Querol, E. Monfort, A. Alastuey, A. Escrig, I. Celades, and J.V. Miró

Monday 7 September 2009	**16:15 - 18:15**	**Neuer Chemie Hörsaal**

Aerosol Modelling - Transport, Transformation and Nucleation

Chairs: Leon Gradon and Veli-Matti Kerminen

16:15	T037A01	**Detecting airborne microorganisms by experimental and numerical tools: application to the spreading of Legionella pneumophila from cooling towers**
		T.L. Ha, E. Robine, E. Tarnaud, F. Tognet, C. Turmeau, Y. Morel, and L. Rouil
16:35	T033A09	**Computational study of aerosol flow in bifurcations**
		M. Pilou, V. Gkanis, P. Neofytou, and C. Housiadas
16:55	T033A10	**HCl-aerosols in industrial gas cleaning processes**
		G. Brosig, M. Bittig, J. Lindermann, S. Haep, M. Luckas, and K.-G. Schmidt
17:15	T033A13	**Morphology of rod-like nanoparticle aggregates by Monte Carlo simulations**
		G. Skillas, A. Maisels, and C.J. Klasen
17:35	T032A01	**Unraveling the "Pressure-Effect" in unary condensation**
		J. Wedekind, A.P. Hyvärinen, D. Brus, and D. Reguera
17:55	T032A04	**Modelling the sign preference in heterogeneous nucleation**
		K. Ruusuvuori, T. Kurtén, H. Vehkamäki, I.K. Ortega, M. Toivola, and M. Kulmala
Back-up Paper	T032A03	**Molecular mechanisms behind nocturnal new particle formation**
		I.K. Ortega, T. Suni, M. Boy, T. Grönholm, M. Kulmala, H. Junninen, M. Ehn, D. Worsnop, H. Maninnen, H. Vehkamäki, H. Hakola, H. Hellén, T. Valmari, and H. Arvela

Monday 7 September 2009	**16:15 - 18:15**	**HSI-Hörsaal**

Fundamentals - Filtration

Chairs: Michael Shapiro and Jose L. Castillo

16:15	T077A02	**Loading of soot nanoparticle agglomerates on air filters**
		J. Wang, S.-C. Kim, and D.Y.H. Pui
16:35	T077A03	**Dependence of the filter efficiency on nanoparticle velocity and shape**
		Z.Y. Zhang and Z.Z. Zhang
16:55	T077A06	**Impact of electrostatic forces on collection of charged nanoparticles aerosols by dielectric wire screens**
		G. Mouret, S. Chazelet, D. Thomas, and D. Bémer
17:15	T077A09	**Multi-scale modelling and experimental measurements of soot filtration in diesel particulate filters**
		S. Bensaid, D.L. Marchisio, and D. Fino
17:35	T077A11	**The effect of porosity on deposition on fibrous filters**
		Sarah J. Dunnett and Charles F. Clement
17:55	T077A19	**Filtration of aerosol particles in structurally inhomogeneous fibrous filters. II – Experimental results**
		A. Jackiewicz and A. Podgórski
Back-up Paper	T077A07	**Experimental results and modelling of the clogging of pleated fibrous filters in presence of humidity**
		A. Joubert, J.C. Laborde, L. Bouilloux, D. Thomas, S. Callé-Chazelet

Monday 7 September 2009	**16:15 - 18:15**	**Hörsaal 3**

Special Session 3: Aerosol Sampling and Aerosol Analytics

Chairs:	Yoshi Iinuma and Thorsten Hoffmann	
16:15	T150A09	**Development and first application of an Aerosol Collection Module (ACM) for quasi online compound specific aerosol measurements**
		T. Hohaus, A. Kiendler-Scharr, D. Trimborn, J. Jayne, and D. Worsnop
16:35	T150A30	**A novel particle sampling system for toxicological characterization of emissions**
		J. Ruusunen, H. Lamberg, M. Tapanainen, K. Hytönen, O. Sippula, J. Tissari, M. Ihalainen, T. Karhunen, A.S. Pennanen, P. Willman, M-R. Hirvonen, R.O. Salonen, and J. Jokiniemi
16:55	T150A07	**MoLa – A new mobile laboratory for atmospheric aerosol research**
		F. Drewnick, S.-L. von der Weiden, J. Schneider, S.R. Zorn, S. Borrmann
17:15	T150A24	**A photoacoustic aerosol absorption spectrometer working from 420 nm to 2200 nm**
		C. Haisch, P. Menzenbach, and R. Niessner
17:35	T150A27	**Assessment of fossil and non-fossil primary and secondary organic aerosol**
		A.S.H. Prévôt, S. Szidat, N. Perron, V. Lanz, M.R. Alfarra, P. DeCarlo, C. Mohr, and U. Baltensperger
17:55	T150A20	**Towards reference-free quantitation in multielemental TXRF analysis of nanoparticles – Effects of particle dimensions and load**
		J. Osán, F. Reinhardt, B. Beckhoff, A. Pap, and S. Török
Back-up Paper	T150A01	**Evaporative loss of accumulated semi-volatile liquid aerosol from fibrous filter**
		B. Sutter, J.C. Appert-Collin, D. Bémer, and D. Thomas

Monday 7 September 2009	16:15 - 18:15	Hörsaal 1
Special Session 7: Test Materials in Toxicological and Health Effect Studies		
Chairs:	Michael Riediker and Athanasios Konstandopoulos	
16:15	T190A11 invited 40min	**Minimal analytical characterisation of engineered nanomaterials need for hazard assessment in biological matrices**
		H. Bouwmeester, I. Lynch, M. Riediker, and F.R. Cassee
16:55	T190A07	**Comprehensive characterisation of manufactured nanoscaled powders following soft dispersion**
		K. Wittmaack
17:15	T190A04	**Intrinsic toxicity and inflammatory potency and/or health damage of Particulate Material (PM) in physiologic and pathologic conditions**
		R. Zangari, F. Cetta, M. Sala, A. Dhamo, P. Laviano, F. Cisternino, G. Malagnino, G. Schiraldi, and E. Bolzacchini
17:35	T190A08	**A new exposure system for an efficient and controlled deposition of aerosol particles onto cell cultures**
		M. Kalberer, M. Geiser, M. Savi, D. Lang, A. Gaschen, M Ryser, J. Ricka, and M. Fierz
17:55	T190A10	**Cellular responses after exposure of lung cell cultures to secondary organic aerosols**
		M. Geiser, M. Kalberer, A. Gaschen, D. Lang, M. Savi, T. Geiser, A. Gazdhar, C.M. Lehr, M. Bur, J. Dommen, and U. Baltensperger
Back-up Paper	T190A01	**Synthesis and characterization of titanium dioxide particles for toxicity tests**
		A.J. Koivisto, H. Alenius, J. Joutsensaari, H. Norppa, M. Miettinen, P. Pasanen, L. Pylkkänen, E. Rossi, T. Tuomi, M. Vippola, J. Jokiniemi, and K. Hämeri

Monday 7 September 2009	**18:15**	**End of Conference Day**
Monday 7 September 2009	**18:15 - 19:30**	**Journal of Aerosol Science- Editorial Board Meeting**
Monday 7 September 2009	**18:15 - 19:30**	**Meeting of Hellenic Association for Aerosol Research (HAAR)**

Tuesday 8 September 2009

Tuesday 8 September 2009	08:00 - 16:15	Registration

Tuesday 8 September 2009	08:45 - 09:45	Audimax

Plenary Lecture II

Chair:	Heinz Burtscher

08:45	Plenary Lecture	**Automotive emissions and how aerosol science contributes to reducing them**
		Matti Maricq

Tuesday 8 September 2009	09:45 - 10:15	Coffee Break and Exhibition

Tuesday 8 September 2009	10:15 - 12:15	Audimax

Aerosol-based Nanotechnology - Fundamentals and Charged Nanoparticles

Chairs:	Alfred Weber and Andreas Schmidt-Ott

10:15	T011A01	**Ionic liquids as a source of positive and negative standard ions in the sub 3 nm range**
		M. Attoui
10:35	T011A02	**A nano-DMA of rectangular planar plates**
		E. Hontañón, M. Alonso, A. Rivero, D. Fuentes, and E. Ramiro
10:55	T110A03	**Disagreement of classical theory for the friction resistance of nanoparticles in low-pressure flows**
		T. Wu and A. P. Weber
11:15	T011A05	**Light scattering by sintered aggregates using T-Matrix method**
		T. Wriedt and R. Schuh
11:35	T011A07	**Formation of ionic molecular clusters in the presence of spurious gases in a bipolar charger**
		G. Steiner, D. Wimmer, and G.P. Reischl
11:55	T011A10	**Refined classical viewpoint on coagulation of charged nanoparticles**
		V.Y. Smorodin
Back-up Paper	T011A04	**Comparison of agglomerate stability of different nanopowders**
		B. Stahlmecke, S. Wagener, C. Asbach, H. Kaminski, H. Fissan, and T.A.J. Kuhlbusch

Tuesday 8 September 2009	10:15 - 12:15	Neuer Chemie Hörsaal

Aerosol Chemistry - Smog Chamber and Laboratory SOA Studies

Chairs:	Mattias Hallquist and Yoshi Iinuma

10:15	T021A03	**CMUCHACHAS: MUltiple CHamber Aerosol CHemical Aging experimentS**
		N. M. Donahue, H. Saathoff, U. Baltensperger, A. Prevot, J. Dommen, T. Brauers, Th. F. Mentel, M. Hallquist, M. Bilde, and T. Hoffmann
10:35	T021A07	**Volatility of aged secondary organic aerosol (SOA) from ozonolysis of monoterpenes**
		K. Salo, M. Hallquist, Å.M. Jonsson, H. Saathoff , C. Spindler, Th F. Mentel, and N. Donahue
10:55	T024A03	**Controlled OH radical induced aerosol ageing in the ADIA simulation chamber**
		H. Saathoff, K.-H. Naumann, O. Möhler, N. Donahue, T. Mentel, R. Tillmann, and T. Leisner
11:15	T021A01	**Uptake of ambient organic gaseous mixtures to laboratory generated aerosols**
		J. Liggio and S.-M. Li
11:35	T021A02	**Gas-phase products and secondary aerosol yields from the ozonolysis of (E)-ß-farnesene**

		I. Kourtchev, I. Bejan, J.R. Sodeau, and J.C. Wenger
11:55	T021A08	**Secondary organic aerosol formation from the OH initiated oxidation of tolualdehydes and dimethylphenols**
		I. Bejan, I. Kourtchev, J.C. Wenger, I. Barnes, and J.R. Sodeau
Back-up Paper	T024A08	**Study of nucleation processes involved in SOA formation from the ozonolysis of a biogenic compound in a smog chamber**
		Y. Katrib, J. Boulon, K. Miet, J. Wang, M. Attoui, K. Sellegri, and J.F. Doussin

Tuesday 8 September 2009		**10:15 - 12:15**	**HSI-Hörsaal**
Special Session 4: Origin, Properties and Impact on Regional and Global Climate			
Chairs:	**Konstantinos Eleftheriadis and Jose Castillo**		
10:15	T160A09	**Study of atmospheric aerosol and columnar water vapor in Antarctic region during 53 Russian Antarctic expedition in 2007-2008**	
		S.A.Terpugova, V.V. Polkin, S.M. Sakerin, D.M. Kabanov, B.N. Holben, I.A. Slutsker, A.V. Smirnov, and V.F. Radionov	
10:35	T160A03	**Measurements of concentrations and deposition velocity of ultrafine aerosol over the Nansen Ice Sheet (Antarctica)**	
		A.Donateo, D.Contini, F.Belosi , F.M.Grasso, G.Santachiara, and F.Prodi	
10:55	T160A13	**Volatility of nuclei mode arctic aerosol particles during summer**	
		G. Biskos, S. Vratolis, J. Ondrácek, A.A. Karanasiou, and K. Eleftheriadis	
11:15	T160A02	**Effects of relative humidity on aerosol light scattering in the Arctic region**	
		P. Zieger, R. Schmidhauser, E. Weingartner, J. Ström, and U. Baltensperger	
11:35	T160A12	**Organic hydroxyl and organosulfate groups in atmospheric particles during ICEALOT 2008**	
		L.M. Russell, P.M. Shaw, A. Frossard, J.H. Kroll, P.K. Quinn, and T.S. Bates	
11:55	T160A07	**Results of a pilot study on the climate relevant particle burden on Greenland**	
		E. Schultz, S. Norra, N. Schleicher,V. Dietze, M. Fricker, U. Kaminski, C.H. Pedersen, and B. Sittler	
Back-up Paper	T160A01	**Surface-atmosphere exchange of aerosol particles in the high Arctic - Results from ASCOS**	
		A. Held, D. Orsini, and C. Leck	

Tuesday 8 September 2009		**10:15 - 12:15**	**Hörsaal 3**
Aerosol Modelling - Atmospheric Applications			
Chairs:	**Sabine Wurzler and Liisa Pirjola**		
10:15	T045A03	**Effect of aerosol mixing state on optical and CCN activation properties in an evolving urban plume**	
		N. Riemer, M. West, R.A. Zaveri, J.C. Barnard, and R.C. Easter	
10:35	T031A17	**Urban PM10 modelling using neural network with weather forecast**	
		K.B. Ang, G. Baumbach, and K.G. Gutbrod	
10:55	T031A18	**Evaluation of model simulated atmospheric constituents with observations over an urban area affected by natural sources**	
		E. Athanasopoulou, M. Tombrou, A.A. Karanasiou , K. Eleftheriadis, and A.G. Russell	
11:15	T031A05	**Enhanced aerosol formation in coastal regions caused by ship emissions**	
		V.Matthias, I. Bewersdorff, A. Aulinger, and M. Quante	
11:35	T180A04	**Simulation of aerosol and clouds on the regional scale**	
		M. Bangert, B. Vogel, H.Vogel, K. Lundgren, R. Rinke and A. Seifert	
11:55	T031A04	**Monitoring the 4-D aerosol distribution: Synergetic use of MODIS AOT, in-situ PM observations and the chemical transport model LOTOS-EUROS**	
		E.C.J.Hendriks, R. Timmermans, A. Segers, and M. Schaap	
Back-up Paper	T031A03	**Determination of the contribution of different groups of emission sources on the concentration of PM10, PM2.5, and NO2 in North Rhine-Westphalia – a whodunnit**	

H. Hebbinghaus, S. Wurzler , M. Memmesheimer, G. Piekorz, E. Friese, H. J. Jakobs, C. Kessler, A. Ebel, and P. Bruckmann

Tuesday 8 September 2009	10:15 - 12:15	Hörsaal 1

High Temperature Aerosols - Combustion Aerosols

Chairs:	Cristina Gutierrez-Canas and Hanns-Rudolf Paur	

10:15	T083A26	The case of on-line measurements vs. gravimetric sampling for quantifying the particulate emissions from biomass combustion
		A. Keller, A. Lauber, A. Doberer, J. Good, T. Nussbaumer, A. Richards, M.F. Heringa, R. Chirico, P.F. DeCarlo, A.S.H. Prevot, U. Baltensperger, and H. Burtscher
10:35	T083A13	Reduction of alkali aerosol formation by addition of peat during combustion of ash rich biomass fuels
		C. Boman, I. Nyström, L. Pommer, D. Boström, and M. Öhman
10:55	T081A04	Characterization of high-temperature aerosols as emission precursors from a MSWI
		E. Peña, S. Astarloa, E. Garcia, S. Elcoroaristizabal, J.A. Legarreta, and C. Gutiérrez-Cañas
11:15	T083A16	Generation of nano-particles during the burnt-out phase of the wood stove burning cycle
		A. Bologa, H.-R. Paur, K. Woletz, and H. Bhangu
11:35	T083A34	Ultrafine particle emission from modern diesel engines: effects of engine conditions and combustion cycle
		C. Beatrice, S. Di Iorio, C. Guido, V. Fraioli, M. Lazzaro, M. Sirignano, and A. D'Anna
11:55	T083A15	Characteristics of particles emitted by turbine engine and in-plume conversion
		M.-D. Cheng, E. Corporan, and M.J. DeWitt
Back-up Paper	T083A25	Dependence between heavy duty diesel engine exhaust nucleation and soot concentration
		T. Lähde, T. Rönkkö, A. Virtanen, A. Solla, M. Kytö, C. Söderström, and J. Keskinen

Tuesday 8 September 2009	12:15 - 13:45	Lunch Break
Tuesday 8 September 2009	12:15 - 13:45 (Meeting Room)	GAeF Board Meeting

Tuesday 8 September 2009	13:45 - 15:45	Poster and Exhibition Area

Poster Session Part I and Exhibition. For details see below

Tuesday 8 September 2009	15:45 - 16:15	Coffee Break and Exhibition

Tuesday 8 September 2009	16:15 - 18:15	Audimax

Aerosol-based Nanotechnology - Modelling of Nanoparticle Formation and Gas Phase Synthesis

Chairs:	Einar Kruis and Sotiris Pratsinis	

16:15	T015A02	Experimental and numerical study of gasdynamically induced particle synthesis
		V. Goertz, N.S. Al-Hasan, M. Dannehl, M.Roeck, A. Maisels, H. Nirschl, and G.H. Schnerr
16:35	T015A23	Nanostructure evolution: Form aggregated to spherical SiO_2 particles made in diffusion flames
		A. Camenzind, H. Schulz, A. Teleki, G. Beaucage, T. Narayanan, and S.E. Pratsinis
16:55	T015A27	Synthesis of Zirconia-Alumina core-shell nanoparticles by liquid flame spray
		M. Aromaa, J.-P. Nikkanen, J.B. Wagner, E. Levänen, T. Mäntylä, and J.M. Mäkelä
17:15	T140A01	Nanoparticle monitoring and modelling in microwave plasmas
		H. Mätzing, W. Baumann, H.-R. Paur, and H. Seifert

17:35	T140A03	**Modelling nanoparticle production in a turbulent diffusion flame**
		A.J. Gröhn, J.K. Jokiniemi, and S.E. Pratsinis
17:55	T140A04	**A spatio-temporal population balance-Monte Carlo method for diffusion and coagulation of nanoparticles in plug-flow aerosol reactors**
		H. Zhao, F.E. Kruis, J. Wei, T. van der Zwaag, S. Haep, and C. Zheng
Back-up Paper	T015A22	**Synthesis and functionalisation of copper and titanium nanoparticles in a spark discharge generator**
		H. Förster, C. Funk, and W. Peukert

Tuesday 8 September 2009	16:15 - 18:15	Neuer Chemie Hörsaal

Atmospheric Aerosols - Remote sensing of Aerosol Properties

Chairs:	Matthias Wiegner and Paul Zieger

16:15	T046A08	**Active and passive remote sensing: analysis of an extreme event over Southern Iberian Peninsula**
		*J. L. Guerrero-Rascado, F. J. Olmo, F. Navas-Guzmán, D. Pérez, H. Lyamani, and **L. Alados-Arboledas***
16:35	T046A07	**Columnar aerosol properties over Italy from MODIS products in the year 2007**
		***P. Burlizzi**, F. DeTomasi, and M. R. Perrone*
16:55	T046A06	**Night-time remote sensing of aerosols in the near ground atmosphere by ground-based hyperspectral imaging**
		***Y. Etzion**, D.M. Broday, T. Kolatt, and M. Shoshany*
17:15	T046A04	**Estimating spectral optical depth of cirrus clouds in the visible domain by synergistic use of Spectrometric and Lidar techniques**
		*M.R. Calvello, P. Di Girolamo, T. Di Iorio , F. Esposito, **G. Pavese**, D. Summa*
17:35	T046A10	**Aerosol profiling within the Ceilometer Network of the German Meteorological Service**
		***H. Flentje**, D. Engelbart, and W. Thomas*
17:55	T046A21	**EARLINET: integration approach for aerosol study**
		***L. Mona**, G. Pappalardo, A. Amodeo, G. D'Amico, I. Mattis, C. Perez, and U. Wandinger*
Back-up Paper	T046A03	**One-year measurements of aerosol vertical profiles in Gual Pahari, India**
		***M. Komppula**, T. Mielonen, H. Lihavainen, A.-P. Hyvärinen, V.-M. Kerminen, H. Baars, R. Engelmann, B. Heese, D. Althausen, T.S. Panwar, R.K. Hooda, V.P. Sharma, and Y. Viisanen*

Tuesday 8 September 2009	16:15 - 18:15	HSI-Hörsaal

Aerosol Chemistry - Multiphase Chemical Mechanisms, Transformation Processes and Interactions

Chairs:	Laurent Deguillaume and Andreas Tilgner

16:15	T028A10	**Determination of the bulk accommodation coefficient of NO_2 and O_3 on deliquesced aerosol particles and the effect of surfactants**
		*A. Rouvière, Y. Sosedova, H.W. Gäggeler, and **M. Ammann***
16:35	T027A06	**Radical, humidity and temperature effects on SOA formation from ozonolysis of monoterpenes**
		***M. Hallquist**, Å. M. Jonsson, K. Salo, and E. Emanuelsson*
16:55	T028A02	**Heterogeneous Reactions of $(NH_4)_2SO_4$ particles with chlorine reactive species: coated wall flow tube studies**
		***R. Ciuraru**, N. Visez, S. Gosselin, and D. Petitprez*
17:15	T028A01	**Heterogeneous reactions of a pyrethroid insecticide with OH radicals and ozone: In-situ measurement of airborne particles using FTIR**
		***M. Segal-Rosenheimer**, R. Linker, and Y.Dubowski*
17:35	T024A09	**Oligomerization from methylglyoxal: a potential mechanism for secondary organic aerosol formation in a simulated cloud model**
		***Y. Farhat**, N. Sauret, M. Claeys, P.C. Maria, and L. Massi*

17:55	T028A07	**Laboratory studies of sulphuric acid and water binary homogeneous nucleation**
		S.-H. Lee, D.R. Benson, L.-H. Young, F.R. Kameel, J.R. Pierce, H. Juninnen, and M. Kulmala
Back-up Paper	T028A03	**Acid-catalyzed reactions of limonene and terpineol and their implication in secondary organic aerosol (SOA) formation**
		Y.J. Li, G.Y.L. Cheong, A.K.Y. Lee, A.P.S. Lau, and C.K. Chan

Tuesday 8 September 2009		**16:15 - 18:15**		**Hörsaal 3**

Aerosol Instrumentation I

Chairs:	**Hans Grimm and Igor Agranovski**

16:15	T091A11	**Evaporation kinetics of a non-spherical, levitated aerosol particle sing optical resonance spectroscopy for precision sizing**
		U.K. Krieger and A.A. Zardinia
16:35	T091A07	**New data of dry deposition velocity of sub-micron aerosol on several rural substrates and comparison with models**
		P. E. Damay, D. Maro, A. Coppalle, E. Lamaud, O. Connan, D. Hébert, and M. Talbaut
16:55	T091A05	**A new calibration method for optical particle counters in the size range of 0.2 to 8 µm**
		M. Weiß and L. Mölter
17:15	T091A06	**Fluorescent test particles for the determination of protection factor of safety work benches**
		S. Opiolka, A. Bankodad, S. Haep, M. Abele, and L. Mölter
17:35	T091A09	**Measurement of nanoparticle agglomerates by combined measurement of electrical mobility and charging properties**
		D.Y.H. Pui, H. Fissan, J. Wang, W.G. Shin, M. Mertler, and B. Sachweh
17:55	T091A03	**In-situ Small Angle X-Ray Scattering (SAXS) characterization of SiO_2 nanoparticles synthesized in a microwave-plasma reactor**
		V. Goertz, A. Abdali, H. Wiggers, C. Schulz, and H. Nirschl

Tuesday 8 September 2009		**16:15 - 18:15**		**Hörsaal 1**

Special Session 5: Special EUCAARI Session

Chairs:	**Urs Baltensperger and NN**

16:15	T170A02	**The European Integrated project on Aerosol Cloud Climate and Air Quality Interactions - EUCAARI – Progress in 2007-2008**
		A. Asmi, M. Kulmala, H. Lappalainen, and EUCAARI team
16:35	T170A05	**SOA formation from stress induced BVOC emissions**
		E. Kleist, M. dal Maso, A. Kiendler-Scharr, T. Hoffmann, T. Hohaus, N. Lang-Yona T. F. Mentel, C. Reinnig, Y. Rudich, R. Tillmann, R. Uerlings, J. Warnke, and J. Wild
16:55	T170A15	**The Mace Head EUCAARI intensive campaign**
		M. Dall'Osto, C. O'Dowd, D. Ceburnis, J. Bialek, R. Dupuy, D. Worsnop, R. Healy, and J. Wenger
17:15	T170A11	**Origin, composition and volatility of aerosol in the Mediterranean during the EUCAARI intensive campaigns: The Finokalia Aerosol Measurement Experiments**
		L. Hildebrandt, E. Kostenidou, B.-H. Lee, G.J. Engelhart, C. Mohr, K. Bougiatioti, P.F. DeCarlo, A.S.H. Prevot, U. Baltensperger, N. Mihalopoulos, N.M. Donahue, and S.N. Pandis
17:35	T170A18	**The EUCAARI LONG- RANGE Experiment (LONGREX)**
		H. Coe, W. T. Morgan, G. McMeeking, P.I. Williams, J.D. Allan, M.J. Northway, C. McConnell, E.J. Highwood, J. Haywood, S Osborne, R. Krecji, T. Hamburger, A. Minnikin, M. Frontoso, C. Reddington, and K.S. Carslaw
17:55	T170A09	**Black carbon ageing over Europe during LONGREX-EUCAARI campaign**
		M.G. Frontoso, K.S. Carslaw, G.W. Mann, D.V. Spracklen, D. Liu, G. McMeeking, G. McMeeking, H. Coe, and A. Stohl
Back-up Paper	T170A17	**Size dependency of ice nucleating properties of various mineral dust samples**
		O. Stetzer, A. Welti, F. Lüönd, and U. Lohmann

Tuesday 8 September 2009	18:15	End of Conference Day
Tuesday 8 September 2009	18:25 - 19:00	General Assembly of GAeF

Tuesday 8 September 2009	20:00 - 21:00	Audimax
Public Lecture		
Chair:	**Peter McMurry**	

20:00	Public Lecture	**Geo-Engineering**
		Rolf Müller

Wednesday 9 September 2009

Wednesday 9 September 2009	08:30 - 12:30	Registration

Wednesday 9 September 2009	08:45 - 09:55	Audimax
Plenary Lecture III		
Chair:	**Gerhard Kasper**	

08:45	Plenary Lecture	**Closing the gap between nanoparticles and molecules**
		Juan Fernandez de la Mora
09:45	Award Ceremony	**Presentation of the Smoluchowski Award**
		Alfred P. Weber

Wednesday 9 September 2009	09:55 - 10:15	Coffee Break and Exhibition

Wednesday 9 September 2009	10:15 - 12:15	Audimax
Atmospheric Aerosols - Urban Aerosols II		
Chairs:	**Alex Huffmann and Oliver Bischof**	

10:15	T051A04	**Aerosol exposure at schools during morning hours: effect of school buses**
		S.A. Grinshpun, C. Li, Q. Nguyen, P.H. Ryan, G.K. LeMasters, H. Spitz, M. Lobaugh, and S. Glover
10:35	T051A34	**Seasonal diurnal concentrations of suspended particulate matter in Mombasa City, Kenya**
		W. Kimani, M.J. Gatari, J.K. Ng'anga', and J. Boman
10:55	T051A28	**Winter particulate pollution and source apportionment in Central India**
		K.S. Patel, N.K. Jaiswal, H. Saathoff, T. Leisner, J.F.N. Aguilera, E.Y Funes, S. Nava, F. Lucarelli, M. Viana, and M. Pandolfi
11:15	T051A06	**Chemical species of transition metals in the aerosol particles of a metropolitan underground railway station**
		I. Salma, M. Pósfai, K. Kovács, E. Kuzman, Z. Homonnay, and J. Posta

11:35	T051A35	**Experimental observations of in-vehicle exposure to particles in real-world driving**
		*I.D. Longley, G.Olivares, **G.F. Coulson**, and N.Talbot*
11:55	T051A20	**Mass size distribution of trace metals at a traffic site and evaluation of a tracer for brake dust**
		***J.K. Gietl**, A.J. Thorpe, R. Lawrence, and R.M. Harrison*
Back-up Paper	T051A40	**Impact of local traffic on NOx and PM: urban background versus traffic locations**
		***M. Van Poppel**, N. Bleux, and P. Berghmans*

Wednesday 9 September 2009	10:15 - 12:15	Neuer Chemie Hörsaal

Particle-Lung-Interactions I

Chairs:	**Otmar Schmid and Lidia Morawska**

10:15	T101A05	**Computer modelling of transport and deposition of detrimental and therapeutic aerosols in three-dimensional realistic airways**
		*Á. Farkas, **I. Balásházy**, I. Szoke, and B.G. Madas*
10:35	T101A01	**Inter- and intra-lobar deposition of inhaled particles**
		***R. Winkler-Heil** and W. Hofmann*
10:55	T106A01	**Investigations into the size distribution of droplets from expiratory activities**
		***L. Morawska**, G.R. Johnson, Z.D. Ristovski, M. Hargreaves, K. Mengersen, S. Corbett, C.Y.H. Chao, Y. Li, and D. Katoshevski*
11:15	T101A10	**Respiratory tract deposition of particles at a busy street**
		***J. Löndahl**, A. Massling, E. Bräuner, E. Swietlicki, M. Ketzel, J. Pagels, and S. Loft*
11:35	T101A13	**A stochastic Lagrangian model for predicting turbulent aerosol deposition in an idealized mouth-throat geometry**
		A. Dehbi
11:55	T101A03	**Real-time deposition measurements of particle size, concentration and breathing profile during particle deposition studies in the human lung**
		***C.J. McGrath** and C.J. Dickens*
Back-up Paper	T101A02	**Effect of intersubject variability of nasal airway dimensions on particle deposition**
		***M. Hussain**, R. Winker-Heil, and W. Hofmann*

Wednesday 9 September 2009	10:15 - 12:15	HSI-Hörsaal

Aerosol-based Nanotechnology - Gas Phase Synthesis

Chairs:	**Wendelin Stark and Vincent Vons**

10:15	T015A01	**Surface processing of aerosol nanoparticles for materials applications:Growth of organic monolayers and multilayers on nanoparticle silicon**
		***J.T Roberts**, S. Calder, and J. Holm*
10:35	T015A05	**Gas phase synthesis of iron carbide nanoparticles for large scale magnetic separations**
		***I.K. Herrmann**, R.N. Grass, and W. J. Stark*
10:55	T015A07	**Hermetically-coated superparamagnetic Fe_2O_3 particles with SiO_2 nanofilms**
		*A. Teleki, M. Suter, P.R. Kidambi, O. Ergeneman, F. Krumeich, B.J. Nelson, and **S.E. Pratsinis***
11:15	T015A09	**Comparative SMPS-/TEM-analyses on laser-generated nanoparticle-aerosols**
		*M. Pesch, J. Spielvogel, **L. Keck**, H.-D. Kurland, J. Grabow, I. Zink, G. Staupendahl, and F. A. Müller*
11:35	T015A15	**Synthesis of Silicon nanoparticles by Laser assisted Chemical Vapor Pyrolysis for Li-ion battery electrodes**
		***D. Munaò**, E.M. Kelder, J.W.M. van Erven, M. Valvo, and J.C.M. Marijnissen*
11:55	T015A28	**Magnetic nanoparticles by chemical vapour synthesis**
		***J. Hukkamäki**, R. Niiranen, and J. Jokiniemi*
Back-up	T015A21	**SiO_2 coating of aerosolized nanoparticles by photoinduced chemical vapor deposition**

Paper		*A.M. Boies*, J.T. Roberts, and S.L. Girshick

Wednesday 9 September 2009	10:15 - 12:15	Hörsaal 3

Aerosol Instrumentation II

Chairs:	E. James Davis and Jorma Keskinen

10:15	T091A12	**Laser-induced breakdown spectroscopy for on-line measurements of particle composition**
		C. Fricke-Begemann, N. Strauß, and R. Nol
10:35	T091A14	**MiniDiSC for personal monitoring and high-resolution monitoring**
		M.Fierz, P. Steigmeier, C.Houle, and H. Burtscher
10:55	T091A23	**Parallel-DMA (PDMA) – a tool for characterization and enrichment of aerosol nanoparticles**
		A. Maißer, G. Allmaier, and W.W. Szymanski
11:15	T091A19	**NanoCheck, a valuable tool for size range expansions of optical particle counters for environmental applications**
		M. Pesch, H. Grimm, R. Hagler, and X. Guo
11:35	T091A18	**Retrieval of aerosol profiles using Multi Axis Differential Absorption Spectroscopy (MAX-DOAS)**
		S. Yilmaz, U. Frieß, A. Apituley, G. de Leeuw, and U. Platt
11:55	T023A01	**Development of an aircraft-based Laser Ablation Aerosol Mass Spectrometer (ALABAMA)**
		M. Brands, M. Kamphus, J. Schneider, C. Voigt, F. Drewnick, and S. Borrmann
Back-up Paper	T091A13	**A Synchronized Hybrid Real-Time Particulate monitor**
		K.J. Goohs, P. Lilienfeld, and J. Wilbertz

Wednesday 9 September 2009	10:15 - 12:15	Hörsaal 1

Aerosol Modelling - Climate and Transport

Chairs:	Elisabetta Vignati and Bernhard Vogel

10:15	T034A01	**Geoengineering climate with controlled sea spray emissions: feasibility and effects on natural marine sulphur cycle**
		H. Korhonen and K.S. Carslaw
10:35	T035A01	**Improvement of biogenic and wood burning emission inventories for air quality modelling in Switzerland**
		D.C. Oderbolz, S. Andreani-Aksoyoglu, J. Keller, I. Barmpadimos, A.S.H. Prévôt, and U. Baltensperger
10:55	T034A06	**Radiative impact of aerosol on the state of the atmosphere on the regional scale**
		H. Vogel, B. Vogel, R. Rinke, and M. Bangert
11:15	T033A02	**Process tracking of particle sulfate formation during the BAQS-Met Experiment in Southern Ontario**
		P.A. Makar, C. Stroud, J. Zhang, W. Gong, M. Moran, D. Sills, S. Gong, K. Hayden, J. Brook, J. Liggio, S.M. Li, J. Murphy, J. Abbatt, and G. Evans
11:35	T033A04	**Episodes of high particle concentrations over Central Europe with emphasis on the Benelux/Rhine-Ruhr area as simulated with a complex chemistry transport model**
		M. Memmesheimer, S. Wurzler, E. Friese, H.J. Jakobs, G. Piekorz, C. Kessler, A. Ebel, and H. Hebbinghaus
11:55	T035A03	**Evaluating the impact of particle emissions from natural sources in the Balkan region**
		K. Markakis, T. Giannaros, A. Poupkou, D. Melas, M. Sofiev, and J. Soares

Wednesday 9 September 2009	12:15 - 13:45	Lunch Break
Wednesday 9 September 2009	12:15 - 13:45 (Meeting Room)	IARA Committee Meeting

Wednesday 9 September 2009	13:45	End of Conference Day

14:30	Visiting the Majolika manufactory
15:00	Guided tour of historic KARLSRUHE
14:00	Laboratory Tours
19:00	Oktoberfest at the Festhalle-Durlach

Thursday 10 September 2009

Thursday 10 September 2009	08:30 - 16:15	Registration

Thursday 10 September 2009	08:45 - 09:45	Audimax

Plenary Lecture IV

Chair:	Wolfgang G. Kreyling

08:45	Plenary Lecture	**Modelling inhaled particle deposition in the human lung**
		Werner Hofmann

Thursday 10 September 2009	09:45 - 10:15	Coffee Break and Exhibition

Thursday 10 September 2009	10:15 - 12:15	Audimax

Atmospheric Aerosols - Hygroscopicity, CCN, and Clouds

Chairs:	Martin Gysel and Chak Keung Chan

10:15	T044A08	**CCN activation and hygroscopic growth measurements of secondary organic aerosols from boreal forest emissions**
		A. Buchholz, Th.F. Mentel, A: Kiendler-Scharr, C. Spindler, R: Tillmann, E. Kleist, and J. Wildt
10:35	T044A19	**CCN ability of mixed organic-inorganic particles**
		M. Frosch, N.L. Prisle, M. Bilde, Z. Varga, and G. Kiss
10:55	T170A04	**Measuring and modeling cloud condensation nuclei concentrations at the Jungfraujoch high alpine site**
		Z. Jurányi, M. Gysel, E. Weingartner, P.F. DeCarlo, M. F. Heringa, R. Chirico, and U. Baltensperger

11:15	T044A18	**Hygroscopic growth of tropospheric particle number size distributions over the North China Plain**
		A.Nowak, P. Achtert, W. Birmili, and A.Wiedensohler
11:35	T044A22	**Measured and modelled hygroscopic properties of the background ambient aerosol in the southern part of Sweden**
		E. Nilsson, P. Roldin, and E. Swietlicki
11:55	T044A03	**Aerosol- and updraft-limited regimes of cloud droplet formation: influence of particle number, size and hygroscopicity on the activation of cloud condensation nuclei (CCN) under pyro-convective conditions**
		Ph. Reutter, J. Trentmann, H. Su, M. Simmel, D. Rose, H. Wernli, M.O. Andreae, and U. Pöschl
Back-up Paper	T044A01	**Aerosol cloud interaction in northern Finland**
		H. Lihavainen and L. Remer

Thursday 10 September 2009	10:15 - 12:15	Neuer Chemie Hörsaal

Particle-Lung-Interactions II

Chairs: **Werner Hofmann and Sonja Mülhopt**

10:15	T105A10	**Analgesic effect from ibuprofen nanoparticles inhaled by male mice**
		*A.A. Onischuk, T.G. Tolstikova, **I.V. Sorokina**, N.A. Zhukova, A.M. Baklanov, V.V. Karasev, O.V. Borovkova, G.G. Dultseva, V.V. Boldyrev, and V.M. Fomin*
11:55	T105A01	**Physico-chemical differences between particle and molecule derived toxicity: Influence of small molecule adsorption on engineered nanoparticles**
		*L.K. Limbach, E.K. Athanassiou, R.N. Grass, and **W.J. Stark***
10:55	T103A01	**The QCM - online dose measurement with high relative humidity**
		***S. Mülhopt**, A. Comouth, A. Grotz, T. Krebs, and H.-R. Paur*
11:15	T105A07	**Oxidative potential of logwood and pellet burning particles assessed by a novel profluorescent nitroxide probe**
		***B. Miljevic**, N.K. Meyer, A. Keller, H. Burtscher, J. Good, A. Dober, T. Nussbaumer, M.F. Heringa, A. Richard ,P.F. DeCarlo ,A.S.H. Prevot, K.E. Fairfull-Smith, U. Baltensperger, S.E.Bottle, and Z.D.Ristovski*
11:35	T104A06	**Towards in vitro nanoparticle toxicity screening: Quantitative prediction of soot-induced pulmonary inflammation from in vitro assays**
		*T. Stoeger, D. Dittberner, S. Takenaka, H. Schulz, and **O. Schmid***
11:55	T105A11	**Physicochemical and in vitro oxidative characterisation of size fractionated PM at microenvironments with contrasting local emissions scenarios**
		***K.J. Godr**i, I.S. Mudway, F.J. Kelly, R.M. Harrison, M. Strak, M. Steenhof, P. Fokkens, A. Boere, D. Leseman, K. Meliefste, G. Hoek, B. Brunekreef, E. Lebret, F. Cassee, I. Gosens, and N.A.H. Janssen*
Back-up Paper	T105A03	**Acute cardiovascular effects associated with air pollution: a new pathogenetic pathway in patients with chronic obstructive pulmonary diseases (COPD)**
		***F. Cetta**, G. Schiraldi, M. Sala, R. Zangari, A. Dhamo, L. Moltoni, P. Laviano, F. Cisternino, A. Azzarà, G. Malagnino, P. Favini, and L. Allegra*

Thursday 10 September 2009	10:15 - 12:15	HSI-Hörsaal

Special Session 1: Atmospheric Aerosol Processes in a Developed Mega-City: The REPARTEE Study in London

Chairs: Roy M. Harrison and Eiko Nemitz

10:15	T130A07	**REPARTEE-I and REPARTEE-II (Regent's Park and Tower Environmental Experiment)**
		***Roy M. Harrison**, M. Dall'Osto, M. Gallagher, P. Williams, H. Coe, J. Allan, E. Nemitz, G. Phillips, R. Jones, J. Barlow, A. Thorpe, W. Bloss, A. Benton, C. Di Marco, S. Ball, C. Martin, A. Lewis, D. Martin, F. Davies, R. Kinnersley, D. Green*
10:35	T130A05	**The effect of boundary layer dynamics on the aerosol size distributions over London**
		***M. Dall'Osto**, J. F. Barlow, Roy. M. Harrison, D. Beddows, and T. Dunbar*

10:55	T130A03	**Attribution of organic aerosols in UK cities**
		J.D. Allan, P.I. Williams, J. Crosier, M.W. Gallagher, and H. Coe
11:15	T130A02	**Chemically-speciated aerosol fluxes above three UK cities**
		G.J. Phillips, E. Nemitz, R. Thomas, D. Famulari, P. Williams, J. Allan, C. Di Marco, H. Coe, R.M. Harrison, and D. Fowler
11:35	T130A08	**Physico-chemical aerosol dispersion in urban environments**
		B.K.Tay, G.M. McFiggans, M.W.Gallagher, C. Martin, M.J. Flynn, P. Harris, S. Lindley, R. Agius, and R.M. Harrison
11:55	T130A10	**Nitrate dynamics in UK urban environments**
		E. Nemitz, G.J. Phillips, R. Thomas, C.F. Di Marco, S. Tang, H. Coe, J. Allan, R.M. Harrison, and D. Fowler
Back-up Paper	T130A01	**Measurements using broadband cavity-enhanced absorption spectroscopy of the sum of NO_3 and N_2O_5 during REPARTEE II and associated model studies**
		A.K. Benton, J.M. Langridge, O. Dessens, S.M. Ball, and R.L. Jones

Thursday 10 September 2009	10:15 - 12:15	Hörsaal 3

Aerosol Instrumentation III

Chairs: Wladyslaw Szymanski and Oliver Bischof

10:15	T091A29	**Thermal desorption/laser photo-ionisation aerosol mass spectrometry for on-line monitoring of molecular organic compounds from individual aerosol particles**
		M. Bente, M. Sklorz, T. Streibel, and R. Zimmermann
10:35	T092A03	**A new personal thermophoretic sampler with simplified analysis routines for nanoparticle exposure studies**
		N. Azong-Wara, C. Asbach, B. Stahlmecke, H. Fissan, H. Kaminski, S. Plitzko, T.A.J. Kuhlbusch
10:55	T092A08	**Novel photoacoustic aerosol monitor for optical absorption coefficient determination. Laboratory and field test**
		T. Ajtai, M. Schnaiter, C. Linke, M. Vragel, Á. Filep, L. Födi, G. Motika, Z. Bozóki, and G. Szabó
11:15	T092A10	**First steps towards a photophoretic mobility analyzer**
		C. Haisch, L. Opilik, M. Oster, and R. Niessner
11:35	T093A03	**Characterization of a newly developed particle detector, NanoCheck 1320**
		J. Seo, R. Hagler, M. Kim, and T. Kim
11:55	T093A01	**Dependence of the performance of condensation particle counter (CPC) on particle number concentration**
		Z.Z. Zhang
Back-up Paper	T092A05	**Development of new instrumentation for aerosol angular light scattering and spectral absorption measurements**
		G. Dolgos, J.V. Martins, L.A. Remer, and A.L. Correia

Thursday 10 September 2009	10:15 - 12:15	Hörsaal 1

Electrical Effects - Electrostatic Discharge and Related Phenomena

Chairs: Caner Yurteri and Jean-Pascal Borra

10:15	T062A02	**The drained DBD electrode as a charger for highly concentrated aerosols**
		M. Wild, J. Meyer, and G. Kasper
10:35	T062A04	**Aerosol charge distributions in Dielectric Barrier Discharges**
		N. Jidenko, E. Bourgeois, and JP. Borra
10:55	T063A06	**Motion of diffusing particles in electric fields**
		V.A. Zagaynov, A.A. Lushnikov, D.V. Vodyanik, and Yu.S. Lyubovtseva
11:15	T062A05	**Influence of gas velocity, particle concentration and electrode geometry on corona discharge characteristics in small electrode gaps**
		A. Bologa, H.-R. Paur, and K. Woletz

11:35	T065A03	The effect of particle pre-existing charge on unipolar charging and its implication on electrical aerosol measurements
		C. Asbach, C. Qi, W.G. Shin, D.Y.H. Pui, and H. Fissan
11:55	T063A05	Measurement of small ions near a busy motorway
		X. Ling, R. Jayaratne, and L. Morawska
Back-up Paper	T068A04	Corona-Quenching by submicrometer particles in turbulent tube-wire electrostatic precipitators
		C. Luebbert and U. Riebel

Thursday 10 September 2009	12:15 - 13:45	Lunch Break

Thursday 10 September 2009	13:45 - 15:45	Poster and Exhibition Area
Poster Session Part II and Exhibition. For details see below		

Thursday 10 September 2009	15:45 - 16:15	Coffee Break and Exhibition

Thursday 10 September 2009	16:15 - 18:00	
Working Group Sessions		

Thursday 10 September 2009	16:15 - 17:00	Audimax
Working Group: Atmospheric Aerosols		
Chair:	Martin Gysel	

Thursday 10 September 2009	16:15 - 17:00	Neuer Chemie Hörsaal
Working Group: PMx		
Chair:	Harry ten Brink	

Thursday 10 September 2009	16:15 - 17:00	HSI-Hörsaal
Working Group: Aerosol based nanotechnology		
Chair:	Hanns-Rudolf Paur	

Thursday 10 September 2009	16:15 - 17:00	Hörsaal 3
Working Group: Aerosol Modelling		
Chair:	Elisabetta Vignati	

Thursday 10 September 2009	16:15 - 17:00	Hörsaal 1

Working Group: Fundamentals		
Chair:	**Jose Castillo**	

Thursday 10 September 2009	**17:15 - 18:00**	**Audimax**
Working Group: Instrumentation		
Chair:	**Aladar Czitrovski**	

Thursday 10 September 2009	**17:15 - 18:00**	**Neuer Chemie Hörsaal**
Working Group: Aerosol Chemistry		
Chair:	**Yoshi Iinuma**	

Thursday 10 September 2009	**17:15 - 18:00**	**HSI-Hörsaal**
Working Group: Particle-Lung-Interaction		
Chair:	**Werner Hofmann**	

Thursday 10 September 2009	**17:15 - 18:00**	**Hörsaal 3**
Working Group: High-Temperature-Aerosols		
Chair:	**Cristina Gutierrez-Canas**	

Thursday 10 September 2009	**17:15 - 18:00**	**Hörsaal 1**
Working Group: Electrical Effects		
Chair:	**Andrei Bologa**	

Thursday 10 September 2009	**18:00**	**End of Conference Day**

Thursday 10 September 2009	**19:00**	**Conference Dinner**

Friday 11 September 2009

Friday 11 September 2009	**08:30 - 15:00**	**Registration**

Friday 11 September 2009	08:45 - 09:55	Audimax

Plenary Lecture V

Chair:	Mats Bohgard

08:45	Plenary Lecture	**Aerosol exposure and health effects: Do we know the basis?**
		Thomas Kuhlbusch
09:45	Award Ceremony	**Presentation of the Poster Awards**
		Johanna Gietl and Hanns-Rudolf Paur

Friday 11 September 2009	09:55 - 10:15	Coffee Break and Exhibition

Friday 11 September 2009	10:15 - 12:15	Audimax

Atmospheric Aerosols - Transport and Transformation, Optical Properties

Chairs:	Darrel Baumgardner and Wolfgang Junkermann

10:15	T042A07	**From fresh exhaust to CCN: Transformation of particles from shipping**
		L. Pfaffenberger, R. Baumann, J. Moldanová, T. Hamburger, B. Weinzierl, A. Minikin, H. Schlager, and A. Petzold
10:35	T042A08	**Effect of Tar burning on UFP size distribution at a background site at Mol, Belgium**
		V.K. Mishra, E. Frijnsa , P. Berghmansa, , N. Bleuxa, and J. Kretzschmar
10:55	T042A10	**Number size distribution and chemical composition changes along vertical profiles in the Po Valley, implications for aerosol optical properties**
		L. Ferrero, E. Bolzacchini, M.G. Perrone, B.S. Ferrini, Z. Lazzati, F. Bruno, D. Cocchi, F. Greco, G. Mocnick, D. Cappelletti, L. Barcherini, S. Ortu, and B. Moroni
11:15	T047A05	**Study of transformation of aerosol optical and microphysical parameters at heating**
		S.A.Terpugova, M.V. Panchenko, T.A. Dokukina, and E.P. Yausheva
11:35	T047A09	**Testing Koschmieder visibility theory in a town**
		D. Strigl and H. Horvath
11:55	T047A04	**Single scattering Albedo variation in the Indian continental tropical and convergence zone during premonsoon and monsoon seasons of 2008**
		J. Jai Devi, S.N. Tripathi, T. Gupta, and V. Gopalakrishnan
Back-up Paper	T042A05	**Planetary boundary layer influence at the Jungfraujoch depending on synoptic weather types**
		M. Collaud Coen, E. Weingartner, and U. Baltensperger

Friday 11 September 2009	10:15 - 12:15	Neuer Chemie Hörsaal

Particle-Lung-Interactions - Indoor Aerosols and Children

Chairs:	Francesco Cetta and Joakim H. Pagels

10:15	T108A04	**The effect of human activity on coarse aerosol levels in a school gymnasium**
		M. Braniš, J. Šafránek, and A. Hytychová
10:35	T108A03	**Ultrafine particle release from hardcopy devices: comparison of test chamber and real room measurement**
		T. Salthammer, E. Uhde, T. Schripp, M. Wensing, C. He, and L. Morawska
10:55	T104A04	**Cytotoxic and inflammatory effects of indoor PM10 compared to outdoor PM10 from German schools**
		S. Oeder, W. Schober, I. Weichenmeier, S. Dietrich, H. Fromme, H. Behrendt, and J.T.M. Buters
11:15	T105A02	**Seasonal and dimensional differences in the proinflammatory potency of atmospheric particulate matter. Comparison of in vitro results with clinical effects in children exposed to the same particles from the same urban area. The Milan Prolife Project**
		F. Cetta, M. Sala, R. Accinni, A. Dhamo, R. Zangari, L. Moltoni, E. Bolzacchini, M. Gualtieri, P. Mantecca, and M. Camatini

11:35	T108A14	**Assessment of indoor aerosol sources from measurements of Number Size Distribution and Chemical Composition by means of Positive Matrix Factorization**
		A.A. Karanasiou, S. Vratolis, M. Lazaridis, and K. Eleftheriadis
11:55	T108A02	**Science behind particles from printer and copier operation: do we understand it?**
		L. Morawska, C. He, G. Johnson, R. Jayaratne, T. Salthammer, H. Wang, E. Uhde, T. Bostrom, R. Modini, G. Ayoko, P. McGarry, and M. Wensing
Back-up Paper	T108A06	**Development of continuous inspection of indoor aerosol in classroom of Peoples Friendship University of Russia**
		T. Aljazar and A. Syroeshkin

Friday 11 September 2009	10:15 - 12:15	HSI-Hörsaal

Aerosol-based Nanotechnology - Application and Structuring

Chairs:	Bernd Sachweh and Martin Seipenbusch

10:15	T014A01	**Antibacterial activity of flame-made Ag/SiO$_2$ nanoparticles**
		G.A. Sotiriou, A. Camenzind, A. Meyer, S. Panke, and S.E. Pratsinis
10:35	T014A05	**Nanoparticles for Li-ion battery electrodes by electrospray-assisted aerosol routes**
		M. Valvo, U. Lafont, D. Munaò, J. C. M. Marijnissen, and E. M. Kelder
10:55	T014A06	**Size-selected agglomerates as ultrasensitive gas sensors**
		H. Keskinen, A.Tricoli, M. Marjamäki, J.M. Mäkelä, and S.E. Pratsinis
11:15	T014A08	**Are gold aerosols superior to other types of gold particles for seeding of semiconductor nanowires?**
		M.E. Messing, K. Hillerich, J. Bolinsson, K.A. Dick, K. Nilsson, J. Johansson, and K. Deppert
11:35	T016A02	**Aerosol synthesis and stabilization of supported metal nanoparticles**
		A. Binder, M. Seipenbusch, and G. Kasper
11:55	T016A04	**One-step synthesis of core-shell porous nanoparticles by an aerosol route**
		G. Kastrinaki, S. Lorentzou, and A.G. Konstandopoulos
Back-up Paper	T014A10	**Application of magnetic cobalt nanoparticles to enhance permeability of metal-polymer composite substrates**
		P. Koskela, U. Tapper, A. Auvinen, J. Jokiniemi, A. Alastalo, H. Seppä, M. Aronniemi, M. Teirikangas, J. Juuti, and H. Jantunen

Friday 11 September 2009	10:15 - 12:15	Hörsaal 3

Atmospheric Aerosols - Specific Aerosol Types I

Chairs:	Martina Krämer and Martin Schnaiter

10:15	T054A07	**Ice nucleation of soot particles with variable organic and sulphuric acid coating**
		O. Möhler, S. Benz, A. Buchholz, J.Crosier, S. Henning, T. Leisner, Th. F. Mentel, V. Michaud, H. Saathoff, M. Schnaiter, R. Wagner, and M. Ziese
10:35	T054A01	**Freezing and activation measurements of coated and uncoated Arizona Test Dust particles**
		D. Niedermeier, S. Hartmann, R. Shaw, D. Covert, Th. F. Mentel, J. Schneider, L. Poulain, T. Clauss, A. Kiselev, E. Hallbauer, H. Wex, and F. Stratmann
10:55	T054A14	**Water to Ice Transition experiments at the AIDA - chamber: first results from the novel ice experiment NIXE-CAPS**
		J. Meyer, M. Krämer, A. Afchine, M. Schnaiter, R. Newton, and D. Baumgardner
11:15	T054A05	**Correlations between particulate sulfate and ozone observed in the UT/LS over Greenland and Central/Western Europe in 2008**
		J. Schmale, J. Schneider, M. Brands, G. Ancellet, H. Schlager, M. Lichtenstern, M. Scheibe, S.R. Arnold, K.S. Law, C. Voigt, and S. Borrmann
11:35	T057A11	**Parameterization of biomass burning particle emissions from wildfires**
		S. Janhäll, M.O. Andreae, and U. Pöschl
11:55	T057A03	**Probing the composition, mixing state and hygroscopic properties of aerosol particles emitted from a wood pellet burner by coupling a SP2 and a SI-AMS with a H-TDMA**

		M. Gysel, T. Tritscher, M.F. Heringa, P.F. DeCarlo, J. Noda, T. Gustafsson, J.B.C. Pettersson, J. Dommen, E Weingartner, A.S.H. Prévôt, and U. Baltensperger
Back-up Paper	T054A11	**Black carbon scavenging by mountain cloud**
		D. Baumgardner, R. Subramanian, C. Twohy, and G. Kok

Friday 11 September 2009	10:15 - 12:15	Hörsaal 1
Atmospheric Aerosols - Mineral Dust		
Chairs:	**Lothar Schütz and Thomas Müller**	

10:15	T052A17	**Composition of Saharan dust and its possible source regions – a review**
		D. Scheuvens, L. Schütz, K. Kandler, M. Ebert, and S. Weinbruch
10:35	T052A16	**Determination of aerosol particle size distribution for mineral dust during the SAMUM campaign**
		M. Diouri, W. von Hoyningen-Huene, T. Zarrouk, T. Dinter, A. Kokhanovsky, and J.P Burrows
10:55	T052A07	**African and local wind-blown dust contributions at three rural sites in SE Spain: aerosol size distribution**
		J.A.G. Orza, M. Cabello, V. Lidón, and J. Martínez
11:15	T052A13	**PM10 source apportionment using factor analysis: Eastern Mediterranean Case**
		F. Öztürk and G. Tuncel
11:35	T052A14	**Simulation of the impact of mineral dust on the monsoon flow and the easterly jet above Western Africa**
		T. Stanelle, B. Vogel, V. Klüpfel, H. Vogel, Ch. Grams, and S. Jones
11:55	T052A18	**Have Saharan dust plumes any impact on ozone retrieval from UV nadir satellite spectrometers?**
		J. Andrey, M. Gil, A. Redondas, M. Navarro, M. Schneider, and E. Cuevas
Back-up Paper	T052A09	**Single particle chemical composition, state of mixing and shape of fresh and aged Saharan dust in Morocco and at Cape Verde Islands during SAMUM I and II**
		K. Kandler, C. Deutscher, M. Ebert, K. Lieke, D. Müller-Ebert, L. Schütz, and S. Weinbruch

Friday 11 September 2009	12:15 - 13:45	Lunch Break
Friday 11 September 2009	**12:15 - 13:45 (Meeting Room)**	**Working Group Chairs Meeting**

Friday 11 September 2009	13:45 - 15:45	Audimax
Atmospheric Aerosols - Physical and Chemical Properties		
Chairs:	**David Topping and Andreas Maßling**	

13:45	T043A03	**Single particle studies of the kinetic and thermodynamic factors governing the size and composition of inorganic/organic/aqueous aerosol**
		J.P. Reid, K.L. Hanford, G. Hargreaves, K.J. Knox, N. Kwamena, A. Laurain, and J.B. Wills
14:05	T043A02	**Combined volatility and mass spectrometric measurements of biogenic secondary organic aerosol**
		E. Emanuelsson , M. Hallquist, A. Buchholz, A. Kiendler-Scharr, **Th. F. Mentel**, and C. Spindler
14:25	T043A11	**Source apportionment studies for trace elements based on hourly size-segregated data**
		A. Richard, M. Furger, N. Bukowiecki, P. Lienemann , M. Nachtegaal, A. Prevot, and U. Baltensperger
14:45	T043A06	**Physical, chemical and hygroscopic properties of activating particles in Northern Finland**
		N. Kivekäs, V.-M. Kerminen, T. Raatikainen, P. Vaattovaara, A.Laaksonen, and H. Lihavainen
15:05	T043A09	**N. Kivekäs, V.-M. Kerminen, T. Raatikainen, P. Vaattovaara, A.Laaksonen, and H. Lihavainen**
		K. Schäfer, S. Emeis, P. Suppan, S. Norra, N. Schleicher, J. Vogt, V. Dietze, U. Kaminski, Y. Wang, J. Xin, F. Chai, and Y. Chen
15:25	T043A15	**Efflorescence, deliquescence and crystal structures of ternary aerosols**

		L. Treuel, S. Pederzani and R. Zellner
Back-up Paper	T043A13	**Chemical and morphological characterization of dustfall (dry deposition) in Vitória-ES Brazil**
		M.M. Conti, L.R. Menegussi, **N.C. Reis** Jr., J.M. Santos, F.J. Silva, and C. Scandian

Friday 11 September 2009		**13:45 - 15:45**		**Neuer Chemie Hörsaal**

Particle-Lung-Interactions - Indoor and Outdoor Aerosols

Chairs:	**Otto O. Hänninen and Conor J. McGrath**

13:45	T104A08	**Seasonal chemical composition and biological effects for fine particles (PM1 and PM2.5) of a Milan urban site (North of Italy)**
		M.G. Perrone, M. Gualtieri, L. Ferrero, C. Lo Porto, E. Bolzacchini, R. Udisti, and M. Camatini
14:05	T108A18	**Ozone initiated SOA formation of combustion aerosols**
		J. Pagels, M. Lindskog, E. Nilsson, E. Swietlicki, and M. Bilde
14:25	T108A17	**Pathways of ultrafine particles generated by laser printers**
		H. Wang, L. Morawska, C. He, G. Johnson, R. Jayaratne, T. Salthammer, E. Uhde, T. Bostrom, R. L. Modini, G. Ayoko, P. McGarry, and M. Wensing
14:45	T106A03	**Ambient concentrations of the major birch allergen Bet v 1 and birch pollen count in Munich, Germany, in 2004 till 2008, and the new EU-HIALINE project**
		J.T.M. Buters, C. Huber, I. Weichenmeier, G. Pusch, W. Kreyling, W. Schober, H. Behrendt, and the HIALINE working group
15:05	T108A16	**Hygroscopic and volatility properties of particles emitted by office equipments**
		H. Wang, G. Johnson, R. L. Modini, C. He, L. Morawska, R. Jayaratne, T. Salthammer, E. Uhde, T. Bostrom, G. Ayoko, P. McGarry, and M. Wensing
15:25	T105A13	**Comparison of in-vitro toxicity and epidemiologically determined mortality risk for ambient particles using alternative particle metrics**
		O.O. Hänninen, I.Brüske-Hohlfeld, O. Schmid, W. Kreyling, T. Stoeger, P.E. Schwarze, J. Cyrys, M. Pitz, A. Peters, and H.-E. Wichman
Back-up Paper	T108A09	**Impact of outdoor combustion emissions on indoor air in a pulmonary hospital**
		M. Vardjan, M. Bajic, A. Zrimec, and **G. Mocnik**

Friday 11 September 2009		**13:45 - 15:45**		**HSI-Hörsaal**

Aerosol Instrumentation IV

Chairs:	**David Pui and Christoph Asbach**

13:45	T094A03	**Mass concentration of PM2.5, nitrate and sulfate measured by automatic instruments and manual sampler during various meteorological conditions**
		J.H. Tsai, C.H. Lin, C.C. Liu, W.F. Lai, and Y.C Yao
14:05	T094A05	**Comparison of the Thermo Scientific TEOM 1405-DF monitor to Reference Method Sampling Results for the Measurement of PM2.5**
		J.L. Ambs
14:25	T095A01	**Ion-induced solvation and nucleation studies in a sonic DMA**
		M. Attoui and J. Fernandez de la Mora
14:45	T095A02	**Construction of a biofluorescence optical particle counter**
		R. Greaney, O. Ryan, S.G. Jennings, and C.D. O'Dowd
15:05	T096A01	**ISO 15900 – A new international standard for differential electrical mobility analysis**
		H.-G. Horn, K. Ehara, N. Fukushima, K. Ichijo, I. Marshal, Y. Otani, M. Owen, C. Peters, P. Quincey, H. Sakurai, J. Schlatter, G.J. Sem, J. Spielvogel, C. Tsunoda, and J. Vasiliou
15:25	T096A03	**Best practices in European aerosol monitoring: the EUSAAR ground-based observation network**
		P. Laj, S. Philippin, A. Wiedensohler, U. Baltensperger, G. de Leeuw, J.-P. Putaud, A.M. Fjaeraa, M. Fiebig, and U. Platt
Back-up Paper	T094A04	**Performance of a new condensation particle counter**
		H. Kim, J. Spielvogel, and T. Kim

Friday 11 September 2009	13:45 - 15:45	Hörsaal 3

Atmospheric Aerosols - Specific Aerosol Types II

Chairs:	Martin Ebert and Konrad Kandler	

13:45	T057A13	**The contribution of biomass burning to PM: a comparison between an Alpine valley and the Po Valley**
		C.A. Belis, A. Piazzalunga, C. Colombi, P. Fermo, B. Larsen, R. Vecchi, C. Carugo, and V. Gianelle
14:05	T057A09	**Strong wintertime influences of residential wood burning aerosols in urban environments: Grenoble and Paris, France**
		O. Favez, B. d'Anna, A. Boréave, I. el Haddad, N. Marchand, C. Piot, J.L. Besombes, D. Voisin, J.L. Jaffrezo, J. Sciare, H. Cachier, and C. George
14:25	T059A07	**Optimized separation of OC and EC for radiocarbon source apportionment**
		S. Szidat, N. Perron, S. Fahrni, M. Ruff, L. Wacker, A. S. H. Prévôt, and U. Baltensperger
14:45	T059A13	**Using a multi-wavelength Aethalometer to determine the contributions of fossil fuel and biomass burning to aerosols in Ispra, Italy**
		C. Gruening, F. Cavalli, Dell'Acqua, S. Dos Santos, and J.-P. Putaud
15:05	T059A02	**Sources and components of organic aerosols in Central Europe**
		V.A. Lanz, A.S.H. Prévôt, M.R. Alfarra, C. Hüglin, C. Mohr, S. Weimer, and U. Baltensperger
15:25	T059A06	**Black carbon aerosols in urban air in South Asia**
		L. Husain, S. Alvi, and V.A. Dutkiewicz
Back-up Paper	T059A09	**OC, EC, and SOA contribution to PM in Lombardy (Italy): results of three winter campaigns (2005-2007)**
		A. Piazzalunga, P. Fermo, R. Vecchi, G. Valli, S. Comero, V. Bernardoni, O. Cazzuli, A.Giudici, and G.Lanzani

Friday 11 September 2009	13:45 - 15:45	Hörsaal 1

Electrical Effects - Charged Aerosols and Their Application

Chairs:	Andrei Bologa and Jan Marijnissen	

13:45	T063A07	**Experimental demonstration of the role of the image force in diffusion charging**
		M. Fierz and H. Burtscher
14:05	T063A11	**Electrospray droplets transport in the extractor-collector configuration. Inertial effects**
		M. Lallave, D. Galán, J. Ortega-Casanova, A. Barrero, and *I.G. Loscertales*
14:25	T061A01	**Controlling progeny droplets emitted during the Coulombic fission of a charged drop**
		H.H. Hunter and *A.K. Ray*
14:45	T063A09	**Phenomenology of salt water electrosprays**
		L.L.F. Agostinho, J.C.M. Marijnissen, C. U. Yurteri, E.C. Fuchs, and S. Metz
15:05	T063A02	**Electrospray aerosol discharge by corona effect: Influence on droplets size and velocity**
		M. Pierobon, M. Sausse Lhernould, D. Zimmermann, P. Mathys, and P. Lambert
15:25	T064A02	**Nano pharmaceutical particle production by EHDA**
		C.U. Yurteri and J.M. Marijnissen
Back-up Paper	T063A03	**Neutralization of Tetraalkylammonium Halide Clusters**
		D. Wimmer, G. Steiner, and G.P. Reischl

Friday 11 September 2009	15:45 - 16:00	Audimax

Closing Remarks

Friday 11 September 2009	16:00	End of Conference

Saturday 12 September 2009

09:00	**Bus tour to STRASBOURG**
09:00	**Bus tour to KLOSTER MAULBRONN and HEIDELBERG**

Poster Session Part I

Aerosol Chemistry

Atmospheric Aerosols - specific aerosol types High

Temperature Aerosols

Aerosol Instrumentation Particle-

Lung-Interactions Radioactive

Aerosols

Special Session 1: Atmospheric Aerosol Processes in a Developed Mega-City: The REPARTEE Study in London

Special Session 5: Special EUCAARI Session

Tuesday 8 September 2009	13:45 - 15:45	Poster Hall
Poster Session Part I		

Aerosol Chemistry

T021A04	**Formation of peroxides in the gas and particle phase during photochemical aging experiments of secondary organic aerosol from alpha-pinene**
	P. Mertes, J. Dommen, T. Tritscher, A.P. Praplan, P.B. Barmet, P.F. DeCarlo, A.S.H. Prévôt, N.M. Donahue, and U. Baltensperger
T021A05	**SOA aging with different OH sources**
	P.B. Barmet, P.F. DeCarlo, J. Dommen, T. Tritscher, A.P Praplan, P. Mertes, A.S.H. Prevot, N.M. Donahue, and U. Baltensperger
T021A06	**Aerosol and gas phase organic acids in smog chamber aging experiments of secondary organic aerosol from α-pinene**
	A.P. Praplan, T. Tritscher, P. Barmet, P. Mertes, P.F. DeCarlo, J. Dommen, A.S.H. Prévôt, N.M. Donahue, and U. Baltensperger
T021A09	**Characterisation of the AIDA aerosol chamber by means of commercial computational fluid dynamics (CFD) software**
	S. Benz, H. Bunz, J. Meinen, O. Möhler, and T. Leisner
T021A10	**H_2O_2 and organic peroxides from the ozonolysis of α-humulene and β-caryophylleney**
	J. Valverde-Canossa, G. Moortgat, A. Sadezky, and R. Winterhalter
T022A02	**Organic composition of PM2.5 aerosols in Cork Harbour, Ireland**
	I. Kourtchev, J. Bell, S. Hellebust, I.P. O'Connor, A. Allanic, R.M. Healy, J.C. Wenger, and J.R. Sodeau
T022A03	**Chemical and physical characterization of diesel emissions from EURO 2, 3 and 4 vehicles fuelled by reference diesel and a 20% biofuel blend**
	J. Klenø Nøjgaard, A. Massling, B. Jensen, A. G. Hemmersam, C. Raahede, and P. Wåhlini

T022A04	**Indicatory polychlorinated dibenzo-p-dioxins and dibenzofurans in the Surrounding Ambient Air of rural/traffic/industrial areas in Taiwan**
	M.-W. Chen, W.-J. Lee, L.-C. Wang, and G.-P. Chang-Chien
T022A05	**Sources assignation of PM2.5 atmospheric aerosol in a rural area of Spain**
	O. Pindado, R.Mª. Pérez, S. García, M. Sánchez, P. Galán, and M. Fernández
T022A06	**Characteristics of dicarboxylic acids in Pearl River Delta Region**

		S.C. Lee, K F. Ho, K. Kawamura, and J.J. Cao
T022A09	**Analysis of low and high molecular weight water-soluble organic aerosol components by LC-MS**	
	Y. Zhang, R. Winterhalter, H. Yang, G.K. Moortgat, and U. Pöschl	
T022A10	**PM1 chemical characterization and source apportionment in two background sites with different anthropic impact near Florence, Italy. Results from all year-round campaigns**	
	R. Udisti, S. Becagli, R. Traversi, F. Rugi, C. Ghedini, E. Castellano, F. Marino, S. Nava, F. Lucarelli, M. Chiari, and G. Calzolai	
T022A11	**Natural and Anthropogenic contributions to PM10 in the L'Alacantí region in the South-East of Spain**	
	M. Santacatalina, E. Yubero, and A. Carratala	
T022A12	**Chemical characterization of a seasonal cycle of PM10 samples collected in Lunz am See, Austria**	
	C. Ramírez-Santa Cruz, A. Kasper-Giebl, H. Bauer, H. Puxbaum, W. Wanek, and M. Dorninger	
T022A13	**Raman spectral analysis of multicomponent aerosols from the environment of sugar factory**	
	V.M.Harpale and R.S.Gosavi	
T022A15	**Evaluation of airborne polycyclic aromatic hydrocarbons from Itaparica Island, Bahia, Brazil**	
	A. L. N. Guarieiro, G. O. da Rocha, L. dos S. Conceição, W. A. Lopes, P. A. de P. Pereira, and J. B. de Andrade	
T022A16	**Indoor air monitoring in service-flats**	
	A.J. Buczynska, A.Worobiec, E.A. Stefaniak, Y. Makarovska, A. Krata, B. Horemans, V. Novakovic, R. Van Grieken, and S. Potgieter-Vermaak	
T022A18	**Analytical methods for quantification and characterization of HULIS (HUmic Like Substances) in atmospheric aerosol**	
	***P. Fermo**, A. Piazzalunga, F. Tuccillo, L. Brambilla, O. Cazzuli, R. Vecchi, and G. Valli*	
T022A19	**Determination of azaarenes in particulate matter using liquid chromatography-tandem mass spectrometry**	
	J.Lintelmann, M. Heil-França, E. Hübner, and G. Matuschek	
T022A20	**Chemical characterization of particulate matter at the Sonnblick Observatory**	
	M.W. Koller, C. Effenberger, A. Kaiser, A. Kranabetter, G. Schauer, and A. Kasper-Giebl	
T022A21	**Influence of fireworks on atmospheric levels of trace metals**	
	N. Galindo, E. Yubero, F. Lucarelli, S. Nava, M. Chiari, G. Calzolai, J. Nicolás, and J. Crespo	
T022A22	**Polycyclic Aromatic Hydrocarbons and carbon-containing species in ambient aerosols in Thessaloniki, Greece**	
	L.P. Chrysikou, C. Samara, A. Bougiatioti, and N. Mihalopoulos	
T022A23	**A systematic chemical and morphological characterization of particulate matter in the main cities of Umbria (Italy) in the years 2006-2009**	
	L.Barcherini, D.Cappelletti, S.Ortu, F.Scardazza, F.Marmottini, B.Moroni, M.Angelucci, M.Galletti, L.Mascelloni, and M.Vecchiocattivi	
T022A27	**Aerosol source apportionment in Cork Harbour, Ireland, based on continuous, real-time measurements, Aerosol Time of Flight Mass Spectrometry and factor analysis**	
	S. Hellebust, R. Healy, I. Kourtchev, A. Allanic, I.P. O'Connor, J. Wenger, and J. Sodeau	
T022A28	**Organic compounds in Secondary Organic Aerosol measured by Direct Thermal Extraction-Gas Chromatography/Mass Spectrometry/Flame Ionization Detection**	
	S. Langer and K. Arrhenius	
T022A29	**Determination of carbon particle fluxes by combination of micro-meteorology and single particle mass spectrometry**	
	E. Gelhausen, K.-P. Hinz, A. Schmidt, O. Klemm and B. Spengler	
T024A04	**Primary organic aerosol and secondary aerosol formation potential from a Euro 3 diesel car during smog chamber experiments**	
	R. Chirico, P.F. DeCarlo, M.F. Heringa, T. Tritscher, E. Weingartner, A.S.H. Prevot, and U. Baltensperger	
T024A05	**HULIS characterisation and attribution to potential source by UV-Vis measurement**	
	C. Baduel, D. Voisin, J.L. Jaffrezo, I. El Haddad, and N. March	
T024A06	**Size distribution of EC and OC in the aerosol of urban areas in France during summer and winter**	
	J.L. Jaffrezo, D. Voisin, C Baduel, N. Marchand, M.B. Personnaz, and D. Robin	

T024A07	**Formation of secondary organic aerosol in the presence of organic seeds: Evaluating the mixing of organic aerosol components using high-resolution aerosol mass spectrometry**
	Lea Hildebrandt, Kaytlin M. Henry, Jesse H. Kroll, Marissa Miracolo, Allen L. Robinson, Spyros N. Pandis, Neil M. Donahue
T024A08	**Study of nucleation processes involved in SOA formation from the ozonolysis of a biogenic compound in a smog chamber**
	Y. Katrib, J. Boulon, K. Miet, J. Wang, M. Attoui, K. Sellegri, and J.F. Doussin
T024A10	**Nucleation processes during the ozonolysis of alkenes and carboxylic acids under kinetically controlled conditions**
	J.L. Wolf, C. Keunecke, and T. Zeuch
T024A11	**Photochemical strength index of size-segregated suburban aerosol during the different air qualities**
	S.-Ch. Kuo, Ch.-L. Chen, L.-Y. Hsieh, and Y.I. Tsai
T025A01	**Sources of fine particulate organic matter in a Mediterranean urban area: Marseilles**
	I. El Haddad, N. Marchand, B. Temime-Roussel, H. Wortham, C. Piot, A. Albinet, J.L. Besombes, and J.L. Jaffrezo
T025A02	**Determination of low-molecular-weight dicarboxylic acids in atmospheric aerosols: comparison between silylation and esterification derivatisation procedures for GC-MS analysis**
	D. Bacco and M.C. Pietrogrande
T026A03	**Biogenic contribution to particulate matter in Northern Italy**
	F. Bianchi, C. Abate, O. Cazzuli, P. Fermo, M. Ferri, A. Giudici, M. Lasagni, A. Piazzalunga, and D. Pitea
T026A05	**Source Apportionment for PM samples: study of n-alkanes distribution as organic tracer using a chemometric approach for GC-MS analysis data handling**
	M. Mercuriali and M.C. Pietrogrande
T027A01	**Modeling aerosol surface chemistry and gas-particle interaction kinetics with a kinetic double-layer model: PAH oxidation by ozone, nitrogen dioxide, and water vapor**
	M. Shiraiwa, R.M. Graland, and U. Pöschl
T027A02	**Acetonitrile and new charged clusters formation**
	T.-E. Parts, A. Luts, U. Hõrrak, and K. Komsaare
T027A04	**The « HUmic LIke Substances » in biomass burning emissions**
	C. Baduel, D. Voisin, J.L. Jaffrezo,I. El Haddad, N. Marchand, and M.B. Personnaz
T027A05	**Detection and kinetics of protein nitration in aerosols by NO_2 and O_3**
	H. Yang, Y. Zhang, and U. Pöschl
T028A03	**Acid-catalyzed reactions of limonene and terpineol and their implication in secondary organic aerosol (SOA) formation**
	Y.J. Li, G.Y.L. Cheong, A.K.Y. Lee, A.P.S. Lau, and C.K. Chan
T028A04	**Effect of water vapour concentration on photonucleation in aromatic aldehydes**
	S.N. Dubtsov, G.G. Dultseva, M.V. Bykova, and F.N. Dultsev
T028A06	**Multiphase processing of isoprene oxidation products – kinetic and product studies**
	D. Hoffmann and H. Herrmann
T028A08	**Multiphase processing of tropospheric halogen species: Mechanism development and modelling**
	P. Bräuer, A. Tilgner, R. Wolke, and H. Herrmann
T028A09	**Development and application of a Reduced Aqueous Phase Chemistry Mechanism**
	A. Tilgner, L. Deguillaume, R. Schrödner, R. Wolke, and H. Herrmann
T028A11	**Development of a mixed phase cloud chemistry model**
	Y. Long, N. Chaumerliac, L. Deguillaume, M. Leriche, and F. Champeau
T055A01	**Comparative overview of PM2.5 mass concentrations and elemental profiles in indoor environments**
	B. Horemans, M. Stranger, S. Potgieter-Vermaak, A. Worobiec, and R. Van Grieken

Atmospheric Aerosols - specific aerosol types

T051A01	**Physicochemical and toxicological profiles of particulate patter (PM) in Los Angeles during the October 2007 Southern California wildfires**
	V. Verma, A. Polidori, J.J. Schauer, M.M. Shafer, F.R. Cassee, and C. Sioutas

T058A05	**The concentration and variation of fungi diversity in atmospheric aerosol of Southwestern Siberia**
	A.S. Safatov, T.V. Teplyakova, B.D. Belan, G.A. Buryak, I.G. Vorob'eva, I.N. Mikhailovskaya, M.V. Panchenko, and A.N. Sergeev

T058A06	**The effect of two types of photocatalysts on aerosols of stable and labile microorganisms**
	A.S. Safatov, S.A. Kiselev, G.A. Buryak, V.Yu. Marchenko, A.A. Sergeev, M.O. Skarnovich, E.K. Emel'yanova, Yu.V. Marchenko, and A.V. Vorontsov

T058A08	**Removal of bioaerosols by using membrane-less electrolyzed water in swinery**
	S.H. Yang, M.Y. Chang, C.Y. Chuang, L.C. Chen, W. Fang, P.H. Wu, and S.W. Kong

T058A09	**Experimental study on pollen settling characteristics in isotropic homogeneous turbulence**
	R. van Hout and L. Sabban

T058A10	**Concentrations and size distributions of ambient fluorescent biological aerosol particles measured with an ultraviolet aerodynamic particle sizer (UVAPS)**
	J.A. Huffman, B. Treutlein, and U. Pöschl

T058A11	**Time resolved measurements of primary biogenic aerosol particles in Amazonia**
	A.G. Wollny, R. Garland, A. Huffman, and U. Pöschl

T058A12	**Dispersion of Ambrosia pollen with the model system COSMO-ART**
	K. Zink, H. Vogel and B. Vogel

T058A14	**Evaluation method of spore concentration uniformity on a fungal substrate using a real-time aerosolization technique**
	J.H. Jung, J.E. Lee, and S.S. Kim

T058A15	**Endotoxins loading in atmospheric aerosols in the Pearl River Delta cities**
	A.P.S. Lau and J.Y.W. Cheng

T058A16	**DEHM-Pollen: A regional scale pollen dispersion model**
	C.A.Skjøth, J.Brandt, J.Christensen, L. M. Frohn, C. Geels, A.B.Hansen, K.M.Hansen, G.B.Hedegaard, and J. Sommer

T058A18	**Disinfection of fungal spores on fibrous filters by Melaleuca alternifolia mist**
	R. Huang, O.V. Pyankov, B. Yu, and I.E. Agranovski

T058A19	**Measurement of subway bioaerosols and removal of bioaerosols using thermal energy**
	B.U. Lee, G.B. Hwang, and H.G. Kim

T150A19	**Allergenic Asteraceae in urban air: DNA- based analysis and relevance for human health**
	I. Germann, J. Froehlich-Nowoisky, U. Poeschl, and V. R. Després

T051A03	**PMx exposition of Prague city transport passengers**
	B. Kotlík, V. Tydlitát, M. Mikešová, and H. Kazmarová

T051A05	**Selected organic and inorganic compounds in atmospheric samples over five South American sites**
	P.C.Vasconcellos, D.Z. Souza, K. H. Nascimento, F.C. Santos, M.P. Araújo, H. Lee, J.B. Andrade, A.L.N. Guarieiro, L.L.N. Guarieiro, O.V. Bustillos, E. Beherentz

T051A07	**Influence of the dilution effect on atmospheric particle size distributions**
	F.J. Gómez-Moreno, M. Pujadas, J. Plaza, J.J. Rodríguez-Maroto, and B. Artíñano

T051A08	**Influence of traffic and meteorology on the TSP, PM10, PM2.5 and PM1 urban aerosol fractions**
	St. Pateraki, D.N. Asimakopoulos, Th. Maggos, H.A. Flocas, S. Tsakanikas, and Ch.Vasilakos

T051A09	**Correlation of near-traffic particle number concentrations and ambient noise**
	S. Weber

T051A10	**Characterization of particle number concentration increases during fireworks**

		J. Crespo, J. Gimenez, R. Castañer, S. Caballero, M. Varea, J. Gil-Moltó, J. Nicolás and, A. Carratalá
T051A11	**Levels of PM1, PM2.5 and PM10 in an urban location in the western Mediterranean**	
	M. Varea, J. Gil-Moltó, C. Chofre, N. Galindo, R. Esclapez, C. Pastor, and J. Crespo	
T051A12	**Two years of continuous measurements of surface and columnar atmospheric aerosol properties at Granada, an urban site in Spain**	
	H. Lyamani, F.J. Olmo, and L. Alados-Arboledas	
T051A13	**Pavement type influence on particulate matter composition**	
	R. Licbinsky, D. Durcanska, V. Adamec, and J. Huzlik	
T051A15	**The spatio-temporal distribution of atmospheric pollution in Beijing, China – Assessment of mass and elemental concentrations of PM2.5 and TSP**	
	N. Schleicher, S. Norra, Y. Chen, F. Chai, K. Cen, and D. Stüben	
T051A17	**Particle emissions of railway traffic determined by detailed single particle analysis**	
	M.F. Meier, B. Grobéty, M. Heuberger-Vernooij, R. Lorenzo, and K. Moser	
T051A18	**Time-resolved analysis of urban air pollution**	
	B. Alföldy and R. Steib	
T051A19	**Rain effect on the size distributions of traffic-related particles and particle-bounded PAHs**	
	C.C. Lin, S.J. Chen, K.L. Huang, W.J. Lee, H.R. Chao, W.Y. Lin, and J.H. Tsai	
T051A21	**Spectral analysis of particle count and mass in ambient air of Ankara, Turkey**	
	D.D. Genç Tokgöz, W. Brunnhuber, and G. Tuncel	
T051A22	**Source apportionment study for dustfall (dry deposition) in Vitória-ES Brazil**	
	N.C. Reis Jr, J.M. Santos, L.R. Menegussi, M. Rigo, and A.L.G.P.O. Souza	
T051A23	**Air quality studies using a measurement system mounted on a tramway in an urban region in Germany**	
	R. Rinke, A. Wieser, B. Vogel, U. Corsmeier, and Ch. Kottmeier	
T051A24	**Atmospheric particles in an urban tunnel under extreme conditions**	
	C.M.Oliveira, M.F. Camões, M. Matos, P. Cantinho, H. Silva , C. Oliveira, N. Martins, J. Tavares, M. Cerqueira, and C. Pio	
T051A27	**Chemical composition of submicron particles in Marseille (summer 2008): insights into sources and processes of urban aerosols**	
	B. D'Anna, A. Boreave, and C. George	
T051A30	**Atmospheric aerosols in the suburb of Prague**	
	D. Rimnácová, V. Ždímal, J. Schwarz,and J. Smolík	
T051A33	**Mobile aerosol mass spectrometer measurements of submicron particulate matter including source apportionment in urban areas**	
	M. Crippa, C. Mohr, P. DeCarlo, V. Lanz, R. Chirico, M. Heringa, A.S.H. Prévôt, and U. Baltensperger	
T051A37	**Reduction of PM industrial ceramic emissions reflected on key components concentrations of ambient PM10**	
	M.C. Minguillón, X. Querol, E. Monfort, A. Alastuey, A. Escrig, I. Celades, and J.V. Miró	
T051A38	**Ten days of intensive air quality measurement at the international airport of Budapest**	
	B. Alföldy, J. Osán, E. Börcsök, A. Nagy, A. Czitrovszky, S. Török, and S. Kugler	
T051A39	**Evaluation of seasonal behaviour of atmospheric PM10 levels in the Basque Country**	
	M.A. Barrero and L. Cantón	
T051A40	**Impact of local traffic on NOx and PM: urban background versus traffic locations**	
	M. Van Poppel, N. Bleux, and P. Berghmans	
T051A41	**Citizen's exposure and urban shape: a tight relationship**	
	M. Filice and P. De Luca	
T051A42	**Indoor to outdoor ratios of PM and PAH related to traffic and street maintenance emissions**	
	D. Martuzevicius, L. Kliucininkas, E. Krugly, T. Prasauskas, I. Vaskeviciute, and B. Strandberg	
T052A01	**Dust events in Beijing, China (2004-2006): Comparison of ground based measurements and**	

	columnar integrated observations
	Z.J. Wu, Y.F. Cheng, M. Hu, B. Wehner, and A. Wiedensohler
T052A02	**Deposition of PM10 mineral dust into the Atlantic Ocean at Cape Verde Islands**
	N. Kaaden, T. Mueller, A. Held, S. Lehmann, K. Mueller, K. Kandler, and A. Wiedensohler
T052A03	**Absorption of mineral dust: comparison between measurement and effective media theories**
	M. Vragel, C. Linke , M. Schnaiter, R. Wagner, and T. Leisner
T052A04	**Spectral absorption coefficients of mineral dust measured at Cape Verde**
	C. Meusinger, A. Wiedensohler, and Th. Müller
T052A05	**Lidar observations of extinction-to-backscatter ratio of long-range transported mineral dust at 355 nm and 532 nm during SAMUM 2**
	S. Gross, J. Gasteiger, V. Freudenthaler, and M. Wiegner
T052A06	**The African dust event of October 2008**
	J.A.G. Orza, M. Cabello, C. Dueñas, M.C. Fernández, E. Gordo, L. Cantón, and M.A. Barrero
T052A08	**Chemical composition and shape of single aerosol particles generated from different Saharan soil samples during the "Mineral Dust Campaign 2008 – AIDA chamber facility, Karlsruhe"**
	K. Kandler, M. Ebert, S. Jäckel, K. Lieke, and S. Weinbruch
T052A09	**Single particle chemical composition, state of mixing and shape of fresh and aged Saharan dust in Morocco and at Cape Verde Islands during SAMUM I and II**
	K. Kandler, C. Deutscher, M. Ebert, K. Lieke, D. Müller-Ebert, L. Schütz, and S. Weinbruch
T052A10	**Microphysical and optical properties of Mineral Dust Aerosols – Investigations during the Mineral Dust campaign 2008 at the AIDA facility, Forschungszentrum Karlsruhe**
	C. Linke , M. Vragel , M. Schnaiter, K. Kandler , T. Müller , C. Verhaege, and A. Petzold
T052A11	**Heterogeneous immersion freezing efficiencies of ice on mineral dust and bacteria**
	M. Brinkmann, D. Rzesanke, and T. Leisner
T052A12	**Spectral absorption of mineral dust: Results of the Mineral Dust Campaign 2008 at the AIDA facility, Forschungszentrum Karlsruhe**
	T. Müller, A. Petzold, K. Rasp, A. Schladitz, M. Vragel, M. Schnaiter, and C. Linke
T052A15	**Particle size distributions of dust during the Mineral Dust Campaign 2008 at the AIDA facility Karlsruhe – How well compare different sizing methods?**
	A. Petzold, A.Veira, K. Rasp, D. Delhaye, T. Müller, K. Kandler, C. Verhaege, M. Vragel, and C. Linke
T053A01	**Measured vertical profiles of aerosol number concentrations inside the PBL over the boreal forest in Finland**
	A.S. Staroverova, M. Boy, T. Gronholm, L. Laakso, A. Guenther, A. Sogachev, and M. Kulmala
T053A02	**Aerosol chemical composition at the Island of Lampedusa (Central Mediterranean): a strategic site for studying aerosol-climate interactions**
	S. Becagli, C. Bommarito, G. Calzolai, M. Chiari, A. di Sarra, F. Lucarelli, S. Nava, F. Rugi, M. Severi, D.M. Sferlazzo, R. Traversi, and R. Udisti
T053A03	**Supermicron aerosol particles near open-pit lignite mine**
	P. Pokorná, J. Hovorka, and J. Brejcha
T053A04	**Pollution levels in fog at the Chilean coast**
	E. Sträter, A. Westbeld, H. Larrain, P. Osses, P. Cereceda, and O. Klemm
T053A05	**First measurements on the carbonaceous fraction in central Antarctic aerosol**
	P. Fermo, A. Piazzalunga, R. Vecchi, S. Becagli, R. Traversi, and R. Udisti
T054A02	**Oxalic acid as a heterogeneous ice nucleus in the deposition and immersion mode**
	R. Wagner, S. Benz, O. Möhler, H. Saathoff, M. Schnaiter, and T. Leisner
T054A03	**Development of cumulus clouds over Europe: High-resolution measurements of aerosol and cloud properties at condensation level**
	F. Ditas, B. Wehner, A. Wiedensohler, R.A. Shaw and, H. Siebert
T054A04	**LACIS Simulations Concerning Heterogeneous Ice Nucleation with Fluent/FPM**
	S. Hartmann, D. Niedermeier, J. Voigtländer, R.A. Shaw, H. Wex, and F. Stratmann

T054A06	**Detection of thin coatings on refractory particles with an aerosol mass spectrometer and application in laboratory studies of hygroscopic growth, CCN and IN activation**
	P. Reitz, J. Schneider, H. Wex, F. Stratmann, D. Niedermeier, K. Mildenberger, D. Covert, Th. F. Mentel, C. Spindler, L. Poulain, and S. Borrmann

T054A08	**Polar light scattering function measurements and stereo imaging of single ice particles**
	A. AbdElMonem, M. Schnaiter, and T. Leisner

T054A09	**Characterisation of a pumped counterflow virtual impactor for ice particle residue sampling from the AIDA cloud chamber**
	C. Oehm, M. Niemand , O. Möhler, and T. Leisner

T054A10	**The microphysical and optical properties of small ice crystals**
	M. Schnaiter, A. AbdELMonem, D. Baumgardner, S. Benz, A. Heymsfield, M. Krämer, T. Leisner, J. Meyer, O. Möhler, C. Oehm, H. Saathoff, C. Schmitt, Z. Ulanowski, and R. Wagner

T054A11	**Black carbon scavenging by mountain clouds**
	D. Baumgardner, R. Subramanian, C. Twohy, and G. Kok

T054A12	**Deposition mode ice nucleation on atmospheric dust aerosols – A comparison of laboratory studies with detailed process model calculations**
	M. Niemand, H.Bunz, S. Benz, O. Möhler, R. Wagner, and T. Leisner

T054A13	**Aircraft contrail conditions: do they live longer?**
	M. Krämer, M. Kübbeler, J. Meyer, M. Hildebrandt, C. Schiller, M. Fiebig, A. Minikin, A.Petzold, H.Schlager, Ch. Voigt, and J.-F. Gayet

T057A01	**Apportioning the wood burning source in an urban area by Positive Matrix Factorization using 4-hour resolved PM10 data**
	R. Vecchi, G. Valli, V. Bernardoni, A. Piazzalunga, and P. Fermo

T057A02	**Contribution of wood smoke to PM2.5 in a Swedish community during the winter season 2007-08**
	P. Molnár and G. Sällsten

T057A04	**Influence of wood burning on the aerosol status in a Saxonian health resort**
	K. Müller, Y. Iinuma, T. Gnauk, E. Brüggemann, L. Poulain, and H. Herrmann

T057A05	**Comparison between LC-MS and GC-MS measurements for the determination of levoglucosan and its application to rural and urban atmospheric samples**
	C. Piot, J.L. Jaffrezo, and J.L. Besombes

T057A06	**PAHs and energy efficiency of soy-biodiesel blends fueled on a diesel generator**
	J.H. Tsai, S.J. Chen, K.L. Huang, and W.J. Lee

T057A07	**Alkali-content of individual aerosol particles in South-West Sweden: Influence of meteorological conditions and air mass origin**
	T.L. Gustafsson, B. Kovacevik, J. Noda, J. Boman and J.B.C. Pettersson

T057A08	**Humic-like substances in transported biomass burning plume at Mt. Lulin in Taiwan**
	C.T. Lee, N.H. Lin, and Y.H. Hou

T057A10	**Chemical characterisation of PM10 emissions from common Portuguese tree species in a wood burning stove**
	C.A. Alves, C. Gonçalves, C. Pio, M. Evtyugina, A.C. Rocha, A. Caseiro, F. Mirante, H. Puxbaum, C. Schmidl, F. Carvalho, and J. Oliveira

T057A12	**Diurnal variation of wood combustion related compounds and impact on urban PM10**
	J. Schnelle-Kreis, G. Abbaszade, R. Kunde, J. Orasche, and R. Zimmermann

T059A01	**Relationship between OC/EC data and meteorological and inorganic trace gas data for a forested site in Brasschaat, Belgium**
	X. Chi, W. Maenhaut, and J. Neirynck

T059A03	**PM emissions from a CFM56 gas turbine engine burning alternate fuels**
	D.E. Hagen, P.D. Whitefield, P. Lobo, and M.B. Trueblood

T059A04	**δ13C measurements of size segregated aerosols from urban site in wintertime**
	A. Garbaras, I. Rimselyte, K. Kvietkus, and V. Remeikis

T059A05	**Seasonal trend of atmospheric organic and elemental carbon mass concentrations over south-eastern Italy**

	A. Dinoi, I. Carofalo, and M. R. Perrone
T059A08	**Radiocarbon measurements on aerosol samples at LABEC (Florence, Italy)**
	V. Bernardoni, G. Calzolai, M. Chiari, M. Fedi, F. Lucarelli, S. Nava, F. Riccobono, G. Valli, and R Vecchi
T059A09	**OC, EC, and SOA contribution to PM in Lombardy (Italy): results of three winter campaigns (2005-2007)**
	A. Piazzalunga, P. Fermo, R. Vecchi, G. Valli, S. Comero, V. Bernardoni, O. Cazzuli, A.Giudici, and G.Lanzani
T059A10	**The importance of organic and elemental carbon in the fine particles over China**
	J.J. Cao, J.C. Chow, J.G. Watson , and S.C. Lee
T059A11	**Semi-continuous EC/OC measurements at the "Demokritos" urban background site in Athens, Greece**
	A.A. Karanasiou and K. Eleftheriadis
T059A12	**Hygroscopicity of combustion aerosols after photochemical aging in a smog chamber**
	T. Tritscher, E. Weingartner, M.F. Heringa, R. Chirico, M. Gysel, P.F. DeCarlo, J. Dommen, A.S.H. Prevot, and U. Baltensperger
T059A14	**Organic compound characterization and source apportionment of indoor and outdoor quasi-ultrafine PM in retirement homes of the Los Angeles Basin**
	M. Arhami, M.C. Minguillón, A. Polidori, J.J. Schauer, R.J. Delphino, and C. Sioutas
T059A15	**Characterisation of diesel exhaust from military vehicles**
	T.H. Gan, P.J. Hanhela, W. Mazurek, M. Keywood, and R. Gillett
T059A16	**One-year record of carbonaceous aerosols from urban location (Kanpur) in the Indo-Gangetic Plain (IGP)**
	K. Ram, M.M. Sarin, and S.N. Tripathi
T059A17	**Compensation of Aethalometer black carbon data for the optical loading effect**
	J.H. Jung, S.S. Park, S.Y. Cho, and S.J. Kim
T059A18	**Water soluble organic carbon in fine particulate matter measured at an urban site during two different seasons**
	S.S. Park, D.H. Kim, S.Y. Cho, and S.J. Kim

Top of Program		**Top of Poster Session Part I**

High Temperature Aerosols	
T037A02	**Effect of air flow distribution on dust emission and efficiency of local exhaust ventilation during wood grinding**
	T. Jankowski
T037A03	**Evaluation of the emissions of airborne pollutants from machines using trace gas technique**
	T. Jankowski
T081A01	**Modeling of mesoscale vortices structure near to a powerful hot source of impurity in a boundary layer of atmosphere**
	K.G. Shvarts and A.V. Shatrov
T081A05	**Contribution of polychlorinated dibenzo-p-dioxins and dibenzofurans from electric arc furnace dust treatment plant to duck farms**
	S.I. Shih, W.J. Lee, H.W. Li, L.F. Lin, L.C. Wang, and G.P. Chang-Chien
T081A06	**Characterization of PCDD/Fs in a secondary aluminum smelter**
	C. Lin and Y.H. Wang
T082A01	**Distribution of metallic traces by size, PM10, PM2.5 and PM1-Emission from secondary aluminium smelters**
	J.J. Rodríguez-Maroto, J.L. Dorronsoro, M. Fernández-Díaz, P. Galán-Valera, and E. Conde Vilda
T082A02	**Aerosol modelling in gasification flue gas containing solid particles and inorganic condensable vapour**
	M. Petit, K. Froment, F. Patisson, J.-M. Seiler,and M. Peyrot

| T083A01 | **Aerosol-size-spectra of a wood-burning furnace** |
| | *P. Madl, W. Hofmann, and H.J. Brandt* |

| T083A02 | **Environmental impact of aerosol particles from a coal-fired power plant** |
| | *I. Grgic, J. Turšic, J. Škantar, and A. Berner* |

| T083A03 | **Salt condensation on simulated superheater tubes** |
| | *M. Broström, S. Enestam, R. Backman, and K. Mäkelä* |

| T083A05 | **Particle and gas emission for a EURO 4 light duty engine using 1st and 2nd generation biodiesel** |
| | *A.G. Hemmersam, C. Raahede, J. Klenø Nøjgaard, A. Massling, P. Wåhlin, H.O. Hansen, and S. Nygaard* |

| T083A06 | **Diesel PM collection performance of a combined system with an electrostatic device and a partial-flow diesel particulate filter** |
| | *H.J. Kim, B. Han, D.K. Song, W.S. Hong, W.H. Shin, S.H. Jung, and Y.J. Kim* |

| T083A07 | **Emissions of polybrominated diphenyl ethers (PBDEs) and polybrominated dibenzo-p-dioxins and dibenzofurans (PBDD/Fs) from ferrous foundries** |
| | *L.-C. Wang, Y.-F. Wang, C.-H. Tsai, G.-P. Chang-Chien* |

| T083A08 | **Nano-particle formation in modern diesel vehicle exhaust: Implications from first measurements of precursor gases** |
| | *F. Arnold, U. Reichl, C.H. Muschik, A. Roiger, H. Schlager, L. Pirjola, T. Rönkkö, J. Keskinen, and D. Rothe* |

| T083A09 | **Mass-mobility relationship of soot generator and diesel soot** |
| | *J. Rissler, H. Abdulhamid, J. Pagels, P. Nilsson, M. Sanati, and M. Boghard* |

| T083A10 | **Non-regulated emissions speciation in diesel and bio- diesel vehicles exhaust** |
| | *M. Petrea, M. Kapernaum, and C. Wahl* |

| T083A11 | **Soot particles and gas phase characterisation on simulating a Diesel Particulate Filter charge** |
| | *L. Mazri, A. Boreave, B. D'Anna, C. George, A. Giroir-Fendler, M. Guth, and P. Vernoux* |

| T083A12 | **Effect of different raw materials on fine particle emissions from small-scale pellet combustion** |
| | *H. Lamberg, O. Sippula, and J. Jokiniemi* |

| T083A14 | **Emulsified palm-biodiesel blends for saving energy and reducing emissions from diesel engines** |
| | *Y.C. Lin, K.S. Chen, L.T. Hsieh, L.F. Lin, and K.H. Hsu* |

| T083A17 | **A reliable method for generation of size selected soot using aerosol technology and detection by sensor device** |
| | *H. Abdulhamid, A. Malik, J. Pagels, R. Bjorklund, P. Josza, J.H. Visser, A. Lloyd Spetz, and M. Sanati* |

| T083A18 | **Effect of air staging on emissions from masonry heaters** |
| | *J. Tissari, V. Suonmaa, J. Sutinen, P. Horttanainen, and J. Jokiniemi* |

| T083A20 | **Influence of road traffic conditions and street characteristics in Madrid City on nanoparticle vehicular emissions** |
| | *A. Domínguez, J.R. Rubio, and C.C. Barrios* |

| T083A21 | **Design and implementation of an on-board real time particle measurement system** |
| | *J. R. Rubio, A. Domínguez, and C.C. Barrios* |

| T083A22 | **Number and mass concentrations and surface area of particles in Diesel exhaust fumes** |
| | *E. Jankowska and M. Posniak* |

| T083A23 | **Size distribution of hazardous chemical compounds in diesel exhaust particles** |
| | *M. Posniak, E. Jankowska, and M. Szewczynska* |

| T083A24 | **Formation of diesel exhaust nucleation mode particles: laboratory and on-road studies** |
| | *T. Rönkkö, A. Virtanen, T. Lähde, L. Pirjola, M. Lappi, D. Rothe, F.Arnold, and J. Keskinen* |

| T083A25 | **Dependence between heavy duty diesel engine exhaust nucleation and soot concentration** |
| | *, and Y.J. Kim* |

| T083A27 | **Effect of biofuels on the diesel particulate emissions and toxicity** |
| | *K. Kuuspalo, M. Ihalainen, T. Karhunen, J. Ruusunen, P. Willman, M. Tapanainen, P. Jalava, R.O. Salonen, A. Pennanen, M. Happo, M-R. Hirvonen, and J. Jokiniemi* |

T083A28	**Multi-Functional Reactor for emission reduction of future diesel engine exhaust**
	S. Lorentzou, D. Zarvalis, and A.G. Konstandopoulos

T083A30	**Abatement of fine particles emissions from wood combustion stoves by electrostatic precipitators**
	A. Bologa, H.-R. Paur, H. Seifert, K. Woletz,and H. Bhangu

T083A31	**Fast evaluation method of the ash aging effect on catalyzed Diesel Particulate Filters**
	D. Zarvalis, S. Lorentzou, and A.G. Konstandopoulos

T083A32	**Carbonyl compound emissions from a heavy-duty diesel engine fueled with biodiesel blends**
	Y.C. Lin, C.S. Yuan, T.Y. Wu, W.C. Ou-Yang, C.B. Chen, and K.H. Hsu

T083A33	**Emission of particles from practical combustion devices burning methane/natural gas**
	P. Minutolo, M.V. Prati, M. Sirignano, and A. D'Anna

T083A35	**PCDD/F reductions from a biodiesel-fueled diesel engine under US transient cycle**
	C.S. Yuan, Y.C. Lin, C.H. Tsai , and Y.S. Lin

Top of
Program

Top of Poster Session
Part I

Aerosol Instrumentation

T023A02	**Performance comparison of two different Laser Ablation Time-of-Flight Mass Spectrometers**
	T. Klimach, M. Brands, F. Drewnick, J. Schneider, M. Kamphus, and S. Borrmann

T091A01	**Efficient sampling and collection of atmospheric aerosols with a novel particle concentrator – Electrostatic Precipitator System**
	B. Han, N. Hudda, Z. Ning, Y.J. Kim, and C. Sioutas

T091A02	**Modeling of mesoscale vortices structure near to a powerful hot source of impurity in a boundary layer of atmospher**
	J. Meinen, S. Khasminskaya, and T. Leisner

T091A04	**Source apportionment of particle number and PM10 concentration**
	E. Cuccia, F. Mazzei, V. Bernardoni, P. Prati, G. Valli, and R. Vecchi

T091A10	**Experimental study on collision efficiency for aerosol particles scavenged by cloud drops**
	L. Ladino, O. Stetzer, U. Lohmann, and B. Hattendorf

T091A13	**A Synchronized Hybrid Real-Time Particulate monitor**
	K.J. Goohs, P. Lilienfeld, and J. Wilbertz

T091A15	**Probing nanoparticles deposited on flat surfaces by X-ray spectrometry at grazing incidence**
	F. Reinhardt, B. Beckhoff, H. Bresch, and S. Seeger

T091A16	**Quantification of carbonate carbon in atmospheric aerosol by means of ATR (Attenuated Total Reflection) spectroscopy and a multivariate calibration method**
	P. Fermo , A. Piazzalunga, F. Tuccillo, L. Brambilla , F. Mazzei, and P. Prati

T091A20	**Application of computer software for airborne particles counting**
	B. Trivuncevic, G. Jereb, B. Poljšak, M. Bizjak, and S.A. Katz

T091A21	**Program controlled gear complex for aerosol monitoring**
	T.E. Ovchinnikova, A.M. Baklanov, S.N. Dubtsov, and I.V. Melekhov

T091A22	**Validation of a new Atmospheric Pressure Interface Time-of-Flight mass spectrometer (API-TOF) to measure the composition of sub-2 nm aerosol particles**
	M. Ehn, H. Junninen, K. Neitola, M. Sipilä, H. Manninen, T. Petäjä, K. Fuhrer, M. Gonin, U. Rohner, S. Graf, M. Kulmala, and D.R. Worsnop

T091A24	**Diffusion based nanoparticle monitor using QCM-technology**
	J. Leskinen, J. Joutsensaari, A. Jakorinne, M. Laasanen, and J. Jokiniemi

T091A25	**Determination of particulate ammonium (NH$_4$+) by thermal dissociation and detection of the generated gaseous ammonia**

Ch. Hueglin, H. Burtscher, P. Graf, C. Houle, D. Meier, and E. Rochat

T091A26	**Characterization of the Hermann and Attoui DMA in the super 3 nm range**
	M. Attoui

T091A28	**Challenges and barriers for the development of SiC nanoparticle measurement technology in Laser Pyrolysis reactors**
	A. Asimakopoulou, M. Kostoglou, and A.G. Konstandopoulos

T091A30	**Monitoring of growth of cloud droplets ensembles with soot and salt condensation nuclei**
	L. Vámos and P. Jani

T091A31	**Application of on-line time-of-flight aerosol mass spectrometry for the determination of molecular iodine**
	M. Kundel, M. Schott, M. Ries and T. Hoffmann

T091A32	**Preview on Nanoparticle Monitors**
	A. Dahl, A. Gudmundsson, and M. Bohgard

T092A01	**Nanoparticles sampling techniques for an aerosol- / particle mass spectrometer**
	J. Meinen, W. Baumann, H.-R. Paur, and T. Leisner

T092A02	**Design and performance of an automatic regenerating adsorption aerosol dryer for continuous operation at monitoring sites**
	Th. M. Tuch, A. Haudek, Th. Müller, A. Nowak, H. Wex, and A. Wiedensohler

T092A04	**A miniature impactor for aerosol collection with emphasis on single particle analysis**
	K. Kandler

T092A05	**Development of new instrumentation for aerosol angular light scattering and spectral absorption measurements**
	G. Dolgos, J.V. Martins, L.A. Remer, and A.L. Correia

T092A06	**Response of the DustTrak DRX to aerosols of different materials**
	X. L. Wang, A. Hase, G. Olson, A. Sreenath, and J. Agarwal

T092A07	**Development of an optical particle counter for in-situ detection of single ice particles in LACIS**
	T. Clauß, A. Kiselev, D. Niedermeier, S. Hartmann, H. Wex, and F. Stratmann

T092A09	**Monitoring of indoor air quality and workplace aerosols - one compact portable system for dust mass, number concentration and Nano particles**
	F. Schneider, R. Hagler, and H. Grimm

T092A11	**Measurement of the wavelength dependence of the extinction coefficient for studying the aerosol contamination of the atmosphere**
	A. Czitrovszky, A. Nagy, and A. Kerekes

T093A02	**Method for the characterization of nanoparticle release from surface coatings**
	M. Vorbau, L. Hillemann, D. Göhler, and M. Stintz

T094A01	**DMA-FMPS aerosol spectrometers laboratory intercomparison**
	F. Belosi, V. Poluzzi, S. Ferrari, G. Santachiara, F. Scotto, A. Trentini, and F. Prodi

T094A02	**Intercomparison of two types of portable optical particle counters (Grimm model 1.109 and 1.108) at an urban aerosol measurement station**
	J. Burkart, H. Moshammer, M. Neuberger, G. Steiner, G. Reischl, and R. Hitzenberger

T094A04	**Performance of a new condensation particle counter**
	H. Kim, J. Spielvogel, S. Ha, and T. Kim

T094A06	**Comparison of the performance of the Thermo Scientific TEOM 1400a with 8500C FDMS and the TEOM 1400a with 8500B FDMS monitors for the measurement of PM2.5**
	J.L. Ambs

T094A07	**Integrated water vapor (IWV) climatology with RIMA-AERONET sunphotometers, GPS and Radiosondes in the Southwestern of Spain**
	B. Torres, V.E. Cachorro, C. Toledano, J.P. Ortiz de Galisteo, A. Berjón, and A.M. de Frutos

T095A03	**Design and characterization of the screw-assisted rotary feeder with ultra low feeding rate**
	K.S. Lee, J.H. Jung, and S.S. Kim

T095A04	**Density analyzing method of atmospheric particles: reliability and limitations using a new ELPI stage**
	J. Kannosto, J. Yli-Ojanperä, M. Marjamäki, A. Virtanen, and J. Keskinen
T095A05	**First tests of thermophoretic trap in short duration microgravity conditions**
	A.A. Vedernikov1 A.M. Markovich, A.V. Kokoreva, N. Bastin, P. Queeckers, N.V. Kozlov, J. Blum, I. von Borstel, and R. Schräpler
T096A02	**Distortions of the DMA transfer function due to geometrical and flow pattern non-ideality and gravit**
	E. Tamm and J. Uin
T096A04	**Effect of size dispersion on the lattice parameters of two-dimensional particle arrays: A possible uncertainty source in AFM size measurement of monodisperse particles**
	K. Shirono and K. Ehara

Top of Program　　　　　　　　　　　　　　　　　　　　　　**Top of Poster Session Part I**

Particle-Lung-Interactions	
T093A04	**Exposure of cyclists to air pollution: a pilot study**
	N. Bleux, B. de Geus, B. Degraeuwe, G. Vandenbulcke, R. Torfs, I. Thomas, R. Meeusen, and L. Int Panis
T101A02	**Effect of intersubject variability of nasal airway dimensions on particle deposition**
	M. Hussain , R. Winker-Heil, and W. Hofmann
T101A04	**Study of aerosol transport and air flow in transparent human airways model**
	J. Jedelsky, F. Lizal, M. Jicha, J. Stetina, and J. Kosner
T101A06	**Hit probability of lung-cancer-sensitive epithelial cells by asbestos fibers with different aspect ratios**
	R. Sturm and W. Hofmann
T101A07	**Modelling dynamic shape factors and lung deposition of small particle aggregates originating from combustion processes**
	R. Sturm and W. Hofmann
T101A08	**A compartment model for the simulation of fiber-cell-interaction in the alveolar region of the human respiratory tract**
	R. Sturm and W. Hofmann
T101A09	**Respiratory tract deposition of diesel engine exhaust particles for healthy subjects and subjects with COPD**
	J. Löndahl, A. Bengtsson, J. Pagels, E. Swietlicki, C. Boman, A. Blomberg, and T. Sandström
T101A11	**Air flow and particle deposition experiments with hollow bronchial airway models**
	A. Czitrovszky, A. Nagy and A. Kerekes
T101A12	**An assessment of time changes of the health risk of PM10 based on GRIMM analyzer data and respiratory deposition model**
	J. Keder
T102A01	**Exhaled breath particles – a biomarker for detection of lung disease?**
	K. Schwarz, J.M. Hohlfeld, H. Biller, H. Windt, and W. Koch
T103A02	**Kinetic of carbon black and TiO2 nanoparticles internalization in two respiratory cellular models**
	E. Belade, L. Martinon, J. Fleury-Feith, M.-A. Billon-Galland, L. Kheuang, S. Lanone, J. Boczkowski, A. Baeza, F. Marano, and J.-C. Pairon
T104A02	**Can a short-term inhalation study be predictive for long-term study outcomes? – First experience with nano-TiO$_2$, Carbon black and Multiwall carbon nanotubes**
	L. Ma-Hock, S. Treumann, V. Strauss, A.O. Gamer, K. Wiench, B. van Ravenzwaay, and R. Landsiedel
T104A03	**Toxic effects of nanoparticles from biomass combustion**
	W.F. Dreher, F. Weise, K. Böhme, S.Lutz, M. Struschka, J. Brodbeck, S. Mülhopt, H.-R. Paur, and S. Diabaté
T104A05	**Action of Fe$_2$O$_3$ nanoparticles on MRC5 lung fibroblasts**

	M.C. Munteanu, O. Zarnescu, C. Sima, M. Radu, M. Costache, C. Grigoriu, and A. Dinischiotu	
T104A07	**Response of a human alveolar cell line to urban fine particles**	
	E. Longhin, P. Mantecca, M. Gualtieri, V. Corvaja, A. Altana, L. Piazzoni, and M. Camatini	
T104A09	**Inflammatory effects of Milan coarse particulate matter on human cell lines**	
	V. Corvaja, M. Gualtieri, and M. Camatini	
T104A10	**Effects induced by metal oxide nanoparticles on in vivo and in vitro systemsl**	
	E. Moschini, R. Bacchetta, D. Gallinotti, P. Magni, M. Camatini, and P. Mantecca	
T105A03	**Acute cardiovascular effects associated with air pollution: a new pathogenetic pathway in patients with chronic obstructive pulmonary diseases (COPD)**	
	F. Cetta, G. Schiraldi, M. Sala, R. Zangari, A. Dhamo, L. Moltoni, P. Laviano, F. Cisternino, A. Azzarà, G. Malagnino, P. Favini, and L. Allegra	
T105A04	**"Aging" of ultrafine particles (UFP), and quantitative daily estimation of UFP determining severe adverse health effects, because of increased surface reactivity of nanoparticles**	
	A. Dhamo, F. Cetta, M. Sala, E. Bolzacchini, R. Zangari, F. Cisternino, A. Azzarà, G. Malagnino, and G. Schiraldi	
T105A05	**Particle-extract-induced cytotoxicity of traffic-related particles**	
	H.C. Chaung, S.J. Chen, K.L. Huang, T.H. Yang, C.C. Lin, W.Y. Lin, and J.H. Tsai	
T105A06	**Air pollution from Milan affects in vitro sperm quality more individuals with previous varicocele than in normal subjects or in rabbit sperm cells**	
	F. Cetta, G. Collodel, E. Moretti, M. Geminiani, C. Castellini, A. Dhamo, G. Malagnino, A. Azzarà, F. Tani, E. Bolzacchini, and M. Camatini	
T105A08	**Quantification of ROS related to particle emissions generated by a diesel engine using ethanol substitution**	
	B. Miljevic, N. Surawski, R. Situ, K.E. Fairfull-Smith, S.E. Bottle, R. Brown, and Z.D. Ristovski	
T105A09	**Physico-chemical and toxicological characterization of welding fumes from different processes**	
	A.C. John, H. Kaminski, M. Wiemann, J. Bruch, C. Eisenbeis, R. Winkler, M. Gube, P. Brand, T. Kraus, and T.A.J. Kuhlbusch	
T105A12	**Morphochemical characteristics and toxic potential of quartz particles in clay bricks factories and foundry plants**	
	B. Moroni	
T105A14	**Levels of dioxins and furans in blood of the residents living in the vicinity of a municipal solid waste incinerator and electric arc furnace**	
	Y.C. Lin, Y.M. Chen, T.Y. Wu, G.P. Chang-Chien, W.F. Ma, and C.H. Hung	
T106A02	**Optimization of airway deposition of inhaled bacteria**	
	A. Horváth, I. Balásházy, Z. Sárkány, Á. Farkas, and W. Hofmann	
T106A04	**Concentration and size distribution of bioaerosols in different residential categories**	
	I. Colbeck and Z. Ahmad Nasir	
T108A01	**Characterisation of the dustiness of highly effective pharmaceutical substances**	
	S. Bach, U. Eickmann, and E. Schmidt	
T108A05	**Evaluation of the overall particle emission reduction efficiencies of commercially available laser printer filters**	
	G. Steiner, D. Wimmer, G.P. Reischl, E. Peteln, and M. Vojta	
T108A06	**Development of continuous inspection of indoor aerosol in classroom of Peoples Friendship University of Russia**	
	T. Aljazar and A. Syroeshkin	
T108A07	**Influence of the window exchange on the aerosol particle in a lived-in city flat**	
	A. Hruška and J. Hemerka	
T108A08	**Generation of nano size particles from limonene/ozone reactions, for controlled human exposures in a chamber**	
	C. Isaxon, J. Pagels, A. Wiertzbicka, A. Eriksson, A..Gudmundsson, J. Nielsen, K. Dierschke, E. Assarsson, U. Andersson, J. Klenö Nöjgaard, and M. Bohgard	
T108A09	**Impact of outdoor combustion emissions on indoor air in a pulmonary hospital**	
	M. Vardjan, M. Bajic, A. Zrimec, and G. Mocnik	
T108A10	**Aerosol particles in the Baroque library hall of the National Library in Prague**	

	L. Ondráčková and J. Smolík
T108A11	**Indoor levels of particulate pollution in urban and rural environment in Pakistan**
	I. Colbeck, Z. Ahmad Nasir, and Z. Ali
T108A12	**Particulate matter size distribution of main indoor sources: measurements in a real scale chamber**
	D.E. Saraga, T. Maggos, C. G. Helmis , A. Passa, C. Vasilakos, and J. G. Bartzis
T108A13	**Behaviour of well defined aerosol particles in a test chamber**
	J. Ondráček, M. Brand, M. Barták, L. Džumbová, and J. Smolík
T108A15	**Determining the effect of a car park on the indoor air quality of a hospital**
	N. Bleux, R. Brabers, M. Van Poppel, P. Berghmans, M. Stranger, R. Torfs, and L. Int Panis
T108A19	**Indoor and outdoor PM concentrations measured in schools and in retirement homes in Milan**
	B.S. Ferrini, L. Ferrero, z. Lazzati, C. Lo Porto, M.G. Perrone, S. Petraccone, G. Sangiorgi, E. Bolzacchini, F. Cetta, and M. Sala
T108A21	**The portable cleaner device for filtration and sterilization of indoor air**
	J.S. Pastuszka, W. Mucha, and E. Marchwinska-Wyrwal
T108A22	**Physical characterization of particulate from laser printer emission**
	M. Filice and P. De Luca
T180A01	**Detection of Cell Homeostasis Imbalance in Subjects Exposed toTraffic Related Air Pollution**
	R. Accinni, F. Cetta, G. Schiraldi, M. Guinea Montalvo, G. Giussani, M. Parolini, C. Dellanoce, R. Zangari, E. Bolzacchi, L. Allegra
T180A02	**Relationship between paediatric hospital admissions for respiratory diseases and air pollution (PM10) in Milan during 2 one year periods (2007 vs 2008)**
	M. Sala, F.Cetta, S. Argirò, S. Palazzo, P. Ballista, L. Dahdah, R. Zangari, G. Rettani, M. Mandelli, and M. Giovannini
T180A03	**Traffic can be responsible for different respiratory adverse effects in schoolchildren. A prospective study in Milan, Italy**
	F. Cetta, M. Sala, S. Argirò, P. Ballista, G. Perrone, R. Zangari, A. Dhamo, P. Laviano, E. Bolzacchini, and M. Giovannini

Radioactive Aerosols	
T121A02	**Factors controlling 7Be and 210Pb atmospheric deposition at Malaga (Spain)**
	C. Dueñas, M.C. Fernández, S. Cañete, E. Gordo, and M. Pérez
T121A03	**Deposition velocities and washout ratios on a coastal site calculated from Gross Alpha and Gross Beta measurements**
	C. Dueñas, M.C. Fernández, E. Gordo, S. Cañete, and M. Pérez
T121A04	**Assesment of air mass transport of Chernobyl originated radionuclides using clustering approach**
	G. Lujaniene, S. Bycenkiene, and V. Aninkevicius
T121A05	**Monitoring of 7Be and heavy metals at the Basic Environmental Observatory "MOUSSALA"**
	I. Penev, J. Stamenov, M.Drenska, B. Damyanov, and Ch. Angelov
T122A01	**Radiation burden of the up clearing deeply deposited radon progenies in the central airways**
	I. Balásházy and G. Kudela
T122A02	**Airway deposition and health effects of inhaled radon progenies**
	I. Balásházy, Á. Farkas, and I. Szoke
T123A02	**The solubility and leaching of aerosol particles – radionuclide carriers – collected on filters in the ventilation system of the Ignalina Nuclear Power Plant**
	R. Jasiulionis and A. Rožkov
T123A04	**Experimental determination of correction factors for assessment of the activity discharges of radionuclides bound to aerosol particles from nuclear facilities**
	K. Vogl

T123A05	**Resuspension of particles inside packages containing radioactive powders**
	F. Gensdarmes, H.E. Thyebault, J. Vendel, B. Eckert, and S. Fourgeaud

**Top of
Program**   **Top of Poster Session
Part I**

Special Session 1: Atmospheric Aerosol Processes in a Developed Mega-City: The REPARTEE Study in London

T130A01	**Measurements using broadband cavity-enhanced absorption spectroscopy of the sum of NO_3 and N_2O_5 during REPARTEE II and associated model studies**
	A.K. Benton, J.M. Langridge, O. Dessens, S.M. Ball, and R.L. Jones
T130A04	**Real time chemical characterisation of aerosols via ATOFMS and ToF-AMS during REPARTEE I**
	M. Dall'Osto, Roy M. Harrison, J. Allan, P. Williams, H. Coe, and E. Nemitz
T130A06	**Remarkable dynamics of nanoparticle in the urban atmosphere**
	M. Dall'Osto, Roy M. Harrison, A. Thorpe, P. Williams, and H. Coe
T130A09	**Lidar data analysis from REPARTEE II campaign**
	T.M. Dunbar, J.F. Barlow, and C.R.Wood

**Top of
Program**   **Top of Poster Session
Part I**

Special Session 5: Special EUCAARI Session

T170A01	**One-year climatology of the aerosol hygroscopicity at the High Alpine Research Station Jungfraujoch (3580 m asl.)**
	L. Kammermann, M. Gysel, E. Weingartner, and U. Baltensperger
T170A03	**Aerosol regional background in developing countries**
	E. Vignati, S. Gilardoni, and F. Cavalli
T170A06	**Chemical characterization of fine and coarse aerosols in a pristine rainforest site during EUCAARI**
	M. Chiruta, D.L. Roberts, and F.J. Romay
T170A07	**AMS measurements of aerosol composition at Cabauw tower during IMPACT 2008**
	A.A. Mensah, A. Kiendler Scharr, H. M. ten Brink, J. S. Henzing, R. Holzinger, Th.F. Mentel, M. Moerman, R.P. Otjes, and G.J. van Zadelhoff
T170A08	**Global model simulations of particle concentrations over Europe during the EUCAARI Intensive Observation Period**
	C.L. Reddington, M.G. Frontoso, K.S. Carslaw, D.V. Spracklen, A. Minikin, T. Hamburger, H. Coe, and J. Trembath
T170A10	**Meeting the challenge of multi-scale integration in EUCAARI: sectional bin versus modal aerosol scheme for large scale modelling**
	M.G. Frontoso, K.S. Carslaw, G.W. Mann, and D.V. Spracklen
T170A12	**Measurements of the Volatility Distribution and Density of Ambient Organic Aerosols during the Finokalia Aerosol Measurement Experiment – 2008**
	E. Kostenidou, L. Hildebrant, G. J. Engelhart, B. Lee, C. Mohr, A. Bougiatioti, U. Baltensperger, N. Mihalopoulos, and S.N. Pandis
T170A13	**Inside an air pollution plume – first results from EUCAARI-station in South Africa**
	L. Laakso, A. Virkkula, H. Laakso, V. Vakkari, P. Beukes, P. Van Zyl, K. Pienaar, K. Chiloane, G. Fourier, S. Piketh, K. Ferguson, T. Tuch, A. Wiedensohler, and M. Kulmala
T170A14	**Mass spectrometric investigations on OH-radical induced ageing of biogenic secondary organic aerosol**
	L. Müller, M.-C. Reinnig, Th. F. Mentel, R. Tillmann, E. Schlosser, A. Wahner, H. Saathoff, N.M. Donahue, and T. Hoffmann
T170A16	**Evaporation of organic and inorganic/organic particles**
	A.A. Zardini, I. Riipinen, I.K. Koponen, M. Kulmala, and M. Bilde

T170A17	**Size dependency of ice nucleating properties of various mineral dust samples**
	O. Stetzer, A. Welti, F. Lüönd, and U. Lohmann

T170A19	**A diluter for a PSAP at an EUCAARI-station in South Africa**
	A. Virkkula, L. Laakso, H. Laakso, V. Vakkari, P. Beukes, P. Van Zyl, K. Pienaar, K. Ferguson, G. Fourier, S. Piketh, T. Tuch, A. Wiedensohler, and M. Kulmala

T170A20	**Aerosol classification by airborne in-situ and high spectral resolution lidar measurements during EUCAARI**
	F. Abicht, M. Esselborn, T. Hamburger, B.Y. Liu, A. Minikin, and A. Petzold

T170A21	**Aerosol microphysics during anticyclonic conditions over Europe during EUCAARI-LONGREX**
	T. Hamburger, A. Minikin, A. Dörnbrack, A. Petzold, H. Rüba, H. Schlager, M. Scheibe, A. Ibrahim, H. Coe, G. McMeeking, W. T. Morgan, and A. Stohl

T170A22	**Characterization of the sources of organic aerosol collected at K-Puszta**
	A. Hoffer, G. Kiss, C. Alves, C. Pio, A. Vicente, E. Finessi, S. Decesari, J. Genberg, K. Stenström, and E. Swietlicki

T170A23	**Photosensitized transformation of dicarboxylic acid in aerosols**
	A. Rouvière, P.F. DeCarlo, A. Schlierf, O. Favez, B. D'Anna, C. George, A. Prévôt, and M. Ammann

T170A24	**Terpenes as potential precursors of humic-like substances in the atmosphere?**
	N. Töro, V. Domján, A. Hoffer, G. Kiss, R. Fisseha, A. Kiendler-Scharr, T. Brauers, and T.F. Mentel

Poster Session Part II

Aerosol-based Nanotechnology Aerosol

modelling

Atmosperic Aerosols - aerosol processes and properties Electrical Effects

Fundamentals PMx

Special Session 3: Aerosol Sampling and Aerosol Analytics

Special Session 4: Origin, Properties and Impact on Regional and Global Climate Special Session 7:

Test Materials in Toxicological and Health Effect Studies Special Session 8: - Artifacts in Measuring PM

Thursday 10 September 2009	**13:45 - 15:45**	**Poster Hall**
Poster Session Part II		

Aerosol-based Nanotechnology	
T011A04	**Comparison of agglomerate stability of different nanopowders**
	B. Stahlmecke, S. Wagener, C. Asbach, H. Kaminski, H. Fissan, and T.A.J. Kuhlbusch
T011A06	**Predominance of soot-mode ultrafine particles in Santiago de Chile: Possible sources**
	E. Gramsch, L. Gidhagen, P. Wahlin, P. Oyola, and F. Moreno
T011A08	**Physico- and electro-chemical characterizations of microwave-assisted polyol preparation of Pt/CNTs**
	Y.-C. Chiang, F.-P. Tsao, and C.-C. Lee
T011A09	**Nanoparticles emitted in the process of Nanofil®5 blending**
	E. Jankowska and W. Zatorski
T012A01	**Nanoparticle film formation by means of an electrostatic precipitator**
	M. Rouenhoff and F.E. Kruis

T012A02	**Penetration of monodisperse, singly-charged nanoparticles through fibrous filters. I - Experimental assessment**
	A. Maißer, W.W. Szymanski, A. Podgórski, A. Jackiewicz, L. Gradon, and G. Allmaier
T012A03	**Penetration of monodisperse, singly-charged nanoparticles through fibrous filters. II – Model validation**
	A. Podgórski, A. Jackiewicz, L. Gradon, W.W. Szymanski, and A. Meisser
T012A04	**Charge distribution of incipient nanoparticles in laboratory flames**
	L.A. Sgro, A. D'Anna, and P. Minutolo
T013A02	**Biological effects in human lung cells exposed to platinum nanoparticle aerosol**
	S. Diabaté, C. Weiss, S. Mülhopt, H.-R. Paur, V. Niedetzky, and M. Seipenbusch

T013A03	**Generation of airborne nanoparticles for in vitro health studies**
	A. Comouth, S. Mülhopt, H. Saathoff, W. Baumann, H.-R. Paur, H. Seifert, and T. Leisnera

T014A02	**Aerosol-derived graphene/copper nanoparticles as an air-stable alternative to metal ink-jet printing for electronics**
	N.A. Luechinger, E.K. Athanassiou, R.N. Grass, and W.J. Stark

T014A03	**Novel nanostructures for solid state alcohol breath analyzers**
	A. Tricoli, M. Righettoni, and S.E. Pratsinis

T014A04	**Anti-fogging coatings by flame synthesis and deposition**
	A. Tricoli, M. Righettoni, and S.E. Pratsinis

T014A07	**Pt-based alloy/carbon nanotubes electrocatalysts for unitized regenerative polymer electrolyte fuel cells**
	Y.-C. Chian, C.-H. Chang, J.-P. Hung, and C.-C. Lee

T014A09	**Rapid aerosol deposition of super-hydrophilic coatings**
	A. Tricoli, M. Righettoni, and S.E. Pratsinis

T014A10	**Application of magnetic cobalt nanoparticles to enhance permeability of metal-polymer composite substrates**
	P. Koskela, U. Tapper, A. Auvinen, J. Jokiniemi, A. Alastalo, H. Seppä, M. Aronniemi, M. Teirikangas, J. Juuti, and H. Jantunen

T015A03	**Design of in-situ coating of aerosols: Efficiency, thickness & texture**
	B. Buesser and S.E. Pratsinis

T015A04	**CO_2 CW laser-driven reactions in pure acetylene flow for generation of nanoparticles**
	P.V. Pikhitsa, D. Kim, and M. Choi

T015A06	**Synthesis of silica nanoparticles in a hybrid microwave-plasma hot-wall reactor under well-controlled conditions**
	A. Abdali, B. Moritz, A. Gupta, H. Wiggers, and C. Schulz

T015A08	**Experiments concerning gasdynamically induced nanoparticle synthesis**
	A. Grzona, A. Weiß, H. Olivier, T. Gawehn, and A. Gülhan

T015A10	**In-situ carbon coating of flame made $LiMn_2O_4$ nano-particles for batteries**
	O. Waser, R. Büchel, F. Krumeich, and S.E. Pratsinis

T015A11	**Reactive 3-D simulations of continuous shock induced particle synthesis**
	N.S. Al-Hasan, M. Giglmaier, and G.H. Schnerr

T015A12	**Size analysis of composite nanoparticles by mixing of Ag and C60 in the gas phase**
	F. Maeda, N. Hashimoto, H. Murayama, and H. Tanaka

T015A13	**Novel nanocolloids production using diameter-selected Ag nanoparticles formed in the gas phase**
	N. Hashimoto, H. Murayama, and H. Tanaka

T015A14	**Investigation of structure and chemical composition analysis of ionic-liquid coated Ag nanoparticles**
	Y. Sekiguchi, M. Shigeyasu, H. Murayama,and H. Tanaka

T015A16	**The effect of flame spray configuration on synthesis of inhomogeneous nanoparticles**
	T. Rudin and S.E. Pratsinis

T015A17	**Generation characteristics of nanoparticles by evaporation/condensation**
	W.Y. Lin, K.H. Chang, Y.Y. Chang, C.Y. Wu, and Y.C. Lee

T015A18	**Synthesis of nano-sized Iron Oxide particles in low-pressure hydrogen flames**
	O.O. Nalcaci, E. Ruzin, and H. Bockhorn

T015A19	**Novel arc plasma system for the aerosol synthesis of metal nanoparticles**
	H. Förster, D. Kilian, H.-J. Schmid, and W. Peukert

T015A20	**Synthesis of monodisperse gadolinium oxide nanoparticles having single monoclinic phase using spark discharge generation**
	I. Aruna, R. Theissmann, and F.E. Kruis

T015A21	**SiO₂ coating of aerosolized nanoparticles by photoinduced chemical vapor deposition**
	A.M. Boies, J.T. Roberts, and S.L. Girshick

T015A22	**Synthesis and functionalisation of copper and titanium nanoparticles in a spark discharge generator**
	H. Förster, C. Funk, and W. Peukert

T015A24	**Synthesis of aerosol nanoparticles by spark generation and their applications**
	R.H. Lee, J.H. Byeon, J.H. Park, and J. Hwang

T015A25	**Decomposition and formation of Si nanoparticles in the chemical vapour synthesis process**
	A. Lähde, K. Vuorikari, U. Tapper, and J.J. Jokiniemi

T015A26	**Nucleation of ibuprofen nanoparticles from supersaturated vapor**
	A. A. Onischuk, A. V. Samodurov, E. E. Elantseva, V. V. Karasev, and A.M. Baklanov

T015A29	**Composite CuOₓ-SiO₂ nanoparticle synthesis by MOCVD**
	P. Moravec, J. Smolík, V.V. Levdansky, and M. Klementová

T015A30	**Production and characterization of Silicon nanoparticles via spark discharge**
	A. Evirgen, V.A. Vons, D. Munao, U. Lafont, L.C.P.M. de Smet, E. M. Kelder, and A. Schmidt-Ott

T015A32	**Production of metallic magnesium using spark discharge**
	V.A. Vons, H. Leegwater, W. Legerstee, S. Eijt, and A. Schmidt-Ott

T015A34	**Gas-phase synthesis of highly-specific nanoparticles on the pilot-plant scale**
	T.P. Hülser, S.M. Schnurre, H. Wiggers, and C. Schulz

T016A01	**Structural stabilization of metal nanoparticles**
	M. Seipenbusch, A. Binder, and H. Shi

T016A03	**Coated highly porous metal hydride nanoparticle layers for hydrogen storage**
	V.A. Vons, H. Leegwater, W. Legerstee, S. Eijt, and A. Schmidt-Ott

T017A01	**Nanoscale particulate emissions from car-brakes**
	H. Bresch, S. Seeger, I. Dörfel, C. Prietzel, and W. Österle

T018A01	**Nanoinventory: a representative survey of nanoparticle usage in Suisse industry**
	K. Schmid, B. Danuser,and M. Riediker

T018A02	**Modelling of accidental nanoparticle release into a workplace**
	C. Asbach, U. Rating, T. van der Zwaag, H. Fissan, T.A.J. Kuhlbusch

T140A02	**Grid-based kinetic Monte-Carlo technique for modelling high-temperature particle formation**
	F.E. Kruis, J. Wei, T. van der Zwaag, S. Haep, and H. Zhao

T140A05	**Modelling Agglomeration and Coalescence of SiO₂ particles in an industrially scaled turbulent flame**
	S. Horender and M. Sommerfeld

T150A05	**Implementation of sampling and characterization methods for nanoparticles**
	C. Dion, A. Noël, J. Boucher, Y. Cloutier, and G. Truchon

Top of Program   **Top of Poster Session Part II**

Aerosol modelling

T031A12	**Role of the charged particles in atmospheric nucleation**
	V.A. Zagaynov, A.A. Lushnikov, Yu.G. Biryukov, T.V. Khodzher, and Yu.S. Lyubovtseva

T032A02	**Homogeneous water nucleation in a laminar flow diffusion chamber**
	A. Manka, D. Brus, A.-P. Hyvärinen, H. Lihavainen, J. Wölk, and R. Strey

T032A03	**Molecular mechanisms behind nocturnal new particle formation**
	I.K. Ortega, T. Suni, M. Boy, T. Grönholm, M. Kulmala, H. Junninen, M. Ehn, D. Worsnop, H. Maninnen, H. Vehkamäki, H. Hakola, H. Hellén, T. Valmari, and H. Arvela

T032A05	**Quantum chemical studies on hydration of HSO_5 and participation of $H_2S_2O_8$ in nucleation**
	M. Toivola, T. Kurtén, T. Berndt, I.K. Ortega, V. Loukonen, H. Vehkamäki, and M. Kulmala

T033A05	**User influence on indoor aerosol model simulation results**
	B. Mølgaard and T. Hussein

T033A07	**Mathematical modelling of clusters and nanoparticles transport in narrow tubes**
	L.A. Uvarova, T.V. Kazarova, and K.V. Vnukova

T033A08	**Mathematical modelling of heat and mass transfer in disperse systems with drops and agglomerates at different external conditions**
	L.A. Uvarova, O.V. Nikitina, and T.V. Kazarova

T033A11	**A methodology to use the flow field from Ansys CFX® software in an in-house sectional aerosol dynamics code**
	E. Makris, V. Gkanis, and C. Housiadas

T033A12	**Thermophoretic deposition of aerosol particles in the plane – parallel channel with considerable transversal temperature drops**
	E.R.Shchukin, Z.L.Shoulimanova, T.N. Bryansteva, and N.V.Malay

T031A01	**Simulation of transport processes of aerosol impurity in a ground boundary layer of above industrial centers**
	K.G. Shvarts and A.V. Shatrov

T031A02	**Scavenging of gaseous pollutants by falling liquid droplets in inhomogeneous atmosphere**
	T. Elperin, B. Krasovitov, and A. Fominykh

T031A03	**Determination of the contribution of different groups of emission sources on the concentration of PM10, PM2.5, and NO_2 in North Rhine-Westphalia – a whodunnit**
	H. Hebbinghaus, S. Wurzler , M. Memmesheimer, G. Piekorz, E. Friese, H. J. Jakobs, C. Kessler, A. Ebel, and P. Bruckmann

T031A06	**Photophoretic motion of absorbing aerosols: updated and advanced model for stratospheric applications**
	S.A. Beresnev, L.B. Kochneva, and V.I. Gryazin

T031A07	**Intercomparison of aerosol microphysics modules in the framework of the ECHAM5 climate model**
	R. Hommel, H. Kokkola, J. Kazil, U. Niemeier, A.-I. Partanen, J. Feichter, and C. Timmreck

T031A08	**The middle atmosphere aerosol-climate model MAECHAM5-SAM2**
	R. Hommel, C. Timmreck, and H.-F. Graf

T031A09	**Model calculations of free tropospheric aerosol and cloud condensation nuclei formation in an SO_2 rich pollution plume**
	L. Pirjola, V. Fiedler, F. Arnold, and H. Schlager

T031A11	**Parameterisation of the aerosol washout process using a moment model**
	R. Rinke, H.Vogel, and B. Vogel

T031A13	**Surface momentum flux in NWP modelling sensitivity studies relevant for dust emission estimation**
	A.C. Carvalho, J. Ferreira, J. Sousa, A. Rocha, and J. Castanheira

T031A14	**Production of water from the environment through simulation of atmospheric water cycle**
	M.K. Bologa, F.P. Grosu, A.A. Policarpov, and O.V. Motorin

T031A15	**Particulate matter from wildfires and its local/regional impacts over Portugal**
	M. Tomé, E. Nunes, C.A. Alves, and J.M. Alonso

T031A16	**Emission contributions of PM10 at an industrial park in southern Taiwan**
	Ch.-L. Chen and Y.I. Tsai

T031A19	**Structure and evolution of the atmospheric boundary layer in Buenos Aires and its relationship with Air Quality**
	A.G. Ulke, M. Arkouli, W. Endlicher, G. Baumbach, E. Schultz, U. Vogt, M. Müller, L. Dawidowski, and A. Faggi

T056A02	**Modelling the sea salt aerosol direct radiative forcing on the regional scale**
	K. Lundgren, H.Vogel, and B. Vogel

T033A01	**Numeric experiment and mesoscale structure of the atmospheric aerosol**
	O.G. Khutorova, D.P. Zinin, and G.M. Teptin

T033A03	**Field measurements of particle number emission factors for freeways**
	C. Nickel, H. Kaminski, U. Quass, A. John, and T.A.J. Kuhlbusch

T033A06	**The interannual variability of the stratospheric aerosol layer as seen in MAECHAM5-SAM2**
	R. Hommel, C. Timmreck, M. Giorgetta, and H.-F. Graf

T034A03	**Simulation of the indirect effect of Austrian background aerosol:Description of the model**
	D. Neubauer, A. Vrtala, H. Puxbaum, and R. Hitzenberger

T034A04	**Seasonal variations of characteristics of atmospheric aerosol optical depth and aerosol radiative forcing in Siberia**
	T.B. Zhuravleva, D.M.Kabanov, and S.M.Sakerin

T034A05	**New particle formation in past, present and future conditions**
	R. Makkonen, A. Asmi, V.-M. Kerminen, A. Arneth, P. Hari, and M. Kulmala

T035A02	**Fugitive PM10/PM2.5 emission factors for coal fired power plants**
	A. Hugo, M. Beyer, T.A.J. Kuhlbusch, C.J. Richter, F. Braun, and A. Wiegele

T035A04	**Developing per smoker emission rates from Environmental Tobacco Smoke**
	V. Agranovski and D. Wainwright

T036A01	**Deposition of pollens in the human respiratory system**
	Z. Sárkány, I. Balásházy, A. Horváth, Á. Farkas, E. Dobos, A. Czitrovszky, W. Hofmann, G. Kudela, and P. Magyar

T036A02	**Comparing lung deposition of ultrafine particles caused by fireworks and traffic**
	F. Kwasny, P. Madl, and W. Hofmann

T056A01	**Increased aerosol cooling from high sea spray emissions in changing climate**
	H. Korhonen, K. S. Carslaw, H.Kokkola, and S. Mikkonen

**Top of
Program**

**Top of Poster
Session Part II**

Atmosperic Aerosols - aerosol processes and properties	
T031A10	**Application of trajectory cluster analysis to Eastern Mediterranean aerosol data**
	F. Öztürk and G. Tunceln

T041A02	**Integrated measurements for aerosol properties detection in a rural site in South-Italy**
	M. Calvello, F. Esposito, and G. Pavese

T041A04	**New particle formation in elevated heights above continental Europe**
	B. Wehner, F. Ditas, A. Wiedensohler, A. Apituley, R.A. Shaw, and H. Siebert

T041A05	**Factors influencing ion-induced nucleation in a Finnish boreal forest**
	S. Gagné, T. Kurtén, T. Nieminen, M. Boy, T. Petäjä, L. Laakso, and M. Kulmala

T041A07	**Why does high relative humidity suppress continental nucleation events?**
	A. Hamed, H. Korhonen, S. L. Sihto, J. Joutsensaari, H. Järvinen, K.E.J. Lehtinen, M. Kulmala, and A. Laaksonen

T041A10	**Ultrafine aerosol and the first observed nucleation burst in Budapest**
	T. Borsós, I. Salma, T. Weidinger, P.A. Aalto, T. Hussein, and M. Kulmala

T041A11	**What are the key players in SOA formation over rural areas?**
	M. Boy, A. Sogachev, S. Smolander, J. Lauros, H. Vuollekoski, S.-L. Sihto, T. Suni, L. Laakso, A. Guenther, and M. Kulmala

T041A13	**Cluster Spectrometers in intensive field measurements within the EUCAARI Project**

H.E. Manninen, S. Gagné, E. Asmi, M. Sipilä, I. Riipinen, L. Laakso, M. Vana, A. Mirme, S. Mirme, U. Hõrrak, C. Plass-Dülmer, G. Stange, G. Kiss, A. Hoffer, M. Moerman, M. Brinkenberg, G.N. Kouvarakis, A. Bougiatioti, C. O'Dowd, D. Ceburnis, B. Svenningsson, L. Tarozzi, S. Decesari, W. Birmili, J. Heseman, A. Wiedensohler, K. Sellegri, V.-M. Kerminen,and M. Kulmala

T041A15	**Sulfuric acid in a deciduous forest during NIFTy Project**
	T. Petäjä, R.L. Mauldin, J. McGrath, E. Kosciuch, J.N. Smith, and S.C. Pryor

T041A18	**Parameterization of new particle formation starting from OH + SO₂**
	T. Berndt, F. Stratmann, M. Sipilä, T. Petäjä, R. Lee Mauldin III, M. Kulmala, J. Curtius, and J. Heintzenberg

T041A19	**Classification of intermediate air ion formation events at urban area**
	K. Komsaare, U. Hõrrak, and H. Tammet

T042A01	**Below cloud snow scavenging: a parameterization for low-intensity snowfalls**
	E.-M. Kyrö, T. Grönholm, H. Vuollekoski, A. Virkkula, M. Kulmala, and L. Laakso

T042A02	**Possible markers of aqueous aerosol of Lake Baikal in the region's atmospheric aerosol**
	A.N. Sergeev, A.S. Safatov, A.P. Agafonov, I.S. Andreeva, M.Yu. Arshinov, B.D. Belan, G.A. Buryak, V.M. Generalov, Yu.R. Zakharova, N.A. Lapteva, S.E. Olkin, M.V. Panchenko, V.V. Parfeneva, I.K. Reznikova, V.B. Simonenkov, T.B. Teplyakova, and V.A. Ternovoi

T042A03	**Comprehensive aerosol size distribution measurements at the Meteorological Observatory Hohenpeissenberg**
	M. Pesch, L. Keck, H. Grimm, A. Wollny, U. Pöschl, and H. Flentje

T042A04	**Transport of stratospheric aerosols in the field of averaged vertical wind**
	V.I. Gryazin and S.A. Beresnev

T042A05	**Planetary boundary layer influence at the Jungfraujoch depending on synoptic weather types**
	M. Collaud Coen, E. Weingartner, and U. Baltensperger

T042A06	**Origin of the high fine aerosol particle concentration event in the boundary layer over Lithuania**
	J. Kilpys, V. Ulevicius, D. Jasineviciene, and S. Bycenkiene

T042A09	**Chemical characteristics of aerosols during foggy and clear days: Case study from northern India**
	K. Ram, A.K. Sudheer, and M.M. Sarin

T042A11	**Nucleation mode particles in the Karlsruhe city plume, the COPS / TRACKS - Lagrange experiment**
	W. Junkermann, R. Hagemann, and B. Vogel

T042A12	**An episode of Saharan dust north of the Alps**
	W. Straub, S. Wurzler, and P. Bruckmann

T043A01	**Contribution of traffic-emitted pollutants at a busy Danish highway compared to a major street in central Copenhagen**
	A. Massling, F. Wang, M. Ketzel, T. Ellermann, S.S. Jensen, and P. Wåhlin

T043A04	**Comparison of particle number concentrations between different environmentsl**
	L. Morawska, X. Ling, and R. Jayaratne

T043A05	**Influence of vehicular traffic on airborne particle surface composition in Zabrze, Poland**
	J.S. Pastuszka, E.Talik, and W. Rogula-Kozlowska

T043A07	**Description of the mesoscale atmospheric aerosol: observation and model**
	C. Engler, W. Birmili, R. Wolke, and A. Wiedensohler

T043A08	**Size distribution of carbonaceous compounds and inorganic ion concentrations in background aerosol, Hungary**
	D. Benko, Á. Molnár, K. Imre, G. Kiss, and A. Hoffer

T043A10	**Oxidative potential of a panel of Carbonaceous and Metallic Nanoparticles**
	M. Sánchez Sandoval Hohl, J.J. Sauvain, K. Donaldson, and M. Riediker

T043A12	**Crystallization of micro droplets observed with Raman spectroscopy**
	Chr. Wender, R. Müller, and Th. Leisner

T043A13	**Chemical and morphological characterization of dustfall (dry deposition) in Vitória-ES Brazil**
	M.M. Conti, L.R. Menegussi, N.C. Reis Jr., J.M. Santos, F.J. Silva, and C. Scandian

T043A14	**Chemical and physical properties of oxalic acid and oxalate aerosol particles**

	A. A. Mensah, A. Buchholz, A. Kiendler-Scharr, and Th. F. Mentel
T044A01	**Aerosol cloud interaction in northern Finland**
	H. Lihavainen and L. Remer
T044A02	**Hygroscopic growth and activation of uncoated and coated soot particles and their relation to ice nucleation**
	M. Ziese, S. Henning, K. Mildenberger, F. Stratmann, O. Möhler, S. Benz, A. Buchholz, Th. Mentel, and the AIDA/LACIS-mobile-team
T044A04	**Luni-solar interaction in precipitation over Europe**
	L. Hejkrlik
T044A05	**Hygroscopic aerosol properties at Cape Verde Islands during the SAMUM-2 field campaign in 2008**
	A.Schladitz, T. Müller, A.Nowak, A.Massling, N.Kaaden, K.Kandler, K.Lieke, A.Wiedensohler
T044A06	**Laboratory investigations of contact and immersion freezing of mineral dust using an acoustic levitator**
	L. Schütz, S.K. Mitra, K. Diehl, F. Berkes, H. Schmithüsen, H. Bingemer, M. Ebert, and S. Weinbruch
T044A07	**Closure between hygroscopic growth and CCN activation of photochemical aged secondary organic aerosols**
	K. Mildenberger, A. Buchholz, T. Clauss, S. Henning, A. Kiselev, Th.F. Mentel, E. Schlosser, F. Stratmann, and R. Tillmann
T044A09	**Ice nuclei and cloud condensation nuclei measurements in a rural area**
	G.Santachiara, L. Di Matteo, F.Prodi, and F. Belosi
T044A10	**Cloud Condensation Nuclei (CCN) at an urban location**
	J. Burkart, G. Steiner, G. Reischl, and R. Hitzenberger
T044A11	**Cloud condensation nuclei in polluted air and biomass burning smoke: Size-resolved measurements and implications for the modeling of aerosol particle hygroscopicity and CCN activity**
	D. Rose, A. Nowak, P. Achtert, A. Wiedensohler, M. Hu, M. Shao, Y. Zhang, M. O. Andreae, and U. Pöschl
T044A12	**Ice residue characterization by aerosol mass spectrometry at the AIDA chamber**
	S.J. Gallavardin, D.J. Cziczo, O. Möhler, and U. Lohmann
T044A13	**Cloud condensation nuclei in pristine tropical rainforest air of Amazonia: measurements and modeling of atmospheric aerosol composition and CCN activity**
	S. S. Gunthe, S. M. King, D. Rose, Q. Chen, P. Roldin, D. K. Farmer, J. L. Jimenez, P. Artaxo, M. O. Andreae, S. T. Martin, and U. Pöschl
T044A15	**Hygroscopicity and activation properties of ambient aerosol particles in the Beijing area**
	S. Henning, A. Nowak, K. Mildenberger, E. Sommerhage, E. Hallbauer, D. van Pinxteren, H. Herrmann, D. Zhaoze, L. Pengfei, C. Zhao, A. Wiedensohler, and F. Stratmann
T044A16	**Studies of the relation between cloud droplet size and dry residual particle size with the Droplet Aerosol Analyser**
	M. Berghof, G.P. Frank, S. Sjogren, and B.G. Martinssonr
T044A17	**Nitrate and the regional Indirect Aerosol Effect**
	H.M. ten Brink, R. Otjes, and P. Jongejan
T044A20	**Quantitative study of the water content and phase transition behaviors of aerosol particles deposited on a hydrophobic substrate using micro-Raman spectroscopy**
	M.C. Yeung and C.K. Chan
T045A01	**Aerosol radiative forcing over an urban Indian city**
	A.S. Panicker and G. Pandithurai
T045A02	**Determination of the aerosol shortwave radiative forcing in the Mediterranenan from ground based and satellite observations**
	C. Di Biagio, A. G. di Sarra, and D. Meloni
T045A04	**Observations of aerosol-cloud interactions at Puijo semi-urban measurement station**
	H.J. Portin, M. Komppula, A.P. Leskinen, S. Romakkaniemi, A. Laaksonen, and K.E.J. Lehtinen
T046A01	**Weighting aerosol with MERIS**
	A.A. Kokhanovsky, A.S. Prikhach, I.L. Katsev, E.P. Zege, and A.P. Ivanov
T046A02	**Estimating PM2.5 over southern Sweden using satellite measurements**

		P. Glantz, A. Kokhanovsky, W. von Hoyningen-Huene, and C. Johansson
T046A03	**One-year measurements of aerosol vertical profiles in Gual Pahari, India**	
	M. Komppula, T. Mielonen, H. Lihavainen, A.-P. Hyvärinen, V.-M. Kerminen, H. Baars, R. Engelmann, B. Heese, D. Althausen, T.S. Panwar, R.K. Hooda, V.P. Sharma, and Y. Viisanen	
T046A05	**Aerosol products from GOME-2 on the Metop-A satellite: first impression**	
	L.G. Tilstra, O.N.E. Tuinder, O.P. Hasekamp, M. de Graaf, and P. Stammes	
T046A09	**Retrieval of biomass burning aerosols over Amazonas using AATSR with AERONET aerosol models**	
	P. Kolmonen, A.-M. Sundström, L. Sogacheva, and G. de Leeuw	
T046A11	**Systematizing MODIS, TOMS and MISR satellite datasets with HYSPLIT model for monitoring regional pattern of aerosol and its seasonal variability in Pakistan**	
	K. Alam and S. Qureshi	
T046A12	**Specific features of angular characteristics of diffuse solar radiation in little-cloud atmosphere**	
	T.B. Zhuravleva, T.V.Bedareva, D.M. Kabanov, I.M. Nasrtdinov, and S.M. Sakerin	
T046A13	**Analyses of MODIS aerosol products over the Iberian Peninsula**	
	M.J. Granados and L. Alados-Arboledas	
T046A14	**How satellite retrievals of NO_2 vertical columns can be improved using aerosol measurements**	
	J. Leitao, A. Richter, A. Kokhanovsky, and J.P. Burrows	
T046A15	**Calibrated CCD imager for aerosol optical and physical properties estimation**	
	A. Cazorla, F.J. Olmo, L. Alados-Arboledas, R. Wagener, and J.E.Shields	
T046A16	**EARLINET for long term observations of aerosol over Europe**	
	G.Pappalardo, U. Wandinger, H. Linnè, A. Amodeo, L. Mona, A. Apituley, L. Alados Arboledas, D. Balis, A. Chaikovsky, A. Comeron, V. Freudenthaler, I. Grigorov, O. Gustafsson, S. Kinne, D. Nicolae, I. Mattis, V. Mitev, A. Papayannis, M.R. Perrone, A. Pietruczuk, M.Pujadas, J.P. Putaud, F. Ravetta, V. Rizi, V. Simeonov, N. Spinelli, K. Stebel T. Trickl, and M. Wiegner	
T046A17	**Vertical characterization of Saharan dust intrusions over Tenerife by ground-based lidar and airborne measurements**	
	C. Cordoba-Jabonero, J. Andrey, M. Gil, and E. Cuevas	
T046A18	**Differences of the aerosol load between an urban and suburban site using remote sensing measurements and model estimates**	
	D. Balis, E. Giannakaki, E. Katragkou, M. Wiegner, K. Markakis, T. Giannaros, and V. Amiridis	
T046A19	**Microphysical and optical properties of aerosols at Thessaloniki, Greece: Comparison of two different inversion algorithms**	
	E. Giannakaki, M. Detlef, and D. Balis	
T046A20	**Aerosol characterization in the North-Center (Castilla y Léon) of Spain**	
	R. Rodrigo, V. Cachorro, A. Berjón, B. Torres, C. Toledano, and A. de Frutos	
T047A01	**Infrared optical constants of highly diluted sulfuric acid solution droplets at cirrus temperatures**	
	R. Wagner, S. Benz, H. Bunz, V. Ebert, O. Möhler, H. Saathoff, M. Schnaiter, and T. Leisner	
T047A02	**Optical properties of different-shaped synthetic hematite particles: A laboratory study**	
	M. Vragel, C. Linke, M. Schnaiter, G. Beuchle, and T. Leisner	
T047A03	**Effects of complex shapes on radiative properties of mineral dust aerosol: Implications on sun photometry**	
	J. Gasteiger, M. Wiegner, C. Toledano, and P. Koepke	
T047A06	**Climate relevant aerosol properties measured at Évora, Portugal, from 2002 to 2008**	
	S.N. Pereira, F. Wagner, and A.M. Silva	
T047A07	**Aerosol light scattering at high relative humidity at a high alpine site (Jungfraujoch)**	
	R. Schmidhauser, P. Zieger, E. Weingartner, M. Gysel, P.F. DeCarlo, and U. Baltensperger	
T047A08	**Comparison of near-surface and columnar aerosol optical and microphysical properties**	
	M.A. Sviridenkov and A.A. Isakov	
T047A10	**Influence of relative humidity on the Angström coefficient values of atmospheric aerosols**	
	J. Kusmierczyk-Michulec	

T047A11	**Comparison between MODIS and GADS aerosols asymmetry factor on a planetary scale**
	C.D. Papadimas, N. Hatzianastassiou, C. Matsoukas, and I. Vardavas

T047A12	**Cavity Ringdown Spectroscopy Measurements of Extinction by Aerosol Particles**
	T.J.A. Butler, D. Mellon, J. Kim, J. Litman, and A.J. Orr-Ewing

T055A02	**Impacts of dust storms on dioxins and furans in a basin area, Taiwan**
	T.Y. Wu, Y.M. Chen, Y.C. Lin, G.P. Chang-Chien, and C.H. Hung

T056A03	**Experimental data interpretation by means of computational fluid dynamics results: Dynamic growth of Sea-Salt particles**
	J. Voigtländer, D. Niedermeier, and F. Stratmann

T056A04	**Highly time-resolved observation of a particle growth event**
	O. Klemm, L.D. Ziemba, B.C. Sive, R.J. Griffin, and R.W. Talbot

T056A05	**Seasonal variation of aliphatic amines at the Cape Verde Islands**
	C. Müller, Y. Iinuma, K. Müller, S. Lehmann, and H. Herrmann

T076A06	**The effect of aerosol characteristics on optical properties in Hong Kong**
	E.Q.J. Bian, R. Zhang, Z.B. Yuan, A.K.H. Lau, and J.Z. Yu

T091A27	**Absorption properties of atmospheric aerosols from a high-altitude site in northern India**
	K. Ram, M.M. Sarin, and P. Hegde

Top of Program   **Top of Poster Session Part II**

Electrical Effects

T062A01	**Observation of formation of secondary plasma spheres in water aerosol-plasma clouds by electric discharge spraying**
	M.V. Jouravlev and A.V. Tovmash

T062A03	**Atmospheric pressure production of Carbon nano-particles by Dielectric Barrier Discharges**
	A. Elcik, N. Jidenko, A.P. Weber, and J-P. Borra

T062A06	**Conversion of methanol vapour in a microwave discharge reactor**
	C.-H. Tsai, Y.-R. Chen, Y.-W. Wang, and Y.-F. Wang

T062A07	**Nano carbon powders produced by microwave plasma methane steam reforming**
	Y.-M. Kuo, C.-H. Tsai, K.-T. Chen, and Y.-C. Lin

T063A01	**Electrostatic removal of submicron particles under CO_2-rich atmosphere**
	Y.J. Kim, H.J. Kim, B. Han, D.K. Song, S.H. Jung, W.S. Hong, and W.H Shin

T063A03	**Neutralization of Tetraalkylammonium Halide Clusters**
	D. Wimmer, G. Steiner, and G.P. Reischl

T063A04	**Dispersion of corona ions downwind from a high-voltage power line**
	X. Ling, R. Jayaratne, and L. Morawska

T063A08	**Energy electroaerosol generation through simulation of atmospheric water cycle**
	M.K. Bologa, T.P.Grosu, A.A. Policarpov, and O.V. Motorin

T063A10	**Droplet size distribution of Electro-hydrodynamic Atomization (EHDA): Parametric dependencies**
	S. Singh, A. Khan, B.K. Sapra, and Y.S. Mayya

T063A12	**Bipolar Diffusion Charging of Aerosol Particles in the Transition Regime**
	K. Barbounis, S. Vratolis, K. Eleftheriadis, and G. Biskos

T064A01	**Multiple electrospray unit with circular symmetry**
	Y. Arnanthigo, C.U. Yurteri, J.M. Marijnissen, and A. Schmidt-Ott

T064A03	**Electrospraying method to prepare ultra-low Pt loading cathodes for PEM fuel cells**

	S. Martin, P.L. Garcia-Ybarra, and J.L. Castillo
T065A01	**Determination of EHD generated droplet size: Review of models and experimental tools**
	M. Sausse Lhernould, M. Pierobon, P. Mathys, and P. Lambert
T065A02	**Electrostatic diagnostics of charged aerosol particles in gasdynamic devices**
	A. Vatazhin, D.Golentsov, and V. Likhter
T065A04	**Method for the estimation of mass concentration in automotive exhaust**
	L. Hillemann, N. Senftleben, and M. Stintz
T068A01	**Prevention of aerosol particle deposition on wafers by means of gas ionization**
	P. Gefter, J. Menear, S. Gehlke, J. Salm, and E. Tamm
T068A02	**Scavenging efficiencies and contact freezing of supercooled cloud droplets for charged aerosol particles: Laboratory experiments**
	D. Rzesanke and T. Leisner
T068A03	**Aerosol charging room: a simple model**
	J. Salm
T068A04	**Corona-Quenching by submicrometer particles in turbulent tube-wire electrostatic precipitators**
	C. Luebbert and U. Riebel

Top of Program   **Top of Poster Session Part II**

Fundamentals	
T027A03	**Mass transfer to a chemically active particle in the transition regime**
	A.A. Lushnikov
T071A01	**Statistical analysis of different proxy values for sulphuric acid concentration**
	S. Mikkonen, J. Joutsensaari, S. Romakkaniemi, T. Petäjä, T. Nieminen, R.L. Mauldin III, M. Kulmala, and A. Laaksonen
T071A02	**Critical size of charged aerosol particles in the presence of adsorbable foreign gas**
	V.V. Levdansky, J. Smolik, and P. Moravec
T071A03	**The role of optical radiation in the homogeneous nucleation**
	V.G. Chernyak and E.S. Evgrafova
T071A04	**Particle formation close to supersaturated droplets**
	B. Svenningsson and M. Bilde
T073A01	**Temperature dependence of the contact angle for n-propanol on silver and on sodium chloride substrate**
	T. Pinterich, S. Schobesberger, A. Vrtala, P. M. Winkler, and P. E. Wagner
T073A02	**Evaporation and particle shape factor of succinic acid particles: Combined analysis of experimental data and computational fluid dynamics results**
	J. Voigtländer and F. Stratmann
T073A03	**Discontinuous hygroscopic growth of an aqueous surfactant/salt aerosol particle levitated in an electrodynamic balance**
	V. Soonsin, U.K. Krieger and Th. Peter
T073A04	**Deposition probability of nanoparticles on inverse surfaces at low pressure**
	C. Asbach, H. Fissan, T.A.J. Kuhlbusch, D.Y.H. Pui, and J. Wang
T073A05	**Reanalyzed n-nonane nucleation experiments conducted in an expansion chamber**
	D. Ghosh and R. Strey
T074A04	**Aerosol Clustering Patterns in Oscillating Flows**
	D. Katoshevski
T074A05	**Droplet bouncing effects in salt water electrospray**

		E.C. Fuchs, L.L.F. Aghostinho, C.U. Yurteri, and J.C.M Marijnissen
T075A01	**Experimental study of dew condensation influence on dust deposition rate**	
	S.A. Biryukov and L.I. Yarmolinsky	
T076A01	**Effects of the non-measured Mid-IR spectral range of the imaginary refractive index on the derivation of the real refractive index using the Kramers-Kronig transformation**	
	M. Segal-Rosenheimer and R. Linker	
T076A02	**Scattering data base for nonspherical particle**	
	J. Wauer, T. Rother, and K. Schmidt	
T076A03	**Polar scattering from fractal like soot agglomerates**	
	K.-H. Naumann, M. Gangl, M. Schnaiter, and H. Horvath	
T076A04		**Aerosol optical depth and its connection with macrometeorological features**
		A. Ponczkowska, T. Zielinski, T. Petelski, J. Piskozub, G. Chourdakis, S. Malinowski, T. Stacewicz, K. Markowicz, A.K. Jagodnicka, M. Posyniak, A. Kardas, I. Stachlewska, M. Gausa, S. Blindheim, A. Smirnov, and B. Holben
T076A05	**Effective dielectric permeability of fractal cluster**	
	V.V. Maksimenko	
T076A07	**Measurements of aerosol optical properties at urban sites to determine aerosol direct radiative effect**	
	S. Stefan, R. Barladeanu, and L. Mihai	
T077A01	**Effect of a hydrocyclone and a centrifugal separator in purifying rolling lubricant**	
	Y. Seo and S.-J. Lee	
T077A04	**Dust concentrators for cost effective gas cleaning**	
	V. Galperin, O. Elport, and M. Shapiro	
T077A05	**A model for steady-state oil transport and saturation in a mist**	
	D. Kampa, J. Meyer, B. Mullins, and G. Kasper	
T077A07	**Experimental results and modelling of the clogging of pleated fibrous filters in presence of humidity**	
	A. Joubert, J.C. Laborde, L. Bouilloux, D. Thomas, S. Callé-Chazelet	
T077A08	**Inactivation of airborne viruses by tea tree oil**	
	O.V. Pyankov, O. Pyankova, B. Mullins, R. Huang, and I.E. Agranovski	
T077A10	**Nanoparticle filtration through capillaries by Langevin dynamics**	
	T.D. Elmøe, A. Tricoli, and S.E. Pratsinis	
T077A12	**Applied the filter pretreated with berberine for removal of bioaerosols**	
	S.H. Yang, Y.C. Huang, C.H. Luo, and C.Y. Chuang	
T077A13	**Deposition of aerosol particles in dense array of spheres**	
	W. Holländer and T. Zaripov	
T077A14	**Factors Affecting CADR (Clean Air Delivery Rate) Measurement**	
	S.H. Huang, K.N. Chang, K.T. Hou, C.W. Chen, C.P. Chang, and C.C. Chen	
T077A15	**Characteristics of commercial antimicrobial filter media for removal of bioaerosols**	
	KY. Yoon, Y.S. Kim, J.H. Park, and J. Hwang	
T077A16	**Collection of submicron aerosol particles and inactivation of bioaerosols by simultaneously using carbon fiber type unipolar charger and fibrous medium filter**	
	J.H. Park, K.Y. Yoon, Y.S. Kim, J.H. Byeon, and J. Hwang	
T077A17	**Filtration of oil mists in multilayer filter fabrics composed from PES and PP fibres**	
	T. Jankowski and W. Gador	
T077A18	**Filtration of aerosol particles in structurally inhomogeneous fibrous filters. I – Model formulation**	
	A. Podgórski and A. Jackiewicz	
T077A20	**Filtration of aerosol particles in structurally inhomogeneous fibrous filters.III – Effect of gas velocity on segregation intensity**	

	A. Jackiewicz and A. Podgórski
T077A21	**Analysis of the influence of a fibrous filter structure used for filtration of nanoaggregates on its quality factor**
	A. Podgórski and M. Goszczynska
T077A22	**Application of the Steam Jet Aerosol Collector (SJAC) for the semi volatile organic compounds gas / particle portioning measurements**
	D. Antkowiak, J. Schnelle-Kreis, W.G. Kreyling, and G. Matuschek
T077A23	**Aerosol based functionalization of porous substrates for diesel particulate emission control applications within the ATLANTIS project**
	A. Asimakopoulou, S. Lorentzou, E. Papaioannou, C. Agrafiotis, and A.G. Konstandopoulos
T079A01	**Mixing state of bi-component mixtures under coagulation from scaling solutions**
	J.M. Fernández-Díaz, G. Gómez-García, M.A. Rodríguez-Braña, M. Domat, and I.A. SanJuan

<table>
<tr><td>**Top of Program**</td><td>**Top of Poster Session Part II**</td></tr>
</table>

PMx

T045A05	**Seasonal PM variation in Cosenza, South Italy**
	M. Filice and P. De Luca
T091A17	**A miniature collector for the concentrated collection of fine airborne particles**
	S.V. Hering and G.S. Lewis
T111A01	**Emission of submicron aerosol particles during the operation of a laser beam printer**
	J.H. Byeon, S.Y. Kim, Y. Kim, D.Y. Lee, and J. Hwang
T111A02	**Wind direction versus sampling point: a real case study**
	M. Filice and P. De Luca
T112A01	**Biodiesel (soy-bean FAME) effect on particulate and gaseous pollutants from a passenger car**
	G. Fontaras, T. Tzamkiozis, L. Ntziachristos, and Z. Samaras
T112A03	**Background concentrations of PAH:s in precipitation and air in Finland**
	M. Vestenius, H. Hellen, and H. Hakola
T112A04	**Indoor versus outdoor air quality measurements: number, mass concentrations and chemical composition of PM at the University of Perugia, Italy**
	S. Ortu, L. Barcherini, D. Cappelletti, F. Marmottini, F. Scardazza, B. Moroni, and B. Sebastiani
T112A05	**Characterization of fine aerosol particle (PM1) and trace element concentrations: assessment of the contribution of local sources and long-range transport**
	R. Caggiano, M. Macchiato, S. Sabia, G.A. Scardaccione, and S. Trippetta
T112A07	**Influence of a Saharan dust outbreak on PM2.5 observations at a Mediterranean sampling site**
	S. Trippetta, R. Caggiano, and M. Macchiato
T113A01	**Assessing the contribution of steel works to PM10 at nearby monitoring station using magnetic particles as tracers**
	E. Petrovský, A. Kapicka, B. Kotlík, R. Zboril, J. Novák, and H. Fialová
T113A06	**Evaluation of the contribution of ship traffic to PM2.5, PM0 concentration in the Venice harbour area**
	D. Contini, A. Gambaro, A. Donateo, F. Belosi, G. Santachiara, D. Cesari, S. De Pieri, and F. Prodi
T113A07	**Integrated approach in the monitoring of particulate matter: relevant parameters for high pollution events**
	M. Amodio, E. Andriani, M. Caselli, B.E. Daresta, G. de Gennaro, A. Di Gilio, P. Ielpo, C.M. Placentino, and M. Tutino
T113A08	**Seasonal variation in trace elemental concentrations in PM2.5 particles in Nairobi, Kenya**
	J. Boman, M.J. Gatari, S.M. Gaita, X. Zhang, B. Xue, and A. Wagner
T113A09	**Diurnal variations in the particle size distribution in Ouagadougou, Burkina Faso**

	J. Boman, B. Xue, X. Zhang, and S. Thorsson
T113A10	**Emissions of PM1 from silent surface road cover in Gothenburg, Sweden**
	J. Boman, S. Janhäll, and E. Björkman
T113A11	**A summertime study of PM10 and PM2.5 mass concentrations in urban and industrialized cities in Turkey**
	E.O. Gaga, A. Ari, J. Argante, K. Meliefste, O.D. Yay, G. Demirel, S. Örnektekin, T. Dögeroglu, W. van Doorn
T113A12	**As, Cd, Cr, Cu, Ni and Pb in PM2.5 in Gothenburg, Sweden**
	A. Wagner, J. Boman, and M.J. Gatari
T113A13	**Use of several receptor models - CMB, APCS and PMF - as a tool to interpret air quality data**
	M. Amodio, E. Andriani, M. Caselli, B.E. Daresta, G. de Gennaro, A. Di Gilio, P. Ielpo, C.M. Placentino, M. Tutino, and L. Trizio
T113A14	**Evaluation of the characteristics of PM10 time series in relation to the type of air monitoring station**
	M.A. Barrero, M. Cabello, J.A.G. Orza, and L. Cantón
T113A15	**Measurements of hydroxy and nitro PAHs in atmospheric urban aerosols**
	A.I. Barrado Olmedo, S. García Alonso, R. Pérez Pastor, and O. Pindado Jiménez
T114A01	**The use of air quality indices to evaluate atmospheric pollution in urban areas**
	A. Di Menno di Bucchianico, G. Cattani, R. Aceto, S. Bartoletti, A. Gaeta, and A.M. Caricchia

Top of Program   **Top of Poster Session Part II**

Special Session 3: Aerosol Sampling and Aerosol Analytics

T150A01	**Evaporative loss of accumulated semi-volatile liquid aerosol from fibrous filter**
	B. Sutter, J.C. Appert-Collin, D. Bémer, and D. Thomas
T150A02	**Role of nitrogen-containing organics in secondary aerosol formation – identification of methylamine in ambient 31 nm – particles by ion trap TDCIMS**
	A. Held, G.J. Rathbone, and J.N Smith
T150A03	**Comparison of 4 temperature protocols for differentiating between OC and EC in thermal-optical transmission analysis of aerosol samples collected on quartz fibre filters**
	W. Maenhaut, X. Chi, and S. Dunphy
T150A04	**Energy saving and pollution reduction of industrial boiler by using methanol- and isopropanol-contained wastewater emulsified heavy fuel-oil**
	S.-L. Lin and W.-J. Lee
T150A06	**Monitoring of particles PM10 and PM2.5 in the Mitrovica urban atmosphere**
	A. Syla, A. Veliu, M. Musa, and B. Kafexholli
T150A08	**"Particle Loss Calculator" – A new software tool for the assessment of sampling and transport efficiencies of aerosol inlet systems**
	S.-L. von der Weiden, F. Drewnick, and S. Borrmann
T150A10	**Stable carbon isotopic composition of PM2.5 in Taiwan**
	A. Kiendler-Scharr, G. Engling, R. Fisseha, W. Laumer, I. Gensch, Y. C. Wu, and Y. T. Chen
T150A11	**AMS aerosols characterization at Seiffen (Germany)**
	L. Poulain, Y. Iinuma, and H. Herrmann
T150A12	**Studies of PM2.5 elemental composition in Venice Lagoon area**
	A.M. Stortinia, A. Freda, D. Cesaric, S. De Pieri, W. Cairnsa, D. Continic, and A. Gambaro
T150A13	**Calculating particle concentration fields for steady and unsteady aerosol sampling**
	A.K. Gilfanov, D.V. Maklakov, and S.K. Zaripov
T150A14	**Numerical study of thin-walled sampler performance for aerosols in low windspeed environments**
	S.K. Zaripov, A.K. Gilfanov, and D.V. Maklakov

T150A15	**Analysis of oligomeric glyoxal using HPLC-ESI-MS – Challenges and possibilities**
	C.J. Kampf and T. Hoffmann
T150A16	**Artifacts in size distributions from low time-resolution mobility sizers in varying particle concentrations**
	M. D. Wright and D. L. Henshaw
T150A17	**Source apportionment and partitioning of persistent organic pollutans in rural site of Turkey**
	S. Yenisoy-Karakas, M. Öz, E.O. Gaga, and A. Ari
T150A18	**Airborne fungi concentrations in trains**
	Y.F. Wang, L.C. Wang, C. H. Tsai, and H.H. Yang
T150A21	**Atmospheric pollution and particulate matter concentration at petrol station in semi-urban site**
	A. Akachat
T150A22	**Particulate matter deposition monitoring in the surroundings of the port of Koper**
	G. Jereb, B. Poljšak, B. Marzi, F. Cepak, G. Dražic, N. Ogrinc, M. Bizjak, and S.A. Katz
T150A23	**Investigation of a Denuder-Filter Sampling Technique for the determination of carbonyl compounds from monoterpene oxidation**
	A. Kahnt, Y. Iinuma, O. Böge, and H. Herrmann
T150A25	**Indoor and outdoor carbon composition of PM2.5 aerosol in Mumbai, India**
	A. Elizabeth Joseph, S. Unnikrishnan, and R. Kumar
T150A26	**Molecular characterisation of biogenic secondary organic aerosols using ion mobility spectrometry - quadrupole time-of-flight mass spectrometry**
	Y. Iinuma and H. Herrmann
T150A29	**Tuning of Sunset EC/OC field instruments to obtain more than comparable data**
	J. Schwarz and P. Vodicka

Top of Program   **Top of Poster Session Part II**

Special Session 4: Origin, Properties and Impact on Regional and Global Climate
T160A01	**Surface-atmosphere exchange of aerosol particles in the high Arctic - Results from ASCOS**
	A. Held, D. Orsini, and C. Leck
T160A04	**Impact of marine aerosol on Arctic Haze**
	T. Petelski, A. Rozwadowska, T. Zielinski, M. Stock, R. Neuber, and R. Treffeisen
T160A05	**Impact of air mass history on aerosol optical thickness at Hornsund station, Spitsbergen**
	A.Rozwadowska, T.Petelski, P.Sobolewski, and T. Zielinski
T160A06	**Geochemical characterization of mineral aerosol at Dome Concordia East Antarctic Plateau (Station Concordia project)**
	F. Marino, E. Castellano, S. Nava, M. Chiari, G. Calzolai, S. Becagli, F. Rugi, M. Severi, R. Traversi, F. Lucarelli, R. Udisti, D. Gaiero, and S. Gassò
T160A08	**Investigation of aerosol microphysical and chemical composition over White and Kara Seas**
	S.A.Terpugova, V.V. Polkin, M.V. Panchenko, L.P. Golobokova, T.V. Khodzher, U.G. Filippova, V.S. Kozlov, V.P. Shmargunov, V.P. Shevchenko, and A.P. Lisitzin
T160A10	**Central Arctic atmosphere pollution by smelter generated SO$_2$: Airborne detection and implications for Arctic Haze and clouds**
	F. Arnold, R. Nau, T. Jurkat, H. Schlager, A. Minikin, A. Dörnbrack, L. Pirjola, and A. Stohl
T160A11	**Physicochemical characteristics of marine aerosols of Western Arctic**
	A.V. Syroeshkin and M.A. Chichaeva
T160A14	**Analyses of laboratory-grown frost flowers, brine and the resultant sea-salt aerosol**
	A.V. Jackson, S.J. Walker, J.J.N. Lingard, B.J. Brooks, R. Obbard, H. Roscoe, and M. H. Smith

T160A15	**Absorption properties of atmospheric aerosols in the ALOMAR station (summer 2008)**
	E. Montilla-Rosero, S. Mogo, J. F López, V. E. Cachorro, R. Rodrigo, and A. De Frutos
T160A16	**Aerosol type comparison among three sub-arctic sites: ALOMAR-Andenes, Abisko and Sodankylä in late spring and summer 2007**
	E. Rodríguez, C. Toledano, V. Cachorro, A. De Frutos, A. Berjón, B. Torres, M. Gausa, and G. de Leeuw
T160A17	**Possible role of internally mixed crustal materials in the enrichments in sulphur of supermicrometric Antarctic coastal aerosol particles**
	P. Mittner, D. Biancato, D. Ceccato, and F. Chiminello

Top of Program   **Top of Poster Session Part II**

Special Session 7: Test Materials in Toxicological and Health Effect Studies

T190A01	**Synthesis and characterization of titanium dioxide particles for toxicity tests**
	A.J. Koivisto, H. Alenius, J. Joutsensaari, H. Norppa, M. Miettinen, P. Pasanen, L. Pylkkänen, E. Rossi, T. Tuomi, M. Vippola, J. Jokiniemi, and K. Hämeri
T190A02	**Characterization of polychlorinated dibenzo-p-dioxin/dibenzofuran emissions from joss paper burned in a furnace**
	M.T. Hu, S.J. Chen, K.L. Huang, Y.C. Lin, G.P. Chang-Chien, and J.H. Tsai
T190A03	**Human type B synoviocytes, as a cellular model for a better knowledge of the pro-inflammatory effects of environmental PM**
	F. Cetta, F. Laghi Pasini, E. Selvi, A. Dhamo, M. Natale, R. Zangari, P. Laviano, L. Cantarini, E. Bolzacchini, M. Camatini, and M. Galeazzi
T190A05	**Redox balance of Thiols in the exhaled breath condensate (BEC) in 2 populations with different exposure to traffic related pollutants**
	F. Cetta, R. Accinni, G. Schiraldi, M. Sala, R. Zangari, P. Laviano, M. Guinea Montalvo, G. Giussani, C. Dellanoce, F. Minardi, and L.Allegra
T190A06	**The possible impact of "sequential co-exposure" on ozone associated adverse health effects. Preliminary data from cumulative cross sectional and prospective studies in Milan**
	F. Cetta, M. Sala, G. Schiraldi, E. Bolzacchini, A. Dhamo, L. Moltoni, G. Gerosa, A. Ballarin-Denti, and L. Allegra
T190A09	**Trace element analyses of spark discharge particles**
	E. Karg, B. Lentner, W.G. Kreyling, and O. Schmid

Top of Program   **Top of Poster Session Part II**

Special Sesion 8: - Artifacts in Measuring PM

T200A03	**Determination of vertical distribution of air pollution over Budapest by aircraft based measurements**
	B. Alföldy, V. Groma, E. Börcsök, A. Nagy, A. Czitrovszky, and S. Török
T200A08	**Organic carbon in Whatman-QMA field-blanks**
	H.M. ten Brink and F. van Arkel
T200A10	**Level of uncertainty on PM2.5 mass concentrations introduced by inorganic sampling artifacts**
	L. Rondo and K. Eleftheriadis

Abstracts

T01 Aerosol-based nanotechnology

Ionic liquids as a source of positive and negative standard ions in the sub 3 nm range.

M. ATTOUI

Department of Physics, Paris XII University, France

Keywords: nanoparticles, DMA, ions, mobility

Positive standards (mass and mobility), stable singly charged ions in the sub 3 nm range of tetra-alkyl ammonium halides, introduced by Ude & Fernandez de la Mora 2005, produced by electrospray atomization of their dilute solutions in ethanol or methanol are widely used in aerosol studies (high flow DMAs and mass spectrometers calibration, experimental measurement of DMAs transfer function, CPCs efficiency detection, ions induced nucleation, nano filtration etc…). Contrary to the calibration experiments, filtration & DMA transfer function measurement, the ions induced nucleation and particle grow in CPCs measurement, ions and or charged particles polarities and charges number are important. This means that we need a source of positive and negative stable ions, standards in mobility and mass in the sub 3 nm range. Ionic liquids (molten salts at room temperature) are good candidates to come up to these expectations.

This paper presents experimental results of acetonitrile seeded with some ionic liquids atomized with electrospray technique coupled to a high flow and high resolution DMA (Fernandez de la Mora & Attoui 2007). A home made electrospray source with 360 µm OD and 40 µm ID silica sharpened needle (New Objective USA) is used to atomize 1mM solution of ILs in acetonitrile. Bottled air gaz of breathing quality carry the ions from the electro spray source to the high resolution DMA. More details on the experimental set up are given by Ude & Fernandez de la Mora 2005. Several ionic liquids are tested during this study. Figure 1 and 2 give respectively an example of the size distribution (if the ions are singly charged!) of ethyl methyl imidazolium bis trifluorosulfamide (EMI TFA) measured by the DMA with an electrometer as detector, without charge reduction nor neutralisation.
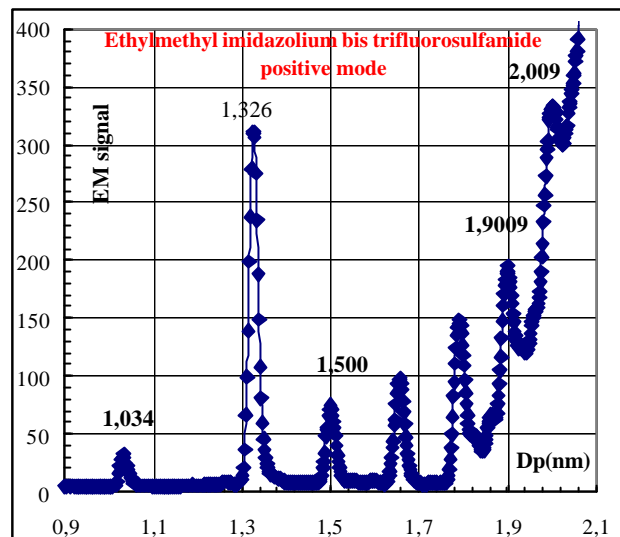
Fig 1 Mobility diameter distribution of positive ions of EMI TFA.
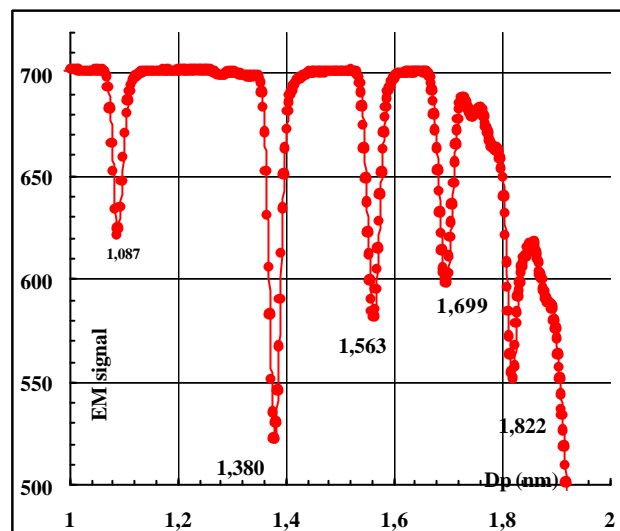
Fig 2 - Mobility diameter distribution of negative ions of EMI TFA.

References :

Fernandez de la Mora J., Attoui, M. (2007) Abstract T02A029 European Aerosol Conference , Salzburg, Austria
Ude, S, Fernandez de la Mora J. (2005),. Journal Aerosol Sci., 36, 1224–1237.

A nano-DMA of rectangular planar plates

E. Hontañón[1], M. Alonso[2], A. Rivero[3], D. Fuentes[1] and E. Ramiro[1]

[1]RAMEM S. A., Sambara 33, 28027, Madrid, Spain
[2]National Center for Metallurgical Research (CSIC), Gregorio del Amo 8, 28040, Madrid, Spain
[3]SIMPPLE, S. L., Països Catalans 15, 43007, Tarragona, Spain

Keywords: Nanoparticles, Planar DMA, Rectangular Plates, Resolution

A novel differential mobility analyzer (DMA) of rectangular planar plates has been developed for the sizing of nanoparticles in the range of 1 to 100 nm (IONER® N1).

A major concern in conventional cylindrical DMAs is the centering of the electrodes, since a very small misalignment can result in a severe degradation of the resolving power of the instrument. To avoid this difficulty, we have chosen a planar geometry, so that electrode centering is no longer an issue. In addition, parallel plates result also in a uniform electric field between the electrodes reducing the diffusional broadening of the transfer function in comparison to cylindrical DMAs. The machining and assembly of the electrodes are also easier and more precise for planar DMAs than for cylindrical DMAs, thereby reducing the cost of the instrument.

Recently a DMA of rectangular planar plates has been demonstrated for analyzing with high resolution ions of mobility in the range of 1 to 2 $cm^2 \cdot V^{-1} \cdot s^{-1}$ (IONER® X1, Santos *et al.* 2008). The successful performance of this instrument has motivated the development of the nano-DMA of parallel rectangular plates presented here. The IONER N1 has been designed to classify non-diffusive nanoparticles with a resolution of 10 when operating at aerosol and sheath flow rates of 2 and 20 $l \cdot min^{-1}$, respectively. Prevision has been done to keep laminar flow conditions at sheath flow rates up to 200 $l \cdot min^{-1}$ to enhance the resolution in the diffusive size range (<10 nm) for specific applications.

The working region of the IONER N1 is a rectangular duct formed of the electrodes (aluminium) and the insulating walls (PET). It has a height of 8 mm (separation between electrodes), a width of 90 mm (distance between insulators), and a length of 110 mm (distance between aerosol inlet and outlet). The aerosol flow enters and exits the classification zone through rectangular slits of 54 mm in length and 1.5 mm in width.

Preliminary experiments were conducted to test flow behaviour and the resolution of the IONER N1. Ions of tetraheptylammonium (THA) were generated by electrospraying a solution of tetraheptylammonium bromide (THABr) in ethanol (10^3 ppm w/v) and carried in a stream of synthetic air into the IONER N1. The current of the ions leaving the DMA was measured with an electrometer (IONER® EL-5010). In the experiments, the IONER N1 operated in open circuit mode with a HEPA filter followed by a mesh at the entrance of the sheath air to the DMA. The spectrum of THA ions was measured at an aerosol flow rate (q) of 2 Nl·min^{-1} and sheath flow rates (Q) of 10 to 50 Nl·min^{-1}. The peaks correspondent to THA monomer (p = +1, Z = 0.96 $cm^2 \cdot V^{-1} \cdot s^{-1}$, d_E = 1.44 nm) are displayed in Fig. 1. The peaks were fitted to Gaussian functions and from these the resolution (R) of the DMA was calculated as the inverse of the Full Width at Half Height (*FWHH*) normalized with respect to the peak voltage (V_p), i.e. $R = V_p/FWHH$. Fig. 2 shows the resolution of the IONER N1 for THA monomer found in the experiments. The points follow fairly well the linear trend predicted by the theory ($R \sim V^{1/2}$) up to sheath flow rates of 50 Nl·min^{-1}. Experiments with ions at higher sheath flow rates and with monodisperse non-diffusive particles are in progress.
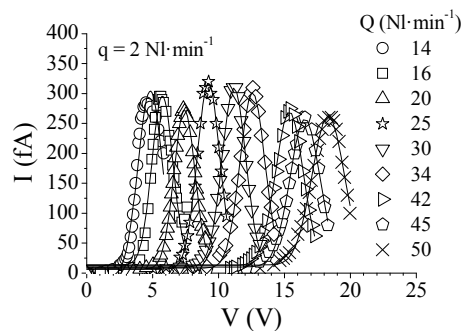
Figure 1. Spectra of THA monomer measured with IONER N1.
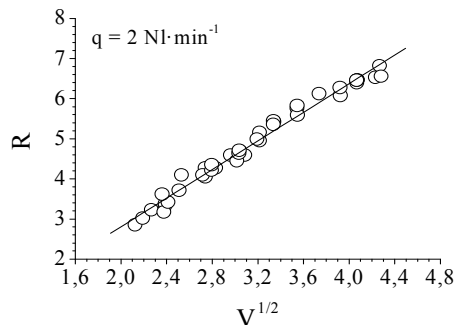
Figure 2. Resolution of IONER N1 for THA monomer.

Santos, J. P., Hontañón, E., Ramiro, E., & Alonso, M. (2008). *Atmos. Chem. Phys. Discuss.*, 8, 17631-17660.

Disagreement of classical theory for the friction resistance of nanoparticles in low-pressure flows

T. Wu[1], A. P. Weber[1]

[1]Institute for Mechanical Process Engineering, Clausthal University of Technology, Leibnizstrasse 19, D-38678 Clausthal-Zellerfeld, Germany

Keywords: CFD, Cunningham correction, Low-pressure-impactor, Measurement, Nanoparticles.

At sufficiently small Reynolds numbers the friction resistance of particles with the carrier gas is described in the continuum region by means of the Stokes formula assuming no slip of the gas molecules on the particle surface. However, at large mean free paths of the carrier gas, this assumption does not hold anymore and the deviation from the continuum character is considered with the slip or Cunningham correction. Recent results for the accelerated movement and electrophoretic transfer of nanoparticles indicate significant deviations from the classical Cunningham correction. This includes the direct measurement of nanoparticle velocities in rectilineal acceleration by means of LDA (Laser-Doppler-Anemometry) (Reuter-Hack et al., 2007) and the investigation of the density of nanoparticles from measurement in a low-pressure curvilinear flow (Skillas et al., 1999).

In the following work, the recent measurements of the separation curve of nanoparticles in a single-stage low-pressure impactor are presented to investigate the disagreement of classical theory for the friction resistance of nanoparticles in low-pressure flows. It was implemented in the following process with electronic procedures.

Nanoparticles, which were singly charged and classified, impacted in a low-pressure impactor. The charges in the aerosol were measured by means of a FCE (Faraday Cup Electrometer) before and after the impaction of particles. For a given particle size, the separation probability increases with increasing particle velocity, leading to a decrease of the concentration of charged particles in the aerosol exit and also measured aerosol charges (Fig. 1). The particle velocity is controlled through the chamber pressure in the impactor. The smaller the chamber pressure, the higher the gas and particle velocity.
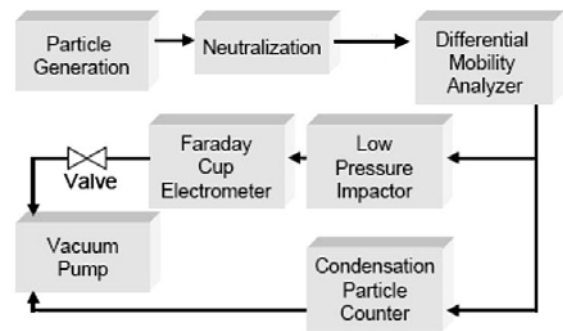
Figure 1. Measurement process of the exit aerosol charges in order to investigate the separation probability of nanoparticles by low-pressure impaction.

At the same time the impaction process of nanoparticles was simulated with CFD procedure, which is based on the classical theory. It was compared with the experiment results. If there is a difference between the both, the calculation of simulation can also be fitted to the measurement results, in order that a varied and effective Cunningham correction is placed in the simulation. The results for single spherical particles and for agglomerates will be presented and discussed.

Reuter-Hack, K., Weber, A. P., Rösler, S., & Kasper, G. (2007). *First LDA Measurements of Nanoparticle Velocities in a Low-Pressure Impacting Jet*, Aerosol Sci. and Technol., 41: 277-283, 2007.

Skillas, G., Tobler, L., Beeli, C., Burtscher, H., Siegmann, K., & Baltensperger, U. (1999). *On the Density of Silver Nanoparticles. A Comparison*, J. Aerosol Sci. Vol. 30, Suppl. I, pp. S493-S494, 1999.

Comparison of Agglomerate Stability of Different Nanopowders

Burkhard Stahlmecke[1], Sandra Wagener[1, 2], Christof Asbach[1], Heinz Kaminski[1], Heinz Fissan[1], and Thomas A. J. Kuhlbusch[1]

[1]Institute of Energy and Environmental Technology (IUTA), Air Quality & Sustainable Nanotechnology Unit, Bliersheimer Str. 60, 47229 Duisburg, Germany
[2]now at Humboldt University Berlin, Department of Geography, Rudower Chaussee 16, 12489 Berlin, Germany

Keywords: Nanoparticles, Agglomerates, Aggregates, Dispersion

The stability of agglomerates made of primary particles in the nanometer size range is an important material parameter of powders. Furthermore, the agglomerate stability is also of interest for estimating the resulting particle size distribution upon accidental release into the atmosphere. Micron-sized agglomerates can be emitted if a leak occurs during particle production or transport in a pressurized vessel,. Due to shear forces within the leak the agglomerates may break up into smaller fragments (e.g. Kurkela et al., 2008). These shear forces can be experimentally simulated by the use of an orifice. In this study, we compared the deagglomeration behaviour of different aerosolized nanoparticle powders during passage of an orifice under various differential pressure conditions.

After aerosolization of nanoparticle agglomerates within a pressurized beaker the aerosol passes an orifice with an aperture of about 500 µm diameter and sharp edges under various differential pressure conditions. The resulting particle size distributions were measured by a scanning mobility particle sizer (SMPS) and were normalized with respect to the total concentration within the size range of the SMPS spectra. This was necessary because of differences in the total concentration for each substance and each pressure step. The resulting relative size distributions were then compared to the case of an "unstressed" aerosol (reference distribution), i.e. the corresponding size distribution obtained at minimal differential pressure without an orifice.

Fig. 1 shows an example of the resulting relative size distributions for four differential pressure steps with regard to the reference size distribution in case of cerium dioxide agglomerates. Values above one indicate increasing concentrations of particles within the corresponding size class. Values below one indicate decreasing concentrations und thus a fragmentation of agglomerates within these size classes. Fig. 1 shows that agglomerates above approximately 300 nm electrical mobility diameter were fragmented which leads to an increase of the relative particle concentration in the size classes below 300 nm. The results furthermore show that a higher differential pressure across an orifice leads to an enhanced fragmentation of airborne nanoparticle agglomerates
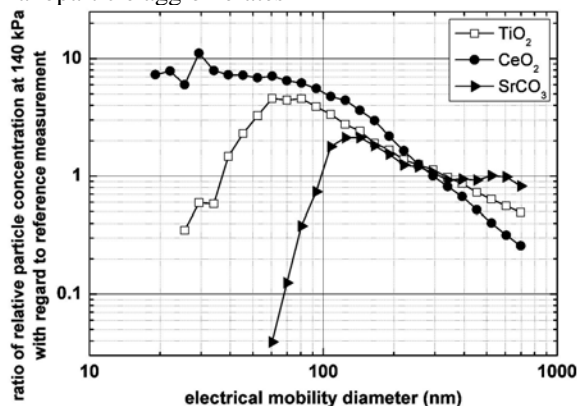
Fig. 2: Comparison of the stability of three different nanoparticle agglomerates.

Fig. 2 shows a comparison of three different particle materials for a differential pressure of 140 kPa across the orifice. As Fig. 2 shows, the fragmentation of the agglomerates seems to be material dependent with the highest degree of fragmentation taking place in case of the cerium dioxide. These results will be discussed in the presentation in view of particle properties like e.g. morphology and BET-surface.

Kurkela, J.A. et al., (2008), Powder Technol., 180, 164-171.

Fig. 1: Influence of an orifice on the relative number size distribution of cerium dioxide agglomerates.

Light scattering by sintered aggregates using T-Matrix method

T. Wriedt[1] and R. Schuh[2]

[1]Institut für Werkstofftechnik, Badgasteiner Str. 3, 28359 Bremen, Germany
[2]Process and Chemical Engineering, University of Bremen, PO Box 330440, 28334 Bremen, Germany

Keywords: aerosol measurement, light scattering, nanoparticle aggregates, sintering.

Methods for the quantitative assessment of the sintering morphology of aggregates are of recent interest in aerosol science. Optical methods for characterization of aggregates of nanoparticles commonly involve scattering measurements at multiple wavelengths or at multiple scattering angles. To develop such optical characterization methods for aggregates of nanoparticles effective methods for the simulation of light scattering of such aggregates are needed. The multiple-scattering T-Matrix method is an effective method to simulated light scattering by aggregates consisting of spherical primary particles (Doicu *et al.*, 2006).

In the multiple scattering T-Matrix method the T-Matrices of spherical primary particles are combined to compute the T-Matrix of the aggregate. This method is however limited to spherical primary particles, such that light scattering of sintered aggregates can not be accurately simulated.

A recent extension of the T-Matrix method allows computing light scattering of aggregates consisting of nonspherical primary particles (Wriedt, *et al.*, 2008; Wriedt & Schuh, 2008). This method has been adopted to compute light scattering by sintered aggregates.

In order to generate aggregates of spheres, a Diffusion Limited Aggregation (DLA) algorithm has been used. Then a phenomenological method based on the Metaball algorithm was used to model the shape of sintered aggregates. A figure of the three dimensional shape of such a sintered aggregate is shown in Fig. 1.

To use the multiple scattering T-Matrix method to compute light scattering by such a sintered aggregate this model has to be decomposed into individual subparticles, which can be nonspherical. Then a multiple scattering method can be applied for the simulation of light scattering of the entire aggregate. The individual subparticles of the sintered aggregate model are depicted using different colours in Fig. 1

In the lecture the algorithm will be presented together with some sample computations to investigate whether light scattering measurements can be used to characterize the morphology of sintered aggregates or to distinguish between aggregates and sintered aggregates.

To validate the light scattering computations the DDSCAT algorithm based on the discrete dipole approximation has been used (Draine & Flatau, 1994).
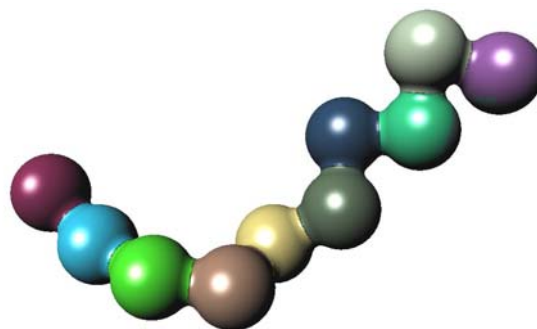
Figure 1. Figure of sintered aggregate decomposed into subparticles for T-matrix computation.

Doicu, A., Wriedt, T., & Eremin, Y. (2006). *Light Scattering by Systems of Particles. Null-Field Method with Discrete Sources - Theory and Programs.* Berlin, Heidelberg, New York: Springer Verlag.

Wriedt, T., Schuh, R., & Doicu, A. (2008). *Part. Part. Syst. Charact.,* 25, 74-83.

Wriedt, T., & Schuh, R., (2008). *J. Quant. Spectrosc. Radiat. Transfer*, 109, 2315-2328.

Draine, B.T., & Flatau, P.J. (1994). *J. Opt. Soc. Am. A,* 11, 1491-1499.

Predominance of soot-mode ultrafine particles in Santiago de Chile: Possible sources

Ernesto Gramsch[1], Lars Gidhagen[2], Peter Wahlin[3], Pedro Oyola[4] and Francisco Moreno[1]

[1]*Physics Department, Universidad de Santiago, Santiago, Chile*
[2]*Swedish Meteorological and Hydrological Institute, Norrköping, Sweden*
[3]*National Environmental Research Institute, Roskilde, Denmark*
[4]*Centro Mario Molina Chile, Santiago, Chile*

Keywords: ultrafine particle, size distribution, $PM_{2.5}$, soot particles.

A monitoring campaign was performed in Santiago de Chile during a winter month of 2003 and 2006 (July) using several instruments to measure the size distribution of particulate material. For the first time, the size distribution of ultrafine particles was measured in Santiago, and an estimation of its sources was done by analyzing its temporal variation. The study was performed in three sites; one of them is located in the eastern part of Santiago, a sector with low particle concentration and about 100 m from a busy street. The other site is located in the western part, which is the sector that has the highest concentration of fine and coarse particle matter during winter, also located far from a street. The third site is located within 5 m from the busiest street in Santiago.

In all stations traffic is the dominating source for fine and ultrafine particles and the size distribution is peaked towards 60 – 100 nm (soot mode). Figure 1 presents the particle size distribution in the three sites during morning rush hour.
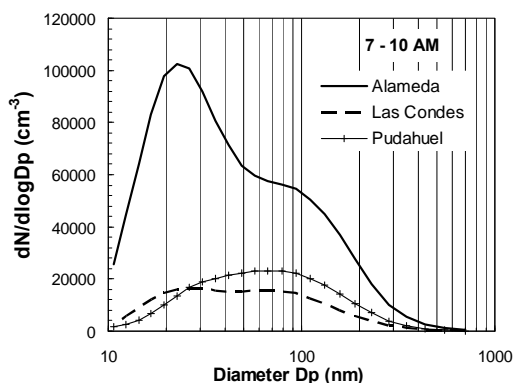
Figure 10. Particle size distributions for Alameda, Pudahuel and Las Condes during the morning rush.

Only in the site near the street, it is possible to see a clear peak towards smaller sizes (10 – 30 nm). The sites far from the street (Pudahuel and Las Condes) show a predominance of the soot mode particle size (60 – 100 nm) even during rush hour. The size distribution measurements presented here indicate that aerosol dynamics play a more important role for the Santiago case as compared to cleaner cities in Europe. Changes in the particle size during different hours of the day reflect both variations in meteorological mixing conditions as well as effects of aerosol dynamic processes such as coagulation, condensation and dry deposition. The size distribution seen in Santiago is more like large polluted cities in Asia (Li et al., 2007, Mönkkönen et al, 2005). The size distribution at sites outside the vicinity of trafficked streets is peaked at 70-100 nm during most of the day, indicating that there is a dominance of the soot mode over the nuclei mode.

The size distributions registered at the three locations, as well as a time series analysis of number concentrations of some particle sizes together with $PM_{2.5}$ mass measurements, indicate that small nuclei size mode particles (20-30 nm) are rapidly removed by coagulation with larger soot mode particles. Only very close to the source, or during special conditions with low aerosol concentrations, can nuclei mode particles survive the transport from the streets to the urban background stations that forms the Santiago monitoring network

A relative increase in the number of the larger ultrafine particles (d $\geq$ 70 nm), as compared to the number of smaller particles (d < 70 nm) correlated with wind speed is an indication of pollution transport with aged particles from other parts of the city..

Li, X. L., Wang, J. S., Tu, X. D., Liu, W. and Huang, Z., "Vertical variations of particle number concentration and size distribution in a street canyon in Shanghai, China". Sci. Tot. Env. 378, 306 – 316 (2007).

Mönkkönen, P., Kaponen, I. K., Lehtienen, K. E. J., Hämeri, K., Uma, R. and Kulmala, M., "Measurements in a highly polluted Asian mega city; observations of aerosol number size distribution, modal parameters and nucleation events", Atmos. Chem and Phys. 5, 57 – 66 (2005).

Formation Of Ionic Molecular Clusters
In The Presence Of Spurious Gases In A Bipolar Charger

G. Steiner, D. Wimmer, G.P. Reischl

Faculty of Physics, University of Vienna, Boltzmanngasse 5, 1090 Wien, Austria

Keywords: Charging efficiency, Ion clusters, Ion mobility, Particle Charging.

This work focuses on the experimental evaluation of the Number Size Distribution (NSD) of ionic clusters, produced by ionizing radiation of an [241]Am α-source, depending on different trace gas contaminations within the carrier gas. The measurements were performed using the Vienna Type UDMA high resolution DMA running in closed-loop (Steiner et al., 2008). The contaminations were added to the carrier gas by using 2 meters of different tubing material in front of an [241]Am Charger.

The properties of small ionic clusters are of special interest since they form a fundamental basis of the EMS method when inverting a measured mobility distribution into a corresponding NSD. This calculation requires a detailed knowledge of the correct charging state of the particles. When it is not known a priori, this, for example, can be achieved by charging the particles in a bipolar ionic atmosphere (neutralization). The particle charging theory by Fuchs (1963) is presently the standard method to calculate the charging probabilities for ultrafine particles (Reischl et al., 1996). Fuchs' theory requires mass and mobility of the charging ions to be known. Whereas the mobility of the charging ions can be directly measured by the EMS method, the Kilpatrick relation (1971) gives the most widely used empirical relationship between ion mass and ion mobility but only allows a rough estimation of the corresponding ion mass.

Figure 1 shows two extremata of measured NSDs of positive ions produced in purified pressurized air, using 2m of Polycarbonate tubing and 2m of a Net hose respectively.
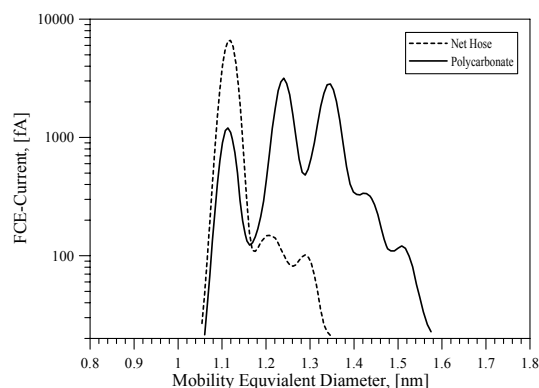
Fig. 1. NSD of pos. ionic clusters produced in purified pressurized air by [241]Am.

In the case of the Polycarbonate tubing, the mean electrical mobility equivalent diameter is shifted towards bigger diameters, resulting in an overall lower mean electrical mobility compared to the use of a net hose. It has to be noted, that no major differences in the spectra of the produced cluster species were observed by using other carrier gases such as nitrogen, argon or artificial air.

Table 1 lists the different properties of positively charged ionic clusters produced by α-radiation depending on the tubing material used in front of the Charger and the most commonly used values obtained by Reischl et al. (1996). The mean mass of the ions was derived by using Kilpatrick's relationship. Similar results were obtained for negative ion species.

tubing material	mean el. Mobility [cm²/Vs]	mean mass, [amu]
Net Hose	1.61	160
Polycarbonate	1.27	303
Polyurethane	1.41	248
PTFE	1.52	199
Stainless Steel	1.51	202
Anodized aluminium	1.55	186
Aged copper	1.58	173
Reischl et al. 1996	1.15	290

Table 1: Comparison of the properties of pos. ions

It can be assumed that the calculated charging probability for aerosol particles strongly differs, depending on the presence of spurious gases in the carrier gas flow passed through the charging device. Furthermore, the measured particle number concentration will be under- or overestimated if the appropriate charging probability is not applied.

Steiner, G. et al. (2008) *Abstract T04A009O EAC 2008, Thessaloniki, Greece*

Fuchs, N.A. (1963), *Geofis. Pura Appl. 56, 185*

Reischl, G.P., Mäkelä, J.M. & Necid, J. (1996), *J. Aerosol Sci. 27, 931*

Kilpatrick, W.D. (1971), In *Proc. Ann. Conf. Mass Spectrosc. 19th, p. 320-326*

Physico- and electro-chemical characterizations of microwave-assisted polyol preparation of Pt/CNTs

Yu-Chun Chiang[1], Fang-Pin Tsao[1] and Chien-Cheng Lee[2]

[1] Department of Mechanical Engineering and Yuan Ze Fuel Cell Center, Yuan Ze University. 135 Yuan-Tung Rd., Chung-Li, Taoyuan 320, Taiwan
[2] Department of Communications Engineering, Yuan Ze University. 135 Yuan-Tung Rd., Chung-Li, Taoyuan 320, Taiwan

Keywords: metal nanoparticles, nanotubes, generation, characterization.

The catalytic activity of the metal particles is known strongly dependent on their size and size distribution. Pt particles with 3-4 nm have been reported to have better electrochemical activities for oxygen reduction. Based on the disadvantages of the conventional methods, microwave heating has received much attention as a new promising technique for the preparation of metal nanoparticles with narrow size distributions. Therefore, the microwave-assisted polyol technique was utilized in this study to prepare the Pt/CNTs catalysts (Li et al., 2005; Han et al., 2008).

The CNTs used in this study was the multi-walled carbon nanotubes, which was provided by Conyuan Biochemical Technology Co. of Taiwan. First, 2 ml aqueous solution of H_2PtCl_6 (50 mM) and 80 mg CNTs were added into 50 ml ethylene glycol (EG). The pH value was adjusted by KOH. The mixture was ultrasonically treated to ensure the CNTs uniformly dispersed in EG solution. Next, the mixture was placed in a household microwave oven (Tatung, 2450 MHz, 800 W) and heated for 60 s. The the solution was centrifuged, and the collected solids were washed with acetone and de-ionized water, then dried in a vacuum oven at 373 K for 24 h. After adjustment of pH value, some samples were impregnated for 2 days. Thus, the effects of pH value, the impregnation were discussed. The physicochemical properties of the products were probed by ICP-AES, TEM/HRTEM, XRD and XPS, and their electrochemical measurements were investigated by cyclic voltammetry (CV).

Based on the experimental design, the Pt: CNTs = 1: 4. The data from ICP-MS measurement revealed that the microwave heating method could prepare the Pt/CBT catalysts with a very well accurate ratio under a pH value between 6 and 9. However, at pH = 2 or 11, the reduction of Pt was really poor. The TEM/HRTEM images show that the mean particle size of Pt catalyst prepared by microwave heating ranged from 2-5 nm. The size decreased as the pH value increased, and that the solution impregnated 2 d might promote the particle growth. In addition, the effect of impregnation on dispersion of Pt particles seemed not significant.

Figure 1 shows the XRD patterns of Pt/CNT and CNT samples. Except for the samples prepared at pH = 2 or 11, all showed C (002) and five characteristic f.c.c. Pt peaks, indexed as Pt (111), Pt (200), Pt (220), Pt (311) and Pt (222). The XRD data were as well consistent with the ICP-MS measurements. High resolution XPS Pt 4f data (e.g., Figure 2) indicate that the pH value and the impregnation exactly make varying chemical states of Pt on the samples. The CV measurements showed that the electrochemical activity was poor when Pt/CNT prepared at pH = 2, and the impregnation would delay the peak location and decrease the activity.
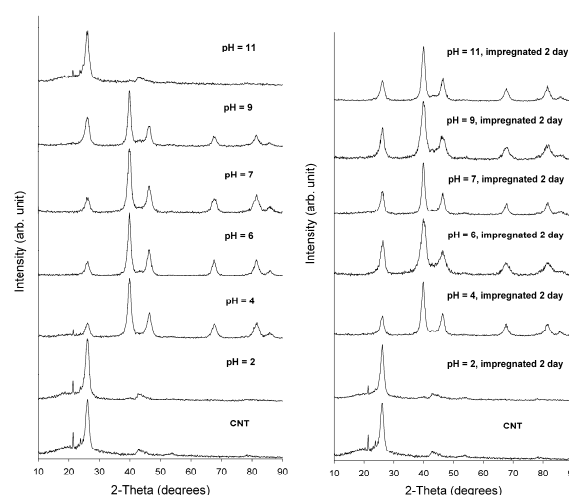
Figure 1. XRD patterns of Pt/CNT samples without (left) or with (right) impregnation.
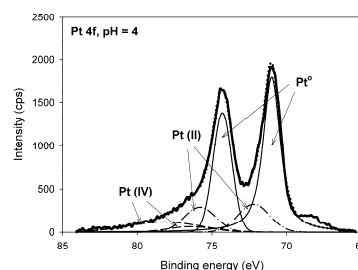
Figure 2. High-resolution fitted Pt 4f spectra of Pt/CNT (pH = 4, without impregnation)

Han, D. M., Guo, Z. P., Zhao, Z. W., Zeng, R., Meng, Y. Z., Shu, D., & Liu, H. K. (2008). *Journal of Power Sources*, 184, 361-369.
Li, X., Chen, W. X., Zhao, J., Xing, W., & Xu, Z. D. (2005). *Carbon*, 43, 2168-2174.

Nanoparticles emitted in the process of Nanofil®5 blending

E. Jankowska and W. Zatorski

Department of Chemical and Aerosol Hazards, Central Institute for Labour Protection
– National Research Institute, Czerniakowska 16, 00-701 Warsaw, Poland

Blending is an operation used in the process of developing new fire-safe polyurethane foams. It is the dustiest of the following operations: cleaning and preparing a form, weighing chemicals and Nanofil®5, blending chemicals and Nanofil®5, and taking out the polymer from the form (Jankowska *et al.*, 2007).

This abstract presents results of research on the concentration and size distribution of nanosize particles before, during and after Nanofil®5 blending. Two 10 g samples of Nanofil®5 were blended for 60 s (scenario B1) and 180 s (scenario B2). Nanosize particle levels were monitored continuously over a 4-hour period using a P-TRAK to measure particle number concentrations in the 20–1000 nm range and an SMPS with a nano DMA to measure particle number concentrations and size distributions in the 5–143 nm range. Particles that settled on different surfaces in the laboratory when samples of Nanofil®5 were blended were not removed. The parameters of laboratory air were: temperature 22–25 °C, humidity 21–32%.

The number concentrations determined with SMPS were higher than those obtained with P-TRAK during blending only. Otherwise, P-TRAK gave significantly higher concentrations (Figure 1).
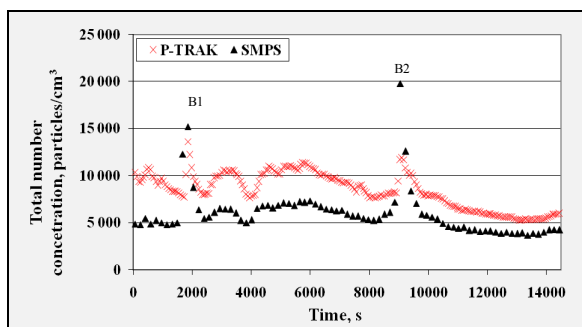
Figure 1. Number concentrations of particles from the 20–1000 nm (P-TRAK) and 5–143 nm (SMPS with nano DMA) ranges in two scenarios:
B1: 10 g Nanofil®5 for 60 s,
B2: 10 g Nanofil®5 for 180 s.

During blending, nanosize particles 5–34 nm in diameter were emitted (Figure 2). The increase in the number concentrations of nanosize particles between the two samples of Nanofil®5 compared to those before blending can be explained by their agglomerations.
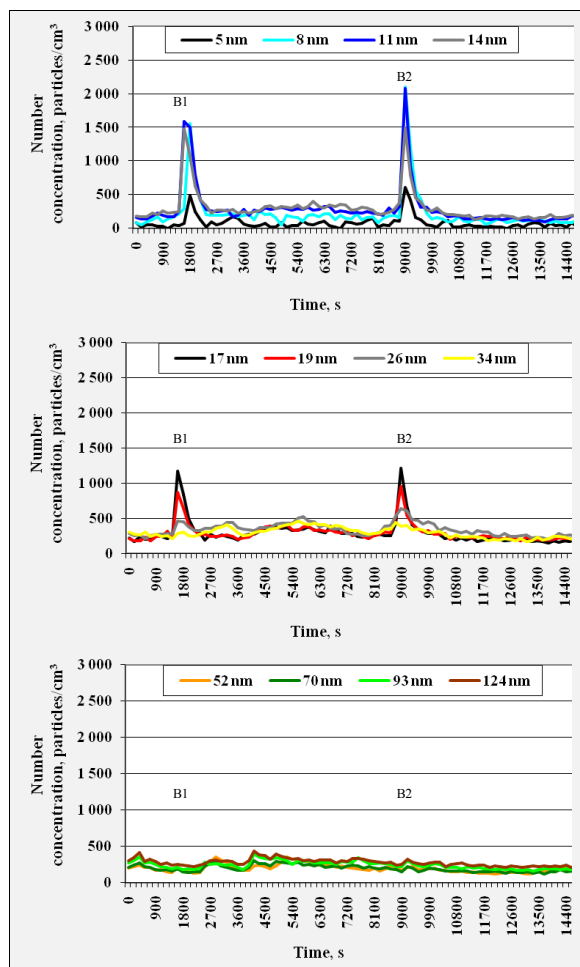
Figure 2. Number concentrations and size distributions of particles from the 5–124 nm range before, during and after blending Nanofil®5 (SMPS with nano DMA) in two scenarios:
B1: 10 g Nanofil®5 for 60 s,
B2: 10 g Nanofil®5 for 180 s.

Jankowska E., Zatorski W. & Pośniak M. (2007) in *European NanOSH Conference – Nanotechnologies: A Critical Area in Occupational Safety and Health*, 3–5 December 2007, Helsinki, Finland, p. 64.

Refined Classical Viewpoint on Coagulation of Charged Nanoparticles

V.Y. Smorodin

Climate Change Institute, 316 Global Sciences Center, University of Maine, Orono, ME 04469, USA

Knudsen numbers for aerosol particles for radii 1-100 nm belong to the range: $Kn_p \approx 0.1 \div 46.4$. We focus on the transition Knudsen regime, $0.1 < Kn_p < 10$. As known, Fuchs' classical theory (Fuchs, 1964) describes the transition from diffusive to gas-kinetic coagulation regime. But it dropped an effect of viscous forces in the relative particle motion. This effect is to reduce collision efficiency and thereby retard the coagulation rate in the continuum and the transition regime (Williams and Loyalka, 1991). One has to complete Fuchs's theory by adding the effect of viscous forces. Such exacted theory can be called as a "refined classical theory" of coagulation (RCTC) in the transition regime. In the frame of RCTC one can exact the electro-Brownian coagulation coefficient and the enhancement factor in the transition regime, as well as obtain useful criteria of coagulation of nanoparticles.

For Boltzmann's equilibrium charge distribution on aerosols in the bipolar ion atmosphere instead of an conventional approximate formula (Reist,1987), $\overline{Z} \approx \sqrt{dkT / \pi e^2}$, $d \geq 50 nm$, we propose an exact expression that can be employed (up to zero) for nanoparticles: $\overline{Z} = \{x \vartheta_3(0, Exp(-x))\}^{-1}$, $x = e^2 / dkT$, $d \geq 0$, where $\vartheta_3(u,q)$ is the known elliptic theta function.

Using RCTC we expanded criteria of the "slow" coagulation of hydrosols formulated in the Derjaguin-Landau-Verway-Overbeek theory for electro-Brownian coagulation of aerosol particles. E.g., for an important case of two like charged particles driven with molecular, Coulomb's, and "image" forces, a criterion of coagulation is: $0.544 eZ / aA < 1$, where A is the Hamaker constant.

As it follows from RCTC, an observed fast decreasing of the coagulation efficiency while particle size goes down, especially in a range of d less than 10-20 nm, is explained with a strong influence of the viscous forces, a prevailing of Brownian diffusion effect over the molecular attraction, and the quantum size dependence of Hamaker's constant. From this viewpoint we interpret data on fast decreasing of the nanosoot coagulation rate (Sagro et al., 2003). By (Maricq, 2004), the soot nanoparticle fraction in bipolar ion atmosphere can have charges: $Z = \pm 1, \pm 2$. Applying our charge distribution formula for these data shows a good agreement. Also analysis of the charge effect on the coagulation half-time in the frame of RCTC demonstrated well fitting data on coagulation of the charged organic carbon nanoparticles (Kim et al., 2005).

We conclude that RCTC, in the area of its validity, is adequate for analyzing peculiarities of coagulation of charged nanoparticles.

Fuchs, N.A. (1964), The Mechanics of Aerosols. Pergamon Press, New York

Kim, S.H. et al. (2005), *J. Coll. Interface Sci.*, 201, pp. 21-39

Maricq, M.M. (2004), *Combustion and Flame.* V.137, No 3, pp. 340-350

Sagro, L.A. et al. (2003), *Chemosphere,* 51 (10), pp. 1079-1090

Williams, M.M.R. and Loyalka, S.K. (1991), Aerosol Science. Theory and Practice. Pergamon Press. -446p.

Nanoparticle film formation by means of an electrostatic precipitator

M. Rouenhoff, F.E. Kruis

Institute for Nanostructures and Technology and CeNIDE (Center for Nanointegration), University of Duisburg-Essen, Bismarckstr. 81, 47057, Duisburg, Germany

In the last ten years, the use of nanoparticles for functional applications has seen a tremendous development. Examples are the use of quantum dots in electronic applications, magnetic dots for high-density magnetic recording, metal oxide nanoparticles for thin gas-sensitive films, thermoelectric films and hybrid inorganic-organic films for solar cells. Apart from these applications, a thin nanoparticle layer is often necessary for characterisation of properties such as particle size, shape, chemical composition and crystallinity. A growing group of applications requires the use of a thin, high-quality film composed of monodisperse nanoparticles, as the specific size-dependent properties will then be the most prominent.

Depending on the application or characterisation technique, spot diameter, thickness, homogeneity of the deposit and porosity of the film have to be controlled.

Other important parameters are the particle size and charge level as well as the deposition efficiency of the process. For production purposes, the film growth rate (unit nm/s) is important. This is the result of the particle concentration, flow rate, deposition efficiency and spot diameter.

There are three main methods for collecting nanoparticles out of the gas phase on a substrate, i.e. low-pressure impaction, thermophoretic deposition and electrostatic precipitation.

In this study, we optimize the design of an electrostatic precipitator starting from the geometry used by Dixkens and Fissan (1999) in order to solve problems with reproducibility caused by unwanted charging effects and inhomogeneity of the deposit. An experimental study of the deposition efficiency and spot topography was performed, which allows to choose the optimal condition to obtain a given spot size as function of particle diameter. We obtained information about the deposit by scanning the spot with a profilometer Ambios XP-200 (see figure 1).
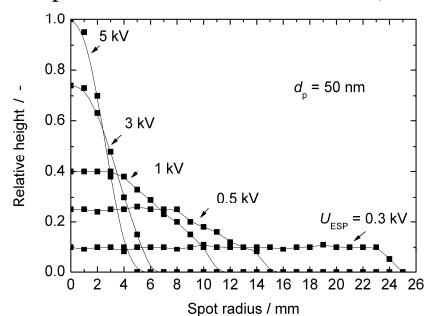
Figure 1. The relative height of the deposition spot formed out of PbS nanoparticles with diameter of 50 nm as a function of spot radius and electrode voltage.

The final ESP design offering a homogenous deposition of nanoparticles can be seen in figure 2.
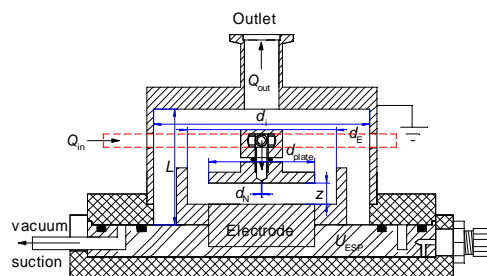
Figure 2. The optimized ESP

Dixkens, J., Fissan, H. (1999). *Aerosol Science and Technology 30* (1999)

Penetration of monodisperse, singly-charged nanoparticles through fibrous filters. Part I – Experimental assessment

A. Maißer[1], W.W. Szymanski[1], A. Podgórski[2], A. Jackiewicz[2], L. Gradoń[2] and G. Allmaier[3]

[1]Faculty of Physics, University of Vienna, Boltzmanngasse 5, 1090 Vienna, Austria
[2]Faculty of Chemical and Process Engineering, Warsaw University of Technology,
ul. Waryńskiego 1, 00-645 Warsaw, Poland
[3]Institute of Chemical Technologies and Analytics, Vienna University of Technology, Getreidemarkt 9, A-1060 Vienna, Austria

Particle filtration is a very efficient, cost effective and widely applied method of gas cleaning, hence many filtration studies were carried out determining the behaviour of particles in filter media. Most of this research however was made for micrometer sized particles. The extension of filter performance to nanometer sized particles needs still attention and the experimental basis is limited. Some recent studies indicate that the conferment of the classical filtration behaviour based on macroscopic filter and filtration parameters and diffusive deposition is feasible into the nanometer size range (Wang et al. 2007).

We addressed the nanoparticle filtration in fibrous filter media made of melt-blown, polydispersed polypropylene fibers. Challenge aerosols were size classified globular particles (proteins, silica particles) from 3.2 – 27.2 nm. They were aerosolized from appropriate suspensions by means of the electrospray (EAG Mod. 3480, TSI, Inc.). The sizing and preparation of challenge particles was done using the PDMA (Parallel Differential Mobility Analyzer). This technique allows a simultaneous measurement of the size distribution of particles in question and in parallel an extraction of a narrow, specific size fraction (Allmaier et al., 2008), which was then used in the penetration study. Particles were carrying one elementary charge; width of the distribution was below about 5%.

The investigated filters were carefully defined by their structural characteristics, such as arithmetic mean fiber diameter, d_{Fa}, filter packing density, α, filter thickness, L, and the geometric mean, d_{Fg}, and the geometric standard deviation, σ_{gdF}, of the fiber diameter distribution. Detailed values are shown in the table within the Fig. 1. In order to minimize the influence of particle diffusion losses on the penetration measurements a test rig containing two identical stainless steel Sartorius™ filter holders connected in parallel was used. One filter holder was furnished with the investigated filter; the other one was used to obtain the upstream concentration at same flow conditions in both branches connected via a 3-way valve to the CPC (Mod. 3025, TSI, Inc.). The flow rate of 1.5 l/min resulted in the gas face velocity of 8.96 cm/s. Typically 30 alternating upstream and downstream measurements for each particle size were made to obtain good statistics.

Results in Fig. 1 show a decrease in penetration not explainable within the classical filtration theory but with the partially segregated flow model (Podgorski, 2009). We anticipated to see even some increase in penetration due to the thermal rebound and re-entrainment of sub-10nm particles, supposing that here the filtration process particles could be influenced by this phenomenon. Possible theoretical model is given in Part II on the penetration model validation.

Filter Symbol	d_{Fa} [µm]	α [-]	L [mm]	d_{Fg} [µm]	σ_{gdF} [-]
O	2.55	0.016	3.5	1.98	1.58
▲	2.91	0.024	2.0	1.91	2.04
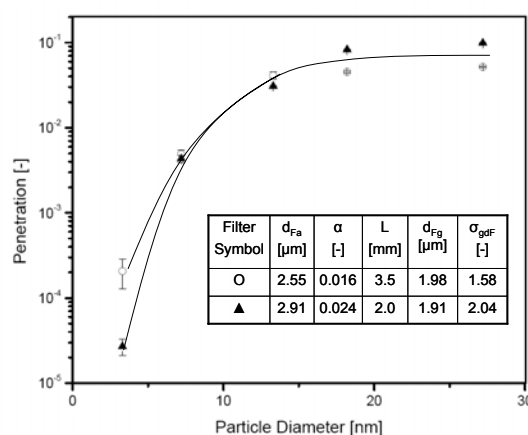
Figure 1. Summary of experimental results.

Wang J. et al. (2007). *J. Nanoprt. Res.* 9, 109-115.
Allmaier G. et al. (2008). *J. Amer. Soc. Mass Spectrometry* 19, 1062-1068.
Podgórski, A. (2009). *J. Nanopart. Res*. 11, 197–207.

Penetration of monodisperse, singly-charged nanoparticles through fibrous filters. Part II – Model validation.

A. Podgórski[1], A. Jackiewicz[1], L. Gradoń[1], W.W. Szymanski[2] and A. Maißer[2]

[1]Faculty of Chemical and Process Engineering, Warsaw University of Technology, Waryńskiego 1, 00-645 Warsaw, Poland
[2]Faculty of Physics, University of Vienna, Boltzmanngasse 5, 1090 Vienna, Austria

Keywords: aerosol filtration, fibrous filter, nanoparticles, penetration

Experimental results of penetration of monodisperse, singly-charged aerosol nanoparticles through electrically neutral fibrous filters made of fibers with various diameters reported in our previous abstract are compared now with theoretical predictions. In the considered case of particles smaller than 30nm in diameter there are only two mechanisms responsible for particle deposition, namely Brownian diffusion (D) and electrostatic attraction due to image forces (IF), and the corresponding single-fiber efficiencies can be estimated as:

$$E_D = 2.9\,[(1-\alpha)/Ku]^{1/3}\,Pe^{-2/3} \qquad (1)$$

$$E_{IF} = 2(N_{IF}/Ku)^{1/2} \qquad (2)$$

where: $Ku = -0.5\ln\alpha - 0.75 - 0.25\alpha^2 + \alpha$ is the Kuwabara number, $Pe = Ud_F/D$ is the Peclet number and $N_{IF} = (\varepsilon_F - 1)q_P^2/[(\varepsilon_F + 1)12\pi^2\mu U\varepsilon_0 d_P d_F^2]$ denotes the dimensionless parameter describing particle capture by image forces. Other symbols have the following meaning: U – the superficial gas velocity, D – the coefficient of Brownian diffusion, α – the filter packing density, μ – the gas viscosity, d_P and q_P – the particle diameter and electric charge, d_F and ε_F – the fiber diameter and dielectric constant, and ε_0 – vacuum permittivity. Note that deposition efficiency for both these mechanisms increases with the particle diameter decrease. Assuming that they are additive, the penetration, P, of charged nanoparticles through a non-charged, monodisperse fibrous filter (made of identical fibers) can be calculated as:

$$P = \exp[-4\alpha L(E_D + E_{IF})/\pi d_F(1-\alpha)] \qquad (3)$$

wherein L denotes the filter thickness. In order to account for fibers polydispersity (distribution of fibers' diameters) in real fibrous filters, we proposed the Partially Segregated Flow Model (hereinafter referred to PSFM), Podgórski and Jackiewicz (2008), for which penetration is calculated from the formula:

$$P_{PSFM} = sP_{FSFM} + (1-s)P_{PMFM} \qquad (4)$$

wherein $0 \le s \le 1$ is the dimensionless empirical parameter called the flow segregation intensity. As seen from Eq. (4), s is the weighting factor for penetrations calculated for two limiting models. P_{PMFM} is the penetration obtained with the use of the Perfectly Mixed Flow Model (PMFM) by means of averaging the ratio $[(E_D(d_F) + E_{IF}(d_F))]/d_F$ that appears in Eq. (3) over the fiber size distribution and this model is considered as an estimate of a lower possible limit of the aerosol penetration through polydisperse fibrous filters.

On the other hand, P_{FSFM} is an estimation of an upper limit of penetration obtained using the Fully Segregated Flow Model (FSFM), see Podgórski (2009). This model assumes that gas velocities for various Kuwabara cells (containing fibers with diverse diameters) are different, but the pressure drop per unit filter thickness is the same for all cells. Results of theoretical calculations of nanoparticles penetration obtained with the use of the PSFM were compared with experimental data for a fibrous filter having following structural characteristics: arithmetic and geometric mean fiber diameter d_{Fa}=2.55μm and d_{Fg}=1.98μm, respectively, filter packing density α=0.016, filter thickness L=3.5mm, and the geometric standard deviation of the fiber diameter distribution σ_{gdF}=1.58. The air face velocity was equal to 8.96cm/s. As seen in Fig. 1, it was possible to obtain a reasonable agreement between the experiment and the theory based on the PSFM for the segregation intensity s=0.43. Contrary to that, the classical theory applied to the mean fiber diameter resulted in drastic underestimation of penetration. It clearly indicates how strong can be effect of the fibers' polydispersity on nanoaerosols filtration.
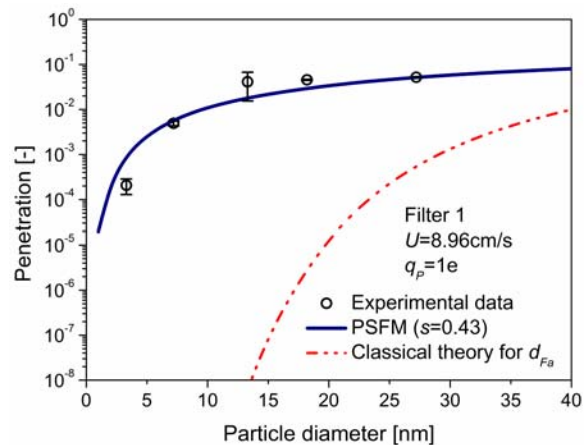
Figure 1. Comparison of experimental results with theoretical calculations.

Podgórski, A. (2009). *J. Nanopart. Res.* 11, 197–207.
Podgórski, A., & Jackiewicz, A. (2008). P*roc. EAC'2008*, Thessaloniki, Abstract T03A064O.

Charge distribution of incipient nanoparticles in laboratory flames

L.A. Sgro[1], A. D'Anna[1], and P. Minutolo[2]

[1]Department of Chemical Engineering, Università di Napoli "Federico II", Naples, Italy 80125
[2]Institute for Research on Combustion, CNR, Naples, Italy 80125

Keywords: charging efficiency, coagulation, DMA, size distribution, measurement (combustion aeros.)

It is well known that a relevant fraction of particles produced in combustion is charged. The charging mechanism in flames is thought to be diffusion charging by ions produced in chemical reactions in the flame front. Particle size and charge state affect aerosol growth dynamics and particle motion within a gas flow subject to an electric field. Nanoparticle manufacturing or control strategies can exploit these phenomena if the detailed size and charge distribution is known.

Maricq (2005, 2008) showed that particles larger than about 13 nm attain a symmetric charge distribution in flames that agrees with Boltzmann theory and depends only on particle size and temperature. This result was explained as a consequence of particle coagulation, which equilibrates the charge distribution to the surrounding gas temperature. However, d<13 nm particles were either totally neutral or had a significantly lower charged fraction than the one predicted by Boltzmann theory (Maricq 2005). Instead, d>20 nm particles attain the Boltzmann charge fraction by diffusion charging at 300K, and the charge fraction of smaller particles is higher than Boltzmann and agrees better with Fuchs' theory (Reischle, et al. 1996). Here, we extend Maricq's work and investigate the charge and size of nanoparticles in ethylene-air flames near and below the onset of soot. These flames produce 1-20 nm particles that have chemical structures ranging from organic carbon to more graphitic or elemental carbon (D'Alessio, et al. 2009).

Size distributions measured with a Differential Mobility Analyzer (DMA) without a particle charger describe only the charged fraction of flame-generated particles. Assuming that the charger effectively charges the aerosol to the Fuchs' distribution, measurements using a particle charger give the size distribution of all flame-generated nanoparticles. Figure 1 plots the current measured by the Faraday Cup Electrometer (FCE) detector without the charger divided by that measured with the charger as a function of the mass equivalent diameter (Fernández de la Mora, et al. 2003) for different flames (Carbon/Oxygen, C/O, ratio) and at various heights, H, above the burner surface. The measurements agree well with the ratio of the charged fraction determined by Boltzmann theory at high temperature divided by that predicted by Fuchs' theory at 300K for all sizes (1-20 nm). The charge distribution of particles measured nearer to the flame front agrees with that predicted by Boltzmann theory near the flame temperature (1700 K). Particles measured later in the flame have cooler Boltzmann distributions (1200 or 1000 K), which coincide with the drop in the temperature that occurs due to probe cooling near its surface. Particle coagulation in the cooled region near the probe is probably the main cause of thermal 'cooling' of the charge distribution, first explained by Maricq (2008). We also note that in flame conditions with bimodal size distributions (C/O=0.65,0.67H15) the charge fraction of the smallest particles agrees with the Boltzmann prediction at flame temperature while the charge fractions of larger particles agree with Boltzmann theory at 1000 K. This observation indicates a size dependent coagulation efficiency (D'Alessio, et al. 2009). The smaller particles (with higher number concentration) retain their charge fraction (predicted by Boltzmann T=1700 K) because they do not coagulate while the charge fraction of larger particles is lowered as they coagulate near the probe surface.
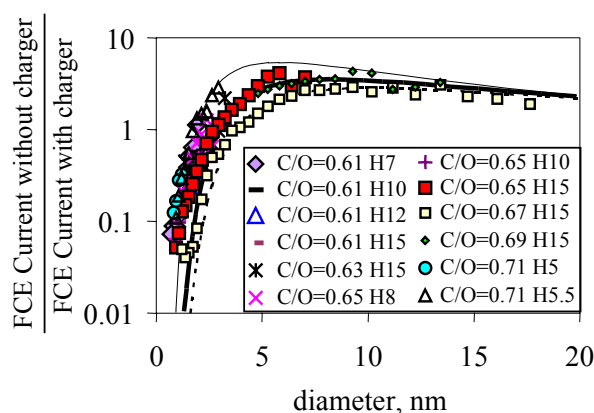
Figure 1. Ratio of the FCE current measured without/with a particle charger (symbols) and the value predicted by Boltzmann theory at 1700 K (thin line), 1200 K (thick line) and 1000 K (dashed line) divided by Fuchs theory at 300K.

D'Alessio, A., D'Anna, A., Minutolo, P., Sgro, L. A. (2009) in Combustion Generated Fine Carbonaceous Particles. Karlsruhe, Germany, Karlsruhe University Press.

Fernández de la Mora, J., de Juan, L., Liedtke, K., Schmidt-Ott, A. (2003). J. Aerosol Sci. 34: 79-98.

Maricq, M. M. (2005). Combust. Flame 141, 406–416. Maricq, M. M. (2008) J. Aerosol Sci. 39, 141-149.

Reischl, G.P., Makelti, J.M., Karch, R., Necid, J. (1996) J. Aerosol Sci. 27, 931-949

Tailor-made nanoparticles as testing materials with changing chemical composition and similar physical properties

L.K. Limbach[1], N.A. Luechinger[1], R.N. Grass[1] and W.J. Stark[1]

[1]Institute for Chemical and Bioengineering, ETH Zurich, 8093, Switzerland

Keywords: Health effects of aerosols, lung/particle interaction, nanoparticles, reactive oxygen species, health aspects of aerosols.

The astonishing physical and chemical properties of engineered nanomaterials have provoked an exponential growth of nano-products on the free market. Growing concerns over the impact of such materials on human health and the environment have initiated first in depth studies on the effect of nanomaterial exposure to biological systems and showed a high mobility of such materials in organisms or cells.

Comparisons of nanoparticles studies are only reasonable if the different nanoparticle compositions are of similar appearance, e.g. particle size, particle size distribution, morphology etc. Certainly, it would be ideal for comparison studies if such nanoparticles could be produced by one single technology to rule out process variability.

This contribution presents a nanoparticles preparation method exceptionally suited for nanotoxicology research (Limbach et al. 2005, 2007, Brunner et al. 2006). Using flame spray pyrolysis (FSP) nanoparticles with virtually any chemical composition can now be readily produced within days and gram quantities (single oxides, mixed oxides, salts and metals). Besides the freedom of composition the here presented synthesis method yields particles with similar morphology, very narrow size distributions and high purity. FSP is derived from the largest industrial process for nanoparticles manufacturing as used to annually produce multitons of some of the most widespread nanomaterials, e.g. carbon black, silica or titania. This makes the here presented materials most relevant for toxicological studies as it represents the closed possible match to industrial manufacturing.

***In vitro* cytotoxicity tests.** We compared the cytotoxicity of seven industrially most important nanoparticles using rhodent and human cell lines. (Brunner et al., 2006) Comparison of the cytotoxicity with known toxic materials such as asbestos or negative controls such as amorphous silica allow a preliminary estimate of oxide nanoparticle toxicity. While a correlation between in vitro and in vivo data is always difficult, the proposed cell based assays may serve as early indicators for sustainable and safe nanoparticle product development. The role of nanoparticle solubility and surface charge illustrates how physical properties are influencing in vitro behavior of nanoparticles. Possible implications on regulation are used to illustrate implementation of these findings.

ROS generation and catalytic activity. We have investigated how chemical composition affects the generation of reactive oxygen species inside living cells. More specifically, twelve industrially important oxide nanoparticle samples containing Fe, Mn, Ti or Co and silica were exposed to lung epithelial cells (A549) (Limbach et al., 2007). The intracellular generation of reactive oxygen species (ROS) was measured using an in vitro assay. In order to distinguish between effects arising from the presence of transition metals ions and nanoparticle-derived effects, the ROS formation was compared to the corresponding ion concentration (supplied as aqueous solutions) of these transition metals.

Soluble heavy metal oxides were up to 10 times more toxic if supplied to cells in the form of nanoparticles compared to exposure of to same metal concentration in form of dissolved ions. This illustrates a Trojan-horse type of uptake mechanism for nanoparticles exposure to mammalian cells.

References

Limbach L.K., R. Bereiter, E. Müller, R. Krebs, R. Gälli, W.J. Stark, Envrion. Sci. Technol, 42 (15), 5828-5833 (2008).

Limbach L.K., P. Wick, P. Manser, R.N. Grass, A. Bruinink, W.J. Stark, Environ. Sci. Technol., 41, 4084-9 (2007).

Brunner T.J., P. Wick, P. Manser, P. Spohn, R.N. Grass, L.K. Limbach, A. Bruinink, W.J. Stark, Environ. Sci. Technol., 40, 4374-81 (2006).

Limbach L.K., Y. Li, R.N. Grass, T.J. Brunner, M.A. Hintermann, M. Muller, D. Gunther, W.J. Stark, Environ. Sci. Technol., 39, 9370-76 (2005).

Biological effects in human lung cells exposed to platinum nanoparticle aerosol

S. Diabaté[1], C. Weiss[1], S. Mülhopt[2], H.-R. Paur[2], V. Niedetzky[3], M. Seipenbusch[3]

[1] Institute for Toxicology and Genetics, Forschungszentrum Karlsruhe, 76021, Karlsruhe, Germany
[2] Institute for Technical Chemistry, Forschungszentrum Karlsruhe, 76021, Karlsruhe, Germany
[3] Institute for Mechanical Process Engineering and Mechanics, University Karlsruhe, 76131, Karlsruhe, Germany

Keywords: platinum nanoparticles, particle characterization, health effects of aerosols, inhalation

Platinum nanoparticles (Pt NPs) are under intense study because of their unique catalytic properties, however, Pt and other platinum group elements are released by cars at an increasing rate. Pt concentrations of 135-303 ng/g have been determined in street dust along highways in Germany (Djingova et al., 2003). Potential health effects of inhaled Pt NPs have not been studied so far. In order to evaluate the potential risk for human health *in vitro* cell-based assays have been performed under submerged conditions and at the air-liquid interface modelling the situation during inhalation.

Methods

A platinum nanoparticle aerosol was generated using a spark discharge generator in nitrogen as the carrier gas. The Pt nanoparticles were diluted by the factor of 10 directly after the generation process. Synthetic air was used for dilution so the oxygen necessary for the cells was added. The aerosol was directed to the Karlsruhe Exposure system (Paur et al., 2008; Diabaté et al., 2008) to analyze the toxicological potential of the freshly generated platinum nanoparticles.

For the bioassay we employed the human bronchial epithelial cell line BEAS-2B and the alveolar epithelial cell A549, both co-cultured with differentiated THP-1 macrophages, growing on Transwell inserts. The responses of the cells were analyzed by measuring the viability, the release of lactate dehydrogenase (LDH test) as an indicator of membrane integrity and release of Interleukin-8 (IL-8) as an indicator of a pro-inflammatory response.

Pt NPs collected on polycarbonate filters (pore diameter 0.4 µm) were used to study cell responses under submerged conditions. The particles were removed from the filters by carefully scraping and a stock solution of 1 mg/ml in cell culture medium containing 10% (v/v) fetal bovine serum was prepared. The solution was vortexed and sonicated to ensure complete dispersion. The cells were exposed to the indicated particle concentrations via the culture medium.

Results

The aerosol was characterized by scanning mobility particle sizing (SMPS 3071, TSI) and TEM (Fig. 1). The particle number concentration in the Karlsruhe Exposure system was determined to 8E+06 1/cm³ with a geometric mean diameter of 25 nm and a standard deviation of $\sigma_g = 1.5$. The mass concentration was 8.13 mg/m³.
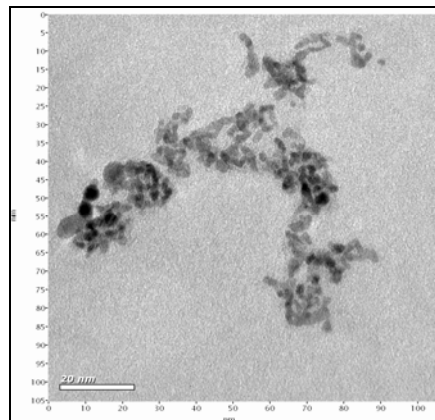
Figure 1. TEM image of Pt particles collected in one exposure chamber while a 2h experiment.

Submerged treatment of A549 cells for 24 h resulted in a loss of viability in dependence of Pt NP concentration. The no observed adverse effect level was 0.1 µg/ml (0.031 µg/cm²) and the lowest observed adverse effect level 1 µg/ml (0.31 µg/cm²) in the LDH as well as in the viability test. BEAS-2B cells seemed to be not as sensitive to Pt NPs as A549 cells (preliminary result).

Exposure to Pt NP aerosol for 2 and 4 hours with a post-incubation period of 20 h under submerged conditions resulted in a moderate increase of LDH leakage in comparison to clean air exposed controls of A549, not for BEAS-2B cells. The viability was not affected in both cell lines, however a remarkable increase of IL-8 release (up to 15 fold of the clean air exposed controls) was observed due to Pt NP exposure in both cell lines. The increase of IL-8 release was also dependent on the time of exposure which is related to the deposited mass.

Conclusion

In summary, the exposure technique at the air-liquid interface and the bioassay described can be used for screening the toxicological potential of a Pt NP aerosol to identify health-related effects.

Diabaté, S., Mülhopt, S., Paur, H.R., & Krug, H.F. (2008). *Altern. Lab. Anim.* 36, 285-298.
Djingova, R., Kovacheva, P., Wagner, G., & Markert, B. (2003). *Sci. Total Environ.* 308, 235-246.
Paur, H.R., Mülhopt, S., Weiss, C., & Diabaté, S. (2008). *J. Verbr. Lebensm.* 3, 319-329.

Generation of airborne nanoparticles for in vitro health studies on lung cells

A. Comouth[1], S. Mülhopt[2], H. Saathoff[1], W. Baumann[2], H.-R. Paur[2], H. Seifert[2],and T. Leisner[1]

[1]Institute for Meteorology and Climate Research and [2]Institute for Technical Chemistry, Forschungszentrum Karlsruhe, Hermann-von-Helmholtz-Platz 1, 76344 Eggenstein-Leopoldshafen, Germany

Metal oxide nanoparticles are currently the largest fraction of industrially generated nanoparticles (Wegner, Pratsinis 2004) besides soot. With the increasing use of engineered nanoparticles a higher exposure to the environment and humans is unavoidable. Hence it is important to know which risks result on human health from an increased exposure. For this reason in vitro toxicity studies on lung cells at the air/liquid interface are necessary. Since nanoparticle synthesis often happens at hostile conditions a direct exposure to cells is impossible. On this account collected nanoparticle powders often are resuspended and afterwards either applied submergerd to cells or atomized and applied at the air liquid interface. However dispersing collected nanoparticle powders can deliver large nanoparticle agglomerates and aggregates with broad size distributions. In this contribution the deagglomeration of resuspended metal oxide nanoparticles and their conversion to airborne nanoparticles via electrospraying will be discussed and a deposition system for in vitro studies at the air liquid interface is presented.

The metal oxide nanoparticles investigated in this work were generated by flame synthesis (Bockhorn et al., 2004), in microwave plasma reactions (Vollath et al. 1992), and in liquid phase processes (commercial samples). The nanoparticle powders collected are suspended in an aqueous solution and treated by an ultrasonic transducer. Employing a commercial Electrospray Aerosol Generator (TSI 3480) the particle suspension is atomized into highly charged droplets with diameters of about 150 nm. After a certain distance the charged droplets are neutralized by a polonium α−source. The particles generated in this way are analyzed by a scanning mobility particle sizer (TSI, 3080 & 3071) for determining the particle size distributions. Further samples are collected with an electrostatic precipitator for microscopic analysis.

Graph 1 shows typical size distributions of SiO_2 nanoparticles generated by electrospraying particles synthesized in a microwave plasma. For comparison a commercial nanoparticle suspension (GRACE, Ludox) has been atomized.

The size distribution of the commercial sample with stabilized SiO_2 particles shows a strong and narrow peak at 29nm. By contrast the size distributions of the resuspended particles from the microwave plasma are very broad and a high amount

of particles are still agglomerated in sizes larger than 100 nm.
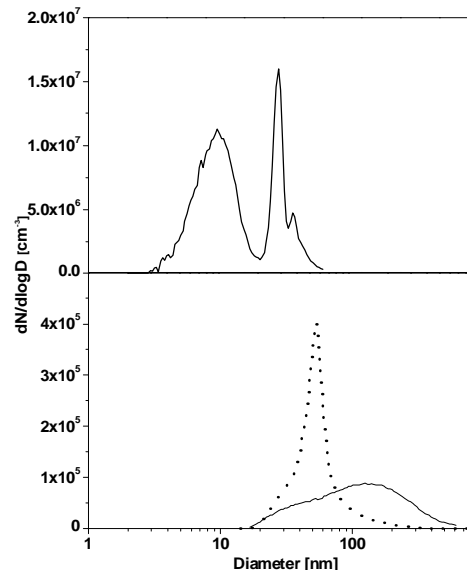
Graph1. Size distributions (SMPS) of airborne SiO_2 nanoparticles generated by electrospraying a commercial available stabilized particle solution with 22nm monomer particle size (Ludox, upper) and resuspended particles generated by microwave plasma synthesis with 10nm (dashed line) and 25nm (straight line) primary particle size (lower).

Nevertheless also particles with sizes down to 20nm clearly can be identified. This may in part be due to deagglomeration during the electrospraying process, probably due to the stress of the highly charged particles.

Possible ways of optimising the deagglomeration process e.g. by investigating the influence of neutralising the particles will be discussed.

H. Bockhorn, H. Dörr, and R. Suntz (2004), VDI-Berichte 1839, 185, VDI-Verlag Düsseldorf

Vollath, D. and K. E. Sickafus (1992), Nanostructured Materials 1(5), 427-437.

Wegner K., Pratsinis S. (2004): Winnacker/Küchler, Chemische Technik: Prozesse und Produkte; WILEY-VCH Verlag GmbH&Co.KGaA, Weinheim, ISBN: 3-527-31032-0

Nanoparticles: Synthesis, characterisation and cellular effects-
The NANO-SYNCC- Project

H.-R. Paur[1], W. Baumann[1], H. Bockhorn[4], A. Comouth[2], S. Diabate[3], H.Mätzing[1], S. Mülhopt[1], O. Nalcaci[4], A. Panas[3], E. Ruzin[4], H. Saathoff[2], H. Seifert[1], C. Weiss[3]

Forschungszentrum Karlsruhe: [1]Institut für Technische Chemie; [2] Institut für Metereologie und Klimaforschung, [3] Institut für Toxikologie und Genetik; Postfach 3640; 76021 Karlsruhe,Germany [4] Universität Karlsruhe (TH): Institut für Technische Chemie und Polymerchemie; 76131 Karlsruhe, Germany

Keywords: particle synthesis, agglomerate, nanoparticles characterization, human lung cells

Introduction

Metal-oxide nanoparticles are widely used in industry, food technology, personal hygiene and are expected to find major applications in medicine in the future. Although there is clear experimental and epidemiological evidence that particles can induce inflammation and cancer in some instances, little is known about the underlying mechanisms. Biological effects of particles depend on their chemical composition, their size which is correlated with the specific surface area (Oberdörster et al., 1994), reactivity of the surface, and other parameters (Nel et al. 2006). In order to predict the biological activity of new nanoparticles, it is necessary to know which parameters induce which effects. For this purpose ,in-vitro experiments have been started to screen defined nanoparticles with different sizes and surface properties for their biological effects. Here we discuss the synthesis of metal oxide nanoparticles by flame synthesis and microwave plasma, their physico-chemical characterization and the first assessment of their toxicity by bioassays.

Experimental

Low Pressure Flame Synthesis (LPF) was carried out by combustion of iron pentacarbonyl at 30 mbar in a premixed hydrogen/oxygen flame in argon under carefully controlled flow conditions. The particles were collected on a teflon-membrane filter.

Microwave plasma synthesis (MWP) is a low-temperature process, which was previously described by Vollath et.al. (1992). Silane (SiH_4) in Argon/Oxygen was oxidized in the microwave plasma at temperatures of about 500 K at p = 20 mbar. The nanoparticles were characterized on-line by Particle Mass Spectroscopy (PMS). The particles were collected thermophoretically by impingers.

The nanoparticles collected were characterised by transmission electron microscopy (TEM) and by dynamic light scattering (DLS, Horiba). Nanoparticle suspensions were prepared and dispersed by electrospray (TSI) and the airborne size distributions were measured by mobility sizing (SMPS, TSI).

Bioassays were conducted by suspending the collected iron and silicon oxide nanoparticles in medium and applying the suspensions to cell cultures. The effects on viability and production of intracellular reactive oxygen species (ROS) were analyzed and compared to those of commercial iron and silicon oxide NPs. Primary particle sizes are 12 and 40 nm for SiO_2 and 20-40 nm for Fe_2O_3 NPs.

Results

Tab. 1 summarizes the primary size of silicon and iron oxide nanoparticles measured downstream of the microwave plasma by PMS and by electron microscopy. These particles when suspended in water show significantly higher particle sizes in DLS-measurement. As the particles were produced at low temperature the agglomeration is probably not due to sintering of the primary particles. IR-spectra of the iron oxide particles show strong OH-bonds, which may indicate agglomeration of primary particles by hydrogen bridge induced bonding.

Particle Source	Precursor	Primary Part.size	Agglomerate size
MWP	200 ppm SiH_4	10 nm[a]	53 nm[d]
MWP	2000 ppm SiH_4	25 nm[b]	150 nm[c]/126 nm[d]
LPF	800-2500ppm $Fe(CO)_5$	11 nm[b]	208 nm[c]

Table 1. Size of primary metal-oxide nanoparticles measured by [a]PMS and [b]TEM as well as agglomerate sizes in liquid suspension measured with [c]DLS and by [d]SMPS.

The first results of the bioassays using commercial silicon and iron oxide NPs are summarized as follows:

- Toxicity in human lung epithelial cells was found for silicon and iron oxide NPs at high concentrations only.
- Silicon dioxide NPs showed high toxicity in mouse macrophages, however iron oxide was not toxic in this test system.
- No ROS formation was detected for both particle species.

Iron oxide NPs synthesized by LPF showed similar effects as commercial iron oxide NPs.

Further work will concentrate on the influence of particle size, agglomeration state and chemical composition on biological effects. Furthermore, the response of cells exposed to NPs at the air-liquid interface and under submerged conditions will be compared.

Nel, A., Xia, T., Madler, L., and Li, N. (2006) Science 311, 622-627

Oberdörster, G., Ferin, J., and Lehnert, B.E. (1994) Environ. Health Perspect. 102 Suppl 5, 173-179

Vollath, D. and K. E. Sickafus (1992). *Nanostructured Materials* **1**(5): 427-437.

Integration of two mathematical models for monitoring of biological doses from inhalation exposure to nano and fine particles in industrial workplace

A. Nikolopoulou[1], P. Neofytou[1], C. Housiadas[1], P. Papazafiri[2], K. Eleftheriadis[1] and L. Tran[3]

[1]National Centre for Scientific Research "Demokritos", Athens, Greece,
[2]School of Biology, University of Athens, Greece,
[3]Institute of Occupational Medicine, Edinburgh, UK.

Keywords: Aerosol dynamics, Deposition, Exposure, Clearance, Modelling.

Inhalation of nanoparticles is one of the great concerns in the area of nanomaterials and nanotechnology safety. Characterization of worker dose includes the chemical and physical characterization of particles, the determination of inhaled doses, and their biological characterization. We present a study addressing these steps for the case of industrial manufacturing of detergent and cosmetics (powders) by combining two models of consecutive simulation: (i) for lung deposition and (ii) for lung clearance. Both models are transformed into computational codes using FORTRAN.

Internal dosimetry is accomplished with an appropriate biomathematical model, consisted of two sub-models, which calculates with a full mechanistic description lung deposition with continuous clearance. The first model is a mechanistic, respiratory deposition model including aerosol and breathing dynamics (Mitsakou et al., 2005 & 2007). It is based on a one-dimensional representation of the aerosol flow along the whole respiratory tract, i.e. the extrathoracic part and all generations of the thoracic part. The second model is a compartmental, mechanistic, model that calculates retention/translocation of deposited particles. (Tran et al., 1999 & 2007). The considered mechanisms include phagocytosis, macrophage life cycle, interstitialization and transfer to the lymph nodes. The integrated model of coupled deposition and clearance ultimately provides effective biological doses to the lung, namely deposited amount minus cleared amount.

Experimental monitoring data of airborne exposure levels during detergent manufacturing in a major chemical plant are used as input to the model to translate the exposure concentrations to effective biological doses to the lung of the workers. In determining internally delivered biological doses worst case scenarios are assumed, *i.e.* workers are not using protective means.

We examined if measurements made by convenient, inexpensive on-line monitors based on light scattering can assess adequately the particles concentration and size characteristics in the workplace (*i.e.* close to the gravimetric methods). Focus is given in assessing the impact on the calculated dose of the measurement uncertainty when monitoring is based on optical ("user-friendly") aerosol measurements.

Dosimetric data are numerically generated by simulating chronic exposure conditions, i.e. running the model over the working life of a worker assuming typical exposure scenarios based on the measurement data (Figure 1). Such chronic simulated doses can be compared with DNELs (derived no-effect limits) from in-vitro biological assays and, therefore, recommend possible safe workplace exposure levels.
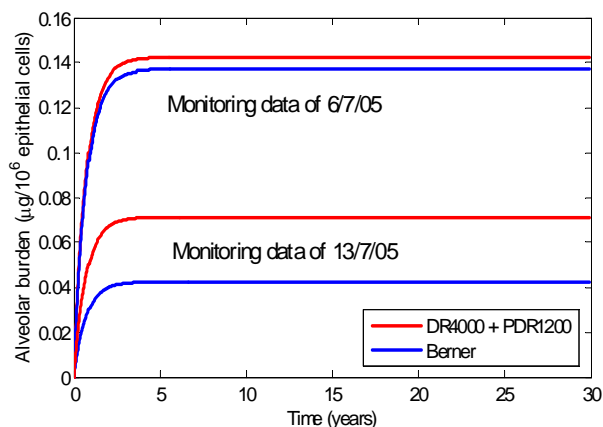
Figure 1. Time evolution of the alveolar burden, under continuous deposition and clearance, assuming a chronic exposure scenario for over a typical working period of 30 years.

The present study illustrates the effectiveness of combining the two mathematical models. Furthermore, we illustrate the feasibility of combining mechanistic mathematical modelling with data from user-friendly monitors and data from in-vitro toxicological assays to derive limits and assess risk.

Mitsakou C., Helmis C., Housiadas C. (2005). *J. Aerosol Sci.*, 36, 75-94.

Mitsakou C, Mitrakos D., Neofytou P., Housiadas C. (2007). *J. Aerosol Medicine*, 20, 519-529.

Tran L., Jones A. D., Cullen R. T., Donaldson K. (1999). *Inhalation Toxicology*, 11, 1059-1076.

Tran L. & Kuempel E., in: *Particle Toxicology* (eds. K. Donaldson, P. Born), 351-386, CRC Press, 2007.

NanoImpactNet – building a multi-stakeholder dialogue on the health and environmental impact of nanomaterials

N. Boschung[1], D. Hart[1] and M. Riediker[1]

[1]Institute for Work and Health, Université de Lausanne + Université de Genève, Bugnon 21, CH-1011, Lausanne, Switzerland

Keywords: Communication, Nanoparticles, Regulation, Stakeholder.

NanoImpactNet (NIN) is a multidisciplinary European Commission funded network on the environmental, health and safety (EHS) impact of nanomaterials. The 24 founding scientific institutes are leading European research groups active in the fields of nanosafety, nanorisk assessment and nanotoxicology. This 4-year project is the new focal point for information exchange within the research community. Contact with other stakeholders is vital and their needs are being surveyed.

NIN is communicating with 100s of stakeholders: businesses; internet platforms; industry associations; regulators; policy makers; national ministries; international agencies; standard-setting bodies and NGOs concerned by labour rights, EHS or animal welfare. To improve this communication, internet research, a questionnaire distributed via partners and targeted phone calls were used to identify stakeholders' interests and needs.

Knowledge gaps and the necessity for further data mentioned by representatives of all stakeholder groups in the targeted phone calls concerned:

- the potential toxic and safety hazards of nanomaterials throughout their lifecycles;
- the fate and persistence of nanoparticles in humans, animals and the environment;
- the associated risks of nanoparticle exposure;
- greater participation in: the preparation of nomenclature, standards, methodologies, protocols and benchmarks;
- the development of best practice guidelines;
- voluntary schemes on responsibility;
- databases of materials, research topics and themes, but also of expertise.

These findings suggested that stakeholders and NIN researchers share very similar knowledge needs, and that open communication and free movement of knowledge will benefit both researchers and industry.

Subsequently a workshop was organised by NIN focused on building a sustainable multi-stakeholder dialogue. Specific questions were asked to different stakeholder groups to encourage discussions and open communication.

1. What information do stakeholders need from researchers and why?
The discussions about this question confirmed the needs identified in the targeted phone calls.

2. How to communicate information?
While it was agreed that reporting should be enhanced, commercial confidentiality and economic competition were identified as major obstacles. It was recognised that expertise was needed in the areas of commercial law and economics for a well-informed treatment of this communication issue.

3. Can engineered nanomaterials be used safely?
The idea that nanomaterials are probably safe because some of them have been produced 'for a long time', was questioned, since many materials in common use have been proved to be unsafe. The question of safety is also about whether the public has confidence. New legislation like REACH could help with this issue. Hazards do not materialise if exposure can be avoided or at least significantly reduced. Thus, there is a need for information on what can be regarded as acceptable levels of exposure. Finally, it was noted that there is no such thing as a perfectly safe material but only boundaries. At this moment we do not know where these boundaries lie.
The matter of labelling of products containing nanomaterials was raised, as in the public mind safety and labelling are connected. This may need to be addressed since the issue of nanomaterials in food, drink and food packaging may be the first safety issue to attract public and media attention, and this may have an impact on 'nanotechnology as a whole.

4. Do we need more or other regulation?
Any decision making process should accommodate the changing level of uncertainty. To address the uncertainties, adaptations of frameworks such as REACH may be indicated for nanomaterials.
Regulation is often needed even if voluntary measures are welcome because it mitigates the effects of competition between industries. Data cannot be collected on voluntary bases for example.
NIN will continue with an active stakeholder dialogue to further build on interdisciplinary relationships towards a healthy future with nanotechnology.

Antibacterial activity of flame-made Ag/SiO$_2$ nanoparticles

[1]Georgios A. Sotiriou, [1]Adrian Camenzind,
[2]Andreas Meyer, [2]Sven Panke and [1]Sotiris E. Pratsinis

[1]Particle Technology Laboratory, [2]Bioprocess Laboratory, Institute of Process Engineering
Department of Mechanical and Process Engineering
Swiss Federal Institute of Technology Zurich (ETH Zurich)
CH-8092 Zurich, Switzerland

Keywords: silver, silica, nanoparticles, antibacterial.

Nano-sized silver (Ag) particles are known that they exhibit antibacterial properties (Feng *et al.*, 2000). The Ag nanoparticles damage either the cell's membrane and, in case of penetration, interact with sulfur and phosphor containing compounds (DNA, proteins) within the cell, thus affecting cell vitality (Morones *et al.*, 2005). Additionally, it has been also suggested that Ag$^+$ are released from the *Ag SSA*, which have an additional contribution to their antibacterial effect (Feng *et al.*, 2000; Morones *et al.*, 2005). That antibacterial effect is enhanced by decreasing the particle size as more Ag surface becomes accessible.

Here, Ag nanoparticles supported on SiO$_2$ with various Ag contents (x= 0 to 25 wt%: *xAg/SiO$_2$*) and from different precursors have been produced by flame spray pyrolysis (FSP), a dry, fast, scalable and versatile method of producing nanoparticles (Madler *et al.*, 2002). Solutions of appropriate amounts of Ag and SiO$_2$ precursors in alcohols were used as precursors of the *xAg/SiO$_2$* particles, that were characterized by TEM/STEM, X-ray diffraction (XRD), nitrogen and oxygen chemisorption. Additionally, the produced *xAg/SiO$_2$* nanoparticles were tested for antibacterial activity against the gram negative bacterium *Escherichia coli*.

The effect of precursor composition on the morphology of the product *Ag/SiO$_2$* nanoparticles was studied. Independent of the precursor which was used, Ag nanoparticles distributed within an amorphous SiO$_2$ matrix were obtained. However, the particle size and the particle size homogeneity are influenced by the precursor selection. Smaller and more homogeneous Ag particles are obtained for Ag precursor with low melting point, most probably because the formation of Ag starts earlier, along with the formation of SiO$_2$. This also leads to the fact that these nanoparticles have less exposed Ag surface area (*Ag SSA*).

The antibacterial activity was also studied for the produced nanoparticles. More pronounced with increasing Ag content, showing the highest effect for the *25Ag/SiO$_2$* particles, however, on the basis of equivalent Ag mass, the more effective particles were the low Ag content ones. Comparison to the existing literature was made and direct correlation between the Ag content and the antibacterial activity was established. Figure 1 shows the growth of *E. coli* in 100 μl LB medium at 37°C, with an initial amount of 10^7 colony forming units (CFU)/ml in the presence of 8 μg/ml of the different *xAg/SiO$_2$* nanoparticles (x=0-25 wt%). It can be observed that for low Ag contents, there is almost no effect on the growth curves. However, as the Ag content is increased, there is a more enhanced antibacterial activity observed, having the highest one for the *25Ag/SiO$_2$*.
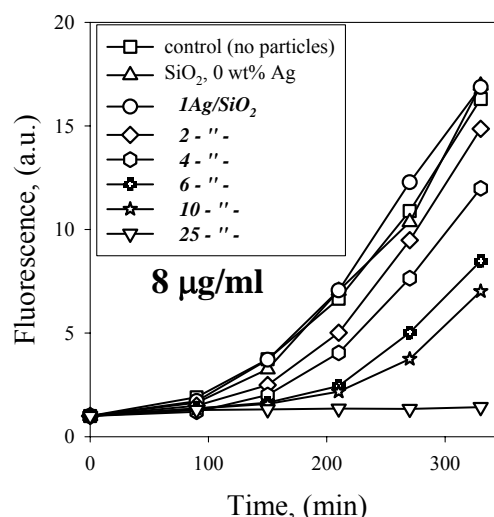
Figure 1: The growth curves of the bacteria at 37 °C, in the presence of 8 μg/ml of all the different Ag content particles.

Feng, Q. L., J. Wu, G. Q. Chen, F. Z. Cui, T. N. Kim and J. O. Kim, "A mechanistic study of the antibacterial effect of silver ions on Escherichia coli and Staphylococcus aureus," *Journal of Biomedical Materials Research* **52**, 662 (2000).

Madler, L., H. K. Kammler, R. Mueller and S. E. Pratsinis, "Controlled synthesis of nanostructured particles by flame spray pyrolysis," *Journal of Aerosol Science* **33**, 369 (2002).

Morones, J. R., J. L. Elechiguerra, A. Camacho, K. Holt, J. B. Kouri, J. T. Ramirez and M. J. Yacaman, "The bactericidal effect of silver nanoparticles," *Nanotechnology* **16**, 2346 (2005).

Aerosol-derived graphene/copper nanoparticles as an air-stable alternative to metal ink-jet printing for electronics

Norman A. Luechinger, Evagelos K. Athanassiou, Robert N. Grass and Wendelin J. Stark

Department of Chemistry and Applied Biosciences, Swiss Federal Institute of Technology (ETH Zurich), Wolfgang-Pauli-Str. 10, HCI E 107, ETH Hönggerberg, Zurich 8093, Switzerland

Keywords: ink-jet printing, copper nanoparticles, graphene, conductive, air-stable.

Metal nanocolloids or metal inks have received tremendous attention for a wide range of applications. The ease of the simple application of metal inks allows ultra-high-volume applications of metallic patterns and strongly affects their fabrication costs. Radio frequency identification (RFID) tags are a very promising application which is assumed to substitute the traditional barcode technology in the near future. Metal oxidation, however, has traditionally restricted the range of useful nano-metals to noble-metals such as silver, platinum, palladium or gold. Technical low cost applications such as ink jet printing of flexible conductors and RFID tags, however, require manufacturing costs of typically less than one cent per tag. The most evident candidate to substitute silver or gold would be copper, but nano-copper rapidly oxidizes under ambient conditions resulting in a loss of electronic performance.

We demonstrate the synthesis of metallic copper nanoparticles by reducing flame spray synthesis (a) at large scale. By a modification of the synthesis setup, the nanoparticles are in-situ coated with protective shells of graphene (c, d). The resulting black nanopowder (Figure 1 b) exhibits high air-stability and chemical inertness which allows easy handling at ambient conditions.

Using an amphiphilic surfactant, a water-based copper nanocolloid could be prepared and successfully printed on to a polymer substrates by conventional ink-jet printing using household-printers. The dried printed patterns exhibited strong metallic gloss (e) and an electrical conductivity of > 100 S m^{-1} (f) without the need of a sintering or densification step. This conductivity currently limits use in electronics to low current applications, electromagnetic shielding and decorative effects. The high stability of graphene-coated copper nanoparticles makes them an economically most attractive alternative to silver or gold nanocolloids and will strongly facilitate the industrial use of metal nanocolloids in consumer goods.
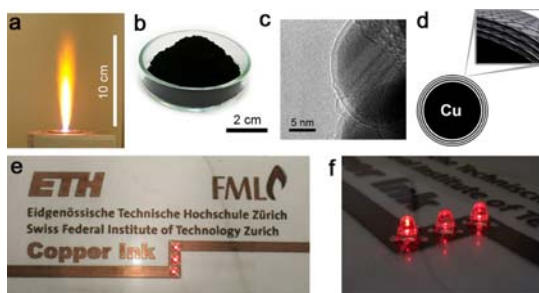
Figure 1. Flame spray synthesis under reducing conditions (a). As-prepared air-stable copper nanoparticles (b). Transmission electron micrograph (c) and schematic (d) showing protecting graphene layers on individual copper nanoparticles. Ink-jet printed conductive patterns on a flexible polymer substrate exhibiting electrical conductivity which was demonstrated by operating light emitting diodes (e, f).

1. N. A. Luechinger, E. K. Athanassiou, W. J. Stark, **Nanotechnology**, 19 445201 (2008).

2. N. A. Luechinger, N. Booth, G. Heness, S. Bandyopadhyay, R. N. Grass, W. J. Stark, **Advanced Materials**, 20, 3044-3049, (2008).

3. N. A. Luechinger, S. Loher, E. K. Athanassiou, R. N. Grass, W. J. Stark, **Langmuir**, 23, 3473-7 (2007).

Novel Nanostructures for Solid State Alcohol Breath Analyzers

Antonio Tricoli, Marco Righettoni and Sotiris E. Pratsinis

Particle Technology Laboratory, ETH Zurich, CH-8092 Zurich, Switzerland, tricoli@ptl.mavt.ethz.ch, tel: +41 44 632 8503, fax: +41 44 632 1595

Keywords: solid solution, gas sensor, ethanol, humidity, selectivity

Solid state alcohol breath analyzers are commonly used by the law enforcement authorities, due to high sensitivity toward ethanol, their portability and fair response and recovery times.[1] Common materials for the synthesis of the sensitive element are SnO_2 nanoparticles with an average size below 15 nm. The main drawback of the exploitation of SnO_2 as sensing material is its high cross-sensitivity to humidity, which requires expensive and elaborated systems for preparation of the gas probe.[2] The cross-sensitivity issue can be solved in some extent by utilizing other oxides such as TiO_2.[3] Nevertheless, such semiconductors have from less sensitivity to EtOH than SnO_2 and may have some stability problems. In fact, it has been reported that flame-made TiO_2 nanoparticles undergo crystallographic phase transition from anatase to rutile while heated at sufficient temperatures thus drastically reducing sensitivity.[3]

SnO_2[4] and TiO_2[3] nanoparticles can be readily made in flame reactors leading to small size and thus high sensitivity. These nanoparticles can also be deposited directly from the hot aerosol on a target substrate placed above the flame and *in situ* stabilized reducing process times.[5] Here, synthesis of novel SnO_2-TiO_2 nanostructures with drastically reduced cross-sensitivity to humidity and high sensitivity to ethanol have been obtained by flame spray pyrolysis. First a liquid precursor is combusted and evaporated forming a super saturation of the target oxides. Nucleation, condensation and coagulation lead to formation of a solid solution of SnO_2/TiO_2 nanocrystals (Fig. 1) with a predominant rutile phase. The solid solution properties, such as the band gap, crystal size and morphology, are correlated to the sensing performance. In particular, the cross-sensitivity to humidity during EtOH detection is investigated at different relative humidity and compared to real operating conditions. In conclusion, the SnO_2/TiO_2 nanostructures are a highly performing material for alcohol breath analyzers with the potential of strongly reducing the cost of such devices.
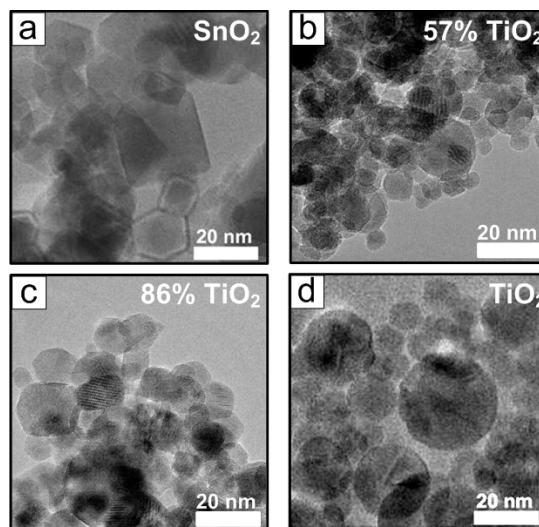
Figure 1: TEM images of pure SnO_2 and TiO_2 and SnO_2/TiO_2 nanoparticles as a function of the TiO_2 content.

References
[1] G. Eranna, B. C. Joshi, D. P. Runthala, R. P. Gupta, *Crit. Rev. Solid State Mat. Sci.*, **2004,** 29, 111.
[2] G. Korotcenkov, *Sens. Actuators, B*, **2005,** 107, 209.
[3] A. Teleki, S. E. Pratsinis, K. Kalyanasundaram, P. I. Gouma, *Sens. Actuators, B*, **2006,** 119, 683.
[4] L. Madler, A. Roessler, S. E. Pratsinis, T. Sahm, A. Gurlo, N. Barsan, U. Weimar, *Sens. Actuators, B*, **2006,** 114, 283.
[5] A. Tricoli, M. Graf, F. Mayer, S. Kühne, A. Hierlemann, S. E. Pratsinis, *Adv. Mater.*, **2008,** 20, 3005.

Anti - Fogging Coatings by Flame Synthesis and Deposition

Antonio Tricoli, Marco Righettoni and Sotiris E. Pratsinis

Particle Technology Laboratory, ETH Zurich, CH-8092 Zurich, Switzerland, tricoli@ptl.mavt.ethz.ch,
tel: +41 44 632 8503, fax: +41 44 632 1595

Keywords: Anti - Fogging, Super - Hydrophilic, SiO_2 - TiO_2, Flame Synthesis and Deposition

The wetting properties of surfaces greatly influence their interaction with the environment.[1] Recently, many studies have focused on the development of efficient coating methods for extreme wetting of surfaces features. Self-cleaning,[2] bacteria-resistant, and anti-fogging[3] surfaces are made by depositing either super - hydrophobic or super - hydrophilic coatings. That impact several applications such as sport and sanitary equipment, lenses for optical devices, reading glasses, automobile windscreens, windows and mirrors to name a few. In particular, anti - fogging coatings are feasible by preventing formation of small water droplets on the substrate surface by a high performing super - hydrophilic coating.[3] Furthermore, such coatings should be transparent, mechanically stable and low cost to promote commercialization.

The coating synthesis method and material properties greatly influence film performance in terms of transparency, stability and anti - fogging effect. Metal - oxide coating processes can be subdivided in wet - and dry - methods. Wet - methods have the advantage of relatively high coating mechanical stability, due to utilization of binders, but require long process time (hours / days), large number of steps and may have poor reproducibility of coating morphology. In contrast, dry methods can deposit highly porous nanostructured coatings in short times with good control and reproducibility of coating morphology.[4] In fact, dry synthesis and deposition of nanostructures is obtainable by several methods such as sputtering, spray pyrolysis, cluster beam deposition, classified aerosol deposition, combustion chemical vapor deposition or flame spray pyrolysis

(FSP), but only few can be scaled easily to deposit on large surfaces and at low cost.

Here, silica and silica - titanium oxide nanostructured coatings have been deposited by FSP onto glass substrates and *in situ* stabilized by flame annealing. The coatings synthesis mechanism has been investigated for the different materials by analysis of the aerosol and coating properties. The coating transparency, stability and wetting features have been characterized as a function of deposition time (thickness and surface coverage) for each material and correlated to their anti - fogging performance.
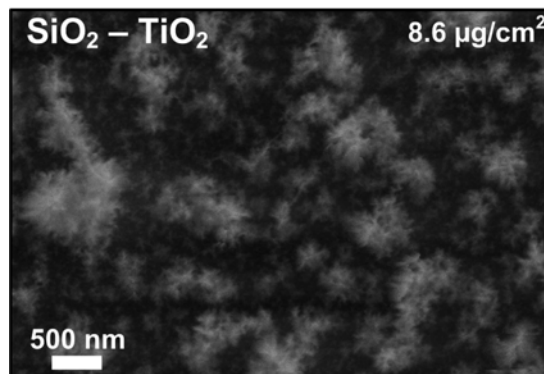
Figure 1: SEM top view of a 8.6 μg/cm^2 SiO_2 - TiO_2 coating. The coating consists of lace - like structures made of air born particles with spike - like endings.

References

[1] R. Wang, K. Hashimoto, A. Fujishima, M. Chikuni, E. Kojima, A. Kitamura, M. Shimohigoshi, T. Watanabe, *Nature*, **1997,** 388, 431.

[2] L. Feng, Y. A. Zhang, J. M. Xi, Y. Zhu, N. Wang, F. Xia, L. Jiang, *Langmuir*, **2008,** 24, 4114.

[3] F. C. Cebeci, Z. Z. Wu, L. Zhai, R. E. Cohen, M. F. Rubner, *Langmuir*, **2006,** 22, 2856.

[4] A. Tricoli, M. Graf, F. Mayer, S. Kühne, A. Hierlemann, S. E. Pratsinis, *Adv. Mater.*, **2008,** 20, 3005.

Nanoparticles for Li-ion battery electrodes by electrospray-assisted aerosol routes

M. Valvo, U. Lafont, D. Munaò, J. C. M. Marijnissen, E. M. Kelder

Nanostructured Materials, Delft University of Technology, Julianalaan 136, 2628 BL, Delft, The Netherlands

Keywords: Nanoparticles, Electrospray, Li-ion batteries.

Nanoparticles are nowadays widely applied to an ever-increasing number of research areas and to different technological fields thanks to their special properties which arise from their compact size. Nanostructured materials are particularly attractive in all those applications where mechanical strength, surface reactivity, enhanced transport properties, and extended interfaces are relevant.

Energy storage and conversion are emerging fields that have been experiencing an extensive use of nanostructures during the last years. The research on novel devices with improved performances regards nanoparticles as powerful tools for tailoring the physichemical properties of the materials that have been commonly employed for these purposes.

Li-ion batteries are currently receiving a considerable attention due to their applications, not only to portable electronics, but also to high-power devices, such as electric vehicles and storage modules for energy produced via renewable sources. A key factor for improving their gravimetric and volumetric energy densities, as well as their power delivery and charging rates - without neglecting fabrication costs and sustainability - is the use of nanoparticles and nanocomposites. Electrode kinetics can be no longer an issue by conveniently using nanoparticles, which yield reduced migration lengths for charge carriers (i.e. Li^+ ions, electrons) and better acceptance of the strains related to Li uptake and removal during electrochemical cycling. This holds particularly true for a class of novel negative electrodes (i.e. metals, metal oxides, alloys, intermetallics), which can store a remarkable amount of Li, but which also suffer from severe volume changes upon charge and discharge.

Electrospray is a versatile technique for atomizing liquids that is increasingly applied to materials technologies [1]. It allows a fine dispersion of the charged emitted droplets, which possibly retain their monodispersity. Different droplet sizes can be achieved by adjusting the experimental parameters. Besides, tuning of the electrostatic fields enables an additional control on the droplets motion. The generated droplets can be collected onto a substrate, or even in a liquid environment where they can eventually undergo further chemical reaction [2]. Depending on the different precursors and conditions employed, several reactions can take place, (i.e. hydrolysis and condensation, pyrolysis, precipitation, etc.), which generally exhibit a characteristic kinetics, due to the evaporation rate of the droplets.

A convenient choice of the parameters (i.e. flow rate, viscosity, temperature, conductivity etc.) enables the fabrication of different structures with various morphologies, which span from nanoparticles to nanostructured thin films [4, 5]. These materials are interesting for advanced Li-ion battery electrodes, since they can inherently meet the requirements for improving the existing technology. Two examples of advanced synthesis methods of nanoparticles for Li-ion battery negative electrodes by electrospray are schematically shown in Figure 1.
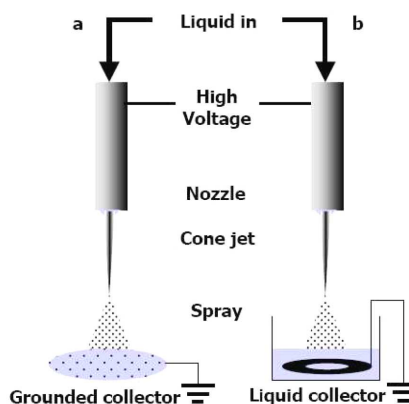
Figure 1. Schematic drawing of electrospray-assisted syntheses. Electrostatic Spray Deposition/Pyrolysis (a). Electrostatic Spray Reductive Precipitation (b).

Metal oxides and metallic-like nanoparticles are typical materials that can fabricated by these techniques, depending on the characteristic reactions involved in the gas/liquid phases and the gaseous atmosphere employed for the synthesis process. Different materials will be considered and their performances in Li-ion battery electrodes will be assessed.

1. Jaworek A. (2007). *J. Mater. Sci.* 42, 266-297.
2. Valvo M., Lafont U., Munaò D. Kelder E. M. (2008). *J. Power Sources* – In Press.
3. van Erven J., Moerman R., Marijnessen J. C. M. (2005). *Aerosol Sci. and Techn.* 39, 941-946.
4. Chen C., Kelder E. M., Schoonman J. (1997). *J. Electrochem. Soc.* 144, L289-L291.
5. van Zomeren A. A., Kelder E. M., Marijnissen J. C. M., Schoonman J. (1994). *J. Aerosol Sci.* 25, 1229-1235.

Size-selected Agglomerates as Ultrasensitive Gas Sensors

Helmi Keskinen[1], Antonio Tricoli[1], Marko Marjamäki[2], Jyrki M. Mäkelä[2] and Sotiris E. Pratsinis[1]

[1] Particle Technology Laboratory, Institute of Process Engineering, Department of Mechanical and Process Engineering, ETH Zürich, CH-8092 Zürich, Switzerland.
[2] Institute of Physics, Aerosol Physics Laboratory, Tampere University of Technology, P.O. Box 692, FIN-33101, Tampere, Finland.

Highly sensitive and, most importantly, very selective gas sensors are desired for sophisticated gas detection e.g. for security or non-invasive and early detection of illnesses such as diabetes or asthma by acetone vapor (Deng *et al.*, 2004) or CO (Horvath *et al.*, 1998) concentrations, respectively, in patients' breath. Metal oxides such as SnO_2 are widely applied for gas detection as their sensitivity and low detection limit can be enhanced by decreasing particle size below 10 nm (Shimizu and Egashira, 1999). Kennedy *et al.* (2003) selected nearly monodisperse SnO_2 nanoparticles by a differential mobility classifier (DMC, TSI) and observed that by decreasing their size from 35 to 10 nm the sensitivity to 1000 ppm ethanol was nearly tripled. However, the sensitivity improvement by reducing the particle size is usually short-lived as the thermal stability of nanoparticles is very low (Xu *et al.*, 1991). As the polydisperse particles have lower thermal stability than monodisperse of equal average size, by narrowing the size distribution, the thermal stability of nanoparticles could be enhanced.

Here, Flame Spray Pyrolysis (FSP) was used to produce SnO_2 particles (Sahm *et al.*, 2004), from which nearly monodisperse agglomerate fractions were selected by a cascade Berner low pressure impactor (BLPI) (Berner and Lurzer, 1980). The polydisperse particles generated by FSP were collected also by glass-fiber filter as well as thermophoretically on TEM-grids along the FSP axis. The thermal stability of collected particles was measured by heating them to 400 - 900 °C in an oven. The X-ray diffraction patterns were measured and crystallite characteristics were obtained using Topas 3.0 software (Bruker). Selected Area Electron Diffraction (SAED) and TEM were carried out with a Phillips CM30ST microscope (LaB6 cathode, 300 kV). The image analysis for primary particle size distribution was carried out with Optimas software (Media Cybernetics, USA).

For fabrication of sensors, the paste of FSP-made or commercial (Sigma-Aldrich, d_{XRD}= 50 nm) SnO_2 particles was stirred and doctor-bladed on Al_2O_3 substrates with interdigitated Au electrodes (10 × 10 mm). The paste was dried slowly by step-wise heating up to 600 °C. The change in sensor resistance upon exposure to CO (4 - 50 ppm) and ethanol vapor (4 - 100 ppm) in dry air (79% N_2, 21% O_2, PanGas) at 320 or 420 °C was measured in DC mode.

By controlling the polydispersity of these agglomerates, the sensing performance can be greatly enhanced. In fact, polydisperse agglomerates of 0.4 - 12 µm in aerodynamic diameter consisting of SnO_2 primary particles about 10 nm in grain and crystal size were produced by flame spray pyrolysis (FSP). Narrowly distributed agglomerates of different sizes (70 – 240 nm) exhibited outstanding sensing performance to CO and ethanol vapor and were more thermally stable than polydisperse ones containing nearly equisized SnO_2 crystals by sintering (Heine and Pratsinis, 2007). The sensor responses (S) to 100 ppm ethanol vapor are extremely high, e.g. S = 640 for sensors made with the smallest agglomerates (70 nm) which is 80 times higher than the response for sensors made with commercial powder. This superior performance is attributed to aggregates of optimal neck size (comparable to twice the Debye length of tin oxide) between the SnO_2 primary particles leading to sintering inhibition and "bottle-neck" (Tricoli *et al.*, 2008) aggregate morphology. In fact, further sintering these agglomerates above 600 °C increased the neck size between primary particles that drastically reduced their sensor response.

Berner, A., and C. Lurzer. (1980). *J. Phys. Chem.*. 84:2079-2083.

Deng, C.H., J. Zhang, X.F. Yu, W. Zhang, and X.M. Zhang. (2004). *J. Chromatogr. B*. 810:269-275.

Heine, M.C., and S.E. Pratsinis. (2007). *J. Aerosol Sci.*, 38:17-38.

Horvath, I., L.E. Donnelly, A. Kiss, P. Paredi, S.A.

Kennedy, M.K., F.E. Kruis, H. Fissan, B.R. Mehta, S. Stappert, and G. Dumpich.(2003). *J. Appl. Phys.*. 93:551-560.

Sahm, T., L. Madler, A. Gurlo, N. Barsan, S.E. Pratsinis and U. Weimar. (2004). *Sens. Actuat. B-Chem.*. 98:148-153.

Shimizu, Y., and M. Egashira. (1999). *MRS Bull.* 4:18-24.

Tricoli, A., M. Graf, and S.E. Pratsinis. (2008). *Adv. Funct. Mater.* 18:1969-1976.

Xu, C., J. Tamaki, N. Miura, and N. Yamazoe. (1991). *Sens. Actuat. B-Chem.*. 3:147-155.

Pt-based alloy/carbon nanotubes electrocatalysts for unitized regenerative polymer electrolyte fuel cells

Yu-Chun Chiang[1], Cheng-Hsiung Chang[1], Jui-Pai Hung[1] and Chien-Cheng Lee[2]

[1] Department of Mechanical Engineering and Yuan Ze Fuel Cell Center, Yuan Ze University. 135 Yuan-Tung Rd., Chung-Li, Taoyuan 320, Taiwan

[2] Department of Communications Engineering, Yuan Ze University. 135 Yuan-Tung Rd., Chung-Li, Taoyuan 320, Taiwan

Unitized regenerative fuel cell (URFC) system combines fuel cell and water electrolyzer with advantages of lower cost, weight, and volume. Up to date, the key technical problem for developing the URFC is optimization of the structure and composition of oxygen electrode for water electrolysis and fuel cell operations. Due to the corrosion of carbon materials by oxygen evolved during water electrolysis, the Pt/C electrocatalysts widely used in fuel cell electrodes is not suitable for the oxygen electrode of URFC. In addition, the alloys of Pt and oxophillic metals, giving rise to a bi-functional mechanism, are known to be superior to Pt-only catalysts (Chen *et al.*, 2001). Therefore, in this study Pt, PtIr, and their composites with carbon nanotubes (CNTs) were prepared and characterized, and their applications on URFC were discussed.

The impregnation method was used to prepare the electrocatalysts (Deivaraj and Lee, 2005). $H_2PtCl_6 \cdot 6H_2O$ and $IrCl_3 \cdot nH_2O$ were used as the precursors of Pt and Ir, respectively, and $NaBH_4$ was used as the reductant. Two multi-walled CNTs were selected, one was provided by Conyuan Biochemical Technology Co. of Taiwan (CNT1) and the other one was synthesized by chemical vapor deposition in our laboratory (CNT2). In order to determine the surface effect, the CNTs were oxidized with H_2SO_4/H_2O_2. HRTEM, XRD, XPS, BET, and cyclic voltammetry were used to characterize the samples. Membrane electrode assembly (MEA) was prepared and the performance of URFC was tested.

Results show that the particle size of PtIr was less than Pt, which implies PtIr should have a better electrochemical activity. The XRD patterns for Pt, PtIr and the composites all showed characteristic f.c.c. Pt or Ir structure. Pt was present in three different oxidation states in Pt/CNT1, but only in two different oxidation states in PtIr/CNT1. The specific surface areas of Pt and PtIr were about 30.26 and 37.11 m^2/g. The cyclic voltammograms (Figure 1) displayed a well-defined hydrogen oxidation region (0.0–0.4V versus SCE). The current densities in the double layer region (between 0.4 and 0.85V) of PtIr were larger than that on Pt, which was characteristic of binary electrocatalysts containing transition metals. The calculated electrochemical surface area for Pt was about 40.5 cm^2/mg. The data in water

electrolysis mode and fuel cell mode show that adding CNTs on oxygen electrode or on both electrodes could produce a better performance than that of pure Pt electrode. Table 1 shows the generation of hydrogen with different MEAs through water electrolysis mode in URFC system. It can be seen that adding CNTs only in oxygen electrode can promote the hydrogen yield effectively.
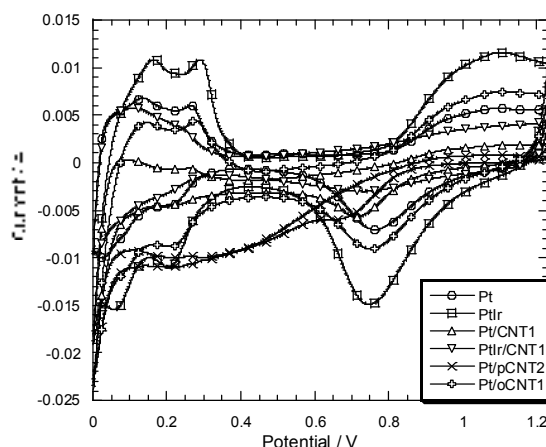
Figure 1. Cyclic voltammograms of Pt-based alloy/carbon nanotubes electrocatalysts.

Table 1. Hydrogen yields of the MEAs prepared by different catalysts.

Catalyst		Hydrogen yield (ml/min)	Specific hydrogen yield (ml/min/g)
Hydrogen electrode	Oxygen electrode		
Pt	PtIr	4.45~4.52	164.81~167.22
Pt/CNT1	PtIr	2.91~3.03	64.67~67.33
Pt/oCNT1	PtIr	2.65~2.73	58.89~60.67
Pt	PtIr/CNT1	6.97~6.90	191.67~193.61
Pt	PtIr/oCNT1	1.73~1.83	48.06~50.83
Pt/CNT1	PtIr/CNT1	2.90~3.01	80.56~83.61
Pt/pCNT2	PtIr/pCNT2	6.04~6.88	167.78~191.11
Pt/oCNT1	PtIr/oCNT1	2.86~3.03	79.44~84.17

Chen, G., Delafuente, D. A., Sarangapani, S. and Mallouk, T. E. (2001) *Catalysis Today*, 67, 341-355.

Deivaraj, T. C. and Lee, J. Y. (2005) *Journal of Power Sources*, 142, 43-49.

Are gold aerosols superior to other types of gold particles for seeding of semiconductor nanowires?

M. E. Messing, K. Hillerich, J. Bolinsson, K. A. Dick, K. Nilsson, J. Johansson and K. Deppert

Solid State Physics, Lund University, Box 118, S-221 00 Lund, Sweden

Electronic devices are soon reaching the physical limits of miniaturization and hence new concepts must be developed. To facilitate further down-scaling of devices one-dimensional semiconductor nanowires is a promising technology [Thelander et al., 2006]. Their unique properties compared to their bulk counterparts, i.e. a large surface-to-volume ratio and quantum confinement effects, make them highly promising for use in device applications. Several electronic and optoelectronic devices have already been demonstrated, including biosensors, light emitting diodes, solar cells, and wrap gate field-effect transistors. However, before nanowire devices can be used for industrial large-scale production a number of issues remain to be solved. One of the most important concerns nanowire syntheses. A complete control over crystal quality, growth rate, and doping levels need to be obtained.

The most common approach to fabricate perfect nanowires, a bottom up method, uses self assembly to build up the structure atom by atom. To initiate the epitaxial growth of a highly perfect ordered nanowire a nanometer-sized metal seed particle, usually gold, is used. The diameter of the seed particle determines the diameter of the nanowire. Many different types of gold particles have been used to initiate nanowire growth. The most common ones are particles made from thin films, colloidal particles, lithographically defined particles, and aerosol particles. In this work we investigate whether aerosol particles are superior to these other common particles used, for seeding growth of epitaxial nanowires. In addition we compare the effect of aerosol particles produced with two different methods on nanowire growth.

Agglomerate aerosol gold particles were produced both by the evaporation/condensation method and by spark discharge between two gold electrodes. In either case the generated agglomerate particles were fed into an aerosol nanoparticle system to enable reshaping of the agglomerate particles and controlled depositions of the produced particles. This system includes a neutralizer, a tandem-DMA setup for size selection and size distribution measurements, a compaction furnace for reshaping of the particles and an electrostatic precipitator for deposition of the particles. The as-produced particles are crystalline, have a high purity, and were deposited onto substrates with high control of diameter and surface number concentration. Furthermore, commercially available colloid particles with a given diameter were deposited onto substrates using two different methods. In the first method a droplet of colloid solution was placed on the substrate followed by the use of a spinner to evenly distribute the particles over the substrate surface. In the second method an electrospray setup, including an electrostatic precipitator, was used to obtain a higher control of the number concentration and coverage of the deposited colloids. Electron beam lithography (EBL) was used to produce gold particles of a given diameter and surface density at an exact location on the substrate. The ability to precisely control were the particles are deposited are beneficial, but the EBL method is much more time consuming compared to the aerosol methods. Finally a 1 nm thin gold film was evaporated onto substrates and by heating at 650^oC for six minutes, particles were formed.

From scanning electron microscopy (SEM) investigations of the deposited particles it is clear that the aerosol particles offer advantages compared to both the colloidal particles and the thin film particles. For the colloids it is not possible to obtain the same control of surface number concentration as for the aerosols. In addition, the particles are surrounded by residues from the solution, something that introduce contaminations that possibly affect the nanowire growth. Regarding the particles made from thin films not only is the surface number concentration uncontrollable, the control of particle diameter is lost as well.

Semiconductor nanowires seeded from the different types of particles were grown by metal organic vapor phase epitaxy (MOVPE). Growth was carried out at three different temperatures for at least five different times at each temperature. Analysis of nanowire growth rates were performed by measuring the lengths of at least 100 wires on each sample from high resolution SEM images. From this analysis it can be seen that the aerosol particles have a shorter nucleation time, i.e. the time it takes before the wires start to grow, compared to the EBL particles, something that might be advantageous. Moreover there seem to be a difference in nucleation time between the two different types of aerosol particles.

Thelander C et al., (2006), *Mater. Today*, 9, 28-35

Rapid Aerosol Deposition of Super-hydrophilic Coatings

Antonio Tricoli, Marco Righettoni and Sotiris E. Pratsinis

Particle Technology Laboratory, ETH Zurich, CH-8092 Zurich, Switzerland, tricoli@ptl.mavt.ethz.ch, tel: +41 44 632 8503, fax: +41 44 632 1595

Keywords: Super-hydrophilic, coatings, SiO_2, TiO_2, Flame Synthesis and Deposition

Utilization of nanostructured materials in surface engineering has enabled several new functionalities for standard products such as anti-fogging (super-hydrophilic) (Ogawa et al., 2003), anti-reflection (Zhang et al., 2006) and self-cleaning (Wu et al., 2007) glasses and mirrors. While a wide number of processes can be utilized to obtain each of these functionalities, new challenges arise during their scale-up. In fact, several of the published patents and studies are based on multi-steps, wet-phase methods which require long time or high costs. Therefore, the development of these new technologies has been limited to few applications and countries.

Morphology and chemical composition of these nanoparticles coatings are the main parameters controlling their functionalities. Flame reactors offer several parameters to control each of these properties and achieve innovative, time saving solutions. Nevertheless several of these parameters such a precursor concentrations and composition, deposition time and distance, temperature of the substrate and in situ stabilization require to be tailored to the final products requirements.

To create super-hydrophilic surfaces, two basic approaches have been explored. The first involves the use of photochemically active materials such as TiO_2. Recently, ultraviolet (UV) irradiation on titania has been found to induce a highly hydrophilic surface with a 0° contact angle for both water and oily liquid. The contact angle is switchable between 0° (after UV irradiation) and 50-60° (after exposure to visible light or storage in the dark) (Stevens et al., 2003). The TiO_2 thin film is transparent, making it possible to be used for glass coating. Other applications requiring transparency include self-cleaning and anti-fogging materials used in cars, buildings, and household glazing. The second case involves the use of textured surfaces to promote super-wetting behavior (Cebeci et al., 2006).

Here, Flame Spray Pyrolysis has been used to rapidly deposit super-hydrophilic coatings on glass surfaces. The materials utilized were TiO_2 and SiO_2 compounds and mixed solution in order to increase both hydrophilic and catalytic properties of the coatings. All materials showed, already after 20 seconds deposition, super-hydrophilic behavior under normal solar irradiation. However TiO_2 did not preserve the super-hydrophilic properties without UV irradiation. In contrast silica doped titania maintained the super-hydrophilic behavior also without UV irradiation. The mechanical stability of all the coatings was improved by in situ annealing. The coating stability and wetting features have been characterized as a function of deposition time (thickness and surface coverage) for each material and correlated to their super-hydrophilic performance. Transmittance analysis of the coated glasses showed completely transparency. Flame route represent a very rapid way to deposit stable super-hydrophilic coatings onto glass surface with very low costs and amount of materials.
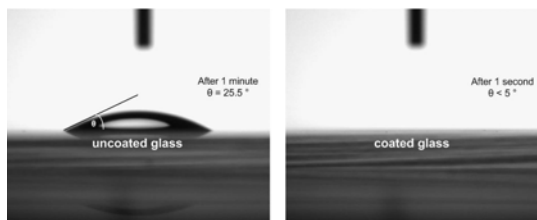
Figure 1: Contact angle measurement of uncoated glass (a) and 0° contact angle of coated glass after 1 s (b).

References

Cebeci, F. C., Wu, Z. Z., Zhai, L., Cohen, R. E., Rubner, M. F. (2006) *Langmuir*, 22, 2856-2862.

Ogawa, T., Murata, N., Yamazaki, S. (2003) *Journal of Sol-Gel Science and Technology*, 27, 237-238.

Stevens, N., Priest, C. I., Sedev, R., Ralston, J. (2003) *Langmuir*, 19, 3272-3275.

Wu, Z., Lee, D., Rubner, M. F., Cohen, R. E. (2007) *Small*, 3, 1445-1451.

Zhang, X. T., Fujishima, A., Jin, M., Emeline, A. V., Murakami, T. (2006) *Journal of Physical Chemistry B*, 110, 25142-25148.

Application of magnetic cobalt nanoparticles to enhance permeability of metal-polymer composite substrates

P. Koskela[1], U. Tapper[1], A. Auvinen[1], J. Jokiniemi[1,2], A. Alastalo[1], H. Seppä[1], M. Aronniemi[1], M. Teirikangas[3], J. Juuti[3] and H. Jantunen[3]

[1]VTT Technical Research Centre of Finland, P.O. Box 1000, 02044 VTT, Espoo, Finland
[2]Department of Environmental Science, University of Kuopio, P.O. Box 1627, FI-70211 Kuopio, Finland
[3]Department of Electrical and Information Engineering, EMPART Research Group of Infotech Oulu, University of Oulu, P.O. Box 4500, FI-90014 University of Oulu, Finland

Keywords: nanoparticles, magnetic nanoparticles, nanocomposites, metal nanocomposite.

High throughput printing techniques offers direct patterning and reduced material and processing costs compared to silicon technology. For example radio-frequency identification (RFID) and security codes are expected to be among the first commercially viable applications of printed electronics. To enable their sophisticated proof-of-concept structures thermoplastic magnetic substrates and magnetic inks need to be developed.

The objectives of this work were synthesis of separated magnetic nanoparticles and their influence in permeability in thermoplastic substrate as a embedded inclusions. Furthermore, expected magnetic properties as a function of filler loading were evaluated by reluctance and Bruggeman theory.

Altogether 50 g of Co nanoparticles were produced by hydrogen (H_2/N_2 23 %) reduction of cobalt chloride at the temperature of 950 $^{\circ}$C (Forsman et al. 2008). Fourier transformation infrared spectroscopy was used to monitor concentrations of reaction product HCl and gas phase impurities. Mass concentration of particles determined with filter samplings was 17 g/m^3. The number size distribution of the primary particles was determined with TEM analysis to be normal with median diameter of 76 nm and standard deviation of 20 nm.

To enable material characterisation and magnetic substrates for further testing metal-polymer composite with 5 vol.% of Co nanoparticles in a thermoplastic polymer ER182 matrix (NOF Corporation, Japan) were compounded using mixing extruder. Furthermore the samples were made by injection moulding system, details are reported elsewhere (Hu et al. 2007). The microstructure was checked by FESEM (Zeiss ULTRA plus, Germany) verifying homogenous distribution of the Co inclusions. Majority of the particles were separated but also some short particle chains were observed. Magnetic properties of the composite were analyzed with Agilent E4991A RF Impedance/Material analyzer (Agilent Technologies Inc., USA) at 1 GHz.

A simple model was developed for the effective relative permeability μ_r^{eff} of the composite substrate. The model is based on equivalence of magnetic (reluctance) and electric (resistance) circuits. The model assumes periodically distributed cubic non-interacting nanoparticles. This model is compared with the well-known Bruggeman's effective medium theory (Starostenko et al.; Ramprasad et al. 2004).
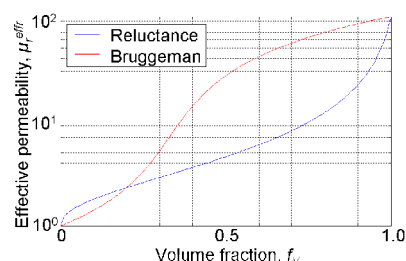
Fig. 1. Effective relative permeability as a function of nanoparticle volume fraction by the two theories. Here $\mu_r = 100$ for Co and $\mu_r = 1$ for the polymer.

In Fig. 1 the two theories are compared and for small volume fractions the reluctance theory becomes close to the Bruggeman theory, as expected, but for large volume fractions models exhibit a significant discrepancies. For the fabricated composites the reluctance theory gives $\mu_r^{eff} = 1.62$ and the Bruggeman's theory 1.24 while the measured permeability was about 1.20, thus close to Bruggeman's prediction. However, taking demagnetization into account also the reluctance theory can be fitted to experiments by assuming that the particles are agglomerated with an average agglomerate aspect ratio of 2. Moreover, magnetic losses can be included in the models by using complex permeabilities.

Forsman, J., Tapper, U., Auvinen, A., & Jokiniemi, J. (2008). *J. Nanopart. Res.*, 10, 745-759.

Rozanov, K., Osipov, A., Petrov, D., Starostenko, S., & Yelsukov, E. (2009) *J. Magn. Magn. Mater.*, doi:10.1016/j.jmmm.2008.11.039.

Ramprasad, R., Zurcher, P., Petras, M., Miller, M., & Renaud, P. (2004) *J. Applied Phys.*, 96, 519-529.

Hu, T., Juuti, J., Jantunen, H., & Vilkman, T. (2007) *J. Eur. Ceram. Soc.*, 27, 3997-4001.

Surface Processing of Aerosol Nanoparticles for Materials Applications: Growth of Organic Monolayers and Multilayers on Nanoparticle Silicon

J.T Roberts[1], S. Calder[1] and J. Holm[2]

[1]Department of Chemistry, University of Minnesota, Minneapolis, MN, 55455, USA
[2]Department of Mechanical Engineering, University of Minnesota, Minneapolis, MN, 55455 USA

For nanoparticles to be components of new materials and devices, methods must be developed to control their surface properties. Much of the research has focused on solution-based chemical processing. However, solution-based methods have numerous disadvantages from both engineering and environmental perspectives. This presentation will discuss recent progress in the development of thermal and photochemical methods for functionalizing and passivating the surfaces of aerosol nanoparticles. Aerosol-based processing circumvents some of the problems that are inherent in solution synthesis. It also provides routes to novel materials, including hybrid core-shell structures that would be difficult to synthesize otherwise.

This presentation will describe recent progress in the deposition of organic monolayers and multilayers on Si nanoparticles that had been produced in a low-pressure RF plasma. In one set of experiments, isotopic labeling techniques were employed to study the mechanism of hydrosilylation on hydrogen- and deuterium-terminated silicon nanoparticles. Fresh, unoxidized particles were reacted with 1,3,5-trimethylbenzene [$C_6H_3(CH_3)_3$], 1-dodecene [$CH_2=CH-(CH_2)_9-CH_3$], and mixtures of mesitylene and 1-dodecene. Fourier transform infrared (FTIR) spectra (Fig. 1) of particles that were reacted with 1-dodecene and mesitylene / 1-dodecene showed strong evidence of CD bond formation, while those particles refluxed in neat mesitylene did not. Careful analysis of the Si-H stretching / D-D stretching region between 2000 and 2300 cm^{-1}, including spectra obtained as a function ambient aging for up to two months, definitively establish new C-D bond formation. These results are consistent with a radical chain mechanism for hydrosilylation. They provide the first incontrovertible evidence, in any system involving solid silicon, of surface hydrosilylation.

In another set of measuremnts, photo-assisted chemical vapor deposition, driven by ultraviolet radiation from mercury vapor lamps, was used to activate methyl methacrylate [$CH_2=C(CH_3)CO_2CH_3$, MMA], resulting in the growth of coatings on silicon nanoparticles. Initial work has established, using FTIR and transmission electron microscopy (TEM), that particles are uniformly coated by an organic layer, presumably polymethyl methacrylate (poly-MMA). We have also established the ranges of flow rates and light fluence that lead to uniform coatings without homogeneous nucleation poly-MMA particles. Further work will address the kinetics of coating formation, the chemical composition of the coating, and the extent to which poly-MMA coatings perturb nanoparticle chemical and photophysical properties. Preliminary work suggests that particles coated with poly-MMA are strongly resistant to oxidation relative to uncoated particles.
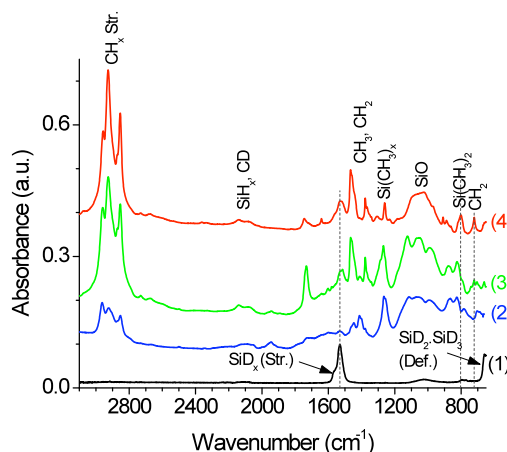
Figure 1. Representative FTIR spectra of deuterium-terminated particles: (1) untreated, (2) reacted in neat mesitylene, (3) reacted with 1-dodecene / mesitylene, and (4) reacted with neat 1-dodecene.

Experimental and Numerical Study of Gasdynamically Induced Particle Synthesis

V. Goertz[1], N.S. Al-Hasan[2], M. Dannehl[3], M.Roeck[3], A. Maisels[3], H. Nirschl[1] and G.H. Schnerr[2]

[1]Institut f. Mechanische Verfahrenstechnik u. Mechanik, Universität Karlsruhe (TH), 76131 Karlsruhe, Germany
[2]FLM - Fachgebiet Gasdynamik, Technische Universität München, 85747 Garching, Germany
[3]Evonik Degussa GmbH, Rodenbacher Chaussee 4, 63457 Hanau-Wolfgang, Germany

Keywords: Generation of Nanoparticles, Nanoparticles, Numerical Simulation, Particle Sampling, SiO_2

Recently, an innovative concept of high throughput gas phase particle reactor has been proposed (Dannehl *et al.*, 2007). The initiation of the chemical reaction is realized by a stationary shock system. The quenching of the high-temperature gas flow is achieved by gas-dynamic quenching i.e. accelerating the flow from subsonic to supersonic speed which decreases the static temperature below the sinter temperature. Because of a homogeneous flow field and high heating and quenching rates narrow size distribution with low aggregation are achieved (Grzona *et. al.*, 2007). Therefore, this method is a high potential alternative to the flame and hot-wall synthesis.

An important aspect of the novel reactor is the characterization of the particles during their formation and growth as well as the end product. In order to describe particle dynamics, samples are taken at different positions in the reactor, i.e. in the reaction chamber and downstream of the quenching.
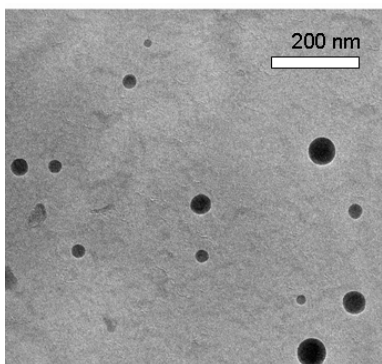
Figure 1. TEM image of SiO_2 particles which were produced in the novel reactor. The sample was extracted downstream of the quenching process.

A particle sample is extracted from the reaction chamber by a water-cooled sampling probe. Since the nanoparticles are not affected by inertia forces ($d_P < 1 \cdot 10^{-7}$ m), an isokinetic sampling is not necessary. Nitrogen is used to dilute the sample at the entrance of the probe. Thus, fast quenching of the sample is possible and chemical reactions as well as particle coagulation are stopped immediately.

Due to the geometry of the reactor and of the sampling probe, it is not possible to exhaust the sample directly in flow direction. However, to avoid extracting particles from the stagnation region of the sampling probe or from the recirculation area behind the probe, the sampling is numerically simulated.

Based on the simulation results the geometry of the sampling probe and the integration in the reactor are adjusted to ensure the particle sampling from the undisturbed flow in the reactor.

Numerical simulations are also used to calculate the particle coagulation inside the sampling probe. The simulations show that due to the short residence time coagulation can be neglected.

The quenching process suppresses the particle growth instantaneously. By taking a sample at this position the influence of the quenching process on the particle morphology can be examined. Since the temperature is lower than the SiO_2 sintering temperature, the sample need not to be frozen at the entrance of the probe. Instead of that the probe must be insulated and heated to avoid condensation of the water vapour of the carrier gas. The extracted particles are separated on a filter. TEM analysis is used to study particle morphology at different stages of production process.

Fig. 1 demonstrates an example TEM-micrograph of the product which was extracted downstream of the quenching system ($\dot{m}_{total} = 90$ g/s; $\dot{m}_{precursor} = 0.14$ g/s, $p_{01} = 10$ bar, $T_{01} = 1450$ K). Even though particle sizes are strongly dissimilar (10-100 nm), the nearly spherical particle shape throughout the sample is remarkable. Though more detailed studies are needed, CFD-simulations with an implemented bimodal particle model accurately predict the mean diameter of the particles (Al-Hasan *et al.*, 2009).

The further analysis of application-relevant properties of the final product is carried out on comparative basis. For this purpose, gasdynamically synthesized particles are compared with commercial fumed silica (AEROSIL ®) with respect to their rheological activity, optical and reinforcement properties

Al-Hasan, N.S. et al. (2009). *EAC 2009*, Karlsruhe.
Dannehl, M. *et al. EAC 2007*, Salzburg, Abstract T09A039.
Grzona, A. et. al. (2007). *Proceedings 26th International Symposium on Shock Waves (ISSW26)*, 15.-20. Juli 2007, Göttingen.

Design of in-situ coating of aerosols: Efficiency, thickness & texture

B. Buesser and S.E. Pratsinis

Particle Technology Laboratory, Institute of Process Engineering,
Department of Mechanical and Process Engineering, ETH Zürich, 8092 Zürich, Switzerland

Keywords: modelling, nanoparticles, coatings, combustion synthesis, sintering

Particles are coated to make them compatible to their host matrices. With such core-shell particles, desirable properties of core (e.g. dielectric, scattering or opacifying performance) particles are conserved while modifying their surface by the shell material.

Aerosol coating is attractive as it contributes to gas-phase synthesis of functionalized nanoparticles in one-step facilitating their economic manufacture. Here aerosol coating of TiO_2 particles with SiO_2 films is investigated theoretically, accounting for SiO_2 monomer generation, coagulation and sintering. At industrial scale manufacture of nanoparticles, such aerosols can encounter high concentration dynamics resulting in much faster growth kinetics and even gelation (Buesser *et al.*, 2009). The evolution of the SiO_2 coating particle population is simulated distinguishing a fine and a coarse mode. The fine mode deposits fast onto TiO_2 particles forming a rather smooth coating while the coarse deposits further downstream and may contribute to rough coatings depending on SiO_2 sintering kinetics (Teleki *et al.*, 2005).

Coating starts by injecting vapor of HMDSO (hexamethyldisiloxane) after the TiO_2 particles have reached their optimal primary particle size that no longer changes by sintering (Teleki *et al.*, 2009). That way TiO_2 primary particles and aggregates have attained a self-preserving distribution that can be represented by a single size facilitating the simulations. Sintering may take place on the surface of TiO_2 particles and transform rough into smooth coatings depending on process conditions.

Figure 1 shows the modeled pathways of coating. The flame-made, uncoated core particles, N_c, (white) enter the reactor at the bottom, followed by injection of the coating film precursor vapor, C, through a torus ring, generating coating monomers (black), N_{f1}, by oxidation in gas-phase. Monomers coagulating with core particles create smooth coating films, V_s, on the core particles. Further, monomers grow by coagulation and sintering to coating particles, N_{f2}, which create rough coating films, V_r, by coagulation with core particles. Rough coatings are transformed to smooth ones by sintering.

The aerosol coating model is combined with computational fluid dynamics (CFD) to account for gas phase reaction of the coating precursor vapor, flow and temperature fields defining the aerosol mixing inside of the coating reactor (Teleki *et al.*, 2009). The influence of TiO_2 particle size and concentration, process temperature, cooling rate, mixing time and HMDSO precursor concentration on SiO_2 coating thickness and texture are investigated.

Especially the evolution of SiO_2 coating thickness and surface area of the rough SiO_2 coating on the TiO_2 core particles surface are discussed. The simulations are compared to data of nanothin SiO_2-coated flame-made rutile TiO_2 particles.
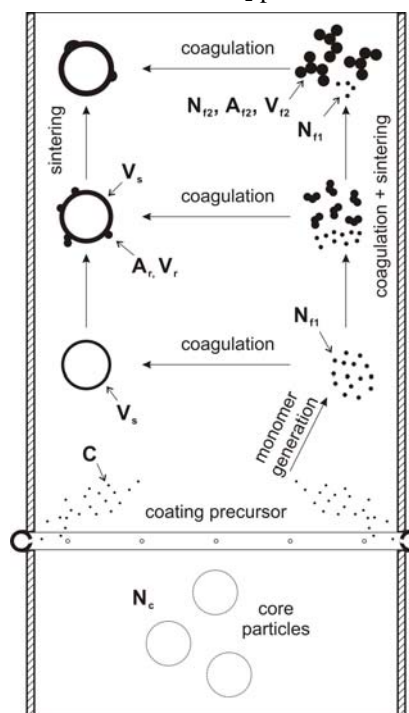
Figure 1. Schematic of the modeled pathways of aerosol coating processes.

Buesser, B., Heine, M.C., Pratsinis, S.E (2009), "Coagulation of highly concentrated aerosols" *J. Aerosol Sci.*, **40**, 89-100

Teleki, A., Pratsinis, S. E., Wegner, K., Jossen R. & Krumeich, F. (2005), "Flame-coating of titania particles with silica" *J. Mater. Res.,* **20**, 1336-1347.

Teleki, A., Buesser, B., Heine, M. C., Krumeich, F., Akhtar, M. K. & Pratsinis, S. E. (2009), "Role of gas-aerosol mixing during in situ coating of flame-made titania particles" *Ind. Eng. Chem. Res.*, **48**, 85-92.

CO₂ CW laser-driven reactions in pure acetylene flow for generation of nanoparticles

P.V. Pikhitsa, D. Kim and M. Choi

National CRI Center for Nano Particle Control, Institute of Advanced, Machinery and Design, School of Mechanical and Aerospace Engineering, Seoul National University, 151-742, Seoul, Korea

Keywords: black carbon, generation of nanoparticles, laser pyrolysis.

It was reported (Choi *et al.*, 2004) that pure acetylene flow inside a diffusion O_2/H_2 flame generated carbon shell-shaped nanoparticles when irradiated with a CO₂ CW laser. We show that the infrared multi-photon absorption of feedback intermediates generated in pure acetylene flow (no O_2/H_2 flame) provides self-sustained conditions where polyatomic molecules (ethylene, vinylidene), excited to the electronic energies, decompose to carbon dimers and excited molecular and atomic hydrogen through 1,2 H-elimination. The latter associates with downstream acetylene to reproduce those absorbing intermediates thus making the reactions self-sustained. A theoretical description of the process is given and compared to experiment where CO₂ CW laser is applied to pure acetylene flow shielded from air by nitrogen or argon (Fig. 1). Possible thermal acetylene decomposition and surface reactions are ignored.

The simplified reaction scheme can be the following:

$$C_2H_2 + H_2^* \rightarrow C_2H_4^*. \quad (1)$$
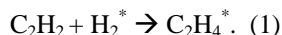
This addition reaction occurs with the rate an where a is the rate constant and n is the acetylene concentration. Then C_2H_4 decomposes under the CO₂ laser irradiation into $CH_2=C: +H_2$ and further vinylidene decomposes into C_2 and H_2 as was described in (Chekalin *et al.*, 1979). Thus the parent H_2 molecule produces two molecules in the branching:

$$C_2H_4^* + h\nu \rightarrow C_2 + 2H_2^*. \quad (2)$$
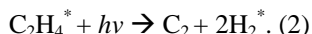
A system of differential equations that follows from (1) and (2) predicts a critical behaviour with the critical gas velocity v_c that can terminate the reaction even at arbitrary high laser power (Fig. 1). There are three relevant parameters: gas velocity v, acetylene dilution ratio x, and laser power w. The exact solution of the corresponding equations gives the relative position Z of the reaction zone to be compared with experiment (Fig. 2). We obtained for Z:

$$Z = Z_0 - (2D/v_c) \ln[2(1-v/v_c)], \quad (3)$$

where D is the hydrogen diffusion coefficient and n_0 is the concentration of pure acetylene; $v_c = 2(Dan_0x)^{1/2}$. Fitting the experimental dependency of Z on gas velocity at different dilutions (not shown) gives an accurate determination of $D = 3.57$ cm²/s and $an_0 = 770$ s⁻¹. At dilution $x=0.6$ $v_c = 81.2$ cm/s. Reasonable values for these parameters support the mechanism for the acetylene conversion to carbon through laser absorbing gaseous intermediates.
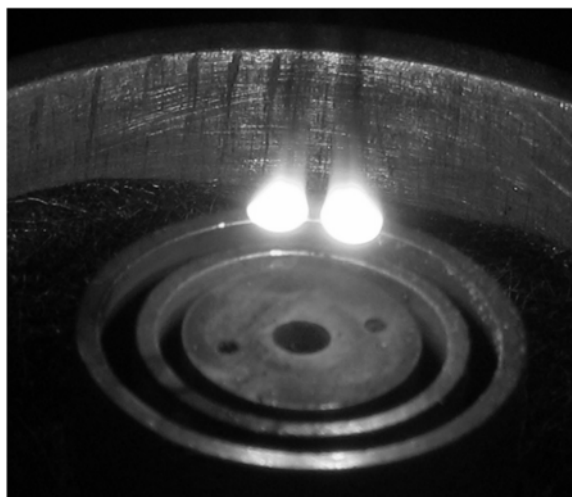
Figure 1. The splitting of the reaction zone of acetylene conversion into carbon in the CO₂ CW laser at high acetylene flow rates. Two streams of carbon nanoparticles are seen. There is no reaction in the centre when the velocity is above the critical v_c.
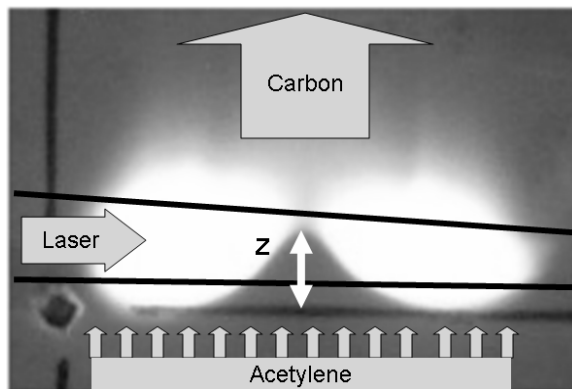
Figure 2. The evolution of the reaction zone. Z is the position of the reaction depending on the gas velocity in the centre. Convergent lines mark the laser beam geometry.

Choi, M. *et al.*, (2004). *Adv. Mater.* 16, 1721-1725.
Chekalin, N. V., Letokhov, V. S., Lokhman, V. N. & A. N. Shibanov, (1979) *Chem. Physics,* 36, 415-421.

Gas Phase Synthesis of Iron Carbide Nanoparticles for Large Scale Magnetic Separations

I. K. Herrmann[1], R. N. Grass[1] and W. J. Stark[1]

[1]Department of Chemistry and Applied Biosciences, Swiss Federal Institute of Technology (ETH Zurich), Wolfgang-Pauli-Str. 10, HCI E 107, ETH Hönggerberg, Zurich 8093, Switzerland

Keywords: Core-shell nanoparticle, Flame spray synthesis, Metal nanoparticles, Magnetic nanoparticles

Nanomagnets are of great interest for a wide variety of applications ranging from magnetic fluids, data storage, and environmental remediation to medicinal imaging and drug delivery. The rapidly growing applications of nanomagnets draw more and more attention to a cost-effective large scale synthesis method for nanomagnets. A great number of suitable methods for the synthesis of magnetic nanoparticles of different compositions and phases, having distinct magnetic properties, has been developed. Nanomagnets with optimal magnetic properties for above applications can be obtained by the use of metals (Co, Fe, saturation magnetization $M_{s, bulk} \leq$ 220 emu g^{-1}) or metal alloys (CoFe, CoNiFe, $M_{s, bulk} \leq$ 245 emu g^{-1}). However, naked metallic nanoparticles are chemically highly active (typically pyrophoric) and are readily oxidized upon contact with air, generally resulting in loss of magnetism and dispersibility. Up to now, this has promoted the widespread use of moderately magnetic oxide nanoparticles, such as magnetite ($M_{s, bulk} \leq 92$ emu g^{-1}).

In this work we show the production of a palette of iron-based nanoparticles, ranging from iron carbide to metallic iron ending up at iron oxide, by a flame spray synthesis process. The herein described process has substantial similarity to the well-established industrial flame spray pyrolysis process, making it particularly suitable for large scale productions of nanoparticles. Grass et al. (2007) and Athanassiou et al. (2007) recently demonstrated how suitable modifications of the conventional flame spray process give access to the preparation of a much broader range of products, including metallic nanomagnets and metal alloy nanoparticles.

The reducing flame spray synthesis setup allows the continuous production of carbon coated iron carbide particles with a mean diameter of 30 nm at a production rate of > 20 g h^{-1}. The carbon-encapsulated iron carbide (Fe_3C/C) nanoparticles have an exceptionally high saturation magnetization of 140 emu g^{-1} and are highly air stable (up to 200°C).
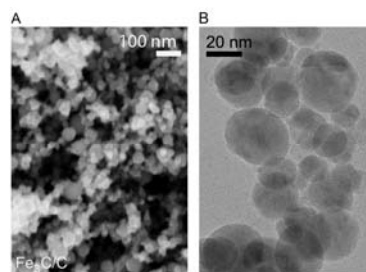
Figure 1. Scanning Electron Micrograph (A) and Transmission Electron Micrograph (B) of carbon encapsulated iron carbide nanomagnets.

Additionally, the carbon surface of these iron carbide nanomagnets could be covalently functionalized with various linkers by following the procedures initially described by Grass et al. (2007) for carbon coated cobalt nanoparticles.
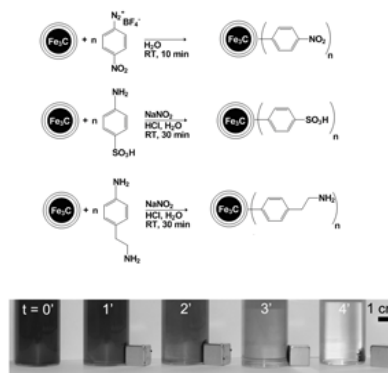
Figure 2. Covalent functionalization of nanomagnets (top) and magnetic recovery of the nanomagnets form aqueous suspension (bottom).

The high saturation magnetization, thermal and chemical stability, low raw material costs, and the efficient synthesis process make the herein described carbon encapsulated iron carbide nanoparticles an attractive low cost alternative for currently applied nanomagnets.

Grass R. N., Athanassiou E.K., Stark W.J., (2007), *Angew. Chem. Int. Ed.*, 46, 4909-12.
Athanassiou E.K., Grass R.N., Osterwalder N., Stark W.J., (2007) , *Chem. Mater.*, 19 (20), 4847-53.

Synthesis of silica nanoparticles in a hybrid microwave-plasma hot-wall reactor under well-controlled conditions

A. Abdali[1], B. Moritz[1], A. Gupta[1], H. Wiggers[1,2], C. Schulz[1,2]

[1]IVG, University of Duisburg-Essen, 47055 Duisburg, Germany
[2]CeNIDE, Center for Nanointegration Duisburg-Essen, 47055 Duisburg, Germany

Keywords: Microwave-plasma reactor, TEOS, SiO_2, nanoparticles characterization, particle growth

Silica nanoparticles have a large range of practical applications. They are widely used as fillers in plastics and coatings to improve material properties such as hardness and thermal stability. Especially applications with a demand for high transparency require silica particles with a specific size, morphology, and surface coating. Therefore, the synthesis of particles with highly-defined particle-size distributions is desired. Most of the silica powder worldwide is produced by gas-phase processes such as flame reactors. However, these methods require exact knowledge of the kinetics of precursor decomposition, particle formation and particle growth. Tetra-ethoxysilane (TEOS) as a halide-free and inexpensive precursor material is subject to growing interest for particle formation from the gas-phase.

A microwave-induced plasma reactor combined with a hot-wall furnace has been constructed for gas-phase synthesis of high-purity silica nanoparticles. The microwave heats the injected gas mixture including TEOS vapor within few microseconds. This initiates the chemical reactions of the precursor decomposition which is then followed by particle formation. The hot-wall furnace allows to achieve longer and variable residence times at high temperature which allows further particle growth such as coalescence, agglomeration as well as sintering of particle agglomerates. The combined use of a plasma and hot-wall reactor allows studying particle growth in detail. Information about the growth kinetics can then be used for the reactor design. The plasma reactor can be initiated and the plasma can be maintained using precursor gaseous TEOS in the presence of O_2 and Ar or N_2. In order to obtain reproducible synthesis conditions the current apparatus has been designed to allow the control of gas flow rates, gas composition, pressure and temperature of the hot-wall furnace.

Particle sizes, shapes and morphologies have been characterized by transmission electron microscopy (TEM). For TEM measurements, the sample was collected through thermophoretic deposition of nanoparticles inside the reaction chamber. TEM results reveal that particles are spherical in shape with a high degree of agglomeration. The size of the primary silica nanoparticles was modified by varying the process parameters, such as TEOS concentration,

reactor pressure, residence time and the furnace temperature. With TEOS concentration of 1.2% by mass, reactor pressure of 40 mbar and the furnace temperature of 800°C, the particles with mean diameter of 9.8 nm were synthesized. The mean particle size was found to increase linearly with increasing the reactor pressure (fig. 1). The degree of agglomeration depends very strongly on the furnace temperature and the resident time. The maximum degree of agglomeration was observed at 400°C while varying the furnace temperature from 200°C to 1000°C. An additional ex-situ analysis was carried out by means of isothermal Brunauer-Emmett-Teller (BET) adsorption. The primary average BET particle diameter was calculated from the determined powder surface area.
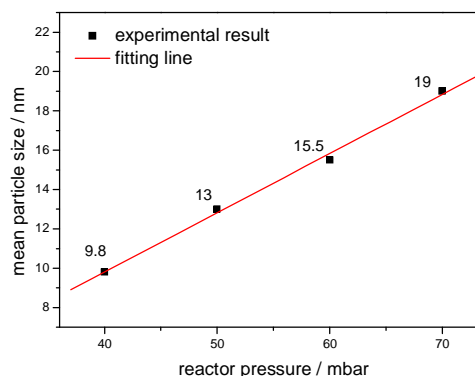
Figure 1. Influence of reactor pressure on the particle size at 800°C furnace temperature

Mueller, R., Kammler, H. K., Pratsinis, S. E., Vital, A., Beaucage, G., Burtscher, P. (2004). *Powder Technology*, 140, 40-48

Gutsch, A., Mühlenweg, H., Krämer, M. (2005). *Small* 1, 30.

Hermetically-coated superparamagnetic Fe_2O_3 particles with SiO_2 nanofilms

A. Teleki[1], M. Suter[2], P.R. Kidambi[1], O. Ergeneman[3], F. Krumeich[1], B.J. Nelson and S.E. Pratsinis[1]

[1]Particle Technology Laboratory, [2]Micro- and Nanosystems, [3]Institute of Robotics and Intelligent Systems, Department of Mechanical and Process Engineering, ETH Zurich, Sonneggstrasse 3, CH-8092 Zurich, Switzerland

Keywords: nanoparticles, oxides, flame spray pyrolysis, core-shell nanoparticle.

Magnetic nanoparticles are frequently coated with SiO_2 to improve their functionality and bio-compatibility in a range of biomedical and polymer nanocomposite applications (Gupta & Gupta, 2005). Silica is stable in aqueous conditions and prevents magnetically-induced self-agglomeration of magnetic cores. Silanol groups on the silica surface react with alcohols and silane coupling agents to produce stable dispersions in non-aqueous solvents and can be further modified by covalent bonding of specific ligands. Furthermore, silica-coated or -embedded γ-Fe_2O_3 (maghemite) nanoparticles exhibit improved thermal stability. Typically iron oxide nanoparticles are coated with SiO_2 by a sol-gel process that involves several steps, similar to the SiO_2-coating of pigmentary titania. Co-oxidized, flame-made SiO_2/Fe_2O_3 particles typically consist of several, small maghemite nanoparticles embedded in larger silica particles or aggregates (Li $et~al.$, 2006). The reduction of Fe_xO_y particle size by adding relatively large amounts of non-magnetic SiO_2 to ensure complete encapsulation significantly decreases the magnetic performance of these composite materials. Clearly, it is important to develop a scalable process for the synthesis of maghemite particles encapsulated by thin SiO_2 layers, thereby minimizing the non-magnetic silica content.

Thus, iron oxide nanoparticles were produced by FSP and the resulting aerosol was in-$situ$ coated with SiO_2 by oxidation of swirling HMDSO vapour (Teleki $et~al.$, 2008a). The process allows independent control of core Fe_2O_3 particle properties and the thickness of their silica coating film. The complete encapsulation of the core particles (22 nm) at > 12 wt% SiO_2 (Figure 1) was demonstrated by isopropanol chemisorption as had been developed for SiO_2-coated TiO_2 (Teleki $et~al.$, 2008b). The silica content in the product can be minimized to decrease the negative impact of silica on the saturation magnetization of γ-Fe_2O_3. The magnetization of flame-made nanoparticles was measured by a vibrating sample magnetometer at room temperature. The highest magnetization corresponds to pure Fe_2O_3, as expected. The addition of 23 – 46 wt% SiO_2 by FSP co-oxidation reduces the magnetization by the presence of silica, and by the reduction of Fe_2O_3 crystallite size for SiO_2/Fe_2O_3 particles. In contrast, the magnetization of 23 wt% SiO_2 in-$situ$ coated Fe_2O_3 is very close to pure Fe_2O_3 and higher than that of commercially available MagSilica. This demonstrates that Fe_2O_3 nanoparticles coated in-$situ$ by thin SiO_2 films retain most of their magnetic properties. The coercivity and remanence of all samples is low indicating superparamagnetism.

Also these particles exhibited excellent dispersibility compared to flame-made co-oxidized silica-iron oxide and commercially available particles. The low isoelectric point of SiO_2 facilitates the dispersion of such particles in aqueous solutions even in the absence of surfactants. A ferrofluid was prepared from 23 wt% SiO_2-coated Fe_2O_3 suspended in water and exposed to a magnetic field. The superparamagnetic properties can be observed as the fluid returns to the original state after removal of the magnet. Such suspensions can facilitate the contrast of MRI as they interact with external magnetic fields and can be positioned in a specific area. Thus, the FSP in-$situ$ coating process enables complete encapsulation of Fe_2O_3 nanoparticles at relatively low SiO_2 contents resulting in highly superparamagnetic Fe_2O_3 particles at reduced cost (as less Si is needed compared to co-oxidized products).
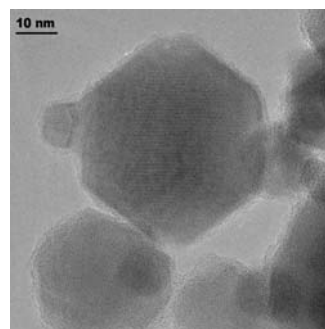
Figure 1. TEM image of γ-Fe_2O_3 in-$situ$ FSP-coated with 23 wt% SiO_2.

Gupta, A.K., & Gupta, M. (1975). $Biomaterials,$ 26, 3995-4021.

Li, D., Teoh, W.Y., Selomulya, C., Woodward, R.C., Amal, R., & Rosche, B. (2006). $Chem.~Mater.$, 18, 6403-6413.

Teleki, A., Heine, M.C., Krumeich, F., Akhtar, M.K. & Pratsinis, S.E. (2008a). $Langmuir$, 24, 12553-12558.

Teleki, A., Akhtar, M.K., & Pratsinis, S.E. (2008b). $J.~Mater.~Chem.$, 18, 3547-3555.

Experiments concerning gasdynamically induced nanoparticle synthesis

A. Grzona[1], A. Weiß[1], H. Olivier[1], T. Gawehn[2] and A. Gülhan[2]

[1]Shock Wave Laboratory, RWTH Aachen University, 52056, Aachen, Germany
[2]German Aerospace Center, Wind Tunnel Department, Linder Höhe, 51147 Cologne, Germany

Keywords: Nanoparticle production, Gasdynamic, Generation of nanoparticles, SiO_2

Recently a new pilot facility for the gas phase synthesis of narrow distributed and low aggregated silica nanoparticles has been established at Evonik Degussa in Hanau. The current work deals with first experiences operating the facility and describes experimental results for a variation of the basic parameters. Since previous work indicates that homogeneity of the flow field and the temperature profile as well as fast heating and quenching are of mayor importance for the particle size distribution the current facility is based on a new method to achieve these objectives (Grzona et al., 2007).

The gaseous precursor is injected in the converging part of a laval nozzle into a high-enthalpy gas flow with inlet conditions $p_0 = 10$ bar and $T_0 = 1450$ K. Downstream the injection the gas mixture is accelerated through the throat of the first nozzle (A_1* in Fig. 1) to supersonic flow conditions and afterwards quasi instantaneously heated by a system of shock waves. Numerical simulation by part of the project team (Al Hasan et al., 2009) predicts a heating time of 70 µs to ignition temperature of 1200 K. Following the initiation of the reaction, different molecular and intermolecular processes lead to the generation and growth of nanoparticles. After a defined reaction time, that is adjustable by varying the overall length of the reaction chamber, the expansion in a second supersonic nozzle with cross section A_2* rapidly cools the flow down to 600 K within 80 µs, which is below the sintering temperature. After this, the total enthalpy of the flow is reduced by water injection in the diverging part of the second nozzle. The quenching rate is fast enough to terminate all inter particle reactions.

In order to determine the particle quality and to describe the growing process, samples are extracted from the reaction chamber and downstream the quenching system by a particle sampling probe and are separated on a filter for detailed TEM analysis (Goertz et. al., 2009).

Figure 1 compares the experimentally measured static pressure distribution with numerical results. Overall agreement is good but the appropriate pressure distribution directly downstream the nozzle throat was not predicted by the simulation. The aberration may be due to slight imperfections in the geometry of the experimental facility. Additionally wall roughness and a complex high temperature sealing system inside the facility certainly influence the pressure distribution.
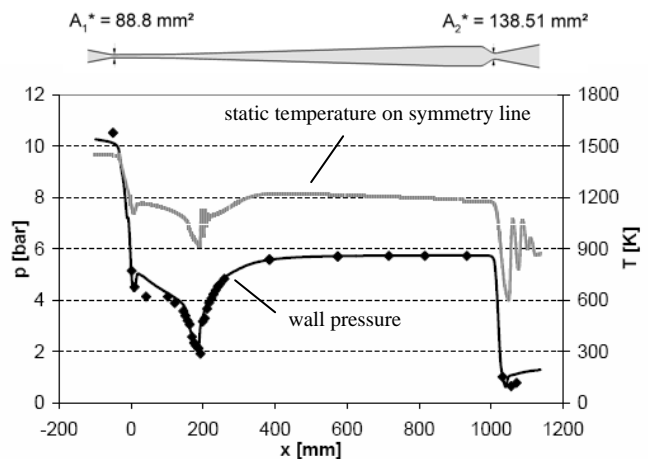
Figure 1. Reactor geometry and wall pressure and static temperature profile, solid lines numerical result

Position and shape of the shock system in the first nozzle have strong influence on the flow inside the reaction chamber. Main flow parameters like shock Mach number, mass flow of precursor and carrier gas as well as second nozzle throat diameter have been varied and their effect on the shock system has been investigated. Additionally theoretical considerations help to understand the occurring phenomena and accompany the improvement of flow conditions with existing models.

The produced particles show a remarkably spherical shape and low aggregation, but size distribution is so far relatively broad. The concept has proven to be a promising method for the production of high quality nanoparticles, but increasing the production rate is one main task of future work.

Grzona, A. et al. (2007). *Proceedings 26th International Symposium on Shock Waves (ISSW 26)*, 15.-20. Juli 2007, Göttingen
Goertz, V. et al. (2009). *EAC 2009*, Karlsruhe
Al-Hasan, N.S. et al. (2009). *EAC 2009*, Karlsruhe

Comparative SMPS-/TEM-analyses on laser-generated nanoparticle-aerosols

M. Pesch[1], J. Spielvogel[1], L. Keck[1], H.-D. Kurland[2], J. Grabow[2], I. Zink[2], G. Staupendahl[2] and F. A. Müller[2]

[1]GRIMM AEROSOL Technik GmbH & Co. KG, Dorfstraße 9, 83404 Ainring, Germany
[2]Friedrich-Schiller-University, Institute of Materials Science and Technology, Loebdergraben 32, 07743 Jena, Germany

Keywords: SMPS, TEM, nanoparticles generation, particle size distribution, agglomerates.

The laser vaporization (LAVA) technique is a highly versatile method for the generation of a multiplicity of nanoparticle-aerosols. In our special implementation (Staupendahl *et al.*, 2003) of this principle, coarse (µm…mm) starting powders are evaporated into a plasma in the focus of a CO_2 laser beam. Evaporation and plasma generation proceed in a continuously flowing condensation gas under atmospheric pressure. Due to the very steep temperature gradient between the hot evaporation zone and the surrounding atmosphere, nucleation, condensation, and coagulation are proceeding very fast, resulting in aerosols of ultrafine particles.

The LAVA process allows for the generation of a broad spectrum of various nanoparticle-aerosols whose properties can be controlled by its process parameters. These features qualify this process as basis for a versatile parametrizable generator for nanoparticle-aerosols. Therefore, the detailed knowledge of the size distribution dependency of the primary particles and their agglomerates on the process parameters is an important prerequisite.

These dependences have been determined mainly by statistical analyses of TEM (transmission electron microscopy) images. However, TEM analyses are extremely time-consuming and their statistical evidence can be unreliable. By contrast the scanning mobility particle sizer (SMPS) permits measurements of statistically reliable mobility diameter distributions in almost real-time. In order to use the SMPS system for the parameterization of the LAVA process and for different material classes the mobility diameter distributions have to be correlated with particle and agglomerate size distributions (Naumann, 2003) resulting from TEM analyses. This long-term objective in mind, first measurements with the GRIMM SMPS+C system compared to TEM analyses were accomplished for zirconia (ZrO_2) nanoparticle-aerosols. These were generated with pulsed CO_2 laser radiation (pulse frequency 100 Hz, pulse length 500 µs, average radiant power 200 W) in air as carrier gas. An additional jet of air (volume flow rates 0 m³/h, 2 m³/h, and 6 m³/h) was led through the condensation zone.

The results of both the SMPS measurements and the TEM analyses (see figure 1 and table 1) clearly indicate that with increasing flow rates the mobility diameters as well as the geometrical diameters of the primary particles are decreasing.

The systematic discrepancies between TEM and SMPS diameter distributions probably result from agglomerates being classified by the differential mobility analyzer (DMA) of the SMPS. Nevertheless depending on the gas volume flow rate the relative shifts of the SMPS distribution curves on one hand and of the TEM distribution curves on the other hand are similar (table 1). This might indicate a correlation between SMPS and TEM results with respect to particle size distributions in LAVA generated nanoparticle-aerosols.
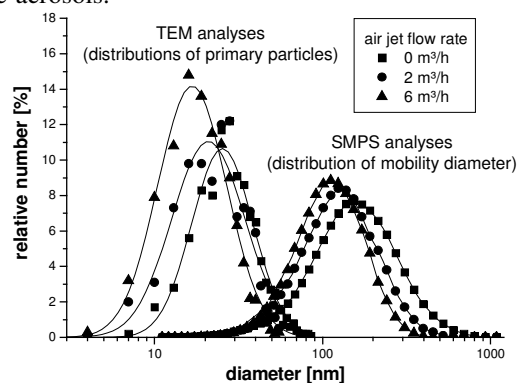
Figure 1. Distributions curves of primary particle sizes and mobility diameters.

In order to derivate a correlation function, which allows for the transfer of mobility diameter distributions into size distributions of primary particles and their agglomerates, these first comparative investigations have to be detailed and expanded on further process parameters as well as on additional material classes.

Table 1. Data of the distribution profiles: Full width at half maximum (fwhm), position of the maximum on the diameter scale (M), and relative shift ($\Delta M/M$) of the maximum position related to the maximum position without additional air jet.

	air jet flow rate	fwhm	maximum	relative shift
		[nm]	M [nm]	$\Delta M/M$ [%]
primary particle diameter	0 m³/h	26	25	-
	2 m³/h	26	20	17
	6 m³/h	20	17	32
mobility diameter	0 m³/h	218	156	-
	2 m³/h	158	131	16
	6 m³/h	130	113	27

Staupendahl, G., Kurland, H.-D., Grabow, J. (2003). *IEEE LEOS Newslett.* 17, 3.

Naumann, K.-H. (2003): *J. Aerosol Sci.* 34 1277-1479.

In-situ carbon coating of flame made LiMn$_2$O$_4$ nano-particles for batteries

O. Waser, R. Büchel, F. Krumeich and S.E. Pratsinis

Particle Technology Laboratory, Department of Mechanical and Process Engineering, ETH Zurich, Sonneggstrasse 3, CH-8092, Zurich, Switzerland

Keywords: flame spray pyrolysis, nanocomposites, coatings, carbon black.

Mobile, safe and non-toxic energy storage with higher specific energy and power is demanded for evolving devices. Rechargeable Li-ion batteries with nanosized LiMn$_2$O$_4$ as active cathode material can fulfil these requirements (Shen *et al.,* 2001). The capacity fading, however, by material decomposition (Amine *et al*., 2004) currently limits its life cycle. Its carbon coating can prevent the Mn-ion dissolution into the electrolyte (Han *et al.,* 2007).

Here, a fast and single-step synthesis method to continuously produce carbon coated nano-LiMn$_2$O$_4$ is presented (Ernst *et al.* 2008). Figure 1 shows the setup that can be divided into an oxygen rich particle formation zone in the bottom and an oxygen lean coating zone at the top, after acetylene injection. In the oxygen rich zone a flame spray pyrolysis (FSP) unit produces core LiMn$_2$O$_4$ particles (Ernst *et al*. 2007) which are in-situ coated upstream in the tube with carbon black by partially oxidizing acetylene. Enclosing the FSP reactor is needed to precisely control the oxygen content otherwise no carbon black can be formed because of air entrainment form the turbulent FSP flame (Ernst *et al*. 2008). To avoid post combustion of carbon the hot off-gas is cooled with nitrogen quench gas. The coated particles were collected on a glass-fibre (GF) filter with the aid of a vacuum pump.

The resulting powders were analyzed by XRD, BET, TGA and TEM. Multiple phases of Li-Mn-O were detected by XRD (LiMn$_2$O$_4$, LiMnO$_2$, Mn$_3$O$_4$ and MnO) as a result of LiMn$_2$O$_4$ reduction in the presence of acetylene at elevated temperatures whereby the degree of reduction could be controlled by the length of the coating zone. Particles with d$_{BET}$ of approximately 50 nm and a coating-layer thickness of 5 to 15 nm (evaluated from TEM images) were produced.
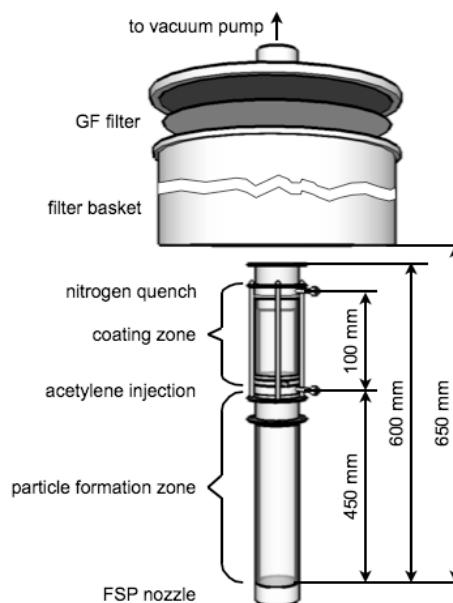
Figure 1. FSP setup for single-step synthesis of CB coated Li-Mn-O nano particles.

Amine, K., Liu, J., Kang, S., Belharouak, I., Hyung, Y., Vissers, D., & Henriksen, G. (2004). *Improved Lithium Manganese Oxide Spinel/Graphite Li-ion Cells for High Power Applications.* Journal of Power Sources, 192(1), 14-19.

Ernst, F. O. Kammler, H. K., Roessler, A., Pratsinis, S. E., Stark, W. J., Ufheil, J., Novak, P. (2007). *Electrochemically active flame-made nanosized spinels:LiMn$_2$O$_4$, Li$_4$Ti$_5$O$_{12}$ and LiFe$_5$O$_8$* Materials Chemistry and Physics 101(2-3), 372–378.

Ernst, F. O., Buechel, R., Strobel, R., Pratsinis, S. E., (2008). *One-step flame-synthesis of carbon-embedded and -supported platinum clusters* Chemistry of Materials 20(6), 2117–2123.

Han, A. R., Kim, T. W., Park, D. H., Hwang, S. J. & Choy, J. H. (2007). *Soft Chemical Dehydration Route to Carbon Coating of Metal Oxides: Its Application for Spinel Lithium Manganate.* Journal of Physical Chemistry C, 111(30), 11347-11352.

Shen, C. H., Liu, R. S., Gundakaram, R., Chen, J. M., Huang, S. M., Chen, J. S., & Wang C. M. (2001). *Effect of Co doping in LiMn$_2$O$_4$.* Journal of Power Sources, 102(1-2), 21-28.

Reactive 3-D Simulations of Continuous Shock Induced Particle Synthesis

N.S. Al-Hasan, M. Giglmaier and G.H. Schnerr

Technische Universität München, FLM-Fachgebiet Gasdynamik, D-85747 Garching
Keywords: CFD, Aerosol modelling, Particle formation and growth, SiO_2, Coagulation.

The scope of the joint project PAK 75/2 (Deutsche Forschungsgemeinschaft DFG) is the development of a novel process of "Gasdynamically induced nanoparticle synthesis". The continuous shock induced particle production is achieved by a setup of two choked Laval nozzles with a subsonic reaction domain in between (Grzona et al., 2007). At the inlet of the primary nozzle the total pressure is p_{01}=10 bar, the total temperature is T_{01}=1400 K and the wall temperature of the pilot facility is T_W=1073 K. The mixture of the injected precursor and the carrier gas is accelerated from subsonic to supersonic speed within a convergent-divergent nozzle. The mixing of the precursor with the carrier gas is depicted in Fig. 1. The precursor concentration levels at the cross sections (Fig. 1) confirm that a homogenous mixture is achieved upstream of the ignition. The steady shock system in the divergent part of the primary nozzle leads to the instantaneous rise of the static temperature T>1200 K and therefore, to ignition of the precursor. The turbulent shock boundary layer interaction with a pre-shock Reynolds number Re_x=9·10^6 and a ratio of the boundary layer thickness to the channel height δ/h=0.14 at the shock location causes a series of weak compression and expansion regions, the so called pseudo shock system.

the particles are instantaneously suppressed. The numerical simulation of the process is realized by the coupled solution of the 3-D Reynolds averaged compressible Navier-Stokes equations together with the arising balance laws for the particle size, for the heat release and for the decomposition of the precursor. The coupling is necessarily a two-way coupling in order to account for the effect of the heat addition to the flow. In this investigation we apply a bimodal and monodisperse particle model. The first mode of the particle model describes the number density of the monomers and the second mode corresponds to the number density of the particles. The boundary layers are resolved by at least 20 finite volumes normal to the corresponding walls, resulting in a resolution of the dimensionless wall distance of y^+<1 (Al-Hasan & Schnerr, 2008). The use of an explicit algebraic Reynolds stress turbulence model ensures that the secondary instabilities in the reactor with a square cross section are resolved. A detailed comparison of the simulation with the experimental results of the pilot facility that are obtained by the project team will be presented in the talk. The sampled particles are spherical non aggregated and have a mean diameter of d_p=4·10^{-8} m which agrees with the numerically predicted particle diameter.
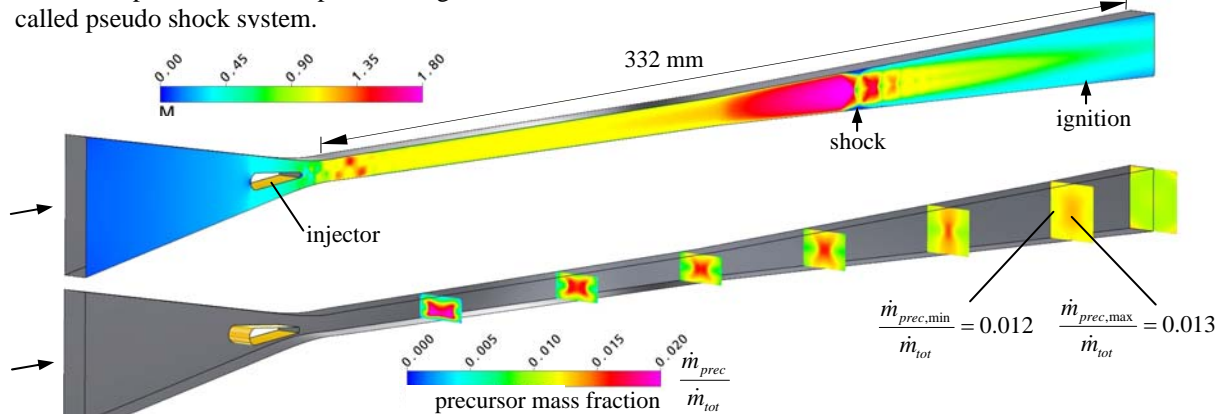
Fig. 1 Primary nozzle, Mach number visualization - top, precursor mass fraction - bottom, CFX, transient 3-D Navier-Stokes simulation (EARSM-model), T_{01} = 1400 K, p_{01} = 10 bar, T_w=1073 K, pre-shock conditions: Mach number M = 1.76, Re_x = 9 · 10^6, δ = 2.2 mm

Heating rates of $dT/dt=10^6$ K/s provide a homogeneous ignition and decomposition of the precursor TEOS (Tetraethoxysilan). The particle growth at constant thermodynamic conditions (T=1300 K, p=6 bar) in the constant area reactor part leads to spherical non aggregated particles. Subsequently the flow is accelerated to a Mach number M=2 through a secondary Laval nozzle. Thereby the particle growth and the agglomeration of

Grzona et al., Proceedings ISSW26 2007 - 26th International Symposium on ShockWaves, Göttingen, Germany,(ed. in chief Hannemann, K.), (2007)

Al-Hasan, N.S., Schnerr, G.H., Proc. GAMM 2008, Bremen, Germany, (ed. Rath, H.J.). To appear in PAMM (2008)

Size analysis of composite nanoparticles by mixing of Ag and C_{60} in the gas phase

F. Maeda, N. Hashimoto, H. Murayama, and H. Tanaka

Institute of Science and Engineering, Chuo University, Tokyo, Japan
1-13-27 Kasuga, Bunkyo-ku, 112-8551, Tokyo, Japan

Keywords: Size analysis, Ag-C_{60} composite nanoparticles, Ag nanoparticles, C_{60} nanoparticles, DMA

Nanoparticles using as building units have much attract attention for the production of novel composite nanoparticle in the gas phase. However, in the gas phase, the nanoparticles are so surface-reactive that it is difficult to keep their individual shape. In this study, we examined to produce composite nanoparticles by mixing of Ag and C_{60} in the gas phase. Diameter of composite nanoparticles was measured using a differential mobility analyzer (DMA), and a field-emission scanning electronic microscope (FESEM).

Ag nanoparticles were produced by a gas aggregation method and were passed through C_{60} vapor. The produced nanoparticles were admitted into an ionizer equipped with a radioactive [241]Am and were diameter-selected by a DMA. The diameter-selected nanoparticles were electrically collected onto a collodion-coated Cu grid. Scanning transmission electron microscope (STEM) images for the collected nanoparticles were observed using an FESEM.

Aggregates of small nanoparticles, which were clearly isolated each other, were observed by STEM images. Figure 1 (a) shows observed diameter for the aggregates plotted as a function of the selected diameter. It was found that each observed diameter was the almost same to the selected diameter. This coincidence suggests that the observed aggregates were produced in the gas phase, not by the coagulation induced by migration of the Ag nanoparticles on the Cu grid. Figure 1 (b) shows observed diameter for the constituent small nanoparticles plotted as a function of the selected diameter. The observed diameter keeps to be constant at approximately 3 nm as the selected diameter increases. This suggests that the small nanoparticles were Ag, were deposited on the C_{60} nanoparticle. Consequently, the production process of the composite nanoparticles can be explained in the following : Ag nanoparticles with approximately 3 nm diameter were produced around the outlet of the heating furnace for the Ag metal, and the Ag nanoparticles were subsequently deposited on a C_{60} nanoparticle produced around the outlet of the heating furnace for the C_{60} powder.
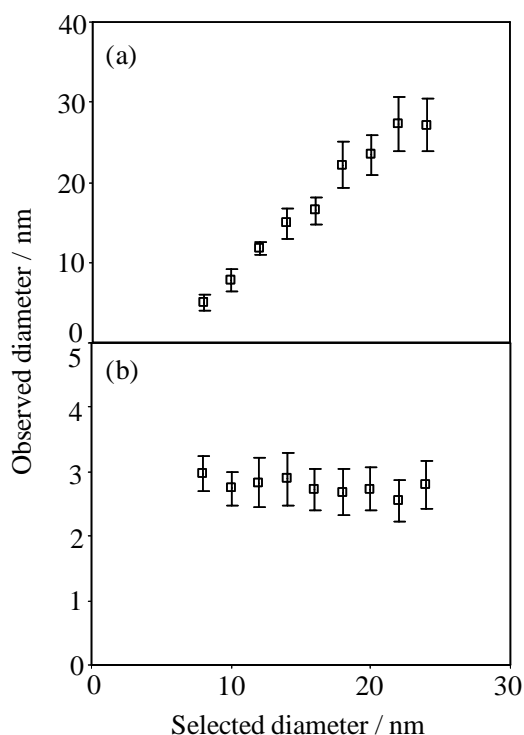
Figure 1. Diameter observed by a STEM plotted as a function of diameter selected by a DMA; (a) observed diameter for the aggregates, (b) observed diameter for the small nanoparticles.

Novel nanocolloids production using diameter-selected Ag nanoparticles formed in the gas phase

N. Hashimoto, H. Murayama, and H. Tanaka

Institute of Science and Engineering, Chuo University
1-13-27 Kasuga, Bunkyo-ku, 112-8551, Tokyo, Japan

Keywords: Ag nanoparticles, DMA, Size analysis, XPS, Chemical composition

Synthesis of nanocolloids has attracted considerable attention due to their specific chemical, physical, electronic and optical properties compared to their corresponding bulk materials. In particular, such properties are so size-dependent that size control of the nanocolloids is essentially important while it is difficult to control the size of the nanocolloids in the synthesis process in general. In this study, we investigated the production of novel nanocolloids using diameter-selected Ag nanoparticles. Size selection of the nanoparticle was carried out using a DMA. Chemical composition of the produced nanoparticles was analyzed by X-ray photoelectron spectroscopy (XPS).

A detailed description of the experimental setup for particle production has been given elsewhere [1]. Ag grains loaded on an alumina boat were heated up to 1100 ^{o}C by a furnace. The vaporized Ag was then passed through ^{241}Am for ionization with N_2 gas flow under the atmospheric condition. The Ag nanoparticles were size-selected at 10 nm by a DMA (Wyckoff G3-LPDMA). The diameter selected Ag nanoparticles were introduced into the PVP solution of which concentration was adjusted to $0.125 gL^{-1}$. A droplet of the solution thus prepared was deposited on a Si substrate, and was dried. The substrate thus prepared was analyzed by XPS.

Figure 1(a) shows Ag 3d spectrum. The peak is observed at 367.9 eV. When the observed binding energy was compared with that for the reference materials such as bulk Ag (368.2 eV), Ag-PVP (367.5 eV), and Ag_2O (368.0 eV), the observed binding energy was close to that for the Ag-PVP. Fig. 1(b) shows O 1s spectrum. The peak is observed at 530.6 eV with broad tail toward higher binding energy. This peak distribution can be peak-fitted under the assumption of two peaks at 530.6 eV and 532.5 eV. When binding energies were compared with those for the reference materials such as O (PVP) (530.7 eV), O (PVP)-Ag (531.6 eV), and Ag_2O (530.0 eV), the binding energies for the fitted peaks were close to those for the O (PVP) and O (PVP)-Ag. In addition, when

the detection efficiency was considered, it was revealed that the number of the Ag atoms is almost equal to that of the O atoms derived from the O (PVP)-Ag peak. This suggests that Ag nanoparticles were completely coated with PVP molecules.

On the other hand, in a survey spectrum, only Ag, N, O, and C atoms were detected which no signals due to Si atoms composed of the substrate were detected. This confirms the present analysis described above.

In conclusion, we succeeded to produce the Ag nanocolloids using the diameter-selected Ag nanoparticles formed in the gas phase. The XPS analysis revealed that the produced Ag nanocolloids were completely coated with PVP molecules.
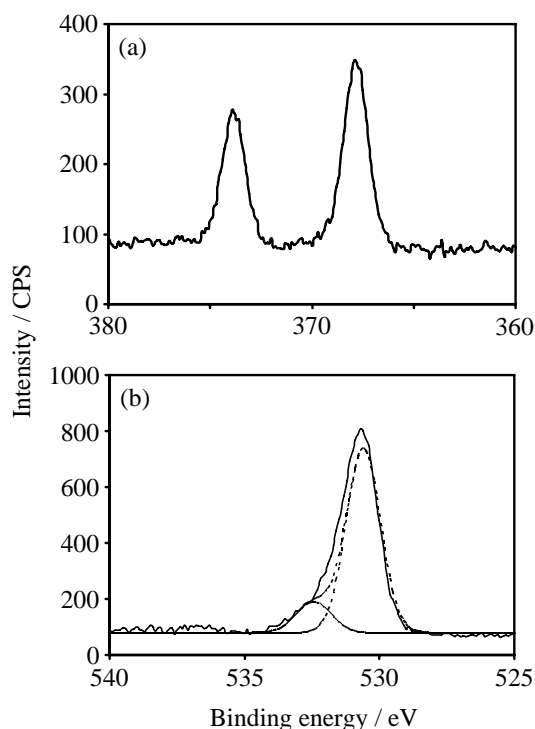
Figure 1. XPS high-resolution spectra for (a) Ag 3d, and (b) O 1s regions.

[1] N.Hashimoto, H.Murayama, and H.Tanaka *Jpn. J. Appl. Phys.* 47 (2008) 4777.

Investigation of structure and chemical composition analysis of ionic-liquid coated Ag nanoparticles

Y. Sekiguchi, M. Shigeyasu, H. Murayama, H. Tanaka

Institute of Science and Engineering, Chuo University
1-13-27 Kasuga, Bunkyo-ku, 112-8551, Tokyo, Japan

Keywords: Ionic liquid, Ag nanoparticle, DMA, SEM, XPS

Production of metal nanoparticles in ionic liquid has attracted much attention because of the production of high surface-reactive metal nanoparticles. However, the production process of the Ag nanoparticles in the ionic liquid has not been recognized clearly. In this study, we investigated Ag nanoparticles formation in ionic-liquid nanoparticles in the gas phase. Gas aggregation technique was used for the production of nanoparticles. A differential mobility analyzer (DMA) and a field-emission type scanning electronic microscope (FESEM) was used for the diameter determination of the produced nanoparticles. X-ray photoelectron spectroscopy (XPS) was used for the chemical composition analysis for the produced nanoparticles.

Ag nanoparticles produced by evaporation of Ag metal were passed through ionic liquid [C_4mpyrr][NTf_2] vapor, of which production method was described elsewhere [1]. The produced nanoparticles were admitted into an ionizer equipped with a radioactive [241]Am, were diameter-selected by a DMA, and were electrically collected onto a collodion-coated Cu grid. Scanning transmission electron microscope (STEM) images of the collected nanoparticles were observed using an FESEM. On the other hand, the diameter-selected nanoparticles were electrically collected onto an Au-coated Si substrate, and were also analyzed by an XPS.

Figure 1 shows diameter observed in the STEM image plotted as a function of diameter measured by the DMA. It was found that the observed diameter was much smaller than the selected diameter. Considering the detection efficiency of the FESEM, the nanoparticles observed in the STEM image are considered to be the Ag nanoparticles. This indicates that diameter difference between the observed and the selected diameter is due to the existence of the ionic liquid layer.

Figure 2 shows survey spectrum of the collected nanoparticles measured by the XPS. The peaks originated from Ag, Au, F, O, N, C, and S atoms are observed in the spectrum. Except of the Au

atoms due to the substrate Au atoms, it is highly probable that the Ag atoms are due to the Ag nanoparticles and F, O, N, C, and S atoms are due to the ionic liquid which is composed of the same atoms. In addition, relative amount of the F, O, N, C, and S atoms estimated from the intensities are quite similar to the stoichiometry of the ionic liquid used in this experiment. These results confirm that the collected nanoparticles are composed of Ag atoms and ionic liquid molecules.

In summary, it is found that the ionic liquid coated Ag nanopaticles are produced by the present method.
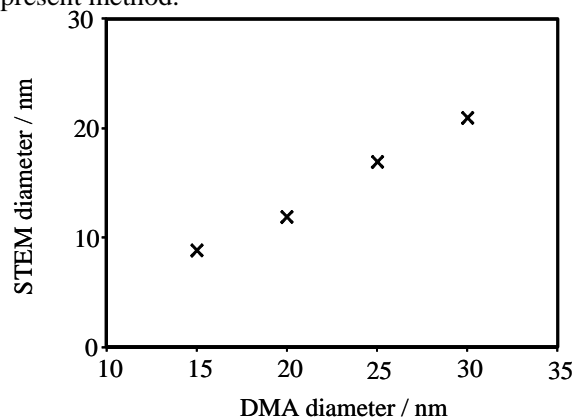
Figure 1. Diameter observed in the STEM image plotted as a function of diameter measured by the DMA
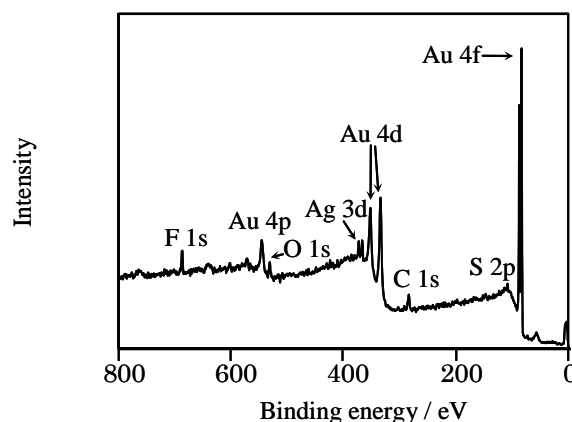
Figure 2. survey spectrum for the collected Nanoparticles measured by XPS

[1] M. Shigeyasu, H. Murayama, and H. Tanaka: Chem. Phys. Lett. **463** (2008) 373.

Synthesis of Silicon nanoparticles by Laser assisted Chemical Vapor Pyrolysis for Li-ion battery electrodes

D. Munao , E.M. Kelder, J.W.M. van Erven, M. Valvo, J.C.M. Marijnissen

Delft ChemTech, NanoStructured Material, TU Delft, Julianalaan 136, 2628 BL, Delft, The Netherlands

Keywords: Generation of nanoparticles, Laser Pyrolysis, Li-Ion batteries.

Nanosized particles are of interest due to various potential applications in several fields (i.e. biomedics, optics and electronics). In this work, the attention is focussed on materials for energy storage, namely negative electrodes for rechargeable Li-Ion batteries.

During the last decades various methods and approaches emerged to produce nanoparticles. These include wet and dry production processes having their own benefits. One of the most promising routes to produce nanoparticles on industrial interesting rates is gas phase synthesis, such as flame pyrolysis and plasma synthesis. Another interesting gas phase production processes is Laser Assisted Chemical Vapour Pyrolysis (LaCVP).

In this process a CO_2 laser is employed to heat a continuous reactant flow which will form nanoparticles. It is shown that this process is capable to produce nanosized powders with particle size from 5 to 50 nanometer. Moreover, depending on synthesis parameters, the particles can be spherical, not agglomerated, highly pure and have a narrow size distribution.

This system has been extensively studied at the TU Delft during the last 20 years. In this research a new CO_2 laser assisted aerosol reactor was developed, with a particular to the design.

A special attention is given to the reaction zone, in order to narrow the particle size distribution. The reaction zone is identified by the intersection between the gas stream and laser beam. Both of them exhibit a rectangular geometry. This combination leads to a perfect matching between the gas velocity profile and the laser intensity profile. In this way different gas molecules have equal probability to absorb the same amount of energy from the laser source. The reactor includes also a wide range of windows for optical analysis purpose. A schematic of the new reactor is shown in figure 1. The details of the design can be found elsewhere (van Erven et al., 2006).

The construction of the reactor is completed and currently the first experiments are carried out. These include the production of silicon nanoparticles from silane gas precursor.

Due to its remarkable lithium storage capacity silicon is envisaged as one of the most promising anode materials for Li-Ion batteries. However, Si suffers from poor mechanical stability upon charging and discharging. This major drawback could be overcome by reducing the size of the active particles down to a few nanometers. In this way it is possible to alleviate considerably the total strain that occurs during the electrochemical process. Moreover, improving the electrode manufacture is widely seen as a technological key-issue. In this respect we are investigating possible alternative methods that can be easily coupled with the LaCVP.

The produced particles are currently under characterization and results concerning Li-ion battery performances will be presented during the conference.
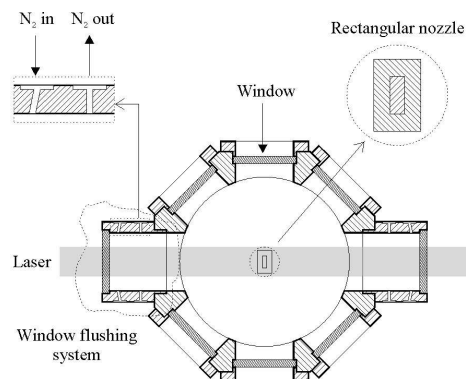
Figure 1. 2-D top view of the reactor. The nozzle geometry and the window flushing system are represented in the magnified details.

Haggerty, J. S. and Cannon, W. R. (1981) 3. *Sinterable powders from laser-driven reactions in Laser-Induced Chemical Processes* 165-241. (ed by Steinfeld, J. I.). New York: Plenum Press.

Van Erven, J.W.M., Trzeciak, T.M., Fu, F., Marijnissen, J.C.M. (2006). *Design of a Laser Assisted Aerosol Reactor for Production of Nanoparticles on Semi-Industrial Scale.* Proceedings of the World Congress on Particle Technology V 2006, Orlando USA. Paper nr. 202D.

Graetz, J. and Ahn, C. C. and Yazami, R. and Fultz, B. (2003). *Electrochemical And Solid State Letters*, 6, A194-A197

The effect of flame spray configuration on synthesis of inhomogeneous nanoparticles

T. Rudin and S.E. Pratsinis

Particle Technology Laboratory, Department of Mechanical and Process Engineering, ETH Zürich,
8092 Zürich, Switzerland

Keywords: Flame spray pyrolysis, Aerosol formation, Size distribution, Powder inhomogeneity.

Particle synthesis from liquid fed flame reactors is known to produce inhomogeneous product under certain process conditions and liquid precursors (Jossen et al., 2005).

Here the effect of flame structure and synthesis parameters on the morphology of inhomogeneous metal oxide nanoparticles made by liquid-fed spray flames is investigated. Two such spray flames are considered here: First, the solvent containing metal-precursor is combusted by the flame spray pyrolysis (FSP) (Madler et al., 2002) where energy is provided by the solvent only. In the second, precursor solution is combusted with additional external acetylene gas feed by the so-called flame assisted spray pyrolysis (FASP). The effect of flame enthalpy density on the metal oxides nanoparticle made from hydrated metal-nitrates precursor in low enthalpy density solvent ethanol is explored. The advantage of such precursors is their ease of preparation and low cost that makes them attractive for industrial applications.

The FASP-nozzle was designed to allow better control of spray combustion condition of the precursor. The design allows the control of all gas flow parameters as well as spray parameters by control of the height of spray ignition above the precursor feed nozzle. The main advantage of such a system is the decoupling of solvent composition from enthalpy density of the flame, which allows greater choice of precursor compositions and access of more economic and ecologic solvents and precursors.

As a first candidate, Bi_2O_3 was chosen as it produces inhomogeneous product (consisting of hollow, large solid and nanograined particles) by FSP (Madler & Pratsinis, 2002) from bismuth-nitrate precursors for different precursor compositions. The effect of flame enthalpy density on the Bi_2O_3 nanoparticle homogeneity is systematically explored. All powders were produced at 2 ml/min precursor flow and 6 l/min dispersion oxygen flow. Injection height of the acetylene gas was 10 mm above spray nozzle.

The particle inhomogeneity was characterized by crystallite size measurements from X-ray diffraction by matching single phase spectra of various average crystallite sizes to the product powder spectrum. Also X-ray disc centrifuge and nitrogen adsorption measurements have been taken to further characterize particle homogeneity.

One of the main results is the possibility to use precursor the above mentioned metal-nitrate ethanol precursors for synthesis of homogeneous product by control of enthalpy addition by the fuel gas in FASP.
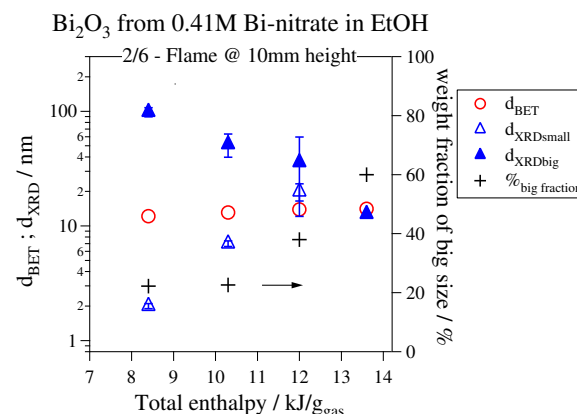
Figure: Particles crystallite sizes measured by XRD and BET- surface equivalent diameters are plotted against total enthalpy of the flame. For XRD, a small (open triangles) and large (filled triangles) size was determined. An estimation of the amount of the big size fraction is plotted on the right axis. For the product at 13.6 kJ/g_{gas} a single crystallite size fits the spectrum best. BET measured particle diameters are plotted for comparison (circles) showing the limited sensitivity of nitrogen adsorption for characterization of inhomogeneous powders (Jossen et al., 2005).

The figure shows the trend to more homogeneous product for higher enthalpy contribution by acetylene. For larger enthalpy densities, the two crystallite sizes fitted to the spectra cannot be separated anymore.

Jossen, R., S. E. Pratsinis, W. J. Stark & L. Madler (2005). Criteria for flame-spray synthesis of hollow, shell-like, or inhomogeneous oxides. *J Am Ceram Soc, 88,* 1388-1393.

Madler, L., H. K. Kammler, R. Mueller & S. E. Pratsinis (2002). Controlled synthesis of nanostructured particles by flame spray pyrolysis. *J Aerosol Sci, 33,* 369-389.

Madler, L. & S. E. Pratsinis (2002). Bismuth oxide nanoparticles by flame spray pyrolysis. *J Am Ceram Soc, 85,* 1713-1718.

Generation Characteristics of Nanoparticles by Evaporation/Condensation

W.Y. Lin[1], K.H. Chang[2], Y.Y. Chang[1], C.Y. Wu[1] and Y.C. Lee[3]

[1]Institute of Environmental Engineering and Management, National Taipei University of Technology, Taipei, Taiwan
[2]Department of Safety Health and Environment Engineering, National Yunlin University of Science & Technology, Yunlin, Taiwan
[3]Department of Safety, Health and Environment, Tungnan University, Taipei, Taiwan

Keywords: silver nanoparticle, aerosol generation, evaporation/condensation.

The purpose of this study is to develop an aerosol generating system that can produce particles of nanometer size in a convenient and efficient way. Stable source of particles is a primary step in evaluating the health effect of nanoparticles deposited in the respiratory tract.

Major factors affect the particle size generated by evaporation/condensation include furnace temperature, quenching gradient and carrier gas flow rate (Damour, 2005; Jung *et al.*, 2006; Ku & Maynard, 2006). Although the method of silver particle generation and sintering characterization has been studied, a systematically investigated and regressed data for predicting particle size generated for easy applications has not been reported.

The generation system included high temperature furnace, ceramic tube reactor, silver powder, cylinder nitrogen gas as carrier gas, and dry-filtered air used as dilution gas. The size-resolved number concentration of aerosols was continuously monitored by a Scanning Mobility Particle Sizer (SMPS, Model 3936, TSI Inc.).

The first objective was to assure that the system could generate a series of specific size of nanoparticles for comparison of the effect of different size. While setting a series of particle size ranges from 10 to 100 nm, the actual particle generated could be very close the objective size by simply adjusting the furnace temperature, carrier gas and dilution gas flow rate. The experimental results were shown in Table 1.

Table 1. Mode of silver nanoparticle generated by the system (5 g silver powder).

Furnace temperature (℃)	Carrier gas (L/min)	Dilution gas (L/min)	Mode (nm)	GSD
1000	1.7	2.0	10.5	1.38
1051	2	2	21.1	1.50
1132	2	2	31.1	1.57
1235	2	2	50.5	1.61
1315	2	2	69.8	1.55
1250*	4	--	109.4	1.50

*10g silver powder

While setting the furnace temperature at 1063℃, a series of experiments were conducted to obtain corresponding particles shown in Figure 1. It provides a reference for obtaining a specific particle size by simply adjusting carrier gas and dilution gas flow rate.
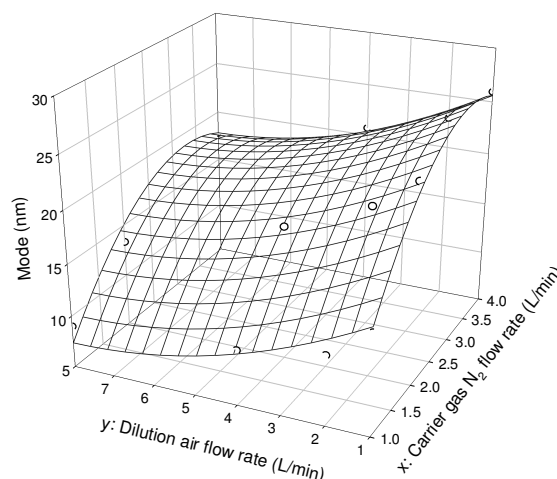
Particle size regression
Mode=5.65+13.95*x-2.52*y-2.09*x^2+0.16*y^2

Figure 1. Particle size of the silver nanoparticle generated as furnace temperature at 1063℃.

Another way to adjust the particle size is to control the furnace temperature. A series of data was obtained by setting carrier gas and dilution gas flow rate in 2 L/min. In addition to the particle size discussed as above, the particle size change and the agglomeration characteristics observed by TEM after sintering was also investigated in this study.

Damour T. M., Ehrman S. H., Karlsson M. N. A., Karlsson L. S., & Deppert K. (2005) Aerosol Sci. Technol, 39, 444–451.

Jung J. H., Oh H. C., Ji J. H., & Kim S. S. (2006). *J. Aerosol Science*, 37, 1662-1670.

Ku B. K., & Maynard A. D. (2006). *J. Aerosol Science*, 37, 452-470.

Synthesis of nano-sized Iron Oxide particles in low-pressure hydrogen flames

O.O. Nalcaci, E. Ruzin and H. Bockhorn

Institute of Chemical Technology and Polymer Chemistry, Karlsruhe University, Engesserstr. 20, 76131, Karlsruhe, Germany

Keywords: Combustion synthesis, Fe-oxides, Particle size distribution, Electron microscopy

Today flame technology is considered to be a scalable, continuous and well-established method for the production of nanoparticles in large quantities. (Strobel *et al.*, 2006)

Gas phase combustion synthesis of inorganic particles is used to make a variety of commodities like SiO_2, TiO_2, Al_2O_3, etc., amounting to millions of tons annually. They are used industrially as pigments, opacities, catalysts, flowing aids, for optical fibres and telecommunication (Roth, 2007)

In this study we have investigated the low pressure flame synthesis of nano-sized iron oxide particles. For comparison an industrial sample (NanoArc, Alfa Aesar) was also investigated.
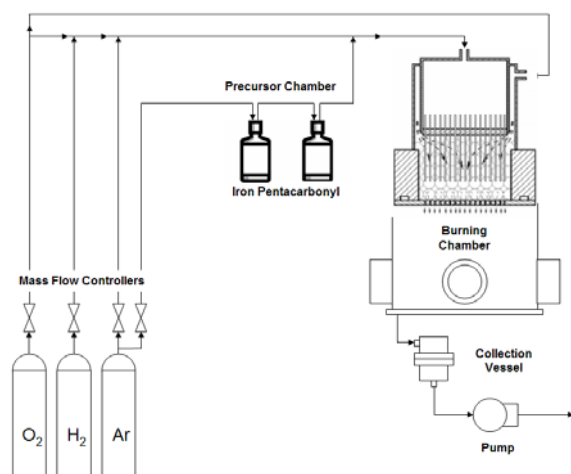
Figure 1: Experimental Setup

The experimental setup is schematically depicted in Figure 1. It consists of a low pressure flat flame burner in an optically accessible chamber for the laser diagnostic measurements. The burner is adjustable in height.

Iron pentacarbonyl ($Fe(CO)_5$) is delivered at widely variable concentrations from a pressure and temperature controlled bubbler unit as saturated vapor in Ar and introduced after a small mixing chamber below the burner matrix into the flame. In the lean premixed $H_2/O_2/Ar$ low pressure flame $Fe(CO)_5$ is oxidized to iron oxide. Gas flows were controlled by calibrated thermal mass flow controllers and the pressure of the burner chamber is held constant at 70 ± 1 hPa.

The resulting material (Iron Oxide) and the industrial sample were characterized by various methods including BET, XRD, electron microscopy, infrared spectroscopy, dynamic light scattering and thermogravimetry.

BET analysis show that the produced particles have a particle size of 12,5 nm and specific surface area of 138 m^2/g compared to 21,6 nm and 35,5 m^2/g of NanoArc. SEM analysis exhibits that the flame synthesis produces particles with a narrow particle size distribution (8-12 nm). The industrial sample due to the different method of synthesis differs in size between 8-200 nm. TEM analysis shows both iron oxides have partially crystalline structures.

The NanoArc sample is clearly identified as Iron Oxide by XRD, whereas for the flame synthesized particles the small particle sizes are prohibiting the identification by XRD. DLS analysis exhibits agglomerated iron oxide particles which cannot be easily separated due to their small particle sizes.
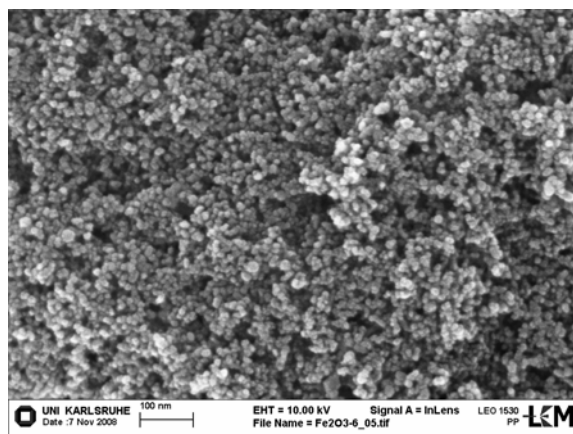
Figure 2: SEM Picture Of Iron Oxide particles

Strobel, R., Alfons, A., Pratsinis, S.E., (2006), *Advanced Powder Technology*, 17(5), 457-480.

Roth, P., (2007), *Proceedings of the Combustion Institute*, 31(2), 1773-178

Novel arc plasma system for the aerosol synthesis of metal nanoparticles

H. Förster[1], D. Kilian[1], H.-J. Schmid[2] and W. Peukert[1]

[1]Institute of Particle Technology, Friedrich-Alexander-University Erlangen-Nürnberg, Cauerstr. 4, 91058 Erlangen, Germany
[2]Institute of Mechanical and Environmental Process Engineering, University of Paderborn, Pohlweg 22, 33098 Paderborn, Germany

Keywords: metal nanoparticles, generation, arc plasma.

Metal nanoparticles exhibit special properties which make them favourable for numerous applications in different fields, such as electronics, sensor technology, catalysis and optics. The synthesis of nanoparticles by arc plasma evaporation of a metal target and subsequent condensation combines the advantage of high production rates with low precursor costs.

The focus of this work lay on the generation of copper and titanium nanoparticles. A schematic sketch of the newly constructed arc plasma furnace is shown in Figure 1. The design was partly inspired by constructions of Mahoney et al. (1995) and Fort (1997). The arc "burns" between a sharpened tungsten rod (cathode) and the metal target (anode) contained in a graphite crucible. A process gas stream carries the metal vapour through an alumina tube surrounding the cathode to the quenching region. There the hot process gas stream is quickly cooled by mixing with cold quench gas which initiates nucleation and dilutes the generated aerosol to reduce agglomeration. To adjust the arc length the anode can be moved in vertical direction. As power supply the DC source of a commercial TIG welder is used.
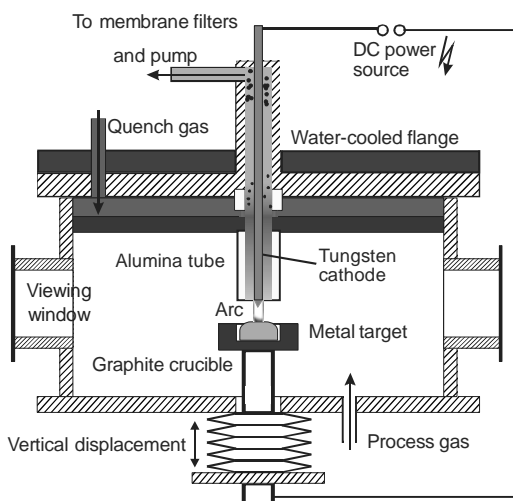
Figure 1. Sketch of the arc plasma furnace.

In order to prevent any oxidation of the particles in the process, argon and nitrogen (both grade 5.0) were used as process respectively quench gas and special attention was turned to a leak-tight design of the system.

The novel arc system features excellent arc stability for a wide range of process conditions. It delivers aerosols with high reproducibility (± 5 % of mean particle size). The influences of process and quench gas flow rates as well as arc current, arc length and system pressure on the mean particle size and agglomerate structure were investigated in detail by SMPS, SEM, TEM and BET measurements. Material analysis was done by XRD, EDX and XPS.

Copper nanoparticles are shown exemplarily in Figure 2. The SMPS mean particle mobility diameter for this sample was 42 nm, which is in good agreement with the analysis of the particle sizes on the SEM image. By systematic variation of system parameters the particle size can be varied between 20 and 80 nm.
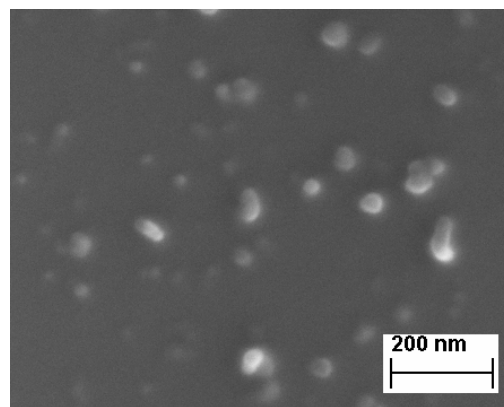
Figure 2. SEM picture of copper nanoparticles.

The experimental work is supplemented by CFD analysis of fluid flow around the plasma torch and population balance modelling of the evolving particle size distribution.

Mahoney, W., & Andres, R. P. (1995). *Materials Science and Engineering*, A204, 160-164.
Fort, D. (1997). *Rev. Sci. Instruments*, 68, 3504-3511.

Synthesis of monodisperse gadolinium oxide nanoparticles having single monoclinic phase using spark discharge generation

I. Aruna, R. Theissmann and F.E. Kruis

Faculty of Engineering and Center for Nanointegration Duisburg-Essen (CeNIDE),
University of Duisburg-Essen, Bismarckstr. 81, 47057, Duisburg, Germany

Keywords: gadolinium oxide nanoparticles, spark discharge generation, monodisperse, monoclinic.

Gadolinium oxide (Gd_2O_3), a lanthanide sesquioxide, has drawn considerable attention recently for its unique properties which can be utilized in a wide range of technological applications. Properties such as its transmission coefficient in the visible region of solar spectrum, wide bandgap, effective emission of radiation source, chemical stability, high neutron absorption cross-section and very high relaxivity make it suitable for use in solar cells, as gate dielectric in semiconductor devices, as phosphors in the color television tubes and display devices, in reactors, neutron detectors, neutron capture cancer therapy, and as a good contrast agent for medical imaging. (Adachi et al. 2004)

In comparison to the studies on bulk and thin films, synthesis of Gd_2O_3 nanoparticles and study of the size-dependent properties is seldom encountered in literature. The present study, thus, aims at synthesis of monodisperse Gd_2O_3 nanoparticles and investigating the modified properties at nanodimensions. For this, monodispersed Gd nanoparticles are synthesized by spark discharge generation. The schematic diagram of the set up is shown in Figure 1. It consists mainly of a spark

Figure 1. Schematic diagram of the synthesis setup for gadolinium oxide nanoparticles. The details of various components are discussed in the text

generator (GFG 1000, PALAS, Karlsruhe, Germany) for growing Gd nanoparticles, a differential mobility analyzer (DMA) for size selection, a oxidation and sintering furnace, and the deposition chamber (Electrostatic precipitator/Low pressure impactor). The commercially available spark generator for growing carbon soot has been modified to grow Gd_2O_3 nanoparticles in the present setup. Graphite rods in the spark generator were replaced by Gd rods (purity 99.9 %) having a diameter of 6.3 mm. One of

the electrodes is connected to the high voltage supply in parallel with the capacitor (20nF). A standard method to produce a sequence of sparks is achieved by charging the high-voltage capacitor via a constant current source. When the voltage reaches the breakdown voltage, spark discharge takes place between the electrodes, which results in ionization of the process gas between the electrodes. The ions are accelerated towards the electrodes resulting in sputter erosion and formation of Gd species. Due to very short duration of the pulsed discharge, Gd species cools down rapidly which results in supersaturation, leading to nucleation and condensation thereby forming primary particles. The charged Gd aerosol generated by the spark generator is passed through the DMA. In-flight sintering in controlled oxygen atmosphere of the agglomerates is performed in order to form quasi spherical Gd_2O_3 nanoparticles after size- selection by the DMA. The effect of process parameters viz, the spark frequency, flow rate of process gas and dilution gas, flow rate of oxygen in the sintering furnace and the annealing temperatures have been studied in detail. Detailed structural analysis revealed the formation of Gd_2O_3 nanoparticles with single monoclinic phase. Figure 2 shows a typical transmission electron microscopy (TEM) image and high resolution transmission electron micrograph of monoclinic Gd_2O_3 nanoparticles of average mobility diameter of 10 nm.

Figure 2 (a) TEM and (b) HRTEM micrographs of Gd3O3 nanoparticles having single monoclinic phase.

Adachi, G, Imanaka, N, & Kang, Z. C. (2004). *Binary rare earth oxides*. Springer-Verlag New York, LLC

SiO$_2$ Coating of Aerosolized Nanoparticles by Photoinduced Chemical Vapor Deposition

A.M. Boies[1], J.T. Roberts[2] and S.L. Girshick[1]

[1]Department of Mechanical Engineering, University of Minnesota, 55455, Minneapolis, U.S.A.
[2]Department of Chemistry, University of Minnesota, 55455, Minneapolis, U.S.A.

Keywords: Aerosol coating, CVD, Core-shell nanoparticle, Photochemical processes, and TDMA.

Nanoparticle composites, consisting of core-shell structures, combine functional properties of several materials, producing particles that are of interest for a range of applications. Recent work by Zhang *et al.* (2008) demonstrated that photoinduced chemical vapor deposition (photo-CVD) can be used to produce organic coatings on sodium chloride particles in a gas-phase process. The present study expands this method for producing core-shell nanoparticle aerosols with a variety of chemical compositions. Aerosols consisting of magnetic iron oxide, sodium chloride, and silver were produced by means of plasma synthesis, nebulization, and inert gas condensation, respectively. Each aerosol was mixed in a reaction chamber with a SiO$_2$ precursor, tetraethyl orthosilicate (TEOS), and then exposed to vacuum ultraviolet (VUV) radiation. The VUV light initiated a reaction by activating TEOS which in turn produced a coating on the particle surface by means of photo-CVD. Experiments were conducted for an array of chamber pressures, temperatures and configurations.

The coating properties were evaluated with a variety of techniques, including in-flight measurement of coating thickness using a tandem differential mobility analyzer (TDMA). Particle coating thickness was obtained by taking the difference in particle radius, as determined by the measured particle size distribution, between coated and uncoated particles. Real-time measurements of particle coating thicknesses allowed for evaluation of critical system parameters that include residence time, precursor concentration, aerosol concentration, and VUV intensity. As shown in Figure 1, the particle coating thickness was influenced by both the flowrate of precursor into the system as well as the flowrate of nitrogen, the dominant system flow. In general, coatings were thicker with increased TEOS flow, which increased the precursor concentration, and decreased with increased nitrogen flow, which served to dilute the precursor concentration and lower the particle residence time.

The coated particles were also imaged using transmission electron microscopy (TEM) and elemental composition was gathered using electron energy dispersive x-ray (EDX) spectroscopy. Particle coating chemistry was determined by Fourier-transform infrared radiation (FTIR) and
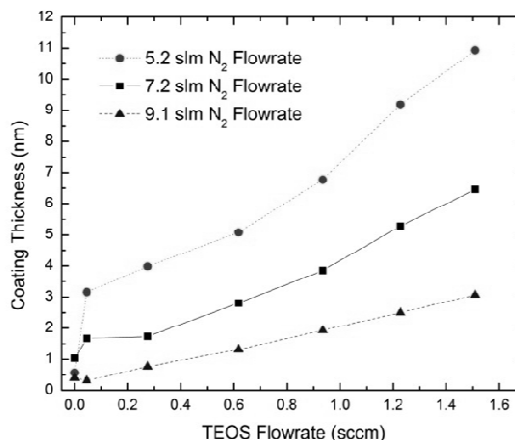
Figure 1: Coating thickness of silver particles for varying TEOS precursor and nitrogen flow rates.

X-ray photo spectroscopy (XPS). As shown in Figure 2, TEM images of coated polydisperse aerosols indicate that increasing coating chamber temperature serves to increase the coating thickness for a given precursor concentration and residence time. However, high chamber temperatures also increase the likelihood of precursor self-nucleation as seen by the nanometer sized spherical inclusions in the coatings at 600˚C.
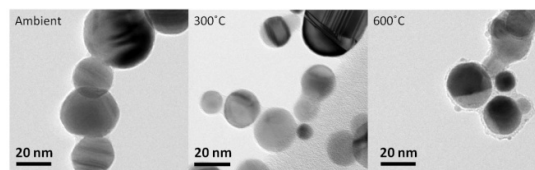
Figure 2:   TEM images of Ag particles coated at varying chamber temperatures.

These studies indicate that photo-CVD is an attractive, general method for producing high quality SiO$_2$ coatings on aerosolized particles produced in a variety of ways. The decoupling of the particle production and coating allows for core-shell structures that would be unlikely to form if produced together, thus providing a method to generate novel nanoparticle composites for a variety of applications.

Zhang, B., Liao, Y.-C., Girshick, S. L., & Roberts, J. T. (2008). *J. Nanopart. Res.* **10**(1), 173-178.

Synthesis and functionalisation of copper and titanium nanoparticles in a spark discharge generator

H. Förster[1], C. Funk[1] and W. Peukert[1]

[1]Institute of Particle Technology, Friedrich-Alexander-University Erlangen-Nürnberg, Cauerstr. 4, 91058 Erlangen, Germany

Keywords: metal nanoparticles, generation, functionalisation, spark discharge.

The synthesis of nanoparticles by the spark discharge method which was first introduced by Schwyn et. al. (1988) offers great versatility as it can be applied for all conducting and semiconducting materials, including those with a high melting point. It delivers ultrafine aerosols (down to atomic cluster size) with narrow size distributions, which makes it interesting for many applications in science and technology.

A schematic sketch of the spark discharge generator used in our studies is displayed in Figure 1. A double cross vacuum flange serves as housing for the spark discharge process. In the experiments either copper or titanium rods of 2 mm diameter were used as electrodes. The rods are fixed in a holder to allow precise adjustment of the electrode gap. The electrical circuit to generate pulsed sparks consists of a high voltage power source (max. 20 kV, max. 6 mA) operated in constant current mode, a capacitor of 4,7 nF and a resistor of 0,5 MΩ that enhances the sparking stability. These specifications enable sparking frequencies of 0 to 700 Hz. The evaporated electrode material, which serves as the material source for particle synthesis, rapidly cools by adiabatic expansion and radiation leading to high supersaturations and nucleation.

transports the generated aerosol out of the sparking zone and the chamber.

The influences of carrier gas flow rate as well as spark frequency, spark gap, system pressure and gas atmosphere on the mean particle size and agglomerate structure were investigated by SMPS, SEM and TEM measurements. Material analysis was done by EDX and TEM in diffraction mode.

A selection of the results obtained by SMPS measurements is shown in Figure 2. By appropriate setting of the system parameters mean particle sizes in the range of 4 to 30 nm can be achieved.
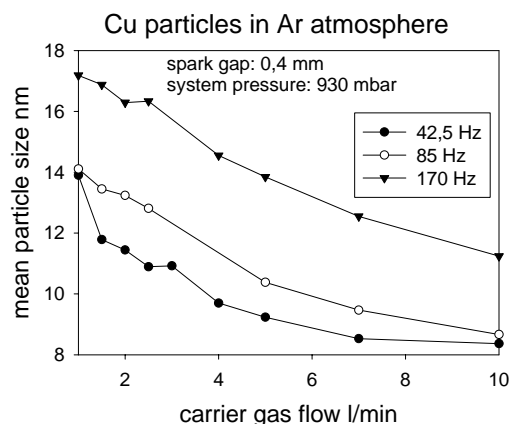
Figure 2. Influence of carrier gas flow rate and spark frequency on the mean size of copper nanoparticles.

For an easy transfer of the metal particles from the gas to the liquid phase it is planned to combine the synthesis process with an in-situ functionalisation of the particle surface. Therefore a precursor gas is added to the carrier gas. The high temperatures in the spark channel should provide enough energy for the decomposition of the precursor. The functionalised surfaces are characterised by HRTEM, XPS and Raman spectroscopy.

Schwyn, S., Garwin, E. & Schmidt-Ott, A. (1988). *J. Aerosol Science*, 19 (5), 639-642.

Byeon, J. H., Park, J.H. & Hwang, J. (2008). *J. Aerosol Science*, 39 (10), 888-896.

Tabrizi, N. S., Ullmann, M.. Vons, V.A., Lafont, U., Schmidt-Ott, A. (2008). *J. Nanoparticle Research*, Article in Press.

Figure 1. Sketch of the spark discharge generator.

To avoid any oxidation in the system an inert gas stream of argon or nitrogen (both grade 5.0)

Nanostructure Evolution: Form Aggregated to Spherical SiO$_2$ Particles Made in Diffusion Flames

A. Camenzind[1], H. Schulz[1], A. Teleki[1], G. Beaucage[2], T. Narayanan[3] and S.E. Pratsinis[1]

[1]Particle Technology Laboratory, Departement of Mechanical and Process Engineering, ETH Zurich, Sonneggstrasse 3, 8092 Zurich, Switzerland
[2]Department of Chemical and Materials Engineering, University of Cincinnati, Ohio 45221-0012, USA
[3]European Synchrotron Radiation Facility (ESRF), 38043 Grenoble, France

Keywords: Nanoparticles, Particle formation and growth, SAXS, In-situ measurements, SiO$_2$.

The formation of nanostructured silica particles by oxidation of hexamethyldisiloxane (HMDSO) in co-annular diffusion flames is investigated by in-situ small-angle X-ray scattering (SAXS) (Camenzind *et al.* 2008). This enabled the nonintrusive monitoring of the mass fractal dimension, the aggregate size, and the number of primary particles per aggregate, along with the silica volume fraction, the primary particle diameter, the geometric standard deviation, and the number density (Beaucage *et al.* 2004) along the flame axis. Parallel to this, thermophoretic sampling (TS) of the particles and analysis by transmission electron microscopy (TEM) allowed for direct comparison of particle morphology to that obtained from the above SAXS analysis, which were compared also to the ultra-small-angle X-ray scattering (USAXS) data for product particles collected from the filter. The flame temperature was measured by in-situ Fourier transform infrared (FTIR) spectroscopy. By increasing the oxygen flow rate, the laminar diffusion flame changed to a turbulent, premixed-like flame. Non-aggregated, spherical particles were formed in the former, while aggregates were formed in the latter flame. The relatively long high-temperature particle residence times in the laminar diffusion flame facilitated sintering of the aggregates formed earlier into compact spherical particles at later stages of the flame.

Table 1. Gas flow rates and product particle sizes (determined by BET) for the diffusion flames producing SiO$_2$ (*S-y*) with *y* being the flow rate of oxygen (l/min) (Camenzind *et al.* 2008).

Flame – O$_2$ flow	CH$_4$	total flow	d_{BET}
	l/min	l/min	nm
S-2		3.3	47
S-4	0.5	5.3	23
S-7		8.3	16
S-10		11.3	13

Beaucage, G., H. K. Kammler, R. Mueller, R. Strobel, N. Agashe, S. E. Pratsinis and T. Narayanan (2004). *Nature Mater.*, 3, 370-374.

Camenzind, A., H. Schulz, A. Teleki, G. Beaucage, T. Narayanan and S. E. Pratsinis (2008). *Eur. J. Inorg. Chem.*, 2008, 911-918.
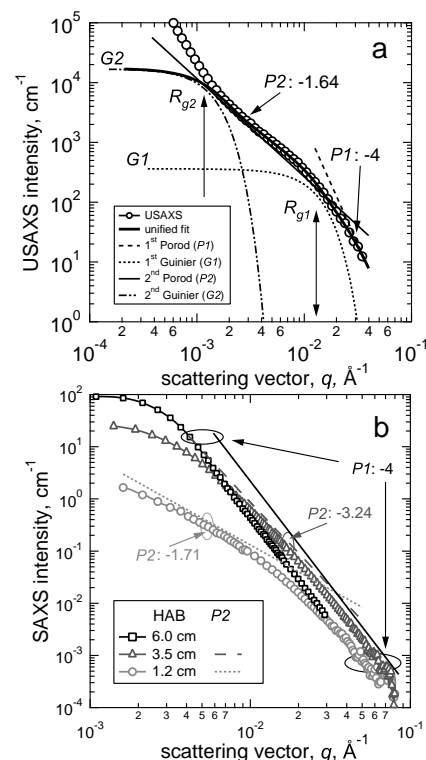
Figure 2. Scattering intensities as a function of scattering vector *q*: (a) *ex-situ* USAXS of particles (*S-10*) collected from the filter and unified fit (bold solid line) along two Guinier (*G1*, *G2*) and Porod (*P1*, *P2*) regimes showing D_f = 1.64 and smooth primary particle surface (slope = -4) and two characteristic sizes, R_{g2} and R_{g1} corresponding to aggregate and primary particle sizes. (b) *in-situ* SAXS of particles of the *S-2* flame at HAB = 1.2, 3.5 and 6 cm. Slopes of the 2nd Porod regime (*P2*) depicting the fractal dimension increase from D_f = 1.71 (mass fractal, HAB = 1.2 cm) to D_s = 2.76 (surface fractal, HAB = 3.5). Two slopes can be distinguished corresponding to the two size lengths of aggregates. At HAB = 6 cm large primary particles having smooth surface (slope equal to -4) are formed. The single slope is obtained indicative of non-aggregated particles which can be described by a single size (Camenzind *et al.* 2008).

Synthesis of aerosol nanoparticles by spark generation and their applications

Ryang Hwa Lee[1], Jeong Hoon Byeon[2], Jae Hong Park[1] and Jungho Hwang[1]

[1]Department of Mechanical engineering, Yonsei University, Seoul 120-749, Korea

[b]Digital Printing Division, Samsung Electronics Co., Ltd., Suwon 443-742, Republic of Korea

Spark generation has been used to generate monometallic particles of a wide range of conducting materials with particles sizes ranging from several nanometers up to ~ 100m in an aerosol state because spark generation is simple. A spark was generated between two either identical or different metal rods inside a reactor under a pure nitrogen environment. The flow rate of nitrogen gas, which was controlled using a mass flow controller was set to 3 L/min. The electrical circuit specifications are as follows: a resistance of 0.5M, a capacitance of 10 nF, a loading current of 2 mA, an applied voltage of 3.0 kV, and a frequency of 667 Hz.
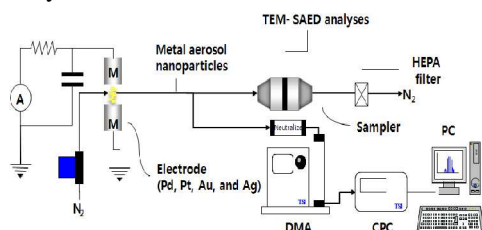
Figure 1. Setup for spark generation

This paper reports the generation and characterization of monometallic (palladium (Pd), platinum (Pt), gold (Au), and silver (Ag) from electrodes of the same material) and bimetallic (Pd–Pt, Pd–Au, and Pd–Ag from electrodes of different materials) aerosol particles produced using a spark discharge. The compositions of the bimetallic particles were measured at different combinations of materials and polarity of the spark electrode.
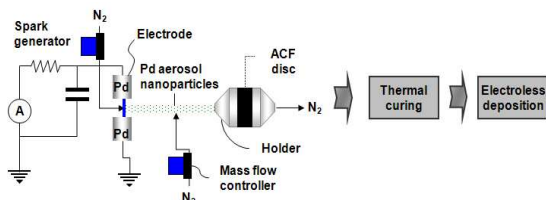
Figure 2. Procedures of conventional and aerosol activation

A method of catalytic activation with palladium aerosol nanoparticles produced by spark generation was introduced. These catalytic particles were deposited onto the surfaces of activated carbon fibers (ACFs). After thermal curing, the catalytically activated ACFs were placed into a solution for electroless deposition (ELD) of silver.
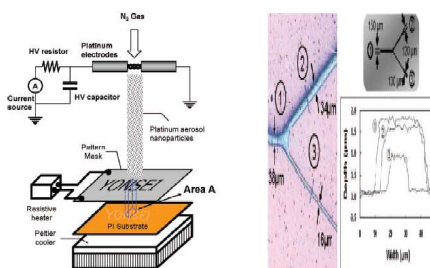
Figure3. Site-Selective Catalytic Surface Activation via Aerosol Nanoparticles for Use in Metal Micropatterning

Figure 3 shows an overview of our surface activation. The platinum nanoparticles were generated via spark discharge and carried by N2 gas to a PI substrate through the pattern hole (width, 100 μm; depth, 100 μm) of the "YONSEI" mask (Debora Electronics Co., Ltd., Korea) for a duration of 5 min
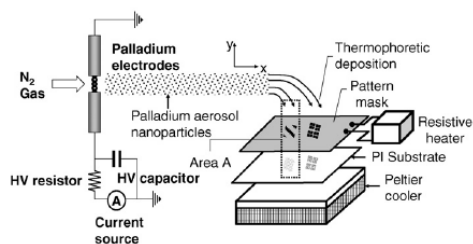
Figure4. Thermophoretic deposition of palladium aerosol nanoparticles for electroless micropatterning of copper

As shown in Fig. 4, the particles were detached from the horizontal flow streamlines and deposited on the PI substrate by thermophoresis due to the temperature distribution inside the dotted area A in Fig. 4

Byeon. J. H., Park, J. H., Hwang, J. (2008) *J. Aerosol Science* 39, pp 888 – 896

Byeon. J. H., Ko, B. J., Hwang, J. (2008) *J. Phys. Chem C* 112, pp 3627 - 3632

Byeon. J. H., Park, J. H., Yoon, K. Y., Hwang, J. (2008) *Langmuir* 24, pp 5949 – 5954

Byeon. J. H., Yoon, K. Y., Jung, Y. K, Hwang, J. (2008) *Elec. communications* 10, pp 1272 - 1275

Decomposition and formation of Si nanoparticles in the chemical vapour synthesis process

A. Lähde[1], K. Vuorikari[1], U. Tapper[2] and J.J. Jokiniemi[1,2]

[1]University of Kuopio, Department of Environmental Science, Fine Particle and Aerosol Technology Laboratory, P.O. Box 1627, FI-70211 Kuopio, Finland.
[2]VTT Technical Research Centre of Finland, Fine Particles, P.O. Box 1000, 02044 VTT, Espoo, Finland

Keywords: silicon, nanoparticles, chemical vapour synthesis.

Silicon nanoparticles have many applications including LEDs (Lee et al. 2004), bioprobes (Dubertret et al. 2002), semiconductors (Bapat et al. 2004) and solar cells (Raniero et al. 2005). However, the full exploitation of solid nanocrystalline powders such as nano-sized silicon particles require powders of narrow size distribution, low agglomeration and high purity (Winterer 2002). This paper presents a chemical vapour synthesis method (CVS) for the preparation of Si- nanoparticles. CVS is based on the vaporisation of the precursor material and the subsequent decomposition in the high temperature aerosol reactor. It enables the preparation of ultrafine particles with a narrow size distribution.

The silicon particles were produced with the CVS at temperatures between 400 and 800 $^{\circ}$C. Hexamethyldisilane (HMDS) was used as precursor with the addition of toluene at temperatures between 400 and 600 $^{\circ}$C. The precursor solution was atomized to droplets with a constant output atomizer (TSI, model 3076). The carrier gas (N_2/H_2 10%) flow rate varied between 2.2 l/min and 3.3 l/min. The aerosol exiting the heated zone of the reactor was diluted with N_2 with a flow rate of 15 l/min using an axial diluter.

The decomposition products of HMDS at different temperatures were monitored directly from the gas phase with the aerosol mass spectrometer (AMS) and Fourier transform infrared (FTIR). Furthermore, the amount of elemental and organic carbon on the particles was analysed from the filter samples. The particle number size distribution was measured with a SMPS (TSI 3081, CPC 3775). The structure and composition of the particles was analysed with transmission (TEM, Philips CN-200 FEG/STEM) and scanning electron microscopes (FE-SEM, Leo Gemini DSM 982).

The decomposition of the precursor, particle formation and final particle composition was dependent on the reactor temperature. The amount of methane and ethylene increased with the increasing reactor temperature indicating the decomposition of HMDS at high temperatures. However, around 29% of organic carbon was observed in the filter samples collected at 800 $^{\circ}$C according the analysis of carbonaceous materials. This is either due to the incomplete decomposition of HMDS or recondensation of some organic species in the sampling.

CVS enables the preparation of nanoparticles with the narrow size distribution with the geometric standard deviation below 1.5. According the SMPS measurements the geometric mean diameter of particles varied between 20 nm and 100 nm depending on the amount of HMDS fed to the reactor and the reactor parameters. Figure 1. shows the shape of Si-particles. The particles were mainly spherical and agglomerated. According the elemental analysis the particles consisted both Si and SiO_2.
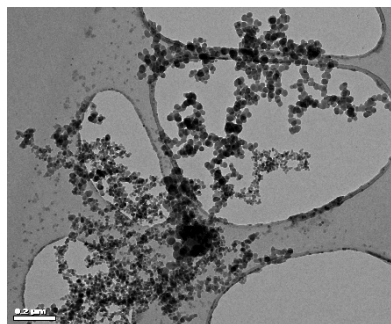
Figure 1. TEM image of silicon particles produced at 700 $^{\circ}$C from HMDS.

The formation of silicon nanoparticles by the chemical vapour synthesis was studied. Silicon particles with a narrow size distribution were obtained. The primary size of particles was around 20 nm. The decomposition of HMDS and subsequently the composition of particles was dependent on the operation temperature of the reactor.

Lee, S., Cho, W., Han, I. K., Choi, W. J. and Lee, J. I. (2004). *Phys. Status Solid B*, 241, 2767.
Dubertret, B, Skourides, P., Norris, D. J., Noireaux, V., Brivanlou, A. H. and Libchaber, A. (2002). *Science*, 298, 1759.
Bapat, A., Anderson, C., Perrey, C. R., Carter, C. B., Campbell, S. A. and Korsthagen, U. (2005). *Plasma Phys. Controlled Fusion*, 46, B97.
Raniero, L., Zhang, S., Aguas, H., Ferreira, I., Igreja, R., Fortunato, E. and Martins, R. (2005). *Thin Solid Films*, 487, 170.Winterer, M. (2002). *Nanocrystalline Ceramics*, Springer, New York.

Nucleation of ibuprofen nanoparticles from supersaturated vapor

A. A. Onischuk, A. V. Samodurov, E. E. Elantseva, V. V. Karasev, A.M. Baklanov

Institute of Chemical Kinetics & Combustion, RAS, Novosibirsk, 630090, Russia

Nucleation of water insoluble drugs is of high interest now in the light of numerous advantages which gives the nanoparticle lung administration with respect to the traditional oral therapy or injection delivery. Ibuprofen is a nonsteroidal, chiral, anti-inflammatory drug with poor water solubility. Here we study the mechanism of ibuprofen nanoparticle formation via nucleation from supersaturated vapour in a horisontal flow chamber. The chamber is made of a molybdenum glass tube (with the inner diameter of 0.8 cm) with an outer heater. Argon flow is supplied to the inlet of the generator through the Petrianov's high efficiency aerosol filter at the rate of 8 cm^3/s (at standard temperature and pressure). The original substance (racemic ibuprofen from Ratiopharm, Germany) is put to the hot zone inside the tube. The saturated vapor is formed inside the chamber. The temperature drops down at the outlet of the heated zone resulting in vapor supersaturation and nucleation. The aerosol concentration and size distribution (Fig. 1) were measured with the Automatic Diffusion Battery designed and built at the Institute of Chemical Kinetics and Combustion, Novosibirsk, Russia.

Fig. 1. Mean particle diameter and number concentration vs. temperature in the saturated vapor zone of flow chamber (as measured by the Automatic Diffusion Battery).

The powder X-ray diffraction patterns of nanoparticles and original powder are compared in Fig. 2. Both XRD patterns from nanoparticles and

original substance correspond to racemic ibuprofen, i.e. the nanoparticles form the same crystal phase as the original substance. The small difference in the peak relative intensities between the curves a and b in the range $17 < 2\theta < 21$ is probably related to the difference in distribution of crystallographic orientations in the micro-sized original powder and nanoparticles.

Fig. 2. X-ray diffraction patterns of a) original ibuprofen powder, b) ibuprofen nanoparticles formed *via* evaporation-nucleation route (mean particle diameter $d = 85$ nm).

The nucleation rate was determined by the video observation of the light scattered from the nucleation zone particles to be 10^6 cm^{-3}s^{-1}. The surface tension of critical nucleus was determined from the experimentally measured nucleation rate as a function of radius (Fig. 3).

Fig. 3. Surface tension of critical nucleus vs. radius.

Synthesis of Zirconia-Alumina Core-Shell Nanoparticles by Liquid Flame Spray

M. Aromaa[1], J.-P. Nikkanen[2], J.B. Wagner[3], E. Levänen[2], T. Mäntylä[2] and J.M. Mäkelä[1]

[1]Aerosol Physics Laboratory, Tampere University of Technology, Tampere, Finland
[2]Department of Materials Science, Tampere University of Technology, Tampere, Finland
[3]Center for Electron Nanoscopy, Technical University of Denmark, Lyngby, Denmark

Keywords: Aluminum oxide nanoparticles, Core-shell nanoparticle, Liquid Flame Spray, Nanoparticle production, Zirconia.

Liquid Flame Spray technique (LFS) can be applied in synthesis of multi-component systems of nanoparticles from liquid precursors. (Mäkelä et al.) It can be utilised for a great variety of materials. Here, we have synthesised zirconia-alumina nanoparticles and characterised.

The particles were synthesised by Liquid Flame Spray from aluminum isopropoxide and zirconium n-propoxide dissolved in xylene. (Nikkanen et al.) The oxygen and hydrogen gas flows in LFS were 20 l/min and 40 l/min, respectively. The liquid feed rate was 5.2 ml/min. The mass concentrations of one component liquids were 1:10. Synthesised nanoparticles were measured using scanning mobility particle sizer (SMPS, TSI Inc.). The particles were also deposited in flame on tunnelling electron microscopy (TEM) grids and collected using electrostatic precipitator for X-ray diffraction analysis (XRD).

SMPS measurements of the nanoparticles (Fig. 1) show mean particle sizes for zirconia and alumina 56 nm and 62 nm, respectively. For binary system of zirconia-alumina particles, the mean particle size is 72 nm. SMPS data also shows that the total particle concentration of the individual systems and two-component system are approximately the same.
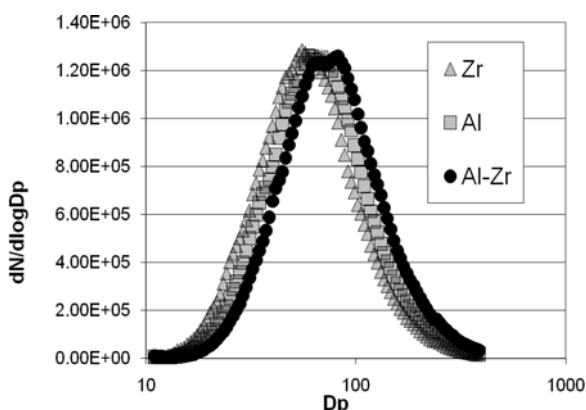
Figure 1. SMPS distributions of one component zirconia (triangle) and alumina (square) nanoparticles and two-component zirconia-alumina (sphere) nanoparticles

From SMPS data, it can be concluded that the particles may have a core-shell structure. High resolution TEM analyses of deposited particles (Fig. 2) show a clear core-shell structure. More thorough analysis reveals that the core is formed of zirconia and therefore the shell is alumina. In all images, a uniform alumina shell is observed.
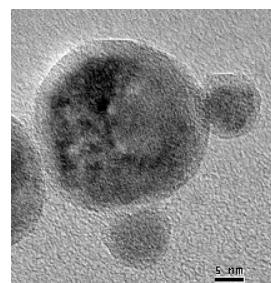
Figure 2. High resolution TEM image of the deposited zirconia-alumina core-shell particles. Scale bar 5 nm.

XRD analysis of the collected powder confirms the TEM observation of crystalline zirconia. Tetragonal phase of zirconia is observed in XRD. There are no peaks of crystalline alumina in XRD spectrum. Alumina shell is amorphous on top of tetragonal zirconia core.

It needs to be noted that we obtain crystalline alumina when synthesizing it in one component system alone. Also, the ZrO_2–Al_2O_3 core-shell particles obtained in literature (Kim and Laine, Chandradass and Bae) consist of crystalline alumina (δ and α, respectively). Interestingly, our particles have an amorphous alumina shell.

Mäkelä, J.M. et al. (2004). J. Mater. Sci., 39, 2783-2788.
Nikkanen, J.-P. et al. (2008). *Research Letters in Nanotechnology*, 516478, 4p.
Kim, M. and Laine, R.M. (2007). *J. Ceram. Proc. Res.*, 36, 129-136.
Chandradass, J. and Bae, D.-S. (2009). *J. Alloys and Comp.*, 469, L10-L12.

Magnetic nanoparticles by chemical vapour synthesis

J. Hukkamäki[1], R. Niiranen[1] and J. Jokiniemi[1,2]

[1]University of Kuopio, Department of Environmental Science, Fine Particle and Aerosol Technology Laboratory, P.O. Box 1627, FI-70211 Kuopio, Finland
[2]VTT Technical Research Centre of Finland, Fine Particles, P.O. Box 1000, FI-02044 VTT, Finland

Keywords: gasphase synthesis, magnetic nanoparticles, ferrocene, size distribution.

Magnetic nanoparticles are widely studied because of their interesting and versatile properties that are desirable in many applications, including for example magnetic fluids, catalysis, biotechnology, biomedicine, magnetic resonance imaging, data storage and environmental remediation (Lu *et al*., 2007). Distinctive chemical, electronic, optical, magnetic and mechanical properties of nanoparticles arise from large fraction of surface atoms (i.e. high surface-to-volume ratio) as well as their size effects.

Aim of this research is to study the effect of reaction conditions on the formation of magnetic nanoparticles. Preliminary results are presented in this abstract.

The method used for production of magnetic nanoparticles is Metal Organic Chemical Vapour Synthesis (MOCVS). In MOCVS a gaseous precursor decomposes thermally or due to reaction to form a low vapour pressure metal or metaloxide molecules, which start to form clusters and grow to larger "droplets" before crystallisation. After crystallisation the formed nanoparticles may still collide and stick together. Due to their small size and thermal effects the collided nanoparticles partly fuse together forming "necks" between the primary particles. In this study, ferrocene was used as a volatile organometallic precursor. According to Moisala *et al*. (2006) formation of iron particles start to take place in N_2 atmosphere at temperatures above 500 °C, but ferrocene vapour decomposition is incomplete at temperatures below 700 °C.

Experiments were performed with a tubular flow furnace. The furnace was operated at atmospheric pressure using temperatures of 700, 800 and 850 °C. The ferrocene precursor was mixed with silica gel in order to enhance nitrogen flow through the precursor bed and placed in a stainless steel container below the reactor tube. Nitrogen as carrier gas flowed through the precursor container at ambient temperature and atmospheric pressure. Except the temperature, experimental setup and conditions were the same in all experiments.

Number size distributions (presented in Figure 1) of the nanoparticles produced at different temperatures were measured with differential mobility analyser (DMA; TSI 3085) and ultrafine condensation particle counter (CPC; TSI 3025A). Prior to size distribution analysis all samples were diluted with nitrogen gas by the factor of 13.
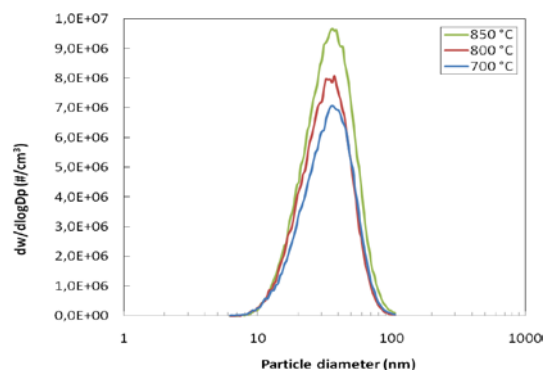
Figure 1. Number size distributions as a function of particle diameter for the diluted samples.

Transmission electron microscope (TEM; JEOL JEM-1200EX) samples were collected from the gas phase on carbon-coated copper grids. TEM image of the nanoparticles produced at 850 °C is shown in Figure 2.
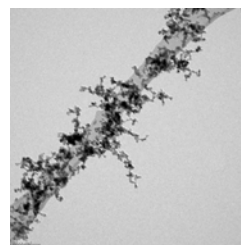
Figure 2. TEM micrograph of nanoparticles formed at 850 °C (magnification 150k).

At higher furnace temperatures concentration of nanoparticles increased, while average particle diameter remained almost intact. Nanoparticles produced at different temperatures all formed similar chainlike structures as shown in Figure 2.

Lu, A.-H., Salabas, E. L. & Schüth, F. (2007) *Angew. Chem. Int. Ed.*, 46, 1222-1244.
Moisala, A., Nasibulin, A. G., Brown, D. P., Jiang, H., Khriachtchev, L. & Kauppinen, E. I. (2006) *Chem. Eng. Sci.*, 61, 4393-4402.

Composite CuO$_x$-SiO$_2$ nanoparticle synthesis by MOCVD

P. Moravec[1], J. Smolík[1], V.V. Levdansky[2] and M. Klementová[3]

[1]Laboratory of Aerosol Chemistry and Physics, Institute of Chemical Process Fundamentals AS CR, v.v.i., 165 02, Prague, Czech Republic

[2]Heat and Mass Transfer Institute NASB, 220072, Minsk, Belarus

[3]Institute of Inorganic Chemistry AS CR, v.v.i., 250 68, Husinec-Řež 1001, Czech Republic

Keywords: hot wall reactor, nanoparticles-generation, MOCVD.

Copper oxide particles have a wide field of applications as catalysts, sensors, semiconductors, etc. Silica composite materials containing different metal oxide particles present a variety interesting magnetic, electric and catalytic properties, and have attracted considerable attention (Yu *et al.*, 2008). In this work, we studied CuO$_x$-SiO$_2$ nanoparticle synthesis by metal organics chemical vapor deposition (MOCVD) using organo-compound precursors copper acetyl acetonate (CuAA) and tetraethyl orthosilicate (TEOS).

Particles were prepared in an externally heated glass tube flow reactor of the length 55 cm and i.d. 27 mm using nitrogen as a carrier gas. Particle synthesis was studied in the presence of oxygen in the reaction mixture (oxidation) and, in some experiments, also in the presence of water vapor. Experiments were performed at moderate reactor temperature (T_R) 500°C and particle production and their characteristics were studied in dependence on precursor concentrations (c_{CuAA}, c_{TEOS}), oxygen concentration (c_O), reactor flow rate (Q_R), and inlet section arrangement. Precursor concentrations were controlled either by the variation of the saturator temperature (T_S), or by the flow rate through the saturator. The particle production was monitored by SMPS and samples for particle characterization were deposited onto TEM grids and Sterlitech Ag filters. Particle characteristics were studied by SEM, TEM, HRTEM, SAED, EDS and XRD.

Particle production was influenced most of all by CuAA concentration, further by the process of precursor decomposition and the reactor flow rate, whereas the influence of TEOS concentration hardly exceeded reproducibility of the experiment. An addition of TEOS to CuAA in the reaction mixture did not result in formation of any new fraction of particles. That indicates binary particles (mixed or coated) were produced by the process.

Morphology of particles varied with experimental parameters of the process. Generally, primary particle size was at about 20 or 30 nm, they were more or less aggregated into clusters or chains, and they had a composite structure, see Figure 1. Also crystalline structure was significantly dependent on experimental conditions: concentration of precursors, oxygen concentration and also inlet section arrangement. In Figure 1 one can see electron diffraction pattern of monoclinic CuO (PDF ICDD 05-0661). At higher c_{CuAA} and/or lower c_O Cu$_2$O crystalline phase prevailed in the particles. At specific conditions, metallic Cu particles encased in the SiO$_2$ layer were prepared.
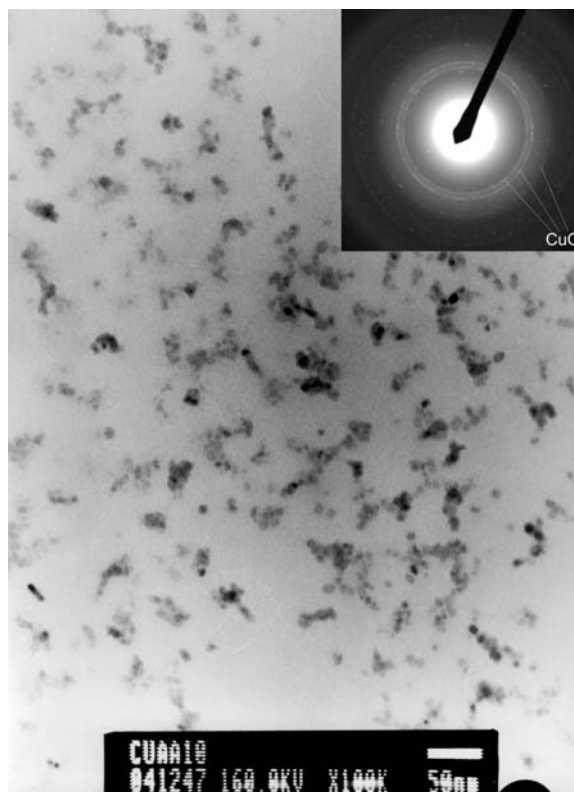
Figure 1. Bright field TEM image and SAED pattern of particles prepared at T_R=500°C, c_{CuAA}=2.5·10^{-7} mol/l, c_{TEOS}=2.4·10^{-6} mol/l, c_O= 10 vol. %.

Yu, Q., Ma, X., Wang, M., Yu, C., & Bai, T. (2008). *Appl. Surf. Sci.*, 254, 5089-5094.

Production and Characterization of Silicon Nanoparticles via Spark Discharge

A. Evirgen, V.A. Vons, D. Munao, U. Lafont, L.C.P.M. de Smet, E. M. Kelder and A. Schmidt-Ott

Faculty of Applied Sciences, DelftChemTech, TU Delft, Julianalaan 136, NL-2628 BL Delft, The Netherlands

Keywords: Spark discharge, nanoparticle production, silicon

In the last decade, nanoparticles have drawn great attention for applications in catalysis, energy storage, solar technology, nanoelectronics and sensor technologies. Although there are various methods to synthesize nanoparticles, the spark discharge generation (SDG) method has been recognized as a versatile technique to produce a wide range of metallic nanoparticles as it is clean and continuous (Schwyn *et al.*, 1988). However, up to now, there is no literature on aerosol generation of non-metallic or semi-conducting nanoparticles via spark discharge. The present work reports on synthesis of Silicon (Si) nanoparticles via SDG, which are very promising for Li-ion battery anodes and sensor applications through inertial impaction.

In this technique, a capacitor with a power supply is connected to the electrodes forming a spark gap. The SDG chamber confines these electrodes, one of which is in a high voltage and the other one is on ground potential. The breakdown of the carrier gas is followed by formation of a conducting channel. The rapid discharge of the capacitor via the gap results in a very high temperature and evaporation of electrode material. Nanoparticle formation takes place by rapid cooling of the vapour by the means of thermal radiation and expansion. In the case of semiconductor electrodes, the resistance of the source material limits the discharge current and therefore the spark energy and therewith the production rate (Tabrizi *et al.*, 2008).

At TU Delft, several studies on applications of spark-generated particles are ongoing. Currently, we are investigating the optimum conditions of the SDG for Si nanoparticles, by a variety of techniques, including transmission electron microscopy (TEM), Differential Mobility Analysis (DMA), and by looking at the electrical properties of the discharge.

In the present study, several different Si source configurations like silicon rods (intrinsic and boron-doped) and pieces of thin silicon wafers (intrinsic and boron-doped) were used, in order to optimize the process. The results showed that the resistance of intrinsic Si rods was quite high compared to boron-doped rods. Although, nanoparticles with primary particle sizes between 2.5-6 nm (Fig.1) were synthesized, the production rate was insufficient for further applications. In order to minimize the resistance in the case of intrinsic silicon, round wafers 2 mm in diameter and 0.5 mm thick were conductively bonded to the end of metallic rods perpendicular to these. This configuration substantially increased the production

rate with respect to intrinsic Si rods, but after the first few sparks, holes through the wafers formed. Thus, continuous production of Si nanoparticles was not possible with this configuration.
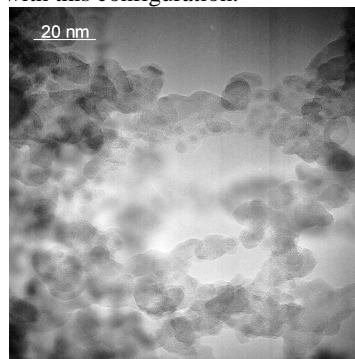
Figure 1. TEM image of produced Si nanoparticles

As compared to intrinsic Si electrodes, the use of lower resistance boron-doped Si rods (resistivity < 0.1 Ω.cm) resulted in a much higher discharge current and accordingly a much higher production rate. This is shown by the particle size distribution curves in Figure 2. The red curve is very promising, because it shows the feasibility of the SDG for Si nanoparticle production, in particular in view of sensor applications and anode material in Li-ion batteries. We plan to use low pressure impaction, as described by Peineke and Schmidt-Ott, 2007, to produce porous Si layers for both applications.
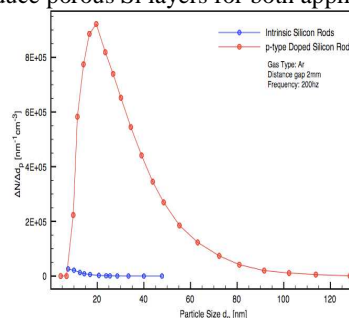
Figure 2. Particle size distributions of Si nanoparticles

Schwyn, S., Garwin, E., Schmidt-Ott, A. (1988). *Aerosol Generation by Spark Discharge*. J. Aerosol Sci., 19, 639.

Tabrizi, N.S., Ullman, M., Vons, V.A., Schmidt-Ott, A. (2008), *Generation of nanoparticles by Spark Discharge*, J. Nanoparticle Res., 11, 315.

Peineke, C., Schmidt-Ott, A., Proc. of PARTEC, Nuremberg, 2007

Analysing the electrical behaviour of the Spark Generator in view of novel applications

V.A.Vons[1], A. Evirgen[1], A. Schmidt-Ott[1]

[1]Nanostructured Materials, DelftChemTech, Faculty of Applied Physics, Delft University of Technology, Julianalaan 136, NL-2628 BL, Delft, The Netherlands

Keywords: Spark discharge generation, Nanoparticle production, Metal nanoparticles, Silicon

The spark discharge generator (SDG) is used to generate nanoparticles by evaporating electrode material using a repetitive discharge (Schwyn et.al., 1988, Tabrizi, Ullman et. al. 2008). Previous work (Tabrizi, Ullman et. al., 2008) has shown that the electrical behaviour of the spark can be modelled according to a simple RLC (resistance inductance capacitance) network. The inductance in the circuit is low, relatively small capacitances are used (20 nF), and the circuit resistance is negligeable. Since the resistance of the plasma quickly reaches a low and constant value (~2-5 Ω), this results in an underdamped oscillation of current and voltage (figure 1). In the same figure a fit of the data is displayed. Deviation between the fit and actual data at the onset of the discharge is due to the fact that the plasma resistance reaches a steady state value only after ~0.2 μs. This can be accounted for only in a numerical solution, not in the analytical form used here. For the remainder of the discharge however, the fit corresponds very well to the data. The same holds for the current.
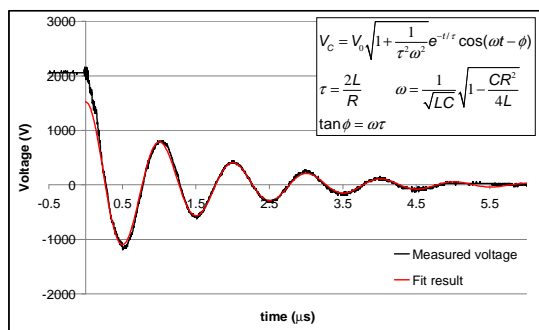
Figure 1: Voltage over capacitorbank. Mg electrodes, 2mm gap, 1 L/min Ar gas. Formulas used for the fit are given in the figure.

Results of applying this simple model to the production of particles using the SDG are presented here. Firstly, the SDG is exceptionally well suited for mixing different materials (Tabrizi, Xu et. al., 2008). One way of doing this is to use electrodes of two different materials. Normally the ratio between the two materials in the resulting nanoparticles cannot be altered except by switching high voltage and ground electrode materials, resulting in two fixed ratios. By adding external resistances to the discharge circuit however, we were able to change the waveform and thus the erosion rates of the electrodes and consequently the composition of the end product.

The resultant waveforms again fit the model very well.

Secondly, the production rate for the semiconductor silicon in the SDG was disappointing so far. Analysis of the waveforms obtained for intrinsic silicon with the model showed that the resistance in the RLC network was very high (~140 Ω) due to the limited conductivity of the silicon rods, resulting in a non-oscillating overdamped discharge. Instead of a high current short duration discharge, a much longer lasting low current discharge is obtained. Visual observation confirmed this.

Doped silicon has a much lower resistance compared to intrinsic silicon. When doped rods were used instead, we were able to increase the production rate by a factor of 10^2-10^3, based on measurements using a TSI3071 Differential Mobility Analyzer (with a new TSI3077A Kr-85 neutralizer) and a Faraday Cup Electrometer or a TSI 3085 Condensation Particle Counter. This result is expected from the model. A comparison between two typical size distributions is given in figure 2. Clearly the production rate for doped silicon is much higher.
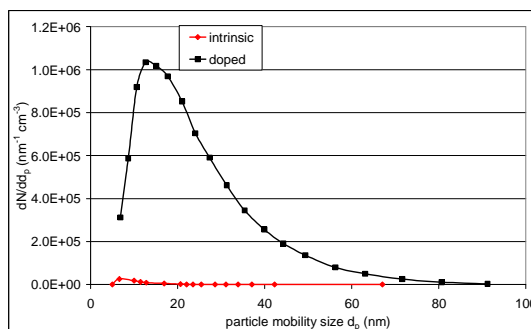
Figure 2: particle size distributions for intrinsic and doped Si. 2 mm gap, 1 L/min Ar.

Tabrizi, N.S., Ullman, M., Vons, V.A., Schmidt-Ott, A. (2008), *Generation of nanoparticles by Spark Dicharge*, J. Nanoparticle Res., 11, 315

Tabrizi, N.S., Xu, Q., Van der Pers, N.M., Lafont, U., Schmidt-Ott, A. (2008). *Synthesis of mixed metallic nanoparticles by Spark Discharge*, J. Nanoparticle Res., accepted.

Schwyn, S., Garwin, E., Schmidt-Ott, A. (1988). *Aerosol Generation by Spark Discharge*. J. Aerosol Sci., 19, 639.

Production of metallic magnesium using Spark Discharge

V.A. Vons[1], H. Leegwater[2], W. Legerstee[2], S. Eijt[2], A. Schmidt-Ott[1]

[1]Nanostructured Materials, DelftChemTech, Faculty of Applied Physics, Delft University of Technology, Julianalaan 136, NL-2628 BL, Delft, The Netherlands
[2]Fundamental Aspects of Materials and Energy, Department of Radiation, Radionuclides and Reactors, Faculty of Applied Physics, Delft University of Technology, Mekelweg 15, NL-2629 JB, Delft, The Netherlands

Keywords: Spark Discharge Generation, Metal nanoparticles, Metalhydrides, Hydrogen Storage, Magnesium

Many types of light metal nanoparticles are interesting for hydrogen storage (Schlapbach & Zuttel, 2001). However, light metal nanoparticles are readily oxidised by both oxygen and water. We investigated the possibility of producing *metallic* nanoparticles from magnesium using spark discharge generation (SDG, Tabrizi et. al. 2008). Particles made using this method are small, crystalline, and can be mixed very well with for instance catalysts and modifiers.

Argon carrier gas was first purified to <1 ppb using molecular sieve and copper catalyst. The entire setup was carefully leak tested, and outgassed to remove any adsorbed water. Before collection of the particles on a 0.45 μm pore size PVDF membrane filter, the spark generator was left to run for at least one hour to remove any traces of water and oxygen. The filter holder was sealed off and carried to an argon filled glovebox. Particles were analysed using Differential Mobility Analysis (DMA) and Transmission Electron Microscopy (TEM), the latter in combination with Electron Dispersive X-ray Spectroscopy (EDX) and electron diffraction. Samples could be inserted into the TEM without exposure to air due to a special sample holder. The hydrogen storage capacity was measured using a thermal desorption spectroscopy (TDS) setup.

The TDS experiments showed that the nanoparticles were capable of absorbing up to 3.5 wt% of hydrogen. The loss in capacity from the maximum of 7.6 wt% for bulk Mg is certainly due in part to oxidation, but we expect that longer loading times (so far, the particles were exposed to hydrogen for relatively short times at low pressures) and the addition of catalysts will raise the measured wt% significantly. Furthermore, for very small particles the actual maximum is reportedly lower due to narrowing of the pressure plateau (Eastman et. al., 1993). A very interesting observation is that when hydrogen is present in a small concentration (5 vol.% @ 1 atm. Ar) in the spark generator, the particles take up a significant amount of hydrogen (3 wt%) in or directly after the spark, even though normally much higher hydrogen pressures are required for any significant uptake by Mg.

A representative TEM micrograph of the particles is shown in figure 1. The particles are highly agglomerated, and there is a large variation in the primary particle sizes. EDX clearly shows the presence of Mg, but also oxygen, and the electron diffractograms only show MgO. Most of the lattice spacings observed can also be assigned to MgO, only some Mg could be found.

However, TDS results (as well as the colour of the obtained powder, pitch-black) suggest the presence of much more metallic Mg. In the micrographs, the outer layer of primary particles seems darker (i.e. more dense) that the core, and most visible lattice spacing are located in the outer layer. Since MgO is much denser than Mg (3.58 g/cm^3 vs. 1.78 g/cm^3) and always forms from the outside inwards, it is highly likely that these darker layers are MgO, whereas the lighter core is Mg. Also, the Mg forms very rapidly during the spark, whereas the MgO forms from the Mg in a much slower oxidation process. Therefore, it is expected that MgO domains are larger than Mg domains, and thus more likely large enough to diffract electrons and to show visible lattice spacings.
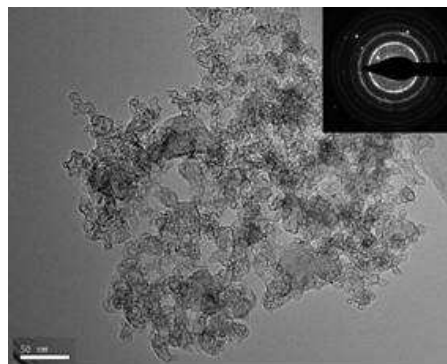
Figure 1: TEM micrograph of produced particles.

Concluding, this work demonstrates the possibility of producing at least partly metallic nanoparticles of a sensitive light metal using SDG.

Schlapbach, L., Zuttel, A. (2001). *Hydrogen-storage materials for mobile applications*, Nature, 414, 353.

Tabrizi, N.S., Ullman, M., Vons, V.A., Schmidt-Ott, A. (2008), *Generation of nanoparticles by Spark Dicharge*, J. Nanoparticle Res., 11, 315.

Eastman, J.A., Thompson, L.J., Kestel, B.J., *Narrowing of the palladium hydrogen miscibility gap in nanocrystalline palladium*, Phys. Rev. B, 48, 84.

Production of Equally Sized Atomic Clusters by a Glowing Wire

C. Peineke[1], M. Attoui[2], R. Robles[3], A.C. Reber[3], S.N. Khanna[3], A. Schmidt-Ott[1]

[1] Nanostructured Materials, Faculty of Applied Sciences, Delft University of Technology, Julianalaan 136, NL-2628BL Delft, The Netherlands
[2] Département de Physique, Faculté des Sciences et Technologie, Université Paris XII, France
[3] Department of Physics, Virginia Commonwealth University, Richmond, Virginia 23284.

Keywords: atomic clusters, superatoms, nano-DMA, wire generator.

Unexpected behavior is found as the particle size is reduced to the atomic cluster range. For example, clusters of non-magnetic solids are found to be magnetic and clusters of noble metals are found to be strong catalysts. Every atom counts in the cluster regime. Using stable clusters, it will be possible to form cluster assembled materials as demonstrated in the case of the fullerenes. Certain stable species mimic the chemical behavior of atoms. These *superatoms* form a new dimension of the periodic table (Khanna et al., 1995). A major challenge in experimental studies on atomic clusters is to produce *arbitrary pure and well defined samples*. In view of cluster assembled materials, increase of the production rate with respect to existing vacuum technology is desired. The present study, to be published shortly in more detail (Peineke et al., 2009), represents a major step regarding these challenges.

In 2007, Peineke and Schmidt-Ott had shown that charged species emitted from a glowing wire produce spikes in the mobility distribution attributed to clusters of outstanding stability (magic numbers). Improved differential mobility classifiers have been applied to nanoparticles, gas ions and large molecules in the past, but not to metallic atomic clusters, in lack of a suitable source of charged clusters.

A resistively heated metal wire is shown to be such a source. Ag_nK^+ clusters are obtained from wires containing silver, with traces of potassium. They are size classified with a differential mobility analyzer, and their relative abundance is determined as a function of the inverse mobility (Upper curve, fig. 1). First principles calculations yield the stability of Ag_n in terms of the removal energy of Ag (fig. 1 (lower curve)). We assign the first peak of the mobility curve to K^+ and the first prominent one to the first stable cluster, Ag_2K^+. These species were also observed in a mass spectrum. The pronounced odd-even oscillation of the calculation then agrees well with the mobility distribution. The distance between the peaks decreases with growing number of atoms, n, in agreement with an estimated relation for $Z^{-1}(n)$.

The calculated Ag_nK^+ cluster properties are similar with respect to the pure Ag_n clusters in terms of energetic and electronic stability and cluster structure. Thus K^+ attachment is an ideal, non-invasive way of charging, which enables mobility classification. Using the heated wire as the source of atomic clusters and simultaneously as the source of K^+ ions leads to selective charging of the clusters, while contaminants in the inert gas remain uncharged. This explains the absence of "gas ion" peaks, which normally occur in mobility spectra in the present size range. As the equally-sized clusters are available for reactivity, coalescence and deposition studies, the method presented demonstrates the power of aerosol technology in the field of atomic clusters.
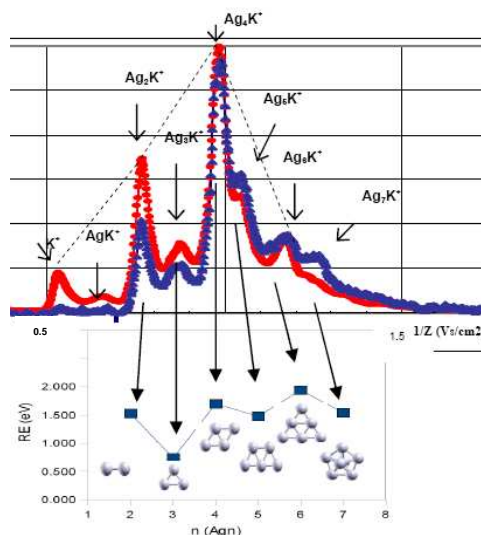
Figure 1. Mobility distribution of Ag_nK^+ (red: Pd wire containing Ag and K; blue: Ag wire containing K) and calculated stability in terms of Ag removal energy.

Fournier, R., J. (2001), Chem. Phys. 115, 2165.
Fernández de la Mora, J., de Juan L., Eichler, T., & Rosell, J. (1998). Trends in Anal. Chem., 17, 328-339.
Khanna, S. N. & Jena, P. (1995). Phys. Rev. B 51, 13705.
Peineke, C., Schmidt-Ott, A. (2007) PARTEC 2007, Nurnberg, Germany, 27.3. – 29.3.2007.
Peineke, C., Attoui, M., Robles, R., Reber, A.C., Khanna, S.N., & Schmidt-Ott, A. (2009). To be publ. J. Aerosol Sci.

Gas-phase synthesis of highly-specific nanoparticles on the pilot-plant scale

T.P. Hülser[1], S.M. Schnurre[1], H. Wiggers [1-3], C. Schulz [1-3]

[1]IUTA, Institute for Energy and Environmental Technology, 47229 Duisburg, Germany
[2]IVG, Institute for Combustion and Gas Dynamics, University of Duisburg-Essen, 47057 Duisburg, Germany
[3]CeNIDE, Center for NanoIntegration Duisburg-Essen, 47057 Duisburg, Germany

Keywords: Nanoparticles, Particle characterization, Particle formation and growth, pilot-plant

Highly-specific nanoparticles provide promising properties for a large variety of applications as the size dependence of their properties allows to tailor materials for specific applications. Synthesis of nanoparticles can follow two fundamentally different routes: wet-chemical and gas-phase synthesis. While wet-chemical synthesis usually ends up in materials grown by thermodynamic control, gas-phase processes enable for a kinetic control of nanoparticle formation. Therefore, this method is favoured for the formation of metastable materials liked doped nanoparticles and nanocomposites. A variety of different reactor concepts like hot-wall reactors, plasma reactors, flame reactors, and laser reactor have been described in literature. Industrial nanoparticle production, however, is covered by flame processes as they enable cost-effective production with high throughput. The quality of the resulting materials is limited and often agglomerates with a broad size distribution are formed. Highly specific nanomaterials, however, are synthesized in specific lab-scale reactors – and are often available in minute quantities only. Therefore, subsequent processing steps cannot be studied and many nanomaterials that require sophisticated synthesis technologies have not yet found their way into practical applications.

Based on our experience with different types of lab-scale reactors, we designed a unique pilot-plant-scale particle synthesis plant enabling for three different synthesis routes using either a hot-wall reactor, a flame reactor or a plasma reactor. In these reactors the energy required for precursor decomposition is provided by either an electrical heat source, a flame, or a microwave-supported plasma. Depending on precursor and gas-phase composition, materials like metals, metal oxides or semiconductors are generated. The chemical composition of the nanoparticles can be adjusted to pure, doped, mixed and composite materials. Pressure, precursor concentration, and residence time can be varied over a wide range to fine-tune particle size and morphology.

The facility generates passivated pure and doped silicon nanoparticles, passivated iron particles, iron-oxide and different metal oxides like titanium dioxide with structures sizing between a few nm and a few μm.

The reactors provide ample opportunities for sampling and in-situ measurements like in-situ laser diagnostics, molecular-beam particle mass spectrometry, and gas chromatography with subsequent mass spectrometry (GC/MS). Based on the multiple characterization methods we are able to fully characterize the reaction processes and to provide information for the development and validation of numerical simulations describing particle formation and growth. Due to the ability of continuous synthesis and on-line diagnostics, nanoparticulate materials with different size-distributions and degrees of agglomeration can be produced.

The reactors enable for the synthesis of significant amounts of nanoparticles, which can be up to kg/h without losing their specification. Therefore, we are able to produce sufficient amounts for first approaches in industrial processes to develop and enable nanoparticle-based materials with new properties.

Figure 1: 3-level Nanoparticle synthesis plant: Filter system in front of the image on the ground level; reactors on the first and second level.

Structural Stabilization of Metal Nanoparticles

M. Seipenbusch, A. Binder, H. Shi

Institut für Mechanische Verfahrenstechnik und Mechanik Universität Karlsruhe (TH), Am Forum 8, 76131 Karlsruhe, Germany. Phone: +49 721 6082416; Fax: +49 721 608 6563

Keywords: sintering, nanoparticles, agglomerates, aerosol microstructure

The increase of particle size and the loss of surface area of nanostructured systems are problematic whenever the retention of these characteristics is necessary to maintain their functionality. A prominent example for this is heterogeneous catalysis where the activity of a catalyst depends on the specific surface area but in many cases also inherently on the particle size. Particle growth and the loss of surface area following sintering therefore lead to a loss in activity and eventually to a deactivation of the catalyst (Bartholomew 2001).

Stabilization of the nanostructure of particulate systems has received increased attention in recent years (Gabaldon 2007; Sault et al 2002; Hayashi et al. 2002). Experimental work has been done on the stabilization of oxides with respect to particle size and crystal phase, for materials like titania, zirconia and alumina, used in photocalytic applications or as catalytic support materials (Hayashi et al. 2002).

In agglomerates of metal nanoparticles the presence of impurities on the surfaces of the particles had a very strong effect on the kinetics of sintering (Seipenbusch et al. 2003) as well as on the kinetics of the restructuring of the agglomerates (Weber and Friedlander 1997).

In this work the structure of aerosol Pd nanoparticle agglomerates was stabilized against a loss of surface area during tempering by application of a thin silica coating using chemical vapour deposition in the gas-borne state. The coating was applied to the surfaces of particles prior to agglomeration and to the already formed structure, yielding two different types of structures. The pure Pd and the stabilized structures were tempered at varied residence times and temperatures to analyze the sintering kinetics as a function of the type of structure. Stabilization of the primary structural elements, the nanoparticles, was accomplished for both coating approaches. A stabilization of the superordinate structure of the ensemble however was only possible by a coating of the agglomerate as a whole. Fig 1 shows the diameters of the primary particles and the agglomerate mobility diameter at various sintering temperatures for clean and silica coated Pd particles. For uncoated Pd particles the decrease of agglomerate size is paralleled by an increase of the primary particle size due to sintering. At 600°C the equilibrium particle size of complete coalescence is reached. At higher temperatures evaporation sets in leading to a decrease of the primary particle size after re-condensation, but an increase of the agglomerate size due to agglomeration of the newly formed particles at room temperature. The coated agglomerates however are effectively stabilized both against restructuring and primary particle coalescence (see Fig 1). Only a slight increase of the primary particle size was observed at 800°C.

The Koch/Friedlander model proved to be in reasonable agreement with all experimental data using one set of parameters in the fit. Although the time scale of the aerosol experiments were limited, the kinetics derived thereof could be extrapolated to higher temperatures and particle sizes in agreement with the experimental data.

The structural stabilisation by surface coating leads to a loss in available metal surface area, as could be shown in catalytic experiments. This loss of about one fourth of the catalytic activity however is small compared to the fourfold loss of surface area by sintering which is prevented by the coating.
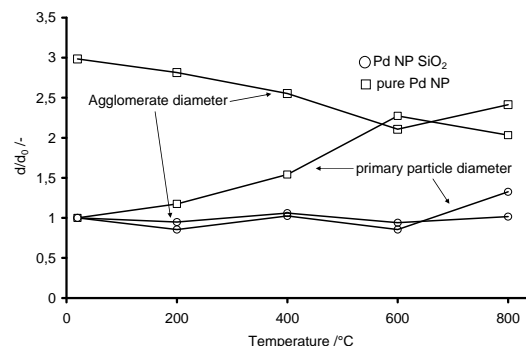
Fig. 1: Sintering of Pd agglomerates as produced and coated in the agglomerated state.

Bartholomew CH (2001). *Appl. Catal*. A 212:17–60.

Gabaldon JP, Bore M, Datye AK (2007) *Top. Catal.* 44:253-262.

Hayashi K, Horiuchi T, Suzuki K et al. (2002) *Catalysis Letters* 78:43-47.

Koch W, Friedlander SK (1990). *J. Aerosol Sci.* 21:S73–S76.

Seipenbusch M, Weber AP, Schiel A et al. (2003). *J. Aerosol Sci*. 34:1699–1709.

Weber AP, Friedlander SK (1997). *J. Aerosol Sci.* 28:179-192.

Aerosol synthesis and stabilization of supported metal nanoparticles

A. Binder[1], M. Seipenbusch[1] and G. Kasper[1]

[1] Institut für Mechanische Verfahrenstechnik und Mechanik , Universität Karlsruhe (TH), Strasse am Forum 8, 76131, Karlsruhe, Germany

Keywords: aerosol coating, CVD, metal nanoparticles, sintering, Nanoparticle generations

In heterogeneous catalysis the decrease of active surface area due to sintering at high process temperatures and the consequent loss of activity is still a huge problem, particularly if the activity also depends on the size of the active particles (for so-called structure-sensitive reactions). Therefore, sintering behaviour and stabilization of supported nanostructured particles is intensively studied in recent years (Gabaldon 2007, Lu 2007).

In this work, highly dispersed palladium was deposited on oxide nanoparticles like SiO_2 or TiO_2 from metal-organic precursors by a continuous gas phase process at atmospheric pressure (Binder 2007). The support particles were generated by chemical vapour synthesis (CVS) in a nitrogen-oxygen mixture in a hot-wall reactor. Downstream, the carrier particles were directly coated with palladium in the aerosol state by metal-organic chemical vapour deposition (MOCVD). In order to study the sintering kinetics of the supported Pd particles, the functionalised particles were fed through an oven directly after the coating reactor and sintered in the aerosol state. The sintering behaviour of the Pd supported on SiO_2 and TiO_2 were investigated by HR-TEM image analysis and the kinetic data were compared. The structure of the Pd particles was stabilized against coalescence by immobilization of the particles in one case by a modification of the carrier particles by doping with a second oxide phase and in another by application of a thin HfO_2-film using a second CVD process in the aerosol state. The influence of the stabilization on the catalytic activity was tested by the hydrogenation of ethene.
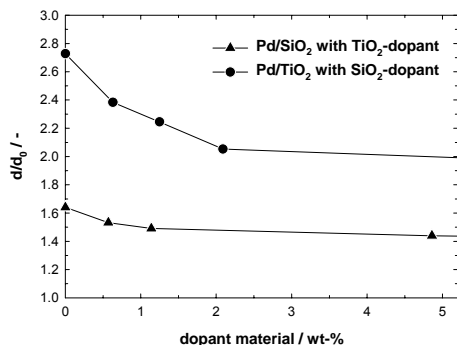
Fig. 1 shows the influence of the modification of the support particles on the sintering behaviour at 800°C. The integration of a second oxide phase into the matrix of the support particles results in a defect of the surface structure which affects the mobility of the Pd particles (Landes 1999). As can be seen from fig 1, a small amount of a second oxide phase on the support has a great influence on the sintering behaviour of the Pd particles, especially for the TiO_2 support, on which the Pd is less stable than on the SiO_2 support. For example, 2 wt% of SiO_2 in the TiO_2 matrix reduces the change in relative Pd particle size from 2.8 to 2.

Because the modification of the support is not applicable for all catalytic systems, the Pd particles are also stabilized by depositing small amounts of HfO_2, which acts as impurity and diffusion and coalescence barriers. In fig. 2 the sintering kinetics of Pd/SiO_2 and with HfO_2 stabilized Pd/SiO_2 particles at 400°C. One can see that the unstabilized Pd particles resulted in a nearly threefold increase of the particle size after 14s, while the coating of the Pd/SiO_2 particles with HfO_2 slows down the sintering process. At higher Hf-precursor concentrations even a prevention of sintering was achieved at conditions which result in a threefold Pd particle size without stabilization.
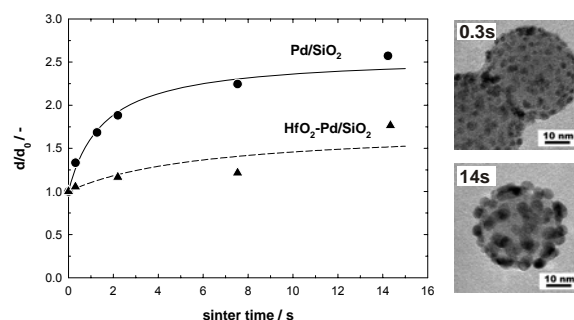
Fig. 2. Sintering of SiO_2 supported Pd particles (●) with corresponding TEM images on the right and with HfO_2 stabilized Pd/SiO_2 (▲) at 400°C.

Binder, A., Heel, A., Kasper, G. (2007) *Chem. Vap. Deposition*, 13:48–54.

Gabaldon, J.P., Bore, M., Datye, A.K. (2007) *Top. Catal.* 44:253-262

Landes, H. (1999) *PhD thesis* LMU München

Lu, J.-L., Weissenrieder, J., Kaya, S., Gao, H.-J., Shaikhutdinov, S., Freud, H.-J. (2007) *Surf. Rev. Lett.* 14:927-934

Fig. 1. Change of the Pd particle diameter d relative to the initial particle size d_0 on modified SiO_2 (▲) and modified TiO_2 (●) particles.

Coated highly porous metal hydride nanoparticle layers for hydrogen storage

V.A. Vons[1], H. Leegwater[2], W. Legerstee[2], S. Eijt[2], A. Schmidt-Ott[1]

[1]Nanostructured Materials, DelftChemTech, Faculty of Applied Physics, Delft University of Technology, Julianalaan 136, NL-2628 BL, Delft, The Netherlands
[2]Fundamental Aspects of Materials and Energy, Department of Radiation, Radionuclides and Reactors, Faculty of Applied Physics, Delft University of Technology, Mekelweg 15, NL-2629 JB, Delft, The Netherlands

Keywords: Inertial Impaction, Nanoparticle production, Metal nanoparticles, Hydrogen Storage, Magnesium

In inertial impaction, an aerosol stream is accelerated by a large pressure differential across a nozzle and directed at a perpendicular substrate, where the particles deposit due to their inertia. Despite being rigid enough to support large structures with high aspect ratios (figure 1), the nanostructure of the particles is maintained to a large degree, and Brunauer Emmett Teller (BET) results showed that more than 80 % of the primary nanoparticle surface remains accessible. Electron micrographs revealed that sintering induced by the impact is the explanation for rigidity. The advantages of our rigid impacted structures are evident for many applications. We used inertially impacted materials as catalysts and hydrogen sensors, both with extremely good results. This clearly demonstrates the accessibility of these structures for different gases, and the capability of absorbing hydrogen.
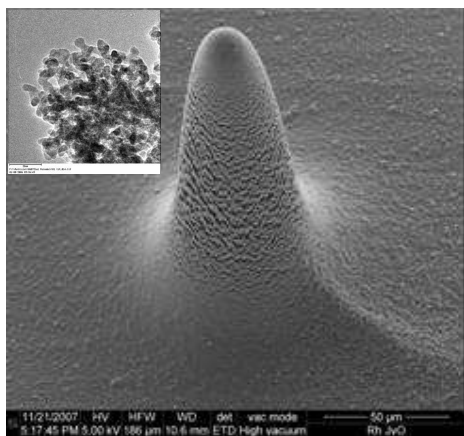
Figure 1: SEM micrograph of a nanoparticle 'tower' made by inertial impaction of Pd-particles. The insert show a TEM micrograph of the 4-5 nm particles.

Many types of light metal nanoparticles are interesting for hydrogen storage (Schlapbach & Zuttel, 2001). Spark discharge generation (SDG, Tabrizi et. al. 2008) can be used to generate particles that are small and crystalline. They can be mixed very well with for instance catalysts and modifiers. We have successfully produced *metallic* nanoparticles powders from magnesium using spark discharge generation and observed that it is possible to store hydrogen in these particles. However, light metal nanoparticles are readily oxidised by both oxygen and water, and nanoparticulate powders are very hard to handle. Due to electrostatic charging they tend to be scattered very easily.

To tackle passivation in addition to rigidity, we investigated the production of coated nanoparticle layers from light metal nanoparticles. A silicon substrate is first cleaned in a plasma sputter deposition (PSD) setup by sputtering and then sputter coated with a uniform layer of palladium. Metal nanoparticles are then impacted on this substrate; the palladium layer helps to improve adherence of the metal nanoparticles to the substrate. Large numbers of parallel lines are impacted close together by moving the impaction nozzle through two dimensions, resulting in a layer of variable geometry (figure 2). The black colour of the layer suggests that the particles are at least partly metallic, as both magnesium oxide and magnesium hydroxide nanoparticles have a white appearance.
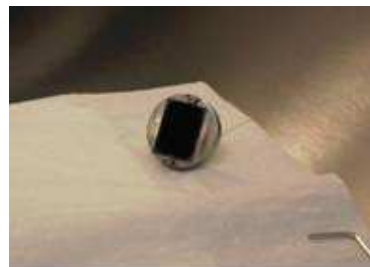
Figure 2: magnesium layer generated by impaction of nanoparticles (shown inside a glovebox)

Afterwards, the generated layer is transferred back to the PDS setup for coating with a second layer of palladium. Palladium is used because it is impermeable to oxygen, protecting the sensitive light metal nanoparticles from oxidation, whereas hydrogen can diffuse through it easily. The first coating attempts were successful, and analysis of the hydrogen storage potential of the layers will be performed using Thermal Desorption Spectroscopy (TDS).

Schlapbach, L., Zuttel, A. (2001). *Hydrogen-storage materials for mobile applications*, Nature, 414, 353.

Tabrizi, N.S., Ullman, M., Vons, V.A., Schmidt-Ott, A. (2008), *Generation of nanoparticles by Spark Dicharge*, J. Nanoparticle Res., 11, 315.

One-step Synthesis of Core-Shell Porous Nanoparticles by an Aerosol Route

G. Kastrinaki[1,3], S. Lorentzou[1,2] and A.G. Konstandopoulos[1,2]

[1]Aerosol &Particle Technology Laboratory, CERTH/CPERI, P.O. Box 60361, 57001, Thessaloniki, Greece
[2] Department of Chemical Engineering, Aristotle University, PO. Box 1517, 54006, Thessaloniki, Greece
[3] Department of Eng. & Management of Energy Resources, University of W. Macedonia, 50100, Kozani, Greece

Keywords: porous nanoparticles, nanoparticles oxides, aerosol spray pyrolysis

Nanostructured composite particles, exhibiting high surface area, well-defined pore sizes and pore connectivity are of great interest for multiway catalytic processes such as in the automotive catalytic converter. One multifunctional nanoparticle, through different pore sizes and doped layer structures can act as a gaseous and particulate (soot) catalyst performing adsorption and oxidation processes. The short procedure of Aerosol Spray Pyrolysis (ASP) (Messing, 1993; Karadimitra, 2001) can begin from a primary solution and end up in building multiple structures at the nanoscale, which can be used for automotive applications.

Primary structures of core-shell nanoparticles were synthesized by ASP. An aqueous solution containing surfactant, tetraorthosilicate (TEOS) and appropriate salt ions is atomized into nano-sized droplets by an air assisted atomizer. The droplets are carried via air inside a heated (400^0C) tubular reactor and the produced particles are collected on a glass fiber filter located at the exit of the reactor. In the silica droplet, the surfactant is located towards the external surface (Ward, 2003) forming micelles, which self assemble into ordered structures, while the water-ion solution is captured in the core undergoing crystallization of the ions when the concentration reaches saturation point. Calcination of the synthesized particles at 450^0C for 5hrs removes the surfactant leaving the final product particles with a porous shell behind.

Further investigation involves synthesis of silica porous particles enriched with catalytic agents by mixing their precursor compounds together in an aqueous solution with surfactant, achieving high dispersion of the dopant and large surface area on each particle. Various combinations of oxides and surfactants are tested, in order to improve nanoparticles durability towards thermal treatment and soot oxidation performance, as well as create complex structures able to shield precious metals from undesirable reactions in the exhaust.

The nanoparticles are tested for soot oxidation efficiency at a Thermogravimetric Analysis device (TGA, Pyris 6), for the determination of surface area and the pore size distribution by BET analysis (Autosorb-1) and particle size distribution by an Aerosizer (TSI 3603) and are morphologically characterized by Transmitting Electron Microscopy (TEM, JEOL JEM 2010).
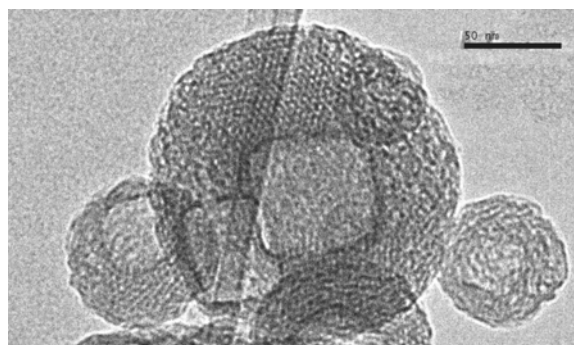
Figure 1. Crystalline core and 2.9 nm porous shell nanoparticle

In the preliminary experiments successful synthesis of crystal core porous shell particles was achieved. The BET analysis measures high surface area (78-326 m^2/g) and continuous pore connectivity while the pore size varies from 2-8 nm depending on the surfactant/s used, while in the case of the oxides the dopant was highly dispersed on the whole particle area exhibiting even higher particle surface areas (289-1115 m^2/g)

Porous silica nanoparticles having multiple morphology and composition are synthesized from one primary solution by ASP. The particles have a well defined pore size shell exhibiting high surface area and are applicable in catalytic processes.

Messing G. L., Shi-Chang Zhang and Jayanthi G. V., *J. American Ceramic Society,* (1993) 76, 2707-2726

Ward T., Datye A., Lopez G., Brinker J., and van Swol F., *NSF NIRT* No. 0210835 (2003)

Karadimitra K., Papaioannou E., Konstandopoulos A.G, J. Aerosol Sci. 32, Suppl. 1, (2001), S233-234

Nanoscale Particulate Emissions from Car-Brakes

H. Bresch[1], S. Seeger[1], I. Dörfel[1], C. Prietzel[1] and W. Österle[1]

[1]BAM Federal Institute for Materials Research and Testing, Unter den Eichen 87, 12205, Berlin, Germany

Keywords: Source identification, Vehicles emissions, Traffic emissions, Brakes, Industrial aerosols.

Emissions from vehicles are a very well investigated research subject. In addition to engine emissions most outdoor studies also found a lot of particulate emissions from wheels and brakes (Thorpe 2008). Furthermore, studies in subway stations reveal metal particle aerosols which are supposed to come from braking interactions. The observed high amount of metallic elements in brake emissions accentuates the need to study health effects of traffic emissions especially in the nanoscale regime. The first step in the evaluation of health effects for nanoscale particulate brake emissions is the characterisation of the emissions under controlled conditions in the laboratory. In our study we analysed the nanoscale particle number distribution and examined differences in the metal content depending on size and temperature.

The experiments were performed in a test chamber for brake-pads in cooperation with a prominent producer of brake pads (Österle 2009). The chamber had a volume of 30 m^3 and the dynamometer was driven by an electric motor in a separate chamber. The test chamber was vented through a 20 cm^3 cross-section ventilation shaft. In order to characterize the particulate emissions, several instruments were used: APS, DustMonitor, SMPS, EEPS, Cascade-Impactor and Nanosampler. The sampling points for all instruments were located in plane with the brake disc at approximately 0.7 m distance from the wheel axis.

The test procedure of the dynamometer was computer-controlled from outside of the chamber. Throughout the different test cycles the brake-pressure and the brake disk surface temperature were recorded together with rpm and other parameters.

With first measurements we characterized the size distribution of the emitted particles. To our surprise and in contrast to previous measurements (Iijima 2007) the maximum of the measured particle number concentration was clearly below 500 nm particle diameter. In most cases it was around 120 nm and even below. Consequently in the next step we focused on particles below 500 nm and compared the performance of the SMPS-System and the EEPS-System (Figure 1).

Both instruments measured the emissions with good correlation to the braking events. Because of the excellent time resolution the EEPS was able to distinguish nearly each single braking event. On the other hand the SMPS with its good size resolution delivered some very useful information about the particle size structure.

Detailed data analysis of the measured results revealed some interesting correlations between braking pressure, temperature, brake-pad composition, particle number concentration, particle size and particle composition. The parameters pressure, temperature and brake-pad composition have a strong influence on the nano particulate emission spectrum. The measured particle number concentration may differ over several decades in intensity.

As a final result we have evidence for a broad emission spectrum of nanoparticles containing metallic elements from commonly used brake-pads. Under special conditions we found evidence for an intense emission of very small metal containing nanoparticles. Considering the discussion about health risks of metal nanoparticles our findings could serve as a basis for the evaluation of outdoor nanoparticle exposures from traffic and further toxicological research and assessments.
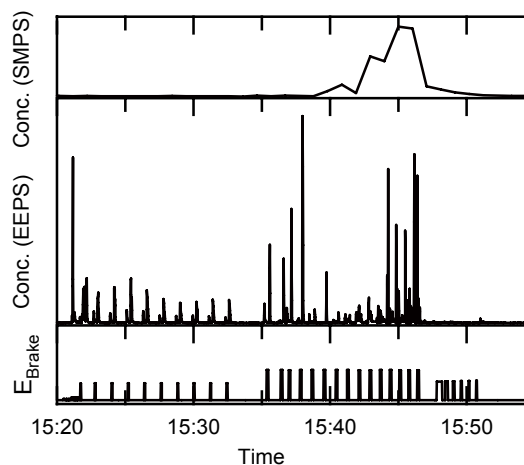
Fig. 1: Comparison of time structure between SMPS and EEPS in relation to braking events.

Iijima, A., et al. (2007). *J. Aerosol Science*, 36, 3456-3467.

Österle,W., Bresch, H., Dörfel, I., Prietzel, C., Seeger, S., Fink, C., Giese, A., Walter, J. (2009). *Proc. IMech Eng. Braking 2009*, accepted.

Thorpe, A., Harrison, R.M. (2008). *Sci. Total. Environ.*, 400, 270-282.

Nanoinventory: a representative survey of nanoparticle usage in Suisse industry

K. Schmid[1], B. Danuser[1], M. Riediker[1]

[1] Institute for Work and Health, University of Lausanne, 1011 Lausanne, Switzerland

Background

Addressing the risks of nanoparticles requires knowledge about their hazards, which is generated progressively, but also about occupational exposure and liberation into the environment. However, currently such information is not systematically collected, therefore the risk assessment of this exposure or liberation lacks quantitative data.

In 2006 a targeted telephone survey among Swiss companies (1) showed the usage of nanoparticles in a few selected companies but did not provide data to extrapolate on the totality of the Swiss workforce. The goal of this study was to evaluate in a representative way the current prevalence and level of nanoparticle usage in Swiss industry, the health, safety and environment measures, and the number of potentially exposed workers.

Results

A representative, stratified mail survey was conducted among 1,626 clients of the Swiss National Accident Insurance Fund (SUVA). SUVA insures about 80,000 manufacturing firms, which represent 84% of all Swiss manufacturing companies.

947 companies answered the survey (58.3% response rate). Extrapolation to all Swiss manufacturing companies results in 1,309 workers (95%-confidence interval, 1,073 to 1,545) across the Swiss manufacturing sector being potentially exposed to nanoparticles in 586 companies (95%-CI: 145 to 1'027). This corresponds to 0.08% (95%-CI: 0.06% to 0.09%) of all Swiss manufacturing sector workers and to 0.6% (95%-CI: 0.2% to 1.1%) of companies.

The industrial chemistry sector showed the highest percentage of companies using nanoparticles (21.2% of those surveyed) and a high percentage of potentially exposed workers (0.5% of workers in these companies), but many other important sectors also reported nanoparticles.

Personal protection equipment was the predominant protection strategy. Only a minority applied specific environmental protection measures.

Conclusions

This is the first representative nationwide study on the prevalence of nanoparticle usage across a manufacturing sector.

The information about the number of companies can be used for quantitative risk assessment. Furthermore it can help policy makers designing strategies to support companies in the responsible development of safer nanomaterial use.

Noting the low prevalence of nanoparticle usage, there would still seem to be time to introduce necessary protection methods in a proactive and cost effective way in Swiss industry. But if the predicted "nano-revolution" becomes true, now is the time to take action.
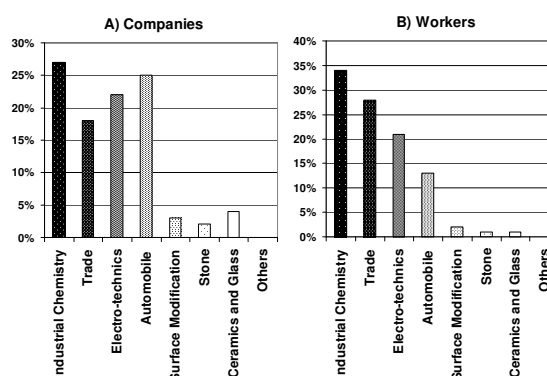
Figure 1. Distribution of companies with nanoparticle applications within the Swiss production sector: A) by company from the different branches, B) by number of workers in these branches.

Schmid, K.; Riediker, M. **2008**, Use of Nanoparticles in Swiss Industry: A Targeted Survey, *Environ. Sci. Technol.*, (7), 2253-2260.

Modelling of accidental nanoparticle release into a workplace

Christof Asbach, Uwe Rating, Till van der Zwaag, Heinz Fissan, and Thomas A.J. Kuhlbusch

Institute of Energy and Environmental Technology (IUTA), Air Quality & Sustainable Nanotechnology Unit, Bliersheimer Str. 60, 47229 Duisburg, Germany

Keywords: Nanoparticles, Exposure, Workplace, Modelling, CFD

Exposure to nanoparticles is currently discussed within the framework of risk assessment. A potential risk may arise, if an exposure to toxic particles exists. Besides investigations of the toxicity of nanoparticles, the study and eventually the prevention of possible exposure to nanoparticles is thus a major step towards sustainable development of nanotechnology. As of now, exposure has mainly been measured with stationary measurement equipment, such as mobility particle sizers, particle counters or surface area monitors. Some papers have recently been published (e.g. Peters et al., 2006; Evans et al., 2008) that describe mapping of submicron and nanoscale particles using mobile equipment in order to obtain higher spatial resolution of the measurements. Only a few personal sampling devices that determine the personal exposure specifically to nanoparticles exist (e.g. Azong-Wara et al., 2009). However all the abovementioned methods have in common that they can only deliver results with limited or no temporal and/or spatial resolution. Modelling of particle dispersion in a workplace can provide information on temporal and spatial variations of aerosol or particle properties. Furthermore modelling can enable the study of the effects of single particle dynamic processes, such as coagulation or Brownian diffusion on the variation of aerosol and particle parameters. Another advantage of modelling is that boundary conditions, such as wall temperatures or ventilation scenarios can be varied in order to study their effect on particle dispersion and consequently possible exposure to particles in a workplace.

We have developed a simulation grid for a realistic, virtual workplace, including a reactor, transport pipes, furniture, gates and a door. A leak is assumed in the reactor and particle dispersion is studied with the CFD software FLUENT along with the Fine Particle Model. The simulation domain is illustrated in Figure 1.

In a basic case, all temperatures in the room were assumed to be 300 K, gates and doors were left open 10 cm at the bottom. The size distribution emitted through the leak was assumed to be lognormal with a median diameter of 50 nm and a concentration of $10^{16}\,m^{-3}$. Parameters affecting particle size distribution and dispersion, including emitted size distributions, ventilation scenarios, background aerosol, and temperatures of floor, reactor wall and leak flow were systematically varied. Figure 2 shows an example of how the size distributions at the three points change, when the temperature of the reactor wall was increased from 300 K to 350 K. In that case, thermophoresis and buoyancy effects can affect particle dispersion in the room.
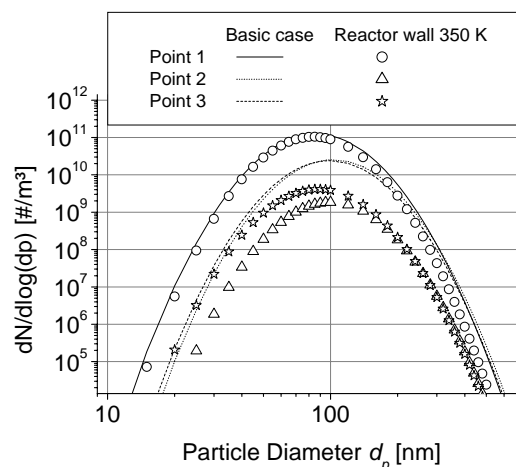
Fig. 2: Change of particle size distribution at three points (see Fig. 1) when the reactor wall temperature was increased from 300 K (basic case) to 350 K

The results show that modelling can be a very efficient tool for studying dispersion and changes of particles during airborne transportation in workplaces. The effect of the modelled variations will be quantitatively discussed in view of importance for exposure assessments and applicability for the design of a safer working environment.

Fig. 1: Simulation domain including reactor with leak, pipes, furniture, gates, and a door

References
Peters et al., *Ann. Occup. Hyg.* **50**: 249-257, 2006
Evans et al., *Ann. Occup. Hyg.* **52**: 9-21, 2008
Azong-Wara et al. *J. Nanopart. Res.*, submitted

Nucleation of ibuprofen nanoparticles from supersaturated vapor

A. A. Onischuk, A. V. Samodurov, E. E. Elantseva, V. V. Karasev, A.M. Baklanov

Institute of Chemical Kinetics & Combustion, RAS, Novosibirsk, 630090, Russia

Keywords: Nucleation, organic aerosols, surface tension.

Nucleation of water insoluble drugs is of high interest now in the light of numerous advantages which gives the nanoparticle lung administration with respect to the traditional oral therapy or injection delivery. Ibuprofen is a nonsteroidal, chiral, anti-inflammatory drug with poor water solubility. Here we study the mechanism of ibuprofen nanoparticle formation via nucleation from supersaturated vapour in a horisontal flow chamber. The chamber is made of a molybdenum glass tube (with the inner diameter of 0.8 cm) with an outer heater. Argon flow is supplied to the inlet of the generator through the Petrianov's high efficiency aerosol filter at the rate of 8 cm^3/s (at standard temperature and pressure). The original substance (racemic ibuprofen from Ratiopharm, Germany) is put to the hot zone inside the tube. The saturated vapor is formed inside the chamber. The temperature drops down at the outlet of the heated zone resulting in vapor supersaturation and nucleation. The aerosol concentration and size distribution (Fig. 1) were measured with the Automatic Diffusion Battery designed and built at the Institute of Chemical Kinetics and Combustion, Novosibirsk, Russia.

Fig. 1. Mean particle diameter and number concentration vs. temperature in the saturated vapor zone of flow chamber (as measured by the Automatic Diffusion Battery).

The powder X-ray diffraction patterns of nanoparticles and original powder are compared in Fig. 2. Both XRD patterns from nanoparticles and

original substance correspond to racemic ibuprofen, i.e. the nanoparticles form the same crystal phase as the original substance. The small difference in the peak relative intensities between the curves *a* and *b* in the range $17 < 2\theta < 21$ is probably related to the difference in distribution of crystallographic orientations in the micro-sized original powder and nanoparticles.

Fig. 2. X-ray diffraction patterns of a) original ibuprofen powder, b) ibuprofen nanoparticles formed *via* evaporation-nucleation route (mean particle diameter d = 85 nm).

The nucleation rate was determined by the video observation of the light scattered from the nucleation zone particles to be 10^6 $cm^{-3}s^{-1}$. The surface tension of critical nucleus was determined from the experimentally measured nucleation rate as a function of radius (Fig. 3).

Fig. 3. Surface tension of critical nucleus vs. radius.

Nanoparticle monitoring and modelling in microwave plasmas

H. Mätzing, W. Baumann, H.-R. Paur and H. Seifert

Forschungszentrum Karlsruhe GmbH,
Institut für Technische Chemie, Bereich Thermische Abfallbehandlung,
Postfach 3640, D-76021 Karlsruhe, Germany

Keywords: nanoparticles, mass spectrometry, particle formation, microwave plasma, modelling

Nanoparticles can be formed from chemical reactions in the gas phase over a wide range of conditions, e.g. at low, ambient and high temperatures and pressures. Therefore, nanoparticles can be formed in natural (atmospheric) processes as well as in industrial processes, where they may be just unwanted by-products, while in other context they may be desired as valuable intermediates or final products. Hence there is great interest and need to provide appropriate measurement devices and to understand the kinetics of nanoparticle formation in detail. This paper reports the measurement of metal oxide particles formed in microwave plasmas by particle mass spectrometry and presents chemical kinetic models for the formation of metal oxide nanoparticles.

The particle mass spectrometer has a two stage molecular beam sampling system which allows in-situ probing. The particles pass a capacitor with variable electric field and the charged particle fraction is separated according to the polarity and to the ratio of kinetic energy to charge. The charged particles are collected at Faraday cups and the resulting intensity is proportional to the number concentration. The particle velocity is measured simultaneously and allows to derive the mass and size spectra from the mass to charge spectrum with the assumption of single charge and with the known material density (Mätzing et al., 2003).

The metal oxide particles were generated in an Ar/O_2 microwave plasma from iron pentacarbonyl and silane, which were added to the inlet gas. Parameters were the input concentration (up to 500 ppm), the pressure P in the plug flow reactor (10 – 40) mbar, the applied microwave power P_{MW} (255 – 595 W) and the residence time t (up to 100 msec). The reaction temperature was around 200 °C. Charged particles of Fe_2O_3 or SiO_2, resp., were detected. The measured signal intensity usually had two peaks at deflection voltages which differed by a factor of two. Since TEM micrographs showed a monodisperse size distribution, the two peaks were due to singly and doubly charged particles. The particle size was found to increase with increasing input concentration, pressure and residence time, but to decrease a little with increasing microwave power.

A volume averaged, 1-dimensional chemical kinetic model was developed to calculate time profiles of the gaseous and particulate species in the Ar/O_2 plasma (Mätzing et al., 2009). The model includes the absorption of microwave energy by free electrons, ionization by energetic electrons and radical formation by the recombination of ions. The decomposition of the precursors and the formation of product species and particles is due to radical reactions as described earlier for flame conditions (Paur et al., 2005), but under microwave conditions the available radical pool is significantly smaller than under flame conditions. Therefore, heterogeneous surface reactions may become important under microwave conditions. Particles are assumed to nucleate from approx. ten metal oxide molecules forming solid clusters of 1 nm diameter which coagulate subsequently. Fig. 1 shows good agreement between measured and calculated particle diameters as function of input concentration.
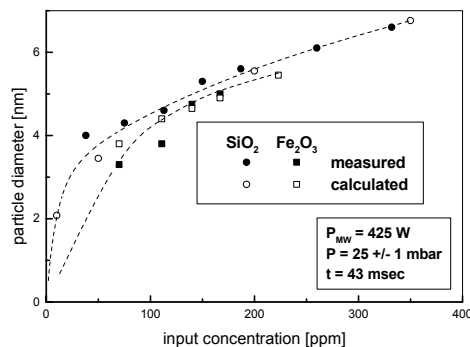
Figure 1. Formation of Fe_2O_3 and SiO_2 nanoparticles in microwave plasma.

Mätzing, H., Baumann, W., Hauser, M., van Raaij, A., Paur, H.-R., Seifert, H., & Roth, P. (2003). *J. Aerosol Sci.*, 34, S277-S278.

Mätzing, H., Baumann, W., Paur, H.-R., & Seifert, H. (2009), *Proc. 19th Int. Symp. Plasma Chemistry*, Bochum, Germany, July 26 – 31, 2009.

Paur, H.-R., Baumann, W., Mätzing, H., & Seifert, H. (2005). *Nanotechnology*, 16, S354 – S361.

Grid-based kinetic Monte-Carlo technique for modelling high-temperature particle formation

F.E. Kruis[1], J. Wei[1] , T. van der Zwaag[2] , S. Haep[2] and H. Zhao[1,3]

[1]Nanostrukturtechnik (NST) and Center for Nanointegration (CeNIDE), Universität Duisburg-Essen, 47057 Duisburg, Germany
[2]Institut für Energie- und Umwelttechnik (IUTA), 47229 Duisburg , Germany
[3] State Key Laboratory of Coal Combustion, Huazhong University of Science and Technology, Wuhan, 430074 Hubei, PR China

Keywords: coagulation, Brownian diffusion, Monte Carlo simulations, CFD, aerosol dynamics

The modelling of industrial nanoparticle-producing reactors is complicated due to the strong gradients of the temperature and velocities, as well as the highly dynamic character of the aerosol. Coupling of dynamic methods such as (discrete-) sectional models and CFD solvers has been demonstrated, but these models have the disadvantage that they do not allow the modelling of multivariate particle properties. Examples of such properties are distributed properties other than particle size, such as charge, form and composition.

Population balance-Monte Carlo techniques (PB-MC) are especially suited for modelling multivariate properties. They can be clearly distinguished from MC methods that describe the Brownian or turbulent particle trajectories by stochastic means because no information about the particle spatial position is needed. The PBE-MC methods are advantageous because of their simplicity and, more importantly, their stochastic and discrete nature that adapts naturally to coagulation which has the same nature.

However, until now there existed no strategy to combine PB-MC models with transport models relevant for aerosol reactor modelling. A new method is proposed which is cell-based and allows to model the particle convection-diffusion transport stochastically. The model uses the information obtained by a CFD solver such as Fluent for the local velocity and temperature distribution. The method is time-driven, and the time step is chosen such that only the simulation particles can only move into the neightbouring cells. After each transport step, a kinetic MC step is done to simulate aerosol dynamics

A series of case studies is performed in well-defined model systems, such as plug-flow reactors. After this validation, a real reactor was modelled, in which indium nanoparticles are formed (Damour et al., 2005). The method is compared with a commercial solver for joint particle dynamic transport simulation (FPM, Particle Dynamics GmbH). In each cell, the particle dynamics was simulated by means of 500 simulation particles.

Figure 1 shows the results of the comparison between the FPM model and the kinetic MC method.
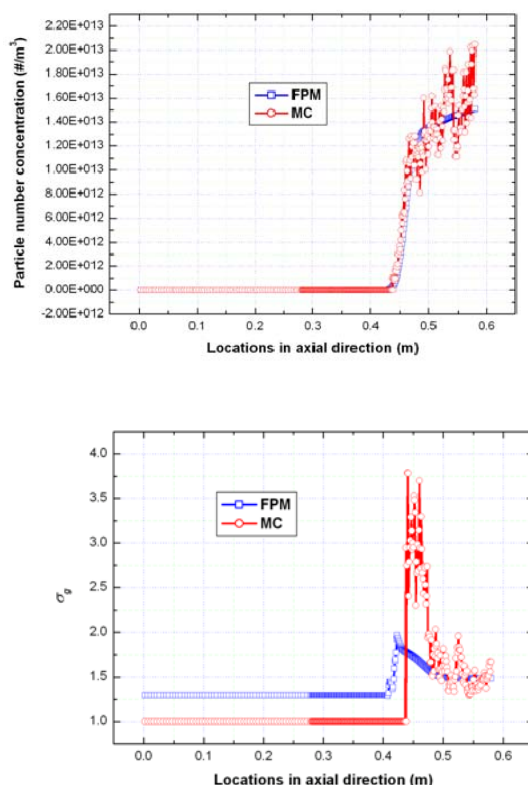
Figure 1. Comparison between the FPM model and the coupled transport-MC model: a) particle number concentration and b) geometric standard deviation as function of the position on the central reactor axis.

Damour, T., Ehrmann, S., Karlsson, M.N. Deppert, K. (2005) Aersol Science Technology 39(5) 444.
Kruis, F.E., Maisels, A., Fissan, H. (2000) AIChE Journal 46(9) 1735.

Modelling Nanoparticle Production in a Turbulent Diffusion Flame

A.J. Gröhn[1,2], J.K. Jokiniemi[2,3] and S.E. Pratsinis[1]

[1]MAVT, ETH Zürich, Particle Technology Laboratory, CH-8092, Zürich, Switzerland
[2]Department of Environmental Sciences, University of Kuopio, Fine Particle and Aerosol Technology Laboratory, P.O. Box 1627, FI-70211 Kuopio, Finland
[3]Fine Particles, VTT Technical Research Centre of Finland, P.O. Box 1000, FI-02044 VTT, Espoo, Finland

Keywords: Aerosol Dynamics, CFD, Flame, Nanoparticle Production.

The goal of this study was to investigate nanoparticle production in turbulent diffusion flames accounting for fluid- and aerosol dynamics (Johanessen *et al.*, 2000) as well as the detailed thermal history of the process. This enables accurate process control, design and optimization to facilitate scale-up of flame aerosol reactors (Pratsinis, 1998). The model results were compared to data of SiO_2 production by combustion of hexamethyldisiloxane (Mueller *et al.*, 2004).

The gas-to-particle formation reactions are considered infinitely fast so a mixing limited combustion model could be used. The combustion model solves a transport equation for mixture fraction, defined as the mass fraction originating from the fuel stream (Sivathanu *et al.*, 1990), so temperature and molar concentrations of the species included in the reaction can be obtained.

The particle formation rate was extracted from the gaseous SiO_2 concentration field by solving a transport equation for particulate SiO_2. The source term, representing particle formation, was solved by minimizing the difference between the gaseous and particulate concentrations. This method can be used when molecular diffusion is negligible compared to turbulent diffusion as the diffusion- and the convection terms of the transport equations are equal.

The aerosol dynamics were solved following characteristic particle trajectories (Johanessen *et al.*, 2000). Temperature, particle formation and velocity along five trajectories were extracted from CFD. The dilution caused by radial turbulent mixing was accounted by comparing the total volume concentration of aerosol from CFD simulations to that from particle formation along a single trajectory.
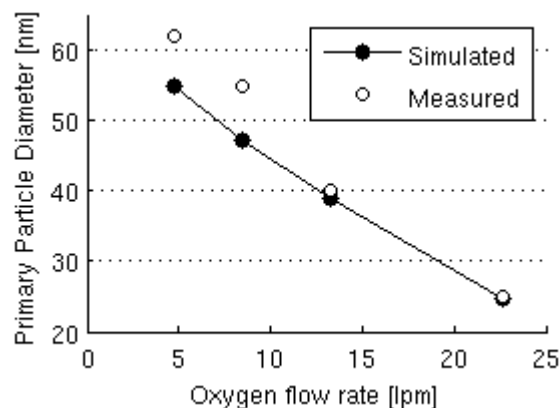
The dilution factor is the difference of these concentrations. Compared to Johannessen *et al.* (2000) this method allows including the particle formation along the trajectories.

The evolution of particle size-, area- and volume concentration were modelled neglecting the spread of the size distribution as flame-made aerosols rapidly attain their self-preserving distribution. The effects of agglomeration, sintering and particle formation were accounted for.

Simulations made with different turbulence models were compared to FTIR measured (line of sight) temperature profiles and fuel conversion rates for different oxidizer flow rates (Mueller *et al.*, 2004). The relatively new realizable k-ε model (Shih *et al.*, 1995) had the best correspondence with the experiments. The realizable formulation can fix the round-jet anomaly and it also sets physical constraints on Reynolds stress components.

The aerosol dynamics simulations were compared to measured primary particle diameters at the outlet (Fig. 1). Measured sintering rate couldn't be explained with previously published values, so the sintering activation energy term was estimated by fitting primary particle diameter to measured data.

The advantage of the used combustion model is its independence of experimental parameters, such as Arrhenius type coefficients, which can be often difficult to acquire. It is possible to obtain the temperature of the flame as well as the formation rate- and volume concentration of the particles from the current reaction model. These variables define directly the agglomeration- and the sintering rate of the aerosol. This suggests that the most important mechanisms influencing the properties of the produced nanoparticles can be explained by the spatial evolution of the mixture fraction.

Figure 1. Primary particle diameter at filter.

Johannessen T., Pratsinis S.E., & Livbjerg H. (2000). *Chem. Eng. Sci.*, 55, 177-191.

Mueller R., Kammler H.K., Pratsinis S.E., Vital A., Beaucage G. & Burtscher P. (2004). *Powder Tech.*, 140, 40-48.

Pratsinis S.E. (1998). *Prog. Energy Combust. Sci.*, 24, 197-219.

Shih T-H., Liou W.W., Shabbir A., Yang Z. & Zhu J. (1995). *Comput. Fluids*, 24, 227-238.

Sivathanu Y.R. & Faeth G.M. (1990). *Combustion and Flame*, 82, 211-230.

A spatio-temporal population balance-Monte Carlo method for diffusion and coagulation of nanoparticles in plug-flow aerosol reactors

H. Zhao[1,2], F.E. Kruis[2], J. Wei[2], T. van der Zwaag[3], S. Haep[3] and C. Zheng[1]

[1]State Key Laboratory of Coal Combustion, Huazhong University of Science and Technology, Wuhan 430074, Hubei, PR China
[2]Nanostrukturtechnik (NST) and Center for Nanointegration (CeNIDE), Universität Duisburg-Essen, 47057 Duisburg,Germany
[3]Institut für Energie- und Umwelttechnik (IUTA), 47229 Duisburg,Germany

Keywords: Aerosol modelling, Nanoparticle production, Coagulation, Diffusion, Monte Carlo simulations.

Plug-flow aerosol reactors are widely used in nanoparticles (NPs) synthesis in the gas phase. Population balance modelling has been a general strategy to simulate the dynamic evolution of NPs (usually, fractal agglomerates) considering nucleation, surface growth, coagulation and sintering. Up to now the task modelling the time (or axial-direction) evolution of nanoparticle volume and surface area distributions had been overcome. However ones have little knowledge about the spatio-temporal dynamics of NPs in gas-phase synthesis, which is important to design new synthesis methods, improve old synthesis techniques, and tailor functional NPs.

Some deterministic methods for population balance modelling, such as (discrete-) sectional method, monodisperse method, (direct) quadrature method of moments, have been coupled with CFD solvers for gas fields to simulate spatially-dependent nanoparticle dynamics. However these dynamic methods are generally formulated by complicated mathematical equations, and more unfortunately, are at the disadvantage of the modelling of more than two internal variables of NPs. In fact, the fractal structure, multicomponent, charging and other functional properties of NPs can not be characterized by commonly-used volume and surface area.

Population balance-Monte Carlo methods (PB-MC) perform ability to deal with high-dimensionality problems in a simple and straightforward manner. And their simplicity, stochastic and discrete nature, particle trajectory tracking make them suit for NPs dynamics, even in spatially anisotropic aerosol reactors. However, MC is generally trapped into the larger CPU time and statistical noise inherent to MC methods.

A new MC, which uses the concept of differentially weighting simulation particles, is proposed to capture the temporally-dependent coagulation dynamics simultaneously having low noise and being able to track the size distribution over the full size range (Zhao et al., 2009). In this work, the proposed differentially weighted time-driven (DWTD) MC method is further coupled with a grid-based particle diffusion model which adopts random walk method to model the particle convection-diffusion transport stochastically (Wei et al. 2007). When the gas fields (gas velocities, temperature, et al.) from CFD solvers (FLUENT in this work) are inputted, the spatio-temporal evolution of NPs in aerosol reactors is obtained.

Fig.1a shows geometric mean diameter (d_{pg}) of NPs along with the central reactor axis, the temporal PB-MC can be used as a benchmark solution; and Fig.1b shows the spatial distribution of d_{pg} at time $t=90$ s.
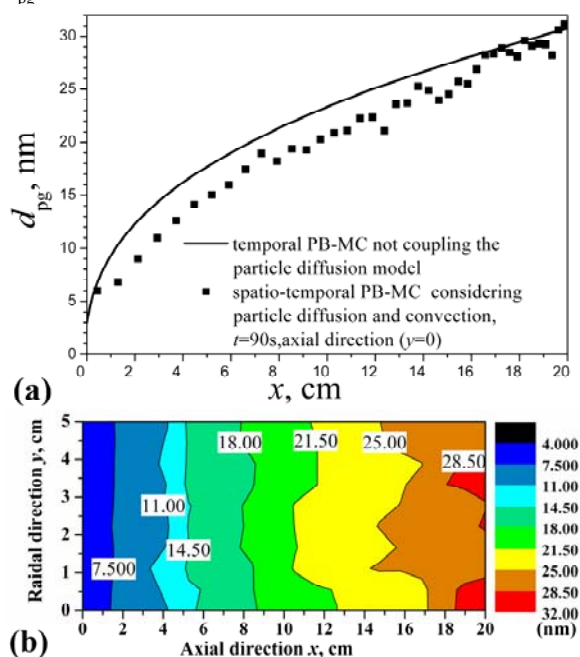
Figure 1. Spatial distribution of nanoparticle diameter in a plug-flow aerosol reactor with initial monodispersed 3 nm and 10^{17} m^{-3} NPs

Zhao, H., Kruis, F. E., & Zheng, C. (2009). *Aerosol Sci. Tech.*, in submission
Wei, J., & Kruis, F. E. (2007). in *6th International Conference on Multiphase Flow, ICMF 2007, Leipzig, Germany, July 9-13*

Modelling Agglomeration and Coalescence of SiO_2 particles in an industrially scaled turbulent flame

S. Horender and M. Sommerfeld

Zentrum für Ingenieurwissenschaften, Martin-Luther Universität Halle-Wittenberg, Merseburg, 06217, Germany

Keywords: Turbulence, CFD, SiO_2, Particle formation and growth.

This contribution deals with an industrially scaled flame synthesis of SiO_2 nanoparticles form the raw material for optical fibers at a rate of ~500g/h. A burner with 3 concentric rings is used, with hydrogen supplied to the outermost ring, oxygen supplied in the middle ring and $SiCl_4$ plus oxygen in the inner tube. Fig. 1 shows produced particles and a laser sheet visualization of the particles in the flame. To further improve the understanding of the flame deposition process we modeled the nucleation and agglomeration of the particles using a validated CFD calculation of the flame and Lagrangian particle tracking, see Horender et al. (2008). Based on this work which focused on particle deposition we developed a model for nucleation based on kinetic theory: the precursor molecules were tracked and allowed to collide due to Brownian motion in regions of the flame with sufficient temperatures so that the $SiCl_4$ precursor had reacted. Additionally, collisions of these growing particles were allowed.

Figure 2. top: Size distribution measured 190 mm above the burner exit, bottom: prediction.

Figure 1. TEM image of sampled particles and laser sheet visualisation of particles in the flame.

The simulated particle size distribution, see fig. 2 was compared with particle sizes obtained by thermophoretic sampling and Transmission electron microscopy. It was found that the simulation predicted that nearly all particles were coalesced to spheres, which was not the case for the measurements. The current contribution tries to identify the reasons for that deviation between model and measurements.

Since the flame has temperatures around 2600 K, which is far above the melting point of SiO_2 of around 1900 K, the experimental finding of incomplete coalescence is surprising. We made an estimation of heat losses due to radiation which gave that approximately 20 % of the total combustion energy would be emitted as radiation. This would lead to a decreased temperature from 2600 K to 2100 K. However, the particles may locally cool the flame even more, due to their segregated non-random distribution, see fig. 1. Currently a model is implemented in our calculation to take these segregated structures and their effect on radiative heat loss and subsequent cooling of the flame into account.

Horender, S., Lipowsky, J., Schwerin, M., Badeke, K.U., & Sommerfeld, M. (2008) *Aerosol Sci. Tech.*, 42, 873-883.

Implementation of sampling and characterization methods for nanoparticles

C. Dion[1], A. Noël[2], J. Boucher[1], Y. Cloutier[1] and G. Truchon[1]

[1]IRSST, 505 De Maisonneuve Blvd. West, H3A 3C2, Montréal, Canada

[2] Department of Environmental and Occupational Health. University of Montréal. 2375, chemin de la Côte-Ste-Catherine, H3T 1A8, Montréal, Canada

Keywords: Aerosol characterization, ELPI, TiO_2 nanoparticles, Electron microscopy

Introduction

The use of nanoparticles (NP) and nanotechnology is growing and workers exposure assessment to nanomaterials poses new challenges to agencies involved in the field of health and safety at work. Little is known on the risk related to the workplace environment (Seipenbusch *et al,* 2008). Characterization of exposure is an important factor of toxicological studies. Electron microscopy (EM) is one of the main tools used to characterize NP (Jarausch & Leonard, 2008; Shin *et al*, 2009). The aim of this study was to develop an optimal characterization method through NP air sampling. This presentation describes the implementation of EM methods based on sampling by two impactors (an electrical low pressure impactor (ELPI) from Dekati Corp and a micro orifice uniform deposition impactor (MOUDI) from MSP Corp).

Methodology

TiO_2 NP of 5 nm were generated in an inhalation chamber at a concentration of 2 mg/m³. TiO_2 NP suspensions (2.5 and 5 g/L) prepared with deionized water were nebulized with a constant output atomizer (TSI model 3076) and a Collison nebulizers. The suspensions were sonicated and filtered to remove large aggregates. NP were collected by ELPI and MOUDI impactors. The ELPI has a lowest stage cut diameter of 7 nm and gives a direct reading allowing a comparison with electron microscopy data. MOUDI impactor has rotating plates allowing a better distribution of the particles. Copper grids were glued on substrates placed on impaction plates using templates created specifically for this purpose. Then the copper grids were analysed by EM.

Results

EM characterization of the initial bulk powder (figure 1a), as well as the TiO_2 suspensions (figure 1b), revealed that NP were agglomerated and had spherical and rod morphologies. The microscopic analysis showed that NP collected on grids were in agglomerated state. Furthermore, the size of the particles and agglomerates present in the aerosols were larger and sometimes beyond the nanometric range (1 – 100 nm).
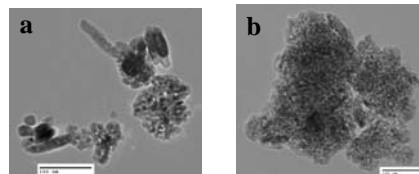
Figure 1 : a) bulk TiO_2; b) TiO_2 suspension

Discussion and conclusion

When analysing a grid from an impactor stage, a representative analysis of the population of the particles needs to be performed in order to get significative statistics and establish, for example, the median diameter. An image analysis software is a useful complementary tool for the characterization of particles. Many similarities can be drawn between the problematic posed by characterization of asbestos fibers and NP. Some of the counting rules for asbestos fibres by EM could be appropriate for the counting of NP. For example, the number of NP that needs to be counted to obtain representative data from the population of NP in the air.

In order to understand and to infer results evolving from nanotoxicological studies, a thorough characterization at each step of the experimentation is necessary. Since characterization of NP will get widely used, we should think about applying the expertise and the knowledge developed with other contaminants like asbestos and other mineralogical dust. There might be a need for harmonization between analytical methods.

Seipenbusch, M., Binder, A. and Kasper, G. *Temporal evolution of nanoparticle aerosols in workplace exposure*, 2008, Annals of Occupational Hygiene, vol. 52, p. 707-716.

Jarausch, K. and Leonard, D. N. *Three-dimensional electron microscopy of individual nanoparticles*, 2008, Journal of Electron Microscopy, *advance access*, 1-9.

Shin, W. G., Wang, J., Mertier, M., Sachweh, B., Fissan, H., Pui, D. Y. H. *Structural properties of silver nanoparticle agglomerates based on transmission electron microscopy: relationship to particle mobility analysis*, 2009, Journal of Nanoparticle Research, vol. 11, p. 163-173.

T02 Aerosol chemistry

Uptake of ambient organic gaseous mixtures to laboratory generated aerosols

John Liggio[1] and Shao-Meng Li[1]

[1]Air Quality Research Division, Atmospheric Science and Technology Directorate, Science and Technology Branch, Environment Canada, 4905 Dufferin Street, Toronto, Ontario M3H 5T4 Canada

Keywords: Organic aerosols, Aerosol chemistry, Aerosol mass spectrometry, Smog chamber, SOA.

The formation of secondary organic aerosols (SOA) in the atmosphere has been an area of significant interest due to its climatic relevance, its effects on air quality and human health. Due largely to the underestimation of SOA by regional and global models, there has been an increasing number of studies focusing on alternate pathways leading to SOA. In this regard, recent work has shown that heterogeneous and liquid phase reactions, often leading to oligomeric material, may be a route to SOA via products of biogenic and anthropogenic origin (Kroll et al., 2005; Kalberer et al., 2004).

Although oligomer formation in chamber studies has been frequently observed, the applicability of these experiments to ambient conditions, and thus the overall importance of oligomerization reactions remain unclear. Specifically, the importance of aerosol acidity, the reversibility of reactions upon neutralization, and the effect of realistic gas phase composition and concentration on the uptake is uncertain and will in part determine the importance to SOA formation.

In the present study, ambient air is drawn into a $2m^3$ Teflon smog chamber and exposed to acidic sulfate aerosols, which have been formed in situ via the reaction of SO_3 with water vapor. The aerosol composition is continuously measured with a High Resolution Aerodyne Aerosol Mass Spectrometer (HR-ToF-AMS), and particle size distributions are monitored with a scanning mobility particle sizer (SMPS). The use of ambient air and relatively low inorganic particle loading potentially provides clearer insight into the importance of heterogeneous reactions. Particularly, the effect of aerosol neutralization arising from the ammonia present in the ambient air, and the reversibility of the organic uptake under such circumstances can be studied.

Results of experiments, with a range of sulfate loadings show that there are several competing processes occurring on different timescales. A significant uptake of ambient organic gases to the particles is observed immediately, possibly associated with the condensational uptake of ambient organics. The increase in organic aerosol mass due to this process increases as a function of the original input SO_4 mass (Figure 1A).

On the other hand, during a period of several hours there is a shift in the organic mass spectrum towards fragments greater than 300 amu, indicating that higher molecular weight products (possibly oligomers) are being formed through a reactive process. This process continues regardless of the fact that the particles are continuously being neutralized.

Measurements with the HR-ToF-AMS during this time also indicate that there is a slow volatilization of organic mass from the aerosols possibly due to the formation of volatile by-products of oligomer forming reactions. This volatilization is primarily associated with hydrocarbon fragments (C_xH_y) (Figure 1B), resulting in an overall reduction in the molar ratio of Carbon to Oxygen (C/O).

The results suggest that both condensation and heterogeneous reactions can occur with ambient organic gases, resulting in significant increases in organic mass, which can occur even in the presence of ammonia. This may have significant implications to the ambient atmosphere where particles may be fully neutralized after their formation.
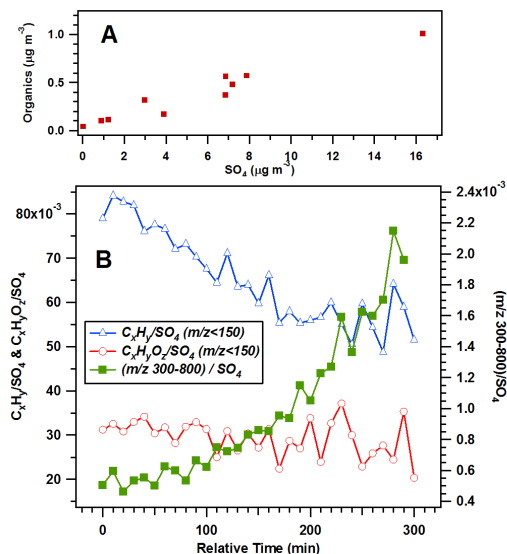
Figure 1. **A.** Immediate organic uptake relative to added sulphate. **B.** Normalized organic fragments as a function of time from sulphate addition.

Kroll, J.H., Ng, N.L., Murphy, S.M., Varutbangkul, V., Flagan, R.C., and Seinfeld, J.H. (2005). *J. Geophys. Res.*,110, D23207.

Kalberer, M., Paulsen, D., Sax, M., Steinbacher, M., Dommen, J., Prevot, A.S.H., Fisseha, R., Weingartner, E., Frankevich, V., Zenobi, R., and Baltensperger, (2004). U., *Science*, 303, 1659-1662.

Gas-Phase Products and Secondary Aerosol Yields from the Ozonolysis of (*E*)-β-farnesene

I. Kourtchev, I. Bejan, J.R. Sodeau and J.C. Wenger

Department of Chemistry and Environmental Research Institute, University College Cork, Cork, Ireland

Keywords: Sesquiterpenes, SOA, smog chamber, aerosol formation.

Vegetation emits a variety of biogenic volatile organic compounds (BVOCs) including isoprene, monoterpenes and sesquiterpenes into the atmosphere. Sesquiterpenes are amongst the shortest lived species due to their high reactivity toward the atmospheric oxidants (O_3, OH and NO_3 radicals) and have shown to give remarkably high aerosol yields.

To date, a number of laboratory studies have been performed on a series of sesquiterpenes with cyclic structures, including β-caryophellene, α-humulene, α-cedrene and α-copaene; however, there is a lack of information concerning the atmospheric reactivity of (*E*)-β-farnesene, an acyclic compound emitted from a wide range of plants (Duhl et al., 2008). (*E*)-β-farnesene contains four double bonds (Structure 1) and is therefore expected to be highly reactive towards atmospheric oxidation and a likely source of free radicals, oxygenated organic compounds and secondary organic aerosol (SOA) in the Earth's atmosphere.

This study presents, for the first time, results from the ozonolysis of (*E*)-β–farnesene. The experiments were performed in a 3.91 m^3 atmospheric simulation chamber at 296 ±2 K to determine gas phase oxidation products and SOA yields in a presence and absence of OH scavengers (i.e., CO, cyclohexane and 2-butanol), aerosol seed and at different humidity levels. The decay of (*E*)-β-farnesene was determined by in situ FTIR spectroscopy. The size distribution of the organic aerosol was measured using a scanning mobility particle sizer (SMPS). SOA-masses were calculated from the measured size distribution assuming an aerosol density of 1 g/cm^3. Gas phase carbonyl products were collected using a denuder sampling technique and analyzed with gas chromatography/mass spectrometry (GC/MS) after subsequent derivatization with O-(2,3,4,5,6-pentafluorobenzyl) hydroxylamine (PFBHA).

A number of carbonyl compounds have been observed as gas phase reaction products and included acetone, 4-methylenehex-5-enal, 6-methylhept-5-en-2-one, *(E)*-4-methyl-8-methylenedeca-4,9-dienal, methylglyoxal, and 4-oxopentanal. A plausible reaction mechanism has been proposed to explain these experimental observations.

During experiments with equal concentrations of (*E*)-β-farnesene and ozone performed under dry conditions in the absence of scavenger, the SOA yield was found to be approximately 30%. When the starting concentration of ozone was in excess of that for the sesquiterpene the aerosol yield increased up to 42%. This could be explained by further oxidation of gas-phase oxidation products containing double bonds and suggested the importance of the contribution of second generation products to the SOA yield. The yield of SOA was found to decreases at high relative humidity and in the presence of OH scavengers.

The results obtained in this study provide additional insights into the role of biogenic emissions in the chemistry of the atmosphere. They indicate that (*E*)-β-farnesene is a source of the ubiquitous carbonyls acetone and 4-oxopentanal and also an efficient precursor for the formation of biogenic SOA.
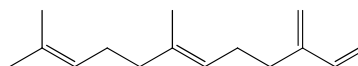
Structure 1. (*E*)-β-farnesene

Duhl, T.R., Helmig, D., & Guenther, A. (2008). *Biogeosciences*, 5, 761-777.

MUCHACHAS: MUltiple CHamber Aerosol CHemical Aging experimentS

N. M. Donahue[1], H. Saathoff[2],
U. Baltensperger[3], A. Prevot[3], J. Dommen[3],
T. Brauers[4], Th. F. Mentel[4],
M. Hallquist[5], M. Bilde[6], T. Hoffmann[7]

[1] Center for Atmospheric Particle Studies, Carnegie Mellon University, Pittsburgh, USA
[2] Institute for Meteorology and Climate Research, Forschungszentrum Karlsruhe, Germany
[3] Laboratory for Atmospheric Chemistry, Paul Scherrer Institut, Villigen, Switzerland
[4] Institut fur Chemie und Dynamik der Geosphäre, ICG-2, Forschungszentrum Jülich, Germany
[5] Atmospheric Science, Department of Chemistry, University of Gothenburg, Sweden
[6] Department of Chemistry, University of Copenhagen, Copenhagen, Denmark
[7] Institut für Anorganische und Analytische Chemie, Johannes Gutenberg-Universität, Mainz, Germany

Keywords: Organic Aerosol, SOA, Aerosol Evolution, Aerosol Chemistry, Aerosol Component Chemistry

The Multiple Chamber Aerosol Chemical Aging ExperimentS (MUCHACHAS) were designed to study the effect of aging by the OH radical on SOA formed from monoterpene ozonolysis. The central hypothesis was that OH oxidation of SOA vapours produced from a 'traditional' SOA reaction such as ozone + α-pinene would significantly alter SOA mass concentrations and other important properties.

It is widely accepted that SOA exists in a phase equilibrium between condensed (particulate) and vapour (gas) phases. For most SOA precursors, but bulk of the carbon mass is believed to reside in the vapour phase: for example, ozone + α-pinene, results in 5-25% of carbon as SOC and thus 95-75% of the carbon as vapours. Those vapours will all react with the OH radical – some may also photolyse or react with other oxidants. This photochemical aging will almost certainly change SOA levels.

Aerosols are thought to remain in the atmosphere for at least one week, on average. The timescale for gas-phase oxidation of SOA vapours is one day or less, and the heterogeneous oxidation timescale is a few days or less. If these oxidation reactions tend to result in more polar, more functionalized organic products, their result will be an increase in SOA; conversely, if these reactions result in C-C bond fragmentation that overwhelms any increase in functionalization, their result will be a decrease in SOA. In either direction, it is likely that these aging reactions control ambient organic aerosol properties.

MUCHACHAS was designed to study this aging phenomenon under a wide range of atmospherically relevant conditions. Different major chamber facilities have complementary capabilities, and so MUCHACHAS was designed to exploit these capabilities to develop a comprehensive picture of ozone + α-pinene SOA aging. Initial experiments in the CMU chamber employed near-UV HOOH photolysis to produce OH radicals; experiments in the AIDA chamber were conducted over a wide range of temperatures (253 – 313 K) using a dark (ozonolysis) OH source; experiments at the PSI chamber with pseudo-solar illumination and both HOOH and ozonolysis OH production under a wide range of NO_x and SOA levels; experiments in the SAPHIR chamber covered multiple-day timescales with ambient illumination.

The end result of these experiments is that aging reactions do dramatically alter SOA levels from ozone + α-pinene: depending on the circumstances, SOA formation can be changed by more than a factor of two. Far over and above simple mass measurements, numerous measurements of SOA composition and properties, reported in other presentations, document significant changes in SOA properties due to aging by OH radicals. This talk will provide a general overview of MUCHACHAS, context for the individual findings, and place the evolution of mass and oxidation state in the context of a two-dimensional volatility basis set incorporating saturation concentration (C*) and the oxidation state (O:C) of the organic aerosol.

Formation of peroxides in the gas and particle phase during photochemical aging experiments of secondary organic aerosol from α-pinene

P. Mertes[1], J. Dommen[1], T. Tritscher[1], A.P. Praplan[1], P.B. Barmet[1], P.F. DeCarlo[1], A.S.H. Prévôt[1], N.M. Donahue[2] and U. Baltensperger[1]

[1]Laboratory of Atmospheric Chemistry, Paul Scherrer Institute, 5232, Villigen, Switzerland
[2]Center for Atmospheric Particle Studies, Carnegie Mellon University, Pittsburgh, Pennsylvania 15213, USA

Keywords: α-pinene oxidation, peroxides, smog chamber, SOA.

Ambient fine and ultrafine particles play a decisive role in atmospheric processes, but have also an important impact on human health, predominantly on respiratory and cardiovascular systems (Pope & Dockery, 2006). Up to about 70% of these ambient particles are composed of organic material. However, the highly complex organic mixture is chemically still poorly characterized. The reaction of terpenes with ozone in the polluted troposphere mainly generates aldehydes, carboxylic acids and organic peroxides. The contribution of these peroxides to health risk is assumed to be especially important because of their high reactivity and oxidation potential.

We are engaged in a project aiming to quantify peroxides present in aerosols (H_2O_2, ROOH and ROOR) generated under controlled conditions. In an accompanying project, lung cells are then examined for morphologic, biochemical and physiological changes after exposure to these aerosol particles. Using iodometry quantification of peroxides could be performed (Gaschen et al., 2008) and interesting time trends could be observed. However, experiments had to be performed at very high aerosol concentrations and time resolution was low (2 hours). Here we undertook an exploratory study with a more sensitive on-line method, but which is not quantitative yet.

The experiments were done in the PSI smog chamber consisting of a 27-m^3 flexible teflon bag suspended in a temperature controlled wooden enclosure. Four xenon arc lamps are used to simulate the solar light spectrum. All experiments were performed at 20°C and 50 % relative humidity. The experiments were performed within the MUCHACHAS (Multiple CHamber Aerosol Chemistry and Aging Studies) experimental series. They were designed to study the aging of secondary organic aerosols by means of OH radicals. First, SOA was produced by the ozonolysis of 10 ppb of the biogenic precursor α-pinene. Thereafter, the SOA was aged by means of OH, which was produced by photolysis of HONO or ozonolysis of tetramethyl ethene (TME). Pentanol was added to trace the OH concentration.

For the peroxide determination we used the AL2002 H_2O_2-ANALYZER (AERO-LASER GmbH). The detection method is based on the reaction of peroxides with p-hydroxyphenylacetic acid catalyzed by peroxidase (from horseradish). The resulting reaction produces a fluorescent dimer that can be excited at 326 nm (Cd-lamp) and detected between 400 and 420 nm (Lazrus et al., 1985). To distinguish between hydrogen peroxide (H_2O_2) (HP) and organic peroxides (ROOH & ROOR) (OPs) two different channels are used. While one channel measures total peroxides, in the other channel HP is destroyed selectively by catalase. The method offers quantitative analysis of HP due to 100 % stripping efficiency. However, due to lower solubility the stripping efficiency of OPs is lower, resulting in a lower limit of their concentration only.

We did measurements for the determination of peroxides in the gas phase and the aerosols. Peroxides from the gas phase were extracted in a stripping coil using pH buffered water (stripping solution). Particle samples were collected behind a charcoal denuder on teflon filters (pore size 5 μm) and extracted with the stripping solution for 45 minutes.

HP and OPs were detected in the gas and aerosol phase directly after the ozonolysis and under both aging procedures. In the case of dark OH large amounts of peroxides were produced. The influence of TME on this needs to be investigated yet. We also explored the influence of light on the peroxide production during ozonolysis and dark-OH aging. First results show that light appears to have a distinct effect on OP formation.

Gaschen, A., Kalberer, M., Dommen, J., Duplissy, J., & Baltensperger, U. (2008). *Geophysical Research Abstracts, EGU General Assembly*, 10, EGU2008-A-09959.

Lazrus, A. L., Kok, G. L., Gitlin, S. N., & Lind, J. A. (1985). *Anal. Chem.*, 57, 917-922.

Pope III, C. A., & Dockery, D. W. (2006). *J. Air Waste Manage. Assoc.*, 56, 709-742.

SOA aging with different OH sources

P.B. Barmet[1], P.F. DeCarlo[1], J. Dommen[1], T. Tritscher[1], A.P Praplan[1], P. Mertes[1], A.S.H. Prevot[1], N.M. Donahue[2], U. Baltensperger[1]

[1]Laboratory of Atmospheric Chemistry, Paul Scherrer Institut, CH-5232, Villigen PSI, Switzerland
[2]Center for Atmospheric Particle Studies, Carnegie Mellon University, Pittsburgh, Pennsylvania 15213, USA

Keywords: secondary organic aerosol, AMS, aerosol aging, gas/particle partitioning, smog chamber.

Understanding secondary organic aerosols (SOA) - their formation, composition and aging - is a major task in today's atmospheric research: SOA present a major fraction of the total organic aerosol and plays an important role in the global climate system due to their radiative properties and their influence on the hydrological system, e.g. on cloud or fog formation. In addition to their climatic relevance aerosols exert an adverse impact on the human health.

Within the MUCHACHAS (Multiple Chamber Aerosol Chemistry and Aging Studies) experimental series SOA was generated by ozonolysis of α-pinene and then aged further by OH exposure.

The experiments were performed in the environmental chamber at the Paul Scherrer Institute (PSI). The chamber consists of a 27-m^3 fluorinated ethylene propylene (FEP) bag suspended in a temperature-controlled enclosure (Paulsen et al., 1995). Four xenon arc lamps (16 kW total) are used to irradiate the chamber. Several instruments monitor the gas phase (VOC, NO/NO$_x$, O$_3$, CO) in the chamber. A PTRMS (proton transfer reaction mass spectrometer) monitors the temporal evolution of the gaseous reactant and a variety of products. The particle phase is characterized by the particle number size distribution (SMPS, scanning mobility particle sizer), the total particle number (CPC, condensation particle counter), and the chemical composition (HR-ToF-AMS, high-resolution time-of-flight aerosol mass spectrometer).

In all experiments SOA was initially formed from the ozonolysis of α-pinene. The aging of the SOA and gaseous products from ozonolysis were then investigated under different conditions: (1) high NO$_x$ concentration, (2) low NO$_x$ concentration and (3) exposure to OH radicals in both dark and lighted environment. The OH production was provided by the addition of tetramethyl ethylene (TME) and ozone - as a dark OH source - or by photolysis of HONO.

Preliminary results of the AMS and PTRMS show that – after turning on the lights – the ratio of m/z 44 (commonly associated with carboxylic acid functional groups) with total organics exhibits a linear correlation to the natural logarithm of the ratio between the measured pinonaldehyde concentration ([PA]) and the maximum pinonaldehyde concentration ([PA$_0$]), a proxy for OH exposure (Fig. 1).
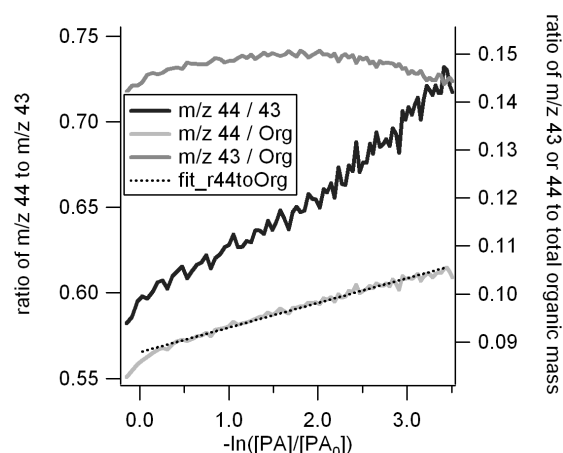
Figure 1. Natural logarithm of the ratio between the measured pinonaldehyde concentration ([PA]) and the maximum pinonaldehyde concentration ([PA$_0$]) vs different m/z - organic ratios.

Moreover, the total aerosol mass concentration (after correction for wall losses) is increased during aging with the OH radicals. This indicates that the production of less volatile products during the oxidation process is favored over fragmentation in these experiments.

Paulsen, D., Dommen J., Kalberer M., Prevot, A. S. H., Richter, R., Sax, M., Steinbacher, M., Weingartner, E., & Baltensperger, U. (2005). *Environ. Sci. Technol.,* 39(8), 2668-2678.

Aerosol and gas phase organic acids in smog chamber aging experiments of secondary organic aerosol from α-pinene

A.P. Praplan[1], T. Tritscher[1], P. Barmet[1], P. Mertes[1], P.F. DeCarlo[1],
J. Dommen[1], A.S.H. Prévôt[1], N.M. Donahue2, U. Baltensperger[1]

[1]Laboratory of Atmospheric Chemistry, Paul Scherrer Institut, 5232 Villigen PSI, Switzerland
[2]Center for Atmospheric Particle Studies, Carnegie Mellon University, Pittsburgh, Pennsylvania 15213, USA

Keywords: organic acids, ion chromatography, smog chamber, SOA, gas-particle distribution

Organic acids represent an important class of organic compounds in the atmosphere for both the gas and aerosol phase. They are either emitted directly from both biogenic and anthropogenic sources or formed as oxidation products from volatile organic compounds (VOCs) and precursors in the aqueous, gaseous and particle phase (Chebbi & Carlier, 1996)

Monoterpenes are a prominent class of VOCs with annual emissions of 127 Tg per year (Guenther *et al.*, 1995). Because of their high formation potential of secondary organic aerosols, several compounds of this class, particularly α-pinene, have been investigated extensively in many laboratory studies.

Among other acids, *cis*-pinic and *cis*-pinonic acid have been found as products of α-pinene ozonolysis. Ma *et al.* (2007) published evidence that these organic acids are formed in the gas phase via Criegee Intermediates (CIs). Recently, Szmigielski *et al.* (2007) identified 3-methyl-1,2,3-butanetricarboxylic acid (MBTCA) as a product from α-pinene photooxidation. This compound has been proposed as a marker species for α-pinene in ambient samples. The formation of this compound was explained by further reaction of *cis*-pinonic acid involving participation of the OH radical (Szmigielski *et al.*, 2007). In general, the formation mechanism of the organic acids from α-pinene is still not well understood.

The present work sets its focus on the fate of α-pinene SOA organic acids under different aging conditions. (1) low NOx concentration (2) high NOx concentration (3) exposure to OH radicals in both dark and lighted environments. α-pinene SOA is produced by ozonolysis without OH scavenger in the PSI smog chamber. It consists of a 27m^3 Teflon® bag that can be irradiated by four Xe arc lamps to simulate sunlight. (Paulsen *et al.*, 2004)

The organic acids are sampled with a wet effluent diffusion denuder (WEDD) and an aerosol collector (AC) for the gas phase and the aerosol particles, respectively. WEDD and AC samples are alternatively concentrated for 30 minutes on a trace anion concentrator (TAC) column (Dionex, Switzerland) and subsequently analyzed by ion chromatography coupled to mass spectrometry (IC/MS). This system is described in more details by Fisseha *et al.* (2004).

The results show that the *cis*-pinonic acid gas phase concentration increases rapidly in the presence of NOx, while it stays more or less constant upon OH exposure. On the other hand, *cis*-pinic acid concentration in aerosol decreases in presence of NOx but is nearly constant during OH exposure. 3-Methyl-1,2,3-butanetricarboxylic acid (MBTCA) is also formed during ozonolysis and demonstrates a strong concentration increase for all aging conditions. This partially agrees with a recent publication of Szmigielski *et al.* (2007), where MBTCA is thought to be formed in the presence of NOx, but this gives evidence that MBTCA can also be formed via another mechanism without NOx.

Overall, the total organic acids concentration is higher after aging processes for both the gas and particle phase. This work furthers our understanding of these oxidized species in the troposphere and in aging SOA.

Comparison with predictions of the Master Chemical Mechanism (MCM) and inclusion of new reaction mechanisms will help to improve the present knowledge of the organic acids formation pathways.

Chebbi, A., & Carlier, P. (1996). *Atmos. Environ.,* 30, 4233-4249.

Fisseha, R., *et al.* (2004). *Anal. Chem.*, 76, 6535-6540.

Guenther, A., *et al.* (1995). *J Geophys Res.,* 100, 8873-8892.

Jang, M. J., & Kamens, R. M. (1999). *Atmos. Environ.,* 33, 459-474.

Lee, S., & Kamens, R. M. (2005). *Atmos Environ.*, 39, 6822-6832.

Ma, Y., *et al.* (2007). *Phys. Chem. Chem. Phys.,* 9, 5084-5087.

Paulsen, D., *et al.* (2005). *Environ. Sci. Technol.,* 39, 2668-2678.

Szmigielski, R., *et al.* (2007). *Geophys Res. Lett.*, 34, L24811, doi:10.1029/2007GL031338.

Yu, J., *et al.* (1999). *J. Atmos. Chem.,* 34, 207-258.

Volatility of aged secondary organic aerosol (SOA) from ozonolysis of monoterpenes.

K. Salo[1], M. Hallquist[1], Å. M. Jonsson[1,2], H. Saathoff[3], C. Spindler[4], Th. F. Mentel[4] and N. Donahue[5]

[1] Atmospheric Science, Department of Chemistry, University of Gothenburg, Sweden.
[2] IVL, Swedish Environmental Research Institute, P.O. Box 5302, Sweden
[3] Institute for Meteorology and Climate Research, Forschungszentrum Karlsruhe, Germany
[4] Institut fur Chemie und Dynamik der Geosphäre, ICG-2, Forschungszentrum Jülich, Germany
[5] Center for Atmospheric Particle Studies, Carnegie Mellon University, Pittsburgh, USA

Keywords : Aerosol Chemistry, SOA (Secondary Organic Aerosols), TDMA Volatility

In this work a Volatility Tandem DMA (VTDMA) was used to monitor changes in particle volatility due to dark hydroxyl radical ageing of Secondary Organic Aerosols (SOA). The overriding aim of this study was to investigate later-generation oxidation of `traditional' SOA formed from ozone + terpene reactions. One important aspect was the determination of the evolution of the volatility of especially the higher-volatility products over a range of temperatures.

The fresh SOA was produced from ozonolysis of α-pinene and limonene both with and without the use of ammonium sulphate seed aerosol. As an OH-radical source the ozonolysis of tetramethylethylene (TME) was used (Lambe et al., 2007). The experiments were done at the AIDA chamber facility at the Institute for Meteorology and Climate Research (Saathoff *et al.* 2003). The AIDA chamber is a 84.5 m^3 large aluminium vessel with a surface to volume ratio of 1.22 m^{-1} and the current experiments were done at four temperatures (253 K, 273 K, 293 K and 313 K).

The VTDMA system used consists mainly of three parts; an initial DMA (differential mobility analyser TSI 3071), a conditioning unit and a SMPS-system. The initial DMA is operated in a recirculating mode, where a monodisperse aerosol fraction is selected. The conditioning unit is made of eight individually stainless steel tubes with 40 cm length and an inner diameter of 6 mm set at independent temperatures. The tubes are mounted in heated aluminium blocks in line with charcoal denuders. This system has been described in detail by Jonsson *et al.* (2007). The SMPS-system (TSI 3096) was used to monitor the change in particle diameter. In addition, a thermodenuder/AMS (Aerodyne TOF-AMS) combination was used for chemical characterisation (cf. Figure 1). Using this system it was possible to follow the general change in SOA chemical composition due to ageing for SOA material of different volatility (all SOA and fraction remaining at 383 K).

The results from these measurements showed clearly that the chemical composition and corresponding volatility changed due to the ageing induced by OH chemistry.
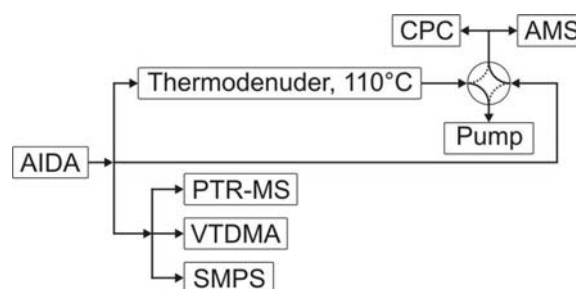
Figure 1. Schematic of the experimental setup showing the most relevant instruments.

As an example Figure 2 shows the volatility changes observed by the VTDMA system, as volume fraction remaining (VFR), before and after generating OH radicals in the aerosol system by oxidising TME.
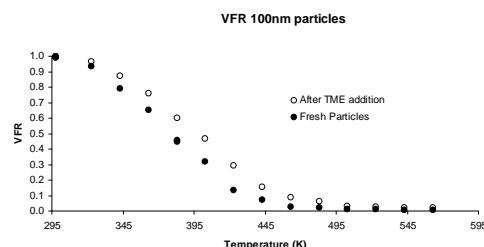
Figure 2. Increase in volume fraction remaining (VFR) after OH-radical ageing.

Jonsson, A. M., Hallquist, M. & Saathoff, H. (2007) *J. Aerosol Science,* **38,** 843-852.

Lambe, A. T., Zhang, J. Y., Sage, A. M. & Donahue, N. M. (2007) *Environ. Sci., & Technol.,* 41, 2357-2363.

Saathoff , H., Naumann, K. H., Schnaiter, M., Schock, W., Mohler, O., Schurath, U., Weingartner, E., Gysel, M. & Baltensperger, U. (2003) *J. Aerosol Science, 34,* 1297-1321.

Secondary organic aerosol formation from the OH initiated oxidation of tolualdehydes and dimethylphenols

I. Bejan[1], I. Kourtchev[1], J.C. Wenger[1], I. Barnes[2] and J.R. Sodeau[1]

[1]Department of Chemistry and Environmental Research Institute, University College Cork, Cork, Ireland
[2] Department of Physical Chemistry, Bergische University Wuppertal, 42097, Wuppertal, Germany

Keywords: hydroxyl radical, secondary organic aerosol, dimethylphenol, m-tolualdehyde, simulation chamber.

Secondary organic aerosol (SOA) is formed in the atmosphere via the gas-phase oxidation of organic compounds of natural or anthropogenic origin (Hallquist et al., 2009). Aromatic hydrocarbons, which are important organic constituents found in gasoline, vehicle exhaust and urban air, are believed to be the most important anthropogenic precursors of SOA formation in the atmosphere. The atmospheric oxidation of the major aromatic compounds, benzene, toluene and xylenes (BTX), proceeds by reaction with OH radicals: H-atom abstraction from the methyl groups results in the formation of benzaldehydes, whilst addition of OH to the aromatic ring yields phenolic products (Calvert et al., 2002).

It has been suggested that BTX oxidation products may make an important contribution to SOA formation observed in aromatic photooxidation systems, however, the SOA formation from the reaction of these compounds has not been investigated. The identification of the products mainly responsible for the SOA formation is, despite years of intensive research, still highly uncertain.

In an attempt to improve our knowledge of the details governing SOA formation from aromatic compounds, we have performed a series of atmospheric simulation chamber experiments to investigate secondary organic aerosol formation from the OH radical initiated oxidation of m-tolualdehyde and 2,6-dimethylphenol. Both of these compounds are important gas-phase products of the oxidation of m-xylene and recent work has indicated that they may be significant contributors to SOA formation.

A series of experiments has been performed in a 3.91 m^3 atmospheric simulation chamber at 296 ±2 K to determine the yield of SOA under conditions of high and low NOx. Hydroxyl radicals were generated from the ozonolysis of 2,3-dimethyl-2-butene and the photolysis of HONO to generate low and high NOx conditions respectively. The decay of the oxygenated aromatics was determined by in situ FTIR spectroscopy. The size distribution of the organic aerosol was measured using a scanning mobility particle sizer (SMPS). SOA-masses were calculated from the measured size distribution assuming an aerosol density of 1.4 g/cm^3. Gas and particle phase carbonyl products were collected using a denuder-filter sampling technique and analyzed with gas chromatography/mass spectrometry (GC/MS) after subsequent derivatization with O-(2,3,4,5,6-pentafluorobenzyl) hydroxylamine (PFBHA).

Preliminary investigations on SOA formation from the OH-initiated oxidation of m-tolualdehyde produced yields of 7-18% under low NOx conditions. The yield of SOA from 2,6-dimethylphenol was in the range 18-32%. In the presence of NOx, the yields were considerably lower, in agreement with other studies (Hallquist et al., 2009). There results indicate that both oxygenated aromatics are likely to contribute to SOA formation under atmospheric conditions.

Hallquist, M., J. C. Wenger, U. Baltensperger, Y. Rudich, D. Simpson, M. Claeys, J. Dommen, N. M. Donahue, C. George, A. H. Goldstein, J. F. Hamilton, H. Herrmann, T. Hoffmann, Y. Iinuma, M. Jang, M. Jenkin, J. L. Jimenez, A. Kiendler-Scharr, W. Maenhaut, G. McFiggans, Th. F. Mentel, A. Monod, A. S. H. Prévôt, J. H. Seinfeld, J. D. Surratt, R. Szmigielski, and J. Wildt (2009). *Atmos. Chem. Phys. Discuss.*, 9, 3555-3762.

Calvert, J., R. Atkinson, K.H. Becker, R. Kamens, J. Seinfeld, T. Wallington, and G. Yarwood (2002) *The Mechanism of Atmospheric Oxidation of Aromatic Hydrocarbon.* Oxford University Press.

Characterisation of the AIDA aerosol chamber by means of commercial computational fluid dynamics (CFD) software

S. Benz, H. Bunz, J. Meinen, O. Möhler and T. Leisner

Institute of Meteorology and Climate Research, Forschungszentrum Karlsruhe, Hermann-von-Helmholtz-Platz, 76344 Eggenstein-Leopoldshafen, Germany

Keywords: CFD, aerosol chamber

The aerosol and cloud chamber AIDA of Forschungszentrum Karlsruhe has shown in the past decade to be a powerful tool simulating atmospheric aerosol and cloud processes (e.g. Möhler et al., 2005, Saathoff et al., 2008). We used a computational fluid dynamics (CFD) code to simulate the coupled fields of velocity, temperature, water vapour and particle number concentration inside the chamber during an expansion experiment. The aim of the presented study is to check the degree of homogeneity by numerical means. We present comparisons of numerical simulations with available experimental data sets.

AIDA consists in principle of an evacuable aluminium vessel (volume 84 m^3, diameter 4m) which is surrounded by a coolable housing. The temperature can be set to any temperature down to –90°C. By controlled pumping the pressure inside the vessel can be reduced inducing a further cooling. This additional cooling – which is adiabatic only in the first stage – is limited by an increasing flux of heat from the chamber wall. The wall rests at almost constant temperature due to its high heat capacity. The gas temperature inside the vessel is monitored by arrays of vertically and horizontally arranged temperature sensors. The inhomogeneity throughout the entire vessel is estimated to +/– 0.3 K. The isothermal wall is internally covered by a thin ice layer which evaporates during the expansion process. This source of water vapour reduces the decrease of the partial pressure of water vapour during reduction of pressure inside the vessel. Thereby the maximum achievable super-saturation is increased. Water vapour is measured in situ using a tuneable diode laser absorption spectroscopy (TDLAS). The sensitivity of the measurement is enhanced by a White–type multiple reflection cell. The measurement delivers a mean value at medium height of the aerosol vessel. Currently no experimental device is available at AIDA to determine the nature of the turbulent flow field inside the vessel.

For our simulations we used the commercial CFD code ANSYS CFX 11.0. The geometry of the AIDA aerosol vessel was highly simplified neglecting details as the above mentioned reflection cell in order to get a rotationally symmetric geometry. Thereby the computational costs could be reduced extremely as solely a segment of 2° had to be modeled. The mixing fan was implemented by an artificial source of momentum. A hexahedral mesh with 24,300 nodes was generated by means of the software ANSYS ICEM CFD. In the boundary layers the mesh was refined to resolve high gradients near the walls.
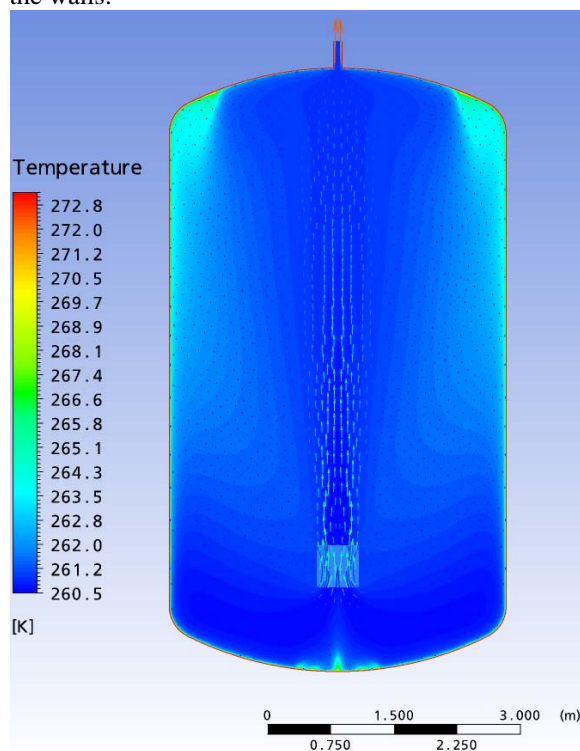
Figure1. Cross section of AIDA vessel with contour plot of temperature after the pressure was reduced from 1000 hPa to 800 hPa within 250s. The vectors illustrate the flow field. The pressure inside the chamber is reduced via a tube which is mounted at the top of the chamber. The air speed directly above the mixing fan amounts to 3 m/s. The mixing fan is enclosed by a baffle (brightly shaded area at the lower part of the chamber).

Möhler, O. et al. (2005), *J. Geophys. Res.,* 110, 3456-3467.
Saathoff, H. et al. (2008), *Atmos. Chem. Phys. Discuss.*, 8, 15595-15664

H$_2$O$_2$ and organic peroxides in the gas and aerosol phase from the ozonolysis of the sesquiterpenes α-humulene and β-caryophyllene

J. Valverde-Canossa[1], G.K. Moortgat[2], A. Sadezky[2] and R. Winterhalter[2]

[1]Laboratorio de Análisis Ambientales, Universidad Nacional, Campus Omar Dengo, 83-6000, Heredia, Costa Rica.
[2]Atmospheric Chemistry Department, Max Planck Institute for Chemistry, P.O. Box 3060, D-55020 Mainz, Germany

Hydrogen peroxide and hydroperoxides are key compounds regarding the chemical composition of the Earth's atmosphere. They are secondary products formed during in the photo-oxidation of volatile organic compounds, acting as precursors of odd-oxygen as well as reservoirs of odd-hydrogen radical and thus influence the HO$_x$ (HO + HO$_2$) cycle (Logan *et al.*, 1981). Hydroperoxides, with sufficiently low vapor pressures, could contribute a large fraction to SOA (Bonn *et al.,* 2004*)*. Production of H$_2$O$_2$ and hydroperoxides occurs mainly in the gas phase by recombination of two HO$_2$ radicals, or HO$_2$ and RO$_2$ radicals, respectively. Furthermore laboratory studies indicate that hydroperoxides are also produced in the ozonolysis reaction of anthropogenic and biogenic alkenes (Großmann, 1999; Valverde-Canossa, 2004). The efficiency of the ozone-alkene reaction with respect to peroxide formation depends on the relative humidity and the chemical structure of the alkene. The sesquiterpenes show a high SOA yield in general and therefore, α-humulene and β-caryophyllene where selected to investigate their chemical degradation, aerosol formation and peroxide yields.

Ozonolysis experiments were performed in synthetic air in a 570 L spherical glass vessel at T = 296 ± 1 K and 730 ± 2 Torr (Winterhalter *et al.,* 2009).

The experiments were performed with and without addition of cyclohexane to scavenge > 95% of the formed OH radicals. The relative humidity was between 50 to 60 %. Initial reactants mixing ratios were about 400 ppb of sesquiterpene and 270 ppb, 860 ppb and 1200 ppb of ozone.

Samples were taken from the gas phase by drawing the air samples through a modified thermostatted helix-shaped coil collector at 5 ± 0.3 °C (Neeb *et al.*, 1997). Additionally, filter samples of the formed SOA were collected at the end of each experiment and extracted. Both types of samples were analysed for peroxides by a combination of two HPLC systems which differ mainly on the mobile phase. Both methods use post-column derivatisation with horseradish peroxidase and fluorescence detection (Valverde-Canossa, 2004).

The experimental results show that for β-caryophyllene, yields of H$_2$O$_2$ were found to be 2 % with excess alkene and 4 % with excess ozone. Moreover, 0.2 % of hydroxymethyl hydroperoxide (HMHP) were formed with excess ozone, while its concentrations were below the quantification limit with excess alkene. Under similar initial conditions, α-humulene produced four times more H$_2$O$_2$. The addition of excess cyclohexane as an OH scavenger did not have any detectable influence on H$_2$O$_2$ yields for both sesquiterpenes. Extracted filter samples of secondary organic aerosol showed significant quantities of hydroperoxides, with a relative percentage of long-chain (C$_6$ to C$_{12}$) organic hydroperoxides to H$_2$O$_2$ of up to 12 %.

Bonn, B. and Moortgat G.K. (2003). *Geophys. Res. Lett.*, 30 (11), 1585-1588.

Großmann, D. (1999). *Die Gasphasenozonolyse von Alkenen in Gegenwart von Wasserdampf als Quelle für Wasserstoffperoxid und organische Peroxide in der Atmosphäre.* Ph.D. Thesis, Johannes Gutenberg University, Mainz, Germany.

Logan, J.A., Prather, M.A., Wofsy, S.C. and McElroy, M.B. (1981). *J. Geophys. Res.*, 86, 7210-7254.

Neeb, P., Sauer, F., Horie, O. and Moortgat, G.K. (1997). *Atmos. Environ.*, 31, 1417-1423.

Valverde-Canossa, J. (2004). *Sources and sinks of organic peroxides in the planetary boundary layer.* Ph.D. Thesis, Johannes Gutenberg University Mainz, Germany.

Winterhalter, R., Herrmann, F., Kanawati, B., Nguyen, T.L., Peeters, J., Vereecken, L. and Moortgat, G.K., *Phys. Chem. Chem. Phys.*, DOI: 10.1039/B817824A, 2009.

Chemical characterisation of PM2.5 aerosols collected during a 2007 summer campaign at a forested site in Brasschaat, Belgium

W. Wang, X. Chi and W. Maenhaut

Dept. of Anal. Chem., Inst. for Nuclear Sci., Ghent University, Proeftuinstraat 86, BE-9000 Gent, Belgium

Keywords: biogenic particles, chemical composition, organic compounds, ion chromatography, PM2.5.

Within the framework of the project "Formation mechanisms, marker compounds, and source apportionment for biogenic atmospheric aerosols" (BIOSOL) aerosol samples are collected at three forested sites in Europe. One of the sites is the state forest "De Inslag" in Brasschaat, Belgium. This forest is located at 51º18'33"N, 4º35'14"E, 15 m above sea level. It is at about 12 km NE of the center of the city of Antwerp and at about 9 km to the east of the Antwerp harbour area, so that the aerosol composition is expected to be strongly impacted by anthropogenic emissions in addition to the biogenic emissions from the forest. During a 2007 summer campaign, aerosol samples were collected from 5 June until 13 July. A high-volume dichotomous sampler (HVDS) was deployed for separate day and night aerosol collections in two size fractions (fine: <2.5 µm; coarse: >2.5 µm). The HVDS was located on a tower at about 9 m above ground level. Double (i.e., front and back) pre-fired Gelman Pall quartz fibre filters were used as collection surfaces for each of the two size fractions. The purpose of the back filters was to assess sampling artifacts, in particular for the carbonaceous aerosol constituents. A total of 71 HVDS samples and 10 field blanks were taken. All filters were analysed for organic carbon and elemental carbon (OC and EC) with a thermal-optical transmission technique (Birch & Cary, 1996) and those from the PM2.5 size fraction were analysed for water-soluble OC (WSOC) as described by Viana *et al.* (2006) and for water-soluble inorganic cationic and organic and inorganic anionic species by suppressed ion chromatography with conductometric detection (thereby using an hydroxide gradient eluent for the anionic species and an isocratic methanesulphonic acid eluent for the cationic species). The campaign median concentrations and interquartile ranges for the various components, as obtained from the front filters of the PM2.5 size fraction, and the median back/front filter concentration ratios for PM2.5 are given in Table 1. The back/front filter ratios are small for most species measured, suggesting that sampling artifacts are negligible for these species. It is known that some of the species measured (i.e., OC, WSOC, NO_3^-) are subject to both positive and negative artifacts (e.g., Turpin *et al.*, 2000) and substantial back/front ratios are obtained for them. Sulphate, which is essentially from anthropogenic sources at our site, is by far the major component, followed by OC and NH_4^+. The relative concentrations of the 3 species are quite similar to those found at urban sites in Belgium (Maenhaut, 2007), thus indicating that the site is indeed strongly impacted by anthropogenic emissions. Consequently, substantial concentrations of particulate-phase organic compounds from mixed biogenic/anthropogenic origin, such as organosulphates and nitrooxy-organosulphates, are expected (Surratt *et al.*, 2008). The measured organic compounds accounted, on average, for 8% of the WSOC and the latter represented 51% of the OC. This latter percentage is intermediate between the percentages of around 40% found for Ghent and of 60% found for the other two (and much less anthropogenically disturbed) forested sites studied within BIOSOL.

Table 1. Front filter median concentrations and interquartile ranges and median back/front filter concentration ratios (all for PM2.5).

Species	Front filter conc. (ng/m³)		Median back/ front ratio
	median	(interq. range)	
OC	1730	(1270 – 2200)	0.17
EC	400	(280 – 620)	0.00
WSOC	810	(570 – 1170)	0.21
NH_4^+	1080	(650 – 2100)	0.04
SO_4^{2-}	2700	(1840 – 3900)	0.00
NO_3^-	650	(400 – 2200)	0.24
Na^+	108	(65 – 210)	0.01
Mg^{2+}	2.7	(1.42 – 6.7)	0.00
K^+	38	(18.7 – 93)	0.12
Ca^{2+}	27	(14.7 – 36)	0.00
MSA	79	(46 – 119)	0.03
Oxalic	75	(50 – 140)	0.01
Malonic	49	(28 – 82)	0.02
Succinic	11.0	(5.7 – 54)	0.02
Glutaric	4.7	(3.3 – 9.7)	0.26

Birch, M. E., & Cary, R. A. (1996). *Aerosol Sci. Technol.* 25, 221-241.

Maenhaut, W. (2007). in *EMEP Particulate Matter Assessment Report*, EMEP/CCC-Report 8/2007, O-7726, NILU, Kjeller (Norway), 95-108.

Surratt, J. D., et al. (2008). *J. Phys. Chem. A* 112, 8345-8378.

Turpin, B. J., Saxena, P., & Andrews, E. (2000). *Atmos. Environ.* 34, 2983-3013.

Viana, M., et al. (2006). *Atmos. Environ.* 40, 2180-2193.

Organic Composition of PM$_{2.5}$ Aerosols in Cork Harbour, Ireland

I. Kourtchev, J. Bell, S. Hellebust, I.P. O'Connor, A. Allanic, R.M. Healy, J.C. Wenger and J.R. Sodeau

Department of Chemistry and Environmental Research Institute, University College Cork, Cork, Ireland

Keywords: PM2.5, chemical composition, organic tracer, source identification, GC-MS.

Atmospheric particles with diameters less than 2.5 μm (PM$_{2.5}$) have adverse effects on human health, visibility and climate. A substantial fraction (20-90%) of atmospheric fine particulate matter are comprised of organic compounds (Kanakidou *et al.*, 2005), which cover a wide range of polarities, volatilities and masses. Our knowledge on the organic chemical composition of atmospheric aerosols is rather limited; only about 30% of the organic matter has been characterised at the molecular level. Nevertheless, some of the identified compounds are source specific and can provide important information on aerosol sources and source processes.

In this study, PM$_{2.5}$ aerosol samples were collected during summer and autumn 2008 periods in the Tivoli Industrial and Dock Estate (Cork, Ireland). The sampling site is characterised as a very complex environment supporting a variety of industrial and domestic activities and representing many emission sources. Aerosol samples were analysed for non-polar and polar organic compounds that are useful markers for the aerosol source characterisation. Non polar organic compounds were determined using thermal desorption gas chromatography/mass spectrometry (TD-GC/MS) and included polycyclic aromatic hydrocarbons (PAHs) and n-alkanes (C$_{20}$-C$_{30}$). The carbon preference index (odd to even ratio) of identified n-alkanes corresponded to diesel and smoke emissions and was comparable with those reported from other urban areas. Major PAHs included naphthalene, acenaphthylene, acenaphthene, phenanthrene, fluoranthene, and pyrene. All detected PAHs are of major health concern due to their well-known carcinogenic and mutagenic properties.

Polar compounds were determined with GC/MS after extraction with $CH_3OH-CH_2Cl_2$ mixtures and a derivatization process that converts carboxylic and hydroxylic groups of the organic compounds to trimethylsilyl (TMS) derivatives. Major polar compounds identified in the summer samples were oxidation products of isoprene, including the 2-methyltetrols and C$_5$ alkene triols. Other identified water-soluble compounds were: malic acid, levoglucosan, galactosan, mannosan, glyceric acid, arabitol and mannitol. Of the latter compounds, galactosan and mannosan are markers for biomass burning that are formed during the pyrolysis of cellulose at temperatures >300°C. Levoglucosan is another biomass burning marker that is formed during combustion and found in both cellulose and lignite pyrolysates (Fabbri *et al.*, 2008).

Arabitol and mannitol are markers for fungal spores, while the origins of malic acid and glyceric acid are still not clear. During the autumn and late autumn periods the atmospheric concentrations of the isoprene oxidation products, as well as the markers for fungal spores, decreased to undetectable levels. This observation can be explained by the occurrence of colder temperatures and lower photochemical activity. In contrast, the average concentrations of biomass burning markers (levoglucosan, mannosan and galactosan) increased substantially from 10 ng/m^3 during summer to 116 ng/m^3 (reaching up to 550 ng/m^3) during the late autumn period. For the late autumn campaign, biomass burning markers exhibited diel variations with the highest concentrations during night-time. The regression analysis demonstrated excellent correlation (R^2>0.99) between galactosan, mannosan and levoglucosan concentrations suggesting that the main source of the biomass burning is cellulose-containing solid fuel (e.g., firewood or peat).

The contributions of different aerosol sources to the organic carbon (OC) mass were assessed based on the available source profile data and average concentrations of the detected polar organic compounds. The average atmospheric concentration of wood smoke was estimated at 59 ng C/m^3 (or 5.5% of the OC) during the summer period and increased up to 650 ng C/m^3 (or 28.5% of the OC) during the late autumn period. During the summer campaign the average atmospheric concentration of fungal spores was 11 ng C/m^3, which corresponds to 1% of the OC, while that of isoprene SOA was estimated at 19.5 ng C/m^3 and 1.8% of the OC.

Kanakidou, M., Seinfeld, J. H., Pandis, S. N., Barnes, I., Dentener, F. J., Facchini, M. C., van Dingenen, R., Ervens, B., Nenes, A., Nielsen, C. J., Swietlicki, E., Putaud, J. P., Balkanski, Y., Fuzzi, S., Horth, J., Moortgat, G. K., Winterhalter, R., Myhre, C. E. L, Tsigaridis, K., Vignati, E., Stephanou, E. G., & Wilson, J. (2005). *Atmos. Chem. Phys.,* 5, 1053-1123.

Fabbri, D., Marynowski, L., Fabianska, M.J., Zaton, M., & Simoneit, B. R. T. (2008). *Environ. Sci. Technol.*, 42, 2957-2963.

Chemical and physical characterization of diesel emissions from EURO 2, 3 and 4 vehicles fuelled by reference diesel and a 20% biofuel blend.

J. Klenø Nøjgaard[1], A. Massling[1], B. Jensen[1], A. G. Hemmersam[2], C. Raahede[2] and P. Wåhlin[1]

[1]Department of Atmospheric Environment, National Environmental Research Institute, University of Århus, Frederiksborgvej 399, 4000 Roskilde, Denmark
[2]Danish Technological Institute, Kongsvang Allé 29, 8000 Århus, Denmark

Keywords: aerosol chemistry, diesel exhaust, particle size distribution, PAHs, aerosol spectrometry.

INTRODUCTION

It is well known, that diesel fuelled vehicles emit high amounts of sub-micrometer aerosol, which in turn is expected to cause adverse health effects. It is envisaged that future regulations will control particulate emissions also in terms of size (Tsolakis, 2006). This work presents a study on diesel exhaust emissions covering different engine types (EURO norm 2-4) operated with a blend (20% w/w biodiesel) and a reference fossil diesel. The study aims at identifying differences in emissions for engines representative for the present car population in Denmark.

METHODS

Gas-phase and particle-phase emissions were measured in different operation modes, that is mode 1 (idle), mode 2 (max torque; 25% load), mode 3 (max torque; 50% load), mode 4 (max torque; 100% load), and mode 5 (max power; 100% load). The raw exhaust from the engine was mixed with particle-free air (1:10) in a dilution tunnel.

NO, NO_2, CO, CO_2, and Total Volatile Organic Compounds (TVOC) were measured in the raw gas exhaust. Carbonyls and filter samples for chemical analysis (EC/OC, PAH, hopanes and steranes) were obtained from the dilution tunnel.

A rotating disc diluter (Matter Engineering, Switzerland) provided variable dilution (15-300 times) and connected the raw gas and a Differential Mobility Particle Sizer (DMPS with size range between 10 – 700nm), which measured the sub-micrometer particle number size distribution (PNSD).

Table 1. Overview of experiment runs and determined parameters (3 replicate measurements).

Type of engine	EURO Norm	Particles	Particle phase	Gas phase
Audi 1,9 TDI	EURO 2	PNSD	PAH, steranes, hopanes	NO, NO2, CO, CO2, TVOC, carbonyls
Peugeot 1,6 HDI	EURO 3	PNSD	steranes, hopanes	NO, NO2, CO, CO2, TVOC
Peugeot 1,6 HDI (Particle Filter)	EURO 4	PNSD	PAH, EC/OC, steranes, hopanes	NO, NO2, CO, CO2, TVOC

The chemical measurements were conducted in mode 4, which is representative for driving on a country road (80 km/hour for Danish conditions).

RESULTS

The particle volume and thereby particle mass of sub-micrometer particles was two orders of magnitude lower for the EURO 4 engine (with particle filter) compared to the EURO 2 and 3 engines. Also, substantial differences in particle number size distribution were observed when using different fuels, but the same engine. In Figure 1, the particle number size distribution of a mode mix (18% mode 1, 25% mode 2, 16% mode 3, 16% mode 4, 25% mode 5) representative for typical driving conditions is presented.
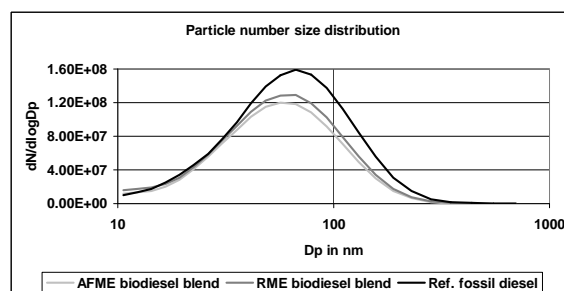
Figure 1. Particle number size distribution (mode mix, EURO 3) for different fuels.

Operating the EURO 3 engine with either of the biodiesel blends resulted in a decrease of emitted sub-micrometer particle volume of about 56% compared to the reference fossil diesel.

For the EURO 2 engine, emission of the individual PAH's were 11-56 % lower when fuelled by the biodiesel blend relative to operation with the reference fossil diesel. For example, the emission of benzo[a]pyrene was 18% lower. Similar and in some cases larger differences were measured for gas-phase carbonyls, e.g. formaldehyde, acetaldehyde and methacrolein were 25, 19 and 30% lower when biodiesel was added to the fuel.

ACKNOWLEDGEMENT

REFERENCES

Tsolakis, A. (2006). Effects on particle size distribution from diesel engine operating on RME biodiesel with EGR. *Energy and Fuels*, 20, 1418-1424.

Indicatory polychlorinated dibenzo-p-dioxins and dibenzofurans in the Surrounding Ambient Air of rural/traffic/industrial areas in Taiwan

Ming-Wei Chen[1], Wen-Jhy Lee[1*], Lin-Chi Wang[2], Guo-Ping Chang-Chien[2]

[1]Department of Environmental Engineering, National Cheng Kung University, Tainan, 70101, Taiwan
[2]Department of Chemical and Materials Engineering, Chengshiu University, Kaohsiung, 83347, Taiwan
*E-mail Address: wjlee@mail.ncku.edu.tw

Keywords: Traffic, Open burning straw, PCDD/Fs, incinerator,rural

This study set out to identify major emission sources of polychlorinated dibenzo-p-dioxins and dibenzofurans (PCDD/Fs) for different atmospheric environments near the Taipei city located in northern Taiwan. Each ambient air sample was collected using a PS-1 sampler (Graseby Andersen, GA) according to the revised EPA Reference Method T09A. The sampling flow rate was specified at ~0.225 m^3 min^{-1}. Each sample was collected continuously on three consecutive days (sampling volume = ~972 m^3). Seventeen PCDD/F congeners were analyzed primarily by using a high resolution gas chromatograph/mass spectrometer (HRGC/MS). There are three sampling sites in this study, site A, B and C are at rural, traffic, and industrial area respectively.

Figure 1 shows the congener profiles of the seventeen 2,3,7,8-chlorinated substituted PCDD/Fs detected from the stack flue gases of municipal solid waste incinerators (MSWIs), gas-fueled Sports Utility Vehicle (GSUV) and open burning straw (straw), respectively. The highest three ratio values of PCDD/Fs for each source were recognized as the indicatory PCDD/Fs and were listed in Table 1.

In this study, the top two congeners (Octachlorinated dibenzo-p-dioxin and 1,2,3,4,6,7,8-Heptachlornated dibenzofuran) of the seventeen 2,3,7,8 chlorinated substituted PCDD/Fs detected from the stack flue gases of MSWIs and GSUV were the same. On the same basis, we combined the atmosphere samples with indicatory PCDD/Fs of emission sources (Table 1), to determine indicatory PCDD/Fs for each selected ambient environment. The above results were able to determine the major emission sources for all investigated ambient-air samples as listed in Table 2.

Therefore, the most significant contributors from PCDD/F emission sources for the rural, traffic and industrial atmospheres were open burning straw, GSUV, and MSWIs, respectively.
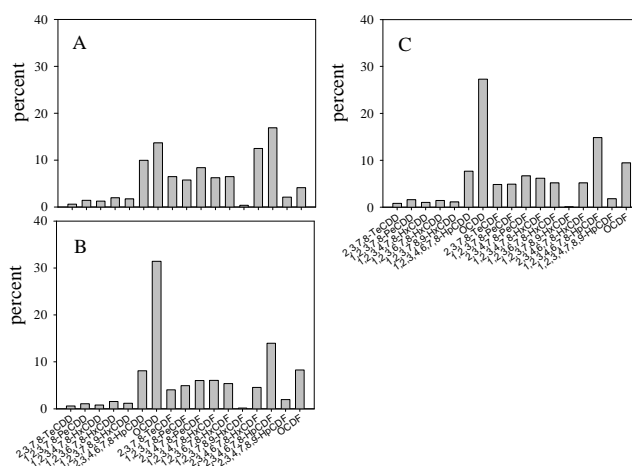
Figure 1 **Congener profiles of seventeen 2,3,7,8 chlorinated substituted PCDD/Fs in ambient air.**

Table 1 Indicatory PCDD/Fs of Several PCDD/F Emission Sources

PCDD/F emission sources	indicatory PCDD/Fs (the highest three ratio values)
MSWIs	1,2,3,4,6,7,8-HpCDF (23.5) OCDF (17.5) OCDD (13.0)
GSUV	OCDD (18.6) OCDF (11.8) 2,3,7,8-TeCDD (5.7)
straw	1,2,3,4,7,8-HxCDF (17.1) 1,2,3,4,6,7,8-HpCDF (14.9) 1,2,3,7,8-PeCDF (11.8)

TABLE 2. Indicatory PCDD/Fs of Ambient Air Sampling Sites and Its Suspected PCDD/F Emission Sources

sampling sites	indicatory PCDD/Fs (the highest three ratio values)	Major PCDD/F emission sources
A(rural area)	1,2,3,4,6,7,8-HpCDF (16.9)、 OCDD (13.7)、 2,3,4,6,7,8-HxCDF (12.5)	Straw
B(traffic area)	OCDD (31.4)、 1,2,3,4,6,7,8-HpCDF (13.9)、 1,2,3,4,6,7,8-HpCDD (8.10)	GSUV
C(industrial area)	OCDD (27.3)、 1,2,3,4,6,7,8-HpCDF (14.8)、 OCDF (9.43)	MSWIs

Sources assignation of PM2.5 atmospheric aerosol in a rural area of Spain

O. Pindado, R.Mª. Pérez, S. García, M. Sánchez, P. Galán and M. Fernández

Chemistry Division, Department of Technology, CIEMAT, Av. Complutense 22, 28040, Madrid, Spain

During last years much attention has been paid to the study of atmospheric aerosol because the particulate matter is associated with hazardous effects on human health as well as adverse effects on environment. Specifically, organic compounds associated to particulate matter are partly to blame for these health problems. There are different emission sources responsible for the presence of organic compounds in atmospheric aerosols, among them anthropogenic and natural sources.

The results from a year-long study of PM2.5 of atmospheric aerosol collected in a rural area of Spain influenced by a highway are reported. This study is pioneer in Spain, because none of studies previously published analyse polar compounds and SOA constituents together PAHs and aliphatic compounds. A total of 89 samples were taken between April 2004 and April 2005 using a high volume sampler. Sampling area was placed in Chapinería, a little village with less than 2000 habitants with a highway 500 meters away sampling point.

This work has been able to characterize the main organic components of atmospheric aerosols (alkanes, PAHs, alcohols and acids) as well as inorganic components. Moreover, it has been performed a multivariate study to assign origin for particulate matter.

For organic fraction, analytical procedure involves Soxhlet extraction with DCM/acetone, a clean up step with silica gel column using solvent of increasing polarity and a derivation reaction with N,O-bis-(trimethylsilyl)-trifluoracetamide (BSTFA). Finally, abundance of n-alkanes, polycyclic aromatic hydrocarbons (PAHs), alcohols and acids were separately determined using gas chromatography/mass spectrometry and high performance liquid chromatography analysis. Inorganic fraction was analysed by ion chromatography, ICP-OES and ICP-MS.

PM2.5 concentrations ranging from 3 to 64 $\mu g \cdot m^{-3}$ with a seasonal median of 13, 15, 18 and 22 $\mu g \cdot m^{-3}$ for spring, summer, autumn and winter, respectively. The Sn-alkanes and SPAHs in air ranged from 3 to 81 $ng \cdot m^{-3}$ and 125 to 6100 $pg \cdot m^{-3}$ respectively, with higher concentrations during winter. Diagnostic parameters suggest that alkanes were predominantly of an anthropogenic origin. However, there are sign that part of alkanes originated from wax plants. The Salcohols were 87 $ng \cdot m^{-3}$ and highest values during summer; while Sacids were 214 $ng \cdot m^{-3}$ and highest values during winter. In both cases, the CPI values are highest in summer and lowest in winter, indicating that emissions of plant waxes are the main source of alcohols and fatty acids. Identification of a-pinene degradation products confirm the biogenic contribution to aerosol. Generally, concentrations of organic compounds were above those other rural areas, confirming the anthropogenic contribution to rural area of Chapinería.

The first stage in this statistical study was to develop a correlation analysis between all variables involved. There have proved high correlation coefficients between some components of atmospheric aerosol. For instance, correlations between NO_x, NO_3^-, NH_4^+, also correlations between Ca, Mg, Al, Fe and Sr, or correlations between oleic, linoleic azelaic and pineno degradation products, and eventually correlations between alcohols and acids higher than C_{20}.

Factor analysis was used to reveal origin of particulate matter of Chapinería. This analysis include 36 input variables, among organic compounds, some inorganic compounds, atmospheric gases, total PM2.5, total carbon and meteorological parameters. Eight factors were extracted accounting more than 83 % of the variability in the original data. These factors were assigned to a typical high pollution episode by anthropogenic particles, crustal material, plant wax emissions, fossil fuel combustion, temperature, microbiological emissions, SOA and dispersion of pollutants by wind action. Also, this analysis has been able to allocate the origin of the six PM2.5 exceedances. Three samples were assigned to a Sahara dust intrusion and three samples were due to an anthropogenic origin.

Finally, a cluster analysis was used to compare the organic composition between the four seasons, being identified six different clusters. According to these results, one of the clusters include the samples, which transport processes of desert dust from North Africa have been registered, and another cluster was comprised by samples characterized by high concentrations of SOA.

Characteristics of Dicarboxylic Acids in Pearl River Delta Region

S. C. Lee[1], K. F. Ho[1], K. Kawamura[2], J. J. Cao[3]

[1] Department of Civil and Structural Engineering, The Hong Kong Polytechnic University, Hong Kong
[2] Institute of Low Temperature Science, Hokkaido University, Sapporo, Japan
[3] State Key Laboratory of Loess and Quaternary Geology, Institute of Earth Environment, Chinese Academy of Sciences, Xi'an, China

Pearl River Delta (PRD) is one of the three areas in China which have experienced extremely fast economic development. Economy in this region has expanded with breathtaking speed for three decades. Air pollution has become a serious environmental problem in PRD. Dicarboxylic acids are an important group of water-soluble organic compounds (WSOC) in the atmospheric aerosols (Jacobson et al., 2000; Kawamura and Yasui, 2005). They have received much attention because of their potential roles in affecting the global climate.

$PM_{2.5}$ samples were collected at 4 sampling locations (Guangzhou [GZ], Zhaoqing [ZQ], PolyU Campus [PU] and Hok Tsui [HT]) in PRD simultaneously during winter (December, 2006 to January, 2007) and summer (July, 2007 to August, 2007). Samples were collected on pre-fired quartz filters by medium volume samplers with a flow rate of 113 L/min. The loaded samples were analyzed for organic carbon (OC) and water-soluble organic carbon (WSOC) at The Hong Kong Polytechnic University and analyzed for water-soluble dicarboxylic acids, ketoacids and dicarbonyls at Hokkaido University using the methods of Kawamura and Yasui (2005).

A homologous series of dicarboxylic acids (C_2-C_{12}) including straight-chain saturated, unsaturated, branched-chain, and hydroxylated as well as ketocarboxylic acids (C_2-C_9) were detected in the aerosol samples. Total measured water-soluble organic species contributed 12% of WSOC in PRD. Molecular distributions of the diacids demonstrated that oxalic (C_2) acid was the most abundant species (except the summer time in HT), followed by phthalic acids (Ph). The C_2 diacid comprised ~30% of the total measured species while Ph comprised ~15%. The diacids with more carbon numbers were less abundant, although C_9 diacids were relatively abundant. Total concentrations of diacids ranged from 119-2617 ng m^{-3} which are similar as other studies in urban areas. Significant seasonal variations of diacids were observed in PRD, with highest concentrations in winter than in summer (except in GZ). In winter, the highest concentrations of total measured water-soluble organic species were observed at PU; while in summer, the highest concentrations of total measured water-soluble organic species were observed at GZ. Diacids are emitted from primary urban sources (e.g. vehicular exhaust) and produced by secondary photochemical oxidation of their precursors in PRD. High concentrations of diacids observed in roadside sampling location (PU) in winter were mainly due to the primary emission of vehicular exhaust. And the lower mixing heights, the formation of the inversion layers, and the less chance of wet deposition can also contribute to the accumulation of air pollutants in the winter at PU. While in summer, the concentrations at PU declined significantly. Low concentrations of diacids in summer can be explained by dilution of polluted air by the inflow of marine air mass (in summer marine air masses are transported from South China Sea)

This study provides the spatial variations of water-soluble organic species in PRD. High water-soluble organic species were determined in down-wind areas in both seasons.
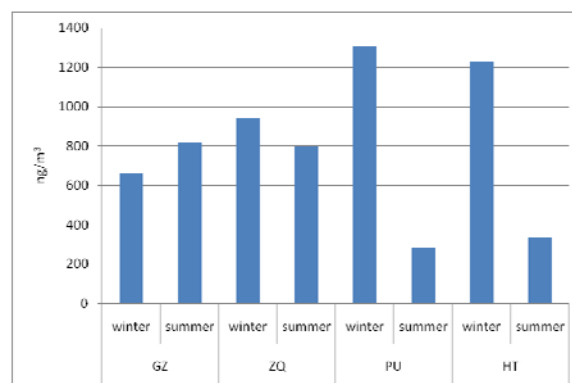
Figure 1. Seasonal variations of total measured water-soluble organic species in PRD.

Jacobson, M.C., Hanson, H.C., Noone, K.J., Charlson, R.J. (2000). *Rev. Geophys.,* 38, 267–294.
Kawamura, K. and Yasui, O., 2005. *Atmos. Environ.*, 39, 1945–1960.

An AMS/TDMA study of organic aerosol properties at a Finnish background site

T. Raatikainen[1], P. Vaattovaara[2], P. Tiitta[2], J. Rautiainen[3],
M. Ehn[4], M. Kulmala[4], A. Laaksonen[1,2] and D.R. Worsnop[5]

[1]Finnish Meteorological Institute, 00101 Helsinki, Finland
[2]Department of Physics, University of Kuopio, 70211 Kuopio, Finland
[3]Department of Chemistry, 00014 University of Helsinki, Finland
[4]Division of Atmospheric Sciences, Department of Physical Sciences, 00014 University of Helsinki, Finland
[5]Aerodyne Research Inc., 45 Manning Road, Billerica, Massachusetts, USA

An Aerodyne Quadrupole Aerosol Mass Spectrometer (AMS) was one of the instruments used during the Hyytiälä spring 2005 measurement campaign. Hyytiälä is a forested rural measurement site in southern Finland. The AMS can measure mass concentrations of non-refractory species including sulphate, nitrate, ammonia and organics from submicron particles (Jayne *et al.*, 2000). A non-negative matrix factorisation method (Paatero and Tapper, 1994; Lanz *et al.*, 2007) was used in identifying two oxidized organic aerosol groups, highly oxidized OOA1 and less oxidized OOA2, from the total organic mass. Properties of the groups were estimated based on their mass spectra, diurnal concentration variations and correlations with measured mass concentrations and other additional data such as air mass history, particle size distributions and different growth factors.

Correlation coefficients showed that concentrations of OOA1 and the inorganic species are correlated. Their concentrations, which can be related to anthropogenic sources and long range transport, depend strongly on air mass history. On the other hand, OOA2 concentration seems to be independent of air mass history, but it has a clear diurnal cycle. This suggests that OOA2 is mainly from local sources and its lifetime is short, possibly less than a day. Commonly OOA2 has the highest concentration in clean air masses, but the other species dominate polluted air masses.

Physical and chemical properties of the organic groups were estimated by correlating their mass concentrations with measured growth factors (GF). Ethanol (EGF) and hygroscopic (HGF) growth factors are defined as equilibrium droplet size in ethanol or water vapour divided by the initial dry size. Volatility growth factors (VGF), which are less than or equal to one, are defined as size after heating divided by the initial dry size. Pure component growth factors of OOA1, OOA2 and the inorganic species (sum of sulphate, nitrate and ammonia) were fitting parameters when a simple linear model was fitted to experimental water and ethanol growth factors. Measured and predicted growth factors as well as mass fractions used in the predictions are shown in Figure 1. In good agreement with the

expectations, the fitted pure component growth factors show that OOA1 is fairly hygroscopic, but OOA2 is mostly water insoluble. On the other hand, OOA2 ethanol solubility is higher than that of OOA1. Preliminary results from the volatility growth factor analysis show that OOA2 is completely evaporated at 150 ºC, but higher temperatures are needed for some OOA1 species.
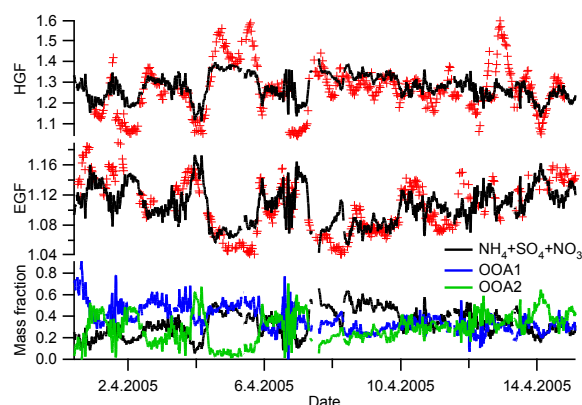
Figure 1. Measured (markers) and predicted (lines) hygroscopic and ethanol growth factors, and mass fractions from the AMS measurements.

The findings here are in good agreement with previous studies. However, it must be kept in mind that current data set is only about two weeks long. It is possible that findings would be somewhat different for some other time period.

Lanz, V. A., Alfarra, M. R., Baltensperger, U., Buchmann, B., Hueglin, C., & Prévôt, A. (2007). *Atmos. Chem. Phys.*, 7, 1503-1522.

Paatero, P., & Tapper, U. (1994). *Environmetrics*, 5, 111-126.

Jayne, J., Leard, D., Zhang, X., Davidovits, P., Smith, K., Kolb, C.E., & Worsnop, D. (2000). *Aerosol Sci. Tech.*, 33, 49-70.

High-time-resolution chemistry measurements of fine particles at an urban site in Helsinki, Finland

M. Aurela[1], S. Carbone[1], S. Saarikoski[1], K. Saarnio[1], T. Mäkelä[1], P. Keronen[2], M. Kulmala[2], D. Worsnop[1,2], and R. Hillamo[1]

[1] Finnish Meteorological Institute, Air Quality Research, P.O. Box 503, FI-00101 Helsinki, Finland
[2] Department of Physical Sciences, FI-00014 University of Helsinki, Finland

Keywords: urban aerosols, on-line measurement, chemical composition, AMS

High-time-resolution chemical measurements of fine particles has been conducted at an urban site in Helsinki, Finland to complete the previous studies focusing mainly on organic carbon, and made using 24 h filter sampling (Saarikoski et al., 2008). Using fast on-line methods the origin and source of individual short events can be more easily specified with the help of ancillary information like backward air-mass trajectories, wind direction or model simulations. The objectives of this study were to specify the chemical composition during different events, to assess the particle source and origin, and finally to identify the atmospheric processes that particles have experienced during the transport.

The measurements were started on December 2008 in Helsinki, Finland at an urban background station (SMEARIII, 60°12'N, 24°58'E, 26 m above sea level). The site is located 5 km northeast from the centre of Helsinki. The most important local source of fine particulate matter is traffic since a densely trafficked major road (60 000 vehicles/day) is situated at a distance of 200 m to the east. However, the contribution of regional residential wood combustion may be substantial during winter.

The chemical composition of aerosol particles in the submicron size range was measured with an aerosol mass spectrometer (HR-ToF-AMS, Aerodyne Research Inc.; Jayne *et al.*, 2000), a semi-continuous organic and elemental carbon analyzer (OC/EC; Bae *et al.*, 2004), and two Particle-Into-Liquid -Samplers (PILS, Orsini *et al.,* 2003) one coupled with two ion chromatographs (IC) (for cation and anion analysis) and the other coupled with a total organic carbon analyzer (TOC analyzer, Shimadzu, Model TOC-V_{CPH})

The AMS measured organics, sulfate, nitrate, ammonium, and non-refractory chloride of which sulfate, nitrate, ammonium and chloride were also analyzed by the PILS-IC. In addition, the PILS-IC was able to measure also oxalate, sodium and potassium. Water-soluble organic carbon was determined by a PILS coupled to the TOC analyzer. Gaseous components, SO_2, NO, NO_x, CO and O_3, were also measured at the station. The time-resolution of aerosol and gas measurements varied from 1 min to 2 h.

As an example of the collected data, two cases are shown in Figure 1 where sulphate concentrations are quite high during a few hours, while the other components such as organics, ammonium and nitrate were not elevated. Sulphate was only partly neutralized and seemed to be mainly in the form of sulphuric acid. According to the backward air mass trajectories the first events were originated most probably from oil shale fuelled power plants in Narva, Estonia. The other high sulphate event seemed to be transported from Saint Petersburg area. Local short-time events dominated by traffic related or biomass burning particles affected mainly the concentrations of organics, nitrate and chloride. These events were often related to the low atmospheric mixing due to the temperature inversion.
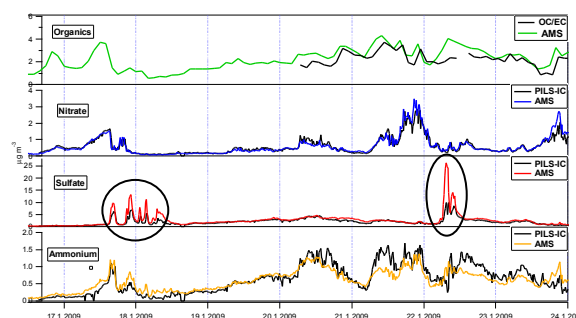
Figure 1. Time-series of organics, nitrate, sulphate, and ammonium measured by AMS or PILS-IC or OC/EC-analyzer in January 16-23, 2009 in Helsinki, Finland. The units are in µg m^{-3}. In the AMS data constant 50% collection efficiency is assumed causing an obvious overestimation for the cases were sulphate is acidic.

Bae, M., Schauer, J., DeMinter, J., Smith, D., & Carry, R. (2004). *Atmos. Environ.* 38, 2885-2893.

Jayne, J.T., Leard, D.C., Zhang, X., Davidovits, P., Smith, K.A., Kolb, C.E. & Worsnop, D.R. (2000) *Aerosol Sci. Technol.*, *33*, 49-70.

Orsini, D., My, Y., Sullivan, A., Sierau, B., Baumann, K., & Weber, R. (2003). *Atmos. Environ.* 37, 1243-1259.

Saarikoski, S., Timonen, H., Saarnio, K., Aurela, M., Järvi, L., Keronen, P., Kerminen, V.-M., & Hillamo, R. (2008). *Atmos. Chem. Phys.* 8, 6281–6295.

Analysis of Low and High Molecular Weight
Water-Soluble Organic Aerosol Components by LC-MS

Y. Zhang, R. Winterhalter, H. Yang, G.K. Moortgat, U. Pöschl

Max-Planck-Institute for Chemistry, P. O. Box 3060, D-55020 Mainz, Germany

Keyword: Aerosol chemistry; Water soluble organic compounds; LC-MS

Water soluble organic compounds (WSOCs), including low (e.g. dicarboxylic acids, nitrophenols et al.) and high (e.g. proteins, DNA et al.) molecular weight compounds, play an important role in the ambient atmosphere. WSOCs not only directly affect the atmosphere's radiation balance by scattering and absorbing solar and infrared radiation, but also modify the radiative properties and lifetimes of clouds by enhancing aerosol mass concentrations and increasing cloud droplet formation.

In this study, liquid chromatography coupled to mass spectrometry (LC-MS) was used to characterize low and high molecular weight WSOCs.

The small molecular weight WSOCs in fine and coarse aerosol particles were collected on glass fibre filters with a high-volume dichotomous sampler. After water extraction, the WSOCs were analyzed by LC-MS with electrospray ionization. The detected and quantified compounds comprise nitrophenols, aliphatic and aromatic dicarboxylic acids, pinic, pinonic and a C_8-tricarboxylic acid (204 Da). The latter acid is found as a major component of pinene SOA in tropical rainforest aerosol from the Amazon basin and in summertime aerosol from Ghent, Belgium (Kubatova et al., 2000). Recently, Szmigielski et al. (Szmigielski et al., 2007) identified this tricarboxylic acid as 3-methyl-1,2,3-butanetricarboxylic acid and suggested an oxidation mechanism involving pinonic acid. However, our findings that C_8-tricarboxylic acid showed no correlation with pinonic acid in both coarse and fine particle samples, could not support the mechanism proposed by Szmigielski et al. (2007).

The high molecular weight WSOCs in aerosol particles include DNA and proteins. Several studies indicated that proteins could be nitrated by the gas phase reaction with NO_2 and O_3 in the atmosphere and that the nitration takes place at the tyrosine site (Franze et al., 2003; Franze et al., 2005). Some recent studies suggested that nitrated proteins might cause and enhance allergic diseases and asthma (Gruijthuijsen et al., 2006). Native protein bovine serum albumin (BSA) was nitrated by tetranitromethane (TNM) in the liquid phase and with NO_2 and O_3 in the gas phase. The characteristic of nitrated BSA was studied using LC-MS.

References:

Franze, T., Weller, M.G., Niessner, R. & Pöschl, U., 2003. *Analyst*, 128(7): 824-831.

Franze, T., Weller, M.G., Niessner, R. & Pöschl, U., 2005. *Environ. Sci. Technol.*, 39(6): 1673-1678.

Gruijthuijsen, Y.K. et al., 2006. *Int. Arch. Allergy Immunol.*, 141(3): 265-275.

Kubatova, A. et al., 2000. *Atmos. Environ.*, 34(29-30): 5037-5051.

Szmigielski, R. et al., 2007. *Geophys. Res. Lett.*, 34(24).

PM1 chemical characterization and source apportionment in two background sites with different anthropic impact near Florence, Italy. Results from all year-round campaigns.

R. Udisti[1], S. Becagli[1], R. Traversi[1], F. Rugi[1], C. Ghedini[1], E. Castellano[1], F. Marino[1], S. Nava[2], F. Lucarelli[2,3], M. Chiari[2], G. Calzolai[3].

[1]Department of Chemistry, University of Florence – I-50019 Sesto F.no (Florence), Italy
[2]INFN - I-50019 Sesto F.no (Florence), Italy
[3]Department of Physics, University of Florence – I-50019 Sesto F.no (Florence), Italy

Keywords: PM1, chemical composition, ions, metals, source apportionment.

Atmospheric load, physical features and chemical composition of micrometric and sub-micrometric aerosol particles are supposed to play a relevant role in air-quality assessment involving human health and environmental conservation. Recently, an increasing attention was devoted in understanding if sub-micrometric fraction (PM1) could be a marker of atmospheric pollution better than PM10 or PM2.5. On one side, the lower size and specific sources, more related to anthropic processes, makes PM1 a potentially selective indicator of anthropic emissions. On the other hand, a significant fraction of some relevant components, even coming from secondary processes (such as nitrate, for instance), could be under evaluated in sampling only sub-micrometric particle. In order to better understanding atmospheric concentrations and chemical composition of PM1 in background (urban and remote) sites, an all-year round campaign was carried out in two sites near the city of Florence, central Italy. We have chosen a background urban site in a residential area of Sesto Fiorentino, a small city (about 50,000 people) about 10 km far from the centre of Florence, and a remote site few km apart, but located on the top of a 750 m hill, in a forested area. Both samplers were located at several meters over the soil level. The background urban site was on the top of a 20 m tower (Villa San Lorenzo, a Renaissance building - VSL); the forestal site (Fonte dei Seppi, Monte Morello - MFS) was on the top of a 12-m tower for fire sighting. This site is located in the hilly area north of Sesto F.no, about 8 km (as the crow lies) far from the first site. Its geographical setting, above possible inversion layers occurring in winter over the Florence valley, makes it particularly useful for the evaluation of the atmospheric concentrations of the mid-scale background aerosol. Samplings were carried out daily (00:00 – 24:00) from 21 March 2007 to 26 May 2008.

In both stations, sampling devices following the EN 12341 European Rule were used. PM1 aerosol samples were contemporaneously collected on Teflon and quartz filters at the flow of 2.3 m^3/h by a two-head FAI-Hydra samplers.

Teflon filters, weighed in standard conditions before and after aerosol collecting, were analysed for ionic content and for selected metals. Quartz filters, pre-fired before exposition, were devoted to the carbon analysis. Ionic composition was measured on a quarter of the Teflon filter by a system built with three ion chromatographs connected with an autosampler. After extraction with 10 ml of ultra pure water in ultrasonic bath (20 minutes), ICs measured inorganic anions (F^-, Cl^-, NO_3^-, SO_4^{2-}) plus oxalate, inorganic cations (Na^+, NH_4^+, K^+, Mg^{2+} and Ca^{2+}) and selected organic anions (acetate, glycolate, propionate, formate, methanesulphonate -MSA and pyruvate) plus F^-. Another quart of the Teflon filters was analysed by ICP-AES with ultra-sonic nebuliser for selected metals: Al, Fe, Mn, Zn, Cu, Cr, Ni, V, Pb, Cd, Mo and As. Filter extraction was carried out following the EN 14902 rule (HNO_3 and H_2O_2 in a Teflon micro-wave digestor).

On a 1.5 cm^2 punch of the quartz filter was analyzed for total carbon (TC), elemental carbon (EC) and organic carbon (OC) with a Thermal/Optical Carbon analyser, Sunset Lab Inc., based on a NIOSH method. Primary and secondary Particulate Organic Matter (POM) fractions were reconstructed.

Here, we report the results of the campaign, enlightening differences between atmospheric load and chemical composition of samples collected in the two stations, located in differently anthropised areas and at different altitude (50 and 750 m a.s.l.). In particular, seasonal patterns of anthropic and biogenic markers were identified and evaluated, also in consideration of the formation of temperature inversion layers in winter in the lower station.

Multiparametric statistical approaches (Absolute Principal Component Analysis – APCA – and Positive Matrix Factorization – PMF) were applied to the large data set in order to carry out a reliable source apportionment of PM1 in the two stations.

Finally, a detailed comparison was performed between PM1, here obtained, and PM2.5 data coming from a previous sampling campaign carried out in the VSL station (about 1.5 years from Sept. 2005 to March 2007) and, for a shorter period (January - March 2007) at MFS station.

Natural and Anthropogenic contributions to PM10 in the L'Alacantí region in the South-East of Spain.

M. Santacatalina[1], E. Yubero[2], A. Carratala[1]

[1]Department of Chemical Engineering, University of Alicante. 03080 Alicante, Spain
[2]LAP, Laboratory of Atmospheric Pollution
Department of Physics, University Miguel Hernández of Elche. 03202 Elche, Spain

Keywords: Chemical composition, air quality, industrial minerals, PM10, source apportionment.

This work is an estimation of the main sources contributing to PM10 in L'Alacantí region, covering a long period (2004 to 2006) and a dataset of 173 samples. The region of L' Alacantí has, at national level, an important production of cement and ceramic, due in part to the presence of important reservoirs of clays, gypsum, and calcareous rocks also derived and related activities: quarries, grinding, transport, construction are present. These activities together with the condition of being an arid area (rain < 300 mm/yr) play an important role on atmospheric particulate matter inmisions.

The sampling has been done at the University of Alicante, which is situated in between the growing residential areas of two main cities in the L'Alacantí region, Alicante and San Vicente. The area is opened to the Mediterranean Sea (East) and surrounded by mountains in the other directions (from S to N) forming a basin. Mild climatology, long periods without complete renovation of air mass, favours the accumulation of local emissions and the development of episodes of regional contamination.

The analysis of NO_3^-, SO_4^{-2}, and Cl^- were made by ionic chromatography on water extracts of a quarter of the fibre quartz filters. NH_4^+ was analysed in water extracts by indophenol method. For the metal analysis half of the filter was digested using an acidic oxidant digestion (HNO_3 (65%) + H_2O_2 (30%)) on a microwave oven reaching high temperature (170ºC) and analysed by ICP-Mass spectrometry. C was determined directly on the filters by a LECO CN analyser. SiO_2 and Al_2O_3 were calculated according to the equations described in Querol et al. (2002).

In the factor analysis performed on the dataset five factors (with factor loadings =>0.5) were found. The first factor has as main tracers SiO_2, Al_2O_3, Mn, Fe, Mg, Sr, Ca, Ba and Zn. This suggests a mineral origin of the atmospheric particles, probably originated from natural sources (regional-scale re-suspension and African Outbreaks). The second factor represents a traffic source (traced by Mo, Sb, Cu, Pb, Cr). Cu is a known tracer of break-wear and carbonaceous particles are tracers of exhaust emissions (mostly diesel). The tracers of the third factor are V, Ni, Tl and K. V, Ni are generally known as tracers for oil combustion emissions and Tl and K are tracers for cement compounds. Hereby this factor suggests cement plant emissions as the underlying PM source. In factor 4, SO_4^{-2}, NH_4^+ and NO_3^- suggests that this source was associated with secondary aerosols and regional or long-range air mass transport, given the prolonged atmospheric residence time of $(NH_4)_2SO_4$. Furthermore, secondary aerosols may also originate from local NO_x and SO_2 from industry or traffic on a city scale (regional-scale). Finally, the last factor may be easily identified as sea salt with Cl^- and Na^+ as main tracers.

Quantification of the contributions to PM10 of the sources described above was carried out by means of MLRA. A good correspondence was achieved between the modelled and the gravimetric PM10 results with R^2 value >0.85. Mineral source constitutes the major source of PM10 with a 41.5% (18.63 µg/m^3) of the PM10 mass. Industrial combustion contribution represents the second highest PM10 fraction with a percentage of 14.79% (6.64 µg/m^3). The traffic source accounted for 12% of the PM10 mass with 5.38 µg/m^3. The secondary aerosol source constitutes only 4.41 % (~2 µg/m^3) of the mass due to the selection of the days explained above. Finally, sea-salt accounted for 2.71% the mass (~1.22 µg/m^3) (Figure 1).
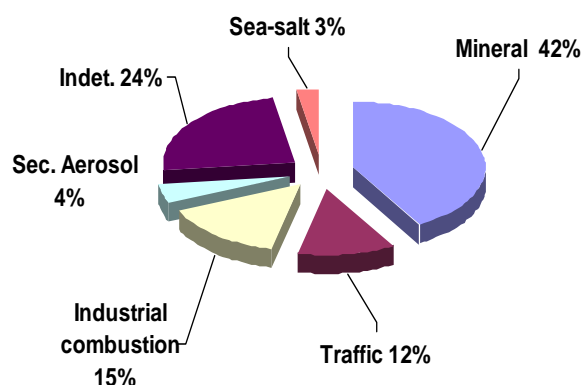
Figure 1. Quantification of the contributions to PM10 of the sources by means of MLRA.

Querol, X., Alastuey, A., De la Rosa, J., Sánchez de la Campa, A., Plana, F., Ruiz, C. (2002). Source apportionment analysis of atmospheric particulares in an industrialised urban site in southwestern Spain. Atmospheric Environment 36, 3113-3125.

Seasonal variation of PM10 source contributions at a rural site in Eastern Austria (Lunz am See)

C. Ramírez-Santa Cruz[1], A.Kasper-Giebl[1], H.Bauer[1], H.Puxbaum[1], W.Wanek[2], M.Dorninger[3]

[1]Department of Chemical Technologies and Analytics, Vienna University of Technology, Getreidemarkt 9/164AC, A-1040, Vienna, Austria

[2]Department of Chemical Ecology and Ecosystem Research, University of Vienna, Althanstrasse 14, A-1090, Vienna, Austria

[3]Department of Meteorology and Geophysics, Althanstrasse 14, A-1090, Vienna, Austria

Starting in spring 2007 a seasonal cycle of aerosol samples was collected at a rural site in Lower Austria with a Digitel High Volume sampler. The sampling site was located at the edge of a small town (Lunz am See, 47° 51′ N, 15° 3′ O, Elevation: 601 m) with no major emissions sources like industry or busy roads nearby, thus representing a rural background station. PM10 samples were collected on quartz fiber filters. Sampling was carried out on a daily basis. Analyses comprised the determination of water soluble major anions and cations, carbonaceous species (TC – total carbon, EC – elemental carbon, OC – organic carbon and CC – carbonate carbon), anhydrosugars and HULIS. During a limited number of days additional aerosol samples were collected on cellulose acetate filters for the determination of mineral dust and trace metals.

Here the seasonal cycles of the main aerosol components will be shown with focus on their concentration ranges and their behavior against external influences, like temperature or precipitation. Aerosol mass ranged from 8.6 – 23.5 µg/m³ considering monthly averages and exceeded the 50 µg/m³ limit given EU-Guideline 1999/30/EG of 1999 only once. The secondary inorganic aerosols represented up to 35 % of the aerosol mass. Organic material rose up to 45% in the late summer. Furthermore a macro tracer model (Puxbaum, 2004) was used for source apportionment. Levoglucosan concentration was used to estimate the contribution of wood smoke to aerosol mass (Schmidl, 2008) as well as organic matter concentrations. Levoglucosan was quantified using anion-exchange high-performance liquid chromatography with pulsed-amperometric

detection (Caseiro, 2007). Biomass burning represented between 2 and 22% of aerosol mass depending on air temperature. Generally the source apportionment varied considerably between different seasons.
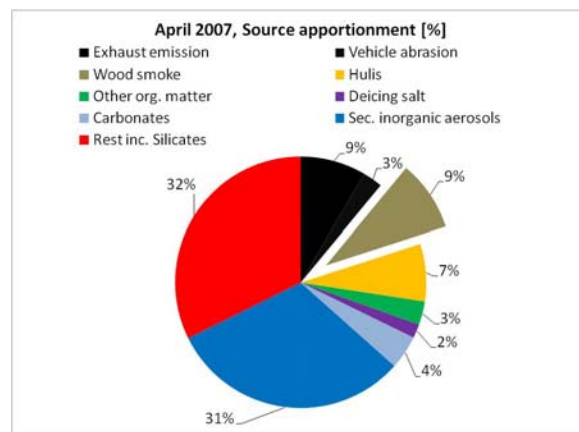
Figure 1: Source apportionment for the month of April 2007, percentage of the total mass.

Schmidl, C. (2008). *Chemical characterisation of particulate matter (PM) emissions from biomass combustion sources*. Vienna, Austria: Doctoral Thesis.

Puxbaum, H. & Bauer, H. (2007). *Aquella Wien – Bestimmung von Immisionsbeiträgen in Feinstaubproben*. Vienna, Austria: Scientific Report for the Government of Vienna.

Caseiro, A. *et al*. (2007). *Determination of saccharides in atmospheric aerosol using anion-exchange high-performance liquid chromatography and pulsed-amperometric detection*. Journal of Chromatography A, 1171, S. 37 - 45.

Raman Spectral Analysis of Multicomponent Aerosols from the Environment of Sugar Factory.

V.M.Harpale[1]., R.S.Gosavi[2]

.

[1]Department of Physics Ahmednagar College, Ahmednagar,414001,(INDIA)
[2]Arts Science and Commerce College Rahuri, 413705,(INDIA)

Keywords: Raman scattering, Aerosols, Raman Spectra, Sugar Factory, Human health.

It is wel understood fact that the increase in the aerosol emissions in the atmosphere of the urban and rural area is great concern to human health and reduction of visibility. The presence of aerosol can cause respiratory and cardiovascular diseases, enhance the formation of cloud precipitation and affect the earth scattering and absorption of radiation (Ramnathan V.et al.2001,Finlayson pitts J.N.2000.ScienfieldJ.H. and Pandis S.N; 1998) Because of the public health dangers, it is important to have accurate and sensitive analytical method for the detection and chemical speciation of those particles. In this paper, we will asses the laser Raman Scattering technique and its applications for the chemical identification of atmospheric aerosols collected from the environment of sugar factory in the month of March 2008. at the Rahuri in the state of Maharashtra (INDIA).

The Spectroscopic measurements carried out in the investigation are performed with laser Raman Spectrometer. In the application of Raman spectroscopic technique, a beam of monochromatic visible laser light is focused on the aerosol sample to obtain Raman spectra. These measurements were carried out using Raman spectrometer (Not Shown). It uses double monochromator with diffraction grating having groove density 1800 grooves per mm and diode laser (532nm wave length) with 25 mW power. The light scattered by aerosol sample is collected and transferred into a double monochromator which is detected by cooled photomultiplier with S-20 response and processed by photon counting electronics.

Raman Spectrum of aerosol samples are collected from the environment of sugar factory during 8th March to 12th March 2008.The spectra provide the qualitative estimate of the chemical species present in the aerosol sample. The Raman frequencies of chemical species, obtained by comparing the frequencies reported in the literature(Degan,I.A.1997). These include 25 independent Raman peaks representing 25Raman frequencies, identifying various chemical elements present in the sample. As documented, all Raman peaks are found within Raman frequency range 521 cm^{-1} to 3396 $cm.^{-1}$ As illustrated in Spectra,(Not shown) three Raman peaks observed at 521 cm^{-1},572 cm^{-1} and 760 $cm.^{-1}$ show the presence of Aryl nitro compounds, however Raman peaks at 1015 cm^{-1} ,1066 $cm^{-1}$and 1275 cm^{-1}exhibit the occurrence of mono and di-sub compounds. Similarly, two peaks which are visible at 2367cm^{-1},2344$cm^{-1}$are recognized as P-H str compounds. There are total nine Raman peaks ranging between 2514 cm^{-1} to3396 cm^{-1}which are characterized as primary and secondary amides which seem to be the major composition of the aerosol samples. In addition to these, alkyl isocynate, Diesters are also found as trace elements which are the compounds of Amonia and Nitrogen. Thus, the aerosol samples constitute different types of elements which are far from being single component system. In fact, the chemical compositions at atmospheric aerosol is highly complex and vary considerably with time and location. Therefore, it is quite obvious that aerosols encountered in the environment occurs as a mixture of substances of nuclei coated with dissimilar materials.

Thus, these results suggest a positive potential for the Laser Raman technique as a analytical tool. The technique developed in the present work has made it possible to identify the mixed salts which may be present in ambient aerosols, as a result of changing atmosphere conditions. The Raman frequencies documented in the present study serve as useful guide to chemical and physical characterization of aerosol particles

Ramnathan V.et.al(2001), Aerosols, climate and the Hydrological cycles, Science 294;2119-2124
Finlqayson Pitt J.N.(2000) Chemistry of the upper and lower Atmosphere; Theory, Experiment and application.Academic Press, san Diego
Scienfield J.H.and Pandis S.N. (1998). Atmospheric Chemistry and Physics, Wiley, New York.
Degan, I.A.(1997). Tables of Characteristics Group Frequency for the interpretation of infrared and Raman spectra Acolyte colyte Publication, U.K..

OC and EC determination in aerosol samples collected on Teflon filters by Particle Elastic Scattering Analysis (PESA) and Ion Chromatography (IC)

L. Bonanni[1], G. Calzolai[1], M. Chiari[2], F. Lucarelli[1], S. Nava[2], S. Becagli[3], R. Udisti[3]

[1]University of Florence, Department of Physics and INFN, Florence, Italy
[2]INFN, National Institute of Nuclear Physics, Florence, Italy
[3]University of Florence, Department of Chemistry, Florence, Italy

Keywords: chemical mass closure, carbonaceous aerosol, PESA, IC

Ion beam analysis (IBA) techniques have proven to be a reliable tool to study the composition of atmospheric aerosol in a fast, non-destructive way. In particular, Particle Induced X-ray Emission (PIXE) is widely used to determine the aerosol elemental composition, simultaneously detecting elements from Na to Pb. Less used, Particle elastic scattering analysis (PESA) technique detects the beam particles elastically scattered by the target nuclei and allows obtaining quantitative information about the elemental composition of the sample as regards low Z atoms like C, H, N and O (Chiari et al., 2005). By IBA techniques (PIXE and PESA) it is possible to obtain a complete reconstruction of the aerosol mass for samples collected on Teflon filters.

If particulate matter is simultaneously collected on Teflon and on Quartz fibre filters, the application of complementary techniques allows a quite complete mass closure and chemical characterisation: Teflon filters can be analysed by PIXE and IC to measure the elemental and ionic composition, while quartz fibre filters can be used to determine EC and OC by thermo-optical-transmittance (TOT) analyses. This approach has been extensively used by the authors, and, in particular, it has been applied in the PATOS project, the first extensive field campaign for the PM10 characterisation in Tuscany.

However, it is not always possible to collect the aerosol by two samplers simultaneously for long periods. When only Teflon filters are used EC and OC can not be measured by TOT analysis. We will show that by the use of PESA and IC it possible to approach this problem.

The measurement of Nitrates and Ammonium by IC allows calculating the H content in these compounds: subtracting this contribution to the total H concentration, measured by PESA, it is possible to estimate the H content in the organic compounds (H_{POM}). If the OC/H ration in organic matter, which is characteristic of the sampling region and sampling season, is known, the OC concentration can be thus estimated. The EC concentration can be then obtained subtracting the OC contribution to the TC, measured by PESA.

To verify the reliability of this procedure, we used samples collected in parallel on both Teflon and Quartz fibre filters, in different typology of sampling sites (urban background, urban traffic and regional background) and during different seasons. These samples have been analysed by PESA, IC and TOT (NIOSH5040) to determine the H, C, Nitrate, Ammonium, EC and OC concentrations to investigate the OC/H_{POM} ratio for the different sampling sites/periods and to verify the accordance between the estimated and the measured EC. The obtained results, that indicate a quite stable OC/H_{POM} ratio for each site, will be described in detail.

The improvements in PESA analysis accomplished with the new Tandem accelerator of LABEC-INFN will be also illustrated: in particular we will show that H can be easily measured on a large number of samples, simultaneously with PIXE (in the same external beam set-up). The results of the first inter-comparison between PESA and TOT analyses for TC measuring will be also presented (Figure 1).
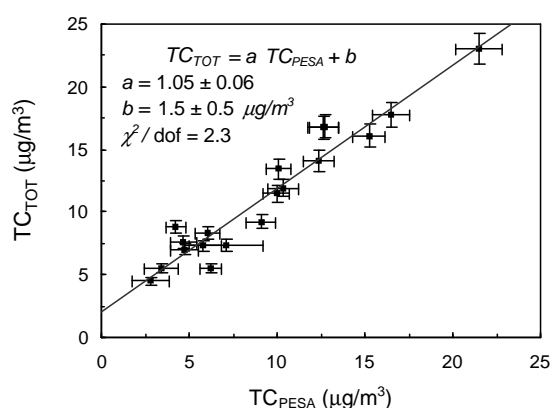
Figure 1. Inter-comparison between PESA and TOT analyses for TC measuring.

M. Chiari, M, Lucarelli, F., Mazzei, F., Nava, S., Paperetti, L., Prati, P., Valli, G., Vecchi, R. (2005), *X-Ray Spectrometry*, 34, 323.

Evaluation of airborne polycyclic aromatic hydrocarbons from Itaparica Island, Bahia, Brazil

A. L. N. Guarieiro, G. O. da Rocha, L. dos S. Conceição, W. A. Lopes, P. A. de P. Pereira and J. B. de Andrade

[1] Chemistry Institute, Universidade Federal da Bahia, Campus de Ondina, 40170-029, Salvador-BA, Brazil

Keywords: Aerosol chemistry, airborne particles, measurements, PAHs, PM10

Particulate matter plays a significant role in the chemistry of the atmosphere and in human health. Several epidemiological studies have associated daily exposures to particulate matter with increased incidence of premature death, chronic asthma, increased hospital admissions and respiratory problems in children (Cho *et al.*, 2005). Polycyclic aromatic hydrocarbons (PAHs) are ubiquitous and abundant pollutants that are emitted from several natural or anthropic sources and may be present in the atmosphere (also hydrosphere and lithosphere). The widespread occurrence of PAHs is largely due to their formation and emission during incomplete combustion of petrogenic materials such as oil, coal and wood as well as biomass burning due to agricultural practices. In urban areas, exhausts from diesel and gasoline vehicles play an important role to the PAH emissions (da Rocha *et al.,* 2009).

The PAHs are regarded as priority pollutants by both the US EPA and the European Community. While no standard currently exists in Brazil for PAH concentrations in ambient air, the U.K. government Expert Panel on Air Quality Standards is considering an air quality standard for PAHs of 0.25 ng m^{-3} (annual mean), to be achieved on December 2010 (da Rocha *et al.,* 2009).

The aim of this work was to determine the 16 priority PAHs in PM_{10} samples collected from Itaparica County (12° 53' 18" S - 38° 41' 43" W) in Itaparica Island, Todos os Santos Bay (Northeastern Region of Brazil). Itaparica Island is a warm (annual temperature: 21.9 – 28.1° C), humid (annual pluviometric index: 1,800 a 2,200 mm yr^{-1}) and remote site, close to Salvador City (707 km^2 and 2,892,625 inhabitants) as well as the Petrochemical Pole of Camaçari (PPC). Depending on wind direction, Itaparica may receive air masses from these urban and/or industrial sites, respectively. 24hr PM_{10} sampling was performed on 25th Apr to 3rd May 2008 (n=7).

Mean PM_{10} concentration was 11.7 μg m^{-3} what is below Brazilian Standards (50 μg m^{-3} for 24 hr). Among all PAHs studied, only fluoranthene (FLT), pyrene (PYR), benz[a]anthracene (BaA), chrysene (CRY), benzo[b]fluoranthene (BbF), benzo[k]fluoranthene (BkF), benzo[a]pyrene (BaP), indene[123-cd]pyrene (IND), dibenz[ah]anthracene (DBA), and benzo[ghi]perylene (BgP) were above limit of detection. Total mean PAH level was 1.36 ng m^{-3}. Individual mean PAH levels are found in Table 1. Total PAH dry deposition flux was achieved to be 0.417 μg m^{-2} day^{-1} (Table 1).

Table 1. PAH atmospheric levels (ng m^{-3}) and dry deposition flux (F_d) (μg m^{-2} day^{-1}) found in the PM_{10} from Itaparica County.

Species	Atmospheric level (ng m^{-3})	Dry deposition flux (μg m^{-2} day^{-1})
FLT	0.031	0.024
PYR	0.034	0.013
BaA	0.047	0.033
CRY	0.099	0.097
BbF	0.441	0.011
BkF	0.111	0.039
BaP	0.087	0.047
IND	0.210	0.148
DBA	0.048	0.067
BgP	0.199	0.104
PM_{10} (μg m^{-3})	11.7	-

According to literature data, the ratios FLT/PYR (0.92), BgP/IND (0.95), and BaP/BgP (0.44), and IND/(IND + BgP) (0.54) were indicative of both heavy-duty and light-duty vehicles' releases as well as (BbF + BkF)/BgP (2.78) has shown domestic soot contribution to the found PAH levels. These ratio scores are in good agreement to those found in other previously studied sites also located in the Todos os Santos Bay (da Rocha *et al.,* 2009). Since Itaparica is a remote place having a very low automobile traffic and no other relevant PAH anthropic sourcers, we can conclude that it probably is a receptor site of PAH impacted air masses coming from Salvador City and/or Petrochemical Pole of Camaçari. However more investigations are being performed in this region to a better understanding of the topic.

Cho, A. K., Sioutas, C., Miguel, A. H., Kumagai, Y., Schmitz, D. A., Singh, M., Eiguren-Fernandez, A., & Froines, J. R. (2005). *Environ. Res., 99*(1), 40-47.

da Rocha, G. O., Lopes, W. A., Pereira, P. A. P., Vasconcellos, P. C., Oliveira, F. S., Carvalho, L. S., Conceição, & de Andrade, J. B. (2009). *J. of the Braz. Chem. Society*, submitted.

Indoor air monitoring in service-flats

A. J. Buczyńska, A. Worobiec, E. A. Stefaniak, Y. Makarovska, A. Krata, B. Horemans, V. Novakovic,
R. Van Grieken and S. Potgieter-Vermaak

Department of Chemistry, University of Antwerp, Universiteitsplein 1, B-2610 Antwerp, Belgium

Keywords: Indoor aerosols, PM2.5, PM1, chemical analysis, elemental carbon.

Belgium has the highest estimated life expectancy loss (14.9 months, compared with 9.0 months as the European average) due to the fact that it has the highest annual mass PM concentrations in Europe as it has been reported in 2004 (Amann et al., 2004). These effects are more pronounced in summer (Nawrot et al., 2006) and adversely affect especially the elderly and juvenile parts of the population.

The study presented in this paper focuses on the elderly and is a part of the PARHEALTH project, which aims to investigate the short-term effects of particulates (both mass and physical-chemical characteristics) on human health in two susceptible segments of the population (children and elderly).

The residents of old age homes have been chosen as the subjects of the research. Since they spend most of their time indoors, special attention was paid to the indoor air quality. Four old age homes located in Antwerp (Belgium) have been monitored during a two-week sampling campaign. Two of them were conducted in summer periods (June, September) and two of them in winter (February), during the years of 2007-2009. The choice of sampling periods was based on the model predictions of high aerosol concentration. The air investigation consisted of the measurements of the mass, elemental and ionic concentrations of size segregated PM1, PM2.5, PM10 (Harvard-type impactors) sampled with the use of teflon membrane filters for 24-h periods. In addition, elemental carbon (EC) monitoring (Aethalometer, Magee Scientific Company, USA) and single particle analysis (PM collected with a 9 stage Berner impactor) were performed. The concentration of gasses such as NO_2, SO_2, ozone and BTEX has also been investigated (Radiello diffusive samplers). Bulk elemental composition was determined with the use of energy-dispersive x-ray fluorescence (EDXRF) analysis and the water-soluble ionic concentrations with ion chromatography (IC). Single particle analysis was performed on size segregated particulate matter for particle size ranges equal to 0.25, 0.5, 1, 2, 4 and 8 μm, respectively using a SEM (JEOL 733, Japan) coupled with EDX detector (Oxford Instruments, CA). The gaseous compounds were analysed by means of IC and UV-VIS.

The indoor PM2.5 mass concentration was in the range of 9-19 $\mu g/m^3$ in summer and 11-54 $\mu g/m^3$ in winter. The PM1 content in PM2.5 was, on the average, 74% during summer months and 64% during winter. The indoor concentrations were generally lower than outdoor, with some exceptions, e.g. for toluene, what can indicate the indoor sources of this pollutant. The highest elemental carbon was noted during one of the winter campaigns and was equal to 27 $\mu g/m^3$. The concentration indoors reflected the outdoor concentration of EC (Figure 1). As also shown below, morning and evening peaks were often noticed suggesting the increased traffic as a source of elevated EC concentrations.
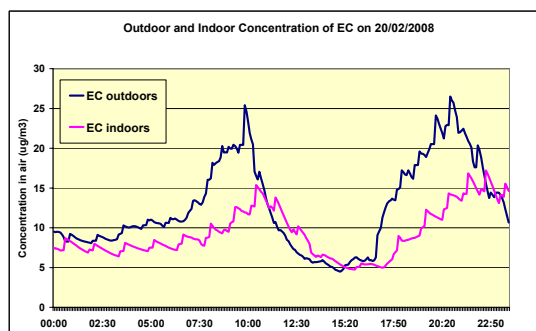
Figure 1. Outdoor and indoor comparison of EC concentration in one of the selected locations.

The events with the highest and the lowest mass concentrations were chosen for a detailed comparison.

Amann, M., Cabala, R., Cofala, J., Heyes, Ch., Klimont, Z., Schöpp, W. (2004). The current legislation and the maximal feasible reduction cases for the café baseline emissions projections. Café Scenario Analysis report nr. 2. (http://www.iiasa.ac.at/rains/CAFE_files/CAFE-MFR3.pdf).

Nawrot, T., Torfs, R., Fierens, F., De Henauw, Hoet, P., Van Kersschaever, G., De Backer, G., Nemery, B. (2006), Epidemiology, vol.17 (6), S262-S262.

Towards single particle surface analysis using fluorescence labelling

M. Putkiranta[1], M. Seipenbusch[2], M. Marjamäki[1] and J. Keskinen[1]

[1]Tampere University of Technology, Department of Physics, Aerosol Physics Laboratory,
Korkeakoulunkatu 3, FI-33720 Tampere, Finland
[2]Universität Karlsruhe (TH), Institut für Mechanische Verfahrenstechnik und Mechanik,
Am Forum 8, 76131 Karlsruhe, Germany

Keywords: aerosol chemistry, fluorescence, chemical properties.

In surface science there are a wide variety of methods used for identification and quantification of functional chemical groups. Xing and Borguet (2007) amass detection limits of different methods: fluorescence labeling 10^{-5} molecules/nm^2, X-ray photoelectron spectroscopy (XPS) and infrared spectroscopy (IR) 10^{-2} molecules/nm^2, time-of-flight secondary ion mass spectrometry (ToF-SIMS) 10^{-1} molecules/nm^2. Our idea is to apply the fluorescence labeling method in real time aerosol particle surface analysis of the functional groups. One of the key questions is whether the fluorescent label material can be detected at low enough concentrations on the surfaces of airborne particles.

A laboratory setup was constructed to analyze the sensitivity of the method. A tailor-made optical chamber was used for scattering and fluorescence measurement from individual test particles. Wide collection solid angle optics with a dichroic mirror and a long-wave-pass optical filter enabled the measurement of scattering and low intensity fluorescence separately. The light detectors were photomultiplier tube modules (PMT). The excitation light source was a blue laser diode of 405 nm wavelength and 60 mW maximum output power. It was driven in the continuous wave mode. The signals from the PMTs were measured by two pulse height analyzers and saved to a PC. The test aerosol size distribution was measured by TSI APS 3321 aerodynamic particle sizer.

The test aerosol was made by coating monodisperse silica or polystyrene latex particles with different fluorescent dye surface concentrations using a custom-made ink jet aerosol generator. The silica particles were 1.2 μm in diameter and polystyrene latex 5.0 μm. The fluorescent dye was riboflavin-5'-phosphate monosodium salt (FMN). The dye surface concentration on the particles was varied from 1 to 200 molecules/nm^2. The scattering and fluorescence signals were measured from 5 000 individual particles per each dye concentration.

In the figure 1 the fluorescence geometric mean signals are shown as a function of the dye surface concentration on the test particles. The error bars are the geometric standard deviations of the fluorescence signals. For the silica particles fluorescence signal depends on the dye concentration linearly in logarithmic scale. The slope given by the least squares method is 1.2 as it was expected to be close to 1. The lower detection limit was 5 molecules/nm^2 and the highest measured concentration about 200 molecules/nm^2.

For polystyrene latex particles the fluorescence signal depends on the dye concentration almost linearly in logarithmic scale. If seven of the highest dye concentrations are considered, the slope given by the least squares method is 0.9. The pure polystyrene latex particles absorb some blue light and fluoresce by themselves also. The effect of this autofluorescence can be seen on low surface concentrations. The lower detection limit was 1 molecules/nm^2 and the highest measured concentration about 200 molecules/nm^2.

The detection limit was higher compared to the methods in surface science. However, if autofluorescence does not occur, it is possible to improve the sensitivity substantially e.g. using a more intense laser or even a pulsed laser as done by Agranovski $et\ al.$ (2004) when testing the performance of the UVAPS using e.g. riboflavin dye. They were able to detect the amount of 10^{-17} g riboflavin in particles of 1.7 μm in diameter compared to 10^{-14} g FMN detected on the surface of 1.2 μm particles in this work.
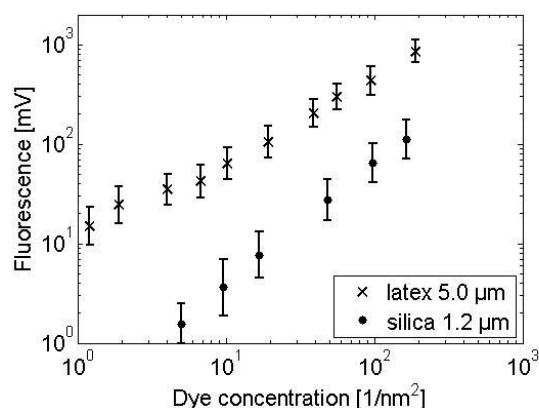
Figure 1. Fluorescence signal as a function of the dye surface concentration on the test particles.

Xing, Y. & Borguet, E. (2007). $Langmuir$, 23, 684-688.

Agranovski, V., Ristovski, Z. D., Ayoko, G. A. & Morawska, L. (2004). $Aerosol\ Science\ and\ Technology$, 38, 354-364.

Analytical methods for quantification and characterization of HULIS (HUmic Like Substances) in atmospheric aerosol

P. Fermo[1] ,A. Piazzalunga[1,*], F. Tuccillo[1], L. Brambilla[1], O. Cazzuli[2], R. Vecchi[3], G. Valli[3]

[1]Dep. Inorganic, Metallorganic and Analytical Chem., University of Milan, Via Venezian 21, 20133, Milan, Italy
[2]ARPA Lombardia-Department of Milan, via Restelli 3/1, 20124, Milan, Italy
[3]Department of Physics, University of Milan ,Via Celoria 16, 20133, Milan, Italy
[*] Now: Dep. of Env. Sc., University of Milano-Bicocca, Piazza della Scienza 1, 20126, Milan, Italy

Keywords: HULIS, atmospheric aerosol, UV-VIS, TOT, ATR-FTIR

Atmospheric HULIS (HUmic Like Substances) represent one of the most important classes of water soluble organic compounds (Salma et al., 2008). HULIS are ubiquitous pollutants and are regarded as a polymeric material with poly-acidic properties (Graber et al., 2006). They are optically active (yellow-brown coloured), are involved in the CCN forming processes and influence the optical properties of the aerosol particles. HULIS have been so termed because they resemble to terrestrial and aquatic fulvic and humic acids. They can originate from oxidation reactions of organic precursors (both biogenic and anthropogenic) even if a debate on their origin is still open. Data set on atmospheric HULIS are quite scarce and time series are not available (Feczko et al., 2007). In the literature they have been characterized by means of different analytical methods (Graber et al., 2006). Here we propose the use of UV-VIS spectroscopy and TOT (Thermal Optical Transmittance) (Birch et al., 1996) for their quantification. Samples were prepared by means of SPE extraction of PM10 samples collected in urban and rural sites in Lombardy region.

The UV-VIS spectrophotometer has been calibrated using a standard of humic acid (Fluka, 53680) or of fulvic acid (SRFA, International Humic Substances Society - IHSS). TOT measurements have been performed spiking known quantities of the solutions containing the samples on punches of quartz fibre filters. A very good accordance has been obtained between the two methods. In the examined sites HULIS on average represents up to the 50% of OC.
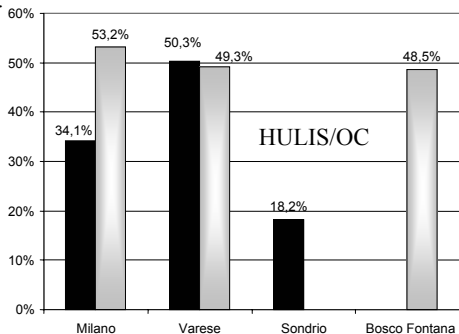
Figure 1- HULIS/OC concentrations for some sites in Lombardy region during winter (black) and summer (grey).

TOT measurements have also allowed to estimate OM/OC ratio which resulted to be in the range 1.5 – 3. For Milan, during winter time, OM/OC is lower than in summer confirming that the chemical nature of HULIS changes with the season probably because changing in the sources and in the processes of formation. These differences in the chemical nature have been also observed by ATR (attenuated total reflection)-FTIR spectroscopy. For Milan the FTIR spectra acquired on winter samples show the signals characteristic of fulvic acid (in particular the absorption at 1720 cm^{-1} due to C=O stretching of the carboxylic group) while summer samples resemble more to humic acid (absorption at 2850 e 2950 cm^{-1} due to methyl and methylene groups of aliphatic chains). Winter times samples are also characterized by higher values of the ratio E_{250}/E_{365} (which is inversely correlated with aromaticity and molecular weight, Graber et al., 2006), in accordance with a predominance a fulvic like molecules. For the rural sites the FTIR spectra have shown a contribution due to polysaccharides.

The chemical speciation of HULIS by FTIR together with the quantification of their contribution to OC and the estimation of OM/OC ratio, allows to deep the knowledge of these ubiquitous pollutants.

Birch, M.E., Cary, R.A., (1996) *Aeros. Sci. & Technol.*, 25, 3, 221-241.
Feczko, T., Puxbaum, H., Kasper-Giebl, A., Handler, M., Limbeck, A., Gelencsèr, A., Pio, C., Preunkert, S., Legrand, M., (2007) *J. Geophys. Res.*, 1123, D23S10
Graber, E. R., Rudich, Y., (2006) *Atmos. Chem. Phys.*, 6, 729 – 753
Salma, I., Ocskay, R., Làng, G. G., (2008), *Atmos. Chem. Phys.*, 8, 2243 – 2254

Determination of azaarenes in particulate matter using liquid chromatography-tandem mass spectrometry

J.Lintelmann, M. Heil-França, E. Hübner G. Matuschek

Institute of Ecological Chemistry, HelmholtzZentrum münchen, D-85758 Neuherberg, Germany

Keywords: azaarenes, APPI, LC-MS/MS, particulate matter.

Amino- and azaarenes are nitrogen-containing derivatives of polycyclic aromatic hydrocarbons (PAH). One main anthropogenic source of these compounds is the incomplete combustion or pyrolysis of organic matter. They have therefore been identified in tobacco smoke, automobile exhaust and in urban air particulate matter (Finlayson-Pitts, 2000)

Due to their noxious potential, PAH content and behaviour in aerosols was focus in many studies during the last years. By contrast the knowledge about the comparable hazardous aza- and amino-arenes is very limited. One reason for this lack of information can be that fast, simple and reliable analytical methods are rare.

Most methods described until now are based on liquid chromatography with fluorescence detection or gas chromatography with mass spectrometric detection (Delhomme and Millet, 2008; Chen and Preston, 1998). Often time-consuming and tedious sample processing steps like extraction and prefractionation are needed before analytical separation and quantification.

To overcome problems involved applying these tools a liquid chromatography-tandem mass spectrometry method (LC-MS/MS) method for the determination of 22 amino- and azaarenes was developed (Pantiru et al.), optimized and validated.

The resulting protocol can be described as follows:
Loaded quartz fiber filters are extracted using Accelerated solvent extraction (ASE) (3 cycles with methanol/dichloromethane, 50/50, 106 bar, 100°C), extracts are carefully evaporated, the residue is dissolved in 1 ml acetonitrile and 20 µl are injected into the LC-MS/MS-system. Separation of the analytes is performed on a Gemini C18 column (5 µm, 250 x 2.0 mm I.D.) with a methanol/formic acid gradient at 0.4 ml/min and 45°C. Ionization is achieved in an atmospheric pressure photoionization interface, detection and quantification is done using the multiple reaction monitoring mode (MRM) with one precursor ion and two daughter ions per analyte. Applying this method, low detection limits, good recoveries and high reproducibility for azaarenes was shown. For the amino-arenes investigated, recoveries were bad, probably due to evaporation and degeneration processes during sample processing.

To verify applicability of the method ten samples of particulate matter (PM$_{2.5}$, 24 h) were collected with an Anderson high-volume sampler on the campus of HelmholtzZentrum in Munich in December 2008. Quartz fiber filters were divided, treated as described above and the concentrations of azaarenes, PAH and selected nitro-PAH were determined and compared under different points of view.

PAH and nitro-PAH were analyzed using laboratory established HPLC-fluorescence methods (Lintelmann et al.).

In the samples analyzed concentrations of azaarenes between ca. 4 pg/m^3 and 370 pg/m^3 were found. As expected, amino-arenes could not be quantified. Highest concentrations – considering the azaarenes – were found for acridine.
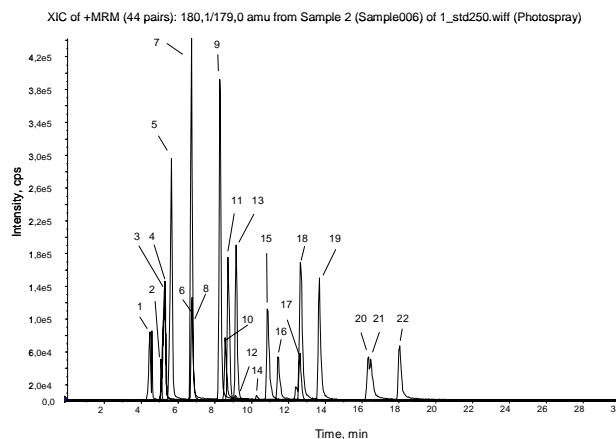
Figure 1. Overlaid MRM-chromatogramm of amino- and azaarenes.

B.J. Finlayson-Pitts, B.J. & Pitts, J.N. (2000). *Chemistry of the Upper and Lower Atmosphere. Theory, Experiments and Applications.* Academic Press, San Diego

Delhomme, O., Millet, M. (2008). *Polycyclic Aromatic Compounds*, 28, 5128-532.

Chen, H-Y., & Preston, M.R. (1998). *Environ. Sci. Technol.*, 32, 577-538.

Pantiru, M., J. Lintelmann, & Matuschek, G. (2005). Determination of nitrogen-containing PAH`s in aerosols by LC/MS/MS. In: *Proceedings of the Third International Symposium on Air Quality Management.* ISBN 975-00331-1-6, 53

Lintelmann, J., Fischer, K., Karg, E., & Schröppel, A. *Anal. Bioanal. Chem.* 381 (2005) 508-519.

Chemical characterization of particulate matter at the Sonnblick Observatory

M.W. Koller[1], C. Effenberger[1,] A. Kaiser[2], A. Kranabetter[3], G. Schauer[4], A. Kasper-Giebl[1]

[1]Institute of Chemical Technologies and Analytics, Vienna University of Technology, Getreidemarkt 9, A-1060, Vienna, Austria
[2]Central Institute for Meteorology and Geodynamics (ZAMG), Hohe Warte 38, A-1190, Vienna, Austria
[3]Abteilung 16 – Umweltschutz, Michael-Pacher-Straße 36, A-5020, Salzburg, Austria
[4]Wetterdienststelle Salzburg, Freisaalweg (ZAMG) 16, A-5020 Salzburg, Austria

Keywords: Atmospheric aerosols, ambient aerosols, chemical analysis, PM10, optic particle counter.

Located in the main ridge of the Austrian Alps (12°57'E, 47°03'N, Hohe Tauern) at the top of Sonnblick (3106 m a.s.l.) the Sonnblick Observatory (SBO) offers a great opportunity for scientific research, e.g. to get information about the background situation above Central Europe.

Aerosol sampling performed since 2005 included sampling of PM10 with a Digitel High Volume Sampler on quartz fibre filters (Pallflex, 150mm) and determination of the CP-count with both a TSI 3022A and a TSI 3781 instrument. Filter sampling was performed with sampling intervals of one week to assure sufficient filter loadings. Water soluble anions and cations were determined by ion chromatography using standard methods. Carbon parameters are analysed by combustion (Cachier et al., 1989 and Effenberger, 2009) and thermooptical methods. In addition selected filters were analysed for selected tracer compounds, i.e. levoglucosan or cellulose. Furthermore aerosol mass was determined.

Sulfate concentrations range from 0.2 to 2 $\mu g/m^3$ (all given volumes are related to 0 °C and 1013.25 mbar) in summer and 0.1 to 1 $\mu g/m^3$ in winter. Based on the available data there is a ratio of 1:5 between the concentrations of the major components during summer- and wintertime, consistent with earlier measurements (Kasper & Puxbaum, 1994). Results of TC are 0.2 to 2.5 $\mu g/m^3$ in summer and around 0.3 $\mu g/m^3$ in winter. The average ratio for TC / SO_4 is about 1.5. Monthly averages of the TC / SO_4 ratio range from 0.9 to 3 and no specific trend was observed throughout the seasons. The analysis of a limited number of samples showed small amounts of levoglucosan, 4 to 26 ng/m^3 (contribution to OC: 3 to 19 %) and cellulose 25 to 85 ng/m^3 (equal to 6 to 22 % of OC), again being similar to former measurements (Puxbaum et al., 2007 and Sanchez-Ochoa et al., 2007).

Although aerosol mass loadings of the filters were quite low, the aerosol mass could reach up above 10 $\mu g/m^3$. Several times these elevated values could be explained by long range transport of Saharan dust, which was also obvious by the colour of the filter, the chemical analysis and the calculation of backward trajectories.

Regarding particle count measurements, long term datasets are available for the butanol-based TSI 3022A. They show a distinct seasonal difference with the average value being close to 800 ccm^{-1} for the warm season, thus being about twice as high as during the cold season. Furthermore the Saharan dust event of spring 2008 has been monitored and will be shown.

A one month study in January 2008 compared this CPC to the water-based TSI 3781. Ratios and trends as well as discrepancies in standard deviation will be discussed.

Cachier, H., Bremond, Marie Pierre, Buat-Menard, P., (1989). *Determination of atmospheric soot carbon with a simple thermal method*, Tellus 41B, 379-390

Effenberger, C. (2008) *Chemische Massenbilanz der PM10-Fraktion am Hohen Sonnblick*, Diploma Thesis, Vienna University of Technology

Kasper, A. & Puxbaum, H., (1994). *Determination of SO2, HNO3, NH3 and aerosol components at a high alpine background site with a filter pack method.* Analytica Chimica Acta, 291(3), 297-304

Sanchez-Ochoa, A., (2007). *Concentration of atmospheric cellulose: A proxy for plant debris across west-east transect over Europe.* Journal of atmospheric research Vol. 112

Puxbaum, H., Caseiro, A., Sanchez Ochoa, A., Kasper-Giebl, A., Claeys, M., Gelencser, A., Legrand, M., Preunkert, S., & Pio, C., (2007). *Levoglucosan levels at background sites in Europe for assessing the impact of biomass combustion on the European background aerosol.* Journal of Geophysical Research-Atmosheres, *112*, D23S05; S. 1- 11.

Influence of fireworks on atmospheric levels of trace metals

N. Galindo[1], E. Yubero[1], F. Lucarelli[2], S. Nava[2], M. Chiari[2], G. Calzolai[2], J. Nicolás[1], and J. Crespo[1]

[1]Department of Physics, Miguel Hernández University, Avda. de la Universidad s/n, 03202, Elche, Spain
[2]Department of Physics, University of Florence and INFN, via Sansone 1, I-50019, Sesto Fiorentino, Italy

Keywords: Aerosol Chemistry, Fireworks, PIXE, PM2.5, Trace elements.

Las Hogueras de San Juan is the biggest festival in the city of Alicante (southeastern Spain) celebrated every June 17-25. Throughout this festival, large quantities of firecrakers and sparklers are burnt everyday in the city centre during a few minutes. This event represents an unusual but important source of atmospheric particles, especially metals. To evaluate the impact of the firecraker and sparkler burning upon the levels and composition of atmospheric particles, daily PM2.5 samples were collected from two sites in Alicante with low volume samplers (2.3 m^3/h). Site 1, located less than 50 m from the pyrotechnic displays, was under the direct influence of the firework plume. Site 2 was chosen as representative of the urban background environment. Elemental analysis was carried out by the Particle Induced X-ray (PIXE) technique.

Figure 1 shows the variations of chloride and different metals linked to firework ignition at both sites. Samples collected from 18-23 June were influenced by pyrotechnic displays close to Site 1 (at 14:00). The remaining days (17 and 25 June), fireworks were displayed at midnight 3-4 km away from both sampling sites. On 24 June a singular event took place (*La Cremà*), when bonfires were lit all over the city.
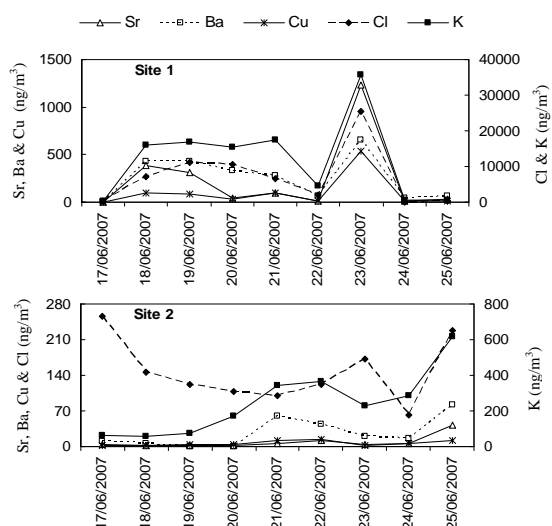
Figure 1. Daily concentrations of Sr, Ba, Cu, Cl and K during *Las Hogueras* in June 2007.

The contribution of firework displays at Site 1 is clear since the levels of Cl and metals were much higher on the days of firecracker and sparkler displays, with a very sharp peak on 23 June. The marked decrease observed afterwards suggests that the sea breeze favours the quick dispersion of atmospheric pollutants from the ignition point. The levels of all elements showed a very similar variation throughout the measurement period, which is indicative of a common source.

The concentrations registered at Site 2 presented very different variations with respect to Site 1 but, in general, all measured elements seemed to be affected by firework displays.

To evaluate the influence of such events on PM levels and elemental composition, average concentrations were calculated for the days with and without pyrotechnic activity (excluding the samples collected on 24 June). For the urban background location two additional samples were collected on 30 June and 1 July. Average concentrations on these two days were taken as a reference of a firework-free period at Site 2. The results are shown in Table 1.

Table 1. Comparison between concentrations measured on firework (FW) and non-firework (NFW) days.

	Site 1 (ng/m^3)		Site 2 (ng/m^3)	
	NFW	FW	NFW	FW
PM2.5	26900	82600	24700	28600
Sr	17	350	3	9
Ba	35	365	19	28
Cu	8	142	3	7
Cl	215	10500	27	157
K	420	17700	124	240

During fireworks, Cl and Sr reached very high values, with averages in Site 1 of 10.5 μg/m^3 and 17.7 μg/m^3, respectively (increment factors: ~40-50). Sr and Cu FW averages are ~ 20 times greater than NFW values. In contrast to what have been reported in other studies (Moreno et al., 2007, Vecchi et al., 2008), Ba showed the lowest factor increment at both sites.

Moreno, T., Querol, X., Alastuey, A. Minguillón, M.C., Pey, J., Rodríguez, S., Miró, J.V., Felis, C. & Gibbons, W. (2007). *Atmos. Environ.*, 41, 913-922.
Vecchi, R., Bernardoni, V., Cricchio, D., D'Alessandro, A., Fermo, P., Lucarelli, F., Nava, S., Piazzalunga, A. & Valli, G.. (2004). *Atmos. Environ.*, 42, 1121-1132.

Polycyclic Aromatic Hydrocarbons and carbon-containing species in ambient aerosols in Thessaloniki, Greece

L.P. Chrysikou[1], C. Samara[1], A. Bougiatioti[2], N. Mihalopoulos[2]

[1]Department of Chemistry, Environmental Pollution Control Laboratory, Aristotle University, Thessaloniki, 54124, Greece
[2] Environmental Chemical Processes Laboratory, Department of Chemistry, University of Crete
PO Box 2208, 71003 Voutes, Heraklion, Greece

Keywords: elemental carbon, organic carbon, PAHs, PM_1, water soluble organic compounds

Carbonaceous compounds constitute a significant fraction of the ambient particulate matter (PM) in the fine size mode (d<1μm) (Temesi *et al.,* 2003). An important part of the carbon mass of aerosols is soluble in water. Polycyclic aromatic hydrocarbons (PAHs) are among the carbonaceous constituents of greatest concern because some of these compounds are carcinogenic (Temesi *et al.*, 2003; Yu *et al*., 2004).

Organic (OC), elemental (EC) and water soluble organic carbon (WSOC), as well as PAHs were determined in the $PM_{0.95}$ particle fraction collected at an urban location within the city of Thessaloniki during winter of 2007 and summer of 2008. $PM_{0.95}$ was sampled using an Andersen high-volume cascade impactor on high purity quartz filters (Environmental Tisch TE-230QZ), baked at 450°C for 8 hours. OC and EC were determined by the Thermal Optical Transmission method in a Sunset Laboratory OCEC Analyser. WSOC was determined in aqueous filter extracts using a Shimadzu TOC-VCSH Analyzer. Filter portions were also extracted with dichloromethane/n-hexane (3:2, v/v). PAHs (Np, Ace, Acy, Fl, Ph, An, F, Py, B[a]An, Chry, B[b]Fl, B[k]Fl, B[a]Py, IPy, dB[a,h]An, B[ghi]Pe, B[e]Py and Per) were analysed by GC-MS. Table 1 lists the concentrations of $PM_{0.95}$ and the targeted aerosol components.

Table 1. Mean±SD concentrations of $PM_{0.95}$ (μg m^{-3}), PAHs (ng m^{-3}), and carbonaceous species (μg m^{-3}) in sampling periods

	Winter	Summer
OC	12.3±9.67	8.37±1.65
EC	6.18±3.16	3.73±1.65
OC/EC	2.71±0.5	2.67±1.45
WSOC	3.76±0.56	2.87±0.71
$PM_{0.95}$	128±54.8	103±56.4
B[a]Py	0.79±0.71	0.05±0.02
BaPE	1.07	0.14
ΣPAHs	15.7±14.1	3.21±1.17

ΣPAHs: Sum of 18 PAHs
BaPE=BaPy + (B[a]An x 0.06) + (B[k]Fl + B[b]Fl) x 0.07 + (IPy x 0.08)

ΣPAHs concentrations in $PM_{0.95}$ were significantly higher in winter than in summer ($P<0.05$ in the non-parametric Mann Whitney U test). The BaPE index indicating the carcinogenic potency of aerosol was also significantly higher in winter (Table 1).

Mean WSOC concentrations were 3.76 μg m^{-3} in winter and 2.87 μgm^{-3} in summer, exhibiting statistically significant seasonal variations. WSOC values were comparable to those reported for fine particles at other locations (Yu *et al*., 2004). WSOC accounted for 12-16% of the TC.

OC content exceeded EC in both sampling seasons, as previously observed at the same site for PM_{10} (Flarountzou *et al*., 2008). Total Carbon (TC) concentrations accounted for about 25% and 17% of $PM_{0.95}$ in cold and warm period, respectively. Although the highest concentrations were noticed in winter, the seasonal differences were not statistically significant.

Strong correlation was observed between OC and EC (Pearson correlation coefficient r was 0.95 in cold and 0.89 in warm season, respectively), indicative of common sources (possibly traffic emissions). OC/EC mean ratios were higher than 2 in both sampling campaigns, revealing the existence of secondary organic carbon (Duan *et al*., 2005). Strong correlation was also found in the cold period between $PM_{0.95}$ and ΣPAHs (r =0.78) as well as for $PM_{0.95}$ and EC in the warm period, (r =0.89), suggesting fresh inputs of small particles from combustion emissions, such as central heating and vehicle exhausts.

Duan, F., He, K., Ma, Y., Jia, Y., Yang, F., Lei, Y., Tanaka, S., & Okuta, T., (2005). *Chemosphere,* 60, 355-364.

Flarountzou, A., Terzi, E., Camara C., Bougiatioti, K., Mihalopoulos N., Nikolaou K., (2008). *Proceedings of EAC,* Thessaloniki, T02A053P.

Temesi, D., Molnár, A., Meśzáros, E., & Feczkơ T., (2003). *Atmospheric Environment* 37, 139–146.

Yu, J.Z., Yanga, H., Zhanga, H., & Laub A.K.H., (2004). *Atmospheric Environment* 38, 1061–1071.

A systematic chemical and morphological characterization of particulate matter in the main cities of Umbria (Italy) in the years 2006-2009

L.Barcherini[1], D.Cappelletti[1], S.Ortu[1], F.Scardazza[1], F.Marmottini[2], B.Moroni[3], M.Angelucci[4], M.Galletti[4], L.Mascelloni[4] and M.Vecchiocattivi[4].

[1]Dipartimento di Ingegneria Civile ed Ambietale, Università degli Studi di Perugia, Italy
[2]Dipartimento di Chimica, , Università degli Studi di Perugia, Italy
[3]Dipartimento di Scienze della Terra, Università degli Studi di Perugia, Italy
[4]ARPA Umbria, via Pievaiola San Sisto, 06132, Perugia, Italy

The aim of this work was to carry out a systematic chemical and morphological characterization of PM in the main cities in Umbria (Central Italy), and to evaluate the impact of biogenic and anthropogenic sources on the air quality at regional scale.

The first stage of the project was dedicated to optimize and integrate various analytical procedures and to plan the sampling campaign. In the second stage, developed between May 2006 and April 2007, sampling was carried out in different urban sites in the two main cities of Umbria, Perugia and Terni. More than 200 PM10 and PM2.5 samples were collected on PTFE filters using low volume air samplers. The samples were analyzed by different techniques of chemical and morphological analysis (ICP-AES, IC, UV-VIS, XRF, SEM-EDS). Considerable morphological and compositional differences among the PM collected in the two sites were evidenced. These differences delineate two different emissive contexts in Perugia and Terni, the former being strongly influenced by motor traffic and the latter resulting from a mixing of natural, roadside and industrial inputs. In addition, potential sources and modes of distribution of fine aerosol in the environment were outlined [1, 2].

In order to further deepen the understanding of these aspects a third stage of the project was planned. This third phase of the project started in December 2008 and will last till Dec 2009. At this stage sampling has been extended to other industrial (Gubbio, Narni Scalo, Spoleto) and to a regional remote background (Martani mountains) sites.

In addition to the equipments employed in the previous stages, herein, two high volume air samplers with cascade impactor are employed to obtain multi-stage particulate size resolution of fine and course fractions. Also, an optical particle counter is used to define the dimensional distribution of fine and ultrafine fractions.

The regional remote background site was located at an altitude of 800 m. on the ridge of a small mountain system (monti Martani) in the center of the Umbria region. The site was equipped with a SWAM 5a Dual Channel Monitor (FAI instruments) with PM10 and PM2.5 selective inlets. The apparatus is controlled remotely and allows to determine the mass concentration of PM by operating on operating and spy filters, comprising a beta radiation emitter and detector.

Seasonal samples on quartz fiber and polycarbonate filters will undergo similar chemical analysis as in stages 1 and 2 of the project.

Data will be presented at the conference also by means of results from multivariate statistical analysis.

Bibliography:
[1] D.Cappelletti et al.(2009), *La Chimica e l'Industria,* 3 (2009) 104-111.
[2] B.Moroni et al. (2008). in *Geology and Health*, Quaderni del Centro di Geobiologia dell'Università degli Studi di Urbino, Ed. R. Coccioni) 5, 81--89 (2008).

Results of the first EC/OC intercomparison exercise for National Air Quality Reference Laboratories

L. Emblico and A. Borowiak

Joint Research Centre, Institute for Environment and Sustainability, 21027 Ispra (VA), Italy

Keywords: Air quality, Elemental carbon, Laboratory experiments, Organic carbon, PM.

Fine particulate matter is a pollutant of increasing concern due to its role in health effects (Pope et al, 2002) and impact on climate change (Seinfeld and Pandis, 1998). The Air Quality Directive 2008/50/EC, published in June 2008, reflects this increased concern and regulates as a novelty ambient air concentrations of fine particulate matter PM2.5. The novelties around the PM2.5 regulation are three fold: an exposure reduction target, a limit value (applicable from 2015 onwards) and the chemical speciation of PM2.5 at urban background sites to provide information on the content of cations, anions, elemental carbon (EC) and organic carbon (OC).

The Joint Research Centre of the European Commission, Institute for Environment and Sustainability, is running the "European Reference Laboratory for Air Pollution (ERLAP)", being the Commission's responsible body for organizing Community quality assurance programmes. ERLAP has been organizing already on a regular basis or on demand intercomparison exercises for inorganic and organic air pollutants, and heavy metals in PM (Gerboles and Buzica, 2008). In order to prepare the Community for the new challenge on PM speciation, ERLAP organized a first EC/OC intercomparison exercise within the AQUILA Network of National Air Quality Reference Laboratories during autumn 2008. Aim of the study was to assess the comparability and quality of TC (total carbon), OC and EC measurements among AQUILA laboratories and to quantify differences in the results. Since no common analytical protocol is currently available for EC/OC determination, each participant was requested to perform the analysis using his own standard procedure.

Filters (diameter 150 mm) have been sampled with a High Volume PM Samplers at three different sites: Ispra (rural background site), Vienna and Essen (urban background sites). 14 punches (including one blank) of 4 cm² have been sent to each of the 16 participating laboratories. Most of the laboratories measured the punches by means of thermo-optical analysis, but using different protocols: NIOSH (NMAM 5040) or similar, and EUSAAR (Cavalli and Putaud, 2008).

First results show that, regardless of sample origin or TC filter loading, a good agreement is found for TC measurements (r.s.d. below 10%), but discrepancies up to 40% were reported on EC measurements.

As one error source filter inhomogeneity has been identified: punches taken close to the filter edge are less homogeneous in carbon content with respect to punches taken in the central part of the filter. Nevertheless, EC data provided by laboratories using the same protocol are in excellent agreement (r.s.d about 10%).

The statistical data treatment of the results will be presented, to quantify differences between analytical protocols, repeatability and reproducibility of measurements and the capacity to meet the data quality objective required by the Air Quality Directive.

AQUILA Network: http://ies.jrc.ec.europa.eu/aquila-homepage.html

Directive 2008/50/EC of the European Parliament and of the Council of 21 May 2008 on ambient air quality and cleaner air for Europe. OJ L152, 11.6.2008,

Cavalli F, Putaud J., 2008. Toward a Standardized Thermal-optical Protocol for Measuring Atmospheric Organic and Elemental Carbon: The EUSAAR Protocol . EUR 23441 EN.

Gerboles, M., and Buzica ,D., 2008. Intercomparison exercise for heavy metals in PM10; EUR 23219 EN.

NIOSH Manual of Analytical Methods (NMAM) http://www.cdc.gov/niosh/nmam/pdfs/5040.pdf

Pope, C.A., Burnett, R., Thun, M.J., Calle, E.E., Krewski, D. Ito, K., Thurston, G.D., 2002. Lung cancer, cardiopulmonary mortality and long-term exposure to fine particulate air pollution. JAMA 287,1132-1141.

Seinfeld, J.H., Pandis, S.N., 1998. Atmospheric Chemistry and Physics; From Air Pollution to Climate Change. John Wiley & Sons INC, New York; Chichester (US).

Identification of homologous series as organic tracers in PM samples: a signal processing method for studying complex GC-MS signals

M.C. Pietrogrande[1], M. Mercuriali[1], L. Pasti[1], D. Bacco[1], F. Dondi[1]

[1]Department of Chemistry, University of Ferrara, Ferrara, I-44100, Italy

Keywords: alkanes, chemical composition, GC-MS, organic tracers, signal processing

Homologous series of n-alkanes and n-alcanoic acids are especially suited as molecular markers to give information relevant to trace the origin and fate of atmospheric aerosols. Two main parameters are used as chemical signature to differentiate anthropogenic vs. biogenic sources: the number of terms of the series (n_{max}) and the carbon preference index (CPI) which represents the prevalence of odd/even carbon number terms of the series.

Gas chromatography-mass spectrometry (GC-MS), the best analytical technique for these organics, generates extensive amounts of data when applied to such complex mixtures as polluted environmental samples, which are complicated by a vast amount of noise, artefacts, and data redundancy.

In the present paper, a signal processing procedure based on the AutoCovariance Function ($ACVF_{tot}$) is applied to GC-MS signals of atmospheric aerosols. This is a computer-assisted signal processing procedure able to transform GC data into usable information by extracting all the analytical results hidden in the complex chromatogram (Pietrogrande *et al.*, 2007). The method is further extended by deriving new mathematical equations and implementing a new computation algorithm to extract information on the homologous series -- n_{max} and CPI -- directly from the experimental $EACVF_{tot}$ computed on the acquired chromatographic signal (Pietrogrande *et al.*, 2008, Pietrogrande *et al.*, 2009).

The procedure was validated on simulated chromatograms with known distribution of the terms of the series: the obtained results prove that the parameters n_{max} and CPI of the homologous series can be estimated with good accuracy and precision.

The method was applied to experimental chromatograms of real samples: aerosol samples ($PM_{2.5}$ and PM_{10}) were collected daily in urban and rural sites. The information on distribution pattern of n-alkanes and n-alkanoic can be directly obtained from the $EACVF_{tot}$ computed on the acquired chromatogram, thus reducing the labour and data handling time and removing the subjective step of peak integration. The advantages of the method can be singled out by comparison with the traditional procedure based on GC peak identification and integration.

The procedure was used to investigate the distribution profile of n-alkane (C_{14}–C_{33} terms) and n-alcanoic acid (C_{14}–C_{26} terms) homologous series. The number of terms and CPI_{tot} values were computed directly from the $EACVF_{tot}$ from the whole chromatogram. Moreover, the procedure can be separately applied to the chromatographic region containing the biogenic heavier terms of the series to compute the $EACVF_{plant}$: the obtained parameters n_{plant} and CPI_{plant} give quantitative information on the role played by the biogenic vs. anthropogenic sources.

The series of n-alkanoic acids was investigated as useful marker in discriminating sources contribution to the aerosol organics: high CPI_{tot} values, confirming the even prevalence of acid isomers mostly derived from plant waxes, were found for rural and urban samples. Information on the biological sources of n-alkanoic acids can be simply extracted by computing $ACVF_{plant}$ on the selected chromatographic region containing the C_{20}–C_{26} terms: the estimated CPI_{plant} reflects the vascular plant wax signature. A simple graphical comparison of $EACVF_{plant}$ with $EACVF_{tot}$ gives quantitative information on the contribution of the biological sources of atmospheric n-alkanoic acids.

Bold line: $EACVF_{tot}$ plot computed on the whole chromatogram to estimate total parameters (**blue** values);
Solid line: $EACVF_{plant}$ plot computed on the chromatogram region containing C_{20}–C_{26} terms to estimate parameters of biogenic contribution (**red** values).
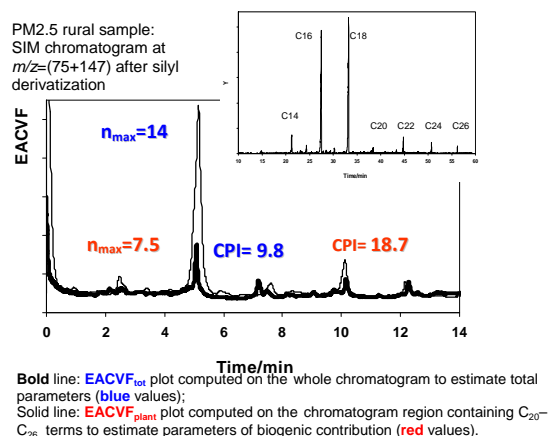
The described signal processing method seems promising for high-throughput analysis of the large data sets generated by chemical monitoring in environmental analysis.

Pietrogrande, M.C., Mercuriali M., Pasti L. (2007) *Anal. Chim. Acta*, 594, 128-138.

Pietrogrande, M.C., Mercuriali M., Bacco, D. (2008) *Air Pollution XVI*, Skiathos (WITPress, Southhampton), 335-343

Pietrogrande, M.C., Mercuriali M., Pasti L., Dondi F. (2009) *Analyst*, DOI: 10.1039/b815317e.

On-line measurements of fine organic aerosols in the region of Paris (France): Evidence of a major source of domestic wood burning

O. d'Argouges, J. Sciare, R. Sarda-Estève

LSCE (CNRS/CEA), CEA Orme des Merisiers, 91191, Gif-sur-Yvette, France

Keywords: Aerosol chemistry, biomass burning, on-line measurements, water soluble organic carbon

Factors controlling fast changes in levels and chemical/optical properties of carbonaceous aerosols were investigated in the region of Paris (France) during wintertime from a wide variety of on-line instruments. All the measurements were performed in the fine mode (A.D. $< 2.5 \mu m$) for a period of 2 weeks (in February 2009) on the roof platform of LSCE, 30km south-west of Paris city.

Levels of water soluble organic carbon (WSOC) were investigated from 4-min time resolution on-line measurements obtained from a PILS-TOC system (Sullivan *et al.*, 2004). The PILS instrument used here was the one described by Sorooshian *et al.* (2006) and was equipped with a Total Organic Carbon (TOC) system Model 900 (Sievers Ltd).
Hourly concentrations of Elemental Carbon (EC) and Organic Carbon (OC) in the fine fraction were obtained from a semi-continuous ECOC field analyzer (Sunset Laboratory, Forest Grove, OR; Bae *et al.*, 2004).
Equivalent Black Carbon (EBC) measurements were obtained from 5-min integrated light absorption measurements performed by a seven-wavelength Aethalometer (Model AE-31, Magee Scientific).
These measurements were completed by fast (15-min time resolution) measurements of the major ions in aerosols using a PILS-IC instrument (Orsini *et al.*, 2003). Continuous (6-min time resolution) measurements of $PM_{2.5}$ (nonvolatile + semivolatile) were performed by a Tapered Element Oscillating Microbalance (TEOM) Model 1400 from Rupprecht & Pataschnik equipped with a Sample Equilibration System (SES) and a Filter Dynamic Measurement System (FDMS, 8500 model series) (Grover *et al.*, 2005).

RESULTS AND DISCUSSION: On-line measurements of WSOC, OC, and EC were first compared with similar measurements performed from VOC denuded filter sampling operating in parallel (R&P Partisol Model 2025, Thermo Scientific). Comparison between these two datasets (on-line vs integrated filter-based) has shown very good agreement, cross-validating the consistency of sampling & analytical techniques.

High Angstrom absorption exponents (derived from Aethalometer measurements) were observed at night pointing out a significant influence of residential wood burning aerosols. Maxima observed in the (babs $_{370nm}$/babs $_{880nm}$) ratio were also observed for potassium (known as a tracer of biomass burning), bringing further confidence on the role of domestic wood burning in the region of Paris.

A very good agreement (r^2=0.76; N=172); was found between (babs $_{370nm}$/babs $_{880nm}$) ratio and (WSOC/BC) ratios suggesting a significant source of WSOC (relatively to BC) for wood burning. By contrast, no correlation was found with WIOC/BC ratio, suggesting that domestic wood burning is a poor emitter of WIOC. These observations are consistent with commonly reported water soluble properties of organics emitted by biomass burning. Also, they clearly show that organic material absorbing in the UV and originating from wood burning is mainly water soluble.

Hourly WSOC/OC ratio was only 0.38±0.14 on average, suggesting a strong contribution of primary organics in the region of Paris for this period of the year. Although WSOC/OC ratio has shown relatively high values during wood burning periods, its variability seemed to be controlled by other mechanisms. The highest ratios were observed systematically at night (e.g. at low temperatures) and would suggest semi-volatile properties for WSOC as proposed recently by Hennigan *et al.* (2008).

Bae, M.S., Schauer, J.J., DeMinter, J.T., Turner, J.R., Smith, D., Cary, R.A. (2004), *Atmospheric Environment*, 38, 2885-2893.

Grover, B.D., Kleinman, M., Eatough, N.L., Eatough, D.J., Hopke, P.K., Long, R.W., Wilson, W.E., Meyer, M.B., Ambs, J.L., Grover, B.D., et al., (2005), *Journal of Geophysical Research*, 110.

Hennigan, C. J., A. P. Sullivan, C. I. Fountoukis, et al., (2008), *Atmos. Chem. Phys. Discuss.*, 8, 4811–4829

Sullivan, A. P., R. J. Weber, A. L. Clements, J. R. Turner, M. S. Bae, and J. J. Schauer (2004), *Geophys. Res. Lett.*, 31, L13105, doi:10.1029/2004GL019681

Sorooshian, A., .F. J. Brechtel, Y. Ma, R. J. Weber, A. Corless, R. C. Flagan, and J. H. Seinfeld1 (2006), *Aerosol Science and Technology*, 40:396–409.

Aerosol source apportionment in Cork Harbour, Ireland, based on continuous, real-time measurements, Aerosol Time of Flight Mass Spectrometry and factor analysis.

S. Hellebust*, R. Healy, I. Kourtchev, A. Allanic, I.P. O'Connor, J. Wenger and J. Sodeau

Department of Chemistry, University College Cork, College Road, Cork, Ireland

Keywords: PM and source apportionment, Organic aerosols, Aerosol spectrometry, shipping emissions.

Cork Harbour is home to Ireland's second largest port and several chemical industries. This study presents a source apportionment model for Cork Harbour developed on four levels, with the objective of quantifying the contribution of shipping emissions to local air pollution. Air quality data and samples of atmospheric aerosols were collected near the main container berth, close to the shipping channel and about 3 km from the centre of Cork City. The data includes a three month record of real-time measurements of gases NO_x, SO_2 and O_3, particulate sulfate and particulate elemental and organic carbon (ECOC) and ambient levels of PM_{25}, acquired in the summer of 2008. During the same period, PM collections were made continuously using a High-Volume Cascade Impactor, sampling at 900 litres of air per minute (lpm) and capturing PM on polyurethane foam (PUF) substrate in two size fractions, $PM_{10-2.5}$ and $PM_{2.5-0.1}$. Two samples were obtained per week. The $PM_{2.5-0.1}$ size fraction was analysed for inorganic ions and metals using ion chromatography and inductively coupled plasma – optical emission spectroscopy. The campaign also included collection of $PM_{2.5}$ on quartz fibre filters over 24 hour periods for one month, using a Digitel DHA-80 high volume sampler collecting 500 lpm, which were subsequently analysed for the presence of organic molecular markers by GC-MS. Finally, over a three week overlapping period an Aerosol Time of Flight Mass Spectrometer (TSI-ATOFMS) was used to characterise chemical composition of several hundred thousand individual particles, which were subsequently clustered into some 30 particle types by a K-means clustering algorithm.

The source apportionment model was developed in stages by initially subjecting each data set to factor analysis by principal component analysis and positive matrix factorisation (PMF) to resolve the main likely sources. This approach combines several independent methods and analytical protocols and allows for robust conclusions regarding likely sources to be made, because each collection method is optimised to the subsequent analysis.

The real-time record can be resolved into four main likely contributors, i.e. traffic, coal/biomass burning, regional/aged traffic emissions and a small shipping contribution to carbonaceous aerosol and sulfate. The organic content of $PM_{2.5}$ collected in daily samples could be attributed to 3 separate sources, one of which coincided with the biomass burning factor and 2 further biogenic factors, which were identified as fungal spores and secondary organic aerosols from biogenic emissions of sVOC.

Likewise, sources of inorganic ions and metals were resolved by a PMF model based on 3 and 4 day collection periods. These include traffic, sea salt, crustal materials and secondary inorganic aerosols. Finally, a model based on the temporal record of individual particle types identified by ATOFMS was able to both resolve factors that coincided with the other models (e.g. fungal spores, biomass burning, sea salt and crustal materials) as well as identifying sources not resolved by the other data. The temporal trends of the latter were highly correlated to the real-time measurements and chemical content of the PM collections. The final factor profiles include ions, metals, organic markers and particle types identified by ATOFMS.

The particle types identified by ATOFMS include clusters that were unequivocally identified with ship plumes, by a combination of size, chemical composition, concurrence with ship times as of schedule provided by the Port of Cork and as identified by peak events in the NO_x, SO_2 and EC records. Real-time, continuous measurements and collections of PM on PUF for determination of inorganic ions and metals have been made for a period exceeding one calendar year. The shipping particle types identified this campaign are used to "calibrate" a shipping emissions factor profile in terms of ions, metals and organic markers and allows for an estimate of the contribution of shipping over the course of the entire record available for the inorganic and organic contents.

V. A. Lanz, M. R. Alfarra, U. Baltensperger, B. Buchmann, C. Hueglin, and A. S. H. Prévôt (2007). *Atmos. Chem. Phys., 7, 1503–1522*.

Delbert J. Eatough, Brett D. Grover, Woods R. Woolwine, Norman L. Eatough, Russell Long, Robert Farber (2008), *Atmospheric Environment* 42, 2706–2719.

J. G. Hemann, G. L. Brinkman, S. J. Dutton, M. P. Hannigan, J. B. Milford, and S. L. Miller (2009), *Atmos. Chem. Phys.*, 9, 497–513.

Organic compounds in Secondary Organic Aerosol measured by Direct Thermal Extraction-Gas Chromatography/Mass Spectrometry/Flame Ionization Detection

S. Langer and K. Arrhenius

SP Technical Research Institute of Sweden, Dept. of Chemistry and Materials Technology, P.O.Box 857, SE-501 15 Borås, Sweden

Keywords: Chemical composition, Organic compounds, Smog chamber, SOA.

Atmospheric aerosols play a key role in many environmental processes. They can affect the optical properties and lifetime of clouds and thus alter the radiative balance in Earth's atmosphere. Atmospheric aerosols are also important because of their impact on human health. Atmospheric particles typically contain 30-80% by mass of organic compounds. Some of the compounds are primary in origin and serve as markers for specific processes such as biomass burning or automotive exhaust and can be used to identify the origin of the particles. Many other species are secondary in origin (secondary organic aerosol, SOA) and are formed as a result of the atmospheric oxidation of volatile organic compounds. Detailed information on the organic content of atmospheric aerosol is thus required in order to fully understand its impact on climate and human health.

Here we present the results of DTE-GC/MS/FID analysis, calibration and method validation of the NIST Standard Reference Material 1649a "Urban Dust (Organics)" with respect to some selected Polycyclic Aromatic Hydrocarbons. A known amount of the sample is placed in an empty glass thermodesorption tube stopped on both sides by glass wool. The tube is subjected to two-stage thermal desorption process (Perkin-Elmer ATD 400), sample components are first swept onto a cold trap packed with an adsorbent, which is held at -30°C and then the cold trap is then flash heated to transfer the components to the GC/MS/FID system.

Table 1. Comparison between NIST certified values and SP results for three selected PAH in the Standard Reference Material "Urban Dust (Organics)".

	Concentration ng/mg	
	SP	Certified
Phenanthrene	4.2 ± 0.6	4.1 ± 0.4
Fluoranthene	5.9 ± 0.5	6.5 ± 0.2
Pyrene	5.3 ± 0.4	5.3 ± 0.3

The instrument is Agilent Technologies Gas Chromatograph 6890 (GC) equipped with flame ionization- (FID), and MSD 5973 mass selective detectiors (MS). The capillary column BPX-5 (5% phenyl polysilphenylene-siloxane, SGE), 50 m, 0.32 mm i.d., 1.0 μm film thickness, was placed in the chromatographic oven that was temperature programmed from 30°C for 2 minutes, 4°C/ min to 150°C, 8°C/min to 300°C, hold time 30 minutes. The injector temperature was set to 280°C. The carrier gas was ultra-high purity helium. The compounds of interest were calibrated, when commercially available, by injection of microliter amounts of the compounds in-methanol standards onto adsorbent tubes that were then analyzed in the same way as the samples. The FID is normally used for calculation of the total organic content in the aerosols using toluene equivalents The MS is used for both identification and quantification of the organic compounds..

The method has been used for analysis of organic compounds in the particles, formed in ozonolysis of various volatile some terpenes such as sabinene, α-pinene or limonene and 2-methyl styrene, and collected in environmental (smog) chambers (LISA-Paris and SP) on glass-fibre filters. A large number of chromatographic peaks were observed in each chromatogram. However, not all the compounds could be identified using the NIST 98 Mass Spectral Library. The presentation will summarize the advantages and disadvantages of the technique.
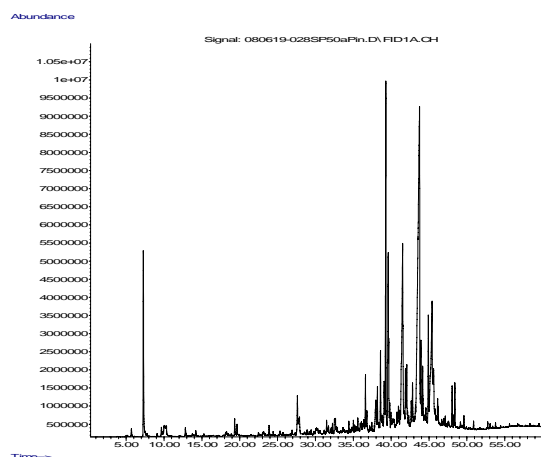
Figure 1. Example of experimental data. FID chromatogram of the organic compounds found in particles from ozone/α-pinene reaction

Determination of carbon particle fluxes by combination of micro-meteorology and single particle mass spectrometry

E. Gelhausen[1], K.-P. Hinz[1], A. Schmidt[2], O. Klemm[2] and B. Spengler[1]

[1]Institute of Inorganic and Analytical Chemistry, Justus-Liebig-University Giessen,
Schubertstr. 60, D-35392 Giessen, Germany
[2] Institute for Landscape Ecology - Climatology, University of Muenster,
Robert-Koch-Str. 26, D-48149 Muenster, Germany

Keywords: Aerosol mass spectrometry, Atmospheric aerosols, Chemical composition, Single particle analysis

Transportable on-line mass spectrometers are well proven to determine chemical and physical properties of aerosols on single particle level during ambient measurements at sites of interest (e.g. rural or urban sites). Size-resolved chemical analysis of ambient particles provides detailed information within the aerosol particle population with high temporal resolution and can be employed under highly variable ambient conditions. In combination with other measurement methods, secondary information about nature and composition of the particles can be obtained. The fast measurement of vertical wind components using an ultrasonic anemometer, in combination with an on-line single particle mass spectrometer, allows the determination of the deposition and emission of particles from / to surfaces.

The mobile, bipolar on-line laser mass spectrometer "LAMPAS 2" (Trimborn *et al.*, 2000) provides for the characterization of individual airborne micro- and nanoparticles. The instrument uses an impact-free, differentially pumped particle inlet system into the mass spectrometer. Inside the instrument particles are first optically detected by two cw-laser beams and their size is determined. In a second step an actively triggered UV laser evaporates and ionizes the detected particles. Bipolar time-of-flight mass spectrometry is used to chemically analyze the generated ions. Synchronously, turbulent wind fluxes are determined using an ultrasonic anemometer (YOUNG Inc.). Correlated evaluation of the data sets from anemometer and mass spectrometer are used for determination of the vertical direction of fluxes of single particle components (Held *et al.*, 2003).

During a measuring campaign in fall 2007 (September, 19th - October, 5th) on a research area near Giessen (Germany) ambient aerosol particles were measured with the LAMPAS 2 instrument. Size and chemical composition were determined for thousands of single particles. Parallel recordings of the vertical wind component, of ambient temperature and of other meteorological conditions were performed as well as bulk collections of particles with a Berner Impactor. Measurement of wind fluxes with the ultrasonic anemometer was achieved with a time resolution of 1/10 s. Mass spectra were sorted by statistical processing (Hinz et al., 1999) and assigned to different classes (groups of chemically similar particles). In a second step of data evaluation, particle spectra of the different classes were sorted according to the synchronously measured vertical wind component. The obtained data set represented the raw data for a determination of deposition / emission fluxes of specific particles and their compounds. For this purpose the chosen method was Eddy Covariance which correlates fluctuation of vertical wind speed with fluctuation of corresponding particle component concentration to receive components flux. During the field campaign a very high amount of carbon containing particles was observed. Therefore, this particle group was chosen to determine the flux of carbon compounds, referring to the approach of Held *et al.*, 2003.

Three (of six) particle classes show a similarity of a dominance of carbon cluster ions. Therefore these classes were summarized and a timeframe of highest amount of carbon containing particles was selected: 02.10.07 17:00h - 03.10.07, 16:00h. In this time range these particles had a portion of more than 89 % of all detected particles. Between 21:30h (02.10.) and 01:30h (03.10.) the number of this carbon containing particles was high enough for flux determination with Eddy Covariance. So for every single particle in this timeframe the carbon concentration is required. Therefore, a relative sensitivity factor by correlating totalized peak areas of carbon cluster ions with the off-line collected bulk measurement of total carbon was calculated. By means of this factor for every single particle the carbon concentration could be assigned.

Results of time-resolved evaluation of carbon containing particles and further calculations for carbon flux determination will be shown.

Held, A. Hinz, K.-P., Trimborn, A, Spengler, B. Klemm, O. (2003). *Geophys. Res. Lett.* 30, 2016
Trimborn, A., Hinz, K.-P., Spengler, B. (2000). *Aerosol Sci. Technol.* 33, 191-201
Hinz, K.-P., Greweling, M., Drews, F., Spengler, B. (1999). *J. Am. Soc. Mass Spectrom.* 10:648-660

Cluster analysis on mass spectra of biogenic secondary organic aerosol

C. Spindler[1], A. Kiendler-Scharr[1], E. Kleist[2], A. Mensah[1], Th. F. Mentel[1], R. Tillmann[1] and J. Wildt[2]

[1] Institut für Chemie und Dynamik der Geosphäre, ICG-2, Forschungszentrum Jülich, Germany
[2] Institut für Chemie und Dynamik der Geosphäre, ICG-3, Forschungszentrum Jülich, Germany

Keywords: Statistical analysis, Aerosol mass spectrometry, SOA, Biogenic Particles

Biogenic secondary organic aerosols (BSOA) are of high importance in the atmosphere. The formation of BSOA from the volatile organic compound (VOC) emissions of selected trees was investigated in the JPAC (Jülich Plant Aerosol Chamber) facility (Mentel et. al., 2009). The tree emissions mainly consist of monoterpenes, sesquiterpenes and organic VOC. The gases were transferred into a reaction chamber and BSOA was formed by OH and O_3 oxidation. The chemical composition of the aerosol was characterized by aerosol mass spectrometry (Aerodyne Quadrupol-AMS, Jayne et. al., 2000). Inside the AMS, the aerosol particles are flash-vaporized at 600°C and the evaporated molecules undergo electron impact ionization at 70 eV. These processes cause a high fragmentation of the organic compounds which is reflected in complex mass spectrometric patterns.

Here, we present a classification of the aerosol mass spectra via cluster analysis (Marcolli et. al., 2006). This method computes a mathematically defined distance between all pairs of mass spectra in a dataset (Figure 1). Similar mass spectra have smaller distances than unlike mass spectra. Average mass spectra are produced by combination of single mass spectra to so-called clusters. The clustering starts with the two closest mass spectra and progresses with increasing distance. This process is visualized with a dendrogramm (Figure 2), where the single clustering steps can be retraced.

The mass spectra presented here were similar compared to ambient mass spectra due to the similarity of the precursor substances. However, we can show that there are differences in the BSOA mass spectra of different tree species. Furthermore we can distinguish the influence of the precursor chemistry and chemical aging. BSOA formed from plants exposed to stress can be distinguished from BSOA formed under non stressed conditions. Significance and limitations of the clustering method for very similar mass spectra will be demonstrated and discussed.
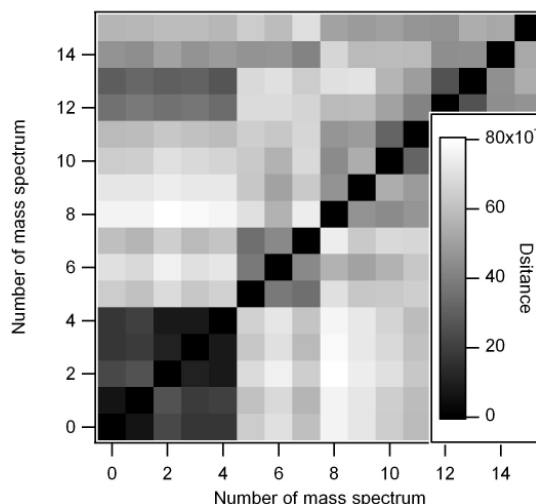
Figure 1. Pairwise distance of mass spectra
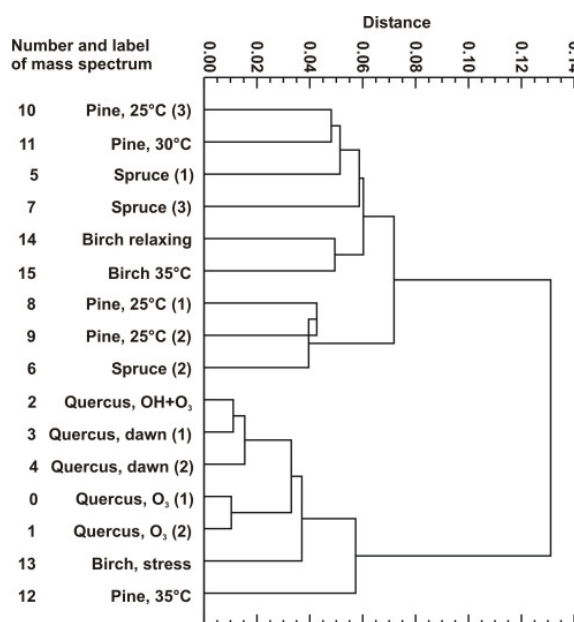
Figure 2. Dendrogramm of cluster analysis

Jayne, J. T., et. al. (2000). *Aerosol Science and Technology*, 33, 49-70.

Marcolli, C., et. al. (2006). *Atmospheric Chemistry and Physics*, 6, 5649-5666.

Mentel, Th. F., et. al. (2009). *Atmospheric Chemistry and Physics Discussions*, 9, 3041-3094.

Formation of secondary organic particles in elementary school classrooms

Congrong He[1], Lidia Morawska[1], Graham Johnson[1], Hai Guo[1], Erik Uhde[2], Godwin Ayoko[1]

[1]International Laboratory for Air Quality and Health, Queensland University of Technology, Brisbane, Australia
[2]Fraunhofer Wilhelm-Klauditz-Institute (WKI), Material Analysis & Indoor Chemistry, Braunschweig, Germany

Keywords: Secondary Organic Aerosols, Ultrafine particles, $PM_{2.5}$, VOCs, Indoor air quality.

Indoor secondary organic aerosol (SOA) formation events in offices (Weschler and Shields 1999, Alshawa et al. 2007) and residential houses (Long, et al., 2000) have been reported in previous studies, however, there are currently no studies that have investigated SOA formation in a naturally ventilated classroom.

In order to determine whether VOCs emitted from the detergents used in a classroom could lead to SOA formation with O_3, experiments were conducted in a classroom, including mopping the floor with water or diluted detergent, monitoring particle number (PN) and mass concentrations, and collecting VOC samples for analysis. In order to quantify particle formation rates, controlled experiments were conducted in which varying numbers of trays, each containing the detergent used in the school, were placed on a bench in a naturally ventilated lecture theatre. Indoor O_3 concentrations were set at a stable level in the range 0.010 – 0.020 ppm.

The results of GC-MS analysis showed that d-limonene was one of the main organic compounds in the detergent used in the school. Outdoor 1 hour average O_3 concentration during the classroom tests was in the range from 0.012 ppm to 0.020 ppm. The results of the experiments are presented in Figure 1, from which it can be seen that, after mopping, particle number concentration started to increase almost immediately. When the same experiment was repeated using pure tap water, there was no increase in particle concentration. We suggest that it was d-limonene which evaporated from the detergent, and after reacting with O_3, this created the indoor SOA during the first experiment.

The results of the controlled experiments confirmed SOA formation in an indoor environment. It was found that when O_3 concentration levels were lower than 0.005 ppm, there was no clear increase in PN concentration when using one tray of detergent. However, rapid particle formation occurred above this concentration. Figure 2 presents an example of time series of PN concentration and the count median diameter (CMD), which shows that, as soon as the detergent trays were placed on the bench in the lecture theatre, the PN concentration increased. The peak values for PN concentration using four and five detergent trays reached 5.89×10^4 and 6.85×10^4 particles cm^{-3}, respectively. These peak values were approximately 20 times higher than background concentration. Average O_3 concentration during these measurements was 0.010

ppm, while the d-limonene concentration was 398 and 525 µg m^{-3}, for four trays and five trays, respectively. It can be seen from Figure 2 that the CMD varied over time, ranging from 24-80 nm and that it decreased immediately after the introduction of the trays, which was followed by a subsequent increase. It also indicates that a large number of nano sized new SOA particles were formed, and these subsequently grew in size.
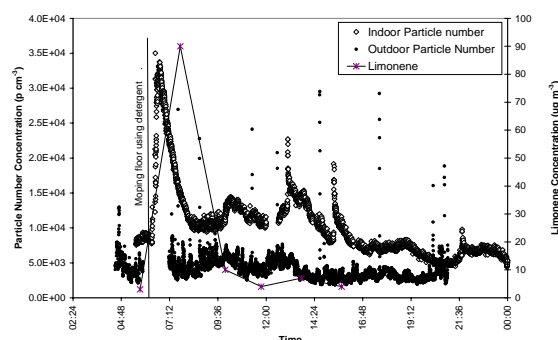
Figure 1 Indoor PN, $PM_{2.5}$ and 30 min average limonene concentrations measured in a classroom.
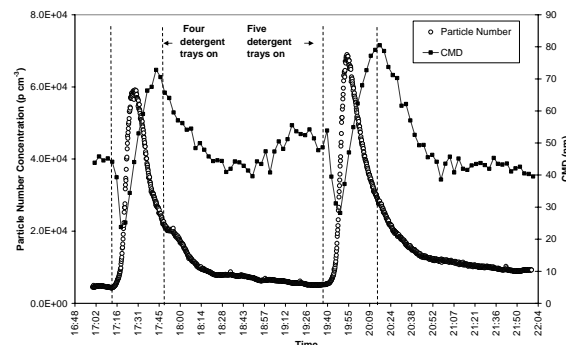
Figure 2 An example of SOA formation in the lecture theatre, when a 4 or 5 detergent trays were present for 34 minutes.

Alshawa, A., Russell, A., Nizkorodov, S. (2007). *Environ. Sci. Technol.*, 41, 2498-2504.

Long, CM., Suh, HH., Koutrakis, P. (2000) *J Air Waste Manag Assoc.*, 50, 1236-50.

Weschler, C. J., Shields, H. C. (1999). *Atmos. Environ.*, 33, 2301-2312.

Controlled OH radical induced aerosol ageing in the ADIA simulation chamber

H. Saathoff[1], K.-H. Naumann[1], O. Möhler[1], N. Donahue[2], T. Mentel[3], R. Tillmann[3], and T. Leisner[1]

[1]Institute for Meteorology and Climate Research, Forschungszentrum Karlsruhe, Hermann-von-Helmholtz-Platz 76344 Eggenstein-Leopoldshafen, Germany
[2]Carnegie Mellon Univ, Ctr Atmospher Particle Studies, Pittsburgh, PA 15213 USA
[3] Institute of Chemistry and Dynamic of the Geosphere, Forschungszentrum Jülich, Leo-Brandt-Str. 52428 Jülich, Germany

Keywords: aerosol chemistry, reaction chamber, aerosol evolution, aerosol modelling, SOA ageing

OH radicals are the most important agents for oxidation of atmospheric pollutants. Furthermore they play an important role in formation and ageing of atmospheric aerosol particles e.g. like secondary organic aerosols (SOA). Since the influence of temperature on aerosol formation and ageing is one of the major uncertainties for understanding aerosol transformations (Tsigaridis et al., 2005) it seems useful to have an OH radical source in the large temperature controlled but dark AIDA aerosol chamber (Saathoff et al., 2008).

Therefore we employed controlled ozonolysis of 2,3-dimethyl-2-butene (TME) to generate OH radicals in a similar way as described by Lambe et al., (2007). Since no direct measurement of OH radicals was available the OH radical concentrations generated in the simulation chamber were calculated from the measured depletion of the OH tracer 3-pentanol. Once characterised the dark OH source was used in ageing experiments on SOA material formed by ozonolysis of α-pinene and limonene under simulated tropospheric conditions in the large aerosol & cloud chamber AIDA on time scales of up to 30 hours and at temperatures between 253 and 313 K. The organic aerosol was generated by controlled oxidation with an excess of ozone and the aerosol mass concentrations were calculated from size distributions measured with differential mobility analysers (SMPS, TSI, 3071). Various instruments were used to measure the time evolutions of hydrocarbons (PTR-MS, FTIR), ozone (UV-absorption), aerosol mass & size (TOF-AMS, SMPS), number concentrations (CPC), and volatility (VTDMA). The experimental results were analysed using the aerosol behaviour code COSIMA (Naumann, 2003), supplemented by a recently developed SOA module.

According to the model analysis the OH radical levels in the AIDA chamber from ozonolysis of TME have been around some times 10^6 cm^{-3} depending on the experimental conditions. Generating the OH radicals this way in the presence of SOA from ozonolysis of α-pinene and limonene resulted in additional formation of SOA mass in the order of 10-20% within two hours or less, in agreement with the predictions of numerical simulations. The additional mass formed is smaller for lower temperatures.
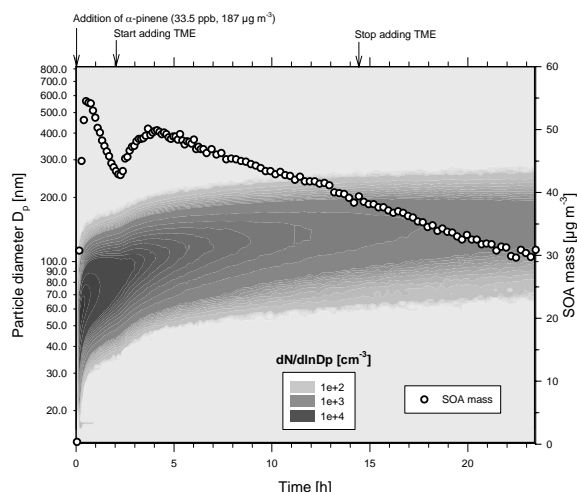
Figure 1. Evolution of size distribution and mass concentration of SOA formed by ozonolysis of α-pinene and aged with OH radicals from TME oxidation at 293.4 K.

For an experiment with SOA from α-pinene ozonolysis Figure 1 shows the evolution of the particle size distribution measured (SMPS) and the particle mass concentration calculated by integration of the volume size distribution using a particle density of 1.25 g cm^{-3}. Arrows indicate the start and end of OH radical generation by TME ozonolysis with an excess of 500 ppb of ozone. Please note that already during ozonolysis of the terpene OH radicals are formed which strongly influence yield and properties of the SOA particles.

Lambe, A. T., Zhang, J. Y., Sage, A. M., Donahue, N. M. (2007) *Environ. Sci., & Technol.,* 41, 2357-2363.

Naumann, K.-H. (2003) *J. Aerosol Science*, 34, 1371-1397.

Saathof f H., Naumann K.-H., Möhler O., Jonsson Å. M., Hallquist M., Kiendler-Scharr A., Mentel T., Tillmann R., Schurath U. (2008) *Atmos. Chem. Phys. Discuss.* 8, 15595-15664.

Tsigaridis, K., Lathiere, J., Kanakidou, M., Hauglustaine, D. A. (2005). *Atmospheric Chemistry and Physics*, 5, 1891-1904.

Primary organic aerosol and secondary aerosol formation potential from a Euro 3 diesel car during smog chamber experiments

R. Chirico, P.F. DeCarlo, M.F. Heringa, T. Tritscher, E. Weingartner, A.S.H. Prevot, and U. Baltensperger

Laboratory of Atmospheric Chemistry, Paul Scherrer Institut, 5232 Villigen PSI, Switzerland

Keywords: diesel emissions; primary organic aerosols; secondary organic aerosols; aerosol mass spectrometry

Particulate matter (PM) measurements operated with low dilution ratios likely overestimate the emitted fine particle mass: Recent findings have shown that the PM mass concentration of particles with a diameter lower than 2.5 µm ($PM_{2.5}$) emitted by a diesel power generator can decrease by 50% when the dilution ratio is increased from 20:1 to 350:1 (Lipsky and Robinson, 2006). The reason for the $PM_{2.5}$ mass reduction has been associated to the repartitioning of semi-volatile organic compounds (SVOCs) to the gas phase (Lipsky and Robinson, 2006). In the atmosphere SVOCs are involved in photochemical reactions and the products generated with low vapor pressure will partition to the particulate phase and contribute to the mass of the secondary organic aerosol (SOA).

Investigations of the contribution of exhaust from a EURO 3 diesel passenger car to primary organic aerosol (POA) and to SOA during smog chamber experiments will be presented. The experiments were carried out in the smog chamber of the Paul Scherrer Institute (PSI) where diesel exhaust was introduced into the chamber with an injection system developed to obtain a representative sample of the diesel exhaust into the chamber. An Aerodyne high-resolution time-of-flight aerosol mass spectrometer (HR-ToF-AMS) was used for the experiments to quantify the organic aerosol while black carbon (BC) concentrations were measured with an aethalometer (Magee Scientific Company, Berkeley, CA).

Primary diesel emissions at idle mode and 60 km/h speed consist mainly of BC with a low fraction of organic aerosol. Figure 1 shows the temporal evolution of the wall loss corrected organic aerosol mass loading for a typical experiment at idle mode. To take into account the wall losses, the organic aerosol produced by photo-oxidation was calculated by multiplying the OA concentration, measured at time t, by a factor calculated from the ratio of the initial BC concentration versus BC concentration at time t. The initial BC concentration was 27.5 µg/m^3 and the initial OM concentration, corresponding to POA, was ~7.5 µg/m^3. At time zero,

the lights were turned on and the photochemistry started producing SOA. After around 3 hours a plateau was reached and the organic matter estimated was ~30 µg/m^3. The temporal evolution of the OM/BC ratio is also shown. At time zero the OM/BC ratio was 0.3. With the lights on this ratio increased by nearly a factor of 3.6 until a constant value around 1.1 was reached.
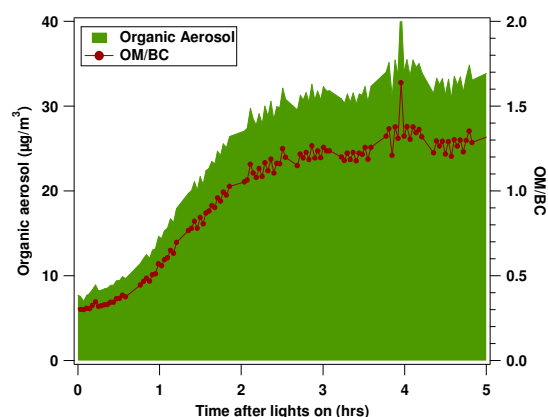
Figure 1. Temporal evolution of OA and of OM/BC ratio during a photo-oxidation experiment at idle mode

Even if newer European directives have introduced increasingly stringent standards for primary PM emissions, gaseous organics emitted from a Euro 3 diesel car could still lead to large amounts of SOA in today's atmosphere. The formation of SOA is much higher than previously thought leading to the question if in addition to the primary aerosol emissions also the emissions of precursors for organic aerosols should be regulated.

References
Lipsky, E. M., and Robinson, A. L. (2006). Environ. Sci. Technol., 40, 155-162.

HULIS characterisation and attribution to potential source by UV-Vis measurement

C. Baduel[1] , D. Voisin[1] , J.L. Jaffrezo[1], I. El Haddad[2], N. Marchand[2], M.B. Perrtsonnaz[3] , and D. Robin[4]

[1]Laboratoire de Glaciologie et Géophysique de l'Environnement, Université Joseph Fourier, 54 rue Molière, 38402, Saint Martin d'Hères, France.
[2]Laboratoire Chimie Provence, Universités d'Aix-Marseille, 3 place Victor Hugo, 13331, Marseilles, France.
[3]ASCOPARG, 44 av. Marcellin Berthelot, 38100, Grenoble, France.
[4]Atmo PACA, 146 rue Paradis, 13006, Marseilles, France.

Keywords: HULIS, Water Soluble Organic Carbon, Absorption, Source identification, Aerosol evolution.

Many studies have shown that "HUmic LIke Substances" (HULIS) may represent a significant fraction (between 15 and 40 % in mass) of the organic carbon (OC) of atmospheric aerosols. Research on atmospheric HULIS is characterized by the lack of knowledge of their sources. Variations of their concentration and characteristic during yearly monitoring are ascribed to variability in the sources and formation processes, with the hypotheses that HULIS may be generated through various chemical pathways and consist in a mixture of primary and secondary products (Graber & Rudich, 2006).

In this study we investigate the temporal and structural variation of the HULIS fraction collected in different environments and the possibility of using UV-Vis measurement to identify the potential sources of HULIS.

HULIS fractions are isolated with a selective extraction scheme with DEAE anionic exchange resin complemented by carbon quantification with DOC analyser. UV spectroscopy is performed on line for the chemical characterisation of HULIS. UV absorbance of theses compounds in function of their carbon mass give an indication on their chemical structure (relative aromaticity). Strong difference of the optical properties and therefore of the chemical structure between HULIS formed during summer- and wintertime is found for urban background samples. This difference highlights the different seasonal processes responsible for emissions and formation of HULIS (Figure 1).

Characteristic specific absorbencies of HULIS compounds were also observed for different aerosol sources: biomass burning, fossil fuel combustion, marine, and secondary formation from anthropogenic and biogenic. Backward trajectory analysis allowed the selection of a representative sample set of marine and anthropogenic conditions for samples collected in Marseilles during the FORMES program. Other samples representative of biomass burning aerosol were collected in very close proximity to combustion-generated aerosol activity.

Functional analysis was performed by APCI/MS/MS to investigate the chemical composition of organic aerosol in terms of functional group quantification. This new approach enables to group chemical compounds by their ability to loose a known neutral molecular fragment for neutral loss

mode or to produce a characteristic ion in the collision cell for the precursor ion scanning mode. This analysis allows a quantitative determination of total carbonyls, carboxylic and nitro groups and provides an apparent molecular weight distribution of the compounds bearing the function under study. Comparisons between functional groups contents and UV absorbance of HULIS will be presented in order to investigate chemical modification of high molecular weight compounds as a function of sources and ageing processes.
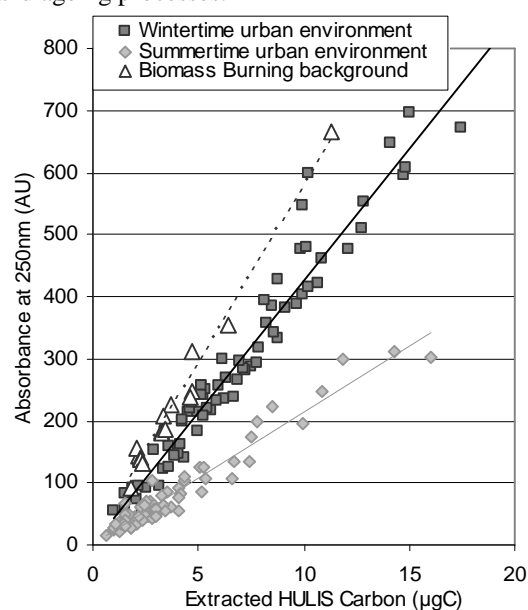
Figure 1: Variation of HULIS structure (relative aromaticity) in function of the extracted HULIS carbon mass for different backgrounds.

Graber, E. R., & Rudich, Y. (2006). *Atmos. Chem. Phys.,* 6, 729-753.

Size distribution of EC and OC in the aerosol of urban areas in France during summer and winter.

J.L. Jaffrezo[1], D. Voisin[1], C Baduel[1], N. Marchand[2], M.B. Personnaz[3], and D Robin[4]

[1]Laboratoire de Glaciologie et Géophysique de l'Environnement, Université Joseph Fourier, 54 rue Molière, 38402, Saint Martin d'Hères, France.
[2]Laboratoire Chimie Provence, Universités d'Aix-Marseille, 3 place Victor Hugo, 13331, Marseilles, France.
[3]ASCOPARG, 44 av Marcellin Berthelot, 38100, Grenoble, France.
[4]Atmo PACA, 146 rue Paradis, 13006, Marseilles, France.

Keywords: Secondary organic aerosols, Special field campaigns, Physical properties

Samples were collected for the determination of EC and OC size distributions during the intensive sampling campaigns of the FORMES program, in urban background areas, in summer 2008 in Marseilles and in winter 08-09 in Grenoble. The comparison of concentrations obtained for samples collected in parallel with impactor- and filter-based methods indicates that the correction of pyrolysis seems to work for the impactor samples despite non even deposits. The size distributions of EC and OC present large differences between the two campaigns. In winter, an overwhelming proportion of the mass fraction for both species is found in the droplet and accumulation modes. In summer, the changes are more drastic with a much larger fraction in the supermicron / coarse mode. The calculation of the EC/OC ratio gives some indications that the different modes are related to various emission / evolution processes. In much the same way, the evolution, according to size distribution, of the fraction of the OC of decreasing volatility obtained during the thermal analysis is an indication of pronounced changes in the characteristics of the carbonaceous matter in each mode.

Acknowledgements
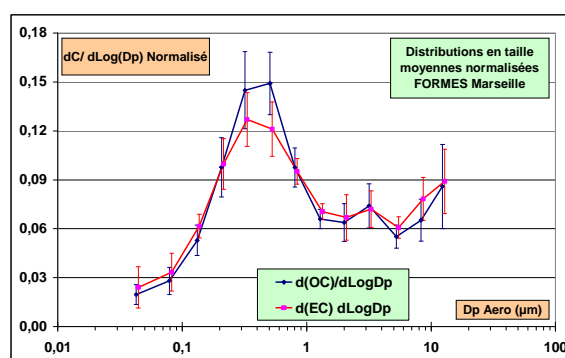
Figure 1: average normalized daily size distribution of OC and EC concentrations for 15 daily samples collected in suburban Marseilles (France) during summer 2008.
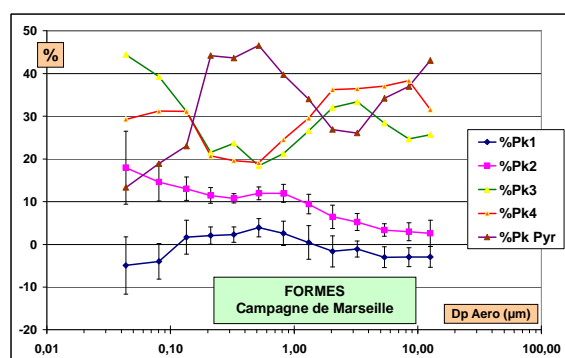
Figure 2: average size distribution of fraction of OC thermal peaks for 15 daily samples collected in suburban Marseilles (France) during summer 2008.

Formation of secondary organic aerosol in the presence of organic seeds: Evaluating the mixing of organic aerosol components using high-resolution aerosol mass spectrometry

Lea Hildebrandt*[1], Kaytlin Henry[1], Jesse H. Kroll[2], Marissa A. Miracolo[1], Allen L. Robinson[1], Spyros N. Pandis[1,3], Neil M. Donahue[1]

[1] Center for Atmospheric Particle Studies, Carnegie Mellon University, Pittsburgh, PA 15213, USA
[2] Dept. of Civil and Environmental Eng., Massachusetts Institute of Technology, Cambridge, MA 02139, USA
[3] Institute of Chemical Engineering and High Temperature Chemical Processes (ICE-HT), Foundation of Research and Technology (FORTH), Patra, Greece

Keywords: AMS, laboratory experiments, mixing state, organic aerosols, PMF

According to the pseudo-ideal-mixing assumption employed in practically all chemical transport models, organic-aerosol components from different sources mix ideally. As a result of this assumption, secondary organic aerosol (SOA) yields predicted by models depend strongly on the amount of total organic aerosol present in the system and not on the origin or chemical nature of the components e.g. biogenic SOA (BSOA), anthropogenic SOA (ASOA) or primary organic aerosol (POA). Recent studies measuring SOA yields in the presence of POA have challenged this assumption (Song *et al.*, 2007). We investigate the mixing of different types of organic aerosol using an isotopically labeled compound and a High Resolution Time-of-Flight Aerosol Mass Spectrometer (HR-AMS) from Aerodyne, Inc. (DeCarlo *et al.*, 2006). The HR-AMS is able to distinguish between mass spectral peaks at the same nominal *m/z*. We use this capability to distinguish ^{13}C-containing and ^{12}C-containing mass fragments.

Experiments were performed in Carnegie Mellon's environmental chamber to form ASOA from isotopically labeled toluene (^{13}C-toluene), and non-labeled BSOA from α-pinene or limonene, or non-labeled POA from diesel exhaust. These experiments thus allow us to investigate the mixing of ASOA/BSOA and ASOA/POA by comparing SOA yields in the presence of organic precursor seed to the yields in the presence of inorganic, non-reactive seed.

We use, compare and discuss three approaches to extract the labeled and non-labeled organic mass spectra. The first method identifies all of the peaks corresponding to organic fragments containing ^{13}C, and those containing only ^{12}C. The sum of these fragments should correspond to the ^{13}C-toluene aerosol vs. the non-labeled organic aerosol, respectively. The second method uses positive matrix factorization (PMF) on the mass spectra, an increasingly popular method used to extract the mass spectra of different types of

organic aerosol (Ulbrich *et al*., 2008; Zhang *et al.*, 2005; Zhang *et al.*, 2007). By applying PMF to the unit mass resolution (UMR) data and the high resolution (HR) data, we can infer how much additional information the HR data provide and whether these experiments could also be conducted with a UMR instrument. Finally, the third method separates the organic mass spectra by using the known organic mass spectra of the different types of organic aerosol (e.g. the ^{13}C-toluene spectrum and the α-pinene spectrum) and reconstructing the observed, mixed organic mass spectrum as a linear combination of the two known mass spectra.

Preliminary results suggest that the separation of the organic mass spectra is possible and that the results from the three methods agree. We can thus calculate the mass yield of one type of aerosol in the presence of the other and compare these yields to the yields in the presence of inorganic seed (Hildebrandt *et al.*, 2009). This allows us to infer the extent of mixing of the different types of organic aerosol. The results of this analysis for the different mixtures investigated will be discussed.

DeCarlo, P. F. *et al.* Analytical Chemistry, 78, 8281-8289, 2006.

Hildebrandt, L., Donahue, N.M., and Pandis, S.N. Atmospheric Chemistry and Physics Discussions, 693-733, 2009.

Song, C. *et al.* Geophysical Research Letters, 34, 2007.

Ulbrich, I. M. *et al.* Atmospheric Chemistry and Physics Discussions, 8, 6729-6791, 2008.

Zhang, Q. *et al.* Atmospheric Chemistry and Physics, 5, 3289-3311, 2005.

Zhang Q. *et al.* Geophysical Research Letters, 34, 2007.

Study of Nucleation Processes Involved in SOA Formation

From the Ozonolysis of a Biogenic Compound in a Smog Chamber

Y. Katrib[1], J. Boulon[2], K. Miet[1], J. Wang[1], M. Attoui[3], K. Sellegri[2] and J.F. Doussin[1]

[1] Laboratoire Inter-Universitaire des Systèmes Atmosphériques , Universités Paris 7 et 12, 94010 Créteil, France
[2] Laboratoire de Météorologie Physique, UBP/CNRS/OPGC, 63177 Aubière, City, France
[3] Département de Physique, Université Paris 12, 94010 Créteil, France

Keywords: SOA, yields, growth, nucleation.

In this study the nucleation processes involved in new particle formation in smog chambers are investigated. Secondary Organic Aerosols (SOA) are formed from the ozonolysis of a biogenic compound, sabinene, using two different ozone generating systems: a UV lamp and a corona barrier discharge. The studies are conducted in a 4.2m^3 stainless steal simulation chamber called CESAM (Multiphase Atmospheric Experimental Simulation Chamber). (Wang et al) A Scanning Mobility Particle Sizer (SMPS) and a Neutral Air Ion Spectrometer (NAIS) are directly connected to the chamber (in parallel to different gas analysers).

In all experiments, 100ppb of sabinene and 100ppb of ozone are mixed in the chamber. Two types of ozone are produced: "fresh" ozone is referred to experiments where sabinene is rapidly injected afterwards in the chamber whereas "aged" ozone corresponds to experiments where sabinene is injected much later (several hours). In addition, the ionisation power of the ozone generating systems is varied while keeping all experimental conditions identical (concentrations, etc.)

The ozone generating system and its ionisation power are found to have a strong impact on SOA properties (e.g. SOA mass yields can vary up to a factor of 3 while increasing the ionisation power). Ozone ageing experiments also impact SOA properties (e.g. the mass yields decrease with ageing).

Furthermore, since the NAIS is capable of detecting neutral particles from 2 nm (Figure 1), we also provide calculations of nucleation rates (J_2) and growth rates (GR). The impact of the ozone type and age is examined for both parameters separately. In addition to that, the use of the NAIS gives us insight on the very first steps of the nucleation process.

To our knowledge, this is the first time that such information is obtained in a well defined smog chamber.
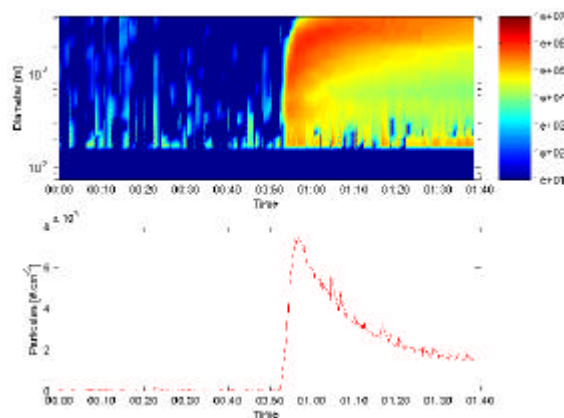
Figure 1: Aerosol size distribution as a function of time measured with a NAIS during the ozonolysis of sabinene, when ozone is produced by a 2W corona barrier discharge.e

Wang et al, *Design of an Experimental Simulation Chamber for Investigating Atmospheric Multi-Phase Chemistry*. In press.

Oligomerization from methylglyoxal: a potential mechanism for secondary organic aerosol formation in a simulated cloud model

Y. Farhat[1], N. Sauret[1], M. Claeys[2], P.C. Maria[1], L. Massi[1]

[1]Laboratoire de Radiochimie, Sciences Analytiques et Environnement (LRSAE),
Université de Nice Sophie-Antipolis, Institut de Chimie de Nice, Parc Valrose, F-06108 Nice, France
[2] Department of Pharmaceutical Sciences, University of Antwerp (Campus Drie Eiken),
Universiteitsplein 1, BE-2610 Antwerp, Belgium

Keywords: secondary organic aerosol, oligomers, β-hydroxy ketone, mass spectrometry, clouds.

Methylglyoxal is an important intermediate in in-cloud reactions of many reactive organics (Lim et al., 2005). Fu et al. (2008) have constructed a global budget of atmospheric glyoxal and methylglyoxal with the goal of quantifying their potential for global secondary organic aerosol (SOA) formation via irreversible uptake by aqueous aerosols and clouds and estimated an annual production of 140 Tg for methylglyoxal. Biogenic isoprene is the most important precursor of methylglyoxal and contributes globally with about 79%, while the second most important precursor is acetone (mostly of biogenic origin). The atmospheric lifetime of methylglyoxal is estimated at ~1.6 h; it undergoes photolysis and oxidation by the OH radical, but can also be taken up in the aqueous aerosol phase and cloud droplets on account of its high water solubility (Betterton et al., 1988; Zhou et al., 1990).

To ascertain the fate of methylglyoxal (MG) in view of its short life time in the atmosphere, dark chamber experiments were carried out in a light protected conductivity cell (175 mL) under simulated cloud conditions (pH = 2-4, T = 14-15 ºC, [MG] = 10^{-3} M, [SO_4^{2-}] = 10^{-4} M, [NH_4^+] = 10^{-3} M). Sample aliquots were collected at regular intervals, diluted with methanol (1:1 ratio) and analyzed by electrospray ionization - mass spectrometry (ESI-MS) in both negative and positive ion modes with an LCQ ion trap instrument (Thermo Fisher). The samples were introduced by direct infusion at a flow rate of 5 µL/min. Other instrumental parameters were: ion spray voltage, 4 kV; and capillary temperature, 250 ºC. In addition, liquid chromatography(LC)/ESI-MS data was acquired using an LXQ linear ion trap instrument (Thermo Fisher). A classical reverse phase C18 column (ODS Hypersil; 3 x 250 mm, 3 µm bonded silica) with a gradient profile was used to achieve chromatographic separation of the oligomers.

Soluble oligomers (n=1-12) formed in the course of acid-catalyzed aldol condensation were detected and identified by positive and negative ion ESI-MS as shown in Figure 1. Their relative abundance was estimated from the full-scan mass spectra. Special emphasis was given to the structural elucidation of abundant oligomers and their corresponding adduct products. The oligomer series starts with a β-hydroxy ketone via aldol condensation and oligomers are formed by multiple addition of

$C_3H_4O_2$ units (72 Da) to the parent β-hydroxy ketone. Furthermore, MS^2 ion trap experiments were performed to structurally characterize the oligomers.

It was found that oligomers form under conditions encountered in clouds even at micromolar concentrations and thus could result in significant SOA formation after cloud droplet evaporation. It is proposed that oligomer formation does not only occur during droplet evaporation when the concentrations of products increase but could also be an in-cloud process and substantially enhance in-cloud SOA yields.
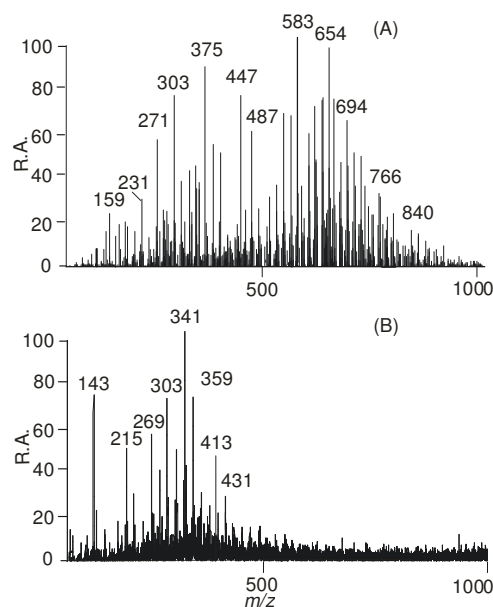
Figure 1. (A): (+)ESI-MS and (B): (-)ESI-MS spectra after reacting methylglyoxal for 1 h.

Betterton, E. A., et al. (1988). *Environ. Sci. Technol.*, 22, 1415-1418.

Lim, H. J., et al. (2005). *Environ. Sci. Technol.* 2005, 39, 4441-4446.

Fu, T. M., et al. (2008). *J. Geophys. Res.* 113, D15303, doi:10.1029/2007JD009505, 2008.

Zhou, X., et al. (1990). *Environ. Sci. Technol.*, 24, 1482-1485.

Nucleation processes during the ozonolysis of alkenes and carboxylic acids under kinetically controlled conditions

J.L. Wolf, C. Keunecke and T. Zeuch

Institut für Physikalische Chemie, Georg-August Universität, Tammannstr. 6, 37077 Göttingen, Germany

Keywords: Aerosol Chemistry, Organic Aerosols, Nucleation, Numerical Simulation.

Over the years, many efforts have been made to unravel the nucleation mechanisms during alkene ozonolysis in laboratory or smog chamber studies. Most of the studies were focussed on terpene ozonolysis with respect to their high biogenic abundances. For α-pinene and β-pinene effects on secondary organic aerosol (SOA) formation have been studied with respect to alkene structure, OH initiated or influenced oxidation, humidity, and seed aerosol. It has been shown that simplified oxidation and nucleation models can predict some of these effects. In most of these studies the secondary organic aerosol formation mechanism is assumed to follow the traditional picture, where multifunctional low volatility products are formed during ozonolysis under supersaturated vapour conditions, high enough to initiate homogenous nucleation.

In the past decade the role of heterogeneous chemistry in aerosol formation emerged. Recently, Bonn et al. proposed a mechanism for organic nucleation involving secondary ozonides as nuclei being activated by heterogeneous reactions with peroxy radicals (RO_2). Heaton et al. showed that oligomers are formed in very early stages of SOA formation suggesting that a mechanism of only a few steps is governing the gas to particle phase transfer.

In order to evaluate kinetic aspects of the gas phase chemistry for organic particle formation, we performed a series of ozonolysis experiments with the model alkenes methylcyclohexene (endocyclic double bond, abbreviated as "MCHe" in figure 1) and methylenecyclohexane (exocyclic double bond, "MCHa"). The use of these alkenes instead of terpenes is appropriate for our objective owing to their comparable reaction rate constants for ozonolysis but much larger vapour pressures at room temperature. This allows the use of much higher initial reactant concentrations compared to pinenes. Aditionally, the rate constants for both alkenes differ by a factor of 15, making them ideal candidates for studying kinetic effects.

The experiments were performed in a 5 L reactor using FTIR spectroscopy (Bruker IFS66) for gas phase educt and product analysis and a SMPS (TSI 3936) for the identification of particle size distributions. Either synthetic air or nitrogen were used as bath gas (1bar). Our experiments reveal an unexpected feature of alkene gas phase ozonolysis, which has not been reported yet. For both alkenes a drastic drop in total particle number density is seen for increased relative alkene concentrations (figure 1).
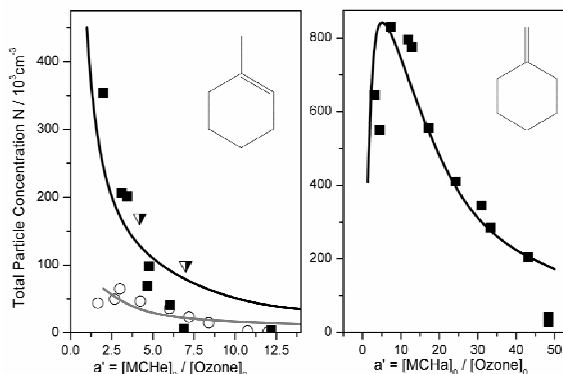
Figure 1. This figure illustrates the dependence of the newly formed total particle concentration on the alkene / ozone concentration ratio (5 ppm ozone constant). Squares stand for experiments, the line for numerical simulation based on simplified nucleation mechanism (for more detail see ref. Wolf et al).

These observations can be rationalized by assuming that ozone or transient species closely coupled to ozone concentrations are involved in the nucleation process. Peroxyradicals as proposed by Bonn et al. can fulfil this capacity. By following this proposal we were able to develop a simplified nucleation mechanism, which nicely predicted the experimental results (lines in figure 1). In contrast to these findings ozonolysis experiments with unsaturated carboxylic acids (methacrylic acid) show a different behaviour, indicating, that a different nucleation mechanism, applies much less depending on RO_2 radicals.

Bonn, B., Korhonen, H., Petäjä, T., Boy, M., Kulmala, M. (2007). *Atmos. Chem. Phys. Discuss.*, 7, 3901-3939.

Heaton, K. J., Dreyfus, M. A., Wang, S., Johnston, M. V. (2007). *Environ. Sci Technol, 41,* 6129-6136.

Wolf, J. L., Suhm, M. A., Zeuch, T. (2009). *Angew. Chem.*, DOI:10.1002/anie.200805189.

Photochemical strength index of size-segregated suburban aerosol during the different air qualities

Su-Ching Kuo[1], Chien-Lung Chen[2], Li-Ying Hsieh[3] and Ying I. Tsai [4,*]

[1] Department of Applied Chemistry, Chia Nan University of Pharmacy and Science, Tainan 717, Taiwan
[2] Department of Finance, Fortune Institute of Technology, Kaohsiung 831, Taiwan
[3] Department of Chemistry, National Cheng Kung University, Tainan 701, Taiwan
[4,*] Department of Environmental Engineering and Science, Chia Nan University of Pharmacy and Science, Tainan 717, Taiwan

Keywords: Dicarboxylic acids; Nanoparticles; Oxalic acid; Malonic acid; Succinic acid; Suburban Aerosol.

1. Introduction

Atmospheric aerosol water-soluble species content in the nano/micron size range has received much attention (Sun and Ariya, 2006; Hsieh et al., 2007; Zhao and Gao, 2008). In this study, two indices were used for judging photochemical strength. One, the mass ratio of malonic acid to succinic acid (M:S mass ratio), indicates the atmospheric photochemical formation potential or the traffic-related emission potential. An M:S mass ratio > 3.0 indicates that photochemical formation potential is higher whilst one between 0.3-0.5 indicates that traffic-related emission potential is higher. The other parameter is the concentration ratio of oxalic acid to sulfate (ox/sulfate ratio).

2. Methodology

The sampling location was in suburban Tainan, southern Taiwan. Size-segregated aerosol sample sets were collected in a non-episodic pollution period (September to October 2004) and during a PM episode (late November 2004). Samples were collected using a MOUDI (Model 110, MSP), combined with a downstream Nano-MOUDI (Model 115). Collected particles were divided into four size modes: the *nuclei* mode, the *condensation* mode, the *droplet* mode, and the *coarse* mode, representing particle sizes of 5-100 nm, 0.10-0.32 μm, 0.32-2.5 μm, and 2.5-100 μm, respectively. Samples were analyzed following the method of Hsieh et al. (2007).

3. Results and Discussion

Figure 1 shows M:S mass ratios in the four size distribution modes and the nano/micron size range during both periods. The mean nano/micron M:S ratio was 0.89 for the non-episodic period and 0.92 for the PM episode, indicating potential for both photochemical formation and onset of traffic-related emission. Of the four size modes, the higher potential photochemical formation was seen mainly in the droplet mode. Higher traffic-related formation potential was observed in the condensation mode. Intermediate M:S mass ratios in the nuclei mode indicate that both photochemical end products and traffic-related pollutants co-exist in this mode.

Figure 2 shows the ox/sulfate ratio for nano/micron particulate. Oxalic acid accounted for 6.23% of the total oxalic acid – sulfate during the PM episode and 5.88% during the non-episodic period. This indicates that the atmospheric photochemical environment was more favorable to the formation of oxalic acid during the PM episode than during non-episodic pollution. Furthermore, during the PM episode, the ox/sulfate ratio for all particle sizes except 18 nm in the 5-100 nm particle size range was 40.2-82.3%, suggesting a stronger potential for oxalic acid formation in the nuclei mode than sulfate. Additionally, the ox/sulfate ratio at 32 nm suddenly increased to 82.3%, higher than in the nano/micron particle size range, suggesting that the production and accumulation of sulfate and oxalic acid was very different. The final product of photochemical reaction, i.e. sulfate, mainly forms and accumulates in these condensation and droplet modes.
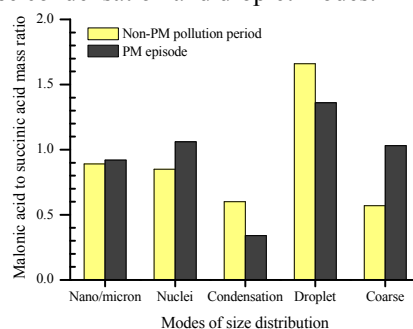
Figure 1. M:S mass ratio in suburban atmospheric aerosols.
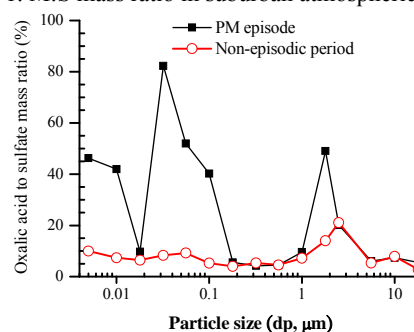
Figure 2. Comparison of mean mass ratio of oxalic acid to sulfate in suburban aerosols.

Hsieh, L.-Y., Kuo, S.-C., Chen C.-L., & Tsai, Y.I. (2007). *Atmos. Environ.* 41, 6648-6661.
Sun, J., & Ariya, P.A. (2006). *Atmos. Environ.* 40, 795-820.
Zhao, Y., & Gao, Y. (2008). *Atmos. Environ.* 42, 4063-4078.

Sources of fine particulate organic matter in a Mediterranean urban area: Marseilles

I. El Haddad[1], N. Marchand[1], B. Temime-Roussel[1], H. Wortham[1], C. Piot[2], A. Albinet[2], J.L. Besombes[2], J.L. Jaffrezo[3]

[1] Laboratoire Chimie Provence (UMR 6264), équipe Instrumentation et Réactivité Atmosphérique, Universités d'Aix-Marseille I, II et III-CNRS, 3 place Victor Hugo, 13331 Marseille Cedex 3
[2] Laboratoire de Chimie Moléculaire et Environnement, Polytech'Savoie- Université de Savoie, Campus Scientifique, 73376 Le Bourget du Lac Cedex, France
[3] Laboratoire de Glaciologie et Géophysique de l'Environnement (UMR 5183), Université Joseph Fourier-CNRS, Rue Molière, BP 96, 38 402 St Martin d'Hères Cedex France.

Keywords: Source apportionment, molecular tracer, Mediterranean urban area

Particulate organic matter (POM) in atmospheric aerosols contributes in approximately 20 to 50% of the total fine aerosol mass at continental mid-latitude (Kanakidou *et al.*, 2005). Several epidemiological studies had associated this class of particulate material with adverse effects on human health (Grahame and Schlesinger, 2007). POM results from primary emissions as well as in situ formation through oxidative processes of gas-phase organic compounds. In order to reduce ambient particles concentrations, an accurate knowledge of the relative contribution of their different sources is required.

During the ESCOMPTE-2001 experiment, evidence has been brought of a large fraction of secondary organic aerosols (SOA) photo chemically produced in the region of Marseilles, a French Mediterranean urban area, pointing out the need for a better characterization of these particles. In this context, a field campaign was carried out at an urban background site of Marseilles in July 2008, within the FORMES program, to estimate the respective influences of the main aerosol sources. More than 70 organic markers including hopanes/steranes, PAH, n-alkanes, phthalate esters, steroids, sugars and sugar anhydrides, and various carboxylic acids were measured.

Figure1 shows the variation of two selected individual organic compounds, Hopane (vehicular marker) and Bis(2-ethylhexyl)phthalate (plasticizer) plotted along with the $PM_{2.5}$ concentrations. The Bis(2-ethylhexyl)phthalate was one of the most abundant organic compounds with concentrations ranging between 1.7 and 25.6 $ng.m^{-3}$. This compound shows a diurnal variation, with higher concentrations during the day, which may be caused by its enhanced emission from plastics with the ambient temperature (Staples *et al.*, 1997). Hopane concentrations present a large variation during the measurement period with concentrations ranging from 0.09 and 0.54 $ng.m^{-3}$, accounting for 0.02 and 0.07 $mg.g^{-1}$ of OC. These are relatively small contributions to OC in an urban area, with no impact from wood combustion. This indicates the inputs from other sources to OC, including most likely primary emissions from regional activities such as ports, industries and petrochemical complex in addition to secondary processes.
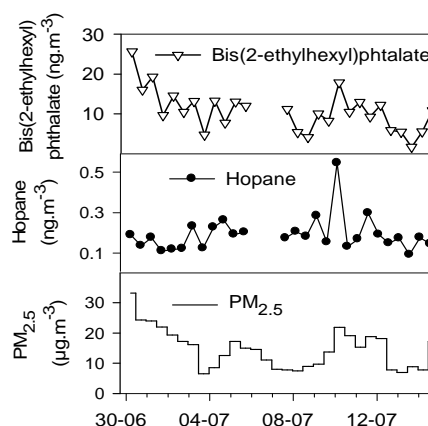
Figure1: $PM_{2.5}$, Hopane and Bis(2-ethylhexyl)phthalate concentrations during the field campaign in Marseilles, July 2008.

Results of source apportionment using receptor based models will be presented together with the variations of secondary organic markers encountered during different meteorological conditions in the campaign.

Kanakidou,M., Seinfeld,J.H., Pandis,S.N., Barnes,I., Dentener,F.J., Facchini,M.C., Van-DingenenR., Ervens,B., Nenes,A., Nielsen,C.J., Swietlicki,E., Putaud,J.P., Balkanski,Y., Fuzzi,S., et al. (2005). *Organic aerosol and global climate modelling: a review.* Atmospheric Chemistry and Physics, 5, 1053-1123.

Grahame,T.J., Schlesinger,R.B. (2007). *Health effects of airborne particulate matter: Do we know enough to consider regulating specific particle types or sources?* Inhalation Toxicology, 19 (6-7), 457-481.

Staples,C.A., Peterson,D.R., Parkerton,T.F., Adams W.J. (1997). *The environmental fate of phthalate esters: a literature review.* Chemosphere, 35 (4), 667-749.

Determination of low-molecular-weight dicarboxylic acids in atmospheric aerosols: comparison between silylation and esterification derivatisation procedures for GC-MS analysis

D. Bacco[1], M.C. Pietrogrande[1],

[1]Department of Chemistry, University of Ferrara, Ferrara, I-44100, Italy

Keywords: dicarboxylic acids, derivatisation, GC-MS, PM, source apportionment.

Aliphatic dicarboxylic acids are one of most important components of water-soluble organics in atmospheric aerosol: they can derive from primary emissions from biomass burning and fossil fuel combustion, as well as photochemical oxidation of organic precursors of both anthropogenic and biogenic origin. Therefore, a detailed investigation on concentrations and relative abundance of these compounds can help us to evaluate the importance of secondary photochemical reactions.

In particular low-molecular-weight (LMW) dicarboxylic acids (C_3-C_{10}) gives important chemical information for source apportioning of aerosol organics and for studying atmospheric processes leading to secondary organic aerosol formation: the C_3/C_4 ratio has been suggested as indicator of enhanced photochemical production of dicarboxylic acids in the atmosphere and the C_6/C_9 ratio may be assumed as a potential indicator of source strength of anthropogenic and biogenic precursors to the aerosol diacids (Kawamura et al., 2005).

To date, GC-MS is the method of choice for characterizing individual organic compounds within aerosol samples, primarily because shows sensitivity, precision and accuracy required in environmental studies. The high polarity and low levels of carboxylic acids pose special challenges for their identification and quantification because require preliminary chemical derivatisation, i.e., conversion to less polar compounds to be eluted through a GC column.

Two derivatisation processes using different reagents and catalysts have been developed and widely used over the years for dicarboxylic acid determination in PM samples (Manish et al., 2007):
1) esterification of the acid groups using methanol or 1-butanol as derivatising agents in the presence of a Lewis acids (often BF_3) as catalyst:
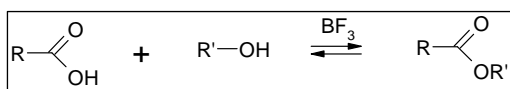
2) silylation based on a silylation reagent that introduces $-Si(CH_3)_3$ groups in the molecules, (Figure 2), i.e., N,O-bis(trimethylsilyl)-trifluoroacetamide (BSTFA) to form trimethylsilyl (TMS) derivatives (Zampolli et al., 2006).
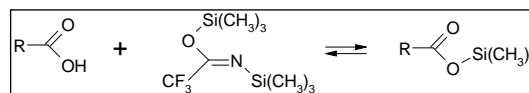
This paper is focused on the determination of LMW dicarboxylic acids (C_3-C_{10}): the most widely used procedures, i.e., esterification with butyl alcohol and BF3 like catalyst and a silylation with N,O-bis-(Trimethylsilyl)trifluoroacetamide (BSTFA) and trimethylchlorosilane (TMCS), were investigated. For each method, the effect of various experimental parameters on the reaction yield has been investigated and optimized: time and temperature, or amount of reagents. The better procedure was searched for the faster one-step derivatisation to determine C_3-C_{10} dicarboxylic acids as target compounds.

The advantages and drawbacks of the methods are investigated and compared in terms of precision and accuracy of the obtained results, sensitivity and detection limit of the procedure.

The obtained results show that the silylation procedure is the method more compatible with application to chemical analysis in PM samples: satisfactory precision and accuracy are obtained for all the studied acids at the sub-nmol level at which the dicarboxylic acids are expected to be present in trace levels (Manish et al., 2007). Butyl esters of low molecular weight dicarboxylic acids are too volatile to yield evaporative losses and too unstable to be accurately quantified so that quantification was possible for the C_4-C_9 dicarboxylic acids.

The precision and accuracy were investigated by comparing results obtained by the two procedures from the simultaneous analysis of dicarboxylic acids in the same $PM_{2.5}$ and PM_{10} samples.

Kawamura, A.K., Yasui, O. Atmospheric Environment, 39 (2005) 1945– 1960

Manish K. Shrivastava, M. K., Subramanian, R., Rogge, W.F., Robinson, A.L. Atmospheric Environment, 41 (2007) 9353–9369

Zampolli, M.G., Meunier, D., Sternberg, R., Raulin, F., Szopa, C., Pietrogrande, M.C., Dondi, F. Chirality, 18 (2006) 279-295.

Characterisation of particle-phase wood smoke tracer compounds in ambient air of a residential area

M.A. Bari[1], G. Baumbach[1], G. Scheffknecht[1] and B. Kuch[2]

[1] Department of Air Quality Control, Institute of Process Engineering and Power Plant Technology, Universitaet Stuttgart, Pfaffenwaldring 23, 70569 Stuttgart, Germany
[2] Institute of Sanitary Engineering, Water Quality and Solid Waste Management, Universitaet Stuttgart, Bandtaele 2, 70569 Stuttgart, Germany

Keywords: wood smoke, organic tracer, GC-MS, ambient air pollution.

With the increasing concern of global climate change, the interest in using wood as renewable fuel has been considered as sustainable energy source for domestic heating in every part of the world during winter especially, where wood is available. In residential villages of Germany, located in forest-rich areas, wood burning causes regional haze with high PM_{10} concentrations in the ambient air, resulting in significant annoyance and nuisance with complains among the inhabitants. To justify measures against this pollution, it was important to determine and characterise different wood smoke tracer compounds in the ambient air during winter in a residential area.

From November 2005 to March 2006 particle-phase PM_{10} samples were collected at a residential site Dettenhausen located in the "Naturepark Schoenbuch" near Stuttgart, Germany. Samples were extracted using toluene with ultrasonic bath and analysed by gas chromatograph-mass spectrometry (GC-MS). Altogether 26 organic compounds inlcuding retene, methoxyphenols, levoglucosan and dehydroabietic acid were detected and quantified in this study. The total methoxyphenol levels were in the range of 2–451 ng/m^3 with the highest concentrations occurring during winter inversion episodes ($PM_{10} = 60$–95 $\mu g/m^3$) in Dettenhausen. The ambient concentrations of different wood smoke tracers are shown in Table 1. Syringol and its derivatives are found in large amounts in hardwood combustion but no significant quantities are detected in softwood emissions. Whereas, guaiacol and its derivatives are emitted from both softwood and hardwood combustion with varying emission rates (Schauer *et al.,* 2001) and the concentrations of guaiacol derivatives are higher in the softwood smoke compared to hardwood smoke (Bari *et al.*, 2008). It was evident that in the ambient air, high concentrations of syringol derivatives and significant concentrations of guaiacol derivatives, dehydroabietic acid and retene were found, indicating the dominant influence of hardwood and softwood combustion to ambient PM_{10} load in the residential area. Levoglucosan was detected in all particle-phase ambient PM_{10} samples (Figure 1).

The characterisation of different wood smoke organic tracers allows to better assess the contribution of wood smoke to the winter ambient PM_{10} loadings in residential areas.

Table 1. Ambient concentrations of wood smoke tracer compounds.

Tracers	Mean (ng/m^3)	Range (ng/m^3)
Syringaldehyde	15.2	0.01–61
Acetosyringone	48.8	0.02–214
Syringylacetone	9.4	0.08–109
Propionylsyringol	9.9	0.01–46
Sinapylaldehyde	5.9	0.66–32
Vanillin	0.3	0.02–1.02
Acetovanillone	0.08	0.01–0.31
Guaiacylacetone	3.9	0.01–19
Coniferyldehyde	1.4	0.02–5.2
Levoglucosan	806	35–3223
Dehydroabietic acid	3.8	0.02–15
Retene	0.7	0.02–3.4
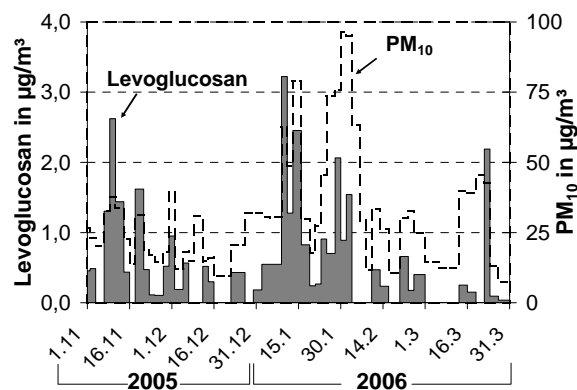
Figure 1. Temporal profile of ambient concentrations of levoglucosan and PM_{10}.

Schauer, J. J., Kleeman, M. J., Cass, G. R., & Simoneit, B. R. T. (2001). *Environ. Sci. Technol.*, 35, 1716-1728.
Bari, M. A., Baumbach, G., Kuch, B., & Scheffknecht, G. (2008). Atmos. Environ., Doi:10.1016/j.atmosenv.2008.09.006.

Biogenic contribution to particulate matter in Northern Italy

F. Bianchi[1], C. Abate[1], O. Cazzuli[3], P. Fermo[1], M. Ferri[2], A. Giudici[3], M. Lasagni[2], A. Piazzalunga[2], D. Pitea[2]

[1]Dep. Inorganic, Metallorganic and Analytical Chem., University of Milan, Via Venezian 21, 20133, Milan, Italy

[2]Dep. of Environmental Sciences, University of Milano-Bicocca, Piazza della Scienza 1, 20126, Milan, Italy
[3]ARPA Lombardia-Department of Milan, via Restelli 3/1, 20124, Milan, Italy

Keywords: biogenic contribution, alkenes, fatty acids, carbon, organic marker

Aerosol particulate matter carbonaceous fraction contains organic tracers that are characteristic of the sources, the formation and the transformation during atmospheric processes.

Organic matter in aerosol particles is due to four major sources depending on environmental conditions: (1) natural biogenic detritus (e.g. plant waxes, microbes, pollens, etc.), (2) anthropogenic emissions (oil combustion, soot, etc.), (3) biomass burning (natural and anthropogenic) and, in minor quantity, (4) soil organic matter.

Biogenic organic matter consists mainly of lipids, humic and fulvic acids, sterols, triterpenoids, sugars, n-alkanes, n-alkanols and n-alkanoic acids (Simoneit, 1999).

In this study we compare some approaches in order to estimate biogenic sources contribution using different bio-aerosol tracers: n-alkanes, fatty acids and Water Soluble Organic Compounds (WSOC).

High volume PM10 aerosol samples were collected during winter and spring in Milan and other sites placed in the Lombardy region (Northern Italy) having different geographical characteristics.

GC-MS analysis is a useful tool for the identification, characterization and quantification of homologous series (like n-alkanes and fatty acids) and it provides very relevant information on organic compounds in complex mixtures.

n-Alkanes and fatty acids can originate from both man-made and natural sources and the distribution patterns of the homologous constituents can help one to assess the contributors (Rogge et al., 1993).

Some preliminary results have shown that PM samples collected in Milan in a background site are characterized by higher concentration of odd carbon number alkanes. From the literature (Rogge et al., 1993) it is well known that biogenic sources are enriched in odd alkanes. An estimation of biogenic aerosol contribution can be obtained by the calculation of CPI_{odd} (carbon preference index).

For Milan, in the background site, during autumn, this value was about 1.7 confirming the contribution of the biogenic source (when only anthropogenic emissions are present $CPI_{odd}=1$). The background site has shown different alkanes concentrations with respect to a site affected by traffic placed in the centre of Milan.

As a comparison the contribution of biogenic aerosol has been studied also in some rural sites of the Po Valley.

Another parameter that can be correlated to the contribution of biogenic sources is WSOC concentration which is strongly dependent on the site (urban or rural) (Poschol 2005). WSOC concentration was estimated by TOT (Thermal Optical Transmittance) method.

Simoneit, B.R.T., (1999) *Environ. Sci. & Pollut. Res*. 6 (3) 159-169.

Rogge, W.F., Mazurek, M.A., Hildemann, L.M., Cass, G.R., Simoneit, B.R.T., (1993) *Atmospheric Environment*, 27A, 1309-1330.

Poschol, U., (2005) *Angewandte,* 44, 7520-7540

Source Apportionment for PM samples: study of n-alkanes distribution as organic tracer using a chemometric approach for GC-MS analysis data handling

M. Mercuriali[1] and M.C. Pietrogrande[1]

[1]Department of Chemistry, University of Ferrara, Ferrara, I-44100, Italy

Keywords: GC-MS, n-alkanes, organic tracers, PM, source apportionment.

Atmospheric aerosols consist of a complex mixture of hundreds of compounds belonging to many different classes: despite this complexity, in environmental monitoring and assessment studies, the more useful choice consists in the sample chemical analysis limited to selected compounds, in order to represent a chemical fingerprint of the possible input sources and to give informations about their fate.

Homologous series of n-alkanes and n-alcanoic acids are usually used as molecular tracers: they are common to multiple sources and they help to differentiate aerosols of anthropogenic origin (i.e. associated with industrial and urban activities) from those of natural, biogenic origin (i.e. epicuticular waxes and pollens) (Oliveira *et al.*, 2007).

The key parameters useful for a good source apportionment are the number of terms (n_{max}) and the carbon preference index (*CPI*) which represents the prevalence of odd/even carbon number terms of the series (Simoneit, 1986).

This is a fundamental parameter for the identification of a biogenic contribute (which is represented by a strong prevalence of odd/even terms, with high values of *CPI*) versus an anthtropogenic one (represented by the lack of a prevalence of odd/even terms, with a CPI value close to 1).

Gas Chromatography-Mass Spectrometry (GC-MS) is the best analytical technique for the determination of these organic compounds but it produces large amount of data when it is applied on such complex mixtures like environmental samples. Moreover there could be even interfering substances, artifacts, noise and data redundancy.

This work describes the application of a signal processing method to GC–MS chromatograms of PM_{10} and $PM_{2.5}$ samples collected in rural and urban areas.

The method is focused on the computation of the two relevant parameters n_{max} and *CPI* that can be directly estimated from the AutoCoVariance Function (ACVF) computed on the acquired chromatogram (Pietrogrande et *al.*, 2007). The procedure makes it possible to extract usable information hidden in the chromatogram thus reducing the labour and time required and increasing the quality and objectivity of the results. Experimental chromatograms of real samples of atmosferic aerosols were investigated (Figure 1).

The CPI_{tot} value is obtained from $EACVF_{tot}$ by evaluating all the n-alkane components, i.e., the C_{12}-C_{35} range (Figure 2). Moreover, the CPI_{plant} can be calculated on the heavier C_{25}-C_{35} n-alkanes in order to describe the contribution of plant waxes. CPI_{plant} is directly estimated from the $EACVF_{plant}$ computed on the partial region of the chromatogram containing the terms.

For each sample, the comparison between $EACVF_{tot}$ related to the total amount of the terms of homologous series, and $EACVF_{plant}$, describing the relative contribution of plant waxes, can be used to quantified the percentages of plant wax fraction in the total n-alkanes.
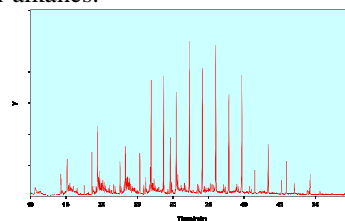
Figure 1. GC-MS chromatogram of a $PM_{2.5}$ sample collected in spring in a rural area
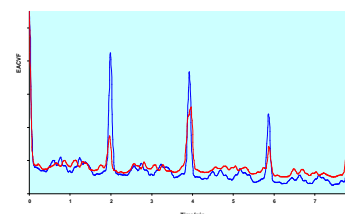
Figure 2. EACVF plot calculated on the whole n-alkane range (C_{21}–C_{35}): blue line; EACVF plot calculated on the heavier n-alkanes (C_{25}–C_{35}): red line.

Oliveira C., Pio C., Alves C., Evtyugina M., Santos P., Goncalves V., Nunes T., Silvestre J.D., Palmgren F., Wahlinc P., Harrad S. (2007) *Atmospheric Environment*, 41, 5555-5570

Simoneit B.R.T. (1986) *International Journey of Environmental Analytical Chemistry*, 23, 207-237

Pietrogrande, M.C., Mercuriali M., Pasti L. (2007) *Anal. Chim. Acta*, 594, 128-138.

Pietrogrande, M.C., Mercuriali M., Pasti L., Dondi F. (2009) *Analyst*, DOI: 10.1039/b815317e

Modeling aerosol surface chemistry and gas-particle interaction kinetics with a kinetic double-layer model: PAH oxidation by ozone, nitrogen dioxide, and water vapor

M. Shiraiwa[1], R. M. Graland[1] and U. Pöschl [1]

[1]Department of Biogeochemistry, Max Planck Institute for Chemistry, J. J. Becherweg 27, D55128, Mainz, Germany

Keywords: PAH, Aerosol modeling, Surface reaction, Aerosol-surface reaction, Health effects of aeorosls.

Atmospheric aerosols have the ability to impact cloud properties, radiative balance and provide surfaces for heterogeneous reactions. Some aerosols are hazardous and pose a threat to human health. One of the most important hazardous compounds is polycyclic aromatic hydrocarbons (PAHs). These aerosols can penetrate deep into lungs, leading to allergenic, mutagenic, and carcinogenic response to human health. Moreover, chemical transformation of PAHs can lead to increase or decrease their potential for adverse health effects. Therefore, for improved evaluations of health risks and air quality, it is necessary to characterize the formation and decomposition kinetics of PAHs on the surface. However, this heterogeneous reaction, as well as the impact on the aerosol, is not fully understood. This uncertainty is due not only to limited measurement data, but also a dearth of comprehensive and applicable modeling formalizations. Without a common model framework, comparing and extrapolating experimental data is difficult.
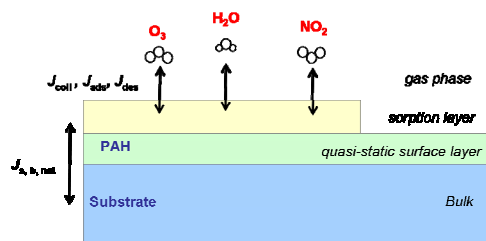
Figure 1. Schematics of double-layer surface model.

In this study, the interaction of ozone, water, and nitrogen dioxide with polycyclic aromatic hydrocarbons was investigated using a novel kinetic surface model (K2-SURF), which enables a detailed description of mass transport (adsorption and desorption) and chemical reaction on the surface [Pöschl et al. 2007; Ammann and Pöschl, 2007]. The results from a variety of published experimental studies of PAH degradation were analyzed and compared utilizing K2-SURF. The heterogeneous reaction of PAH and O_3 follow a Langmuir-Hinshelwood mechanism. The Langmuir equilibrium constants (K) and second-order-rate coefficients of surface reaction were estimated. The differences in adsorption of O_3 were much larger than surface

reaction. K_{O3} value varies significantly by almost 3 orders of magnitude (10^{-15} - 10^{-13} cm3). In contrast, k_{SLR}, PAH, O_3 are almost in the same order of 10^{-17} cm^2 s^{-1} for PAH on solid substrates. The mean residence time and adsorption enthalpy suggest chemisorption of ozone and NO_2 and physisorption of H_2O.
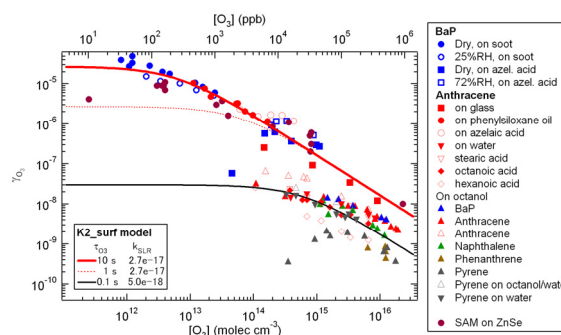
Figure 2. Uptake coefficients of O_3 by PAH on various substrates.

Temporal evolution of surface composition and uptake coefficient of O_3 (γ_{O3}) was modelled, showing the effects of reversible competitive adsorption and chemical aging of PAH. The steady-state model explained strong dependence of γ_{O3} on gas phase ozone concentration in five order range as shown in Figure 2. We suggest the order of 10^{-6} - 10^{-5} for PAH on solid aerosol such as soot and solid organics at atmospheric condition. The lifetime of PAH on the surface depends strongly on gas-phase ozone concentration and substrate, also influenced by co-adsorbing gases. It was estimated to be ~20 min on soot surface and ~10 h on solid organics at typical atmospheric condition. The basic parameter presented in this study can be easily incorporated in atmospheric model to describe PAH degradation process.

Ammann, M. and U. Pöschl (2007) *Atmos. Chem. and Phys*, 7, 6025-6045.
Pöschl, U., Y. Rudich, and M. Ammann (2007) *Atmos. Chem. and Phys*, 7, 5989-6023.

Acetonitrile and new charged clusters formation

T.-E. Parts, A. Luts, U. Hõrrak, K. Komsaare

Institute of Physics, University of Tartu, Ülikooli 18, 50090 Tartu, Estonia

Keywords: aerosol chemistry, ion mobility, ions, particle formation, trace gases.

Volatile organic compounds (VOCs) are a significant fraction of atmospheric aerosol and their impact into ion-induced aerosol nucleation events could be considered (Enghoff & Svensmark, 2008). Acetonitrile (methyl cyanide, CH_3CN) is one of the atmospheric pollutants, VOC, emitted from biomass burning. Acetonitrile can reach the stratosphere where it is characteristically associated in positive ion clusters $H^+(CH_3CN)_n(H_2O)_m$ in the upper regions (Arijs et al., 1983). Previously we reported some results of young (about 1 second age) small positive air ions measurement including effect of CH_3CN on the mobility spectra (Parts & Luts, 2004). These experiments were done in laboratory conditions. Now we measured the spectra of ions in natural air and try to elucidate the relation between young ions and natural ones measured at the same time.

The continuous measurements of the mobility distribution of air ions were carried out in urban environment, in the centre of Tartu, Estonia. The improved version of a unique small air ion mobility spectrometer - KAIS, developed at the University of Tartu, measured the mobility spectra of young ions, produced by corona discharge, in the mobility range from 0.6 to 2.6 $cm^2V^{-1}s^{-1}$ (sizes <1.6 nm). Concurrently the BSMA (Balanced Scanning Mobility Analyzer) measured the mobility spectra of natural ions in the mobility range of 0.032 - 3.2 $cm^2V^{-1}s^{-1}$ (the size range 0.4 - 7.5 nm). In addition, the BSMA can provide the data about aerosol nucleation burst events (Tammet, 2004).
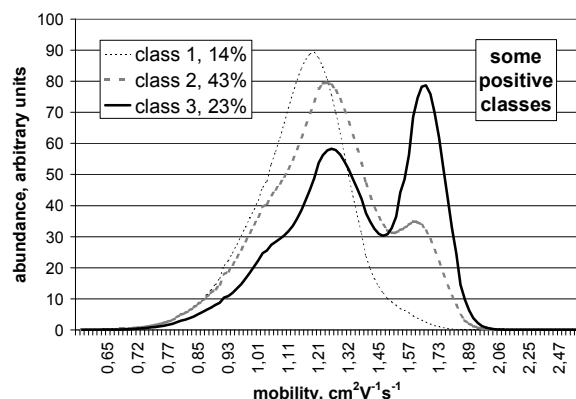
Figure 1. Background spectra of young positive ions.

The common young positive air ion spectra outdoors can have several shapes (Figure 1) depending on the atmospheric conditions (Luts &Parts, 2008).

Acetonitrile, added to natural air, apparently changes the size distribution and masses of ions and in this way the mobility spectra (Figures 2, 3).
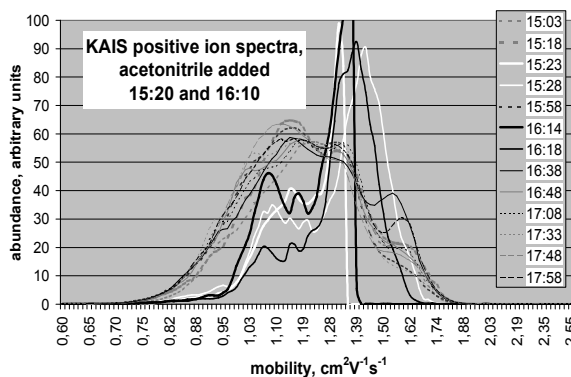
Figure 2. Temporal evolution of KAIS spectra.
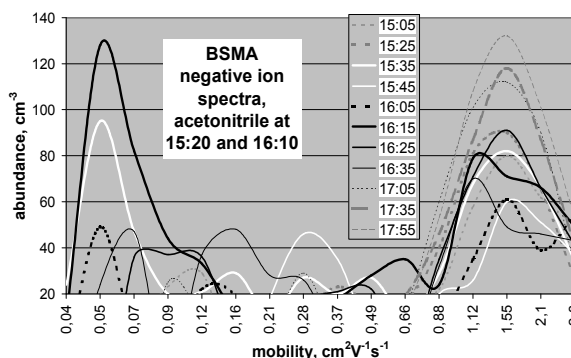
Figure 3. Temporal evolution of BSMA spectra.

Preliminary results show that acetonitrile could be considered responsible for new charged particles formation at some burst events.

Enghoff, M. B., & Svensmark, H. (2008). *Atmos. Chem. Phys.,* 8, 4911-4923.

Arijs, E., Nevejans, D., & Ingels, J. (1983). *Nature* (Lond), 303, 314-316.

Luts, A., & Parts, T.-E. (2008). *Report Series in Aerosol Science*, 92**,** 123-126.

Parts, T., & Luts, A. (2004). *Atm. Envir.,* 38, 1283-1289.

Tammet, H. (2004). In *Nucleation and Atmospheric Aerosols 2004: 16th Int'l Conf., Kyoto, Japan,* 294–297.

The « HUmic LIke Substances » in biomass burning emissions

C. Baduel[1] , D. Voisin[1] , J.L. Jaffrezo[1],I. El Haddad[2], N. Marchand[2], M.B. Personnaz[3]

[1]Laboratoire de Glaciologie et Géophysique de l'Environnement, Université Joseph Fourier, 54 rue Molière, 38402, Saint Martin d'Hères, France.
[2]Laboratoire Chimie Provence, Universités d'Aix-Marseille, 3 place Victor Hugo, 13331, Marseilles, France.
[3]ASCOPARG, 44 av Marcellin Berthelot, 38100, Grenoble, France.

Several studies have shown that "HUmic LIke Substances" (HULIS) may represent a significant fraction (15 and 40 % in mass) of the organic carbon (OC) of atmospheric aerosols. Recently, a seasonal evolution of their concentrations was demonstrated, for six background sites, with one maximum in summer and another one in winter (Fezcko et al., 2007). These variations are ascribed to a variability in the sources and formation processes, with the hypotheses that HULIS may be generated though various chemical pathways and consist in a mixture of primary and secondary products.

Many recent papers tentatively ascribed biomass burning as one potential origin of aerosol water soluble HULIS. Incomplete breakdown of polymeric carbohydrates and lignin during such combustion could generate organics present in the HULIS fraction. Pyrogenic semi-volatile organic compounds could also produce HULIS through condensation reactions with other molecules (Mayol-Bracero et al.; 2002). Decesari et al. (2002) also proposed that HULIS can derive from the reaction of soot particles with atmospheric oxidants, which can be important for any combustion-generated aerosol.

This work is focused on HULIS in samples impacted by combustion processes. It presents results obtained for two HULIS fractions: water soluble HULIS and "Total" HULIS, the fraction extracted in alkali media to extract the more hydrophobic compounds. HULIS analysis was performed with a selective isolation scheme with DEAE anionic exchange resin complemented by carbon determination (Baduel et al., 2009). UV spectroscopy was performed on line for the chemical characterisation of HULIS. Samplings were carried out in very close proximity to combustion-generated aerosol: in a tunnel and nearby garden fires; in cities during burning season and with cascade impactor. The results indicate some variability in the characteristics of HULIS obtained from these different sources.

Series of ozone experiments in chamber was performed with samples collected nearby garden fires. Functional analysis by APCI/MS/MS was then performed on this sample set to investigate the chemical composition of organic aerosol in terms of functional group quantification. This new approach enables to group chemical compounds by their ability to loose a known neutral molecular fragment for neutral loss mode or to produce a characteristic ion in the collision cell for the precursor ion scanning mode. This analysis allows a quantitative determination of total carbonyls, carboxylic and nitro groups and provides an apparent molecular weight distribution of the compounds bearing the function under study.

Determination of functional groups contents will be presented in order to investigate chemical modification and oxidation processes which lead to the formation of polar groups on soot particle and will tentatively be related to modification of HULIS absorption spectra.

Baduel, C. et al. (2009), Submitted to Atmos. Chem. Phys.

Decesari, S. et al. (2002). Atmos. Environ., 36, 1827–1832.

Feczko, T. et al. (2007). *J. Geophys. Res.*, *112*(D23S10), doi:10.1029/2006JD008331.

Mayol-Bracero, O. L. et al. (2002). *J. Geophys. Res.*, *107* (D20 8091), doi:10.1029/2001JD000522.

Detection and kinetics of protein nitration in aerosols by NO_2 and O_3

H. Yang, Y. Zhang, U. Pöschl

Max Planck Institute for Chemistry, Department of Biogeochemistry, Mainz, Germany

Keywords: aerosol chemistry, protein nitration, kinetics, NO_2, O_3.

The effects of air pollution on allergic diseases are not yet well-understood, but recent studies have shown that proteins are efficiently nitrated by polluted air (Franze et al., 2005) and that nitration enhances the allergenic potential of proteins such as the prominent birch pollen allergen Bet v 1 (Gruijthuijsen et al., 2006). Accordingly, the nitration of proteins in bioaerosol particles such as pollen and spores by NO_2 and O_3 might be a reason why allergies are on the increase in areas with traffic-related air pollution such as mega-cities and city clusters.

In this study we have developed a method to determine the nitrotyrosine residue number per molecule in nitrated model proteins (bovine serum albumin, BSA; ovalbumin, OVA) by liquid chromatography coupled to UV-Vis photometry and mass spectrometry detectors (LC-DAD and LC-ESI-MS). Nitration experiments were carried out by exposing proteins to synthetic gas mixtures of nitrogen dioxide, ozone, nitrogen, synthetic air and water vapor. Reaction rates were measured at different concentration levels of NO_2 and O_3, and rate coefficients for the heterogeneous chemical reaction were determined. The implications for atmospheric aging and chemical transformation of bioaerosol particles and their potential effects on public health will be discussed.

Franze, T., Weller, M.G., Niessner, R., & Pöschl, U. (2005). *Environ. Sci. Technol.* 39, 1673-1678.

Gruijthuijsen, Y.K., Grieshuber, I., Stöcklinger, A., Tischler, U., Fehrenbach, T., Weller, M.G., Vogel, L., Vieths, S., Pöschl, U., & Duschl, A. (2006). *Int. Arch. Allergy Immunol.* 141, 265-275.

Radical, Humidity and Temperature effects on SOA Formation from Ozonolysis of Monoterpenes

M. Hallquist[1], Å. M. Jonsson [1,2], K. Salo[1] and E. Emanuelsson[1]

[1] Atmospheric Science, Department of Chemistry, University of Gothenburg, Sweden.
[2] IVL, Swedish Environmental Research Institute, P.O. Box 5302, Sweden

Keywords : Keywords : Aerosol Formation, Ozone ,Alpha pinene oxidation, SOA, Temperature

Secondary organic aerosol (SOA) formation accounts for a significant fraction of ambient tropospheric aerosol (Hallquist *et. al.,* 2009). In this work special emphasis is on SOA produced from oxidation of biogenic compounds. In the atmosphere these compounds are oxidised primarily by ozone, OH radicals and NO_3 radicals. In the degradation process compounds with low volatility can be formed which may undergo gas-to-particle conversion, hence contributing to the formation of SOA. One important group of compounds contributing to SOA formation is the monoterpenes ($C_{10}H_{16}$), where globally α-pinene and limonene are the most abundant. In this work the impact of temperature, relative humidity (RH) and radical chemistry on the aerosol formation from ozonolysis of limonene, Δ^3-carene, α-pinene and β-pinene have been investigated.

The experiments were conducted by using the G-FROST (**G**öteborg-**F**low **R**eactor for **O**xidation **S**tudies at low **T**emperatures) set-up. This set-up consists mainly of a laminar flow reactor (length: 1.9 m and i.d:10 cm) and a scanning mobility particle sizer (SMPS) system where particle number and mass size distributions were obtained. This is a set-up where temperature, relative humidity and concentrations can be carefully controlled (e.g. Jonsson *et al.,* 2008). Figure 1 illustrates the effect of water and scavenger on SOA formation.
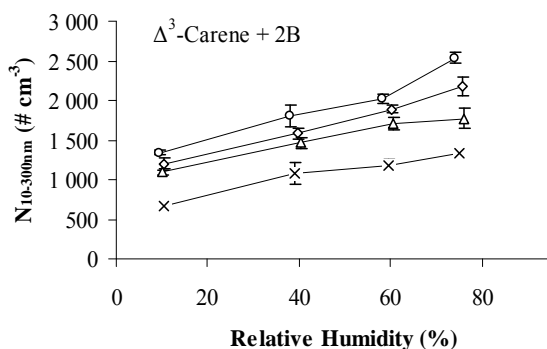
Figure 1. Effect of OH scavenger concentration on the number of particles formed in the ozonolysis of Δ^3-carene. The concentration is increasing in the order circles, diamonds, triangles and crosses.

The results presented are for different reaction temperatures (243 - 298 K) and for a range of relative humidities (0 - 80%). In addition, the use of OH-scavengers, 2-butanol or cyclohexane and without any scavenger in the system, will demonstrate another important topic showing the evidence of OH radical production from the ozonolysis at low temperatures. The results are discussed in relation to the current knowledge of the degradation mechanism and structural differences between the monoterpenes investigated.

References
Hallquist M., J. C. Wenger, U. Baltensperger, Y. Rudich, D. Simpson, M. Claeys, J. Dommen, N. M. Donahue, C. George, A. H. Goldstein, J. F. Hamilton, H. Herrmann, T. Hoffmann, Y. Iinuma, M. Jang, M. Jenkin, J. L. Jimenez, A. Kiendler-Scharr, W. Maenhaut, G. McFiggans, Th. F. Mentel, A. Monod, A. S. H. Prévôt, J. H. Seinfeld, J. D. Surratt, R. Szmigielski, and J. Wildt. The formation, properties and impact of secondary organic aerosol: current and emerging issues, *Atmos. Chem. Phys. Discuss.*, 9, 3555-3762, 2009.

Jonsson Å. M., Hallquist M, and Ljungström E, Influence of OH Scavenger on the Water Effect on Secondary Organic Aerosol Formation from Ozonolysis of Limonene, Δ^3-Carene, and α-Pinene, *Environ. Sci. and Tech.*, 42 (16): 5938–5944 (2008)

Heterogeneous reactions of a pyrethroid insecticide with OH radicals and ozone: In-situ measurement of airborne particles using FTIR

M. Segal-Rosenheimer[1], R. Linker[1], and Y.Dubowski[1]

[1]Department of Civil and Environmental Engineering, Technion-Israel Institute of Technology , Technion City, 32000, Haifa, Israel

Keywords: *in-situ* measurement, degradation processes, toxic aerosols, FTIR

Pesticides are highly toxic compounds. They may be promoted into the atmosphere during their application via drift of aerosols, as well as by volatilization or dust erosion from treated surfaces after application. Transport of pesticides and their degradation products are likely to introduce them to non-target and widespread areas. Although previous studies indicate that a major portion of applied pesticides ends up in the atmosphere, this is the medium about which we know the least regarding pesticides' fate.

Pyrethroids are synthetic pyrethrins, which are gaining popularity in replacing the organophosphate insecticides due to their low avian and mammalian toxicity. As such, they are widely used, both indoor and outdoor. Having low vapour pressure, they are likely to reside in the atmosphere in the airborne particulate phase or adsorbed upon stagnant surfaces. While adsorbed on atmospheric interfaces, these compounds interact with solar radiation and atmospheric oxidants, yielding product that may be more toxic or hydrophilic (Segal-Rosenheimer and Dubowski, 2007).

The main goal of the present study was to gain a quantitative insight regarding atmospheric degradation process of such materials, using α-cypermethrin as a model material. The present investigation focused on the heterogeneous reactions of airborne cypermethrin with ozone and OH radicals using FTIR spectroscopy to monitor simultaneously both condensed and gas-phases, and to extract reaction kinetics and product identification. An additional goal was to examine the effect of the pesticides' purity (analytical standard versus technical grade material), and of the state of the substrate (airborne, adsorbed on stagnant surface as a film or deposited as aerosols) on the reaction kinetics. This was done in order to estimate the applicability of such laboratory data to outdoor conditions and their usage in exposure assessments.

Film and deposited aerosols measurements were done using an ATR-FTIR set-up, as described in detail elsewhere (Segal-Rosenheimer and Dubowski, 2007).

Airborne experiments were performed as follows: aerosols were generated by atomizing aqueous solution of technical grade cypermethrin (0.1% w/w, like in field applications). After drying, the aerosols were introduced into a long path IR cell (Optical path 22 meters, V=8.5L), where the reaction took place. A small N_2 purge flow was used to reduce deposition on the cell's mirrors. Ozone was generated by radiating O_2/N_2 mixture with a 185 nm UV light. OH radicals were generated via a dark reaction of 2,3 dimethyl 2-butene with ozone as described in Atkinson and Aschmann (1993). The reaction monitoring started after reaching steady state of the oxidants and aerosols levels, as determined by the IR spectra. Ozone and (in the OH experiments) 2,3 dimethyl 2-butene were purged constantly in small flows through the cell, while aerosols were inserted and reacted as batch. Complimentary product analysis using GC-MS was carried on the films extracts and aerosol residues collected on filters at the reactor's outlet.

Among the products that were identified by the IR spectra were carbon monoxide and two condensed phase carbonyls. The formation rates of the two carbonyls were shown to be different, suggesting that some of them are products of secondary surface reactions. The main products identified by the GC-MS analysis were 3-phenoxybenzaldehyde and 1,2 benzenedicarboxyl. The latter was observed only as the product of the technical grade compound. With regard to kinetics, the technical grade cypermethrin was found to be less reactive toward these gaseous oxidants than its analytical standard. Furthermore, airborne particles seemed to yield higher degradation rates in comparison to the rates obtained on stagnant surface (both film and deposited aerosols). No significant difference was found, however, between the reactions of cypermethrin deposited on stagnant surface as aerosols or as a film. These results emphasize the importance of a dedicated investigation of pesticides degradation in the airborne phase.

Atkinson, R. & Aschmann, S. M. (1993). *Environ. Sci. Tech.*, 27, 1357-1363.

Segal-Rosenheimer, M. & Dubowski, Y. (2007). *J. Phys. Chem. C.,* 111, 11682-11691.

Heterogeneous Reactions of $(NH_4)_2SO_4$ particles with chlorine reactive species: coated wall flow tube studies

Raluca CIURARU, Nicolas VISEZ, Sylvie GOSSELIN, Denis PETITPREZ

Laboratoire de Physico-Chimie des Processus de Combustion et de l'Atmosphère (PC2A), UMR 8522, Universite de Lille 1, Cité Scientifique - Bâtiment C11, 59655 Villeneuve d'Ascq, France

Keywords: aerosol chemistry, ammonium sulphate, multiphase processes

INTRODUCTION

The chlorine atoms could be the most important oxidant in the marine boundary layer at dawn when the OH concentration is small. The chlorine species will be photolyzed at sunrise to generate Cl atoms at concentrations estimated to be on the order of 10^5 atoms cm^{-3} [1]. It can modify the acidity budget (HCl), oxidize various volatile organic compounds (VOCs), contribute to sulphur oxidation in the aqueous phase. It can also participate to ozone destruction or production, depending on the (VOCs) concentrations [2].

The sulfates represent the majority compounds of the particles of aerosols, which are produced from the anthropic SO_2 emissions. The presence of ammonium salts in the troposphere has a significant influence upon the atmospheric concentrations of their acid constituents, which can be regenerated during transport. Ammonium sulfate concentration ranges from 2.78 to 23.7 μg m^{-3} in fine particles, and from 0.15 to 1.39 μg m^{-3} in coarse particles [3].

In order to better understand the heterogeneous reactivity between these aerosol particles and chlorine reactive species, kinetic studies are in progress in our laboratory.

EXPERIMENTAL

The heterogeneous uptake of some chlorine reactive species by ammonium sulfate particles has been investigated at room temperature and low pressure. Studies were performed in a laminar coated wall flow tube reactor coupled to a quadrupole mass spectrometer.

Our experimental set-up and techniques to prepare coated surfaces will be detailed. Salt samples of ammonium sulfate are prepared in two different ways: as spray deposited substrates, using a constant output atomizer and as powder substrates.

The measurement of the first order rate constant, k is achieved by changing the contact time between the surface and the gas, using a movable injector. From the rate constant, we can determine the uptake coefficient, γ, which represents the ratio between the number of gas molecules removed by the condensed phase and the number of gas molecules striking the interface per unit time.

Chlorine atoms are produced within a DC microwave discharge in a mixture of molecular chlorine and helium.

RESULTS

The uptake of Cl atoms on ammonium sulfate particles was found to be fast with an uptake coefficient of $\gamma = (5 \pm 2) \times 10^{-4}$. This result is in agreement with the only available data from Martin et al, 1980 [4].

The secondary product, molecular chlorine, Cl_2, was observed, owing to the heterogeneous recombination of halogen atoms on the surface of the particles. Studies below room temperature are now in progress.

These measurements will be also extended to other particles of atmospheric interest such as ammonium bisulfate (NH_4HSO_4) and ammonium nitrate (NH_4NO_3).

REFERENCES

(1) Spicer C. W., Chapman E. G., Finlayson-Pitts B. J., Plastridge R. A., Hubbe J.M., Fast J. D., Berkowitz C. M. (1998), *Letters To Nature*, 394(6691), pp 353-356
(2) Pechtl, S., von Glasow (2007), R., *J. Geophys. Res. Letters*, vol. 34, L11813
(3) Xiaoxiu L., Xiaoshan Z., Yujing M., Anpu N and Guibin J.(2003), *Atm. Environ.*, 37, 2581-2588
(4) Martin L.R., Judeikis H.S., Wun M. (1980) , *J. Geophys. Res.*, 85, 5511-5518

Acid-catalyzed reactions of limonene and terpineol and their implication in secondary organic aerosol (SOA) formation

Y.J. Li[2], Gema Y.L. Cheong[2], Alex K.Y. Lee[1], Arthur P.S. Lau[3] and C.K. Chan[1*]

[1]Department of Chemical and Biomolecular Engineering, [2]Environmental Engineering Program, [3]Institute for the Environment, Hong Kong University of Science and Technology, Clear Water Bay, Kowloon, Hong Kong

Keywords: organic aerosols, aerosol chemistry, multi-phase chemistry, sulfuric acid, SVOC.

It has been reported that acid-catalyzed reactions of some semi-volatile organic compounds can affect their partitioning between the gas phase and the particle phase, hence the properties of atmospheric particles. These particle-phase reactions can enhance secondary organic aerosol (SOA) formation via accretion reactions including polymerization, aldol condensation etc. (Jang et al., 2003; Liggio & Li, 2008) and addition reactions (Surratt et al., 2007) such as organosulfate formation from volatile/semi-volatile organics (e.g. carbonyls, alcohols and alkenes). Other studies, however, found that acid-catalyzed reactions are either thermodynamically unfavourable (Basanti & Pankow, 2004) or kinetically too slow (Zhao et al., 2004) to contribute to substantial amount of SOA formation in the troposphere. The discrepancy is largely due to the fact that both mechanisms and kinetics for those acid-catalyzed reactions are still unclear, and even the product identities of which remain poorly understood.

In the present study, we investigated the acid-catalyzed reactions of biogenic volatile organic compounds by a flow cell reactor with acidic particles deposited onto a hydrophobic substrate. Limonene (LN) and a mixture of terpineols (3 isomers of limonene hydroxyls, TL) were used as the model VOC compounds to study the acid-catalyzed reactions. Reaction products were identified from experiments under different acidity conditions by controlling the relative humidity (RH). For both LN and TL experiments, limonene dimers (LND) and limonene trimers (LNT) were formed under low RH conditions (<20%) and high VOC concentration level (~30 ppmv for LN and ~1 ppmv for TL). At lower VOC concentrations (~1 ppmv for LN and ~0.1 ppmv for TL), dimer and trimer formation for LN experiments was less significant (only found in 2% RH conditions), while dimers and trimers were still observable in TL experiments at RH=2% and 20%. A limonene ketone (carvenone, LNK) was also observed in most of the low RH experiments with LN or TL. The amount of these products (LND, LNT and LNK) increased with decreasing RH. Under higher RH conditions (>20%), both LN and TL gave monomer derivatives as the reaction products, i.e., several unidentified monomers (probably carboxylic derivatives of limonene, LNM) for LN or limonene

dihydroxyls (LNOH2) for TL. The formation of these monomer derivatives was also dependent on RH, with increasing amounts of products formed at higher RH conditions. The acidity-dependent reaction pathways (Fig. 1) were proposed based on product information from the flow cell reactor experiments and bulk solution experiments.
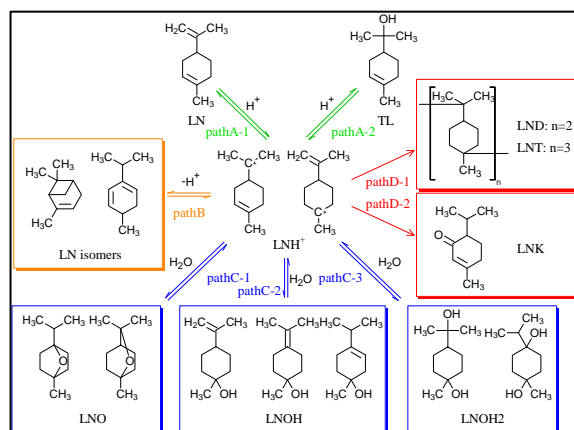
Fig. 1 Acidity-dependent reaction pathways of limonene (LN) and terpeneols (TL). Products are shown by typical structures while isomers of them were also observed in the experiments.

Barsanti, K.C. & Pankow, J.F. (2004), *Atmos. Environ.*, 38, 4371-4382.

Clegg, S.L., Brimblecombe, P. & Wexler, A.S. (1998) *J. Phys. Chem. A.*, 102, 2137-2154.

Jang, M.S., Carroll, B., Chandramouli, B. & Kamens, R.M. (2003), Environ. Sci. & Tech., 37, 3828-3837.

Kazansky V.B. (2001), *Catal. Rev.*, 43, 199-232.

Liggio J. & Li S.M. (2008), *Atmos. Chem. Phys.*, 8, 2039-2055.

Surratt, J.D., Kroll, J.H., Kleindienst, T.E., Edney, E.O., Claeys, M., Sorooshian, A., Ng, N.L., Offenberg, J.H., Lewandowski, M., Jaoui, M., Flagan, R.C. & Seinfeld, J.H. (2007), *Environ. Sci. & Tech.*, 41, 517-527.

Zhao J., Levitt N.P. & Zhang R.Y. (2005), *Geophys. Res. Lett.*, 32, L09802, doi:10.1029/2004GL022200.

Effect of Water Vapour Concentration on Photonucleation in Aromatic Aldehydes

S.N. Dubtsov[1], G.G. Dultseva[1], M.V. Bykova[1] and F.N. Dultsev[2]

[1]Institute of Chemical Kinetics and Combustion, Institutskaya, 3, 630090, Novosibirsk, Russia
[2]Institute of Semiconductor Physics, Lavrentiev ave., 13, 630090, Novosibirsk, Russia

Keywords: particle formation and growth, photochemical processes, organic compounds, molecular clusters.

Aromatic aldehydes are common urban air pollutants. Their photolysis under sunlight is accompanied by the formation of the organic particulate matter. An investigation of the mechanism of gas-to-particle conversion in aromatic aldehyde vapour under laboratory conditions allowed us to reveal the dependence of photolysis rate, photonucleation efficiency, and chemical composition of gaseous and aerosol products on the concentration of water vapour in the initial gas mixture. Since water vapour is an inevitable component of the atmosphere, participation of H_2O in the formation of secondary organic aerosol is of atmospheric significance.

Benzaldehyde, the most important atmospheric aromatic aldehyde, and salicylic aldehyde which is an analogue of many biogenic (plant-emitted) aldehydes were chosen as the primary compounds for the investigation. The initial stages of aldehyde photolysis were studied by means of spin trapping using specially synthesized dihydropirazine derivatives with nitrone groups to trap free radicals and to identify their spin adducts with the help of EPR. Gas-phase products of aldehyde photolysis were analyzed using liquid chromatography, UV spectroscopy, IR-FTIR, NMR and GC-MS. The kinetics of photonucleation was studied with a Diffusion Aerosol Spectrometer (Ankilov, 2002).

To explain the observed dependencies on water vapour concentration, semi-empirical calculation of clusterization in the gas phase was carried out by means of MNDO/PM3 and MM2 using the CS Chem 3D Pro, Version 5.0 software (Cambridge Soft Corporation, USA).

Experimental results indicate that the rates of photolysis of aromatic aldehydes depend on water vapour concentration. In the case of benzaldehyde, the chemical composition of the products is also dependent on H_2O concentration (Dultseva, 2008). For example, glyoxal and biphenyl, expected only in the absence of oxygen, were detected as the products of aldehyde photolysis in the air as a carrier gas. Modeling showed that the reason is the formation of a cluster in which two benzaldehyde molecules and one water molecule are held together by hydrogen bonds. Though this is only a weakly bound cluster, its formation allows the formyl radical generated primarily in photolysis to react with the neighbouring aldehyde molecule rather than with oxygen which is now an outer component with respect to the formed cluster.

The rate of benzaldehyde photolysis was observed to increase with an increase in $[H_2O]$, while photonucleation rate decreased. For salicylic aldehyde, photolysis rate decreased with an increase in water vapour concentration as shown in Fig. 1. Thus, the presence of a hydroxyl group in the aromatic ring brings about severe changes of cluster formation, and the entire mechanism changes.

It is demonstrated in the present work that clusterization of the primary products of aldehyde photolysis plays an important part in subsequent reaction pathways leading to aerosol formation.
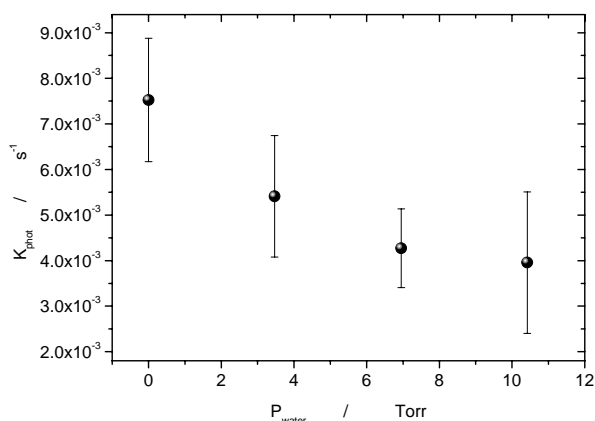
Figure 1. Dependence of the photolysis rate of salicylic aldehyde on water vapour concentration.

Ankilov, A. N. et al. (2002). *Atmospheric Research* 62, 177–207.
Dultseva, G.G., Dubtsov, S.N., & Dultsev, F.N. (2008). *J. Phys. Chem. A,* 112, No. 23, 5264–5268.

Multiphase Processing of Isoprene Oxidation Products – Kinetic and Product Studies

D. Hoffmann and H. Herrmann

Department of Chemistry, Leibniz-Institute for Tropospheric Research, Permoserstr. 15, 04318, Leipzig, Germany

Keywords: Isoprene, Multiphase chemistry, SOA (Second. Organic Aerosols), Water soluble organic compounds

Isoprene represents a significant fraction of non-methane hydrocarbon in the troposphere. Its emissions have recently been estimated to be in the range of 500 and 750 TgC yr^{-1} (Guenther et al., 2006). Due to its enormous source strength, the atmospheric fates of isoprene and all of its degradation products are very important in atmospheric processes. For example, isoprene oxidation processes can influence the regional ozone and secondary organic aerosol (SOA) formation.

Some aspects of SOA formation from isoprene and its oxidation products were studied by a number of chamber studies in the past (Kroll et al., 2006, Surratt et al., 2007). However, aqueous phase oxidation processes which may occur after phase transfer of 'early' oxidation product are often neglected. These processes are a potentially important source for organic particle mass constituents such as carboxylic acids. Most of the existing aqueous phase modelling studies, related to the isoprene oxidation sequence, focus only on 'later' oxidation products such as methylglyoxal, hydroxyacetone, pyruvic acid and oxalic acid. However, a recent field study reports much higher aqueous phase concentration of some 'earlier' isoprene oxidation products including methacrolein and methyl vinyl ketone than expected concentrations (van Pinxteren et al., 2005). This indicates that the importance of multiphase chemical processes in the course of the isoprene oxidation is possibly underestimated as a source for the production of organic particle mass together with known 'heterogeneous processes', such as the direct condensation of low-volatility products from gas phase processes onto existing particle surfaces.

In order to implement the isoprene multiphase chemistry in atmospheric models detailed kinetic and mechanistic studies are needed. Therefore, the aqueous phase oxidation of isoprene oxidation products such as methacrolein, methacrylic acid and methyl vinyl ketone by atmospheric radicals (such as OH and NO$_3$) was systematically investigated within this contribution.

Kinetic measurements were carried out as a function of the temperature and the pH of the measurement solution. All kinetic experiments were done applying the laser-photolysis-long-path-absorption (LP-LPA) technique. Rate constants were measured either directly or using competition kinetic methods.

Table 1 summarizes the kinetic results obtained for OH radical reactions at T = 298 K.

Table 1. Measured second order rate constants (k_{2nd}, T = 298K) and activation energies (E_A) for OH radical reactions in aqueous solution.

Compound	pH	k_{2nd} M^{-1}s^{-1}	E_A kJ/mol
Methacrolein	7	$(1.0\pm0.1)\cdot10^{10}$	(10 ± 6)
Methyl vinyl ketone	7	$(7.4\pm0.7)\cdot10^{9}$	(8 ± 6)
Methacrylic acid	3	$(1.2\pm0.1)\cdot10^{10}$	(11 ± 4)
Methacrylate	8	$(1.2\pm0.1)\cdot10^{10}$	(12 ± 5)

Oxidation products were identified applying different analytical techniques such as HPLC-UV, CE-UV and HPLC-MS after laser flash photolysis. All samples were analyzed offline with and without prior derivatization steps. In order to purify and enrich the samples, a solid phase extraction (SPE) was performed before analysis. Identified reaction products are mainly functionalized carbonyl compounds and carboxylic acids.

The kinetic and mechanistic data obtained in this study will be used to improve and extend existing aqueous phase isoprene oxidation mechanism. With the updated and extended mechanism the role of multiphase processes for the formation of organic particle constituents such as carboxylic acids from the isoprene oxidation can be much better assessed in the future.

Guenther, A., Karl, T., Harley, P., Wiedinmyer, C., Palmer, P. I., & Geron C. (2006). *Atmospheric Chemical Physics,* 6, 3181–3210.

Kroll, J. H., Ng, N. L., Murphy, S. M., Flagan, R. C., & Seinfeld, J. H. (2006). *Environmental Science & Technology*, 40, 1869-1877.

Surratt, J. D., Kleindienst, T. E., Edney, E. O., Lewandowski, M., Offenberg, J. H., Jaoui, M., & Seinfeld, J. H. (2007). *Environmental Science & Technology,* 41, 5363– 5367.

van Pinxteren, D., Plewka, A., Hofmann, D., Müller, K., Kramberger, H., Svrcina, B., Bächmann, K., Jaeschke, W., Mertes, S., Collett, J.L., & Herrmann, H. (2005). *Atmospheric Environment,* 39, 4305-4320.

Laboratory Studies of Sulfuric Acid and Water Binary Homogeneous Nucleation

Shan-Hu Lee[1], David R. Benson[1], Li-Hao Young[1,2], F. Rifkha Kameel[1], Jeffrey R. Pierce[3], Heikki Juninnen[4], and Markku Kulmala[4]

[1]Kent State University, Department of Chemistry, Kent, OH, USA
[2]Now at China Medical University, Department of Occupational Safety and Health, Taichung, Taiwan
[3] NASA Goddard Space Flight Center, MD, USA
[4]University of Helsinki, Department of Physical Sciences, Helsinki, Finland

Keywords: Binary homogeneous nucleation, Aerosol formation and Growth, Sulfuric acid

Binary homogeneous nucleation (BHN) of sulfuric acid and water (H_2SO_4/H_2O) is one of the most important atmospheric nucleation processes, but laboratory observations of this nucleation process are very limited and there are also large discrepancies between different laboratory studies. The difficulties associated with these experiments include wall loss of H_2SO_4 and uncertainties in estimation of H_2SO_4 concentrations ([H_2SO_4]) involved in nucleation.

We have developed a very unique laboratory experimental set up to study H_2SO_4/H_2O BHN with two chemical ionization mass spectrometers (CIMSs) to measure [H_2SO_4] (initial and residual) and aerosols sizing spectrometers. We produce H_2SO_4 vapor at in-situ from the $SO_2 + OH \rightarrow HSO_3$ reaction as occurring in the atmosphere, as opposed to most of previous nucleation studies where H_2SO_4 vapor is produced from liquid H_2SO_4 samples.   OH is produced from the water UV absorption, which also allows for direct measurements of [OH] with accurate photon flux measurements and thus the initial [H_2SO_4] when [SO_2] $\gg$ [OH]. We also used numerical simulations to characterize the nucleation zone based on the measured [H_2SO_4] and particle sizes. These results indicate that the nucleation zone is a half of the nucleation reactor. Wall loss factors of H_2SO_4 were determined from calculations by assuming that wall loss is diffusion limited and also from simultaneous measurements of the initial and residual [H_2SO_4] with two CIMSs and these wall loss results are consistent each other – this is the first time that wall loss of H_2SO_4 is quantitatively characterized with experiments. We also made comprehensive tests in order understand how our nucleation system becomes stabilized over a long time, so that we can provide reproducible particle concentrations and aerosol nucleation rates.

We have measured H_2SO_4-H_2O BHN nucleation rates at atmospheric pressure, 288 K and 10 - 55 % RH. The CIMS-measured residual [H_2SO_4] that is required to produce the unit J range from $10^7 – 10^8$ cm^{-3}, but if wall loss is taken into account the threshold values for initial [H_2SO_4] are at the $10^8 – 10^9$ cm^{-3} range, much higher than the atmospheric conditions.   Furthermore, the measured J is proportional to [H_2SO_4] with the second to tenth powers and proportional to RH with the eleventh to fifteenth powers. These results indicate that there are two to ten molecules of H_2SO_4 in the critical clusters, more than those derived from atmospheric observations (1-2). These results thus suggest that H_2SO_4-H_2O BHN alone is insufficient to explain atmospheric aerosol formation and other ternary species can be important.   Aerosol growth rates derived from the measured H_2SO_4 and aerosol sizes range from 100-500 nm hour^{-1}, much higher than those found in the atmosphere, because of the high [H_2SO_4] used in our experiments. The measured aerosol sizes are proportional to log RH, showing a weak dependence of aerosol growth on RH. But the RH effects are more pronounced at higher [H_2SO_4], indicating that RH is more important for aerosol growth in the H_2SO_4 rich environment.

These results are summarized in Benson et al. (2008) and Young et al. (2008).

Benson, D.. R. Young, L. H., Kameel, F. R. Lee, and S.-H. Lee, Laboratory-Measured Sulfuric Acid and Water Homogeneous Nucleation Rates from the SO_2 + OH Reaction, *Geophys. Res. Lett.*, 35, L11801, Doi:2008GL033387 (2008).

Young, L.-H., Benson, D. R., Kameel, F. R., Pierce, J. R., Juninnen, H., Kulmala, M., Lee, S.-H., Laboratory studies of sulfric acid and water binary homogeneous nucleation: Evaluation of laboratory setup and preliminary results, *Atmos. Chem. Phys.* 8, 1-20 (2008).

Multiphase processing of tropospheric halogen species: Mechanism development and modelling

P. Bräuer[1], A. Tilgner[1], R. Wolke[1], and H. Herrmann[1]

[1]Leibniz Institute for Tropospheric Reasearch, Permoser Str. 15, 04318 Leipzig, Germany

Keywords: Multiphase chemistry, Modelling, Aerosol cloud interaction, MBL.

Halogens play a key role in marine chemistry. There has been a great effort to understand the mechanisms of halogen chemistry in the atmosphere. Research is done in field experiments (e.g. Pszenny *et al*., 2007), laboratory studies (e.g. Burkholder *et al.*, 2004), as well as modelling studies (e.g. Pechtl *et al.*, 2007).

In the present study we developed a comprehensive halogen module for the use with the multiphase mechanism RACM MIM2ext/ CAPRAM 3.0i. The mechanism includes reactions of inorganic chlorine, bromine, and iodine species in the gas phase as well as in the aqueous phase. There was a special emphasis on reactions of halogen species with organic compounds. Reactions are included in both phases and in contrast to other models are calculated explicitly in the aqueous phase. In the developed halogen module a total number of 205 species have been adopted which take part in 594 reactions. There are 356 gas phase reactions of which 156 belong to the chlorine chemistry, 103 to the bromine, and 97 to the iodine chemistry. In the aqueos phase 201 reactions have been added with 60, 87, and 54 new reactions for the chlorine, bromine, and iodine chemistry, respectively. The implemented kinetic data is based on the latest recommendations and the most recent literature data.

The mechanism was constructed for the use of a great variety of different scenarios in tropospheric chemistry modelling. For the simulations the model SPACCIM (Wolke *et al.*, 2005) was used. The model was initialized with an scenario for the open ocean where cloud chemistry is considered by non-permanent clouds. To evaluate the importance of the chlorine, bromine, and iodine chemistry as well as interactions of cloud droplets and particles with the multiphase chemistry of halogens in the troposphere sensitivity runs were performed where iodine, iodine plus bromine and aqueous phase chemistry, respectively, were omitted. Progress is continuing to develop a scenario where anthropogenic polluted air masses mix with marine influenced air masses to study the influence of halogens on coastal cities.

First model results seem reasonable. The calculated concentrations of halogen species are in good agreement with measurements. Typical profiles and concentrations of the oxidants ozone, OH radical, and HO_2 radical could be produced. For the first time a detailed time resolved analysis of the source and sink fluxes for most important halogen species has been done. Those fluxes are necessary for a better understanding of the tropospheric multiphase chemistry of halogens and give more information than just the evaluation of concentration profiles. There has also been a determination of the primary sources of halogens in the atmosphere. Results are shown for the case of iodine in Figure 1.
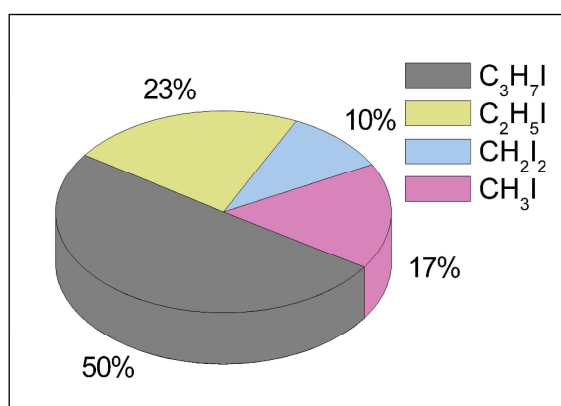
Figure 1. Calculated relative contributions of iodoalkanes to the tropospheric iodine atom budget averaged over the whole modelling period of 108 hours.

Burkholder, J. B., Curtius, J., Ravishankara, A. R. & Lovejoy, E. R. (2004). *Laboratory studies of the homogeneous nucleation of iodine oxides.* Atmospheric Chemistry and Physics, 4, 19-34.

Pechtl, S., Schmitz, G., & von Glasow, R. (2007). *Modelling iodide – iodate speciation in atmospheric aerosol: Contributions of inorganic and organic iodine chemistry.* Atmospheric Chemistry and Physics, 7, 1381-1393.

Pszenny, A. A. P., Fischer, E. V., Russo, R. S., Sive, B. C., & Varner R. K. (2007). *Estimates of Cl atom concentrations and hydrocarbon kinetic reactivity in surface air at Appledore Island, Maine (USA), during International Consortium for Atmospheric Research on Transport an Transformation/Chemistry of Halogens at the Isles of Shoals.* J. of Geophysical Research, 112, D10S13.

Wolke, R., Sehili, A. M., Simmel, M., Knoth, O., Tilgner, A., Herrmann, H. (2005). *SPACCIM. A parcel model with detailed microphysics and complex multiphase chemistry.* Atmospheric Envivronment, 39, 4375-4388.

Development and Application of a Reduced Aqueous Phase Chemistry Mechanism

A. Tilgner[1], L. Deguillaume[2], R. Schrödner[1], R. Wolke[1] and H. Herrmann[1]

[1]Department of Chemistry, Leibniz Institute for Tropospheric Research, Permoserstr. 15, Leipzig, 04318, Germany, (tilgner@tropos.de)
[2]Observatoire de Physique du Globe de Clermont Ferrand, Université Blaise Pascal 24, Avenue des Landais, 63177 Aubière cedex, France

Keywords: Multiphase chemistry, Modelling, Aerosol cloud interaction.

Recent model studies have implicated the necessity of more complex aqueous phase processes to be considered in future higher scale chemistry transport models (CTMs). Important chemical cloud effects are mainly not yet considered or less represented in currently available regional scale CTMs. To this end, a mechanism reduction of the detailed aqueous phase chemistry mechanism CAPRAM 3.0i (Chemical Aqueous Phase RAdical Mechanism; Herrmann et al., 2005) with about 777 reactions have been performed to develop simplified mechanism with less than 250 processes.

For the mechanism reduction manual methods including detailed process investigations and automatic techniques (see Mauersberger, 2005) were applied. Both investigations have been done in order to provide a less computationally intensive mechanism which is operational in higher scale CTMs and accurately represents the main chemical aqueous phase processes. The results of the manual reduction have been compared with the output of an automatic reduction. This comparison showed a quite good agreement. Based on the restrictions of both reduction methods, a final reduced mechanism was derived which describes the main characteristics of inorganic and organic aqueous phase processes occurring in tropospheric warm clouds. With less than 200 reactions, the reduced mechanism is nearly a factor of 4 smaller than the detailed CAPRAM 3.0i mechanism (see Table 1). Most of the chemical reduction potential has been realised in the organic chemistry with 393 unimportant reactions. Moreover, the number of aqueous phase species decreased from 380 in the full CAPRAM 3.0i mechanism to 130 in the final reduced version. Furthermore, 11 unimportant phase transfer processes and 36 insignificant chemical equilibriums have been identified according to their minor relevance for the preselected reduction key species. The calculated percentage deviations between the full and reduced mechanism are mostly below 5 % for the most important target compounds.

Additionally, numerical sensitivity tests were performed focusing on the relevance of both the relative and absolute integration error tolerances for an accurate and efficient modelling. The studies have shown that cloud formation and particularly evaporation periods are circa three times more computationally intensive than in-cloud conditions.

This indicates the requirement for sufficiently accurate tolerances particularly there. Comparisons of the required CPU times between the full and reduced mechanism showed reductions of approximately 40 %.

Table 1. Number of processes and chemical species considered in the full (C30i) and the reduced (C30i-r) CAPRAM 3.0i mechanism.

Aqueous phase mechanism	C3.0i	C3.0i-r
Number of aqueous reactions	676	140
Number of photolysis reactions	12	5
Mass transfer processes	51	37
Equilibriums	89	53
Total number of chemical processes	777	198
Number of aqueous species	380	130

In order to examine the applicability of the developed reduced mechanism for later regional scale CTM applications, 2-D test simulations have been performed using fixed meteorological conditions. For the model runs, the CTM MUSCAT (Wolke et al., 2004) in its 2-D offline mode has been applied. Simulations with the reduced CAPRAM 3.0i mechanism and a less complex inorganic aqueous phase chemistry mechanism (INORG) have been compared to evaluate the effects of more detailed chemistry. The model results show considerable differences in the multiphase oxidation budget and the inorganic mass processing. Moreover, the studies pointed out that entrainment/detrainment cloud zones are very chemically effective due to the permanent mixing input from the surrounded air.

Prospectively, the reduced mechanism represents the basis for studying chemical cloud effects on regional scale with future CTMs and will be important for a better understanding of the multiphase aerosol cloud processing effects on regional scale and the interpretation of field data.

Herrmann, H., et al. (2005), *Atmospheric Environment*, 39(23-24), 4351-4363.

Mauersberger, G. (2005), *Atmospheric Environment*, 39(23-24), 4341-4350.

Wolke, R., et al. (2004), in *Parallel computing: Software technology, algorithms, architectures and applications*, edited by G. R. Joubert, et al., pp. 363-370, Elsevier, Amsterdam, The Netherlands.

Determination of the bulk accommodation coefficient of NO_2 and O_3 on deliquesced aerosol particles and the effect of surfactants

A. Rouvière[1], Y. Sosedova[1], H.W. Gäggeler[1] and M. Ammann[1]

[1] Laboratory for Radiochemistry and Environmental Chemistry, Paul Scherrer Institut, 5232, Villigen, Switzerland

Keywords: mass accommodation; aerosol modelling; coatings; aerosol chemistry; NO_2

Atmospheric aerosol particles are continuously processed by gas phase oxidants, which affects their life time and climate effect. The aim of this work is to understand uptake of O_3 or NO_2 from the gas phase to deliquesced aerosol particles, with a specific eye on the bulk accommodation coefficient, α_b, i.e., the gas kinetic probability that the gas phase molecules enter the liquid phase. Experiments were performed in an aerosol flow tube, and the analysis is assisted by kinetic modelling to track reactants both in the gas and aerosol phase. We also investigated the effect organic surfactants have on the uptake of O_3.

NO_2 uptake to gentisic acid sodium salt particles. Gentisic acid trisodium salt (Na_3GA), a proxy for biomass burning derived aromatic compounds, was used as a model compound to provide a fast aerosol phase sink for NO_2. The NO_2 uptake was investigated using the ^{13}N tracer technique, by which the transfer of ^{13}N labelled NO_2 to the particles is followed as function of time in an aerosol flow reactor. Figure 1 shows typical kinetic data of the disappearance of NO_2 from the gas phase and of the appearance of the products in the aerosol phase as a function of time in the aerosol flow tube. Adjusting the corresponding simulations all available experimental data leads to a best estimate for α_b of 0.025 and for k_2 of 3.6×10^8 $M^{-1}s^{-1}$, which is the second order liquid phase rate constant for the reaction between NO_2 and Na_3GA.
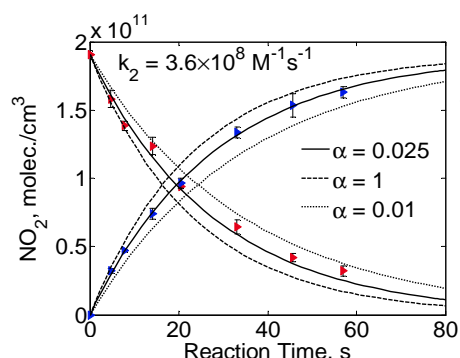
Figure 1. Typical results and simulations of an aerosol flow tube experiment of the reaction of NO_2 with gentisic acid sodium salt. Red symbols: Gas phase NO_2 concentration; blue symbols: aerosol phase nitrite product. Solid lines kinetic model simulations.

O_3 uptake to deliquesced potassium iodide particles. Similar experiments were performed with O_3 reacting with deliquesced KI particles, shown in Figure 2. The kinetic model simulations of this and similar experiments show that α_b is close to 1, if we assume that the second order rate constant between iodide and ozone is $k_b=1.2\times10^9$ $M^{-1}s^{-1}$ (Liu et al, 2001).

The values obtained for α_b for O_3 and NO_2 are significantly larger than previous estimates. This indicates that also only slightly soluble molecules are able to very rapidly enter the aqueous phase.
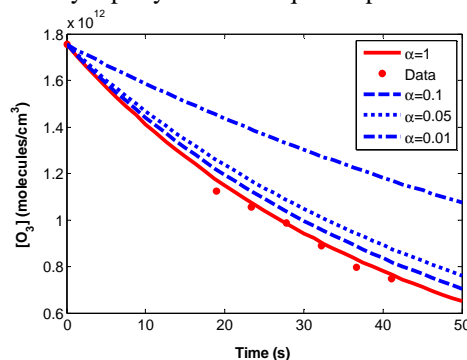
Figure 2: Temporal evolution of O_3 in the aerosol flow tube as a function of reaction time with deliquesced KI aerosol (red symbols). Kinetic model simulations are shown for different values of α_b (lines).

In a previous study, we have shown that organic coatings can reduce the mass transfer of HNO_3 between the gas and the aerosol phases (Stemmler et al, 2008). In this work, we studied the effects of fatty acids (C_9-C_{20}) on the ozone uptake to deliquesced KI particles. The results show that the degree to which ozone uptake is inhibited as a function of the fatty acid mass fraction is consistent with trends of the monolayer properties especially for C_{15}-C_{20} acids, i.e., density and surface phase state.

Acknowledgement

References

Liu, Q. et al., (2001). Inorg Chem.,40, 4436-4442.
Stemmler, K. et al., (2008). Atmos. Chem. Phys. 8, 687-725.

Development of a mixed phase cloud chemistry model

Y. Long[1], N. Chaumerliac[1], L. Deguillaume[1], M. Leriche[2], F. Champeau[1]

[1]LaMP/CNRS, Blaise Pascal University, 24 Av. des Landais, 63177, Aubière, France
[2]LA/CNRS, Paul Sabatier University, 14 Av. E. Belin, 31400, Toulouse, France

Since several years, significant efforts have been made by the scientific community to understand and characterize the tropospheric chemistry. The evaluation of multiphase chemistry versus the overall tropospheric chemistry and its role in the earth's radiative budget is challenging because the physical nature and reactivity of condensed phases are still poorly known. However, it has been shown that multiphase chemistry within clouds has two major effects:
(1) An indirect effect by modifying cloud radiative properties;
(2) A direct effect on atmospheric chemistry.

More specifically, mixed-phase convective clouds have been recognized as an important means for vertical transport of pollutants from the boundary layer to the upper troposphere but very little is known about how chemical composition are modified due to chemical and microphysical processes occurring in the course of transport.

Only cloud process models allow studying these complex microphysical and chemical interactions. In this context, the M2C2 model (Model of Multiphase Cloud Chemistry) has been developed at the LaMP laboratory coupling chemical explicit reactivity together with detailed microphysical processes (Deguillaume et al., 2004, Leriche et al., 2007).

The cloud parametrization considers a two-moment scheme with warm processes for cloud water and rain water. This model integrates a multiphase chemistry module witch is explicit and valid for any environment. It describes the chemistry of H_xO_y, sulfur, chlorine, carbonates, NO_y, transition metals and organic compounds. Variable photolysis is also considered both in gaseous and aqueous phases. Liquid drops pH is calculated at each time step by solving the electroneutrality equation. This model has been recently updated to consider more realistic dynamic (i.e. entrainment) and different ice hydrometeors.

Indeed, entrainment has been implemented in the M2C2 model that dynamically modifies the simulated liquid water content and the parcel temperature. Mixed phase processes describe pristine formation, vapor deposition and collision/coalescence growth, evaporation, sedimentation and all complex conversions between hydrometeor categories, such as aggregation, accretion, riming, freezing, melting and sublimation. Ice retention and the burial during riming and crystal growth by vapor deposition respectively are considered to conclude in favor of the major role of ice phase in the trace compounds budget.

To assess the importance of ice phase and of crystal habit for the cloud chemical composition, two different air masses have been simulated (maritime vs. continental). The setup for simulations are derived from Audiffren et al. (1999) with chemical initialization taken from Williams et al. (2002) for the maritime case and Voisin et al. (2000) for the continental one.

First, microphysical properties of simulated convective clouds will be fully described looking specifically at the differences between simulated continental and marine clouds (ice distributions and contents, precipitation, processes at work). Second, direct freezing of droplets and their hydrodynamical collection by falling ice particles will be analysed because they constitute alternative ways for the removal of species, disturbing the transfer between only gas and liquid phases. Finally, sensitivity tests are performed on uncertain parameters such as burial efficiency for example.

By this study, the mixed phase cloud formation influence on chemical and dynamical processes will be evaluated by comparison with a warm cloud reference case. Results will be compared to previous numerical studies on this topic (Audiffren et al., 1999, Yin et al., 2005, Stuart et al., 2006).

Audiffren N., Cautenet S., Chaumerliac N. (1999). *Journal of Applied Meteorology*, 38, 1149-1160.

Deguillaume, L., M. Leriche, A. Monod & N. Chaumerliac (2004). *Atmos. Chem. Phys.*, 4, 95-110.

Leriche, M., R.L. Curier, L. Deguillaume, D. Caro, K. Sellegri, N. Chaumerliac (2007). *J. Atmos. Chem.,* 57-3, 281-297.

Stuart, L. A. & M. Z. Jacobson (2006) *J. of Atmos. Chem.*, 53, 13-42.

Voisin, D., & M. Legrand (2000). *J. of Geophys. Res.*, 105, 6817-6835.

Williams, J.E., F.J. Dentener & A.R. van den Berg, (2002) *Atmos. Chem. Phys.*, 2, 277-302.

Yin Y., Carslaw K.S. & Feingold G. (2005) *Quarterly Journal of the Royal Meteorological Society*, 131, 221-245.

Comparative overview of PM$_{2.5}$ mass concentrations and elemental profiles in indoor environments

B. Horemans[1], M. Stranger[1,2], S. Potgieter-Vermaak[1,3], A. Worobiec[1], R. Van Grieken[1]

[1]Department of Chemistry, University of Antwerp, Universiteitsplein 1, B-2610, Antwerp, Belgium
[2]VITO, Environmental Risk and Health, Air Quality Measurements, Boeretang 200, B-2400 Mol, Belgium,
[3]University of the Witswatersrand, Molecular Science Institute, Private Bag X3, PO Wits, 2050, South Africa

Keywords: PM$_{2.5}$, indoor-outdoor particles, elemental composition.

People in temperate or cold countries spend about 90% of their time indoors and exposure to elevated indoor particulate matter (PM) is a global concern. Moreover, epidemiological studies have indicated a strong correlation between personal exposure to fine thoracic airborne particulate matter (equivalent aerodynamic diameter < 2.5 µm, PM$_{2.5}$) and lung and cardiovascular disorders. Policy makers aim to regulate and control the emission of environmental aerosols, but the main focus is to regulate emission levels for ambient conditions, based on the association of indoor air pollutant concentrations with that of the outdoor. Currently, the Flemish Policy for Indoor Environment advices an annual PM$_{2.5}$ guideline value of 15 µg.m^{-3}, while the European guideline for ambient air recommends a maximum 24h averaged concentration of 25 µg.m^{-3}. Indoor PM is however often present at levels which equal or exceed the outdoor concentrations and can have a significantly different chemical composition and particle size distribution compared to outdoors.

The data presented are the result of a large scale study of PM$_{2.5}$ in 4 different types of indoor environments including residences, schools, offices, and daytime care centres. In total, approximately 76 different locations in Flanders (Belgium) have been monitored using Harvard type impactor units. The lowest PM$_{2.5}$ concentration levels were found in non-smoking offices, with PM$_{2.5}$ levels ranging from 8 to 24 µg.m^{-3} with an average of 15 µg m^{-3}. Higher concentrations were found in nurseries (31 µg.m^{-3}, range 13-49 µg.m^{-3}) as well as in non-smoking residences (29 µg.m^{-3}, range 11-74 µg.m^{-3}) and schools (61 µg.m^{-3}, range 11-166 µg.m^{-3}). Smoking environments contained significantly elevated levels of PM$_{2.5}$, with indoor/outdoor (I/O) ratios ranging from 0.7 to 5. Except for some isolated cases, I/O ratios for non-smoking offices and daytime care centres stayed below unity (average of 0.83 and 0.77, respectively). In primary schools, however, indoor sources caused on average I/O mass ratios higher than 1, reaching a maximum value of 8.8. The high concentrations for soil dust elements in PM$_{2.5}$ collected in the classrooms, particularly those with carpets, indicated that resuspension contributed considerably to the increased mass concentrations. Moreover, it was thought that the use of chalk in the classrooms was responsible for the high Ca concentrations indoors.

About 85% of the present data set represents real time exposure mass concentrations for PM$_{2.5}$, which is unique for Flanders. Except for offices, averages were noticeably higher than the current Flemish guideline value (2 – 5 times higher). Elemental concentrations can provide insight to establish the source of elevated indoor levels and should be used in conjunction with mass concentrations to evaluate the indoor air quality.

Polar organic compounds in PM$_{2.5}$ aerosols from Brasschaat, Belgium, during a 2007 summer campaign: Sources and diel variations

Y. Gómez-González[1], R. Vermeylen[1], W. Maenhaut[2] and M. Claeys[1]

[1]Department of Pharmaceutical Sciences, University of Antwerp (Campus Drie Eiken),
Universiteitsplein 1, BE-2610 Antwerp, Belgium
[2]Department of Analytical Chemistry, Institute for Nuclear Sciences, Ghent University, BE-9000 Gent, Belgium

In recent secondary organic aerosol (SOA) research several novel tracers from the photooxidation of α-/β-pinene have been structurally characterized that are also detected at significant concentrations in ambient fine aerosol and are thus useful for aerosol source characterization. These tracers include organosulfates and nitrooxy organosulfates (Surratt et al., 2007; 2008; Iinuma et al., 2007; Gómez-González et al., 2008), which have a mixed biogenic/anthropogenic origin since their formation requires sulfuric acid which is mainly from anthropogenic origin. In addition, a novel C$_8$-tricarboxylic acid, i.e., 3-methyl-1,2,3-butanetricarboxylic acid (MBTCA), was elucidated and identified as a stable endproduct from the photooxidation of α-/β-pinene in the presence of NO$_x$ (Szmigielski et al., 2007). In the present study, the concentrations of known and novel α-/β-pinene SOA tracers were determined in fine (PM$_{2.5}$; particulate matter with a diameter ≤2.5 μm) aerosol samples from a mixed pine/oak forest in Belgium that is heavily impacted by pollution, their time series and diel variations were examined, and the effects of meteorological parameters (temperature) and trace gas concentrations (ozone, SO$_2$ and NO$_x$) were assessed.

Separate day and night PM$_{2.5}$ aerosol samples were collected during a 2007 summer field campaign in the state forest "De Inslag", located in Brasschaat, Belgium, about 12 km to the northwest of the center of the city of Antwerp. The samples were collected on quartz fiber filters with a high-volume dichotomous sampler and extracted with methanol. Separation of the terpenoic acids was achieved using a T3 Atlantis (Waters) column and methanol as organic modifier. A second LC method using a Gold (Thermo Fisher) column and acetonitrile as organic modifier was developed to achieve separation for the isomeric α-pinene related nitrooxy organosulfates with molecular weight 295 (5 peaks). The LC/MS analyses were performed with an LXQ linear ion trap instrument (Thermo Fisher) in the negative ion electrospray ionization and full scan modes. For quantitation, use was made of two internal recovery standards (sebacic acid and octanesulfate) and calibration with reference standards. As to known α-/β-pinene SOA tracers, cis-pinic (MW 186) and cis-pinonic acid (MW 184) were included, as well as the recently characterized MBTCA. Other targeted terpenoic acids were the limonene SOA products ketolimononic and limonic acid, both with a MW of 186, and the Δ^3-carene SOA tracers caric (MW 186) and caronic acid (MW 184).

MBTCA, cis-pinic and cis-pinonic acid showed average concentrations of 4.9, 0.9 and 2.8 ng m^{-3}, and in total represented 0.23% of the organic carbon (OC). Of the targeted terpenoic acids, MBTCA exhibited the highest concentrations during the first days of the campaign that were characterized by high maximum temperatures (> 22ºC), while cis-pinonic acid showed the lowest concentrations, a result consistent with the formation of MBTCA through further oxidation of cis-pinonic acid (Szmigielski et al., 2007). MBTCA and cis-pinonic acid (expressed as %C of OC) showed diel variations with maxima mostly during daytime, while cis-pinic acid mainly peaked at night.

The five α-pinene-related MW 295 nitrooxy organosulfates showed an average total concentration of 3.1 ng m^{-3}, and represented 0.07% of the OC. They exhibited clear diel variations with maxima at night, consistent with observations first reported by Iinuma et al. (2007) and nighttime NO$_3$ radical chemistry as supported by Surratt et al. (2008). Interestingly, rather low concentrations of the MW 295 α-pinene SOA tracers were found during the first nights of the campaign (with maximum daytime temperatures > 22ºC). These results hint that the latter α-pinene SOA tracers are formed during nights following days where α-pinene was not fully consumed by photooxidation, leaving a portion of the emitted α-pinene available for processing by nighttime NO$_3$ chemistry.

Gómez-González, Y., et al. (2008). J. Mass Spectrom., 43, 371-382.
Iinuma, Y., et al. (2007). Environ. Sci. Technol., 41, 6678-6683.
Surratt, J. D., et al. (2007). Environ. Sci. Technol., 41, 517-527.
Surratt, J. D., et al. (2008). J. Phys. Chem. A, 112, 8345-8378.
Szmigielski, R., et al. (2007). Geophys. Res. Lett., 34, L24811, doi:10.1029/2007GL031338.

T03 Aerosol modelling

Simulation of transport processes of aerosol impurity in a ground boundary layer of above industrial centers

K.G. Shvarts[1], A.V. Shatrov[2]

[1] Department of Mathematics and Mechanics, Perm State University, 614990, Bukirev Str., 15, Perm, Russia
[2] Department of Mathematical Modeling, Vyatka State University, 610000, Moskovskaya Str., 36, Kirov, Russia

The new quasi two-dimensional model of mesoscale processes of transport and diffusion of an impurity in under layer of atmosphere with allowance of its temperature non-uniformity is submitted. Its conclusion is based on a technique described by [1-3]. The model represents development of the theory of "shallow water" on baroclinic atmosphere. With the help of a designed numerical scheme was calculated the structure of an impurity cloud from a point source arranged in large town with allowance for a thermal-uniformity of an underlying surface and an advection. The site by the sizes 100 km on 100 km in neighborhood of city Kirov (Russia) undertook is demonstrated that at a rather gentle western wind (speed of 2 m\s) the horizontal temperature non-uniformity introduces essential change to a current of traffic of a plume of an impurity (see Figure 1).
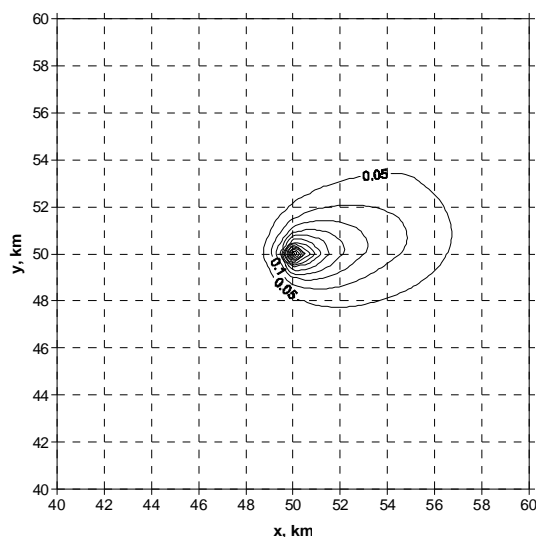
Figure 1. Distribution of concentration of an Impurity in lobes of marginal concentration

The count of interplay of an aerosol impurity with an underlying surface was made ground of non-uniformity of distribution of a coupling coefficient, which calculated with the help of the information of a map of land of computational area. The parallel implementation of algorithm of calculation is executed on the programming language Intel Fortran v.10.023 in medium LAM-MPI under control OS Linux Red Hat 7.0, established on the cluster supercomputer HP HPC Enigma X000 of Vyatka state university.

Also the approach given in this work helps to organize on-line monitoring of intensify of pollution emission into the atmosphere. Step-by-step regularization and serial functional approximation are used to solve the inverse problem.

Aristov, S.N., Frik, P.G. (1988) *Fluid Dynamics,* 4. 48-55.
Schwarz, K.G. (1995) *Computing technologies*, 13, 326-335.
Schwarz, K.G.(1998), *AIAA Progr*. Ser. 182, .271-279.

Scavenging of Gaseous Pollutants by Falling Liquid Droplets in Inhomogeneous Atmosphere

Tov Elperin, Boris Krasovitov and Andrew Fominykh

Department of Mechanical Engineering, The Pearlstone Center for Aeronautical Engineering Studies
Ben-Gurion University of the Negev, P. O. B. 653, 84105, Beer-Sheva, Israel

Keywords: scavenging, wet removal, absorption, atmospheric pollution, solubility

Concentration measurements of CO_2, SO_2, NH_3 and other gases in the atmosphere revealed altitudinal dependence of the concentrations. In this study we analyze mass transfer during absorption of soluble atmospheric gases by falling rain droplets with internal circulation taking into account altitudinal dependence of concentrations of soluble trace gases and temperature distribution in the atmosphere. Concentration of soluble gas and temperature distribution in the droplet are governed by a system of unsteady convective diffusion and energy conservation equations with time-dependent boundary conditions (Elperin et al. 2007; 2008, 2009). It is shown that gas absorption by falling droplets is described by a system of Volterra integral equations (Elperin and Fominykh 2005) that are solved numerically. We compare the results obtained using the model of gas absorption in the case of uniform distribution of soluble gases and temperature with those obtained when concentration of soluble gases and temperature vary with altitude. The comparison showed that vertical concentration and temperature profiles in atmosphere have a profound effect on mass transfer during gas absorption by a falling rain droplet. When concentration of soluble trace gases in the atmosphere is assumed constant, their content in the droplet attains saturation after a certain time elapsed, and at the final stage of their fall droplets do not absorb soluble trace gases. When concentration of soluble gases in the atmosphere decreases with altitude, droplets absorb trace gases during all the fall period. Consequently, concentration of soluble gases inside droplets at the ground which fall in the atmosphere with a homogeneous distribution of trace gases is lower than the concentration inside the droplet falling in the atmosphere with altitude dependent concentrations. When concentration of soluble gases increases with altitude, after a certain time interval droplets begin to release the dissolved gases. Consequently droplets have a lower concentration of trace gases at the ground level as compared with droplets falling in an atmosphere with a homogeneous distribution of trace gases. Dependence of the concentration of the dissolved gas in the bulk of a water droplet vs. time for absorption of CO_2 by water (average concentration of CO_2 in the atmosphere is 300 ppm) is shown in Fig. 1. Calculations are performed for a case when initial concentration of dissolved gas in a droplet is negligibly small and for different values of gradients of concentration of a soluble gas. The derived solution can be used in calculations of scavenging of hazardous gases in atmosphere by rain or gas absorption in spray absorbers and incorporated into the computer codes. The simple form of the obtained solutions allows to use them to analyze the dependence of the rate of mass transfer on different parameters, e.g., upon a radius of a droplet, diffusion coefficient, gradient of absorbate concentration in a gaseous phase etc. The obtained solution can be used for validating modeling procedures for solving more complicated problems of gas absorption by falling liquid droplets.
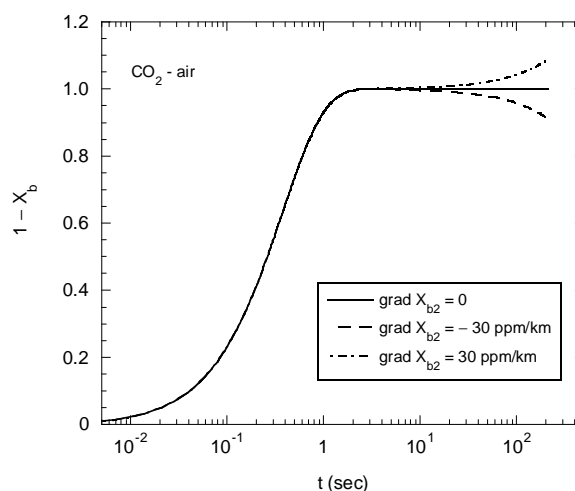
Figure 1. Dependence of the concentration of the dissolved gas in the bulk of a water droplet vs. time.

References

Elperin, T. & Fominykh, A. (2005) Atmospheric Environment, 39, 4575-4582.
Elperin, T., Fominykh, A. & Krasovitov, B., (2007). Journal of the Atmospheric Sciences, 64, 983–995.
Elperin, T., Fominykh, A., & Krasovitov B. (2008) Atmospheric Environment, 42, 3076–3086.
Elperin, T., Fominykh, A. & Krasovitov, B., (2009). Journal of the Atmospheric Sciences, (in press).

Determination of the contribution of different groups of emission sources on the concentration of PM10, PM2.5, and NO$_2$ in North Rhine-Westphalia – a whodunnit

H. Hebbinghaus[1], S. Wurzler[1] , M. Memmesheimer[2], G. Piekorz[2], E. Friese[2], H. J. Jakobs[2], C. Kessler[2], A. Ebel[2], and P. Bruckmann[1]

[1] North Rhine Westphalia State Agency for Nature, Environment and Consumer Protection (LANUV), P.O. Box 101052, D-45610 Recklinghausen, Germany

[2] Rhenish Institute for Environmental Research (RIU), EURAD-Project, University of Cologne, Aachener Strasse 201-209, D-50931 Cologne, Germany

High levels of particle (PM10, PM2.5) and NO$_2$ concentrations are known to cause adverse health effects. Therefore, the EC air quality directives set limit and target values for various pollutants, such as PM10 and NO$_2$. Where these limit values are exceeded, plans and programmes have to be set up to meet the limit values in future. One important part of these plans is the source apportionment: Identifying the main contributors and thus enabling specific actions to reduce the load. Measurements have been showing high levels of background concentrations in North Rhine-Westphalia (NRW) of up to 50 % of the limit values, contributing to exceedances of the limit values. Therefore, model simulations have been performed to assess the main contributors to the background concentrations.

The background concentration of PM10, PM2.5, and NO$_2$ was simulated with the European Air Pollution Dispersion Model (EURAD, Memmesheimer et al., 2004). The EURAD model simulates the concentration due to emissions, transport, and chemical transformation. The meteorological data stem from the MM5, transport is modelled by solving the 3-D advection and diffusion equation. The chemical model CTM2 treats chemical processes and the Modal Aerosol Dynamics Model (MADE) is used to account for secondary aerosol (Schell et al., 2001). The model is run in a one-way nesting with three grids, the largest domain spanning Europe in a horizontal resolution of 125 x 125 km². Nested in this is the area of Germany with 25 x 25 km² horizontal resolution. The smallest domain spans NRW with a horizontal resolution of 5 x 5 km². This nesting allows the consideration of long-distance transport.

The simulations have been performed for the year 2006 with different emission sources switched off. In this paper we present the results for four scenarios, focused on NRW: Basic case (no changes in emissions), no anthropogenic emissions in NRW, no industrial emissions in NRW, no emissions from vehicles in NRW.

The basic simulation yields similar results for all parameters. The highest concentrations are found in the highly populated, industrially influenced conurbation of the Ruhr area and along the river Rhine with values of about 26 µg/m³ (PM10) and 30 µg/m³ (NO$_2$), while the rural areas show lower values, about 10 µg/m³ (NO$_2$) and 15 µg/m³ (PM10). The model yields good to satisfactory results in comparison to measurements. For PM10, problems mainly occur at Duisburg which is governed by a complex structure of sources and diffuse emissions. Here, the model overestimates the pollution burden.

The results for the scenarios differ, depending on the parameter and the regarded area. In general, in NRW the influence of long-distance transport is highest in the western parts and lower in the eastern. This is to be expected, due to the prevailing West winds, but can be different for special episodes. On average, for PM10 and PM2.5 about two-thirds of the background concentrations stem from long-distance transport, while for NO$_2$ it is roughly one third to one half.

Concerning emission sources in NRW, for NO$_2$ the largest contribution comes from vehicle traffic. In the conurbations, the vehicles yield approximately 70 % of the load due to anthropogenic emissions in NRW, which corresponds to about 50 % of the total background concentration there. In the rural areas, the load due to vehicle emissions in NRW is about twice as much as the load due to industry emissions in NRW, about 20 % of the background concentration.

For the particles, the main factor in the conurbations are industrial emissions, accounting for about twice as much of the background concentration as vehicles. In the rural areas the contributions of industrial and vehicle emissions more or less equal each other. It has to be kept in mind, though, that the model only yields the background concentration. At, e.g., street canyons with a high density of traffic, the local traffic has a large contribution to the total concentration (20 to 40 %) which can lead to exceedances of limit values. To meet the limit values for PM10 and NO$_2$, actions have to be taken towards vehicle emissions as well as industrial emissions.

Memmesheimer, M., Friese, E., Ebel, A., Jakobs, H. J., Feldmann, H., Kessler, C., Piekorz, G. (2004), IJEP, **22**, 108 – 132.

Schell, B., Ackermann, I.J., Hass, H., Binkowski, F.S., and Ebel, A. (2001) *J. Geophys. Res.,* 106, 28275-28293.

Monitoring the 4-D aerosol distribution: Synergetic use of MODIS AOT, in-situ PM observations and the chemical transport model LOTOS-EUROS

E.C.J.Hendriks, R. Timmermans, A. Segers and M. Schaap

TNO Built Environment and Geosciences, PO-Box 80015, 3508 TA, Utrecht, The Netherlands

Keywords: aerosol modelling, AOD, PM measurements data-assimilation, Ensemble Kalman Filter

Monitoring aerosols over wide areas is important both for the assessment of exposure of the population to PM and for the assessment of climate forcing by aerosols. Present monitoring techniques – when independently used- are not sufficient to capture the high variability of aerosol fields in space and time. Synergetic use of ground-based observations (in-situ and surface remote sensing), satellite instruments and models is useful to increase the knowledge on the 4-D distribution of aerosols.

In the line of striving for an optimal synergy between the available tools for the monitoring of the 4-D aerosol field over the European region, we investigate the impact of the use of ground-based PM observations and MODIS AOT in combination with the LOTOS-EUROS chemistry transport model (Schaap et al., 2008). For this purpose we use the ensemble Kalman filter (EnKF) data-assimilation technique where we have applied random noise to the emissions of aerosol precursors to define the ensemble and therewith the model uncertainty.

Previous studies have shown the added value of data-assimilation of in-situ PM observations (Denby *et al.*, 2008) and that of MODIS AOT (Schaap, *et al.*, 2006) in the LOTOS-EUROS model for PM2.5 and PM10. In this work, we evaluate the added value of combining the assimilation of both in-situ observations and MODIS AOT for the construction of the 4-D the aerosol distribution. In addition, we explore the possibilities for assimilation of EARLINET data, which will provide more detailed information on the vertical aerosol profile.

During the first stage of this study, we have determined the quality and suitability of the MODIS observations for assimilation in the LOTOS-EUROS model. For this, we have compared the collection 5 datasets from Terra and Aqua MODIS for the year 2006 over Europe with ground-based observations from the AERONET network. In comparison to the earlier study on MODIS collection 4 for 2003, the quality of the satellite data has improved and the bias is removed (see Fig. 1). Temporal correlation between MODIS AOT and AERONET data is 0.80 for both instruments, the spatial correlation is 0.81 and 0.73 for terra and aqua MODIS respectively. The improved quality is promising for succesfull results on the data-assimilation.

Further details on this comparison and the results of the synergetic data-assimilation technique will be presented at the conference.
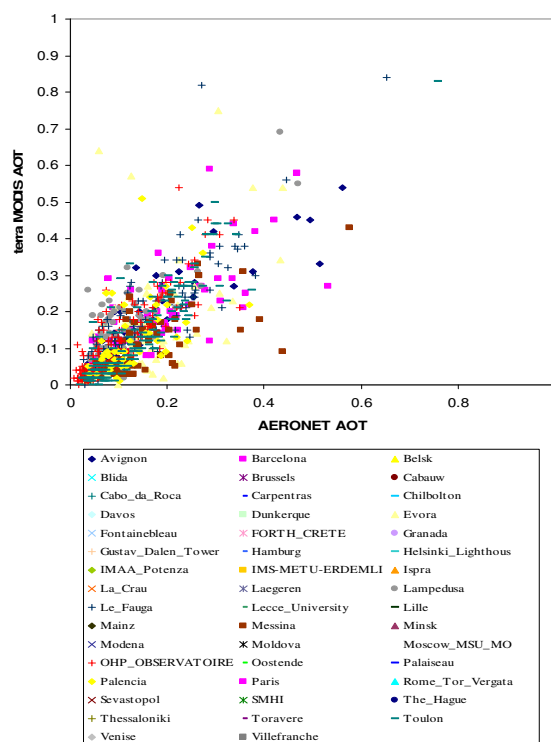
Figure 1. terra MODIS AOT versus AERONET AOT

Denby, B., Schaap, M., Segers, A., Builtjes, P. & Horálek, J., *Comparison of two data assimilation methods for assessing PM10 exceedances on the European scale*, in *Atmospheric Environment,* 42, 7122–7134, 2008.

Schaap, M., Timmermans, R. M. A. , Sauter F.J., Roemer, M., Velders, G. J. M, Boersen, G. A. C., Beck, J. P. & Builtjes P. J. H., *The LOTOS-EUROS model: description, validation and latest developments*, *Int. J. of Environ. and Pollution*, 32, No. 2, pp.270–290, 2008.

Schaap, M., de Leeuw, G., Henzing, B. & Builtjes, P. J. H., Assimilation of aerosol optical depth over Europe in a regional chemistry transport model, in *Proceedings of the 7th International Aerosol Conference, September 10-15, 2006, St. Paul (MN), Abstract Book Volume 2*, 1839-1840, 2006.

Enhanced aerosol formation in coastal regions caused by ship emissions

V.Matthias[1], I. Bewersdorff[2], A. Aulinger[1], and M. Quante[1]

[1] GKSS Research Centre Geesthacht GmbH, Institute for Coastal Research, Max-Planck-Strasse 1, 21502 Geesthacht, Germany
[2] During this work at GKSS Research Centre Geesthacht GmbH, Institute for Coastal Research, Max-Planck-Strasse 1, 21502 Geesthacht, Germany

Keywords: aerosol modelling, shipping emissions, coastal area.

As a consequence of the global distribution of manufacturing sites and the increasing international division of labor, ship traffic is becoming more and more important as an origin of air pollution. Particularly contamination due to the emissions from large cruise and cargo ships was subjected to be responsible for pollution of the sea as well as the urban harbour environment (Endresen et al., 2003, Tsyro and Berge, 1997). However, the effects of ship traffic on air pollution have up to now only been studied on rather coarse horizontal model resolution.

This study is based on a detailed ship traffic statistics of Lloyd's Marine Intelligence Unit (LMIU) for the North and Baltic Seas for the year 2000. It consists of a vessel characteristic database and a vessel movement database and it includes all commercial vessels equal to or greater than 100 gross tonnages (GT). Emission factors (power-based in g/kWh) used in this study are obtained from Cooper and Gustafsson (2004). The procedure how to obtain the ship emission dataset is displayed in Figure 1.
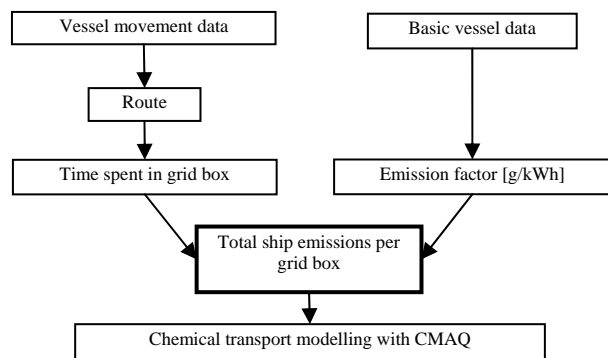
Figure1: Outline of the procedure to generate the ship emission dataset

The high spatial and temporal emission fields that were derived reveal a recognizable dependence of the ship emissions on season. The contribution of ship emissions to the modelled concentration and deposition distribution of sulfur and nitrogen containing aerosol compounds as well as PM10 in North Sea coastal areas is investigated. The modelling is performed with the Community Multiscale Air Quality modelling system (CMAQ). It is applied on a 54 x 54 km^2 grid for over Europe and on an 18 x 18 km^2 nested grid for the North Sea area.

In this study we investigate which regions are highly influenced by ship emissions and under which meteorological conditions the effect is most pronounced. For this purpose, CMAQ model runs with and without the inclusion of ship emissions are performed and compared to each other.
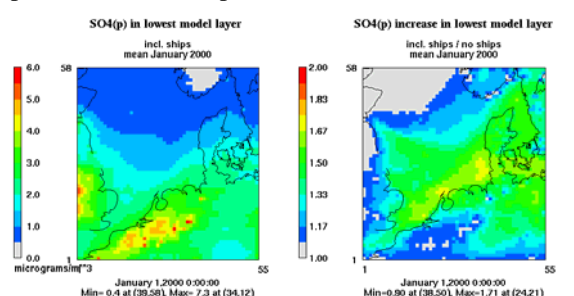
Fig. 2: Modelled sulphate aerosol concentrations in North Sea coastal regions and their increase due to ship emissions in January 2000.

The results show that northern Germany, Denmark and southern Sweden are highly affected by increased concentrations of nitrate and sulphate aerosols that originate from emissions of NO_x and SO_2 from ships travelling in the North Sea (Fig. 2). This effect is larger in summer than in winter because of lower nitrate concentrations in summer. Land based sulphur emissions show a seasonal cycle with lower emissions in summer than in winter while ship emissions are higher in the summer months. Subsequent effects on eutrophication are also investigated in this study.

Cooper, D.A., T. Gustafsson (2004). Methodology for Calculating Emissions from Ship: 1. Update of Emission Factors. SMHI Swedish Metrological and Hydrological Institute. Norrköping, Sweden.

Endresen, Ø., E. Sørgård, J.K. Sundet, S.B. Dalsøren, I.S.A. Isaksen, T.F. Berglen, G. Gravir (2003). *J. Geophys. Res.* 108 (D17), 4560.

Tsyro, S.G., E. Berge (1997). The Contribution of Ship Emission from the North Sea and the North-eastern Atlantic Ocean to Acidification in Europe. EMEP/MSC-W Note 4/97. Norwegian Meteorological Institute. Oslo, Norway.

Photophoretic motion of absorbing aerosols: updated and advanced model for stratospheric applications

S.A. Beresnev, L.B. Kochneva, V.I. Gryazin

Aerosol Physics Laboratory, Ural State University, 620083, Ekaterinburg, Russia

Keywords: aerosol modelling, carbonaceous aerosol, light absorption, photophoresis, stratospheric aerosols

One of possible mechanisms of vertical transport of absorbing aerosol particles in stratosphere can be radiometric photophoresis (Beresnev *et al.*, 2003 *a*, *b*). The offered earlier model predicts, in particular, that for certain types of absorbing carbonaceous aerosol the negative "solar" photophoresis (motion of particles in the field of short-wave solar radiation against gravity) and positive "thermal" photophoresis (motion of particles in the field of long-wave outgoing thermal radiation) can lead to the vertical lifting and levitation of sub-micrometer and micrometer particles at altitudes of the lower and middle stratosphere at the assumption of stationary atmosphere (Figures 1,2). This transport mechanism is sufficiently effective for the light and low-conductivity compact and fractal-like particles (for example, for carbonaceous and volcanic fly-ash particles). Furthermore, radiometric photophoresis is the regular and permanent factor of vertical aerosol motion on synoptic and global time scales. In thermally and mechanically stable stratosphere the given long-term transport mode can lead, for example, to unexpected and uncontrollable accumulation of soot particles from aircraft engines and biomass burning.

In this report we present the updated model for radiometric photophoresis of atmospheric aerosols.

Firstly, the results for "solar" photophoretic characteristics are calculated in the framework of advanced model for short-wave solar radiation (Zhuravleva & Firsov, 2004).

Secondly, the characteristics for "thermal" photophoresis are specified taking into account the downward long-wave thermal radiation (Gribanov *et al.*, 1999).

The third important generalization concerns the form and structure of considered aerosol particles. In early model the particle was assumed spherical with homogeneous thermal-physics and optical properties. Experiments with fractal-like soot particles discussed by Beresnev *et al.* (2005) show a possible direction in transferring earlier received results on the more complex particle geometry by the account of gas-kinetic transport form-factor and estimation of the photophoretic asymmetry factor J_1 on the basis of optical mean-field theory.

We discuss also the known facts of soot particles accumulation in the upper troposphere and low stratosphere with the purpose of clearing of probable physical mechanisms of the given phenomenon.
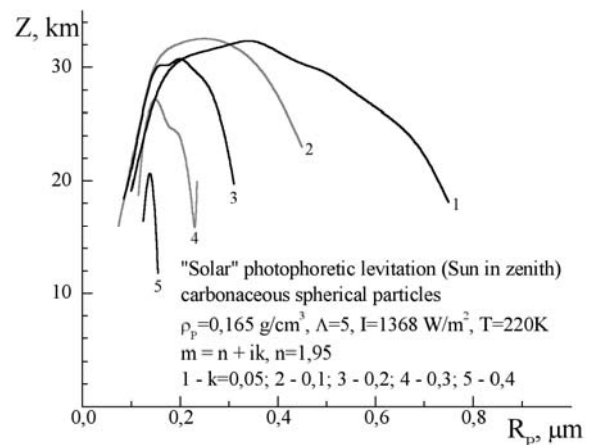
Figure 1. The photophoretic levitation altitudes for carbonaceous spherical particles in the case of "solar" photophoresis.
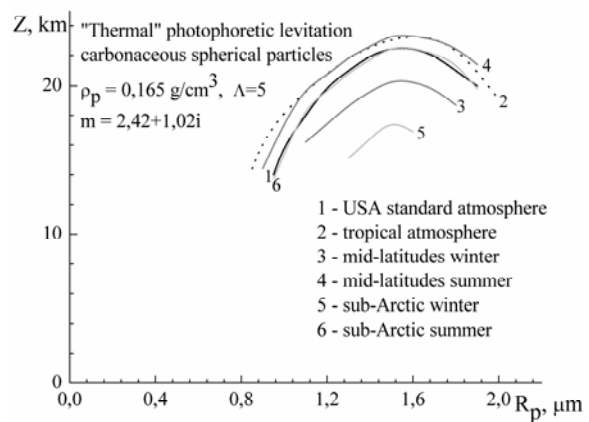
Figure 2. The photophoretic levitation altitudes for carbonaceous spherical particles in the case of "thermal" photophoresis.

Beresnev, S. A., Kovalev, F. D., Kochneva, L. B. *et al.* (2003). *Atmos. Oceanic Opt.*, 16(1), 44-48.

Beresnev, S. A., Kochneva, L. B., Suetin, P. E. *et al.* (2003). *Atmos. Oceanic Opt.*, 16(5-6), 431-438.

Beresnev S. A., Kochneva L. B., Gryazin V. I., & Gribanov, K. G. (2005). *Proc. SPIE*, 6160, 797-807.

Zhuravleva, T. B., & Firsov, K. M. (2004). *Atmos. Oceanic Opt.*, 17(11), 799-806.

Gribanov, K. G., Zakharov, V. I., & Tashkun S. A. (1999). *Atmos. Oceanic Opt.*, 12(4), 358-361.

Intercomparison of aerosol microphysics modules in the framework of the ECHAM5 climate model

R. Hommel[1,2], H. Kokkola[2,3], J. Kazil[2,6], U. Niemeier[2], A.-I. Partanen[2,4,5], J. Feichter[2] and C. Timmreck[2]

[1]Centre for Atmospheric Science, Department of Chemistry, Cambridge University, Cambridge, UK
[2] Max Planck Institute for Meteorology, Hamburg, Germany
[3]Finnish Meteorological Institute, Kuopio, Finland
[4]Tampere University of Technology, Tampere, Finland
[5]University of Kuopio, Department of Physics, Finland
[6]National Oceanic and Atmospheric Administration (NOAA), Chemical Sciences Division, Boulder, USA

Keywords: Aerosol dynamics, Atmospheric aerosols, Modelling, Sulfur particles, Volcanic particles**.**

Aerosols in the atmosphere are an elementary constituent of the atmospheric composition and affect the global climate through a variety of physical and chemical interactions in the troposphere and stratosphere (IPCC, 2007). Large volcanic eruptions alter the Earth's radiative balance and interfere with the catalytic cycles of ozone depletion mainly by the formation of micrometer size aerosol particles above the tropopause.

Recent experimental and numerical investigations of process oriented aerosol-climate interactions revealed that appropriate climate effects can only be modeled when informations about the aerosol size and number spectra are provided (e.g. Zhang et al., 2002; Dusek et al., 2006). Nevertheless in the majority of climate models volcanic perturbations of the stratosphere are either prescribed based on the aerosol parameters of interested (surface area, optical depth) or the aerosol microphysics is considered explicitly but with a heavily reduced number of degrees of freedom (Timmreck et al., 1999; Dameris et al., 2005). This yields e.g. to underestimations of surface temperature effects in the fade of an eruption. To overcome that weakness, we tested three aerosol modules currently available in the framework of the climate model ECHAM5 (Roeckner et al., 2003) in environmental conditions assumed to be representative in the stratosphere after the injection of SO_2 from modest to large volcanic eruptions. The study focuses on the evolution of liquid H_2SO_4/H_2O aerosol.

The modal modal M7 (Vignati et al., 2004; Stier et al., 2005), currently the default aerosol scheme in ECHAM5, is compared with two sectional aerosol schemes: the moving centre sectional aerosol scheme SALSA (Kokkola et al., 2008), and the fixed sectional scheme SAM2 (Hommel 2008). Since direct measurements of particle size informations during the initial stage of a volcanic injection in the stratosphere are not available, the detailed sectional aerosol model MAIA (Kazil and Lovejoy, 2007) is used as a reference in this study.

It is shown that all modules are able to represent a "typical" stratospheric background aerosol distribution when the particles are formed via the oxidation pathway of SO_2. However, the modules differ strongly and their setup have to be changed to be applied in global model simulations capturing respective volcanic episodes.

Dameris, M., Grewe, V., Ponater, M., Deckert, R., Eyring, V., Mager, F., Matthes, S., Schnadt, C., Stenke, A., Steil, B., Brühl, C., & Giorgetta, M. A., Atmos. Chem. Phys., 5, 2121-2145, 2005.

Dusek, U., Frank, G. P., Hildebrandt, L., Curtius, J., Schneider, J., Walter, S., Chand, D., Drewnick, F., Hings, S., Jung, D., Borrmann, S., & Andreae, M. O., Science, 312, 2006.

Hommel, R., Reports on Earth System Science 57, Max Planck Institute for Meteorology, 2008

IPCC: Climate Change 2007: The scientific basis., Cambridge University Press, New York, 2007.

Kazil, J. & Lovejoy, E. R., Atmos. Chem. Phys., 7, 3447–3459, 2007.

Kokkola, H., Korhonen, H., Lehtinen, K. E. J., Makkonen, R., Asmi, A., Järvenoja, S., Anttila, T., Partanen, A.-I., Kulmala, M., Järvinen, H., Laaksonen, A., & Kerminen, V.-M. Atmos. Chem. Phys., 8, 2469–2483, 2008.

Roeckner, E., Bäuml, G., Bonaventura, L., Brokopf, R., Esch, M., Giorgetta, M., Hagemann, S., Kirchner, I., Kornblueh, L., Manzini, E., Rhodin, A., Schlese, U., Schulzweida, U., & Tompkins, A., MPI-Report, 349, 2003.

Stier, P., Feichter, J., Kinne, S., Kloster, S., Vignati, E., Wilson, J., Ganzeveld, L., Tegen, I., Werner, M., Balkanski, Y., Schulz, M., Boucher, O., Minikin, A., & Petzold, A., Atmos. Chem. Phys., 5, 1125–1156, 2005.

Timmreck, C., Graf, H.-F., & Kirchner, I., J. Geophys. Res., 104, 9337–9360, 1999.

Vignati, E., Wilson, J., & Stier, P., J. Geophys. Res., 109, doi:10.1029/2003JD004485, 2004.

Zhang, Y., Easter, R. C., Ghan, S. J., and Abdul-Razzak, H., J. Geophys. Res., 107, 4558, 2002.

The middle atmosphere aerosol-climate model MAECHAM5-SAM2

R. Hommel[1,2], C. Timmreck[2], and H.-F. Graf[1]

[1]Centre for Atmospheric Science, Cambridge University, Cambridge, UK
[2]Max Planck Institute for Meteorology, Hamburg, Germany

Keywords: aerosol modelling, in-situ measurements, satellites, stratospheric aerosols, sulfur particles.

We are presenting a new global aerosol-climate model MAECHAM5-SAM2 (Hommel, 2008) to study the aerosol dynamics in the UTLS under background and volcanic conditions.

The microphysical core module SAM2 is an extension of the aerosol module SAM (Timmreck & Graf, 2000), previously used by Timmreck (2001) in conjugation with the predecessor climate model ECHAM4 to investigate the size distribution of stratospheric background aerosol. SAM2 treats the formation, the evolution and the transport of stratospheric sulphuric acid aerosol. The aerosol size distribution and the weight percentage of the sulphuric acid solution is calculated dependent on the concentrations of H_2SO_4 and H_2O, their vapor pressures, the atmospheric temperature and pressure. The fixed sectional method (e.g. Gelbard et al., 1980) is used to resolve an aerosol distribution between 1 nm and 2.6 μm. Homogeneous nucleation, condensation and evaporation, coagulation, water-vapor growth, sedimentation, dry and wet deposition are considered. The applied stratospheric sulfur chemistry scheme is based on an extension of the chemical transport model CHEM (Steil et al., 2003, Dameris et al., 2005), using offline oxidants (OH, O_3, NO_2) derived from the earth system model MESSy (e.g. Jöckel et al., 2005).

The aerosol module is applied in the middle-atmosphere climate model MAECHAM5, resolving the atmosphere up to 0.01 hPa (~80 km) in 39 layers (Manzini et al., 2006).

Our simulations reveal that MAECHAM5-SAM2 well represents in-situ measured (Deshler et al., 2003) size distributions of stratospheric background aerosol in the northern hemisphere mid-latitudes. Distinct differences can be seen when derived integrated aerosol parameters (surface area, effective radius) are compared with aerosol climatologies based on the SAGE II satellite instrument. In this study we used SAGE II retrievals compiled by the University of Oxford (PARTS, 2004) and the NASA AMES laboratory (Bauman et al., 2003). It can be shown that the bias between the model and the SAGE II data increases as the moment of the aerosol size distribution decreases. Thus the modeled effective radius show the strongest bias, followed by the aerosol surface area density. Correspondingly less biased are the higher moments volume area density and the mass density of the global stratospheric aerosol coverage. This finding supports the key finding No. 2 of the SPARC Assessment of Stratospheric Aerosol Properties (2006), where it was shown that during periods of very low aerosol load in the stratosphere, the consistency between in-situ and satellite measurements, which exist in a volcanically perturbed stratosphere, breaks down and significant differences exist between the systems for key aerosol parameters including the aerosol surface area density.

Bauman, J. J., Russell, P. B., Geller, M. A., & Hamill, P., J. Geophys. Res., 108, 2003.

Dameris, M., Grewe, V., Ponater, M., Deckert, R., Eyring, V., Mager, F., Matthes, S., Schnadt, C., Stenke, A., Steil, B., Brühl, C., & Giorgetta, M. A., Atmos. Chem. Phys., 5, 2121-2145, 2005.

Deshler, T., Hervig, M. E., Hofmann, D. J., Rosen, J. M., & Liley, J. B., J. Geophys. Res., 108, 2003.

Gelbard, F., Tambour, Y., & Seinfeld, J. H., J. Colloid Interface Sci., 76, 541–556, 1980.

Hommel, R., Reports on Earth System Science 57, Max Planck Institute for Meteorology, 2008.

Jöckel, P., Sander, R., Kerkweg, A., Tost, H., und Lelieveld, J., Atmos. Chem. Phys., 5, 433-444, 2005.

Manzini, E., Giorgetta, M. A., Esch, M., Kornblueh, L., & Roeckner, E., J. Climate, 19, 3863-3881, 2006.

PARTS: Particles in the upper troposphere and lower stratosphere and their role in the climate system, Project Report, European Commission, eds. H.-F. Graf, 2004.

SPARC: Stratospheric Processes and their Role in Climate: Assessment of Stratospheric Aerosol Properties (ASAP),WCRP–124, WMO/TD No. 1295, SPARC Report No. 4, eds. L. Thomason & T. Peter, 2006.

Steil, B., Brühl, C., Manzini, E., Crutzen, P. J., Lelieveld, J., Rasch, P. J., Roeckner, E., & Krueger, K., J. Geophys. Res., 108, 2003.

Timmreck, C. & Graf, H.-F., Meteorol. Zeitschr., 9, 263–282, 2000.

Timmreck, C.:, J. Geophys. Res., 106, 28313–28332, 2001.

Model calculations of free tropospheric aerosol and cloud condensation nuclei formation in an SO_2 rich pollution plume

L. Pirjola[1,2], V. Fiedler[3,4], F. Arnold[3,4], and H. Schlager[3]

[1]Department of Physics, University of Helsinki, P.O. Box 64, 00014 Helsinki, Finland
[2]Department of Technology, Metropolia University of Applied Sciences, P.O. Box 4000, 00180 Helsinki, Finland
[3]Institut für Physik der Atmosphere, Deutsches Zentrum für Luft- und Raumfahrt, Oberpfaffenhofen, 82234 Wessling, Germany
[4]Atmospheric Physics Division, Max Planck Institute for Nuclear Physics, P.O. Box 103980, 69029 Heidelberg, Germany

Fossil fuel combustion represents the most important source of atmospheric sulfur dioxide (SO_2), a major air pollutant. Presently most atmospheric SO_2 is released in Europe and in East Asia from combustion of relatively sulfur rich coal. After the release from ground level combustion sources substantial amounts of SO_2 may be transported to the middle and upper troposphere where SO_2 is removed preferably by OH induced gas-phase conversion to gaseous sulfuric acid (GSA). Depending on the efficiency of photochemical OH formation, a SO_2 lifetime of 7–14 days is sufficiently long to allow SO_2 long-range transport. At low temperatures typical of the middle and upper troposphere, GSA may undergo binary (H_2SO_4-H_2O) nucleation leading to new aerosol particles. These grow by condensation and coagulation, and ultimately may become CCN.

In this work we report on model investigations of particle formation and growth in an SO_2 rich aged pollution plume detected at 5-7 km altitude over the East Altantic on 3 May 2006 (Fiedler *et al.*, 2009a). The peak SO_2 concentration was 900 pmol/mol, measured by chemical ionization mass spectrometry CIMS. A sectional aerosol model AEROFOR (e.g. Pirjola & Kulmala, 2001) is a Lagrangian type box model that includes gas-phase chemistry along with aerosol dynamics; in this work particles were formed by homogeneous binary H_2SO_4-H_2O nucleation and grown by coagulation and condensation of H_2SO_4 and H_2O. Gaseous sulphuric acid was formed via the oxidation of OH and SO_2 under clear sky conditions, in accordance with a satellite cloud top temperature data analysis. Simulations started 8.5 days before the measurements over the Eastern Asia, where the origin of the plume was predicted by a particle dispersion model FLEXPART (Stohl *et al.*, 2005). Four different scenarios for the amount of pre-existing particles were studied, and sensitivity tests of CCN concentrations were performed.

As an example, Fig. 1 shows the number concentrations Nd of aerosol particles with diameters larger than d nm as a function of time when the initial particle number concentration was 250 cm^{-3} (Fiedler *et al.*, 2009b). Freshly nucleated particles were formed during the first two days leading to the maximum particle concentration of 6×10^6 cm^{-3}. Condensational and coagulational growth formed particles with diameters larger than 50 nm already after the first day. Particles of these sizes may act as CCN at 0.5% supersaturation and are therefor available for cloud formation.
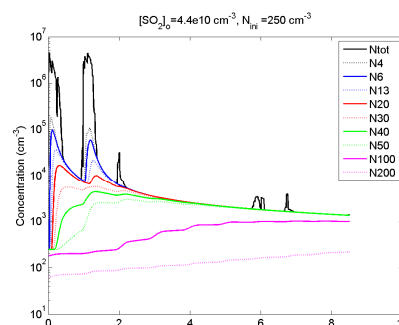
Figure 1. Time evolution of particle number concentrations of different size classes.

After 8 days and at a distance of about 20 000 km from its birthplace, the plume had very suitable conditions for the formation of whiter clouds possibly possessing a reduced tendency for rainout. The Asian pollution plume reported here represents a striking example of an environmental impact of long range transport of fossil fuel combustion generated SO_2.

Fiedler, V., Nau, R., Ludmann, S., Arnold, F., Schager, H. and Stohl, A. (2009a). *Atmos. Chem. Phys. Discuss.*, 9, 1377-1405.

Fiedler, V., Arnold, F., Schager, H. and Pirjola, L (2009b). *Atmos. Chem. Phys. Discuss.*, 9, 2763-2790.

Pirjola, L. and Kulmala, M. (2001) Tellus, 53B, 491-509.

Stohl, A., Forster, C., Frank, A., Seibert, P., and Wotawa, G. *Atmos. Chem. Phys.*, 5, 2461–2474, 2005.

Parameterisation of the aerosol washout process using a moment model

R. Rinke, H.Vogel and B. Vogel

Institute for Meteorology and Climate Research,
Karlsruhe Institute for Technology

Keywords: Aerosol modelling, Washout, Wet deposition

The scavenging of particles by precipitation is one of the major processes by which the atmosphere is cleansed and the balance between the sources and sinks of atmospheric aerosol particles is maintained. While significant experimental and theoretical work has been dedicated to estimate the particle lost due to the washout mechanism under a variety of conditions (Wang and Pruppacher, 1977; Slinn, 1983), recent reports show that the representation of aerosol removal processes in current aerosol transport models remains a source of uncertainty (Rasch et al., 2000). Particles may be scavenged by precipitation due to inertial impaction Brownian motion, electrical and phoretic effects.

Theoretical and numerical studies of the washout mechanisms have led to the predictions of a functional dependence of the scavenging collision efficiency on the aerosol size. Although there are some numerical microphysical models that prescribed meteorological parameters coupled with the cloud microphysics and aerosol removal processes, these models are too complex, and require huge computational resources to be used in comprehensive three dimensional models.. Thus, various scavenging coefficients, expressed as constants or functions of the precipitation intensity, are used in regional or mesoscale Lagrangian and Eulerian models to describe the precipitation and wet removal of pollutants (Seinfeld and Pandis 1998). However, the dependence of the scavenging process on the aerosol particle and drop size distribution and also the drop settling velocity can not be considered. Thus, for practical purposes, the development of a more simple and accurate model, which describes the particle removal process by wet precipitation, coupled with an air quality model, is needed.

The main purpose of our study is the development of a moment model for the simulation of particle scavenging by raindrops under consideration of the physical scavenging mechanisms Brownian diffusion, interception, impaction, thermophoresis, diffusiophoresis and electrical attraction. The evolution of the particle size distribution by a wet scavenging process for the entire ambient aerosol size range is investigated using the moment method, which is easy to handle and computationally efficient, compared with other numerical methods, such as sectional size representation. A log-normal aerosol distribution was assumed, and the collision efficiency formula given by Davenport and Peters (1978) was modified for use in the moment method. The parameterisation scheme was used to simulate the particle lost due to the washout mechanism in the regional air quality model COSMO-ART (Vogel et Al., 2009). The parameterisation scheme and the results of our simulations will be presented.
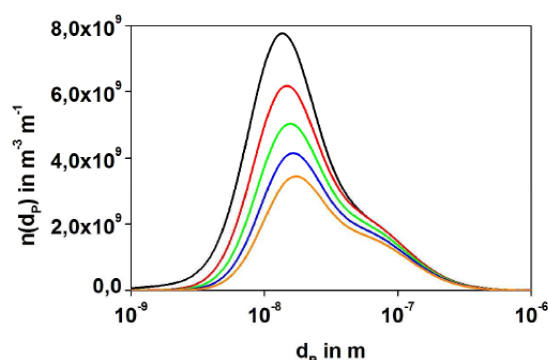
Figure 1 Particle number as function of particle diameter for an urban aerosol (black curve before rain; red curve after 15 min rain; green curve after 30 min rain; blue curve after 45 min rain; yellow curve after 60 min rain).

Davenport, H. M. und L. K. Peters (1978). Field studies of atmospheric particulate concentration changes during precipitation. Atmos. Environ., 12, 997–1008.

Rasch, P. J., Feichter, J., Law, K., et al. (2000). A comparison of scavenging and deposition processes in global models: results from the WCRP Cambridge Workshop of 1995, Tellus, 52B, 1025–1056.

Seinfeld, J. H. and Pandis, S. N. (1998). Atmospheric Chemistry and Physics, Wiley, New York, pp. 1326.

Slinn,W. G. N. (1983). Precipitation scavenging, in Atmospheric Sciences and Power Production 1979, Chap 11. Division of Biomedical Environmental Research, U.S. Department of Energy, Washington, D.C..

Vogel, B., H. Vogel, D. Bäumer, M. Bangert, K. Lundgren, R. Rinke, T. Stanelle, (2009) submitted to APCD.

Wang, P. K. and Pruppacher, H. R. (1977). An experimental determination of the efficiency with which aerosol particles are collected by water drops in sub saturated air, J. Atmos. Sci., 34, 1664–1669.

Role of the charged particles in atmospheric nucleation

V.A. Zagaynov[1], A.A. Lushnikov[1], Yu.G. Biryukov[1], T.V. Khodzher[2], Yu.S. Lyubovtseva[3]

[1]Department of Aerosols, Karpov Institute of Physical Chemistry, 10, Vorontsovo Pole, 105064 Moscow, Russia
[2]Limnological Institute, 3, Ulanbatorskauy, Irkutsk, Russia
[3]Geophysical Center RAS, Moscow, Russia

Atmospheric nucleation is a very complicated process. There are several factors that influence on nucleation rate: chemical reactions, photo-chemical reactions, ionization and so on. Classic nucleation theory based on the consideration of fluctuations of vapour concentration is unable to account for the particle generation in the atmosphere. The matter is that the atmospheric air contains many kinds of nuclei: large molecules, molecular clusters, ions and so on. The source of atmospheric ions is well known: it is the cosmic rays and the and the earth radiation. The efficiency of collisions between vapor molecules and ions is higher than between neutral molecules. Thus the nucleation rate on charged vapor molecules should be faster. We tried to test this fact.

To this end the diffusion aerosol spectrometer (DAS) was used to measure the particle concentrations and the particle size distributions (Zagaynov, 2006). In DAS the screen type diffusion batteries were used. To enlarge the particles whose size cannot be measured by optical counters the particle amplifier was used. In this amplifier particles with size from 3 up to 200 nm grew up to 600 nm, and after that their concentration was measured by the optical counter. Measured penetrations through diffusion batteries were converted into particle size distribution (Zagaynov *et al., 2008*). One measurement took from 2 to 3 min., each measurement point contains the data on the concentration of particles with sizes exceeding 3 nm, the averaged particle size, the particle distribution width, and the size histogram of particles larger than 200 nm. To select neutral particles from all atmospheric particles the electric planar capacitor was used. The voltage applied to the capacitor was chosen to cut all charged particles. Measurements were carried out continuously, aerosol particles passed trough the capacitor steadily, and a periodical voltage was applied to the capacitor.

The measurements were carried out on the shore of the Baikal Lake (East Siberia). This region may be considered as a background one where the anthropogenic pollution in the atmosphere may be neglected. Aerosol investigations were performed during June – July. At that time the nucleation bursts were expected to be observed.

Nucleation bursts may be identified by abrupt growth of particle concentration, decrease in the averaged particle size, and increase in the concentration of the smallest particles. Sometimes these nucleation bursts are followed by increased concentrations of some gas admixtures, for example SO_2, sometimes these correlations with the gas concentrations growth were absent. The example of our measurements is shown in the fig. 1.
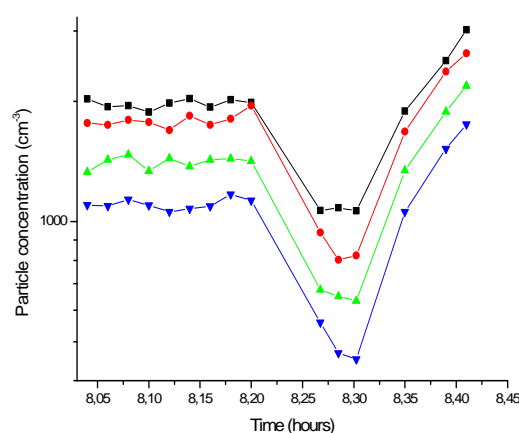
Figure 1. Particle concentrations of different sizes during the measurements.

In fig.1 black line is the total particle concentration, the concentration of particles in the range 3-5 nm is shown in red, the green color corresponds to the particles of 5-10 nm in diameter, and the blue one displays larger particles of 10 – 20 nm. From fig.1. one sees that when charged particles are removed (three points in the center of the figure), the particle concentration decreases. This concentration drop is due to the generation of the smallest particles in the system. At the same time we have to keep in mind that small particles of the size lower than 3 nm might have much higher concentration, and if we would be able to check them, the effect could be more clearly expressed. This means that most of particles observed in our experiments were nucleated on ions.

Zagaynov, V.A., (2006). *Nanotechnics (in Russian),* 1, 141-145.

Zagaynov, V.A., Biryukov, Yu.G., Lushnikov, A.A. (2008). *Patent of Russian Federation, #2006137791/28(041133).*

Surface momentum flux in NWP modelling sensitivity studies relevant for dust emission estimation

A. C. Carvalho, J. Ferreira, J. Sousa, A. Rocha and J. Castanheira

Department of Physics, University of Aveiro. Campus Universitário de Santiago. 3810-193 Aveiro, Portugal.

Keywords: aerosol modelling, atmospheric applications, dust fluxes

Previous studies regarding particulate matter (PM) sources into the atmosphere (Rodríguez et al, 2001; Koçak et al., 2007), and its importance on measured PM concentrations show that natural sources can provide important PM loads during PM episodes (an episode corresponds to the daily average concentrations greater then 50 µg m^{-3}). Over the Iberian Peninsula, these PM natural sources are often associated with forest fires, marine aerosols and aerosols generated during surface erosion processes, which are very efficient over surfaces with low vegetation cover and small amounts of precipitation and very typical of this region. The air quality networks of Portugal and Spain have PM concentrations records that show the influence of a major desertic source of dust in the Sahara (Querol et al, 2004; Pereira, et al., 2005).

The PM dust emissions to the atmosphere from desertic sources can be considered as a phenomenon that depends first on the intensity of the horizontal wind (Bouet et al, 2006). However, if there isn't some turbulence and instability present in the atmosphere the particles tend to deposit and do not remain in suspension. Thus, the calculation of concentration of particulate matter in the atmosphere produced through wind erosion starts by determining the flow of material by the surface. The processes that move the soil particles into the atmosphere include: i) aerodynamics suspension, (ii) saltation and (iii) sandblasting. The flow of particulate matter is dependent on the soil composition, the characteristics of the crust, vegetation cover, and soil moisture. As previously mentioned, after the emission, the processes that are involved on getting the material in suspension in the atmosphere for further advection are related with the atmospheric turbulence. The parameter that gathers the information relating the average wind speed, turbulence and atmospheric stability is the friction velocity. Shaw et al., 2008 (and references in it) state the importance of the friction velocity and soil moisture on vertical dust flux.

Mesoscale weather forecast models are important tools in order to obtain meteorological states of the atmosphere for further applications on dust models. In this sense, it is extremely important to know how mesoscale models respond to different physical parameterisations, regarding dust studies, through sensitivity studies.

The present work regards a sensitivity study to different PBL parameterisations and soil moisture data applied in two mesoscale meteorological numerical models namely, the MM5 and WRF-ARW. Since wind velocity and friction velocity are the main meteorological parameters for the calculation of dust flux and suspension of the particulate matter into the atmosphere, the influence of the different physical parameterisations and data on surface wind and friction velocity will be shown.

The influence of vertical and horizontal resolution of the model will also be explored over parts of the domains that overlap in the nested configuration considered.

The simulation period includes the period from the 15th and 31st of July 2004. During this period several air quality and research measuring stations have recorded high PM concentration levels, above 700 µg m^{-3} over Algarve and 400 µg m^{-3} over the Lisbon airsehd region, which make it an interesting period for numerical studies experiments.

Bouet C., F. Lasserre, G. Cautenet, B. Laurent, B. Marticorena and G. Bergametti (2006). *Geophysical Research Abstracts*, Vol. 8.

Querol, X.; A. Alastuey, C.R. Ruiz, B. Artiñano, H.C. Hansson, R.M. Harrison, E. Buringh, H.M. ten Brink, M. Lutz, P. Bruckmann, P. Straehl, J. Schneider (2004). *Atmosph. Environ,* 38, 6547-6555.

Pereira, Sérgio; Ana Maria Silva, Thierry Elias e Frank Wagner (2005). in Proc. of *6º Encontro Luso-Espanhol de Meteorologia. Sesimbra*, Portugal, 116-118.

Shaw, William J.; K. Jerry Allwine, Bradley G. Fritz, Frederick C. Rutz, Jeremy P. Rishel, Elaine G. Chapman (2008). *Atmosph. Environ,* 42, pp 1907–1921.

Rodríguez, S.; X. Querol, A. Alastuey, G. Kallos and O. Kakaliagou (2001). *Atmosph. Environ,* 35, 2433-2447.

Koçak, Mustafa; Nikos Mihalopoulos, Nilgün Kubilay (2007). *Atmosph. Environ,* 41, 3806-3818.

Production of water from the environment through simulation of atmospheric water cycle

M.K. Bologa[1], F.P. Grosu[2], A.A. Policarpov[1], O.V. Motorin[1]

[1]Institute of Applied Physics, 5 Academiei str., MD 2028, Chisinau, Moldova
[2]Agrarian State University, 44 Mircesti str., MD 2049, Chisinau, Moldova,

Keywords: atmospheric aerosols, condensation, modelling, vapour

It is simulated the atmospheric water cycle consisting in the evaporation of water from the earth surface, its ascent in the form of vapours, condensation in the upper cold layers of the atmosphere and falling out as precipitations back on the earth surface to remove fresh water from ground and atmosphere. Under natural conditions it can be brought about through the cycle "localization" creating the necessary conditions of its existence in the limited space, for instance, in the form of a hothouse placed on the sunny side of a hill wet slope (Cojuhari & Bologa, 2003). Water evaporating from the ground in the hothouse under the action of the heat sun radiation ascends in the form of vapour to the hothouse upper edge where there is provided a metal capacitor where vapour is condensed at the expense of cooling by the surrounding air (wind). The obtained water may be used as technical one or can be returned into the ground to complete the water cycle.

The examination of the mentioned physical concepts has been carried out under laboratory conditions.

The experimental model is a solar vapour collector (SVC) in the form of a trough with constant length and width b and controlled height h of the wet air layer. The trough is half-filled with soil layer (mainly with mixture of sand and "keramzit"). Drain pipes to transfer the obtained condensate back into the soil and to imitate the moisture circulation are placed in the middle of the layer. The trough is covered by the polyethylene film. Electric photo lamp imitates solar radiation. The outer air supply and the angle of inclination α to the horizon are the controlled parameter. The soil is moistened with water.

The problem on the transport of wet air into SVC has been solved and the formula for the vapour (water) flow rate

$$G_v = \gamma b \left[(s_0 / b)G + (Ah^3 r_s / 120) \right], \qquad (1)$$

where γ is the wet air density, s_0 is the average relative air humidity at the level $z = 0$ (the figure), G is the volume flow rate, m^3/sec determined by the formula

$$G = b \int_{-h/2}^{h/2} v(z)dz = -\frac{\Delta P}{l} \cdot \frac{bh^3}{12\eta}$$

where $\Delta P / l$ is the pressure gradient along the canal with length l, η is the air viscosity dynamic coefficient. Parameter A characterizes the natural convection (NC) of the mixed character (thermal $\beta\theta_s$ and humidity $\beta_s r_s$) and is

$$A \equiv g(\beta\theta_s + \beta_s r_s)\sin\alpha / (6v),$$

where $\beta = -\gamma_0^{-1}(\partial\gamma / \partial T)_o$; $\beta_s = -\gamma_0^{-1}(\partial\gamma / \partial s)_o$; $v \equiv \eta / \gamma$, and differences of temperatures θ_s and humidities r_s on the layer lower and upper bases are presented by the expressions:

$$\theta_s \equiv T_2 - T_1 = T(-h/2) - T(h/2);$$
$$r_s \equiv s_2 - s_1 = s(-h/2) - s(h/2).$$

The first addend of formula (1) describes the vapour flow caused by the pressure unbalanced gradient $\Delta P / l$, for example by the wind head, and if the canal is closed at the face planes then $G = 0$ and according to formula (1) vapour mass transfer takes place only due to NC:

$$G_v = \frac{\gamma g(\beta\theta_s + \beta_s r_s)bh^3 r_s \sin\alpha}{720v}$$

precisely moisture factor ($r_s \neq 0$) causing moisture transfer ($G_v \neq 0$). Moisture convective transfer unlike hydrodynamic one is one of the peculiarities of the vapour solar collector operation under laboratory conditions.

Wet air flow from the collector enters the vapour condenser consisting in a thin- walled metal cylinder with height h_c and diameter d_c. The outside of the condenser is air-blasted by the conventional room fan imitating wind and cooling the condenser. It should be noted that cooling occurs only due to the natural convection. Condensate flow rate is determined by the generalized formula:

$$G_c / G_{co} = 5.88 \times 10^{-3} \cdot \Pi \cdot (Gr\,Pr)^{0.25} \cdot Re^{0.6},$$

where G_{co} is the vapour mass flow rate at the entrance into the condenser, $\Pi \equiv \dfrac{\lambda\theta_o s}{rdG_{co}}$, $Re \equiv \dfrac{vd}{v}$, $Pr \equiv \dfrac{v}{a}$, s is the condenser lateral area; d is the diameter; v is the fan air-blasting rate; θ_o is the difference of temperatures of the condenser and the surrounding air.

Under laminar conditions at $h = 0.07$ m, $\alpha = 27^o$ it was obtained $G_c \approx 10^{-4}$ kg/sec in average. Use of the condensate for obtaining of aerosols opens wide possibilities of applied applications including electric energy generation. Under natural conditions these effects should be tenfold stronger.

Cojuhari I., Bologa M. (2003) EHD wind installation, Patent of Moldova, MD-2199 (13) B.I. (in Romanian).

Particulate matter from wildfires and its local/regional impacts over Portugal

M. Tomé[1], E. Nunes[2], C.A. Alves[3]and J.M. Alonso[2]

[1]Escola Superior de Tecnologia e Gestão, IPVC, Avenida do Atlântico, 4900-348 Viana do Castelo; Portugal
[2]Escola Superior Agrária, IPVC, Refóios do Lima, 4990-706Ponte do Lima; Portugal
[3]Centre for Environmental and Marine Studies (CESAM), Department of Environment, University of Aveiro, 3810-193 Aveiro, Portugal

Keywords: Forest fire, Atmospheric Pollution, Coastal area, Chemistry transport model, 3D.

Between 20 and 23 August 2005, a large wildfire occurred close to Viana do Castelo city, in the North-west of Portugal. High emissions and wind direction have favoured the transport of both primary and secondary air pollutants to the city centre. This was one of the most critical events in terms of air pollution affecting directly thousands of inhabitants during more than 24 hours. The health impact upon population was significant, increasing the number of hospital admissions due to respiratory problems. It was considered the possibility of evacuation of the district hospital due to bad indoor air quality.

Taking into account that there was only one nearby rural background air quality station, several studies to characterise the 3D meteorology, emissions and transport/dispersion have been made in order to assess, with high resolution, the air quality in a more broad area. These studies involved field data from the national air quality network (as the impact was extended hundreds of kilometers from the fire location), field data from the fire propagation each 12 hours, meteorology data, fuel cover and topography. Records of several air quality stations in the North and Central regions of Portugal registered atypical PM_{10} levels exceeding 200 µg.m^{-3} during these days

In order to model this air quality event, several numerical tools were used, namely: i) Farsite model (for fire progression); ii) Nuatmos model (prognostic wind model accounting for local topography effect); iii) lagrangian code (transport and dispersion of passive pollutants). Moreover, it was used ADMS-Urban to assess the impact of traffic emissions upon the air quality in Viana do Castelo. Aiming to confirm easily the smoke plume trajectory, forward trajectories HYSPLIT have been computed. This event is being further studied by using WRF model and its chemistry module in order to better assess the real photochemical impact of such a suburban forest fire. Indeed, during a typical summer day, the high biogenic emissions from regional vegetation reacting with the anthropogenic and forest fire emissions can produce extreme levels of ozone and related oxidants. During this event, there were not records of ozone in the city centre and the nearby regional station was not influenced by this episode of bad air quality.

Figure 1 shows the forest fire progression, wind and PM_{10} field concentration at 15h00, 20 August 2005. One can see high levels of particles whose effects have synergies with those of other pollutants emitted by wildfires. According to our simulations, there were PM_{10} levels exceeding 100 µg.m^{-3}. Figure 2 illustrates the trajectories of the smoke plume above the Atlantic Ocean and Iberian Peninsula released by several simultaneous fires.
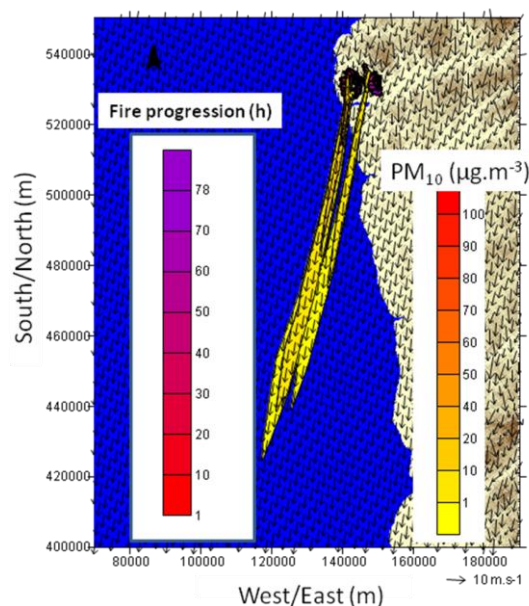
Figure 1. Fire progression, wind and PM_{10} field concentrations at 15h00, 20 August 2005.
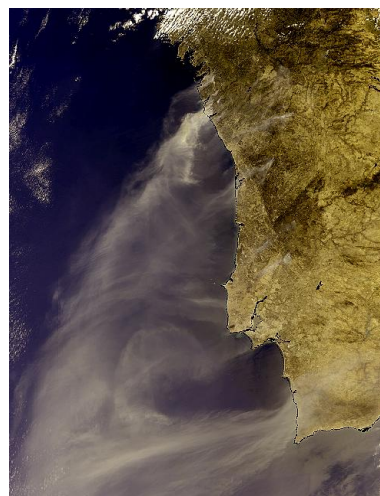
Figure 2. Satellite view of forest fires smoke above Iberian Peninsula on 21 August 2005 (Source: www.esa.int).

Emission contributions of PM$_{10}$ at an industrial park in southern Taiwan

Chien-Lung Chen[1] and Ying I. Tsai [2],*

[1] Department of Finance, Fortune Institute of Technology, Kaohsiung 831, Taiwan
[2] Department of Environmental Engineering and Science, Chia Nan University of Pharmacy and Science, Tainan 717, Taiwan

Keywords: source apportionment, air pollution - modelling, PM10

Source-oriented air quality models have been used to predict the pollutant concentrations by using a chemical dispersion model and different source categories as input (Ying et al., 2007). This study applied a Gaussian trajectory transfer-coefficient model (GTx) to estimate the source apportionment (Tsuang, 2003; Tsuang et al., 2003). The GTx model is a Lagrangian-type gridding trajectory model coupled with physical-chemical mechanisms.

This study uses the GTx model at Daliao air quality station, southern Taiwan, in Nov-Dec, 2007. A petrochemical and metals' industrial park was about 200 m north from Daliao air quality station. Hourly observed PM$_{10}$ concentrations were measured continuously by the Environmental Protection Administration in Taiwan (EPA/Taiwan). The observed and calculated daily concentrations of PM$_{10}$ are shown in Figure 1 and the correlation coefficient (r) is 0.36. The simulated PM$_{10}$ shows a fair agreement with observed data during the study time. The bias of the PM$_{10}$ concentrations for the receptor is -3.6% and RMSE is 44.2 µg m^{-3}.
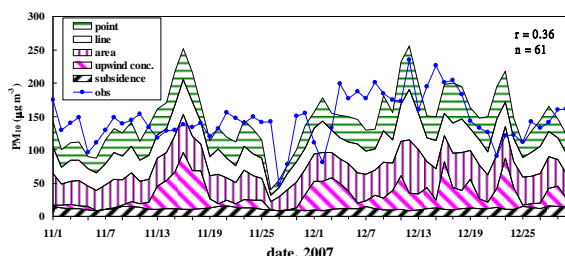
Figure 1. Observed and calculated daily concentrations at Daliao.

The PM$_{10}$ emission source distributions to Daliao air quality station is showed in Figure 2. Pollution sources include point sources, line sources, area sources, upwind boundary concentrations and subsidence. The major sources of PM$_{10}$ to Daliao are area sources (29%), line sources (25%), and then point sources (24%). We define the PM$_{10}$ episode as the observed daily PM$_{10}$ concentration is greater than 125 µg m^{-3}. There are 49 PM$_{10}$ episode days and 12 PM$_{10}$ non-episode days at Daliao station during Nov-Dec, 2007.

The differences of source apportionments between PM$_{10}$ episode and non-episode days are showed in Figure 3. It is obvious that the point

sources increase about 4% PM$_{10}$ contributions in episode days. The other sources decrease 1% PM$_{10}$ contributions in episode days each. These results can provide the estimation for air quality abatement strategy.
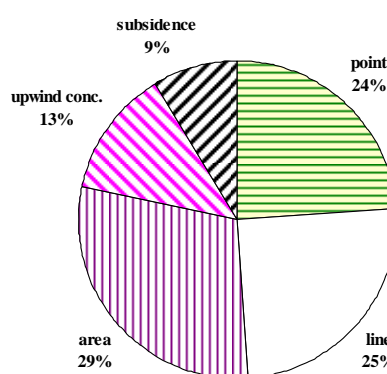
Figure 2. Emission contributions for Daliao air quality station from Nov to Dec 2007.
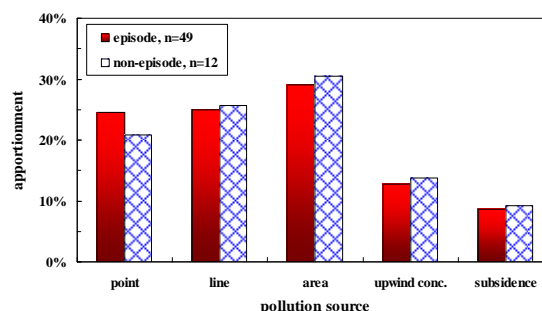
Figure 3. Differences of source apportionments between PM$_{10}$ episode and non-episode days at Daliao.

Tsuang, B.-J. (2003). *Atmospheric Environment*, 37, 3981-3991.

Tsuang, B.-J., Chen, C.-L., Lin, C.-H., Cheng, M.-T., Tsai, Y.-I., Chio, C.-P., Pan, R.-C. & Kuo, P.-H. (2003). *Atmospheric Environment*, 37, 3993-4006.

Ying, Q., Fraser, M.P., Griffin, R.J., Chen, J., Kleeman, M.J. (2007). *Atmospheric Environment* 41, 1521-1538.

Urban PM_{10} modelling using neural network with weather forecast

K.B. Ang[1], G. Baumbach[1] and K.G. Gutbrod[2]

[1]Institute of Process Engineering and Power Plant Technology (IVD), Department of Air Quality Control (RdL), Universitaet Stuttgart, Pfaffenwaldring 23, 70569 Stuttgart, Germany
[2]meteoblue AG, Clarastrasse 2, CH-4058 Basel, Switzerland
Keywords: PM_{10}, neural network, weather forecaster, air quality modelling

Weather forecasters provide information on meteorological parameters, such as probable wind characteristics and precipitation amount for an area, which would generally suffice for the general population. If such forecasters could be extended to provide additional information on probable ambient PM_{10} concentrations in a day in advance, the benefits would be two-fold. First, such extended weather forecaster could act as both an alarm for the quality of ambient air and bad weather. Second, the information derived from the extended weather forecaster could aid in public education.

The potential of using neural network models to predict the daily average PM_{10} concentrations one day ahead at an urban background site and a heavily trafficked site in Stuttgart (Germany) was evaluated. The two developed neural network models can be simplified as follow:

Input parameters from 1 May 2007 to 1 May 2008:

$PM_{10, \, day \, 0}$	(Measurements from PM_{10} gravimetric analyses)
Mixing height$_{, \, day \, 0}$	(Measurements from radio soundings)
Temperature$_{, \, day \, 1}$	Weather forecast
Wind velocity$_{, \, day \, 1}$	Weather forecast
Wind direction$_{, \, day \, 1}$	Weather forecast
Precipitation$_{, \, day \, 1}$	Weather forecast

Target parameter: $PM_{10, \, day \, 1}$

The entire data set was divided into three separate subsets (training, validation and test sets) for the needs of the neural network model's development and evaluation. The early stopping technique was implemented during the training of the neural network. The training process was finalised when the selected measure of errors for the validation data set reached a minimum. For the evaluation of the neural network models' performance, several performance indicators were computed, namely the mean absolute error (MAE), the root mean square error (RMSE), the fractional bias (FB), the index of agreement (IA) and the squared correlation coefficient (R^2).The results for the developed neural network models' for the two sites are summarised in Table 1.

The time-series of predicted and observed 24 h PM_{10} concentrations at the two sites are presented in Figure 1 to illustrate the models' performance. In the urban background site, the results obtained with the model demonstrate good agreement with the observed PM_{10} concentrations, with the IA and R^2 values of 0.79 and 0.73 respectively. In contrast to the results obtained at the urban background site, the corresponding IA and R^2 values are clearly lower at the traffic site. In general, the model for the traffic site was able to reasonably reproduce the day-to-day variation of PM_{10} concentrations. However, part of the lower measured values was underpredicted. This result was expected, as the PM_{10} concentrations at the traffic site is strongly influenced by the local road dust and thus making it more difficult for PM_{10} prediction. At both sites, the local PM_{10} pollution episode during late December 2007 was also not fully captured by the models.

Table 1. Performance indicators for the neural network models

Site	Urban Background	Traffic
MAE in µg/m³	6.57	12.42
RMSE in µg/m³	1.51	0.29
FB in %	-11.00	0.19
IA	0.79	0.67
R^2	0.73	0.66
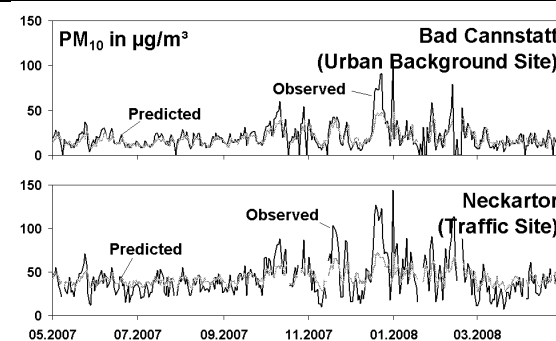
Figure 1. Time series of predicted and observed PM_{10} concentrations at Bad Cannstatt and Neckartor

The overall models' results illustrates a possibility of effective use on the operational level for forecasting PM_{10} concentrations one day in advance using Numerical Mesoscale Model (NMM) weather forecasts as input parameters. The existence of quality meteorological forecasts is an important factor for the models' successful implementation for real-time predictions. With appropriate input data sets, such models could be modified and adopted to other locations as well.

Evaluation of model simulated atmospheric constituents with observations over an urban area affected by natural sources

E. Athanasopoulou[1], M. Tombrou[1], A.A. Karanasiou [2], K. Eleftheriadis[2] and A.G. Russell[3]

[1]Department of Physics, University of Athens, Zografou, 15784, Athens, Greece
[2]Inst.of Nuclear Tech. & Radiation Protection, N.C.S.R. "Demokritos", Ag. Paraskevi, 15310, Athens, Greece
[3]School of Civil and Environmental Engineering, Georgia Inst. of Tech., 311Ferst Drive NW, Atlanta, USA

Keywords: aerosol modelling, marine aerosols, dust.

New parameterizations of both marine and dust aerosol dynamics in a regional scale model are evaluated using observations in Athens, GR.

Data from size distribution measurements for the aerosol mass concentration and the concentrations determined for water soluble inorganic species were utilised in this study. Samples were obtained by means of an 11 stage Berner cascade impactor at the "Demokritos" urban background site (DEM) during April 10 & 11, 2006. Complementary data include 24-hour average PM_{10} measurements at 5 network stations of the National Ministry of the Environment (ARI, LYK, THR, MAR, AGP). Hourly PM_{10} measurements from 2 stations adjacent to the highway (COL, IRA) are also used.

All chemical constituents are simulated using the PMCAMx chemical transport model (Environ, 2003). An important model update is that calcium, potassium and magnesium are explicitly treated inside ISORROPIA II (Fountoukis and Nenes, 2007). The new parameterizations for marine and dust emissions were described in Athanasopoulou et al. (2008a).

The conventional comparison between PMCAMx results and bulk PM_{10} measurements show that discrepancies are rather small (Table 1). This indicates that most of the emission sources are being captured. Larger under predictions (LYK, THR, COL, IRA) are likely due to locally and temporally intense emissions, also evident from hour to hour aerosol comparisons.

Sodium concentrations are well simulated (0.9 $\mu g/m^3$) compared to measurements (1.2 $\mu g/m^3$) suggesting the marine parameterization used is providing reasonable estimates, since sodium is well suited to characterize marine aerosol.

Performance for calcium, potassium and magnesium (predicted: 3.5, 0.3, 0.2 $\mu g/m^3$, observed: 2.4, 0.6, 0.3 $\mu g/m^3$) suggest that the dust parameterization is capturing those emissions, since these species can be used as soil tracers for Attica (Karanasiou et al, 2007).

Fine nitrate concentrations are well simulated (2.2 $\mu g/m^3$) compared to measurements (2.5 $\mu g/m^3$), indicating that the recent changes have substantially improved in the ammonia emission inventory, after its poor evaluation in a preceding study (Athanasopoulou et al., 2008b). The over prediction of coarse nitrates (predicted: 7.6 $\mu g/m^3$, observed: 1.8 $\mu g/m^3$) is likely due to the overestimation of the calcium ratio in crustal dust inside the model.

A comparison of the aerosol size distribution of the simulations with the measurements shows the need for revising the size distribution of fine aerosol emissions from most sources, with their peak around 0.3 – 0.5 μm.

Table 1. PM_{10} in Athens for 10, 11 April, 2006.

Station	Measurements ($\mu g/m^3$)	Predictions ($\mu g/m^3$)	Fractional Bias (%)
DEM	34.3	37.1	1.9
ARI	54, 67	59.1, 67.7	2.2, 0.2
LYK	55, 102	38.5, 50.6	-8.8, -16.8
THR	34, 56	18.8, 26.9	-14, -17.5
MAR	42, 56	38.6, 48.1	-2.1, -3.7
AGP	32, 46	29.6, 34.1	-1.9, -7.4
COL	41.9, 65.2	32.5, 41.5	-6.3, -11
IRA	64.1, 89.6	38.5, 50.6	-12.4, -14

Athanasopoulou, E., Tombrou, M., Pandis, S. N., Russell, A. G. & Dandou, A. (2008a). *Modelling the effects of heterogeneous chemistry in the air quality of Athens, Greece: marine and dust aerosol*, in *Proc. European Aerosol Conference*, Thessaloniki.

Athanasopoulou, E., Tombrou, M., Pandis, S. N., and Russell, A. G. (2008b). *The role of sea-salt emissions and heterogeneous chemistry in the air quality of polluted coastal areas*, Atmos. Chem. Phys., 8, 5755-5769.

Environ (2003). *Development of an Advanced Photochemical Model for Particulate Matter: PMCAMx*. Final Report, ENVIRON Int. Corp.,Novato, Calif.

Fountoukis, C., and Nenes, A. (2007). *ISORROPIA II: a computationally efficient thermodynamic equilibrium model for $K^+–Ca^{2+}–Mg^{2+}–NH^+_4–Na^+–SO_2^{-4}–NO^-_3–Cl^-–H_2O$ aerosols*, Atmos. Chem. Phys., 7, 4639–4659.

Karanasiou A. A., Siskos P. A. & Eleftheriadis K. (2007). *Source apportionment of fine and coarse aerosol in the Athens Metropolitan area*. in *Proc. European Aerosol Conference*, Salzburg, Abstract T19A033

Structure and evolution of the atmospheric boundary layer in Buenos Aires and its relationship with Air Quality

Ana Graciela Ulke[1], Marcelina Arkouli[2], Wilfried Endlicher[3], Günter Baumbach[2], Eckart Schultz[4], Ulrich Vogt[2], Marlén Müller[3], Laura Dawidowski[5], Ana Faggi[6]

[1] Universidad de Buenos Aires, Depto. de Ciencias de la Atmósfera y los Océanos, Argentina
[2] Universität Stuttgart, Institute of Process Engineering and Power Plant Technology, Dept. of Air Quality Control, Germany
[3] Humboldt Universität zu Berlin – Institute of Geography, Dept. of Climatology, Germany
[4] Deutscher Wetterdienst, Dept. of Human – Biometeorology, Germany
[5] Comisión Nacional de Energía Atómica, Depto. de Monitoreo Ambiental, Argentina
[6] Universidad de Flores, Facultad de Ingeniería Ecológica, Argentina
Corresponding Author: ulke@at.fcen.uba.ar

Keywords: PM, horizontal and vertical distribution, local flow, RAMS model

Buenos Aires has a population of approximately three-million inhabitants and an area of 203 km^2. The city is a part of the metropolitan region of Buenos Aires, which is the third largest metropolis in Latin America. The vehicle traffic (the main source of pollutants) has an increasing trend that in conjunction with the lack of urban planning and the scarce knowledge on the local climate and circulation, stress the relevance of the issue of the air quality and urban atmosphere. Buenos Aires does not yet have an effective air pollution monitoring network.

The Buenos Aires Research in Urban Climate and Air Pollution project (BARUCA) was established to contribute to the assessment of the air pollution situation in Buenos Aires and the advance in the characterization of the urban climate.

During one year, from May 2006 to June 2007, continuous measurements at seven sites and random measurements on ground at 60 sites were done. Air pollutants like particulate matter, nitrogen dioxide, and volatile organic compounds as well as relevant meteorological variables were measured. Special intensive observations using tethered balloons during selected periods were also made. In the soundings, meteorological variables (temperature, humidity, wind speed and direction) and particulate matter concentrations were observed.

In this contribution, some results of the project are presented and analyzed. A study of the measurements of two special observation periods is presented. One campaign took place in winter and the other in summer. The vertical structure and evolution of the atmospheric boundary layer and meteorological parameters is discussed. The greater scale meteorological setting and its impact on the development of local circulation is explored. The aim was to study the role of the local and synoptic flow systems on the dispersion of air pollutants. In addition to the data of the project, the routine surface and upper air measurements from the Argentine National Weather Service were used in the study.

The special observation periods documented for the first time in Buenos Aires city the detailed vertical structure of the atmospheric boundary layer and its evolution. The greater scale synoptic environment was characterized. The variation of the meteorological parameters and mixing conditions showed consistent results when compared with the pollutants concentration and behavior. The results of the winter campaign showed a greater scale synoptic environment favorable to the development of local circulation and the growth of the mixing layer. The winter period was simulated using a high resolution mesoscale RAMS model. Nested grids with two-way interactive nesting were used in order to capture the three-dimensional details of the flow and its evolution. The structure of the modeled atmospheric boundary layer is compared with the sounding data. The joint analysis of the wind fields and related dispersion conditions along with the measured concentrations is performed.
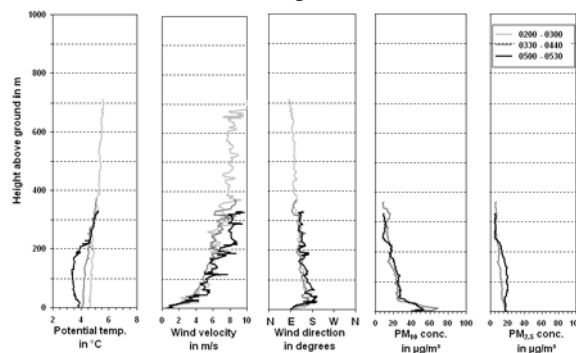
Figure 1. Vertical profiles of meteorological parameters, PM$_{10}$ and PM$_{2.5}$ performed on 03 August 2006.

Unraveling the "Pressure-Effect" in Unary Condensation

J. Wedekind[1], A.P. Hyvärinen[2], D. Brus[2,3] and D. Reguera[1]

[1]Departament de Física Fonamental, Universitat de Barcelona, Martí i Franquès 1, 08028 Barcelona, Spain
[2]Finnish Meteorological Institute, Erik Palménin aukio 1, P.O. Box 503, F1-00101 Helsinki, Finland
[3]Laboratory of Aerosol Chemistry and Physics, Institute of Chemical Process Fundamentals, Academy of Sciences of the Czech Republic, Rozvojová 135, CZ-16502 Prague 6, Czech Republic

Keywords: condensation, vapor-liquid nucleation, pressure-effect, molecular dynamics.

A gas phase can be supersaturated considerably beyond its equilibrium condensation point before liquid drops form spontaneously. The pathway of the phase transition is blocked because microscopic droplets are thermodynamically less favorable than the bulk vapor. Therefore, the transition can only be initiated by rare fluctuations exceeding a critical size, called the *critical nucleus*. The formation of such a critical nucleus is the limiting step in the transition and its frequency of occurrence is called the *nucleation rate* (Debenedetti, 1996). Nucleation is behind most phase transitions and plays a crucial role in atmospheric processes such as the formation of aerosols or the condensation of water vapor into clouds (Kulmala, 2003; Tunved *et al.*, 2006). An accurate experimental evaluation of the nucleation of atmospherically relevant substances and its correct theoretical prediction are essential for a better understanding of climate change and are the subject of intense investigations (Winkler *et al.*, 2008).

Nucleation is highly sensitive to small changes in the state variables describing the system, most notably to temperature. However, condensation is always connected with the release of latent heat. In experiments this latent heat is removed by the presence of a large background of ambient carrier-gas. This carrier-gas should be noncondensing and chemically inert and should have no influence on the nucleation except serving as the desired heat bath. But many experiments suggest that there is an influence on the nucleation rate that can span some orders of magnitude, depending on the pressure and type of the carrier-gas (Brus *et al.*, 2008; Brus *et al.*, 2006). Unfortunately, the overall picture is far from clear. Comparisons of experimental findings cover all possibilities: no effect, increase, or decrease of the nucleation rate with carrier-gas pressure. Continuous improvements in the experimental setups rather confirmed than remedied this undesirable and elusive effect.

Here we present a simple yet physically very appealing model that resolves many of the apparent contradictions of ths "pressure-effect" (Wedekind et al., 2008). We take a deliberate step back and incorporate the presence of a carrier-gas into classical theory in a most natural manner that accounts for the two primal contributions of the carrier-gas: the efficiency of thermalization and the additional work that a cluster has to spend for growing in its presence. These contributions have opposite trends and we show how this may be responsible for the existence of apparently contradictory results. Molecular dynamics (MD) simulations of Lennard-Jones argon nucleation with helium as carrier-gas confirm the predictions of our model quite impressively.

The model does not discard the influence of other factors on the observed pressure-effect. But these factors (if applicable) can be added easily to as secondary contributions to the more fundamental and inevitable physical roles of a physically ideal and chemically inert carrier-gas in nucleation and which are accounted for in our model. We deliberately separated the influence of a truly inert carrier-gas pressure from e.g. binary nucleation or surface adsorption. It is somehow misleading to include these under the same "pressure-effect" tag because even though the strength of them may depend on pressure, their origin certainly is not the pressure of the carrier-gas. In any case, the insights provided by our model will undoubtedly be very helpful to quantify and remove the influence of ambient gas on experiments. This opens the door to a more accurate evaluation of nucleation rates with important implications on many atmospheric and technological processes.

Brus, D.*et al.* (2008), *J. Chem. Phys.*, 128, 134312.

Brus, D., Zdimal, V., and Stratmann, F. (2006), *J. Chem. Phys.*, 124, 164306-164314.

Debenedetti, P. G., *Metastable Liquids: Concepts and Principles*. (Princeton University Press, Princeton, 1996).

Kulmala, M. (2003), *Science*, 302, 1000-1001.

Tunved, P.*et al.* (2006), *Science*, 312, 261-263.

Wedekind, J.*et al.* (2008), *Phys. Rev. Lett.*, 101, 125703.

Winkler, P. M.*et al.* (2008), *Science*, 319, 1374-1377.

Homogeneous Water Nucleation in a Laminar Flow Diffusion Chamber

A. Manka[1], D. Brus[2,3], A.-P. Hyvärinen[2], H. Lihavainen[2], J. Wölk[1] and R. Strey[1]

[1]Institut für Physikalische Chemie, Universität zu Köln, Luxemburger Str. 116, 50939 Köln, Germany
[2]Finnish Meteorological Institute, Erik Palménin aukio, P.O. Box 503, FI-00101 Helsinki, Finland
[3]Laboratory of Aerosol Chemistry and Physics, Institute of Chemical Process Fundamentals Academy of Sciences of the Czech Republic, Rozvojová 135, CZ-165 02 Prague 6, Czech Republic

Keywords: homogeneous nucleation, water, nucleation rate, supersaturation.

Nucleation and condensation of water takes place in many industrial processes and plays a major role in the atmosphere and climate change. Therefore it is of great interest to clarify the physics of water nucleation in order to make accurate predictions for the condensation process. In order to complete the available data we measured homogeneous nucleation of water in a laminar flow diffusion chamber (LFDC). A detailed description of the experimental device can be found in Lihavainen & Viisanen (2001). The homogeneous nucleation rates are measured in helium as carrier gas at ambient pressure and for four different temperatures (240, 250, 260 and 270 K). Obtaining isothermal nucleation rates as a function of supersaturation enables us to compare our data with theoretical predictions (Becker & Döring, 1935;Wölk & Strey, 2001) and literature data measured by other groups in different devices (Miller *et al.*, 1983, Luijten *et al.*, 1997, Wölk & Strey, 2001, Mikheev *et al.*, 2002, Holten *et al.*, 2005).

In Figure 1 the homogeneous nucleation rates J of water measured in the LFDC (filled circles) are shown as a function of supersaturation S between 240 and 270 K.
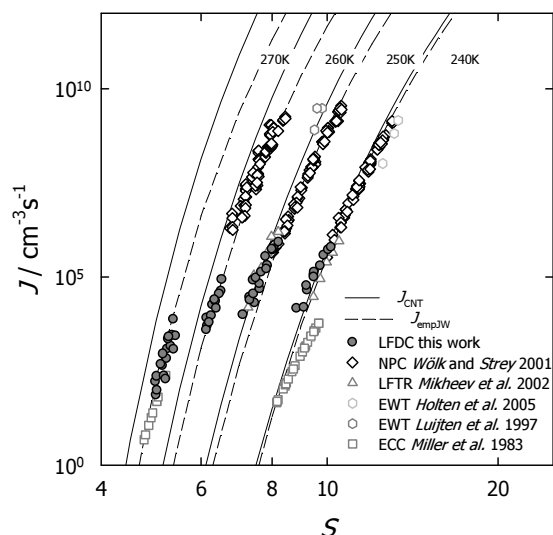
For comparison we also include experimental data measured in a nucleation pulse chamber (NPC; diamonds), in a laminar flow tube reactor (LFTR; triangles), in an expansion wave tube (EWT; hexagons), as well as in an expansion cloud chamber (ECC; rectangles). Certainly there are more experimental data available (Brus *et al.*, 2008,Kim *et al.*, 2004) but here we confine ourselves to comparisons to data measured at exactly the same temperatures. The LFDC data extend the NPC-data to lower rates with a slight overlap in the 240 and 250 K isotherm. Furthermore, we also find a rather good agreement with the LFTR-data by Mikheev *et al.* (2002). We also show the predictions by classic nucleation theory (CNT; solid lines) and the empirical correction function to CNT (dotted lines) by Wölk & Strey (2001). The agreement with CNT at 240 and 250 K seems to be quite good, but at higher temperatures CNT predicts too high nucleation rates. This disparate temperature dependence has been analyzed by Wölk & Strey (2001) and accounted for with the empirical correction function. Hence it shows a good agreement with all data sets.

Becker, R., & Döring, W. (1935), *Ann. Phys. (Leipzig)* 24, 719.

Brus, D., Ždímal, V., & Smolík, J. (2008), *J. Chem. Phys.* 129, 174501.

Holten, V., Labetski, D. G., & van Dongen, M. E. H. (2005), *J. Chem. Phys.* 123, 104505.

Kim, Y. J., Wyslouzil, B. E., Wilemski, G., Wölk, J., & Strey, R. (2004), *J. Phys. Chem.* 108, 4365.

Lihavainen, H., & Viisanen, Y. (2001), *J. Phys. Chem. B* 105, 11619.

Luijten, C. C. M., Bosschaart, K. J., & van Dongen, M. E. H. (1997), *J. Chem. Phys.* 106, 8116.

Mikheev, V. B., Irving, P. M., Laulainen, N. S., Barlow, S. E., & Pervukhin, V. V. (2002), *J. Chem. Phys.* 116, 10772.

Miller, R. C., Anderson, R. J., Kassner, J. L., Hagen, J., & Hagen, D. E. (1983), *J. Chem. Phys.* 78, 3204.

Wölk, J., & Strey, R. (2001), *J. Phys. Chem. B* 105, 11683.

Figure 1. Comparison of all available experimental homogeneous nucleation rate data for water at 240-270 K with CNT (solid lines) and the empirical correction function to CNT by Wölk & Strey (2001) (dashed lines).

Molecular mechanisms behind nocturnal new particle formation

I.K. Ortega[1], T. Suni[1], M. Boy[1], T. Grönholm[1], M. Kulmala[1], H. Junninen[1], M. Ehn[1], D. Worsnop[1], H. Maninnen[1], H. Vehkamäki[1], H. Hakola[2], H. Hellén[2], T. Valmari[3] and H. Arvela[3]

1 Department of Physics, P.O. Box 64, FI-00014 University of Helsinki, Finland.
2 Finnish meteorology institute, Air Chemistry Laboratory,P.O. Box 503, 00 101 Helsinki, Finland
3 STUK, Radiation and nuclear safety authority, P O Box 14, 00881 Helsinki, Finland

Keywords: Organic, Nucleation, Modelling, SOA, Quantum Mechanic.

Atmospheric aerosols influence climate directly and indirectly. Unfortunately the role of atmospheric aerosols is still the forcing with the lowest level of scientific understanding, as reported in the newest report by the Intergovernmental Panel on Climate Change (IPCC 2007).

Nucleation events are in most cases observed during daytime but in some locations they can occur also during the night. In Tumbarumba in New South Wales, Australia, these nocturnal events are very intense and frequently observed (Suni et al. 200).

The objective of this study is to evaluate the role of different VOCs in nocturnal nucleation events. The selected VOCs are limonene, alpha-pinene, beta-pinene and 3-carene; these are the most abundant VOCs in Tumbarumba and in Hyytiälä.

We performed a series of chamber experiments with the objective to reproduce the nocturnal events observed in Australia. Additionally we used quantum chemical calculations to study the molecular mechanism behind the nocturnal nucleation events. Finally we have used the quantum chemical results in aerosol formation models to check if the proposed mechanism could explain the observed nucleation events.

Our quantum chemical calculations were performed using a systematic multi-step method recently developed by our group (Ortega et al. 2008).

Table 1. Formation energies calculated for various clusters containing 1 sulphuric acid and different VOCs oxidation products at 298K and 1 atm

Organic Acid	ΔG (kcal/mol)
Caric acid	-10.5
Caronic acid	-14.4
7- hydroxy caronic acid	-19.3
Pinic acid	-7.2
Pinonic acid	-9.4
7- hydroxy pinonic	-11.1
Limonic acid	-4.6
Limononic acid	-10.6
7- hydroxy limononic	-6.9

As we can see in Table 1, the formation energies differences between different compounds are quite important in some cases. If we compare those energies with the formation energy of sulfuric acid dimer, 6.3 kcal/mol, we can see how the most of organic acids studied forms more stable cluster than sulfuric acid on its own, so their presence should enhance nucleation.

During the experiments we were able to produce particles in dark conditions using ozone and different monoterpenes. The results show that the oxidation rate plays a crucial role in the formation of particles, confirming that the oxidation products of monoterpenes rather that the monoterpenes it selves are involved in the formation of new particles.

Model simulations with SOSA show that nucleation rates calculated with the mechanism explained above are in good agreement with nucleation rates based on measured particle size distributions.

Our results show that the oxidation products of VOCs play an important role in nucleation events. Not all these compounds have the same importance, so characterizing the particle formation potential with, for example, the total concentration of VOCs is probably an unsatisfactory approximation. Taking into account the different emission of VOCs in different environments (like Tumbarumba and Hyytiälä) probably can explain the differences in observed nucleation events.

T. Suni, M. Kulmala, A. Hirsikko, T. Bergmaa, L Laakso, P.P. Aalto, R. Luning, H. Cleugh, S Zegelin, D. Hughes, E. Gorsel, M. Kitchen, M Vana., U. Hörrak, A. Mirme, S. Sevanto., K. Twining and C. Tadros (2008) *Atmos. Chem. Phys.* 8, 129

I.K. Ortega, T. Kurtén, H Vehkamäki and M. Kulmala, (2008) *Atmos. Chem. Phys.* 8, 2859

Modelling the sign preference in heterogeneous nucleation

K. Ruusuvuori[1], T. Kurtén[1], H. Vehkamäki[1], I.K. Ortega[1], M. Toivola[1], M. Kulmala[1]

[1]Division of Atmospheric Sciences and Geophysics, Department of Physics, University of Helsinki, P.O.Box 64, 00014, Helsinki, Finland

Keywords: Modelling, Heterogeneous nucleation, Ions.

Nucleation on ions is an important process in the atmosphere. Ions of opposite sign were observed to exhibit different nucleation rates as early as 1897 (Wilson, 1897) but the reason for this sign preference remained a mystery for more than a century. In a recent paper by Nadykto *et al.* (2006) it was demonstrated that the sign effect can be predicted by carrying out relatively simple quantum chemical calculations. This means we can use quantum chemical methods to help us understand the role of ion-induced nucleation in atmospheric nucleation reactions. However, the computational methods in use today are generally iterative methods that employ a variety of approximations in order to keep the cost in computational resources reasonable. Because of this, we must compare the theoretical predictions with high quality experimental results in order to gain reliable insight on the initial steps of ion-induced nucleation.

We studied the binding energies of small charged and neutral n-propanol – tungsten oxide and n-propanol - silver clusters. The objective of our study was to replicate the experimental results obtained by Winkler *et. al.* (2008), which indicated a negative sign preference for both cases. This was done to get quantitative results which could be used to explain the experimental data and to test the limits and reliability of the used quantum chemical methods.

Silver and tungsten atoms are relatively large, so out of computational considerations we began our studies by considering very small, neutral or singly charged seed molecules (WO_3, W_3O_9, Ag_2 and Ag_3) and a single n-propanol molecule. This choice was also supported by the fact that the experimentally observed sign effect was stronger for smaller seed particles. However, even in these simple cases we experienced computational difficulties and were unable to replicate the sign preference on a qualitative level. The absolute values of the electronic energies for the positively charged clusters were not only larger than for the negatively charged clusters in all cases (which would imply a positive sign preference), but the difference was also as much as one order of magnitude in the worst cases. We also noted that cations proved to be computationally more demanding than anions. Different programs, methods and levels of accuracy have been employed in the computations, but the qualitative results of the computations have so far stayed unchanged.

While the exact reasons for both the computational problems and the results remain at this time unknown, we suspect that the computational methods used are too approximate to model clusters and molecules where constituent atoms have such a large number of electrons accurately enough to provide qualitatively reliable results. Different methods and levels of accuracy are not equally suitable even for all the cases tested here, so further studies are still required. Another plausible explanation is the difference between the size of the seed molecules in our simulations and the size of the actual nucleating clusters observed in the experiment, which were approximated to contain around 20 to 25 molecules based on the heterogeneous nucleation theorem (Vehkamäki *et al.*, 2007). In addition to trying to solve the computational difficulties, we have started to model a case where the n-propanol molecule is adsorbed on a neutral or singly charged seed molecule consisting of 20 silver atoms (Ag_{20}).

Our calculations have been performed using the Gaussian 03 (Frisch *et al.*, 2004), SIESTA (Soler *et al.*, 2002) and TURBOMOLE (Ahlrichs *et al.*, 1989; versions 5.9 & 5.10) quantum chemistry programs.

Wilson, C.T.R., *Phil. Trans. R. Soc. A* 189, 265 (1897).

Nadykto, A.B., Natsheh, A.A., Yu, F., Mikkelsen, K.V. and Ruuskanen, J., *Phys. Rev. Lett.* 96, 125701 (2006).

Ahlrichs, R., Bär, M., Häser, M., Horn, H. and Kölmel, C., *Chem. Phys. Lett.* 162, 165 (1989).

Frisch, M.J. *et al.*, Gaussian 03, Revision C.02, Gaussian, Inc., Wallingford CT (2004).

Soler, J.M., Artacho, E., Gale, J.D., García, A., Junquera, J., Ordejón, P. and Sánchez-Portal, D., *J. Phys. Condens. Matt.* 14, 2745 (2002).

Winkler, P.M., Steiner, G., Vrtala, A., Vehkamäki, H., Noppel, M., Lehtinen, K.E.J., Reischl, G.P., Wagner, P.E. and Kulmala, M., *Science* 319, 1374 (2008).

Vehkamäki, H., Määttänen, A., Lauri, A., Kulmala, M., Winkler, P., Vrtala, A. and Wagner, P.E., *J. Chem. Phys.* 126, 174707 (2007).

Quantum chemical studies on hydration of HSO_5 and participation of $H_2S_2O_8$ in nucleation

M. Toivola[1], T. Kurtén[1], T. Berndt[2], I. K. Ortega[1], V. Loukonen[1], H. Vehkamäki[1], M. Kulmala[1]

[1]Department of Physics, University of Helsinki, Finland
[2]Leibniz-Institut für Troposphärenforschung e. V. Leipzig, Germany

Keywords: homogeneous nucleation; sulfuric acid; quantum chemistry.

Sulfuric acid is a key component in atmospheric aerosol formation. However, the experimental results give reason to expect (Berndt *et al.*, 2008) that reaction intermediates of sulfuric acid formation and their alternative reaction products could be involved in particle formation. The observations indicate, on one hand, that no direct photochemistry of sulfur – containing molecules is likely explain the observed nucleation rate, and on the other hand that the key steps must involve reactants that lie before SO_3 on the SO_2 oxidation chain.

Based on the known mechanism of SO_2 oxidation, there are thus only two alternatives: the HSO_3 and HSO_5 radicals. Since the concentration of HSO_3 is almost certainly very low due to its efficient reaction with O_2 to form HSO_5, the observed nucleation mechanism is thus very likely to involve as a key step the reaction of HSO_5 with some other molecule, leading (either directly or via more steps) to the formation of efficiently nucleating products. For example, self-reaction of HSO_5 would form $H_2S_2O_8$ (plus an oxygen molecule).

A central uncertainty in any nucleation mechanism involving HSO_5 is the lifetime of this metastable intermediate radical. Previous modeling studies have predicted the dissociation of HSO_5 into SO_3 and HO_2 to be very rapid, leading to a short lifetime of HSO_5, and a low net yield for the pathways forming alternative reaction products such as $H_2S_2O_8$. According to calculations by Salonen *et al.* (2009), the sulfuric acid-peroxo disulfuric acid ($H_2S_2O_8$) dimer is more stable than the sulfuric acid dimer with respect to the electronic energy. However, these studies have not accounted for the effect of hydration on the stability of HSO_5.

In this study, we have investigated both the growth energetics of H_2SO_4-$H_2S_2O_8$ clusters, and studied the effect of hydration on the stability (and thus, lifetime) of HSO_5.

Calculations on larger clusters have been performed using a systematic multi-step method. The initial molecule and cluster geometries are taken from earlier computational studies, or generated with the DL_POLY_2 molecular dynamics program. The structures are optimized with the SIESTA program, using the BLYP functional with a DZP basis set and corresponding pseudopotentials. The single point energies were computed at the RI-MP2/aug-cc-pV(T+d)Z level using TURBOMOL program suite.

Hydrates of HSO_3, HSO_5, HO_2 and SO_3 have been studied at the G3B3 (mono- and dihydrates) and UCCSD(T)/aug-cc-pV(T+d)Z//UB3LYP/6-311++G(3d,3p) level (monohydrates only) using the Molpro 2006.1 program for the coupled-cluster energy calculations and the Gaussian 03 program suite for all other steps.

Table 1. Free electronic energies of sulfuric acid addition reaction in units of kcal mol-1.

Reaction	ΔE
$(H_2SO_4)_3$+ H_2SO_4	-18,7
$(H_2S_2O_8)\cdot(H_2SO_4)_2$+ H_2SO_4	-19,7
$(H_2S_2O_8)_2\cdot(H_2SO_4)$ + H_2SO_4	-20,9

The electronic energies for the addition of sulfuric acid to various cluster types are shown in Table 1. It can be seen that the addition of sulfuric acid to a cluster containing peroxodisulfuric acid is more favorable than the addition to a pure sulfuric acid cluster. We are in the process of calculating the Gibbs free energy values for the addition reactions.

High-level quantum chemical calculations (Kurtén *et al.*, 2009) demonstrate that HSO_5 is much more strongly hydrated than SO_3 and HO_2, leading to a significant increase in its lifetime with respect to dissociation. Due to hydration, the stability of HSO_5 with respect to dissociation is increased by several kcal/mol in ambient conditions. At least partial proton transfer from HSO_5 to H_2O is predicted to occur in the $HSO_5(H_2O)_2$ cluster, which may have important implications for the reactivity of hydrated HSO_5. Kinetic modeling assuming an efficient self-reaction for $HSO_5(H_2O)_2$ indicates that this mechanism could, in principle, explain the experimentally observed particle formation rate.

Berndt, T., Stratmann, F., Bräsel, S., Heintzenberg, J., Laaksonen, A., and Kulmala M. (2008) *Atmos. Chem. Phys.*, 8, 6365-6374 .

Kurtén, T., Berndt, T., and Stratmann, F. (2009) *Atmos. Chem. Phys. Discuss.* 9, 2823-2853 .

Salonen, M., Kurten, T., Vehkamaki, H., Berndt, T., and Kulmala, M. (2009) *Atmospheric Research* **91** (1), 47-52.

Numeric experiment and mesoscale structure of the atmospheric aerosol

O.G. Khutorova, D.P. Zinin and G.M. Teptin

Kazan State University, 18 Kremlevskaya St., Kazan, 420008, Russia

This paper is devoted to the application of mesoscale WRF-CHEM model for researching of vertical and horizontal inhomogeneous structure of pollutant concentration in the East Europe region

For this region the numerical model was built. The numerical model of tropospheric mesoscale inhomogeneities is created on the basis of numerical WRF meteomodel (Stockwell et al., 1990). The modelling parameters are meteoparameters and small gases. The model take into account pollutant transfer, including an aerosol, in view of local geographical particularity: real relief and land use categories maps, optimum numerical schemes of atmospheric processes are chosen.

For comparison we used a databank of measurements of aerosol and gaseous impurities concentrations by the net of automatic stations in urban region of Eastern Europe (54° N, 49° E), (53° N, 51° E) and the data of air density measured by GPS-GLONASS station.

The NCEP/NCAR data of a global state and dynamics of atmosphere (NNRP project) were used as an initial and boundary approximation to real weather conditions.

Horizontal scale of territory is 800x600 km. Horizontal space resolution is 10 km. Height of gained atmospheric layer is 17-20 km with 31 layers of data discretization. Time resolution of outcomes is 30 min with internal integration step is 60 sec.

Comparison with real observational has shown good correspondence for temperature and wind velocities.

The outcomes show the complicated vertical and horizontal structure of formed inhomogeneities in aerosol concentration field and others pollutants (Fig.1). These results match to observational results about mesoscale atmospheric inhomogeneities.

On the basis of the gained data the analysis of the wave's effects in time variable inhomogeneous structure of troposphere fields revealed the basic regularities for vertical and horizontal waves.

These results of numerical wave researching were compared with experimental wave researching results for the same territory and time period.

An analysis of long time measurements of aerosol and minor gaseous impurities by atmospheric monitoring stations displayed mesoscale time and space variations.

The measurement of the mass concentration of the aerosol by filter has the measurement accuracy - 1 μg/m3. Measurements are made at height of 2.4 m. The same point simultaneously wind velocity and direction, temperature, relative humidity, minor gas impurities concentrations are measured.

By the wavelet transform we analyze the series of aerosol concentrations simultaneously in temporal - frequency space. All kind of impurities and meteoparameters has the same spectra of wave disturbances. So, the mesoscale variations of atmospheric impurities are determined by atmospheric dynamics. Horizontal length of mesoscale waves is 1-160 km. Waves direction depend on the wind direction (Fig.2).

Figure 1. Aerosol concentration deflection from mean vertical profile. Vertical cross section.
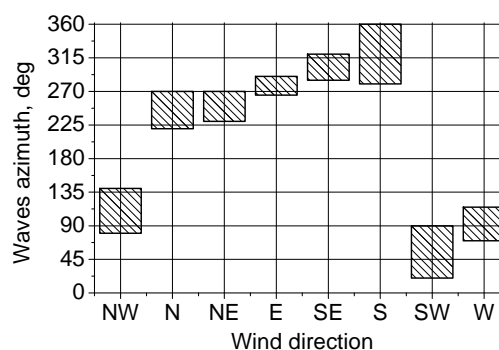
Fig.2 Waves azimuth versus wind direction

Stockwell, W.R., Middleton, P., Chang, J. S., Tang, X. (1990) *J. Geophys. Res.*, 95, 16343-16367.

Process Tracking of Particle Sulfate Formation
During the BAQS-Met Experiment in Southern Ontario

P. A. Makar[1], C. Stroud[1], J. Zhang[1], W. Gong[1], M. Moran[1], D. Sills[2],
S. Gong[1], K. Hayden[1], J. Brook[1], J. Liggio[1], S.M. Li[1], J. Murphy[3], J. Abbatt[3], G. Evans[3]

[1]Air Quality Research Division, Environment Canada
[2]Cloud Physics and Severe Weather Research Section, Environment Canada
[3]Chemistry Department, University of Toronto, Toronto, Canada

Keywords: Sulfate, Modelling (regional), Measurements, Aerosol Formation, AMS.

The Border Air-Quality Study – Meteorology (BAQS-Met) took place in the summer of 2007 in the southern-most part of Canada, the region bordered by Lakes Erie, St. Clair, Huron and Ontario. Aircraft and surface observations were made to determine the effects of local meteorology (land and lake breezes) on particulate matter formation. The Environment Canada AURAMS (A Unified Regional Air-Quality Modelling System) was used in forecast mode during the study to help direct aircraft and ground-based mobile laboratories. AURAMS includes size-resolved speciated particulate matter formation (12 bin sectional approach).

Subsequent to the measurement campaign, a nested version of the AURAMS model was developed to examine the impact of lake breezes on particulate matter formation. Three levels of nesting were employed: an outer nest with 42 km resolution extending over North America, a 15km intermediate grid centered over eastern North America, and a 2.5 km grid focused on the study domain. The model output on the highest resolution 2.5 km domain will be the focus of this discussion. The model shows the capability to resolve very small-scale features in the measurements, with good timing for the capture of plumes from major particulate events at fixed sites in the area, though variable ability to resolve some local features from aircraft and mobile ground-based laboratories.

A formal statistical comparison between observations and both aircraft and ground-based observations has been prepared. Figure 1 shows an example comparison between Aerosol Mass Spectrometer measured sulfate and model-predicted sulfate for the same size range, at one of the fixed super-sites in the study (Harrow). The agreement is good, with the timing of sulfate peaks and lows being well captured by the model.

An example comparison from the surface mobile laboratory CRUISER is shown in Figure 2. This is followed by a comparison of the statistics for this drive along the highway (R =correlation coefficient, B = slope, A = intercept, MB = mean bias, NMB = normalized mean bias(%), ME = mean error, NME = normalized mean error(%)).

A diagnostic package has been added to the high resolution model to track the changes in particle
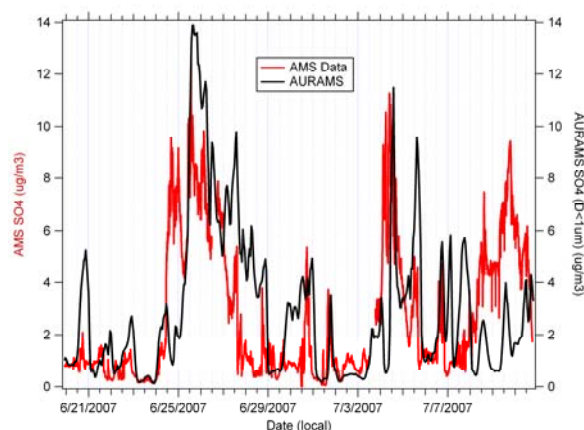
Figure 1. Comparison between AURAMS PM_1 SO_4 and AMS SO_4, Harrow.
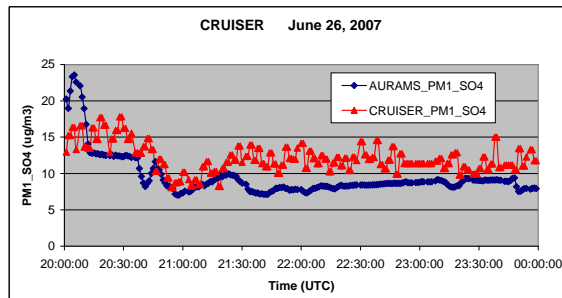
Figure 2. Comparison between AURAMS PM_1 SO_4 and AMS SO_4, CRUISER.

Table 1.Statistical analysis of comparison depicted in Figure 2.

R	B	A	MB
0.535	0.768	0.184	-2.63
NMB	ME	NME	
-21.7	3.19	26.3	

sulfate due to each of the model's chemical and physical processes. This in turn has allowed the relative importance of different model processes towards the resulting sulfate concentrations to be evaluated for different particle sizes. The relative importance of advection, diffusion, chemical formation, chemical transformation, and the different components of particle microphysics will be presented for different periods during the measurement intensive.

Field measurements of particle number emission factors for freeways

Carmen Nickel, Heinz Kaminski, Ulrich Quass, Astrid John, Thomas A.J. Kuhlbusch

IUTA e.V., Air Quality & Sustainable Nanotechnology Unit, Bliersheimer Str. 60, 47229 Duisburg, Germany

Keywords: emission factor, particle size, vehicle emissions

Particle number concentration measurements have recently been introduced into European traffic exhaust regulations (Euro VI; COM 2007). Therefore one of the goals of the 3 weeks upwind and downwind measurements at a German motorway (A61) was to derive particle number emission factors.

So far most studies were conducted at busy and highly polluted traffic sites within city limits or used the effect of pollution accumulation in tunnels (Rautberger-Wulff, 2000; Luhana et al., 2004). Results from these studies are not directly transferable to the emissions of motorways with free air flow and high speed conditions. Hence information on number emissions from motorway traffic is very limited.

In this project, scanning mobility particle sizers (SMPS) were installed on both sides of the motorway, i.e. upwind and downwind, to measure the particle number size distribution. The values from both SMPS were used to generate the emission factors of vehicles for particle number by using the NOx tracer method (Gehrig et al., 2003). Hereby the dilution factor is calculated from the measurement concentration differences of nitrogen oxides, the number of vehicles, and tabulated NOx emission factors.

Only data during clear up/downwind and dry meteorological conditions were used for the calculation. At first the emission factor (EF) for particle number emission per vehicle were generated. Then a multiple regression model was used to apportion the emission factors to the fraction emitted by light duty vehicles - LDV (i.e. petrol and diesel passenger cars, vans, motorcycles) and heavy duty vehicles – HDV (i.e. lorries and busses), respectively. The particle size dependence of the EFs is shown in Fig. 1, with highest factors for the smallest particles.
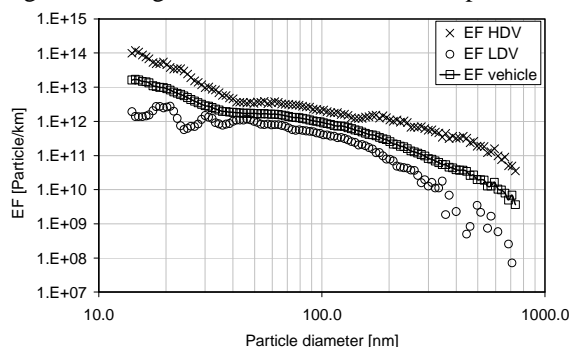
Fig 1: Emission factors for particle number emission per vehicle, LDV and HDV

Fig. 1 also shows that the emission factor for the HDV was higher than the emission factor for LDV for every particle size. Especially EFs for particles with a diameter < 30 nm show enhanced emissions. EF for particles between 30 and 200 nm show similar decrease for HDV and LDV while for larger particles (> 200nm) EF's decrease steeper for LDV than for HDV.

In order to give specific information on size resolved emission factors, the following size ranges were evaluated: < 50 nm, < 100 nm, 50 - 200 nm and total number concentration (TNC) and presented in Fig. 2.

Vehicles emitted mainly smaller particles, < 50 nm. These particles are mainly formed by homogeneous nucleation when the exhaust of the vehicles is rapidly cooled upon emission. Another emphasis is in the range of 50 - 200 nm. Soot particles are mainly emitted in this size range.

Emission factor for total number concentration for HDV were calculated to be 1,25E+15 Particle / km and 6,64E+13 Particle / km for LDV.
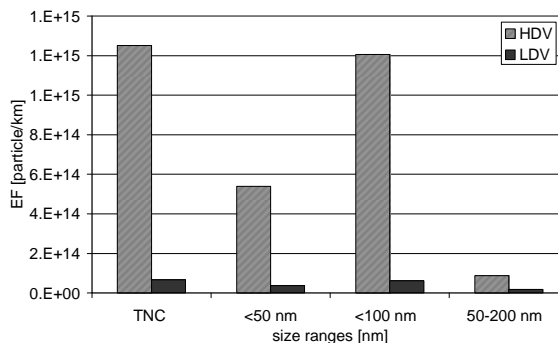
Fig. 2 emission factor for the different size ranges itemised for HDV and LDV

Rauterberg-Wulff, A. (2000). *Untersuchung über die Bedeutung der Staubaufwirbelung für die PM10-Immission an einer Hauptverkehrsstraße.* Final report: TU Berlin, Germany.

Gehrig, R., Hill, M., Buchmann, B., Imhof, D., Weingartner, E. H., Baltensperger, U. (2003). *Verifikation von PM10-Emissionsfaktoren des Strassenverkehrs.* Final report: research project ASTRA 2000/415, Switzerland.

Episodes of high particle concentrations over Central Europe with emphasis on the Benelux/Rhine-Ruhr area as simulated with a complex chemistry transport model

M. Memmesheimer[1], S. Wurzler[2], E. Friese[1], H.J. Jakobs[1], G. Piekorz[1], C. Kessler[1], A. Ebel[1], H. Hebbinghaus[2]

[1]Rhenish Institute for Environmental Research (RIU), University of Cologne,
Aachener Strasse 209, D-50931 Cologne, Germany

[2]North Rhine Westphalia State Agency for Nature, Environment and Consumer Protection (LANUV), P.O. Box 101052, D-45610 Recklinghausen, Germany

Keywords: Air pollution modelling, Chemistry transport model – 3D, Modelling (regional), PM_{10}, NO_2

The Rhine-Ruhr area with its 10 Million inhabitants, located in the federal state of North-Rhine-Westphalia, is one of the regions in Europe which has the characteristics of a mega-city. Together with the nearby urban agglomerations in the Benelux area, including Brussels, Amsterdam and Rotterdam, it forms a region which is heavily burdened by air pollutants as PM_{10} and NO_2, mainly due to industry and traffic. Emissions of NH_3, which is an important gaseous precursors for secondary particles formed in the atmosphere, are also quite high in this region. It might be difficult to achieve the limit values as given in the EC air quality directive within parts of the Benelux/Rhine-Ruhr area.

Calculations with the EURAD model (Memmesheimer *et al., 2004, 2007)* have been performed to investigate characteristic features of air pollution episodes with high particle concentrations in the Benelux/Rhine-Ruhr area. Comparison of base case simulations with emission scenarios are used to illustrate the transport of air pollutants over long distances and to demonstrate the interactions between different areas. An example, including a scenario without anthropogenic emissions in Germany, is shown in Figure 1. It can clearly be seen that the high particle concentrations in the Benelux and France partly can be attributed to emissions from Germany. Other examples for different emission scenarios will be shown for the local as well as for the European scale. Air pollution episodes with high concentrations of PM_{10} are characterized by anticyclone conditions over Central Europe leading to accumulation of gaseous precursors and secondary aerosols as well as primary emitted particles. The frequency of those weather situations can influence the number of exceedances of the daily limit value for PM_{10} of 50 $\mu g/m^3$ for the year considered and therefore might lead to interannual variations caused by changing meteorological conditions. PM_{10} concentrations are to a larger extent influenced by transport than NO_2.

Future extensions of the model applications aim at the coupling to the global scale and the performance of long-term runs on the time-scale of a decade. The fluxes of atmospheric trace constituents will be considered in more detail within the recently established FP7 project Cityzen.
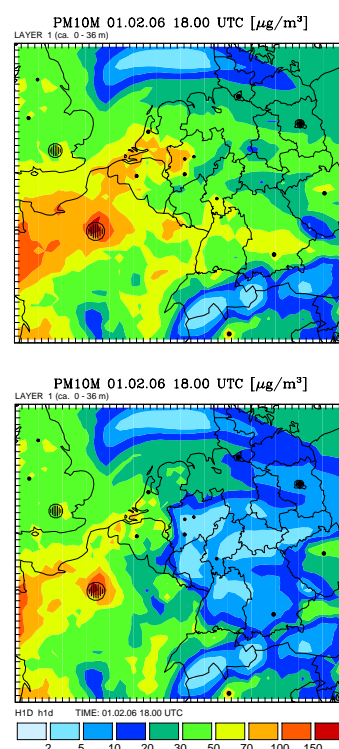
Figure 1. PM_{10} concentrations, upper part: base case, lower part: no anthropogenic emissions in Germany

Memmesheimer, M., Friese, E., Ebel, A., Jakobs, H.J., Feldmann, H., Kessler, C., Piekorz, G. (2004): Long-term simulations of particulate matter in Europe on different scales using sequential nesting of a regional model, IJEP, 22, 108-132.

Memmesheimer, M., Wurzler, S., Friese, E., Jakobs, H.J., Feldmann, H., Ebel, A., Kessler, C., Geiger, J., Hartmann, U., Brandt, A., Pfeffer, U., Dorn, H:P. (2007): Long-term simulations of photo-oxidants and particulate matter over Europe with emphasis on North-Rhine-Westphalia. Air Pollution Modelling and Its Application XVIII, Ed. C. Borrego, E. Renner, Elsevier, Amsterdam, 158–167, DOI:10,1016/S1474-8177(07)06028-7.

User influence on indoor aerosol model simulation results.

B. Mølgaard[1] and T. Hussein[1]

[1]Department of Physics, University of Helsinki, Helsinki, FIN-00014, Helsinki, Finland

Keywords: indoor aerosols, aerosol modelling, penetration, deposition.

A size resolved indoor aerosol model should at least take ventilation rate, outdoor particle size distribution, penetration factor, and deposition rate into account. Depending on the application also resuspension, coagulation, evaporation, condensation, nucleation and indoor sources might be of importance. In a multi compartment model transport between the compartments should also be included. Even in a rather simple case, there might be several unknowns to find. Iteration of these unknowns often leads to several solutions (group of input parameters) that simulate the indoor particle size distribution almost equally well when compared to the measurement.

We have constructed a single compartment model that simulates the indoor particle size distribution in an office with mechanical ventilation. The office consists of a main room, a small shower room, and a small bath room. Coagulation, evaporation, condensation and nucleation were ignored. We have incorporated a deposition model by (Lai & Nazaroff, 2000), which predicts the deposition rate based on the average friction velocity. By using data from a measurement campaign at an office (G3, 3 air changes/h, no indoor sources or activity, surface/volume = 3.6), we aimed at finding a solution that best-fits the model simulation with the measurement.

It turns out that the simulation works well with very different sets of input parameters. The four different sets of input parameters in figure 1 all give a rather good simulation of the measured data. Where there are differences between simulation and data, it is not obvious which set of input parameters gives the best prediction most often. The penetration factor that corresponds to a friction velocity of 15 cm/s is not realistic as it is higher than the penetration factor of a G3 filter for particles diameters smaller than 25 nm. The penetration factor corresponding to 8 cm/s might be the most realistic one as it allows for some particle loss in the ventilation pipes for all particle sizes except the largest ones.
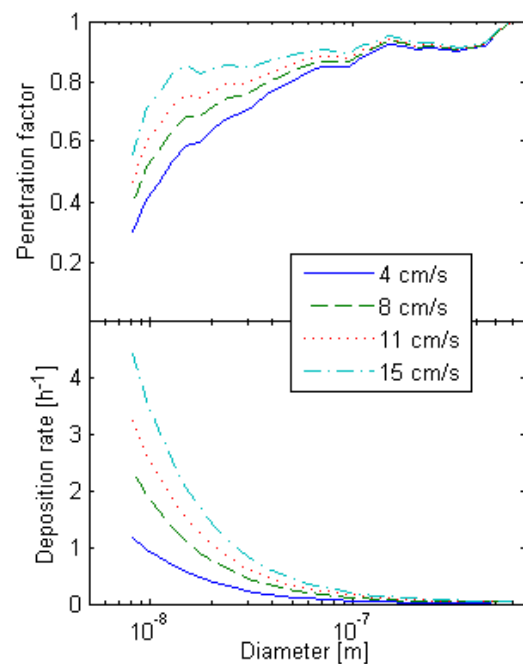
Figure 1: Deposition rates according to (Lai & Nazaroff, 2000) and best fit penetration factors for four different friction velocities.

Lai, A. C. K & Nazaroff, W. W. (2000) *J. Aerosol Science,* 31, 463-476.

The interannual variability of the stratospheric aerosol layer as seen in MAECHAM5-SAM2

R. Hommel[1,2], C. Timmreck[2], M. Giorgetta[2] and H.-F. Graf[1]

[1]Centre for Atmospheric Science, Cambridge University, Cambridge, UK
[2]Max Planck Institute for Meteorology, Hamburg, Germany

Keywords: Aerosol dynamics, aerosol modelling, stratospheric aerosols, sulfur particles.

In the lower stratosphere the interannual variability of gaseous constituents is dominated by the quasi-biennial oscillation (QBO; see Baldwin et al., 2001). Although the QBO is a phenomenon of the equatorial stratosphere, the QBO affects the atmospheric dynamics and thus trace gas concentrations in all latitudes, from the tropical stratospheric reservoir (TSR) to the polar vortex (e.g. Gray & Chipperfield, 1990). In tracers such effects are reflected by concentration gradients and by the formation of characteristic concentration patterns dependent on the phase of the QBO (e.g. Randel et al., 1998), the annual cycle (e.g. Mote et al., 1996), planetary wave mixing (e.g. Randel et al., 1993), tropopause exchange processes (Holton et al., 1995) and chemical pathways. In recent years QBO effects e.g. in CH_4 and O_3 were studied widely (e.g. Schoeberl et al., 2008). Little attention was given to QBO modulations in lower stratospheric particulate matter. However, SAGE (Trepte & Hitchman, 1992) and HALOE (e.g. Choi et al., 1998, 2002) observations of the tropical stratospheric aerosol exposed a typical biennial signal that could be linked to the QBO.

We are presenting the first comprehensive modeling study of QBO effects in the global stratospheric aerosol layer under non-volcanic conditions, using the size resolved aerosol-climate model of the middle and upper atmosphere MAECHAM5-SAM2 (Hommel, 2008). Our model studies show that in the vicinity of descending equatorial zonal winds QBO induced anomalies were found in all prognostic and diagnostic aerosol parameters as well as in concentrations of sulphate aerosol precursor gases. Qualitatively QBO modulations in the modeled aerosol mixing ratio correspond to modulations found in spaceborne observations of the aerosol extinction (Trepte & Hitchman, 1992; Hasebe, 1994; Choi et al., 1998). Phase shifts and phase inversions in the modelled aerosol parameter anomalies are caused by non-linearities in QBO controlled process interactions. QBO induced anomalies in the aerosol number concentration are a function of particle size. Enhanced reversible gas-to-particle partitioning (condensation, evaporation of H_2SO_4) has been found in regions above the aerosol concentration maximum, which is linked to QBO modulations in both thermodynamic quantities and advective transport. Observational findings (Trepte & Hitchman, 1992) of the upper and lower transport regimes for stratospheric tracers out of the TSR are reproduced by the model, while the secondary circulation associated with the QBO (e.g. Plumb & Bell, 1982) can be identified by the modelled aerosol concentration gradients according to observational findings of Choi et al. (1998).

The QBO modulates the uplift of gaseous aerosol precursors through the tropical tropopause region into the stratosphere, which is enhanced in easterly QBO phases by ~15 % for SO_2. Respective modulations in the uplift of sulfur aerosol with tropospheric origin could not be seen. Instead our simulations reveal that QBO modulations in TSR aerosols are caused by modulations in aerosol formation and growth processes and modulations in the advective transport of those particles. Therefore QBO induced anomalies in the TSR aerosol concentration are directly linked to the QBO modulated cross-tropopause transport of SO_2.

Baldwin, M. P., et al., Rev. Geophys., 39, 179-229, 2001.

Choi, W., Grant, W. B., Park, J. H., Lee, K., Lee, H., & Russell III, J. M., J. Geophys. Res., 103, 6033-6042, 1998.

Choi, W., Lee, H., Grant, W. B., Park, J. H., Holton, J. R., Lee, K.-M., & Naujokat, B., Tellus B 54/4, 395–406, 2002.

Gray, L. J. & Chipperfield, M. P., Geophys. Res. Lett., 17, 933–936, 1990.

Hasebe, F., J. Atmos. Sci., 51, 1994.

Holton, J. R., Haynes, P. H., McIntyre, M. E., Douglass, A. R., Rood, R. R., & Pfister, L., Rev. Geophys., 33, 403–439, 1995.

Hommel, R., Reports on Earth System Science 57, Max Planck Institute for Meteorology, 2008.

Mote, P. W., et al., J. Geophys. Res., 101, 3989–4006, 1996.

Randel, W. J., Gille, J. C., Roche, A. E., Kumer, J. B., Mergenthaler, J. L., Waters, J. W., Fishbein, E. F., & Lahoz, W. A., Nature, 365, 533–535, 1993.

Randel, W. J., Wu, F., Russell III, J. M., Roche, A., & Waters, J. W., J. Atmos. Sci., 55, 163–185, 1998.

Schoeberl, M. R., et al., Geophys. Res., 113, 2008.

Trepte, C. R. & Hitchman, M. H., Nature, 355, 626-628, 1992.

Mathematical modelling of clusters and nanoparticles transport in narrow tubes

L.A. Uvarova[1], T.V. Kazarova[2] and K.V. Vnukova

[1]Department of Applied Mathematics, Moscow State University of Technology "STANKIN",
3a Vadkovskii lane, 127994, Moscow, Russia
[2]Department of Philosophy, Moscow State University of Technology "STANKIN",
3a Vadkovskii lane, 127994, Moscow, Russia

Keywords: modelling, molecular clusters, density functional theory, metal nanoparticles

The modeling of a transport of clusters and nanoparticles in different systems and structures is one from actual modern problems. It is application in such areas as control, nano-electronics, medicines and other scientific areas

We considered the transport of the clusters and the nanoparticles in narrow tubes by the molecular dynamics methods. On the surface of the tube was set potential.

The famous potentials of the interaction were considered: the Lenard – Jones potential, the Bukingem modification potential, the Lenard – Jones modification potential allowed consider an interaction of molecules or small particles with a surface,
$$U(r_{ij}) = \pi \rho \varepsilon_{ij} \left(\frac{\sigma_{ij}^{12}}{45 r_{ij}^9} - \frac{\sigma_{ij}^6}{9 r_{ij}} \right),$$

where ε_{ij} is a depth of a potential pit, σ_{ij} is a effective diameter of particles, ρ is a density of a matter wall. In general case it is necessary to take into account the Casimir force at the consideration a very small distance. In this case the energy interaction can be describe by the Casimir –Polder potential.

$$U(r_{ij}) = -\frac{\hbar c}{4\pi r_{ij}^7} (23(\alpha_E^{(i)} \alpha_E^{(j)} + \alpha_M^{(i)} \alpha_M^{(j)}) -$$
$$7(\alpha_E^{(i)} \alpha_M^{(j)} + \alpha_M^{(i)} \alpha_E^{(j)}))$$

where $\alpha_E^{(i)}, \alpha_M^{(i)}$ express a electric and a magnetic polarization i- molecule or i- particle correspondingly, c is light velocity.

In work [Nadykto et al., 2006] by the quantum-chemical methods with the help the modern applications packages Gaussian, Gromacs, HyperChem is received values of the density for small clusters of water. There are considered water clusters $(H_2O)_n$, $n=2 – 10$ and it is showed that ratio $\frac{\rho}{\rho_0}$ (where ρ is the density of the cluster and ρ_0 is the density of the liquid) changes from 0.93 (for $n=2$) to 1.45 (for $n=10$). In given work we carried out the calculations for transport of the water clusters with the using Verle's algorithm. However value for density of the cluster (which includes in the expression for potential) was determined by the quantum-chemical methods. Consequently, it was close to real value. Some the results of the calculation experiments are presented in Table 1. Here in the numerator of fraction is wrote number of the flying particles and in the denominator is wrote number of the precipitating particles. The particles transport takes place in the narrow conical tube (diameters are 10 - 12 nm). The denominator increases with the increase of the length of the moving. The energy for drops and agglomerates was considered (for the different matter) with the using the density functional theory. The results allowed assess the adoption of the classic methods for such systems.

Table 1. The example of the transport and the precipitating for the water clusters at $n=3$

Number of particles	Number of experiments	Distance in the tube for moving particles, nm		
		10	100	1000
3	50	51/99	9/141	0/150
4	50	59/141	13/187	0/200
5	50	72/178	22/228	2/248

In this work is received that such nanoparticles precipitate on the surface more quickly then clusters of the appropriate diameter with the water density.

We considered the transport of the metallic nanoparticles under the acting of the different potentials. In the calculations we considered the real nanoparticles got at the different experimental conditions. For the consideration the moving of the magnetic nanoparticles and its interaction with the surfaces it is necessary to find the spin orientation. The spin evolution may be found on basis the Landau – Lifshits –Gilbert equation:
$$\hbar S_{af} \frac{d\vec{s}_{ni,j}}{dt} = \vec{s}_{ni,j} \times \vec{H}_{eff} + \mu \vec{H}_{eff}$$ (where μ is died out signal, $H_{eff} = -\frac{\partial W}{\partial s_{ni,j}}$, and W is total energy).

Such results can use for the external and internal control in the environment physics (for example for a cell).

Nadykto, A.B., et al (2006). *Physical Review Letters,* 96, 125701-4.

Mathematical modelling of heat and mass transfer in disperse systems with drops and agglomerates at different external conditions

L.A. Uvarova[1], O.V. Nikitina[1] and T.V. Kazarova[2]

[1]Department of Applied Mathematics, Moscow State University of Technology "STANKIN",
3a Vadkovskii lane, 127994, Moscow, Russia
[2]Department of Philosophy, Moscow State University of Technology "STANKIN",
3a Vadkovskii lane, 127994, Moscow, Russia

Keywords: aerosol modelling, droplets, agglomerates, evaporation, heat and mass transfer

The evaporation in drops and agglomerates aerosol collections in the electromagnetic fields is considered. This problem for evaporation and heat and mass transfer was solved by the methods of infinite elements. Heat and mass transfer in these systems induced by the action of electromagnetic radiation. Thermo-physics model has the following form

$$C_{pi}\rho_i \frac{\partial T_i}{\partial t} = \vec{\nabla}\chi_i(\vec{\nabla} T_i) + q_i(T_i), \; C_e\rho_e \frac{\partial T_e}{\partial t} = \vec{\nabla}\chi_e(\vec{\nabla} T_e),$$

$$T_i(\vec{S}_i, t) = T_e(\vec{S}_i, t), \; -\chi_i \frac{\partial T_i}{\partial \vec{n}}(\vec{S}_i, t) = -\chi_i \frac{\partial T_e}{\partial \vec{n}}(\vec{S}_i, t) +$$

$$L_i J_i(R(t), t,), T_e(\infty, t) = T_\infty,$$

$$\frac{\partial C_i}{\partial t} = \nabla D_i(\nabla C_i), \; i = 1 \div N,$$

$$-\frac{dM_i}{dt} = \oint_{S_i} D_i \nabla C_i dS_i,$$

where S_i is a surface of i-particle, T_e is the temperature outside of a particle, C_{pi} is the heat capacity of i-particle, C_e -is the heat capacity of the environment, t is the time, T_∞ is the temperature of the environment undisturbed by the presence of particles, ρ_i is the density of substance of a particle, ρ_e is the density of substance of the environment, $\vec{n}$ is a surface normal, $q_i(T_i)$ is heat source of electromagnetic nature, N is number of particles, C-concentration, D-diffusion coefficient "agglomerate matter – external medium ", M_i –mass of i-matter, I is flux, L- the heat capacity of the phase moving.
We believe that heat physical characteristics depend on temperature.

The modeling carried out as in quasi-stationary regime (at a small overheat) as and in non-stationary regimes. The heat transfer modelling for spherical carbonaceous aerosol collective of particles was carried out in [Uvarova et al, .2006]. In work [Nikitina, 2008] was investigated non-stationary evaporation of single drop with the consideration of the border moving by heat potential method.

The heart source $q_i(T_i)$ was determined from the solving of the corresponding electrodynamics problem. At the consideration of a collective of spherical particles it was used exact solution for two particles; that is substantiated by the importance of a pair influences [Krivenko & Uvarova, 2004]. At the consideration of a collectives agglomerates was used T-matrix method.

We considered the different external conditions and investigated the influence of the atmospheric factors on the heat and mass transfer and the evaporation velocity.

The calculations for different configurations and atmospheres were carried out. In particular, for the water drops with initial radiuses 1-5 micron in the collective from 3 drops at corresponding powers of electromagnetic radiation it was received the following correlation:

$$R_0 - R = kt,$$

where for the Earth atmosphere $k=0{,}625*10^{-3}$ and for the Venus atmosphere $k=12{,}5$.
The middle temperatures in the drops for the Venus atmosphere and for the Earth atmosphere equal correspondingly:

$$T_m(R) = 1{,}045 \cdot 10^{15} R^2 + 500,$$

$$T_m(R) = 4{,}66 \cdot 10^{11} R^2 + 293.$$

In general case the drops and agglomerates configurations and atmospheric factors have the influences on the evaporation velocities, and quantitative results different significanty at the qualitative coincidence of the laws even.

Uvarova L.A., Krivenko I.V.,& Smirnova M.A. (2006). *Chemical Engineering Transactions,* 10, 251-256.
Nikitina O.V. (2008). In *Proc. of Scientific conference MSUT "Stankin",* Moscow, 46-49 (*in Russian*).
Krivenko I.V.,& Uvarova L.A. (2004). *Russ. J. Phys. Chem.* 78, 894-898.

Computational study of aerosol flow in bifurcations

M. Pilou[1,2], V. Gkanis[2], P. Neofytou[2] and C. Housiadas[2]

[1]Laboratory of Biofluid Mechanics & Biomedical Engineering, School of Mechanical Engineering, National Technical University of Athens, 15773 Athens, Greece
[2]Thermal Hydraulics & Multiphase Flow Laboratory, National Centre for Scientific Research "Demokritos", 15310 Agia Paraskevi, Greece

Keywords: aerosol modelling, deposition, CFD

INTRODUCTION

Aerosol flows within the respiratory system are of great importance in order to assess the risk of airborne micro- and nano- particles deposition in the system and the benefit of pharmaceutical drugs inhalation. The former is related to the toxicity of the particles and possible lesions in the deposition sites and the latter to the efficiency and optimization of inhalation devices and pharmacologic aerosol therapy. In order to identify the aerosol mechanisms, which are most important for these flows, many researchers studied aerosol flows in bifurcations, since the shape of the bronchial trees can be approximated by successive bifurcations up to the alveolus. Thus, there are experimental (Myojo, 1987), theoretical (Gradon & Orlicki, 1990) and computational studies (Balásházy & Hofmann, 1993; Farkas & Balásházy, 2008; Zhang et al., 2009) of aerosol flows in a bifurcation. In the majority of the latter studies commercial Computational Fluid Dynamics (CFD) software are used to obtain the fluid flow field combined with user defined equations in the same codes (Nowak et al, 2003), Monte Carlo techniques (Balásházy & Hofmann, 1993) or Lagrangian formulation (Longest & Xi, 2007; Farkas & Balásházy, 2008) to solve for particle dynamics.

In the present work, a parametric study of aerosol flow in bifurcations is performed. In particular, the flow of monodisperse aerosol populations in a bifurcation is simulated using non-commercial CFD codes for the continuous and the particulate phase, where both particle diffusion and inertial effects are taken into account, using an Eulerian formulation of the particle General Dynamic Equation (GDE).

METHODS

The effect of inertia on Brownian diffusional transport, in isothermal aerosol flows, under steady state conditions, is explicitly considered through the low Stokes number expansion of the average momentum equation (Fernandez De La Mora & Rosner, 1982). As a result, a first-order correction to the particle velocity field due to particle inertia is obtained:

$$\vec{v}_p = \vec{v} - D\nabla \ln c - \tau_p (\vec{v} \cdot \nabla)\vec{v} + O(\tau_p^2), (1)$$

where $\vec{v}$ is the carrier gas velocity, c the particle concentration, D the Brownian diffusion coefficient and τ_p the particle relaxation time. In this case the GDE that describes the particle concentration c and its variation in space and time takes the form:

$$\frac{\partial c}{\partial t} + \nabla \cdot (c\vec{v}) - \tau_p \nabla \cdot \left[c(\vec{v} \cdot \nabla)\vec{v} \right] = \nabla \cdot D\nabla c, (2)$$

that incorporates effects due to particle inertia to first order in the particle relaxation time, in an Eulerian description.

The non-commercial CFD code developed by Neofytou, 2005, which is used in the current study, utilises the finite volume method and is applied to the solution of the velocity and pressure fields of the carrier gas and subsequently the GDE (eq.(2)) for the particle size distribution. High order upwind discretisation schemes are used for the second and third term on the left hand side of eq.(2), whereas for the term on the right hand side central difference schemes are preferred.

With the use of the aforementioned computational tools, a parametric study of the aerosol flow in the bifurcation is performed. Inlet fluid and concentration profiles, fluid Reynolds number, bifurcation geometry and size and shape of the particles serve as parameters of our study. The numerical results of the present study are compared with solutions available in literature.

Balásházy, I. & Hofmann, W. (1993). *J. Aerosol Science*, 24, 745-772.

Farkas, A. & Balásházy, I. (2008). *Computers in Biology and Medicine*, 38, 508-518.

Fernandez de la Mora, J. & Rosner, D. E. (1982). J. *Fluid Mechanics*, 125, 379-395.

Gradon, L. & Orlicki, D. (1990). *J. Aerosol Science*, 21, 3-19.

Longest, P. W. & Xi, J. (2007). *Aerosol Science and Technology*, 41, 380-397.

Myojo, T. (1987). *J. Aerosol Science*, 18, 337-347.

Neofytou, P. (2005). *Advances in Engineering Software*, 36, 664-680.

Zhang, Z.,Kleinstreuer, C. & Kim, C. S. (2009). *J. Aerosol Science*, 40, 16-28.

HCl-Aerosols in Industrial Gas Cleaning Processes

G. Brosig[1], M. Bittig[1], J. Lindermann[1], S. Haep[1], M. Luckas[2] and K.-G. Schmidt[1]

[1]Institute of Energy and Environmental Technology, Bliersheimer Straße 60, 47229 Duisburg, Germany
[2]Thermal Process Engineering, University Duisburg-Essen, Lotharstraße 1, 47057 Duisburg, Germany

Keywords: absorption, aerosol modelling, heterogeneous condensation.

The aim of this work was to examine and to model the behavior of flue gases from incineration processes during the passage of wet scrubbers. At waste incineration plants equiped with a wet scrubber system to absorb HCl it was observed that the emitted gas contained significantly higher concentrations of HCl than expected and designed. The reason for this increase in HCl-amount could be traced back to the generation of fine HCl-droplets generated during the passage of the scrubber.
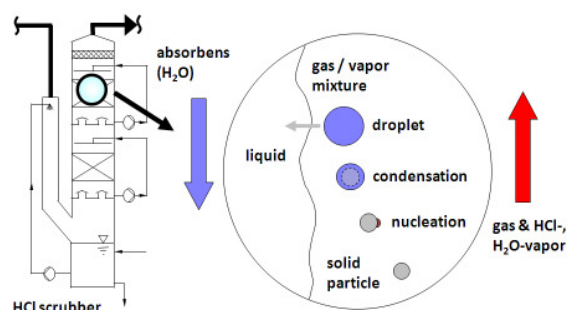
Figure 1. Physical model of the droplet generation during the passage in a HCl-scrubber.

In spite of modern separating systems the discharge of fine dust cannot be eliminated completely. The very tiny particles remaining in the exhaust gas are seeds for the fog formation. This nucleated seeds will grow inside the scrubber because of condensation to micron droplets (Fig. 1) but remain in a growth class where the droplets are very difficult to separate. Because of this carrier effect the HCl-fog passing the scrubber can cause problems of precipitation, damage the catalysator and cause corrosion in following plant units. Eventually there is the risk that the specification limits of the exhaust gas concerning HCl cannot be hold.

To support the plant manufacturer of scrubbing systems a flexible and broad applicable simulation program based on a rigorous process model was developed. The program has the ability to model the thermodynamical states and complex transfer processes in the scrubber. For this the balance equations for mass, components and energy was established according to a segmented non-equilibrium-stage-model. This model contains correlations for mass and energy transfer between gas, liquid, and particle phase. For computing the stationary solution the numerical equation solver LIMEX from ZIB (Zuse Institute Berlin, Ehrig *et al.*, 2002) was used.

The program was then successively validated. Initially the physical consistency of the model and the exactness of the program were checked by means of more simple units like heat exchanger, humidifier and HCl-absorber. Finally validating calculations of the total complex process model were carried out. Therefor experimental data from literature (Vogt, 2001; Haep, 2000; Ofenloch, 2005) were utilised as well as measurement results obtained from experiments at the technical scale plant erected for this purpose at IUTA (Institute for Energy and Environmental Technology). In all cases the simulation showed a good agreement with the experimental results. As one example the measured particle diameter at the end of the scrubber is compared with the calculated one (Fig. 2).
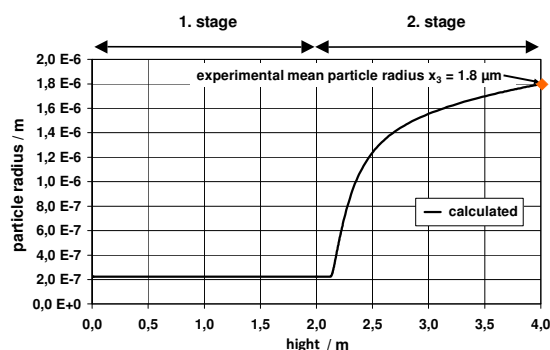
Figure 2. Good agreement for the particle radius between simulation and experiment

Ehrig, R, Ofenloch, O., Schaber, K. & Deuflhard, P. (2002). *Chem. Eng. Science*, 57, 1151-1163

Vogt, U. (2001). *Konditionierung und Abscheidung submikroner Partikeln in Füllkörperkolonnen*. Kaiserslautern, Germany: Fortschritt-Berichte Mechanische Verfahrenstechnik und Strömungsmechanik, Band 4, Aerosolabscheidung

Haep, S. (2000). *Bildung und Wachstum von Aerosolen unter Bedingungen der nassen Rauchgasreinigung*. Düsseldorf, Germany: Fortschritt-Berichte VDI, Reihe 3, Verfahrenstechnik, Nr. 641, VDI-Verlag.

Ofenloch, O. (2005). *Entstehung und Verhalten von Aerosolen in Gaswaschanlagen*. Düsseldorf, Germany: Fortschritt-Berichte VDI, Reihe 3, Verfahrenstechnik, Nr. 832, VDI-Verlag.

A methodology to use the flow field from Ansys CFX® software in an in-house sectional aerosol dynamics code

E.Makris[1,2], V. Gkanis[2] and C. Housiadas[2]

[1]Department of Mechanical Engineering, National Technical University of Athens, 15773 Athens, Greece

[2]Thermal Hydraulics & Multiphase Flow Laboratory, National Centre for Scientific Research "Demokritos",

15310 Agia Paraskevi, Greece

Keywords: CFD, aerosols dynamics, Ansys CFX®

INTRODUCTION

In order to model the aerosol dynamics in a given geometry one needs to solve for the flow field in that geometry, and often, one has to deal with complex geometries, such as flow of air in the human respiratory organ. Therefore, the construction of the mesh and the subsequent solution of the governing equations for the fluid flow, and the solution of the general dynamic equation for the particles can be a difficult task. In this work we develop a methodology to use the flow field obtained with a commercial software, Ansys CFX®, in our in-house sectional aerosol dynamics code.

The commercial software Ansys CFX® has tools that help the scientist to easily construct any geometry, no matter how complicated this geometry may be. More importantly, Ansys CFX® will solve for the flow field in that geometry. This software is also capable of working in parallel mode, which would significantly reduce the computational time, and thus it would allow the scientists to obtain high-resolution results. Nevertheless, Ansys CFX® has a limited number of built in functions. Although Ansys CFX® can solve the general dynamic equation for the particles, it is not capable of modeling the cases were nucleation, coagulation or agglomeration of particles take place.

Therefore, in this work we propose a methodology to use the flow field from Ansys CFX® in an in-house sectional aerosol dynamics code. With this method, we manage to construct the mesh, solve for the flow field, and model the aerosol dynamics in complex geometries.

METHOD

The aerosol dynamics are modeled with a Fortran code that was developed by Mitrakos(2007, 2008). This code not only solves the Eulerian form of the general dynamic equation for the particles, but it is also capable of modeling the nucleation, growth and coagulation of particles. This code incorporates the sectional approach, and it uses the Finite Volume Method.

The software Ansys CFX® is used to construct the mesh and solve the Navier-Stokes equations. Although Ansys CFX® exports the solution in the form: node, coordinates, solution, we do not know how Ansys CFX® is numbering the nodes of the mesh. For example, from the exported file we can read which nodes are on the boundaries, but we do not know where exactly these nodes on the boundary are. Therefore, we read this file by utilizing the CGNS (CFD General Notation System) protocol. This protocol was developed in an effort to standardize CFD input and output format, and it provides an enormous amount of information about the mesh. For example, it gives for each node the adjacent nodes, extremely useful information to reconstruct the mesh. Once we have the mesh and the flow field at each node, we use Mitrakos' code to solve the general dynamic equation for the particles. More importantly the developed code is capable of solving not only steady state, but also time dependent flow fields. The difficulty about this type of flow fields, is, however that we need to develop a code for data communication between, Ansys CFX® software and our in house code, at each time step. The results obtained with this methodology are validate by comparing them against those derived by Mitrakos et all. (2008).

REFERENCES

Mitrakos et al. (2007). *Aerosol and Technology, 41:1076 – 1088, 2007* American Association for Aerosol Research

Mitrakos, D. (2008). Thesis Title: *Numerical Simulation of multiphase flow in dispersion – Application in the dynamics of particle flow.* National Technology University of Athens, Mechanical Engineering Department

Mitrakos D. & Jokiniemi J. & Backman U. & Housiadas C. *J. Nanonparts Res (2008) 10:153-161*

Thermophoretic deposition of aerosol particles in the plane – parallel channel with considerable transversal temperature drops

E.R.Shchukin, Z.L.Shoulimanova, T.N. Bryansteva, N.V.Malay

Institute for High Temperature RAS, Izorskaya, 13/19,Moscow,127412, Russia

Keywords: aerosol modeling, heat and mass transfer, high temperature aerosols, industrial aerosols

Aerosol particles suspended in a non-isothermal gas acquire a mean velocity relative to the gas and move in the direction opposite to the temperature gradient. This effect, known as thermophoresis, occurs whenever the size of the particles is comparable to the mean-free-path of the background gas and is caused by the differential momentum transfer to the particles following collisions with molecules that originate in regions of the gas that differ in temperature. For particles with nearly spherical shape, the thermophoretic velocity is given by

$$U_T = -f_T \nu \nabla T / T ,$$

where ν is the coefficient of cinematic viscosity and T is the gas temperature. The scalar coefficient value $f_T \le 1$ depends on the particle and gas thermal conductivities and the Knudsen number (based on particle radius and gas mean free path).

A theoretical model was developed describing the thermophoretic deposition of aerosol particles in fully-developed laminar flow through channels with their walls at different fixed temperatures. Precipitation of particles occurs under the considerable transversal temperature drops. Gas flow takes place when the density, the dynamic viscosity and the thermal conductivity depend on the temperature of the gas. The nonlinear system of equations of gas dynamics describing the distribution of the temperature and the longitudinal component of the mass velocity was solved analytically [Shchukin E.R., e*t al*]. The expression for the distributions of the temperature and longitudinal component of the velocity in the gas flow enabled us to obtain formulae for direct estimation of the channel length l_c at which the complete thermophoretic precipitation of particles occurs.

With the constant value of f_T (as, for instance, for small particles) and the degree dependence of the thermal conductivity $K = K^{(1)} \theta^{\alpha}$ and the dynamic viscosity $\mu = \mu^{(1)} \theta^{\beta}$ upon $\theta = T / T_1$, the expression for l_c is equaled to

$$l_c = l_c^{(0)} \psi, \qquad l_c^{(0)} = QH / bn^{(2)} \nu^{(2)} ,$$

where $\nu^{(2)} = \nu^{(1)} \theta_2^{1+\beta}$, $\mu^{(2)} = \mu^{(1)} \theta_2^{\beta}$, $n^{(2)} = n^{(1)} / \theta_2$ are the kinematics viscosity, the dynamic viscosity and concentration of molecules at the upper heating plate; $\theta_2 = T_2 / T_1$; T_1 and T_2 are the temperatures at the upper and lower plate surface; Q is the expenditure of molecules in the cross-sections of the channel; H is the distance between the plates; b is the width of the plates.

$$\psi = \left((1+\alpha) \theta_2^{\beta} / f_T \gamma_1 \varphi \right) \times$$

$$\psi = \left((1+\alpha) \theta_2^{\beta} / f_T \gamma_1 \varphi \right) \times$$

$$\times \left\{ \frac{\left(1 - \theta_2^{2+3\alpha-2\beta}\right)}{\left(2+3\alpha-2\beta\right)} \frac{\left(1 - \theta_2^{2+2\alpha-\beta}\right)}{\left(1 - \theta_2^{1+\alpha-\beta}\right)} - \frac{\left(1 - \theta_2^{3+4\alpha-2\beta}\right)}{\left(3+4\alpha-2\beta\right)} - \gamma_1 \gamma_2 \theta_2^{1+\alpha-\beta} / \left(1 - \theta_2^{1+\alpha-\beta}\right) \right\}$$

$$\varphi = \left\{ \gamma_2 \frac{\left(1-\theta_2^{2+2\alpha-\beta}\right)}{\left(1-\theta_2^{1+\alpha-\beta}\right)} - \frac{\left(1-\theta_2^{2+3\alpha-\beta}\right)}{\left(2+3\alpha-\beta\right)} - \gamma_1 \theta_2^{1+\alpha-\beta} / \alpha \left(1-\theta_2^{1+\alpha-\beta}\right) \right\}$$

where $\gamma_1 = \left(1 - \theta_2^{1+\alpha}\right)$, $\gamma_2 = \left(1 - \theta_2^{1+2\alpha-\beta}\right) / (1+2\alpha-\beta)$

Numerical evaluation has shown that the increase of the upper plate temperature causes a decrease in the length of complete thermophoretic entrapment of particles.

Shchukin E.R., *et al.* (1996). *Physica Scripta.*, 53, 478-483.

Morphology of Rod-Like Nanoparticle Aggregates by Monte Carlo Simulations

G. Skillas[1], A. Maisels[2] and C.J. Klasen[3]

[1]Process Technology, Evonik Degussa GmbH, Hanau-Wolfgang, Germany
[2]Inorganic Materials, Evonik Degussa GmbH, Hanau-Wolfgang, Germany
[3]Performance Polymers, Evonik Degussa GmbH, Darmstadt, Germany

Keywords: nanotubes, rods, morphology, fractals, modelling.

Powders have a broad application in science and technology as pigments, ceramics, fillers, composites, carriers to name some. Powder properties depend on properties of powder particle material and on physical properties of particle collective i.e. are determined by the integral behaviour of a vast quantity of individual particles. As result, particle morphology becomes decisive.

The particle morphology depends on peculiarities of powder synthesis and processing. Synthesis procedures are based on sequences of chemical and physical processes, therefore, analytical description of powder particle morphology becomes a challenging task. For powders obtained through high temperature gas-processes, through precipitation in liquids, through sol-gel route, the concept of fractal dimension found a wide recognition (Samson et al., 1987). This approach is based on assumption, that powder particles are fractal-like aggregates composed of equally sized, spherical primary particles. No theoretical approach for non-spherical primary particles is known.

In the actual work morphology of aggregates consisting of rod-like primary particles is studied by means of Monte Carlo simulations. Examples of such primary particles are nano-crystals, -tubes, -rods, proteins, etc (Knipping et al., 2004; Bandorowicz-Pikula et al., 2004). In simulations, the aspect ratio of primary particles is varied from 1 (spheres) to 16.

For aggregates of rod-like primary particles with the aspect ratio $\alpha = 4$, dependency of the number of primary particles n_p on the diameter of gyration D_g is shown in Fig. 1.

As follows from Fig. 1, the relation between n_p and D_g introduced by Samson *et al.*, 1987

$$n_p = c_0 \left(\frac{D_g}{D_p} \right)^{d_f}$$

for aggregates of spherical primary particles can be extended for rod-like primary particles aggregates with known aspect ratio to

$$n_p = c_0 \left(\frac{D_g}{(1+\alpha)D_p} \right)^{d_f}$$

with c_0 being some constant. It is remarkable, that the fractal dimension d_f is nearly the same for aspect ratios 1 and 4.
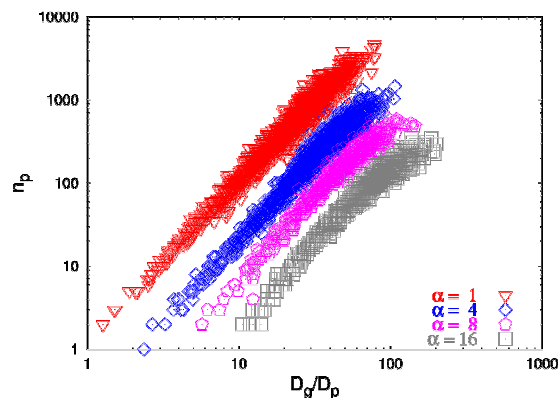
Figure 1. Primary particle number vs. diameter of gyration for different rod-like primary particle aggregates ($\alpha = 4 - 16$, $D_p = 2$ nm) and for aggregates of spherical primary particles ($\alpha = 1$). Generated at temperature of 1523 K and a pressure of 101325 Pa.

Bandorowicz-Pikula, J., Konopka, D., Hennig, J. *et al.* (2004). *Annexins*, 1, 68-78.
Knipping, J., Wiggers, H., Kock, B. F. *et al.* (2004). *Nanotechnology*, 15, 1665-1670.
Samson, R. J., Mulholland, G. W., & Gentry, J. W. (1987). *Langmuir*, 3, 272-281.

Geoengineering climate with controlled sea spray emissions: feasibility and effects on natural marine sulphur cycle

H. Korhonen[1] and K. S. Carslaw[2]

[1]Department of Physics, University of Kuopio, POB 1627, 70211 Kuopio, Finland
[2]School of Earth and Environment, University of Leeds, Leeds LS2 9JT, United Kingdom

Keywords: climate effect, CCN, emissions, marine aerosol, aerosol modelling.

As dramatic cuts in greenhouse gas emissions in the near future seem unlikely, several geoengineering ideas involving aerosol particles have been proposed in recent years as a method to combat climate warming. One of the more feasible proposals is controlled emissions of sea spray particles in an effort to increase marine low-cloud albedo. Neglecting all explicit treatment of aerosol processes, the few published climate model studies up till now (e.g. Latham et al., 2008) have assumed that this method is capable of globally doubling the cloud droplet number concentration. However, the wind speed dependence of both natural and geoengineered (planned spray vessels are wind powered) sea spray flux, transport of sprayed particles to cloud base level and enhanced heterogeneous reaction of natural DMS-derived SO_2 on freshly emitted alkaline sea spray particles are just some factors that could affect the relative increase of cloud droplets at any geoengineered location.

This work presents for the first time an investigation of the feasibility and side effects of controlled sea spray emissions using an explicit size-resolved aerosol model. We use the global model GLOMAP (Spracklen et al., 2005) and add a wind-speed dependent geoengineering sea spray flux to four separate regions of the world's oceans (Fig. 1). In these regions the natural CCN concentration is low (due to low local wind speeds and little anthropogenic pollution) and low-level cloud cover frequent making them potential target regions for possible future geoengineering experiments. In accordance with the plans for spray vessel prototype (personal communication with S. Salter, 2008), we assume that the injected man-made sea spray flux is proportional to $u^{1.5}$ (where u is 10-metre wind speed).

Our simulations suggest that CCN(0.2%) enhancement of 20-60% at cloud base level of 1 km is realistic when using the flux specified above (Fig 1). Note that this is a clearly lower enhancement than assumed in previous climate model studies, mainly because we simulate explicitly transport of the injected particles from the ocean surface to the cloud base level and thus account for dry and wet deposition as well as dispersion. Although some enhancement is seen outside the geoengineered regions, it is clear that the climate effects of this method are fairly local and it would therefore be necessary to build a very large fleet of vessels in order to alter the cloud droplet number globally.

On the other hand, we find that the additional sea spray flux has a relatively small effect on marine boundary layer natural sulphur cycle, which we have recently shown to be an important source of CCN over remote oceans (Korhonen et al., 2008). This is because the injected sea spray particles are small (dry size ~250 nm) and contribute only a minor fraction to pH buffered heterogeneous oxidation of SO_2 since supermicron sea spray particles have a much larger buffering capacity. While the injected sea spray significantly reduces DMS-derived sulphuric acid concentration in the lower atmosphere, the H_2SO_4 concentration in the free troposphere, and thus CCN from binary nucleation, is practically unaffected.
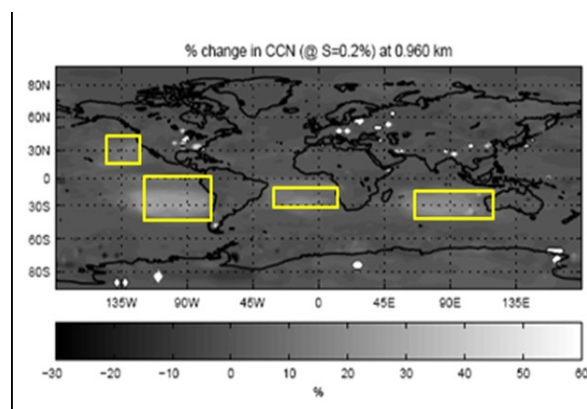
Figure 1. Percent increase in CCN at 0.2% supersaturation due to controlled sea spray emissions.

Korhonen, H., K. Carslaw, D. Spracklen, G. Mann & M. Woodhouse. (2008). *J. Geophys. Res.*, 113, D15204.

Latham, J., P. Rasch, C.-C. Chen, L. Kettles, A. Gadian, A. Gettelman, H. Morrison, K. Bower & T. Choularton (2008), *Phil. Trans. T. Soc. A.*, 366, 3969-3987.

Spracklen, D., Pringle, K., Carslaw, K., Chipperfield, M. & Mann, G. (2005). *Atmos. Chem. Phys.*, 5, 2227-2252.

Optimization of sulfur injections to the stratosphere: 1-D model study of geoengineering

A.-I. Partanen[1,2], H. Korhonen[1], J. Kazil[3], U. Niemeier[3], C. Timmreck[3], K.E.J. Lehtinen[1,2], J. Feichter[3], H. Kokkola[2]

[1]Department of Physics, University of Kuopio, P.O.Box 1627, 70211 Kuopio, Finland
[2]Finnish Meteorological Institute, Kuopio Unit, P.O.Box 1627, 70211 Kuopio, Finland
[3]Max Planck Institute for Meteorology, Bundesstraße 53, 20146 Hamburg, Germany

Keywords: geoengineering, aerosol modelling, sulfur dioxide, stratospheric aerosols

During the recent years deliberately altering the climate system has been a target for extensive research. Model studies show that injecting sulfur dioxide into the stratosphere could counteract global warming caused by the increased concentrations of green house gases (eg. Robock et al. 2008). Previous model studies of sulfate geoengineering with climate models have used fairly simple aerosol population description. For example Rasch et al. (2008) and Robock et al. (2008) used a prescribed aerosol size distribution for the generated sulfate aerosol.

In order to give a more realistic and detailed view on the evolution of the stratospheric aerosol we use single column model (SCM) version of the aerosol-climate model ECHAM5-HAM (Stier et al., 2005), whose size-segregated microphysical core M7 takes into account nucleation, condensation and coagulation. Computational efficiency of the SCM makes it possible to test a large range of different injection scenarios.

Our goal is to optimize sulfur dioxide injections to create a given radiative forcing with the lowest possible mass flux into the atmosphere. Interesting parameters for injections are for example injection height and interval between injections. We use offline atmospheric dynamics from a preceding full three dimensional model run without additional sulfur dioxide injections. This approach allows us to avoid the interference from the chaotic behavior of the climate system and concentrate fully on the aerosol dynamics.

The difference in meteorological conditions between tropics and the Arctic creates differences in the geoengineered aerosol. Nucleation of new particles is continuous in tropics if sufficient sulfur dioxide injections are provided but in the Arctic there are periods with length of months without nucleation taking place. This makes it harder to maintain constant aerosol population in the arctic stratosphere. Residence times in the Arctic are also shorter than in tropics as shown in Figure 1.

Sulfur injections make the stratospheric particles grow and these bigger particles form a coagulation sink for the new particles in the nucleation mode. As a result, concentrations in the nucleation mode are lower compared to the control run in all locations.

Time-averaged radiative forcing due to the sulfate aerosol is stronger in tropics than in the Arctic. Both have considerable temporal variation. Based on preliminary results a global amount of 2 Tg(S) per year of sulfur dioxide provides a forcing of about -0.4 W/m^2 in tropics and about -0.3 W/m^2 in the Arctic.

The reliability of the SCM is evaluated by comparing results with a full 3-D model run. The SCM can reproduce fairly well the evolution of the aerosol population given by the full model in tropics. It can also be used in other locations to emulate the full model although it underestimates the vertical mixing and the residence time of the sulfate aerosol.

Comparison between several model runs with different injection heights shows that for example in tropics aerosol forcing is strongest if the sulfur dioxide is injected at a level of about 30 hPa, but there are no significant differences in a modest mass flux range. The most effective ratio between aerosol forcing and injected mass is found with a low mass flux.
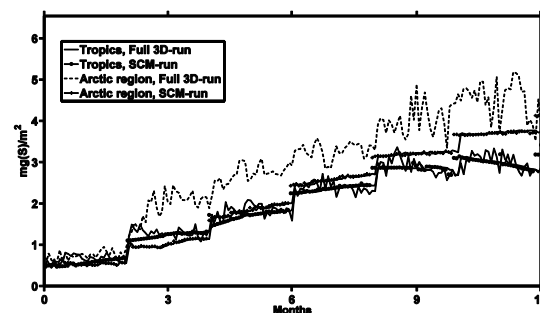
Figure 1. Stratospheric total sulfuric burden in tropics (bottom two lines) and in an arctic region (top two lines) simulated by the SCM and the full model.

Rasch, P. J., Crutzen, P. J. & Coleman, D. B. (2008). Geophys. Res. Lett., 35, L02809, doi:10.1029/2007GL032179.

Robock, A., Oman, L. & Stenchikov, G. L. (2008). J. Geophys. Res., 113, D16101, doi:10.1029/2008JD0.

Stier, P., Feichter, J., Kinne, S., et al. (2005). Atmos. Chem. Phys., 5,1125-1156.

Simulation of the indirect effect of Austrian background aerosol: Description of the model

D. Neubauer[1], A. Vrtala[1], H. Puxbaum[2], R. Hitzenberger[1]

[1]Faculty of Physics, University of Vienna, Boltzmanngasse 5, 1090, Vienna, Austria
[2]Institute of Chemical Technologies and Analytics, Vienna University of Technology, Getreidemarkt 9/164, 1060, Vienna, Austria

Keywords: indirect effect, carbonaceous aerosol, cloud microphysics, black carbon.

Aerosols and greenhouse gases are the two most important contributors to the anthropogenic climate change (IPCC, 2007). Usually, models (Rotstayn, 1999; Lohmann *et al.*, 2000) use measured aerosol data as input, and their predictions are compared to cloud parameters measured independently from the aerosol measurements. The model developed in this study uses simultaneously measured values for the aerosol and the subsequent cloud. This way, more realistic predictions for the indirect aerosol effect can be expected. The model uses data from an earlier intensive measurement campaign at an Austrian background site which allows predictions of the indirect effect for regional continental aerosols in Central Europe. The effects of black carbon are investigated.

The aerosol and cloud data are taken from the FWF project P 131 43 – CHE and had been collected in 2000 at a measurement site on a mountain in the proximity of Vienna (Rax, 1680 m a.s.l.). In the study by Iorga *et al.*, 2007 the direct effect of the aerosol in Austria on the radiative balance was calculated and the influence of the surface albedo on radiative forcing and its direction (warming or cooling) was investigated.

The simulation model consists of two parts, a cloud droplet growth model and a radiative transfer model (Key & Schweiger, 1998). The growth model for cloud droplets computes the cloud droplet distribution originating from a measured aerosol distribution. The changes in measured liquid water content of the real-world cloud are continually compared with the liquid water content of the simulated cloud containing the growing droplets. The radiative transfer model then computes the radiative forcing using the calculated cloud droplet size distribution.

The cloud model is a cloud parcel model which describes an ascending air parcel containing the droplets. Turbulent diffusion (important for stratiform clouds) is realized through a simple approach. The model includes nucleation, condensation, coagulation and radiative effects. Because of radiative heating/cooling of the cloud droplets the ambient temperature and the critical super-saturation of the droplets can change. The absorption of solar radiation of a cloud droplet can be significantly increased by black carbon.

For radiative transfer calculations, the radiative transfer code of the public domain program 'Streamer' (Key & Schweiger, 1998) was adapted to our purposes. 'Streamer' accounts for scattering and absorption of radiation in the whole spectral region by gases and particles. Built-in types of surface albedo as well as other values can be chosen. The radiative transfer equation can be solved by two different numerical methods to increase the precision of the calculation.

The radiative properties of the cloud depend on the single scattering properties of the cloud droplets, which in turn depend on the composition of the cloud droplets. In this study the cloud droplets are assumed to consist of water and black carbon. Different mixing types of black carbon in the cloud droplets are used for the calculations (Lesins *et al.*, 2002).

Test runs for a pure water cloud with an average liquid water content of 0.33 g/m^3 indicate that the first indirect aerosol effect might result in a negative radiative forcing (cooling) between -0.14 and -1.39 W/m^2.

IPCC, [Solomon, S. et al. (eds.)] (2007). *The Physical Science Basis. Contribution of Working Group I to the Fourth Assessment Report of the Intergovernmental Panel on Climate Change*, Cambridge, U.K. and New York, NY, USA: Cambridge University Press.

Rotstayn, L. D. (1999). *J. Geophys. Res.*, 104(D8), 9369–9380.

Lohmann, U. & Feichter, J. (2000). *J. Geophys. Res.*, 105(D10), 12,193–12,206.

Iorga, G., Hitzenberger, R., Kasper-Giebl, A. & Puxbaum, H. (2007). *J. Geophys. Res.*, 112, D01204.

Key, J. & Schweiger, A. J. (1998). *Computers & Geosciences*, 24(5), 443-451.

Lesins, G., Chýlek, P. & Lohmann, U. (2002), *J. Geophys. Res.*, 107(D10), 4094.

Seasonal variations of characteristics of atmospheric aerosol optical depth and aerosol radiative forcing in Siberia

T.B. Zhuravleva, Kabanov D.M., S.M. Sakerin

Institute of Atmospheric Optics, 634021, Tomsk, Russia

In the report, we consider the seasonal variations of aerosol optical depth (AOD) and shortwave component of direct aerosol radiative forcing (*ARF*) in boreal zone of Siberia. The specific features of *ARF* formation under typical conditions of Siberian region are determined by comparatively low atmospheric turbidity, in contrast to the radiation effects of biomass burning and industrial and desert aerosol.

1. Analysis of annual AOD behavior for different Siberian regions is performed on the basis of multiyear measurements of spectral atmospheric transparency. In the region of Tomsk, these data are obtained for a longer observation period and extended spectral range 0.34-4 μm. Among the key features of annual AOD behavior, we revealed that: (a) AOD maxima are observed in April-May ($\tau_{0.5}^a \geq 0.18$) and July (with a local minimum in June), and minimum AOD values are observed in October-November ($\tau_{0.5}^a \leq 0.11$); (b) annual AOD behavior is more pronounced in the UV region of the spectrum: the $\tau_{0.37}^a$ variability range is 0.11 with average value 0.21; (c) Angström parameter is maximum in July (α=1.5) and minimum in winter (α=1). Average spectral AOD dependences for characteristic periods are presented in Fig. 1.
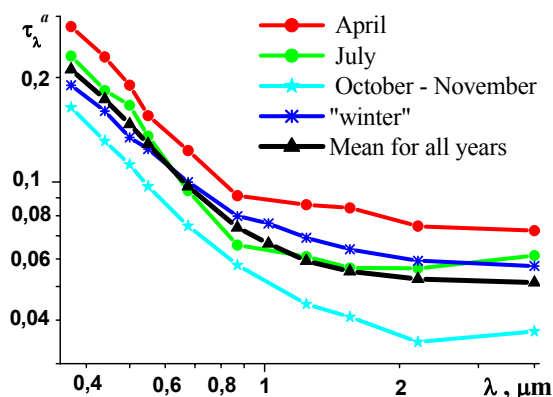
grounds to study shorter-term observation series in other Siberian regions and to estimate the specific features of the spatial AOD distribution. It is shown that the general pattern of annual AOD behavior is the same in Tomsk and Siberia, also supported by the results of the satellite observations (MODIS).

Comparative analysis showed common character of annual variations of τ_λ^a, α, and atmospheric moisture content *W*: growth of the values in warm period and drop in the cold period. Differences in the variations of these characteristics are manifested in differing relative amplitude of annual behavior; crossing times through annually mean level, first observed for $\tau_{0.5}^a$ (March-September) and then for α (April-October) and *W* (May-October); and additional springtime spike of AOD, observed neither for α nor for W.

2. For simulation of integrated radiative fluxes, we used the method according to which the spectral interval 0.2-5 μm is divided into 30 bands. Within each subinterval, the solar radiative fluxes were calculated on the basis of algorithms of the Monte Carlo method; the absorption by atmospheric gases is accounted for on the basis of the *k*-distribution method.

In specification of input parameters in *ARF* calculations, we used a combined approach, incorporating the results of measurements (AOD and *W*) and data, presented in well-known models of aerosol (single scattering albedo and scattering phase function), atmospheric gas constituents, and underlying surface.

The calculations of *ARF* are made taking into account the seasonal variations of the spectral AOD, W, and surface albedo. It is shown that the larger cooling at the surface level in spring months compared with autumn months is caused by the seasonal AOD variations. The cause for the *ARF* differences between summer and winter periods, for comparable AOD values, is the substantial change of surface reflectance: appearance of snow cover leads, in particular, to change of ARF sign at the top of the atmosphere.

Figure 1. Average spectral dependences of atmospheric AOD in characteristic months of year.

Closeness of the annual AOD behavior in Tomsk, calculated for the multiyear (1995-2008) and shorter (2003-2008) observation periods, gave us

New particle formation in past, present and future conditions

Risto Makkonen[1], Ari Asmi[1], Veli-Matti Kerminen[2], Almut Arneth[3], Pertti Hari[4] and Markku Kulmala[1]

[1]Department of Physics, University of Helsinki, 00560, Helsinki, Finland
[2]Finnish Meteorological Institute, 00560, Helsinki, Finland
[3]Department of Physical Geography and Ecosystems Analysis, Lund University, 223 62, Lund, Sweden
[4]Department of Forest Ecology, University of Helsinki, 00790, Helsinki, Finland

Keywords: Aerosol modelling, Nucleation, Particle formation and growth, SOA.

New particle formation can effectively alter cloud properties by increasing the number of cloud droplets. Clouds with higher cloud droplet number concentration (CDNC) have increased cloud albedo, and high CDNC might even hinder precipitation. However, the importance of aerosol nucleation on climate on a global scale is difficult to estimate, since precursors for nucleation vary from location to another. Sulphuric acid is known to participate in the initial nucleation process, but for example the roles of ammonia and organic compounds are still rather uncertain.

The role of aerosols on climate has been changing dramatically since the beginning of industrialization. Emissions of anthropogenic primary particles and sulphur dioxide have been rather steadily increasing. Today, emission regulations and efficient filtering techniques help to reduce these emissions except in rapidly developing countries. But the biosphere can also play a major role in the evolving aerosol-climate. With the changing geographic patterns and overall anthropogenic emissions the relative role of biogenic vs. anthropogenic aerosol precursors are becoming increasingly important for the overall understanding of the system behavior. For instance, emission estimates for biogenic VOCs are 702 Tg(C)/yr, 725 Tg(C)/yr and 1251 Tg(C)/yr for preindustrial, present-day and future conditions, respectively, when considering only climate change and the generally more productive vegetation (Lathière *et al.,* 2005). Due to several interacting and changing factors (e.g. the role of atmospheric CO_2 concentration, land use/land cover change) and possible feedback mechanisms, the importance of new particle formation in different conditions is impossible to quantify without a comprehensive global model.

The aim of this study is to explore changes in patterns and magnitude of new particle formation due to industrialization, changes in vegetation and climate change. We focus on the role of biogenic organic compounds on aerosol growth and the actual nucleation process. We use ECHAM5-HAM (Stier *et al.*, 2005) aerosol-climate model with T42 resolution (~2.8°x2.8°) for global simulations for three time periods: pre-industrial (1750), present (2000), and future (2100). In simulating BSOA formation, both thermodynamic gas-particle partitioning and condensational transport from gas to particle phase are considered. We also consider organic vapors to participate the actual nucleation process.

Emissions of pre-industrial and present-day primary aerosol and precursor gases (other than biogenic organics) are described in Dentener *et al.* (2006). For future emissions IPCC scenario B2 is used. To account for changes in emissions of biogenic volatile organic compound, we use emission maps of Lathière *et al.* (2005) as a starting point. Lathière *et al.* calculated emissions for the Last Glacial Maximum, the pre-industrial (1850s), present-day (1990s) and the future. These are based on climate change and effects of changing atmospheric CO_2 concentration on vegetation.

Due to the low anthropogenic emissions of sulphur dioxide during the pre-industrial period, aerosol nucleation from biogenic organic vapors is relatively significant source of new particles. On the other hand, low condensation sink makes it easy for nucleation sized particles to reach CCN sizes. Since also the concentrations of condensing vapors are low, aerosol growth rates are lower than in present day. In our future scenario, global sulphur dioxide emissions are lower than present-day, but regionally emissions are even higher. Increasing emissions of biogenic volatile organic compounds stress the role of biosphere in future climate but additional processes (CO_2 inhibition, land cover change) complicate this picture.

Lathière, J., Hauglustaine, D. A., De Noblet-Ducoudré, N., Krinner, G., and Folberth, G. A. (2005). *Geophys. Res. Lett.*, 32, L20818, doi:10.1029/2005GL024164.

Stier P., Feichter J., Kinne S., Kloster S., Vignati E., Wilson J., Ganzeveld L., Tegen I., Werner M. , Schulz M., Balkanski Y., Boucher O., Minikin A., Petzold A. (2005). *Atmos. Chem. Phys.*, 5, 1125-1156.

Dentener, F., Kinne, S., Bond, T., Boucher, O., Cofala, J., Generoso, S., Ginoux, P., Gong, S., Hoelzemann, J. J., Ito, A., Marelli, L., Penner, J. E., Putaud, J.-P., Textor, C., Schulz, M., van der Werf, G. R., and Wilson (2006). *J. Atmos. Chem. Phys.*, 6, 4321-4344.

Radiative impact of aerosol on the state of the atmosphere on the regional scale

H. Vogel, B. Vogel, R. Rinke, M. Bangert

Institut für Meteorologie und Klimaforschung, Forschungszentrum Karlsruhe / Universität Karlsruhe, 76021 Karlsruhe, Germany

Keywords: modelling(regional), aerosol radiative forcing, natural and anthropogenic aerosol, soot particles

The role of natural and anthropogenic aerosol particles for the atmosphere on the regional scale is still under discussion.

In this study we use the comprehensive fully online coupled model system COSMO-ART (Vogel et al., 2009) to quantify feedback processes that are initialized by changes in the radiative fluxes by anthropogenic and natural aerosol particles on the regional to the continental scale. The meteorological driver is COSMO (Steppeler *et al.*, 2003), the operational weather forecast model of the German weather service (DWD). ART stands for **A**erosols and **R**eactive **T**race gases. Beside physical processes like transport, turbulent diffusion, and dry and wet deposition it includes photochemistry and aerosol dynamics applying the modal approach. The optical properties of aerosols as the extinction coefficient and the single scattering albedo are accounted for in COSMO-ART according to the parameterization of Bäumer *et al.* (2004).

In order to quantify the impact of anthropogenic aerosols on the state of the atmosphere over Central Europe we carried out simulations for two episodes in August 2005. The first episode is characterized by a high pressure situation with almost cloud free conditions over Central Europe whereas during the second episode a frontal passage results in cloudiness for most parts of the model domain. The comparison of the simulations with and without feedback processes shows that the anthropogenic aerosol load causes a reduction of the global radiation in the order of 10-15 W m^2 for the cloud free episode. Additionally a clear link between aerosol concentration and the decrease of radiation is found. The reduction of radiation is followed by a mean temperature reduction up to 0.3 K (Fig. 1, top). For the second episode the situation is quite different. On the one hand side the changes of the global radiation for the feedback run a even larger, on the other hand no clear correlation between aerosol load and modifications in radiation is visible. Concerning the temperature the results show not a uniform temperature decrease but also areas with higher temperatures in case of the feedback run (Fig. 1, bottom). This is caused by modifications of the cloud cover as a consequence of the aerosol impact.

Although we have so far neglected the interaction of the aerosol particles with the microphysics of clouds the results of the two sensitivity studies demonstrate that anthropogenic and natural aerosol have a remarkable influence not only on the global climate but also on the regional scale during episodes of a few days.
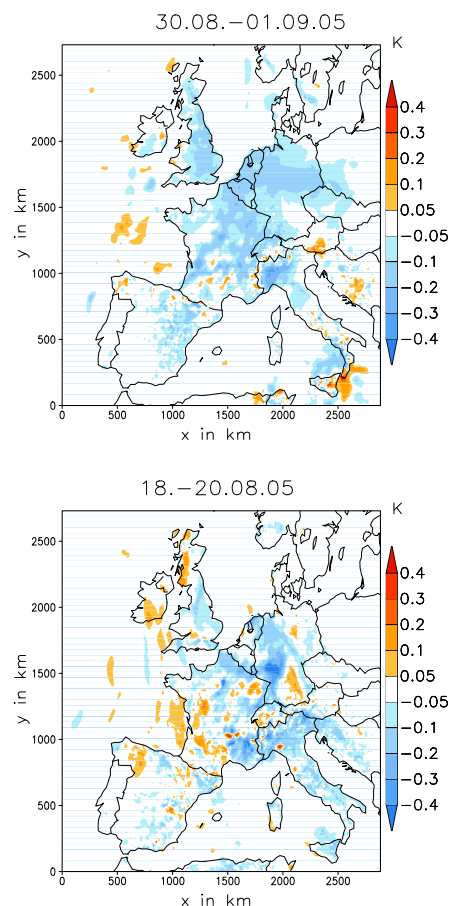
Figure 1. Averaged ΔT2m (with feedback – no feedback) for the cloud free episode (top) and cloudy episode (bottom).

Bäumer, D., B. Vogel, Ch. Kottmeier (2004), *J. of Aerosol Sci.*, pp. 1195-1196.

Steppeler, J., G. Doms, U. Schättler, H. W. Bitzer, A. Gassmann, U. Damrath and G. Gregoric (2003), *Meteorology and Atmospheric Physics*, 82, 75-96.

Vogel, B., H. Vogel, D. Bäumer, M. Bangert, K. Lundgren, R. Rinke, T. Stanelle, (2009) *submitted to APCD*.

Improvement of biogenic and wood burning emission inventories for air quality modelling in Switzerland

D. C. Oderbolz, Ş. Andreani-Aksoyoğlu, J. Keller, I. Barmpadimos, A.S.H. Prévôt, U. Baltensperger

Laboratory of Atmospheric Chemistry (LAC), Paul Scherrer Institut, Switzerland

Keywords: Aerosol modelling, Organic aerosols, Biogenic emissions

Chemical transport models can be used to better understand the processes leading to secondary organic aerosols and other air pollutants. A chemical transport model connects many single atmospheric processes into a unified framework, which allows studying the complex interactions between them better.

However, current models tend to drastically underestimate particulate matter, especially secondary organic aerosol (SOA) (Volkamer *et al.*, 2006).

Switzerland experiences high levels of particulate matter especially during winter time. One of the challenges for aerosol modelling in this region is the complex topography that creates many sub-grid effects which make vertical transport and hence dilution of air pollutants hard to predict.

Recent measurements (Lanz *et al.*, 2008; Sandradewi *et al.*, 2008) show that both in mountainous regions as well as in the Swiss plateau, wood burning is an important source for particulate matter in winter. Biogenic volatile organic compounds (BVOCs) that undergo oxidation are suspected to contribute substantially to particulate matter in summer in Switzerland. In this study, we address the need to better account for both wood burning and BVOC emissions in Switzerland.

We use CAMx version 4.51 with the Carbon Bond 2005 (CBM 05) chemical mechanism and an improved aerosol module that includes SOA formation from isoprene and sesquiterpenes as well as oligomerisation (Morris *et al.*, 2006). The meteorological input is prepared using MM5 version 3.7.4.

The emission inventory was updated using data from a recent study (Steinbrecher *et al.*, 2009).

A special focus of this work is on sesquiterpenes ($C_{15}H_{24}$), a large subgroup of alkenes. Chamber studies show that these chemical compounds have an aerosol yield close to 100% (Ng *et al.*, 2006). However, emission data is scarce and highly uncertain. Sesquiterpenes are emitted by both coniferous and deciduous plants during day- and night time. The emission flux in our new inventory is modelled as leaf temperature dependent without taking into account radiation, because of the currently limited knowledge.

In addition, the wood burning inventory was improved with respect to wood used for heating purposes in Switzerland. In the original inventory, wood burning was not represented explicitly, but treated together with all heating emissions. Also, the effect of altitude on heating was not considered.

In this study, the influence of improved emission inventory on the modelling of aerosols will be discussed.

Lanz, V. A., Alfarra, M. R., Baltensperger, U., Buchmann, B., Hueglin, C., Szidat, S., Wehrli, M. N., Wacker, L., Weimer, S., Caseiro, A., Puxbaum, H., & Prevot, A. S. H. (2008). *Environ. Sci. Technol*, 42, 214-220.

Morris, R. E., McNally, D., Tesche, T. W., Tonnesen, G., Boylan, J., & Brewer, P. (2006). *Atmos. Environ.*, 40, 4960-4972.

Ng, N. L., Kroll, J. H., Keywood, M. D., Bahreini, R., Varutbangkul, V., Flagan, R. C., Seinfeld, J. H., Lee, A., & Goldstein, A. H. (2006). *Environ. Sci. Technol*, 40, 2283-2297.

Sandradewi, J., Prévôt, A. S. H., Weingartner, E., Schmidhauser, R., Gysel, M., & Baltensperger, U. (2008). *Atmos. Environ.*, 42, 101-112.

Steinbrecher, R., Smiatek, G., Köble, R., Seufert, G., Theloke, J., Hauff, K., Ciccioli, P., Vautard, R., & Curci, G. (2009). *Atmos. Environ.*, 43, 1380-1391.

Volkamer, R., Jimenez, J. L., San Martini, F., Dzepina, K., Zhang, Q., Salcedo, D., Molina, L. T., Worsnop, D. R., & Molina, M. J. (2006). *Geophys. Res. Lett.*, 33.

Fugitive PM_{10}/$PM_{2.5}$ Emission Factors for Coal fired power plants

A. Hugo[1], M. Beyer[1], T.A.J. Kuhlbusch[1], C. J. Richter[2], F. Braun[2], A. Wiegele[2]

[1]Institute of Energy and Environmental Technology (IUTA), 47229 Duisburg, Germany
[2]iMA Richter & Röckle GmbH & Co.KG, 79098 Freiburg, Germany

Keywords: Emission Factor, Industrial Aerosols, PM_{10}/$PM_{2.5}$, Reverse Dispersion Modelling.

PM_{10} and $PM_{2.5}$ mass concentrations are currently of particular concern when extensions of existing power plants or new power plants are planned.

To estimate the contribution of fugitive dust sources like stockpiles, transhipment and transportation of coal material, certain calculation methods can be used. Data provided by the German engineering standard, VDI guideline VDI 3790 Part 3 (1999), are limited to emission factors for total suspended particles (TSP) for bulk material handling and windblown emission. The available data on PM_{10} and $PM_{2.5}$ emission factors are poor and disputed among experts.

A project studying windblown dust emission from open coal handling and coal stockpiles of power plants started with the aim to derive validated fine dust emission factors (PM_{10} and $PM_{2.5}$) by the use of ambient air monitoring and reverse dispersion modelling (EN 15445, 2008).

The work is covering the following working steps in order to derive reliable PMx-emission factors:

- Assortment of power plant sites with "typical technology",
- Estimating the dustiness of the coal,
- Conducting measurement campaigns determining PM_{10}, $PM_{2.5}$, TSP and meteorological conditions,
- Development of measurement data evaluation procedure,
- Dispersion modelling: Lattice model, testing by tracer gas experiments (SF6),
- Statistical data analysis, Reverse dispersion modelling (RDM),
- Emission factor evaluation, Comparison with results of other studies.

For hard coal and brown coal fired power plant sites, the "typical technology" for coal handling on each type of site is identified. Based on this data, appropriate measurement sites were chosen.

The "dustiness" of a material is an important modelling parameter. The dustiness of the coals was characterized by use of a standardized continuous drop apparatus (IGF, Bochum), different impactors and optical particle monitors, .

The measurement campaign has started at a hard coal power plant site in May 2008, with PM_{10} and $PM_{2.5}$ monitors (TEOM) at five sites with a time resolution of 5 minutes. In addition three monitors have been installed for TSP measurements. The monitoring will run until the end of March 2009, allowing the assessment of the influence of varying meteorological conditions on emission factors. Meteorological data is measured at different points and heights. In addition, the data is linked with webcam and GPS data of sources like dump pits to identify specific emission situations. For quality assurance, different data assorting routines are used.

The dispersion factors between dust sources and the measurement sites are calculated with a Lagrangian dispersion model using time series of local meteorological data. The movement of the sources along the stockpiles has been considered during the modelling calculations.

The emission factors are derived by the application of upwind/downwind differences and the reverse dispersion modelling method (RDM) according to international and German standards (VDI Guideline 4285 and EN 15445, 2008). Main steps of the method are carried out by the application of statistical analysis (e.g. multiple linear regression analysis) on the measured ambient air data and on the calculated dispersion factors.

A main advantage of the chosen experimental setup is the high time resolution for measured and modelled data, so short-time effects can be investigated. The contemporaneous PMx- and TSP-measurement allow the re-evaluation of emission factors currently used.

The benefits of the chosen measurement setup will be presented in comparison to other estimation strategies. The first estimation of the PM_{10}-Emission factor will be presented.

EN 15445: Fugitive and diffuse emissions of common concern to industry sectors - Qualification of fugitive dust sources by Reverse Dispersion Modelling, 2008-04

VDI 3790 Part 3: Environmental meteorology: Emission of gases, odours and dusts from diffuse sources: Storage, transhipment and transportation of bulk materials, 1999-05

Evaluating the impact of particle emissions from natural sources in the Balkan region

K. Markakis[1], T. Giannaros[1], A. Poupkou[1], D. Melas[1], M. Sofiev[2] and J. Soares[2].

[1]Aristotle University of Thessaloniki, Department of Physics, Laboratory of Atmospheric Physics, P.O. Box 149, 54124 Thessaloniki, Greece
[2]Finnish Meteorological Institute, Helsinki, Finland

Keywords: sea salt, dust, emissions, natural aerosols

Natural emissions of particles play a major role in air quality especially for areas which are close to the Saharan reservoir. The studies which employ modeling approaches in order to evaluate the contribution of those sources in the Balkan area are limited.

To study the impact of natural emissions of particles in the region, the NEMO emission model was employed. NEMO is integrated into the operational MM5/CAMx modeling system operated and developed by the laboratory of atmospheric physics in the Aristotle University of Thessaloniki. Emissions of wind erosion dust, sea salt and pollen are calculated according to the operational model setup having hourly basis and 10km spatial resolution. The meteorological parameters necessary to calculate the emission rates derive from the GFS database.

The methodology of NATAIR was implemented for the calculation of pollen and wind erosion dust emissions employing the high resolution landcover database of USGS and the soil texture maps of Webb et al., 2000 and van Liedekerke and Panagos. Sea salt emissions were calculated (Figure 1) based on the original formulas of Monahan et al., 1986 and Martensson et al., 2003 according to the modifications of Mikhail Sofiev.

Preliminary results in the Greater area of Athens, Greece indicate that sea salt emissions represent a considerable emitter of particles in the area. A simulation performed for a period of one week in June 2007 showed that sea salt, wind erosion dust and pollen emissions are in the order of 25 per cent compared to the PM_{10} emissions having anthropogenic origin for the same period (Markakis et al., 2009).

U.S.Geological Survey, Global Land Cover Charateristics Data Base.

van Liedekerke M., Panagos P., Soil Texture Map 10 km x 10 km (ETRS_LAEA version) ESDBv2 Raster Archive - a set of rasters derived from the European Soil Database distribution version 2 (published by the European Commission and the European Soil Bureau Network, CD-ROM, EUR 19945 EN)

Webb, R.W., Rosenzweig, C.E., & E. R. Levine. (2000). Global Soil Texture and Derived Water-Holding Capacities (Webb et al.). National Laboratory Distributed Active Archive Centre, Oak Ridge, Tennessee, U.S.A.

Markakis, K., Poupkou, A., Melas, D., Zerefos, D., (2009). A GIS based anthropogenic PM_{10} emission inventory for Greece. Submitted in Atmospheric Research.

Marrtensson, E.M., Nilsson, E.D., de Leeuw, G., Cohen, L.H., Hansson, H.C. (2003). Laboratory simulations and parameterization of the primary marine aerosol production. Journal of Geophysical Research 108, NO. D9, 4297.

Monahan, E. C., D. E. Spiel, and K. L. Davidson, A model of marine aerosol generation via whitecaps and wave disruption, in Oceanic White-caps, edited by E. C. Monahan and G. MacNiochaill, pp. 167 – 193,D. Reidel, Norwell, Mass., 1986.

Figure 1. Spatial distribution of Sea Salt PM_{10} emissions for a period of one week in June 2007

Developing per smoker emission rates from Environmental Tobacco Smoke

V. Agranovski and D. Wainwright

Environmental (Air) Sciences Division, Environmental Protection Agency, 80 Meiers Rd., 4068, Brisbane, Queensland, Australia

Keywords: Air pollution modelling, emissions, cigarette smoke, inventory

Environmental Tobacco Smoke (ETS) emissions are the complex mixture of gases and fine particles, with thousands of individual toxic air contaminants (Daisey et al, 1998) emitted by the burning of tobacco products (cigarettes, cigars, and pipes) and from smoke exhaled by the smokers. The composition of ETS emissions vary depending on the tobacco content, additives present and the type of paper and filter material used. In Australia, cigarettes are the principal source of ETS emissions (ABS, 2000). The environmental and health impacts of ETS emissions from cigarettes are of concern to regulatory agencies.

In recent years, there has been an increasing interest in developing emission inventories as a tool for regional air quality management. Development of emission inventories is, however, an expensive and time-consuming task due to diversity and large number of individual emission sources. Techniques for estimating emissions using readily available data and simplifications are therefore highly desirable. For example, locally-specific default emission rates can be used to estimate emissions for developing national emission inventories.

The purpose of this research was developing per smoker emission rates (PSER) from cigarette smoke for using them as a cost-effective means of estimating emissions over large geographic areas containing many pollution sources.

The PSER, in kilograms per year, were estimated from the total annual amounts of a pollutant emitted during smoking cigarettes, divided by the number of cigarette smokers in the inventory year. Total annual ETS emissions were estimated using smoking prevalence data from the Australian tobacco surveys and cigarette sales data from the manufacturers. The emissions factors (μg/cigarette) used for calculations (for the pollutants of interest) were specific to the Australian conditions; they were based on the most recent data available for cigarette brand variants manufactured and sold in Australia.

A selection of the default per smoker emission rates (kg/smoker/yr) derived from this research is presented in Table 1. These figures are the mean values (plus SD) for the last seven years, for which data were available (up to 2007).

Table 1. Selection of per smoker emission rates (PSER) from cigarette smoke

Compound	PSER (kg/smoker/yr)	
	Mean	SD
1,3 Butadiene	2.06E+00	8.67E-02
Acetaldehyde	9.60E+00	4.04E-01
Acetone	5.96E+00	2.51E-01
Acrolein	1.96E+00	8.24E-02
Acrylonitrile	5.57E-01	2.35E-02
Benzene	1.70E+00	7.16E-02
Benzo[a]pyrene	6.24E-04	2.63E-05
Cadmium	2.17E-03	9.12E-05
Carbon monoxide	3.28E+02	1.38E+01
Catechol	6.37E-01	2.68E-02
Chromium	1.05E-03	4.44E-05
Ethylbenzene	7.24E-01	3.05E-02
Formaldehyde	2.63E+00	1.11E-01
Hydrogen cyanide	7.00E-01	2.95E-02
Methyl ethyl ketone	1.03E+00	4.32E-02
Oxides of nitrogen	1.16E+01	4.90E-01
PM$_{2.5}$	7.60E+01	3.20E+00
Phenol	1.61E+00	6.79E-02
Styrene	5.92E-01	2.49E-02
Toluene	3.39E+00	1.43E-01
Volatile organic compounds	2.44E+01	1.03E+00
Xylenes	2.62E+00	1.11E-01

It has to be noted that the derived default PSER values (in Table 1) are based on the assumption that, following the results of the national population surveys, the average Australian adult (older than 15 years) smoker consumes approximately 5150 cigarettes annually, over the most recent years.

Daisey, J.M., K.R.R. Mahanama and A.T. Hodgson. (1998). *J. Exposure Analysis and Environmental Epidemiology*, 8, 313-334.

ABS (2000). Australian Social Trends, Australian Bureau of Statistics 2000, Cat. No. 4102, Canberra.

Deposition of pollens in the human respiratory system

Z. Sárkány[1], I. Balásházy[2], A. Horváth[3], Á. Farkas[4], E. Dobos[5], A. Czitrovszky[6], W. Hofmann[7], G. Kudela[8], P. Magyar[9]

[1]Discipline of Physiology, University of Medicine and Pharmacy of Targu Mures, Gheorghe Marinescu 38, 540000 Targu Mures, Romania
[2]Hungarian Academy of Sciences, KFKI Atomic Energy Research Institute, P.O. Box 49, 1525 Budapest, Hungary
[3]GlaxoSmithKline, Csörsz u. 43, 1124 Budapest, Hungary
[5]Institute of Nuclear Research, Hungarian Academy of Sciences, H-4001 Debrecen, P.O. Box 51, Hungary
[6]Department of Laser Applications, Research Institute for Solid State Physics and Optics, H-1525 Budapest, P.O. Box 49, Hungary
[7]Department of Materials Engineering and Physics, Division of Physics and Biophysics, University of Salzburg, Hellbrunner Str. 34, 5020 Salzburg, Austria
[8]Aerohealth Scientific Research Development and Servicing Ltd., 2090 Remeteszőlős, Csillag sétány 7, Hungary
[9]Department of Pulmonology, Semmelweis University, Diós árok út 1/C, 1125 Budapest, Hungary

Allergies are on the increase worldwide, and diseases like hay fever or asthma are more and more common. Pollen is one of the most widespread factors that can cause an allergy, and while increasing effort is focused on revealing the physiological and immuno-pathological aspects of pollen induced reactions, their airway transport and deposition is far to be fully explored.

The objective of this study is to characterize the total, regional and generation number specific deposition of pollens in the size range of 0.1-50 μm at different breathing modes in case of healthy subjects and asthmatic patients. Furthermore, the work aims to examine the effect of gender and age on pollen deposition. In addition, it proposes to contribute to the debate related to the increasing number of asthma attacks following thunderstorms by providing useful information concerning the lung deposition of intact and fragmented pollens.

For the modelling of transport and deposition of inhaled pollen particles in the airways of healthy adult males the stochastic lung deposition model of Koblinger and Hofmann was developed and applied. The same mathematical model was applied in the case of adults and children, but the airways were scaled down, taking into consideration the functional residual capacity (FRC) ratios. Tidal volume and breathing cycle values were corresponding to specific breathing modes, namely resting, light physical exercise and heavy physical exercise. For modelling of pollen transport and deposition in asthmatic airways a severe asthma attack was simulated, characterized by 4500 ml functional residual capacity, 600 ml tidal volume, 35 min^{-1} breathing frequency and an exhalation time/inhalation time ratio of 2/1. Airway narrowing was simulated by applying a random degree of airway constriction for each particle trajectory in each bronchial airway generation, using Monte Carlo calculations based on experimental data.

Our simulation results demonstrate that although the upper airways (especially the nasal passages) act as an efficient filter for most particles with diameters between 20-50 μm, some smaller and fragmented pollen particles may penetrate into the thoracic airways, where they can deposit with efficiencies depending on breathing parameters and pollen characteristics. Fragmented pollens between 1 and 10 μm have the highest probability to deposit in the lung, supporting the theory, which states that fragmented pollen particles are responsible for the increase in the incidence of asthma attacks following thunderstorms.

Bronchial deposition fractions computed in the airways of children, normalised to unit time and total inner surface area of the bronchial airways, were systematically higher than the corresponding values of adult subjects, suggesting that children are the most exposed to the allergic effects of pollens. Gender issues seem not to influence significantly the airway deposition of pollen particles. However, particles between 0.5 and 20 μm deposit more efficiently in the lung of asthmatics than in the healthy lung, especially in the bronchial region.

Comparing lung deposition of ultrafine particles caused by fireworks and traffic

F. Kwasny, P. Madl and W. Hofmann

Department of Materials Engineering and Physics, University of Salzburg, 5020 Salzburg, Austria

Keywords: Lung deposition, particle size distribution, fireworks, ultrafine particles

Every year New Years celebrations are carried out across the world by individuals as well as official organizations involving fireworks, creating concern about an estimated intense particle load in densely populated areas.

This campaign investigated the size distribution of aerosols in the range below 1 µm, comparing its influence on lung deposition. Sampling sites were located in the downtown area of Salzburg, Austria, measuring New Years fireworks particle load and burden of traffic exhaust during a typical work day under winter weather conditions.

Most environmental monitoring campaigns rely on measuring PM_1, $PM_{2.5}$ or PM_{10}. This does not reflect the actual impact on humans, as depositions vary widely depending on the particle size distribution and the amount of ultrafine particles. Although PM_{10} seemed to be correlated with trends in ultrafine particles, it did not provide enough evidence that ultrafine particle behavior can be considered simply as a fraction of PM_{10} (Rosenbohm et al., 2005).
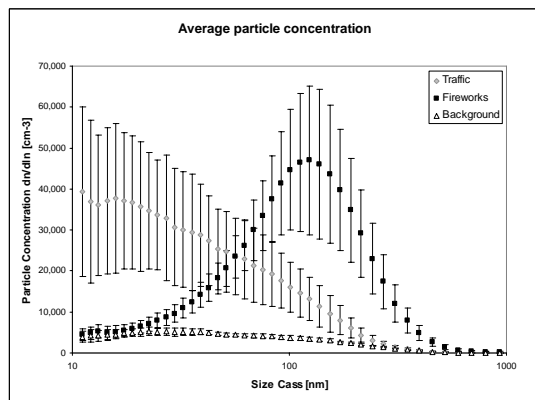
Figure 1. Particle size distribution averages comparing fireworks, traffic exhaust and a background value.

The sampled nano-particle inventory shows a great difference in its distribution. We found that the main burden in ultrafine particles originated from traffic exhaust. Although both fireworks and traffic show a similar total particle concentration of 78,790 $[N/cm^3]$ (fireworks) and 75,518 $[N/cm^3]$ (traffic) respectively, traffic creates significantly more particles below 100 nm with a broadened distribution

within that range. Fireworks particles fingerprint peaks past the 100 nm range. This difference in distribution is of great influence for the deposition in the human lungs.
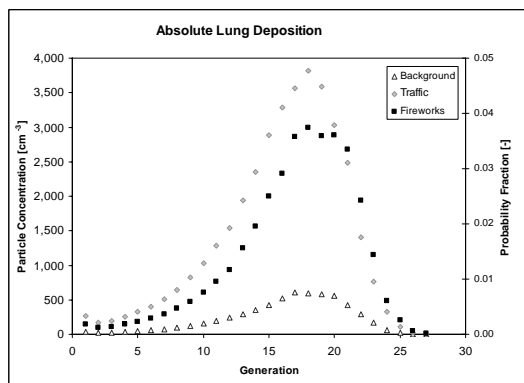
Figure 2. Modeled lung deposition patterns using the Monte Carlo code IDEAL. Plotted are simulations for fireworks, traffic and background measurements.

We used the gathered data on size distribution in the stochastic lung deposition model developed by Koblinger & Hofmann (1990), which shows distinct lung depositions past the 15th generation. Figure 2 shows a distinct higher particle deposition from traffic exhaust in this alveolar region. Deposition here is associated with increased cardio-circulatory problems, as the immune system is the primary organ to remove entrapped particles (Donaldson et al., 1988).

Although fireworks increase PM_{10} (Barman et al., 2008), this study found a less heavy impact on human lung deposition from fireworks versus average downtown traffic.

Barman, S.C., Ramesh, S., & M. P. S. Negi, M. P. S., & Bhargava, S. K. (2008). Environ Monit Assess 137:495 – 504

Donaldson, K., Li, X. Y., & MacNee, W. (1988). *Journal of Aerosol Science*, 29. 5 - 6.

Hofmann, W. & Koblinger, L. (1990). *Journal of Aerosol Science*, 21. 675 - 688.

Koblinger L. & Hofmann, W. (1990). *Journal of Aerosol Science*, 21. 661 - 674

Rosenbohm, E., R. Vogt, R., Scheer, V., Nielsen, O.J., Dreiseidler, A., Baumbach, G., Imhof, D., U. Baltensperger, U., Fuchs, J., Jaeschke, W.(2005). *Atmospheric Environment*, 39, 5696 - 5709.

Detecting airborne microorganisms by experimental and numerical tools: application to the spreading of *Legionella pneumophila* from cooling towers.

T.L. Ha[1], E. Robine[1], E. Tarnaud[2], F. Tognet[2], C. Turmeau[3], Y. Morel[3] and L. Rouil[2]

[1]Centre Scientifique et Technique du Bâtiment (CSTB), Marne La Vallée, France
[2]Institut National de l'Environnement Industriel et des Risques (INERIS), Verneuil en Halatte, France
[3]Centre d'Etudes du Bouchet (CEB), Vert-le-Petit, France

Keywords: bioaerosols, dispersion, modelling, *in situ* measurements, *Legionella pneumophila*.

Legionella pneumophila is a causative agent of respiratory illness in humans. Most of community outbreaks of legionellosis have been linked with an airborne transmission of pathogen from cooling towers. During the outbreak in Pas-de-Calais, France, 2003, it was observed that *L. pneumophila* could be transported in air at least 6 km from the source (Nguyen *et al.*, 2006). To support investigations during epidemics, dispersion models could be used to optimize air sampling strategy for detecting airborne *L. pneumophila* and evaluate how far contaminated aerosols would be spread from cooling towers. The objective of this research is to investigate the performance of available plume models for predicting concentrations of airborne microbes, by iterative model-to-experimental data comparisons.

A dispersion field campaign of biological aerosols was performed at CSTB during August 25 to 29, 2008. Spores of *Bacillus globigii* were disseminated from the roof of a building on site. Air was sampled at 5 various locations from the source as showed on the Figure 1.

Figure 1. Sampling sites selected from predictions of the distribution of aerosols generated from the source (S). A, B, C were located at 50 m from the emission, D at 70 m on another roof and E at 70 m at the ground.

The sampling sites were selected from preliminary numerical simulations performed with ADMS, developed by CERC (Cambridge Environmental Research Consultants (http://www.cerc.co.uk/software/adms4.htm), a Gaussian dispersion model using current understanding of the structure of the atmospheric boundary layer. To simplify calculations, paths of biological aerosols were estimated by assuming the bioaerosol is an inert particle. Atmospheric dispersion of aerosols was computed following local daily weather forecasts (temperature, humidity, wind speed and direction). Topography and buildings surrounding the emission source were also taken into account by the model. Slit and six-stage Andersen samplers were used for collecting the airborne microorganisms directly onto TSA agar. Wetted-wall cyclones and SKC Biosamplers were also runned for sampling air into distilled water. Liquid samples obtained in this way were then plated on TSA agar. Typical colonies of *B. globigii* were enumerated after 16-20 hours at 37°C.
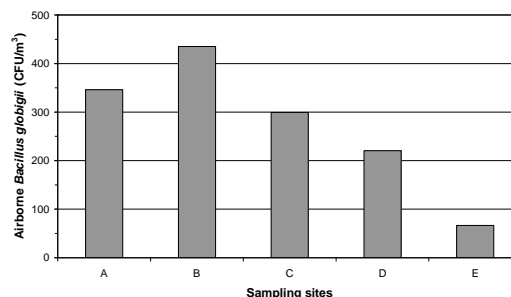
Figure 2. Concentrations of airborne *B. globigii* detected at sampling sites

The results showed a good correlation between predictions and *in situ* measurements. Spores of *B. globigii* were detected at all sampling locations selected following simulations with the ADMS4. These first observations suggest the potential operational use of models in case of epidemics of legionellosis or all another threat linked to biological aerosols dispersion.

Nguyen, T. M. N., Ilef, D., Jarraud, S., Rouil, L., Campese, C., Che, D., Haeghebaert, S., Ganiayre, F., Marcel, F., Etienne, J. & Desenclos, J.-C. (2006). *The Journal of Infectious Diseases*, 193, 102-111.

Effect of aerosol mixing state on optical and CCN activation properties in an evolving urban plume

N. Riemer[1], M. West[2], R.A. Zaveri[3], J.C. Barnard[3], and R.C. Easter[3]

[1]Department of Atmospheric Sciences, University of Illinois at Urbana-Champaign, Urbana, IL, 61801, USA
[2]Department of Mechanical Science and Engineering, University of Illinois at Urbana-Champaign, IL, Urbana, 61801, USA
[3]Atmospheric Science and Global Change Division, Pacific Northwest National Laboratory, Richland, WA, 99352, USA

Keywords: soot, aging, particle-resolved model

The mixing state of atmospheric aerosol particles is of crucial importance for assessing their macroscopic impact, since it governs their chemical reactivity, cloud condensation nuclei activity and radiative properties. A prominent example for this is soot, which can be present in the atmosphere in external as well as in internal mixture (Okada & Hitzenberger, 2001). To represent soot and its impacts in atmospheric models, the transfer of soot from external to internal mixture, called "aging", needs to be represented adequately.

However, tracking the mixing state in conventional aerosol models requires treating a multidimensional size distribution, which is computationally prohibitive. Therefore current models adopt certain simplifications, which usually translate into the assumption of an internal mixture within one mode or size section. The uncertainties associated with this assumption, which artificially ages freshly emitted particles instantly, are not well quantified.

In this study, we present a new approach, the stochastic particle resolved model PartMC, which explicitly resolves the composition of individual particles in a given population of different types of aerosol particles, and accurately tracks their evolution due to emission, dilution, and coagulation (Riemer et al., 2009). PartMC was coupled with the new state-of-the-art aerosol chemistry model MOSAIC (Zaveri et al., 2008), which simulates the gas- and particle-phase chemistries, particle-phase thermodynamics and dynamic gas-particle mass transfer in a deterministic manner. The coupled model system PartMC-MOSAIC predicts number, mass and full composition distribution, and is therefore suited for applications where any or all of these quantities are required.

PartMC-MOSAIC was applied to an idealized urban plume case to simulate the evolution of urban aerosols of different types (diesel soot, gasoline soot, meat-cooking aerosol). Figure 1 shows a two-dimensional projection of the size distribution that illustrates the mixing state with respect to black carbon (BC) after 24 hours of simulation. We see that at a given size, a continuum of mixing states exists with different BC fractions.

For this urban plume scenario we quantified the individual processes that contribute to the aging of the aerosol distribution, illustrating the capabilities of our model approach. We analyzed the effect of aerosol mixing state on optical and CCN activation properties in such an evolving urban plume. The results show that urban aerosols can still have widely different mixing states even after 24 hours of processing, highlighting the importance of accurately resolving mixing state in aerosol optical and CCN prediction studies.
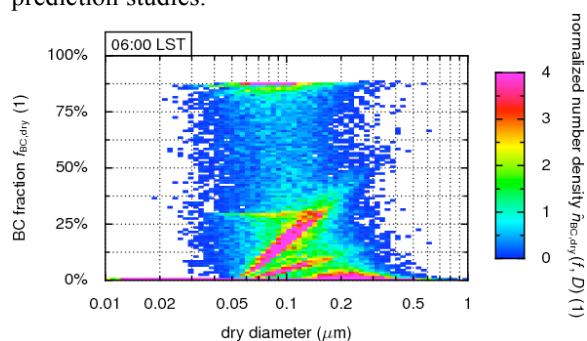
Figure 1. Normalized two-dimensional number distribution after 24 hours of simulation.

Okada, K. & Hitzenberger, R.M. (2001). Atmos. Environ., 35, 5617-5628.
Riemer, N., West, M., Zaveri, R.A., Easter, R.C. (2009), J. Geophys. Res., in press.
Zaveri, R.A., Easter, R.C., Fast, J.D., Peters, L.K. (2008), J. Geophys. Res., D02210.

Increased aerosol cooling from high sea spray emissions in changing climate

H. Korhonen[1], K. S. Carslaw[2], H.Kokkola[3] and S. Mikkonen[1]

[1]Department of Physics, University of Kuopio, POB 1627, 70211 Kuopio, Finland
[2]School of Earth and Environment, University of Leeds, Leeds LS2 9JT, United Kingdom
[3]Finnish Meteorological Institute, Kuopio Unit, POB 1627, 70211 Kuopio, Finland

Keywords: marine aerosol, emissions, aerosol modelling, CCN, climate effect.

Emission rates of many natural aerosol types depend strongly on local meteorological parameters, which implies that the projected climate change is very likely to change natural aerosol concentrations in the coming decades. These changes can significantly alter the magnitude of aerosol radiative effects, especially in remote regions with little anthropogenic influence. One such region is the Southern Ocean where observations have already shown a statistically significant increase in low level wind speeds since the 1970s. However, the effect of this change on marine aerosol concentrations has not been quantified although recent research suggests that wind-speed driven flux of sea spray is an important, if not dominant, CCN source in the remote marine atmosphere (Korhonen et al., 2008).

This work presents for the first time an estimate of the change in sea spray emissions and thus in natural aerosol radiative effect over the Southern Ocean in the past 30 years. We run global size-segregated aerosol microphysics model GLOMAP (Spracklen et al., 2005) forced with ECMWF winds for two periods: 1980-1982 and 2000-2002. The model runs include wind-dependent sea spray and DMS emissions together with anthropogenic SO_2, sulphate and OC/BC emissions.

We predict significant changes in Southern Ocean zonal mean CCN concentrations that correspond well with changes in surface level zonal mean wind speeds (Fig. 1). In certain regions of the high-wind-speed belt in the 40-60° S latitude band, we predict up to 50% increase in CCN corresponding to a significant 1% local cloud albedo increase. On the other hand, in some regions around the 40° S latitude, decrease in wind speeds has led to a drop in CCN concentration by up to 30% since the 80s. This change has created optically thinner clouds and thus a warming effect due to natural processes.

It is also noteworthy that the good correlation between CCN and wind speed changes is evident in almost all latitude bands south of 30° N. The significant drop in CCN in the mid- and high latitudes of the northern hemisphere is due to radical reduction of SO_2 (and corresponding sulphate aerosol) emissions in Europe and North America in the 80s and 90s motivated by the acid rain problem.

In fact, the correlation between CCN and SO_2 holds for all latitude bands especially in summer months (not shown) but does not imply causality in the remote marine regions south of 30° N. This is because in these regions, the increased SO_2 is from DMS whose ocean-to-atmosphere flux is also controlled by surface level wind speed. While DMS-derived SO_2 can have a large influence on CCN, this influence is via nucleation and subsequent growth in the free troposphere (Korhonen et al., 2008), a process that takes several days and thus involves long-range transport. Therefore the effects of increased DMS emissions on CCN are rarely local but are seen hundreds or thousands of kilometres from DMS source regions (Woodhouse et al., 2008).

We therefore conclude that the observed increase of wind speeds in the Southern Ocean in the past 30 years has led to a significant increase in CCN and cloud albedo, and that this natural cooling effect is due to increased sea spray emissions. The next step is to extend this study and quantify the radiative cooling from projected higher sea spray emissions in the future climate.
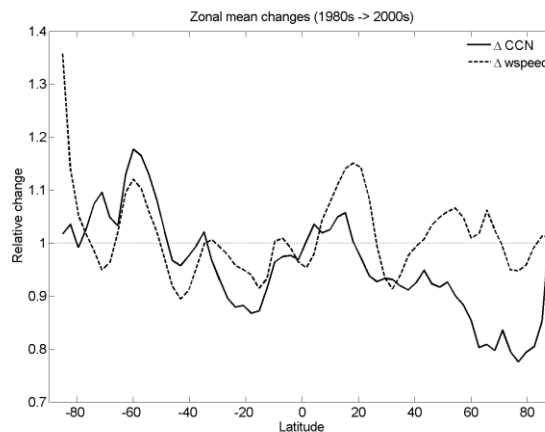
Figure 1. Relative change in zonal mean CCN and surface wind speed from early 1980s to early 2000s (marine regions only).

Korhonen, H., Carslaw, K., Spracklen, D., Mann, G. & Woodhouse, M. (2008). J. Geophys. Res., 113, D15204.

Spracklen, D., Pringle, K., Carslaw, K., Chipperfield, M. & Mann, G. (2005). Atmos. Chem. Phys., 5, 2227-2252.

Woodhouse, M., Mann, G., Carslaw, K. & Boucher, O. (2008), Atmos. Env., 42, 5728-5730.

Modelling the Sea Salt Aerosol Direct Radiative Forcing on the Regional Scale

K. Lundgren, H.Vogel and B. Vogel

Institut für Meteorologie und Klimaforschung, Forschungszentrum Karlsruhe/Universität Karlsruhe, Postfach 3640, 76021 Karlsruhe, Germany

Keywords: Aerosol radiative forcing, AOD, Modelling (regional), Sea Salt.

About 70 % of the Earth's surface is covered by ocean, which is why the flux of sea salt is one of the largest aerosol sources. Sea salt influences atmospheric processes over ocean and sometimes also over land. The direct radiative forcing due to sea salt is mainly investigated on the global scale, but still shows great uncertainties ranging from -0.08 to -6.2 W m^{-2} (Lewis and Schwartz, 2004 and references there in) globally and annually averaged. On the regional scale investigations are very rare and the physics behind the forcing has seldom been analyzed.

For the purpose to improve the understanding of the direct forcing due to sea salt, the regional scale model COSMO-ART (Vogel et al., 2009) is applied. The meteorological driver is COSMO, the operational weather forecast model of the German weather service (DWD). ART stands for Aerosols and Reactive Trace gases.

Recently the emission of oceanic dimethyl sulphide and the relevant photochemical reactions have been included into the model. The emissions of DMS are parameterized as described by Nightingale (2000). Optical properties are accounted for following Bäumer et al., 2004.

The emission of dry sea salt is described by a composition of three parameterizations (Mårtensson et al., 2003, Monahan et al., 1986 and Smith et al., 1993) as function of 10m-level wind speed and sea surface temperature.

A simulation of sea salt with radiation feedback is performed for the Mediterranean region for a high level pressure situation in January 2003. Figure 1 illustrates the simulated dry sea salt aerosol optical depth at 12 UTC the 27th of January.
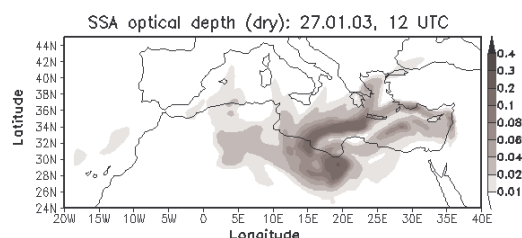
Figure 1. Simulated AOD of sea salt in the Mediterranean Region. Example at 12 UTC the 27th of January.

The maximum simulated AOD of is in the order of 0.4. The corresponding change in surface reached shortwave radiation is influenced by the sea salt particles due to two effects. There is one direct cooling effect due to the scattering of sunlight in the order of magnitude of 5 W m^{-2}. Due to this direct cooling effect the thermodynamic properties of the atmosphere is modified, which in turn affect the cloud cover. Changes in cloud cover have in turn impact on the short wave radiation at the surface, which can be called a semi-direct effect on the radiation by the particles. This semi-direct effect is simulated in the order of 20 W m^{-2}.

COSMO-ART accounts for wet sea salt particles. Condensation of H_2SO_4 on the dry sodium chloride particles is treated and the uptake of water is considered. First results from simulations of wet sea salt particles will be presented and the radiative forcing due to sea salt particles on the regional scale will be discussed.

From the simulations we have already performed with the dry sea salt aerosol we can expect that the sea salt particles have an impact on the state of the atmosphere not only above the sea but also at the adjacent land masses.

Bäumer, D., B. Vogel, & Kottmeier, Ch. (2004). *J. Aerosol Science*, pp. 1195-1196.

Lewis, E.R., & Schwartz, S. E. (2004). *Sea salt aerosol production.* Washington, DC: American Geophysical Union.

Lundgren, K. (2006). *Numerical simulation of the spatial and temporal distribution of sea salt particles on the regional scale.* Thesis for M.Sc., Stockholm University.

Mårtensson, E.M., Nilsson, D., De Leeuw, G., Cohen, L.H., & Hansson, H.-C.(2003) *J. Geophys.Res.*108, 4297, doi:10.1029/2002JD00226.

Monahan, E. C., Spiel, D. E., & Davidson, K. L. (1986). *Oceanic Whitecaps*, Monahan, E. C., & Mac Niocaill, G. Eds., D. Reidel, pp. 167-174.

Nightingale, P. D., Malin, G., Law, C. S., Watson, A. J., Liss, P. S., Liddicoat, M. I., Boutin, J., & Upstill-Goddard, R. C. (2000). *Global Biogeochem. Cycles,* 14, pp. 373-387.

Riemer, N., Vogel, H., Vogel, B., & Fiedler, F. (2003). *J. Geophys. Res.*, 108, D19, 4601, doi:10.1029/2003JD003448.

Smith, M. H., Park, P. M. & Consterdine, I. E. (1993). *Q. J. R. Met. Society* 119, pp. 809-824.

Vogel, B., H. Vogel, D. Bäumer, M. Bangert, K. Lundgren, R. Rinke, T. Stanelle, (2009) submitted to APCD.

Simulation of aerosol and clouds on the regional scale

M. Bangert[1], B. Vogel[1], H.Vogel[1], K. Lundgren[1], R. Rinke[1] and A. Seifert[2]

[1] Institut für Meteorologie und Klimaforschung, Forschungszentrum/Universität Karlsruhe, 76021 Karlsruhe, Germany
[2]Deutscher Wetterdienst, 63067, Offenbach, Germany

Keywords: Aerosol cloud interaction, CCN, Modelling (regional), Tropospheric aerosols, Clouds.

The interaction of aerosol and clouds is a multi-scale problem. Modelling studies followed a variety of approaches to improve the understanding of this interaction. Most studies had their focus either on the interaction with single clouds or on the global forcing of the aerosol. On these scales the inhomogeneous and variable distribution of the aerosol and of the clouds can not be sufficiently represented. To investigate the interaction between the aerosol and the atmosphere on the regional to continental scale the variations in the distribution of aerosol particles caused by the spatial and temporal variation of the emissions the ongoing physical, and chemical processes have to be considered.

To fulfil these requirements we developed the model system COSMO-ART. It is based on the non-hydrostatic weather forecast model COSMO (Consortium for Small-scale Modeling, Doms & Schättler, 2002) of the German Weather Service (DWD) and is online coupled with comprehensive modules for gas phase chemistry and aerosol dynamics. ART stands for Aerosols and Reactive Trace gases. COSMO-ART includes complex photochemistry to calculate the temporal and spatial distribution of the gaseous precursors of the secondary aerosol particles. For submicron particles five internally mixed modes with log-normal size distributions are used. All modes are subject to condensation and coagulation. A detailed description of the model formulation and of the representation of the natural and the anthropogenic emissions can be found in Vogel et al. (2009).

The activation of particles is calculated by integrating the size distribution of the individual modes. The critical radius for the integration is determined with the Köhler theory and the parameterization of Abdul-Razzak & Ghan (2000) with respect to the size distribution and the chemical composition of the individual modes. The cloud scheme is an extended version of the operational scheme used for the weather forecast with the COSMO model. For the representation of autoconversion, accretion, and selfcollection of cloud drops the double-moment parameterization of Seifert & Beheng (2001) is used for cloud water and droplet number.

In this study the influence of the aerosol particles on cloud properties and precipitation formation was simulated for Central Europe with a spatial resolution of 7 km.

The simulated distribution of the available CCN is very variable and depends strongly on the properties of the aerosol particles. The results of the simulations show that in the area of a forming cloud the availability of CCN is higher than in the surrounding area because of local vertical transport processes and high humidity. Therefore the distributions of CCN and clouds are related to each other on the regional scale.
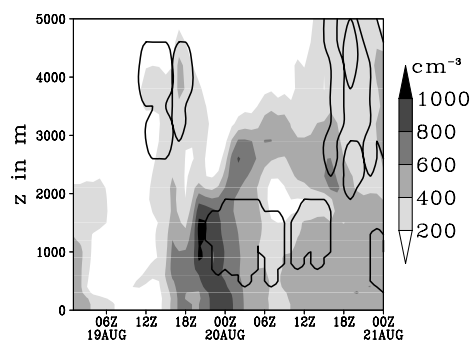
Figure 1. Evolution in time of CCN for 0.1% supersaturation (greyscale) and clouds (contours) at Karlsruhe.

The comparison with a simulation that was performed with a fixed homogenous aerosol distribution shows that the simulation allowing variable aerosol distributions leads to changes in cloud droplet number density. Consequently, this has also an influence on the warm rain process. High CCN-concentrations weaken the initial formation of rain and tend to delay the rain initiation in warm clouds. Depending on the lifetime of the cloud system the net precipitation amount can be the same, but with temporal and spatial shifts in the distribution of precipitation.

Abdul-Razzak, H. & Ghan, S. J. (2000). *J. Geophys. Res.*, 105, 6837–6844.

Doms, G. & Schättler, U. (2002). *A description of the nonhydrostatic regional model LM part I: Dynamics and numerics*. Offenbach, Germany: available at: www.cosmomodel.org.

Seifert, A. & Beheng, K. D. (2001). *Atmos. Res.*, 59-60, 265–281.

Vogel, B., Vogel, H., Bäumer, D., Bangert, M., Lundgren, K., Rinke, R. & Stanelle, T. (2009). *Atmos. Chem. Phys. Discussion*, submitted.

T04 AA aerosol processes and properties

Application of Trajectory Cluster Analysis to Eastern Mediterranean Aerosol Data

F. Öztürk, G. Tuncel

Middle East Technical University, Environmental Engineering Department, 06531, Ankara, TURKEY

Eastern Mediterranean region attracts the researchers for many years since it is covered by highly industrialized European countries on West and North West, developing countries on South and North and Saharan dessert on South. In addition to receiving different composition of atmospheric material from these regions, its unique climate characteristics make the atmosphere of region more complex to understand. The objective of this study is to find the variation of chemical composition of aerosols with air masses transported from different directions before intercepting at our station.

Daily PM_{10} aerosol samples were collected at Turkish Mediterranean coast between 1993 and 2001. SIERRA ANDERSEN model Hi-Vol sampler was used to collect aerosols on Whatman-41 filters. Approximately 2000 aerosol samples were analyzed by a combination of three analytical techniques. Inductively Coupled Plasma Mass Spectrometry (ICPMS) and Energy Dispersive X-Ray Spectrometry (EDXRF) were employed to find trace element content of the samples. Besides, collected samples were analyzed by means of Ion Chromatography (IC) to determine SO_4^{2-} and NO_3^- concentrations.

In this study, airmass backward trajectories were calculated using the HYSPLIT (HYbrid Single-Particle Lagrangian Integrated Trajectory) Version 4.0 model, which is a online service developed by the National Oceanic and Atmospheric Administration (NOAA) Air Resources Laboratory (ARL) (Draxler, R.R. and Rolph, G.D., 2003). Five days-long backward trajectories at 1500 m starting altitude were requested for each day between 1993 and 2001. K-means clustering, which was previously proposed by Dorling et al. (1992), was used to classify the trajectories. After application of cluster analysis, 9 clusters were retained to further interpret the origin of air masses influencing the chemical composition of aerosols collected at our station. The percentage of trajectories assigned to each cluster along with their corresponding cluster centroids was depicted in Figure 1.

Since there is one trajectory corresponding to each sampling day, the average concentrations of measured parameters were calculated for each cluster. Variation of SO_4^{2-} concentration with respect to cluster was shown in Figure 2 as an example. Highest SO_4^{2-} concentration, about 10 μgm^{-3}, was associated with air mass trajectories traveled over Balkans before intercepting at our station.

Figure 1. Cluster centroids and percentage of trajectories assigned to each cluster
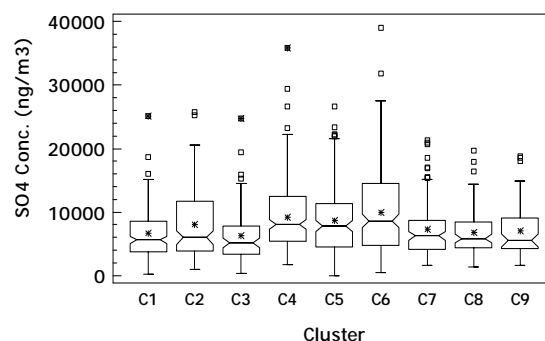
Figure 2. Sulfate concentration in each cluster

Kruskal-Wallis test was employed to test the whether the concentrations corresponding in one of the clusters is statistically different from rest of the clusters. Applied test has revealed that all of the parameters are statistically different at least in one of the sectors with the exception of Pb, NO_3^-, NH_4^+, Cl, W, Pt, Au, Ca and Cr. These elements seem not to vary from one to another at 95 % confidence interval.

Draxler, R.R. and Rolph, G.D., (2003). *HYSPLIT (HYbrid Single-Particle Lagrangian Integrated Trajectory) Model access via NOAA ARL READY Website*. NOAA Air Resources Laboratory, Silver Spring, MD.

Dorling, S.R., Davies, T.D., and Pierce, C.E. (1992).*Cluster analysis: a technique for estimating the synoptic meteorological controls on air and precipitation chemistry-method and applications*. Atmospheric Environment 26A (14), 2575-2581

Integrated measurements for aerosol properties detection in a rural site in South-Italy.

M. Calvello[1,2], F. Esposito[1] and G. Pavese[2]

[1] DIFA- Università della Basilicata, C. da Macchia Romana, 85100, Potenza, Italy
[2] CNR-IMAA, C. da S. Loya, 85050, Tito Scalo (PZ), Italy

Keywords: black carbon, columnar properties, mass size distribution, , optical properties.

The possibility of an integration of surface and columnar measurements for atmospheric aerosols optical and physical properties detection, has been investigated in a rural site in Southwest Italy (Tito Scalo, 40° 35' N, 15° 41' E, 750m a.s.l).

The measurements site is a very small industrial zone placed in a large rural area with some anthropogenic aerosol local source impacting the sampling location (some little plants and a main road passing near the site). Moreover, the site is exposed to receive aerosol loading that can be anthropogenic from North-Eastern Europe or dust intrusion from Sahara desert.

Surface measurements have been obtained by a 13 stages DLPI impactor (0.03 to 10.0 μm mounted with polycarbonate filters) and an AE31 aethalometer (7 wavelenghts from 370 to 950 nm), while columnar ones by a high resolution (1.5 nm) spectroradiometer Ocean Optics (spectral range 400nm-900nm). In particular, daily averaged values of AOD and Ångström turbidity parameters from radiometric data together with mass-size distributions from impactor data and black carbon concentrations from aethalometer have been analyzed from May to October 2008. Furthermore, from inverted direct solar radiance, aerosol columnar number and volume size distributions have been obtained for the same period.

To support data interpretation, trajectories analysis has been performed with HYSPLIT4 (Draxler & Rolph, 2003). Back- trajectories for 12 different endpoints (from 500 m to 6000 m) have been calculated for a better monitoring of aerosol distribution through atmosphere vertical structure. As a further support, maps from NAAPS and DREAM models have been used.

Both surface and columnar measurements lead to the same classification of aerosol impacting on the measurement site based on different retrieved aerosol size distributions and optical parameters : anthropogenic aerosol from North-Eastern Europe, Saharan dust from Africa, and background aerosol from local sources such as soil dust for the coarse mode and traffic for the fine one.

As an example, in the following graphic, temporal variations of daily averaged values of v_1 (columnar fine fraction concentration) as obtained from radiometric measurements, of BC (surface black carbon concentration, 800nm) as measured by aethalometer, and of V_1 (surface fine fraction mass) as obtained from DLPI measurements, are reported.
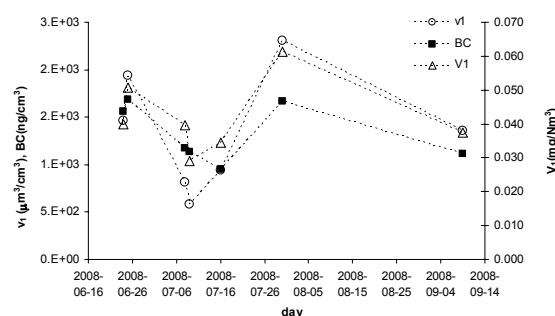
Figure 1. Temporal variations of v_1 (daily averaged columnar fine fraction concentration), of BC (daily averaged surface black carbon concentration, 800nm), and of V_1(daily averaged surface fine fraction mass) for measurement period.

Lower values of N_1, v_1 and BC are found during dust event (July, 8th) and for back-ground aerosol (July, 16th and September, 9th). Maximum values correspond to anthropogenic loading due to air masses transport from Eastern Europe (June, 24th and 25th, July 30th) .

Comparing surface and columnar measurements, better agreement has been found in the case of anthropogenic aerosol loading and back-ground aerosol than in the case of Saharan dust intrusions. It could been explained by the presence of a high dust layer affecting columnar data in a more intense way than surface ones (Lyamani *et al.*, 2008). Good agreement for anthropogenic and back-ground aerosols suggests that in these cases, surface aerosols radiative properties dominate columnar integrated data.

Draxler, R. R., Rolph, G. D., (2003). *HYSPLIT Model access via NOAA ARL READY Website,* NOAA Air Resources Laboratory, Silver Spring, MD.,(http://www.ready.noaa.gov/ready/open/hysplit4.html).

Lyamani, H., Olmo, F., J., Alados-Arboledas, L., (2008). *Atmos. Envir.*, 42, 2630-2642.

Simulation experiments studying the influence of plant VOC emission patterns on the formation of new particles

A. Kiendler-Scharr[1], J. Wildt[2], M. Dal Maso[1], T. Hohaus[1], E. Kleist[2], T. F. Mentel[1], R. Tillmann[1], R. Uerlings[2], U. Schurr[2], and A. Wahner[1]

[1]ICG-2: Troposphäre, Forschungszentrum Jülich, Jülich, Germany
[2]ICG-3: Phytosphäre, Forschungszentrum Jülich, Jülich, Germany

Keywords: Biogenic SOA, Nucleation rate, VOC, Plant chamber

Roughly 90 percent of the global volatile organic compounds (VOC) are emitted from land vegetation (Guenther et al, 1995). VOCs influence atmospheric oxidation capacity and serve as precursors for secondary organic aerosol (SOA).

In regions with low primary aerosol concentrations, biogenic SOA production proceeds via nucleation of gas phase species. Investigations of the mechanism underlying the frequently observed nucleation events in the European boreal forest demonstrate a straightforward relation between monoterpene emissions and gas-to-particle formation (Tunved et al, 2006). This is important because nucleation can provide substantial numbers of aerosols.

Number density and size distribution of aerosols are sensitive quantities that determine direct and indirect climate effects of aerosols. Kerminen et al. (2005) estimated a current radiative forcing by new particle formation in Boreal regions of about -0.2 to -0.9 Wm^{-2}. Extrapolating current monoterpene emission rates into the year 2100, Tunved et al. (2008) predict a 40% increase of cloud condensation nuclei (CCN) over Boreal forests caused by a temperature increase of 5.8°C.

Here we present results from simulation experiments conducted under atmospherically relevant conditions using VOC emissions from a variety of tree species. Specific emission patterns and total VOC concentrations were varied and nucleation rates from photochemical degradation of these mixes were determined.

Experiments were conducted in the Jülich Plant Atmosphere Chamber (JPAC, Mentel et. al, 2009). The system consists of two temperature controlled chambers, one housing the plants the second one used for photochemical SOA production. Ambient conditions such as temperature, relative humidity, photosynthetic active radiation (PAR), CO_2, O_3, and NO_x levels can be controlled in the chambers. OH is produced photochemically from O_3 and H_2O and typically reaches values of $1\text{-}5\times10^7$ cm^{-3}.

The emissions of trees (spruce, pine, birch, beech and oak) were taken as gas phase SOA precursors. The formation of new particles was observed to depend on OH and VOC concentration. Nucleation rates observed in this set up are generally larger than found in field measurements (Kulmala et al, 2004). This is due to the very low condensational sink in the JPAC experiments. Growth rates are at the upper end of ambient observations.

Of the tree species investigated oak emissions were observed to lead to the lowest nucleation rates. Dependencies of the nucleation rate on VOC emission patterns will be discussed. Furthermore we will discuss implications of these dependencies for new particle formation in response to climate change.

A. Guenther et al., *J. Geophys. Res.*, 100 (D5), 8873, 1995

V. M. Kerminen et. al, *Geophys. Res. Let.*, 32, L1480, 2005

M. Kulmala et al., *Journal of Aerosol Science*, 35, 143, 2004

T. F. Mentel, et. al, *Atmosph. Chem. Phys. Discuss.*, 9, 3041, 2009

P. Tunved et- al, *Sience*, 312, 261, 2006

P. Tunved et. al, *Tellus B*, 60, 473, 2008

New particle formation in elevated heights above continental Europe

B. Wehner[1], F. Ditas[1], A. Wiedensohler[1],
A. Apituley[2], R.A. Shaw[1], H. Siebert[1]

[1]Leibniz Institute for Tropospheric Research, 04318 Leipzig, Germany
[2]RIVM - National Institute for Public Health and the Environment Environment and Safety Division
3720 Bilthoven, The Netherlands

Keywords: nucleation, number size distributions, vertical distribution, particle formation and growth

The formation of ultrafine particles (with a diameter < 20 nm) from gaseous precursors provides a significant source of new atmospheric nuclei in the atmosphere. Although new particle formation has been examined through various atmospheric aerosol studies, there is still a number of open question concerning process, location, and involved precursor gases.

A selection of instruments to measure aerosol and cloud microphysics has been operated on the helicopter-borne platform ACTOS (Siebert et al., 2006). The most significant improvement compared to former aircraft measurements is the low flight speed of the helicopter (15 m s^{-1}) leading to a higher spatial resolution. Aerosol number size distributions (NSD) were measured between 6 nm and 2.5 μm. A small and light SMPS (Scanning Mobility Particle Sizer) has been developed measuring particle diameters from 6 to 255 nm with a time resolution of 2 min. An OPC (Model 1.129, Grimm Aerosol Technik, Ainring, Germany) has been used to measure larger particles with diameters from 250 nm to 2.5 μm with 1 Hz resolution. In addition total particle number concentrations (D_p > 6 nm) have been measured with a resolution of 1 Hz. Turbulence and cloud microphysical parameters have been measured with the instruments described in Siebert et al., 2006. To describe the development of the boundary layer, data from the Raman lidar CAELI which was operated in Cabauw during selected periods have been considered.

These instruments have been used during the IMPACT campaign near Cabauw (NL) in May 2008. During a few measurement flights significantly increased particle number concentrations have been observed above the well mixed boundary layer. Here, exemplarily the measurements from May 13, 2008 will be presented.

Figure 1 shows vertical profiles of potential temperature, water vapour mixing ratio, particle number concentration (N), and CO_2 concentration between 7:30 and 8:45 UTC. The well-mixed boundary layer was developed up to a height of approximately 200 m capped by a strong inversion. Increased particle number concentrations were observed between 550 and 800 m, the strongest maximum occurs in the second profile.
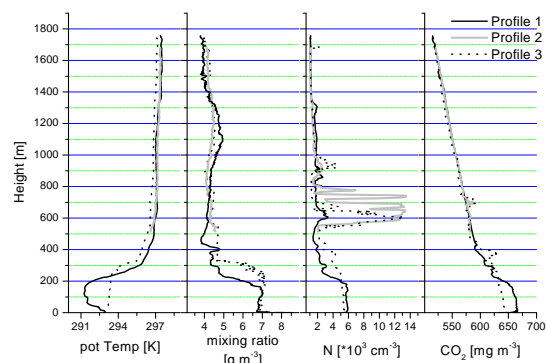
Figure 1: Vertical profiles of potential temperature, mixing ratio, particle number concentration (N), and CO_2 concentration during flight on May 13, 2008.
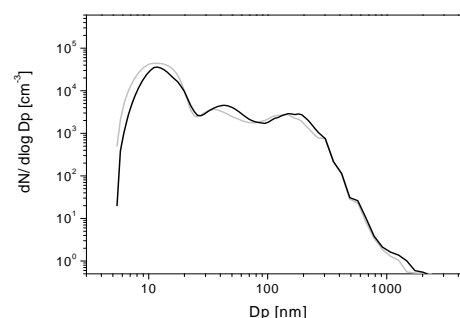
Figure 2: Selected number size distributions measured during a horizontal leg in 800 m.

In addition to vertical profiles also horizontal legs in selected heights were flown. Figure 2 shows two NSD measured by SMPS and OPC in a height of 800 m showing a significant mode of ultrafine particles. Obviously new particle formation occurred at higher altitudes significantly above the well mixed boundary layer. New particle formation at the ground has not been observed at this time. Therefore, the ultrafine particles cannot be vertically mixed from ground level to higher levels by convection such as often claimed.

Reference
Siebert, H., H. Franke, K. Lehmann, R. Maser, E. W. Saw, D. Schell, R. A. Shaw, and M. Wendisch (2006) Probing Fine-Scale Dynamics and Microphysics of Clouds with Helicopter-Borne Measurements, Bull. Amer. Met. Soc., 87, 1727 – 1738.

Factors influencing ion-induced nucleation in a Finnish boreal forest

S. Gagné[1], T. Kurtén[1], T. Nieminen[1], M. Boy[1], T. Petäjä[1], L. Laakso[1] and M. Kulmala[1]

[1]Department of Physics, University of Helsinki, P.O. box 64, Helsinki, Finland

Keywords: Ion-induced nucleation, field measurements, Ion-DMPS.

New particle formation (NPF) and growth has been observed to take place frequently and in a wide range of environments (Kulmala et al., 2004). The exact nucleation mechanisms and their respective contributions to particle formation are still unknown. Many mechanisms have been proposed: for example homogeneous, heterogeneous, binary, ternary, activation, kinetic and ion-induced nucleation (IIN). The contribution of IIN to new particle formation varies from one place to another and from one day to another (Iida et al., 2006; Gagné et al., 2008). In this work, we investigate the factors influencing on the importance of ion-induced nucleation based on Ion-DMPS measurements in the SMEAR II station (Hyytiälä, Finland; Vesala et al., 1998) from April 2005 until the end of 2007.

The NPF event days were divided into two categories (overcharged and undercharged) based on Ion-DMPS data (Laakso et al., 2007). Overcharged events (implying some participation of IIN) are the days on which there were more charged particles observed then there would be in a charge steady-state, for both the negative and positive polarity. Undercharged events (implying no or very low IIN participation) were those for which positively and negatively charged particle concentrations were equal or lower than those observed at charge steady-state. We found 164 overcharged days and 42 undercharged days. Overcharged and undercharged days were compared with particle concentration, charged cluster and particle concentration, temperature, relative humidity, absolute humidity, modelled sulphuric acid concentration and saturation ratio and condensation sink.

Very few undercharged events took place during summer months while overcharged events were taking place. In order to make sure that there was no seasonal bias we removed the summer month events from the data before analysing temperature and relative humidity. Overcharged events occurred at an average of 5°C warmer temperatures than undercharged events. Undercharged days yielded higher concentrations of nucleation mode particles which is in agreement with Vana et al. (2006) (see Figure 1). The modelled sulphuric acid concentration was on average equal during overcharged and undercharged events; however the saturation ratio of sulphuric acid was around 4 times higher for undercharged events. The temperature difference can only explain a saturation ratio of around 2 times higher.

We hypothesize that warmer temperatures affect the activation of neutral clusters while it has only a minor effect on IIN. This would explain changes in the fraction of particle formed through IIN (IIN contribution).
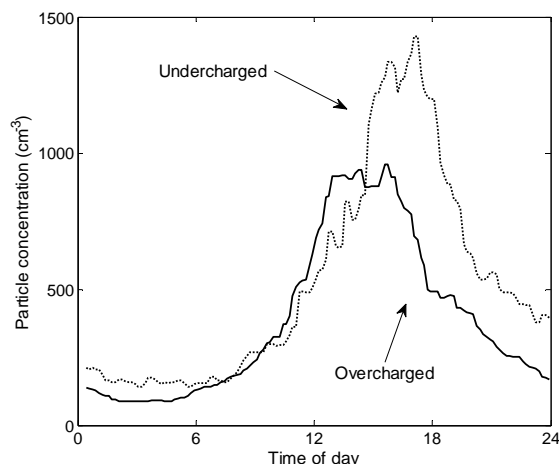
Figure 1. Median nucleation mode particle concentration (3 to 20nm, taken from the DMPS) as a function of time of day during over- and undercharged days (full and dashed line resp.).

Gagné, S., Laakso, L., Petäjä, T., Kerminen, V.-M. and Kulmala, M. (2008). Tellus, 60, 318-329.

Iida, K., Stolzenburg, M., McMurry, P., Dunn, M. J., Smith, J. N., Eisele, F. and Keady, P., J. (2006). Geophys. Res., 111, D23201, doi:10.1029/2006JD007167.

Kulmala, M., Vehkamäki, H., Petäjä, T., Dal Maso, M., Lauri, A., Kerminen, V.-M., Birmili, W., and McMurry, P. (2004). J. Aerosol Sci., 35, 143–176.

Laakso, L., Gagné, S., Petäjä, T., Hirsikko, A., Aalto, P.P., Kulmala, M. and Kerminen, V.-M. (2007). Atmos. Chem. Phys. 7, 1333-1345.

Vana, M., Tamm, E., Hõrrak, U, Mirme, A., Tammet, H., Laakso, L., Aalto, P., and Kulmala, M. (2006). Atmos. Res., 82, 536-546.

Vesala, T., et al.. (1998). Trends in Heat, Mass & Momentum Transfer, 4, 17–35.

Why does high relative humidity suppress continental nucleation events?

A. Hamed[1], H. Korhonen[1], S. L. Sihto[2], J. Joutsensaari[1], H. Järvinen[3], K. E.J. Lehtinen[1,4], M. Kulmala[2] and A. Laaksonen[1,3]

[1]Department of Physics, University of Kuopio, P. O. Box 70211, Finland
[2]Department of Physics, University of Helsinki, P. O. Box 64, 00014 Helsinki, Finland
[3]Finnish Meteorological Institute, P.O. Box 503, 00101 Helsinki, Finland
[4]Finnish Meteorological Institute, Kuopio Unit, P.O. Box 1627, FIN-70210 Kuopio, Finland

Keywords: Nucleation, Sulphuric acid, Condensation sink, Relative humidity

It has been observed in different continental locations that nucleation events take preferentially place at low relative humidities (RH) (e.g. Hyvönen at al., 2005; Hamed et al., 2007; Laaksonen et al., 2008). Several possibilities have been suggested for the RH dependence of nucleation, but no firm conclusions have been drawn so far. These possibilities include enhanced coagulation scavenging of sub 3-nm clusters at high RH, interference of water vapour with gas-phase chemistry producing condensable organics, diminished solar radiation at high RH leading to diminished gas-phase oxidation chemistry, and increased condensation sink (CS) of condensable gases due to hygroscopic growth of pre-existing particles. In this presentation we study the 2003 QUEST spring campaign data from Hyytiälä measurement station in Finland to examine some of these possibilities in detail.

Figure 1a shows the observed decrease of solar radiation at high RH during the 2003 campaign. Both RH and solar irradiation show a clear diurnal cycle: in the morning, as sunlight warms the ground layer, RH often starts to decrease, and will increase again when sunset approaches and air begins to cool. Hence, there is an anti-correlation between RH and solar irradiation. At an annual level this anti-correlation may be smeared, as the daily peak intensity of the irradiation varies strongly from midwinter to midsummer, but at a monthly level it should be detectable. In addition, solar irradiation can be attenuated at high relative humidity, both due to increased cloudiness, and due to enhanced scattering of sunlight by hygroscopicity grown particles (haze). This causes the production of OH radicals to decrease, and thus the production term of H_2SO_4 decreases (the same is valid of course for the production terms of condensable organics species).

It can be readily seen from Fig. 1a that the highest radiation values are limited to about 60% RH and below, and that at higher humidities the maximum values decrease as a function of RH quite steeply, especially above 90% RH. It is thus evident that high RH's limit the production of H_2SO_4 and other condensable gases, as is also seen in Figure 1b.

Figure 1b shows that the maximum H_2SO_4 concentrations decrease by more than an order of magnitude between 60-90% RH. This strongly suggests that the main reason for the suppression of nucleation at humid conditions is due to the effects by which high RH tends to decrease the source term and increase the sink term of H_2SO_4. Very likely high RH poses similar influences on condensable organics. However, it depends on the role of the organics in new particle formation whether RH's suppressing action on new particle formation is mediated also via them. If the organics participate only in particle growth, then there is only relatively minor influence on the observed nucleation rate "J_3" (at higher growth rate "GR", the probability of a cluster to survive to 3 nm increases). However, if they participate in the actual nucleation, increasing J_1, then there should be a similar influence as via H_2SO_4. Moreover, we have studied RH effect on CS and coagulation sink and they cannot explain event suppression

(a)   (b)
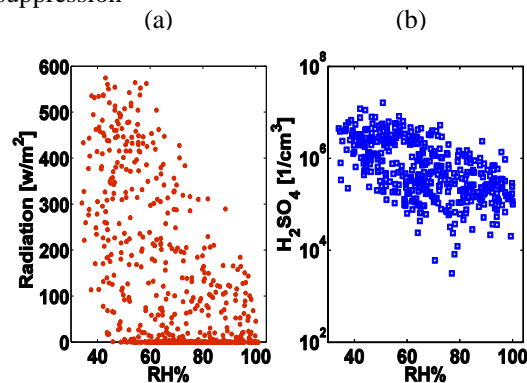
Figure1.(a) RH% versus solar irradiation (Wm^{-2}) (red colour) and (b) RH% versus H_2SO_4 concentrations (1/cm^3) (blue colour) observed during spring 2003 QUEST field campaign in Hyytiälä, Finland.

Hyvönen, S., et al. (2005). *Atmos. Chem. Phys,* 5, 3345– 3356.

Hamed, A ., et al. (2007). *Atmos. Chem. Phys*, 7, 355- 376.

Laaksonen, A ., et al. (2008). *Atmos. Chem. Phys,* 8, 2657-2665.

On the connection between new particle formation rate, sulphuric acid and organic compounds in Hohenpeissenberg (Germany)

P. Paasonen[1], S.-L. Sihto[1], T. Nieminen[1], H. Vuollekoski[1], I. Riipinen[1], E. Asmi[2], C. Plass-Dülmer[3], H. Berresheim[3,4], W. Birmili[5], and M. Kulmala[1]

[1]University of Helsinki, Department of Physics, P.O. Box 64, FI-00014 University of Helsinki, Finland
[2]Finnish Meteorological Institute, P.O. Box 503, FI-00101 Helsinki, Finland
[3]German Weather Service, Meteorological Observatory Hohenpeissenberg, Germany
[4]Now at: Dept of Physics, Environmental Change Institute, National Univ. of Ireland, Galway, Ireland.
[5]Leibniz Institute for Tropospheric Research, Permoserstrasse 15, D-04318 Leipzig, Germany

Keywords: Particle formation, nucleation, sulphuric acid, VOC.

Field measurements have shown that the coupling of the new particle formation rate and the sulphuric acid concentration can be described with power-law functions with exponent between one and two (Riipinen et al. 2007, Kuang et al. 2008). Here we analyse this coupling from two large data sets measured in rural southern Germany. We also examine the connection between the particle formation rate and concentrations of oxidation products of volatile organic compounds (VOC).

The data sets were measured at the Hohenpeissenberg Meteorological Observatory, operated by the German National Meteorological Service (DWD), the first in 1998-2000 during the Hohenpeissenberg Aerosol Formation Experiment (HAFEX, Birmili et al. 2003) and the second in 2007-2008 during the EUCAARI-campaign. The particle number size distributions were measured with Differential Mobility Particle Sizer (DMPS) during HAFEX and Neutral Air Ion Spectrometer (NAIS) during EUCAARI. The monoterpene and aromatic hydrocarbon concentrations were measured with Gas Chromatography ion-trap Mass Spectrometer (GC-MS), and the sulphuric acid concentration with Chemical Ionisation Mass Spectrometer (CIMS, Berresheim et al. 2000).

The particle formation rate J was calculated from the size distributions on the days on which a regional particle formation event was observed. J was compared to the sulphuric acid concentration $[H_2SO_4]$ in order to determine the daily nucleation coefficients A and K connecting J and $[H_2SO_4]$ in the activation theory ($J=A[H_2SO_4]$, Kulmala et al. 2006) and in the kinetic theory ($J=K[H_2SO_4]^2$). The momentary values of A and K ($A=J/[H_2SO_4]$ and $K=J/[H_2SO_4]^2$) were compared to meteorological variables, trace gas concentrations and estimated concentrations of VOC oxidation products.

In the HAFEX data set we found a clear correlation between the nucleation rate J and the sulphuric acid concentration to the power from one to two. Linear coupling between J and $[H_2SO_4]$ was slightly more frequent than squared. The medians of the daily nucleation coefficients were 1.8×10^{-7} s^{-1} for A and 3.3×10^{-14} cm^{3}s^{-1} for K. However, the daily values of A and K varied within two orders of magnitude and even during one day the observed formation rates fluctuated around the rates predicted by the theories. Additionally, the daily kinetic coefficient correlated negatively with median $[H_2SO_4]$, although according to the kinetic theory they should be independent.

We observed a correlation between the momentary values of A and K and the oxidation product concentrations of VOCs originating from coniferous trees (see Fig. 1). This correlation could be the reason for the variations in both daily and momentary values of the nucleation coefficients. Our results suggest that both sulphuric acid and VOCs take part in atmospheric particle formation.

The results from the EUCAARI 2007-2008 campaign will be presented as well.
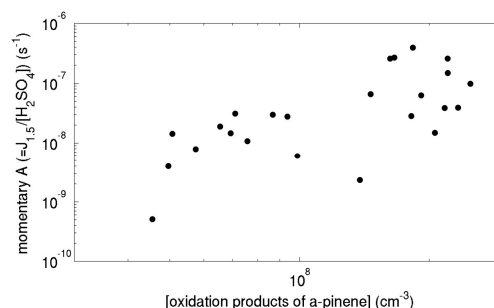
Figure 1. Momentary values of the activation coefficient A versus the estimated oxidation product concentration of α-pinene (HAFEX campaign).

Birmili, W. et al. (2003). *Atmos. Chem. Phys.*, 3, 361-376.
Berresheim, H. et al. (2000). *Int. J. Mass Spectrom*, 202, 91-109.
Kuang C. et al (2008). *J. Geophys. Res.*, 113, D10209.
Kulmala, M. et al. (2006). *Atmos. Chem. Phys.*, 6, 787-793.
Riipinen, I. et al. (2007). *Atmos. Chem. Phys.*, 7, 1899-1914.

Nucleation in boreal forest environments: How biogenic terpenes govern the correlation of formation rates with sulphuric acid

Boris Bonn[1], Michael Boy[2], Markku Kulmala[2], Ilona Riipinen[2] and Sanna-Liisa Sihto[2]

[1]Institute for Atmospheric and Environmental Sciences, Frankfurt University, D-60438 Frankfurt/Main, Germany
[2]Department of Physical Sciences, Helsinki University, P.O. Box 64, FI-00014 Helsinki, Finland

Keywords: Nucleation mechanism; sesquiterpenes; sulphuric acid; boreal forest; particle formation.

Abstract. Atmospheric new particle formation is a general phenomenon observed over coniferous forests. So far nucleation is described as a function of gaseous sulphuric acid concentration with two different types of correlation between particle formation rates and measured sulphuric acid concentrations. One has been found linear and one squared to H_2SO_4 known as activation and kinetic nucleation. We explain the observed "correlation coefficients" A and K by the contribution of biogenic terpenes to the process of new particle formation acting as nucleation inducing molecules in reacting with ambient ozone. One aspect of interest is the variation of the observed A and K coefficients in different environments and at different times at the very same place. According to the mechanism presented this variation is caused by variable ambient concentration of sesquiterpenes, the ambient water vapour and available carbonyl compounds. Especially the highly reactive sesquiterpenes, released as a stress response by the vegetation have strong impact on the changes in A and K.

While binary and ternary nucleation mechanisms involving sulphuric acid dominate nucleation in the upper troposphere other compounds such as terpenoids emitted by the biosphere as a stress response are believed to contribute to the new particle formation process in the meteorological boundary layer too. Here we formulate a mechanism[1], which combines the sulphuric acid related observations and smog chamber studies of biogenic terpenes. In there a reactive terpene such as a sesquiterpene reacts with ozone leading to substantial productions of a stabilized Criegee biradical (sCI). Its predominant atmospheric reaction is the one with atmospheric water vapour forming hydroxy-hydroperoxides not nucleating. On the contrary reactions with sulphuric acid and carbonyl compounds produce unstable and reactive intermediate species that can take up more sulphuric acid molecules and start the cluster formation process. Depending on which pathway is used predominantly one can observe either a squared or a linear relationship to sulphuric acid.

This leads to a formulation of the correlation coefficients A (linear) and K (squared relationship) as follows:

$$A = k_{coll.,SOZ+H_2SO_4} \cdot k_{sCI}^{aldehyde} \cdot [sCI][aldehyde] \cdot \tau_{SOZ}$$

$$K = \frac{k_{coll.,org.sulfate+H_2SO_4} \cdot k_{sCI}^{H_2SO_4} \cdot [sCI]}{CS_{org.sulfate}}$$

Intercomparison with field measurements result in a picture as shown in Figure 1. Assuming a radical like reaction rate of sulphuric acid with secondary ozonides or organo sulphates matches observations best. However, there are a lot of open questions remaining.
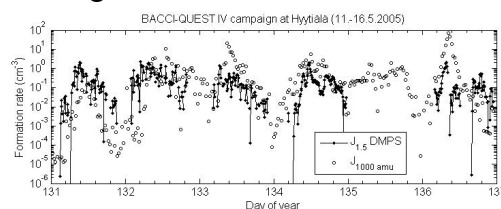
Figure 1. Intercomparison of measured formation rates at Dp = 1.5 nm at 11.-16.5.2005 and the calculated ones of the new mechanism.

References:

Bonn, B., Kulmala, M., Riipinen, I., Sihto, S.-L. and Ruuskanen, T.M., *J. Geophys. Res.*, **113**, D12209, doi:10.1029/2007JD009327, 2008.

Ultrafine aerosol and the first observed nucleation burst in Budapest

T. Borsós[1], I. Salma[1], T. Weidinger[2], P.A. Aalto[3], T. Hussein[3] and M. Kulmala[3]

[1] Institute of Chemistry, Eötvös University, H-1525 Budapest, P.O. Box 32, Hungary
[2] Department of Meteorology, Eötvös University, H-1525 Budapest, P.O. Box 32, Hungary
[3] Department of Physical Sciences, University of Helsinki, FIN-00014 Helsinki, P.O. Box 64, Finland

Keywords: DMPS, number size distribution, nucleation rate, urban aerosols.

Ultrafine aerosol plays an important role in urban environments as far as its health, climate and other environmental effects are concerned. A research was initiated to study the source processes, formation, growth, properties and effects of ultrafine aerosol particles at various places in Budapest including a kerbside, central urban sites, a tunnel and an urban background. On-line measurements have been performed using a differential mobility particle sizer (DMPS; Aalto et al., 2001) for determining particle number concentration in 30 bins in the 6–1 000 nm mobility diameter range, a tapered element oscillating microbalance (TEOM) for obtaining aerosol mass concentrations in the PM2.5 size fraction, and a mobile meteorological monitoring station for recording basic meteorological parameters. The time resolution of the measurements is about 10 min. The instruments were set up at the campus of the Eötvös University in central Budapest, Hungary near the river Danube, and they have been measuring continuously since 1 November 2008.

Number size distributions are inverted from the DMPS data, the size distributions are fitted by lognormal distributions using DoFit algorithm (Hussein et al., 2005), and time series are assembled from various derived quantities. Temporal evolution of and changes in the nucleation mode, Aitken mode and accumulation mode are utilized for classification the atmospheric processes and for identification of nucleation events.

The total number of particles in the measured size range varied from 1 300 to 71 000 cm^{-3} with a median value of 14 300 cm^{-3} for the winter season. The variability is related to micrometeorological conditions, emission and formation processes. Each day was classified into groups referred as banana type event, apple type even, non-event, featureless/undefined or missing/test data, and their occurrence was derived. Preliminary results show that new aerosol particle formation and consecutive growth (banana type nucleation) were only observed on three days. Time series for the size distribution and for the total particle number concentration for one day of them, i.e., for Saturday, 8 November 2008 are shown in Figs. 1 and 2, respectively. Relationships between the nucleation mode parameters and micrometeorological conditions have been investigated. Growth rate of the nucleation mode particles was also determined and will be presented and further discussed.
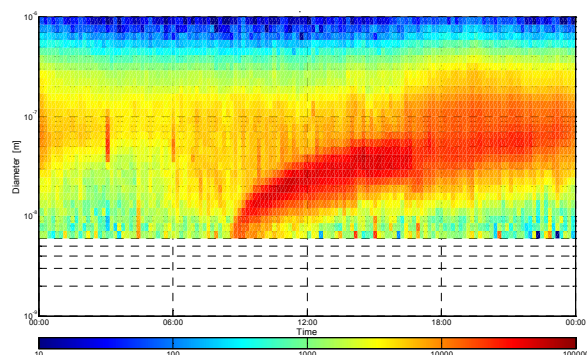
Figure 1. The first observed new particle formation event and consecutive growth in central Budapest on Saturday, 8 November 2008.
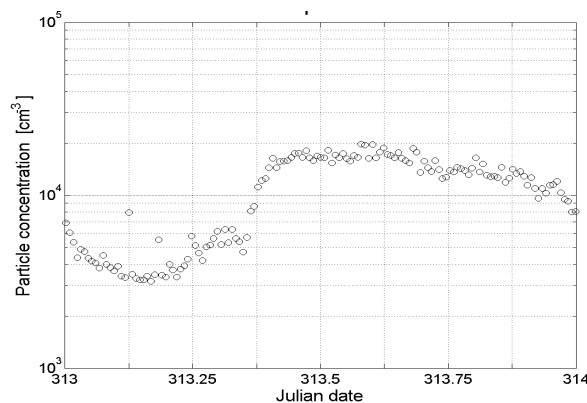
Figure 2. Diurnal variation of the total particle number concentration in the 6–1000 nm diameter range in central Budapest on 8 November 2008.

Aalto, P., Hämeri, K., Becker, E., Weber, R., Salm, J., Mäkelä, J., Hoell, C., O'Dowd, C., Karlsson, H., Väkevä, M., Koponen, I.K., Buzorius, G. & Kulmala, M. (2001). Tellus, 53B, 344–358.
Hussein, T., Dal Maso, M., Petäjä, T., Koponen, I.K., Paatero, P., Aalto, P.P., Hämeri, K. & Kulmala, M. (2005). Boreal Env. Res., 10, 337–355.

What are the key players in SOA formation over rural areas?

Michael Boy[1], Andrey Sogachev[2], Sampo Smolander[1], Johanna, Lauros[1], Henri Vuollekoski[1], Sanna-Liisa Sihto[1], Tanja Suni[1], Lauri Laakso[3], Alex Guenther[4], Markku Kulmala[1]

[1]Department of Physics, University of Helsinki, P.O. Box 64, 00014 Helsinki, Finland
[2]Wind Energy Division, Risø National Laboratory for Sustainable Energy, Technical University of Denmark, P.O. Box 49, DK-4000 Roskilde, Denmark
[3]School of Physical and Chemical Sciences, North-West University, Private Bag x6001, Potchefstroom 2520, Republic of South Africa
[4]ACD, NCAR, 3450 Mitchell Lane, Boulder, CO 80301, USA

Keywords: atmospheric aerosols, aerosol modelling, nucleation, chemistry, boundary layer.

The role of atmospheric aerosols is perhaps the biggest unknown concerning our climate and greenhouse warming. Most of these issues are linked to the composition of the newly formed particles, which is currently not understood entirely.

Organic compounds and their reaction products can participate in the formation and growth processes of atmospheric particles (Boy et al., 2003). Recent research results with a new nucleation parameter including organic vapours explained the seasonal and annual variability of observed nucleation events at different sites (Bonn et al., 2009). Using this parameter it seems very likely that nucleation events will increase in number over the entire boreal regions and several mid-latitude areas, thus impacting both ambient aerosol number concentrations and cloud properties.

Although many field campaigns, laboratory experiments and new modelling approaches have led to increased understanding, detailed mechanisms responsible for the formation of new particles in the troposphere and their influence on health, environment and climate have still not been completely elucidated. In MALTE (Model to predict new Aerosol formation in the Lower Troposphere, Boy et al., 2006) individually developed codes from different institutes around the globe are merged into a one-dimensional model including aerosol dynamics, boundary layer meteorology, biology and chemistry in order to investigate the formation and growth processes of (SOA) under realistic atmospheric conditions.

Four background field stations in different ecosystems were selected for our model runs:

- Boreal forest - SMEAR II in Hyytiälä, Finland
- Temperate forest - Manitou Forest Station, Colorado, USA
- Eucalypt forest - Tumbarumba, South-East Australia
- Savannah – Botsalano game reserve, South Africa

It is likely that different nucleation mechanisms are at work in different conditions. In the past the main candidates for nucleation in the lower troposphere have been thought to be binary sulphuric acid – water, ternary sulphuric acid – water – ammonia mixtures or ion induced nucleation of sulphuric acid and water. All of these nucleation theories were implemented in MALTE and tested for different locations with the result that none could satisfactorily explain the observed particle formation events.

Which molecules are the really important key players in atmospheric particle formation processes is still unsure, however limonene which has been highlighted in several publications for the highest nucleation potential of all monoterpenes could inherit this role. Until now limonene was never seriously considered in atmospheric nucleation because of its low fraction of the total monoterpenes mass. However, new quantum chemical calculations and chamber experiments with different monoterpenes showed that the reaction products of limonene could be involved in the formation of new particles. Including these new findings in MALTE by calculating an organic nucleation rate based on the activation of limononic acid through sulphuric acid resulted in high agreement with the nucleation rates based on measured particle size distributions.

The big open question today and for the near future is to what extend organic vapours are involved in the nucleation mechanism and is sulphuric acid still one main steering parameter for the formation of new clusters or activating the organic compounds or is sulphuric acid not involved at all in the nucleation of atmospheric particles.

Bonn, B. et al. (2009), *Atmos. Chem. Phys. Discuss.* 9, 673-691
Boy M., et al. (2003), *J. Geophys. Res.* 108 (D21), 4667
Boy, M., et al. (2006), *Atmos. Chem. Phys.*, 6, 1-19

Aerosol particle characteristics in a semi-clean savannah environment

Ville Vakkari[1], Heikki Laakso[1], Desmond Mabaso[2], Moses Molefe[2], Nnenesi Kgabi[2], Markku Kulmala[1] and Lauri Laakso[1,3]

[1]University of Helsinki, Dept. Physics, P. O. Box 64, 00014 Univ. of Helsinki, Finland
[2]Department of Physics, North-West University, Private Bag X 2046, Mmabatho, Republic of South Africa
[3]School of Physical and Chemical Sciences, North-West University, Potchefstroom, Republic of South Africa

Keywords: atmospheric aerosols, biomass burning, nucleation, Southern Africa, savannah.

Despite some previous observations, in Africa combined long-term measurements of trace gas concentrations, aerosol particle mass concentrations and number size distributions (especially in ultrafine size range), air ion number size distributions and meteorological variables are practically non-existent, (Piketh et al., 2005; Laakso et al., 2008). We will describe here some preliminary results of 1.5 years measurements with a transportable measurement trailer (Petäjä et al., 2007) in a relatively clean savannah environment in Botsalano game reserve from the period 20 July 2006 to 30 January 2008.

The aerosol particle size distribution from 10 to 840 nm was measured using a DMPS system and air ion and charged particle distribution from 0.4 to 40 nm using an Air Ion Spectrometer. In addition to the measurements in the trailer 96-hour back-trajectories were calculated for each hour during the measurement period using HYSPLIT 4.8 model (Draxler and Hess, 2004). Satellite information on biomass burning was obtained from MODIS Thermal anomalies product (Kaufman et al., 2003).

New particle formation events were classified and formation and growth rates calculated according to Dal Maso et al. (2005). The strong and frequent – on 83% of days – new particle formation during morning hours is clearly visible in the averaged diurnal behaviour of the three-modal log-normal distribution fitted in the DMPS data, Figure 1.
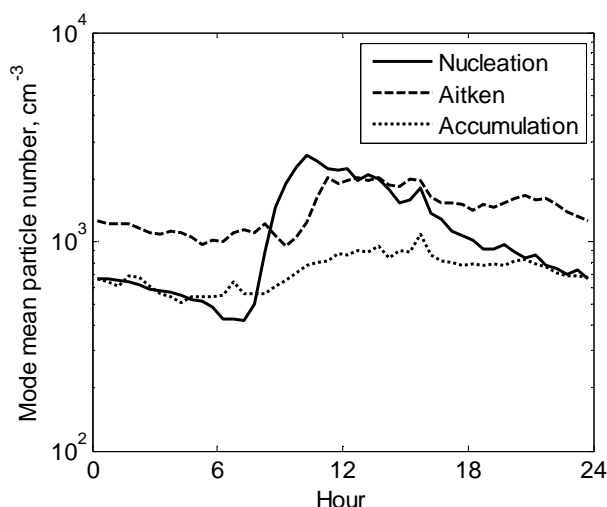
The average particle growth rate for particle size range 10-30 nm was 9.2 nm h^{-1} and average formation rate of 10nm particles, J_{10}, 4.7 $cm^{-3}s^{-1}$. The average ion (or charged particle) growth rates for size ranges 1.5-3 nm, 3-7 nm and 7-20 nm were 7.6 nm h^{-1}, 10.1 nm h^{-1}, and 8.6 nm h^{-1}, respectively. The average ion J_2 was 0.6 $cm^{-3}s^{-1}$. Both DMPS and AIS growth rates show a weak minimum during winter and maximum at spring and summer, as do observations from other sites (Kulmala et al., 2004). The levels of growth rates and formation rates are among the highest observed in continental areas (Kulmala et al., 2004).

MODIS fire observations combined to measurements via back-trajectories indicate the fires to increase in the observed Aitken mode diameter from 56nm to 73nm and carbon monoxide concentration from 110 ppb to 150 ppb when average distance to 100 neasrest fire observations along the trajectory was less than 50km.

Dal Maso, M., Kulmala, M., Riipinen, I., Wagner, R., Hussein, T., Aalto, P. P., and Lehtinen, K. E. J. (2005), Boreal Environ. Res., 10, 323–336.

Draxler R.R., and Hess, G.D. (2004), NOAA Technical Memorandum ERL ARL-224.

Kaufman, Y., Ichoku, C., Giglio, L., Korontzi, S., Chu, D. A., Hao, W. M., Li, R.-R., and Justice, C. O., (2003), International Journal of Remote Sensing, 24:1765-1781.

Kulmala, M., Vehkamäki, H., Petäjä, T., Dal Maso, M., Lauri, A., Kerminen, V.-M., Birmili, W., and McMurry, P. H. (2004), J. Aerosol Sci., 35, 143-176.

Laakso, L., Laakso, H., Aalto, P. P., Keronen, P., Petäjä, T., Nieminen, T., Pohja, T., Siivola, E., Kulmala, M., Kgabi, N., Molefe, M., Mabaso, D., Phalatse, D., Pienaar, K. and Kerminen, V.-M. (2008), Atmos Chem Phys 8, 4823-4839.

Petäjä, T., Laakso, L., Pohja, T., Siivola, E., Laakso, H., Aalto, P.P., Keronen, P., Kgabi, N.A. and Kulmala, M. (2007), Proceedings of International Conference on Nucleation and Atmospheric Aerosols 2007, Galway, Ireland, August.

Piketh, S., van Nierop, M., Rautenbach, C., Walton, N., Ross, K., Holmes, S., Richards, T. (2005), Palace consulting engineers ltd., Republic of South Africa.

Figure 1 Averaged diurnal behaviour of fitted modal peak.

Cluster Spectrometers in intensive field measurements within the EUCAARI Project

Hanna E. Manninen, Stéphanie Gagné, Eija Asmi, Mikko Sipilä, Ilona Riipinen, Lauri Laakso, Marko Vana, Aadu Mirme, Sander Mirme, Urmas Hõrrak, Christian Plass-Dülmer, George Stange, Gyula Kiss, András Hoffer, Marcel Moerman, Marcel Brinkenberg, Giorgos N. Kouvarakis, Aikaterini Bougiatioti , Colin O'Dowd, Darius Ceburnis, Birgitta Svenningsson, Leone Tarozzi, Stefano Decesari, Wolfram Birmili, Jonas Heseman, Alfred Wiedensohler, Karine Sellegri, Veli-Matti Kerminen and Markku Kulmala

*Members in the European Integrated project on Cloud Climate and Air Quality Interactions (EUCAARI) Project Office, Division of Atmospheric Sciences, University of Helsinki

Keywords: Aerosol formation, Atmospheric aerosols, Ion clusters, Nucleation.

Aerosol particles influence the climate both directly by interacting with the incoming radiation, and indirectly acting as seeds for the formation of cloud droplets. The secondary aerosol formation by nucleation and subsequent growth to cloud condensation nuclei sizes of atmospheric aerosol particles has been observed at various locations around the world (Kulmala et al., 2004). Despite the growing number of locations where frequent aerosol formation has been observed, the overall magnitude of this source of aerosol is still not well understood. Field measurements play a key role in understanding the particle formation events and the processes behind the atmospheric nucleation.

Within the EUCAARI project (Kulmala et al., 2008) cluster spectrometers have been operating continuously in 12 field sites in Europe in various environments. The different types of air ion and cluster spectrometers started measuring during the Intensive Observation Period in March 2008 and will continue measuring till May 2009 (Table 1). Roughly 12 months of continuous cluster measurements will be obtained from each field site for studying the processes leading to the atmospheric nucleation.

Table 1. Continuous field measurements associated with EUCAARI Intensive Observation Period (IOP).

Field site	Instrument	IOP started
Cabauw, the Netherlands	AIS, NAIS	April 2008
Finokalia, Greece	AIS	April 2008
Hohenpeissenberg, Germany	NAIS	March 2008
Hyytiälä, Finland	BSMA	March 2007
Jungfraujoch, Switzerland	AIS	March 2008
K-puszta, Hungary	AIS	March 2008
Mace Head, Ireland	NAIS	June 2008
Melpitz, Germany	NAIS	March 2008
Puy de Dôme, France	NAIS	March 2008
Pallas, Finland	NAIS	May 2008
San Pietro Capofiume, Italy	BSMA	March 2008
Vavihill, Sweden	AIS	March 2008

The different spectrometers were Air Ion Spectrometer (AIS, Mirme et al. 2007), Balanced scanning Mobility Analyzer (BSMA, Tammet 2006), Neutral cluster and Air Ion Spectrometer (NAIS, Manninen et al. 2009) and Airborne-NAIS (A-NAIS). They measured the number size distribution of >0.8 nm ions and, in the case of the NAIS, >1.8 nm particles.

New particle formation (NPF) events were seen on every one of the 12 sites where cluster spectrometers were measuring, allowing estimations of the contribution of the events on the total aerosol load in the atmosphere. The monthly NPF event distribution varied from one station to another, which was expected because the stations are influenced by different environments and are in different climates. In K-Puszta, the number of NPF events was the highest amongst the studied stations. The most non-event days were seen in Finokalia, which is a Mediterranean coastal site. In Mace Head, particularly, many different types of NPF events were observed.

Intensive EUCAARI cluster spectrometer measurements allowed us to calculate reliable estimates for the atmospheric nucleation and growth rates in various environments. In case of parallel ion and neutral cluster measurements, we could also estimate the contribution of ions to particle formation. In the future, this database will be integrated to regional and global scale climate models. To estimate regional aerosol source apportionment and long range transport also trajectory analysis will be included into the study.

Kulmala, M. et al. (2004). J. Aerosol Sci., 35, 143-176.
Kulmala, M. et al. (2008). Atmos. Chem. Phys. Discuss., 8, 19415-19455.
Manninen, H.E. et al. (2009) submitted to Boreal Environ. Res.
Mirme, A. et al. (2007). Boreal Environ. Res., 12, 247-264.
Tammet, H. (2006) Atmos. Res., 82: 523–535.

Ambient Measurements of Sulfuric Acid, Ammonia and Aerosol Size in Kent, Ohio

Jingmin Li, David Benson, Victoria Cunningham, Flavia Frimpong, William Montanaro, Brian Dailey, and Shan-Hu Lee

Kent State University, Department of Chemistry, Kent, OH, USA

Keywords: Ambient sampling, New particle formation, Sulfuric acid, Ammonia, Aerosol size

In order to investigate how aerosol precursors affect aerosol nucleation and which nucleation mechanisms dominate in the lower troposphere, we have conducted long-term, ground-based observations of aerosol size and precursors (sulfuric acid and ammonia) in Kent, OH. At present, there are a very limited number of simultaneous measurements of these two major aerosol precursors and aerosol size at the ground level.

Kent is a college town with a population of about 30,000, located in Northeastern Ohio. Kent is less polluted compared to EPA SuperSites (e.g, Atlanta, Pittsburgh, and Detroit) where typically new particle formation studies were made, but is also surrounded by three urban cities within 80 km. Ohio is also famous for the gray sky due to haze in winter. Northeastern Ohio has rich vegetation with numerous large forests and farms and has many natural lakes.

Particles are sampled from a near isokinetic, laminar flow aerosol sampling inlet with an electrically grounded stainless tube from a window in our lab (room 304 of Williams Hall at the Kent State University main campus). Particle concentrations are measured with two scanning mobility particle sizers (SMPS, TSI) consisting of a differential mobility analyzer (NDMA, TSI 3080) and a condensation particle counter (CPC, TSI 3772) and consisting of a differential mobility analyzer (DMA, TSI 3080) and a condensation particle counter (CPC, TSI 3776). These two sets of SMPSs together cover the ambient aerosol size range from 2.5-1000 nm.

In parallel to a butanol CPC, we also run a water CPC to identify the relative amount of sulfuric acid vs. organic compounds in small particles. Previously we made comparisons with water CPC and butanol-CPC and found that the water-CPC concentrations about 8 times higher than the butanol-CPC concentrations for pure sulfuric acid particles, whereas when sampling the laboratory room air, the concentrations measured from WCPC were only ~ 7% higher than those measured by the butanol-CPC CPC [Young et al., 2008].

Two chemical ionization mass spectrometers are used to measure H_2SO_4 and NH_3 simultaneously. For H_2SO_4, we use an atmospheric pressure ion-molecule reaction with negative NO_3^- ions and detection limit of H_2SO_4 is as low as 1×10^5 cm^{-3}. For NH_3, we use low pressure positive proton transfer ion chemistry using protonated acetone or ethanol ions and the background concentration of ammonia detection is < 0.1 ppbv. Temperature and RH are monitored simultaneously.

New particle formation observed in Kent showed the highest frequency in summer (>50%) and the lowest frequency in winter (<10%). Aerosol growth rates measured during new particle formation events ranged from 5-10 nm $hour^{-1}$. Sulfuric acid concentrations were higher during the summer (at the 10^7 cm^{-3} range at noontime) than in winter (10^6 cm^{-3}) and this trend seemed to be correlated with the measured frequency and magnitude of new particles. Ammonia concentrations measured during the winter were at the sub ppbv level (i.g., 10^9 cm^{-3}). Surface areas were not strongly anti-correlated to new particle concentrations. From these results, we conclude that sulfuric acid is important for aerosol formation but other ternary species are also necessary.

In this presentation, we will discuss how aerosol nucleation and growth rates are correlated to sulfuric acid and ammonia concentrations and how atmospheric conditions (sun flux, precipitation, and air mass history etc.) affect aerosol nucleation.

Young, L.-H., Benson, D. R., Kameel, F. R., Pierce, J. R., Juninnen, H., Kulmala, M., Lee, S.-H., Laboratory studies of sulfric acid and water binary homogeneous nucleation: Evaluation of laboratory setup and preliminary results, *Atmos. Chem. Phys.* 8, 1-20 (2008).

Sulfuric Acid in a Deciduous Forest during NIFTy Project

T. Petäjä[1], R.L. Mauldin, III[2], J. McGrath,[2,3] E. Kosciuch[2], J.N. Smith[2] and S.C. Pryor[4]

[1]Atmospheric Chemistry Division, National Center for Atmospheric Research, Boulder, CO, USA
[2]Department of Physics, University of Helsinki, Finland
[3]Department of Atmospheric and Oceanic Sciences, University of Colorado at Boulder, CO, USA
[4]Atmospheric Science Program, Department of Geography, Indiana University, Bloomington, IN, USA

Keywords: Atmospheric aerosols; Sulfuric acid; Measurements; Particle formation and Growth

As demonstrated in a number of investigations (Kulmala et al. 2004), new particle formation occurs readily in the boundary layer, including a deciduous forested region in Denmark (Pryor et al. 2005). Gaseous sulfuric acid is considered to play a central role in atmospheric aerosol formation (Weber et al. 1996). A technique for measuring the gas-phase sulfuric acid concentration even down to about 10^4 molecules cm-3 has already been available for more than a decade (Eisele and Tanner, 1993. As a result, a number of field campaigns have been performed that allow us to look at connections between the gas-phase sulfuric acid concentration and aerosol formation or growth rates. Although sulfuric acid seems to be a key component in the formation (Weber et al. 1996, Sihto et al. 2006), there are strong indications that condensing vapors other than sulfuric acid are frequently needed to explain the observed particle growth rates (Kulmala et al. 2001, Fiedler et al. 2005).

The aim of this study is to present measurements of sulfuric acid in the gas phase during a field campaign at Morgan Monroe state forest near Bloomington, IN, USA in May, 2008. We measured gaseous phase sulfuric acid and hydroxyl radical concentrations with a Chemical Ionization Mass Spectrometer (CIMS).

Sulfuric acid in the gas phase was measured with a technique utilizing selected chemical ionization and subsequent detection with a mass spectrometer. The CIMS instrument was operated inside a garden shed at Morgan Monroe State forest. The site is also an AmeriFlux tower site (Pryor and Barthelmie, 2007). The measurements were performed from May 10 to May 31, 2008.

Measurement of sulfuric acid with the CIMS consists of several steps, including sample transport, chemical ionization, ion reactions, mass filtering and signal detection. The measurement of hydroxyl radical relies on the detection of isotopically labeled sulfuric acid with the CIMS-technique. More details can be found elsewhere (Eisele and Tanner, 1993, Mauldin et al. 1998, Mauldin et al. 2001)

During a CIMS measurement cycle, H2SO4 was measured 10 times followed by 20 measurements of combined OH and H2SO4 concentrations each lasting typically 30 s. The concentrations were averaged over 5 minutes.

The concentration of sulfuric acid varied approximately four orders of magnitude, from 10^4 molec cm-3 up to 10^8 molec cm-3 as a five minute average. Due to the photochemical production, the highest sulfuric acid concentrations were reached around noon. New particle formation was observed during the field campaign on several days.

The median noon concentration during the whole time period was 10^7 molec cm-3, which is clearly higher than for example the corresponding maxima in a boreal forest site Hyytiälä during spring 2007 obtained with a similar CIMS instrument (Petäjä et al., 2008). The measurement site is in the Ohio river valley, where there are many coal fired power plants, which emit large amounts of SO_2, so depending on the back trajectories, the measurement site is occasionally in the plume, which results on average higher sulfuric acid concentrations. The levels are comparable with the values observed in the central Europe (Birmili et al. 2003)

Birmili et al. (2003) *Atmos. Chem. Phys.*, **3**, 361–376.

Eisele, F. & Tanner, D. (1993) *J. Geophys. Res.* **98**, 9001–9010.

Fiedler et al. (2005) At*mos. Chem. Phys.*, **5**, 1773–1785.

Kulmala et al. (2001) *Tellus,* **53B**, 324–343.

Kulmala et al. (2004) *J. Aerosol Sci.,* **35**, 143-176.

Mauldin et al. (1998) *J. Geophys. Res.*, **103**, 16 713–16 729.

Mauldin et al. (2001) *Geophys. Res. Lett.*, **28**, 3629–3632.

Petäjä et al. (2008) *Atmos. Chem. Phys. Discuss.* **8**, 20193-20221.

Pryor et al. (2005) Geophys. Res. Lett., 32:L06804.

Pryor, S.C. & Barthelmie, R.J. Proceedings of 17th International Conference, Galway, Ireland, doi: 10.1007/978-1-4020-6475-3_184, 2007.

Sihto et al. (2006) *Atmos. Chem. Phys.* **6**, 4079-4091.

Weber et al. (1996) *Chem. Eng. Comm.* **151**, 53-64.

Modelling of aerosol dynamics and particle chemistry using a new nucleation theory

Pontus Roldin[1], Guy Schurgers[2], Birgitta Svenningson[1], Erik Swietlicki[1], Axel Eriksson[1], Joakim Pagels[3], Erik Nilsson[1], Matthias Ketzel[4] and Susanna Gustafson[5]

[1]Div. of Nuclear Physics, Lund University, SE-221 00, Lund, Sweden, [2]Dept. of Physical Geography and Ecosystem Analysis, Lund University, [3]Div. of Ergonomics and Aerosol Technology, Lund University, [4]NERI, Dept. of Atmospheric Environment, Aarhus University, [5]Environmental Dept., City of Malmö.

Keywords: nucleation, organosulphates, surfactants, sulphuric acid, AMS

For this work a coupled column trajectory model for aerosol dynamics, gas phase chemistry and radiative transfer calculations (ADCHEM[1]) has been applied. The model is an updated version of the model described by Roldin et al., (2008). The main updates since the previous version are: 1) more detailed organic and inorganic particle chemistry with sulphate, nitrate, ammonium, sodium, chloride, EC, POA, anthropogenic and natural SOA, 2) in cloud processing of the aerosol particles including SO_2 and H_2O_2 condensation.

The aim of this work is to study the particle chemistry in the sub-micrometers size range and test a new nucleation theory developed in this work. The modelled results have been compared with measurements from DMPS, AIS, AMS and HTDMA at the Vavihill rural background station in Southern Sweden (13°09´E, 56°01´N).

The model study was focused on an 11 day period between 29th of September and 9th of October 2008. Air mass trajectories were retrieved from the internet based HYSPLIT model. Anthropogenic gas and PM2.5 emissions from EMEP were included along the trajectories. For Denmark and Southern Sweden regional emission inventories from the Danish National Environmental Research Institute and Malmö Environmental Department were used instead of the EMEP data. Isoprene and monoterpene emissions over Europe were derived with the vegetation model LPJ-GUESS (Schurgers et al., 2009).

The new nucleation mechanism included in the model assumes that stable organosulphate nucleation clusters (XSO_x), forms from reactions between gas phase sulphuric acid and an organic surfactant (X) at the particle surface water film (eq. 1). In the model the organic surfactants are formed exclusively by condensation of oxidation products from monoterpenes, reacting with OH. After the organosulphate molecules have been formed they can evaporate out into the gas phase (eq. 2), and immediately form stable nucleation clusters with one organosulfate molecule as core (eq. 3). Decreasing RH promotes nucleation since the particle water in the surface film get more concentrated on organosulphates, which then are

---

1 Aerosol Dynamics CHEmistry Model

forced out to the gas phase. The number of clusters formed, also depends on the particle surface area concentration *(A),* in each diameter size bin *i (eq. 3).* The proposed nucleation theory has been compared with simulations using the kinetic nucleation theory. Examples from the model and measurements can be seen in figure 1.

1) $X(surf.film) + H_2SO_4(g) \rightarrow XSO_x(surf.film)$

2) $XSO_x(surf.film) \rightarrow XSO_x(g)$
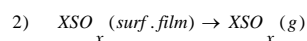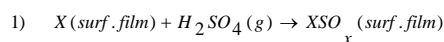
3) $J_{1nm} = k\left[H_2SO_4(g)\right] \sum\limits_{i=1}^{N}\left(A_i\left[X(aq,bulk)\right]_i\right)$

     $k = k_1 k_2 \exp\left(-\Delta G^O_{surf-bulk}\middle/(RT)\right)$

4) $\left[X(surf.film)\right] = \left[X(aq,bulk)\right]\exp\left(-\Delta G^O_{surf-bulk}\middle/(RT)\right)$
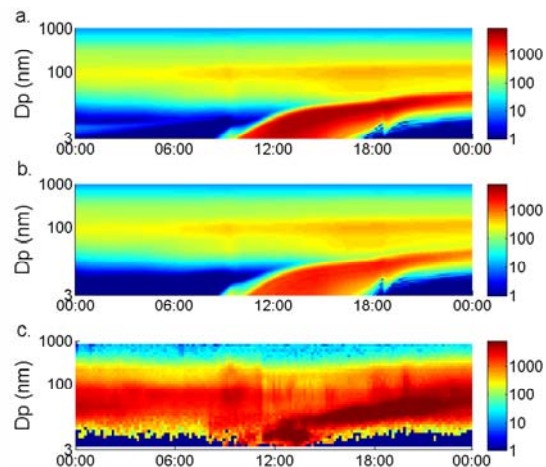
Figure 1: Particle number size distributions (dN/dlogDp cm^{-3}) for a. kinetic nucleation theory, b. nucleation theory proposed in this work, and c. measured with DMPS at Vavihill, 6th of Oct., 2008.

Roldin P., Swietlicki E., Löndahl J., Massling A., Kristensson A., Nilsson E. and Hussein T., 2008. Aerosol dynamics in the continental boundary layer in Southern Sweden. Conference Proceedings, EAC, 2008.

Schurgers G., Arneth A., Holzinger R., and Goldstein A., 2009. Process-based modelling of biogenic monoterpene emissions: sensitivity to temperature and light. Atmos. Chem. Phys. Discuss., 9, 271–307.

Parameterization of new particle formation starting from OH + SO$_2$

Torsten Berndt[1], Frank Stratmann[1], Mikko Sipilä[2,4], Tuukka Petäjä[2], R. Lee Mauldin III[3], Markku Kulmala[2], Joachim Curtius[5] and Jost Heintzenberg[1]

[1]Leibniz-Institut für Troposphärenforschung e.V., Permoserstr. 15, 04318 Leipzig, Germany
[2]Department of Physics, University of Helsinki, P.O. Box 64, FIN-00014, Finland
[3]Atmospheric Chemistry Division, Earth and Sun Systems Laboratory, National Center for Atmospheric Research, P.O. Box 3000, Boulder, CO 80307-5000, USA
[4]Also at: Helsinki Institute of Physics, University of Helsinki, P.O. Box 64, FIN-00014, Finland
[5]Institute for Atmospheric and Environmental Sciences, Goethe-University Frankfurt am Main, 60438 Frankfurt am Main, Germany

Simultaneous measurements of newly formed ultra-fine particles and H$_2$SO$_4$ in the lower troposphere reveal that new particle formation is strongly connected to the occurrence of H$_2$SO$_4$ with concentrations of about 10^5 - 10^7 molecule cm^{-3} and the production rate of new particles can be described by a power law equation for H$_2$SO$_4$ with an exponent in the range of 1 – 2 (Weber et al., 1996, Kulmala et al., 2006).

From our laboratory, using the reaction of OH radicals with SO$_2$ for "H$_2$SO$_4$" formation (Berndt et al., 2005), experimental evidence for the formation of new particles was found for "H$_2$SO$_4$" concentrations of ~10^7 molecule cm^{-3}. Here, "H$_2$SO$_4$" stands for all products arising from the reaction of OH radicals with SO$_2$. The analysis of integral number measurements by means of commercially available UCPCs revealed that measured slopes of log(N) vs. log(["H$_2$SO$_4$"]) were affected by the decreasing size-dependent counting efficiency of the UCPCs used for dp < 3nm leading to an overestimation of the slopes.

The aim of this study is to find out the optimal experimental conditions for the detection of the majority of nucleated particles with appropriate methods. Such data represent the basis for a reliable description of the overall process of nucleation in term of a power equation.

The nucleation experiments have been carried out in the atmospheric pressure flow-tube *IfT*-LFT (i.d. 8 cm; length 505 cm) at 293 ± 0.5 K. For integral particle measurements a butanol-based UCPC (TSI 3025), a H$_2$O-based UCPC (TSI 3786) as well as a pulse height condensation particle counter (PH-CPC) have been used. In order to measure particle size distributions a differential mobility particle sizer (DMPS) consisting of a Vienna-type DMA and a butanol-based UCPC (TSI 3025) came into operation.

In Figure 1 experimental data of measured particle numbers vs. ["H$_2$SO$_4$"] are depicted measured simultaneously by means of three different UCPCs (TSI 3025, TSI 3786, PH-CPC) as well as by DMPS (dp ≥ 3 nm). The IfT-LFT was operated with a residence time of 290 sec and r.h. = 22%.
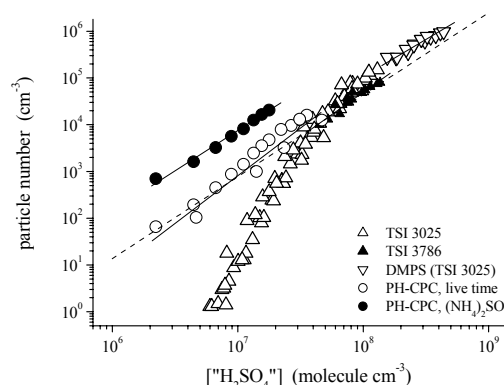
Figure 1. Measured particle numbers as a function of "H2SO4" concentration at r.h. = 22 % for a residence time of 290 sec.

The slopes log(N) vs. log(["H$_2$SO$_4$"]) span a range of 1.58 - 2.03 (DMPS: 1.58 ± 0.05; TSI 3786: 1.91 ± 0.11; PH-CPC, live time: 2.03 ± 0.01; PH-CPC, (NH$_4$)$_2$SO$_4$: 1.70 ± 0.06).

In further experiments, for several fixed "H$_2$SO$_4$" concentrations new particle formation was investigated as a function of relative humidity (or H$_2$O vapour concentration). Putting all measurements together, the overall best fit according to equation

$$N = k \, (["H_2SO_4"] \, / \, \text{molecule cm}^{-3})^{\alpha} \, ([H_2O] \, / \, \text{molecule cm}^{-3})^{\beta}$$

yielded $\alpha = 1.76 \pm 0.02$ and $\beta = 1.54 \pm 0.04$.

Berndt, T., O. Böge, F. Stratmann, J. Heintzenberg, and M. Kulmala (2005), *Science* 307, 698-700.

Kulmala, M., K. E. J. Lehtinen, and A. Laaksonen, (2006), *Atmos. Chem. Phys.* 6, 787–793.

Weber, R. J., J. J. Marti, P. H. McMurry, F. L. Eisele, D. J. Tanner, and A. Jefferson (1996), *Chem. Eng. Comm.* **151**, 53-64.

Classification of intermediate air ion formation events at urban area

K. Komsaare, U. Hõrrak, H. Tammet

Institute of Physics, University of Tartu, Ülikooli 18, 50090 Tartu, Estonia

Keywords: air ions, ion-induced nucleation, particle formation, urban areas

The importance of new particle formation on the Earth climate has been discussed in many of the recent papers (Enghoff & Svensmark, 2008), but the mechanism and species responsible for the nucleation are not well known so far. Air ions (cluster ions and electrically charged aerosol particles) mainly determine the electrical state of the atmosphere, but they can be involved also in the nucleation process.

In this paper we present the results of a statistical analysis of the nucleation events based on long-term measurements of air ion mobility distributions from April 2004 to December 2008 in urban environment, in the centre of Tartu, Estonia (58°22'N, 26°43'E).

The BSMA (Balanced Scanning Mobility Analyzer) measured the mobility spectra of natural ions in the mobility range of 0.032 - 3.2 $cm^2V^{-1}s^{-1}$ (the size range 0.4 - 7.5 nm). In addition, the BSMA can provide the data about aerosol nucleation burst events (Tammet, 2006).

We have classified the intermediate air ion (or 1.6 - 7.4 nm charged particle) formation events at Tartu using similar classification principles as given by (Hirsikko et al., 2007), modified by (Komsaare et al., 2007).

Class 1. The formation and subsequent growth of particles had a clear shape. The concentration of new generated particles was sufficiently high and their growth starting from the cluster ion mode up to the upper size of 7.5 nm was clearly seen during several hours. The gap between the cluster ion mode and larger ions was filled with ions indicating that cluster ions were involved in the nucleation process.

Class 2. Similarly to class 1, the formation of particles started from the cluster ion mode, but due to some reason, the growth of particles was suppressed in the size range about 3 - 5 nm. The reason might be consumption of nucleating vapours.

Class 3. The particle formation did not start from the cluster ion mode and we saw a gap between cluster ions and larger ions at about 1.6 - 3 nm. The event might be due to the particle formation by homogeneous nucleation with a subsequent charging of neutral particles by cluster ions. Those particles may contain VOC substances.

Class 4. During the nucleation event the concentrations of intermediate ions was quite low. The event lasted for 1 - 6 hours. These events can be considered also as uncertain cases.

Results of the statistical analysis of all categories of events are given in Table 1 and

Figure 1. As follows, the most pronounced events (class 1) with clear formation and growth of nanometer particles occurred most frequently during spring, the second maximum was recorded in autumn. Class 2 events occurred preferably first half-year and class 3 events mainly during warm period, when vegetation was most active. Class 4 events, as weak and sometimes uncertain events, occurred throughout a year, preferably in spring.

Table 1. Summary of nucleation events (+ ions/-ions) according to event classes (cl.1...cl.4) and total measurement days during year.

Year	cl.1	cl.2	cl.3	cl.4	days
2004	7/7	8/10	4/4	19/19	140
2005	13/13	17/25	8/9	42/42	305
2006	8/8	12/22	2/3	36/39	279
2007	28/31	16/21	11/11	41/41	310
2008	9/13	21/32	7/6	31/36	346
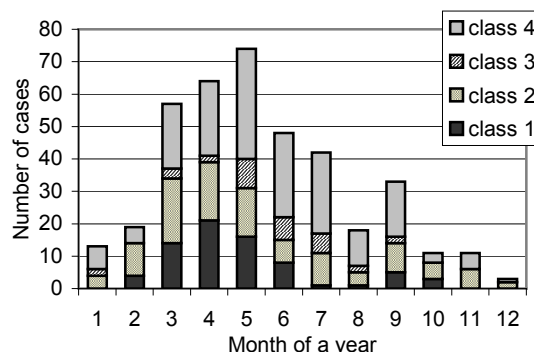
Figure 1. Cumulative monthly distribution of the number of cases when the nucleation event of negative ions was observed.

Enghoff, M. B., & Svensmark, H. (2008). *Atmos. Chem. Phys.,* 8, 4911-4923.

Tammet, H. (2006). *Atmos. Res.,* 82, 523-535.

Hirsikko, A., Bergman, T., Laakso, L., Dal Maso, M., Riipinen, I., Hõrrak, U., & Kulmala, M. (2007). *Atmos. Chem. Phys.,* 7, 201-210.

Komsaare, K., Hõrrak, U., Tammet, H., Siingh, D., Vana, M., Hirsikko, A., and Kulmala, M. (2007). In *Atmospheric Electricity: 13th Int'l Conf., Beijing,* CAS, 2007, 116-119.

Below cloud snow scavenging: a parameterization for low-intensity snowfalls

E.-M. Kyrö[1], T. Grönholm[1], H. Vuollekoski[1], A. Virkkula[1], M. Kulmala[1], L. Laakso[1,2]

[1] Department of Physics, P.O. Box 64, FI-00014 University of Helsinki, Finland
[2] current address: School of Physical and Chemical Sciences, North-West University, Private Bag x6001, Potchefstroom 2520, Republic of South Africa.

Keywords: scavenging, particle deposition, deposition efficiency, aerosol modelling

Sub-nanometre below cloud snow scavenging is very poorly known compared to rain scavenging, yet it is an important aerosol removal mechanism in the polar regions, in mountainous areas, as well as in the upper troposphere and in mid-latitudes in wintertime. The few studies that exist prove the great importance of snow scavenging as a deposition mechanism (Martin *et al.*, 1980, Sauter & Wang, 1989). We studied snow scavenging coefficients for 10 nm – 1 µm particles using 4 years of DMPS (Differential Mobility Particle Sizer) and Vaisala FD12P weather sensor data from SMEAR II –station in Hyytiälä, Southern Finland. The results will be compared with rain scavenging coefficients calculated by Laakso *et al.* (2003) in the similar way.

The snow scavenging coefficients (Λ_s) were calculated using following formula

$$\Lambda_s(D_p) = -\frac{1}{t_1 - t_0} \ln\left(\frac{c_1(D_p)}{c_0(D_p)}\right), \qquad (1)$$

where t is time, c particle concentration and D_p the diameter of the particle. From the 4 years of data (2005-2008) in total of 160 hours of snowfall were chosen.

The monthly and yearly distributions of the selected snowfalls were rather similar to all occurred snowfalls. Most represented snowfall types were slight continuous snowfall and snow grains and the median intensity was 0.2 mm h^{-1}. Due to the small amount of data and very similar snowfalls, the intensity-dependence of Λ_s could not be calculated

The median Λ_s was found to be $1.8 \cdot 10^{-5}$ s^{-1} and the medians for each DMPS size bin varied between $8.7 \cdot 10^{-6}$ s^{-1} and $5.2 \cdot 10^{-5}$ s^{-1}. The values were slightly higher than those of rain scavenging (Laakso *et al.*, 2003).

We parameterized the results using the same equation as Laakso *et al.* (2003) for rain scavenging (Fig. 1). Compared with their parameterization, snow scavenging parameterization gave similar values to rain scavenging with intensities around 3 mm h^{-1}, although snowfalls were dominated by intensities below 0.2 mm h^{-1}. A case study of a snowfall that occurred in Hyytiälä on 23 Nov 2008 and had intensities higher than 5 mm h^{-1} showed that snowfalls with higher intensity scavenge particles more efficiently, as expected. The median Λ_s for the snowfall was $8 \cdot 10^{-5}$ s^{-1}.
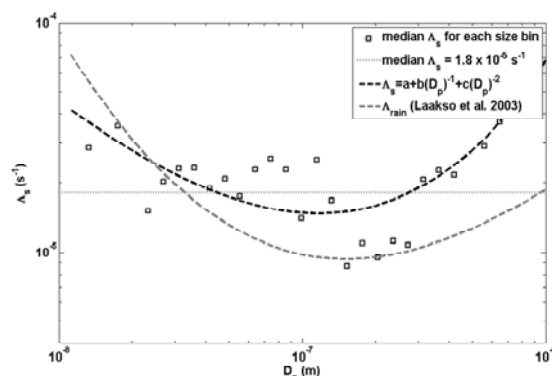
Figure 1. Median snow scavenging coefficients for each DMPS size bin as well as the parameterization for median. The median Λ_s for the whole dataset was $1.8 \cdot 10^{-5}$ s^{-1}. In addition, the parameterization by Laakso *et al.* (2003) for rain scavenging is shown.

The functionality of the parameterization was tested in the University of Helsinki Multicomponent Aerosol Model (UHMA) and it showed good agreement with the measurements (Fig. 2).
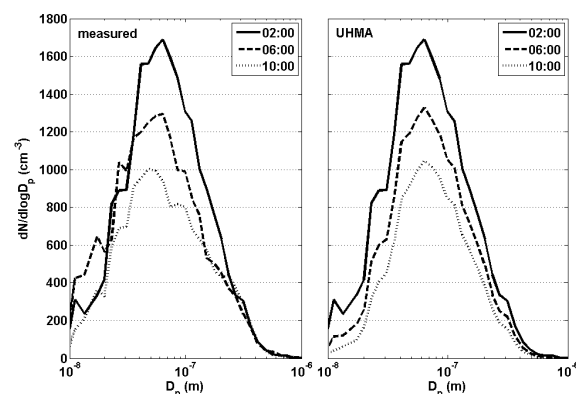
Figure 2. Measured and modelled particle size spectra during a snowfall 21.1.2007 02:00 – 10:00 (+2 UTC)

Laakso, L., Grönholm, T., Rannik, Ü., Kosmale, M., Fiedler, V., Vehkamäki, H. & Kulmala, M. (2003). *Atm. Env.*, 37, 3605–3613.

Martin, J.J., Wang, P.K & Pruppacher, H.R. (1980). *J. Atmos. Sci.*, 37, 1628–1638.

Sauter, D. & Wang, P.K. (1989). *J. Atmos. Sci.*, 46, 1650–1655.

Possible markers of aqueous aerosol of Lake Baikal in the region's atmospheric aerosol

A.N. Sergeev[1], A.S. Safatov[1], A.P. Agafonov[1], I.S. Andreeva[1], M.Yu. Arshinov[2], B.D. Belan[2], G.A. Buryak[1], V.M. Generalov[1], Yu.R. Zakharova[3], N.A. Lapteva[1], S.E. Olkin[1], M.V. Panchenko[2], V.V. Parfeneva[3], I.K. Reznikova[1], V.B. Simonenkov[2], T.B. Teplyakova[1] and V.A. Ternovoi[1]

[1]Federal State Research Institution SRC VB "Vector", Koltsovo, Novosibirsk region, 630559, Russia
[2]IAO SB RAS, 1, Square of Academician V. Zuev, Tomsk, 634021, Russia
[3]Institute of Limnology SB RAS, 3, Ulan-Batorskaya, Irkutsk, 664033, Russia

Keywords: atmospheric aerosols, bioaerosols, chemical composition, source identification.

INTRODUCTION

Atmospheric aerosols, which are simultaneously present in the region's air, usually originate from different sources and, correspondingly, have different component and chemical compositions. The analysis of its element composition and chemical and biological markers is the most informative method to determine a possible source of atmospheric aerosol. It's well known that water aerosol originates from water surface layer. The goal of the present work was to compare chemical and biological markers present in atmospheric aerosol and the surface microlayer (SML) of Lake Baikal water.

MATERIAL AND METODS

Sampling was performed in the summer of 2008 in the vicinities of Listvyanka, Sakhyurty settlement, Peschanaya Bay and above the water area of the lake. Equipment registering hydrometeorological parameters during the experiments was installed in a central point on the bank at right angle to the wind direction: an aerosol particle counter and 3 independent devices with volumetric flow of 50 l/min for collecting air samples on filters. Identical triples of independent devices were located at the distance of approximately 100 m to the left and to the right of the central point. A research ship with 3 independent devices for air sampling on filters was located at the distance of 700 m from the bank; 200 and 1000 μm - thick samples of the water SML were collected from the ship. An Antonov-30D airplane carrying an aircraft laboratory flew above the water area of Baikal.

The concentration of different chemical elements in the samples was determined with atomic absorption method on Shimadzu AA-6300 device with a flame and a thermoelectron atomizers. A fluorescent method using the reagent described in You *et al.* (1997) was employed to determine the total protein concentration. Polycyclic aromatic hydrocarbons (PAH) in samples of atmospheric air and water SML were determined with the method of high-performance liquid chromatography.

The presence of proteobacteria in the tested samples was used as a biomarker. They usually make up a rather large portion of bacteria in water systems (Bel'kova, 2004; Kemp & Aller, 2004). Their genetic material was detected with PCR method using primers for 16s RNA fragment described in Mercier *et al.* (1999).

RESULTS AND DISCUSSION

Atmospheric air of Lake Baikal practically does not contain particles with a diameter of more than 10 μm, and most particles were concentrated within the range of less than 1 μm. The total mass of aerosol particles does not exceed 2 μg/m^3.

The element analysis results show that all samples of aerosol and water SML contain maximal concentrations of the same chemical elements. Consequently, SML of Baikal water was the source of a portion of aerosol collected in this period. This is also confirmed by the detection of genetic material of water microorganisms in most studied aerosol samples of Lake Baikal including altitude samples collected above the water area of the lake. The total protein was found in the studied aerosols in lower concentration than in regions without a powerful water source. PAH pollutants were detected in none of the samples within the method sensitivity.

Thus, the performed work did not allow us to reveal a unique marker belonging only to aerosol of water origin in the studied region.

You W.W., et al. (1997). *Annal. Biochem.*, 244, 277-282.

Bel'kova, N.L. (2004). *Baikal water column microbiologic community's taxonomic diversity.* PhD Thesis. Vladivostok.

Kemp, P. F., & Alle,r J. Y. (2004). *FEMS Microbiol. Ecol.*, 47, 161-177.

Mercier, B., Burlot, L., & Ferec, C. (1999). *J. of Virol. Methods*, 77, 1-9.

Comprehensive aerosol size distribution measurements at the Meteorological Observatory Hohenpeissenberg

M. Pesch[1], L. Keck[1], H. Grimm[1], A. Wollny[2], U. Pöschl[2], H. Flentje[3]

[1]GRIMM Aerosol Technik GmbH & Co. KG, Dorfstrasse 9, D-83404 Ainring, Bayern, Germany
[2]Max Planck Institute for Chemistry, Becherweg 27/29, D-55128 Mainz, Germany
[3]Deutscher Wetterdienst, Albin-Schwaiger-Weg 10, D_82383 Hohenpeissenberg, Germany

Keywords: particle size distribution, aerosol instrumentation, trajectory, tropospheric aerosols.

Particle size distributions are crucial for the climate and health effects of atmospheric aerosols. In this study we apply a new mobile instrument package for comprehensive characterization of atmospheric aerosol size distributions ranging from a few nanometers (ultrafine particles) up to several micrometers (coarse particles).

This Wide Range Aerosol Spectrometer (WRAS, Grimm Aerosol Technik, Model 565) combines a Scanning Mobility Particle Sizer with Condensation Particle Counter (SMPS+C) covering the particle diameter range of 5.5 – 350 nm with an optical aerosol spectrometer covering the range of 250 nm – 32 µm. The two datasets are automatically synchronized and combined as illustrated in Fig. 1. The complete system is mounted in a stand-alone stainless steel outdoor housing and includes a sampling probe with a Nafion dryer.
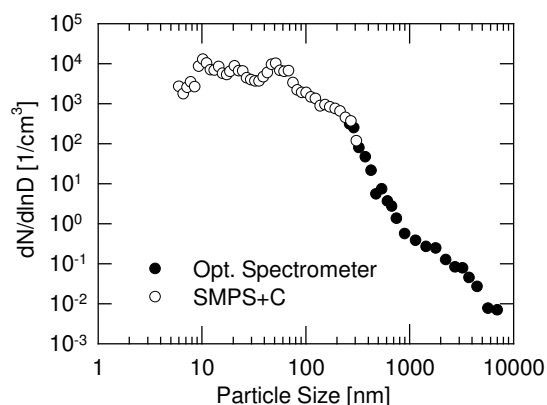
Figure 1. Particle size distribution measured with the WRAS system.

In this study, the WRAS system has been set up on the roof deck of the Meteorological Observatory Hohenpeissenberg (MOHp, 47°48' N, 11°20' E, 985m a.s.l.) which is operated by the German Weather Service (DWD) and is part of the Global Atmosphere Watch (GAW) program of the World Meteorological Organization (WMO). The observatory is located on a hill with about 300 m elevation above a rural area in Bavaria, Germany. A broad range of meteorological, trace gas, and aerosol parameters is continuously measured at the MOHp. Together with back trajectory analyses, these data shall be correlated with the aerosol size distribution measurements to obtain information about particle sources, transport and transformation.

Figure 2. Installation of the WRAS system on the roof platform of the GAW station Hohenpeissenberg

The WRAS measurements have been started in January 2009 and shall be continued over one year to characterize annual cycles, including the seasonal variability of primary biological aerosol particles such as fungal spores, which are major components of the coarse fraction of rural aerosols (~3-5 µm; Held et al., 2008). Another goal is the differentiation of photochemically formed particles and combustion particles by integrative analysis of particle size distributions, volatile organic compounds like terpenes and photooxidants such as ozone and nitrogen oxides (Hock et al, 2008). The comparison with the long time series of particle size distribution at Hohenpeissenberg allows for mutual quality control and putting the campaign data into longer perspective.

Held, A., Zerrath, A., McKeon, U., Fehrenbach, T., Niessner, R., Plass-Dülmer, C., Kaminski, U., Berresheim, H., Pöschl, U. (2008). *Atmospheric Environment*, 42 8502–8512.
Hock, N., Schneider, J., Borrmann, S., Römpp, A., Moortgat, G., Franze, T., Schauer, C., Pöschl, U., Plass-Dülmer, C., and Berresheim, H. (2008). *Atmospheric Chemistry and Physics*, 8, 603-623.

Transport of stratospheric aerosols in the field of averaged vertical wind

V.I. Gryazin, S.A. Beresnev

Aerosol Physics Laboratory, Ural State University, 620083, Ekaterinburg, Russia

Keywords: aerosol dynamics, aerosol modelling, atmospheric aerosols, stratospheric aerosols, vertical wind

The latitudinal and seasonal dependences of vertical profiles of the averaged vertical wind for different time intervals from 1992 to 2006 based on the data of the UKMO atmosphere general circulation model are analyzed.

We used in calculations the 13-year averaged data for the vertical wind. The positive values of velocities correspond to the lifting of particles against gravity, while negative ones correspond to the sedimentation of particles. One can see that the vertical wind is a determining factor for the particle motion up to altitudes of about 30–40 km. At altitudes above 40 km the gravitational sedimentation becomes a determining factor, while the vertical wind can only accelerate or slow down the sedimentation process (Beresnev & Gryazin, 2007; Beresnev et al., 2008). Calculations of the velocities for some standard particle in the middle atmosphere are presented in Figure 1.
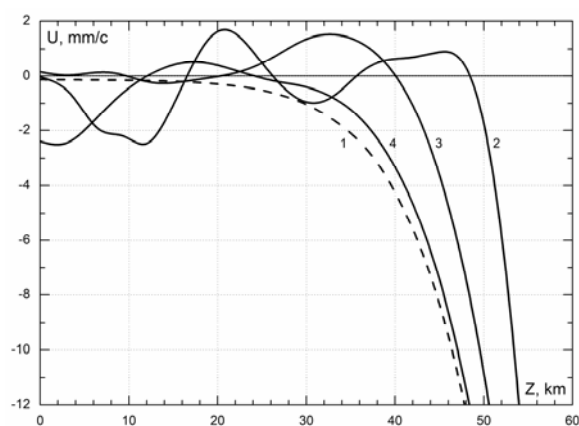
Figure 1. Velocities of particles with $\rho = 1$ g/cm^3 and $R_p = 1$ μm in the middle atmosphere: gravitational sedimentation only (1); total velocity of particles under action of the annual-averaged vertical wind for equator (2), North pole (3), and South pole (4).

The estimates of the times of lifting or sedimentation of particles from some fixed altitude to possible limiting boundaries are of principal significance. From Figure 2 follows, in particular, that vertical wind can be a potential mechanism for the formation of dynamically stable aerosol layers in the middle atmosphere at altitudes corresponding to the alternation of the vertical wind velocity sign from positive to negative. More detailed analysis of the vertical wind fields supposes long-term existence of aerosol clouds and clears up possible mechanisms of penetration and accumulation aerosols in stratosphere and mesosphere.
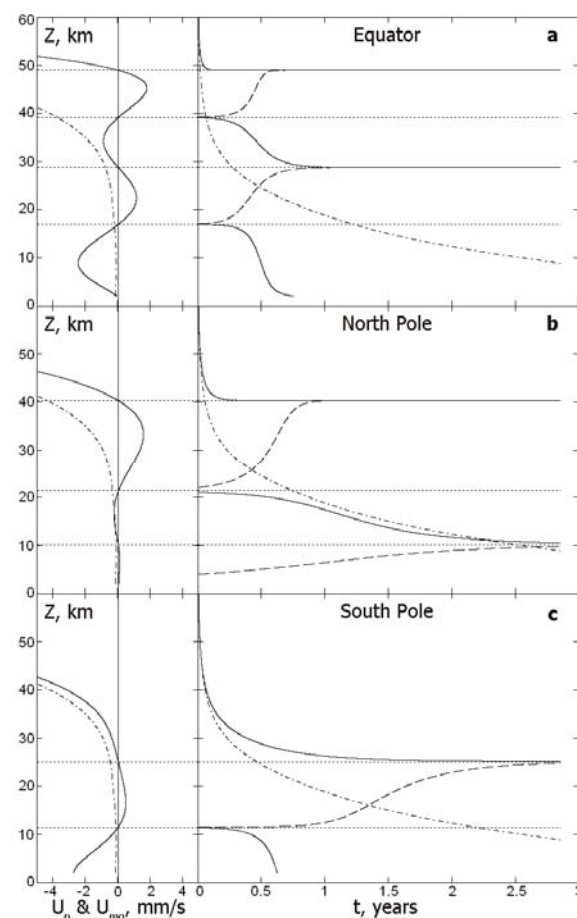
Figure 2. Times of particle lifting (solid curves) and sedimentation (dashed curves) taking into account vertical wind: the equator (a), North pole (b), South pole (c). Dot-and-dash curves correspond to the action of gravitational sedimentation only.

Beresnev, S. A., Gryazin, V. I. (2007). Atmos. Oceanic Opt., 20(6), 492-498.
Beresnev, S. A., Gryazin, V. I., Gribanov, K. G. (2008). Atmos. Oceanic Opt., 21(6), 448-454.

Planetary boundary layer influence at the Jungfraujoch depending on synoptic weather types

M. Collaud Coen[1], E. Weingartner[2] and U. Baltensperger[2]

[1]MeteoSwiss, CH-1530 Payerne, Switzerland.
[2] Laboratory of Atmospheric Chemistry, Paul Scherrer Institut, CH-5232 Villigen, Switzerland.

Keywords: Atmospheric aerosol, seasonal patterns, synoptic weather types, Jungfraujoch, free troposphere.

The high alpine research station Jungfraujoch (JFJ) is situated at 3580 m asl in the middle of the Swiss Alps. As stated by Lugauer et al. (1998) on the base of epiphaniometer data, the JFJ is prevalently situated in the free troposphere (FT), but is often influenced by injection of planetary boundary layer (PBL) air by thermal convection. The continuous measurements of the main aerosol optical properties since 1995 allow corroborating and further developing the previously published atmospheric transport processes relevant to high Alpine configurations.

The yearly and daily cycles of aerosol absorption and scattering coefficients, condensation nuclei concentration, backscatter fraction, single scattering albedo, as well as of all Ångström exponents have been analyzed as a function of different synoptic weather types. The used Alpine Weather Statistics (AWS) from Schüepp (1979) is based on the diurnal analysis of the pressure distribution at the surface and at 500 hPa and classifies the weather into 40 situations that can be subdivided in 8 groups or three mains synoptic groups (convective (51%), advective (43%) and mixed (6%)). The convective anticyclonic weather type is characterized by subsidence and cloud dissipation, whereas the convective cyclonic weather type leads to an ascent of air and cloud formation. Advective weather types are characterized by horizontal motion and can be subdivided by wind direction at 500 hPa.

The seasonal cycles of all aerosol optical properties show great variations depending on the synoptic weather types (Fig. 1a). When the weather is characterized by subsidence (convective anti-cyclonic), the scattering coefficient is very low from October to April, increases rapidly in April reaches its maximum at the end of July and then rapidly decreases. During the cold months the inversion level stays under the JFJ altitude and no injection of PBL air to the altitude of the JFJ occurs, such that the JFJ stays in the undisturbed FT. During summer, aerosol transport by thermally driven convection during subsidence leads to the greatest aerosol load.

During advective weather types, the scattering coefficient seasonal cycle is similar to the subsidence case, but with less sharp limits between the FT and the PBL influenced periods, as well as lower CN concentrations and scattering and absorption coefficients. The PBL influence can be also traced by

the scattering Ångström exponent becoming greater (particles becoming smaller) in the presence of more polluted air masses. Fig.1b confirms the above described seasonal cycle, advective weather types leading to smaller aerosols than subsidence.

The scattering coefficient seasonal cycle has completely different features during lifting weather type (convective cyclonic), with maximal values in February-April period and a rather monotonous decreases from June to January. The aerosol transport by lifting is maximal at the end of winter (Fig. 1a), leading to occasional PBL influence at the JFJ also during winter. Convective cyclonic weather type occurs however only for 2.5% of time during these months. The scattering Ångström exponent (Fig. 1b) is high (about 2) for the whole year except one month around the winter solstice. The corresponding prevalence of small particles during most of the year might be due to preferential scavenging by precipitation of larger particles during this weather type, however this needs further investigation.
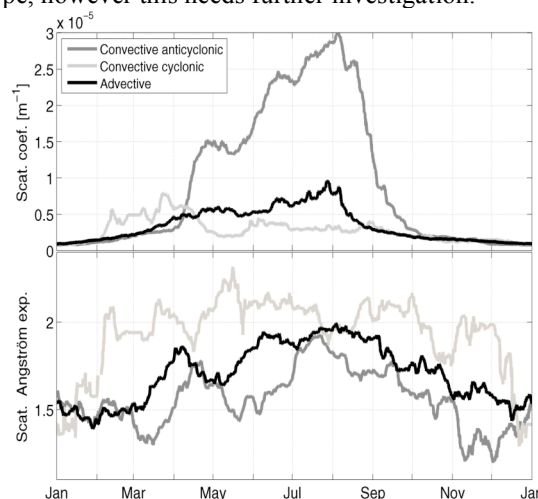
Figure 1. 12.5 years mean seasonal cycle of a) scattering coefficient and b) scattering Ångström exponent for three synoptic weather types.

Wanner, H., Salvisberg, E., Rickli, R., & Schüepp, M. (1998). *Meteorol. Zeitschrift*, N.F. 7, 99-111.

Lugauer, M., Baltensperger, U., Furger, M., Gäggeler, H.W., Jost, D.T., Schwikowski, M., & Wanner, H. (1998). *Tellus*, 50B, 76-92.

Schüepp, M. (1979), *Beilage zu den Annalen 1978*, (available from MeteoSwiss, Zürich, Switzerland).

Origin of the high fine aerosol particle concentration event in the boundary layer over Lithuania

J. Kilpys, V. Ulevicius, D. Jasineviciene and S. Bycenkiene

[1]Institute of Physics, Savanorių av. 231, LT-02300, Vilnius, Lithuania

Keywords: Atmospheric aerosols, fine particles, black carbon, long-range transport.

Aerosol particles plays important role in the atmospheric radiation balance and can influence global and regional climate. Moreover, it can cause a variety of respiratory and cardiovascular system diseases. The main sources of fine particles are their primary emissions and secondary formation by gas-to-particle conversion process in the atmosphere. However, if local emissions are low, high aerosol particle concentration levels could be associated with long-range transport of such particles (Andriejauskiene *et al.*, 2008, Wuzler *et al.*, 2008).The goal of this study is to examine the unusual high aerosol particle concentration event caused by long-range transport.

We analyzed data from the Preila environmental pollution research station and Vilnius air quality stations. Preila station is located on the coast of Baltic Sea, on the Curonian Spit, and is far from substantial local sources or airborne pollutants and thus can be characterized as a regionally representative background site. Continuous BC measurements were performed using the Aethalometer AE31 (Magee Scientific Company). The optical transmission of carbonaceous aerosol particles was measured sequentially at seven   (370, 450, 520, 590, 660, 880 and 950 nm). The total aerosol particle concentration was measured by using the Condensation Particle Counter (CPC) UF-02 (Institute of Physics), which can register 4.5 nm particles. The air mass backward trajectories were calculated to find out the origin of air mass during this event. The series of three-day air mass backward trajectories were calculated for the entire period using the Hybrid Single - Particle Lagrangian Integrated Trajectories model Version 4 (HY-SPLIT)(NOAA, www.arl.noaa.gov/ready.html). Fire maps were used to show burning of biomass, because the March 31 – April 3 event is characterized by high BC concentration. Fire maps were collected using FIRMS (Fire Information for Resource Management System) .

Aerosol particle and BC concentrations reached very high levels during the event on March 31 – April 3, 2008. The 1-hour average value of aerosol concentration reached 30 000 cm^{-3}, BC – 19 000 ng/m^3; usually average particle concentration values vary in the range from 500 to 4000 cm^{-3}, BC – 300 to 1500 ng/m^3. BC measurements are performed at seven wavelengths, and during this high concentration event measurements at different wavelengths had significant differences. This shows that there is high organic material content in aerosol. BC is a tracer of primary anthropogenic emissions, and its variability reflects changes in source strengths, long-range transport and atmospheric mixing characteristics. Atmospheric black carbon is always primary in origin since it is not formed by atmospheric reactions but is emitted directly into atmosphere as a result of fossil fuel or biomass burning. Analysis of backward trajectories and fire maps from FIRMS confirmed that there were a lot fires in Ukraine and Russia at the end of March and beginning of April. Most probably it was grass fires in steppes and agricultural areas. It produced a high number of fine particles with significant BC content. These particles due to long-range transport air masses were brought to the territory of Lithuania in 3 days and caused high peaks of aerosol particle (fig. 1) and BC concentrations.
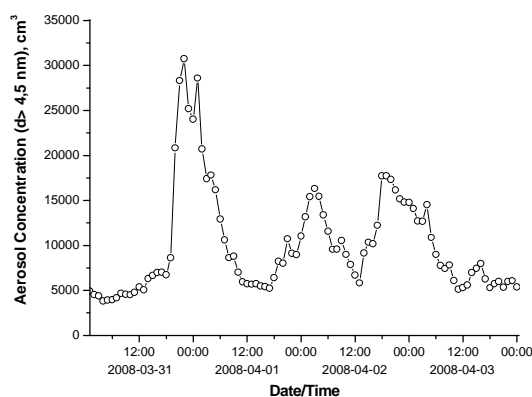
Figure 1. Hourly variation of high aerosol concentration at Preila station on March 31–April 3.

1. Andriejauskiene J., Ulevicius V., Bizjak M., Spirkauskaite N., Bycenkiene S. (2008). *Lithuanian Journal of Physics*, 48, 183-194.
2. Wuzler S., Niemann K., Engel I., Garus G., Olschewski A., Friesel J., Pfeffer U., Hoogerbrugge R., Bruckmann P. (2008). *Abstracts of European Aerosol Conference 2008*, Thessaloniki, Abstract T06A1790.

From fresh exhaust to CCN: Transformation of particles from shipping

L. Pfaffenberger[1], R. Baumann[1], J. Moldanová[2], T. Hamburger[1], B. Weinzierl[1],
A. Minikin[1], H. Schlager[1] and A. Petzold[1]

[1] DLR, Institut für Physik der Atmosphäre, Oberpfaffenhofen, 82234 Wessling, Germany
[2] IVL Swedish Environmental Research Institute, SE 400 14 Göteborg, Sweden

Keywords: CCN, emission factor, MBL, shipping emissions.

The impact of shipping emissions on climate change and chemical composition of the marine boundary layer is important since shipping represents a major element of international transportation. Currently only few emission data exist from ships, including the atmospheric transformation (Murphy et al., 2008; Petzold et al., 2008). Almost no aerosol emission data are available on a model grid scale.

The aims of this study are to characterise the properties of aerosol particles from emission during plume processing in the atmosphere to deposition, and to determine the spreading of superposed ship plumes over sea lanes. Within the QUANTIFY field study in June 2007 particle emissions from ship engines and their atmospheric transformation were studied. Airborne measurements of a single ship plume were combined with simultaneous measurements of fresh exhaust onboard the source vessel (Moldanová et al., 2008). Additionally, aged aerosol in highly frequented sea lanes was measured.

Onboard the DLR Falcon 20 E-5, a set of instruments was operated for the in situ measurements of secondary volatile aerosol, primary combustion particles, marine background aerosol, trace gases and meteorological parameters.

To obtain an emission index (EI), i.e. particle number exhausted by the engine per kg fuel, the measured number of particles is related to the amount of a chemically inert combustion tracer like CO_2 in order to neglect dilution due to expansion and dispersion of the ship plume (Petzold et al., 2008).
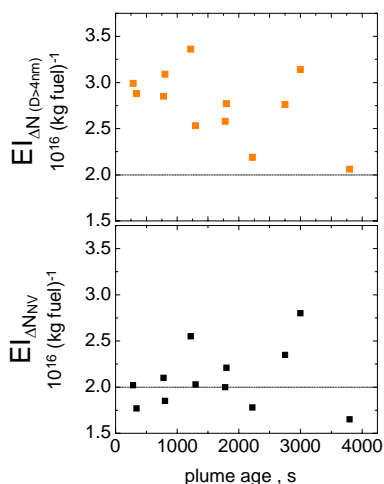
Figure 1. EIs of total aerosol (top panel) and non-volatile Aitken mode aerosol (bottom panel).

EIs of total aerosol, non-volatile Aitken mode aerosol and accumulation mode aerosol of young plumes have been analysed. As shown in Figure 1 the EI for total aerosol decays during plume expansion to an approximate value of 2×10^{16} (kg fuel)$^{-1}$ due to coagulation processes during plume expansion. The respective EI of the non-volatile Aitken mode aerosol however remains at a constant value of similar magnitude, indicating that combustion aerosol is processed to less extent than the total aerosol.

Figure 2 shows a time series of number concentrations of total aerosol, non-volatile Aitken particles and accumulation mode aerosol at 233 ± 4 m above sea level. Marine background aerosol is superposed by ship plumes of different age. Narrow peaks represent fresh plumes while the broad regions of enhanced aerosol concentration indicate highly frequented shipping corridors.

The mixing state of fresh ship exhaust aerosol and corridor aerosol will be presented. The potential impact of processed particles from shipping on the cloud condensation nuclei budget in ship traffic corridors and its climate effect will be discussed.
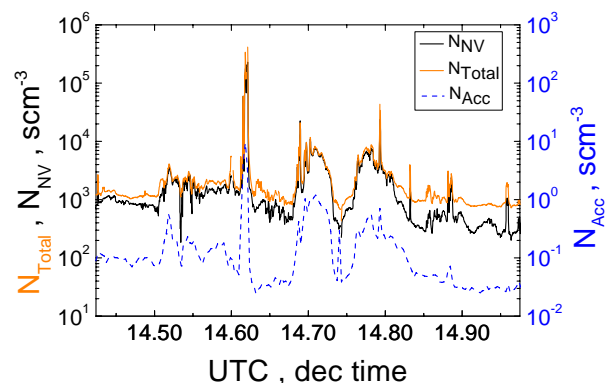
Figure 2. Time series of total aerosol, non-volatile Aitken mode aerosol and accumulation mode aerosol at a constant flight level of 233 ± 4 m above sea level.

Moldanová J., et al. (2009). *Atmos. Environ.*, accepted.
Murphy, S. M. et al. (2009). *Environ. Sci. Technol.*, 43, in press.
Petzold A., et al. (2008). *Atmos. Chem. Phys.*, 8, 2387–2403.

Effect of Tar burning on UFP size distribution at a background site at Mol, Belgium

V.K.Mishra[ab*], E. Frijns[a] , P. Berghmans[a], , N. Bleux[a], , J. Kretzschmar[b]

[a]VITO, Flemish Institute for Technological Research Boeretang 200, B-2400 Mol, Belgium

[b]Department of Bioscience Engineering, University of Antwerp, Antwerp, Belgium

Key words: Ultrafine particles; size distribution; SMPS; nucleation mode; number concentration.

Ultrafine particles (UFP), which are defined as particles <0.1 μm in diameter, are on a mass basis only a minor component of the atmospheric aerosol (∼1% by weight), but on a number basis they are a major constituent (∼86% by count). Because of their increased number and large surface area as well as their high pulmonary deposition efficiency, UFPs are particularly important in atmospheric chemistry and environmental health. To date, there has been rapidly increasing epidemiological evidence linking respiratory and cardiovascular health effects and exposures to UFPs (Morawska et al., 2008).

In the present study a detailed analysis of a two days diurnal variation of size resolved UFP number concentration data have been presented, in order to study the impact of local tar burning on UFP size distribution at a background site in Mol, Belgium. After careful analysis of particle size distribution patterns, for ease of comparison, the entire UFP fraction was divided into two size modes, i.e., nucleation mode (<25 nm), aitken/accumulation mode (30–100 nm). Particles in different size modes are formed in different ways: nucleation mode particles result from gas-to-particle conversion of different chemical compounds like sulphuric acid and ammonia. Aitken mode particles are directly emitted from combustion processes. They may also result from condensational growth and coagulation of nucleation mode particles. An extensive analysis of small time scale changes in UFP size distribution was utilized to study the dynamics of aerosols.

A two days sampling (26 & 27 January 2009) was performed, with a TSI model 3034 scanning mobility particle sizer (SMPS) (TSI Inc., Shoreview, MN, USA) and an aerodynamic particle sizer (APS) (model 3321, TSI Inc., Shoreview, MN, USA). The SMPS–APS system has the advantage over other continuous mass monitors of generating mass concentrations at discrete size intervals near-continuously.

The mean particle number size distributions during Tar burning were compared with early morning and nighttime hours, when there was no tar burning..

The tar burning not only caused substantial increase (>4 fold) in total UFP number concentration but also shifted the dominant size (Fig. 1 &2) mode towards the lower size range,
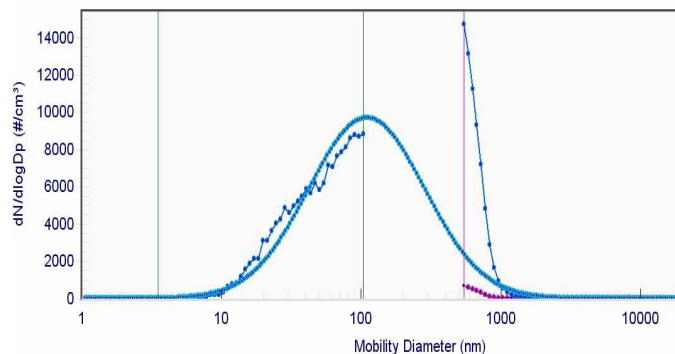
Fig.1 Number Size distribution during early morning hours (6:00am) without tar burning.
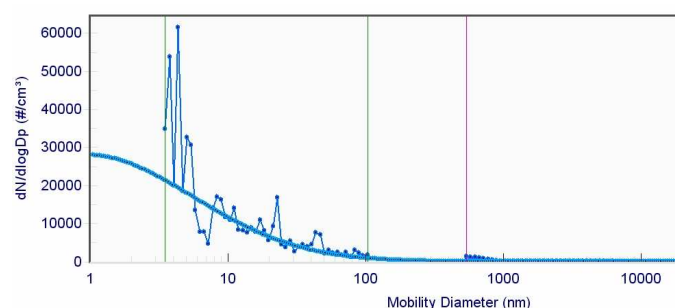
Fig.1 Number Size distribution early afternoon (11:00am) with tar burning.

i.e., the maxima now shifted into nucleation mode which was in Aitken mode when there was no tar burning. The formation rate of nucleation mode particles were also increased by a factor of 10^3, so tar burning caused a local nucleation burst in a background site which otherwise has a low UFP levels (<8,000 cm^{-3}).

Another important results was deviations between different characteristics diameters increase with increasing σ_g. For example, for a log normal distribution with $\sigma_g=2.0$ the condensation sink diameter was 1.52 times larger than the number mean diameter but only 1.25 times larger for $\sigma_g=1.6$.

Reference:

Morawska, L., Ristovski, Z.,Jayaratne,E.R.,Keogh, D.U., Ling, X., 2008. Ambient nano and ultrafine particles from motor vehicle emission: Charcteristics, ambient processing and implications on human exposure. Atmospheric Environment. 42, 8113-8138.

Chemical characteristics of aerosols during foggy and clear days:

Case study from northern India

Kirpa Ram[1], A.K. Sudheer[1] and M.M. Sarin[1]

[1]Physical Research Laboratory, Ahmedabad-38009, India

Keywords: Urban Aerosol, Foggy period, Chemical composition, Water-soluble organic carbon

A significant fraction of particulate matter (PM) consists of water-soluble species (both organic as well as inorganic) and have tendency to act as cloud condensation nuclei (CCN). In addition, inorganic species (SO_4^{2-} and NH_4^+), formed by chemical transformation processes, affect the regional atmospheric chemistry (Rastogi and Sarin, 2006). Thus, abundance pattern, chemical and optical properties of aerosols can be very different during foggy days and non-foggy (clear) days because of the differences in atmospheric parameters such as relative humidity (RH) and temperature. Results from a case study on the chemical composition (organic and inorganic constituents) of atmospheric aerosols during foggy and non-foggy days from an urban site, Allahabad (25.4 °N, 81.9 °E, 123 m amsl), in the IGP during wintertime (Dec 2004) are presented.

Table 1. Chemical composition of aerosols during foggy (F-1 and F-2) and non-foggy (non-F) days. Concentrations are in $\mu g \ m^{-3}$.

	TSP	NH_4^+	SO_4^{2-}	WSOC	WSF	EC	OC
F-1	301	9.8	28.4	21.1	0.38	6.5	57
F-2	264	9.0	24.1	17.4	0.37	5.2	43
non-F	319	4.8	15.0	15.6	0.28	6.2	48

The inorganic constituents, cations (Na^+, K^+, NH_4^+, Ca^{2+} and Mg^{2+}) and anions (Cl^-, SO_4^{2-} and NO_3^-), were measured on Ion-Chromatograph and water-soluble organic carbon (WSOC) was analyzed on TOC analyzer whereas EC and OC content in aerosols were assessed on EC-OC analyzer using TOT protocol (Rengarajan et al, 2007). On average, the abundance of total suspended particulate (TSP) matter and water-soluble inorganic species (WSIS, sum of cations and anions) are 300 $\mu g \ m^{-3}$ and 60 $\mu g \ m^{-3}$ (~20% of PM), respectively; and SO_4^{2-}, NO_3^- and HCO_3^- were the major anions whereas NH_4^+ and Ca^{2+} dominate among cations. The abundances of NH_4^+ and SO_4^{2-} increased by a factor of two during foggy days (F-1 and F-2, Fig. 1) compared to non-foggy days (non-F), WSOC content also increased significantly (Table-1 and Fig. 1). The production of these inorganic species depends on the availability of the precursor gases (SO_2 and NH_3), surface area (i.e.

abundances of fine and accumulation mode particles), RH and reacting species such as H^+ ions and OH free radicals. RH and surface area are relatively higher during foggy days and precursor gases are confined to smaller volume, thus, increasing the formation of SO_4^{2-} and NH_4^+. The RH dependence on the formation of these species is further supported by an increase in the water-soluble fraction (WSF) during foggy periods. The increase in SO_4^{2-} and NH_4^+ concentrations during the foggy-days due to increase in PM can be ruled out as the ratios of these species to PM shows similar increasing trend. The increase in WSOC abundance and WSOC/OC ratios (Table-1) is attributable to enrichment of WSOC during fog conditions than the particulate OC. The role of regional emission sources and atmospheric chemical constituents in the fog formation and subsequent change in optical properties of aerosols are very crucial and needs detailed investigation in order to understand their impact on radiation budget and regional climate.
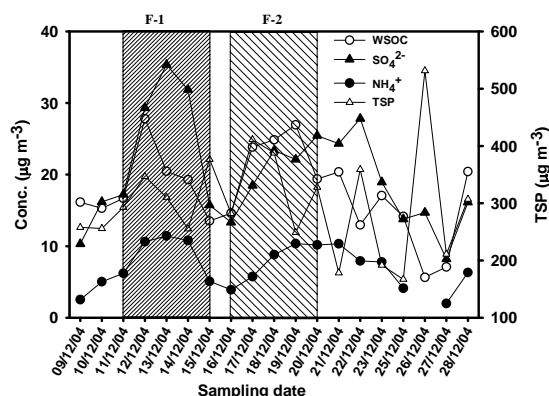
Figure 1. Temporal variability of chemical species at Allahabad. F-1 and F-2 represent the two foggy-periods observed during sampling period (Dec 2004).

Rastogi & Sarin (2006). *Geophysical Research Letters,* doi:10.1029/2006GL027708.
Rengarajan R. et al (2007). *J. Geophysical Research-Atmosphere,* doi: 10.1029/2006JD008150

Number size distribution and chemical composition changes along vertical profiles in the Po Valley, implications for aerosol optical properties

L. Ferrero[1], E. Bolzacchini[1], M. G. Perrone[1], B.S. Ferrini[1], Z. Lazzati[1], F. Bruno[2], D. Cocchi[2], F. Greco[2], G. Mocnick[3], D. Cappelletti[4], L. Barcherini[4], S. Ortu[4], B. Moroni[5]

[1] POLARIS research center, DISAT, University of Milano-Bicocca, Piazza della Scienza 1, 20126, Milano, Italy
[2] Department of Statistics "P. Fortunati", University of Bologna, Via delle Belle Arti 41, 40126, Bologna, Italy
[3] Magee Scientific, Aerosol d.o.o. Kamniska 41 SI-1000 Ljubljana, Slovenia
[4] Department of Engineering, University of Perugia, Via G. Duranti 93, 06125 Perugia, Italy
[5] Department of Earth Science, University of Perugia, Via G. Duranti 93, 06125 Perugia, Italy

Keywords: Atmospheric aerosols, vertical distribution, mixing layer, aerosol evolution, size analysis

Atmospheric particulate matter is crucial in environmental pollution problems, health hazard and climate changes. On one hand particulate matter is one of the most important atmospheric pollutants, specially in urban areas (Rodriguez et al., 2007). A typical example is found in the Po Valley cities (North Italy) where ventilation is scarce and stagnant conditions often occur causing a marked seasonally influenced PM trend (Ferrero et al., 2007).

On the other hand, it has been found that aerosols influence also the climatic system for they ability to scatter and absorb sunlight (direct effect). Globally they are opposed to greenhouse gases in global warming, cooling the earth-atmosphere system. The number size distribution and the chemical composition of the particles in the atmosphere are all parameters that can influence this process (IPCC, 2007). A knowledge of the vertical distribution of aerosol can give a direct estimation of the influence of atmospheric dispersion conditions on PM pollution levels; while a knowledge of the vertical distribution of aerosol properties, like number concentration, size distribution and chemical composition are key parameters in order to derive aerosol optical properties with height and, at the opposite, to apply inversion algorithms used to retrieve the aerosol characteristics from optical measurements (Dubovik et al., 2000).

Pollution levels and changes in aerosol properties along height were jointly investigated in the Po Valley (north Italy) and in Terni Valley (middle Italy) in order to asses the influence of meteorology on them, paying attention to the role of the mixing layer.

To do that vertical profiles of particle number size distribution (15 size classes between 0.3 to 20 μm) were monitored at Torre Sarca site (45°31'19"N, 9°12'46"E) in Milan, using an optical particle counter (OPC GRIMM *1.108 "Dustcheck"*) and a portable meteorological station deployed on a 4 m tethered balloon (Ferrero et al., 2007). This method provides the direct measure of the PM profile along height, with a direct evaluation of the Mixing Layer (ML) height (Seibert et al., 2000). In addition special sampling campaigns were carried out using a miniaturized cascade impactor (Sioutas SKC, 5 impaction stages: >2.5 μm, 1.0-2.5 μm, 0.5-1.0 μm, 0.25-0.5 μm, <0.25 μm). PM massive samples were collected during the day along vertical profiles: at ground level, into the mixing layer and over it. The ionic inorganic fraction was quantified by ion chromatography (Dionex ICS-90) system. Shape, size and elemental composition were assessed by SEM-EDX system.

Vertical profiles of black carbon (BC) were measured too with a prototype AE-51 microAeth Aethalometer (Magee Scientific) with a time resolution of 1 second.

Here we present three years of vertical profile measurements (2005-2008). More than 300 PM vertical profiles were measured both during winter and summer times, mainly in clear and dry sky conditions. Under these conditions, no significative changes in aerosol content of NO_3^-, SO_4^{2-} and NH_4^+ into and over the mixing layer were found. On average, taking into account the total particle number concentration measured at ground and over the ML (in the OPC size range), quite steady PM concentrations were found over the ML, representing the 28 ± 2 % during winter and 35 ± 2 % during summer. The same was observed fro black carbon concentrations.

From experimental measurements we observed also changes in size distribution along height. An increase of the mean particle diameter, in the accumulation mode, passing through the mixing layer was evidenced under stable conditions; the mean relative growth was 2.1 ± 0.1% during winter and 3.9 ± 0.3% during summer. At the same time, sedimentation processes occurred across the ML height for coarse particles leading to a mean particle diameter reduction: 14.9 ± 0.6% during winter and 10.7 ± 1.0% in summer. In order to explore better the physical behaviour of finest particles along height, a cluster analysis of the vertical profiles was carried out allowing to distinguish four group: group A and B formed mainly by winter launches whereas groups C and D contained mainly measured in summer days. A hierarchical statistical model, following the theory of compositional data (Aitchison, 1986), for the particle size distribution has been developed for each group to describe the aging process of the finest PM fraction along height. A third-order degree polynomial was adequate for describing fine particle growth along height in atmospheric stable conditions. A mean growth estimated on the basis of the model was respectively of 1.92% during winter and 6.05% during summer, in accordance to experimental evidences.

Group C was the only one that exibithed an opposite behaviour; vertical profiles influenced by transport events were clustered into it. In these situations a decrease in the mean particle diameter for fine particles was observed over the mixing layer. At the same time a sharp change, referred to the ground, in the relative contribution of SO_4^{2-}, NO_3^- and NH_4^+ to the ionic inorganic fraction was observed over it. At the same time NOAA Hysplit backtrajectories showed the presence of transport event for example from East Europe and Mediterranean sea.

So ML height appeared in most cases as a critical parameter for splitting the lower troposphere into two areas: one, into the ML, in which fresh aerosol from anthropogenic emissions and secondary origin was present, and another one over the ML influenced by background conditions with aged aerosols (especially during winter) or by aerosols long-range transported.

These data were mainly carried out in clear and dry sky conditions, in which usually aerosol properties can be also derived by satellite remote sensing using different sensors (i.e. MODIS). In this cases a knolwedge of the mean measured changes in aerosol size distribution and so in optical ptoperties could be very useful (Levy et al., 2007; Chu et al., 2003)

Rodriguez et al., Atmos. Chem. Phys, 7, 2217-2232, 2007
Ferrero L. & al. (2007), *FEB*, Vol. 16 N° 6.
IPCC: Climate Change 2007.
Dubovik et al., JGR, 105, 9791–9806, 2000.
Seibert P. & al. (2000), *Atm. Env.*, 34, 1001-1027.
Aitchison J. (1986), Chapman and Hall.

Nucleation mode particles in the Karlsruhe city plume, the COPS / TRACKS - Lagrange experiment

W. Junkermann[1], R. Hagemann[2] and B. Vogel[2]

[1]Forschungszentrum Karlsruhe, IMK-IFU, Kreuzeckbahnstr. 19, 82467 Garmisch-Partenkirchen, Germany
[2]Forschungszentrum Karlsruhe, IMK-TRO, 76021 Karlsruhe, Germany

Keywords: nucleation, size distribution, airborne particles

Within the COPS/TRACKS (Kottmeier et al., 2008) campaign in the Rhine valley and northern Black Forest an airborne Lagrange experiment was performed to investigate the fate of a single city plume and its chemical aging during transport over remote areas of the Kraichgau. Measurements of aerosols and aerosol size distributions were performed using an ultralight aircraft equipped with fast condensation particle counters, scanning mobility particle sizers and optical particle counters for the characterisation of the whole spectrum of particle sizes from ultrafine aerosols to coarse particles.

An aerosol plume of nanometer size particles was detected with a source region above the city of Karlsruhe and aging and growth of the particles during three hours transport time. The temporal evolution of size distributions within this plume was generally in agreement with the behaviour of size distributions of nucleation events with a subsequent growth of about 5 nm/h (Laaksonen et al, 2005) but the diurnal timing of the particle generation was several hours delayed compared to typical nucleation events observed elsewhere (Wu et al, 2008). Though nucleation events have occasionally been reported to happen later during the day the weather patterns during the campaign rather favoured early morning nucleation.

We use a 1-D version of the comprehensive model system COSMO-ART (Vogel et al., 2009) to test individual hypothesis that could explain the unexpected nucleation time shift behaviour of the observed temporal development of the size distributions. We found that either a direct emission of nanometre size particles (< 5 nm) or a strong source of SO_2 would be required to explain the observations. Sufficient emissions of ultrafine particles have not been reported up to now neither from traffic exhaust, nor from city emissions or from polluted rural conditions (Wu et al. 2008). An elevated source of SO_2 in our model simulations produced rapidly new particles with a similar temporal evolution of the size distributions as observed. SO_2 emission from a nearby power plant thus might be responsible for the particle plume.
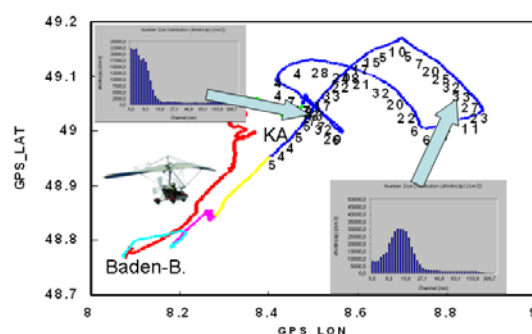
Fig. 1, Flight track, size distributions and total number of particles > 10 nm (/1000) during the Lagrange flight. Particle numbers outside the plume were ~ 4-6000 / cm3.
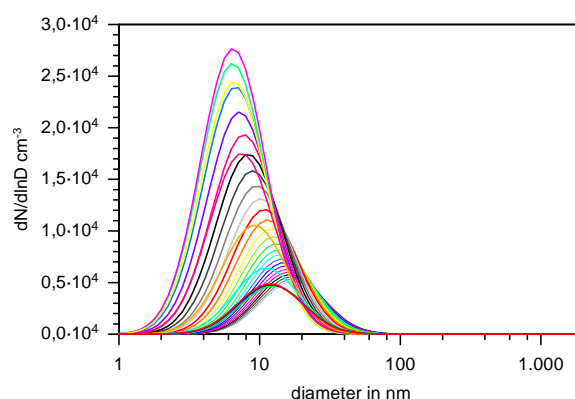
Fig. 2, Simulated temporal evolution of the size distribution with five minutes time intervals.

Wu, Z., Hu, M., Lin, P., Liu, S., Wehner, B., Wiedensohler, A., (2008), Atmos. Environ., 42, 7967-7980.

Kottmeier Ch. et al., (2008), Meteorol. Z., 17, 931-948.

Laaksonen, A., Hamed, A. Joutsensaari, J., Hiltunen, L., Cavalli, F., Junkermann, W., Asmi, A., Fuzzi S., and Facchini,M.C, Geophys. Res. Lett., 32, L06812, 10.1029/2004GL022092, (2005)

Vogel, B., H. Vogel, D. Bäumer, M. Bangert, K. Lundgren, R. Rinke, T. Stanelle, (2009) submitted to APCD.

An episode of Saharan dust north of the Alps

W. Straub, S. Wurzler, and P. Bruckmann

North Rhine-Westphalia State Agency for Nature, Environment and Consumer Production, P.O. Box 101052, D-45610 Recklinghausen, Germany

Keywords: Saharan dust, PM_{10}, $PM_{10}/PM_{2.5}$.

From May 27 to June 1 2008 a pronounced episode of long range transport of Saharan dust has been observed over central Europe causing high PM_{10} values especially in the Alps and also in several regions of northern Germany (Fig. 1). Elevated PM_{10} concentrations were observed as the particle cloud travelled from Southern France (Hyeres) via parts of Italy, Austria (Brixlegg), Switzerland (Rigi) and Southern Germany (Andechs) to North-West Germany (Netphen) (Tab. 1). The PM_{10} and $PM_{2.5}$ data originate from the monitoring networks of the countries, states and provinces affected.
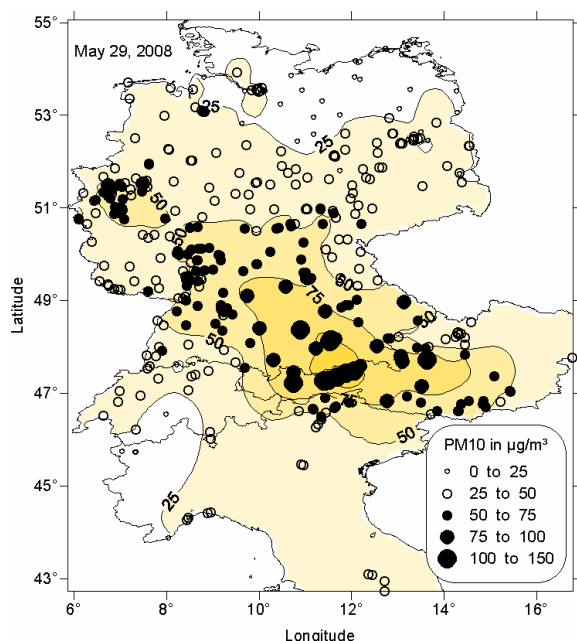
Figure 1: PM_{10} daily means at monitoring stations in the Alpine region and Germany on May 29, 2008.

Table 1: Elevated PM_{10} daily and hourly means at selected background stations in central Europe.

Station	Date	Daily / hourly means of PM_{10} ($\mu g/m^3$)
Hyeres	5/27/08 (9PM)	46 / 69
Brixlegg	5/28/08 (9AM)	135 / 196
Rigi	5/28/08 (9PM)	61 / 143
Andechs	5/29/08 (4PM)	94 / 155
Netphen	5/30/08 (8AM)	63 / 107

During this time, the weather conditions were characterized by a pronounced trough over Western Europe, directing a strong southerly flow of extremely warm tropical air masses from the Mediterranean Sea. Weather reports from this period hinted to the transport of Saharan dust.

While $PM_{2.5}$ to PM_{10} ratios in the Alps and Southern Germany showed only small values (around 0.3) typically for Saharan dust, in Essen-Vogelheim, a typical urban background station in Northern Germany, considerably higher values of 0.5 to 0.6 has been observed (Fig. 2). Further chemical analysis of the particles collected in Essen-Vogelheim and comparison of the $PM_{2.5}$ to PM_{10} ratios revealed a change in aerosol composition during the transport over Germany. Especially in the region of the Rhine Ruhr conurbation a high share of secondary aerosols could be identified.
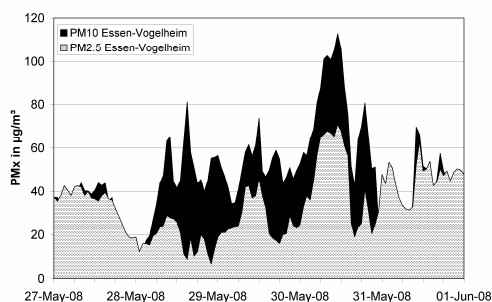
Figure 2: Time series of simultaneously measured PM10 and PM2.5 data ($\mu g/m^3$) from Essen (urban background station).

Within the presentation, the analysis of the episode of long range transport of Saharan dust and the various meteorological and chemical processes which come into play and which impede simple conclusions based only on PM_{10} ground based measurements are presented. It is shown that an integrated approach is needed to observe changes in aerosol during long range transport which combines a whole array of different methods.

Bruckmann, P., Birmili, W., Straub, W., Pitz, M., Gladtke, D., Pfeffer, U., Hebbinghaus, H., Wurzler, S., & Olschewski, A. (2008). *Gefahrstoffe – Reinhaltung der Luft*, 68, 490-498.

Contribution of traffic-emitted pollutants at a busy Danish highway compared to a major street in central Copenhagen

A. Massling[1], F. Wang[1,2], M. Ketzel[1], T. Ellermann[1], S. S. Jensen[1] and P. Wåhlin[1]

[1]Department of Atmospheric Environment, National Environmental Research Institute, University of Aarhus, Frederiksborgvej 399, 4000 Roskilde, Denmark
[2]Institute of Nuclear and New Energy Technology, Tsinghua University, 100084 Beijing, China

Keywords: Aerosol measurement, particle size distribution, PM2.5/PM10, NO_x, traffic emissions.

INTRODUCTION

Light and heavy duty vehicles emit high amounts of ultrafine aerosol particles, but contribute also significantly to PM2.5 due to re-suspension of road dust and wear from brakes and road surface. NO_x has been used as tracer for many studies to quantify particulate emissions from traffic. However, only limited data are available on particulate emissions on highway traffic. This study presents a comparison of traffic emitted particulate pollutants between a busy Danish highway and a major street in central Copenhagen.

METHODS

Two field sites were chosen for the study: an urban site consisting of a kerbside station located at a major road (mean vehicle speed 50 km/h) and a highway site (at highway 21, 30km east of Copenhagen, mean vehicle speed 100 km/h). At both sites a corresponding background station was available. The parameters monitored during an eight week period at these four stations are listed in Table 1.

Table 1. Measured pollutants simultaneously monitored at four field stations.

Station	Particles	Particle phase	Gas phase
Urban kerbside	PNSD[1], PM2.5	Elements, BTX[2], PAHs[3]	NO, NO_2, O_3, CO, SO_2
Urban background	PNSD, PM2.5, PM10	Elements	NO, NO_2, O_3, CO
Highway kerbside	PNSD, PM2.5, PM10	-	NO, NO_2, CO
Highway background	PNSD, PM2.5, PM10	-	NO, NO_2, CO,

[1]Particle number size distribution; [2]Polycyclic aromatic hydrocarbons; [3]Benzene, toluene, and xylene.

After selecting for wind direction, the difference of kerbside minus background concentrations was used to address the traffic contribution from both sites. A total dataset of four weeks was analyzed and particulate concentrations were linked to NO_x emissions and traffic volume measurements.

RESULTS

At working days, the daily average contribution from traffic of NO_x was 197 and 131 ($\mu g/m^3$) and in total particle number 32480 and 26240($\#/cm^3$), at the highway and at the urban site, respectively. Corresponding values for PM2.5 were 3.8 and 5.0 ($\mu g/m^3$). Figure 1 shows the diurnal variation of the traffic contribution at both sites during workdays, Saturdays and Sundays.
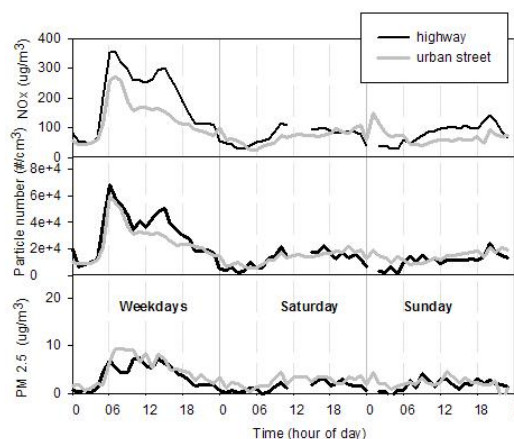
Figure 1. Diurnal variation of the traffic contribution during workdays, Saturdays and Sundays.

The diurnal pattern of NO_x and total particle number are observed to be quite similar for the highway and urban site. The rush hours (7:00 and around 15:00) can clearly be identified at both sites during working days and concentrations also correspond well with the traffic volume. The afternoon rush hour is much more pronounced at the highway site as traffic is strongly linked to commuting people. In comparison, the urban rush hour appears more smeared due to additional traffic in the downtown area. As particle number (10 − 700 nm) during working days is always smaller at the urban site compared to the highway, PM2.5 is always a bit larger giving the hint that road dust emissions are obviously higher at lower vehicle speed.

During the early morning hours on Sundays, NO_x, total particle number and PM2.5 exhibit small concentration maxima due to the high share of taxis in traffic volume. This finding is only valid for the urban site as expected.

ACKNOWLEDGEMENT

Combined volatility and mass spectrometric measurements of biogenic secondary organic aerosol

E. Emanuelsson [1], M. Hallquist[1], A. Buchholz[2], A. Kiendler-Scharr[2], Th. F. Mentel[2] and C. Spindler[2]

[1] Atmospheric Science, Department of Chemistry, University of Gothenburg, Göteborg, Sweden
[2] Institut für Chemie und Dynamik der Geosphäre, ICG-2, Forschungszentrum Jülich, Germany

The volatility of secondary organic aerosol (SOA) from the oxidation of mixtures of biogenic Volatile Organic Compounds (VOC) has been investigated in the SAPHIR facility in Forschungszentrum Jülich, Germany, by using a Volatility Tandem Differential Mobility Analyser (VTDMA). The standard VTDMA setup comprises three main parts (Jonsson et al. 2007): 1) An initial DMA, where a nearly monodispers size fraction of the aerosol particles is selected (typically 100 or 150 nm), 2) the oven unit, i.e. four ovens in parallel where each oven includes a heating and adsorption section where the evaporation and adsorption of the volatile fraction occurs and 3) a final SMPS (Scanning Mobility Particle Sizer) system where the residual particle number distribution is measured. For this measurement campaign the set-up also contained a Quadrupol Aerosol Mass Spectrometer (Aerodyne QAMS, Jayne et. al, 2000). The temperature of the ovens can be varied between 298 and well above 573 K. In parallel to the final SMPS the AMS was used for chemical composition and density measurements. When the system was dedicated for AMS measurements the initial DMA was bypassed to improve the aerosol concentration. However, the produced SOA has a narrow size distribution still making it possible to follow small changes in the aerosol peak diameter. A general feature of the thermo-denuder system is that a less volatile SOA gives a larger residual particle size distribution compared to more volatile SOA.

The experiments conduced were based on photochemical oxidation of a reference boreal mixture (BMT) of terpenes, consisting of α-pinene, β-pinene, limonene, Δ^3-carene, and ocimene. In further studies, the sesquiterpenes β-caryophyllene and α-farnesene were added (BMT+SQT). Secondary organic aerosol was formed from the precursor compounds by reaction with $O_3/H_2O/OH$ in SAPHIR on the first day. The particles were kept in the chamber for up to two further days and were exposed to natural sunlight and OH radicals to initiate close to natural chemical aging.

The VTDMA results show that SOA becomes less volatile during ageing and this ageing was further enhanced when the mixtures were exposed to sunlight. The volatility, measured as normalised mode particle diameter (NMDp), was also affected by changes in the terpene mixtures (Figure 1).

With the AMS we measured mass spectra of the organic aerosol particles at a reference temperature of 298 K and two additional elevated temperatures. Size distributions of the particles were obtained from the particle-time-of-flight mode of the AMS at sixteen representative m/z values. The residual total mass measured at the elevated oven temperatures was related to the total mass at the reference temperature to obtain the mass fraction remaining (MFR), which is higher for less volatile SOA. In agreement with the decreasing volatility during aging measured with the VTDMA, the MFR increases with time. An effective density of the particles was calculated comparing the mode position of the size distributions measured with the AMS and the SMPS. The effective density increases with ongoing photochemical ageing. In addition, the density of the low volatile residual particles that passed a high-temperature oven is higher than the density of particles at reference temperature. In order to investigate if the observed changes in density and volatility can be attributed to changes of the chemical composition of the particles, the mass spectra obtained at different oven temperatures and different chemical age were compared. We found that the ratio of heavy fragments (m/z > 90) increases with higher temperatures. Furthermore the fraction of the CO_2^+-fragment at m/z 44 to the total mass increases during the ageing process.
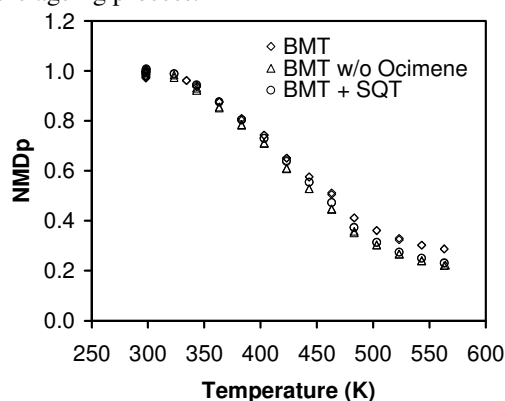
Figure 1. Volatility of freshly nucleated SOA for different precursor mixtures.

Jayne, J. T., et. al. (2000). *Aerosol Science and Technology*, 33, 49-70.
Jonsson Å. M., Hallquist M, and Saathoff H., (2007), *Journal of Aerosol Science*, 38, 843-852.

Single Particle Studies of the Kinetic and Thermodynamic Factors Governing the Size and Composition of Inorganic/Organic/Aqueous Aerosol

J.P. Reid[1], K.L. Hanford[1], G. Hargreaves[1], K.J. Knox[1], N. Kwamena[1], A. Laurain[1] and J.B. Wills[1]

[1]School of Chemistry, University of Bristol, Bristol, BS8 1TS, United Kingdom

Keywords: single particle analysis, Raman spectroscopy, thermodynamic equilibrium, dicarboxylic acids, mass accommodation.

The kinetic and thermodynamic factors regulating the equilibrium size and composition of aerosol must be understood if their influence on climate and atmospheric chemistry is to be fully understood. In particular, the influence of organic components on the hygroscopicity of mixed component aerosol and on the kinetics of mass accommodation must be investigated.

Recently, we have developed a range of novel optical techniques for trapping and manipulating single aerosol particles or arrays of up to 12 particles (Mitchem and Reid, 2008). A single-beam gradient force optical trap (optical tweezers) provides a strong restoring force that allows an aerosol particle to be retained within a gas or aerosol flow, to low pressure and during coalescence with moving aerosol particles. When coupled with linear and non-linear spectroscopic techniques, the size, composition, mixing state, phase and refractive index of multiple aerosol particles can be compared and contrasted within the same gas phase environment, with high time-resolution and with spatial resolution. In particular, the evolution in the size of a liquid droplet can be determined with nanometre accuracy from the unique fingerprint of enhanced Raman scattering at wavelengths which match whispering gallery modes.

The opportunity provided by aerosol optical tweezers to perform comparative measurements allows highly accurate measurements of the evolving equilibrium wet particle size with change in relative humidity (RH), an investigation of the thermodynamic factors governing particle size (Hanford et al., 2008). More specifically, an aqueous sodium chloride droplet can be used as a control droplet i.e. as a microprobe of the gas phase RH (Butler et al., 2008). From the evolving size of the aqueous sodium chloride droplet, the surrounding RH can be determined with an accuracy of better than ±0.09 %. In this paper we will report on studies of the equilibrium variation in wet droplet size from close to saturation (approaching 100% RH) down to RHs at which a liquid droplet exists in a supersaturated state. In particular, we will describe how aerosol optical tweezers can be used to interrogate the thermodynamic properties of mixed particles containing inorganic salts and organic diacids, typical of water soluble organics found in the atmosphere, under conditions of low RH.

The opportunity to characterise the equilibrium properties of mixed phase aerosol particles using aerosol optical tweezers will also be considered, examining in particular the variation in microphysical structure of particles containing hydrophobic and hydrophilic phases, specifically oleic acid and palmitic acid.

Finally, we will present the first comparative measurements of the kinetics of mass transfer between the gas and condensed phases during particle growth or evaporation. The change in size of two droplets, one an inorganic control droplet and a second organic doped droplet, measured under the same environmental conditions at the same time, will be described (Knox et al., 2008). Measurements have been undertaken over a range of pressures, from atmospheric pressure down to 2 kPa, allowing the mass accommodation of water on aerosol particle surfaces to be probed directly through highly accurate measurements of evolving particle size during growth. In particular, we will consider the influence of surface active organic components on the mass accommodation coefficient of water adsorbing to an aqueous surface.

It is anticipated that such comparative measurements could provide invaluable information as we seek to resolve the difference between the thermodynamic and kinetic factors that regulate the size and composition of aerosol particles.

Mitchem, L. & Reid, J.P. (2008). Chem. Soc. Rev. 37 (2008), 756-769.

Hanford, K., Mitchem, L., Reid, J.P., Clegg, S.L., Topping, D.O., & McFiggans G.B. (2008), J. Phys. Chem. A. 112 (2008) 9413-9422.

Butler, J.R. , Mitchem, L., Hanford, K.L., Treuel, L. & Reid, J.P. (2008), Faraday Discussions 137 (2008), 351-366.

Knox, K.J. & Reid, J.P. (2008), J. Phys. Chem. A. 112 (2008) 10439-10441.

Comparison of Particle Number Concentrations between Different Environments

Lidia Morawska, Xuan Ling and Rohan Jayaratne

International Laboratory for Air Quality and Health,
Queensland University of Technology, GPO Box 2434, Brisbane, QLD 4001, Australia

Keywords: Air Quality, Atmospheric Aerosols, Particle Concentration, Vehicle Emissions

Particle number concentrations vary significantly with environment and, in this study, we attempt to assess the significance of these differences. Towards this aim, we reviewed 85 papers that have reported particle number concentrations levels at 126 sites covering different environments. We grouped the results into eight categories according to measurement location including: road tunnel, on-road, road-side, street canyon, urban, urban background, rural, and clean background. Median values were calculated for each category. This review was restricted to papers that presented concentrations numerically. The majority of the reports were based on either CPC or SMPS measurements, with a limited number of papers reporting results from both instruments at the same site. Hence there were several overlaps between the number of CPC and SMPS measuring sites. Most of the studies reported multiple measurements at a given study site, while some studies included results from more than one site. From these reports, the overall median value for each location category was calculated.

Overall, there were 4 road tunnel studies (with 1 site using the CPC and 4 using the SMPS), 7 on-road studies (with 14 sites using the CPC and 2 using SMPS), 20 road-side studies (with 5 sites using the CPC and 22 using the SMPS), 7 street canyon studies (with 1 site using the CPC and 7 using the SMPS), 28 urban studies (with 1 site using the CPC and 31 sites using the SMPS), 4 urban background studies (with 3 sites using the SMPS), 8 rural studies (with 2 sites using the CPC and 11 sites using the SMPS) and 5 clean background studies (with 9 sites using the SMPS). The corresponding median number concentrations for the eight site categories are shown in Figure 1.

The eight location categories may be classified into four distinct groups. The mean median particle number locations for these four types were found to be statistically different from each other and are shown by the horizontal lines in Figure 1. Rural and clean background sites had the lowest concentrations of about 3×10^3 cm^{-3}. Urban and urban background sites showed concentrations that were three times higher (9×10^3 cm^{-3}). The mean concentration for the street canyon, roadside and on-road measurement sites was 4.6×10^4 cm^{-3}, while the highest concentrations were observed in the road tunnels (8.6×10^4 cm^{-3}).
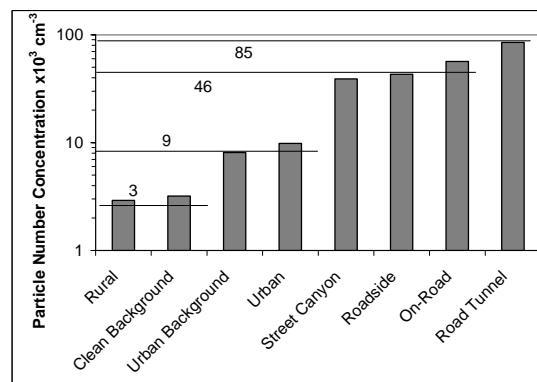
Figure 1: Median particle number concentrations at the eight classified location categories.

The median particle number concentrations measured at all sites by the CPC's and DMPS/SMPS's were 2.8×10^4 cm^{-3} and 2.1×10^4 cm^{-3}, respectively, indicating that the median CPC measurements were 32% greater than the DMPS/SMPS's measurements. The difference in the means was tested using a Students t-test and found to be statistically significant at a confidence level of over 99%. This result is in agreement with Morawska et al (2008) whose conclusion was based on a smaller number of studies.

What is the explanation for this? Random instrument error may be ruled out as the result was based on over 60 separate studies. However, it was noted that the lower particle size cut-off for the CPC was generally lower than for the SMPS. Thus, CPCs are likely to count nanoparticles smaller than 15 nm more effectively than SMPSs. Also, we expect the difference to be larger for environments where a nucleation mode is present and smaller where aged aerosols dominate. The comparison shows the overall magnitude of difference that can be expected when comparing results using these two different measuring techniques. Further, it is important to keep these differences in mind when attempting to establish quantitative understanding of variations in particle concentration for different environments, which is of significance for human exposure and epidemiological studies.

Morawska, L., Z. Ristovski, E.R. Jayaratne, D.U. Keogh and X. Ling. Ambient nano and ultrafine particles from motor vehicle emissions: characteristics, ambient processing and implications on human exposure. Atmos. Environ. 42, 8113-8138, 2008.

Influence of vehicular traffic on airborne particle surface composition in Zabrze, Poland

J.S. Pastuszka[1], E.Talik[2] and W. Rogula-Kozlowska[1,3]

[1]Department of Air Protection, Silesian University of Technology, 2 Akademicka St., 44-100, Gliwice, Poland
[2]Institute of Physics, University of Silesia, 4 Uniwersytecka St., 40-007 Katowice, Poland
[3]Institute of Environmental Engineering, Polish Academy of Sciences, Zabrze, Poland

Keywords: traffic, PM2.5, PM10, XPS.

Although the toxicity of airborne particles is still not clearly understood, it should be noted that the chemical composition of the surface of particles play also the important role in determining health effects, because the surface is directly accessible to biological fluids after inhalation.

In this work the results of the PM10 and PM2.5 study in Zabrze, Upper Silesia, Poland, near a very busy city street intersection and in a site representing urban background air are presented.

The samples were taken in pairs; a pair consisted of two samples of the same aerosol fraction (PM10 or PM2.5) taken simultaneously at the roadside site and at the background site.

Next, the surface elemental composition was determined for 5 selected pairs of parallel exposed PM10 filters and 4 pairs of parallel exposed PM2.5 filters, by applying the X-ray photoelectron spectroscopy (XPS) technique. The PHI 5700/660 Photoelectron Spectrometer (Physical Electronics, USA) with the monochromatic Al K_{α} source of X rays (1486 eV) was used.

Example of the XPS spectra for the roadside and background aerosol in Zabrze is shown in Fig. 1.
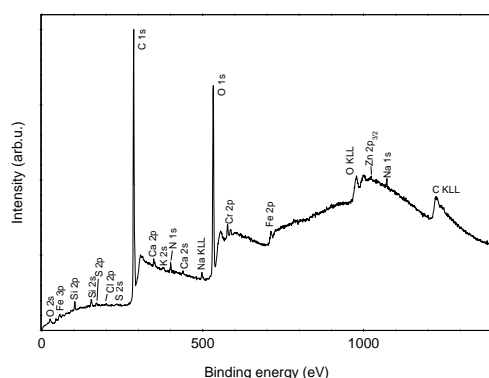
Figure 1. Example of the XPS spectrum for the PM2.5 sample from the crossroads site.

Before the detailed analysis of these data it should be noted that XPS yields information on the particle surface rather than the average composition of the whole particles. An important limitation is also the loss of volatile species under UHV conditions. As shown in Fig. 1, the spectra indicate strong peaks of carbon and oxygen what seems to be the typical picture for the urban aerosol. The relative content of the elements determined from the XPS analysis is presented in Table 1. It can be seen that the surface layer of PM2.5 from the roadside contains significantly more carbon and less oxygen than the airborne particles collected at the background site what might be explained by the high emission of carbon, mainly soot, from vehicles.

Table 1. Surface elemental composition of PM2.5 collected near the crossroads and the background site (Monthly means of selected elements for August).

Element	Concentration in (%)	
	Crossroads	Background
C	82.53	74.59
N	1.290	2.270
O	12.41	20.78
Na	0.215	0.215
Si	1.045	1.760
S	0.275	0.135
Cl	0.390	0.100
Pb	0.020	0.005
Ca	0.265	0.090

Generally, this analysis showed that the main components of the surface layer of all studied airborne particles were carbon, nitrogen and oxygen. Besides, the typical surface layer is composed of sodium, potassium, silicon, magnesium and aluminum. In some samples also zinc and calcium occurred. It has been documented that the surface layer of the airborne particles near the crossroads contained more carbon and less oxygen comparing with particles from the background site.

Physical, chemical and hygroscopic properties of activating particles in Northern Finland

N. Kivekäs[1], V.-M. Kerminen[1], T. Raatikainen[1], P. Vaattovaara[2], A.Laaksonen[1,2] and H. Lihavainen[1]

[1] Finnish Meteorological Institute, PO Box 503, FI-00101 Helsinki, Finland
[2] Department of Applied Physics, University of Kuopio, P.O. Box 1627, FIN-70211 Kuopio, Finland

Keywords: Aerosol chemistry, Aerosol size distribution, Hygroscopic growth, Cloud microphysics

Particle and cloud droplet properties were studied in at the Pallas GAW station in northern Finland from September 16th to October 6th 2005. The station is located on the top of a hill, and was inside cloud for 25% of the measurement period. This allowed us to measure the cloud activation in situ. (Kivekäs *et al.*, 2009)

The dry particle size distribution was measured with two DMPS:s, one measuring the total particle population including the cloud droplets, the other measuring only the non-activated particles. The chemical composition and mass concentration of the particles was measured with an AMS, the measured components being SO_4, NO_3, NH_4 and organics. Particle hygroscopicity was measured with HTDMA from particles having dry diameter of 30, 50, 80, 100 and 150 nm. Cloud droplet number concentration and size distribution were measured with FSSP. Besides these, the meteorological parameters were measured at the site, and air mass back trajectories were calculated for the measurement period. The air masses were classified into three groups according to their arriving path, the groups being clean marine, polluted European and mixed air mass.

The FSSP was running only for a two days during the measurement period. Therefore the main source of information for the number concentration of activated particles was the calculated activated fraction from the difference between the two DMPSs (Komppula et al., 2005). A thorough activation analysis was made only for particles with dry diameter > 100 nm. This was done because the method is vulnerable to differences in the counting efficiency of the DMPS:s, and the activation of smaller particles was found to be within the error. The calculated number concentration of activated particles was compared to the measured one for the time period when the FSSP was running, and a good agreement was found.

The aerosol mass concentration (m_{tot}), as well as number concentration of particles with diameter 100 nm or larger (N_{acc}) depended on the air mass type. European air masses contained the highest amount particulate matter and marine air masses the lowest. The inorganic fraction of m_{tot} (IO) depended on the air mass type as well, being highest in the European and lowest in the marine air masses. The hygroscopic growth factor (GF) depended on solubility, as expected, and had therefore correlation with the air mass as well. Because of the N_{acc}, IO and GF all correlated positively with each other, it was difficult to separate the effects of these three in the cloud droplet activation.

For activation analysis the data was divided in three categories according to visibility at the measurement site. These categories were cloud (visibility < 200 m), unclear (visibility 200 – 3000 m) and no cloud (visibility > 3000 m). In category cloud the activated fraction of N_{acc} (Act_{100}) was on average 65%. The value of Act_{100} in category cloud decreased slightly with increasing Nacc, and did not show any systematic dependency on IO. However, there was a clear difference in the N_{acc} vs IO dependency between the categories cloud and no cloud, as can be seen in figure 1.
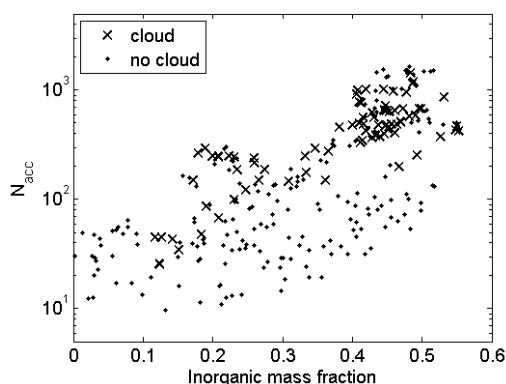
Figure 1. Number concentration of accumulatiun mode particles for cloud and no cloud cases as function of inorganic mass fraction of the particles.

In conclusion we say that the effects of particle number or mass concentration and chemical composition at Pallas are difficult to separate, as the parameters are highly correlated. The air masses arriving to the site are highly different, but cloud activation was observed in all air mass types, meaning that activation happens in very different aerosol conditions.

References:
Kivekäs N., Kerminen V.-M., Raatikainen T., Vaattovaara P. & Lihavainen H. (2009) *Boreal Env. Res*. (submitted)
Komppula M., Lihavainen H. & Kerminen V.-M. (2005) *J. Geophys. Res.*, 110(D0), 6204, doi:10.1029/2004JD005200.

Description of the mesoscale atmospheric aerosol: observation and model

C. Engler[1], W. Birmili[1], R. Wolke[1] and A. Wiedensohler[1]

[1]Leibniz-Institute for Tropospheric Research, Permoserstraße 15, 04318 Leipzig, Germany

Because of the proven connection between fine particle number concentration and human health effects (e.g. Pope *et al.*, 2002), there is a high necessity to quantify the distinct contributions of urban aerosol particle number concentrations. For this purpose, atmospheric chemistry transport models (CTM) are suitable, but the level of accuracy is unclear. Thus, a systematic model validation with experimentally determined data is needed.

Atmospheric particle measurements were carried out between September 2006 and July 2007 at seven observation sites in Saxony, Germany (two street, two urban background, two rural background and one mountain station). The measurements include particle number size distributions (3 to 800 nm), PM_{10} mass, PM_{10} chemical composition (every fourth day, 24 hours sampling duration), trace gas concentrations and meteorological parameters.

The modeling system COSMO-MUSCAT is a coupling between the meteorological forecast model COSMO of the German Weather Service (DWD) and the chemistry transport model (CTM) MUSCAT (Wolke *et al.*, 2004). To describe the gas phase chemical and aerosol dynamic processes, MUSCAT consists of a chemistry, an aerosol, and a complex emission module. For comparing the number size distributions with the observed ones, the size-resolved aerosol module M7 (Vignati *et al.*, 2004) will be used in the model.

The level of urban PM_{10} mass has been described as a superposition of three contributions: rural background, urban background and traffic increment (Lenschow *et al.*, 2001). Depending on the location (type) of the observation site, one, two or all fractions contribute to the local concentration. In this work, the urban increment has been estimated for the PM_{10} mass as well as for the particle number concentration for each measured size bin (3 to 800 nm) using the experimentally determined particle number size distributions. The daily variation of the PM_{10} and the particle number concentration urban increment is shown in Fig. 1 for the two German cities Leipzig and Dresden. For both PM_{10} mass and size resolved particle number, the values were higher in Dresden than in Leipzig. Possible reasons for this finding could be the different location of the stations in each city (city center and suburbs, respectively) or the special orographic situation of Dresden in the Elbe-valley.
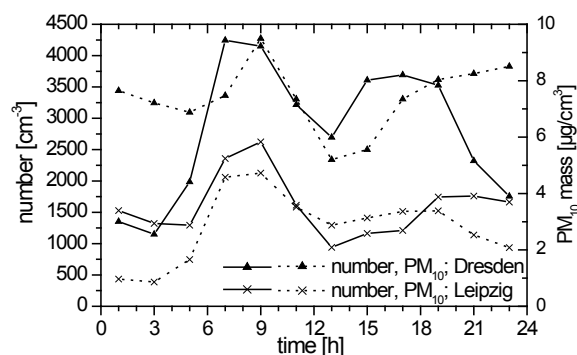
Figure 1. Daily variation of the urban increment concentration (urban – rural background) of the total particle number (3-800 nm) for two German cities.

In a first episode of ten days, several meteorological parameters, trace gas concentrations, PM_{10} mass and the chemical composition of PM_{10} have been compared for all observation sites. The simulation of the meteorology was as comparable to the observations as expected. The comparison of the trace gas concentrations and aerosol parameters showed partly difficulties of the model to simulate the real conditions correctly. For some parameters, only the mean values or the trends, for others only individual days were predicted correctly. Reasons for this are manifold and will be investigated in the future.

Lenschow, P., Abraham, H.-J., Kutzner, K., Lutz, M., Preuß, J.D. & Reichenbacher, W. (2001). *Atmospheric Environment*, 35 (1), 23-33.

Pope III, C.A., Burnett, R.T., Thun, M.J., Calle, E.E., Krewski, D., Ito, K. & Thurnston, G.D.. (2002). *American Medical Association*, 287, 1132-1140.

Vignati, E., Wilson, J. & Stier, P. (2004). *Journal of Geophysical Research*, 109, doi: 10.1029/2003JD004485.

Wolke, R., Knoth, O., Hellmuth, O., Schröder, W. & Renner, E. (2004). in *Parallel Computing: Software Technology, Algorithms, Architectures and Applications.* (Elsevier; Amsterdam), 367-370.

SIZE DISTRIBUTION OF CARBONACEOUS COMPOUNDS AND INORGANIC ION CONCENTRATIONS IN BACKGROUND AEROSOL, HUNGARY

Diána Benkő[1], Ágnes Molnár[2], Kornélia Imre[1], Gyula Kiss[2], András Hoffer[2]

[1]University of Pannonia, Dept. Earth and Environmental Sciences, P. O. Box 158, H-8201 Veszprém, Hungary
[2]Air Chemistry Group of Hungarian Academy of Sciences, P. O. Box 158, H-8201 Veszprém, Hungary

Keywords: fine aerosol, size distribution, organic carbon, inorganics, seasonal patterns

The role of aerosol particles in visibility regulation is of great importance. It is well known that these processes depend on the size and on the chemical composition of the particles. Beside inorganic constituents, carbon containing species give the most important fraction of atmospheric aerosol in the fine particle size range. The results obtained during the last decade show that significant part of these species is water soluble. Recently the effect of organic material on aerosol activation is in the focus of considerable attention (Varga et al, 2007). Since the above mentioned processes are controlled mainly by the fine particles, in this work the size distributions of inorganic ions and carbonaceous (total carbon, water soluble carbon) compounds are presented for the fine mode aerosol. On the other hand, the seasonal variation of these components is discussed.

The aerosol sampling was performed at the Hungarian background air-pollution monitoring station at K-puszta. The samples were collected on weekly basis in 2008, from January to October. Sampling was carried out by an electrical low pressure impactor (ELPI). The air was sampled at a height of 10m above the surface, under ambient temperature and humidity conditions. The lower cut-off diameters of stages were 0.03, 0.06, 0.11, 0.18, 0.27, 0.42, 0.68, 1.05, 1.70μm. The aerosol samples of different size ranges were chemically analyzed. Measurement of total carbon (TC) was carried out by using an Astro Model 2100 TOC solid-analyzer (Temesi et al., 2003). The concentrations of inorganic ions were determined by ion chromatography (Imre and Molnár, 2008).

The results show that in the fine size range sulfate (except in summer), nitrate and TC were characterized by bimodal size distributions. The highest concentrations were found in the droplet mode, while a second peak was obtained in the condensation mode. These two modes indicate that– in the majority of cases – at K-puszta aged aerosol can be measured. However, in summer, in the size distribution of sulfate three modes could be distinguished. The third peak appeared below 0.1μm, showing the evidence of new particle formation.

In the size distributions of the compounds important seasonality could be observed. The lowest nitrate concentration was found in summer, due likely to the volatility of NH_4NO_3. Nitrate/sulfate ratio may indicate the importance of nitrate compared to sulfate ions. The seasonal changes in the nitrate concentration are clearly shown by this ratio. In winter the nitrate/sulfate ratio is high around 1. On the other hand in spring and summer this ratio generally decreased and showed slight size dependence. Seasonal variation of sulfate concentration was not found very important. Total carbon (TC) content of the fine particles was found to be important in all seasons. Similar to nitrate, TC concentration was significantly higher in winter than in spring or summer. To compare the possible role of sulfate and organic particles in different size ranges, the values of carbon/sulfate ratio were also calculated.

Imre, K., Molnár, A. (2008): Hygroscopic behavior of Central European atmospheric background aerosol particles in summer. Időjárás **112**, 63-82.

Temesi, D., Molnár, A., Mészáros, E., Feczkó, T. (2003): Seasonal and diurnal variation in the size distribution of fine carbonaceous particles over rural Hungary. Atmospheric Environment **37**, 139–146.

Varga, Z., Kiss, G., Hansson, H.C. (2007): Modelling the cloud condensation nucleus activity of organic acids on the basis of surface tension and osmolality measurements. Atmospheric Chemistry and Physics **7**, 4601-4611.

Air pollution by particulate matter in various heights, the example of Beijing

Klaus Schäfer[1], Stefan Emeis[1], Peter Suppan[1], Stefan Norra[2], Nina Schleicher[2], Joachim Vogt[3], Volker Dietze[4], Uwe Kaminski[4], Yuesi Wang[5], Jinyuan Xin[5], Fahe Chai[6], Yizhen Chen[6]

[1]Institute of Meteorology and Climate Research, Atmospheric Environmental Research Division (IMK-FU), Forschungszentrum Karlsruhe, Kreuzeckbahnstr. 19, 82467 Garmisch-Partenkirchen, Germany
[2]Institute of Mineralogy and Geochemistry (IMG), Universität Karlsruhe, Karlsruhe, Germany
[3]Institute of Regional Science (IRS), Universität Karlsruhe, Karlsruhe Germany
[4]Competence Center Biometeorology, Air Pollution Department German Weather Service (DWD), Freiburg, Germany
[5]LAPC, Institute of Atmospheric Physics (IAP), Chinese Academy of Sciences (CAS), Beijing People's Republic of China
[6]Laboratory for Urban and Regional Atmospheric Environmental Research, Chinese Research Academy of Environmental Sciences, Beijing, People's Republic of China

Keywords: air quality, air pollution, mixing layer height, emissions, transport

Beijing is one of the Megacities showing the worst air quality conditions on the globe and additionally facing seasonal dust storms. The IMG is currently carrying out a DFG research project on the spatial distribution of urban aerosol pollution in Beijing. On the basis of these experiences, a KIT start-up project was launched in 2008/2009 to characterize the vertical composition of the Beijing atmosphere with special respect to the occurrence of particles.

Beijing air quality suffers frequently occurring air pollution events. Local and regional wind systems are able to refresh the air masses or stabilize air pollution over Beijing. One main local wind systems can be suggested to occur in Beijing, which is a mountain-valley wind system. This is induced by the more than 2000m high mountain ridge of the north-western Yundu and Xishan Mountains. On the other hand, this mountain ridge acts as barrier for air masses coming from southern directions with low velocities. During those meteorological conditions, air pollution can accumulate in the region of Beijing. The objective of this campaign is to investigate the strengths of wind systems during different weather situations by direct measurements and to assess their potential impacts on Beijing's atmosphere and air pollution.

Two field visits are carried out in end of winter 2008/2009 and beginning of spring 2009 to analyse the vertical distribution of atmospheric particles by various methods. Coarse geogenic, biogenic and anthropogenic particles were sampled by passive sampling methods on adhesive acceptor plates in various heights. PM2.5 is sampled by active samplers. The collected coarse particles will be analysed by automated optical microscopy at the DWD for size fraction distribution between 2.5 and 80µm. Under supervision of IMG, shape and major elemental composition of coarse particles will be documented by means of scanning electron microscopy at the Laboratory for Electron Microscopy (LEM) of the Universität Karlsruhe. Mass concentration and elemental composition of PM2.5 will be analysed by IMG. Furthermore, a ceilometer is used to analyse the actual development of the height of inversion and boundary layers and the distribution of aerosols and particles. The vertical distribution of atmosphere layers is additionally investigated with a weather zeppelin measuring air temperature, relative humidity, wind velocity and direction in various heights up to 300 m AGL. Additionally, similar data is available from meteorological masts in Beijing and around.

It is suggested that the results of these two field visits will exemplarily highlight the vertical distribution of atmospheric layers in combination with particulate concentrations at selected sites and for specific times. However, it is essential for the future development of the quality of Beijing's atmosphere to intensify research for a comprehensive understanding of the air mass movements throughout the year.

Oxidative potential of a panel of Carbonaceous and Metallic Nanoparticles.

M. Sánchez Sandoval Hohl[1], J.J. Sauvain[1], K. Donaldson[2], and M. Riediker[1]

[1]Institute for Work and Health, Rue du Bugnon 21, 1011 Lausanne, Switzerland
[2]University of Edinburgh Centre for Inflammation Research, 47 Little France Crescent Edinburgh, EH16 4TJ

Characterisation of nanoparticles (NP) based on size distribution, surface area, reactivity, and aggregation status of nanoparticles (NP) are of prime importance because they are usually closely related to toxicity. To date, most of the toxicity studies are quite time and money consuming.

In the present study we report the oxidative properties of a panel of various NP (four Carbonaceous, nine Metal oxides, and one Metal as showed in Table 1) assessed with an acellular reactivity test measuring dithiothreitol (DTT) consumption (Sauvain *et al.* 2008). Such a test allows determining the ability of NP to catalyse the transfer of electrons from DTT to oxygen. DTT is used as a reductant species.

NP were diluted and sonicated in Tween 80® to a final concentration of 50 μg/mL. *Printex 90* was diluted 5 times before doing the DTT assay because of its expected higher activity. Suspensions were characterised for NP size distribution by Nanoparticle Tracking Analysis (Nanosight©). Fresh solutions were incubated with DTT (100 μM). Aliquots were taken every 5 min and the remaining DTT was determined by reacting it with DTNB. The reaction rate was determined for NP suspensions and blank in parallel.

The mean Brownian size distribution of NP agglomerates in suspension is presented in Table 1. D values correspond to 10th, and 50th percentiles of the particle diameters. All the NP agglomerated in Tween 80 with a D50 size corresponding to at least twice their primary size, except for *Al₂O₃ (300 nm).*

The DTT test showed *Printex 90* sample to be the most reactive one, followed by *Diesel EPA* and *Nanotubes*. Most of the metallic NP was non-responding toward this test, except for *NiO* and *Ag* which reacted positively and *ZnO* which presented the most negative reactivity (see Figure 1). This last observation suggests that electron transfer between DTT and oxygen is hindered in presence of *ZnO* compared with the blank. Such "stabilization" could be attributable to *ZnO* dissolution and complexation between Zn2+ ions and DTT.

Sauvain JJ, Deslarzes S, & Riediker M. (2008). *Nanotoxicology* 2: 121-129.

Table 1. Size distribution means of NP suspensions (in Tween 80®)

NANOSAR short name	NP/Tween [μg.ml⁻¹]	Primary size [nm]	D10 [nm]	D50 [nm]
Carbonaceous				
Printex 90	1.00	14	117±13	214±22
Diesel EPA	0.10		148±3	221±8
Nanotubes	0.75		211±19	294±22
Fullerene	5.00		70±7	125±3
Metal oxides				
Al₂O₃ (7 nm)	0.05	7	36±1	59±6
Al₂O₃ (50 nm)	5.00	50	38±1	106±8
Al₂O₃ (300 nm)	0.05	300	115±3	179±10
CeO₂	5.00	20-30	28±3	115±9
NiO	5.00	10-20	50±4	113±7
SiO₂	5.00	10	15±2	51±6
ZnO	1.00	20	53±8	119±12
TiO₂ (anatase)	2.00	5	9±1	30±5
TiO₂ (rutile)	2.00	30-40	24±5	57±17
Metal				
Ag	5.00		13±4	58±21
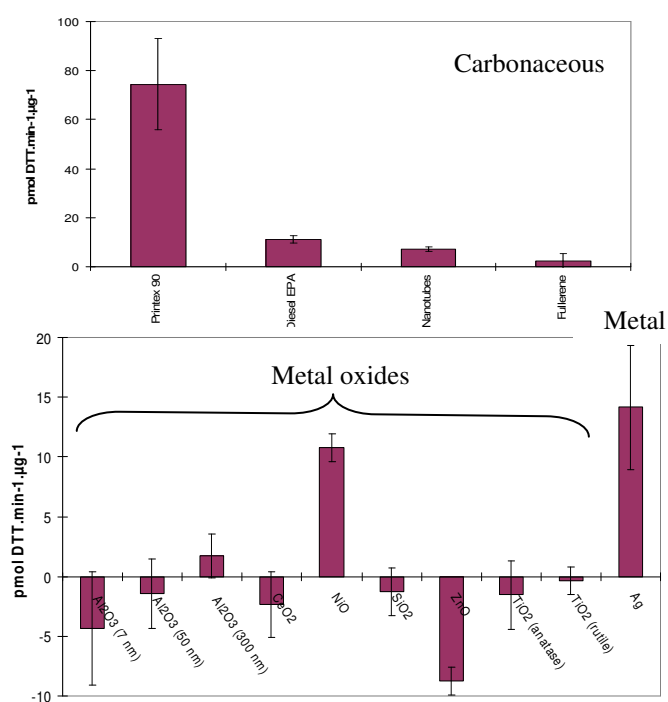
Figure 1. DTT consumption of different NP suspensions in Tween 80.

Source apportionment studies for trace elements based on hourly size-segregated data

A. Richard[1], M. Furger[1], N. Bukowiecki[2], P. Lienemann [2], M. Nachtegaal[1], A. Prevot[1] and U. Baltensperger [1]

[1]Paul Scherrer Institut, Labor für Atmosphärenchemie, CH-5232 Villigen PSI, Switzerland
[2]Empa, Swiss Federal Laboratories for Materials Testing and Research, Ueberlandstrasse 129, CH-860 Dübendorf, Switzerland

Keywords: trace elements, impactor, XRF, source apportionment

Trace element concentrations in ambient aerosol were measured at different sites in Switzerland as well as in the Mediterranean area with the objective to conduct source apportionment studies.

Sampling was performed in three different size ranges (0.1-1 µm, 1-2.5 µm and 2.5-10 µm) with a rotating drum impactor onto thin mylar or polypropylene foils. These samples were subsequently analyzed with synchrotron radiation X-ray fluorescence spectroscopy (SR-XRF). This allows for the detection of such low mass concentrations of elements (a few ng/m^3) without further sample treatment. For SR-XRF the sampling time can be significantly reduced compared to wet-chemical and conventional filter analysis and the investigation of diurnal variations becomes feasible. Samples were analyzed with XRF at different synchrotron beam lines (PSI-SLS superXAS beamline, Hasylab, beamline L and ALS, Berkeley, beamline 10.3.1) at different incident energies ranging from 11.5 – 60 keV. With the analysis at lower excitation energies the range of elements from Al – Zn could be detected while at higher energies elements up to Ba were detectable.

Although trace elements do not appear in high concentrations they can provide indications about the origin of different kinds of air pollution (e.g. traffic, wood burning, mineral dust etc). Specific groups of elements with similar temporal behaviour lead to assumptions on source compositions. Without a-priori knowledge about the sources positive matrix factorisation (PMF) was employed to mimic their contribution as well as their time evolution. The PMF2 program uses a stable algorithm to estimate source strengths and profiles from multivariate data sets (bilinear receptor-model).

For 0.1-1 µm particles one typical factor is wood burning showing contributions of sulphur, potassium, calcium and zinc (Figure 1). Furthermore there is also a fraction related to soil and terrestrial elements, and a single peak of sulphur presumably representing secondary sulphate. Another factor leads to the assumption of a vehicle/traffic related exhaust/abrasion source. For 2.5-10 µm particles on the other hand one main factor consists of calcium, silicon and iron, obviously components of mineral dust. A second factor is attributed to mechanical abrasion, and in winter time chlorine from de-icing salt could be identified. Different measurement sites and different seasons show however varying strengths of emission sources.

The final goal is to combine for the first time the SR-XRF data set with aerosol mass spectrometer (AMS) data, providing information on the composition of the particles over an extended range of elements and chemical compounds, including organics. Results will be interpreted in the context of meteorological parameters and will finally help in formulating mitigation strategies against air pollution.

Bukowiecki, N. et al. (2005) *Environ. Sci. Technol.*, 39, 5754-5762.
Bukowiecki, N. et al., (2008) *Spectrochim. Acta,* B 63, 929-938.
Paatero, P. (2007): *User's guide for positive matrix factorization programs PMF2 and PMF3, part 1: tutorial*, University of Helsinki, Finland

Fig. 1. Factor profile of 0.1-1 µm fraction

Crystallization of micro droplets observed with Raman spectroscopy

Christiane Wender[1,2], Rene Müller[3] and Thomas Leisner[1,2]

1Forschungszentrum Karlsruhe, Institute of Meteorology and Climate Research,
Atmospheric Aerosol Research Department, POB 3640, 76021 Karlsruhe, Germany
2University of Heidelberg, Institute of Environmental Physics,
Im Neuenheimer Feld 229, 69120 Heidelberg, Germany
3TU Ilmenau, Institute of Physics, POB 100565, 98684 Ilmenau, Germany

Keywords: Cloud microphysics, Crystallization, Droplets, Levitation, Raman microscopy

Phase transitions between the liquid and the solid state play an important role in atmospheric processes. Freezing of droplets is a very important mechanism for cirrus cloud formation and precipitation. But it is suggested that other process next to freezing like glass transition can occur. (Zobrist *et al*. 2002) Gao (Gao *et al* 2006) found during contrail studies in the upper troposphere relative humidity around 130% but droplet formation was inhibited. One possible explanation for this high RH can be glassy particles. Glass transition at atmospheric conditions occurs easily with organic compounds. Due to their high viscosity the inner diffusion is so slow that water uptake is nearly inhibited. (Angell, 2002) (Murray, 2008) To understand the process of glass transition in the atmosphere helps to understand also the nucleation and growth of ice, chemical reactions and the uptake of water from aerosols.

In our experiment we apply Raman spectroscopy to probe phase transitions of micro particles under simulated atmospheric conditions.

We use an electrodynamic balance to trap single droplets for further processing. This trap consists of a ring and two cap electrodes which hyperboloidal geometry provides a field where charged particle can be levitated. Due to non-contacting storage also particles in metastable states (supercooling, supersaturation) can be handled without unrequested effect of surfaces

The trap is mounted into a climate chamber to realize electrical and thermal insulation. With this setup temperatures up to -80°C can be obtained. In principle the experiments are temperature jump experiments. But also slow temperature ramps are possible. The droplet generation is realized with a piezo injector. It is possible to vary the size of the initial droplet between 40µm and 90µm.

We use CCD camera to observe the trapped particle and get information about size and state. The chemical composition of the probe is determined by Raman spectroscopy to monitor chemical aspects at the phase transitions. In our setup the spectrometer is combined with a microscope that we can use confocal Raman spectroscopy which allows to probe with high spatial resolution. The two wavelength of 786nm and 532nm provide the possibility to access a wide range of probes.

In this work we present first results of freezing behavior of citric acid solution droplets.

C. A. Angell (2002), *Chem. Rev*., 102, 2627650

B. Zobrist, C. Marcolli, D. A. Pedernera, and T. Koop (2008), *Atmos. Chem. Phys*., 8, 5221–5244

B. J. Murray, *Atmos. Chem. Phys*. (2008), 8, 5423–5433

R.S. Gao, D.W. Fahey,_, P.J. Popp, T.P. Marcy, R.L. Herman, E.M. Weinstock, J.B. Smith, D.S. Sayres, J.V. Pittman, K.H. Rosenlof, T.L. Thompsona, P.T. Bui, D.G. Baumgardner, B.E. Anderson, G. Kok, A.J. Weinheimer (2006), *Atmospheric Environment* 40 1590–1600

Chemical and morphological characterization of dustfall (dry deposition) in Vitória-ES Brazil

M. M. Conti[1]; L. R. Menegussi[1]; N. C. Reis Jr[1]; J. M. Santos[1]; F. J. Silva[2] and C. Scandian[2]

[1]Departamento de Engenharia Ambiental, Universidade Federal do Espirito Santo, 29.060-910, Vitoria, Brazil
[2]Departamento de Engenharia Mecânica, Universidade Federal do Espirito Santo, 29.060-910, Vitoria, Brazil

Keywords: chemical analysis, deposition; Particle characterization; dustfall particles.

The interest for fine and ultra-fine particles is mainly related to the hazard to human health, due to deep penetration in the respiratory system. However, larger particles (> 10 µm) are also a matter of concern, since dustfall is a considerable source of nuisance for urban population (Vallack & Shillito, 1998; Farfel et al, 2005). In spite of its importance, there are very few source apportionment studies targeting dustfall particles.

In this work, dustfall samples were collected in 10 monitoring points in the Metropolitan Region of Vitória, in the State of Espírito Santo, Brazil (Figure 1). These locations were chosen based on the results of an atmospheric dispersion model. Settled particles samples were collected periodically starting from January 2008, by using an ASTM D 1739 dustfall collectors and 10 x 10 cm flat plates covered with an adhesive tape.
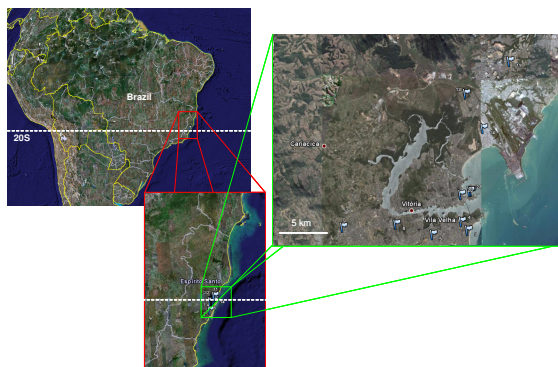
Figure 1. Schematic representation of the Metropolitan Region of Vitória and the location of the 10 monitoring points.

The particulate matter samples were analyzed by using SEM/EDS (Scanning Electron Microscope/Energy Dispersive Spectroscopy). In order to prevent imaging artifacts or other scanning faults, due to electrostatic charging, the samples were coated with a thin Pt-Au layer.

Figure 2 is an example of the images obtained during this study, where a wide distribution of particle size can be observed. The majority of the particles collected range from 5 to 100 µm, but some particles smaller than 5 µm were also collected. In general smaller particles appear agglomerated in the collected samples. This fact can be observed in Figure 3, where a SEM image of a sample is displayed together with an EDS characterization of 6 individual particles.
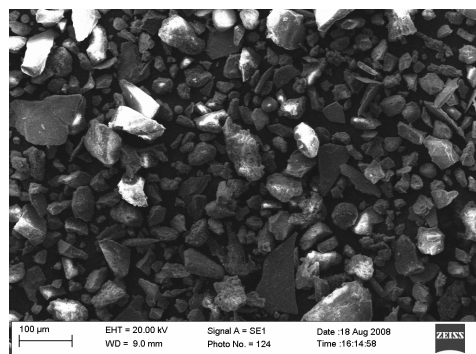
Figure 2. SEM image of a settled particle sample.

The composition of the settled particles can be traced to the main industrial sources and natural sources of the region, such as iron ore, soil, coal and marine aerosol. In is possible to note, in Figure 3, the morphological differences between particles from different sources, where particles labeled 1 and 5 were characterized as coal; particles 2, 4 and 6 were characterized as iron ore and 3 as soil.
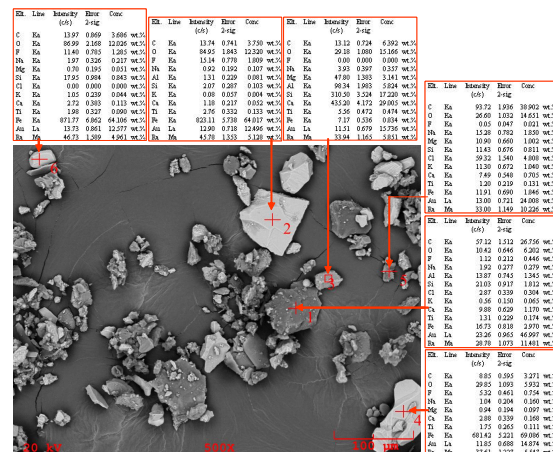
Figure 3. SEM image of a sample and a quantitative analysis of EDS spectra for 6 individual particles.

Farfel, M. R. et al. (2005) *Environmental Research*, Volume 99, Issue 2, 204-213.
Vallack, H. W., Shillito, D. E. (1998) *Atmospheric Environment*, Volume 32, Issue 16, 2737-2744.

Chemical and physical properties of oxalic acid and oxalate aerosol particles

A. A. Mensah[1], A. Buchholz[1], A. Kiendler-Scharr[1], Th. F. Mentel[1]

[1]Institut für Chemie und Dynamik der Geosphäre, ICG-2, Forschungszentrum Jülich, Germany

Keywords: AMS, Hygroscopic growth, H-TDMA, Oxalic acid.

We present aerosol mass spectrometric and hygroscopic growth measurements of oxalic acid and some of its derivates. A Hygroscopic Tandem Differential Mobility Analyzer (HTDMA) and two Aerodyne Aerosol Mass Spectrometers (AMS, (Jayne, J. T. *et al.*, 2000)) were used to investigate physical and chemical properties of oxalic acid (OxAc, $H_2C_2O_4 \times 2 H_2O$), ammonium oxalate (AmOx, $(NH_4)_2C_2O_4 \times 1 H_2O$), potassium oxalate (KOx, $K_2C_2O_4 \times 1 H_2O$), and sodium oxalate (NaOx, $Na_2C_2O_4$). The chemical composition, especially the crystal water content was determined by use of the two AMSs. Hygroscopic growth properties in the range of 0% to 95% relative humidity (RH) were determined by an HTDMA.

Aqueous solutions of the oxalates were atomized, dried, and size selected prior to the measurements. MilliQ-water with a total organic carbon content below 10 ppb and a resistance of 18.2 MΩ was used to prepare the solutions. The salts were of purity grade puriss. (>99%, Sigma Aldrich). Aerosol particles were generated in an atomizer (TSI 3076) with filtered (< 1 #/cm^3) and dried ($< 0.2\%$ RH) synthetic air. The aerosol stream was dried with a silica gel and a nafion drier to below 1% RH. Aerosol particles were size selected by a DMA (TSI 3071) operated at a RH below 1%.

Two experimental setups were used. First, size selected particles were directly introduced into the AMS and the Scanning Mobility Particle Sizer (SMPS) of the HTDMA. The complete aerosol path was held below 1% RH. Second, dry size selected particles were humidified at different RH in a nafion humidifier before introduction into the AMS and SMPS. The sheath air of the SMPS was kept at the same RH as the humidifier.

The chemical composition of all four oxalates was determined by a Quadrupole-AMS (Q-AMS) and a High-Resolution Time of Flight AMS (HR-ToF AMS). Basic analysis of the oxalates with the Q-AMS showed expected composition and water content except for oxalic acid. High resolution analysis of oxalic acid revealed a significant fraction of the cat ions to be ammonium instead of hydrogen. Additionally, and in agreement with the interpretation of substantial ammonium uptake, the measured crystal water content of oxalic acid was substantially lower then theoretically expected.

A series of experiments of oxalic acid was performed to investigate the absorption of ammonium. Only oxalic acid salt taken directly from a sealed container was free of ammonium. If atmospheric air was allowed to enter the container, oxalic acid had an ammonium content of 10% and higher within less then 1 day. This means, special care (protective gas) is essential for the storage of oxalic acid solid or in aqueous solution to ensure the purity of oxalic acid.

The deliquescence and the efflorescence branch of the growth curve of all four substances were measured and deliquescence (DRH) and efflorescence points (ERH) were determined with the HTDMA (Table 1). KOx and NaOx show normal behavior of slightly soluble inorganic salts. In contrast, OxAc and AmOx exhibited some irregularities at the theoretical points of efflorescence (Figure 1). The particles grew instead of shrank with decreasing RH. This behavior can be explained by the formation of crystal hydrates. Additionally, Oxalic acid particles did not deliquesce at a specific RH but grew continuously.

Table 1. Measured deliquescence (DRH) and efflorescence points (ERH) of the investigated salts.

	DRH (%)	ERH (%)
KOx	84.8±1.0	50.5±1.0
NaOx	92.2±1.4	83.3±1.0
AmOx	93.3±1.4	irregular
OxAc	continuous growth	irregular
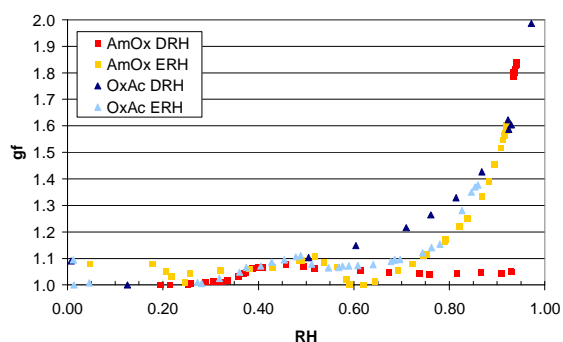
Figure 1. hygroscopic growth curves for AmOx (squares) and OxAc (triangles). (Error bars are smaller than symbols (ΔRH = ±1.0, Δgf = 0.005)

Jayne, J. T., D. C. Leard, *et al.*, (2000). *Aerosol Science and Technology*, 33, 49-70.

Efflorescence, deliquescence and crystal structures of ternary aerosols

L. Treuel, S. Pederzani and R. Zellner,

University of Duisburg-Essen, 45141 Essen, Germany

Keywords: Ammonium Sulfate, Dicarboxylic acids, Deliquescence, Raman Microscopy, Electron Microscopy.

Atmospheric aerosols have a significant influence on human health, chemical component deposition, cloud albedo, cloud condensation (CCN) and atmospheric turbidity. An extremely important property of such aerosols is their response towards changes in the relative humidities. Not only do the changes impact on the water content of the aerosol, they also modify their size and hence their surface area and scattering behaviour.

The work presented here combines experimental and theoretical studies of the thermodynamics of atmospherically relevant aerosols. The phase behaviour of ammonium salts and their ternary mixtures with water and a range of selected dicarboxylic acids have been experimentally investigated and the results have been modelled with current state of the art thermodynamic aerosol models (Clegg and Seinfeld, 2006 a,b). A new surface aerosol microscope (SAM) setup was developed as a robust and reliable research tool.

The influence of the dicarboxylic acid concentration on the deliquescence relative humidity (DRH) has been studied for a multitude of dicarboxylic acids. Moreover, the temperature dependence of the deliquescence was studied in electrodynamic balance (EDB) (Treuel et al., 2008) and SAM experiments. Figure 1 (Treuel et al., 2008) shows a typical example of a single aerosol particle before, during and after the deliquescence in these experiments.
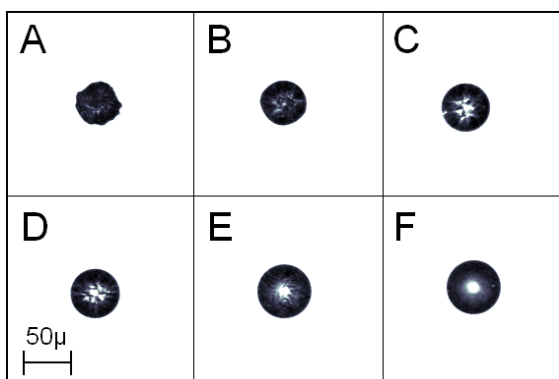
Figure1. Series of micro-photographs taken before (A), during (B-E) and after (F) the deliquescence of a pure ammonium sulphate particle.

Furthermore, the influence of hydrophilic and hydrophobic insoluble substances on the efflorescence and subsequent deliquescence was investigated and atmospheric implications of these findings are discussed.

In addition to the measurements on the dependence of the DRH on temperature and concentration, the crystal structures resulting from the efflorescence of highly supersaturated binary and ternary aerosols have also been determined for the first time using Raman Scanning Microscopy and Environmental Scanning Electron Microscopy (ESEM).
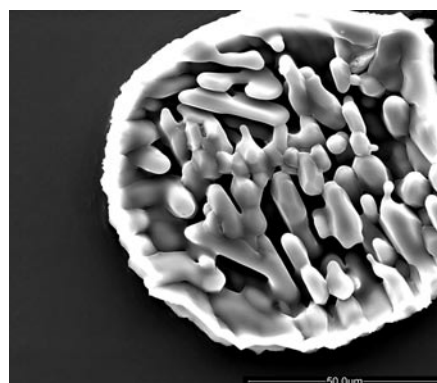
Figure 2. ESEM micrograph of a single, effloresced ammonium sulphate aerosol particle (Treuel, 2009).

The results from these studies elucidate the crystal structures and the spatial distribution of crystals formed during the efflorescence process of complex ternary mixtures.

This leads to an enhanced understanding of the thermodynamics governing the deliquescence process and sheds some light on the special dependences and the kinetics of crystallisation in complex solutions.

Clegg, SL and Seinfeld, JH (2006a)
    J. Phys. Chem. A 110, 5692-5717.
Clegg, SL and Seinfeld, JH (2006b)
    J. Phys. Chem. A 110, 5718-5734.
Treuel, L, Schulze, S, Leisner, T, Zellner, R (2008).
    Faraday Discuss. 137, 265 – 278.
Treuel, L (2009), *"On the Phase Behaviour of Binary and Ternary Aerosols"*, Verlag Mensch&Buch, Berlin, *in press.*

Aerosol cloud interaction in northern Finland

H. Lihavainen[1] and L. Remer[2]

[1]Finnish Meteorological Institute, P.O.Box 503, FIN-00101, Finland
[2]NASA Goddard Space Flight Center, Greenbelt, MD 20771, Finland

Clouds constitute perhaps the largest source of uncertainty in predicting the behavior of the Earth's climate system (IPCC, 2007; Baker and Peter, 2008). Many of the climatically important cloud properties, including the reflectivity, lifetime and precipitation patterns of clouds, depend strongly on atmospheric aerosol particles. While aerosols may have multiple effects on clouds, the fundamental role of aerosol particles acting as cloud condensation nuclei and thus directly affecting cloud microphysical particles and cloud optical properties are known as aerosol indirect effects. Narrowing uncertainties in representations of the indirect effect and developing well-constrained parameterizations for models must proceed through diligent analysis of aerosol-cloud interactions from all available platforms (McComiskey and Feingold, 2008).

Data analysed here are based on in-situ measurements at the Pallas Global Atmosphere Watch station. The basic equation behind the analyses is

$$ACI = \frac{d \ln \tau_d}{d \ln \alpha}\bigg|_{LWP} = -\frac{d \ln r_e}{d \ln \alpha}\bigg|_{LWP} = \frac{1}{3}\frac{d \ln N_d}{d \ln \alpha}, \qquad (1)$$

where N_d is number concentration of cloud droplets, LWP means liquid water path, and α in some proxy for the aerosol burden, such as the aerosol optical depth, number concentration of aerosol particles or aerosol light scattering coefficient.

Several different measurement schemes, cases, are compared with the aid of equation (1); 1. in-situ measurements of number concentration of aerosols and cloud droplets, 2. in- situ measurements of aerosol number concentrations and cloud microphysical properties from remote sensing data (MODIS Terra and Aqua) and 3. aerosol and cloud properties from remote sensing data (MODIS Terra and Aqua).

The results are summarized in figure 1. The ACI values for data sets 1 and 2 described above have been calculated by taking the sum over a number size distribution. The starting bin of the sum is changed from smaller sizes to larger sizes to see how the size of aerosols affects ACI. It can be seen that when the sum is taken over the whole size distribution, from 10 nm to 500 nm, the differences between the cases 1 and 2 are largest. This is most probably due to a fact that data set in case 2 includes lot of new particles formation events and thus the variation of concentration in the size range which does not contribute to cloud droplet population is

large. The data sets in case 1 does not include new particle formation events.

When the sum is taken from larger sized cases, 1 and 2 approach each other. The ACI from cloud optical thickness is almost the same as that from in-situ measurements in case 1. The ACI calculated from cloud r_{eff} shows clearly lower values than from COT. A similar effect is also seen when using only remote sensing data, the ACI calculated from COT is higher than that calculated from r_{eff}. The reason for this is unknown.
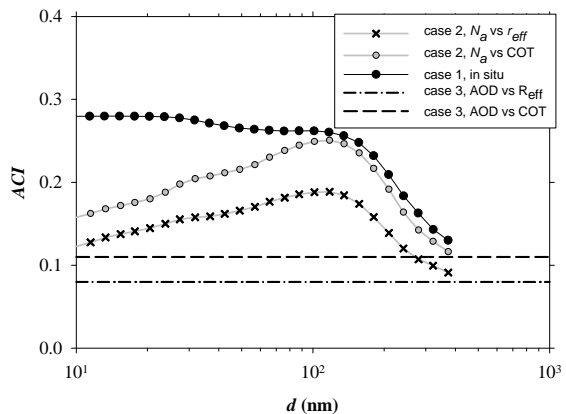
Figure1. Comparison of different approaches to calculate ACI from equation one. N_a is the number concentration of aerosols and AOD is aerosol optical depth.

It is interesting to observe that ACI calculated from different measurement approaches the same value when the sum is taken from larger sizes. The fact that larger sizes are optically more active and thus contribute the most to AOD from remote sensing data could at least partly explain this. However this raises the question of how good are satellite based estimates of aerosol indirect effects.

IPCC: Summary for Policymakers Cambridge University Press, Cambridge, United Kingdom and New York, NY, USA, 2007.
Baker, M. B., and Peter, T. (2008) *Nature*, 451, 299-300.
McComiskey, A., and Feingold, G. (2008) *Geophys. Res. Lett.*, 35, L02810, doi:10.1029/2007 GL032667

Hygroscopic growth and activation of uncoated and coated soot particles and their relation to ice nucleation

M. Ziese[1], S. Henning[1], K. Mildenberger[1], F. Stratmann[1], O. Möhler[2], S. Benz[2], A. Buchholz[3], Th. Mentel[3] and the AIDA/LACIS-mobile-team

(1) Leibniz-Institute for Tropospheric Research, Cloud Group, Leipzig, Germany
(2) Forschungszentrum Karlsruhe, IMK-AAF, Karlsruhe, Germany
(3) Forschungszentrum Jülich, ICG-II: Troposphere, Jülich, Germany

Keywords: activation, coatings, hygroscopic growth, LACIS-mobile, soot particles.

Soot particles, which are insoluble in water, are emitted by biomass burning and fossil fuel combustion. During their presence in the atmosphere, soluble substances condense on these particles and alter their cloud-forming potential (Andreae & Rosenfeld, 2008). Thus measurements of the hygroscopic growth (HTDMA, LACIS-mobile), activation behavior (DMT-CCNC) - scope of this paper - and ice nucleation (AIDA chamber (Möhler et al., 2001)) were performed to estimate the cloud-forming potential of pure and coated soot particles. Globally, soot particles contribute up to 2.5 % to the atmospheric aerosol (Horvath, 1993). In the framework of the investigations described here, soot particles were generated either applying a graphite-spark-generator (GFG1000) or a flame-soot-generator (Mini-CAST). With respect to the hygroscopic growth and activation behavior, the influences of the carrier-gas (GFG-soot), the OC-content (CAST-soot) and of different coating materials were investigated.

soot-type	coating	growth factor
GFG-Ar	non	1.03
GFG-N$_2$	non	n. d.
CAST-min OC	non	1.04
CAST-med OC	non	1.04
CAST-max OC	non	n. d.
CAST-min OC	sulfuric acid	1.15
CAST-med OC	sulfuric acid	1.4
CAST-max OC	sulfuric acid	1.9

Table 1: Measured growth factors applying LACIS-mobile for different soot types at 98.4% relative humidity (n. d. - not detected).

Differences in the hygroscopic growth and activation behavior of GFG generated soot particles were found for the two carrier-gases considered. If nitrogen was used, neither hygroscopic growth nor activation were observed. In contrast, when argon was used, particles featured a slight hygroscopic growth and were easier to activate. Hygroscopic growth increases with decreasing OC-content of the CAST-soot, up to growth factor (GF) 1.04 at 98.4 % relative humidity (see also table 1). Lower OC-contents also result in the particles being activated more easily.

Coating with sulfuric acid enhances the hygroscopic growth (table 1) and activation behavior of CAST-soot for different OC-contents (figure 1). Attempts of coating the soot particles (CAST and GFG) with oxalic and succinic acid resulted in no measurable change in their hygroscopic growth and activation behavior. This is most likely due to evaporation of the coating material.
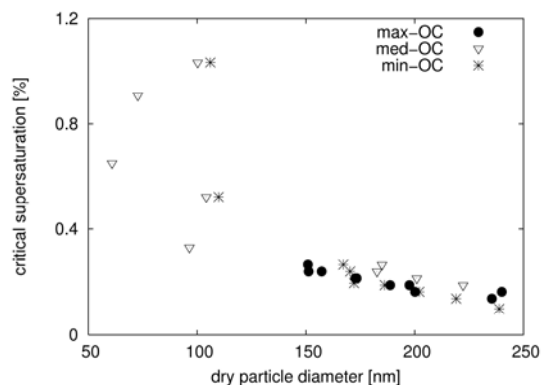
Figure 1: Measured activation behavior of CAST soot coated with sulfuric acid and different OC-contents.

Comparing hygroscopic growth and activation to ice-nucleation behavior similar trends were observed. GFG-soot with argon as carrier-gas acts as a better ice nuclei than GFG-soot with nitrogen. For the CAST-soot the ice-nucleation activity decreases with increasing OC-content. Coating of the CAST soot particles with sulfuric acid shows different effects on the ice nucleation behavior with a trend to less ice formation in the deposition mode at lower ice saturation ratios, but the occurrence of an immersion freezing mode was observed close to the thresholds for homogeneous freezing of pure sulfuric acid particles.

Andreae, M.O., Rosenfeld, D. (2008), Earth-Science Reviews, 89, 13-41
Horvath, H. (1993), *Atmos. Environ.*, 27A, 293-317.
Möhler, O. et al. (2001), Proceedings of Workshop on Ion-Aerosol-Cloud-Interactions (IACA).

Aerosol- and updraft-limited regimes of cloud droplet formation: influence of particle number, size and hygroscopicity on the activation of cloud condensation nuclei (CCN) under pyro-convective conditions

Philipp Reutter[1,2], Jörg Trentmann[2], Hang Su[1], Martin Simmel[3], Diana Rose[1], Heini Wernli[2], Meinrat O. Andreae[1] and Ulrich Pöschl[1]

[1] Biogeochemistry Department, Max Planck Institute for Chemistry, Mainz, 55128 Mainz, Germany
[2] Institute for Atmospheric Physics, Johannes Gutenberg University, Mainz, 55099 Mainz, Germany
[3] Leibniz Institute for Tropospheric Research, Leipzig, 04318 Leipzig, Germany

Keywords: CCN, Activation, Hygroscopicity, Modelling, Biomass burning.

We have investigated the formation of cloud droplets under (pyro-)convective conditions using a cloud parcel model with detailed spectral microphysics and with the κ-Köhler model approach for efficient and realistic description of the cloud condensation nucleus (CCN) activity of aerosol particles.

Assuming a typical biomass burning aerosol size distribution (accumulation mode at 120 nm), we have calculated initial cloud droplet number concentrations (N_{CD}) for a wide range of updraft velocities (w = 0.5-20 m s^{-1}) and aerosol particle number concentrations ($N_{CN} = 10^3 - 10^5$ cm^{-3}) at the cloud base. Depending on the ratio between updraft velocity and particle number concentration (w/N_{CN}), we found three distinctly different regimes of CCN activation and cloud droplet formation:

(1) An aerosol-limited regime that is characterized by high w/N_{CN} ratios ($>\approx 10^{-3}$ m s^{-1}/(cm^{-3})), high maximum values of water vapour supersaturation ($S_{max} > \approx 0.5\%$), and high activated fractions of aerosol particles ($N_{CD}/N_{CN} > \approx 90\%$). In this regime N_{CD} is directly proportional to N_{CN} and practically independent of w.

(2) An updraft-limited regime that is characterized by low w/N_{CN} ratios ($<\approx 10^{-4}$ m s^{-1}/(cm^{-3})), low maximum values of water vapour supersaturation ($S_{max} < \approx 0.2\%$), and low activated fractions of aerosol particles ($N_{CD}/N_{CN} < \approx 20\%$). In this regime N_{CD} is directly proportional to w and practically independent of N_{CN}.

(3) An aerosol- and updraft-sensitive regime, which is characterized by parameter values in between the two other regimes and covers most of the conditions relevant for pyro-convection. In this regime N_{CD} depends non-linearly on both N_{CN} and w.

In sensitivity studies we have tested the influence of aerosol particle hygroscopicity on N_{CD}. Within the range of effective hygroscopicity parameters that is characteristic for continental atmospheric aerosols ($\kappa \approx 0.05\text{-}0.6$), we found that N_{CD} depends rather weakly on the actual value of κ. Only for aerosols with very low hygroscopicity ($\kappa < 0.05$) and in the updraft-limited regime also for aerosols with higher than average hygroscopicity (κ > 0.3) did the relative differential quotients ($\Delta N_{CD}/N_{CD}$)/($\Delta \kappa/\kappa$) exceed values of ~0.2, indicating that a 50% difference in κ would change N_{CD} by more than 10%. Realistic changes in the aerosol particle size distribution had practically no effect on the aerosol-limited regime and limited influence on the aerosol- and updraft sensitive regime ($\Delta N_{CD}/N_{CD}$ < 30%) but can have strong effects at low supersaturation in the updraft-limited regime ($\Delta N_{CD}/N_{CD}$ > 30% at $S_{max} < 0.1\%$).

Overall, the results of this and related studies suggest that the variability of initial cloud droplet number concentration in (pyro-)convective clouds is mostly dominated by the variability of updraft velocity and aerosol particle number concentration in the accumulation mode. Coarse mode particles and the variability of particle composition and hygroscopicity appear to be play major roles only at low supersaturation in the updraft-limited regime of CCN activation ($S_{max} < 0.2\%$).

Simmel, M. and Wurzler, S. (2005): *Atmos. Res.,* 80, 218-236.

Petters, M. D. and Kreidenweis, S. M. (2007): *Atmos. Chem. Phys.,* 7, 1961-1971.

Rose, D., Nowak, A., Achtert, P., Wiedensohler, A., Hu, M., Shao, M., Zhang, Y., Andreae, M. O., and Pöschl, U. (2008): *Atmos. Chem. Phys. Discuss.,* 8, 17343–17392.

Gunthe, S. S., S. M. King, D. Rose, Q. Chen, P. Roldin, D. K. Farmer, J. L. Jimenez, P. Artaxo, M. O. Andreae, S. T. Martin, and U. Pöschl (2008): *Atmos. Chem. Phys. Discuss.,* 9, 3811-3870, 2009

Luni-solar interaction in precipitation over Europe

L. Hejkrlik

Czech Hydrometeorological Institute, 400 11, Ustí nad Labem, Czech Republic

A great deal of attention has been given in literature to variation of precipitation related to lunar phase. Semi-synodic wave has been discovered in the 1960's, known as Bowen's signal, but in reality similar studies were published even decades before (Camuffo, 2001). In our previous studies we tried to verify the hypothesis that the phenomenon was transient and that the typical wave could be identified only in some periods. We have found that in very long series of rainfall data at Praha-Klementinum (1804-2007) the possibility to demonstrate the Bowen's signal varied quasi-periodically. The extremes of the long-term course appeared mostly two years before solar minima in nearly 22-year rhythm. We concluded that there was relationship to solar magnetic cycle and suggested a null-hypothesis about teleconnections between Sun, Moon and Earth's atmosphere (Hejkrlik, 2008).

This paper is an extension of previous study onto 13 European 100-year series (1901-2000) of daily precipitation amounts. The area of interest ranged from Dublin to Bucuresti and from Marseille to Nord Odal. Monthly precipitation series were created with respect to lunar phase and analysed by superposed epochs method. For every single year in period 1903-1998 a matrix of 61-62 synodic series was composited, ranging two years before and after the middle year. Similarity of resulting signal to the Bowen's model (simple semi-lunar cosinus wave, shifted by 4 days) was measured by correlation coefficient and plotted against time.

The resulting series, smoothed by 5-year moving average, exhibit probable Hale-cycle modulation which is partly asynchronous for various stations across the continent (Fig. 1). Although mutual correspondence of the graphs is sometimes very impressive, the possibility that their appearance is due to a combination of the smoothing procedure and the temporal and spatial correlation among the observations cannot be ignored (Lund, 1965).

Presented results support the idea about possible relationship between solar variability and the Moon's influence on processes in cloud formation. Variability of galactic cosmic rays as an effect of changing conditions inside the heliosphere and the lunar distortion of the Earth's magnetic field may control the number of CCN and consequently the precipitation amount.
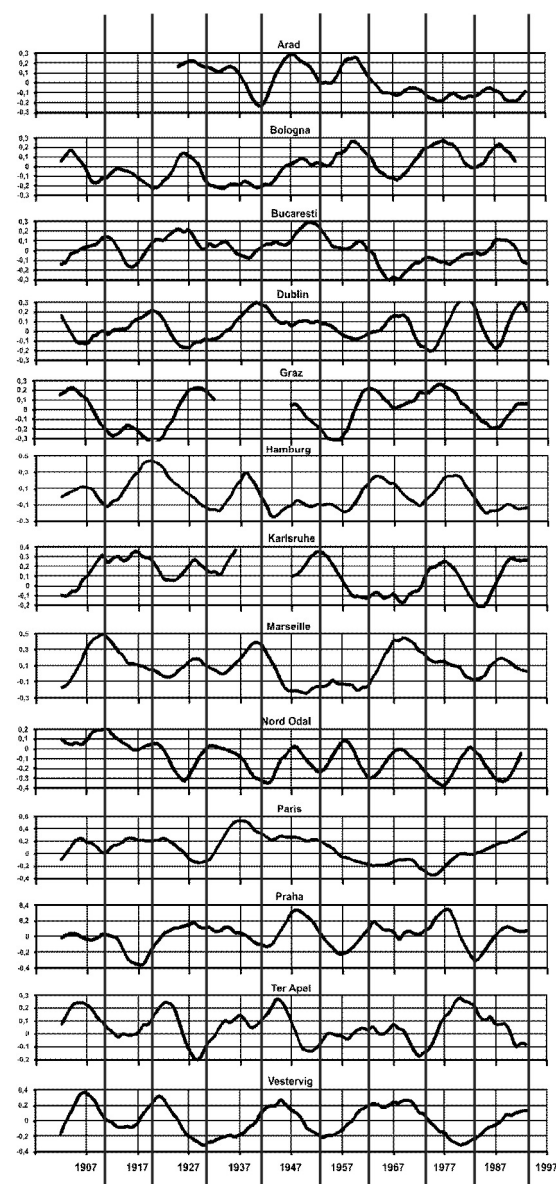
Figure 1. Expression of Bowen's signal against moments of solar minima (vertical lines).

Camuffo, D. (2001). *Earth, Moon and Planets,* **85-86**, 99-113.

Hejkrlik, L. (2008). European Aerosol Conference 2008, Thessaloniki, Abstract T06A015P

Lund, I. A. (1965). *J. Atmos. Sci.*, **22**, 24-39.

HYGROSCOPIC AEROSOL PROPERTIES AT CAPE VERDE ISLANDS DURING THE SAMUM-2 FIELD CAMPAIGN IN 2008

A. Schladitz[1], T. Müller[1], A. Nowak[1], A. Massling[1,2], N. Kaaden[1], K. Kandler[3], K. Lieke[3] and A. Wiedensohler[1]

[1]Leibniz Institute for Tropospheric Research (IfT), 04318, Leipzig, Germany
[2]National Environmental Research Institute, Aarhus University, 4000, Roskilde, Denmark
[3]Institute for Applied Geosciences, Technical University Darmstadt, 64287, Darmstadt, Germany

Keywords: Hygroscopicity, Saharan dust, Marine aerosols, Chemical composition

The SAMUM-2 field campaign was carried out to investigate aerosol physical properties of a mixture of transported mineral dust particles from the Saharan desert, sea salt aerosol from the Atlantics, and biomass burning aerosol from central Africa. Hygroscopic properties in terms of growth factors (HGF) in dependence on particle diameter (Dp) and relative humidity (RH) were measured at Praia, Cape Verde Islands from Jan 17th to Feb 10th 2008.

For determination of hygroscopic growth of the sample aerosol, an H-TDMA (Hygroscopicity - Tandem Differential Mobility Analyzer) was operated at 85% RH selecting distinct particle diameters in the size range from Dp = 30 – 350 nm. In addition to the dry particle number size distribution (RH < 20%, Dp = 20 – 570nm) measured by a DMPS (Differential Mobility Particle Sizer), the humidified particle number size distribution at RH = 30, 55, 75 and 90% was measured by an H-DMPS (Humidified - Differential Mobility Particle Sizer) in the same size range.

Descriptive hygroscopic growth factors (DHGFs) were determined from dry and humidified particle number size distributions, applying the summation method (Birmili et al., 2004). The size dependent DHGFs were parameterized in terms of relative humidity by fitting a power law function:

$$\text{DHGF} = \left(1 - \frac{RH}{100}\right)^{-\gamma}$$ (Swietlicki et al., 2000) to the

data adapting the free parameter γ.

Chemical composition of aerosol samples taken during the field study was conducted by electron – microscopical single particle analysis.

The hygroscopic properties of sub micrometer particles show a subdivision into three different particle groups, namely "more hygroscopic" (HGF > 1.6), "less hygroscopic" (1.3< HGF <1.6) and "hydrophobic" (HGF < 1.3) particles. Figure 1 illustrates the average frequency of the different particle groups at 30, 50, 80, 150, 250 and 350nm for the entire measurement period. It was found, that the larger the particles are the higher is the hydrophobic number fraction. From the comparison of chemical and hygroscopic data it was found, that hydrophobic particles are mineral dust particles with respect to the larger particles while smaller particles are most likely soot agglomerates. More hygroscopic sea salt particles originated from the surrounding Atlantics.

Figure 2 shows a function of the median γ values in the size range from Dp = 30 – 350nm for the entire measurement period. From the chemical analysis it is assumed that the maximum number fraction of non - sea salt sulphate particles (NSS) is responsible for the maximum of γ and thus the resulting DHGF.
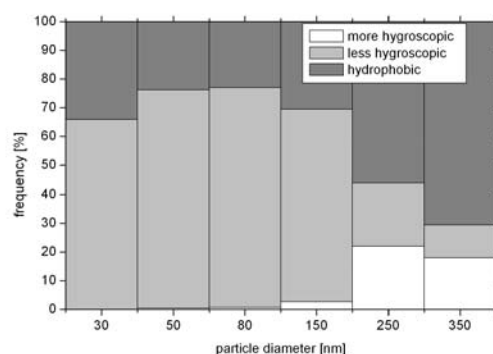
Figure 1: Average frequency of more hygroscopic particles (white), less hygroscopic particles (light gray) and hydrophobic particles (gray).
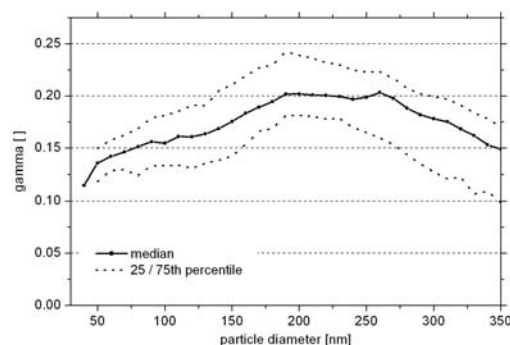
Figure 2: Median γ value and corresponding 25th and 75th percentile values for 30 – 350 nm particles for the entire measurement period.

Birmili, W., Nowak, A., Schwirn, K., Lehmann, K.et al. (2004) A new method to accurately relate dry and humidified number size distributions of atmospheric aerosols. *Journal of Aerosol Science* 1, 15–16, Abstracts of EAC, Budapest 2004.
Swietlicki, E., Zhou, J., Covert, D.S., Hämeri, K. et al. (2000) Hygroscopic properties of aerosol particles in the north-eastern Atlantic during ACE-2. *Tellus*, 52B, 201-227.

Laboratory investigations of contact and immersion freezing of mineral dust using an acoustic levitator

L. Schütz[1], S. K. Mitra[1], K. Diehl[1], F. Berkes[1], H. Schmithüsen[1], H. Bingemer[2], M. Ebert[3], and S. Weinbruch[3]

[1]Institute for Atmospheric Physics, Johannes-Gutenberg University, 55099 Mainz, Germany
[2]Institute for Atmosphere and Environment, J.-W.-Goethe-University, 60438 Frankfurt, Germany
[3]Institute of Applied Geosciences, Technical University Darmstadt, 64287 Darmstadt, Germany

Keywords: heterogeneous ice nucleation, mineral dust

Introduction

The influence of aerosol particles on heterogeneous ice formation is currently insufficiently understood although this information is strongly required to study the role of ice nuclei in clouds (Levin *et al.*, 2007). Modelling studies have shown that the type and quantity of atmospheric aerosol particles acting as ice nuclei can affect ice cloud microphysical and radiative properties as well as their precipitation efficiency (e.g. Lohmann and Diehl, 2006; Storelvmo et al., 2008). Therefore, a quantitative description of the ice nucleation processes is crucial for a better understanding of formation, life cycles, and the optical properties of clouds as well as for the numerical precipitation forecast.

Mineral dust particles are efficient ice nuclei (Pruppacher and Klett, 1997). The ice nucleation properties of the most abundant minerals occurring in desert aerosols were investigated by environmental scanning electron microscopy (Zimmermann *et al.*, 2007 and 2008). Such investigations are restricted to heterogeneous ice nucleation via deposition and condensation mode freezing. However, in immersion and contact modes, laboratory experiments were performed mainly with two mineral dust types, kaolinite and montmorillonite (e.g., Pitter and Pruppacher, 1973) while data for quartz, calcite, orthoclase, albite, hematite, and gypsum are not available at all. In order to close this gap attempts were made utilizing an acoustic levitator (Ettner *et al*, 2004) operated in a cold chamber.

Experimental Methods

Freezing experiments are carried out inside a walk-in cold chamber where temperatures down to -40°C are achieved. Pure water drops are levitated using an ultrasonic trap in order to have the drop suspended without any container contacts in a setup similar to what has been described by Ettner *et. al.* (2004). The temperature of the drop was continuously monitored by an in-situ calibrated Infrared thermometer from the instant of its placement in the trap until the drop froze completely. During investigations on the initiation of immersion freezing by specific materials, particles from those are added to the drop prior to its placement in the trap. For the study of nucleation by contact the material in powdered form is blown towards a pre-cooled drop. The onset of activation is indicated by a rapid rise of the drop temperature to about 0°C, which subsequently remains constant as long as the drop is not completely frozen. Afterwards, the temperature drops again to ambient levels.

Results

Preliminary studies are carried out with materials whose ice nucleation properties are available from the literature, in order to standardize the experiment for application to new materials. Measurements with silver iodide gave an activation temperature between -4 and -6°C, which is in good agreement with values from earlier studies (Pruppacher and Klett, 1997). Experiments will be continued with mineral particles which have not been investigated so far, such as quartz, calcite, orthoclase, albite, hematite, and gypsum. Results will be presented at the conference.

Acknowledgements

References

Ettner, M., S. K. Mitra, and S. Borrmann, 2004: Atmos. Chem. Phys., 4, 1925–1932.

Levin, Z., et al., 2007: The WMO/IUGG International Aerosol Precipitation Science Assessment Group (IAPSAG).

Lohmann, U., and K. Diehl, 2006: J. Atmos. Sci., 63, 968-982

Pitter, R. L., and H. R. Pruppacher, 1973: *Quart. J. Roy. Meteor. Soc., 99,* 540-550.

Pruppacher, H.R., J.D. Klett, 1997: *Microphysics of Clouds and Precipitation*, 2nd ed., Kluwer Academic Publishers, Dordrecht.

Storelvmo, T., J. E. Kristjannson, and U. Lohmann: J. Atmos. Sci., 60, 3214-3230

Zimmermann, F., M. Ebert, A. Worringen, L. Schütz, and S. Weinbruch, 2007: Atmos. Environ., 41, 8219-8227

Zimmermann, F., S. Weinbruch, L. Schütz, H. Hofmann, M. Ebert, K. Kandler, and A. Worringen, 2008: J. Geophys. Res., 113, D23204.

Closure between Hygroscopic Growth and CCN Activation of Photochemical Aged Secondary Organic Aerosols

Mildenberger, K. (1), Buchholz, A. (2), Clauss, T. (1), Henning, S. (1), Kiselev, A. (1), Mentel, Th. F. (2), Schlosser, E.(2), Stratmann, F. (1), Tillmann, R. (2)

(1) Institute for Tropospheric Research, Permoser Str. 15, 04318 Leipzig, Germany
(2) Forschungszentrum Jülich, ICG-II: Troposphere, Jülich, Germany

Keywords: activation, hygroscopic growth, secondary organic aerosol, aging, LACIS-mobile.

The effects of organics on the hygroscopic properties of particles has not yet been fully understood. There is still a discrepancy between the observed cloud condensation nucleus (CCN) activation and hygroscopic growth measurements when predicting CCN activity with κ-Köhler theory following Petters & Kreidenweis (2007). In this study the ability of secondary organic aerosol (SOA) particles, produced from photooxidation and ozonolysis of different monoterpene mixtures (MT), to absorb water and activate to cloud droplets during aging was investigated. Hygroscopic growth measurements were performed with a HTDMA (RH <97%, FZ Jülich) and LACIS-mobile (RH >97%, IfT) while the CCN activity was measured with a CCNC (RH >100%, DMT). All experiments took place at the SAPHIR-chamber at the research centre Jülich in summer 2008 under near atmospheric conditions such as natural sunlight, low precursor and O_3 concentrations (4-100 ppb) and long reaction times (2 days). As precursor we used a monoterpene mixture (cis-ocimene, limonene, α-pinene, β-pinene, Δ3-carene). Alternatively, we added the sesqui-terpenes trans-caryophyllene and farnesene. All mixtures had been identified as major constituents of plant emissions in previous experiments.

Differences in the hygroscopic growth and activation behaviour were found for different radiation intensities. At sunny days the SOA particles were more hygroscopic than on cloudy days. The weather effect was even stronger than the observed aging which takes mainly place during the first hours of an experiment. We also found that different precursor concentrations do not significantly effect the hygroscopic growth of the formed particles.

Tab. 1: κ-values were calculated from hygroscopic growth and activation measurements. The κ values derived from hygroscopic growth measurements were used to calculate the critical supersaturation (Sc) for activation, 08/06/10, 100 ppb MT, D_{dry} = 150 nm.

D_{dry} [nm]	κ		calculated Sc [%]	measured Sc [%]
150	minimum[1]	0.05	0.29	-
150	maximum[1]	0.11	0.20	-
150	average[1]	0.07	0.24	-
150	variable σ[2]	0.05	0.23	-
154	activation	0.11	-	0.2

[1]calculated from hygroscopic growth measurements, σ=72 mN m^{-1}
[2]calculated from hygroscopic growth and activation measurements, σ=variable (Ziese et al., 2008)

The hygroscopicity parameter κ following Petters & Kreidenweis (2007) was determined from all hygroscopic growth measurements. Tab. 1 shows the averaged, minimum and maximum κ-values. Afterwards the theoretical Köhler-curves were calculated with these κ (Fig. 1) using a constant surface tension of water. From this curves, values for the critical supersaturation (Sc) were derived, too. Also a method for calculating Köhler curves with a concentration dependent surface tension following Ziese et al. (2008) was utilized. The insert in figure 1 shows κ as a function of relative humidity (RH).
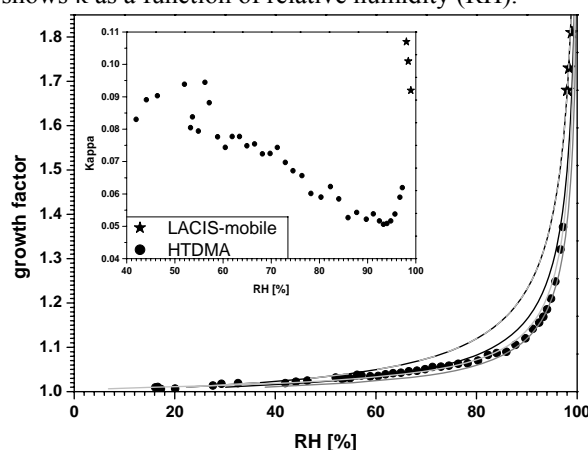
Fig. 1: Closure of CCNC and hygroscopic growth for a sunny day at the SAPHIR chamber, 08/06/10, 100 ppb MT, D_{dry} = 150 nm. Köhler curves for κ max and activation (grey-black dashed line), κ average (black line), κ min (dark grey line) and variable σ (light grey line).

At a fixed RH, the calculated growth factor increases with increasing κ. The calculated Köhler curves for the highest κ derived from hygroscopic growth measurements and from the activation measurements are identical. In contrast to this there is a gap between the averaged κ and the CCN activation. This shows that the assumption of a constant κ (Petters & Kreidenweis, 2007) is not valid if we are using a constant surface tension. Using the concentration dependent surface tension method following Ziese et al. (2008) for calculating the Köhler curve a closure between hygroscopic growth and CCNC activation can be achieved.

Ziese, M., *et al.* (2008). *Atmos. Chem. Phys.*, 8, 1855-1866.

Petters, M.D. & Kreidenweis, S.M. (2007). *Atmos. Chem. Phys.*, 7, 1961-1971.

CCN activation and hygroscopic growth measurements of secondary organic aerosols from boreal forest emissions

Buchholz, A. (1), Mentel, Th. F. (1), Kiendler-Scharr, A. (1), Spindler, C. (1), Tillmann, R. (1), Kleist, E.(2), Wildt, J. (2)

(1) Institut für Chemie und Dynamik der Geosphäre, ICG-2, Forschungszentrum Jülich, Germany
(2) Institut für Chemie und Dynamik der Geosphäre, ICG-3, Forschungszentrum Jülich, Germany

Keywords: hygroscopic growth, CCN, secondary organic aerosol, cloud microphysics

Plant emitted volatile organic carbons (VOCs) are a major precursor of secondary organic aerosols (SOA), an important constituent of atmospheric aerosols. The precursors are oxidized via ozonolysis, photooxidation, or by NO_3 and form aerosol particles. To investigate the physical properties of aerosol that are produced from this complex natural mixtures of VOC the Juelich Plant Atmosphere Chamber (JPAC) at the Research center Juelich was used. Trees which are typical for the boreal forest were set in the temperature controlled plant chamber (PC). The emissions of the trees were then transmitted into a coupled reaction chamber (RC) containing 80 ppb of ozone and a relative humidity (RH) of 60%. The particle formation was started by switching on UV lights generating several times $10^7 \, cm^{-3}$ OH radicals. For these experiments the RC temperature was kept constant at 17°C and PC temperature was tuned between 15 and 30°C to change the VOC emissions coming from the trees.

Both the tree emissions and the composition of the gas phase in the RC were monitored with GC-MS and PTR-MS. Particle number concentration and size distribution were determined by CPC (TSI 3025) and SMPS (TSI 3080). The chemical composition of the aerosol was measured with a high resolution aerosol mass spectrometer (WToF-AMS). Hygroscopic growth factors (GF) were determined with a humidity tandem differential mobility analyzer (HTDMA) for different particle sizes at RH = 0 - 97%. Cloud condensation nuclei (CCN) activation was measured with a continuous flow CCN counter (DMT).

Different emission pattern of the trees (e.g. induced by heat stress) changed the measured GF and activation diameter (D_{crit}). However, up to 80% RH the GF changes are within the range of the measurement error. The GF(RH = 90%) are between 1.08 and 1.15.

Koehler theory was applied to combine CCN activation measurements with GF. The κ parameter according to Petters & Kreidenweis, (2007) was calculated. κ(CCN) was determined for the different measured super saturations (SS). The κ(GF) decrease with increasing RH but levels off at RH > 95% and κ(GF) calculated from GF for RH > 95% are listed in table 1. If the surface tension (σ = 72.8 mN/m) of water and a constant κ (κ(CCN) or κ(GF) at highest measured RH) are assumed then the Köhler curve calculated from κ(CCN) does not agree with the measured growth curve. If σ is reduced to 54.6 mN/m the calculated curve fits very well with the measured data (see red line and open squares in figure 1). Thus, with the assumption of a surface tension lower than that of water closure between HTDMA and CCN data was achieved.
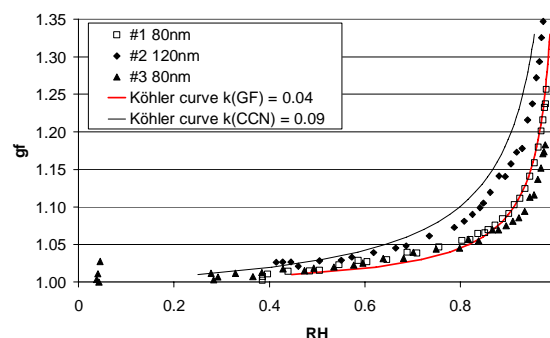
Figure 1: GF curve for different dry sizes TC temperature 30°C; calculated Köhler curves with κ(CCN) = 0.09 and σ = 72.8 mN/m (black line) and κ(GF) = 0.04 and σ = 54.6 mN/m (red line).

Table 1: κ values calculated from HTDMA and CCN measurements using the surface tension of water (σ = 72.8 mN/m). For κ(GF) the last measured value is given (at RH = 97%)

	κ	D_{crit} / nm	dry size / nm
HTDMA			
#1	0.040	-	80
#2	0.052	-	120
#3	0.030	-	80
CCN			-
0.4% SS	0.099	58.92	-
0.6% SS	0.094	65.67	-
0.8% SS	0.075	74.67	-
1.0% SS	0.068	96.50	-

Petters, M. D. & Kreidenweis, S. M. (2007). *Atmos. Chem. Phys.*, 7, 1961-1971.

Ice nuclei and cloud condensation nuclei measurements in a rural area

G.Santachiara[1], L. Di Matteo[1], F.Prodi[1,2] and F. Belosi[1]

[1]Institute ISAC-CNR, Clouds and Precipitation Group, Bologna, Italy
[2]Department of Physics, University of Ferrara, Dept. of Physics, Ferrara, Italy

Key Words: Ice nuclei, cloud condensation nuclei, ice supersaturation, water supersaturation

Introduction

Aerosol particles that catalyze the formation of ice crystals in cloud are called Ice Nuclei (IN) and can form ice through different thermodynamic mechanisms or modes: deposition, condensation-freezing, immersion and contact. It is generally agreed that ice will form on nuclei in response to different kinds of thermodynamic forcing, the primary variables being temperature and supersaturation with respect to ice and water (S_{ice} and S_w, respectively).

Cloud condensation nuclei (CCN) play a crucial role in determining the microphysical and radiative properties of clouds. The main goals of the presented experimental campaign can be summarized as follow: a) compare IN concentration in different size ranges, supersaturations and temperatures b) check for a diurnal trend in the IN and CCN concentrations c) investigate the relationship between IN and condensation nuclei (CN).

Experimental

Experimental campaigns were performed at a rural site (S.Pietro Capofiume, near Bologna) during summer (09 -12 July 2007) and winter (07-10 February 2008). Simultaneous samplings were collected on nitrocellulose membrane of various aerosol fractions, i.e. PM1, PM2.5, PM10 and total suspended particles (TSP), four times a day (period 06 -22 h), at 3 m above ground level.

Simultaneous measurements of particle number concentrations (CNC-TSI) and particle concentrations in different size classes starting from d>0.3 µm (Grimm, Mod.1.108) were also performed. Meteorological data (air temperature, wind speed, pressure) were recorded. Concentrations of IN were detected by the membrane filter technique, using a continuous diffusion chamber, which allows the control of the filter and air temperature.

Measurements were made at S_{ice} from 9.6 to 34%, and S_w from -8% to 10% (winter campaign), and S_{ice} from 20 to 32%, and S_w from 0% to 10% (summer campaign). The device used was a thermal diffusion chamber, which consists of two parallel circular plates of aluminium joined together by a non-conducting glass. The chamber is illuminated by a laser (He-Ne, λ= 632 nm). An optical system and videocamera detect the droplets in a volume of approximately $6x10^{-3}$ cm^3 and record images every second during the supersaturation cycle. During the winter experimental campaign addition measurements of CCN were made. The device used is a thermal diffusion chamber consisting of two parallel circular plates of aluminium joined together by a non-conducting glass.

A temperature difference is applied by thermoelectrically cooling the bottom plate, while the upper plate is maintained at ambient temperature. The upper surface of the chamber is covered with a sintered porous glass imbued with water. In this way, a thermal and vapour density linear gradient is created within the chamber, with a maximum supersaturation near the center of the chamber.

Results and discussion

Both the summer and winter campaigns reveal no correlation between particle numbers measured by the optical counter and CN concentration, nor between IN measured in the different size ranges, by either the counter spectrometer (d>0.3micron) or the condensation nuclei counter .

The fraction of all particles active as IN constitutes a very small part of the aerosol population. Both in the summer and winter campaigns the ratio of IN to CN concentration, depending on T, S_{ice} and S_w , ranges from about $1:10^8$ to $1:10^7$. By comparing the mean value of IN concentrations during summer and winter campaigns , it is noted, by considering the same values of S_{ice} and S_w, that higher values are measured in the summer campaign. The measured concentrations turns out lower than those reported in rural areas (Castro et al., 1998).

Cloud condensation nuclei during the winter campaign show a diurnal trend, with lower values at about midday and higher ones during night. The trend emerging in the measurements excludes the possibility of CCN originating from a photochemical nucleation process. It could be the effect of the inversion layer due to the infrared radiation emitted by the Earth's surface in clear sky conditions. In addition there could be an SO_2 oxidation process on the surface of aerosol during night-time, due to high relative humidity (about 90%).

Concerning the CCN concentration, the mean value measured at S_w= 0.36% is 1294 cm^{-3}. Published papers report a wide range of CCN concentrations, from several thousand per cubic centimeter (Baumgardner, 2004) to less than 10 cm^{-3} (Radke and Hobbs, 1969).

Castro, A. et al., *Atmos. Res*. **47-48**, 155-167 (1998)
Baumgardner, D. et al., *Atmos.Env*., 38 , 357-367 (2004)
Radke, L.F..et al., *J.App.Meteor*. **26**, 281-288 (1969).

Cloud Condensation Nuclei (CCN) at an urban location

J. Burkart, G. Steiner, G. Reischl and R. Hitzenberger

University of Vienna
Faculty of Physics, Aerosol, Bio- and Environmental Physics, Boltzmanng. 5, A-1090 Vienna, Austria

Keywords: ambient aerosols, CCN

By acting as Cloud Condensation Nuclei (CCN) aerosol particles can alter the microphysical properties of clouds and cause radiative forcing. The so called indirect aerosol effect is still subject to great uncertainties (IPCC 2007) mainly due to a lack of information on the CCN behaviour of real world aerosols. Especially a longer-term data base is missing.

In our long-term study the cloud condensation nucleation ability of the atmospheric aerosol in Vienna was investigated with the University of Vienna CCN counter (Giebl et al. 2002, Dusek et al. 2006). The measurements were performed at the roof laboratory of the Physics Building of the University of Vienna from July 2007 to December 2008.

The University of Vienna CCN counter was used to measure the CCN concentration every five minutes. In parallel the CN concentration was measured in the bypass flow of the CCN counter with a TSI CPC (model 3010) and activation ratios were obtained (A=CCN/CN). The University of Vienna CCN counter operates on the principle of a static thermal diffusion cloud chamber. Within the cylindrical cloud chamber formed by two parallel plates separated by a glass ring low supersaturations (0.2-2%) can be established. The supersaturation is controlled by the temperature difference between the plates and was set to 0.5% for this study. In addition to the CCN parameters the number size distribution was measured with a Vienna type DMA operated in a closed loop arrangement and a commercially available portable optical particle counter (Grimm Model 1.109). So information on the size distribution from 0.01 to 32 µm could be obtained.

In this presentation we want to concentrate on the behaviour of the CCN parameters throughout the year including data on aerosol number size distribution and meteorological information.

Figure 1 shows a typical example of a measurement month. CN concentrations, CCN concentrations and activation ratios are plotted against time. A strong variation of the CCN concentration, the activation ratio and the CN concentration can be observed. This is even true when looking at single measurement days.

Mean, maximum and minimum values for CN and CCN concentrations and activation ratios where calculated for the whole measurement period and are listed in Table 1. It is noteworthy that for each parameter the span between minimum and maximum value is quite large indicating again a strong variation of the parameters. Meteorological information will be included to check for typical aerosol behavior under similar meteorological conditions.

A first evaluation of the aerosol size distribution was performed as well. Comparing the CCN concentration with the concentration of the particles with a diameter greater than 250nm demonstrated that during summer time much smaller particles could be activated than during winter time.
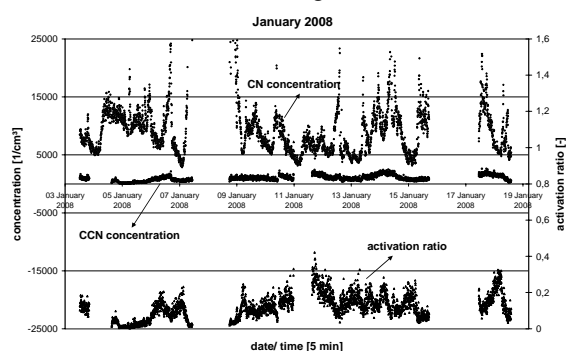
Figure 1. Typical example of a measured time series of CN and CCN concentration and activation ratio.

	CN conc. $(1/cm^3)$	CCN conc. $(1/cm^3)$	activation ratio (-)
mean	7300	810	0.13
max	51600	3600	0.47
min	910	160	0.02

Tabel 1 Mean, maximum and minimum values for CN and CCN concentrations and activation ratios over the whole measurement period

Giebl, H., A. Berner, G. Reischl, H. Puxbaum, A. Kasper-Giebl and R. Hitzenberger, *Journal of Aerosol Science* 33 (2002), 1623-1634

IPCC (2007): *Climate Change 2007 - The Physical Science Basis.* Cambridge and New York. (Cambridge University Press)

Dusek, U., Reischl, G. P., Hitzenberger, R., *Environ. Sci Technol.* 40 (2006), 1223 – 1230

Cloud condensation nuclei in polluted air and biomass burning smoke: Size-resolved measurements and implications for the modeling of aerosol particle hygroscopicity and CCN activity

D. Rose[1], A. Nowak[2], P. Achtert[2], A. Wiedensohler[2], M. Hu[3], M. Shao[3], Y. Zhang[3], M. O. Andreae[1], and U. Pöschl[1]

[1]Max Planck Institute for Chemistry, Biogeochemistry Department, Mainz, Germany
[2]Leibniz Institute for Tropospheric Research, Leipzig, Germany
[3]State Key Joint Laboratory of Environmental Simulation and Pollution Control, College of Environmental Sciences and Engineering, Peking University, Beijing, China

Keywords: CCN, hygroscopicity, megacity, biomass burning,, air pollution.

Atmospheric aerosol particles serving as cloud condensation nuclei (CCN) are key elements of the hydrological cycle and climate, but their abundance, properties and sources are highly variable and not well known. We have measured and characterized CCN in polluted air and biomass burning smoke during the PRIDE-PRD2006 campaign on 1–30 July 2006 at a rural site ~60 km northwest of the mega-city Guangzhou in southeastern China.

CCN efficiency spectra (activated fraction vs. dry particle diameter; 20–300 nm) were recorded at water vapor supersaturations (S) in the range of 0.07% to 1.27%. Depending on S, the dry CCN activation diameters were in the range of 30–200 nm, corresponding to effective hygroscopicity parameters kappa in the range of 0.1–0.5. The hygroscopicity of particles in the accumulation size range was generally higher than that of particles in the nucleation and Aitken size range. The campaign average value of kappa for all aerosol particles across the investigated size range was 0.3, which equals the average value of kappa for other continental locations.

During a strong local biomass burning event, the activation diameters increased by ~10% and the average value of kappa dropped to 0.2, which can be considered as characteristic for freshly emitted smoke from the burning of agricultural waste. At low S (~0.27%), the maximum activated fraction remained generally well below one, which indicates substantial proportions of externally mixed CCN-inactive particles with much lower hygroscopicity – most likely soot particles (up to ~60% at ~250 nm). The mean CCN number concentrations ($N_{CCN,S}$) ranged from 1100 cm^{-3} at S=0.07% to 16 000 cm^{-3} at S=1.27%, representing ~7% to ~85% of the total aerosol particle number concentration. Based on the measurement data, we have tested different model approaches (power laws and κ-Köhler model) for the approximation/prediction of $N_{CCN,S}$ as a function of water vapor supersaturation, aerosol particle number concentration, size distribution and hygroscopicity. Depending on S and on the model approach, the relative deviations between measured and predicted $N_{CCN,S}$ ranged from a few percent to several hundred percent.

The largest deviations occurred at low S and with power laws based on particle number concentration. With the κ-Köhler model and a constant hygroscopicity parameter of 0.3, the deviations were on average less than ~20%, which confirms that κ=0.3 may be suitable for approximating the hygroscopicity and CCN activity of continental aerosols in large scale models of the atmosphere and climate. On the other hand, the temporal variations of $N_{CCN,S}$ observed during the biomass burning event and in diurnal cycles could not be captured with constant κ (deviations up to ~80%). With variable values obtained from individual CCN efficiency spectra, the relative deviations were on average less than ~10% and hardly exceeded 20%, confirming the applicability of the κ-Köhler model approach for efficient description of the CCN activity of atmospheric aerosols. Note, however, that different types of κ-parameters have to be distinguished for external mixtures of CCN-active and -inactive aerosol particles.

References:
Rose, D., S. S. Gunthe, E. Mikhailov, G. P. Frank, U. Dusek, M. O. Andreae, U. Pöschl, Calibration and measurement uncertainties of a continuous-flow cloud condensation nuclei counter (DMT-CCNC): CCN activation of ammonium sulfate and sodium chloride aerosol particles in theory and experiment, Atmospheric Chemistry and Physics, 8, 1153-1179, 2008.
Rose, D., Nowak, A., Achtert, P., Wiedensohler, A., Hu, M., Shao, M., Zhang, Y., Andreae, M. O., and Pöschl, U.: Cloud condensation nuclei in polluted air and biomass burning smoke near the mega-city Guangzhou, China – Part 1: Size-resolved measurements and implications for the modeling of aerosol particle hygroscopicity and CCN activity, Atmospheric Chemistry and Physics Discussions, 8, 17343-17392, 2008.

Ice residue characterization by aerosol mass spectrometry at the AIDA chamber

S.J. Gallavardin[1,2], D.J. Cziczo[1,3], O. Möhler[4], and U. Lohmann[1]

[1] Institute for Atmospheric and Climate Science, ETH Zurich, Zurich, Switzerland
[2] now at Institute for Atmospheric Physics, Johannes Gutenberg-University Mainz, Mainz, Germany
[3] now at Atmospheric Science and Global Change Division, Pacific Northwest National Laboratory, Richland, Washington, USA
[4] Institute for Meteorology & Climate Research, Forschungszentrum Karlsruhe, Karlsruhe, Germany

Aerosols affect climate both directly and indirectly. Indirect effects of aerosols are due to the interactions of particles with clouds. Particles that trigger the formation of ice are termed ice nuclei (IN) while those inducing cloud water droplets are denominated cloud condensation nuclei (CCN). Mineral particles are known to be good ice nuclei although their nucleation capabilities are nevertheless still poorly understood. To better assess the global impact of mineral dusts on climate, a better knowledge of the particle properties and nucleation conditions is needed. During the International workshop on Comparing Ice nucleation Systems (ICIS) at the AIDA chamber facility in Karlsruhe in September 2007, 4 different mineral dusts were tested in different ice nucleation systems and characterized in details. For example, by determining the size and composition of the residue from an ice particle produced in a nucleating system, it is possible to deduce some key characteristics of mineral ice nuclei.

Thus, for a given test aerosol, ice particles were generated in the AIDA chamber by a rapid adiabatic air expansion starting at the temperature range to be investigated (-18°C for example). By defining appropriate expansion speeds and cycles of the AIDA chamber, it was possible to perform particle pre-activation studies. The resulting ice particles were then inertially separated from the interstitial aerosol with a pumped counter-flow virtual impactor. Once the water has evaporated, the ice particle left a residue which was led to the Particle Analysis by Laser Mass Spectrometry instrument (PALMS). The residue was then size and chemically analyzed online at single particle level. The whole method and setup are detailed in Gallavardin *et al.*, (2008).

Mass spectra of ice nuclei with a mineral composition were sorted in different classes over the experiment course. Thus the mass spectra pattern of the more efficient ice nuclei of a given test mineral dust can be identified. Figure 1 presents results for a typical experiment with Saharan Dust. It was observed more ice residues having the mass spectrum pattern B than A since its proportion decreases with time though both ice residues A and B were found in

similar amount when the nucleation started. The mass spectra patterns A and B (named arbitrarily) both had a clear mineral dust signature but were significantly different from each other. It is however not possible yet to associate the pattern difference to a given chemical composition or mineralogy of the mineral dust particles. Additional data taken during ICIS are available to address this issue. Finally, a different frequency of mass spectra with pattern A and B in ice residues can be noted for the second nucleation event. This might suggest pre-activation or particle water processing of the mineral dusts.
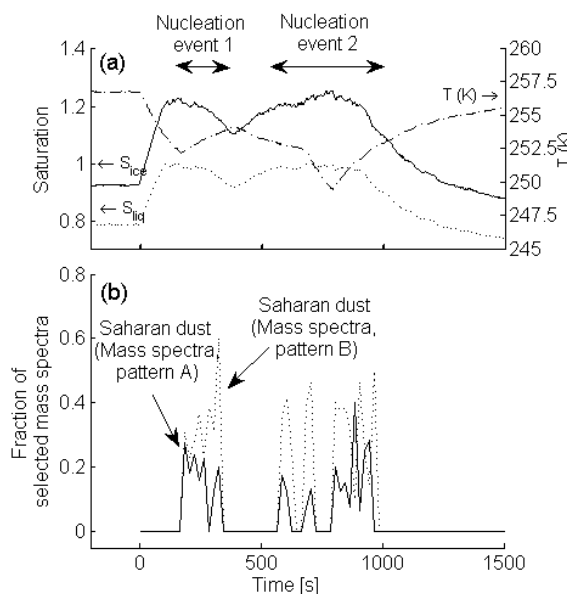
Figure 1. Ice nucleation experiment ICIS07-20 with Saharan Dust. (a) Temporal evolution of the water saturation and temperature in the AIDA chamber. (b) Temporal evolution of the fraction of 2 mass spectrum patterns A and B of the ice residues from Saharan dust.

Gallavardin, S. J. et al (2008). *Aerosol Sci. and Technol.*, 42, 773-791

Cloud condensation nuclei in pristine tropical rainforest air of Amazonia: size-resolved measurements and modeling of atmospheric aerosol composition and CCN activity

S. S. Gunthe[1], S. M. King[2], D. Rose[1], Q. Chen[2], P. Roldin[3], D. K. Farmer[4], J. L. Jimenez[4], P. Artaxo[5], M. O. Andreae[1], S. T. Martin[2], and U. Pöschl[1]

[1] Max Planck Institute for Chemistry, Biogeochemistry Department, Mainz, Germany
[2] Harvard University, School of Engineering and Applied Sciences & Department of Earth and Planetary Sciences, Cambridge, MA, USA
[3] Lund University, Nuclear Physics, Faculty of Technology, Lund, Sweden
[4] University of Colorado, Dept. of Chemistry & Biochemistry and CIRES, Boulder, CO, USA
[5] Instituto de Fisica, Universidade de Sao Paulo, Sao Paulo, Brazil

Atmospheric aerosol particles serving as cloud condensation nuclei (CCN) are key elements of the hydrological cycle and climate. We have measured and characterized CCN at water vapor supersaturations in the range of $S = 0.10\text{-}0.82\%$ in pristine tropical rainforest air during the AMAZE-08 campaign in central Amazonia.

The effective hygroscopicity parameters describing the influence of chemical composition on the CCN activity of aerosol particles varied in the range of $\kappa = 0.05\text{-}0.45$. The overall median value of $\kappa \approx 0.15$ was only half of the value typically observed for continental aerosols in other regions of the world. Aitken mode particles were less hygroscopic than accumulation mode particles ($\kappa \approx 0.1$ at $D \approx 50$ nm; $\kappa \approx 0.2$ at $D \approx 200$ nm).

The CCN measurement results were fully consistent with aerosol mass spectrometry (AMS) data, which showed that the organic mass fraction ($X_{m,org}$) was on average as high as ~90% in the Aitken mode ($D \leq 100$ nm) and decreased with increasing particle diameter in the accumulation mode (~80% at $D \approx 200$ nm).

The κ values exhibited a close linear correlation with $X_{m,org}$ and extrapolation yielded the following effective hygroscopicity parameters for organic and inorganic particle components: $\kappa_{org} \approx 0.1$ which is consistent with laboratory measurements of secondary organic aerosols and $\kappa_{inorg} \approx 0.6$ which is characteristic for ammonium sulfate and related salts.

Both the size-dependence and the temporal variability of effective particle hygroscopicity could be parameterized as a function of AMS-based organic and inorganic mass fractions $\kappa_p = 0.1 \, X_{m,org} + 0.6 \, X_{m,inorg}$, and the CCN number concentrations predicted with κ_p were in fair agreement with the measurement results.

The median CCN number concentrations at $S = 0.1\text{-}0.82\%$ ranged from $N_{CCN,0.10} \approx 30$ cm^{-3} to $N_{CCN,0.82} \approx 150$ cm^{-3}, the median concentration of aerosol particles larger than 30 nm was $N_{CN,30} \approx 180$ cm^{-3}, and the corresponding integral CCN efficien-

cies were in the range of $N_{CCN,0.10}/N_{CN,30} \approx 0.1$ to $N_{CCN,0.82}/N_{CN,30} \approx 0.8$.

Although the number concentrations and hygroscopicity parameters were much lower, the integral CCN efficiencies observed in pristine rainforest air were similar to those in highly polluted mega-city air. Moreover, model calculations of $N_{CCN,S}$ with a global average value of $\kappa = 0.3$ led to systematic overpredictions, but the relative deviations exceeded ~50% only at low water vapor supersaturation (0.1%) and low particle number concentrations (≤ 100 cm^{-3}).

These findings confirm earlier studies suggesting that aerosol particle number and size are the major predictors for the variability of the CCN concentration in continental boundary layer air, followed by particle composition and hygroscopicity as relatively minor modulators.

Depending on the required and applicable level of detail, the information and parameterizations presented in this paper should enable efficient description of the CCN properties of pristine tropical rainforest aerosols in detailed process models as well as in large-scale atmospheric and climate models.

Gunthe, S. S., King, S. M., Rose, D., Chen, Q., Roldin, P., Farmer, D. K., Jimenez, J. L., Artaxo, P., Andreae, M. O., Martin, S. T., and Pöschl, U. (2009) *Atmos. Chem. Phys. Discuss.*, 9, 3811-3870.

Rose, D., Gunthe, S. S., Mikhailov, E., Frank, G. P., Dusek, U., Andreae, M. O. and Pöschl, U. (2008) Atmos. Chem. Phys., 8, 1153-1179.

Rose, D., Nowak, A., Achtert, P., Wiedensohler, A., Hu, M., Shao, M., Zhang, Y., Andreae, M. O. and Pöschl, U. (2008) Atmos. Chem. Phys. Discuss., 8, 17343-17392.

Hygroscopicity and activation properties of ambient aerosol particles in the Beijing area

S. Henning[1], A. Nowak[1], K. Mildenberger[1], E. Sommerhage[1], E. Hallbauer[1], D. van Pinxteren[1], H. Herrmann[1], D. Zhaoze[2], L. Pengfei[2], C. Zhao[2], A. Wiedensohler[1] and F. Stratmann[1]

[1]Leibniz-Insitute for Tropospheric Research, Leipzig, 04318, Leipzig, Germany
[2]Department of Atmospheric Science, School of Physics, Peking University, Beijing 100871, China

Keywords: Ambient aerosols, hygroscopic growth, CCN, LACIS-mobile, HH-TDMA.

Large areas of China suffer from heavy air pollution caused by the strong economic growth in the last two decades. Especially, regions such as the Pearl River Delta in Southern China and the eastern central region around Beijing underlie haze layers clearly visible from satellite observations. The reduced visibility and the large optical depth caused from high aerosol concentrations are strongly dependent on the ability to take up water (hygroscopicity). At relative humidities between 90 and 99%, the aerosol particles grow exponentially. The hygroscopic behaviour at relative humidities close to 100% is strongly linked to the particles ability to grow into cloud droplets at supersaturation. The strong anthropogenic emission of aerosol particles implies a change of the cloud droplet size distribution which increases the cloud albedo. This indirect aerosol effect leads to a general cooling of the atmosphere and is one of the most uncertain parameters with respect to global change.

The HaChi project is performed in March and July 2009 at the Wuqing Meteorological station, 100 km south-east of Beijing. The particle number size distribution, the particle optical properties and their hygroscopic properties at high RH is characterized as well as their cloud nucleating properties above supersaturation. In addition the particles chemical composition is size-resolved analysed. In the here presented work we focus on the hygroscopicity and activation measurements.

HH-TDMA measurements [*Hennig, et al.*, 2005]: These data provides hygroscopic growth factors and number fractions of different externally mixed groups of aerosol particles. The hygroscopic growth at different particle sizes and several different relative humidities (e.g. 90, 94, 98%) will be measured.

LACIS-mobile measurements [*Stratmann, et al.*, 2004; *Wex, et al.*, 2006]: LACIS-mobile is operated at slightly subsaturated (e.g. 98-99.5%) conditions. Particle growth factors is determined as function of dry particle size for a highly interesting RH region with the strongest size effect.
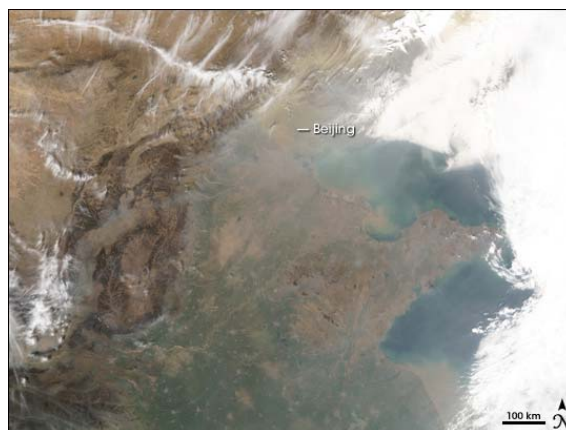
Figure 1. The grayish haze spread across most of the centre of the image (around Beijing) is likely a mixture of urban, industrial, and residential air pollution, possibly mixed with smoke from agricultural and other fires.

Size selected CCN measurements: A DMT-CCNC instrument [*Roberts and Nenes*, 2005] is operated in combination with a DMA. Applying this set-up, synchronising the selected dry diameters and the obtained CCNC supersaturation, allows for size scans as well as supersaturations scans. From these the activation points of the aerosol particles are determined.

The combination of the hygroscopic growth information of HH-TDMA and LACIS-mobile provides the tool to calculate the ambient number size distribution at high relative humidities. Using a Mie-model, the optical properties are calculated and the hygroscopic growth, the absorption and scattering coefficients are determined as a function of air mass.

Hennig, T., et al. (2005), *J. Aerosol Sci.*, *36*, 1210-1223.

Roberts, G. C., & A. Nenes (2005), *Aerosol Sci. Technol.*, *39*, 206-221.

Stratmann, F., et al. (2004), *J. Atmos. Oceanic Technol.*, *21*, 876-887.

Wex, H., et al. (2006), *Atmospheric Chemistry and Physics*, *6*, 4519-4527.

Studies of the relation between cloud droplet size and dry residual particle size with the Droplet Aerosol Analyser

M. Berghof, G.P. Frank, S. Sjogren and B.G. Martinsson

Department of Physics, Lund University, Lund, Sweden

Keywords: aerosol cloud interaction, cloud microphysics, clouds, DAA (Droplet aerosol analyser), droplets

INTRODUCTION

The influence of aerosols on clouds is one of the central topics in today's atmospheric and climate research. The intricate interaction of aerosol properties and meteorology in cloud development is a challenging task to investigate. In addition, every single cloud is unique, since the aerosol properties and meteorological conditions are highly variable in space and time. Thus, generalizations and inclusions in models of factors controlling cloud formation, cloud evolution, precipitation initiation and cloud radiative properties are extremely difficult, although of great importance in order to understand and model atmospheric processes and climate effects.

Here, we will present the features and capabilities of the Droplet Aerosol Analyser (DAA) [1] by showing first results obtained at the summit of Mt. Brocken (51.80º N, 10.67º E, 1142 m asl) in the Harz region in central Germany in 2009.

INSTRUMENTATION

The Droplet Aerosol Analyser (DAA) is an instrument especially developed for studies of the interaction between aerosol particles, cloud/fog droplets and interstitial particles. It is based on a concept where the aerosol is processed in several steps by aerosol charging mechanisms, diffusion drying, and electrostatic aerosol spectrometry (using Differential Mobility Analysers, DMAs). This gives a unique three-parameter data-set (ambient diameter, dry residual particle diameter and number concentration) and a number of related aerosol/cloud parameters can be determined:

• Number size distribution of ambient cloud/fog droplets and interstitial particles at ambient conditions
• Number size distribution of dry residual particles
• The relation between ambient diameter and dry (residual) diameter on a single droplet/particle basis
• Characterization of the droplet activation as defined by the Köhler equation
• The size dependent scavenging of particles due to activation
• Concentration of soluble matter in the individual droplets (solute concentration)
• Liquid water concentration

A second generation of the instrument has now been developed. The new instrument has a higher time resolution, and is more suited for long-term measurements, which is favourable in order to obtain results with high statistical confidence.

LONG TERM CLOUD MEASUREMENT

With the improved version of the DAA, long-term measurements at the summit of the Mt. Brocken (Germany) will be performed starting in 2009. The project is in collaboration with the Air chemistry group of the Technical University of Brandenburg (BTU Cottbus), who has a cloud measurement site at Mt. Brocken since many years. Long-term measurements provide the possibility for a variety of air masses with different aerosol properties to reach the site. Also different cloud types with different dynamical properties immerse at the site, such as orographically induced clouds (high updraft velocity) and stratiform clouds (low updraft velocity). The combinations of different aerosol properties, air masses, and cloud types can be classified, and the results for each main combination can thus be described with high statistical confidence. Focus will be on warm clouds.

Figure 1. Weather station of the German Meteorological Service DWD (left) and measurement site (right) on Mt. Brocken.

Descriptions of the aerosol-cloud relation will then be derived in relation to the aerosol present and to the cloud dynamics. The results can be used for validations of cloud model results, and to undertake parameterizations for inclusion of the results in large-scale models.

ACKNOWLEDGEMENTS

REFERENCES

[1]   Martinsson, J. Aerosol Sci., 27, 7, 997-1013, 1996

Nitrate and the regional Indirect Aerosol Effect

H.M. ten Brink, R. Otjes, P. Jongejan

Netherlands Energy Research Foundation (ECN), P.O. Box 1, 1755 ZG Petten, The Netherlands

The Indirect Aerosol Effect (IAE) has a maximum in coastal regions like The Netherlands (Roelofs, 2006). The responsible manmade CCN are thought to be dominated by the component sulphate. The concentration of sulphate is drastically declining at the moment and as a consequence the regional IAE should fade out.

The projection of a drastic decline in the IAE can be erroneous, because manmade nitrate may be an important CCN-agent. Moreover, it is projected that its decrease is much less than that of sulphate.

The number of data on nitrate in the CCN-range in our region is limited and the values are often underestimates, because evaporative losses of nitrate occur during sampling.

We investigated the possible role of nitrate as CCN-agent in a process study in our cloud-chamber, of which the results were presented at EAC2008. We concluded that nitrate was present and often dominant in the particles that act as CCN, especially at the low super saturations occurring in the stratocumulus clouds that are most relevant for the IAE.

Most of the particles that activated in our cloud chamber had a size in a narrow range of 120 to 200 nm mobility diameter. This range corresponds to an aerodynamic diameter range of approximately 160 to 280 nm, assuming a (dry) particle density of 1.6 g cm-3.

Longer-term data that can be combined with other aerosol characteristics were absent in our process study. For that reason we performed a year-long monitoring

Monitoring study

We deployed our new monitor, the MARGA-sizer. This instrument allows representative sampling of the semi-volatile ammonium nitrate. The aerosol is size-classified before sampling in a number of (aerodynamic) size fractions.

Monitoring took place during the whole year 2008, encompassing the EUCAARI-campaign in May. The sampling occurred at ground level of the meteo-observation tower of CESAR at Cabauw in the centre of the country.

As sampling line a 2 meter Teflon-tubing was used, in which evaporation of the semi-volatile ammonium nitrate is negligible.

To put the concentration of nitrate in perspective we compare its concentration with that of sulphate, which is also measured with the instrument.

We present here the data obtained in that month. Not only a MARGA-sizer was deployed, but also a standard MARGA, with a better time-resolution was operated. This latter instrument measures the same components without size-classification. This helped in improving the quality of the size-fractionated data.

The size-range that corresponded best with the one in which probably the most numerous CCN reside is that between 180 and 320 um (aerodynamic diameter). For that reason we provide the concentration of nitrate in that size range here, in figure 1.

To appreciate the importance of nitrate also the concentration of sulphate in the same size-range is shown. Noticeable is the much larger variations in the concentration of nitrate which is a characteristic that is also found for the rest of the year.
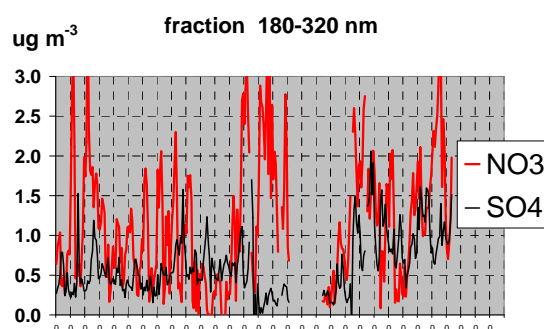
Figure 1. Concentrations of the indicated components in the "CCN-range" during the month of May at the CESAR-site of Cabauw, in the centre of the Netherlands.

In addition to the composition there are data on the CCN-concentration and of the size-spectra in 2008 obtained by partners in the CESAR-consortium. These data should be jointly evaluated to further assess the importance of nitrate as regional CCN-component.

Roelofs, G.J. (2006) *Simulation of the anthropogenic influence on CDNC over Europe. http://www. phys.uu.nl/~roelofs/werk/pdf_papers/roelofs_accent .pdf*

Hygroscopic Growth of Tropospheric Particle Number Size Distributions over the North China Plain

A.Nowak[1], P. Achtert[2], W. Birmili[1] and A.Wiedensohler[1]

[1] Leibniz-Institute for Tropospheric Research, Leipzig, 04318, Leipzig, Germany
[2] Department of Meteorology, Stockholm University, Stockholm, 106 91, Stockholm, Sweden

Keywords: Ambient aerosols, hygroscopic growth, CCN, megacity, air pollution

Atmospheric aerosol particles absorb water vapor at relative humidities well below supersaturation. This hygroscopic growth has consequences on atmospheric visibility and the scattering of downwelling and upwelling solar radiation. The hygroscopicity of particles is furthermore connect with their ability to act as cloud condensation nuclei.

A relatively new experimental method (HDMPS, see Fig. 1) to determine particle hygroscopic growth is the comparison of complete dry and humidified particle size distributions measured by electrical mobility spectrometer, [Birmili et al., 2008; Eichler et al., 2008]. We apply this recently developed technique to obtain growth factors of tropospheric particles over the North China Plain, i.e. in a region where anthropogenic sources highly contribute to the tropospheric aerosol.

Our atmospheric in-situ measurements were conducted between August 10 and September 9, 2006, within the framework of CAREBEIJING (Campaigns of Air Quality Research in Beijing, 2006). The overall goals of CAREBEIJING included the quantification of pollution transport from the southern provinces of the North China Plain into the agglomeration of Beijing to identify and characterize the atmospheric conditions that lead to a degradation of air quality and visibility in the entire region.

Figure 2 provides a comprehensive view of the observation of the atmospheric in-situ measurements at Yufa during CAREBEIJING [Achtert et al., 2009]. Over the 22 day period, dramatic variations occurred in the PM1 mass concentration. Also contains the descriptive hygroscopic particle growth factors (DHGF) obtained at Yufa. DHGFs were extracted for the diameters Dp = 50, 150 and 250 nm — representing key diameters in the size-dependent behaviour of the particles, although the data provided by the summation method allows to extract any particle diameter between 30 and 300 nm. Among the three diameters investigated, the highest DHGFs were obtained for Dp = 250 nm, i.e. the accumulation mode.

Because the influence of different synoptic-scale air masses was highly evident, the entire measurement period was divided into appropriate sub-periods based on back-trajectories as well as the level of total particle mass.
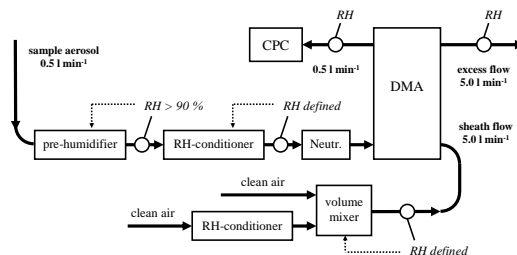
Figure 1: Sketch of the HDMPS. Lines indicate flow scheme. CPC: Condensation particle counter; DMA: Differential mobility analyser.
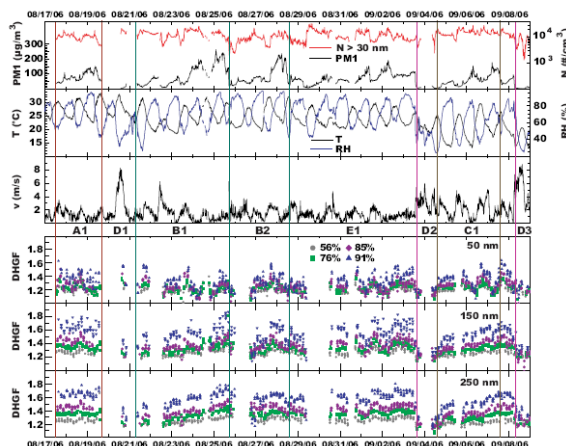
Figure 2: Atmospheric measurements at the Yufa site during CAREBEIJING: PM1 mass concentration, particle number concentration (N) (Dp >30 nm), temperature (T), relative humidity (RH), wind speed (v), and DHGFs extracted for Dp = 50, 150 and 250 nm.

Birmili, W., K. Schwirn, A. Nowak, et al. (2008), Hygroscopic growth of atmospheric particle number size distributions in the Finnish boreal forest region, manuscript submitted to Bor. Env. Res., 19/5/2008.
Eichler, H., Y. F. Cheng, W. Birmili, et al. (2008), Hygroscopic properties and extinction of aerosol particles at ambient relative humidity in South-Eastern China, Atmos.Env.,inpress,doi:10.1016/j.atmosenv.2008.05.007.
Achtert, P., W. Birmili, A. Nowak, et al. (2009), Hygroscopic Growth of Tropospheric Particle Number Size Distributions over the North China Plain, J. Geophys. Res., doi:10.1029/2008JD010921, in press.

CCN ability of mixed organic-inorganic particles

M. Frosch[1], N.L. Prisle[1], M. Bilde[1], Z. Varga[2] and G. Kiss[3]

[1]Department of Chemistry, University of Copenhagen, Universitetsparken 5, DK-2100 Copenhagen, Denmark
[2]Department of Earth and Environmental Sciences, University of Pannonia, Egyetem 10, 8200 Veszprém, Hungary
[3]Air Chemistry Group of Hung. Acad. Sci. at University of Pannonia, Egyetem 10, 8200 Veszprém, Hungary

Keywords: CCN, carbonaceous aerosol, Köhler theory, CCNC measurements

Organic compounds often account for the majority of fine aerosol mass and therefore may play an important role in cloud formation. The CCN ability, surface tension effect and water activity depression of pure organic compounds have been examined in a number of studies. However, in most cases, ambient aerosol particles are composed of both organic compounds and inorganic components. In this study different mixtures of organic acids and inorganic salts were investigated (see Table 1).

Table 1. Composition of the mixtures studied

Components of the mixture	Mass %
Oxalic acid – Ammonium sulfate	50-50
Oxalic acid – Ammonium sulfate	80-20
Succinic acid – Ammonium sulfate	50-50
Adipic acid – Ammonium sulfate	50-50
Citric acid – Ammonium sulfate	50-50
cis-Pinonic acid – Ammonium sulfate	50-50
Nordic Reference Fulvic Acid (NRFA) – Ammonium sulfate	50-50
Oxalic acid – Sodium Chloride	50-50
Oxalic acid – Sodium Chloride	80-20

First, solutions were prepared that corresponded to different growth factors. Then surface tension and water activity of these solutions were determined by using pendant drop shape analysis and freezing point osmometry, respectively. Finally, critical supersaturations corresponding to different dry particle sizes were calculated using Köhler theory. In a parallel set of experiments critical supersaturations were determined with a cloud condensation nucleus counter (CCNC).

The surface tension depression caused by most of the studied organic acids was negligible in the concentration range that is relevant at activation. Consequently, only the very early phase of droplet growth is influenced by the surface tension effect of these compounds but there is no effect on the critical supersaturation. However, this statement does not apply for NRFA and cis-pinonic acid which decreased the surface tension of the solution by 6-20% in solutions corresponding to activation conditions. The surface tension depression of these surfactants had a reducing effect on critical supersaturation as well. The surface tension of the droplet solutions composed of organic surfactant + ammonium sulfate mixtures at a given growth factor was higher than for the pure surfactant but lower than for the pure inorganic salt.

Water activity of the solutions was determined by the inorganic salts due to the higher degree of dissociation. At a given growth factor water activity of an organic acid + inorganic salt mixture was in most cases higher than for the pure inorganic salt but lower than for the pure organic compound. The type and relative quantity of the inorganic salt significantly influenced the water activity of the droplet solutions and thus activation as well. In this respect the oxalic acid + ammonium sulfate mixtures are exceptions because these mixtures activate at very similar critical supersaturations independent of the ratio of oxalic acid and ammonium sulfate.

Critical supersaturations of particles composed of the above mixtures and having different dry diameters were experimentally determined with a cloud condensation nucleus counter as well. Results for oxalic acid and ammonium sulfate (50-50) are shown in Figure 1. Continuous lines were obtained from surface tension and osmometry measurements by applying Köhler theory while individual data points were measured with the CCNC. For most mixtures similarly good agreement was experienced.
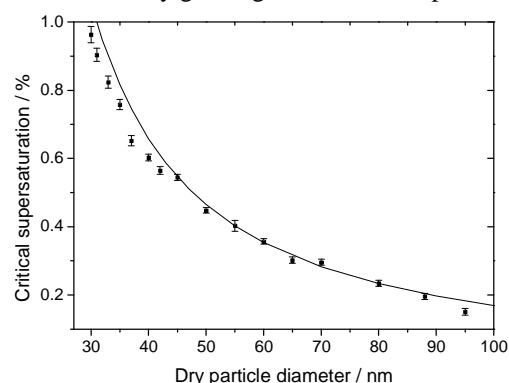
Figure 1. Oxalic acid and ammonium sulphate, 50-50

Quantitative study of the water content and phase transition behaviors of aerosol particles deposited on a hydrophobic substrate using micro-Raman spectroscopy

M.C. Yeung[1, 2] and C.K. Chan[2]

[1]Environmental Engineering Program, Hong Kong University of Science and Technology, Clear Water Bay
Kowloon, Hong Kong
[2]Department of Chemical and Biomolecular Engineering, Hong Kong University of Science and Technology, Clear Water Bay, Kowloon, Hong Kong

Keywords: phase transitions, hygroscopicity, Raman microscopy, particle characterization

The role of atmospheric particles in global climate change has been recognized due to their effects on radiative forcing (Charlson *et al.*, 1992; Haywood & Boucher, 2000). The forcing mechanisms always depend on the physical properties of the particles, such as the hygroscopic properties and phase states, Hence, knowledge of the hygroscopic and phase transition behaviors of particles is essential to understanding their effects on the climate.

In this study, we used micro-Raman spectroscopy to investigate the hygroscopicity and phase transition behaviors of in situ particles of various compositions, including pure inorganic (ammonium sulfate (see Figures 1 and 2) and ammonium nitrate), pure organic (malonic acid, glutaric acid and glyoxylic acid), as well as ammonium sulfate particles mixed with dicarboxylic acid particles. Particles deposited on a hydrophobic substrate were exposed to changing relative humidity. Raman spectra measured at different relative humidities were used to determine the water content and phase of the particles.

We present hygroscopicity in terms of water-to-solute mass ratios, which are obtained from the integrated area ratios of the water band to a distinct solute peak. Deliquescence and crystallization can be confirmed by abrupt changes in the Raman peak position and the full-width-half-height of distinct solute peaks. The results in this study agree well with literature findings (Lightstone *et al.*, 2000; Peng *et al.*, 2001; Ling & Chan, 2008) and model predictions (Clegg *et al.*, 2006), demonstrating the capability of the micro Raman spectroscopic approach in studying the hygroscopicity and phase transition behaviors of particles, including supersaturated droplets.

Charlson, R. J., Schwartz, S. E., Hales, J. M., Cess, R.D., Coakley, J. A., Hansen, Jr., J. E. & Hofmann, D. J. (1992). *Science*, 255, 423-430.
Haywood, J. & Boucher, O. (2000). *Rev. Geophys*, 38, 513-543.
Lightstone, J. M.; Onasch, T. B.; Imre, D. & Oatis, S. (2000). *J. Phys. Chem. A*, 104, 9337-9346.
Peng, C., Chan, M. N. & Chan, C. K. (2001). *Environ. Sci. Technol.*, 35, 4495-4501.
Ling, T. Y. & Chan, C. K. (2008). *J. Geophys. Res.*, 113, D14205, doi:10.1029/2008JD009779.
Clegg, S. L. & Seinfeld, J. H. (2006). *J. Phys. Chem. A,* 110, 5692-5717.
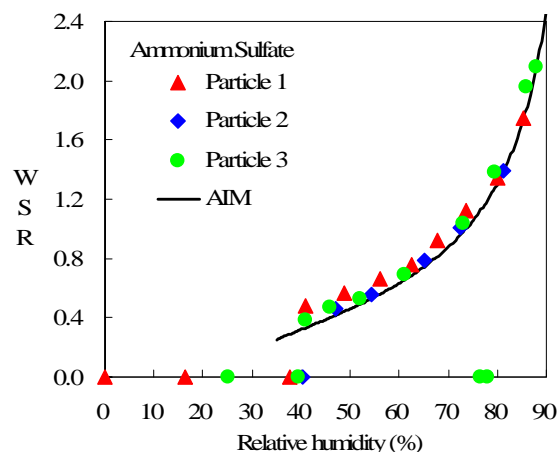
Figure 1. Change in the water content of pure AS particles. The WSRs calculated from the AIM model are also included (black curve).
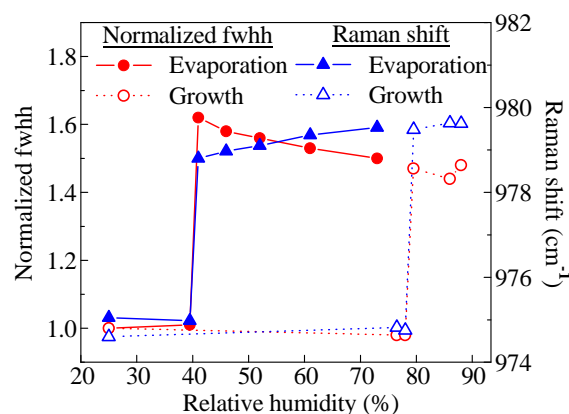
Figure 2. Changes in normalized fwhh and Raman shift of the sulfate peak (980 cm^{-1}) of a pure AS particle under a humidity cycle.

Measured and Modelled Hygroscopic Properties of the Background Ambient Aerosol in the Southern Part of Sweden

E. Nilsson[1], P. Roldin[1], E. Swietlicki[1]

[1]Department of Physics, University of Lund, SE 221 00, Lund, Sweden

Keywords: H-TDMA, HYSPLIT model, Modelling, Ambient aerosols

The hygroscopic properties of the atmospheric aerosol are of great importance to the global climate. Not only do they have an influence on the direct aerosol effect by altering the particle size with water uptake, but they also affect the point of activation and the number of clod droplets which in turn affect cloud albedo and lifetime (the so called indirect effect) (Kaufmann *et al*., 2002).

One way to measure the hygroscopic properties of the aerosol is with a Hygroscopic Tandem Differential Mobility Analyser (H-TDMA), which measures the mobility diameter growth. This technique gives information both on the water uptake of the individual particles and on the degree of external mixing, as different separated modes of hygroscopicity can be isolated. An H-TDMA designed for long term measurements of the ambient aerosol has been constructed within the frameworks of the EU FP6 Infrastructure Project EUSAAR and was deployed at the Swedish background site Vavihill in May 2008. It has been in operation since then, measuring dry particle size diameters between 35 nm and 265 nm and continuously validating data with daily automated measurements of ammonium sulphate.

In this work, HYSPLIT trajectory analysis will be used on ~ 1 year of H-TDMA data to quantify the hygroscopic properties of particles originating from different sectors during different seasons, chosen because of their respective classes of possible particle sources. The sectors represent e.g. clean air from the northern sea, clean air from the boreal forests, polluted air from the Baltic region, etc.

Case model studies have been carried out for each sector. An aerosol dynamics model including particle phase chemistry (ADCHEM), developed at Lund University has been used to attempt to link the modelled particle chemistry to the hygroscopic properties measured at ground level.

The example presented in this abstract is from the 6th of October 2008 at 16:00. This relatively clean air mass with respect to anthropogenic emissions originated from the Atlantic sea 24 hours earlier and passed over northern Denmark before reaching Sweden and Vavihill (Fig 1.). The measured and modelled hygroscopic growth factors correspond well with each other (Fig 2.). The model predicted an increasing water uptake for the larger dry particle sizes at this particular day, which was confirmed by

the H-TDMA measurements. This is in the model results mostly due to an increasing fraction of NaCl for the larger sizes, originating from sea spray.

Figure 1. 24 h backwards trajectory from 16:00 on the 6th of October 2008.
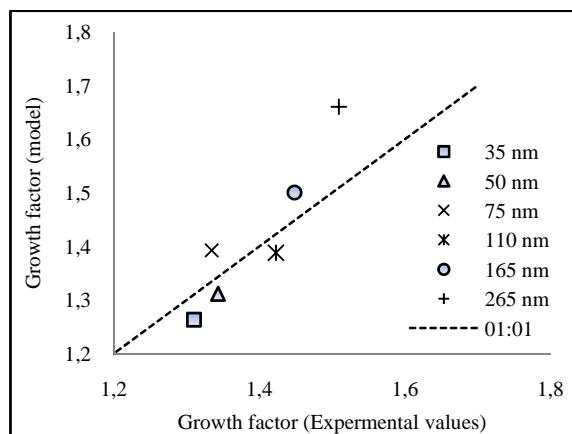
Figure 2. Modelled and measured hygroscopic growth at Vavihill.

Kaufman, Y. J., Tanre, D., and Boucher, O. (2002). *A satellite view of aerosols in the climate system*, Nature, 419, 215-223.

Aerosol Radiative forcing over an Urban Indian City

A.S. Panicker [1] and G. Pandithurai [1]

[1] Indian Institute of Tropical Meteorology, Pashan, Pune-411008, India

Key words: AOD, Atmospheric aerosols, Single scattering albedo

Collocated observations of aerosol optical parameters, radiative fluxes in the longwave (0.4-50µm), shortwave (0.3-3 µm) spectral regions and aerosol chemical composition data has been used to quantify aerosol radiative forcing in the longwave (LW) and shortwave (SW) spectral regions over an Indian urban site, Pune during a dry winter [Dec2004 to Feb2005]. Aerosol optical parameters derived from a Prede Sun/Sky radiometer (Prede Inc., POM-01L) such as aerosol optical depth(AOD) , single scattering albedo(SSA), asymmetry parameter (ASP), OMI column ozone and MODIS water vapor have been incorporated in the Santa Barbara Discrete-ordinate Atmospheric Radiative Transfer model (SBDART) to derive short wave fluxes. The derived shortwave fluxes compared well with the Pyranometer-observed short wave fluxes.

Since no direct observations of aerosol optical properties are available in the longwave spectral region (above 1.2 µm), observed aerosol chemical composition data sets such as water-insoluble, water-soluble components and soot values were incorporated in the software package OPAC to derive the optical properties of aerosols in the longwave region (1.2-40 µm). OPAC-derived aerosol optical properties were compared with those of Skyradiometer-derived and found to be matching well at visible and near IR wavelengths (Figure 1).

The sky radiometer observed aerosol properties in the short-wave region and OPAC derived aerosol optical properties in the longwave region along with OMI column ozone, MODIS water vapor and 6-hourly NCEP profiles of temperature and humidity have been incorporated in SBDART to derive Long wave fluxes. Simulated LW fluxes found to be matching well with the Pyrgeometer observed LW fluxes. Fluxes in SW and LW regions also has been derived for aerosol free conditions also to calculate radiative forcing, which is the difference in fluxes with and with out aerosols. The short wave forcing is found to be around -35 Wm^{-2} at the surface while in the longwave domain forcing value found to be around +8 Wm^{-2} at the surface. The net forcing (LW+SW) at the surface found to be -27 Wm^{-2}. The study suggests that on contrary to the cooling in the shortwave region, aerosols increases surface warming in the long wave domain, enhancing green house effect. The results obtained here agree with the study conducted by vogelmann et al., (2003).
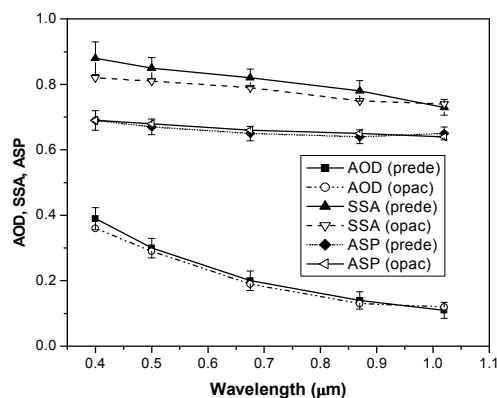
Figure.1: Comparison of Sky radiometer observed and OPAC derived aerosol optical properties.

Reference:

Vogelmann, A, M., P. J. Flatau, M. Szczodrak, K. M. Markowicz, and P. J. Minnett (2003), Observations of large aerosol infrared forcing at the surface, *Geophy. Res .Lett, 30(12),* 1655, doi:10.1029/2002GL016829.

Determination of the aerosol shortwave radiative forcing in the Mediterranenan from ground based and satellite observations

C. Di Biagio, A. G. di Sarra and D. Meloni

ENEA-ACS, via Anguillarese 301, 00123, S. Maria di Galeria (Roma), Italy
Keywords: aerosol radiative forcing, optical depth, african dust, marine aerosols.

Atmospheric aerosols play a relvant role in the detrmination of the Mediterranean radiative budget, and its climate. They may intervene in the hydrologic cycle through different mechanisms, and may influence cloud properties and the vertical structure of the atmosphere.

Measurements of aerosol optical properties, solar radiation, and other parameters relevant for climate are routinely carried out at the Mediterranean island of Lampedusa (35.5°N, 12.6°E). Data from the period June 2004 – August 2006 are used in this study. A multifilter rotating shadowband radiometer (MFRSR) (Harrison *et al.*, 1994) and several pyranometers (PSP) are used to derive the aerosol optical depth, τ, at 500 nm and the shortwave irradiance at the surface. The ground-based observations are combined with satellite determinations of the outgoing shortwave flux obtained with the Clouds and the Earth's Radiant Energy System (CERES) (Wielicki *et al.*, 1996) on board Terra and Aqua satellites.

The measurements are used to estimate the surface and the top of atmosphere (TOA) shortwave aerosol direct radiative forcing. The direct method (Satheesh & Ramanathan, 2000) is here applied to derive the radiative forcing efficiency (FE), i.e. the forcing produced by aerosol with $\tau=1$. The radiative forcing is then obtained by multiplying FE by τ.

Two different aerosol types are discriminated on the basis of their optical properties and on backward airmass trajectories (Pace *et al.*, 2006): desert dust, DD, and mixed aerosol, MA. DD are aerosols transported from the Sahara desert to Lampedusa, while MA includes marine, marine polluted, and mixtures of different types of particles. The average aerosol optical depth over the period June 2004 – August 2006 is (0.265 ± 0.085) for DD, and (0.143 ± 0.065) for MA.

The surface and TOA forcing efficiency are derived, for solar zenith angles θ between 15° and 45°, for DD, MA, and for the whole dataset, WD. The atmospheric forcing efficiency is also derived as the difference between TOA and surface forcing.

Table 1 shows the retrieved values of the instantaneous shortwave radiative forcing at TOA (RF_{TOA}) and at the surface (RF_S) for solar zenith angles of 15°-25°, 25°-35° and 35°-45° for DD, MA, and WD.

The forcings at the surface and TOA are larger for DD (about -60 and -25 Wm^{-2}, respectively) than for MA (about -45 and -10 Wm^{-2}). This is due to

the high value of both forcing efficiency and average optical depth for DD with respect to MA. FE at the surface is comprised between -220 and -240 Wm^{-2} for DD, and between -250 and -310 Wm^{-2} for MA; the forcing efficiency at TOA is between -100 and -77 Wm^{-2} for DD, and between -70 and -57 Wm^{-2} for MA.

Table 1. Instantaneous shortwave TOA (RF_{TOA}), and surface (RF_S) radiative forcing (Wm^{-2}) retrieved at different intervals of θ for DD, MA, and WD.

	θ	$(RF_{TOA} \pm \sigma_{RF})$	$(RF_S \pm \sigma_{RF})$
DD	15°-25°	-26.5 ± 5.4	-62 ± 13
	25°-35°	-33.1 ± 5.7	-59 ± 11
	35°-45°	-20.4 ± 9.2	-
MA	15°-25°	-8.2 ± 2.6	-45 ± 12
	25°-35°	-10.0 ± 2.9	-43 ± 12
	35°-45°	-9.4 ± 2.6	-36 ± 10
WD	15°-25°	-11.3 ± 2.7	-43 ± 12
	25°-35°	-13.2 ± 3.2	-42 ± 11
	35°-45°	-10.7 ± 2.6	-

The atmospheric forcing is between +26 and 37 Wm^{-2}. These results indicate that the atmospheric forcing is more than 50% of the surface forcing. This large radiative effect may induce a significant perturbation to the atmospheric thermal structure, stability, and to cloud properties.

Harrison, L., Michalsky J., and Berndt J. (1994). *Appl. Opt.,* 33, 5118-5125.

Pace, G., di Sarra A., Meloni D., Piacentino S., & Chamard P. (2006). *Atmos. Chem. Phys.*, 6, 697-713.

Satheesh, S. K., & Ramanathan V. (2000). *Nature*, 405, 60-63.

Wielicki, B. A., Barkstrom B. R., Harrison E. F., Lee III R. B., Smith G. L., & Cooper J. E. (1996). *Bull. Amer. Meteorol. Soc.*, 77, 853-868.

Observations of aerosol-cloud interactions at Puijo semi-urban measurement station

H.J. Portin[1], M. Komppula[1], A.P. Leskinen[1], S. Romakkaniemi[2], A. Laaksonen[3,2] and K.E.J. Lehtinen[1,2]

[1]Finnish Meteorological Institute, Kuopio unit, P.O. Box 1627, FI-70211, Kuopio, Finland
[2]University of Kuopio, Department of Physics, P.O. Box 1627, FI-70211, Kuopio, Finland
[3]Finnish Meteorological Institute, Research and Development, P.O. Box 503, FI-00101 Helsinki, Finland.

Keywords: aerosol cloud interaction, atmospheric aerosols, clouds, indirect effect.

In 2006, a new measurement station for aerosol-cloud interactions was established in Kuopio, Finland (Leskinen *et al.*, submitted to *Boreal Env. Res.*). The station is located on top of the Puijo observation tower (306 m a.s.l, 224 m above the surrounding lake level), offering good conditions for particle and cloud measurements.

We are using a twin-DMPS system for particle size distribution measurement with a size range of 10-500 nm until March 2007 and 7-800 nm thereafter. We have a heating in the sample inlet for drying the cloud droplets, so we observe the total (interstitial+residual) size distribution. Cloud droplet size distribution (3-50 µm) is measured with a cloud droplet probe (Droplet Measurement Technologies).

We calculated hourly averages of weather parameters, particle and cloud droplet size distribution data. We classified all hourly averages with visibility below 200 m and rain intensity below 0.2 mm/h as cloud event hours. We use the limit for rain intensity, since rain drops remove unactivated aerosol particles and would disturb analysis.

We classified this data into four groups based on the particle number concentration in order to distinguish the correlations between concentration and parameters involved in cloud-particle interaction. We found three indications of the aerosol indirect effects (Table 1): 1) Cloud droplet concentration N_d increased with the increasing particle concentration N_p. 2) N_d and average droplet diameter d_d were inversely proportional, as previous studies have shown (e.g. Komppula *et al.*, 2005; Twohy *et al.* 2005). 3) Ratio of N_d to accumulation mode particle concentration N_{acc} was smaller when N_p is higher.

We did trajectory analysis to classify the air masses into marine and continental. It should be noted that the marine air masses can not be considered purely marine since they spent on average 40 hours over the continent before arriving to Puijo. Marine air masses were characterized by the higher N_p, higher N_{ait}/N_{acc} ratio and smaller N_d compared to continental (Table 2). The higher N_{ait}/N_{acc} ratio in the marine air masses is consistent with the pronounced Aitken mode of usual marine size distributions (e.g. Anttila *et al.*, 2008). The lower N_p in continental air masses compared to marine was not what one would expect. It seems that during the cloud events, the continental air masses were relatively clean, the average N_p being below the annual average.

Table 1. Total particle concentration N_p, cloud droplet concentration N_d, droplet diameter d_d (µm), accumulation mode particle concentration N_{acc}, N_d/N_{acc} and ratio of Aitken mode particle concentration to accumulation mode particle concentration N_{ait}/N_{acc} during the observed cloud events. Last line shows average values during all cloud events. All concentrations are in cm^{-3}.

N_p	N_d	d_d	N_{acc}	N_d/N_{acc}	N_{ait}/N_{acc}
< 700	160	7.77	130	1.23	2.41
700-1300	248	6.16	326	0.76	1.80
1300-2200	261	5.95	389	0.67	2.72
> 2200	294	5.37	502	0.59	3.50
1375	239	6.33	328	0.72	2.47

Table 2. Same as table 1, but data is classified into marine and continental according to air mass origin.

class	N_d	d_d	N_p	N_{acc}	N_d/N_{acc}	N_{ait}/N_{acc}
marine	203	6.82	1313	191	1.06	4.08
cont.	231	6.55	1160	334	0.69	1.90

Anttila, T., Vaattovaara, P., Komppula, M., Hyvärinen, A.-P., Lihavainen, H., Kerminen, V.-M., & Laaksonen, A. (2008) *Atmos. Chem. Phys. Discuss.*, 8, 14519-14556.

Komppula, M., Lihavainen, H., Kerminen, V.-M., Kulmala, M., & Viisanen, Y. (2005) *J. Geophys. Res.*, 110, D06204, doi: 10.1029/2004JD005200.

Leskinen A.P., Portin H.J., Komppula M., Lihavainen H., Laaksonen A. & Lehtinen K.E.J. submitted to *Boreal Env. Res.*

Twohy, C.H., Petters, M.D., Snider, J.R., Stevens, B., Tahnk, W., Wetzel, M., Russell, L., & Burnet, F. (2005) *J. Geophys. Res.*, 110, D08203, doi:10.1029/2004JD005116.

Weighting aerosol with MERIS

A. A. Kokhanovsky[1,2], A. S. Prikhach[2], I. L. Katsev[2], E. P. Zege[2], A. P. Ivanov[2]

[1]Institute of Environmental Physics, University of Bremen, O. Hahn Allee 1, D-28334, Bremen, Germany
[2]Institute of Physics, National Academy of Sciences of Belarus, Nezaleznasti Avenue 68, 22068, Minsk, Belarus

The measurements of the mass concentration of aerosol in terrestrial atmosphere is of great importance for a number scientific disciplines, climate studies, pollution monitoring, and aerosol transport. Therefore, the aerosol particulate matter mass concentration (e.g. PM10, particulate matter with diameters of aerosol particles smaller than 10 microns) is measured in thousands locations worldwide on a regular basis. Ground measurements, however, are quite expensive and limited with respect to the spatial coverage. On the other hand, satellite measurements enable the observation of large areas (e.g., Europe) in a short time interval with varying resolution depending on the instrument. In particular, the MEdium Resolution Imaging Spectrometer (MERIS) onboard ENVISAT has the resolution $0.3 \text{km} \times 0.3 \text{km}$, which is sufficient for pollution monitoring on a fine scale. The task of this paper is to present a novel technique for the determination of the aerosol mass concentration from spaceborne observations. The idea of the technique is quite simple. The proposed method is based on the retrieval of the Aerosol Optical Thickness (AOT) in the spectral range 412-670nm, from satellite data. The most recent family of these algorithms is presented and discussed by Kokhanovsky and de Leeuw (2009). The derived spectral AOT can be presented in the following form:

$$\tau(\lambda) = \beta \lambda^{-\alpha}. \qquad (1)$$

Here λ is the wavelength, β is the value of AOT at $\lambda = 1\mu m$ and α is so – called Angstrom parameter. Clearly, α is determined by the size of particles being larger for smaller scatterers. It approaches 4.0 for molecular scattering and zero for large particles such as in dust clouds uplifted from the desert surfaces during dust storms. In this work we propose simple parameterizations for dependencies of α and average extinction cross section of particles C_{ext} on the effective radius of particles defined as the ratio of the third to the second moment of the aerosol size distribution. This enables to relate the columnar number of particles n (measured in m^{-2}) to the retrieved values of AOT (its value at 412nm is used) and the derived parameter α. In particular, it follows:

$$n = \tau C_{ext}^{-1}. \qquad (2)$$

Here n can be related to some average number concentration of aerosol particles N and the aerosol layer thickness L with the following simple equation: $n = NL$. Therefore, if L can be estimated, then also the particulate matter concentration $m = NV\rho$ (in $\mu g/m^3$) can be derived. Here ρ is the density of aerosol particles and V is their average volume. It is difficult to estimate L from space. Therefore, it is proposed to retrieve the columnar particulate matter concentration $M = mL$, which does not depend on the vertical extent and the position of the aerosol layer in atmosphere, in the absence of information on the aerosol position and thickness.

The corresponding retrieval technique was implemented in the C++ code and run using MERIS data, provided by the European Space Agency, for a single day over Germany (October 13th, 2005). The maps of AOT, Angstrom parameter, effective radius of particles, and particulate matter vertical columns (PMVC) were prepared. It was found that measurements from a satellite correlate well with ground measurements of AOT and Angstrom parameter. The good enough correlation between satellites derived PM values and ground measured PM values averaged over a large area was observed. But correlation of the local ground measured and satellite derived PM is quite poor, which can be explained by different spatial scales of corresponding techniques. Nevertheless, the derived PMVC maps represent spatial patterns of the aerosol distribution on a large scale in a correct way. They can be used by environmental agencies for assessing related environmental risks and health indices in a fast and reliable way.

Kokhanovsky, A.A., & de Leeuw, G. (2009). *Satellite Aerosol Remote Sensing Over Land*, Berlin: Springer-Praxis.

Estimating PM$_{2.5}$ over southern Sweden using satellite measurements

P. Glantz[1], A. Kokhanovsky[2], W. von Hoyningen-Huene[2] and C. Johansson[1]

[1]Department of Applied Environmental Science, Stockholm University, Frescativägen 50, SE-106 91, Stockholm, Sweden
[2]Institute of Environmental Physics, University of Bremen, Otto-Hahn-Allee 1, 28359, Bremen, Germany

Retrievals of aerosol optical thickness (AOT) using spaceborne MERIS ENVISAT and MODIS AQUA observations in central Europe for the days 26 March to 1 April 2007 are compared with AERONET (Aerosol Robotic NETwork. The retrievals are performed using the algorithm described by von Hoyningen-Huene et al. (2003). On the whole the agreement between satellite and ground retrievals is good (MERIS, R^2=0.86; MODIS, R^2=0.92). However, for higher values the satellite instruments somewhat underestimate AOT compared to AERONET. This could be caused by aerosol absorption effects that are not included in the present approach. Polluted air masses contain significant quantities of soot particles and have therefore a lower single scattering albedo compared with 0.98, which is assumed in the present work. Furthermore, for low aerosol loadings (AOT < 0.15) the satellite retrieved AOT is a factor of 2 higher than AERONET. This is probably caused by too low surface reflections described in the retrieval model.

Here we have also combined satellite retrievals of AOT over southern Sweden with ground measured PM$_{2.5}$. MODIS (~1 km) mean AOT versus in-situ PM$_{2.5}$ over southern Sweden for the days 26 March to 1 April 2007. Results are shown in Figure 1. The AOT and PM$_{2.5}$ have been averaged according to eight pixels surrounding the pixel corresponding to

the in-situ station and approximately half an hour before and after the satellite overpass, respectively. The relative humidity (ECMWF) was low over the southern Sweden during these days and hygroscopic growth of the aerosols has therefore been neglected in this study. Figure 1 shows that a relatively good correlation ($R^2 = 0.59$) is obtained between satellite retrieved AOT and ground measured PM$_{2.5}$. Similar slope (with $R^2 = 0.58$) as the one shown in Fig.1 is obtained between MERIS full resolution (FR) data (300 m) and in-situ PM$_{2.5}$ (not shown). The slope values (0.012 µg^{-1} m^3 and 0.013 µg^{-1} m^3 for MERIS and MODIS, respectively) agree reasonable well with 0.014 µg^{-1} m^3 and 0.019 µg^{-1} m^3 found by Wang and Christopher (2003) and Shinozuka et al. (2007), respectively. A relative humidity value of 80% (Shinozuka et al., 2007) and a growth factor according to polluted aerosol are assumed in the present estimations.

The relationship between satellite estimated and ground measured PM$_{2.5}$ has been applied on MERIS FR data over Stockholm and surrounding area. Our preliminary analysis shows that the geographic variations in particle emissions from road traffic in Stockholm correlate with satellite derived measurements of PM$_{2.5}$.
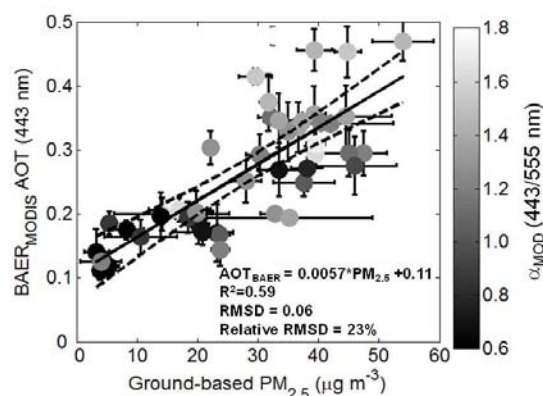
Figure 1. MODIS retrieved AOT (443 nm) versus ground measured PM$_{2.5}$ over southern Sweden for the days 26 March to 1 April 2007. The solid line is a linear fit and the corresponding 95% confidence interval is denoted with dashed lines. The gray colors denote MODIS alpha exponent (α_{MOD} (443/555 nm)).

Shinozuka, Y., Clarke, A. D., Howell, S. G., Kapustin, V. N., McNaughton, C. S., Zhou, J., and Anderson, B. E., (2007), Aircraft profiles of aerosol microphysics and optical properties over North America: Aerosol optical depth and its association with PM2.5 and water uptake, *J. Geophys. Res.*, 112, D12S20.

von Hoyningen-Huene, W., Freitag, M., and Burrows, J. B. (2003), Retrieval of aerosol optical thickness over land surface from top-of-atmosphere radiance, *J. Geophys. Res*, 108, D9, 4260.

Wang, J. and Christopher, S. A., (2003), Intercomparison between satellite-derived aerosol optical thickness and PM2.5 mass: Implications for air quality studies, *Geophys. Res. Lett.*, 30, 2095.

One-year measurements of aerosol vertical profiles in Gual Pahari, India

M. Komppula[1], T. Mielonen[1], H. Lihavainen[2], A.-P. Hyvärinen[2], V.-M. Kerminen[2], H. Baars[3], R. Engelmann[3], B. Heese[3], D. Althausen[3], T.S. Panwar[4], R.K. Hooda[4], V.P. Sharma[4] and Y. Viisanen[2]

[1]Finnish Meteorological Institute, P.O.Box 1627, FI-70211, Kuopio, Finland.
[2]Finnish Meteorological Institute, P.O.Box 503, FI-00101, Helsinki, Finland.
[3]Leibniz Institute for Tropospheric Research, Permoserstr. 15, D-04318, Leipzig, Germany.
[4]The Energy and Resource Institute, Dabari Seth Block, IHC Complex, Lodhi Road, 110 003, New Delhi, India.

Keywords: lidar, lidar ratio, extinction, remote sensing, air pollution.

The effects of atmospheric aerosols and their interactions with clouds have the largest uncertainty in climate forcing estimates (e.g. Ramanathan *et al.*, 2001; Lohmann & Feichter, 2005). Particles affect and change various climatically important factors, like the cloud reflectivity and lifetime. The influence of particles on radiative balance is depending on their properties and vertical profiles.

In Southern Asia only few measurements of aerosol vertical profiles have been carried out, and mostly during short campaigns. Though, these countries have an important role in the battle against pollution and climate change. The largest and most persistent of pollution-caused hazes, the "brown cloud", covers an area of 10 million km^2 over the Southern Asia and concerns more than 50 % of the world's population. This particulate air pollution is assumed to originate from fossil fuel and biomass burning. The polluted air is likely to have significant harmful effects on human health and regional climate over Southern Asia (e.g. Pandey *et al.*, 2005; Lau & Kim, 2006; Ramanathan *et al.*, 2007). It is suggested that the atmospheric brown cloud in Asia contributes to the regional lower-tropospheric warming as much as the recent increase of the anthropogenic greenhouse gases (Ramanathan *et al.*, 2007).

We have established a one year campaign of lidar measurements to measure aerosol vertical profiles in Gual Pahari (28º26'N, 77º09'E, 243 m a.s.l.), India. The station is surrounded by agricultural farm fields and forests, about 30 km south of Delhi. The lidar measurements were conducted from March 2008 to March 2009. The measurements belong to the frame of the EUCAARI (European Integrated project on Aerosol Cloud Climate and Air Quality interactions) project.

The instrument used, is a seven-channel Raman-lidar called "POLLY XT–POrtabLe Lidar sYstem eXTended" (Althausen *et al.*, 2008). The output of the instrument includes vertical profiles of the particle backscattering coefficient at three wavelengths (355, 532 & 1064 nm) and of the particle extinction coefficient at two wavelengths (355 & 532 nm). The vertically integrated extinction coefficient gives the AOD (Aerosol Optical Depth). Also such size/composition-dependent, intensive particle quantities as the Ångstrom exponents of the backscatter and the extinction coefficients, the lidar ratio and depolarisation can be determined. With this optical data it is possible to get information about the particle size distribution and chemical composition with an inversion. The height and the evolution of the boundary layer and night-time residual layer can be defined together with the height and thickness of different cloud and aerosol layers. The depolarisation channel (355 nm) of the lidar enables us to estimate the ratio of ice crystals and water droplets in clouds. The vertical resolution of the system is 30 meters. Depending on the cloudiness the whole troposphere can be monitored (up to few tens of kilometres).

Preliminary results reveal up to 5 km thick aerosol layers, with AODs well above one. The lidar-based AOD values were in line with the values obtained from MODIS (The Moderate Resolution Imaging Spectroradiometer) satellite instrument. Often multi-layer aerosol structure is observed and with backward trajectories the sources areas of various layers can be defined. Furthermore, statistics of the boundary layer evolution will be defined and the measurements will be compared with ground-based measurements at the site. A detailed comparison with AOD obtained from lidar and MODIS will be done. The typical backscattering and extinction profiles for the different seasons will be provided. Attempts to characterize the share of biomass burning aerosol and dust will be done.

Althausen, D., Engelmann, R., Baars, H., Heese, B., & Komppula, M. (2008). In *Conf. Proceedings of The 24th International Laser Radar Conference*, Boulder, 23.-27.6.2008, Abstract S01P-04.

Lau, K.-M., & Kim, K.-M. (2006). *Geophys. Res. Lett.*, 33, L21810, doi:10.1029/2006GL027546.

Lohmann, U., & Feichter J. (2005). *Atmos. Chem. Phys.*, 5, 715–737.

Pandey, J. S., Kumar, R., & Devotta, S. (2005). *Atmos. Environ.*, 39, 6868–6874.

Ramanathan V., Crutzen P.J., Kiehl J.T., & Rosenfeld D. (2001). *Science*, 294, 2119–2124.

Ramanathan, V., Ramana, M.V., Roberts, G., Kim, D., Corrigan, C., Chung, C., & Winker, D. (2007). *Nature*, 448, 575–579.

Estimating spectral optical depth of cirrus clouds in the visible domain by synergistic use of Spectrometric and Lidar techniques

M.R. Calvello[12], P. Di Girolamo[1], T. Di Iorio[3], F. Esposito[12], G. Pavese[2], D. Summa[1]

[1]Dipartimento di Ingegneria e Fisica dell'Ambiente, Università della Basilicata, Potenza, I-85100, Italy
[2]CNR-IMAA, Tito Scalo (PZ), I-85055, Italy
[3]Dipartimento di Fisica, Università La Sapienza, 00100 Roma, Italy

This paper presents an experimental technique to estimate the spectral optical depth of a cirrus cloud obtained from the synergistic use of Lidar and Spectrometric measurements. The technique has been applied on the dataset collected in Cervinia (about 2000 m a.s.l.) on 13 March 2007 during COBRA-Ecowar campaign (Bhawar et al., 2008).

The considered Lidar system measured, besides other atmospheric parameters, the particle backscattering coefficients at 355, 532 and 1064 nm and the particle extinction coefficients at 355 and 532 nm, allowing aerosol and cirrus optical depth estimation.

Spectral columnar atmospheric optical depth values were derived from solar irradiance spectra measured at ground level with 1.5 nm of resolution, by using an Avantes AVS-USB 2000 radiometer.

Using these two experimental techniques in a synergistic way means that lidar data are used to distinguish and separate aerosol and cirrus contribution to the atmospheric optical depth, while the radiometric measurements are used to extend throughout the visible domain the cirrus optical depths previously measured at 532 nm.

In fact, on 13 March 2007 the lidar system detected, from 10:00 to 12:00 UTC, a thin cloud at 9 km a.g.l. together with a stable aerosol component near the ground, as shown in figure 1.
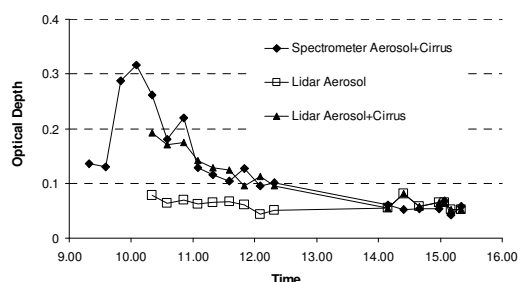
Figure 1. Comparison between Lidar and Spectrometric aerosol + cloud optical depths at 500 nm: a good agreement has been found. Squares represent Lidar aerosol optical depth only, which are stable during the day.

Moreover, in the same figure it is verified that atmospheric optical depth measured by lidar and radiometers are in good agreement. This allows to obtain cirrus spectral optical depth by subtracting both aerosol and Rayleigh contributions from radiometric atmospheric optical depth.
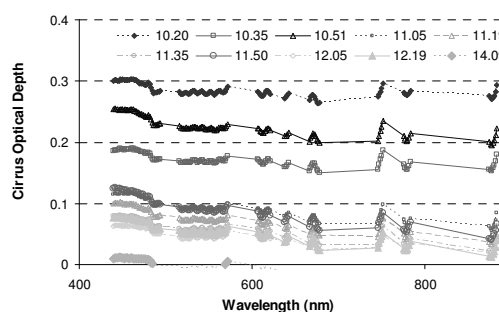
Figure 2. Time variation of the spectral cirrus optical depth for 13 March 2007.

In figure 2 is reported the time variation of the spectral cirrus optical depth, as estimated with this synergistic technique. It can be easily seen the amplitude decrease with time, until the thin cloud dissolution.

Esposito, F., Leone, L., Pavese, G., Restieri, R., Serio, C. (2004). *Atm.Env.* 38, 1605 – 1614

R. Bhawar, G. Bianchini, A. Bozzo, M. R. Calvello, M. Cacciani, M. Carlotti, F. Castagnoli, V. Cuomo, P. Di Girolamo, T. Di Iorio, L. Di Liberto, A. di Sarra, F. Esposito, G. Fiocco, D. Fuà, G. Grieco, T. Maestri, G. Masiello, G. Muscari, L. Palchetti, E. Papandrea, G. Pavese, R. Restieri, R. Rizzi, F. Romano, C. Serio, D. Summa, G. Todini, E. Tosi: "Spectrally Resolved Observations of Earth's Emission Spectrum in the H2O Rotational Band". *Geop. Res. Lett.*, VOL. 35, L04812, doi:10.1029/2007GL032207, (2008)

Aerosol products from GOME-2 on the Metop-A satellite: first impression

L.G. Tilstra[1], O.N.E. Tuinder[1], O.P. Hasekamp[2], M. de Graaf[1] and P. Stammes[1]

[1]Climate Research and Seismology Department, Royal Netherlands Meteorological Institute (KNMI),
Wilhelminalaan 10, 3732 GK, De Bilt, The Netherlands
[2]Earth Oriented Science Division, Netherlands Institute for Space Research (SRON),
Sorbonnelaan 2, 3584 CA, Utrecht, The Netherlands

Keywords: aerosol detection, satellites, remote sensing

In the framework of the O3MSAF (Satellite Application Facility on Ozone and Atmospheric Chemistry Monitoring) of EUMETSAT we produce two aerosol products from observations of the satellite instrument Global Ozone Monitoring Experiment (GOME-2) onboard Metop-A (Callies *et al.*, 2000). From the Earth reflectances measured at 340 and 380 nm we calculate the Absorbing Aerosol Index (AAI), which is an index that indicates the presence of UV-absorbing aerosols like desert dust or smoke. The AAI is capable of detecting aerosols over land and sea surfaces, even in the presence of clouds when the absorbing aerosol layer overlies the cloud.

As a reference, we can make use of the AAI determined from satellite measurements taken by the spectrometer SCIAMACHY onboard the Envisat satellite. The SCIAMACHY AAI is available since July 2002 and can serve as a very reliable reference (Tilstra *et al.*, 2007). Also see Figure 1. The aerosol plumes seen in this picture are desert dust and biomass burning aerosols. By focusing on specific regions, and inspection of time series of the AAI, we can validate the GOME-2 AAI by direct comparison with the SCIAMACHY AAI. In this way, we will be able to report on the quality of the GOME-2 AAI.

The second aerosol product we produce is the Aerosol Optical Thickness (AOT). For this product, we make use of the polarisation measurements that are performed by GOME-2. Special Polarisation Measurement Devices (PMDs) are available onboard, measuring both components of the incoming radiation. Information about the polarisation of the detected radiation can be used to detect the microphysical characteristics of aerosols. The AOT currently has an experimental status. We will report on the status of both GOME-2 aerosol products.

References:

Callies, J., Corpacciolli, E., Eisinger, M., Hahne, A., & Lefebvre, A. (2000). GOME-2 - Metop's second-generation sensor for operational ozone-monitoring, *ESA Bull.*, 102, 28-36.

Tilstra, L. G., de Graaf, M., Aben, I., & Stammes, P. (2007). Analysis of 5 years SCIAMACHY Absorbing Aerosol Index data, in *Proceedings of the 2007 Envisat Symposium, ESA Special publication SP-636*, Montreux, Switzerland.
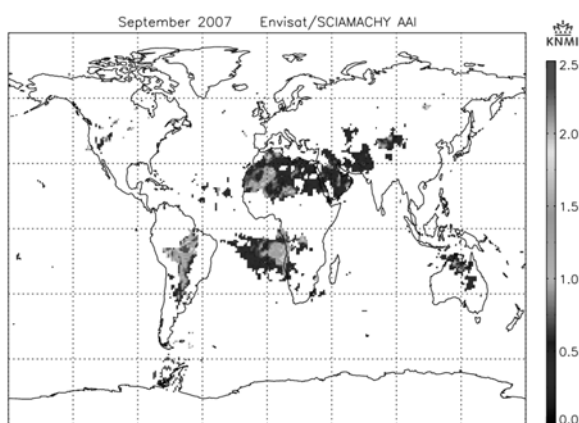
Figure 1. Global monthly aerosol distribution for September 2007, according to the Absorbing Aerosol Index (AAI) measured by the satellite instrument SCIAMACHY onboard the Envisat satellite. Only positive AAI values are shown. They are indicative of the presence of (UV-absorbing) aerosols.

Night-time remote sensing of aerosols in the near ground atmosphere by ground-based hyperspectral imaging

Y. Etzion[1], D.M. Broday[1], T. Kolatt[3], and M. Shoshany[2]

[1] Department of Environmental and Water Resources Engineering, Technion - Israel Institute of Technology,   Haifa 32000, Israel
[2] Department of Transportation and Geo-Information Engineering, Technion - Israel Institute of Technology, Haifa 32000, Israel
[3] ASI – Applied Spectral Imaging Ltd. Migdal-HaEmek 10511, Israel

Keywords: remote sensing, urban pollution, fine particles, aerosol measurement, hyperspectral imaging

Spatiotemporal variations in size attributes of ambient aerosols, in particular fine PM, are important estimates for public health risk assessment. Both satellite and ground remote sensing (RS) are applied for characterizing atmospheric aerosols by analyzing the aerosol interactions with electromagnetic radiation in different visible-NIR wavelengths or multiple angles. Relying on solar radiation, these methods are limited by the sun elevation angle and the cloud cover, and also by the revisit periods for satellite-borne sensors.

Current RS procedures can provide estimates of bi-modal size distributions in vertical atmospheric columns (Wang *et al.,* 1996). However, the correlation between the vertical aerosol profiles and ground-level particulate matter (PM) distribution at the urban-scale resolution is highly influenced by the geo-site specific seasonality and the corresponding mixing layer height (Schäfer *et al.*, 2008). Standard ground-level stations that monitor ambient PM provide only integrated concentrations in discrete and sparse locations. Consequently, their data is susceptible to sporadic readings.

A ground hyperspectral camera (VDS Vosskühler Cool-1300Q), originally used for biomedical applications, has been adapted for ground environmental remote sensing. The camera acquires signals in the visible-NIR range (λ=400-1100nm, 160 channels), thus having a prospective aptitude to trace spectral signatures of urban PM in the accumulation mode (Kuzmanoski *et al.*, 2007). The aim of this study was to extract the size attributes of PM in the accumulation mode obtained by hyperspectral imaging through horizontal open paths of 1-4km between the camera and the imaged targets. The study focused on implementing an innovative night-time imaging procedure by using remote street lights as spectral emission sources. This procedure offers a new concept for simultaneous measurements of aerosols in multiple ambient air columns when solar radiation cannot be used.

A laboratory scale feasibility study has been conducted using controlled conditions of aerosol loadings in a dedicated optic chamber. Aerosol optical thicknesses (AOT) in between 0.05-1.00 were emulated according to reported levels of AOT in urban regions (Erlick & Frederick, 1998). Spectral imaging was experimented with a halogen source which emits radiation in the range of λ=500-900nm.

The optical thickness derived from the hyperspectral sensor response in the laboratory experiments was comparable to Mie calculations of spectral extinction based on simultaneous size measurement by scanning mobility particle sizer (TSI, SMPS™ 3936). Periodical field imaging of remote street lights was performed next. Significant changes in the hyperspectral signature were acquired during dust storm events.
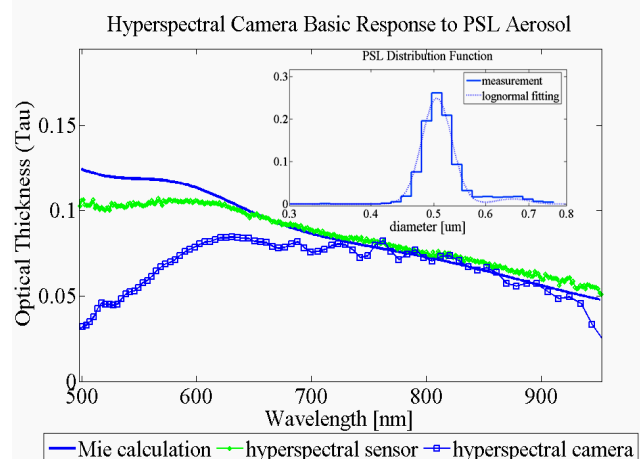
Figure 1. Hyperspectral camera response to a monodisperse 0.5µm PSL aerosol.

Erlick, C. & Frederick, J. E. (1998). *J. Geophysical Research-Atmospheres* 103(D18), 23275-23285.

Kuzmanoski, M., Box, M. A., Schmid, B., Box, G. P., Wang, J., Russell, P. B., Bates, D., Jonsson, H. H., Welton, E. J., & Seinfeld, J. H. (2007). *Aerosol Science and Technology* 41, 231-243.

Schäfer, K., Harbusch, A., Emeisa, S., Koepke, P., & Wiegner, M (2008). *Atmospheric Environment* 42, 4036–4046.

Wang, P., Kent, G. S., McCormick, M. P., Thompson, L. W., & Yue, G. K. (1996).*Applied Optics* 35, 433-440.

Columnar Aerosol Properties over Italy from MODIS Products in the year 2007

P. Burlizzi, F. DeTomasi and M. R. Perrone

CNISM, Department of Physics, Universita' del Salento, 73100, Lecce, Italy

Keywords: atmospheric aerosol, remote sensing of aerosol, satellites, aerosol measurement

Aerosol particles affect the climate directly by scattering and absorbing solar radiation and indirectly by modifying cloud microphysical properties. But, as a consequence of their high spatial and temporal variability, these effects can be strongly regional and the current uncertainty in the quantitative assessment of the Earth's radiative balance, is a direct consequence of the variable nature of aerosols on regional and seasonal scales. A multiple-measurement approach is currently used to characterize aerosol optical and microphysical properties and assess aerosol impact on global climate. Specifically, long-term continuous observations from satellites, networks of ground-based instruments and dedicated field experiments in clean and polluted environments are used to feed global aerosol and climate models.

The aerosol remote sensing from long-term operation satellites represents the best way to achieve a global characterization of aerosol properties and the launch of the NASA Earth Observing System (EOS) reveals the great effort of the scientific community to reduce the existing uncertainty on aerosol distribution and properties. Specifically, the Moderate Resolution Imaging Spectroradiometer (MODIS), onboard the EOS Terra and Aqua polar-orbiting satellites since December 1999 and May 2002, respectively, has been designed for multidisciplinary studies of the earth-atmosphere and ocean-atmosphere interactions (King et al., 1992).

In this paper aerosol optical depths (AODs) and corresponding fine-mode fractions (ηs) from MODIS observations in 2007 are used to investigate over Italy the spatial and temporal dependence of mean AOD and η values. In particular, AOD and η values have been retrieved in square boxes of variable size (from 10 km x 10 km up to 300 km x 300 km) centered at Rome, Lecce and Lampedusa, which are representative of sites differently affected by pollution and the dependence of AOD and η mean values on box size is investigated.

The spatial sensitivity of aerosol products retrieved from MODIS observations is demonstrated. In fact, the data analysis has allowed inferring source and sinks areas and defying when and to which extent local data can be representative of larger areas. Figures 1a-b show the Frequency Distribution (FD) of daily AOD mean values at 550 nm calculated by averaging all available daily values of a 20 km- and 300 km-wide square box, respectively centered at Rome (dotted black line), Lecce (full grey line) and Lampedusa (full black line). Figure 1a shows that daily AOD mean values of 20 km-wide square boxes are quite dependent on monitoring area location: the AOD-FD centered at Rome (dotted black line) is wider and peaked at higher AOD values with respect to the one centered at Lecce and Lampedusa, as a consequence of the larger contribution of anthropogenic pollution. Conversely, Fig. 1b reveals that daily AOD mean values of 300 km x 300 km areas are poorly dependent on monitoring area location. The above results, which clearly reveal that aerosol properties exhibit a pronounced spatial variability at scales of few tens of kilometers, i.e. smaller than the resolution of most current global models, allow inferring that only high-resolution regional climate models (RCMs) offer useful tools to evaluate regional impacts of aerosols and reduce the current uncertainty in the quantitative assessment of aerosol effects on climate.
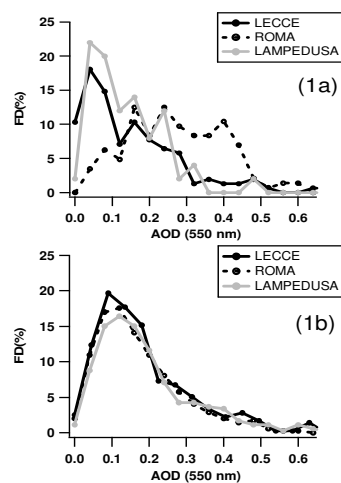
Fig. 1   AOD frequency distribution plots for (a) 20 km- and (b) 300 km-wide square box.

King, M. D., Kaufman Y. J., Menzel W. P., and Tanré D. (1992). *IEEE Transactions On Geoscience and Remote Sensing*, 30, 1-27.

Active and passive remote sensing: analysis of an extreme event over Southern Iberian Peninsula

J. L. Guerrero-Rascado, F. J. Olmo, F. Navas-Guzmán, D. Pérez, H. Lyamani, and L. Alados-Arboledas

Departamento de Física Aplicada, Universidad de Granada, Fuentenueva s/n, 18071, Granada, Spain.
Centro Andaluz de Medio Ambiente (CEAMA), Av. del Mediterráneo s/n, 18071, Granada, Spain

Keywords: Lidar, Saharan dust, optical depth, optical properties, satellites.

In this work we present an analysis of the extreme Saharan dust event detected from 3 to 7 September 2007 over Granada, Southern Iberian Peninsula. The event has been monitored by the Atmospheric Physics Group of the University of Granada. Special emphasis is paid to the singularity of this event over our region, which was monitored with both active and passive remote sensing instrumentation.

This especial Saharan dust event is characterized for its extreme intensity over Southern Iberian Peninsula. The intensity of the event was visualized on the aerosol optical depth series obtained by the sun-photometer Cimel CE 318-4 operated at Granada in the framework of AERONET network using level 2 data. Figure 1 shows the temporal series of the instantaneous values of aerosol optical depth at 500 nm and the Angström exponent (i.e., the spectral dependency of aerosol optical depth) calculated in the range 440-870 nm. This Saharan dust event affected also other Iberian Peninsula stations included in AERONET (El Arenosillo and Évora stations).

To obtain additional information about this event, several tools were explored. Extreme values of different aerosol optical properties were recorded on 6 September. For this day, back-trajectories analysis indicates air masses coming from North Africa fundamentally. In addition, NAAPS and DREAM models forecast the presence of a mineral dust plume over Southern Iberian Peninsula.

Lidar profiles were obtained during daytime using the Klett-Fernald-Sasano algorithm in combination with sun-photometer data (Guerrero-Rascado et al., 2008). The profiles show the aerosol vertical distribution evolution during the Saharan dust event and are in agreement with the results obtained by passive remote sensing. During the most intense stage, 6 September (Figure 2), the maximum aerosol backscatter values are around a factor of 8 respects to the others maximum showed in this Saharan dust event. The temporal evolutions of the aerosol optical properties are in coincidence for passive and active remote sensing.
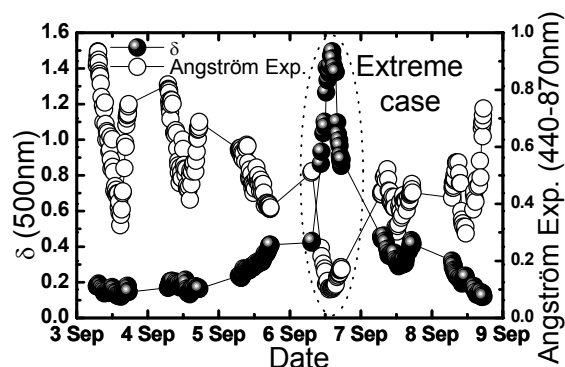
Figure 1. Aerosol optical depth and Angström exponent series during the analyzed period.
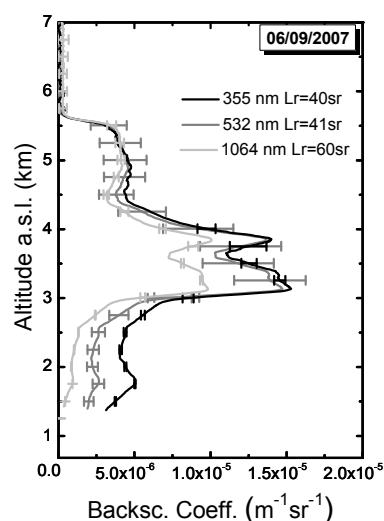
Figure 2. Aerosol backscatter coefficient profiles on 6 September 2007 at noon.

Guerrero-Rascado, J. L., B. Ruiz, L. Alados-Arboledas (2008), *Atmos. Environ.*, 42, 2668–2681.

Retrieval of biomass burning aerosols over Amazonas using AATSR with AERONET aerosol models

P. Kolmonen[1], A.-M. Sundström[2], L. Sogacheva[1] and G. de Leeuw[1,2]

[1]Finnish Meteorological Institute, Climate Change Unit, PL 503, 00101, Helsinki, Finland
[2]Department of Physics, University of Helsinki, PL 64, 00014, Helsinki, Finland

Keywords: remote sensing, biomass burning, satellites.

The AATSR Dual-View (ADV) algorithm for ATSR-2 (Along Track Scanning Radiometer 2) and AATSR (Advanced Along Track Scanning Radiometer) has been used for retrieving aerosol properties over land for over a decade (Veefkind *et al.*, 1998). Retrievals have been made over various locations globally. This study presents the first results from the application of the ADV over the Amazonas region. The special emphasis of the study is on distinguishing biomass burning aerosols from background aerosols near biomass burning sites.

The ADV algorithm takes advantage of the two views (near nadir and 55º forward) of the AATSR instrument. By assuming that aerosol optical depth (AOD) is small at the 1.6 μm channel of the instrument, the so-called k-ratio between the forward and nadir surface reflectances of the a pixel is determined from the measured top-of-atmosphere radiance. This ratio is then assumed to be wavelength independent, thus enabling the computation of the AOD for the AATSR aerosol retrieval channels which are 555 nm, 659 nm and 1.6 μm (Flowerdew & Haigh, 1995). The aerosol model used in the retrieval is a mixture of two aerosol types typically consisting of small and coarse particles, respectively. The mixing ratio is decided during the retrieval and it is a retrieval result.

AERONET (AErosol RObotic NETwork) is a network of ground based sun photometers (Holben *et al.*, 1998). It can be used to find feasible aerosol models globally. In a study by Omar *et al.* (2005) AERONET data was clustered in order to categorize aerosol models. Two of the clusters that were mostly found at the AERONET sites in the Amazonas region were biomass burning and industrial pollution.

ADV retrievals of the mixture of the biomass burning and industrial pollution aerosol types were made for the period from July to October 2007. To localize biomass burning sites during the time period Ionia ATSR world fire atlas was employed. The retrieved aerosol mixtures over pixels that were closer than 10 km to a fire event and no more than 1 hour from the event were judged to present biomass burning aerosol mixtures. A reference group was composed of aerosol mixtures that were retrieved over pixels that were more than 100 km and 48 hours from all fire sites.

The main result of the study was determined by averaging aerosol mixtures for both the biomass burning mixture group and the reference group. These results are presented in table 1.

Group	Average fraction of bm type	Standard deviation of the bm type fraction
Biomass burning	0.45	0.43
Reference	0.14	0.32

Table 1. The comparison of the fraction of biomass burning aerosol type (bm) in the retrieved aerosol mixtures for the biomass burning group and the reference group.

It can be seen from the results that while the standard deviations of the average fractions of the biomass types are large, there is a clear distinction between the two groups. Mixtures retrieved close to biomass burning event sites contain more biomass burning aerosol type.

Other results of the study include comparisons between ADV and AERONET AOD at AERONET sites in the Amazonas region. In these comparisons ADV AOD was generally higher than AERONET AOD. This is mainly due to the used mixture. Only small particle type for the biomass burning and industrial pollution was used. This means that the lack of coarse particles had to be compensated by higher concentration of small particles, thus leading to high AOD.

Flowerdew, R. J., & Haigh, J. D. (1995). *Geophys. Res. Lett.*, 23, 1693-1696.
Holben, B. N *et al.* (1998). *Remote Sens. Environ.,* 66, 1-16.
Omar, A. H., *et al.* (2005). *J. Geophys. Res.,* 110, D10S14.
Veefkind, J P. *et al.* (1998). *J. Geophys. Res.,* 104, D2253-2260.

Aerosol Profiling within the Ceilometer Network of the German Meteorological Service

Harald Flentje[1], Dirk Engelbart[2], Werner Thomas[1]

Deutscher Wetterdienst (DWD), Albin-Schwaiger-Weg 10, D-82383 Hohenpeissenberg, Germany

Email: harald.flentje@dwd.de

Keywords: Lidar, backscatter, tropospheric aerosols.

So far, aerosol profiles are operationally sampled with intermittent spatio-temporal resolution within lidar networks (cf. GAW Aerosol Lidar Observation Network – GALION, 2007) or by few regular backscatter sondes. However, in praxi this does often not capture the 3-D aerosol distribution close enough to allow for tracking transport and micro-physical processes, radiation interaction and air-quality (e.g. visibility) during specific events or on a routine basis, not to mention a possible assimilation into (chemical) weather models. Recently, ceilometers (i.e. relatively low-cost and robust mini lidars for continuous operation), have been upgraded such that one may retrieve significant aerosol information though being not as quantitative as the sophisticated lidar systems. The German Met. Service (DWD) currently installs Jenoptik CHM15K (www.jenoptik-los.com) ceilometers at more than 40 meteorological network stations for mainly cloud detection purposes (Fig. 1).

The CHM15K uses a diode-pumped Nd-YAG laser (1064 nm) yielding about 8 µJ per pulse at 5-7 KHz repetition rate. Divergence is 100 µrad, the vertical resolution is 15m. Though originally designed for cloud detection, hitherto data indicate the applicability for mixing layer detection and even aerosol profiling. The invertibility with respect to backscatter coefficients is about to be investigated and an intercomparison campaign with a micro pulse lidar is envisaged for spring/summer 2009.
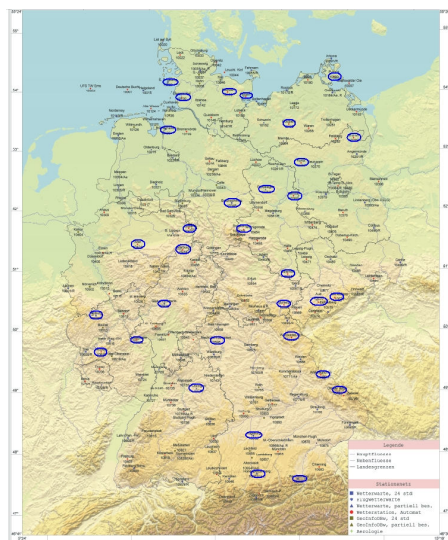
Figure 1: Stations equipped with CHM15K ceilometers within the DWD meteorological network

An example for the offset/range-corrected raw signal of the CHM15K ceilometer is shown in Fig. 2. It reveals Saharan dust layers above the meteorological observatory Lindenberg during a Saharan dust episode from 25-30 May 2008. The qualitative backscatter section shows the PBL as well as scattered clouds (black) and the Saharan particles (green-yellow-red) above, reaching an altitude up to 4-5 km. Complete overlap of laser beam and receiving telescope is reached around 1200 m.a.g.l. but can be reasonably corrected down to ≈500 m.
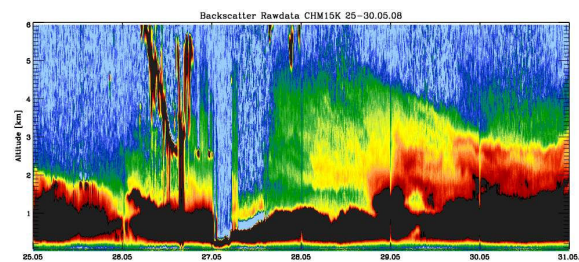
Figure 2: Raw backscatter at Lindenberg from 25-30 May 2008

In this study, we will evaluate first ceilometer measurements at the Global AtmosphereWatch (GAW) station Hohenpeissenberg (MOHp, 47°48' N, 11°02' E, 985m a.s.l.) with collocated Micropulse Lidar measurements. Further the information content of the data set will be discussed with focus on deriving backscatter coefficient profiles, characterizing the overlap and stability of the optical system as well as the possibility of applying sunphotometer measurements for atmospheric calibration (i.e. conversion to extinction coefficients). Finally, the integration of all the ceilometer's data from the network into a single data set and it's potential applications will be investigated.

References:
Mehnert, J. and M. Pesch, Locating the mixing layer – algorithms to identify the MLH using lidar signals, personal communication, 2009.
Teschke, G., A Wavelet algorithm for the estimation of mixing layer heights with lidar ceilometer, Report for DWD sub-contract, Met. Obs. Lindenberg, 22pp, May 2008.
WMO, GAW Aerosol Lidar Observation Network (GALION), Draft outline, GAW report no. 178 (ftp://ftp.wmo.int/Documents/PublicWeb/arep/gaw/gaw178-galion-27-Oct.pdf)

Systematizing MODIS, TOMS and MISR satellite datasets with HYSPLIT model for monitoring regional pattern of aerosol and its seasonal variability in Pakistan

Khan Alam[1], Salman Qureshi[1,2]

[1]Department of Geography & Geology, University of Salzburg, Hellbrunnerstrasse 34, Salzburg 5020, Austria.
[2]Department of Geography, University of Karachi, University Road, Karachi 75270, Pakistan

Key word: TOMS; MODIS; MISR; HYSPLIT; AOD; Pakistan

Atmospheric aerosols play an important role in the energy balance of earth-atmosphere system. Aerosols vary in time in space and can lead to variations in cloud microphysics. The aerosol concentration is increasing day-by-day because of growing population, urbanization, and industrialization. In this paper we used Total Ozone Mapping Spectrometer (TOMS), Moderate Resolution Imaging Spectro-radiometer (MODIS), and Multi-angle Imaging Spectroradiometer (MISR) aerosol data in order to understand the spatial and temporal variations of aerosols in the different cities of Pakistan.

Hybrid Single Particle Lagrangian Integrated Trajectory (HYSPLIT) model has been used for trajectory analysis to obtain origin of air masses in order to understand the variability of aerosol concentrations. We analyzed that the current MODIS aerosol data (2005-2008) and previous TOMS data (1981-1992) show increasing concentration of aerosol load in the vicinity of Pakistan.

We inter-compared MODIS and MISR aerosol optical depth (AOD) to validate satellite retrievals and found that there is strong positive correlation between MODIS-MISR AOD (Table.1). Annual and seasonal variability of AOD has been assessed in industrial, urban, semi-urban, semi-arid and rural cities of Pakistan. Our analysis shows that maximum value of AOD is found in summer season over all study areas (See Fig.1 for Karachi only). Furthermore, with the back trajectory analysis, we analyzed that winter air masses reaching to the localities of Pakistan have traveled long distance, whereas the summer air masses traveled short distances. Therefore the air masses spent more time over land during summer time than winter, which legitimately explains the higher concentration aerosol observed during summer as compared to winter.

Table.1 Pearson Correlation for MODIS-MISR AOD for the period 2001-2005.

Name of Cities	Pearson Correlation
Karachi	0.845
Rohri	0.862
DG Khan	0.871
Multan	0.746
Lahore	0.676
Faisal Abad	0.716
Rawalpindi	0.818
Peshawar	0.892
Swabi	0.768
Zhob	0.675
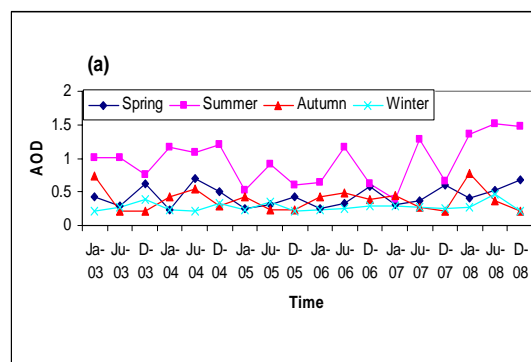
Figure.1 Seasonal variation of AOD for Karachi.

Dey, S., Tripathi, S. N., Singh, R. P. & Holben, B. N. (2005). Seasonal variability of aerosol parametes over Kanpur, an urban site in Indo-Gangetic basin. J. *Advances in Space Research,* 36, 778-782.

Prasad, A.K., & Singh, R.P. (2007). Comparison of MODIS-MISR aerosol optical depth over the Indo-Gangetic basin during winter and summer seasons (2000-2005). *Remote Sensing of Environment*, 107, 109-119.

Specific features of angular characteristics of diffuse solar radiation in little-cloud atmosphere

Zhuravleva T.B., Bedareva T.V., Kabanov D.M., Nasrtdinov I.M., Sakerin S.M.

Institute of Atmospheric Optics, 634021, Tomsk, Russia

Keywords: aerosol optics, clouds, Monte Carlo simulations, Sun photometer, diffuse radiation

As is well known, the spectral measurements of direct and diffuse solar radiation make it possible to retrieve many optical and microphysical characteristics of atmospheric aerosol. The existing methods are developed for application under clear-sky conditions, seriously reducing the possibility of their use in many regions of the globe. For instance, in Siberia a full implementation of familiar AERONET methods covers 2% of cases out of the total number of observational situations, predominately due to the presence of clouds. One of the possible methods of solution of this problem is to extend – under certain conditions – the applicability limits of the known methods to *little-cloud* situations.

As a first step, we initiated the studies of transformation of angular structure of downward diffuse radiation during appearance of separate clouds. In the report, we present the algorithms of the Monte Carlo method, developed for brightness calculations in the molecular-aerosol (B_{clr}) and cloudy (B_{cld}) atmosphere under assumption that clouds are approximated by simplest geometric bodies (ellipsoids). We present the results of numerical simulation and measurements of diffuse radiation in solar almucantar for four spectral channels of Sun photometer CE-318 0.44, 0.67, 0.87, and 1.02 μm.

It is shown that that the variations of sky brightness during appearance of separate cloud take place in three ranges of viewing azimuth angles φ: in geometric zone of cloud location, a small region "before the cloud" on sun-facing side, and a more extended region "behind the cloud" (Fig. 1). The scattered radiation nearby the cloud is affected by the following factors. First of all, $B_{cld}(\varphi)$ increases under impact of extra illumination due to reflection off the cloud. However, in the behind-cloud zone, due to the shadowing effect, the solar radiation, reaching this region, is attenuated to a larger degree than in the cloud absence. A net effect of the two competing factors is that, in a certain angular range φ of the shadowed zone, the following relation holds: $K(\varphi) = B_{cld}(\varphi)/B_{clr}(\varphi) < 1$.

We discuss the variations of spectral-angular characteristics of diffuse radiation in the zone of cloud radiation effect for different optical-geometric cloud parameters and conditions of experiment (cloud extinction coefficient, cloud position relative to line of sight, viewing zenith and azimuth angles, etc.). In particular, brightness spike within the cloud $K(\varphi)$ increases with decreasing wavelength because the cloud optical characteristics, in contrast to molecular-aerosol ones, are practically unchanged in the considered spectral range. The obtained estimates qualitatively agree with data of field experiments.
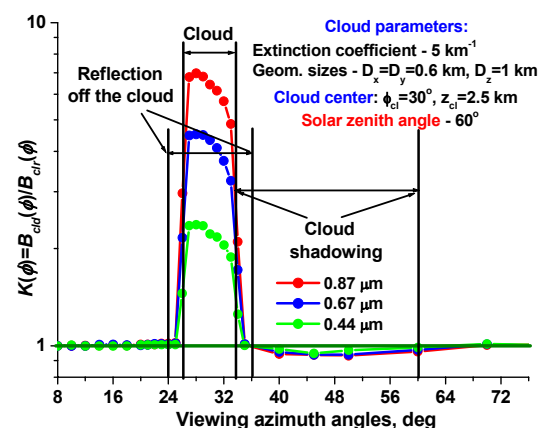
Figure 1. Azimuthal dependence of $K(\varphi)$ in the region of cloud radiation effect.

It is shown that, in the wide range of input parameters, outside the cloud and in near-cloud zone, change of sky brightness during appearance of cloud turns out *insignificant*: in most considered cases, the relative difference between $B_{cld}(\varphi)$ and $B_{clr}(\varphi)$ does not exceed the radiation calculation error 1.5-2%. This circumstance determines the potential possibility of implementing certain methods of retrieval of aerosol optical/microphysical characteristics in little-cloud situations.

ANALYSES OF MODIS AEROSOL PRODUCTS OVER THE IBERIAN PENINSULA

M.J. Granados Muñoz and L. Alados-Arboledas

Departamento de Física Aplicada, Facultad de Ciencias, Universidad de Granada, Fuentenueva s/n, 18071, Granada, Spain.
Centro Andaluz de Medio Ambiente (CEAMA), Junta de Andalucía-Universidad de Granada, Av. del Mediterráneo s/n, 18071, Granada, Spain

Keywords: MODIS, aerosol optical depth, regional variability, seasonal variability.

In order to investigate the optical properties of atmospheric aerosol over the Iberian Peninsula we use almost 9 years of MODIS aerosol derived products. The Moderate Resolution Imaging Spectroradiometer (MODIS) sensor on the Terra and Aqua satellites is retrieving daily global aerosol products over land and ocean in a variety of spectral bands from blue to thermal infrared every 1–2 days with a 16-day repeat cycle. Terra and Aqua (both with a 705km orbit) are in a sun-synchronous, near polar, circular orbit. Aqua crosses the equator daily at 01:30 p.m. LT as it moves north (ascending mode) in contrast to Terra, which crosses the equator at 10:30 a.m. daily (descending mode). Since its first launch (18 December 1999), the MODIS aerosol algorithm has been continuously updated and evaluated by the MODIS scientific team. This resulted in a complete set of products, being the last version that called Collection 005 (C005), that are based on MODIS algorithm version Global time-series of aerosol parameters have been produced from MODIS/Terra (EOS AM-1) since its launch in December 18, 1999 and from MODIS/Aqua (EOS PM-1) since 4 May 2002. The pre-launch uncertainty (theoretical error) of the MODIS aerosol optical depth (AOD) is $\pm0.05\pm0.15$ (AOD) over land and $\pm0.03\pm0.05$(AOD) over ocean. The spatial resolution of MODIS (pixel size at nadir) is 250 m, 500m and 1000 m, depending on the spectral band. The aerosol C005 dataset used in this study is part of the MODIS Terra Level-3 daily gridded atmospheric data product available on the MODIS web site http://modis.gsfc.nasa.gov/. The data cover the broader Iberian Peninsula (35ºN–45º N and 10ºW–5º E) for the period 1 March 2000 to 28 February 2009 (almost 9 complete years). The MODIS Atmosphere Daily Global Product is stored on an equal angle latitude-longitude grid with a horizontal resolution of 1º×1º. Thus, 150 cells are available for each day of the 9-year study period.

The present study focuses on the AOD at the wavelength of 550nm (AOD550) and Angström exponent over land, because it is near the peak of the solar spectrum and thus associated with large radiative effects, and because AOD is usually given at this wavelength by the various available aerosol datasets. Spatial and temporal features of the aerosol optical properties have been analyzed.

This region is of particular importance because it is a crossroad where aerosols from different sources are superimposed and mixtures of different kinds of particles converge (e.g. Lyamani et al., 2006) such as fine anthropogenic aerosols from Europe, desert dust from North Africa and maritime aerosols from the Mediterranean Sea. In addition, in the Mediterranean basin aerosols exert a strong climatic effect especially in summer, due to the cloud-free conditions and high solar radiation intensity.

Marked spatial gradients have been evidenced due to the existence of different climatic regions and the influence of different source regions for aerosol particles. On the other hand, the seasonal features reveal large aerosol load in summer, with particles coming from North Africa, specially in the South-eastern (SE) part of the Iberian Peninsula, and a relevant contribution of biomass burning particles specially in the North-western (NW) of the Iberian Peninsula (IP).
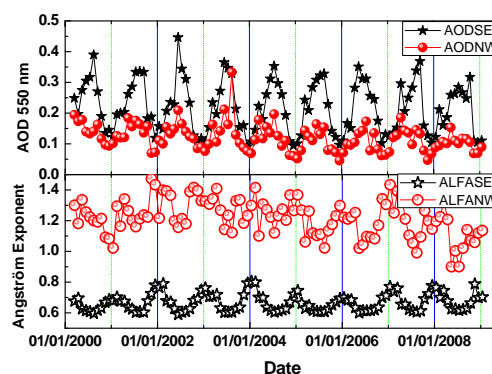
Figure 1. Aerosol optical depth (550 nm) and Angström exponent series for SE IP and NW IP for the period 2000-2009.

Lyamani, H. et al. (2006), *Atmos. Environ.*, 40, 6465-6476.

How satellite retrievals of NO_2 vertical columns can be improved using aerosol measurements

J.Leitao[1], A. Richter [1], A. Kokhanovsky[1] and J.P. Burrows[1]

[1] Institute of Environmental Physics, University of Bremen, Otto-Hahn-Allee 1, D-28359 Bremen, Germany

Keywords: Airmass factor, NO_2, remote sensing, satellite, tropospheric aerosol.

Satellite instruments measuring backscattered solar radiation, such as the Global Ozone Monitoring Experiment (GOME and GOME-2), the SCanning Imaging Absorption spectroMeter for Atmospheric CHartographY (SCIAMACHY) or the Ozone Monitoring Instrument (OMI) provide an unique opportunity to measure several atmospheric trace gases (including ozone (O_3), nitrogen dioxide (NO_2), and sulphur dioxide (SO_2)) from space and determine their global distribution. These data are essential to identify emission sources, investigate pollution hot-spots (e.g. megacities) and also to analyse long-term trends of pollutant concentrations.

Tropospheric columns of trace gases can be retrieved from UV/vis satellite measurements using the Differential Optical Absorption Spectroscopy (DOAS) method. NO_2, in particular, is retrieved usually in the wavelength window of 425-450nm. By removing the stratospheric contribution from the total slant column (SC) (Richter *et al.*, 2005) a tropospheric slant column is obtained. Finally, the vertical tropospheric column of NO_2 is calculated with the division of the SC by an airmass factor (AMF) that is computed with a radiative transfer model (RTM), e.g. SCIATRAN (Rozanov *et al.*, 2005). Proper choice of the a priori assumptions (such as absorber profile, surface albedo and aerosol characteristics) used for these calculations is necessary to obtain the correct values of NO_2 present in the troposphere. Knowing this, a sensitivity study was performed in order to find the key factors in terms of uncertainties in AMF calculations, and consequently on the NO_2 tropospheric vertical column determination.

In current retrieval methods of satellite data products, the aerosol effects are accounted for in different ways, e.g. by including them in the cloud treatment used (Boersma *et al.*, 2004) or by relying on model results (Martin *et al.*, 2002). The method currently applied at the University of Bremen includes the aerosol in the retrieval using a static map derived from CO_2 emission which attributes urban aerosols to "polluted" regions, rural aerosols elsewhere over continents, and, maritime aerosols over the oceans. These three types of aerosols are then combined in scenarios built with the LOWTRAN model (Nüß, 2005; Richter *et al.*, 2005). This methodology does not capture the full spatial and time variability of aerosols and their characteristics. In addition, the effect of aerosol scattering in the atmosphere is quite complex depending not only on their profile (vertical distribution and optical depth (AOD)) but also on the optical properties (e.g., size distribution and refractive index).

The presence of aerosols can have quite contrasting effects on the satellite measurements of tropospheric NO2 (Leitão *et al.*, 2008). The NO_2 signal can be enhanced by multiple scattering within an aerosol layer or by an increase of the effective albedo when the NO_2 layer is above the aerosol. On the other hand, the aerosol will act as a shield, decreasing the SC measured, if it is located above the trace gas. The use of independent satellite measurements (e.g., from MERIS or CALIPSO) and ground-based measurements (from AERONET stations) allows for determination of AOD, aerosol vertical profile and aerosol physical properties. This data can then be used in the computation of AMFs offering the possibility for improvement of SCIAMACHY NO_2 retrievals. Here we present some results of the overall sensitivity study and an example on how improvements can be achieved and what could be the overall impact on the global NO_2 retrieval.

Boersma, F. K., Eskes, H. J., & Brinksma, E. J. (2004). *J. Geophys. Res.*, 109, D04311.

Leitão, J., Richter, A., Heckel, A., & Burrows, J. P. (2008). *Geophysical Research Abstracts*, **10**.

Martin, R. V., Chance, K.D., Jacob, J., Kurosu, T. P., Spurr, R. J. D., Bucsela, E., Gleason, J. F., Palmer, P. I., Bey, I., Fiore, A. M., Li, Q., Yantosca, R. M., & Koelemeijer, R. B. (2002). *J. Geophys. Res*, **107**, 4437-4456.

Nüß, H. (2005). *Verbesserungen des troposphärischen NO2-Retrievals aus GOME- und SCIAMACHY-Daten*, Ph.D. Thesis, Bremen University.

Richter, A., Burrows, J. P., Nüß, H., Granier, C., & Niemeier, U. (2005). *Nature*, 437, 129-132.

Rozanov, A., Rozanov, V., Buchwitz, M., Kokhanovsky, A., & Burrows, J. P. (2005). *Adv.Space Res.*, 36(5), 1015-1019.

Calibrated CCD imager for aerosol optical and physical properties estimation

A. Cazorla[1,2], F..J. Olmo[1,2], L. Alados-Arboledas[1,2], R. Wagener[3] and J.E.Shields[4]

[1]Departamento de Física Aplicada. Universidad de Granada. Fuentenueva s/n. 18071, Granada. Spain
[2]Centro Andaluz de Medio Ambiente (CEAMA). Avda. del Mediterraneo s/n. 18006. Granada. Spain
[3]Environmental Sciences Department. Brookhaven National Laboratory. BLDG 490D, 30 Bell Ave., Upton, NY 11973
[4]Marine Physical Lab, Scripps Institution of Oceanography, University of California San Diego, 9500 Gilman Dr., La Jolla CA 92093-0701

Ground-based sky imagery has been used for years for cloud cover assessment. Previous work with the All-Sky Imager developed in the Atmospheric Physics Group at University of Granada (Cazorla et al, 2008) revealed the potential of the ground-based sky imagery for aerosol optical properties characterization. Considering the increasing interest in automatic ground-based devices that could provide solutions that combine the cloud and aerosol characterization in the same instrument, the development of techniques to extract aerosol characteristics from sky imagers can help the existing aerosol data bases such as AERONET (Holben et al, 1998).

The Whole Sky Imager (WSI) (Shields et al., 1998), a calibrated ground-based sky imager has been tested to determine optical properties and a preliminary test has been performed to determine physical properties of the atmospheric aerosol. Different neural network models estimate the aerosol optical depth (AOD) for three wavelengths using the radiance extracted from the principal plane of sky images from the WSI as input parameters. The models use data from a CIMEL CE318 (Holben at al., 1998) radiometer for training and validation.

The data set selected in this work comprises the period from October 1st 2001 to September 29th 2002. This data set let us model the seasonal variability of the atmospheric aerosol. Using the cloud decision images from the WSI we removed all the cases with clouds, to work with the clear-sky results. A total of 1047 clear-sky image sets (i.e. 3 spectral images acquired in one set) were associated with a synchronous CIMEL measurement, applying a ±2 minutes margin for the AOD estimation. We also associate the WSI wavelengths (450, 650 and 800 nm) with the nearest CIMEL wavelength (440, 675 and 870 nm, respectively). A total of 84 principal planes from the WSI were associated with synchronous CIMEL principal plane measurements applying the same margin and the same wavelengths association. Figure 1 shows and example of the agreement of the WSI and CIMEL principal planes.

The AODs and radiance over the principal plane are compared to those retrieved by the CIMEL. The correlation reveals that an inversion code can be applied using the images from the WSI to provide physical properties of the aerosol (size distribution).
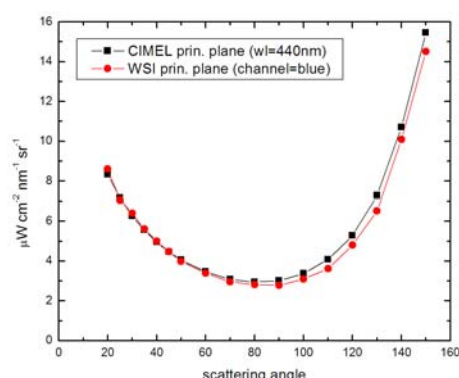
Figure 1.The agreement of the CIMEL and WSI principal planes can be see in this graph. The 440nm and blue filters of the instruments were used respectively.

The deviations between the WSI derived AOD and the AOD retrieved by AERONET are within the nominal uncertainty assigned to the AERONET AOD calculation (±0.01), in 80% of the cases. The explanation of data variance by the model is over 92% in all cases. The correlation between the WSI and CIMEL principal planes is over 95% for the 450 and 650 nm and 88% for the 800 nm channel.

Cazorla, A., Olmo, F.J. & Alados-Arboledas, L. (2008). *Atmospheric Environment,* 42 (11), 2739-2745

Holben, B.N., . (1998). *Remote Sensing of Environment,* 66 (1), 1–16

Shields, J.E., Johnson, R.W., Karr, M.E. & Wertz, J.L. (1998). in *Proc. 10th Symposium on Meteorological Observations and Instrumentations*, Phoenix, AZ.

EARLINET for long term observations of aerosol over Europe

G.Pappalardo[1], U. Wandinger[2], H. Linnè[3], A. Amodeo[1], L. Mona[1], A. Apituley[4], L. Alados Arboledas[5], D. Balis[6], A. Chaikovsky[7], A. Comeron[8], V. Freudenthaler[9], I. Grigorov[10], O. Gustafsson[11], S. Kinne[3], D. Nicolae[12], I. Mattis[2], V. Mitev[13], A. Papayannis[14], M.R. Perrone[15], A. Pietruczuk[16], M.Pujadas[17], J.P. Putaud[18], F. Ravetta[19], V. Rizi[20], V. Simeonov[21], N. Spinelli[22], K. Stebel[23], T. Trickl[24], M. Wiegner[9]

[1]Istituto di Metodologie per l'Analisi Ambientale CNR-IMAA, Potenza, I-85050, Italy
[2]Institut für Troposphärenforschung, Leipzig, Germany
[3]Max-Planck-Institut für Meteorologie, Hamburg, Germany
[4]Rijksinstituut voor Volksgezondheid en Milieu, Bilthoven, The Netherlands
[5]Universidad de Granada, Granada, Spain
[6]Aristoteleio Panepistimio, Thessalonikis, Greece
[7]Institute of Physics, National Academy of Sciences, Minsk, Bjelarus
[8]Universitat Politècnica de Catalunya, Barcelona, Spain
[9]Ludwig-Maximilians-Universität, München, Germany
[10]Institute of Electronics, Bulgarian Academy of Sciences, Sofia, Bulgaria
[11]Swedish Defence Research Agency (FOI), Linköping, Sweden
[12]National Institute of R&D for Optoelectronics, Magurele-Bucharest, Romania
[13]CSEM, Centre Suisse d'Electronique et de Microtechnique SA, Neuchâtel, Switzerland
[14]National Technical University of Athens, Department of Physics, Athens, Greece
[15]Università del Salento, Department of Physics, Lecce, Italy
[16]Institute of Geophysics, Polish Academy of Sciences, Warsaw, Poland
[17]Centro de Investigaciones Energéticas, Medioambientales y Tecnológicas, Madrid, Spain
[18]EC Joint Research Centre, Ispra (VA), Italy
[19]Université Pierre et Maris Curie-Institut Pierre Simon Laplace, Paris, France
[20]Università degli Studi dell'Aquila - Dipartimento di Fisica - CETEMPS, L'Aquila, Italy
[21]Ecole Polytechnique Fédérale de Lausanne, Switzerland
[22]Consorzio Nazionale Interuniversitario per le Scienze Fisiche della Materia, Napoli, Italy
[23]Norwegian Institute for Air Research (NILU), Kjeller, Norway
[24]Forschungszentrum Karlsruhe IMK-IFU, Garmisch-Partenkirchen, Germany

Keywords: lidar, lidar ratio, tropospheric aerosols, network, EARLINET.

Lidar networks are fundamental to study aerosol on large spatial scale and to investigate transport and modification phenomena. These are the motivations why EARLINET, the European Aerosol Research Lidar Network, was established in 2000, as a research program funded by the European Commission in the frame of the 5th framework program. After the end of the project, the network activity continued on the base of a voluntary association.

At present, EARLINET consists of 25 lidar stations: 10 single backscatter lidar stations, 8 Raman lidar stations with the UV Raman channel for independent measurements of aerosol extinction and backscatter, and 7 multiwavelength Raman lidar stations for the retrieval of aerosol microphysical properties.

On March 2006, the EC Project EARLINET-ASOS (Advanced Sustainable Observation System) started on the base of the EARLINET infrastructure. This infrastructure project will enhance the operation of the network.

EARLINET observations are performed on a regular schedule of one daytime measurement per week around noon, when the boundary layer is usually well developed, and two night-time measurements per week, with low background light, in order to perform Raman extinction measurements. In addition to the routine measurements, further observations are devoted to monitor special events such as Saharan dust outbreaks, forest fires, photochemical smog and volcano eruptions.

Data quality has been assured by instrument intercomparisons using the available transportable systems. The quality assurance also included the intercomparison of the retrieval algorithms for both backscatter and Raman lidar data. Moreover, tools for the continuous quality check of the instruments and algorithms used have been developed.

EARLINET data can contribute significantly to the quantification of aerosol concentrations, radiative properties, long-range transport and budget, and prediction of future trends on European and global scale. It can also contribute to improve model treatment on a wide range of scales and to a better exploitation of present and future satellite data.

Vertical characterization of Saharan dust intrusions over Tenerife by ground-based lidar and airborne measurements

C. Cordoba-Jabonero[1,2], J. Andrey[1], M. Gil[1] and E. Cuevas[3]

[1]Instituto Nacional de Técnica Aeroespacial (INTA), Atmospheric Research and Instrumentation Branch, Ctra. Ajalvir km.4, Torrejon de Ardoz, 28850-Madrid, Spain
[2]Universitdad de Granada (UGR), Group of Atmospheric Physics, Granada, Spain
[3]Agencia Estatal de Meteorología (AEMET), Atmospheric Research Centre of Izaña, Sta. Cruz de Tenerife, Spain

Keywords: Saharan dust, lidar, airborne measurements, vertical distribution, AOD.

Large extensions of suspended dust particles upwelled from the Sahara desert can remain in the atmosphere during days and suffer long-range transport.

In recent years a number of effects of aerosols have been identified no only in the radiative balance but also in fitoplancton production or long-distance potential transport of virus, all of them having relevant impact on several socio-economic sectors. Dust clouds significantly modify the radiative transfer throughout the atmosphere and perturb the UV retrieval of nadir-looking aircraft or satellite boarded instrumentation. In addition, suspended dust can modify the thermal balance of the lower atmosphere.

In spite of a great attention has been paid in last years to the aerosol in global scale and, in particular, to Saharan aerosols, a large uncertainty on the sign of the radiative forcing still remains.

Canary Islands offer the most favourable site with high-quality instrumentation installed at different heights, and located downwind of the outbreaks sources for dust monitoring.

Saharan dust intrusions over Tenerife are frequently observed in summertime, arriving at high altitudes, resulting from strong convective activity over the Sahara under favourable meteorological conditions. In this sense, the vertical distribution of dust is a key parameter on the understanding of the aerosol-ozone-UV interactions, and even on aerosol modelling, unlike both ground-based 'in-situ' and columnar measurements performed by other techniques can offer. The vertical characterization of individual dust events is significant for the determination of the Saharan Air Layer (SAL) and for assessing the climate impact of such phenomena, even at local scales.

In the frame of TROMPETA (TROpical Monitoring PhasE of The Atmosphere) project (Gil et al., 2006) height-resolved measurements were performed in July 2005 over Tenerife surroundings by using a ground-based lidar: Micropulse Lidar v. 3 (MPL-3) whose measurements are routinely performed since 2005 at AEMET's Santa Cruz de Tenerife (28.5ºN 16.2ºW, 52 m a.s.l.) subtropical station within the NASA MPLNET; and airborne instrumentation: Passive Cavity Aerosol SPectrometer (PCASP-100X) aboard INTA's C-212 aircraft for vertical in-situ particle size classification.

A clearly observed dusty event was monitored for 3 days (19-21 July 2005). These observations were also confirmed with AERONET data, which reflected both high Aerosol Optical Thickness (AOT) and low Angstrom exponent values for these days.

In this work we will present the results of the vertical characterization of dust by using the observations performed by ground-based lidar (MPL) and airborne instrumentation (PCASP) under TROMPETA 2005 campaign. Extinction coefficient profiles were retrieved, estimating the AOT as well, for each set of measurements (MPL and PCASP). AOT values were reported ranging between 0.5 and 0.7 for the analysed period. MPL hourly integrated AOT values were also compared with the AERONET one, showing a good agreement and a similar evolution along the day. Dust events corresponded to intrusions differing in vertical extension distribution and maximal reached altitude as well as in its temporal behaviour. These results can be directly applied in aerosol radiative forcing assessment and aerosol modelling.

Moreover, results also revealed the strength and weakness on aerosol vertical characterization for each type of instrumentation (MPL and PCASP).

Gil, M., J. F. Lopez-Herreros, S. Chueca, O. Serrano, S. Alonso, E. Cuevas, P. M., Romero, M. Navarro, J. Andrey, C. Córdoba-Jabonero, M. Yela, A. Redondas, S., Rodriguez, M. Schneider, I. Kramer, T. Blumenstock and C. Pérez, A. (2006), TROMPETA (TROpical Monitoring PhasE in The Atmosphere) Project: Aerosols-Radiation-Ozone interaction in the Subtropics, *Proc. 5ª Asamblea Hispano-Portuguesa de Geodesia y Geofísica*, 30/1-3/2, Sevilla 2006.

Differences of the aerosol load between an urban and suburban site using remote sensing measurements and model estimates

D. Balis[1], E. Giannakaki[1], E. Katragkou[1], M. Wiegner[2], K. Markakis[1], T. Giannaros[1] and V. Amiridis[3]
[1]Laboratory of Atmospheric Physics, Thessaloniki, Greece
[2]Meteorological Institute of the Ludwig-Maximilian-University, Munich, Germany
[3]Institute for Space Applications and Remote Sensing, National Observatory of Athens, Greece

Keywords: Lidar, Aerosol modelling, PM10.

A UV-aerosol campaign was held from July 14-25, 2006, at Thessaloniki, Greece, as part of the integrated project SCOUT-O3 (Stratosphere-Climate Links with Emphasis on the Upper Troposphere and Lower Stratosphere). In this study we have compared aerosol optical depth derived from cimel with PM10 concentration as derived with the Comprehensive Air quality Model with extensions (CAMx) for an urban (Thessaloniki center) and rural area (Epanomi). Moreover, backscatter and extinction profiles from ground-based and airborne lidars were also used in order to estimate the free tropospheric contribution of aerosols in the greater area of Thessaloniki. The dataset was used to study the spatial variability of the aerosols and their optical properties, as well as to compare and investigate the difference in the diurnal variability between the centre if the city and the suburbs. Both lidar systems were successfully intercompared in the frame of the European Aerosol Research Lidar Network (EARLINET).

CAMx (http://www.camx.com/) is an Eulerian photochemical dispersion model that allows for an integrated "one-atmosphere" assessment of gaseous and particulate air pollution (ozone, PM2.5, PM10, air toxics, mercury) over many scales ranging from sub-urban to continental. CAMx incorporates two-way grid nesting, which means that pollutant concentration information propagates into and out of all grid nests during model integration. Meteorological fields are supplied to the model to quantify the state of the atmosphere in each grid cell for the purposes of calculating transport and chemistry. For this work CAMx (v4.42) has been off-line coupled to the mesoscale meteorological model MM5. Two-dimensional gridded low-level emissions are defined by space – and time- varying rates for each individual gas and PM species to be modelled. Emissions from industry and power plants are included as elevated point sources. Chemistry is parameterized according to the CB-IV chemical mechanism.

Aerosol Robotic Network (AERONET) is a network of globally distributed Sun photometers (http://www.aeronet.com). Aerosol optical depths were used for the campaign period and correlated with the weighted average of pm10 concentration as shown in figure 1.

During the campaign, the aerosol burden over Thessaloniki experienced large variations in load and nature, especially due to the variable prevailing meteorological conditions, which resulted in the advection of air masses from different sources. Variations of the aerosol optical depth between 0.2 and 1.0 at 340 nm were recorded. The aerosol optical depth at 340 nm along with the PM 10 concentration calculations as derived from the model are presented in Figure 1 for Thessaloniki and in Figure 2 for Epanomi.
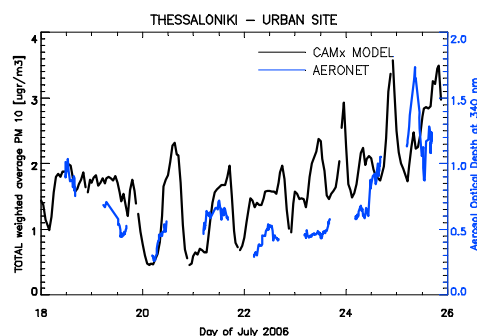
Figure 1. Total weighted average of PM 10 concentration (black) derived with CAMx model and aerosol optical depth at 340 nm (blue) as given by AERONET for Thessaloniki.
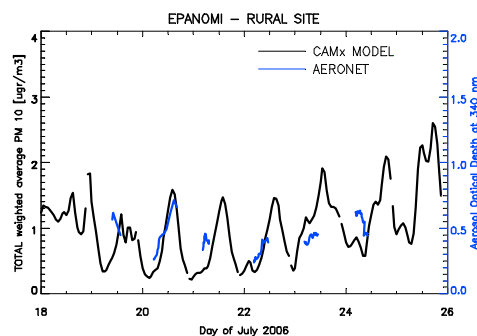
Figure 2. Total weighted average of PM 10 concentration (black) derived with CAMx model and aerosol optical depth at 340 nm (blue) as given by AERONET for Epanomi.

Amiridis, V., Balis, D.S., Kazadzis, S., Bais, A., Giannakaki, E., Papayannis A., and Zerefos, C.(2005), J. Geophys. Res., 110, D21203, doi:10.1029/2005JD006190, 2005.

Microphysical and optical properties of aerosols at Thessaloniki, Greece: Comparison of two different inversion algorithms

E. Giannakaki[1], D. Müller[2] and D. Balis[1]

[1]Laboratory of Atmospheric Physics, Thessaloniki, Greece
[2]Leibniz Institute for Tropospheric Research, Leipzig, Germany

Keywords: Atmospheric aerosol, Aerosol size distribution, CIMEL

A UV-aerosol campaign was held from July 14-25, 2006, at Thessaloniki, Greece, as part of the integrated project SCOUT-O3 (Stratosphere-Climate Links with Emphasis on the Upper Troposphere and Lower Stratosphere). A number of in-situ, remote sensing and aircraft measurements were performed. Among the goals of the campaign was to derive microphysical aerosol properties by the usage of in-situ and remote sensing aerosol measurements.

At the Laboratory of Atmospheric Physics (LAP) a two wavelength combined Raman elastic-backscatter lidar is used to perform continuous measurements of suspended aerosols particles in the planetary boundary layer (PBL) and the lower free troposphere (Amiridis et al., 2005). The lidar system of LAP and the algorithms implemented were successfully intercompared in the frame of the European Aerosol Research Lidar Network (EARLINET).

During the campaign, the aerosol burden over Thessaloniki experienced large variations in load and nature, especially due to the variable prevailing meteorological conditions, which resulted in the advection of air masses from different sources. Variations of the optical depth between 0.2 and 1.0 at 340 nm and of the Angstrom exponent between 0.7 and 2.0 were recorded. Different aerosol microphysical properties are expected for the boundary layer and the free tropospheric region over Thessaloniki.

Microphysical particle properties are derived with an inversion algorithm that has been developed at the Leibniz Institute for Tropospheric Research (IfT). A detailed description of the original version of the algorithm is given by Müller et al., 1999. Modifications concerning the selection of the optimum solution space were made by Veselovskii et al. 2002. Changes concerning the minimum number of measurement wavelengths which are needed for the inversion can be found in Müller et al. 2001 and Veselovskii et al., 2002.

Aerosol Robotic Network (AERONET) is a network of globally distributed Sun photometers. AERONET provides microphysical properties in systematic base using an inversion algorithm (Dubovik et al., 2000). The combined use of lidar and sunphotometer measurements with the inversion algorithm has been used to retrieve effective radius. The comparison shows a good agreement for the fine mode of size distribution.
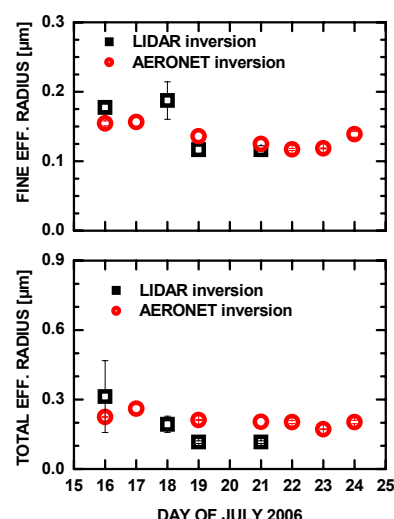
Figure 1. Comparison of effective radius with IFT algorithim inversion anf AERONET inversion for the fine mode (top) and total (bottom).

Inversion-based retrieval products from AERONET have not yet systematically been validated by comparison to in-situ measurements. In this study aerosol optical data from cimel taken during the SCOUT-O3 campaign were used to estimate the microphysical properties of aerosols using the inversion algorithm from IFT. The results were compared with the corresponding microphysical aerosol properties as given by AERONET. For the period of SCOUT-O3 campaign, effective radii from the well-known AERONET inversion algorithm seem to be consistent with our results in the case of fine mode size distributions.

Amiridis, V., Balis, D.S., Kazadzis, S., Bais, A., Giannakaki, E., Papayannis A., and Zerefos, C.(2005), J. Geophys. Res., 110, D21203, doi:10.1029/2005JD006190, 2005

Giannakaki, E., D. Balis, D. Müller, V. Amiridis, S. Rapsomanikis, and A. Bais (2008), 24th ILRC 22.

Dubovik, O., M. D. King, (2000), J. Geophys. Res., 105, pp. 673 - 696

Müller, D, U. Wandinger and A. Ansmann (1999), Appl. Op., 37, pp. 2346 – 2357.

Veselovskii, I., Kolgotin, A., Griaznov., V., Müller, D, Wandinger, U., and Whiteman D., Appl. Opt., 41, pp. 3685-3699.

Aerosol characterization in the North-Center (Castilla y Léon) of Spain

Rubén Rodrigo, Victoria Cachorro, Alberto Berjón, Benjamín Torres, Carlos Toledano, Angel de Frutos

[1] GOA -Group of Atmospheric Optics, University of Valladolid, 47071 Valladolid – Spain

Keywords: Aerosol characterization, AOD, Optical properties, Angström coefficient, Aerosol size distribution,

The Atmospheric Optic Group (GOA-UVa) at the University of Valladolid is the responsible of the photometric Palencia site belonging to AERONET-PHOTONS-RIMA, which is located in the Castilla y León region, in the north-center of Spain. Routine measurements are carried out since 2003. We take for our study the time period between 23-Jan-2003 and 01-Jul-2008. The instrument which has been taking measurements is a CIMEL sun photometer that provides the necessary data for a complete statistics. The data from Palencia site are included in AERONET at level 2.0 (Holben et al 1998), except the period 02-Aug-2006 until 10-Apr-2007 that are still in 1.5 level.

We have carried out a characterization of the aerosol in Palencia site. This classification is based on the aerosol optical properties derived from direct sun and sky radiance measurements: Aerosol Optical Depth (AOD), Angström exponent (AE) between 440 and 870 nm and inversion products, e.g. size distribution, phase function, single scattering albedo, etc.

The total number of measurement days was 1518 out of 2192 days since its deployment, which represent the 69.2% of the analysed period.

The background aerosol at the site presents low turbidity, especially in autumn (figure 1). The predominant type is clean continental aerosol. At Palencia most of the high AOD events were registered in summer (mostly June and July), but some episodes were also observed in spring. These episodes were analyzed following the methodology described in Toledano et al. (2007), using threshold values in AOD and AE to discriminate aerosol types. From this analysis we found that the events not corresponding with the background aerosol in our station are due to desert dust events that arrive from Sahara (9.6% of days), contamination events that reach the site from Europe or due to recirculation of polluted air masses from our own country (11.6% of days), or both mixed (7.0% of days). Also few episodes of biomass burning from forest fires (1% of days) are detected, with high values of the AOD and AE.

The mean AOD (440 nm) is 0.15 (STD 0.12). The maximum AOD achieves 1.2 during a desert dust event in July 2004. The majority of AOD data (79% of days) are below 0.2.

Figure 2 shows the monthly means of the AE. The mean value is 1.34 (STD 0.45) with almost no variation along the year. This parameter indicates fine particle predominance which is typical of the continental aerosol.
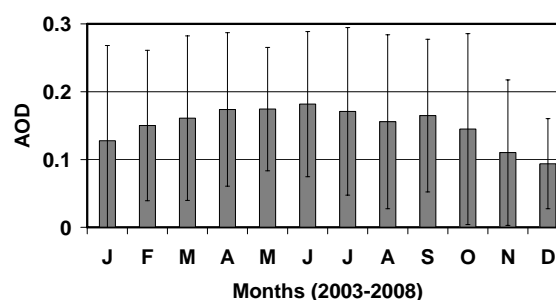
Figure 1. Monthly average of the Aerosol Optical Depth (AOD) during 2003-2008 at Palencia site. Bars in boxes are the standard deviation.
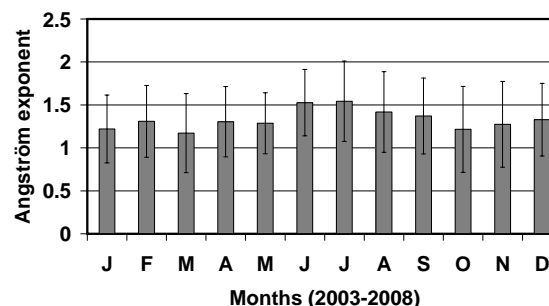
Figure 2. Monthly average of the Angström exponent during 2003-2008 at Palencia site. Bars in boxes are the standard deviation.

Bibliography
Holben B., et al Remote Sens. Environ., 66,1-16, 1998 (http://aeronet.gsfc.nasa.gov/).
Toledano, C., V.E. Cachorro, A.M. de Frutos, M. Sorribas, N. Prats and B.A. de la Morena. Desert dust events over the south-western Iberian Peninsula in 2000-2005 inventoried with an AERONET Cimel sun photometer. J. Geophys. Res.,112, D21201, doi:10.1029/2006JD008307, 2007.

EARLINET: integration approach for aerosol study

L. Mona[1], G. Pappalardo[1], A. Amodeo[1], G. D'Amico[1], I. Mattis[2], C. Perez[3], U. Wandinger[2]

[1]Istituto di Metodologie per l'Analisi Ambientale – Consiglio Nazionale delle Ricerche (IMAA-CNR), C.da S. Loja, Tito Scalo, Potenza, I-85050, Italy
[2]Institut für Troposphärenforschung, Leipzig, Germany
[3] Earth Sciences Division, Barcelona Supercomputing Centre, Barcelona, Spain

Keywords: lidar, tropospheric aerosol, remote sensing, vertical distribution.

The recent IPCC (Forster et al., 2007) reports that the uncertainty about aerosol direct and indirect effects is still too high to draw a conclusion about the effect of human activities on radiation budget. More observations, and in particular altitude resolved measurements, are needed in order to further reduce this uncertainty. Nowadays, lidar techniques are an indispensable tool to study the vertical structure of aerosol field and to investigate aerosol optical properties, because they allow us to obtain direct measurements of aerosol extinction (and therefore optical depth) without critical assumptions and to describe the aerosol vertical distribution. At European level, systematic lidar measurements are performed within EARLINET (European Aerosol Research Lidar NETwork) since May 2000, providing a long-term database of aerosol lidar measurements (Pappalardo et al., 2009a).

The complexity of the problem requires a synergistic approach of satellite and ground-based observations together with model calculations in order to achieve an accurate quantification of aerosol and cloud radiative forcing (e.g. Diner et al., 2004). In this context, EARLINET consortium is exploring possibilities about scientific study based on the integration of different datasets.

EARLINET lidar network together with a large number of AERONET sites provides an optimal benchmark for comparison and integration of passive and active remote sensing techniques for study of aerosol impact on radiation budget. First comparisons of aerosol optical depth at a subset of AERONET /EARLINET sites were carried out, allowing us also to discuss the representativeness of the data.

For what concerns the impact on air quality, EARLINET measurements performed during the EMEP intensive measurements period (17 Sept – 16 Oct 2008) are a good starting point for the integration of PM measurements and vertical profiles.

Since June 2006, CALIPSO (Cloud-Aerosol Lidar and Infrared Pathfinder Satellite Observations) mission provides a first unique opportunity to address the study the 4-dimensional distribution of aerosols and clouds on a global scale. Because of its geographic coverage and its high quality, the EARLINET network can be considered an optimal single instrument to increase and validate the accuracy of aerosol optical properties retrieved from the CALIPSO pure backscatter lidar. In addition, EARLINET correlative measurements provide a unique opportunity to investigate the representativeness of CALIPSO observations, thanks to the well-established high quality of EARLINET data and to the geographical distribution of EARLINET stations over Europe, covering a large variety of different aerosol contents in the free troposphere and the local planetary boundary layer (Mona et al., 2009; Pappalardo et al., 2009b).

Finally, EARLINET data will be used for aerosol models validation. In this context, first systematic quantitative comparisons with the DREAM (Dust REgional Atmospheric Model) dust forecast model have been carried out for selected stations with large number of dust observations.

Diner, D. J., et al. (2004), *PARAGON: An integrated approach for characterizing aerosol climatic and environmental interactions*, Bull. American Meteorol. Soc., 85, 1491–1501.

Forster, P., et al. (2007), in *Climate Change 2007: The Physical Science Basis,* edited by S. Solomon, D. Qin, M. Manning, Z. Chen, M. Marquis, K. B. Averyt, M. Tignor, and H. L. Miller, Cambridge Univ. Press, New York.

Mona, L., et al. (2009), *One year of CNR-IMAA multi-wavelength Raman lidar measurements in correspondence of CALIPSO overpass: Level 1 products comparison*, submitted to Atmos. Chem. And Phys.

Pappalardo, G., et al. (2009a)*, EARLINET for long term observations of aerosol over Europe*, EAC.

Pappalardo, G., et al. (2009b), *EARLINET correlative measurements for CALIPSO: first intercomparison results*, to be submitted to Jour. Geo. Res.

Infrared optical constants of highly diluted sulfuric acid solution droplets at cirrus temperatures

R. Wagner[1], S. Benz[1], H. Bunz[1], V. Ebert[2], O. Möhler[1], H. Saathoff[1], M. Schnaiter[1], and T. Leisner[1]

[1]Forschungszentrum Karlsruhe, Institute for Meteorology and Climate Research (IMK-AAF), Karlsruhe, Germany
[2] University of Heidelberg, Physical Chemistry Institute, Heidelberg, Germany

Keywords: sulfuric acid, infrared spectroscopy, refractive index.

Complex refractive indices for supercooled sulfuric acid solution droplets in the mid-infrared spectral regime (wavenumber range 6000 – 800 cm^{-1}) have been retrieved for acid concentrations ranging from 33 to 10 wt% H_2SO_4 at temperatures between 235 and 230 K, from 36 to 15 wt% H_2SO_4 at temperatures between 225 and 219 K, and from 37 to 20 wt% H_2SO_4 at temperatures between 211 and 205 K. These measurements cover for the first time the composition regime which is involved when supercooled H_2SO_4/H_2O solution droplets enter an environment that is supersaturated with respect to the ice phase at temperatures below 235 K. The optical constants were derived with a Mie inversion technique from measured H_2SO_4/H_2O aerosol extinction spectra which were recorded during controlled expansion cooling experiments in the large coolable aerosol chamber AIDA of Forschungszentrum Karlsruhe (Wagner et al., 2008).

The experimental trajectories of these expansion cooling cycles closely follow an atmospheric composition trajectory (Fig. 1). Initially concentrated H_2SO_4/H_2O solution droplets are subjected to a gradually increasing relative humidity upon cooling. Thereby, the sulfuric acid solution droplets continuously dilute until they finally freeze at some threshold composition.
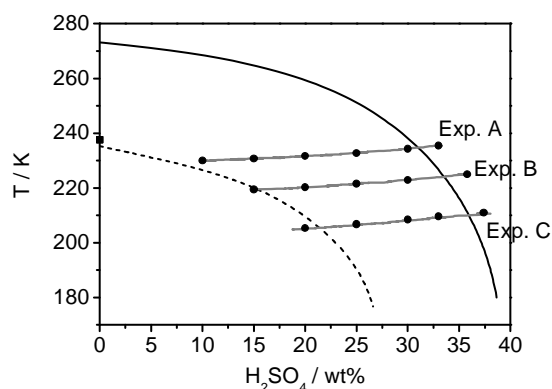
Figure 1: Experimental trajectories of three expansion cooling experiments with supercooled sulfuric acid solution droplets within the sulfuric acid – water phase diagram. Highlighted by black dots on the trajectories are the specific acid concentrations for which the optical constants were determined (see Fig. 11 in Wagner et al., 2008).

Model calculations of the condensational growth of the sulfuric acid solution droplets were performed with the computer model MAID (Bunz et al., 2008). These calculations demonstrated that the aerosol particles had sufficient time to reach equilibrium with temperature and water vapor to possess a well-defined composition during the expansion cooling cycles. Fast and highly accurate water vapor measurements by means of direct tunable diode laser absorption spectroscopy were used in combination with the Aerosol Inorganics Model (AIM) to infer the composition of the sulfuric acid solution droplets.

The new low-temperature optical constants for highly diluted sulfuric acid droplets reveal significant temperature-induced spectral variations in comparison with the refractive indices for higher temperatures, which are associated with a change in the equilibrium between sulfate and bisulfate ions (Fig. 2).
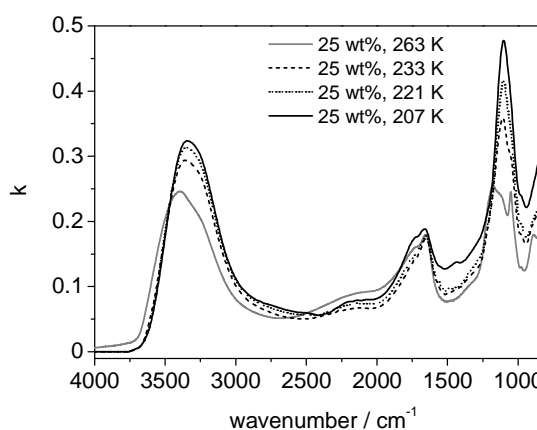
Figure 2: Temperature dependence of the spectrum of the imaginary part of the complex refractive index (k) of H_2SO_4/H_2O for an acid concentration of 25 wt% H_2SO_4 (see Fig. 12 in Wagner et al., 2008)

Bunz, H., Benz, S., Gensch, I. & Krämer, M. (2008). *Environ. Res. Letters*, 3, 035001.

Wagner R., Benz S., Bunz H., Möhler O., Saathoff H., Schnaiter M., Leisner T. & Ebert V. (2008). *J. Phys. Chem. A*, 112, 11661-11676.

Optical Properties of Different-Shaped Synthetic Hematite Particles: A Laboratory Study

M. Vragel [1], C. Linke [1], M. Schnaiter [1], G. Beuchle[2], and T. Leisner [1]

1) Institut für Meteorologie und Klimaforschung (IMK-AAF), Forschungszentrum Karlsruhe, Germany
2) Institut für Technische Chemie (ITC-TAB), Forschungszentrum Karlsruhe, Germany

Keywords: Fe-oxides, Mie scattering, Optical Properties, Shape

In order to retrieve microphysical aerosol properties from remote sensing measurements, one important question is whether the optical properties depend on the shape of the aerosol particles. Natural mineral dust particles show a wide range of aspherical shapes that cannot be described analytically, but in model studies usually have to be approached as spheroidal particles.

In our laboratory experiments we use synthesized nonspherical hematite particles of different morphologies, which serve as model aerosols (Table 1). Each type of hematite particles has a nearly monodisperse size distribution and a well-defined particle shape.

Shape	Aspect ratio	Large axis [nm]
Pseudo-spheres	1.1	135-200
Spheroidal, small	1.9	320-350
Spheroidal, large	2.8	480-570

Table 1. Shape, aspect ratio and size of synthetical hematite particles investigated in an aerosol chamber.

At the Institute of Meteorology and Climate Research of Forschungszentrum Karlsruhe, Germany, the optical properties of the above mentioned hematite aerosols were investigated experimentally. The particles were dispersed into a 3.7 m³ aerosol chamber, reaching initial particle concentrations of 10^3 - 10^4 cm^{-3}. During three to four hours the particle concentration decreased by one order of magnitude. Table 2 lists the optical quantities measured at the aerosol chamber. Detailed descriptions of the instruments are given in Schnaiter et al., 2005 and Linke et al., 2006.

Instrument	Optical Quantity	Wavelength [nm]
Extinction Spectrometer LOPES	extinction coefficient	200 – 1000 $\Delta\lambda$ = 2.5 nm
Integrating Nephelometer	scattering coefficient	450, 550, 700
Photoacoustic Spectrometer MuWaPAS	absorption coefficient	266, 355, 532, 1064
Laser Light Scattering Instrument SIMONE	near backscatter linear depolarisation ratio and forward to backward scattering ratio	488
deduced	singles scattering albedo angström exponents	450, 550, 700

Table 2. Some optical quantities measured at the aerosol chamber and their corresponding wavelengths.

The talk presents spectral extinction and absorption cross section measurements and depolarisation measurements. The data are compared with results of Mie and T-Matrix calculations. Since it is not possible to synthesize larger hematite particles and for technical limitations concerning the instrument design, the study is limited to sphere equivalent diameters of several hundred nanometers. Results show no definite shape dependence of the spectral extinction behaviour, because it can be reproduced with both Mie and T-matrix models.

Schnaiter et al., *Measurement of Wavelength-Resolved Light Absorption by Aerosols Utilizing a UV-VIS Extinction Cell*, Aerosol Sc. and Techn., 39, 249, 2005

Linke, C. et al., *Opt. Properties and Mineralogical Compos. of Different Saharan Mineral Dust Samples: A Laboratory Study*, At. Ch. and Phys. Disc., 6, 3315, 2006

Effects of complex shapes on radiative properties of mineral dust aerosol: Implications on sun photometry

J. Gasteiger[1], M. Wiegner[1], C. Toledano[2] and P. Koepke[1]

[1]Meteorologisches Institut, Ludwig-Maximilians-Universität, Theresienstraße 37, 80333 München, Germany
[2]Grupo de Óptica Atmosférica, University of Valladolid, Prado de la Magdalena, 47071 Valladolid, Spain

Keywords: mineral dust, particle shape, optical properties, extinction, remote sensing.

Mineral dust aerosol is a component of earth's atmosphere that is important with respect to radiative forcing and thus for climate. The complex microphysics of this aerosol component, however, introduces problems in the field of light scattering and subsequently in remote sensing (and in-situ) measurements. Each dust particle has an individual shape. Thus for modelling of radiative properties and their inversion, assumptions are not only needed for the size distribution and refractive index, as for other aerosol types, but also for the particle shape. Usually spheres or spheroids are assumed as simplification.

To assess the uncertainties introduced by these assumptions, the influence of the particle shape on light scattering is simulated. Using the Amsterdam DDA code (Yurkin *et al.*, 2007) complex shapes are compared to spheres and spheroids.
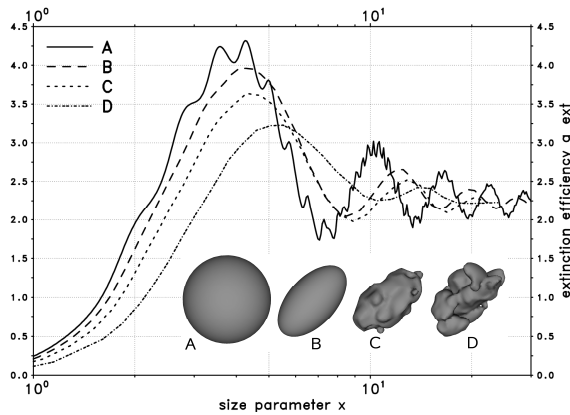
Figure 1. q_{ext} vs. x for four different shapes

Fig. 1 shows the extinction efficiency $q_{ext}=C_{ext}/(\pi r^2)$ for four different shapes, depending on their size relative to the wavelength (defined as the size parameter $x=2\pi r/\lambda$), with r related to a sphere with an equivalent projected area. The refractive index is assumed as $m=1.52+0.0043i$. The extinction efficiency q_{ext} together with the column-integrated size distribution $n(r)$ results in spectral variations of the aerosol optical depth τ_p, which is given by

$$\tau_p(\lambda) = \int\limits_0^\infty \pi \cdot r^2 \cdot q_{ext}(2\pi \cdot r / \lambda) \cdot n(r) \cdot dr$$

τ_p values at different wavelengths are used to define the Angstrom exponent α as a qualitative indicator of aerosol particle size, which is used for the interpretation of sun photometer measurements:

$$\alpha_{\lambda_1,\lambda_2} = \frac{\ln(\tau_p(\lambda_1)/\tau_p(\lambda_2))}{\ln(\lambda_2/\lambda_1)}$$

As Fig. 1 indicates, the optical depth not only depends on the size, but also on the shape of the particles. The variation of α, resulting for particles with a log-normal size distribution ($r_{mod}=0.1\mu$m; $\sigma=2.7$; $r_{max}=10\mu$m; $r_{eff}=1.125\mu$m), but different shape are shown in Tab. 1 (particles larger than $r=1.5$ μm are assumed to be spherical in all cases).

Table 1. Angstrom exponent $\alpha_{440,870}$ of four different shapes (see Fig. 1).

Shape	$\alpha_{440/870}$
A (spheres)	0.0184
B (spheroids)	0.0394
C (deformed spheroids)	0.0757
D (aggregates)	0.1572

The α for the aggregate particles is comparable to the α of spheres, however only if the radius of the spherers is changed to $r_{mod}=0.0667\mu$m (and unchanged σ, resulting in $\alpha=0.1562$). This means, that the size of the particles is underestimated by a factor of 1.5, if spherical shape was assumed in the inversion model, while the "real-world" aerosol particles were aggregates as shown in Fig. 1 (D).

Further investigations with an ensemble of representative particle shapes are needed to better quantify the uncertainties in sun photometric inversions. Furthermore, it is well known, that the shape of aerosol particles significantly influences sideward and backward scattering (Koepke and Hess, 1988; Mishchenko *et al.*, 1997). Investigations on how the angle-dependent optical parameters of the simplified shapes compare to those of complex shapes are planned. These investigations can be helpful e.g. for the interpretation of sky radiometer and lidar measurements.

Yurkin, M. A. *et al.* (2007), *JQSRT*, 106, 546-557.
Koepke a. Hess (1988), *Appl. Opt.*, 27, 2422-2430.
Mishchenko, M. I. *et al.* (1997), *JGR*, 102, 16831-16847.

Single Scattering Albedo Variation in the Indian Continental Tropical Convergence Zone during Pre-monsoon and Monsoon Seasons of Year 2008

J. Jai Devi[1], S.N. Tripathi[1], Tarun Gupta[1], V.Gopalakrishnan[2]

[1] Department of Civil Engineering, Indian Institute of Technology Kanpur, 208016, Kanpur, India
[2] Instruments and Observational Techniques Division, Indian Institute of Tropical Meteorology Pune, 411008, Pune, India

Monsoon rainfall over Indian subcontinent is the lifeline for more than hundreds of million people. Therefore, any climatological changes in its characteristics warrant investigation. Recent global modeling studies, albeit few only, that estimated the aerosol effects on monsoon show conflicting results- one group of investigators report enhancement of rainfall in the pre-monsoon season (May-June) and reduction during the main monsoon (July-September) phase (Lau et al., 2006); while others (Ramanathan et al., 2006) show an overall rainfall reduction in whole India during May-September months.

The continental tropical convergence zone (CTCZ) over India has a complicated atmospheric structure due to uneven terrain which rises from sea level to ~6 km. In the I-CTCZ (Indian CTCZ) lies the great Indian Desert in the west, heavily polluted Indo-Gangetic basin in the North-Central India, high altitude Himalayas in the North East and peninsular region towards South. Elevated terrains act both as preferred centres for local convection and barriers to the transcontinental free flow of air at lower levels (Hills, 1978).

An extensive aircraft experiment over I-CTCZ was performed during pre-monsoon (May '08) and late monsoon (September '08) seasons to study aerosol microphysical and optical properties. During the study, based on the striking differences in physical, optical and chemical properties of aerosols present over I-CTCZ, the region was divided into five zones- The Himalayan foothills; The Indo Gangetic (IG) basin; the desert region; The Central India; and the marine region. Knowledge of the spatial and vertical structure of the aerosol layer will help to verify and constrain the modeled results for Indian monsoon.

Results on the vertical and spatial distribution of aerosol optical properties e.g. SSA obtained during the airborne measurements using an onboard Photoacoustic Soot Spectrometer (PASS-1) which was integrated with photomultiplier tube for measuring scattering coefficient will be presented together with black carbon mass fraction obtained using Aethalometer, Scanning Mobility Particle Sizer and Aerodynamic Particle Sizer.

Interesting results for other zones with strikingly different aerosol properties will also be presented to give overall variation in the optical properties of aerosols within and above the mixed layer during pre-monsoon and monsoon with vertical variation at selected stations.

Hills, R. C. (1979). Inst. Brit. Geogr. 4, 3, 329–352.

Lau, K.M., Lau, M.K., & Kim, K.M (2006). Climate Dynamics 26: 855-864

Ramanathan, V., Chung, C., Kim, D., Bettge, T., Buja, L., Kiehl, J.T., Washington, W. M., Fu, Q., Sikka, D.R., & Wild, M. (2006). Proc. Nat. Acad. Sci. 102(15): 5326-33

Study of transformation of aerosol optical and microphysical parameters at heating

S.A. Terpugova, M.V. Panchenko, T.A. Dokukina and E.P. Yausheva

V.E. Zuev Institute of Atmospheric Optics, 1, Ak. Zuev square, 634021, Tomsk, Russia

Thermooptics, i.e. measurements of the response of the optical properties to the controlled heating is one of the operative techniques for study of the aerosol composition. One of the merits of this experimental approach is possibility to carry out measurements immediately in the air flow without sampling on the filters which may cause change of the aerosol properties. In the present paper, the results of the thermooptical measurements carried out in 2004–2007 in the Institute of Atmospheric Optics in Tomsk are analyzed.

Thermooptical measurements were performed with complex experimental setup based on the nephelometer-polarimeter PhAN. Prior to thermooptical measurements, transformation of the aerosol optical characteristics with relative humidity was measured. So the thermooptical aerosol properties could be compared with parameters of the aerosol condensation activity. The range of the heating was $25 - 250°C$. At heating, the angular scattering coefficient μ at wavelength of 510 nm and scattering angle of 45° was recorded continuously. At temperatures of 25°C, 100°C, and 175°C, seven parameters of the aerosol scattering (angular scattering coefficients at 45° and wavelengths of 410, 510 and 630 nm and their orthogonally polarized components at scattering angle of 90° and wavelengths of 450 and 520 nm were registered.

As quantitative optical characteristics of the aerosol volatility we have chosen three parameters:

$$F = \frac{\mu(25°C) - \mu(100°C)}{\mu(25°C)}, \quad Q = \frac{\mu(100°C) - \mu(250°C)}{\mu(25°C)},$$

and $S = \frac{\mu(250°C)}{\mu(25°C)}$,

where $\mu(T)$ is the angular scattering coefficient at the scattering angle of 45° for aerosol heated up to the noted temperature. If accept $\mu(25°C)=1$, then the parameters F and Q describe the fractions of the components evaporated in the respective temperature range, and the parameter S characterizes the incombustible residue. Thermooptical measurements are the part of regular observations of the aerosol optical characteristics, which also include measurements of angular and polarization characteristics of light scattering by dry matter of aerosol particles in visible wavelength range. The inverse problem was solved for the data of these measurements, and the aerosol size spectra and the particle refractive indices were retrieved.

A positive correlation of S with black carbon fraction was revealed. Peculiarities of the seasonal behavior of the thermooptical parameters were analyzed. It was found that the parameter F has minimum in spring (March-April) and maximum in summer (June-August), the parameter Q is maximum in spring (April) and minimum in the end of summer (August-September), and the parameter S is minimum in summer (June-July) and maximum in winter (November-January).

The results of the measurements of the seven optical parameters at three air temperatures were inverted to the aerosol distributions at the particle's radius range $0.05 - 0.6$ μm. Particle's refractive indices were also retrieved. It must be noted that the level of aerosol scattering at 90° at background conditions after heating is often the same order, or even less, than Rayleigh scattering. It leads to significant uncertainties in the separation of the aerosol scattering from the measured signals. So, the reliable inversion can be carried out only at situations with rather high aerosol loading. At initial temperature limitations are not so rigorous. It was found that greater values of the refractive index at 25° correspond on average, greater values of the residue S.

Inversion of the measurement data at different stages of heating allows estimating the size dependence of the volatility factor VF comparing the cumulative number concentrations. Volatility factor can be introduced as the ratio of the size of the heated particle to initial size. Examples of the VF retrieved are presented in Figure 1.
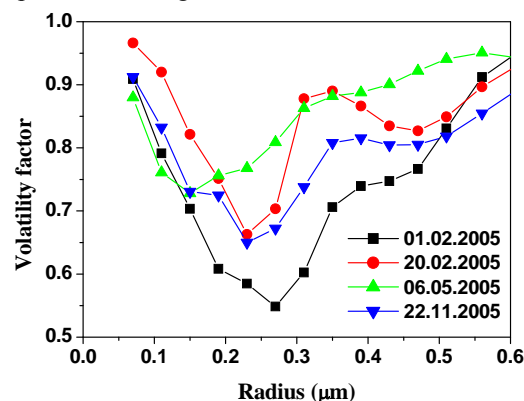
Figure 1. Volatility factors at temperature of 175°C as functions of the particle radius.

The main extremum of VF is usually located in the size region $0.2 - 0.3$ μm. In some cases, the second minimum is observed at $0.4 - 0.5$ μm.

Climate relevant aerosol properties measured at Évora, Portugal, from 2002 to 2008

S.N. Pereira[1], F. Wagner[1] and A.M. Silva[1,2]

[1]Évora Geophysics Centre, Rua Romão Ramalho, 59, 7000 Évora, Portugal
[2]Department of Physics, University of Évora, Rua Romão Ramalho, 59, 7000 Évora, Portugal

Keywords: optical properties, aerosol characterization, measurements.

The assessment of the direct effect of aerosols on climate (due to their interaction with solar and terrestrial radiation via scattering and absorption processes) requires quantitative information on the optical properties of atmospheric aerosols. Long term measurements at different locations are essential for characterizing both the aerosol field and climatology in order to decrease the uncertainties in radiative forcing estimations. Routine measurements of spectral scattering coefficients, $\sigma_{sp}(\lambda)$, and backscattering coefficients, $\sigma_{bsp}(\lambda)$, were carried out at Évora Geophysics Centre's Observatory since 2002. Near surface measurements were made with an Integrating Nephelometer (TSI-3563) at the wavelengths λ = 450, 550 and 700 nm. In addition, measurements of absorption coefficient, $\sigma_{ap}(\lambda)$, at 670 nm, were performed since 2007 with a Multi-Angle Absorption Photometer (Thermo Scientific, Model 5012). The former extensive properties are used to compute the extinction coefficient, $\sigma_{ep}(\lambda)$. Additional intensive climate relevant properties are derived, namely the backscattering ratio, b, single scattering albedo, ω, and Ångstrom exponent, α (which is related to size distribution).

Évora is a small sized city (~60000 inhabitants) within a rural area and is located on the south-western sector of the Iberian Peninsula. No major polluting industries are present in the area; therefore the local anthropogenic production is essentially related to traffic and biomass burning for heating during the colder fall and winter periods. On the other hand, the aerosol load is frequently of moderate to low magnitude, hence the site is suitable for monitoring long-range transported particles from other regions, namely dust from Sahara and pollution from major industrial/urban areas or due to forest fires (Elias *et al*., 2006; Pereira *et al*., 2008).

Daily averaged values are used to investigate the time evolution and variability of the measured quantities aiming to obtain aerosol climatology for the site. Figure 1 shows the time evolution of σ_{sp}(550nm) and σ_{bsp}(550nm) along the seven years period. A seasonal variation is observed with higher values in winter (likely due to the combined effect of biomass burning due to heating added to the usual traffic and a low mixing layer height) and also in summer whose peaks are related to forest fires and desert dust aerosols transported to the site. In 2008, the lack of extreme values can be attributed to the absence of important dust episodes and forest fires.

Figure 2 shows the time evolution of σ_{ap}(670nm) in 2007 and 2008, with a significant increase during winter, and a simultaneous decrease in ω (not shown) which are in agreement with the increase in the fraction of absorbing material in winter.
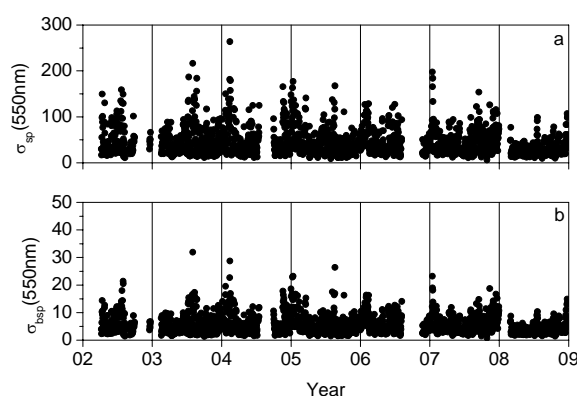
Figure 1. Time evolution of (a) σ_{sp}(550 nm) and (b) σ_{bsp}(550 nm) daily values between 2002 and 2009.

Figure 2. Time evolution of σ_{ap}(670 nm) daily values.

Elias, T., Silva, A. M., Belo, N., Pereira, S., Formenti, P. 2006. Aerosol extinction in a remote continental region of the Iberian Peninsula during summer. *J. Geophys. Res*, **111**, D14204, doi: 10.1029/2005JD006610.

Pereira et al., Scattering properties and mass concentration of local and long-range transported aerosols over the South Western Iberian Peninsula, *Atmospheric Environment* (2008), doi:10.1016/j.atmosenv.2008.06.008.

Aerosol light scattering at high relative humidity at a high alpine site (Jungfraujoch)

R. Schmidhauser, P. Zieger, E. Weingartner, M. Gysel, P.F. DeCarlo and U. Baltensperger

Laboratory of Atmospheric Chemistry, Paul Scherrer Institut, 5232, Villigen PSI, Switzerland

Keywords: light scattering, relative humidity, nephelometer, optical properties, single scattering albedo.

All aerosol parameters measured within the Global Atmosphere Watch aerosol monitoring program (GAW) have to be measured under dry conditions (<40% relative humidity (RH)). This is necessary to compare different measurement sites. However, aerosol particles experience high RH conditions in the atmosphere. The ambient RH determines the water content of aerosol particles and therefore has an important influence on the particles' ability to scatter visible light. The RH dependence of the particle light scattering coefficient (σ_s) is therefore an important measure for climate forcing calculations.

We built a novel humidification system for an integrating nephelometer to measure the RH dependence of σ_s. σ_s can be measured at a defined and controlled RH in the range of 40-90%. This RH conditioner consists of a humidifier, followed by a dryer, which enables us to measure the hysteresis behavior of deliquescent aerosol particles (Schmidhauser *et al.*, 2009). The factor quantifying the influence of RH on σ_s is called light scattering enhancement factor f(RH) and is the ratio between σ_s at high and low RH.

The humidified nephelometer measured σ_s at varying RH in May 2008 at the high alpine GAW station Jungfraujoch, Switzerland (3580m asl). To calculate f(RH) the dry σ_s of the GAW nephelometer was used. In May 2008 the f(RH) at 85% RH ranged from 1.2 to 3.5. Figure 1 shows a typical humidogram measured on May 13, 2008. Light scattering enhancement factors at 85% RH and at a wavelength of 550 nm are higher than 2.5. A comparison model study (Nessler *et al.*, 2005a) predicted 0-30% lower f(RH=85%) values.
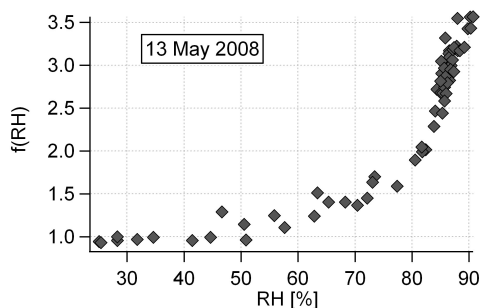
Figure 1. Light scattering enhancement factor f(RH) at 550 nm wavelength versus RH for one day of the measurement campaign at Jungfraujoch.

Water uptake by the aerosol particles not only increases aerosol light scattering, but also changes other variables important for calculating aerosol climate forcing such as the single scattering albedo (SSA). The SSA is the ratio of σ_s and the extinction coefficient σ_e ($\sigma_e=\sigma_s+\sigma_a$, σ_a: absorption coefficient).

Figure 2 presents histograms of the SSA at 10% and 85% RH, respectively, at a wavelength of 550 nm. The dry SSA at Jungfraujoch is already relatively high, with a peak at 0.91, indicating that the aerosol is ten times less absorbing than scattering ($\sigma_a <5\cdot10^{-6}$ m^{-1}). The humid SSA was calculated with σ_s at 85% RH and dry σ_a assuming that the absorption does not change with RH (Nessler *et al.*, 2005b). By including the water uptake of aerosol particles, the peak of the SSA in the histogram is at 0.96.
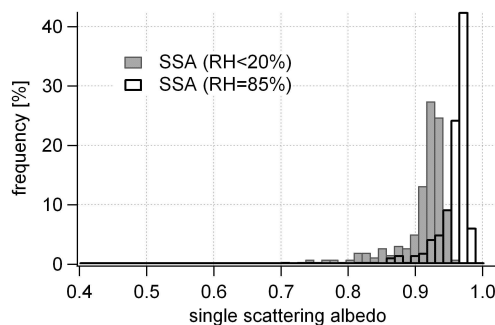
Figure 2. Histogram of the single scattering albedo (SSA) at Jungfraujoch in May 2008 at dry (~10% RH) and humid (85% RH) conditions (1h averages).

This work demonstrates that the water uptake of aerosol particles has an important influence on radiative forcing calculations because it enhances the particles scattering coefficient and therefore changes their optical properties (such as the SSA or the backscatter fraction).

Nessler, R., Weingartner, E. & Baltensperger, U. (2005a). *Environ. Sci. Technol.*, 39 (7), 2219-2228.

Nessler, R., Weingartner, E. & Baltensperger, U. (2005b). *J. Aerosol Sci.*, 36, (8), 958-972.

Schmidhauser, R., Zieger, P., et al. (2009). Submitted to *Environ. Sci. Technol.*

Comparison of near-surface and columnar aerosol optical and microphysical properties

M.A. Sviridenkov and A.A. Isakov

A.M. Obukhov Institute of Atmospheric Physics, 3, Pyzhevsky, 119017, Moscow, Russia

Aerosol properties retrieval from the data on sun-sky radiance is a complicated problem. At large angular distances from the sun, the contribution of the Rayleigh and multiple scattering into the measured radiance is predominant. It leads to significant errors in determination of the characteristics of the aerosol single scattering. Polarimetric measurements in local scattering volumes allow to obtain all the aerosol scattering characteristics needed for solution of the inverse problem. Another advantage of the local optical aerosol measurements is the possibility to modify artificially state of the aerosol, e.g. to humidify the airflow, and thus to study aerosol condensation activity important for the estimation of the aerosol climatic effects. However, validity of the expansion of the aerosol properties from the near-ground layer to the atmospheric column is not completely investigated yet. In the present paper, the AErosol RObotic NETwork (AERONET) data are compared with the results of the procession of ground-based polarimetric measurements.

Observations were made at Zvenigorod Scientific Station of the Institute of Atmospheric Physics (IAP), located at 50 km from the centre of Moscow in March – September, 2007. The AERONET data of the 2.0 level were used for comparison. Optical characteristics of the near-ground aerosol were measured by spectral polarimeter designed in IAP. The instrument measures the orthogonally polarized components of the angular scattering coefficients at the scattering angles of 45°, 90° and 135° in the spectral interval 400 – 700 nm. Polarimetric data were inverted to the aerosol size distributions using the iterative technique. The obtained size spectra of the near-ground aerosol are compared with AERONET retrievals (Dubovik & King, 2000) in Figure 1. Since the minimal scattering angle in polarimeter used is equal to 45°, comparison was limited by the submicrometer radius range Positions of modes of the column averaged size distributions are close to those for the ground layer. The units of the size spectra are chosen in such a way that they coincide when the effective height is equal to 1 km for all particle radii. It can be seen from Figure 1 that effective height of the aerosol layer varies in wide limits. It causes the break of correlation between the aerosol volume concentration near ground and the volume columnar content. The relation between qualitative aerosol parameters, such as effective radii

of the fine fraction, is also appearing only as a tendency.

To check the possible effect of the applied techniques of the inverse problem solution on the results of retrieval, we inverted the AERONET data on the aerosol optical depth (AOD) using the iterative technique. Inversion of the AOD only does not allow estimating the particle refractive index n. So the inverse problem was solved at *a priori* assumption n =1.5. Erroneous assignment of the refractive index does not affect severely the shape of the size distributions. Results of our inversions of the AOD do not contradict the AERONET retrievals of the fine aerosol friction. However, in general, they are wider and more similar to the polarimetric data
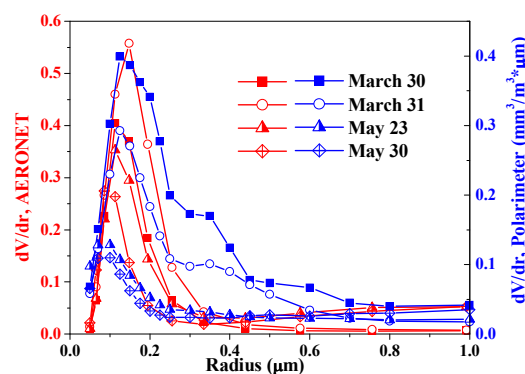
Figure 1. Volume size distributions obtained from the data of polarimetric measurements and AERONET retrievals. Zvenigorod, 2007.

Dubovik, O., & King, M. D. (2000). *J. Geoph. Res.*, 105, 20673-20696.

Testing Koschmieder Visibility Theory in a Town

Daniela STRIGL and Helmuth HORVATH

Faculty of Physics, Aerosol Bio and Environmental Physics, University of Vienna, 1090 Vienna, Austria

Keywords: Visibility, extinction coefficient, aerosol scale height, inhomgeneity, atmospheric aerosol

During a three month period the horizontal extinction coefficient was measured with a University of Vienna Telephotometer. The measuring path was over the central part of Vienna. The visibility was observed by establishing a set of visibility targets at the full horizon and recording all visible objects. The targets were both within Vienna and outside Vienna. Due to the surrounding hills a full visibility observation was not possible in all directions. The far away targets were at a higher altitude than the location of the observer and the telephotometer.

The Koschmieder visibility formula is a simple means to obtain the visibility from the atmospheric extinction coefficient. But it postulates a homogeneous atmosphere, ideal black visibility targets, and a standard contrast threshold of the eye. All these conditions do not hold in a town, thus a relation between observed visibility and calculated visibility has considerable scatter, as shown in the figure below.

But additional information for adjusting Koschmieder's formula was available. The relative radiance of the targets was known, thus non-black targets were not a problem. The visibility of the non-black targets was converted to the visibility of an ideal black target which obviously was larger. The homogeneous atmosphere obviously does not hold in a town. Thus the observed visibility of targets located outside of the town is larger than under homogeneous conditions. Another source of discrepancies is the decrease in aerosol particles concentration with increasing altitude. This makes targets at a higher altitude better visible than anticipated. During part of the visibility observations the vertical optical depth was measured with a CIMEL sun photometer. Thus information on the scale height was available. This could be used to adjust for vertical inhomogeneity.

Appling all these additional information it was possible to reduce the scatter of the data points. Therefore it can be concluded, that a modified Koschmieder relation between visibility and atmospheric extinction can characterize well observed visibility.
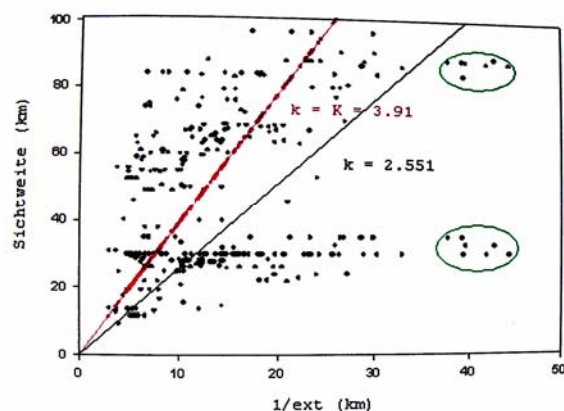
Influence of relative humidity on the Angström coefficient values of atmospheric aerosols

J. Kusmierczyk-Michulec

The Netherlands Organization for Applied Scientific Research, TNO, The Hague, The Netherlands

Relative humidity (RH) modifies the optical properties not only of hygroscopic atmospheric aerosols but also of mixtures containing non-hygroscopic aerosols like organic carbon or black carbon. As a result of wetting the hydroscopic particles grow, thereby changing the effective radius of an aerosol mixture and subsequently the aerosol extinction or aerosol optical thickness.

The variation of the extinction coefficient or the aerosol optical thickness with the wavelength can be presented as a power law function with a constant (related to the power factor) known as the Ångström coefficient (Ångström 1929). When the particle size distribution is dominated by small particles, a situation usually associated with pollution, the Ångström coefficients are high; in clear conditions they are usually low. Kusmierczyk-Michulec & Van Eijk (2007) demonstrated that the Ångström coefficient can be used as a tracer of continental aerosols. With changing atmospheric conditions and rising or falling RH, the measured aerosol optical thickness/extinction likewise changes, and so does the Ångström coefficient. The question is whether these changes can be quantified.

This paper presents the theory of the relations between the Ångström coefficient and the composition of atmospheric aerosol mixtures for various RH conditions. A change in RH alters the size distribution of hygroscopic aerosols like sea-salts (NaCl) and anthropogenic salts, e.g. NH_4NO_3 and $(NH_4)_2SO_4$. The main aerosol components of natural atmospheric mixtures include sea-salts (SSA), black carbon (BC), organic carbon (OC), and anthropogenic salts like ammonium hydrogen sulphate (NH_4HSO_4), ammonium nitrate (NH_4NO_3) and ammonium sulphate (($NH_4)_2SO_4$), which belong to a large group of water-soluble particles (WS). To model the physical and optical properties of these aerosol components both literature and experimental data were used.

The optical properties of the aerosol mixture can be represented by the aerosol extinction or by the aerosol optical thickness. Both parameters can be modelled using the external mixing approach. This means that each aerosol component of a given natural aerosol mixture is represented by a different substance with its own single mode size distribution and single complex index of refraction. The spectral values of the aerosol extinction for a given aerosol component are found from Mie calculations.

The results of a laboratory study of the changes in the optical properties of single-salt and mixed-salt aerosols caused by wetting are presented by Tang (1997) and Tang & Munkelwitz (1994). It is interesting to apply these results to atmospheric aerosols, which can contain both soluble and insoluble particles.

The observed variations in Ångström coefficients can be explained by changes in the effective radius of a mixture resulting from changes in RH and/or aerosol composition: the larger the number of small aerosol particles, the smaller the effective radius and the larger the Ångström coefficient. However, the change in Ångström coefficient due to variation in RH is far less than that caused by differences in aerosol mixture composition.

Ångström, A., (1929). *On the atmospheric transmission of sun radiation and on dust in the air.* Geogr. Ann., 11, 156-166.

Kusmierczyk-Michulec J. and A.M.J. van Eijk, (2007), *Ångström coefficient as a tracer of the continental aerosols,* Proceedings SPIE vol. 6708-25, Atmospheric Optics: Models, Measurements, and Target-in the-Loop Propagation, 27-28 August 2007, San Diego, CA, USA.

Tang, I.N., and H. R. Munkelwitz, (1994), *Water activities, densities, and refractive indices of aqueous sulfates and sodium nitrate droplets of atmospheric importance*, J. Geophys. Res., 99, D9, 18801-18808.

Tang, I.N., (1997), *Thermodynamic and optical properties of mixed-salt aerosols of atmospheric importance*, J. Geophys. Res., Vol. 102, D2, pp.1883-1893.

Comparison between MODIS and GADS aerosols asymmetry factor on a planetary scale

C.D. Papadimas[1], N. Hatzianastassiou[1], C. Matsoukas[2] and I.Vardavas[3]

[1]Laboratory of Meteorology, Department of Physics, University of Ioannina, 45110 Ioannina, Greece
[2]Department of Environment, University of the Aegean, 81100 Mytilene, Greece
[3]Department of Physics, University of Crete, 71110 Heraklion, Crete, Greece

Keywords: Atmospheric aerosols, Aerosol radiative effect, Aerosol optical properties, Satellites, MODIS

Aerosol particles are important to the climate of the earth–atmosphere system since they perturb its radiation budget through their direct, indirect and semi-direct effects. Their potential to warm or cool the Earth significantly depends on their physical and chemical properties, and on the wavelength and direction of the incident radiation. The radiative properties of an aerosol layer are dependent, for example, on the chemical composition that mainly affects absorption, and on their physical properties, such as particle shape and orientation, size and size distribution, density of particles and refractive index. The radiative impact of an aerosol layer is thus determined by the aerosol optical properties and its altitude and physical thickness. The three key radiative properties, considered in climate models, are the aerosol extinction optical thickness, single scattering albedo and asymmetry factor.

The aerosol asymmetry factor, g_{aer}, is a measure of the preferred scattering direction by the aerosol particles. In radiative transfer studies, the g_{aer} is equal to the mean value of μ (the cosine of the scattering angle), obtained by using the angular scattering phase function $P(\mu)$ as weight. The g_{aer} approaches +1 for scattering strongly peaked in the forward direction and -1 for scattering strongly peaked in the backward direction, whereas $g_{aer} = 0$ for either isotropic or symmetric scattering. Although g is required by climate and radiative transfer codes, the available data are not comprehensive, especially for global coverage and adequate spectral resolution.

In the present study, we evaluate the differences between the 7-year (2000–2007) MODIS (MODerate resolution Imaging Spectroradiometer of National Aeronautics and Space Administration) and GADS (Global Aerosol Data Set) g_{aer} products. The evaluation is performed at the geographical cell (2.5×2.5 latitude-longitude) level on a planetary scale by comparing MODIS g_{aer} data over ocean at 470 nm and GADS g_{aer} data at 500 nm, for winter and summer conditions. The GADS g_{aer} data are originally given at fixed relative humidity values, and were re-computed (Hatzianastassiou et al., 2004), for each pixel, for realistic humidity values taken from the National Centers for Environmental Prediction (NCEP) and National Center for Atmospheric Research (NCAR) Global Reanalysis Project.

The global distribution of long-term average GADS g_{aer}, over both land and ocean, is shown in Fig. 1a with values varying between about 0.67 and 0.79, indicating mainly forward scattering by aerosols at 500 nm. The mean annual global GADS g_{aer} value over ocean is 0.76. Figure 1b displays the geographical distribution of relative percentage differences between the GADS and MODIS g_{aer} data averaged over the MODIS 7-year period. In general, the differences are mostly positive indicating that the GADS g_{aer} data are mainly overestimated with respect to those of MODIS. The computed mean annual global value of MODIS g_{aer} over ocean is equal to 0.73 and the global mean differences between the two data sets is 3.8%. The differences mostly range from +1% to +5%. However, over most coastal locations there are either small negative differences (down to -5%) or large positive ones (10%-15%), respectively.

Our results indicate that, in general, the GADS-based g_{aer} data are quite similar to those of MODIS and thus can be used in radiative transfer models. Their advantage is their high spectral resolution that satisfies the requirements of detailed spectral radiative transfer models. Nevertheless, care must be taken in using them when examining inter-annual variations. Our results indicate that the GADS g_{aer} inter-annual variability is smaller than that of MODIS. This has to be considered given that our model results show that a 5% increase in g_{aer} causes a decrease in the magnitude of aerosol direct radiative effect at the Earth's surface of about 11%.

(a)   (b)
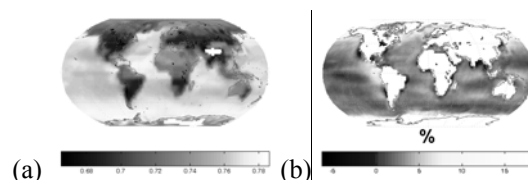
Figure 1. (a) Global distribution of 7-year (2000–2007) average GADS g_{aer} at 470 nm. (b) Relative percentage differences between the GADS and MODIS 7-year averages of g_{aer}.

Hatzianastassiou et al. (2004b). *Tellus*, 56B, 51–71.

Cavity Ringdown Spectroscopy Measurements of Extinction by Aerosol Particles

T.J.A. Butler[1], D. Mellon[1], J. Kim[1], J. Litman[2] and A.J. Orr-Ewing[1]

[1]School of Chemistry, University of Bristol, Cantock's Close, Bristol BS8 1TS, United Kingdom
[2]Department of Chemistry, Queen's University, Kingston, Ontario K7L 3N6, Canada

Keywords: cavity ringdown spectroscopy, light extinction, optical properties, statistical analysis.

Atmospheric aerosols play an important role in determining the Earth's radiation balance but the extent of their effect on the global climate is poorly determined and needs to be studied further. Cavity ringdown spectroscopy (CRDS) is gaining in popularity as a sensitive technique to measure optical properties of aerosols. So far, in most of the CRDS measurements of aerosols such as that by Pettersson *et al.* (2004), the aerosol extinction cross section (σ) was extracted by using Beer-Lambert law and relied on the use of a condensation particle counter to measure the particle concentration.

Recently, we proposed a statistical model based on the random fluctuations of particle numbers, which allows determination of σ without prior knowledge of particle concentration (Butler *et al.*, 2009). The model is based on the linear relationship between the extinction coefficient (α) and its variance ($Var(\alpha)$):

$$Var(\alpha) = \frac{\sigma}{V} < \alpha > + \alpha_{min}^2$$

where V is the intracavity laser volume and α_{min} is the minimum detectable extinction coefficient, determined by the inherent noise in the system. For a TEM_{00} cavity mode, V can be straightforwardly calculated from Gaussian beam theory.

The statistical model was tested by measuring the extinction caused by an ensemble of monodisperse polystyrene spheres with optical feedback CRDS (OF-CRDS). α and corresponding values of $Var(\alpha)$ were measured at various particle concentrations and they were plotted against each other as shown in Figure 1. The value of σ was obtained from the gradient of the line of the best fit. The extinction cross sections of polystyrene spheres determined from the experiment were in good agreement with the predictions of Mie theory calculations as presented in Table 1.

Table 1. Comparison of experimentally determined and calculated extinction cross sections for the samples of polystyrene spheres.

Nominal particle diameter/nm	$\sigma_{exp}/10^{-9}$ cm^2	$\sigma_{calc}/10^{-9}$ cm^2
700	2.63 ± 0.05	2.97 ± 0.18
500	0.45 ± 0.12	0.485 ± 0.036
400	0.15 ± 0.07	0.146 ± 0.013

The relationship between α and $Var(\alpha)$ deviated from linearity at high particle concentration. An additional variance coming from the ringdown fitting method could partly account for this deviation.

Monte Carlo simulations incorporating the Brownian motion and gravitational settling of particles showed that extinction cross sections can be underestimated if the measurements are made too rapidly and consecutive measurements become correlated. The reason for using an OF-CRDS apparatus was to exploit its fast acquisition rate (1.25 kHz) but if such fast acquisition is not needed or causes problem with correlation in measurements, a normal CRDS apparatus with slower acquisition rate (~10 Hz) can be used. The use of conventional CRDS setups using either pulsed or continuous wave lasers is underway.
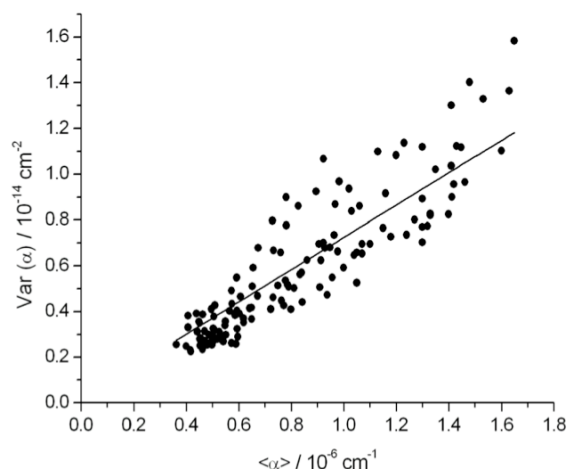
Figure 1. Plot of $Var(\alpha)$ against $<\alpha>$ for polystyrene spheres 700 nm in diameter.

Butler, T.J.A., Mellon, D., Kim, J., Litman, J., & Orr-Ewing, A.J. (2009). *J. Phys. Chem. A*, 113, 3963-3972.

Pettersson, A., Lovejoy, E.R., Brock, C.A., Brown, S.S., & Ravishankara, A.R. (2004). *J. Aerosol Science*, 35, 995-1011

Impacts of dust storms on dioxins and furans in a basin area, Taiwan

Tzi-yi Wu[1], Yan-Min Chen[2*], Yuan-Chung Lin[3], Guo-Ping Chang-Chien[4,5], Chung-Hsien Hung[4]

[1] Department of Chemistry, National Cheng Kung University, Tainan 70101, Taiwan.
[2] Sustainable Environment Research Center, National Cheng Kung University, Tainan 701, Taiwan.
[3] Institute of Environmental Engineering, National Sun Yat-Sen University, Kaohsiung 804, Taiwan.
[4] Department of Chemical and Materials Engineering, and Super Micro Mass Research & Technology Center, Cheng Shiu University, Kaohsiung County 833, Taiwan.
[5] Graduate Institute of Medicine, College of Medicine, Kaohsiung Medical University, Kaohsiung County 807, Taiwan

Keywords: PCDD/Fs; dust storm; ambient air pollution; basin area

Few studies have been conducted on the relationship between the high levels of dust particles and the concentrations of atmospheric PCDD/F during dust storm episodes. However, they did not investigate the impact of dust storm on basin areas.

In March, 2008, a dust storm from China had a serious impact on Taiwanese air quality. During this period, a cold air mass from China moved south and the cold front at its leading edge passed over Taiwan. PCDD/F emissions are expected to be directly influenced by dust storms. Some studies have been conducted on the relationship between the high levels of dust particles and the concentrations of atmospheric PCDD/F during Asian dust storm episodes (Lee *et al.*, 2007; Chi *et al.*, 2008; Liu *et al.*, 2009; Lin *et al.*, 2008). However, they did not investigate the impact of dust storms in basin areas. Taking this into account, the main goal of this study is to assess PCDD/Fs before and during dust storms in basin areas of northern Taiwan.

This present study shows the dust storm effect on regulated harmful matter and polychlorinated dibenzo-*p*-dioxin/dibenzofuran (PCDD/F) concentrations in basin areas. The results indicate that the average PM_{10} (aerodynamic diameter less than 10 μm), SO_2 (sulfur dioxide), NO_2 (nitrogen oxides), CO (carbon monoxide) and O_3 (ozone) levels during the dust storm were 3.43, 2.03, 1.17, 1.05 and 1.79 times higher than those before the dust storm, respectively. Mean PCDD/F concentrations during the dust storm (0.639 pg Nm^{-3}; 0.0323 pg I-TEQ Nm^{-3}) were significantly higher than those before the dust storm (0.240 pg Nm^{-3}; 0.00705 pg I-TEQ Nm^{-3}). The PCDDs concentration during the dust storm was 1.23 times larger than that before the dust storm, and the PCDFs concentration was 6.82 times larger.

Therefore, the dominant contribution of PCDD/Fs concentration during dust storm in the basin areas of northern Taiwan is PCDFs. The above results indicate that the impact of a dust storm on regulated harmful matter and PCDD/F concentrations in the basin area is significant.
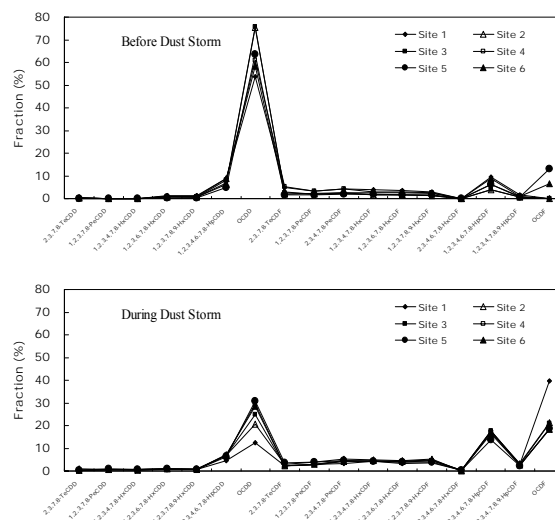
Figure 1. Congener profiles of 17 PCDD/F species from different sites ambient air before and during dust storm.

Lee, S.J. Park, H., Choi, S.-D., Lee, J.-M., Chang, Y.-S. (2007). *Atmospheric Environment* 41, 5876-5886.

Chi, K.H., Hsu, S.C., Wang, S.H., Chang, M.B. (2008). *Science of the Total Environment* 401, 100-108.

Liu, T.-H., Tsai, F., Hsu, S.-C., Hsu, C.-W., Shiu, C.-J., Chen, W.-N., Tu, J.-Y. (2009). *Atmospheric Environment* 43, 458-467.

Lin, M., Oki, T., Holloway, T., Streets, D.G., Bengtsson, M., Kanae, S. (2008). *Atmospheric Environment* 42, 5939-5955.

Experimental data interpretation by means of computational fluid dynamics results: Dynamic growth of Sea-Salt particles

J. Voigtländer[1], D. Niedermeier[1], F. Stratmann[1]

[1]Leibniz Institute for Tropospheric Research, Leipzig, Germany

Keywords: sea salt, marine aerosols, particle growth, dynamic growth, modelling

Sea-Salt particles represent a significant fraction of all particulate matter in the atmosphere. Because of the atmospheric relevance, hygroscopic particle growth, cloud condensation nuclei (CCN) activation and dynamic particle growth of three different Sea-Water samples, originated from the Baltic Sea and the Atlantic Ocean, was measured and theoretical modelled. Investigations regarding hygroscopic growth and CCN activation were already published in Niedermeier et al., 2008 and only data concerning dynamic particle growth are considered here.

Experiments were performed at the Leipzig Aerosol Cloud Interaction Simulator (LACIS, Stratmann et al., 2004), a laminar flow diffusion chamber for measurements of hygroscopic particle growth, cloud condensation nuclei (CCN) activation and dynamic particle growth. In the experiments, quasi-monodispersed particles with mobility equivalent sizes between 40 nm and 120 nm, selected by means of a DMA, were used. All measurements were performed at least three times for each measurement point. Mean values and standard derivations were calculated. It was assumed, that the standard derivation represents the experimental uncertainty. Differences were found between the measurements of the three different samples (Fig. 1).

To discuss these differences, the experimental data only are not sufficient and numerical simulations were therefore included in the investigations. For the simulations, the Computational Fluid Dynamics Code (CFD-Code) FLUENT6 combined with an Eulerian particle model (Fine Particle Model (FPM), Wilck et al., 2002) was used. The model was already validated (Voigtländer et al., 2007b) and successfully applied for various applications (e.g., Voigtländer et al., 2007b). It allows an accurate simulation of the droplet growth in LACIS. For the simulation of the Sea-Salt particles, the model was extended to account for relevant thermo dynamical and material properties (e.g., Pitzer activity coefficient model, particle density, surface tension, particle shape factor). The experimental data then were simulated, including a sensitivity analysis concerning relevant properties and boundary conditions (e.g., inlet temperature, operation pressure).

The results of the numerical simulations allowed a detailed discussion of the experimental data. It could be proven, that the observed different behaviour between the different Sea-Water samples were not caused by the different chemical composition of the extracted particles. In fact, small fluctuations of thermo dynamic properties during the experiments (operation pressure, inlet temperature) resulted in variations of the vapour mass diffusion and the saturation profiles inside LACIS. Such variations were found to be of higher importance than the particle composition.
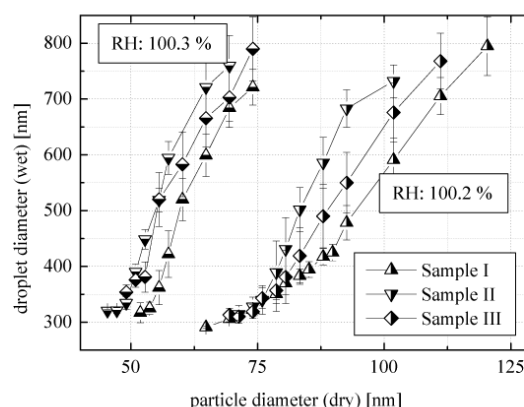
Figure 1: Measured dynamic particle growth of the extracted Sea-Salt particles. Measurements at two different super-saturation ratios are shown.

The investigations demonstrate the necessity of accurate simulations in addition to experimental data, because the simulation results largely enhance the quality of experimental data interpretation.

Niedermeier, D. & Wex, H. & Voigtländer, J. & Stratmann, F. & Brüggemann, E. & Kiselev, A. & Henk, H. & Heintzenberg, J. (2008), Atm. Chem. Phys., 8, 579-590.

Stratmann, F. & Kiselev, A. & Wurzler, S. & Wendisch, M. & Heintzenberg, J. & Charlson, R.J. & Diehl, K. & Wex, H. & Schmidt, S. (2004). *J. Atmos. Ocean Tech., 21, 876-887.*

Voigtländer, J & Stratmann, F. (2007a), J. Geophys. Res., 112, D20208, doi: 10.1019/2007/JD008604.

Voigtländer, J & Riipinen, I. & Stratmann, F. & Kulmala, M. (2007b), European Aerosol Conference, Salzburg, Austria, T12A004.

Wilck, M. & Stratmann, F. & Whitby, E.R. (2002). in *Proc. Sixth Int. Aerosol Conf.,* Taipei, Taiwan, 1269-1270.

Highly Time-Resolved Observation of a Particle Growth Event

O. Klemm[1], L.D. Ziemba[2], B.C. Sive[2], R.J. Griffin[2], R.W. Talbot[2]

[1]University of Münster, Climatology Working Group, Robert-Koch-Str. 26, 48149 Münster, Germany
[2]University of New Hampshire, Climate Change Research Center, Morse Hall, Durham, N.H. 03824, USA

Keywords: aerosol chemistry, aerosol mass spectrometry, field measurements, nucleation

We observed particle dynamics in the marine boundary layer during an experiment in July 2006 on Appledore Island, 10 km offshore the NE United States Atlantic coast, at the border between the states of Maine and New Hampshire (42.97N, 70.62W). The experiments were part of the New England AIRMAP program (http://airmap.unh.edu). Particle physics and chemistry were studied by using an SMPS (TSI Inc., Shoreview, MN, USA) particle sizer, a Q-AMS (Aerodyne Research, Inc., Billerica, MA, USA) aerosol mass spectrometer, and various instrumentation for gas (including CO, CO_2, O_3, VOCs) and particle concentrations.

We present results of an aerosol growth event during the night of 14 / 15 July, 2006. Particle growth was identified and quantified through an increase of the geometric mean of the number distribution and lasted over a period of approximately 13 hours (Fig. 1). The back trajectories (not shown here) indicate continental outflow with influence of from both biogenic and industrial emissions on air chemistry.

Analysis of the development of the geometric means of particle number distribution and the individual component mass size distributions, as well as the development of total and specific mass concentrations, lead to separation of three distinct phases of the growth event (Fig. 1).

A detailed analysis of processes driving the particle dynamics will be presented. Briefly, during Phase I from 02:45 through 05:35 UTC, no significant increase of aerosol mass or mass components (except sulfate) was observed. Most likely it is the change of air mass history with varying relative importance of biogenic and industrial emissions that govern the observed aerosol dynamics. During Phase II (05:35–12:50 UTC), gas-to-particle conversion was clearly detected and quantified for each particle component. The geometric mean diameter (SMPS) increased with 3.9 nm hr^{-1}. Most of the aerosol mass increase was attributable to organic carbon, followed by sulfate, nitrate, and ammonium. Phase III (12:50–15:30 UTC) represents a completely different situation. Well after sunrise, the geometric mean diameter of the aerosol number distribution or the individual mass components did not increase significantly any more (exception again: sulfate). The total and individual mass components decreased. Apparently it is mainly entrainment of cleaner air into the plume that drives particle dynamics.

The combination of SMPS and Q-AMS in a field experiment allows to separate various aerosol processes (gas-to-particle conversion, coagulation, emissions, entrainment) from each other. Stationary conditions during a growth event (here: Phase II) can be identified and analyzed separately. This allows precise analysis of particle growth processes. Details on the VOC concentrations and their potential contribution on particle growth will be shown.
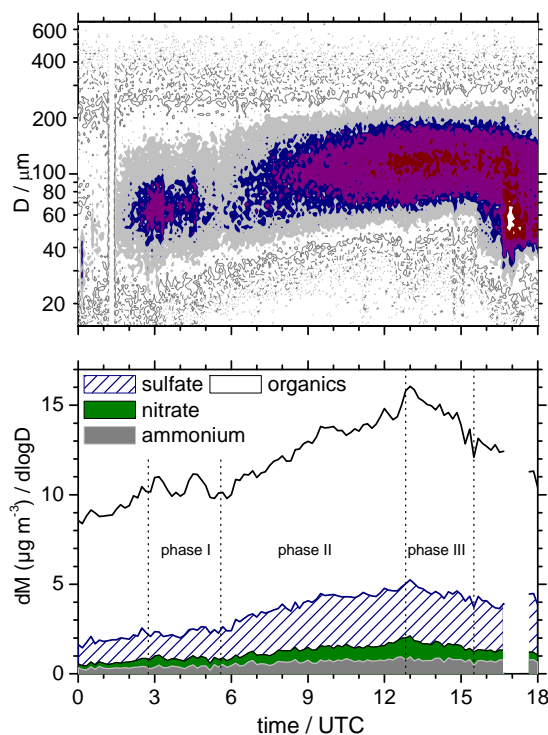
Figure 1. Physical and chemical characterization of the particle growth event on 14/15 July 2006 at Appledore Island. The time axis (UTC) is four hours ahead of local time (EDT). Upper panel: number size distribution with grey area shading indicating dN/dlogD > 4000 cm^{-3}, blue > 8000, purple > 10000, dark red > 15000, and white > 20000, respectively, as measured with SMPS. Lower panel: Stacked concentrations of major components, as measured with Q-AMS. Growth event phases are indicated

Seasonal variation of aliphatic amines at the Cape Verde Islands

C. Müller, Y. Iinuma, K. Müller, S. Lehmann and H. Herrmann

Chemistry Department, Leibniz-Institute for Tropospheric Research (IfT), Permoserstr. 15,
04318 Leipzig, Germany

Keywords: chemical composition, field measurements, marine aerosol, amines

Ammonium sulphate plays an important role in new particle formation, especially in the remote marine environment. However, smaller aliphatic amines such as methylamine can compete with ammonium in the marine environment. Theoretical calculations have shown that alkyl ammonium sulphate formation is preferred over ammonium sulphate when both ammonium and amines are present [Kurten et al. (2008); Barsanti et al. (2008)]. The detection of aliphatic amines in submicron size range particles in the marine environment suggests that organic salt formation processes may be of significant importance in aerosol formation in the marine environment [Facchini et al. (2008)]. However, their roles in atmospheric processes, exact biogenic origins and the formation process are still not well known.

The seasonal variability of new particle formation was studied during one year field campaign in the Cape Verde Islands. Aerosol samples were collected with a high volume sampler (DIGITEL DAH 80) from May 2007 to June 2008. During two intensive campaigns (first in May/June2007 and second in December/January2007/08), size resolved aerosol samples were collected with a five stage Impactor (Berner Impactor) in parallel to the Hi-Vol sampling.

To determine the alkyl amines, filters were extracted with methanol and derivatised with ACQ (6-aminoquinolyl-N-hydroxy-succinimidyl, Waters). Derivatised amines were analysed using high performance liquid chromatography coupled to electrospray ionisation ion trap mass spectrometer (HPLC/ESI-ITMS).

Methylamine (MA), dimethylamine (DMA) and diethylamine (DEA) were detected mainly in smaller particles. On the stage two (0.14-0.42µm) the average concentrations of MA were 21±5 pg m^{-3} in summer months and 185±121 pg m^{-3} in the winter months. Similar trends were observed for DMA and DEA with lower concentrations in summer (216±78 pg m^{-3} for DMA and 67±29 pg m^{-3} for DEA) and higher concentrations in winter (567±317 pg m^{-3} for DMA, 320±160 pg m^{-3} for DEA). These high amine concentrations in winter are in contrast to the normal marine biological cycle with high biological activity in spring/summer months. There are two possibilities that may have an influence on high amine concentrations in winter months. First possibility is the influence of mineral dust on the Island (Fig. 1) in winter months and second is high biological activity which was observed in winter. The high biological activity may be caused by upwelling processes or Sahara dust deposition in the Cape Verde region.
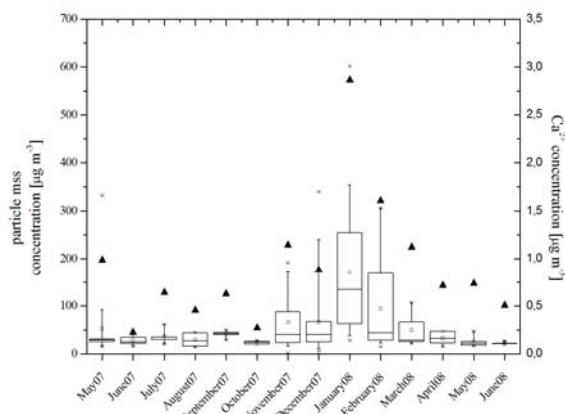
Figure 1: Seasonal particle mass concentration and calcium determined from Digitel quartz fibre filters.

Barsanti, K. C., McMurry, P. H., & Smith, J. N. (2008). *Atmospheric Chemistry and Physics Discussion*, 8, 20723-20748.

Facchini, M. C., Decesari, S., Rinaldit, M., Carbone, C., Finessi, E., Mircea, M., et al. (2008). *Environmental Science & Technology*, 42, 9116-9121.

Kurten, T., Loukonen, V., Vehkamaki, H., & Kulmala, M. (2008). *Atmospheric Chemistry and Physics*, 8, 4095-4103.

The effect of aerosol characteristics on optical properties in Hong Kong

Emily Q.J. Bian[1], R. Zhang[2], Z.B. Yuan[3], Alexis K.H. Lau[1], J.Z. Yu[1]

[1]Atmospheric, Marine and Coastal Environment Program, Hong Kong University of Science and Technology, Kowloon, Hong Kong
[2]Department of Mathematics, Hong Kong University of Science and Technology, Kowloon, Hong Kong
[3]Environmental Central Facility, Hong Kong University of Science and Technology, Kowloon, Hong Kong

PM_{10} sampling was conducted at Tung Chung station (TC) in Hong Kong every six days from Jan. 8th, 2006 to Dec. 28th, 2006. Particulate mass, major ions (sulphate, nitrate, ammonium, sodium and chloride), organic carbon (OC) and elemental carbon (EC) were analyzed. Light scattering coefficients ($\sigma_{obs,sp,890nm}$) were also measured by a Belford visibility sensor (model 6000) at this site. During the same period, light extinction coefficients ($\sigma_{obs,ext,550nm}$) were also observed by a transmissionmeter (model LPV-3) at the Hong Kong International Airport (HKIA). As HKIA is approximately 2km away from the TC sampling site, we believe HKIA and TC should be impacted by the same air mass for most of the time.

Optimum size distribution of aerosols with two log-normal modes superimposed, condensation mode (C-mode) and droplet mode (D-mode), were retrieved from the enumeration method by applying the ISORRPIA-Mie model (Malm, 2003). First, PM_{10} species were converted to $PM_{2.5}$ by empirical ratios derived from MOUDI data sampled in an adjacent region, Shenzhen. Sulphate was assumed in the form of $(NH_4)_2SO_4$ and nitrate in the form of NH_4NO_3. Second, chemical species were assumed to have the same size distribution. $\sigma_{cal,sp,890nm}$ and $\sigma_{cal,ext,550nm}$, were calculated based on the enumerated size distributions with five parameters, including geometric mean diameter (D) and geometric standard deviation (σ) of the C-mode and the D-mode and the mass ratio of the two modes to total $PM_{2.5}$. The ranges of D, σ and mass ratio for C-mode are 0.20-0.40μm with an interval of 0.05, 1.50-2.40 with an interval of 0.05 and 20-30% with an interval of 5%, respectively. The ranges of D, σ and mass ratio for D-mode are 0.50-1.20μm with an interval of 0.05, 1.25-2.50 with an interval of 0.05 and 70-80% with an interval of 5%, respectively. Additionally, the particles were assumed to be internally mixed (Huang et al., 2008). The primary goal is to find the 'representative' size distribution with the minimum deviation between the two calculated optical properties ($\sigma_{cal,ext,550nm,}$ and $\sigma_{cal,sp,890nm}$) and their corresponding measured values. The deviation χ^2 was quantified by the linear least squares with the form:

$$\chi^2 = \frac{(\sigma_{cal,ext,550nm} - \sigma_{obs,ext,550nm})^2}{\sigma_{obs,ext,550nm}^2} + \frac{(\sigma_{cal,sp,890nm} - \sigma_{obs,sp,890nm})^2}{\sigma_{obs,sp,890nm}^2}$$

The results are reasonable since calculated $\sigma_{sp,890nm}$ and $\sigma_{ext,550nm}$ have a good correlation with their corresponding observations (R^2=0.91 and 0.82, respectively).

In the revised IMPROVE formula, different mass scattering efficiencies (MSEs, in the unit of m^2/g) were adopted for chemical species depending on their mass concentration (Pitchford, 2007). Our results show that ratio of non-EC/EC (non-EC includes sulphate, nitrate and OC) is a better parameter to describe the variation of MSE. In the model result, mass concentration, the ratio of non-EC/EC, $\sigma_{cal,sp,890nm}$ and $\sigma_{cal,ext,550nm}$ increase with the increase in diameter of D-mode. This can be explained by the aerosol size increase due to in-cloud processing during the regional transport on severely polluted days. The high ratio of non-EC to EC is also an indicator aged and regionally transported aerosols. In addition, as the diameter increases, mass scattering efficiency (MSE) increases while mass extinction efficiency (MEE) decreases. Theoretical calculation shows that both MSE and MEE decrease when the diameter of aerosols having the same non-EC/EC ratio varies from 0.6 to 1.0μm. But for particles, of a given size, but having different non-EC/EC ratios, MSE increases with the non-EC/EC ratio. The combined effect of size growth and non-EC/EC increase is the increase of MSE, which suggests the non-EC/EC ratio is a more appropriate parameter to describe the variation of MSE and MEE in this region.

Based on the formula (I), the increase of $\sigma_{obs,sp,890nm}$ during severely polluted days is mainly caused by the combined effects of MSE and mass concentration while the increase of $\sigma_{obs,ext,550nm}$ is mainly caused by mass concentration enhancement.

$$B_{sc} = \sum_i MSE_i \times f_i(RH) \times Mass_i \qquad (I)$$
$$B_{ext} = \sum_i MEE_i \times f_i(RH) \times Mass_i$$

Huang, X.F. et al (2008). *Atmospheric Chemistry and Physics*, 8, 5843-5853

Malm, W.C. et al (2003). *J. Geophysical Research*, 108, D9, 4279.

Pitchford, M. et al (2007) *J. Air Waste Manage. Assoc.*, 57, 1326-1336

Absorption properties of atmospheric aerosols from a high-altitude site in northern India

Kirpa Ram[1], M.M. Sarin[1] and P. Hegde[2]

[1]Physical Research Laboratory, Ahmedabad-38009, India
[2]Space Physics Laboratory, Trivandrum - 695022 Kerala, India

Black carbon (BC), one of the major absorbing aerosol species in after GHGs, is being considered as driver of the global warming due to increase in anthropogenic emissions on a regional to global scale. BC is produced during incomplete combustion processes from fossil-fuel and biomass burning and forms a primary constituent of "soot" particles in the atmosphere. Light absorbing carbon (LAC) mass in atmospheric aerosols is either assessed by optical method (as BC mass) or by thermal methods (referred as elemental carbon; EC). The LAC mass determined by the two analytical methods can differ by a factor of two to four (or even more). Thus, search for an absolute method for LAC mass determination is still a debatable issue in atmospheric scientific community. The measurement via optical methods is convenient and rapid but requires knowledge of mass absorption efficiency (σ_{abs}, in unit of m^2g^{-1}) in order to convert the measured absorption coefficient (b_{abs}, Mm^{-1}) into BC mass concentration. Using thermo-optical EC-OC analyzer, we propose a novel and unique approach for the determination of b_{abs} and σ_{abs} in aerosol samples, collected from a high-altitude site Manora Peak (29.4°N, 79.5°E, ~1950 m amsl) in northern India.

The optical properties (b_{abs} and σ_{abs}) were simultaneously assessed using the measured optical-attenuation (ATN) at 678 nm laser source employed in the thermo-optical EC-OC analyzer. The measurement of ATN is primarily used to define the split-point between organic and elemental carbon (OC and EC) (Ram et al, 2008). The measured b_{abs} (equivalent to measured ATN values) shows a strong linear dependence on thermal EC concentration ($R^2=0.75$, n=65) indicating the validity of Beer-Lambert's law. The b_{abs} exhibit a large temporal variability with higher values typical of winter (Dec-Feb) and post-monsoon (Sept-Nov) and lower were associated with the summer (Apr-May) and monsoon (June-Aug). Further, the slope of the linear plot (Fig. 1) provides a value of 10.4 m^2g^{-1} for σ_{abs} at Manora Peak; however, a large temporal variability for σ_{abs} has been observed during sampling period (range: 6.1-18.8 m^2g^{-1}). The σ_{abs} value obtained in this study is similar to that used in the PSAP (10.0 m^2g^{-1}) for

the determination of BC mass concentration. As σ_{abs} shows a large temporal and spatial variability and depends on the source, aerosol composition and mixing state of BC in aerosols, the use of 'site-specific' σ_{abs} values has been suggested (Liousse et al, 1993; Sharma et al, 2002). However, use of 'site-specific' σ_{abs} values for BC determination is not a very common practise because it requires two independent measurements of absorption (from optical methods) and EC concentration (from thermal methods). The analytical approach used in this study involves the use of only one instrument (thermo-optical EC-OC analyzer) to infer b_{abs} and 'site-specific' σ_{abs} values which can be used in optical methods for BC mass determination.
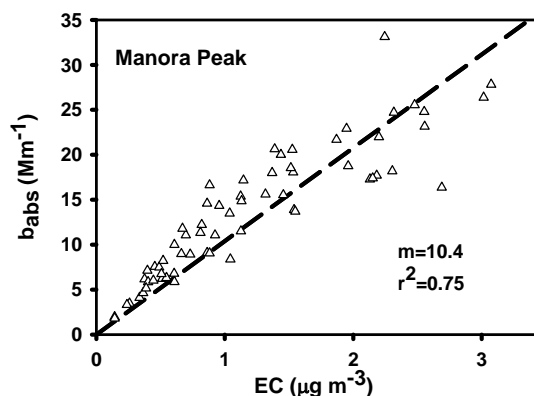
Figure 1. The linear regression plot of absorption coefficient (b_{abs}, Mm^{-1}; 1 $Mm^{-1}=10^{-6}$ m^{-1}) vs. EC concentration.

Ram K., et al (2008). *Atmospheric Environment,* 42, 6785-6796.
Liousse et al. (1993). *Atmospheric Environment,* 27A, 1203-1211.
Sharma S., et al (2002). *J. Geophysical Research-Atmosphere,* doi: 10.1029/2002JD002496.

Measuring and modeling cloud condensation nuclei concentrations at the Jungfraujoch high alpine site

Z. Jurányi, M. Gysel, E. Weingartner, P.F. DeCarlo, M. F. Heringa, R. Chirico and U. Baltensperger

Laboratory of Atmospheric Chemistry, Paul Scherrer Institut, CH-5232 Villigen PSI, Switzerland

Keywords: CCN, Aerosol size distribution, Aerosol mass spectrometry, Aerosol cloud interaction

Atmospheric aerosol particles that are able to act as cloud condensation nuclei (CCN) are important for the climate and the hydrological cycle, but their properties are not fully understood. Total CCN concentration at different supersaturations was measured during CLACE 2008 (CLoud and Aerosol Characterization Experiments) in May 2008 at the high alpine measurement site, Jungfraujoch (3580 m asl.). Simultaneously, an aerosol mass spectrometer (AMS) and a scanning mobility particle sizer (SMPS) were providing information on the chemical composition and size distribution of the measured aerosol.

Number size distribution and chemical composition data were used to model CCN concentrations using a simplified Köhler theory. This theory uses the water activity parameterization of Petters and Kreidenweis (2007) with the assumption that the surface tension of the solution droplet at the activation can be substituted with the value of pure water and the Zdanovskii-Stokes-Robinson (Stokes and Robinson, 1966) mixing rule. Solving the Köhler equation, the critical dry diameters (D_{crit}) as a function of time and the supersaturation in the CCN counter were derived. This information was then used to predict the CCN concentration by integrating the size distribution for D>Dcrit.

The predicted and the measured CCN concentration is highly correlated (R^2 ~0.98) and they agree within ±15% at every supersaturation, though a systematic underprediction is generally observed (Fig. 1, blue points). Closure test with polydisperse ammonium sulphate (AS) aerosols indicate that the prediction bias is just beyond measurement uncertainty. One would need to assume very hygroscopic aerosol, pure AS or even more hygroscopic (kappa = 0.55-0.75), which is unlikely to be present at Jungfraujoch, in order to fully match the prediction with the measurement. Contrary to this an average 15 % of surface tension depression is able to explain the difference between the predicted and measured CCN concentration.

Neglecting the time variation of the chemistry data by averaging it for the whole one month measurement period (Fig. 1, green points) gives almost identical results as the full model, and does not significantly decrease the quality of the prediction. To further investigate the importance of the chemical composition a sensitivity study was performed where changes in the predicted CCN concentration were calculated while the chemical composition was varied. The study showed that knowledge of the average chemical composition is enough to reliably model the CCN concentration at sites with similarly aged and internally mixed aerosols as encountered at the Jungfraujoch.
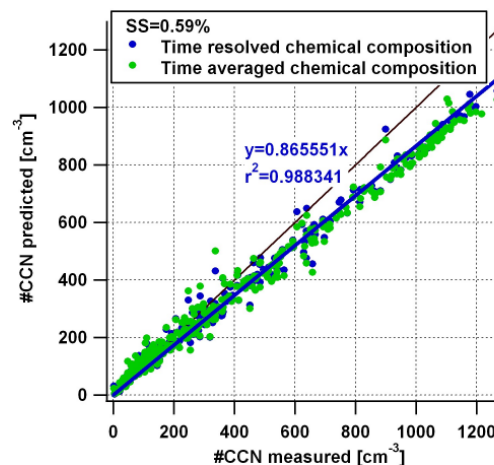
Figure 1. The predicted CCN concentration as function of the measured at 0.59% supersaturation. Blue points were calculated using time resolved chemical information, for the green ones time averaged chemistry data was used.

Petters, M.D., and S.M. Kreidenweis 2007 A single parameter representation of hygroscopic growth and cloud condensation nucleus activity, *Atmos. Chem. Phys.,* **7,** 1961-1971.
Stokes, R.H., and R.A. Robinson 1966 Interactions in aqueous nonelectrolyte solutions. I. Solute-solvent equilibria, *J. Phys. Chem.,* **70,** 2126-2130.

T05 AA specific aerosol types

Physicochemical and toxicological profiles of particulate patter (PM) in Los Angeles during the October 2007 Southern California wildfires

Vishal Verma[1], Andrea Polidori[1], James J. Schauer[2], Martin M. Shafer[2], Flemming R. Cassee[3] and Constantinos Sioutas[1]

[1]Department of Civil and Environmental Engineering, University of Southern California, Los Angeles, CA, USA
[2]Department of Civil and Environmental Engineering, University of Wisconsin, Madison, WI, USA
[3] Center of Environmental Health Research, National Institute for Public Health and the Environment (RIVM), the Netherlands

To characterize the impact of the October 2007 wildfires on the air quality of Los Angeles, integrated ambient particulate matter (PM) samples were collected near the University of Southern California between October 24 and November 14, 2007. Samples were analyzed for different chemical species (i.e., water-soluble organic carbon, water-soluble elements, and several organic compounds), and the redox activity of PM was evaluated using two different assays, the Dithiothreitol (DTT) and Macrophage Reactive Oxygen Species (ROS) assays. Tracers of biomass burning such as potassium and levoglucosan were elevated by 2-fold during the fire period (October 24-28), compared to the post-fire period (November 1-14). Water-soluble organic carbon (WSOC) concentrations were also higher during the fire event (170 and 78 µg/mg of PM, during fire and post-fire, respectively). While the DTT activity (on a per PM mass basis) increased for samples collected during the fire event (0.024 nmol DTT / min × µg on October 24) compared to the post-fire samples (0.005 nmol DTT / min × µg on November 14), the ROS activity did not increase during the wildfires, probably because these two assays are driven by different PM species. While the DTT assay reflected the redox potential of polar organic compounds, which are abundant in wood-smoke, the ROS assay was mainly influenced by transition metals (e.g. Fe, Cu, Cr, Zn, Ni, and V), emitted mostly by vehicular traffic and other combustion sources, but not by the wildfires.

The particle size distribution variation in fine particle to the inland area of South Kanto from the coastal line of Tokyo bay

Hiroaki Minoura and Nobuo Shimo

Japan Petroleum Energy Center, Minato-ku, Tokyo, 105-0001, Japan

1. Introduction   Particle concentration in downtown Tokyo showed decreased tendency from the middle in 90's (Minoura et. al., 2006), and it was in a situation that the SPM environmental standard was satisfied. According to the report of the Administration (e.g. Tokyo Metropolis white paper on environment 2006), $PM_{2.5}$ concentration at Tokyo urban background area shows around $20\mu g/m^3$, and a countermeasure for the concentration reduction is examined. Pollutants accumulate during the sea breeze circulation between the inland area of South Kanto and the Tokyo bay, and generate the secondary PMs. However, these processes were investigated only by several points of ground observation or air quality simulation, and our knowledges are limited. An aircraft observation by using a helicopter from the coastal line of Tokyo bay to inland area of South Kanto was carried out, and PM size distribution was measured consecutively.

2. Observation   The flight commuted between Kisei (inland town in South Kanto) from Tokyo Bay in two hours (1km m^{-1}), and we made a round trip nine times during August 1 from July 30, 2008. Except the coast line of 200m altitude, the flight altitude was navigated with 600m uniformity. The PM was measured by APS3321 (TSI, Inc.). For the measurement of the pollutant gas, NOx monitor (Thermo 42C/J) and O_3 monitor (Dylec 1150) were equipped with. Meteorological sonde was launched at Saitama Univ. (inland area in South Kanto) and Urayasu (coastal town of Tokyo bay) every three hours, and the mixing height and upper wind condition were measured.

3. Results
(1) From the measured results of the meteorological sonde, all flights were carried out in the mixing layer. The number of PM concentration increased so as to move ahead to the inland, and the average PM diameter decreased. The ozone concentration also showed increase tendency, but, as for the NOx, a clear variation was not provided. The number concentration and the relationship with the mean PM diameter provided between nine flights of three days showed the correlations shown in Figure 1 which could be approximate as straight lines similar

in the coast line of 200m altitude and the inland area of 600m altitude in each.
 (2)   The variation of the PM size distribution was shown in Figure2. When we move ahead inland, decrease number in coarse PM and increase in fine PM were observed, and the deposition of sea salt PM and the addition of the secondary PM were suggested.
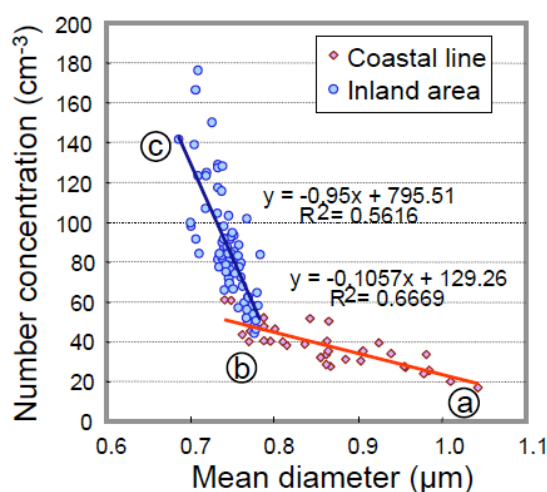
Figure 1: Number concentration and relations with the mean particle diameter
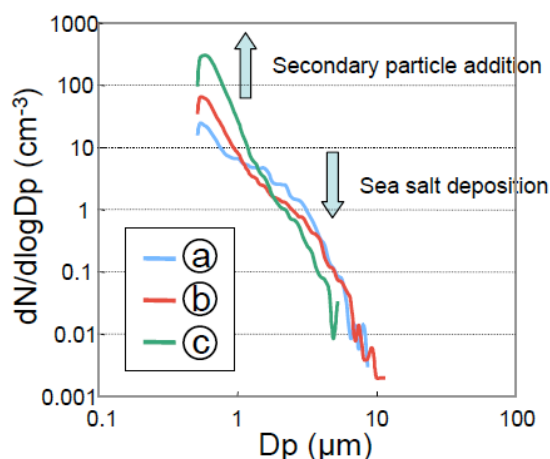
Figure 2: Particle size distribution in the representative spots

Minoura H., K. Takahashi, J. Chow, and J. Watson (2006) Atmospheric Environment, 40, 2478-2487.

PMx exposition of Prague city transport passengers

B. Kotlík[1], V. Tydlitát[2], M. Mikešová[1] and H. Kazmarová[1]

[1] National Institute of Public Health, Šrobárova 48, 100 42, Prague 10, Czech Republic
[2] Institute of Chemical Process Fundamentals AS CR, v.v.i., Rozvojová 135, 165 02, Prague 6, Czech Republic

Keywords: indoor air quality, PM, PAU, exposure, traffic

Environment air of big agglomerations contains a variety of contaminating substances with potential adverse influence on health of the citizens. The contamination is usually measured by a net of monitoring stations, which during the day record values of controlled harmful substances in each place. However, representativness of the measured values is often limited only to closest vicinity.

The estimated exposition scenarios imply that an average Prague citizen usually spends, depending on season, from 2 to 7 hours a day in outdoor environment and at least one hour in public transport.

Table 1. Weight concentrations of PM_{10}, $PM_{2,5}$ and $PM_{1,0}$ (v $\mu g/m^3$) for particular modes of transport.

	From - till	PM_{10}	$PM_{2,5}$	$PM_{1,0}$
Break in ride and backgroun locations	8:40-9:14	107,1	103,1	56,7
	9:31-9:54	139,9	109,1	56,0
	10:40-11:28	155,6	120,6	60,2
	12:18-13:11	119,5	86,3	42,3
	13:57-14:39	169,5	103,7	45,5
IN TOTAL	180 min.	**138,3**	**104,6**	**52,1**
Central City	From - till	PM_{10}	$PM_{2,5}$	$PM_{1,0}$
	7:50-8:39	124,0	110,8	60,3
	9:15-9:30	145,3	113,7	60,3
	9:55-10:39	202,2	137,1	66,1
	11:29-12:17	184,6	120,1	55,3
	13:12-13:56	176,9	110,0	49,3
	14:40-16:06	164,2	100,3	44,6
IN TOTAL	286 min.	**174,6**	**116,3**	**55,1**
With developing doors		PM_{10}	$PM_{2,5}$	$PM_{1,0}$
Without developing doors		123,4	108,5	58,6
With developing doors on stages		177,9	117,1	54,5

The presented results of PM and PAU measured in heating season (from 5th to 19th November) 2008 describe the load of indoor environment in trams, on various routes in Prague in east-west and north-south directions.

In the parts of the city most exposed to contamination by transport the measured immediate (minute integral) values of weight concentrations of monitored fractions of aerosol particles went up to a level of 84 $\mu g/m^3$ ($PM_{1,0}$), 200 $\mu g/m^3$ ($PM_{2,5}$) a 480 $\mu g/m^3$ (PM_{10}).

While the level of load of tram indoor environment by weight concentrations of $PM_{1,0}$ fraction is more or less stable, the variability of measured values of aerosol particles belonging to $PM_{2,5}$ a PM_{10} is significantly higher. This variability depends both on meteorological conditions and on the door opening frequency at stations and also on the type of locality (viz tab. #1).

Accredited procedures were used for measurement (Grimm 1.109, Testo 442) and sample acquisition (Digitel FH-77).

The measured values can be used to estimate the amount of harmful substance (BaP, PM_{10}, $PM_{2,5}$, $PM_{1,0}$) to which the passenger of Prague tram transport is exposed. Measured values were used as input values, where the mean value of aerosol particles of PM_{10} fraction is (5.11/19.11) 165/66 $\mu g/m^3$, $PM_{2,5}$ 115/34 $\mu g/m^3$, $PM_{1,0}$ 55/10 $\mu g/m^3$ and BaP 0,64/0,30 ng/m^3.

We can estimate that in Prague it takes approximately two minutes for a tram to travel one kilometer, an adult breathes (in a calm state) approximately from 10 to 15 times a minute and the amount of inhaled air is approximately 0,5 liter. In one minute an average passenger of Prague tram transport inhales from 5 to 7,5 liters of air and with it he inhales:

- 0,33 to 0,83 µg aerosol particles of PM_{10} fraction
- 0,17 to 0,58 µg aerosol particles of $PM_{2,5}$ fraction
- 0,05 to 0,28 µg aerosol particles of $PM_{1,0}$ fraction
- 1,5 to 3,2 pg of benzo[a]pyrene.

When traveling one kilometer an average Prague tram passenger inhales from 10 to 15 liters of air and with it he inhales:

- 0,66 to 1,65 µg aerosol particles of PM_{10} fraction
- 0,34 to 1,15 µg aerosol particles of $PM_{2,5}$ fraction
- 0,10 to 0,55 µg aerosol particles of $PM_{1,0}$ fraction
- 3,0 to 6,4 pg benzo[a]pyrene.

Exposure depends on the amount of time spent in the vehicle or on the number of kilometers traveled. Measurements have proved the significance of this type of exposition environment, particularly in the case of aerosol particles of PM_{10} a $PM_{2,5}$ fractions infiltrated to tram from line sources. An almost area nature of load from outdoor air environment PAU and significance of car transport as a source of emissions of these substances have been confirmed. There is an obvious difference between the load in the centre of the city and in the suburbs and a significant influence of actual meteorological conditions which influences the dispersion of the emitted substances.

Aerosol exposure at schools during morning hours: effect of school buses

S.A. Grinshpun[1], C. Li[1], Q. Nguyen[1], P.H. Ryan[1], G.K. LeMasters[1], H. Spitz[2], M. Lobaugh[2], S. Glover[2]

[1]Department of Environmental Health, University of Cincinnati, Cincinnati, OH 45267, USA
[2]Nuclear & Radiological Engineering Program, University of Cincinnati, Cincinnati, OH 45267, USA

Keywords: aerosol emission, concentration, carbon, traffic, school bus.

About 25 million public and private school students in the USA are transported to and from school daily by diesel fuel powered buses Wargo et al., 2002). Among various traffic pollutants, diesel exhaust particles exhibit a respirable size fraction with a peak size in the ultrafine range (<0.1 µm) that is capable of penetrating the lower airways (Ban-Weiss et al., 2008). There is no established safe level of diesel exposure for children, especially those with respiratory illnesses, such as asthma. Children's short-term exposure associated with aerosol emission from school buses has not been adequately investigated. This case study was conducted in a major metropolitan area (Cincinnati, Ohio, USA) to determine the particle concentration and elemental composition in the school vicinity during the intense bus traffic period (6 AM to 9 AM).

Identical measurements were performed at a test and control sites. The ambient aerosol was initially characterized using a real-time Wide Range Particle Spectrometer (WPS) and then continuously monitored at each site with a real-time non-size-selective P-Trak, which detected particles of 20 nm to >1 µm. In addition, air samples were collected on filters using PM2.5 Harvard Impactors and analyzed by the X-ray fluorescence technique (for 38 elements) and by thermal-optical transmittance (for carbon). The measurements were performed during two seasons: winter (at ambient temperatures around 0°C) and spring (between 10 and 20°C).

The particle size distribution measured with a WPS identified the presence of a considerable ultrafine particle size fraction at the school location. The school bus traffic was found to significantly increase the local aerosol background across the entire range of particle sizes (p<0.01). While the difference was especially high for the smallest WPS-measured particles (about 5-fold of the background level), no significant difference was shown with particle sizes in excess of ~ 25 nm.

The number concentration of aerosol particles at the test site was pronouncedly time-dependent while at the control site it was essentially flat. A common occurrence at the test site was low (background) particle number concentration during the first 15 min of sampling that increased substantially thereafter. It exhibited a series of spikes as high as >500,000 cm^{-3} over the next 2.5 hours and returned to background by ~ 9 AM. The particle count at the school site exceeded that at the control site almost by 5-fold in winter when buses were continuously idling and over 2-fold in spring (less idling). On some days, a 15 min-averaged particle number concentration exhibited significant correlation with the number of school bus arrivals and departures during these time intervals. On other days, the correlation was not statistically significant, which pointed out to an increased influence of mobile and stationary PM sources unrelated to school buses. As expected, the 3-h-averaged particle concentrations determined in the test site on days, when the school buses operated, were significantly different and more than 2-fold higher (on average) than those measured on bus-free days. Overall, the data suggested an association between the number of detected aerosol particles and school bus traffic intensity. At the same time, the results of the multiple regression modeling showed no statistically significant association between the particle concentration and the commuter traffic intensity at the school site and may have been masked by the school bus emission. Analysis of the filter samples collected at the test site between 6 AM and 9 AM revealed elevated levels of elemental carbon (2.8 times in winter and 3.1 times in spring) as compared to the control site. The PM2.5 mass concentrations of other relevant elements were also higher; on average, the difference ranged from 1.7-fold (As, winter) to 13.8-fold (Ti, spring). The data suggest that particulate emission from school bus exhaust (including ultrafine diesel particles) significantly contributes to the children's exposure in the school vicinity.

Wargo, J. Brown, D., Cullen, M., Addiss, S., Alderman, N. (2002). *Children's Exposure to Diesel Exhaust on School Buses*. North Haven, CT: Environment & Human Health, Inc. [Report] http://www.ehhi.org/reports/diesel/dieselintro.pdf

Ban-Weiss, G. A., McLaughlin, J. P., Harley, R.A., Lunden, M. M., Kirchstetter, T. W., Kean, A. J., Strawa, A. W., Stevenson, E. D., Kendall, G. R. (2008). *Atmos. Environ.*, 42, 220-232.

Selected organic and inorganic compounds in atmospheric samples over five South American sites

P.C.Vasconcellos[1], D.Z. Souza[2], K. H. Nascimento[1], F.C. Santos[1], M.P. Araújo[2], H. Lee[1], J.B. Andrade[3], A.L.N. Guarieiro[3], L.L.N. Guarieiro[3], O.V. Bustillos[2], E. Beherentz[4].

[1]Institute of Chemistry, University of São Paulo, 05508-900, São Paulo, Brazil
[2]National Institute of Nuclear Energy, 05508-000, São Paulo, Brazil
[3]Institute of Chemistry, Federal University of Bahia, 40170-290, Salvador, Brazil
[4] Universidad de Los Andes, Bogotá, Colombia.

Keywords: chemical tracers, organic compounds, water-soluble ions, n-alkanals, PAH.

The atmosphere over Latin American cities is influenced by a variety of emissions sources. Brazilian cities are impacted by different kind of emissions since different fuels are used. Alcohol-fueled motor vehicle, gasoline, diesel and recently, biodiesel emit to the atmosphere a variety of compounds. In addition to this mix, biomass burning is often observed in tropical forest and sugarcane plantations, and these plumes are often observed far from the emission sources affecting the air composition. This paper discuss the results of several compounds (water-soluble ions, levoglucosan, PAH, n-alkanes, n-alkanones and n-alkanals) in aerosols collected in Brazil: São Paulo (SPA, urban), Piracicaba (PRB, biomass burning) and Mata Atlântica (MAT, forest) and in Colombia (Bogota), two sites: industrial (BOI) and vehicular emissions (BOV).

Water-soluble ions were analysed by Ion Chromatography, n-alkanes and PAH by Gas Chromatography and Flame Ionization Detection, n-alkanals, n-alkanones and levoglucosan by Gas Chromatography and Mass Spectrometry Detection.

In the average PM_{10} concentrations presented at SPA site were lower than BOI (industrial area) and comparable to BOV (vehicular emissions predominance) (Table 1).

Table 1. Average total concentrations of compounds groups identified in ambient air.

$ng\ m^{-3}$	Brazil sites			Colombia sites	
	SPA	PRB	MAT	BOI	BOV
inorganic anions	8870	6142	1660	4809	2713
organic acids	534	963	199	403	332
cations	3506	2975	2479	1626	1445
levoglucosan	37	114	11	*	*
n-alkanes	209	92	17	212	*
PAH	42	20	3	26	*
n-alkanals	2	2	1	37	*
n-alkanones	25	10	3	209	*
PM_{10} ($\mu g\ m^{-3}$)	38±14	49±24	9±3	106±47	46± 6

* in analysis

The overall distribution of n-alkanes ranges in carbon chain from C_{16} to C_{35}. The odd to even carbon number predominance is $>C_{25}$ and the Carbon Preference Index ranges from 0.7 to 1.0 in all sites.

The n-alkan-2-ones were determined ranging C_{10} to C_{20}, with predominance of 2-hexadecanone. The n-alkanals ranged from C_8 to C_{14} and tetradecanal was the predominat. The n-alkanals $< C_{20}$ may in part be derived from anthropogenic activity or from atmospheric oxidative processes (Alves et al. 2008).

Oxalic acid was the most abundant compound in the three sites and PRB site presented the highest level in the sugarcane burning season (377 ng m^{-3}).

Good correlations between sulfate and, oxalate and formate corroborate the strong vehicular emission influence at SPA site and between sulfate and potassium at BOV may be attributted to biomass or waste burnings.

Formic/acetic ratios have been used to suggest emissions sources or photochemical reactions. Values higher than 1 were found in all samples indicating high photochemical formation in the atmosphere.

The presence of sulfate and nitrate as predominant ions confirm the vehicular influence in all sites. At MAT site (forest) long range transport and/or local biomass burning can impact the site atmosphere.

Chloride may be transported from sea and in particular in São Paulo site can be formed during waste burning (Vasconcellos et al., 2007).

The highest average total PAH levels were found at SPA site (42 ng m^{-3}).This value is two times higher than those found at burning site (20 ng m^{-3}). PAH of lower molecular weight (from phenanthrene to pyrene) were found in higher levels at PRB (biomass burning); in the other side, the higher ones (benz(a)anthracene to benzo(g,h,i)perilene) were found at SPA site (urban).

Levoglucosan, a tracer for cellulose in biomass burning (Simoneit et al., 1999), as expected, was found in higher concentrations at PRB site (114 ng m^{-3}).

Alves, C. (2008). *Annals of The Brazilian Academy of Sciences*, 80, 21-82.
Simoneit, B.R.T. (1999). *Atmos. Environ.* 33,173-182.
Vasconcellos et al. (2007). *WASP* 186, 63-73.

Chemical species of transition metals
in the aerosol particles of a metropolitan underground railway station

I. Salma[1], M. Pósfai[2], K. Kovács[2], E. Kuzman[1], Z. Homonnay[1], J. Posta[3]

[1] Eötvös University, Budapest, Hungary
[2] University of Pannonia, Veszprém, Hungary
[3] Debrecen University, Debrecen, Hungary

Aerosol mass concentrations are usually larger (often several times) in underground railways than in corresponding outdoor areas. Furthermore, the particles are larger and heavier, are mainly composed of Fe, and contain less soot. Transition metals, i.e., Fe, Mn, Ni, Cu and Cr exhibit the largest crustal enrichment factors in metros. The underground aerosol particles were shown to be eight times more genotoxic and four times more likely to cause oxidative stress than the particles collected on a busy street. It is suspected that the chemical forms of the transition metals and their capability to release radicals play a role in the increased adverse health effects of the underground aerosol particles.

Aerosol samples were collected on the platform of a metro station in central Budapest by a stacked-filter unit sampler in $PM_{10-2.0}$ and $PM_{2.0}$ size fractions on polycarbonate filters. The filters were studied by individual particle analysis, i.e., by atomic force microscopy, scanning electron microscopy and transmission electron microscopy with energy-dispersive X-ray spectrometry and selected-area electron diffraction. The bulk aerosol samples were investigated by ^{57}Fe Mössbauer spectroscopy at temperatures of 20 and 297 K, and they were subjected to chemical speciation analysis based on sequential leaching and atomic absorption spectrometry with graphite furnace for Cr in order to determine the abundances of Cr(III) and Cr(VI).

Images of particles obtained for the $PM_{10-2.0}$ size fraction showed irregular and angular shapes, suggesting that they originated from primary emission sources. Atomic force microscopy images showed that the $PM_{2.0}$-fraction particles typically had a rather rugged surface and appeared to have either layered or granular morphologies. The surfaces of the most common particles typically exhibited globular features. The individual particles were classified into five groups that were each characterized by large concentrations of: 1) Fe and O, 2) Ca, Mg and C, 3) Si, Ca, Mg, Cl and Fe, 4) Si, and 5) C. The compositions of the groups are consistent with particles of iron oxides, carbonates, silicates, quartz and carbonaceous (possibly plastic and anthropogenic) debris, respectively. The images also revealed that Fe-rich particles in the $PM_{2.0}$ size fraction were aggregates of nano-sized crystal grains. Selected-area electron diffraction patterns exhibited diffraction rings, indicating the polycrystalline nature of the aggregates and a random crystallographic orientation of the nanocrystals. Hematite (Fe_2O_3) was the major phase in all iron oxide particles, and in some particles, minor amounts of magnetite (Fe_3O_4) were also present. It is suggested that these aggregated Fe-rich aerosol particles were generated by sparking between the electric conducting rail and collectors. Mössbauer spectroscopy indicated that hematite was a major Fe-bearing species in the $PM_{10-2.0}$ size fraction; its mass contribution to the Fe was 36%. Further constituents (magnetite, ferrite, carbides and FeOOH) were also identified.

Chromium in the $PM_{2.0}$ size fraction could be dissolved completely, while Cr in the $PM_{10-2.0}$ size fraction was partially soluble. The difference in the water solubility for the two size fractions indicates that the abundance of their major chemical forms is discrepant, and that their source processes are diverse. The insoluble Cr - which was 2.7% of the total amount in the $PM_{10-2.0}$ size fraction - can partially be associated with some non-soluble Cr-compounds originating from the Earth's crust. The remaining insoluble Cr contains Cr_2O_3 and metallic Cr. In addition, Cr in the PM_{10} size fraction was substantially less water soluble for the metro than for ambient urban aerosol (2% vs. 12%). In the $PM_{10-2.0}$ size fraction, practically all dissolved Cr had an oxidation state of three. This corresponds to ambient conditions. In the $PM_{2.0}$ size fraction, however, approximately 7% of the dissolved Cr consisted of Cr(VI). This can be of concern since Cr(VI) is one of the most harmful metallic components.

The present research demonstrates that the aerosol in underground railways differs not only in mass concentration, size distribution and chemical composition from the ambient outdoor urban aerosol but substantial differences occur in chemical speciation of some relevant transition metals. The increased harmful health effects are likely more related to surface chemistry influenced by the location and coordination of the metals on particle surfaces, perfection of the crystals on the surfaces and the surface size distribution than to the dissolved amounts of transition metals.

Influence of the dilution effect on atmospheric particle size distributions

F.J. Gómez-Moreno, M. Pujadas, J. Plaza, J.J. Rodríguez-Maroto and B. Artíñano

CIEMAT, Dept. Medio Ambiente, Av. Complutense, 22, E-28040 Madrid, Spain.

Keywords: Atmospheric aerosols, Urban aerosols, Particle size distribution.

Atmospheric particle size distributions have been measured in an urban background site in Madrid by means of an SMPS (TSI) instrument in the size range 15-600 nm. Evolution of particle size distribution has been identified for different meteorological scenarios. In this work, the influence of the wind speed on the particle size distributions of atmospheric aerosols will be analyzed.

A statistical analysis was done averaging the size distribution during continuous periods with wind velocity below and above 3 m/s. Since Madrid industrial activity consists essentially of light factories, its plume is typically urban, fed by traffic emission and also by heating devices in winter. The high wind speeds produce the plume dilution and reduce the time for particle aging. The analysis has shown a general decrease in the particle number concentration as the emission produced by the city is diluted. At the same time, the typical increase of the mode between 80-100 nm observed in previous works under episodic days (Pujadas et al, 2007) disappeared, and the emission mode was characterized by smaller particle sizes.

To illustrate this behavior the period 4-11 February 2007 has been selected for analysis among the different situation studied. During this period, there were 3 days with a wind speed under 3 m/s, 2 transition days with an increasing wind speed and 3 more days with a wind speed above 5 m/s. During these last days, the wind direction remained approximately constant from the west-southwest. Other meteorological parameters with possible influence in the size distribution did not vary significantly.

A clear decrease in particle number concentration was observed as the wind speed increased and produced a dilution effect, such that on 5 February there was a mean number concentration of 3.2 10^4 part/cm^3 and on 11 February it was 3.9 10^3 part/cm^3, a full order of magnitude smaller. More interesting than the number concentration was the mode displacement. During the stagnation period (low wind speed), the particle mode was around 30 nm and after a period of time it was possible to surmise a second mode around 80 nm, caused by the particle aging. During the vented period the only mode observed was the one generated by the emissions, as these particles did not have time to age before being transported to the experimental suburban site. This particle mode was shifted to smaller sizes than under non-vented conditions, even smaller than 15 nm, and only a branch of the distribution is seen.

A possible reason for this behavior is that the dilution effect produced by high wind speeds reduces the organic concentrations in the gas phase and produces a higher volatilization of the organic compounds from the particulate phase, thereby reducing particle size. This is in agreement with Robinson et al. (2007), who established that the dilution effect on diesel particles was more intense than previously considered and that an important mass fraction of these particles is shifted to the gas phase as the dilution factor increases.
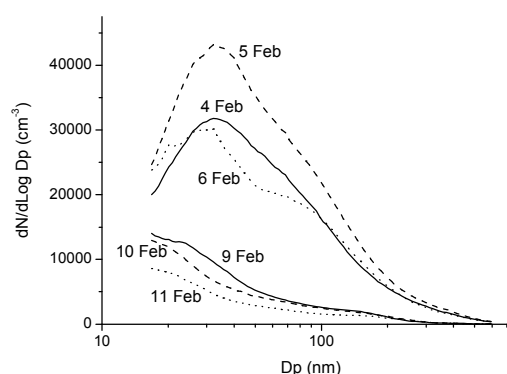
Figure 1. Evolution of the daily averaged size distributions for the period 4-11 February 2007

Pujadas, M., Gómez-Moreno, F.J., Plaza, J., Rodríguez-Maroto, J., Sánchez, M., Coz, E., Artíñano, B., 2007. Time evolution of fine and ultrafine ambient particle in a Madrid suburban site. European Aerosol Conference 2007, Salzburg, abstract T13A170.

Robinson, A. L., Donahue, N. M., Shrivastava, M. K., Weitkamp, E. A., Sage, A. M., Grieshop, A. P., Lane, T. E., Pierce, J. R., Pandis, S. N., 2007. Rethinking organic aerosols: semivolatile emissions and photochemical aging. Science 315, 1259-1262.

Influence of traffic and meteorology on the TSP, PM10, PM2.5 and PM1 urban aerosol fractions

St. Pateraki[1,2], D. N. Asimakopoulos[2], Th. Maggos[1], H. A. Flocas[2], S. Tsakanikas[2] and Ch.Vasilakos[1]

[1]Environmental Research Laboratory/INT-RP, National Centre for Scientific Research "DEMOKRITOS", 153 10 Aghia Paraskevi Attikis, P.O.B. 60228 Athens, GREECE

[2]Department of Environmental Physics and Meteorology, Faculty of Physics, University of Athens, University Campus, building PHYS-5, 157 84, Athens, GREECE

Keywords: Aerosol size distribution, Traffic, Meteorology, Air Pollution,

High levels of ambient traffic – related particulate matter (PM) have been reported to be associated with increased human morbidity and mortality (Valavanidis et al., 2009).

A winter (3/3-9/3/08) and a summer campaign (14/6-6/6/08) deployed simultaneously in two different sites in Athens, Greece. Measurements took place for TSP, PM_{10}, $PM_{2.5}$, PM_1 at two sites: 1) Varipompi, which is located northeasterly of the centre of Athens and around 16 Km away, (hereafter will be referred as site 1). It is characterized as an industrial, traffic area, sited in close (approximately 100 m) to the national road Athinon-Lamias. 2) Aghia Paraskevi, which is located easterly of the Athens basin in the National Center of Scientific Research (NCSR) 'Demokritos' (hereafter will be referred as site 2). This is a suburban area, at the outskirts of a highly populated area, on the foot of Hymettos mountain within a forest of pine trees. The Hymettos mountain peripheral road is crossing the eastern part of the NCSR area at a distance of approximately 200 m. The two sampling sites were selected taking under consideration their variability concerning the pollution characteristics and sources.

This study addresses three objectives: (i) to determine the mean levels of TSP, PM_{10}, $PM_{2.5}$ and PM_1 (ii) to investigate the relationship between PM and traffic (iii) to investigate the correlation with other priority air pollutants (O_3, NO, NO_2) as well as with meteorology and atmospheric circulation.

Particles at site 1 were collected using Osiris Dust Monitor which provides continuous and simultaneous indication of the different mass fractions PM_1, $PM_{2.5}$, PM_{10} and TSP. At site 2 $PM_{2.5}$ were collected using Teom 1400a while PM_{10}, PM_1 with the use of 2 low-volume (Derenda (LVS3.1/PNS3.1-15)) controlled flow rate (2.3 m^3/h) samplers. Hourly data for O_3, NO and NO_2 were provided by the Ministry of Environment. National Meteorological Service provide the meteorological data (WD, WS, T, RH) for site 1 while at site 2 there is a meteorological mast, operating under the responsibility of NCSR 'Demokritos'.

Table 1 presents the mean values of mass concentrations for the air pollutants mentioned above.

Table 1: Statistical values ($\mu g/m^3$) for the experimental sites

Site1				
($\mu g/m^3$)	TSP	PM_{10}	$PM_{2.5}$	PM_1
Max	213	159	38.1	14.2
Min	21.0	13.9	3.06	0.82
Avg	93.2	66.4	14.9	4.58
St.dev	61.7	48.2	12.2	4.51
Site 2				
($\mu g/m^3$)		PM_{10}	$PM_{2.5}$	PM_1
Max		40.0	24.7	21.2
Min		18.9	8.46	5.12
Avg		26.1	16.7	11.7
St.dev		6.89	5.28	6.28

At site 1, the four PM fractions presented higher concentrations early in the morning (winter: 5:00 am, 7:00am, and summer: 7:00 am, 8:00 am) concurring with the rush traffic hours. At site 2 the $PM_{2.5}$ peaks presented in the midday (12:00pm, 13:00 pm), go along with the assumption that fine particles" are favoured of the transformations, which take place in the atmosphere with the presence of solar radiation.

The average values for the $PM_{2.5}/PM_{10}$ ratio indicate great variability between the two sites. The ratios ranged from 0.22 to 0.28 and from 0.35 to 0.70 for sites 1 and 2 respectively. The results proved that site 2 is predominantly affected by secondary aerosol sources.

The regression analysis which was used revealed the existence of common sources for the PM fractions at both sites (R: 0.85-1.00).

Valavanidis A., Loridas S., Vlahogianni T., Fiotakis K. (2009). J Hazard Mater., 162, 886-8

Correlation of near-traffic particle number concentrations and ambient noise

S. Weber

Department of Applied Climatology and Landscape Ecology, University of Duisburg-Essen, Essen, 45141, Essen, Germany
Keywords: urban, particle number, ambient noise

Urban areas are prone to significant concentrations of different environmental stressors due to the large number of potential emission sources, e.g. traffic, industry and households. Two stressors receiving increased attention during recent years are particulate air pollution and environmental noise. In a number of studies both were associated with significant effects on human health. In an earlier study the correlation between noise and particle mass concentrations was evaluated (Weber and Litschke, 2008).

The intention of the present research is to study the spatio-temporal variation of particle number concentrations and ambient noise on the local scale within an urban residential environment close to a busy major road.

Study area and methods

Measurements were performed within a busy urban street canyon and its surrounding neighbourhood in Essen, Germany. The street canyon 'Gladbecker Straße' (federal road B224) is characterised by a long-term average daily traffic intensity (ADT) of about 49 000 vehicles 24 h^{-1}.

To study the spatio-temporal variability of particle number concentration and ambient noise both quantities were gathered at 50 fixed measurement points (MP) along the 3.5 km measurement route during four consecutive days from Monday 28 July to Thursday 31 July, 2008. This results in a spatial resolution of about one measurement every 70 m.

Total particle number concentration (TNC) was measured by a handheld condensational particle counter (CPC, TSI Inc., USA, Model 3007). According to the manufacturer the CPC is able to measure particles above a cut-off of 10 nm. The CPC measures the total number concentration with a time resolution of 1 s.

Ambient noise was evaluated by a handheld noise level meter (Norsonic, Norway; Mod. Norsonic 118). The device is able to sample the noise level with a resolution of 1 s.

Results

Average particle number concentrations measured by handheld CPC during twelve mobile measurements vary between 12,500 cm^{-3} and 29,500 cm^{-3} on average. However, the 20 s maximum TNC along the measurement route can reach concentrations of more than 100,000 cm^{-3}.

When comparing the 12 measurements conducted in Essen a range of about 17,000 cm^{-3} (range of median = 12,000 cm^{-3}) is covered. The significant difference between median and average values indicates the degree of spatial variability of number concentrations between and within measurements.

The spatial distribution of noise and TNC is significantly coupled to road traffic on B224 (Fig. 1). The values at every single MP in the vicinity of the major road (MP 15, 21, 25, 29, 49, 50, cf. Fig. 1) as well as the contiguous MP along the street canyon (MP 33 to 43) are considerably elevated above those located at some distance to B224. Within the street canyon TNC reaches mean maxima of up to 40,000 cm^{-3}. On average the street canyon TNC are larger by a factor of up to 2.4 in comparison to the local background within the residential neighbourhood streets.

The close spatio-temporal covariation of both quantities is supported by a correlation analysis. Significant positive correlations between TNC and noise are demonstrated by Pearson and Spearman rank-correlation coefficients (r > 0.5).
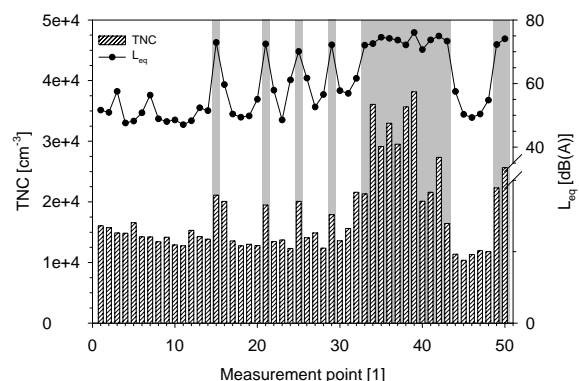
Fig. 1: Median TNC and Leq at the 50 measurement points along the route. Grey shadings indicate the points that are situated in close proximity to road traffic on B224.

Weber, S. and Litschke, T. (2008) *Atmos Environ*, 42(30), 7179-7183.

Characterization of particle number concentration increases during fireworks

J. Crespo[1], J. Gimenez[1], R. Castañer[1], S. Caballero[1], M. Varea[1], J. Gil-Moltó[1], J. Nicolás[1], A. Carratalá[2]

[1]Department of Applied Physics, Miguel Hernández University, 03202, Elche, Spain
[2]Department of Chemical Engineering, University of Alicante, 03080, Alicante, Spain

Every year, during the second half of June, the festival *Las Hogueras de San Juan* is celebrated in Alicante (38°20´43´´N, 0°28´59´´W), located in southeast Spain on the Mediterranean coast.

During this festival, there are three types of short-duration spectacles characterized by elevated emissions of particles into the atmosphere. These events are:

- Fireworks: displays take place between 25-29 June, beginning every evening at midnight. Their duration does not exceed 30 minutes.

- Cremá: Beginning at midnight on 24 June, it consists in burning monuments built from combustible materials (wood, cardboard and Styrofoam) all over the city, reducing them to ashes.

- Mascletás: Noise spectacles take place daily from 19-24 June, beginning at 14:00h. During this event, huge quantities of firecrackers are lit.

Particle size distribution of each event is characterized by a Grimm 1108 optical particle counter. This instrument determines the particle number concentration in 15 particle size channels, from 0.3 µm to >20 µm. The measurements began in mid-June and lasted until early July, at 1 min intervals.

Figure 1 represents the particle size distribution obtained for each event. In order to realize these profiles, the average particle concentration was selected from one hour of measurements, beginning with the commencement of these events.
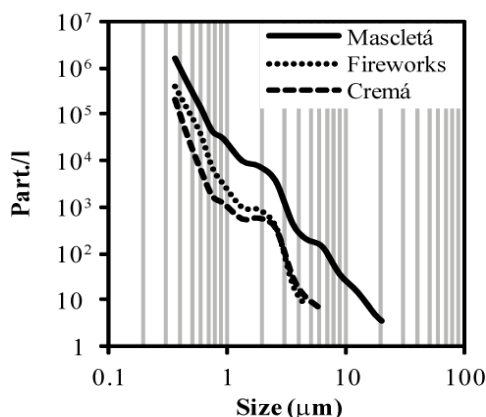
Figure 1. Particle size distribution during Fireworks, Mascletá and Cremá events.

Larger numbers of particles of all sizes were registered during the Mascletá. This may be due to the sampling point being located less than 100 m from the Mascletá launching site. The Fireworks displays took place some 3 km away.

Figure 2 shows the increase factor (number of times the concentration increases) to quantify the particle concentration increases each event causes. It is calculated between the hourly number particle average for each event and the same temporal period on a day without.
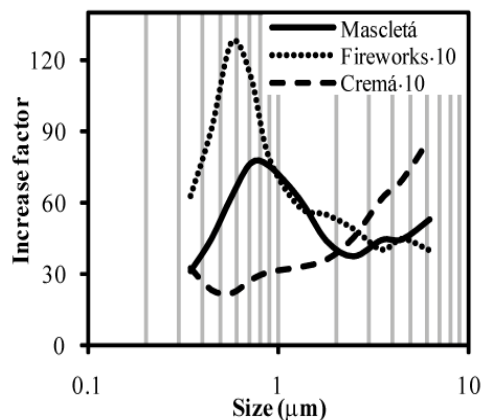
Figure 2. Increase factor between size distributions during Fireworks, Mascletá and Cremá events.

Figure 2 shows Mascletás are the event producing the greatest increase when compared to similar periods without events. Distribution increases are similar for the Mascletá and Fireworks, and in both cases, it is primarily the accumulation mode where the distribution rises. The increase profile for Fireworks is similar to that found in other cities (Vecchi et al., 2004), registering maximums around 0.5-1 µm. For the Cremá, the distribution increase grows along with particle size, and is greater in the coarse mode.

Vecchi, R., Bernardoni, V., Cricchio, D., D´Alessandro, A., Fermo, P., Lucarelli, F., Nava, S., Piazzalunga, A., Valli, G. (2004). *Atmos. Environ.*, 42, 1121-1132.

Levels of PM1, PM2.5 and PM10 in an urban location in the western Mediterranean

M. Varea, J. Gil-Moltó, C. Chofre, N. Galindo, R. Esclapez, C. Pastor and J. Crespo

Department of Physics, Miguel Hernández University, Avda. de la Universidad s/n, 03202, Elche, Spain

Keywords: PM1, PM2.5, PM10, Saharan dust, Urban areas.

From July 2008 until February 2009, twenty daily samples of PM10, PM2.5 and PM1 were simultaneously collected in the urban atmosphere of Elche (southeastern Spain) by means of low volume samplers (2.3 m^3/h). The sampling site was located on the roof of a building of the Miguel Hernández University, adjacent to a major city avenue, in a highly ventilated area.

Figure 1 shows the daily variability of each fraction during the study period along with rain, wind and Saharan dust (shaded in grey) events.
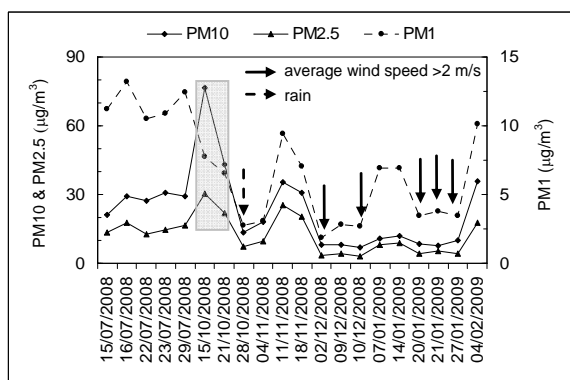
Figure 1. Evolution of daily PM concentrations in Elche (southeastern Spain).

The levels of PM1 were higher in summer when solar radiation is much more intense. This could be explained considering the photochemical formation of secondary particles as the main source of submicron aerosol in the study area. The highest PM10 and PM2.5 concentrations were measured on days with Saharan dust intrusions. The influence of such events upon the PM1 fraction seems to be much lower, as has been previously reported for other Mediterranean locations (Pérez *et al.,* 2008). However, a small set of samples collected in the beginning of summer 2008 under the influence of African dust episodes at the same sampling site showed PM1 levels $\geq$ 25 μg/m^3. A possible explanation for this discrepancy could be the formation of secondary inorganic compounds by reactions on fine dust particles (Usher *et al.*, 2003) favoured by the higher solar radiation in summer than in the fall and winter months. Further investigations have to be done to confirm the previous hypothesis. Other PM peaks observed during fall and winter might have been caused by high atmospheric stability conditions (lower wind speed and mixing height). During December 2008

and January 2009 exceptionally low PM levels were registered, in particular for the PM2.5 and PM10 fractions (< 9 and 12 μg/m^3 daily averages, respectively) compared with previous data obtained at the same location (annual mean levels of 15 μg/m^3 for PM2.5 and >30 μg/m^3 for PM10, Galindo *et al.*, 2008). One of the reasons for this reduction may be meteorological factors, mainly wind speed. The relationship between PM concentrations and the daily average wind speed is shown in Figure 2. Although, in general, higher wind speeds favour the dispersion of atmospheric pollutants and reduce PM levels, the PM1 fraction seems to be less affected indicating that other factors such as solar radiation may also have a major influence on PM1 concentrations.
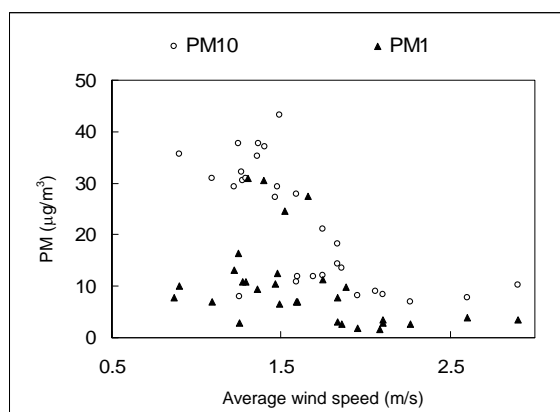
Figure 2. Relationship between PM1 and PM10, and the daily average wind speed.

Regarding the PM1/PM2.5 and PM1/PM10 ratios, average values of 0.63 and 0.35 were obtained for the period considered. These values are lower than those registered at more populated and industrialised areas (Pérez *et al,* 2008).

Galindo, N., Nicolas, J. F., Yubero, E., Caballero, S., Pastor, C. & Crespo, J. (2008). *Atmos. Res.*, 88, 305-313.

Pérez, N., Pey, J., Querol, X., Alastuey, A., López, J. M. & Viana, M. (2008). *Atmos. Environ.*, 42, 1677-1691.

Usher, C. R., Michel, A.. E. & Grassian, V. H. (2003). *Chem. Rev.*, 103, 4883-4939.

Two years of continuous measurements of surface and columnar atmospheric aerosol properties at Granada, an urban site in Spain.

H. Lyamani, F.J. Olmo and L. Alados-Arboledas

Departamento de Física Aplicada. Facultad de Ciencias. Universidad de Granada.
Fuentenueva s/n. 18071-Granada. Spain.
CEAMA-Centro Andaluz de Medio Ambiente. Av. del Mediterráneo s/n. 18006-Granada, Spain

Aerosol particles affect the Earth's radiative balance, climate and human health. However, despite the significant progress in understanding aerosol effects, these aerosol effects still contain considerable uncertainties due to the poor understanding of aerosol properties and their high spatial and temporal variability (Forster et al., 2007). In this work two years (from December 2005 to November 2007) of continuous measurements of various surface and columnar aerosol properties at Granada (37.18º N, 3.58º W, 680 m a.s.l), Spain, are analyzed.

The scattering coefficient, σ_{sp}, was measured with an integrating nephelometer (TSI, model 3563) in three wavelengths: 450, 550 and 700 nm. Light absorption coefficient at 670 nm, σ_{ap}, was recorded with a Multi-Angle Absorption Photometer (MAAP). Particle size distribution in the diameter range 0.50-20 μm was obtained by an aerodynamic aerosol sizer (APS-3222, TSI). The columnar aerosol optical depth, $\delta_{a\lambda}$, was retrieved using a CIMEL CE-318 Sun photometer.

The daily average values of σ_{sp} at 550 nm range from 12 to 234 Mm^{-1} with an average of 60±30 Mm^{-1}, while the daily average values of σ_{ap} (670 nm) vary from 4 to 57 Mm^{-1}, averaging 21±10 Mm^{-1}. The lowest of σ_{sp} and σ_{ap} values are associated with rain event and the largest values are linked to long range transport from North Africa. Both σ_{sp} and σ_{ap} show a clear seasonal cycle with summer minimum and winter maximum. This seasonal pattern in σ_{sp} and σ_{ap} is opposite to the seasonal cycle showed by $\delta_{a\lambda}$ (Figure 1). The difference in the seasonal features of the surface and column-integrated data is related to seasonal variation in the aerosol vertical distribution, aerosol sources and boundary layer height. The scattering Angström exponent is found to be 1.8±0.2, 1.6±0.3, 1.3±0.3 and 1.4±0.3 during winter, spring, summer and autumn, respectively, suggesting a large fraction of submicron particles at the site, especially during winter. These observations are supported by aerosol size distribution measurements made by the APS. Urban aerosols in Granada contain a large fraction of absorbing material as indicated by the average single-scattering albedo of 0.65±0.07, 0.66±0.06, 0.70±0.06 and 0.73±0.06 obtained during autumn, winter, spring and summer, respectively.

The aerosol scattering albedo is below the critical value of 0.86 that determines the shift from cooling to warming. A clear diurnal pattern is observed, in all seasons, in σ_{sp} and σ_{ap} with two local maxima occurring in early morning and late evening. This diurnal cycle is mainly attributed to the diurnal evolution of atmospheric boundary layer and local anthropogenic activities. In all seasons, σ_{sp} and σ_{ap} show significant decrease on weekends compared to weekdays, indicating a strong impact of traffic emissions.
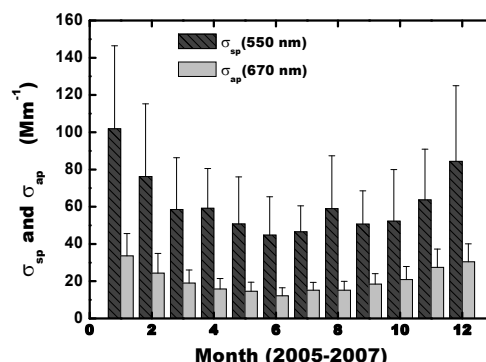
Figure 1. Monthly variations of σ_{sp} (550 nm) and σ_{ap}.(670 nm). The error bars are the standard deviations.

Forster, P., et al.: *Changes in Atmospheric Constituents and in Radiative Forcing. In: Climate Change 2007: The Physical Science Basis. Contribution of Working Group I to the Fourth Assessment Report of the Intergovernmental Panel on Climate Change* [Solomon, S., D. Qin, M. Manning, Z. Chen, M. Marquis, K. B. Averyt, M. Tignor and H. L. Miller (eds.)]. *Cambridge University Press, Cambridge, United Kingdom and New York, NY, USA, 2007.*

Pavement type influence on particulate matter composition

R. Licbinsky[1], D. Durcanska[2], V. Adamec[1], J. Huzlik[1]

[1]Transport Research Centre, Lisenska 33a, 636 00, Brno, Czech Republic
[2]Faculty of Civil Engineering, University of Zilina, Komenskeho 52, 01026, Zilina ,Slovakia

Particulate matters (PM) are an actual part of research not only due to increasing concentrations in the ambient air but primarily because of their negative effects on human health (respiratory and cardiovascular diseases). 347,900 European died in accordance with the EU study (Watkiss et al., 2005) due to air pollution. Especially in the large cities PM can be a problem due to the road transport that is an important source of these particles.

Two localities were chosen for active PM sampling (LECKEL MVS6) to determine the differences in the PM concentrations and chemical composition near roads with different pavements. The first locality represents highway near town Zilina with stone mastic asphalt pavement (SMA) and approximately 20,000 vehicles per day. Second one is the part of Zilina town circuit with asphalt concrete pavement (AC) and approximately 14,000 vehicles per day. PM_{10}, $PM_{2.5}$ and $PM_{1.0}$ concentrations using gravimetric analysis (Mettler-Toledo MX5/A) of each exposed filter were measured and the content of selected metals (ICP/MS, Agilent 7500ce) and polyaromatic hydrocarbons (GS/MS, Shimadzu QP2010) were determined. Meteorological conditions and current traffic intensity were also observed during the sampling campaigns. The first sampling campaign took place in July 2008, the second one in October 2008.

It is assumed that inorganic particles originate purely because of cement concrete pavement abrasion. Thus these particles also represent 90 % of particles from asphalt pavement abrasion (Snilsberg et al., 2007) and their main content is in the coarse PM fraction. The share of this coarse fraction on overall PM_{10} concentrations was higher on the locality with AC pavement (town circuit road) determined during both sampling campaigns. $PM_{1.0}$ fraction was dominant in both campaigns on locality next to highway with SMA pavement. These results indicate higher production of coarse PM fraction due to abrasion of AC pavement. Selected metals contents that represent some source connected with particle mechanical separation such as Zn, Sb, Cu, Ba and others were determined in both course and fine PM fractions.

$PM_{2.5}$ fraction was also observed using different methodology to determine the content of polyaromatic hydrocarbons. These results will also be presented in this paper.
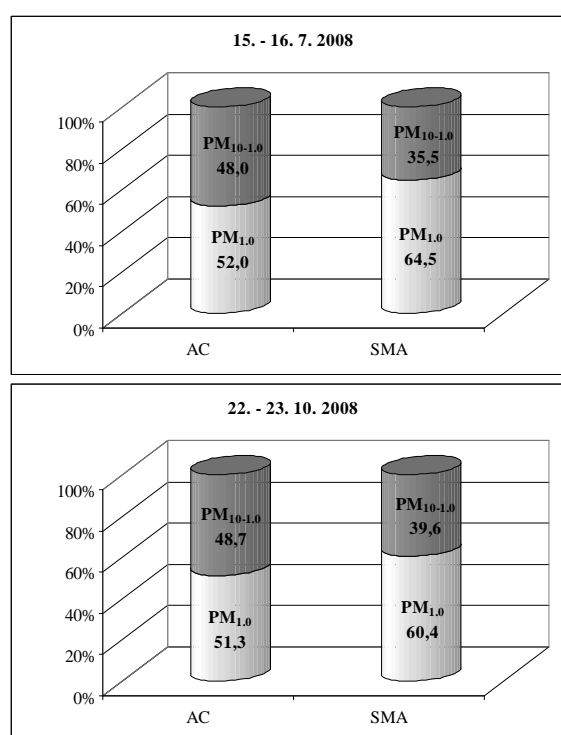
Figure 1. The share of PM fractions

Watkiss, P., Pye, S., & Holland, M. (2005). *CAFE CBA: Baseline analysis 2000 to 2020*, CAFE Programme, EAE Technology Environment, Didcot, Oxon, United Kingdom, 112 p.

Snilsberg, B., Myran, T. Uthus, N. & Erichsen, E. (2007). Characterization of road dust In *Symposium Proceedings. The 8th International Symposium on Cold Region Development, ISCORD*. Trondheim, Norway. Tampere, Finland.

Improvement in ambient air quality in East Germany after the German reunification: Analysis of the trends in exposure and their implications

J.Cyrys[1,2], M. Pitz[2], S. Breitner[1], M. Stölzel[1], W. Kreyling[1], J. Heinrich[1], H-Erich Wichmann[1,3] and A. Peters[1]

[1] Helmholtz Zentrum München-German Research Center for Environmental Health, 85764 Neuherberg, Germany
[2] University of Augsburg, Environment Science Center, 86159 Augsburg, Germany
[3] Ludwig-Maximilians-University, IBE, Chair of Epidemiology, 81377 Munich, Germany

Keywords: air quality, ambient aerosols, source structure, German reunification, long-term trends.

In recent years, ambient air pollution concentrations have been reduced Europe-wide by emission controls and fuel replacement. These measures are of particular interest for the regulating agencies as well as for the regulated entities.

One of the main objectives of our study carried out in Erfurt, Germany, was to assess the changes in ambient air quality and in the emission source structure after the German reunification, when air quality dramatically improved. For the same period we also report on selected results showing associations between decreasing air pollutant levels and short-term mortality.

We obtained data on gaseous pollutants SO_2, O_3, NO_2 and CO, mass concentrations of particulate matter (PM) < 10 µm (PM_{10}), and meteorology for the whole study period between October 1991 and March 2002. Ultrafine particle number (UFP) and $PM_{2.5}$ mass concentrations were measured during the winter 1991/92 and from September 1995 to March 2002 at a research monitoring site.
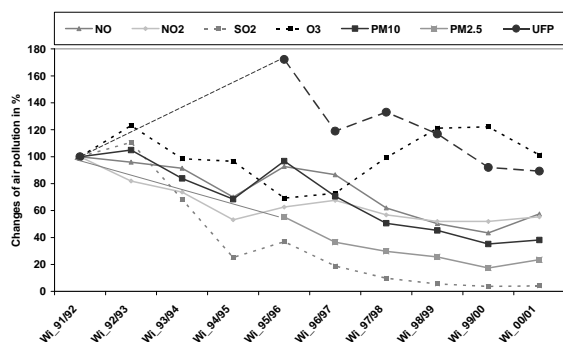
Figure 1. Changes of winter mean concentrations of air pollutants in Erfurt from winter 1991/92 to winter 2000/01 (expressed in %, the air pollutants levels in winter 1991/92 were assumed to be 100%).

As shown in Figure 1 the most rapid decrease of winter mean concentrations over the study period was observed for SO_2. The decrease of the particle mass concentration in the winter seasons was 80% and 70% for $PM_{2.5}$ and PM_{10}, respectively. In contrast, the trend for UFP was less clear. Except of a strong increase in winter 95/96, rather stable UFP levels were observed in the following period.

An analysis of correlations and ratios between the air pollutants showed that the pollution mixture has changed during the 90ties towards a mixture much like "Western European" urban air pollution, which is characterized by elevated concentrations of NO_x, O_3 and UFP and lower concentrations of SO_2 and TSP. Two source categories that have undergone significant changes in East Germany after the reunification include energy production (by power plants and by local heating) and the number and type of vehicles. For example, prior to the reunification many homes used individual coal furnaces for heating. This practice has nearly been eliminated after the reunification, with coal-burning ovens being replaced mostly by natural gas heating systems (Figure 2).
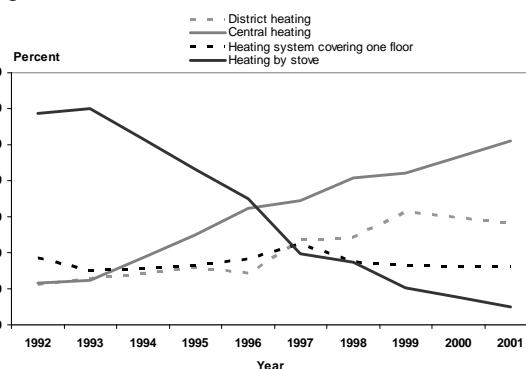
Figure 2. Changes of energy use patterns in Erfurt 1992 – 2001 (urban area).

The strongest health effects of the mortality study were observed in the transition period 1995-1997 (Breitner et al. (2009)) when changes in source characteristics took place and the benefits of ambient air quality were not yet completely achieved. Furthermore, it seems that the improved ambient air quality in East Germany after the reunification led to lower health effects at the end of the 90's than during the 90's.

S. Breitner, M. Stölzel, J. Cyrys, M. Pitz, G. Wölke, W. Kreyling, H. Küchenhoff, J. Heinrich, H.E. Wichmann, and A. Peters (2009). *Environmental Health Perspectives*, doi: 10.1289/ehp.11711 (available at http://dx.doi.org/).

The spatio-temporal distribution of atmospheric pollution in Beijing, China – Assessment of mass and elemental concentrations of PM$_{2.5}$ and TSP

N. Schleicher[1], S. Norra[1], Y. Chen[2], F. Chai[2], K. Cen[3], D. Stüben[1]

[1]Institute of Mineralogy and Geochemistry, Universität Karlsruhe, Adenauerring 20, 76131, Karlsruhe, Germany
[2]Institute of Urban and Regional Atmospheric Environmental Research, Chinese Research Academy of Environmental Sciences, 8 Yangfang Anwai, 100012, Beijing, China
[3]Department of Geology and Mineral Resources, China University of Geosciences, Xueyuan Road 29, 100083, Beijing, China

Keywords: urban aerosols, PM$_{2.5}$, TSP, elemental composition, megacity.

The megacity Beijing accounts to the most polluted cities in the world. Atmospheric particulate pollution is of major concern since it affects the health of the 15 million inhabitants. Sources for particulate matter are numerous and interferences between anthropogenic and geogenic particles are abundant.

Active sampling of PM$_{2.5}$ was carried out on a weekly basis continuously for 2 years (from August 2005 till August 2007) using Mini-Volume samplers (Leckel, Berlin) at a flow rate of 200 L/h. Five sampling sites were established along a transect through Beijing and sampling was done separately for day and night. At one site, additional TSP samples (flow rate of 1 m²/h) were collected.

Mass concentrations were calculated gravimetrically (Sartorius MP2). For analysis of trace metals one quarter of quartz filters was digested with concentrated HNO$_3$ (Merck, sp), concentrated HF (Merck, sp) and concentrated HClO$_4$ (Merck, sp). Determination of elements was performed by a high-resolution inductively coupled plasma mass spectrometer (HR-ICP-MS, Axiom).

PM$_{2.5}$ mass concentrations varied between 65 and 209 µg/m³ with an average concentration of 87 µg/m³, while TSP concentrations ranged from 76 to 1028 µg/m³ with an average concentration of 370 µg/m³ for the whole period. However, the mass and also the concentrations of single elements varied strongly over the course of the year (Figure 1).
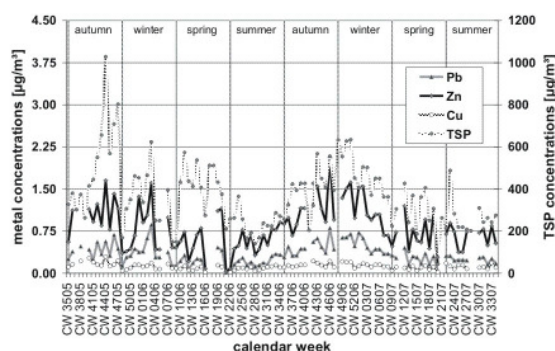
Figure 1. Yearly course for Pb, Zn and Cu concentrations in TSP samples together with TSP mass concentrations between 08/2005 till 08/2007.

Element ratios, such as Pb/Ti, supported the distinction between periods of predominant geogenic or anthropogenic caused pollution (Figure 2).
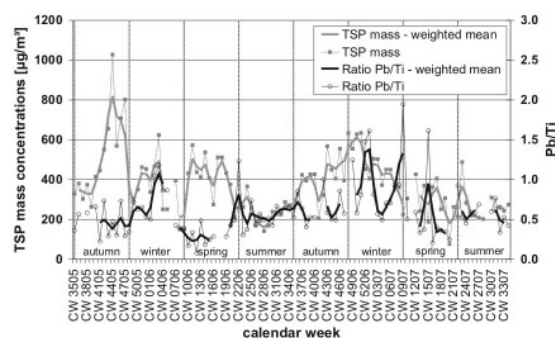
Figure 2. TSP mass concentration and the ratio of Pb and Ti concentrations between 08/2005 and 08/2007.

Lowest aerosol concentrations occurred during summer, due to meteorological conditions (e.g. rainfall during summer months) and the lack of certain sources (especially emissions from heating processes). In spring, high aerosol concentrations are predominantly caused by geogenic particles, whereas winter is a time of high aerosol concentrations caused by anthropogenic emission processes (heating period) and favoured by winterly inversion situations.

Besides temporal variations, also spatial differences occurred within the city, with higher PM concentrations in the southern parts of Beijing. This observation is reflected in the differences in land-use.

Sequential extractions were used to gain more detailed information about bioavailability of trace metals. Some hazardous metals such as Cd and Ni showed a relatively high bioavailability

Further knowledge of the temporal and spatial aerosol distribution and the corresponding sources is important for the detailed assessment of the pollution of Beijing's atmosphere. Moreover, besides the total mass concentrations, health studies should consider harmful metal concentrations and their solubility and toxicity state. This provides important additional information for the assessment of the particular chemistry of atmospheric particles.

First measurements of aerosols on a ZEPPELIN airship

R. Tillmann[1], Th..F. Mentel[1], A. Kiendler-Scharr[1] and A. Wahner[1]

[1] Institut für Chemie und Dynamik der Geosphäre, ICG-2, Forschungszentrum Jülich, Germany

Keywords: tropospheric aerosol, field measurements, vertical distribution, CPC, SMPS

In summer 2007 and autumn 2008 the airship ZEPPELIN NT was equipped with a suite of instruments to measure the distribution of different trace gases, short-lived radicals and aerosols in the planetary boundary layer together with radiation fluxes and meteorological parameters. A condensation particle counter (CPC, TSI Inc.) and a scanning mobility particle sizer (SMPS, TSI Inc.) were used to measure the total number concentration of atmospheric aerosols and their number size distribution. The measurements were carried out over forested, rural and urban areas in southern Germany as well as over Lake Constance. The performed flight patterns were vertical profiles above selected areas (e.g. figure 1) and regional flight tracks within a defined height above the ground (e.g. figure 2).

Height resolved measurements of aerosol number concentrations show predominately that aerosol concentration decreases with height independent of the area investigated. Since primary aerosols and precursors of secondary aerosols have their sources near the surface, aerosol concentrations are expected normally to be lower at higher altitudes.

As an example figure 1 presents the flight profiles above the city of Ravensburg and a forested area nearby as observed in autumn 2008. Above the forest (green shaded part) at altitudes below 700 m - 100 m above the ground and within the planetary boundary layer - high particle number concentrations > 5000 cm^{-3} were observed. The concentrations well above the planetary boundary layer at altitudes between 800 and 1150 m were overall stable around 2000 cm^{-3}. Shaded in red presents data measured over the city of Ravensburg 10 km south of the forest. The lowest flight height was about 350 m above ground. The observed number concentrations were in the same range as over the forested area above the planetary boundary layer.

Figure 2 presents particle number concentrations measured in a height of 230 – 400 m above the ground in the region of Lake Constance. Particle number concentrations up to 15000 cm^{-3} were observed at the eastern part of the flight track presumably dominated by anthropogenic emissions e.g. a nearby motorway. During the remaining time of the flight number concentrations were mostly < 6000 cm^{-3}.

In general the observed aerosol number concentration during the two campaign periods covers a range between 500 and 40000 cm^{-3}. Results of the SMPS-measurements show bi- and tri-modal aerosol size distributions in a particle diameter range of 13 – 750 nm.
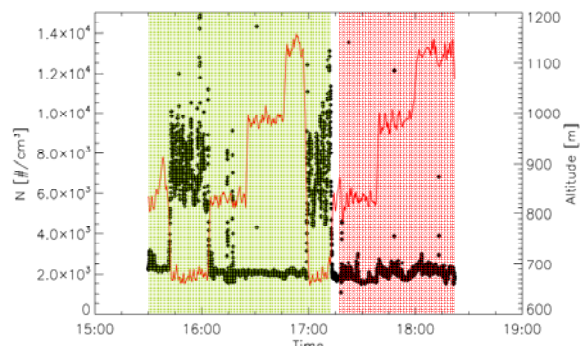
Figure 1. Flight profiles above a forested area (green shade) and the city of Ravensburg (red shade). The particle number concentration is presented as black dots, the altitude of the measurement as a red line.
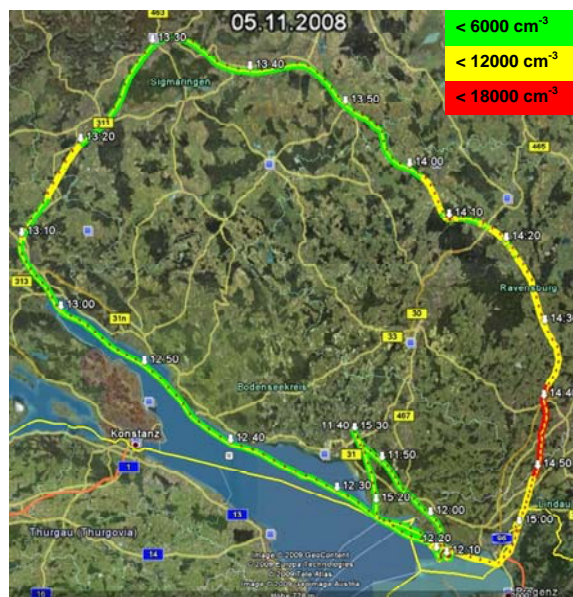
Figure 2. Particle number concentrations measured on the flight track of the ZEPPELIN in November 2008. During most time of the flight the height was within a range of 230 - 400 m above the ground. Particle concentrations along the flight track are indicated by colors.

Particle emissions of railway traffic determined by detailed single particle analysis

M.F. Meier[1], B. Grobéty[1], M. Heuberger-Vernooij[1], R. Lorenzo[1], K. Moser[1]

[1]Department of Geosciences, University of Fribourg, Chemin du Musée 6, 1700, Fribourg, Switzerland

Keywords: Anthropogenic aerosols, CCSEM, SEM/EDX, Single particle analysis, Traffic.

The goal of this study was to estimate the particulate emissions from railway traffic. For that purpose PM10 samples were actively collected at two different locations. The first sampling point at Juchhof, Zürich, was along a straight stretch with overland traffic mode i.e. no excessive breaking or accelerating. The train density is with 700 trains a day among the highest in Switzerland. This site was equipped with 5 stations, 3 at 10 m from the tracks, one at 36m and one site at 120m. Sampling was wind controlled i.e. collection was allowed only with wind blowing from the tracks. Total sampling time was 4 hours spread over one week in December 2004 The second location was in a curve at the entrance of the railway station of Fribourg. Trains change speed and break along this stretch. Train density is about 150 trains per day. Two collectors were placed 10 meters from the tracks. No wind control was used and total sampling time was 4 times 12 hours in November and December 2007. The slightly entrenched location and the house wall in the back of the samplers guarantee, nevertheless, that mainly particles originating from the railway traffic reach the samplers. Both sites are at a large distance from important roads. Particles were also collected simultaneously within an apartment adjacent to the railway lines at the second location. The sampler was positioned in a sleeping room and the windows were opened 2 times a day for 10 minutes.

Morphology and chemistry of single particles were analyzed by computer controlled scanning electron microscopy (SEM) and energy dispersive spectroscopy (EDS). Based on chemistry three particle classes were defined and assigned to their sources: 1. iron and iron oxide class, 2. silicate class and 3. calcium carbonate and sulfate class. The amount of particles that could not be attributed to one of theses three classes was less than 10% of the total particle mass. The mass of the individual particles was determined by multiplying their calculated volumes with the densities of the class they were assigned to. The iron dominated particles were either irregularly shaped pointing to pure mechanical wear or had spherical shapes characteristic for products of a melt process. To estimate the PM10 emissions of the railway lines, the mass from the 120m distant sampling point at the first location and from a sampler separated by a raw of buildings from the tracks at the second location were subtracted from the values at 10m. The source strength at the first location, normalized to the number of trains, was $4.3\mu g\ m^{-3}$ from all classes and $2.9\ \mu g\ m^{-3}$ in the iron class. In Fribourg the source strength was $2.87\ \mu g\ m^{-3}$ and $1.24\mu g\ m^{-3}$ respectively. When taking into account the train density these values are roughly three times higher than in the first location. This is attributed to the increased abrasion due to the curve geometry of the tracks and the acceleration respectively deceleration of the trains. The values for Juchhof fit well with analyses made at the same location based on gravimetric methods and bulk chemical analysis (Gehrig et al., 2005). Soot and copper bearing particles are among the particles, which do not fit one of the three classes. The latter are certainly derived from friction between the electric line and the bow collector.

The total particle mass concentration found inside the apartment was about 20% of the outdoor mass concentration. The proportion of the iron class was, however, below the proportion found outdoors. The average particle size of the indoor iron particles is smaller. Measurements made in an apartment in the city away from the railway lines do not differ substantially from the above values. Iron particles, derived from mechanical wear in car engines, are present in similar concentrations.

Railway traffic is a source of PM10, but the dense nature of the particles confines their impact to the region in direct vicinity of the railway track.

Gehrig, R., Hill, M., Lienemann, P., Zwicky, C. N., Bukowiecki, N., Weingartner, E., Baltensperger, U. & Buchmann, B. (2005). *Railway traffic - a source of fine particles? Contributions of railway traffic to local PM10 concentrations*. European Aerosol Conference 2005, Ghent, Belgium, pp. 256.

Time-resolved analysis of urban air pollution

B. Alföldy[1] and R. Steib[2]

[1]KFKI Atomic Energy Research Institute, Konkoly-Th. M. u. 29-33., 1121, Budapest, Hungary
[2]Hungarian Meteorological Service, Kitaibel P. u. 1., 1024, Budapest, Hungary

Keywords: air pollution, columnar mass, PM_{10}, mixing layer, urban aerosols.

Air pollution directly affects the quality of life, human and other being's health, climate, and mediately has an effect on the water and soil pollution. Because of its general environmental and health impact air pollution is continuously monitored worldwide in the bigger cities. In Budapest 12 monitoring station are operating that provide hourly concentration data for the main urban air pollutants namely: carbon monoxide (CO), nitrogen monoxide (NO), nitrogen dioxide (NO_2), sulphur dioxide (SO_2), particle mass under diameter of 10 μm (PM_{10}) and ozone (O_3).

Generally, air pollutions is characterised by the atmospheric concentrations of the pollutants. While the majority of the receptors (eg. human beings) are affected by the concentration, study of the total columnar mass of the pollutants has similar importance. Columnar mass (CM) can be defined as the pollution mass contained by an air column over $1 m^2$ ground surface in the boundary layer. Mathematically it can be expressed from the next formulation of the concentration:

$$c(t)=CM(t)/MH(t), \qquad (1)$$

where $c(t)$, $CM(t)$ and $MH(t)$ are the time functions of the concentration, the columnar mass and the thickness of the boundary layer that will be referred as mixing height (MH) in the following. Consequently, the dimension of the columnar mass is $\mu g/m^2$.

Columnar mass characterizes the emission more direct than the concentration, namely its time dependence is devoid from the variation of the thickness of the boundary layer. Based on the time-resolved analysis of the columnar mass, information about the time profile of the emission, as well as chemical modifications occurred after the emission can be obtained. Since climate effect of specific pollutants depends on the numbers of particles or molecules being in the light path, which is related to the columnar mass; CM in addition is the fitting parameter for quantification of climate effect of air pollution.

Relation between the concentration and columnar mass is determined by the volume, within which pollutants are mixed that can be characterized by its vertical dimension, the so called mixing height (MH). In this work hourly averages of mixing height was calculated by AERMOD for a monthly period in June, 2007. Columnar mass was calculated for the pollutants listed above based on Eq.1. Mass fluxes of the pollutants that were calculated as the time derivative of CM are presented in the following figures.
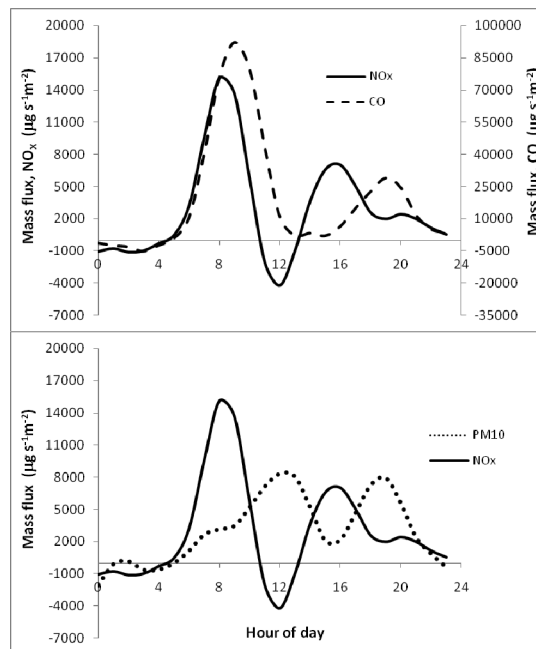
Figure 1. Average daily profiles of CO and NO_X mass fluxes (top panel) as well as NO_X and PM_{10} mass fluxes (bottom panel)

It can be seen from the figures that around 5:00, when the urban traffic starts, the mass flux is positive for all pollutants. The traffic's intensity, and as parallel the emission increase until 9:00, then start to decrease as it can be found from the curve of CO. Mass flux of NO_X reaches its maximum one hour before at 8:00 and has a minimum at 12:00 in the negative range. At the same time mass flux of PM_{10} has a maximum. In the following period NO_X and PM_{10} have complementary variation. This pheno-menon can be interpreted by secondary aerosol production from nitrogen compounds as precursor agents. Comparing the local maximum of PM_{10} mass flux at 8:00 by the maxima at 12:00 and 19:00, it can be deducted that the secondary formation of the aerosol has higher contribution to the urban PM_{10} load than the primary emission.

Rain effect on the size distributions of traffic-related particles and particle-bounded PAHs

C.C. Lin[1], S.J. Chen[1,*], K.L. Huang[1], W.J. Lee[2], H.R. Chao[1], W.Y. Lin[3] and J.H. Tsai[1]

[1] Department of Environmental Engineering and Science, National Pingtung University of Science and Technology, 91201, Taiwan.
[2] Department of Environmental Engineering, National Cheng Kung University, 70101, Taiwan.
[3] Institute of Environmental Planning and Management, National Taipei University of Technology, 10608, Taiwan.

Keywords: traffic source, PAHs, nanoparticles, ultrafine particles, size distribution.

Polycyclic aromatic hydrocarbons (PAHs) bound in nano/ultrafine particles from vehicle emissions may cause adverse health effects. However, little is known about the characteristics of the nanoparticle-bound PAHs and the PAH-associated carcinogenic potency/cytotoxicity; therefore, this study characterizes traffic-related nano/ultrafine particles collected beside a busy road using a micro-orifice uniform deposition impactor (MOUDI) and a nano-MOUDI equipped with quartz filters (with diameters of 37 and 47 mm, respectively).

Before and after each sampling, the filters were dried for 24 h in a desiccator at 25 °C in 40% relative humidity. They were then weighed on an electronic balance (AND HM202) with a resolution of 10 μg. The particulate matter (PM) concentration was determined by dividing the mass with the volume of sampled air. All PAHs samples were Soxhlet-extracted with a mixed solvent (1:1 (v/v) n-hexane/dichloromethane) for 24 hours. The extracts were then concentrated, cleaned using a silica column, and reconcentrated with ultra-pure nitrogen to 1.0 mL before analysis by GC/MS (Hewlett-Packard 5972).

One of our earlier papers indicated that most of the nano and ultrafine particles collected at the same sampling site were mainly contributed by traffic (Lin et al., 2005). The mass concentration of traffic-related particles exhibited a tri-modal distribution, with a major, a secondary, and a minor peak in the coarse (3.2–5.6 μm), fine (1–1.8 μm), and nano (0.018–0.032 μm) size ranges, respectively. The particles collected on sunny days (mean of S2–S4) displayed a bi-modal distribution with a secondary peak that was larger (1.0–1.8 μm) than that (0.18–0.32 μm) of the particles sampled on sunny days after rain (mean of S1 and S5) (Figure 1). The difference between PM size distributions before and after rain was significant in the
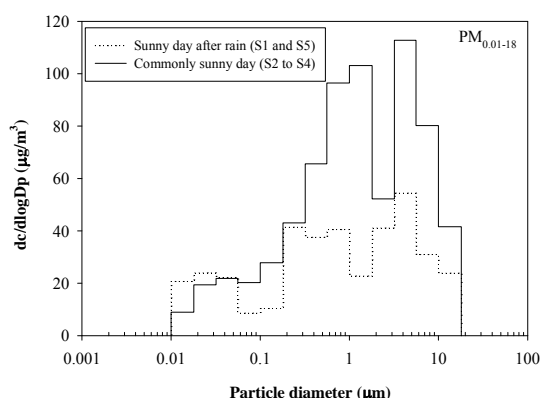
size range 0.056–18 μm ($p = 0.0094$) but insignificant in the range 0.01–0.056 μm ($p = 0.237$) at a significance level of $\alpha = 0.05$. The latter result may be associated with the fact that the sampling site was close to the traffic emission source and most of the collected nanoparticles were freshly emitted from vehicle tailpipes. Therefore, the effect of rain on the nanoparticle size distribution was not significant.

Both the with/without rain sampling cases in this study displayed tri-modal size distributions for particulate total-PAHs (Figure 2); furthermore, the peak in the Aitken size range is wider in this study than that in the work by Miguel et al. (2005). On sunny days, the major, secondary, and minor peaks were within the ranges 0.018–0.032, 0.56–1, and 3.2–5.6 μm, respectively (Figure 2), while those for sunny days after rain were within 0.032–0.056, 0.18–0.32, and 5.6–10 μm, respectively. The two cases exhibited a size distribution difference for particle-bound total-PAHs, which was significant in the size range of 0.056–18 μm ($p = 0.013$, $\alpha = 0.05$) but insignificant in the 0.01–0.056 μm range ($p = 0.192$, $\alpha = 0.05$). Clearly, rain only weakly influenced the size distributions of the PM and particle-bound total-PAHs for the nano particles; in contrast, rain affected the larger sampled particles although some other environmental conditions (such as wind direction/speed, height of the mixing layer, and source strength) must also be considered.
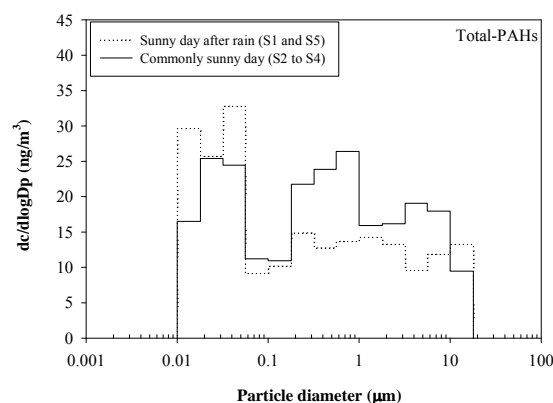
Figure 2. Size distributions of the particle-bound mean total-PAHs collected on sunny days and sunny days after rain.

Lin, C.C., Chen, S.J., Huang, K.L., Hwang, W.I., Chang-Chien, G.P., & Lin, W.Y. (2005). Environ. Sci. Technol., 39, 8113–8122.
Miguel, A.H., Eiguren-Fernandez, A., Sioutas, C., Fine, P.M., Geller, M., & Mayo, P.R. (2005). Aerosol Sci. Technol., 39, 415–418.

Figure 1. Size distributions of the mean PM collected on sunny days and sunny days after rain.

Mass size distribution of trace metals at a traffic site and evaluation of a tracer for brake dust

J.K. Gietl, A.J. Thorpe, R. Lawrence and R.M. Harrison

Division of Environmental Health and Risk Management, School of Geography, Earth and Environmental Sciences, University of Birmingham, B15 2TT, United Kingdom

Keywords: Emission Factor, Road Dust, Size Distribution, Traffic Emissions.

Road traffic emissions comprise not only exhaust emissions but also resuspension of road dust, brake and tyre wear. The material of brake linings consists of many different components in variable compositions, depending on the manufacturer. Schauer *et al.* (2006) suggested amongst others Barium (Ba) as a potential tracer for soils contaminated with road dust since Ba, in the form of barite is used as filler material in brakes. The aim of this study is to calculate by means of Ba the ratio of brake wear to traffic emissions.

Our measurements took place at two sites in London, at Marylebone Road (heavily trafficked roadside) and at Regents College (urban background) with an 8-stage MOUDI impactor and a Partisol sampler ($PM_{2.5}$ and PM_{10}) in March 2007. The MOUDI samples, collected on Teflon filters, were analyzed by ICP-MS for Al, Ba, Cu, Fe, Sb, Ti, V, and Zn and by IC for Ca^{2+}, K^+, Mg^{2+}, Na^+, and NH_4^+.

The data was analysed based on their mass concentration and size distribution.

By comparing the mass concentrations we detected a clear roadside increment for Ba, Ca^{2+}, Cu, Fe, Na^+, and Sb. The concentrations of Al and Ti were only higher in the coarse fraction at Marylebone Road due to road dust resuspension. The distributions of the trace metals Ba, Cu, Fe, and Sb were similar. Their main mass concentration can be found in the prime mode with a sometimes bimodal distribution at particle diameter (Dp) of 3.6 µm (Figure 1).
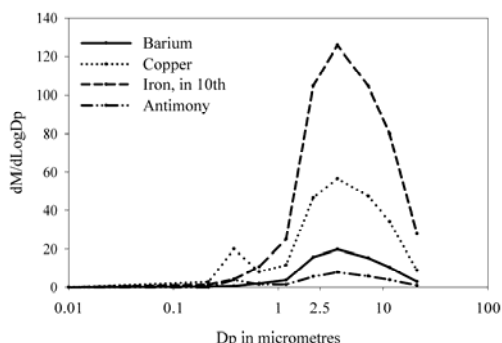
Figure 1: Mean size distribution of trace metals at Marylebone Road, March 2007.

The distribution at Regents College was in this size range unimodal with a clearly lower mass concentration (Figure 2).
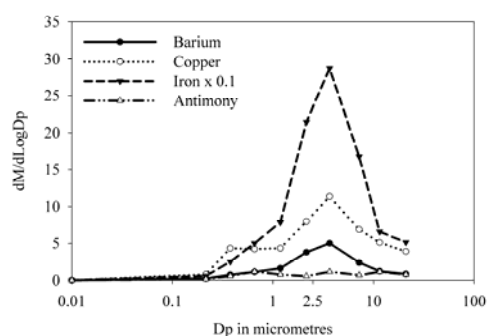
Figure 2: Mean mass size distribution of trace metals at Regents College, March 2007.

At the roadside Ba, Cu, Fe, and Sb have a common source, which is brake dust. That we are dealing with a traffic related source is affirmed by the comparison with the ratios of gas phase pollutants, CO and NO_x, for Marylebone Road to an urban background site (London North Kensington). These ratios are similar to those found for the metallic elements typical of traffic.

Further work is aimed at quantifying the ratio of barium to brake dust mass so as to use barium as a quantitative tracer of brake dust particles. This will be done by taking the roadside increments of particulate matter (in average 9.2 µg/m^3 for PM_{10} and 4.6 µg/m^3 for $PM_{2.5}$) and data for the vehicle fleet, number, composition, and speed averages, into account.

Schauer, J. J., Lough, G. C., Shafer, M.M., Christensen, W., Arndt, M.F., DeMinter J.T., et al. (2006). *Characterization of metals emitted from motor vehicles*. Health Effects Institute.

Wolfenbarger, J. K., & Seinfeld, J. H. (1990). *J. Aerosol Science*, 21, 227-247.

SPECTRAL ANALYSIS OF PARTICLE COUNT AND MASS IN AMBIENT AIR OF ANKARA, TURKEY

Deniz D. Genç Tokgöz[1], Wolfgang Brunnhuber[2] and Gürdal Tuncel[1]

[1] Department of Environmental Engineering, Middle East Technical University, 06531, Ankara, Turkey
[2] Technik GmbH & Co. KG, Dorfstraβe 9- D- 83404 Ainring, Germany

Particulate matters are emitted into atmosphere from various sources including combustion, industrial and natural processes. Particulate matters have adverse effects on human health (Anderson, 2009 and references therein), materials (Grossi and Brimblecombe, 2002), visibility (Watson, 2002) and earth's climate (IPCC, 2001). Size, concentration and chemical composition are the main properties of particulate matter; and particles are generally characterized by their size (aerodynamic diameter). Total suspended particles (TSP) is the most comprehensive term including particles of any size suspended in air and defined as the particulate matter with an aerodynamic diameter less than 100 µm. PM_{10} and $PM_{2.5}$ is particulate matter with an aerodynamic diameter less than 10 µm and 2.5 µm, respectively. The PM_{10} fraction is called as respirable suspended particulate (RSP) and the $PM_{2.5}$ fraction is called as fine particles. The fraction between 10 µm and 2.5 µm are called as coarse particles. Up to now the mechanism by which particles influence human health are poorly understood, however it is believed that health effects are more closely associated with particle size. Particle size is also important in climatic aspect as small particles have longer residence time in the atmosphere and have more radiative forcing (IPCC, 2001).

Fine fraction of particulate matter is composed of non-volatile and semi-volatile components. Non-volatile components include sulphate, trace metals and elemental carbon. Semi-volatile components include ammonium nitrate, some organic species and water. While the non-volatile components are always in solid phase, semi-volatile components are in dynamic equilibrium between gas and solid phase. Determination of fine particulate matter with $PM_{2.5}$ Federal Reference Method (FRM) has some artifacts because some fraction of semi-volatile components collected on the filter may evaporate (Grover et al., 2006; Wilson et al., 2006).

In this study size distribution of atmospheric particles was investigated at a suburban site in Ankara in August 2008 and January 2009. An aerosol spectrometer (GRIMM, model 265), which can optically measure particle number concentrations in 32 size bins, between 0.25 and > 32 µm was operated at the Middle East Technical University, which is located at a suburban area in Ankara. Mass concentrations were calculated from number concentrations using particle densities obtained from parallel gravimetric measurements. Diurnal and week day – weekend differences in particle number concentrations and mass concentrations of PM_1, $PM_{2.5}$ and PM_{10} particles were investigated. Significantly lower particle counts were observed, particularly in large particle sizes at night and at weekends. This was attributed to less soil dust resuspension at night and at weekends. Higher day-time fine particle number and mass was attributed to traffic activity at a nearby road. Number of semi-volatile material was determined by heating the sampling pipe to 80°C. A heated measurement period lasted for 10 minutes and it was followed by another 10 minutes of non-heated measurement period. The particle number concentration difference between the two periods was taken as the number concentration of semi-volatile material. Data indicated that approximately 10% of particles at submicron range are semi-volatile. However contribution of semi-volatile materials decrease to 5% at around 5 µm and <1 % at particle diameters > 10 µm. Although these numbers are typical, semi-volatile content of atmospheric particles did show significant variation in time.

Anderson, H. R. (2009). Air Pollution and Mortality: A History. Atmospheric Environment, 43(1), 142-152

Grossi, C. M., Brimblecombe, P. (2002). The effect of atmospheric pollution on building materials. Journal De Physique. IV : JP 12 (10), Pr10/197-Pr10/210

Grover, B. D., Eatough, N. L., Eatough, D. J., Chow, J. C., Watson, J. G., Ambs, J. L., Meyer, M. B., Hopke, P. K., Al-Horr, Rida, Later, D. W. and Wilson, W. E. (2006). Measurement of both Nonvolatile and Semi-Volatile Fractions of Fine Particulate Matter in Fresno, CA, Aerosol Science and Technology, 40:10, 811- 826

IPCC, 2001. Climate Change 2001. Intergovernmental Panel on Climate Change. Cambridge University Press, London.

Watson, J. G. (2002).Visibility: Science and Regulation, Journal of the Air and Waste Management Association, 52, 628–713.

Wilson, W. E., Grover, B. D., Long, R. W., Eatough, N. L., Eatough, D.J. (2006). The measurement of fine particulate semivolatile material in urban aerosols. Journal of the Air and Waste Management Association, 56 (4), 384-397

Source apportionment study for dustfall (dry deposition) in Vitória-ES Brazil

N. C. Reis Jr[1]; J. M. Santos[1]; M. Rigo[1]; L. R. Menegussi[1], A. L. G. P. O. Souza[1]

[1]Departamento de Engenharia Ambiental, Universidade Federal do Espirito Santo, 29.060-910, Vitória, Brazil

Keywords: deposition; dust; source apportionment; receptor model; PIXE.

The problem of source apportionment of ambient particulate matter has been a subject of growing interest in the last decade. This class of studies is conventionally based on the use of receptor-oriented models, which infer source contributions by determining the best-fit combination of emission source chemical composition profiles needed to reconstruct the chemical composition of ambient samples. Several source apportionment studies regarding total suspended particulates (TSP) and PM with the aerodynamics diameter less than 10 µm (PM10) and 2.5 µm (PM2.5) have been published in the specialized literature, among others Watson et al (2002), Garcia et al (2006), Gupta et al. (2007).

The interest for fine and ultra-fine particles is mainly related to the hazard to human health, due to deep penetration in the respiratory system. However, larger particles (> 10 µm) are also a matter of concern, since dustfall is a considerable source of nuisance for urban population (Vallack & Shillito, 1998; Farfel et al, 2005). In spite of its importance, there are very few source apportionment studies targeting dustfall particles.

In this work a source apportionment study for dustfall in the Metropolitan Region of Vitória, in the State of Espírito Santo, Brazil, is performed. Settled particles samples were collected monthly, starting from January 2007, at 10 different locations. These locations were chosen based on the results of a dispersion model (Figure 1).
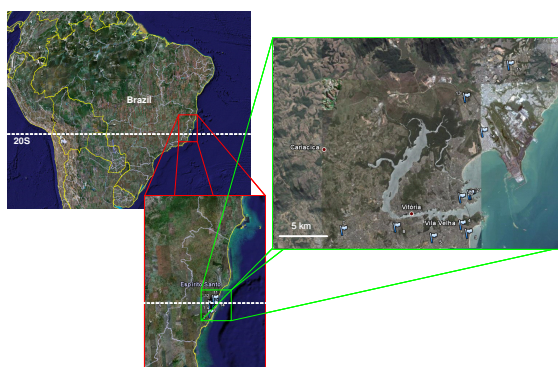
Figure 1. Schematic representation of the Metropolitan Region of Vitória and the location of the 10 monitoring points.

The samples were collected by using two ASTM D 1739 dustfall collectors, with 25 cm diameter colleting buckets, at each monitoring site. Settled particles samples were analyzed by using Thermal Optical Transmittance (TOT) to identify and quantify organic carbon and elemental carbon, Proton Particle induced X-Ray Emission method (PIXE). The species present in the majority of samples were: Na, Mg, Al, Si, P, S, Cl, K, Ca, Ti, Mn, Fe, OC e EC.

Chemical profiles of the sources of the region were constructed by using CETESB (Environmental Agency of the State of São Paulo) and USEPA databases, as well as, PIXE and TOT analyses of particle samples collected from the main sources of the region (Figure 2).
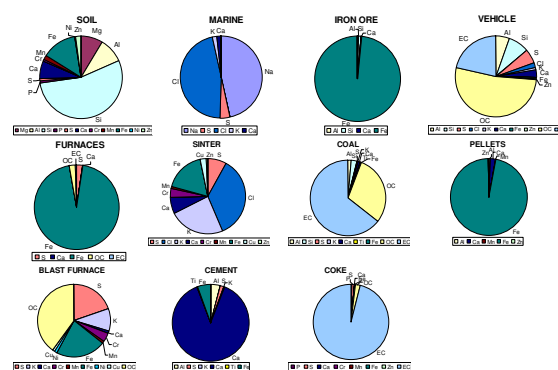
Figure 2. Chemical profiles of the main sources of the region.

EPA-CMB 8.2 was used to identify and quantify the contributions from emission sources to each monitoring site. Soil, iron ore, coal, vehicular emissions and marine aerosol were the sources responsible for the largest contributions, and could be clearly traced to anthropogenic activities in the region, which are closely related to siderurgical plants and Metropolitan Region traffic.

Watson, J. G. et al. (2002) *Energy & Fuels*, v.16, p. 311-324.

Gupta, A. K. et al. (2007) *Journal of Hazardous Materials*, Volume 142, Issues 1-2, 2, 279-287.

Garcıa, J. H. et al (2006) *Chemosphere* 65, 2018–2027.

Farfel, M. R. et al. (2005) *Environmental Research*, Volume 99, Issue 2, 204-213.

Vallack, H. W., Shillito, D. E. (1998) *Atmospheric Environment*, Volume 32, Issue 16, 2737-2744.

Air quality studies using a measurement system mounted on a tramway in an urban region in Germany

R. Rinke, A. Wieser, B. Vogel, U. Corsmeier, Ch. Kottmeier

Institute for Meteorology and Climate Research,
Karlsruhe Institute for Technology

Keywords: Air Quality, Particle measurements, Ultrafine particles, Urban Aerosols

The spatial and temporal variability of air quality in an urban area and its surrounding will be measured with an automated measurement system mounted on a tramway. For the project we developed a new measurement system (Figure 1) including a new aerosol inlet in respect to the special conditions on the tramway. The measurements will be conducted on selected above-ground tramway lines including the urban region of Karlsruhe in Germany and the remote areas around the city. For those measurements the Karlsruhe tramway is one of the most attractive in Europe because of the high dense rail network. The rail network is not only located in the city of Karlsruhe, it also reaches a wide distance of about 50 km in each direction from the city centre. The measurements will be taken on one tram along two selected tramway lines (Figure 2). The first one connects the northern Black Forest southwards from Karlsruhe, far from industrial installations, with the city centre of Karlsruhe and the Rhine valley northwards of Karlsruhe. The second one connects the rural areas north-east of the city with the western rural areas close to the Rhine river. Both lines operate from the hinterland through the city centre back into the hinterland and are crossing areas with very high concentrations of particles and trace gases as well as areas where only background concentrations are expected. Therefore, the measurements are useful for determining urban effects of distribution of pollutants as well as for the identification of source areas. The data from these measurements are used for the assessment of the representativeness of already existing measurement

stations and for the selection of suitable locations for future measurement stations. The ascertained dataset will be used to develop and verify mitigation strategies. They will also serve for the evaluation of numerical models on the urban and regional scale. The measurements will start in May 2009. The concept of the measurement system and first results will be presented. It is also possible to visit the equipped tramway during EAC2009 in Karlsruhe.
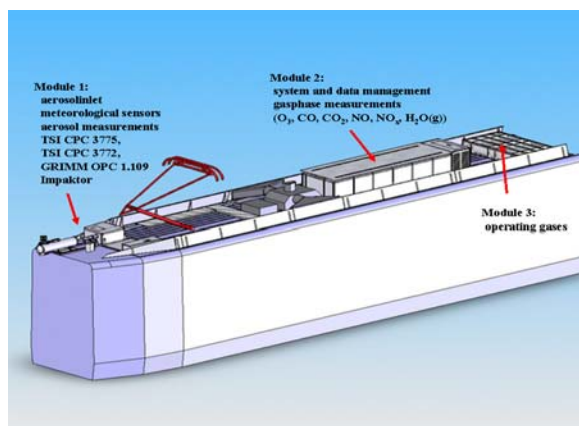
Figure 1. Study of the measurement system on the tramway.
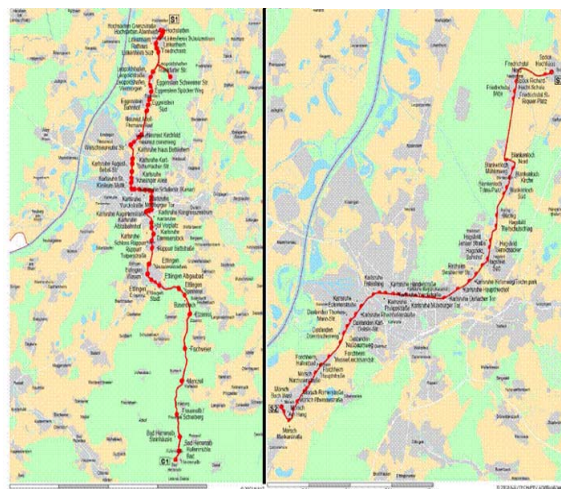
Figure 2. Selected tramway lines.

Atmospheric particles in an urban tunnel under extreme conditions

C.M.Oliveira[1], M.F. Camões[1], M. Matos[2], P. Cantinho[2], H. Silva[2], C. Oliveira[3], N. Martins[3], J. Tavares[3], M. Cerqueira[3] and C. Pio[3]

[1] CCMM/DQB-Faculty of Science, University of Lisbon, Edifício C8, Campo Grande, 1749-016 Lisboa, Portugal
[2] Chemistry Department, ISEL, R. Cons. Emídio Navarro, 1, 1959-007 Lisbon, Portugal
[3] Centre for Environmental and Marine Studies, Department of Environment and Planning, Aveiro University, Campus Universitário de Santiago, 3810-193 Aveiro, Portugal

Keywords: aerosol characterization, air quality, tunnel, traffic.

In order to improve car access and circulation a new tunnel has been recently built in the urban area of the city of Lisbon, namely Praça Marquês de Pombal. This tunnel is 1725 meters long and has three entrances and five exits. The tunnel makes the connection between the city centre and the highway to Estoril and to all the urban area between this village and Lisbon. Due to the particular relief of Lisbon (also know as "the city of the seven hills") this tunnel has a very high slope, 10% at the maximum with an average of 9%. This slope is a matter of concern and has originated several restrictions like a speed limit of 50 km/h and the prohibition of circulation of trucks and transport of dangerous goods. The Directive 2004/54/CE, that enunciates the principles of tunnel operation and construction in Europe, states that "Longitudinal gradients above 5% shall not be permitted in new tunnels, unless no other solution is geographically possible." This tunnel does not respect the longitudinal gradient above 5% because it was geographically impossible" which is the situation of this one. It has a heavy incoming traffic in the morning (descending and Lisbon entrance) and a heavy outgoing traffic at the end of the day (ascending and Lisbon exit). Frequently, the traffic in these two periods is jammed. The traffic has been estimated in 30.000 vehicles per day in each way.

In this work a sampling campaign in the tunnel was carried out in collaboration with the Lisbon Town Hall. The sampling campaign has been planned and implemented in order to identify the atmospheric particles concentration and composition with particulate matter being collected in four size fractions (less than 0.5 µm, between 0.5 and 1.0 µm, between 1.0 and 2.5 µm, and finally between 2.5 and 10.0 µm) on quartz fibre filters using Hi-Vol samplers. One sampler was located at the down-hill traffic direction (entering into the city) and worked continuously between 8 and 10 a.m., and other one, at the ascendant direction (getting out of the city) between 5 and 7 p.m.. Both equipments were located at the middle of the tunnel in a common chunk to all the traffic in the tunnel.

Sampling was performed during two weeks in October 2008, covering every days of the week, aiming at acquiring information on sampled atmospheric particles, which were further submitted to physical observation and chemical analysis. The effect of road slope, up-hill or down-hill traffic that affects motor regime and traffic density, are additional parameters whose impact on air composition is also critically evaluated.

The results may be used by the responsible authorities to help take new measures to improve the automatic ventilation system of the tunnel, if necessary.

Spatial and temporal variability of ultrafine particles within an urban agglomeration, the Ruhr-Area, Germany

Carmen Nickel[1], Stephan Weber[2], Heinz Kaminski[1], Ulrich Pfeffer[3],
Peter Bruckmann[3], Thomas A.J. Kuhlbusch[1]

[1] IUTA e.V., Air Quality & Sustainable Nanotechnology, Duisburg, Germany
[2] Department of Applied Climatology, University of Duisburg-Essen, Germany
[3] Landesamt für Umwelt, Natur und Verbraucherschutz Nordrhein-Westfalen, Recklinghausen, Germany

Keywords: ultrafine particles, urban aerosols, vehicles emissions

Due to the large number and heterogeneity of pollutant sources in urban environments, particle number concentrations and size distributions are subject to significant spatial and temporal variability. While recent research indicated some correlation between number concentrations of larger particles across cities, the spatial-temporal variation of ultrafine particle number concentrations is significantly larger (Costabile et al., 2008; Tuch et al., 2006). Additionally, differences in aerosol size distributions between multiple urban measurement sites are much less understood.

The present study analyses ongoing measurements of particle number and particle size distributions in the size range $14 < Dp < 740$ nm from three different sites within the urban agglomeration 'Ruhr-Area'.

Measurement locations comprise: An urban background site (Mülheim-Styrum), situated in a light traffic residential zone and a traffic site close to a major road (Gladbeckerstrasse) with about 50,000 vehicles per day.

The outcomes of the measurements reflect the traffic flow of the different areas. The total number concentration provide an indication that there is a significant difference between the two areas (Fig.1), caused by the higher traffic flow.

Fig. 2 demonstrates that the values for traffic station are clearly higher than the values for the urban background. Mainly the ultrafine particles illustrate a clear aggrandisement and the values suggest that higher concentrations are due to traffic.
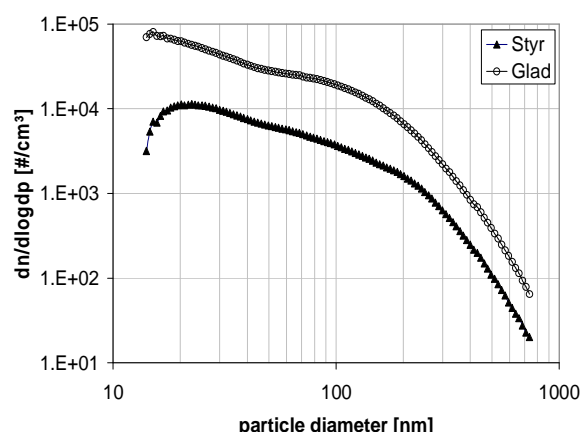
Fig 2: Average of the number size distribution for the two stations.

In the vicinity to the latter site a 'near-traffic' site is installed to evaluate especially the spatial differences coupled to temporal changes in concentrations and size distributions. The representativeness of the stationary measurements are backed up by mobile measurements of particle number concentrations by handheld condensational particle counters ($Dp > 10$ nm). First results indicate a good correlation between total number concentrations and distance of the measurement to road traffic. Further data interpretations in view of, e.g. absolute number concentrations, temporal patterns, small scale representativeness all in view of relevance for exposure of the population, will be presented and discussed.

Fig. 1: Median (error bars represent 25 and 75 percentiles) and Midpoint (red circle) of Total Number concentration of particles at the two different areas, urban background (Styr.) and traffic zone (Glad.)

Costabile, F. Birmili, W., Klose, S. Tuch, T., Wehner, B., Wiedensohler, A., Franck, U., König. K. & Sonntag, A., (2008) *Atmospheric Chemistry and Physics Discussions*, 8(5): 18155.

Tuch, T.M., Herbarth, O., Franck, U. Peters, A., Wehner, B., Wiedensohler, A., Heintzenberg (2006). *Journal Expos Sci Environ Epidemiol*, 16(6): 486.

Chemically-resolved aerosol volatility measurements from two megacity field studies

J.A. Huffman[1,2], K.S. Docherty[1], A.C. Aiken[1], M.J. Cubison[1], I.M. Ulbrich[1], P.F. DeCarlo[1,3], D. Sueper[1,4], J.T. Jayne[4], D.R. Worsnop[4], P.J. Ziemann[5] and J.L. Jimenez[1]

[1]Cooperative Institute for Research in Environmental Sciences (CIRES), 80309, Boulder, Colorado, USA
[2]Now at Max Planck Institute for Chemistry, Biogeochemistry Department, 55128, Mainz, Germany
[3]Now at Paul Scherrer Institute (PSI), 5232, Villigen, Switzerland
[4]Aerodyne Research Inc., 01821, Billerica, MA, USA
[5]Air Pollution Research Center, University of California, 92521, Riverside, California, USA

Keywords: Volatility, Thermodenuder, Aerosol Mass Spectrometry, Field Measurements, Submicron Particles

The volatilities of different chemical species within ambient aerosols are important in order to be able to more accurately understand their reaction and deposition rates, but also remain poorly characterized. The coupling of a recently modified rapid, temperature-stepping thermodenuder (TD, operated in the range 54–230°C, ~21s heated residence time) with a High-Resolution Time-of-Flight Aerosol Mass Spectrometer (HR-ToF-AMS) during field studies in two polluted megacities has enabled the first direct characterization of chemically-resolved urban particle volatility on a timescale shorter than most changes in ambient particle composition. Measurements were conducted for approximately two weeks each in Riverside, CA as a part of the SOAR-1 study (Study of Organic Aerosols in Riverside – Phase 1, July-August 2005) and Mexico City as a part of MILAGRO (Megacity Initiative: Local And Global Research Observations, March-April 2006). Volatility measurements are generally consistent and show ambient nitrate as having the highest volatility of any AMS aerosol species while sulfate showed the lowest volatility. Total organic aerosol (OA) showed volatility intermediate between nitrate and sulfate, with an evaporation rate of $0.6\% \cdot K^{-1}$ near ambient temperature, although OA dominates the residual species at the highest temperatures. Different types of OA were characterized with marker ions, diurnal cycles, and positive matrix factorization (PMF) and show significant differences in volatility. Reduced hydrocarbon-like OA (HOA, a surrogate for primary OA, POA), oxygenated OA (OOA, a surrogate for secondary OA, SOA), and biomass-burning OA (BBOA) separated with PMF were all determined to be semi-volatile. The most aged OOA-1 and its dominant ion, CO_2^+, consistently exhibited the lowest volatility, with HOA, BBOA, and associated ions for each among the highest. The similar or higher volatility of HOA/POA compared to OOA/SOA contradicts the current representations of OA volatility in most atmospheric models and has important implications for aerosol growth and

lifetime. Our results strongly imply that all OA types should be considered semivolatile in models.

The study in Riverside identified organosulfur species (e.g. $CH_3HSO_3^+$ ion, likely from methanesulfonic acid), while both studies identified ions indicative of amines (e.g. $C_5H_{12}N^+$) with very different volatility behaviors than inorganic-dominated ions. The oxygen-to-carbon ratio of OA in each ambient study was shown to increase both with TD temperature and from morning to afternoon, while the hydrogen-to-carbon ratio showed the opposite trend.
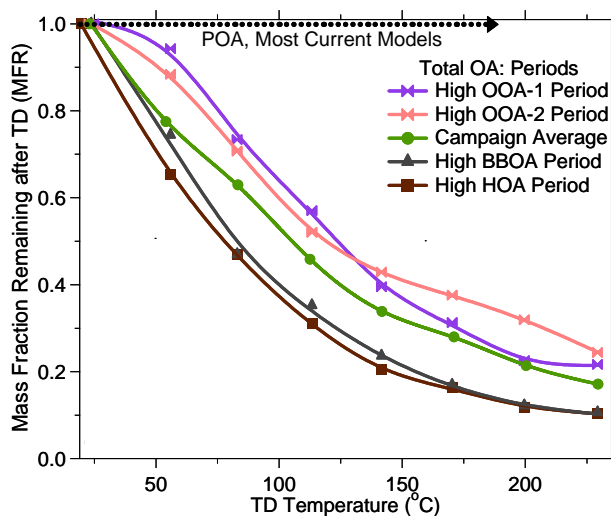
Figure 1. Particle mass fraction remaining (MFR) after passing through TD is shown as a function of TD-processing temperature ("thermogram"-style plots). As temperature increases, MFR decreases from a defined value of unity at ambient temperature with a larger negative slope showing more rapid evaporation. Aerosol from periods (1-2 hours) during MILAGRO when different OA types were dominant are shown as different colored lines. HOA and BBOA are shown to decrease more rapidly with increasing temperature than the average OA or than periods of OA dominated by aged, oxygenated aerosol.

Chemical composition of submicron particles in Marseille (summer 2008): insights into sources and processes of urban aerosols.

B. D'Anna,[1] A. Boreave,[1] and C. George[1]

[1]Institut de Recherches sur la Catalyse et l'Environnement, IRCELYON-CNRS, Université Lyon 1, Villeurbanne, France

Keywords: Urban pollution, Particle caracterization, Aerosol Mass Spectrometer, Aerosol chemical composition, Ultrafine particles.

A Time of Flight Aerodyne aerosol mass spectrometer (AMS) was deployed from 30 June to 15 July 2008 in the frame of the project FORMES (Fraction Organique de l'aérosol urbain: Méthodologie d'Estimation des Sources).

The main objectives of this deployment were to characterize the concentrations, size distributions, and temporal variations of nonrefractory (NR) chemical species in submicron particles (approximately PM1) and in particular to quantify and investigate the organic fraction of the urban aerosol. Further analysis of the organic fraction has been performed using positive matrix factorization (PMF) for aerosol mass spectra to identify the main components of the total organic aerosol and their related sources. Reasonably good agreement was observed on particle concentrations, composition, and size distributions between the AMS data and measurements from collocated instruments (given the difference between the PM1 and PM2.5 size cuts), including TEOM,12-hour- and 24-hour-averaged organic carbon, sulphate, nitrate and SMPS.
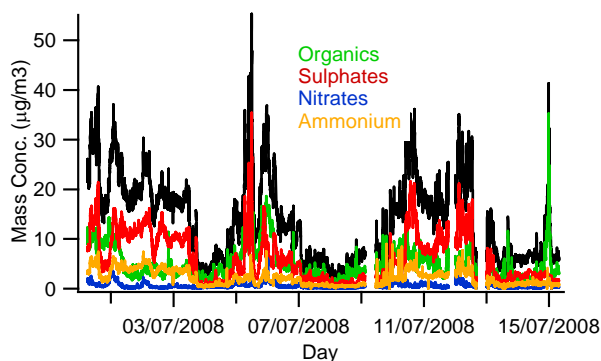
Figure 1. Times series of the mass concentrations of PM1: total, sulphate, organic, ammonium, nitrate.

Total NR-PM1 mass concentration in Marseille accumulates over days and rapid cleaning occurred when the meteorological conditions changed, due mainly to the Mistral wind. Sulfate and organics are the major NR-PM1 components while the concentrations of nitrate and chloride are generally quite low. Significant amounts of ammonium, which most of the time are consistent with sulfate present as ammonium sulfate, are also present in particles. However, there are several periods when the aerosols are acidic and more than 40% of sulfate is in the form of ammonium bisulfate.

The accumulation mode (350–600 nm in vacuum aerodynamic diameter for the mass distributions) and the ultrafine mode (<100 nm) are observed most frequently. The accumulation mode was dominated by sulfate that appears to be internally mixed with organics, while combustion-emitted organics are often the main component of the ultrafine particles (except during nucleation events). The ultrafine-mode organic aerosols are mainly associated with combustion sources (likely traffic). A single exception occurred during a nucleation event the 5th of July when very high concentration of small acidic sulphate particles has been measured. The nucleation event was preceded by very high concentration of SO_2 (industrial source nearby the city of Marseille).

Positive matrix factorization (PMF) was used for the aerosol mass spectra to identify the main components of the total organic aerosol and their sources. The PMF retrieved factors were compared to measured reference mass. Three main factors were found to explain the variance in the data and could be assigned either to sources or to aerosol components such non oxygenated fraction (HOA), and two other partly and highly oxygenated organic aerosol fractions (OOAI and OOAII).

WINTER PARTICULATE POLLUTION AND SOURCE APPORTIONMENT IN CENTRAL INDIA

K. S. Patel[1*], N. K. Jaiswal[1], H. Saathoff[2], T. Leisner[2], J. F. N. Aguilera[3], E. Y Funes[3], S. Nava[4], F. Lucarelli[5], M. Viana[6], M. Pandolfi[6]

[1]School of Studies in Chemistry, Pt. Ravishankar Shukla University, Raipur, CG, India, E. Mail: patelks_55@hotmail.com
[2]Institute for Meteorology and Climate Research (IMK-AAF), Forschungszentrum Karlsruhe, Germany
[3]Dipartimento di Fisica and Istituto Nazionale di Fisica Nucleare, Firenze, Italy
[4]Dipartimento di Fisica and Istituto Nazionale di Fisica Nucleare, Genova, Italy
[5]Universidad Miguel Hernández-Elche, División de Física Aplicada, Dpto. Física y Arquitectura de Computadores, Av. del Ferrocarril s/n. Edificio Alcudia, Spain
[6]Institute of Earth Sciences "Jaume Almera",Spanish Research Council - CSIC
C/ Lluís Solé i Sabarís s/n,08028 Barcelona, Spain

Keywords: particulate pollution, particle composition, source apportionment

Aerosols play an important role in climate change, precipitation, and health hazards (Brunekreef & Holgate, 2002; Ramanathan & Carmichael, 2008). Particulate matter is the most serious pollutant in various cities of Asian countries like India and China mainly due to huge coal burning (Menon *et al.*, 2002). The severe winter particulate pollution is observed in several urban parts of the central India due to emissions of steel and cement industries, rice mills, thermal power plants, etc. The sampling campaigns of particulate matters) in the winter (December, 2006 - February, 2007) were carried out in Raipur city (latitude: 21°24'N and longitude: 81°63'E), one of the most industrialized parts of India, to characterize the ambient mass concentrations of coarse particulate matter (PM_{10}) and their sources. Fifteen coarse particulate matter (PM_{10}) and three suspended particulate matter (SPM) samples from 15 different locations of Raipur city were collected. Techniques i.e. thermal method, proton induced X-ray emission spectrophotometry and ion chromatography were used for monitoring the species i.e. carbons, trace elements and water soluble ions, respectively.

The mass concentrations of PM_{10} and SPM in the ambient air ranged from 221 - 760 and 1150 - 1577 $\mu g\ m^{-3}$ with mean values of 435±85 and 1331±250 $\mu g\ m^{-3}$, respectively. The mean mass concentration ratio of $[PM_{10}]/[SPM]$ was found to be 0.33. The PM_{10} concentration in Raipur city in the winter exceeded the limit of 50 $\mu g\ m^{-3}$ by a factor of eight.

The mass concentrations of OC_{10} and EC_{10} ranged from 20 – 153 and 11 - 114 $\mu g\ m^{-3}$ with mean values of 51±17 and 41±15 $\mu g\ m^{-3}$, respectively. The mean mass concentration ratio of $[EC_{10}]/[EC_{SPM}]$ and $[OC_{10}]/[OC_{SPM}]$ was found to be 0.6 and 1.4, respectively.

The total mass concentrations of nine trace elements (i.e. Al, P, Ti, Cr, Mn, Fe, Cu, Zn and Zr), $\sum PM_{10}TE_9$ and $\sum SPMTE_9$ ranged from 23.2 - 105.4 and 73.7 - 119.2 $\mu g\ m^{-3}$ with mean values of 42.2±10.5 and 101±27 $\mu g\ m^{-3}$, respectively.

The sum of total mass concentrations of the water soluble ions (i.e. Cl^-, NO_3^-, SO_4^{2-}, NH_4^+, Na^+, K^+, Mg^{2+} and Ca^{2+}), $\sum PM_{10}WSI_8$ and $\sum SPMWSI_8$ ranged from 34.6 - 114.4 and 25.2 - 47.4 $\mu g\ m^{-3}$ with mean values of 64±11 and 34.4±13 $\mu g\ m^{-3}$, respectively. All ions have higher concentrations in the coarse fraction. Among them, the mass concentrations of Ca^{2+} were the highest whereas the mass concentrations of NH_4^+ were the smallest.

Species like Ca, Al, Fe, and sulphate contributed significantly and their mass concentrations ranged from 11.5 – 31.0, 6.5 – 20.3, 14.0 – 78.0 and 8.5 – 38.4 $\mu g\ m^{-3}$ with mean values of 10.9±1.9, 20.6±3.5, 27.5±8.0 and 17.4±4.1 $\mu g\ m^{-3}$, respectively.

The highest mass concentrations of PM_{10} or EC_{10} and OC_{10} or WSI_{10} were observed in the industrial area and surroundings, respectively, probably due to difference in the origin.

The coarse particulates are accompanied by high fractions of elemental carbon (8.6%), organic carbon (11.2%), trace elements (9.7%) and water soluble ions (15.5%). The total mass concentration of the carbons, trace elements and water soluble ions in the PM_{10} and SPM includes 45.0 and 17.6%, respectively. The uncertainty in the PM_{10} and SPM accounts 55.0 and 82.4%, respectively. Four sources: anthropogenic, mineral, cement plants and secondary source for emission of the following species OC, BC, K, Mg, SO_4^{2-}, NO_3^- and Cl^-; trace elements, Na/Ca; and NH_4^+, NO_3^- and SO_4^{2-} were apportioned by the principal component analysis (PCA) model.

Brunekreef B. & Holgate S. T. (2002), *Lancet*, 360, 1233-1242.
Menon S., Hansen J., Nazarenko L. & Luo Y. F. (2002), *Science*, 297, 2250-2253.
Ramanathan V. & Carmichael G. (2008), *Nature Geoscience*, 1, 221 - 227.

Atmospheric aerosols in the suburb of Prague

D. Řimnáčová, V. Ždímal, J. Schwarz, J. Smolík

Laboratory of Aerosol Chemistry and Physics, Institute of Chemical Process Fundamentals of the ASCR v.v.i.,
Rozvojová 2, 165 02, Prague 6 - Suchdol, Czech Republic

Keywords: Atmospheric Aerosols, Measurement, Particle Size Distribution, Particle Formation.

Atmospheric aerosols are very complicated systems; their physical and chemical properties vary greatly due to variation in meteorological parameters, aerosol sources or sinks. During last years many measurements were carried out at various conditions concerning site or season. The campaigns aimed at finding conditions which affect aerosol dynamics and formation of new aerosol particles.

Formation of new aerosol particles (nucleation event) was found to take place all over the world and may have significant effect for climate. Nucleation events have been studied in detail during last decade (Kulmala et al., 2004).

So far no long-term measurements have been carried out at background sites in the Czech Republic. Seasonal campaigns were performed in Prague in the period 2004/2005 (Hovorka et al, 2007, Schwarz et al, 2006).

In this work we summarize results from the first year of a continuous sampling at the suburban background site in Prague - Suchdol. The site is located in the campus of the Academy of Sciences of the Czech Republic.

The measurement consisted of synchronous sampling by two aerosol spectrometers, one SMPS (model 3034, TSI Inc.) and an APS (3321, TSI Inc.). These instruments covered the particle size range from 10 nm to 10 µm and sampled with a time resolution of 5 minutes. Meteo data (temperature, pressure, relative humidity, wind direction and velocity, total solar radiation etc.) and concentrations of gaseous pollutants (NO, NO_2, NO_x, O_3, SO_2) were monitored using a weather-station operated by the Czech Hydrometeorological Institute (CHMI).

The one-year series of particle number size distributions provided these results: The average concentration was found to be 6500 particles/cm^3. Size distributions were mostly monomodal with mode in the Aitken range (25-100 nm). During rush hours, enhanced concentrations were observed mostly in the Aitken mode, and correlated well with an increase of concentrations of gaseous pollutants. Other events were revealed as well, like biomass burning from local combustion sources, or long range transport of coarse aerosol particles.

New particle formation of the type "Banana event" was identified frequently. Concentration of ultrafine particles and their surface would drop before the event started and relative humidity would decrease to 25-40 %. Wind would usually blow from the N or NW sector. The average values of formation rate (J_3) were estimated to be 1.8 cm^{-3}s^{-1} and the growth rate (GR) 6.6 nm h^{-1}.

One example of such an event, detected on August 30, 2008, is illustrated in Figure 1. It was cloudy and windy the night and the morning before. Around 11 o'clock it cleared up and wind changed its direction (from SW, and W to N). Then new particles appeared and, subsequently, began to grow. Number concentration of particles under 25 nm rose rapidly, while concentrations of other fractions stayed. Later, concentration of nucleation mode particles dropped as the already formed particles grew to bigger sizes. Concentrations of NO and NO_2 were around 5 µg/m^3, while that of O_3 stayed close to 100 µg/m^3.
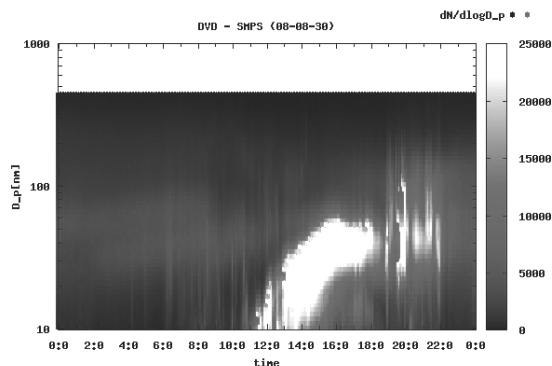
Figure 1. „Banana Event" on 30.08.2008 (x - time, y – particle size, grey scale – number concentration)

Kulmala M., Vehkamäki H., Petäjä T., Dal Maso M., Lauri A., Kerminen V.-M., Birmili W., & McMurry P.H.: (2004), *J. Aerosol Sci.*, 35, 143-176.

Hovorka J., Ždímal V., Schwarz J., Wagner Z., Doháyosová P., Braniš M., Smolík J.: *European Aerosol Conference*, Program and Abstracts, p. T13A229, (Salzburg, Austria).

Schwarz J., Chi X., Maenhaut W., Hovorka J., Smolík J.: (2006), (Eng) *NOSA 2006 Aerosol Symposium*, Book of Abstracts, pp. 335-339, (Helsinki, Finland).

Influence of petrochemical activities on fine particles and VOC observed in a Mediterranean urban area

N. Marchand[1], B. d'Anna[2], J.L. Jaffrezo[3], Sellegri K.[4], J.L. Besombes[5], I. El Haddad[1], V. Michaud[3], C. Piot[5], B. Temime-Roussel[1], C. George[2], P. Laj[4], H. Wortham[1], D. Voisin[3], A. Armengaud[6], G. Gille[6], D. Robin[6]

[1] Laboratoire Chimie Provence (UMR 6264), équipe Instrumentation et Réactivité Atmosphérique, Universités d'Aix-Marseille I, II et III-CNRS, 3 place Victor Hugo, 13331 Marseilles Cedex 3, France.
[2] Institut de Recherches sur la Catalyse et l'Environnement de Lyon (UMR 5256), Université Claude Bernard Lyon 2, Avenue Albert Einstein F-69629,Villeurbanne cedex, France.
[3] Laboratoire de Glaciologie et Géophysique de l'Environnement (UMR 5183), Université Joseph Fourier-CNRS, Rue Molière, BP 96, 38 402 St Martin d'Hères Cedex, France.
[4] Laboratoire de Météorologie Physique (UMR 6016) Université Blaise Pascal, 24 av des Landais, 63177 Aubière cedex, France.
[5] Laboratoire de Chimie Moléculaire et Environnement, Polytech'Savoie- Université de Savoie, Campus Scientifique, 73376 Le Bourget du Lac Cedex, France.
[6] Atmo PACA, 146 rue Paradis, 13006, Marseilles, France

Keywords: Ambient urban aerosol, AMS, PTRMS, Particles size distribution, industrial aerosol

With traffic of about 97 million tons (Mt) (62.5% of crude oil and oil products) in 2007, the autonomous port of Marseilles is the most important port of the Mediterranean Sea. It handles twice the traffic compared to Genes, and nearly three times the traffic of Barcelona or Valencia. A huge petrochemical area among other industrial plants (steel mill, coke plant,..) is also located close to Marseilles, the second most populated city in France with more than 1 million inhabitants. This area is also well known for its photochemical pollution especially regarding ozone, and evidence of rapid formation of secondary organic aerosol have been pointed out within the framework of the ESCOMPTE experiments.

In this context, an intensive field campaign was carried out at an urban background site in July 2008, within the FORMES program. C-TOF-AMS, HS-PTR-MS, SMPS, and VHTDMA were connected together to a common inlet in order to investigate in detail fine particles and VOC's with high temporal resolution.

In addition to local sources, high concentrations of particles reaching 140 000 cm^{-3}, most of the time associated with SO_2, were observed during the campaign. These particles had diameter less than 20 nm when the sampling site was directly downwind the main industrial area and their composition were dominated by sulphates and organics. Results presented in figure 1 were acquired during a typical sea breeze event. An increase of the particles diameter, of ozone and secondary VOCs (such as MEK) associated to a longer transit time of the air masses above the Mediterranean Sea were observed. During these events, particles present acidic conditions (30-40% of sulphates were in the form of bisulphate HSO_4^-) and VHDTMA results show an external mixing state of the aerosol (Dp=25 and 100 nm) with one hydrophobic mode (GF at 90% =1.05-1.30) and one hydrophilic mode (GF=1.35-1.70).
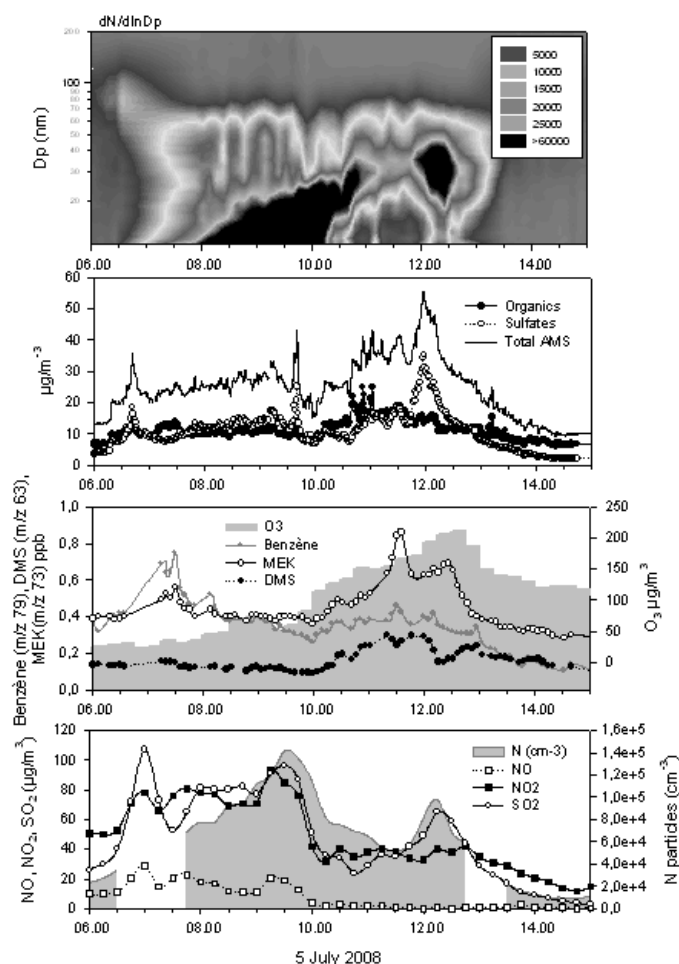
Figure 1: Evolutions of properties of aerosol and selected VOCs during typical sea breeze event heavily impacted by industrial emissions.

Mobile aerosol mass spectrometer measurements of submicron particulate matter including source apportionment in urban areas

M. Crippa, C. Mohr, P. DeCarlo, V. Lanz, R. Chirico, M. Heringa, A.S.H. Prévôt and U. Baltensperger

[1]Laboratory of Atmospheric Chemistry, Paul Scherrer Institut, Villigen, Switzerland

Keywords: AMS, Organic aerosols, Source apportionment

The Aerodyne aerosol mass spectrometer (AMS) was used in a mobile laboratory in order to assess spatial variability of submicron particulate matter composition. The measurements include the inorganic components ammonium, chloride, sulfate, and nitrate and the organic mass. The use of positive matrix factorization (PMF) of the organic aerosol mass spectra allows the quantitative distinction of different source to organic mass, especially biomass burning, hydrocarbon-like organic aerosol (from fossil fuel combustion) and oxidized organic aerosol (can often be interpreted as secondary organic aerosol) (Lanz et al., 2007; Ulbrich et al., 2008).

Measurements were performed in Zürich, Milan and will be performed in Barcelona in Paris. From the latter two, only preliminary analysis will be available. The measurements in Milano showed that HOA was the dominant OA fraction while in Zürich OOA was often the most important one. A new method was developed to distinguish between regional and local contributions to the submicron mass. In Zürich, it was found that in most areas, traffic was the main local source. In some residential areas, a significant contribution of wood smoke could be detected.

Lanz, V. A., M.R. Alfarra, U. Baltensperger, B. Buchmann, C. Hueglin, & A.S.H. Prevot (2007), *Atmos. Chem. Phys.*, 7, 1503-1522.

Ulbrich, I.M., M.R. Canagaratna, Q. Zhang, D.R. Worsnop & J.L. Jimenez (2008), *Atmos. Chem. Phys. Discuss.*, 8, 6729-6791.

Seasonal diurnal concentrations of suspended particulate matter in Mombasa City, Kenya

W. Kimani[1], M. J. Gatari[1], J. K. Ng'anga'[2] and J. Boman[3]

[1]Institute of Nuclear Science and Technology, University of Nairobi, P. O. Box 30197, Nairobi, Kenya
[2]Department of Meteorology, University of Nairobi, P. O. box 30197-00100, Nairobi, Kenya
[3]Chemistry Department, Atmospheric Science, Göteborg University, 412 96 Göteborg, Sweden

Key words: Urban pollution, developing countries, Mombasa sea port, TSP, measurements

Air pollution research in developed countries reveals scenarios of heavy indirect costs emanating from adverse effects on human health and ecosystems. The main dynamic emission source of air pollution is the transport industry and its growth in Kenya is high in the midst of poor infrastructure and increasing inability to sustain proper vehicle maintenance. The work reported here is from an air measurement campaign that covered three distinct seasons from October 1988 to May 1989. It is the first campaign that investigated total suspended particulate (TSP) matter in the city of Mombasa, the second largest town in Kenya and largest regional sea port. Mombasa is an island located at 5^0 S 38^0 E and lies on the path of the cool southwest and dry northeast monsoons. The weather is mainly hot and humid except for the cool months of July and August.
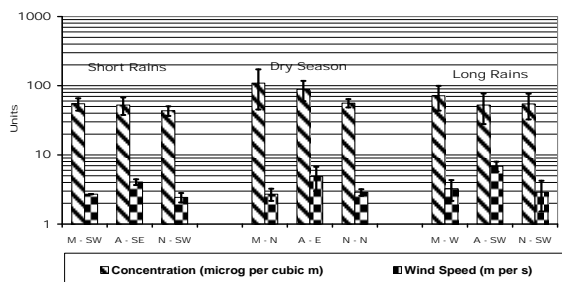
Figure 1. Mean Seasonal Diurnal concentrations of TSP matter and wind speed. M-SW indicates morning period and dominating southwesterly winds. A indicates afternoon and N night. They are all labeled with wind direction as described for M - SW.

The rainfall regime in Mombasa is tri-modal with maximum falls in April-May, followed by rain in July-August and October-November. A high volume sampler type SH-69 (Staplex Co., New York, USA) was used to sample air particles on Whiteman glass fiber filters (0.20 m by 0.25 m). Samples were taken from 0300–0900, 1130 -1730 and 2030-0230 h per day. The filters were weighed using a semi micro-balance, Ainsworth type 24 (Ainsworth Division, Denver, Colorado, USA). The measured

concentrations were highest during the dry season and in the morning periods in all the seasons. They were below the WHO recommended integrated mass over 24 h, of PM_{10}. However it might not be a representative comparison since the sampling period was only 6 h per sample.

Similar concentrations were observed during the rain seasons. However, the higher wind speeds during the long rains implied higher scavenging of suspended particles. One would expect more particles due to the stronger wind transport and dust production. The results also implied that the early morning sea breeze had a pronounced influence on Mombasa aerosol. It means that the marine aerosol has an unknown sizeable contribution to the ambient air pollution in Mombasa. More studies are recommended in this coastal city.
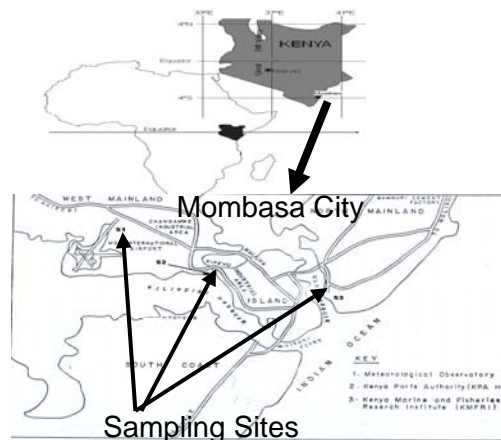
Figure 2. Map of Mombasa with location shown relative to maps of Kenya and Africa.

Künzli et al., (2000). The Lancet 356, 795-801.
Akeredolu, F. (1989). *Atmos. Environ.* 36, No.4, 783-792.

Experimental observations of in-vehicle exposure to particles in real-world driving

I.D. Longley, G.Olivares, G.F. Coulson, N.Talbot

National Institute of Water & Atmospheric Research Ltd, Auckland 1149, New Zealand

Very high particle number concentrations (PNC) are observed in vehicle plumes and at busy roadsides, especially relative to urban and remote background concentrations. This leads us to hypothesise that total exposure to ultrafine particles of much of the urban population is disproportionately influenced by the relatively short time that most people spend in close proximity (order of metres) to vehicle exhausts. Much of that time is spent inside vehicles, especially cars. In busy urban driving the entry point of air into a vehicle cabin is close behind the exhaust of the vehicle in front. In this sense a car's internal volume can be considered to be a vessel for collecting and trapping polluted air, thus potentially increasing the exposure of the occupants relative to those travelling without the aid of a cabin (e.g. cyclists, motorcyclists).

We designed a research programme aiming to quantify in-car exposure The first stage involves characterising the air exchange rate of a small pool of test vehicles, and the dependence of that rate on ventilation settings (windows open/closed, vents open/closed, air conditioning on/off/variable, fan off/variable speed) and vehicle speed. The second stage involves choosing a limited number of ventilation scenarios and driving the test vehicles over a number of typical commuting routes in Auckland whilst simultaneously measuring pollutant concentrations inside and outside of the test vehicle. The third stage involves using air exchange rate data to develop a semi-empirical car ventilation model to predict interior concentrations from a knowledge of exterior concentrations.

We investigated the air exchange rate in two cars driven in controlled conditions. Smoke was generated inside the cabin and indoor/outdoor concentrations measured using a matched pair of P-Traks (TSI Inc.). Exponential decay curves were fitted to interior-exterior PNC. We found influences of cabin volume, vehicle speed, fan speed, vent setting and air conditioning which were consistent with literature values and anticipated mechanisms of particle mixing and deposition, and air exchange.

In on-road tests we found that interior PNC responded to exterior PNC in a manner indicative of the cabin acting like a buffer, smoothing external variability. The "trapping" phenomenon was very apparent, with brief encounters with a single gross-emitting vehicle leading to extended high interior exposure lasting many minutes after the encounter. Figure 1 shows this effect in a Honda Civic Hybrid driving on a commuting route in north Auckland with the windows closed, and air conditioning on low
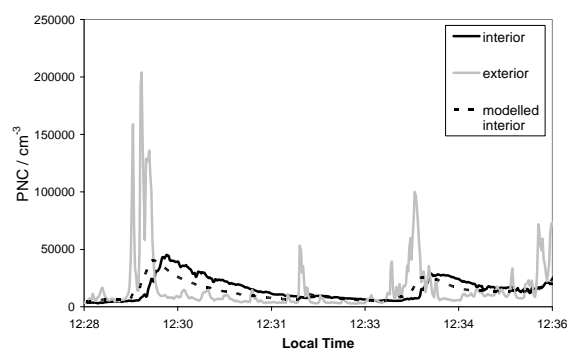
Figure 1. Interior/exterior PNC concentrations in a car driving in N Auckland. (windows closed, AC low) and modelled interior concentrations.

We found that a ventilation model based on a simple speed-dependent first-order difference function performed well in describing the time series of interior PNC. Small improvements in model performance were achieved by introducing a variable deposition rate driven by estimated changes in particle size modes. Model results are also shown in Figure 1.

Reduction of PM industrial ceramic emissions reflected on key components concentrations of ambient PM_{10}

M.C. Minguillón[1],*, X. Querol[1], E. Monfort[2], A. Alastuey[1], A. Escrig[2], I. Celades[2], J.V. Miró[3]

[1] Institute for Environmental Assessment and Water Research, CSIC, C/Jordi Girona 18-26, 08034, Barcelona, Spain
[2] Instituto de Tecnología Cerámica, Campus Riu Sec, Universitat Jaume I, 12006, Castellón, Spain
[3] Generalitat Valenciana, Conselleria de Medio Ambiente, Agua, Urbanismo y Vivienda, C/Francesc Cubells 7, 46011, Valencia, Spain

The relationship between the reduction of specific ceramic particulate emissions and ambient levels of some PM_{10} components, such as Zn, As, Pb, Cs and Tl, was evaluated. To this end, the industrial area of Castellón (Eastern Spain) was selected, where around 40% of the EU glazed ceramic tiles and a high proportion of EU ceramic frits (middle product for the manufacture of ceramic glaze) are produced.

The PM_{10} emissions from the ceramic processes (tile and frit manufacture) were calculated over the period 2000 to 2007 taking into account the evolution of the degree of implementation of corrective measures throughout the study period. Whereas the emissions from tile manufacture didn't undergo significant changes during the study period, the emissions from frit manufacture showed a marked decrease. This decrease is mainly due to the implementation of abatement systems (mainly bag filters) in the majority of the fusion kilns for frit manufacture in the area as a result of the application of the Directive 1996/61/CE, IPPC.

On the other hand, ambient PM_{10} sampling was carried out from April 2002 to July 2008 at three urban sites and one suburban site of the area and a complete chemical analysis was made for about 35 % of the collected samples, by means of different techniques (ICP-AES, ICP-MS, Ion Chromatography, selective electrode and elemental analyser). The series of chemical composition of PM_{10} allowed us to apply a source contribution model (Principal Component Analysis), followed by a multilinear regression analysis, so that PM_{10} sources were identified: mineral, soil, industrial #1, industrial #2, road traffic, regional background and sea spray. The contribution of these sources to bulk ambient PM10 was quantified on a daily basis, as well as the contribution to bulk ambient concentrations of the identified key components (Zn, As, Pb, Cs, Tl). The contribution of the sources identified as the manufacture and use of ceramic glaze components (industrial #1 and industrial #2), including the manufacture of ceramic frits, accounted for more than 65, 75, 58, 53, and 53% of ambient Zn, As, Pb, Cs and Tl levels, respectively (with the exception of Tl contribution at one of the sites). The

important emission reductions of these sources during the study period had an impact on ambient key components levels, such that these were reduced significantly during the study period. A simple statistical analysis showed that there was a high correlation between PM_{10} emissions from the ceramic sources and ambient key components levels (R^2= 0.61-0.98).

Ten days of intensive air quality measurement at the international airport of Budapest

B. Alföldy[1], J. Osán[1], E. Börcsök[1], A. Nagy[2], A. Czitrovszky[2], S. Török[1], S. Kugler[3]

[1]KFKI Atomic Energy Research Institute, Konkoly-Th. M. u. 29-33., 1121, Budapest, Hungary
[2]Research Institute for Solid State Physics and Optics, Konkoly-Th. M. u. 29-33., 1121, Budapest, Hungary
[3]Environmental Department of Budapest Airport Pte Ltd., P.O.B. 53., 1675, Budapest, Hungary

A ten days long intensive air pollution measurement campaign was performed at the international airport of Budapest from 26 June to 5 July, 2008. A monitoring station was installed at terminal 2A. The monitored components were: CO, NO_x, SO_2, O_3, measured by Horiba gas monitors; $PM_{2.5}$, PM_{10} by Rupprecht& Patashnick TEOM monitors; black carbon by Magee Scientific aethalometer; size fractionated aerosol above 250 nm by a Grimm 1.108 aerosol spectrometer; and the total particle number by a TSI 3775 CPC. In addition, hourly aerosol samples were collected onto Teflon filters that later were chemically analysed.

The airport traffic is the highest at Terminal 2, consequently the air quality is the worst there (Schürmann, 2006). Mainly PM exceedances were registered during previous campaigns (Groma, 2008). For this reason the main goal of the campaign was to study the chemical composition of the aerosol for the deduction of the possible sources. Ionic composition of the aerosol was determined after dissolving the $PM_{2.5}$ samples by ion chromatography. Atmospheric concentration of sulphate, nitrate, ammonium and chloride ions were determined. Prior to the sample destruction, elemental composition was measured by XRF that provided quantitative elemental composition from S to Pb. Table 1 contains the correlation coefficients between $PM_{2.5}$ mass and the chemically/optically determined mass balance.

Table 1. Correlation of total elemental mass (E), total ionic mass (I), black carbon mass (BC) with the total $PM_{2.5}$ mass.

$\mu g/m^3$	E	I	BC	E+I	E+BC	I+BC	E+I+BC
$PM_{2.5}$	0.21	0.27	0.28	0.52	0.38	0.49	0.57

It can be seen from the table that none of E, I or BC correlates with the total $PM_{2.5}$ mass. However, their sum shows a weak correlation. This result arises from the difference in time evolution of the three aerosol components' concentrations that indicate difference of the sources. Although sulphate/nitrate concentration does not correlate by the BC, it is not impossible that they have the same sources, such as aircraft and service vehicles. Namely BC originates directly from combustion; the sulphate/nitrate aerosol is a product of atmospheric chemical reactions that delay its appearance after the emission occurs.

Figure 1 shows the correlation between $PM_{2.5}$ mass and the analytically determined mass balance (E+I+BC). It can be seen that in addition to the weak correlation, only 20% of the total $PM_{2.5}$ mass could be detected by the above mentioned analytical methods. Organic aerosol or fine fraction of silicates could be assumed to be responsible for the non-detected 80% of the total $PM_{2.5}$ mass.
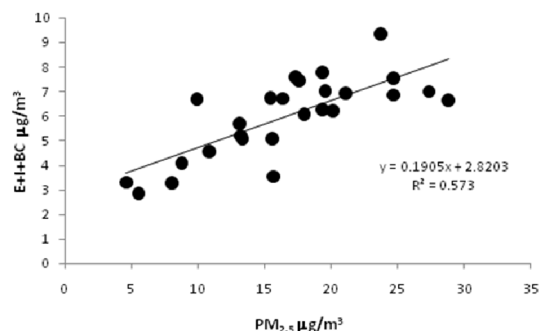
Figure 1. Correlation between TEOM measurements and the analytically determined masses of the aerosol
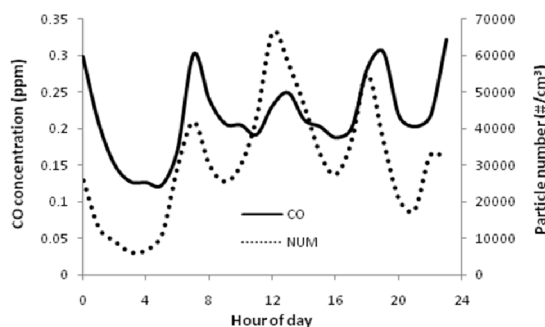
Figure 2. Daily cycles of particle number and CO concentrations.

Figure 2 presents the average daily cycles of total particle number ($d > 10$ nm) and CO concentrations. Both curves have three peaks in agreement with the three rush periods of the airport's traffic. Even though the three traffic peaks have similar maximal intensites, the middle CO peak is smaller, while the total particle number peak is higher than the outer ones. Since the mixing height is maximal around noon, the lower middle CO peak is clear, while the high particle number values around noon can be elucidated by secondary aerosol formation.

Groma, V., Osán, J., Török, S., Meirer, F., Streli, C., Wobrauschek, P., Falkenberg, G. (2008). *Időjárás*, 112, 83-97.

Schürmann, G., Schäfer, K., Jahn, C., Hoffmann, H., Groma, V., Török, S. Emeis, S. (2006). in *Proc. of SPIE, Vol. 6362*. Bellingham, WA, USA.

Evaluation of seasonal behaviour of atmospheric PM$_{10}$ levels in the Basque Country

M.A. Barrero and L. Cantón

Department of Applied Chemistry, University of the Basque Country, 20018, San Sebastián, Spain

Keywords: monitoring network, PM$_{10}$ time series, regional background, seasonal patterns, urban areas.

PM$_{10}$ is the main measurements found to exceed prescribed limits in the urban areas of the Basque Country. In order to correct data for the contributions due to natural events like African dust outbreaks, the regional background has to be estimated. This work focuses on the seasonal behaviour of the regional background and how it affects PM$_{10}$ levels in urban areas.

The Basque Government Air Quality Monitoring Network is composed of ~70 monitoring stations covering the main urban areas as well as some remote (background) sites. Air quality data from these automatic stations were collected and processed between 2005 and 2008. The data consisted of hourly concentrations of carbon monoxide, nitrogen oxides (NO and NO$_2$), ozone, PM$_{10}$, PM$_{2.5}$, and sulphur dioxide.

Data matrices were processed and relevant statistics extracted leading to daily, monthly, seasonal and yearly averages for each monitoring station.

Applying the methodology described by Escudero et al. (2007), PM$_{10}$ regional background was estimated on a daily basis and subtracted from each daily PM$_{10}$ data point.

A seasonal cycle in the regional background time series was detected showing maximum values in summer and minima in winter. The opposite was found for urban and industrial sites, once the regional background contributions were subtracted. The resulting PM$_{10}$ "corrected" data correlated better with primary pollutants, providing stronger evidence for relationships to urban emission sources.

Furthermore, these calculations allowed estimates of the contribution of marine aerosol and African dust outbreaks to the average PM$_{10}$ concentrations detected at each station.

In addition, differences between regional background sites were found to be dependent upon their proximity to the coast, with the coastal sites showing higher background levels, especially in winter.

Finally, the evaluation of four years of corrected data reveals a trend of improving air quality in the Basque Country with decreasing trends observed for most primary pollutant concentrations, most notably PM$_{10}$.
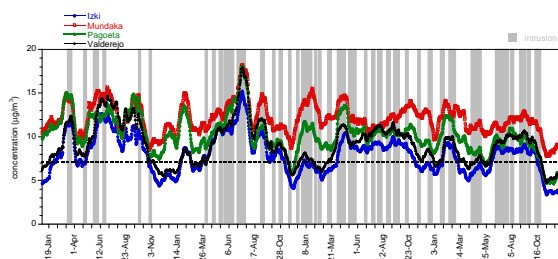
Figure 1. Evolution of PM$_{10}$ regional background levels in the Basque Country, estimated at four locations.
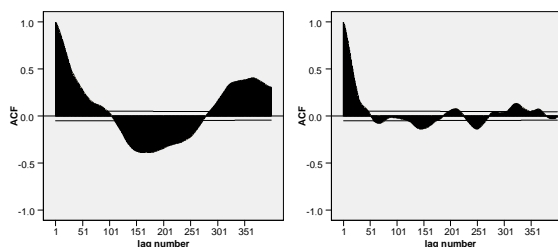
Figure 2. Autocorrelation functions of regional background PM$_{10}$ values from an interior site (left) and a coastal one (right).

Escudero, M.; Querol, X.; Pey, J.; Alastuey, A.; Pérez, N.; Ferreira, F.; Alonso, S.; Rodríguez, S.; Cuevas, E. (2007). *Atmos. Environ.,* 41, 5516-5524.

Impact of local traffic on NOx and PM: urban background versus traffic locations

M. Van Poppel, N. Bleux and P. Berghmans

Flemish Institute for Technological Research (VITO), Boeretang 200, 2400 Mol, Belgium
email : martine.vanpoppel@vito.be

Keywords: traffic, NOx, PM, EC.

Introduction

Road transport is one of the main sources of urban air pollution, especially PM and NOx. The knowledge that these traffic related emissions induce adverse health effects, is an incentive for cities to evaluate the urban air quality and look for actions that can be taken. Before cost effective measures can be taken, the actual air quality of the city has to be assessed in order to identify hot spot locations.

Existing air quality measurement networks measure air pollution at different sites and give an 'average value' for the surrounding area. However, most of these measurement stations are not located at hot spot locations e.g. close to busy roads. The aim of this study is to assess the air quality at urban (curb site) locations. The measurement campaign presented here, is part of an extensive study, including measurements and modeling to assess the current situation and evaluate potential measures.

Methodology

Monitoring was performed in June – August 2008 at some typical locations in the centre of Antwerp. The selected monitoring locations are characterised by different exposure to traffic e.g. ring road, access road, street canyon, bus location and urban background. Traffic oriented locations are compared to the urban background location to assess the contribution of traffic. Measurements include PM (PM_{10}, $PM_{2.5}$ and PM_1), black smoke, EC (Elemental Carbon) and NOx. PM_{10} daily average values are measured according to the EU reference method (EN 12341) using a sequential low volume sampler. A mobile imission laboratory – equipped with a TEOM-FDMS, Grimm 1.108 and NOx analyzer - is used during two weeks (at three of these locations) to measure the size fractions of PM and the weekly profile of NO_x and PM_{10}. In addition, diffusive samplers are used to measure 2-weekly average NO_2 concentrations. The measured concentrations are also compared to data of nearby monitoring stations of the air quality monitoring network.

Results

Highest concentrations are measured in the street canyon. The average difference in PM_{10} concentrations compared to the background location was 22 µg/m^3 in the street canyon and respectively 4, 5 and 6 µg/m^3 at the ring location, bus location and access road. A major part (60%) of the PM_{10} concentration at the street canyon location can be attributed to the coarse fraction ($PM_{10-2.5}$).

A selection of the filters were analysed to determine EC concentrations by the TOT. Lowest concentrations (average of 1.31 µg/m3 EC) are measured at the urban background location. This was expected since this site is not directly exposed to traffic. The average value are typical values for urban background stations. Highest concentrations are measured in the street canyon and at the access road, respectively 5.4 and 3.9 µg/m^3. Intermediate concentrations are measured at the bus location and the ring road, respectively 2.8 and 2.6 µg/m^3. It must be mentioned that at this part of the campaign, the bus traffic was somewhat less than normal due to nearby road works. Lower EC concentrations are measured on Sundays at the traffic locations. The traffic flows are 10 to 40 % lower on Sunday, depending on the location.

Lowest NO_2 concentrations are measured at the urban background locations. Extrapolated NO_2 concentrations are below the annual limit value at background locations. However, at all other locations, NO_2 concentrations are very close to or above the annual limit value of 40 µg/m^3. Highest concentrations are measured at bus locations and street canyon. Also access road show high concentrations followed by ring location. Ring locations are open locations, which improves the dilution of the pollution.

NOx profiles are measured at access road, street canyon, bus location and compared to urban background. A clear daily pattern for the traffic locations can be seen for NO concentrations. The pattern for NO_2 is less pronounced. NO_2 is more distributed over the city. A plausible explanation is that most of NOx from traffic is emitted as NO and transformed in the atmosphere into NO_2.

A good correlation was found for the access road when comparing daily average NOx to EC. This was not valid for NOx and PM_{10}. Both pollutants (NOx and EC) are directly related to combustion sources as traffic.

Citizen's exposure and urban shape: a tight relationship.

M. Filice[1], P. De Luca[1]

[1]Department of Pianificazione Territoriale, University of Calabria, Rende, 87036, Cosenza, Italy

Air pollution question lies in the health effects due to inhalation of pollutants, except for coincidence of a family disease. It is well documented that there are different points of view to reduce urban pollution: transport and urban planning, improvement to road network, use of renewable energy. Several studies underlined that urban shape can affect air quality (Borrego *et al.*, 2006; Filice, 2007), as well land use (Marshall *et al.*, 2005) and source apportionment. Urban particles have changeable properties that could influence citizen exposure, especially fine and ultrafine particles with greater penetration in human lung (Asgharian *et al.*, 2006). Our work is focused on the idea that the dislocation of buildings could influence citizen exposure. For this purpose PM10 was collected in two adjacent sites: a canyon street and an open street with hourly sampling time (8 a.m-1 p.m.) and a frequency of 5 filters/day during April 2006 in Cosenza urban area. At the same time we observed traffic flow trend. The characterisation of filters was obtained by gravimetric method coupled with Scanning Electron Microscopy (SEM).

From a gravimetric point of view we observed a relationship between consecutive hourly concentrations. Canyon street showed a moderate relation between PM10 concentration in the time i and PM10 concentration in consecutive time i+1 (fig.1), while open street showed a weak relation (fig.2). Image analysis (SEM, Jeol Stereo Scan 360) showed two different trends. We observed a time increasing of fine particles in Canyon Street, as opposed to Open Street.

This result suggests us that citizen's exposure could be due to several parameters, such as urban shape. We propose following exposure relation:

$$[PM10_h](\mu g/m^3) = f\ (Ftr, K, S)$$

Where:

Ftr, function of traffic flow;
K, function of hourly meteorological condition;
S, function of urban shape.
Urban shape could influence particles dispersion, especially fine particles with a long residence time.
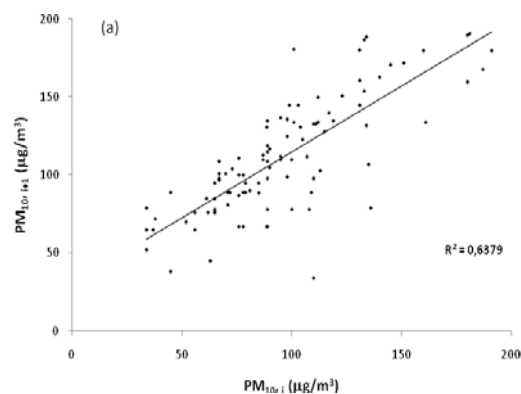
Figure 1. Canyon street: relation between PM10 concentration in consecutive time *i, i+1*.
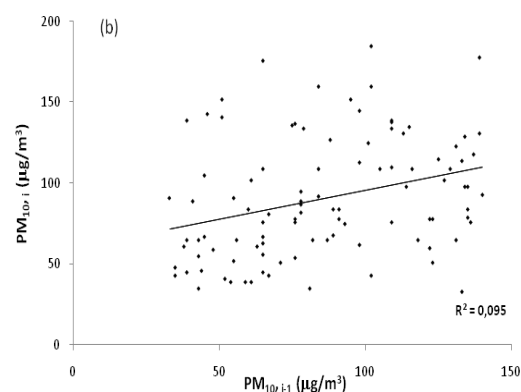
Figure 2. Open street: relation between PM10 concentration in consecutive time *i, i+1*.

Further works will be focusing to define shape factor and its role to reduce urban particulate pollution.

Asgharian B., Price O.T., Hofmann W., (2006), *J. of Aerosol Science*, 37, 1209 – 1221

Borrego C., Martins H., Tchepel O., Salmin L., Monteiro A. e Miranda A.I. (2006), *Environm. Modelling & Software*, 21, 461-467

Filice M., (2007), *Inquinamento atmosferico. Monitoraggio ambientale e caratterizzazione chimico-fisica di polveri sottili. PhD Thesis in Environmental Planning and Technologies*, University of Calabria (in Italian)

Marshall J. D., McKone T. E. e Deakin E., (2005), *Atmospheric Environment*, 39, 283-295

Indoor to Outdoor Ratios of PM and PAH Related to Traffic and Street Maintenance Emissions

D. Martuzevicius[1], L. Kliucininkas[1], E. Krugly[1], T. Prasauskas[1], I. Vaskeviciute[1], and B. Strandberg[2]

[1]Department of Environmental Engineering, Kaunas University of Technology, Radvilenu pl. 19, LT50254 Kaunas, Lithuania
[2]Occupational and Environmental Medicine, Sahlgrenska Academy at Goteborg University, Box 414, SE40530 Goteborg, Sweden

Keywords: PM10/PM2.5, PAH(s), traffic, road dust, resuspension.

Introduction

The objective of the study was to assess the influence of road traffic and street maintenance services to the air pollution by direct emissions and resuspended particles. Kaunas similarly to many other Eastern European cities is facing extreme levels of air pollution by particulate matter during winter and especially early spring season. This is attributed to the fact that city maintenance service companies utilize sand and salt mixture for street de-icing. Since the deposits of sand are not effectively removed in the end of cold season, passing traffic and wind gusts cause excessive fugitive dust emission. As a result, cities have problems complying with the PM10 annual exceedance limits. In addition to PM10 and PM2.5, we aimed at assessing behaviour of PAHs with respect to the road dust associated pollution both outdoors and indoors.

Methods

Field experiments were performed in two locations in Kaunas city. The first site was located at a 3rd floor balcony and a room of the 5-story university dormitory, located 8 meters from a busy two lane street. The room was occupied by two non-smoking students who carried out their routine activities (no thermal aerosol generation was expected). The second site was established at first floor storage premises of a university faculty building, located 4 meters from a busy three lane one-way city centre street. The room was unoccupied and only visited briefly by sampling crew and other university staff.

The outdoor samples were taken by PM10 and PM2.5 cyclones (URG Inc., 16.7 lpm). Indoor and outdoor comparison samples were taken by SKC PM4 cyclones (2.2 lpm). Samples were taken on Whatman GFA glass microfiber filters. PM mass concentration was determined by gravimetric method. Afterwards, samples were shipped to Sahlgrenska Academy at Goteborg University for PAH analysis by GC-MS. In total, 32 PAHs were determined. The indoor particle number concentration was monitored by Lighthouse 3016 OPC.

Results

The results of the campaign conducted during months of January-February revealed a very minor difference in PM2.5 and PM10 concentrations (average PM2.5/PM10 ratio was 0.95 at Site #1 and 0.90 at site #2). This phenomenon reflects that both fractions were generated by the same source. The most of PM10 mass was comprised of fine particles and these particles were likely originated from direct traffic emissions. This is also confirmed by PAH measurement results, where PAH compounds were very close for both PM2.5 and PM10 fractions. The PAH concentration in PM2.5 was slightly higher. On the other hand, indoor and outdoor measurement comparison revealed a significant reduction of PAHs after penetrating the indoor environment (Fig. 1). It must be noted that both selected locations featured wooden window frames that were relatively lose in terms of air circulation. This suggested that near-street residents of older buildings may be significantly exposed to PAHs and PM in general.
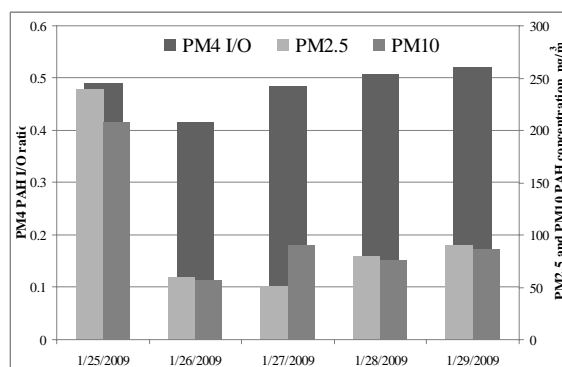
Figure 1. I/O ratio of total PAHs in PM4 fraction and total PAHs in PM2.5 and PM10 fractions

The sensitivity of indoor air concentrations in the sampling locations was clearly revealed by the street maintenance (night time sweeping) episode, registered by the OPC. During this event, the total particle number concentration (0.3-10 μm) has increased by 20%. This suggests that maintenance works may alone be responsible for a significant increase of particle concentration both outdoors and indoors.

Dust events in Beijing, China (2004-2006):
Comparison of ground based measurements and columnar integrated observations

Zhi Jun Wu[1,2], Ya Fang Cheng[2], Min Hu[1], Birgit Wehner[2], Alfred Wiedensohler[2]

1   State Key Joint Laboratory of Environmental Simulation and Pollution Control,
College of Environmental Sciences and Engineering, Peking University, Beijing, P. R. China
2   Leibniz Institute for Tropospheric Research, 04318 Leipzig, Germany
Keywords: Aerosol size distribution, Asian dust, aerosol optical depth, Ångström exponent

Three-year particle number size distribution (PNSD) measurements were performed in the urban atmosphere of Beijing, China during the dust events in the springs of 2004-2006. In this work, the PNSD data are analyzed to characterize the particle size distributions and optical properties of the particles by combining with AERONET sun/sky radiometer data.

In total, 18 dust events were identified and further categorized as two different types (group 1 and 2), which are associated with different weather conditions. Figure 1 shows the evolution of PNSD during two single dust events representing group 1 and group 2.
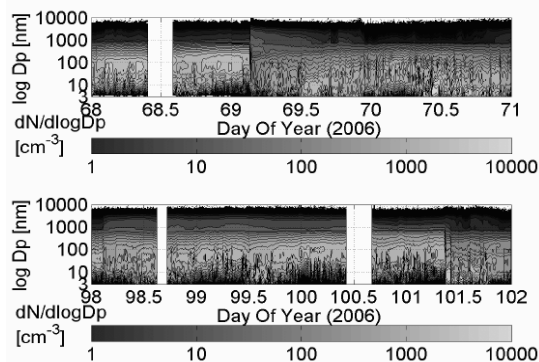
Figure 1: Time series of PNSD during dust events for group 1 (Upper panel) and group 2 (Lower panel).

The dust events in group1 were associated with unstable weather conditions. The high wind speeds (on average, > 4 m s^{-1}) lead to an effective removal of anthropogenic aerosols. As a result, dust particles dominated the total particle volume concentration (3 nm-10 μm) for over 70%.

The events in group 2 with a longer duration time and lower ratios of coarse mode particles to the total particle volume concentration occurred under stable local weather conditions. The stable meteorological conditions, which did favor the accumulation of urban pollutants, led to the superposition of dust particles and anthropogenic aerosols.

Figure 2 presents the correlation between AOD and Ångström exponent for group 1, group 2, and heavy polluted days. The Ångström exponents for group 1 varied between -0.07 and 0.29 being smaller than those for group 2 with the range of 0.31-0.87. On average, the AOD of the dust events in group 2 (0.76-2.47) were higher than those of group 1 (0.23-1.31). We found that the superposition of dust particles and urban aerosols may result in higher AOD for group 2 than anthropogenic heavy polluted episodes.
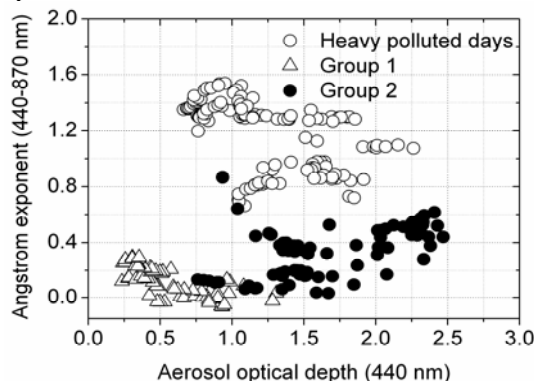
Figure 2: Ångström exponent versus AOD for group 1, group 2, and heavy polluted days.

In this study, a comparison between the particle volume size distributions retrieved from AERONET and the ones obtained by the TDMPS measurements were performed to gain insight into the differences in the ground based and column integrated measurements. The results are shown in Figure 3. The peak diameters of coarse mode particles from the ground based measurement are smaller than those from AERONET retrieved ones.
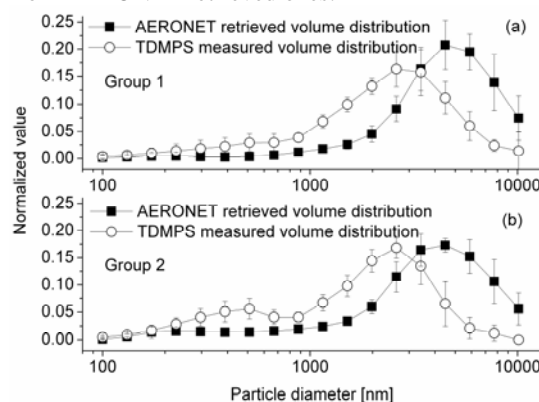
Figure 3: Average normalized particle volume size distribution derived from AERONET and from TDMPS measurements for group 1 and 2.

Deposition of PM10 mineral dust into the Atlantic Ocean at Cape Verde Islands

N. Kaaden[1], T. Mueller[1], A. Held[1], S. Lehmann[1], K. Mueller[1], K. Kandler[2] and A. Wiedensohler[1]

[1] Department of Physics, Leibniz Institute for Tropospheric Research, Leipzig, Germany
[2] Institute of Applied Geosciences, Darmstadt University of Technology, Darmstadt, Germany

Keywords: Deposition, Eddy covariance fluxes, Passive Sampler, Saharan dust, SMPS.

Soluble iron has a large impact on ocean bioavailability. One of the largest sources of iron to deposit into the ocean is the transport and deposition of Aeolian dust (Jickells *et al.*, 2005). Emission rates of dust mass can be predicted in good agreement with observations, but the transport of dust and therefore its deposition rates cannot be modelled accurately. There is still a lack in understanding of how much dust is deposited into the ocean and how the temporal variability of dust deposition can be described (Aumont *et al.*, 2008).

From January 10th to February 6th, 2009, an extensive field study within the project SOPRAN (Surface Ocean PRocesses in the ANthropocene) was conducted at the Cape Verde Islands. The main goal was to estimate the deposition of Saharan Mineral dust into the tropical North eastern Atlantic Ocean. Two different methods were used to measure and calculate the deposition rates.

The first method is the eddy covariance method. A sonic anemometer was used to measure turbulence parameters including friction velocity to parameterize size dependent particle deposition velocities. A SMPS (Scanning Mobility Particle Sizer) and an APS (Aerodynamic Particle Sizer) were utilized to determine the particle number size distribution for particles up to 10 µm, which can be converted into a mass size distribution after assuming a density. To obtain the dust fraction from the mass size distribution, the number fraction of dust particles was determined with a H-DMA-APS (Hygroscopicity Differential Mobility Sizer Aerodynamic Particle Sizer). Size dependent particle deposition velocities and size dependent mass concentrations were combined to obtain the particle mass flux.

Within the second method, two Sigma_II passive samplers were mounted on a tower in 10 and 30 m height. Nuclepore filters and glassy carbon disks were used as sample base. They were used in each sampler to determine the net mass of dust and elemental composition that was fallen within one week and the dust size distribution, respectively. The samples were analyzed with a TXRF (Total X-ray Reflectory Fluorescence spectrometer) and with an electron microscope, respectively. An overview over the used instrumentation to obtain the dust mass deposition rates is given in Table 1.

Table 1: Instrumentation and derived parameters.

Method one – eddy covariance measurements	
Sonic anemometer	3D Wind velocity and wind direction in high temporal resolution
SMPS + APS	Particle number size distribution
H-DMA-APS	Number fraction of dust particles at Dp = 600, 800 and 1000 nm
Method two – Sigma II Passive samplers	
Nuclepore filters	Net dust mass and dust elemental composition
Carbon disks	Dust size distribution

During the four week field study, dust events changed with times free of dust. A first result of dust deposition obtained with method one is presented for January 14th, 2009. The preliminary deposition mass fluxes for dust particles smaller than 10 µm in diameter for this day varied between 0.01 and 0.08 $\mu g \cdot m^{-2} \cdot s^{-1}$.
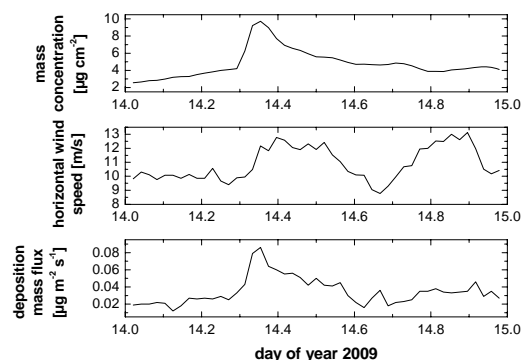
Figure 1: Timeseries of the mass concentration (upper figure), the horizontal wind speed (middle figure) and the deposition mass flux (lower figure) for the 14th of January 2009.

In Figure 1, the mass fluxes, the horizontal wind speed and the mass concentration for January 14th, 2009 are presented. This figure clearly shows that the deposition flux varies over the day due to changing meteorological conditions and the total available dust mass.

Jickells et al. (2005). *Science*, 308, 67 – 71
Aumont et al. (2008), *Geophys. Res. Let.*, 35, 1-5

Absorption of Mineral Dust: Comparison between Measurement and Effective Media Theories

M. Vragel, C. Linke , M. Schnaiter, R. Wagner and T. Leisner

Institut für Meteorologie und Klimaforschung (IMK-AAF), Forschungszentrum Karlsruhe, Germany

Keywords: Absorption, Refractive Index, Saharan Dust

Mineral dust paricles are irregular formed particles containing a heterogeneous internal mixture of silicates, clay minerals, iron oxides and many other components. There are indications that dark mineral phases, e.g. iron oxides like hematite, increase the absorption of mineral dust towards the UV-wavelengths. Because of the mineralogical complexity of the particle system it is difficult to determine the complex refractive index of mineral dust.

For our laboratory study we used two soil samples from the field campaigns SAMUM and AMMA. The optical properties of these two dusts were determined experimentally during the "Mineral Dust Campaign 2008" at the AIDA facility at the Institute of Meteorology and Climate Research of Forschungszentrum Karlsruhe, Germany. Detailed description of the instruments are given in Schnaiter et al., 2005 and Linke et al., 2006.

Particles of the size fraction < 20 μm or 20 – 75 μm were dispersed into the 3.7 m³ big aerosol chamber, reaching initial particle concentrations of approximately 10^3 - 10^4 cm^{-3} and median particle diameters of approximately 300 nm. During three to four hours the particle concentration decreased by one order of magnitude. Table 1 shows an extract of the optical quantities measured at the aerosol chamber.

Instrument	Optical Quantity	Wavelength [nm]
Extinction Spectrometer LOPES	extinction coefficient	200 – 1000 $\Delta\lambda$ = 2.5 nm
Integrating Nephelometer	scattering coefficient	450, 550, 700
Photoacoustic Spectrometer MuWaPAS	absorption coefficient	266, 355, 532, 1064
deduced	singles scattering albedo angström exponents	450, 550, 700

Table 1. Some optical quantities measured at the aerosol chamber and their corresponding wavelengths.

With data from the laboratory study we tried to estimate an effective complex refractive index for the two dust aerosols. For simplification of the complex system we assumed the dust consisting of only two minerals. Illite representing a component that causes only scattering in the considered wavelength range and hematite causing absorption. The optical constants of illite and hematite were mixed following the Bruggeman and volume mean effective medium approximations. With the obtained set of effective optical constants we performed Mie calculations. The received spectral absorption behaviour was compared to measured absorption cross sections. The poster shows that employing the Bruggeman and volume mean effective medium approximations results in slightly different hematite contents.

Schnaiter et al., *Measurement of Wavelength-Resolved Light Absorption by Aerosols Utilizing a UV-VIS Extinction Cell*, Aerosol Science. and Technology, 39, 249, 2005

Linke, C. et al., Optical Properties and Mineralogical Composition of Different Saharan Mineral Dust Samples: A Laboratory Study, Atmospheric Chemistry and Physics Discussions, 6,3315, 2006

Spectral absorption coefficients of mineral dust measured at Cape Verde

C. Meusinger, A. Wiedensohler and Th. Müller

Leibniz Institute for Tropospheric Research, Leipzig, Germany

Keywords: Optical instrumentation, Absorption coefficient, Mineral dust.

Absorption measurements are essential in aerosol science, as they are important for estimating the earth's radiative budget. An Optical Spectral Absorption Photometer (SOAP) was newly developed at the Leibniz Institute for Tropospheric Research in Leipzig (Müller et al. 2009). This instrument allows in-situ determination of different kinds of absorbers, e.g. mineral dust and soot. A SOAP installed at Cape Verde worked in several campaigns so far, embedded in the project SOPRAN (Surface Ocean Processes in the Anthropocene). Here, dust transported from the mainland of Africa (Saharan desert) is of special interest, being expected to fertilize marine flora and fauna. Using the SOAP dust concentrations will be determined.

Simultaneous, filter-based measurements of transmission and reflection over a wavelength range from 350nm to 960nm are performed using a deuterium lamp as source and two spectrometers as detectors. An additional reference channel is optionally available, measuring without any loading. Filters are changed manually at least once a day or if transmission is less than 50%. The aerosol flow is regulated by a flow controller to a constant rate of 1.5 l/min and the sample spot area has a diameter of 6.1 mm on the filter.

SOAP was calibrated using highly absorbing (soot) and strongly scattering (ammonium sulphate) particles. The corresponding reference instruments for optical depths in scattering and absorption were Nephelometer and MAAP, respectively. According to a two-stream radiative transfer model (Arnott, et al., 2005), absorption was calculated from the measured data, providing the basis for further discussions.
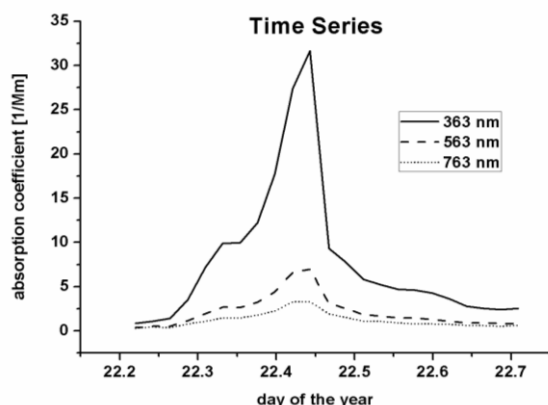
Figure 1. Time series of absorption coefficients of several wavelengths during a dust event

At Cape Verde islands, the SOAP was localized near the shore on São Vicente. The use of an inlet installed on a tower of 30 m height ensured a minor part of sea spray in the measured aerosol compared to an inlet near the ground. Absorption coefficients during a dust event in January 2009 are shown in figures 1 and 2.
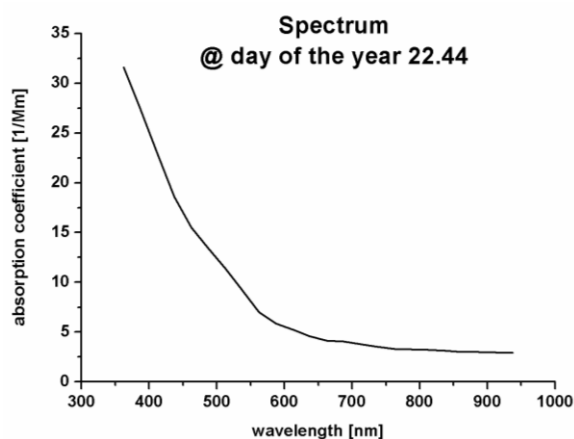
Figure 2. Spectrum of absorption coefficient of a dust event (same as figure 1)

Figure 1 exemplifies a significant change of the absorption coefficient (factor >30 at 350nm) in relatively short time (half a day). Whereas data in figure 2 shows typical spectral absorption of dust as they were found in other campaigns before, e.g. Morocco (Müller et al., 2009). For a more detailed explanation, future experiments in the lab are planned to determine specific spectra of the most commonly found compounds of mineral dust.

Arnott, P.W. et al. (2005). Towards Aerosol Light-Absorption Measurements with a 7-Wavelength Aethalometer: Evaluation with a Photoacoustic Instrument and 3-Wavelength Nephelometer. *Aerosol Sci. Technol.*, **39**, 17-29.

Müller, T., et al. (2009). Spectral absorption coefficients and imaginary parts of refractive indices of Saharan dust during SAMUM-1, *Tellus*, **61B** (1), 79-95.

Lidar observations of extinction-to-backscatter ratio of long-range transported mineral dust at 355 nm and 532 nm during SAMUM 2

S. Gross[1], J. Gasteiger[1], V. Freudenthaler[1] and M. Wiegner[1]

[1]Meteorological Institute, Ludwig-Maximilians-Universität, Munich, 80333 Munich, Germany

Mineral dust is one of the major aerosol components of the troposphere. However, the radiative forcing of mineral dust is still uncertain, because it strongly depends on the spatial distribution and optical properties of the particles. To improve the knowledge of Saharan Dust the SAharan Mineral dUst experiMent SAMUM took place. During the first field campaign (Heintzenberg, 2009) in May and June 2006 measurements of pure, not aged Saharan Dust were made in Morocco close to the Saharan desert. The second field campaign in January and February 2008 (SAMUM 2) was located in Praia at the Cape Verde islands to investigate the properties of long-range transported Saharan Dust. This site is affected by Saharan Dust transported over the Atlantic Ocean and often mixed with African biomass burning aerosols.

An important parameter with respect to radiative forcing is the profile of the particle extinction coefficient. To derive it from a standard backscatter lidar, a trustworthy value of the extinction-to-backscatter ratio, also called lidar ratio, is required. However, until now the number of observations of the lidar ratio for Saharan Dust is very limited. For the spaceborne backscatter lidar mission Calipso, e.g., a lidar ratio of 40 sr at 532 nm is assumed for layers identified as mineral dust, whereas during the first field campaign of SAMUM a lidar ratio for pure, not aged Saharan Dust was found to be in the range of 55 sr at 355 nm and 532 nm (Tesche et al., 2009).

In this paper we discuss observations from the two lidar systems POLIS and MULIS of the Meteorological Institute in Munich during SAMUM 2. They cover profiles of backscatter and extinction coefficients, lidar ratios and linear particle depolarization ratios (δ_A), thus allowing a thorough characterisation of the aerosols. A preliminary error analysis shows that the relative errors of the particle backscatter and linear particle depolarization ratio are below 5% and about 10%, respectively; for the particle extinction and lidar ratio they are between 10 and 15%.

As an example, results of a major Saharan dust plume crossing Cape Verde from January 28 – 30, 2008 are presented. The dust layer mainly extended from the top of the boundary layer at about 500 m to about 1000 m height above ground level. The aerosol optical depth of this layer was about 0.13 – 0.14 at 355 nm. Measurement values of δ_A from 25% - 28% at 355 nm, and 29% - 31% at 532 nm clearly indicated non-spherical Saharan Dust

particles (Freudenthaler et al., 2009) in this layer. Lidar ratios of about 70 sr at 355 nm were observed and seem to be smaller at 532 nm.
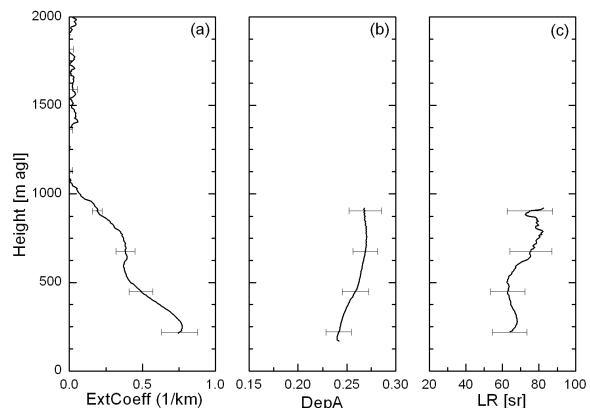
Figure 1. Particle extinction coefficient(a), δ_A (b) and lidar ratio(c) at 355 nm of Saharan Dust measured on January 29, 2008, 18:00 – 20:00 UTC (b) and 21:00 – 22:30 UTC (a, c) with POLIS. The signal profiles were vertically smoothed over 200 m (b) and 400 m (a, c). The error bars indicate the statistical and systematic errors.

These values are consistent with model calculations considering the non-spherical shape of dust particles (Wiegner et al., 2009). Whether the wavelength dependence of the lidar ratio and δ_A will allow conclusions about the size distribution of the dust particles is under investigation. Comparisons with results of the first SAMUM field campaign will be used to study their modification during the transport from the sources. Validation of these finding is provided with in-situ size measurements from the research aircraft FALCON from the German Space Centre (DLR), which are available for both SAMUM field campaigns.

Freudenthaler, V., et al. (2009). *Tellus, 61B,* 165-179
Heintzenberg, J., (2009). *Tellus, 61B,* 2-11
Mattis, I., Ansmann, A., Mueller, D., Wandinger, U. & Althausen, D. (2002). *Geophysical Research Letters*, VOL. 29, NO. 0.
Tesche, M., et al. (2009). *Tellus, 61B,* 144-164
Wiegner, M., et al. (2009). *Tellus, 61B,* 180-194

The African dust event of October 2008

J.A.G. Orza[1], M. Cabello[1], C. Dueñas[2], M.C. Fernández[2], E. Gordo[2], L. Cantón[3] and M.A. Barrero[3]

[1]SCOLAb, Física Aplicada, Universidad Miguel Hernández, 03202, Elche, Spain
[2]Department of Applied Physics I, Faculty of Science, University of Málaga, 29071, Málaga, Spain
[3]Chemical Engineering Group, Department of Applied Chemistry, University of the Basque Country, 20018, San Sebastián, Spain

An intense African dust outbreak (ADO) was detected in southern Spain beginning October 10, 2008. After a northward displacement across the Iberian Peninsula (IP) the dust plume swept most of continental Europe. Daily PM10 levels up to 378 µg/m^3 and daily horizontal visibility values (in absence of rainfall) down to 4.8 km were recorded in Spain. The dust was also observed on the daily SeaWiFS satellite images and by the OMI satellite sensor.

Synoptic charts of 850 hPa geopotential height (NCEP reanalysis), the output of dust dispersion models (DREAM, NAAPS, SKIRON) and backtrajectory analysis (HYSPLIT) show that the dust episode was driven by a relative low in western Algeria combined with a high pressure system in the Central Mediterranean that mobilized a dust plume out of Algeria towards SE Spain on October 9. In the two days following the low intensified and displaced westward to the SW of the San Vicente Cape while the high pressure concentrated over Italy and Tunisia. The synoptic situation changed on October 12: the intense high in the Mediterranean continued injecting dust northward to the IP, while the low to the west of Africa weakened and the combination of the Azores high and the Icelandic low induced NW stream flows that transported dust to France and in subsequent days across continental Europe. On October 14 the high pressure over the Mediterranean weakened and the input of African dust ended. The IP was gradually influenced by the NW flows as the Azores high moved southwestward; correspondingly, the dust was displaced to the east and the aerosol load was reduced from October 16 till 19. From October 20 to 28 two less-intense ADOs were registered, but their influence was limited mainly to southern and eastern Spain.

The evolution of the ADO has been followed according to hourly PM10 data from a considerable number of stations belonging to regional air quality networks in Spain. Maximum daily PM10 levels decrease with latitude (Fig. 1). Such maxima are found to occur on October 11-12 in southern Spain and on October 13-15 in the northern part. At some of the northern locations levels remained just below 50 µg/m^3.

Hourly PM10/PM2.5 ratios for a number of the locations are discussed. A significant increase is found for PM10 and PM2.5 during the dust event. PM10/PM2.5 ratios show an increase not restricted to the traffic hours but extended to the whole diurnal period.

The features of the aerosol number size distributions obtained with an optical particle counter (Grimm 190) in a site on SE Spain are presented as well.
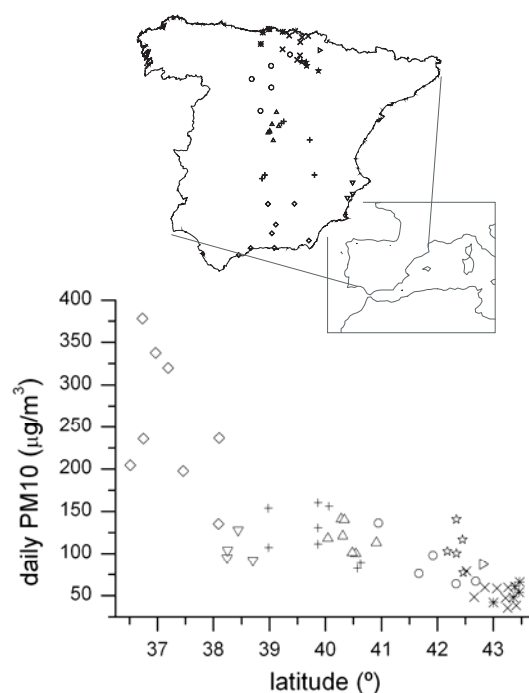
Figure 1. Location of a subset of the monitoring stations (up) and registered maximum daily PM10 levels as a function of the latitude (down).

African and local wind-blown dust contributions at three rural sites in SE Spain: aerosol size distribution

J.A.G. Orza[1,2], M. Cabello[1,2], V. Lidón[2], J. Martínez[2]

[1]SCOLAb, Física Aplicada, Universidad Miguel Hernández. 03202 Elche, Spain
[2]Aeolian Erosion Research Group, Universidad Miguel Hernández. 03202 Elche, Spain

Aerosol number size distribution and meteorological parameters were measured at three rural sites in semiarid southeastern Spain. The influence of both the wind speed and the arrival of air masses loaded with African dust on the airborne particulate distribution was assessed.

Number concentrations of suspended particles in 31 size bins between 0.25 and 32 μm diameter were continuously recorded with a GRIMM 190 aerosol spectrometer at: *(i)* a rural background (RB) location in a perennial tussock grassland, from July to October 2006; *(ii)* a rural site surrounded by abandoned crop lands, and influenced by mineral industries and by a small paved road having a small traffic load located 30 m to the East (RA), from June to December 2007; *(iii)* a rural (R) location in an agricultural plot previously cleared and then lightly leveled and compacted for future lemon-tree cultivation, from February to June 2008.

Events of long range transport from North Africa (African dust outbreaks, ADO) to the study area were identified by the output of aerosol dispersion models, air back-trajectories, satellite imagery and synoptic charts of 850 hPa geopotential height.

Three main findings are reported:

There is an increase in the concentration of particles larger than 2 μm with increasing wind speed while the concentrations decrease for smaller particles. At the RA location, that increase is observed for particles in the range 1.6 – 3.5 μm, the precise value depending on the wind speed, with West winds.

Particulate resuspension is found to occur at all wind speeds, although wind threshold values can be identified by a sharp increase in particulate concentrations for a range of particle sizes. Wind speed thresholds for particle entrainment increase with decreasing particle size (down to 2.5 μm for the highest winds) as interparticle cohesion becomes more important.

The size distributions present maxima at 1.6 and 3 μm on ADOs. Dependence with the season and the pathway followed by the backtrajectories is discussed.

Chemical composition and shape of single aerosol particles generated from different Saharan soil samples during the "Mineral Dust Campaign 2008 – AIDA chamber facility, Karlsruhe"

K. Kandler[1], M. Ebert[1], S. Jäckel[1], K. Lieke[1], S. Weinbruch[1]

[1]Institute für Angewandte Geowissenschaften, Technische Universität Darmstadt, Germany

Keywords: mineral dust, chemical composition, optical properties, electron microscopy.

Detailed knowledge of the mineralogical composition and morphology of particles is important to derive their optical properties and to interpret integral optical measurements of the aerosol ensemble. For this reason, samples from the aerosol chamber were collected with a miniature impactor system on a carbon adhesive. The size-resolved particle aspect ratio and chemical composition is determined by means of scanning and transmission electron microscopy and energy-dispersive X-ray micro analysis for particles between 50 nm and 1 µm in diameter. Mineralogical bulk composition of the parent soils was analyzed by X-ray diffraction analysis.

This work focuses on the aerosol generated from two soil samples. The first one originates from Burkina Faso (BF). X-ray diffraction of sieved fractions shows a very high content of iron oxides (10 to 50 % mass for particles larger than 20 µm) with a hematite:goethite ratio of approximately 2:1. A quartz content of approximately 50 % was measured; the clay minerals illite, kaolinite and muscovite were identified, with kaolinite dominating. The second sample (MO) originates from a hamada NE of the Erg Chegaga, S Morocco. Besides a quartz content of approximately 40 %, 30 % of feldspars (albite and microcline) and 30 % clay minerals are found. The iron oxides content is below the detection limit (2 %).

The variation in the aerosol composition is significantly smaller than in the parent soils. While the bulk BF sample has an iron oxide content more than one order of magnitude higher than the MO sample, this relation decreases to a factor of approximately 2 for the aerosol. In the MO sample, about 10 % of the particles are calcium-rich minerals (gypsum/anhydrite, dolomite and calcite). In contrast, these minerals are not observed in the BF sample. In general, the iron content of the silicate particles of the BF sample is higher than that of the MO silicates by about 50 % relative (see Fig. 1, cluster around Si index 0.4). In addition, in the BF sample a group of particles with approximately 200 nm diameter is observed which show a very high iron content. These particles probably consist of a nano-crystalline iron oxide core with an amorphous silicate coating. The mineralogical phases of the crystallites in the core still have to be determined.

Assuming a constant hematite:goethite ratio (as measured in the BF sample) and a ratio of oxidic iron to total iron of 1:3 (value averaged from litera-ture), a total "absorbing hematite-equivalent" volume abundance of 3.2 % for the BF sample and 1.7 % for the MO sample is estimated.

The shape of the particles is quite complex. However, it can be expressed as a two-dimensional aspect ratio by fitting an ellipse to the particle image outline. The overall resulting median value is 1.8 with low variations between the samples. This is significantly higher than values found for atmospheric mineral dust (1.6, see Fig. 2), which is explained by the presence of chain-like particle aggregates in the former case. The iron-rich 200 nm particles mentioned above exhibit lower aspect ratios (1.57), and thus, the median aspect ratio of the BF sample is slightly lower than that of the MO sample.
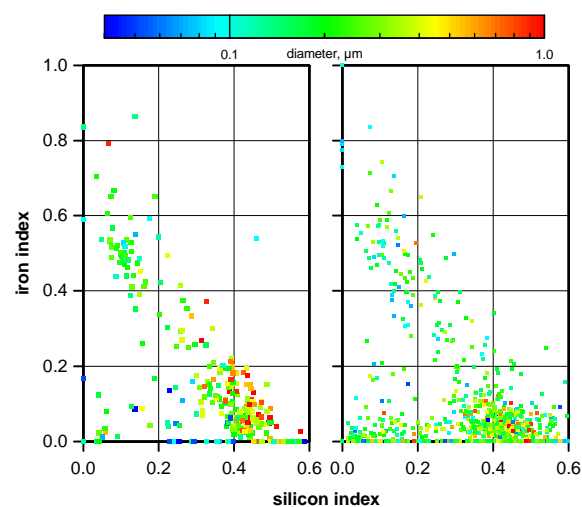
Fig. 1: Comparison of Fe/Si indices for the Burkina Faso (left) and the Morocco (right) sample
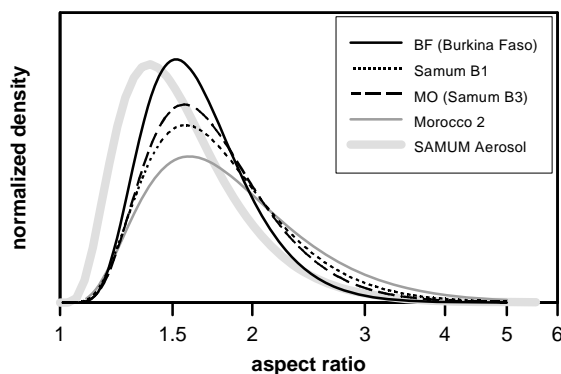
Fig. 2: aspect ratio density distribution

Single particle chemical composition, state of mixing and shape
of fresh and aged Saharan dust
in Morocco and at Cape Verde Islands during SAMUM I and II

K. Kandler[1], C. Deutscher[2], M. Ebert[1], K. Lieke[1], D. Müller-Ebert[1], L. Schütz[2], S. Weinbruch[1]

[1]Institute für Angewandte Geowissenschaften, Technische Universität Darmstadt, Germany
[2]Institute für Physik der Atmosphäre, Johannes-Gutenberg-Universität Mainz, Germany

The Saharan Mineral Dust Experiment (SAMUM) is focussed to the understanding of the radiative effects of mineral dust. During the SAMUM 2006 field campaign at Tinfou, southern Morocco, chemical and mineralogical properties of fresh desert aerosol was measured. The winter campaign of Saharan Mineral Dust Experiment II in 2008 was based in Praia, Island of Santiago, Cape Verde. This second field campaign was dedicated to the investigation of transported Saharan Mineral Dust. Ground-based and airborne measurements were performed in the winter season, where mineral dust from the Western Sahara and biomass burning aerosol from the Sahel region occurred.

Samples were collected with a miniature impactor system, a sedimentation trap, a free-wing impactor, and a filter sampler. Beryllium discs as well as carbon coated nickel discs, carbon foils, and nuclepore and fiber filters were used as sampling substrates. The size-resolved particle aspect ratio and the chemical composition are determined by scanning electron microscopy and energy-dispersive X-ray microanalysis of single particles. Mineralogical bulk composition is determined by X-ray diffraction analysis.

In Morocco, three size regimes are identified in the aerosol: Smaller than 500 nm in diameter, the aerosol consists of sulfates and mineral dust. Larger than 500 nm up to 50 µm, mineral dust dominates, consisting mainly of silicates, and – to a lesser extent – carbonates and quartz. Larger than 50 µm, approximately half of the particles consist of quartz. Time series of the elemental composition show a moderate temporal variability of the major compounds. Calcium-dominated particles are enhanced during advection from a prominent dust source in Northern Africa (Chott El Djerid and surroundings). More detailed results are found in Kandler et al. (2009)

At Praia, Cape Verde, the boundary layer aerosol consists of a superposition of mineral dust, marine aerosol and ammonium sulfate, soot, and other sulfates as well as mixtures of these components. During low-dust periods, the aerosol is dominated by sea salt. During dust events, mineral dust dominates the particle mass (more than 90 %). Particles smaller 500 nm in diameter always show a significant abundance of ammonium sulfate.

Comparing a high dust period at Cape Verde with the total data from Morocco, it is found that the atomic ratio distributions of Al/Si, K/Si and Fe/Si for the single particles are very similar for the dust component. This indicates that the dominating silicate minerals are the same. In contrast, the content of calcium rich minerals at Cape Verde is significantly lower than in Morocco which is in agreement with the source regions for the Cape Verde dust (E Mali and W Niger) derived from trajectory analysis.

The sulfur content of super-micron aerosol particles at Cape Verde scales with the particle surface, indicating the presence of sulfate coatings. For the submicron particles, the sulfur content scales with particle volume, which can be attributed to the large amount of particles identified as ammonium sulfate. In contrast to findings in Japan (Zhang et al., 2006), no internal mixtures between pristine seasalt and mineral dust are present during this dust period at Cape Verde. However, for a significant number of particles a small amount of sodium and chlorine is associated with internal mixtures of dust and sulfate, what may indicate that these particles started as internal mixture of dust with a sea water droplet before taking up more sulfur from the gas phase.

In general, the shape of the particles in Morocco and Cape Verde is rather similar: The distributions of the two-dimensional aspect ratio of an ellipse fitted to each particle's shape for the total aerosol show no significant differences. A median value of 1.6 is found for both locations.

References
Kandler, K., Schütz, L., Deutscher, C., Hofmann, H., Jäckel, S. and co-authors 2009. *Tellus B*, submitted.
Zhang, D., Iwasaka, Y., Matsuki, A., Ueno, K. and Matsuzaki, T. 2006. *Atmos. Environ.* 40, 1205-1215.

Microphysical and optical properties of Mineral Dust Aerosols –

Investigations during the Mineral Dust campaign 2008 at the AIDA facility, Forschungszentrum Karlsruhe

C. Linke[1] , M. Vragel[1] , M. Schnaiter[1], K. Kandler[2] , T. Müller[3] , C. Verhaege[4], A. Petzold[5]

[1]Institute of Meteorology and Climate Research, Forschungszentrum Karlsruhe, Germany
[2]Institut für Angewandte Geowissenschaften, Technische Universität Darmstadt, Germany
[3]Leibniz Institute for Tropospheric Research, Leipzig, Germany
[4]Laboratoire de Météorologie Physique, Clermont-Ferrand, France
[5]German Aerospace Center, Institute of Atmospheric Physics, Oberpfaffenhofen-Wessling, Germany

Keywords: mineral dust, optical properties, size distribution.

Mineral dust aerosols from desert regions affect the earth's radiative budget. The assessment of dust aerosols contribution to the direct radiative forcing is difficult, due to the fact that the dust particles do not only scatter but also absorb electromagnetic radiation over a broad spectral range. Furthermore mineral dusts are complex mixtures of different mineralogical compositions, with broad variations in particle size distribution and particle morphology.

Due to uncertainties in the relation between the microphysical and optical properties of mineral dust aerosols, the Mineral Dust Campaign 2008, at the aerosol and cloud chamber facility AIDA, Forschungszentrum Karlsruhe, was initiated to investigate several mineral dust samples of naturally occurring composition. Aerosol samples from different geographical regions of Africa are investigated. Among these samples, two samples were taken during the field campaigns AMMA/SOP2 and SAMUM-I.

The aim of this chamber experiment was to provide a dust aerosol of defined size distribution and known mineralogical composition. The experimental set-up was intended to realize both inter-comparison of instruments and the closure between micro-physical and optical measurements. Finally, a model for the determination of effective refractive indices of the investigated dust aerosols should be derived.

For aerosol generation, the soil dust samples were sieved first and the fraction of 20 to 75 μm was dry dispersed by a rotating brush generator (RGB 1000, PALAS) in combination with a dispersion nozzle. The re-dispersed aerosol then passes through a stage cyclone with a cut off size of about 1 μm. Altogether six different pure dust aerosols were investigated.

During the experiments the microphysical characterization was performed by APS (TSI), SMPS (TSI), and OPC (Grimm) instruments. For chemical and mineralogical characterization aerosol samples for single particle analysis were taken directly from the chamber.

The optical properties were determined by extinction, scattering and absorption measurements. The extinction coefficients of the dust aerosol were determined by the Long Path Extinction Spectrometer LOPES (FZK). The scattering phase function as well as the total scattering coefficient was determined by a Dual polarization Polar Nephelo-meter D2PN (LaMP). An integrating nephelometer (TSI) measured the total scattering and back-scattering coefficients simultaneously. Absorption coefficients were determined by the three filter based methods PSAP, MAAP and SOAP and by photoacoustic spectroscopy of airborne particles. The 3λ-PSAP (DLR) and the 1λ-MAAP (DLR) measured the absorption at 660nm, 550nm, 467nm and 670nm, respectively. The SOAP (IfT) determined the absorption coefficients between 800-300nm, with a spectral resolution of 50nm. The 4λ-PAS (FZK) measured the absorption coefficient at 1064nm, 532nm, 355nm and 266nm.
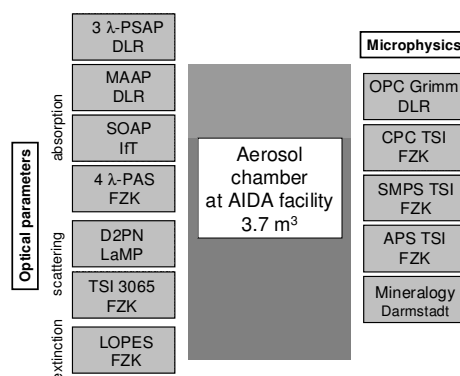
Figure 1. Instrumentation of the aerosol chamber during the Mineral Dust Campaign 2008.

Heterogeneous immersion freezing efficiencies of ice on mineral dust and bacteria

Maren Brinkmann[1], Daniel Rzesanke[1] and Thomas Leisner[1,2]

[1]Institute of Meteorology and Climate Research, Atmospheric Aerosol Research Department, Forschungszentrum Karlsruhe, POB 3640, 76021 Karlsruhe Germany
[2]Institut of Environmental Physics, University of Heidelberg, Im Neuenheimer Feld 229, D-69120 Heidelberg

Formation of cirrus clouds and the initiation of precipitation from tropospheric clouds depend strongly on the liquid to solid phase transition of supercooled cloud droplets. Due to the high aerosol particle concentration in the lower atmosphere, ice particle formation is dominated by heterogeneous freezing processes (Pruppacher & Klett, 1997). This secondary aerosol effect influences the global cloud albedo with high impact to the climate (IPCC, 2007). So far, the nature of these mechanisms is barely understood.

In this work, the heterogeneous immersion freezing of droplets was studied on typical atmospheric aerosols, such as mineral dust particles and *Pseudomonas syringae* bacteria.

To characterise the different nuclei regarding their freezing behaviour, we studied large numbers of individual droplets with an average diameter of 100µm, levitated in an electrodynamic balance inside a miniaturised climate chamber under realistic atmospheric conditions (Davis, 1997 and Duft *et al.*, 2002). The main methods of investigation were microscopy, microspectroscopy and light scattering analysis (Duft & Leisner, 2004).

In contrast to temperature ramp experiments, we repeat the experiment several thousand times at constant temperature, recording the time until a droplet freezes. According to classical nucleation theory, plotting the logarithm of the fraction of unfrozen droplets as a function of time (as shown in Figure 1) allows the determination of the heterogeneous freezing rate J_{het}, which corresponds to the slope of the freezing curve.

As suspensions of realistic heterogeneous nuclei contain particles of various sizes and nucleating abilities, a distribution of J_{het} has to be expected. In our data, this is reflected by the fact that the freezing curves do not exhibit a constant slope, but a steep initial decrease, followed by a much shallower slope at later times. This indicates a broad range of "freezing abilities" amongst the dust particles.

In order to quantify the freezing ability of a certain type of nucleus, we compare the nucleation rate J_{het} of an ensemble of droplets that froze at temperature T_{het} with the nucleation rate J_{hom} of a homogeneously frozen ensemble of droplets at temperature T_{hom}. The difference between the actual temperature T_{het} and T_{hom} is a convenient and descriptive measure for the ice nucleating power of specific germs.

Figure 1. Freezing curves for droplets containing ATD particles. Each data point corresponds to one freezing event. The rapid increase in nucleation rate within a temperature range of only 1°C is clearly visible.

Davis, E.J. (1997). *A history of single aerosol particle levitation*, Aerosol Science and Technology **26**

Duft, D. et al. (2002). *Shape oscillations and stability of charged microdroplets*, Physical Review Letters **89** (8)

Duft, D and Leisner, T. (2004) *The index of refraction of supercooled solutions determined by the analysis of optical rainbow scattering from levitated droplets*, International Journal of Mass Spectrometry **233** (1-3)

IPCC: *Climate Change 2007: Synthesis Report.* [Core Writing Team, Pachauri, R.K and Reisinger, A.(eds.)]. IPCC, Geneva, Switzerland, p.39

Pruppacher, H.R. & Klett, J.D. (1997). *Microphysics of Clouds and Precipitation*; 2nd rev. Edition, Kluwer Academic Publishers; Dordrecht

Spectral absorption of mineral dust: Results of the Mineral Dust Campaign 2008 at the AIDA facility, Forschungszentrum Karlsruhe

T. Müller[1], A. Petzold[2], K. Rasp[2], A. Schladitz[1], M. Vragel[3], M. Schnaiter[3], and C. Linke[3]

[1]Leibniz Institute for Tropospheric Research, 04318, Leipzig, Germany
[2] German Aerospace Center, Institute of Atmospheric Physics, Oberpfaffenhofen, Germany
[3]Institute for Meteorology and Climate Research, Karlsruhe, Germany

Keywords: absorption coefficient, mineral dust, optical properties.

Mineral dust aerosols contribute significantly to the total atmospheric aerosol load. Dust transported over long distances affect the earth's radiative budget by absorption and scattering light in the near ultraviolet, visible and infrared spectral ranges. Optical properties of mineral dust may vary with particle size and mineralogical composition.

The Mineral Dust Campaign 2008 (cf. accompanying contributions to EAC2009), held at the NAUA chamber (IMK, Karlsruhe), was conducted to determine optical and physical properties of re-suspended dust. One of the goals of the experiment was to determine absorption coefficients of different dusts, especially the wavelength dependence in the ultraviolet and the visible spectral range. Several types of systems to measure the absorption coefficient were available. These are filter-based absorption photometers (PSAP, MAAP, and SOAP) and a photoacoustic absorption spectrometer (PAS).

An overview of the systems and methods used in the workshop is given in Table 1. Details on the measurement principles and data evaluation methods can be found in the references. The combined use of these instruments offers a great wavelength range.

Table 1. Systems used for measuring the absorption coefficient of mineral dust. [1]German Aerospace Center (DLR), [2]Leibniz Institute for Tropospheric Research (IfT), [3] Institute for Meteorology and Climate Research (IMK)

Photometer	Wavelengths [nm]	References
PSAP[1]	467, 530, 660	Virkkula et al., 2005
MAAP[1]	637	Petzold et al., 2005
SOAP[2]	300 to 960	Mueller et al., 2009
PAS[3]	266, 355, 532, 1064	Linke et al., 2006

Mineral dust of several sources was investigated. An example of the spectral absorption coefficients ($\sigma_{abs}(\lambda)$) of two different dust samples, collected in Burkina Faso and Morocco, is shown in Figure 1. Both types of dust show a similar dependence on the wavelength. The Ångström absorption exponent, which is a measure of the steepness of the wavelength dependent absorption, is defined by

$$\alpha = -\frac{\ln(\sigma_{abs}(\lambda_1)/\sigma_{abs}(\lambda_2))}{\ln(\lambda_1/\lambda_2)} \ .$$

The Ångström absorption exponent (at wavelengths λ_1=530nm and λ_2=637nm) are 4.35 and 6.41 for the Morocco and Burkina Faso samples, respectively. Measurements of the optical properties of mineral dust in Morocco during the field campaign SAMUM-1 revealed, that the Ångström absorption exponent is between 4.07 and 4.73 for high dust concentrations (Schladitz, 2009).
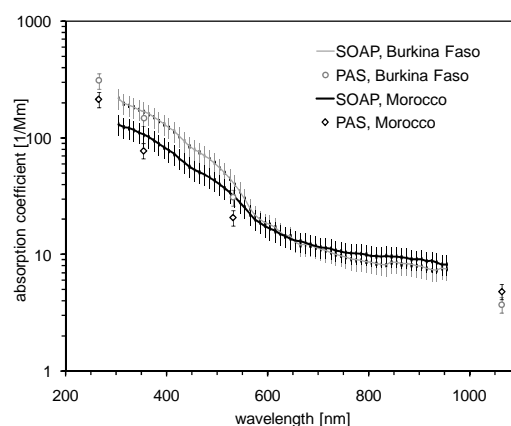
Figure 1. Spectral absorption coefficient of two dust samples measured with SOAP and PAS.

Measurements of spectral absorption and extinction coefficients and the particle number size distribution will be used to estimate effective refractive indices. Derived refractive indices will be related to the mineralogical particle composition.

Virkkula, A., et al. (2005). *Aerosol Sci. Technol.* **39**, 68-83.

Linke, C. et al. (2006). *Atmos. Chem. Phys.* **6**, 3315-3323.

Müller T., et al. (2009). *Tellus* **61B** (1), 79-95.

Petzold et al. (2005). *Aerosol Science & Technology*, **39**, 40-51.

Schladitz, et al. (2009). *Tellus* **61B** (1), 64-78

PM$_{10}$ Source Apportionment Using Factor Analysis: Eastern Mediterranean Case

F.Öztürk, G.Tuncel

Middle East Technical University, Environmental Engineering Department, 06531, Ankara, TURKEY,

Aerosol samples evaluated in this manuscript was collected in a rural station located at Turkish Mediterranean coast between 1992 and 2001. PM$_{10}$ samples were collected on Whatman 41 filters using SIERRA ANDERSEN Hi-Vol sampler. Approximately 2000 samples were gathered within this time frame. Analytical techniques employed in the analysis of collected samples were Inductively Coupled Plasma Mass Spectrometry (ICPMS), Energy Dispersive X-Ray Fluorescence (EDXRF) Spectrometry and Ion Chromatography (IC). Samples were analyzed both in terms of their major ion contents including NH_4^+, NO_3^-, SO_4^{2-} and Cl^-, and also trace element contents from Li to U. This study is unique for Eastern Mediterranean not only for the number of parameters investigated but also time period covered.

In this study, factor analysis with varimax rotation was used to find the sources affecting chemical composition of Eastern Mediterranean aerosols. Scree plot obtained from factor analysis was depicted in Figure 1.
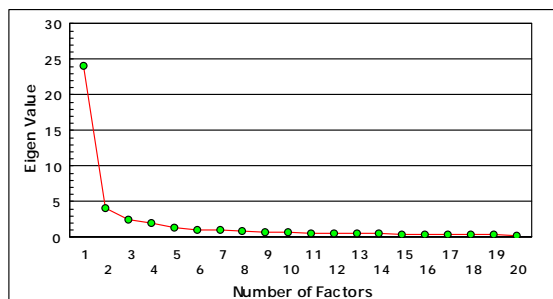
Figure 1.Scree plot obtained from factor analysis

Factors having eigenvalues greater than 1 should be retained in the factor analysis since eigenvalues less than 1 indicate insignificant contribution to system variance. Following these criteria, seven factors were retained in the analysis. Seven extracted factors account for $\wp$ 80 % of the total variance. It is obvious that factor one is a crustal factor since it includes considerably high loadings of soil derived elements such as Al, Ca, Fe and rare earths (e.g., La, Lu, Gd, Tm and Tb). This factor accounts for $\wp$ 54 % of the system variance alone. Recently, Trapp et al. (2008) analyzed the samples collected at Barbados in terms of their lanthanides (Ce, Dy, Eu, Er, Gd, Ho, Lu, Nd, Pr, Sm and Tm) content and tried to use the lanthanides

as marker of dust transported from Africa. Since high loadings of these elements were not observed in other factors, it can be suitable to call this factor as "Saharan Dust" factor. High loadings of SO_4^{2-}, V and Zn implied that this factor is sort of anthropogenic in origin. These elements are well known markers of coal (SO_4^{2-}, Zn) and oil combustion (V). It was previously shown by Güllü et al. (2004) that long range transported material to Eastern Mediterranean had similar composition with one observed here. This factor is responsible for $\wp$ 9 % of the system variance. Third factor has high loadings of Na, Cl, and Mg and moderate loading of K. These elements are markers of sea salt and hence, this factor is called as "sea salt" factor, which responsible for $\wp$ 5.4 % of the total variance. Moderate loadings of Y, V, Ti, Rb, Mn, K, Fe, Cs, Co and Ca in addition to high loadings of Cr and Ni implied that fourth factor is crustal factor. Local soil around the sampling station contains considerable quantities of Cr and Ni (Güllü et al., 2004). Fifth factor accounts for about 3 % of the total variance and has high loadings of As and Ge along with moderate loadings of Cs, Co, Cd, Bi and Be are observed. Arsenic and Ge are typical tracers of coal combustion. For this reason, is called as coal combustion factor. Sixth factor is highly loaded in Pb, Pt, Sb, Sn and W. Lead is the major signature of gasoline use from motor vehicle emissions in the atmosphere. Consequently, we called this factor as motor vehicle emission factor. This factor accounts for 2.5 % of system variance. Last factor contains high loadings of Se and weak loadings of As and Bi. Selenium is mainly emitted from coal combustion. Consequently, this factor is another coal combustion factor.

John Michael Trapp, Frank J. Millero, Joseph M. Prospero, (2008). *Temporal Variability of the Elemental Composition of African Dust Measured in TradeWind Aerosols at Barbados and Miami*. Marine Chemistry, doi: 10.1016/j.marchem.2008.10.004

Güllü, G.(1996). *Long Range Transport of Aerosols.* Ph.D. Thesis, Environmental Engineering Department, Middle East Technical University, Turkey, Ankara

Güllü, G., Ölmez, I., and Tuncel, G. (2004). *Source apportionment of trace elements in the Eastern Mediterranean atmosphere*. Journal of Radioanalytical and Nuclear Chemistry 259 (1), 163-171

Simulation of the impact of mineral dust on the monsoon flow and the easterly jet above Western Africa

T. Stanelle, B. Vogel, V. Klüpfel, H. Vogel, Ch. Grams, S. Jones

Institut für Meteorologie und Klimaforschung, Forschungszentrum Karlsruhe / Universität Karlsruhe, 76021 Karlsruhe, Germany

Beside sea salt mineral dust is the most important source of aerosols for the atmosphere. One of the earth's largest sources of mineral dust is the Saharan desert in West Africa. The impact of mineral dust on the state of the atmosphere and especially with the dynamics on the regional scale is currently not very well quantified. We are applying the numerical model system COSMO-ART (Vogel et al., 2009, Stanelle, 2009) for a dust episode that occurred during the GERBILS campaign to study feedback processes of mineral dust and the state of the atmosphere on the regional scale. The meteorological driver of the model system is the operational weather forecast model COSMO (former LM, Steppeler *et al.*, 2003) of the German Weather Service. The current version of COSMO-ART allows an estimation of the direct effect caused by natural and anthropogenic aerosols. The calculated radiative fluxes are modified by the correspondingly simulated aerosol load at each time step. Since the model system is fully online coupled it allows the estimation of the feedback processes of the aerosol and the atmosphere.

The field campaign GERBILS (Marsham et al., 2008) was organized by the UK Met Office and took place in June 2007. During an episode that lasts from June 19th -25th, 2007 dust was emitted at the western side of a heat low and transported southward by the thereby strengthened Harmattan. At the inner tropical depression zone (ITD) which separates the southerly Harmattan flow from the northerly monsoon flow the emitted dust particles are lifted upward. At higher elevations the dust is transported further southward and finally gets incorporated in the easterly African jet (Figure 1).

We carried out two sets of simulations one taking into account the feedback processes initialized by the mineral dust and a second one where the feedback was switched of and the radiative effects of the mineral dust particles are therefore neglected. North of the ITD the mineral dust layer is attached to the surface. This leads to an increase of the temperature in the boundary layer and a decrease of the temperature at higher elevations. South of the ITD the elevated dust layer leads to a cooling inside of the monsoon flow and to a warming above it. This dipole like temperature difference (Figure 2) caused by the mineral dust intensifies the flow systems including the vertical uplift of the mineral dust particles. This is an impressive example of a feedback mechanism that is currently not accounted for numerical weather forecast models.
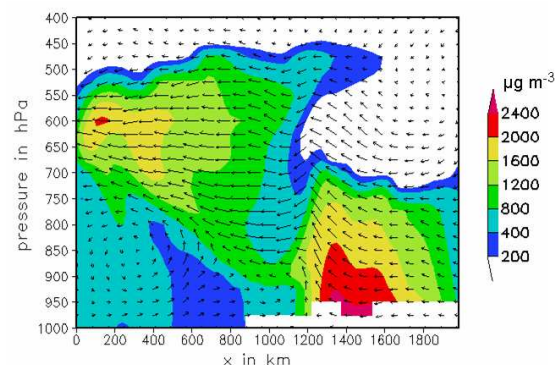
Figure 1. Simulated wind vectors and dust concentration at 15:00 UTC, June 21st, 2007.
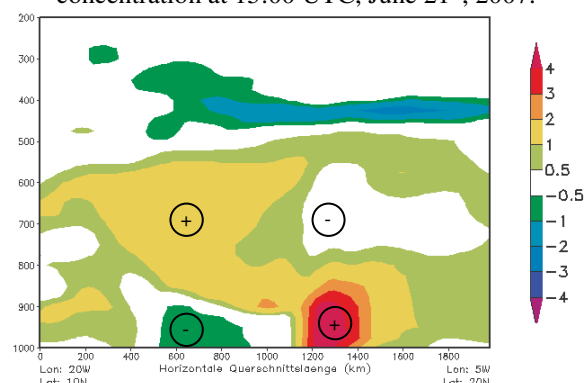
Figure 2. Simulated temperature difference due to mineral dust in K at 15:00 UTC, June 21st, 2007.

Marsham, J.H., Parker, D.J., Grams, C.M., Taylor, C.M., Haywood, J.M. (2008), J. Geophys. Res., 113 (D21102), 1-14, DOI 10.1029/2008 JD009844.

Steppeler, J., G. Doms, U. Schättler, H. W. Bitzer, A. Gassmann, U. Damrath and G. Gregoric (2003), *Meteorology and Atmospheric Physics*, 82, 75-96.

Stanelle, T. (2009), PhD Thesis, Universität Karlsruhe, Germany.

Vogel, B., H. Vogel, D. Bäumer, M. Bangert, K. Lundgren, R. Rinke, T. Stanelle, (2009) *submitted to APCD*.

Particle size distributions of dust during the Mineral Dust Campaign 2008 at the AIDA facility Karslruhe – How well compare different sizing methods?

A. Petzold[1], A.Veira[1], K. Rasp[1], D. Delhaye[1], T. Müller[2], K. Kandler[3], C. Verhaege[4], M. Vragel[5], and C. Linke[5]

[1]Institut für Physik der Atmosphäre, DLR, Oberpfaffenhofen, 82234 Wessling, Germany
[2]Leibniz Institut für Troposphärenforschung, Permoserstrasse 15, 04318 Leipzig, Germany
[3] Institut für Angewandte Geowissenschaften, TU Darmstadt, 64287 Darmstadt, Germany
[4] Laboratoire de Météorologie Physique, Clermont-Ferrand, France
[5] Institut für Meteorologie und Klimaforschung, Forschungszentrum Karlsruhe, 76021 Karlsruhe, Germany

Keywords: mineral dust, optical properties, size distribution.

Dust particle size distributions and information on dust refractive index and particle shape are key input parameters for the determination of optical and radiative properties of airborne dust. Climate models require this data together with information on the vertical distribution of desert dust. During the Mineral Dust Campaign 2008 at the AIDA facility, special emphasis was put on the measurement of dust size distributions and mass with different methods in order to assess the uncertainties in dust size distribution measurement.

Measuring particle size distributions of airborne dust is still a challenge. The main reasons for the existing measurement uncertainties are

1. the wide size ranged of mineral dust particles extending from the sub-µm accumulation mode to giant dust particles larger than 100 µm,
2. the irregular shape of dust particles, and
3. the limited number of measurement methods available for this application.

Airborne dust particles can be sized by optical methods such as light scattering techniques, and by aerodynamic sizing methods such as Aerodynamic Particle Sizers or Impactors. Sizing by morphological methods using microscopy analyses of particles collected on appropriate matrices is only of limited applicability to airborne measurements due to detection limit issues. The available methods measure different properties such as aerodynamic equivalent diameters, optical equivalent diameters, or geometric diameters. Table 1 summarises the methods used during our studies.

Table 1. Methods for measuring particle size and mass during the Mineral Dust Campaign 2008.

Instrument	Property
Optical Particle Counter GRIMM 1.109	Light scattering, optical equivalent diameter
SMPS	Electrical mobility, mobility diameter
APS	Aerodynamic sizing, aerodynamic equivalent diameter
Filter sampling	Total mass, morphology
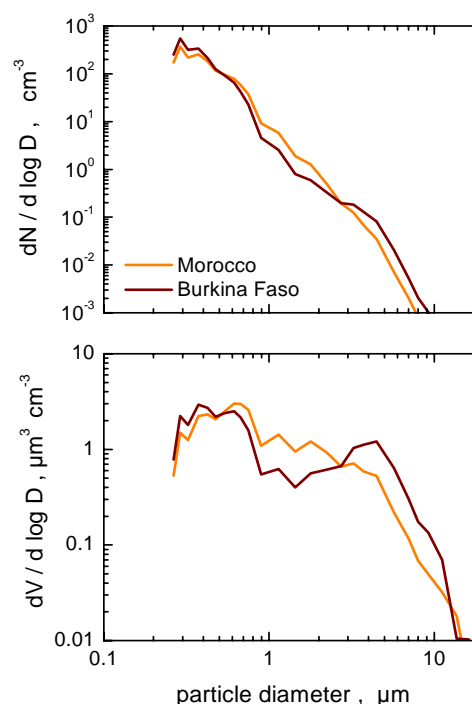
Figure 1. Size distribution of dust from Morocco and Burkina, re-suspended in the aerosol chamber of AIDA and measured downstream a cyclone.

As is shown in Figure 1, the dust re-suspended from bulk samples shows different number (top) and volume (bottom) size distributions depending on its origin, which will be compared to measurements in Morocco with airborne dust of similar origin (Petzold et al., 2009; Weinzierl et al., 2009). The results from closure studies on the methods applied at AIDA (Table 1) will be used to quantify uncertainties of dust size measurements in airborne field studies.

Petzold, A., et al. (2009). *Tellus* 61B, 118-130.

Weinzierl, B., et al. (2009). *Tellus* 61B, 96-117.

Determination of aerosol particle size distribution for mineral dust during the SAMUM campaign

M. Diouri[1], W. von Hoyningen-Huene[2], T. Zarrouk[1], T. Dinter[2], A. Kokhanovsky[2], J.P Burrows[2]

[1]LPA, University Mohamed 1st, Oujda, Morocco, [2]IUP, University of Bremen, Bremen, Germany

Keywords: Aerosol optical depth, Almucantar, Inverse problems, Particle size distribution, Sunphotometer

Ground closure measurements of Aerosol Optical Thickness in Morocco on May-June 2006 under AERosol VALidation project (AERVAL) which is a part of SAharan Mineral dUst experiMent (SAMUM) consortium research projects has permitted the determination of the corresponding columnar particle size distribution characteristics. The measurements, consisting of spectral sun photometer measurements of direct solar radiation, angular and spectral sky radiance in the almucantar have been made using a CIMEL CE 318 sun photometer at the site TINFOU (30.237°N, 5.607°W, 750m of altitude), a plane desert with free horizon near the main source of mineral dust over the word, 30 Km south of the city Zagora. The instrument was calibrated by numerous Langley-plot measurements at various locations and at various temperature conditions. For measurements in the desert region of Morocco with diurnal temperature changes from 20 to 45°C the temperature correction was essential to get correct spectral behaviour of AOT. Linear temperature sensitivities have to be accounted for all channels. The largest temperature sensitivities are in the UV and the NIR channels. The AOT is derived from corrected total optical thickness by making corrections for Raleigh scattering and gas absorption which is considered for ozone and water vapour, for the desert case in Morocco NO_2 absorption is not considered.

For the retrieval of particle size distribution, the coupled inversion radiation transfer CIRATRA approach (von Hoyningen-Huene and Posse, 1997) and CLEOPATRE code of calculus (Diouri and Sanda, 1997) are used. The tow inversion problem algorithms are based on non linear inversion method where the columnar PSD is deduced from spectral AOT and a fixed refractive index for CLEOPATRE and from spectral AOT and sky radiance in the almucantar and unknown refractive index in the range 1.31 to 1.70 with convergence constraint for CIRATRA. For the latter one we give below an example of results obtained with mean characteristics. The particle sphericity approach is discussed versus different representation models.
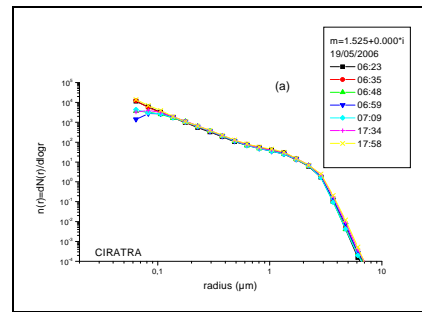
Radius (µm)	σ	N
0.044	1.98	4476
0.525	1.39	81
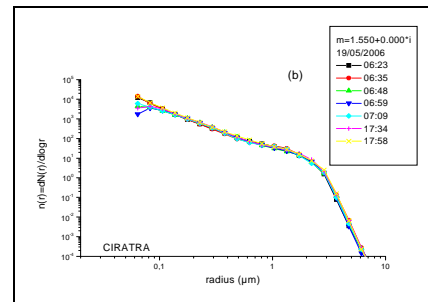
Radius (µm)	σ	N
0.069	2.02	5373
0.54	1.94	294

Example of distribution obtained at TINFOU for m = 1,525+ 0000i (a) and for m= 1,550 + 0000i (b)

Von Hoyningen-Huene et all. (2009). Measurements of desert dust optical characteristics at Porte au Sahara during SAMUM Tellus, **61B**, 206-215

Diouri, M. and Sanda I.S. (1997). Deduction of particle size distribution from aerosol optical depth CLEOPATRE-1 code *J. Aerosol Sci. 28, S459-S460*

von Hoyningen-Huene W. and P. Posse (1997) Non sphericity of aerosol particles and their contribution to radiative forcing. J. Quant. Spectr. Rad. Trans. 57, 651-668

Composition of Saharan dust and its possible source regions – a review

D. Scheuvens[1], L. Schütz[2], K. Kandler[1], M. Ebert[1] and S. Weinbruch[1]

[1]Institut für Angewandte Geowissenschaften, Schnittspahnstraße 9, TU Darmstadt, 64287, Darmstadt, Germany
[2]Institut für Physik der Atmosphäre, Universtiät Mainz, Becherweg 21, 55128, Mainz, Germany

Keywords: Saharan dust, source identification, composition.

The Sahara is the strongest source on earth for mineral dust, supplying up to 10^9 t per year of material to the atmosphere (about 50 % of the total mineral dust burden). Saharan dust is subject to long-range transport and may be transported over thousands of kilometers (e.g., across the Atlantic Ocean). The exact consequences of Saharan dust input into the atmosphere are still a matter of debate (Heintzenberg, 2009), but it is generally accepted, that the introduction of mineral matter into the atmosphere has large impacts on the global radiation balance (direct and indirect forcing), thus influencing the climate system from a global to a local scale. Furthermore, the uplift, transport and settling of Saharan and Sahelian dust significantly changes the terrestrial and oceanic systems in the regions of dust entrainment and settling. Hence, a better knowledge of the potential source areas in the northern part of Africa may lead to an improvement of (paleo)climate models. We have compiled the available bulk analysis data (mineralogy, elemental and isotope composition) of Saharan and Sahelian aerosols and soils in order to distinguish source regions with specific compositional characteristics.

Region 1: Atlas region
The bulk mineralogical data of dusts that originated in the Atlas region clearly shows a general high amount of carbonates (with calcite > dolomite) in good agreement with the geology and the outcropping soils. Dusts from the Atlas region are also characterized by the highest illite/kaolinite ratios in northern Africa (> 2.0). Furthermore, palygorskite has been detected in many soil samples in this area and may be also present as an additional marker in the uplifted dust. The high carbonate content and the low content of Fe-bearing minerals (hematite, goethite) of the potential source sediments leads to very low Fe/Ca ratios in the dust. Based on the available isotopic data (Grousset *et al.*, 2005), a further sub-division into a northern Atlas source region with lower ^{87}Sr/^{86}Sr ratios (< 0.725) and higher $\varepsilon_{Nd}(0)$ values (> -15) and a southern Atlas source region with relatively high ^{87}Sr/^{86}Sr ratios (> 0.725) and low $\varepsilon_{Nd}(0)$ values (< -15) is possible.

Region 2: Libya, Egypt
Compared to the Atlas region, dusts that originated in Libya or Egypt are characterized by a lower but still significant carbonate content and a scarcity of palygorskite. Illite/kaolinite ratios show a general decrease from west to east and hence are relatively low in NE Africa (< 1.0). $\varepsilon_{Nd}(0)$ values of potential source sediments in Libya and Egypt are of the same order as the $\varepsilon_{Nd}(0)$ values of source sediments from the northern Atlas source region, but show increasing values from western Libya (< -15) towards Egypt (> -11). More diagnostic are the low ^{87}Sr/^{86}Sr ratios (< 0.720) that are characteristic for source sediments from Tunisia, Egypt and Libya.

Region 3: Sahelian region (Chad, Niger, central Mali, Mauritania)
The most characteristic criteria for the Sahelian (or Sub-Saharan) region are the general absence of carbonates and palygorskite in the analyzed soil and dust samples and the very low illite/kaolinite ratios of < 0.5. Again, on the basis of the isotope data this very large potential source region can be sub-divided into an eastern sector with lower ^{87}Sr/^{86}Sr ratios (< 0.720) and higher $\varepsilon_{Nd}(0)$ values (around -12) and a western area with higher ^{87}Sr/^{86}Sr ratios and lower $\varepsilon_{Nd}(0)$ values (around -15).

Region 4: southern Algeria, northern Mali
This area is located in an intermediate position between the Sahelian and Atlas region. Dust and soil samples from this area exhibit relatively low illite/kaolinite ratios (c. 0.5), clearly discriminating it from samples from the Atlas region. Calcite contents are variable, probably depending on the exact location of dust entrainment. Palygorskite is generally rare. Isotope data is scarce, but ^{87}Sr/^{86}Sr ratios are probably higher than 0.720 and extrapolated $\varepsilon_{Nd}(0)$ values fall in the range between -15.0 and -12.0.

Our review of the available compositional data of Saharan and Sahelian dusts and soils reveals that a combination of different methods leads to an improved characterization of potential source areas. However, it has to be claimed that the areal density of the data is still far from satisfactory.

Grousset, F. E. & Biscaye, P.E. (2005). *Chem. Geol.*, 222, 149-167.
Heintzenberg, J. (2009). *Tellus*, 61B, 2-11.

Have Saharan dust plumes any impact on Ozone retrieval from UV nadir satellite spectrometers?

J. Andrey[1], M. Gil[1], A. Redondas[2], M. Navarro[1], M. Schneider[3] E. Cuevas[2]

[1]Instituto Nacional de Técnica Aeroespacial (INTA), Ctra. Ajalvir km. 4, Torrejón de Ardoz, 28850, Spain
[2]Agencia Estatal de Meteorología (AEMET), Observatorio de Izaña, La Marina 20, 28071, Sta. Cruz de Tenerife, Spain
[3]Institute for Meteorology and Climate Research, Trace Constituents in the Stratosphere and Tropopause Region, University of Karlsruhe and Karlsruhe Research Centre, Germany

Keywords: Dust, Ozone, Satellites, Aerosol impacts, Columnar properties.

Saharan aerosols containing iron absorb radiation in the UV at a somewhat uncertain rate (Torres et al., 2005). It has been reported that large extensions of absorbing aerosols might degrade the accuracy of the column of gases in satellite nadir-viewing spectrometers operating in the UV by introducing artifacts in the retrieval associated to changes in the weighting functions that cannot be properly accounted for (Torres & Bhartia, 1999).

Two airborne campaigns in the frame of the TROMPETA project have been designed to scan the atmosphere in the Canary Islands area in order to characterise the optical properties of the aerosol layer. Extinctions were used to feed LIBRADTRAN transfer radiative model with the aim of clarification the degree of perturbation of ozone measurements in satellite nadir configuration. INTA C212 atmospheric aircraft, ground based and satellite instrumentation have been used to achieve project goals.

Instruments operating in different spectral ranges (Brewer UV-direct sun, DOAS in the visible at zenith and FTIR direct sun) at Izaña Observatory (28N, 16W, 2360 m.a.s.l.) have been compared with on-board SCIAMACHY, TOMS in versions 7 and 8, OMI and GOME spectrometers datasets from 1999 to 2008. Special attention has been paid to the days on which TROMPETA campaigns were carried out. Methodology applied is independent for every instrument. Aerosol Optical Depth (AOD) at 440 nm measured by AERONET at Izaña observatory has been used to validate a "dust index" defined as two-wavelength ratio colour index from DOAS measurement. Colour index allows extending the period of study from 1999 to nowadays.

Preliminary results do not show the expected large discrepancies between the different techniques (UV and Vis) and observations modes (direct sun, diffuse-nadir, diffuse-zenith) expected under large aerosol loading. All instruments show ozone reductions during the campaigns days as compared to "non-dust" days, ranging from of -1.4% (DOAS) to -2.1% (OMI) which is half of what was predicted by radiative transfer models for the loading and vertical distribution of the dust. Statistic of the ozone departures from low-pass filter versus AOD show no tendency for visible spectrometer operating in Chappuis, slight negative for Brewer, TOMS-V8 and OMI and largest negative for TOMS-V7. However, even in this later case, the observed reduction is smaller than that predicted by the models. Models can fit the observations if Saharan dust single scattering albedo is increased from the WMO recommended values to the suggested ones by recent measurements.

Torres O., P. K. Bhartia, A. Sinyuk, E.J. Welton and B. Holben, *Total Ozone Mapping Spectrometer measurements of aerosol absorption from space: Comparison to SAFARI 2000 ground-based observations.* J. Geophys. Res., 110, D10S18, doi: 10.1029/2004JD004611, 2005.

Torres O. and P. K. Bhartia, *Impact of tropospheric aerosol absorption on ozone retrieval from backscattered ultraviolet measurements.* Journal of Geophysical Research D:Atmospheres, 104(D17): 21569-21577, 1999.

Measured vertical profiles of aerosol number concentrations inside the PBL over the boreal forest in Finland

A.S. Staroverova [1], M. Boy[1], T. Gronholm[1], L. Laakso[1], A. Guenther[2], A. Sogachev[1] and M. Kulmala[1]

[1]University of Helsinki, Dept. Physics, P. O. Box 64, 00014 Univ. of Helsinki, Finland
[2]ACD, NCAR, P.O. Box 3000, 80307 Boulder, Colorado, USA

Keywords: atmospheric aerosols, aerosol measurements, boundary layer, CPC, vertical distribution.

The daily pattern of particle concentrations in the lower atmosphere is in rural areas strongly affected by the emissions of volatile organic compounds (VOC) from the biosphere (Guenther *et al*., 2000). These VOCs are believed to play an important role in new atmosphere particle formation events (Boy *et al*., 2003). The aerosol particles have essential impacts (such as cloud formation, scattering and absorbing of radiation) on the atmosphere radiation balance and hence the climate (Lohmann & Feichter, 2005). Therefore a wide understanding about the vertical structure of aerosols is important.

In this study we measured aerosol particle concentrations in the planetary boundary layer with a tethered balloon and a portable condensation particle counter (CPC TSI 3007). The measurements took place in Hyytiälä, Southern Finland, above a boreal forest in four seasons.

The vertical structure of the aerosol particles were dominated by the temperature inversion and mixed layer height. We found that the measurements at the ground are good estimate for the whole mixed layer. In our experiments the concentrations inside and above the mixed layer were approximately constant, decreasing with height and showed small gradients. On the top of mixed layer the concentrations sharply decreased with height (see Fig. 1). When the atmosphere was not mixed, concentrations showed the same distribution with height in stable and in the residual layers, with large gradient between them. When MLH developed in the morning or decreased in the evening aerosol concentration profiles followed this change: and aerosol particles were diluted to the higher layers or deposited to the lower layers of the atmosphere. This enables the use of ground-based measurements to represent the concentration within the boundary layer. Aerosol concentration distinctly increased within all measurement height when air mass changed from clean northern or western to polluted southern or eastern origin. We also noticed that (in autumn and spring) the aerosol particle concentration measurements from the evening were a good estimate for the next morning's concentration in the residual layer, in conditions where no change of air mass and no rainfall was observed. This enables the use of ground-based measurements to represent the concentration within the boundary layer. These results can be important for initializing aerosol background concentration vertical profiles in chemical and aerosol models.
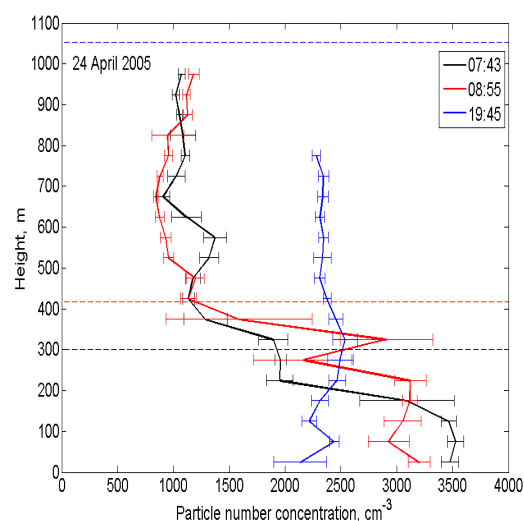
Figure 1. Aerosol particle concentration measured during soundings on 24th April 2005. Solid horizontal lines are error bars. Dashed horizontal lines are mixed layer heights predicted by the model SCADIS (Sogachev *et al*., 2002)

Boy M., Rannik Ü., Lehtinen K.E.J., Tarvainen V., Hakola H., & Kulmala M. (2003). *J. Geophys. Res.* 108 (D21), 4667.

Guenther A., Geron C., Pierce T., Lamb B., Harley P., & Fall R. (2000). *Atmos. Environ.* 34, 2205-2230.

Lohmann U., & Feichter J. (2005). *Atmos. Chem. Phys.*, 5, 715-737.

Sogachev, A., Menzhulin, G., Heimann, M., & J. Lloyd, (2002). *Tellus* 54B (5), 784-819.

Aerosol chemical composition at the Island of Lampedusa (Central Mediterranean): a strategic site for studying aerosol-climate interactions

S. Becagli[1], C. Bommarito[2], G. Calzolai[3], M. Chiari[4], A. di Sarra[5], F. Lucarelli[3], S. Nava[4], F. Rugi[1], M. Severi[1] D.M. Sferlazzo[2], R. Traversi[1] and R. Udisti[1]

[1]Department of Chemistry, University of Florence, Sesto F.no, I-50019, Florence, Italy
[2] ENEA, Climate Laboratory, I-90141, Palermo, Italy
[3]Department of Physics, University of Florence, Sesto F.no, I-50019, Florence, Italy
[4]INFN, Sesto F.no, I-50019, Florence, Italy
[5]ENEA, Climate Laboratory, I-00123, S. Maria di Galeria, Italy

Marine aerosols contribute significantly to the global aerosol budget, considering that about 70% of the Earth is covered by oceans. Significant impact of secondary marine aerosols (mainly $nssSO_4^{2-}$ and methanesulphonic acid – MSA) on global climate was first demonstrated by Charlson *et al.* (1987). In addition, significant amounts of submicron and large sea salt particles can be found in the marine atmosphere, also affecting the properties of marine CCN (O'Dowd *et al.* 2004). Due to the relevant role of aerosol in affecting climate, studies of variability in aerosol chemical composition at marine sites coupled with optical properties are requested in order to understand the complex aerosol-climate interactions, and reduce the uncertainty in the determination of the aerosol radiative forcing (IPCC, 2007).

To this purpose, a sampling campaign was carried out at the Station for Climate Observations at the island of Lampedusa (35° N, 12.6° E). Continuous observations of greenhouse gases concentration, aerosol properties, total ozone, ultraviolet irradiance, and other climatic parameters are routinely carried out (di Sarra *et al.*, 2002) at Lampedusa. Since June 2004, a continuous aerosol sampling has been performed with daily resolution by pre-selected cut-off sampler equipped with PM10 sampling head. After mass determination, each filter was analyzed for main and trace ions (Na^+, NH_4^+, K^+, Mg^{2+}, Ca^{2+}, F^-, Cl^-, NO_3^-, SO_4^{2-}, MSA, acetate, formate, glycolate, oxalate), and selected metals (soluble fraction at pH = 1.5). Half filter was analysed by PIXE for total (soluble and insoluble) elemental content.

The Positive Matrix Factorization (PMF) model has been applied to the chemical data in order to obtain the source apportionment of the PM10 at Lampedusa. The dominant sources have been found to be primary marine, crustal, secondary and continental-anthropic.

The source temporal profiles, obtained by PMF, allow to identify events in which one of the sources is mainly evident, making possible the correlation between source chemical composition and column-integrated aerosol optical properties (optical thickness and Angstrom exponent). In particular, Saharan dust intense events have been detected from the temporal evolution of the crustal component, and their attribution is confirmed by back-trajectory analysis. For these events, some ratio (w/w) between crustal markers have been calculated and reported in table 1 together with mean ratios in Earth's crust.

Table 1. Ratio of selected marker calculated in Saharan dust events and mean Earth crust.

Ratio	Saharan dust events (w/w)	Mean crust (w/w)
Al/Si	0.4	0.30
Ca/Si	1.1	0.15
Fe/Si	0.4	0.20
Ti/Si	0.04	0.02

Also the soluble fraction of selected markers has been calculated showing different percentages as a function of source. For iron, this percentage in Saharan dust aerosol is about 5% but can reach 50% in aerosol coming from anthropized areas. The determination of soluble fraction of oligo-elements in aerosol deserve particular attention in the study of biogenic productivity as an answer to dust deposition over marine areas. The correlation between Saharan dust deposition and marine phytoplanktonic productivity, as revealed by atmospheric concentration of MSA, was also investigated. Higher MSA concentration occurs about one week later than intense Saharan dust event, even if the relationship between MSA concentration and intensity of Saharan dust event is not linear.

Charlson, R.J., & 3 others (1987), , *Nature*, 326, 655–661.

IPCC, 2007. The physical science basis. Contribution to the Forth Assessment Report of the Intergovernmental Panel on Climate Change, Cambridge University Press, Cambridge, UK.

di Sarra, A., & 9 others. (2002), *J. Geophys. Res.*, 107(D18), 8135, doi:10.1029/2000JD000139.

O'Dowd, C.D. and 8 others (2004), *Nature*, 431, 676– 680.

Supermicron aerosol particles near open-pit lignite mine

P. Pokorná[1], J. Hovorka[1] and J. Brejcha[2]

[1] Institute for Environmental Studies, Faculty of Science, Charles University in Prague, Benátská 2,
128 01, Prague 2, Czech Republic
[2] The Brown Coal Research Institute, j. s. c., Budovatelů 2830, 434 37, Most, Czech Republic

Keywords: PM₁₀, PM₂.₅, aerosol size distribution, fugitive dust, rural air quality

Exploitation of lignite deposits usually lead to deterioration of air quality (Jones, 2001). Large coal basin in the Northern Bohemia in the Central Europe, besides the mining industry, also attracted large technology complexes. Such cumulation of potential air pollution sources caused serious problems of air quality not only in the past, but also in lesser extent, at nowadays.

The purpose of this study was to contribute to the estimation of possible sources of the coarse fraction of aerosol in rural areas close to opencast lignite-mine.

Measurements were conducted in the Northern Bohemia in proximity to an open-pit coal mine Nástup of area near 45 km². Five sampling localities were chosen around the perimeter of the mine (Table. 1.) Summer sampling campaign went from the 11th Jul to the 27th Jul 2008. The 24 hour PM₁₀ by Harvard Impactor (HI) and PM2.5 by Sioutas Cascade Impactor (SCI) were sampled in the study. 5 minute data on meteorology (wind speed/direction, temperature, relative humidity, global radiation) and 30 minute PM₁₀ by Beta-attenuation monitors were also concurrently measured at each station.

Table 1. List of the sampling stations.

Sampling station / Sampler	Geographic coordinates	Location to the mine
Březno- Kontejner (HI-K, SCI)	50° 24' N 13° 25' E	SE
Březno – Čistička (HI-C)	50° 23' N 13° 24' E	SE
Výsypka (HI-V)	50° 26' N 13° 19' E	SW
Málkov (HI-M)	50° 23' N 13° 19' E	NW
Spořice (HI-S)	50° 26' N 13° 23' E	NE

There are several sources of the aerosol particles distinguished according to particle size in the study area. Coarse particles are emitted by lignite mining/transportation/pulverization, and by dumping arable land, gypsum and fly ash. Fine particle are generated by large combustion processes, i.e. coal power stations, ironworks, local heating and transportation.

Contrary to our expectations there was not a significant difference in PM₁₀ among all of the five sampling stations during the study period (Figure 1.) though their different distance and orientation with respect to mining activity.
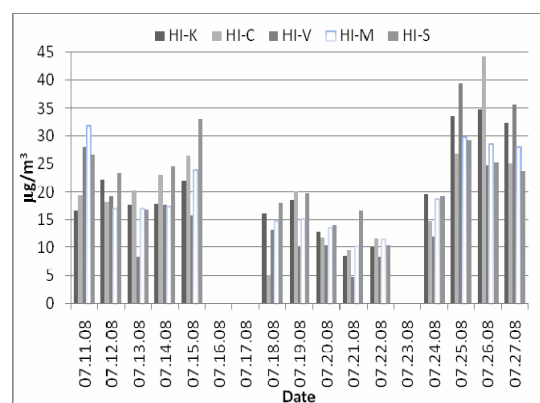
Figure 1. Temporal variation of PM₁₀ by HI round the mine during summer sampling campaign.

Also correlation between meteorology parameters and aerosol mass, which points to fugitive dust sources, was weak. The reason is, that coarse fraction formed on average 24% of total aerosol mass while particles below 250 nm of aerodynamic diameter surprisingly formed on average 67% of total aerosol mass. So we concluded that high temperature processes surpassed fugitive aerosol sources during the study period. Our conclusions were also confirmed by concurrent measurements of 5 minute integrates of aerosol size distribution from 14-10000 nm size. Particle size distribution is important for human exposure and risk assessment, as well as for aerosol particle reconnaissance and understanding the mechanisms of atmospheric processes (Morawska, 1999).

Jones, T., Blackmore, P. Leach, M., Bérubé, K., Sexton, K. & Richards, R. (2002). *Environ.Monit. Asses.*, 75, 293-312.

Morawska, L., Stephen, Th. Jamriska, M. & Johnson, G. (1999). *Atmos. Environ.*, 33, 4401-4411.

Pollution Levels in Fog at the Chilean Coast

E. Sträter[1], A. Westbeld[1], H. Larrain[2], P. Osses[3], P. Cereceda[3], O. Klemm[1]

[1]University of Münster, Climatology Working Group, Robert-Koch-Str. 26, 48149 Münster, Germany
[2]Atacama Desert Center ADC, Pontificia Universidad Católica de Chile and Universidad Bolivariana, Iquique.
[3] Institute of Geography, Pontificia Universidad Católica de Chile, Santiago de Chile, Chile.

Keywords: air pollution, fog, enrichment factor, back trajectories

During July and August 2008 fog water was collected for chemical analysis in Patache, at the coast of northern Chile, 60 km south of Iquique (20°49'S, 70°09'W). Advective and orographic fog events occur regularly at the cliff in the coastal range at about 800 m above MSL. People collect these types of fog water at some places along the coast with Large Fog Collectors (LFC) for domestic use and for watering field crops. So far, no chemical analysis of fog water was performed in Patache. Pure fogwater samples were taken by using a passive Scientific Cylindrical Fog Collector. Major ions and trace metals were quantified.

	median μeq/l	median %	mean μeq/l	min μeq/l	max μeq/l
pH	3.3		3.2	2.4	3.8
H^+	500	16	710	150	3600
NH_4^+	77	2.4	100	12	410
K^+	27	0.8	35	2.7	240
Na^+	700	22	880	120	3900
Ca^{2+}	100	3.2	140	27	560
Mg^{2+}	180	5.7	220	35	1000
Cl^-	610	19	810	110	3300
NO_3^-	230	7.1	390	42	2400
PO_4^{3-}	< 3.0	0.0	< 3.0	1.6	220
SO_4^{2-}	780	24	1200	119	7600
total	3204		4485		

Table 1. Statistical summary for pH (without unit) and major ion concentrations in the fogwater samples as collected in Patache, Chile.

The analyses indicate very high median ionic concentrations (3204 μeq/l, Tab. 1). Observed pH's range between 2.4 and 3.8. The median H^+-concentration represents 16 % of the total ionic equivalent concentration. Sulfate is the anion exhibiting the highest concentrations. A median value of 780 μeq/l was found, which accounts for 24 % of the total median concentration. In contrast to sulfate, nitrate shows only a low percentage of 7.1 %. Further major ions are sodium and chloride, which are typical seasalt ions in coastal fog.

High correlations between the measured ions suggest a causal link between concentration in the fog samples and the liquid water content (LWC) of the cloud. The higher the liquid water content the lower are the ionic concentrations. During our measurement period orographic fog led to higher concentrations in fog water than advective fog.

Enrichment factors with sodium as reference ion were calculated to identify potential emission sources contributing to the observed pollutant levels. We found that K^+, Na^+, Mg^{2+} and Cl^- mainly result from seaspray. Sulfate, however, is enriched by a factor of 9. The measured trace elements are highly enriched by factors up to hundreds of thousands (Zn: 30, Ni: 1700, As: 2100, Cd: 3200, Fe: 81000, Cu: 82000, Pb: 207000). A cluster analysis supports the conclusion that sulfate and the trace elements originate from anthropogenic activities. The sulfate cannot primarily originate from oceanic dimethylsulfide (DMS).

With regard to the back trajectories, the air masses generally reach the study site from southerly directions after travelling along the Chilean coast. A typical back trajectory is shown in Fig. 1. Presumably the air masses pick up pollutants in the densely populated cities, industrial plants and power plants along the Chilean coast and transport them over hundreds of kilometers to Patache. Here, they were detected as ingredients in fog water and lead to high pollution levels therein.
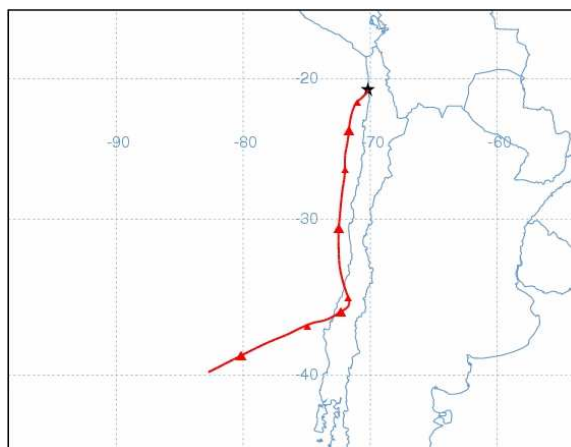
Figure 1. A typical 96 hour back trajectory of the air masses reaching Patache.

First measurements on the carbonaceous fraction in central Antarctic aerosol

P. Fermo[1], A. Piazzalunga[1,2], R. Vecchi[3], S. Becagli[4], R. Traversi[4], R. Udisti[4]

[1]Univ. of Milan Dept. of Inorganic, Metallorganic and Analytic Chemistry, via Venezian 21, 20133, Milan, Italy
[2]University of Milan-Bicocca Dept. of Environmntal Sciences, Pza. della scienza,1 20126, Milan, Italy
[3] University of Milan Dept. of Physics, via Celoria 16, 20133, Milan, Italy
[4] University of Florence, Dept. of Chemistry, Via della Lastruccia, 3 – I-50019 Sesto F.no - Italy

Keywords: Antarctic aerosol, organic carbon, elementary carbon, aerosol chemistry, PM

In industrialised and continental areas, the atmospheric aerosol carbonaceous fraction, such as Elemental Carbon (EC) and Organic Carbon (OC), are currently used in identifying and quantifying primary and secondary sources from natural and anthropogenic emissions (biomass burning, vegetation and marine emissions, combustion processes etc.). In urban sites, the TC contribution can be dominant in the aerosol mass budget.

On the contrary, very few data were obtained from polar regions, especially from Central Antarctica, where atmospheric concentrations are very low and the main contributions come from long-range transport of partially oxidised C-cycle compounds from marine biogenic emissions.

In this study we show the first results of the OC and EC atmospheric concentration in aerosol samples collected at Station Concordia, Dome C (East Antarctica, 75 °S, 123 °E, 3220 m a.s.l., about 1100 km away from the nearest coast).

Aerosol sampling were carried out in the framework of the "Station Concordia" international project, during the 2006/07 austral summer campaign (Nov 06 – Feb 07) and the following 2007 wintertime period (Mar 07 – Oct 07).

Bulk aerosol samples were collected on pre-fired quartz filter 47 mm diameter, 2 µm nominal pore size, by using a Tecora Echo-PM sampler operating at 2.3 m^3/h local conditions. Samplings lasted from 1 to 2 weeks, corresponding to air volumes ranging from 250 to 700 m^3 (local conditions: P around 640 mbar, T° ranging from -30 to -70 °C), in order to collect a sufficient aerosol quantity. Sampler hardware and software were improved in order to correct external/internal temperature gradient.

The sampling site was located in the "clean air zone" of Station Concordia area, about 1 km upwind with respect buildings and human activities. In order to prevent the contamination from power plants and base activity, a meteorological trigger was set up to stop the sampling when air masses were coming from a selected angular sector facing the base camp.

Filter holders were pre-washed prior sampling under a laminar flow hood and filters were stored in pre-cleaned polycarbonate Petri dishes, sealed in polyethylene bags, at – 25 °C until the analysis.

Parallel collections of size-segregated aerosol samples were carried out by several devices (PM10 and PM2.5 samplers, 8-stage Andersen impactor) and the results have been already published (Becagli et al., 2009; Jourdain et al., 2008; Preunkert et al., 2008; Udisti et al., 2008).

Here we present the first quantification of the carbonaceous component on aerosol samples collected all year round at Dome C. In our knowledge, no other data are available up to now on OC and EC aerosol concentrations in the central Antarctic region, at least in winter period.

TOT (Thermal Optical Transmittance) method was used for OC/EC quantification (Birch and Cary 1996).

Preliminary results show that OC concentration during winter is about 50 ng/m^3 while EC values are generally below the detection limit of the technique. The analysis of the complete data set in comparison with others biogenic marker (e.g. methanesulphonic acid, low molecular weight carboxylic acid, non sea salt sulphate) will allow to establish possible sources of OC.

Becagli S., Castellano E., Cerri O., Chiari M., Lucarelli F., Marino F., Morganti A., Nava S., Rugi F., Severi M., Traversi R., Vitale V., Udisti R. (2009) "Italian Research on Antarctic Atmosphere", SIF – Bologna. In press.
Birch, M.E., Cary, R.A., (1996) *Aeros. Sci. & Technol.*, 25, 3, 221-241.
Jourdain B., Preunkert S., Cerri O., Castebrunet H., Udisti R., Legrand M., (2008). *J. Geophys. Res.*, 113, D14308, doi: 10.1029/2007JD009584.
Preunkert S., Jourdain B., Legrand M., Udisti R., Becagli S., Cerri O. (2008). *J. Geophys. Res.*, 113, D15302, doi: 10.1029/2008JD009937.
Udisti R., S. Becagli, E. Castellano, O. Cerri, A. Mannini, F. Marino, A. Morganti, E. Salvietti, M. Severi, R. Traversi. 2008. *Terra Antarctica Report*, 14, 187-198.

Freezing and Activation Measurements of Coated and Uncoated Arizona Test Dust Particles

D. Niedermeier[1], S. Hartmann[1], R. Shaw[1, 2], D. Covert[3], Th. F. Mentel[4], J. Schneider[5], L. Poulain[1], T. Clauss[1], A. Kiselev[1], E. Hallbauer[1], H. Wex[1], and F. Stratmann[1]

[1]Department of Physics, Leibniz Institute for Tropospheric Research, 04318 Leipzig, Germany
[2]Department of Physics, Michigan Technological University, Houghton, Michigan 49931, USA
[3]Joint Institute for the Study of the Atmosphere and Ocean, University of Washington, Seattle, Washington 98195, USA
[4]ICG-2: Troposphäre, Forschungszentrum Jülich, 52425 Jülich, Germany
[5]Particle Chemistry Department, Max Planck Institute for Chemistry, 55128 Mainz, Germany

Keywords: heterogeneous ice nucleation, ice nuclei, hygroscopic growth, activation, dust

Ice particles are formed in the atmosphere through homogenous and heterogeneous ice nucleation. For heterogeneous nucleation still open questions exist concerning the controlling factors (Kärcher and Lohmann, 2003).

During the FROST (FReezing and activation abilities Of coated and uncoated duST particles) campaign, the Leipzig Aerosol Cloud Interaction Simulator (LACIS, Stratmann *et al.*, 2004) was used to investigate the immersion freezing behavior of coated and uncoated Arizona Test Dust (ATD) particles with a quasi-monodisperse mobility size of 300 nm. The ATD particles were coated with succinic acid ($C_4H_6O_4$), ammonium sulfate ((NH_4)$_2SO_4$), and sulfuric acid (H_2SO_4, at two different coating thicknesses). The particles were characterized with respect to shape, chemical composition, hygroscopic growth and droplet activation.

The ATD particles were found to contain water soluble materials, however, in small quantities. Using aerosol mass spectrometry, it was possible to distinguish different H_2SO_4 coating thicknesses.
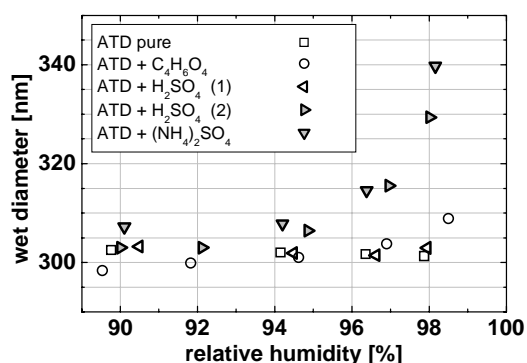
Figure 1. Hygroscopic growth of pure ATD particles and the different coatings.

In general, uncoated particles and those with thin H_2SO_4 (1) or with $C_4H_6O_4$ coatings showed almost no hygroscopic growth. Only particles coated with thick H_2SO_4 (2) and with (NH_4)$_2SO_4$ grew noticeably above 95% RH (see Figure 1). All types

of particles were activated at atmospherically relevant super-saturations (0.1 – 0.4 %), with particles coated with thick H_2SO_4 or with (NH_4)$_2SO_4$ being the most effective CCN.

Uncoated particles and those with $C_4H_6O_4$ or with thin H_2SO_4 coatings started to serve as ice nuclei (IN) at higher temperatures compared to particles with thick H_2SO_4 or with (NH_4)$_2SO_4$ coatings. Although the latter two showed similar hygroscopic growth and droplet activation behavior, they differed in their ability to act as IN, with ATD particles coated with (NH_4)$_2SO_4$ being the most ineffective IN (see Figure 2).
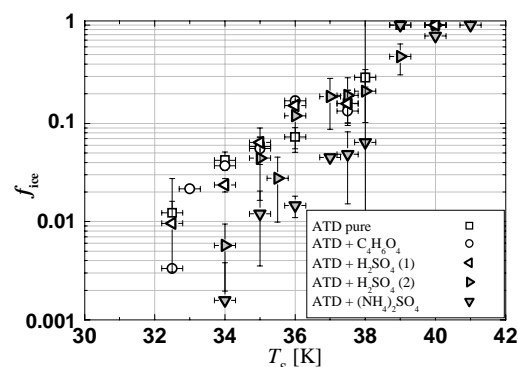
Figure 2. Freezing behavior of pure ATD and the different coated particles. The ice fraction f_{ice} is plotted versus the supercooling temperature T_s. The line at T_s = 38K separates the heterogeneous (on the left) and homogeneous (on the right) freezing modes.

It seems that the ability of the investigated particles to act as IN is not related to water activity at least for the freezing process investigated in this study. However, it should be noted that the supercooled droplets were activated and highly diluted before freezing occurred.

Kärcher, B., and Lohmann, U. (2003). *J. Geophys. Res.*, 108, 4402, doi:10.1029/2002JD003220.
Stratmann, F. *et al.* (2004). *J. Atmos. Oceanic Technol.*, 21, 876-887.

Oxalic acid as a heterogeneous ice nucleus in the deposition and immersion mode

R. Wagner, S. Benz, O. Möhler, H. Saathoff, M. Schnaiter, and T. Leisner

Forschungszentrum Karlsruhe, Institute for Meteorology and Climate Research (IMK-AAF), Karlsruhe, Germany

Keywords: oxalic acid, heterogeneous ice nucleation.

Several recent studies have addressed the potential of dicarboxylic acids to act as ice nuclei in the deposition and immersion mode. Parsons et al. (2004) have shown that solid malonic, succinic, glutaric, and adipic acid particles are inefficient ice nuclei in the deposition mode at temperatures above 243 K. Prenni et al. (2001) also investigated the ice nucleation efficiency of oxalic acid which usually is the prevalent dicarboxylic acid in atmospheric aerosol particles. A continuous flow diffusion chamber was used to measure ice formation from dry, near-monodisperse 50 and 100 nm diameter oxalic acid particles. It was shown that the threshold relative humidity to freeze 1% of the particles was close to water saturation at temperatures between 228 and 213 K. Zobrist et al. (2006) specifically addressed the ability of oxalic acid as a heterogeneous ice nucleus in the immersion mode, thereby considering that dicarboxylic acids will be part of a multi-component mixture in atmospheric aerosol particles. If precipitating from these mixtures, the organic crystals will be included in an aqueous solution with other inorganic/organic solutes and thus can only act as immersion ice nuclei. The freezing experiments were performed with emulsified binary oxalic acid/water solutions of different solute concentrations and selected ternary solutions with e.g. sulfuric acid, sodium chloride, and ammonium sulfate as additional solute species. Freezing temperatures were detected with a differential scanning calorimeter. The authors demonstrated that in several of the emulsified aqueous solutions homogeneous ice nucleation can trigger the precipitation of the organic solute as presumably oxalic acid dihydrate crystals. These embedded crystals then acted as immersion mode ice nuclei in a second freezing cycle, as evidenced by a higher ice freezing temperature in comparison with the preceding homogeneous freezing cycle.

In this contribution, we will present selected results from heterogeneous ice nucleation experiments with airborne particles of oxalic acid (either as pure crystals or as crystals embedded in aqueous solutions with other solutes) which were performed in the large coolable aerosol chamber AIDA of Forschungszentrum Karlsruhe. During the recent years, the AIDA chamber has been improved and widely used for controlled expansion cooling experiments which mimic the adiabatic expansion cooling of rising air parcels in the atmosphere. The change of relative humidity and the formation of ice crystals are monitored with a comprehensive set of in situ and sampling instruments, including e.g. fast and highly accurate water vapor measurements by means of direct tunable diode laser absorption spectroscopy and in situ scattering and depolarisation measurements to detect the phase change from spherical aqueous solution droplets to aspherical ice crystals. In addition, the phase and composition of the aerosol and cloud particles can also be deduced from in situ infrared extinction measurements (Fig. 1).
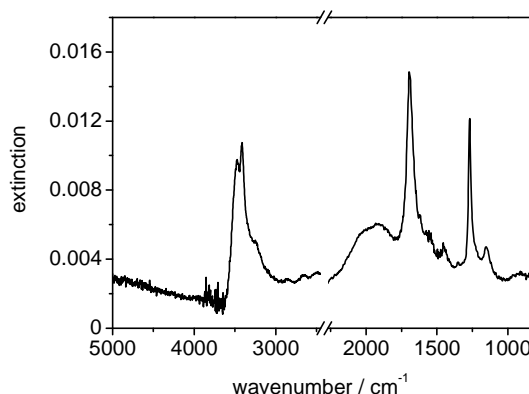
Figure 1: Infrared extinction spectrum of solid crystals of oxalic acid dihydrate, recorded at $T = 243$ K in the AIDA chamber, see Fig. 10 in Braban et al. (2003) as a comparison.

Our preliminary results indicate that the efficiency of oxalic acid as a heterogeneous ice nucleus depends on the pathway leading to the nucleation of its crystalline form, meaning that the crystal microstructure might be an important factor.

Braban, C. F., Carroll, M. F., Styler, S. A. & Abbatt, J. P.D. (2003). *J. Phys. Chem. A*, 107, 6594-6602.

Parsons, M. T., Mak, J., Lipetz, S. R. & Bertram, A. K. (2004). *J. Geophys. Res. (Atmos.)*, 109, D06212.

Prenni, A. J., DeMott, P. J., Kreidenweis, S. M., Sherman, D. E., Russell, L. M. & Ming, Y. (2001). *J. Phys. Chem. A*, 105, 11240-11248.

Zobrist, B., Marcolli, C., Koop, T., Luo, B. P., Murphy, D. M., Lohmann, U., Zardini, A. A., Krieger, U. K., Corti, T., Cziczo, D. J., Fueglistaler, S., Hudson, P. K., Thomson, D. S. & Peter, T. (2006). *Atmos. Chem. Phys.*, 6, 3115-3129.

Development of cumulus clouds over Europe:
High-resolution measurements of aerosol and cloud properties at condensation level

F. Ditas[1], B. Wehner[1], A. Wiedensohler[1],
R.A. Shaw[1], H. Siebert[1]

[1]Leibniz Institute for Tropospheric Research, 04318 Leipzig, Germany

Keywords: cloud formation, aerosol-cloud interaction

Variations in aerosol number size distributions play an important role in Earth's radiation budget. In particular the interaction of aerosols and clouds still causes the largest uncertainty concerning radiative forcing. In contrast to various ground-based measurements concerning spatial variations of aerosol number size distributions the knowledge about aerosol processes in cloud regions is still rare.

A selection of instruments to measure aerosol and cloud microphysics has been operated on the helicopter-borne platform ACTOS (Siebert et al., 2006). Aerosol number size distributions were measured between 6 nm and 2.5 μm using a small and light SMPS (6 to 255 nm, time resolution 2 min) and an OPC (250 nm to 2.5 μm, time resolution 1 s). In addition total particle number concentrations ($D_p > 6$ nm) have been measured with a resolution of 1 Hz. Droplet size distributions were measured by a Phase Doppler Interferometer for Cloud Turbulence (PICT). Turbulence and cloud microphysical instrumentation was described in detail in Siebert et al., 2006.

This equipment has been used during the IMPACT campaign near Cabauw (NL) in May 2008. Here, results from a measurement flight on May 20 during the beginning of development of cumulus clouds are presented.
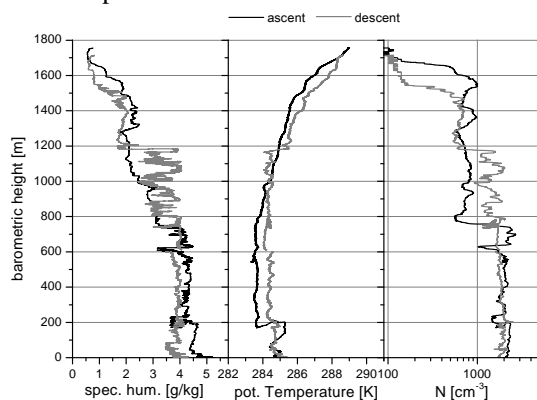
Figure 1: Vertical profiles of specific humidity, potential temperature, and particle number concentration (N) during ascent and descent on May 20, 2008.

Figure 1 shows vertical profiles of specific humidity, potential temperature, and total particle number concentration (N) during ascent and descent on May 20, 2008. The well-mixed boundary layer was still under development which is obvious in the increasing height from 750 m during ascent to 1170 m during descent.
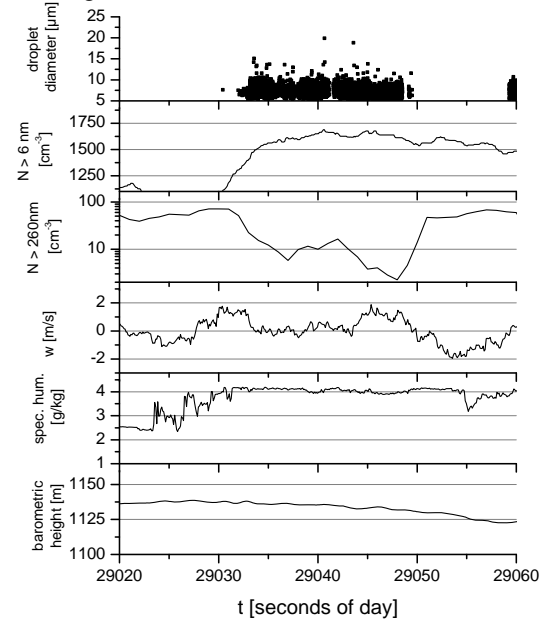
Figure 2: Horizontal variation of selected parameters during cumulus development on May 20, 2008.

Figure 2 shows selected parameters measured during a section of a horizontal flight leg in the height where onset of cumulus convection has been observed. The occurrence of dots in the upper plot (droplet diameters) marks the region where a fresh cumulus was observed. Increasing N and specific humidity as well as positive vertical wind speed w indicate that air from the boundary layer has been lifted into the cumulus condensation level. The number concentration of particles > 260 nm decreases due to activation of CCN.

The mean concentration of cloud droplets during this particular section was 600 cm^{-3} while 99% of these droplets where < 10 μm. Particle number size distributions show that particles down to 40 nm have been activated as CCN. This might be due to the high supersaturations occurring on very small scales due to turbulent convective transport of humid boundary layer air and mixing with the drier residual layer.

Reference
Siebert, H., H. Franke, K. Lehmann, R. Maser, E. W. Saw, D. Schell, R. A. Shaw, and M. Wendisch (2006) Probing Fine-Scale Dynamics and Microphysics of Clouds with Helicopter-Borne Measurements, Bull. Amer. Met. Soc., 87, 1727 – 1738.

LACIS Simulations Concerning Heterogeneous Ice Nucleation with Fluent/FPM

S. Hartmann[1], D. Niedermeier[1], J. Voigtländer[1], R. A. Shaw[1, 2], H. Wex[1] and F. Stratmann[1]

[1]Department of Physics, Leibniz Institute for Tropospheric Research, 04318 Leipzig, Germany
[2]Department of Physics, Michigan Technological University, Houghton, Michigan 49931, USA

Keywords: heterogeneous ice nucleation, mineral dust, ice nuclei, modelling

Atmospheric ice particles are generated through homogenous and heterogeneous ice nucleation. Especially for the latter process open questions concerning the controlling parameters or mechanisms still exist (Kärcher and Lohmann, 2003). In order to simulate the water-to-ice phase transition in the Leipzig Aerosol Cloud Interaction Simulator (LACIS, Stratmann *et al.*, 2004), the Fine Particle Model (FPM, Wilck *et al.*, 2002) in connection with the CFD code Fluent 6 (Fluent Inc., 2001) was extended to account for homogeneous and heterogeneous nucleation processes, as well as suitable boundary conditions. Ice nucleation was implemented following classical nucleation theory (CNT) according to Zobrist (2006). Fluent/FPM is used to find suitable thermodynamic conditions such as temperature, and water and ice saturation ratios to perform the first freezing experiments with the newly-built long version of LACIS, and for interpretation of experimental results from the FROST campaign (FReezing and activation abilities Of coated and uncoated duST particles, Niedermeier *et al.*, 2009).

To simulate ice nucleation processes in terms of a temperature dependent freezing rate J^* derived from the nucleation rate, 300 nm spherical monodisperse Arizona Test Dust (ATD) particles internally mixed with a small amount of ammonium sulfate were used. The homogeneous freezing rate J^*_{hom} also account for the amount of liquid water on the particles and the heterogeneous freezing rate J^*_{het} depends on the total insoluble particle surface.
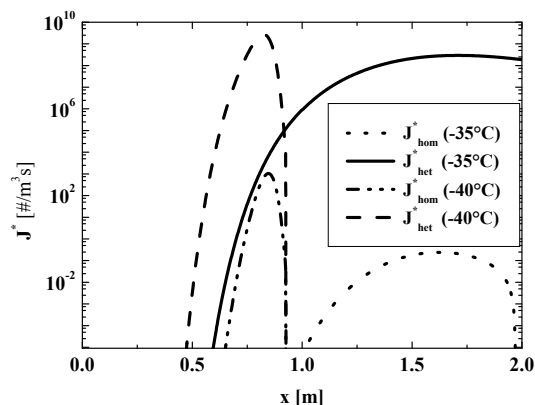
Fig. 1: Homogeneous and heterogeneous freezing rate J^* for different wall temperatures at LACIS centerline with ice boundary condition.

The heterogeneous freezing rate is always several orders of magnitude higher than the homogenous freezing rate over the considered temperature range, see Figure 1. The phase transition of supercooled water droplets to ice crystals is determined by J^*. Figure 2 presents the number concentration of seed particle-droplets and ice crystals in the particle-containing region of flow along the centerline.
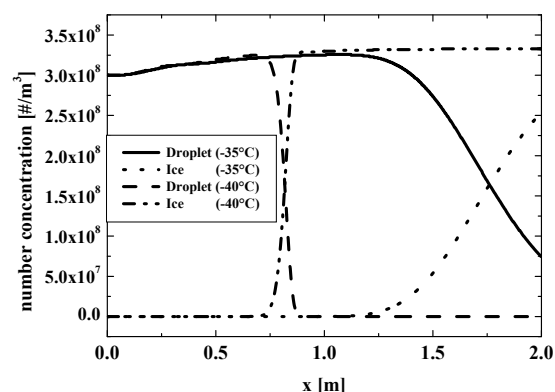
Fig. 2: Number concentration of seed particle-droplets and ice crystals for different wall temperatures.

At an externally adjusted wall temperature of -35°C, not all supercooled water droplets are transformed to ice at the LACIS outlet (x=2.0m), because the temperature is not sufficiently low and the resulting J^* is not large enough to transform all droplets to ice prior to total evaporation of the supercooled water droplets in the ice super- and water subsaturated environment. As can be seen in Figures 1 and 2, the homogeneous and especially the heterogeneous freezing rates become sufficiently large at -40°C adjusted wall temperature such that all supercooled water droplets freeze within a narrow distance (x range). As a result J^* falls to zero.

By comparing Fluent/FPM simulations with experimental results the ability of CNT to capture the observed behavior will be evaluated, and this will aid in developing suitable parameterizations of microphysical properties concerning ice nucleation.

Kärcher, B., and Lohmann, U. (2003). *J. Geophys. Res.*, 108, 4402, doi:10.1029/2002JD003220..

Stratmann, F. *et al.* (2004). *J. Atmos. Oceanic Technol.*, 21, 876-887.

Niedermeier *et al.* (2009). *submitted Abstract at EAC 2008*, Karlsruhe, Germany

Wilck, M. *et al.* (2002). *Proc. Sixth Int. Aerosol Conf.*, Taipei, Taiwan, 1269–1270.

Zobrist (2006), *Ph.D. Thesis*, 13-18

Correlations between Particulate Sulfate and Ozone Observed in the UT/LS over Greenland and Central/Western Europe in 2008

J. Schmale[1], J. Schneider[1], M. Brands[1,2], G. Ancellet[3], H. Schlager[4], M. Lichtenstern[4], M. Scheibe[4], S.R. Arnold[5], K.S. Law[3], C. Voigt[4] and S. Borrmann[1,2]

[1] Particle Chemistry Dept., Max Planck Institute for Chemistry, J.-J. Becher Weg 27, 55128, Mainz, Germany
[2] Institute for Atmospheric Physics, J. Gutenberg University, J.-J. Becher Weg 21, 55128, Mainz, Germany
[3] LATMOS, Université Pierre et Marie Curie, 4 Place Jussieu, 75005 Paris, France
[4] Institute for Physics of the Atmosphere, German Aerospace Center (DLR), Münchner Straße 20, 82234 Oberpfaffenhofen, Germany
[5] Institute for Climate and Atmospheric Science, School of Earth and Environment, University of Leeds, LS2 9JT Leeds, UK

Keywords: UT/LS Aerosols, AMS, Sulfate, Ozone, Arctic Aerosols

Mass spectrometric aerosol measurements were conducted on board of the French research aircraft "ATR-42" during the POLARCAT-France campaign in July 2008 from Kangerlussuaq, Greenland, and on board the German "DLR-Falcon" during the CONCERT-Chemistry study in October 2008 over Central and Western Europe.

The in-situ aerosol data presented here were measured by an Aerodyne C-ToF-AMS during eight flights in the Arctic region and six flights over Europe. The AMS analyzes particles in a size range between 60 and 800 nm vacuum aerodynamic diameter with respect to their chemical components that evaporate at 600 °C. The instrument was operated with a time resolution of 30 seconds during POLARCAT and ten seconds during CONCERT, thus providing a spatial resolution of approximately 3 and 2 km, respectively. This study mainly refers to sulfate containing particles. Further instrumentation on board of the "ATR-42" included in-situ ozone and CO measurements, as well as aerosol and ozone LIDARs. The "Falcon" aircraft was equipped with in-situ ozone and CO detectors, and an NO_y instrument among others. Flight altitudes in the Arctic ranged from 400 m above the Northern Atlantic up to 7,000 m over sea and land (ice) in the free troposphere, while measurements over Europe took mainly place between 9,000 m and 12,000 m, i.e. in the UT/LS region.

Sulfate aerosol concentrations over Greenland ranged between 0.1 and to 0.5 µg m^{-3} (STP) while ozone concentrations reached up to a maximum of 160 nmol mol^{-1} (ppbv). High particulate sulfate masses were almost always accompanied by increasing ozone mixing ratios. During the measurements over Europe, particulate sulfate concentrations were highest in the UT/LS region with values around 1.5 µg m^{-3} (STP). Ozone mixing ratios reached up to about 350 nmol mol^{-1}. Again, both species reveal a pronounced correlation. Figure 1 shows a representative plot with 1 min average values for October 31, 2008 for a flight from Shannon, Ireland to Oberpfaffenhofen, Germany.

The three boxes indicate values from the troposphere (including the boundary layer), the UT/LS region and the lower stratosphere. For lower altitudes, ozone mixing ratios ranged between almost 0 and 50 ppbv while particulate sulfate matter reached peak concentrations in the boundary layer and background concentrations below 0.2 µg m^{-3} in the free troposphere. In the tropopause region, sulfate aerosol mass increases again together with ozone to values comparable to those measured in the boundary layer. The same is observed for stratospheric air, however, with a less steep slope and lower sulfate concentrations. In general, higher ozone values also corresponded to higher potential temperature (theta) values which indicates influence from stratospheric air masses.
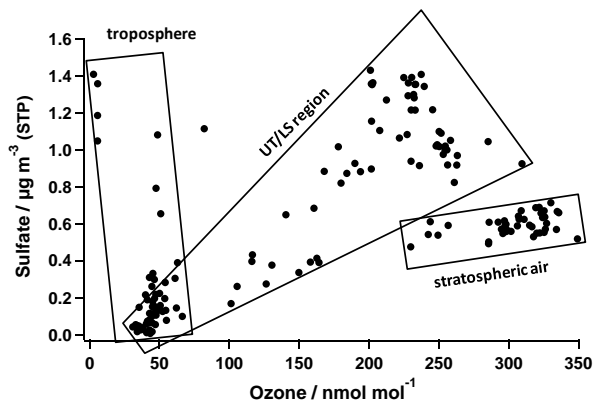
Figure 1. Sulfate aerosol concentration vs ozone mixing ratio on October 31, 2008 crossing the North Atlantic Flight Corridor

Possible origins of the probed air masses are currently being investigated. North American, Siberian and European anthropogenic pollution as well as influences from biomass burning are taken into account in the case of Greenland arctic aerosol, while air-traffic, stratospheric intrusions, and also possible volcanic emissions are considered for the measurements over Europe in October.

Detection of thin coatings on refractory particles with an aerosol mass spectrometer and application in laboratory studies of hygroscopic growth, CCN and IN activation

P. Reitz[1,2], J. Schneider[1], H. Wex[3], F. Stratmann[3], D. Niedermeier[3],
K. Mildenberger[3], D. Covert[4], Th. F. Mentel[5], C. Spindler[5], L. Poulain[3], and S. Borrmann[2,1]

[1]Particle Chemistry Department, Max Planck Institute for Chemistry, Mainz, Germany
[2]Institute for Atmospheric Physics, Johannes Gutenberg University, Mainz, Germany
[3]Leibniz Institute for Tropospheric Research, Leipzig, Germany
[4]University of Washington, Seattle, USA
[5]Institute for Chemistry and Dynamics of the Geosphere II: Troposphere, Research Center Jülich, Jülich, Germany

Keywords: Aerosol cloud interaction, Aerosol mass spectrometry, AMS, CCN, Ice nuclei.

Activation studies with refractory Arizona Test Dust (ATD) particles of 200, 300, and 400 nm size diameter coated by thin layers of inorganic and organic material have been performed at the LACIS facility, Leipzig. The detection and quantification of the coating was done by aerosol mass spectrometry. Here we discuss the possibilities and limitations of the method with respect to the detection of coatings in the nm range. The results show that even coatings thicknesses in the order of 0.1 nm can be detected. Furthermore, it was found that (ATD) contains significant amounts of organic and inorganic compounds.

Insoluble aerosol particles like mineral dust or soot are not efficient cloud condensation nuclei (CCN) in their pure state, but their CCN efficiency can be enhanced by coatings of soluble material. This process is regarded to be of great importance in the atmosphere (Lohmann et al., 2004). On the other hand, coating an insoluble particle with soluble material can decrease the ice nucleation efficiency of these particles (Möhler et al., 2008). In order to understand and quantify these effects, test particles (e.g., ATD, pure minerals, soot) are coated in laboratory experiments with species as H_2SO_4, secondary organic material, or ammonium sulfate in order to enhance their CCN efficiency, to study their hygroscopic growth, and their ice nucleation efficiency (Möhler et al., 2008). From modified Köhler theory it is known that the number of water soluble molecules contained on an insoluble particle determines hygroscopic growth as well as CCN activation of the coated particles.

Atmospherically relevant coating thicknesses are on the order of a few nanometers on dust particles of a few hundred nanometers diameter. These thin coatings contain therefore only a small mass fraction of the whole particle and the coating mass is in the order of a few hundred attograms (1 ag = 10^{-18} g) per particle. In laboratory activation experiments, experimental closure can only be obtained if the measured mass of the coating corresponds to the coating mass inferred from hygroscopic growth and/or critical supersaturation. The measurement of

such a small quantity can only be realized by averaging over a large number of particles, but still highly sensitive instrumentation and careful data analysis is required. Here we report on activation experiments with coated ATD particles in the LACIS facility (Stratmann et al., 2004) during the FROST experiment (April 2008) and the experimental issues connected with detection and quantification of such coating with an Aerodyne Aerosol Mass Spectrometer (AMS).
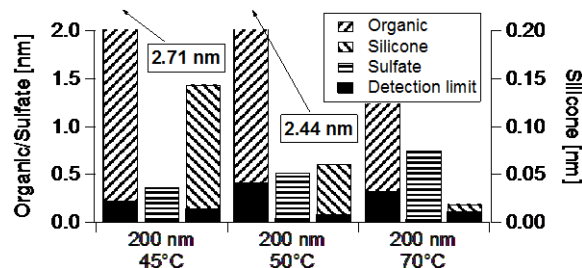
Figure 1. Coating thicknesses for ATD particles of 200 nm geometric size coated with sulfuric acid as a function of temperature assuming spherical particle shape. Organic material and silicone (right scale) were found to be components of the Test Dust.

Lohmann, U., K. Broekhuizen, R. Leaitch, N. Shantz, and J. Abbatt, Geophys. Res. Lett., 31, L05108 (2004).
Möhler, O., S. Benz, H. Saathoff, M. Schnaiter, R. Wagner, J. Schneider, W. Walter, V. Ebert, and S. Wagner, et al., Environ. Res. Lett., 3, 025007 (2008).
Stratmann, F., A. Kiselev, S. Wurzler, M. Wendisch, J. Heintzenberg, R. J. Charlson, K. Diehl, H. Wex, and S. Schmidt, J. Atmos. Ocean. Technol. 21, 876-887 (2004).

Ice nucleation of soot particles with variable organic and sulphuric acid coating

O. Möhler[1], S. Benz[1], A. Buchholz[3], J.Crosier[5], S. Henning[2], T. Leisner[1], Th. F. Mentel[3], V. Michaud[4], H. Saathoff[1], M. Schnaiter[1], R. Wagner[1], and M. Ziese[2]

[1]Karlsruhe Institute of Technology, Postfach 3640, 76021 Karlsruhe, Germany
[2]Leibnitz Institute for Tropospheric Research, Permoserstrasse 15, 04318 Leipzig, Germany
[3]Forschungszentrum Jülich GmbH, ICG-2, 52425 Jülich, Germany
[4]Université Blaise Pascal, LaMP, 24, Avenue des Landais, 63177 Aubière Cedex, France
[5]University of Manchester, Center for Atmospheric Science, Oxford Road, Manchester M13 9P, UK

Keywords: Atmospheric aerosols, cloud microphysics, ice nucleation, organic aerosols

The consumption of fossil fuel in vehicle motors or aircraft engines induces the emission of large numbers of soot particles internally mixed with variable amounts of organic compounds and sulphuric acid. If these particles are involved in cloud formation processes, the insoluble soot core may induce heterogeneous ice nucleation and therefore affect the formation, life cycle and radiative properties of mixed-phase and cirrus clouds. Recent experiment series at the AIDA (Aerosol Interaction and Dynamics in the Atmosphere) cloud chamber investigated both the cloud condensation and ice nucleation behaviour of soot particles coated with variable amounts of secondary organics and sulphuric acid.

The soot particles were generated with in a propane diffusion flame (CAST) at variable fuel-to-air ratio and thus variable fractions of elemental and organic carbon. Additional sulphuric acid coating was achieved by saturation of the flame soot aerosol flow with sulphuric acid vapour at temperatures between 50°C and 70°C and subsequent condensation of the vapours to the soot particles by passive cooling of the aerosol in a flow tube before entering the aerosol chambers. The chemical composition of the aerosol was analysed by aerosol mass spectrometry, the hygroscopic growth was measured with three instruments (HTDMA, VHTDMA, LACIS-mobile), and the cloud activation (CCN) behaviour was measured with two DMT-CCNC instruments.

This contribution investigates how coating with sulphuric acid affects the ice nucleation efficiency of flame soot particles with different organic carbon content at temperatures between -45°C and -55°C. This was achieved with series of AIDA cloud expansion experiments with different aerosols prepared as indicated above. Figure 1 shows a typical example of time series from an experiment with sulphuric acid coated soot particles. After starting the experiment at t = 0, the relative humidity increases due to expansion cooling of the cloud chamber volume. After about 20 s of pumping the relative humidity with respect to ice (solid line in panel 2) exceeds the ice saturation line, but almost no ice

particles are formed in the ice supersaturated regime until the relative humidity approaches water saturation (dashed lines in panel 2). At this point, ice is formed either by immersion freezing or homogeneous freezing of particles taking up water depending on the hygroscopic behaviour of their mixed sulphuric acid and organic carbon coating. The freezing starts at higher ice supersaturations than for pure sulphuric acid particles.
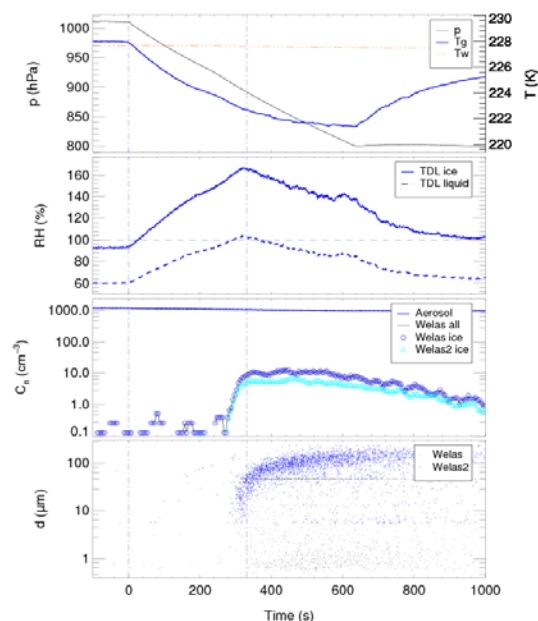
Figure 1. Typical course of an AIDA cloud expansion experiment with sulphuric acid coated flame soot particles. Panel 1: pressure (black line), wall temperature (orange line), and gas temperature (blue line); panel 2: relative humidity with respect to water (dashed line) and ice (solid line); panel 3: aerosol (blue line) and ice particle (symbols) number concentration; panel 4: optical sizes of single particles detected with the welas and welas2 optical particle counters.

Polar light scattering function measurements and stereo imaging of single ice particles

A. AbdElMonem[1], M. Schnaiter[1] and T. Leisner[1]

[1]Forschungszentrum Karlsruhe, Institute of Meteorology and Climate Research, Karlsruhe, Germany

Keywords: cloud microphysics, ice crystals, light scattering, optical instrumentation

Better understanding of the influence of Cirrus clouds on the radiative properties of the atmosphere requires a smart determination of microphysical and optical properties of ice cloud particles. This requires *in situ* measurements of the microphysical properties of the ice particles in conjunction with a suitable modelling of their optical properties. The latter, however, demands the existence of reliable optical models for the polar scattering function of different pristine and complex ice crystal habits.

Our technique, **PHIPS**, is a new experimental device for the stereo-imaging of individual cloud particles and the simultaneous measurement of the polar scattering function of the *same* particle. The resolution power of the microscope unit is about 3 µm with the facility to image the same particle under an angular viewing distance of 30° by a second identical microscope unit. This facilitates a 3D morphology impression of the ice crystals. The scattering part of PHIPS enables the measurement of the polar light scattering function of cloud particles with an angular resolution of 1° for forward scattering directions (from 1° to 10°) and 8° for side and backscattering directions (from 18° to 170°), Figure (1).

The presented results were collected in the ice cloud characterisation campaign HALO-02 which was conducted in December 2008 at the AIDA cloud chamber in the temperature range from -5°C to -70°C. In a series of experiments small externally generated seed ice crystals were grown in AIDA at distinct temperature and saturation ratio conditions. The temperature dependent morphology changes and the supersaturation dependent structural complexity were monitored by PHIPS. Habit classification, structural details, and particle orientation were deduced from the image data and were discussed in the context of the corresponding scattering data. The scattering function measurements reveal ice particle orientation dependent specular reflection peaks which might contain information about the surface roughness (Sherbakov *et al.*, 2006).

The presentation will demonstrate the advantage of coupling the polar scattering measurements to the stereo imaging.
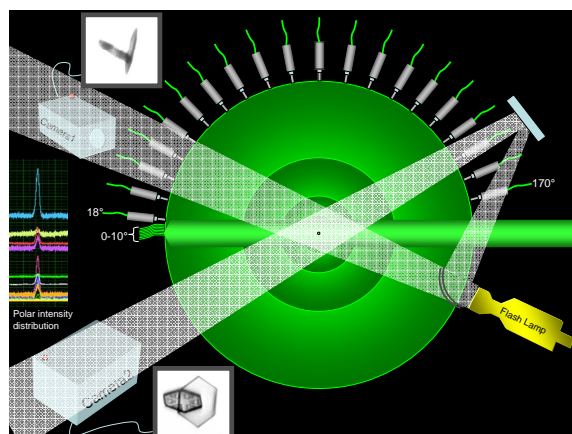
Figure 1. A drawing illustrates the principle of PHIPS. Inset, mid-left, is a sample row data of the scattering phase function. The corresponding scattered crystal is viewed at two different angles which enhance the morphology of the image.

Sherbakov, V., Gayet, J.-F., Baker, B., and Lawson, P. (2006). *J. Atmos. Sci.*, 63, 1513-1525

Characterisation of a Pumped Counterflow Virtual Impactor for Ice Particle Residue Sampling from the AIDA Cloud Chamber

C. Oehm[1,2] , M. Niemand[1] , O. Möhler[1] and T. Leisner[1,2]

[1]Institute for Meteorology and Climate Research (IMK-AAF), Forschungszentrum Karlsruhe, 76344 Eggenstein-Leopoldshafen, Germany
[2]Institute for Environmental Physics (IUP), Ruprecht-Karls-Universität Heidelberg, 69120 Heidelberg, Germany

Keywords: Virtual impactor, Cut-off diameter, Droplets, Ice nuclei, Cloud microphysics.

At the aerosol and cloud simulation chamber facility AIDA (Aerosol Interaction and Dynamics in the Atmosphere) of Forschungszentrum Karlsruhe both droplet and ice clouds can be generated and observed at realistic atmospheric conditions. Thus, microphysical cloud processes can be investigated in the laboratory, especially heterogeneous ice nucleation of mineral dust, soot, organic and biological particles.

To analyse the generated droplet and ice particles they have to be separated from interstitial aerosol particles. This is achieved by a Pumped Counterflow Virtual Impactor (PCVI), which separates the incoming particles according to their inertia. In traditional counterflow impactors (CVI), the required air flow velocity is generated by wind tunnels or the motion of aircrafts. In the pumped CVI, these methods have been replaced by using a vacuum pump to provide the flow.
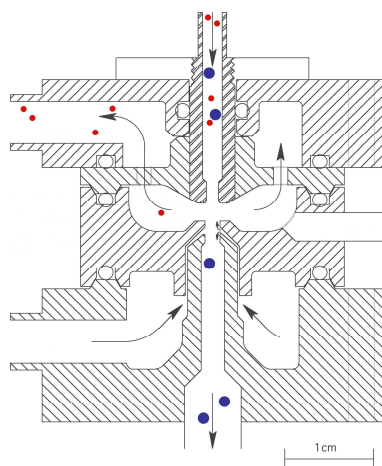
Figure 1. Schematic drawing of the PCVI
(Boulter *et al.*, 2006)

The input flow from the cloud chamber, induced by the vacuum pump, is turned and discarded sideways. Low inertia particles are pumped away, but particles with high inertia cannot follow the streamlines and impact into a minor particle-free counterflow. This minor flow replaces the solid impaction surface of conventional impactors.

Only ice particles and cloud droplets with sufficient high inertia can penetrate the counterflow,

enter the sample flow and can be analysed afterwards. The strength of the counterflow and the kinetic stopping distance of the incoming particles determine the 50% cut-off diameter for a given pump flow. The 50% cut-off diameter is the particle diameter at which 50% of particles were transmitted into the sample flow. The minimal cut-off diameter of the impactor depends on his geometric dimension as well as the adjusted pressures and flows.

To measure the 50% cut-off diameter, a new optical particle spectrometer, a WELAS_3 instrument, was installed behind the PCVI. A second WELAS_1 instrument directly samples from the chamber to measure the actual number density and size distribution of cloud droplets and ice particles before entering the PCVI. The PCVI cut-off curves are determined from the difference of the size distributions measured with WELAS_1 and WELAS_3.
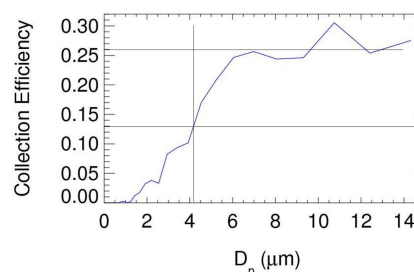
Figure 2. PCVI cut-off curve

The poster shows the setup and process of a typical AIDA experiment. Furthermore it explains the functionality and the principle of operation of the Pumped Counterflow Virtual Impactor, and describes first results for determination of the minimal 50% cut-off diameter. Processes of cloud microphysics have an important influence on life cycles of clouds, as well as on formation of precipitation and the climate.

J. E. Boulter, D. J. Cziczo, A. M. Middlebrook, D. S. Thomson, & D. M. Murphy (2006). Design and Performance of a Pumped Counterflow Virtual Impactor, *Aerosol Science and Technology*, 40:969-976

The microphysical and optical properties of small ice crystals

M. Schnaiter[1], A. AbdELMonem[1], D. Baumgardner[2], S. Benz[1], A. Heymsfield[3], M. Krämer[4], T. Leisner[1], J. Meyer[4], O. Möhler[1], C. Oehm[1], H. Saathoff[1], C. Schmitt[3], Z. Ulanowski[5], R. Wagner[1]

[1] Forschungszentrum Karlsruhe, Institute of Meteorology and Climate Reseach, Karlsruhe, Germany
[2] Universidad Nacional Autónoma de México, Centro de Ciencias de la Atmósfera, México City, México
[3] National Center for Atmospheric Research, Boulder, USA
[4] Forschungszentrum Jülich, Institute of Chemistry and Dynamics of the Geosphere, Jülich, Germany
[5] University of Hertfordshire, Science and Technology Research Institute, Hatfield, UK

The importance of small ice crystals with sizes smaller than 50µm to the microphysical and optical properties of cirrus clouds are currently controversially discussed (McFarquhar *et al.,* 2007). This is because some *in situ* cloud probes seem to clearly overestimate the number concentrations of small ice particles due to particle shattering on their protruding shrouds or inlets. On the other hand, if these small ice crystals are real they can have a substantial impact on the radiative properties of the clouds (Mitchell *et al.*, 2008).

In order to unravel the microphysical nature of small ice particles, we started to run dedicated ice cloud characterisation experiments at the aerosol and cloud chamber AIDA of Forschungszentrum Karlsruhe. Ice particles are nucleated homogeneously and heterogeneously on different aerosols by expansion cooling experiments in the -28C to -80C temperature range. The emerging and disappearing ice clouds are probed routinely by FTIR extinction spectroscopy, laser light scattering and depolarisation measurements, and single particle optical counting and sizing (Wagner *et al.*, 2009). For a series of AIDA experiments the light scattering and depolarisation measurements were analysed in the context of size and shape parameters retrieved from FTIR extinction spectroscopy using theoretical T-matrix computations for compact ice cylinders. Although the measured trends in the size dependence of the depolarisation properties could be reproduced by the simplified ice particle model, remaining discrepancies are likely caused by the missing details of the ice crystal morphologies. That's why we employed a set of additional *in situ* cloud particle probes, like the Cloud Aerosol and Precipitation Spectrometer CAPS, the Small Ice Detectors SID-2H and SID-3, and the Video Ice Particle Sampler VIPS in the recent AIDA ice cloud characterisation campaign HALO02.

Figure 1 gives an example of a HALO02 expansion cooling experiment started at an initial temperature of -68C. The generated cloud was composed of two size-separated ice particle modes corresponding to homogeneous and heterogeneous ice nucleation. The two ice nucleation modes have distinct backscattering linear depolarisation properties with higher depolarisation ratios for the homogenously nucleated small ice particle mode.

Such experiments offer the possibility to investigate the link of the bulk optical and ice mass properties of the cloud to the microphysical details of the constituent ice particles. Moreover, *in situ* cloud probes can be compared under defined laboratory conditions and without any particle shattering artefacts for clouds composed entirely of small ice particles.
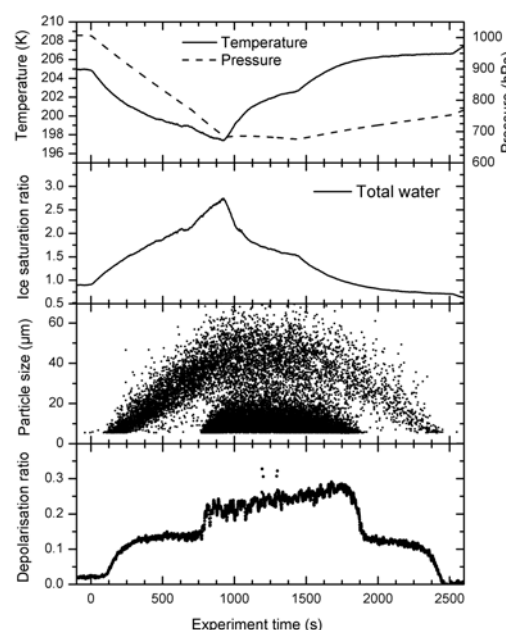
Figure 1. AIDA ice cloud experiment with subsequent heterogeneous and homogeneous ice nucleation events. Note that the given optical particle size overestimates the ice particle geometry.

Mitchell, D.L., Rasch, P., Ivanova, D., McFarquhar, G., Nousiainen, T. (2008). *Geophys. Res. Lett.*, 35, L09806, doi:10.1029/2008GL033552.

McFarquhar, G.M., Um, J., Freer, M., Baumgardner, D., Kok, G.L., Mace, G. (2007). *Geophys. Res. Lett.*, 34, L13803, doi:10.1029/2007GL029865.

Wagner, R., Linke, C., Naumann, K.-H., Schnaiter, M., Vragel, M., Gangl, M., Horvath, H. (2009). *JQSRT*, accepted.

Black carbon scavenging by mountain clouds

D. Baumgardner[1], R. Subramanian[2], C. Twohy[3], G. Kok[2]
[1]Universidad Nacional Autónoma de México, Centro de Ciencias de la Atmósfera, Mexico
[2]Droplet Measurement Technologies, Boulder, CO
[3]Oregon State University, Corvallis, OR

The removal of black carbon (BC) by clouds by way of nucleation and inertial scavenging is the most efficient mechanism for cleansing the atmosphere of one of the most ubiquitous components of primary emissions of pollutants. However, our understanding of the physical mechanism behind this removal process remains limited. By definition, there are two processes that lead to the removal of aerosol particles by clouds. The formation of cloud hydrometeors from aerosols by nucleation is one process; the removal by inertial impaction is another.

Recent studies of clouds over the northern Pacific, using a counterflow virtual impactor (CVI) to separate cloud particles from interstitial aerosols, and a single particle soot photometer (SP2) to measure the BC mass of individual cloud particle residuals, provided compelling evidence that inertial scavenging could not be ruled out as a mechanism for removing BC in upper tropospheric cirrus clouds (Baumgardner et al., 2008).

This same approach has been carried out in mountain upslope and wave clouds over Rocky Mountains. By following the trajectory of air parcels through these clouds, it is observed that the mass of BC in cloud particle residuals increases with the age of the air mass, as shown in Fig. 1, where the cloud boundaries are given by the ice water content (IWC) derived from the CVI. The IWC is nearly but the BC in the cloud particle residuals increases from 3 to 15 ng m^{-3}. This means that the ratio of BC mass to ice water content also increases as shown in Fig. 2. Nucleation scavenging cannot explain these trends but inertial scavenging is a reasonable explanation. An inertial scavenging rate of 36 ng of BC per hour for each gram of water is estimated from this particular cloud pass.
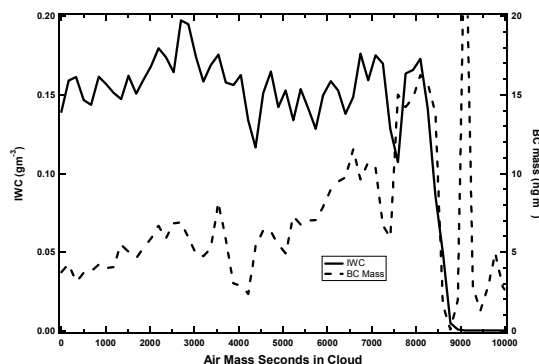
Figure 1
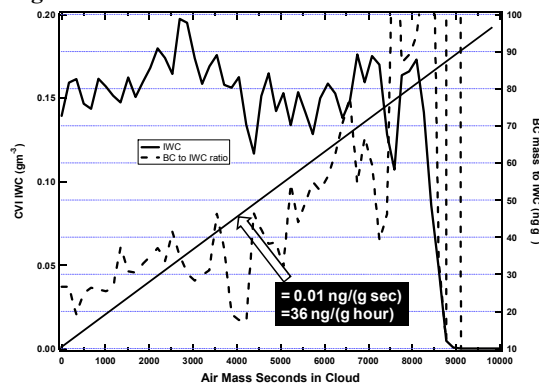
Figure 2 –

References

Baumgardner, D., R. Subramanian, C. Twohy, J. Stith and G. Kok, 2008: Scavenging of Black Carbon by Ice Crystals Over the Northern Pacific, *Geophys. Res. Letters*, 35, L22815, doi:10.1029/2008GL035764.

Deposition mode ice nucleation on atmospheric dust aerosols – A comparison of laboratory studies with detailed process model calculations

M. Niemand[1], H. Bunz[1], S. Benz[1], O. Möhler[1], R. Wagner[1] and T. Leisner[1, 2]

[1]Institute of Meteorology and Climate Research, Forschungszentrum Karlsruhe, Hermann-von-Helmholtz-Platz, 76344 Eggenstein-Leopoldshafen, Germany
[2]Institute of Environmental Physics, Heidelberg University, Im Neuenheimer Feld 229, 69120 Heidelberg, Germany

Keywords: heterogeneous ice nucleation, aerosol model, cirrus clouds, atmospheric dust aerosols

Cirrus clouds are known to play an important role in the global energy balance through their interactions with solar and terrestrial radiation. Whether cirrus clouds have a net heating or cooling effect on climate strongly depends on their microphysical structure such as size, shape and number concentration of the ice crystals and therefore on the cirrus cloud formation mechanisms. Cirrus clouds form by homogenous freezing of super-cooled liquid aerosol particles or by heterogeneous ice nucleation mechanisms involving solid particles. To predict the climate impact of cirrus clouds correctly, models need appropriate parameterizations for heterogeneous ice nucleation by atmospheric aerosols. Existing parameterizations of heterogeneous ice nucleation were tested by a combined experimental and modelling study.

The experiments were carried out at the aerosol and cloud chamber facility AIDA (Aerosol Interaction and Dynamics in the Atmosphere) of Forschungszentrum Karlsruhe. AIDA allows a realistic simulation of tropospheric and stratospheric cloud conditions covering a wide range of temperature and pressure. The comprehensive model MAID (model for aerosol and ice dynamics) (Bunz et al., 2008) was used to calculate the temperature and saturation inside the cloud chamber. Temperature and saturation are directly coupled to the aerosol behaviour. MAID is especially suitable to study the evolution of ice clouds, because it balances the implemented trace gas components accurately and is based on elementary aerosol physics without restrictions regarding size distributions and composition.

Figure 1 shows a typical AIDA cloud expansion experiment with Arizona test dust (ATD). After starting the expansion at t = 0, the relative humidity increases due to the expansion cooling. The relative humidity with respect to ice exceeds the ice saturation line after about 20 s and ice particles are formed via deposition nucleation. The model calculations are indicated by solid red and dashed red lines. The parameterization of Kärcher & Lohmann (2003) for heterogeneous ice nucleation was used.

This contribution investigates how competing parameterizations for heterogeneous ice nucleation agree with the experiment.
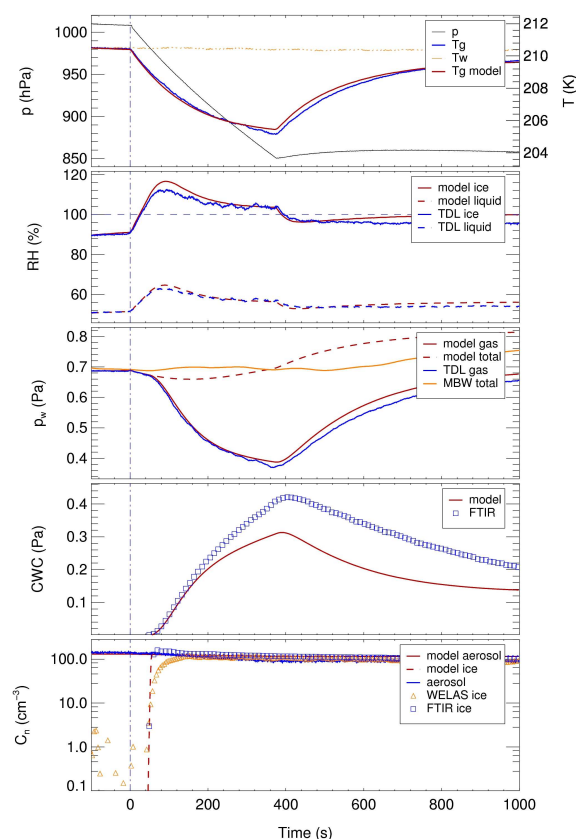
Figure 1. Comparison of an AIDA cloud expansion experiment with ATD to MAID model calculations. Panel 1: pressure p, wall temperature T_w, gas temperature T_g; panel 2: relative humidity with respect to water and ice; panel 3: water vapour pressure, total water; panel 4: ice water content; panel 5: aerosol and ice particle number concentration.

Bunz, H., Benz, S., Gensch, I., & Krämer, M. (2008). *Environ. Res. Lett.*, 3, 035001 (8pp).

Kärcher, B., & Lohmann, U. (2003). *J. Geophys. Res.*, 108 D14, 4402-4416.

Wagner, R., Benz, S., Möhler, O., Saathof, H., & Schurath, U. (2006). *Atmos. Chem. Phys.*, 6, 4775.

Aircraft contrails: do they live longer?

M. Krämer[1], M. Kübbeler[1], J. Meyer[1], M. Hildebrandt[1], C. Schiller[1], M. Fiebig[2],
A. Minikin[3], A.Petzold[3], H.Schlager[3], Ch. Voigt[3], J.-F. Gayet[4]

[1]ICG1, Forschungszentrum Jülich, 52425, Jülich, Germany
[2]Norwegian Institute for Air Research (NILU), Dept. Atmospheric and Climate Research, Kjeller , Norway
[3]DLR Oberpfaffenhofen, Institute for Physics of the Atmosphere, Weßling, Germany
[4]LaMP, UMR/CNRS, Universite Blaise Pascal, Clermont-Fd, France
Keywords: Cirrus clouds, cloud microphysics, ice crystals, evaporation

Aircraft contrails frequently occur in the upper troposphere. They consist of ice particles having the potential to directly affect the Earth´ climate. The frequency, life time, ice crystal size spectra and thus radiative properties of contrails depend strongly on the ambient distribution of the relative humidity with respect to ice (RHi). In air with RHi below 100% contrails are believed to be short-lived, while persistent contrails require an ambient RHi of at least 100% (Gao et al., 2006).

During the mid-latitude aircraft experiments CONCERT (*CON*trail and *C*irrus E*xpeR*imen*T*, 6 flights, Oct./Nov. 2008), CIRRUS (1 flight, Nov. 2006) and PAZI (`*PA*rtikel und *ZI*rren´, 2 flights, May 2003), RHi inside of contrails were measured using the high precision *F*ast *I*n-situ *S*tratospheric Lyman-alpha *H*ygrometer FISH. Ice crystals were detected using an FSSP300, a Polar Nephelometer and a Cloud Particle Imager. Enhanced signals of gas phase NOy or nonvolatile particle concentration are used to distiguish contrails from natural cirrus.

Contrails were probed in most cases above cirrus appearing together with warm fronts of low pressure systems. Figure 1 (bottom) shows RHi frequencies of occurrence from about 1 hour of observation time in 52 contrails during the 9 flights. The peak of the RHi frequency distribution is at 90%, i.e. most of the contrails were embedded in subsaturated air. For comparison, the most frequent RHi of natural cirrus is 100% in cold as well as in warmer cirrus (Figure 1, top: blue and red curves; Krämer et al., 2008).

The age of the observed contrails was between 3 and 20 minutes. First, observation based model simulations with the detailed kinetical ice cloud model MAID (Bunz et al., 2008) show that contrails, consisting of many small ice crystals,   should disappear in between 1-2 minutes and that the longer lifetimes might be caused by very few larger ice crystals evaporting only slowly under   subsaturated conditions.

Our results imply that, to date, the lifetime of contrails below 100% RHi may be underestimated. Further analysis of the observations will be performed to confirm and explain these results.
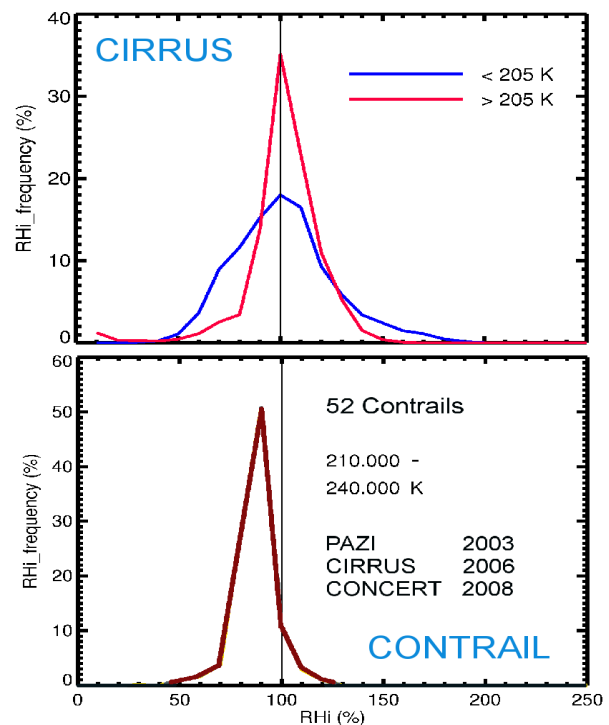
Figure 1. RHi frequency of occurrence in cirrus clouds (from Krämer et al., 2008) and in contrails.

Bunz et al. (2008). MAID: a model to simulate UT/LS aerosols and ice clouds. *Envir. Res. Lett.,* 3, 10.1088/1748-9326/3/3/035001.

Gao et al. (2006). Measurements of relative humidity in a persistent contrail. *Atmos. Env.,* 40, 1590 - 1600.

Krämer et al. (2008). Ice supersaturations and cirrus cloud crystal numbers. *ACPD*, 8, 21089-21128.

Water to Ice Transition experiments at the AIDA - chamber:
first results from the novel ice experiment NIXE-CAPS

J. Meyer[1], M. Krämer[1] ,A. Afchine[1] , M. Schnaiter[2], R. Newton[3] and D. Baumgardner[3,4]

[1]ICG1, Forschungszentrum Jülich, 52425, Jülich, Germany
[2]IMK-AAF, Forschungszentrum Karlsruhe, Karlsruhe, 76344, Karlsruhe, Germany
[3]Droplet Measurement Technologies, Boulder, CO 80308, USA
[4]Universidad Nacional Autónoma de México, Mexico City, Mexico

Keywords: ice clouds, cloud microphysics, light scattering, depolarization, instrument development

For the understanding of cloud microphysical processes, in-situ ice crystal measurements are crucial. A new feature has been added to the Cloud Aerosol Spectrometer (CAS, Baumgardner *et al*., 2001), namely the measurement of depolarisation of scattered light from cloud particles that now allows the distinction between water and ice.

The CAS has been flown on aircraft to determine cloud properties since 2002. The standard instrument is based on scattering of light in near forward (4-12 degrees) and near backward angles (168-176) for sizing and refractive index determination. By comparing forward and backward signals, spherical and aspherical particles in a narrow size range can be separated. The new CAS includes an additional detector placed in the backward direction and behind a polarized filter which is rotated 90 degrees to the incident light. Thus, the amount of light a particle depolarises can now be detected. The ratio of depolarized to non-depolarized backscattered light (D2N), over a range of sizes (3-50 µm) is proportional to the asphericity. The extended CAS is a part of a new instrument called NIXE-CAPS.

Here, we show laboratory experiments where water drops and ice crystals are nucleated from soot, sulphuric acid and other aerosol particles. From these experiments, we investigate D2N to determine particle aspericity. The experiments took place in December 2008 at the AIDA cloud chamber in Karlsruhe, Germany, in the context of an intercomparison of ice spectrometers that will be operated on the new German aircraft HALO.

During the experiment, as shown in Figure 1, the transition from water to ice could be observed. CCN were activated to water drops that then froze at temperatures around -35C. The D2N for different size ranges is shown in the top panel of figure 1, the bottom panel shows the corresponding drop/ice concentrations.
First, small water drops up to 5 um form (black line). These drops freeze at around 60160 UTC seconds, which can be seen from the significant increase in the D2N ratio. The evaluation of the signals of the larger size ranges (blue, red, green) show an inverse trend of the fraction of water converting to ice:

The larger the drops, the earlier they freeze. This can be seen in Figure 1, where the D2N ratio of the larger drops increases earlier than the ratio of the smaller drops. The scatter ratio of the largest drops (20-25 um, green) increased nearly instantaneously

.
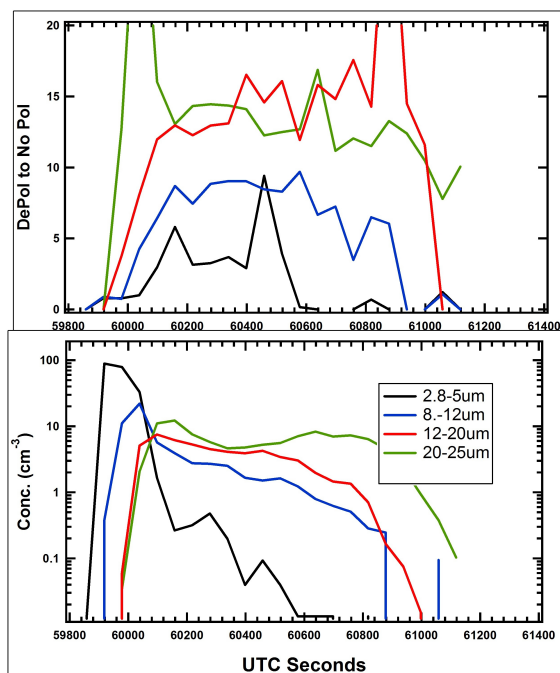
Figure 1. AIDA water to ice transition experiment on December 09, 2008, at 238 -240K with soot particles as ice nuclei; bottom: concentration of water drops and ice in different size ranges, top: ratio of depolarised to non-polarised backscattered light as indicator for ice crystals.

Baumgardner D. & Jonsson H. & Dawson W. & O'Connor D. & Newton R. (2001). *Atmos. Res.,* 59-60, 251-264

Apportioning the wood burning source in an urban area by Positive Matrix Factorization using 4-hour resolved PM10 data

R. Vecchi[1], G. Valli[1], V. Bernardoni[1], A. Piazzalunga[2], and P. Fermo[3]

[1]Department of Physics, University of Milan, and INFN, via Celoria 16, 20133, Milan, Italy
[2]Department of Environmental Sciences, University of Milan-Bicocca, p.za della Scienza 1, 20126, Milan, Italy
[2]Department of Inorg., Metall. and Analytical Chemistry, University of Milan, via Venezian 21, 20133, Milan, Italy

Keywords: biomass burning, receptor model, levoglucosan.

Particles produced during biomass and wood burning impact global climate (Crutzen and Andreae, 1990) and affect often regional and local air quality. Particles emission from residential wood combustion can increase ambient particle concentrations to high levels reducing the possibility of attaining PM10 air quality standard (EU-Directive 1999/30/EC). Indeed, the daily PM10 legislative limit is frequently exceeded at many urban sites in Europe, especially during wintertime.

Aiming at pollution mitigation strategies, an important step is identifying major emission sources. Multivariate receptor models have been widely used for particulate matter source apportionment (e.g. Viana et al., 2008; and therein cited literature) because, contrarily to other approaches, they do not need require accurate and representative source emission profiles. Generally, source chemical profiles are available for the combustion of specific types of wood under controlled conditions and, unfortunately, significant variations were observed in the emission profiles of different chemical markers as a function of fuel type and combustion conditions (among others, Fine et al., 2001).

Levoglucosan is a major component of aerosol particles emitted by biomass combustion. It is a pyrolysis product from cellulose (i.e. combustion of fossil fuels or biodegradation and hydrolysis of cellulose do not produce levoglucosan) and has been proposed as a unique tracer of wood smoke because of its stable properties in the atmosphere (Simoneit et al., 1999). In Italy, as in many other countries, in latest years there has been an increasing diffusion of residential wood burning for domestic heating because of its compatibility with environmental sustainable policies (i.e. it has almost neutral CO_2 emissions and is renewable) and for economic reasons (it is much cheaper than other heating fuels and systems). At present, 25.6 % of the Italian families use wood as fuel for domestic heating with a national wood consumption of about 20 million tons (APAT-ARPA Lombardia, 2007).

The main purpose of this work was using a receptor model (Positive Matrix Factorization, PMF) to resolve the wood burning source and to determine its chemical profile in a data set from Milan, the major urban site in Lombardy. Furthermore, a comparison between our modelled results and the ones detected by other authors in laboratory-controlled conditions was carried out.

A peculiarity of this work is also the availability of a 4-hour resolution PM10 data set chemically characterised for elements, ions, elemental and organic carbon as well as for levoglucosan concentrations. The receptor-model approach can be a powerful tool not only to assess the wood burning impact but also to verify the effectiveness of mitigation strategies.

APAT-ARPALombardia, 2007. Stima dei consumi di legna da ardere ed uso domestico in Italia, ricerca commissionata da APAT ad ARPA Lombardia - *Rapporto finale*, Marzo 2007.   (in Italian)

Crutzen, P.J. & Andreae, M.O. (1990). *Science* 250, 1669-1678

Fine, P.M., Cass, G.M., Simoneit, B.R.T. (2001). *Environ. Sci. & Technol.*, 35, 2665-2675

Simoneit, B.R.T. (1999). *Environmen Sci. & Poll. Res.*, 6, 159-169

Viana, M., Kuhlbusch, T.A.J., Querol, X., Alastuey, A., Harrison, R.M., Hopke, P.K., Winiwarter, W., Vallius, M., Szidat, S., Prévôt, A.S.H., Hueglin, C., Bloemen, H., Wåhlin, P., Vecchi, R., Miranda, A.I., Kasper-Giebl, A., Maenhaut, W., Hitzenberger, R. (2008). *J. Aerosol Science*, 39, 827-849

Contribution of wood smoke to PM$_{2.5}$ in a Swedish community during the winter season 2007-08

Peter Molnár, Gerd Sällsten

Department of Occupational and Environmental Medicine, Sahlgrenska Academy, University of Gothenburg, SE-405 30 Gothenburg, Sweden
Keywords: Back trajectories, Biomass burning, PM$_{2.5}$, Wood smoke.

Domestic wood burning for residential heating is quite common in the Nordic countries and can be a major local contributor to PM$_{2.5}$. Wood smoke often gives rise to complaints regarding annoyance and health concerns.

We measured daily PM$_{2.5}$ levels using IVLs auto changer (Ferm *et al.*, 2001) in two areas in Tanumshede, a small community in Sweden. Sampling took place during the winter 2007-08 in one wood burning area with regular complaints regarding wood smoke, and a reference area without any nearby wood burning sources. Temperature measurements with one hour resolution at two heights, 3 and 10 m, were sampled during the whole period. Air mass back trajectories were computed daily and each day was classified into one of four categories (Nordic, Marine, Continental or UK) according to Molnár *et al.*, (2006). In addition, all adult residents in the wood burning area were asked to complete a questionnaire regarding their homes and any annoyance.

The measured PM$_{2.5}$ levels (Table 1) were low in the wood burning area (mean 5.6 µg m^{-3}) and comparable with levels at Swedish background stations within the urban measurement network. The winter season of 2007-08 was characterised by mild temperatures, high frequency of windy days and plenty of precipitation (mostly rain). The monthly mean temperatures ranged 1.6–4.8 °C, and only 30 days had a mean temperature below freezing. No periods with strong inversions were found, but periods of weak inversion were frequent. In table 1, mean mass concentrations of PM$_{2.5}$ in the wood burning and the reference area are presented together with mean differences, for the whole winter, for cold and warm days, for days with or without temperature inversion, and for the four trajectory classes.

On cold days (mean temperature <0°C) higher concentrations were found in the wood burning area compared to the reference area, while no difference was found for warmer days. Days with temperature inversion (vertical temperature gradient >0.1°C m^{-1}) also showed higher concentrations compared to the reference area, but the difference was small. Trajectory analysis showed that air masses originating from continental Europe gave rise to higher concentrations in both areas, while the smallest long range contribution was from marine air masses. The difference between the two areas was about 1 µg m^{-3} for cold days and for air masses

originating from the north and the Atlantic Ocean. This wood smoke contribution is lower than reported in other studies (BHM, 2003; Glasius *et al.*, 2006), 2–4 µg m^{-3}, possibly because of the unusual mild and rainy winter season this year.

The reported annoyance due to wood smoke was still detectable, in spite of the mild winter, 10 % weekly annoyance compared to 3 % in a national health survey (2001). This demonstrates that local wood smoke can cause annoyance even at a contribution to PM$_{2.5}$ of about 1 µg m^{-3}.

Table 1. Mean concentration to PM$_{2.5}$ in the wood burning area and the reference area, the mean difference and number of days for the various subgroups. Statistical significant differences (p<0.05, Wilcoxon signed rank test) are marked in bold.

	Wood (µg m^{-3})	Ref. (µg m^{-3})	Diff. (µg m^{-3})	# of Days
All Days	5.6	5.5	0.1	151
Cold Days	6.2	5.3	**0.9**	28
Warm Days	5.5	5.6	− 0.1	107
Inversion	5.6	5.3	**0.3**	87
No Inversion	5.7	6.0	− 0.3	48
Nordic	5.7	5.0	**0.7**	32
Marine	4.7	3.6	**1.1**	33
Continental	7.9	7.6	0.2	33
UK	5.2	6.0	− 0.8	27

BHM, Biofuel-Health-Environment: Final report (In Swedish). (2003).

Ferm, M., Gudmunsson, A. and Persson, K., Measurements of PM$_{10}$ and PM$_{2.5}$ within the Swedish urban network. *NOSA Aerosol symposium*, Lund, Sweden (2001).

Glasius, M. *et al.*, Impact of wood combustion on particle levels in a residential area in Denmark, *Atmos Environment* **40**(2006), pp. 7115-7124.

Miljöhälsorapport (Environmental health report, in Swedish). The National Board of Health and Welfare, Stockholm, Sweden (2001).

Molnár, P., Johannesson, S., Boman, J., Barregard, L. and Sallsten, G., Personal exposures and indoor, residential outdoor, and urban background levels of fine particle trace elements in the general population, *J Environ Mon* **8**(2006), pp. 543-551.

Probing the composition, mixing state and hygroscopic properties of aerosol particles emitted from a wood pellet burner by coupling a SP2 and a SI-AMS with a H-TDMA

M. Gysel[1], T. Tritscher[1], M.F. Heringa[1], P.F. DeCarlo[1], J. Noda[2], T. Gustafsson[2], J.B.C. Pettersson[2], J. Dommen[1], E Weingartner[1], A.S.H. Prévôt[1], and U. Baltensperger[1]

[1]Laboratory of Atmospheric Chemistry, Paul Scherrer Institut, 5232, Villigen, Switzerland
[2]Department of Chemistry, Atmospheric Science, University of Gothenburg, SE-412 96, Göteborg, Sweden

Keywords: Biomass burning, Black carbon, H-TDMA, Aerosol mass spectrometry, Single particle analysis.

In recent years wood pellet burners, using a renewable energy source, have become increasingly popular because of their low net CO_2 emissions. However, pellet burners are known to have higher particle emissions compared to fossil fuel burners, which may raise air quality and health concerns.

The exhaust from a pellet oven emitted during the first 4 minutes after ignition was sampled into a Teflon bag, followed by the photochemical oxidation of gaseous exhaust constituents with simulated sunlight. This process led to formation of additional low volatile organic compounds condensing onto the existing primary aerosol. Resulting particle properties were investigated with a suite of aerosol instrumentation. As a novelty a single particle soot photometer (SP2; Stephens *et al.*, 2003) and a surface ionisation aerosol mass spectrometer (SI-AMS, Svane *et al.*, 2009) were operated downstream of a hygroscopicity tandem differential mobility analyser (H-TDMA, Duplissy *et al.*, 2008) in order to probe the chemical composition of individual particles in dependence of their hygroscopic growth factor (GF).

Selected particle properties after about 4 hours of photochemical processing are shown in Fig. 1. The inverted GF probability density function (GF-PDF) at 95% RH reveals an external mixture of distinct less (GF<1.25) and more (GF>1.25) hygroscopic modes (Fig. 1A). The SP2 shows that in either growth mode ~6% of the 150-nm-particles contain a black carbon (BC) core (lower BC cut-off ~60 nm), whereas in the less and more hygroscopic modes of the 200-nm-particles ~15% and ~45%, respectively, contain BC (Fig. 1B). The mean BC mass per particle is larger for the bigger particles (Fig. 1C). The corresponding mean BC volume fraction is ~16-20% and independent of dry size and growth factor (Fig. 1D). The latter is at first surprising because one would expect a decreasing fraction of water-insoluble material with increasing growth factor. However, the two growth modes possibly differ mainly in the relative amounts of organic matter (OM) and inorganic salts. The aim of further data analysis including the SI-AMS is to test this hypothesis. Final results will be presented in a broader context including results from all instruments, temporal trends imposed by photochemical processing and samples taken during the stable burning phase characterised by lower OM emissions.
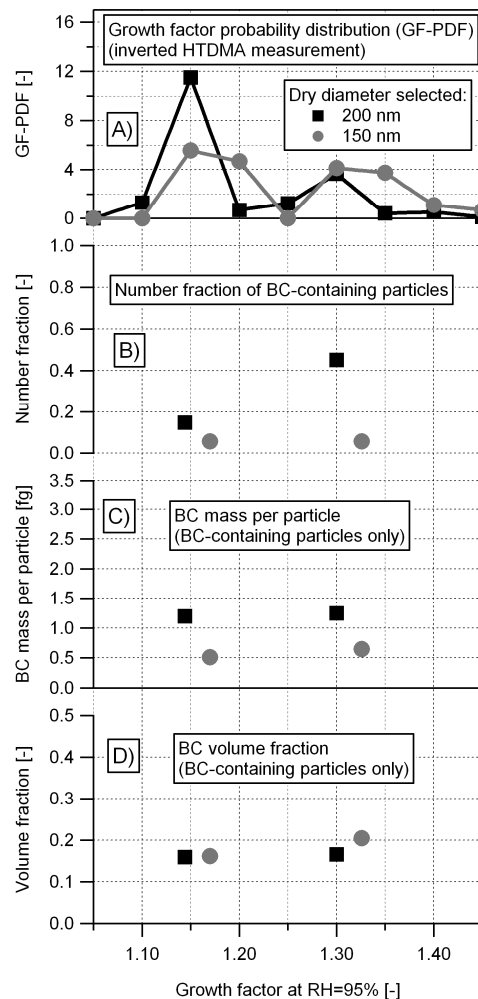
Figure 1. Growth factor resolved mixing state of BC.

Duplissy, J., Gysel, M., Sjogren, S., *et al.* (2008). *Atmos. Meas. Techniques Discuss.*, 1, 127–168.
Stephens, M., Turner, N., & Sandberg, J. (2003). *Appl. Opt.*, 42, 3726-3736.
Svane, M., Gustafsson, T., & Pettersson, J. B. C. (2009). *Aerosol Sci. Technol.*, in press.

Influence of wood burning on the aerosol status in a Saxonian health resort

K. Müller, Y. Iinuma, T. Gnauk, E. Brüggemann, L. Poulain, H. Herrmann

Leibniz-Institut für Troposphärenforschung, Permoserstr. 15, 04318 Leipzig, Germany

Keywords: HV-filter sampling, chemical characterization, tracers

In Seiffen, a health resort in Saxonian Ore mountains, aerosol samples were collected during the winter (October 2007 till March 2008) and during three weeks in August 2008 to characterize the influence of wood burning on the air quality. Seiffen is known for their use of different types of wood burning systems and consequently the air quality is significantly impacted by a number and types of wood burning units installed in the village.

The sampling was carried out every fourth day using PM_1-, $PM_{2.5}$- and PM_{10}- HV-samplers during the winter. An identical set of instruments was installed at the nearby Schwartenberg site which is part of the air quality network for the Saxonian Ministry of Agriculture, Environment and Geology. Data from the Schwartenberg site, which is not directly influenced by the emissions of Seiffen, are used as the background for the region.

Three winter episodes were selected for the detailed charcterization of the influence of wood burning in Seiffen. The concentrations of levoglucosan were compared to the summer sampling days and some winter days with extremely low levoglucosan values. Other known wood burning or combustion tracers (retene, benzo(a)pyrene and potassium) were compared to the levoglucosan data. Fig. 1 shows a correlation between the observed PM_{10} concentrations for levoglucosan and retene for all sampling day.

$y = 0.0037x + 0.5898$
$R^2 = 0.7164$
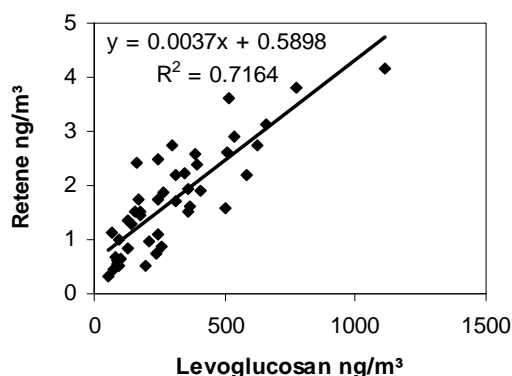
Figure 1.   Correlation of PM10 data between retene and levoglucosan.

A good correlation between levoglucosan and benzo(a)pyrene concentrations suggests that they mostly originated from the same source, likely domestic wood combustion. Wood burning was identified as an important additional PM source in winter aerosol. However, the influence of wood combustion was also observed in summer aerosols, most likely from the production of domestic hot water using wood combustion boilers.

Table 1 summarises the contributions of biomass burning to PM1, PM10, K, TC, benzo(a)pyrane and retene levels in Seiffen. Due to a high background level of biomass burning aerosols in Seiffen during summer months, the numbers shown in Tables 1 are likely biased towards the lower end and actual contribution of biomass burning in Seiffen might be higher than the numbers shown in Table 1.

Table 1. Average contribution of wood burning in Seiffen based on the levoglucosan data from the three intensive periods in winter and the winter/summer background levels

	Contribution of wood burning [%]
PM_{10} mass	11 / 18
PM_1 mass	12 / 28
K in PM_{10}	17 / 43
TC in PM_{10}	24 / 26
B(a)Pyrene in PM_{10}	51 / 53
Retene in PM_{10}	31 / 36

Aerosol mass spectrometer measurements in January 2008 have shown that the daily variation of the levoglucosan correlates well with the heating behaviour of people. The measurements showed two daily peaks, one in the morning hours (7:00-9:00) and the other major peak in the evening (17:00-21:00). Additional contributions to PM_{10} from wood combustion were 21.3, 12.0 and 1.3 µg/m³ for the three intensive measurement periods in Seiffen.

Observed results are in good agreement with data published in the "AQUELLA" Steiermark report (Bauer et al., 2007).

Reference

Bauer, H., Marr, I., Kasper-Giebl, A., Limbeck, A., Caseiro, A., Handler, M., Jankowski, N., Klatzer, B., Kotianova, P., Pouresmaeil, P., Schmidl, Ch., Sageder, M., Puxbaum, H., 2007. *"Aquella" Steiermark Bestimmung von Immissionsbeiträgen in Feinstaubproben* (http://umwelt.steiermark.at/).

Comparison between LC-MS and GC-MS measurements for the determination of levoglucosan and its application to rural and urban atmospheric samples

C. Piot[1,2], J.L. Jaffrezo[1] and J.L. Besombes[2]

[1]Laboratoire de Glaciologie et Géophysique de l'Environnement (UMR 5183), Université Joseph Fourier-CNRS, Rue Molière, BP 96, 38402 St Martin d'Hères Cedex, France
[2]Laboratoire de Chimie Moléculaire et Environnement, Polytech'Savoie- Université de Savoie, Campus Scientifique, 73376 Le Bourget du Lac Cedex, France

Keywords: levoglucosan, LC-MS, organic aerosols.

The determination of atmospheric concentrations of levoglucosan, an unambiguous tracer of biomass burning emissions, becomes all the more important with the development of wood as a renewable energy for domestic heating. Indeed, wood smoke contains many toxic compounds, like polycyclic aromatic hydrocarbons (PAHs) and fine particular matter (PM). In consequence, it has an impact on the ambient air quality and many researches demonstrated the increase of atmospheric PM load due to domestic biomass combustion in developed countries.

Fast, cheap, and reliable measurements are needed for an improved survey of the impacts of these emissions. Analysis of this tracer is traditionally performed with Gas Chromatography-Mass Spectrometry (GC-MS) techniques after derivatization (Bergauff *et al*., 2008). But this method requires several labour intensive and solvent-consuming steps of extraction and derivatization before analysis.

Simpler and faster techniques using Liquid Chromatography-Mass Spectrometry (LC-MS) emerged in the last few years (Schkolnik & Rudich, 2006). The LC-MS analysis of levoglucosan does not require the use of derivatization reagent and can be carried out starting from an aqueous extraction of the samples. However, the two techniques have not been intercompared so far for measurements performed on the same samples. In this work, an LC-MS2 method is described, coupling two techniques in order to deliver an appropriate separation of levoglucosan isomers and a sensitive detection : High Performance Liquid Chromatography (HPLC), in conditions close to those described in Caseiro *et al.* (2007), and Electrospray Ionisation-tandem Mass Spectrometry (ESI-MS/MS) in negative polarity (Gambaro *et al.,* 2008).

This work presents a comparison of simultaneous measurements of levoglucosan for samples coming from different types of sampling sites and seasons. Particularly, it includes samples from Marseilles (summer 2008) and Grenoble (winter 2009), two French urban areas, with collection performed within the FORMES program (Fraction ORganique de l'aérosol urbain : Méthodologie d'Estimation des Sources). Other samples are coming from rural areas and emissions sources in an regional context. The LC-MS allows an analysis in less than 3 minutes (Fig.1) with a very simple extraction but only levoglusoan and its isomers are analysed. The run is longer with the GC-MS (up to 20 min) but allows the detection of many compounds. LC-MS must be used for analyses of many measurements campaigns in routine and GC-MS for global and diversify analyses.
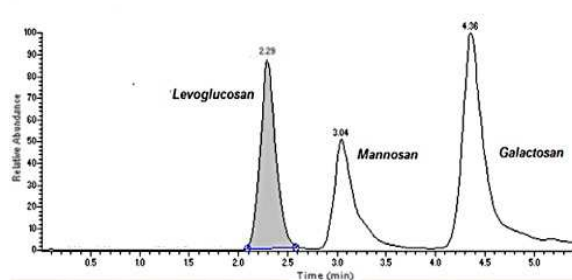
Figure 1 : LC-MS chromatogram

Bergauff, M., Ward, T., Noonan, C., & Palmer, C.P. (2008). *Intern. J. Environ. Anal. Chem.*, 88(7), 473-486.

Caseiro, A., Marr, I.L., Claeys, M., Kasper-Giebl, A., Puxbaum, H., & Pio, C.A. (2007). *Journal of Chromatography A*, 1171, 37-45.

Gambaro, A., Zangrando, R., Gabrielli, P., Barbante, C., & Cescon, P. (2008). *Anal. Chem.*, 80 (5), 1649-1655.

Schkolnik, G., & Rudich, Y. (2006). Anal. Bioanal. Chem., 385, 26-33.

PAHs emission and energy efficiency of a generator fueled by soy-biodiesel blends

J.H. Tsai[1], S.J. Chen[1*], K.L. Huang[1] and W.J. Lee[2]

1 Department of Environmental Science and Engineering, National Pingtung University of Science and Technology, 91201, Taiwan.
[2] Department of Environmental Engineering, National Cheng Kung University, 70101, Taiwan.

Keywords: biodiesels, PAHs, energy efficiency, generators.

Increasing attention has been paid to biodiesels used as alternative fuels for diesel engines and generators. The use of biodiesels in diesel engines has been extensively studied. However, little is known about the reduction mechanism of polycyclic aromatic hydrocarbons (PAHs) emission from diesel generators fueled with soy-biodiesel blends. In this study, therefore, the PAHs emissions and energy efficiencies of a biodiesel-fueled generator under different addition ratios of biodiesel were investigated. A pure petroleum diesel (B0) and three soy-biodiesel blends (B10 (v/v = 10% soy-biodiesel/90% B0), B20 (v/v = 20% soy-biodiesel/80% B0), and B50 (v/v = 50% soy-biodiesel/50% B0)) were tested at four loads (unload, 5 kW, 7 kW, and 10 kW).

Despite of the load of bearing power, the average concentrations of total-PAHs emitted from the generator using B10 and B20 were lower (by 38% and 28%, respectively) than that using B0 (Figure 1). When compared to B0, the emission factors of total-PAHs were significantly lowered (average 72%) as the addition ratios of soybean biodiesel increased. This finding indicates that the use of biodiesel fuel containing soybean oil methyl ester reduced PAHs emission from the generator. In addition to the lower amounts of PAHs in soybean biodiesel than in B0, soybean oil methyl ester has higher oxygen content (11 wt%) and cetane number than pure petroleum diesel. The addition of soybean oil in pure petroleum diesel might increase the self-ignition propensity and decrease the ignition delay of diesel resulting in the improvement of fuel combustion efficiency and the reduction of PAHs production/emission. Kameda *et al.* (2007)
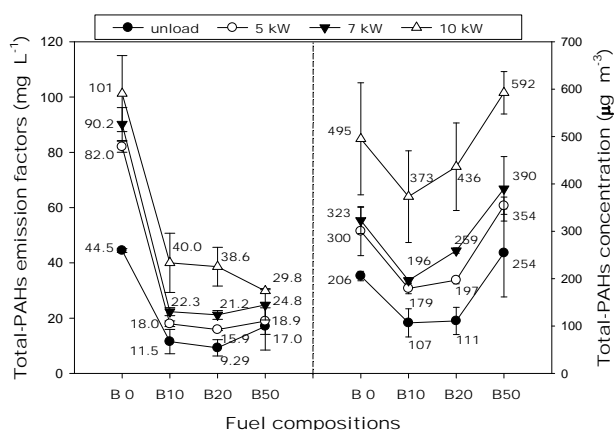
found that the PAH and nitro-PAH emissions from the biodiesel with 20% toluene addition were not higher than those from the one without toluene addition. They suggested that trace amounts of aromatic hydrocarbons in biodiesel were not the major factor for the reduction of PAHs and nitro-PAHs emissions; instead, the higher oxygen content in biodiesel was probably responsible for such a reduction.

In this study, the energy efficiency (EE) of generator is defined as the ratio of the output energy divided by the input energy. Under the same bearing power, the EE of generator increased at the additions of 10% and 20% soybean biodiesel (B10 and B20, respectively), with the greatest EE increase when using the B20 (average increase 0.34%) (Table 1). The phenomena might be associated with the higher oxygen content and cetane number for the B10 and B20 than for the B0 (pure petroleum diesel) (Dorado *et al.*, 2003; Kalligeros *et al.*, 2003), which increased the fuel combustion efficiency of the diesel engine. However, when the soybean biodiesel addition was up to 50% (B50), the EE of generator decreased by an average of 1.09% at 5–10 kW (Table 1), probably resulted from incomplete combustion of fuel and obstruction of energy release (Lin *et al.*, 2006). Therefore, the addition ratio of soybean biodiesel to pure petroleum diesel is critical for the EE of generator.

Table 1. The energy efficiencies of generator under different addition ratios of biodiesel

	EEs (%) (n=3)		
	5 kW	7 kW	10 kW
B0	19.53±0.05	23.15±0.02	25.04±0.11
B10	19.57±0.06	23.18±0.05	25.09±0.02
B20	19.59±0.02	23.24±0.33	25.12±0.02
B50	19.45±0.08	22.90±0.09	24.59±0.35

Dorado, M.P., Ballesteros, E., Arnal, J.M., Gómez, J., & López, F.J. (2003). *Fuel*, 82, 1311–1315.

Kalligeros S., Zannikos, F., Stournas, S., Lois, E., Anastopoulos, G., Teas, Ch., & Sakellaropoulos, F. (2003). *Biomass Bioenergy*, 24, 141–149.

Kameda, T., Nakao, T., Stavarache, C., Maeda, Y., Hien, T.T., Takenaka, N., Okitsu, K., & Bandow, H. (2007). *Bunseki Kagaku*, 56, 241-248.

Lin, Y.C., Lee, W.J., Hou, H.C. (2006). *Atmos. Environ.*, 40, 3930-3940.

Figure 1. Concentrations and emission rates of the total-PAHs emitted from the generator.

Alkali-content of individual aerosol particles in South-West Sweden: Influence of meteorological conditions and air mass origin

Torbjörn L. Gustafsson, B. Kovacevik, J. Noda, J.Boman and Jan B. C. Pettersson

Department of Chemistry, Atmospheric Science, University of Gothenburg, S-412 96 Gothenburg, Sweden

The influence of atmospheric transport patterns and meteorology on observed levels of potassium- and sodium-containing submicron particles has been examined in Gothenburg, Sweden, during the winter and spring seasons from February 16 to May 20, 2007. Gothenburg is located on the west coast of Sweden and the urban area has a population of about 600,000 people.

An aerosol mass spectrometer (AMS) was used to measure the alkali metal content in single submicron particles. The AMS is based on orthogonal acceleration time-of-flight mass spectrometry combined with surface ionization (Svane et al. 2004; 2005; 2009) and it provides semi-quantitative measurements of the alkali content of individual particles in the size range from 20 to 1000 nm. The aerodynamic lens system of the AMS produces a narrow particle beam that is directed towards a restively heated (1500 K) platinum surface in the AMS vacuum system. The particles are efficiently ionised at the hot surface by surface ionisation (Svane et al 2004). The ions are accelerated into a time-of-flight unit and ions with different mass to charge ratio (m/z) reaches the ion detector separated in time. Ions are detected with a multi channel plate (MCP) and amplified and counted by a computer-controlled Fastflight-2 Digital Signal Avarager.

The Na and K concentrations were typically in the range 1-50 ng m^{-3} and showed large variability on the time scale of a few hours for both elements with peak concentrations above 100 ng m^{-3} for Na. The time series indicate that the two concentrations were correlated during some periods, but this was not generally true and the Na:K ratio usually varied in the range from 0.1 to 20. The local temperature, wind speed and wind direction were observed to influence the alkali concentrations, and cluster analysis of air mass back trajectories showed that the concentrations also depended on the origin of the air mass.

High concentrations of sodium-containing particles were favoured by westerly winds and high wind speeds, and were related to sea spray particles in air masses originating from the Atlantic. Weak diurnal variations in Na concentration where attributed to sea breeze.

High concentration of potassium-containing particles correlated with low temperatures and low wind speeds, and was related to air masses originating from continental Europe. Low Na:K ratios suggested that these particles originated from solid fuel combustion including biomass burning.

High K concentrations were observed in air masses transported from regions in Eastern Europe during a period with extensive agricultural burns. Diurnal variations and the importance of wind direction suggested that sources in the near region made significant contributions to the observed K concentrations, see Fig. 1. The observed alkali concentrations were concluded to be affect both by emissions from the near region and by long-range transport. The study also illustrates the capacity of the developed AMS for selective and sensitive detection of specific types of particles in ambient air.
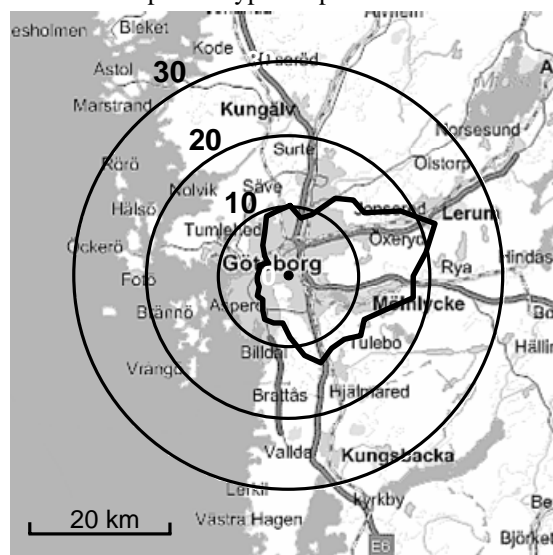
Fig. 1 Potassium concentration (ng m^{-3}) in submicron particles as a function of wind direction measured in Gothenburg from February 16 to May 20, 2007.

References

Svane, M., Hagström, M., and Pettersson, J. B. C. (2004). Chemical Analysis of Individual Alkali-Containing Aerosol Particles: Design and Performance of a Surface Ionization Particle Beam Mass Spectrometer. *Aerosol Sci. Technol.* 38:655-663.

Svane, M., Janhäll, S., Hagström, M., Hallquist, M., and Pettersson, J. B. C. (2005). On-line Alkali Analysis of Individual Aerosol Particles in Urban Air. *Atmos. Environ..* 39:6919-6930.

Svane, M., Gustafsson, T. L., Kocevik, B., Noda, J., Andersson , P. U., Nilsson D. E., and Pettersson, J. B. C. (2009). On-line chemical analysis of individual alkali-containing aerosol particles by surface ionization combined with time-of-flight mass spectrometry. *Aerosol Sci. Technol., in press.*

Humic-like substances in transported biomass burning plume at Mt. Lulin in Taiwan

C.T. Lee[1], N.H. Lin[2], Y.H. Hou[1] and S.Y. Chang[3]

[1]Graduate Institute of Environmental Engineering, National Central University, Jhongli, 32001, Taiwan
[2]Department of Atmospheric Sciences, National Central University, Jhongli, 32001, Taiwan
[3]Department of Public Health, Chung Shan Medical University, Taichung, 40201, Taiwan

Keywords: humic-like substances, atmospheric aerosols, biomass burning, $PM_{2.5}$.

HULIS (HUmic LIke Substances) in water-soluble organic aerosol drew a lot of attentions recently. The sources of HULIS can be varied from photochemical reactions, biomass burning (BB) plume, and microorganisms in soil or sea water. In cloud or fog samples, HULIS is found the most active species in reducing surface tension of a droplet. The effect may result in increasing droplet numbers in clouds. In this study the observation of HULIS in aerosol at Mt. Lulin is reported and is found associated with transported BB plume.

The aerosol was collected by using Graseby Andersen/GMW Model 1200 High-Volume Air Sampler at Mt. Lulin (2,862 m a.s.l.) in Taiwan in March 2008. The preparation of filter samples is similar to Varga et al. (2001) including solid phase extraction (Chrom Tech SPE-12 column), addition of 1 M HCl, and elution with 5 ml MeOH. The effluent was added with 5 ml purified water (>18 MΩ) after nitrogen drying. The samples were analyzed by a high-performance liquid chromatography (Hitachi Model 890-0443) when they were ready.

The US NASA Earth Observatory (http://earthobservatory.nasa.gov/NaturalHazards/) provides satellite pictures of fire spots for big-scale BB. In addition, the flow streamlines and the transport pathways of air masses to the observation site were checked by using the HYSPLIT back trajectory model (Draxler and Rolph, 2003). The transport of BB plume to Mt. Lulin was thus confirmed for aerosol collected in March 2008.

Figure 1 shows a linear relationship between HULIS and water-soluble organic carbon (WSOC) in the collected aerosol. It indicates that HULIS at Mt. Lulin was about 49% of WSOC.
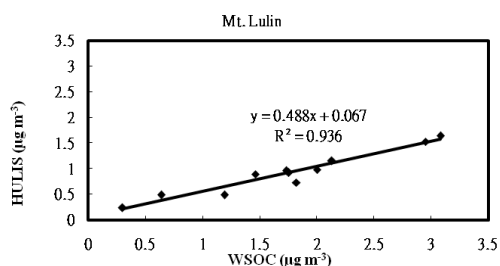
Figure 1. Linear correlation between aerosol WSOC and HULIS collected at Mt Lulin in March 2008.

In addition, HULIS is highly associated with organic carbon fraction 3 (OC3, a high-temperature evolved carbon category) in Figure 2, which implies that it is a less volatile species in aerosol organics.
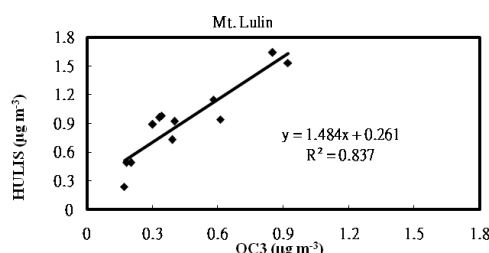
Figure 2. Linear correlation between aerosol OC3 and HULIS collected at Mt Lulin in March 2008.

As mentioned previously, several sources contributed to HULIS in aerosol. Figure 3 shows a strong association of potassium ion with HULIS. Since potassium ion is well acknowledged as a BB tracer (Andreae et al., 1983), it clearly indicates that the collected HULIS in aerosol was contributed from the air masses transported from BB source region.
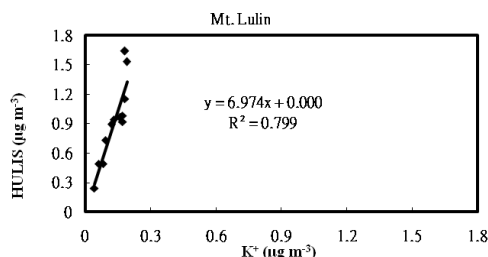
Figure 3. Linear correlation between aerosol potassium ion and HULIS collected at Mt Lulin in March 2008.

Andreae, M. (1983). Science, 220, 1148-1151.

Draxer, R.R., & Rolph, G. (2003). HYSPLIT4 model, NOAA Air Resources Laboratory, Silver Spring, MD, U.S.A.

Varga, B., Kiss, G., Ganszky, I., Gelencsér, A. & Krivácsy, Z. (2001). Talanta, 55, 561–572.

Strong wintertime influences of residential wood burning aerosols in urban environments: Grenoble and Paris, France

O. Favez[1,5], B. d'Anna[1], A. Boréave[1], I. el Haddad[2], N. Marchand[2], C. Piot[3,4], J.L. Besombes[3], D. Voisin[4], J.L. Jaffrezo[4], J. Sciare[5], H. Cachier[5], C. George[1]

[1]Institut de Recherches sur la Catalyse et l'Environnement, CNRS-Université Lyon1, Villeurbanne, France
[2]Laboratoire de Chimie Provence, CNRS-Université d'Aix-Marseille, Marseille, France
[3]Laboratoire de Chimie Moléculaire et Environnement, Université Savoie-Polytech'Savoie, Chambéry, France
[4]Laboratoire de Glaciologie et Géophysique de l'Environnement, CNRS-Université Grenoble, Grenoble, France
[5]Laboratoire des Sciences du Climat et de l'Environnement, CNRS-CEA, Gif sur Yvette, France

Keywords: urban pollution, wood combustion, carbonaceous aerosols, source apportionment, absorption

Carbonaceous aerosols originating from biomass burning are known to contain high amounts of carcinogenetic polycyclic aromatic hydrocarbons as well as light-absorbing species (black and brown carbon) which significantly influence the aerosol radiative forcing and atmospheric photochemistry. It is thus of prime importance to evaluate their contribution to particulate matter in the ambient air. However, residential wood burning emissions have been generally disregarded until recently, and data related to their influence on the air quality of large European urban centres are still very scarce.

We investigate here the impact of residential wood burning aerosols on the air pollution of two French cities: Grenoble, located in an Alpine valley, and Greater Paris, one of the few European megacities. These studies were notably conducted using aerosol filter-based measurements, a c-ToF Aerosol Mass Spectrometer, and a multi-wavelength Aethalometer.

In particular, the latter instrument was used to investigate the spectral dependence of the aerosol light absorption, and subsequently to track the presence of brown carbon of biomass burning origin in the atmosphere of both cities. Relatively high Angstrom absorption exponents were observed during the winter season (Figure 1), suggesting a significant influence of residential wood burning aerosols in these urban environments. This hypothesis was confirmed by high amounts of (water-soluble) organic carbon, of humic-like substances, and of levoglucosan.

Various source apportionment exercises, including Positive Matrix Factorization (Lanz et al., 2007) and an Aethalometer model (Sandradewi et al., 2008), were then achieved to evaluate the contribution of wood burning aerosols to total particulate matter (Figure 2). Results notably indicate that residential wood burning emissions accounted on average for more than 50% and 25% of fine carbonaceous aerosols at wintertime in Grenoble and Paris respectively. Such results underline the significant impact potentially played by residential wood burning emissions on particulate air pollution in large European urban centres.

	Paris summer	Paris winter	Grenoble winter
Absorption exponent	1.07	1.25	1.31
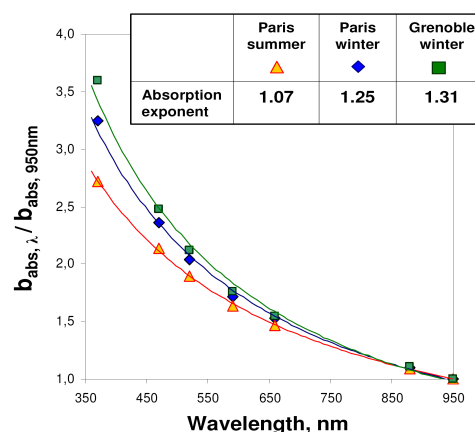
Figure 1. Mean spectral shape of aerosol light absorption in Paris and Grenoble.

Figure 2. Contribution of wood burning emissions to carbonaceous aerosols during a winter pollution episode in Grenoble.

Lanz et al. (2007). *Atmos. Chem. Phys.*, 7, 1503-1522.
Sandradewi et al. (2008). *Environ. Sci. Technol.*, 42, 3316-3323.

Chemical characterisation of PM$_{10}$ emissions from common Portuguese tree species in a wood burning stove

C.A. Alves[1], C. Gonçalves[1], C. Pio[1], M. Evtyugina[1], A.C. Rocha[1], A. Caseiro[1], F. Mirante[1], H. Puxbaum[2], C. Schmidl[2], F. Carvalho[3] and J. Oliveira[3]

[1]Centre for Environmental and Marine Studies (CESAM), Department of Environment, University of Aveiro, 3810-193 Aveiro, Portugal
[2]Institute of Chemical Technologies and Analytics, Vienna University of Technology, Getreidemarkt 9/164-UPA, 1060 Vienna, Austria
[3]Nuclear and Technological Institute, Unit of Radiological Protection and Safety, E.N. 10, 2686-953 Sacavém, Portugal

Keywords: biomass burning, wood stove, particulate emissions, OC/EC, radionuclides

A recent study has pointed out residential wood combustion as a major contributor to particulate pollution in Europe during winter (Legrand & Puxbaum, 2007). One goal of detailed analysis of biomass burning emissions is the potential use in receptor models for particulate matter source apportionment. Since the distribution of compounds emitted differs by species and burning conditions and there are many variations among published profiles (e.g. Fine *et al*., 2004; Schmidl *et al*., 2008), it is desirable to obtain specific data at a regional level on the chemical characterisation of wood smoke.

To characterise the PM$_{10}$ emissions from wood stoves and compare the emission profiles to those obtained from previous experiments in other countries, a series of source tests were carried out on the burning of some of the most prevalent Portuguese tree species (Table 1). Analysis of the wood smoke included particle mass emission factors and the determination of its carbonaceous content (OC/EC) by a thermal optical technique (Carvalho *et al*., 2006). The trace metal speciation has been performed by ICP-OES and XRF (Schmidl *et al*., 2008). Radionuclides have been measured by α-spectrometry (Carvalho *et al*., 2007). PM$_{10}$ samples were also analysed for the main water-soluble ion species.

Table 1. Portuguese tree species selected for wood stove combustion tests

Tree species	kha forest	% cover	Moisture (%)
Pinus pinaster	911	27.3	38.5
Eucalyptus globulos	541	16.3	41.6
Quercus suber	331	9.9	41.2
Acacia longifolia	19	0.6	41.5

Results suggest that eucalyptus and oak contribute with similar PM$_{10}$ (Figure 1) and carbonaceous emissions (Table 2), while pine and acacia smoke present some resemblances. The comparison of chemical profiles from this study with literature showed quite different concentrations, in spite of some qualitative similarities.
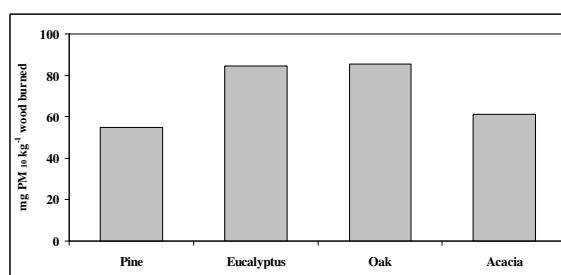
Figure 1. PM$_{10}$ emission factors from the combustion of Portuguese tree species in a stove

Table 2. Emission factors for wood stove combustion (w/w % of PM$_{10}$)

	OC	EC	OC/EC
Pine (sw)	26±10	37±12	0.9
Eucalyptus (hw)	32±5	13±8	3.1
Oak (hw)	43±2	11±4	4.4
Acacia (hw)	20±10	25±10	1.0
Ref. (a)	41-55	10-31	1.3-5.7
Ref. (b)	51-59 (hw)	3-23 (hw)	2.6-17.3 (hw)
	44-78 (sw)	8-22 (sw)	3.0-10.2 (sw)

(sw) – softwood; (hw) – hardwood; (a) Schmidl et al. (2008); (b) Fine et al. (2004)

Carvalho *et al*. (2006) *Atmos. Res*., 80, 133-150.
Carvalho *et al*. (2007) *J. Environ. Radioactiv*., 98, 298-314.
Fine *et al*. (2004) *Environ. Eng. Sci*., 21, 705-721.
Legrand, M. & Puxbaum, H. (2007). *J. Geophys. Res*., 112, D23S01.
Schmidl *et al*. (2008) *Atmos. Environ*., 42, 126-141.

Parameterization of biomass burning particle emissions from wildfires

S. Janhäll, M.O. Andreae and U. Pöschl

Department of Biogeochemistry, Max Planck Institute for Chemistry, D-55128, Mainz, Germany

Keywords: Biomass burning, Emission factor, Combustion aerosols, PM, Particle size distribution.

Aerosol particle emissions from wildfires have a large impact on air quality and climate. For burning seasons the visibility in the affected areas can be heavily reduced, and the health effect on the local population can be vast. Biomass burning particles are efficient cloud condensation nuclei (CCN) and the probability of activation is thus mainly related to the particle size and particle number concentrations.

In this study we use published experimental data and different fitting procedures to derive particle number and mass emission factors (EF_{PN}, EF_{PM}) related to fuel category and mass of dry fuel burned as well as characteristic scaling ratios between particle and carbon monoxide emissions (PN/CO, PM/CO). Moreover, we explore and characterize the variability of the smoke particle size distribution, which is typically dominated by a lognormal accumulation mode with count median diameters in the range of 100-150 nm (depending on age, fuel and combustion efficiency).

The emissions of particles are mainly described by linear relations to the modified combustion efficiency, MCE, defined as the ratio between the carbon emitted from the fire as carbon dioxide and the carbon emitted from the fire as carbon dioxide and carbon monoxide as a total (Yokelson et al., 1996).

$$MCE = (\Delta C_{CO2}) / (\Delta C_{CO2} + \Delta C_{CO})$$

An example of the fittings is shown in Fig. 1, for the emission factor for particle number, EF_{PN}, from different fuels. A standard fitting method is used and the dotted lines show the y-error from the fitting. The forest data is taken directly as published, while savanna and grass data were measured only above 100 nm diameter and thus corrected for the lack of smaller particles, assuming a varying particle size distribution.

This fitting procedure is repeated on particle mass data for different fuels and on particle size distributions, described by a lognormal size distribution, with geometric mean and geometric standard deviation given. This data varies with MCE and is used to show that our results for particle mass emissions, particle number emissions and particle size distribution data together give a good description of the particle emissions.
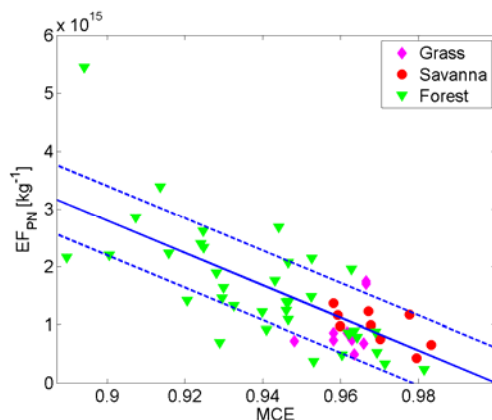
Figure 1. Emission factor of particle number versus modified combustion efficiency (MCE) for three studies, Guyon et al., 2005 (forest) and LeCanut et al., 1996 (savanna, grass).

The result of this study is a description of the particle emissions from biomass burning, relating the variables to modified combustion efficiency and fuel, and describes both the particle number, particle mass and particle size distribution of the emissions.

Guyon, P., Frank, G. P., Welling, M., Chand, D., Artaxo, P., Rizzo, L., Nishioka, G., Kolle, O., Fritsch, H., Dias, M. A. F. S., Gatti, L. V., Cordova, A. M., & Andreae, M. O. (2005). *Atmospheric Chemistry and Physics*, 5, 2989-3002.

LeCanut, P., Andreae, M. O., Harris, G. W., Wienhold, F. G., & Zenker, T. (1996) *J. of Geophysical Research,* 101, 23615-23630.

Yokelson, R. J., Griffith, D. W. T., & Ward, D. E. (1996) *J. of Geophysical Research*, 101, 21067-21080.

Diurnal variation of wood combustion related compounds and impact on urban PM$_{10}$

J. Schnelle - Kreis[1], G. Abbaszade[1], R. Kunde[2], J. Orasche[1] and R. Zimmermann[1,2,3]

[1] Ecological Chemistry Helmholtz Zentrum München, Ingolstädter Landstrasse 1, 86573 Neuherberg, Germany
[2] Bavarian Center for Applied Energy Research, Walther - Meißner - Str. 6, 85748 Garching, Germany
[3] Department of Analytical Chemistry, University of Rostock, Dr. Lorenz Weg 1, 18051 Rostock, Germany

Keywords: Ambient Aerosol, PM10, Biomass burning, Modelling (regional), Source apportionment.

The use of wood as renewable energy source is discussed contradictorily. On one hand the favourable CO_2 balance does not enhance the global warming problem whereas on the other hand biomass combustion significantly contributes to ambient PM mass loading and ambient concentrations of polycyclic aromatic hydrocarbons (PAH).

The study presented here was carried out in Augsburg, Germany. It consisted of four main parts: update of emission inventory for domestic heating, emission measurements, emission and aerosol dispersion modelling and ambient monitoring. The data presented focus on the results of the ambient monitoring.

High volume ambient PM$_{10}$ samples have been collected during the heating periods 2006/7 and 2007/8. In order to distinguish sources within the city from regional background, daily sampling was carried out simultaneously at five sites within and three sites outside of the town in February and March 2008. Samples were analysed for inorganic ions, elements, EC/OC and organic tracer compounds. During a 10 day period in February 2008 additional low volume samples were taken with 3 h time resolution and analysed for organic compounds.

At the traffic related site PM$_{10}$ mass concentrations were in the range of 8.7 - 93.2 µg/m³ (average 31.8 µg/m³) in winter 2006/7 and 5.1 - 98.0 µg/m³ (average 36.7 µg/m³) in winter 2007/8. The limit value of 50 µg/m³ was exceeded 15 times in winter 2006/7 and 26 times in winter 2007/8 respectively.

The concentrations of Levoglucosan, an organic tracer for biomass combustion, were in the range of 29 - 1922 ng/m³. Dehydroabietic acid, a specific tracer for coniferous wood combustion, showed concentrations in the range of 13 - 708 ng/m³. Concentrations of Potassium, which is commonly used as inorganic tracer for biomass combustion, were in the range of < 50 - 875 ng/m³.

Concentrations of all tracers for biomass combustion are highly correlated (r > 0.85; p<0.005) independent of the year and sampling site. Just like in our long term monitoring study (Schnelle-Kreis 2007) PAH concentrations are higher correlated to source factors of solid fuel combustion (wood and coal) than to traffic related source factors.

Based on emission factors of PM and trace compounds determined within the study, the fraction of ambient PM$_{10}$ originating from (primary) wood combustion particles was calculated. Highest concentrations of PM from wood combustion were found during periods with low air exchange (low wind speed and low mixing layer height). In these periods up to 4 µg/m³ higher concentrations of particles from wood combustion were found in an inner city residential area compared to the city centre. Based on the measurements near the city and in 100 m above ground level up to 75 % of the wood combustion particles could be assigned to local sources, depending on the meteorological conditions in the atmospheric boundary layer.

The measurements with time resolution of 3 h showed a clear diurnal variation with high concentrations of wood combustion tracers at night (Figure 1). Peak concentrations of more than 17 µg/m³ PM$_{10}$ from primary wood combustion particles were detected between 9 p.m. and midnight
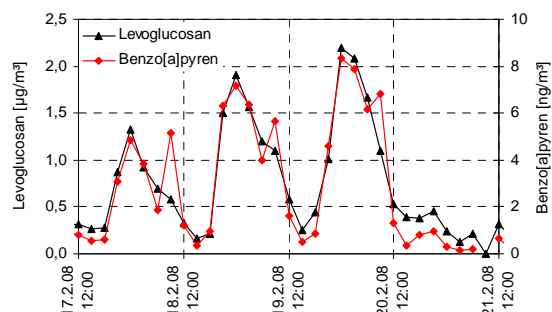
Figure 1. Diurnal variation of Levoglucosan and Benzo[a]pyren concentrations in a period with low air exchange. Traffic site. 3h samples.

Schnelle - Kreis, J., Sklorz, M., Orasche, J., Stölzel, M., Peters, A., Zimmermann, R. (2007) *Environ. Sci. Technol*. 41, 3821 - 3828

Sklorz, M, Briedé, J.J., Schnelle - Kreis, J., Liu, Y., Cyrys, J., de Kok, T.M., Zimmermann, R.. (2007) *J. Toxicol. Env. Health A* **70**, 1866 - 1869

The contribution of biomass burning to PM: a comparison between an Alpine valley and the Po Valley

C. A. Belis[1,2], A. Piazzalunga[3], C. Colombi[4], P. Fermo[5], B. Larsen[2], R. Vecchi[6], C. Carugo[1], V. Gianelle[4]

[1] Environmental Protection Agency of Lombardy Dept. of Sondrio, via Stelvio, 35, 23100, Sondrio, Italy
[2] European Commission Joint Research Centre - Institute for Environment and Sustainability, 21027, Ispra, Italy
[3] University of Milan-Bicocca Dept. of Environmental Sciences, Pza. della Scienza,1 20126, Milan, Italy
[4] Environmental Protection Agency of Lombardy Dept. of Milan, via Juvara, 22, 20122, Milan, Italy
[5] Univ. of Milan Dept. of Inorganic, Metallorganic and Analytic Chemistry, via Venezian 21, 20133, Milan, Italy
[6] University of Milan Dept. of Physics, via Celoria 16, 20133, Milan, Italy

Keywords: biomass burning, source apportionment, levoglucosan, PAH, modelling.

Levels of PM10 exceed limit values not only in the densely populated and industrialized Po Valley but also in the nearby Alpine valleys. In addition, annual means of benzo(a)pyrene in the valley floor in the southern Alps are higher than those observed in the adjacent Po Valley and exceed the target value set by EU Directive 2004/107/EC.

In a recent study, it has been observed that despite the very small differences in winter concentrations of PM from different sites of the valley floor (kerbside, urban background and rural background), levels of this pollutant decrease significantly with height (Belis et al., 2008). These authors indicated that the orography and the meteorology of the cited Alpine area strongly contribute to the accumulation of local emissions in the air layer influenced by the winter ground level thermal inversion.

According to the emission inventory of the Lombardy Region the main sources of primary PM10 in the Alpine city of Sondrio are biomass burning (42%) and transport (36%) compared to 10% and 64% respectively of primary PM10 in the city of Milan.

In order to check these estimations source apportionment has been carried out with the receptor model CMB 8.2 using the concentration of 20 elements in PM10 measured in a three years survey (2004 – 2007). In addition to the source profiles available in literature, local source profiles were obtained for soil, biomass burning, brakes, tyres, etc. (Colombi et al., 2008). The results indicate that in the Alpine city 25% of PM10 derives on average from biomass burning while the contribution of this source in the city of Milan is <10%. The contribution from biomass burning is relevant also in areas where carpentry is the main economic activity.

The concentrations of levoglucosan, a chemical marker for biomass burning (Simoneit et al., 1999), measured between 2005 and 2007 in 4 sites distributed across the Po Valley and the Alpine area strongly support the hypothesis of a higher contribution of this source to the PM in the Alpine valley floors. In Sondrio, biomass burning contributes to 20-45% of EC and to 40-55% of OC (Piazzalunga et al., 2008).

Similar indications come from the comparison of K levels in 11 sites from different areas (rural, urban and suburban) between the Po Valley, and the southern slope of the Alps. However, interpretation of K as tracer of wood smoke is not straightforward since its emission factor varies with the temperature of combustion and since the uptake from the soils into roots is also subject to variability (Hays et al., 2005).

In the Alpine valley floor the winter concentration of 6 PAH with 5 - 6 rings (benzo(b)fluoranthene, benzo(k)fluoranthene, benzo(a)pyrene, benzo(g,h,i) perylene, indeno(1,2,3-c,d)pyrene, and dibenzo (a,h)anthracene) in a kerbside site is 25% lower than that in the background sites (rural and urban) while levels of these compounds above the inversion layer fall to 20% of those observed in the valley floor.

Moreover, it has been observed in three short term winter campaigns carried out between 2005 and 2007 contemporaneously in Sondrio and Milan that concentrations of benzo(a)pyrene presented a significant correlation with those of levoglucosan (R^2=0.89) in both sites.

These results point to biomass burning as an important source of PAH to the urban PM in both the Alpine and the Po Valley areas.

Belis C.A., Gianelle V., De Stefani G., Colombi C., & Magnani T. (2008). *Chemical Engineering Transactions* 16, 153-160.

Colombi, C., Mossetti S., Belis C., Gianelle V., Lazzarini M., Angelino E., Peroni E., & Della Mora S. (2008). in *Proc. 3rd National Conference on Particulate Matter* (Bari, Italy) 90.

Hays M.D., Fine P.M., Geron C.D., Kleeman M.J. Gullett B.K. (2005). *Atmospheric Environment*, 39, 6747-6764.

Piazzalunga A., Fermo P., Vecchi R., Valli G., Belis C. & Cazzuli O. (2008). in *Proc. European Aerosol Conference* (Thessaloniki, Greece) abstract T12A014P.

Simoneit B.R.T., Schauer J.J.,. Nolte C.G, Oros D.R., Elias V.O., Fraser M.P., Rogge W. F. and Cass G. R. (1999). *Atmospheric Environment*, 33, 173-182.

Primary biological aerosol particles: Detection and identification of characteristic compounds by aerosol mass spectrometry

F. Freutel[1], J. Schneider[1], S. R. Zorn[1,2], F. Drewnick[1], S. Borrmann[1,2] and T. Hoffmann[3]

[1]Particle Chemistry Dept., Max Planck Institute for Chemistry, Joh.-J.-Becherweg 27, 55128 Mainz, Germany
[2]Institute for Atmospheric Physics, University Mainz, Joh.-J.-Becherweg 21, 55128 Mainz, Germany
[3] Institute of Inorganic and Analytical Chemistry, University of Mainz, Duesbergweg 10-14, 55099 Mainz, Germany

Keywords: primary organic aerosols, bioaerosols, aerosol mass spectrometry.

The contribution of primary biological aerosol (PBA) to the total aerosol particle concentration is estimated to range between 25% and 80%, depending on location and season (e.g., Matthias-Maser and Jaenicke, 1995; Jaenicke, 2005). Especially in the tropical rain forest PBA is expected to be a major fraction of aerosol particles in the supermicron range, and also an important part of the submicron aerosol. PBA particles consist of species as plant fragments, pollen, spores, fungi and viruses. Therefore, they contain a wide variety of different chemical compounds and substance classes, such as amino acids and proteins, sugars and cellulose, lipids or chlorophyll.

For this reason we have performed mass spectrometric laboratory measurements (Aerodyne C-ToF and HR-ToF AMS, single particle laser ablation instrument SPLAT) on pure submicron aerosol particles containing typical PBA compounds, such as carbohydrates and amino acids. Our aim was to identify typical mass spectral patterns of these compounds, and to explain the observed fragmentation patterns on the basis of molecular structures. In doing so, the emphasis was set on determining several typical mass spectrometric markers or patterns which would enable us to identify in ambient data these substance classes typical for PBA. Therefore, the laboratory data were compared to submicron particle mass spectra obtained during AMAZE-08 (Amazonian Aerosol CharacteriZation Experiment, Brazil, February/March 2008). During this campaign ambient aerosol was measured with a HR-ToF AMS in the remote Brazilian rainforest, where a comparatively large amount of PBA is suspected to contribute to the total submicron organic mass.

The laboratory results indicate that characteristic m/z ratios for carbohydrates (e.g., glucose, saccharose, mannitol) can be identified, for example $m/z = 60$ ($C_2H_4O_2^+$) or $m/z = 61$ ($C_2H_5O_2^+$). For amino acids certain typical nitrogen-containing fragments were found (e.g. $m/z = 30$ from the fragment CH_4N^+), which also occur in the mass spectra of peptides and small proteins. Large proteins, however, seem to become oxidized to CO_2^+ to a large extent in the vaporization process of the

AMS, seemingly making it difficult to detect such proteins in atmospheric aerosol particles with this instrument.

The field data from AMAZE-08 were examined with respect to these markers, and their presence could be verified. The contribution of carbohydrates and of amino acids and proteins to the total organic mass for this data set is estimated to about 5% for each of both examined substance classes.

Interestingly, the typical markers of sugars are identical to those of levoglucosan, a known and commonly used marker for biomass burning. As levoglucosan is formed from burning of cellular material, this comes as no surprise, but at the same time raises the question to which extent these markers for biomass burning may be affected by PBA (and vice versa), and how the two sources can or cannot be distinguished by means of mass spectrometry alone.

Another challenge for the positive identification of carbohydrates in organic matter may arise from overlap with oxygen-containing secondary organic aerosol components, which probably could not be distinguished from PBA-related signals by mass spectrometric markers. Here, the nitrogen-containing substances seem to be a more promising approach. In high resolution mass spectra, such as obtained by the HR-ToF AMS the peaks from nitrogen-containing fragments can be well determined, and the respective markers can more clearly be contributed to PBA than it is the case with the markers for the oxygen-containing compounds, because the sources for the former fragments are much more unique. Nevertheless, the uncertainty inherent in the complete vaporization of the proteins in the AMS remains open. Thus, it is still questionable if the quantification of PBA using AMS field data can be more than a rough estimation.

Jaenicke, R. (2005), *Science*, 308, 73.
Matthias-Maser, S., and R. Jaenicke (1995), *Atm. Res.* 39, 279-286.

High Diversity of Fungi in Air Particulate Matter

J. Fröhlich-Nowoisky[1,2], V. R. Després[1,3], and U. Pöschl[1]

[1,1]Biogeochemistry, Max Planck Institute for Chemistry, P.O. Box 3060, D-55020 Mainz, Germany
[2] Geosciences, Johannes Gutenberg University, Saarstraße 1, D-55099 Mainz, Germany
[3]General Botany, Johannes Gutenberg University, Saarstraße 1, D-55099 Mainz, Germany

Fungal spores account for large proportions of air particulate matter, and they influence the hydrological cycle and climate as nuclei for water droplets and ice crystals in clouds, fog and precipitation (Elbert et al., 2007). Moreover, some fungi are major pathogens and allergens. The diversity of airborne fungi is, however, hardly known. The use of molecular genetic methods resolves many limitations of traditional detection methods for the analysis of biological aerosol particles (Després et al., 2007).

In this study, air filter samples were collected with a High Volume Sampler separating fine and coarse particles (aerodynamic cut-off diameter ~3 µm) for one year 2006/2007 in Mainz, Germany. The samples were analyzed for the presence of fungal deoxyribonucleic acid (DNA). All PCR products were cloned and several clones sequenced. The obtained sequences were blasted in the National Center for Biotechnology Information databank to find the closest match and determine the taxonomic identity of the organisms from which the DNA on the filter samples had most likely originated.

We found pronounced differences in the relative abundance and seasonal cycles of various groups of fungi in coarse and fine particulate matter, with more plant pathogens in the coarse and more human pathogens and allergens in the respirable fine particle fraction (< 3 µm). Moreover, the ratio of Basidiomycota to Ascomycota was found to be much higher than previously assumed, which might also apply to the biosphere.

Després V.R., Nowoisky J.F., Klose M., Conrad R., Andreae M.O., Pöschl U. (2007). Characterization of primary biogenic aerosol particles in urban, rural, and high-alpine air by DNA sequence and restriction fragment analysis of ribosomal RNA genes, *Biogeosciences*, 4, 1127–1141.

Elbert W., Taylor P. E., Andreae M. O., Pöschl U. (2007). Contribution of fungi to primary biogenic aerosols in the atmosphere: wet and dry discharged spores, carbohydrates, and inorganic ions, *Atmospheric Chemistry and Physics*, 7, 4569–4588.

Fröhlich-Nowoisky, J. Després, V.R., Pöschl, U.: High diversity of fungi in air particulate matter, submitted, 2008.

Antibiotic-resistant microorganisms in atmospheric aerosol of Southwestern Siberia

A.S. Safatov, L.I. Puchkova, G.A. Buryak and I.S. Andreeva

Federal State Research Institution SRC VB "Vector", Koltsovo, Novosibirsk region, 630559, Russia

Keywords: atmospheric aerosols, bacteria, bioaerosols - monitoring.

It is known that microorganisms influenced by antibiotics can become antibiotic-resistance. Recently a large variety of antibiotics are used in the world, which ultimately can get into the environment causing the development of microorganisms' resistance to them.

The study of antibiotic resistance of bacteria found in atmospheric aerosol of Southwestern Siberia was performed in 2006 – 2008. More than 500 samples were collected in the vicinities of Novosibirsk in two on-ground points and one altitude point (from 500 to 7000 m using aircraft sampling). Sampling places and method using liquid impingers are described in more detail in Safatov *et al.* (2008).

Standard methods were employed to detect culturable microorganisms. Samples were seeded onto Petri dishes containing different agarized media. Successive sample dilutions were prepared if necessary. The seedings were incubated in a thermostat at the temperature of 28 - 30°C for 3-14 days. Morphological peculiarities of colonies of detected bacteria and the cell morphology were examined visually and with light microscopy, respectively. Fixed preparations of Gram-stained cells and vital preparations of cell suspensions observed with the phase contrast method were used for this purpose. Taxonomic groups the detected bacteria referred to were determined up to the genus according to the classifier (The Prokaryotes, 1981).

The sensitivity of microorganisms to antibiotics was determined on solid media using paper disks (Research Center of Pharmacology, Saint-Petersburg, Russia). The method is based on determining the diameter of zones of delayed growth of the studied microorganism round the disk with antibiotic (Methods …, 1984). Fifteen antibiotics widely used in medical practice were tested in the work: ampicillin (10 μg/disk), neomycin (30 μg/disk), benzylpenicillin (100 U/disk), levomycetin (30 μg/disk), carbenicillin (100 μg/disk), canamycin (30 μg/disk), oleandomycin (15 μg/disk), rifampicin (5 μg/disk), streptomycin (30 μg/disk), polymyxin (300 U), erythromycin (15 μg/disk), lincomycin (15 μg/disk), oxacillin (10 μg/disk), gentamycin (10 μg/disk), tetracycline (30 μg/disk).

A total of more than 1500 strains of culturabble bacteria were found in the samples (bacteria of the same genera detected in different samples were considered to belong to different strains); antibiotic resistance was determined for more than 800 of them. Research results show that only 12.8% of the studied bacteria found in atmospheric aerosol of Southwestern Siberia are susceptible to all the used antibiotics. Correspondingly, more than 87% of the studied bacteria display resistance at least to one antibiotic. Approximately 26.8% of bacteria are resistant to the effect of only one antibiotic, and approximately 29.3% are resistant to the effect of two out of 15 different antibiotics. Less than 6% of bacteria display resistance to more than five antibiotics, and one bacterium is resistant to nine antibiotics. No bacteria resistant to a large number of antibiotics were detected.

Approximately 80% of the studied bacteria displayed resistance to polymyxin, and approximately 60% displayed resistance to oxacillin. Wide use of these antibiotics in medical practice in previous years could have made a large variety of bacteria in the environment resistant to them. On average, from 5 to 30% of the studied bacteria are resistant to the effect of other antibiotics. Bacteria resistance to neomycin, rifampicin and gentamycin are being minimal.

The carried out research demonstrated that atmospheric aerosol of Southwestern Siberia contains a surprisingly high percentage of bacteria displaying antibiotic resistance. Consequently, more strict administrative measures should be elaborated to preserve the existing ecosystems. The use of antibiotics in medical practice should be performed with great care to exclude their getting into the environment and replacing strains by antibiotic resistance ones.

Methods of General Bacteriology. (1984). Ed. F. Gerhardt. Moscow: Mir Publishers, Vol. 3. (in *Russian*).

The Prokaryotes. A Handbook on Habitats, Isolation, and Identification of Bacteria (1981). Eds. M. P. Starr, H. Stolp, H. G. Truper, *et al*. Berlin, Heidelberg, New York, Tokyo: Springer-Verlag.

Safatov, A. S., Andreeva, I. S., Belan, B. D., *et al.* (2008). *Clean*, 36, 564-571.

The concentration and variation of fungi diversity in atmospheric aerosol of Southwestern Siberia

A.S. Safatov[1], T.V. Teplyakova[1], B.D. Belan[2], G.A. Buryak[1], I.G. Vorob'eva[1], I.N. Mikhailovskaya[1], M.V. Panchenko[2] and A.N. Sergeev[1]

[1]Federal State Research Institution SRC VB "Vector", Koltsovo, Novosibirsk region, 630559, Russia
[2]Insdtitute of Atmospheric Optics SB RAS, 1, Square of Academician V. Zuev, Tomsk, 634021, Russia

Keywords: atmospheric aerosols, bioaerosols - monitoring, fungi.

Fungi make up a large portion of culturable microorganisms in atmospheric aerosol. They can spread with aerosols causing different diseases in humans, animals and plants. The present work describes a detailed two-year observation of the concentration and representation of different genera of culturable fungi in atmospheric air of Southwestern Siberia.

Samples were collected during the last ten days of each month at the altitudes of 500 – 7000 m (point **A**) using aircraft sampling. Air samples were collected for 8–10 minutes in sterile impingers. On-ground air samples were collected on the same impingers for 30 minutes with the airflow of 50 l/min on the sites of FSRI SCR VB "Vector" (point **B**, four samplings during 24 hours) and in Klyuchi settlement (point **C**, 7 successive days of each season). The concentration of culturable fungi was determined with standard methods on Saburaud medium. The concentration of culturable fungi in samples was expressed in colony-forming units (CFU). The minimal detection threshold for the concentration of culturable fungi in atmosphere was 40 CFU/m^3 for altitude samples and 11 CFU/m^3 for surface samples. The standard error of determination of culturable fungi concentration under such conditions does not exceed $\pm 0.2 \log_{10}$ of the value. The determination of the genera of fungi was performed according to Hibbert *et al.* (2007).

The performed works showed that the concentrations of culturable fungi in atmospheric air samples were very variable, Table 1. The obtained results did not allow us to reveal the dependence of the seasonal variation of their concentration and diversity in on-ground and altitude samples of atmospheric air of Southwestern Siberia.

It was shown that atmospheric air samples contained culturable fungi from numerous genera. During the first year, from 11 to 16 genera were detected in different sampling points, and from 9 to 16 genera were detected during the second year. A total of more than 20 different genera of culturable fungi were detected in the samples. Among them, the representatives of the genera including culturable fungi potentially pathogenic for man (such as *Aspergillus, Cladosporium, Penicillium, Alternria, Aspergillus, Trichodema*, etc.) were found. At the same time, the representatives of the genera of culturable fungi whose useful properties can be used in modern biotechnology were detected in the same samples (such as *Aspergillus, Aureobasidium, Ganoderma*).

Table 1. Fungi concentrations in atmosphere in three sampling points, CFU/m^3, averaged over all measurements of the month.

Months of Sampling	Point **A**	Point **B**	Point **C**
June 2006	41.6	302.8	
July 2006	107.1	433.3	173.9
August 2006	229.1	527.8	
September 2006	187.5	530.3	
October 2006	114.6	41.5	37.7
November 2006	20.8	94.3	
December 2006	10.5	91.5	
January 2007	0.0	108.5	34.9
February 2007	78.1	41.5	
March 2007	46.9	13.8	
April 2007	36.4	77.8	52.0
May 2007	135.5	633.0	
June 2007	52.3	286.3	
July 2007	-	291.8	88.4
August 2007	31.4	339.0	
September 2007	31.3	75.3	
October 2007	26.0	169.3	41.3
November 2007	10.4	47.3	
December 2007	5.3	289.0	
January 2008	10.4	13.8	6.1
February 2008	36.4	83.3	
March 2008	10.4	11.0	
April 2008	-	52.8	19.1
May 2008	47.0	38.8	

Note: «-» - no data available.

Hibbert, D. S., *et al.* (2007). *Mycol. Res.*, 111, 509-547.

The effect of two types of photocatalysts on aerosols of stable and labile microorganisms

A.S. Safatov[1], S.A. Kiselev[1], G.A. Buryak[1], V.Yu. Marchenko[1], A.A. Sergeev[1], M.O. Skarnovich[1], E.K. Emel'yanova[1], Yu.V. Marchenko[1] and A.V. Vorontsov[2]

[1]Federal State Research Institution SRC VB "Vector", Koltsovo, Novosibirsk region, 630559, Russia
[2] Boreskov Institute of Catalysis SB RAS, 5, Academician Lavrent'ev av., Novosibirsk, 630090, Russia

Keywords: bioaerosols, photocatalyst, TiO_2 nanoparticles, bacteria, viruses.

INTRODUCTION

Previously we presented a new method to evaluate photocatalyst activity at inactivation/ disintegration of microorganism aerosols at early stages of development of new photocatalysts when they are not tested in air cleaners yet (Safatov *et al.*, 2008a). This method was employed to compare photocatalytic activities of two types of photocatalysts at inactivation/disintegration of *Mycobacterium smegmatis* aerosols: those based on "pure" and platinized titanium dioxide. The present work is devoted to the comparison of photocatalytic activities of these two photocatalysts at inactivation/disintegration of aerosols of four different microorganisms.

MATERIALS AND METHODS

Two representatives of each kingdom (bacterial and viral) were selected for the study: one which is more stable in the environment and a more labile one. They are the stable soporiferous *Bacillus thuringiensis* and the labile *Mycobacterium smegmatis* as well as the stable vaccinia virus and the labile influenza virus A/Aichi/2/68 (H3N2). Biological activity of bacterial samples was determined by the number of colony-forming units in 1 ml of the sample that of vaccinia virus was determined by the number of plaque-forming units on *Vero* cell culture in 1 ml of the sample and that of influenza virus - by the number of doses infecting 50% of embryonated chicken eggs in 1 ml.

Microorganism aerosol samples deposited on glass slides were exposed to ultraviolet light for 1-30 minutes using a PHILIPS PL-S 11W/10/2P lamp; irradiation power was 0.65 ± 0.05 mW/cm^2. All experiments with samples and controls were performed in not less than 3 repeats at room temperature and $30 - 50\%$ relative humidity. The details of the experiment and the construction of the plant used to deposit microorganism aerosols onto the support are described in Safatov *et al.* (2008b).

RESULTS AND DICUSSION

Photocatalytic activity of the catalyst (K) was determined as the ratio between biological activity of microorganism after 30 minutes of irradiation with the above power on the control slide (without photocatalyst), $T_{control}$, and that after 30 minutes of irradiation on the slide with photocatalyst, $T_{photocatalyst}$.

The results of the carried out experiments are summarized in Table 1. The accuracy of determining K value taking into account the repeats was not lower than 45%.

Table 1. The comparison of photocatalysts photocatalytic activities ($K = T_{control}/T_{photocatalyst}$) for four different microorganisms

Microorganism in aerosol deposited to slides	Photocatalyst's type	
	«Pure» TiO$_2$	Platinized TiO$_2$
Bacillus thuringiensis	2.0	4.2
Mycobacterium smegmatis	6.3	30.0
Vaccinia virus	13.3	22.9
Influenza virus A/Aichi/2/68 (H3N2)	3.3	57.5

As follows from the data of Table 1, all the studied microorganisms are effectively inactivated by both types of photocatalysts. Microorganisms, which are more stable in the environment, display a larger resistance and to the effect of photocatalysts. The studied bacteria, which have their own reparation systems, are more resistant to the effect of photocatalysts than the studied viruses. Under the same conditions, catalysts based on platinized TiO_2 cause a greater loss of biological activity of all the studied microorganisms than those based on "pure" TiO_2.

Safatov, A. S., Kiselev, S. A., Marchenko, V. Yu., *et al.* (2008a). in *Abstracts European Aerosol Conference, 24-29 August, 2008,* Thessaloniki, Greece, T02A073P.
Safatov, A., Kiselev, S., Marchenko, V., *et al.* (2008b). *Chemical engineering transactions,* 16, 275-282.

Collection of airborne spores from combustion environments

S.A. Grinshpun[1], A.Adhikari[1], C. Li[1], T. Reponen[1], M. Schoenitz[2], E.L. Dreizin[2], M. Trunov[3]

[1] Center for Health-Related Aerosol Studies, University of Cincinnati, Cincinnati, OH 45267, USA
[2] Department of Chemical, Biological and Pharmaceutical Engineering, NJIT, Newark, NJ 07102, USA
[3] Reactive Metals, Inc., Newark, NJ 07103, USA

Keywords: aerosolization, bacteria, spore, combustion, temperature, filter collection

Destruction of biological agents is the subject of increasingly active research and development. Energetic materials are currently being developed with the added capability to effectively inactivate stress-resistant microorganisms. This is of particular interest, as in a military/counterterrorism situation biological agents may become aerosolized and should be neutralized rapidly, before larger areas become contaminated. Consequently, there is a need in developing and validating adequate methods and protocols for testing the biocidal effectiveness of such energetic materials. We have recently designed and built a state-of-the-art experimental facility for assessing the survival of aerosolized microorganisms exposed to the combustion of various materials. The facility includes an aerosolization chamber, a combustion chamber, and a system for measuring the physical (through real-time monitoring) and biological (through collection and viability analysis) characteristics of bioaerosol particles. Particles passing through the chambers are collected on a filter, which is continuously exposed to combustion products during the entire test. There is currently no data on microbial inactivation occurring on the collection filter due to this exposure. This study addresses this knowledge gap.

A challenge bioaerosol of *Bacillus subtilis* endospores, generated from suspension with a six-jet Collison nebulizer was mixed with HEPA-filtered dry air. Charge-equilibrated by passing through a 10 mCi Kr[85] neutralizer (TSI, Inc., USA), the bioaerosol was measured with an optical size spectrometer (Grimm Technologies, Inc., Germany). Following a 10-min nebulization period, a stable concentration was achieved in the range of 10^2–10^3 spores/cm^3. The spores were collected on five polycarbonate filters with no burning in the combustion chamber. After deposition on the filters, two pre-loaded filters served as controls, while three others were exposed to combustion products as a strand (diameter=1/2", length=10") burned in the combustion chamber for up to 2 min. The strand consisted of an energetic Al-MoO$_3$ nanocomposite and paraffin wax as a binder. Combustion products were aluminum oxide, molybdenum oxide, water, carbon oxides and soot. Estimates derived from continuous monitoring of the chamber wall temperature suggest that the air inside the chamber was heated well in excess of 200°C. However, gaseous combustion products were cooled down prior to reaching the filters so that the pre-loaded spores were not exposed to high temperatures. Filter collection from the combustion environment was conducted at time intervals ranging from 20 to 80 s. *B. subtilis* spores were extracted from the filters using a standard extraction method and cultivated on TSA agar. After incubation for 18 h, the surviving spore fraction was calculated based on the bacterial colony forming units in control and treated samples.

The microbial inactivation occurring on the collection filters was found to depend on the time for which the filter was exposed to combustion products. The data suggest that the surviving fraction of spores decreases exponentially with time (see Figure). It is seen that a significant fraction of microorganisms that were viable when collected on the filter, may lose viability as a result of the exposure to the combustion products. Inactivation of more than 50% of initially viable spores was observed for collection times as short as 20 s.

The data suggest that distinguishing the biological inactivation in the aerosol from that occurring on the collection filter poses a considerable challenge. To minimize the detrimental effect of the combustion products on the viability of spores collected on a filter, the collection time should not exceed a few seconds. This is impractical in many cases, which in turn raises a question of the suitability of filter collection for these experimental conditions. Samplers with liquid collection medium, such as impingers and wet cyclones, are currently being examined as possible alternatives.
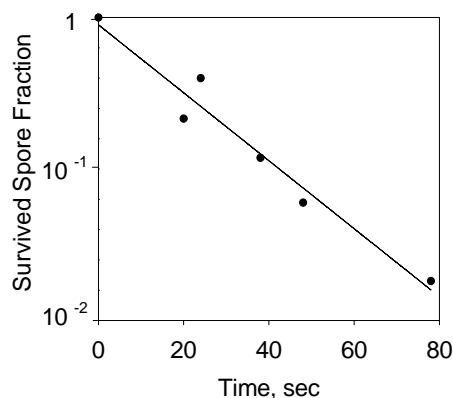
Removal of bioaerosols by using membrane-less electrolyzed water in swinery

S.H. Yang[1], M.Y. Chang[2], C.Y. Chuang[3], L.C. Chen[3], W. Fang[3], P.H. Wu[2], S.W. Kong[3]

[1]Department of Environmental and Occupational Health, Toko University, Chia Yi County 613, Taiwan, R.O.C
[2] Department of Bio-lndustrial Mechatronics Engineering, National Ilan University, Ilan 260, Taiwan, R.O.C
[3]Department of Bio-lndustrial Mechatronics Engineering, National Taiwan University, Taipei 106, Taiwan, R.O.C.

Keywords: removal efficiency, bioaerosols, electrolyzed water, swinery

There are higher concentrations of fungi and bacteria in the agriculture poultry and cattle farms (Thorne *et al.*, 1992; Predicala *et al.*, 2002; Venter *et al.*, 2004). Some of those fungi and bacteria would cause respiratory and hypersensitive diseases. Accordingly, air quality of these farms is an increasingly important issue. Therefore, an increasing number of air-cleaning technologies are being adopted to remove bioaerosols.

Currently, electrolyzed water (HOCl) has been applied in the agriculture and food industries for removal of fungi and bacteria (AL-HAQ *et al.*, 2005; Huang *et al.*, 2008; Kim & Huang, 2000).

This work aims to use a new membrane-less electrolyzed water produced system to generate the electrolyzed water spray for removal of bioaerosols. The electrolyzed water, generated by membrane-less electrolysis of the sodium chloride solution, is a disinfectant with the properties of near-neuture and low corrosiveness. Thus, this work used the electrolyzed water spray in the swinery for removal of fungi and bacteria bioaerosols.

In the experimental setup, a swinery was chosen as the tested site. We used the membrane-less electrolyzed water produced system to generate the electrolyzed water spray. The concentration of the electrolyzed water spray was about 200 ppm. For understanding the removal efficiency of bioaerosols by using electrolyzed water spray, we sampled the bioaerosols concentrations before and after using the electrolyzed water spray in the swinery. The concentrations of fungi and bacteria bioaerosols were measured by MAS100 Air Sampler (MAS 100, Merck Ltd., Germany). The operation time of electrolyzed water sprayed in the swinery was about 30 minutes.

Figure 1 shows that the concentration changes of fungi and bacteria bioaerosols by using the electrolyzed water spray in the tested swinery. Before the electrolyzed water spray, the concentration of the bacteria bioaerosol concentration is about 3×10^5 CFU/m^3. After the electrolyzed water spray, the concentration of the bacteria bioaerosol was decreasing obviously in the beginning, and the removal efficiency of the bacteria bioaerosols is about 40%. And then the concentration of the bacteria increased with time increasing. Before the electrolyzed water spray, the concentration of the

fungi bioaerosol concentration is about 2×10^4 CFU/m^3. After the electrolyzed water spray, the concentration of the fungi bioaerosol was decreasing obviously in the beginning, and the removal efficiency of the fungi bioaerosols is about 52%. And then the concentration of the fungi increased with time increasing. Those findings indicated that the electrolyzed water spray could remove the bioaerosols obviously, and the removal ability would decrease with time increasing.
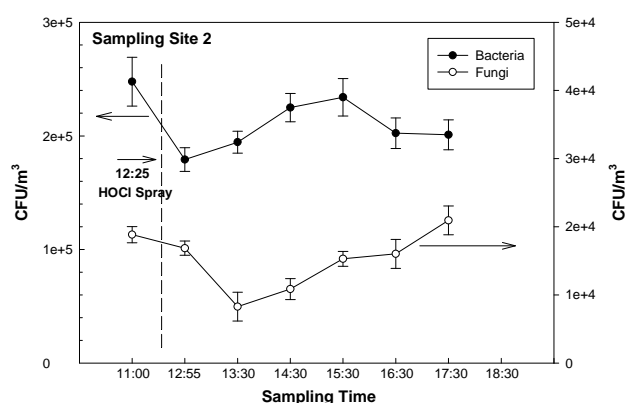
Figure 1.Concentration changes of bioaerosols in the swinery.

AL-HAQ, M. I., Sugiyama, J., & Isobe S. (2005). *Food Science and Technology*, 11(2), 135-50.

Huang, Y. R., Hung, Y. C., Hsu, S.Y., Huang, Y. W., & Hwang, D. F. (2008). *Food Control*, 19, 329-45.

Kim, C., & Hung, Y. C. (2000). *Intentional Journal of food Microbiology*, 61, 199-207.

Predicala, B. Z., Urban, J. E., Maghirang, R. G., Jerez, S. B., & Goodband, R. D. (2002). *Curr Microbiol*, 44, 136-140.

Thorne, P. S., Kiekhaefer, M. S., Whitten, P, & Donham, K. J. (1992). *Appl Environ Microbiol*, 58, 2543–2551.

Venter, P., Lues, J. F. R., & Theron, H. (2004). *Poultry Science*, 83, 1226–1231.

Experimental study on pollen settling characteristics in isotropic homogeneous turbulence

R. van Hout[1] and L. Sabban[1]

[1]Faculty of Mechanical Engineering, Technion-IIT, Technion city, 32000, Haifa, Israel

Keywords: Bioaerosols, Laboratory experiments, Non-spherical particles, Turbulence.

In models of atmospheric pollen dispersal, the pollen grains are generally modeled as small spheres and any morphological features are thought to be irrelevant to their dispersal characteristics (Jarosz et al. 2004, Boehm & Aylor 2005). However, most pollen grains have interesting morphological features. For example, ragweed (*Ambrosia*) pollen have characteristic "spikes" (Fig. 1) while in pine pollen grains, the main body is attached to air-filled "bladders" called sacci (see Fig. 2). It has since long been suggested (Wodehouse 1935) that the addition of the sacci (i.e. low-density volume) would improve long distance pollen dispersal.
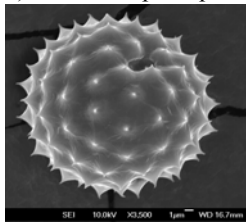
Figure 1. Ragweed pollen

The effect of the sacci on the <u>still-air</u> settling velocity of pine pollen was studied by Schwendemann et al. (2007) using Stroboscopic photography experiments. However, pollen release and dispersal occurs in turbulent atmospheric flows that are known to affect the still-air settling velocity of small particles (Maxey 1987). The effect of turbulent eddies on pollen dispersal can be estimated by considering the Stokes number, defined as the ratio between the particle response time $\tau_p \approx \rho_p D^2 / 18\mu$, and a characteristic time scale of the flow, e.g. the Kolmogorov time scale, $\tau_k \equiv (\nu/\varepsilon)^{1/2}$. Here ρ_p is the pollen density, D the pollen diameter, μ and ν are the dynamic and kinematic air viscosity, respectively, and ε is the dissipation rate of turbulent kinetic energy. Typical dissipation rates around canopy height are $\varepsilon \approx 0.1 - 0.2$ m^{2}s^{-3} (van Hout et al. 2007). Taking into account a range of pollen densities, Stokes numbers of order one are obtained, indicating that pollen response to turbulence is of the same order as the Kolmogorov time scale. Thus, the pollen grains should respond to a substantial fraction of turbulent fluctuations (Wang and Maxey 1993), especially the larger ones, whose time scales extend to orders of magnitude larger than the Kolmogorov
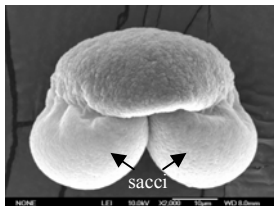
Figure 2.   Pine pollen.

time scale. Therefore, the pollen settling velocity in a turbulent flow field, an essential input parameter to any dispersal model, is expected to be significantly different from the still-air settling velocity.

In the present study we experimentally measure the settling behavior of non-spherical pollen grains in isotropic homogeneous air turbulence and make a comparison with the settling behavior of similarly sized spherical particles. A 40 cm^3 closed, transparent cube was constructed and isotropic, homogeneous turbulence with near zero mean flow is generated in the center part by 8 woofers mounted on each of the cube's corners. Each of the woofers is independently controlled by a randomly changing frequency signal. The generated turbulence flow field inside the cube as well as the pollen grains descending in it, are measured by high-speed Particle Image Velocimetry (PIV) and high-speed digital holographic cinematography. Preliminary results on the effect of isotropic homogeneous turbulence on the settling velocity of non-spherical particles in comparison to spherical ones will be presented. In addition, using the high-speed digital holographic movies that provide both spatially as well as temporarily resolved data, detailed information on pollen spatial distributions and trajectories will be presented.

Jarosz, N., Loubet, B., & Huber, L. (2004). *Atmospheric Environment*, 38, 5555-5566.

Boehm, M. T., & Aylor, D. E. (2005). *Atmospheric Environment*, 39, 4841-4850.

Maxey, M. R. (1987). *J. Fluid Mech.*, 174, 441-465.

Schwendemann, A. B., Wang, G., Mertz, M. L., McWilliams, R. T., Thatcher, S. L., & Osborn, J. M. (2007). *Amer. J. Bot.*, 94, 1371-1381.

Van Hout, R., Zhu, W., Luznik, L., Katz, J., Kleissl, J., & Parlange, M. (2007). *J. Atmos. Sci.*, 64, 2805-2824. DOI: 10.1175/JAS3989.1

Wang, L. P., & Maxey, M. R. (1993). *J. Fluid Mech.*, 256, 27-68.

Wodehouse, R. P. (1935). *Pollen grains: their structure, identification and significance in science and medicine.* Hafner Publishing, New York, USA.

Concentrations and size distributions of ambient fluorescent biological aerosol particles measured with an ultraviolet aerodynamic particle sizer (UVAPS)

J.A. Huffman[1], B. Treutlein[1,2], and U. Pöschl[1*]

[1]Max Planck Institute for Chemistry, Biogeochemistry Department, 55128, Mainz, Germany
[2]Now at Ludwig Maximilians University, Institute for Physical Chemistry, 80799, Munich, Germany

Keywords: Bioaerosols, Field Measurements, Fluorescence, Fungal Spores, Ambient PM

Biological particles suspended in the atmosphere may constitute a large fraction of the total atmospheric particulate matter, but ambient measurements have been limited by sampling difficulties and are therefore few. In this study, atmospheric particle concentrations and size distributions in the diameter range of 0.5–20 μm were measured over a period of four months from August to November 2006 in the city of Mainz, Germany using an ultraviolet aerodynamic particle sizer (UVAPS). In this instrument, particle counting and aerodynamic sizing by light scattering and time-of-flight measurements are complemented by the measurement of fluorescence emission (420–575 nm) after excitation by a 355 nm laser. The range of emission wavelengths contains a region characteristic of molecules involved in the metabolism of biological organisms, such as reduced pyridine nucleotides (e.g. NAD(P)H) and riboflavin. Thus, particles exhibiting fluorescence at these wavelengths can be regarded as "fluorescent biological aerosol particles" (FBAPs) or "viable aerosol particles," and their concentration can be considered as a lower limit for the ambient abundance of primary biogenic aerosol particles (PBAPs).

Over the four-month measurement period the number concentration of FBAPs varied in the range of 0.002–2 cm^{-3} with an arithmetic mean value of 0.03 cm^{-3}. They accounted for 0.5–21% (mean value 1%) of the total aerosol particle number concentration in the investigated size range. The mass concentration of FBAPs varied in the range of 10^{-2}–10^{2} μg m^{-3} with an arithmetic mean value of 1.3 μg m^{-3} and corresponding to a mean value of 17% (0.08–94% range) of total particle mass, significantly affected by both a constant background and FBAP events increasing in mass concentration by several orders of magnitude.

The observed total aerosol particle number distributions were typically monomodal with a maximum at 0.6–0.75 μm in aerodynamic particle diameter. In contrast, the number distribution of FBAPs exhibited events with alternating mono-, bi-, and trimodal patterns and maxima at various diameters – most commonly 0.75 and 2.5–5 μm, but occasionally also at 1.5 and 13 μm. The number and position of the peaks in the total particle mass distributions were highly variable; they were mostly observed at 0.6–0.8, 3–5, and ~7 μm. Maxima of the FBAP mass distributions most often occurred at 3–5 μm and ~7.5–9 μm; small peaks also occurred at 0.7–1.5 μm.

The ratio of FBAP to total aerosol particle number and mass exhibited pronounced peaks at ~4–5 μm (mean ratio 0.3 FBAP/Total) and 9-10 μm (mean ratio 0.3). The poster will present time series of the number and mass concentrations of particles measured with the UVAPS during the 4-month sampling period as well as size distributions of both total particles and fluorescent bioparticles. Overall, the work highlights the UVAPS ability to continuously measure atmospheric bioparticles with at least 5-minute time resolution at a European site influenced by alternating urban and rural air. Measurement results confirm that primary biogenic aerosol particles account for a major fraction of course atmospheric aerosol particles, especially in the range of 3-10 μm.
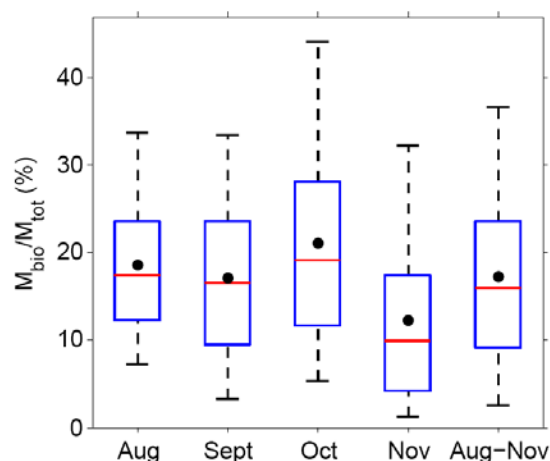
Figure 1. Fraction of FBAP mass to total particle mass shown as a whisker plot of 5-minute data points. Black dot shows arithmetic mean, red bar shows median, blue bars show 25 and 75%, and black bars show 5 and 95% variations. Sampling months of August-November are each shown individually, as well as for the total measurement campaign.

Time Resolved Measurements of Primary Biogenic Aerosol Particles in Amazonia

A.G. Wollny[1], R. Garland[1], A. Huffman[1], and U. Pöschl[1]

[1]Max Planck Institute for Chemistry, Biogeochemistry Department, Mainz, Germany

Keywords: bioaerosols, coarse particles.

Biogenic aerosols are ubiquitous in the Earth's atmosphere and they influence atmospheric chemistry and physics, the biosphere, climate, and public health. They play an important role in the spread of biological organisms and reproductive materials, and they can cause or enhance human, animal, and plant diseases. Moreover, they influence the Earth's energy budget by scattering and absorbing radiation, and they can initiate the formation of clouds and precipitation as cloud condensation and ice nuclei. The composition, abundance, and origin of biogenic aerosol particles and components are, however, still not well understood and poorly quantified. Prominent examples of primary biogenic aerosol particles, which are directly emitted from the biosphere to the atmosphere, are pollen, bacteria, fungal spores, viruses, and fragments of animals and plants.

During the Amazonian Aerosol Characterization Experiment (AMAZE-08) a large number of aerosol and gas-phase measurements were taken on a remote site close to Manaus, Brazil, during a period of five weeks in February and March 2008. This presented study is focused on data from an ultraviolet aerodynamic particle sizer (UVAPS,

TSI inc.) that has been deployed for the first time in Amazonia. In this instrument, particle counting and aerodynamic sizing over the range of 0.5-20 µm are complemented by the measurement of UV fluorescence at 355 nm (excitation) and 420-575 nm (emission), respectively. Fluorescence at these wavelengths is characteristic for reduced pyridine nucleotides (e.g., NAD(P)H) and for riboflavin, which are specific for living cells. Thus particles exhibiting fluorescence signals can be regarded as 'viable aerosols' or 'fluorescent bioparticles' (FBAP), and their concentration can be considered as lower limit for the actual abundance of primary biogenic aerosol particles. Data from the UVAPS were averaged over 5 minute time intervals. The presence of bioparticles in the observed size range has been confirmed by filter samples.

First data analyses show a pronounced peak of FBAP at diameters around 2-3 µm. In this size range the biogenic particle fraction was generally higher than 50%. Additionally, bursts of FBAP have been observed nearly every day just before sunrise. During these periods the coarse (super-micron) aerosol consisted almost completely out of fluorescent bioparticles.

Dispersion of Ambrosia pollen with the model system COSMO-ART

K. Zink, H. Vogel, B. Vogel

Institut für Meteorologie und Klimaforschung, Forschungszentrum Karlsruhe/Universität Karlsruhe,
Postfach 3640, 76021 Karlsruhe, Germany

Keywords: Bioaerosols, Aerosol Modelling (regional), Dispersion

Ambrosia artemisiifolia L. (in the following: Ambrosia) originates in North America but has been spreading in Europe for more than a century. The most polluted areas include southern Hungary and the area of Lyon in France (Laaidi et al., 2003). There are also populations of this species reported throughout Central and Eastern Europe including Germany (Alberternst et al., 2006), Switzerland (Taramarcaz et al., 2005), Austria, Poland and several more. Meanwhile the plant is spreading even in countries with cooler climates like Sweden (Dahl et al., 1999).

Pollen grains of Ambrosia are highly allergenic. Even numbers down to 5 to 10 pollen per cubic meter can lead to health problems for sensitive persons (Taramarcaz et al., 2005). The threshold for most of the other allergenic pollen in Europe lies at about 50 pollen per cubic meter. Ambrosia flowers late in the year compared to most other allergenic plants, therefore prolonging the season in which allergies occur. Symptoms of the allergy to Ambrosia include pollinosis, conjunctivitis, asthma, and abnormal fatigue. Touching the plant with bare skin can cause allergic contact dermatitis. The consequential costs for the treatment of patients allergic to Ambrosia are estimated for Germany to lie between 19 and 50 million € (Reinhardt et al., 2003).

In most studies up to now, only back-trajectory analyses and daily cycles of pollen concentration measurements were used to study the origin of Ambrosia pollen. In our study we implemented an emission module of Ambrosia pollen in the non-hydrostatic model system COSMO-ART (Vogel et al., 2009) and calculated their distribution. COSMO is part of the forecast system of the German Weather Service (DWD). ART stands for Aerosol and Reactive Trace gases and describes the chemical reactions and the aerosol dynamics. In contrast to several other CTM model systems our model system is fully online coupled, which means that for the transport processes consistent numerical methods for all variables are used. It has a modular structure and therefore it is easily possible to run it in a forecast mode. Several modules were implemented to describe the primary emission of aerosols which are a function of different meteorological variables like temperature and wind speed. To describe the emissions flux of pollen the model includes the parameterisation of Helbig et al. (2004) with adjustments concerning the Ambrosia.

We apply our parameterisation to simulate an Ambrosia pollen episode in mid-September 2006. It is noticeable that between September 12th and September 21st, uncommonly high numbers of Ambrosia pollen were found at several sites throughout North-eastern Germany. Sensitivity runs taking into account different source regions were performed to quantify the specific contributions to the observed pollen concentrations.
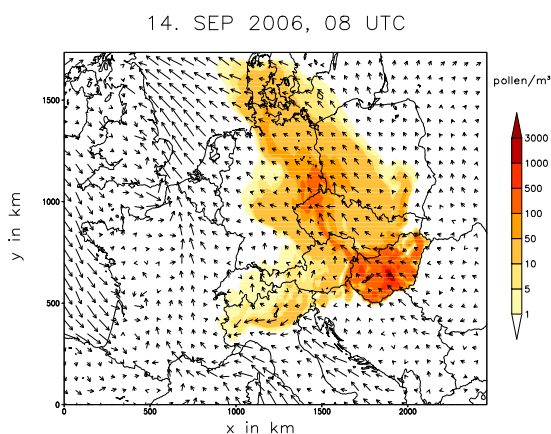
Figure 1: Pollen concentration and wind field in Central Europe, Sep 14th, 2006

Alberternst, B., Nawrath, S. & Klingenstein, F. (2006). *Nachrichtenbl. Deut. Pflanzenschutzd.,* 58 (11), 279-285.

Dahl, A., Strandhede, S.-O. & Wihl, J.-A. (1999). *Aerobiologia,* 15, 293-297.

Helbig, N., Vogel, B., Vogel, H. & Fiedler, F. (2004). *Aerobiologia*, 20, 3-19.

Laaidi, M., Thibaudon, M. & Besancenot, J.-P. (2003). *Int. J. Biometeorol.,* 48, 65-73.

Reinhardt, F., Herle, M., Bastiansen, F. & Streit, B. (2003). *Umweltforschungsplan des Bundesministeriums für Umwelt, Naturschutz und Reaktorsicherheit,* Forschungsbericht 201 686 211, UBA-FB 000441.

Taramarcaz, P., Lambelet, C., Clot, B., Keimer, C. & Hauser, C. (2005). *SWISS MED WKLY.,* 135, 538-548.

Vogel, B., H. Vogel, D. Bäumer, M. Bangert, K. Lundgren, R. Rinke, T. Stanelle, (2009) *submitted to APCD.*

Characteristics of biological particles in indoor environment

M. Moustafa, M. Abd El-Hady and A. Mohamed

Department of Physics, Faculty of Science, Minia University, El-Minia, Egypt

(mona_moustafa9@yahoo.com)

Keywords: size distribution, bacterial particles, fungal particles, Andersen impactor

Introduction

Currently, characterization of biological particles has become an important issue because of related health effects (Chih-Shan Li & Po-An Hou, 2003). Since many people spend most of their time indoors, in locations, homes, offices and other occupational environments, concern regarding the health effects of indoor air quality has growth. Therefore the aim of this study was to characterize the concentration and size distribution of the indoor biological particles (bacterial and fungal particles) using Andersen impactor as bioaerosol sampler at two heights and two different ventilation conditions.

Materials and methods

Six stage Andersen impactor (operates at 28 l/min) was used for collecting biological particles. 27 ml of NA and PDA plates are used for bacterial and fungal collection, respectively. Sampling time was 15 minutes to avoid overestimated number of particles. The samples were incubated at 37 ^{o}C for 2-5 days. Measurements were performed at research laboratories of Physics department, Faculty of Science, Minia university at different heights; first and second floor. Runs were taken under two different ventilation conditions; minimum ventilation where all windows and doors kept closed and the second ventilation using air-conditioning system (ACV).

Results

Concentration and size distribution of bacterial and fungal particles were measured at two heights and two different ventilation conditions. It was found that the mean concentration of total bacterial particles is higher than the total fungal particles in all the studied conditions, which might be related to the human sources. This is in agreement with the results of Jozef S. Pastuszka et al., (2000) and Chih-Shan Li & Po-An Hou (2003). As an example of the determining size distributions in this study, figure (1) and figure (2) illustrate the size distribution of fungal particles under different ventilations at the second floor. The highest concentration was found at size range 3.3 to 4.7 µm at minimum ventilation while it shifts to the lower size range 2.1 to 3.3 µm under ACV condition. These could be attributed to the reduction of residence time of these indoor particles with ventilation factor (Hussein Kanaani et al., 2008).
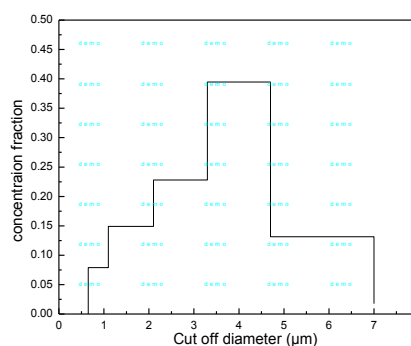
Figure (1). size distribution of fungal particles at minimum ventilation
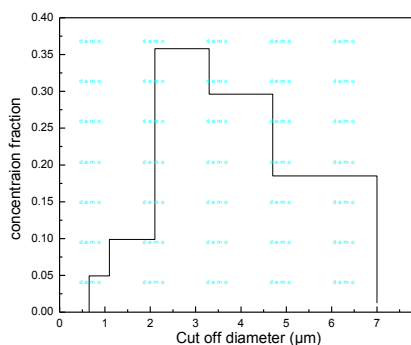
Figure (2). size distribution of fungal particles at ACV

References

Chih-Shan Li & Po-An Hou (2003). Bioaerosol characteristics in hospital clean rooms. J. the Science of the Total Environment, 305, 169-176.

Jozef S. Pastuszka, U. Kyaw Tha Paw, Danuta O. Lis, Agnieszka Wlazlo and Krzysztof Ulfig (2000). Bacterial and fungal aerosol in indoor environment in Upper Silesia, Poland. J. Atmospheric Environment, 34,3833-3842.

Hussein Kanaani, Megan Hargreaves, Zoran Ristovski and Lidia Morawska (2008). Deposition rates of fungal spores in indoor environments, factors effecting them and comparison with non-biological aerosols. J. Atmospheric environment, 42, 7141-7154.

Evaluation method of Spore Concentration Uniformity on a Fungal Substrate Using a Real-time Aerosolization Technique

J.H. Jung[1], J.E. Lee[2] and S.S. Kim[1]

[1]Department of Mechanical Engineering, Korea Advanced Institute of Science and Technology (KAIST), Guseong-dong, Yuseong-gu, Daejeon 305-701, Republic of Korea
[2]Department of Environmental Health, Graduate School of Public Health, Seoul National University, Yeongeon-Dong, Jongro-Gu, Seoul 110-799, Republic of Korea

Keywords: Bioaerosols, Fungi, Fungal spores, Aerosolization, Particle concentration, Spore uniformity.

Fungal bioaerosols constitute the major component of ambient airborne microorganisms and are well-known for their harmful effects on human health. Several studies have reported that the concentration of airborne fungal particles contribute to the occurrence of human diseases and public health problems associated with acute toxicity, such as allergies and asthma. These public health problems have raised concerns over airborne fungal particles, and finding effective methods of controlling fungal bioaerosols has become a priority.

The aerosolization characteristics of the fungal spores are affected by many environmental variables such as air velocity, release time from agar, and relative humidity (Pasanen et al., 2000; Górny et al., 2002). The uniformity and distribution of spore concentrations on a fungal substrate is an important parameter for the stable and constant generation of fungal bioaerosols over long time periods. However, traditional method using a light microscope is very slow and inefficient in evaluating the uniformity of spores on fungal substrates.

In this study, we proposed an evaluation method for spore concentration uniformity on fungal substrates using the real-time aerosolization characteristics of the fungal spores. A fungal bioaerosol generator, developed previously (Jung et al., 2009a, 2009b), was used for the steady aerosolization of fungal spores. As shown in Fig. 1, the multi-orifice air jets and the rotating substrate inside the generator were used to scan a fungal culture Petri plate and to aerosolize the fungal spores. Experimental tests on *Cladosporium cladosporioides* were conducted. The particle size distribution and total spore concentration of aerosolized fungal spores were measured using a particle size distribution analyzer and a condensation particle counter.

The results demonstrate that it is possible to evaluate the uniformity of the spore concentration of fungi on a substrate by measuring the variance of the particle concentration in real time (Fig. 2). In addition, the uniformity of the fungal spore concentration has little effect on the particle size distribution under the selected experimental conditions.
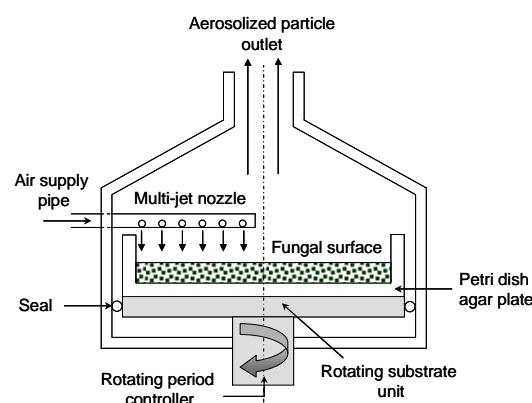
Figure 1. Design of fungal bioaerosol generator (Jung et al., 2009a, 2009b).
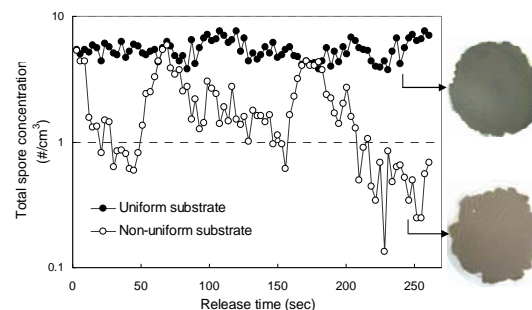
Figure 2. Variations in the total concentration of aerosolized spores with respect to the same growth and aerosolization condition.

Górny, R.L., Reponen, T., Willeke, K., Schmechel, D., Robine, E., Boissier, M. & Grinshpun, S.A. (2002). *Appl. Environ. Microbiol.* 68, 3522-3531.

Jung, J.H., Lee, C.H., Lee, J.E. Lee, J.H., Kim, S.S. & Lee, B.U. (2009a). *J. Aerosol Sci.* 40, 72-80.

Jung, J.H., Lee, J.E. & Kim, S.S. (2009b). *Environ. Eng. Sci.* doi:10.1016/j.envres.2008.12.010.

Pasanen, A.L., Rautiala, S., Kasanen, J.P., Raunio, P., Rantamaki, J. & Kalliokoski, P. (2000). *Indoor Air* 10, 111-120.

Endotoxins loading in atmospheric aerosols in the Pearl River Delta cities

Arthur P.S. Lau and Jessica Y.W. Cheng

Institute for the Environment,
Hong Kong University of Science and Technology, Clear Water Bay, Kowloon, Hong Kong

Endotoxins are known for their strong pro-inflammatory responses and considered to be common aero-allergens. The bacterial endotoxins are associated with the phospholipid A moiety on the outer membrane of the Gram negative group bacteria. Since the 3-OH fatty acids (3-OHFAs) are unique structural components associated with the phospholipid A moiety on the membrane, 3-OHFAs have been deployed as biomarker to quantify the loading of the gram negative bacteria in the atmospheric aerosols (Lee et al., 2004). The Pearl River Delta has been urbanized and industrialized rapidly in the past twenty years. Air quality and its health implication in the PRD are gaining more concern. The present study aimed to characterize the allergenic potential of the coarse ($PM_{2.5-10}$) and fine ($PM_{2.5}$) ambient aerosols in terms of concentration of the 3-OHFAs and the standard Limulus Amebocyte Lysate (LAL) test collected from major cities, Guangzhou (GZ) and Nansha (NS) in PRD.

Aerosols were collected on quartz filters through the high volume samplers (Graseby) on 24-hour basis at three cities in the PRD Hong Kong, Nansha and Guangzhou since August 2007. Filter samples were analyzed for 3-OHFAs following the procedures reported by Lee et al. (2004) using GC-MS. The LAL assay followed the standard procedures of the PolarScan protocol.

Figure 1. The profiles of total 3-OHFAs in the coarse ($PM_{2.5-10}$) and fine ($PM_{2.5}$) aerosols.
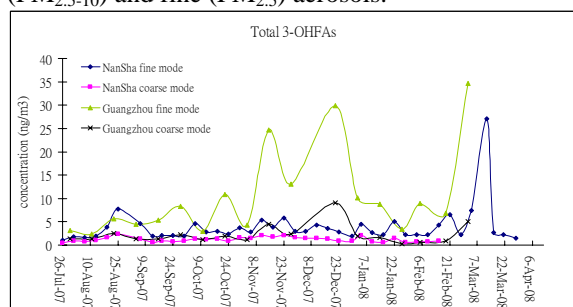
Figure 1 shows that amount of total 3-OHFAs is highly site- and size-dependent. GZ had generally higher 3-OHFAs than NS. 72.5% and 80.4% of the total 3-OHFAs was associated with $PM_{2.5}$ in NS and GZ respectively. Table 1 summarizes some of the results on the endotoxin level from the LAL assay. The allergenic potential reflected from LAL results shows that coarse aerosols (>2.5µm) had a similar level as the fine aerosols (<2.5 µm); while at GZ, the allergenic potential of the coarse aerosols was two and a half fold of the fine ones. As the 3-OHFAs comprises a family species from C10 to C18 on the parent chain. The differential toxicity in relation to the distribution of these member species, as well as the seasonal and spatial distribution of the 3-OHFAs and the endotoxin profiles will be discussed.

Table 1. Summary of the preliminary results on LAL

City	LAL Mean, EU/m^3 (range)	
	$PM_{2.5-10}$	$PM_{2.5}$
Nan Sha	0.18 L: 0.01 H: 0.91	0.16 L: 0.01 H: 0.50
Guang Zhou	0.32 L: 0.08 H: 0.88	0.12 L: 0.04 H: 0.36

Range: L – lowest measured value, H – highest measured value
EU: endotoxin units

Lee, Alex K.Y., Chan, Chak K., Fang, Ming and Lau, Arthur P.S. (2004). *Atmo. Environ.* 38, 6307-6317.

DEHM-Pollen: A regional scale pollen dispersion model

C.A.Skjøth[1], J.Brandt[1],J.Christensen[1], L. M. Frohn[1], C. Geels[1], A.B.Hansen[1], K.M.Hansen[1], G.B.Hedegaard[1] and J. Sommer[2]

[1]Department of atmospheric Environment, National Environmental Research Institute, University of Aarhus, Frederiksborgvej 399 DK-4000, Roskilde, Denmark
[2]Astma-Allergy Association, Universitetsparken 4, DK-4000 Roskilde, Denmark
Keywords: bioaerosols, biospheric processes, emissions, long-range transport, modelling.

In Europe, allergy and sensibility to pollen has increased dramatically since the middle of the 20th century. In Denmark, this sensibility has increased from 12.9% to 22.5% during the period 1990-1998. The reasons for this increase in Denmark and other European countries are unknown. There is therefore a big need for improved knowledge within this area. This can be done by introducing biological based atmospheric transport models (BTM). BTMs are similar to chemical transport models (CTM). A BTM can be used for research in aerobiology such as dispersion of pathogens, bacteria or pollen. The use of BTM in atmospheric biology looks promising but is rarely done compared to the use of CTMs in atmospheric chemistry. In this study we present a BTM model DEHM-Pollen, where DEHM-Pollen is based on the DEHM model, which is a hemispheric scale CTM model with 63 chemical species and nesting options. Two important components in a CTM model is the emission inventory and a chemical scheme. Similarily a BTM needs an emission inventory and a "biological scheme", where this scheme can take into account biological mechanisms such as viability or growth of species. In DEHM-Pollen the emission inventory is based on a species inventory and the biological scheme is based on a combination of a phenological model and a flowering model. We show how DEHM-Pollen can be used to extend the knowledge of distribution obtained from a single pollen monitoring trap located in Denmark.

We also show, how the assimilation of biological observations such as the development of the pollen season affects the biological modules in the model and therefore also the model calculations.
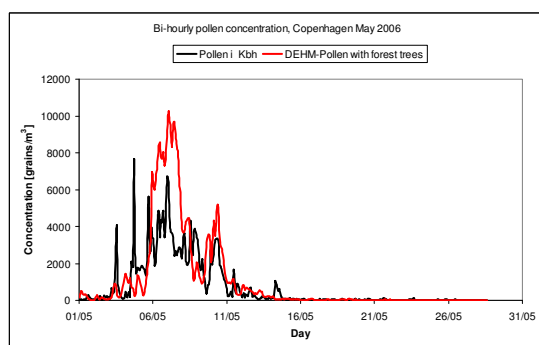
Figure 1. Comparison of measured and modelled bi-hourly birch pollen concentration for the year 2006.

As an example, it is shown how long-range transport of high levels of birch pollen (Fig 1) have arrived in Copenhagen from the Baltic countries and Russia and are further distributed out into the North Sea within a time frame of one week (Fig 2).
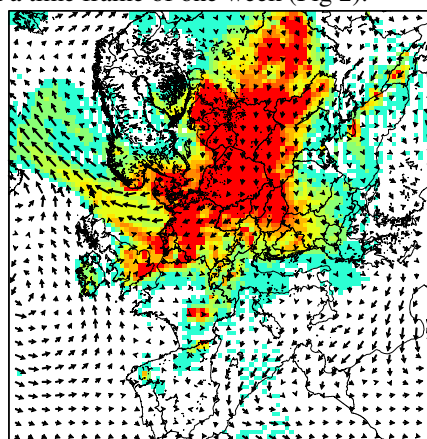
Figure 2. Birch pollen concentration on European scale as simulated with DEHM-Pollen, May 5 2006.

The results show, how the DEHM-Pollen model can be used to extend the information obtained from a single point. As such, the biological based atmospheric transport model can improve knowledge within research related allergy.

Long-range transport of birch pollen to Denmark may come from the surrounding countries such as Sweden, Poland, Germany, Baltic countries and Russia. Such episodes may arrive during the local pollen season, pre-season or post-season. During pre-season, pollen allergy patients are in general medically unprotected. Such episodes will therefore have a full impact with respect to allergic reactions among the allergy patients. DEHM-Pollen can be used to calculate variations in human exposure of pre-seasonal allergenic pollen. Such calculations have the potential to explain pre-seasonal outbreaks of allergic reactions among sensitized patients

DEHM-Pollen is a new component in the THOR integrated air quality and forecast system. The use of DEHM-Pollen in forecast mode can supplement pollen forecasting systems based on a few measurement stations by providing early warnings of severe pre-seasonal pollen episodes by showing how far and how severe a possible pre-seasonal birch pollen cloud will progress into Denmark

Modelling mineral dust and airborne micro-organisms with the Danish Eulerian Hemispheric Model

L.M. Frohn, C. Geels, C.A. Skjøth, K.M. Hansen, J.H.Christensen, J. Brandt, G.B. Hedegaard, A.B. Hansen, O., Hertel.

Department of Atmospheric Environment, National Environmental Research Institute, University of Aarhus, Frederiksborgvej 399, DK-4000, Roskilde, Denmark

Keywords: Aerosol modelling, Airborne particles, Bioaerosols, Long-range transport, Mineral dust.

Sensor systems for bioterror must be able to distinguish natural occurrences from real attacks. For this they require quantitative input about the natural background of micro-organisms and environmental pathogenic traits. However, knowledge of numbers, species, viability and pathogenicity of airborne micro-organisms is extremely scarce, and models to predict background fluctuations are inadequate. Recent studies indicate that significant concentrations of viable micro-organisms are routinely transported by dust and marine aerosols over intercontinental distances (Prospero et al., 2005). The understanding and subsequently modelling of the aerial dispersion of such episodes will improve knowledge with respect to atmospheric transport of micro-organisms and pathogens. However it is not known, which degree of detail is necessary for assessing the risks associated with airborne micro-organisms.

Comprehensive knowledge about the characteristics controlling the process of long-range transport of viable micro-organisms is therefore needed. The AeroBactics project is designed to close these gaps of knowledge. The project started in March 2007 and a short overview of the project-activities will be given in the presentation.

One of the main tasks of the project has been to further develop the Danish Eulerian Hemispheric Model (Christensen, 1997, Frohn et al., 2002) to include emission, transport and deposition of micro-organisms from three different source categories; anthropogenic (applications of pesticides), marine (sea-spray driven emissions) and natural land-based (dust uplift driven emissions).

A dust emission module obtained from the University of Athens (Nickovic et al., 2001) has been implemented in the DEHM model and validations with available dust measurements will be presented. A parameterisation describing the relation between dust uplift and estimated micro-organism concentrations will also be described, together with comparisons between measured and modelled air concentrations of micro-organisms obtained within the project.

Prospero, J. M., Blades, E., Mathison, G. & Naidu, R. (2005). *Aerobiologica,* 21, 1, 1-19.

Christensen, J. H. (1997). *Atmospheric Environment*, 31, 24, 4169-4191.

Frohn, L. M., Christensen, J.H. & Brandt, J. (2002). *Journal of Computational Physics*, 179, 68-94.

Nickovic, S., Kallos, G., Papadopoulos, A., Kakaliagou, O. (2001). *Journal of Geophysical Research*, 106, D16, 18,113-18,129.

Disinfection of fungal spores on fibrous filters by *Melaleuca alternifolia* mist

Ruth Huang, Oleg V. Pyankov, Bofu Yu and Igor E. Agranovski,

Griffith School of Engineering, Griffith University, Nathan, 4111 Australia

Keywords: bioaerosol, filtration, particle re-entrainment, microbial inactivation

Various infectious microorganisms are transmitted via airborne route and may cause a wide range of illnesses, especially when deposited in the respiratory tract. Commercial HVAC systems could therefore be ones of the entry points for hazardous contaminants such as biological weapon agents (BWA). Cleaning of air by domestic HVAC systems is usually performed on the filters with a range of efficiencies starting from relatively low values. However, when filters are used for collection of biological aerosols, capturing of viable particles on its own is not sufficient for effective control of environment. The reason for it is based on a fact that collected particles could be detached from the filter surface and re-entry the air stream causing contamination of ambient air and corresponding human and animal diseases. This issue call for further investigations related to development of mechanisms of rapid and reliable inactivation of collected particles on the filter surface. Our previous investigations confirmed that bacterial aerosols could be efficiently inactivated if fibres of the filter are coated with *Melaleuca alternifolia*, known as tea tree oil (TTO). The essential oil of, is commonly used as a topical antiseptic, and also as a complementary medicine for bacterial and fungal infections. Several investigations have confirmed the in-vitro activity of TTO against a wide range of common postharvest pathogens. Even a robust strain of *Bacillus subtilis var niger* bacteria was efficiently inactivated during short residence time periods (Pyankov et al., 2008). The current project is focused on the investigation of the possibility of inactivation of robust fungi by TTO coated fibres of common HVAC fibrous filter. Considering the fact that fungal spores are very robust and resistant to chemical and physical stresses, the conclusion about the possibility of their inactivation by TTO could not be simply drawn from the results obtained for bacterial strains.

The experimental program was similar to the one described in detail in Pyankov et al. (2008). In brief, four HVAC filters were installed in parallel in a holder and the TTO was applied onto their surfaces for 5 minutes through the Collison nebulizer. Parallel arrangement of the filters and equal flow rate across all of them ensured uniform distribution of TTO and fungal spores on their surfaces. After 5 minutes run, the nebulizer flow was discontinued and fungal spores, aerosolized from the surface of an agar plate, were mixed with HEPA filtered and dried air and passed through the parallel filter assembly for 3 minutes. On completion of this procedure, filter holder was disconnected and the first filter was immediately placed in a vessel containing 50 ml of sterile water to eliminate any further influence of TTO. The vessel was sonicated in a bath for 2 minutes and then centrifugated for 3minutes. Water and oil were carefully pored from the vessel leaving the entire amount of fungal spores at the bottom. Ten milliliters of fresh distilled water were then added to the vessel and sonicated for five minutes ensuring uniform distribution of the microorganism in it. Then, the liquid was decimally diluted and 100 µl of each dilution was spread on the surface of the agar plate to obtain counts of viable fingi. Three plates were used for each dilution to ensure statistically reliable results. The second filter was undergone though the same procedure 15 minutes after to evaluate the inactivation effect of TTO over this time period. The third and fourth filters were analyzed after 30 and 60 minutes respectively. The final results were then obtained as ratios of 15, 30 and 60 minut results by the result obtained for zero time period (first filter).

For comparison of the results, the experiment was repeated identically for biologically inactive light mineral oil (LMO, Sigma Chemicals M3516).

Obviously, it was impossible to keep the concentration of airborne fungi identical for all experimental runs. To make the concentration related correction, the total concentration was monitored in all experiments by APS (TSI, USA) and viable particle concentration by personal bioaerosol sampler (Agranovski et al., 2005).

The results were obtained for two common environmental fungal strains, i.e. *Aspergillus Niger* and *Rhizopus Stolonifer*. It was found that the TTO is capable to disinfect robust fungal strains collected on the filter surface. The rate of inactivation, however, was not very high and did not exceed 50% for the entire duration of 60 minutes exposure.

Pyankov, O., et al. (2008). *CLEAN, (Special Bioaerosol Issue)*, **36(7),** 609-614

Agranovski, I., et al. (2005). *J. Aerosol Sci. (Special Bioaerosol Issue)*, **36**, 609-617.

Measurement of subway bioaerosols and removal of bioaerosols using thermal energy

B. U. Lee, G. B. Hwang, and H. G. Kim

Department of Mechanical Engineering, Konkuk University, Hwayang Dong, Gwang-Jin Gu, 143-701, Seoul, Republic of Korea

Keywords: bioaerosols, subway, removal, temperature.

Seoul has huge subway systems, which are several hundreds kilo-meter long. Also, currently, the construction to lengthen the subway system continues. Several millions of people are using the subway systems everyday in Seoul, Korea.

As the concerns over the indoor pollutants grow, there is a demand to measure the concentration of indoor air pollutants and to control the pollutants in the subway system.

Especially, there is ongoing innovation in the subway system, which is to build screen doors between the train tracks and the platforms. The original purpose of the screen door is to protect passengers from falling to the train tract while trains approach. In addition to the safety problems, the screen doors also have great impact on the indoor environmental conditions in the platforms, therefore, it is necessary to newly monitor and to control indoor pollutants under the screen door conditions.

In this study, among various indoor pollutants, we focus on the airborne microorganisms in the subway systems, which are known as etiological agents for respiratory and skin diseases.

We first measured the concentration of bioaerosols in the platform of the subway system. We prepared two kinds of culture medias for bioaerosols, one is for bacteria, and the other is for fungi. We used the Anderson impactor with varying the sampling time depending on the expected concentration of the bioaerosols, to sample airborne microorganisms.

The sampled bioaerosols on the culture media inside the Anderson impactor are incubated and the colonies on the culture media are enumerated. We can calculate the concentration of bioaerosols by using the sampling time, the sample flow rate, and the number of colonies in the media.

We also develop a control equipment for bioaerosols in the subway system. We use the thermal energy as a major principle in the equipment, because the thermal energy produce minimum amount of side effects in indoor environments compared to the ultraviolet and electric ion emissions (Lee & Lee, 2006). However, the thermal energy has disadvantage such as energy consumption. Recently, our team found that less than 1 second residence time is enough to inactivate airborne microorganisms (Jung *et al.*, 2009), therefore, we designed low energy consuming equipment.

We measured airborne bacteria and fungi from March, 2008 to May, 2008. The concentration of airborne bacteria ranged from 600 CFU/m^3 to 900 CFU/m^3. The concentration of airborne fungi ranged from 5 CFU/m^3 to 70 CFU/m^3. The concentration varied with locations of measurements.

We tested the designed control system in the platform of the subway system. We measured the bacteria bioaerosol concentrations at the inlet and the outlet of the control system and calculated the efficiency of the system. The inactivation efficiency against bacteria bioaerosols ranged from 13% to 49%. We can control the efficiency by varying the temperature conditions and the flow rate through the control equipment.

We expect that the concentrations of bioaerosols highly depend on the population of passengers and the outside weather conditions. Therefore, we plan to conduct additional measurements under various conditions in the subway system. Also, we will revise the control systems to increase the inactivation efficiency against bacteria bioaerosols. And we plan to test it for fungal bioaerosols.

Jung, J.H., Lee, J.E., Lee, C.H., Kim, S.S., & Lee, B.U. (2009). High-temperature short-time process of fungal bioaerosols in a continuous-flow system. *Applied & Environmental Microbiology* (in press).

Lee, Y. H., & Lee, B. U. (2006). *J. Microbiol. Biotechnol.* 16, 1684-1689.

Relationship between OC/EC data and meteorological and inorganic trace gas data for a forested site in Brasschaat, Belgium

X. Chi[1], W. Maenhaut[1] and J. Neirynck[2]

[1]Dept. of Anal. Chem., Inst. for Nuclear Sci., Ghent University, Proeftuinstraat 86, BE-9000 Gent, Belgium
[2]Research Institute for Nature and Forest (INBO), Gaverstraat 4, BE-9500 Geraardsbergen, Belgium

Keywords: carbonaceous particles, organic carbon, elemental carbon, PM2.5, meteorology, trace gases.

Last year we reported on the measurement of PM2.5 carbonaceous aerosols with a semi-continuous, real-time carbon aerosol analysis instrument at three forested sites in Europe (Maenhaut & Chi, 2008). One of the sites was the state forest "De Inslag", Brasschaat, Belgium. Here, we report on additional measurements at this site and on the relationship of the organic, elemental, and total carbon data (OC, EC, and TC) with meteorological and inorganic trace gas data and with time of day. As last year, we will discuss the optical OC (OptOC) and optical EC (OptEC) data, together with the data for TC (with TC = OptOC + OptEC). The data at Brasschaat were acquired in three different periods, i.e. (1) from 25 April to 13 July 2007, (2) from 19 September to 12 November 2007, and (3) from 15 July to 6 November 2008. The time resolution of the measurements was 1 h during the first period and 2 h during the other two periods. During the first period, TC ranged from 0.3 to 9.2 µg/m^3 (median 2.5 µg/m^3) and the average OptEC/TC ratio was 0.26±0.11; during the second period, the range in TC was 0.4 – 14 µg/m^3 (median 3.4 µg/m^3) and the average OptEC/TC ratio was 0.36±0.12; and during the third period TC ranged from 0.6 to 16 µg/m^3 (median 2.8 µg/m^3) whereas the average OptEC/TC ratio was 0.38±0.13. The OptEC/TC ratios at Brasschaat are substantially higher than those found at our two other forested sites (i.e., K-puszta, with a ratio of 0.15±0.05 and Hyytiälä, with a ratio of 0.08±0.04). The EC/TC ratio at Brasschaat is similar to that observed at Ghent and other urban sites in Europe (e.g., Viana *et al.*, 2007). This indicates that our site at Brasschaat is seriously impacted by carbonaceous aerosols from anthropogenic origin. This is not surprising considering that the site is at about 12 km NE of the center of the city of Antwerp and at about 9 km to the east of the Antwerp harbour area. There was a clear tendency for TC to exhibit higher levels during the night than during the day, which is likely due to a shallower boundary layer during night. There was, however, also a weak maximum in TC at around 8:30 a.m., which was due to higher levels in OptEC because of the morning rush hour traffic. The impact of this rush hour was particularly apparent in the diurnal OptEC/TC ratio, which is shown in Figure 1 for the first period, and separately for working-days and weekend days/holidays.
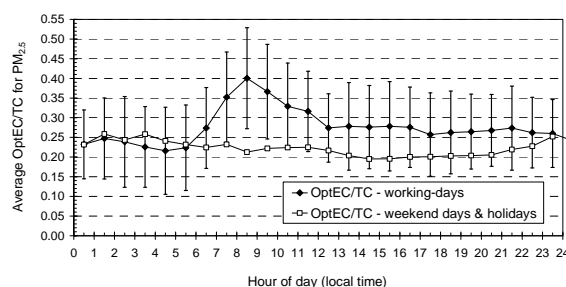
Figure 1. Diurnal variation of OptEC/TC ratio.

The relationships between the OptOC, OptEC, and TC data and the meteorological and inorganic trace gas data were examined. The meteorological data included were pressure, temperature, relative humidity, wind speed, wind direction, sunshine, and precipitation, whereas the trace gases were SO_2, O_3, NO, NO_2, and CO_2. For the 2007 data (combination of periods 1 and 2), OptEC was highly correlated with NO (r = 0.75) and NO_2 (r = 0.66), but even better with NO_x (r = 0.83). This is clearly a reflection of the common origin of OptEC and these trace gases, which is the combustion of fossil fuels and in particular automotive exhaust emissions. OptOC, OptEC, and TC were also highly correlated with CO_2 (all r around 0.7). Furthermore, there was a clear tendency for the particulate carbonaceous species, NO, NO_2, NO_x, and CO_2 to be negatively correlated with wind speed. This is rather logical as low wind speeds are common during periods of stagnation, when the levels of pollutants can build up. As to the relationship between the particulate carbonaceous species and wind direction, this was examined by making polar plots (wind roses) for OptOC and OptEC. OptOC was highest for winds from the east; periods of easterly winds are frequently periods of air mass stagnation and low wind speeds. OptEC, in contrast, showed highest levels for the wind direction range from 112.5° to 270°, which corresponds roughly with the sector where the center of Antwerp and the harbour are located. There was, however, a clear peak in OptEC for winds from the SSE. Incidentally, in this direction, a major highway passes within less than 2 km from our sampling site.

Maenhaut, W., & Chi, X. (2008). *European Aerosol Conference 2008*, Abstract T06A035P.

Viana, M., et al. (2007). *Atmos. Environ.* 41, 5972-5983.

Sources and Components of Organic Aerosols in Central Europe

V.A. Lanz[1], A.S.H. Prévôt[1], M.R. Alfarra[2], C. Hüglin[3], C. Mohr[1], S. Weimer[3], and U. Baltensperger[1]

[1]Paul Scherrer Institut, Laboratory for Atmospheric Chemistry, 5232, Villigen PSI, Switzerland
[2]University of Manchester, Centre for Atmospheric Science, Manchester (UK)
[3]Empa, Swiss Federal Laboratories for Materials Testing and Research, Überlandstrasse 139, 8600, Dübendorf, Switzerland

The quadrupole version of the Aerodyne Aerosol Mass Spectrometer (q-AMS) was deployed at several places in Switzerland, Austria, and Liechtenstein. The q-AMS provides real-time information on mass concentration and composition of the non-refractory species in particulate matter smaller than 1 μm (NR-PM$_1$) with high time- and size-resolution at unit mass resolution. The combination of factor analysis and ambient AMS data represents a relatively new approach to identify organic aerosol (OA) sources/components (Zhang *et al.*, 2005). In this study, such an approach (PMF – positive matrix factorization; Lanz *et al.*, 2007, 2008) was applied to various OA data sets covering a wide range of pollution levels (mobile measurements on motorways, urban, rural, and even a high-alpine location) as well as all seasons of the year.

Dominating aerosol components were representing oxygenated and secondary organic aerosol (OOA-I and OOA-II), primary particles from wood burning (P-BBOA; especially in residential areas in wintertime with abundances of ~50% OA and more) and primary traffic-related aerosols (usually ~10% of OA, but up to 60% on motorways). Close to sources, charbroiling and potentially food cooking aerosols could be distinguished as well.

The OOAs' time series were compared to measurements of AMS inorganics (sulphate, nitrate, and ammonium) in order to facilitate their interpretation as secondary OA (SOA). Diurnal cycles of the estimated source strengths, ancillary gas-phase and meteorological data, estimated emission ratios etc. were also used to validate the interpretations of the factor analytical results.

Lanz, V. A. *et al.* (2007). *Atmos. Chem. Phys.*, 7, 1503–1522.
Lanz, V. A. *et al.* (2008), *Environ. Sci. Technol.*, 42, 214–220.
Zhang, Q. et al. (2005), *Environ. Sci. Technol.*, 39, 4938–4952.

PM Emissions from a CFM56 Gas Turbine Engine Burning Alternate Fuels

D.E. Hagen[1], P.D. Whitefield[1], P. Lobo[1], and M.B. Trueblood[1]

[1]Center of Excellence for Aerospace Particulate Emissions Reduction Research, Missouri University of Science and Technology, 65409, Rolla MO, USA

Keywords: Combustion aerosols, Measurement (combustion aeros.), PM measurements, Soot size distribution.

There is a growing concern for the environmental impact of jet engine exhaust emissions on the atmosphere. The anticipated growth in commercial air traffic, rising fuel costs, an increasing desire to reduce reliance on fossil fuels produced in politically unstable regions, and the possibility of reduced emissions has driven research into alternate renewable fuels suitable for gas turbine engines, either from biomass (Biofuels) or synthesis from coal, natural gas and other renewable feedstocks (Fischer-Tropsch (FT) fuels). Industry and government have recently sponsored (Dec 07, Jan 09) two engine emission tests led in part by the Missouri S&T team. The test focused on burning alternative and conventional fuels and associated blends in a CFM56- type commercial gas turbine engine. The CFM56 engine type is the most common engine in the global commercial fleet powering more than 70% of the US domestic fleet.
The purpose of these emission tests was to quantify any differences in particulate matter (PM) and hazardous air pollutants (HAP) emissions observed between the different fuels, and assess the environmental impacts that may result from these differences. This paper will focus on the Dec. 2007 PM emissions test conducted at the General Electric test facility at Peebles, Ohio. Alternate fuels offer a possible means for reducing engine emissions and hence their environmental impact.

The emissions measurement campaign involved the characterization of the PM exhaust emissions at a point 1m behind the engine exhaust plane, for various fuel types, under similar engine operating conditions. The engine was mounted in a fixed test stand and an extractive sampling probe was held in a probe rake mounted behind the engine. The probe allowed for immediate sample dilution with dry nitrogen at an approximate dilution ratio of 10 to 1. A sample train of length ~ 43m carried the sample to instrumentation housed in a trailer. The fuels studied were: Jet-A, Jet-A1, 20% Fatty Acid Methyl Ester / 80% Jet-A1, 40% Fatty Acid Methyl Ester / 60% Jet-A1 (40% Biojet), 50% FT / 50% Jet-A1, and 100% FT. The Jet-A and Jet-A1 fuels were supplied by General Electric, the Fatty Acid Methyl Ester fuel by Imperium, and the FT fuel by the US Air Force.
Changes in the PM emissions were determined relative to the Jet-A1 fuel. The preliminary emissions changes corresponding to the 40% Biojet and 100% FT fuel are shown in Figures 1 and 2.
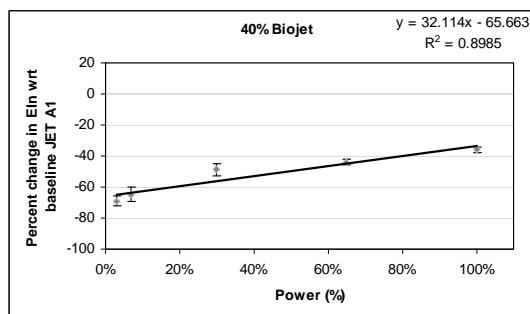
Figure 1. Reduction in number based emissions index given by the 40% Biojet fuel.
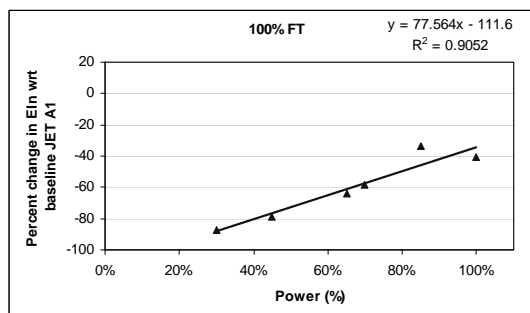
Figure 2. Reduction in number based emissions index given by the 100% FT fuel.

The PM measurements indicate that, especially for the 100% FT fuel, PM number and mass are diminished at all powers relative to conventional fuels.

$\delta^{13}C$ measurements of size segregated aerosols from urban site in wintertime

A. Garbaras, I. Rimselyte, K. Kvietkus and V. Remeikis

Institute of Physics, Vilnius, LT-02300, Vilnius, Lithuania

Keywords: cascade impactor, elemental carbon, mass size distribution, PM and source apportionment, urban aerosol.

Aerosol samples were collected with MOUDI during a winter season (2008 – 2009) at an urban site in Vilnius (54°38' N, 25°11' E), Lithuania. Several samples were collected; one sampling duration was 1 week. Parallel to MOUDI sampling, $PM_{2.5}$ samples on quartz fiber filters were collected every 24 h. For all samples the carbon concentration was measured with the Elemental analyzer (EA). The total carbon (TC) and elemental carbon (EC) isotopic ratio was measured with EA coupled to the isotope ratio mass spectrometer (*ThermoFinnigan*) in all MOUDI cascades. Isotopic ratio analysis methodology is presented in (Garbaras *et al*., 2008).

Size segregated aerosol samples had unimodal distribution for TC with the maximum in the 0.56 – 1 μm size range (Table 1), typical of urban sites (Chow *et al*., 2008).

Table 1. Total carbon concentrations on MOUDI stages.

Stage No.	D_p (μm)	TC (μg/m³)
1	18	0.04
2	10	0.02
3	5.6	0.03
4	3.2	0.06
5	1.8	0.09
6	1	0.41
7	0.56	0.83
8	0.32	0.77
9	0.18	0.45
10	0.10	0.12
11	0.056	0.12

TC isotopic value -26.5 ‰ was measured in ultrafine mode (D_p = 0.056 – 0.1 μm). Delta values differ in accumulation and coarse modes significantly (Fig. 1). The isotopic ratio varied from -26.6‰ to -25.5 ‰ in accumulation mode (D_p = 0.1 – 1.8 μm) and from -25.5 ‰ to -23.7 ‰ in coarse mode (D_p = 1.8 – 18 μm).

Domestic heating and transportation are main sources of carbonaceous aerosols during wintertime. TC isotopic value -26.3 ‰ in ultrafine mode is in agreement with published data for fuel (Widory *et al*., 2004). Measured TC isotopic values in accumulation mode were similar to black carbon measurements in Zurich city during wintertime

which had isotopic value about -26.5 ‰ (Fisseha *et al*., 2008).
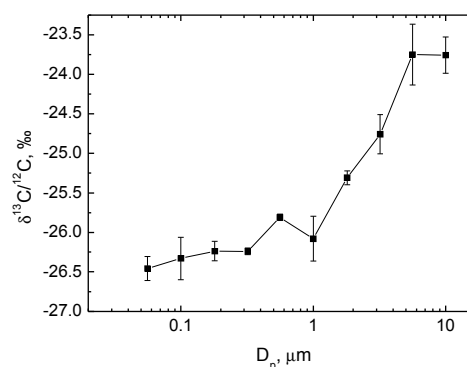
Figure 1. $\delta^{13}C/^{12}C$ of size segregated TC in Vilnius, during 02-08 December 2008.

Garbaras, A., Andriejauskiene, J., Bariseviciute, R. and Remeikis, V. (2008). *Lithuanian J. Phys.*, 48, 259-264.

Chow, J. C., Watson, J. G., Lowenthal, D. H. and Magliano, K. L. (2008). *Atmospheric Research*, 90, 243-252.

Widory, D., Roy, S., Le Moullec, Y., Goupil, G., Cocherie, A. and Guerrot, C. (2004). *Atmospheric Environmen*, 38, 953–961.

Fisseha, R., Saurer, M., Jäggi, M., Siegwolf, R.T.W., Dommen, J., Szidat, S., Samburova, V. and Baltensperger, U. (2008). *Atmospheric Environment*, 43, 431-437.

Seasonal trend of atmospheric organic and elemental carbon mass concentrations over south-eastern Italy

A. Dinoi, I. Carofalo, and M. R. Perrone

CNISM, Department of Physics, University of Salento, Via per Arnesano, 73100, Lecce, Italy

Keywords: elemental carbon, organic carbon, atmospheric aerosol, PM2.5, PM1.

Atmospheric carbonaceous particles are an important component of fine particulate matter (PM) and play a primary role both in adverse health effects and in global climate change by affecting radiative forcing. Elemental carbon (EC) and organic carbon (OC) are the main fractions of carbonaceous particles. EC is emitted directly from combustion sources and it's a good indicator of primary anthropogenic air pollutants. OC can be emitted from primary emission sources or produced by chemical reactions occurring in the atmosphere (Turpin and Huntzicker, 1995).

Results on OC and EC mass concentrations determined by the thermal-optical transmission technique (Sunset Laboratory OCEC Analyzer) on PM2.5 and PM1 samples are reported in this paper. PM2.5 and PM1 samples have been collected from July to December, 2008 at a suburban site of southeastern Italy.

Table 1 provides main statistics on tested parameters. In addition to PM2.5 and PM1 mass concentrations ± 1 standard deviation (SD) for July, August, and September (JAS) and for October and November (OND), respectively, mean values ± 1 SD of EC and OC mass concentrations are also provided. OC/EC mass ratios and TC/PM mass percentages ± 1 SD are also given in Table 1. TC represents the total mass carbon that is calculated by adding OC and EC mass concentrations.

It is worth noting from Table 1 that 65% and 57% of the PM2.5 mass concentration is due to PM1 particles on JAS and OND, respectively. Table 1 does not reveal any marked dependence on season of tested parameters, at least within ± 1 SD of mean values and within the investigated time of the year. However, PM2.5 and PM1 mean mass concentrations are larger on JAS. As a consequence, TC/PM mass percentages are slightly larger on OND. In particular, the mass percentage of carbonaceous particles is 30% and 40% of the collected mass on PM2.5 and PM1 samples on JAS and OND, respectively. These last results show that the mass contribution of carbonaceous particles is quite large over the monitoring site.

We also observe from Table 1 that the OC/EC mass ratio exceeds 2.0 both in PM2.5 and PM1 samples. This last result allows inferring the presence of secondary organic aerosols according to Cao et al. (2004).

Figure 1a-b showing OC versus EC scatter plots reveals that both species are well correlated. In fact, the Pearson coefficient is 0.6 and 0.7 for OC-EC mass concentrations monitored in PM2.5 and PM1 samples, respectively. These results may suggest that mass concentration levels of both carbonaceous species are controlled by similar atmospheric processes and that OC and EC can be attributable to common dominant sources.

Work is on progress to address main sources of carbonaceous particles over the monitoring site.

Table 1 Average mass concentration (± SD) of PM2.5 PM1, OC, EC, TC/PM percentages and OC/EC mass ratios for JAS and OND.

	PM2.5		PM1	
	JAS	OND	JAS	OND
PM Mass $\mu g/m^3$	26 ± 11	21 ± 5	17 ± 8	12 ± 3
OC $\mu g/m^3$	5 ± 2	6 ± 3	3 ± 1	3 ± 1
EC $\mu g/m^3$	1.9 ± 0.6	2.4 ± 0.9	1.5 ± 0.5	1.7 ± 0.7
TC/PM %	30 ± 10	42 ± 10	30 ± 11	44 ± 9
OC/EC	2.7 ± 0.9	2.7 ± 0.8	2.4 ± 0.7	2.1 ± 0.6
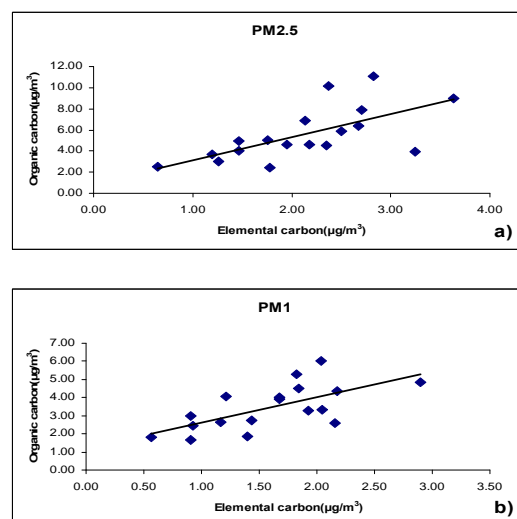
Figure 1 Scatter plots of OC versus EC for (a) PM2.5 samples and for (b) PM1 samples.

Turpin, B.J., Huntzicker, J.J., (1995). *Atmospheric Environment* 29, 3527–3544.

Cao, J.J., Lee, S. C., (2004) *Atmospheric Environment* 38, 4447–4456.

Black Carbon Aerosols in Urban Air in South Asia

Liaquat Husain[1,2], Sofia Alvi[3] and Vincent A. Dutkiewicz[1,2]
[1]Wadsworth Center, NY State Department of Health, Albany, NY 12201-0509.
[2]Department of Environmental Health Sciences, School of Public Health,
State University of New York, Albany, NY, USA 12201-0509.
[3]HEJ Institute of Chemistry, University of Karachi, Karachi, Pakistan.

Black (BC) and organic (OC) carbon bearing aerosols contribute large fractions of fine particle mass. BC represents the fraction that absorbs visible light and cause global warming. South Asia has recently received increased attention due to its rapidly rising pollutant emissions, including carbonaceous aerosols. To assess the regional and global climate change caused by aerosols in South Asia, detailed information is required on the atmospheric concentrations of carbonaceous aerosols in the region. Husain et al. [2007] recently reported extensive measurements of EC, OC and BC in Lahore, Pakistan from November 2005 to January 2006. Briefly, black carbon concentrations, [BC], were very high, ranging from about 5 to 110 μg m^{-3}, **and** daily mean was 21.7μg m^{-3}. Total carbonaceous aerosols averaged 96 μg m^{-3} of carbon, and contributed around 69% of the $PM_{3.2}$ mass. As the overall data on carbonaceous aerosols in South Asia are sparse, we undertook a year long study of BC aerosols in Karachi, the largest city in Pakistan. Results from a full year of Aethalometer BC measurements made in Karachi from April 2006 to April 2007 were used to investigate the temporal trends, diurnal and seasonal variations, and emission sources.

Karachi is a coastal city on the Arabian Sea with a population of about 14 millions, an area around 3,500 km^2 and a large industrial base. The AE21 Aethalometer (Magee Scientific) was operated out the third floor window of the HEJ Research Institute of Chemistry building on the University of Karachi campus (24.941° N, 67.123° E) between 17 April 2006 and 14 April 2007. The AE21 measures [BC] by collecting the particulate matter on rolled quartz filter with a cellulose fiber backing and continuously monitoring the transmission intensity of light beams at 880 and 370 nm wavelengths. The manufacturer's recommended absorption coefficients were used; 16.6 and 39.5 m^2 g^{-1}, respectively for the 880 nm and 370 nm channels. We exclusively report the [BC] from the 880- nm channel. The AE21 was operated with a cyclone inlet (BGI corporation) equipped with a bug and rain guard at a flow rate of 4 lpm (liters per min). This makes the cut-point around 3.2 μm. Five-minute averaging times were used. The instrument was set to advance to a new filter spot when the total attenuation was equivalent to a BC loading of 1,250 ng and it was operated with the 1 in 10 dilution option to minimize frequent filter advances

Daily mean [BC] varied from about 1 to 15 μg m^{-3}. However, short term spikes exceeding 40μg m^{-3} were common, occurring primarily during the morning and evening rush-hours. [BC] concentration was highest during November through February, ~ 10 μg m^{-3}, and lowest during June through September, ~2 μg m^{-3}. Diurnal, seasonal, and day-of-the-week trends are discussed. It is demonstrated that these trends are strongly impacted by meteorological patterns. A simple box model was applied to the concentration profiles to separate the impact of meteorological conditions and elucidate the underlying emissions patterns. Daily emissions varied from 14,000 to 22,000 kg of BC per day, or 6.5 kilometric tons per year. This was based on the area of metropolitan Karachi and 17.5 kilo metric tons emissions per year. Folding in the populations of each area yields a BC footprint of from 0.68 to 1.1 kg per person per year. Expanding the model to previously collected data yields annual emissions of 11.8 to 8.7 kilometric tons per year for Lahore. The higher value includes contributions from regional biomass burning. The lower estimate translated into a BC emission footprint of 1.0 kg per person per year for Lahore, or on the order of the higher estimate for Karachi.

Husain,L., Dutkiewicz, V. A., Khan, A. J., and Ghauri, B. M.,2007. Characterization of Carbonaceous Aerosols in Urban Air, Atmospheric Environment, 41, 6872 –6883.

Optimized separation of OC and EC for radiocarbon source apportionment

S. Szidat[1], N. Perron[2], S. Fahrni[1,2], M. Ruff[3], L. Wacker[3], A. S. H. Prévôt[2] and U. Baltensperger[2]

[1]Department of Chemistry and Biochemistry, University of Berne, Freiestrasse 3, 3012 Bern, Switzerland
[2]Paul Scherrer Institut, 5232 Villigen-PSI, Switzerland
[3]Laboratory of Ion Beam Physics, ETH Zurich, 8093 Zurich, Switzerland

Keywords: Carbonaceous aerosol, elemental carbon, organic carbon, source apportionment, radiocarbon analysis

Carbonaceous aerosols are a major component of the fine particulate matter and, thus, contribute to its climate and health effects. Radiocarbon (^{14}C) determinations offer a unique possibility for unambiguous source apportionment of carbonaceous aerosol particles (Currie, 2000; Szidat, 2009). This isotopic method enables a direct distinction of contemporary and fossil carbon in ambient aerosols, because ^{14}C has decayed in fossil material.

Carbonaceous aerosol (total carbon, TC) is classified into the sub-fractions elemental carbon (EC) and organic carbon (OC). This classification is widely acknowledged, although there is an ongoing debate on the optimum separation procedure of these method-dependent fractions. EC is exceptional among all carbon fractions, because it is introduced to the atmosphere solely as primary particles either from fossil fuel combustion or from biomass burning. Consequently, ^{14}C measurements of EC allow a direct determination of the contributions from biomass and fossil fuel burning to this fraction. Therefore, separation of OC and EC for ^{14}C analysis is desirable, especially because of the fact that opposite isotopic values of both fractions are often observed (Szidat et al., 2004a; Szidat et al., 2006; Szidat et al., 2009).

In previous work (Szidat et al., 2004a; Szidat et al., 2006), we performed chemical separation of OC and EC from quartz fiber filters for ^{14}C measurement using a step-wise oxidation (Szidat et al., 2004b). Here, OC was oxidized at 340°C in a stream of pure oxygen. EC was converted at 650°C after complete removal of OC and interfering water-soluble inorganic compounds, which is done by extraction with diluted hydrochloric acid and water followed by pre-heating in air at 390°C for 4 hours. CO_2 evolving from OC and EC was cryo-trapped and sealed in ampoules for ^{14}C measurement.

For correct ^{14}C analysis of EC, suppression of the positive artifact during OC removal ("charring") is of special importance. Charring will produce additional EC, so the ^{14}C measurement of EC may then be biased. The suppression of charring is optimized especially by the water extraction and the oxidative treatment of the filters. In order to reveal this effect during analysis, we now present sample preparation with a commercial OCEC Analyzer (RT 3080, Sunset Laboratory Inc.) applying on-line monitoring of the optical properties of the filters during the thermal treatment. This shows that the charring-revealing attenuation increase of EC is ≤4% for summer and winter filters from Gothenburg/Sweden (Szidat et al., 2009), if interfering components are removed by water extraction and temperature-controlled oxidation (Fig. 1). Charring becomes more prominent, even under oxidizing conditions, if the water-extraction step is omitted. The highest amount of artificial EC is produced, if OC is evaporated under helium, so that this often-used approach for determination of OC and EC concentrations (NIOSH method) is inappropriate for isolation of EC for ^{14}C analysis.
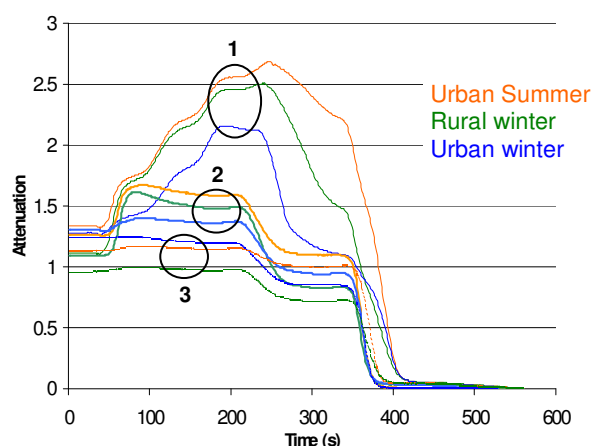
Fig. 1: Attenuation variation for three samples types from Gothenburg analyzed under these conditions: NIOSH method with original filters (1), three-step thermal method under pure O_2 with original filters (2), three-step thermal method under pure O_2 with water-extracted filters (3).

Currie, L. A. (2000). *Radiocarbon*, 42, 115-126.
Szidat, S., et al. (2004a). *Radiocarbon*, 46, 475-484.
Szidat, S., et al. (2004b). *Nucl. Instr. Meth. Phys. Res. B*, 223-224, 829-836.
Szidat, S., et al. (2006). *J. Geophys. Res.*, 111, D07206, doi:10.1029/2005JD006590.
Szidat, S. (2009). *Science*, 323, 470-471.
Szidat, S., et al. (2009). *Atmos. Chem. Phys.*, in press.

Radiocarbon measurements on aerosol samples at LABEC (Florence, Italy)

V. Bernardoni[1], G. Calzolai[2], M. Chiari[3], M. Fedi[2], F. Lucarelli[2], S. Nava[3], F. Riccobono[1], G. Valli[1], R Vecchi[1]

[1]University of Milan, Department of Physics and INFN, Milan, Italy
[2]University of Florence, Department of Physics and INFN, Florence, Italy
[3]INFN, National Institute of Nuclear Physics, Florence, Italy

Keywords: Carbonaceous aerosol, Radiocarbon, Elemental Carbon, Organic Carbon.

Radiocarbon measurements have been shown to be a powerful tool for aerosol source apportionment. As ^{14}C is absent in fossil sources, its quantification in aerosol samples allows the resolution of the biogenic and anthropogenic contributions. It is noteworthy that the non-fossil fraction contains both natural and anthropogenic contributions (for example biomass burning). Thus, in order to resolve all the carbonaceous sources, it is mandatory to perform radiocarbon measurements not only on the Total Carbon (TC) but also on Elemental and Organic fractions.

Since many years, the INFN-LABEC laboratory of Florence (Italy) has been involved in AMS (Accelerator Mass Spectrometry) measurements for radiocarbon dating, carried out with a 3 MV Tandetron accelerator. However, in order to perform radiocarbon measurements on TC, EC and OC in aerosol samples, a new sample preparation line was required, to fulfill all the pretreatment procedures necessary to separate the carbonaceous fractions.

The new sample preparation line was developed to analyse samples characterised by smaller quantity than those typically prepared for to the radiocarbon dating. This improvement is even more important for radiocarbon measurements on EC, as it is only about a quarter of TC.

The new sample preparation line can be briefly described as follows: the carrier gases (He and O_2) after being suitably purified proceed in a combustion oven, where the filter loaded with atmospheric particulate matter is placed. The thermal program and the sample preparation were optimised to allow the EC/OC separation. After the combustion oven, a CuO catalyser ensures that all the combustion products evolve to CO_2. After the removal of alogens, sulphates and nitrates, CO_2 is cryogenically trapped with a newly designed trap. CO_2 is then transferred from the trap to the graphitisation line, which forms the last part of the new sample preparation line. Later on, the produced graphite is pressed in capsules to be inserted in the accelerator ion source for analysis.

Some tests to check the reproducibility and the reliability of the results were carried out, together with blanks evaluation. Measurements were performed on daily PM10 samples collected on quartz fiber filters with a high-volume air sampler. OC and EC concentration, together with TC, were also quantified on these samples by thermo optical transmittance (TOT) analyses.

These preliminary AMS measurements showed that the ion currents obtained with our accelerator were well measurable, and the results were reproducible, thus confirming the feasibility of the measurements on such small samples (at the moment about 500 µg of Carbon).

Figure 1. The new sample preparation line.

Currie, L.A., (2000), Evolution and multidisciplinary frontiers of ^{14}C aerosol science, *Radiocarbon 42*, 115-126.

Szidat, S., Jenk, T.M., Gäggeler, H.W., Synal, H.-A., Hajdas, I, Bonani, G., Saurer, M. (2004), THEODORE, a two-step heating system for the EC/OC determination of radiocarbon (^{14}C) in the environment, *Nucl. Instr. & Meth. B* 223-224, 829–836.

Szidat, S., Ruff, M., Wacker, L., Synal, H.-A., Hallquist, M., Shannigrahi, A.S., Yttri, K.E., Dye, C., Simpson D. (2008), Fossil and non-fossil sources of organic carbon (OC) and elemental carbon (EC) in Göteborg, Sweden, *Atmos. Chem. Phys. Discuss,* 8, 16255-16289.

OC, EC, and SOA contribution to PM in Lombardy (Italy): results of three winter campaigns (2005-2007)

A. Piazzalunga[1,*], P. Fermo[1], R. Vecchi[2], G. Valli[2], S. Comero [2], V. Bernardoni[2], O. Cazzuli[3], A.Giudici[3], G.Lanzani[3]

[1]Dep. Inorganic, Metallorganic and Analytical Chem., University of Milan, Via Venezian 21, 20133, Milan, Italy
[2]Department of Physics, University of Milan ,Via Celoria 16, 20133, Milan, Italy
[3]ARPA Lombardia-Department of Milan, via Restelli 3/1, 20124, Milan, Italy
[*] Now: Dep. of Environmental Sciences, University of Milano-Bicocca, Piazza della Scienza 1, 20126, Milan, Italy

The carbonaceous fraction (OC, organic carbon, ed EC, elemental carbon) represents one of the major components of atmospheric aerosol particulate matter. The new Air Quality Directive 2008/50/EC requires measurements of elemental and organic carbon at selected background sites in each Member State. Until now very scarce data were available for Northern Italy, one of the most polluted area in Europe. OC and EC quantification was carried out in the frame of PARFIL (Particolato Fine in Lombardia) project whose aim was to study air quality in Lombardy region. The study of the carbonaceous fraction allows from one hand to acquire information on sources contribution to PM and from the other hand to enhance the knowledge of health effects and implication on climate changes (EC is responsible of solar radiation absorption while OC plays an important role in the clouds formation).

PM10 and PM2.5 samplings campaigns were carried out, during the three years 2005-2007, in urban, background, rural and remote sites (Milan, Varese, Brescia, Cantù-CO, Boscofontana-MN, Mantova, Alpe S.Colombano-SO, Lodi) representative of the geographical differences present in the region. About 80 samples in total were collected for each site during each year.

TOT (Thermal Optical Transmittance) method was used for OC/EC quantification (Birch and Cary 1996).

Differences in OC and EC concentrations were singled out and were ascribed to the peculiar characteristic of the site (urban, remote-alpine or rural). Nevertheless, all the sites placed in the Po Valley show quite homogeneous values, especially during the warm season, confirming the hypothesis of pollutants dispersion on a regional scale. In figure 1 average OC and EC concentrations in PM10 samples collected during the investigated period (years 2005-2007) at the three types of sites examined (urban, rural and alpine) are shown.

It noteworthy that at urban sites OC is mainly present in PM2.5 representing on average 35 – 40% of the mass while it accounts for 15% - 35% in PM10. Also EC is mostly present in the fine fraction, representing on average 3% - 15% of the mass with higher values in sites affected by traffic.
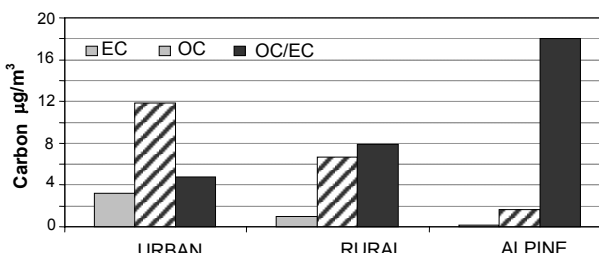
Figure 1- OC, EC and OC/EC in PM10 samples in different sites in Lombardy region as average for the years 2005-2007

The contribution of the biomass burning source was also estimated analyzing the tracer levoglucosan (Simoneit et al., 1999). Wood burning represents on average 15% of PM10 during winter time in urban sites, such as Milan, and 26% in Sondrio, an urban alpine site where the use of wood for residential heating is widespread.

Secondary organic aerosol (SOA) contribution was also quantified since the knowledge of this fraction is important in evaluating policies for PM reduction. In this study SOA was quantified applying the EC tracer method (Turpin et al., 1995) using $(OC/EC)_{prim}$ =1.34 for summer (Giugliano et al., 2005) and a value experimentally determined for winter $((OC/EC_{prim})$ =1.58, Vecchi et al., in press). On average, secondary organic carbon represents about 50% and 70% of total carbon in urban and rural sites, respectively.

Birch, M.E., Cary, R.A., (1996) *Aeros. Sci. & Technol.*, 25, 3, 221-241.
Giugliano, M., Lonati, G., Butelli, P., Romele, L., Tardivo, R., Grosso, M., (2005) *Atmos Env.*, 39, 2421-2431.
Simoneit, B.R.T., Schauer, J.J., Nolte, C.G., Oros, D.R., Elias, V.O., Fraser, M.P., Rogge, W.F., Cass, G.R. (1999) *Atmos. Env.*, 33, 173-182.
Turpin B.J., Huntzicker J.J., (1995) *Atmos. Env.,* 29, 3527-3544.
Vecchi R., Bernardoni V, Fermo P., Lucarelli F., Mazzei F., Nava S., Piazzalunga A., Prati P., Valli G. (in press). *Environ.Monit. & Assess.*

The importance of organic and elemental carbon in the fine particles over China

J.J. CAO[1], J.C. Chow [2], J.G. Watson [2], S.C. Lee [3]

[1] SKLLQG, Institute of Earth Environment, Chinese Academy of Sciences, Xi'an, China
[2] Division of Atmospheric Sciences, Desert of Research Institute, Reno, USA
[3] The Hong Kong Polytechnic University, Hong Kong, China

Keywords: Organic carbon, elemental carbon, OC/EC ratio, China.

Simultaneous measurements of fine particles ($PM_{2.5}$) were taken during winter and summer seasons at 2003 in 14 cities in China. Daily PM samples were analyzed for OC and EC by the IMPROVE thermal/optical reflectance protocol (TOR) and analyzed water-soluble ions by ion chromatogram (IC). Average $PM_{2.5}$ OC concentrations in the 14 cities were 38.1 µg m^{-3} and 13.8 µg m^{-3} for winter and summer periods, and the corresponding EC were 9.9 µg m^{-3} and 3.6 µg m^{-3}, respectively. OC and EC concentrations of had summer minima and winter maxima in all the cities. Carbonaceous matter (CM), the sum of organic matter (OM, = 1.6 × OC) and EC, contributed 44.2% to $PM_{2.5}$ in winter and 38.8% in summer. Compared with carbon species, sulfate, nitrate, and ammonia were three dominant ions, which accounted to 17.7%, 9.0%, and 5.5% in winter and 20.5%, 11.5% and 7.8% in summer, respectively. Therefore, carbonaceous aerosol is the more important contributor to fine particles than sulfate aerosols in urban aerosols. OC was correlated with EC (R^2: 0.56–0.99) in winter, but correlation coefficients were lower in summer (R^2: 0.003-0.90). Using OC/EC enrichment factors, the primary OC, secondary OC and EC accounted for 47.5%, 31.7% and 20.8%, respectively, of total carbon in Chinese urban environments. More than two-thirds of China's urban carbon derived from directly-emitted particles. Average OC/EC ratios ranged from 2.0 to 4.7 among 14 cities during winter and from 2.1 to 5.9 during summer. OC/EC ratios in this study were consistent with a possible cooling effect of carbonaceous aerosols over China.

Table 1 Description of Sampling Site in Each City

Cities	Location	Site description
Hong Kong	South China	Coastal and commercial city
Guangzhou	South China	Commercial and industrial city
Xiamen	Southeast China	Coastal city
Chongqin	Middle Southwest	Industrial city
Wuhan	Middle of China	Industrial city
Hangzhou	East China	Continental city
Shanghai	East China	Megacity
Xian	Middle Northwest	Continental city
Qingdao	East China	Coastal city
Jinchang	Middle Northwest	Asian dust source region
Tianjin	North China	Megacity
Yulin	Middle Northwest	Continental city near a desert
Beijing	North China	Capital, the largest city
Changchun	Northeast China	Industrial city
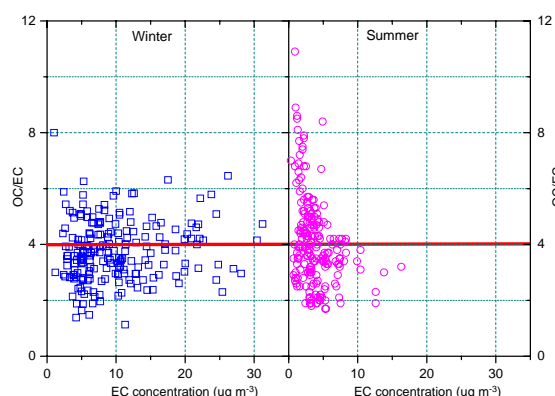
Figure 1. The distribution of OC/EC ratios vs EC concentrations in winter and summer

Semi-Continuous EC/OC measurements at the "Demokritos" urban background site in Athens, Greece

A.A. Karanasiou, K. Eleftheriadis

Institute of Nuclear Technology and Radiation Protection, Environmental Radioactivity Laboratory, National Centre of Scientific Research "Demokritos", 15310 Ag. Paraskevi, Attiki, Greece

Carbonaceous material constitutes a major fraction of atmospheric aerosol. This fraction is thought to be responsible for adverse health effects caused by its reductive potential and the presence of specific organic species. Although a substantial part of carbonaceous material may not be readily identified, two sub fractions of total carbon (TC), namely, elemental carbon (EC) and total organic carbon (OC) have been analytically resolved. It has been observed that particulate organic matter may comprise up to 40% of the atmospheric PM2.5 aerosol mass concentration at European urban and kerbside sites (Putaud et. al., 2004).

The two components, elemental and organic carbon were measured at the "Demokritos" urban background site in the periphery of the Athens Metropolitan area, Greece. A semi-continuous EC/OC analyzer (Sunset Laboratory thermal optical transmittance method) was operated with a sample collection time of 165 minutes followed by a 12 minute analysis period. The samples are collected on quartz filters downstream of a PM2.5 cyclone and a diffusion denuder. Elemental and Organic carbon were determined using the NIOSH Method 5040 protocol.

The origin of carbonaceous particles can be estimated on the basis of the relationship of organic vs elemental carbon, Figure 1. A rather poor correlation between organic and elemental carbon was observed which implied that a variety of sources contributed to the ambient concentrations of carbonaceous particles.

The diurnal variation of the EC and OC concentrations were also studied, Figure 2. As expected, the EC concentrations showed a peak during the morning rush-hour. This result suggests that sources of EC were closely related to motor vehicles, mainly those with diesel engines. In contrast to the diurnal trend of EC, semi-continuous OC slightly increased during night. It seems that sources of OC were less related to traffic sources. Biomass burning, the formation of secondary organic aerosol and long range transport contributed to OC concentration levels.

Thermal EC concentrations determined by the Sunset EC/OC analyzer were compared to Black Carbon, BC measured by means of an Aethalometer. (AE31-Magee Sci.). The relationship between optical and thermally determined black carbon appears

rather complex due to a number of causes ranging from Saharan dust to a variable mixing state of the collected aerosol particles.

An important constituent of carbonaceous material, carbonate carbon (CC) or inorganic carbon causes a positive artifact to organic carbon concentration. Mineral dust and transported desert dust contribute to the presence of atmospheric carbonate. In the used NIOSH methodology carbonate appears as a fourth peak during OC analysis. During this study, carbonate concentrations were determined in order to track dust events.
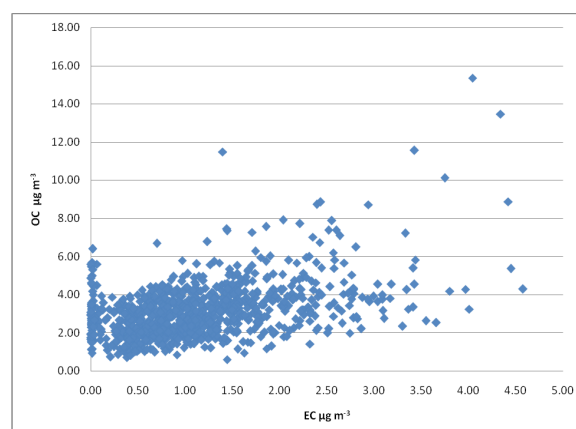
Figure 1. Relationship between OC and EC concentration in PM2.5 samples
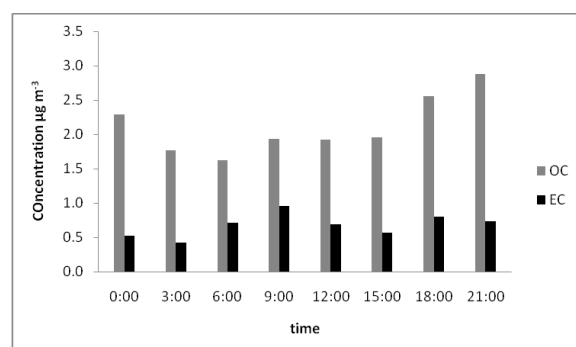
Figure 2. Diurnal variation of the EC and OC concentrations

Putaud, J-P., Raes, F., Van Dingenen, R., et al., (2004). *Atmos. Environ.,* 38, 2579-2595.

Hygroscopicity of combustion aerosols after photochemical aging in a smog chamber

T. Tritscher, E. Weingartner, M.F. Heringa, R. Chirico, M. Gysel, P.F. DeCarlo, J. Dommen, A.S.H. Prevot, U. Baltensperger

Laboratory of Atmospheric Chemistry, Paul Scherrer Institut (PSI), CH-5232 Villigen, Switzerland

Keywords: Hygroscopicity, TDMA, diesel emissions, wood smoke

Combustion emissions are a mixture of black carbon (BC), organics, and other compounds such as inorganic salts. They contribute in several areas to an important fraction of the total aerosol mass. Secondary organic aerosol (SOA) in our atmosphere originates from transformation of primary volatile organic compounds (VOC) over a wide volatility range under the influence of photochemistry. The hygroscopic properties and the contribution to cloud formation of all these complex mixtures are still largely unknown.

The photochemical aging of combustion aerosols was analyzed under almost atmospheric conditions at the PSI smog chamber ($27 \, m^3$) (Paulsen *et al.*, 2005). Different sources of soot aerosols from an Euro 3 diesel passenger car (without particle filter), a log wood oven, and a pellet burner were introduced via heated injection system into the chamber. A hygroscopicity tandem differential mobility analyzer (H-TDMA) measured the hygroscopic properties during photochemical aging, complemented by further aerosol instrumentation. The hygroscopic growth factor (HGF) depends on relative humidity (RH), chemical composition and particle size and is defined as the ratio of the wet particle mobility diameter D to dry diameter (D_0).

As an example, Figure 1 shows the temporal evolution of the particle's HGFs at 90% RH for different log wood burning experiments. HGFs measured during the experiments investigating starting phase emissions showed an increasing trend up to values of about 1.10. Smaller particles (D_0 =

150 nm) showed a slightly higher HGF than the larger ones (D_0 = 250 nm). Particles emitted during the flaming phase exhibited a lower HGF (1.02) and no trend with photochemical aging.

Biomass burning aerosols from a pellet oven showed a completely different hygroscopicity. A more complete combustion process resulted in lower emissions of total organics and soot, whereas inorganic salts became a major component of these aerosols. HGFs up to 1.80 at RH=95% during stable phase burning experiments were observed. Photochemical aging resulted in the formation of additional SOA and the HGF decreased with time to values of about 1.4 (at RH=95%) which were similar to the hygroscopicity of pure biogenic SOA (Duplissy *et al.*, 2008). In some cases an externally mixed aerosol with a less (HGF =1.1) and a more (1.7) hygroscopic mode was observed.

The hygroscopicity of diesel aerosols was generally lower and remained constant with photochemical aging in most experiments (HGF ≈ 1.00 at RH = 90 – 95%) or increased slightly in a few experiments to a HGF of at most 1.06.

Paulsen, D. et al. (2005). *Environ. Sci. Technol.* 39(8), 2668-2678.
Duplissy, J. et al. (2008). *Geophys. Res. Let.* 35(3), 5.
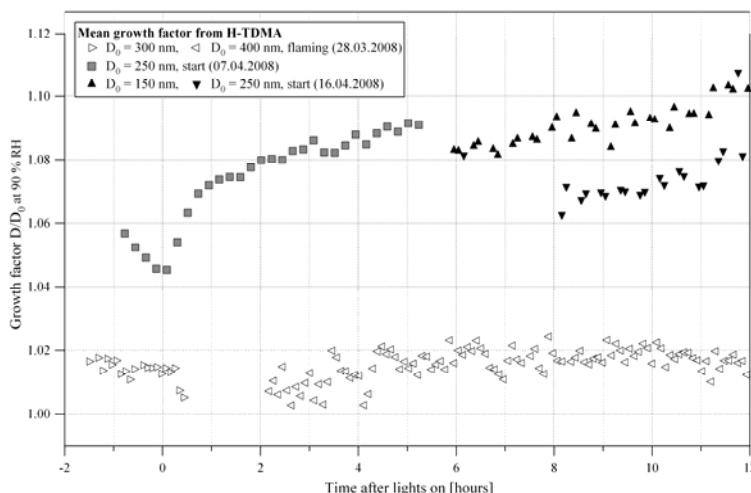
Figure 1. Temporal evolution of the hygroscopic growth factor at 90% RH of combustion particles from a log wood oven during photochemical aging. Particles from the starting phase and flaming phase were investigated.

Using a multi-wavelength Aethalometer to determine the contributions of fossil fuel and biomass burning to aerosols in Ispra, Italy

C. Gruening, F. Cavalli, Dell'Acqua, S. Dos Santos, J.-P. Putaud

European Commission, DG-JRC, Institute for Environment and Sustainability,
Climate Change Unit, T.P. 290, I-21020 Ispra (VA), Italy

Keywords: Absorption, Carbonaceous aerosol, Measurement, Aerosol component composition

Source apportionment of carbonaceous aerosols is important for the development and implementation of action plans for air quality improvements and to assess the impact of carbonaceous aerosols on climate forcing. With the increased use of biomass for residential heating instead of fossil fuel, the contribution of carbonaceous aerosols from biomass burning will certainly increase.

Sandradewi et al. (2008) recently introduced an Aethalometer model to quantitatively attribute the particulate matter contribution from traffic exhaust, i.e. fossil fuel, and wood burning that uses a linear superposition of the different light absorption properties of these sources.

For this study we used a one year time series recorded in 2007 at the EMEP-GAW station in Ispra, Italy (45 °49' N, 8 ° 38' E, 235m asl). The station is located between the Northern edge of the Po valley and the Alpine foothills and it is representative of a semi-rural environment. Due to the topography, this region is characterised by low wind speed conditions. Together with frequent inversion layers near ground in the winter season, the dispersion of pollutants emitted in the region is hindered. This situation results in frequent exceedences of the EU 24 h limit value of 50 μg m^{-3} PM10 (see Van Dingenen et al., 2004).

The aerosol light absorption was measured with a Magee Scientific AE31 Aethalometer at seven wavelengths, i.e. λ= 370, 470, 520, 590, 660, 880, and 950 nm in 10-min cycles during the entire year.

Figure 1 shows the daily averages of the time series of the different aerosol absorptions at the infrared and UV channels of the Aethalometer. Both absorptions follow a seasonal cycle with maximum in winter and minimum in the summer. The cycle for the UV channel though is much more pronounced than the one for the IR.

Looking in figure 2 at the absorption Ångstroem exponent α = -ln(b_{abs}/K) using all seven wavelengths, one observes a very different behaviour in summer and winter. During summer, α lies between 0.8 and 1, whereas during winter it is significantly bigger, averaging around 1.5. Reported values for α vary in the literature between 0.8 and 1.1 for traffic and diesel soot and 0.9 and 2.2 for fresh wood smoke.
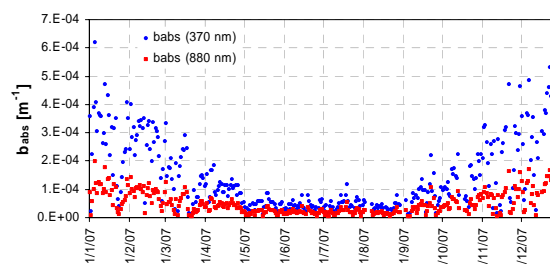
Fig. 1: Daily average of the absorption coefficients for the entire year 2007.

Therefore our findings clearly indicate that during summer time the light absorbing aerosol consists mainly of soot from fossil fuel, whereas in winter also the contribution of aerosols from biomass burning is significant.
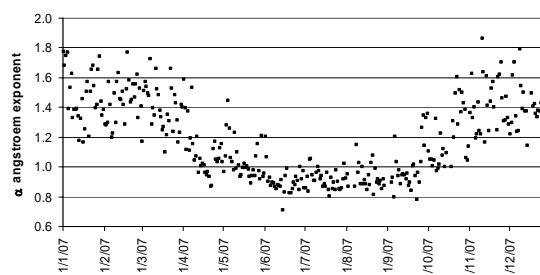
Figure. 2 Daily average of the absorption Angstroem exponent α (λ= 370nm-880 nm) for 2007.

Using the Aethalometer model from Sandradewi et al. (2008), we will present a quantitative estimate of the biomass burning and fossil fuel contribution to the light absorbing aerosol in Ispra.

R. Van Dingenen et al. (2004) A European aerosol phenomenology - 1: physical characteristics of particulate matter at kerbside, urban, rural and background sites in Europe, Atmospheric Environment, **38**, 16, 2561-2577

J. Sandradewi, et al. (2008). Using aerosol light absorption measurements for quantitative determination of wood burning and traffic emission contributions to particulate matter. Environ. Sci. Technol., **42**, 3316-3323.

Organic Compound Characterization and Source Apportionment of Indoor and Outdoor Quasi-ultrafine PM in Retirement Homes of the Los Angeles Basin

M. Arhami[1], M.C. Minguillón[1,*], A. Polidori[1], J.J. Schauer[2], R.J. Delfino[3], C. Sioutas[1]

[1]University of Southern California, Department of Civil and Environmental Engineering, 3620 South Vermont Avenue, Los Angeles, CA 90089, USA
[2]University of Wisconsin-Madison, Environmental Chemistry and Technology Program, 660 North Park Street, Madison, WI 53706, USA
[3]Department of Epidemiology, School of Medicine, University of California, Irvine, Irvine, CA, 92697, USA

* Now at Paul Scherrer Institute, 5232 Villigen PSI, Switzerland

Quasi-ultrafine particulate matter ($PM_{0.25}$) and its components were measured in indoor and outdoor environments at four retirement communities in the Los Angeles basin, CA, as part of the Cardiovascular Health and Air Pollution Study (CHAPS). The present study focuses on the characterization of the sources, organic constituents and indoor and outdoor relationships of quasi-ultrafine PM.

The average indoor / outdoor ratio of most of the measured PAHs, hopanes and steranes were close to- or slightly lower than- 1. The indoor-outdoor correlation coefficients (R) were always positive and for most of these components it was quite high (median R was 0.60 for PAHs and 0.74 for hopanes and steranes). Conversely, indoor n-alkanes and n-alkanoic acids concentrations were generally higher than outdoor levels (in some cases up to ~30 times), and median R values were low (0.27 and 0.19 for n-alkanes and acids, respectively). This suggests that indoor sources influenced the indoor levels of these two important compound classes significantly, whereas indoor PAHs, hopane and steranes were mainly of outdoor origin.

Regarding secondary organic aerosol, generally higher levels were measured indoors than outdoors (up to ~8 times).

The Chemical Mass Balance (CMB) model was applied to speciated chemical measurements of quasi-ultrafine PM for both indoor and outdoor datasets including the following sources: High Duty Vehicles (HDV), Light Duty Vehicles (LDV), Biomass Burning (BB) and Ship emissions. Vehicular sources had the highest contribution among the apportioned sources for both indoor and outdoor particles at all sites (on average 1.67 to 4.86 $\mu g/m^3$ of the quasi-UF mass) (Figure 1). These results highlight the significance of outdoor mobile sources on indoor environments and indicate that particles from mobile sources infiltrate indoors with high efficiency.
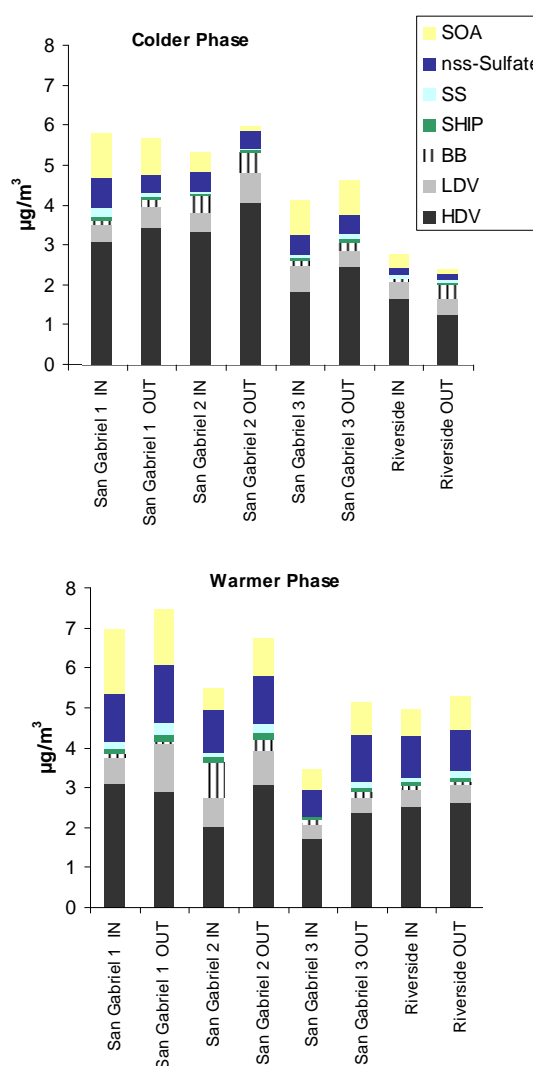
Figure 1. Source apportionment results to quasi-UF PM. SOA: secondary organic aerosol; nss-sulfate: non sea salt sulphate; SS: sea salt.

Characterisation of Diesel Exhaust from Military Vehicles

T.H. Gan[1], P.J. Hanhela[1], W. Mazurek[1], M. Keywood[2] and R. Gillett[2]

[1]Defence Science and Technology Organisation, 506 Lorimer St, Fishermans Bend, Victoria 3207, Australia
[2]CSIRO Marine and Atmospheric Research, Station St., Aspendale, Victoria 3195, Australia

Keywords: diesel exhaust, occupational exposure, PAH(s), particle size distribution, PM_{10}

Introduction

The Australian Defence Force (ADF) operates a large fleet of vehicles fitted with diesel engines of various types and age. They include special purpose vehicles such as tracked (M113A1) and wheeled (ASLAV) armoured personnel carriers with unusual exhaust configurations. This combined with the design of the vehicle and location of personnel can result in atypical exposures to engine exhaust emissions. Thus a study was undertaken to determine the concentrations and characteristics of diesel exhaust particulates (DPM) in the breathing zone of vehicle occupants.

Experimental

Vehicle trials were conducted on test circuits in a rural area, free from vehicular pollution. Continuous measurements of exhaust emissions were made at four locations in the vehicles for PM_{10}, fine particles in the size range 0.3 μm – 20 μm, polynuclear aromatic hydrocarbon (PAH) concentrations, NO_x, CO and VOCs. Quartz and Teflon filter samples were also obtained for PAH and soluble inorganic ion analyses but loadings were insufficient. Mass size distributions using the MOUDI multistage impactor were determined under engine idling conditions.

Results and Discussion

PM_{10} levels were found to vary with passenger location, vehicle speed and load, as expected (CARB 1998). Transient DPM concentrations ranged from 0.05-5 mg m^{-3}.

Mass size distributions, under idling conditions, were bimodal and differed between normally aspirated (M113A1) and turbo-charged engines (ASLAV) as shown in Fig. 1, consistent with findings reported elsewhere (Kittelson 2002). Particle number concentrations generally tracked mass concentrations and varied with time as the engine load and vehicle speed changed (Fig. 2).

PAH measurements (Fig. 3) indicated good correlation with DPM concentrations. DPM levels also correlated with NO_x, CO and VOCs, indicating little interference from road dust.

Progress is underway to determine the size fractionated chemical composition of DPM using the Sioutas design multistage impactor (Misra 2002).

Conclusions

The exposure levels were affected by location of personnel and engine load conditions in both the M113A1 and ASLAV vehicles.
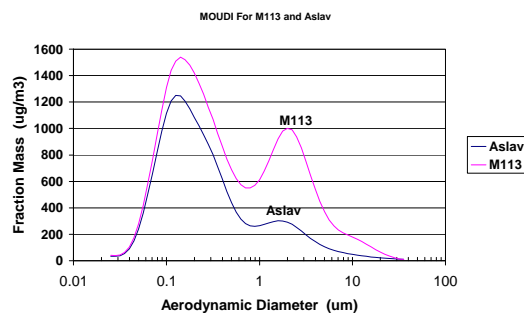
Fig.1. Comparison of MOUDI mass size distributions for the M113A1 and ASLAV vehicles.
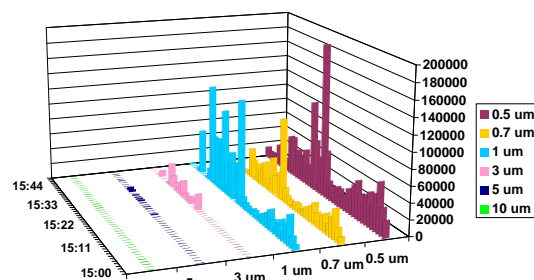
Fig. 2. Dynamic DPM particle size distribution for the M113A1 vehicle.
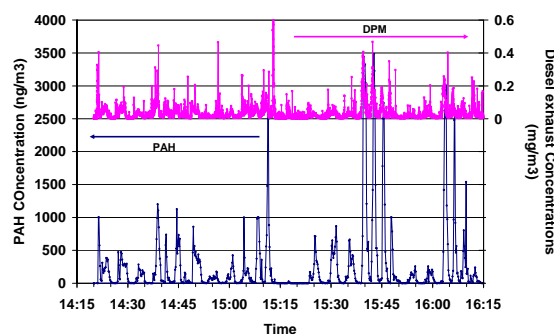
Fig. 3. Correlation of PAHs and DPM for the ASLAV vehicle.

References

CARB (1998). California EPA , Air Resources Board Staff Report, *Proposed Identification of Diesel Exhaust as a Toxic Air Contaminant, Appendix III.ht*tp://www.arb.ca.gov/regact/dieseltac/dieseltac.htm (28 April 1998).

Kittelson, D. (2002). In *CRC Workshop on Vehicle Particulate Emission Measurement Technology,* San Diego, 21 October 2002.

Misra, C., Singh, M., Shen, S., Sioutas, C. & Hall, P. (2002). *J. Aerosol Sci.,* 33, 1027-1047.

One-year record of carbonaceous aerosols from urban location (Kanpur) in the Indo-Gangetic Plain (IGP)

Kirpa Ram[1], M.M. Sarin[1] and S.N. Tripathi[2]

[1]Physical Research Laboratory, Ahmedabad-38009, India
[2]Department of Civil Engineering, Indian Institute of Technology, Kanpur-208016, India
Keywords: Elemental carbon, Organic carbon, Urban aerosol.

The Indo-Gangetic Plain (IGP), extending from 22-31 °N and 74-91 °E, is one of the most polluted regions in northern-India with characteristic emissions from small scale industries, vehicular traffic and biomass burning (woodfuel and agriculture-waste) (Tare et al, 2006; Nair et al, 2007). The entire region experiences extreme climate changes, with severe cold (temperature dipping as low as 0 °C), fog and haze conditions during winter season (Dec-Feb). As a result, dispersion of pollutants is confined within the Boundary Layer (~ 500-800 m) during wintertime. During summer months (Apr-June), temperature reaches as high as 45 °C at certain Plain regions; and emission from fossil-fuel combustion is dominant compared to biomass burning. With a view to study temporal variability of anthropogenic species, a systematic and continuous measurements of organic carbon (OC), elemental carbon (EC) and water-soluble organic carbon (WSOC) have been made from an urban location, Kanpur (26.5 °N, 80.3 °E, 142 m amsl) in the IGP. The details of measurement protocol are described in our recent publication (Ram et al. 2008).

Table 1. Seasonal variation in abundances of carbonaceous species and particulate matter (PM).

Seasons	TSP $\mu g\ m^{-3}$	OC $\mu g\ m^{-3}$	EC $\mu g\ m^{-3}$	WSOC $\mu g\ m^{-3}$
Summer	141±82	13.4±4.3	2.1±1.9	6.5±0.9
Winter	194±60	39.9±16.6	5.1±1.5	12.0±6.9
Post-Monsoon	146±41	29.8±9.5	4.1±1.9	-

The OC, EC and WSOC abundances at Kanpur are about a factor of two higher (Table-1) during winter (Dec-Feb) and post-monsoon (Sept-Nov) compared to those during summer months. Total carbonaceous aerosols (TCA=1.6*OC+EC) contributes ~20% of particulate matter (PM) during summer and ~35% during winter and post-monsoon. The OC and EC abundances exhibit a large scatter, indicating emission from different sources (Fig.1). The OC/EC ratio shows large variability (Av: 7.4±3.5; range: 2.4 to 22.0). The higher OC/EC ratios are associated with high abundance of OC, derived from biomass burning sources, during wintertime and lowest, OC/EC ratios are recorded in the month of March (Fig. 1). The month of March is characterized as a transition period between winter and summer in the IGP; the strength and nature of emission sources changing from biomass burning to fossil-fuel (mainly from vehicular emissions) and hence, resulting in lower OC/EC ratios. The relatively higher WSOC/OC ratios during summer (0.49±0.13) are attributable to enhanced formation of secondary organic aerosol (SOA). The large temporal variability observed in the abundance pattern of OC and EC, due to the seasonal shift in the emission sources, has implications to changes in the physical and optical properties of aerosols within the IGP as well as atmospheric radiative forcing on a regional scale.
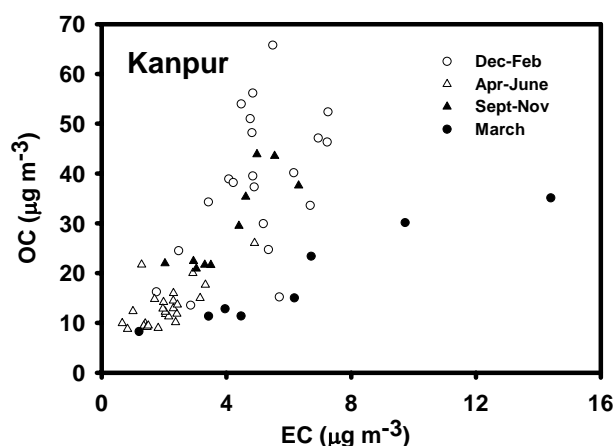
Figure 1. Scatter plot between OC and EC at Kanpur. The relatively high EC abundances (and low OC/EC ratio) obtained during March are also shown.

Tare V., et al. (2006). *J. Geophysical Research-Atmosphere,* doi: 10.1029/2006JD007279
Nair V.S., et al. (2007). *J. Geophysical Research-Atmosphere,* doi: 10.1029/2006JD008099
Ram K., et al. (2008). *Atmospheric Environment,* 42, 6785-6796.

Compensation of Aethalometer black carbon data for the optical loading effect

Jeong-Hoon Jung, Seung Shik Park[*] Sung Y. Cho, and Seung J. Kim

Department of Environmental Engineering, Chonnam National University, 300 Yongbong dong, Buk-ku, 500-757, Gwangju, Republic of Korea

[*]Author to whom correspondences should be addressed: Tel: +82-62-530-1863 Fax: +82-62-530-1859; e-mail: park8162@chonnam.ac.kr

Keywords: Black carbon, optical loading effect, urban area, seasonal variation

Black carbon (BC) concentrations were measured with an Aethalometer (AE-16, 880 nm) at time interval of 5-min at an urban site for one year. Twenty-four hour filter-based integrated measurements of PM2.5 particles were also made at the same site during the winter and summer to test any optical loading bias in the Aethalometer BC results. Monthly average BC concentration was higher in winter than in summer, possibly due to increase in emissions from energy consumption and traffic congestion, and poor dispersion in winter. Also temporal cycles of BC indicate that short-term transient spikes were common, occurring primarily during the morning and evening rush-hour periods.

The BC reported from the Aethalometer show obvious discontinuities at the filter tape advances, indicating a rise in the apparent BC concentrations after the filter tape advances. In the Aethalometer measuring BC concentration in ambient air it is assumed that attenuation (ATN) is linearly proportional to loading of aerosol black carbon. However, recently it has been reported that as the loading of particles on the filter increases, the existing particles may shadow the freshly-collected ones (Hansen *et al.*, 2007; Virkkula *et al.*, 2007). If the non-linear effect between the ATN and BC data is present, the reported BC data may be influenced by the overall loading of BC. This would be seen as a reduction in BC result as a function of ATN. In this study we used a simple method to decide if there was (or was not) an effect on the Aethalometer BC data according to the loading of the filter spot. Average BC in each range of ATN was calculated every month. Figure 1 shows variation of average BC with ATN in June and December. If there is a consistent spot loading effect, it will be seen as a consistent change in ATN versus average BC. The amount of effect is described by the "k" factor proposed by Virkkula *et al.* (2007). Average BC in June was almost constant with ATN value, while a consistent decrease in average BC with increasing ATN was found in December. The k factor according to the statistical fit in June and December was 0.04 and 3.34, respectively, implying the optical loading effect is not seen at all times. It seems that the aerosol collected in December was fresh or dominated by immediate local sources, while the aerosol particles in June was aged in the atmosphere for a long time or

strongly mixed with optically scattering species. A loading compensation to make an adjustment to raw BC data was performed according to a single parameter non-linearity model with the loading effect of k value every month. Our results show that loading compensation process has taken account of the effects of the filter tape, and the simple linear model gives an adequate explanation.
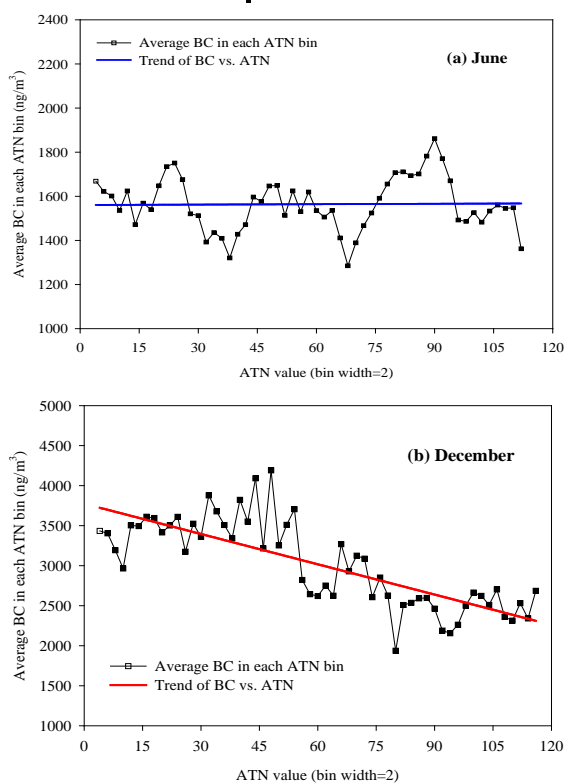
Figure 1. Variation of average BC with each range of ATN during June and December.

Hansen *et al.* (2007). In *Proc.* 5th Asian Aerosol Conference, Kaohsiung, Taiwan.

Virkkula A. *et al.* (2007). *J. Air & Waste Manage. Assoc.*, 57, 1214-1222.

Water soluble organic carbon in fine particulate matter measured at an urban site during two different seasons

Seung Shik Park, Dai Hoon Kim, Sung Y. Cho, and Seung J. Kim

Department of Environmental Engineering, Chonnam National University, 300 Yongbong dong, Buk-ku, 500-757, Gwangju, Republic of Korea

Keywords: Fine particulate matter, water-soluble organic carbon, OC/EC ratio

In recent years, much research interest has been focused on atmospheric carbonaceous particles due to their influence on climate and adverse health effects. The current understanding of the atmospheric carbonaceous particles describes their water-soluble organic carbon (WSOC) fraction as a complex mixture of very soluble organic compounds, slightly soluble organic compounds, surfactants, and some undetermined macromolecular compounds, the chemical determination of which still poses many problems (Sullivan & Weber, 2006). In order to better understand the characteristics of the WSOC, daily $PM_{2.5}$ (particles with aerodynamic diameter less than 2.5 μm) aerosol samples were collected during the winter (Dec. 12, 2007- Feb. 23, 2008) and summer (June 1-Aug 22, 2008) intensive periods at an urban site of Gwangju, Korea. Daily size-fractionated aerosol samples were also collected for WSOC analysis. The samples from the $PM_{2.5}$ samplers were analyzed for organic and elemental carbon (OC and EC), and WSOC contents. WSOC was also separated into two fractions, i.e., hydrophobic and hydrophilic fractions, using XAD solid phase extraction technique, which was adapted from methods developed to separate humic and fulvic acids in aqueous samples (Thurman & Malcolm, 1981). Group-separated fractions were quantified with Total Organic Carbon (TOC) analyzer.

Concentrations of OC and EC were observed to have 4.5 μg/m^3 (0.9-15.7 μg/m^3) and 1.8 μg/m^3 (0.3-7.0 μg/m^3), respectively, during the winter, and 5.0 μg/m^3 (1.4-17.8 μg/m^3) and 1.6 μg/m^3 (0.5-3.1 μg/m^3) during the summer. As expected, higher OC/EC and WSOC/OC ratios were found in summer than in winter (Figure 1). The higher WSOC/OC slope in the summer than in winter suggests that secondary organic aerosol formation processes produce significant amounts of WSOC during the summer. Information on the WSOC partitioning between its primary and secondary fraction can be derived by means of the EC tracer method. Secondary WSOC concentrations estimated using EC tracer method accounted for on average 11.2% (0-51.4%) and 18.9% (0-62.5%) of the measured WSOC concentrations in winter and summer in Gwangju.

Results of WSOC fractionation suggests that processes, such as secondary organic aerosol (SOA) formation, which is likely more vigorous in the summer, produce significant amounts of hydrophilic compounds. Hydrophilic fraction of OC may be even more significant during period of active SOA production. There was a general progression of increasing ratios of WSOC to OC and hydrophilic WSOC to OC from winter to summer.
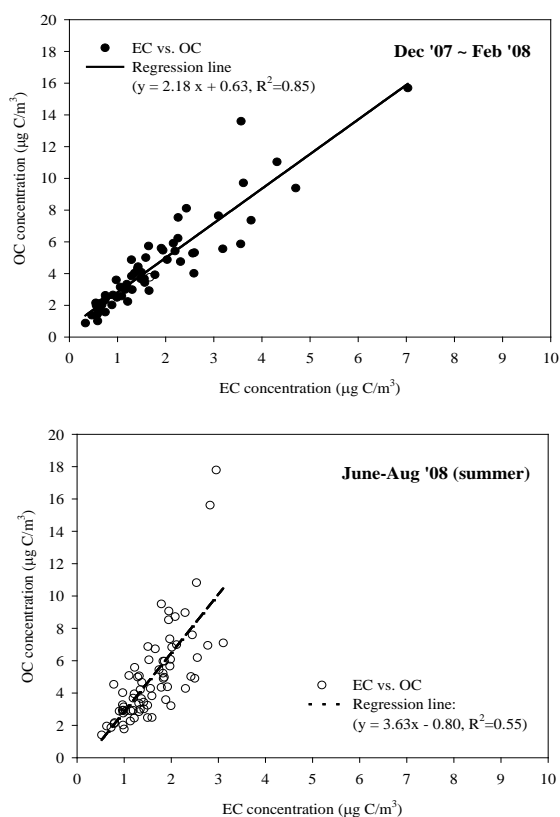
Figure 1. Relationship between OC and EC concentrations during the winter and summer.

Sullivan, A.P. & Weber J.R. (2006). *J. Geophysical Research*, 111, D05314.

Thurman, E.M., & Malcolm, R.L. (1981). *Environmental Science & Technology*, 15, 463-466.

Allergenic *Asteraceae* in urban air: DNA- based analysis and relevance for human health

I.Germann[1], J.Froehlich-Nowoisky[1,2], U. Poeschl[1], V. R. Després[1,3]

[1] Biogeochemistry, Max Planck Institute for Chemistry, P.O. Box 3060, D-55020 Mainz, Germany
[2] Geosciences, Johannes Gutenberg University, Joh.-Joachim- Becher-Weg 21, D-55128 Mainz, Germany
[3] General Botany, Johannes Gutenberg University, Saarstraße 1, D-55099 Mainz, Germany

Keywords: *Ambrosia artemisifolia,* DNA, Bioaerosols

Ragweed (*Ambrosia artemisifolia*) and mugwort (*Artemisia vulgaris*) are highly important allergenic weeds belonging to the Asteaceae plant family (Wopfner et al., 2005). Their pollen are one of the main causes of allergenic reactions accompanied by asthma and other severe health problems in late summer and autumn. While mugwort is a native plant in Europe, ragweed reached Europe e.g. by bird seeds as a neophyte from North America about a hundred years ago and spreads rapidly into new areas of central and southern Europe. It is now abundant in the Rhone valley (France), northern Italy, and eastern parts of Austria, Hungary, Croatia and Bulgaria (D' Amato et al., 1998). A small ragweed plant can produce up to 3000 seeds per year, whereas large plants produce up to 62,000 seeds, causing highest concentrations of ragweed pollen in the air in August and September (800 grains/m^3) (Gadermaier et al., 2004).

As the spread of ragweed has been observed in Germany during the last years, we were interested to see if the DNA of ragweed in air and thus the number of bioaerosols originating from these allergenic plants, also increased during the past years. Mugwort DNA was studied as a control.

As genetic analysis methods have been shown to be a good strategy for analyzing bioaerosols (Després et al 2007), filter samples were collected with a High Volume Sampler separating fine and coarse particles (aerodynamic cut-off diameter ~3 µm) for a period of three years (2006 - 2008) in Mainz, Germany. The samples were analyzed for the presence of ragweed and mugwort deoxyribonucleic acid (DNA).

Real Time PCR was used to quantify the amount of ragweed and mugwort DNA mainly in the pollen seasons during this three year period. While the abundance of mugwort DNA stayed constant in this measurement period - only correlating with the climate conditions during the flowering period - we found a steady increase of the ragweed pollen during the last 3 years, which might be associated with the constant spread of *Ambrosia artemisifolia* over Germany in the course of the last years.

There is a need for a more comprehensive and longer study analyzing the spread of ragweed accompanied by the increase of pollinosis in late summer and autumn in Germany.

Still, the constant increase of ragweed DNA in air illustrates the ongoing expansion of this highly allergenic plant and encourages to closely observe this phenomenon in future for ensuring human health.

D'Amato G., Spieksma F.T., Liccardi G., Jager S., Russo M., Kontou-Fili K., Nikkels H., Wuthrich B., Bonini S. (1998). Pollen-related allergy in Europe, *Allergy*, 53, 567–578.

Després V.R., Nowoisky J.F., Klose M., Conrad R., Andreae, M.O., Pöschl U. (2007). Characterization of primary biogenic aerosol particles in urban, rural, and high-alpine air by DNA sequence and restriction fragment analysis of ribosomal RNA genes, *Biogeosciences*, 4, 1127–1141.

Gaderrmaier, G., Dedic, A., Obermeyer, G., Frank, S., Himly, M., Ferreira, F. (2004). Biology of Weed Pollen Allergens. *Current Allergy and Asthma Reports,* 4, 391-400.

Wopfer, N., Gadermaier, G., Egger, M., Asero, R., Ebner, C., Jahn-Schmidt, B., Ferreira, F. (2005). The spectrum of Allergens in Ragweed and Mugwort Pollen. *Int Arch Allergy Immunol*, 138, 337-346.

T06 Electrical effects

Controlling progeny droplets emitted during the Coulombic fission of a charged drop

H. H. Hunter and A. K. Ray

Department of Chemical and Materials Engineering, University of Kentucky
Lexington, KY 40506-0046, USA

Keywords: charged particles, electrospray, nanoparticles, levitation, light scattering

When the charge on a drop reaches a level, known as the Rayleigh limit, the drop becomes unstable and emits a fraction of its charge and mass in the form of progeny droplets, a process referred to as the Coulombic fission. Although the Rayleigh limit has been confirmed experimentally, two key questions about the fission process remain unresolved. First, what factors control charge and mass losses from a drop, and second, how much charge a progeny droplet carries. The size and number of progeny droplets produced at fission are directly related to the answers of these questions. Empirical models based on the observations on elecrosprays suggest that the electrical conductivity of a drop plays a dominant role in the fission process, but can not explain experimental observations. We have investigated the fractional charge and mass losses at an instability induced breakup, and the factors that control the characteristics of the progeny droplets. In this study we demonstrate that the size and charge-to-mass ratio of progeny droplets can be controlled through the addition of a solute that dissociates into ions.

Experiments were conducted on single charged droplets suspended in an electrodynamic balance, and a high precision light scattering technique based on optical resonances was used to determine the size and the size change of a droplet at a charge instability induced breakup. The charge level and the charge loss at a breakup were obtained from the dc voltages required to gravitationally balance the droplet prior to and following the breakup. We have examined droplets of diethylphthalate (DEP) and dimethylphthalate (DMP) that were doped with either one of the two ionophores: tridodecylmethylammonium chloride (TDMAC), and tridodecylmethyl-ammonium nitrate (TDMAN), or an ionic liquid: 1-ethyl-3-methyl-imidazolium dicyanamide, [EMIM][N(CN)2]. The dissociation of each of these ionic compounds produces two singly charged ions of opposite signs. The concentration of ions in a bulk solution at a given concentration of an ionic compound, and the mobilities of the ions were established from the measurements of conductivities at various concentrations of the ionic compound. To determine the concentration of the ionic compound as a function of size in an evaporating droplet we assumed that the amount of the ionic compound remains constant at the initial known value, that is, no losses occur through evaporation and only negligible losses occur during a fission.

Experimental data show that during fission the mass loss from a drop decreases, while the charge-to-mass ratio of progeny droplets increases as the ion concentration in the drop increases. The results suggest that non-uniform ion distributions created by the presence of charge in a drop play a major role. We show that the charge-to-mass ratio of progeny droplets is proportional to the conductivity, at the surface of the mother drop, but not the conductivity of the bulk solution that can generate the drop. We have calculated the surface conductivity from the mobilities of ions and their concentrations at the surface, determined by solving the Poisson-Boltzmann equation. By minimizing the Gibbs free energy change associated with fission we deduce that a progeny droplet carries 50% of the Rayleigh limit charge, and its size varies inversely to the surface conductivity raised to the power of 2/3. The results of this study suggest a way of synthesizing tailored nanoparticles from charged drops by controlling the fissions through the drop size and the ion concentration level.

Observation of formation of secondary plasma spheres in water aerosol-plasma clouds by electric discharge spraying

M. V. Jouravlev[1] and A. V. Tovmash[2]

[1]Raymond and Beverly Sackler Faculty of Exact Sciences, School of Chemistry, Tel-Aviv University, 69978, Ramat-Aviv. Israel.
[2]State Scientific Center of Russian Federation, Institute of Physical Chemistry named after L.Ya. Karpov, 103064, Vorontsovo pole 10, Moscow, Russia.

Keywords: electric discharge, plasma, water aerosols, ball lightning

The observation of the secondary spherical structures of the aerosol-plasma clouds generated by the electrical discharge is made. The spherical water cloud as a secondary structure consistent with the charged aerosol particles in the plasma cloud is produced in an underwater discharge. This involves igniting a short high-voltage discharge in a water tank, when it decays a plasma jet then emerges from the surface. Flashover from the water enables the current to enter the clay tube, where it causes the water contained there to evaporate. After the current pulse a luminous second plasmoid consisting of charged water particles appears. Spheres continue to be visible about 800 milliseconds during the current has been decayed and the energy input is thus cut off, really be quenched after a few milliseconds at most.

The plasma glows very brightly, although the secondary plasmoids appear to be rather cold. It is measured that the lifetime of the dissipation of the secondary spherical aerosol-plasma particles structure is 0.87 sec. The measured diameter of the sphere is 3 cm.
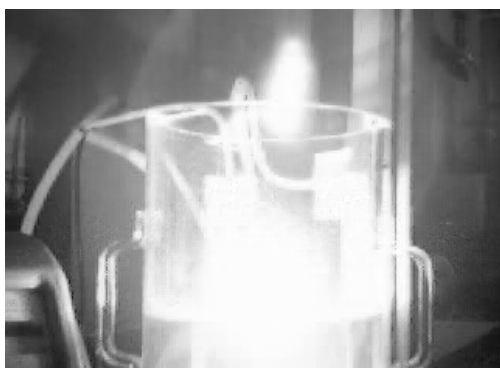
Fig.1. The initial stage of electric discharge under water surface.

The laboratory facility for creating glowing flying plasmoids is described (A.I Egorov, 2004) which allows a number of experiments to be performed to study the main properties of the ball lightning (A.I Riabzev, 1987). We develop new set up for studding the low intensity electric discharge spraying for the formation of charge aerosol particles. Figs 1-3 show the rare phenomena of the temporal behavior of the secondary spheres in initial aerosol-plasma clouds. The pictures were made by digital camera. This research can help new understanding of the nature of ball lightning and coagulation effect of charge aerosol particles.
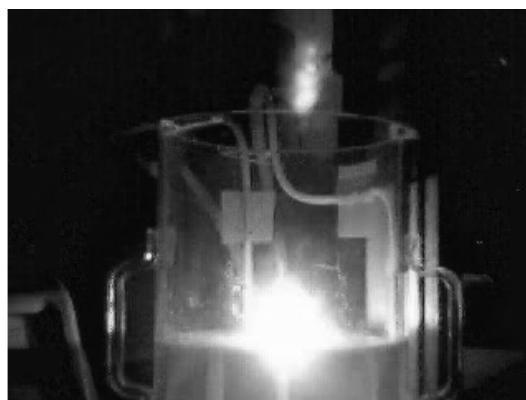
Fig2. The stage of the aerosol-plasma clouds spraying by electric discharge. It is shown the formation of the secondary plasma spheres after 0.3 s (Fig.1).

Fig. 3. The stage of formation of four plasma spheres from electric discharge after 0.07 s. (Fig.2)

A.I. Egorov, S.I. Stepanov, G.D. Shabanov (2004). Laboratory demonstration of ball lightning, Physics-Uspekhi, 174, Issue 1, 107-109
A.I. Riabzev, I.P. Stakhanov (1987). Technical Physics, 57. Issue 8, 1583-1587

The drained DBD electrode as a charger for highly concentrated aerosols

M. Wild, J. Meyer and G. Kasper

Institut für Mechanische Verfahrenstechnik und Mechanik, Universität Karlsruhe (TH),
76131 Karlsruhe, Germany

Keywords: electrical effects, dielectric barrier discharge, charge measurement, charged particles.

This work deals with a concentric drained Dielectric Barrier Discharge (dDBD) electrode arrangement (see Figure 1). The central electrode consists of 3 concentric layers: a metallic core which the excitation voltage is applied to, a dielectric layer and a conductive winding, which acts as the drainage electrode. The central electrode is placed in a grounded cylinder of stainless steel. At the surface of the dielectric a surface plasma is ignited and a superposed electric field due to the drainage voltage drags ions of the selected polarity into the surrounding charging region. The dDBD concept is an evolution of the Masuda boxer charger (Masuda 1978).
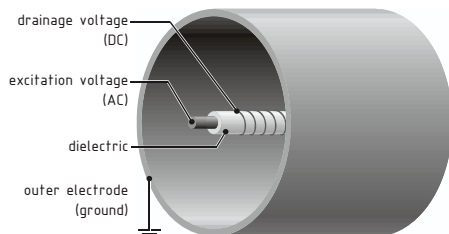
Figure 1. Schematic of the dDBD charger

The dDBD electrode is used for charging aerosols under particle-space-charge-influenced conditions. Regular corona discharges, for example wire-tube or tip-plate configurations, suffer under these conditions from heavy operational disturbances (corona quenching). The dDBD electrode uses internal excitation for the charge emission. Additionally, the core is shielded by the virtual equipotential surface of the applied winding. Therefore, the field conditions in the charging region surrounding the central electrode are only of minor importance for the charge emission behaviour of the electrode.

Due to the advantage of a forced emission of charges, the dDBD technique was chosen for the investigation of the diffusion charging of highly concentrated (HC) aerosols. The dDBD is compared to a wire electrode which acts as the reference system because it's charging behaviour is well known. Therefore the dDBD had to be calibrated to behave like a wire electrode regarding its charging result at a given applied field strength. This calibration is done with an aerosol of low concentration (LC) without the influence of particle space charge. NaCl aerosol was generated and monodisperse fractions of neutral particles were used for the charging experiments. The loss and average particle charge of the wire was analysed as plotted in figure 2 (✦). Afterwards several wire data points were selected (◇) and the applied field strength was calculated. To operate the

dDBD at the same conditions its average field strength was simulated by FEM simulations (Comsol Multiphysics). Appropriate operational parameters for comparable field strengths were selected. Using those parameters, Experiments under variation of the excitation frequency of the electrode (0,1 - 5 kHz) were conducted (○). Lower frequencies resulted in lower average particle charges and hence in lower loss inside the charger. Increasing the frequency delivered a variety of selectable charge/loss data pairs. The charging behaviour of the wire electrode regarding loss and average particle charge at a given mean radial electric field strength can thus be imitated by the dDBD using different excitation frequencies.
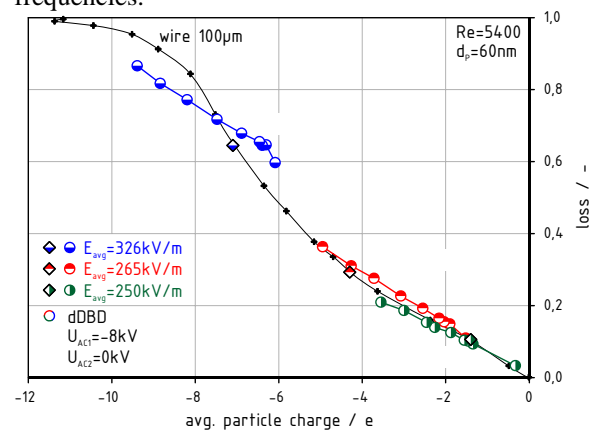
Figure 2. Selected 100µm wire electrode 60 nm data points (◇) of distinctive field strengths and the corresponding charging results for the dDBD (○) with varied excitations frequency

It could be proven that the dDBD electrode is comparable to a wire electrode and it is able to imitate the charging behaviour at LC conditions. Hence the operating range of the charging setup used is extended to HC conditions with pronounced particle space charge effects. Using a novel condensation aerosol source capable to deliver aerosols with number concentrations $> 10^9 \, cm^{-3}$ the diffusion charging in highly concentrated aerosols can be investigated. By comparing dDBD and corona wire data, it is possible to separate the influence of particle space charge effects on ion transport and ion generation.

Masuda, S., M. Washizu, Mizuno A., and Akutsu K. (1978), *Conf. Rec. IEEE/IAS Ann. Meeting Vol. 1B*, pp. 16-22

Atmospheric pressure production of Carbon nano-particles by Dielectric Barrier Discharges

A. Elcik[1], N. Jidenko[2], A.P. Weber[1] and J-P. Borra[2]

[1] Institut für Mechanische Verfahrenstechnik, TU Clausthal 38678 Clausthal-Zellerfeld
[2] Laboratoire de Physique des Gaz et des Plasmas (UMR 8578 CNRS –Univ. Paris Sud Orsay, F-91405)
Equipe Décharges Electriques et Aerosol, SUPELEC, F-91192 Gif sur Yvette Cedex, France

Keywords: Plasma, Dielectric Barrier Discharges, nanoscale carbon particles, Production.

Controlled size nanoparticles are mainly produced by nucleation. The spark generator is commonly used for the production of high concentration of 50 to 200 nm aerosol. The first step is the vaporisation of both electrodes, producing hot vapours that nucleate while cooled down in the surrounding gas at ambient temperature. Then coagulation of high densities of primary nanoparticles leads to agglomerates of 50 to 200 nm (JH Byeon et al. 2008). However, there is a growing demand to produce particles smaller than 50 nm for nano-material production, tools calibration and fundamental study of properties of these nano-particles to evaluate the dispersion and the impacts of these new materials on health of people working in production places as well as in the environment. To do so, we have proposed and tested to reduce the energy of the discharge filament, using dc streamers and prevented sparks produced in point-to-plane geometries polarised in dc or micro-discharges produced in ac-Dielectric Barrier Discharges (DBD), all working at atmospheric pressure (Borra et al., 2008).

The paper focuses on the production of nanoparticles smaller than 50 nm produced by low energy micro-discharges filaments produced in DBD, working at atmospheric pressure (Petit et al., 2002). Here, Carbon nano-particles were produced by using a carbon coating on one of Al_2O_3 dielectric surfaces.

Peak-to peak voltage between 14 and 20 kV at 70 kHz was used to polarise the electrodes covered with an Al_2O_3 dielectric platelets (1mm thick with 5mm^2 area), spaced by a gap of 1mm. The section of the gap of 3mm^2 was fed with Nitrogen flow rate of 0.3 lpm. The so-produced particles were then characterised by post-discharge size distribution performed by classical SMPS with a cutting diameter of 5 nm. Besides, based on the low pressure impaction principle (Abouali and Ahmadi, 2005) was also used for collection of nano-particles down to 2nm sizes for TEM and chemical analysis.

Figures 1 presents the evolution of the size distribution of so-produced Carbon nano-particles.
At first, it has to be underlined that atmospheric pressure Discharges with low energy filaments (from 1 to 10 µJ per filament) allow one to produce nano-particles with an unimodal size distribution with a mean diameter of 15 nm. EDX analysis confirmed that the nanoparticles consisted of carbon. Hence, these results confirm that smaller particles are produced by DBD than with spark generator, as expected from the reduced energy per filament.
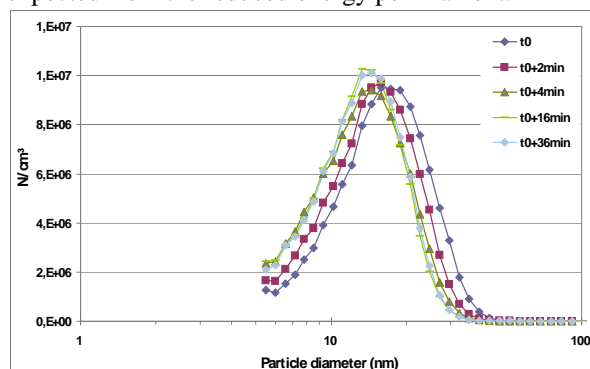
Figure 1. Evolution of the size distribution of nano-particles produced by atmospheric pressure DBD.

After a couple of minutes, the unimodal size distribution with a mean diameter of 15 nm does not evolve anymore for a period depending on the coating thickness. In our experiment with a 1µm thick Carbon coating, the size distribution was constant up to an hour. This initial evolution mainly consists in reducing the mean diameter and increasing the number of smaller particles which probably arises from higher initial vapour fluxes producing higher densities of primary nano-particles, coagulating faster, when the discharge initiate on surface defaults reinforcing the electric field and the energy per filament, than a couple of minutes later, when the surface defaults have been eroded by the discharge.
This process seems promising for the production of nano-particles with any defined composition related to the dielectric coating vaporised or sputtered by the discharge filament from the surface. Moreover, as the initial vapour flux is related to the energy deposited on surface by filament discharge, tunable size can be achieved by controlling the energy per filament.

Borra et al.(2008) *Plasma Phys. CF* **50** 124036.
JH Byeon et al, (2008) *JAS* **39-10** 888-896
Petit M et al (2002) *Rev.Sci. Instrum.* **73** 2705–12
O.Abouali, G.Ahmadi (2005) *J. Nanopart. Res.* **7**: 75–88

Aerosol charge distributions in Dielectric Barrier Discharges

N. Jidenko, E. Bourgeois and JP. Borra

Laboratoire de Physique des Gaz et des Plasmas (UMR 8578 CNRS –Univ. Paris Sud Orsay, F-91405)
Equipe Décharges Electriques et Aerosol, SUPELEC, F-91192 Gif sur Yvette Cedex, France

Keywords: electrical discharge, aerosol charging, electrical mobility.

Aerosol particle charging is involved in many scientific and industrial applications such as electrostatic precipitation, coating, post-production particle assembly, particle self-repulsion to preserve high interfacial areas, neutralization to prevent dust explosion, coulombian agglomeration of bipolar aerosols and measurements based on electrostatic techniques. Depending on the application, high charge level, or high particles penetration through the charger, control charge distribution, a mix of these criteria is required. Non-thermal Atmospheric Pressure Electrical Discharges are an efficient way to charge particles (Borra 2005).

Charging mechanisms by collection of ions and related charging laws are defined and have been validated in quasi-stationary ions densities, especially in DC corona discharges (Fuchs 1963). Dielectric Barrier Discharges (DBD) are constituted of two electrodes that are separated by a gas gap spacing with at least one dielectric material in the gap. The dielectric barrier prevents arc formation but involves an alternative polarization of the system (typically a few kV at 50 Hz–1 MHz). In air, at atmospheric pressure, DBD occur as thin and brief Filaments Discharge (a few 10's of μm, a few 10's of ns) homogeneously distributed over the dielectric surface (Petit et al. 2002). Thus, DBD produce high transient charging conditions (bipolar ions densities and electric field) in which particles charging is investigated.

Post discharge ions densities and mobilities as well as particle charge distributions and losses are investigated versus plasma and hydrodynamics parameters with monodisperse aerosol from 20 nm to 900 nm injected in the DBD.

Table 1. Post DBD positive and negative ions mobilities at 3 lpm.

Electrode temperature (°C)	Positive ions mobilities ($cm^2.V^{-1}.s^{-1}$)	Negative ions mobility ($cm^2.V^{-1}.s^{-1}$)
30-90	0.96/1.41/1.79	1.78
90-160	1.41 / 1.79	0.83/0.9/1.03/ 1.15/1.36

Table 1 shows the peaks position of mobility spectra. Positive ions are independent of gas temperature whereas negative ions depend on the nature of gaseous species produced by the discharge. Indeed at low temperature ozone is the predominant species and above 90°C nitrogen oxides are predominant.
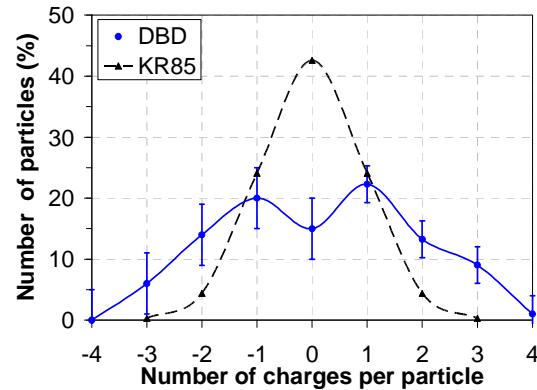
Figure 1. Charge distributions of 102 nm latex particles in Kr85 and 20 kHz DBD at 20 kV with a gas flow rate of 0.3 lpm with 0.6 s before analyses.

Figure 1 proves that particles are charged of both polarities due to ion persistence in the discharge gap induced by dielectric surface polarization. The net charge is slightly positive as a result of higher electrical mobility of negative charges (electrons and negative ions are better collected on the dielectric surfaces than positive ions). Though bipolar charging conditions, charge distributions differ from those obtained in radioactive neutralizer (KR[85]).

Final charge level of particles depends on the different positive and negative ion densities they cross. If charge level acquired by the particle inside the DBD could reach higher level than those measured, charge distributions tend to Boltzmann distribution due to homogeneous bipolar ions density downstream the charger.

As a conclusion, discharge filament can be considered as a local brief and confined ion/electron source, leading to transient charging conditions i.e. in varying electric field and charge densities.

At last, the frequency of the applied voltage controls the amplitude of the oscillating particle trajectory and can be adjust to limit electro-deposition in the DBD. DBD are thus an alternative to corona discharge, preventing the oxidation of metal electrodes inducing particle production and discharge evolution in time.

Petit M et al. (2002) *Review of scientific instruments* **73 (7)**, 2705-2712

Fuchs N A (1963) *Geofisica Pura e Applicata* **56 1,** 185-193

Borra JP (2005) *J. Phys. D : Appl. Phys* **39**, 19-54

Influence of gas velocity, particle concentration and electrode geometry on corona discharge characteristics in small electrode gaps

A. Bologa, H.-R. Paur, K. Woletz

Institut für Technische Chemie, Forschungszentrum Karlsruhe, Postfach 3640, 76021, Karlsruhe Germany

Electrostatic precipitators (ESPs) are one of the most effective control devices for fine particles from exhaust gases. But ESPs often suffer with clogging problems and corona suppression at high particle concentrations.

The influence of particle concentration and ESP operation conditions on the corona discharge characteristics and clogging problems in the ionizing stage with small electrode gap was studied. The ionizing stage consisted of different grounded nozzles with inner diameter from 16 mm to 80 mm and high voltage (HV) needle or star-shaped electrodes. Investigations were carried out with Al_2O_3 particles (gas temperature $T_g=90\text{-}120°C$), oil mist (atmospheric conditions), tar (humid air, $T_g=40\text{-}50°C$) and H_2SO_4, HCl, $(NH_4)_2SO_4$ and NH_4Cl aerosol in wet gases, $T_g=40\text{-}80°C$. The scope was to minimize the clogging of the ionizing stage and to increase the stability of ESP operation.

The tests with Al_2O_3 particles show, that at high particles concentrations the loading of the nozzles (Fig.1) provokes the spark-over discharges which together with back corona decrease ESP collection efficiency. With increase of gas velocity in the nozzles over 15 m/s the electrode gap remains practically clean and the frequency of the spark-over discharges decreases.

Fig.1 The ionizind stage with small electrode gap loaded with Al_2O_3 particles

A pilot ESP was used for treating of water vapour saturated off gas with tar particles at flow rate 250-500 m^3/h and particle mass concentration up to15 mg/m^3. The current-voltage characterisctics of the ionizing stage show a strong decreasing of the spark-over voltage after 8 hours of operation (Fig.2). The descrease took place due to loading of the nozzles with sticky particles. The sharp points on the loaded surface provoked spark-over discharges and

decreased the stability of ESP operation. The loading was observed in the electrode gap and downstrean part of the nozzles. The particle number concentration during the test was below the level of corona suppression.
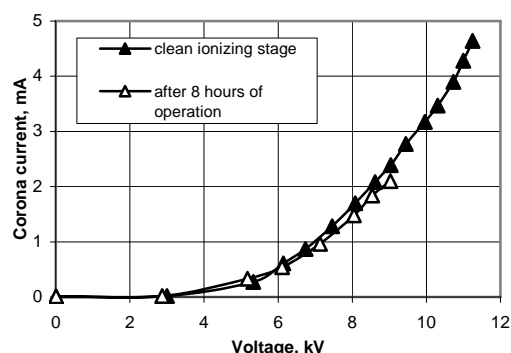
Fig.2 Ionizing stage current-voltage characteristics in the precipitator of tar particles

An ESP was used for collection of lubricant oil mists with particle concentration up to 100 mg/Nm³. After 150 hours of operation, the spark-over discharge decreased from 11,5 kV to 10 kV, The corona current was still $I_{op}>4$ mA and higher than at previous tests (Fig.2). The problem of nozzle loading was solved by changing of nozzle geometry, by use of star-shaped electrodes instead of needles and by increase of gas velocity in the electrode gap.

A pilot wet ESP was used for collection of fine $(NH_4)_2SO_4$ droplets. The high concentration of particles resulted in strong corona suppression in the small electrode gaps. At gas velocity in the nozzle <10 m/s, a liquid ring was built inside of the nozzle opposite to the HV star-shaped electrode. The liquid ring decreased the electrode gap width and provoked spark-over discharges. Also the EHD spraying of liquid was observed from the sharp points of the high voltage electrode. It resulted in decrease of the stability of ESP operation. With increase of applied voltage, the EHD spraying was suppressed. At constant voltage, the increase of gas velocity in the ionizing section up to 18-20 m/s decrease of corona suppression in the charging zone from 70% to 20% and increased the operation current.

The results of the improvement of the corona discharge characteristics in small electrode gaps and the enhancement of the stability of the ESP at high particle number concentrations in the gas flow are proposed for discussion.

Conversion of methanol vapour in a microwave discharge reactor

Cheng-Hsien Tsai[1,*], Yun-Ru Chen[1], Yan-Wen Wang[1], and Ya-Fen Wang[2]

[1]Department of Chemical and Materials Engineering, National Kaohsiung University of Applied Sciences, Kaohsiung 807, Taiwan.
[2]Department of Bioenvironmental Engineering, Chung Yuan Christian University, Chung-Li 320, Taiwan.

Keywords: aerosol spray pyrolysis, high-temperature aerosol, methanol, plasma, hydrogen.

The production of hydrogen from the conversion of methanol (MeOH, CH_3OH) is usually carried out through catalytic steam reforming reaction, oxidative steam reforming reaction, or decomposition processes [Ma, et al., 2000; Geissler, et al., 2001; Boccuzzi, et al., 2003]. H_2 is regarded as a regenerable energy, and will play a key role for applying as the fuel of fuel cell. Hence, this study provides a single-stage, plasmalysis of methanol to produce mainly hydrogen using an atmospheric pressure microwave plasma reactor.

The continue microwave plasma system (Fig. 1) was assembled by a commercially available magnetron (National Electronics YJ-1600, 2.45 GHz) with maximum stationary power of 5 kW. A quartz tube are intersected the waveguide (ASTEX WR340) and the resonator perpendicularly. The compositions of the reactants and gaseous byproducts were identified and quantified by RGA, FTIR and GC/TCD.

The experimental conditions are as follows: inlet molar fraction of MeOH was 3.3% with N_2 as the balanced gas, system pressure was at atmospheric pressure; applied MW power was set at 0.8-1.4 kW; temperature of the feed was at room temperature; and total flow rate was fixed at 12.4 slpm (standard liter/min).

Experimental results showed that the conversion of MeOH was slightly elevated by increasing the applied power and was in the range of 97.0-99.3% (Fig. 2). The addition of a low inlet concentration of MeOH should does not quench apparently the electron concentration in the cavity resonator.

The species of byproducts that produced from the pyrolysis of MeOH were measured. H_2 and CO were the predominant compounds. The minor/trace byproducts were CH_4, C_2H_2, C_2H_4, CO, and nano carbon black particles. HCN was not found. In MW discharge, energetic electrons are generated. Then a large amount of free radicals are produced via the electron impaction dissociation reaction, penning dissociation reaction, or molecule-radical reactions.

Fig. 2 showed that the selectivity of H_2 (H_2O was not included) increased slightly from 96.4% to 99.2% when the applied power elevated from 0.8 to 1.4 kW. A little elevation of H_2 selectivity was found and might be caused by the dissociation of more CH_3

radicals that yielded from the decomposition of MeOH, producing more H atoms, then H_2 and resulting in the reduction of yields of CH_4, C_2H_2, and C_2H_4. The selectivities of H-containing trace byproducts, CH_4, C_2H_4, and C_2H_4, decreased from 2.2% to 0.4%, 1.0% to 0.3%, and 0.5% to 0.1%, respectively, when the powers were elevated from 0.8 to 1.4 kW.

As for the selectivities of carbon-containing components were in the order: CO > carbon black $(C_1) > C_2H_2 > CH_4 > CO_2 \sim C_2H_4$.
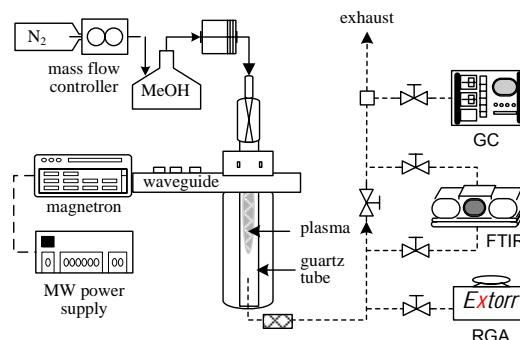
Figure 1. Experimental apparatus
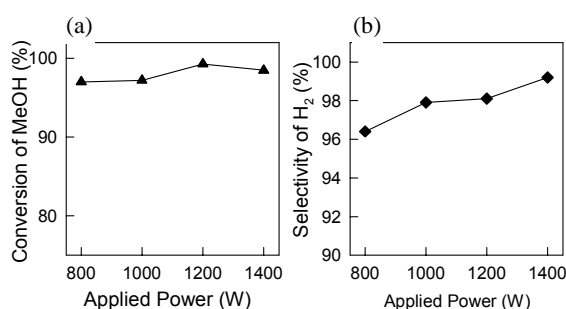
Figure 2. Conversion of MeOH (a) and Selectivity of hydrogen in the effluents (b) at [MeOH]in = 3.3%.

Ma, L., Gong, B., Tran. T., Wainwright, M. S. (2000). *Catal. Today*, **63**, 499-505.

Geissler, K., Newson, E., Vogel, F., Truong, T. B., Hottinger, P., Wokaun, A. (2001). *Phys. Chem. Chem. Phys.*, **3**, 289-293.

Boccuzzi, F., Chiorino, A., Manzoli, M. (2003). *J. Power Sources*, **118**, 304-310.

Nano carbon powders produced by microwave plasma methane steam reforming

Yi-Ming Kuo[1], Cheng-Hsien Tsai[2,*], Kuan-Ting Chen[2], and Yuan-Chung Lin[3]

[1]Department of Environmental and Safety Engineering, Chung Hwa College of Medical Technology, Taiwan
[2]Department of Chemical and Materials Engineering, National Kaohsiung University of Applied Sciences, Taiwan.
[3]Institute of Environmental Engineering, National Sun Yat-Sen University, Taiwan.

For energy resources efficient conversion, methane (CH_4) is generally used to produce the more valuable intermediates or products, such as H_2, syngas (H_2 + CO), C_2H_4, CH_3OH and CH_2O [Periana, et al., 1993]. Especially H_2, is regarded as a regenerable energy, and will play a key role for applying as the fuel of fuel cell. Hence, this study provides a single-stage, steam reforming of methane to produce mainly hydrogen through converting C atoms as carbon black to reduced the emission of CO_2 using an atmospheric-pressure microwave plasma reactor.

The continue microwave plasma system (Figure 1) was assembled by a commercially available magnetron (National Electronics YJ-1600, 2.45 GHz) with maximum stationary power of 5 kW. A quartz tube are intersected the waveguide (ASTEX WR340) and the resonator perpendicularly. The solid carbon depositions were collected by a trap and were analyzed by XRD, SEM, and XPS. The compositions of the gaseous byproducts were identified and quantified by FTIR and GC/TCD

The experimental conditions are as follows: inlet H_2O/CH_4 molar ratio (R) was 0.5-3, inlet molar fraction of CH_4 was 5% with N_2 as the balanced gas, system pressure was at atmospheric pressure; applied MW power was set at 0.8-1.4 kW; temperature of the feed was at room temperature; and total flow rate was fixed at 12 slpm (standard liter/min).

After the steam reforming of CH_4, a large amount of black fine particles were yielded and the major compositions of the solid depositions were high purity of carbon element with the content of carbon atoms was about 100%. Interesting, the selectivity of carbon powders increased from 30.5% (at R = 0, plasma pyrolysis) to about 48.0% (at R = 0.5, 1, 2), then decreased to 13.7% when R reached 3 at 1.0 kW. A large amount of carbon powders were produced at a lower R because the addition the H_2O led to the significant inhibition of C_2H_2 formation, as well as only a little CO/CO_2 being formed.

By XRD, the structure of carbon black was belong to graphite-rhombohedral that was identified at 2θ = 26.3 [JCDPS card No. 75-0444] with a crystalline grain about 8.3 nm. From the XPS spectra, only single peak of C_{1S} could be found at 284.6-284.8 eV that was assigned as the C-C functional group and might attribute to carbon polymers [Portela et al., 1995].

The morphological properties of the synthesized carbon powders were investigated by SEM images (Figure 2). The fine spheroidally shaped particles, whose sizes are about 40-70 nm, are aggregated together to form a cluster of carbon particles.

In sum, a large amount of nano carbon powders could be produced from the steam reforming of methane for producing hydrogen and reducing the emission of greenhouse gas CO_2 through a microwave plasma approach.
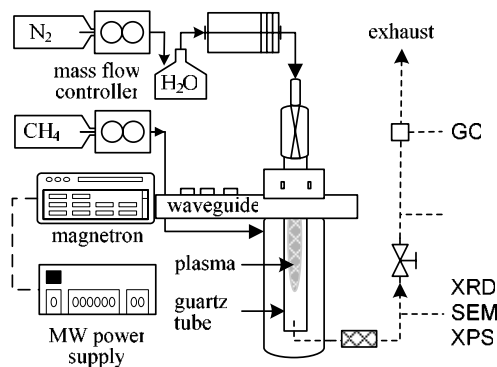
Figure 1. Experimental apparatus
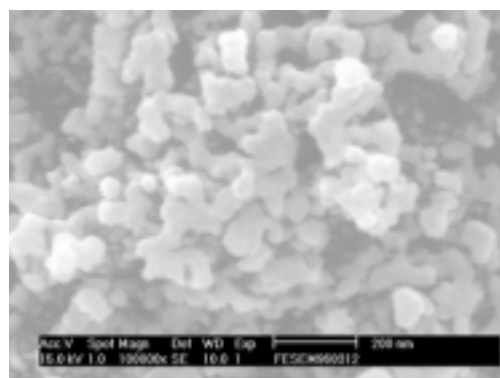
Figure 2. SEM image of the produced nano carbon powders produced at 1.0 kW and R = 3.

Portela, L., Grange, P. & Delmon, B. (1995). *J. Catal.*, 156, 243-254.

Periana, R.A., Taube, D.J., Evitt, E.R., Loffler, D.G., Wentrcek, P.R., Voss, G. & Masuda, T. (1993). *Science*, 259, 340-343.

Electrostatic removal of submicron particles under CO_2-rich atmosphere

Y.J. Kim, H.J. Kim, B. Han, D.K. Song, S.H. Jung, W.S. Hong, and W.H. Shin

Green Environmental System Division, Korea Institute of Machinery and Materials, 305-343, Deajeon, South Korea

Keywords: Electrostatic precipitators, Carbon dioxide, Collection, Submicron particles

The consumption of fossil fuels has attributed to severe global warming due to the emission of green house gases such as carbon dioxide (CO_2). Nevertheless, coal has been highlighted as a future energy source owing to its stable cost and supply (Buhre *et al.*, 2005). However, the use of coal should be accompanied with the reduction of the greenhouse gases for a carbon-constrained future. To separate CO_2 gas in coal combustion, oxy-fuel combustion has been interested in these days. Oxy-fuel combustion uses oxygen as an oxidant and CO_2 gas as a surround gas instead of air and therefore emits mostly CO_2 and water as by-products. It is easy to return and/or capture CO_2 gas in the oxy-fuel combustion. Electrostatic precipitators (ESPs) have been widely used to collect ultrafine particles in the coal combustion. Surrounded gases in the coal combustion chamber probably change the performance of ESPs. Therefore, it needs to investigate the collection characteristics of ESP based on gas compositions, gas flow rate, and particle size etc.

High purity (more than 99.9%) CO_2 gas mixed with air was introduced into an electric tube furnace of about 300°C and passed through an ESP. KCl particles generated by a constant atomizer were supplied upstream the tube furnace. Particle size distributions were measured upstream and downstream of the ESP by a SMPS (Model 3936, TSI, USA). Experimental conditions were shown in Table 1.

Figure 1 shows voltage versus current curves at different gas compositions, gas flow rates and electrical polarities of the applied voltage. As increasing the fraction of CO_2 gas, corona current decreased due to high ionization potential of CO_2 gas compared to O_2 gas. As increasing air velocity, corona current decreased due to shorter residence time in the ESP. The corona current of negative corona was higher than that of positive corona due to different charging mechanism.

Table 1. Experimental conditions

Composition (CO_2:Air)	0:100, 50:50, 80:20
Face velocity	0.3, 0.5 m/s
Applied Voltage	±7~18 kV
Particle size	30~500 nm

Figure 2 shows collection efficiency of 300 nm particles at different gas compositions. Increase

of power consumption led to increase of collection efficiency. At the same power consumption, the collection efficiency was decreased as increasing the fraction of CO_2 gas. This is in a good agreement with the result of corona current. Furthermore, negative applied voltage and low air flow rate led to increase of the collection efficiency due to higher corona currents, that is, higher ion concentration.
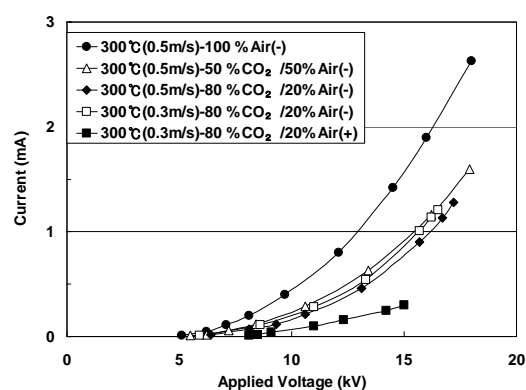
Figure 1. Voltages versus current curves with different gas compositions, velocity and electrical polarity
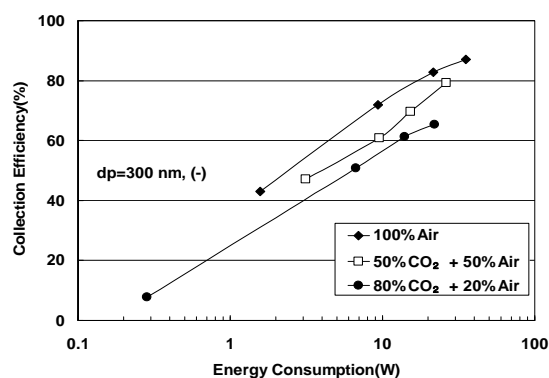
Figure 2. Collection efficiency of 300 nm particles as a function of power consumption with different gas compositions

Buher, B. J. P., Elliott, L. K., Sheng, C. D., Gupta, R. P. & Wall, T. F. (2005). *Prog. Energ. Combust.*, 31, 283-307.

Electrospray Aerosol Discharge by Corona Effect: Influence on Droplets Size and Velocity.

M. Pierobon, M. Sausse Lhernould, D. Zimmermann, P. Mathys and P. Lambert.

Bio, Electrical And Mechanical Systems (BEAMS), Université Libre de Bruxelles,

50, Av. F.D. Roosevelt, CP 165/56, Bruxelles, 1050, Belgium.

Keywords: *Electrospray, corona discharge, electrohydrodynamic (EHD).*

This paper reports on an experimental study of electrosprays, including the use of corona effect in order to discharge generated aerosol. The main contribution is, in particular, the study of the influence of corona effect on droplets size and speed, as well as on the influence of electrospray on corona current. Beside piezoelectric and ultrasonic nebulization methods, electrospray achieves liquid atomization by inducing electrical stress in a liquid meniscus, subjected to an electrical potential ($\sim$3.5kV), so as to produce a so-called "Taylor cone" (see Fig. 1.a). A thin liquid jet (of a preset diameter) appears at cone apex, which subsequently generates droplets as a result of Rayleigh instabilities. This physical event had been first investigated by J. Zeleny [1] and fully described by G. Taylor, both mathematically [2] and physically [3]. Electrospray offers several advantages: droplets diameter ranging from a few nanometers to several hundreds of micrometers; close distribution of droplet size; and risk of recombination prevented by the intrinsic electrical charge of each droplet.

However, there remains a major disadvantage for some applications, i.e. the electrical charge carried by drops. This article presents a way to counter this disadvantage by effecting discharge of such generated droplets, by means of a corona current which is applied to the droplets flow in the opposite direction (see Fig. 1.a). This procedure has already been implemented by K. Tang and A. Gomez [4], according to Noakes *et al.* US Patent [5]. A corona discharge is set up with a potential difference (~-3.5kV) between a sharp electrode and a counter plate electrode, electrically grounded. By fringe effect on sharp needle tip, obtained electrostatic field is huge (~0.2MV/m) and therefore air is ionized, giving birth to ions motion and subsequently an electrical current. The latter is then used to discharge droplets, as it goes counter liquid flow direction.

The simplicity of implementation is one of work originalities: liquid column to produce hydrostatic pressure, hypodermic needle and two EMCO high voltage supplies. The topology used is presented in Fig. 1.b. In order to observe generated droplets, we used a high-speed camera (up to 12kHz) with backlighting and a laser refractometer. Those image capture devices are coupled with a simple numerical post processing, using Matlab environment. Results generated by this image capture set-up concern electrospray influence on steady corona current as well as corona influence on electro-
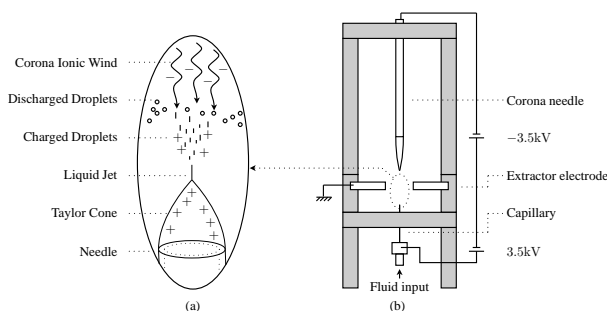
Figure 1: Sketch of a simple discharged EHD.

spray behavior and droplets size. Charged droplets are moving very fast (about 1.5m/s) within the intense electrical field (~0.2MV/m) needed to create electrospray. Once they are discharged, their speed is much lower ($\sim$2cm/s), and they become much easier to observe.

Finally, we highlight a promising feature concerning the spindle mode (oscillating between dripping and cone jet modes), based on a spraying mode nomenclature made by Cloupeau and Prunet-Foch [6]: using corona discharge, we may efficiently separate sporadic cone jet mode generated droplets and micro dripping mode droplets. This is made possible using the fact that dripping droplets are much more charged than thin cone jet droplets; as a consequence, they are not completely discharged as compared to cone jet droplets: spindle mode drops are still electrically attracted by ground and therefore they are expelled from the system while cone jet drops are gradually generating a cloud. Perspectives of this work are the influence quantization of corona effect on electrospray current and droplets intrinsic electrical charge.

References

[1] J. Zeleny. *Phys. Rev.*, 10(1):1–6, 1917.

[2] G. Taylor. *Proc. R. Soc. London*, 280:383–397, 1964.

[3] G. Taylor. *Proc. R. Soc. London*, 313:453–475, 1969.

[4] K. Tang and A. Gomez. *J. Colloid Interface Sci.*, 175:326–332, 1995.

[5] T.J. Noakes, I.D. Pavey, D. Bray, and R.C. Rowe. US4829996, 1989.

[6] M. Cloupeau and B. Prunet-Foch. *J. Aerosol Sci.*, 25(6):1021–1036, 1994.

Neutralization of Tetraalkylammonium Halide Clusters

D. Wimmer, G. Steiner, G.P. Reischl

Faculty of Physics, University of Vienna, Boltzmanngasse 5, 1090 Wien, Austria

Keywords: Cluster ions, Charging efficiency, Electrospray, Neutralization.

For basic studies performed under laboratory conditions, the characterization as well as the generation of well defined nano-aerosols with sizes down to single molecules is of crucial importance. Furthermore, the chemical nature, the structure and the properties of the molecular clusters have to be known and controlled as well. Especially studies related to heterogeneous nucleation strongly depend on the mean size and the size distribution of seed particles and demand the precise knowledge of cluster sizes and charging states.

Therefore, this work focuses on the evaluation of the Number Size Distribution (NSD) of well defined, singly charged Tetraalkylammonium Halide Clusters, generated by the electro spray atomization method. The latter yield unique size distributions of several distinctly separated cluster species (Ude & Fernández de la Mora, 2006). As they can be considered as strictly monodisperse / monomobile clusters, they are well qualified for various laboratory studies.

As it is often necessary to produce neutral particles, this study further concentrates on the neutralization of the latter ionic molecules. The neutralization of aerosols can be achieved by passing the particles / clusters through a bipolar ionic atmosphere. Fuchs' (1963) particle charging theory is until know the standard method to calculate the charging probabilities for ultrafine particles The diffusion charging / neutralization process occurs as a result of random thermal motion of ions and particles in their electrostatic field, which leads to ion-particle collisions. As for large particles the charging process is dominated by Brownian diffusion and the coulomb field of the net-charge of particle and ions. For very small particles in the size range of molecular clusters the combination process is dominated by the influence of the multipole moments caused by the structure of the charged and/or neutral clusters (Nadykto et al., 2006).

Figure 1 shows the measured NSD of Tetrabutylammonium Iodide (black line) (TBAI) represented by three sharply separated molecule species at 1.2nm (monomere), 1.53nm (dimere) and 1.73nm (trimere).

The blue line indicates positive ionic cluster produced by the ionizing radiation of the [241]Am neutralizer. The red line gives the size spectrum of TBAI after passing the neutralizer.
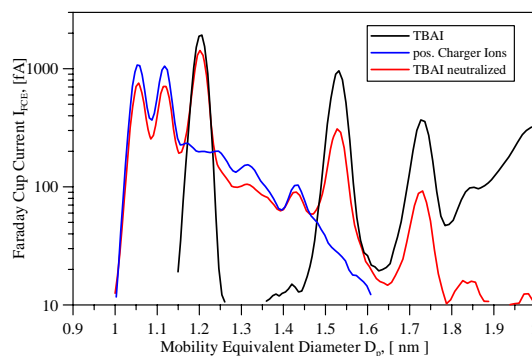
Fig. 1: NSD of TBAI, pos. ions and neutralized TBAI clusters.

According to Fuchs' charging theory, most of the TBAI clusters should be neutral after passing the neutralizer, only a fraction around a few percent should carry one elementary charge. In contrast to that we find that most of the TBAI clusters remain charged. This effect could be observed for several other Tetraalkylammonium Halide molecules.

We think that the positive charge of the Tetraalkylammonium Halides localized on the nitrogen atom, deeply inside the molecular structure, is shielded by the numerous electron shells of the surrounding hydrogen atoms. The potential neutralizing incoming negative ion has therefore to overcome a potential barrier. Therefore we investigated the neutralization process at different temperatures. Figure 2 shows the dependency of the neutralization process on the neutralizer temperature and therefore on the charging ions kinetic energy.
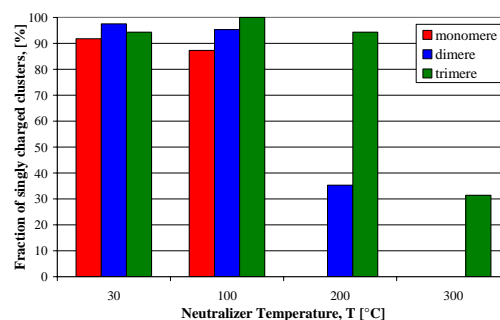
Fig. 2: Neutralization deficiency vs. ion temperature

Fuchs, N.A. (1963), *Geofis. Pura Appl. 56, 185*

Ude, S., Fernández de la Mora, J. (2005), *J. Aerosol Sci. 36, 1224-1237*

Nadykto, A. et al., J., Phys. Rev. Lett., 96, 125701, (2006)

Dispersion of Corona Ions Downwind from a High-Voltage Power line

Xuan Ling, Rohan Jayaratne and Lidia Morawska

International Laboratory for Air Quality and Health,
Queensland University of Technology, GPO Box 2434, Brisbane, QLD 4001, Australia

Keywords: air ions, charged particles, electrical effects, ion mobility, power lines.

Corona discharge is responsible for the small ions found near overhead power lines, and these are capable of modifying the ambient electrical environment such as the dc electric field at ground level (Fews, Wilding et al. 2002). Once produced, small ions quickly attach to aerosol particles in the air, producing 'large ions' which are roughly 1 nm to 1 μm in diameter. However, very few studies have reported measurements of ions produced by power lines and its impact on particle charge concentrations. In this present study, the measurements were conducted as a function of normal downwind distance from a 275kV power line for investigating the effect of corona ions on air ions, aerosol particle charge concentration and dc e-filed.

In this study, both positive and negative small ion concentrations (<1.6nm), net large ion concentration (2nm-5μm), ultrafine particle number concentration, dc electric field (EF) and ac magnetic field (MF)were measured at one upwind location and several downwind locations of the power line (Fig.1), as well as (Fig2). The results indicate that ions of both signs were produced by the power line and show that the negative air ion concentration was dominant. The value of the net charge particle concentration and the EF also showed a negative polarity.

The maximum ion concentration was located at a downwind distance of about 20m from the line, suggesting that the corona ions produced by the

Figure 2. EF and MF value as a function of distance from the power line in the direction of the wind.
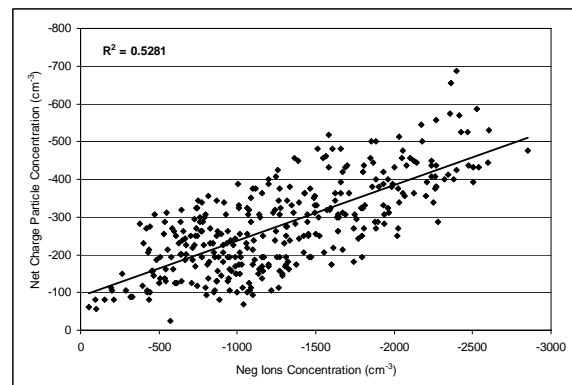
Figure 3. The negative air ion concentration plotted against the net particle charge concentration.

power line were transported in the wind and did not reach the ground directly under the line. Fig 3 shows the negative air ion and net particle charge concentrations at a point 40m downwind were monitored simultaneously at 1s intervals over a period of 5 min. These two parameters showed a significant correlation with a correlation coefficient of 0.73.

Fews, A.P., Wilding, R.J. et al. (2002). "Modification of atmospheric DC fields by space charge from high-voltage power lines." Atmospheric Research 63: 271-289.

Figure 1. Median average values of positive and negative small ion concentrations and net charge particle (large ion) concentration as a function of distance from the power line in the direction of the wind.

Measurement of Small Ions near a Busy Motorway

Xuan Ling, Rohan Jayaratne and Lidia Morawska

International Laboratory for Air Quality and Health,
Queensland University of Technology, GPO Box 2434, Brisbane, QLD 4001, Australia

Keywords: air ions, ion mobility, vehicle emissions, traffic emissions

Combustion sources are well-known sources of electrical ions (Howard, J.B. et al. 1973). Motor vehicles emissions are one of the main sources of ions in urban environments. The presence of charged particles in motor vehicle emissions has been known for many years (Kittelson, 1986; Yu et al, 2004; Jung and Kittelson, 2005). Although these particles are probably charged by the attachment of air ions, there is very little information on the nature, sign and magnitude of the small ions (diameter < 1.6 nm) emitted by motor vehicles and/or present by the sides of roads.

Experiments were conducted near a busy motorway with the aim of quantifying the concentration of small ions. Two air ion counters were utilized to determine positive and negative small ion concentrations. Wind speeds, wind direction and traffic density and composition were also recorded. Measurements were conducted with a steady wind of about 15 kmph, blowing normal to the road. The traffic density on the road was about 100 vehicles per min in each direction. Approximately 15-20% of the vehicles were heavy duty diesel. The instruments were located on the upwind and downwind sides of the road at a distance of approximately 2m from the edge of the road at a height of about 1 m. Background ion concentrations were measured in an open park, well away from vehicular traffic.

A summary of the results are shown in Table 1. Total ion concentrations on the upwind side were approximately 1.6 times higher than at the background site. The concentrations on the downwind side were approximately 1.9 times higher than on the upwind side. Median positive and negative ion concentration differences between the two sides of the road were 442 and 527 cm^{-3} respectively. Time series of the positive and negative air ion concentrations at background, upwind and downwind of the road are shown graphically in Fig 1.

Although Kittelson et al (1986) and Maricq (2006) showed that motor vehicle emissions contain equal magnitudes of positive and negatively charged particles, this is the first time that it has been shown that motor vehicles emit small ions of both signs, of approximately equal magnitude. Note the sharp concentration spikes observed in both charge signs, especially on the downwind side of

Table 1. Positive and negative small ion concentrations at background, upwind and downwind of the motorway in units of ions/cm^{-3}.

		Background	Upwind	Downwind
Mean	+	427	629	1163
	-	-312	-468	-1053
Median	+	401	669	1111
	-	-277	-463	-990
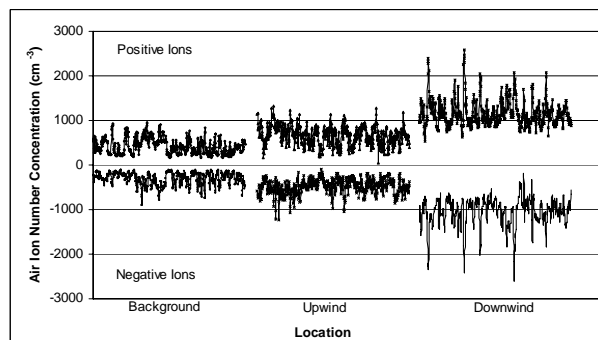
Figure 1. Positive and negative small ion concentrations at background, upwind and downwind of the motorway.

the road. Closer inspection showed that these spikes almost always coincided with diesel heavy duty vehicles. The results suggest that most of the observed ions arise from heavy duty vehicles.

Howard, J.B., Wersborg, B.L. and Williams, G.C. (1973). "Goagulation of carbon particles in premixed flames." Faraday Symposia of the Chemical Society, 7: 109-119.

Kittelson, D.B. and Pui, D.Y.H. (1986). "Electrostatic collection of diesel particles." SAE Technical Paper, 860009.

Yu, F. (2001). "Measurements of ion concentration in gasoline and diesel engine exhaust" Atmospheric Environment, 38:1417-1423.

Jung, H. and Kittelson, D.B. (2005). "Measurement of electrical charge on diesel particles." Aerosol Science and Technology 39: 1129-1135.

Maricq, M.M. (2006). "On the electrical charge of motor vehicle exhaust particles." Journal of Aerosol Science 37(7): 858-874.

Motion of diffusing particles in electric fields

V.A. Zagaynov[1], A.A. Lushnikov[1], D.V. Vodyanik[1], Yu.S. Lyubovtseva[2]

[1]Department of Aerosols, Karpov Institute of Physical Chemistry, 10, Vorontsovo Pole, 105064 Moscow, Russia
[2]Geophysical Center RAS, Moscow, Russia

Motion of aerosol particles in gas phase is complicated by the collisions between particles and gas molecules. At the same time the external fields make the particles to move in the definite direction. The collisions of particles with gas molecules deviate them from their trajectories.

Let us consider the motion of charged particles in electric fields. At the same time the influence of charged particles on the external electric field is supposed to be negligible. To simplify the problem we assume that each particle is charged with one elementary charge. In this case the particles motion can be described by the continuity equation:

$$\frac{\partial c}{\partial t} + div\vec{j} = 0 \qquad (1)$$

where $c(t,\vec{r})$ is the particle concentration, which is much lower than the concentration of the carrier gas molecules c_0.

Only stationary cases will be considered: $\frac{\partial c}{\partial t} = 0$

We studied the planar   and the cylindrical geometries. In the planar case the flow of carrier gas with charged particles moves between two plates. The distance between plates is much less than the width and the length of the channel. The electric field may be considered as homogeneous. In the case of cylindrical geometry the carrier gas with charged particles moves between two coaxial cylinders. Let us suppose the charged aerosol flow enters into the space between charged surfaces by a thin $\Delta x \ll (x_2 - x_1)$ layer, where x_1 and x_2 are the positions of the surfaces. Aerosol flow is repulsed from the plate wth the similar polarity. We denote the velocity of the flow v. The charged particles shift from one charged surface to another as they move along the plates. Let us find the distribution of the particle concentration. To write the equation for particle concentration $c(\vec{r})$ let us define the particle flows:

$$\vec{j} = \vec{j}_D + \vec{j}_E + \vec{j}_v \qquad (2)$$

Here: $\vec{j}_D = -\vec{\nabla}c(\vec{r})$ is the diffusion flow;

$\vec{j}_E = D\frac{e\vec{E}}{kT}c(\vec{r})$ is the flow defined by the electric field;

$\vec{j}_v = \vec{v}c(\vec{r})$ is the transport flow;

here D is the diffusion coefficient, e is the electron charge, $\vec{E}$ is the electric field.

Substituting flow (2) into equation (1) gives the diffusion equation:

$$-D\Delta c + D\frac{e\vec{E}}{kT}\vec{\nabla}c + \vec{v}\vec{\nabla}c = 0 \qquad (3)$$

with the boundary condition:

$$c(\vec{r})\,|_S = 0 \qquad (4)$$

The boundary condition (4) means that the particles approaching the surface deposit on it. Equation (3) and boundary conditions (4) have to be supplemented with the initial conditions:

$$c(z = 0) = c^0(\vartheta(x) - \vartheta(x + \Delta x)) \qquad (5)$$

where $\vartheta(x)$ is the Heaviside step function. Equation (3) with boundary and initial conditions (4) and (5) was solved for planar and cylindrical geometries. An example of the solution is shown in fig. 1.
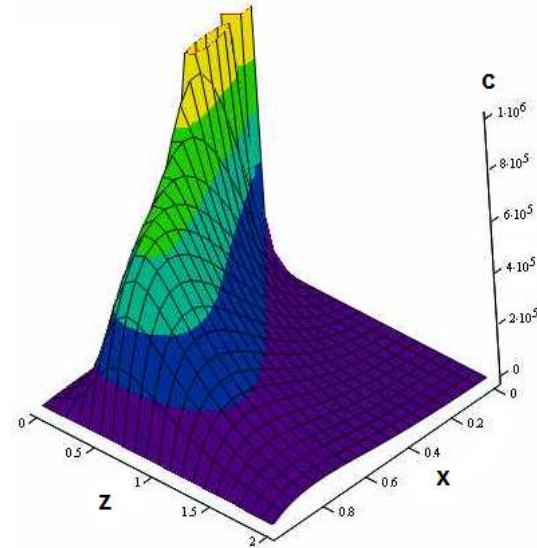
Figure 1. Spacial distribution of particle concentration during transport along plane parallel channel. Scales along axes x and z are given in cm and c in cm^{-3}.

As is seen from fig.1, the diffusion spreads the particle distribution along the longitudinal axis z .

Experimental demonstration of the role of the image force in diffusion charging

M. Fierz and H. Burtscher

University of Applied Sciences Northwestern Switzerland, 5210 Windisch, Switzerland

Keywords: charging efficiency, corona discharge, electrometer, particle charging.

Unipolar diffusion chargers (DCs) are used in an increasing number of aerosol instruments. In simpler devices, the total charge acquired by the aerosol is measured with an electrometer (e.g. Matter LQ1-DC, TSI EAD/NSAM), while in more complex instruments, the DC is used prior to particle sizing (e.g. TSI EEPS/FMPS/UFP330, Dekati ELPI, Matter DiSC, Grimm NanoCheck 1.300). All of these instruments - in particular the sizing instruments - rely on the DC to impart a well-defined charge on the particles. It is often assumed that the particle charge only depends on the particle diameter. If this is not the case, particles of equal mobility diameter will be sized or counted differently depending on their other properties.

One of the properties influencing diffusion charging is the dielectric constant of the particle. The image force which attracts ions to particles is larger for metallic particles than for particles with low dielectric constant. In particular, PSL particles which are often used for instrument calibration have a very low dielectric constant.

The influence of particle material on diffusion charging has not been investigated systematically in the past. To fill this gap, we measured the diffusion charging efficiency for spherical particles of two different materials, silver and ammonium sulphate. These two materials were chosen, because spherical particles can be produced easily. We performed experiments with a unipolar diffusion charger with a low Nt-product (Nt ~ 4E11 m^{-3}s) to avoid multiple charging as far as possible, where Coulomb repulsion complicates matters further. The charge acquired per particle was measured by simultaneously measuring the particle concentration with a CPC and the charge acquired by the particles after the DC. Measurements were corrected for doubly charged particles, coincidence errors in the CPC and losses in the DC. The charge per particle was measured in the size range of 20 to 100 nm. Silver particles were generated by heating silver in a furnace, and sintered at 1200°C to yield spherical particles. Ammonium sulphate was dissolved in ultrapure water and nebulised, also yielding spherical particles. The particles were collected on TEM grids to verify that they were indeed spherical (See Figure 1).

We found that the charge per particle is about 10% higher for silver particles than for ammonium sulphate particles (see Figure 2) in the entire size range investigated.
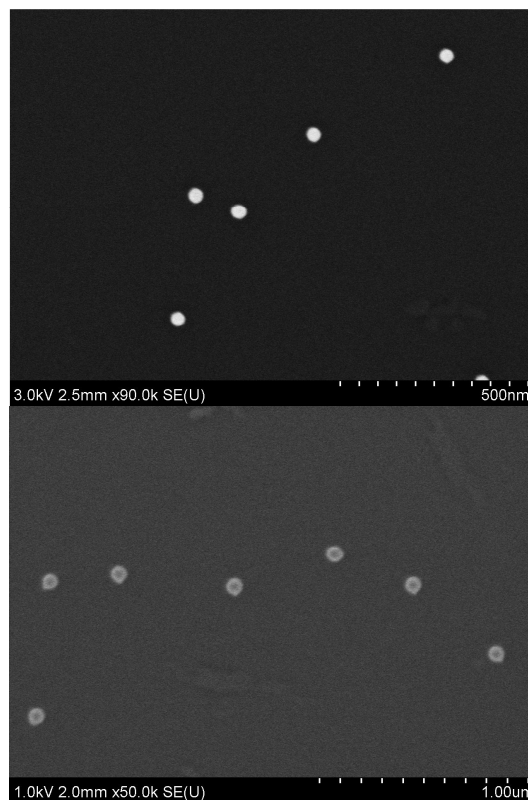
Figure 1: Monodisperse silver particles (40nm, top) and ammonium sulphate particles (80nm, bottom).
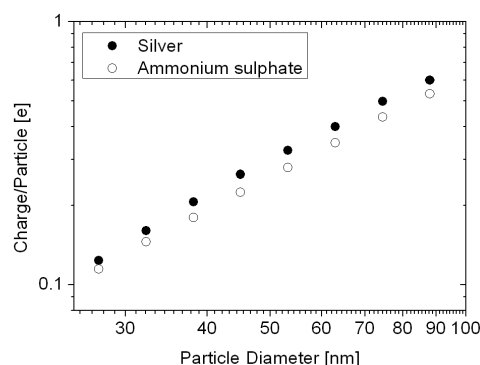
Figure 2. Charge per particle acquired by spherical silver and ammonium sulphate particles

Energy electroaerosol generation through simulation of atmospheric water cycle

M.K. Bologa[1], T.P.Grosu[2], A.A. Policarpov[1], O.V. Motorin[1]

[1]Institute of Applied Physics, 5 Academiei str., MD 2028, Chisinau, Moldova
[2]Agrarian State University, 44 Mircesti str., MD 2049, Chisinau, Moldova,

The possibility to get electric energy through simulation of the atmospheric water cycle (AWC) consisting in the evaporation of water from the earth surface, its ascent in the form of vapours, condensation in the atmosphere upper cold layers and falling out as precipitations back on the earth surface is analyzed. The very presence of electric phenomena under the conditions of the considered cycle points to such a possibility. Electrohydrodynamic (EHD) methods could be additionally used to obtain electric energy.

Three variants of such applications are examined: 1) aerosol wind generator using corona discharge for charging the aerosol particles obtained at the mixing of vapour from AWC with cold air flows; 2) condensate from AWC sprinkles the spiked spherical electrode connected to the high voltage source , as a result the condensate is dispersed under the action of both hydrodynamic (wind) factors and electrostatic forces being simultaneously charged; 3) condensate got in AWC serves as the working medium for Kelvin generator (KG) (Hill & Iacobs, 1997).
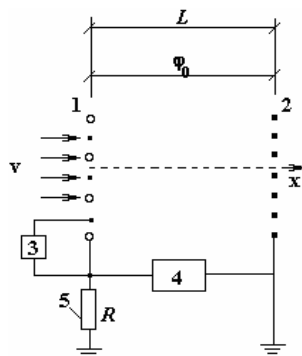
Schematics of EHD wind generator

Generator specific design is presented for the first case. The scheme is shown in the figure and includes the emitter of charged aerosol particles 1, playing the part of the first cloud, the charge accumulator 2, playing the part of the second cloud; high voltage power source to create corona discharge and to charge the particles 3; control system 4; loading 5. It is obtained the solution for potential and intensity and formulas for main generator characteristics.

Generator specific design is presented for the first case. Its scheme includes the emitter of charged aerosol particles, playing the part of the first cloud, the charge accumulator, playing the part of the second cloud; high voltage power source to create corona discharge and to charge the particles; control system; and loading. It is obtained the solution for potential and intensity and formulas for generator characteristics.

In the second case the generator is more effective as the charges and sizes ("sail effect") of particles are larger. Both variants require the presence of the additional source of direct-current voltage: to induce corona discharge necessary to charge aerosol particles in the first case and to charge the spiked electrode creating charged medium in the second one. After achieving the stable operating conditions of the generator it is possible to use a part of the generated energy with the aim to change the primary source. Kelvin generator is devoid of this drawback as doesn't require the additional voltage sources. This is one of its most important merits. Two KG circuits are considered: conventional circuit and combined one. In the report the principles of their work are considered. In the combined circuit the additional generating effect is obtained at the expense of the blowing aerosol drops by the air flow.

The system of vessels and electrodes is a capacitor, the charge accumulated by it is determined from the formula

$$Q = C \cdot \varepsilon,$$

where C is the system electric capacity, ε is the electromotive force (EMF) of KG.

The capacitor charging current intensity is:

$$I = dQ/dt = Cd\varepsilon/dt.$$

As the size of drops increasing they merge together and there occurs the KG jet operation when the potential difference grows substantially. Under the drop conditions the generator provides EMF up to 10-15 kV during several minutes. Under jet conditions the charging occurs during several seconds. Combined EHD generator turns to be more efficient when the drops are blown away by the air flow (wind). A hypothesis is proposed that auto-increasing of electric fields is possible in the clouds according to the electric circuits analyzed in the report.

Hill M., Iacobs D. (1997). *Phys. Education*, 32, 60-63.

Phenomenology of Salt Water Electrosprays

L.L.F. Agostinho[1,2], J. C. M. Marijnissen [1,2], C. U. Yurteri [1,2], E.C. Fuchs[2] and S. Metz[2]

[1] NanoStructured Materials Department, Technological University of Delft, 2628 BL Delft, The Netherlands
[2] Wetsus Centre of Excellence for Sustainable Water Technology, 8900 CC Leeuwarden, The Netherlands

Keywords: Electrospray, Morphology, NaCl, EHDA

Electrohydrodynamic atomization (EHDA) of salt water exhibits intrinsic limitations due to its high surface tension and electrical conductivity (Tang & Gomez, 1994). The formation of stable spray from such fluids in the cone-jet mode requires special ambient conditions like gas blankets with specific dielectric constants to avoid corona formation (Grace, 1994). We report the generation of stable sprays with salt water in the micro-dripping mode rather than the cone-jet mode. For the data presented, a NaCl solution with concentration of 35g/L was used. Under certain conditions, narrow size distributions with main droplets of about 100µm in diameter and RSD of ~0.06 can be achieved with such liquids using a nozzle with inner diameter of 410µm.

The spray characterization was carried out using a capillary-plate configuration with a nozzle to plate distance of 5cm. Different flow rates and potentials were tested in order to find stable sprays. Such modes were identified using both, oscilloscope signals (Fig. 1) and high speed imaging (Fig. 2), droplets and sprays were characterized using high speed image analysis.

Table 1: Characteristics of stable spray modes in terms of flow rate, applied potential, measured current and measured cone pulsation frequency.

Flow (mL/h)	U (kV)	d (cm)	Current (uA)	Frequency (Hz)
2	6	5	0.4	450
	7	5	0.8	800
	-6.5	5	0.8	675
	-7.3	5	1.1	750
5	7	5	0.9	650
	8	5	1.3	690
	11	5	3	570
	12	5	3.9	580
	13	5	4.9	540
	-8.2	5	1.8	620
	-9	5	2.4	750
10	6.5	5	0.6	370
	7	5	0.9	470
	8	5	1.3	560
	9	5	1.8	640
	12	5	3.8	450
	13	5	4.9	470
	14	5	6	440
	-8	5	1.7	625
	-9	5	2.4	735
	-10	5	3.4	780
	-11	5	4.4	806

Figure 2 shows three different configurations for stable salt water electrosprays generated with 2, 5 and 10mL/h at a potential of 6, 11 and 6.5kV, respectively.

Figure 1: Electric current deposited on the counter electrode converted from the oscilloscope signal (R_o=1MΩ, 2mL/h, 6kV and 35 g(NaCl)/L).

The flow rates, electric potentials, electric current, cone pulsation frequency and nozzle to plate distance for stable sprays in micro dripping mode are given in table 1. The droplet diameter varies between 40µm (2mL/6kV) and 200µm (10mL/14kV) with good size distribution.

Figure 2: Salt water electrospray characteristics for different flow rate and potentials.

An overview of the observed stable configurations of salt water electrosprays is presented and compared with similar spray configurations reported in the literature, and a possible future application of such sprays for desalination purposes is introduced.

J. Grace & J.C.M Marijnissen (1994), *J. Aeorsol Sci.* **25**, 1005-1019.
K. Tang & A. Gomez (1994), *J. Aeorsol Sci.* **25**, 1237-1249.

Droplet Size Distribution of Electro-hydrodynamic Atomization (EHDA): Parametric Dependencies

Sanjay Singh, Arshad Khan, B.K. Sapra and Y.S. Mayya

Health, Safety and Environment Group
Bhabha Atomic Research Centre, Mumbai, India

Introduction

Electro-hydrodynamic atomization (EHDA) is a technique employed to generate well defined droplets ranging from nanometre size upto several micrometers by the action of electrostatic force. Technologically, this is achieved by feeding a conducting liquid in to a metal capillary maintained at a high potential with respect to a ground electrode. At the outlet of the capillary, the liquid forms a conical meniscus, through the apex of which a fine liquid ligament is ejected which breaks up farther downstream to disperse into a spray. The spray formed has several unique features like a) high net charge, which prevents coalescence, b) flexibility to generate a wide size range of droplets and c) control of droplet size distribution to near monodispersity (Keqi *et al*. 1996). The variables which control the dispersion process include voltage to the capillary, liquid flow rate and liquid physical properties like, electrical conductivity, viscosity, dielectric constant etc. The present study illustrates the dependencies of these process variables on particle generation with a view to develop robust scaling laws.

Results and Discussions
Applied voltage vs. particle size distribution
In EHDA, jet break up pattern within the cone jet mode heavily depends on applied voltage to the capillary. Different modes of operation can be seen by gradually increasing the applied voltage to the capillary. Fig. 1 shows the size distribution of the ethylene glycol droplets, generated by EHDA and neutralized using the Am-241 source before sampling. As may be seen the size distribution is virtually independent of the voltage subsequent to the formation of the stable cone-jet.

Effect of Liquid Conductivity
The electrical conductivity of the liquid is the most important parameter governing the stability of the cone jet and the droplet size distribution (Hayati et al, 1987; Fernandez de la Mora et al 1994). Our experiments showed that mean droplet diameter increases as the conductivity increases. This trend was consistent for a liquid flow rate in the range of of 2 ml/h to 5 ml/h.

Effect of Liquid flow rate
It is observed that the mean droplet diameter increases monotonically with flow rate of the liquid, although the geometric standard deviation is not sensitive to the flow rate with in the range of operating voltage ensuring the stable cone jet mode of the EHDA. This observation is consistent with that of other investigators (Ganon-Calvo et al. 1997). However, to establish the scaling laws additional experiments need to be conducted.
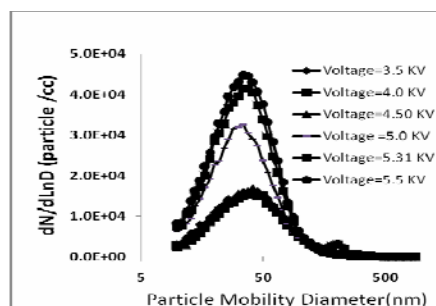
Fig.1 Size distribution of Ethylene glycol spray at varying voltages
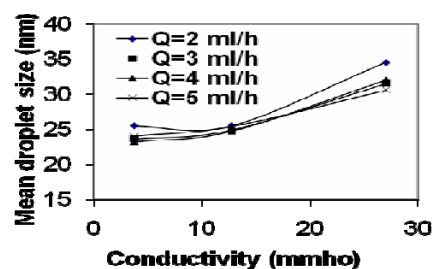
Fig.2 Variation in the Mean droplet diameter with conductivity for varying flowrates

Table 1: Size distribution of Ethylene Glycol spray generated by EHDA at varying flow rates

Liquid flow rate (ml/h)	Mean droplet diameter (nm)	Geometric Standard deviation
1	27	1.65
2	33	1.73
3	37	1.80

References
Keqi Tang and Alessandro Gomez (1996), *J. Colloid and Interface Science*, 184, 500 – 511.
Hayati I., Bayley A.I. and Tadros Th. F. (1987a) *J. Colloid Interface Sci.*, 117, 205-221.
Fernandez de la Mora, J., and Loscertales, I.G (1994), *J. Fluid Mech,*. 260,155.
Ganon-Calvo A.M., Davila J. and Barrerro A. (1997), *J. Aerosol Sci.*, 28(2), 249 – 275.

Electrospray droplets transport in the extractor-collector configuration. Inertial effects.

M. Lallave[1], D. Galán[1], J. Ortega-Casanova[2], A. Barrero[3] and I. G. Loscertales[2]

[1]Yflow, Marie Curie 4, 29590 Campanillas, Malaga, Spain
[2]Dep. Ing. Mecánica y Mecánica de Fluidos, Universidad de Málaga, Plaza El Ejido s/n, 29013 Málaga, Spain
[3]Dep. Ingeniería Aeroespacial, Universidad de Sevilla, Camino de los Descubridores s/n, 41092 Sevilla, Spain

Keywords: electrospray, aerosol dynamics, charged particles, electrical effects.

In this presentation we report, by means of numerical simulations and experimental results, on the key role played by the aerosol inertia on the dynamics of a fine, highly charged monodisperse particles (i.e. electrospray), when they are injected at a given fixed rate (i.e. fixed current I) through a tiny hole of radius a in an initially aerosol-free region limited by two parallel, infinite, conducting planes at a distance L apart, subjected to a potential difference $\Delta\phi$ (Bocanegra *et al*., 2005). Previous work focused in the axysimmetric lagrangian description of the problem (Loscertales *et al*., 2007); in the present case, the aerosol is modelled as a continuous, non-diffusing, phase. The dimensionless steady-state equations for the aerosol number density $n,$ its velocity $\vec{v},$ the electric potential $\psi,$ and the gas velocity and pressure $\vec{u}$ *and* $p,$ are

$$\nabla.\vec{u} = 0; \quad \vec{u}.\nabla\vec{u} = -\nabla p + \frac{1}{Re}\nabla^2\vec{u} + \alpha n(\vec{v} - \vec{u}), \quad (1)$$

$$\vec{v}.\nabla\vec{v} = \delta\,\vec{\in} - \lambda(\vec{v} - \vec{u}); \quad \nabla.(n\vec{v}) = 0, \quad (2)$$

$$\nabla^2\psi = \beta n, \text{ where } \vec{\in} = \nabla\psi, \quad (3)$$

The problem is described by five dimensionless parameters: $\alpha, Re, \delta, \lambda, \beta$, where Re is the Reynolds number. For particles number densities not too high ($\alpha \ll 1$), the aerosol and gas motion decouples, and the solution of the motion for the gas phase (equations in (1)) is simply $\vec{u} = 0$ and $p = cte$. For aerosol particles sufficiently small (i.e. less than few microns), the inertia appears to be irrelevant ($\delta \approx \lambda \gg 1$), and so the momentum conservation equation for the aerosol becomes $\vec{\in} = \vec{v}$. Thus, the equations describing the aerosol dynamics are reduced to

$$\nabla.(n\nabla\psi) = 0, \nabla^2\psi = \beta n. \quad (4)$$

The problem is solved subject to the boundary conditions for the potential, which are

$$\psi\left(r \geq \frac{a}{L}, 0\right) = 0, \psi(r,1) = 1, \frac{\partial\psi}{\partial r}(0,z) = \frac{\partial\psi}{\partial r}(\infty,z) = 0,$$

and the constant aerosol input flux,

$$\frac{I}{2\pi Z q_p \rho_o \Delta\phi L} = \int_0^{a/L} n(r,0)\frac{\partial\psi}{\partial r}(r,0)dr \,.$$

This latter condition allows defining the only left parameter, $\beta = \frac{IL^2}{4\pi^2\varepsilon_o\Delta\phi V_o a^2}$, where ρ_o is the typical aerosol number density, q_p is the charge per aerosol particle, ε_o is the vacuum permittivity, Z is the aerosol electric mobility and V_o is a characteristic particle electric velocity based on Z and on the imposed field. The solution of this model does not agree with the experimental results on the current I_c that reaches the end plate: $I_c/I \neq f(\beta)$. However, as shown in figure 1, the solution shows that, in the

vicinity of the injection hole rim, the characteristics followed by the aerosol abruptly bend backwards, exhibiting rather small radii of curvature: within this region, the aerosol particles cannot follow the characteristics and the inertia sets in.
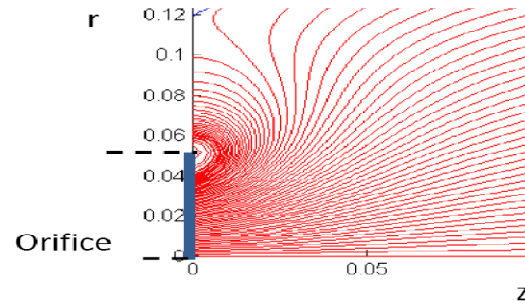
Figure 1. Characteristic followed by the aerosol.

The typical value of such a tiny length l is provided by making the inertial term in (2) of the order of the right hand side, which leads to $l \sim \frac{L}{\lambda} \ll L$. Rewriting the equations in term of this new length, the parameter β in (3) becomes $\beta/\lambda \approx \frac{I}{\varepsilon_o\Delta\phi V_o} \times \frac{L}{l_p}$, where l_p is the particle stopping distance. This parameter collapses the otherwise scattered data for more than ten experiments run with electrosprays of liquids having conductivities from 10^{-5} to 10^{-3} S/m, in a single curve, as shown in figure 2.
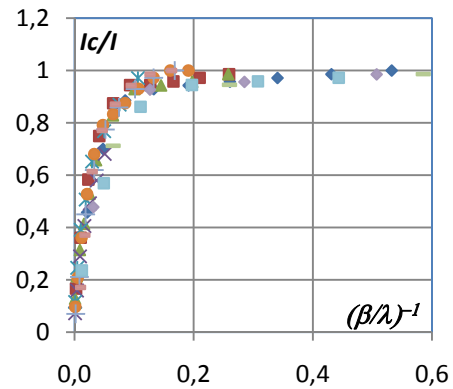
Figure 2. Current reaching the collector versus $(\beta/\lambda)^{-1}$.

Bocanegra, R., Galán, D., Marquez, M., Loscertales, I.G. & Barrero, A. (2005), *J. Aerosol Science*, 36, 1387-1399.

Loscertales, I.G., Rodríguez, E. A., Galán, D., Marquez, M. & Barrero, A. (2007), *EAC 2007, Salzburgh*, Abstract T05A005.

Bipolar Diffusion Charging of Aerosol Particles in the Transition Regime

K. Barbounis[1], S. Vratolis[2], K. Eleftheriadis[2], and G. Biskos[1]

[1]University of the Aegean, Department of Environment, Mytilene, 81100, Greece
[2]N.C.S.R. ''Demokritos'', Institute of Nuclear Technology & Radiation Protection, 15310 Ag. Paraskevi, Athens, Greece

Keywords: Bipolar Ions, Diffusion Charging, Nanoparticles

Bipolar diffusion charging is by far the most common technique for neutralizing aerosols in particle mobility spectrometers, e.g., Scanning Mobility Particle Sizers (SMPSs). The greatest advantage of bipolar charge neutralizers is that a well-defined Boltzmann-type charge distribution can be set to the particles after some equilibration time (Fuchs 1963; Wiedensohler 1988). This is particularly important when inverting the electrical mobility distributions to particle size distributions when using electrical mobility spectrometers.

The charge distribution that the particles acquire when passing through an aerosol neutralizer depends, among other parameters, on the ion concentration, N_i, and residence time, t, of the particles in the neutralizer, as well as on the ion mobility of the generated ions. Most theoretical models assume that the $N_i t$ product is high enough to achieve charge equilibrium, and a specific ion species having average properties to be responsible for the charging process. In practice, however, the $N_i t$ product may not be high enough to achieve charge equilibrium. In addition, the spectrum of ions, having a wide range of mobilities, that exists in such neutralizers can further affect the final charging state of the particles.

The concentration of ions in the neutralizer depends on the ion source whereas the residence time on the design and the operating conditions of the neutralizers. The distribution of ion species depends on the age of the ions and the concentration of trace gases, (e.g., SO_2 and H_2O) in the air.

In this paper we report measurements that explore the dependency of the charging probability upon the type of neutralizer and the concentration of water vapor. The type of neutralizer (ion source, and design) was used to investigate the sensitivity of the $N_i t$ product to the charging probability. The concentration of water vapor was varied to investigate changes in the mobility of bipolar ions, which lead to changes on the charge state of the aerosol particles.

Various radioactive aerosol neutralizers were tested: a [85]Kr neutralizer (TSI model 3077, 74 MBq), a high activity [210]Po neutralizer (NRD model P-2031, 740 MBq), and a low activity [210]Po neutralizer (house-made case equipped with [210]Po source filaments, NRD model 2U500, 18.5 MBq). The relative humidity levels varied in the range of 5 % - 80 % .

Measurements were performed with laboratory-generated particles that were passed throught a Tandem Differential Mobility Analyzer (TDMA) setup coupled with a CPC. The neutralizer upstream of the first DMA was a Po-210 source (NRD model P-2031, 740 MBq). This neutralizer was kept through out the whole measurements. The test neutralizers were placed between the two DMAs, and their performance was evaluated at different operating conditions. Differences of the charging probability of the examined chargers were observed, depending on the concentration and residence time of the aerosol particles in the neutralizer, as well as on the concentration of water vapor of the sample. These differences were more pronounced for particles having diameters less than 50 nm. In many cases the use of Po-210 sources led to new particle formation, possibly due to ion-induced nucleation.

Theoretical calculations using Fuchs limiting sphere theory equations (Fuchs, 1963) and the charged particle concentration balance equations (Alonso, 1997) showed good agreement with the measured charging probability on the particles, as shown in Figure 1 for the case of Po-210 neutralizers.
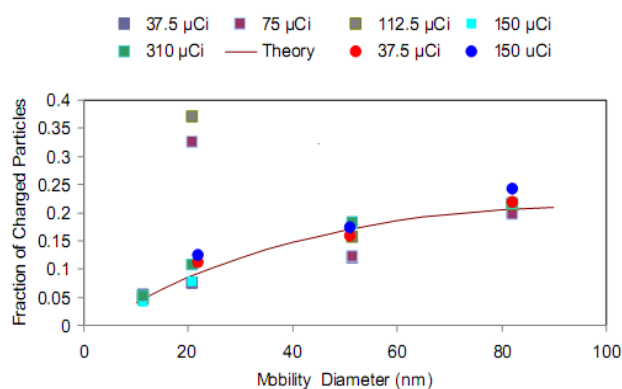
Fig1. Charging efficiency of the Po-210 neutralizers having variable activity. Measurements were performed at 0.3 lpm (circles) and 1.5 lpm (squares) aerosol sample flow rate.

References

Fuchs, N. A. (1963). *Geof. Pura Appl.*, 56, 185-193.
Wiedensohler, A. (1988). *J. Aerosol Sci.*, 19, 387-389.
Alonso M, Kousaka Y. ,Nomura T., Hashimoto N., and Hasimoto T., (1997) . *J. Aerosol Sci, 28, 1479-1490.*

Multiple Electrospray Unit with Circular Symmetry

Y. Arnanthigo, C. U. Yurteri, J.M. Marijnissen, A. Schmidt-Ott

NanoStructured Materials, DelftChemTech, Delft University of Technology, Delft, 2628 BL, The Netherlands

Keywords: EHDA, Electrospray, Electrical effects, Monodispersed droplets

A high production rate of monodispersed like droplets by electrohydrodynamic atomization (EHDA) from a single nozzle is limited by the fact that the expected droplet diameter is mainly a function of the flow rate. Outscaling of EHDA by using multiple nozzles is possible. However, factors such as electrical interference between the neighbouring sprays, and liquid flow rate variations from nozzle to nozzle are problems to overcome for industrially acceptable stable systems (Tang and Gomez, 1996; Bocanegra et al., 2005).

Providing a uniform flow rate and a uniform electric field to each nozzle is essential for getting uniform droplet from an outscaled electrospray assembly. Bocanegra et al. (2005) reported that multi-hole electrosprays provided no large dispersion in the droplet size distribution from nozzle to nozzle when the flow rate throughout each hole was the same.

The minimum distance between the different nozzles is determined by the interference of the electric field at the nozzles and the interference at the nozzles created by the space charge, originate from the different sprays. So, a model is required to optimize this distance.

This work is the continuation of our previous design of a hole-based electrospray system (Arnanthigo et al., 2008), which uses a series of holes drilled through a PTFE body. The large reservoir was filled with a porous medium in order to achieve uniform delivery to each nozzle. However, non-uniform flow of solution at low flow rates was still observed. To overcome this limitation, in the new design, a reservoir providing equal flow paths and flow resistances to each nozzle is considered, so that flow is equally distributed. (Fig. 1)

The performance of the nozzle is being studied in an attempt to optimise the design of a multiple electrospray system. Fig. 1, the reservoir is made of Delrin® and the ejector nozzles are made from Peek®. Each nozzle is provided with an injection room to minimize spray interferences as described by Hartman, (1998). The bottom view of whole chamber is shown in Fig. 2. The extractor and grounded plates are made of brass. Experiments are performed in order to determine the optimum diameter, d, distance between holes, x, *and* the distance between the hole and the extractor plates, h. In addition, a number of liquids with a range of properties were investigated.
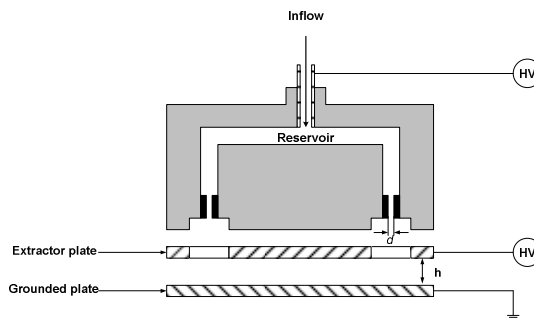
Figure 1. Schematic of the multi-hole electrospray atomiser.
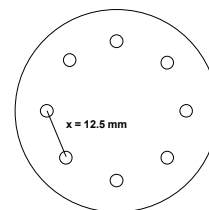
Figure 2. Schematic of the multi-hole electrospray atomiser (bottom view).

The different solutions were a mixture of ethanol and ethylene glycol and pure ethanol. The flow rates were varied between 0.1ml/hr and 5 ml/hr. Tests results including size and current measurements and comparisons with scaling laws will be presented and discussed.

Arnanthigo Y., Biskos G., Yurteri C., Marijnissen J. M., & Schmidt-Ott. A (2008). in *Proc. Conf. on European Aerosol*, Greece

Bocanegra, R., Galán D., Márquez M., Loscertales I. G. & Barrero A. (2005). *J. Aerosol Science*, 36, 1387-1399.

Hartman R.P.A. (1998). *Electrohydrodynamic Atomization in the cone-jet mode from physical modelling to powder production*. Delft University of Technology, Netherlands.

Tang K. and Gomez A. (1996). *J. Colloid and Interface Science,* 184, 500-511.

NANO PHARMACEUTICAL PARTICLE PRODUCTION BY EHDA

C. U. Yurteri, and J.M. Marijnissen,

NanoStructured Materials, DelftChemTech, Delft University of Technology, Delft, 2628 BL, The Netherlands

Keywords: EHDA, Electrospray, Micro Droplets, Nanoparticles

Manufacturing of pharmaceutical products generally requires a liquid or gas phase process. However for most pharmaceuticals, due to their sophisticated molecular structure, the liquid route will be the most appropriate one. Production of pharmaceutical particles in the form of nanoparticles can also be done via the wet route (colloids) or a dry route. Separating nanoparticles from the liquid phase without some contamination will be almost impossible. In order to avoid contamination a dry method might be favourable. Formation of particles requires reduction of bulk into smaller i.e. "nano" fractions. Different disintegration techniques exist, such as grinding, liquid atomization, lithography, and evaporation /condensation depending on either the liquid or solid phase involved.

We only consider liquid atomization where droplet formation is followed by particle conversion. From the several atomization methods we are only interested in methods which break up into quasi uniform droplets, so we limit ourselves to jet breakup in the laminar flow region followed by Rayleigh breakup (Lefebvre, 1989). Another limitation is the size of the initially generated droplets. To produce nanoparticles the initial droplet size should be already fairly small, because otherwise the begin concentration has to be unacceptably low. One should realize that the diameter of the final particle after drying equals the diameter of the initial droplet times the cube root of the volumetric concentration of the non-volatile material (van Erven et al. 2005). In case of very low concentrations of the product material, the role of impurities might become very important. The best option is a method, which produces mono sized droplets with a diameter smaller than the inside nozzle diameter. Such a method is found in: ElectroHydrodynamic Atomization (EHDA) or Electrospraying. EHDA is a method to produce very fine droplets from a liquid (atomization) by using an electric field. By applying the right conditions, monodisperse droplets from nanometers to several micrometers can be produced.

By means of an example, i.e., the production of nano Taxol particles (See Figure 1), a generic way to produce nanoparticles from a multitude of different precursors will be discussed. Several examples of medicine particles made by EHDA will be given, in the nano- and micro- range, with different properties, such as controlled release, high porosity and elongated shape. Also a method, bipolar coagulation, where two sprays of opposite electrical potential are used will be discussed. Bipolar coagulation can also be used to apply nanoparticles on a carrier (see Figure 2). Finally some attention will be given on EHDA instrumentation and out-scaling methods.
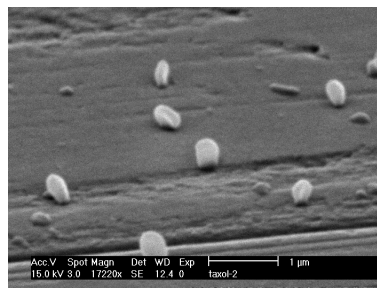
Figure 1. Taxol ; 1.0% in EtoH at 22 µL/h (21 $^{\circ}$C/ 38% RH), 60 sec (spray time), 3 cm (spray to substrate distance), -2.1 kV (High Voltage)
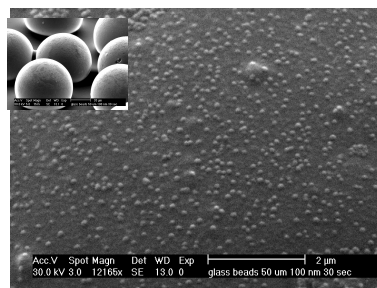
Figure 2. 45 µm glass beads stationary coated with 100 nm PS spheres

Lefebvre, A.H., (1989) Atomization and Sprays, Hemisphere Publishing Company

Van Erven J., Moerman R., and Marijnissen J. C. M. (2005), Aero. Sci. and Tech. , vol. 39, no 10, pp. 929-934

Electrospraying method to prepare ultra-low Pt loading cathodes for PEM fuel cells

S. Martin, P.L. Garcia-Ybarra and J.L. Castillo

Dept. Fisica Matematica y de Fluidos, Facultad de Ciencias, UNED, 28040, Madrid, Spain

Keywords: electrospray, fuel cell, nanoparticle applications, particle deposition, deposit morphology.

Recently, an electrospray method has been applied to generate catalyst layers for fuel cells with high dispersion of the catalyst (Baturina & Wnek, 2005). The purpose of the present work is to explore the potential of this method for achieving ultra-low Pt loadings (less than 0.1 mg_{Pt} cm^{-2}). Although vacuum deposition methods (CVD, PVD, sputtering, etc) have been successful in achieving ultra-low Pt loading, the vacuum conditions make them relatively expensive and not easily adaptable to serial production. Unlike these methods, the electrospray technique has not vacuum requirements; it is easily scalable and based on a simple experimental set up.

Catalyst inks were prepared as suspensions of Pt/C 10 wt.% nanoparticle catalyst in Nafion-alcohol solutions. The electrospray setup consists of a needle and a collector connected to a DC high voltage power supply (Bertan 205B-10R). A syringe pump (KDS 100) drives the catalyst ink through a capillary tube into the needle at the selected flow rate. Charged droplets are formed at the needle tip and forced by the electric field to move toward the collector while the alcohol content evaporates during the flight. Depending on the operating conditions, aggregates or even single particles can be deposited leading to catalytic layers with different morphologies (Loscertales *et al.*, 2007). Suspensions of 7 $mg_{Pt/C}$ ml^{-1} were electrosprayed at 0.3 ml h^{-1} flow rates in the steady cone-jet mode, the needle to collector distance was 7 cm and the potential difference was 9 kV. Fractal-like catalytic layers of 5 cm^2 area were built on carbon paper sheets and used as cathodes in PEM fuel cells. Cathodes with platinum loads of 0.1, 0.05, 0.025 and 0.0125 mg_{Pt} cm^{-2} were made in this way.
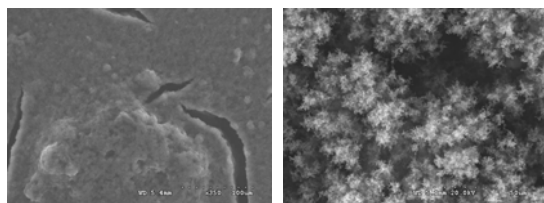
Figure 1. SEM micrographs of electrodes prepared by impregnation (left) and by electrospray (right).

On the other hand, some reference electrodes (anodes) were prepared by impregnation with 1 mg_{Pt} cm^{-2} loading and 30% Nafion content. For comparison, magnified views of the surface of both types of electrodes are shown in Figure 1.

Depending on the platinum loading, the surface of the electrosprayed catalytic layers shows different characteristics as seen in Figure 2. For 0.1 mg_{Pt} cm^{-2} the catalyst covers completely the carbon paper resulting in a rough but continuous catalytic layer. However for a lower loading of 0.0125 mg_{Pt} cm^{-2}, the catalyst covers individually the carbon fibres that constitute the paper, resulting in large unused portions of the cathode area.
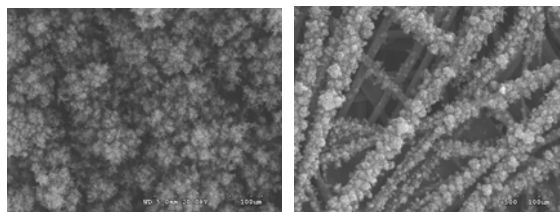
Figure 2. SEM images of the catalyst layer applied by electrospray with platinum loading of 0.1 mg_{Pt} cm^{-2} (left) and 0.0125 mg_{Pt} cm^{-2} (right).

Membrane-electrode assemblies (MEAs) were prepared with these electrodes by hot-pressing each anode-cathode pair with a Nafion 112 membrane sheet sandwiched between them at 10 MPa and 120º C for 2 min. These MEAs were tested in a commercial single fuel cell hardware (FC05-01SP Electrochem, inc.) connected with an external electronic load (Hocher & Hackl PL306).

The electrosprayed cathode performance turns out to be a function of the Nafion content in the catalyst ink showing a maximum performance at a given Nafion content which depends on the platinum loading.

Baturina, O.A. & Wnek, G.E. (2005). *Electrochem. Solid-State Lett.*, 8, A267-A269.
Loscertales, I.G., González, J.C., Galan, D., Perea, A., Garcia-Ybarra, P.L., Castillo, J.L., Marquez, M. & Barrero, A. (2007), *EAC2007*, Salzburg, Abstract T05A006.

Determination of EHD Generated Droplet Size:
Review of Models and Experimental Tools

M. Sausse Lhernould, M. Pierobon, P. Mathys and P. Lambert

Bio, Electrical And Mechanical Systems (BEAMS), Université Libre de Bruxelles,

Bruxelles, 1050, Belgium.

Keywords: Electrospray, droplets

Electrospraying, i.e. atomizing a liquid using electrical forces, allows the production of very fine droplets, down to the nanometer size. Applications of the electrospray are multiple: biological and organic nanoparticles production, nanocoating, pulmonary drug delivery, fuel injection... In most applications, droplets size is a very important constraint. It is thus of the utmost importance to be able to accurately measure droplets sizes and their distribution for spray optimization and determine how parameters such as voltage, flow rate and liquid properties affect the size distribution in the aim of being able to control it. This article proposes a brief review of literature models for determining electrosprayed droplets sizes depending on operating parameters and a review of droplets size measurement techniques available and their performances. Finally results obtained experimentally are presented before concluding on applicative methods for droplets size control.

Some authors [1] provide models for calculating droplets diameter based on the electrospray operating parameters and liquid properties. It is known for example that the radius of the electrosprayed droplet is correlated to voltage but also a function of surface tension γ, liquid density ρ and liquid flow rate ν_F:

$$R \propto (\rho \nu_F^2 \gamma)^{1/3} \qquad (1)$$

Tang et al. [2] studied the effect of liquid flow rate, applied voltage and electric liquid conductivity on droplet size and spray monodisperity. Droplet size was found to be dominantly controlled by the liquid flow rate and secondly by the applied voltage. Study showed no dependence on capillary size and no dependence of the electrode configuration.

Technique	Principle	Use	Cost	User
Shadowgraphy	Backlighting	++	++	[3]
Laser Diffraction	Diffraction	+	- -	[4]
PDA	Doppler	-	- -	[5]
ILIDS/IPI/MSI	Interferometry	- -	- -	

Table 1: Techniques and users

Techniques available for droplets sizing and reviewed in the article include backlighting, laser diffraction, Phaser Doppler Anemometry (PDA), Glare Points Velocimetry and Sizing (GPVS) and Interferometric Laser Imaging for Droplet Sizing (ILIDS), also called Interferometric Particle Imaging (IPI) or Mie Scattering Imaging (MSI). Techniques are compared depending on the difficulty of their implementation and their performances.

An experimental measurement station for droplets size using shadowgraphy which is the most cost effective solution has been set up. It allows images capture and treatment. Using this technique, droplets coming from an EHD Generated Aerosol by Corona Effect were imaged and measured, their size ranging between between 15 and 25 μm. Comparison is then made with commercial equipments using laser diffraction and PDA in order to determine performances of the technique, the goal being here to present the reader with some advice on choosing adequate droplet sizing equipments in the EHD context.

Identifying the parameters on which electrosprayed droplets size depend is the main goal of this work through literature review. Quantifying the impact of these parameters on droplets size is the second aim through literature models and observations. Different techniques are available for experimental droplet sizing that are also reviewed and compared. Finally, an experimental set-up has been tested on an electrospray developed in our facilities.

References

[1] Oleg. V. Salata. *Current Nanoscience*, 1:25–33, 2005.

[2] K. Tang and A. Gomez. *J. Colloid Interface Sci.*, 184:500–511, 1996.

[3] R. Ragucci, F. Fabiani, A. Cavaliere, P. Muscetta, and C. Noviello. *Experimental Thermal And Fluid Science*, 21:156–161, 2000.

[4] R. Bocanegra, D Galán, M. Márquez, I.G. Loscertales, and A. Barrero. *J. Aerosol Sci.*, 36:1387–1399, 1995.

[5] A.M. Gañán-Calvo, J. Dávila, and A. Barrero. *J. Aerosol Sci.*, 28(2):249–275, 1996.

Electrostatic diagnostics of charged aerosol particles in gasdynamic devices

A.Vatazhin, D.Golentsov, V. Likhter

Central Institute of Aviation Motors, Aviamotornaya St. 2, 111116, Moscow, Russia

In the report the new summarized results of experimental and theoretical researches of a method of registration of the charged particles (over the range 10^{-2} - 10 mkm) in a gas flow before, inside and on an exit of aircraft engine and power devices are presented. The particles in these devices appear charged for the following reasons. They become charged as a result of their taking-off the ground and injection into the air-inlets of aircraft engines (Vatazhin, 1997). The particles are formed charged due to destruction of metal elements of equipment (Vatazhin, 2008). The ice particles appear charged in their coming off the surfaces in interior or exterior gasdynamic flows. The "foreign", as a rule charged, particles coming into inlets of engines or test benches from exterior atmosphere.

It's necessary to detect these particles both to estimate the current state of devises and to predict their future one. To do it we developed a method and a system of non-intrusive electrostatic diagnostic. The method is grounded on the detection (with special antennae) the electrostatic signals generated by the charged particles which there are in the device gasdynamic flow. The methodology of the analysis of the registered signals was created.

The system of electrostatic diagnostic is used in two directions. The first one: the system allows to determine the abnormal operational conditions of gasdynamic devices. The indication of the abnormal conditions is the appearance of additional solid or liquid aerosol particles in the gasdynamic flow. The second direction is related to making strategy of use of the diagnostic method. The strategy consists in definition both of initial, *basis* "electric portrait" of gasdynamic device or aircraft engine and subsequent, *current* "portrait" and then in their comparison. The difference between these "portraits" is the integral sign of abnormal situation.

The method of diagnostic was used in various laboratory, airfield, test bench operation conditions. Let's consider some examples of the method using.

1) *Coming the "foreign" particles into engine inlet.* On fig. 1 the signals generated by the particles coming into an inlet of the aircraft engine are presented. The signals were registered by two antennae fixed in enter and exit of the engine. The time shift of the signals is related to moving of the particles inside of the engine. The analysis of the signals shows, that a charge of the particles is positive and they may be the metal ones.
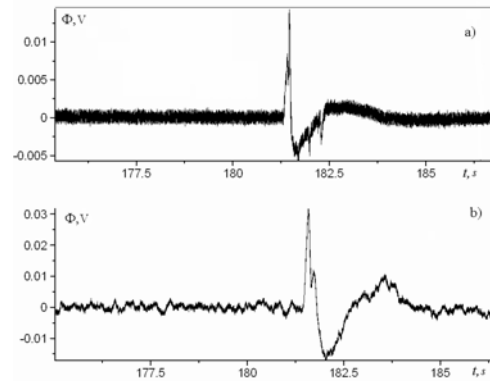
Figure 1. The signals of "enter" (a) and "exit" (b) antennae generated by "foreign" particles, coming into the engine

2) Appearance in the engine tract the charged particles due to the engine element destruction.
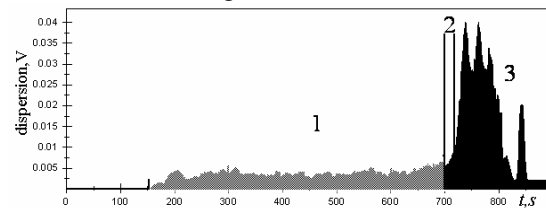
Figure 2. The dispersion of the antenna signal in normal (1) and abnormal (2,3) engine operation modes.

On fig. 2 the change of the antenna signal dispersion from normal (1) up to abnormal (2,3), when the dispersion increases by the order, is shown. In the flow appears a great number of positively charged particles that are the sign of destruction of an interior engine element. This assumption was confirmed by the subsequent inspection of engine.

The presented examples show, that the developed theory and construction of the diagnostic system allow to register both the current state of gasdynamic devices or aircraft engines and to predict the evolution of the abnormal operational modes of devices.

Vatazhin, A.B. (1997) *J. of Electrostatics*, 40&41, 711-716

Vatazhin, A.B. (2008) *Electrogasdynamic in aviation applications* // In book "The problems of mechanics". Moscow, "Omega-L

The effect of particle pre-existing charge on unipolar charging and its implication on electrical aerosol measurements

Christof Asbach[1], Chaolong Qi[2,3], Weon Gyu Shin[2], David Y.H. Pui[2], Heinz Fissan[1]

[1] Institute of Energy and Environmental Technology (IUTA), Air Quality & Sustainable Nanotechnology Unit, Bliersheimer Str. 60, 47229 Duisburg, Germany

[2] Department of Mechanical Engineering, University of Minnesota, 111 Church Street SE Minneapolis, MN, 55455, USA

[3] now at: National Institute for Occupational Safety and Health, 4676 Columbia Parkway, Cincinnati, Ohio 45226, USA

Electrical particle chargers are commonly used devices in aerosol measurement technology. Recently, unipolar diffusion chargers have raised increased attention, because the electrical current resulting from the deposition of the charged particles can be tuned to be proportional to either the particle length (TSI EAD model 3070A), the total active surface area ("Fuchs surface area") of particles (Matter engineering, LQ1-DC), or the lung deposited surface area (TSI Nanoparticle Surface Area Monitor, NSAM model 3550 and Aerotrak 9000). Particularly the possibility of measuring particle surface area is of major interest, because several researchers proposed particle surface area to be the most health relevant measure. These instruments are commonly calibrated with uncharged or neutralized particles, which can be considered as representative for aged atmospheric particles. However, if particles are freshly produced or sampled near electrical powerlines or substations or during thunderstorms, they can bear unipolar charges. These pre-existing charges on the particles may interfere with the unipolar charging process in the abovementioned instruments and therefore bias the results.
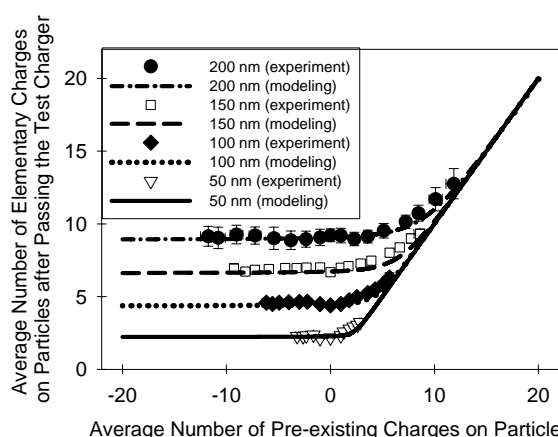
(positive or negative) charge level by using a charger (Chen et al. 1999) before passing them through the tested unipolar diffusion charger from a TSI NSAM. Figure 1 shows that the particles initially carrying negative charges carry almost the same amount of positive charges as the initially uncharged particles after passing the test charger whereas the particles initially carrying positive charges show an increased final charge level. An analytical solution of a model for particle charge distribution of initially charged particles was provided for unipolar charging based on Fuchs' theory and the birth-and-death theory. The Nt value used in this model was obtained by fitting the experimental data of average charge on particles for initially uncharged particles. The results from the analytical solution show very good agreement (see Fig. 1) with experimental data regarding the relationship between the pre-existing charge and the final charge on particles (50 - 200 nm in this study). Experimental tests of the response of the Nanoparticle Surface Area Monitor (NSAM) against initially charged particles demonstrated that NSAM could have a large response deviation of up to 20% in the tested charge level depending on the particle size and the amount of pre-existing positive charges on particles. Modeling of NSAM response showed similar deviation and predicted that when pre-existing charge is high enough, the NSAM response can be as much as 5 to 9 times higher than the response to uncharged particles.

Fig. 1: Effect of pre-existing positive and negative charge on the final particle charge after passing the unipolar test charger

We investigated the effect of particle pre-existing charges on unipolar charging (Qi et al., 2009). Particles were pre-charged to a known unipolar

References

C. Qi , C. Asbach, W.G. Shin, H. Fissan, D.Y.H. Pui (2009): The effect of particle pre-existing charge on unipolar charging and ist implications on electrical measurement, *Aerosol Sci. Technol.* **43** 232-240

D.R. Chen and D.Y.H. Pui (1999): A high efficiency, high throughput unipolar diffusion aerosol charger for nanoparticles, *J. Nanoparticle Res.* **1**:115-126

Method for the estimation of mass concentration in automotive exhaust

L. Hillemann, N. Senftleben, M. Stintz

Institute of Process Engineering and Environmental Technology, TU Dresden, 01062 Dresden, Germany

Keywords: Charge measurement, Instrumentation, Particulate mass, Diesel exhaust

In the field of aerosol technology exist several scientific methods for the measurement of size distributions of aerosols. In technical applications often not the detailed size distribution but only a mean size or a concentration information is required.

For the detection and quantification of particles electrometer are widely used, if the average number of charges per particle $n_e(x)$ is known. The measured electrical current is given by the following equation:

$$I = eQc_n \int n_e(x) q_0(x) dx$$

A single electrometer delivers only the number concentration. To acquire an additional size information several methods are possible: the combination with another measurement principle (Park et al., 2007), the size dependent removal of particle fractions (Burtscher et al., 2008) or the parallel use of different charging mechanisms (Park et al., 2007). The latter method bases on the different relation between the average number of charges per particle and the particle size. For unipolar diffusion and field charging Park et al. (2007) give:

$$n_{e,Diff}(x) \sim x^{1.17}$$

$$n_{e,Field}(x) \sim x^{1.91}$$

In the present work the combination of two corona-jet-chargers is used, employed as diffusion and field charger, respectively. From the measured electrical currents the mean particle size considering a lognormal size distribution is calculated according to Park et al. (2007) (Figure 1).
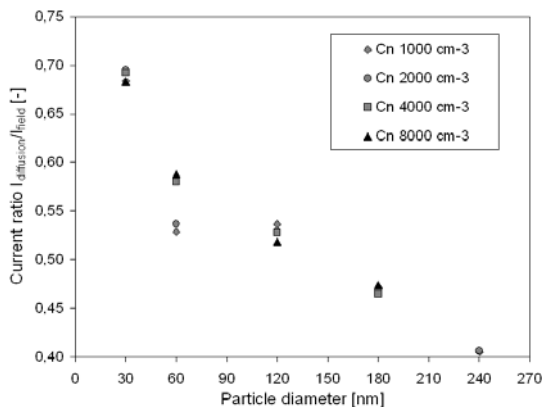
Figure 1. Ratio of the currents measured by both electrometers using different charging mechanisms plotted versus particle size.

Using this data the mass concentration of the aerosol is calculated by:

$$c_m = \frac{K\pi c_n}{6} \int q_0(x) x^3 dx$$

The contribution will show first experimental results. The calculated mass concentration based on the measurement of the electrical currents is compared to direct gravimetric measurement. Additionally the measurement error is estimated (Figure 2).
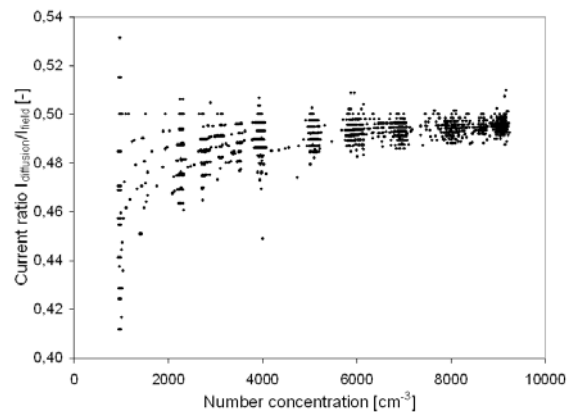
Figure 2. Ratio of the currents versus number concentration, the increasing deviation for lower concentration illustrates the lower limit of the method (particle size 100 nm).

Burtscher, H.; Fierz, M.; Schmidt-Ott, A. (2008), Particle measurement based on diffusion charging, European Aerosol Conference 2008, Thessaloniki, Abstract T04A004O

Park, D.; An, M.; Hwang, J.: Development and performance test of a unipolar diffusion charger for real-time measurements of submicron aerosol particles having a log-normal size distribution (2007). J. Aerosol Science, 38, 420-430.

Park, D.; Kim, S.; An, M.; Hwang, J.: Real-time measurement of submicron aerosol particles having a log-normal size distribution by simultaneously using unipolar diffusion charger and unipolar field charger (2007). J. Aerosol Science, 38, 1240-1245.

Prevention of aerosol particle deposition on wafers by means of gas ionization

P. Gefter[1], J. Menear[1], S. Gehlke[1], J. Salm[2], and E. Tamm[2]

[1]MKS, Ion Systems, 1750 North Loop Road, 94502, Alameda, USA
[2]Institute of Physics, University of Tartu, 18 Ülikooli St., 50090, Tartu, Estonia

Keywords: nanoparticles, air ions, charged particles, particle deposition.

In semiconductor industry, the 45 nm and 33 nm technology nodes move from the development phase to full scale manufacturing, and micro contamination control becomes increasingly important. Nanoparticles with diameters between 16 and 23 nm cause wafer defects because they are half of the feature size. Further, cleaning 16–50 nm particles from a wafer surface is problematic. Beyond time consumption, cleaning has been shown to destroy fragile multi-layer structures.

The presentation discusses several models of an electrostatically charged wafer and different methods of wafer charge measurement. Wafer charge (in nanocoulombs) is directly measured with a Faraday Cup or a Faraday FOUP. Both measurement tools serve well to quantify total accumulated charge. The Faraday FOUP offers two practical advantages: First, the measurement can be automated, because the Faraday FOUP fits onto a SEMI standard load port. Second, background measurement noise is less because manual wafer handling is avoided. Lower noise permits accurate measurement of the low charge levels that affect nanoparticles deposition.

The environment inside a SEMI tool plays a dominant role in micro contamination control efficiency. Temperature, humidity, air velocity and pressure are normally used to characterize the tool environment. More specific contamination control parameters are proposed. They are: (1) aerosol particle size distribution, (2) time variation of particle concentration, (3) particle charge distribution, (4) positive and negative air ion concentration, (5) electrostatic field strength created by charged wafers, and (6) electrostatic field strength created by equipment (robotic) parts.

The focus of this presentation is that (1) air-borne nanoparticles concentrations and (2) electrostatic field strength should be considered together. First, as the concentration of airborne nanoparticles decreases, the probability of deposition onto the wafer decreases. Second, electrostatic attraction of charged nanoparticles is the dominant deposition mechanism. Electrostatic attraction is roughly 100 times more important than diffusion or impaction.

Analysis and control of nanoparticles (particularly, 10–50 nm) differs from the control of particles greater than 100 nm. When the technology node was 180 nm, laser particle counters with 100 nm sensitivity provided information on defect-causing particles. And controlling electrostatic fields above 250 V/cm was normally sufficient. For 45 nm technology, 100 nm particle counters no longer suffice since killer particles are well below the counter's detection threshold. And electrostatic fields below 50 V/cm affect nanoparticles deposition rates. For a given charge level, small particles move faster than large particles in an electrostatic field. Hence, small particles deposit in a shorter period of time.

One of the most reliable and efficient ways to prevent small particle deposition is to control positive and negative air (gas) ion concentration inside the tool. Pulsed gas ionization with alternating polarity provides a double-fold effect on particle deposition rate. First, high ion concentration prevents charge accumulation on wafers and ungrounded machine parts. Second, air (gas) ionization decreases particle concentration inside the processing chamber, as preliminary experiments have shown.

Measurements of 10 nm particle concentration and control of electrostatic field levels (guidelines SEMI E78-0708) are recommended. Semiconductor equipment that passes a test at 10 nm has an extended lifetime that ranges from the 90 nm technology node to the 22 nm technology node, provided that the E78-0708 guidelines are met.

Equipment vendors and chip fabricators do not have to redesign for each technology node. This positively affects profitability by eliminating redundant equipment qualifications and reducing downtime for equipment upgrades.

Corresponding author: Dr. Jaan Salm
E-mail: jaan.salm@ut.ee

Scavenging efficiencies and contact freezing of supercooled cloud droplets for charged aerosol particles: Laboratory experiments

Daniel Rzesanke and Thomas Leisner

Forschungszentrum Karlsruhe, Institute of Meteorology and Climate Research,
Atmospheric Aerosol Research Department, POB 3640, 76021 Karlsruhe, Germany

Keywords: Aerosol cloud interactions, Charged particles, Climate effect, Heterogeneous ice nucleation

The global electric circuit is one of the candidates for a potential coupling of terrestrial climate with solar activity (Friis-Christensen, 2000). It has been suggested that the vertical electric currents in the atmosphere, which are carried by ions, ionic clusters and electrified aerosol particles can modify the cloud microphysics and thereby can link the atmospheric layers (Tinsley, 2000).

In the framework of the DFG priority program CAWSES ["*Climate And Weather of the Sun-Earth System*"] (CAWSES, 2009) we conduct laboratory experiments which quantify the interaction between electrified aerosol particles and cloud droplets in order to assess the atmospheric relevance of this link between the higher and lower atmosphere. More specific, we quantify the influence of charges, electrical fields and ionizing radiation on the heterogeneous and homogeneous freezing nucleation in cloud droplets.

These experiments are carried out under realistic atmospheric conditions on individual particles in electrodynamic levitation inside a miniaturized climate chamber (Davis, 1997; Duft *et al.*, 2002). The main methods of investigations are microscopy, microspectroscopy and light scattering analysis (Duft & Leisner, 2004).

Inside an electrodynamic balance (EDB) a supercooled cloud droplet can be exposed to a high laminar and cooled aerosol flow. Thereby high number concentrations of atmospheric representative aerosol particles carrying a single elementary charge can be provided.

As seen in Fig. 1 a charged droplet will be discharged in an oppositely charged aerosol flow. We are able to specify the collection rate for charged cloud droplets, which efficient collection diameter is much larger then the geometrical, as a function of charge. With this setup it is also possible to provide aerosol particles acting as heterogeneous freezing nuclei (contact freezing). Thereby the aerosols ice nucleation ability is a function of size and composition.

We will present results on the scavenging efficiency, discharging rate and freezing ability of charged droplets exposed to an aerosol flow as a function of droplet charge and aerosol size and composition.
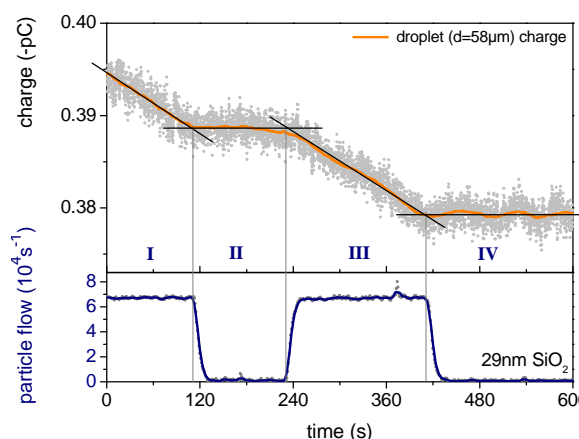
Figure 1. Upper panel: Aerosol uptake (SiO_2 particles, 29 nm in diameter) by a charged 58 µm droplet seen by droplet discharge. From the slope of the curve in regions 1 and 3, the effective scavenging efficiency of the droplet can be determined to be 79 ($d_{effective}$=516 µm).
Lower panel: Aerosol flow past the droplet. All aerosol particles carry one positive elementary charge.

CAWSES, 2009. www.bu.edu/cawses/, (Feb., 2009)

Davis, E. J. (1997). *A history of single aerosol particle levitation*, Aerosol Science and Technology **26**

Duft, D., et al. (2002). *Shape oscillations and stability of charged microdroplets*, Physical Review Letters **89** (8)

Duft, D., & Leisner, T. (2004). *The index of refraction of supercooled solutions determined by the analysis of optical rainbow scattering from levitated droplets*, International Journal of Mass Spectrometry **233** (1-3)

Friis-Christensen, E. (2000). *Solar variability and climate*, Space Science Reviews **94**

Tinsley, B. (2000). *Influence of solar wind on the global electric circuit, and inferred effects an cloud microphysics, temperature, and dynamics in the troposphere*, Space Science Reviews **94**

Aerosol charging room: a simple model

J. Salm

Institute of Physics, University of Tartu, 18 Ülikooli St., 50090, Tartu, Estonia

Charging of aerosol particles is used in several appliances: in aerosol precipitators, in aerosol measuring apparatus etc. Diffusion charging by means of small air ions is mainly applied. Unipolar air ions are generated for the charging in most cases. The aerosol particles to be charged should sojourn in a room enriched with air ions for certain time. In order to design a charger, it is necessary to know the air ion parameters in the room, first of all the space charge density of air ions.

Let us consider a simplified one-dimensional steady state model according to Figure 1. There are two parallel plane electrodes that do not hinder gas flow, e.g. conductive grids. A potential difference U is maintained between the electrodes. The ions of one polarity are generated with a constant rate at the plane $x = 0$. Further the ions are transported towards x-direction by means of gas flow and of electric field.
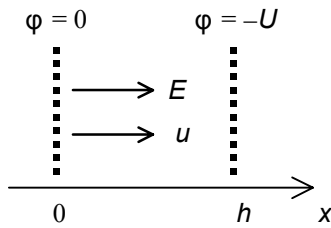
Figure 1. Schema of the charging room.

The current density j is proportional to the gas flow speed u and to the electric field strength E:

$$j = \rho(u + ZE), \qquad (1)$$

where ρ is the space charge density and Z is the electrical mobility of small air ions. The current density is considered as independent of flow speed and electric field strength.

The space charge modifies the electric field, and therefore the quantities ρ and E are not independent of x. The changes of E are determined by means of the Poisson equation

$$\varepsilon_0 \frac{dE}{dx} = \rho , \qquad (2)$$

where ε_0 is the electric constant.

In principle, it is possible to solve the system of Equations (1) and (2) in order to find ρ and E at any distance between the electrodes. However, due to non-linearity, the solution is complicated. Let us consider the limiting cases: (1) the electric current density is determined mainly by the gas flow or by the electric field, but the effect of space charge is negligible; (2) the current density is considerably limited by space charge.

In the first case, the current density is approximately expressed as

$$j \approx \rho \left(u + Z \frac{U}{h} \right). \qquad (3)$$

The space charge density can be found from Equation (3), but the current density should have a low value:

$$j \ll \frac{\varepsilon_0}{Zh} \left(u + Z \frac{U}{h} \right)^2 . \qquad (4)$$

In the second case, the current density is mainly determined by the electric field originated from the space charge,

$$j = \rho Z E, \qquad (5)$$

and

$$j \gg \frac{\varepsilon_0}{Zh} \left(u + Z \frac{U}{h} \right)^2 . \qquad (6)$$

It is possible to solve the system of Equations (2) and (5) and to express ρ and E. In the extreme case, $\rho \to \infty$ and $E \to 0$ at $x = 0$. Then

$$\rho = \sqrt{\frac{\varepsilon_0 j}{2Zx}} , \qquad (7)$$

and

$$E = \sqrt{\frac{2 j x}{\varepsilon_0 Z}} . \qquad (8)$$

Integrating the function (8) from 0 to h, it is possible to find the potential difference U, and to express the current density:

$$j = \frac{9 \varepsilon_0 Z U^2}{8 h^3} . \qquad (9)$$

Similar equation has been published by Mott and Gurney in 1940 for conductive current in ionic crystals.

Corona-Quenching by submicrometer particles in turbulent tube-wire electrostatic precipitators

C. Luebbert[1], U. Riebel[1]

[1]Lehrstuhl Mechanische Verfahrenstechnik, Brandenburgische Technische Universitaet Cottbus, 03046, Cottbus, Germany

The suppression of current uptake in electrostatic precipitators by space charge attached to low mobility particles is known as corona-quenching. A physical model is developed which allows the description of this effect by equations which can be solved analytically. In contrast to space charge simulations done by many other authors (Talaie (2005), Elmoursi & Castle (1984), Lindau & Matts (1984)) our model directly shows the dependence of corona-quenching on particle size and concentration, on geometry and electric parameters.

The model departs from a superposition of externally imposed electric field the space charge electric field in the quenched state, whereby the contribution of gas ions is neglected. This allows establishing a balance equation for space charge, whereby the deposition of charged particles to the walls is directly connected to the increase of charge on individual particles during the quench process.

$$c \cdot \left(\frac{dn}{dt}(\bar{n}) \right) = \bar{n} \cdot \left(\frac{dc}{dt} \right)$$

c: Particle number concentration
n: Number of elementary charges per particle
t: time

Macroscopic charging kinetics and current uptake in the quenched regime are derived from a Lambert-Beer-style extinction function for the gas ions passing through the aerosol, whereby the extinction coefficient considers the mechanisms of single particle charging kinetics and electric field strength.

$$I(r_{tube}) = I(r_{wire}) \cdot \exp\left\{ -\frac{c}{Z_i} \cdot \int_{r_{wire}}^{r_{tube}} \frac{\Lambda(r)}{E(r)} \cdot dr \right\}$$

I: Current
n: Z_i Ion mobility
E: Electric field strength
r: radius coordinate
Λ: ion-particle combination coefficient

A well mixed tube-wire electrostatic precipitator operated in a batch-wise mode was used to verify the basic assumptions as well as the complete time dependent current uptake by highly resolving measurements.
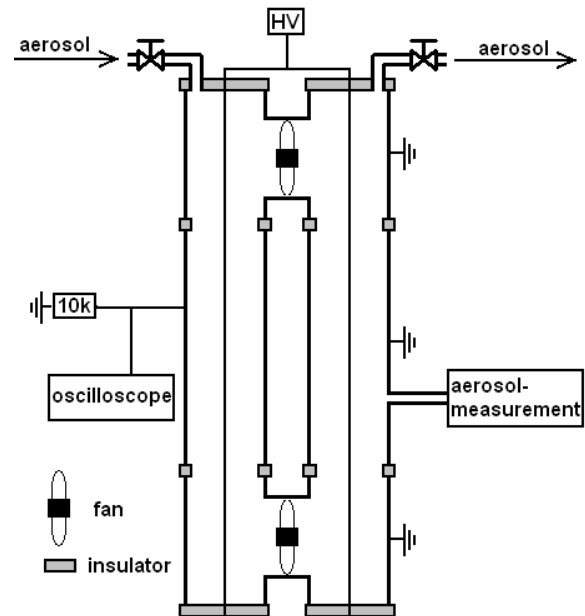
Fig.1: Experimental setup for corona-quenching measurement
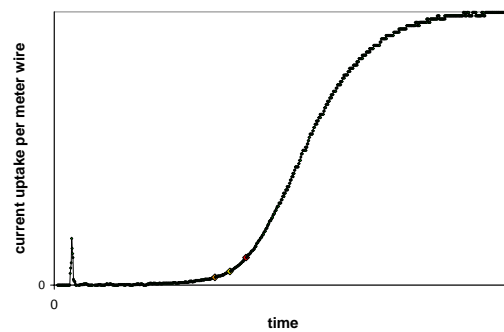
Fig.2: Typical time time dependent current uptake measured the setup in Fig.1

Talaie, M. R. (2005). *J. Hazardous Materials*, (B124), 44-52.

Elmoursi, A. A. & Castle, G. S. P. (1984). Second international conference on electrostatic precipitation, Kyoto, Nov. 1984, 911-919.

Lindau, L. & Matts, S. (1984). Second international conference on electrostatic precipitation, Kyoto, Nov. 1984, 911-919.

T07 Fundamentals

Mass transfer to a chemically active particle in the transition regime

A.A. Lushnikov

Karpov Institute of Physical Chemistry, 10, Vorontsovo pole, 105064 Moscow, Russia

Keywords: absorption, aerosol chemistry, condensation, evaporation, sticking probability.

A theory of chemical uptake of gaseous reactants by aerosol particles is developed for arbitrary regimes of reactant transport. The size dependence of uptake efficiency is found for non-unity values of sticking probabilities of the reactant molecules to the particle surface. Three key points of the present consideration are:

i. A modification of Maxwell's boundary condition for the distribution of condensing molecules over coordinates and velocities. This modified boundary condition allows accounting for the transport of reactants across the particle surface.

ii. The solution of the collisionless Boltzmann's equation for the distribution function of reactant molecules in the free molecule zone and matching thus found concentration profile with that in the diffusion zone.

iii. The flux conservation in the form "the reactant flux from outside = consumption of the reactant inside" is used for formulating a set of rather simple equations describing the kinetics of chemical uptake. The following processes are considered:

i. kinetics of particle growth in absence of chemical reactions,

ii. kinetics of uptake by a particle containing active reactant (the first and the second order kinetics)

iii. Reactant dissociates inside the particle.

The final output of the present consideration:

i. estimation of the characteristic times for uptake in a variety of situation,

ii. kinetic curves (the dependence of reactant population inside the particle on time, on the sticking probability, Knudsen number etc.).

In contrast to "normal" condensation and evaporation no simple formulas exist so far describing the mass transfer to (from) a chemically active aerosol particle in the transition regime.. The attempts grounded on the numerical solution of the Boltzmann equation presented in Williams & Loyalka, 1991 are too complicated for everyday use. It is very desirable to have something similar to the Fuchs-Sutugin formula for the condensational efficiency of aerosol particles. Below we present our attempt to derive such a formula. To this end we apply the scheme developed in Lushnikov & Kulmala, 2004.

Let $J(a)$ be the mass flux onto the particle of radius a. We introduce the particle mass transfer efficiency $\gamma(a)$ as follows:

$$J(a) = \gamma(a)(n_\infty - n_a^+ / \beta), \qquad (1)$$

Here β is the mass accommodation coefficient, a is the particle radius, and $n_a^{+,-}$ stands for the reactant concentration above (+) or beneath (-) the particle surface. In contrast to "normal" case these concentrations are regulated by the diffusion-reaction process inside the particle and the diffusion of the reactant in the gas phase. The boundary concentrations of the reactant are linked by the Henri law $n_a^- = H n_a^+$, with H being the dimensionless Henri constant. The efficiency $\gamma(a)$ can be expressed in terms of the diffusivity D of the gaseous reactant and the thermal velocity of the gas molecules as follows:

$$\gamma(a) = \frac{\gamma_{fm}}{1 + \beta S(a v_T / 2D)}, \qquad (2)$$

where $S(x) = \sqrt{1 + x^2}$ and $\gamma_{fm} = \beta \pi a^2 v_T$ is the uptake efficiency in the free-molecule regime.

Lushnikov, A.A., & Kulmala, M. (2004) *Phys. Rev. E 70*, 046413-1 – 9.

Williams, M.M.R. & Loyalka, S.K. (1991). *Aerosol Science. Theory & Practice*, Oxford, New York, Seoul, Tokyo, Pergamon P ress.

Statistical analysis of different proxy values for sulphuric acid concentration

S. Mikkonen[1], J. Joutsensaari[1], S. Romakkaniemi[1], T. Petäjä[2], T. Nieminen[2], R.L. Mauldin III[3], M. Kulmala[2], and A. Laaksonen[1]

[1] Department of Physics, University of Kuopio, P.O.B 1627, FIN-70211 Kuopio, Finland
[2] Department of Physics, University of Helsinki, P.O.B 64, FIN-00014 Helsinki, Finland
[3] Atmospheric Chemistry Division, National Center for Atmospheric Research, Boulder, CO, USA

Keywords: solar radiation, statistical analysis, sulphur dioxide, sulphuric acid.

Sulphuric acid is known to be a significant factor in the new particle formation in the atmosphere (e.g. Kulmala et al., 2006) and the number concentration of freshly nucleated particles is found to have a strong dependency on sulphuric acid (Sihto et al., 2006). The problem is that gas phase sulphuric acid concentration is difficult to measure and in many measurement sites no H_2SO_4 data is available. The purpose of this study is to test how the different proxies predict the real sulphuric acid concentration in two different datasets measured in Hyytiälä, Finland, in 2003 and 2007.

Using a proxy for sulphuric acid concentration is based on chemical reaction $SO_2 + OH \rightarrow H_2SO_4 + HO_2$. Integrating the differential equation for sulphuric acid concentration $d[H_2SO_4]/dt = k \cdot [OH] \cdot [SO_2] - [H_2SO_4] \cdot CS$, where CS is condensation sink and k is temperature dependent reaction constant, gives the sulphuric acid concentration at given time. To simplify the problem, it can be assumed that the sulphuric acid production is in steady-state with its loss, i.e. $d[H_2SO_4]/dt = 0$, which leads to a proxy function given by $[H_2SO_4] = k \cdot [OH] \cdot [SO_2] \cdot CS^{-1}$. Measurements show that OH concentration is highly correlated with intensity of solar radiation, and if OH is not available, it is possible to use a proxy given by $[H_2SO_4] = k \cdot Radiation \cdot [SO_2] \cdot CS^{-1}$.

Petäjä et al. (2008) used some proxies to dataset measured in Hyytiälä, Finland during EUCAARI 2007 campaign. Their results suggest that the best approximation for sulphuric acid concentration is a product of SO_2 and either OH or solar radiation divided by condensation sink. The results of our study indicate that from the statistical point of view, the role of CS in the proxy is either minor, or in some cases it may even decrease the prediction ability of the proxy.

Nonlinear fitting procedure was conducted to both datasets, with a fit function given by $[H_2SO_4] = a \cdot Radiation^b \cdot [SO_2]^c \cdot CS^d$, and it suggests that the power c for SO_2 concentration is approximately 0.5. Using the square root of SO_2 in the proxy increased the prediction ability significantly (Table 1.) and the best results were gained in Hyytiälä 2007 data with $[H_2SO_4] = a \cdot k \cdot [OH] \cdot [SO_2]^{0.5}$, where a is regression slope and k is temperature dependent reaction constant. OH was not measured during the Hyytiälä 2003 campaign, so that we had to use calculated OH values. As can be seen, the prediction results with calculated OH were not very good. The best prediction was attained with $[H_2SO_4] = a \cdot k \cdot Radiation \cdot [SO_2]^{0.5}$ which was also the best proxy in the 2007 data if OH was left out. Beside global radiation, we were also tested UV-A and UV-B in the proxy but the prediction ability did not improve significantly. The reason for the better performance of proxies with square root of SO_2 can only be speculated, but it is possible that it has to do with the somewhat unrealistic steady-state approximation.

Table 1. Coefficient of determination R^2 for different proxies in both datasets. Note that OH in 2003 data is a calculated value. Glob refers to global radiation.

Proxy $H_2SO_4=$	R^2 2003	R^2 2007
k*Glob*$[SO_2]$*CS^{-1}	0.77	0.59
k*OH*$[SO_2]$*CS^{-1}	0.69	0.71
k*Glob*$[SO_2]$	0.75	0.62
k*OH*$[SO_2]$	0.76	0.65
k*Glob*$[SO_2]^{0.5}$*CS^{-1}	0.55	0.43
k*OH*$[SO_2]^{0.5}$*CS^{-1}	0.47	0.55
k*Glob*$[SO_2]^{0.5}$	0.88	0.71
k*OH*$[SO_2]^{0.5}$	0.71	0.78

Brief tests were also made to long term data measured in Hohenpeissenberg, Germany (Birmili et al., 2003) and the results were similar as for Hyytiälä.

Birmili, W., et al. (2003), Atmos. Chem. Phys., 3, 361-376
Kulmala, M., et al. (2006). Atmos. Chem. Phys., 6, 787-793.
Petäjä, T. et al. (2008). Atmos. Chem. Phys. Discuss, 8, 20193-20221.
Sihto, S.-L., et al. (2006). Atmos. Chem. Phys., 6, 4079-4091.

Critical size of charged aerosol particles in the presence of adsorbable foreign gas

V.V. Levdansky[1], J. Smolik[2] and P. Moravec[2]

[1]Heat and Mass Transfer Institute NASB, 15 P. Brovka Str., 220072 Minsk, Belarus
[2]Institute of Chemical Process Fundamentals AS CR, v.v.i., Rozvojova 135, 165 02 Prague 6, Czech Republic

Keywords: charged particles, condensation, adsorption.

The processes of nucleation and condensation growth of particles (clusters) are of interest both for atmospheric phenomena and for different fields of new technology related to the production and use of nanoparticles. It is known that the charge of particles (clusters) can essentially affect the critical size of particles and the rate of homogeneous nucleation (Reist, 1993).

Let us consider the joint effect of the particle charge and the presence of adsorbable foreign gases on the critical size of particles. Further, we for simplicity do not examine the effect related to a change of the concentration of polar molecules of the vapor near the particle surface due to the particle charge (Nadykto *et al.*, 2003).

Taking into account the dependence of the surface tension on the pressure of the adsorbable foreign gas according to (Luijten *et al.*, 1997), we can obtain following equation for the critical diameter d_{cr} of the particle with the elementary charge q:

$$\ln S = \frac{V_m}{kT}\left[\frac{4\sigma_0}{d_{cr}} - \frac{2q^2}{\pi d_{cr}^4}\left(\frac{1}{\varepsilon_g} - \frac{1}{\varepsilon_p}\right)\right]$$

$$+ \frac{4V_m n_a}{d_{cr}}\ln\left(\frac{P_L}{P_a + P_L}\right) - \ln\left(\frac{\alpha_c}{\alpha_e}\right), \qquad (1)$$

where S is the saturation ratio, k is the Boltzmann constant, T is the temperature, V_m is the volume per molecule in the particle, ε_p and ε_g are respectively the dielectric constants of the particle substance and the gas phase, α_c is the condensation coefficient, α_e is the evaporation coefficient, σ_0 is the surface tension of the pure substance (i.e. the substance without adsorbed molecules of the foreign gas), n_a is the number of adsorption sites per unit area, P_a is the foreign gas pressure; the value of P_L can be written as

$$P_L = \frac{n_a(2\pi m_a kT)^{1/2}}{\beta\tau}. \qquad (2)$$

Here τ is the adsorption time of foreign gas molecules (it can depend in the general case on the particle charge), m_a is the mass of the molecule of the foreign gas, β is the sticking coefficient of the foreign gas molecules for the part of the surface not occupied by adsorbed molecules.

It is seen from Eq. (1) that in the case, when $\alpha_c/\alpha_e < 1$, the effect of the adsorbable foreign gas can compensate to some extent the effect related to a difference in the condensation and evaporation coefficients (e.g. in the case of the size-dependent condensation coefficient).

Figure 1 shows the dependence of $\ln S$ on the critical diameter of the charged water drop.
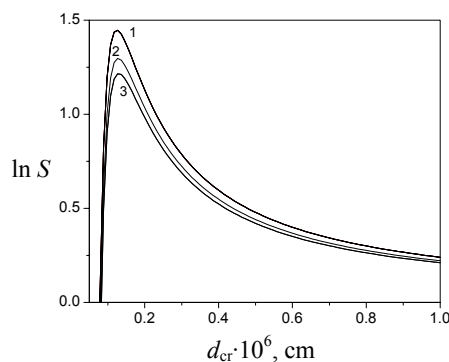
Figure 1. Dependence of $\ln S$ on the critical diameter of the water drop with the elementary charge at $T = 273$ K and $\alpha_c = \alpha_e$; 1: $P_a = 0$, 2: $P_a/P_L = 0.3$, 3: $P_a/P_L = 0.5$.

It is seen from Fig. 1 that with the increase of P_a/P_L the value of S corresponding to the definite value of d_{cr} decreases.

Reist, P. C. (1993). *Aerosol Science and Technology.* New York: McGraw-Hill.
Nadykto, A. B., Makela, J. M., Yu, F., Kulmala, M., & Laaksonen, A. (2003). *Chem. Phys. Lett.*, 382, 6-11.
Luijten, C. C. M., Bosschaart, K. J., & van Dongen, M. E. H. (1997). *J. Chem. Phys.*, 106, 8116-8123.

The role of optical radiation in the homogeneous nucleation

V.G. Chernyak and E.S. Evgrafova

Department of Physics, Ural State University, 620083 Yekaterinburg, Russia

The physical and mathematical model of homogeneous nucleation kinetics in a supersaturated vapor in an optical radiation field has been developed. It is of interest for the modern atmosphere research techniques and also from the standpoint of partial control of the nucleation process. A feature of this problem lies in the fact that the temperature of nucleus differs from the equilibrium temperature of a vapor, a fact that can be explained either by the absorption of the light by the particle or by removal of the latent heat of phase transition. Expression for change of the free energy has the form (Bashkirov and Fisenko, 1981)

$$\Delta\Phi = \Delta\Phi_0 + cg\left(\langle T_p \rangle - T_0\right)\left(\frac{L}{cT_0} - 1\right), \quad (1)$$

where $\Delta\Phi_0$ is the isothermal work of nucleation, c is the heat capacity of particle, T_0 is the equilibrium temperature of a vapor, c is the heat capacity per condensed phase molecule, $\langle T_p \rangle$ is the particle temperature averaged over the particle volume and L is the latent heat of phase transition per condensed phase molecule. The second term in Eq. (1) takes into account the change of free energy due to the absorption of the radiation by the particle and due to the removal of the latent heat of phase transition. The nucleus is macroscopic particle. The wave length of radiation is much greater than the radius of nucleus.

We assume that the relative change of nucleus temperature is small, i.e. $\left(T_p - T_0\right)/T_0 \ll 1$. The temperature of the nucleus was defined from the solution of the heat conductivity equation considering the absorption of radiation by the particle. The boundary conditions to the heat conductivity equation require the temperature limit at the particle centre and continuity of radial heat flux at its surface. It has allowed taking into account the thermal physical and optical properties of the nucleus.

We consider the free-molecule regime, in which the mean free path of molecules in vapor is much greater than the radius of nucleus. In addition, it has been assumed that the radius of the particle is much less than the wavelength of radiation. For further calculations the Frenkel-Zeldovich's classical method (Lifshitz & Pitaevskii, L. P. (1981) was used and the expressions for radius of a critical nucleation center and nucleation rate have been obtained. Dependencies of these quantities on intensity and frequency of radiation, optical properties of the

nucleus and thermophysical parameters of a vapor have been calculated. It is shown that with a increase of intensity or frequency of radiation, the radius of a critical nucleus value also increases, however the nucleation rate value decreases. The absorption of radiation by the formed nucleus stimulates its evaporation and hence leads to increase in the minimal size at which this nucleus appears viable and continues to grow. At particular value of radiation intensity $I = I_m$ the radius of critical nucleus should be the infinite. Physically it means that occurrence of viable nucleation centers in supersaturated vapor at $I \geq I_m$ is impossible.

We made some numerical estimates for water vapor under typical experimental conditions. The source of light is a tunable dye CO_2 – laser with wave length ~ 10.6 μm. The result of calculation for relative nucleation rate J/J_0 (J_0 is the isothermal nucleation rate at I=0) depending on radiation intensity is presented in Fig.1.
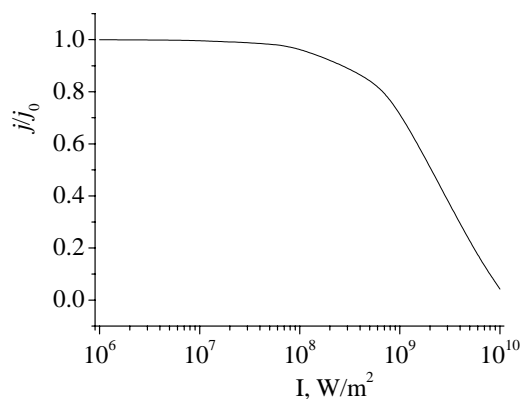
Figure 1. The nucleation rate in supersaturated water vapor as a function of the radiation intensity.

As is seen from the Figure 1, the influence of radiation becomes essential at $I > 10^8 \ W/m^2$.

Bashkirov A.G. and Fisenko S.P. (1981) Teor. and Matemat. Fizika **48**, 106.

Lifshitz, E. M., & Pitaevskii, L. P. (1981). *Physical Kinetics*: *Course of Theoretical Physics by L. Landau and E.M. Lifshitz.* Oxford: Pergamon, Vol. 10.

Particle formation close to supersaturated droplets

B. Svenningsson[1,2] and M. Bilde [2]

[1]Department of Physics, Lund University, Box 118, S-221 00, Lund, Sweden
[2]Department of Chemistry, University of Copenhagen, Universitetsparken 5, DK-2100, Copenhagen, Denmark

Keywords: particle formation, solubility, droplets, deliquescence, dicarboxylic acids,

The aim of this contribution is to describe a mechanism by which supersaturations, high enough to activate clusters and initiate the early particle growth, can be created locally, in the vicinity of supersaturated droplets. As examples of candidate substances, the calculations are made for succinic acid, adipic acid, and cis-pinonic acid, the later is an oxidation product of alpha-terpene. The calculations made are estimates made to illustrate principles and trends, not aiming at exact values.

By applying the Kelvin effect on some organic acids we estimate that saturation ratios of 4-50 are needed to activating clusters, 1.5 nm in diameter, with compounds having surface free energies in the range 0.073-0.2 N/m^2.

The mechanism presented here, by which high vapour saturation ratios can be achieved in the vicinity of droplets, applies to hygroscopic compounds with stable crystal structures that result in low solubilities and low solid state equilibrium vapour pressures.

At its deliquescence relative humidity, an organic acid in a saturated solution is in equilibrium with its solid. They should thus both be in equilibrium with the same gas phase concentration of the organic acid. It is well known that aqueous solution aerosol particles most often remain in aqueous phase, forming supersaturated solutions, when the relative humidity is decreased below the deliquescence point. The organic acid equilibrium vapour pressure over such a solution increases with increasing concentration of the organic acid in the aqueous solution, resulting in higher equilibrium vapour pressures over a supersaturated solution than over a saturated solution and over a solid particle of the same organic acid. Small solid state particles can thus grow by condensation of the organic compound, at the same time as the compound evaporates from the aqueous solution. The mechanism is somewhat analogous to growth of ice crystals at the expense of liquid water droplets in mixed phase clouds.

Laboratory studies investigating the mechanism has been performed and will be presented.

The relevance of the proposed mechanism for laboratory studies and risks for artefacts will be discussed.

The atmospheric importance of the mechanism is not clear. Arguments acting in favour as well as against it will be presented.. Also, atmospheric conditions during which the mechanism possibly can play a role will be discussed.
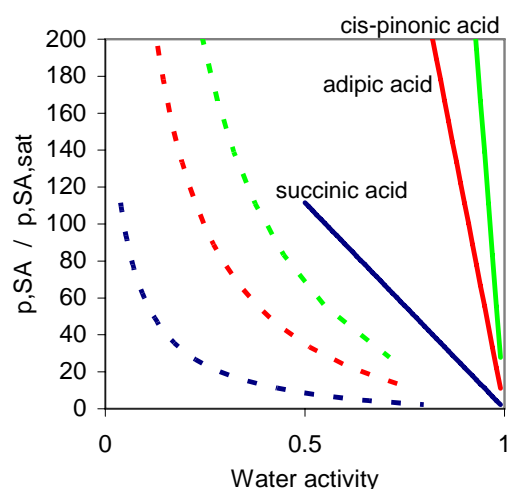
Figure 1. : Ratios between the saturation vapour pressure over the solid state and that over an aqueous solution of the organic acid only (solid lines) and aqueous solutions with organic acid and ammonium sulphate (dotted lines, mass ratio 1:9) for succinic (blue), adipic (red) and cis-pinonic acid (green), respectively. The curves are obtained by assuming Raoults law for both the water activity and the activity of the organic acid.

Riipinen, I., B. Svenningsson, I. Koponen, M. Bilde, K. E. J. Lehtinen, and M. Kulmala (2006), *Atmospheric Research*, 82, 579-590.

Size dependent nanoparticle transport in rising bubbles

M. Hermeling[1] and A.P. Weber[1]

[1] Institute of Mechanical Process Engineering. Clausthal University of Technology, 38678, Clausthal-Zellerfeld, Germany

High product purity and good bioavailability of substances are important in the pharmaceutical industry. Several conventional techniques, like milling or high-pressure homogenization, reduces the particle size, what improves the bioavailability, but the disadvantages are contamination and morphology changes of the product (Juhnke , 2006).

As an alternative supercritical fluids may be used in the form of RESSAS (Türk & Lietzow, 2004; Young *et al.*, 2003). The Rapid Expansion of a Supercritical Solution (CO_2 and solved pharmaceutical substance) into an Aqueous Solution (with added surface active substances) leads to small bubbles, in which the nanoparticles were produced. Due to the high material concentration, the particles tend to form agglomerates by diffusion in the gas phase of the rising bubbles.

Beside the agglomeration, the particles (agglomerates or primary particles) could be transported to the interface and then transferred into the suspension. There the particles are stabilized against further agglomeration by surface active substances.

To investigate the mass transfer of nanoparticles from the gas phase into the suspension depending on the particle size a model system was used, consisting of a bubble column and carbon particles (see Figure 1).
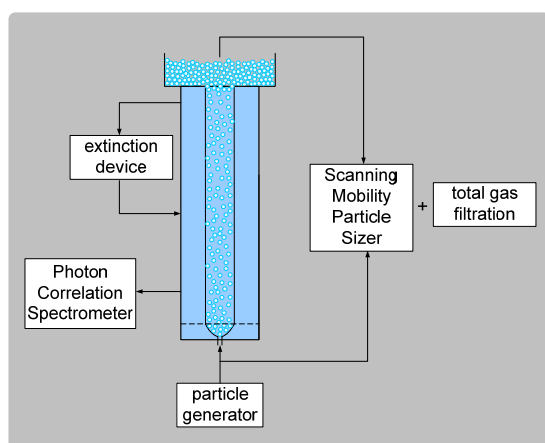
Figure 1. Model system for the investigation of the size depending separation efficiency

For different mean mobility equivalent diameters carbon-nanoparticles were produced with constant number concentrations. The particle mass concentration was determined by filter measurements and compared with the particle mass in the suspension as measured by extinction. Table 1 show the separation efficiency for constant residence time of the bubbles in the liquid (t = 0.75 s). As expected om the basis of existing models for the transfer of aerosol particles to the interface in rising bubbles (Fuchs, 1964; Pich & Schütz, 1991), the separation efficiency of smaller particles is higher than for larger particles.

Table 1. separation efficiency depending on particle size

Particle size (nm)	Total produced particle mass (mg/h)	Particle mass in suspension (mg/h)	Separation efficiency (%)
48	0,114	0,104	91
82	0,174	0,135	77,5

Separation efficiency of further particle sizes, especial smaller mobility equivalent diameter (about 20 nm) will be presented in this contribution. In addition, the results for the overall mass balance will be presented. Therefore, the aerosol behind the bubble column will be measured and compared with the aerosol in front of the bubble column.

Fuchs, N. A. (1964). *The Mechanics of Aerosols*. Pergamon Press. Oxford

Juhnke, M. (2006). *Dissertation*. Cuvillier Verlag Göttingen.

Pich, J. & Schütz, W. (1991). *J. Aerosol Science*, 22, 267-272.

Türk, M. & Lietzow, R. (2004). *AAPS PharmSciTech* 5 (4) Article 56.

Young, T., Johnston, K.P., Pace, G.W. & Mishra, A.K. (2003). *AAPS PharmSciTech* 5 (1) Article 11.

Temperature dependence of the contact angle for n-propanol on silver and on sodium chloride substrate

T. Pinterich, S. Schobesberger, A. Vrtala, P. M. Winkler and P. E. Wagner

Faculty of Physics, University of Vienna, Boltzmanngasse 5, A-1090
Wien, Austria

Keywords: Contact Angle, Heterogeneous Nucleation, Physical Vapour Deposition

According to the classical nucleation theory (Fletcher, 1958) heterogeneous nucleation on aerosol particles strongly depends on the contact angle. Recently Schobesberger (2008) measured the temperature dependence for heterogeneous nucleation of n-propanol vapour on NaCl-particles and on silver-particles. A strange temperature dependence for the nucleation process of n-propanol vapour on NaCl was found. This unexpected behaviour may be explained by a temperature dependence of the contact angle. Consequently we studied the contact angle as a function of temperature.

Measurements were performed using a modified Krüss K12 Tensiometer, featuring a refrigerated double-walled glass top. This allows a precise setting of the temperature of the immersed probe and the surface of the observed liquid and thus the temperature both of the surrounding air and of the liquid is well defined.

Contact angle measurements between silver and n-propanol were performed using the dynamic Wilhelmy-method, where a probe with well defined dimensions is immersed into or withdrawn from a liquid with known surface tension. Since a uniform geometry for the analysed silver probes is required, multiple cutting and polishing stages were performed up to the accomplishment of a 0.04 µm grain size. The probes were made out of a 925 sterling silver plate. Influences on measurements related to the 7.5% residual copper-content are additionally avoided by making use of 99.9% silver-powder evaporation process via Physical Vapour Deposition (PVD). The investigated temperatures were ranging from 0°C to 30°C. The immersion-depth of the probes amounted to 3 mm. This depth was found to be an optimal compromise satisfying both sufficient immersion and short measuring time.

Results show that the number of PVD-steps influences the contact angle and its temperature dependence. With increasing number of PVD-processes not only the value of the contact angle is reduced but also its temperature dependence changes. Figure 1 illustrates the temperature dependence for the case of 1 PVD-step.
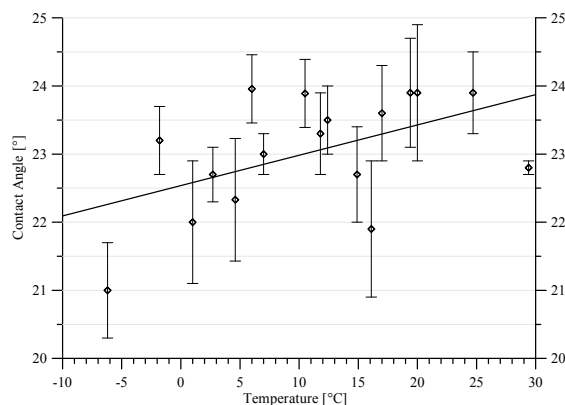
Figure 1. Temperature dependence of the contact angle for n-propanol on silver using a one time vaporised plate (1 PVD-step)

For the determination of the contact angle between organic liquids and sodium chloride substrate, the Washburn-method was used. This sorption method makes contact angle measurements between liquids and powder-form solids possible. Based on the experimental determination of the capillary climbing speed of the liquid the contact angle is calculated assuming the observed powder to be a bundle of capillaries. This approximation requires an experimental determination of the observed powders material constant. For every measurement 4 g NaCl-powder was filled into a glass tube with a filter base and this was suspended from the balance of the Tensiometer.

Experimental results indicate an angle of 0° at 20°C, in agreement with the value reported by Ortner (2000). Investigations with a Goniometer further confirm this result. Implications of the obtained results for heterogeneous nucleation processes will be reported later.

Schobesberger S. (2008). *Strange Temperature Dependence Observed For Heterogeneous Nucleation of n-Propanol Vapor On NaCl Particles,* Diplomathesis at University of Vienna.

Fletcher, N. H., (1958). *J. Chem. Phys.* 29, 572

Ortner R. (2000). Diplomathesis at University of Vienna.

Evaporation and particle shape factor of succinic acid particles:
Combined analysis of experimental data and computational fluid dynamics results

J. Voigtländer[1], F. Stratmann[1]

[1]Leibniz Institute for Tropospheric Research, Leipzig, Germany

Keywords: succinic acid, organic aerosol, particle shape, evaporation, modelling

Because of the atmospheric relevance, much effort has been spent on the experimental and theoretical investigation of hygroscopic and dynamic particle growth. In this study, a combined analysis of experimental data and computational fluid dynamics modelling has been employed to determine evaporation rates and particle shape factors of succinic acid ($C_4H_6O_4$).

Experiments were performed at the Leipzig Aerosol Cloud Interaction Simulator (LACIS, Stratmann et al., 2004), which is a laminar flow diffusion chamber for measurements at sub- and super-saturated conditions. The numerical simulations were performed using the Computational Fluid Dynamics Code (CFD-Code) FLUENT6 combined with an Eulerian particle model (Fine Particle Model (FPM), Wilck et al., 2002).

In the experiments, quasi-monodispersed particles, aerosolized from diluted water - $C_4H_6O_4$ solutions by means of an atomizer, were used. The particles were dried and selected by means of a DMA. $C_4H_6O_4$ particles with mobility diameters of 200 nm and 250 nm were used in this study. Measurements were performed at high RH up to 99.6 percent and at least three times for each measurement point. Mean values and standard derivation were calculated for each data point. It was assumed, that the standard derivation represents the experimental uncertainty.

To investigate the evaporation of succinic acid, the selected and dried particles were exposed to various residence times in upstream direction of the laminar flow chamber (Fig. 1). The evaporated mass then was determined from the reduced observed hygroscopic particle growth compared to particles, which flow directly through the chamber.

The larger the residence time under dried conditions, the more succinic acid evaporated and the smaller were the observed sizes of the hygroscopically grown particles (Fig. 1). The observed evaporation of succinic acid was significant, but slightly smaller than reported by Riipinen et al., 2006.

For the simulations, all relevant thermo dynamical properties (diffusion coefficients, activity model (UNIFAC), densities, thermal conductivity, surface tension, vapour pressure) and physical processes (fluid dynamics, particle dynamics, including condensation/evaporation of water and also of succinic acid) for the considered system were implemented and considered in the model. The model was also validated for succinic acid (Voigtländer et al., 2007). Differences were found between numerical calculations and experimental data.

To describe the difference between mobility equivalent diameter selected by the DMA and the mass equivalent diameter used in the calculations, a particle shape factor for the dry $C_4H_6O_4$ particles was therefore additionally introduced and fitted to the experimental data.
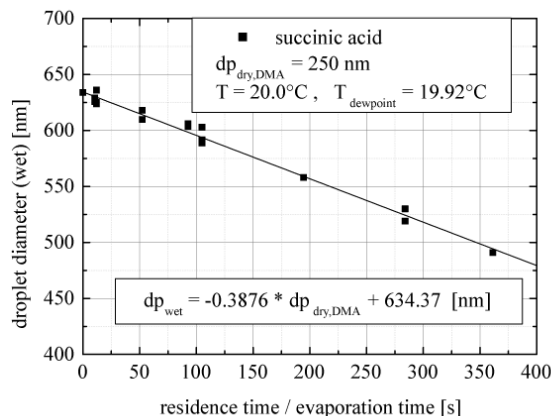
Figure 1: Measured hygroscopic growth of $C_4H_6O_4$ particles with 250 nm in diameter (electrical mobility equivalent) at 20°C and 99 percent RH. The residence time in front of the laminar flow chamber was varied to determine the evaporation of $C_4H_6O_4$.

Values for the DSF of 1.06 for particles with mobility diameters of 200 nm and 1.10 for particles with 250 nm were found. The results are in good agreement with the values published in a recent study (Zelenyuk et al, 2006).

Riipinen, I. & Svenningsson, B. & Bilde, B. & Gaman, A. & Lehtinen, K.E.J. & Kulmala, M. (2006). *Atmos. Res., 82,579-590.*

Stratmann, F. & Kiselev, A. & Wurzler, S. & Wendisch, M. & Heintzenberg, J. & Charlson, R.J. & Diehl, K. & Wex, H. & Schmidt, S. (2004). *J. Atmos. Ocean Tech., 21, 876-887.*

Wilck, M. & Stratmann, F. & Whitby, E.R. (2002). in *Proc. Sixth Int. Aerosol Conf.,* Taipei, Taiwan, 1269-1270.

Zelenyuk, A. & Imre, D.. (2006). *Aerosol Sci. Tech.,* 40, 197-217.

Discontinuous hygroscopic growth of an aqueous surfactant/salt aerosol particle levitated in an electrodynamic balance

V. Soonsin, U.K. Krieger and Th. Peter

Institute for Atmospheric and Climate Science, ETH Zurich, 8092, Zurich, Switzerland

Keywords: surfactants, hygroscopicity, growth, size analysis, light scattering

Organic compounds are a major fraction of tropspheric aerosol. The organic fraction is usually internally mixed with inorganic salts within the particles so the phases of the aerosol will be influenced by both mixing the organic substances with each other and mixing between organic and inorganic constituents (Marcolli et al., 2004) in an aqueous aerosol particle. If the organic substance is a surfactant, it will lower the surface tension. In addition aggregates of the organic monomers, called micelles, may be formed if the concentration of the organic exceeds a certain limit (critical micelle concentration). These aggregates may have different morphology (spheres or cylindrical tubes etc.) and size, depending on the nature of the organic molecule, its concentration and the concentration of inorganic salts. These aggregates will lead to solubilisation of organic compounds in aqueous atmospheric aerosol.

In our experiment an electrically charged particle is levitated in an electrodynamic balance (EDB) (Krieger et al., 2000). Five independent methods to characterize the aerosol particle: (i) mass from DC voltage, (ii) radius from Mie phase functions, (iii) composition from Raman spectroscopy, (iv) radius and refractive index from LED-white light source (Zardini et al., 2006) and Mie resonance spectra analysis, and (v) particle shape and morphology from temporal light-scattering fluctuation.

We performed measurements using ternary aqueous solution particles consisting of tetraethylene glycol monooctyl ether ($CH_3(CH_2)_7(OCH_2CH_2)_4OH$ or C_8E_4) as organic surfactant and sodium chloride (NaCl) as inorganic salt at different temperatures and compositions.

From Mie theory, tracking a specific mode during growth or shrinkage allows the measure of the radius change. Mie resonance spectra of ternary droplets show discontinuous growth with increasing relative humidity (RH) and also discontinuous shrinkage at temperatures and RHs at which the salt is completely deliquesced and the concentration of the organic surfactant is larger than the critical micelle concentration, see Figure 1, panel (b). The voltage compensating the gravitational force, which proportional to the particles mass, panel (d), shows also discontinuous water uptake, but its precision is smaller than that of the radius measurement.
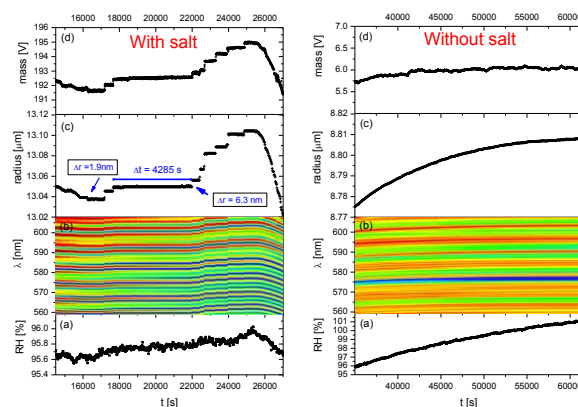
Figure 1 Experimental results for Ternary C_8E_4/NaCl/H_2O and Binary C_8E_4/H_2O (a) RH (b) Resonance spectra (c) Particle radius (d) DC voltage

We speculate that this discontinuous, step-like, growth is caused by disaggregation of a micelle needed to conserve the monolayer of surfactant molecules on the aqueous aerosol particle surface upon growing as shown in Figure 2.
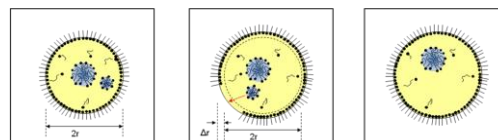
Figure 2 Micelle disaggregation

The number of molecules of the disaggregating micelle can be deduced using the polar surface area of a C_8E_4 molecule and the surface area increase of the aerosol particle calculated from the step increase of the radius. For the particle of Fig. 1 this leads to an aggregation of about 10^6 molecules, which might be due to high salt concentration of the particle, since we did not observe the discontinuous growth with binary C_8E_4/water particles.

Marcolli, C., Luo, B., &. Peter, T. (2004). *J. Phys. Chem. A*, 108, 2216-2224.

Krieger, U.K., Colberg, C.A., Weers, U., Koop, T., and Peter, Th. (2000). *Geophys. Res. Lett.*, 27, 2097-2100.

Zardini, A.A., Krieger, U.K., & Marcolli, C. (2006). *Optics Express*, 14, 6951-6962.

Deposition probability of nanoparticles on inverse surfaces at low pressure

Christof Asbach[1], Heinz Fissan[1], Thomas A.J. Kuhlusch[1], David Y.H. Pui[2], Jing Wang[2]

[1] Institute of Energy and Environmental Technology (IUTA), Air Quality & Sustainable Nanotechnology Unit, Bliersheimer Str. 60, 47229 Duisburg, Germany

[2] Department of Mechanical Engineering, University of Minnesota, 111 Church Street SE, Minneapolis, MN, 55455, USA

Keywords: nanoparticles, contamination, diffusion, inertia, thermophoresis

The prevention of particulate contamination on critical surfaces is becoming a major challenge in semiconductor manufacturing. Due to decreasing feature sizes of the integrated circuits, the size range of interest for contamination control is continuously extended towards smaller particles. Extreme ultraviolet lithography (EUVL), a very prominent candidate for the production of the next generation of computer processors, is expected to produce feature sizes of 32 nm and below. EUVL utilizes reflective photomasks that are maintained facing down during chip production, which occurs at a low pressure level of 10 Pa or below. These photomasks are particularly vulnerable, because they cannot be covered by any protective materials. In case of particle deposition on its surface, the particle(s) will be sharply reproduced onto the wafer, where this may cause damages such as a short circuit on the produced chips. A contaminated photomask has to be replaced, which causes a long downtime of the production. Photomasks therefore have to be protected against particle deposition. Previously we have published protection schemes for EUVL photomasks (Asbach et al, 2005a), which comprise the establishment of a thermal gradient underneath the critical surface in order to thermophoretically repel particles. In quiescent gas, particles may approach the critical surface due to inertial and/or diffusional particle motion. In a previous publication (Asbach et al., 2005b), we focused on the deterministic inertial particle motion and could show that thermophoresis is mainly effective against slowly traveling particles. The model was experimentally verified and found to be in good agreement. The early model was now extended to include the effect of diffusional motion on particle deposition, which makes it a combined analytical-statistical model (Asbach et al., 2008). The model delivers the probability that a particle with known initial velocity and known initial distance to the critical surface contaminates the mask. It is assumed that after time t the particle is within a sphere which expands with time and whose radius can be described by means of the diffusional displacement. The center point of the sphere moves according to the deterministic particle motion, caused by inertia, gravity and/or thermophoresis. The exact location of the particle within the sphere cannot be calculated, but only a spatial probability estimated by weighting the sphere's cross sectional area with a Gaussian distribution function. The resulting contamination probability is shown in Fig. 1 for particles with an initial distance of 1 mm and initial velocities between 0.01 m/s and 10 m/s.
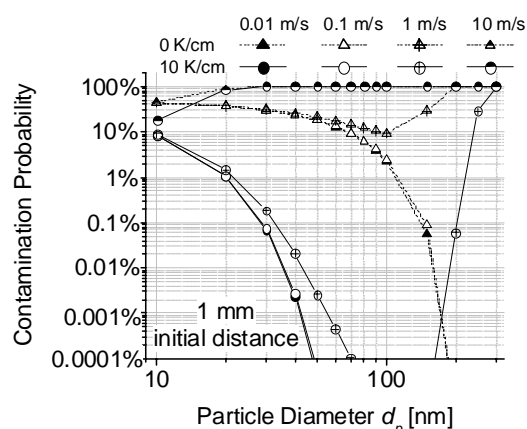
Fig. 1: Contamination probability of particles with 1 mm initial distance to critical surface, with (10 K/cm) and without (0 K/cm) thermophoretic protection (Asbach et al., 2008).

It was shown that the deposition of particles with high inertia is always likely, whereas the probability of diffusion driven particle deposition can be significantly reduced. The modeling results were experimentally verified, using a vacuum chamber with capabilities to inject particles into a quiescent gas with known velocity (Kim et al., 2006). Experimental results will be presented and compared with calculated contamination probabilities.

References
C. Asbach, H. Fissan, J.H. Kim, S.J. Yook, D.Y.H. Pui (2005a) *J. Nanoparticle Res.* **8**: 705-708

C. Asbach, J.H. Kim, S.J. Yook, D.Y.H. Pui, H. Fissan (2005b) *Appl. Phys. Lett.* **87**: 234111

C. Asbach, H. Fissan, T.A.J. Kuhlbusch, J. Wang, D.Y.H. Pui (2008) *Appl. Phys. Lett.* **93**: 054104

J.H Kim, H. Fissan, C. Asbach, S.J. Yook, D.Y.H. Pui (2006) *J. Vac. Sci. Technol.* **A24:**229-234

Reanalyzed *n*-nonane nucleation experiments conducted in an expansion chamber

David Ghosh[1,2] and Reinhard Strey[1]

[1]Institut für Physikalische Chemie, Universität zu Köln, Luxemburgerstr. 116, 50939 Köln, Germany
[2]Philip Morris Research Laboratories GmbH, Fuggerstr. 3, 51149 Köln, Germany

Understanding particle formation for the *n*-alkanes can contribute to a more environmentally benign separation process of longer chained *n*-alkanes and impurities from raw natural gas mainly containing CH_4. For scientists who are interested to enhance our fundamental knowledge concerning particle formation and growth it is of advantage that the nucleation process for the *n*-alkanes occurs well above the triple point where the physical properties of these compounds are well known. Most of the experimental investigations of the nucleation process for the *n*-alkanes are focused on *n*-nonane and the earliest accessible nucleation investigations for *n*-nonane were conducted in 1970 by Katz. The majority of the experimentally accessible nucleation data including the early investigations by Katz in 1970 have treated the constant pressure heat capacity c_p of *n*-nonane in a temperature dependent manner. For long chained *n*-alkanes the increasing number of freedoms of rotation and vibration compared to simple molecules like argon or even water where c_p is often assumed to be constant justifies the importance of treating the constant pressure heat capacity c_p in a temperature dependent manner.

In this work we have reanalyzed the nucleation data for *n*-nonane conducted by Wagner & Strey (1984), and Viisanen *et al.* (1998) in an expansion chamber because it was assumed that during the rapid expansion of a mixture consisting of carrier gas (argon) and condensible specie (*n*-nonane) the gas could be treated for simplicity reasons with a constant pressure heat capacity ($c_p = $const., $\gamma = c_p / c_v = 1.1$) using the Poisson equation. The more accurate equations given by Witte & Tatum who were able to present how to correctly analyze gas expansions for gases with non constant heat capacities were used in this work. In Figure 1 & 2 the deviation in the nucleation temperature, and consequently, in the supersaturation between a temperature independent heat capacity ($c_p = $const., $\gamma = c_p / c_v = 1.1$) and a temperature dependent heat capacity $c_p(T)$ is demonstrated. For the Wagner and Strey data (Figure 1) the nucleation temperatures are increased by ~3 K - ~0.1 K, while for the Viisanen *et al.* data (Figure 2) the nucleation temperature T shifts up from $T = 230$ K to $T \sim 231.15$ K when treating c_p in a temperature dependent manner. This increase in nucleation temperature is accompanied by an increase in equilibrium vapor pressure, and consequently, by a decrease in supersaturation.

Clearly the effect is amplified as the expansion path is increased.
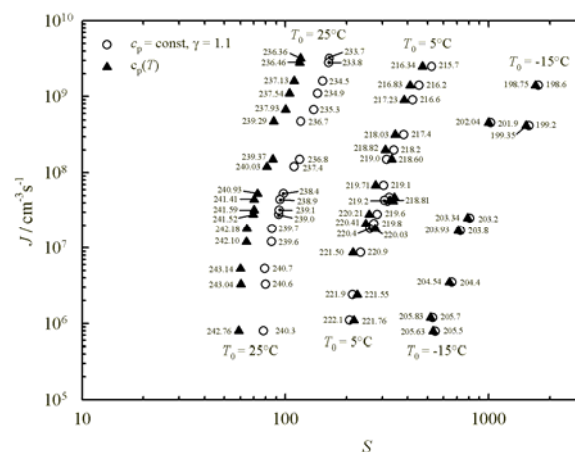
Figure 1. The nucleation rate *J* plotted *vs.* the supersaturation *S* for the nucleation data given by Wagner & Strey (1984) in the literature (c_p=const.) (empty circles) and the reanalysis ($c_p(T)$) (filled triangles) of their data.
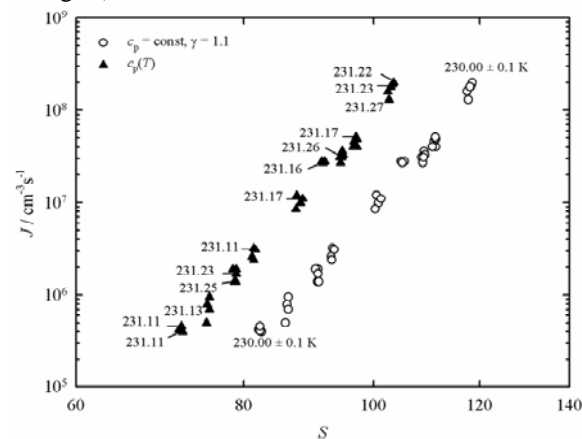
Figure 2. The nucleation rate *J* plotted *vs.* the supersaturation *S* for the nucleation data given by Viisanen *et al.* (1998) in the literature (c_p=const.) (empty circles) and the reanalysis ($c_p(T)$) (filled triangles) of their data.

Katz, J. L., (1970). *J. Chem. Phys.* **52** (9) 4733-4748.
Wagner, P. E. & R. Strey, (1984) *J. Chen. Phys.* **80** (10) 5266-5275.
Viisanen, Y., P. E. Wagner, & R. Strey, (1998). *J. Chen. Phys.* **108** (10) 4257-4266.
Witte, D. W. and E. K. Tatum, (1994) *Computer Code for Determination of Thermally Perfect Gas Properties*, National Aeronautics and Space Administration, Hampton.

An acoustic trap for submicron aerosol particles

P. Vainshtein and M. Shapiro

Faculty of Mechanical Engineering, Technion – Israel Institute of Technology, Haifa, Israel

Keywords: trap, acoustics, particle, motion, camera, random

Submicron and nanometer particle levitation and trapping have important applications in physical research including mass spectrometry, light scattering measurements for particle sizing and others[1]. Acoustic levitation in gases in a standing wave generated in levitators consisting of a plane transducer and reflector is limited to mm-size particles[2]. This is because secondary streaming appearing within such levitators prevents positioning micrometer and submicron particles[3]. In our previous study[4], we investigated quadrupole acoustic aerosol particle focusing in a three-dimensional channel of hyperbolic cross-section. Here we introduce adaptation of that wall configuration for quadrupole trap (Fig. 1)
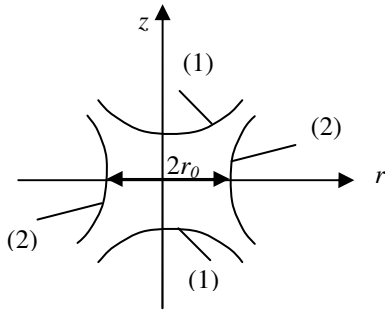
Fig. 1. Quadrupole axisymmetric acoustic chamber of hyperbolic configuration. The endcap transducers (1) and the ring transducer (2) generate acoustic pressure waves with amplitude p_s and frequency ω.

A similar quadrupole chamber with hyperbolic electrodes was employed for ions trap by means of an ac electric field[5].

We consider a quadrupole acoustic chamber with wavelength, λ satisfying condition $\lambda >> 2r_0$ (see Fig. 1). Under this condition and for small oscillations amplitudes the flow within the chamber may be considered incompressible and creeping.

Under such simplification we solve the unsteady Stokes creeping flow equations within the chamber. The obtained flow velocity pattern does not contain secondary streaming, normally present in oscillating flows[2]. This situation is similar to that of the quadrupole acoustic channel[4]. The fluid velocity field is linearly distributed and vanishing at the chamber centre. This leads to particle drifting motion towards the centre.

For the particle trajectories we solve the three-dimensional Langevin equation

$$\frac{d\mathbf{u}_p}{dt} = \frac{\mathbf{u} - \mathbf{u}_p}{\tau} + \Xi_{Br}, \quad \tau = \frac{2}{9}\frac{a^2 C}{\nu \Pi_\rho}, \quad (1)$$

Here $\omega = 2\pi f$ is the angular frequency, f is the acoustic frequency, $\mathbf{u}$ and $\mathbf{u}_p$ are the velocities of fluid and particles, respectively, τ is the Stokes relaxation time, a is the particle radius, ν is the fluid kinematic viscosity, Π_ρ is the fluid-to particle-density ratio and C is the Cunningham's slip correction factor, Ξ_{Br} is the Brownian acceleration. In the present circumstances where $\Pi_\rho \omega \tau << 1$, the Basset and added mass forces are negligible.

Figure 2 shows mapping of a 100 nm particle trajectory on the plane $z, r = \sqrt{x^2 + y^2}$. The particle is seeded at two locations $x_0 = y_0 = z_0 = 0.5$ and $x_0 = x_0 = z_0 = 0.25$ with the initial velocity coinciding with that of air.
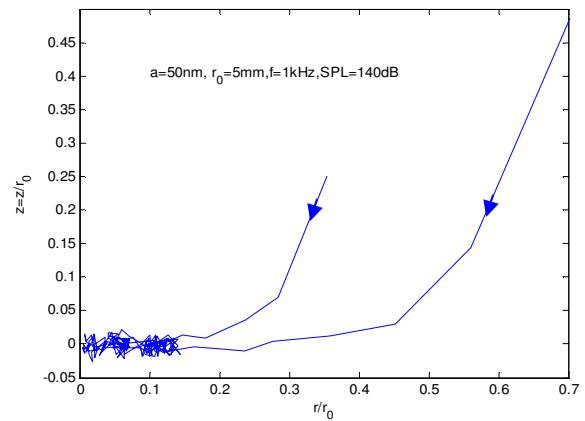
Fig. 2. Simulated random particle trajectories in a quadrupole acoustic chamber. r-radial particle distance from the origin.

It is seen that the particle approaches the chamber center and performs random walk there within a diffusion-broaden spot. We also show that the size of the spot decreases with increasing intensity of the acoustic field. Thus the acoustic field controls the particle's effective trapping volume.

[1]Davis, E.J. (1997) Aerosol Sci. Techn., 26, 212-254.
[2]Trinh, E.H. and Robey, J.L. (1994) Phys. Fluids 6 (11), 3567-3579.
[3]Vainshtein, P., Fichman, M., Shuster, K., and Gutfinger, C. (1996) J Fluid Mech. 306, 31-42.
[4]Vainshtein, P. and Shapiro, M. (2008) EAC Abstracts, Thessaloniki, Greece, August 2008, Abstract T05A007P.
[5] Wueker, R.F., Shelton, H., and Langmuir, R.V. (1959) J. Appl. Phys. 30, 342-349.

Modeling source strength modification due to coagulation in a diffusing aerosol puff

Y. S. Mayya[1] and S. Anand[2]

[1] Radiological Physics & Advisory Division, Bhabha Atomic Research Centre, Mumbai-400 085, India.
[2] Health Physics Division, Bhabha Atomic Research Centre, Mumbai-400 085, India.

The particles released into the atmosphere from combustion and explosive sources are concentrated at the release point ($>10^6$-10^7 particles/cc) with sizes predominantly less than 50 nm. The concentration decreases rapidly due to the combined effect of coagulation and dispersion as the plume spreads and becomes a part of the background aerosol. It is important to estimate the fraction of the emitted particles surviving coagulation along with the modification in the size spectra, by the time they are completely dispersed in the atmosphere. Although realistic situation can only be addressed after due considerations are given to the details of meteorology and source characteristics, model studies will be useful in understanding the relative importance of coagulation vis-à-vis dispersion in governing survival fraction (Turco & Yu, 1997). To this end, we have examined coagulation-diffusion problems from an analytical and numerical framework.

In a recent study (Anand & Mayya, 2009), we employed Jaffe approximation technique, borrowed from ion-recombination theory, to obtain approximate analytical solutions to coagulation-diffusion equation. If N_a particles are emitted from a Gaussian puff of radius of gyration R_g, and if K is the mean coagulation coefficient of particles and D is diffusion coefficient in the atmosphere, then the fraction of particles surviving coagulation as the puff completely disperses may be shown to be

$$F_\infty = (1+A)^{-1} \qquad (1)$$

$$A = 3^{1/2} K N_a / \left(16 \left(\pi\right)^{3/2} R_g D\right).$$

While this formula captures the qualitative features of the processes, it under-predicts the survival fraction as compared to that obtained by accurate numerical computations. This calls for seeking more accurate approximations. For this we have now developed what may be called as beyond-Jaffe approximation. The Jaffe technique assumes the validity of diffusion laws for the spatial dispersion of the puff. In the beyond Jaffe approximation, allowance is made for a non-diffusive evolution of spatial variance due to coagulation. We illustrate the technique for the decay of the total number concentration $N(r,t)$ in a spherically symmetric puff for constant diffusion coefficient and coagulation kernel. The equation is

$$\frac{\partial N(r,t)}{\partial t} = D \nabla^2 N(r,t) - \frac{1}{2} K \left[N(r,t)\right]^2 \qquad (2)$$

Given an initial Gaussian puff, we assume the following functional form for its evolution:

$$N(r,t) = \frac{N_a}{\pi^{3/2} \xi(t)^{3/2}} \exp\left(-r^2/\xi(t)\right) F(t) \qquad (3)$$

where, $\xi(t)$ (measure of variance) and $F(t)$ (survival fraction) are yet to be determined. Upon taking spatial moments of Eq.(2), we obtain coupled equations for $\xi(t)$ and $F(t)$, which may be exactly solved in the limit, $t \to \infty$, to yield

$$F_\infty = \left(1 + \frac{5A}{4}\right)^{-4/5} \qquad (4)$$

For small A, Eq.(4) approaches Eq.(1). As the parameter A increases, the two equations differ noticeably. In figure 1, we have compared the two solutions with numerical solutions of Eq.(2) obtained using Mathematica (Wolfram, 2005). As may be seen the "beyond Jaffe approximation" is quite close to the accurate solutions even for very large values of A.
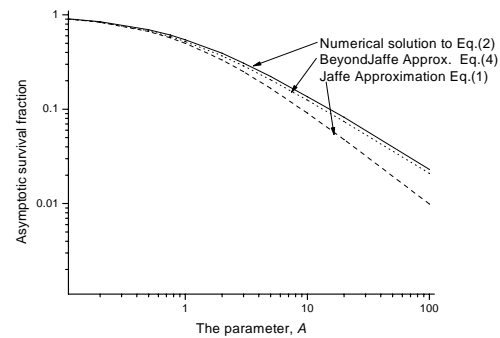
Figure 1: Variation of survival fraction with A.

The approach proposed may be extended for estimating modification of the size spectra during dispersion. It is also possible to include homogeneous non-constant kernels and space and time dependent diffusion coefficients. From a practical point of view, the A value will be low (~0.1) for dilute puffs in highly dispersive atmospheres and can be large (1-10) for dense puffs in calm atmospheres such as those arising from intense fireworks in festive seasons. In general, the formulae can be viewed as environmental source modifiers for particle releases from localized sources.

Anand, S., & Mayya, Y.S. (2009). *J. Aerosol Sci.*, (*in press*).

Wolfram Research, Inc. (2005). *Mathematica, Version 5.2*, Champaign, IL.

Turco, R.P, & Yu, F. (1997). *Geoph. Res. Letters*, **24**, 1223-1226.

Dynamics of aerosols at nonlinear oscillations in tubes. The theory and experiment

D.A. Gubaidullin, R.G. Zaripov, A.L. Tukmakov and L.A. Tkachenko

Institute of Mechanics and Engineering, Kazan Science Center, Russian Academy of Sciences,
2/31, Lobachevsky str., 420111, Kazan, Russia

Keywords: aerosol, coagulation, deposition, experiment, oscillations.

In the present work, nonlinear oscillations of an aerosol of different initial concentration and dynamics of particles is considered in closed and open tubes of different length near to sub-harmonic resonances.

Experimental investigations were carried out for length of tubes $L_0 = 2,7; 3,7; 4,7; 6,7$ m in a range of oscillation frequency of an aerosol from 0 to 18 Hz. For making an aerosol the fluid Di-ethyl-hexyl-sebacate $C_{26}H_{50}O_4$ (DEHS) was used. On the average geometrical diameter of droplets DEHS aerosol in undisturbed state is 0,8 μm. Dependences of concentration of droplets of an aerosol on time for various frequencies of excitation, times of an enlightenment (coagulation) of an aerosol from frequency and intensity of oscillations have been received.

Concentration of drops for all experiments monotonously decreases in due course and with growth of frequency of excitation. In case of the closed tube this process is caused by coagulation of an aerosol and deposition of drops on walls of a tube and it is well approximated by a Boltzmann distribution low. In an open tube alongside with coagulation of an aerosol and deposition of drops on walls of a tube emission of an aerosol in environmental space takes place also. In this case, dependences of concentration of drops of an aerosol on time is approximated by an exponential distribution. Dependences of time of enlightenment (coagulation) of an aerosol on frequency of excitation also have non-monotonic character with a minimum and a maximum at transition through a resonance. Thus time of an enlightenment of an aerosol in an open tube decreases in two and more times in comparison in due course coagulations in the closed tube. Nonlinear association of time of enlightenment (coagulation) of drops is established at nonlinear oscillations of an aerosol in a tube from initial concentration of an aerosol. It is revealed, that reduction of length of a tube also increase in intensity of piston oscillation results in decreases of an enlightenment (coagulation) time of an aerosol. The ordered existential structures (alternation of the condensed and rarefied sites of an aerosol) in visual area about the middle of the closed tube are found out.

The numerical modeling of a drift of the solid spherical particles were in a suspension in a nonlinear wave field of the closed tube and open flat channel at excitation of oscillations of a gas column on three first fundamental frequencies is executed. It is obtained, that easy particles drift under an operation of acoustical current, and heavy are displaced under an action of wave pressure. In result easy and heavy particles concentrate in different areas of the resonator: easy are displaced to antinodes of a standing wave of velocity, heavy - to nodes. Depending on a steepness of a wave front of compression, the same particles can behave as easy at small nonlinearity, or as heavy at steep enough fast-head wave front. Drift of heavy particles in the open channel proceeds in two stages. The first quickly proceeding stage is connected to the mechanism of drift due to asymmetry of a wave, and the second with drift under action of developed acoustic stream.

Dynamics of a single particle with various physical and geometrical parameters is experimentally investigated at the longitudinal oscillations of gas generated by the flat piston, in a tube with various conditions on the ends. It is revealed, that a particle, both from closed, and from the open end of a tube moves to the piston, near to a wall of the closed pipe - to the return side, making longitudinal oscillations with increase in the oscillations swing that is caused by acoustic streaming. In a radial direction, the oscillating particle goes from an axis to a wall of the closed tube up to a boundary point. It is revealed, that the increase in lengths of a tube and frequency of excitation of gas in up to - resonant modes gives in growth of an oscillations swing of a particle and increase of its medial velocity. Nonmonotonic character of dependence of medial velocity of a motion of a spherical particle from frequency of excitation of gas is detected. At approach to a resonance medial velocity is incremented and attains the peak value on a resonant frequency. Behind a resonance medial velocity decreases. Effect of a weight and diameter of a particle on its oscillations swing and medial velocity is investigated. Shift of a maximum of a curve of dependence of medial velocity of a motion of a particle from an oscillation frequency aside magnifications of frequency is shown at increase of a weight or diameter of a particle.

Aerosol Clustering Patterns in Oscillating Flows

D. Katoshevski

Department of Biotechnology and Environmental Engineering, Ben-Gurion University of the Negev, Beer-Sheva 84105, Israel

Keywords: Grouping, Clustering, Aerosol Dynamics, Aerosol Modelling, Aerosol Fundamentals

It is well known that the interaction of particles and droplets with the ambient gas is important for various problems of aerosol mechanics, such as, engineering, environmental and medical applications including those related to modeling of dynamics of atmospheric particles, marine particles (Winter et al., 2007), modeling of inhaled particles, modeling of sprays in internal combustion engines (Katshevski et al.,2008), and other applications. Numerous experimental and numerical studies of free shear flows showed that in many cases a flow has a large-scale vortex structure which has a periodic form and moves in the direction of the flow. Owing to this fact, the flow velocity field is fairly periodic both in time and in the direction of the flow. This problem is challenging from the point of view of mathematical analysis. We present a qualitative mathematical analysis of particle dynamics in periodically changing flows. It reveals various modes of particle dynamics, which shed light on particle behavior in more general and complex configurations. We term here the tendency to form groups and clusters as "**grouping**". The grouping/clustering phenomenon is illustrated schematically in Fig. 1.
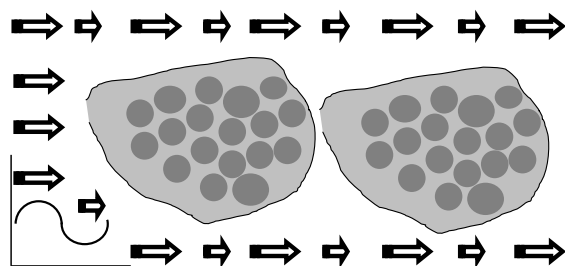
Figure 1. Schematic description of travel-grouping of aerosol particles in an oscillating flow field.

Particle grouping/clustering patterns

Our calculations reveal that there are three modes of grouping behavior. These modes include: I) Stable grouping, II) Weak Grouping, and III) Non-Grouping.

Particle trajectories in stable and weak grouping are presented in Fig. 2. The first mode of behaviour, "*Mode I*" is characterized by the formation of particle groups and a subsequently stable conjoint motion. In "*Mode II*" which stands for *weak grouping*, temporarily joined particles shift from one group to the other or groups break up. In contrast "*Mode III*" defines a clear *non-grouping* situation where there is very little tendency, if any, to aggregate. As grouping is associated with conditions, such as the host-flow velocity, the frequency of the oscillations as well as particle/droplet size, we may say that in certain range of conditions we expect to observe one of these modes. This will be elucidated in the presentation.

In the case where we use a frame of reference moving at the phase velocity we find a different outocme for grouping and non-grouping representation of the trajectories. Grouping trajectoires converge into a dot when the grouping is clearly stable and non-stable grouping results in an osscilating trajectory behavior. The stable grouping implies that the stable groups in Fig. 2 (left) may later in time break. This will not be the case according to the second represntation.
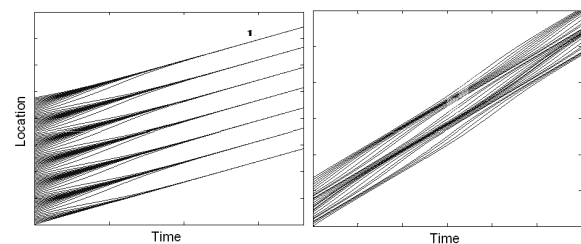
Figure 2. Left-stable grouping, Right-weak grouping

Grouping may lead to aerosol coagulation and this should have an effect on the coagulation modelling included in the aerosl general Dynamic Equation (Katoshevski and Seinfeld, 1997).

Katoshevski, D. and Seinfeld, J. H. (1997) *Aerosol, Science and Technology*, 27, 550-556.

Katoshevski, D., Shakked, T., Sazhin, S.S., Crua, C., Heikal, M.R. (2008) *International J of Heat and Fluid Flow*, 29, 415-426.

Winter, C., Katoshevski, D., Bartholomä, A., Flemming, B., (2007), *J. Geophysical Research* (*JGR-Oceans*) 112: doi:10.1029/2005JC003423. August 2007

Droplet Bouncing Effects in Salt Water Electrospray

E.C. Fuchs[1], L.L.F. Aghostinho[1], C.U. Yurteri[2] and J.C.M Marijnissen[1,2]

[1]Wetsus Excellence Centre of Sustainable Water Research, Agora 1, 8900 CC Leeuwarden, The Netherlands
[2]Delft University of Technology, Faculty of Chemical Technology, Laboratory of Particle Technology,
Julianalaan 136, 2628 BL Delft, The Netherlands

Keywords: electrospray, noncoalescence, bouncing

The fact that droplets of the same liquid may come into contact without coalescing has been investigated thoroughly in the past, a comprehensive review on the topic is given by e.g. Neitzel & Pasqual (2002). We found that similar phenomena can also be observed in electrospraying, where droplets are ejected from a nozzle under the application of a high electric field (see e.g. the reviews by Grace & Marijnissen (1994) or Shin *et al* 2004).

We report the observation of semi-coalescent bouncing effects of droplets in salt water electrospray while the spray is operating in the micro-dripping mode. In the given examples, the NaCl concentration is 35g/L, the flow rate 5mL/h, and the working distance between nozzle and grounded counter-electrode is 5cm. An example for a semi-coalescent droplet bouncing is given in Fig. 1.
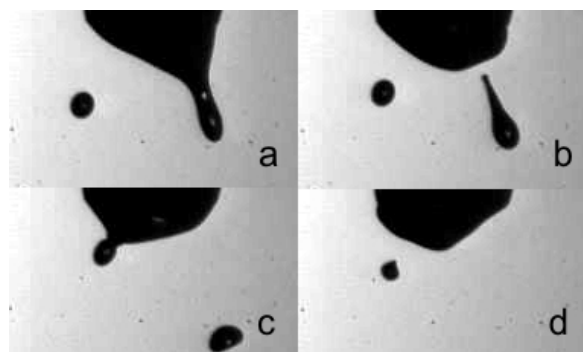
Fig. 1: Semi-coalescent droplet bouncing in salt water electrospray (+12kV). While the right droplet is being ejected from a cone (a,b,c), the previously ejected left droplet returns (a,b), loses mass (c) and is ejected again (d). The images were recorded with 6250 frames/s, the droplet diameter is ~ 100µm.

Three independent effects have to be considered in order to properly describe the phenomenon: The mechanism for the return of the ejected droplet against gravity due to electrokinetic forces, the mass and charge transfer on contact with the liquid surface on the nozzle, and the subsequent re-ejection of the droplet.

Additional, we report the observation of non-tangent bouncing of electrospray droplets. Here, the droplet is repelled by the field without touching the surface of the cone. An example is given in Fig. 2.
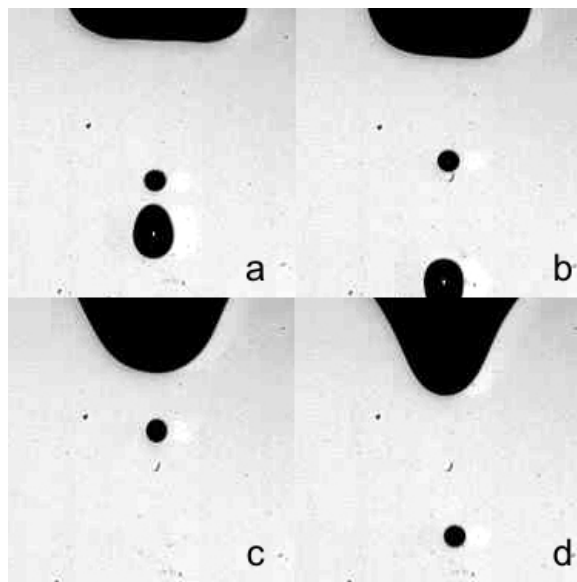
Fig. 2: Non-tangent droplet bouncing in salt water electrospray (-9kV). After two droplets have been formed from a liquid cone (a), one moves away (b) while the other is moving back (b,c) where it finally bounces off the electric field around the growing cone (d). The images were recorded with 5400 frames/s, the droplet diameter is ~ 100µm.

In the case of non-tangent droplet bouncing as shown in Fig. 2, it is assumed that the smaller droplet is first repelled by the bigger one below pushing it back upwards to the cone which finally repels it again. This is plausible because both droplets and cone are negatively charged. However, since the non-tangent bouncing has also been observed without a second droplet, attractive electric forces have to be considered as well.

Based on the works of Hartman *et al* (1999), the principles of non-coalescence and EHD, a possible explanation of the observed effects will be proposed.

G. P. Neitzel & P. Dell'Aversana (2002), *Annu. Rev. Fluid. Mech.* **34** 267-89

J.M. Grace & J.C.M. Marijnissen (1994), *J. Aerosol Sci.* **25**. No. 6, 1005-1019

W.-T. Shin, S. Yiacoumi, C. Tsouris (2004), *Cur. Op. Coll. & Interf. Sc.* **9,** 249-255

R.P.A. Hartman, D.J. Brunner, D.M.A. Camelot, J.C.M. Marijnissen & B. Scarlett (1999), *J. Aerosol Sci.* **30** No. 7, 823-849

Calculation of Aggregate Friction Coefficient from Active Surface

L. Isella and Y. Drossinos

European Commission, Joint Research Centre, I-21027 Ispra (VA), Italy

Keywords: active surface, fractal, aggregates, mobility, friction.

The hydrodynamic behaviour of fractal-like soot aggregates suspended in a viscous fluid is of considerable importance for their transport and depositional properties. The calculation of the drag force on a fractal aggregate consisting of n primary spherules, henceforth called monomers, involves solving numerically Stokes equation for a low Reynolds number steady flow past the aggregate (Filippov, 2000). Analytical treatments usually require simplifying assumptions like aggregate spherical symmetry.

In this study we suggest an agile, albeit approximate, method to determine the aggregate friction coefficient β_n in the continuum regime relying on aggregate active surface A, defined as the fraction of aggregate geometrical surface available for gas absorption. Experimentally, A can be measured by evaluating the fluid-molecule-to-aggregate integral collision cross section.

Experimental findings (Siegmann & Siegmann, 2000) show that the product of aggregate mobility (inversely proportional to aggregate friction coefficient) times active surface is constant over a wide range of mobilities. This is not unexpected since the drag force (fixing aggregate mobility) felt by an aggregate in a viscous fluid is also due to collisions with the carrier flow.

The approach we follow tracks closely the experimental method. We solve the steady-state diffusion equation for fluid molecules surrounding the aggregate assuming molecule concentration $\rho = 0$ on aggregate geometrical surface (absorption of colliding molecules) and $\rho = \rho_\infty$ far away from aggregate surface. This amounts to neglecting the possibility of multiple scattering of fluid molecules by the aggregate. The calculated diffusive flux can then be integrated along the aggregate geometrical surface, to determine the overall fluid-molecule-to-aggregate collision rate, proportional to the active surface and hence to the aggregate friction coefficient. Though the proportionally constant is still unknown, one can take the ratio of the aggregate collision rate to n times the collision rate on an isolated monomer, where n is the number of monomers in the aggregate. This yields the ratio between the aggregate and the monomer friction coefficients. The method neglects that momentum transferred to the aggregate by the fluid is only approximately proportional to the number of collisions underwent by fluid molecules, since the velocities of molecules approaching the aggregate are in general position-dependent, hence not all the collisions transfer the same momentum.

In order to test the goodness of the approximation, we calculated the friction coefficients of linear chains, for which there are theoretical and experimental results in literature. The simulations were performed in cylindrical coordinates with the finite element software Comsol Multiphysics. We calculated also the friction coefficients along the direction parallel and orthogonal to the symmetry axis, $\beta_n^{\uparrow}$ and $\beta_n^{\rightarrow}$, by integrating on the aggregate surface the projected diffusive flux along the axial and radial direction, respectively.

Diffusive Flux around Linear Chain — Max: 4.122, Min: 0
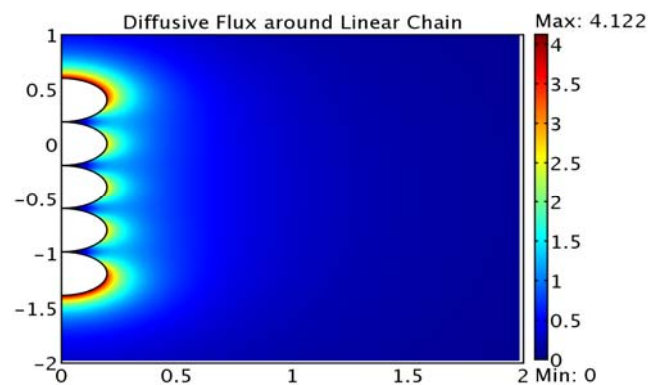
The calculated friction coefficients for different values of n are in within a few percents from the findings illustrated in other studies, a few of which are reported in the table below.

	Filippov	Happel & Brenner	Diffusion
$\beta_2^{\uparrow} / \beta_1^{\uparrow}$		0.645	0.633
$\beta_2^{\rightarrow} / \beta_1^{\rightarrow}$		0.716	0.725
$\beta_8^{\rightarrow} / \beta_1^{\rightarrow}$	0.435		0.428

Although validated on linear chains, the method can be applied to aggregates of arbitrary shape. This means e.g. that whenever high-resolution images of an aggregate are available, it is possible to estimate its active area and friction coefficient, thus gaining valuable insight on aggregate catalytic activity and diffusional properties.

Filippov, A. V. (2000). *J. Colloid and Interface Science*, 229, 184-195.

Siegmann, K. & Siegmann, H.C. (2000). *Society of Automotive Engineers*, 2000-01-1995.

Happel, J. & Brenner, H. (1983). *Low Reynolds number hydrodynamics.* Dordrecht, Holland: Kluwer Academic Publishers.

Experimental study of dew condensation influence on dust deposition rate

S.A. Biryukov[1] and L.I. Yarmolinsky[2]

[1]The Jacob Blaustein Institutes for Desert Research, Department of Solar Energy and Environmental Physics, Ben-Gurion University of the Negev, Sede Boqer Campus, 84990, Israel
[2]The Jacob Blaustein Institutes for Desert Research, Albert Katz International School for Desert Studies, Ben-Gurion University of the Negev, Sede Boqer Campus, 84990, Israel

Keywords: dew condensation, dust, deposition velocity, solar collectors

Dew condensation is known to have a negative effect on removal of dust from solar collectors due to growth of adhesion of particles to surface after water evaporation. But the process of condensation may be important also from another point of view: the gradient of temperature and relative humidity in pre-surface interface may meaningfully influence the process of dust deposition on surface from the air, probably enhancing it. The goal of the reported investigation was a laboratory study of dew condensation influence on the process of dust deposition.

Environmental dust was dispersed in a deposition chamber and deposited on two horizontal glass samples by gravity and natural convection. One of two samples was preliminarily cooled down to the temperature lower than the dew point; the second (reference) sample was kept at the room temperature, which was much higher than the dew point. After the exposure, the particle size distributions on the glass surface and the corresponding deposition rates have been compared for both samples. Numerical enhancement E of deposition for each group of particle sizes was calculated as the ratio of corresponding deposition rates:

$$E = \frac{N_{cooled}}{N_{reference}}$$

It was found that the dew condensation process has led to the growth of deposition rates both on the top and on the bottom sides of the cooled sample. This enhancement of dust deposition positively correlated with the level of atmospheric relative humidity. The value of enhancement was found to be dependent on size of dust particles. As it is illustrated by the diagram (Fig.1), this dependence was different for top and bottom sides.

The enhancement was more significant for deposition on the top surface than on the bottom one.

The most significant enhancement coefficient ($E > 40$) was found for particles smaller than 3 micron in size in the case of deposition on the top surface (relative humidity=55%: T=25˚C).

For the bottom surface effect of enhancement of dust deposition rates by condensation was practically independent on particle size.
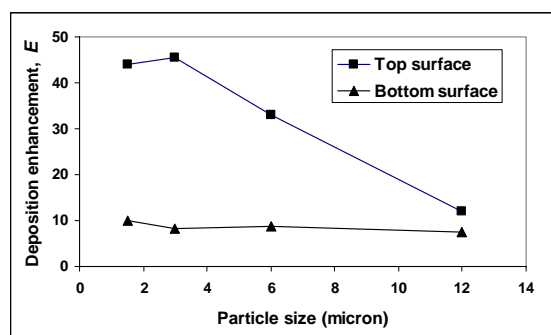
Figure 1 Enhancement of deposition rates for the top and for the bottom surfaces of preliminarily cooled glass sample.

The additional enhancement for small particles deposition on the top surface may be related to conditions of super-saturation in pre-surface interface, resulting in condensation of water vapor on dust particles and the corresponding growth of their masses. This effect has to lead to higher relative growth of masses of smaller particles and, correspondingly, to the higher increase of their deposition velocity under gravity.

Effects of the non-measured Mid-IR spectral range of the imaginary refractive index on the derivation of the real refractive index using the Kramers-Kronig transformation

M. Segal-Rosenheimer[1], and R. Linker[1]

[1]Department of Civil and Environmental Engineering, Technion-Israel Institute of Technology, Technion City, 32000, Haifa, Israel

Keywords: Atmospheric aerosols, Refractive index, Truncation error, Spectrum extrapolation, Ammonium sulphate,

Quantitative analysis of remote sensing and laboratory broadband spectroscopic measurements of aerosols relies on the accurate knowledge of their complex refractive index ($N(\nu) = n(\nu) + ik(\nu)$) in the spectral region of interest.

In the derivation of the refractive index, the imaginary part ($k(\nu)$) is usually estimated using spectra of a thin film of the investigated material or transmission spectra of small particles. The real part ($n(\nu)$) can then by derived for instance using the Kramers-Kronig transform (KKT) that relates n and k according to (Bohren and Huffman, 2004):

$$(1) \qquad n(\tilde{\nu}_0) - 1 = \frac{2}{\pi} P \int_0^\infty \frac{k(\tilde{\nu})\tilde{\nu}}{\tilde{\nu}^2 - \tilde{\nu}_0^2} d\tilde{\nu}$$

However, the use of Equation 1 requires the knowledge of k over the whole spectral range - from zero to infinity. In practice, of course, this demand cannot be satisfied, as the transmission or absorption measurements are made over a finite spectral range. Therefore, when performing the KKT calculation on a measured k spectrum, one needs to assume its behavior beyond the measured spectral range. As the KKT procedure is a common method for the extraction of optical constants, a general approach to asses the influence of the absorption features in the spectral range beyond the measurement limits would be useful. Such a tool would provide a quantitative criterion for deciding whether extrapolation of the k spectrum beyond the actual measurement's range is desirable and what type of extrapolation would be most appropriate. Also, in remote sensing applications, such a tool would show whether a set of optical constants measured at a given spectral range is accurate enough to serve as an input for extracting aerosol data (e.g. size distribution and concentration) from another finite transmission spectrum.

In the present study, we investigate the influence of bands of various locations and bandwidths in the non-measured IR spectral region ($0-800$ cm^{-1}) on the n values obtained by the computational procedure of the KKT. Specifically, the quantitative effect of the spectral truncation in the implementation of the KK integral to derive n was assessed. The net contribution of the non-measured spectral range was calculated under different scenarios (i.e. different band locations and band widths). The bands were represented by Gaussian- or Lorentzian-shaped analytical functions. Additional analysis was conducted to estimate the relevance of different assumptions that are commonly made with regard to the non-measured range (e.g. linear extrapolation or the effect of uncertainty in the precise band location). The results were implemented on two optical constants' datasets of ammonium sulfate and water in the Mid-IR range.

In general, it was shown that neglecting the low wavenumber range causes an overestimation of n. Linear extrapolation of the k spectrum, although widely used, was shown to have a negligible effect on the n correction. As different band locations and widths were tested, it was possible to derive an analytical function that describes the influence of the non-measured band on the final n values within the measured spectral range:

$$(2) \qquad n(\tilde{\nu}_0) = -\frac{35.14 \cdot \exp\left(-4.75 \cdot 10^{-3}\mu\right)}{\left(\tilde{\nu}_0 - \mu\right)^{\left(1.95 - 1.06 \cdot 10^{-3}\mu\right)}}$$

where $n(\nu)$ is the real index value within the measured range (i.e. 4500-800 cm^{-1}), and μ is the location of the neglected (unmeasured) band. The band width (for example σ in the Gaussian band shape) was found to have very little influence on the final results and was not incorporated into the relationship given in Equation 2. Similar analysis was done for a linear extrapolation scenario, to yield its correction on the real index under different slopes. In addition, a third function was derived to describe the influence of uncertainty in the non-measured band location (i.e. the precise μ). The above functions were shown to be effective in reproducing the correction factors of n in the measured range, given the specific band location and scale, without the need to extend the KKT to the non-measured spectral range.

Bohren, C. F., & Huffman, D. R. (2004). *Absorption and scattering of light by small particles*. Weinheim, Wiley-VCH.

Scattering data base for nonspherical particle

J. Wauer[1], T. Rother[2] and K. Schmidt[2]

[1]Institute for Meteorology, University of Leipzig, D-04103 Leipzig, Germany
[2]Remote Sensing Technology Institute, German Aerospace Center, D-17235 Neustrelitz, Germany

Keywords: light scattering, nonspherical particle, aerosol optics, optical properties, backscatter

Light scattering on nonspherical dielectric particles becomes of growing importance in remote sensing of the earth's atmosphere. Studying the influence of desert dust is only an example in this context. The existence of nonspherical particles can be checked directly with modern LIDAR systems by detecting the depolarisation in back scattering direction. But also indirect measurements provide several hints for the necessity to take light scattering on nonspherical particles into account. Therefore we have to consider nonspherical mineral scatterer.

But there are especially two aspects which makes this necessity a complex task. First, the numerical effort is much higher as compared to the case for spherical particles within the Mie theory. The time of calculations strongly depends on the morphology of particles and can be performed on-line only in very specific situations. Second, the convergence procedures of the existing approaches are more complex as compared to Mie theory. To obtain reliable results, one needs a detailed knowledge of the methodology behind a certain approach. Otherwise, one can run into a lot of pitfalls. Therefore we present a scattering database for nonspherical particles of a certain accuracy that releases the users from dealing with numerical aspects of the light scattering problem.

The data base contains orientation averaged scattering quantities of spheroids. With respect to spheres, the aspect ratio av=a/b (a, b- semi axes of the spheroid, av>1 belongs to prolate spheroids) is an additional parameter to describe the light scattering.

In table 1 the range of the data base parameters is given.

aspect ratio	refractive index n		size parameter
	Re(n)	Im(n)	
0.67-1.5	1.31-1.8	0-0.1	≤ 40

Table 1. Parameter range of the data base for spheroidal particles.

Currently, the data base contains more then 145.000 data sets. To get easy access to this data, we have developed an user interface. This user interface provides also some additional functionalities going beyond the simple readout of data. These are consistency tests of the user requests, interpolation between data and the computation of size averaged scattering quantities.

In figure 1 and 2 two examples are presented to illustrate the usage of the data base. In figure 1 some scattering quantities of single, randomly oriented particles are plotted and in figure 2 size averaged phase functions are given.
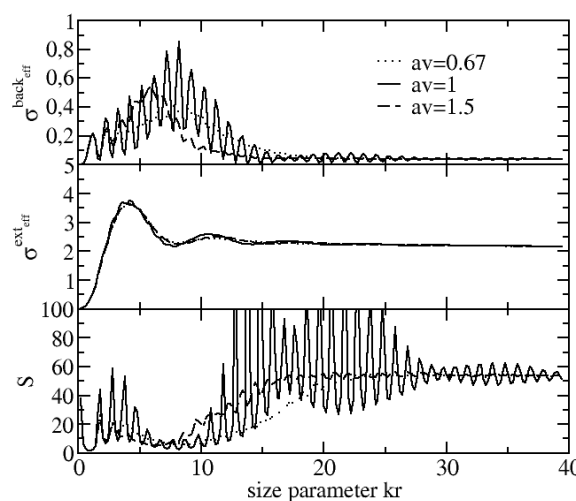
Figure 1. Back scattering efficiency σ^{back}_{eff}, extinction efficiency σ^{ext}_{eff} and LIDAR ratio S of a randomly oriented oblate spheroid (dotted lines), a sphere (solid lines), and of a prolate spheroid (dashed lines), all having a refractive index n=1.5+0.05i, as a function of the volume equivalent size parameter kr.
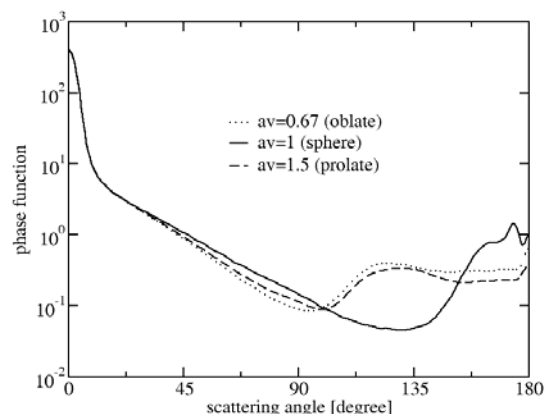
Figure 2. Size averaged phase function of randomly oriented oblate spheroids (dotted lines), spheres (solid lines), and of prolate spheroids (dashed lines) with λ=0.355μm, n=1.5, and a log-norm distribution function with a mode radius r_m= 1.2 μm and σ_m=1.4 μm.

Polar scattering from fractal like soot agglomerates

K.-H. Naumann[1], M. Gangl[2], M. Schnaiter[1], and H. Horvath[2]

[1]Institute for Meteorology und Climate Research, Atmospheric Aerosol Research Division,
Research Centre Karlsruhe, Germany
[2]Faculty of Physics, University of Vienna, Austria

Keywords: aerosol optics, light scattering, soot agglomerates, fractals, aerosol modelling

For fractal-like agglomerates with volume fractal dimensions $D_f \leq 2$ multiple scattering of incident light may be neglected to a good approximation. Therefore the Rayleigh-Debye-Gans (RDG) theory provides a reliable yet convenient route towards computing the differential and total scattering cross sections of fractal particles (Sorensen, 2001). So far, however, besides assuming spherical isotropy additional simplifications regarding the form of the radial pair distribution function g(r) of the monomers like exponential or Gaussian cutoff had to be employed when calculating the structure factor S(q). For example, by interpolating between the well-known small-q and large-q limiting expressions, Dobbins and Megarides (1991) derived simple analytical approximations for S(q) and the total specific scattering cross section σ_{sca}. This paper, however, considers a statistical mechanical procedure based on an exact analytical expression for g(r) recently developed by Naumann (2003).

In order to evaluate the performance of the treatment based on the exact form of g(r), reference T-matrix calculations for model clusters of various sizes generated by a ballistic aggregation algorithm and resembling the properties of Diesel soot ($D_f = 1.8$; diameter of monomers: 25 nm; $\lambda = 450$ nm) were performed using Daniel Mackowki's code (http://www.giss.nasa.gov/~crmim/t_matrix.html) including and excluding multiple scattering. The latter case is equivalent to the RDG treatment of a discrete arrangement of monomers. We observed good agreement between the T-matrix predictions and the statistical approach based on the exact form of g(r) for both the normalized angle dependent scattering cross section and the total specific scattering cross section as a function of cluster size. Following Dobbins and Megarides (1991) the total scattering cross section should reach a constant plateau in the large particle regime. Clearly this prediction is not supported by the T-matrix and rigorous RDG calculations for Diesel soot clusters up to 1024 monomers.

During the AIDA soot campaign 2002 conducted at the Research Centre Karlsruhe a polar nephelometer developed at the University of Vienna was employed to measure the scattering intensity of Diesel soot and graphite spark (Palas) soot agglomerate particles at a wavelength of 501 nm angularly resolved over 28 channels covering the range from 16 to 164 degrees. As an example, Figure 1 compares the measured and the simulated differential scattering cross section for Palas soot. Altogether, the experimental results could be well reproduced by the statistical approach, thereby allowing to determine the fractal dimensions of Diesel and Palas soot to 1.95±0.10 and 2.2±0.2, respectively. These findings are consistent with results obtained by analysing aerosol dynamics experiments using the fractal aerosol behaviour code COSIMA (Naumann, 2003) and by combining particle mobility sizing with low pressure impaction (Weingartner et al., 1995), while the analysis of TEM images appears to lead to systematically lower values.
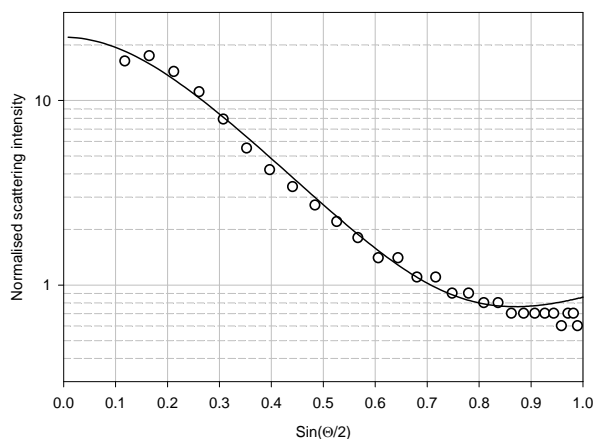
Figure 1. Measured and simulated differential scattering cross section for Palas soot, normalized to the value at 90 degrees.

Dobbins, R. A. and Megarides, C. (1991) Absorption and scattering of light by polydisperse aggregates. *Applied Optics* 30, 4747-4754.

Naumann, K.-H. (2003). COSIMA – a computer program simulating the dynamics of fractal aerosols. *J. Aerosol Science*, 34, 1371-1397.

Sorensen, C. M. (2001) Light scattering by fractal aggregates: A review. *Aerosol Sci. Technol.,* 35, 648-687.

Weingartner E., Baltensperger U., and Burtscher H. (1995) Growth and structural change of combustion aerosols at high relative humidity. *Environ. Sci. Technol.* 29, 2982-2986.

Aerosol optical depth and its connection with macrometeorological features

A. Ponczkowska[1], T. Zielinski[1], T. Petelski[1], J. Piskozub[1], G. Chourdakis[2], , S. Malinowski[3], T. Stacewicz[3], K. Markowicz[3], A. K. Jagodnicka[3], M. Posyniak[3], A. Kardas[3], I. Stachlewska[3], M. Gausa[4], S. Blindheim[4], A. Smirnov[5], B. Holben[5]

[1] Institute of Oceanology, PAS, Poland
[2] Raymetrics SA, Greece
[3] University of Warsaw, Poland
[4] ALOMAR Laboratory, Norway
[5] Goddard Space Flight Center, NASA, USA

Keywords: marine aerosol, optical properties, coastal sites, Arctic.

The contribution of aerosol particles to moisture and energy exchange processes at the sea surface, to the global salt flux, their role in cloud droplet formation processes and their influence both upon the maritime atmospheric radiation balance and propagation at visible and infra-red wavelengths or visibility assessment are of increasing concern (Sakerin *et al.*, 2007).

This has a significant influence on both the performance of electro-optical systems and our experience in everyday life. A thorough understanding of such phenomena is essential to an accurate assessment of many processes important for the development of coupled ocean-atmosphere global circulation models, including the pollution problem. Due to its light attenuation properties, aerosols are important in satellite investigations of the ocean surface (Smirnov *et al.*, 2009).

The aerosol studies during the AREX campaigns were carried out onboard the r/v *Oceania* between 2000 and 2008. During each campaign the vessel cruised for six weeks in the European Arctic between 0 and 14°E and 69 and 79°N. In 2006 the ship cruised in the area of ALOMAR laboratory on Island Andoya in northern Norway (16°E and 69°N). Data were also collected during the SOAP experiment in 2006 in Crete.

The studies were conducted using an ensemble of instruments, including lidars, ceilometers, laser particle counters, CPC and sunphotometers. The full meteorological coverage (wind speed, direction, air mass backtrajectories, relative humidity, air temperature, etc.) was provided by the ship meteo station, which collected data every 10s, from the British Atmospheric Data Center and using HYSPLIT (Zielinski *et al.*, 2005).

In order to find the relationships between the aerosol variability in the marine boundary layer and above we compared our data against the pressure levels charts (850, 700, 500 hPa). We observed that the state of the atmosphere between 1 to 3 kilometers above sea level can reflect the changes in the marine boundary layer.

We examined the spatial and temporal variation of aerosol optical depth in different marine areas (including coastal zones) using the upper troposphere charts for the northern hemisphere. Comparison of manual analysis charts with empirical data facilitates detection of different behavior patterns of aerosol optical depth and the characterization of the influence of vertical water vapor distribution on AOD values (present as atypical spectral behavior). During our investigations the calculation of useful backscatter coefficient parameter was made at above 1.5 km altitude and it occurred that the columnar AOD can be significantly affected by the ridges of northern hemisphere circulation. The principal conclusions are also combined with detection of jet stream event over Lofoten Islands. The range of changes between the "Before" and "During" state of AOD was significant.

The results show that local emissions are not always most important factors, which influence the composition of marine aerosol in the near water atmospheric layer, even for the coarse mode aerosols, also known as the sea salt mode. The air mass history must be taken into consideration.

Sakerin, S.M., Smirnov, A., Kabanov, D.M., Pol'kin, V.V., Panchenko, M.V., Holben, B.N., Kopelevich, O.V. (2007). *Aerosol optical and microphysical properties over the Atlantic Ocean during the 19th cruise of the Research Vessel Akademik Sergey Vavilov,* J. Geophys. Res.112 (D10): art. no. D10220.

Zielinski, T., Piskozub, J. (2005). *Studies of aerosols in the marine boundary layer in the coastal area during the EOPACE'9.* Boundary-Layer Meteorology, Vol. 116, No. 3, 533-541.

Smirnov, A., Holben B., et al., (2009). *Maritime Aerosol Network (MAN) as a component of AERONET.* J. Geophys. Res. 100: 16,639-16,650.

Effective dielectric permeability
of fractal cluster

V.V.Maksimenko

Karpov Institute of Physical Chemistry, Moscow, 10, ul. Vorontsovo Pole, 105064, Russia.

An interest to transparent media with anomalous high value of effective dielectric permeability is continuously increased because of problems of modern nanophotonics. Such media allow to reduce light velocity, to screen external electromagnetic fields, to reduce wave length of radiation etc. Typical example of such systems is fractal cluster (FC) consisting of nonabsorbing particles.

Due to the power decrease of the cluster density, the effective dielectric permeability of FC must be function of coordinate. This essentially complicates the problem because just the possibility of replacement of real non uniform medium by some homogeneous medium defines all advantages of introduction of effective permeability $\bar{\varepsilon}$. Fortunately, one more approach to the problem is possible.

Is shown that FC is characterized by some set of values of $\bar{\varepsilon}_N$ instead only one value $\bar{\varepsilon}$. These values are uniformly distributed along the circle of radius

$$\left| \bar{\varepsilon}_N \right| \simeq \left| \varepsilon - 1 \right| N^{\frac{3-2d}{4d}N}$$

of complex plane $\operatorname{Re}\bar{\varepsilon}, \operatorname{Im}\bar{\varepsilon}$. Here, ε is the dielectric permeability of material, d is the fractal dimension, and $N \gg 1$ is the number of particle inside correlation block of the cluster. Is assumed that space correlations between particles are defined by power law and correlation length is defined by upper limit of integral expressing the normalization requirement for binary correlator $g_2(r)$:

$$\int g_2(r)d\mathbf{r} = 1/n_0 ,$$

where n_0 is the mean concentration of particles inside cluster.

At $d < 3/2$ and $N \gg 1$ the effective dielectric permeability of cluster becomes very large. An exclusiveness of the magnitude $d = 3/2$ is not accident. The number of particles inside cluster with characteristic size r grows as r^d. Using approximation that all particles inside the correlation block are correlated, the number of binary correlators grows as $N^2 \sim r^{2d}$ and at $d > 3/2$ the correlated particles cannot be placed inside the volume $\sim r^3$.

Wave length of virtual photon inside cluster λ_{int} differs from that of incident photon λ,

λ_{int} becomes essentially smaller. This process is called the renormalization of λ. The physical reason is very simple. The dielectric permeability of any system increases in vicinity of any electromagnetic resonance. FC is characterized by set of cavities with power distribution over sizes. The incident photon finds the initial resonance cavity whose size is comparable with its wave length. An initial increase of $\bar{\varepsilon}$ occurs. Owing to this, the wave length of radiation inside medium decreases because $\lambda \to \lambda_{int} = \lambda / \sqrt{\bar{\varepsilon}}$. At the same time the photon velocity is also decreased ($c \to \mathrm{v} = c / \sqrt{\bar{\varepsilon}}$) but the frequency $\omega = 2\pi \mathrm{v} / \lambda_{int}$ remains constant (c is the light velocity in vacuum). The photon with renormalized wave length λ_{int} again finds the resonance cavity with characteristic size comparable with λ_{int} and so on. As a result, all cavities inside cluster can be filled by renormalized photons. The photons with $\lambda_{int} \to 0$ will be among them. Their effective velocity is zero. Such photons are called the localized ones. The external electromagnetic field stops penetrates inside the cluster. In other words, the effective dielectric permeability of cluster tends to infinity. We met here with just this situation. Set of values $\bar{\varepsilon}$ reflects existence of corresponding set of values λ_{int}.

In order the phonon can penetrates inside the cluster the latter must has an initial "resonance" cavity. If the characteristic size of cluster is order of one micron the characteristic size of such cavity is fractions of the micron. So, in order the above mentioned processes can have a place the frequency of incident photon must belongs to visible range of spectrum.

Above mentioned program was realized using the methods of multiple scattering theory. The effective dielectric permeability was founded from analysis of averaged photon propagator inside FC (Lushnikov & Maksimenko,1993).

It is possible, the above mentioned features of fractal clusters with low fractal dimension allow to use aerogels as Cherenkov's detectors of elementary particles – very high effective dielectric permeability makes local velocity of light lower than velocity of detected particles.

Lushnikov A.A., Maksimenko V.V. (1993), JETP, 497 -503.

Measurements of aerosol optical properties at urban sites to determine aerosol direct radiative effect

Sabina Ştefan[1], Raluca Barladeanu[1] and Laura Mihai[1]

[1]University of Bucharest, Faculty of Physics, Dept. of Atmospheric Physics, P.O.BOX MG-11, Bucharest, Romania

Keywords: optical properties, physical properties, in – situ measurements, urban pollution

The aim of the present work is to obtain aerosol physical and optical properties that will allow evaluation of the direct climate forcing at surface. For this we have used *in situ* measurements of PM (Particulate Matter) in three sites in Bucharest (Romania) area, during 2007 year: rural suburban and industrial.

The OPAC soft (Hess et al., 1998) helped us to obtain optical parameters of the aerosol *versus* wave length.

The optical properties were also determined by using sun-photometer (Holben et al. 2001) and nephelometer equipments.

Meteorological data are used referring to the selected sites to test dependence of the parameters on atmosphere state. The Aerosol optical Depth (AOD) and Single Scattering Albedo (SSA) values are strongly dependent on the type of site, industrial, suburban or rural (Fig1a, b). The differences between AOD values for rural and industrial site, for example are very large. One can observe the largest AOD values during summertime for the both sites. For urban the AOD values are larger than over rural site indicating a polluted urban zone. The dependence of AOD on relative humidity was also demonstrated (Fig.1a, b).

Compared with the scattering, the absorption ability of particles are relatively more significant over industrial site. Consequently, the low values of SSA in observed in autumn and winter months (not shown) over industrial area are attributed to the relative dominance of absorbing aerosols.

The both, Single Scattering Albedo (SSA) and asymmetry factor showed a low sensitivity to AOD at the wavelengths in all seasons.
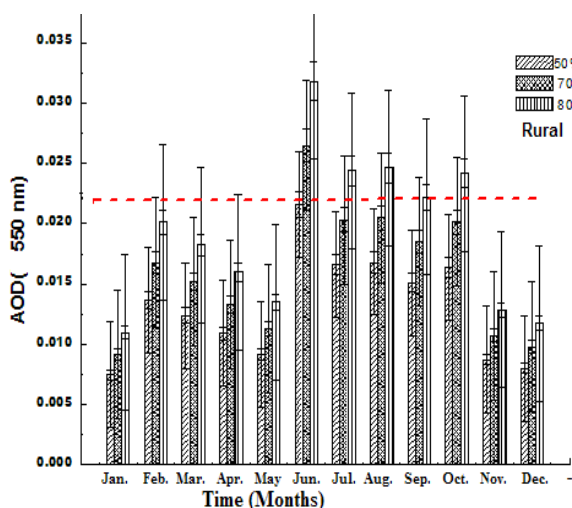
Fig1a. Temporal variation of monthly means AOD at 550nm for urban site.
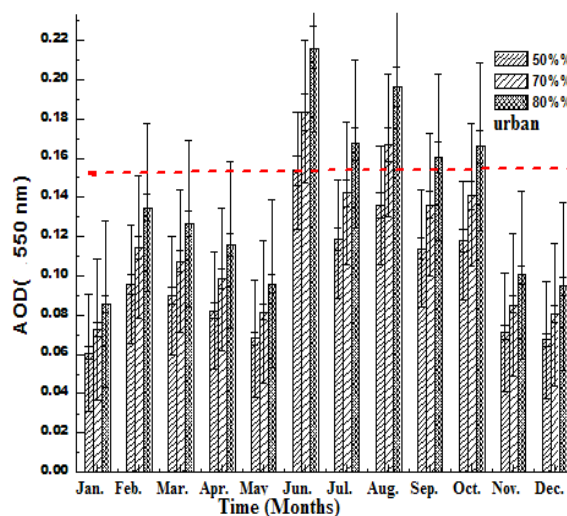
Fig1b. Temporal variation of monthly mean AOD at 550nm for rural site (error bars represent the standard error of the monthly ensembles).

Hess M., Koepke P. and Schult I. (1998). *Optical properties of aerosol and clouds*, the software package, Bulletin of American Meteorological Society 79, 831-844.

Holben, B. N., Tanr´e, D., Smirnov, A., et al.: *An emerging ground-based aerosol climatology: aerosol optical depth from AERONET*, J. Geophys. Res. 106, 12 067–12 097, 2001.

Effect of a Hydrocyclone and a Centrifugal Separator in Purifying Rolling Lubricant

Youngjin Seo and Sung-Jin Lee

Rolling Technology Research Group, POSCO Technical Research Laboratories,
POSCO, Gwangyang-si, Jeonnam, Korea 545-090

Keywords: Hydrocyclone, Centrifugal separator, Rolling lubricant, Iron concentration.

In general, steel makers [i.e., POSCO (Korea)] are nowadays required to produce high quality and high strength steel. In order to produce such steel, it requires additional process after hot-rolling, which is called, "cold-rolling". The main difference between hot-rolling and cold-rolling is the temperature of rolled materials. Rolling lubricant that is used during cold-rolling is very important because it has direct relevance to the degree of lubrication and cleanliness of final products.

The current system for purifying rolling lubricant consists of nonwoven fabric whose porous size is about 50 μm and magnetic filters. The fabric is to remove coarse particulate matter and fine iron content's particles are supposed to adhere to the magnetic filters. However, the efficiency of the filtration system has been poor. For example, there has been an overflow of the lubricant through the fabric and the magnetic filters have been inefficient. Thus, renovated methodology to clean the lubricant is in need.

In the paper, two common devices such as a hydrocyclone and a centrifugal separator have been evaluated as to particle extraction efficiency, iron (Fe) concentration, and oiliness in the lubricant. The three items are extremely important in terms of economical efficiency and quality of final products.

A hydrocyclone is a size classification device that separates solid particles from operating liquid based on the difference of specific gravity between the solid and the liquid. It could be used for separating liquid from liquid when there is density difference between the two liquids. The principle of a centrigual separator is very similar to that of a hydrocyclone. The main difference between the two is that there is no moving part in a hydrocyclone.

Particle distribution was measured by a particle size analyzer (Model number: Mastersizer 2000, Malvern, United Kingdom). Special chemical analysis is required to quantify Iron (Fe) concentration and oiliness in the lubricant, which will not be described in the paper.

Prior to the test, volume fraction of particles below 10 μm among particles was approximately 91.6% and the largest particle size was 34.7 μm. The median size in terms of volume fraction was about 2.9 μm.

After test using a hydrocyclone (Model number: gMax2, Krebs Engineering, AZ, USA), most particles, smaller than 10 μm, were extracted so that volume fraction of particles, larger than 10 μm among particles was only 1.9% and that the largest particle in the sample (Overflow) was 17.4 μm. The median size with respect to volume fraction was about 2.5 μm. Figure 1 shows the measured data.

On the other hand, the effectiveness of a centrifugal separator (Model number: BABY2, Pieralisi, Netherland) in terms of particle extraction efficiency was much enhanced compared to the hydrocyclone. After test with the separator, most particles, larger than 6.6 μm, were eliminated (Figure 2). The operating flow rate was 0.067 ton/min and rotating RPM (revolutions per minutes) was 3300.

Regarding reduction of iron (Fe) concentration, the hydrocyclone was of no effect. However, there was about 50% reduction by the centrifugal separator.

On the subject of oiliness, both devices produced a beneficial result. That is because specific gravity of oil is smaller than 1.

Further studies will be conducted to verify why the centrifugal separator generated better result in terms of reduction of iron (Fe) concentration.
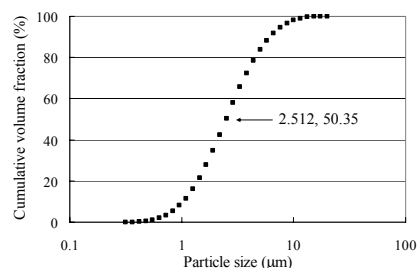
Figure 1. Particle distribution in the lubricant after test with the hydrocyclone
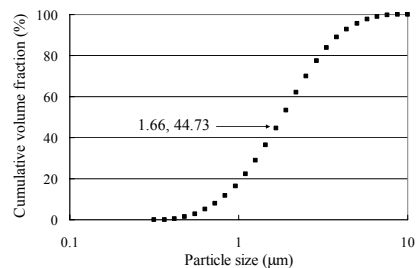
Figure 2. Particle distribution in the lubricant after test with the centrifugal separator

Alliott, E. A. (2006), *Centrifugal Dryers and Separators*. Wexford College Press.

Svarovsky, L. and Thew, M. T. (1992), *Hydrocyclones Analysis and Application*. Kluwer Academic Publishers.

Loading of Soot Nanoparticle Agglomerates on Air Filters

J. Wang, S-C. Kim and D.Y.H. Pui

Particle Technology Laboratory, Department of Mechanical Engineering, University of Minnesota, Minneapolis, MN, USA, 55455

Keywords: filtration, filter loading, cake filtration, soot agglomerates.

Studies for filtration of nanoparticle agglomerates are still scarce compared to those for spherical particles. Lange et al. (1999) measured the filtration efficiency of fibrous filters for carbon agglomerates and for spherical particles as a function of the mobility diameter. Kim et al. (2009) studied filtration of silver nanoparticle agglomerates by fibrous filters.

The pressure drop across a filter can rise rapidly under heavy particle loading conditions. Endo et al. (1998) performed experiments to measure the pressure drop and the height of dust cake in real time. They derived an analytical expression to correlate the pressure drop with the particle size distribution and particle shape.

We investigate loading of soot nanoparticle agglomerates on fibrous air filter media. The soot agglomerates were generated from a diffusion burner with propane gas as fuel and compressed air as oidant/sheath. The mode of the number distribution was determined to be 120 nm. A Differential Mobility Analyzer (DMA) - Aerosol Particle Mass Analyzer (APM) system was used to measure the mass of agglomerates as a function of the mobility size, which gave a fractal dimension of 1.90±0.1.

We performed extensive studies using electron microscopy. The agglomerates were composed of primary particles of nearly spherical shape. From the sizes of 190 primary spheres analyzed, we found that the mean diameter was 28 nm with a geometric standard deviation of 1.26.

Loading experiments with soot agglomerates were performed with the face velocity of 10 cm/s. The filter used in the loading experiments was HE 1071, a fiberglass media manufactured by Hollingsworth and Vose. A total number of 12 tests were carried out; the loading time was varied in these tests but other conditions were kept the same. Filter mass changes were measured after the loading tests with the accuracy of 0.1 mg. We measured the cake thickness using a video enhanced microscope. The 12 tests had similar values of cake porosity and the average value was 0.95. The pressure drop across the filter was monitored during the loading process and the final pressure drop when the test ended was recorded. We plot the final increased pressure drop as a function of the loading mass in Figure 1. It can be seen that the pressure drop increases approximately linearly with the loading mass.

To better understand the results, we look at the analytical expression derived by Endo et al.

(1998):

$$\Delta P_c = 18\mu U_f H \frac{(1-\varepsilon)\upsilon(\varepsilon)}{\varepsilon^2} \frac{\kappa}{d_{vg}^2 \exp(4\ln^2 \sigma_g)}$$

where μ is the gas viscosity; U_f is the face velocity; H is the cake thickness; ε is the porosity; $\upsilon(\varepsilon)$ is the void function; d_{vg} is the geometric mean of the volume equivalent diameter of the loading particles and σ_g is the geometric standard deviation; κ is the dynamic shape factor. The cake could be regarded as formed by primary particles in soot agglomerates. When the size distribution of the primary particles was used in the model of Endo et al., good agreement between the experimental and computed results was obtained as shown in Figure 1.
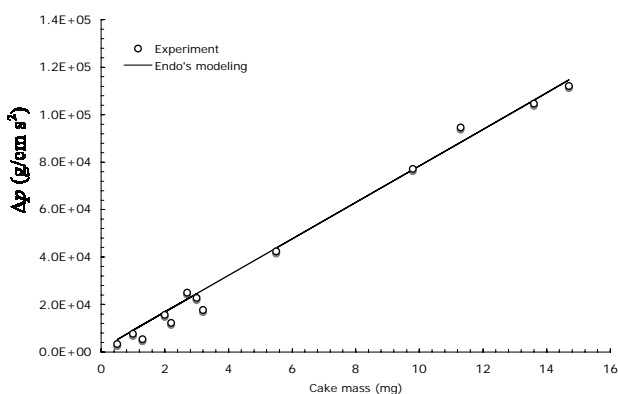
Figure 1. The pressure drop at the end of the loading test as a function of the cake mass.

Endo, Y., Chen, D-R and Pui, D.Y.H. (1998) *Powder Technology*, 98(3), 241 – 249.

Lange, R., Fissan, H. and Schmidt-Ott, A. (1999). *Particle & Particle Systems Characterization* 16, 60- 65.

Kim, S.C., J. Wang, J, Emery, M., Shin, W-G, Mullholand, G. and Pui, D.Y.H. (2009), in print, *Aerosol Sci. & Technology*.

Dependence of the filter efficiency on nanoparticle velocity and shape

Z.Y. Zhang[1] and Z.Z. Zhang[2]

[1]Department of General Surgery, Digestive Medical Center, the First Affiliated Hospital of Tsinghua University, 100016, Beijing, P.R.China
[2]Institute of Nuclear and New Energy Technology, Tsinghua University, 100084, Beijing, P.R.China

Keywords: filtration efficiency, re-entrainment, particle roll and tumble.

The filtration efficiency of fibrous filters may decrease because of particle bounce from the fibers (Ellenbecker et al, 1980). Boskovic et al. (2008) showed the influence of the face velocity on the filtration efficiency for three types of particles of different shape (PSL, NaCl and MgO), at the velocity of 5cm/s, the shape of the particles plays a significant role, but for the velocity of 10 and 20 cm/s, the effect of particle shape is less obvious because inertial removal mechanism is becoming dominant.

Based on the experimental data, Boskovic et al (2008) further calculated the probability of NaCl particles to roll or to tumble. They considered that inertial impaction is the key factor and got the rolling probability of particle due to inertia.

But diffuison is another important filtration mechanism, the thermal velocities of the particles of different shape are calculated according to Hinds. 1999 and listed in Table1.

Table 1. Thermal velocities of the particles of 50nm and 300nm.

Particle type	Size (nm)	Thermal velocity (cm/s)
PSL	50	15.8
	300	1.08
NaCl	50	11.0
	300	0.748
MgO	50	8.54
	300	0.501

As shown in Table 1, the thermal velocity is larger than the face velocity of 5cm/s for all types of particles of 50nm, so only considering the inertia mechanism is not sufficient, and at least the diffusion mechanism should be added to investigate the probability of NaCl to roll or to tumble.

In this paper, the equations provided by Boskovic et al. (2008) would be modified as the equation (1), α and β are two parameters determined by the number, position and kinetic energy, etc. of particles come into contact with the filter fiber. So, it is very complicated to get α and β, here, for simplicity, α and β are assumed as 0.5.

$$\frac{\left[q_{sngl}^{exp}/\left(\alpha\varepsilon_{sngl-impa}^{thr} + \beta\varepsilon_{sngl-diff}^{thr}\right)\right]_{MgO}}{\left[q_{sngl}^{exp}/\left(\alpha\varepsilon_{sngl-impa}^{thr} + \beta\varepsilon_{sngl-diff}^{thr}\right)\right]_{NaCl}} \quad (1)$$

$$= \frac{\left[\ln\left(1-E_f\right)/\left(\alpha\varepsilon_{sngl-impa}^{thr} + \beta\varepsilon_{sngl-diff}^{thr}\right)\right]_{MgO}}{\left[\ln\left(1-E_f\right)/\left(\alpha\varepsilon_{sngl-impa}^{thr} + \beta\varepsilon_{sngl-diff}^{thr}\right)\right]_{NaCl}}$$

According to the equation (1), the calculated results are listed in Table 2 and different from those got by Boskovic et al. (2008).

Table 2. Rolling probability of NaCl versus MgO calculated by equation (1) and Boskovic et al. (2008)

Calculated equation	5cm/s face velocity	
	50nm	300nm
Equation (1)	1.06	0.65
Boskovic et al. (2008)	0.64	0.42

In conclusion, inertial impaction, diffusion and interception are all capture mechanisms of fibrous filter. The possiblities of particle rolling or tumbling should consider all of them. In fact, it is very complicated to descibe the rolling probability of particles in detail and need further research.

Boskovic, L., Agranovski, I. E., Altman, I. S., & Braddok R. D. (2008). *Journal of Aerosol Science*, 39, 635-644.
Ellenbecker, M. J., Leith, D., & Price, J. M. (1980). *Journal of the Air Pollution Control Association*, 30, 1224-1227.
Hinds, W. C. (1999). *Aerosol Technology: Properties, Behavior, and Measurement of Airborne Particles*. New York, John Willey & Sons, Inc.

DUST CONCENTRATORS FOR COST EFFECTIVE GAS CLEANING

V. Galperin, O. Elport, M. Shapiro

Laboratory of Transport Processes in Porous Materials, Faculty of Mechanical Engineering,
Technion – Israel Institute of Technology
Haifa, 32000, Israel

Keywords: dust removal, virtual impactor, concentration, collection efficiency, cyclone

Among modern industrial gas cleaning methods from dust particles, inertial separators (mainly cyclones) are the simplest and less expensive devices. They however inefficiently collect particles with sizes below 5 μm. So the cyclones are normally used for coarse or preliminary gas cleaning. To satisfy the environmental standards' requirements for particulate emissions into the atmosphere, scrubbers, electrostatic precipitators (ESP) and fabric filters are used. Figure 1 illustrates efficient dust collection zones of these dust separation equipment, all of which are rather expensive compared to cyclones.

During several last years we have been investigating dust concentration in cyclone-type devices to improve the efficiency of dust collection and decreasing the expenses. The idea of using concentrators (virtual impactors) for environmental control is to divide the dusty gas stream in two portions: a smaller (minor) portion, where most of the dust mass is contained and the major one. The latter is aimed to be cleaned to a degree that satisfies the environmental standards' requirements and thus may be released to atmosphere without further cleaning. Gas cleaning expenses are proportional to the gas volume. Hence cleaning the remaining minor gas portion is much less expensive than the whole inlet stream. We studied the influence of different aerodynamic parameters and initial dust concentration on the efficiency of cyclone-type concentrators. For this purpose we designed, constructed and tested several concentrators' prototypes. The results reveal that tangential reverse flow cyclone-

type concentrators with minor gas volume of about 20% enable one to diminish the modern power stations' outlet dust concentration (emission rate) by about 60% (see broken line in fig. 1). Further reducing the outlet concentration may be achieved by improving the aerodynamic characteristics of dust concentrators and optimizing their design parameters.
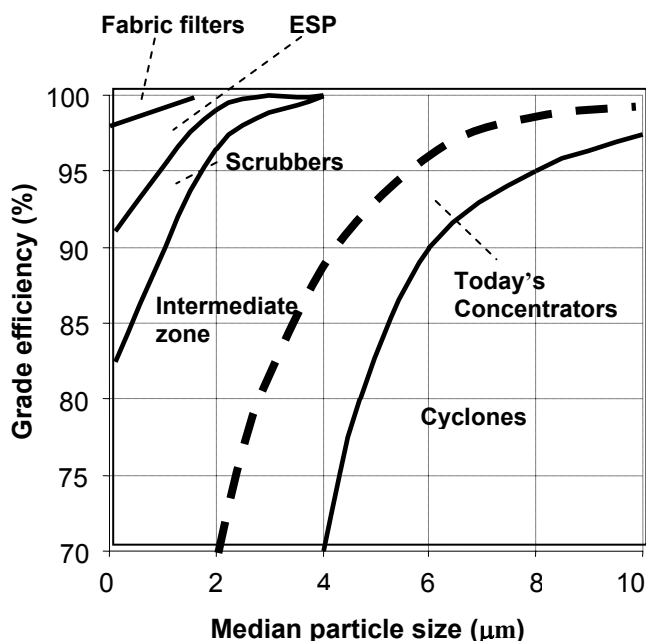
Figure 1. Dust concentrator efficiency compared with traditional dust collection devices. Broken line: grade efficiency of the tested reverse-flow tangential cyclone-type concentrator

1. Galperin, V., & Shapiro, M. (1999). Cyclones as dust concentrators, *J. Aerosol Science* 30, S897 – S898.
2. Bohnet M., Gottschalk O. (1998). Calculation of grade efficiency and pressure drop of aerocyclones with suction of a partial gas stream, *Chem. Eng. Technol., PARTEC* **98**, 95-109.
3. Elport O. (2008). *Collection of dust particles in cyclone-type concentrators*, M.Sc thesis, Technion, Haifa, Israel.

A Model for Steady-State Oil Transport and Saturation in a Mist

D.Kampa[1], J. Meyer[1], B. Mullins[2] and G. Kasper[1]

[1]Institut für Mechanische Verfahrenstechnik und Mechanik, Universität Karlsruhe (TH), 76128 Karlsruhe, Germany
[2]Centre of Excellence in Cleaner Production, Curtin University of Technology, Perth, WA 6845, Australia

Keywords: Aerosol filtration, Coalescence filtration, Modelling, Oil Mist

This paper deals with the functioning of oil mist filters typically used to remove small oil droplets from gas flowing from the crankcase of an automotive engine or an oil lubricated compressor. In principle, such mist filters become entrained with oil in the early stages of operation, until they reach a stationary state where oil accumulation equals entrainment and drainage rates.

A kinetic model has been developed to describe the spatial distribution of oil within the filter in terms of a steady-state saturation $S(x)$, where x is the filter depth in flow direction. The model is based on a balance of oil accumulation and transport rates within each infinitesimal layer. Solution of the resulting differential equation leads to the well-known U profile for $S(x)$ (Figure 1).
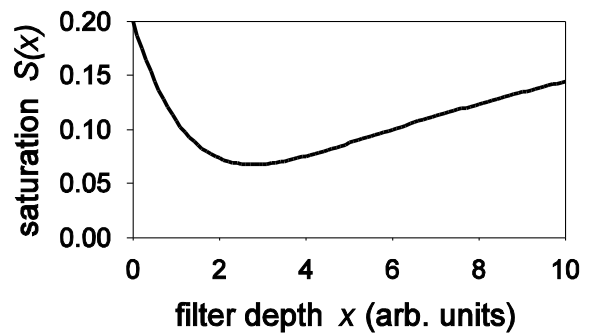
Figure 1. U profile of the saturation $S(x)$ as a function of the filter depth x.

Impact of Electrostatic Forces on Collection
of Charged Nanoparticles Aerosols by Dielectric Wire Screens

G. Mouret[1,2], S. Chazelet[1], D. Thomas[1], D. Bémer[2]

[1] Nancy-Université/LSGC/CNRS – 1, rue Grandville – BP 20451 – 54001 Nancy Cedex, France
[2] INRS – Ingénierie des Procédés – Avenue de Bourgogne 54501 Vandoeuvre les Nancy Cedex, France

Key words: nanoparticles, aerosol filtration, electrostatic forces, wire screen, Boltzmann equilibrium

Considering the numerous works that have been carried out for the last few decades, it seems to be unambiguous today that because of Brownian diffusion, penetration of uncharged nanoparticles through wire screens continuously decreases as the aerosol diameter does, and that experimental points can be well represented by the Cheng and Yeh's model (Alonso *et al.*, 1997; Shin *et al.*, 2008). It is no longer the case however with charged aerosols. Indeed, this paper presents results of penetration of nanoparticles aerosols at Boltzmann equilibrium through a plastic wire screen.

The test monodisperse aerosol of copper or carbon nanoparticles, the electrical mobility diameter of which was varied from 4 to 80 nm, was produced from a commercial spark-generator and a nano-DMA for diameter selection. Before challenging the screen in a dummy chamber device (Heim *et al.*, 2005), the aerosols were electrically-neutralized (Boltzmann equilibrium) thanks to a ^{85}Kr radioactive source. Both upstream and downstream concentrations were measured using the same CPC.
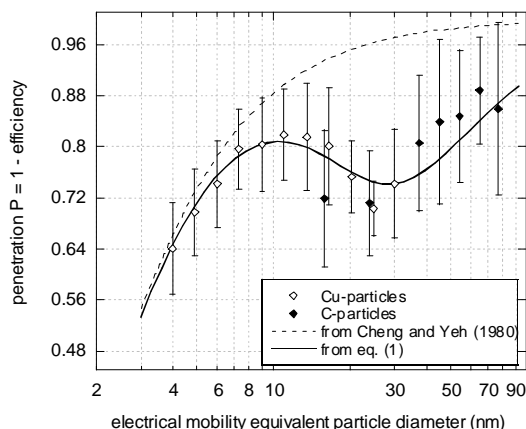
Figure 1 – Penetration of nanoparticles at Boltzmann equilibrium through the wire screen, at 5 cm/s

As it can be seen on figure 1, the experimental points clearly give a "wave-shaped" curve, with a local minimum for P at 25 nm about. This can in fact be well represented taking into account the collection probability of each kind of particles composing the Boltzmann equilibrium aerosol. Such a consideration leads to:

$$P = \sum_i x_i \times P_i \qquad \text{eq. (1)}$$

where x_i is the numeric fraction of particles carrying i elementary charges (i varies from –2 to 2 below 100 nm) and can be estimated from Wiedensohler's equations. P_i is the penetration value of the i-particles through the screen.
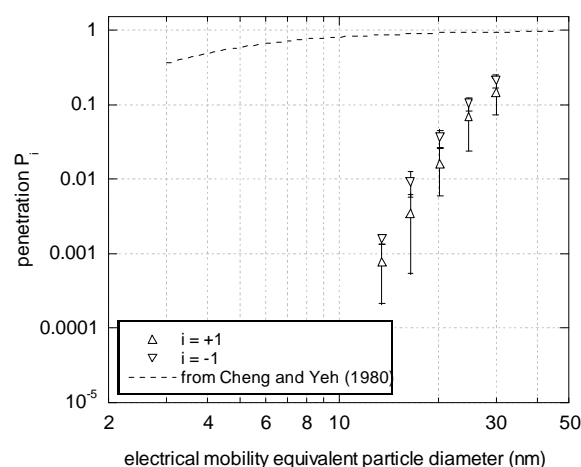
Figure 2 – Penetration of unipolarly charged nanoparticles through the wire screen at 5 cm/s

Figure 2 shows the penetration of unipolarly charged aerosols through the screen. Charged particles are clearly more efficiently captured than uncharged particles, which would only be trapped by Brownian diffusion (theory of Cheng and Yeh). This increased collection efficiency is due to electrostatic forces, the effect of which can be mathematically estimated knowing the electrical charge density carried by the fibers of the screen. Added to the fact that $x_{i \text{ for } i \neq 0}$ increases while x_0 decreases as the particle diameter increases, this leads to the situation reported on figure 1. The same kind of behaviour is currently experimentally-observed at the lab with another wire screen.

Cheng, Y. S. and Yeh, H. C. (1980). *Journal of Aerosol Science*, 11, 313-320.
Alonso, M. *et al.* (1997). *Aerosol Science and Technology*, 27, 471-480.
Shin, W. G. *et al.* (2008). *Journal of Aerosol Science*, 39, 488-499.
Heim M. *et al.* (2005). *Aerosol Science and Technology*, 39, 782-789.
Wiedensohler, A. (1988). *Journal of Aerosol Science*, 19, 387-389.

Experimental results and modelling of the clogging of pleated fibrous filters in presence of humidity

A. Joubert[*,1,2], J.C. Laborde[1], L. Bouilloux[1], D. Thomas[2], S. Callé-Chazelet[2]

[1] IRSN/Laboratoire d'Expérimentations en Confinement, Epuration et Ventilation, BP 68, 91192 Gif-sur-Yvette, France
[2] Nancy Université/Laboratoire des Sciences du Génie Chimique/CNRS, BP 20451, 54001 Nancy cedex, France

Pleated High Efficiency Particulate Air (HEPA) filters, made up of glass fibers, are used in general ventilation and particularly in nuclear facilities for the containment of radioactivity. In conditions of dry air, the increase in pressure drop across a pleated HEPA filter during clogging by solid particles has already been studied (Del Fabbro et al., 2000). Nevertheless, some accidental situations, such as the emergence of a hole on a pipe with release of steam, can lead to a sharp increase of the air humidity. Studies in literature with plane HEPA filters (Gupta et al., 1993) reveal that air humidity affects the increase in pressure drop. But concerning pleated filters, there is no analytical study in the literature to predict the influence of humidity on their characteristics.

The aims of this study is first, to fill the lack of analytical data on the behaviour of pleated HEPA filters during clogging in presence of humidity and then, to purpose a model to predict the experimental results.

Pleated HEPA filters were tested in an experimental test bench located in the Institut de Radioprotection et de Sûreté Nucléaire (IRSN). The characteristics of pleating of the filters are: length of pleat 26 mm and distance between two pleats 2.1 mm, and the filtration area is 0.42 m^2. Two different aerosols were used to clog the filters: one consist of non-hygroscopic alumina particles (mass median aerodynamic diameter: 4.2 µm) and the other is made up of hygroscopic sodium chloride particles (mass median aerodynamic diameter: 1.1 µm). The influence of humidity on the growth factor of the two aerosols has been studied. Clogging tests were carried out at relative humidity varying between 5% and 100% and at three different filtration velocities: 1.4, 2.9 and 5.7 cm/s. During each clogging, filtration velocity and relative humidity of air were maintained constant and air temperature was fixed at 25 ± 2°C. The pressure drop across the filters and the particles mass generated were recorded during the tests.

Results of clogging tests with alumina particles have shown that the effect of humidity on the evolution of pressure drop depends on the geometry of the filter. Indeed, for plane filters, mostly used in laboratories for experimental studies, the increase in pressure drop during clogging is linear and lower with increasing air humidity. This effect of humidity can be attributed to an increase in the particle to particle adhesive forces when the air humidity increases, leading to a more open particulate cake (Gupta et al., 1993). For pleated filters, the pressure drop, for a given particles mass loading, is higher with increasing humidity. This effect of humidity observed for pleated filters can be explained by acceleration in reduction of filtration area, which is specific to pleated filters, with increasing humidity. For a given rate of humidity and particles mass loading, increase in filtration velocity leads to a lower aeraulic resistance (which is proportional to the ratio between the pressure drop and the filtration velocity) across pleated HEPA filter.

With hygroscopic sodium chloride particles, the presence of humidity can affect the structure of particles. For humidity below the deliquescent point of particles (75% at 25°C) and during the formation of cake, the increase in pressure drop across pleated filters is lower with increasing humidity. Reduction of filtration area is difficult to obtain due to the small particles flow. For humidity over deliquescent point, particles are transformed into droplets and the evolution of pressure drop is indicative of clogging with liquid aerosol.

Experimental data have permit to develop a semi-empirical model to predict the evolution of pressure drop across pleated HEPA fibrous filter during clogging by solid particles and in presence of humidity. The model is based on Kozeny's equation, describing the pressure drop across particulate cake, and on the reduction of filtration area, specific to pleated filters (Laborde et al., 2002).

Del Fabbro, L., Brun, P., Laborde, J.C., Lacan, J., Renoux, A., & Ricciardi, L. (2000) *J. Aerosol Science*, 31, 210-211.

Gupta, A., Novick, V.J., Biswas, P., & Monson, P.R. (1993) *Aerosol Science and Technology*, 19, 94-107.

Laborde, J.C., Del Fabbro, L., Mocho, V.M., & Ricciardi, L., (2002) *International Workshop on particle loading and filtration kinetics in fibrous aerosol filters*, University of Karlsruhe (Germany).

Inactivation of airborne viruses by tea tree oil

O.V. Pyankov[1], O.Pyankova[1], B.Mullins[2], R.Huang[1] and I.E. Agranovski[1]

[1] Faculty of Environmental Sciences, Griffith University, Brisbane, 4111, QLD, Australia
[2] Centre of Excellence in Cleaner Production, Curtin University of Technology, Bentley, 6102, WA, Australia

Keywords: bioaerosols, airborne virus, air quality control, tea tree oil, filtration.

As discussed in our previous publications (Pyankov et al., 2008), although filtration remains the most efficient method of removal of airborne particles, some issues related to possible re-entrainment of captured particles from the rear face of the filter back into the carrier gas need to be addressed. Obviously, viable biological particles blown off from the filter surface could still cause substantial damage to human and animal health and contaminate the ambient environment. We suggested a new technology utilizing coating of filter fibres by biologically active tea tree oil (TTO). It was found (Pyankov et al., 2008) that pre-wetting the filter fibres with TTO, prior to its usage for bacterial aerosol control, could provide significant benefits in terms of rapid inactivation of captured microorganisms, thereby minimizing the number of live/viable particles which could be reentrained from the filter by the air.

In this project we investigate some performance characteristics of TTO for control of viable airborne viruses, using the H11N9 non-pathogenic (to humans) Influenza strain. Two strategies are suggested:

1. Using TTO to coat the filter fibres, followed by their utilization for the control of viral particles. In this case, the removal efficiency of the filter would not be significantly enhanced, due to the very small alteration of the filter properties by a thin TTO film/droplets. However, such a system would inactivate collected particles, thereby minimizing/eliminating any risk of re-entrainment to the gas carrier. The experiments were performed according to the procedure described in detail in (Pyankov et al., 2008). In brief, four TTO coated filters were installed in parallel in a special holder and used for the removal of concentrated airborne viral particles, generated using a Collison nebulizer over a 1 min period. Then, one of the filters was immediately placed into 50 ml vessel containing sterile water, to wash all collected viral particles from the filter surface and eliminate any further action of the TTO to inactivate the captured virons. The second filter was placed into the similar water container 5 minutes after the first one, then the third and fourth at 30 and 60 minutes respectively. All liquids were then analyzed by plaque assay to enumerate viable particles remaining on the filter after the above time periods. Biologically neutral light mineral oil (LMO) was used for control

purposes *i.e.*, the above experimental program was identically repeated for LMO coated fibrous filter.

2. A second method of utilizing the TTO was to add TTO mist to the H11N9 contaminated air, to evaluate microbial inactivation in the natural ambient air environment. To perform the experiments, viral particles were generated using a Collison nebulizer and fed into a rotating aerosol chamber (~200 liters) capable of holding submicron particles in airborne form for up to 6-8 hours with low settling losses. A sample of the air was extracted by a personal bioaerosol sampler (Agranovski et al., 2005), at 5, 15, 30 and 60 minute intervals after commencement of the experiment. These samples were then analyzed by viral assay. LMO was again used as a control case. Additionally, the natural inactivation of H11N9 in air was examined with no oil aerosol present. The results of the natural inactivation of H11N9 in the rotating aerosol chamber are presented in the figure.
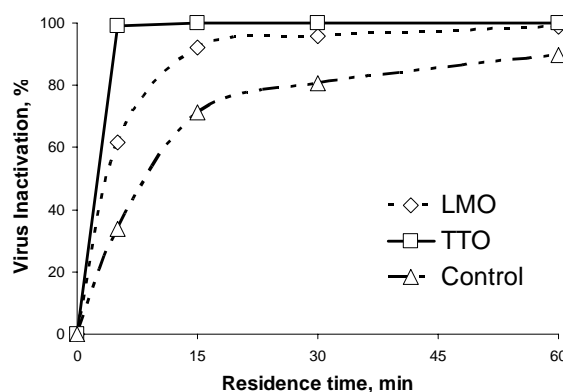
As can be seen, almost 100% of the viral particles were inactivated 5 minutes after the discharge of TTO into the chamber. Inactivation was much less rapid with LMO and slower still for the control experiments. Without oil aerosol, some viable particles remained after 60 minutes duration. Similar results were obtained for fibre coating experiments when almost all viral particles were inactivated within the first 5 minutes (for TTO). The efficiency was much lower for LMO, which was not significantly distinctive from the "no oil" case.

Pyankov, O., et al. (2008). *CLEAN, (Special Bioaerosol Issue)*, **36(7),** 609-614
Agranovski, I., et al. (2005). *J. Aerosol Sci. (Special Bioaerosol Issue)*, **36**, 609-617.

Multi-scale modelling and experimental measurements of soot filtration in diesel particulate filters

S. Bensaid, D.L. Marchisio and D. Fino

Department of Materials Science and Chemical Engineering,
Politecnico di Torino, c.so Duca degli Abruzzi 24, 10129, Turin, Italy

Keywords: Aerosol filtration, CFD, Diesel soot particles, Filters, Modelling.

Nowadays, soot emissions in the automotive sector can be reduced by physically trapping the particles within on-board Diesel Particulate Filters (DPF). The filter gets progressively loaded by filtering the soot laden flue gases, thus causing an increasing pressure drop, until regeneration of the filter is carried out via the oxidation of the trapped particles.

The main objective of this work is to investigate the features of soot particles deposition inside the channels of wall-flow DPFs, since they are responsible for the pressure drop evolution across the filter, and they are bound to influence the dynamics of the soot oxidation process. This aim is achieved by carrying out both experimental observations and CFD simulations.

Laboratory scale filters (300 cpsi, 17.7 cm long and 2.54 cm in diameter) were loaded with a synthetic soot generator (Aerosol Generator GFG-1000-PALAS), and the pressure drop across the filter was recorded during the loading process (Fig. 1).
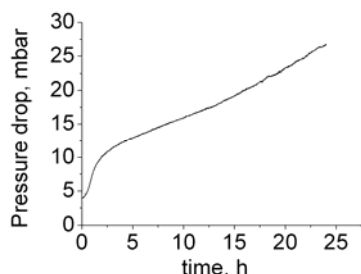
Figure 1. Experimental curve of soot loading.

The profiles of particles deposition inside the channels were evaluated at different filtration times. The measurements included channels from the centre to the periphery of the filter, at different axial positions. This was done by cutting the filter in segments, and Fig. 2 reports the experimental results for a channel in section at 2 cm from the gas inlet.
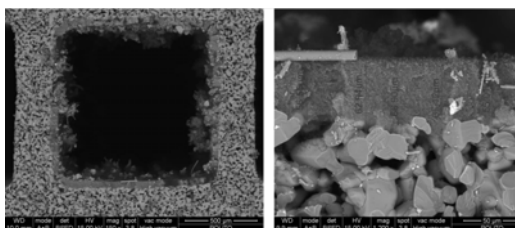
Figure 2. Measured thickness of the soot layer along the filter (section at z=2cm): 150X and 1200X.

Experimental SEM observations revealed that the soot layer thickness is not constant along the axial coordinate (see Fig.3-left), being minimum at around half of the channel length. In addition, the amount of soot deposited is affected by the channel position along the filter diameter with respect to the inlet flow, since central channels (see channel 1 in Fig.3-right) result in higher deposition rates rather than those in the periphery (channels 2 to 4 and 5 to 7).
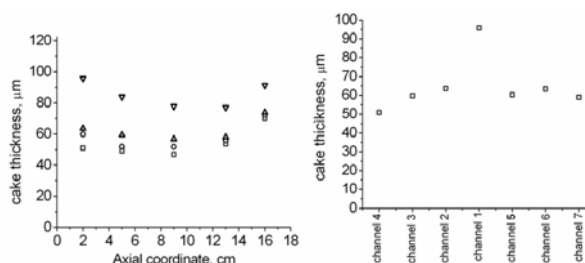
Figure 3. Experimental thickness of the soot layer along the filter. Left: different axial positions (▼- channel 1, ▲- channel 2, •- channel 3, ▪- channel 4); right: channel locations (section at z=2cm).

The obtained experimental measurements were then reproduced through a three-dimensional mathematical model based on CFD simulations: two grids at different scales were used to this end. A "single channel" grid (Bensaid et al., 2008) was used to describe the soot deposition process into a channel of the filter, the consequent gradual modification of the properties of the porous media (i.e. permeability and porosity, Konstandopoulos et al., 2000), and the formation of a soot layer on the top of it.

In order to compute the volumetric flow rates entering the different channels, a "full scale filter" model was adopted (Figure 3), aimed at taking into account the maldistribution of the flow occurring at the inlet cross sectional area.

The ongoing investigation is focused on optimizing computational costs arising from the coupling of the two scales models.

Bensaid, S., Marchisio, D.L., Fino, D., Saracco, G. & Specchia, V., (2008). in *Proc. 10th World Filtration Congress*, Leipzig, Germany 13-18 April 2008, pp. 328-332, Vol. 3.

Konstandopoulos, A.G., Skaperdas, E., Papaioannou, E., Zarvalis, D. & Kladopoulou, E., (2000). *SAE 2000-01-1016*.

Nanoparticle filtration through capillaries by Langevin dynamics

T.D. Elmøe, A. Tricoli and S.E. Pratsinis

Particle Technology Laboratory, Department of Mechanical and Process Engineering, ETH Zürich,
8092 Zürich, Switzerland

Keywords: Langevin dynamics, Fractals, Deposition, Morphology, Filtration.

Filtering a nanoparticle-laden gas through a porous substrate results in the formation of a homogenous and highly porous film (Andersen et al., 2002). An important parameter in filtration is the pressure-drop evolution (Stenhouse and Trottier, 1991). Three regimes have been identified experimentally (Japuntich et al., 1994): In the first regime, particles deposit within the filter (deep bed filtration) and pressure-drop slightly increases with mass-loading. In the second, the captured particles start collecting incoming particles and clogging commences increasing the pressure-drop. In the third regime, the filter cake is formed and the pressure-drop increases rapidly.

Another important parameter is the clogging mass, which yields the filtered mass required until the onset of cake-filtration. Once this filtration mode occurs, the growing cake begins to act as a highly effective filter removing all incoming particles (Schmidt, 1996). Operation of the filter should take place near the clogging point, where high efficiency is obtained, without the expense of a too high pressure-drop. In filtration processes the Peclet number (Pe), the ratio of the convective to the diffusive transport (Przekop et al, 2003) determines the physical properties of the filter-cake.

Here, the complete evolution from deep bed filtration to cake growth is obtained by first princples using Langevin dynamics (Ermak and Buckholz, 1980; Heine and Pratsinis, 2007) for a wide range of Pe numbers (0.01 – 10). From the detailed evolution of the deposit morphology, the change in pressure-drop, as well as the filtration efficiency, is obtained for a highly porous filter. That way the detailed structure of such deposits is revealed and most importantly, the fraction of particles penetrating is calculated from first principles. The model is validated in the limits of purely diffusional deposition (Pe $\rightarrow$ 0) and purely ballistic deposition (Pe $\rightarrow$ ∞), as well as against classic filtration theory. Structures (deposit) grown for intermediate Pe numbers are also examined.

Figure 1 shows the evolution of the filtration efficiency (dotted line), as well as the pressure-drop (solid line) for filtration of monodisperse particles in a highly porous (> 90 %) filter at Pe =1. Filtration conditions can be seen in the figure caption. The pressure-drop calculated by cake filtration theory (Ruth, 1935) using the clogging mass, and cake solid volume fraction estimated from the present work is also shown (broken line).
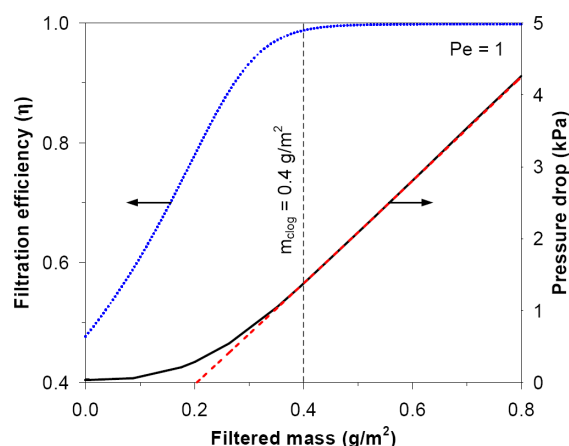
Figure 1: Evolution of the filtration efficiency (dotted line) and pressure-drop (solid line) with the total mass of particles filtered. Comparison with cake filtration theory is also shown (broken line). Physical properties used: particle diameter: 50 nm, solid density 1000 kg/m^3, concentration: 10^{14} #/m^3, pore radius: 2 µm, filter thickness: 10 µm.

The figure shows, that once the filter is clogged and cake filtration commences, all incoming particles are removed on top of the growing cake. Furthermore, the experimentally observed evolution of the pressure-drop is also seen qualitatively on Fig. 1. As expected, the application of cake filtration theory is seen to be valid after clogging, using the clogging mass and the cake solid volume fraction evaluated from the time-dependant morphology. Both of which are obtained in this work.

Andersen, S.K., Johannessen, T., Mosleh, M., Wedel S., Tranto, J. & Livbjerg H. (2002), *J. Nano-particle Res.*, 4(5), 405-416

Ermak, D.L., & Buckholz, H., (1980), *J. Comp. Phys.*, 35, 169-182

Heine, M.C. & Pratsinis S.E. (2007) *Langmuir*, 23, 9882-9890

Japuntich, D.A., Stenhouse, J.I.T. & Liu, B.Y.H. (1994), *J. Aerosol Sci.,* 25 (2), 385-393

Przekop, R., Moskal, A. & Gradoń, L. (2003), *Aerosol Science*, 34, 133-147

Ruth, B.F. (1935), *Industrial and Engineering Chemistry*, 27 (6), 708-723

Schmidt, E. (1996), *Powder Technology*, 86, 113-117

Stenhouse, J.I.T., & Trottier, R. (1991), *J. Aerosol Sci.*, 22, S777-S780

The effect of porosity on deposition on fibrous filters.

Sarah J. Dunnett[1], Charles F. Clement[2]

[1]Department of Aeronautical and Automotive Engineering, Loughborough University, Loughborough, Leics. LE11 3TU, U.K.
[2]15 Witan Way, Wantage, Oxon, OX12 9EU, U.K.

Keywords: fibrous filter, filtration, numerical simulation, particle deposition

INTRODUCTION

Fibrous filters generally consist of many threadlike fibres oriented more or less normal to the fluid flow which passes through them. Particles carried by the fluid flow may impact upon the fibres and become removed from the flow. The collected particles accumulate forming complex structures which influence the fluid flow and further deposition. Understanding the process of particle deposition and its effects upon further deposition are crucial in understanding the performances of fibrous filters. We have been developing a numerical model of fibrous filtration aimed at investigating deposition due to various mechanisms and the effect filter properties and particle characteristics have upon it, Dunnett and Clement 2006, 2009. We have shown that deposit porosity does not influence further deposition for small particles where diffusion is dominant, Dunnett and Clement 2009. However, in this work, we show that deposition by interception can be strongly affected by porosity to produce deposit shapes observed previously Kanaoka et al (1986).

NUMERICAL MODEL

In earlier work, Dunnett and Clement (2009), a numerical model has been developed which determines the flow field, and particle motion, around a single fibre which has a porous deposit made up of collected particles on its surface. Neighbouring fibres are taken into account by the application of boundary conditions on the computational domain. The deposition of particles onto the porous surface can be determined and hence the growth of the deposit modelled. The shape of the deposit is affected by the size of the particles considered. For small particles diffusion is the main mechanism by which they deposit on the surface and in this case deposit is collected around the majority of the fibre. The main non-dimensional parameters to consider when solving for the particle concentration, n, in this case are the Peclet number, Pe, given by $Pe=U_0 d/D$, and κ the ratio of the particle to fibre diameters . U_0 is the mean flow velocity, d the fibre diameter and D the coefficient of diffusion of the particles. The effects of particle interception with the surface are accounted for when solving for n by the application of boundary conditions. Interception becomes more important as the size of the particle increases and dominates

when $s = \dfrac{\kappa}{\delta} \geq 1$. In this expression $\delta = (4k/Pe)^{1/3}$, where k is the hydrodynamic factor, is the non-dimensional thickness of the diffusion layer.

For still larger particles inertial impaction is the dominant mechanism of capture.

An example of a deposit formed, where interception is the method of deposition, .is shown in Figure 1 In the figure the fibre initially has a layer of deposit on it. The value of s is approximately unity hence we are in the region where interception has just become the dominant deposition mechanism. The surface formed by particles depositing due to interception is shown for the cases when the initial deposit is assumed to be solid and when it is porous with a porosity of $\varphi=0.92$, where φ is the fraction of the porous media that is occupied by void space. The value of κ is 0.025.

initial deposit --- solid ····· $\varphi=0.92$ ----
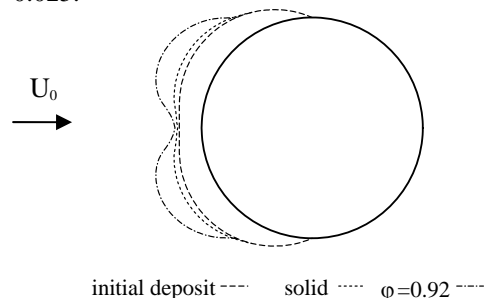
Figure 1. Surface formed by interception.

It is found here that for deposition due to interception the porosity of the initial deposit does not become significant until $\varphi>0.8$. After this value the deposit surface grows rapidly as the flow moves through the deposit already formed. The resulting formation of "ears" on the deposit is a characteristic feature of some of the deposits observed by Kanaoka et al (1986).

We have already shown that the porosity of the deposit does not affect the deposition pattern when diffusion is dominant, but its value is clearly important in the interception region.

REFERENCES

Dunnett, S.J. and Clement, C.F. (2006) J. Aerosol Sci., 37, 1116-1139.
Dunnett, S.J. and Clement, C.F. (2009) Eng. Anal. Boundary Elem., In press
Kanaoka, C.,Emi,H.Hirage,S.,Myojo,T.(1986) Aerosols,formation and reactivity 2nd Int. Con. Berlin

Applied the filter pretreated with berberine for removal of bioaerosols

S.H. Yang[1], Y.C. Huang[2], C.H. Luo[3] and C.Y. Chuang[4]

[1]Department of Environmental and Occupational Health, Toko University, Chia Yi County 613, Taiwan, R.O.C
[2]Graduate Institute of Environmental Engineering, National Taiwan University, Taipei 106, Taiwan, R.O.C
[3]Department of Environmental Engineering, Hung-Kuang University, Taichung County 433, Taiwan, R.O.C.
[4]Department of Bio-lndustrial Mechatronics Engineering, National Taiwan University, Taipei 106, Taiwan, R.O.C.

Keywords: filtration efficiency, bioaerosols, berberine, antiseptic

Most people typically spend around 87.2% of their time indoors (Lance, 1996). Accordingly, indoor air quality is an increasingly important issue. Bioaerosols importantly affect indoor air quality because they cause various respiratory diseases (Eduard et al., 1993; Melbostad et al., 1994). Higher concentrations of bioaerosols were found in indoors because of higher temperature and relative humidity all round year in Taiwan. Many epidemiological studies have inferred that sick building syndrome (SBS) was related to bioaerosols. Therefore, it cannot be neglected that the problem of indoor air pollution caused by bioaerosols in Taiwan. The purpose of this study is desired to develop of antiseptic filters by using the herbal medicine-coptidis rhizoma extract (berberine) and to explore the filtration efficiency of bioaerosols. Many studies have demonstrated that berberine has been used as an antiseptic material (Wang, 1998). Therefore this work applied the berberine-pretreated filter as the antiseptic filter.

This work applied the fibrous filter coated with the berberine to explore the feasibility of removing bioaerosols. Bioaerosols are generated from a microbial suspension liquid using a Collison Nebulizer. Bioaerosols are mixed with a clean air and then are filtered using fibrous filter pretreated with berberine. To assess collection efficiency of fibrous filter, several factors were investigated, including the microbial species, berberine concentrations, higher and lower relative humidity, and different face velocities. The filtration efficiency of bioaerosols was assessed by sampling, incubation, and counting the numbers of viable colony before and after filtration. In addition, the aerodynamic particle sizer was used to explore different removal mechanisms for bioaerosols. This work will show the results of the feasibility of removal different bioaerosols by berberine coated on fibrous filter.

Figure 1 plots the aerosol penetration through the untreated filter and 1.0% berberine-pretreated filters using 1.0-μm PSL aerosols and E. coli bioaerosols at face velocities of 10 cm/s (RH 30%). The experimental results reveal that the aerosol penetrations through the untreated filter and 1.0% berberine pretreated filters at a face velocity of 10 cm/s are approximately 65%, and 64%, respectively. The results also show that penetration of E. coli bioaerosols through the untreated filter and the 1.0% berberine-pretreated filters are around 65% and 24%, respectively. A comparison of the results of the penetration of the PSL aerosol through the 1.0% berberine-pretreated filters indicates that penetrations of the E. coli bioaerosol and the PSL aerosol through the untreated filter were similar, while penetration through the 1.0% berberine-pretreated filters with E. coli bioaerosol were much lower than that with PSL aerosol, indicating that berberine has an antiseptic effect on E. coli bioaerosol.
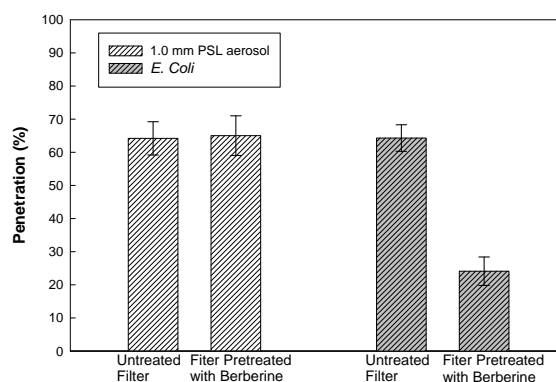
Figure 1. Penetration through untreated and berberine pretreated filter with 1.0 μm PSL aerosols and E.coli bioaerosols

Eduard, W., Sandven, P., & Levy, F. (1993). Am. J. Ind. Med., 24, 207-222

Lance, W. (1996). Journal of Air and Waste Manage. Assoc., 46, 98-126.

Melbostad, E., Eduard, W., Skogstad, A., Sandven, P., Lassen, J., Sostrand, P., & Heldal, K. (1994). Am. J. Ind. Med., 25, 59-63.

Wnag, B. X. (1998). Chinese herbal medicine pharmacology. Tianjin, China: Tianjin Science and Technology Press.

Deposition of aerosol particles in dense array of spheres

W. Holländer[1], T. Zaripov[2]

[1]Fraunhofer Institute Toxikologie und Experimentelle Medizin, Nikolai-Fuchs 1, D-30625, Hannover, Germany
[2]Institute of Mathematics and Mechanics, Kazan State University, Prof. Nuzina 1, 420008, Kazan, Russia

Keywords: aerosol filtration, deposition efficiency, charged particles, CFD

In this work deposition of aerosol particles in a packed bed has been studied experimentally and theoretically. The bed consists of spheres of diameter d=500μm packed into the cylinder (fig.1). The studied range of particle sizes is 0.5-3 μm.

Fig.1. Photo of packed bed

To calculate the deposition efficiency 3D mathematical model of aerosol flow through the filter is developed. The periodically repeating arrangements of spheres such as 3D cubic close packing with porosity $\varepsilon = 0.26$ are studied (fig.2). The fluid flow through the array of spheres is calculated using unit-cell approach. The carrier phase velocity field in the void space of periodic unit-cell is found within the steady incompressible fluid flow approximation by means of CFD program FLUENT. At the left and right boundaries of the cell the components of the velocity vectors are set to be periodic. At the fluid/solid boundaries no-slip boundary conditions are fulfilled. At the up and down fluid boundaries as well as at the left and right ones the slip-symmetry conditions are applied.
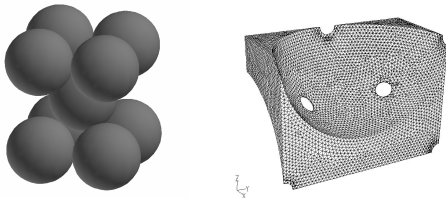
Fig.2. Element of sphere packing and the smallest periodic unit-cell

The trajectory of an aerosol particle is determined by numerical integration of particle motion equations

$$\frac{d\overline{v}}{dt} = \beta\left(\overline{u} - \overline{v}\right) + g + \frac{F_e}{m}$$

where $\overline{v}$, $\overline{u}$ are the particle and air velocities, $\beta = 3\pi\mu d / c_s m$, μ is the air viscosity, d and m

are the particle diameter and mass, c_s is the Cunningham correction factor, $\overline{F_e}$ is the image force for charged particles.

To trace the particle paths the air velocity vector $\overline{u}$ in the current point of particle location must be known. To interpolate the velocity components found in nodes of a tetrahedral mesh the method described by Schafer and Breuer [1] is used.

Deposition of uncharged and charged aerosol particles is studied taking into account the inertial impaction, gravity and image force actions. A fair agreement of the results obtained in calculations with the corresponding experimental data is observed.

For the given range of particle sizes a noticeable amount of uncharged particles penetrate through the packed bed. This means that the diffusion, impaction and gravity actions are not enough for total deposition of particles. The charged particles totally deposit on 40-50 periodic unit-cells (fig.3, N is the number of elementary units of charge of particle).
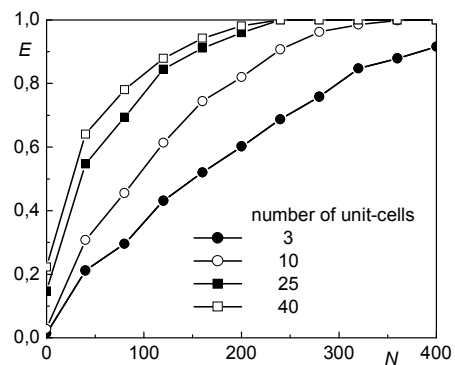
Fig.3. Deposition efficiency of charged particles for d=0.6 μm at various number of unit-cells (filter lengths)

Schafer, F., Breuer, M. (2002) Int. J. Num. Meth. Fluids, 39, 277-299.

Factors Affecting CADR (Clean Air Delivery Rate) Measurement

S.H. Huang[1], K.N. Chang[2], K.T. Hou[2] C.W. Chen[3], C.P. Chang[3], C.M. Chiang[4] and C.C. Chen[2]

[1]Institute of Environmental Health, National Taiwan University, Taipei, Taiwan
[2]Institute of Occupational Medicine and Industrial Hygiene, National Taiwan University, Taipei, Taiwan
[3]Institute of Occupational Safety and Health, Council of Labor Affairs, Taipei, Taiwan
[4]Department of Architecture, National Cheng-Kung University, Tainan, Taiwan

Keywords: Indoor air cleaner, Aerosol generation, Clean air delivery rate

Indoor air pollutant levels, depending on the emission intensity, may be two to five times higher than the pollutant level outdoors, according to a previous survey of U.S. Environmental Protection Agency. The facts that people are likely to spend 90 percent of their time indoors, and some of the indoor air pollutants such as tobacco smoke, pollen, mold and dust could create asthmatic and allergic reactions, it is important to implement an effective indoor air quality management program. The best control strategy for good indoor air quality is to remove the contaminant at the source. It is the most cost effective approach because the volumetric flow rate to be treated is the lowest. When source removal is not feasible, ventilation to dilute and collect contaminants becomes the preferred option,. However, often the residual houses may not be equipped with a mechanical ventilation system and may have to rely on portable air cleaning appliances.

In ANSI/AHAM AC-1-2006 (Method for Measuring Performance of Portable Household Electric Room Air Cleaners), Clean Air Delivery Rate (CADR) is a measure of the appliance's ability to reduce aerosol particles in the 0.10 to 11 μm size range. In the present study, the effects of test chamber size, aerosol size (distribution), aerosol number concentration, position and flow rate of aerosol spectrometer, and leak rate of the test chamber on the CADR measurements were investigated. Two types (ESP and filter) of commercially available indoor air cleaners were tested in a standard certification chamber, and a chamber 1/8 of the volume of a standard chamber. Polydisperse aerosol particles were generated using a constant output aerosol generator and an ultrasonic atomizer. Aerosol outputs from both generators were then neutralized using a radioactive source (Kr-85) to neutralize the aerosol particle to the Boltzmann charge equilibrium. The main aerosol size-spectrometers were a Scanning Mobility Particle Sizer and an Aerodynamic Particle. The background decay rates were measured using real time aerosol

instruments and a Mini Infra-Red Analyzer (MIRAN) was used when SF_6 was the test agent.

The results showed that CADR value is a function of aerosol size. The ESP- and filter-type air cleaners had obviously different characteristic CADR curves. In general, the ESP air cleaner performed better in aerosol collection, air resistance, and power usage. The relative location and orientation of the air cleaner and aerosol spectrometer in the test chamber had little effect on the CADR measurements. The measured CADR values decreased with increasing aerosol number concentration apparently due to coagulation effects during the natural decay. The coagulation effect became less significant if aerosol number concentration was lower than 1.0×10^5 #/cm^3. Use of smaller test chamber is possible. However, only the data collected before infiltrated aerosols became dominant should be used for calculating the CADR value. Room air cleaners with multi-level performance fan settings normally delivered higher CADR when operated under higher air cleaning mode setting, but not necessarily the CADR/watt value, probably due to the difference in the fan performance curve.

AHAM (2006) Method for Measuring Performance of Portable Household Electric Room Air Cleaners. Standard AC-1-2006, Association of Home Appliance Manufacturers, Chicago.

Characteristics of commercial antimicrobial filter media for removal of bioaerosols

K.Y. Yoon, Y.S. Kim, J.H. Park and J. Hwang

Department of Mechanical Engineering, Yonsei University, 120-749, Seoul, Republic of Korea

Keywords: antimicrobial, bacteria, bioaerosols, filters, indoor air quality

Antimicrobial filters, which contain antimicrobial agents on the surface of air filters, are widely used to control bioaerosols. Yoon et al. (2003) prepared silver-deposited activated carbon fiber filters. Chitosan and iodine were also used for preparation of antimicrobial filters (Hou et al., 2008; Lee et al., 2008). Performances of antimicrobial filters are determined by both filtration and antimicrobial performances. In this study, characteristics of commercial antimicrobial filter media for bioaerosol removal were estimated.
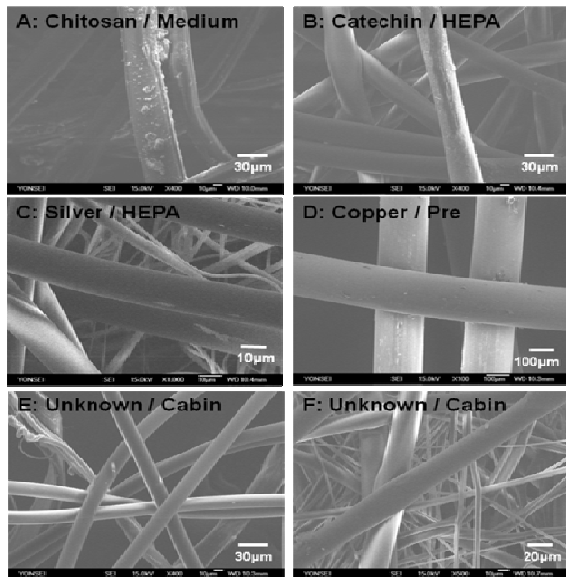
Figure 1. SEM images of antimicrobial filters used in this study.

To estimate the filtration efficiencies of antimicrobial filters, *Escherichia coli* and *Staphylococcus epidermidis* were dispersed into air and measured using a nebulizer (BGI Inc., U.S.) and APS (Aerodynamic Particle Sizer; model 3321, TSI Inc. U.S.), respectively. The filtration efficiency (η_{filt}) was calculated by following equation

$$\eta_{filt} = 1 - \frac{C_{down}}{C_{up}} \quad (1)$$

where, C_{up} and C_{down} are number concentrations of bioaerosols at upstream and downstream of test filters.

For estimation of the antimicrobial efficiencies of filters against *E. coli* and *S. epidermidis*, suspension test method was used. The antimicrobial efficiencies (η_{anti}) was calculated using following equation

$$\eta_{anti} = 1 - \frac{CFU_{sample}}{CFU_{control}} \quad (2)$$

where, $CFU_{control}$ and CFU_{sample} are colony numbers of control and test samples.
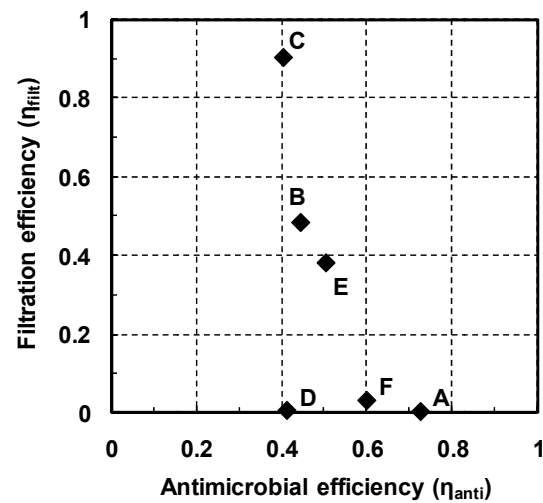
Figure 2. Filtration and antimicrobial efficiencies of antimicrobial filters.

Filter C and filter A showed the highest filtration and antimicrobial efficiencies, respectively.

Hou, Q., Liu, Z., Duan, B., and Bai, L. (2008) Characteristics of antimicrobial fibers prepared with wood periodate oxycellulose, Carbohydrate polymers, 74, 235-240.

Lee, J. H., Wu, C. Y., Wysocki, K. M., Farrah, S., and Wander, J. (2008) Efficacy of iodine-treated biocidal filter media against bacterial spore aerosols, Journal of Applied Microbiology, 105, 1318-1326.

Yoon, K. Y., Byeon, J. H., Park, C. W., and Hwang, J. (2008) Antimicrobial effect of silver particles on bacterial contamination of activated carbon fibers, Environmental Science and Technology, 42, 1251-1255.

Collection of submicron aerosol particles and inactivation of bioaerosols by simultaneously using carbon fiber type unipolar charger and fibrous medium filter

J.H. Park[1], K.Y. Yoon[1], Y.S. Kim[1], J.H. Byeon[2] and J. Hwang[1]

[1] School of Mechanical Engineering, Yonsei University, 120-749, Seoul, Republic of Korea
[2] Digital Printing Division, Samsung Electronics Co., Ltd., 443-742, Suwon, Republic of Korea

Keywords: Filtration, Submicron Particle, Bioaerosols, Particle charging, Fibrous filter.

Bioaerosols which are airborne particles of biological origins, including viruses, bacteria, fungi, and all varieties of living materials, are also known as etiological agents of many diseases. To remove these aerosol particles, fibrous filter is used traditionally. But submicron particles are difficult to be removed by fibrous filter and bioaerosol collected on the fibrous filter surfaces can be cultivated and release bad odors (Schleibinger & Rüden, 1999). Our study proposes fibrous medium filter with carbon fiber type charger to enhance the removal of submicron particles and bioaerosols. Carbon fiber type charger was simple and ozone free device (Han et al., 2008).

A sample of fibrous medium filter was installed at the middle of the test duct. Two carbon fiber type chargers were fixed on the top and bottom of test duct 10cm ahead of the filter media. The operation voltage was saw tooth wave form of peak-to-peak 4kV, 60Hz. The concentration of ions was controlled by a rheostat. Potassium chloride (KCl) particles sized 50-400nm were supplied into the test duct for particle removal test. Aerosolized *E.coli* was supplied into the test duct and deposited on the filter media for antimicrobial test. The face velocities at the filter media were varied as 0.5, 1.0 and 1.5m/s for particle removal test. Number concentration of test particles was measured by a scanning mobility particle sizer (SMPS). The average charge per particle was estimated with an aerosol electrometer by current measurement.

Bioaerosols were deposited for 5 minutes. Deposited bioaerosols exposed to unipolar ions and air. Ion exposure rate was 4×10^7 ions/(cm^2·min). Ion exposure time was 0, 1, 5, and 10 minutes. Then bacteria were extracted from filter media for incubation. The sampled filter media, cut into 20 mm diameter, was put into corning tube with nutrient broth. Corning tube that included the sampled filter media and nutrient broth were ultra-sonicated for 30 min. Then, this corning tube was incubated in a shaking incubator at 37°C for 3 hours. After then, the bacteria were spread on a nutrient agar plate and incubated at 37°C for 12hour. Number of bacteria was measured by colony counting.

The results of submicron removal test and antimicrobial test are documented in Table 1 and Table 2. The average removal efficiency of filter media was 62.0%, and it was increased to 74.8% with the chargers at 0.5m/s. When the face velocity was increased, average removal efficiencies were decreased. The average removal efficiency of the filter media at 1.0m/s and 1.5m/s, were 55.4% and 48.4%, respectively. The average removal efficiency of the filter media with chargers at 1.0m/s and 1.5m/s, were 63.9% and 53.1%, respectively. The survival fractions of *E. coli* exposed to positive air ions for periods of 1, 5 and 10 minutes, were 76.3%, 34.1% and 7.3%, respectively.

Table 1. Particle removal efficiencies with face velocities.

Face velocity	Particle size	Particle removal efficiency (%)				
		50	100	200	300	400
0.5m/s	Filter only	42.5	31.4	46.4	67.6	78.9
	/w charger	59.5	46.9	59.9	80.5	90.5
1.0m/s	Filter only	33.4	22.6	39.0	61.3	73.7
	/w charger	44.3	32.4	48.5	69.8	81.4
1.5m/s	Filter only	21.4	14.8	33.0	55.8	68.1
	/w charger	27.3	20.6	38.1	60.6	72.6

Table 2. Survival efficiencies of bioaerosol.

Ion exposure time (min)	0	1	5	10
Ion exposure rate ($\times 10^7$ ions/(cm^2·min))	0	4	20	40
Survival efficiency (%)	100	76.3	34.1	7.3

Han, B., Kim, H.J., Kim, Y.J., & Sioutas, C. (2008) *Aerosol Science and Technology*, 42, 793-800
Schleibinger, H. & Rüden, H. (1999) *Atmospheric Environment*, 33, 4571-4577.

Filtration of oil mists in multilayer filter fabrics composed from PES and PP fibres

T. Jankowski, W. Gądor

Department of Chemical and Aerosol Hazards, Central Institute for Labour Protection – National Research Institute, 00-701 Warsaw, Poland

Keywords: nonwovens, oil mist, filtration efficiency, particle size distribution

Most metal working operations call for the use coolant liquids to lubricate the surface between the work piece and the tool, and to remove heat generated by the process. Health problems have been reported among workers exposed to coolants. The multilayer filter fabrics are important part of collection protective equipment used in machining and grinding operations.

This article presents results of investigations of the influence of changes of particle and fiber diameter on the pressure drop and filtration efficiency of multilayer filter fabrics used to filtration of oil mists.

Tests were conducted using the spunlace and melt-blown nonwovens manufactured from polyester (PES) and polypropylene (PP) fibers (table 1 and figure 1).

Table 1. Structural characteristic of tested nonwovens.

Filter No.	Filter thickness	Fiber diameter	Porosity	Main pore size
	[mm]	[μm]	[%]	[μm]
A1	2.85	3.16	96.49	5.99
A2	2.13	6.42	95.86	38.22
A3	2.23	12.22	94.77	91.55
B	5.32	54.72	96.03	215.79
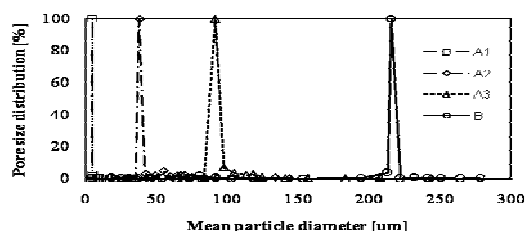
Figure 1. Pore size distribution of tested nonwovens.

Tests were carried on using a setup composed of aerosol generator AGF 2.0 iP and SMPS 3936. The DEHS was used for aerosol generation. Particle number concentrations were determined in the range of particle size from 40 to 300 nm and at different values of aerosol concentration (C) and velocity (U) (figure 2).
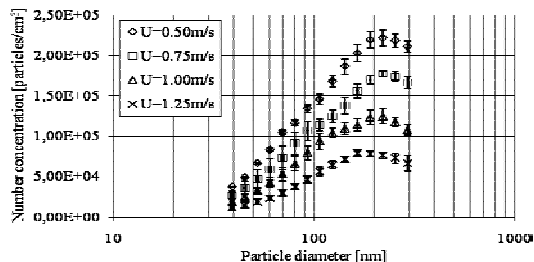
Figure 2. Inlet particle size distributions of DEHS.

The results of tests of pressure drop of nonwovens at different aerosol velocities are shown in figure 3.

It was found that pressure drop of tested nonwovens increases (but filtration efficiency decreases - figure 4 and 5) as the fiber diameter of back filter layer decreases and as aerosol velocity increases.
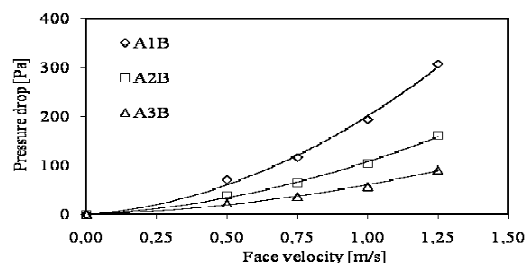
Figure 3. Pressure drop of multilayer filter fabrics.

Figure 4 and 5 illustrate the results of changes in filtration efficiency depending on the aerosol velocity, fiber and particle diameter.
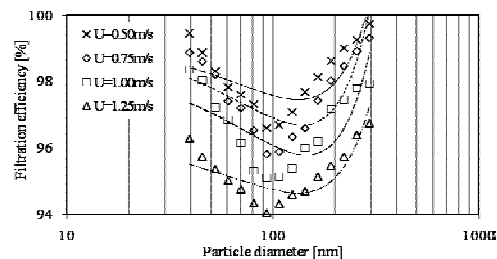
Figure 4. Filtration efficiency of A1B filter fabric.
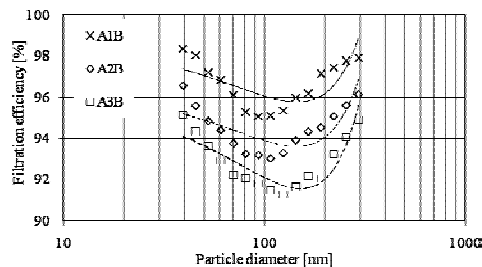
Figure 5. Efficiency of tested filter fabrics as a function of fibres diameter of back filter layer at U=1.00 m/s.

The diameter of most penetration particles (MPPS) was increases from 93.1 nm to 124 nm as the fiber diameter of back filter layer increases.

Filtration of aerosol particles in structurally inhomogeneous fibrous filters.
I – Model formulation.

A. Podgórski, A. Jackiewicz

Faculty of Chemical and Process Engineering, Warsaw University of Technology,
Waryńskiego 1, 00-645 Warsaw, Poland

According to the theory of depth filtration in fibrous filters, aerosol penetration, P, through a filter with thickness L and packing density α is given by:

$$P = \exp\left[-\frac{4\alpha L}{\pi(1-\alpha)}\left(\sum_m \frac{E_m(d_F)}{d_F}\right)\right] \quad (1)$$

where $E_m(d_F)$ is the single fiber efficiency due to m^{th} mechanism of deposition (i.e., diffusion, interception, inertial impaction, coupling of diffusion and interception), which depends on the fiber diameter, d_F. In the case of a polydisperse filter made of fibers with various diameters, Eq. (1) is usually utilized by applying a certain equivalent fiber diameter, e.g., the arithmetic mean diameter determined by image analysis or the equivalent diameter obtained from the pressure drop measurements. However, such simple approach is not well-grounded and it may result in serious errors. Instead, the entire fiber diameter distribution should be taken into account. Moreover, aerosol penetration through a polydisperse filter depends on the relative distribution of various fibers. We can consider two limiting cases. When fibers with different sizes are distributed evenly in space and flow in a filter is well mixed on the mesosclae, Eq. (1) can be simply averaged using the fiber diameter distribution function $g(d_F)$. Such approach is based on the assumption that superficial gas velocity is the same for all Kuwabara cells containing various fibers and let us call this method Perfectly Mixed Flow Model (PMFM). Thus, aerosol penetration according to PMFM can be calculated as:

$$P_{PMFM} = \exp\left[-\frac{4\alpha L}{\pi(1-\alpha)}\int_0^\infty \sum_m \frac{E_m(d_F)}{d_F}g(d_F)\mathrm{d}d_F\right] \quad (2)$$

PMFM represents estimation of the lower limit of aerosol penetration through a polydisperse filter. In the second extreme, one can consider the situation when fibers with different diameters are completely separated from each other. Assuming that the pressure drop per unit filter thickness is the same for all Kuwabara cells with various fibers, we can formulate Fully Segregated Flow Model (FSFM) and calculate penetration as:

$$P_{FSFM} = \int_0^\infty d_F^2 P(d_F)g(d_F)\mathrm{d}d_F \Big/ \int_0^\infty d_F^2 g(d_F)\mathrm{d}d_F \quad (3)$$

$P(d_F)$ in Eq. (3) denotes penetration calculated using Eq. (1) as for a monodisperse filter with fibers of diameter d_F, and the single fiber deposition efficiencies $E_m(d_F)$ for particular fibers' diameters should be computed for individual superficial gas

velocities $U_0(d_F)$, corresponding to various Kuwabara cells with different fibers:

$$U_0(d_F) = \overline{U}_0 d_F^2 \Big/ \int_0^\infty d_F^2 g(d_F)\mathrm{d}d_F \quad (4)$$

$\overline{U}_0$ denotes mean superficial gas velocity for entire filter. FSFM is anticipated to be the estimate of the upper limit of aerosol penetration through a polydisperse filter. Real situation lies somewhere in between PMFM and FSFM, thus, we finally postulate general Partially Segregated Flow Model (PSFM), for which the penetration is calculated as a linear combination of penetrations computed from the two limiting models – Eq. (2) and (3):

$$P_{PSFM} = sP_{FSFM} + (1-s)P_{PMFM} \quad (5)$$

where we introduced dimensionless parameter s that can be named segregation intensity. It can vary between zero (perfect mixing) and one (full segregation). Fig. 1 shows an example of calculations for a filter with thickness L=3.5mm, packing density α=0.016, having the log-normal fiber diameter distribution with geometric mean d_{Fg}=1.98 μm and geometric standard deviation σ_{gdF}=1.58, at superficial gas velocity 0.2m/s. It can be seen that the penetration calculated using PSFM can be either higher or lower than the one predicted on the basis of the arithmetic mean fiber diameter, depending on the value of s. The two following abstracts present method of determination of s based on experimental data and validation of the proposed models.
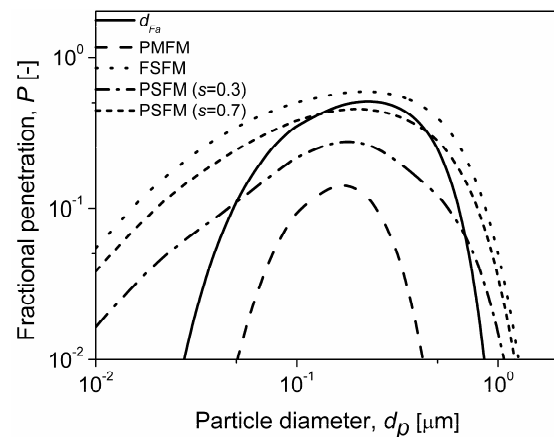
Fig. 1. Penetration calculated for arithmetic mean fiber diameter d_{Fa} (solid line) and for the models PMFM, FSFM and PSFM (for s=0.3 and s=0.7).

Filtration of aerosol particles in structurally inhomogeneous fibrous filters.
II – Experimental results.

A. Jackiewicz, A. Podgórski

Faculty of Chemical and Process Engineering, Warsaw University of Technology,
Waryńskiego 1, 00-645 Warsaw, Poland

Keywords: aerosol filtration, fibrous filter, inhomogeneity, penetration.

The Partially Segregated Flow Model, *PSFM*, formulated in our previous abstract in order to describe aerosol penetration through polydisperse fibrous filters was verified experimentally for eight polypropylene melt-blown filters. It was found that the fiber size distribution of all tested filters can be satisfactory described by the log-normal distribution, see an example for the filter #3 in Fig. 1.
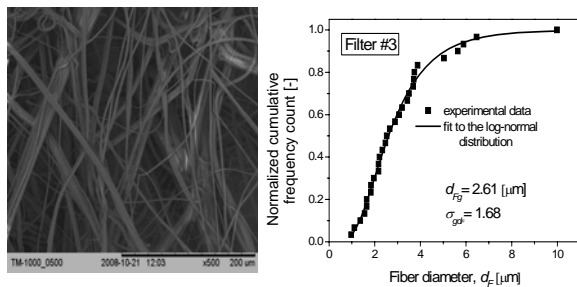
Fig. 1. Fiber diameter distribution for the filter #3.

Structural characteristics of these filters (arithmetic mean fiber diameter, d_{Fa}, filter packing density, α, filter thickness, L, and the geometric mean, d_{Fg}, and the geometric standard deviation, σ_{gdF}, of the fiber diameter distribution) are collected in Table 1.

Table 1. Characteristics of the analyzed filters.

Filter No.	d_{Fa} [μm]	α [-]	L [mm]	d_{Fg} [μm]	σ_{gdF} [-]
1	2.55	0.016	3.5	1.98	1.58
2	2.91	0.024	2.0	1.91	2.04
3	3.15	0.030	1.9	2.61	1.68
4	2.33	0.024	1.3	1.90	1.81
5	2.06	0.019	5.6	1.46	1.80
6	1.53	0.027	5.1	1.22	1.82
7	1.72	0.023	6.4	1.47	1.82
8	3.63	0.039	3.7	2.78	1.87

All filters were examined in terms of the initial penetration, P, of polydisperse solid particles utilizing the modular filter test system (Palas MFP-2000). The measurements were carried out for air velocity U_0=0.15 m/s.

The experimental results were compared with theoretical calculations done by applying: *PSFM* for polydisperse filters and with classical theory developed for monodisperse filters used in line with the arithmetic mean fiber diameter, d_{Fa}. For all investigated filters it was possible to obtain a reasonable agreement with experimental data using the *PSFM*, whilst the penetration computed on the basis of the mean fiber diameter significantly differed from them, see Fig. 2. Determined values of the dimensionless phenomenological parameter, called the segregation intensity, s, were in the broad range 0.08 - 0.55 in the case of the eight investigated filters for superficial gas velocity U_0=0.15 m/s. Under those conditions the lowest values of s were observed for filters #6 and #7, which belonged to the thickest ones and were made of the finest fibers. On the other hand, the thinnest filters (#3 and #4) containing larger fibers had much higher values of s.
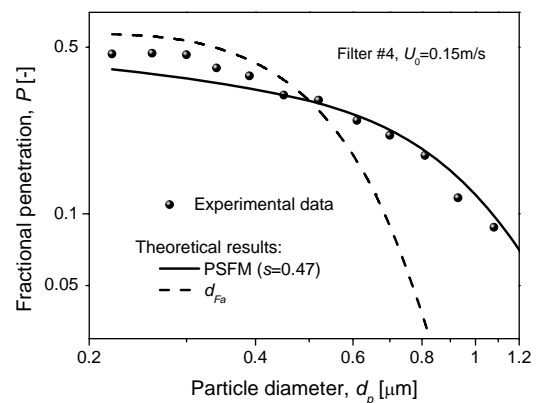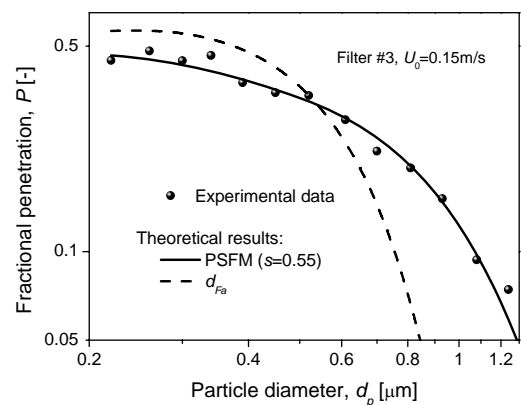
Fig. 2. Comparison of the experimental values of the penetration with theoretical results for filter #3 and #4 (dashed lines – classical theory for arithmetic mean fiber diameter; solid lines – model *PSFM*).

Filtration of aerosol particles in structurally inhomogeneous fibrous filters.
III – Effect of gas velocity on segregation intensity.

A. Jackiewicz, A. Podgórski

Faculty of Chemical and Process Engineering, Warsaw University of Technology,
Waryńskiego 1, 00-645 Warsaw, Poland

Keywords: aerosol filtration, fibrous filter, inhomogeneity, penetration.

As it has been shown in our previous abstract, the Partially Segregated Flow Model (PSFM) can be sucessfully used to describe fractional penetration of aerosol particles through polydisperse fibrous filters if the segregation intensity, s, is determined on the basis of experimental data. The aim of this work is to analyze effect of gas velocity on s.
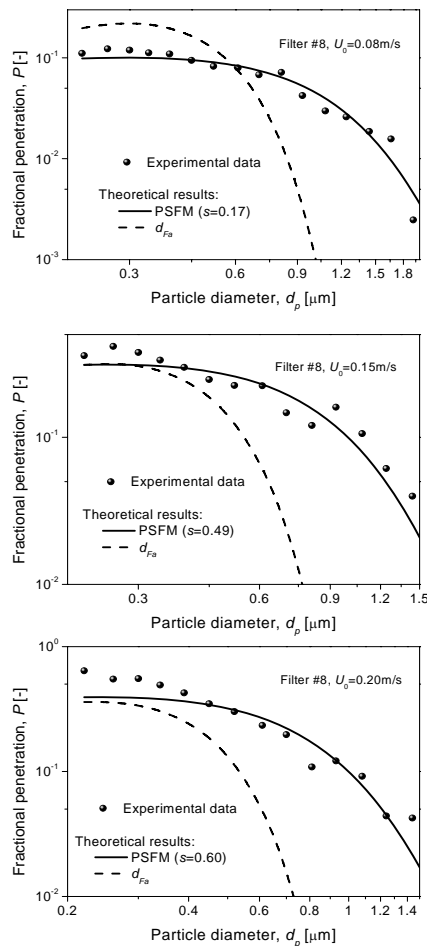
Figure 1. Comparison of the experimental values of the penetration with theoretical results for filter #8 for different superficial air velocities (dashed lines – classical theory for arithmetic mean fiber diameter; solid lines – model *PSFM*).

Parameter s was determined for eight polydisperse fibrous filters characterized in our previous abstract according to the Eq. (1), wherein P_{FSFM} denotes the penetration for the fully segregated flow model,

P_{PMFM} is the penetration for the perfectly mixed flow model, P_{exp} means the experimental penetration and the summation index „i" goes over all experimental data for particular filter and for fixed air velocity obtained for various particle diameters. Eq. (1) was derived using the method of least squares applied to relative residuals.

$$s = \frac{\sum_i \frac{\left(P_{FSFM_i} - P_{PMFM_i}\right)\left(P_{exp_i} - P_{PMFM_i}\right)}{P_{exp_i}^2}}{\sum_i \left(\frac{P_{FSFM_i} - P_{PMFM_i}}{P_{exp_i}}\right)^2} \qquad (1)$$

All filters were tested at four air velocities to check the influence of the superficial gas velocity on the segregation intensity, see one example in Fig. 1 for the filter #8. The results of calculations for eight filters are collected in Table 1. They indicate that the segregation intensity increases with the increase of gas velocity and this relationship is close to linear in the considered range of air velocities, see Fig. 2.

Table 1. Segregation intensity, s, for all tested filters.

Filter No.	Segregation intensity, s, for four superficial gas velocities, U_0 [m/s]			
	0.08	0.12	0.15	0.20
1	0.13	0.31	0.22	0.69
2	0.13	0.22	0.45	0.53
3	0.17	0.63	0.55	0.63
4	0.21	0.37	0.47	0.42
5	0.19	0.21	0.32	0.70
6	0.018	0.11	0.08	0.24
7	0.027	0.049	0.11	0.11
8	0.17	0.27	0.49	0.60
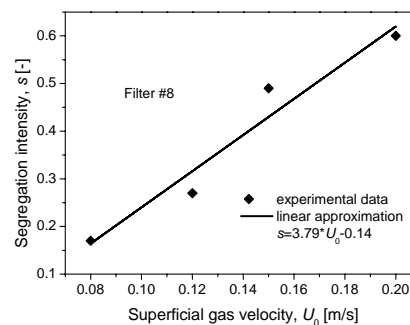
Figure 2. Effect of the superficial air velocity, U_0, on the segregation intensity, s, for the filter #8.

Analysis of the influence of a fibrous filter structure used for filtration of nanoaggregates on its quality factor

A. Podgórski and M. Goszczyńska

Faculty of Chemical and Process Engineering, Warsaw University of Technology,
Waryńskiego 1, PL-00-645 Warsaw, Poland

Keywords: aerosol filtration, aggregates, fibrous filter, soot particles.

The aim of this work is to analyze theoretically possibility of optimization of a fibrous filter structure (fiber diameter, d_F, and filter packing density, α) in order to maximize the initial value of the quality factor, QF, for a filter to be used for removal of fractal-like nanoaggregates (e.g., soot particles); this quality factor is generally defined as: $QF = -\ln P/\Delta p$, wherein P is the initial penetration of aerosol particles through the filter and Δp denotes the initial pressure drop across the filter. When calculating P and Δp, classical single-fiber theory based on the Kuwabara flow model extended for slip effect in the case of nanofibrous media was used. To estimate the single fiber deposition efficiencies for various mechanisms (Brownian diffusion, direct interception, inertial impaction) in the case of aggregates, the model of Lattuada et al. was employed in order to determine the characteristic aggregate radii: aerodynamic radius to calculate coefficient of Brownian diffusion, outer (collision) radius to determine interception parameter, and mass-equivalent radius necessary for the Stokes number calculations. Simulations were performed for air at STP condition at superficial gas velocity 0.2 m/s. Radius of a primary particle in the aggregate was 10 nm and its density 1000 kg/m^3. We considered the aggregates with three various values of the fractal dimension, namely: D_f = 1.65, 2.10 and 2.80, and consisting of different numbers of primary particles: N_{pp} = 100, 1000 and 10000. All calculations were performed for several values of the fiber diameter in the range 0.01–100 μm and various filters packing densities between 0.001 and 0.1. Figure 1a shows sample results of calculations of $QF(d_F,\alpha)$ for the aggregate composed of N_{pp}=1000 primary particles, which has the fractal dimension D_f=1.65, and Fig. 1b for the aggregate with D_f=2.80. It can be observed that in both cases an optimal fiber diameter, d_{Fopt}, (for which QF reaches a local maximum, QF_{max}) can be determined, depending on the value of α, and the more porous filter is, the d_{Fopt} should be smaller. Comparing values of QF_{max} determined for various filter packing densities we can conclude that they decrease with an increase of α, thus, the best performance of a filter – from the QF viewpoint – may be expected for possibly porous one and composed of the finest fibers. Of course, such a filter has to meet a user requirements concerning initial efficiency and mechanical strength. It can be also noted than for more open aggregates (i.e., for

D_f=1.65, Fig. 1), the range of optimal fiber diameters (d_{Fopt} between 0.1 μm for α=0.001 and 1.4 μm for α=0.1) is shifted towards greater sizes compared to the case of a more compact aggregate with D_f=2.80 (d_{Fopt} between 0.01 μm for α=0.001 and 0.3 μm for α=0.1). Although optimal values of QF are greater for aggregates with smaller values of fractal dimension, the variability of the function $QF(d_F,\alpha)$ is more pronounced then. Thus, we can finally conclude that it is possible to estimate optimal structural parameters of a fibrous filter to be used for removal of aggregated aerosol particles and the result depends strongly on the aggregate's parameters (size and number of primary particles, fractal dimension).
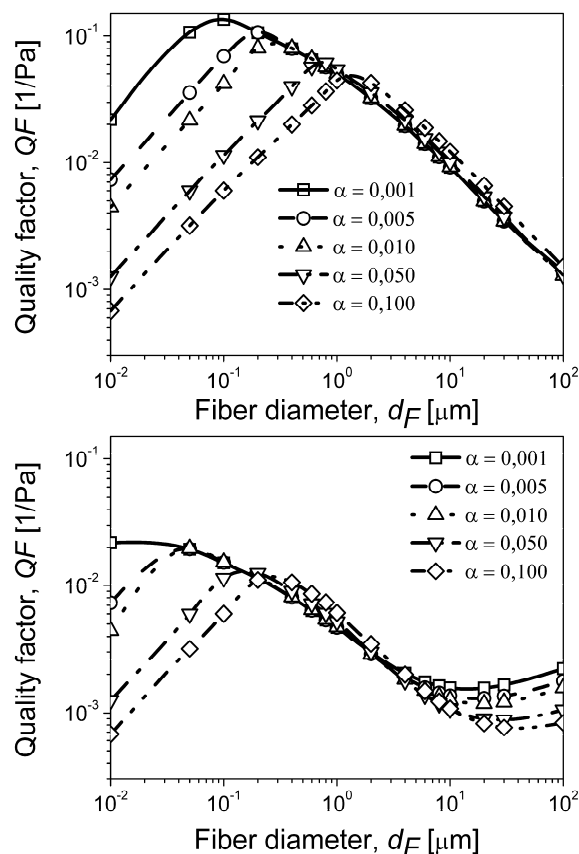
Figure 1. Filter quality factor, QF, as a function of the fiber diameter, d_F, and the filter packing density, α, calculated for aggregates with:
a) D_f=1.65 and N_{pp}=1000; b) D_f=2.80 and N_{pp}=1000.

Application of the Steam Jet Aerosol Collector (SJAC) for the semi volatile organic compounds gas / particle portioning measurements

D. Antkowiak[1], J. Schnelle-Kreis[1], W.G. Kreyling[2], G. Matuschek[1]

[1]Institute of Ecological Chemistry, Helmholtzzentrum München, Ingolstädter Landstrasse 1, 85764, Neuherberg, Germany
[2]Institute of Inhalation Biology, Helmholtzzentrum München, Ingolstädter Landstrasse 1, 85764, Neuherberg, Germany

Keywords: Aerosol filtration, Aerosol sampling, Measurement errors, SVOC.

Aerosol collection, especially for semi volatile compounds, is subject to significant artefacts due to evaporation, adsorption processes and chemical degradation. Nevertheless, since both health and ecological impacts of certain compounds depend on their appearance form it is very important to distinguish between their concentration in the gas- and particle phase. Therefore, finding a proper sampling technique is not an easy issue.

The Steam Jet Aerosol Collector (SJAC) was originally designed for the online determination of inorganic compounds from the particle phase (Slanina et al., 2001). In our work we concentrate on the adaptation of the original SJAC for sampling organic compounds in both particle and gas phase.

Particle collection efficiency was examined with different non-polar particles by means of Scanning Mobility Particle Sizer (TSI Model 3936 SMPS) and the optimum working conditions were obtained for two kind of regarded steamers. The applied cyclone with preceding mixing chamber working with original boiling pot were found to remove over 99% of graphite particles (Palas Generator GFG 1000) as well as octacosane-particles from homogeneous nucleation of the gas phase and candle- soot particles. Application of alternative steam injection technique yielded in much lower particle collection efficiency ca. 66% of particle number.

Pure gas phase streams of four individual organic compounds (heptadecane (1), undecanol (2), naphthalene (3) and methoxyacetophenone (4)) were applied in order to estimate the amount of bias caused by the transfer of components from gas phase to the particle fraction. The water solubility of these compounds was in the range from $3*10^{-4}$ for heptadecane to $2*10^{3}$ mg/l for methoxyacetophenone (see Table 1).

Table 1: Water solubility and K_{ow} values for the organic test compounds.

Substance No.	Water solubility (mg/l)	Log P (octanol-water)
1	0.00029	8.7
2	19.1	4.3
3	31	3.3
4	2030	1.8

The concentration in the particle fraction varied from below 0.1% of the gas sample for heptadecane to below 3% for methoxyacetophenone (see Fig. 1).
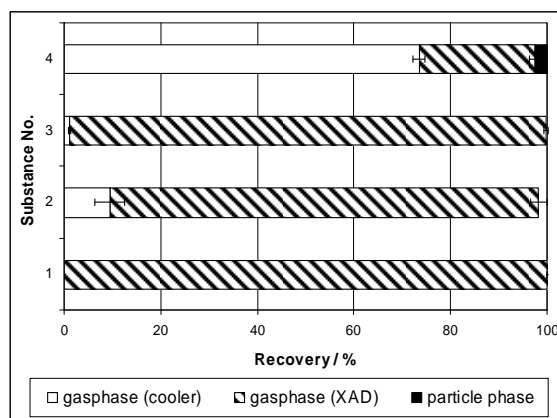
Figure 1. Average fractionation of gaseous test compounds between the three samples (gas phase 1, gas phase 2 and particle phase of the modified SJAC during gas phase measurements;

The analytical procedure includes the liquid-liquid extraction with dichloromethane (for water samples) and Accelerated Solvent Extraction (ASE) with acetone/hexane mixture (for XAD4 samples) both followed by cleanup, evaporation and GC-MS analysis.

J. Slanina, H.M. ten Brink, R.P. Otjes, A. Even, P. Jongejan, A. Khlystov, A. Waijers-Ijpelaan, M. Hu, Y. Lu (2001). *The continuous analysis of nitrate and ammonium in aerosols by the steam jet aerosol collector (SJAC): extension and validation of the methodology.* Atmospheric Environment 35, 2319 - 2330.

Aerosol Based Functionalization of Porous Substrates
for Diesel Particulate Emission Control Applications within the ATLANTIS project

A. Asimakopoulou[1], S. Lorentzou[1], E. Papaioannou[1], C. Agrafiotis[1] and A.G. Konstandopoulos[1,2]

[1]Aerosol & Particle Technology Laboratory, CERTH/CPERI, PO Box 60361, 57001 Thermi, Thessaloniki, Greece
[2]Department of Chemical Engineering, Aristotle University, PO Box 1517, 54006, Thessaloniki, Greece

Keywords: porous substrates, material synthesis, catalysts, diesel emissions, filtration.

A great number of porous media based on various materials (oxide and non-oxide ceramics, sintered metal powders and metal and ceramic textile/fabrics) have been developed for diesel particulate emission control applications, such as diesel particulate filters (DPF). However, certain problems (e.g. inadequate durability, short lifetime and high cost) continue to represent important challenges that trigger the development of new filter materials. Suitably engineered and functionalised porous materials can therefore bring important breakthroughs in the above areas. Motivated by this fact, the European project ATLANTIS is underway, in which the goal is to develop a highly efficient and multifunctional (simultaneous gaseous and particulate pollutants removal) emission control system for future Diesel powered engines.

The present work reports on one of the objectives of the ATLANTIS project, namely the creation of a data base of porous materials/structures (characterized with an array of techniques) that will provide the building blocks for future Diesel emission control applications, including DPFs. The base materials for these porous building blocks are ceramic powders, metal fibers and ceramic fibers of different compositions. These can then be used in various (2-D and 3-D) shaping processes to produce sintered sheets and textile fabrics, foams and multichannel structures, with spatially tuned pore structure and geometries.

The developed porous media are being evaluated for automotive applications in two steps firstly as bare samples and secondly as functionalized samples via Aerosol Infiltration-Deposition (AID) processes, originally introduced in this field by Karadimitra et al. (2001).

Screening tests are performed at the laboratory scale and in Diesel engine exhaust to evaluate the following properties of the porous samples: a) flow resistance, b) filtration efficiency and c) soot loading behaviour d) direct (oxygen-based) and e) indirect (NO_2-assisted) soot oxidation activity. This creates a five-dimensional space where, regions of "acceptable" and "unacceptable" performance can be identified and trade-offs with respect to different performance criteria may be assessed. A set of promising porous materials and structures has thus been identified for further functionalization. The functionalization at the present stage focuses on identifying a suitable soot oxidation catalyst, while gas treatment catalytic functions will follow soon after. A wide variety of soot oxidation catalyst formulations has been synthesized via aerosol synthesis routes, and the most promising formulations were subsequently coated on the selected porous structures and evaluated on a Diesel engine exhaust set-up.

Indicative results with respect to indirect soot oxidation are shown in Figure 1 for AID-coated SiC and Al_2O_3 wall-flow monoliths. It can be seen that both monoliths reduce the soot oxidation temperature from the uncoated sample, however, the reduction on the SiC monolith, is higher.
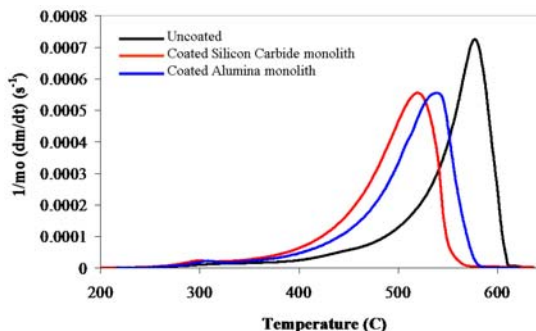
Figure 1. Indirect soot oxidation on coated SiC and Al_2O_3 wall flow monoliths by a flow containing 300 ppm of NO.

Karadimitra, K., Macheridou, G., Papaioannou, E. & Konstandopoulos, A. G. (2001). in *Proc. Partec 2001,* Paper No 135.

Dust cloud manipulation in microgravity: positioning, squeezing and trapping

A.A. Vedernikov

Microgravity Research Centre, Université Libre de Bruxelles, 50, av. F.D. Roosevelt, 1050, Brussels, Belgium

Keywords: aerosol dynamics, cloud dust, dynamic balancing, instrument development, microgravity

Interaction in Cosmic and Atmospheric Particle Systems (ICAPS) is one of the main projects of the European Space Agency in physical sciences (Boon at al., 2008, Blum at al., 2008). Its part related to astrophysical experiments in microgravity deals with investigation of dust particle interaction, kinetics of agglomeration, formation of extended extremely fluffy agglomerates and their detailed microstructure. Microgravity is a necessity for these experiments because of relatively low gas pressure. Even individual micrometer size particles fall down too quickly in a rarefied gas at normal gravity to form agglomerates by Brownian mechanisms. Extended agglomerates, would they appear in such conditions, will not sustain their own weight.

After formation in microgravity conditions, the dust cloud requires different manipulations, most important are positioning, squeezing and trapping. First of all, one has to counterbalance external perturbations – residual gravity, thermophoretic force and gas flow driven by thermal creep. Two latter effects arise as a result of temperature differences along the chamber walls. Tiny temperature gradients as low as about 1mK/cm sweep away the cloud from the observation area. Solution of this problem is rather straightforward using static three-dimensional force with active feed back: a Cloud Positioning System analyzes regularly cloud images and works out a force that moves the whole cloud in such a way that the reference group of particles stays around the same fixed position in the chamber.

Cloud trapping and/or squeezing are more challenging tasks for a cloud containing millions of particles per cubic centimeter in a volume of tens of cubic centimeters. Trapping (without squeezing) assumes creation of a flat potential well with steep enough walls preventing a cloud from dispersion due to Brownian motion or sweeping away by external perturbation forces. Cloud squeezing requires extended central potential. Ideally the gradient should be high enough to move most of the cloud particles to a fixed point in the chamber to form single agglomerate within a reasonable time interval. Modeling and microgravity experiments showed that cloud trapping and squeezing can not be provided by known instrumentation based on electro dynamic balancing of the Paul trap type (Davis, 2002).

In the Microgravity Research Centre we develop a set of new approaches and instruments for cloud positioning, trapping and squeezing, which for simplicity termed "traps" – thermophoretic, photophoretic, diffusiophoretic, gas density variation, fluid velocity profiling, and magnetic. The thermophoretic trap passed the first tests in microgravity conditions (Vedernikov et al., 2007 and 2009). Its advantage is in the fact that positioning, trapping and squeezing properties do not require electrical charge on the particles and all these "trap" functions in the free molecular regime are much less sensitive to particle sizes as compared to the electro dynamic balancing. Such property is particularly interesting for agglomeration experiments. The progress in the development of the efficient thermophoretic traps bases on appropriate geometry of the trap and rapid temperature variation. We developed rapid thermoelectric heaters (Vedernikov et al., ICT & ECT 2009) making more than 500 K/s on the working surface that allows using the thermophoretic trap at frequencies up to about 20 Hz.

The traps under development have different properties: stabilized temperature or on the contrary highest possible temperature variation in the trapping volume (up to about hundred degrees), particle preferential trapping based on particle size, optical, magnetic or other properties, formation of intensive three-dimensional periodic shear flow or three-dimensional gas density pulsations of the contraction-expansion type with minimal shear flow intensity, etc. Their choice and/or combination (also including electro dynamic balancing) depends upon the task for dust cloud manipulation system. Their use at normal gravity is also possible.

Boon, J. P., Kvick, Å. & Minster, O. (2008). *Europhysicsnews*, 39/3, 25-26.

Blum, J. et al. (2008). *Europhysicsnews*, 39/3, 27-29.

Davis, E. J. & Schweiger, G. (2002). *The Airborne Microparticle: Its Physics, Chemistry, Optics, and Transport Phenomena.* Springer, 833 p.

Vedernikov, A. A., Markovich, A. V., & Blum, J. (2007). In *European Aerosol Conference*, Salzburg (Austria), Abstracts, LP35.

Vedernikov, A. A., et al. (2009). In *European Aerosol Conference*, Karlsruhe (Germany), Poster

Vedernikov, A. A., Markovich, A. V., Kokoreva, A. V. (2009). In *Proc. 28th International Conference on Thermoelectrics and 7th European Conference on Thermoelectrics*, Frieburg, Germany

Mixing state of bi-component mixtures under coagulation from scaling solutions

J.M. Fernández-Díaz, G. Gómez-García, M.A. Rodríguez-Braña, M. Domat, I.A. SanJuan

Department of Physics, University of Oviedo, C/Calvo Sotelo, s/n, E-33007 Oviedo, SPAIN

Keywords: bi-component aggregate, coagulation, mixing state

Smoluchowski coagulation equation gives a mean field description of many aggregation processes: aerosol and cloud physics, polymer chemistry, colloidal chemistry, etc. This equation describes the evolution of the particle size distribution (PSD). For mono-component systems one size variable is needed (particle diameter or mass). However, when several species are necessary to the description of the system, a multicomponent approach has to be used: the independent variables are the masses of every species in the particles.

The simplest multicomponent system is a bi-component mixture: each particle is described by the mass of the first (m) and the second (n) component. Apart from the PSD, $c(m,n,t)$ (t is time) some others (derived) properties can be analysed in the evolution. Among these, Lushnikov (1976) introduced two important magnitudes to characterise coagulation mixtures: the total number, N, of particles having a given concentration $C = m/(m+n)$ of the first component, and the total mass, M, with the same concentration (expressions for M not shown for brevity). By putting $\chi = m+n$, the total mass in a particle, it is obtained:

$$N(C,t) = \int_0^\infty \chi c(m(\chi,C),n(\chi,C),t)\, d\chi.$$

In the evolution of the systems we are often interested in their long time (asymptotical) behaviour. This leads to the so called scaling solutions, which describe approximately the system, and are sometimes obtained from a discrete case: i.e., the PSD is composed by two kind of monomers, with an initial number M_{10} of the first component and M_{01} of the second one ($M_T = M_{10}+M_{01}$). For coagulating systems with kernel independent from the composition of the colliding particles, Lushnikov showed that:

$$c(m,n,t) = P(m,n)c_{\text{homo}}(m+n,t),$$

being c_{homo} the PSD corresponding to the homogeneous case (if we were not able to distinguish the monomers). For long time and large particles, Vigil and Ziff (1998) showed (expressed with our nomenclature) that:

$$P(m,n) \approx \frac{M_T}{\sqrt{2\pi M_{10}M_{01}}} \exp\left(-\frac{M_T^2(C-C_o)^2\chi}{2M_{10}M_{01}}\right),$$

being $C_o = M_{10}/M_T$ the overall concentration of the first component.

We will use the scaling solutions and previous equations to study the values of N (and M) for long time, for the cases with constant, additive and product kernel, for which c_{homo} are known. Time t is normally expressed in function of other equivalent variable: a critical cluster size (s), increasing with time, and depending on the initial PSD and the kernel.

For the constant kernel, $s = b_0 t/2$, by using the known homogeneous case solution, we obtain:

$$N_{\text{cons}}(C,s) \approx \frac{M_T}{2\sqrt{2M_{10}M_{01}}} s^{-2}[E_0(C,s)]^{-3/2},$$

$$E_0(C,s) = \frac{M_T^2}{2M_{10}M_{01}}(C-C_o)^2 + \log(1+1/s).$$

This expression has the adequate form: the total area between $C=0$ and $C=1$ under N is the total number of particles (variable with time) (For M the area is the total mass—constant.) Moreover, curves for N and M tend to a Dirac-δ: particles with concentration away from C_o are removed from the system.

For the additive kernel (with the proper s definition) M obtained through the exposed methodology is good. However, N cannot be obtained because an improper integral appears. For the product kernel the problem is greater: it shows gelation, and the total mass in the system is no more conserved from certain instant. For time tending to gelation time the scaling solution is known, and from this we obtain M and N as before. Both expressions show bizarre behaviour: N increases as C tends to 0 and 1, and M (with an apparently correct form) encloses an infinite area. In both cases non-physical behaviour is found.

In conclusion, we think that scaling solutions are good enough to analyse the mixing state of mixtures for PSDs that have not grit (small particles) for long time (i.e., constant and Brownian kernels). On the contrary, if small particles remain in the system mixing states could be only obtained from the actual (and not approximate) solutions.

Lushnikov, A.A. (1976) Evolution of coagulating systems. III. Coagulating mixtures. *J. Colloid Interface Sci.*, 54:94–101.

Vigil, R.D., & Ziff, R.M. (1998) On the scaling theory of two-component aggregation. *Chem. Engr. Sci.*, 53:1725–1729.

T08 High temperature aerosols

Effect of air flow distribution on dust emission and efficiency of local exhaust ventilation during wood grinding

T. Jankowski

Department of Chemical and Aerosol Hazards, Central Institute for Labour Protection – National Research Institute, 00-701 Warsaw, Poland

Keywords: wood dust, emissions, ventilation, air flow distribution

The concentration of hazardous substances in air during industrial process is very important factor for occupational safety and health. Typical example of process, which has the potential to dangerous workers, is wood grinding. Particles of wood dust are pathogenic and very dangerous for human health. They penetrate into the lungs – or to be more precise – to the alveoli.

This article presents some aspects of influence of air flow conditions on dust emission and efficiency of local exhaust ventilation (LEV) during wood grinding.

Tests were conducted in accordance with Standard No. EN 1093-2:2006 at a test stand – a chamber. A dual-disc bench grinder with two grinding wheels - diameter of 250 mm - was used for processing soft (pine) wood. The bench grinder co-operated with an immovable LEV connected with a dust separator.

Tests were carried on using two methods:
- the anemometric method for measuring air flow velocity with Vivo Draught 20T35 Transducers,
- the tracer gas method for measuring:
  - real pollutant concentration with a DustTrak 8520,
  - tracer gas concentration with a MIRAN SapphIRe 100E Portable Gas Analyzer.

Sulfur hexafluoride (SF_6) was used as a tracer gas simulating a real pollutant in defined air flow conditions. The tracer was introduced into a real pollutant emission source. Measurements of the tracer concentration were carried out by taking samples continually over at least 30 minutes. Measurement points were positioned at vertical and horizontal planes at the three heights. Both real pollutant and tracer concentrations were measured at four measurement points around the bench grinder, when the LEV was turned on and turned off.
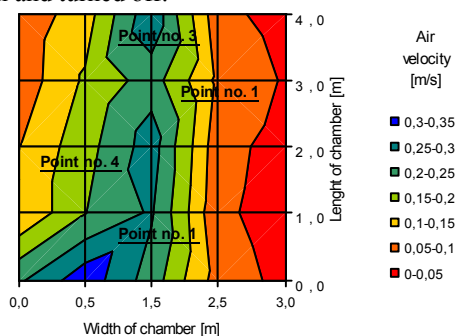
Figure 1. Air flow velocity distribution in the chamber during wood grinding.
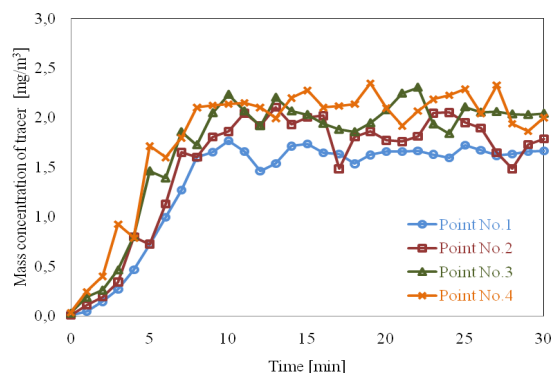
Figure 2. Distribution of the tracer concentrations around the bench grinder.

Figure 1 and 2 illustrates the results of distribution of air flow velocity and tracer gas concentration. Tests shows that values and directions of air streams resulting from the bench grinder significantly influenced air velocity distribution around the wood grinding. The process of the distribution of the wood dust and tracer gas around the bench grinder was similar and consisted of three stages: a short, non-spreading stage; a quick increase of dust and tracer concentration; a stabilization state of concentration.

Table 1. Effect of air flow conditions on the mass soft wood dust emission rate and efficiency of the LEV.

| | | Mass pollutant emission rate [mg/s] | | | |
| | | Nominal volume air flow rate [m³/h] | | | |
		500	1000	2000	3000
LEV turned	off	1.002	0.905	0.774	0.636
	on	0.036	0.032	0.028	0.026
Efficiency of LEV [%]		96.38	96.45	96.44	95.83

It was found that mass pollutant emission rate decreases as the volume air flow rate around the bench grinder increases (table 1). Mass pollutant emission rate decreased and it was 24.5 ÷ 28.3 times lower than that measured when the LEV was turned off.

Standard No. EN 1093-2 (2006).

Evaluation of the emissions of airborne pollutants from machines using trace gas technique

T. Jankowski

Department of Chemical and Aerosol Hazards, Central Institute for Labour Protection – National Research Institute, 00-701 Warsaw, Poland

Keywords: emissions, tracer method, bench test method, ventilation system

One of the most basic working conditions that conform to occupational safety requirements is a prevention of employees against exposure to pollutants within their working rooms. For relationship with EU directives, machine (M) causing pollutant emission hazard must be equipped with proper means of collection protective equipment against aerosols, i.e. housings or local exhaust ventilation (LEV).

Methods of determining emission of pollutants from machines have been described. It complies with EN 1093-2:2006. This standard specifies the methods to enable measurements of the emission rates of airborne pollutants from a single machine, whose operation can be controlled, using trace gas techniques.

The experiments are carried out using a setup composed of following elements: the purpose-built chamber (1) with filtering unit (2), the venture tube (3), pressure transducer (4), air regulating damper (5), fan (6), switch box (7), hygrometer (8); sampling probes kit for air parameters (9, 10, 11), PC (13), accessories (12); cylinder of tracer gas (14), flow meter (15), sampling tubes (20) for dust monitor (21), dosing (16) and sampling tubes (17) for tracer gas analyzer (18).

The scheme of the set-up is shown in figure 1.
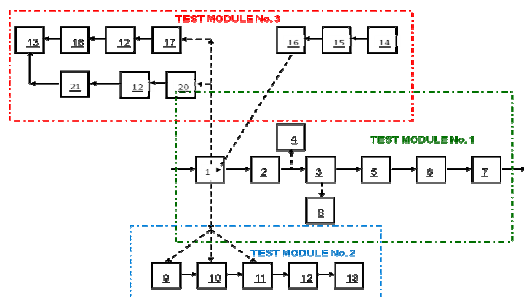
Figure 1. Scheme of the instrumental set-up.

The following measurement methods are applied to determine pollutants dispersion from a machine with the LEV: anemometric and tracer gas method.

The anemometric method is based on determining air velocity distribution by measurements make in different points located on horizontal and vertical dimensions within a chamber. These situate 1.7, 1.1, 0.1 m above the floor, which reflects the standing employees' head, middle and feet (figure 2). For the sitting employees - 1.1, 0.6, 0.1m.

The principle of the tracer gas method is based on the use of a tracer gas generated at a known and constant emission rate to provide the best representation of the real pollutant source. The mean tracer gas and pollutant concentrations are measured in the pollutants dispersion area in a chamber. Concentration measurements of the tracer gas are made in four measurement points, as presented in figure 2.
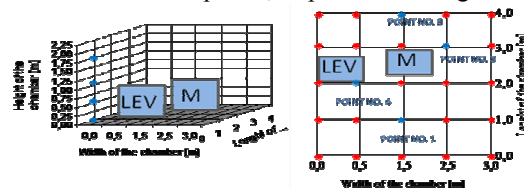
Figure 2. Measurement points at a test stand.

The index of the emission airborne pollutants from machines are levels of dust and tracer gas concentration determined when LEV was turned on and turned off.

The mass tracer gas emission rate $(q_{T,i})_m$ [mg/s] at measurement point "i" is determined on the basis of the following formula:

$$(q_{T,i})_m = (q_{T,i})_V \cdot \frac{M_T \cdot 1000}{V_{m(t,p)} \cdot 60}$$

The mass real pollutant emission rate $(q_{p,i})_m$ [mg/s] can be described by:

$$(q_{p,i})_m = (q_{T,i})_m \cdot \frac{\sum_i (\bar{C}_{p,i})_m / (\bar{C}_{T,i})_m}{n}$$

where: $(q_{T,i})_V$ – volume tracer gas flow rate [l/min], M_T – molar mass of the tracer gas [g/mol], $V_{m(t,p)}$ – molar volume of gas at the temperature (t) and pressure (p) of the experiment [l/mol], $(\hat{C}_{p,i})_m$ – mean mass concentration of pollutant [mg/m³], $(\hat{C}_{T,i})_m$ – mean mass concentration of tracer gas [mg/m³] and n – number of measurement points.

The example results concerning only one tested wood grinder without LEV are shown below (table 1).

Table 1. The mass dust emission rate from a machine.

Point No.	$\bar{C}_{p,i}$ [mg/m³]	$\bar{C}_{T,i}$ [mg/m³]	$\dfrac{\sum_i (\bar{C}_{p,i})_m / (\bar{C}_{T,i})_m}{n}$	$(q_{p,i})_m$ [mg/s]
1	7.11	7.48		
2	7.28	7.95	1.05	1.61
3	8.45	8.88		
4	9.24	9.45		

Gliński M. (2002). JOSE, 1(8), 97-105.

Modeling of mesoscale vortices structure near to a powerful hot source of impurity in a boundary layer of atmosphere

K.G. Shvarts[1], V.A. Shklyaev[2]

[1]Department of Mathematics and Mechanics, Perm State University, 614990, Bukirev Str., 15, Perm, Russia

[2] Department of Meteorology, Perm State University, 614990, Bukirev Str., 15, Perm, Russia

Keywords: boundary layer, cyclonic vortex, heat-mass transfer, heat source, turbulent diffusion

We obtained the new quasi–two–dimensional model of impurity propagation from a powerful thermal source with allowing for heterogeneity of turbulent diffusion above a source and outside of it [1,2]. The equations are deduced with the help of three–dimensional model of convection on an example of oil ignition. Boundary conditions and coefficients of the model are defined by a method of parameterization of small–scale turbulence. Results of numerical calculations are presented. They have shown that the powerful vortices motion is formed in the bottom atmosphere above a place of oil ignition as result of linear and nonlinear influence of a non–uniform horizontal gradient of temperature near the thermal torch. The physical characteristics of vortices and their quantity are defined by the values of turbulence factors outside and above of a heat source. The formed field of a wind essentially influences on a character of distribution of oil impurity in vicinity of a source.

Numerical solution was received by means of the explicit finite-difference scheme, on a grid 250 x 250 knots, for a square plate in length 100 km. Fields of concentration of an impurity, temperatures of air, function of a current and indignations of function of a current have been received. The field of perturbation of stream-function, field of concentration of oil impurity and field of temperature are demonstrated at Figure 1, Figure 2 and Figure 3.

Figure 2 Field of concentrations at development cyclonic vortex.
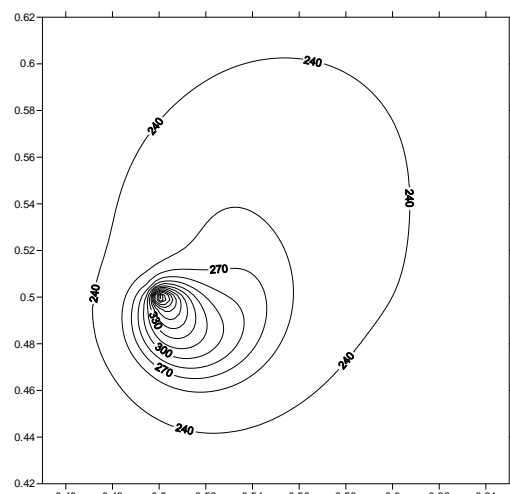
Figure 3 Field of temperature at development cyclonic vortex.

Shvarts, K.G., Shklyaev, B.A. (1994) *Russian Meteorology and Hydrology*, No.9, 21-29.
Shvarts, K.G., Shklyaev, V.A. (2008) Int. Conf. "Fluxes and structures in Fluids", July 2–7, 2007, St.–Petersburg, *Selected Papers*, 185–190.

Figure 1 Field of perturbation of stream-function at development cyclonic vortex.

Gas phase synthesis of zinc sulfide nanoparticles

E.K. Athanassiou[1*], R.N. Grass[1] and W.J. Stark[1]

[1]Department of Chemistry and Applied Biosciences, ETH Zurich, Wolfgang-Pauli-Strasse 10, 8093, Zurich, CH

Keywords: combustion synthesis, flame spray synthesis, nanocrystalline material, nanoparticles application.

Flame synthesis has been applied for several decades for the large-scale manufacturing of metal oxides such as silica and titania. Recent developments including flame spray pyrolysis have allowed the large scale production of functional nanometerials starting from nano-gypsum[1], calcium-phosphate[2] for bio applications, to non-noble metal[3, 4] nanoparticles, complex alloys[6] and metallic / ceramic[7] nanocomposites for mechanical, magnetic, electronic or sensor applications[8].

Here we present how thermodynamics allowed us to further extend the principle of flame synthesis for the production of sulfide nanoparticles. The oxygen-limiting conditions in collaboration with sufficient amounts of a sulfur source allowed the production of zinc sulfide nanoparticles (10 to 40 nm, Figure 1) at much higher production rates (in a lab-scale reactor: 5 to 10 g h^{-1}) than typical wet-based processes of quantum dots. The zinc sulfide nanoparticles could be further doped with other elements to further enhance its electrical properties such as photoluminescence. We demonstrate how versatile gas phase processes are and how thermodynamic and chemical reactions in high temperature flames could offer an interesting alternative for the large-scale production of photoluminescent materials.
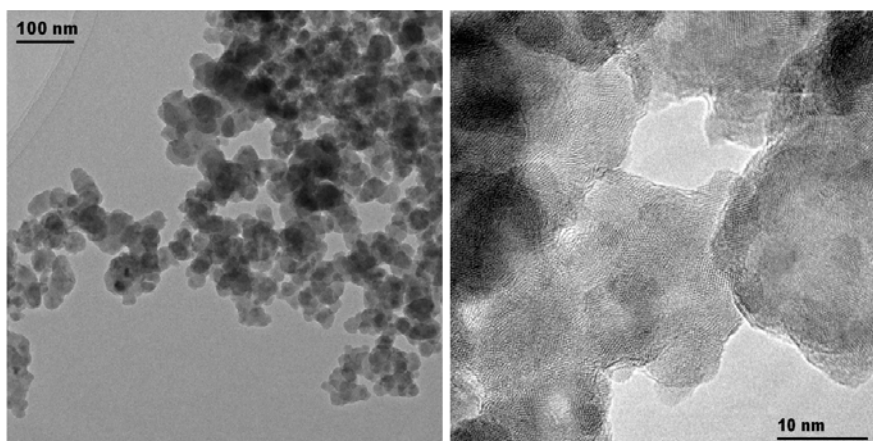
Figure 1. The principle of flame spray pyrolysis has been further extended for the preparation of zinc sulfide nanoparticles. Transmission electron microscopy images of zinc sulfide nanoparticles show that the as prepared particles have an average size of 10 to 40 nm (left) and exhibit high crystallinity (right).

References:
[1] Osterwalder, N., Loher, S., Grass, R.N., Brunner, T.J., Limbach, L.K., Halim, S.C., & Stark, W. J. (2007). *J. Nanopart. Res.*, 9, 275-281.
[2] Brunner, T.J., Bohner, M., Dora, C., Gerber, C., & Stark, W. J. (2007). *J. Biomed. Res. Part B,* 83B(2) 400-407.
[3] Athanassiou, E.K., Grass, R.N., & Stark, W. J. (2006). *Nanotechnology*, 17, 1668-1673.
[4] Grass, R. N., Athanassiou, E.K., & Stark, W. J. (2007). *Angew. Chem. Int. Ed.*, 46, 4909-4912.
[5] Athanassiou, E.K., Grass, R.N., Osterwalder, N., & Stark, W. J. (2007). *Chem. Mater.*, 19(20), 4847-4853.
[6] Grass, R.N., Albrecht, T.F., Krumeich, F., & Stark, W. J. (2007). *J. Mater. Chem.,* 17, 1485-1490.
[7] Athanassiou, E.K., Krumeich, F., Grass, R.N., & Stark, W. J. (2008). *Phys. Rev. Lett.*, 101, 166804.

Temperature-induced reduction of the work function of submicron aerosol particles and its implication on thermionic particle charging

K. Reuter-Hack[1], G. Kasper[1] and A.P. Weber[2]

[1]Institute of Mechanical Process Engineering and Applied Mechanics, Karlsruhe Institute of Technology, 76128, Karlsruhe, Germany
[2]Institute of Mechanical Process Engineering. Clausthal University of Technology, 38678, Clausthal-Zellerfeld, Germany

Keywords: high temperature aerosols, charged particles, in situ measurements.

Aerosol particles have been found to exhibit very high charge levels at elevated temperatures (Schiel et al., 2003). The reason for this enhanced charging was supposed to be due a work function reduction. However, measurements in a high temperature tube furnace showed that the particle charging by direct electron emission is superimposed by diffusional charging with negative ions originating from the tube wall. In fact, at very high temperatures the polarity of the particle charge changes from positive to negative. Therefore, the reliability of the effective work function as deduced from the particle charge was rather uncertain so far. Therefore, photoemission spectroscopy was employed to measure the work function of aerosol particles as a function of temperature for conditions where thermoemission from the walls was negligible. Since the particles were between 70nm and 220nm they exhibit solid state behaviour of the bulk material. In addition, also electrostatic corrections accounting for the image charge correction for very small sizes were not necessary (Müller et al., 1988).

Aerosol particles of Pt and TiO2 were produced by spark discharge and thermal decomposition, respectively, and size classified in a Differential Mobility Analyzer (DMA). The negatively singly charged particles entered the UV illumination chamber which was heated to temperatures up to 700°C. From a broad band UV source monochromatic a narrow wavelength was selected with a monochromator and the resulting photon flux was measured with a photomultiplier tube (PMT). Using a combination of electrostatic precipitator (ESP) and Condensation Particle Counter (CPC) single electron counting efficiency was obtained.

In Figure 1 the results for platinum and titanium dioxide particles are shown. For temperatures above 500°C thermionic emission from the walls of the illumination chamber overwhelm the aerosol charge rendering direct photoelectric measurements of the particle work function impossible. However, for the determination of the aerosol charge at high temperatures it was found that for the used quartz tubes electron emissions from the walls could be neclected at least up to 800°C.
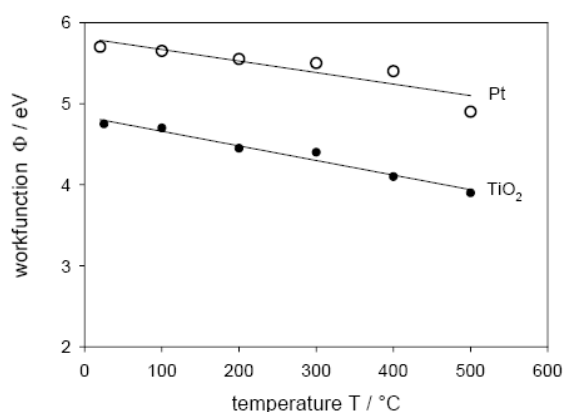
Figure 1. Temperature-induced reduction of the work function of Pt and TiO2 nanoparticles

Therefore, the work function was extrapolated to 800°C and the resulting particle charge state was calculated using a model outlined in Schiel (2007). The calculated and the measured particle charge agree very well so that the results of the work function determination and the charge measurement corroborate each other. Thus, the work function behaviour allows to predict the charging behaviour of aerosol particles at high temperatures for cases where secondary effects such as thermionic emission from the walls are insignificant.

Müller, U., Schmidt-Ott, A., Burtscher, H. (1988) Z. Phys. B – Condensed Matter, 73, 103
Schiel, A., Weber, A.P., Kasper, G., Schmid H.-J. (2002), *Part. Part. Syst. Charact*., 19, 410-418.
Schiel, A. (2007) Ph.D. Thesis, University of Karlsruhe, Germany

Characterization of high-temperature aerosols as emission precursors from a MSWI

E. Peña[1], S. Astarloa[2], E. Garcia[2], S. Elcoroaristizabal[2], J.A. Legarreta[1], C. Gutiérrez-Cañas[1].

[1] Dpt. Chemical and Environmental Eng., U. of the Basque Country, A. de Urquijo s/n, 48013, Bilbao, Spain
[2] AIRg María Díaz de Haro, 48920, Portugalete, Spain

Keywords: Solid Waste Incineration, Heavy metals, Fine particles, Electrostatic Precipitator.

Trace emissions of both heavy metals (HM) and PCDDs/PCDFs from municipal sewage sludge incineration (MSWI) are subjected to tighten regulations (Directive 94/67/EC). Some heavy metals –Cu and Fe- could play a catalytic effect and then, enhance the "de novo" synthesis pathways (Chang *et al*, 2004) along the final process stages. Moreover, the emission of volatile metals –Zn, Cu and in less amount Pb- are linked with the presence of a secondary mode around 0.7 μm -aerodynamic diameter number distribution- (Gutierrez-Cañas et al, 2006). Electrostatic precipitators directly downstream of the boiler show a penetration window in the size range of trace metals occurrence; therefore this work aims to ascertain how the fractional efficiency is related to metal concentration and how this efficiency can be improved through manipulation of operation variables, such as the applied voltage.

The experimental study covers the seasonal variations all over the year 2006. Mean values were 116 t sludge/day; 2212 tons gas/day; 21 t fly ash/day. Combustion temperature under standard operating conditions in the furnace is maintained slightly over 925 ºC. Directly downstream of the boiler a two-field electrofilter operates from 85 up to 105 kV (200ºC gas temperature). After the electrofilter are two scrubbers and finally the stack.

Experimental methods are reported elsewhere (Gutierrez-Canas, 2006). Essentially, a picture of the metals partitioning is achieved by analysis of all the process streams. Interpretation of such a data set must include a careful estimation of the uncertainty of flow measurements. For this reason, mass balance closure is not reported. However, joint discussion of chemical and morphological analysis together with thermodynamic prediction allows to improve the understanding about the metal behaviour. Sludge supply and characteristics, operation parameters – filtration system and process variables, such as fuel-to-air ratio and temperature profile within the furnace-boiler system- and process streams were also analyzed. Size distribution dynamics was monitored using real time aerosol analyzers - ELPI (Dekati) and APS 3321 (TSI, Inc)- and in-duct cascade impactors - Kalman KS 220 and Dekati-, were used as sample separators for further analysis (chemical –ICP/MS- and morphological/chemical –SEM/EDS); aerosol sampling and monitoring cover from the boiler outlet to the stack.
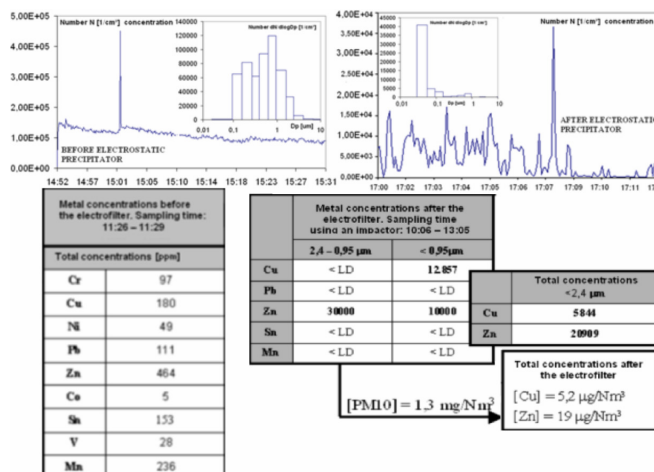
Figure 1: Temporal evolution of the total number concentration and size distribution. Size-segregated metal concentrations (ppm wt).
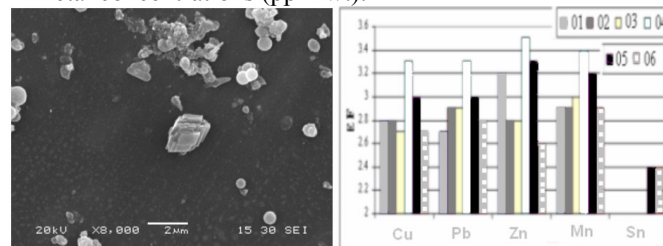
Figure 2: Particle morphology typical of halides at the electrofilter inlet–SEM- and analysis of HM Enrichment Factors "EF" –ICP mass-.

Total concentrations of HM emissions are very low; therefore the current configuration and control of this line is adequate. Size distribution is highly displaced to the fine fraction. The volatile HM series for this specific solid waste are: Cu, Zn, Pb, Sn and Mn –These series can be changed with different concentrations of alkalis-. A correct control of these series must be done at the outlet of the electrofilter and their concentrations are not linked with PM10 which are thermodynamically linked with influence of anions, fractionation of these metals and with the theoretical condensation of the aerosol –Cu and Zn in the ultrafine range (PM1)- -there are connections with the size distributions at the outlet of the electrofilter-.

References
Chang M.B. et al. / Chemosphere 55 (2004) 1457- 1467
Ferge T., Maguhn J., Felber H. and Zimmerman R., (2004), Environ. Sci. Technol, 38,1545-1553.
Gutierrez-Cañas C. et al. (2006) Int. Aerosol Conf., St Paul, MN.
Lind T., Hokkinen J. and Jokiniemi J. (2003) Environ. Sci. Technol., 37, 2482-2846.

Contribution of polychlorinated dibenzo-*p*-dioxins and dibenzofurans from electric arc furnace dust treatment plant to duck farms

S.I. Shih[1*], W.J. Lee[2], H.W. Li[2], L.F. Lin[1], L.C. Wang[3] and G.P. Chang-Chien[3]

[1]Department of Environmental Engineering, Kun Shan University, Yung Kang, 710, Tainan County, Taiwan
[2]Department of Environmental Engineering, National Cheng Kung University, Tainan, 701, Tainan City, Taiwan
[3]Department of Chemical and Materials Engineering, Cheng Shiu University, Niaosong, 833, Kaohsiung County, Taiwan

Keywords: PCDD/Fs, Air pollution, Dry deposition, Dust.

A high level of polychlorinated dibenzo-*p*-dioxins and dibenzofurans (PCDD/Fs) in duck eggs (30.0-45.0 pg WHO/g-fat) was found in central Taiwan. Several reports were suspecting a specific electric arc furnace dust treatment (EAFDT) plant, locating near the duck farm, to be responsible for the "Toxic Egg Event". The present study primarily aimed at evaluating the impact from EAFDT plant on the duck total-PCDD/F daily intake by using both Industrial Source Complex Short Term model (ISCST) and dry/wet deposition models.

The EAFDT plant was established in 1999 to recover zinc oxide via the Waelz process. [Mager, et al., 2003] Basic information of EAFDT plant is shown in Table 1. The dry deposition flux of PCDD/Fs in the atmosphere is a combination of both gas- and particle-phase fluxes, which is given by: $F_T = F_g+F_p$. F_T is the summation of PCDD/F deposition fluxes from both gas and the particle phases; F_g is the PCDD/F deposition flux from the gas phase, F_p is the PCDD/F deposition flux from the particle phase. The wet deposition flux of PCDD/Fs is a combination of both vapor dissolution into rain and the removal of suspended particulate by precipitation.

Two high-resolution gas chromatographs/high-resolution mass spectrometers (HRGC/HRMS) were used for PCDD/F analysis. The HRGC was equipped with a DB-5 fused silica capillary column with a splitless injection, while the HRMS had a positive electron impact (EI+) source. The analyzer mode of the selected ion monitoring was used with the resolving power at 10,000. The electron energy and source temperature were specified at 35 eV and

Table 1. Basic information of the EAFDT plant

Feed materials	EAF fly ash, coke, sand
Furnace type	Waelz rotary kiln
Air pollution control devices	Dust settling chamber, venturi tower, cyclones, bag filters
Stack height (m)	35
Flue gas rate (Nm^3/h)	52,200
Treatment capacity (t/year)	Approximately 70,000

250 ^{o}C, respectively. The oven temperature program was set according to the following: initially at 150 ^{o}C (held for 1 min), then increased by 30 ^{o}C/min to 220 ^{o}C (held for 12min), and finally increased by 1.5 ^{o}C/min to 310 ^{o}C (held for 20min). Helium was used as the carrier gas. [Wang, et al., 2003]

Congener profile of 17 2,3,7,8-substituted PCDD/Fs in feed was shown in Figure 1. The dominant congeners were OCDD, OCDF 1,2,3,4,6,7,8-HpCDF and 1,2,3,4,6,7,8-HpCDD.

After different scenario simulations, the worst case occurred at duck farm A and at 200 g feed and 5 g soil for duck intake, where 47.81% of the PCDD/Fs came from the original soil, 44.92% from feed and 6.58% from stack flue gas. Considering different uncertainty factors, such as the flow rate variation of stack flue gas and errors from modelling and measurement, the PCDD/F contribution fraction from the stack flue gas of EAFDT plant may increase up to twice as that for the worst case (6.58%) and become 13.2%, which was still much lower than that from the total contribution fraction (86.8%) of both feed and original soil. Dust contained purposely in duck feed by the farmers was a potential major source for the duck daily intake. While the impact from EAFDT plant has been proven very minor, the PCDD/F content in the feed and soil, which was contaminated by illegal fly ash landfills, requires more attention.

Figure 1. Congener profile of 17 2,3,7,8-substituted PCDD/Fs in feed.

Mager, K., Meurer, U., Wirling, J. (2003). *JOM*, 55, 20–25.
Wang, L. C., Lee, W. J., Lee, W. S., Chang-Chien, G. P., & Tsai, P. J. (2003). *Environ. Sci. Technol.*, 37, 62-67.

Characterization of PCDD/Fs in a secondary aluminum smelter

C. Lin and Y.H. Wang

[1] Department of Environmental Engineering and Science, National Pingtung University of Science and Technology, Pingtung County, Taiwan.

Keywords: Dioxin, Secondary ALS.

Aluminum is commonly used in food packaging, construction, transportation, and industry. Aluminum is recovered by secondary aluminum smelters (secondary ALSs). Waste and recycled aluminium are used in recovery. However, scrap and dross may contain organic impurities such as plastics, paints, and solvents. Furthermore, secondary ALSs use such chemicals as NaCl, KCl, and other salts as flux. Taiwan has approximately 196 secondary ALSs. The annual gross output of aluminium from these ALSs is as high as 670 ktons.

This study characterizes polychlorinated dibenzo-p-dioxins/dibenzofurans (PCDD/Fs) concentrations in workplace air and ambient air of a secondary aluminum smelter. The secondary ALS has operated in southern Taiwan for 7 years. Its annual aluminum output is about 5,000 tones. The smelting process is conducted in batches; processing each batch takes approximately 3-4 h. Five or six batches are processed daily. Three furnaces are smelt the aluminum. Furnace 1 smelts recycled aluminum; furnace 2 adjusts the metal content for different products; and furnace 3 removes impurities and then casts the aluminum. Gas exhaust is then treated by APCDs including air cooling, cyclones, injected powder activated carbon (PAC), and bag filters. Each furnace operates at 750-800° C

Each workplace and ambient air sample was collected using a PS-1 sampler (Graseby Andersen, GA, USA) and sampled for 24 h. PCDD/F sampling followed the US EPA Reference Method TO9A and analysis followed the Method 8290A. All chemical analyses were conducted at the Super Micro Mass Research and Technology Center, Cheng-Shiu University, which is an accredited laboratory in Taiwan.

During the operation of the secondary ALS, the PCDD/F concentrations in workplace air and ambient air were 0.352 and 0.0704 pg I-TEQ/Nm^3, respectively. The PCDD/Fs concentration in workplace air is 5 fold higher than that in ambient air. The PCDD/PCDF ratios in workplace air and ambient air were all <1, indicating *de novo* mechanisms in formation of PCDD/Fs. The highest concentrations for PCDD/F congeners were OCDD, 1,2,3,4,6,7,8-HpCDF, OCDF, 1,2,3,4,6,7,8-HpCDD, and 2,3,4,7,8-PeCDF. The operation of secondary aluminum smelter affects the pollutant concentrations and surrounding air quality. Experimental results suggest that besides the terminal control technologies for stack flue gases, engineering control technologies in the workplace need further improvement. Chen *et al*. reported the PCDD/F concentrations in the surrounding environment and workplace during operation of the secondary ALS were 0.141–0.670 and 0.571 pg I-TEQ/Nm^3, respectively, which are higher than our findings.
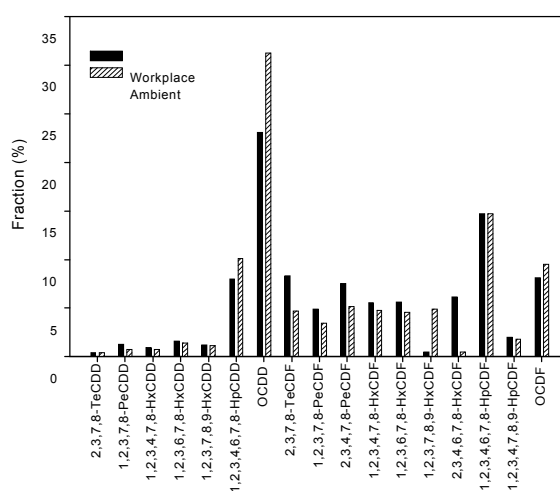
Figure 1. Homologues of PCDD/Fs in the secondary aluminum smeltering workplace and ambient air.

Aittola, J.P.. Paasivirta, J., Vattulainen, A., Sinkkonen, S., Koistinen, J., & Tarhanen, J. (1996). *Chemosphere*, 32, 99-108.
Chen, S.J., Lee, W.S., Chang-Chien, G.P., Wang, L.C., Lee, W.J., Kao, J.H., & Hu, M.T. (2004). *Atmos. Environ*, 38, 3729-3732.

Distribution of metallic traces by size, PM_{10}, $PM_{2.5}$ and PM_1- Emission from secondary aluminium smelters

J.J. Rodríguez-Maroto[1], J.L. Dorronsoro[1], M. Fernández-Díaz[2], P. Galán-Valera[2] and E. Conde Vilda[2].

[1] Departamento de Medioambiente, CIEMAT, Avda. Complutense 22, 28040, Madrid, Spain
[2] Departamento de Tecnología, CIEMAT, Avda. Complutense 22, 28040, Madrid, Spain

Keywords: Aluminium smelter, emissions, heavy metal, PM10, PM2.5, PM1.

In the metallurgical industry, the emissions to air arise from the storage, handling, pre-treatment, pyro-metallurgical and hydrometallurgical stages. With the purpose to obtain a data base of emissions from non ferrous metal smelting in Spain, a measurement program was planned and is being carried out. One of its objectives is to determine the distribution of the particulate matter PM, by sizes: PM_{10}, $PM_{2.5}$ and PM_1, as well as the metals that could accompany it in these emissions. In a first stage of this project, the industrial sector of secondary aluminum was chosen to be evaluated. With this aim thirteen secondary aluminium smelters, which suppose ~70% of the secondary aluminium production in Spain, have participated in the study.

Secondary aluminium production involves a pre-treatment (sorting, processing, and cleaning scrap) and smelting/refining operations (cleaning, melting, refining, alloying, and pouring of aluminium). One of the mean potential emission sources of dust and metal compound in the metallurgic process is the stage of smelting. A series of campaigns was made to sample, to evaluate the dust fractionation and to analyze the metallic traces in emissions coming from this stage.

The sampling and measurement was carried out in accordance with US EPA 201A and VDI 2066/5 procedures (1994) using two types of cascade impactors: Mark III with eight collection stages or a three-stage KS207 Kalman System GMBH. The samples of collection substrates were chemically analyzed according to method EPA IO-3.1 (Selection, preparation and extraction of materials from filters) as previous step to the determination by ICP-OES (inductively coupled plasma emission spectroscopy) and/or ICP-MS (inductively coupled plasma mass spectrometry) and FAAS (flame atomic absorption spectroscopy). The operating conditions of each installation were determined during the sampling. All measurements took place during the process was operated normally.

For the four intervals of aerodynamic diameter particle, dp (in microns): dp>10, 10>dp>2.5; 2.5>dp>1; dp<1, the predominant interval is the one of submicron particles. Al, Zn and Cu were found to be the main metal by mass in PM.

The distribution of metallic traces by size not always agrees with the distribution in total mass of particles in the same size range for a same facility. It was observed significant dispersions in the metals size distribution data.
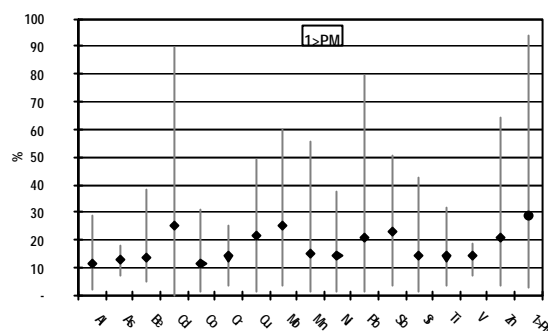
Figure 1. Percentage of partition in the size range dp<1, with respect to the total mass of each metal and PM. (maximum, minimum and average values).

Most of these effects have its origin in the heterogeneity into the furnace bed and the differences in the emission gas cleaning systems. The first one is mainly due to selection and pre-treatment of raw material used (scrap and other secondary, also the addiction of fused salt and recovered from skimmings and salt slag) with diversity of shapes and chemical compositions. The second one is due to the different cooling system technologies (air injection, heat exchanger etc.) and separators (cyclone, scrubbers, bag filter…) used in each smelter.

European Commission, (2001). Document on Best Available Techniques in the Non Ferrous Metals Industries.

Ehrlich C. *et al.* (2007). *Atmospheric Environment 41 (2007) 6236–6254.*

Su-Ching Kuoa *et al.* (2007). *Atmospheric Environment 41 (2007) 6884–6900.*

Aerosol modelling in gasification flue gas containing solid particles and inorganic condensable vapour.

Martin Petit[1], Karine Froment[1], Fabrice Patisson[2], Jean-Marie Seiler[1],Marine Peyrot[1]
[1] CEA Grenoble - DEN/DTN/SE2T/LPTM, 17 rue des Martyrs; 38054 Grenoble Cedex 9; France
[2] LSG2M, Ecole Mines Nancy Parc de Saurupt, F-54042 Nancy, France
Corresponding author: Martin Petit: martin.petit@cea.fr
tel :33-(0)4 38 78 96 75 – fax:33-(0)4 38 78 52 51

Keywords: Industrial aerosol, Carbonaceous particles, Aerosol modelling, Biofuel, ELPI

Biomass gasification allows producing a synthetic gas called biogas that can be used for Fischer-Tropsch biofuels synthesis or for feeding a SOFC. However, there may be many pollutants in the obtained biogas since biomass feedstock contains many inorganic compounds that are volatilised during the high temperature treatment. These inorganic species can harm reactor walls, deactivate catalysts or foul pipes. That is why, it is very important to know how these species behave in the process. Then, it will be possible to know how they can be filtered.

After the high temperature process, many species are in gas phase and can condense to form solid particles during gas cooling. Depending on the cooling rate of the flow, the temperature, the flow rate, the concentration of vapour species or seed particles, the phenomena describing the condensation of vapour will not have the same impact on the final state of the particles.

Some studies already exist concerning the aerosol formed in combustion facilities. But, most of them focus on the formation of alkali sulphates which are not present in gasification. Indeed, due to different oxygen partial pressure in the biogas during gasification, the species released in gas phase are not the same that those released during combustion. In particular, alkali components that are released as solid sulphates are released in gas phase linked with chlorine whereas sulphur is released in gas phase with hydrogen (H_2S) (Petit et al. 2009). During gas cooling, thermodynamic calculations show the formation of solid alkali chlorides.

Besides, studies performed on the laboratory small scale fluidised bed reactor showed that inorganic vapours condense on soot particles formed in large amount in the reactor. Yet, in an entrained flow reactor, no soot particles should be formed, the particles shape and composition will then be different in that case and that may alter the conclusions.

In the paper, the different phenomenological models that exist to describe the condensation of vapour to form particles will be first reviewed. These models explain how particles appear thanks to nucleation, how they grow through coagulation and heterogeneous condensation and how they deposit on wall through co-deposition phenomena. The most adequate models will then be used in a global model (sectional or using the moment method).

One difficulty is that model validation is not available in the physical conditions of our application, as they are generally used for different applications (atmospheric dispersion of pollutants).

That is why we had to develop the following experimental setting (see figure 1): solid particles are mixed with condensable vapour of KCl or NaCl and the flow is cooled at different cooling speeds. A dilution probe will be then used to cool the gas and an Electrical Low Pressure Impactor (ELPI) will measure the particles size distribution. Thanks to the analysis of particles collected on the different stages of the ELPI, the chemical composition of particles will be given.
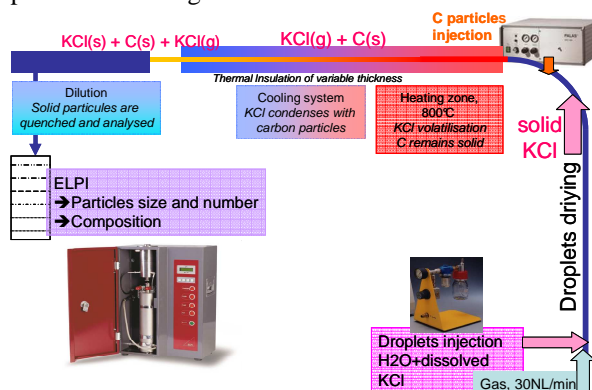
Figure 1 Schematic view of the experimental device

First calculations have been made using a simplified model to get general trends. The results will be compared with the first experimental data obtained with the device.

————————————
Petit M., Froment K. et al. *Relation between oxygen partial pressure in the syngaz and inorganic releases during biomass gasification.* Proceedings of the European biomass Conference 2009

Rapid Characterization of Agglomerate Aerosols by in situ Mass-Mobility Measurements

J.H. Scheckman[1], S.E. Pratsinis[2] and P.H. McMurry[1]

[1]Particle Technology Laboratory, Department of Mechanical Engineering,
University of Minnesota, 55455, Minneapolis, MN, USA
[2]Particle Technology Laboratory, Institute of Process Engineering,
Department of Mechanical and Process Engineering, ETH Zürich, 8092 Zürich, Switzerland

Keywords: Aerosol Characterization, SiO_2, Agglomerates, Aerosol Particle Mass Analyzer

Transport and physical/chemical properties of nanoparticle agglomerates depend on primary particle size and agglomerate structure (size, fractal dimension and number of primary particles). Today, such particles are characterized reasonably well with respect to primary particle size (counting microscopic images, nitrogen adsorption, x-ray diffraction, light scattering) but rather poorly when it comes to agglomerate size and structure. This research reports on in situ techniques for measuring such properties.

Nanoparticle agglomerates of silica with a broad spectrum of primary particle and agglomerate sizes were generated by oxidizing hexamethyldisiloxane in a methane/oxygen diffusion flame. Upon leaving the flame, agglomerates of known electrical mobility size were selected with a differential mobility analyzer (DMA) and their mass was measured with an aerosol particle mass analyzer (APM) resulting in their mass fractal dimension, D_f, and dynamic shape factor, χ. Scanning and transmission electron microscopy (SEM/TEM) images were used to determine primary particle diameter, and to qualitatively investigate agglomerate morphology.

The DMA-APM measurements were reproducible within 5%, as determined by multiple measurements on different days under the same flame conditions. The effects of flame process variables (oxygen flow rate and mass production rate) on particle characteristics (single particle mass, D_f, and χ) were determined.

All generated particles were fractal-like agglomerates with average primary particle diameters of 12–93 nm and $D_f = 1.7$–2.4. Increasing the oxygen flow rate decreased primary particle size and D_f (Figure 1), while it increased χ. Increasing the production rate increased the agglomerate and primary particle sizes, and decreased χ without affecting D_f. The effects of oxygen flow rate and particle production rate on primary particle size reported here are in agreement with ex situ measurements in the literature (Mueller *et al*., 2004, Wegner & Pratsinis, 2003) while the effect of process variables on extent of agglomeration (χ) is demonstrated for the first time to our knowledge.
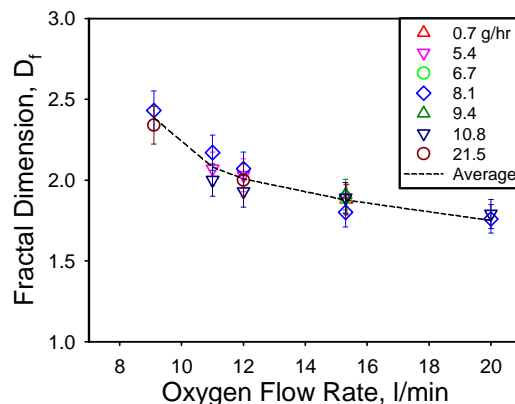
Figure 1. Fractal dimension vs O_2 flow rate for production rates from 0.7 to 21.5 g/hr. Dotted line connects the average of the measured fractal dimensions for each burner configuration. Error bars show 5% uncertainty in fractal dimension.

Mueller, R., Kammler, H.K., Pratsinis, H.K., Vital, A., Beucage, G., & Burtscher, P. (2004). *Powder Technology*, 140, 40-48.
Scheckman, J.H., Pratsinis, S.E., McMurry, P.H. (2009). *Langmuir*, submitted.
Wegner, K. & Pratsinis, S.E. (2003). *Chemical Engineering Science*, 58, 4581-4589.

Aerosol-Size-Spectra of a Wood-Burning Furnace

P. Madl[1]. W. Hofmann[1], H. J. Brandt[2]

[1]Department of Materials Engineering & Physics, University of Salzburg, 5020 Salzburg, Austria
[2]Windhager Zentralheizung Technik GmbH, 5201 Seekirchen, Austria

Keywords: biofuels, wood combustion, wood smoke, nanoparticles, lung deposition

Wood is the most important carrier of solar / renewable energy. The fuel characteristics with low ash and low sulfur content challenges coal, oil, and gas heating systems.

The emitted particle inventory of a LogWIN 30kW solid fuel, wood heating systems was monitored during the start-up-, continuous phase and burnout- phase. The furnace is characterized by a discontinuous charging of roughly 50 cm long logs into combustion chamber.

Upon loading the feeder with beech-logs, the furnace was booted according to a strict protocol for either automatic or manual start-up routine. The aerosol inventory was sampled with a wide-range aerosol monitor consisting of an SMPS and an OPC operated in tandem mode. Besides a typical calorific value of around 15.3 MJ/kg, dry wood still contains up to 15% water (Strehler, 2000). Therefore, a condensation trap was placed inbetween the sample outlet and the measurement devices. Due to the extremely high aerosol concentrations during the start-up procedure, both instruments have been provided with a 1:100 dilution system. Once in normal combustion mode, the furnace's particle inventory is equivalent to a state-of-the-art pellet burner.

downstream the chimney. The continuous combustion mode is characterized by a drastic particle-size shift from a coarse range around 300 nm to a finer range of about 70 nm.

Once the furnace switched over into a continuous combustion mode, the generated aerosol was again monitored at the end-of-stack (roof-top) of the test-site. The slightly altered particle concentration emitted into the environment was gathered and used for particle deposition calculations with the stochastic lung deposition model developed by Koblinger & Hofmann (1990).

The model revealed deposition peaks past the 15th generation (Fig. 2), which belong to the pulmonary or alveolar region (Yeh & Schum, 1980). This alveolar deposition is common for combustion aerosols. It has been proposed that alveolar deposition is associated with increased cardio-circulatory problems, as the immune system is the primary organ to remove entrapped particles (Donaldson et al., 1988).
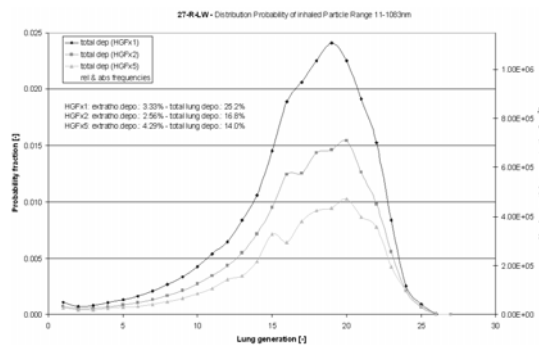
Figure 2. Modelled deposition pattern of the end-of-stack aerosol, using the Monte Carlo code IDEAL. Plotted are three individual simulations for various Hygroscopic Growth Factors (HGF).

Donaldson, K., Li, X. Y., MacNee, W. (1988). *Journal of Aerosol Science*, 29. 5-6.

Hofmann, W. & Koblinger, L. (1990). *Journal of Aerosol Science*, 21. 675-688.

Koblinger L. & Hofmann, W. (1990). *Journal of Aerosol Science*, 21. 661-674.

Strehler, A. (2000). Technologies of wood combustion. *Ecological Engineering*, Volume 16, Supplement 1: 25-40.

Yeh, H. C. & Schum, G. M. (1980). Bull. Math. Biol. 42: 461-480.

Figure 1. Time-resolved aerosol distribution during start-up and normal combustion mode.

Figure 1 displays the particle distribution for both the start-up and the continuous combustion mode measured at the exhaust outlet some 90 cm

Environmental impact of aerosol particles from a coal-fired power plant

I. Grgić[1], J. Turšič[2], J. Škantar[3] and A. Berner[4]

[1]Laboratory for Analytical Chemistry, National Institute of Chemistry, Hajdrihova 19, SI-1000 Ljubljana, Slovenia
[2]Environmental Agency of the Republic of Slovenia, Vojkova 1b, 1000 Ljubljana, Slovenia
[3]Environmental Department, Electroinstitute Milan Vidmar, Hajdrihova 2 SI-1000 Ljubljana, Slovenia
[4]Faculty of Physics, University of Vienna, Boltzmanngasse 5, A-1090 Vienna, Austria

Keywords: Chemical composition, Combustion particles, Mass size distribution, Size-segregated aerosols, Source identification.

One of the major pollution problems for urban and remote environments is the industrial combustion process where the quality of the fuel and combustion technology is of great importance. Coal is still the most commonly used fuel for commercial power generation (Xu *et al.,* 2003). The transport, transformation and deposition of emitted pollutants depend on regional climatic conditions. Thus, specific studies for the individual power plants are essential to evaluate their environmental impact.

New aerosol measurement techniques enable size-dependent analyses of aerosol particles, thus better classifications and more comprehensive studies of the effect of ambient aerosols are possible. A special sampling system for measurements of size segregated particles directly at the source of emission was developed (Turšič et al., 2008).

In this work, the size segregated sampling of particles at the largest coal-fired power station in Slovenia (capacity of about 750 MW and consumption of about 4×10^6 t of lignite coal) by the newly developed system was performed. In addition, simultaneous measurements of particles were performed in the surrounding environment to estimate the contribution of this source to the actual ambient concentrations.

Measurements were carried out in June 2005 and May 2006. Sampling at the source was conducted from the 50 m platform on the stack using the existing sample ports. The central part of our system is a ten stage low-pressure cascade impactor (Berner type, size ranges from 15 nm to 16 µm), which was positioned outside the chimney stack, while a sampling probe was placed into the chimney. On the basis of long term monitoring of SO_2 in the influential area of power plant two sampling sites were chosen, i.e. Velenje where the influence of power plant is usually the lowest and Veliki vrh where the influence should be the highest. At both locations parallel sampling of particles using two identical Berner type four stage low-pressure cascade impactors was performed (size range: 0.17 – 10 µm). Sampling times were about 12 h. After acid extraction of aerosol deposits on Tedlar foils measurements of selected elements were performed by inductively coupled plasma mass spectrometry (ICP-MS), while SO_4^{2-} was determined by ion exchange chromatography (IC) after extraction of deposits on aluminum foils in Milli-Q water.

The results of mass size distribution of particles sampled at the source showed, that for most typical elements (As, Mo, Pb,) the highest concentrations were observed in the size range between 1 and 4 µm. For Se and Ga two modes were identified, first near 0.25 µm and second one at around 2µm. Figure 1 shows the ratio between the concentrations of selected elements measured at high and low SO_2 concentrations at Veliki vrh. Elements typical for coal combustion are connected with the ratios significantly higher than 1 (As, Se in Figure 1).

Velenje is a typical urban background location with strong influence of traffic. Concentrations of particles as well as concentrations of some typical traffic related elements (e.g. Cd, Fe, Zn, Mn) were higher at this sampling site than at Veliki vrh.
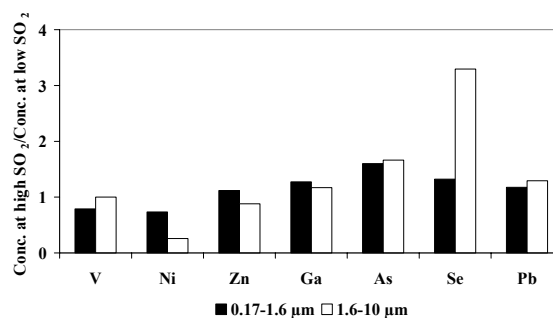
Figure 1: Ratios of concentrations for selected elements at elevated concentration of SO_2 and low concentration of SO_2 at location Veliki vrh.

Xu, M., Yan, R., Zheng, C., Qiao, Y., Han, J. & Sheng, C, (2003). *Fuel Process. Technol.* 85, 215-237.
Turšič, J., Grgić, I., Berner, A., Škantar, J., Čuhalev, I. (2008). *Environ. Sci. Technol.* 42, 878-883.

Salt condensation on simulated superheater tubes

M. Broström[1], S. Enestam[2], R. Backman[1] and K. Mäkelä[2]

[1]Department of Energy Technology and Thermal Process Chemistry, Umeå University, S-901 87, Umeå, Sweden
[2]Metso Power Oy, Finland Box 109, 33101 Tampere, Finland

Keywords: salt aerosol, condensation, combustion aerosols, particle deposition.

Condensation of gaseous KCl and NaCl is known to participate in deposit formation and high temperature corrosion processes of superheater tubes. Little is known about interactions between the two salts, which are of interest in for instance black liquor recovery boilers or waste incinerators where the fuels contain relatively high amounts of both salts. Within this work, salt condensation on simulated superheaters at different steel temperatures, salt vapor concentrations and mixtures was investigated.

Salt vapors of 1 to 1000 ppm were prepared by controlled evaporation and dilution by a continuous flow of N_2 in a high temperature (800-900*C) furnace. An air cooled condensation probe with controllable temperature gradient was inserted in the hot gas stream. The probe surface was kept at temperatures around where condensation was expected. After exposure, the probe surface was analyzed with SEM/EDS and XRD.

The results of the analyzes probe surfaces together with temperature and concentration information revealed information about condensation temperatures, phase compositions of the condensed salts and also the effects of mixing the two salts. The results are discussed in connection to basic mechanisms in deposit formation and high temperature corrosion.

Measurement of soot in atmospheric and low pressure flames with a novel particle mass spectrometer

H. Mätzing, W. Baumann, O. Bayode, T. Felleisen, H.-R. Paur and H. Seifert

Forschungszentrum Karlsruhe GmbH,
Institut für Technische Chemie, Bereich Thermische Abfallbehandlung,
Postfach 3640, D-76021 Karlsruhe, Germany

The formation and growth of soot particles in flames are difficult to measure since the surrounding gas is highly reactive, the particle size is in the range of a few nanometers and the particle concentrations are higher than 10^{10} cm^{-3}.

Soot particle sizing methods involve (a) sampling and off-line analysis like transmission electron microscopy (TEM), (b) sampling and on-line analysis like mobility analyzers (SMPS) which require high sample dilution or, (c) non-intrusive methods like light scattering and extinction or laser-induced incandescence (LII). Often, preference is given to the non-intrusive optical methods, but they are associated with averaging over the particle size distribution rather than resolving it.

In this study, soot formation was measured in low and atmospheric pressure flames with a novel particle mass spectrometer (PMS).
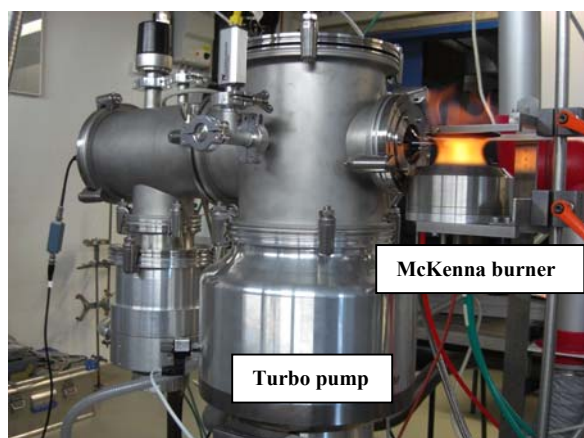
Figure 1. Particle mass spectrometer (ATMO-PMS)

The PMS has a two stage molecular beam sampling system which allows a probing inside of the flame. Due to the supercritical expansion in the molecular beam, the incoming gas is quenched down very quickly and all interactions between the particles or between particles and gas molecules are blocked within the shortest possible time. Behind the two stage inlet system, the particles pass a capacitor with variable electric field and the charged particle fraction is separated according to the polarity and to the ratio of kinetic energy to charge. The charged particles are collected at faraday cups and the resulting intensity is proportional to the number concentration. The particle velocity is measured simultaneously and allows to derive the mass and size spectra from the m/z spectrum with the assumption of single charge (z = 1) and with the known material density.

Soot particles were generated in laminar, flat premixed acetylene or ethylene / air flames burning at low (25 mbar) and ambient pressure. The McKenna burner consists of an inner cylindrical chamber of 7.5 cm in diameter with a water-cooled sintered bronze plate and around this plate there is an outer concentric annulus for sheet gas to stabilise the flame. Both positively and negatively charged soot particles with diameters between 2 and 10 nm were detected and their growth along the flame axis for different C/O ratios was measured. At low pressure, the soot particles show charge distributions with three peaks, while at ambient pressure four to five peaks appear which are partly overlap (Fig. 2). Under the assumption that peak 1 is induced from single charged and the other peaks from higher charged particles, we calculate a mean particle diameter of 7 nm which is comparable to Maricq (2003) measured with SMPS.
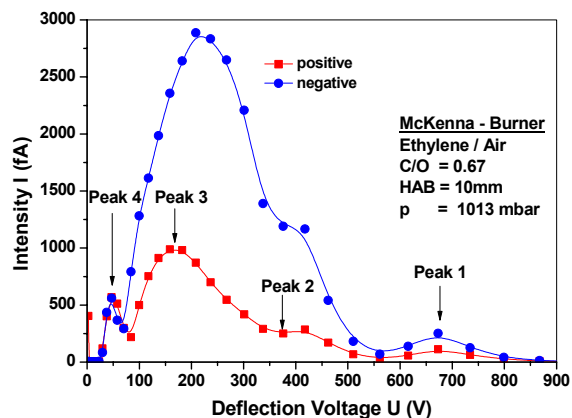
Figure 2. Charge distribution of soot particles in ambient ethylene / air flame

The absolute particle mass was detected with a quartz crystal microbalance (QCM) installed in the molecular beam and by deflection of the charged particles with a capacitor it is possible to measure the ratio of charged to uncharged particles. The results of measurements in the atmospheric flames show that up to 40 % of the soot particles are charged.

Paur, H.-R., Baumann, W., Mätzing, H. & Seifert, H. (2005). *Nanotechnology*, 16, S355 – S361.

Maricq, M. (2003). *Combustion and Flame*, 132, 328-342.

Particle and gas emission for a EURO 4 light duty engine using 1st and 2nd generation biodiesel

A.G. Hemmersam[1], C. Raahede[2], J. Klenø Nøjgaard[3], A. Massling[3], P. Wåhlin[3] H.O. Hansen[2] and S. Nygaard[1]

[1]Department of Chemistry and Water technology, Danish Technological Institute, Kongsvang Alle 29,8000, Aarhus C, Denmark
[2]Department of sustainable energy and Transportation, Danish Technological Institute, Kongsvang Alle 29, 8000, Aarhus C, Denmark
[3]Department of Atmospheric Environment, National Environmental Research Institute, University of Århus, Frederiksborgvej 399, 4000 Roskilde, Denmark

Keywords: Diesel emissions, Combustion particles, biofuels, number size distribution, SMPS.

A significant source of particle emission in the urban areas originates from diesel driven vehicles and the impact of different types of diesel on the particle and gas emission is a subject of increasing importance, due to the increase in the use of biodiesel (Swanson et al., 2007). The increase in usage of biodiesel is motivated by the whish to limit the dependency and environmental impact that is associated with the use of fossil diesel. 2nd generation biodiesel is based from on a feedstock that originates from non food or waste products and is therefore from a sustainability as well as economical point of view an interesting source of biodiesel (Taylor, 2008). However not much data comparing particle and gas emission from vehicles using 1st and 2nd generation biodiesel exists, it is therefore of scientific, as well as from an applied interest to compare emission from diesel vehicles using 1st and 2nd generation biodiesel.

This study presents the particle and gas emission from a Euro 4 light duty engine using standard petrochemical diesel, biodiesel blend with 20% (B20) or 100% (B100) biodiesel. The 2nd generation biodiesel was made from a feedstock consisting mainly of animal fat (AFME) and the 1st generation biodiesel was based on rapeseed oil (RME). The engine was operated in 5 different operating modes taken from ISO/EN 8178, which simulate driving conditions of various loads and effect. Specifically were 0 %, 25 %, 50 % and 100 % loads and 100% effect of the engine tested in the current study.

Table 1. Comparison of the weighted gas emission and fuel consumption of a EURO 4 engine.

	NOx (g/kWh)	CO (g/kWh)	Fuel consumption (g/kWh)
Diesel	7.18	0.18	209
B20 RME	6.80	0.13	211
B20 AFME	7.48	0.11	211
B100 AFME	7.86	0.29	235

Both particle number concentration and particle size distribution was characterized using rotating disc diluter followed by a scanning mobility particle sizer (SMPS). The gas emissions were measured using mandatory measuring principles and weighted according to ISO/EN8178.
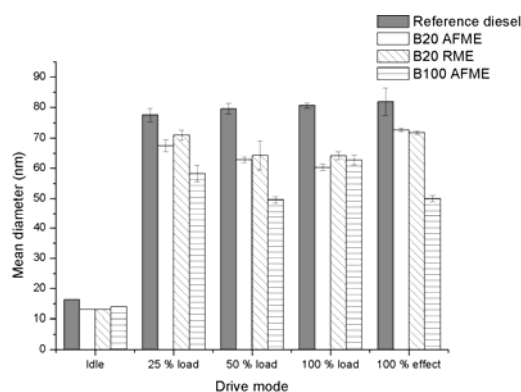
Figure 1.The mean diameter of the particle emissions as a function of biodiesel blend and engine load .

The particle emission results, se figure 1, show that the mean diameter of the particles emitted using biodiesel was found to be smaller than for particles emitted using standard diesel. This trend was seen for both AFME and RME based biodiesel blends. The mean diameter of particles emitted using 1st (RME) and 2nd (AFME) generation biodiesel was not significantly different. The particle concentration emitted was found to be significant lower when using 1st and 2nd generation biodiesel compared to standard diesel, this trend was seen for all 5 driving modes. The lowest particle concentration emission and the smallest particle mean diameter was found when operating at 0% load. The gas emission data, as seen in table 1, show that the NOx emission increase when using blends of AFME biodiesel but seems to decrease when using RME blends. The CO emission decreases when using B20 but raises when using B100.

Swanson K.J., Madden M.C., Ghio A.J., (2008) *Environmental Health Perspectives*, 115, 496- 499.
Taylor G., (2008). *Energy Policy*, 36, 4406-4409.

Diesel PM collection performance of a combined system with an electrostatic device and a partial-flow diesel particulate filter

H.J. Kim, B. Han, D.K. Song, W.S. Hong, W.H. Shin, S.H. Jung and Y.J. Kim

Korea Institute of Machinery and Materials,
171 Jang-dong, Yuseong-gu, Daejeon 305-343, Republic of Korea

Diesel particulate matters are presently regulated in grams per kilometre or grams per kilowatt-hour, but number-based PM regulation is currently being discussed for the future emission standards. In order to meet the coming standards, "wall flow" particulate trap consisting of ceramic substrates with alternately sealed channels have been available for a number of years and have already been installed in mass-produced vehicles. This filter can achieve an efficiency of more than 95 % over the total range of particle sizes. However, the filter still causes problems with excessive amount of deposited soot, which increases back-pressure and mechanical damages due to non-uniformity of the temperature gradients in the filter during regeneration. In order to lower the back-pressure and to increase thermal stability, metallic filters such as partial-flow filters and foam filters have been developed in Germany and South Korea etc. However, the filtration devices have shown lower performance than DPF for removal of diesel PMs.

In this study newly developed diesel PM filtration systems have been developed. One of the developed models (Electrostatic Partial-flow Diesel Particulate Filter, EPDPF 1) was consisted of an ionization part, electrostatic field imposing part and partial-flow diesel particulate matter filter (PDPF) and the other (EPDPF 2) was composed of the same parts as the first model but additionally equipped with air insulation device at the ionization part. Shown in Figure 1, the developed electrostatic partial-flow diesel PM filtration systems have been tested using a 3000 cc diesel engine with an engine dynamo, DMA (Model 3080,TSI, USA), CPC (Model 3076, TSI, USA), a rotary dilutor (Model MD-19, Matt engineering, Switzerland) at steady-state engine operation conditions, idle, 2000, 3000, 3500 rpm, 2000 rpm 25 % and 50% load, 3000 rpm 50 % load, and 3500 rpm 60% load.
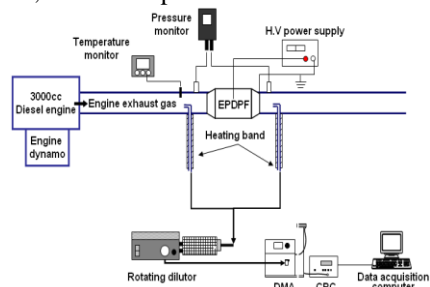
Figure 1. Experimental setup for the performance test with a diesel engine dynamo.
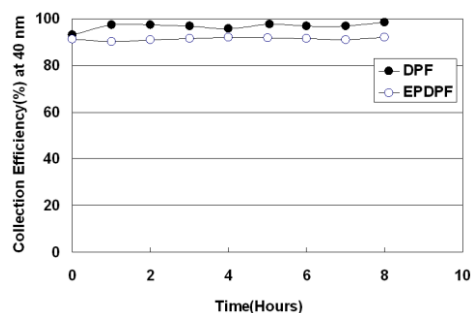
Figure 2. Comparison of removal efficiency of diesel PMs between DPF and EPDPF for 8 hours at 2000rpm 50% load.
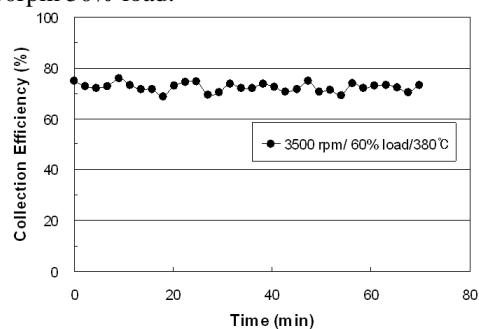
Figure 3. Removal efficiency of diesel PMs of EPDPF for 1 hour at 3500rpm 60% load.

Figure 2 shows the results of the PM collection performance test of DPF and EPDPF 1 at 2000 rpm 50 % load (250℃) for 8 hours. The PM removal efficiency of the EPDPF 1 at a peak diameter, 40 nm, was continuously over 90 %, a similar efficiency of DPF, and the back-pressure of EPDPF 1 was significantly lower than that of DPF by 80%. Figure 3 shows the results of the PM collection performance test of EPDPF 2 at 3500 rpm 60 % load for 1 hour. In order to suppress spark over at an ionization part of the system at high temperature condition of exhaust gas, more than 400℃, 10 L/min air were supplied into the ionization part. Diesel PMs were collected by more than 75 % in the device, even at the high temperature of exhaust gas.

Kim, H. J., Kim, Y. J., Han, B. (2008). *Evaluation on performance of an electrostatic diesel PM trap device and its application to diesel engine after-treatment.*, Transactions of KSAE, Vol 16, No 6, pp 176-183.

Emissions of polybrominated diphenyl ethers (PBDEs) and polybrominated dibenzo-p-dioxins and dibenzofurans (PBDD/Fs) from ferrous foundries

L.C. Wang[1,*], Y.F. Wang[2], C.H. Tsai[3], G.P. Chang-Chien[1]

[1]Department of Chemical and Materials Engineering, Cheng Shiu University,
840, Chengching Rd., Kaohsiung 833, Taiwan, ROC
[2] Department of Bioenvironmental Engineering,
Chung Yuan Christian University, Chung-Li 320, Taiwan
[3]Department of Chemical and Materials Engineering,
Kaohsiung University of Applied Sciences. Kaohsiung 807, Taiwan

Keywords: PBDEs, PBDD/Fs, dioxin, ferrous foundries.

Polybrominated diphenyl ethers (PBDEs) are extensively used as brominated flame retardants (BFRs) in many articles for daily use. Concerns about polybrominated dibenzo-*p*-dioxins and dibenzofurans (PBDD/Fs) increased with the more and more extensive use of BFRs. This study investigated the PBDE and 2,3,7,8-substituted PBDD/F characteristics in the stack flue gases of two ferrous foundries. The stack flue gases were collected isokinetically according to U.S. EPA modified Method 23. Three stack flue gas samples were collected for each facility, and the collection of each stack flue gas sample lasted for about 3 hours. Detailed instrumental analysis parameters of PBDD/Fs and PCDD/Fs are given in our previous work (Wang et al., 2007; 2008).

The mean PCDD/F, PBDD/F and PBDE (30 congeners) concentrations in the stack flue gases of ferrous foundries (Table 1) were 0.0421 ng I-TEQ/Nm^3, 0.00147 ng TEQ/Nm^3 and 36.7 ng/Nm^3, respectively. The PBDD/F concentrations in the stack flue gases of the ferrous foundries were lower than those of MSWIs (2.28 pg/Nm^3, 0.557 pg TEQ/Nm^3) and IWIs (18.2 pg/Nm^3, 4.17 pg TEQ/Nm^3) (Wang et al., 2007). The PBDE concentrations in the stack flue gases of the ferrous foundries were 2-3 orders higher than the atmospheric PBDE concentrations (Cetin et al., 2008; Choi et al., 2008).

PCDD/F, PBDD/F and PBDE congener profiles in the stack flue gases of the ferrous foundries were illustrated in Figure 1. For PCDD/Fs, 2,3,7,8-TeCDF, 1,2,3,7,8-PeCDF, and 2,3,4,7,8-PeCDF, are more prominent congeners in the stack flue gases. Similarly, 2,3,7,8-TeBDF, 1,2,3,7,8-PeBDF and 2,3,4,7,8-PeBDF are the most abundant congeners The comparable distributions of congener profiles between PCDD/Fs and PBDD/Fs indicate similar substitution mechanisms of bromine and chlorine during formation. For PBDEs, the most dominant PBDE congeners in the stack flue gases of the ferrous foundries are highly brominated-substituted congeners, including BDE-209, -208, -207, -206.

Table 1 PCDD/F, PBDD/F and PBDE concentrations in the stack flue gases

		mean	RSD (%)
PCDD/Fs	mass (ng/Nm^3)	0.254	66.3
	I-TEQs (ng I-TEQ/Nm^3)	0.0421	80.7
PBDD/Fs	mass (ng/Nm^3)	0.00670	12.9
	TEQs (ng TEQ/Nm^3)	0.00147	20.9
PBDEs	Total (ng/Nm^3)	36.7	17.7
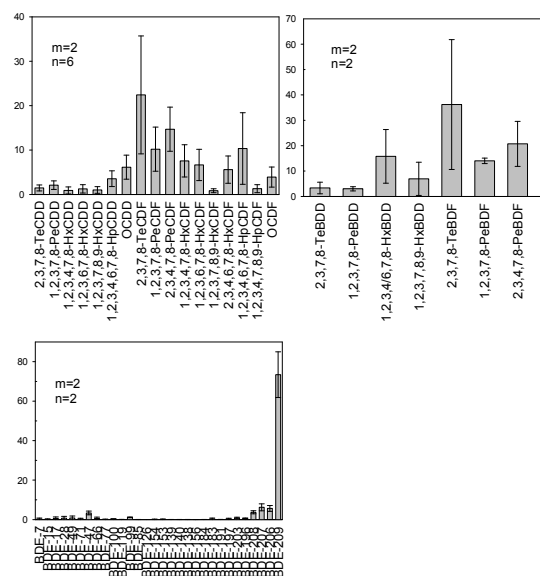
Figure 2 PCDD/F, PBDD/F and PBDE congener profiles in the stack flue gases

Wang, L. C.; Tsai, C. H.; Chang-Chien, G. P.; Hung, C. H. (2008). *Environ. Sci. Technol. 42*, (1), 75-80.

Wang, L. C.; Chang-Chien, G. P. (2007) *Environ. Sci. Technol. 41*, (4), 1159-1165.

Cetin, B.; Odabasi, M. (2008) *Chemosphere*, *71*, 1067-1078.

Choi, S. D.; Baek, S. Y.; Chang, Y. S. (2008) *Atmos. Environ. 42*, 2479-2488.

Nano-particle formation in modern diesel vehicle exhaust: Implications from first measurements of precursor gases

F. Arnold[1,2], U. Reichl[1], C.H. Muschik[1], A. Roiger[2], H. Schlager[2], L. Pirjola[3,4], T. Rönkkö[5], J. Keskinen[5], and D. Rothe[6]

[1]Atmospheric Physics Division, Max Planck Institute for Nuclear Physics (MPIK), P.O. Box 103980, D-69029 Heidelberg, Germany
[2]Institut für Physik der Atmosphäre, Deutsches Zentrum für Luft- und Raumfahrt (DLR), Oberpfaffenhofen, 82234 Wessling, Germany
[3]Department of Technology, Metropolia University of Applied Sciences, P.O. Box 4000, 00180 Helsinki, Finland
[4]Department of Physics, University of Helsinki, P.O. Box 64, FIN-00014 Helsinki, Finland
[5]Institute of Physics, Aerosol Physics Laboratory, Tampere University of Technology, P. O, Box 692, FIN-33101 Tampere, Finland
[6]MAN Nutzfahrzeuge AG, Abt. MTVN, Abgasnachbehandlung / Partikelmesstechnik, Vogelweiherstr. 33, D-90441 Nürnberg, Germany

Keywords: mass spectrometry, diesel exhaust, nucleation, sulphur particles, number concentration.

Aerosol particles generated by diesel vehicles represent major health affecting air pollutants in cities and near motor ways. To mitigate the diesel particle pollution problem, diesel vehicles become fitted or retro-fitted with modern exhaust after treatment systems (ATS), which efficiently remove engine generated primary particles (soot and ash). However, unfortunately these ATS promote the formation of low vapour pressure gases, which may undergo nucleation and condensation leading to secondary nucleation particles (NUP). NUP are substantially smaller than soot particles and can intrude with maximum efficiency the lowest, least protected, and most vulnerable compartment of the human lung, but their chemical nature and mechanism of formation are only poorly explored. Using a novel mass spectrometric method, we have made the first on-line measurements of low vapour pressure gases in the exhaust of a modern heavy duty diesel vehicle engine, operated with and without ATS and combusting low and ultra-low sulphur fuels including also biofuel. In addition, we have made accompanying NUP measurements and NUP model simulations. We find that modern diesel ATS promote NUP formation by promoting the formation of the important NUP precursor gas, sulphuric acid, and by not preventing sufficiently the emission of organic NUP precursor gases.

Modern diesel ATS with quasi-continuous regeneration involve a combination of a diesel particle filter (DPF) and a diesel oxidation catalyst (DOC). The DOC converts engine generated NO to NO_2, which acts as a soot oxidant already at typical diesel exhaust temperatures. Unfortunately however, the DOC may also generate undesired additional oxidation products. A striking example is SO_3, which is formed by oxidation of fuel sulphur and which reacts with water vapour leading to gaseous sulphuric acid. Suphuric acid has a very low saturation vapour pressure and therefore may condense and even nucleate in the cooling exhaust, downstream of the car-tail pipe. This may lead to the formation and growth of NUP. Other undesired oxidation products are partially oxidized hydrocarbons. These may include also condensable gases, particularly organic di-acids, some of which possess very low vapour pressures and therefore would be potential condensing and eventually even nucleating gases.

Our experiments, made in exhausts of a heavy duty diesel vehicle engine combusting low or ultralow sulphur fuels, lead to the following major conclusions: (a) a modern diesel vehicle ATS promote the formation of gaseous sulphuric acid which turned out to be a key nucleating gas involved in NUP formation; (b) an ATS does not prevent sufficiently the formation of organic condensable gases which contribute markedly to NUP growth; (c) NUP precursor gases experience strong storage in and release from the ATS; (d) a modern ATS fitted diesel vehicle, even when combusting ultra-low sulphur fuel with an FSC=10 ppmm, produces as much sulphuric acid as the same vehicle without ATS combusting formerly used fuel with an FSC=300 ppmm.

NUP are not regulated, even not by the most stringent of the presently operational air quality regulations, since these are particle mass rather than particle size and number oriented. Considering their maximum lung intrusion efficiency and role as potential carriers of carcinogenic compounds, NUP deserve increased future attention.

Mass-mobility relationship of soot generator and diesel soot

J. Rissler, H. Abdulhamid, J. Pagels, P. Nilsson, M. Sanati, and M. Boghard

Department of Ergonomics and Aerosol Technology, Lund University, P.O. Box 118, SE-22100, Lund, Sweden

When measuring aerosol particle size distributions many different techniques can be used. For the different techniques particle diameter can be defined differently depending on the principle of the technique. For example, the Differential Mobility Analyzer (DMA) classifies particles according to their mobility diameter (d_{me}), impactors according to the particle aerodynamic diameter, etc. To be able to compare the results, or convert between number and mass size distributions, information about the particle morphology and density is needed.

In this study the DMA–Aerosol Particle Mass Analyzer (DMA-APM) technique was used to study the effective density (ρ_{eff}) and mass fractal dimension of particles resulting from two combustion sources; a combustion soot generator (Abdulhamid et al., 2009) operated at 3 different air-to-fuel ratios, and an idling diesel engine (VF Passat -98, passenger car). Additionally, during all measurements a Scanning Mobility Particle Sizer (SMPS) measured the mobility number size distribution.

The DMA-APM system (Park et al., 2003) consists of a DMA coupled in series with an APM. The DMA selects particles one mobility diameter (50 to 400 nm were characterized). The APM consists of two rotating cylinders rotating at a rotational speed, ω. The mass size distribution of the selected particle size is measured by scanning the APM voltage (V_{APM}) and from the peak voltage, the particle mass (m) is calculated according to (Park et al., 2003):

$$ m = \frac{\pi}{6} d_{ve}^3 \rho_{true} = \frac{\pi}{6} d_{me}^3 \rho_{eff} = \frac{qV_{APM}}{r^2 \omega^2 \ln\left(\frac{r_2}{r_1}\right)} $$

where r is the difference in radius of the APM inner and outer cylinder ($r_2 - r_1$) and q the particle charge.

Making the assumption that the radius of gyration is linearly proportional to the mobility diameter, which should hold for the conditions in this study (Park et al., 2003), the mass fractal dimension (Df_m) is given by $m = C d_{me}^{Df_m}$.

The results of the study are presented in Figure 1 and 2. For the soot generator the aerosol effective densities were found to vary between 0.85 and 0.16 g/cm^3 over the size range studied, indicating that the particles become progressively more irregular as the mobility size increased. The fractal dimension of the burner particles was determined to 2.22, 2.35 and 2.38, increasing with increasing air to fuel ratio.

The particles from the diesel engine had a higher effective density than those resulting from the soot generator, and a fractal dimension of 2.41. This is very similar to the results found in Park et al., 2003 where the fractal dimension of a high-duty diesel engine working at low load was determined to 2.41 and at high load 2.33, see Figure 1 and 2. Assuming an inherent material density of 2 g/cm^3, extrapolation of the densities gave a primary particle size was of 25 nm for the diesel particles and 10-19 nm for the soot generator.
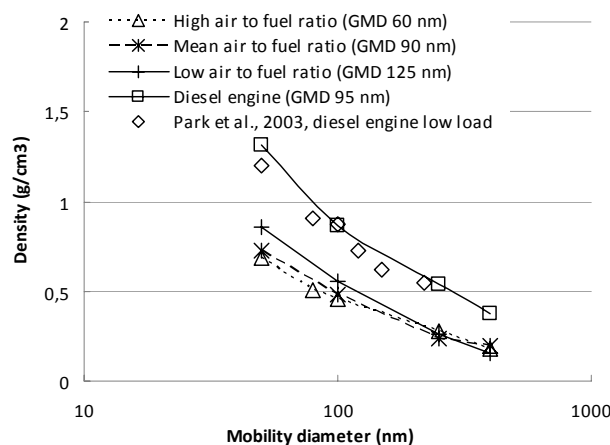
Figure 2. Effective densities for the aerosols studied.

Park K.., Cao F., Kittelson D.B., and McMurry P.H. (2003). Relationship between Particle Mass and Mobility for Diesel Exhaust Particles, Environ. Sci. Technol., 37,577-583.

H. Abdulhamid, J. Pagels, R. Bjorklund, A. Spetz, Peter Josza and M. Sanati. To be submitted. Detection of diesel-like generated soot particles by thermophoretic deposition on a resistivity soot sensor.

Figure 1. Particle mass as a function of mobility diameter.

Non-regulated emissions speciation in diesel and bio- diesel vehicles exhaust

M.Petrea[1], M. Kapernaum[1] and C. Wahl[1]

[1]Institute of Combustion Technology, German Aerospace Center,
Pffaffenwaldring 38-40, 70569, Stuttgart, Germany

Keywords: biofuels, diesel exhaust, emissions.

In order to reduce the emissions of air pollutants, engine, engine management design and fuel formulation have changed. Ultra clean vehicle technologies started to be used in increased number. As a result, the emissions composition is expected to change as well. A large number of comparative studies report results on regulated pollutants emitted by diesel and bio- diesel, but there is a lack of data for the unregulated pollutants. The use of new technologies and new fuels require new emissions tests especially for non-regulated compounds.

In this study, the emissions characteristics of a reference diesel fuel in comparison with reference fuel blended with RME, by different operating conditions are reported.

The test fuels include a reference diesel fuel, and reference diesel fuel (CEC RF-06-03) blended with RME (Rape Methyl Esther) in different percentage (20% and 50%).

The effects of the RME blend (20 and 50%) to a reference diesel fuel on the exhaust emissions (NMVOC, CO_2, NOx, particles) and from an internal combustion engine diesel passenger car (2148 cm^3), equipped with SCR catalyst respecting the Euro 4 emission norm, and direct injection system is presented.

The measurements were conducted on a roller test bench using different driving cycles: ARTEMIS cycle, real world driving cycle, NEDC cycle, the standard European driving cycle and additionally a driving cycle consisting in idle, 30, 50, 90 km/h.

The off line NMVOC'(non methane vehicle compounds) were sampled using cold traps, active carbon tubes, DNPH tubes and analysed by use of GC-MS and HPLC (high performance liquid chromatography), respectively. The particles were monitored by use of an EEPS (Engine Exhaust Particle Sizer). Other 22 components, among them: CO2,. NO, NO2, C6H6 and C6H5CH3 were monitored by use of an on line FTIR (MEXA 6000 FT series analyser).

The sampling positions were before and after passing the catalyst, respectively in the exhaust manifold and in the tailpipe exhaust.

It shows that the operating conditions have great influence on the NMVOC emissions.

Emissions of benzene and aldehydes are increased with the bio- Diesel fuel. The investigations reveal that among the carbonylic compounds 15 oxygenated species were found in engine out exhaust and only 3 in tailpipe emissions (formaldehyde, acetaldehyde and acroleine).

The hydrocarbons emissions decrease by increased RME content.

The nitro-compounds, while unregulated are also known to pose health and environmental problems. The nitro-phenols and nitro-cresols in the combustion process of vehicles were reported by Nojima et al. (1983) and Tremp et al (1993).

These compounds, known as carcinogens, were investigated from their identification in after engine exhaust up to their presence in the tailpipe diesel exhaust.

The influence of the catalyst activity was revealed.

The investigation of these compounds in the exhaust from conventional and alternative fuels allows the evaluation of alternative fuel usage effects.

Nojima ,K.,. Kawaguchi, A., Ohya, T.,. Kanno S.,& Hirobe, M. (1983). *Chemical and Pharmaceutical Bulletin,* 31, 1047–1051.

Tremp, J., Mattrel, P., Fingler, S.,& Giger, W. (1993), *Water, Air, and Soil Pollution,* 68, 113–123.

Soot particles and gas phase characterisation on simulating a Diesel Particulate Filter charge

L. Mazri, A. Boreave, B. D'Anna, C. George, A. Giroir-Fendler, M. Guth, and P. Vernoux

Institut de Recherches sur la Catalyse et l'Environnement de Lyon (IRCELYON), UMR 5256 CNRS Université Claude Bernard Lyon 1, Université Lyon 1, 69626 Villeurbanne, France

Keywords: Aerosol mass spectrometry, Air cleaning, Aerosol, Soot, Diesel exhaust

Diesel engines power major of the trucks, buses and since 2007 more than 50% of cars in France. As Diesel exhaust causes health hazards, the reduction of Diesel pollution has become a public priority. Diesel engines emit large quantities of particulate matters (PM) and nitrogen oxides (NOx), both precursors of photochemical smog. The study of the air quality in urban area, initiated in the fifties, had clearly demonstrated the link between pollution and mortality.

Soot particulates less than 2.5µm in size are most specifically dangerous for human health. Diesel Particulate Filters (DPF, Figure 1a) are the most effective solution for reducing the PM emissions. The filter durability is closely entailed by the successful control of periodic regeneration by combustion of the deposited particulate.

In this study, we investigated the effect of a pressure increase above a DPF on soot composition, while charging it. Soots were generated by using a Combustion Aerosol Standard generator (CAST *Jing* Burner) and we simulated a DPF by using a valve. The gas phase analysis was monitored with a micro Gas Chromatographer (µGC) and the particle phase with an Aerosol Mass Spectrometer coupled to a Scanning Particle Mobility Sizer (AMS, SPMS) (Figure 1). AMS and SMPS give precious information on the particulates concentration, size distribution and also on the chemical composition of the particulates. It allows a real time test with information on the impact of particle size on treatment efficiency and therefore the possibility of key parameters identification for improved particle removal.
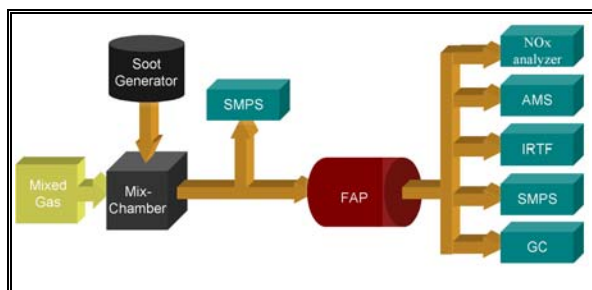
Figure 1. Diagram of experimental Setup

Soot diameters were found in the range of 35 – 180 nm according to the operating conditions of the burner (propane/air ratio).

Since the pressure above the valve increased slowly, the gas phase is slightly changing. New gaseous species appeared that should be related to a less complete combustion process. Simultaneously AMS measurement campaign has shown that organics were mostly present on the soot particles surface. By comparing simultaneously AMS to SMPS data respectively, we can approach the soot particle density. Further analysis of the AMS data is being done (figure 2).
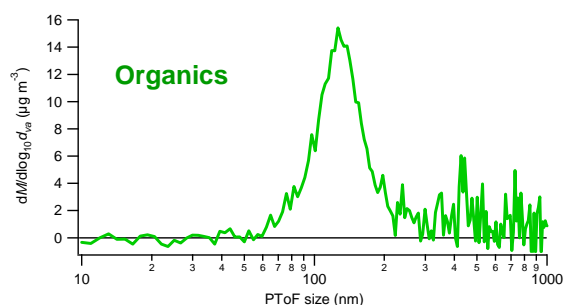
Figure 2. CAST generated soot Particle Time of Flight (PTof).

This study is the introduction of a larger project that aims at developing an Innovative Process for Reducing Emission of Particulates from Diesel exhaust (IPREP), introducing new catalysts based on electrochemical promotion for Diesel particulate filtering. This type of catalyst will enable low temperature filter regeneration, therefore preventing increased fuel consumption during regeneration process (as currently occurring) and reducing the associated costs. IPREP is a 3 year project which involves 5 french laboratories and 2 french companies.

J.G. Slowik et al. (2007). *Aerosol Sci. Technol.*, 41:295–314,

M. Guth et al. (2008). *OREPOC Conferences proceeding*

Effect of different raw materials on fine particle emissions from small-scale pellet combustion

H. Lamberg[1], O. Sippula[1], and J. Jokiniemi [1,2]

[1]Department of Environmental Science, University of Kuopio, Fine Particle and Aerosol Technology Laboratory, P.O. Box 1627, FI-70211 Kuopio, Finland.
[2]VTT, Technical Research Centre of Finland, Fine Particles, P.O. Box 1000, 02044 VTT, Espoo, Finland.

Keywords: biofuels, combustion particles, particulate mass, chemical composition

Biomass fuels are used for heating and energy production to reduce CO_2 emissions and to replace fossil fuels. In the same time, combustion of biomass induces fine particle emissions that cause adverse health effects (Dockery *et al,* 1993). There is a lack of sawdust and cutter chips for pellet production to meet the demand in growing markets. Therefore it is important to study different raw materials effect on particle emissions in pellet combustion.

In this study, fine particle emissions were measured during combustion of pellets made of stem wood, peat, pine bark and unbarked small diameter roundwood and different mixtures of these raw materials.

A Biotech PZ-RL pellet boiler with 25 kW maximum output was used in this study. Particle measurements were done in a dilution tunnel, where part of the flue gas was transferred through a heated sample line. Particle number size distributions and concentrations were measured with an Electrical Low Pressure Impactor (ELPI, Dekati Oy). Particle mass size distributions were measured with Dekati Low Pressure Impactor (DLPI, Dekati Oy). Filter samples were collected from the dilution tunnel for analyses on elemental composition, and organic and elemental carbon (Thermal-optical method). Gaseous analyses were made from undiluted flue gas. ABB Hartman & Braun gas analyzer was used for determining gaseous emissions. CO_2 analyzer (ABB AO2040, Uras 14) measured CO_2 concentration in the dilution tunnel for dilution ratio calculations.

Particle number emissions and mass emissions varied greatly when different pellets were combusted. Particle mass emission from peat pellet was the lowest (5.9 mg/MJ) and the highest from pine bark (46 mg/MJ).

Particle sample analyses showed that the particle emission in a modern pellet boiler is mainly formed of alkali metal salts and the fractions of incomplete combustion (organic material and elemental carbon) were low. The most common fine fly ash forming elements were potassium and sulphate.

The fuels were also analyzed for elemental compositions. When knowing the elemental composition of fuels and elemental composition of particle, the release of different ash forming elements could be evaluated.

It was found out that alkali metal release factors vary significantly between different fuels. Two different factors were identified to explain the observed differences. First, the fuel silicon content and second the fuel chlorine/sulphur ratio (figure 1). Silicates are known to bind alkali metals and prevent their enrichment to fine particles while sulphur in fuel converts alkali metals to sulphates which are less volatile than alkali chlorides.

Pellets raw material affects significantly the fine particle emissions in small-scale pellet combustion. Addition of park to pellets increase fine particle emissions. Fuels containing the most silicon had the lowest emissions of alkali metals to fine particles and also lowest fine particle emissions.
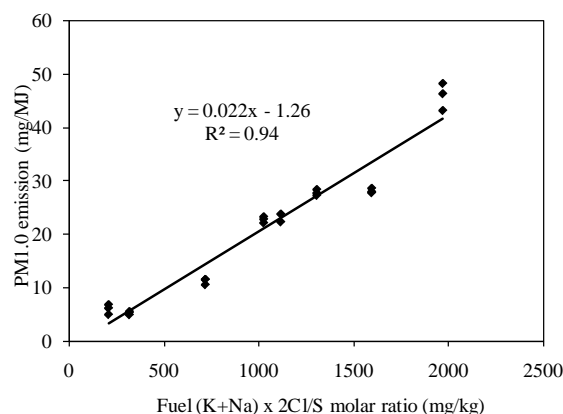
Figure 1. Fine particle emission as function of fuel alkali metal content multiplied by fuel chlorine/sulphur ratio.

Dockery, D.W.; Pope, C.A.; Xu, X.P.; Spengler, J. D.; Ware, J.H.; Fay, M.E.; Ferris, B.G.; Speizer, F.E. *N. Engl. J. Med.* 1993, *329*, 1753–1759.

Reduction of alkali aerosol formation by addition of peat during combustion of ash rich biomass fuels

C. Boman[1], I. Nyström[2], L. Pommer[1], D. Boström[1] and M. Öhman[2]

[1]Energy Technology and Thermal Process Chemistry, Umeå University, SE-901 87 Umeå, Sweden
[2]Division of Energy Engineering, Luleå University of Technology, SE-971 87 Luleå, Sweden

Keywords: combustion aerosols, biomass, peat, alkali metals, ash transformation

Increased demand of new feedstocks for biomass fuels are pushing the market towards potentially more problematic raw materials with high ash content, e g logging residues, energy crops, cereals and waste materials. Compared to stemwood fuels like sawdust, such raw materials generally contain higher concentrations of ash forming elements, where K, Na, Cl, S and P are of special relevance concerning the aerosol chemistry and formation of fine particles and deposits (Jenkins *et al.*, 1998; Knudsen *et al.*, 2004). The present focus on potential health related effects of combustion aerosols will lead to more stringent regulations of particle emission from small stationary combustion sources within EU. Today, combustion units in the range from residential (<50 kW) to mid-size (0.5-3 MW) are usually equiped only with cyclones and as an alternative to more efficient and expensive flue gas cleaning, fuel related measures (additives or co-combustion) may be used to change the ash transformation processes. (Lundholm *et al.*, 2005; Zeuthen *et al.*, 2007; Boman *et al.*, 2008). Earlier studies (Pommer *et al.*, 2009) have shown a high "reactivity" of inorganic elements in peat that gives a good potential to be used to reduce ash related problems. The composition of peat can, however, vary considerably and most important for capture of alkali are the reactions involving Si, Ca and Al.

The objective of the work is to explore and demonstrate the potential to use peat as an additive to ash rich biomass fuels to reduce the formation of alkali aerosols. It is as a part of the general ambitions to make use of ash chemical transformation processes in minimizing technical and environmental problems. The presentation comprises different complementary studies; both experimental (laboratory and full scale) and theoretical (thermochemical modeling). Information from detailed chemical analysis of bottom ash/slag, impactor samples (0.03-10 µm) and deposit probe samples (e g by SEM-EDS and XRD) are used together with gas measurements (SO_2/SO_3, HCl) and compared with chemical equilibrium model calculations using the FactSage program and databases.

Experimental tests in both grate fired boilers and fluidized beds have illustrated the potential of admixing peat to different biomass fuels to reduce the amount of fine particle emissions, as shown by the example in Figure 1.
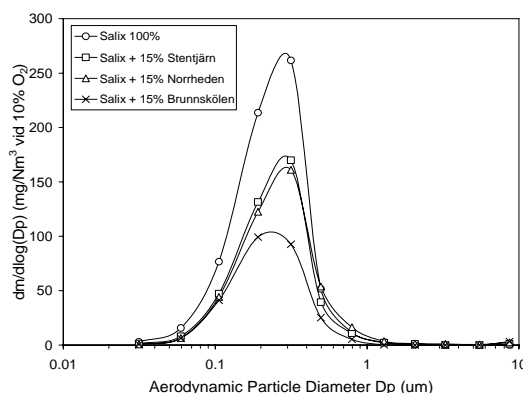
Figure 1. Fine particle emissions during combustion of Salix and admixtures of three different peats in a small pellet boiler (<50 kW).

The vast variation in composition of different peats leads to different influences on the ash transformation. The main process of relevance is the relation between capture of alkali vapours (e g KOH and KCl) in bottom ash as solid and/or melted silicate/oxide phases/slag and the release to the aerosol phase with subsequent condensation processes (e g as KCl and K_2SO_4). The mechanism of transfer and/or removal of alkali in the gas phase is presumably explained by sorption and/or reaction of alkali vapours with reactive peat ash (containing e g Ca and Si). The extensive experimental results are supported by thermochemical calculations and the work will be implemented in semi-empirical models to predict the ash behaviour and aerosol formation during combustion of biomass.

Jenkins, B. M., Baxter, L. L., Miles, T. R. & Miles, T. R. (JR). (1998). *Fuel Process Tech*, 54, 17-46.

Knudsen, J. N., Jensen, P. A. & Johansen, K. D. (2004). *Energy Fuels*, 18, 1385-1399.

Lundholm, K., Nordin, A., Öhman, M. & Boström, D. (2005). *Energy Fuels*, 19, 2273-2278.

Zeuthen, J. H., Jensen, P. A., Jensen, J. P., & Livbjerg, H. (2007). *Energy Fuels*, 21, 699-709.

Boman, C., Öhman, M. & Boström, D. (2008). in *Proc. 16th Euro. Biomass Conf. & Exhibi.*, Valencia, Spain.

Pommer, L., Öhman, M., Boström, D., Burvall, J., Backman, R., Olofsson, I. & Nordin, A. (2009). *Energy Fuels* (submitted).

Emulsified palm-biodiesel blends for saving energy and reducing emissions from diesel engines

Y.C. Lin[1], K.S. Chen[1]*, L.T. Hsieh[2], L.F. Lin[3], K.H. Hsu[1]

[1] Institute of Environmental Engineering, National Sun Yat-Sen University,
Kaohsiung 804, Taiwan.
[2] Department of Environmental Science and Engineering, National Pingtung University of Science and Technology. Pingtung 912, Taiwan.
[3] Department of Environmental Engineering, Kun Shan University,
Tainan County 710, Taiwan.

Keywords: biodiesel, emulsion, bio-solution additive, PAH, diesel engine

Recently, water-in-oil emulsions used in conventional liquid fuel engines have confirmed that water in emulsified diesel plays an important role in the combustion process (Selim and Elfeky, 2001; Samec et al., 2002; Lin and Wang., 2003; Abu-Zaid, 2004; Armas et al., 2005; Kerihuel et al., 2005). Recently, a bio-solution has been used as an additive in emulsified fuels by our research group (Lin et al., 2006; Lin et al., 2008). In order to achieve low emissions and high combustion efficiency from diesel engines, combining the use of emulsified biodiesel/diesel and additive has been considered as promising alternatives. This study probed into the energy saving. Emissions of PM and PAHs from a diesel engine were assessed. The results obtained from this study can provide a feasible energy saving fuel for diesel engines and lessen their resultant environmental impacts.

The brake specific fuel consumption (BSFC) was listed in Table 1. The results reveal that BSFC increased with the increase of palm-biodiesel blends by considering diesel + water as the total fuel. This is because the low GHV of both palm-biodiesel (9353 cal g^{-1}) and water were lower than that of P0 (10524 cal g^{-1}). Therefore, the BSFC must be increased to maintain the same electrical power output. In considering diesel plus palm-biodiesel as total fuel, bio-solution excluded, the energy savings (ESs) were -0.222% for P10, -0.825% for P20, 12.4% for E16P10, and 11.7% for E16P20 in comparison with P0 (Table 1). The experimental results clearly indicate that the emulsified palm-biodiesel with bio-solution can enhance the combustion process. Furthermore, the mean PM reduction fractions were 45.6%, 21.2%, 89.2%, and 90.1% for P10, P20, E16P10, and E16P20, respectively (Table 2). The mean reduction fractions of total PAHs and total BaP_{eq} were P10 (14.7%, 13.6%), P20 (28.0%, 28.5%), P30

(39.1%, 39.5%), E16P10 (53.7%, 54.2%), E16P20 (69.3%, 69.6%) and E16P30 (77.3%, 77.5%) in comparison with P0 (1.16 mg L^{-1}, 1.73 µg L^{-1}) (Table 3). In conclusion, emulsified palm-biodiesel with bio-solution can simultaneously save energy and reduce pollutants. Increased complete combustion results in the generation of fine particles. Therefore, future research investigating the size distributions of particles emitted through combustion of emulsified fuels is needed.

Table 1. brake specific fuel consumption

	P0	P10	P20	E16P10	E16P20
L/kWh	0.3605	0.3613	0.3634	0.3707	0.3817

Table 2. Mean PM emission factor (mg/L)

	P0	P10	P20	E16P10	E16P20
PM mg/L	231	126	182	25.0	23.0

Table 3. Mean PAH emission factor (µg/L)

	P0	P10	P20	E16P10	E16P20
PAH µg/L	1160	990	836	538	357
BaPeq µg/L	1.73	1.49	1.24	0.791	0.525

Selim, M.Y.E., Elfeky, S.M.S. (2001) App. Thermal Eng. 21, 1565-1582.
Samec, N., Kegl, B., Dibble, R.W. (2002) Fue81, 2035-2044.
Lin, C.Y., Wang, K.H. (2003) Fuel 82, 1367-1375.
Abu-Zaid, M. (2004) Energy Conv. Manag. 45, 697-705.
Armas, O., Ballesteros, R., Martos, F.J., Agudelo, J. R. (2005) Fuel 84, 1011-1018.
Kerihuel, A., Kumar, M.S., Bellettre, J., Tazerout, M. (2005) Fuel 84, 1713-1716.
Lin, Y.C., Lee, W.J, Chen, C.C., Chen, C.B. (2006) Environ. Sci. Technol. 40, 5553-5559.
Lin, Y.C., Lee, W. J., Chao, H.R., Wang, S.L., Tsou, T.C., Chang-Chien G.P., Tsai, P.J. (2008) Environ. Sci. Technol. 42, 3849-3855.

Characteristics of Particles Emitted by Turbine Engine and In-Plume Conversion

M.-D. Cheng[1], E. Corporan[2] and M.J. DeWitt[3]

[1]Environmental Sciences Division, Oak Ridge National Laboratory, Oak Ridge, TN, USA
[2]Propulsion Directorate, Wright-Patterson Air Force Research Laboratory, Wright-Patterson, OH, USA
[3]University of Dayton Research Institute, Dayton, OH

Keywords: turbine engine, emissions, nanoparticles, fuel, Fisher-Tropsch

Particulate emissions from two types of helicopter turboshaft engines operated with military JP-8 and paraffinic Fischer-Tropsch (FT) fuels were characterized as an objective of the field campaign held at the Hunter Army Airfield in Savannah, GA in June 2007. In general helicopter engines exhaust particles size distributions observed at the engine nozzle and 4.14m downstream locations showing the geometric mean diameters smaller than 50nm for all engine power settings investigated in this study. For both locations, the geometric mean diameter increased as the engine power setting increased; this trend also holds true for the emitted particle number concentration. The growth of particle geometric mean diameter was found significant, 7nm, only in the case of the idle power setting.

Sulfur-to-sulfate conversion was found to be independent of the engine power setting. Emissions of both sulfur and sulfate increased as the engine power increased. When JP-8 fuel was used, particles smaller than 7nm were found to increase in samples taken at the downstream location. The number concentration in this tail increased as the power setting increased. No such observation was found when FT fuel was used implying that the increased formation of nuclei particles in the plume downstream was likely to be caused by the sulfur and aromatic compounds in the JP-8 fuel. Total particulate carbon emissions increased as the engine power setting increased. Use of FT fuel reduced the elemental carbon emissions as it compared to the JP-8 fuel, and organic carbon emission at idle power but not at the higher powers. The reduction of elemental carbon by the FT fuel was attributed to the absence of aromatics (soot precursors) in the fuel. The OC/EC ratio was found to be in the range of 3 to 50 depending on the engine power setting. The aircraft emitted OC/EC was found to decrease as the engine power increased.
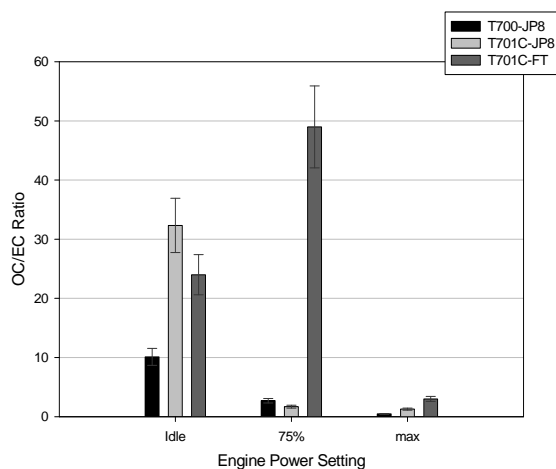
Plot of OC/EC as a function of engine power setting. OC stands for organic carbon, and EC stands for elemental carbon.

M.-D. Cheng, E. Corporan, M.J. DeWitt, and B. Landgraf (2008) Emissions of Volatile Particulate Components from Turboshaft Engines Operated with JP-8 and Fischer-Tropsch Fuels, J. Aerosol and Air Quality Res., in press

Generation of nano-particles during the burnt-out phase of the wood stove burning cycle

A. Bologa, H.-R. Paur, K. Woletz, H. Bhangu

Institut für Technische Chemie, Forschungszentrum Karlsruhe, Postfach 3640, 76021, Karlsruhe Germany

The extensive studies of wood combustion process show that individual wood furnaces are responsible for high emissions of aerosol and hydrocarbons. As fine particles are strongly associated with increased mortality and cardiovascular diseases, there is an increasing need for investigations of the processes of fine particle generation [1], their characterisation and collection to reduce the emissions.

In the report we present the results of investigations of fine, especially nano-size, particles generation during the burnt-out phase of the wood stove burning cycle. The tests were carried out with a small-scale wood stove with normal thermal output 8 kW. The beech-wood and fir-wood logs were burnt during the experiments. The stove was in operation from 5 to 7 hours per day and the average wood dosage was 2,5-3 kg/h.

In the stove the wood burns in three stages. During the first one, wood is heated to evaporate and drive off the moisture. With increase of temperature, during the second stage, the wood breaks down chemically and volatile matter is vaporized and burnt. After the release of the volatile gases, in the third stage, the remaining material which is a charcoal burns. If no more wood is put into the stove, the combustion slows down but the unburned carbon stays in the stove until it burns.

In the Fig.1 are presented the curves for particle size distribution in the gas flow for the end of the burning cycle when the charcoal combustion predominates.

The particle number concentrations in the gas flow were measured by SMPS (Grimm). The measurement point was ca. 3 m downstream of a pilot electrostatic precipitator (ESP) installed between the stove and the chimney. The measurements were carried out with and without particle charging and precipitation in the ESP.

The diagrams show the presence of nano-particles in the gas flow in the burnt-out phase. In time evolution, the number concentration decreases from $(5-6)\cdot10^7$ to $(1-2,5)\cdot10^7$ #/cm³. The mean size of particles is in-between 40 and 50 nm. At the end of
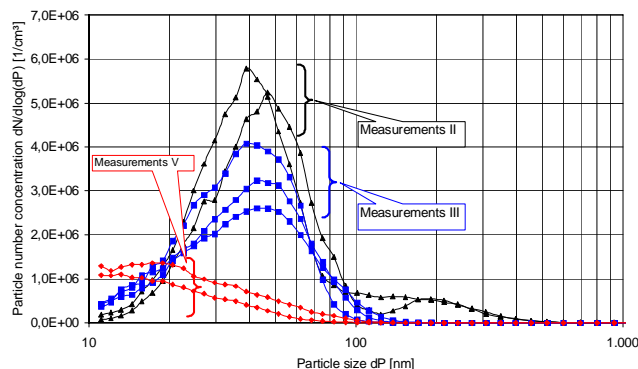
a) ESP is switched off
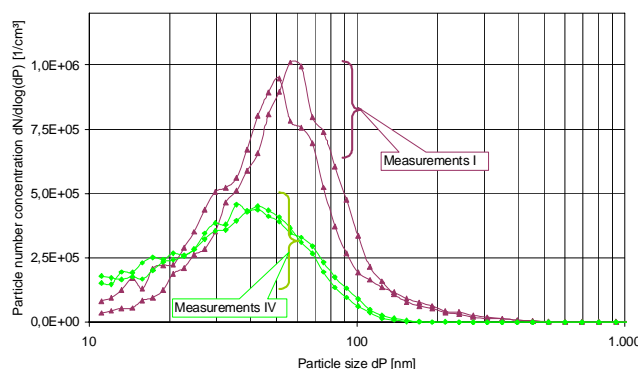
b) ESP is switched on

Evolution of particle size distribution in the gas flow downstream the pilot ESP, dilution factor 1:10, time of measurements: (I) 12:50-13:17, (II) 13:17-13:30, (III) 14:04-14:24, (IV) 14:24-14:45, (V) 14:45-14:59

the combustion cycle, particles mean size decreases to 20-30 nm.

Particle charging in the ESP decreases particle number concentration in the gas flow and changes the mean size of the particles. It increases up to 50-60 nm (Fig.1,b, measurement I) mainly due to particles agglomeration.

In spite of the fact of high number concentration of nano-particle there was no visible corona discharge suppression in the ESP during the burnt-out phase of the wood stove burning cycle.

[1] Hueglin Ch., Gaegauf Ch., Künzel S., Burtscher H., Characterization of wood combustion particles: morphology, mobility, and photoelectric activity. Environ Sci Technol 1997;31:3439–47.

A Reliable Method for Generation of Size Selected Soot using Aerosol Technology and Detection by Sensor Device

H. Abdulhamid[1], A. Malik[1], J. Pagels[1], Robert Bjorklund[2], Peter Josza[3], Jacobus H. Visser[4], Anita Lloyd Spetz[2], and M. Sanati[1]

[1]Department of Ergonomics and Aerosol Technology, Lund University, P.O. Box 118, SE-22100, Lund, Sweden
[2]Department of Physics, Chemistry and Biology, Linköping University, SE-581 83 Linköping, Sweden
[3]Volvo Technology Corporation, Department 06100, CTP, Sven Hultins Gata 9D, SE-41288 Göteborg, Sweden
[4]Ford Motor Company, Dearborn, MI, USA

Keywords: Diesel soot particles, soot generator, thermophoretic sampling, detection of soot, sensor

Realization that particle emissions from diesel engines pose serious health problems has led to regulation and active manufacturer efforts to reduce the particle mass leaving the exhaust pipe. While this has resulted in cleaner air there is concern that modern engines release increased number concentrations of nanoparticles which are potentially more hazardous than previous black smoke emissions. A recent study has shown that Euro IV standard particles at the same mass concentration had higher toxicity than soot from old engines because of their smaller size and more active surfaces (D. S. Su et.al).

In this paper we report the generation of soot having diesel exhaust particle size distributions from liquefied petroleum gas combustion (H. Abdulhamid et.al, D. Lutic et.al). Control of the fuel/oxygen ratio allowed production of a range of particle sizes that exhibited good stability over several hours production time. The particles were characterized by a variety of techniques such as TEM and thermophoretic deposition on sensor surfaces was employed to demonstrate application to analytical method development.

EXPERIMENTAL SET-UP

The combustion soot generator (Fig. 1) had three components: flame, quenching and mixing sections. Particles were generated by a quenched diffusion flame. Propane as fuel was fed into the inner of two co-axial stainless steel pipes while air was introduced through the outer pipe as oxidant. The stability of the flame, and thus the generated soot, was very sensitive to any small variation in the flow characteristics. Two mass flow controllers (Bronkhorst High-Tech, The Netherlands) were used to precisely control the fuel and carrier air flow rates. Additionally, the carrier gas stream was stabilized with a ceramic monolith (honeycomb) flow laminarizer to further enhance the flame stability. By varying the carrier air/fuel flow ratio soot of different concentrations and size distributions could be produced. The carrier air/fuel flow rates necessary to generate soot particle size-distributions with geometrical mean diameters (GMD) of 60, 90 and 120 (nm) soot particles were 3.2/85, 3.1/85 and 3.0/85 (l/ml) respectively.
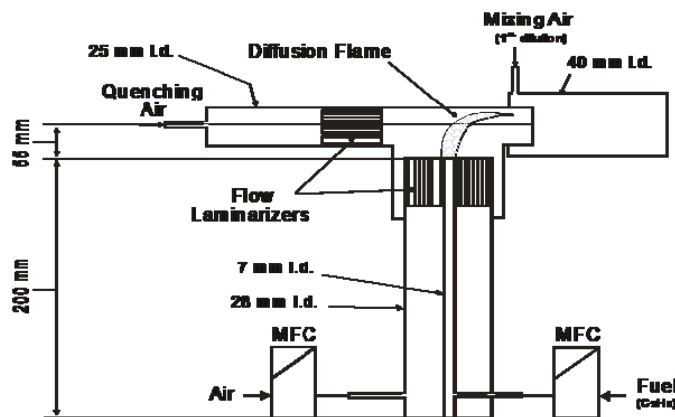
Figure 1: Illustrative sketch showing the soot generator.

The diffusion flame was quenched by the quenching line (using air with a flow of 9 l/min) at a certain height (55 mm) above the flame. The quenching line was also supplied by a flow laminarizer to prevent excessive flame disturbance. The quenching air diluted and cooled the flame which resulted in a significant decrease in soot coagulation and prevented any further oxidation of the generated soot particles. This allowed production of high concentrations of size-controlled soot particles. Thus, quenching played an important role in defining the chemical and physical properties of the produced soot particles.

The soot leaving the quenching section was subsequently diluted and completely mixed in the mixing region using air at 45 l/min. This ensured a uniform soot distribution having controlled concentration out from the burner with no need for any further mixing zone.

As the diffusion flame was completely protected from any environmental influences such as flow variation, humidity and temperature gradient, a highly stable and reproducible soot production was attained.

A scanning mobility particle sizer (SMPS 3934 from TSI Inc., USA) was used to measure the generated soot number size distribution (Fig. 2). Before the soot was analysed with the SMPS system it was diluted using an ejector (DI-1000 Dekati Diluter. Finland) to

a ratio of 1:13 in order not to exceed the measurable range for the SMPS.

After SMPS verification for a certain stable size distribution of generated soot particles, a flow of 300 ml/min was sucked using vacuum either directly from the outlet of the burner to the thermophoretic sampler for high number soot concentration or diluted further, to a ratio of either 1:2.7 or 1:12.8, using another ejector (Q-VDF250 ANVER VACUUM PUMP, USA). The later dilution ratios were quantified by determining the dilution of CO concentration using a flue gas analyzer (testo 350-XL, Testo AG, Germany).

Resistivity sensors having interdigitated electrodes were prepared on 90 nm thick SiO_2 films grown on p-type silicon. The electrode pattern was obtained by lift-off technique after sputtering 5 nm Ti and 200 nm Au films. The electrode gap was 40 μm. Each sensor was mounted on a 16-pin holder and silicon pieces were glued around the sensor to create an aerodynamically smooth surface for the incoming carrier gas. The resistance change during soot deposition was measured using a digital multimeter device (TTI 1604 Thurlby Thandar Instruments, UK) capable of measuring in the resistance range from 1 kOhm to 40 MOhms.

The methods stability presented in Fig. 3.
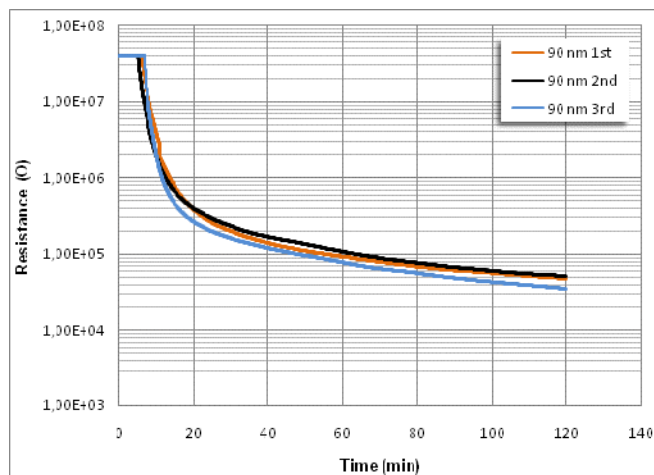
Figure 3: Resistance change for 2 hours exposure to generated soot particles of 90 nm (GMD) using three fresh sensors on different days.

D. S. S u , A L Serafino , J-O Müller, R Jentoft , R Schlögl, S Fiorito Cytotoxicity and Inflammatory Potential of Soot Particles of Low-Emission Diesel Engines Environ. Sci. Technol. 42 (2008)1761–1765
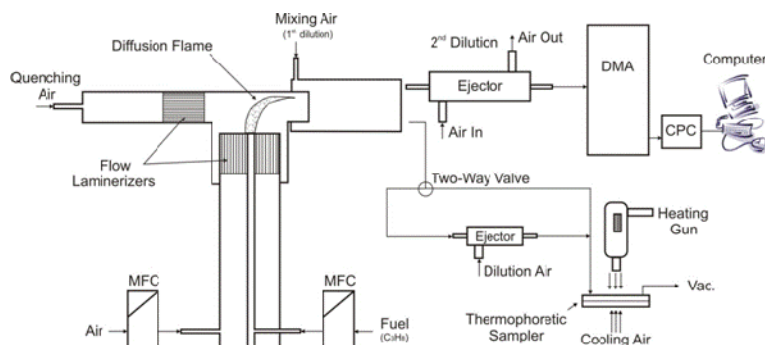
Figure 2: Schematic diagram of the experimental set-up.

H. Abdulhamid, A. Malik, J. Pagels, R. Bjorklund, D. Lutic, Peter Josza, J. H. Visseer, A. Lloyd Spetz, and M. Sanati. Detection of diesel-like generated soot particles by thermophoretic deposition on a resistivity soot sensor. To be submitted.

D. Lutic, A. Lloyd Spetz, M. Sanati, J. Visser, P. Jozsa PCT/SE2008/050215 Method and arrangement for detecting particles, , patent filed by Volvo CC (2008)

Effect of air staging on emissions from masonry heaters

J. Tissari[1], V. Suonmaa[1], J. Sutinen[2], P. Horttanainen[2] and J. Jokiniemi[1,3]

[1]Department of Environmental Science, University of Kuopio, P.O. Box 1627, FIN-70211, Kuopio, Finland
[2]Tulikivi Ltd., FIN-83900, Juuka, Finland
[3]VTT, Technical Research Centre of Finland, Fine Particles, P.O. Box 1000, FIN-02044 VTT, Espoo, Finland

Keywords: wood combustion, emissions, fine particles, elemental carbon.

Residential wood combustion (RWC) for heat production has been assessed to be a major source of e.g. fine particle mass emissions, but also polyaromatic hydrocarbons and several gaseous pollutants such as volatile organic compounds throughout Europe. Due to their health effects, there is a need to reduce these emissions. On the other hand, there is a large potential to decrease emissions by developing the combustion technology particularly in small scale appliances.

One of the basic prerequisites for complete combustion is good mixing of secondary air and pyrolysis gases, and a satisfactory residence time for the flue gas oxidation (e.g. Stehler, 2000). In modern combustion appliances, the combustion air is supplied evenly in three stages to the firebox or burners while in the conventional heaters the air staging are not used. In modern appliances the primary air regulates the combustion rate, whereas the following air supplies enhance secondary combustion.

In this study, two different combustion techniques were studied in masonry heaters. Both particle and gaseous emissions were compared. In comparison, identical structure in heaters and similar operational practice was used. In the conventional masonry heaters (CMH) there was no air staging while in the modern masonry heaters (MMH) the air supply was divided to primary air (through the grate) and secondary air which was led into the top of the primary combustion chamber. Both large (3 tn) and small (1 tn) masonry heaters was used.

For fine particle measurements, a partial sample flow from the stack was led to the two step dilution system (Tissari *et al.*, 2007) with porous tube diluter (PRD) and ejector diluter (ED), giving a total dilution ratio of 45–177. Particle number emissions and number size distributions were measured with an Electrical Low Pressure Impactor (ELPI, Dekati Ltd.), and a Fast Mobility Particle Sizer (FMPS, TSI 3091). Particle mass size distributions were measured using a Dekati Low Pressure Impactor (DLPI, Dekati Ltd.). The PM_1 samples were collected on filters from diluted gas using a pre-impactor and the filter holders. The PM_1 samples for gravimetric and elemental analyses (IC, ICP-MS) were collected on 47 mm Teflon membrane filters and for organic (OC) and elemental carbon (EC) analysis in two parallel lines on 47 mm quartz fiber filters. In addition, total PM were measured from the hot exhaust gas by using standard measurement method. The gaseous compounds were measured continuously with an analyzing rack for CO, CO_2, NO_x and O_2 and the organic gaseous substances (OGC) with a flame ionization detector. In addition, 28 calibrated volatile organic compounds were measured continuously with a Fourier Transform Infrared (FTIR, Gasmet Technologies Ltd.) analyzer.

Air staging in the MMHs reduced the particle and gas emissions remarkably (Figure 1). In PM_1 the reduction was 27% and 55% in small and large MHs, respectively. High reduction was observed in both gaseous and particulate organic emissions. For example, in the CH_4 emissions, the reduction was 76–91%. However, the air staging did not seem to reduce substantially the EC emission. In MMHs the air supply through the grate is lower which possibly decreases the entrainment of coarse particles to the flue gas. The preheating of secondary air at the expense of the grate temperature may decrease the release of alkali metal compounds, but enhances also secondary combustion. It seems that the air staging is effective way to reduce gaseous and organic emissions from batch combustion appliances. However, the factors that affect the EC emissions should be studied more.
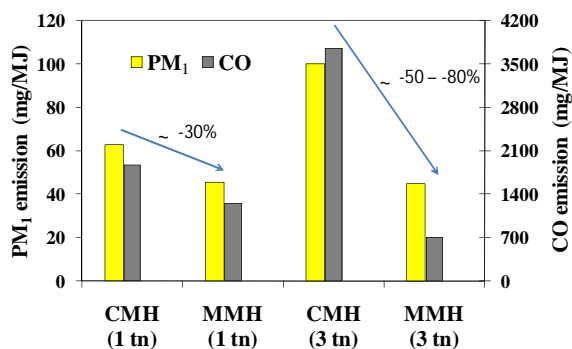
Figure 1. PM_1 and CO emission factors from small (1 tn) and large (3 tn) masonry heaters with old (without air staging, CMH) and new (with air staging, MMH) combustion techniques.

Stehler, A. (2000) *Ecological Engineering,* 16, S25–S40

Tissari, J., Hytönen, K., Lyyränen, J. & Jokiniemi, J. (2007). *Atmospheric Environment,* 41, 8330–8344.

Evaluation of a high temperature aerosol sampling probe

O. Sippula[1] and J.K. Jokiniemi[1,2]

[1]University of Kuopio, Department of Environmental Science, Fine Particle and Aerosol Technology Laboratory, P.O. Box 1627, FI-70211 Kuopio, Finland.
[2]VTT Technical Research Centre of Finland, Fine Particles, P.O. Box 1000, 02044 VTT, Espoo, Finland

Keywords: Aerosol modelling, Aerosol sampling, Combustion aerosol, Nucleation mode.

A general disadvantage in biomass-combustion is the formation of alkali metal rich aerosol. In small boilers the alkali metals are responsible for high fine particle emissions while in power stations the common problems are the alkali metal induced formation of sticky and corrosive deposits on the heat exchangers. In order to get experimental data on the aerosol formation and transformation inside the combustion systems a quench-diluting sampling system has been developed. In this system, the sample is quenched, by rapidly decreasing temperature and concentrations, to freeze the chemical reactions, particle agglomeration and, at the same time, to prepare the sample suitable for different analyzers. However, in many cases, for example due to the large amount of condensable vapours in the samples, considerable changes in the samples cannot be avoided. Thus, a reliable sampling from the hot flue gas is usually challenging.

The aim of this work was to create a test procedure to characterize the operation of different diluting sampling systems. This study focused especially on conditions typical in biomass-fired boilers. The practical interest is to find out optimal sampling parameters and to develop aerosol sampling technologies. The sampling system in this study applies a porous tube diluter, previously used in combustion studies (Sippula et al., 2008).

The experiments were carried out in a laboratory, using a laminar flow reactor to produce an aerosol which consists of principal components present in biomass combustion aerosol (KCl and K_2SO_4). KCl -vapour was supplied into the reactor, using a saturator. K_2SO_4 particles were produced inside the reactor by supplying controlled amounts of SO_2 and H_2O gases into the reactor. The amount of K_2SO_4 formed was tracked by measuring SO_2 and HCl concentrations using an FTIR analyzer (Gasmet). The aerosol sample was drawn into the porous tube diluter at temperatures varying from 500 to 750 ^{o}C. After the porous tube diluter the secondary dilution was conducted in an ejector diluter. The diluted samples were analyzed for particle size distributions using Nano-SMPS (TSI) and FMPS (TSI). To get information on the conditions inside the diluter, axial profiles of sample temperature and mixing with the dilution air were measured. The mixing was measured by moving a thin probe at the centreline of the diluter and measuring the marker-gas (CO_2) concentrations. The experimental results were interpreted using a 1D sectional model (Backman et al., 2002) which solves numerically the particle size distribution, ash chemistry and deposition.

The measurements showed a relatively fast mixing just at the probe tip and cooling rates between 5×10^5 and 8×10^6 ^{o}C/s. The particle size distributions were sensitive to sampling conditions, as expected. Both experiments and model simulations showed that KCl vapour introduced in the probe tends to nucleate and forms a separate particle mode even in the presence of fine K_2SO_4 particles (Fig 1).
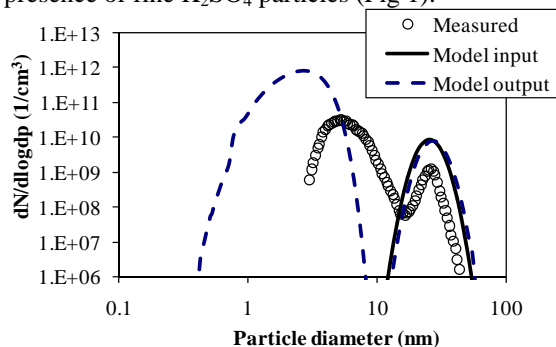
Figure 1. Measured and modelled particle size distributions when KCl = 96 mg/m^3, K_2SO_4 = 113 mg/m^3, dilution ratio = 20, sampling temp. $\approx$ 650 ^{o}C.

The separation of gas-phase and particulate phase fly ash compounds in high temperature sampling is important to avoid significant errors and false interpretation of the results. The used sampling probe was found to favour the formation of nucleation mode from the gas-phase KCl. The experiments and computer simulations were qualitatively in agreement. In future, the model can be used for pre-evaluating different sampling probe constructions.

Sippula, O., Lind, T. & Jokiniemi, J. (2008). *Fuel*, 87, 2425-2436.
Backman, U., Jokiniemi, J. K., Auvinen, A., Lehtinen, K. E. J. (2002). *J. Nanoparticle Research*, 4, 325-335.

Influence of road traffic conditions and street characteristics in Madrid City on nanoparticle vehicular emissions

A. Domínguez[1], J.R. Rubio[2] and C.C. Barrios[1]

[1]Environmental Department, CIEMAT, Avda. Complutense, 22. 28040, Madrid, Spain
[2]Dept. of Energy and Fluidomechanics Engineering, UPM, José Gutiérrez Abascal, 2. 28400, Madrid, Spain

With the variation of traffic conditions and street characteristics, the vehicular emissions suffer changes. During the last years, the number of vehicles running in urban traffic conditions has increased. Due to this, particulate emissions have risen and the relation of street characteristics and road traffic condition on vehicular emissions has been demonstrated (Ericsson et al., 2006). At present, most of the studies about on-board particle measurement analyze the particle emissions from the point of view of total mass. This work studies the total concentration of nanoparticles (in a range of 5.6 to 560 nm) in real driving conditions in an average circuit of Madrid.

The main aim of this work was to determinate the influence of traffic conditions and street characteristics on the variation of nanoparticle number. The input variable was: Street type (26 different stretches of Madrid City, which gathered makes a circuit of which its main characteristic is being the ring of old part of the town with high traffic intensity like it is shown in figure 1), traffic environmental factor (peak and off-peak hours) and direction factor (clockwise and anti-clockwise). The output variable was: velocity (average and standard deviation), average number of particle in each stretch.

Figure 1. Stretches of Madrid selected for the experiments. Source: "*Comunidad de Madrid*".

To develop the experiment, it was used a Seat Alhambra (year 2007, 140CV, TDI, 2.0 litres). In terms of the equipments (figure 2), it used a TSI Thermodilutor 379020 and a TSI EEPS 3090. Such an equipment setup made it possible to keep a 100° C temperature for the entire sampling line and to complete a hot first dilution (100 °C). It is important to keep the sampling line at this temperature in order to avoid distorted results from the appearance of particles of volatile origin (Kasper, 2004). The second dilution was performed by permitting the sample to cool down, as it would under environmental conditions, in order to simulate the conditions surrounding the exhaust outlet.
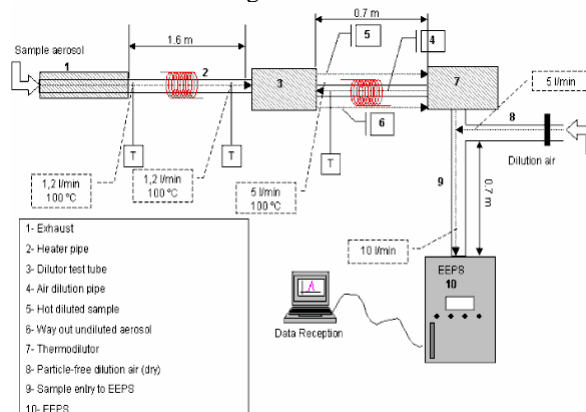
Figure 2. The equipment set-up diagram

An analysis of variance was used to evaluate the influence of road traffic conditions and street characteristics, finding out that street type and traffic environmental factor have more influence than direction factor on particle number, concluding that all the input variables result significant for the output variables. On the other hand, changes in the velocity causes large variation on particle number concentrations.

Ericsson, E., Larsson, H. & Brundell-Freij, K. *Transportation Research Part C*, 14, 369-383. Cambridge, U.K.: Cambridge University Press.
Kasper, M. (2004). *SAE Paper* 2004-01-0960.

Design and implementation of an on-board real time particle measurement system

J. R. Rubio[1], A. Domínguez[2], C. C. Barrios[2]

[1]Dept. of Energy and Fluidomechanics Engineering, UPM, José Gutiérrez Abascal, 2. 28400, Madrid, Spain
[2]Environmental Department, CIEMAT, Avda. Complutense, 22. 28040, Madrid, Spain

Recently, the scientific community has shown its interest in improving the knowledge about the number particle size distribution in internal combustion engines in real traffic conditions. Due to this, we have developed a new technology to adapt laboratory equipment to the modality of on-board equipment and in this way, to quantify the specific contribution of one vehicle in real traffic conditions in urban areas and highway areas.

It used a SEAT minivan, Alhambra model (year 2007, 140CV, TDI, 2.0 litres), emptying out the back of the vehicle and with the resulting area, we assembled the following equipment: Engine Exhaust Particle Sizer[TM] (EEPS[TM]) to measure the particle number and size distribution and Thermodilutor (379020 of TSI), with a heated exhaust probe block (warming temperature of 180 ℃); two heater pipe that guarantee sample aerosol and first particle-free dilution air rise developed flow condition with a temperature higher than 150 ℃ (Desantes et al., 2004); a diaphragm compressor with a 20 litres vacuum chamber needed to cushion the slug flow; a test tube for the exhaust extraction that was designed to avoid any perturbation in the flow caused by recirculation, detachment, etc.
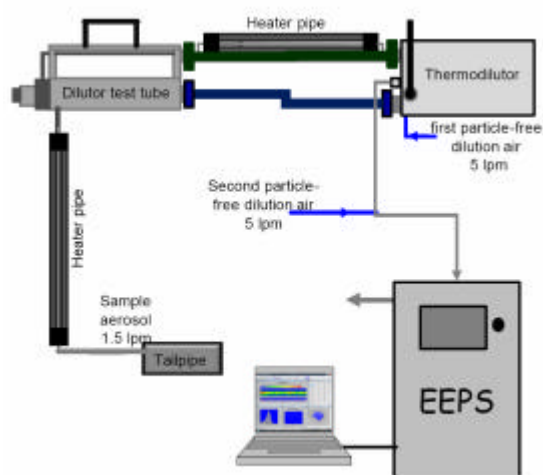
Figure 1- The equipment set-up diagram

The main innovation of this work is the design and implementation of a structure that allows putting the EEPS into the vehicle. The EEPS works with a vertical electrode column which implies a high sensibility to the vibrations and the movement associated to the driving. To prevent and to minimize the influence of these vibrations, it arranged a mechanism that guarantees three degrees of freedom and uses the weight and inertia of the EEPS to keep EEPS vertical position.

The figure 1 shows the set-up and the layout of equipment, it was developed finding out that the mixture between exhaust gases and dilution air carry out the process shown in figure 2. The dilution must not change the sample (Burtscher, 2005) with regard to the tailpipe due to the sample transformations along the different pipes (coagulation, rise in adsorption surface in gaseous phase, formation from volatile compounds and even particle dragging caused by water condensation).
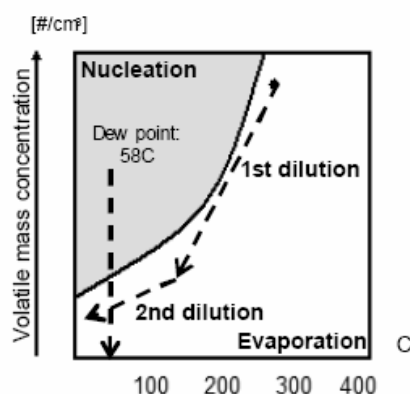
Figure 2- Phase diagram shows the concentration of volatile mass concentration vs its temperature (Kasper et al, 2004)

The developed technology has been checked in ascent/descent highway, sharp loops, with different velocities and in different carriage ways, permitting the correct and safety running of the on-board measurement.

Burtscher, H. (2005). *Journal of Aerosol Science* 36 (7), 896–932.

Desantes, J. M., Bermúdez, V., Pastor, J.V. & Fuentes, E. (2004) *Measurement Science and Technology*. 15 2083–2098

Kasper, M. (2004). *SAE Paper* 2004-01-0960.

Number and mass concentrations and surface area of particles in Diesel exhaust fumes

E. Jankowska and M. Pośniak

Department of Chemical and Aerosol Hazards, Central Institute for Labour Protection
– National Research Institute, Czerniakowska 16, 00-701 Warsaw, Poland

Keywords: Diesel exhaust, concentration, ultrafine particles, surface area.

Diesel exhaust fumes (DEF) are a complex mixture of particulate and gas phase pollutants. Most attention has been focused on particulate phase components of Diesel fumes due to possible acute and chronic respiratory effects.

This abstract presents results of research on mass and number concentrations and surface area of particles (TB) emitted as DEF. Investigations were conducted in a typical garage used for storage and for repairing cars. Sampling points were located 1.4 m from the source of Diesel fumes. Before a Diesel engine switched on, background level was determined (time: 0 s). With the Diesel engine switched on, investigations were conducted for up to 1000 s. Measurements were done with:

- SMPS (CPC 3022A and nano DMA, TSI) – size distribution (Figure 1) and number concentration of particles in the 5-143 nm range (Figure 2a),
- P-TRAK 8525 (TSI) – number concentration of particles in the 20-1000 nm range (Figure 2b),
- DUST TRAK 8520 (TSI) – mass concentration of particles in the 100-10000 nm range (Figure 2c),
- AERO-TRAK 9000 (TSI) surface area of particles in the 10-1000 nm range (Figure 2d).

Figure 1 illustrates size distribution of emitted ultrafine particles characteristic for DEF: with Nuclei Mode (NM) and Accumulation Mode (AcM).
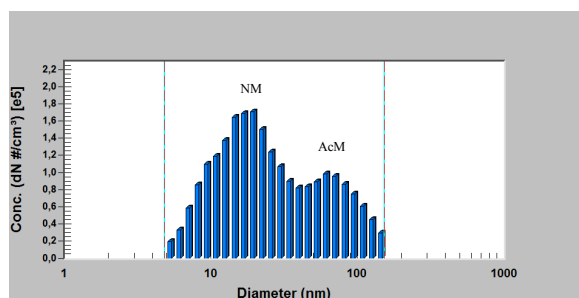
Figure 1. Size distribution of particles in the 5-143 nm range emitted after 540 s of the Diesel engine being switched on (SMPS with nano DMA results).

Compared to the background results the total number concentrations particles in the 5-143 nm range increased from $1.5e^{+4}$ particles/cm^3 to $2.5e^{+6}$ particles/cm^3 (Figure 2a, SMPS), whereas in the 20-1000 nm range from $2.2e^{+4}$ particles/cm^3 up to $3.6e^{+5}$ particles/cm^3 (Figure 2b, P-TRAK). This means that most of the emitted ultrafine particles were less than 20 nm in diameter. Mass concentration of particles in the 100-10000 nm range (some particles from AcM and particles from Coarse Mode - CM) increased from 0.07 mg/m^3 to 0.37 mg/m^3 (Figure 2c, DUST-TRAK).

The surface area of particles deposited in the lungs is a very important parameter of ultrafine particles emitted as DEF. Results (Figure 2d, AERO-TRAK) show that when the Diesel engine was switched on, the surface area of particles in the 10-1000 nm range increased significantly from 22 μm/cm^3 (background) to 2012 μm/cm^3.
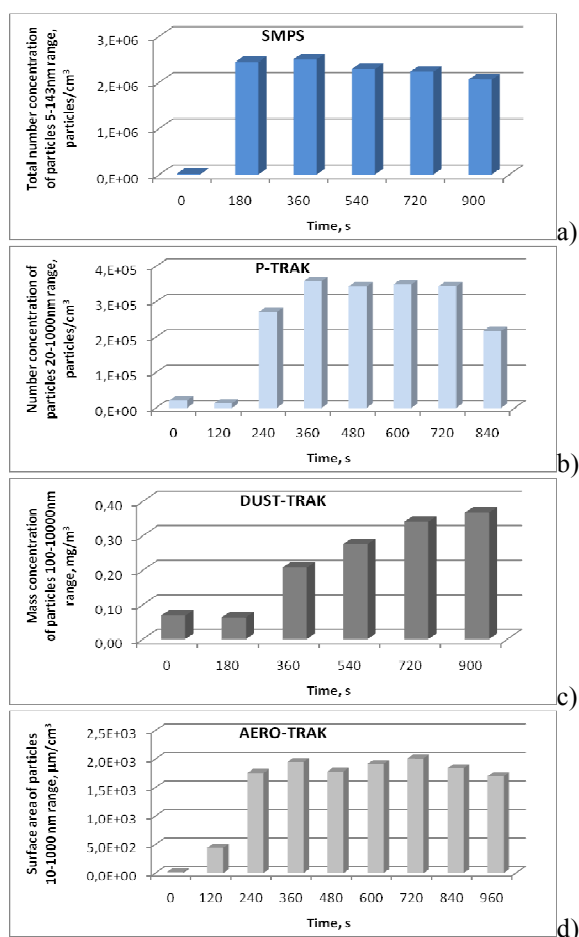
Figure 2. Number and mass concentrations and surface area of Diesel particulate phase obtain with:
a) SMPS,   b) P-TRAK,
c) DUST-TRAK,   d) AERO-TRAK.

Size distribution of hazardous chemical compounds in diesel exhaust particles

M. Pośniak, E. Jankowska, M. Szewczyńska

Department of Chemical and Aerosol Hazards, Central Institute for Labour Protection
– National Research Institute, Czerniakowska 16, 00-701 Warsaw, Poland

Keywords: diesel exhaust fumes; particles concentration; size distribution; PAHs

Combustion in automobile Diesel engines is connected with the production of low solubility carbon-centred fine particles of a complex chemical and physical structure, which contain inorganic and organic fractions. This fraction is comprised of uncombusted fuel, lubricating oil and polycyclic aromatic hydrocarbons (PAHs) along with a range of other xenobiotics, which can condense on the particles. Epidemiological studies have shown that there is a strong link between occupational exposure to Diesel exhaust particles (DEP) and lung cancer. Animal studies generally support these findings and demonstrate that DEP are carcinogenic; however, these findings are complicated by the issue of rat lung overload. Exposure to DEP has also been shown to be highly inflammatory.

The aim of this study was to analyse the concentration level of PAHs condensed on the individual fractions $PM_{0.25}$, $PM_{2.5}$, PM_{10} of DEP and to determinate their mass concentration.

METHODS
- Generation of DEP: laboratory station equipped with a Diesel engine SKODA FABIA TDI/2007 power supplying type CONNON RAIL
- Sampling: DEP were fractioned on PEM10, PEM2.5 and PCIS samplers with PTFE filters
- Determination of $PM_{0.25}$, $PM_{2.5}$, PM_{10} mass concentration: gravimetric methods using microbalance METTLER TOLEDO type UMX2.
- Determination of PAH concentration: HPLC-FL method using a Gyncotek gas chromatograph, Pinnacle II PAH column (15 cm x 3.2 mm), gradient mobile phase - acetonitryl : water.

RESULTS
The results of mass concentrations of fine particles in Diesel exhaust fumes determined with the gravimetric method with PCIS and PEM samplers are introduced in Table 1.

Table 1. Mass concentrations of $PM_{0.25}$, $PM_{2.5}$, and PM_{10}.

Sampler	n	Air volume [dm^3]	Fraction	Concentra - tion [mg/m^3]
PCIS	11	405 ÷ 1089	$PM_{0.25}$	0.26 ÷ 0.48
PEM	5	495 ÷ 1089	PM_{10}	0.39 ÷ 0.58
PEM	7	315 ÷ 1080	$PM_{2.5}$	0.26 ÷ 0.50

Concentrations of PAHs in $PM_{2.5}$, PM_5 and PM_{10} of DEP are shown in Table 2 and Figure 1.

Table 2. Mass concentration of PAHs in $PM_{2.5}$, PM_5 and PM_{10}.

Sampler	n	Air volume [dm^3]	Fraction	Concentration [ng/m^3]
PCIS	11	405 ÷ 1089	$PM_{0.25}$	33 ÷ 188
PCIS	11	405 ÷ 1089	PM_{10}	33 ÷ 258
PEM	5	495 ÷ 1089	PM_{10}	89 ÷ 105
PEM	7	315 ÷ 1080	$PM_{2.5}$	42 ÷ 132
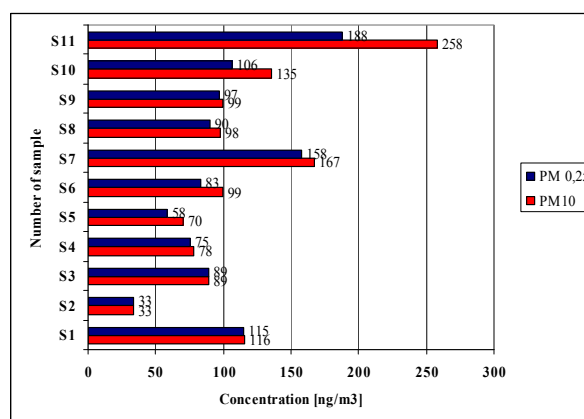
Figure 1. Comparison of PAH concentrations in $PM_{0.25}$, and PM_{10} Diesel exhaust particles.

CONCLUSIONS
An analysis of mass concentrations in fine particle fractions of DEP determined with gravimetric methods has shown that fraction $PM_{0.25}$ constituted 66 ÷ 83% of fraction PM_{10}.

The investigation confirmed that the finest determined fraction $PM_{0.25}$ is the main source of PAHs in Diesel exhaust particles. The percentage contribution of PAH concentrations in $PM_{0.25}$ was in the range 73 ÷ 100% of PAHs in PM_{10}.

Cincinell A., Del Buba M., Martellini T., Gambaro A., Lepri L. (2007) *Gas-particle concentration and distribution of n-alkanes and polycyclic aromatic hydrocarbons in the atmosphere of Prato*, Chemosphere, 68, 3, 472-478

Formation of diesel exhaust nucleation mode particles: laboratory and on-road studies

T. Rönkkö[1], A. Virtanen[1], T. Lähde[1], L. Pirjola[2], M. Lappi[3], D. Rothe[4], F.Arnold[5]
and J. Keskinen[1]

[1]Aerosol Physics Laboratory, Tampere University of Technology, PL599, 33720, Tampere, Finland
[2]Department of Technology, Metropolia University of Applied Sciences, P.O. Box 4000, 00180 Helsinki, Finland
[3] VTT Technical Research Centre of Finland, P.O. Box 1000, 02044 VTT, Finland
[4]MAN Nutzfahrzeuge AG, Abt. MTVN, Abgasnachbehandlung/Partikelmesstechnik, Vogelweiherstr. 33, D-90441 Nürnberg, Germany
[5]Atmospheric Physics Division, Max Planck Institute for Nuclear Physics (MPIK), P.O. Box 103980, D-69029

Submicron diesel exhaust particles can typically be divided into two separate groups depending on particle size and particle properties. In number based size distributions, these two groups are most frequently named as nucleation mode and accumulation mode (Kittelson et al. 1998). Accumulation mode consists of solid agglomerated soot particles and semivolatile compounds adsorbed or condensed on these particles. Nucleation mode particles have been reported to consist mainly of water, sulphuric compounds and hydrocarbons and they are frequently reported to be volatile. The mean particle diameters of the nucleation mode and the accumulation mode are typically between 3-30 nm and 40-100 nm, respectively.

In this study the focus has been on the characteristics and the formation of the nucleation mode particles in exhaust of diesel vehicles. The study aimed to clarify the formation of the nucleation mode in a real exhaust plume and to study the correlation between the particle measurements in laboratory and in real-world conditions. Also the effects of technology parameters (vehicle type, exhaust after-treatment, fuel), the driving conditions and the exhaust dilution on exhaust particles were studied.

Measurements were conducted with two heavy duty diesel vehicles (Rönkkö et al. 2006; Rönkkö et al. 2007) and with two passenger cars. On-road measurements were made by chasing individual vehicles with the laboratory vehicle equipped with aerosol instruments and instruments to measure gaseous pollutants. Laboratory measurements were performed with same vehicles and with a heavy duty diesel engine equipped with different after treatment devices (Lähde et al 2009). The laboratory measurements made it possible to study the effects of dilution parameters, fuels and exhaust after treatment in well-defined sampling and dilution conditions.

Results of both on-road and laboratory measurements indicate that the formation of the diesel exhaust nucleation mode particles can be divided into different paths. Without an exhaust after treatment or with a diesel oxidation catalyst, the particle formation is based on the existence of non-volatile core particles in raw exhaust and on the particle growth by volatile compounds during the exhaust dilution and cooling process (Figure 1). However, in the case of the oxidation catalyst, also the sulphur driven nucleation during the dilution and cooling process is possible. When a diesel particle filter is used, the formation of the nucleation mode particles seems to occur during the dilution and cooling process and the formation seems to be sulphur driven.
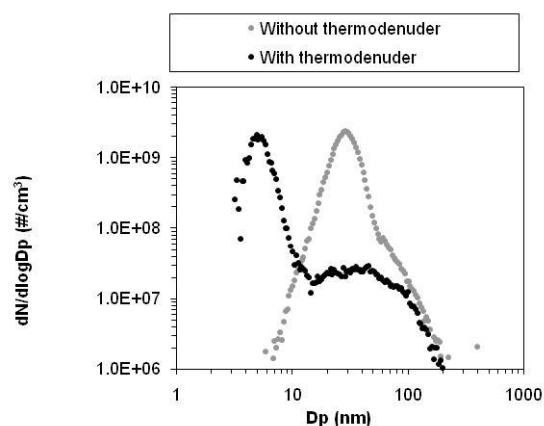
Figure 1. Exhaust particle size distributions of heavy duty diesel vehicle without exhaust after treatment measured with and without thermodenuder treatment (see Rönkkö et al. 2007).

Kittelson, D. B. (1998). *J. Aerosol Science,* 29, 575-88.
Lähde, T., et al. (2009). *Environ. Sci. Technol.,* 43, 163-8.
Rönkkö et al. (2006). *Atm. Env.* 40, 2893-2901.
Rönkkö et al. (2007). *Environ. Sci. Technol.,* 41, 6384-6389.

Dependence between heavy duty diesel engine exhaust nucleation and soot concentration

T. Lähde[1], T. Rönkkö[1], A. Virtanen[1], A. Solla[2], M. Kytö[2], C. Söderström[2] and J. Keskinen[1]

[1]Aerosol Physics Laboratory, Tampere University of Technology, PL599, 33720, Tampere, Finland
[2] VTT Technical Research Centre of Finland ,P.O. Box 1000, 02044 VTT, Finland

Keywords: diesel emission, nucleation mode, engine parameters, heavy duty.

The diesel exhaust particle population includes often two distinctive modes, namely soot and nucleation mode (Kittelson 1998). The soot mode consist of non-volatile, combustion chamber originated, electrically charged carbonaceous agglomerates (Kittelson et al. 1986) and, until recently, the nucleation mode was assumed to be formed solely through nucleation of condensing gases in ambient air or in dilution system (e.g. Shi and Harrison 1999). However, when no aftertreatment or aftertreatment with low deposition efficiency is used also the nucleation mode is shown to possess electrically charged non-volatile core (Lähde et al. 2009; Filippo and Maricq 2008). The diameter of the core is typically below 10 nm, while the soot diameter is around or above 50 nm. However, the composition and the mechanism of formation of the core are still unknown.

The characteristics of the core are studied here in relation to the diesel exhaust soot mode and engine power. The soot mode characteristics are known to respond on engine parameters.

Diesel exhaust emission characteristics were measured in an engine dynamometer. The studied engine was heavy duty turbo compound Euro 4 diesel engine with unit injectors and EGR. The engine was run without aftertreatment with several engine loads. Used diesel fuel sulphur content was below 10 ppm.

Particulate distributions were measured with a SMPS equipped with DMA 3085 and CPC 3025 (Tsi Inc.). Size range measured with the SMPS was between 3 nm and 60 nm. Also ELPI (Dekati ltd.) was used in the study to monitor the exhaust particle concentrations. Sample was diluted first with porous tube type diluter and second with ejector diluter. The particle population was dried with a thermodenuder designed for particles with diameter < 30 nm.

Particle size distributions with volatile compounds and without volatile compounds were bimodal for all measured engine load conditions. The soot mode remained unchanged while sample was treated with the thermodenuder, but the nucleation mode number concentration and GMD decreased. The change of the GMD and the concentration was strongest with low loads. For the low sulphur fuel (<10 ppm) without catalytic converter, the change of the concentration is connected to hydrocarbon growth of the core into the measurable size range.

The core mode total volume increased while the engine power increased; the soot mode total volume behaved oppositely, **Figure 1**.The change in the soot mode volume may be connected to the enhanced oxidation in engine cylinder. The core volume change, however, seems to be too high to be explained with the changes in coagulation processes. Both soot and nucleation mode volume changed only little when the engine torque was changed. However, while the engine speed was changed and the power was kept approximately constant, the total volume between modes changed strongly
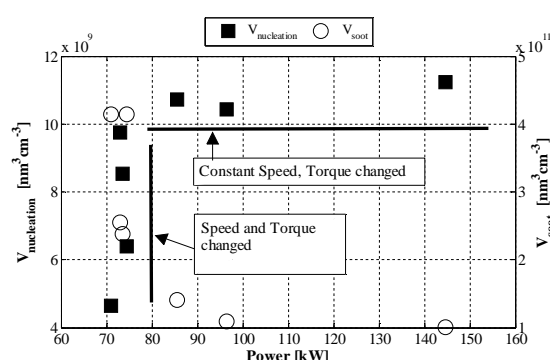
Figure 1. The dry nucleation mode and soot mode total volume as a function of engine power.

The nucleation mode was shown to possess nonvolatile core with all studied engine loads. The core mode characteristics changed along the soot mode characteristics while the engine condition was changed. The change in the core concentration implies an in-cylinder origin also for the core particles

Kittelson, D. B. (1998). *J. Aerosol Science,* 29, 575-88.

Kittelson, D. B., Moon, K. C. & Pui, Y. H. (1986), SAE 860009, 19-30.

Shi, J. P., and Harrison, R. M. (1999), *Environ. Sci. Technol.* 33, (21), 3730-6.

Lähde, T., Rönkkö, T., Virtanen, A., Schuck, T.J., Pirjola, L., Hämeri, K., Kulmala, M., Arnold, F., Rothe, D., and Keskinen, J. (2009). *Environ. Sci. Technol.,* 43, 163-8.

Filippo, A. D., & Maricq, M.M.. (2008). *Environ. Sci. Technol.* 42, (21), 7957-62.

The case of on-line measurements vs. gravimetric sampling for quantifying the particulate emissions from biomass combustion

A. Keller[1], A. Lauber[2], A. Doberer[2], J. Good[2], T. Nussbaumer[2], M.F. Heringa[3], P.F. DeCarlo[3], R. Chirico[3], A. Richard[3], A.S.H. Prevot[3], U. Baltensperger[3] and H. Burtscher[1]

[1] Institute for Aerosol and Sensor Technology, University of Applied Sciences Nordwestern Switzerland, 5210, Windisch, Switzerland
[2] Lucerne School of Engineering and Architecture, Lucerne University of Applied Sciences and Arts, 6048, Horw, Switzerland
[3] Laboratory of Atmospheric Chemistry, Paul Scherrer Institut, 5232, Villigen, Switzerland

Keywords: Wood Combustion, PM measurements, TEOM, Diffusion Battery.

Recent studies have shown that, in industrialized countries like Switzerland, particulate matter emissions from residential wood burning can substantially surpass traffic related emissions even in the proximity of a busy road (Szidat et al., 2007). The emissions from wood burning may therefore have a bigger impact on health than what has previously been thought. However, wood stoves, log wood boilers, pellet boilers and other biomass combustion devices are usually only characterized during type approval measurements. This is problematic specially in the case of log wood combustion because the combustion conditions depend on several parameters (Nussbaumer et al., 2008), and it is difficult to predict their real life emissions based solely on these tests (i.e. mass based gravimetric sampling).

The aim of this study is to evaluate the information obtained using the standard type approval method and propose an alternative to characterize the emissions of wood stoves and boilers in a detailed manner. For that purpose, we have investigated the mass emissions of a log wood burner using a TEOM (accumulated mass), two DiSCs (mass through number conc. & geometrical mean diameter, see Fierz et al., 2007), a Dusttrack and an OPC (mass trough light scattering). As opposed to the gravimetric sampling, all these instruments provide an online and time resolved measurement.

Our measurements raise the question of the validity of the type approval test in its current form. For instance, figure 1 shows four complete burn-cycles during a warm-start test of a conventional wood stove. Typically, 70 to 90% of the emissions are produced during the first third of the burn cycle. But there is no a priori way of knowing when the mass emission rate will change from a steep increase to a near to zero value. Thus, a gravimetric sampling cannot discriminate the two phases. Only a time resolved measurement can fully qualify the emissions and point out which parts of the burning cycle should be optimized.

We also present a detailed comparison between the different instruments. All of them produced consistent data even if they are based on very different principles. The good correlation between the TEOM, which directly measures particle mass, and the other instruments suggests that the DiSC and the Dusttrack are an alternative to the gravimetric sampling. Additionally, these portable instruments can easily be taken to the field to characterize the wood stoves and boilers under real life conditions.

Finally, we discuss the influence of dilution temperature on the measured particulate mass emissions. Our results suggest that a good amount of previously condensed volatile matter may re-evaporate during the dilution process when using the standard dilution temperature of 150 C.
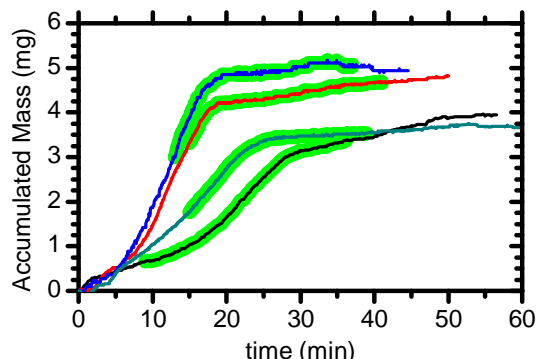
Figure 1. Accumulated total particle mass as sampled by the TEOM against time emitted during four burn cycles of a wood stove. Time zero marks the moment when the wood was placed on the glowing charcoal-bed. The region highlighted in green indicates the period of time when the norm measurements were performed. Sampling rate 3Nlt/min, dilution temperature 150 C. Data corrected for dilution factor.

Fierz, M., Burtscher, H., Steigmeier, P., and Kasper, M. (200). /SAE 2007-08PFL-484/

Nussbaumer, T., Doberer, A., Klippel, N., Bühler, R., Vock, W.: 16th European Biomass Conference and Exhibition, Valencia, 2–6 June 2008, ETA-Florence, ISBN 978-88-89407-58-1

Szidat, S., Prévôt, A. S. H., Sandradewi, J., Alfara, M. R., Synal, H.-A., Wacker, L., Baltensperger, U. (2007). Geophys. Res. Lett., 34, L05820.

Effect of biofuels on the diesel particulate emissions and toxicity

K. Kuuspalo[1], M. Ihalainen[1], T. Karhunen[1], J. Ruusunen[1], P. Willman[1], M. Tapanainen[1,2], P. Jalava[1,2],
R. O. Salonen[2], A. Pennanen[2], M. Happo[2], M-R. Hirvonen[1,2] and J. Jokiniemi[1,3]

[1]Fine Particle and Aerosol Technology Laboratory, Department of Environmental Science, University of Kuopio
P.O. Box 1627, FI-70211 Kuopio, Finland
[2]National Institute for Health and Welfare, Department of Environmental Health, P.O. Box 95 FI-70701 Kuopio,
Finland
[3]VTT Technical Research Centre of Finland, Fine Particles, P.O. Box 1602, 02044 VTT, Espoo, Finland

Keywords: diesel emissions, biofuels, health effects of aerosols, particle size distribution

Multiple types of diesel engines are used in a wide variety of vehicles because of their good fuel efficiency and high power output. Recently growing concern on environmental issues has led to increased interest in alternatives to fossil fuels. New fuels with different properties may change the physical and chemical, and related toxicological characteristics of diesel emission particles. Because diesel engines are one of the major sources of particulate air pollution in urban areas the emissions of new bio based fuels need to be tested in comparison to the conventional ones to avoid unexpected health effects.

The objective of this study was to investigate the differences in the effects of alternative diesel fuels on the physical and chemical characteristics and toxicity of particulate emissions.

A Non-road EURO II diesel engine in combination with an engine dynamometer was employed for the study. Exhaust emissions of three different test fuels Rapeseed Methyl Ester (RME) biodiesel, Hydro treated Vegetable Oil (HVO) bio based diesel and sulfur-free (EN590) diesel were analyzed with and without a catalytic converter. The catalytic converter used in this study is described in detail by Lehtoranta *et al.*, 2007.

For all the fuels, regulated emissions, particle number size distributions and organic and elemental carbon (OC/EC) measurements were made during steady states of C1 (ISO 8178-4) modes. To investigate the toxic activities (inflammation, cytotoxicity) samples were collected from previously chosen four test cycle modes and pooled together to achieve adequate mass.

Sampling and dilution system for particle number size distribution, OC/EC and PM measurements consisted of a porous-tube-type diluter, an ageing chamber and an ejector-type diluter assembled accordingly. Similar system has been used in several other vehicle and engine exhaust studies, eg. Lyyränen *et*. al., 2004.

Analyzers used in the aerosol size distribution measurements were an Electrical Low-Pressure Impactor (ELPI, Dekati, Inc.) with filter stage, nano and long Scanning Mobility Particle Sizers (SMPS, TSI Inc.) and a Fast Mobility Particle Sizer (FMPS, TSI Inc.). OC/EC samples were analyzed with the thermal optical method (Sunset laboratory, Inc.).

Particulate samples for toxicological analysis were collected from a Constant Volume Dilution tunnel (ISO 8178) with a High Volume Cascade Impactor (HVCI). Mouse macrophage cell line (RAW264.7) were exposed for 24hrs in a dose-dependent manner to the PM samples. Production of proinflammatory cytokine TNFα was measured by Enzyme Linked Immunosorbent Assay (ELISA) and acute cytotoxicity (Cell death) by MTT-test.

Preliminary results show that the particulate mass emission was the largest with EN590, followed by RME and HVO. The catalytic converter decreased the particulate emissions with all the fuels. All the exposures triggered cytokine production and cytotoxicity in a dose-dependent manner in macrophages. Cytokine responses to the EN590 and HVO particles were slightly increased after catalyst treatment (fig. 1 A). MTT-test did not reveal any major differences in cytotoxicity between the three diesel fuels with or without the catalytic converter (response to the same amount of mass). When the emitted emission/kWh is taken in to the consideration the cytotoxicity and inflammatory response could be estimated to be roughly the half of that without the catalytic converter as shown in the case of TNFα (fig. 1 B).
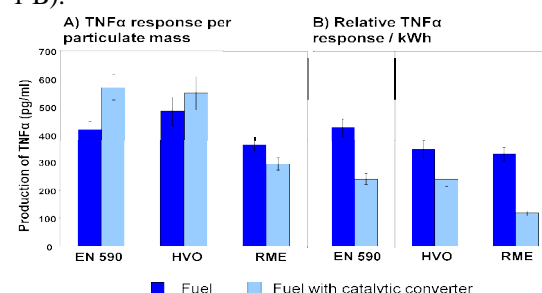
Fig 1. Production of proinflammatory cytokine TNFα

Lehtoranta, K., *et al.,* (2007). *Particle oxidation catalyst in light heavy duty diesel applications.* SAE technical paper series, 2007-24-0093

Lyyränen, J., Jokiniemi, J., Kauppinen, E.I., Backman, U. and Vesala, H., (2004). *Comparison of Different Dilution Methods for Measuring Diesel Particle Emissions.* Aerosol Sci. Technol., 38, 12-23.

Multifunctional Reactor for Emission Reduction of Future Diesel Engine Exhaust

Souzana Lorentzou[1, 2], Dimitrios Zarvalis[1], Athanasios G. Konstandopoulos[1, 2]

[1] Aerosol & Particle Technology Laboratory, CERTH/CPERI, Thermi-Thessaloniki 57001, Greece
[2] Department Chemical Engineering, Aristotle University, Thessaloniki 54006, Greece

Keywords: multifunctional reactor, diesel emissions, diesel exhaust, filtration.

Diesel Low Temperature Combustion (LTC) technologies for passenger cars are considered to be potentially beneficial due to low soot particulate and NOx emissions. However, it is anticipated that they will not remove the necessity of the exhaust emission control systems and especially the Diesel Particualte filters (DPFs). Moreover, LTC mode of engine operation demands tailored emission control systems that would address issues like the low NOx to soot ratio, the elevated HC and CO concentration etc. In this work, the development of a novel Multi-Functional Reactor (MFR) for the diesel engine exhaust is presented. The aim was to build a system that would have increased catalytic direct and indirect (NO$_2$-assisted) soot oxidation activity taking also advantage of thermal heat recovery (Konstandopoulos & Kostoglou, 1999) to minimize, the associated to the filter regeneration, fuel penalty.

The MFR incorporates a metal mixed oxide catalyst (MOC) and barium oxide (BaO) synthesized and deposited via an aerosol route, and a noble metal (Pt) applied via a traditional wet-chemistry technique (Konstandopoulos et al., 2008). MOC was used to enhance the direct soot oxidation rate, while Pt was used for the enhancement of the indirect soot oxidation rate and CO and HC conversion. BaO was included to improve the local availability of NO$_2$ and thus increase the soot oxidation rate.

The combination of aerosol and wet chemistry techniques enabled the optimal distribution of the different catalytic functionalities on the filter substrate wall. Evaluation of the catalysts was conducted at the small scale (catalyst coated small filter samples), with respect to their filtration efficiency, soot loading behaviour and soot oxidation activity at the engine test cell bench and was compared samples obtained from a catalyzed wall-flow Reference Diesel Particulate Filter (Reference DPF).

At the small scale the catalyzed filters demonstrated increased "initial" filtration efficiency compared to the reference DPF. The incorporation of Pt enhanced the indirect soot oxidation activity as well as the HC and CO conversion, with the type of the washcoat and the amount of Pt playing an important role. Addition of BaO has positive impact on the indirect soot oxidation, while the combination of aerosol and wet-chemistry techniques (for the Pt and the washcoat) enabled the production of multifunctional coatings with enhanced direct as well as indirect soot oxidation activity.

Based on the obtained results a full scale prototype MFR was built. The performance of this prototype was examined with respect to its heat recovery capability and to the soot loading and regeneration behaviour.

At the full-scale (prototype MFR) integration of the filtration function and heat exchange was achieved, without the use of an external heat exchanger. The MFR prototype demonstrated significant internal heat recovery capability. On the basis of soot loading and regeneration behaviour, the pressure drop of the MFR during soot loading was at comparable level with the pressure drop of the Reference DPF and even smaller after a certain soot mass load. More significantly, it demonstrated increased soot oxidation rate with respect to the Reference DPF in the temperature area between 450 and 550°C (up to 4 times, Figure 1).
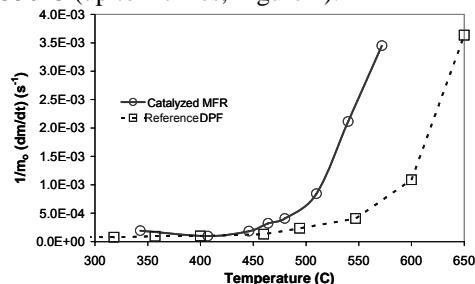
Figure 1. Soot oxidation rate as a function of filter inlet temperature for MFR and reference filters.

With respect to gaseous conversion, the MFR demonstrated significant HC and CO oxidation without notable NO$_2$-slip. However, the HC and CO conversion was less than the one attained by the small-scale filter sample produced initially without the incorporation of the MOC-BaO components, indicating a possible masking of the Pt activity when all catalytic components are integrated.

Konstandopoulos, A.G., & Kostoglou, M. (1999). SAE Tech. Paper, 1999-01-0469, (SP-1414).

Konstandopoulos, A.G., Boettcher, J., Lorentzou, S., Pagkoura, C. (2008). SAE Tech. Paper, 2008-01-0483, (SP-2154).

Raman Study of Nanostructure Evolution of Diesel Soot During Oxidation

A. Zygogianni[1], V. Polatidis[2] and A. Konstandopoulos[1,2]

[1] Aerosol and Particle Technology Laboratory (APTL), Center for Research and Technology Hellas, Chemical Process Engineering Research Institute (CERTH/CPERI), 6th km Charilaou-Thermi rd, 57001, Thessaloniki

[2] Department of Chemical Engineers, Aristotle University of Thessaloniki, PO. Box 517, 54006, Thessaloniki

Keywords: Diesel soot particles, Raman microscopy, Soot structure, Soot reactivity.

During the last decades there has been a major worldwide concern for the protection of the environment that led to the development of numerous associated technologies. In the area of air pollution reduction, serious efforts have been made for the control of automotive emissions, such as soot particulates from diesel engines, which are hazardous environmental pollutants. These particles can be effectively removed from the exhaust by means of a Diesel Particulate Filter (DPF), which has to be regenerated periodically (soot oxidation) in order to avoid undesirable backpressure in the engine (Konstandopoulos *et al.*, 2005). In the present work we perform a microstructural analysis during the oxidation of soot particles to clarify the mechanism of soot oxidation.

Several studies have been conducted on the chemical structure and reactivity of different types of soot and related carbonaceous materials employing Raman spectroscopy (Ivleva *et al.*, 2007; Fang *et al.*, 2004; Sadesky *et al.*, 2005). This method provides fingerprint spectra which allow distinction of a wide range of chemical substances and of order-disorder effects on carbonaceous materials.

The Raman spectra of soot can be divided into areas of first-order (<1800 cm^{-1}) and second-order (2200–3400 cm^{-1}) peaks. The bands that appear at the first region are the G ("Graphite") band at around 1580cm^{-1} which is attributed to the natural vibration mode of the six-member ring planes in the graphite structure, as well as the bands around 1150, 1350, 1500 and 1620 cm^{-1}, known as D_4, D_1, D_3 and D_2, respectively (figure 1).
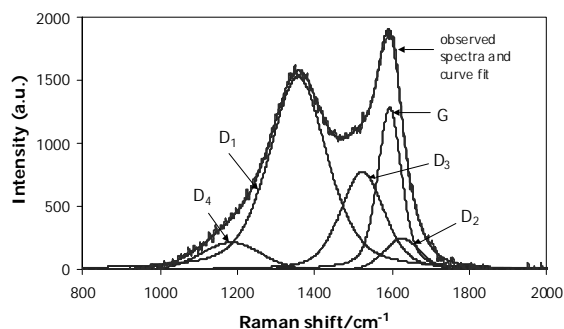
Figure 1. Curve fit for the first-order Raman spectra of soot.

The 1350 cm^{-1} band (D_1 band), commonly called the defect band, is attributed to a graphitic lattice vibration mode with A_{1g} symmetry and is known to be characteristic for disordered graphite. The 1500 cm^{-1} band (D_3) appears between the two maxima peaks and originates from the amorphous carbon fraction of soot.

In the current work, we investigated the use of Raman microspectroscopy in following structural changes in several engine soot samples upon oxidation. The soot particles were acquired from filters exposed in diesel engine exhaust. The effect of the engine type (common rail versus rotary pump engine), the engine operating conditions (varying engine speed and load) and the combustion mode (conventional versus Homogeneous Charge Compression Ignition, HCCI) were studied. For comparison purposes, the structural evolution of a carbon black (synthetic soot) sample was also studied. The soot oxidation experiments were performed under a flow of air (100ml/min) with a temperature increase from 25 to 600°C at a rate of 3°C/min.

The soot samples were morphologically characterized by Transition Electron Microscopy (TEM), while their oxidation rate was determined by Thermogravimetric analysis (TGA). Raman spectra have been recorded before and during the oxidation process with a Raman microscope system using a 514.5 nm laser line as an excitation source (delivering ~7.5 mW). The spectral parameters have been determined by curve fitting with five bands (G, D_1-D_4) as proposed by Sadesky *et al* (2005). The integrated intensity ratio I_{D1}/I_{Ga} and the band width values of D_1 and D_3 were used to investigate the degree of graphitization of soot samples. The synthetic soot indicated higher degree of structural order than the engine soot. Among the different types of engine soot analyzed the more significant differences were noticed among soot particles acquired under different engine combustion modes.

Konstandopoulos, A.G., Papaioannou E., Zarvalis D., Skopa S., Baltzopoulou P., Kladopoulou E., Kostoglou M., Lorentzou S., (2005). *SAE Tech. Paper*, 2005-01-0670 (SP-1942).

Ivleva N., Messerer A., Yang X., Niessner R., Poschl U., (2007) Environ. Sci. Technol., 41, 3702-3707.

Fang H. & Lance M., (2004) SAE, 2004-01-3043.

Sadesky A., Muckenhuber H., Grothe H., Niessner R., Poschl U., (2005) Carbon, 43, 1731-1742.

Abatement of fine particles emissions from wood combustion stoves by electrostatic precipitators

A. Bologa, H.-R. Paur, H. Seifert, K. Woletz, H. Bhangu

Institut für Technische Chemie, Forschungszentrum Karlsruhe, Postfach 3640, 76021, Karlsruhe Germany

Keywords: wood combustion, fine particles, particle concentration, electrostatic precipitators, particle collection efficiency

Wood is often combusted in stove and fireplaces for domestic heating. This process of heat generation produces a great number of fine particles which come with exhaust gases and are strongly associated with increased mortality and cardiovascular diseases. As the wood combustion is a considerable source of indoor and outdoor air pollution, there is an increasing need for fine particle collectors to reduce the emissions.

Electrostatic precipitators (ESPs) are the most common choice ensuring high removal efficiency for the complete particle size range. The known ESPs for exhaust gas cleaning from wood or pellets combustion can be divided into two groups: the first includes the units installed at the exit of the chimney, and the second includes the ESPs installed downstream or integrated to the combustion units.

The over-view of the known electrostatic precipitators for small-scale wood and pellets stoves is presented in the report. The electrostatic precipitators are analyzed from the point of view of their design, operation parameters as voltage and corona current, exhaust gas flow rate and temperature, particle number and mass concentration, ESP collection efficiency, problems, advantages and disadvantages.

The following problems which the ESPs meet during the operations are discussed: cleaning of the high voltage (HV) and grounded electrodes, protection of high voltage isolator from condensate, loading with fine particle and short-currents, dependence of the ESP collection efficiency on particle concentration in the exhaust gas, long-term stability of ESP operation, the investment and operation costs of the electrostatic precipitators.

On the basis of this analysis, the following demands to the design of a new ESP were determined: (i) no openings in the ESP (for example, blowers) from which exhaust gas can come into the indoor atmosphere, (ii) collector stage cleaning without ESP opening, (iii) protection of high voltage isolator without blowing of a purge air (iv) compact design, indoor/outdoor application and retrofitting to existing wood combustion facilities.

The pilot electrostatic precipitator designed and investigated in the Forschungszentrum Karlsruhe is presented in the figure (the direction of the gas flow is shown by arrows).

Pilot electrostatic precipitator
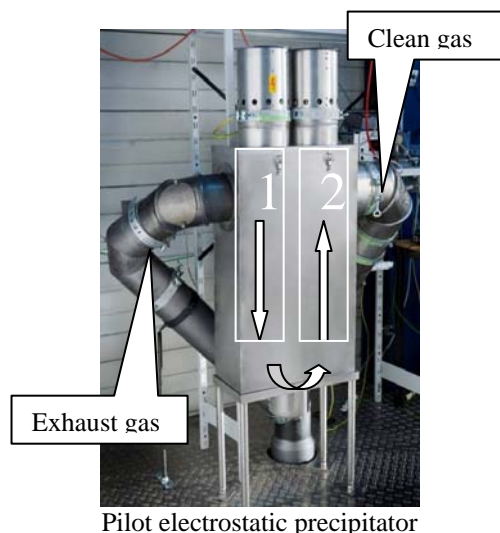
The ESP consists of an ionizing (1) and a collector (2) stages. Fine particles are charged in the DC negative corona discharge formed in the ionizing stage between the gas duct and the shaped disk corona electrode. The use of thin star-form HV electrode ensures stabile corona discharge and particle charging. Charge aerosol is precipitated in the specially designed collector stage which presents the grounded brush electrode installed in the gas duct. The periodical rotation of the brush ensures the effective collection of particles and cleaning of the ESP collector in automatic regime. The use of brush collector ensures compact ESP design.

The ESP was installed downstream a wood-log combustion stove with power 8 KW. The mass concentration in the exhaust gas varied from 20 to 110 mg/Nm³ and particle number concentration from 10^6 to 10^8 #/cm³. The average mass collection efficiency of the ESP is $\eta=62\pm3\%$ for part-time operation in strong corona quenching conditions (at high particle number concentration) and $\eta=72\pm6\%$ for operation without corona quenching. In the special designed ionizing stage, the high voltage isolator is protected without any use of purge air. Last tests have shown over 100 hours of stabile ESP operation without isolator cleaning.

At the end of the report the authors would conclude the main results of the development and would compare the design ESP with known electrostatic precipitators.

Fast Evaluation Method of the Ash Aging Effect on Catalyzed Diesel Particulate Filters

Dimitrios Zarvalis[1], Souzana Lorentzou[1, 2], Athanasios G. Konstandopoulos[1, 2]

[1] Aerosol & Particle Technology Laboratory, CERTH/CPERI, Thermi-Thessaloniki 57001, Greece
[2] Department Chemical Engineering, Aristotle University, Thessaloniki 54006, Greece

Keywords: ash, catalyzed DPF aging.

The employment of Diesel Particulates Filters (DPFs) has increased in the automotive industry in the recent years. Every year innovative catalyzed DPFs appear in the market. Establishing a certain maintenance-free time period regarding the DPF is of major importance. One of the most serious problems the filter manufacturers face concerning system's durability is the performance deterioration due to the filter aging because of the accumulation of the ash particles. The evaluation of the effect of the ash aging on the filter performance is a time and cost consuming task that slows down the process of manufacturing innovative filter structures and designs. Thus, a methodology for the fast evaluation of the effect of ash aging on the DPF performance would easily be appreciated.

The origins of ash are the lubricating oil additives, the engine wear as well as the fuel, especially if it contains additives for regeneration purposes. As fuel additives are decreasingly favoured into the emission control area, the most significant source of ash particles becomes the lube oil. Attempts for the development of rapid ash aging techniques have been reported in the literature. Most of them were based on oil-doping of fuel to decrease the necessary testing time. Methods of artificially increased oil consumption move away from the "natural" engine oil consumption and this movement may lead to unrepresentative results e.g. results concerning the filter backpressure increase due to accumulation of the ash (Sutton et al., 2004).

In the present work the effort was placed in developing a very rapid ash aging technique (ash-aging duration of 1 day) which resembles the real life conditions of ash accumulation. The method can be applied to small-scale filter samples. Small-scale filter sample testing is of particular importance during substrate material or catalyst material developments. The main lube ash formation and deposition pathways are considered to be the following:

- Ash forms as particles and transports/deposits on to the filter.
- Ash forms on the filter by pyrolysis of deposited oil droplets.
- Combination of the above.

In this method the ash particles are formed and deposited on filter samples enclosed into a high-temperature Aerosol-based Synthesis and Deposition (ASD) reactor (Konstandopoulos et al., 2005). Solutions of diesel fuel and engine oil are sprayed into the reactor. Tuning the operating conditions of the ASD unit allows to efficiently control the parameters that primarily affect the oil-derived ash formation and deposition.

The produced ash particles exhibited many morphological and compositional similarities to engine produced ash particles, but more importantly they exhibited the same ash layer flow resistance properties. The latter determine the pressure drop behaviour of the ash-loaded filter. This method was applied for the fast aging of sintered metal filter materials.

Ash-aged filter samples have been evaluated with respect to their soot loading behaviour, regeneration and filtration efficiency. For the uncoated filters, the results showed that an ash mass load up to a certain level leads to decreased overall pressure drop during soot loading. For coated filters the ash deposit may lead to either increased or decreased overall pressure drop depending on the type of the catalytic coating. The ash particle layer caused a significant increase in the filtration efficiency of the samples.

The kind of effect of the ash particles on the soot oxidation rate depends also on the catalyst type. Figure 1 presents the effect of the ash particles on the soot conversion rate for a coated and an uncoated filter sample.
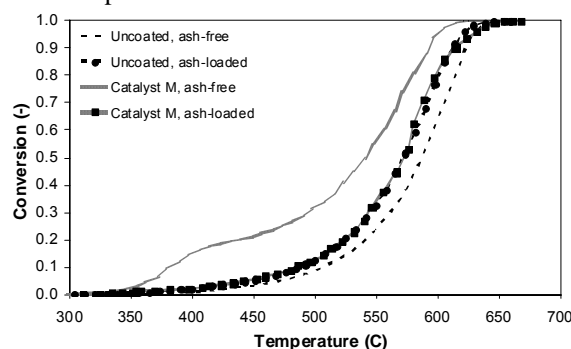
Figure 1. Effect of the ash particle layer on the soot oxidation for coated and uncoated filters.

Sutton M., Britton N., Otterholm B., Tangstrom P., Frennfelt C., Walker A., Murray I., (2004) *Investigation into Lubricant Blocking of Diesel Particulate filters*, SAE Tech. Paper No. 2004-01-3013,.

Konstandopoulos A. G., Vlachos N., Stavropoulos I., Skopa S,. Schumacher U., Woiki D., Frey M., (2005) *Study of a Sintered Metal Particulate Trap*, SAE Tech Paper No. 2005-01-0968.

Carbonyl compound emissions from a heavy-duty diesel engine fueled with biodiesel blends

Y.C. Lin[1]*, C.S. Yuan[1], T.Y. Wu[2], W.C. Ou-Yang[3], C.B. Chen[4], K.H. Hsu[1]

[1] Institute of Environmental Engineering, National Sun Yat-Sen University,
Kaohsiung 804, Taiwan.
[2] Department of Chemistry, National Cheng Kung University, Tainan 70101, Taiwan.
[3] Department of Chemical and Materials Engineering, National Kaohsiung University of Applied Sciences,
Kaohsiung 80778, Taiwan.
[4] Fuel Quality and Automobile Emission Research Division, Refining and Manufacturing Research Institute,
Chinese Petroleum Corp., Chia-Yi 60036, Taiwan.

Keywords: carbonyl compounds, biodiesel, paraffinic fuel, diesel engine

Carbonyl compounds (CBCs) play an important role in atmospheric chemistry and urban air quality because they are important precursors to free radicals, ozone, and peroxyacyl nitrates (Grosjean et al., 1993; Carter, 1995; Grosjean et al., 1996). Formaldehyde and acetaldehyde were main species of carbonyl emissions from the exhaust of diesel engines. Several studies showed that BE-diesel (Shi et al., 2006; Pang et al., 2006; Pang et al., 2008) and waste cooking oil biodiesel (20% vol; Peng et al., 2008) could be used to decrease formaldehyde emission by about 20% ~ 25% and 23%, respectively, but they increase acetaldehyde emission by 20% ~ 30% and 17%, respectively. It should be noted that formaldehyde, acetaldehyde, and acetone are toxic contaminants, mutagens, and carcinogens (Goldmacher et al., 1983; Shepson et al., 1986) so their reductions in diesel-engine emission are desirable.

This study investigated the emissions of CBCs from a HDDE (heavy-duty diesel engine) at one low load steady-state condition, 24.5% of the max load (40 km h^{-1}), using five test fuels: premium diesel fuel (D100), P100 (100% palm biodiesel), P20 (20 % palm-biodiesel + 80 % premium diesel fuel), PF80P20 (80 % paraffinic fuel + 20 % palm-biodiesel), and PF95P05 (95 % paraffinic fuel + 5 % palm-biodiesel). Experimental results indicate that formaldehyde was the major carbonyl in the exhaust, accounting for 70.3% ~ 75.4% of total CBC concentrations for all test fuels (Figure 1). Using P100 and P20 instead of D100 in the HDDE increased CBC concentrations by 9.74% and 2.89%, respectively. However, using PF80P20 and PF95P05 as alternative fuels significantly reduced CBC concentrations by 30.3% and 24.2%, respectively (Table 1). The wide usage of paraffinic-palmbiodiesel blends as alternative

fuels could protect the environment. However, it should be noted that only one engine operated at one low load steady-state condition was investigated.
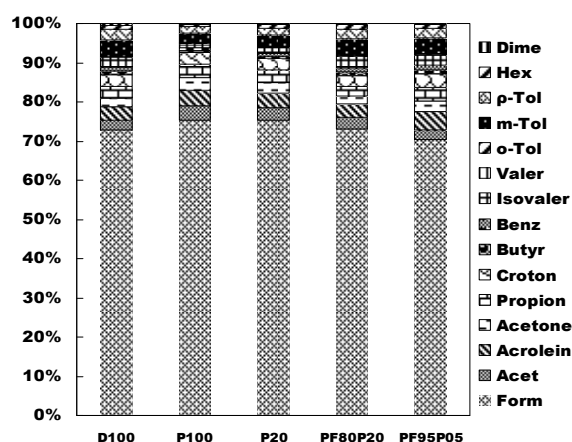
Figure 1. CBC profiles

Table 1. Total CBC emissions

	D100	P100	P20	PF80P20	PF95P05
µg m^{-3}	3800	4170	3910	2880	2650
mg L^{-1}	1360	1440	1370	1070	966

Goldmacher, V.S., Thilly,W.G. (1983). Mural. Res. 116, 417-422.

Shepson, P.B., Klelndlenst, T.E., Edney, E.O., Nero, C. M. (1986). Environ. Sci. Technol. 20, 1008-1013.

Grosjean, E., Williams, II E., Grosjean, D. (1993). Journal of the Air Waste Management Association 43, 469-474.

Carter, W.P.L. (1995). Atmospheric Environment 29, 2513-2527.

Grosjean, D., Grojean, E., Seinfeld, J. H. (1996). Environ. Sci. Technol. 30, 1038-1047.

Shi, X., Pang, X., Mu, Y., He, H., Shuai, S., Wang, J., Chen, H., Li, R. (2006). Atmospheric Environment 40, 2567-2574.

Pang, X., Shi, X., Mu, Y., He, H., Shuai, S., Chen, H., Li, R. (2006). Atmospheric Environment 40, 7057-7065.

Pang, X., Mu, Y., Yuan, J., He, H. (2008). Atmospheric Environment 42, 1349-1358.

Emission of particles from practical combustion devices burning methane/natural gas

Minutolo, P.[1], Prati, M.V.[2], Sirignano, M.[3], D'Anna, A.[3]

[1]Istituto di Ricerche sulla Combustione, CNR, P.le Tecchio 80, 80125, Napoli, Italy
[2] Istituto Motori, CNR, V.le Marconi, 1, 80125, Naples, Italy
[3] Department of Chemical Engineering, University of Naples Federico II, P.le Tecchio 80, 80125, Naples, Italy

Keywords: methane/natural gas, particle size distribution, indoor/outdoor particles, industrial aerosols, CNG car emissions.

Several studies have been conducted in last years on the combustion of methane and natural gas (NG), since they represent one of the source of energy with a low emissions of greenhouse gases, toxic combustion by-products and particulate matter. In addition they can be widely used in different combustion devices. However, recent studies have showed that also these clean fuels can produce a reliable number of particles.

A wide range of measurements on several real combustion systems are here presented: from domestic to industrial heater, together with gas turbine and I.C. engines.

Premixed and diffusive burner configurations used for home heating appliances have been studied under various operating conditions. Advanced in-situ optical diagnostics, based on laser induced emission spectroscopy (LIE), and ex-situ measurements, based on scanning mobility particle size (SMPS) measurements, and particles collection by a water-based sampling technique, have been used in order to evaluate total particulate concentrations and size distribution functions. Water samples, are analyzed by light absorption and UV induced fluorescence measurements. Moreover, also cook stoves and catalytic heaters have been investigated, for their effect on indoor pollution; for this device water sampling and sizing by SMPS have been provided. For all these applications natural gas was employed; it was constituted by about 84% methane, 8% ethane, 2% propane, 5% nitrogen with others larger hydrocarbons in low concentration.

In addition measurements have been conducted on a I.C. engine fuelled with CNG and a gas turbine fuelled with methane. A TapCon (or Vienna) DMA equipped with a Faraday Cup Electrometer (FCE) has been utilized to analyze the exhaust gases. For I.C. engine also ELPI (Electrical Low Pressure Impactor) has been used. The DMA, in the utilized configuration, allows to detect particle, down to 2nm, whereas ELPI is much more sensible for particles larger then 20 nm. Experiments for I.C. engine have been conducted at the exhaust of a Euro 3 S.I. car, driven on a chassis dyno bench. Different regimes have been investigated in order to understand the role of settings on particle production.

For all devices examined, experiments has showed that methane combustion even when it is conducted in overall lean premixed conditions can produce particles; generally these particles have a size of 2-3nm, spectroscopic behaviour typical of small polycyclic aromatic compounds, and a significant water affinity. In particular home burner appliances resulted able to oxidize most part of particle produced; the final effect is low emission in terms of mass concentration, whereas the number of these particles is relatively high. Beside of this, in the 10 nm–100 nm range, typical of primary soot particles, the number concentration of the particles measured at the exhaust of the combustion system is of the same order of magnitude of the number concentration of the particles present in ambient air. Similar results have been found for the cook stoves and catalytic heaters. In particular the partial premixed flame stabilized on cook stoves produces a reliable amount of particle with mean size of 3nm. Finally a large concentration of particles is produced and therefore emitted.

I.C. engine fuelled with CNG resulted to be, as the other combustion devices, a low emission technology. Measurements evidence that particles with dimension larger than 5nm are comparable with atmospheric background. However, in some condition, the exhaust analyzed contained particles with a mean size of 2nm; particles were present in number concentration clearly higher than the air room background, and comparable with values found for the other devices investigated.

In conclusion methane, pure or in natural gas, resulted to be a non-zero emission fuel. Real combustion devices, conducted in their optimal configuration, have showed that particles with size of 2-3nm are produced and emitted in relative high number concentrations.
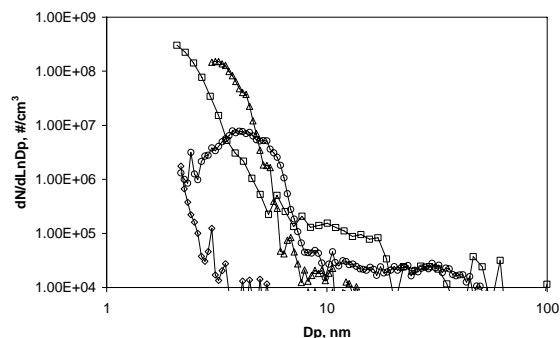

Figure 1. Typical PSDFs from cook stove(Δ), home burner appliance in diffusive ($\circ$) and premixed ($\Diamond$) configuration and I.C. engine at constant speed($\Box$).

Ultrafine particle emission from modern diesel engines: effects of engine conditions and combustion cycle

Beatrice, C.[1], Di Iorio, S.[1], Guido, C.[1], Fraioli, V.[1], Lazzaro, M.[1], Sirignano, M.[2], D'Anna, A.[2]

[1]Istituto Motori – CNR, Viale Marconi, 8, 80125, Naples, Italy
[2]Department of Chemical Engineering, University of Naples Federico II, P.le Tecchio 80, 80125, Naples, Italy

During last years an increased interest on pollution problem has focused the attention on the particulate emission from real combustion systems. According to the studies conducted on laboratory systems, particles in the ultrafine range have been pointed as major responsible for pollution and health risk. These particles are not usually taken into account in the total mass amount, due to their low concentration in mass, but become predominant in a concentration number analysis.

In order to investigate on the mechanism involved in the particle formation and on the influence of combustion characteristics on particle size distribution at the engine exhaust, measurements have been conducted at the exhaust of an EURO5 diesel engine, sampling the particles upstream the particulate filter.

Different analyzers have been adopted, according to their different sensibilities and skills. In particular, a TapCon (or Vienna) DMA equipped with a Faraday Cup Electrometer (FCE) has been utilized for the characterization of size distribution function of particles; at the same time, measurements of soot mass concentration have been performed employing a 483 Microsoot sensor from AVL. The DMA, in the adopted configuration, allows to measure particles down to 2nm.

To investigate the effect of engine combustion, several tests have been conducted in two engine loading points (low and medium) and for different EGR conditions. Varying the EGR from zero to an optimal value able to approach EURO5 NOx emission level at the engine exhaust, a sensitive response of both size distribution function and total amount of particles produced has been observed.

Focusing the attention in the range 1÷100nm, generally is possible to distinguish two peaks in the size distribution function: the first peak is around 2-4nm, the second one has the maximum at 50-60nm. These two modes in the PSDFs are present simultaneously in some combustion conditions, whereas in other cases only the large one is found. This behaviour suggests that the combustion condition can be responsible for the production of particles belonging to the first mode.

The increase of the EGR seems to reduce the production of particles with size up to 5-10nm, but on the other hand it strongly increases total particle amount, although the larger mode does not change in terms of the size of the peak value. However, a direct correlation between EGR and first mode is not possible and needs deeper investigations. The effect of the engine operating condition on particle production is comparable with respect to EGR: the higher is the engine workload, the lower is the first peak value; on the contrary, an higher engine load produces much more particulate matter, as well known, and increases the number of the larger particles.

In conclusion, by means of the use of a DMA, a PSDF sensitivity in the range 1-100nm versus some operating parameters in a modern diesel engine has been checked. An inhibition or reduction of the smallest particles has been detected by increasing both EGR and engine load, i.e. the in-cylinder soot loading level. These are only preliminary investigations on the correlation between diesel combustion conditions and the size function distribution of the emitted nanoparticles. Further studies are necessary in order to better understand if these parameters can be taken as the only responsible for the production of these very small particles, or other factors have to be considered.

In the future attention will be paid in the analysis of the role of the EGR on smallest particle emission, in particular on the effect that EGR has in terms of combustion temperature and of the recirculation of particles in combustion chamber. Other aspects should be also deepened, e.g. the role of the in-cylinder soot loading conditions on the exhaust PSDF shape, since the preliminary results have been evidenced a significant sensitivity.
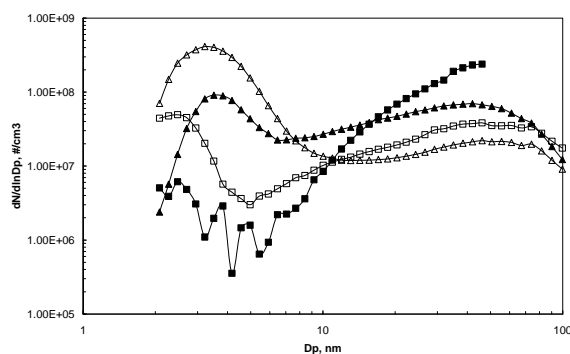
Figure 1. PSDFs with 0% of EGR (empty signs) and optimal EGR (filled signs) for low load (triangles) and medium load (square) engine conditions.

PCDD/F reductions from a biodiesel-fueled diesel engine

under US transient cycle

C.S. Yuan[1], Y.C. Lin[1]*, C.H. Tsai [2], Y.S. Lin[3]

[1] Institute of Environmental Engineering, National Sun Yat-Sen University, Kaohsiung 804, Taiwan.
[2]Department of Chemical and Materials Engineering, National Kaohsiung University of Applied Sciences, Kaohsiung 807, Taiwan.
[3] Department of Safety Health and Environmental Engineering, National Kaohsiung First University of Science and Technology, Kaohsiung 811, Taiwan.

Keywords: PCDD/F, biodiesel, diesel engine, emission

Emission of hydrocarbons and polycyclic aromatic hydrocarbons from diesel vehicles may be consistent with the role of aromatic precursors for polychlorinated dibenzo-p-dioxin/dibenzofuran (PCDD/F) formation and the degenerated graphitic soot structure in de novo synthesis (Huang and Buekens, 1995). PCDD/F concentrations from the diesel engine decreased with increasing load rate (Kim et al, 2003). Ryan and Gullett (2000) concluded that mean PCDD/F emission factors from HDDE operated at highway and city route types were 0.0372 and 0.0893 ng I-TEQ L^{-1}, respectively, with average of 0.0581 ng I-TEQ L^{-1} (Ryan and Gullett, 2000). Furthermore, Gullett and Ryan (2002) found that a high mileage diesel engine caused higher PCDD/F emissions (0.058 ng I-TEQ L^{-1}) as compared to a newly rebuilt one (0.024 ng I-TEQ L^{-1}) (Gullett and Ryan, 2002). However, few researches focused on reduction and/or increase of PCDD/F emissions from HDDEs. Gullett and Ryan (2002) found that diesel fuel with low sulfur, ARCO prototype low sulfur diesel fuel, caused high PCDD/F emissions (0.044 ng I-TEQ L^{-1}) as compared to commercial diesel fuel bought in North Carolina (0.024 ng I-TEQ L^{-1}) (Gullett and Ryan, 2002). PCDD/F emission can be reduced from 0.097 to 0.023 ng I-TEQ L^{-1} when the diesel oxidation catalyst was used (Dyke et al, 2007). Hence, find an alternative fuel to reduce PCDD/F emissions from HDDEs is needed today.

Although PCDD/F emissions from heavy-duty diesel engines (HDDEs) have been investigated in the literature, PCDD/F emissions from HDDEs fueled with palmbiodiesel-diesel blends and paraffinic-palmbiodiesel blends under US Transient Cycle have been rarely addressed in the past. Figure 1 shows PCDD/F congener profiles in the exhaust. Accordingly, the most dominant PCDD/F from HDDEs is

OCDD or OCDF for all test fuels except premium diesel fuel (PDF). Compared with PDF (2.37 pg I-TEQ m^{-3}) fueled Cummins B5.9-160 HDDE, PCDD/Fs reduction are 60.3%, 79.7%, 94.7%, and 97.6%, respectively, for B20 (20 vol% palmbiodiesel + 80 vol% PDF), B100, BP9505, (95 vol% paraffinic fuel + 5 vol% palmbiodiesel) and BP8020. Mean reduction fractions of PCDD/Fs (PDF = 1.08 ng I-TEQ L^{-1}) from the exhaust of Cummins B5.9-160 HDDE were 60.9%, 78.7%, 94.6%, and 97.6% for B20, B100, BP9505, and BP8020, respectively (Table 1). The above results indicate that it is an effective way to reduce PCDD/F emissions from HDDEs by fueling palm-biodiesel or paraffinic fuel because of no aromatic hydrocarbons in the above two fuels.
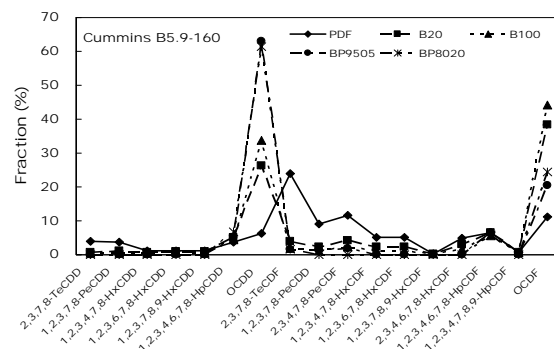
Figure 1. PCDD/F congener profiles

Table 1 PCDD/F emission factor (pg I-TEQ BHP^{-1} h^{-1})

	PDF	B20	B100	BP9505	BP8020
Cummins	274	126	60.9	15.5	7.19

Huang H., Buekens A. (1995) Chemosphere 1995; 31; 4099-4117.

Ryan J.V., Gullett B.K. (2000) Environ. Sci. Technol. 2000; 34; 4483-4489.

Gullett B.K., Ryan J.V. (2002) Environ. Sci. Technol. 2002; 36; 3036-3040

Kim K.S., Hong K.H., Ko Y.H., Yoon K.D., Kim M.G. (2003) Chemosphere 2003; 53; 601–607.

Dyke P.H., Sutton M., Wood D., Marshall J. (2007) Chemosphere 2007; 67; 1275–1286

T09 Instrumentation

Development of an Aircraft-based Laser Ablation Aerosol Mass Spectrometer (ALABAMA)

M. Brands[1,2], M. Kamphus[1,3], J. Schneider[2], C. Voigt[4], F. Drewnick[2] and S. Borrmann[1,2]

[1]Institute for Atmospheric Physics, Johannes Gutenberg University, Mainz, Germany
[2]Particle Chemistry Department, Max Planck Institute for Chemistry, Mainz, Germany
[3]now at: EMERSON Process Management, Hasselroth, Germany
[4]Institute of Atmospheric Physics, German Aerospace Center, Wessling, Germany

Keywords: Aerosol mass spectrometry, Single particle analysis, Laser ablation, Aircraft measurements.

We present here the development of a novel Aircraft-based single particle Laser ABlation time-of-flight MAss spectrometer (ALABAMA), which is capable of measuring the chemical composition and size of ambient aerosol particles in the size range between 200 and 900 nm.

The aerosol particles are sampled from ambient air through a pressure-regulated Liu type aerodynamic lens system and focused to a narrow beam into the vacuum of a sizing chamber. By travelling through two orthogonally aligned 532 nm continuous wave laser beams, particles generate scattered light that is focused onto photomultipliers by means of two elliptical mirrors.

After deriving the aerodynamic size of the particles from their individual flight time, a 266 nm Nd:YAG laser (τ = 5 ns, E = 8 mJ/pulse) is triggered to vaporize and ionize the particles in the extraction region of the mass spectrometer.

The bi-polar Z-shaped time-of-flight mass spectrometer (TOFWERK AG, Thun, Switzerland) generates a complete mass spectrum with a resolution of m/Δm ~450 in the m/z range from 10-300.

All components fit in a 19'' aircraft-compatible rack of approximately 1,60m height, not exceeding a total weight of 150kg. The instrument will be suitable and certified for the new german HALO high altitude and long range research aircraft.

Extensive lab characterizations have been performed, providing detailed information on the instruments performance and limitations.

The lower detection limit is given by the amount of light scattered by the particles and the upper detection limit by the transmission properties of the inlet system.

Detection and ablation efficiencies for polystyrene latex (PSL) monospheres as a function of particle size are shown in Figure 1.

Measurements for different particle shapes and sizes show a decrease in detection efficiency by ~85% for NaCl and even >95% for soot particles, due to a widening and misalignment of the particle beam as well as different optical properties of the particles.

Ablation efficiency varies strongly (up to -60% for mineral dust) due to changes in absorption- and ionization properties for different particle types, as well as decreasing hitrate due to the widening and misalignment of the particle beam.
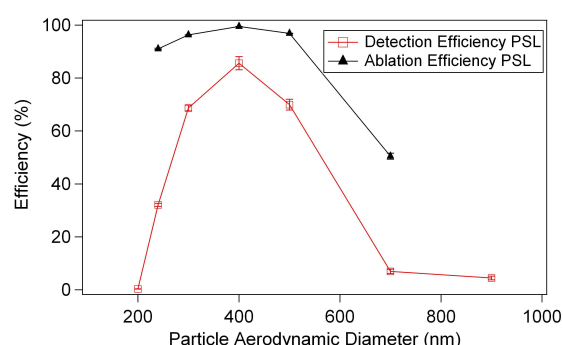
Figure 1. Detection and ablation efficiency of PSL microspheres as a function of size.

Furthermore ALABAMA has been deployed during a four week measurement campaign at the AIDA chamber (Aerosol and Heterogeneous Chemistry in the Atmosphere) at the Research Center in Karlsruhe/Germany. This project focused on ice nuclei and ice formation efficiencies of different particle types and atmospheric conditions and offered excellent opportunity to test the instrument under atmospheric conditions. Additionally an intercomparison with instruments operating on similar methodologies has been performed.

In summer 2009 ALABAMA will be operated on a research aircraft during the MEGAPOLI campaign to perform measurements on urban pollution aerosols within and above the boundary layer above and downwind of large metropolitan areas.

Results on the instruments performance under various pressure and ambient conditions, as well as single particle composition data of the field and laboratory measurements will be presented.

Performance comparison of two different Laser Ablation Time-of-Flight Mass Spectrometers

T. Klimach[2], M. Brands[1,2], F. Drewnick[2], J. Schneider[2], M. Kamphus[1], and S. Borrmann[1,2]

[1]Institute for Atmospheric Physics, Johannes Gutenberg University, Mainz, Germany
[2]Particle Chemistry Department, Max Planck Institute for Chemistry, Mainz, Germany

Keywords: Aerosol mass spectrometry, Single particle analysis, Laser ablation

We present extensive intercomparison measurements between two different single particle laser ablation time-of-flight aerosol mass spectrometers utilizing similar working principles with differences in the inlet and particle detection design and in the ablation laser wavelength: the Single Particle Laser Ablation Time-of-flight aerosol mass spectrometer (SPLAT, Kamphus et al., 2008) and the Aircraft-based Laser Ablation Aerosol Mass spectrometer (ALABAMA).

The general setup of both instruments is as follows. Ambient aerosol is focused by an aerodynamic lens system to a narrow beam. Two orthogonal CW laser beams are used to determine the aerodynamic diameter of the aerosol particles and to trigger the ablation laser. The ablation, which vaporizes and ionizes the particles, takes place in the extraction region of a bi-polar time-of-flight mass spectrometer, resulting in detailed information on the chemical composition of the individual particles.

For comparison of the inlet and particle detection systems of the two instruments detection and ablation efficiencies for different types of aerosol particles, namely PSL (Fig. 1) and glass spheres, broken glass, soot and PAH, were determined as a function of particle size, SPLAT was operated with both, a Schreiner type aerodynamic lens (Schreiner, 1999) focusing particles in a size range between 0.2 and 3 µm and with a Liu type lens with a size range from 50 to 800 nm detecting the forward scattered light with an optical lens assembly and a photomultiplier. ALABAMA was operated with the Liu type aerodynamic lens only, using elliptical mirrors to collect the scattered light.
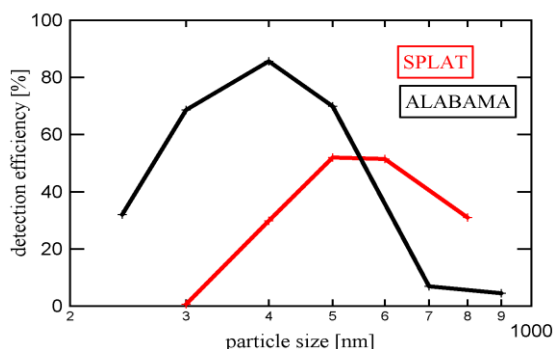
Figure 1: PSL Detection efficiencies of SPLAT and ALABAMA. Both devices equipped with a Liu type lens.

Due to its elliptical mirrors ALABAMA is able to detect smaller particles than SPLAT, which on the other hand detects larger particles more efficiently.

For investigation of the influence of the ablation laser wavelength onto the ion fragmentation a variety of identical aerosol particles has been measured with the two instruments. SPLAT uses an excimer laser for particle ablation, which can be operated at 193 nm and 308 nm, depending on the laser gas; ALABAMA uses a frequency quadrupled Nd:YAG laser, operating at 266 nm. The higher energy of the 193 nm ablation laser is supposed to result in a stronger fragmentation of the vaporized molecules. This was also observed in the mass spectra of Arizona Test Dust particles (Fig. 2).
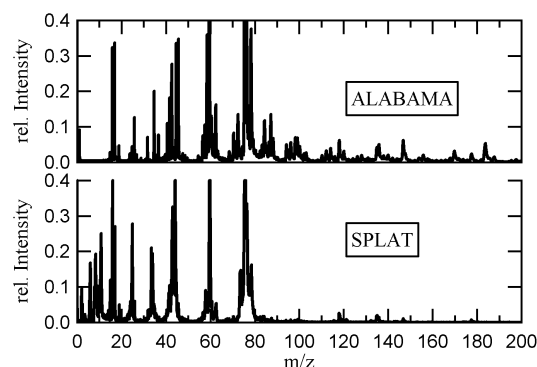
Figure 2: Averaged mass spectra of Arizona Test Dust obtained with SPLAT and ALABAMA.

Further experiments with different mineral dusts and organic substances are conducted to investigate the influence of the ablation wavelength on single-particle mass spectra and to get a better understanding of the underlying laser desorption and ionisation effects.

Kamphus M., et al. (2008), *Aerosol Science and Technology*, 42:11, pp.970-980
Schreiner J., et al. (1999), *Aerosol Science and Technology*, 31, pp. 373-382
Liu P., et al (1995), *Aerosol Science and Technology*, 22, pp. 314-324

Efficient Sampling and Collection of Atmospheric Aerosols with a Novel Particle Concentrator – Electrostatic Precipitator System

B. Han[1], N. Hudda[2], Z. Ning[2], Y. J. Kim[1], C. Sioutas[2]

[1] Eco-machinery Research Division, Korea Institute of Machinery and Materials, Daejeon 305-343, South Korea
[2] Department of Civil and Environmental Engineering, University of Southern California, Los Angeles, CA 90089, USA

A novel particle sampling methodology, combining a versatile aerosol concentrator enrichment system (VACES) and carbon fiber charger developed by our lab (Han *et al*. 2008) was extended to develop prototype electrostatic precipitators (ESP) for the collection of particles on substrate (Particulate Matter-ESP) and direct cell exposure (Cell-ESP) for toxicological analysis.

In our system, particles grown to super-micron droplets via condensation of ultrapure deionized water were concentrated by virtual impaction in VACES and then droplets were charged in a carbon fiber charger with negligible ozone generation, and subsequently diffusion-dried to their original particle size, while preserving the acquired charges. The charged particles were then collected on suitable substrates in two different ESP prototypes for chemical and toxicological analysis.

To minimize possible chemical reactions between sampled particles and ions or negligible amount of ozone generated in the corona region, our previous carbon fiber charger was modified, by separating the charging zone from the ionization zone. Number of charges per particle was about 50 per particle, which was higher than comparative studies (Biskos *et al*, 2005). These charged particles had removal efficiencies (the fraction of particles not penetrating the ESP of the total incoming; based on particle number concentration before and after ESP) greater than 90% for particle sizes smaller than 200 nm, and about 80-90% for particles larger than 200 nm in the PM-ESP at 3 l/min, whereas more than 95% removal was achieved for particles smaller than 200 nm in Cell-ESP at 1.5 l/min. These results imply that ultrafine particles (smaller than 100 nm), which have been traditionally difficult to charge by means of conventional charging techniques, can be effectively charged and removed in both concentrator-ESP systems.

ESPs were further investigated to establish the collection efficiency, i.e., fraction of particles deposited on the target surface from that removed in ESP. Difference between removal and collection efficiency represent losses to tubing and the insulating parts of ESP. Based on the test done on lab generated PSL particles of 100 nm, NaCl and atmospheric aerosol the gravimetric agreement between the parallel filter line and ESP collection substrate was about 80%.

Field test were also conducted to establish the performance of the PM-ESP prototype by comparing the mass and chemical compositions to a filter in a parallel reference line. Samples were composited and offline chemical analyses on the filters/substrates included ion chromatography (IC) for the analysis of inorganic ions (chloride, nitrate, phosphate, ammonium and sulfate), selected trace elements measured via inductively coupled plasma-mass spectroscopy (ICP-MS), and water soluble organic carbon (WSOC). These test results had a concentration agreement for various elements (0.81) and inorganic ions (0.83) similar to the gravimetric agreement or the collection efficiency. The consistent agreement across a variety of PM species indicates that the particle concentrator-electrostatic precipitator system is efficient in collecting ambient aerosols while preserving their chemical composition.

Biskos G., Reavell, K., and Collings, N. (2005). *Unipolar Diffusion Charging of Aerosol Particles in the Transition Regime*. J. Aerosol Sci., 36:247-265.
Han, B., Hudda, N., Ning, Z., and Sioutas, C. (2008*a*) *Enhanced Unipolar Charging of Concentration-Enriched Particles using Water-based Condensation Growth*. J. Aerosol Sci., 39:770-784.

Concentrated atmospheric nanoparticle beams in vacuum for X-ray and optical spectroscopy.

J. Meinen[1,2], S. Khasminskaya[1] and T. Leisner[1,2]

[1] Institute for Meteorology and Climate Research, Aerosols and Heterogeneous Chemistry in the Atmosphere (IMK-AAF), Forschungszentrum Karlsruhe GmbH, Germany

[2] Institute for Environmental Physics (IUP), Atmosphere and Remote Sensing, Ruprecht-Karls-Universität Heidelberg, Germany

Keywords: Atmospheric Nanoparticles, Charge Reversal Spectroscopy, Aerodynamic Lens

The IPCC AR4 points out the important role of aerosol in the radiation budget of the earth. In the model prediction, direct and indirect contribution of the atmospheric aerosol causes a net cooling of the earth. Understanding the fundamental physical and chemical processes of heterogeneous nucleation of water on nanoparticles could help improving the models.

On our poster we present the first stage of the TRAPS apparatus (Trapped Reactive Atmospheric Particle Spectrometer). The apparatus comprises as nanoparticle sources atomizers, electrospray and plasma reactors in order to produce nanoparticle sizes from 20-50nm, 10-20nm and 5-10nm respectively. The nanoparticles are dispersed in helium as carrier gas at high pressure. After passing a critical orifice into rough vacuum a tuneable aerodynamic lens is used to focus the particles into a differential pumping stage. We put high effort in optimizing the aerodynamic lens for particle beams close to the diffusion limit by CFD calculations. Downstream the differential pumping the particle beam is used to continuously refill a linear ion trap. For the trapping of particles in the size range of several kDa to MDa, a radio frequency from 10-150 kHz is. In contrast to the work of other groups, which are using digital ion traps, we developed an amplifier capable to provide an appropriate sinusoidal voltage with amplitude up to 3kV.

This assembly is capable to inject nanoparticles into vacuum chambers in a highly efficient way. The dilution of the particle number concentration arising from the gas expansion from room pressure into vacuum is compensated by concentrating the particles in a small cylindrical volume by electrodynamic trapping. The enlargement of the target density compared to a free molecular beam provides a tool for various techniques of spectroscopy used on smaller ions by routine.

In-situ Small Angle X-Ray Scattering (SAXS) Characterization of SiO$_2$ Nanoparticles Synthesized in a Microwave-Plasma Reactor

V. Goertz[1], A. Abdali[2], H. Wiggers[2], C. Schulz[2] and H. Nirschl[1]

[1]Institut f. Mechanische Verfahrenstechnik u. Mechanik, Universität Karlsruhe (TH), 76131 Karlsruhe, Germany
[2]Institut f. Verbrennung u. Gasdynamik, Universität Duisburg-Essen and CeNIDE, Center for NanoIntegration Duisburg-Essen, 47057 Duisburg, Germany

Keywords: In-situ measurements, Microwave-plasma reactor, Nanoparticle characterization, SiO$_2$, SAXS

Optical, mechanical, thermal or handling properties of coatings as well as bulk materials can be improved by using nanomaterials and nanocomposites containing nanoparticles. Depending on the application, specific properties of the nanomaterials are required. For example if a high transparency of coatings with high mechanical and chemical resistance is demanded, SiO$_2$ nanoparticles with a specific size, morphology and surface coating are particularly suitable. Thus, a detailed characterization of the nanoparticles and also an exact knowledge concerning the particle formation and particle growth is indispensable.

An adequate measuring method is the small-angle X-ray scattering (SAXS), which can be used for in-situ measurements of aerosols as well as suspensions. The technique can determine the particle size and size distribution, the specific surface area, the fractal dimension and the aggregate number within one measurement (Beaucage *et al.*, 2004). Besides the multiplicity of particle describing parameters within a single measurement, the technique offers the opportunity to measure in-situ.

However, laboratory X-ray scattering equipment like Kratky and pinhole cameras has a low scattering intensity and as a consequence, the measurement takes several hours (8h+). To overcome this constraint a Kratky compact camera was modified using a multilayer X-ray mirror (Göbel mirror). The mirror converts a divergent, incoming X-ray beam into a parallel one and was established inside the camera. Additionally, a two-dimensional imaging plate detector replaced the one-dimensional, gas-filled detector. Owing to these changes, intensity and image quality are increased and the required measurement time is decreased by a factor of 20. Due to this, the camera can be used now for in-situ measurements during particle formation.

In order to validate the in-situ measurement technique the synthesis of SiO$_2$ nanoparticles in a microwave-plasma reactor is observed. Inside the plasma a gas mixture including TEOS vapour, oxygen, argon, and nitrogen is decomposed within a few microseconds followed by the formation of silica nanoparticles.

With respect to the reactor design, the SAXS camera body is split in two parts to integrate the reaction chamber into the measurement section and to operate the camera in the particle formation zone. In Figure 1 the in-situ measurement setup is represented.
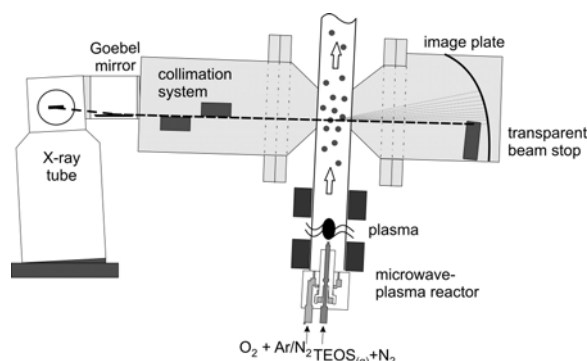
Figure 1. Schematic representation of the in-situ SAXS measurement setup

The in-situ SAXS results are compared with online particle mass spectrometry and TEM measurements (Janzen *et al.*, 2001). For the TEM measurements, particles collected from the PMS molecular beam and through thermophoretic sampling of nanoparticles from the reaction chamber were investigated. The results show a good match between the different measurement techniques and qualify the SAXS method as a non-intrusive possibility for the in-situ characterization of nanoparticle properties.

Beaucage G., Kammler H.K., Mueller R., Strobler R., Agashe N., Pratsinis S.E., Narayanan T. (2004). *Nat. Mater.*, 6, 370-374.

Beaucage G., Kammler H.K., Pratsinis S.E. (2004). *J. Appl. Cryst.*, 37, 523-535.

Janzen C., Wiggers H., Knipping J., Roth P. (2001). *J. Nanosci. Nanotech.*, 1, 221-225.

Source apportionment of particle number and PM10 concentration

E. Cuccia[1], F. Mazzei[1], V. Bernardoni[2], P. Prati[1], G. Valli[2], R. Vecchi[2]

[1]Department of Physics, University of Genova and I.N.F.N., Via Dodecaneso 33, 16146, Genova, Italy
[2]Department of Physics, University of Milano and I.N.F.N.,Via Celoria 16, 20133, Milano, Italy

Keywords: optical counter, PMF, ED-XRF, size-segregated source apportionment, urban aerosol

In a previous work (Mazzei et al., 2007), we described a methodology to apportion particles number in several size classes by receptor models (Gordon, 1988) fed with high time resolution series of elemental concentration values.

In this work the same approach is tested on a set of PM10 daily samples collected in the city of Genoa, during a campaign carried out in the harbour area. Elemental concentrations from Na to Pb were obtained through Energy Dispersive X-Ray Fluorescence (ED-XRF), and the contribution of specific sources to particulate matter (PM) concentration were apportioned by Positive Matrix Factorization, PMF (Paatero and Tapper, 1994). During the PM10 sampling, size segregated particles number distribution was measured by a Grimm 1.108 optical counter (OPC). This device counts atmospheric particles, with diameter, D_p, between 0.25 μm and 32 μm, in 31 size bins. The number of particles in each size bin was apportioned versus the time trends of PM10 sources resolved by PMF, using a multi-linear regression. The result is shown in Figure 1. On average, an absolute uncertainty of ± 5%, must be added to each value reported in Figure 1. As expected, natural sources as "sea salt" and "re-suspended soil" show larger contributions in the coarse fraction, unlike "secondary" compounds that are mainly concentrated in the fine fraction. Traffic emissions contribute to all size bins even if with a smaller contributions between 0.6 μm and 2 μm. Heavy oil combustion shows a flat distribution up to 3 μm but it should be reminded that very fine particles (i.e. with $D_p < 0.25$μm) are not detected by the OPC. Finally, we could identify a "local source", concentrated in particles with Dp > 0.5 μm, which, according to its profile, looks linked to harbour activities.

The apportionment in Figure 1 can be partially tested assuming all particles with the same density and deducing, for each size bin, the corresponding mass concentration apportionment. Summing on all the size bins, a new apportionment of PM10 can be obtained and compared with the standard result based on daily elemental concentration values. Results are presented in Figure 2 where the good agreement of the two methods can be appreciated. This study shows that the contemporary use of daily PM samplers and OPC can give the apportionment of both PM and size-segregated number of particles, provided that the elemental/chemical composition of PM samples is deduced by proper laboratory analysis and used as input of a receptor model as PMF.
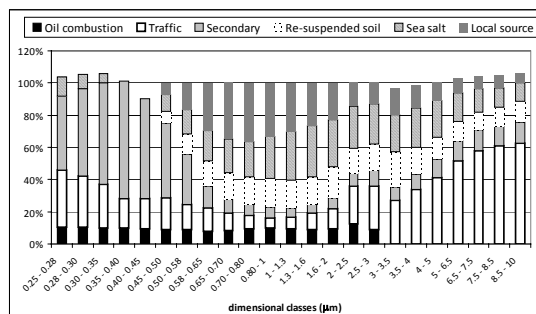
Figure 1: Apportionment of particles number in each size bin versus the PM sources identified by PMF
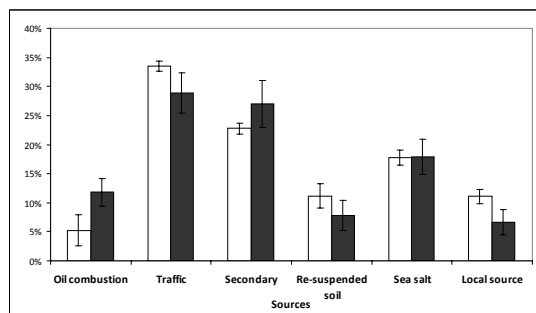
Figure 2: Comparison between "standard" apportionment of PM10 obtained by time series of elemental concentration values measured on daily basis plus PMF analysis (black bars) and the PM10 apportionment deduced with the methodology proposed in this work (white bars)

Mazzei, F., Lucarelli, F., Nava, S., Prati, P., Valli, G., Vecchi, R. (2007). *Atmos. Environ.,* 41, 5525-5535.
Gordon, GE., (1988). *Environ. Sci. Technol.*, 22, 1132−1142.
Paatero, P, Tapper, U., (1994). *Environmetrics*, 5, 11−126.

A new calibration method for optical particle counters in the size range of 0.2 to 8 μm

M. Weiß, L. Mölter[1]

[1]Palas GmbH, 76229, Karlsruhe, Germany

Keywords: optical aerosol spectrometer, calibration, size resolution, monodisperse aerosol generator.

Several papers about the calibration of light-scattering aerosol spectrometers (e.g. Friehmelt, 2000, Heim et al., 2008) already exist. However, the calibration of the Optical Aerosol Spectrometers (OAS) is still extensively discussed and issue of standardization committees (e.g. ISO/FDIS 21501-1). There are three significant reasons for this: 1.) An OAS has to be calibrated with respect to its counting efficiency and its size resolution. 2.) There is still no unique procedure available to calibrate optical particle counters in an expanded size range. A calibration related to the counting efficiency is often limited to a maximum size range of about 800 nm, the maximum mobility diameter that can be classified by commonly used Different Mobility Analysers (DMA). 3.) The effort which is necessary in order to calibrate OAS is large and time-consuming and therefore routinely not applicable for a quality control standard.

For this reason a calibration method has been developed that can be used to calibrate OAS with respect to the counting efficiency and the size resolution (see Fig. 1). The method is based on an improved aerosol generator for DEHS (MAG 3000) which produces monodisperse droplets in the size range of 0.2 to 8 μm. Additionally, the generator is able to keep the concentration constant which makes it suitable for reliable and reproducible measurements. In order to calibrate OAS, the aerosol of the generator is diluted into a channel with clean air to reduce the concentration, to avoid coincidence problems and to enable isokinetic sampling for the OAS. In contrast to a calibration procedure with a DMA as classifier for a monodisperse aerosol (Heim et al, 2008), the method with the MAG 3000 as a constantly producing monodisperse aerosol generator makes the calibration of OAS possible up to 8 μm. Moreover, this method is much cheaper in terms of technical requirements and less time-consuming which makes it applicable for quality standard controls.

The procedures to evaluate the measured distributions in order to characterize the size resolution and to measure the counting efficiency with a reference device are discussed. It is also shown that the described method is suitable for the calibration of OAS and the results are comparable to a calibration method with a DMA as a classifier for a monodisperse aerosol.

The above-described method has been used to characterize the size resolution and to measure the counting efficiency of the newly developed white light aerosol spectrometer welas® digital 2000 in the size range of 0.2 to 8 μm. In contrast to the predecessor welas® 2000 the welas® digital 2000 has a digital signal processing and a logarithmic A/D-converter (the former welas® had an analog signal processing and a linear A/D-converter). This improvement enhances the counting efficiency of the welas® digital and improves the size resolution for particles smaller than 1 μm. Additionally, the method has also been used to characterize the LAS-X II® (PMS) and to compare its size resolution and the counting efficiency with the welas® digital 2000. As the welas® digital 2000 can be equipped with five different sensors for concentrations from 1 P/cm³ to 10^6 P/cm³, it is further shown that all sensors can be calibrated with the described procedure.

Since this calibration method is an accurate and cost-efficient method to calibrate OAS, it is now used as a quality control for all welas® digital systems.
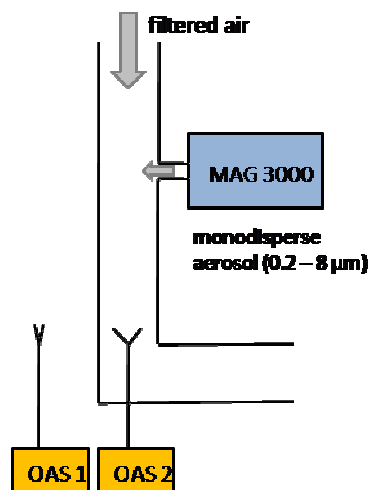

Figure 1. Set-up to calibrate light scattering aerosol spectrometers with a constantly producing monodisperse aerosol generator (MAG 3000). Different OAS are measured consecutively.

Friehmelt, R. (2000). Aerosol-Meßsysteme, Vergleichbarkeit und Kombination ausgewählter o-line Verfahren, *Universität Kaiserslautern, ISBN 3-925178-47-3*

Heim M., Mullins, B.J. Umhauer, H., Kasper, G. (2008). *J. Aerosol Science, 39, 1019-1031*

Fluorescent test particles for the determination of protection factor of safety work benches

S. Opiolka[1], A. Bankodad[1], S. Haep[1], M. Abele[2] and L. Mölter[2]

[1]Institut für Energie- und Umwelttechnk e.V., Bliersheimer Strasse 60, 47229, Duisburg, Germany
[2]Palas GmbH, Greschbachstrasse 3b, 76229, Karlsruhe, Germany

For the handling of dangerous materials in micro-biological and biotechnological laboratories as well as in medical institutions, safety work benches according to EN 12469 and cytostatics work benches according to DIN 12980 are used for the personal, product and diversion protection. In order to guarantee these security functions officially prescribed tests are described in the mentioned standards.

From point of view of the personal protection the examination of the protection factor on the working aperture of the safety work bench is of particular importance. Objective of the test is the evaluation of the number of test particles which enter the work bench' location under overcoming of the air flow on the working aperture.

In addition to the test particles released during the examination, there are also other, naturally existing particles like e. g. dust, abrasion from clothes and devices, danders, etc., within the safety work bench' location. The number of the naturally existing particles in the ambient air normally exceeds the number of the test particles released. A non-selective proof of the test particles by, e. g. optical particle counters supplies, in this case, a number concentration from the sum of the naturally existing particles and the test particles in the ambient air. Thus, the evaluation of the measuring result for the calculation of the protection factor of the work bench is not possible. For this reason, time-consuming micro-biological and chemical procedures with principal disadvantages are currently used for the test described to get the selective proof of the test particles.

New verification procedures for the determination of the protection factor on the working aperture of the safety work benches should comply with particular requirements (EN 12469). The number of released test particles N should not be smaller than 3×10^8 and the suction rate s not smaller than 20 l/min. The number of detected test particles n should not be higher than 4. A protection factor A_{pf} of at least $1,5 \times 10^5$ can be verified with these values. Thereby, the protection factor is calculated with:

$$A_{pf} = (N \times s) / (10^4 \times n)$$

A new verification procedure which complies with these conditions uses fluorescent test particles. These are released within the safety work bench and collected out of the work bench with impactors used as samplers. The plates of the impactors are evaluated under a fluorescence microscope after the test. In the dark field mode all particles collected are visible, in the fluorescence mode exclusively the fluorescent test particles.
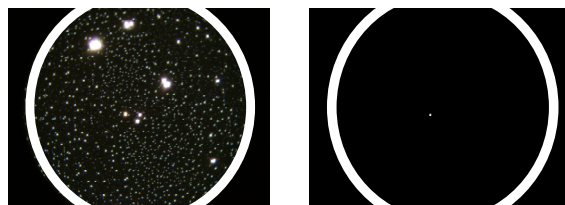
Figure 1. Microscope in the dark field mode (left) and fluorescent mode (right).

Another new verification procedure uses also fluorescent test particles. These are directly detected by an optical particle counter. Exclusive the fluorescence light of the test particles is detected by the selection of suitable light sources, optical filters and photomultipliers. All other particles existing in the ambient air are faded out. A functional prototype of the new particle monitor for fluorescent test particles is introduced.

DIN 12980 *Laboratory furniture - Cabinets for handling cytotoxic drugs - Requirements, testing.*
EN 12469 *Biotechnology - Performance criteria for microbiological safety cabinets.*

New data of dry deposition velocity of sub-micron aerosol on several rural substrates and comparison with models.

P. E. Damay[1], D. Maro[1], A. Coppalle[2], E. Lamaud[3], O. Connan[1], D. Hébert[1] and M. Talbaut[2]

[1]Institut de Radioprotection et de Sûreté Nucléaire, DEI/SECRE/LRC, 50130 Cherbourg Octeville, France
[2]COmplexe de Recherche Interprofessionnel en Aérothermochimie, 76801 Saint Etienne du Rouvray, France
[3] Institut National de la Recherche Agronomique, 33883 Villenave d'Ornon, France

Key words: Dry deposition, ELPI, Atmospheric aerosols

INTRODUCTION

Dry deposition flux is the quantity of particles deposited per unit surface and time. The dry deposition velocity is obtained by dividing the deposit flux by the aerosol concentration measured in the air. The lack of experimental data on dry deposition velocities of sub-micron aerosols in a prairie creates uncertainties larger than one order of magnitude for operational models. In this work we present the new results on several substrates and quantified them as a function of aerosol sizes and atmospheric turbulence parameters.

MATERIAL AND METHODS

Dry deposition flux can be calculated from the covariance between fluctuations of the vertical wind velocity and fluctuations of the atmospheric aerosol concentration. The aerosol concentration was measured with an Electrical Low Pressure Impactor (ELPI, Dekati, Inc.) and the wind by an ultrasonic anemometer for 30 minutes at high frequency. The vertical calibration of parameters to validate measurements (stationarity, integral characteristic of turbulence, Foken & Wichura, 1996), then spectral analysis and the calculation of fluxes were done. Three experimental campaigns were conducted in southwestern France in order to carry out the methodology on several substrates (maize, grass and bare soil).

RESULTS

Measurement provided values of dry deposition velocities (Vd) of sub-micron aerosols. The friction velocity (U*) and the heat sensible flux (H) have simultaneous effect on the deposit phenomena, because they influence the atmospheric turbulence These effects can be taken into account simultaneously by parameterizing Vd/U* as a function of the inverse of Monin-Obukov length (Wesely, 1985).

For neutral and stable atmospheric conditions, the dry deposition velocities are shown on the figure1. Vd is plotted as a function of the aerosol size and normalized by U*. Operational models (Slinn 1982, and Zhang et al. 2002) are also plotted on the same graph. Vd/U* results are very close for every substrates. Furthermore, a discrepancy between models and measurements is observed for aerosol greater than 0.5 µm.
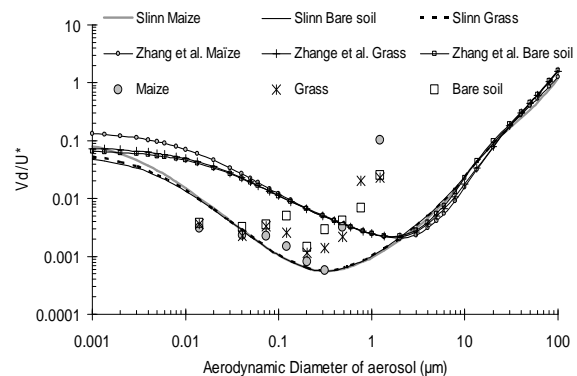
Figure 2. Dry deposition velocity measurements and models on different rural canopies

CONCLUSION

We present our results: discuss the impact of micrometeorological parameters and particle size on the dry deposition velocity. The perspective of work is to apply this method on other substrates: urban, forest or other rural substrates.

Foken Th., & Wichura, B. (1996). Tools for Quality assessment of surface-based flux measurement. *Agricultural and Forest Meteorology*, 78, 83-105

Kaimal J. C. & Finnigan J. J. (1994). Spectra and cospectra over flat uniform terrain. In: Oxford University Press (Eds), *Atmospheric Boundary Layer Flows*, New York, pp. 32-66.

Wesely, M. L., Cook, D. R. et Hart, R. L. (1985) Measurements and parameterization of particulate sulfur dry deposition over grass. *Journal of. Geophysical Research* 90, 2131-2143.

Slinn W. G. N. (1982). Prediction for particle deposition to vegetative canopies. *Atmospheric Environment* 16, 1785-1794.

Zhang L., Gong S., Padro J., Barrie L. (2001). A size-segregated particle dry deposition scheme for an atmospheric aerosol module. *Atmospheric Environment* 35, 549-560.

Measurement of Nanoparticle Agglomerates by Combined Measurement of Electrical Mobility and Charging Properties

D.Y.H. Pui[1], H. Fissan[2], J. Wang[1], W.G. Shin[1], M. Mertler[3] and B. Sachweh[3]

[1]Particle Technology Laboratory, Department of Mechanical Engineering, University of Minnesota, Minneapolis, MN, USA, 55455
[2]Institute of Energy and Environmental Technology e. V. (IUTA), Bhersheimer Strasse 60, 47229, Duisburg, Germany
[3]BASF SE, Fine Particle Technology and Particle Characterization, GCT/P - L540, 67056, Ludwigshafen, Germany

Nanoparticle agglomerates are pervasive in atmospheric sciences, air pollution, and material manufacturing. Combustion processes are used to manufacture a variety of materials in agglomerate form including fumed silica, titanium dioxide, and carbon black. Measurement of agglomerates is of great importance to many applications.

Agglomerates may possess complicated structures, which makes measurement of them a difficult task. One of the most common methods for agglomerate measurement is electron micrograph, which can provide direct measurement of the structural properties (Shin et al. 2009). However, taking electrical micrographs and performing image analysis can be time consuming and expensive. In addition, interpretation of the 2D images for 3D results may rely on assumptions and cause inaccuracy. Fast and online measurement for agglomerates is required in many scenarios including measuring fast changing agglomerates, quality control for material manufacturing, monitoring toxic air-borne agglomerates, etc. Most of the current aerosol instruments are designed for spherical particles. Therefore, there is a need for instruments capable of fast and online measurement of gas-borne nanoparticle agglomerates.

We have developed an instrument, Universal NanoParticle Analyzer (UNPA), for online measurement of gas-borne nanoparticle agglomerates. UNPA utilizes Differential Mobility Analyzer (DMA), Condensation Particle Counter (CPC) and Nanoparticle Surface Area Monitor (NSAM) to characterize airborne nanoparticle morphology and measure the number, surface area and volume distributions of airborne nanoparticles. The key parameter measured is the UNPA sensitivity, which is defined as the current (fA) measured by the NSAM divided by the number concentration measured (#/cm^3)

$$S = I/N \text{ (fA cm}^3\text{)}.$$

Experimental data (Figure 1) have shown that the UNPA sensitivity S depends on the particle morphology. S is larger for loose agglomerates than for spheres at a fixed mobility diameter.

Charging theories of Chang (1981) for aerosol particles of arbitrary shape indicates that geometric surface area and electrical capacitance of particle are two important parameters to determine mean charge of non-spherical particles. Our analysis shows that the electrical capacitance of loose agglomerates is larger than that of spherical particles with the same mobility. Therefore loose agglomerates can gain more charges in a charger, which in turn gives rise to higher values of UNPA sensitivity.
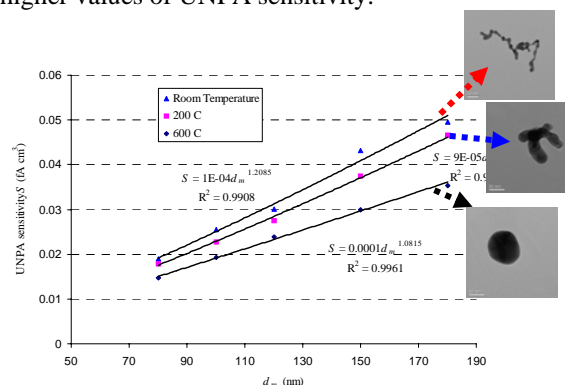
Figure 1. UNPA sensitivity as a function of the mobility size for particles of different morphologies.

UNPA measures the sensitivity S at a specified mobility size, compares it to the values of the loose agglomerates and spheres from calibration to determine the morphology. Agglomerates are modeled as clusters of spherical primary particles. From UNPA sensitivities, the primary particle size is determined using a fitting procedure. Using the models of Lall and Friedlander (2006) for loose agglomerates, the number of primary particles in agglomerates can be computed. Then the surface area and volume of agglomerates can be obtained. Operated under the scanning mode, UNPA can provide the number, surface area and volume distributions of loose agglomerates in the range of 50 – 800 nm in several minutes.

Shin, W-G, Wang, J., Mertler, M., Sachweh, B., Fissan, H., Pui, D.Y.H. (2009), *J. Nanoparticle Research*. 11, 163 – 173.

Chang, J.-S. (1981). *J. Aerosol Science*, 12, 19-26.

Lall, A. A. & Friedlander, S. K. (2006) *J. Aerosol Science*. 37, 260-271.

Experimental study on collision efficiency for aerosol particles scavenged by cloud drops

L. Ladino[1], O. Stetzer[1], U. Lohmann[1] and B. Hattendorf[2]

[1]Institute for Atmospheric and Climate Science, ETH Zürich, 8092, Zürich, Switzerland
[2]Department of Chemistry, ETH Zürich, 8093, Zürich, Switzerland

Keywords: Brownian Diffusion, Collection efficiency, Inertial Impaction, Thermophoresis

Cloud formation is an important issue in atmospheric and climate science. For example the impact of the anthropogenic aerosols on clouds it is still unknown. Aerosol particles can activate as cloud condensation and ice nuclei. In addition, aerosol particles colliding with droplets can be removed from the atmosphere by wet deposition. Collisions below 0°C can initiate freezing of droplets by contact freezing. Therefore, this process can influence cold clouds and hence the global radiation budget and the hydrological cycle.

There are some instruments available to measure the collision efficiency between droplets and aerosol particles. In most of them is not possible to work with small drops. Only few experimental data are available on collision efficiencies and the majority of all experiments were done with particles smaller than 0.4 μm and raindrops (D_d>100 μm).

In figure 1 we can see that all previous experiments were done mainly for rain drops (> 100 μm) with a constant particle diameter and changing drop sizes. Collision efficiencies for varying particle sizes are not well known.

In this study, collision efficiencies are measured with a new experimental setup. Aerosol particles of a known size and concentration can interact with small droplets produced with a piezo droplet generator in a chamber of variable length. The droplets are then collected with a cup impactor. The collected solution is then analyzed for the scavenged aerosol mass by Inductively Coupled Plasma-Mass Spectrometry (ICP-MS).

From this data, collision efficiencies can be derived. We report the first results with particles of $LiBO_2$ (with diameters between 0.4 μm and 0.6 μm) and droplets with a diameter of 32 μm. Our data is then compared to theoretical model calculations (Park *et al.* (2005) and Tinsley *et al.* (2006)) and literature data.

The forces included in our calculation are Brownian diffusion, interception, inertial impaction and thermophoresis.
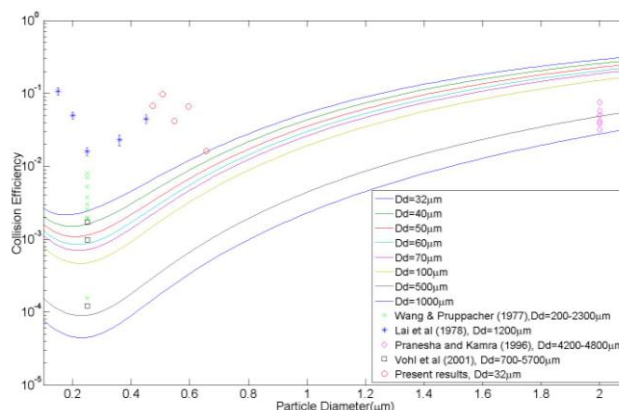
Figure 1. Comparison of theoretical collision efficiencies with experimental data from the literature and with our laboratory experiments.

The theoretical results show that by increasing the droplet diameter the collision efficiency decreases (confirmed experimentally by Vohl *et al.* (2001)). If the model is right previous experimental data drastically overestimate the collision efficieny.

Our data also differ from theory but lie in the range of other experimental data. With some modifications to the experimental setup we expect to get better results in future.

Tinsley B.; Zhou L.; Plemmons A. (2006) "Changes in scavenging of particles by droplets due to weak electrification in clouds". *Atmos. Res.,* 79, 266-295.

Park S.; Jung C.; Jung K.; Lee B.; Lee k. (2005) "Wet scrubbing of polydisperse aerosols by freely falling droplets". *Aerosol Sci.* 36, 1444–1458.

Vohl O.; Mitra S.; Diehl K.;Huber G.; Wurzler S.; Kratz K.; Pruppacher H. (2001) "A wind tunnel of turbulence effect on the scavenging of aersolos particles by water drops". *J. Atmos. Sci.* 58, 3064-3072.

Evaporation kinetics of a non-spherical, levitated aerosol particle using optical resonance spectroscopy for precision sizing

Ulrich K. Krieger[1], and Alessandro A. Zardini[2]

[1]Institute for Atmospheric and Climate Science, ETH Zurich, 8092 Zurich, Switzerland
[2]Department of Chemistry, University of Copenhagen, 2100 Copenhagen, Denmark

Keywords: Aerosol Spectrometry, Single Particle Analysis, Size Measurement, Vapour Pressure.

In atmospheric and climate science there is considerable interest in understanding the partitioning between gas and particle phase of chemical species. In particular, for semi-volatile substances like ammonium nitrate or certain organic species, the partitioning will strongly influence the particulate matter burden in the troposphere, the radiative properties of the aerosol, the cloud processing and the heterogeneous chemistry. In order to predict this partitioning, it is crucial to know the vapour pressure of the compounds under ambient conditions, whereas most established methods rely on high temperatures to achieve detectable vapour pressures. In the present work we use optical resonance spectroscopy (Zardini et al., 2006) to size solid, non-spherical particles during evaporation with a precision superior to direct imaging and mass change monitoring.
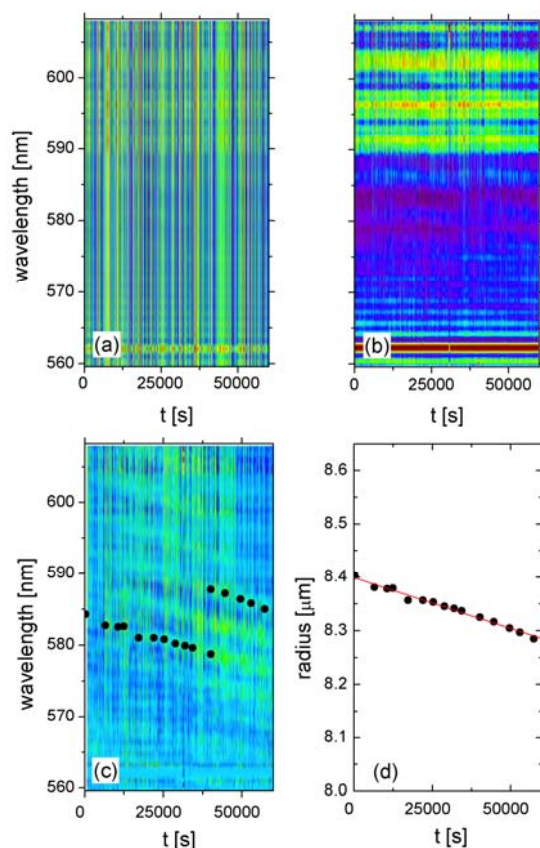
Figure 1. Panel (a) shows the raw spectra of an evaporating ammonium nitrate solid particle versus time (wavelength on vertical axis, colour coded in-

tensity). The intensity of each spectrum is normalized to the same maxima and minima in panel (b). In panel (c) the data of panel (b) are normalized with the mean spectrum of the complete time series. Panel (d) show the radius deduced from panel (c). A linear fit to the data yields: $dr/dt = -1.9 \times 10^{-6}$ µm/s at T = 283 K.

In contrast to evaporating liquid particles, raw resonance spectra do not allow easily to discern a shift in the resonance position, which is related to a size change. To make the size change of an evaporating, non-spherical particle visible in its resonance spectra we proceed as shown in Fig. 1. Panel (a) shows the times series of raw spectra (grey scale coded intensity). Each single spectrum is separately normalized to its own maximum and minimum and the result is plotted in panel (b). The most prominent features here are intensity extrema at certain wavelength (roughly regularly spaced) which are not time dependent and originate from etaloning of the CCD. Therefore, further normalization is performed in panel (c) by dividing each spectrum of panel (b) by the mean spectrum of the complete times series. The non time dependent features are suppressed and optical resonances shifting with time become visible, although not nearly as distinct as in the case of an evaporating liquid, i.e. spherical particle. To deduce quantitative information about the radius change with time, we associate one of the optical resonances with a specific size parameter $x_0 = 2\pi \cdot r_0/\lambda_0$. If we know the initial radius, r_0, we may follow its temporal evolution by measuring the wavelength, $\lambda(t)$, of the time shifting resonance through $r(t) = x_0 \cdot \lambda(t)/2\pi$. For retrieval of the particle radius from the resonance spectra shift of Fig. 1(c) we use visual inspection, i.e. a prominent resonance feature is tracked down as indicated by the black dots. If it leaves the wavelength domain or becomes less distinct with time, we switch to another resonance feature as illustrated in Fig. 1(c) at t ≈ 40000 s.

The vapour pressures deduced from these experiments compare favourably with high temperature effusion measurements of ammonium nitrate.

Zardini, A. A., Krieger, U. K., and Marcolli, C. (2006), *Opt. Express,* 14, 6951–6962.

Laser-induced breakdown spectroscopy for on-line measurements of particle composition

C. Fricke-Begemann[1], N. Strauß[2] and R. Noll[1]

[1]Fraunhofer-Institut für Lasertechnik, Aachen, Germany
[2]Chair for Laser Technology, RWTH Aachen University, Aachen, Germany

For the analysis of particle composition, a measurement technique has been developed using laser-induced breakdown spectroscopy (LIBS). It offers favourable characteristics for applications from emission monitoring to industrial process control.

LIBS is a measurement technology for chemical analysis which uses a focussed pulsed laser beam that evaporates and thermally excites a small portion of material. The radiation emitted from the excited material is measured with a spectrometer and because of the characteristic spectral lines of the elements, the signal allows to determine the composition of the material under investigation. The concentrations of practically all elements can be determined.

LIBS can directly be applied to solids, liquids and gases, and is used today in a wide range of applications. In industrial applications LIBS measurement systems have been proven to be suited for routine automated analytical purposes. For the analysis of aerosol, this technique has been applied before for the elemental analysis of particles deposited on filter substrates with size-classification (Kuhlen *et al.*, 2008).

When applied to an aerosol stream, LIBS can be used to measure the composition of particles in a large size-range from a few nanometers up to the upper micrometer range. Due to the complete dissociation of chemical compounds, the technique can be applied to all types of particles including industrial nanoparticles of metallic oxides.

To measure the composition of particles using LIBS, we demonstrate the realisation of a measurement which transfers an aerosol containing gas stream into a measurement chamber where the particles are evaporated into a laser-induced plasma. The system is characterised and calibration examples are given for some elements. The short response time of the instrument allows measurements with a time resolution below one second. Direct data processing immediately provides analytical results as required for online applications.

Into the measurement system a DMA has been included. When the aerosol gas stream is previously guided through the electrostatic classifier, the particle composition can be determined with respect to the particle size.

Kuhlen, T., Fricke-Begemann C., Strauss N., Noll R. (2008), Analysis of size-classified fine and ultrafine particulate matter on substrates with laser-induced breakdown spectroscopy, *Spectrochimica Acta Part B*, 63, 1171–1176

A Synchronized Hybrid Real-Time Particulate Monitor

K.J. Goohs[1], P. Lilienfeld[1], and J. Wilbertz[2]

[1]Department of Research, Thermo Fisher Scientific, Massachusetts, 27 Forge Parkway, 02038, Franklin, USA
[2]Engineering Department, Thermo Electron GmbH, Frauenauracher Strasse 96, 91056 Erlangen, Germany

Keywords: Aerosol Instrumentation, Light Scattering, Beta Attenuation, Hybrid Methodology

A hybrid nephelometric/radiometric particulate mass monitor capable of providing real-time measurements is described. The SHARP (Synchronized Hybrid Ambient Real-time Particulate) monitor incorporates a light scattering photometer whose output signal is continuously referenced to the time-averaged measurements of an integral beta attenuation mass sensor. This system achieves improved short-term precision and accuracy of both PM_{10} and $PM_{2.5}$ determinations. The SHARP monitor incorporates advanced firmware to optimize the continuous mass calibration of the nephelometric signal, ensuring that the measured mass concentration remains independent of changes in the particle population being sampled.

The SHARP monitor incorporates a "dynamic heater" system designed to maintain the relative humidity of the air passing through the filter tape of the radiometric stage well below the point at which the collected particles accrete and retain liquid water. This heating system minimizes the internal temperature rise ensuring negligible loss of semi-volatiles from the collected sample. The SHARP monitor is operable at ambient temperatures and features an adjustable filter change cycle and relative humidity set point to mitigate aerosol artifacts or more closely match the measurements of gravimetric reference methods.

Transformed field test data from four test sites with varied season, geography and chemical composition indicate that the SHARP monitor provides PM short-term, i.e., one hour-resolved measurements with a precision of better than ±1.0 µg/m3. Yearlong field tests indicate acceptable daily accuracy (1.0 + 0.1) and correlation > 0.97 compared against $PM_{2.5}$ reference samplers.
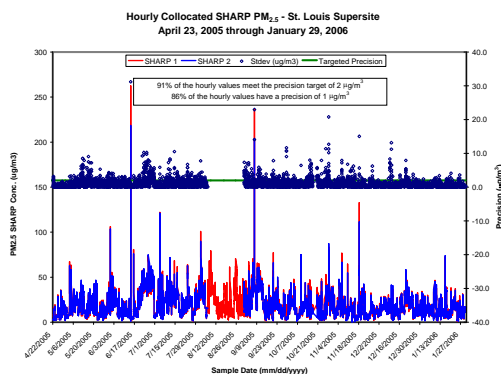
Figure 1. Collocated precision field data
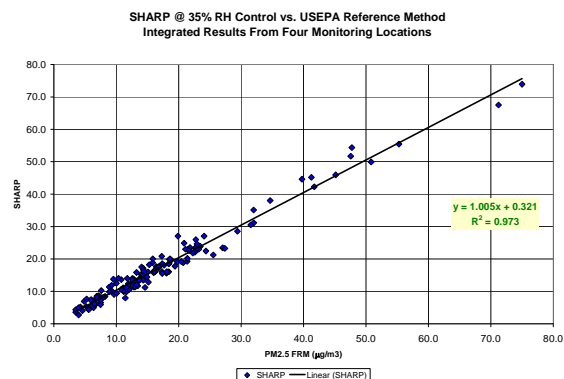
Figure 2. Scatter plot of SHARP Monitor data versus EPA reference method. Data is integrated across four regional monitoring locations of varied chemical composition that include winter and summer testing periods.

Babich, P., Wang, P.-Y., Allen, G., Sioutas, C., Koutrakis, P. (2000). *Development and evaluation of a continuous ambient PM2.5 mass monitor*. Aerosol Science and Technology 32, 309-324.

Chang, C. T. and Tsai, C. J. (2003). *A model for the relative humidity effect on the readings of the PM10 beta-gauge monitor*. Journal of Aerosol Science 34, 1685-1698.

Charron, A., Harrison, R. M., Moorcroft, S., Booker, J. (2004). *Quantitative interpretation of divergence between PM10 and PM2.5 mass measurements by TEOM and gravimetric (Partisol) instruments*. Atmospheric Environment 38, 415-423.

Chung, A., Chang, D. P. Y., Kleeman, M. J., Perry, K. D., Cahill, T. A., Dutcher, D., McDougall, E. M., Stroud, K. (2001). *Comparison of real-time instruments used to monitor airborne particulate matter*. Journal of the Air and Waste Management Association 51, 109-120.

Dresia, H., Fischotter, P., Felden, G. (1964). *Kontinuierliches Messen des Staubgehaltes in Luft und Abgasen mit Betastrahlen (Continuous measurement of the dust concentration in air and in exhausts by means of beta radiation)*. VDI-Z. 106, 1191-1195.

Gebhart, J. (2001). *Optical direct-reading techniques*. Aerosol Measurement, 2nd edition, Baron, P. A., Willeke, K., editors. (Wiley- Interscience). Chapter 15.

miniDiSC for personal monitoring and high-resolution monitoring networks

M. Fierz, P. Steigmeier, C. Houle and H. Burtscher

University of Applied Sciences Northwestern Switzerland, 5210 Windisch, Switzerland

Keywords: ambient air pollution, diffusion battery, field measurements, instrumentation, personal sampling.

Current aerosol instruments capable of measuring ultrafine particles are mostly large, heavy, expensive, which complicates many applications of these instruments. Recently, we introduced the diffusion size classifier (DiSC, Fierz *et al.*, 2007) as a simple instrument capable of simultaneously measuring particle number concentration and mean particle diameter with a time resolution of one second. Since the DiSC is based on a unipolar diffusion charger followed by current detection in two electrometers, it can also measure the total aerosol length or the lung-deposited surface area like the TSI NSAM (Fissan *et al.*, 2006) – a parameter that is likely to be health relevant.

We have now developed a miniaturized version of the DiSC (see Figure 1), which is nearly ten times smaller and lighter than the original instrument – it is truly handheld and weighs less than 1 kg. The entire instrument was also optimized to reduce the number of necessary parts to lower the instrument cost.

Figure 1: an image of the miniaturized diffusion size classifier (miniDiSC) compared to a CPC.

It has often been suggested that particulate mass (proportional to diameter d^3) may not be the most health relevant parameter to measure (e.g. Maynard 2007), and that particle surface area ($\sim d^2$) or number ($\sim d^0$) might be just as relevant. The miniDiSC is small and simple enough to allow personal exposure monitoring. It will allow studies linking particle number concentration and lung-deposited surface area to acute health effects to test the hypothesis that these parameters are highly health-relevant.

Another potential area of application for the new instrument is in monitoring networks. Currently, most monitoring networks consist of a limited number of stations containing bulky and expensive instruments. An alternative approach is to use a much larger number of inexpensive instruments which operate autonomously over extended periods of time, and which transmit their measurements and the instrument status over wireless communications networks. This type of measurement network can be set up with minimal effort on either a very local scale (e.g. to measure transport properties close to an aerosol source) or on a slightly larger scale, e.g. to monitor the temporal and spatial variation of air pollution in a city with very high resolution. Since the miniDiSC is inexpensive and requires very little maintenance, we are working on this type of monitoring network, and the direct integration of results in Google Earth (Figure 2).
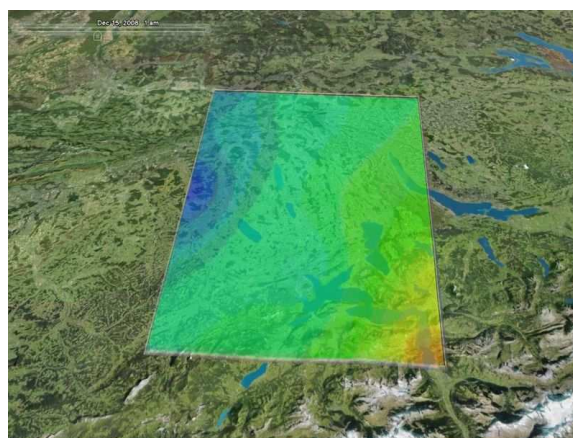
Figure 2. Integration of monitoring network data into Google Earth.

Fierz M., Burtscher H., Steigmeier P. and Kasper M. 2007. *Field measurement of particle size and number concentration with the Diffusion Size Classifier (DiSC)*, SAE 08PFL-484

Fissan H., Neumann S., Trampe A., Pui D.Y.H. and Shin W.G. 2006. *Rationale and principle of an instrument measuring lung deposited nanoparticle surface area.* J. Nanoparticle Research 9:53-59.

Maynard A.D. 2007. *Nanotechnology: The Next Big Thing, or Much Ado about Nothing?* Ann. Occup. Hyg. 51:1-12.

Probing Nanoparticles Deposited on Flat Surfaces by X-ray Spectrometry at Grazing Incidence

Falk Reinhardt[1], Burkhard Beckhoff[1], Harald Bresch[2] und Stefan Seeger[2]

[1]Physikalisch-Technische Bundesanstalt, Abbestr. 2-12, 10587 Berlin
[2]Bundesanstalt für Materialforschung und -prüfung, Unter den Eichen 87, IV.24, 12205 Berlin

Keywords: Aerosol characterization, Cascade impactor, Elemental composition, Particle size distribution, XRF

The strive for advancement in quantitative and qualitative nanoparticle analysis is motivated by multiple questions about potential risks caused by handling of or exposition to nanoscaled particles (interaction with the environment). Among those questions the verification and quantification of the dose-response relationship is a prominent one. Furthermore, improved knowledge of the interactions of nanoparticles with all kind of material surfaces is necessary for evaluating the use of the particle's properties. To answer those questions analysis of nanoparticles has to be developed further with respect to both sampling procedures and analytic techniques aiming on elemental compositions.

The further development of analytic techniques also involves the examination of deposited nanoparticles with synchrotron radiation. Depending on the particle number concentration, size-preselected nanoparticles were sampled on clean and flat silicon wafers either by use of a cascade impactor or by use of an electrostatic sampler. The deposition density on the wafer was approximately 10^5 particles/mm^2 or less. Deposition with the electrostatic sampler led to an approximately evenly distributed deposition.

PTB employs monochromatized synchrotron radiation of well-characterized beamlines, reliable X-ray spectrometry (XRS) instrumentation and absolutely calibrated X-ray detectors for the non-destructive investigation of bulk and layered samples in its laboratory at BESSY II (Beckhoff, 2008).
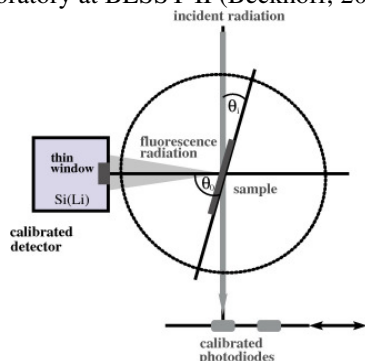
Figure 1: Sketch of grazing incidence XRS beam geometry

Grazing incidence X-ray fluorescence analysis (GIXRF) has the potential to effectively contribute to the characterization of nanoparticles deposited on flat surfaces with respect to elemental compositions, and potentially even depth profiles. Based on total-reflection X-ray fluorescence analysis (TXRF), which offers lower levels of detection in the pg to fg range, in GIXRF the incident angle of the excitation radiation is tuned between 0° and about threefold the critical angle of total-reflection. Therewith the intensity of the X-ray standing wave field (XSW) at a given height above the surface is modified. A particle of a given diameter deposited on the flat surface will be affected by the intensity of excitation radiation varying with the angle of incidence and hence yields a correspondingly varying X-ray fluorescence signal.

Thus, in addition to information on the elementary composition of the particles, which is inherent to XRF, information on the deposited size fraction can be obtained (Fig. 2).
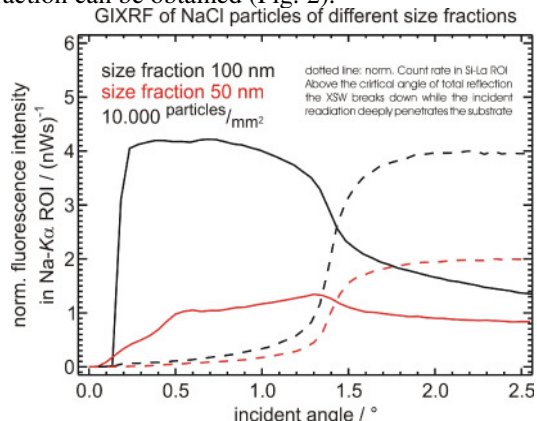
Figure 2: Angular dependence of detected fluorescence radiation dependent on incident angle.

Different specimens were prepared by depositing Zn compounds and NaCl particles with size fractions down to 10 nm on silicon wafer substrates by use of a differential mobility analyzer (DMA). Those particles serve as model systems for current and future reference-free quantitative analysis of size fractioned aerosol particles.

Beckhoff, B. (2008). *J. Anal. At. Spectrom.* 23, 845.

Quantification of carbonate carbon in atmospheric aerosol by means of ATR (Attenuated Total Reflection) spectroscopy and a multivariate calibration method

P. Fermo[1] , A. Piazzalunga[1,*] F. Tuccillo[1], L. Brambilla[1] , F. Mazzei[2], P. Prati[2]

[1]Dep. Inorganic, Metallorganic and Analytical Chem., University of Milan, Via Venezian 21, 20133, Milan, Italy
[*]Now: Dep. of Environmental Sciences, University of Milano-Bicocca, Piazza della Scienza 1, 20126, Milan, Italy
[2] Dipartimento di Fisica and INFN, University of Genova, via Dodecaneso 33, 16146, Genova, ITaly

Particulate matter (PM) carbonaceous fraction contains organic carbon (OC), elemental carbon (EC) as well as carbonate carbon (CC). The contribution of inorganic carbon is often neglected because its concentration is generally low and, moreover, there is not a reference analytical method for its quantification. Nevertheless in same cases, where a specific source of carbonate is present (mineral dust, street dust re-suspension, concrete plant, etc.), this fraction must be determined (Jankowski *et al.,* 2008).

PM10 atmospheric aerosol samples came from Massa Carrara, one of the most famous place in Italy where marble is quarried. The samples were collected on a daily basis (24 hours) along the road followed by the trucks transporting marble rocks form the pit to the sea. PTFE filters were used and characterized for their elemental composition by means of ED-XRF. PM10 concentration on average was 34.6 $\mu g/m^3$ and calcium showed quite high values being on average 17.3 $\mu g/m^3$. Therefore a contribution of the marble pit and/or marble transportation as significant PM sources cannot be ruled out.

In this work $CaCO_3$ was determined by infrared spectroscopy in ATR (Attenuated Total Reflection) mode. This approach, more effective than IR spectroscopy in transmission mode, has already been used in the literature for the quantification of PM organic fraction (Ghauch *et al.,* 2006).

In order to quantify $CaCO_3$ amount by ATR technique, a multivariate calibration method has been employed. For this purpose the program TQ ANALYST 8.0 by Thermo Fisher Scientific was employed. The regression algorithm is PLS (Partial Least Square). The use of chemometric techniques for quantification of some species in PM samples by IR spectroscopy has been already used (Coury et al., 2008) but not for the determination of carbonate content since $CaCO_3$ infrared most intense absorption (at about 1420 cm^{-1} and due to CO_3^{2-} stretching mode) is interfered by the presence of both ammonium sulphate and nitrate. Because of this superposition we investigated only the region center at 871 cm^{-1} which correspond to CO_3^{2-} bending.

Suitable standards were prepared mixing known quantities of calcium carbonate with nujol, which is normally used as a diluting matrix when IR spectra are acquired. In order to obtain for the standard mixtures ATR spectra comparable with those registered for PM samples, the standards were deposited on the diamond crystal, covered with a PTFE filter and then pressurized and scanned as for the ambient samples.

The calibration curve, obtained analyzing 15 standards, has a fit of $R^2=0.99$ and a RMSEC (root mean square error of calibration) of 0.69. Since the model efficiency is based on its performance in prediction (in this case the ability to estimate unknown $CaCO_3$ concentrations in aerosol samples), a validation procedure was applied giving a model Performance Index of 91.3%.

In order to validate the method based on ATR-FTIR, portions of the same PM10 samples have been analyzed by means of IC (Ion Chromatography) following a procedure recently suggested in the literature (Jankowski *et al.,* 2008).

A very good agreement between the two methods has been obtained. Furthermore it has been demonstrated that there is a contribution to PM due to the marble caves even if calcium is not present only as calcium carbonate (on average 50% of Ca is in the form of $CaCO_3$). This evidence has been confirmed also by SEM-EDX (Scanning Electon Microscopy – Energy Dispersion X-ray spectroscopy) analyses carried out on some of the filters where the presence of calcium carbonate together with calcium silicates and calcium sulphate has been pointed out.

In conclusion the method here proposed is an alternative to IC analysis and offers an advantage since it allows to analyze directly carbonate content which is not indirectly derived from the ions balance.

Jankowski, N., Schmidl, C., Marr, I. L., Bauer, H., Puxbaum, H., (2008). *Atmos. Env.*, 42, 8055 – 8064.
Ghauch, A., Deveau, P.A., Jacob, V., Baussand, P. (2006). *Talanta*, 68, 1294 – 1302.
Coury, C., Dillner, A. M., (2008). *Atmos. Env.*, 42, 5923 – 5932.

Retrieval of Aerosol Profiles using
Multi Axis Differential Absorption Spectroscopy (MAX-DOAS)

S. Yilmaz[1], U. Frieß[1], A. Apituley[2], G. de Leeuw[3,4,5] and U. Platt[1]

[1]Institute of Environmental Physics, University of Heidelberg, Germany
[2]National Institute for Public Health and the Environment, Bilthoven, The Netherlands
[3]Finnish Meteorological Institute, Helsinki, Finland
[4]Department of Physics, University of Helsinki, Finland
[5]TNO, Utrecht, The Netherlands

Keywords: Remote sensing, atmospheric aerosols, optical properties, instrument development.

Multi Axis Differential Absorption Spectroscopy (MAX-DOAS) is a well established measurement technique to derive atmospheric trace gas profiles by collecting scattered light spectra at different elevation angles and subsequent inverse modelling of the radiative transfer (Hönninger et al., 2004). Since aerosol particles are significantly involved in the scattering of the detected light, information about their distribution in the atmosphere is vitally important for the modelling procedure. Through MAX-DOAS measurements of trace gases with an already known vertical distribution, like the oxygen dimer O_4, it is possible to retrieve information on atmospheric aerosols (Wagner et al., 2004). Based on the optimal estimation method, we have developed an algorithm (Frieß et al., 2006) which fits simultaneously measured O_4 optical densities at several wavelengths and elevation angles to values simulated by a radiative transfer model. Retrieval parameters are aerosol extinction profile and optical properties like single scattering albedo, phase function and Angström exponent.
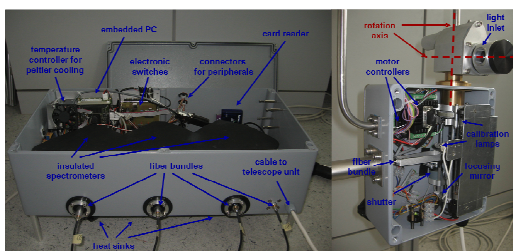
Figure 1. MAX-DOAS instrument with spectrometer (left) and telescope unit (right)

In the scope of a joint research activity of the EU funded project EUSAAR (European Supersites for Atmospheric Aerosol Research) we have developed a new type of DOAS instrument, which uses three miniature spectrometers to cover the near ultraviolet to visible wavelength range (290–790nm), enabling to capture all absorption bands of the oxygen-dimer O_4. Additionally, it is possible to point to any direction in the sky with a 2D telescope unit which is connected to the spectrometers via fibre optics (Figure 1).

In May 2008, an intercomparison campaign with established aerosol measurement techniques took place in Cabauw/Netherlands, where simultaneous DOAS, Lidar, Sun photometer and Nephelometer measurements were performed.

We present first results of selected days from this period (Figure 2). The optical properties of aerosols retrieved by the DOAS technique show qualitative agreement with the established measurement techniques demonstrating the progress towards our goal of establishing the MAX-DOAS technique for retrieving optical properties of atmospheric aerosols. Quantitative comparison is ongoing.
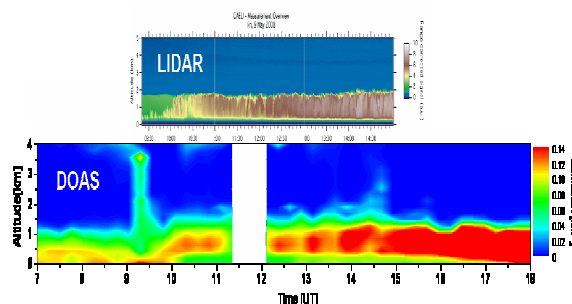
Figure 2. Profiles of aerosol optical properties retrieved from an intercomparison performed in Cabauw/Netherlands on 09.05.2008. Top: range corrected lidar signal. Bottom: aerosol extinction from MAX-DOAS.

Hönninger, G., v. Friedburg, C., & Platt, U. (2004). Multi Axis Differential Absorption Spectroscopy (MAX-DOAS). *Atmospheric Chemistry and Physics*, 4(231-254).

Wagner, T., Dix, B., v. Friedeburg, C., Frieß, U., Sanghavi, S., Sinreich, R., & Platt, U. (2004). MAX-DOAS O4 measurements: A new technique to derive information on atmospheric aerosols - Principles and information content. *Journal of Geophysical Research*, 109(D22205) (doi:10.1029/2004JD004904).

Frieß, U., Monks, P.S., Remedios, J.J., Rozanov, A., Sinreich, R., Wagner, T., & Platt, U. (2006). MAX-DOAS O4 measurements: A new technique to derive information on atmospheric aerosols. (II) Modelling studies. *Journal of Geophysical Research*, 111(D14203) (doi:10.1029/2005JD006618).

NanoCheck, a Valuable Tool for Size Range Expansions of Optical Particle Counters for Environmental Applications

Markus Pesch, Hans Grimm, Roland Hagler and Xiaoai Guo

GRIMM Aerosol Technik GmbH & Co. KG, Dorfstrasse 9, D-83404 Ainring, Bayern, Germany
Email: mp@grimm-aerosol.com

Keywords: Aerosol instrumentation, Nanoparticles, Number concentration, Optical particle counter, PM measurements

A series of GRIMM optical particle counters can be used for continuous measurement of aerosol particles, which can be reported for the various particle size channels down to sub-micron range in various modes, like particle counts in [#/liter] and environmental dust mass distribution in [µg/m³]. These environmental instruments work using the principle of light scattering technology, as shown in Fig.1. A semiconductor laser serves as light source. The signal scattered from the particle passing the laser beam is collected at ca. 90° by a mirror and transferred to a recipient-diode. The signal of the diode passes a multi-channel size classifier after a corresponding amplification. A pulse height analyzer then classifies the signal transmitted in each channel. These counts can be converted to a mass distribution from which different PM values derive.
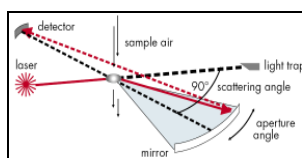
Fig.1 Measurement Principle of GRIMM Spectrometer.

Fig.2 GRIMM NanoCheck 1.320 Sensor.

Since the intensity of the scattered light decreases with the sixth power of the particle size, optical light scattering systems can't detect particles below about 0.1µm. As displayed in Fig.2, a GRIMM patented portable NanoCheck[TM] 1.320 sensor, which combines a unipolar diffusion charger, a time multiplexed electrical conductivity measurement and an aerosol faraday cup electrometer, can measure the total number concentration in the range of about 30nm to 400nm and the mean diameter of the aerosol number distribution in real time and continuously. This new portable NanoCheck[TM] 1.320 Sensor can work with any GRIMM aerosol spectrometer, getting the sample directly from the spectrometer. In this way the combination of both instruments makes it possible to monitor the full aerosol size range from a few nanometers up to 30µm in different size channels. This compactly designed detector can be used as an exposure monitor for indoor and outdoor aerosol nanoparticles.

In this work, by using a GRIMM environmental dust monitor (EDM 365) and a NanoCheck[TM] 1.320 Sensor, various measurements were carried out in a resident's garden in Ainring in Germany and in a traffic measuring station in Salzburg in Austria. EDM 365 reports PM10, PM2.5, PM1.0, particle counts as well as meteorological parameters such as temperature and relative humidity. Fig.3a illustrates the measured PM values of outdoor aerosols in a resident's garden in Ainring in Germany. There appear some peaks in the PM curves. Peak

1 shows that on Friday afternoon more people go back home by car and hold a dinner party or celebration nearby and the high peak is due to the fog and drizzle. Peak 2 and 3 result from traffic on Saturday and house heating by burning wood, respectively. On Sunday people go to church and then in about 1 hour they go back home, as illustrated in Peak 4. Thus, by monitoring PM values one can indentify and study the aerosol sources resulting from human activities, nearby traffic, meteorological effect like fog and drizzle, and so on.

A comparison of the outdoor aerosol number concentrations measured with NanoCheck 1320 and EDM 365 is made in Fig.3b. The difference between two measurements gives the particle number concentration in the size range of 25nm-0.25µm. EDM365 data multiplied by a factor fit well to Nanocheck data and the trend of both measurements seems to be the same. It shows that NanoCheck 1320 is a valuable addition to EDM 365, greatly expanding the size range of optical particle counters.
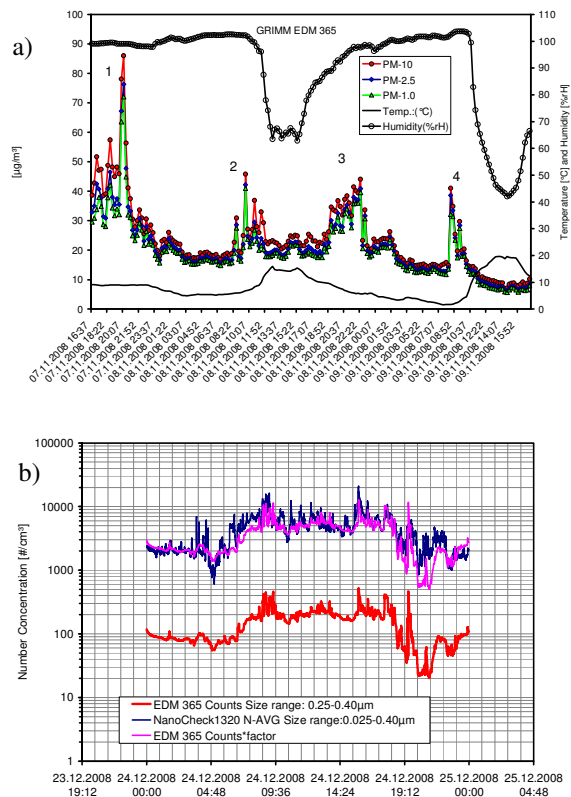

Fig.3 a) Results measured by GRIMM EDM 365; b) Comparison of the outdoor aerosol number concentrations measured with EDM 365 and NanoCheck.

Application of Computer Software for Airborne Particles Counting

B. Trivuncevic[1], G. Jereb[1,4], B. Poljšak[1], M. Bizjak[1,2] and S. A. Katz[3,4]

[1] University of Ljubljana, College of Health Studies, Poljanska 26 a, 1000 Ljubljana, Slovenia
[2] Environmental Agency of the Republic of Slovenia, Vojkova 1b, 1000 Ljubljana, Slovenia
[3] Rutgers University, Department of Chemistry, Camden, NJ 08102-1411, USA
[4] University of Nova Gorica, School of Environmental Sciences, Vipavska 13, Nova Gorica, Slovenia

Keywords: air pollution, TSP, alternative deposition method, particle counting

Dust emissions from various anthropogenic sources such us ore depots, coal pits or even quarries represent nuisance sources in residential areas. The inhabitants of the residential area Rožnik and Ankaran city are located near the Port of Koper have complained for several years now about dust emissions, which they observe in their living environment, on the vegetables, fruits, etc. and attribute to some of the activities at the port.

Particulate matter deposition is usually a complex mixture of particles of different origin, size and chemical composition. Sources of particles can vary; some of anthropogenic and some of terrestrial origin. For that reason simple alternative measurement device for quick estimation of direction and quantity of particulate matter, based on deposition and/or adhesion was developed (1). Two types of sampling devices were constructed. Both of them collect particulate matter from air on adhesive material (medical Vaseline) and enable collection in both the horizontal and vertical directions.

Plastic ball of 20 cm diameter, covered with Vaseline was used for sampling device 1. For sampling device 2 specially designed octagonal prisms in which nine glass plates covered with Vaseline were assembled in a way that collects particles coming from different directions on the adhesive surface (Figure 1). Sampling devices were located around the coal and iron ore depot in Port of Koper (Slovenia).
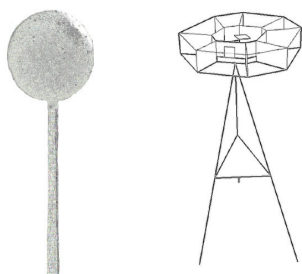
Figure 1. Appearance of sampling device 1 and 2

Previous study (Goličnik et al., 2008) already revealed that these new sampling devices are suitable for rapidly estimating the flow direction of major particulate matter sources. Particulate matter samples, collected in this way could also be analyzed qualitatively. Since the cost of both sampling devices, especially the cost of type 1, is relatively low, many such devices could be used for quick screening of environment in order to find the most representative locations for later placement of more sophisticated, accurate and expensive devices for air monitoring.

Since both methods are not sensitive enough for quantification of particulate mass by gravimetrical analysis counting of particles was used as an alternative method. Samples were analyzed using two different approaches: I) Particles were counted manually by visual approach using magnifying lens. On each side of the ball particles were counted according to template model on total surface of 5 cm^2 (Figure 2). II) From each ball or plate from octagonal sampler digital pictures were made and on them particles on 5 cm^2 surface were analyzed and counted by use of computer software.
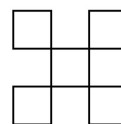

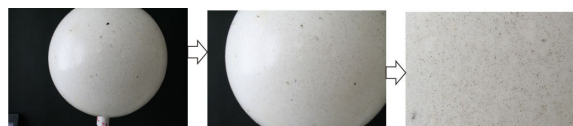Figure 2. Appearance of template model for particles counting

Figure 3. Sampling device 1 after 1 month exposure

The aim of this experiment was to compare visual counting with computer counting in order to evaluate the ease and accuracy with which the particles on the sampling device could be determined. In future we will try to correlate number of particles on surface with other standard methods (VDI, 1996) in order to extrapolate data collected in this manner with regulatory limits.

References

Goličnik B., Jereb G, Poljšak B, Planinšek A., Katz S.A. and Bizjak M. *Alternative method for quick estimation of direction and quantity of particulate matter by its deposition. EAC 2008, Thessaloniki.*

VDI und DIN Guideline VDI 2119 part 2 (1996) - *Measurement of Particulate Precipitations – Determination of dust precipitation with collecting pots made of glass.*

Program controlled gear complex for aerosol monitoring

T. E. Ovchinnikova[1], A. M. Baklanov[2], S. N. Dubtsov[2], I. V. Melekhov[2]

1 Institute for Water and Environmental Problems SB RAS, Morskoy pr. 2, IWEP, 630090 Novosibirsk, Russia
[2]Institute of Chemical Kinetics and Combustion SB RAS, Institutskaya, 3, 630090, Novosibirsk, Russia

Keywords: atmospheric aerosols, diffusion battery, optical particle counter, particle size distribution

A complex of two devices for atmospheric aerosol monitoring was developed in the Institute of Chemical Kinetics and Combustion. First of them is the diffusion spectrometer of aerosol DSA, or diffusion battery created in the institute. It was used for a long time for the analysis of concentrations and particle size distributions. The other one is optical particle counter AZ6. DSA is meant for the analysis of aerosol structure with particle sizes in the range from 3 to 200 nm, and AZ6 is used for aerosols with particle sizes from 200 to 1200 nm.

A specially developed computer program DSA09 controls the complex (separately or together). The program allows to set up measurements regimes, to accept and process data and to save them as files.

Diffusion battery penetration data are obtained as m measured concentration values c_i (m is the total number of battery ports)

To obtain particle size distribution f(r) one needs to solve the set of integral equations

$$c_i + e_i = \int_{r_{min}}^{r_{max}} f(r) p_i(r) dr, \quad i = 1...m \ ,$$

where c_i is measured concentration value, e_i is unknown measurement error and $p_i(r)$ is the penetration function for i-th port of a battery. The method of use is based on the idea that as set of solutions is convex and error distribution is known, resulting solution may be represented as approximate sum of all possible solutions multiplied by their statistical weights. (Ovchinnikova et all, 2006).

As the data error is estimated during measurements particle size distribution can be obtained even under sharp fluctuations of aerosol concentrations resulting to nonmonotonic data.

Graphic interface lets to watch concentrations and structure of aerosol dynamics. On the Fig. 1 the main window of the program of data view and process with the data of one measurements is shown.

Data obtained with DSA include:

- counts values (panel "Counts");
- graph of measured counts, time of measurement beginning, mean values, error assessment, total concentration, (left upper widow); a dashed line represents data reconstructed from calculated distribution;
- calculated particle size distribution (left lower window).

Data obtained with AZ6 include:

- time of measurement beginning, mean values, total concentration, (right upper widow);
- particle concentrations diagram (right lower window).

A panel View Progress is assigned for measurements review (subsequently or in random order).

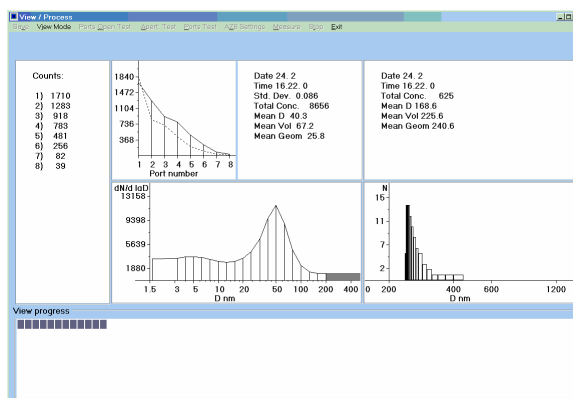The data represented on the figure are the result of laboratory experiment.

Figure 1. Laboratory experiment data.

Ovchinnikova, T. E., Eremenko, S .I. & Baklanov, A.M (2006). in *Proc. 7th Int. Aerosol Conf.* St.Paul, Minnesota, 497-498.

Validation of a new Atmospheric Pressure Interface Time-of-Flight mass spectrometer (API-TOF) to measure the composition of sub-2 nm aerosol particles

M. Ehn[1], H. Junninen[1], K. Neitola[1], M. Sipilä[1], H. Manninen[1], T. Petäjä[1], K. Fuhrer[2], M. Gonin[2], U. Rohner[2], S. Graf[2], M. Kulmala[1], and D.R. Worsnop[1,3]

[1]Department of Physics, University of Helsinki, P.O.Box 64, 00014, Helsinki, Finland
[2]Tofwerk AG, Switzerland
[3]Aerodyne Research Inc., Billerica, MA, USA

Keywords: Cluster ions, mass spectrometry, ion mobility, instrumentation

The lower size limit for aerosol particle detection has long been 3 nm. During recent years, new methods of detection and, also indirect composition measurements, have been presented (e.g. Kulmala *et al.*, 2007). Now, a new Atmospheric Pressure Interface Time-of-Flight mass spectrometer (API-TOF) is being developed at Tofwerk AG, Thun, Switzerland. This instrument will give new insight into particle chemical composition in the range 0-3000 Da, which corresponds roughly to a particle size range up to 2.5 nm in diameter. These are the sizes where atmospheric nucleation takes place, and is therefore of great interest. The API-TOF is currently being tested in the laboratory at the department of physics at University of Helsinki, through comparison with a high resolution Herrmann differential mobility analyzer (HDMA, Herrmann et al., 2000) and a neutral cluster and air ion spectrometer (NAIS).

The API-TOF samples 0.9 L/min of air (through a 300 µm orifice), directly from ambient pressure. Two quadrupoles then guide ions as the gas is pumped away. Finally, an ion lens focuses the ions into the TOFMS extraction region. The TOFMS operates in two modes, V or W, where the letter signifies the flight path of the ions in the TOFMS; i.e. there are one or two reflections in the V and W modes, typical m/Q resolving power of roughly 3000 or 5000, respectively.

The NAIS and HDMA both measure cluster ion mobility. The relationship between ion mobility and mass are somewhat uncertain. Here we have used the empirical fit described in Mäkelä *et al,* 1996. Both the NAIS and HDMA measure the distributions at ambient pressure whereas the API-TOF pressure is reduced to 10^{-6} mbar. Therefore the cluster distribution can be perturbed both due to evaporation at low pressure, and fragmentation in the quadrupole ion guides.

One of the first experiments generated ions by passing laboratory air through a corona charger, measuring the output with all three instruments in parallel. Preliminary results are plotted in Fig. 1. The top panel shows the cluster distribution as measured by the NAIS and HDMA. It is evident that the HDMA has superior resolution compared to the NAIS, but nevertheless, there is an agreement between the instruments. The bottom graph shows an average mass spectrum measured simultaneously by the API-TOF. The pattern of peaks at higher masses, the largest at 610 Th (~1.6 nm), result from a short piece of conductive silicone tubing in the inlet, showing how sensitive the system is to contamination. The mobility spectra and the mass spectrum are not an exact match, but as mentioned, this was not expected.

High resolution analysis of the mass scale and isotope patterns should allow for identification of more peaks in Fig. 1. The detailed analysis of the spectra obtained so far has only begun, and more experiments will be performed during a 3 week intensive. The goal is to use API-TOF to measure aerosol clusters in ambient air, at orders of magnitude lower concentrations.
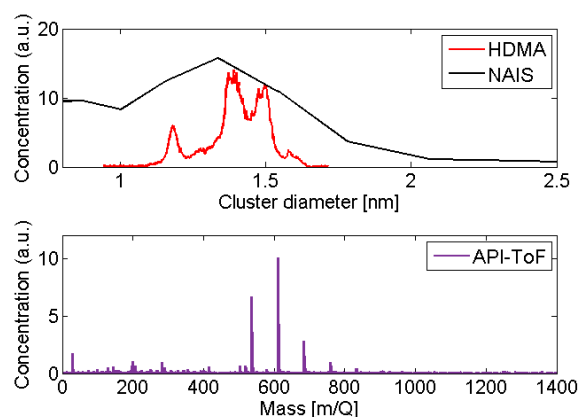

Figure 1. Size distributions of positive ions produced by a corona charger, measured with three different instruments.

Herrmann,W., Eichler, T., Bernardo, N., and Fernandez de la Mora, J. (2000). *Abstract to the annual conference of the AAAR*, St. Louis, MO.

Kulmala, M., Riipinen, I., Sipilä, M., Manninen, H. Petäjä, T., Junninen, H., Dal Maso, M., Mordas, G. Mirme, A., Vana, M., Hirsikko, A., Laakso, L., Harrison, R., Hanson, I., Leung, C., Lehtinen, K., Kerminen, V-M. (2007). *Science*, Vol. 318. No. 5847, pp. 89 - 92.

Mäkelä, J., Jokinen, V., Mattila, T., Ukkonen, A. and Keskinen, J. (1996). *J. Aerosol Sci.*, Vol. 27, No. 2, pp. 175 - 190.

Parallel-DMA (PDMA) – a tool for characterization and enrichment of aerosol nanoparticles

Anne Maißer[1], Günter Allmaier[2] and Wladyslaw W. Szymanski[1]

[1]Faculty of Physics, University of Vienna, 1090, Vienna, Austria
[2]Institute of Chemical Technology and Analytics, Vienna University of Technology, 1060, Vienna, Austria

Keywords: nanoparticles, bioaerosols, collection efficiency, characterization

Electrostatic methods provide numerous options for the characterization and investigation of aerosol nanoparticles. Differential mobility analysis (DMA) has proven its ability to characterize according to size and separate inorganic particles as well as aerosol particles of biological origin such as proteins or viruses. Because it operates under atmospheric pressure it offers an opportunity also to utilize this technique for micro-preparative applications. For that reason a parallel-DMA (PDMA) system was constructed and has proven its feasibility to simultaneously monitor the size distribution of aerosolized nanoparticles and to select one specific fraction particle size fraction (Allmaier et al. 2008). PDMA contains of two identical DMAs working in parallel. The scanning nano-DMA1 delivers the complete size spectrum of the aerosolized particles. The nanoDMA1 is combined with an electrical aerosol detection device working on the Faraday cup principle. An identical separation unit – the nano-DMA2 - running parallel with the nano-DMA1 operates at one given voltage setting (separation) and can be used for sampling or enrichment (collection) of the one selected size class of nanoparticles..

For further physical or chemical investigation of this specific classified size fraction it is necessary to remove the nanoparticles from the gas phase after nano-DMA2 separation. Thus the PDMA was used in combination with an electrostatic nano-sampler (ENS). The ENS was designed specifically for the usage on bionanoaerosol particles but it works equally well for inorganic particles. It uses electrostatic force to collect charged particles exiting the nanoDMA2. The ENS is a kind of an impinger using a liquid as collecting media to provide "soft landing" to the particles. Between the nozzle outlet and the liquid surface an electrostatic field is applied. The appropriate choice of liquid offers both the conductivity and if needed an appropriate environment to preserve biological activity of particles impacted and captured on its surface. Several proteins, dendrimers and silica particles covering equivalent mobility diameters from 5 to 30 nm were chosen to evaluate the collection efficiency of the ENS.

It was shown that the appropriate voltage applied to the liquid could increase the collection efficiency of the ENS up to 100 % for all investigated particles. The ultimate verification of the feasibility of the PDMA-ENS system is to prove the presence and, in the case of bioaerosols, the biological viability of the size-selected nanoparticles in the ENS liquid.

Various nanoparticles were classified and sampled on liquid surface in the ENS over periods of up to 50 hours. The sample was consequently re-injected to the Electrospray Aerosol Generator (Mod. 3480, TSI, Inc.) and again analyzed with the PDMA. Fig.1 shows the size distributions for HS-30 silica particles (Sigma Aldrich). The exactly same location of measured peaks for the stock suspension and in the liquid sampled silica particles proves the feasibility of the approach.
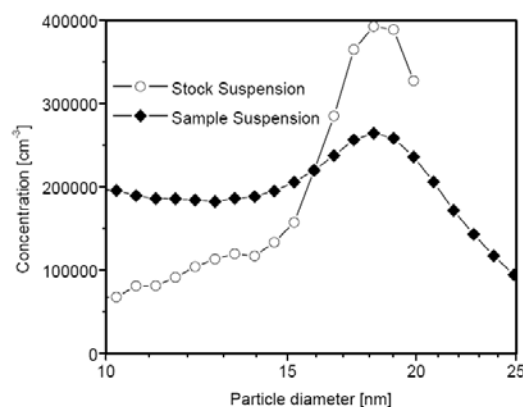

Figure 1. PDMA size distributions of silica particles.

An enzyme activity of the sampled enzyme was tested to answer the question on the preservation of the biological function after the aerosolization, charging, separation and sampling step. The bioactivity of the enzyme β-galactosidase (equivalent mobility diameter 8 nm) was measured before and after the sampling process. The enzyme activity test revealed the existence of activity in the enzyme after the sampling process. This is an evidence for a successful effort combining electrospraying and DMA-technique with "soft landing" collection and enrichment of biological nanoparticles.

Allmaier, G. et al. (2008), *Journal of the American Society of Mass Spectrometry* **19**, 1062-1068.

Diffusion based nanoparticle monitor using QCM-technology

J. Leskinen[1], J. Joutsensaari[3], A. Jakorinne[4], M. Laasanen[4], J. Jokiniemi[1,2]

[1]Univ. of Kuopio, Department of Environmental Science, P.O. Box 1627, FI-70211 Kuopio, Finland.
[2]VTT Technical Research Centre of Finland, P.O. Box 1602, 02044 VTT, Espoo, Finland
[3]Univ. of Kuopio, Department of physics, P.O. Box 1627, FI-70211 Kuopio, Finland.
[4]Savonia Univ. of Appl. Sci., Information Technology R&D Unit, P.O. Box 6, FI 70201 Kuopio, Finland

The use of nanoparticles has increased rapidly over the past decade. Therefore health effects of these ultra fine particles are of public concern and it has become important to monitor concentrations of nanoparticles in the air at workplaces where nanoparticles are handled.

We have developed an inexpensive method and device called nanoparticle monitor to monitor nanoparticle concentrations in the air surrounding employees. At the moment we are in a testing phase, a prototype has been constructed and the device gives a response for high nanoparticle concentrations.

The device is based on two vibrating quartz crystals (QCM) which detect particle mass deposited on them (Ho, 1984). In our current prototype, characteristic frequency of the crystals is around 5 MHz and the frequency change, caused by the deposited mass is detected with a precision of 0.1 Hz. This enables a theoretical mass sensing limit of around 2.2 ng. The crystals are placed between two polyoxymethylene-plastic blocks. The blocks are put together, with the crystals facing each other (fig1). The crystals are separated from each other with a spacer plate. The plate is hollow in the middle and the distance between the crystals can be changed by using spacers with demanded thickness. In the present study, a 0.2 mm foil was used as a spacer. The sample aerosol flows through the device and a fraction of the particles is deposited on the crystals via diffusion.
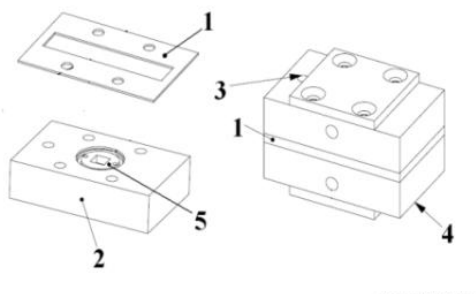
Figure 1. Schematic drawing of the prototype. 1) spacer plate, 2) plastic block, 3) aerosol in, 4) aerosol out and 5) crystal holder.

The aerosol flow rate can be varied from 0 to around 1.5 lpm. Calculations using particle diffusion equations (Hinds, 1999) predict that the greater the flow rate, the more mass will be deposited on the crystals. The 0.2 mm spacing is quite narrow and turbulence would not increase the deposition rate.

A sample aerosol was produced using a constant output atomizer (TSI) with ammonium sulfate-water-solution and was diluted with dry pressured air. The particle distribution was measured by SMPS at the beginning of the test period to get number concentration around 10^6 #/cm^3 and the mode around 50 nm.

The sample aerosol guided to the nanoparticle monitor was dried to remove moisture from the particles. A preimpactor was used to remove large particles. Particle exposure gave a clear response when the impactor's cut 50 % diameter was as low as 355 nm.
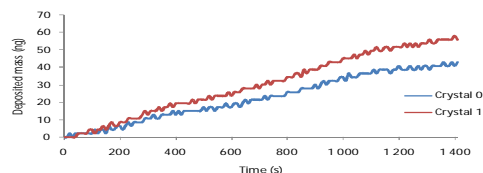

Figure 2. Nanoparticle mass deposited on the crystals with flow rate 1.5 lpm and preimpactor cut 50 % diameter 355 nm.

The nanoparticle monitor will be further developed to enhance the particle deposition. In addition different methods will be tested to prevent larger particles from depositing on the crystal surfaces.

M. H. Ho (1984). Application of Quartz Microbalances in Aerosol Mass Measurements. Application of Piezoelectric Quartz Crystal Microbalances, Elsevier Science Publishers.

Hinds W. C. (1999). Aerosol technology. A Wiley-interscience publication.

Determination of particulate ammonium (NH_4^+) by thermal dissociation and detection of the generated gaseous ammonia

Ch. Hueglin[1], H. Burtscher[2], P. Graf[1], C. Houle[2], D. Meier[2] and E. Rochat[3]

[1] Empa, Swiss Federal Laboratories for Materials Testing and Research, 8600 Duebendorf, Switzerland
[2] University of Applied Sciences Northwestern Switzerland, 5210 Windisch, Switzerland
[3] Omnisens SA, 1110 Morges, Switzerland

Keywords: Ammonia, ammonium nitrate, ammonium sulfate, inorganics, thermal decomposition.

In the continental boundary layer, inorganic salts are main constituents of the atmospheric aerosol. They mainly consist of ammonium (NH_4^+), sulfate (SO_4^{2-}), nitrate (NO_3^-) and small amounts of sodium (Na^+) and chloride (Cl^-) (Putaud et al., 2004). NH_4^+ exists preferably as ammonium sulfate (($NH_4)_2SO_4$) and semi-volatile ammonium nitrate (NH_4NO_3).

Because ammonium is of considerable environmental importance, a variety of measurement techniques have been developed during the past. These include filter-based methods, continuous particle collection systems with subsequent analysis by ion chromatography (IC), as well as aerosol mass spectrometry. However, simple and reliable techniques for time-resolved long-term measurement of ammonium are not readily available.

As mentioned above, NH_4NO_3 is semi-volatile and easily dissociates at ambient conditions, contributing to the well known volatilisation losses often encountered in measurements of ambient particulate matter (PM). In contrast, ($NH_4)_2SO_4$ is non-volatile at atmospheric conditions. To our knowledge, there is no conclusive information about the thermal decomposition mechanism available in the literature. Halstead (1970) studied the thermal dissociation of ammonium sulfate at 400°C and found that volatilisation occurs in two distinct sets of reactions. First, ammonium pyrosulfate (($NH_4)_2S_2O_7$) and NH_3 is formed, in a second stage ammonium pyrosulfate is decomposed forming NH_3, SO_2 and N_2. Kiyoura & Urano (1970) proposed a more complex thermal dissociation process involving ammonium bisulfate (NH_4HSO_4), triammonium sulfate (($NH_4)_3HSO_4)_2$), ammonium pyrosulfate and sulfamic acid (NH_2SO_3H) as intermediates.

In this study, we investigate the potential of a novel approach for quantitative determination of NH_4^+ based on thermal dissociation of ammonium compounds. Our technique is conceptually similar to methods developed for analysis of nitrate in aerosol particles (Yamamoto & Kosaka, 1994). It is based on the collection of dried ambient aerosols on a cold sampling filter maintained at 4°C, followed by controlled thermal dissociation of the collected ammonium compounds and finally, by time resolved detection of gaseous ammonia that results from thermal dissociation.

A prototype sampler and thermal dissociation unit was built and tests of the thermal dissociation of ammonium salt test aerosols (ammonium nitrate, ammonium sulfate and ammonium bisulfate) and ambient aerosols were performed. We found that the used technique is feasible for automated semi-continuous determination of NH_4^+. A major problem was the high adsorptivity and reactivity of NH_3. This requires a very careful selection of materials which are in contact with ammonia. In addition, a trap for acids (i.e. nitric acid and sulfuric acid), which are formed during the dissociation, had to be installed. Otherwise, the formed acids may deposit on available surfaces and act as a sink for NH_3. Some other technical problems still have to be solved. Figure 1 shows results for a laboratory sample (left) and a sample from outdoor aerosol. In both cases the sulfate and the nitrate peak can clearly be resolved.
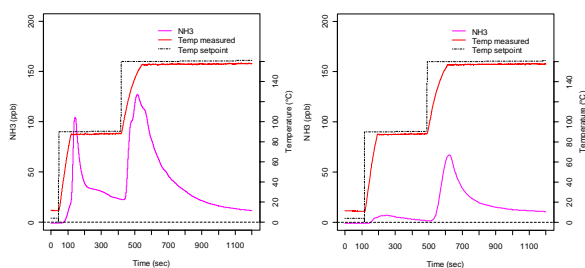

Figure 1. Thermal dissociation of mixed NH_4NO_3 and ($NH_4)_2SO_4$ aerosols generated by atomising an aqueous solution of the two salts (left). Right graph: NH_3 signal from thermal dissociation of ambient aerosol particles collected during 2.5h on a summer afternoon with obviously low NH_4NO_3 concentration (July 24 2008, outdoor temperature = 24°C).

Halstead, W.D. (1970). *J. appl. Chem.*, 20, 129-132.

Kiyoura R., Urano K. (1970). *Ind. Eng. Chem. Process Des. Develop.*, 9, 489-494.

Putaud, J.P. et al. (2004). *Atmos. Environ.*, 38, 2579-2595.

Yamamoto, M., Kosaka, H. (1994). *Anal. Chem.*, 66, 362-367.

Characterization of the Hermann and Attoui DMA in the super 3 nm range.

M. ATTOUI

Physical Department, University Paris XII France

Keywords: DMA, mobility, transfer function, nano particles.

Juan Fernandez de la Mora with various collaborators and colleagues at Yale University (CT. USA) introduced last few decades high resolution DMAs (Hermann, Rosser, Attoui DMAs) for ions and particles in the sub 3 nm range. These DMAs work at high sheath flowrates (around 1000 lmin^{-1} for the HDMA and 4 000 lmin^{-1} for the ADMA for example) to minimize diffusion losses and increase the resolution in terms of mobility diameters. All these DMAs have been tested with standard positive ions (tetra-alkyl ammonium halides) in the sub 3 nm range, produced with electrospray method. This paper presents experimental measurement results of the transfer function of the HDMA and ADMA running at sheath flowrates ranging from 50 to 1 000 1 min^{-1} with particles larger than 3 nm. The super 3 nm particles are produced with a hot wire generator and/or atomizer. A hot wire generator is used for the production of singly charged particles from 3 to 20 nm. Two identical ADMA are used in serial to measure the transfer function with 'large' particles. Unfortunately it was not possible to loan a second HDMA for this study. An ADMA is used as a generator for the HDMA transfer function measurement. Atomizer (for deionised and tape water, polystyrene spheres in clean water and diethyl sebacate in ethanol) is used for particles larger than 20 nm. The first DMA (Attoui type) is used as a generator of monomobile particles at a constant voltage while the voltage of the second (tested) DMA is scanned from 0 to 6 kV.

The particles leaving the atomizer at 3 lmin^{-1} are dried in diffusion dryer and neutralized in Kr 85 TSI neutralizer before their introduction in the first DMA. The particles produced with the wire generator are not neutralized since they are self singly charged. A home-made Faraday cup electrometer (FCE) or CPC is used as a detector for the monodisperse aerosol. The sheath flow rate in the both DMAs is measured with TSI mass flowmeters. The both DMAs run in open loop. The first one runs over pressure by pushing clean air with a blower through a TSI mass flowmeter. The second DMA runs underpressure by sucking with a second blower and second TSI mass flowmeter. A laminar flowmeter is used in the aerosol flow between the two DMAs. The polydisperse aerosol is introduced at 3 lmin in the first DMA. The monodisperse aerosols is sucked at 3 lmin.

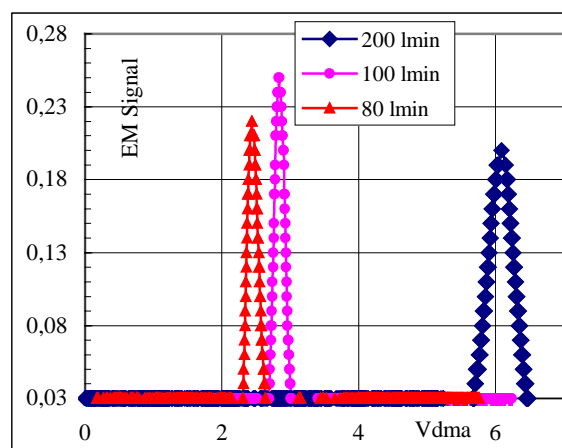Fig 1 gives the results for the ADMA running at different flowrates from 80 to 800 l min^{-1}.

Fig 1 Transfer functionoftheADMAat 3 sheath air flowrates.

Challenges and Barriers for the Development of SiC Nanoparticle Measurement Technology in Laser Pyrolysis Reactors

A. Asimakopoulou[1], M. Kostoglou[1,2] and A.G. Konstandopoulos[1,3]

[1]Aerosol & Particle Technology Laboratory, CERTH/CPERI, P.O. Box 60361, 57001, Thessaloniki, Greece
[2]Department of Chemistry, Aristotle University, Univ. Box 116, 54124, Thessaloniki, Greece.
[3]Department of Chemical Engineering, Aristotle University, PO. Box 1517, 54006, Thessaloniki, Greece

Keywords: silicon carbide, laser pyrolysis, fractal aggregates, on-line measurements, nanoparticles.

The on-line monitoring of aerosol size distribution has proven to be a valuable tool in various applications concerning atmospheric pollution, health effects or industrial nanoparticles production. For the last case, an on-line monitoring system could greatly enhance the process optimization, the constant product quality and the achievement of safe operational conditions. However, several issues must be addressed regarding the aerosol sample handling, the design and location of sampling ports, etc. The aim of the present study is to deal with the challenges that appear during on-line measurements (such as the level and the kind of dilution, particle losses, etc.) in order to proceed with in-situ measurements during the synthesis of SiC nanoparticles by laser pyrolysis.

Proper aerosol sampling procedures presented in the literature (e.g. Burtscher, 2001), alert to the challenges that must be addressed in order not to affect the resulting particle size distribution. Particle losses may occur in the sampling path due to diffusion, impaction, thermophoresis, or even internally in the monitoring instrument. Among them, diffusion losses are more prevalent for smaller particles and, thus, it is important to quantify accurately the nanoparticle losses when sizing aerosol particles on-line. For high concentration aerosols (the case of laser pyrolysis nanoparticle production), care must be taken to properly dilute the sample to minimize any effects of condensible species and coagulation and to effectively "freeze" the size distribution as it is in the process stream. All these factors must be examined before building up an on-line aerosol sampling and measuring system.

In order to study where and how to place sampling ports in a SiC laser pyrolysis reactor, it is necessary to understand the transformations of the particle size distribution caused by the physical and chemical phenomena that occur inside the reactor. For this reason, a theoretical consideration of the laser pyrolysis process is performed. The key feature of the process is the excitation of silane by a CO_2 laser. The resulting species are very reactive and produce solid silica on which acetylene reacts leading to aggregate generation with primary particles consisting of Si and SiC. The above phenomena occur very fast (along few mm of the reactor). In the rest of the reactor only coagulation takes place (irreversibly due to the partial sintering at the necks between the primary particles). A fractal aggregation model is developed to describe the particle dynamics in the second part of the reactor in order to understand better the measured aggregate size distributions.

Apart from the theoretical approach, the aforementioned barriers in on-line aerosol sampling and measuring are examined here, also, in practice. Therefore, for the development of appropriate SiC aggregate nanoparticle measurement methods, an experimental set-up for ex-situ measurements has been created. In this set-up, an aerosol stream of SiC nanoparticles synthesized by laser pyrolysis is generated and, afterwards, properly diluted. An SMPS (TSI Inc. SMPS 3936) is recording several nanoparticle size distributions and useful information is obtained regarding the type of size distribution (unimodal or multimodal), the mean diameter and the standard deviation of each peak. Results obtained with the SMPS are compared with ex-situ characterization techniques (BET, XRD, SEM, TEM). The above set-up forms the basis for a monitoring system (see Figure 1) which will allow the on-line qualitative and quantitative analysis of crucial characteristics of silicon carbide nanoparticles in a laser pyrolysis reactor process.
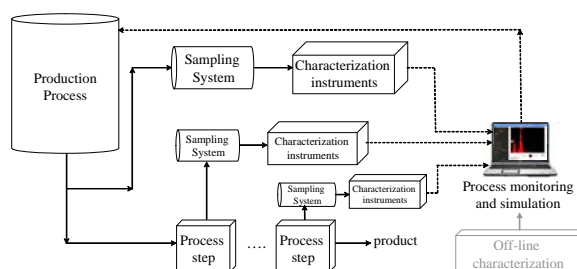

Figure 1. Lay out for SiC nanoparticles measurement.

Burtscher, H., 2001., *Report for Particle Measurement Programme*, BUWAL/GRPE, March 2001.

Thermal desorption/laser photo-ionisation aerosol mass spectrometry for on-line monitoring of molecular organic compounds from individual aerosol particles

M.Bente[1,2], M.Sklorz[1,2], T.Streibel[1,2] and R.Zimmermann[1,2,3]

[1]Institute of Ecological Chemistry, Helmholtz Zentrum München, D-85764, Oberschleißheim, Germany
[2]Chair of Analytical Chemistry, University of Rostock, D- 18051, Rostock, Germany
[3] bifa-Umweltinstitut, D-86167, Augsburg, Germany

Keywords: Aerosol mass spectrometry, Single particle analysis, Polycyclic aromatic compounds, Source identification

Within the last decade, aerosol mass spectrometry has evolved to a versatile tool for applied and fundamental aerosol research. Up to now, however, the detection of molecular organic species by aerosol mass spectrometry is very difficult. Recently a new single particle laser ionisation mass spectrometer, using a two-step laser-desorption photo-ionization approach for detection of aromatic molecular compounds on individual particles was developed and successfully tested (Bente 08). Tracked and sized individual single particles (SP) herein firstly are laser desorbed (LD) on the fly within the ion source of the mass spectrometer by a IR-laser pulse (CO_2-laser, 10.2 µm). After some microseconds the released aromatic molecules are selectively ionized by an intense UV-laser pulse (ArF excimer, 248 nm) in a resonance enhanced multiphoton ionisation process (REMPI). The ions are detected in a time of flight mass spectrometer (TOFMS). With this setup (i.e. laser desorption –REMPI-ionisation – single particle – Time-of-flight mass spectrometry or LD-REMPI-SP-TOFMS) it is possible to detect profiles of polycyclic aromatic hydrocarbons (PAH) and their derivatives which are predominantly bound to the ambient fine particulate matter (PM). It could be shown, that source specific molecular indicators for diesel car emissions, gasoline car emissions as well as for biomass burning (soft/hard wood) are detectable. As PAH and their derivatives may show both, chronic toxicity (i.e. many PAH are potent carcinogens) as well as acute toxicity (i.e. inflammatory effects due to oxidative stress) and are discussed to be relevant for the observed health effects of ambient PM, a better understanding of the occurrence, dynamics and particle size dependence of particle bound-PAH is of particular interest. In this context it was decided to make the LD-REMPI-SP-TOFMS aerosol mass spectrometric technology for organic monitoring more suited for field measurements. For this purpose the laser desorption step (LD) is substituted by a thermal desorption (TD) step, similar as in case of the Aerodyne AMS technology (Bente 2009). However, due to the features of the pulsed REMPI photo-ionisation a single particle detection of molecular organic compounds remains possible. With the current aerosol inlet system particles from about 400 nm to 10 µm are accessible. The novel thermal desorption –

REMPI-ionisation – single particle – Time-of-flight mass spectrometry approach (TD-REMPI-SP-TOFMS) was tested with standard aerosol in the laboratory (re-dispersed wood ash). Furthermore real-world combustion aerosols were investigated (diesel/gasoline car emissions). Finally ambient measurements were performed using a virtual impactor enrichment unit to increase the detection frequency of ambient particles in the covered size range. It was possible to find distinct differences in the pattern of PAH and PAH derivatives in the single particle mass spectra from different sources (e.g. gasoline, wood combustion and diesel emissions). In Figure 1 a TD-REMPI-SP-TOFMS mass spectrum from ambient air (winter) is shown.
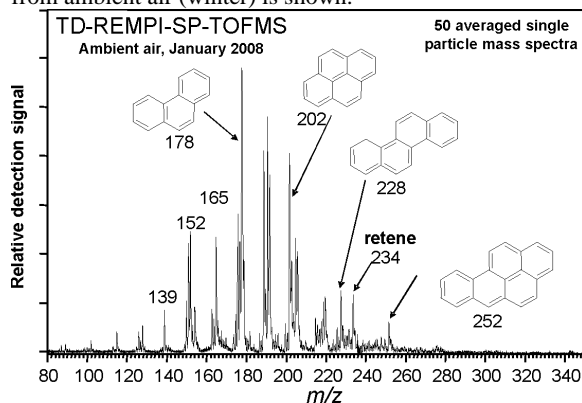

Figure 1: TD-REMPI-SP-TOFMS mass spectrum from ambient air in winter 2008 (50 single particle mass spectra averaged, Oberschleißheim, Germany). Beside several prominent PAH masses, the peak at 234 m/z can be assigned to retene, a wood combustion tracer.

The results obtained with the novel on-line thermal desorption method are comparable to the ones obtained by the earlier, more sophisticated two laser-technology. In conclusion, on-line thermal desorption laser photo-ionization single particle mass spectrometry (TD-RTEMPI-SP-TOFMS) represents a promising technology for field measurements and source apportionment studies based on single particle organic analysis. It is planned to apply the technology at the Augsburg aerosol monitoring super-site of the Helmholtz-Zentrum München.

Bente, M., Sklorz, M., Streibel, T., Zimmermann, R. *Anal. Chem. 80* (2008) 8991–9004
Bente, M., Sklorz, M., Streibel, T., Zimmermann, R. *Anal. Chem.* 81 (2009) in press

Monitoring of growth of cloud droplets ensembles with soot and salt condensation nuclei

L. Vámos, P. Jani

Research Institute for Solid State Physics and Optics, Konkoly-Thege str. 29-33. H-1121. Budapest, Hungary

In a simple experiment the scattered intensity of an ensemble of particles is easily collected during an appropriately short time of the condensation process. While the steady state is reached according to the thermo dynamical conditions the scattered data can be collected in a few milliseconds. This gives an adequately accurate estimate for the mean intensity and the variance intensity.

In an earlier work (Jani et al, 2002) we have shown that the ratio of the mean intensity, $\overline{I}$, to its standard deviation, σ_I, on the particle ensemble is a constant, depending on the number of the scattering particles:

$$\frac{\overline{I}}{\sigma_I} = \sqrt{\overline{N}} \, \frac{\overline{I_1}}{\sqrt{\sigma_{I_1}^2 + \overline{I_1}^2}}, \qquad (1)$$

where $\overline{I_1}$ the mean value and σ_{I_1} is the standard deviation of intensity scattered on single particles.

If we assume that the number of particles in a sensing volume changes according to the Poissonian statistics with constant mean number and deviation, then the change of the scattered intensity can be directly attributed to the condensation/evaporation of the coated water layer. The purpose of this paper is to extract the scattering data from ensemble of particles which can be attributed to the change of the particle radius.

We now consider the scattering properties of single coated soot (n=1.96+i0.66) and salt (n=1.54) particles by Mie computation based on our earlier study in [Jani, P. & Vámos, L., 2006]. The scattered intensity ratio relative to homogenous water droplets is shown in Figure 1. The core size was varied up to
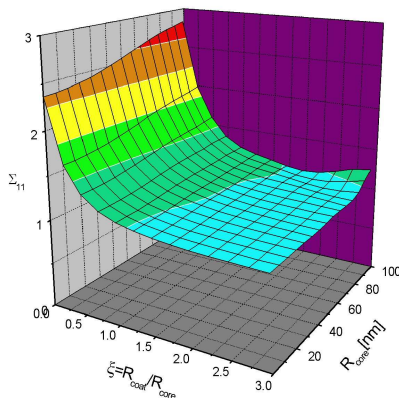

Figure 1. Scattered intensity of cloud droplets with salt nuclei relative to pure water droplets as a function of the core radius and the relative water layer thickness radius.

200nm and the relative coat radius up to three times of the core.

Ensemble data were generated from 1000 particle in average by Monte Carlo method according to the Poissonian distribution. The lognormal drop size distribution was generated for fixed 200nm salt and soot core size. The illumination pulse train consists of 1000 pulses at 1064nm. As the monodispersity is assumed the $\overline{I}/\sigma$ ratio gives directly the square root of the average particle diameter independent of the size and material (refractive index) of the particle or the illumination wavelength.
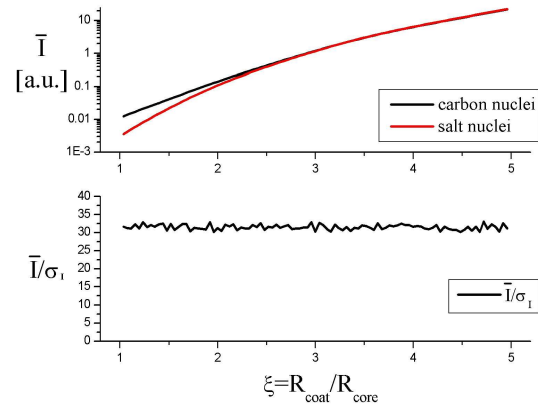

Figure 2. Average scattered intensity for cloud droplets with soot and salt nuclei (top) and the ratio of the average scattered intensity to its standard deviation as a function of the relative radius.

The average scattered intensity has a dynamic range of three orders of magnitude meanwhile the average particle number and so the $\overline{I}/\sigma$ doesn't change. The result gives the possibility of a simple measurement of the layer thickness from the statistics of the scattered intensities. By the way the constant $\overline{I}/\sigma$ ratio gives the average particle number in the sensing volume for monodisperse particles. A non-intrusive optical method was suggested for the online monitoring of the condensation process.

Jani P. et al (2002), *J. Aerosol Science*, 33, 694-707.
Jani, P. & Vámos, L. (2006), in *Proc. 7th International Aerosol Conference IAC2006* St. Paul, Minnesota, USA, 10-15 Sept., 490p.

Application of on-line time-of-flight aerosol mass spectrometry for the determination of molecular iodine

M. Kundel, M. Schott, M. Ries and T. Hoffmann

[1]Department of Inorganic and Analytical Chemistry, Johannes Gutenberg-University, Duesbergweg 10-14, 55128, Mainz, Germany

Keywords: aerosol mass spectrometry, on-line measurements, molecular iodine, MBL

In the last few years, there has been increasing evidence that iodine species do have an important influence on the marine atmospheric chemistry. Recent studies show that iodine species are involved in the tropospheric ozone depletion, the formation of new particles in the marine boundary layer (MBL) and the enrichment of iodine in the marine aerosol.

Numerous laboratory and tropospheric field measurements show that molecular iodine (I_2) and biogenic volatile organoiodine compounds (e.g. CH_3I, CH_2I_2), which are released into marine atmosphere by algae and phytoplankton, are suggested to be the most important precursors for reactive iodine in the MBL (O´Dowd & Hoffmann 2005). During daylight these compounds are rapidly photolyzed to I atoms because of their photochemical instability. Their major fate is the reaction with ozone forming the iodine monoxide radical (IO). Further reactions of IO lead to the formation of higher iodine oxides (Hoffmann et al. 2001), which finally nucleate and form new particles. Natural new particle conversion via gas-to-particle is an important process determining the concentration of atmospheric aerosols. In their evolution aerosols can act as cloud condensation nuclei. Thus aerosols have an indirect effect on the Earth´s radiative budget and consequently on the Earth´s climate.

However, the identification and quantification of reactive iodine containing compounds is still an analytical challenge. This work presents the development of an on-line method for the determination of molecular I_2 using time-of-flight aerosol mass spectrometry (ToF-AMS). Aerosol mass spectrometry (AMS) provides a real-time analysis of the particle size, the particle mass and the chemical composition of non-refractory aerosols.

A direct measurement of gaseous I_2 by ToF-AMS is not possible. Therefore molecular iodine has to be transferred from the gas phase to the particle phase before entering the ToF-AMS. For this purpose α-cyclodextrin was used as a derivatization agent. α-cyclodextrin molecules consist of a hydrophilic surface and a hydrophobic cavity. Due to its hollow cone structure α-cyclodextrin is capable of forming an inclusion complex with I_2.

The derivatization reaction was carried out in a 10L reaction chamber made of glass. A fine spray of α-cyclodextrin, which had been generated by an atomizer, was continuously introduced into the reaction chamber. Gaseous I_2 was added into chamber by using a temperature controlled and nitrogen flushed test gas source, which was based on an open tube diffusion technique. After exiting the reaction chamber, the aerosol was analysed by ToF-AMS.

Hoffmann, T., et al. (2001). *Geophysical Research Letters*, 28, 1949-1952.

O´Dowd, C.D., & Hoffmann, T. (2005). *Environmental Chemistry*, 2, 245-255

Preview on Nanoparticle Monitors

A. Dahl, A. Gudmundsson and M. Bohgard

Ergonomics and Aerosol Technology, Lund University, SE-22100, Lund, Sweden

Keywords: MiniDiSC, NanoCheck, NanoTracer, Indoor Air Quality

MiniDiSC (University of Applied Sciences, Windisch, CH), NanoCheck (Grimm Aerosol) and NanoTracer (Philips Research) are new, light weight, battery powered aerosol instruments that are based on electrical measurement techniques. The MiniDiSC is a handheld version of the DiSC (Fierz et al. 2007). The handheld NanoTracer (Marra 2008) and the portable NanoCheck (Schneider 2009) are based on similar measuring principle. These instruments are developed for measuring nanoparticles and are able give fair estimates on number concentration and particle mean diameter. In this study the instruments were tested on candle smoke.

The NanoTracer and the MiniDiSC was at the time of the study in the final stages of development. The results are, therefore, not necessary representative for the final products.

The three instruments were calibrated by the manufacturers with salt aerosols. During the tests the instruments where run in parallel with a uCPC (model 3025, TSI) and an SMPS-system consisting of a Vienna DMA and a 3760A CPC (TSI). The candle smoke was generated by ten candles and the smoke was then led to a $22m^3$ chamber were the instruments were placed. After reaching a mass concentration of $200\mu g/m^3$ the candles were extinguished. The chamber was continuously ventilated with particle free at an air exchange ratio of $5h^{-1}$.
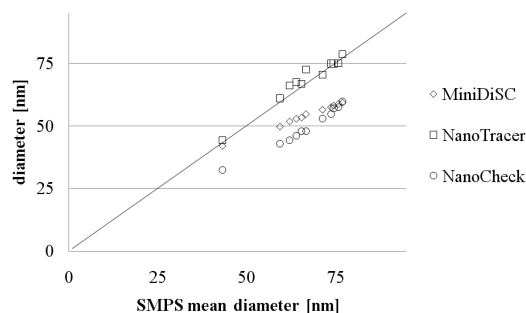

Figure 1. Diameter correlation between SMPS system and the studied instruments. 60s average.

As shown in figure 1, the NanoTracer correlates well with the particle diameter as measured with SMPS (average of 2.5% error). The MiniDiSC and the NanoCheck underestimated the diameter with an average of 19% and 25% respectively. On the other hand as indicated in figure 2, the average error in the NanoCheck particle number concentration is less than 2%, while NanoTracer and the MiniDiSC overestimated the number concentration by an average of 34% and 45% respectively.

Neither of the instruments was calibrated for the aerosol used in this study and errors are expected and since the errors show fairly monotonic relationship, proper calibration would suppress these errors.
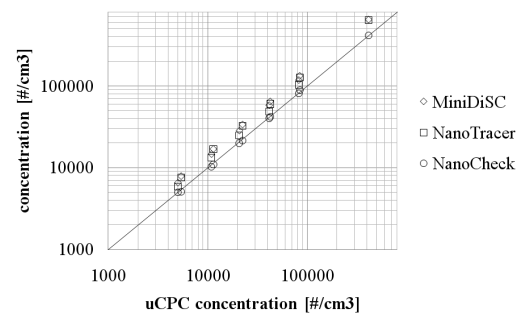

Figure 2. Concentration correlation between uCPC and the studied instruments. 60s average. (At 400 000 $\#/cm^3$ the SMPS was used as reference.)

The SMPS system is the most frequently used instrument for nanoparticles, but the complexity makes field work challenging. Although the instruments in this study provide less accurate data, the simplicity and the battery powered design give them potential to be used extensively in field work.

Fierz M., Burtscher H., Steigmeier P. and Kasper M. (2007). Field measurement of particle size and number concentration with the Diffusion Size Classifier (DiSC). /SAE 2007-08PFL-484/
Marra J. (2008). Ultra-fine particle sensors for indoor air pollution monitoring and control. Proc., Indoor Air, Copenhagen, Denmark.
Schneider F. (2009). New insights in aerosol particle Detection - NanoCheck and Wide Range Aerosol Spectrometer. Proc. 18th Symposium of the NVvA, Zeist, Netherlands.

Nanoparticles Sampling Techniques for an Aerosol- / Particle Mass Spectrometer

J. Meinen[1,2], W. Baumann[3], H.-R. Paur[3] and T. Leisner[1,2]

[1] Institute for Meteorology and Climate Research, Aerosols and Heterogeneous Chemistry in the Atmosphere (IMK-AAF), Forschungszentrum Karlsruhe GmbH, Germany
[2] Institute for Environmental Physics (IUP), Atmosphere and Remote Sensing, Ruprecht-Karls-Universität Heidelberg, Germany
[3] Institute for Technical Chemistry, Thermal Waste Treatment (ITC-TAB), Forschungszentrum Karlsruhe GmbH, Germany

Keywords: Aerosol Mass Spectrometry, Aerodynamic Lens, Microwave Plasma Reactor, CFD

For the measurement of the particle formation kinetics in technical processes, the Research Centre in Karlsruhe developed a particle mass spectrometer (PMS) specifically for the measurement of the size distribution of primary particles in the flames and plasmas with very high concentrations of particle numbers in the range of 108 to 1012 cm-3. Therefore, an intact sampling technique is needed which is suitable for particles in the size range of a few nm.

The particle mass spectrometer uses a classic molecular beam sampling technique with an inlet nozzle and a second nozzle as a skimmer. The system has been tested successfully covering different nanoparticle sources, such as microwave plasma synthesis, a low-pressure flame and a spark generator. These particles sources are characterized by very small primary particles of a size range from 3 to 10 nm and they generate a very high number concentration, which is difficult to measure online with other measurement methods. The molecular beam technique, as a sampling method, offers the following advantage: Due to the supercritical expansion, the incoming gas is frozen very quickly; furthermore, all interactions between the particles or interactions between particles and gas molecules are blocked within the shortest possible time (ms). On the other hand the disadvantages of this sampling technique are bad particle transmission into the measurement chamber and a very high pumping capacity, which has to be provided for supercritical expansion into the molecular range.

For sampling purpose other Aerosol- / Particle Mass Spectrometers use almost exclusively an aerodynamic lens. The first generation of these lenses was designed for a minimum particle size of 300 nm and a second generation of commercially designed lenses are now available down to 30 nm, which are used in the AMS (Aerodyne) and the ATOFMS (TSI). McMurry has designed and tested an aerodynamic lens for particles smaller then 10 nm. An optimized aerodynamic lens system arisen from CFD-Simulations combines the advantage of a supercritical expansion through a critical nozzle and forms a well-defined beam through a multilevel aerodynamic lens, especially for nanoparticles.

The measurement principle of PMS is based on the deflection of a charged nanoparticle beam by a homogeneous field of a capacitor. The deflection capacitor separates the incoming particles according to their polarity in a negative and a positive charged fraction. The deflection voltage is proportional to the ratio of the kinetic particle energy to its charge ($U \sim \frac{1}{2} m v^2 / z$). By varying the deflection voltage, particles of different energy-to-charge ratio are collected at the faraday cups, which are located symmetrically to the left and right of the centre line at the end of the detection chamber. The current generated at the faraday cup is proportional to the incoming number of particles times their total charge and it is measured with a highly sensitive amplifier. The amplification is 10^{10} V/A with an ultra-low-noise 3-dB bandwidth of 7 kHz. The results can be translated to retrieve the ratio of the kinetic particle energy to the number of charges ($\frac{1}{2} m v^2 / z$). To convert this energy spectrum into the particle size distribution, the number of charges (z), the particle velocity and the material density must be known. For an accurate measurement, detailed knowledge of the molecular beam and of the particles included is necessary. Furthermore, the particle speed in the molecular beam, the charge number per particle and the ratio of charged to uncharged particles is also needed.

The quality and the particles transfer of the molecular beam sampling technique were measured with SiO2 - nanoparticles from the microwave plasma synthesis; and the absolute particle mass was detected with a quartz crystal microbalance (QCM) installed in the molecular beam.

Design and performance of an automatic regenerating adsorption aerosol dryer for continuous operation at monitoring sites

Th. M. Tuch, A. Haudek, Th. Müller, A. Nowak, H. Wex, A. Wiedensohler

Leibniz Institute for Tropospheric Research, Leipzig, Germany

Keywords: Aerosol instrumentation, Monitoring.

Physical and optical properties of aerosol particles depend on the relative humidity of their carrier gas. To achieve comparability of measurements from different aerosol monitoring sites, networks usually require that the aerosol is dried to a relative humidity below 50% r.H.. Commercially available aerosol dryers are often not suitable for remote monitoring sites. Diffusion dryers need to be regenerated frequently, Nafion dryers are not designed for high aerosol flow rates. We have developed automatic regenerating adsorption aerosol dryers for a design flow rate of 1 m³/h (figure 1).
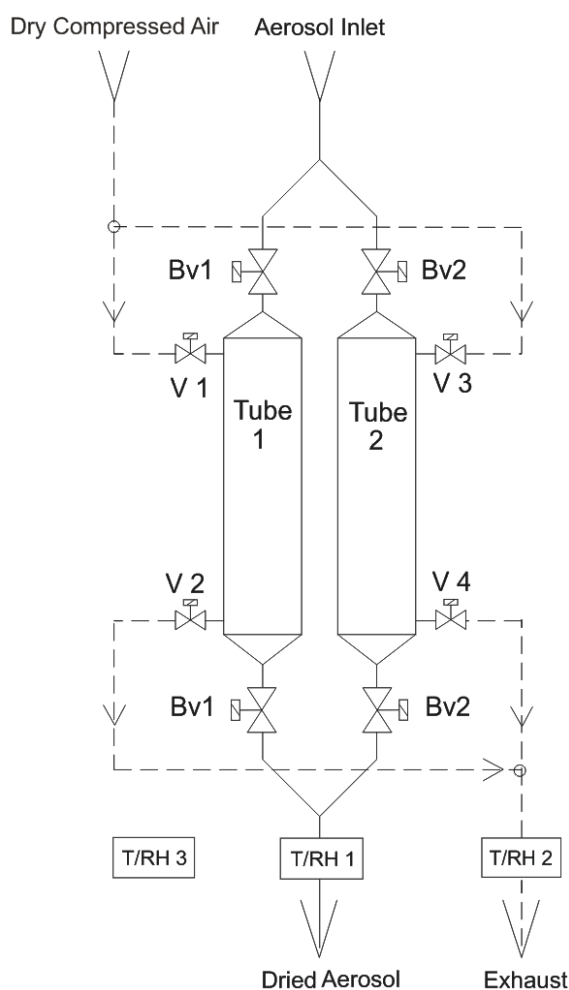
Figure 1: Schematic view of the aerosol dryer

Particle transmission efficiency has been measured during a 3 weeks experiment. The lower 50% transmission efficiency was found to be below 3 nm at this flow rate. Operated at the design flow rate, the aerosol transmission efficiency exceeds 92% in the size range from 10 nm to 800 nm. Measured transmission efficiencies (dots) are in good agreement with theoretical calculations line (figure 2.).
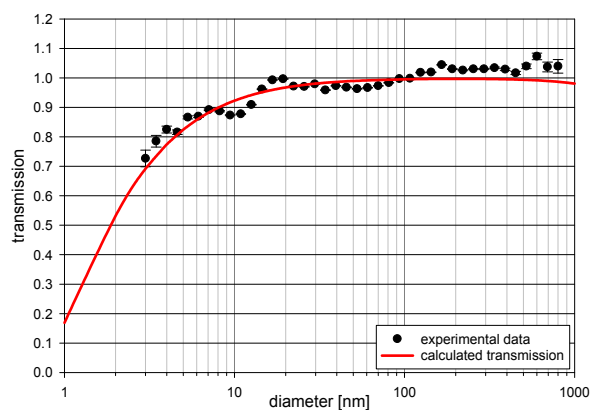

Figure 2: Size dependent transmission of the aerosol dryer (measured and calculated) at 16.7 l/min.

So far seven dryers have been deployed worldwide. The most challenging site for such a dryer is located in the rainforest of the Amazonas river basin about 50 km off the city of Manaus.
Monthly average temperatures at this site range from 24 to 33 deg. C with a daily average humidity of up to 90% r.H.. From February 2008 through August 2008 we measured an average ambient temperature of 30.3 +/- 2.3 deg. C with a relative humidity of 78.5 +/- 3.9%. During the experiment average relative humidity of the dried aerosol was 27.1 +/- 7.5 % r.H.

We demonstrated that the new automatic regenerating aerosol dryer performs well under adverse environmental conditions. Relative humidity of the aerosol at the most challenging site never exceeded design values. Operational parameters of the system need, however, to be set according to site requirements. Routine maintenance of the system did require little effort which makes these dryers suitable to be operated at remote continuous monitoring sites.

A new personal thermophoretic sampler with simplified analysis routines for nanoparticle exposure studies

Nkwenti Azong-Wara[1], Christof Asbach[1], Burkhard Stahlmecke[1], Heinz Fissan[1], Heinz Kaminski[1], Sabine Plitzko[2], Thomas A.J. Kuhlbusch[1]

[1] Institute of Energy and Environmental Technology (IUTA), Air Quality & Sustainable Nanotechnology Unit, Bliersheimer Str. 60, Duisburg, Germany
[2] Federal Institute for Occupational Safety and Health (BAuA), Nölderstrasse 40-42, Berlin, Germany

Keywords: thermophoresis, CFD, modelling, nanoparticles, personal sampling.

Assessing the exposure to airborne nanoparticles, e.g. at workplaces during nanoparticle production, is an important step towards a sustainable nanotechnology. Personal exposure assessments of fine and coarse particles have been predominantly carried out by the use of mass based personal particle samplers. Most common versions of these personal particle samplers consist of a miniaturized impactor with a defined cut off size followed by a filter (e.g. Sioutas *et al.*, 1999). This approach is undesirable for assessing the exposure of nanoparticles where the mass is not a very prominent factor. One suitable way of sampling nanoparticles is by employing the principle of thermophoresis defined as the directed thermal diffusion of aerosol particles that occurs when a temperature gradient is established in the gas.

A new thermophoretic personal sampler, also known as Thermal Precipitator (TP), was developed with the objective to uniformly deposit particles on a substrate, in order to simplify the microscopic analysis e.g. by Scanning Electron Microscopy (SEM). The development builds on an old TP developed by the German Federal Institute for Occupational Safety and Health (BAuA). The non-uniform deposition pattern of this old TP was found to be due to its non-uniform temperature gradient caused by two centrally placed tiny heating coils in the middle of the TP. A uniform temperature gradient is created in the new TP by introducing two plates with different but uniform temperatures with the colder plate acting as the substrate for particle deposition. Analytical calculations were done, considering the interaction and effectiveness of the various forces acting on particles in the TP, assuming a plug flow velocity of 5.5 mm/s (inlet velocity in old TP) and a substrate length of 20 mm. The calculations showed an optimum at a gap distance of 1 mm and temperature gradient of 15 K/mm in order to achieve a uniform deposition of particles. These results set the basis for more complex numerical simulations. The simulations were carried out with the CFD software FLUENT in connection with the Fine Particle Model (FPM). Fig. 1 illustrates the homogeneous particle deposition as a function of particle size for three typical orientations of the TP between 1.5 mm and 8 mm from the start of the substrate. The deposition is fairly homogeneous up to a particle size limit of about 300 nm independent of the orientation. Above 300 nm, gravity causes a deviation of the orientation-dependent deposition rates.
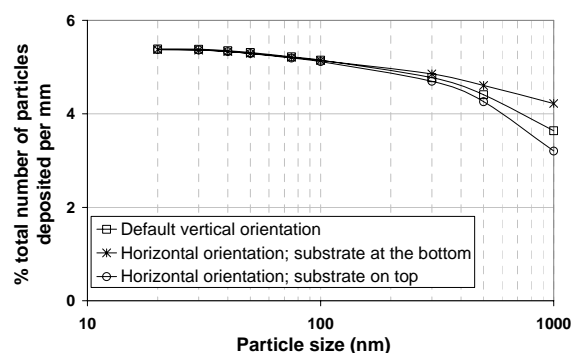

Fig. 1 Particle deposition for three orientation cases of the TP with a temperature gradient of 15 K/mm

The modelling results affirmed that during an eight hour sampling period (standard working shift) sufficient particles will be deposited for SEM analysis.

The new TP was designed based on the modelling results and a first prototype built. Peltier elements were employed on both plates in the TP to create a temperature gradient which is kept constant by a temperature regulation element. The new TP has the dimensions of 4.1 x 4.5 x 9.7 cm³ and weighs approximately 130 grams, and can therefore be comfortably carried by a worker. Fig 2 shows the design of the first prototype. Modelling results and the design of the new TP will be presented.
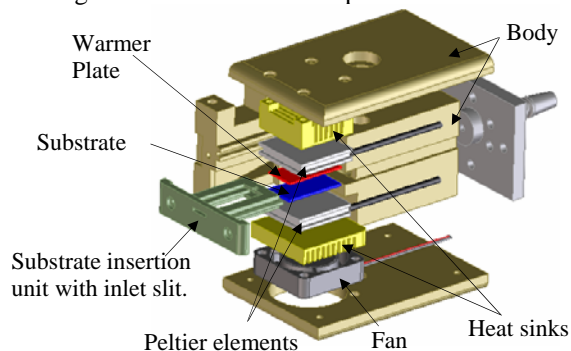

Fig. 2 Design of the new Thermal Precipitator

Reference:
Sioutas *et al. J. Aerosol Sci.* **6**: 693-707, 1999

A miniature impactor for aerosol collection with emphasis on single particle analysis

K. Kandler[1]

[1]Institut für Physik der Atmosphäre, Universität Mainz;
now at: Angewandte Geowissenschaften, Technische Universität Darmstadt, Germany

Keywords: aerosol sampling, impactor, SEM/EDX, single particle analysis

The collection of samples for individual particle analysis differs from those of for example bulk-chemical methods. The particles need to be isolated on the substrate, which should provide as much (chemical or morphological) contrast to the particles as possible. In this work, a micro inertial impactor (MINI) is described, a cascade impactor with single round nozzles designed for a versatile operation for the collection of single particle analysis. Most attention was paid to the small instrument size, ease of use, interchangeability of different substrates, and a collection size range suitable for electron-microscopic particle analysis.

The MINI follows the design of Mercer et al. (1970), but for ease of use each single stage is split into a nozzle and a substrate holder. The MINI outer shell consists of a tube with interior and exterior diameters of 10 mm and 18 mm, respectively and an inner length of 40 mm. It features o-ring fittings at the top and bottom to seal the threads. Construction material is stainless steel.

The split design of the single stages (see Fig. 1) allows the use of nozzles and substrate holders in any combination. O-rings around the nozzles ensure the sealing of the single stages and hold the stages in position through friction. Nozzles from 0.2 to 1.5 mm were constructed with a small interval. The nozzle construction followed the design criteria given by Newton et al. (1977).

The flow rate is usually set by keeping one of the nozzles in critical condition. When the 0.25 mm nozzle is used as critical orifice, a flow of approximately 0.5 l/min is reached. Nozzle diameters and the corresponding approximate cut-off sizes for this case can easily be calculated (e. g., Raabe et al., 1988). Alternatively, the MINI can be used in low-pressure mode. Behind a drop in the pressure on the critical nozzle of significantly more than half of the inlet pressure, particles smaller than 30 nm can be collected. However, the maintenance of the necessary vacuum (typically 50 to 100 hPa at a strongly increased air volume flow) on the impactor outlet requires rather large vacuum pumps.

For each type of substrate the substrate holder needs to be adapted to place the surface of the sampling substrate at the reference height h_0 (Fig. 1) with exactness better than the nozzle diameter w to yield the target cut-off size. The substrate holders can feature magnets to securely hold substrates like transmission electron microscopy grids or nickel plates commonly used in electron microscopy. The

criter.	value
s/w	1.3
l/w	1 for $w > 0.5$ mm, else 0.5 mm
w_s/s	3 for $w > 0.5$ mm, else 1.5 mm
α	45°
D_t	10.0 mm
D_s	9.95 mm
D_f	7.0 mm
D_c	4.0 mm
f_d	0.9 mm
f_h	1.2 mm
O-ring	8 mm x 1 mm

Fig. 1 (right): Design criteria, measures, and schematic drawing

Fig. 2 (below): Substrate holders for 3.05 mm diameter TEM grids with edge to prevent slipping (left), for 4 mm diameter metal discs with or without coating (center), and for 5 mm square silicon plates (right)
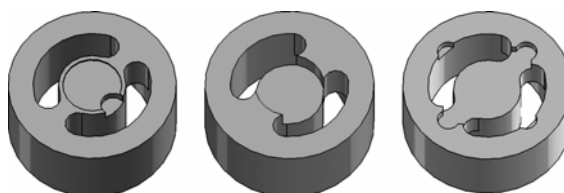
maximum usable substrate size is about 5 mm in square (see Fig 2 for examples).

To facilitate the assembly of the MINI it is recommended to create a rod with two different tips from a softer material (e. g., PTFE) to push the stages in and out. As the nozzles are susceptible to mechanical damage, an annular tip should be used with an outer diameter of 6.5 mm and an inner diameter of 4.5 mm. The other tip used for pushing into the inlet cone of the nozzles should be spherical or tapered. A cap should be built which holds the stages safely while pushing them out of the impactor tube with an inner diameter of 11 mm and a length of 40 mm. An end-to-end slot in the cap facilitates taking out the nozzles and substrate holders with tweezers.

Mercer, T. T., Tillery, M. I., Newton, G. J. (1970). *J. Aerosol Sci.,* 1, 15.

Newton, G. J., Raabe, O. G., Mokler, B. V. (1977). *J. Aerosol Sci.,* 8, 339-347.

Raabe, O. G., Braaten, D. A., Axelbaum, R. L., Teague, S. V., Cahill, T. A. (1988). *J. Aerosol Sci.,* 19, 183-195.

Development of new instrumentation for aerosol angular light scattering and spectral absorption measurements

G. Dolgos[1], J.V. Martins[1,2], L.A. Remer[2] and A.L. Correia[2]

[1]Dep. of Physics, University of Maryland, Baltimore County, 1000 Hilltop Circle, 21250, Baltimore MD, USA
[2]NASA Goddard Space Flight Center, Code 613.2, 20771, Greenbelt MD, USA

Keywords: Light absorption, Chemical composition, Scattering matrix, Hygroscopicity.

In order to quantify the effects of aerosols on the atmospheric radiation budget, absorption and scattering properties of many different aerosol types have to be mapped with considerable accuracy. Remote sensing of aerosol properties from space with current satellite sensors requires knowledge of aerosol optical properties, including phase function (the directional distribution of scattered light), in order to quantify aerosol loading (Mishchenko *et al.*, 2004). Black carbon is the main anthropogenic absorber; its warming effect can be comparable to that of carbon dioxide (Ramanathan & Carmichael, 2008). Other absorbers (mainly organic materials and dust) are also important, and have distinct spectral dependence over the solar spectrum.

We designed, built and calibrated a novel device for aerosol phase function measurements. This device is an imaging nephelometer called I-Neph that is capable of measuring the phase function close to the extreme directions, i.e. from 1.5° to 178.5° in the present configuration. The broad range is crucial for particle size retrievals. The current resolution is less than 1° near the extreme directions, and the angular range and resolution can be improved.
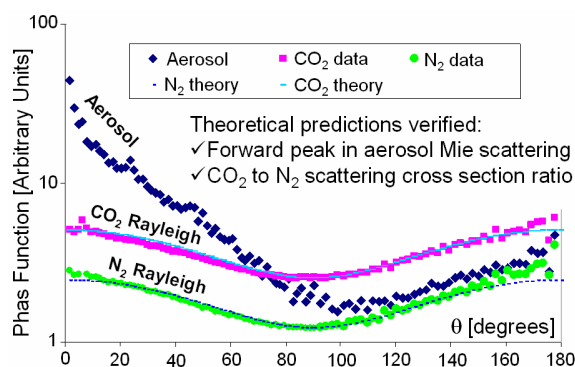
next effort to improve the I-Neph. Aerosol phase functions can be measured already as a function of humidity. The I-Neph has no moving parts, measures in a few seconds and is suitable for the laboratory and the field. We will upgrade the I-Neph to measure polarization and the full phase matrix.

Our goal has been to measure the absorption spectra of black carbon and other aerosols from 200 nm to 2500 nm, using sampled filters. Although the deep UV measurements are not important for the atmospheric radiative balance, they contain important information about the chemical composition of the sample. Measuring the decrease in filter reflectance permits the calculation of spectral absorption cross section of the aerosol particles. We implement multiple ways to measure reflectance (including a stable novel integrating sphere) in order to eliminate systematic errors due to its directional distribution. Preliminary results of spectral aerosol optical depth (AOD) are shown in Figure 2, mass measurements will be carried out in the upcoming months in order to obtain mass absorption coefficient.
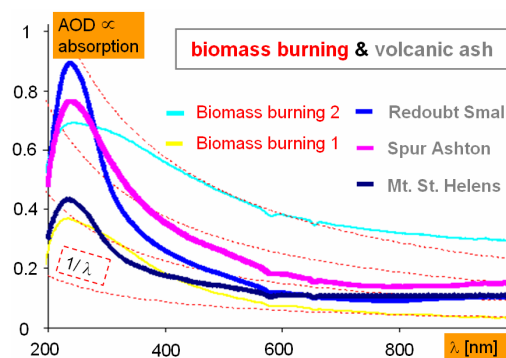

Figure 1. Raw data of direct measurements at 532 nm with the current I-Neph prototype at UMBC. Pure N_2 and CO_2 data are compared with their corresponding theoretical calculations and ambient aerosol data.

The aerosol phase function in Figure 1 has not been corrected for the Rayleigh contribution from air. The angle dependent sensitivity of the system causes the small discrepancy between raw data and Rayleigh theory. We located the cause of the current high frequency noise and it will be eliminated during our

Figure 2. Relative spectral mass absorption coefficient of various aerosols.

Mishchenko, M., B. Cairns, J. E. Hansen, L. D. Travis, R. Burg, Y. J. Kaufman, J. V. Martins, E. P. Shettle (2004), *JQSRT*, 88, 149–161
Ramanathan, V. and G. Carmichael (2008), *nature geoscience,* 1, 221-227

Response of the DustTrak DRX to Aerosols of Different Materials

X. L. Wang, A. Hase, G. Olson, A. Sreenath, J. Agarwal

TSI Inc., St Paul, MN 55126, USA

The DustTrak DRX is a real-time monitor for size segregated aerosol mass concentrations. It combines photometry with single particle sizing to measure PM_1, $PM_{2.5}$, PM_4 and PM_{10}. Since this instrument works on the principle of light scattering, its response depends on aerosol properties, such as particle shape, refractive index, size distribution and density. In this paper, we report the results from four sets of experiments using the DRX to measure different aerosols. Its comparison with a photometer and an optical particle counter (OPC) will be discussed, and its advantages and limitations will be addressed.

The first experiment investigates the DRX photometric response to different aerosols. The DRX was challenged with ultrafine Arizona Road Dust (A1 dust), ammonium sulfate, sodium chloride and Emery oil. The result showed that the DRX photometric response for unit aerosol mass is approximately inversely proportional to the particle density for the aerosols investigated.

The second experiment uses the DRX to measure four different aerosols: ultrafine Arizona Road Dust, coarse Arizona Road Dust (A4 dust), hematite and petroleum coke. The result showed that when the aerosol under measurement is different from the calibration aerosol, the DRX could not predict mass concentrations accurately. This experiment also showed that once calibrated with the aerosol of interest, the DRX can measure mass concentrations quite accurately. An example comparison between the DRX and the Tapered Element Oscillating Microbalance (TEOM) for measuring the light absorbing petroleum coke is shown in Figure 1.

The third experiment compares the DRX with a simple photometer, the TSI DustTrak 8520, for their sensitivities to size distribution change. Both instruments were calibrated with A1 dust. Then they were used to measure A4 dusts. It was shown that the DRX underestimated PM_{10} concentration by 7%, while the DustTrak 8520 underestimated 31%. Therefore the DRX PM_{10} measurement is less sensitive to size distribution change than a photometer due to its single particle measurement feature.

The forth experiment compares the DRX with the TSI 8220 OPC for measuring monodisperse Emery oil particles at various concentrations. The result showed that while the OPC can accurately measure very low concentrations (<0.1 $\mu g/m^3$), it suffered coincidence losses at relatively low concentrations (~10 $\mu g/m^3$). On the other hand, the DRX was not so accurate at very low concentrations (<1 $\mu g/m^3$) due to low signal-to-noise ratio, it can measure high concentrations without coincidence losses. Therefore the DRX is suitable for dusty environments.

In summary, we measured the DustTrak DRX response to different aerosols. It is shown that the DRX could not accurately measure mass concentration if the aerosol of interest is different from the calibration aerosol. However, once calibrated with the measurement aerosol, the DRX can measure size segregated mass concentrations quite accurately. Comparing to a simple photometer, the DRX not only provides particle size information, but also is more accurate for PM_{10} measurement and less sensitive to particle size distribution shift. Comparing an OPC, the DRX can measure higher concentrations, and is more suitable to dusty environment.
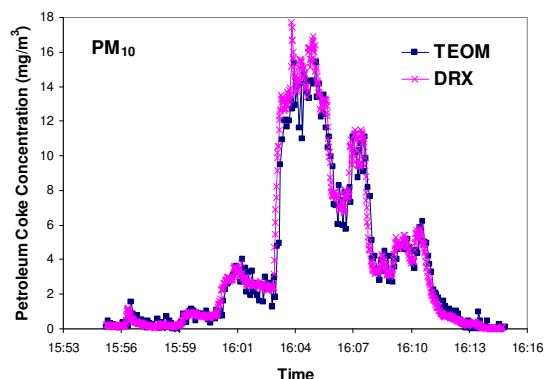

Figure 1. PM_{10} mass concentrations of petroleum coke dust measured by TEOM and DRX. The TEOM had a PM_{10} impactor on it inlet, while the DRX did not have an impactor. The DRX simultaneously measured PM_1, $PM_{2.5}$, PM_4, PM_{10} and TPM. Only PM_{10} is plotted for the sake of clarity.

Development of an optical particle counter for in-situ detection of single ice particles in LACIS

T. Clauß, A. Kiselev, D. Niedermeier, S. Hartmann, H. Wex and F. Stratmann

Leibniz-Institute for Tropospheric Research, 04318 Leipzig, Germany

Keywords: Depolarization, Instrumentation/physical char., Instrument development, Optical counter

Ice particles influence radiation properties and precipitation mechanisms in atmospheric clouds. Therefore the investigation of the freezing behaviour of different aerosol particles which act as ice nuclei (IN) is important and still poses unresolved questions.

The Leipzig Aerosol Cloud Interaction Simulator (LACIS, Stratmann *et al.*, 2004) is used to investigate the IN activity of different natural and artificial aerosol particles, and to learn more about homogenous and different heterogeneous freezing processes.

To support these measurements, a particle detection method able to differentiate between ice particles and droplets in LACIS is needed. The main goal is to determine the fraction of frozen and unfrozen particles in mixed water and ice aerosol systems under different thermodynamic conditions.

An Optical Particle Counter (OPC) was built to detect single particles downstream of the LACIS tube to measure not only a size distribution but also the rotation of the main polarization plane of the backscattered light. The principle is based on the difference in depolarization of particles with different shape.
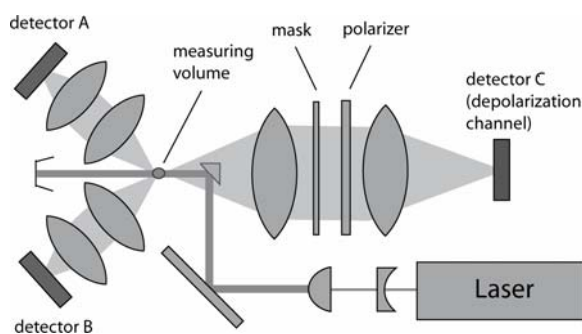

Figure 1. Optical layout of the OPC for the detection of ice particles (top view).

The configuration of the OPC is shown in Figure 1. The vertically polarized laser light at 532 nm is focused on the measuring volume situated downstream of the LACIS tube. The light scattered by a single particle crossing the measuring volume into the near forward direction is detected by two photomultiplier tubes (PMT) "A" and "B". The detected signal of PMT "A" is then used to determine the particle size, whereas the signal of PMT "B" is used to ensure that the particle is crossing the measuring volume exactly in the focal point of the illuminating optics. The backscattered light is filtered by a polarizer and detected by PMT "C". By rotating the polarizer, it is possible to distinguish between different polarization states.

In case of spherical particles, the polarization state of the scattered light can be analytically described by Lorenz-Mie theory. Figure 2 shows an example of a backward scattering pattern for a 5 μm water droplet. It can be clearly seen, that there exist special angular ranges where the parallel polarization component dominates.
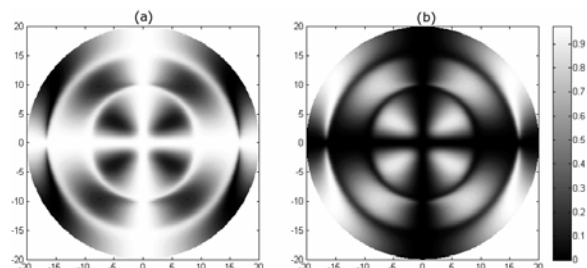

Figure 2. The parallel (a) and perpendicular (b) polarization components normalized to the total scattering intensity and mapped onto the backward scattering detector plane. The zero of the XY-coordinate frame corresponds to the 180° scattering direction. The scattering pattern is calculated by Lorenz-Mie theory for a 5 μm spherical water droplet.

In general, ice particles are not spherical, so that the backscattering patterns of both polarization components are much more complicated. With a mask installed in the backscattering channel it is possible to limit the field of view of the PMT "C", so that the perpendicular component of light scattered by a spherical particle almost vanishes. Thus it is possible to exclude spherical particle from registration. The appearance of this mask is defined by the calculations.

First test measurements of immersion freezing on Arizona Test Dust particles (ATD) were performed with the new OPC. In these experiments it was shown for the first time that an in-situ discrimination of single frozen and unfrozen water droplets is possible.

Stratmann, F. *et al.* (2004). *J. Atmos. Oceanic Technol.*, 21, 876-887.

Novel Photoacoustic Aerosol Monitor for Optical Absorption Coefficient Determination. Laboratory and Field Test.

T.Ajtai[1], M. Schnaiter[2], C. Linke[2], M. Vragel[2], Á. Filep[1], L. Födi[1], G. Motika [4], Z. Bozóki[3], G. Szabó[1]

[1] Department of Optics and Quantum Electronics, University of Szeged, Hungary
[2] Institute of Meteorology and Climate Research, forschungszentrum Karlsruhe
[3] Research Group on Laser Physics of the Hungarian Academy of Science, University of Szeged, Hungary
[4] Lower Tisza Valley Environmental Inspectorate, Szeged, Hungary.

There is an increasing concern for novel methods to determine the optical absorption coefficients of atmospheric aerosol. The available on-line instruments like MAAP (Multi Angle Absorption Photometer) and PS2 (Single Particle Soot Photometer) has weakness of spectral resolution or the sampling artifact of filter matrix. These methods neither suitable for direct determination of light absorption by aerosol nor dispose the capability of the source apportionment. Photoacoustic measurement technique is one of the highly promising method for analysis of aerosols, as it can determine directly the amount of light absorption by aerosols while being largely insensitive to uncharacteristic light scattering.

The Multi Wavelength Photoacoustic System (WaSul-MuWaPas) operating at four different wavelength in wide wavelength range (266nm, 355nm, 532nm, 1064nm) for optical characterisation of artificially generated and atmospheric aerosol was developed.

The system characteristic performances are shown at table 1. (MDOA: Minimum Detectable Optical Absorption Coefficient)

Table 1. Wasul-MuWaPaS system performance

Wavelength (nm)	Power (mW)	MDOA (Mm-1)
1064	360	0,6
532	90	1,2
355	12	9,6
266	6	9,5

The spectral PA response of different type of artificially generated soot and dusts were measured. As a reference the extinction spectrometer and TSI; 3653 Nephelometer was used. From the extinction and scattering measurement the absorption coefficient can be calculated. Good agreement was found between the PA and the reference response. Figure 1.

The WaSul-MuWaPas was deployed at the EMEP-GAW regional station of JRC Ispra and operated parallel with the instrumentation used at the site including Nephelometer, Aethalometer, MAAP, DMPS.
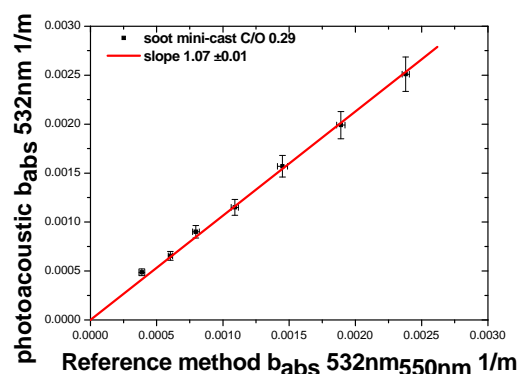

Figure 1: Correlation between the PA and the reference spectral response of CAST soot at 532nm wavelength.

Despite the low EBC mass concentration (below 1μg/m3) occurred at the field station during the experiments excellent agreement was found between the PA and the corrected aethalometer response.
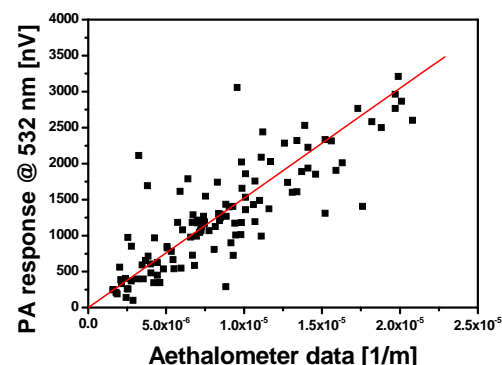

Figure 2. Correlation between the PA response and the corrigated aethalometer data at 532nm wavelength during the one week measurement period.

Monitoring of indoor air quality and workplace aerosols - one compact portable system for dust mass, number concentration and Nano particles

F. Schneider, R. Hagler and H. Grimm

Grimm Aerosol Technik GmbH, 83404 Ainring, Germany

Keywords: indoor air quality, Nanoparticles characterization, occupational health, mass concentration, aerosol measurement, aerosol size distribution,

Laser aerosol spectrometry is a well-proofed techniques for online particle monitoring with very good time and size resolution. Battery powered systems even are suitable portable measurements. One limitation of optical light scattering technique is the limit of particle size detection, due to the strong decrease of scattering intensity with decreasing particle size. A new sensor attachment now enables to measure down to 25nm with high time resolution, and displaying particle concentration and mean particle diameter of Nano sized aerosol particles and keeping all the advantages of laser aerosol spectrometer.

Portable Nano attachment NanoCheck 1320 with adapter 1320-HLX and laser aerosol spectrometer

The sensor attachment exists of a faraday cup electrometer, combined with a charger and a time multiplexed electrode for conductivity measurement. This unique patent pending setup is sensitive to about 10fA, which correlates to an minimum concentration of 5000 particles/ccm and can measure up to about 5 * 10^6 particles/ccm. In addition one can determine the mean particle diameter also and the active surface area of the measured nano sized aerosol.

Indoor air quality and workplace monitoring are historically based on measurements of particles mass fractions according to their penetration depth into the lung. So this system keeps the link to the past, by data output according to the European standard EN 481. Particle mass only has limited significance characterizing health effects due to inhaled particles emitted e.g. by combustion, Nano particle processing or welding.

This setup is unique for monitoring the risk potential of aerosol particles and nano particles in particular, which will become more and more important for indoor air quality and the monitoring of workplace aerosols. The compact and lightweight design of this new device will enable necessary mobile measurements for work place monitoring, inhalation studies, occupational health studies and production inspection.

This contribution reports on a new technique for determination of particle number concentration and mean particle diameter in a size range 25nm up to 300nm in combination with complete characterization number, size can mass distribution of the aerosol particles up to 32µm. Examples of measurements at different indoor environments will be presented in detail, also the possibility to comparisons of indoor and outdoor measurements, e.g. for the fast determination of background concentrations levels.

First Steps Towards a Photophoretic Mobility Analyzer

C. Haisch, L. Opilik, M. Oster, and R. Niessner

Chair for Analytical Chemistry, Technische Universität München, D-81377, Munich, Germany

Keywords: photophoresis, optical properties, particle characterization, separation.

Photophoresis (PP), or more precisely photo-thermophoresis (PTP), occurs when an aerosol particle is illuminated by a strong light from one side, which leads to locally inhomogeneous warming. The heat is transferred to the surrounding gas atmosphere, which gets heated as well. In consequence, the collision rate of the gas molecules with the particle increases, which results in a net force acting on the particle. It reaches an equilibrium velocity, governed by the PP force on the one hand and the Stoke's flow resistance on the other. For semitransparent particles, the PTP force can even act towards the light source, if the light gets focused behind the particle, leading to local warming on the particle's backside. The PTP force depends on the light intensity, on thermal properties of the gas medium and on the geometrical, optical and thermal properties of the particle. As we presented, the evaluation of the PP velocities of different particles can reveal information on their optical and thermal properties, when the gas's properties are known (Haisch et al., 2008). Additionally, direct PP forces act on the particles, which are caused by the momentum transfer of photons being scattered on the particle. Generally, these forces are considered negligible compared to the PTP force, but for certain, highly scattering particles this may not hold true.

We are designing an instrument which employs PTP and PP forces for aerosol characterization and fractionation. As the fundamental operating is similar to the one of a Differential Mobility Analyzer, we chose the name PP Mobility Analyzer for the new instrument. Two similar designs are currently under comparison. Both are based on two coaxial gas flows, the inner one (diameter ~100 µm) containing the particles, the outer one acting as sheath air. Both laminar flows are adjusted to the same flow velocity of few 100 µm s^{-1}. Without the influence of the PP force, particles move with the flow trajectories. Opposite to the aerosol inlet, there is either a narrow wall, splitting the flow into two separate channels. Depending on the flows in these two channels, which are maintained by pumps, the flow trajectories in before the wall are influenced in a way that all particles end in one of the two channels (see Fig. 1). The PP force pushes particles with high PP efficiency into other flow trajectories. If the PP force is sufficiently strong, they end up in the other channel, where they can be counted. Depending on the flow ratio of the two channels, more or less PP force is necessary to push particles into the second channel. As alternative configuration we replaced the separation wall by a second capillary, which is experimentally simpler, but not suitable for the separation of particles exhibiting negative PP.
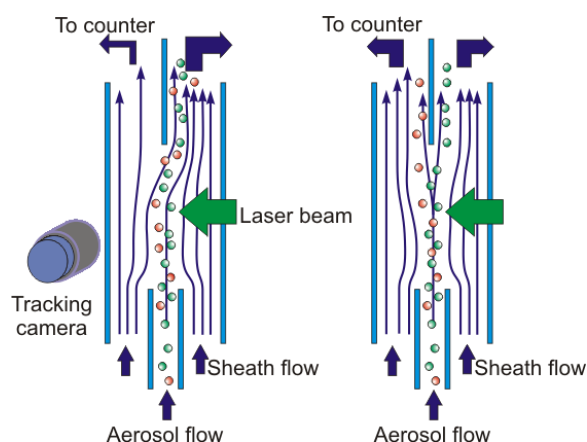

Figure 1 Principle of the PP Mobility Analyzer.

The proposed PPMA system will reveal new information on optical and thermodynamic properties of aerosol particles and will find its way to routine application. The PP velocimetric measurements carried out in parallel indicate, that the PP effect allows distinguishing between particles of identical chemical composition, but different microstructure. One example are the significantly different velocities of NaCl particles generated either by condensation from the gas phase or by drying of nebulised salt solution. We present results of our optimized PP velocimetry setup, which now allows online data evaluation, which means that a continuous monitoring of PP properties is possible.

All PP systems presented here are now coupled to the outlet of a Differential Mobility Analyzer in order to distinguish between the influence of particle's size and opto-thermal properties on the PP force. The PP measurements are carried out only on a limited size fraction of the particles, which can be varied stepwise.

Haisch, C., Kykal, C., & Niessner, R. (2008), *Anal. Chem.* 80, 1546-1551.

Measurement of the wavelength dependence of the extinction coefficient for studying the aerosol contamination of the atmosphere

A. Czitrovszky, A. Nagy, A. Kerekes

Research Institute for Solid State Physics and Optics, Konkoly Thege Miklós st. 29-33.
1121 Budapest, Hungary
Envi-Tech Ltd., , Konkoly Thege M. st. 29-33., 1121 Budapest, Hungary

Keywords: remote sensing, radiation measurement, radiometry,
size distribution, extinction coefficient

Remote sensing of aerosols, retrieval of optical depth and aerosol size distribution in the atmosphere by means of sun photometry has long history and is in the focus of the scientific interest continuously. The relationship between the aerosol contamination of the atmosphere and wavelength dependence of the extinction coefficient has been studied theoretically than experimentally by a number of groups (King *et al.* 1978, Liu *et al.* 1999, Schmid *et al.* 1997 *etc.*). From spectral attenuation measurements the size distribution and the concentration of aerosol can be determined.

Our aim was to develop a multi channel radiometer for the measurement of the extinction coefficient at different wavelengths. The system consists of a three channel detection system with wide spectral range (from UV to IR) in which the selection of the wavelengths can be made using narrow band filters. The central wavelength of the filters was fitted to the characteristic spectral lines corresponding to certain materials.

The system has three detection channels. Two of them has narrow band interference filter holder, for selecting the proper wavelengths. In the third detection channel the incoming light is reflecting from four mirrors which have high reflectivity only in a narrow band around a certain UV line. This four mirror increases the wavelength selectivity by four orders of magnitudes. So this device combines the benefits of the UV radiometer and a wide range spectrometer for the determination of the wavelength dependence of the extinction coefficient.

In addition to the commonly used data retrieval process for the determination the size distribution and concentration of atmospheric aerosols (Liu *et al.* 1999, Schmid *et al.* 1997, King *et al.* 1978, Pearson *et al.* 2007, *etc.*), an evaluation method based on the ratio of the signals obtained in different channels is introduced. This method is independent of the absolute intensity which is varying with the cloud density or meteorological conditions.

After the calibration of the device we made several measurement campaigns at different optical conditions. The measurement results are under evaluation.

Figure 1. The multichannel radiometer device

King M.D., Byrne D.M., Herman B.M., Reagan J.A., (1978) Aerosol size distributions obtained by inversion of spectral optical depth measurements, *J. Atmos. Sci.,* 35, 2153-2167.

Liu Y, Arnott W.P., Hallett H., (1999) Particle size distribution retrieval from multispectral optical depth: influences of particle non-sphericity and refractive index, *J. Geophys. Res.,* 104, 31753-31762.

Schmid, B., Matzler, C., Heimo, A., Kampfer, N., (1997) Retrieval of optical depth and particle size distribution of tropospheric and stratospheric aerosols by means of Sun photometry, Geoscience and Remote Sensing, IEEE Transactions on Volume 35, Issue 1, 172 – 182.

Pearson R., Fitzgerald R.M., Polanco J., (2007) An inverse reconstruction model to retrieve aerosol size distribution from optical depth data, *J. Opt. A: Pure Appl. Opt.* 9 56-59.

Dependence of the performance of condensation particle counter (CPC) on particle number concentration

Z.Z. Zhang

Institute of Nuclear and New Energy Technology, Tsinghua University, 100084, Beijing, P.R.China

Keywords: CPC, counting efficiency, number concentration, particle growth.

The condensation particle counter (CPC) is a widely used instrument for measuring the number concentration of submicrometer and nanometer airborne particles. The instrument operates by producing a supersaturated vapour in the saturator and then condensing on the particles to grow them to a large, detectable size.

The simulated condenser in this paper is that of TSI model 3020 CPC, the length of condenser is 8cm and the diameter is 4mm, the working fluid is n-butyl alcohol, the saturator and condenser temperatures are 35 ℃ and 10 ℃ separately, the sample flow rate is 5cm^3/s (Zhang & Liu, 1990).

The equations of continuity, momentum, particle diffusion, heat and mass transfer are used. Especially, the heat and mass source terms are considered based on the heat release of vapor condensation and the vapor depletion (Barret & Baldwin, 2000; Varghese & Gangamma, 2007).

$$C_p \rho \left(u \frac{\partial T}{\partial x} + v \frac{\partial T}{\partial r} \right) = k \left[\frac{\partial^2 T}{\partial x^2} + \frac{1}{r} \frac{\partial}{\partial r} \left(r \frac{\partial T}{\partial r} \right) \right] + Ln\dot{k}$$

$$u \frac{\partial n}{\partial x} + v \frac{\partial n}{\partial r} = D \left[\frac{\partial^2 n}{\partial x^2} + \frac{1}{r} \frac{\partial}{\partial r} \left(r \frac{\partial n}{\partial r} \right) \right] - n\dot{k}$$

In this paper, the simulated particles are of 100nm diameter and the number concentrations are from 10#/cm3 to 10^7#/cm3.

As shown in Figure 1 and Figure 2, when the number concentrations are smaller than 10^4#/cm^3, the particles growth would be not affected by the particle concentrations. But for the concentration of about 10^5#/cm^3, the growth has a litter different. Because the photodetector of CPC can detect the particles larger than 0.5μm by counting method, the counting efficiency would be equal to that of concentrations smaller than 10^4#/cm^3.

For the concentration of about 10^6#/cm^3, the vapor in the tube isn't enough to grow all of the particles freely following the particle growth law. At the outside of the condenser, the particle size would be smaller than 0.5μm near the condenser wall, so the CPC counting efficiency would be smaller than 100%.

For the concentration of about 10^7#/cm^3, the vapor is so little that the particles wouldn't grow to 0.5μm, and the photodector of CPC cannot detect any particles.

The results above are also applicable to the particles whose diameter is different from 100nm.
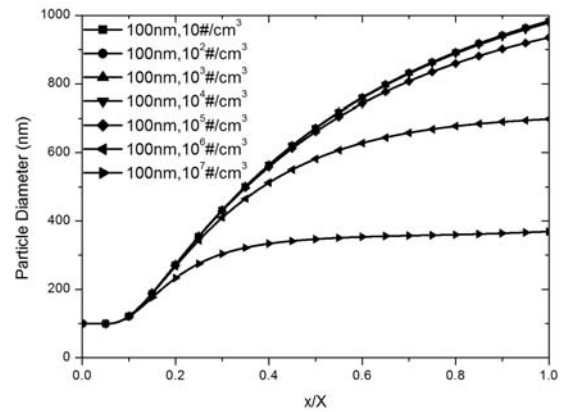

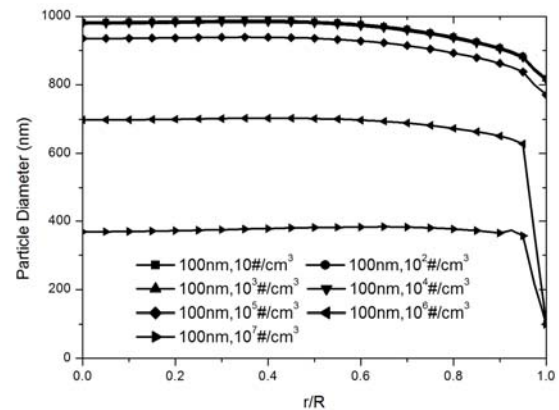Figure 1. Particle diameter along the condenser axis at different number concentrations.

Figure 2. Size distribution of particles at the outside of the condenser at different number concentrations.

Barrett, J. C., & Baldwin, T. J. (2000). *Journal of Aerosol Science,* 31, 633-650.
Varghese, S. K., & Gangamma, S. (2007). *Aerosol and Air Quality Research.* 7, 46-66.
Zhang, Z. Q., & Liu, B. Y. H. (1990). *Aerosol Science and Technology*, 13, 493-504.

Method for the characterization of nanoparticle release from surface coatings

M. Vorbau, L. Hillemann, D. Göhler, M. Stintz

Institute of Process Engineering and Environmental Technology, TU Dresden, 01062 Dresden, Germany

Surface coatings are widely used in industry as well as domestically. Nanoparticles are considered to enhance substantially certain properties of such coatings, e.g. its resistance to mechanical stress or UV-light. Thus they are increasingly employed as additives. The usage of these coatings is subject to investigations regarding the release of nanoparticles into air, which may cause adverse health effects / have an impact on human health. However, suitable methods for the quantification of nanoparticle release have not been established yet.

Investigations in the field of wear resistance were normally made in the area of material science either in dry and in wet environments. One of the most common tests for simulating the abrasive damage during the service life of components is the so called Taber test (see Figure 1).
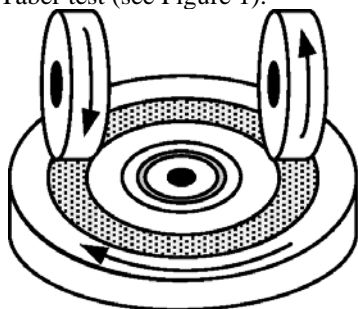

Figure 1. Abrasion scheme of a Taber Abraser with test piece (sample), abraded area, abrasion wheels and the direction of rotation (marked with arrows)

The stress of the Taber test corresponds to the typical stress applied to surface coatings in a domestic scenario, e.g. when walking with sandy shoes on a floor surface coating. With this method an area of 30 cm^2 per revolution is stressed with both wheels. The parameters which have to be specified for the testing method are the material of the abrasion wheels, the normal force and the number of abrasive cycles (number of turntable revolutions).

The Taber test ensures a reproducible and standardized stress of the sample which is important for reproducible measurement results.

The employed test rig bases on an abrasion section and a measurement section. The released particle concentration of the aerosol, generated by the Taber Abraser, is determined by CPC. Also the particle size distribution of the aerosol is measured by SMPS. An Electrostatic Precipitator (ESP) is used for deposition of nanoparticles for subsequent microscopic analysis. The mass loss resulting of the abrasion process is determined gravimetrically.
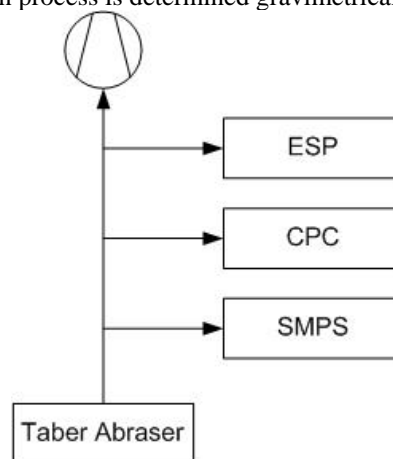

Figure 2. Schematic test rig with aerosol generation (Taber Abraser) and measurement setup (CPC, SMPS and ESP).

In preliminary tests the optimal adjustments of the abrasion tool were determined.

The measured data delivers the mass loss of the sample and the size distribution of the released particles. This enables the specification of the number concentration of the released particles in defined size fractions (< 100 nm, < 625 nm and total) per mass unit of the coating material.

The contribution will explain the developed method in detail and present first data for different coating types. More information are given in Vorbau *et al.*, 2008.

M. Vorbau, L. Hillemann, M. Stintz. Method for the characterization of the abrasion induced nanoparticle release into air from surface coatings. *J Aerosol Science,* (2008), doi: 10.1016/j.jaerosci.2008.10.006

Characterization of a Newly Developed Particle Detector, NanoCheck 1320

Jaejung Seo[1], Hagler Roland[2], Myungjoon Kim[1] and Taesung Kim[1]

[1]SKKU Advanced Institute of Nanotechnology (SAINT), Sungkyunkwan Universiry, Cheoncheon-dong, 440-746, Suwon, Korea

[2]Grimm Aerosol Technik GmbH & Co. KG, DorfstraBe 9 D-83404, Ainring, Germany

Keywords: nanoparticle, calibration, particle detector

Since the scatter intensity decreases with the sixth power of the particle size, it is difficult for an optical light scattering system to detect particles below about 0.1 μm. For this reason, developing the nanoparticle instrumentation with various methods has been attempted for many years.

Recently, Grimm Aerosol Technik developed a new particle detector for aerosol exposure monitoring, which covers nanoparticles and the dust in one portable unit. This particle detector is composed of a unipolar diffusion charger, a new conductivity measurement tool and an aerosol electrometer. The use of an ion attachment by diffusion from an electrical charger with the detection of the total charge is a well known technique for measuring the so-called active surface area. The current is nearly proportional to the particle concentration and mean diameter. In addition, a new method of conductivity measurement is implemented in the sensor. Conductivity measurement combined with the diffusion charging, the current of the aerosol electrometer and calibration factors enable obtaining the total number concentration in the range of 20nm~400nm and the mean diameter of the aerosol number distribution function in real time.
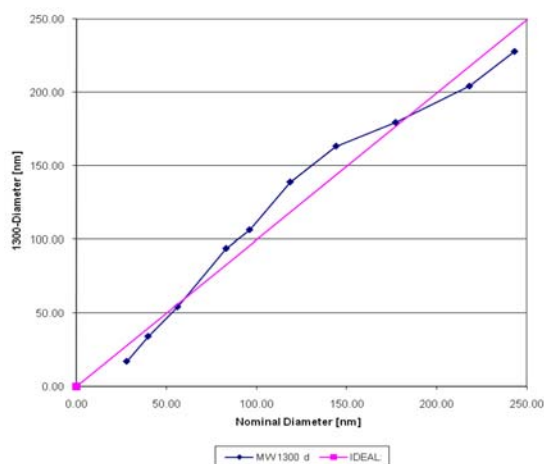

Figure 1. Comparison of experimental results with the ideal

The detector measures two currents I_{tot} and I_{wE} sequentially, from which $\Delta I = I_{tot} - I_{wE}$ can be calculated. These raw data are used to determine a mean particle diameter D_p and the D_p with the measured current I_{tot} is used to calculate the particle number concentration. Hence, by knowing the efficiency curve of the diffusion charger and the particle diameter, the particle concentration can be determined. However, due to the different charging characteristics of particles, the detector response might be different where different correction factor has to be incorporated in the particle detector.

In this study, characterization of NanoCheck was performed with a scanning mobility particle sizer (SMPS), which consists of differential mobility analyzer (DMA) and condensation particle counter (CPC). To obtain the optimum setup for a new particle detector, we first characterized the NaCl particles along with different types of DMA and flow rate were carried out. From this experiment, we found out that the best results were obtained with 1.5l/min of sample flow along with middle DMA for 5lpm of sheath air flow. In addition, different types of aerosols such as indoor and outdoor aerosols were also used for further verification. The routine I_{tot} was measured and knowing the flow rate and the particle concentration measured by a CPC to determine the elementary charge per particle size.

In conclusion, a new particle detector, NanoCheck developed by GRIMM Aerosol Technik showed that the measurement performed in the range of 20nm~ 400nm with correction factor of 1.1 for NaCl, 1.7 for indoor and 1.9 for outdoor aerosol.

Jan DL, Sharpiro AH, Kamm R. (1989). *Journal of Applied Physics*, 67, 147-159.
W.G. Shin, D.Y.H.Pui, H. Fissan, S. Neumann and A. Trampe. (2006). *Journal of Nanoparticle Research*, 9, 61-69.

DMA-FMPS aerosol spectrometers laboratory intercomparison

F.Belosi[1], V. Poluzzi[3], S. Ferrari[3], G. Santachiara[1], F. Scotto[3], A. Trentini[3], F. Prodi[1,2]

[1]Institute ISAC-CNR, Bologna, Italy
[2] Physics Department, University of Ferrara, Italy
[3] Regional Agency for Prevention and Environment (ARPA), Bologna Department, Italy

Keywords: ultrafine particles, DMA, FMPS.

Ultrafine particles could have a strong impact on human health, as several works show. Therefore the need to characterize the aerosol size distribution up to a few nanometers, also in air quality studies, has increased considerable increased over recent years. The most common sampling technique is based on a DMA column coupled with a CPC. The Differential Mobility Analyzer (DMA) technique requires radioactive sources to bring the sampled particles to the Boltzmann equilibrium charge condition. Current regulations, at least in European countries, pose restrictions on the transport and detection of radioactive materials (European Directive 1493/93) even for sealed radionuclide sources, making difficult to perform field DMA measurements or ultrafine primary aerosol emission characterisation at chimneys. TSI has developed a Fast Mobility Particle Sizer Spectrometer (FMPS) whose measurement principle is based on a particle unipolar charger and an electrometer analyzer consisting of a series of electrometers thus avoiding a radioactive source and shortening the sampling time.

This study will present the results of a laboratory comparison between a DMA system (Grimm, DMA Mod. 5.500 and CPC Mod. 5.403) and a FMPS (TSI, Model 3091). The Grimm DMA column is capable of measuring aerosol size distribution in the range from 11 nm up to 1000 nm, while the FMPSS works in the range from 5.6 nm to 560 nm. Therefore, a wide size spectrum overlaps between the instruments. The exercise consists of a simultaneous sampling by the two devices of three different kinds of aerosols generated in the laboratory: Milli-Q water and a Fe_2O_3 colloidal solution, both nebulized in a Collison type atomizer, and indoor particles.

Fig. 1 and 2 show respectively the size distribution obtained with the Grimm-DMA and TSI-FMPS of the three tested aerosols: the Milli-Q water has the lowest particle size distribution (which can not be resolved by DMA), the Fe_2O_3 particles have a maximum at about 30 nm, and indoor particles at about 100 nm. Each aerosol type test consists of 3 replicas of simultaneous samplings (DMA was run in fast mode so that both instruments almost the same sampling time). Fig. 3 shows the relative difference between Grimm and TSI, against the particle diameter. Relative differences are of the order of

100% and tend to increase with aerosol size (dp > 100 nm). Further research on the performance of the new FMPS against the traditional sampler should be encouraged in order to better understand eventual behaviour differences.
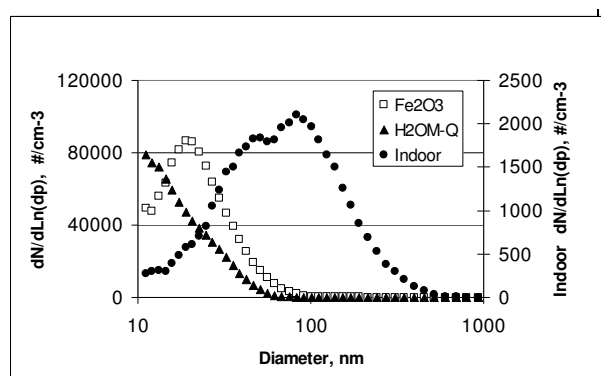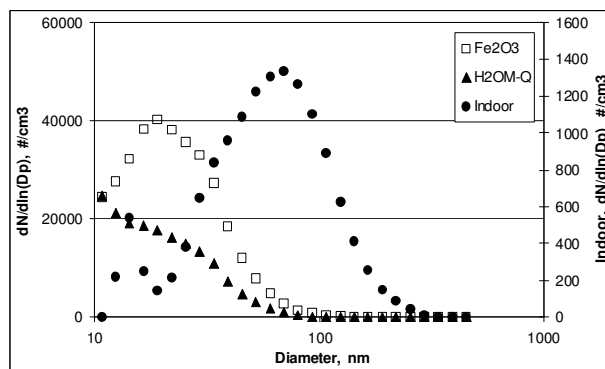

Figure 1. Grimm-DMA aerosol size distribution
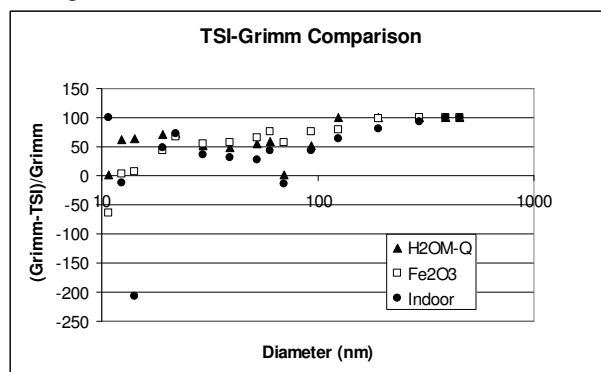

Figure 2. TSI-FMPS aerosol size distribution

Figure 3. Relative difference results

Intercomparison of two types of portable optical particle counters (Grimm model 1.109 and 1.108) at an urban aerosol measurement station

J. Burkart[1], H. Moshammer[2], M. Neuberger[2], G. Steiner[1], G. Reischl[1] and R. Hitzenberger[1]

[1]University of Vienna
Faculty of Physics, Aerosol, Bio- and Environmental Physics, Boltzmanng. 5, A-1090 Vienna, Austria
[2]Medical University of Vienna
Institute of Environmental Health, Kinderspitalgasse 15, A-1090 Vienna, Austria

Keywords: optical particle counter, urban aerosol

Optical particle counters (OPC) are used frequently as online instruments in order to get a quick overview of aerosol parameters such as mass concentration (e.g. PM10 or PM2.5) or number concentration.

In our study the focus was on testing the performance of two different types of optical particle counters when measuring particle number concentration and number size distribution of atmospheric urban aerosols.

Optical particle counters measure the intensity of the light scattered by single particles passing a laser beam. The resulting electrical signal is analysed and particles are classified into different size channels according to the height of the electrical impulse, and a number size distribution is obtained. Scattered light intensity is assumed to be a monotonic function of particle size.

Both OPCs used in this study are produced by Grimm, Ainring, Germany. Model 1.108 (OPC2) has 15 size channels and a lower and upper cut-off diameter of 0.3 and 20μm, respectively. Model 1.109 (OPC1) has 31 size channels and a lower and upper cut-off diameter of 0.25 and 32μm, respectively. The OPCs were connected with a Y-piece to the same inlet tube and sampled atmospheric aerosol with a flowrate of 1.2 L/min. In addition to the OPCs a Vienna type DMA and a TSI CPC were operated to obtain information on the number size distribution in the size range from 10 to 1000nm (DMA) and the total particle concentration (CPC). The measurements were performed at the urban aerosol measurement station at the roof laboratory of the University of Vienna in December 2007 and January 2008.

When comparing total particle concentration measured by OPC1 and OPC2, an average difference of a factor of 2.5 can be found. In all the cases OPC1 could detect more particles than OPC2. A comparison with the DMA data confirms that this is due to the slight difference in the lower cut-off diameter of the two instruments. As illustrated in Figure 1 the concentrations obtained by integration of the DMA size distribution from the upper cut-off diameter to 250 and 300nm agree within 15% to the concentrations measured with the OPCs.

In Figure 1 the total particle concentration as obtained by integration over the whole DMA size distribution is plotted as well. It can be seen that the total particle concentration can be over 20 times larger than the particle concentration obtained by the OPCs. (Please note that there is a factor of ten between the scale on the left y-axis and the scale on the right y-axis. Only total particle concentration (DMA) refers to the left axis.) The total particle concentration does not even follow the pattern of the particle concentrations received by OPC1 and OPC2 and the factor of difference is not constant.

Our comparison shows that using OPCs for estimating particle number concentration can be very misleading and in general underestimates particle number concentration quite severely. Even a slight difference in the lower cut-off diameter can lead to considerable differences in measured particle concentrations.
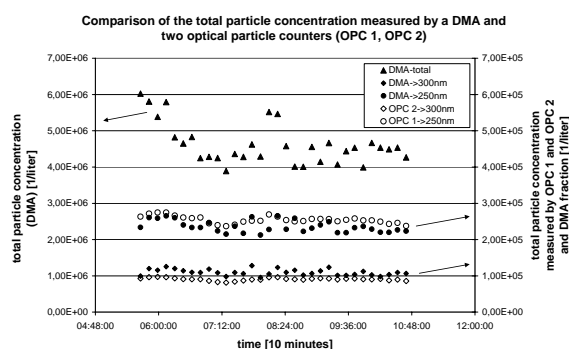

Figure 1 Comparison of the total particle concentration measured by a DMA and two different optical particle counters

Mass concentration of $PM_{2.5}$, nitrate and sulfate measured by automatic instruments and manual sampler during various meteorological conditions

J.H. Tsai[1], C.H. Lin[1], C.C. Liu[2], W.F. Lai[1] and Y.C. Yao[1]

[1]Department of Environmental Engineering, National Cheng Kung University, Tainan, 701, Taiwan, Republic of China
[2]Taiwan Environmental Protection Administration, Taipei, 100, Taiwan, Republic of China

Keywords: fine particulate matter, nitrate, sulfate, TEOM, MOUDI.

In order to characterize of fine particulate matter, Taiwan Environmental Protection Administration (TEPA) has established an air quality monitoring network (aka supersite) in southern Taiwan. Those particulate concentrations are measured by analyzers automatically and continuously in stations, as said TEOM method. This study was undertaken to evaluate the data difference between the automatic monitoring instrument and manual sampler under various meteorological conditions, i.e. temperature and relative humidity, and to understand the accuracy of the automatic monitoring instrument. The instruments are presented in Table 1.

Table1. The sampling instrument of ambient fine PM used at this study.

Item	Automatic		manual	
	Instrument	Data collection period	Instrument	Data collection period
$PM_{2.5}$ mass concentration	R&P 1400	10 min	MOUDI	24 hour
particulate nitrate in $PM_{2.5}$	R&P 8400N	30 min	MOUDI	24 hour
particulate sulfate in $PM_{2.5}$	R&P 8400S	30 min	MOUDI	24 hour

The airborne particulate matter and their precursor gases were collected by MOUDI samplers at an air quality monitoring station located near the supersite during October 2005 to December 2007. This station was one of the stations with highly frequent occurrences of poor air quality days in Taiwan. The NO_3^- and SO_4^{2-} contained in $PM_{2.5}$ particulate were detected by ion chromatography. Totally were 23 sets of daily concentration data measured by manually MOUDI samples, and by automatically measurements (R&P analyzers).

In general, the result of whole data shows that the $PM_{2.5}$ mass concentration by MOUDI sampler is larger than that by R&P automatic analyzers significantly (p value < 0.05 by t-test); the mean concentrations are 53.6 and 38.6 μg/m^3, respectively. Moreover, the R&P 1400 data were related to MOUDI data with a high correlation coefficient (r = 0.89).

The NO_3^- in $PM_{2.5}$ by MOUDI sampler is larger than that by R&P 8400N, however, without statistical significance. The correlation result shows

a medium correlation between the data measured by R&P 8400N and MOUDI. The SO_4^{2-} in $PM_{2.5}$ by MOUDI sampler is close to that by R&P automatic analyzers. The correlation coefficient is 0.73.

At ambient temperature lower than 25 ^{o}C, the mean $PM_{2.5}$ mass concentration by MOUDI sampler (79.4 μg/m^3) is larger than that by R&P automatic analyzers (52.7 μg/m^3) significantly (p<0.05), however, the mean value are close at temperature higher than 25 ^{o}C (25.4 μg/m^3 for MOUDI and 23.3 μg/m^3 for R&P 1400). In contrast, the $PM_{2.5}$ mass concentrations by MOUDI were larger than that by R&P 1400 significantly (p<0.05) regardless of RH condition (lower or higher than 70%). The result also indicated that the R&P 1400 data were related to MOUDI data with a high correlation coefficient, the r value is 0.97 (RH<70%), and 0.82 (RH>70%). Figure 1 illustrated the relative of $PM_{2.5}$ mass concentration measured by automatic instruments and manual sampler at different RH condition.
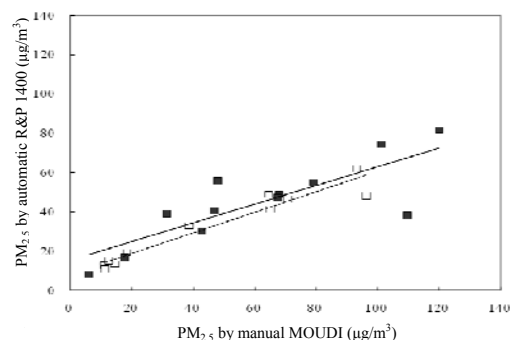

Figure 1. The relative of automatic instruments and manual sampler at different RH condition (□ at RH < 70%, ■ at RH > 70%).

In brief, the study showed that the automatic instruments and manual sampler instruments for fine particulate measurement shall have different result, to some extent. The study would be helpful to develop or evaluated the fine particulate monitoring instrument or method.

Performance of a New Condensation Particle Counter

Hojoong Kim[1], Juergen Spielvogel[2], Soohyun Ha[1], and Taesung Kim[1]

[1]SKKU Advanced Institute of Nanotechnology (SAINT), Sungkyunkwan Universiry, Cheoncheon-dong, 440-746, Suwon, Korea
[2]Grimm Aerosol Technik, Dorfstrasse 9, D-83404, Ainring, Germany

Keywords: CPC, aerosol instrumentation, nanoparticles, measurements

With the increase of submicron or ultrafine particle researches on either atmospheric or nanoscience field, the scanning mobility particle sizer (SMPS) which mainly consists of differential mobility analyzer (DMA) and condensation particle counter (CPC), is one of the most commonly used instruments. As the particle number concentration in a unit aerosol volume is counted by the CPC, its counting efficiency determines overall performance of the SMPS instrument.

From the invention of continuous-flow CPC, a number of CPC measurement methods characterizing performance of the CPC have been carried out, such as the work of Wiedensohler *et al.* (1997) or S Mertes *et al.* (1995). Although, there are a lot of studies related to the CPC measurements, new studies are still performed due to its importance in ultrafine particle research.

Grimm Aerosol Technik, an aerosol instrumentation company in Germany, has recently developed new CPC instrument which has improved performance compared to previously developed CPCs of the company. The instrument has smaller optical volume than that of previous instruments so that higher limit of single particle count per time can be achieved due to less coincidence effect. Larger temperature difference (ΔT) between condenser and saturator, and internal coincidence effect correction function also contribute to the improved performance.

In this study, calibration and characterization were performed with a prototype model of new CPC. List of the measurements is shown in Table 1.

Table 1. List of the measurements.

Name of measurement	Used instruments
Linearity	New CPC, Grimm 5.403, FCE
Square wave input response	New CPC , Grimm 5.403, FCE
Ramp input response	New CPC , Grimm 5.403
Counting efficiency	New CPC , Grimm 5.403

The experimental setup was composed of new CPC, Grimm 5.403 CPC, and faraday cup electrometer (FCE) unit. The FCE unit was considered as a reference to calibrate the prototype and Grimm 5.403 CPCs.

Linearity and square wave input measurements were performed to confirm calibration status of 2 CPCs used in this study. Figure 1 shows the result of linearity measurement of the CPCs. For counting efficiency measurements, we used different conditions of atmospheric pressure, low pressure down to 800 mbar, different ΔT, and particles made of different materials.

The experimental results of efficiency measurement showed that new CPC has smaller d_{50} and higher counting efficiency for ultrafine particles than Grimm 5.403 CPC. Similarly, other experimental results also showed better results than those of Grimm 5.403 CPC.

In conclusion, new CPC showed that it has improved performance than the previously developed CPC.
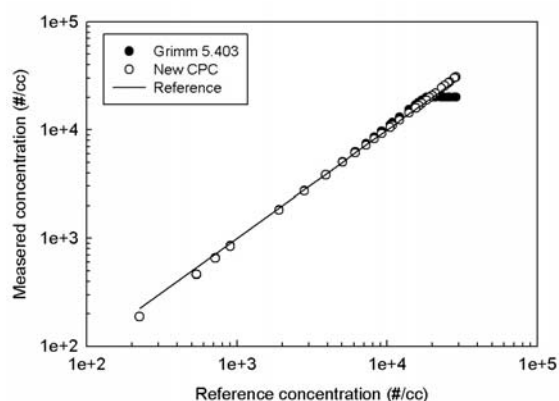

Figure 1. The result from linearity measurement

Wiedensohlet, A., Orsini, D., Covert, D. S., Coffmann, D., Cantrell, W., Havlicek, M., Brechtel, F. J., Russell, L. M., Weber, R. J., Gras, J., Hudson, J. G., & Litchy, M. (1997). *Aerosol Science and Technology,* 27, 224-242.

Mertes, S., Schroder, F., & Wiedensohler, A. (1995). *Aerosol Science and Technology*, 23, 257-261.

Comparison of the Thermo Scientific TEOM 1405-DF monitor to Reference Method Sampling Results for the Measurement of PM$_{2.5}$

J.L. Ambs[1]

[1]Thermo Fisher Scientific, Franklin, Massachusetts, 02038, United States of America

Keywords: TEOM, FDMS, PM2.5, Ambient PM

Thermo Scientific recently conducted PM$_{2.5}$ equivalency testing on the new TEOM 1405-DF Dichotomous Ambient Particulate Monitor with FDMS (TEOM 1405-DF) The TEOM 1405-DF was compared to the US EPA PM$_{2.5}$ reference method and the European reference methods at locations in both the US and Europe.

The TEOM 1405-DF is a dichotomous sampler configured as a dual filter sampler for the simultaneous measurement of both fine (PM$_{2.5}$) and coarse (PM$_{10-2.5}$) particles in PM$_{10}$. A virtual impactor is used to separate the fine and coarse PM into two samples for collection and measurement on two sample filters in the TEOM 1405-DF. The two samples pass through two FDMS modules before being captured and measured by the two inertial micro-balances in the TEOM mass sensor.

The FDMS was designed to take advantage of the TEOM real-time mass measurement system to address these issues by characterizing the semi-volatile and non-volatile portions of ambient PM$_{2.5}$ as present in the atmosphere at the time of collection. When sampling ambient aerosol, the sample filter in the TEOM monitor collects the incoming ambient aerosol, which includes both the non-volatile as well as semi-volatile material. Because of the self-referencing nature of the FDMS equipped TEOM monitors, the FDMS equipped TEOM monitors are able to measure and correct for the presence of semi-volatile material present in the collected sample.

During operation, the FDMS equipped TEOM monitors alternately sample ambient aerosol and then sample through a chilled reference filter for equal time periods. During normal sampling, or the base period, the TEOM sample filter is measuring mass increase from the ambient aerosol as well as any mass changes of collected the semi-volatile material. During the reference period of sampling, the sampled ambient aerosol is filtered in the chilled filter conditioner and no incoming ambient aerosol is measured by the mass sensor and only changes to the amounts of semi-volatile material previously collected on the sample filter are measured. The switch between the base and reference measurement periods occurs every six minutes and the monitor calculates the base and reference mass concentrations

for these switch periods at the end of each successive measurement.

The reference mass concentration is then subtracted from the base mass concentration to determine the near real-time ambient mass concentration. In this way the FDMS system determines the total atmospheric aerosol mass concentration including volatile and semi-volatile components as they exist in the atmosphere at the time of collection. The system then subtracts the calculated reference concentration from the calculated base mass concentration giving a net ambient aerosol mass concentration which represents the mass concentration of ambient aerosol as it exists at the time of sample collection.

During this sample study, multiple reference samplers and multiple TEOM 1405-DF monitors were operated simultaneously at each of the sampling locations. The reference sampler filters were sampled for 23-hour periods and collected daily. The test program provided for a wide range of sampling conditions over multiple seasons of the year, and widely varying environmental conditions. The results presented in Figure 1 are representative of the results obtained over the test program.
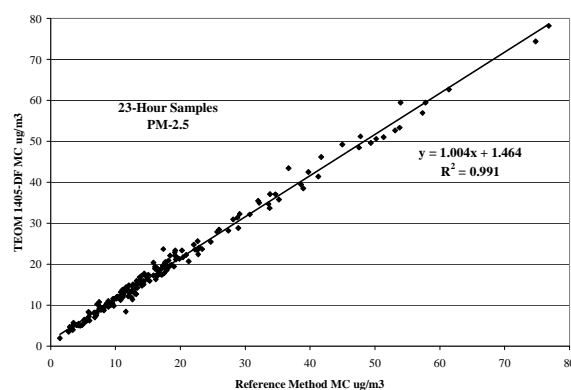

Figure 1. Comparison between the TEOM 1405-DF Dichotomous Ambient Particulate Monitor with FDMS and Reference Method samplers in multiple locations and multiple seasons.

Comparison of the performance of the Thermo Scientific TEOM 1400a with 8500C FDMS and the TEOM 1400a with 8500B FDMS monitors for the measurement of PM$_{2.5}$

J.L. Ambs[1]

[1]Thermo Fisher Scientific, Inc., Franklin, Massachusetts, 02038, United States Of America

Keywords: TEOM, FDMS, PM2.5, Ambient PM

Thermo Scientific released the first Filter Dynamics Measurement System (FDMS) for the TEOM monitor in 2002. The Thermo Scientific TEOM 1400a with 8500C FDMS (8500C FDMS) is the current version of the 8500 FDMS equipped line of TEOM 1400a ambient PM monitors. The "C" version of the FDMS utilizes a more efficient dryer for better performance. This work explored the performance differences between, TEOM monitors using the current version of the dryer with older dryers.

PM$_{2.5}$ is a complex mixture of chemical species in a range of physical sizes that varies significantly with season and location and can include both non-volatile and semi-volatile materials. Ammonium nitrate, semi-volatile organic material, and water are semi-volatile materials, while other components are non-volatile in the context of ambient PM measurements. Many studies show that there is a loss of semi-volatile material from the collected samples using some continuous monitors as well single event filter samples, including the US EPA PM$_{2.5}$ reference method.

The FDMS was designed to take advantage of the TEOM real-time mass measurement system to address these issues by characterizing the semi-volatile and non-volatile portions of ambient PM$_{2.5}$ as present in the atmosphere at the time of collection. When sampling ambient aerosol, the sample filter in the TEOM monitor collects the incoming ambient aerosol, which includes both the non-volatile as well as semi-volatile material. Because of the self-referencing nature of the FDMS equipped TEOM monitors, the monitors are able to measure and correct for the presence of semi-volatile material present in the collected sample.

During operation, the FDMS equipped TEOM monitors alternately sample ambient aerosol and then sample through a chilled reference filter for equal time periods. During normal sampling, or the base period, the TEOM sample filter is measuring mass increase from the ambient aerosol as well as any mass changes of collected the semi-volatile material. During the reference period of sampling, the sampled ambient aerosol is filtered in the chilled filter conditioner and no incoming ambient aerosol is measured by the mass sensor and only changes to the

amounts of semi-volatile material previously collected on the sample filter are measured. The switch between the base and reference measurement periods occurs every six minutes and the monitor calculates the base and reference mass concentrations for these switch periods at the end of each successive measurement.

The reference mass concentration is then subtracted from the base mass concentration to determine the near real-time ambient mass concentration. In this way the FDMS system determines the total atmospheric aerosol mass concentration including volatile and semi-volatile components as they exist in the atmosphere at the time of collection. The system then subtracts the calculated reference concentration from the calculated base mass concentration giving a net ambient aerosol mass concentration which represents the mass concentration of ambient aerosol as it exists at the time of sample collection.

Field comparisons of the two FDMS systems were performed in multiple locations and over multiple seasons to evaluate the effect of the improved dryer on the performance of the FDMS equipped TEOM monitors. Collocated monitors were compared over 24 hour test periods and compared to the results collected from collocated reference samplers.   Comparative results from the collocated FDMS equipped TEOM monitors are presented in Figure 1.
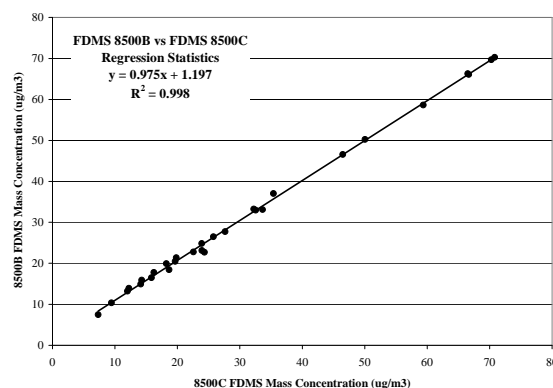

Figure 1. Comparison of FDMS systems with the "B" and "C" types of dryers installed.

Integrated water vapor (IWV) climatology with RIMA-AERONET sunphotometers, GPS and Radiosondes in the Southwestern of Spain

B. Torres[1], V. E. Cachorro[1], C. Toledano[1], J. P. Ortiz de Galisteo[2], A. Berjón[1], A. M. de Frutos[1]

[1]Group of Atmospheric Optics, University of Valladolid, Spain.
[2]Spanish Meteorology Agency (AEMET), Delegación Territorial de Castilla y León, Spain

Keywords: Precipitable water vapor, Sun-Photometer, GPS, Radiosonde, RIMA-AERONET.

Abstract

Column integrated water vapor (IWV) data in the Southwestern of Spain are analyzed during 2001 to 2005 with two aims: 1) to establish the climatology over this area using three different techniques, such as Sun-Photometer (SP), Global Position System (GPS) and Radiosondes, and 2) to take advantage of this comparative process to assess the quality of radiometric IWV data collected at the RIMA-AERONET station. The 5 years of climatological series gives a mean value of about 2 cm (STD=0.72) and a clear seasonal behavior as a general feature, with the highest values in summer and the lowest in winter. In the multi-annual monthly means basis, the highest values are reached in August-September, with a mean value of 2.5-2.6 cm, whereas the lowest are obtained in January-February, with an average of 1.4-1.5. However the most relevant results for this area is the observed local minimum in July, occurring during the maximum of desert dust intrusions in the southern Iberian Peninsula.
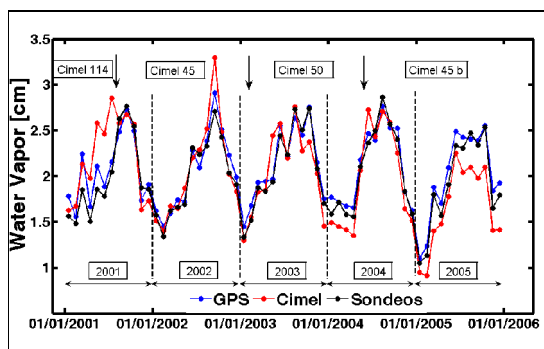
Figure 1. The time series of monthly means of IWV during 2001-2005, for data collected by GPS, SP and Radiosondes. Arrows indicate a change of SP.

A comparison process allows us to evaluate the agreement of IWV data sets between these three different techniques at different temporal scales because of different time sampling. On a daily basis and taking GPS as the reference value (Bokoye et al., 2006) we have a bias or difference between Radiosonde and GPS measurements for the entire data base of 0.07 cm (relative bias of 3%) and RMSE of 0.33. For SP-GPS we have a bias of 0.14 cm (about 7%) and RMSE of 0.37. On a monthly basis the differences between Radiosonde and GPS values varies from summer with 2% to winter with -8% and between SP and GPS values from 3% in summer to −14% in winter.
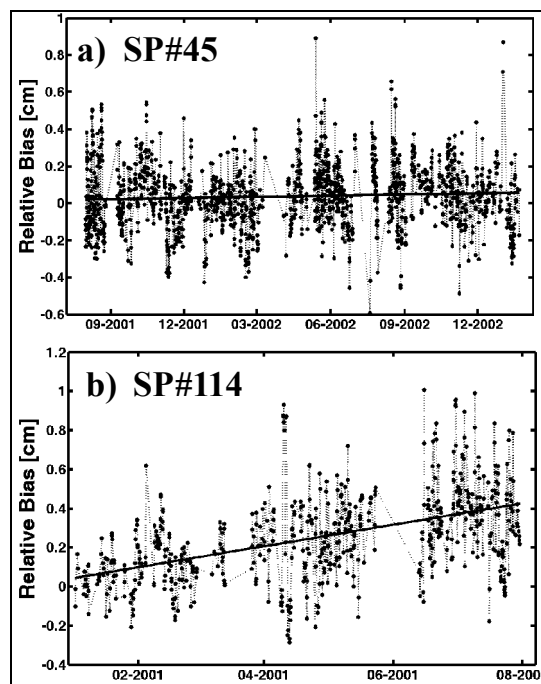

Figure 2. Relative bias values between SP-GPS and the regression line of tendency for a) SP #114 (bad behavior) and b) SP #45(good behavior).

The observed bias between GPS and SP varies during each SP operational period, with lower values at the beginning of the measurements and increasing until the end of its measurement term and with the bias values being quite dependent on each individual SP. The observed differences highlight the importance of drift in each Sun-Photometer, because of filter aging or other calibration problems. Hence the comparison with GPS appears to be a powerful tool to asses the quality of Sun-Photometer for IWV retrieval.

Boyoke, A.I., Royer, A., Cliche, P., & O'Neill, N. (2006). Calibration of Sun Radiometer-Based Atmospheric Water Vapor Retrievals Using GPS Meteorology. *Journal of Atmospheric and Oceanic Technology, 24,* 964-979.

Ion-induced solvation and nucleation studies in a sonic DMA

M. Attoui[1] J. Fernandez de la Mora[2]

[1]Physic Department, Paris XII University France [2]Mechanical Department Yale University USA

Key words: DMA, Mobility, ion induced nucleation

Fernandez de la Mora has recently introduced the *HalfMini DMA*, a miniature high resolution DMA reaching sonic conditions (Mach number = M = 1) at a flow rate of sheath gas of *only* Q~740 lit/min. Due to an efficient diffuser and a negligible flow resistance at the DMA outlet, sonic flow is readily achieved with one or two conventional vacuum cleaner pumps. Our goal is to study ion induced solvation and nucleation (IISN) by running this DMA sonically with a gas containing a vapour. The vapour is below saturation conditions at stagnation conditions, but substantial supersaturation is achieved in the sonic working section by expansion cooling. In order to control gas composition without consuming 750 lpm of purified gas, we operate the sheath flow under closed loop, so that its composition is that of the inlet aerosol. Since the pumps introduce ~ 1 kW into the gas, the main challenge is to cool the circuit such as to achieve a steady state operation with a temperature as uniform as possible (to avoid condensation on cold circuit parts) and as low as possible (to favour IISN over homogeneous nucleation). This we have achieved by closing the flow circuit with a long line of corrugated SS tubing immersed in a slightly cooled water bath at 10°C witch gives sheath air temperature between 18 to 22 °C. The working gas is typically CO_2 into which controlled quantities of alcohol are added continuously at the aerosol inlet, with a syringe pump and in a heated loop, ensuring complete vaporization of the alcohol. This vapour-laden gas is then introduced into an electrospray chamber where tetraheptyl ammonium (THA^+) ions are added, and then enters the DMA. We measure the mobility of these ions as a function of vapour concentration and Mach number. In preliminary experiments with no vapour addition we confirm that sonic conditions are achieved by observing that, above a critical pump power, further increases in power lead to no increase in the voltage V_{DMA} at which the peak of the (dry) ion appears. Figure 1 shows the evolution of V_{DMA} as the methanol concentration is changed at M = 1. The shift in voltage (inverse mobility) is due in part to the increased ion drag associated to the change in composition of the gas, and in part also to growth of the ion by solvation. Only the latter effect provides information on IISN. We plan to isolate the first effect in experiments at low M and higher temperature, to then study quantitatively the second in sonic experiments at lower temperatures.
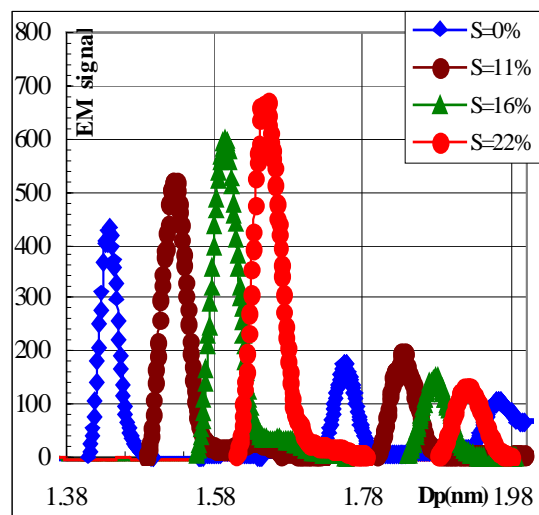

Figure 1 : THA^+ size distribution of THABr at different supersaturation with methanol. The second peak is the dimer ion $(THA^+Br^-)THA^+$

Construction of a Biofluorescence Optical Particle Counter

Russell Greaney[1], Oliver Ryan[1], S. Gerard Jennings,[1] Colin D. O'Dowd,[1]
[1] School of Physics & Centre for Climate and Air Pollution Studies, Environmental Change Institute, National University of Ireland, Galway, University Road, Galway, Ireland.

O'Dowd et al. (2004) found that submicrometer marine spray aerosol contained a significant fraction of organic matter and is associated with the seasonality of plankton biological activity as determined from satellite ocean-colour products. Laser induced fluorescence will probe the organic content of marine aerosols through excitation of fluorescence of chlorophyll-a contained in the phytoplankton. The fluorescence quantum yield is very low for chlorophyll-a in phytoplankton, ranging from 2% to 7% (Lizotte & Priscu, 1994). The fluorescence signature also has a very short lifetime on the order of nanoseconds making the fluorescence output almost simultaneous to the elastic scattered light signal. This necessitates the use of highly sensitive photomultiplier tubes (PMTs) to maximise data signal-to-noise.
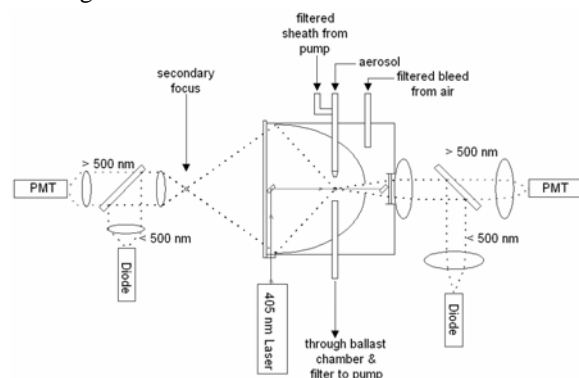

Figure 1: A schematic layout of the instrument.

Figure 1 depicts the layout of the laser induced fluorescence optical particle counter (LIF-OPC) instrument. All flow rates in and out of the chamber are balanced to allow a smooth non-turbulent hydro-dynamically focused air flow. The ellipsoid reflector has a protected silver coating to maximize collection of the scattered 405 nm laser light as well as having high collection efficiency for the chlorophyll-a fluorescence. High efficiency dichroic (long pass) mirrors split the collimated beam at an edge wavelength of 500 nm, passing the scattered light to photodiodes, and the weaker fluorescent emission to highly sensitive Hamamatsu PMTs.

Calibration and testing of the instrument is currently underway and is producing both sizing and fluorescence measurements. The LIF-OPC has sized particles (ammonium sulphate) as low as 167 nm in diameter and also detected fluorescence from 3 µm PSL spheres (Green 510 from Duke Scientific).

Chlorophyll-a powder will be used with the aerosol generator (TSI atomizer and classifier) to produce chlorophyll particles of known diameter to calibrate the PMT fluorescence signal output. A phytoplankton breeding tank will be created to allow in-house measurements of bubble mediated aerosol from seawater enriched with phytoplankton cultures. After validation the instrument will be brought for flux measurements and bioaerosol chlorophyll detection trials on the Atlantic coast at the Mace Head atmospheric research station.

C.D. O'Dowd, M.C. Facchini, F. Cavalli, D. Ceburnis, M. Mircea, S. Decesari, S. Fuzzi, Y.J. Yoon, and J-P. Putaud, "Biogenically-driven organic contribution to marine aerosol", Nature 431, 676-680, 2004.

M.P. Lizotte, and J.C. Priscu, "Natural fluorescence and quantum yields in vertically stationary phytoplankton from perennially ice-covered lakes, Limno". Oceanogr. 39(6), 1399-1410, 1994.

P. H. Kaye, J. E. Barton, E. Hirst, and J. M. Clark, "Simultaneous light scattering and intrinsic fluorescence measurement for the classification of airborne particles", Applied Optics, 39, 3738-3745, 2000.

Design and Characterization of the Screw-Assisted Rotary Feeder with Ultra Low Feeding Rate

K.S. Lee[1], J.H. Jung[1] and S.S. Kim[1]

[1]Department of Mechanical Engineering, Korea Advanced Institute of Science and Technology (KAIST), Guseong-dong, Yuseong-gu, Daejeon 305-701, Republic of Korea

Recently, as the regulation about the emission of the GHG (Green House Gas), such as CO_2 or CH_4, has become more severe, the O_2/CO_2 combustion system, which enables the easy CO_2 recovery from the high concentration of the CO_2 in combustion chamber by the EGR (Exhaust Gas Recirculation), was introduced as one of the promising combustion systems. Furthermore, In-furnace desulfurization technique, which need not additional chamber for the desulfurization, can be applied to the O_2/CO_2 combustion system despite of its low desulfurization efficiency. The O_2/CO_2 combustion system is able to store the exhaust gas using the storage facilities instead of emitting it to the atmosphere. This process is conducted using calcium carbonate ($CaCO_3$) sorbent particles which have wide size range.

In previous studies, various feeding methods, such as rotary feeder, screw feeder, vibration feeder, and turntable feeder, have been used to transport the sorbent particles into the combustion chamber. However, most of these feeders have several drawbacks, such as high feeding rate and the usage of high carrier gas volume rate, when they are applied to the lab-scale researches (Reist *et al.*, 2000; Gundogdu, 2004).

In this study, we investigated the screw-assisted rotary feeder which enables transport small quantity of sorbent. The generation characteristics, such as uniformity and stability, were verified using CPC (Condensation Particle Counter 3022A, TSI Inc., USA), APS (Aerodynamic Particle Sizer 3321, TSI Inc., USA), and SMPS (Scanning Mobility Particle Sizer, TSI Inc., USA) systems. Two rotors which have different number of groove (4- and 12- grooved rotors) were constructed and examined in various

rotation speeds (3, 6, 9, 18, and 27 rpm) with constant air flow rate (23 L/min).

Figure 1 shows the variance of the particle number concentration of 4-grooved rotor at the experimental conditions from 3 to 27 rpm of rotation speed. From real-time method using CPC, the screw-assisted rotary feeder has the pulse-shaped particle generation characteristics repeating on-off operations periodically. As the rotation speed increased, the frequency of discharging sorbent particles increased. At the same time, the amplitudes of the number concentration data decreased.

Table 1. Mean number concentrations ($\#/cm^3$) and COVs of two different grooved rotors in various rotation speeds

		3 rpm	9 rpm	27 rpm
4-grooved rotor	Mean	0.13E6	1.1E6	1.6E6
	COV	0.358	0.127	0.082
12-grooved rotor	Mean	0.29E6	0.61E6	0.39E6
	COV	0.127	0.075	0.312

Table 1 shows the mean of number concentrations and the COVs (Coefficient of Variance) of two different grooved rotors in various rotation speed conditions. For the 4-grooved rotor, both number concentration and COV decreased with increased rotation speed. For 12-grooved rotor, however, they decreased with variance of rotation speed from 9 to 27 rpm. We think that this variance of mean and COV may be caused of the lack of filling time of sorbent particles into the groove.

From this study, the particle generation condition with high uniformity and stability can be established from the screw-assisted rotary feeder. Also, we can control the feeding rates of sorbent particles by adjusting the rotation speeds of the grooved rotor.

Reist, P. C., & Taylor, L. (2000). *Powder Technol.*, 107, 36-42.
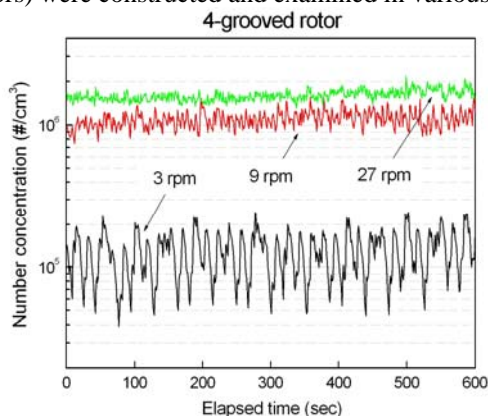Gundogdu, M. Y. (2004). *Powder Technol.*, 139, 76-80.

Figure 1. Number concentration of 4-grooved rotor in rotation speeds from 3 to 27 rpm in real time.

Density analyzing method of atmospheric particles: reliability and limitations using a new ELPI stage

J. Kannosto, J. Yli-Ojanperä, M. Marjamäki, A. Virtanen, J. Keskinen

Aerosol Physics Laboratory, Department of Physics, Tampere University of Technology, P. O. Box 692, FIN-33101 Tampere, Finland

The assessment of climatic and health effects of atmospheric aerosol particles requires detailed information on the particle properties. In addition, the particle chemical composition and other chemical and physical properties carry information concerning sources and formation mechanisms of the particles. Nucleation bursts observed in different environments are producing nucleation mode particles in the atmosphere. There have been intensive and successful efforts to identify different nucleation mechanisms. Regardless of the progress, there are still gaps in the general understanding of the new particle formation.

Our method is based on a simultaneous ("parallel") distribution measurement with an ELPI and a SMPS/DMPS and, further, on the relationship between the aerodynamic size, the mobility size and the effective density of the particles (Ristimäki et al. 2002). We have studied density of boreal forest particles and found the density values for nucleation, Aitken and accumulation modes (Kannosto et al. 2008). Measurements in Kannosto et al. 2008 have been made using normal ELPI impactor with the filter stage. After these measurements, we have developed a new ELPI stage with a lower cut point (Yli-Ojanperä et al. 2009). And we have performed calibration measurements in the laboratory and simulations to clarify the lowest size limits and reliability of the density analyzing method using the old and the new ELPI impactors.

We simulated particle distribution modes with different GMD, GSD and concentration. ELPI currents were calculated using the simulated modes and specific density values. 5% random error was added to these ELPI currents. Density value of each mode was calculated 50 times. Laboratory tests of the density analyzing method were taken using di-octyl sebacate (DOS, density 0.912 g/cm^3) and evaporation-condensation generator to produce polydisperse aerosol distribution. Geometric mean diameter of the particles size distribution varied between 8 nm – 40 nm and the distributions were very narrow.

Results of the reliability simulations show differences between the new and the old impactor setup. The density analyzing method produces densities close to the initial value at high GMD values. With smaller GMD than 15 nm, the density analyses resulted in different values depending on the impactor type. Density values under 15 nm analyzed using the old impactor increases as GMD decreases and variation is very high. Between 8 nm – 15 nm the new impactor setup gives the density values very close to the initial values, indicating lower size limit for density analysis. Also, the variation of the density values was much smaller with the new impactor. Lowest detection limit for the new impactor setup is about 10 nm and for the old setup about 15 nm. These limits are in aerodynamic diameters and they are affected by the particle density.

Results of the laboratory test agree with the results of simulations. The density value of DOS particle distributions calculated with the density analyzing method is very close to bulk density of DOS. The new impactor setup produces the correct result down to about 10 nm when the old impactor setup reaches 15 nm.

Kannosto J., Virtanen A., Lemmetty M., Mäkelä J.M., Keskinen J., Junninen H., Hussein T., Aalto P., Kulmala M. (2008), Mode resolved density of atmospheric aerosol particle, *Atmospheric Chemistry and Physics* 8, 5327-5337

Ristimäki, J., Virtanen, A., Marjamäki, M., Rostedt, A., Keskinen J. (2002): On-line measurement of size distribution and effective density of submicron aerosol particles. *J. Aerosol Sci.*, 33, 1541-1557

Yli-Ojanperä J., Kannosto J., Marjamäki M. Keskinen J. (2009), Improving the nanoparticle resolution of the ELPI, Manuscript in preparation/submitted

First tests of thermophoretic trap in short duration microgravity conditions

A.A. Vedernikov[1], A.M. Markovich[1], A.V. Kokoreva[1], N. Bastin[1], P. Queeckers[1], N.V. Kozlov[2], J. Blum[3], I. von Borstel[3], R. Schräpler[3]

[1]Microgravity Research Centre, Université Libre de Bruxelles, 50, av. F.D. Roosevelt, 1050, Brussels, Belgium
[2]Perm State Pedagogical University, Perm, 614990, Russia
[3]Institut für Geophysik und Extraterrestrische Physik, Technische Universität zu Braunschweig, 38106, Germany

Keywords: aerosol dynamics, cloud dust, dynamic balancing, instrument development, microgravity

The European Space Agency's scientific program Interactions in Cosmic and Atmospheric Particle Systems (ICAPS) is aimed at increasing our knowledge about dust agglomeration in astrophysical processes mostly related to proto-planetary matter formation (Blum et al., 2008). Microgravity conditions are needed to suppress sedimentation, which in the laboratory considerably reduces the experimentation time, thus Brownian motion driven agglomeration can be performed over a much-extended period of time. However, grain diffusion to the walls (at which all dust grains inevitably stick) and residual forces, like e.g. thermophoresis, impose limits to the maximum achievable agglomerate size and the agglomeration rate. The reduction of these adverse effects demands an efficient trapping mechanism for dust ensembles with the following requirements: particle sizes – from monomers of ~1μm to agglomerates of up to ~1mm; particle concentration up to 10^6-10^7 cm^{-3}; fixed pressure in the range 0.1 -10 mbar; room temperature (about 300K); cloud volume in the 'area of interest" – 1 to 40 cm^3; total chamber volume about 1 liter. Prevention of grain diffusion or drift to the walls of the experiment chamber allows long-duration agglomeration studies for the investigation of aggregate morphologies, aggregation rate, aggregate mass distribution, and temporal behavior of the mean aggregate mass for a variety of grain sizes, shapes, compositions and gas pressures.

To meet the requirements of the project, the experimental instrumentation should provide 1) squeezing of such a dense cloud (mostly to compensate particle number lowering due to Brownian agglomeration) and 2) counterbalancing external cloud perturbations. Traditional approach would be using electrodynamic balancing (EDB or Paul trap) taking into account the fact that particles are naturally charged by cog wheel injection. However, this technique has principal disadvantages coming from presence of opposite charges on the particles. Among other drawbacks it leads to quick reduction of the total charge-to-mass ratio of growing agglomerates, lowering of the 'trapping strength' followed by loosing the agglomerates - the most interesting objects of investigation. The use of the thermophoretic force (Vedernikov et al., 2007) should remove most disadvantages of the electrodynamic balancing. Mean particle velocity in a thermophoretic trap is convenient to express as

$$v_{sq} = \langle v_T \rangle_t = -\frac{2\tau_p}{1+(\omega\tau_p)^2}\left[\frac{v_{ref}C_z P_{ref}\omega_{ref}T_{ac}(\omega_{ref})}{\omega\cdot(\nabla T)_{ref}\cdot P}\right]^2 z$$

where τ_p particle relaxation time; ω angular frequency (2-10 Hz); v_{ref} is the value of the particle thermophoretic velocity at known temperature gradient $(\Delta T)_{ref}$ and reference pressure P_{ref}; C_z proportionality coefficient in the temperature profile fit $T=T_0+C_z*T^2$ around equilibrium trap point; T_{ac} is the temperature variation amplitude on heaters at reference frequency ω_{ref} (T_{ac} was 4.2 K for 10 Hz); z mean particle axial coordinate.

First tests in microgravity conditions of the Bremen drop tower (microgravity duration 4.7 s) were performed in a prototype chamber of the ICAPS project that imposed certain geometrical limitations on the trap (two coils, diameter 62 mm separated by 10 mm). Measured motion parameters were in agreement with the theoretical model.
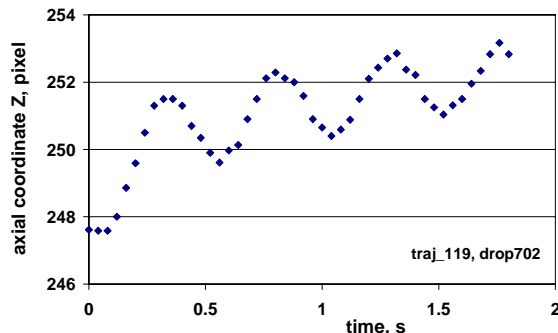
Figure 1. Typical particle trajectory.

The tests allowed identifying 1) necessary modifications in the trap's geometry and heater's functioning to visualize squeezing effect of the dust cloud in short duration experiments and 2) potentials of laboratory use of the thermophoretic trap.

Blum, J. et al. (2008). *Europhysicsnews*, 39/3, 27-29.
Vedernikov, A. A., Markovich, A. V., & Blum, J. (2007). In *European Aerosol Conference*, Salzburg (Austria), Abstracts, LP35.

ISO 15900 – A new international standard for differential electrical mobility analysis

H.-G. Horn, K. Ehara, N. Fukushima, K. Ichijo, I. Marshal, Y. Otani, M. Owen, C. Peters, P. Quincey,
H. Sakurai, J. Schlatter, G.J. Sem, J. Spielvogel, C. Tsunoda, J. Vasiliou

ISO TC 24/SC 4/WG 12

Keywords: Aerosol measurement, Measurement errors, SMPS, DMPS, Electrical Mobility.

Differential electrical mobility analysis is a well established and widely used tool to measure submicrometer particle size distributions. Measurements are made with quite a variety of electrical mobility spectrometers, ranging from several commercial systems and their multiple variations to self built equipment. A new International Standard ISO/DIS 15900 (2008) covers measurements with such devices.

All electrical mobility spectrometers are based on the measurement of particle migration in a gas due to an external electrical force and due to the drag force. Data inversion routines are necessary to convert the raw data (either particle count versus differential electrical mobility classifier voltage or particle count versus time) into particle number as a function of particle size. Several parameters influence the precision of the measurement and of the data inversion; most important are:

- Applied particle charge distribution model
- Applied transfer function model
- Slip correction coefficients
- Correction of particle losses and detector efficiency
- Precision of operating parameters like flow rates, voltages etc.
- Data inversion algorithms

Thus, the comparison of results obtained from measurements with different spectrometers may become less simple than originally expected.

For example, recent comparison measurements of electrical mobility spectrometers by Helsper *et al.* (2008) have shown that the number concentration - integrated from 40 nm to 350 nm - obtained from measurements with five systems (four commercial systems from two manufacturers and a self built system by IfT Leipzig) agreed within 12%. In the size range from 20 nm to 200 nm, all number size distributions compared within 20%. However, deviations increase below and above these size ranges. The authors conclude that the reasons for these differences might be uncertainties from correction functions for particle losses, counting statistics, bipolar charge distributions used in the individual inversion routines, and the size dependent particle losses of the different sampling inlets.

Much higher transparency, especially of the parameters and algorithms used for data inversion, would have been necessary to allow in depth analysis of the reasons for the deviations in the above mentioned study. ISO 15900 intends to deliver such

transparency: For example, standardized common values and calculation algorithms are provided for slip correction and for particle size-dependent equilibrium charge distributions. Use of different values and algorithms is - of course - allowed, but must be reported together with the results to make a measurement ISO compliant.

The key purpose of ISO 15900 is to provide user guidance and thus to improve measurement quality and comparability. The standard does not address the specific instrument design, or the specific requirements of particle size distribution measurement for different applications, but includes the calculation method of uncertainty, in accordance with the guideline given in the ISO/IEC Guide to the expression of uncertainty in measurement.

To support the user and to further improve comparability and quality of results, ISO 15900 offers a general description of electrical mobility spectrometry and the underlying physical principles. It also describes proven measurement procedures, and recommends periodic test procedures and calibrations. Annexes add information about particle chargers and charge distributions, particle detectors, the slip correction factor, data inversion, systems with cylindrical differential electrical mobility classifier, calibration with particle size standards, uncertainty of measurement, and a detailed bibliography.

The new standard ISO 15900 is actually available as Draft International Standard (DIS). It will very soon be published as Final Draft International Standard (FDIS).

ISO/DIS 15900 (2008), *Determination of particle size distribution – Differential electrical mobility analysis for aerosol particles.* ISO/TC 24/SC 4/WG12 (Beuth, Berlin)

Helsper, C., Horn, H.-G., Schneider, F., Wehner, B. & Wiedensohler, A. (2008). *Intercomparison of five mobility size spectrometers for measureing atmospheric submicrometer aerosol particles.* Gefahrstoffe - Reinhaltung der Luft 68(2008) Nr. 11/12 (Springer-VDI, Düsseldorf), 475-481.

ISO/IEC Guide 98-3:2008-09. *Uncertainty of Measurement – Part 3: Guide to the expression of uncertainty in measurement (GUM).* (Beuth, Berlin)

Distortions of the DMA transfer function due to geometrical and flow pattern non-ideality and gravity

E. Tamm and J. Uin

Laboratory of Environmental Physics, Institute of Physics, University of Tartu, Ülikooli 18, 50090, Tartu, Estonia

Keywords: Aerosol instrumentation, DMA, Instrument development, Modelling, Transfer function.

The aim of this work was to investigate the influences of non-ideal properties of the DMA and also gravity on the transfer function (TF) of a DMA. The probability for these effects occurring and the magnitude of their influence increase with the increasing dimensions of the DMA and thus particle size being used. The main motivation for this work comes because of the very long DMA (active length > 1m) that was built by this workgroup. With such dimensions any non-idealities of the construction are more clearly visible.

To investigate the possible effects that the non-ideal geometrical properties of the DMA construction may have on the DMA TF, a series of computer simulations was conducted. As a base model, the above-mentioned very long DMA was used with specific construction and working parameters (i.e. flow rates, voltage etc.). Mainly two problems were investigated – first, the effect of shift between the axes of the cylindrical DMA electrodes and second, the effect of non-uniformly distributed aerosol flow along the perimeter of the DMA inlet. Uniformity of the sheath air along the perimeter is better guaranteed by the construction.

To calculate the DMA TF, the space between the electrodes was divided into vertical sections so that the cross section of the outer was comprised of sectors with equal central angles. The overall TF was calculated as an average of TFs of individual sections. The limiting mobilities and TFs were calculated according to Tammet (1970) and Stolzenburg (1988). This was possible because according to Tammet, the general theory developed for cylindrical aspiration capacitor is applicable to the sector of the cylindrical capacitor as well as to the parallel-plate capacitor. The flow rates in the section were taken to be proportional to the area of its cross section. For finding the capacitance of the section, the corresponding parts of the inner and outer electrode were taken to form a parallel-plate capacitor. The non-uniform aerosol flow was roughly simulated by using 3 periods of a sine function (the DMA has 3 inlets for aerosol flow).

The results of the calculations show that the shift between the DMA cylinders has the effect of widening and lowering the TF (Fig. 1). It can be seen that the TF is already significantly lower with shifts below 0.5 mm. With the increasing shift, the TF deteriorates even further with a second peak appearing

around 0.8 mm. The effect of the non-uniform aerosol flow is also to "soften" the TF, especially the edges of the function while the peak area remains practically unchanged. In such a case where both of described non-idealities are present their effects would combine, with the second one being much less pronounced.
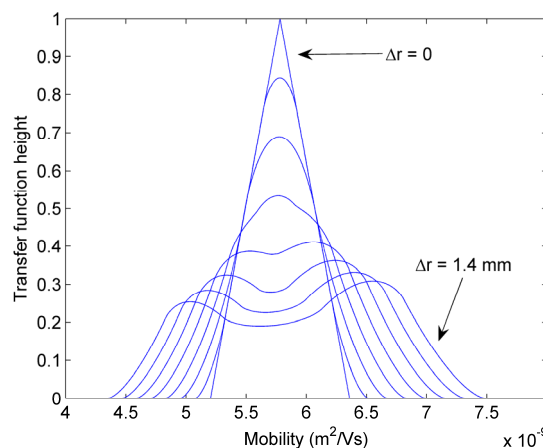

Figure 1. DMA transfer functions in case of different shifts Δr = 0, 0.2, …, 1.4 mm between the axes of the DMA cylindrical electrodes.

The calculations on the effects of gravity show that in case of big particles ($d \geq 1$ μm), when particle settling velocity due to gravity is comparable with its drift velocity in the electric field of the capacitor, the gravity causes shift of the TF in direction of the bigger mobilities (smaller particles) conserving its general shape (triangle). In case of the mentioned very long DMA, the peak mobility of the TF will be shifted up to 20% for particles with d = 10 μm.

Stolzenburg, M.R. (1988). An ultrafine aerosol size distribution measuring system. PhD Thesis, University of Minnesota.
Tammet, H.(1970). The aspiration method for the determination of atmospheric ion-spectra. Israel Program for Scientific Translations, Jerusalem.

Best practices in European aerosol monitoring:
the EUSAAR ground-based observation network

P. Laj (1), S. Philippin (1), A. Wiedensohler (2), U. Baltensperger (3), G. de Leeuw (4, 5),
J.-P. Putaud (6), A.M. Fjaeraa (7), M. Fiebig (7), U. Platt (8)

(1) Laboratoire de Météorologie Physique, Université Blaise Pascal, FR-63177 Clermont-Ferrand, France
(2) Leibniz Institute for Tropospheric Research, DE-04318 Leipzig, Germany
(3) Laboratory of Atmospheric Chemistry, CH-5232 Paul Scherrer Institut, Villigen, Switzerland
(4) Netherlands Organisation for Applied Scientific Research, NL-2597 Den Haag, The Netherlands
(5) Finnish Meteorological Institute, FI-00014 Helsinki, Finnland
(6) Climate Change Unit, Joint Research Centre, IT-21020 Ispra, Italy
(7) Norwegian Institute for Air Research, NO-2027Kjeller, Norway
8) University of Heidelberg, DE-69120 Heidelberg, Germany

The EU-funded project EUSAAR (EUropean Supersites for Atmospheric Aerosol Research) aims at integrating measurements of atmospheric aerosol properties from a distributed network of 20 high-quality European ground-based stations. The objective is to ensure harmonization, validation and data diffusion of current measurements of physical, chemical, and optical properties being critical for quantifying the key processes and the impact of aerosols on climate and air quality. The achievements within the research-based EUSAAR permit to improve the comparability of measurements for data users and to adopt best practices in aerosol monitoring procedures.

Figure 1. Map of Europe with the distribution of all EUSAAR ground-based stations.

Within the network, initiatives were taken to publish recommendations for long-term and routine measurements, operational data analysis, and data structure for the newly developed aerosol observation database EBAS related to the following instruments / techniques: (1) Standard particle mobility size spectrometers (commercially available and custom-made SMPS, DMPS), still associated with large uncertainties due to lack of generally accepted technical standards with respect to instrumental set-up, measurement mode, data

evaluation, and quality control (Wiedensohler et al., 2009); (2) HTDMAs (Hygroscopicity Tandem Differential Mobility Analysers) coupled with a standardized inversion scheme to ensure quality-assured measurements of water uptake of aerosol particles (Duplissy et al., 2008 Gysel et al., 2009); (3) Three different commercially available integrating nephelometers with improved correction mechanisms to account for the non-ideal illumination due to truncation of the sensing volumes and for non-Lambertian illumination from the light sources (Müller et al., 2008); and (4) Standardized procedures for improved thermal-optical discrimination between organic and elemental carbon and for assessing and mitigating major positive and negative biases of different types of carbonaceous particulate matter encountered across Europe (Putaud et al., 2008).

With an increasing number of measurement sites and institutions involved in measuring aerosol parameters, the need for technical standardization and data harmonization of atmospheric aerosols has become a key issue.

Duplissy, J. et al. (2008). *Intercomparison study of six HTDMAs: results and general recommendations for HTDMA operation*, Atm. Meas. Tech. Disc., 1, 1-507.

Gysel, M. et al. (2009). *Inversion of tandem differential mobility analyser (TDMA) measurements*, J. Atm. Sci., 40, 2, 134-151.

Müller, T. et al. (2008). *Performance Characteristics of three Different Integrating Nephelo-meters: Angular Illumination, Empirical and Size-Based Corrections*, Atm. Sci. Tech., submitted.

Putaud, J.-P. et al. (2008). *Toward a standardized thermal-optical protocol for measuring atmospheric organic and elemental carbon: The EUSAAR protocol*, Env. Sci. Tech., submitted.

Wiedensohler, A. et al. (2009). *Particle Mobility Size Spectrometers: Harmonization of Technical Standards and Data Structure to Facilitate High Quality Long-term Observations of Atmospheric Particle Size Distributions*, Atm. Meas. Tech., submitted.

Effect of size dispersion on the lattice parameters of two-dimensional particle arrays: A possible uncertainty source in AFM size measurement of monodisperse particles

Katsuhiro Shirono and Kensei Ehara

National Institute of Advanced Industrial Science and Technology
Tsukuba, Ibaraki 305-8563, Japan

Keywords: size measurement, particle size, measurement errors, atomic force microscopy.

Atomic force microscopy (AFM) is a possible candidate for an accurate method of sizing monodisperse particles for developing nanoparticle size standards (APEC ISTWG Project, 2006). In the AFM method, monodisperse particles such as polystyrene latex spheres are arranged in a two-dimensional closed pack array on a solid surface, and the average particle diameter is determined by measuring the lattice parameter. A systematic bias in the measurement may occur due to the size dispersion of the particles, but this effect has not been studied in detail so far. In the present study, a theoretical simulation of particle arrangement in a two dimensional array was carried out to investigate this effect.

In the simulation, seventy-two particles sampled randomly from a normal size distribution with mean diameter 100 nm and a standard deviation σ were placed onto a $2000\,\text{nm} \times 2000\,\text{nm}$ area. The values of σ were set at 0, 2, 4, and 8 nm. The Markov chain Monte Carlo method was employed to determine possible arrangements of the particles, with assuming that the interparticle potential is given by the sum of van der Waals potential and a hard core repulsive potential. Simulation was carried out more than five times for a specified value of σ.

Examples of particle arrangement obtained in this way are shown in Figure 1. The ideal closed packing is realized for $\sigma = 0$ nm, while a regular periodic structure is barely discernible for $\sigma = 8$ nm. In the intermediate cases of $\sigma = 2$ nm, and 4 nm, it is seen that a local regularity is retained.

For each pair of two adjacent particles i and j, the gap was calculated from

$$g_{ij} = l_{ij} - (D_i + D_j)/2 \,, \qquad (1)$$

where l_{ij} is the distance between the centre of the particles, and D_i and D_j are the particle diameters. It is found that except for the case of $\sigma = 0$ nm, particles in approximately 75 to 80 % pairs are in direct contact (i.e., $g_{ij} = 0$) irrespective of the value of σ. Considering the finite resolution of AFM images, we may assume that in practical AFM measurements the mean particle diameter is determined from

$$\overline{D} = \sum_{(g_{ij} \le g)} l_{ij} \bigg/ \sum_{(g_{ij} \le g)} 1 \,, \qquad (2)$$

where g represents a threshold gap indicating that pairs with $g_{ij} > g$ are excluded from measurement.

Figure 2 shows $\overline{D}$ as a function of g. Even for $g = 0$, a bias in $\overline{D}$ is observed. This occurs because larger particles have higher probability of having adjacent particles in direct contact than smaller particles. Because a sizing error in the order of 0.5 % is considered not negligible in developing particle size standards, the result shown in Figure 2 indicates that the size dispersion can be a non-negligible uncertainty source in particle sizing by AFM.
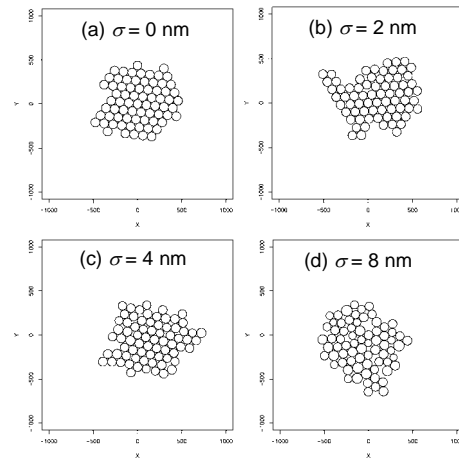

Figure 1. Typical two dimensional arrangements of 100 nm nearly-monodisperse particles with (a) $\sigma = 0$ nm, (b) 2 nm, (c) 4 nm, and (d) 8 nm.
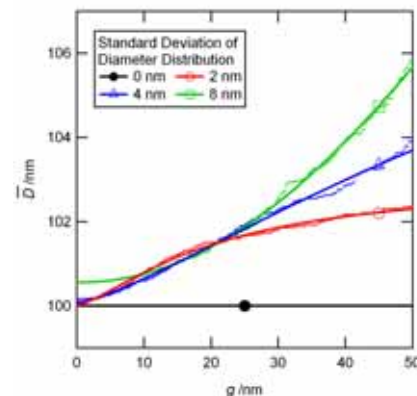

Figure 2. Average diameter $\overline{D}$ as a function of the resolution limit g.

APEC ISTWG Project (2006), *Interlaboratory Comparison on Nanoparticle Size Characterization*, Report on measurement results.

T10 Particle-lung-interaction

Exposure of cyclists to air pollution: a pilot study

N. Bleux*, B. de Geus**, B. Degraeuwe*, G. Vandenbulcke***, R. Torfs*, I. Thomas***, R. Meeusen** & L. Int Panis*,****

* Flemish Institute for Technological Research (VITO), Boeretang 200, 2400 Mol, Belgium
email : nico.bleux@vito.be
**Vrije Universiteit Brussel, Fac. LK, dept. Human Physiology & Sports Medicine, Belgium.
*** C.O.R.E. and Department of Geography, Université Catholique de Louvain (UCL), Belgium
**** Transporation Research Institute, University of Hasselt, Belgium

Keywords: cycling, exposure, vehicles emissions

Cycling is again becoming a favorite mode of transport both in developing and in developed countries due to increasing traffic congestion, environmental concerns and increasing fuel costs. In Europe, it is also considered as a healthy sports activity. However, due to high levels of hazardous pollutants in the road microenvironment the cyclist might be at a higher health risk because of a higher breathing rate and proximity to the vehicular exhaust. Also, accident risk and the lack of an adequate infrastructure are a major hindrances to bicycle use.

The objective of the SHAPES project (A Systematic analysis of Health risks and physical Activity associated with cycling PoliciES) is to assess the total impact on health of commuter cycling compared to commuting by car in Belgium. Three aspects are taken into account: 1) the difference in exposure to air pollution, 2) the difference in accident risk and 3) the positive effect of physical activity of cycling compared to car use.

We will present the SHAPES methodology that allows us to simultaneously measure fine and ultra fine particles (PM_{10}, $PM_{2.5}$, PM_1 and UFP numbers) and breathing (tidal volume) while cycling or driving a car. We first validate this methodology and then demonstrate that the exposure of cyclists to traffic exhaust depends on small scale attributes of the cycling track (e.g. the distance to the road).

We will also present a dust mapping technique which can be a useful tool for town planners and local policy makers.

Our tests in Mol (rural area), Louvain-La-Neuve (urban background) and Brussels (fig. 1) (street canyon) show that even on identical trajectories PM concentrations turn out to be higher inside cars than on bicycles, presumably because of their relative places on the road. But even then cyclists have a higher exposure due to a higher breathing rate while cycling.
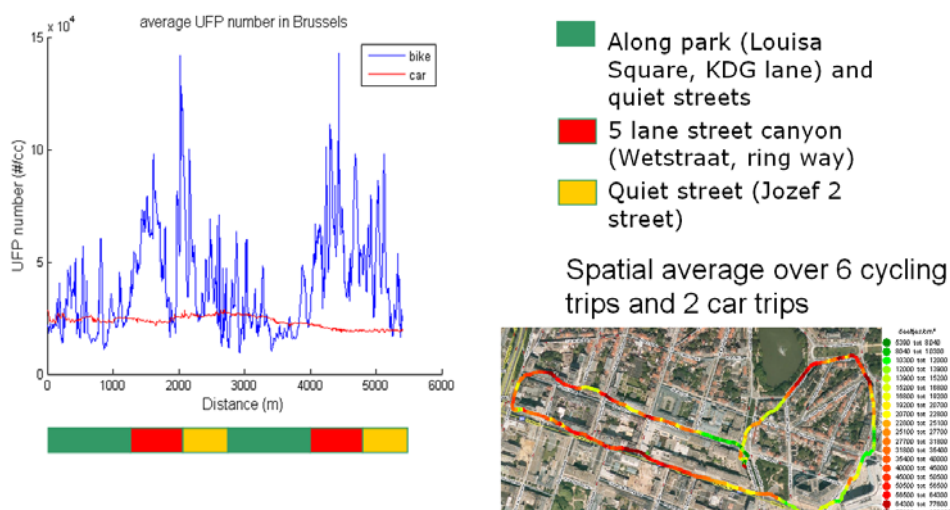

Figure 1: Measurement results from one of the trips in Brussels

Inter- and intra-lobar deposition of inhaled particles

R. Winkler-Heil and W. Hofmann

Department of Materials Engineering and Physics, University of Salzburg, 5020 Salzburg,Austria

Keywords: inhalation, lung deposition, modelling.

Lung diseases caused by the inhalation of particulate matter have often been reported to occur at specific sites in the lung, particularly within specific lobes. For example, Parkash (1977) found that lung carcinomas are more likely to develop in the right than in the left lung, and more likely in the upper than in the lower lobes. He further postulated that this site specificity ought to correlate more with localized deposition patterns than with biological-hematogenic factors. It is therefore important for risk assessment purposes to determine particle deposition patterns between and within the different lobes.

The human lung is composed of 5 lobes, 2 in the left lung and 3 in the right lung: left upper lobe (LUL), left lower lobe (LLL), right upper lobe (RUL), right middle lobe (RML) and right lower lobe (RLL). In the current version of the stochastic deposition model IDEAL (Koblinger and Hofmann, 1990), the random pathway selection of inhaled particles into the different lobes is based on 3 criteria: (1) the ratio of the parent cross-section to the cross-section of both daughters varies from 0.72 (LLL) to 1.70 (RML) (Yeh & Schum, 1980). These differences in cross-section ratios lead to different numbers of bronchial airway generations in each lobe. (2) The airflow into each lobe, and hence the probability of a particle entering a given lobe, depends on lobar volume (Yeh & Schum, 1980). (3) The asymmetry (lower lobes are ventilated more efficiently than upper lobes) and asynchrony (upper lobes are ventilated more rapidly than lower lobes) of lung ventilation is modelled by asymmetry and asynchrony coefficients, derived from experimental data (Hofmann et al., 2008).
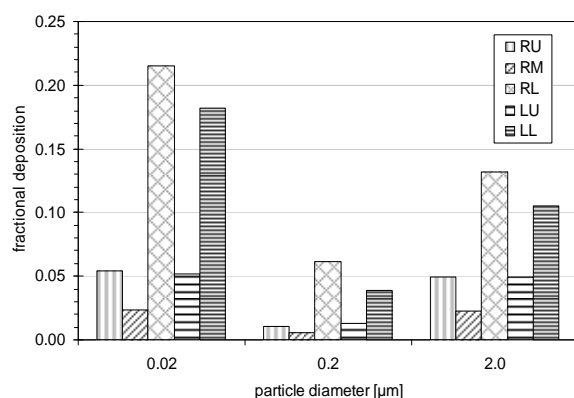
Deposition fractions of 0.02, 0.2 and 2 µm particles in the five lung lobes under sitting breathing conditions (ICRP, 1994) are plotted in Figure 1, exhibiting significant differences among the individual lobes. Consistent with the U-shaped total deposition curve, lobar deposition depends on particle diameter. However, the ratios between the different lobes are quite similar for the three particle sizes.

The corresponding deposition patterns within each lobe are illustrated in Figure 2 for the 0.02 µm particles, where diffusion is the primary deposition mechanism. While absolute deposition values are different among the various lobes (see Figure 1), their relative distribution among the airways of a given lobe is practically same in all lobes. The differences in pathlength within each lobe are caused by differences in corresponding lobar volumes.
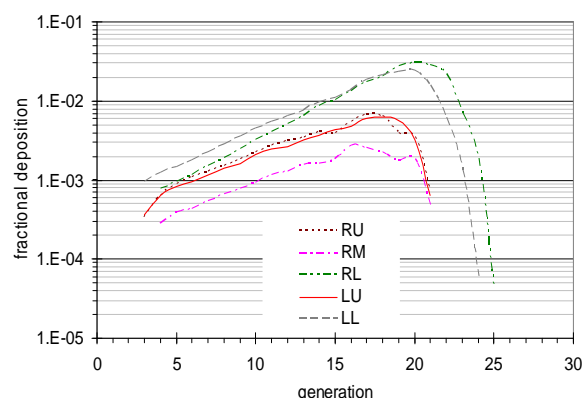
Figure 2. Generational deposition in the five lung lobes for 0.02 µm particles under sitting breathing conditions.

Hofmann, W., Pawlak, E., & Sturm, R. (2008). *Inhal. Toxicol.* 20, 1059-1073.

ICRP (1994). *ICRP Publication 66*. London, UK: Pergamon.

Koblinger, L., & Hofmann, W. (1990). *J. Aerosol Sci.* 21, 661-674.

Parkash, O. (1977). *Respiration* 34:295-304.

Yeh, H.C., & Schum, G.M. (1980). *Bull. Math. Biol.*, 42, 461-480.

Figure 1. Fractional deposition in the five lung lobes for sitting breathing conditions.

Effect of intersubject variability of nasal airway dimensions on particle deposition

M.Hussain[1,2] , R. Winker-heil[1] and W. Hofmann[1]

[1]Department of Physics and Biophysics, University of Salzburg, 5020, Salzburg, Austria
[2] Directorate General of Safety, 44000, Islamabad, Pakistan

Keywords: lung deposition, nasal airways, intersubject variability, modelling,

The Nasal airways are the major route of inhaled particles under normal breathing conditions. Hence the filtering efficiency of nasal airways is an important determinant of doses delivered by inhaled particles to the lung. Since the structure of the nasal airway geometry exhibit significant intersubject variations, it affects both extrathoracic deposition and, in further consequence, the fraction of inhaled particles reaching the lung.

Nasal airway dimensions measured by K.H. Cheng et al. (1996) using MRI technique in 10 adults male were used during current study to measure nasal and total deposition for particle sizes ranging from 1 nm to 10 μm under sitting and light exercise breathing conditions. For diffusion regime (particle size ≤0.2 μm), the inspiratory nasal deposition efficiency as a function diffusion coefficient (D) and flow rate (Q) , was fitted by the equation $E_n = 1 - \exp(-0.355 S_f^{4.14} D^{0.5} Q^{-0.28})$, where $S_{f,}$ is the average shape factor of the nasal turbinate region (Cheng, 2003). For the inertial impaction regime (particle size >0.2μm) deposition efficiency as function of aerodynamic diameter (da) and flow rate (Q) was approximated by the equation $E_n = 1 - \exp(-110 Stk)$, where Stk is dimensionless Stokes number $(Stk = \pi^{0.5} d_a^2 Q / 18 \mu A_{min}^{1.5})$ depends on the minimum nasal cross-sectional area A_{min} (Cheng, 2003). Calculation with the above deposition equations revealed that the range of the experimentally observed deposition efficiencies could be approximated by 2 standard deviations of S_f and A_{min} values. Thus, it was assumed that intersubject variations of the nasal deposition efficiencies are determined primarily by corresponding fluctuations of S_f and A_{min}.

Standard deviations of the nasal deposition efficiencies for any particle diameter from 1 nm to 10 μm were then obtained by fitting empirical functions to the computed standard deviations for defined flow rates. For calculation of thoracic and total deposition, these functions were implemented into the Monte Carlo deposition code IDEAL (Hofmann & Koblinger, 1990)

The simulated effects of intersubject variability of nasal airway on nasal and total deposition are presented in Table 1 and Figure 1.
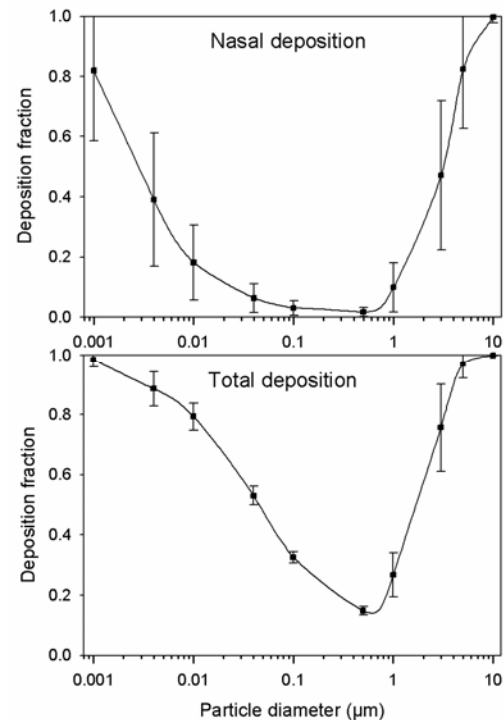
Figure 1. Effect of intersubject variability of nasal airways on nasal and total deposition fraction under sitting breathing conditions.

Cheng, Y. S. (2003). *Aerosol Sci.& Tech.*37:659-671.
Cheng et al. (1996). *J. Aerosol Sci.* 27,785-801.
Hofmann and Kobinger (1990). *J. Aerosol Sci.* 21,675-688.
ICRP Publication 66 (1996). *Human Respiratory Tract Model for Radiation Protection.* Pergamon, London, UK.

Table 1. Effect of intersubject variability, expressed as coefficient of variation (CV), on nasal and total deposition fractions under sitting and light exercise breathing conditions.

Particle diameter (μm)	Nasal deposition (CV)		Total deposition (CV)	
	Sitting	Light exercise	Sitting	Light exercise
0.001	0.29	0.36	0.02	0.02
0.01	0.69	0.71	0.06	0.04
0.1	0.77	0.78	0.06	0.05
1	0.83	0.71	0.27	0.39
10	0.02	0.001	0.001	0.001

Real-Time Deposition Measurements of Particle Size, Concentration and Breathing Profile During Particle Deposition Studies in the Human Lung

C.J. McGrath and C.J. Dickens

British American Tobacco, Group R&D Centre, Southampton SO15 8TL, UK

Three major factors affecting particle deposition in the human lung are particle size, particle growth within the lungs, and breathing profile during inhalation and exhalation of the particles. It is often difficult to measure all of these parameters during particle deposition studies, as the measurements themselves can interfere with the test aerosol, or change the way the subject inhales. This is especially the case when measuring the deposition of tobacco smoke, where the aerosol is sub-500nm in size, highly dynamic and can be changed significantly by small changes to dilution and temperature.

A methodology has been developed that allows real-time measurement of particle size, particle number concentration and breathing profile to be made during tobacco smoke deposition studies, with the measurements having minimal interference on the aerosol or the smoking behavior of the volunteer. This methodology was used to examine the link between inhalation depth, particle size and smoke deposition.

Two current smokers were recruited for this proof of concept study, giving informed consent. The volunteers smoked a commercial King-Size cigarette with 7mg tar yield, as measured by machine smoking at the ISO smoking regime. Puffing behaviour was measured in real-time by a SA7 Smoking Analyser developed in-house, measuring flow, volume and duration using a differential pressure transducer. Inhalation behaviour was measured in real-time using the commercially available Lifeshirt® system (Vivometrics, CA, USA), which utilises a respiratory monitoring technique called inductive plethysmography (Sackner et al. 1980).

After puffing and inhalation the cigarette smoke was exhaled into a sampling system operating at a constant flow of 117 l.min^{-1}. A sampling port was connected to a real-time particulate spectrometer (DMS-500, Cambustion, Cambridge, UK) which measures particle size and concentration by electrical mobility at 10Hz over a size range of 5 – 1000 nm. As the flow through the sampling system is known, the total number of particles exhaled can be calculated, along with the corresponding inhalation depth and time profile.

Inhaled smoke was characterised by replaying the recorded human puffing profiles, as measured by the SA7, on a Smoking Cycle Simulator (McAughey *et al*, 2007) and then sampling through the DMS-500.

The total number of particles inhaled, exhaled and deposited was calculated. Equivalent values for particle surface area and particle volume were also calculated. Table 1 shows the average deposition values for each volunteer together with inhaled particle size and inhaled volume as a percentage of the volunteer's vital capacity. Figure 1 plots the fraction of particles depositing against inhalation as a fraction of the volunteer's vital capacity, on a puff by puff basis.

Table 1: Puff by puff deposition estimates for number, surface area and volume weightings

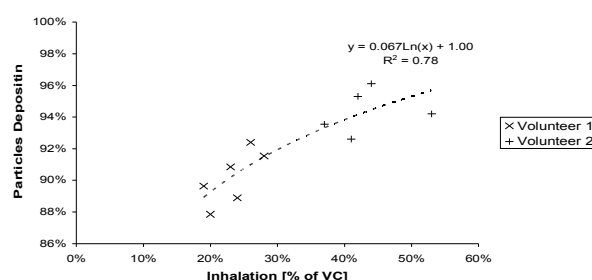| Vol.	Fraction Deposited [%]			Particle Size CMD [nm]	Inhaled Volume [% VC]
	Number	Surface Area	Volume		
1	90.2 ± 1.6	78.0 ± 4.9	69.4 ± 9.9	145.2 ± 19.1	23.3 ± 3.4
2	94.4 ± 1.2	82.6 ± 6.2	70.0 ± 8.4	142.2 ± 11.0	43.4 ± 5.9

Figure 1: Fraction of particle number depositing versus inhalation depth

Table 1 shows that the fraction of particles depositing is greater for particle number than total surface area and total particle volume. This implies that there is a tendency for the smaller particles within the distribution to deposit with a higher efficiency. The values for the volume weighted deposition are comparable to mass weighted deposition in previous studies (Baker & Dixon, 2005). Figure 1 shows a trend of decreasing deposition with decreasing inhalation depth, with a strong correlation ($r^2 = 0.78$).

Future work will seek to quantify the regional deposition of tobacco smoke particles in a larger subject group to estimate the dose to specific areas of the human airways.

Baker, R.R. and Dixon, M. (2006) *Inhal Tox* 18, 255-294
Sackner J. et al. (1980) *Am Rev Respir Dis*, 122(6) 867-71
McAughey J.J. et al (2007) Puff profile simulator for Tobacco Smoke Particle Diameter and Mass Measurement, AAAR 26th Annual Conference, Reno, NV, USA.

Study of Aerosol Transport and Air Flow in Transparent Human Airways Model

J. Jedelsky, F. Lizal, M. Jicha, J. Stetina and J. Kosner

Faculty of Mechanical Engineering, Brno University of Technology, 61669, Brno, Czech Republic

Keywords: lung model, aerosol measurement, lung deposition, Laser Doppler anemometry

The effort to understand how aerosols transport and deposit in lungs drove us to application of a velocity measurement with PDA (Phase Doppler Anemometry). In contrast to common methods we use air as a carrier medium; therefore we had to develop a new thin-walled transparent model of lungs to avoid an optical distortion (Jedelsky *et al.*, 2007).

Before we approach to a measurement with the realistic transparent model we decided to check some questions, which arise in connection with adjustment of experiment. We have to decide how to attach the piston mechanism which simulates breathing to the model, accordingly to control breathing from above the model i. e. the inspiration is in overpressure or from below when the inspiration is in underpressure. The second objective was to ascertain splitting of air flow into particular branches.

For the measurement of breathing control effect we fabricated simplified Plexiglas model of trachea and first bifurcation, diameters are 16 mm and 12 mm, lengths are 15 cm and 11 cm and angles of branches are 138° and 152° measured from trachea.
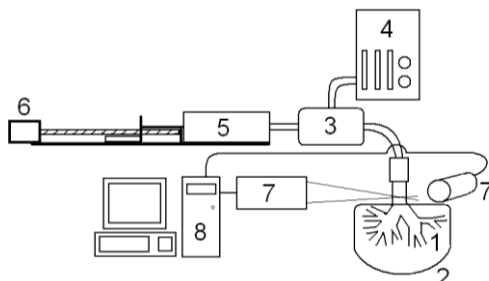

Figure 1. Diagram of a test rig with PDA.

Simplified model was fixed into test rig (see fig. 1). Test rig consists of the motor (6) with piston (5), velocity and diameter of aerosol particles are measured by PDA (7) in seven points in a cross section 22 mm before the carina. All measurement points lie in a plane perpendicular to trachea axis. Air flow and aerosol generated by TSI 3475 aerosol generator (4) were mixed in a mixing chamber (3).

We found some distinctions in a comparison of results measured with the breathing regime controlled from above and from below of the model (see typical behaviour in fig. 1 and 2).

We observed increased value of turbulence intensity especially during expiration phase. The reason of this distinction is different pressure conditions what leads to altered conditions of turbulence generation.
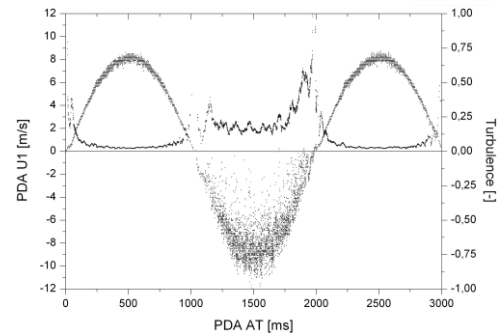

Figure 2. Velocity and turbulence while above breathing control.
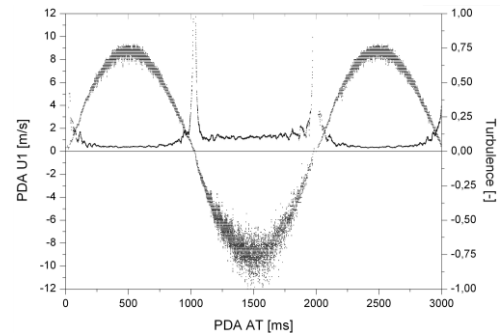
Figure 2. Velocity and turbulence while below breathing control.

For a measurement of an air flow division into particular branches in the realistic transparent model we add Furness Controls FCO flow meters into the test rig. The result of this experiment is airflow distribution through each output branch under different breathing conditions.

We concluded that a way of air supply attachment is important for velocity and turbulence development. The below air supply connection matches the real human lung conditions, as inspiration is in underpressure in both the cases. Turbulence intensity is growing during one breathing cycle in all of measured points. Knowledge of airflow distribution could help us to understand aerosol deposition.

Jedelsky, J., Lizal, F., Jicha, M., Krsek, P., Stetina, J., Kosner, J. (2008). *Experimental model of human airways for flow, particle transport and deposition study*, In European aerosol conference. Thessaloniki, Greece. 2008.

Computer modelling of transport and deposition of detrimental and therapeutic aerosols in three-dimensional realistic airways

Á. Farkas, I. Balásházy, I. Szőke and B. G. Madas

Health and Environmental Physics Department, Hungarian Academy of Sciences KFKI Atomic Energy Research Institute, Konkoly Thege M. ut 29-33, 1121 Budapest, Hungary

Keywords: health effects of aerosols, lung deposition, CFD, deposition efficiency, trajectory

There is constantly accumulating clinical and scientific evidence that a large variety of inhalable aerosols, such as radioactive aerosols, bioaerosols (e.g. bacteria, fungi, and pollens), fly ash particles originating from fossil fuel burning, diesel exhaust particles or particles from cigarette smoke can be associated with several diseases affecting the airways and even with non-lung diseases. At the same time, inhaled therapeutic aerosols can efficiently combat against airway disorders and possibly other diseases by delivering the drug into the systemic circulation via the lung. Hence, study of transport of the inhaled detrimental and therapeutic aerosols and quantification of their deposition within the airways are essential in both understanding the health effects of detrimental aerosols and optimisation of aerosol drug delivery. Computational modelling, as a tool in tracking the inhaled aerosols, holds the advantage of being reproducible, flexible and cost effective. The objective of this work was to apply numerical models to study the fate of the inhaled aerosols and to quantify their deposition in reconstructed human airways.

The geometry of the airways was reconstructed from digital images acquired by medical imaging techniques. Combinations of commercial software (such as 3D-DOCTOR and VGSTUDIO) and user developed codes were used for the segmentation of planar slices of the airways recorded by computer tomography and for the rendering of the three dimensional airway surfaces. The reconstructed geometries were transformed into computational domains by the generation of unstructured, inhomogeneous tetrahedral meshes in the GAMBIT environment. The FLUENT computational fluid dynamics commercial code in conjunction with user supplied programs were applied to simulate the air flow fields, to compute the trajectories and to simulate the deposition of inhaled particles in the airways. To reproduce as many as possible scenarios large ranges of breathing modes and particle sizes were considered. Deposition efficiencies, defined as the ratio of the number of particles depositing in a given airway segment to the number of particles entering the same segment, were computed.

Our simulation results demonstrate that application of morphologically realistic airway geometries is essential in capturing local features of the air flows and in accurate modelling of particle deposition distributions. Deposition in both the upper and central airways is highly inhomogeneous, with preferential deposition sites like the pharynx region in the upper airways and the peaks of the bifurcations in the central airways (see Figure 1). However, the degree of non-uniformity is higher for large particles depositing mostly due to inertial impaction. Our computed deposition efficiency values suggest that particles with aerodynamic diameters around 1 μm produce the least efficient deposition in the trachea and large bronchi. The computed deposition patterns have been tested by the optical method of Czitrovszky et al. (2003).

Present results can provide useful information regarding health consequences of the inhaled detrimental aerosols and might be integrated into future aerosol therapy protocols.
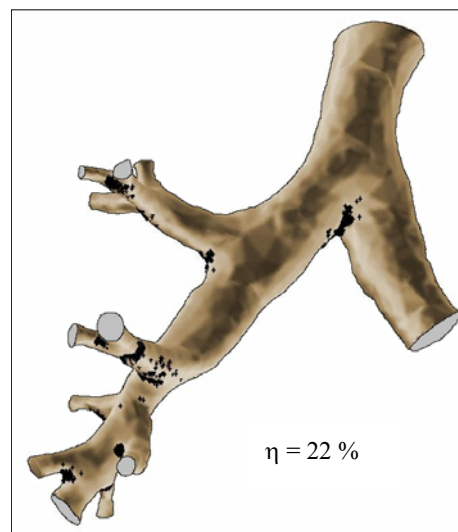

Figure 1. Deposition patterns of 10 μm inhaled particles on a central airway segment during light physical activity. η: deposition efficiency.

Czitrovszky A., Nagy A., & Jani P. (2003). *J. Aerosol Sci.* 2., S953-954.

Hit probability of lung-cancer-sensitive epithelial cells by asbestos fibers with different aspect ratios

R. Sturm and W. Hofmann

Department of Materials Engineering and Physics, Division of Physics and Biophysics
University of Salzburg, Hellbrunnerstrasse 34, A-5020 Salzburg, Austria

Keywords: asbestos, fibers, lung/particle interaction, aspect ratio, modelling.

Exposure to airborne asbestos fibers, and mineral fibers in general, is commonly regarded as a serious health hazard. Numerous medical studies published during the past decades have indicated that the deposition of asbestos fibers in the human respiratory tract increases the risk of asbestosis and other nonmalignant lung and pleural disorders. Moreover, asbestos has been classified as a known human carcinogen, whose inhalation leads to a significant enhancement of the risk of bronchial, alveolar or interstitial lung cancer (e. g. Bernstein et al., 2001).

Extensive medical investigations have revealed that nonciliated secretory cells in the bronchial airways are most susceptible to malignant transformations (Fig. 1). These may be induced either by injuries resulting from the impact of long and thin fibers or by intracellular signalling cascades resulting from the uptake and storage of those biopersistent particles in the cellular compartment. The risk of developing lung cancer increases with the amount of inhaled fibers, the duration of exposure, and the physical characteristics of the fibrous material.
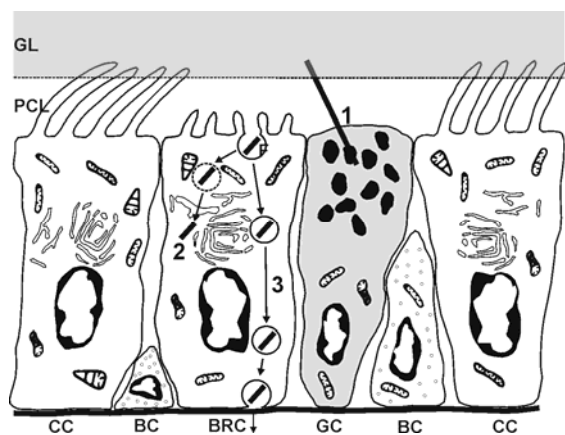

Figure 1. Possible types of fiber-cell interaction in the airway epithelium: 1 – injury by fiber impaction, 2 – uptake and storage, 3 – transcytosis. Abbreviations: BC – basal cell, BRC – brush cell, CC – ciliated cell, GC – goblet cell, GL – gel layer, PCL – periciliary liquid.

The hit probability of cancer-sensitive cells in the airway epithelium was simulated for asbestos fibers (density: 2.6 g cm^{-3}) with a constant diameter of 0.5 µm but variable length. Deposition of these particles was computed with the particle deposition code IDEAL, originally developed by Koblinger & Hofmann (1990), using the aerodynamic diameter concept formerly proposed by Stöber (1972). For these simulations, light work breathing conditions were applied (ICRP (1994). The fraction of nonciliated secretory cells in the tracheal and bronchial epithelium (airway generations 0 – 8) was assumed to be 18 - 40 %, and 22 - 60 % in the bronchiolar epithelium (airway generations 9 – 16) (ICRP, 1994).

Table 1. Hit probability (%) of asbestos fibers (d = 0.5 µm) in the bronchial and bronchiolar region of the human respiratory tract.

Fiber length (µm)	Bronchial	Bronchiolar
5	0.44 – 0.98	1.01 – 2.75
10	0.53 – 1.17	1.18 – 3.21
15	0.56 – 1.24	1.22 – 3.33
25	0.62 – 1.37	1.34 – 3.65
50	0.69 – 1.53	1.46 – 3.97

Preliminary results, summarized in Tab. 1, clearly show an enhancement of both bronchial and bronchiolar hit probabilities with increasing fiber length, i.e. increasing aspect ratio. Asbestos fibers (d = 0.5 µm) with aerodynamic diameters ranging from 0.99 µm (l = 5 µm) to 1.32 µm (l = 50 µm) are generally characterized by a rather low total lung deposition (20 – 30 %), with the highest deposition fractions found in the alveolar region. Nevertheless, hit probabilities in the bronchial region may also become significant for high amounts of inhaled fibers.

Bernstein, D. M., Riego Sintes, J. M., Ersboell, B. K., & Kunert, J. (2001). *Inhal. Toxicol.*, 13, 851-875.
ICRP (1994). *Human respiratory tract model for radiological protection*. Oxford, U.K.: Pergamon Press.
Koblinger, L. & Hofmann, W. (1990). *J. Aerosol Sci.*, 21, 661-674.
Stöber, W. (1972). In *Assessment of Airborne Particles*. Springfield, TN: Thomas, 249-289.

Modelling dynamic shape factors and lung deposition of small particle aggregates originating from combustion processes

R. Sturm and W. Hofmann

Department of Materials Engineering and Physics, Division of Physics and Biophysics, University of Salzburg, Hellbrunnerstrasse 34, A-5020 Salzburg, Austria

Keywords: Combustion aerosols, aggregates, particle shape, lung deposition, modelling.

Diesel exhaust particles and other soot particles originating from combustion processes are irregularily shaped particulate aggregates with diameters of several hundred nanometers. In the past, combustion particles have been increasingly emitted into the atmospheric air, enhancing their significance as a major public health hazard and contributing to the burden of pulmonary and cardiovascular diseases (Bayram et al., 2006).

For an appropriate simulation of non-spherical particle behaviour in the human respiratory tract, the concept of the dynamic shape factor and the aerodynamic diameter has been introduced by Stöber (1972) at the beginning of the 1970s. Dynamic shape factors adopt values >1 for prolate and oblate particle shapes (fibers, disks), whereas they may vary between 2 and 15 for particle clusters consisting of monodisperse spheres (Kasper, 1982). Especially high shape factors have a significant effect on the deposition of such clustered particles. The two main objectives of this study are: 1) to model dynamic shape factors of small particle aggregates, and 2) to apply these factors to inhaled particle deposition..

The dynamic shape factor k of particulate clusters was computed according to the suggestions of Kasper (1982), where the parameter k may be estimated according to the simple formula
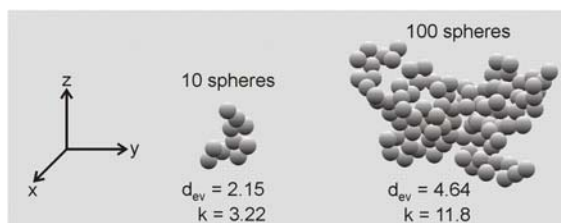
$$k = \frac{d_{es}}{d_{ev}},$$

Figure 1. Mean values for d_{ev} and k for particle clusters consisting of 10 and 100 monodisperse spheres (diameter: 1 unit).

where d_{es} denotes the diameter of the enveloping sphere and d_{ev} the diameter of the equivalent volume sphere. Calculations of k were carried out with a computer program allowing the variation of the number of monodisperse spheres defining the particulate cluster (Fig. 1). Computation of aerodynamic diameters d_{ae} for the simulation of particle deposition in the human respiratory tract was based on the widely applied equation

$$d_{ae} = d_{ev} \cdot \sqrt{\frac{1}{k} \cdot \frac{\rho_p}{\rho_0} \cdot \frac{C_C(d_{ev})}{C_C(d_{ae})}},$$

with ρ_p and ρ_0, respectively, denoting the density of the cluster and unit density (1 g cm^{-3}), and $C_C(d_{ev})$ and $C_C(d_{ae})$ representing the Cunningham slip correction factors of particles with d_{ev} and d_{ae}.

Particle deposition was calculated for light-work breathing conditions (ICRP, 1994), using the stochastic deposition model developed by Koblinger & Hofmann (1990). The diameter of the monodisperse spheres was assumed to be 10 nm, resulting in average cluster diameters of 71.2 (10 spheres) and 587.7 nm (100 spheres). Preliminary deposition results are summarized in Tab. 1.

Table 1. Relative deposition fractions (%) of cluster particles in different regions of the human respiratory tract.

Lung region	10 spheres cl.	100 spheres cl.
Extrathoracic	15.11	11.86
Bronchial	12.17	6.41
Bronchiolar	42.86	26.14
Alveolar	29.86	55.59

Table 1 demonstrates that particulate clusters containing 10 monodisperse spheres are preferably deposited in more proximal lung compartments under the given breathing conditions. Thereby, the uppermost airways serve as efficient filters prohibiting the total penetration of the clusters into deeper lung regions. In contrast, the larger clusters are deposited primarily in the more peripheral lung compartments, underlining their role as important carcinogen for alveolar tumors.

Bayram, H., Ito, K., Issa, R., Ito, M., Sukkar, M., & Chung, K. F. (2006). *Eur. Respir. J.*, 27, 705-713.

ICRP (1994), *Human respiratory tract model for radiological protection.* Oxford, U.K.: Pergamon Press.

Kasper, G. (1982). *Aerosol Sci. Technol.*, 1, 187-199.

Koblinger, L., & Hofmann, W. (1990). *J. Aerosol Sci.*, 21, 661-674.

Stöber, W. (1972). In *Assessment of Airborne Particles*. Springfield, TN: Thomas, 249-289.

A compartment model for the simulation of fiber-cell-interaction in the alveolar region of the human respiratory tract

R. Sturm and W. Hofmann

Department of Materials Engineering and Physics, Division of Physics and Biophysics,
University of Salzburg, Hellbrunnerstrasse 34, A-5020 Salzburg, Austria

Numerous medical studies performed during the past decades (e.g. Lippmann, 1990; Heesterberg & Hart, 2001) have demonstrated that exposure to airborne mineral fibers, and especially to asbestos fibers, presents a significant health hazard. Accumulation of fibers in the lung enhances the risk of lung diseases, such as asbestosis, pneumoconiosis, and asbestos-induced lung cancer. The highest damage by fiber deposition and accumulation occurs in the alveolar region, where the particles are subject to various clearance mechanisms. The efficiency of these mechanisms depends primarily upon two factors, the size of the deposited material, and its degradability due to biological processes (Lippmann, 1990).

In this contribution, a compartment model is presented, which aims to describe the interaction between biopersistent fibers and alveolar cells and tissues (Fig. 1). Inhaled mineral fibers deposited in the alveolar region may hit the surface of the alveolar epithelium which is lined by a thin blanket of the so-called surfactant. Independent of their length all fibrous particles undergo endocytosis by alveolar macrophages. Those fibers exceeding the dimension of the macrophages will not be cleared from their sites of deposition, whilst small fibers will be evacuated along two paths: (1) towards the conductive airways and, in further consequence, to the gastrointestinal tract, and (2) towards the lung parenchyma (interstitium) (ICRP, 1994). Fibers accumulated on the alveolar walls or taken up by macrophages may provoke inflammatory reactions, resulting in a hyperactivity of fibrocytes, while

fibers accumulated in the parenchyma and mesothelium may act as serious carcinogens.

Alveolar fiber deposition was simulated using the stochastic deposition model of Koblinger & Hofmann (1990), assuming light-work breathing conditions (ICRP, 1994). Fibrous particles included in the computations had a uniform diameter of 0.5 µm, a density of 2.6 g cm^{-3} (mean density of asbestos), and an aspect ratio of 10 and 100, resulting in fiber lengths of 5 and 50 µm. Rate constants of the compartment model were estimated from published medical and histological data.
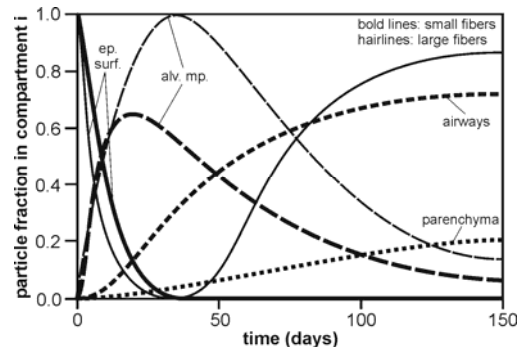
Figure 2. Preliminary results obtained by the compartment model. Computations were carried out for two size classes of biopersistent asbestos fibers.

As shown in Fig. 2, small fibers are subject to a significant clearance by alveolar macrophages, but also to an accumulation in the parenchyma. The first process occurs within several weeks to months, whilst the second process takes presumably much longer due to the penetration of numerous cell layers by the fibrous material. In contrast, large fibers are partly taken up by the macrophages, but are not effectively cleared due to their sizes. This results in an accumulation of the material on the epithelial surface.

Heesterberg, T. W., & Hart, G. A. (2001). *Crit. Rev. Toxicol.*, 31, 1-53.
ICRP (1994), *Human respiratory tract model for radiological protection.* Oxford, U.K.: Pergamon Press.
Koblinger, L., & Hofmann, W. (1990). *J. Aerosol Sci.*, 21, 661-674.
Lippmann, M. (1990). *Environ. Health Perspec.*, 88, 311-317.

Figure 1. (a) Sketch exhibiting the basic cellular components included in the model; (b) Definition of the model compartments and associated rate constants.

Respiratory tract deposition of diesel engine exhaust particles for healthy subjects and subjects with COPD

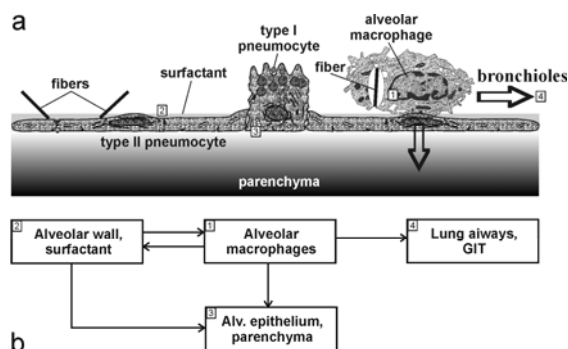J. Löndahl[1], A. Bengtsson[1], J. Pagels[2], E. Swietlicki[1], C. Boman[3], A. Blomberg[4] and T. Sandström[4]

[1]Department of Physics, Lund University, PO Box 118, SE-221 00, Lund, Sweden
[2]Ergonomics and Aerosol Technology, Lund University, PO Box 118, SE-221 00, Lund, Sweden
[3]Energy Technology and Thermal Process Chemistry, Umeå University, SE-901 87 Umeå, Sweden
[4]Department of Respiratory Medicine and Allergy, University Hospital, SE-901 85 Umeå, Sweden

Keywords: lung deposition, diesel exhaust, COPD, health aspects of aerosols

Both epidemiological and toxicological studies have shown a correlation between adverse health responses and exposure to diesel exhaust particles. A key factor for determining the health effects is the deposition of the particles in the respiratory tract during breathing. It is therefore important to investigate the deposited fraction and dose for different aerosol sources during various conditions. It has been suggested that certain sub-populations are more susceptible to adverse health effects of airborne particles. One such group is those diagnosed with chronic obstructive pulmonary disease (COPD). The objective of this study was to examine the deposited fraction and dose of fresh diesel exhaust particles for healthy subjects and subjects with COPD.

The size-resolved deposited fraction and deposited dose of diesel engine exhaust particles were measured with the RESPI instrument (Löndahl et al. 2006). In RESPI particle concentrations in inhaled and exhaled air is measured with a scanning mobility particle sizer (SMPS). The measurements were done on 10 healthy subjects (5m/5f) and 10 subjects (7m/3f) with varying degree of COPD, from mild to moderate. One healthy male was excluded because of difficulties to breathe relaxed in the instrument. A Volvo diesel engine (Volvo TD40 GJE, 4.0 L, four cylinders, 1996) with no exhaust after-treatment was used with a typical MK1 diesel fuel (sulphur content ≤ 10 ppm). The engine was operated in a motor test bench to simulate different operating conditions. The deposited fraction was measured for two different diesel aerosols: idling and transient load conditions according to the urban driving part of the standadized European Transient Cycle (ETC) protocol. The deposited fraction according to the International Comission for Radiological Protection model (ICRP, 1995) was calculated for each subject and compared to the measured values. The deposited dose was calculated (normalized to one hour exposure at 100 μg/m^3 for both aerosols).

The average deposited fraction and dose for the two groups and aerosols are presented in Table 1. The study showed a statistically significant difference in deposited fraction between the groups. For both studied driving conditions, the deposited fraction is lower for the subjects with COPD compared to the healthy subjects, but the deposited dose is higher. The higher deposited dose for the subjects with COPD is expected as they breathed with a higher minute volume than the healthy subjects. The difference in deposited fraction between the two aerosols can most probably be explained by the different size distributions. The aerosol from the idle engine mode contained more nucleation mode particles for which the probability of deposition is high.

Table 1: Average deposited number fraction (DF) and deposited dose for exposure to 100 μg/m^3 of diesel exhaust particles during one hour.

	Idle driving		Transient driving	
	DF	Dose (μg)	DF	Dose (μg)
Healthy	0.65	13.2	0.47	11.5
COPD	0.57	16.6	0.40	14.3

When comparing the measured size-resolved deposited fractions with those of the ICRP model, the measured deposition for the healthy group agrees well with the ICRP model. The measured deposited fractions for the group with COPD show a different pattern compared to the ICRP model, which indicates that the change in lung morphology also may affect the deposition. The difference in deposited fraction between the healthy group and the group with COPD is most significant in the particle size range between 20 nm and 70 nm. In this size range, the ICRP model predicts that most particles are deposited in the alveolar region. COPD affects the alveolar region, for example with emphysema which cause a gradual destruction of the alveolar walls.

ICRP Publication 66. 1995. Human Respiratory Tract Model for Radiological Protection, 66.International Comission on Radiological Protection.

Löndahl J, Pagels J, Swietlicki E, Zhou JC, Ketzel M, Massling A, Bohgard M. 2006. *Journal of Aerosol Science* 37:1152-1163.

Respiratory tract deposition of particles at a busy street

J. Löndahl[1], A. Massling[2], E. Bräuner[3], E. Swietlicki[1], M. Ketzel[2], J. Pagels[4], S. Loft[3]

[1]Department of Physics, Lund University, PO Box 118, SE-221 00, Lund, Sweden
[2]Dep. of Atmospheric Environment, Nat. Env. Res. Inst., Aarhus University, DK-4000 Roskilde, Denmark
[3]Dep. of Occ. and Env. Health, Inst. of Pub. Health, PO Box 2099, DK-1014 Copenhagen, Denmark
[4]Ergonomics and Aerosol Technology, Lund University, PO Box 118, SE-221 00, Lund, Sweden

Traffic is one of the major sources of urban air pollution. To relate exposure to adverse health effects it is important to determine the deposition probability of the inhaled particles in the human respiratory tract. The aims of this study were to: 1) experimentally determine the respiratory tract deposition of a typical urban street aerosol for a group of healthy adults, 2) measure the hygroscopic properties of the particles, and 3) provide a tool/model to estimate particle deposition in other similar environments.

The size dependent deposition of 12-580 nm particles was determined in 9 healthy subjects breathing by mouth on the windward side of a busy street (6 lanes, 65 000 vehicles/day) in Copenhagen, Denmark. Measurements were carried out with a recently developed set-up, RESPI (Löndahl et al. 2006), that was extended with a novel processing unit to account for particle size changes in the lungs (Löndahl et al. 2009). In RESPI particle concentrations in inhaled and exhaled air is measured with a scanning mobility particle sizer (SMPS). The aerosol was characterized both at the curbside and, to obtain the background concentration, at rooftop level. Particle hygroscopicity, a key parameter affecting respiratory tract deposition, was also measured with a hygroscopic tandem differential analyser (H-TDMA) at the same time of exposure. The modelled deposition fraction was determined by adjusting the well-established ICRP model for the measured hygroscopic growth factors.

The size dependent deposition fractions of the particles in the range 12-580 nm is shown in Figure 1.
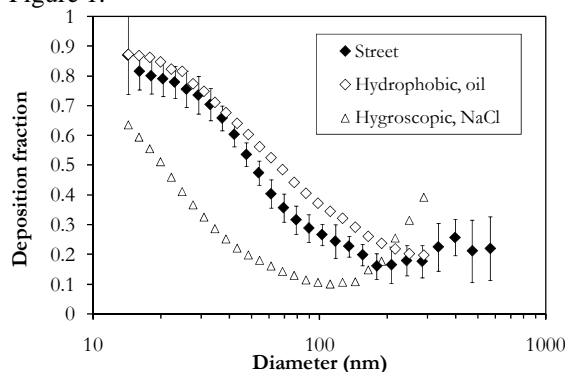

Figure 1. Deposition fractions of the particles at a busy street. Oil and salt were studied previously.

The total fraction of the particles that deposited in the respiratory tract is shown in Table 1. The "traffic exhaust" contribution is assumed to be the hydrophobic fraction of the curbside particles. The deposited amount, or dose, of the traffic exhaust particles was 16 times higher by number and 3 times higher by surface area compared to the deposition of residential biofuel combustion particles investigated previously (equal inhaled mass concentrations). This was because the traffic exhaust particles had both a higher deposition probability and a higher number and surface area concentration per unit mass.

Table 1. Total deposition fractions of particles from the curbside of a busy street, from traffic exhaust and, for comparison, from biomass combustion. Mean values for all subjects

	Total Deposition Fractions		
	Number	Surface area	Mass
Curbside	0.60	0.29	0.23
Traffic exhaust	0.68	0.35	0.28
Biomass combustion	0.22	0.23	0.24

The experimentally estimated deposition could be explained by using the well-established ICRP model and taking the hygroscopic properties of the particle into account.

ICRP Publication 66. 1995. Human Respiratory Tract Model for Radiological Protection, 66.International Comission on Radiological Protection. Publication 66.

Löndahl J, Massling A, Vaclavik Bräuner E, Swietlicki E, Ketzel M, Pagels J, Loft S, 2009, manuscript under review for *Environmental Science & Technology*

Löndahl J, Pagels J, Swietlicki E, Zhou JC, Ketzel M, Massling A, Bohgard M. 2006. *Journal of Aerosol Science* 37:1152-1163.

Air flow and particle deposition experiments with hollow bronchial airway models

A. Czitrovszky, A. Nagy, A. Kerekes

Research Institute for Solid State Physics and Optics, Konkoly Thege M. st. 29-33., 1121 Budapest, Hungary
Envi-Tech Ltd., Konkoly Thege M. st. 29-33., 1121 Budapest, Hungary

Non contact optical measurement methods based on the elastic light scattering from single particles is one of the leading measurement technologies engaged in particle measurement and analysis. This technique combined with the measurement of electric charge on the particles was utilized to experimentally investigate the performance of the stochastic lung deposition model and computational fluid dynamics airway models.

A proportional glass bronchial airway model with one to one scaling (figure 1.) was manufactured based on a resin human lung cast to investigate the deposition of sub and super micron particles in airway generations 1 to 8. The glass airway model makes possible the utilization of optical methods for the measurement of velocity distributions and particle deposition patterns within the airways. Applying these techniques we determined the velocity profiles (e.g. figure 2.) and particle deposition patterns and compared them with numerical simulations of (Hofman *et al.* 2003, 2006, Balásházy *et al.* 1996, Balásházy *et al.* 1999, Balásházy *et al.* 2003, Farkas *et al.* 2006, Farkas *et al.* 2007, Farkas *et al.* 2008,).
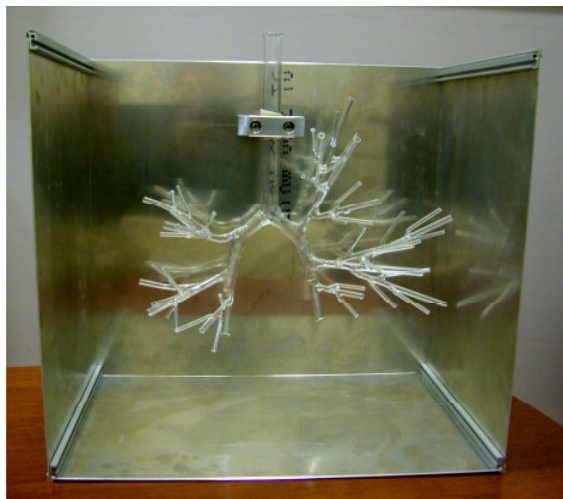
Figure 1. The proportional glass bronchial airway model with one to one scaling

Monodisperse polystyrene latex particles (Duke Scientific) having different sizes were generated using a PG100 aerosol generator and introduced into the model. The ventilation velocity was fitted to the real conditions in a human lung. The concentration of the particles was measured by a GRIMM 1.109 optical particle counter. The velocity profile was determined using a laser Doppler anemometer utilising the benefits of the thin glass wall. The determination of the velocity profile and aerosol concentration in different generations of airways is under process.
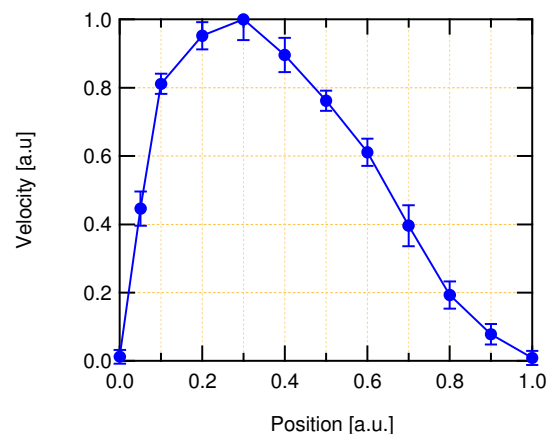
Figure 2. Velocity profile in a second generation airway after the first bifurcation in the glass bronchial airway model.

Hofmann W., Golser R., Balásházy I. (2003) *Aerosol Sci. and Technol.* 37, 988-994.

Hofmann W., Winkler-Heil R., Balásházy I. (2006). *Inhal. Toxicol.* 18, 10, 809-819.

Balásházy I., Heistracher T., Hofmann W. (1996). *J. Aerosol Med*. 9, 3, 287-301.

Balásházy I., Hofmann W., Heistracher T. (1999). *J. Aerosol Sci*. 30, 2, 185-203.

Balásházy I., Hofmann W. Heistracher T. (2003). *J. Appl. Physiol*. 94, 5, 1719-1725.

Farkas Á., Balásházy I., Szőcs K. (2006). *J. Aerosol Med*. 19:3, 329-343.

Farkas Á., Balásházy I. (2007). *J. Aerosol Sci*. 38, 865-884.

Farkas Á., Balásházy I. (2008). *Comp. Biol. Med*. 38, 508-518.

An assessment of time changes of the health risk of PM10 based on GRIMM analyzer data and respiratory deposition model

J.Keder

Czech hydrometeorological Institute, Na Sabatce 17, 14306, Prague, Czech Republic

PM10 particles are considered as one of the most problematical pollutants affecting the human health. Particles comprise typical air pollution burden especially in the urban environment, where they are emitted primarily from the mobile sources. Particles entering human respiratory system are subjected to number of deposition mechanisms. The most important ones are impaction, settling, diffusion and interception. The fraction of particles deposited in different parts of respiratory tract depends on the aerodynamical particle diameter. Thus, identical PM10 concentrations measured by air quality monitoring stations may cause different health effects depending on size distribution of particles whose concentration was detected.

Simultaneous measurements of particle number concentration in 31 size fractions were provided using GRIMM Model 190 analyzer in Prague (capital of the Czech Republic) and in Ostrava industrial region. These enable to assess the proportion of contribution of different fraction to the total PM10 concentration. Collocated PM10 concentration data gathered by the radiometric method are available as well.

Several models have been developed to predict the particle deposition in human respiratory tract. The model developed by the International Commission on Radiological Protection (ICRP) was at the measured data and possible particulate dose assessment has been provided and compared for different locations and time periods.
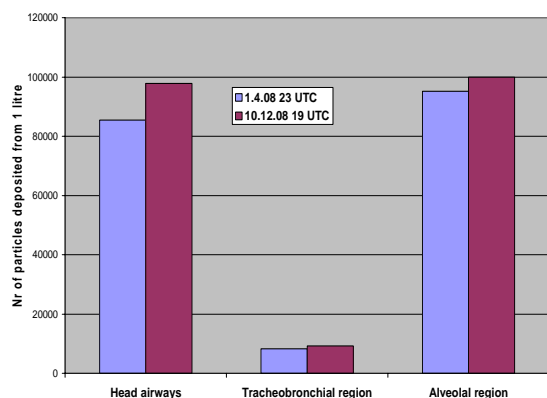
Figure 1. Number of particles deposited in human airways in different hours with the same particle mass concentration 150 µg.m^{-3} (ICRP model)
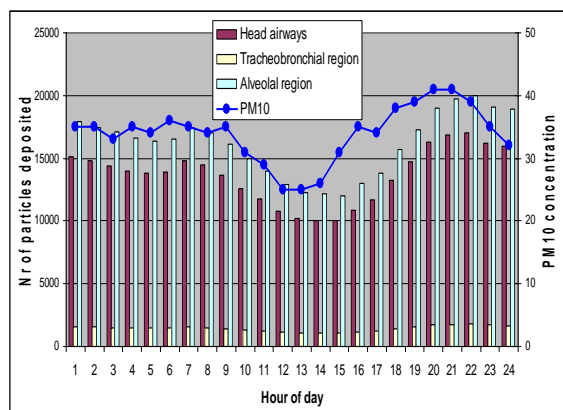
Figure 2. Daily course of number of particles deposited in human airways compared with PM10 concentration (annual medians)
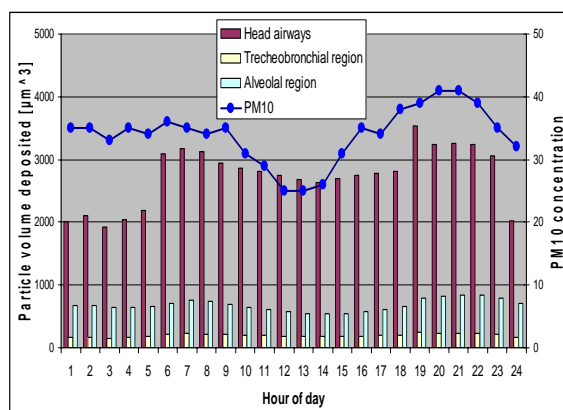
Figure 3. Daily course of particle volume deposited in human airways compared with PM10 concentration (annual medians)

Examples of obtained results are demonstrated on figures. Differences of particle number deposited in particular parts of human airways for different hours with identical particle mass concentration, estimated by the ICRP model, are shown on Fig.1. Figures 2 and 3 demonstrate daily course of this deposition (annual medians), compared with PM10 mass concentration changes.

A stochastic Lagrangian model for predicting turbulent aerosol deposition in an idealized mouth-throat geometry

A. Dehbi

Department of Nuclear Energy and Safety, 5232 Villigen PSI, Switzerland

Keywords: Pulmonary drug delivery, Deposition, Continuous Random Walk, CFD, Turbulence

Solid and liquid aerosols are commonly administered through inhalators to patients with a variety of lung diseases. Understanding and controlling the way these aerosols deposit inside the human mouth, throat and lungs is a primary research area. In recent years, Computational Fluid Dynamics (CFD) has emerged as a powerful and economical alternative to empiricism in the simulation of particle physics inside the mouth-throat geometry (MTG).

One of the main difficulties facing CFD researchers in this area is the specification of turbulent fluid fluctuations experienced by the particles. Recent research has concentrated on Large Eddy Simulations (LES) and Detached Eddy Simulations (DES) in conjunction with Lagrangian Particle Tracking (LPT) to predict particle deposition in the MTG. While providing close agreement with data, LES/DES-LPT approaches are extremely time consuming. It is hence worthwhile to see whether better Lagrangian stochastic models can help Reynolds Averaged Navier Stokes (RANS)-based treatments achieve comparable accuracy. In this investigation, both the RANS Reynolds Stress Model (RSM) and DES are used to obtain the mean carrier flow field, whereas the turbulent fluid velocities are defined through a Continuous Random Walk (CRW) model based on the normalized Langevin equation (Dehbi, 2008).

The geometry employed is derived from the idealized MTG developed at the Aerosol Research Laboratory of Alberta (ARLA) (Grgic et al. (2004)). The CFD mesh consists of 5 prismatic cell layers parallel to the walls, and tetrahedral meshes in the rest of the boundary layer and in the bulk region. Mesh sensitivity studies showed that a grid with 1.4 million cells is adequate to achieve grid-independent results. Simulations were conducted with inhalation flow rates of 30, 60 and 90 L/min, corresponding to Reynolds numbers of respectively 2052, 4105, and 6158, based on an equivalent diameter of 0.021 m.

The RSM and DES models are equally accurate when compared with deposition fraction data produced by Grgic et al. (2004) (see Tables 1 & 2).

In addition, the RSM simulations show (see Figure 1) that the particle deposition fraction scales very well with $Stk \cdot Re^{0.37}$, in agreement with the experimental findings of Grgic et al. (2004).

In conclusion, this investigation demonstrates that RANS-RSM, combined with the state-of-the-art Langevin CRW provides accuracy that compares very favorably with the LES/DES approaches which require computing resources typically two orders of magnitudes greater.

Table 1. Deposited fraction (%) for Q=30 L/min

MMD μm	Experiment (Grgic et al.)	RSM	DES
3.00	2.0 ± 0.5	6.4	5.1
4.98	7.2 ± 2.1	11.8	8.6
5.00	10.0 ± 3.0	11.8	8.6
6.50	32.0 ± 3.0	20.6	16.0
6.59	19.3 ± 2.5	20.9	16.1

Table 2. Deposited fraction (%) for Q=90 L/min

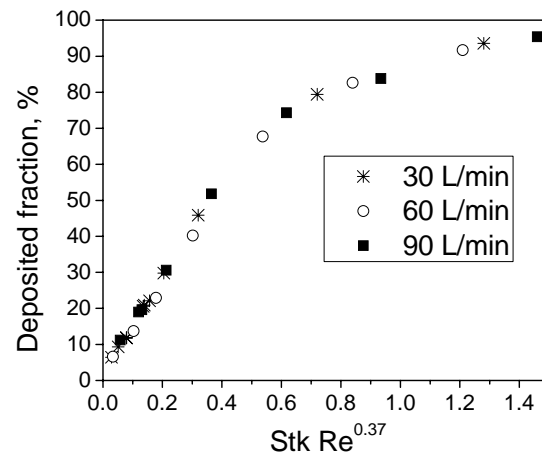| MMD μm	Experiment (Grgic et al.)	RSM	DES
2.87	15.1 ± 1.2	19.0	20.9
3.00	33.0 ± 5.0	19.6	21.0
3.82	40.3 ± 2.7	30.6	34.1
5.00	68.0 ± 3.0	51.8	55.0
6.50	78.0 ± 3.0	74.3	77.1

Figure 1. RSM-based predictions of deposition

Dehbi, A. (2008), *Int. J. Multiphase Flow,* 34, 819-828

Grgic, B., Finlay W.H., & Heenan A.F. (2004), *J. Aerosol Science*, 35, 21–32.

Exhaled breath particles – a biomarker for detection of lung disease?

K. Schwarz[1,3], J.M. Hohlfeld[2,3], H. Biller[2], H. Windt[1], W. Koch[1]

[1]Dep. of Aerosol Technology, Fraunhofer ITEM, Nikolai-Fuchs-Str.1, 30625 Hannover, Germany
[2]Dep. of Clinical Airway Research, Fraunhofer ITEM, Nikolai-Fuchs-Str.1, 30625 Hannover, Germany
[3]Clinic for Pneumology, Hannover Medical School, Carl-Neuberg-Str.1, 30625 Hannover, Germany

Keywords: lung/particle interaction, exhaled breath analysis, aerosol characterization, lung physiology

The chemical analysis of exhaled breath is a convenient and non-invasive method for the examination of the lung that provides information on pulmonary status directly from the airways and alveoli. The exspired air contains small particles generated in the deep lung. Due to lack of systematic data correlating the particle emission flux with respiratory variables it is unclear to which extent the chemical analysis of the particulates could be used for detection and monitoring of airway disease. Therefore we carried out a clinical study to determine the relevant parameters for number and mass flux of the exhaled particles.

An experimental set-up was designed to record the particle concentration, the size distribution and the air flow with high time resolution. The particle concentration was measured by a condensation nuclei counter (TSI 3760), the size distribution was analysed using a laser spectrometer (PMT Lasair II-110) sizing particles in six channels in the range between 0.1 µm and 5 µm. The airflow is recorded simultaneously using a flow sensor. Precautions were taken to prevent water vapour condensation in the measuring system: the flow sensors and the CNC were placed inside a box thermostated to 37 °C. The sample air of the particle sizer was sufficiently diluted.

For 14 healthy volunteers (aged 21 – 55 years) and four patients with moderate-to-severe COPD the properties of the exhaled aerosol were recorded for different tidal volumes.

For all healthy subjects, the number of particle emitted per breath, N, rose exponentially with increasing ventilation ratio, defined as ratio of tidal volume, V_T, to vital capacity, VC,

$$N = A \cdot \exp\left(\beta \frac{V_T}{VC} \right)$$

with β in the range of 6 – 10. A high interday and intraday reproducibility was found for the number of the exhaled particles. However, there was a large inter-individual variability in N covering about two orders of magnitudes (factor A in the range of 0.8 to 103 for healthy subjects).
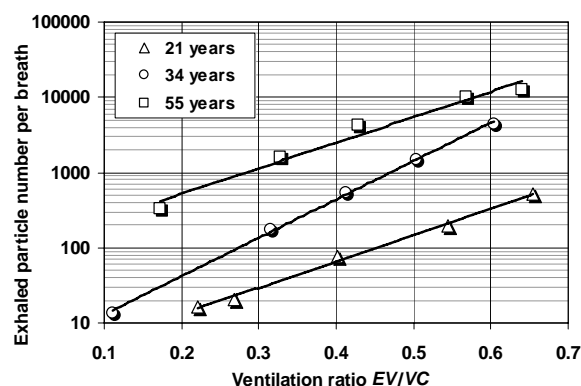
Figure 1. Exhaled particle number for healthy subjects of different age

The number of exhaled particles is determined by the particle generation rate in the lung and the rate of redeposition in the airways during exhalation, mainly due to diffusive and gravitational deposition. For all subjects the particle size was predominantly in the submicron range, with count median diameter at 0.4 µm. Larger particles are deposited by gravitational settling.

The tidal volume turned out to be the most important variable determining the exhaled particle flux of the individual subject. The exponential behaviour of the particle emission flux as function of the ventilation ratio suggests that reopening of collapsed terminal airways linked with a sudden break-up of the surfactant film is the main mechanism for aerosol generation in the lung. Further studies have to be carried out to identify other relevant determinants for the number of exhaled particles and eventually to explain the large inter-subject variability. This is necessary to evaluate the usefulness of exhaled breath particle analysis as a biomarker for detection of lung disease.

The QCM - Online Dose Measurement with high relative Humidity

[1]S. Mülhopt, [2]A. Comouth, [1]A. Grotz, [3]T. Krebs, [1]H.-R. Paur

[1] Institute for Technical Chemistry, Thermal Waste Treatment Division,
Forschungszentrum Karlsruhe GmbH, 76021, Karlsruhe, Germany
[2]Institute for Meteorology and Climate Research, Atmospheric Aerosol Research Department
Forschungszentrum Karlsruhe GmbH, 76021, Karlsruhe, Germany
[3]Vitrocell Systems GmbH, 79183, Waldkirch, Germany

Background: Epidemiological studies show an association between the concentration of fine and ultrafine particles (PM10, PM2.5, PM1.0) in the atmosphere and the rate of mortality or morbidity due to respiratory and cardiovascular diseases. The assessment of the risk of airborne nanoparticles in workplaces or other atmospheres containing ultra fine particles is therefore an urgent task. The causes of the toxicological effects of ultra fine and nanoparticles to the human organism are yet insufficiently known. Besides the chemical composition, the physical properties of the particles seem to be of particular importance for the effects. For the quantitative assessment of the toxicity of airborne nanoparticles the dose–response relationship is tested in *in vitro* test systems using bioassays of cell cultures as sensor.

Material and Methods: For the air-liquid interface exposure of cell cultures towards aerosols the Karlsruhe exposure system was developed (Paur et al., 2008). This system consists of an isokinetic sampling unit to collect the aerosol from the particle loaded atmosphere. Particles bigger than 1 µm are removed by passing a size selective inlet. The aerosol is humidified up to 85 % and temperature controlled to 37 °C. From this aerosol sample flows of 100 ml/min each are directed into VITROCELL® exposure modules, which contain Transwell® inserts with human lung cells on the microporous membrane. The aerosol flows perpendicular onto the surface of the cell culture and the particles deposit on it. After exposure experiments of 1 up to 8 hours the cell cultures were tested for different biological responses like the viability (LDH, AlamarBlue) as well as the release of Interleukin-8 (IL-8) as a marker for pro-inflammatory changes (Diabaté et al, 2008).

For accurate determination a of the particle dose on the cell culture surface a novel online measurement technique was developed (Mülhopt et al, 2008). The sensor of a quartz crystal microbalance is placed in an exposure chamber parallel to the Transwell membrane inserts and exposed to the aerosol in the same geometry as the cell cultures. The deposited mass per area unit is monitored as a function of exposure time showing a linear relationship for a constant aerosol flow with defined particle concentration.

Depending on the kind of aerosol and the investigated conditions of exposure the relative humidity of may increase above 50 %. In these cases adsorption of water at the sensor crystal surface takes place. This results in an increased level of zero frequency for the quartz crystal microbalance depending on the amount of water on the surface which correlates with the relative humidity (Fig. 1).
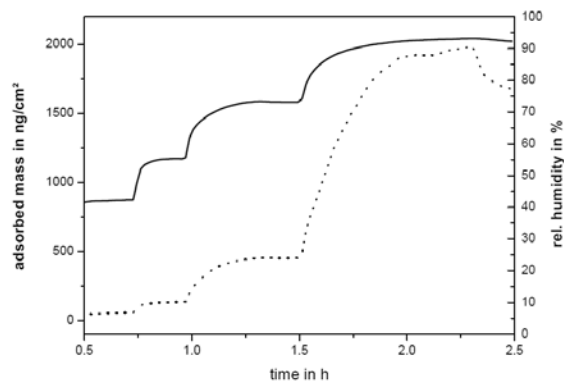
Figure 1. Correlation of mass loading on the quartz crystal microbalance for different relative humidities.
Dotted line = mass loading (left ordinate).
Continuous line = relative humidity (right ordinate)

Results: High relative humidity indicates a loading of the quartz crystal microbalance depending on the relative humidity. For 90 % r.h. it causes a 20 nm layer of water. This has to be considered using the QCM online dose measurement.

Conclusion: The QCM method first time provides an online dose measurement for in vitro exposure experiments at the air liquid interface also under high humidity conditions.

References:
Diabaté, S., Mülhopt, S., Paur, H.-R., Krug, H.F. (2008) *Alternatives To Laboratory Animals* 36, 285
Mülhopt, S.; Paur, H.R.; Wäscher, T. (2008) Vorrichtung zur Messung von Feinstpartikelmassen. DE-OS 10 2007 013 938
Paur, H.R., Mülhopt, S., Diabaté, S., Weiss, C. (2008) *Journal für Verbraucherschutz und Lebensmittelsicherheit* 3, 3, 319-329

Kinetic of carbon black and TiO₂ nanoparticles internalization in two respiratory cellular models

E. Belade[1], L. Martinon[1], J. Fleury-Feith[1], M.-A. Billon-Galland[1], L. Kheuang[2], S. Lanone[2], J. Boczkowski[2], A. Baeza[3], F. Marano[3] and J.-C. Pairon[1, 2]

[1]Laboratoire d'Etude des Particules Inhalées, City of Paris, F-75013, Paris, France
[2]Institut National de la Santé et de la Recherche Médicale, Unité 955, F-94000, Créteil, France
[3]Laboratoire des Réponses Moléculaires et Cellulaires aux Xénobiotiques, Université P7, F-75005 Paris, France

Keywords: nanoparticles, lung/particle interaction, electron microscopy.

The aim of this study was to evaluate the kinetic of internalization of NP (carbon black: FW2 and P60, and dioxide titanium TiO₂) in *in vitro* cellular models : bronchial epithelial cells (16HBE) and fibroblastic cells (MRC5).

Transmission electron microscopy (TEM 1200 EX II JEOL, digital camera GATAN ERLANGSHEN ES500W).was used to study the internalization of NP after exposure of cells to 5 µg/cm² of carbon black NP or TiO₂ NP. This method is recommended to observe the cell/NP interactions (Oberdörster et al., 2005). Internalization was also evaluated after exposure of 16HBE cells to 0,5, 5 and 10 µg/cm² of NP, during 24h.

Internalization was observed in the majority of cells as early as 6h, and seemed to occur earlier in 16HBE cells than in MRC5 cells. Internalization was more important for TiO₂ NP than for carbon black NP in both cell lines, with a higher mean size of NP aggregates for TiO₂, which increased with exposure duration. Internalized NP were mainly in vesicles, with observations suggesting an endocytosis process.

These results suggest that kinetic of NP internalization may depend on the type of cell and NP.
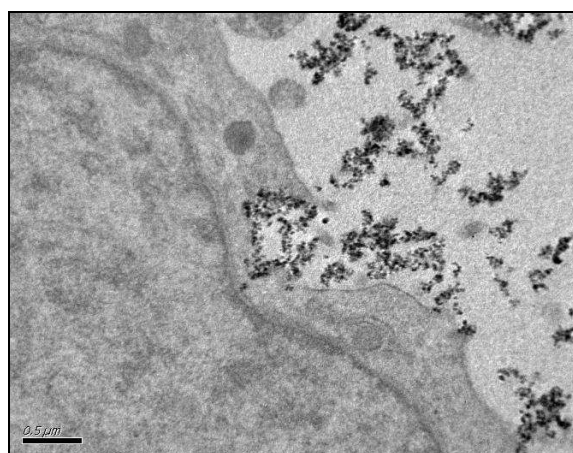
Figure 1. Internalization of Black Carbon FW2 nanoparticles by 16HBE epithelial cell (observed by TEM, X 30000).

Oberdörster G, Maynard A, Donaldson K, et al. (2005). A report from the ILSI Research Foundation/Risk Science Institute Nanomaterial Toxicity Screening Working Group. Principles for characterizing the potential human health effects from exposure to nanomaterials: elements of a screening strategy. *Part Fibre Toxicol.*, 2, 8.

Table 1. Characteristics of nanoparticles.

	Diameter (nm)	Surface (m²/g)	Manufactory
carbon black			
P60	21	115	Degussa
FW2	13	350	Degussa
TiO₂	15	190-290	Sigma

Can a short-term inhalation study be predictive for long-term study outcomes?
– First experience with nano-TiO$_2$, Carbon black and Multiwall carbon nanotubes

Lan Ma-Hock, Silke Treumann, Volker Strauss, Armin O. Gamer, Karin Wiench, , Bennard van Ravenzwaay
and Robert Landsiedel[1]

[1]BASF Product Safety, GV/TB – Z470, 67056 Ludwigshafen, Germany

Keywords: Inhalation, Lung/Particle interaction, Carbonaceous particles, TiO$_2$ nanoparticles.

Inhalation exposure seems to be the application route of highest concern for biopersistent nanoparticles. To meet the urgent needs for toxicological data, we have developed a standard short-term inhalation test in Wistar rats with exposures on five consecutive days (6 hours a day) to well characterized aerosols of nano-powders. The study design comprises the examination of an extensive set of parameters at different time points (at termination of the last exposure or after a recovery period of 2 to 3 weeks). We consider, this short-term inhalation model to be able to predict nanoparticle-derived toxicity in the respiratory tract which may occur after long term exposure.

To evaluate the test design, the inhalation toxicity of several materials with primary particle size in the nano scale was studied in male Wistar rats (Table 1)

Table 1. Physical chemical properties of the test materials

	TiO2	CB	MWCNT
Primary particle size (nm)	25	27	0.286
Particle size range (nm)	13 - 71	11 - 68	Diameter 10-15 nm; length 0.1-10 µm
BET surface area (m2/g)	51	40	179
Purity	99.5 %	99.5 %	91.4
impurities			8.6 % (Al + Fe)

Groups of up to 14 animals were head-nose exposed to dust aerosols for 6 hours a day for five consecutive days. The respiratory tract was evaluated by light microscopy in groups of 6 animals either after the last exposure or after a recovery period of two (TiO2) or three weeks (CB and MWCNT). Bronchoalveolar lavage was performed in satellite animals (5 animals per group and time point) 3 days after the exposure and 2 (TiO2) or 3 weeks (CB and MWCNT) thereafter. Several biochemical, cytological parameters were measured in the in bronchoalveolar lavage fluid (BALF).

The results of the atmospheric concentrations and the particle size analysis are presented in table 2.

Table 2. Characterization of the test atmosphere

	TiO2	CB	MWCNT
Atmosphere concentration (mg/m3)	2.4 ± 0.5 12.1 ± 0.5 50.0 ± 1.6	0.54 ± 0.10 2.53 ± 0.18 10.8 ± 1.53	0.15 ± 0.05 0.57 ± 0.10 2.86 ± 0.82
MMAD (range, µm)	0.7 - 1.1	0.6 – 0.9	0.9 – 2.0
GSD (range)	2.3 – 2.5	2.1 – 4.5	3.0 – 3.8
SMPS CMD (µm)	0.25	0.23	-
OPC CMD (µm)	0.45	0.40	-

The results of our study with TiO$_2$ were overall comparable to those reported for a 90-day study (Bermudez et al. 2004). The low observed adverse effect concentration (LOAEC) in the 90-day study was the atmospheric concentration of 2 mg/m3 determined by cell proliferation rate after the exposure. The same LOAEC was achieved in the current study determined by examination of the lavage fluid.

Concerning Carbon Black, no adverse effect was observed at the tested high concentration of 10 mg/m3. This NOAEC is five times higher than the LOAEC of nano-TiO2, indicating that this material is less potent in causing pulmonary effects.

Our results on MWCNT indicate a high inflammation potency of the test material. The effects were not reversible but progressive. The NOAEC was as low as 0.1 mg/m3, with slight, not significant effects still present at 0.1 mg/m3. There were strong qualitative correlation between our findings after 5-day inhalation exposure with 3 weeks post exposure and those ITI studies after 90 days post exposure observation (Lam et al. 2006).

Our results on nano scale TiO2, CB and MWCNT indicate a qualitative correlation between the outcome of the short-term inhalation test and sub-chronic to chronic inhalation studies. The five day inhalation study appears to be a useful tool to efficiently assess nano materials lung toxicity.

Bermudez, E., Mangum, J.B., Wong, B.A., Asgharian, B., Hext, P.M., Warheit, D.B., Everitt, J.I. (2004). Toxicol. Sci. 77, 347-357

Lam C.W., James J.T., McCluskey R., Arepalli S., Hunter R.L. (2006). Crit. Rev. Toxicol. 36(3):189-217

Toxic effects of nanoparticles from biomass combustion

Werner Fr. Dreher[1], Frank Weise[1], Karen Böhme[1], Steffen Lutz[1], Michael Struschka[2],
Johannes Brodbeck[2], Sonja Mülhopt[3], Hanns-Rudolf Paur[3], Silvia Diabaté[4]

[1]Materials Development and Testing, NMI Naturwissenschaftliches und Medizinisches Institut,
Markwiesenstraße 55, 72770, Reutlingen, Germany
[2]Institute of Process Engineering and Power Plant Technology (IVD), Universität Stuttgart, Pfaffenwaldring 23,
70569, Stuttgart, Germany
[3]Institute for Technical Chemistry, Forschungszentrum Karlsruhe GmbH, 76021, Karlsruhe, Germany
[4]Institute for Toxicology and Genetics, Forschungszentrum Karlsruhe GmbH, 76021, Karlsruhe, Germany

Keywords: soot, toxicity, biomass, exposure, air-liquid interface

Increasing prices for petroleum and natural gas as well as the rising interest in the application of CO_2-neutral raw materials for an energy extraction, lead, in the case of heat generation, to an increased application of biomass. The emitted nanoparticles have a high dwell time in the atmosphere and can penetrate as a component of the particulate emission *via* the airway or the alimentary canal into the human body. However, the main transportation path is the airway, thus the lung. The particulate matter is too small to be detained in the nasal mucosa and the trachea as it is the case for greater particles. This results in cough, an increase in asthmatic attacks and eventually lung cancer. Correlations with cardiovascular diseases have been observed. It has been demonstrated that fine (<2.5 μm) and ultrafine (<0.1μm) particles cause stronger adverse health effects than larger particles.

The consequences of the toxic effects of different particulate matter for example resulting from combustion engines or combustion plants resp. fireplaces with wooden biofuels are still not completely understood. Hence, it is essential to clarify which particulate emissions from combustion processes have a deep toxic influence on human body to optimise these firing processes.

This aspect is investigated in this project on the base of an *in vitro* model for a human lung. This should serve as basis for the development of technical innovations (filter systems) for combustion plants, which minimise or eliminate the emission of soot in order to assure a better protection of humans.

For the air-liquid interface exposure of cell cultures towards aerosols the Karlsruhe exposure system (Mülhopt et al) is used. After sampling the aerosol from the combustion off gas stream, particles above 1 μm are removed by a size selective inlet. The gas humidity is adjusted to 85% by injection of steam. A549 human lung cell cultures are subjected to a constant flow of the conditioned aerosol. After exposure, the responses of the cells are analysed to measure the biological responses such as viability, inflammatory or oxidative stress. An online dose measurement technique monitors the deposited particle mass per cell culture area.
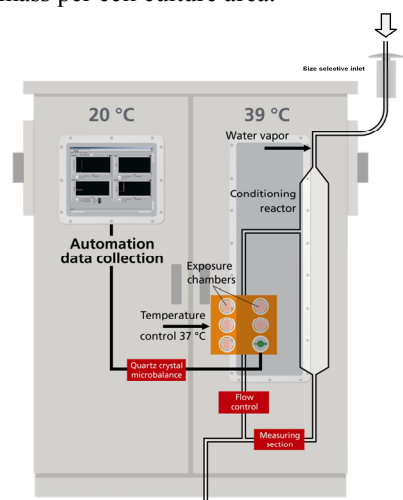
Figure 1. Karlsruhe exposure system for *in vitro* testing of airborne nanoparticle emissions from industrial processes.

The toxicity of particulate matters, from the incomplete combustion of biomass in fire places, will be investigated. The correlation between the incinerator charges, chemical composition, particle emission and toxicity considering various operation parameters will be analysed. The future goal is to contribute to the clarification of particulate matter and its toxicity potential. Hence, we will contribute to fundamentals of technological innovations which will provide a base for the optimisation of the firing process.

Mülhopt, S., Paur, H.R., Diabaté, S., Krug, H.F. (2007). *Advanced Environmental Monitoring*, Y.J. Kim and U. Platt, eds. Springer Netherlands, pp. 402-414.

Cytotoxic and Inflammatory Effects of Indoor PM_{10} compared to Outdoor PM_{10} from German schools

S. Oeder[1], W. Schober[1], I. Weichenmeier[1], S. Dietrich[2], H. Fromme[2], H. Behrendt[1] and J.T.M. Buters[1]

[1]Division of Environmental Dermatology and Allergy, Helmholtz Zentrum München/TUM, ZAUM-Center for Allergy and Environment, Technische Universität München, 80802, Munich, Germany
[2]Bavarian Health and Food Safety Authority, Department of Environmental Health, 85764, Oberschleißheim, Germany

Keywords: health effects of aerosols, indoor/outdoor particles, PM10, lung/particle interaction, human lung cell.

Outdoor particulate matter (PM_{10}) is associated with a wide range of health effects and a European threshold limit of $50\mu g/m^3$ (daily limit) was established in 2005. However, most individuals spend at least 85% of their time indoors where particle concentrations are mostly higher than outdoors. Since children represent a vulnerable group, we investigate the health effects of indoor air PM_{10} collected in elementary school classrooms compared to outdoor air PM_{10}.

PM_{10} was collected on Teflon filters by using medium volume samplers ($2.3m^3/h$; Derenda Inc.) in classrooms of five schools with two classrooms per school in Munich during teaching hours (5.5h/day). In parallel the outdoor air nearby the classrooms was sampled ($30m^3/h$; high volume sampler; Derenda Inc.). Each school was sampled for four weeks. Samples were taken from October 2007 to July 2008. Filter load was determined gravimetrically. Particles were recovered by sonication, lyophilized and resuspended in water. Cytotoxicity was assayed as a decline of cellular ATP concentration in human primary keratinocytes, human lung epithelial A549 cells and Chinese hamster V79 lung fibroblasts at concentrations up to $10\mu g/ml$. In addition, toxicity after metabolic activation was assayed in V79 cells expressing human cytochrome P450 1A1, 1A2, 1B1, 2A6, 2B6, 2C9, 2D6, 2E1, 3A4, 3A5. For a genome wide gene expression analysis BEAS-2B bronchial epithelial cells were incubated with $10\mu g/ml$ PM_{10}. RNA was isolated and analyzed on Affymetrix HG U133A 2.0 expression arrays (14,500 genes).

Indoor PM_{10} in schools occurred at $126\pm48\mu g/m^3$. The corresponding outdoor concentrations were $27\pm15\mu g/m^3$. While in A549 and V79 cells no toxicity was observed, in human primary keratinocytes classroom PM_{10} at a concentration of $10\mu g/ml$, corresponding to an air equivalent of about 40L per cm^2 of cell surface caused a slight (20%, $p<0,05$) decrease in vitality. This cytotoxic effect was also found in V79 cells after metabolic activation by CYP1A1 or CYP2C9 ($p<0.05$). Genome wide analysis of PM_{10} from outdoor and indoor air showed the overexpression of xenobiotic metabolizing genes (CYP1A1, CYP1B1) and of inflammatory cytokines (IL1A, IL1B, IL6, IL8). Indoor PM_{10} caused a lower induction of xenobiotic metabolizing genes but an up to 6 fold higher induction of inflammatory cytokines compared to outdoor PM_{10}.

Direct cytotoxicity and metabolic activation by cytochrome P450 isoforms 1A1 and 2C9 were statistically significant at a PM_{10} concentration of $10\mu g/ml$, which is about 10,000 times higher than exposure encountered in classrooms. We therefore expect no toxic effects of these particles in school children.

Although not toxic, the cells reacted to PM_{10} by an induction of the metabolizing enzyme CYP1A1 and CYP1B1. Indoor air PM_{10} induced less xenobiotic metabolizing enzymes but had a higher level of induction of inflammation than outdoor air PM_{10}. Because outdoor air had a 10 fold lower PM_{10} concentration we think that ventilation practice in schools should be modified.

Action of Fe_2O_3 nanoparticles on MRC5 lung fibroblasts

M.C. Munteanu[1], O. Zărnescu[1], C. Sima[2], M. Radu[1], M. Costache[1], C. Grigoriu[2], A. Dinischiotu[1]

[1]Department of Biochemistry and Molecular Biology, University of Bucharest, 91-95 Spl. Independentei, 050095 Bucharest, Romania
[2]Laser department, National Institute of Laser, Plasma and Radiation Physics, 409 Atomistilor, 077125 Bucharest-Magurele, Romania

Keywords: lung/particle interaction, nanoparticles, chaperones, lung fibroblasts,

Although it is well known that nanoparticles produce adverse health effects, molecular studies on the influence of Fe_2O_3 (hematite) nanoparticles on MRC 5 lung cell lines have not yet been investigated. Chaperones are responsible for protein folding, protein association in oligomeric complexes and the import of protein precursors to intracellular compartments (Gething & Sambrook, 1992). Abundant data demonstrate that the incorrect folding of proteins forms the molecular basis of some human diseases (Thomas et al., 1995).

In the present study, we have investigated the expression of the MRC 5 lung cell line exposed to nanoparticles on the translational level of heat shock proteins of 27, 60, 70 and 90 kD. The primary nanoparticle size distribution was a lognormal function, in the range 10-120 nm, most of them being of 40-60 nm. The nanoparticle high resolution electron microscopy image is presented in figure 1.
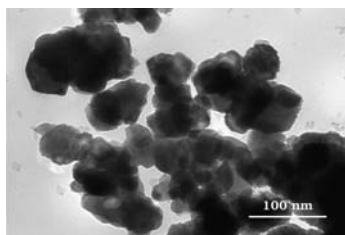
Figure 1. Fe_2O_3 nanoparticles HRTEM images.

The MTT test was used to assess cell viability after MRC5 cell treatment with 6.12×10^6 Fe_2O_3 particles per individual cell for 24, 48 and 72 hours. The gene expression of Hsp 27, Hsp 60, Hsp70, Hsp90 was analyzed through quantitative real time PCR (qRT-PCR) following all three time intervals of exposure.

The viability of the MRC5 lung cell lines in the presence of these nanoparticles decreased by 25% and 40% after 48 and 72h, respectively.

The expression of Hsp27 at the transcriptional level was upregulated after 24h, almost unchanged after 48h and downregulated after 72h of treatment. A very significant increase of Hsp60 mRNA expression occurred after 24, 48 and 72h of exposure. The level of Hsp70 mRNA significantly decreased after 72h, whereas that of Hsp 90 was not affected by the hematite nanoparticles exposure.

Our results suggest that hematite nanoparticles especially affected the mitochondria. The level of Hsp60 mRNA can be correlated with that of the corresponding protein which is remarkably immunogenic. Several *in vivo* studies demonstrated the existence of autoantibodies against Hsp60 which provoke cell death with the development of fibrosis foci.

Gething M.J. & Sambrook J. (1992), *Nature*, 355 (6355), 33-45

Thomas P., Qu B-H. & Pedersen P. (1995), *TIBS*, 20, 456-459

Towards *in vitro* nanoparticle toxicity screening: Quantitative prediction of soot-induced pulmonary inflammation from *in vitro* assays

T. Stoeger, D. Dittberner, S. Takenaka, H. Schulz and O. Schmid

Institute for Inhalation Biology, Helmholtz Zentrum München, Ingolstaedter Landstr. 1, 85764 Neuherberg, Germany

Keywords: health effects of aerosols, lung/particle interaction, nanoscale carbon particles, organics, soot particles

Inhalation of insoluble particles is believed to cause an oxidative cellular stress response, which may lead to pulmonary or even systemic inflammation. In addition to concern about combustion-derived nanoparticles (CDNPs), an increasing number of engineered nanoparticles is expected to be emitted into the atmosphere due to the economic success of nanotechnology. In the interest of consumer and workers' safety fast, reliable and affordable screening techniques for (nano-)particle toxicity are required. In addition, animal protection demands the development of straightforward *in vitro* tests, which are verified against *in vivo* results. Responding to these demands we aimed to reduce our previously published particle toxicity model from mice (*in vivo*) to cells (*in vitro*).

We have previously demonstrated that acute pulmonary inflammation in BALB/cJ mice (influx of polymorphonuclear neutrophils (PMNs) into the lungs) 24h after intratracheal instillation of six types CDNPs (soot) is well correlated with the BET surface area of the particles (Stoeger et al., 2006). Furthermore, pulmonary inflammation due to CDNPs could be attributed to two main mechanisms, the oxidative potency (OxPot) of the carbon core and the bioactivation of organic compounds (such as PAHs) condensed onto the cores (Stoeger et al., 2009). While the former was quantified with a well-established cell-free *in vitro* assay (consumption of ascorbate (antioxidant)), the latter required gene expression analysis (*Cyp1a1*) of lung tissue from the CDNP exposed mice. To replace this *in vivo Cyp1a1* test with an *in vitro* assay different murine lung cell lines were examined for *Cyp1a1* inducibility after CDNP exposure. While the murine alveolar macrophage cell line MHS displayed no *Cyp1a1* responsiveness, the murine alveolar epithelial cell line LA4 showed excellent correlation with the *in vivo Cyp1a1* expression (R^2=0.94).

Our previously described two parameter model for pulmonary inflammatory efficacy (I_{Ef} [%PMN/µg]) (Stoeger et al., 2009), can now be modified to predict *in vivo* I_{Ef} from *in vitro* data according to $I_{Ef} = 5.05 OxPot + 0.033 Cyp1a1_{LA4}$. Figure 1 shows that this simple linear model based on *OxPot* and *Cyp1a1_{LA4}* data explains 94% of the observed variability in I_{Ef} with a slope of 0.99 (forced through the origin). This is particularly remarkable, since the six types of CNDPs used here represent a wide range of the most important physico-chemical properties, namely (primary) particle diameter (10-50nm), organic content (OC; 1-20%) and BET surface area (43-800m^2/g) (Stoeger et al., 2006; Matuschek et al., 2007). Consequently, the data set includes CDNPs which induce oxidative stress predominantly via direct particle-cell interaction (high *OxPot*, low *Cyp1a1_{LA4}* induction) or via *Cyp1a1* mediated detoxification pathways leading to bioactivation of organic compounds.

The *OxPot* and *Cyp1a1_{LA4}* based *in vitro* model presented here accurately predicts acute pulmonary inflammation in mice after instillation of six types of CDNPs. If the model can be expanded to include additional pathways of toxicity (e.g. transition metals), a fast and reliable *in vitro* screening for nanotoxicology may be within reach. This would be a significant step towards consumer and worker's safety, reduction of animal experiments and societal acceptance of novel products containing nanotechnology.
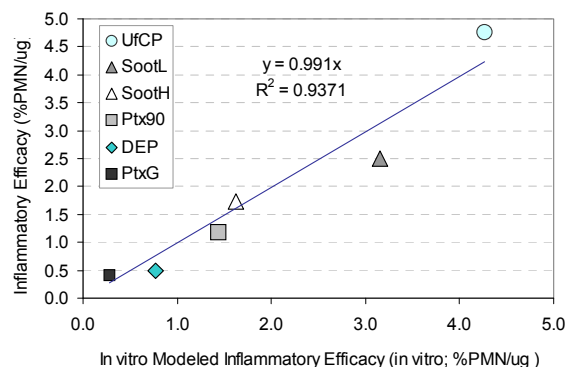
Figure 1. Comparison of measured *in vivo* inflammatory efficacy and an *OxPot- Cyp1a1_{LA4}* based *in vitro* model for six types of CDNPs. (UfCP: spark discharge carbon particles; SootL, SootH: soot from a propane diffusion flame (CAST burner) with low and high organic content; Ptx90, PtxG: commercially available black carbon (Printex90, PrintexG); DEP: Diesel NIST SRM-1650a)

Stoeger et al. (2006). Environ. Health Persp., 114, 328-333.

Stoeger et al. (2009). Environ. Health Persp., 117, 54-60.

Matuschek et al. (2007). Environ. Sci. Technol. 41, 8406-8411.

Response of a human alveolar cell line to urban fine particles

E. Longhin, P. Mantecca, M. Gualtieri, V. Corvaja, A. Altana, L. Piazzoni and M. Camatini

POLARIS Research Center, Department of Environmental Sciences, University of Milano-Bicocca, 1, P.zza della Scienza, 20126, Milan, Italy

Keywords: PM2.5, A549, Carbon Black particles, Cytotoxicity.

Recently, particular attention has been paid to the toxicological properties of PM2.5, the fine fraction of air particulate matter, which penetrates deeply in respiratory tract and can easily reach the alveolar ducts (Billet *et al.*, 2007). PM2.5 was collected in an urban area using a low volume gravimetric sampler. Samples were processed and the particles were detached from filters and used to test their cytotoxic effects on the human alveolar cell line A549.

A549 cells were exposed to urban particle suspensions at the concentrations of 0.1, 1, 10, 25 and 50μg/cm^2. Carbon Black particles (CB) of similar dimension were used at the doses of 1, 10, 25μg/cm^2 as a reference inert particulate matter. Cell viability, intracellular reactive oxygen species (ROS) production, cytochrome P450 CYP1A1 and enzyme HMGB-1 expression, particle internalization with light and transmission electron microscopy were analysed.

A concentration-dependent decrease in cell viability was observed in A549 cells exposed to particle suspensions, showing a significant difference with respect to controls starting from the dose of 10μg/cm^2. Cell viability was not affected by CB until the concentration of 25μg/cm^2.

ROS production was investigated by flow cytometry using the fluorescent probe DCFH-DA. While control cells did not show ROS-linked fluorescence, a significant and concentration-dependent increase of ROS after exposure to 10μg/cm^2 PM was observed. PM-induced ROS always resulted to be significantly higher than those induced by CB.

PM2.5 cell exposure also induced a marked Cytochrome CYP1A1 expression, as revealed by the flow cytometry analyses.

HMGB1 is an enzyme passively released by damaged or necrotic cells and the correlation between the exposure to PM and the release of HMGB1 in the medium from A549 cells is under investigation.

Phagocytosis of particles by A549 cells was morphologically characterized and seemed to depend on both particle concentration and exposure time, with the majority of particles being engulfed in membrane-bound vacuoles after 24h of exposure. Cell-particle interaction is also under investigation for the molecular changes observed in the particle carbonaceous structure (Zerbi et al., 2008). Cytotoxic effects, mainly represented by necrotic changes, were visible at light microscope (Fig. 1). At ultrastructural level, particles clusters onto the outer layer of the cell membrane were observed with the phagocytic structures forming in correspondence of the points of cell-particles interaction. Cell membrane lyses and mitochondrial ultrastructural disruption appeared to be the main modifications induced by PM2.5 on A549 cells (Gualtieri et al., *in press*).

In conclusion urban PM2.5 has a potentially high toxicological impact and can induce cell toxicity in a concentration-dependent manner being able to enter and damage the A549 cells, and even to provoke their death. CB, of an aerodynamic diameter similar to that of PM2.5, was consistently less effective. This finding suggests the leading role of the other components of PM such as transition metals and PAHs adsorbed onto the carbon core.
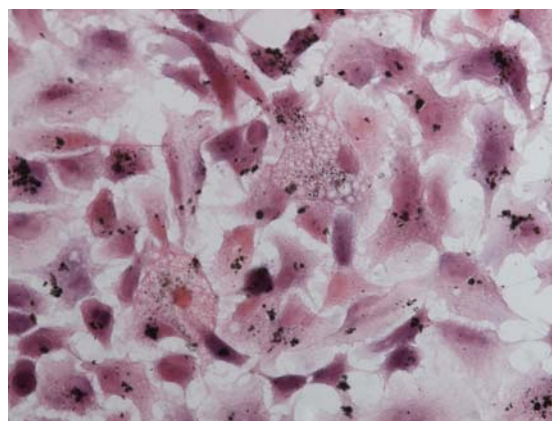
Figure 1. Light microscopy of HE stained A549 monolayers exposed to 25μg/cm^2 PM2.5 for 24h, showing extensive cytoplasmic vacuolations.

Billet, S., Garçon, G., Dagher, Z., Verdin, A., Ledoux, F., Cazier, F., Courcot, D., Aboukais, A. & Shirali, P. (2007). *Environ. Res.* 105, 212–223.

Gualtieri, M., Mantecca, P., Corvaja, V., Longhin, E., Perrone, M.G., Bolzacchini, E., Camatini, M. *Toxicol Letters (in press)*.

Zerbi, G., Ferrugiari, A., Fustella, G., Tommasini, M., Mantecca, P., Gualtieri, M., Camatini, M. 2008. *Chem. Eng. Trans.* 16, 387-394

Seasonal chemical composition and biological effects for fine particles (PM1 and PM2.5) of a Milan urban site (North of Italy)

M.G. Perrone[1], M. Gualtieri[1], L. Ferrero[1], C. Lo Porto[1], E. Bolzacchini[1], R. Udisti[2], M. Camatini[1]

[1]Research Center POLARIS, University of Milano-Bicocca, DISAT, P.zza della Scienza 1, 20126 Milan
[2]Department of Chemistry, University of Florence, Via della Lastruccia 3, 50019 Sesto F.no, Florence

Keywords: PM1, PM2.5, chemical composition, health effects of aerosol

Exposure to fine particulate matter in polluted area is associated with harmful health effects on the exposed population. PM composition, in addition to concentration, plays an important role: *in-vitro* and *in-vivo* studies have shown a correlations between the PM effects and its chemical composition (de Kok, 2006).

In the present study, PM sampling was performed in an urban site of Milan, which is the biggest city in the North of Italy and it results to be one of the most polluted area in the central t Europe.

Fine particles, PM1 and PM2.5, were collected with a low volume gravimetric sampler (38,33 l/min) during summer (August -September) and winter (January-March).

Particles detached from the filters, according to the procedure reported (Gualtieri et al., 2009), were analyzed for the chemical composition and the effects produced on the human lung epithelial cell line A549. PM samples were analyzed for:
- inorganic ions (by IC): Na^+, K^+, Ca^{++}, Mg^{++} NH_4^+, F^-, Cl^-, NO_3^-, $SO_4^{2=}$
- elements (by ICP-optical): Al, As, Ba, Cd, Cr, Cu, Fe, Mn, Mo, Ni, Pb, V, Zn
- polycyclic aromatic hydrocarbons, PAHs (by GC-MS): BaA, CHR, BbF, BkF, BaP, BeP, dBahA, BghiP, IcdP.

In-vitro tests were performed to assess cell viability with the MTT assay, DNA damage with the COMET Assay, and cytokine release (IL-6 and IL-8) with ELISA.

Multivariate data analysis (Principal Component Analysis-PCA) was applied to investigate the relationship between chemical composition and biological response. Chemical composition was expressed as mass contribution to total PM (ug/ug %); biological responses were referred to the concentration of exposure of 12 ug cm^{-2} .

Milan PM chemical composition showed a characteristic seasonal trend.

Summer samples presented a higher mass contribution of $SO_4^=$ originated from a secondary source, in respect to thr winter samples. The percentages were respectively 13% and 7% in PM2.5 samples.

Winter PM was characterized by a higher mass contribution of semi volatile compounds, such as NO_3^-, and chemical compounds from combustion source, like PAHs. PAHs mass contribution in winter

PM samples was 5-6 times higher than summer . K^+ mass contribution was higher in winter PM samples (50 %) than in summer ones, according to the wood combustion source.

A seasonal trend in PM biological effects was observed. Cell viability was affected , since the % of cell death in summer was two times higher in comparison with the one of winter (0.27 ± 0.05 and 0.14± 0.05 respectively)

Significant correlations between biological endpoints and chemical compounds in PM samples were found. PCA analysis (FIG.1) shows that cell death correlates with As (R=0.76), $SO_4^=$ (R=0.68) Zn (R=0.66) Cr (R=0.64) and Cu (R=0.58).
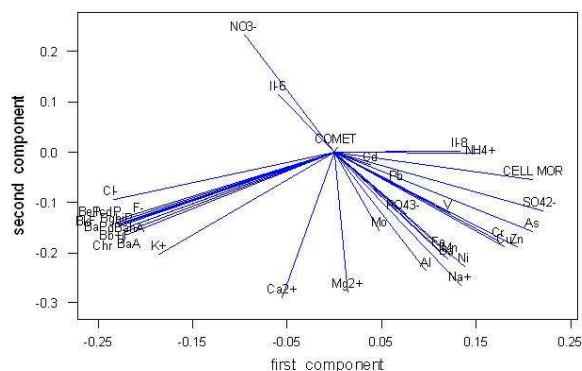
Figure 1. PCA analysis of the chemical composition and biological responses in 16 samples

PM1 and PM2.5 fractions were characterized by a similar chemical composition. PM2.5 samples were enriched in some chemical compounds , mainly present in the intermodal fraction PM(2.5-1), such as Ca^{++} and Mg^{++} (contribution from soil dust), and Fe, Zn, Ba and Mn.

The analysis of PM1 samples showed that cell mortality and IL-8 release may be related to the same chemical properties (R=0.97). The chemical composition of PM2.5 samples seems to have major effects on the cell mortality and DNA damage (R=0.85).

de Kok TMCM, *et al.* (2006). Mutation Research 613, 103-122
Gualtieri M., *et al.*, (2009). Toxic. Letters (in press)

Inflammatory effects of Milan coarse particulate matter on human cell lines

V. Corvaja[1], M. Gualtieri[1], M. Camatini[1]

[1]Research Center POLARIS, University of Milano-Bicocca, DISAT, P.zza della Scienza 1, 20126 Milan

Keywords: PM10, Human lung cell, Biogenic particles

Introduction. The coarse fraction of the particulate matter (PM10) is recognized as having significant adverse effects on the bronchiolar region of conducting airways. In order to improve the understanding on Milan PM10 cellular effects, we collected PM10 samples during summer 2008 in a typical urban site (Torre Sarca).

Endotoxins, such as lipopolysaccharides (LPS), peptoglycan and other lipoprotein, are one component of PM10 fraction of particular interest. These molecules are component of the cell-wall of gram-negative and gram-positive bacteria and when inhaled, they stimulate alveolar macrophages and respiratory epithelial tissue to release cytokines, which thus initiate the inflammatory cascade. Cytokines were found to be more strongly induced by coarse fraction than by fine one (PM2.5) and several studies have shown that the PM-induced cytokine production was partially inhibited by adding polymyxin B (LPS chelator). Moreover toll-like receptors (TLR) are cell membrane receptor involved in microbial pathogens structure recognition and it has been demonstrated they key role in the activation of the inflammatory responses pathways (Becker et al., 2005).

Experimental design. The human alveolar cell line A549 and the monocytic cell line THP-1 were exposed to 1μg/cm² of PM10 for 24h. Endotoxin concentration in PM10 was measured by LAL test. Cell cytotoxicity was assessed by the Alamar Blue assay. Interleukin (IL)-6, which activates the immune system and exerts multiple effects on numerous cell types including synthesis of acute phase proteins, and IL-8, an important chemoattractant for neutrophils, released in the medium of treated cells, was measured by ELISA. Cells viability was slightly affected by PM10 treatment in comparison to control cells. To assess the importance of TLRs in the activation of the PM10-induced inflammatory response cell were also treated with specific antibodies for the toll like receptor (TLR-2; TLR-4) prior the exposure to the particles. Cells were also exposed to LPS as positive control. Fine carbon black particles (CB) were used as reference material and their viability and proinflammatory potential were measured.

The results showed that LPS induced-inflammatory response was significant at the concentration used both on the single cell line than on the coculture system. The response was higher in the THP-1 cell line than in A549 indicating the primary role of monocytes in the pathogenic response. Surprisingly PM10 had minor effects on the single cell lines but in the co-culture system it induced a significant increase of the IL-6 levels (FIG.1). This is probably due to signalling pathway among the monocyte and epithelial cells. CB showed no significant effects in the experiments performed. Pre-treatment with TLR inhibitors was able to reduce IL-6 release in PM10 and LPS treated cells.

Conclusions. The data demonstrate the importance of TLRs in the inflammatory response trigger by PM10, assessing the importance of bacteria-wall component. Moreover the data on IL-6 expression underline the existence of an inter-cellular signalling between the two cell types, which needs further investigation.
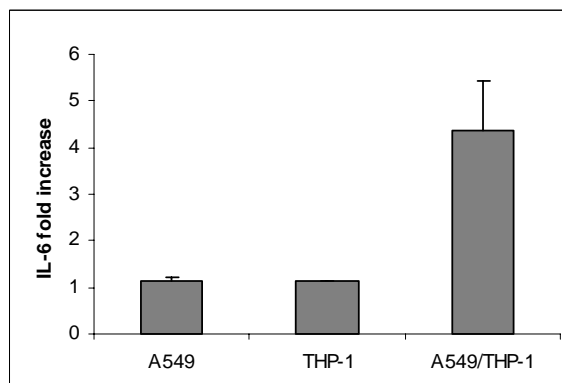
FIG.1 IL-6 release in monocultures (A549, THP-1) and co-cultures (A549/THP-1) exposed to 1μ/cm² of PM10.

Alfaro-Moreno E., Nawrot T.S., Vanaudenaerde B.M., Hoylaerts M.F., Vanoirbeek J.A., Nemery B., Hoet P.H. Eur Respir J. 2008 Nov;32(5):1184-94

Becker S., Dailey L., Soukup J.M., Silbajoris R., Toxicol Appl Pharmacol. 2005 Feb 15;203(1):45-52.

Gualtieri M., Mantecca P., Corvaja V., Bolzacchini E., Fustella G., Zerbi G., Camatini M. Chemical Engineering Transaction 2008 16, 411 – 18

Gualtieri M., Øvrevik J., Mantecca P., Holme j., Corvaja V., Camatini M. Eurotox, 2008

Effects induced by metal oxide nanoparticles on *in vivo* and *in vitro* systems

E. Moschini, D. Gallinotti, P. Magni, M. Camatini and P. Mantecca

POLARIS Research Centre, Department of Environmental Sciences, University of Milano-Bicocca, 1, P.zza della Scienza, 20126, Milan, Italy

Keywords: nanoparticles, metal oxides, ecotoxicity, cytotoxicity, *Xenopus laevis*

Nanomaterials residues can actually represent a source of risks for both environmental and human health. While abundant literature is available on the possible adverse health effects elicited by inhalable nanoparticles (Farrè *et al.*, 2009), there is a huge lack of knowledge regarding the potential toxicity of nanoparticles (NPs) in the aquatic environment. Metal and metal oxide nanomaterials are produced at industrial scale and largely employed for different applications such as environmental remediation, electrical devices and pharmaceuticals (Simonet *et al.*, 2009). So that they may represent a serious hazard for workers, consumers and environment. Moreover, once released in the different environmental matrices, metal and metal oxide NPs may change their properties and reactivity, thanks to the influence of chemical, physical and biological agents.

The present research aims to investigate the potential adverse effects induced by different metal oxide NPs on amphibian (*Xenopus laevis*) development, which represents a very sensible biological model to test aquatic toxicity. Concomitantly, the same NPs have been administered to human cell cultures to compare the toxic mechanisms elicited at cellular level in response to NPs in different biological models. Carbon NPs have been used in the experiments as reference material.

Firstly we have set up the conditions of NPs suspension to define a standard and suitable work procedure. It is indeed already recognized that different methods of NP dispersion can lead to different behaviour and consequently to different biological effects. Moreover it is critical to ascertain if toxic effects are mainly linked to the soluble metal content and/or to the particles themselves. Thus NPs' suspensions have been characterized for dissolved and total metal contents throughout the test time; for the stability of the suspension, for the morphology of the particles and for the aggregation phenomena occurring.

Xenopus exposure to metal oxides resulted in little or no mortality and in low percents of external malformations when compared to the effects of inert carbon particles. Lethal and teratogenic effects of NPs did not reach significant level even at very high NP concentrations. We observed internalization of particles and particles' aggregates in different organs and tissues.

Notable histological lesions were found at the level of CNS, especially in correspondence to the encephalic vesicles, and likely contribute to the abnormal swimming behaviour observed in NP exposed larvae at the end of the tests.
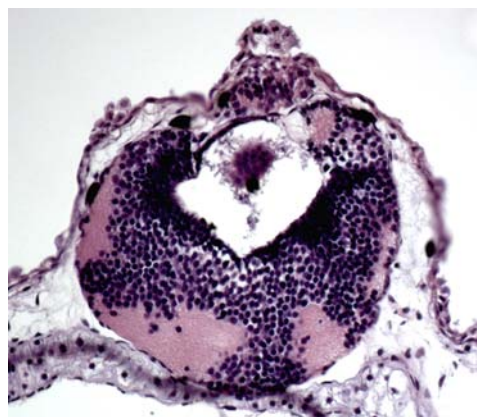
Figure 1. Encephalon of a *X. laevis* embryo showing internalization of CuO NPs and disorganization of the nervous cells.

Such effects seemed to be markedly reduced in embryos exposed to carbon NPs, testifying for the determinant role of the NPs' elemental composition in their own biological activity

Significant decreases in vitality have also been observed in human alveolar epithelial cells in response to metal oxide NPs, in contrast to the results obtained with nano-carbon exposure, that induced lower values of cell mortality. Cellular response to NPs have been mainly attributed to their pro-oxidants generation capacity, as demonstrated by the increased oxidative damages observed in both *in vitro* and *in vivo* systems.

Actually regulations mainly exist for soluble forms of toxic metals. For that, it is crucial to understand if nanomaterials are toxic and, if so, whether the toxicity is quantitatively or mechanicistically different than that of soluble metals (Griffitt *et al.*, 2007).

Griffitt, R. .J., Weil, R., .Hyndman, K. Y., Denslow, N. D., Powers, K., Taylor, D. T., Barber, D. S. (2007). *Environ. Sci. Technol.,* 41, 8178-8186.

Farré, M., Gajda-Schrantz, K., Kantiani, L., Barceló, D. (2009). *Anal. Bioanal. Chem.,* 393, 81-95.

Simonet, B. M., Valcárcel, M. (2009). *Anal. Bioanal. Chem.* 393,17-21.

Physico-chemical differences between particle and molecule derived toxicity: Influence of small molecule adsorption on engineered nanoparticles

L.K. Limbach[1], E.K. Athanassiou[1] R.N. Grass[1] and W.J. Stark[1]

[1]Institute for Chemical and Bioengineering, ETH Zurich, 8093, Switzerland

Keywords: Health effects of aerosols, lung/particle interaction, nanoparticles, health aspects of aerosols.

The rapidly growing applications of nanotechnology require a detailed understanding of benefits and risks, particularly in toxicology. The present study highlights the physical and chemical differences between particles and molecules when interacting with living organisms [1]. In contrast to classical chemicals, the mobility of nanoparticles is governed by agglomeration, a clustering process changing the characteristic size of the nanomaterials during exposure, toxicity tests or in the environment [4]. The current status of nanotoxicology highlights non-classical toxic interactions through catalytic processes inside living cells and the enhanced heavy metal transport into the cytosol through the "Trojan horse mechanism" [2]. The safety of nanoparticles in consumer goods is proposed to be rendered inherently safer by substituting currently applied persistent oxides through biodegradable materials.

The possible negative effects of nanoparticles are correlated to their nano-specific material properties or to the effective uptake mechanism into human cells. The cellular membrane is an evolutionary grown barrier for different molecules and salts [4]. Small molecules tend to adsorb on surfaces. Due to their high specific surface, nanoparticles offer a great potential for molecules adsorption. Within this study we investigated the transport of molecules into human epithelia cells (A549) adsorbed on nanomaterials. Industrially relevant ceria, silica and carbon black were chosen as model nanoparticles with different surface charge and hydrophobicity. A colorimetric adsorption assay showed that under biological relevant conditions only hydrophobic nanomaterials can adsorb small biomolecules. A cell viability assay was preformed after the exposure of two model toxins, paclitaxel and colchicine, together with nanoparticles. For paclitaxel exposure together with carbon black a significant increased toxic effect was found compared to single toxin exposure. For hydrophilic silica and ceria nanomaterials no increased toxic effects were found within the model assay. The effect coming from adsorbed molecules on nanomaterials is expected to gain in importance for larger bio-molecules.
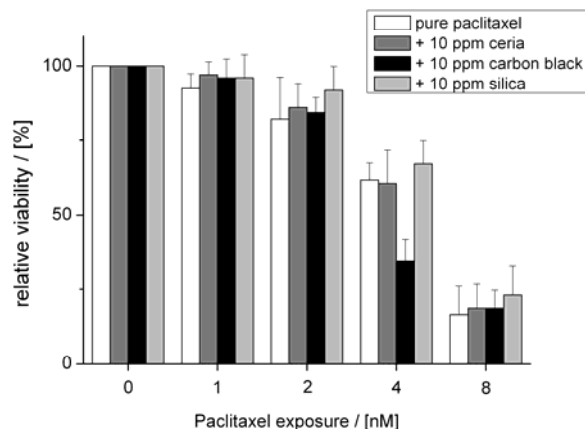
Figure 1: Relative cell viability (MTT) after 3 day of exposure to paclitacel. Additional exposure of 10 ppm ceria (dark gray bars), carbon black (black bars), and silica (light gray bars) were compared to single paclitaxel exposure (white bars). Mean±S.E.M over values of three independent experiments.

This study shows that beyond mere physico-chemical properties, nanoparticle cytotoxicity can also result in complex and unexpected mechanism.
The here presented co-transport of classical toxins on the back of nanoparticles into cells is another most astonishing property of engineered nanoparticles.

References

[1] Limbach, L.K., R.N. Grass, W.J. Stark Chimia, *in print*
[2] Limbach L.K., P. Wick, P. Manser, R.N. Grass, A. Bruinink, W.J. Stark, Environ. Sci. Technol., 41, 4084-9 (2007).
[3] Brunner T.J., P. Wick, P. Manser, P. Spohn, R.N. Grass, L.K. Limbach, A. Bruinink, W.J. Stark, Environ. Sci. Technol., 40, 4374-81 (2006).
[4] Limbach L.K., Y. Li, R.N. Grass, T.J. Brunner, M.A. Hintermann, M. Muller, D. Gunther, W.J. Stark, Environ. Sci. Technol., 39, 9370-76 (2005).

Seasonal and dimensional differences in the proinflammatory potency of atmospheric particulate matter. Comparison of in vitro results with clinical effects in children exposed to the same particles from the same urban area. The Milan Prolife Project.

F. Cetta[1], M. Sala[2], R. Accinni[3], A. Dhamo[1], R. Zangari[1], L. Moltoni[1], E. Bolzacchini[4], M. Gualtieri[4], P. Mantecca[4], M. Camatini[4]

[1] Department of Surgery, Research Doctorate in Oncology and Genetics, University of Siena, 53100,Siena, Italy
[2] Department of Pediatrics, University of Milan, University of Milan ,20122,Milan, Italy
[3] CNR Institute of Clinical Physiology, 20162, Milan, Italy
[4] Department of Environmental Sciences, University of Milano-Bicocca,20126 Milan, Italy

Keywords: air pollution, urban pollution, health effects of aereosols, lung-particle interaction

One issue of major concern in the evolution of adverse health effects from environment pollution is to compare data from in vitro studies and experimental models in animals to clinically evident effects in humans. A wide range of research studies- both basic and clinical studies- have been performed, trying to relate pollution events to hospital admissions and/or major respiratory or cardiovascular adverse effects.

In particular, hospital admissions to the main pediatric service of Milan were recorded, analysed and compared with daily and seasonal variation in PM_{10} and $PM_{2,5}$ concentration, during 4 consecutive periods: winter 2007-summer 2007-winter 2008-summer 2008. There were 390 acute pediatric admissions in 2008. Respiratory disease were classified as follows: asthma or asthma like disorders; upper respiratory diseases (pharyngitis, pharingotonsillitis, otitis); lower respiratory diseases (bronchitis, bronchiolitis and pneumonia).

During 2007, there were in total 391 pediatric admissions for respiratory disease; 192 (99 males and 93 females) during the 1st winter semester, and 199 during the 2nd semester.

The mean age (SD) was 31 months +/- 38.1, range 23 mo-15y. The mean hospital stay was 5 days +/- 2.6, range 1-17 days. There was 12.7% asthma or asthma related admission; mo 55.8% due to lower respiratory illness, and 31.5 % due to upper respiratory disease. The daily coverage of PM_{10} concentration during the 1st semester 2007 was 48.3 +/- 17.9 mcg/m^3 median 47. There were 107 (59.1%) days with at least hospital admission. The mean daily concentration of PM was higher in days with (107) than without (n=74) hospital admissions (p=0.032 or < 0.05).

In addition, the human bronchial epithelial cell-line BEAS-2B and the human alveolar epithelial cell A549 were seeded at a concentration of 80.000 cell/well and treated after 48 hrs with both summer and winter PM 10 and PM 2.5 sampled in the main Milan urban area.

Cytotoxicity was assessed by HOECHST 33342/91 staining. Viability was calculated as the sum of viable mitotic cells. Release of the proinflammatory citockine IL was measured by sandwich ELISA assay. Oxidative stress was evaluated by chemiluminescence and genotoxicity was assessed by comet assay. It was found that whereas A549 cell viability was not significantly reduced after summer and winter PM exposure, summer PM had no significant effects on BEAS-2B viability, whereas winter PM treatment induced a decrease in cell viability, both at the dose of 25 and 50 mcg/cm^2. In addition, whereas both winter and summer $PM_{2.5}$ produced only a slight increase in IL 8 release, winter PM_{10} induced a 5 fold increase in IL 8 release in treated cells, and summer PM_{10} induced a 20 fold increase (p< 0,05) in IL 8 expression, which was reduced to 11- fold- increase after polimixin treatment.

In conclusion, in vitro studies using PM_{10} and $PM_{2,5}$ sampling from different seasonal samples seem to correlate with clinical data in children exposed to the same type and concentration of PM during winter and summer season. In particular, BEAS-2B resulted more responsive to PM treatment than A549. Winter PMs were more cytotoxic than summer PMs; Summer PM_{10} had a higher proinflammatory potential, which could be partly due to biological components (LPS).

Accordingly, children acute admissions were significantly affected by pollution data, with increased admission during winter time, namely for upper air tract infections, whereas lower tract inflammation and acute admission for asthma were more frequent during the spring: summer season.

Even if great caution is required when trying to relate in vitro studies to clinical effects in humans, the present report is the first study in a large urban area trying to compare "in vitro" and clinical effects of the same urban particles in different seasons of the year.

Acute cardiovascular effects associated with air pollution: a new pathogenetic pathway in patients with chronic obstructive pulmonary diseases (COPD)

F. Cetta[1], G. Schiraldi[2], M. Sala[3], R. Zangari[1], A. Dhamo[1], L. Moltoni[1], P. Laviano[1], F. Cisternino[1], A. Azzarà[1], G. Malagnino[1], P. Favini[1,4], L. Allegra[2]

[1] Department of Surgery, Research Doctorate in Oncology and Genetics, University of Siena, Nuovo Policlinico "Le Scotte", viale Bracci, 16, I-53100 Siena, Italy
[2]Toracopulmonary and Cardiovascular Department and [3]Department of Pediatrics, University of Milan, Via Festa del Perdono,7,20122,Milan, Italy
[4]Assessorato alla Salute, Comune di Milano, Italy

keywords: urban pollution, field measurements, health effects of aereosols, hospital, lung-particle interaction

Increased exposure to air pollution causes both acute and chronic inflammation that could adversely affect the cardiovascular system. A working hypothesis to explain PM related cardiovascular (CV) damage includes effects of systemic inflammation, shown by elevated C reactive protein, blood leukocytes, platelet, fibrinogen and increased plasma viscosity. Repeated exposure to PM may exacerbate the vascular inflammation of atherosclerosis and promote plaque development or rupture, so determining acute effects such as angina or myocardial infarction. Another hypothesis, in addition to indirect effects mediated by initial pulmonary inflammation, is direct action of particles that have become blood born, after passing through the alveolar-interstitial filter (Mills, 2009). However, in most of cases, acute severe CV effects occur within 1-2 hours after the PM pollution peak, and it is unlikely that these mechanisms, which require systemic inflammation and activation of liver mechanisms, could be responsible for early cardiac arrest(Cetta, 2008).

The aim of the present study has been to evaluate whether other mechanisms could be responsible or co-responsible for acute CV effects.

Methods: A cross-sectional survey was performed, comparing daily values of PM in Milan, measured by stationary monitors with the rate of hospital admission to all the city hospital because of respiratory and cardiovascular diseases during 2008. In addition, in a small panel study, two 2-week on field campaigns in different seasons of the year were performed to assess PM10, PM2,5 and PM1 concentrations, both by optical and gravimetric samplers. Environment pollution data were compared with the clinical and functional status of two groups of old patients living in public hospices, located close to o far from main cross roads. In addition to patient history, spirometry, ECG, laboratory examination, analysis of exhaled breath condensate (EBC) were performed in all these subjects.

Results: More than 20.000 patients had hospital admission because of respiratory or CV complications during 2008. In particular, acute admissions to hospital for CV diseases during pollution peaks were more frequent in patients with previous COPD. In the panel study, blood samples showed an increased C protein concentration and cytokine production in subjects with COPD. In a small subgroup of these patients (n=38, age 82±9) an increase in plasma total Cysteine (a pro-oxidant substance) and an alteration in redox balance and cell homeostasis were also observed.

Conclusion: We hypothesize that another mechanism could also occur, in addition to ROS mediated systemic inflammation and autonomous system alteration via sensory nerves in the respiratory tract, in patients with COPD, chronic air tract infection or emphysema. In these patients, increased PM inhalation during pollution peaks could determine increased occurrence of endoluminal "plugs", consisting of mucus, bacteria, cellular debris and PM particles, which facilitate acute obstruction of a variable proportion of bronchiolo-alveolar ducts, in already compromised patients. This could determine, in turn, further restriction of the respiratory functions with possible redistribution into a lesser pulmonary area of the blood flow to lung. In addition, because of segmental bronchial obstruction, sudden distension of the bronchial system, cranially to the obstruction site, could also occur with possible irritation, by sudden stretching, of the vagal fibers running over the bronchioli, and possible alteration of the vagal tone and cardiac rhythm.

Mills, N.L., Donaldson, K., Hadoke, P.W., Newby, D.E., et al., (2009). *Nat Clin Pract Cardivasc Med*,6,36-44.
Cetta, F., Laganà, K., Kola, E., Dubini, G., (2008). *European Aerosol Conference, Thessaloniki, AbstractT09A011O*.

"Aging" of ultrafine particles (UFP), and quantitative daily estimation of UFP determining severe adverse health effects, because of increased surface reactivity of nanoparticles.

A. Dhamo[1], F. Cetta[1], M. Sala[2], E. Bolzacchini[3], R. Zangari[1], F. Cisternino[1], A. Azzarà[1], G. Malagnino[1], G. Schiraldi[4]

[1] Department of Surgery, Research Doctorate in Oncology and Genetics, University of Siena, Nuovo Policlinico "Le Scotte", viale Bracci, 53100,Siena,Italy
[2] Department of Pediatrics and [4]Toracopulmonary and Cardiovascular Dept, University of Milan, Via Festa del Perdono,7,20122,Milan,Italy
[3] Department of Environmental Sciences, University of Milano-Bicocca,20126 Milan, Italy
keywords: air pollution, nanoparticles, surface reaction, health effects of aereosols

Ambient ultrafine particles (diameter <100 nm) are currently considered among the most toxic pollutants, due to the increased ratio surface/mass and the increased number of particles (interacting with host tissues), each of which capable of individual intrinsic toxicity. Therefore, particle surface area for particles of different sizes, but of the same chemistry, has been suggested as a better dosimetric than is particle mass or particle number. Nanoparticles have an increased biological activity, due to an increased interaction with cells and subcellular structures than larger – sized particles and their biokinetics is also likely different, because of additional possibility of translocation, such as through skin, lymphatics and neural routes.

The aim of the present study has been to evaluate if "aging" of the various components of PM, i.e. relative their time lapse in one mode, before turning into another could affect health outcome in humans.

In the City of Milan, Italy, both cross sectional and longitudinal studies have been performed, in particular in children attending schools and in old people living in hospices, to relate air pollution to clinical outcomes. In particular, clinical laboratory and instrumental functional data of enrolled subjects were compared with indoor and outdoor measurement of PM, both by optical and gravimetric samplers size differentiation of PM as PM10, PM 2,5, PM1, and PM0,1 and subsequent chemical speciation of the various components, one of our main objective was the daily and seasonal calculation of the rate PM0,1 to PM10 in various areas of the city and comparison with adverse health effects in susceptible populations (children and old people).

The following results were obtained. There was a striking difference in PM_{10}, $PM_{2,5}$ and PM1 concentration not only according to seasons, but also in the various hours of the day. In particular, PM levels varied according to the site of measure (close or far from main crossroads) to day-night alternate or to season (PAH$_S$ were 14 fold less frequent in summer than in winter). Interestingly, during children entrance to their school, sited in a park, in the time lapse between 8,15 and 8,45 in the morning, PM_{10} levels had a peak up to 1000 μg/m^3, i.e. 20 folds greater than the prefixed daily threshold for PM_{10} values. The extreme variability, not only of PM mass concentration, but also of its composition, namely due to the frequent and almost instantaneous turning from one mode to another (UFP to PM1 or PM2,5) in the various hours of the same day, suggesting the necessity of hourly measures in metropolitan areas. It also underlines, once again, the complexity of environmental pollution and of the mutual interactions among various components and various hosts.

It is suggested that, in addition to individual susceptibility (the sum of genetic predisposition plus personal history), which is probably the main determinant of health effects from pollutants, aging of UFP also could be a major determinant of the still unclear health effects of UFP in metropolitan areas. In fact, even if traffic related pollutants are of great importance and differ among various areas of the city, the enormous impact of nanosized particles, which could be inferred by theoretical models, is probable hampered, or dramatically reduced, by the rapid turnover and physicochemical evolution of UFPs. Interestingly, UFPs every 3 min. get out from the UFP scale, so avoiding bulk formation, i.e. the maximum concentration is that relative to a 3 min. lapse and not to 24 h, i.e. the sum of multiple 3 min intervals. In fact, UFP rapidly lapse turn towards the fine and/or coarse mode of accumulation, due to immediate aggregation, so loosing or decreasing their deleterious biological potential, capable of severe health effects from a theoretical point of view, but probably less dangerous at usual and actual ambient concentration of UFP.

Particle-extract-induced cytotoxicity of traffic-related particles

H.C. Chaung[1], S.J. Chen[2],*, K.L. Huang[2], T.H. Yang[3], C.C. Lin[2], W.Y. Lin[4] and J.H. Tsai[2]

[1] Department of Veterinary Medicine, National Pingtung University of Science and Technology, 91201, Taiwan
[2] Department of Environmental Engineering and Science, National Pingtung University of Science and Technology, 91201, Taiwan
[3] Graduate Institute of Biotechnology, National Pingtung University of Science and Technology, 91201, Taiwan
[4] Institute of Environmental Planning and Management, National Taipei University of Technology, 10608, Taiwan

Traffic emission is regarded as one of the major contributors to the high concentrations of polycyclic aromatic compounds (PACs) in urban air (Wild & Jones, 1995). Several epidemiologic studies have demonstrated the association of ambient ultrafine particles (UFPs) with adverse respiratory and cardiovascular effects, resulting in morbidity and mortality in susceptible parts of the population (Peters, et al., 1997; Penttinen et al., 2001; von Klot et al., 2002). Still, little attention has been paid to the cytotoxicities of traffic-related nanoparticle-bound PACs (10–56 nm, with health significance). Accordingly, this work elucidates the particle-extract-induced cytotoxicity in the size-resolved particles that were collected beside a busy road using a micro-orifice uniform deposition impactor (MOUDI) and a Nano-MOUDI. The particle extracts were tested using an alveolar macrophage (AM) assay to examine the cytotoxicities derived from the corresponding reduction in cell viability of AMs.

The cytotoxicity assay was performed using porcine AMs as an in vitro screening system. In the cell screening system, bleomycin (dissolved (2 U mL^{-1}) in a phosphate buffer solution) which can cause alveolar epithelial cell death was used as a positive control. These AMs were stained with propidium iodide (PI) solution. The reduction in cell viability (RCV) of AMs was evaluated by counting the PI-positive cells using a flow cytometer (Beckman Coulter, USA). The RCV of AMs in each treated sample was calculated according to the following formula: RCV (% control) = (% of PI-positive cells in treatment − % of PI-positive cells in control)/% of PI-positive cells in control."

Table 1 shows the cytotoxicity responses induced by particle extracts. The cells treated with extracts from 0.010–0.18 and 5.6–18 µm particles had greater mean RCV values than those from 0.18–5.6 µm particles (p < 0.05). It is interesting to find that the mean RCV value (128±21%) for bleomycin (BLM) was statistically similar to those for the 0.032–0.056, 0.056–0.1, and 0.1–0.18 µm particles. Among the extracts of the tested size-resolved particles, one of the 0.01–0.018 µm (10–18 nm) nanoparticles exhibited the greatest mean RCV value (381±75%), which was also statistically higher than that of BLM (p < 0.05). Accordingly, it is inferred that among the tested particle extracts containing PACs, the one from the 10–18 nm nanoparticles displayed the highest AM cytotoxicity (also higher than the BLM-induced one); furthermore, those from the 0.032–0.056, 0.056–0.1, and 0.1–0.18 µm particles were similar to that from BLM.

For the particles in each of the 13 size ranges, the cytotoxicity of particle extracts was significantly higher ($p < 0.05$) for the nano (particularly the 10–18 nm)/ultrafine particles than for the coarser particles. Mossman et al. (2007) reported that ultrafine particles are more critical than $PM_{2.5-10}$ for particle toxicity although $PM_{2.5-10}$ might also be toxic. The phagocytic activity inhibition of macrophagic cells is higher for ultrafine particles than for coarse particles (Renwick et al., 2001).

Table 1. RCV of alveolar macrophages for the particle extracts.

Particle extracts	RCV (%)
0.010–0.018 µm	382±75.9
0.018–0.032 µm	47.4±5.48
0.032–0.056 µm	63.2±3.67
0.056–0.1 µm	76.0±9.47
0.1–0.18 µm	67.6±12.4
0.18–0.56 µm	15.4±3.15
0.32–0.56 µm	8.42±0.93
0.56–1.0 µm	6.39±0.87
1.0–1.8 µm	7.05±0.75
1.8–3.2 µm	12.6±0.69
3.2–5.6 µm	8.19±1.12
5.6–10 µm	28.2±3.49
10–18 µm	56.3±5.71
BLM	128±21.0

Mossman, B. T., Shukla, A., & Fukagawa, N. K. (2007). Free Radic. Biol. Med., 43, 504–505.

Penttinen, P., Timonen, K.L., Tiittanen, P., Mirme, A., Ruuskanen, J. & Pekkanen, J. (2001). Eur. Resp. J., 17, 428–435.

Peters, A., Wichmann, H.E., Tuch, T., Heinrich, J. & Heyder, J. (1997). Am. Respir. Crit. Care Med., 155, 1376–1383.

Renwick, L. C., Donaldson, K., & Clouter, A. (2001). Toxicol. Appl. Pharmacol., 172, 119–127.

von Klot, S., Wolke, G., Tuch, T., Heinrich, J., Dockery, D.W. & Schwartz, J. (2002). Eur. Respir. J., 20, 691–702.

Wild, S.R. & Jones, K.C. (1995). Environ. Polut., 88, 91–108.

Air pollution from Milan affects *in vitro* sperm quality more in individuals with previous varicocele than in normal subjects or in rabbit sperm cells

F. Cetta[1], G. Collodel[1,2], E. Moretti[1,2], M. Geminiani[2], C. Castellini[3] A. Dhamo[1], G. Malagnino[1], A. Azzarà[1], F. Tani[1], E. Bolzacchini[4], M. Camatini[4].

[1] Department of Surgery, Research Doctorate in Oncology and Genetics and [2]Department of Biomedical Sciences, Center for Research and Therapy of Male Infertility, University of Siena, Nuovo Policlinico "Le Scotte", viale Bracci, 16, I-53100 Siena, Italy
[3]Department of Zootechnical Science, University of Perugia, Perugia, Italy
[4] Department of Environmental Sciences, University of Milano-Bicocca, Piazza dell'Ateneo Nuovo, 1,20126 Milan, Italy

Keywords: air pollution, urban pollution, field measurements, health effects of aereosols.

Aim of the study: The aim of the present study has been to investigate *in vitro* whether environmental pollution, and in particular samples of PM10 and PM 2,5 from Milan, may affect human and/or rabbit sperm quality.

Methods: Daily levels of PM_{10} and $PM_{2.5}$ and PM_1 (diameter <10 μm, 2.5 μm, 1 μm respectively) were measured by an OPC detection unit, both outside primary schools for children and 2 hospices for retired people in Milan, Italy.

In particular, an OPC 1.108 Dustcheck detector (Grimm) was used for indoor measurements, whereas as OPC 1.107 "Environcheck" model (Grimm) was used for outdoor analysis. Both were able to estimate PM1, PM2,5 and PM10 concentration. In addition, samples by low volume gravimetric detectors were also obtained (EPA system 16,67 l/min[-1] Tecora, Milan Italy; or EU system 33,34l/min[-1] , Zambelli, Milan Italy). Usually Teflon filters (47 mmØ, 2 μm, Pall Gilman, USA) were used, but sometimes other supports (quartz, polycarbonate), were also used. Samples from these filters were used after sonication in sterile phosphate buffer saline (PBS).

Aliquots of these samples at a concentration of 10/50/75μg/ml were incubated for 4 or 6 hours at 37°C with rabbits spermatozoa, and sperm cells from humans with normal sperm quality and men with varicocele (Collodel, 2008).

Results: Treatment with PM2,5 at concentration of 10,50 and 75 μg/dl did not show evident damage in rabbit spermatozoa when the samples were incubate for 4 and 6 hrs. On the contrary, 50 μg/dl caused in human samples a decrease in progressive motility and an increase in the percentage of necrosis and apoptosis. Samples from patients with abnormal semen parameters (varicocele) showed even worse semen quality.

In fact, they showed reduced semen quality already after 4hrs of incubation at a concentration of 10μg/ml. The mean ± standard deviation of sperm motility was 11±4.08. Mean values of FI (Fertility Index) also were strongly reduced (from 726004,5 to 340026,75). Moreover, Annexin V/PI assay showed an increase in the percentage of apoptotic and necrotic cells. A further decrease of sperm quality (progressive motility decreasing from 20% to 4%, necrosis from 33% to 53 % and FI from 726004,5 to 162500,25) was observed after 4-hour incubation at a concentration of 50μg/ml.

Conclusion: Present data "*in vitro*" show a progressively greater damage to the reproductive function, passing from rabbit sperm to normal human sperm, and to sperm from men with altered semen.

Sperm alterations and PM related damage to reproductive function could be a suitable model to make comparison of health damage among various types and/or concentrations of pollutants and/or various types of hosts (Cetta, 2009).

Collodel, G., Moretti, E., (2008). *J Androl*. 29,106-114.

Collodel, G., Geminiani, M., Cetta, F., Camatini, M., Bolzacchini, E., Renieri, T., Mourvaki, W., Castellini, C., Moretti, E. (2008). *European Aerosol Conference (EAC), Thessaloniki-Greece, Abstract T09A006O*.

Cetta F., Dhamo A., Moltoni L., Bolzacchini E (2009).. *Environ Health Perspect. In press*

Oxidative potential of logwood and pellet burning particles assessed by a novel profluorescent nitroxide probe

B. Miljevic[1,5], N.K. Meyer[2,6], A. Keller[2], H. Burtscher[2], J. Good[3], A. Doberer[3], A. Lauber[3], T. Nussbaumer[3], M.F. Heringa[4], A. Richard[4], P.F. DeCarlo[4], A.S.H. Prevot[4], K.E. Fairfull-Smith[5], U. Baltensperger[4], S.E.Bottle[5] and Z.D. Ristovski[1]

[1]International Laboratory for Air Quality and Health, Queensland University of Technology, 4001, Brisbane, Australia
[2]Institute for Aerosol and Sensor Technology, University of Applied Sciences, 5210, Windisch, Switzerland
[3]Lucerne School of Engineering and Architecture, Lucerne University of Applied Sciences and Arts, 6048, Horw, Switzerland
[4]Laboratory for Atmospheric Chemistry, Paul Scherrer Institute, 5232, Villigen, Switzerland
[5]ARC Centre of Excellence for Free Radical Chemistry and Biotechnology, Queensland University of Technology, 4001 Brisbane, Australia
[6](now at) Laboratory for Energy Systems Analysis, Paul Scherrer Institute, 5232, Villigen, Switzerland

Keywords: biomass burning, health effects of aerosols, reactive oxygen species, profluorescent nitroxide

As a source of renewable energy, residential biomass combustion is regaining importance. As such, it presents a significant source of aerosol particle emissions in many countries. However, only a limited number of studies evaluating the potential toxicological impact resulting from biomass burning exist (Naeher et al., 2007). In general, ambient particulate matter (PM) has been associated with various adverse health effects. Oxidative stress caused by particle-bound reactive oxygen species (ROS) and generation of ROS at the sites of deposition has been widely accepted as a hypothetical mechanism for PM-related injury.

This study assesses the potential toxicological impact of particles produced by an automatic pellet boiler and a logwood oven, by using a novel profluorescent nitroxide probe BPEAnit. The probe is weakly fluorescent, but yields strong fluorescence emission upon radical trapping or redox activity. This makes it a powerful optical sensor for radicals and redox active compounds. Samples were collected by bubbling aerosol through an impinger containing 20 mL of 4μM BPEAnit solution, followed by fluorescence measurement. The combustion cycle consisted of cold start (startup and stable burning phase), restart (warm start) and bad burning (air inlet closed). During each of combustion phases, both test and HEPA filtered control samples were collected in impingers. PM was characterised using a Tapered Element Oscillating Microbalance (TEOM), a Scanning Mobility Particle Sizer (SMPS), a Diffusion Size Classifier (DiSC), a Fast Mobility Particle Sizer (FMPS) and a High Resolution Time-of-Flight Aerosol Mass Spectrometer (HR-ToF-AMS). The aerosol sample was delivered to the instruments and impingers via a dual stage heated (150°C) ejector dilution system. Based on the difference of fluorescence signal between test and control sample, the amount of ROS for each phase was calculated and normalized to the PM mass measured by the TEOM.

Figure 1 shows the calculated ROS concentration for four distinctive phases of logwood burning. Cold start burning resulted in a much higher amount of reactive species per unit of PM mass than warm start burning. In addition, sampling of logwood burning emissions after passing through a thermodenuder at either $150^{o}C$ or $250^{o}C$ did not result in a significant increase of fluorescence signal. This clearly indicates the importance of organics in PM-related toxicity. Particle emissions from the pellet boiler, although of similar mass concentration, were not observed to lead to an increased fluorescence signal during any of the combustion phases. This indicates a lower toxicological potential for particulate emissions from pellet boilers as opposed to logwood burning.

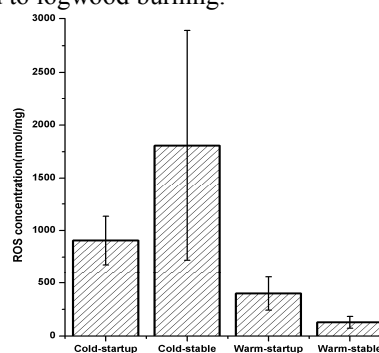Figure 1. Average ROS concentrations for cold and warm start of logwood burning particle emissions.

The obtained values for logwood burning emissions are relatively similar to diesel exhaust particles, but $10-50$ times higher than sidestream cigarette smoke.

Naeher, L.P., Brauer, M., Lipsett, M., Zelikoff, J.T., Simpson, C.D., Koenig, J.Q., Smith, K.R., (2007). *Inhalation Toxicology* 19, 67-106.

Quantification of ROS related to particle emissions generated by a diesel engine using ethanol substitution

B. Miljevic[1,3], N. Surawski[1,2], R. Situ[2], K.E. Fairfull-Smith[3], S.E. Bottle[3], R. Brown[2] and Z.D. Ristovski[1]

[1]International Laboratory for Air Quality and Health, Queensland University of Technology, 4001, Brisbane, Australia
[2]School of Engineering Systems, Queensland University of Technology, 4001, Brisbane, Australia
[3]ARC Centre of Excellence for Free Radical Chemistry and Biotechnology, Queensland University of Technology, 4001 Brisbane, Australia

Keywords: biofuels, health aspects of aerosol, reactive oxygen species, profluorescent nitroxides

The global fuel crisis and the need to reduce greenhouse gases have led to increased efforts to develop alternatives for the current fuel sources. Due to its renewable nature and reduced particulate emissions (reviewed in Hansen et al., 2005 and Ribeiro et al., 2007) biofuels were found to be a good substitute. Despite the significant amount of research related to the emissions characteristics of dual-fuelled diesel engines, not much is known about the health related properties of these emissions.

By detecting and quantifying the amount of PM-related Reactive Oxygen Species (ROS), this study aimed at assessing the potential toxicological impact of particulate matter (PM) coming from ethanol fumigated emissions compared to pure diesel emissions. For this purpose, a novel profluorescent nitroxide probe (BPEAnit) developed at Queensland University of Technology was used. BPEAnit is a weakly fluorescent compound, but yields strong fluorescence upon radical trapping or redox activity. This makes it a powerful optical sensor for radicals and redox active compounds. Samples were collected by bubbling aerosol through an impinger containing 20 mL of 4μM BPEAnit solution and followed by fluorescence measurement.

In this study, a four cylinder Ford 2701C Pre-Euro I diesel engine coupled to a dynamometer was used. Four ethanol fumigation percentages were employed, namely E0 (neat diesel), E10 (10% of ethanol), E20 (20% of ethanol) and E40 (40% of ethanol). The engine was run at idle, 25%, 50% and full (100%) load, all at intermediate speed (1700 rpm). The aerosol sample was delivered to the instruments and impingers via a two stage, unheated dilution system. For each fuel type and test mode, both the test and HEPA filtered control sample were collected in impingers. The size of particulates was characterized using a Scanning Mobility Particle Sizer (SMPS) and gas emissions (NOx, CO, hydrocarbons) were monitored using a gas analyser.

For particle emissions from both neat diesel and ethanol fumigation, generated under different engine loads, a strong nucleation mode was observed, with a CMD in the range of 30-50 nm. The only exception were emissions coming from pure diesel generated under full engine load – in this case particles were in the accumulation mode with a CMD of 83 nm.

Based on the difference of the fluorescence signal between test and control sample, the amount of ROS for each test load and ethanol percentage was calculated and normalised to the mass of PM derived from SMPS scans. Results are shown in Figure 1. As can be seen, there is a decrease of ROS concentration with the increase of engine load with substantially lower ROS concentration of particle emissions generated under 100% engine load (particle in accumulation mode). This suggests that much higher concentration of ROS is present in the nucleation mode. Fumigation of 10 and 20 % ethanol did not result in significant ROS concentration compared to neat diesel (Figure 1 B). In contrast, 40% ethanol substitution resulted in a tripling of the ROS concentration relative to the baseline diesel case.
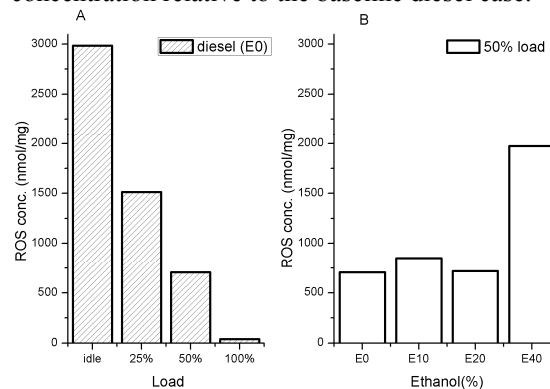
Figure 1. A) ROS concentration related to particle emissions running on pure diesel and four different loads; B) ROS concentrations for 50% engine loads and three different ethanol substitutions.

Results from measurements on a newer EURO III diesel engine will also be presented.

Hansen, A.C., Zhang, Q. ,Lyne, P.W.L., (2005). *Bioresource Technology* 96, 277-285.

Ribeiro, N.M., Pinto, A.C., Quintella, C.M., da Rocha, G.O., Teixeira, L.S.G., Guarieiro, L.L.N., do Carmo Rangel, M., Veloso, M.C.C., Rezende, M.J.C., Serpa da Cruz, R., de Oliveira, A.M., Torres, E.A. ,de Andrade, J.B., (2007). *Energy & Fuels* 21, 2433-2445.

Physico-chemical and toxicological characterization of welding fumes from different processes

A.C. John[1], H. Kaminski[1], M. Wiemann[2], J. Bruch[2], C. Eisenbeis[3], R. Winkler[3], M. Gube[4], P. Brand[4], T. Kraus[4] and T.A.J. Kuhlbusch[1]

[1] IUTA e.V., Air Quality & Sustainable Nanotechnology Unit, 47229 Duisburg, Germany
[2] IBE GmBH, Institute for Lung Health, 45768 Marl, Germany
[3] Schweisstechnische Lehr- und Versuchsanstalt SLV, 47057 Duisburg, Germany
[4] Institute for Occupational Medicine, RWTH Aachen University, 52074 Aachen, Germany

Keywords: occupational exposures, ultrafine particles, $PM_{0.4}$-sampler, FMPS, NSAM.

About one million workers worldwide are engaged in welding processes, where they are exposed to a complex mixture of inhalable pollutants. Adverse effects in the respiratory system can occur due to this occupational exposure. Currently, legislative limits only exist for inhalable and alveolar particles. However, epidemiologic and toxicologic studies show that especially ultrafine particles (UFPs) are related to adverse effects on human health.

Although welders can be exposed to very high concentrations of UFPs, no standards exist concerning metrology or limits. In order to enable an assessment of possible health effects and a risk management for different welding processes and their variations, a study "Nanoscaled particles at welding fume workplaces" was carried out, where different welding processes were investigated with regard to physical and chemical characterization as well as toxicologic effects of the welding fume particles, together with occupational health examinations of the exposed workers.

Twelve different welding processes / process variations where chosen for the analyses, taking into account market share and toxicological relevance, among others. All welding experiments were performed at the welding training and research centre (SLV) in Duisburg, Germany.

As welding produces quickly changing emissions, measurement equipment with a high time resolution is needed. Therefore, a Fast Mobility Particle Sizer (FMPS) was used to determine particle size distributions. The surface area concentration deposited in the alveolar region of the lung was measured with a Nanoparticle Surface Area Monitor (NSAM), and particle number concentrations were monitored with a water-based and a butanol-based condensation particle counter (UWCPC and UCPC). Mass concentrations were determined with a newly designed $PM_{0.4}$-High Volume Sampler, together with occupational standard stationary and personal PM_4-samplers. Chemical analyses were conducted for Fe, Mn, Cr, Ni, Ti, Cu, Zn, Pb, Al, Sn and Mo. Morphological characterization of the particles by REM analyses was carried out on special substrates using a Nanometer Aerosol Sampler (NAS).

During the study, different variations (shielding gases, materials, arc types) of gas and shielded metal arc welding were characterized. $PM_{0.4}$-mass concentrations varied by a factor of ca. 7, whereas alveolar surface area and number concentrations varied by factors of about 70 and 50, respectively. During all welding, particle size distributions showed two modes, but varying in their relative importance (see figure 1). The first mode was consistently at ca. 10 nm and the second one varying from 100-150 nm. The above mentioned analysed metals accounted for 17% to 55% of the $PM_{0.4}$ mass.
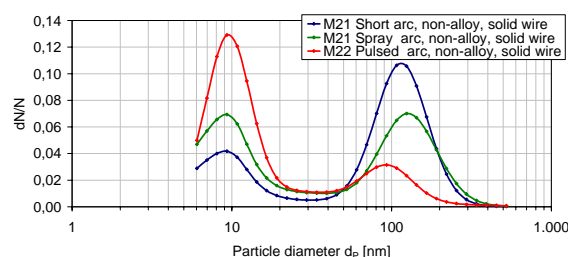

Figure 1. Examples for the three types of size distributions obtained during the welding study.

The toxicity of the welding fumes was tested in a multi dose approach from the $PM_{0.4}$-teflon filter samples. Alveolar macrophages were used for the biological in vitro tests. The results are based on a vector model including the following parameters: release of glucuronidase, functional cell damage, release of mediators (TNFα) and release of reactive oxygen species (ROS). The toxicity of the twelve different welding fumes varied significantly.

In the presentation, the results of the welding particle characterization linked to the in vitro toxicity testing will be discussed in detail. Additional toxicological in vivo and occupational studies will be conducted on three samples which were selected on the basis of the physico-chemical characterization and in vitro toxicity testing.

Analgesic effect from ibuprofen nanoparticles inhaled by male mice

A. A. Onischuk[1], T. G. Tolstikova[2], I. V. Sorokina[2], N. A. Zhukova[2], A.M. Baklanov[1], V. V. Karasev[1], O. V. Borovkova[1], G. G. Dultseva[1] V. V. Boldyrev[3,4], V. M. Fomin[5]

[1]Institute of Chemical Kinetics & Combustion, RAS, Novosibirsk, 630090, Russia
[2]Institute of Organic Chemistry, RAS, Novosibirsk, 630090, Russia.
[3]Scientific and Education Centre "Molecular design and ecologically safe technologies"
    Novosibirsk State University, 630090, Russia.
[4]Institute of Solid State Chemistry & Mechanochemistry, RAS, Novosibirsk, 630090, Russia
[5] Institute of Theoretical and Applied Mechanics, RAS, Novosibirsk, 630090, Russia

Keywords ibuprofen, nanoparticles, aerosol drug administration, particle lung deposition, mice, analgesic effect.

Aerosol lung administration is a convenient way to deliver water-insoluble or poorly soluble drugs, provided that small-sized particles are generated. This work studies the analgesic effect from the aerosolized ibuprofen nanoparticles. Ibuprofen is a nonsteroidal, chiral, anti-inflammatory drug that inhibits the enzyme cyclooxygenase and thus acts as an analgesic. We show for the outbred male mice that the pulmonary administration of ibuprofen nanoparticles requires a dose which is 3 to 5 orders of magnitude less than that for the orally delivered particles at the same analgesic effect.

The inhalation scheme includes a flow aerosol generator, plastic boxes for mice, filters, diluters, flow control equipment and aerosol spectrometer (Fig. 1). The aerosol evaporation - condensation generator consisted of a horizontal cylindrical quartz tube with an outer heater. Argon flow was supplied to the inlet and aerosol was formed at the outlet. The particle mean diameter and number concentration varied from 10 to 100 nm and $10^3 - 10^7$ cm^{-3}, respectively (as measured by an automatic diffusion camera). The chromatographic and UV analysis showed that the aerosol particles were chemically identical to the maternal substance (i.e. there was no thermal decomposition or oxidation during evaporation). The X-ray diffraction analysis showed that the nanoparticle crystal phase (racemic ibuprofen) was identical to that of the original ibuprofen powder. The analgesic effect of ibuprofen was estimated in the "acetic acid writing" test (one hour after the aerosol exposure, 0.1 ml of 0.75% acetic acid solution in water was injected intraperitoneally to the animals; five minutes after the injection, the number of writhes i.e. abdominal constriction followed by dorsiflexion and stretching of hind limbs occurring during a 3 min period was measured). The dose-dependent analgesic effect of aerosolized ibuprofen was studied in comparison with the oral treatment (Fig. 2). It was found that the dose for aerosol treatment is three to five orders of magnitude less than that required for oral treatment at the same analgesic effect. Accompanying effects

were moderate venous hyperemia and some emphysematous signs.
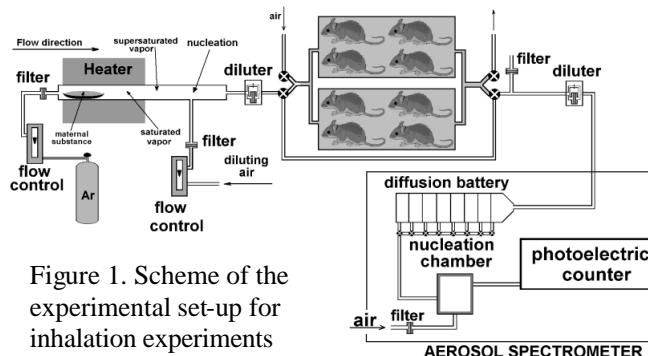
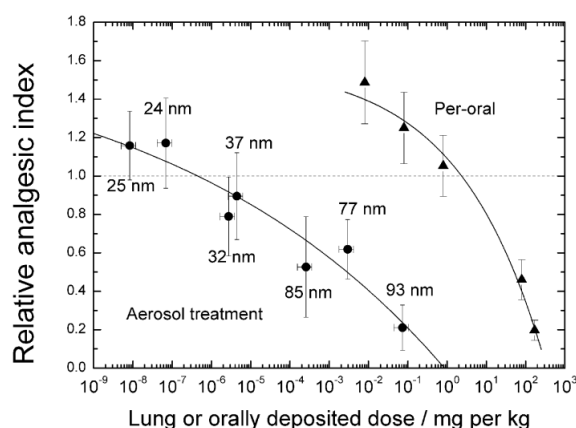Figure 1. Scheme of the experimental set-up for inhalation experiments

Fig. 12. Relative analgesic index (the ratio between the mean number of writhes for the aerosolized group and that for untreated group) vs. the lung deposited dose (circles). Triangles are RAI values for peroral treatment. Bars indicate standard error. Mean particle diameter is indicated for each inhalation point.

Physicochemical and *in vitro* oxidative characterisation of size fractionated PM at microenvironments with contrasting local emissions scenarios

K.J. Godri[1,2], I.S. Mudway[1], F.J. Kelly[1], R.M. Harrison[2], M. Strak[3], M. Steenhof[4], P. Fokkens[3], A. Boere[3], D. Leseman[3], K. Meliefste[4], G. Hoek[4], B. Brunekreef[4], E. Lebret[3], F. Cassee[3], I. Gosens[3], N.A.H. Janssen[3]

[1] King's College London, London, United Kingdom;
[2] University of Birmingham, Edgbaston, United Kingdom;
[3] RIVM (National Institute for Public Health and the Environment), Bilthoven, the Netherlands;
[4] IRAS (Institute for Risk Assessment Sciences), University of Utrecht, Utrecht, the Netherlands

Keywords: oxidative stress, chemical characterisation, lung-particle interactions, health effects of aerosols

The capacity of particulate matter (PM) to induce toxicity (in particular to elicit a respiratory and/or systemic inflammatory response) has been proposed to be a function of its oxidative potential (OP), i.e. the ability of PM to generate reactive oxygen species directly or indirectly resulting in oxidative injury to the lung. RAPTES (Risks of Airborne Particles: a hybrid Toxicological-Epidemiological Study) seeks to evaluate PM OP as a metric of biological activity so as to provide an aggregate measure of the particulate toxicity burden across size fractions in the ambient airshed. A measure of oxidative potential could provide a health relevant PM indicator that could be more informative than mass alone.

RAPTES is a multi-staged project. The aim of the first phase, was to comprehensively characterise the chemical (secondary inorganics, transition metals, elemental and organic carbon, polyaromatic hydrocarbons, quinones), physical and *in vitro* oxidant properties of PM collected at a range of traffic (continuous, stop and go, and diesel), industrial (harbor and steel mill) and rural/background (farm and urban background) microenvironments in the Netherlands. The physiochemical and *in vitro* oxidative signatures in local emission scenarios were compared to select a subset of locations for phase 2. Phase 2 consists of an exposure campaign using healthy young human volunteers and will be supplemented with cell culture experiments. The chemical, physical and oxidative properties of PM will also be assessed as determinants of observed acute respiratory and systemic responses experienced by the exposed populations. Results from the first phase of the RAPTES project will be presented.

Significant chemical composition variations were found between the different sites. The highest total and soluble transition metal concentrations (Cu, Fe, Ba, Sb) were found at the underground site for the fine and coarse fractions. In particular, total iron concentrations were on average very high ($PM_{2.5}$ 28 $\mu g\ m^{-3}$; $PM_{2.5-10}$ 31 $\mu g\ m^{-3}$), likely resulting from train wheel abrasion. Compared to the underground,
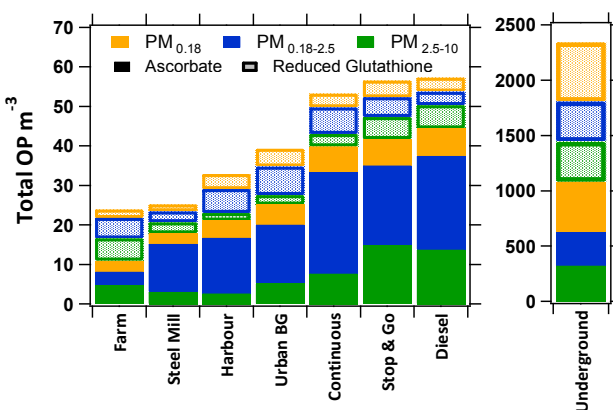

Figure 1 – Stacked size stratified total particulate OP m^{-3} measurements for all RAPTES sampling sites. This metric represents the sum of ascorbate (solid bars) and reduced glutathione (outlined bars) depletion in synthetic respiratory track lining fluid. Note underground measurements are presented on a different y-axis scale.

total and soluble concentrations of these metals, were significantly lower at all traffic sites. Trace metal concentrations were considerably lower at the background/rural and industrial sampling locations.

The OP of size segregated PM samples from RAPTES phase 1 sampling sites were assessed *in vitro*, based on their capacity to deplete ascorbate and reduced glutathione in synthetic respiratory tract lining fluid. An aggregate of these two oxidative potential measurements across all measured PM size fractions was calculated as the total atmospheric particulate toxicity calculated per unit volume of ambient air (OP m^{-3}). A trend to higher OP m^{-3} was identified at traffic sites, specifically the underground, while the lowest OP m^{-3} was found at the farm. Contrasts across microenvironments in PM toxicity were delineated by differing chemical composition profiles; traffic related components were identified as proxies of PM oxidative potential (Cu, Zn, elemental carbon).

Morphochemical characteristics and toxic potential of quartz particles in clay bricks factories and foundry plants

B. Moroni

Dipartimento di Scienze della Terra, University of Perugia, Piazza Università, 06123, Perugia, Italy

Keywords: industrial aerosols, size distribution, shape, electron microscopy, occupational health.

Since 1997 quartz has been classified as a Group 1 carcinogen (IARC, 1997). However, not all kinds of quartz are equally toxic and some distinction has to be made based on the inherent characteristics of the particles and the external factors affecting their biological activity (Donaldson & Borm, 1998; Fubini, 1998). The aim of this work was to characterize the quartz particles from clay brick factories and foundry plants in order to make some inferences on particle toxicology in these fields of industrial activity.

To this purpose, a total number of 35 bulk and aerosol dust samples from different working stations in clay bricks factories and foundry plants were analyzed by scanning electron microscopy coupled with image analysis, surface area measurement by stereoscopic reconstruction, EDS microanalysis and cathodoluminescence spectroscopy. A complete set of morphological parameters (*e.g.* perimeter, area, Feret diameter, axes length, elongation, roundness, compactness) and chemical data on a large number of particles along with a set of surface area measurements and structural informations on selected representative particles were obtained.

In the bulk materials different types of quartz, namely both authigenic (undefective) and igneous (defective) in the foundry quartz sands and from two distinct sedimentary basins in the brick clays, were found. Detailed examination of the morphological characteristics of quartz in the lines of production evidenced a significant reduction of the grain size from bulk material (clay, quartz sand) to airborne dust. In the meanwhile a change of micromorphology towards increasing complexity was evidenced in the foundry plants while the opposite tendency was evidenced in the clay brick factories.

A distinguishing feature of the airborne dust samples from the foundry plants is the presence of conspicuous amounts of fine and ultra-fine iron particles with spinel structure (magnetite, Fe_3O_4). Considering the role of magnetite in the redox cycling, the coexistence of inhalable metal and silica particles within the airborne dust points to a synergistic effect of both kind of particles in promoting cell damage.

Preliminary evaluation of the concentration and the solubility degree of Fe and other metals of potential health effect (Mn, Ni, Zn and Cr) by ICP-AES revealed these elements be enriched in the insoluble fraction. The low levels of solubility along with the small size of the airborne particles in the foundry plants are sufficient matter to consider this class of particles potentially harmful to health through direct diffusion into the cell and chemical release of the toxic elements in the cytosol.

In the light of all these points and in accordance with epidemiological studies (Goldsmith, 1994) greater occupational cancer risk of steel rather than of brick clay workers is postulated.

Donaldson, K. & Borm, P. J. A. (1998). *Ann. occup. Hyg.*, 42, 287-294.
Fubini, B. (1998). *Ann. occup. Hyg.*, 42, 521-530.
Goldsmith, D. F. (1994). In: *Reviews in Mineralogy, Vol. 29: Silica. Physical behaviour, geochemistry and materials applications*, The Mineralogical Society of America, 545-606.
IARC (1997). *IARC Monographs on the Evaluation of Carcinogenic Risks to Humans*, Vol. 68: Silica, some silicates, coal dust and para-aramid fibrils. Lyon, France: IARC Press.

Comparison of *in-vitro* toxicity and epidemiologically determined mortality risk for ambient particles using alternative particle metrics

O.O. Hänninen[1,2], I.Brüske-Hohlfeld[1], O. Schmid[3], W. Kreyling[3], T. Stoeger[3], P.E. Schwarze[4], J. Cyrys[1,5], M. Pitz[5], A. Peters[1], and H-E. Wichman[1]

[1]Helmholtz Zentrum München, Institute of Epidemiology, D-85764 Neuherberg, Germany
[2]National Institute for Health and Welfare, Department of Environmental Health, FI-70701 Kuopio, Finland
[3]Helmholtz Zentrum München, Institute of Inhalation Biology, D-85764 Neuherberg, Germany
[4]Norwegian Institute of Public Health, N-0403 Oslo, Norway
[5]: University of Augsburg, Environment Science Centre, D-86159 Augsburg, Germany

Keywords: Health effects of aerosols, Epidemiology, Particle size distribution, Lung deposition.

Toxicological testing is actively developed for risk assessment of new chemicals and materials including nanoparticles. The actual relationship of in vitro and animal toxicity and human population level health effects remains unknown until wide use of the substance.

The current work uses a known environmental health risk of ambient particles with a large body of epidemiological (Pope&Dockery, 2006) and toxicological (Brown *et al.*, 2004, Duffin *et al.*, 2007) evidence for a quantitative comparison of the toxicological observed effect levels and epidemiological responses for quantification of the protection level provided by a toxicological risk assessment.

Size resolved ambient PM measurements, population exposure attenuation and lung deposition model (Figure 1) are used to estimate ambient to indoor PM concentration and lung deposition relationships and to transform epidemiological relative mortality risk associated with ambient PM concentrations into corresponding dose-response relationship. Allometric scaling model is used for estimating human alveolar doses from the in-vitro toxicological doses.

Substantial epidemiological mortality risk (2-20% increases in daily all-cause mortality; Table 1) was estimated for toxicological lowest observed effect levels (LOEL) from selected studies. These LOELs corresponded to ambient concentrations of 34 – 340 $\mu g\ m^{-3}$, representing values ranging from normal levels to highest peaks observed in central European cities. At background mortality rate of 0.8%, typical for developed countries, these risks are realized at 1.6×10^2-1.6×10^3 deaths per million citizens (Table 1), figures which are 2-3 orders of magnitude higher than an acceptable risk of one in a million.

Toxicological testing has to be accompanied, besides a carefully selected and justified allometric scaling procedure, by an additional safety factor to account for population variation in sensitivity. Without evidence of lower toxicity epidemiological data on ambient particles may be used in a screening level risk assessment to support hazard identification.
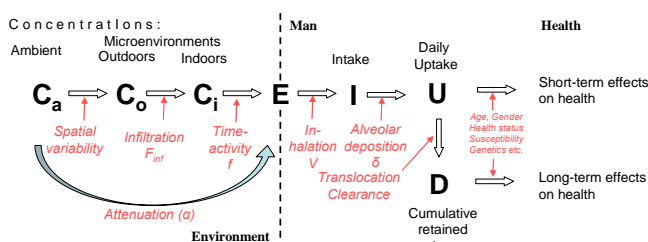
Figure 1. This is the sort of Figure which illustrates good agreement between theory and experiment.

Table 1. Estimation of the epidemiological relative risk corresponding to the experimental lowest observed effect dose of selected toxicological studies.

	Low	Central	High	Unit
Toxicological observed effect level (OEL)	10	30	100	$\mu g\ ml^{-1}$
Allometry (alveolar fluid volume)	5.7	5.7	5.7	ml
Acute human alveolar dose	57	171	570	μg
Epidemiological dose-response (RR)	0.36 %	0.36 %	0.36 %	/10 μg
Risk (R=$RR_D \times D$)	2.05 %	6.2 %	20.5 %	1
Annual background risk (BR)	0.80 %	0.80 %	0.80 %	1
Absolute risk	1.6E-04	4.9E-04	1.6E-03	1
Absolute risk per million	164	492	1642	$/10^6$
Corresponding ambient PM_{10} level	34.2	102.6	342	$\mu g\ m^{-3}$

Brown DM, Donaldson K, Borm PJ, Schins RP, Dehnhardt M, Gilmour P, Jimenez LA, Stone V. (2004). *Am J Physiol Lung Cell Mol Physiol* 286:L344-353.

Duffin, R, Tran, L, Brown, D, Stone, V and Donaldson, K (2007). *Inhalation Toxicology*, 19(10): 849 – 856

Pope C.A., Dockery D. (2006). *J Air Waste Manag Assoc* 56:709–742.

Levels of dioxins and furans in blood of the residents living in the vicinity of a municipal solid waste incinerator and electric arc furnace

Yuan-Chung Lin[1], Yan-Min Chen[2*], Tzi-yi Wu[3], Guo-Ping Chang-Chien[4,5], Wen-Feng Ma[6], Chung-Hsien Hung[4,6]

[1] Institute of Environmental Engineering, National Sun Yat-Sen University, Kaohsiung 804, Taiwan.

[2] Sustainable Environment Research Center, National Cheng Kung University, Tainan 701, Taiwan.

[3]. Department of Chemistry, National Cheng Kung University, Tainan 70101, Taiwan

[4] Department of Chemical and Materials Engineering, and Super Micro Mass Research & Technology Center, Cheng Shiu University, Kaohsiung County 833, Taiwan.

[5] Graduate Institute of Medicine, College of Medicine, Kaohsiung Medical University, Kaohsiung County 807, Taiwan

[6] Super Micro Mass Research & Technology Center, Cheng Shiu University, Kaohsiung County 833, Taiwan.

Keywords: dioxins and furans; human blood; municipal solid waste incinerator; electric arc furnace.

Many human activities have been concluded as the potential sources of PCDD/Fs, such as combustion, manufacturing of organic chloride chemicals and metals smelting processes involving the use of chlorinated or chlorinated-derived chemicals (Stieglitz et al., 1990). Among of these many sources, the emissions from MSWI have been estimated as the major sources in the ambient air in USA (Cleverly et al., 1998). Taiwan got the 12th position in the world for the total output of crude steel in 2007. Hence, both MSWIs and EAFs would be the very important contributors of PCDD/Fs in Taiwan. However, the levels of PCDD/Fs in blood of the non-occupationally exposed residents are not well established in Taiwan. Moreover, the area with adjacent MSWI and EAF is rarely studied.

The participants in this study all lived within the 4 Km radius of the MWI and EAF, as shown in Figure 1(a). The mean levels of total PCDD/Fs in blood were 23.9 pg/g lipid, 32.2 pg/g lipid and 27.4 pg/g lipid on the basis of I-TEQ, 1998-WHO TEQ and 2005-WHO TEQ, respectively.

The data of BMI, age, and I-TEQ were plotted in 2D figure as presented in Figure 1(b) There is no significant relationship among BMI, age, and I-TEQ values. Figure 2 showed the fraction of average I-TEQ levels of 17 PCDD/Fs congeners to total I-TEQ PCDD/Fs in blood. It reveals that dominant dioxins toxicity in blood come from 2,3,4,7,8-PeCDF, 1,2,3,7,8-PeCDD, 2,3,7,8-TCDD, 1,2,3,6,7,8-HxCDD, and OCDD, that contributed 81.7%. Similar results have been found (Lee et al., 2005). It can be attributed to 2,3,4,7,8-PeCDF has a highest half life time (19.6 years) among all 17 congeners, and it is be expect more easy accumulated in the blood.
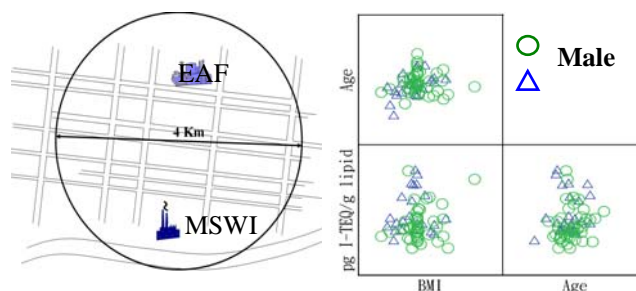
Figure 1. (a) Schematic picture of the sampling location; (b) Dependence of level of PCDD/Fs (pg I-TEQ/g lipid) in human blood on age, and BMI values.
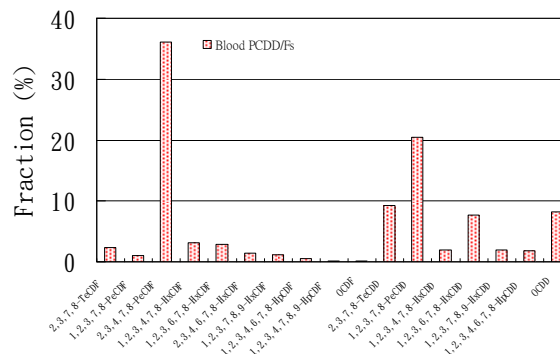
Figure 2. Seventeen PCDD/Fs congener fractions to I-TEQ in the blood samples

Cleverly, D., Schaum, J., Winter, D., Schweer, G., O'Rourke, K., 1998. The inventory of sources of dioxin in the United States. Organohalogen Compd. 36, 1-6.

Lee, C.C., Chen, H.L., Su, H.J., Guo, Y.L., Liao, P.C., 2005. Evaluation of PCDD/F patterns emitted from incinerator via direct ambient sampling and indirect serum levels assessment of Taiwanese. Chemosphere 59, 1465-1474.

Stieglitz, L., Zwick, G., Beck, J., Bautz, H., Roth, W., 1990. The role of particulate carbon in the de-novo synthesis of polychlorinated dibenzodioxins and-furans in fly-ash. Chemosphere 20, 1953-1958.

Investigations into the size distribution of droplets from expiratory activities

L. Morawska[1*], G.R. Johnson[1], Z.D. Ristovski[1], M. Hargreaves[1], K. Mengersen[1], S. Corbett[2], C.Y.H. Chao[3], Y. Li[4], D. Katoshevski[5]

[1]Queensland University of Technology, Brisbane, QLD, Australia
[2]Centre for Public Health, Western Sydney Area Health Service, Sydney, NSW, Australia
[3]Department of Mechanical Engineering, The Hong Kong University of Science and Technology, Hong Kong SAR, China
[4]Department of Mechanical Engineering, The University of Hong Kong, Hong Kong SAR, China
[5]Department of Biotechnology and Environmental Engineering, Ben-Gurion University of the Negev, Beer-Sheva, Israel

The need to obtain a comprehensive understanding of expired aerosols across the entire range of droplet sizes has become an increasingly urgent issue over the past decade. To address this question, investigations of expiratory droplets were conducted using the Expired Droplet Investigation System (EDIS), applying three separate measurement techniques to cover the entire size range from 0.5-2000 µm; Aerodynamic Particle Sizer (APS, $0.5 \leq d \leq 20$ µm, Interferometric Mie Imaging (IMI, $d \geq 2$ µm) and Droplet Deposition Analysis (DDA, $20 \leq d \leq 2000$ µm). A number of the important new findings arising from this work are presented below:

Droplets smaller than 5 µm dry to their equilibrium residual size within 0.8 s, so APS size distributions were dominated by droplet residues. This contrasts with IMI measurements performed immediately in front of the mouth which assess droplets before any change has occurred and with DDA which assesses largeer droplets, which deposit before drying.

The size distributions from these measurement methods have been combined for speech (Figure 1) and coughing, after correcting for evaporation and the detection efficiency of the various methods. It is likely that the newly created droplets detected by IMI at 10 µm become the residue droplet modes seen between 1.8 and 5.5 µm with the APS.
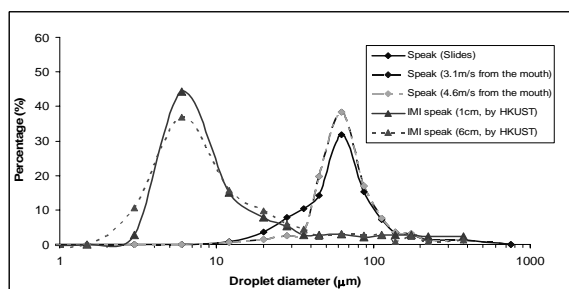

Figure 1. Combined IMI and DDA expired aerosol distributions for speech .

Aerosols produced during expiratory activities arose from at least three distinct mechanisms:

1. A breath aerosol mode with a residual diameter of 0.8 µm occurs during all activities. This mode is produced by the bursting of fluid obstructions in the bronchioles during inhalation, a mechanism dubbed the Bronchiolar Fluid Film Burst (BFFB) mechanism (Johnson & Morawska, 2009). This aerosol is probably composed of bronchial epithelial lining fluid.

2. During vocalised speech and coughing increased aerosol production occurs with residual diameters from 1.8 to 5.5 µm. This aerosol arises from vocal folds vibrations during speech (Morawska et al., 2008) and is probably composed of mucus from the larynx. When measured immediately after production using IMI, what may be the same aerosol mode produced during speech as referred to above, was located at 16 µm (C.Y.H. Chao et al., 2009).

3. Addition aerosol production occurs in the mouth and pharynx, with residual diameters in the range 50-100 µm (Xiaojian Xie et al., 2009). This aerosol is composed of saliva from the mouth and pharynx as was demonstrated by the detection of food dye residues introduced to the volunteer's mouth.

Morawska, L., Johnson, G.R., Ristovski, Z.D., Hargreaves, M., Mengersen, K., Corbett, S., Chao, C. Y. H., Li, Y. Katoshevski, D. (In Press). *Journal of Aerosol Science.*

Johnson, G.R., Morawska, L.. (In Press). *Journal of Aerosol Medicine and Pulmonary Drug Delivery.*

C.Y.H. Chao, M.P.Wan, L. Morawska, G.R. Johnson, Z.D. Ristovski, M. Hargreaves, K. Mengersen, S. Corbett, Y. Li, X. Xie, D. Katoshevski. (2009). *Journal of Aerosol Science,* 40, 122-133.

Xie, X., Morawska, L., Li, Y., Chao, C.Y.H., Wan, M.P., Johnson, G.R., Ristovski, Z.D., Hargreaves, M., Mengersen, K., Corbett, S., and Katoshevski, D. (In Preparation). *Journal of Aerosol Science.*

Optimization of airway deposition of inhaled bacteria

A. Horváth[1], I. Balásházy[2], Z. Sárkány[3], Á. Farkas[2] and W. Hofmann[4]

[1]GlaxoSmithKline, Csörsz u. 43, 1124 Budapest, Hungary
[2]Health and Environmental Physics Department, MTA KFKI Atomic Energy
Research Institute, P.O. Box 49, H-1525 Budapest, Hungary
[3] Discipline of Physiology, University of Medicine and Pharmacy of Targu Mures
Gheorghe Marinescu 38, 540000 Targu Mures, Romania
[4]Department of Materials Engineering and Physics, Division of Physics and Biophysics, University of Salzburg,
Hellbrunner Str. 34, 5020 Salzburg, Austria

Keywords: bacteria, health effects of aerosols, lung deposition, Monte Carlo simulations, bioaerosols

Respiratory infections represent one of the most important bioaerosol-associated health effects. Although a large number of inhalable pathogenic bacteria have been identified and the related respiratory symptoms are well-known, their airway transport and deposition is still not fully explored.

The successful transmission of an infection depends on several factors such as the susceptibility of the individual, duration of exposure, concentration of the infectious agent, breathing rate and the route of infection, but one of the simplest and most economic ways to reduce the chance of getting infected would be to choose a breathing mode, which ensures a low bacterial airway deposition.

The objective of this work was to characterize the deposition of inhaled bacteria in different regions of the lung and to find the optimum breathing modes, which ensure the minimum chance of bacterial infection in a given environment.

For this purpose a stochastic lung deposition model has been applied. In order to find the breathing pattern that yields the lowest deposited fraction of the inhaled bacteria, multiple simulations were carried out with several combinations of tidal volumes ranging from 400 to 2000 ml, and symmetrical breathing cycles ranging from 2 to 10 s, with or without breath-hold before and after exhalation. Particle aerodynamic diameters varied between 1 and 20 μm, the functional residual capacity of the lung was taken as 3300 ml, and simulations were performed for both nose and mouth breathing conditions.

Present computations demonstrated that regional (extrathoracic, tracheobronchial, acinar), lobar and generation number specific deposition distributions of the inhaled bactera are highly sensitive to their aerodynamic diameter and to the breathing parameters. However, different breathing patterns are needed to minimise the total and regional deposited fractions of the inhaled particles.

According to our results, mouth breathing with short breathing periods, no breath-hold and low tidal volumes minimise the total respiratory system deposition. Bronchial deposition values of particles smaller than 2 μm were the lowest in the case of a 2 s breathing cycle and 400 ml tidal volume, while particles larger than 2 μm yielded the lowest deposition values in the case of a 2 s breathing cycle and 2000 ml tidal volume. Although deposition values in the acinar region were higher than tracheobronchial ones for small particles and lower for large particles, there were no significant differences regarding the optimum breathing pattern to achieve the lowest deposition values in these two regions. Our results have shown that bronchial and acinar deposition can be minimised by a breathing mode characterised by short breathing cycles through the nose with long breath-holds after exhalations and high tidal volumes.

When comparing minimum and maximum lobar deposition values it is shown that deposition fractions are the highest in the lower lobes, and the maximum values are two orders of magnitudes higher than the minimum values. Generation number specific minimum and maximum deposition values also prove that the deposited fractions can be significantly reduced even at generation level by the application of appropriate breathing modes.

Ambient concentrations of the major birch allergen Bet v 1 and birch pollen count in Munich, Germany, in 2004 till 2008, and the new EU-HIALINE project

J.T.M. Buters[1], C. Huber[1], I. Weichenmeier[1], G. Pusch[1], W. Kreyling[2], W. Schober[1], H. Behrendt[1]
and the HIALINE working group[3]

[1] Division of Environmental Dermatology and Allergology, Helmholtz Zentrum München/TUM, ZAUM - Center for Allergy and Environment, Technische Universität München, Munich, Germany

[2] Helmholtz Zentrum München, German Research Center for Environmental Health, Institute for Inhalation Biology, Neuherberg, Germany

[3] M. Thibaudon, France, M. Smith, Great Britain, C. Galan, Spain, R. Brandao, Portugal, R. Albertini, Italy, A. Stach, Poland, B. Weber, Germany, A. Rantio-Lehtimäki, Finland, S. Jäger, Austria, M. Sofiev, Finland, I. Sauliene, Lithuania, L. Cecchi, Italy

Background Exposure to allergens is one of several factors determining sensitization and allergic symptoms in individuals. Exposure to aeroallergens from pollen is assessed by counting allergenic pollen in ambient air. However, proof is lacking that pollen count is representative for allergen exposure, also because allergens were found in non-pollen bearing fractions. We therefore monitored simultaneously birch pollen count and the major birch pollen allergen Bet v 1 in different size fractions of ambient air in Munich from 2004 till 2008, and now also in 8 countries in Europe in the HIALINE project.

Methods Ambient air was sampled at 800l/min with a Chemvol high-volume cascade impactor equipped with stages PM>10µm, 10 µm>PM>2.5µm, and in Munich also 2.5 µm>PM>0.12µm. The polyurethane impacting substrate was extracted with 0.1M NH_4HCO_3, pH8.1. The major pollen allergens from birch Bet v 1, grass Phleum P 5 and olive Ole e 1 were determined with allergen specific ELISA´s. Pollen counts were assessed with a Burkard pollen traps.

Results The five studied years were all strong birch pollen flight years for Munich, Germany. In those years 95±3% of Bet v 1 was found in the PM>10 µm fraction, the fraction containing birch pollen. On none of the days did we find any Bet v 1 in the respirable 2.5µm>PM>0.12µm fraction (all <0.5%). We found that Bet v 1 could have absorbed to diesel particles that also deposit in this fraction.

Pollen released 215% more Bet v 1 in 2007 than the same amount of pollen in 2004. Also within one year, the release from the same amount of pollen varied several fold between different days. This variation could be explained by the phenomenon that Bet v 1 from pollen within catkins increased from zero to 9200ng/10 mg pollen in the last week before pollination when each day anthers could have pollinated, depending on the weather. We now started sampling in 8 different European countries to evaluate larger differences in climate.

Conclusion Bet v 1 was only found in the pollen-containing fraction. Pollen from different years, different trees and even different days released up to 10-fold different amounts of Bet v 1 already at one location. Thus exposure to allergen is poorly monitored by only monitoring birch pollen count. We now compare 8 countries in Europe within the EU-HIALINE (Health Impacts of Airborne Allergen Information Network). We think that monitoring the allergens itself in ambient air might be an improvement in allergen exposure assessment.

Concentration and size distribution of bioaerosols in different residential categories

Ian Colbeck and Zaheer Ahmad Nasir

Department of Biological Sciences, University of Essex, Colchester, CO4 3SQ, U K

Keywords: indoor air quality, bioaerosols, size distribution

There has been great concern about the potential health hazards of indoor bioaerosols to humans, with a special focus on allergenic or toxigenic fungi and their association with indoor air quality. In a review on health effects of bioaerosols Douwes et al. (2003) concluded that the potential health effects of bioaerosol exposures were diverse including infectious diseases, acute toxic effects, allergies and cancer. Most of the studies on levels of bioaerosols in various residential settings report only the total concentrations and studies on aerodynamic particle size of bioaerosols are rare. However particle size is critical with regard to their fate in the air and their deposition in the human respiratory system. Hence, the present study was conducted to evaluate the total concentration and size distribution of bioaerosols in various residential houses in South East England.

Three different types of residential houses were sampled: single room in shared accommodation (Type I), single bedroom flat in three storey buildings (Type II) and two bedroom houses (Type III). Five different houses were sampled in each type. The sampling was carried out during the summer of 2007 using an Anderson six stage viable particle sampler, loaded with Malt Extract Agar and Nutrient Agar. The sampling interval was of 5 minutes, and after collection the agar plates were incubated at 25ºC for 48 hours. Data on humidity, temperature, water damage, visible mold, age of home, number of occupants, respiratory illness, and pets was recorded. Colony forming units (CFU/m^3) were enumerated for each stage and the total counts for all the stages were calculated.

The total geometric mean concentration of bacterial aerosols in housing types I, II and III was 1557 CFU/m^3, 2403 CFU/m^3 and 5036 CFU/m^3, respectively. While the mean geometric CFU/m^3 for fungal spores in the same housing type was 925,813 and 2,124 respectively (Table 1). The average temperature in all the three housing types was 22°C. Whereas, Type I and II had the same average relative humidity (47%), in Type III it was 59%. There was an increasing order in the bacterial concentration from housing Type I to III. The highest fungal concentration was found in Type III followed by I and II. The observed differences in concentration and size distribution of biaerosols implied differences in their airborne behaviour and hence varied exposure in different residential settings.

	Bacteria		Fungi	
Housing Type I	GM	GSD	GM	GSD
Total	1557	1.5	925	2.9
7µm & above	279	1.3	176	1.8
4.7-7µm	277	1.7	241	2.3
3.3-4.7µm	434	2.6	192	5.8
2.1-3.3µm	240	1.3	82	9.5
1.1-2.1µm	212	1.5	110	2.0
0.65-1.1µm	19	2.5	15	1.9
Housing Type II				
Total	2403	2.3	813	3.6
7µm & above	471	3.0	63	1.6
4.7-7µm	382	2.3	136	2.2
3.3-4.7µm	451	2.7	232	3.7
2.1-3.3µm	536	2.2	182	8.4
1.1-2.1µm	355	3.5	100	2.1
0.65-1.1µm	64	1.3	7	1.1
Housing Type III				
Total	5036	2.5	2124	1.4
7µm & above	199	1.3	257	4.8
4.7-7µm	311	1.1	294	4.2
3.3-4.7µm	207	2.8	429	1.7
2.1-3.3µm	774	4.2	581	2.2
1.1-2.1µm	2228	1.6	140	1.5
0.65-1.1µm	659	11.1	7	1.0

Table 1. Summary of bioaerosol concentration (geometric mean – GM and geometric standard deviation - GSD) in three different types of residences.

The size distribution of bacterial aerosol varied in all the three housing types. In Type I, II and III houses, the maximum bacterial aerosols were recovered from stage 3 (3.3–4.7µm), stage 4 (2.1–3.3µm) and stage 5 (1.1–2.1µm), respectively. While most of fungal spores were found in stage 2 (4.7-7µm), stage 3 (3.3–4.7µm) and stage 4 (2.1–3.3µm) in housing Type I and II. However, in housing type III, the highest fungal colonies were on stage 5 (1.1-2.1µm).

The bioaerosol concentration varied significantly in different housing types. Size and age of house humidity, water damage and number of occupants showed a significant effect on indoor levels of bioaerosols.

Douwes, J., Thorne, P., Pearce, N. and Heederik, D. 2003. Bioaerosol health effects and exposure assessment: Progress and prospects, *Ann. Occup. Hyg.*, 47: 187–200.

Characterisation of the dustiness of highly effective pharmaceutical substances

S. Bach[1], U. Eickmann[2] and E. Schmidt[1]

[1]Department of Safety Engineering/Environmental Protection, University of Wuppertal, Rainer-Gruenter-Str., 42119, Wuppertal, Germany
[2]Berufsgenossenschaft für Gesundheitsdienst und Wohlfahrtspflege, Bonner Str. 337, 50968, Cologne, Germany

Keywords: dust, health aspects of aerosols, indoor sources.

To determine the dustiness of powders there are various methods available and even more methods have been custom-made for special purposes by universities, research institutes and companies. A good overview is given in BOHS, 1985.

The UNC-CH Dustiness Tester (see figure 1) was specially designed for the purpose of determining the dustiness of highly effective and/or cost-intensive powders. It needs only 10 mg of material per measurement, that is 50 mg per powder assuming a total of five measurements. On the contrary, a minimum of 150 g is used for other commercially available instruments (Bach *et al.*, 2008).
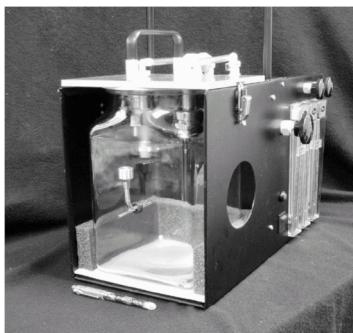

Figure 1. The UNC-CH Dustiness Tester from the University of North Carolina at Chapel Hill

5 mg ± 0.1 mg of dry powder are introduced into the apparatus through a nozzle. The delivery end of the injection nozzle is centred in one side of a 1.5 Gallon glass jar serving as the dust chamber. Air is then drawn from the jar at 60 Lpm for 1.5 seconds; replacement air passes through the injection nozzle and disperses the powder into the jar. The instrument collects the released dust on two different filter devices, one for the total suspended dust and one for the respirable aerosol fraction. After dispersing the powder into the jar, dust-laden air is collected on the filters for 4 minutes with partial flow rates of 4.2 Lpm for the respirable fraction resp. 2 Lpm for the total suspended dust. To increase sensitivity, the cycle of injection and sampling is then repeated with an additional 5 mg of powder so that 10 mg of powder are dispersed in all.

The mass difference of the filters after the measurement in the ratio to the initially introduced powder has to be adjusted to the actual flow rates (Boundy *et al.*, 2006). The dustiness is therefore a percentage of the injected powder.

The Accident Prevention & Insurance Association for health and welfare work wanted to have anaylsed the dustiness of 11 different powders used in pharmacies to produce medicaments. These materials are classified as hazardous and can affect human health strongly. To be able to estimate the workers exposure of these powders, the determination of dustiness is essential.

Because the UNC-CH Dustiness Tester is a very new instrument, there was a lack of reference measurements and there is no possibility to classify the measured values to a specific dustiness, such as "low", "moderate", "high", etc. For that case, reference materials were chosen and their dustiness was determined with two devices conforming to European standards - one continuous drop instrument and one rotating drum device -, another well-accepted single-drop apparatus and the UNC Dustiness Tester. The above named reference devices all provide a classification of the measured values.

All results have been scaled, so that each instrument allocates a value between 0 and 1 to each material, independent from measuring principle and unit. The one reference device showing the best compliance of the scaled results to those of the UNC-CH Dustiness Tester (broken down by the two fractions) was used to transform its classification system to the new instrument.

Bach, S., Schmidt, E. (2008), *Ann. Occup. Hyg.*, 52, 8, pp. 717-725, "Determining the Dustiness of Powders – A Comparison of three Measuring Devices"

Boundy, M., Leith, D., Polton, T. (2006). *Ann. Occup. Hyg.*, 50, pp. 453-458. "Method to evaluate the dustiness of pharmaceutical powders"

British Occupational Hygiene Society (1985), Technical Guide No.4, *Dustiness Estimation Method for Dry Materials*

Science behind particles from printer and copier operation: do we understand it?

Lidia Morawska[1*], Congrong He[1], Graham Johnson[1], Rohan Jayaratne[1], Tunga Salthammer[1,2], Hao Wang[1], Erik Uhde[2], Thor Bostrom[1], Robin Modini[1], Godwin Ayoko[1], Peter McGarry[1], Michael Wensing[2]

1International Laboratory for Air Quality and Health, Queensland University of Technology, GPO 2434, Brisbane QLD, 4001, Australia
[2]Fraunhofer Wilhelm-Klauditz-Institute (WKI), Material Analysis & Indoor Chemistry, Bienroder Weg 54 E, 38108, Braunschweig, Germany

Keywords: Aerosol emissions, Ultrafine particle, Laser printers, VOCs, Indoor air quality.

Background. Recent studies on printer emissions showed that about a third of the popular brands of laser printers emit large numbers of ultrafine particles (<0.1 µm). These numbers are high enough to elevate the concentration in a large office area to levels encountered, for example, near a busy road. These studies did not, however, investigate the nature of the particles, their composition or their formation mechanisms. Therefore, the current study was undertaken with the aim of identifying the source and nature of the emitted particles and the factors that determine whether a specific laser printer is a high or low emitter of particles.

Methods. More than 30 new printers were studied, with the popular HP 1320n and HP 2200 (being a high and low particle emitter, respectively), chosen for more extensive investigations. The printers were operated either in a flow tunnel, to provide information on characteristics of particles approximately 30s after emission (including particle size distribution and concentration measurements using SMPSs and CPCs, as well as ozone and VOC), or in an experimental box chamber, to provide information on particle volatility and hygroscopicity (using a Volatility and Hygroscopicity Tandem Differential Mobility Analyser (VHTDMA), as well as information about particle aging and other emission characteristics. Other characteristics or parameters investigated included particle morphology (scanning and transmission electron microscopy) and fuser temperature. In addition, emissions from the idle belts of the fuser rollers, paper, toner powder and lubricating oil were investigated whilst being heated in a controlled-temperature furnace, to provide insight into particle formation from each of these materials independently from the others. The study involved over 250 emission tests.

Results. Based on the results of this study, the following conclusions were derived:

- The idle belts of the fuser rollers, paper, toner powder and lubricating oil are potential particle sources during printing.
- The particles contain at least two distinct species and these are volatile in air, when heated briefly to 130°C, however they are not water soluble, nor do they become so during thermal treatment. Figure 1 provides some examples of the results of VHTDMA tests.

- The particles are of secondary nature, being formed in the air from volatile organic compounds originating from both the paper and hot toner. Some of the toner is initially deposited on the fuser roller, after which the organic compounds evaporate and then form particles.
- In terms of particle number, 29 of the 30 new office printers were high particle number emitters. On average, 95% of the total submicrometer particles emitted by these printers were ultrafine particles (< 100nm).
- In general, a positive relationship was found between fuser roller temperature and average particle number emission rate. However, this relationship was only clear for some brands of printers, which implies that there are other factors which also play a role in particle emissions.
- Among other factors, an association was found between intense bursts of particles and fuser temperature fluctuations, which suggests that the difference between high and low emitters lies in the speed and sophistication of the temperature control.
- The results of this study imply that fuser roller temperature is the key driving force behind different particle emission levels, however, the chemical and physical characteristics of the fuser roller, as well as its structure, may also play an important role in the particle emission characteristics of individual printers. More research is needed in this area to investigate the science behind particles emitted from printer and copier operation.
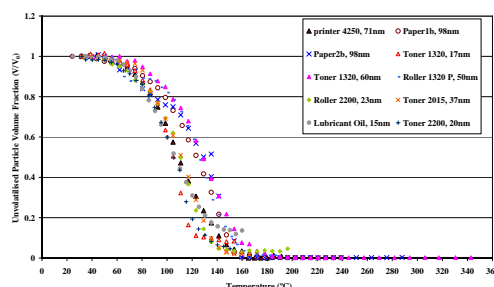

Figure 1: Example of volatilisation temperature curve of the particles generated by the idle belts of the fuser rollers, paper, toner powder and lubricating oil as well as printer, measured by the VH-TDMA. Initial particle sizes are given in the legend.

Ultrafine particle release from hardcopy devices: comparison of test chamber and real room measurement

T. Salthammer[1,2], E. Uhde[1], T. Schripp[1], M. Wensing,[1], C. He[2] and L. Morawska[2]

[1]Fraunhofer Wilhelm-Klauditz-Institute (WKI), 38106 Braunschweig, Germany
[2]Queensland University of Technology (QUT), 4000 Brisbane, Australia

Keywords: Indoor Particles, Ultrafine Particles, Emission Factor, FMPS, Laser Printers,.

The emission of ultrafine particles (UFP) from hardcopy devices is currently in the focus of frequent research activities, because the influence of printer configuration, environmental conditions, and composition of consumables on the emission behavior appears to be complex (Morawska et al., 2008; Schripp et al., 2008, 2009; Wensing et al., 2008).

We have analyzed the release of ultrafine particles (UFP) from laser printers and office equipment using a Fast Mobility Particle Sizer (FMPS) and appropriate mathematical models. Measurements were carried out in a 1m³ chamber, a 24m³ chamber and an office room. The time-dependent emission rates were calculated for these environments using a deconvolution model. The results give a deeper insight to the formation of UFP and lead to a distinction between "initial burst" and "constant emitters". The measurements also indicate that the emitted particles are mainly generated within the heated fuser unit of a laser printer. The combination of heat management and specific ingredients of the fuser unit is suspected to be the main factor governing particle creation. Several semi-volatile organic compounds are possible candidates that could lead to nucleation and aerosol formation during the fusing process.

At the start of the printing process the UFP concentration in air rises sharply. Especially in the emission test chamber with an interior volume of 1m³ this rapid change in concentration can be observed due to the low dilution. The particle concentration development when operating a printer in two different chambers and the office room is displayed in Figure 1. The increase in particle number concentration in a real office environment under the same printing conditions is as fast as in the emission test chamber. The most noticeable difference between the measurements in office and emission test chamber is the dissimilar decay in concentration after the emission from the printer stops. This result also confirms the findings from an earlier study (Wensing et al., 2008).

Due to differences in the environmental parameters (e.g. air exchange rate, air velocity, volume, and air flow pattern) the particle loss-rate coefficient β, which is a function of first order deposition decay constants, the second order coagulation term, and the air exchange rate, is larger in the emission test chambers than in the office.

Test chamber experiments under standardized conditions are useful to study the UFP emissions from laser printers and other hardcopy devices, but the influence of the chamber volume on the particle concentration makes this parameter less applicable for the comparison of different printers in different chambers. Moreover, measured chamber concentrations can not directly be used to estimate real-room exposure scenarios. However, the emission behavior of a printer can in general be characterized by the time-dependent emission rate. This parameter can e.g. be applied be used for modeling purposes.
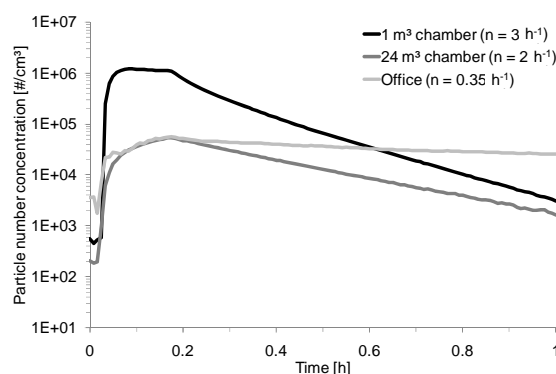

Figure 1. Particle number concentration during the print and post-print operating phases of a laser printer in 1m³ chamber, 24m³ chamber and real room.

Morawska, L., He, C., Johnson, G., Jayaratne, R., Salthammer, T., Wang, H., Uhde, E., Bostrom, T., Modini, R., Ayoko, G., McGarry, P. & Wensing, M. (2009) *Environmental Science & Technology*, available online (DOI: 10.1021/es802193n).

Schripp, T., Uhde, E., Wensing, M., Salthammer, T., He, C., and Morawska, L. (2008). *Environmental Science & Technology*, 42, 4338-4343.

Schripp, T., Mulakampilly, S.J., Delius, W., Uhde, E., Wensing, M., Salthammer, T., Kreuzig, R., Bahadir, M., Wang, L. & Morawska L. (2009) *Gefahrstoffe – Reinhaltung der Luft*, in press.

Wensing, M., Schripp, T., Uhde, E. & Salthammer, T. (2008). *The Science of the Total Environment*, 407, 418-427.

The effect of human activity on coarse aerosol levels in a school gymnasium

M. Braniš[1], J. Šafránek[2], A. Hytychová[1]

[1]Charles University in Prague, Faculty of Science, Albertov 6, 128 43 Prague 2, Czech Republic
[2]Charles University in Prague, Faculty of Physical Education, José Martího 31, 162 52 Prague 6, Czech Republic

The relevance of coarse dust for health was emphasized by Brunekreef and Forsberg (2005), who reviewed epidemiological evidence of the effects of coarse airborne particles on health. In studies of chronic obstructive pulmonary disease, asthma and respiratory admissions, coarse particulate matter (PM) was shown to have a stronger or as strong short-term effect as fine PM, suggesting that coarse PM may lead to adverse responses in the lungs, triggering processes leading to hospital admissions. These findings underline the importance of studies aimed at characterisation of coarse particles generated indoors during human activity, such as exercise in school gyms and sports arenas because higher concentrations of coarse particles are known to be related, among others, to increased prevalence of asthma.

We have analyzed coarse particulate matter content in a school gymnasium during eight campaigns 7-10 days long performed between November and August of the successive year, covering all seasons of a school year. Particulate matter was sampled indoors and outdoors by a pair of personal cascade impactor samplers (PCIS). Indoor and outdoor temperature, relative humidity (RH), ambient wind velocity, ambient $PM_{2.5}$ from the nearest fixed site monitor (FSM) and presence of exercising pupils in the gymnasium were considered as relevant variables. We used principal component analysis (PCA) to ascertain the relationships between the indoor and outdoor factors. Only factors with eigenvalues greater than 1 and factor loadings for each variable above 0.5 were considered important.

The PCA revealed three principal factors explaining over 76% of the data set variability (DSV). The first factor (explaining 42.6% DSV) included both indoor and outdoor PCIS $PM_{2.5}$, negative load of ambient temperature and ambient FSM $PM_{2.5}$ demonstrating that during low temperatures in winter the aerosol concentrations tend to increase and penetrate indoors. The second factor (explaining 23.3% DSV) included outdoor coarse particulate matter between 1 and 10µm in aerodynamic diameter (stages A and B of the PCIS), negative load of ambient RH and weak load of ambient temperature demonstrating that dry and warm conditions are main factors for resuspension of particles outdoor. The third factor included only coarse indoor aerosol between 1 and 10µm in aerodynamic diameter (explaining 10.4% DSV) and a human activity indicator (man-hour counts).

A reasonable correlation coefficient (0.642) between ambient and indoor coarse (A impactor stage) particulates during days without human activity (weekends, holidays) suggests that association between the indoor and outdoor microenvironments exists but low indoor/outdoor ratio (0.33±0.18) showed that contrary to the $PM_{2.5}$ (I/O ratio 0.88±0.29) the outdoor-to-indoor penetration rate of this aerosol fraction was low.

Considering the fact that, during aerobic exercise, inhaled air is taken in predominantly through the mouth the filtration effect of upper respiratory pathways may be limited and increased amount of coarse particles can penetrate deeper in the lungs. As shown by Fox *et al.* (2005), Smedje and Norback (2001) or Daisey *et al.* (2003) higher levels of coarse particles may be responsible for higher bacterial contamination in crowded school areas, which may result in serious health problems including infections, allergies, and respiratory irritation.

We conclude that attention should be paid not only to outdoor but also to specific indoor microenvironments. So far, only outdoor physical activity of school children was considered risky in connection with deteriorated urban air quality (Villarreal et al., 2002).

Brunekreef, B., and Forsberg, B. (2005), *Eur. Respir. J.* 26, 309–318.
Daisey, J.M., Angell W.J., and Apte, M.G. (2003), *Indoor Air.* 13, 53-64.
Fox, A., Harley, W., Feigley, C., Salzberg, D., Toole, C., Sebastianc, A., and Larssonc, L. (2005), *J. Environ. Monitor.* 7, 450 – 456.
Smedje, G., Norback, D. (2001), *Int. J. Tubercul. Lung Dis.* 5(11), 1059-1066.
Villarreal-Calderón, A., Acuña, H., Villarreal-Calderón, J., Garduño, M., Henríquez-Roldán, C.F., Calderón-Garcidueñas, L., Valencia-Salazar, G. (2002), *Arch. Environ. Health* 57(5), 450-460.

Evaluation Of The Overall Particle Emission Reduction Efficiencies Of Commercially Available Laser Printer Filters

G. Steiner[1], D. Wimmer[1], G.P. Reischl[1]
E. Peteln[2], M. Vojta[2]

[1]Faculty of Physics, University of Vienna, Boltzmanngasse 5, 1090 Wien, Austria
[2]Dexwet Technology GmbH, Hauptstrasse 3, 2602 Blumau, Austria

Keywords: Filters, Filtration efficiency, Indoor sources, Laser printer.

The performance of three commercially available filter systems [improved DEXWET filter system Modular Professional 2000 (DW), Filter A and Filter B], specially assigned for office machines was investigated. Therefore, the overall particle emissions evolving from a standard b/w laser printer during a print job were investigated, using a specially designed exposition test chamber with a volume of 0.4 m³. Measurements with and without mounted filter systems were performed.

During the measurements, special attention was paid to investigate the overall reduction of the particle emissions by the installed filter system.

The test chamber comprises eight stainless steel dilution air inlets as well as a conical shaped sample dome on the top of the chamber. Temperatures and relative humidities were measured and monitored at four positions in the setup (see Fig.1). The values obtained at the chamber inlet (purified dilution air T_1, RH_1), chamber outlet (emission sample T_2, RH_2), inside the chamber near the printer fan (T_3, RH_3) and inside of the printer housing near the toner cartridge (T_4, RH_4) were recorded. Additionally, an anemometer was installed at the printer fan outlet to evaluate the streaming velocity of the airflow exiting the printer and thereby the pressure drop caused by an installed filter.
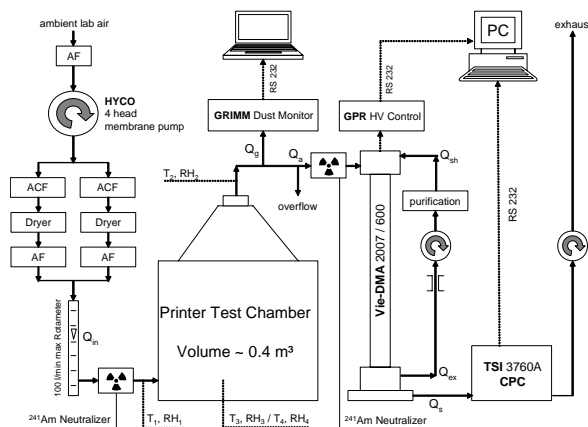

Fig. 1. Experimental Setup

To determine the Number Size Distribution (NSD) of the emitted particles in the size range below 300 nm, Electrostatic Mobility Spectrometry (EMS) with its core part a Differential Mobility Analyzer (DMA) and a Condensation Particle Counter (CPC) as sensor was applied. To minimize charge effects of potentially highly charged aerosols on the sampling and evaluation, the chamber was flushed with bipolar ions produced by an [241]Am neutralizer. A second size analyzing system, based on optical aerosol classification (GRIMM Dust Monitor) was installed inline with the outlet of the sample dome to determine the NSD for particles larger than 300 nm.

One print job was defined by a series of five blocks of consecutively printing 50 sheets with a delay of 15 seconds between the individual blocks. An achromatic template according to Blauer Engel RAL-UZ122:2006-04 with 5% coverage served as test page. Exclusively original toner material from the printer manufacturer and paper brands suggested by the printer manufacturer were used throughout the study.
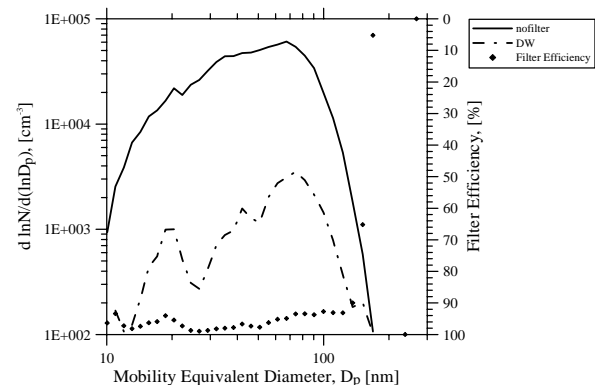
Fig. 2. Example for a typical number size distribution of laser printer emissions; unfiltered (nofilter) and filtered using the Dexewet filter system (DW).

This study shows that the overall retention efficiency of individual filter systems mounted on the air exit of the laser printer strongly depends on their pressure drop. A larger pressure drop causes particulate matter bypassing the filters through the remaining openings of the printer (eg. paper collection tray) and thereby deteriorating the overall filtration efficiencies evaluated by the chosen method.

Development of continuous inspection of indoor aerosol in classroom of Peoples Friendship University of Russia

T. Aljazar, A. Syroeshkin

Department of Biology & General Genetics, Peoples Friendship University of Russia, Miklukho-Maklaya str. 8, 117198, Moscow, Russia

Concerning air pollutants, most attention was invariably directed to the outdoor air quality. Indoor aerosol particles cause a health hazard because most people spend most of their time indoors. (Van Grieken *et al,* 2006). The inhalation way of the entering of particles is most dangerous, since even with the small concentrations of aerosol particles in the atmosphere, the large volume of inhaled air regarding the big surface area of the respiratory tract (about 50 M^3/day and 70 M^2), beside the enter transfer activity of aerosol particles (Vasilenko, 1999). Studies indicate that are more than 30 cancerous materials metal (Pb, As, Be, Ni, Cr, etc.), asbestos, polycyclic, aromatic, hydrocarbons and their derivatives, and radioactive materials, which adhere to the indoor aerosol particles (Jiang *et al*, 2004). Particle size is the most important physical parameter, which influences their behavior before entering the organism; the depressiveness of aerosols can be different - from the thousandths of micron to tens of microns. Usually aerosols are polydispersonal. The divisions of respiratory organs noticeably are distinguished as far as such indices as the precipitation of aerosols, mechanisms and the speed of their removal. Therefore, it is very important to identify the sources of the indoor aerosol particles. This fine dust can penetrate deeply in the respiratory system, be taken up in the blood stream and cause local inflammations, and lead to asthma attacks, bronchitis, lung cancer and heart diseases. Indoor pollutant measurements were carried out to assess the relation between the type and amount of factors which affect indoor air pollutants and the comfort and quality of indoor environments.

We have recently measured size spectra and concentration of aerosols inside in classroom of Medical Faculty of Peoples Friendship University of Russia (PFUR). Around-the-clock work of aerosols counter during many days let to obtain typical regime characteristics of in-door aerosols in background state of classrooms (without students) and during lessons. Two-three times increasing of total aerosol concentration or drastic change in size spectrum comparing with regime data let for professors and tutors to make a resolve about short break in studies and aerate class-room. Also we develop our air-control system for automatic control of air quality by university technical service. We use two type of equipment: laser counter FLUKE 983 (control of particulate matter with a diameters 0.3μ, 0.5μ, 1.0μ,

2.0μ, 5.0μ, 10.0μ) and automatic laser counter IDL-1 (Cluster-1) (control of particulate matter with a diameters from 0.5 μ to 120 μ with 450 size groups). IDL-1 combined two regime: aerosols counter and particle sizer (for high concentration of aerosols) with Low Angle Laser Light Scattering (LALLS) method. IDL-1 was developed by our group combined with A.V. Dumansky Institute of Colloidal Chemistry and Chemistry of Water (Kiev).

We have obtained the data about the total regime concentration of in-door aerosols in the different places and condition in the class rooms. The typical background total aerosol concentration is measured with many days continuous measurement. Back ground time-curve of aerosols concentration presents on figure 1. It is very necessary to fast prevent dramatic changing in aerosols concentration because during winter period some students may be latent carrier of respiratory infection diseases. Now we control the presence in in-door aerosols influenza A virus with nested PCR-detecting of the viruses on aerosols (AFA) filters.
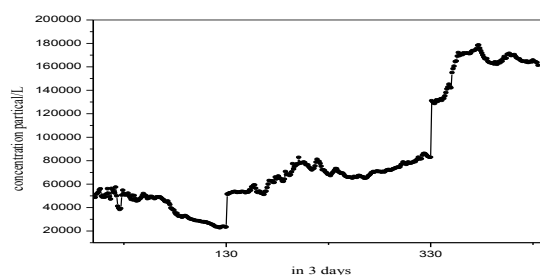
Figure 1. The example of the time-curve of aerosols concentration during three days in classrooms of Medical Faculty of PFUR (December, 2008).

Vasilenko I. Ya. Toxicology of nuclear division products. – 1999. – Moscow: Nauka. 354 p.

Jiang, D., Li., X., Qiu, Z., Lu, R., Li, Y., & Zhang, G. (2004)Journal of Radio Analytical and Nuclear Chemistry, 260, 301-304.

Van Grieken, R., Buczynska, A., Horemans, B., Stranger, M., & Worobiec, A. (2006) University of Antwerp, Belgium.

Influence of the window exchange on the aerosol particle concentrations in a lived-in city flat

A. Hruska, J. Hemerka

Faculty of Mechanical Engineering CTU in Prague, Department of Environmental Engineering, Technicka 4, 166 07 Prague 6 - Dejvice,

Keywords: indoor aerosol, indoor air quality, penetration

The aim of this paper is to present measurements of the aerosol particle concentrations in a lived-in flat.

Particle contaminants in the indoor environment were recognized as a major cause of health problems in Europe. It is therefore important to understand the behaviour of the indoor particle contaminants.

Aerosol particle number size distributions in the range of 0.25–10 μm were measured in two one week long campaigns both indoors and outdoors in a flat in a common panel house with natural ventilation on the fringe of Prague, Czech Rep.

The distributions were measured with Optical Particle Counter GRIMM 1. 109. Automatic switch valve was used for changing between indoor/outdoor sampling. The relative humidity, air temperature and especially carbon dioxide concentration were monitored indoors with the Indoor Air Quality Monitor (Sensotron, model PS31).

The main actual goal of the work is measuring and interpretation of aerosol particles indoor-to-outdoor relationship before and after flat reconstruction. The essential part of reconstruction was replacing of the 25 years old wooden windows by the modern leakproof plastic windows (system TROCAL). Future plan is repetition of experiments with commercial air purifier installed in the flat.

The apartment is on the fifth floor of eight floor house and consisted of a four rooms, a hallway corridor, and two bathrooms. In the time of measurements it was occupied by two adults and an infant. Because the measurements were carried out during winter, the windows were most of the time closed, entrance doors were opened for a short period of time (leaving and arriving).

As can been seen on the Fig. 1, indoor concentration is dependent on outdoor concentration due to infiltration, except during cooking activities. With new windows are indoor concentrations markedly under outdoor ones. The results should provide a better understanding of the particle number size distribution characterizations indoors and generally intensify the knowledge of indoor climate.
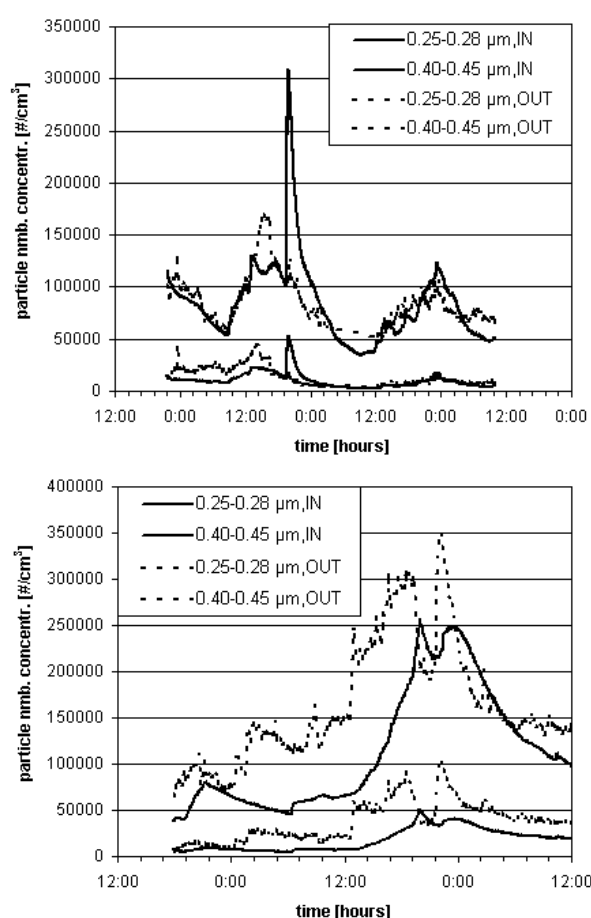

Figure 1. Examples of measured indoor-outdoor concentrations, 2 fractions, old and new windows

Tareq Hussein, Thodoros Glytsos, Jakub Ondráček, Pavla Dohányosová, Vladimír Ždímal, Kaarle Hämeri, Mihalis Lazaridis, Jiří Smolík, Markku Kulmala (2006), *Particle size characterization and emission rates during indoor activities in a house.* Atmospheric Environment, 23, 4285-4307

Generation of nano size particles from limonene/ozone reactions, for controlled human exposures in a chamber

C Isaxon[1], J Pagels[1], A Wiertzbicka[1], A Eriksson[1], A Gudmundsson[1], J Nielsen[2], K Dierschke[2], E Assarsson[2], U Andersson[2], J Klenö Nöjgaard[3] and M Bohgard[1]

[1] Division of Ergonomics and Aerosol Technology (EAT) Lund Institute of Technology, Lund, Sweden
[2] Division of Occupational and Environmental Medicine and Psychiatric Epidemiology, Lund University, Lund, Sweden
[3] Department of Atmospheric Environment, University of Aarhus, Denmark

An aim of this study has been to develop a method to generate a stable, reproducable terpene/ozone aerosol and deliver it to the exposure chamber while the aerosol still is fresh. An additional aim has been to study the detailed and complex reaction chemistry. The aerosol generated in this study is utilized for exposure of healthy human test subjects in a controlled chamber setting, during and after which various medical responses are being investigated.

Limonene is a common terpene constituent in many consumer products used in indoor settings. On reaction with ambient ozone the oxidation species rapidly form condensed-phase products, which significantly elevate the indoor levels of ultra fine aerosol particles. The size range and the complex chemical composition of the various reaction products and intermediaries suggest that they are likely to cause adverse effects human health. (Rohr et al 2003).

Terpene vapor is generated continuously by passing pure nitrogen (2 lpm) through a glass bottle containing 6.7 ml of commercial essential oil (lemon oil, oleum citri, Interlam ab), consisting of 60-95 % *d*-limonene. The VOC level is monitored with a photoinization detector (Photovac 2020) at the outlet of the glass bottle. Ozone is generated by a spark discharge generator using filtered dry air, and is added to the ventilation air flow just downstream the inlet for terpene vapours. The ventilation air passes HEPA and active carbon filter before vapor flow and ozone are added, just prior to entering the 21.6 m^3 stainless steel exposure chamber.

The behaviour of pure limonene in the exposure chamber is studied in separate experiments. During the exposures particle mass concentration in the chamber is monitored with a Tapered Element Oscillating Microbalance (TEOM, Rupprecht & Patashnic Co inc.) and particle number concentration and size distribution by a Scanning Mobility Particle Sizer system (consisting of a CPC 3010, TSI Inc and a long column Hauke DMA). An aerosol mass spectrometer (AMS, Aerodyne research inc.) is used for investigating the oxidation states and the elemental composition, with regards to carbon, hydrogen and oxygen, of the reactants.

Upon reaction with ozone there is an immediate burst of nucleation particles (5-25 nm), which due to condensation and coagulation processes grow in size to 150 nm (air exchange rate of 4.5 h^{-1}). In 2-3 hours the system reaches steady state with mainly a single mode of particles in the mean diameter range of 95-105 nm. Particles are slowly generated by nucleation at steady state. Prior to reacting with limonene vapor the concentration of ozone is 40 ppb. The ozone is almost completely consumed by the terpenes, leaving a residual ozone level in the exposure chamber of 5-8 ppb. Since ozone itself is an airway irritant, a low ozone level inside the chamber is of importance in the exposure studies. After reaching steady state, the generation system delivers a stable aerosol with regards to particle size, number and mass concentration, as shown in figure 1.
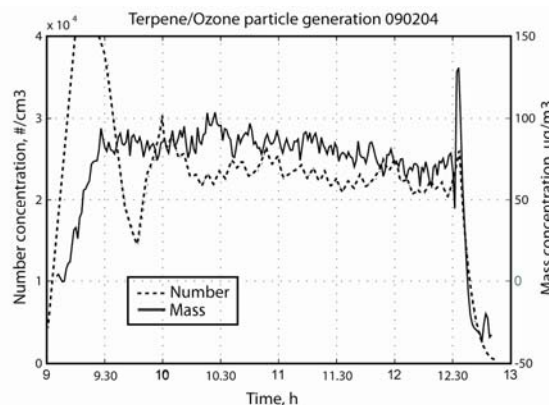
Figure 1. Number and mass concentration during an exposure event. At 12.30 the exposure chamber is evacuated.

The generation method developed resulted in a stable and reproducible terpene/ozone aerosol, and has been successfully used in human exposure studies.

Rohr A C, Weschler C J, Koutrakis P, Spengler J D, *Generation and Quantification of Ultrafine Particles through Terpeen/Ozone Reaction in a Chamber Setting*, Aerosol Science and Technology 37:65-78, 2003

Impact of outdoor combustion emissions on indoor air in a pulmonary hospital

M. Vardjan[1], M. Bajič[2], A. Zrimec[3] and G. Močnik[2]

[1] SETCCE and Optotek d.o.o., SI-1000 Ljubljana, Slovenia
[2] Aerosol d.o.o., SI-1000 Ljubljana, Slovenia
[3] Institute of Physical Biology d.o.o., SI-1000 Ljubljana, Slovenia

Keywords: black carbon, indoor aerosols, indoor / outdoor particles, optical properties, woodsmoke.

Black carbon (BC) concentrations were monitored inside and outside of a pulmonary hospital in Golnik, Slovenia for a month in summer and a month and a half in late autumn and winter 2006. Three dual wavelength (370 nm, 880 nm) Aethalometer™ instruments with size selective inlets were installed to measure aerosolized BC with aerodynamic diameter of 2 μm or less. BC concentration according to the day of week was analyzed. Concentration time series of an outside location (OUT) and two inside locations (hall IN1, and patient room IN2) were cross correlated for both infra-red and ultra-violet channels separately.

Black carbon concentrations inside and outside the Golnik hospital were shown to be low during month and a half long autumn measurements. Median BC concentration was around 1200 ng/m^3.

Indoor and outdoor concentrations are well correlated. Large number of samples and various signal processing gave time delay estimations for the infra-red and ultra-violet channels. Both results are consistent and show that indoor concentrations follow the outdoor concentration. General indoor/outdoor time delay is calculated to be 30 minutes in late autumn / winter and zero in summer (due to open windows). Weekdays and weekends had different diurnal characteristics. Various methods of dealing with loading effects and missing data gave similar time delays between locations.

Table 1. Correlation between locations.

IN1/OUT		IN1/IN2		OUT/IN2	
IR	UV	IR	UV	IR	UV
0.72	0.80	0.82	0.92	0.70	0.79

The ratio of absorption coefficients β at 370 nm and 880 nm is a metric we have used to study the change of composition of light absorbing carbonaceous aerosol. The ratio showed a substantial increase from the summer value of around 2,5 (as expected for a completely black aerosol with β~λ^{-1}) to values higher than 3 in late autumn / winter. This was attributed to increased absorption in the UV due to wood combustion in the village in which the hospital is situated. The increase was characteristic outside and inside the hospital.

The results suggest that outdoor combustion, of which BC is a primary tracer, greatly influences indoor air in the hospital. Concentrations and composition of carbonaceous aerosol outside and inside the hospital appear to be the same.
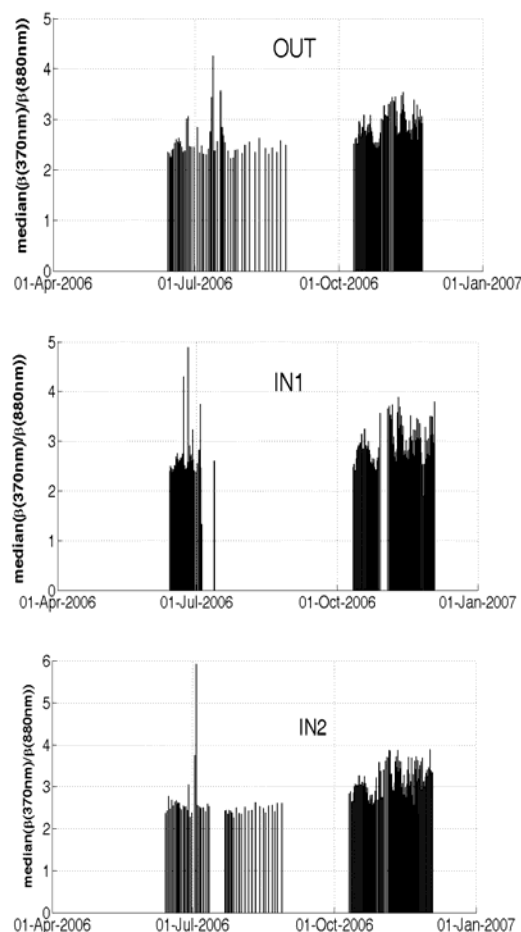

Figure 1. Median ratio of absorption coefficient β at 370 nm and 880 nm for locations OUT, IN1 and IN2.

Aerosol particles in the Baroque library hall of the National Library in Prague

L. Ondráčková and J. Smolík

Laboratory of Aerosol Chemistry and Physics, Institute of Chemical Process Fundamentals AS CR, v.v.i.,
165 02, Prague, Czech Republic

Keywords: particulate matter, indoor air quality.

Aerosol particles are one of the major pollutants in outdoor and indoor air. Together with adverse health effect they may negatively influence also ecosystems and cultural heritage. In outdoor environment particles deposit on the surface of buildings and statues, indoors particles deposit on the objects of art at museums and show rooms and on the surfaces of books and documents in libraries and archives. Coarse particles are abrasive in nature and they can damage works of art by mechanical abrasion when artefacts are moved or handled. Fine particles of acidic or alkaline character may penetrate into the books where they may cause chemical degradation or moistening due to their hygroscopicity (e.g. Bioletti and Goodhue, 2008; Hatchfield, 2002; Nazaroff et al., 1990). The aim of this study was to determine whether and how much visitors influence aerosol concentration in the Baroque library hall.

Measurement was performed during 10 days' intensive campaign. Aerodynamic Particle Sizer (APS) was used for measurement of particle number size distribution, DustTrak measured PM_1 concentration and Indoor Air Quality Monitor PS32 monitored temperature, relative humidity and CO_2 concentration. Sightseeing tours took place every day from 10 a.m. till 7 p.m.; from Monday till Thursday the tours started every hour and from Friday to Sunday every half-hour.

Results of particle number concentration measured with APS were divided into 4 size fractions (≤ 1 μm, 1-2 μm, 2-5 μm a 5-20 μm) and recalculated to the mass concentration (μg·m^{-3}). Recalculation was done on assumption that each size fraction is represented by spherical particles with GMD corresponding to the GMD of the recalculated size interval and with density of 1g·cm^{-3}. This conversion does not provide real mass concentration, but allows us to compare changes of concentration during visiting hours. Time behavior of small particles concentration (≤ 1 μm) showed that visitors did not affect the fine particle concentration and that these particles most likely came from outdoor environment. Concentrations of other size fractions (1-2 μm, 2-5 μm a 5-20 μm) and CO_2 showed periodical rising starting at the beginning of opening hours (about 10 a.m.), with maxima achieved at the end of visiting hours (about 7 p.m.) and subsequent decrease to beginning values (e.g. Fig. 1a). The CO_2 concentration chart (see Fig. 1b) shows the same periodicity like in the case of coarse particle concentration. Influence of visitors on the aerosol concentration in Baroque library hall was determined by comparing of average concentration measured during non-visiting hours and mean value obtained during visiting hours. Aerosol concentration was at an average 6 times higher during visiting hours than during non-visiting hours.
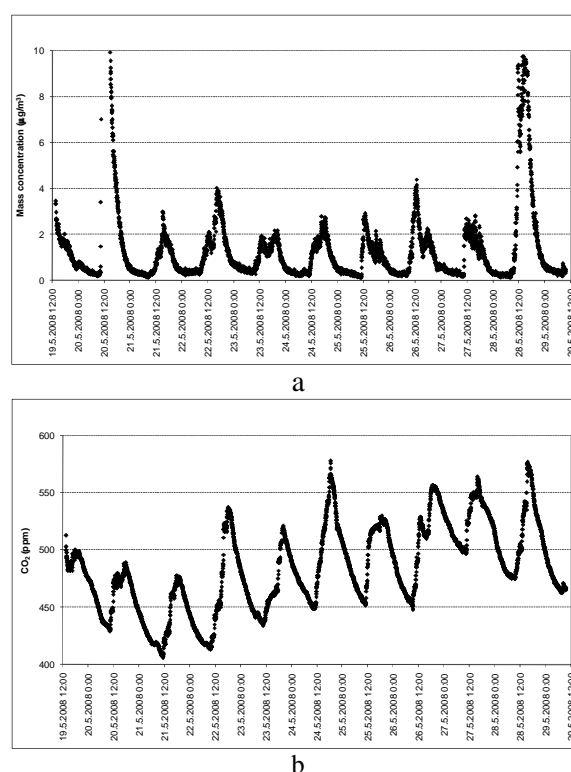
Figure 1. Time series of mass concentration of fraction 2-5 μm (a) and CO_2 concentration (b).

Bioletti, R. and Goodhue, R. (2008). *Proc. 8th Indoor Air Quality 2008 Meeting,* 17th-19th April 2008, Vienna, Austria.

Hatchfield, P. B. (2002). *Pollutants in the Museum Environment: Practical Strategies for Problem Solving in Design, Exhibition and Storage.* Archetype Publications, London.

Nazaroff, W. W., Salmon, L. G. a Cass, G. R. (1990). *Environ. Sci. Technol.*, 24, 66-77.

Indoor levels of particulate pollution in urban and rural environments in Pakistan

Ian Colbeck[1] , Zaheer Ahmad Nasir[1] and Zulfiqar Ali[2]

[1]Department of Biological Sciences, University of Essex, Colchester, CO4 3SQ, U K
[2]Departments of Wildlife and Ecology, University of Veterinary and Animal Sciences Lahore

Keywords: Indoor air quality, mass concentration, number concentration

Particulate pollution has emerged as a serious environmental health concern in Pakistan. The country is suffering from deterioration of air quality due to high population growth, absence of public transport and a significant increase in private vehicles. Additionally, rural areas experience high levels of indoor air pollution due to the use of biofuels as an energy source. In Pakistan, almost 70% of the population lives in rural areas and use wood, dung, crop residue or natural gas as a fuel for cooking and heating. Despite the evidence that air quality, both indoors and outdoors, is deteriorating with enormous speed very little work has been done in this regard.

Measurements of particulate mass and number concentration have been made at two rural sites (Chak NO.35/2.L. and Bhaun) and one urban site (Lahore). Three measurement campaigns were carried out in winter, summer and spring to understand the dynamics of particulate pollution. The sampling was conducted in kitchens (using either biomass fuel or natural gas) and living rooms all the sites continuously for a period of one week in each setting. Mass concentration of particles (PM10, PM2.5, PM1) was monitored using two different GRIMM: analysers (Model 1.108 and Model 1.101) while the number concentration was measured with Condensation Particle Counter (TSI 3010, 3781). The data on temperature, humidity, housing characteristics and occupant activities was also recorded.

The values of the number concentration in a living room at Lahore were in the range 13,771 - 181,029 cm^{-3}. While at rural sites a maximum concentration of 156,056 cm³ was obtained. On the other hand, the highest number concentrations were recorded in the urban kitchen using natural gas (245,803 cm^{-3}) as compared to rural kitchens using biomass fuel (219,609 cm^{-3}) and natural gas (226,231cm^{-3}). With reference to the mass concentration of particulate matter, rural kitchens using biomass fuels had an average concentration of 2,000 – 4,000 µg/m^3 with a maximum of 8,000µg/m^3 (Figure 1). Whilst, in kitchens using natural gas at both rural and urban sites average concentrations were of 900 - 1300 µg/m^3 with the highest of 5,000 µg/m^3.
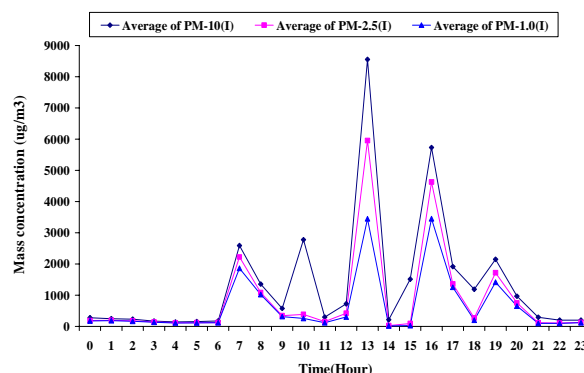
Figure 1. Mass concentration of PM10, PM2.5 and PM1 in a kitchen using solid mass fuel at rural site in Pakistan

While in the living room in Lahore and rural sites it was generally in the range 131 µg/m^3 to 1,200 µg/m^3 (Figure 2). The concentrations were generally higher in rural living rooms as compared to urban ones. During smoking and cleaning the concentration could rose up to 7,854 µg/m^3.
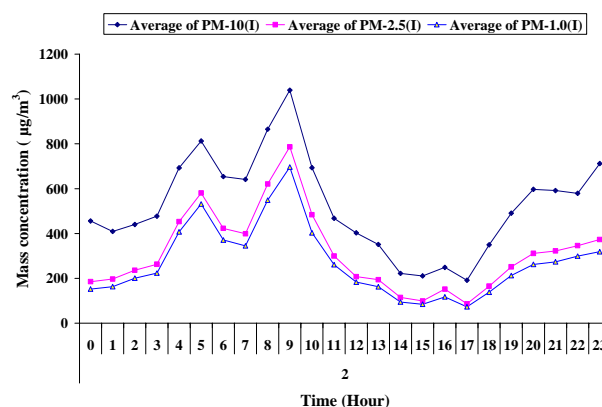
Figure 2. Mass concentration of PM10, PM2.5 and PM1 in a living room at an urban site in Pakistan

The present study showed considerably high concentrations of particulate matter particularly in the kitchen using biomass fuel as compared to living areas. Thus women and children are exposed the most due to amount of time spent in the kitchen. The mass and number concentration of particulate matter in urban and rural settings was well above of any standards for particulate matter pollution

Particulate matter size distribution of main indoor sources: measurements in a real scale chamber

D.E. Saraga[1,3], T. Maggos[1], C. G. Helmis[2] , A. Passa[2], C. Vasilakos[1] and J. G. Bartzis[3]

[1]Environmental Research Laboratory/INT-RP, National Centre for Scientific Research "DEMOKRITOS", Aghia Paraskevi Attikis, P.O.B. 60228, 15310 Athens, Greece
[2]Department of Environmental Physics and Meteorology, Faculty of Physics, University of Athens, University Campus, building PHYS-5, 157-84 Athens, Greece
[3]Department of Energy Resources Engineering, University of Western. Macedonia, 50100 Kozani, Greece

Keywords: indoor sources, size distribution, measurements.

Exposure to fine and ultrafine particles has been identified as an important factor affecting human health. These particles make a very small contribution to the mass distribution, but they represent a major part of the number distribution. Currently, there is a trend to associate respiratory health effects with the number concentration or surface area of particles (Mitsakou et al., 2007).

A specially constructed room in NCSR Demokritos was converted to a full-scale, walk-in chamber of 18 m^3 for the purpose of the measurements. All the experiments were conducted twice, in order to study the mass/volume and particle number/volume concentration in fourteen different size channels. Prior and after each test, intensive cleaning of all the surfaces took place. Furthermore, uniforms and shoe coverings were put on by the technician who was entering the room. A complete mixing of the internal air was ensured by the use of a table fan which was in operation during all the experiments. An automatic portable aerosol spectrometer (Grimm 1.108) was used for measuring particles from 0.23 μm to >20 μm in diameter (for the mass mode) and from 0.30 μm to >20 μm (for the particles number mode). Indoor air temperature, relative humidity and external light intensity were continuously recorded by a HOBO 08 thermometer. The average air exchange rate in the chamber was 0.51 ± 0.05 h^{-1}, measured by the tracer gas decay rate technique. The spectrometer was placed at 1m above the floor level and an 1-minute sampling interval was chosen for monitoring. The sources which were examined are: cigarette smoking, cleaning spray use, hair spray use, scented sticks burning, vacuuming, meat frying, cooking on a grill, making toasts, ironing, walking on a carpet, walking on floor, and pillow dusting.

Results indicated that a number of sources which were tested, produced high particles concentration, measured either as mass/volume or as number of particles/volume (table 1). Of course, concentration levels and size of particles emitted, should be examined simultaneously. Among sources tested, hair spray use produced the largest amount (in mass) of –coarse- particles, followed by grill cooking and pillow dusting. Regarding particle number/volume measurements, meat frying and grill cooking produced the largest amount of particles, mainly of fine and coarse fraction as expected (Afshari et al., 2005).

Table 1. particle size channels influenced during activity and maximum concentrations measurements

activity tested	particles size (μm)	max. concentration (μg/m^3)	max. concentration (particles/cm^3)
toaster	0.8-1.0 and 4.0-5.0	25	141
cleaning spray	1.6-5.0 and 7.5-10.0	52	53
vacuuming	0.4-1.6 and 10.0-15.0	54	42
walking on floor	7.5-10.0	69	2
ironing	0.30-1.6	97	1841
scented sticks	0.65-0.8	102	260
meat frying	0.23-7.5	106	12223
walking on carpet	7.5-10.0	375	8
cigarettes smoking	0.23-0.65	757	3279
pillow dusting	7.5-15.0	3173	2
grill cooking	1.6-20	7278	10569
hair spray	5.0-7.5	36454	2521

Based on the above, sources related to resuspension (walking on a carpet/on floor, pillow dusting and vacuuming) correspond to bigger particles sizes i.e. >7.5μm. Especially for vacuuming, two size modes were noticed, as with the exception of resuspension, emissions from the mechanical part of the vacuum occur. Sources associated with cooking (grill, frying, toasting) emit both fine and coarse particles because of the heated surfaces' emissions and vapor production. A remarkable difference between the two kinds of spray is noticed. Although the same spraying duration, mass and number of particles produced is significantly elevated. Further results and discussion about the sources' profiles tested will be presented.

Afshari A., Matson, U. and Ekberg, L.E. (2005). *Characterization of indoor sources of fine and ultrafine particles: a study conducted in a full-scale chamber.* Indoor Air, 15, 141-150.
Mitsakou C., Housiadas C., Eleftheriadis K., Vratolis S., Helmis C., Asimakopoulos D. (2007). *Lung deposition of fine and ultrafine particles outdoors and indoors during a cooking event and a no activity period.* Indoor Air, 17, 143-152.

Behaviour of well defined aerosol particles in a test chamber

J. Ondráček[1], M. Brand[2], M. Barták[2], L. Džumbová[1] and J. Smolík[1]

[1] Laboratory of Aerosol Chemistry and Physics, Institute of Chemical Process Fundamentals, v.v.i., Academy of Sciences of the Czech Republic, Rozvojova 135, Prague 6, 165 02, Czech Republic
[2] Department of Environmental Engineering, Faculty of Mechanical Engineering, Czech Technical University, Technicka 4, Prague 6, 166 07, Czech Republic

Keywords: indoor aerosols, particle deposition, coagulation, ventilation system.

Deposition of aerosol particles in various test chambers and real indoor environments has been studied extensively during last decades (e.g. Nazaroff and Cass, 1989; Hussein et al., 2009). Several different mechanisms of particle removal from the air exist in the indoor environment (gravitational settling, Brownian and eddy diffusion, thermophoresis, electrostatic drifting and coagulation). Keeping constant temperature and conductive surfaces within the measurement chamber we can concentrate only on the major deposition mechanisms, such as gravitational settling, diffusion and coagulation. This study represents continuation of our previous research in the field of indoor aerosols including the test chamber studies with different surface materials and measurements conducted in the real apartment.

During the study an intensive indoor measurement campaign in a test chamber was conducted. The campaign included measurements of size resolved mass and number concentration, monitoring of temperature, relative humidity and pressure inside and outside the test chamber. Influence of several operational parameters on particle deposition was studied (see Figure 1.). It included different mixing intensity inside the chamber (2), ventilation rates (5) and particle size (7). Two aerosol generators were used as a source of well defined aerosol particles. The data obtained during the study will serve as a basis for consecutive modeling using Multi-Compartment and Size-Resolved Indoor Aerosol Model (MC-SIAM, e.g. Hussein et al., 2009) and Fluent with Fine Particle Model.

The dimensions of measurement chamber were 360x420x300 cm having the total volume of 45.4 m^3. The chamber was carefully sealed and the floor was covered with zinc coated metal plates to increase the conductivity and hence decrease the influence of electrostatic charge on particle deposition rates. The measurement campaign was split into two phases. The first phase covered measurement of coarse particles (> 1 μm). Particle size distribution inside and outside the chamber was measured using aerosol spectrometer APS 3321 (TSI) and the dynamic behaviour of particles inside the chamber was observed using 3 photometers

DustTrak. The photometers were placed in three different locations (vertically and horizontally). Well defined coarse particles were generated using MAG 3000 aerosol generator (DEHS particles with NaCl core). The second phase comprised of fine particle measurements (< 100 nm, $(NH_4)_2SO_4$ particles generated using AGK 2000). Particle size distribution inside and outside the chamber was measured using aerosol spectrometer SMPS 3936 (TSI). The dynamic behaviour of the particles was monitored using particle counter CPC 3775 (TSI) with four inlets placed in different locations within the chamber. Switching among individual sampling places was provided with the controlled system of electrically driven valves. The mixing of the injected aerosol particles was provided with two office fans. The ventilation of the chamber was assured by means of the efficient filter at the inlet and the vacuum pump at the outlet of the chamber.
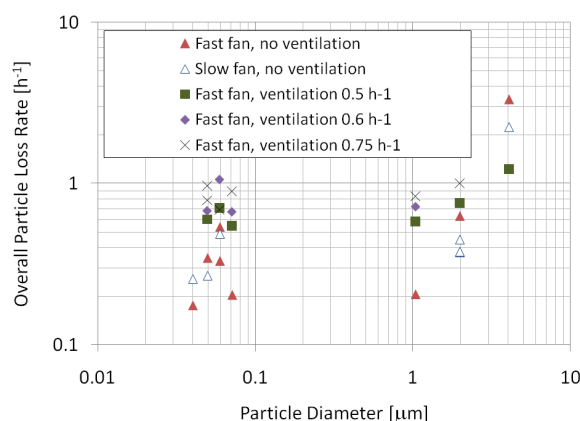
Figure 1. Overall particle loss rate during different experimental scenarios.

Nazaroff, W. W., & Cass, R. G. (1989). *Environment International,* 15, 567-584.
Hussein, T., Hruška, A., Dohányosová, P., Džumbová, L., Hemerka, J., Kulmala, M., Smolík, J. (2009). *Atmospheric Environment*, 43, 905-914.

Assessment of indoor aerosol sources from measurements of Number Size Distribution and Chemical Composition by means of Positive Matrix Factorization

A.A. Karanasiou[1], S. Vratolis[1], M. Lazaridis[2] and K. Eleftheriadis[1]

[1] Institute of Nuclear Technology and Radiation Protection, Environmental Radioactivity Laboratory, National Centre of Scientific Research "Demokritos", 15310 Ag. Paraskevi, Attiki, Greece
[2] Department of Environmental Engineering, Technical University of Crete, Greece

Keywords: PMF, indoor aerosols, indoor particles, indoor sources, source apportionment

Indoor exposure of humans to particulate matter depends on a number of key parameters and processes. Occupants and their activities, the outdoor aerosol concentration and the ventilation rate are those parameters considered highly important in indoor air quality (Lazaridis et al., 2008). The objective of the present study is to identify and characterize indoor aerosol sources using both elemental concentrations and number size distribution data. Positive Matrix Factorization analysis (PMF) was employed in this type of indoor aerosol data.

Measurements of the indoor aerosol size distribution were carried out in three typical apartments located in the Athens urban area. The size resolved aerosol number concentration was obtained at five minutes intervals using a Scanning mobility particle sizer for the fraction between 10 – 550 nm expressed in mobility diameter (SMPS, DMA model 3071 and CPC 3022A, TSI Inc., USA). The indoor aerosol mass concentration was also determined using a three-stage Dekati impactor. Trace metals and water soluble ions were determined on a 24h basis. Black carbon concentrations (BC) were measured by means of an aethalometer. Only non-smoking residents were considered in this study. Human activity (presence of people, ventilation, vacuuming and cooking) in every flat was recorded in a diary.

PMF analysis based on particle size distribution data revealed four sources, Figure 1. The source profiles were identified by relating source contributions with human activity indoors. The first source was assigned to new particle formation mostly associated with cooking (Factor 1). Three outdoor sources were also resolved, related to traffic and other combustion sources (Factor 2, Factor 3), or secondary aerosol in the accumulation mode (Factor 4). High contribution of these outdoor sources to the indoor aerosol number concentrations coincided with periods of increased air exchange between indoors and outdoors. These results suggested that penetration of outdoor particles is the most important parameter significantly affecting the indoor air quality. BC concentrations showed a moderate positive correlation with at least two of those outdoor sources (Factors 3 &4).

Elemental, ionic and black carbon concentrations were also subjected to PMF analysis. The chemical profile of the resolved sources was found to be dominated by Fe, Ca, K and Na. Pearson's correlation coefficient between the resolved source contributions and elemental concentrations suggested possible tracers for indoor aerosol sources. Specific metals like Fe may be released during the cooking process (Chao and Cheng, 2002).

Figure 1. Number size distribution of the resolved sources
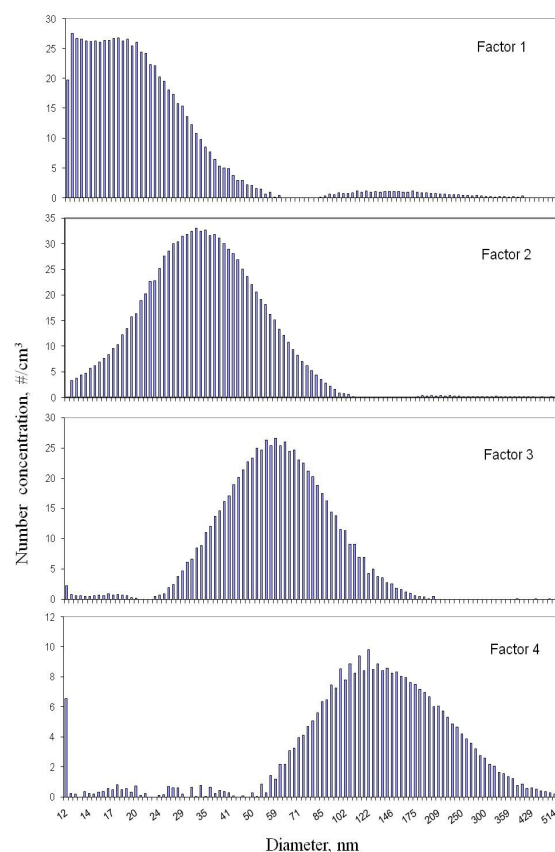
References
Chao C.Y., Cheng E.C., (2002), *Indoor Built Environ*, 11**,** 27-37
Lazaridis M., V. Aleksandropoulou; J.E. Hanssen C. Dye; K. Eleftheriadis; E. Katsivela (2008), *Air & Waste Manage. Assoc.* 58:346-356

Determining the effect of a car park on the indoor air quality of a hospital

N. Bleux*, R. Brabers*, M. Van Poppel*, P. Berghmans*, M. Stranger*, R. Torfs* & L. Int Panis*,**

* Flemish Institute for Technological Research (VITO), Boeretang 200, 2400 Mol, Belgium
email : nico.bleux@vito.be
** Transportation Research Institute, University of Hasselt, Belgium

Keywords: indoor air quality, vehicle emissions, ultra fine aerosols, hospital

Indoor air quality is a special concern in hospitals. Often higher standards of indoor air quality are pursued, not only in specific hospital wings like intensive care but also in patient rooms and public areas. In cases where the hospital's public car park is located close to the hospital, vehicle emissions can cause concerns with respect to the infiltration of air pollutants inside the hospital. In this specific case the department of lung oncology was located within 5 meters of a 2 stories high parking lot. When during the summer certain windows were opened to compensate for the limited capacity of the air-conditioning typical vehicular odors were observed by the medical staff, and there was concern over the health of both medical staff and patients.

The objective of this study was to examine the spatial distribution of the ultra fine particle in the neighborhood of the car park and to asses the possible infiltration of the vehicle emissions inside the hospital.

We performed mobile dust mappings in and around the car park to assess the spatial distribution of the vehicular emissions with a newly developed dust mapping tool (AëroFlex – see fig 1.) which consisted of portable ultra fine monitors and a GPS-logger. We combined these results with indoor air quality measurements of fine and ultra fine particle to examine the effect of open and closed windows.

When all windows were closed we measured indoor ultra fine particle concentrations around 2 000 particles /cm³ when outdoor concentrations were on average around 12 000 partcles/cm³. These low indoor concentrations were attributed to an adequate ventilation system based on overpressure.

Opening windows led to the loss of this overpressure, allowing indoor ultra fine particles levels to approach outdoor particle levels within a few minutes. Measurements in the window slit clearly showed vehicular emissions flowing into the room.
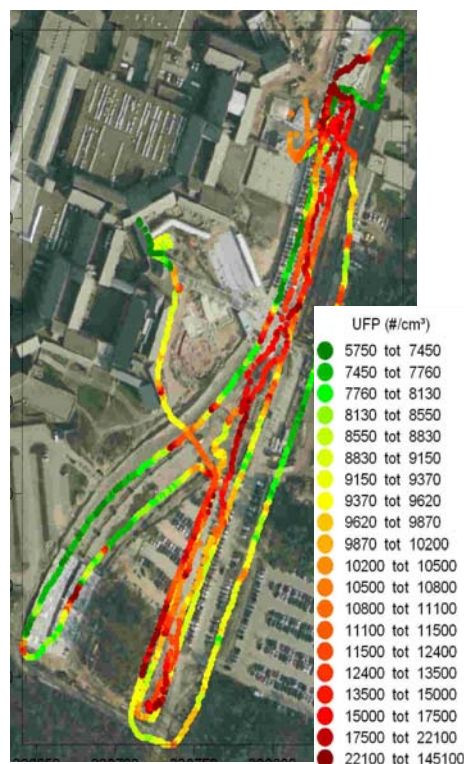

Figure 1: Dust mapping of ultra fine particles on and around a hospital car park

Hygroscopic and volatility properties of particles emitted by office equipments

H. Wang[1], G. Johnson[1], R. L. Modini[1], C. He[1], L. Morawska[1], R. Jayaratne[1], T. Salthammer[1,2], E. Uhde[2], T. Bostrom[1], G. Ayoko[1], P. McGarry[1], M. Wensing[2]

[1]International Laboratory for Air Quality and Health, Queensland University of Technology, GPO 2434, Brisbane QLD, 4001, Australia
[2]Fraunhofer Wilhelm-Klauditz-Institute, Material Analysis & Indoor Chemistry, Bienroder Weg 54 E, 38108, Braunschweig, Germany

Keywords: Indoor aerosols, Particle characterization, Submicron particles, Hygroscopicity, Volatility

Recent studies (Destaillats *et al.*, 2008) have shown that the operation of office equipment can be a significant source of ultrafine particles (<0.1μm). He *et al.* (2007) reported a third of the popular brands of laser printers had emitted large numbers of particles. The nature of the generated particles, however, is still not fully explained.

The hygroscopic and thermal decomposition behavior of particles emitted by a laser printer was investigated for varying levels of toner coverage and when operating without paper and/or toner. The measurements were conducted using a Volatility and Hygroscopic Tandem Differential Mobility Analyzer (VH-TDMA) (Johnson *et al.*, 2004). The hygroscopic and volatility properties of particles in the dominant size range were examined after they were introduced to a box chamber. Particles emitted by fuser rollers, paper, toner powder, and lubricant oil when heated in controlled-temperature flow-through furnace were also studied in this way.

Particle volatilization is shown in Figure 1(a) and Figure 2. The volatilization started at around 60 °C, and 50% volume of the generated particles was lost at about 110 to 130°C. The shape of the volatilization curve for 50% coverage is similar to that for heated toner powder with a volume increase of up to 20% occurring in temperature range of 70 – 105 ^{0}C, which indicates the presence of a species with characteristics different from those of the species produced during experiments where no toner powder was involved. Furthermore, the difference in volatility between 0% coverage and without paper demonstrates that paper made a contribution to particle generation during printing.

Figure 1(b) presents the hygroscopicity of the generated particles at RH = 90%. The particles were non-hygroscopic throughout the volatilization temperature range although in some cases the particle hygroscopic growth factor (Dh/Dv) showed a negative growth as temperatures exceeded 105 ^{0}C. This effect may have resulted from the collapse of the residual internal core when exposed to high humidity.

Therefore, the printer-emitted particles are non-hygroscopic and somewhat volatile.
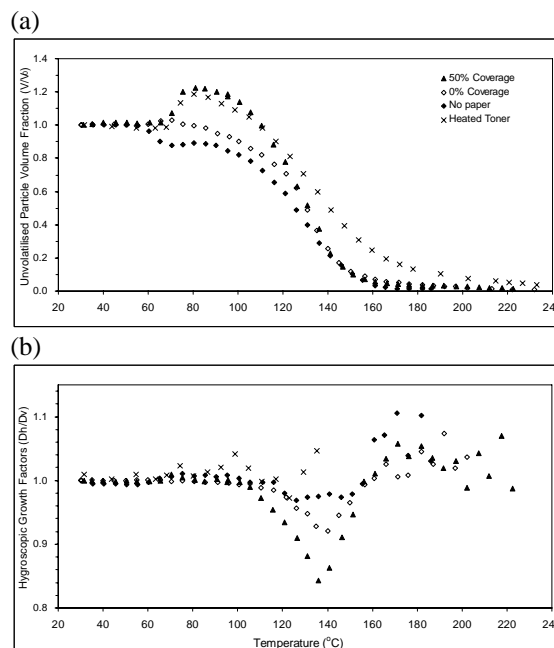
Figure 1. VH-TDMA spectra of 50 nm particles generated by a laser printer or heated toner powder, showing (a) the relative volume after volatilization; and (b) the hygroscopic growth factors versus thermodenuder temperature.
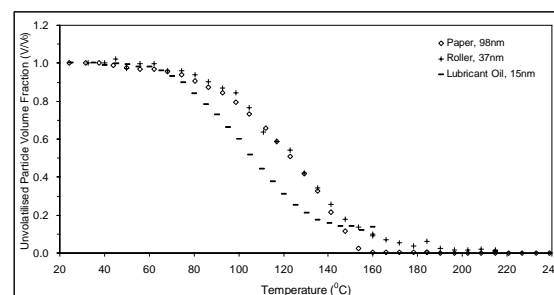
Figure 2. Volatilization temperature curve for particles generated by the paper, fuser roller, and lubricant oil, measured by the VH-TDMA. Initial particle sizes are given in the legend.

Destaillats, H., Maddalena, R. L., et al. (2008). *Atmos. Environ.*, 42 (7), 1371-1388.
He, C., Morawska, L., & Taplin, L., (2007). *Environ. Sci. Technol.*, 41 (17), 6039-6045.
Johnson, G., Ristovski, Z., & Morawska, L. (2004). *J. Aerosol Sci.*, 35 (4), 443-455.

Pathways of ultrafine particles generated by laser printers

H. Wang[1], L. Morawska[1], C. He[1], G. Johnson[1], R. Jayaratne[1], T. Salthammer[1,2], E. Uhde[2], T. Bostrom[1], R. L. Modini[1], G. Ayoko[1], P. McGarry[1], M. Wensing[2]

[1]International Laboratory for Air Quality and Health, Queensland University of Technology, GPO 2434, Brisbane QLD, 4001, Australia
[2]Fraunhofer Wilhelm-Klauditz-Institute, Material Analysis & Indoor Chemistry, Bienroder Weg 54 E, 38108, Braunschweig, Germany

Keywords: Indoor aerosols, Fine aerosol, Particle formation, Generation of nanoparticles

Ultrafine particles (<0.1μm) are emitted from printers, and this may result in an elevation of the particle number concentration in the office environment, as reported in recent years (*He et al.*, 2007; Destaillats *et al.*, 2008). However, no studies have been conducted to reveal the possible pathways of how these particles are generated. From the present study, we propose four possible pathways for producing ultrafine particles during printing.

A series of specially designed experiments were conducted in a box chamber or a flow through tunnel to investigate the formation processes of particles emitted from a "high" emission laser printer. The total particle number concentrations and particle size distributions in the submicrometer size range were measured by a condensation particle counter and a scanning mobility particle sizer, respectively. Ozone and total volatile organic compounds (TVOC) concentrations were also monitored.

No ultrafine particles were observed when the printer was operated without fuser heating in the flow through tunnel. This clearly demonstrates that the temperature is the key factor controlling printer particle generation, and, due to their strong relationship with temperature, suggests that SVOCs and VOCs vaporized from printer components are involved in the particle formation processes.

PATHWAY I: The printer was made to operate without paper (and without the release of toner for printing) in a chamber for consecutive intervals of about 20s. Despite being about one order of magnitude lower than for normal printing, the particle concentration showed a significant increase over the time of the print run. Particle production continued but at lower rates when neither toner nor paper were involved in the process. This suggested that the fuser roller itself was not the main contributor to the particle emission, but that some vaporizable residues on the fuser roller made a contribution to the particle formation. Therefore it is probable that evaporation and then condensation of the residues and/or deposited SVOCs on the fuser roller is a pathway for the formation of particles. The result was confirmed by the flow through tunnel tests, in which the particle count median diameter during the first 2 min after printing was larger than that of subsequent particles due possibly to the contribution of the above pathway during the printer warm-up stage.

PATHWAY II: In the flow through tests, the printer was operated to produce 0% toner coverage on the printed paper with an unused fuser roller (no toner or paper residues). The numbers of particles observed were lower than those in other tests with the used roller, and varied over a range of three orders of magnitude. Assuming that the emission condition of the fuser roller itself and the paper were almost consistent during all the tests, the great variation in particle numbers may have resulted from the random passage of small amounts of toner powder which occasionally fell out of the hopper and were brought to the fuser. It indicated the possibility of particle generation through the condensation of SVOCs volatized from the toner powder when it was heated by the fuser.

PATHWAY III: A chemical reaction was believed to be involved in the particle formation as an important pathway. Two relationships were seen in the chamber tests: (1) the positive correlations between ozone concentrations and submicrometer particles; and (2) the contrasting negative correlation between TVOC concentrations and submicrometer particles (Morawska *et al.*, 2009). They indicated that the reactions between ozone and VOCs also played a significant role in the particle generation. However, its importance relative to direct volatilization and nucleation of SVOCs released directly from toner deposits cannot be quantified at present.

PATHWAY IV: All the chamber and tunnel tests were performed with a particle-free background, which means that no preferential nuclei were supplied and only homogeneous nucleation occurred. Therefore, the fourth pathway of particle formation in relation to printers is heterogeneous nucleation which may be predominant in the real environment.

He, C., Morawska, L., & Taplin, L., (2007). *Environ. Sci. Technol.*, 41 (17), 6039-6045.

Destaillats, H., Maddalena, R. L., et al. (2008). *Atmos. Environ.*, 42 (7), 1371-1388.

Morawska, L., He, C., Johnson, G., et al. (2009). *Environ. Sci. Technol.*, 43 (4), 1015-1022.

OZONE INITIATED SOA FORMATION OF COMBUSTION AEROSOLS

J. PAGELS[1], M. LINDSKOG[1], E. NILSSON[1], E. SWIETLICKI[2], M. BILDE[3] and M. BOHGARD[1]

[1]Ergonomics and Aerosol Technology, Lund University, Box 118, 221 00, Lund, Sweden
[2]Department of Physics, Lund University, PO Box 118, SE-221 00, Lund, Sweden
[3]Department of Chemistry, Univ. of Copenhagen, Universitetsparken 5, 2100 København Ø, Denmark

Keywords: INDOOR AIR, OZONE, AEROSOL MASS SPECTROMETRY, SOA FORMATION

Recently it has been shown that organic aerosols from incomplete combustion such as emissions from diesel engines are significantly transformed upon atmospheric ageing (Robinson et al. 2007). The particle mass emission factors increases due to gas-to-particle conversion upon exposure to UV-light. We hypothesize that these effects are generic also for other types of combustion aerosols and oxidants. The aim of this work is to test this hypothesis by investigating processing of indoor combustion aerosols upon exposure to elevated ozone concentrations.

Incenses and sidestream cigarette smoke of market leading brands were generated in a controlled manner in the Lund aerosol chamber (22 m^3, stainless steel chamber). After a desired particle concentration (30, 60 or 100 μg/m^3) was established, the chamber was sealed. Two types of experiments (each 2-5 hours long) were performed, reference experiments with no added ozone and experiments where 100 or 400 ppb ozone was added after 20 min using an ozone generator (Ozone Technology). The ozone level was monitored using a UV spectrophotometric ozone monitor (model 49, Thermo Andersen). The particle size distribution and number concentration was determined using a scanning mobility particle sizer (model 3934, TSI Inc.). The chemical composition of fresh and aged aerosol particles was studied using a High-Resolution Time-of-Fight Aerosol Mass Spectrometer (HR-TOF-AMS; Aerodyne Research Inc.). The total mass concentration (PM1) was determined from the SMPS number size distribution using particle effective densities, which were empirically determined by comparing mobility (SMPS) and vacuum aerodynamic diameters (AMS).

Decrease in mass concentration over time in reference experiments were due to wall losses and some evaporation during the initial part of the experiment. As ozone was introduced into the chamber a rapid increase in mass concentration took place. For sidestream cigarette smoke the mass increase relative to the reference measurement is about 70% at 400 ppb ozone, and about 40% at 100 ppb ozone. Similar effects were found for incenses. It was found that concentrations of oxidised fragments detected with the AMS increased rapidly as ozone

was added (fig 1). This shows that the condensed material is highly oxidised, compared to the hydrocarbon dominated primary particles. The elemental composition showed increased oxygen to carbon ratio and increased nitrogen concentration after ozone addition.
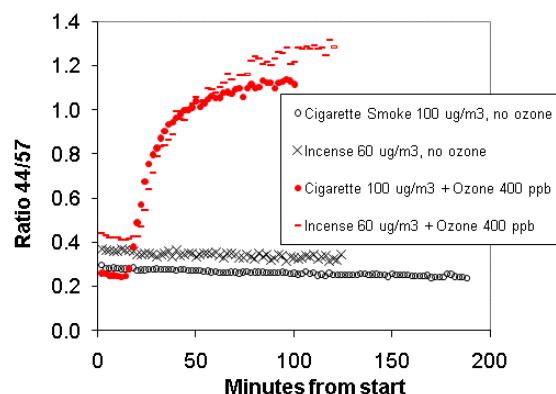
Figure 1. Time dependence of the ratio of two major fragments detected with AMS. m/z 44 (mainly CO_2^+) is a marker for oxidised organics, m/z 57 (mainly $C_4H_9^+$) is a marker for hydrocarbon like organics.

These effects are rapid enough to be relevant for indoor air (10-15 min). Health effects of aged particles are almost certainly different from those of fresh particles. Future experiments are planned to involve other combustion aerosols, such as wood smoke and traffic emissions and other oxidants, for example UV-light.

Robinson AL, Donahue NM, Shrivastava MK, et al. (2007) SCIENCE 315, 1259-1262

Indoor and outdoor PM concentrations measured in schools and in retirement homes in Milan.

B.S. Ferrini[1], L. Ferrero[1], z. Lazzati[1], C. Lo Porto[1], M.G. Perrone[1], S. Petraccone[1], G. Sangiorgi[1], E. Bolzacchini[1], F. Cetta[1], M. Sala[2]

[1]POLARIS research center, DISAT, University of Milano Bicocca, Piazza della Scienza 1, 20126, Milano, Italy
[2]Uiversity of Milan, Clinica Pediatrica Azienda Ospedaliera San Paolo via di Rudinì 8, Milano, Italy

Keywords: indoor/outdoor particles, PM, optical particle counter.

PM concentration in Milan is very high during autumn and winter (Rodriguez et al., 2007), so exposure of children and old people, which are more predisposed to asthma and chronic obstructive pulmonary disease (COPD) (Pope & Dockery, 1999) is crucial. In particular it could be very important to asses the real exposure of such people; in this way it becames very important to combine the ambient PM exposure among the indoor PM exposure where these peoples spend their time mostly in a day. In this study we measured PM concentrations in two primary schools and in two retirement homes located one at the periphery and one in the centre of the city, to define the pollution effects on the health of children and old people.

Simultaneous indoor and outdoor PM10, PM2.5 and PM1 concentration measurements are conducted. Data are collected using an optical particle counter (OPC Grimm 1.108 "Dustcheck") in indoor and an optical particle counter (OPC Grimm 1.107 "Environcheck") in outdoor with a time resolution of 5 minutes. These instruments are choosen because an high temporal resolution is needed to verify the existence of internal emission. Reference instruments are gravimetric sampler, so a correlation between PM daily average values from OPC and daily gravimetric PM downloaded from ARPA Lombardia internet site (www.arpalombardia.it) has been calculated. The correlation is very high ($R^2 = 0.95$ for PM10, $R^2 = 0.89$ for PM2.5) and assure a good valuation of PMx concentration.

Measurements conducted in the schools evidence that indoor concentrations exhibited a great temporal variability, with an increase in concentration in the morning, when children started their school activity, and a decrease in the late afternoon. Data were divided into two set, one from 7.30 in the morning, until 18.30 in the afternoon (day), and the other one for the hours during the closing time of the school (night). Ratio beetween PMx concentration measured during the day and during the night are shown in table 1.

	PM1_i/PM1_o	PM2.5_i/PM2.5_o	PM10_i/PM10_o
Day	1.01	1.48	4.11
Night	0.75	0.78	0.75

Table 1. Ratio between PMx concentration in the day and in the night.

During the day, in both schools, indoor PMx concentration is higher than outdoor, but PM10 is the highest of all. This phenomenon is due to a coarse particle resuspencion by school activity. Infact, the concentration increase simultaneously to the school opening, and mostly in the coarse fraction. During night indoor concentrations decrease because of the particles deposition effect end the relation is the same for all the PMx considered.

In the retirement homes, the day and night trend is present, but during the day the incresing in PMx concentration in not so high as in the schools. Besides, indoor instruments were put in the dining rooms, so high PMx concentration are measured at dinner-time.

The ratio between indoor and outdoor concentration for all the PMx dimensional classes is presented in table 2.

	PM1_i/PM1_o	PM2.5_i/PM2.5_o	PM10_i/PM10_o
Day	0.73	0.81	0.97
Night	0.44	0.48	0.51

Table 2. Ratio between PMx concentration in the day and in the night.

Indoor concentration are always lower than outdoor concentration, contrary to values obtained in the schools analysed data.

In conclusion, PM concentrations in school and retirement homes have similar behaviours, but in school higher concentration are misured because of children activity.

Pope, C., & Dockery, D. (1999). Chapter 31. *Epidemiology of particle effects*. (pp. 673−705). San Diego: Academic Press.
Rodriguez et al. Atmos. Chem. Phys., 7, 2217-2232, 2007.

The portable cleaner device for filtration and sterilization of indoor air

J.S. Pastuszka[1], W. Mucha[2] and E. Marchwinska-Wyrwał[2]

[1]Department of Air Protection, Silesian University of Technology, 2 Akademicka St., 44-100, Gliwice, Poland
[2]School of Public Health, Medical University of Silesia, 18 Piekarska St., 41-902 Bytom, Poland

Keywords: aerosol cleaners, bioaerosols, indoor aerosols, indoor air quality.

Sometimes rapid improvement of the quality of indoor air is needed. In case when indoor environment is polluted by particulate matter and/or bioaerosol the portable air cleaners can be used. It should be noted that for the removing of airborne particles the simple filtration device is enough. However, to reduce the concentration of alive bacteria or fungi some sterilization techniques must be applied. In some areas, for example in Upper Silesia, Poland, some hospital buildings are located near the busy roads what means that the level of airborne particles, mainly PM2.5, is elevated there. Therefore, it is important in such buildings to reduce both the concentration of solid and biological particles.

In our study we tried to use for this purpose the Electron Wind Generator (EWG), made in USA, which is an air purification device using a sophisticated combination of electrode topology and specially designed high voltage power supply. First, the decrease in the concentration of particulate, bacterial and fungal aerosol in the selected rooms due to the work of the EWG device has been estimated. This decrease can be described as $C_{i,2}/ C_{i,1}$, where $C_{i,1}$ is the concentration of pollutant "i" when the cleaner does not work, and $C_{i,2}$ is the concentration of pollutant "i" when the cleaner works but after stabilization (i.e. when the concentration reaches the constant level). In our study the ratio $C_{i,2}/ C_{i,1}$ has been found for the selected rooms (one office room, one clinic waiting-room, two hospital rooms and one surgery room), depending on such parameters like number of persons occupying the room, room volume, ventilation rate, and so on. The example results are shown in Table 1.

Table 1. Example of the airborne bacteria (B) and fungi (F) concentration in the hospital room decreasing due to the work of the EWG cleaner.

	Background [CFU/m³]	After 2 hours [CFU/m³]	After 4 hours [CFU/m³]
(B)	168	63	49
(F)	341	261	84

The obtained results indicate that the EWG portable air cleaner can significantly reduce the concentration of airborne particles as well as the bacterial and fungal aerosols. In general, the investigated cleaner demonstrated the highest efficiencies with respect to bacterial contaminant and was least effective in the particles (TSP and PM5) removal. In the small room (30-40 cubic meters) without mechanical ventilation the ratio $C_{i,2}/ C_{i,1}$ was about 0.15 and 0.20 – 0.30 for the total viable bacteria and fungi respectively. In the large hospital surgery rooms with a heating and air-conditioning (HVAC) system the EWG device was marginally effective.

Unfortunately, due to the high voltage the significant emission of ozone during the work of this cleaner has been observed. Therefore, in the second part of our study we applied the carbon filter in the EWG device to reduce the emission of ozone. For such hybrid device we obtained the emission of ozone without and with the carbon filter 9.175 µg/min and 3.77 µg/min, respectively. This result indicates that the efficiency of the collection of ozone by the used coal filter is 60%. Figure 1 shows the changes of the ozone concentration in some studied room as a function of time of working the EWG cleaner without (upper curve) and with the coal filter (lower curve).
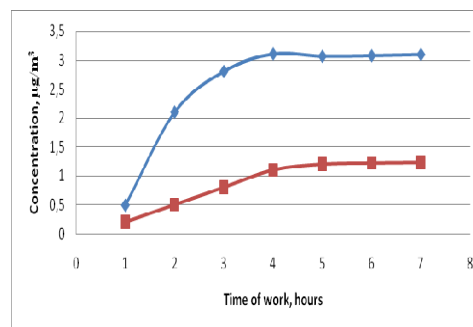

Figure 1. Concentration of ozone in the room as a function of time. The upper curve- the EWG portable cleaner works without the coal filter. The lower curve - the cleaner works with the coal filter.

Physical characterization of particulate from laser printer emission

M.Filice[1], P.De Luca[1]

[1]Department of Pianificazione Territoriale, University of Calabria, Rende, 87036, Cosenza, Italy

Keywords: PM, indoor source, particle characterization, exposure, laser printer.

The growing interest in indoor pollution is due to human health effects (Kotzias, 2005) emphasized by the residence time of people in confined environments (Issarayangyum&Greaves, 2007; Gulliver&Briggs, 2004). Average citizen spends about 80-90% of his time in closed living environment for family reasons (home), utilities (transport) or working (offices). Several studies showed that indoor pollutants concentrations may be greater than outdoor concentrations (Jones, 1999; Chaloulakou&Mavroidis,2002; Chaloulakou *et al.*, 2003). Indoor air pollution is the result of interaction between pollutant properties, characteristics of materials, human activities and air masses change.

In the last year we observed an interesting italian trend, with an increasing of family informatization, for this reason the ratio of *computer&printer* in the italian families is very high. Several studies showed that the printers have a role in indoor pollution, especially laser printers (Kagi *et al.*, 2007).

In this context our study is based on the characterization of particles produced by a laser printer for office and households. Our focus is on particulate matter (PM), for a twice reason. From a physical point of view, there is a correlation between PM small size and a high penetration in the human respiratory system. From a chemical point of view, there is the transport in human organism of incompatible chemical substances. The experiment in this study was carried out to evaluate polluting power of printers. There were three phases. The first step, acquisition and operation of the printer. Second step, used until exhausted toner. Third step, emptying the pocket of particles collection and laboratory analysis. The collected particulates were subsequently analyzed using Simultane Thermo Analysis (Netzsch, modell 429) in order to define PM thermal characteristics. The Thermal Analysis is a technique based on measuring the change in the weight of the sample as a function of temperature in controlled atmosphere. The analysis was conducted by heating the sample (160 mg) from 293-1023°K, with 10°C/min speed in static air. We observed two main variations with a weight loss of about 15%. We observed a weight loss between 623-723°K. DSC curve showed two different peak points (Figure1). The first one is due to exothermic effect with maximum at about 648°C, the second is due to endothermic effect at about 723 °C. We have identified specific ranges of temperature:

- Volatile fraction: mass loss until 623°C
- Combustible fraction: mass lost between 623-723 °C
- Ash: noncombustible material remaining after a combustion until 1023°C.

Around 85% of the mass does not undergo changes during the growth of temperature, this suggests a high percentage of noncombustible material. These ash particles could be due to ink features and additives used to keep it fluid.
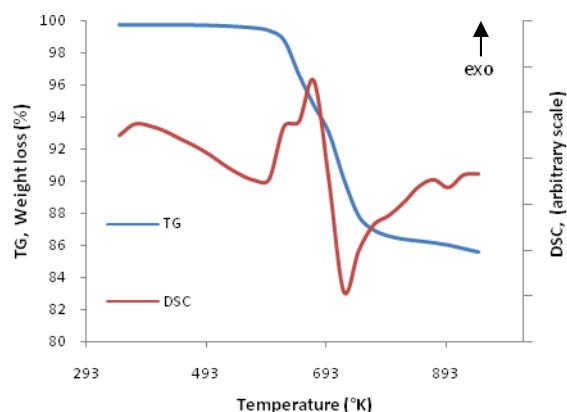
Figure 1. TG and DSC profile for PM sample by a laser printer

Future research will focus on the chemical characterization of emissions, ash particle analysis and evaluation of indoor particles dispersion process.

Chaloulakou A., Mavroidis I., (2002), *Atmospheric Environment,* 36, 1769–1781

Chaloulakou A., Mavroidis I., Duci A.,(2003), *Chemosphere,* 52 ,1007–1019

Gulliver J., Briggs D.J., (2004), *Atmospheric Environment*, 38, 1-8

Issarayangyun T., Greaves S., (2007),*Transportation Research Part D*, 12, 347-357

Jones A.P.,(1999), *Atmospheric Environment*, 33, 4535-4564

Kotzias D., (2005), *Experimental and Toxicologic Pathology*, 57, 5–7

Lee S.C., Lam Sanches, Fai Ho Kin, (2001) *Building and Environment*, 36, 837–842

Naoki Kagi, Shuji Fujii, Youhei Horiba, Norikazu Namiki, Yoshio Ohtani, Hitoshi Emi, Hajime Tamura, Yong Shik Kim, 2007, *Building and Environment*, 42,1949–1954

Detection of Cell Homeostasis Imbalance in Subjects Exposed to Traffic Related Air Pollution

R. Accinni[1], F. Cetta[2], G. Schiraldi[3], M. Guinea Montalvo[1], G. Giussani[1], M. Parolini[1], C. Dellanoce[1], R. Zangari[2], E. Bolzacchini[4], L. Allegra[3]

[1]CNR Clinical Physiology Institute, Niguarda Cà Granda Hospital, 20162, Milan, Italy
[2]Department of Surgery, Research Doctorate in Oncology and Genetics, University of Siena, Nuovo Policlinico "Le Scotte", viale Bracci, 16, I-53100 Siena, Italy
[3]Toracopulmonary and Cardiovascular Dpt., University of Milan,Via Festa del Perdono,7,20122,Milan, Italy.
[4] Department of Environmental Sciences, University of Milano-Bicocca, Piazza dell'Ateneo Nuovo, 1,20126 Milan, Italy

Air-pollution promotes ROS generation and oxidative stress, causing imbalance of the antioxidant endogenous system.

The aim of this study has been to evaluate the role of thiol analysis by HPLC – cysteine (Cys), cysteinylglycine (CG), homocysteine (Hcy) and glutathione (GSH), which are redox balance parameters – for the early recognition of a risk-subject in a population exposed to environmental pollution. In a heavy polluted city, such as Milan, Italy, a group of subjects (n=38, age 82±9) living in hospices for retired people was enrolled and compared to a control population (n=42, age 70±8), living in Aprica, a remote alpine site, (1118 m a.s.l) with low traffic volume, in order to evaluate adverse health effects of traffic related air-pollution.

Daily levels of PM10, PM2,5 and PM1 were measured both by OPC detectors and low volume gravimetric detectors. Information on previous clinical history was collected. Spirometry and HPLC analysis on blood samples were performed for the evaluation of thiols (plasma total and reduced forms PT, PR respectively; erythrocytes total and reduced forms ET, ER respectively).

Results must be considered preliminary, because of the limited number of collected samples.

Table 1. Significantly different parameters. [mean±standard deviations (unpaired data T-test)].

	Milan µM	Aprica µM	p
PR Cys	10,7±4,4	8,0±2,1	0,01
PT Cys	459,8±155,2	286,3±74,8	<0,001
PT Hcy	27,7±19,9	14,5±10,6	0,001
ET Cys	62,2±45,4	33,7±20,5	0,013
ER Cys	2,5±0,8	1,5±0,6	< 0.001
ET CG	6,6±3,0	4,7±2,5	0.005

In order to match the population by age, we excluded patients over the age of 90 and under the age of 70 (table 2). After that, (*) significance increased in comparison with previous statistical analysis.

Table 2. Significant data in populations matched by age (Milan n=21, age 78±7; Aprica n=23, age 77±4). [mean±standard deviations (unpaired data T-test)].

	Milan µM	Aprica µM	p
PR Cys	13,6±3,4	7,7±2,0	0,001*
PT Cys	427,1±152,2	280,4±74,9	<0,001
PT Hcy	28,3±23,6	13,8±7,5	0,012
PR CG	2,4±0,6	1,7±0,6	0,007
PR GSH	2,2±1,0	1,4±0,8	0,025
ET Cys	73,1±31,5	45,8±23,4	0,003*
ER Cys	2,8±0,8	1,4±0,5	< 0.001
ET CG	7,7±3,5	4,9±2,8	0.006
ER CG	2,0±0,9	1,5±0,7	0,047

There was no evident difference in the GSH levels between the two populations. In fact, GSH alteration is a late event, occurring in severe imbalances and no subject in both groups had clinically evident pulmonary diseases. The increase in PT and PR Cys (a pro-oxidant) is likely caused by a lower intake into the erythrocyte. Moreover, the higher concentrations of E-Cys suggest that in the cell there is an obstacle to the condensation of Cys with glutammic acid in the γ-glutamil cycle. In the Milan's group high Hcy levels indicate that it is not being used for cystationine synthesis. Moreover, the excessive presence of P Hcy and P Cys promote the production of ROS, altering redox state and cell homeostasis. At the same time, lower levels of PR GSH show an increase of γ-GT activity and, consequently, of plasmatic GSH peroxidase.

Inhabitants of areas with different traffic volumes show significantly different Cys CG and Hcy levels even if GSH remains unchanged, suggesting a greater- pro-oxidant effect in more exposed populations, affecting Cys CG and Hcy levels, before GSH alterations. Therefore, analysis of thiol redox balance in plasma and erythrocytes is able to distinguish between more and less exposed subjects and could be a useful diagnostic tool for early detection of subjects at higher risk of health effects from environmental pollution.

Relationship between paediatric hospital admissions for respiratory diseases and air pollution (PM$_{10}$) in Milan during 2 one year periods (2007 vs 2008)

M. Sala[1], F.Cetta[2], S. Argirò[1], S. Palazzo[1], P. Ballista[1], L. Dahdah[1], R. Zangari[2], G. Rettani[1], M. Mandelli[1], M. Giovannini[1]

[1]Department of Pediatrics, San Paolo Hospital University of Milan, Via Festa del Perdono,7,20122,Milan, Italy
[2]Department of Surgery, Research Doctorate in Oncology and Genetics, University of Siena, Nuovo Policlinico "Le Scotte", viale Bracci, 16, I-53100,Siena, Italy

keywords: urban pollution, hospital, field measurements, traffic-emission, health effects of aereosols,

Recent studies outlined the possibility of important adverse effects of children health due to air pollutants. In particular, traffic related pollution adversely affects lung function development (Gauderman, 2007).

The aim of the present study has been the evaluation of the association between urban PM10 concentration and hospital admission for respiratory diseases in a paediatric Department (San Paolo Hospital) in Milan.

A comparison was made between years 2007 and 2008. It must be outlined that since January 1, 2008, a municipal order was introduced (ECOPASS pollution charge), reducing vehicular traffic towards the city center.

All hospital admissions for respiratory disease in the Department of Paediatrics, San Paolo Hospital during the study period were 781(463 males and 318 females). The mean duration of hospitalisation was 5 days, range 1-29. The mean daily concentration of PM$_{10}$ was 45,5 μg/m^3, SD 28,85, range 2-185 μg/m^3.

In order to evaluate the effects of pollution on hospital admissions, days of the year were divided into two groups: in the former we included days with at least one hospital admission for respiratory disease, in the latter days without admissions for respiratory illness.

In 445 (60,9%) days, at least one hospital admission occurred, while in 276 (39,1%) days no hospital admission was observed. During the entire study period mean daily concentrations of PM$_{10}$ (μg/m^3) significantly (p<0,001) differed between days with or without hospital admissions, as shown in table 1. When we analysed data considering different threshold values of mean PM$_{10}$ concentrations, we observed that, during both years, the rate of days with hospital admissions increased when increasing thresholds of PM$_{10}$ were considered (p <0,01). This trend became significant in days with mean PM$_{10}$ concentrations exceeding 30 μg/m^3 (p<0,001). As shown in table 1, a significative (p<0,001) difference was found between the mean values of PM$_{10}$ during 2007 and 2008. The mean duration of hospitalisation also significantly (p= 0,009)

decreased from 2007 to 2008 (5 vs 4,34 days) (table 2). All hospital admissions were classified in accordance with ICD-9: 99 (13,5%) asthma or asthma like disorders, 282 (38,6%) lower respiratory illness and 219 (30%) upper respiratory illness. Even if there were no significant differences between hospital admissions for asthma and lower respiratory illness during 2007 and 2008, admissions for lower respiratory illnesses decreased in 2008 (144 vs 138); on the contrary there were more pronounced differences between hospital admissions for upper respiratory illness during 2007 and 2008 (99 vs 120, p=0,50)

	PM$_{10}$	
	2007	2008
Daily mean (μg/m^3) [SD]	49,98 [31,1]	41,6[26,08]

Table 1: Mean values of PM$_{10}$ during 2007 and 2008.

	2007	2008
N. Admission for respiratory disease	391 (male 244, female 147)	390 (male 219, female 171)
Mean duration of hospitalisation in days	5 *	4,34 *

* p= 0,009

Table 2: Distribution of admissions in 2007 and 2008

It is concluded that exposure to air pollutants causes detrimental effects on children respiratory health. The observed improval in year 2008 could be due to meteorological reasons, but also to the introduction of ECOPASS, which determined a reduction of vehicular traffic (-12% private vehicles accessing the ECOPASS LTZ – Limited Traffic Zone). Even if preliminary, present data suggest that a modest reduction of pollutant concentration could have beneficial effects on children's respiratory health.

Gauderman, W.J., Vale, H., Mc Connell, R., et al., (2007). Lancet,369,571-577

Traffic can be responsible for different respiratory adverse effects in schoolchildren. A prospective study in Milan, Italy

F. Cetta[1], M. Sala[2], S. Argirò[2], P. Ballista[2], G. Perrone[2], R. Zangari [1], A. Dhamo [1], P. Laviano [1], E. Bolzacchini[3], M. Giovannini. [2]

[1]Department of Surgery, University of Siena, Nuovo Policlinico "Le Scotte", 53100 Siena, Italy
[2]Department. of Pediatrics, University of Milan,Via Festa del Perdono,7,20122,Milan, Italy
[3] Department of Environmental Sciences, University of Milano-Bicocca, Piazza dell'Ateneo Nuovo, 1,20126 Milan, Italy

keywords: air pollution, field measurements, traffic-emission, health effects of aereosols

Recent studies outlined the possibility of important adverse effects of children health due to air pollutants. In particular, traffic related pollution adversely affects lung function development (Gauderman, 2007).

Two-hundreds and twenty-eight children (127 males and 101 females), mean age 8 years, were enrolled from 2 primary schools, which were located in different sites, for studying pollution related respiratory symptoms and/or diseases in different places of Milan with a different traffic related exposure. The former (School 1) was located near a large park, the latter was located downtown, close to main crossroads (School 2). Daily levels of PM10 and PM 2,5 (diameter < 10 μm and 2,5 μm, respectively) were measured using a mobile detection unit, which was placed either outside the schools (in the school garden) and within common places (corridors), for 7 consecutive days during 2 different campaigns (winter and spring-summer). Children underwent skin prick testing for inhaled allergens, analysis of exhaled nitric oxid FeNO and spirometry.

The distribution of FeNO values was significantly different (p=0,02) between the two schools. In particular, the percentage of children with FeNO values <5 ppb in school 1 was higher (almost double) than in school 2. In 73% of children attending the school located downtown FeNO concentration was between 5 e 20 ppb. This difference, even if within normal values, could reflect a major bronchial eosinophilic inflammation in children exposed to higher concentration of pollutants.

The percentage of asthma exacerbations in the previous 12 months was higher in children from school 2 (p=0.05). On the contrary, the prevalence of persistent allergic rhinitis in children allergic to grass pollen was higher in school 1 (p=0.03). In particular, the latter children also had a greater activity limitation, due to rhinitis and concomitant conjunctivitis (p=0.03).

Interestingly, the highest recorded peak for PM10 occurred between 8,15 and 8,45 in the morning, for 3 consecutive days, and was strictly related to activities concomitant with children arrival. This peak (up to 1000 μg/m^3) didn't seem to produce specific health effects, likely because of the usual PM10 composition in a park site, with a very low content of toxic or reactive components.

In conclusion, symptoms and hospital admissions because of lower respiratory tract diseases (bronchitis, bronchiolitis, pneumonia) were more frequent during the winter campaign and in school 2, located downtown, whereas otitis and allergic rhinitis or conjunctivitis, together with asthma, were more severe during the spring-summer period and in school 1, located near the park (p < 0,05).

Present continuous on field monitoring of the various types of PM clearly shows that:

- short lasting pollution peaks, even reaching concentrations 20 folds above the fixed limits, have no consequences on children health and are easily induced by children themselves, only because of their arrival or movement. They cannot be eliminated, by restriction policies, because they are due to the very presence of the human beings who should be protected.

- these high peaks are going to recur at the same time in consecutive days and are then related to easily detectable factors.

- there is an enormous daily variability, in PM10 concentration among the various hours of the day, and the daily mean value results from the average of values with a very high standard deviation (+30,+1000 μg/m^3) and include various peaks.

Present findings show that, on the basis of the distribution of FeNO values, different degrees of respiratory function and bronchial inflammation were found in the 2 groups of children. Even if great caution is required when relating data from air quality monitoring to clinical outcomes in humans, it can be inferred that: 1) the different air quality in the 2 schools could have a role in determining observed differences; 2) traffic could be, at least in part, responsible for the different air quality; 3) reduction of traffic related pollution should be a logical and suitable objective of policy makers.

Gauderman, W.J., Vale, H., Mc Connell, R., et al., (2007). Lancet,369,571-57

T11 PMx

Seasonal PM variation in Cosenza, South Italy

M.Filice[1], P. De Luca[1]

[1]Department of Pianificazione Territoriale, University of Calabria, Rende, 87036, Cosenza, Italy

Keywords: PM, urban area, seasonal patterns, gravimetric analysis, atomic absorption

Air pollution complexity is a dynamic mechanism due to interaction between pollutants and environment. Several studies showed that pollutants have a seasonal trend in regional scale (Hiena *et al.*, 2002; Filice *et al.*, 2004; Amodio *et al.*, 2008). Other underlined a relationship between air pollution and climate change (Jacob&Winner, 2009).

This paper presents the results obtained during one year period (January-December 2005) to study seasonal footprint in local scale on particulate matter pollution. Measurements were carried out in Cosenza (South Italy), with a total population around 732.869 (110.1 inh./km^2, 155 city-states), is the major province in the Calabria region situated between Tyrrhenian and Ionian Sea. Particulate matter samples were collected at a height of 3 m above the ground for 15 consecutive days/month in a road site. 24-h particulate samples were collected on mixed cellulose membrane filters of 0.8 μm pore size with an air flow rate of approximately 20 l/min The concentration was determined using the gravimetric method, the atomic absorption was used to determine chemical marker in order to find seasonal variation. At same time we observed meteorological trends such as temperature, relative humidity, rainfall and wind direction.

A database has been constructed containing PM concentration data (180samples) from the monitoring site. Average annual PM concentration was around 45.5 ± 10 μg/m^3. We split all gravimetric data into 14 classes with a step of 5 μg/m^3. Annual trend showed a bimodal distribution with two peaks (fig.1). Daily PM variation showed a seasonal trend with greater concentration in winter (table1).

Table 1. Comparison between seasonal data

Period	data	Percentile (μg/m^3)		
		10	50	95
Year	180	32.10	44.45	62.00
Winter	45	41.15	51.60	63.29
Summer	45	28.89	39.00	50.87

We focused our attention in two month group data: summer and winter. The results showed the seasonal influence: first peak was due to summer-effect (30-35 μg/m^3), while second peak was due to winter-effect (45-50 μg/m^3).
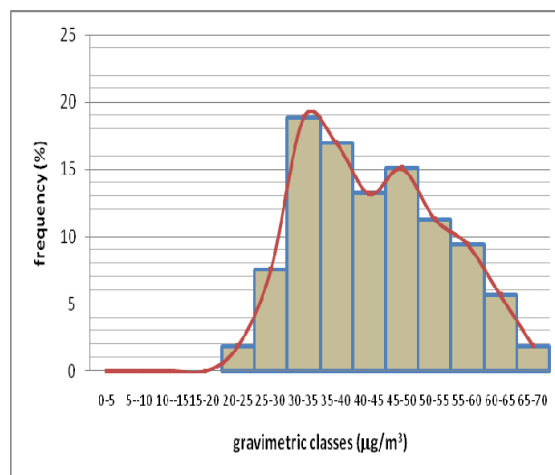

Figure 1. Gravimetric annual frequency.

The chemical speciation was by atomic absorption spectrometry (Shimadzu 6300), using the total digestion with HNO_3. We analyzed a blank filter to determine chemical influence of the filter. Chemical marker showed the seasonal footprint. Summer samples showed a high calcium presence (natural contribution) compared to winter samples. Moreover, in summer we observed more Ni, Cr, Zn and K, while in winter we observed more Pb, S, Ti, Cu, Cs e V. We did not observe Fe seasonal variation. Further works are focused to identify the relationship between cluster particles (morphology, size and chemical composition) and period of sampling to determine the seasonal-effect on particle properties.

Amodio M.,Bruno P.,Caselli M.,de Gennaro G., Dambruoso P.R., Daresta B.E., Ielpo P., Tutino M., (2008), *Atmospheric Research*, 90, 313–325

Filice M., De Luca P., Nastro A. (2004). *Environmental Engineering and Management Journal*, 3, 293-304

Hiena P.D., Bac V.T., Tham H.C., Nhan D.D., Vinh L.D,(2002), *Atmospheric Environment,* 36, 3473–3484

Jacob D.J., Winner D.A.(2009), *Atmospheric Environment,* 43, 51–63

Ten-year measurements of Radon's decay products to study the role of atmospheric dispersion on PM levels

R. Vecchi[1], G. Valli[1], V. Bernardoni[1], and A. Franchin[1]

[1]Department of Physics, University of Milan, and INFN, via Celoria 16, 20133, Milan, Italy

Keywords: radon decay products, dispersion, PM

The measurement of the concentration and temporal behaviour of radioactive aerosol in atmosphere can provide information on atmospheric thermodynamic conditions as well as on atmospheric processes that involve aerosols such as transport, dispersion, removal rates and residence time.

Since 1997 our group has been measured the concentration of Radon's short-lived decay products routinely and continuously in Milan (Italy) with hourly resolution (Marcazzan et al., 1995; Sesana et al., 2003; Vecchi et al., 2004).

Radon activity concentration outdoor is detected through the collection of its short-lived decay products attached to aerosol particles and the spectroscopic evaluation of their alpha activity by a home-made instrument with high sensitivity (detection limit = 0.2 Bq m^{-3}).

Long-term Radon measurements (Kataoka et al., 1998; Perrino et al., 2001; Sesana et al., 2003) show that the temporal variation of its concentration can give immediate information on the evolution of the stability conditions in the boundary layer. The stability conditions of the lower atmospheric layers, on a local scale, are very important as influence pollutants concentration on different time scales. Indeed, the dilution of pollutants in the mixing layer must be ascribed to thermal and dynamic turbulence, whilst the horizontal transport of pollutants is due to the wind field. In the Milan area and in the whole Po valley ventilation is scarce (despite sporadic advection episodes, typically Föhn events) and vertical dispersion plays the main role.

From long-term measurements performed in Milan by our group a typical daily pattern in Radon concentrations can be singled out: it is generally characterised by a minimum in late afternoon and a maximum in the early morning. This pattern is observed on sunny days with clear sky (both during day and night) and low ventilation rate and it occurs very frequently in Milan during both winter and summer months. The nocturnal accumulation of Radon is due to the low mixing layer generally caused by a low-height or ground-based temperature inversion of radiative origin. The variation of Radon concentration observed between the minimum in the afternoon and the maximum in the following day is a good indicator of the nocturnal mixing layer depth. When the sun rises in the morning and heats the ground the inversion is destroyed so that the re-mixing of Radon takes place in layers of increasing heights causing a decrease of its concentration levels. The minimum concentration is registered during the afternoon when the mixing layer reaches its maximum depth. The variation between maximum and minimum Radon concentration in the same day is an index of the maximum height of the mixing layer, which has been evaluated by means of a box model suitably set up (Pacifico, 2005).

The analyses performed on our long-term dataset have been singled out a significant correlation between PM10 and ^{222}Rn daytime concentrations evidencing the dominant role of atmospheric dispersion in determining the temporal variation of PM10 levels. Whenever ^{222}Rn concentrations accumulate during the night (indicating the formation of a nocturnal atmospheric stability), PM10 concentrations show higher values than those registered during the daytime before, despite a nocturnal decrease in emissions from active sources. On the contrary, when ^{222}Rn concentrations do not accumulate during night hours, PM10 levels are lower than those measured the daytime before. It is worth noting that in both cases the aerosols residence time plays a role and has to be taken into account.

Moreover, an analysis of the relationship between PM and atmospheric dispersion over the ten-year data set will be presented.

Kataoka, T., Yunoki, E., Shimizu, M., Mori, T., Tsukamoto, O., Ohhashi, Y., Sahashi, K., Maitani, T., Miyashita, K., Fujikawa, Y., Kudo, A. (1998). *Boundary-Layer Meteor.*, 89, 225–250

Marcazzan G.M., Mantegazza F., Astesani R. (1995). *Life Chemistry Reports* 13, 151-158.

Perrino, C., Pietrodangelo, A., Febo, A. (2001). *Atmos. Environ.*, 35, 5235-5244

Sesana, L., Caprioli, E., Marcazzan, G.M. (2003). *J. Environ. Radioact.*, 65, 147-160

Vecchi, R., Marcazzan, G., Valli, G., Ceriani, M., Antoniazzi, C. (2004). *Atmos. Environ.*, 38, 4437-4446

FACTORS CONTROLLING ^{7}Be AND ^{210}Pb ATMOSPHERIC DEPOSITION AT MALAGA (SPAIN)

C. Dueñas, M.C. Fernández, S. Cañete, E. Gordo and M. Pérez

Department of Applied Physics I, Faculty of Sciences, University of Málaga. 29071 Málaga (SPAIN)

E-mail: mcduenas@uma.es

Keywords: atmospheric aerosol, deposition, ^{7}Be, ^{210}Pb, precipitation

ABSTRACT.-Bulk atmospheric deposition of ^{7}Be and ^{210}Pb has been measured at Málaga (4º 28′ 80″ W; 36º 43′ 40″ N) a coastal Mediterranean station in the south of Spain, from January 2005 through April 2008 for monthly periods. The fluxes of ^{7}Be and ^{210}Pb were mainly correlated with rainfall and correlated one with the other .Concentrations of ^{210}Pb and Ca^{++} in rain were correlated with transport time of air masses over the continent

INTRODUCTION Berylium-7 is one of the radionuclide produced by spallation reactions of cosmic rays with light atmospheric nuclei.^{7}Be rapidly associates primarily with submicron-sized aerosol particles. Lead-210 which is one of the natural radionuclide of the ^{238}U decay series is widely used as a tracer. ^{210}Pb depositional pattern gave us information on continental aerosols in lower troposphere. These two radionuclides with their different sources and therefore are useful to understand the mechanisms of aerosol removal from the atmosphere. These radionuclides have measured routinely in many places of the word in order to study the description of environmental processes such as aerosol transit and residence times in the troposphere, aerosol deposition velocities and aerosol trapping by ground vegetation.

MATERIAL AND METHODS.- The sampling site is one of the environmental radioactivity monitoring network stations operate by the Spanish Nuclear Security Council (CSN). The sampling point was located above the ground, on the roof of the Faculty of Sciences, University of Málaga. Monthly precipitation and dry fallout samples were routinely collected using a steel tray 1m^2 in area as a collecting system and polyethylene vessels of 50 l capacity for rainwater samples reservoirs. Measurements by gamma spectrometry were performed to determine the ^{7}Be and ^{210}Pb activities of the samples using an intrinsic REGe detector. The peak analysis of ^{7}Be (I= 10.52 %, 477.7 KeV) and ^{210}Pb (I = 4%, 45 KeV) was done using SPECTRAN AT peak analysis software. The counting time was 172800s
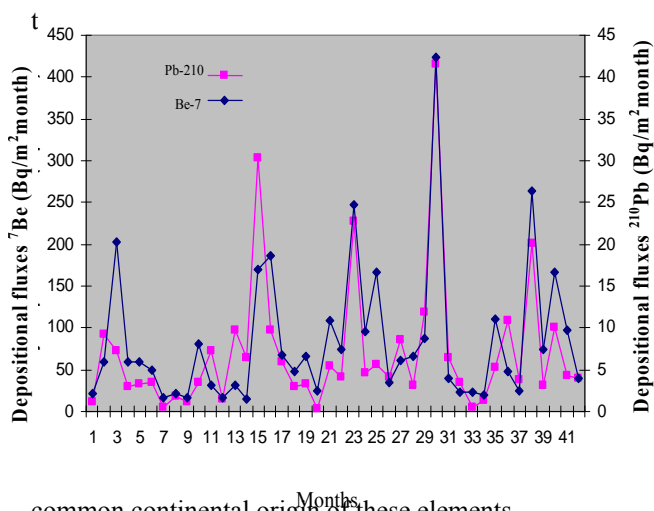
RESULTS The results from depositions of ^{7}Be and ^{210}Pb were correlated with four parameters: rainfall amount, rainfall duration, number of dry days and number of wet days. Table 1 provides the correlation coefficients between the fluxes of and the mentioned parameters.

Table 1. Linear correlations coefficients between fluxes of ^{7}Be and 210Pb and some parameters

	^{7}Be		^{210}Pb	
	r	p	r	p
Rainfall amount	0.80	99	0.70	99
Rainfall duration	0.44	99	0.36	95
Number of dry days	-0.72	99	-0.68	99
Number of wet days	0.74	99	0.71	99

The depositions of ^{7}Be and ^{210}Pb were well correlated with the amount of rainfall . Such relations have been commonly observed and explained by the fact that rainfall constitutes the major depositional pathway of these radionuclides. As previously observed, correlation of rainfall with ^{7}Be seems better than with ^{210}Pb (Caillet el al., 2001) likely due to a relatively greater contribution of ^{210}Pb from dry deposition.

The fluxes of ^{7}Be and ^{210}Pb are correlated one with the other (r = 0.83; p >99 %) . Figure shows the monthly results for period of measurements. There is a relationship between air mass trajectories and the concentrations of ^{210}Pb and Ca $^{++}$ illustrates t

common continental origin of these elements.

Caillet, S., P. Arpagaus, F. Monna and J. Dominik (2001). Factors controlling ^{7}Be and ^{210}Pb atmospheric deposition as revealed by sampling individual rain events in the region of Geneva, Switzerland.J. Environ. Radioactivity 53, 241-256.

DEPOSITION VELOCITIES AND WASHOUT RATIOS ON A COASTAL SITE CALCULATED FROM GROSS ALPHA AND GROSS BETA MEASUREMENTS

C. Dueñas, M.C. Fernández, E. Gordo, S. Cañete, and M. Pérez

Department of Applied Physics I, Faculty of Sciences, University of Málaga. 29071 Málaga (SPAIN)

E-mail: mcduenas@uma.es

Keywords: atmospheric aerosol, deposition velocity, precipitation, washout ratio

INTRODUCTION-The gross-alpha and gross beta activities in aerosols and bulk deposition samples were measured in Málaga, Southeastern Spain (36º43´40´´N; 4º28´8´´W). At the same sampling point, aerosols were colleted weekly on filters and monthly precipitation sampling was carried out to study depositions. Levels of particulate matter fraction were also monitorized in Málaga. Using the gross alpha and beta activities in air and their depositional fluxes, the deposition velocities of aerosols and washout ratios are calculated .The minimum and maximum value of alpha and beta deposition velocities are 0.42 - 7.69 cms^{-1} and 0.09 - 2,12 cms^{-1} respectively and the corresponding washout ratios are 449-6980 and 93-3760 respectively.

MATERIAL AND METHODS

The gross alpha activity was measured by a solid ZnS (Ag) scintillation counter. The gross beta activity was measured with a gas flow proportional counter of the low-background multiple detector type with four sample detectors (Camberra HT-1000) and PM10 concentrations were measured for the beta attenuation method.

RESULTS AND DISCUSSION The dates used in the analysis are means monthly values of concentrations in surface air. The period of measurements was performed from October 2005 to September 2007. The dates were analyzed to derive the statistical estimates characterizing the distribution. Studies of the frequency distribution show lognormal distribution is significant at the 0.01 level assuming these types of distribution, the geometric mean should be used to characterize average values.

Table1 provides the statistical parameters from the measurements of alpha and beta deposition velocities ($V_{d\alpha}$ and $V_{d\beta}$) of aerosols and washout ratios($W_{R\alpha}$ and $W_{R\beta}$).

Variable	$V_{d\alpha}$ (cm/s)	$V_{d\beta}$ (cm/s)	$W_{R\alpha}$	$W_{R\beta}$
Geometric mean	1,26	0,48	2004,6	788,2
Dispersion factor	2,26	2,29	2,24	2,63

Table1. Statistical parameters.

Table 2 shows the correlation coefficients and associated probabilities between and some parameters. Since the p-values are less that 0.01, there is statistically significant relationship between deposition velocities of gross alpha and gross beta activities and the rainfall.

The maximum value of deposition velocities alpha and beta correspond with maximum value of rainfall

Parameters	Vd α (cm/s)	Vd β (cm/s)
Rainfall	0.76(0.01)	0.67(0.01)
PM10	-0.31(0.10)	-0.38(0.10)

Table2. Linear correlations coefficients of Vd and some parameters.

Figure 1 shows the negative correlation of rainfall with the variations of washout ratios alpha and beta. In the figure 2 is reflected in a positive correlation of alpha and beta washout ratios with PM10. The maximum washout ratios values of alpha and beta correspond with a minimum value of rainfall and an increase of the PM10.
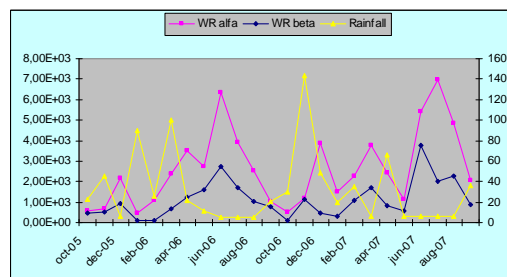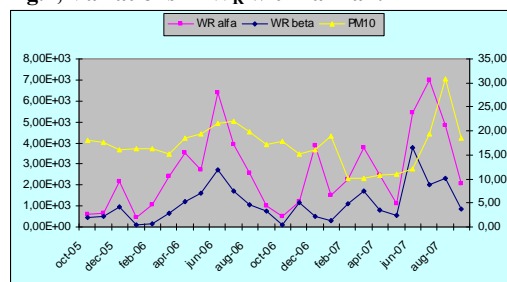

Fig.1, Variations in W_R with rainfall.

Fig.2 Variations in W_R with PM-10.

REFERENCES-.MCNEARY, D. and BASKARAN, M. **Depositional characteristics of ^{7}Be and ^{210}Pb in southeastern Michigan.** J. Geophys. Res. 108, D7, 4210-4225, 2003.

Assesment of air mass transport of Chernobyl originated radionuclides using clustering approach

G. Lujanienė[1], S. Byčenkienė[2], V. Aninkevičius[3]

[1]Nuclear and Environmental Radioactivity Research Laboratory, Institute of Physics,
Savanorių 231, LT-02300 Vilnius, Lithuania

[2]Environmental Physics and Chemistry Laboratory, Institute of Physics,
Savanorių 231, LT-02300 Vilnius, Lithuania

[3]Semiconductor Physics Institute, A. Goštauto 11, LT-01108 Vilnius, Lithuania

The Chernobyl accident caused the release of a great amount of radioactive substances into the atmosphere. Variations in ratio, concentrations and speciation of radionuclides observed after the accident were explained by different proportion of condensed and fuel particles in the Chernobyl fallout. The radioactive aerosols were detected at many locations in Europe more than 1000 km away from the source. Consequences of the Chernobyl accident have been intensively studied in the last two decades. Low activities of the Chernobyl originated radionuclides that are still present in the environment can be used to study the long distance transport of contaminants.

In order to evaluate the contribution of the transport of air masses to the ^{137}Cs air activity concentration, the time series of ^{137}Cs variation in aerosol samples from 1993 to 1999 and 2005-2006 were analysed. The three-dimensional 10-day air mass backward trajectory method was applied to determine possible transport pathways of ^{137}Cs. The relevant air masses were identified by using a filter and Ward's hierarchical clustering algorithm in combination with Euclidean distance (Ward, 1963) was performed on air mass backward trajectories. In this paper, we focus on the study domain, which covers the 30 km Chernobyl zone. The 10-day air mass backward trajectories were clustered and grouped according to season, travelled way, and height over the surface before arrival. The analysis of air mass pathway has indicated the transport of ^{137}Cs from the Chernobyl restricted zone and surrounding areas. A positive correlation was found between the frequency of air masses and the activity concentrations of ^{137}Cs during study periods (1997-1999 and 2005-2006).

The release of plutonium isotopes into the environment after the Chernobyl accident was insignificant: mean (0.224) and median (0.204) ^{240}Pu/^{239}Pu ratio values determined in 1995-2003 were close to those of the global fallout (Lujanienė et al., 2009). The exponential decrease in the ^{240}Pu/^{239}Pu atom ratio from 0.40 to 0.19 was observed (Fig. 1). It can be interpreted as a result of decrease in the amount of the Chernobyl originated plutonium in the environment due to deposition and mixing with plutonium isotopes derived from the global fallout. The mean and median data were fitted by the first order kinetic equation and the residence time of the Chernobyl derived plutonium in the environment was obtained to be about 1.6 -0.4 years.
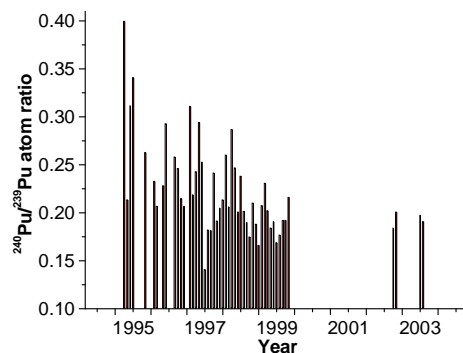

Figure 1. ^{240}Pu/^{239}Pu atom ratio in aerosol samples.

The activity concentrations of plutonium measured in monthly aerosol samples could not be traced back via backward trajectories precisely, however, its transport from contaminated territories can be expected. The comparative correlation analyses of mean monthly and daily activity concentrations of ^{137}Cs as well as ^{240}Pu/^{239}Pu atom ratio with the frequency of air masses was performed in order to approximately estimate the possible transport of the Chernobyl originated plutonium. Preliminary results indicated the identical correlation for the ^{137}Cs mean monthly activity concentrations in comparison with daily ones, while no positive correlation for the plutonium transport from the highly contaminated after the Chernobyl accident region was found in 1997-1999. Data analyses are in progress.

Ward, J. H., (1963). Hierarchical Grouping to Optimize an Objective Function. *Journal of the American Statistical Association*, 58, 236-244.

Lujanienė, G., et al. (2009) *J. of Environ. Radioactivity,* 100, 108-119.

Monitoring of ^{7}Be and heavy metals at the Basic Environmental Observatory "MOUSSALA"

I.Penev, J.Stamenov, M.Drenska, B.Damyanov and Ch.Angelov

Institute for Nuclear Research and Nuclear Energy,
Bulgarian Academy of Sciences, 72 Tscarigradsko shosse, 1784, Sofia, Bulgaria

Keywords: aerosol sampling, radioactive particles, natural radioactivity, man-made radioactivity.

The Basic Environmental Observatory is situated in the vicinity of peak of Moussala, 2971m., the highest point in Balkanian Peninsula. The peak is in the frame of reserve Central Rila, part of the National Park Rila. The observatory has been established by Institute for Nuclear Research and Nuclear Energy of Bulgaria Academy of Sciences. Here, in spite of very harsh conditions a wide spectrum of physical investigations are in full progress – meteo, atmosphere investigations, precipitations, monitoring of space and Earth radiations, different components of cosmic particles and etc., see http://beo-db.inrne.bas.bg/moussala/

A big sampler with capacity 1500-1800m^{3}/h has been mounted according to the program of aerosols investigations on BEO-"Moussala".The sampler is shown on figure 1.
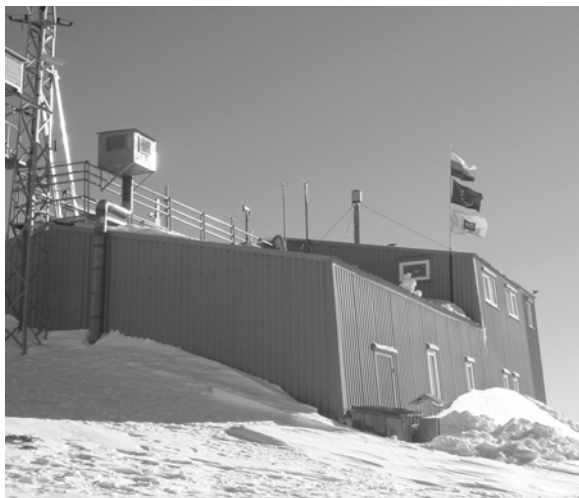

Figure 1 Basic Environmental Observatory, on the roof is house for sampling

The air, ~ 15000m^{3}, is passing through fibber filter with high efficiency. After sampling the filter is pressed to the pill size: diameter 56mm and thickness 13-15mm. The pills are measured by H.P.Ge spectrometer with 30% relative efficiency. More detail description of the device and method are given in Uzunov at al., 2007 and Penev at al., 2007. For 2008 more then 160 samples were analyzed for natural and man made radioactivity. Special attention is paid to the behavior of the ^{7}Be and heavy metals isotopes. The fluctuation of the volume concentration of these isotopes is informative in exchange for the big air mass between different atmosphere strata.

The interval of the above mentioned fluctuations of ^{7}Be at the altitude ~3000m vary in size more then 15 times, see figure 2.
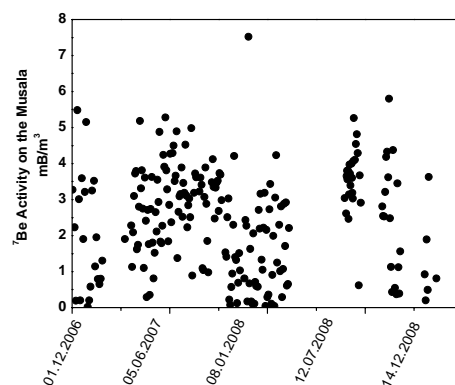

Figure 2. The data ^{7}Be for 2007-2008y at BEO-Moussala

The intensive interchange of very big air mass at Moussala, (wind velocity is in the frame 5 –50m/s) with aerosols with different origin, together with big sampling is a splendid opportunity to control the air quality. The minimal detectable activity of the method is from 10^{5} to 10^{6} times lower, and then max permissible according to the IAAE standards for man-made radioactivity.

It is planned to make an analysis of the aerosols for heavy metals and other elements in the near future. Remoteness of BEO from all kind urban activity gives good opportunity for such investigations.

Some correlations between ^{7}Be and cosmic rays including neutron component is under progress.

This work is done in the frame of BEOBAL EU project.

Uzunov, N., Janminchev, V., Penev, I., Drenska, M., Damyanov, B., Damyanova, A. (2007). in Annual of Constantin Preslavski University, Shumen vol.XVII B2

Penev, I., Stamenov, J., Drenska M., Damyanov, B., Valova, Tsc., Uzunov, N., Arhangelova, N. (2007), *Ecology and Future,* v.VI, n.3, 27-31.

Key issues in radionuclide labeled aerosol monitoring for resuspension studies and short to long-term post-accident characterizations
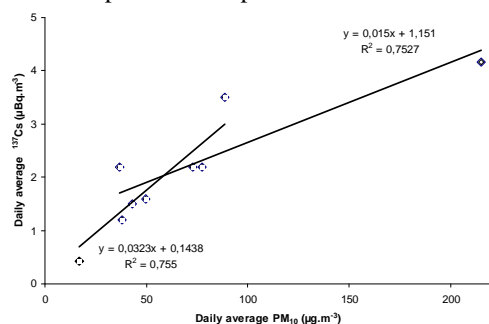
O. Masson[1], D. Piga[1], L. Bourcier[2]

[1] Institute of Radioprotection and Nuclear Safety, IRSN-Cadarache, 13115 Saint Paul lez Durance, France
[2] Laboratory of Physical Meteorology (LaMP), Blaise Pascal University, 24 Av[e] des Landais, 63177 Aubière, France

The French radioactive aerosol monitoring network (OPERA) celebrates its fiftieth anniversary this year. This monitoring was gradually updated both in terms of aerosol sampling (up to 700 m^3/h) and radioactivity measurement in order to determine current airborne levels as low as 0,2 µBq/m^3 for ^{137}Cs. One of the key issues in monitoring is linked to understanding the environmental transfer processes. These processes affect radioactive aerosols inside the atmospheric compartment (rainout, washout, dry deposition and impaction). Radioactive aerosol are also emitted from others compartments of the biosphere that received radionuclide fallout (via resuspension or biomass burnings). The least soil particle resuspension that has ^{137}Cs concentration of some hundreds to tens thousands Bq/m^2 (like in France) is enough to increase airborne levels temporarily. This is especially true during Saharan dust events because of high dust flux, even if the Saharan soil particle activity is lower. About a dozen Saharan events are count every year especially in the southern half of France. During Saharan dust outbreaks the daily airborne activity levels is correlated with PM10 evolution (fig. 1). Moreover the activity levels in deposited dust collected in France are quite concentrated when compared to the Saharan soils. This enrichment is due to the coarse particule segregation loss that have less affinity with ^{137}Cs than fine particles. Our findings show that yearly averaged activity levels are twice to ten times higher for altitude locations (mountainous). The cruising altitude of Saharan plumes is responsible of this.

Fig.1: Relationship between ^{137}Cs activity level and PM_{10} of mineral origin from Sahara

Fires also lead to redistribution of formerly deposited radionuclides, mainly due to the burning of radionuclide-enriched forest litter even over long distances. During winter, temperature inversion in the lower atmospheric layers coupled with wood burning for domestic purposes may also lead to temporary increases in airborne artificial radionuclide levels. Except for these extreme events, routine and local resuspension, regular in time and mainly dependant on season also contributes to the background level. Local resuspension effect can also be found in the better relationship with ^{137}Cs airborne activity when considering coarse particles (PM_{10}) that don't travel far from their emission area, instead of fine particles ($PM_{2.5}$). In France a six year long study shows that oceanic air flux is correlated to a light positive longitudinal airborne activity gradient from west to east whereas there is no background PM_{10} gradient (15 µg.m^{-3}). Thus, the activity gradient can be explained by the soil activity related to the longitudinal Chernobyl fallout distribution. During eastern winds a remote contribution is added from areas more impacted by Chernobyl fallout. This added contribution results in quite the same averaged gradient but with 3 times more pronounced values at both France boundaries and a 4 times enhanced variability. At the scale of France and for the last 8 years, local and remote resuspension can explain about 1/3 of ^{137}Cs rising levels; biomass burnings 1/3 too. The last third corresponds to winter temperature inversion coupled with domestic wood burning emissions. Enhancing knowledge about these mechanisms is useful to mapping territorial radioecological sensitivity and to explain long term post-accident persistence of airborne radionuclides at trace levels. Current needs are concerning the radionuclide aerosol size segregation.

Radiation burden of the up clearing deeply deposited radon progenies in the central airways

I. Balásházy[1,2] and G. Kudela[2]

[1]Health and Environmental Physics Department, Hungarian Academy of Sciences KFKI Atomic Energy Research Institute, Konkoly Thege M. út 29-33, 1121 Budapest, Hungary
[2]Aerohealth Scientific Research Development and Servicing Ltd., 2090 Remeteszőlős, Csillag sétány 7, Hungary

Most of the lung cancers of former uranium miners developed in the large central airways and near 90% of the neoplastic lesions have been found in airway generations 2-5. Current computational fluid dynamics calculations indicate high primary deposition density values in the peaks of the central airways. However, the cellular burden of the radon progenies deposited in the deep regions of the bronchial and acinar sections of the lung and clears up by the mucociliary escalator may contribute to the health effects found in airway generations 2-5. The surface of the airways highly increases and the deposition efficiency does not decrease remarkably with generation number, thus, it looks a reasonable supposition that the dose contribution of the up clearing radon progenies may contribute to the health effects in the large airways.

In the present work, the primary deposition distributions of inhaled radon progenies were computed in the whole respiratory system by the stochastic lung deposition model at different breathing conditions. In addition, a new bronchial clearance model has been elaborated to simulate the up cleared fractions of attached and unattached radon progenies in each of the bronchial airway generations. Finally, the ratio of the up cleared and primarily deposited fractions has been calculated at airway generation level at two different breathing patterns and at two mucus velocities.

The main input data of the clearance model are the deposition data, the velocity of the mucus in a generation, the length of the airways and the half life of radon progenies.

Based on the results, in the central airways, the radiation burden of the up clearing, more deeply deposited, radon progenies can be significantly higher than the burden of the primarily deposited fraction in these airways both at resting and light physical activity breathing conditions in case of unattached and attached radon progenies. The dose contribution of the deeply deposited ^{218}Po and ^{214}Pb isotopes in the large airways are higher than that of ^{214}Bi. The radiation burden of the more deeply deposited ^{214}Po in the central airways is practically zero because of its short half life. The results demonstrate that one of the reasons of radon induced lung cancer may be the dose contributions, in the central airways, of the up clearing, more deeply deposited, radon progenies.

The computed deposition distributions of inhaled particles in bronchial airways have been validated by A. Kerekes et al. (2009).
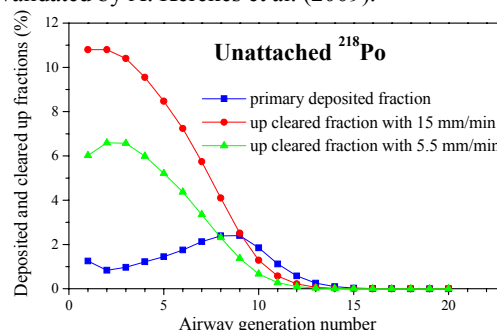

Figure 1. Primary deposition fractions of unattached ^{218}Po at light physical activity breathing condition and cleared up fractions at 15 and 5.5 mm/min mucus velocities.
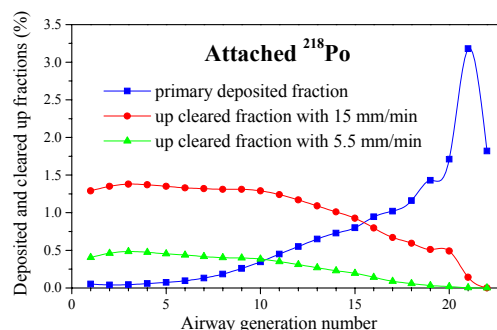

Figure 2. Primary deposition fractions of attached ^{218}Po at light physical activity breathing condition and cleared up fractions at 15 and 5.5 mm/min mucus velocities.

A. Kerekes, A. Nagy and A. Czitrovszky (2009) Experimental flow and deposition studies with hollow bronchial airway models. *17th ISAM Congress 2009*, Montery, California, USA. May 10-14 2009.

Airway deposition and health effects of inhaled radon progenies

I. Balásházy, Á. Farkas and I. Szőke

Health and Environmental Physics Department, Hungarian Academy of Sciences KFKI Atomic Energy Research Institute, Konkoly Thege M. út 29-33, 1121 Budapest, Hungary

Keywords: radon decay products, health effects of aerosols, lung deposition, CFD, deposition efficiency

Inhaled radon progenies provide more than the half of natural radiation exposure. There is increasing evidence that the cellular distribution of radiation burden is an important factor regarding the biological response to ionisation radiation, thus, one of our tasks was the characterisation of the distribution of cellular exposure.

Histological studies of former uranium miners presented strong correlation between primer deposition hot spots and neoplastic lesions. Most of these lesions were located along the carinal regions of the large bronchial airways. In the present work, computational fluid dynamics (CFD) approaches have been applied to simulate the deposition distribution of inhaled radon progenies along central human airways. The geometry and the cellular structure of epithelial lung tissue were numerically reconstructed based on anatomical and histological data. Single and multiple alpha-hit and cellular dose distributions have been computed applying Monte Carlo modelling techniques at different breathing conditions.

light physical activity breathing condition. Size of scanning surface element is a 45μm side triangle.

Values of local per average deposition densities, that is, enhancement factors (Figure 1), hit probabilities (Figure 2) and doses may be up to two-three orders of magnitude higher in the deposition hot spots than the average values. Dose calculations revealed that some cell clusters may receive high doses even at low exposure conditions.

Applying the model to different radiation exposure conditions useful relations can be received regarding the linear-nonthreshold hypothesis.

Ultrafine deposition distributions can be experimentally validated by the measurement technique of Jani et al. 1999.
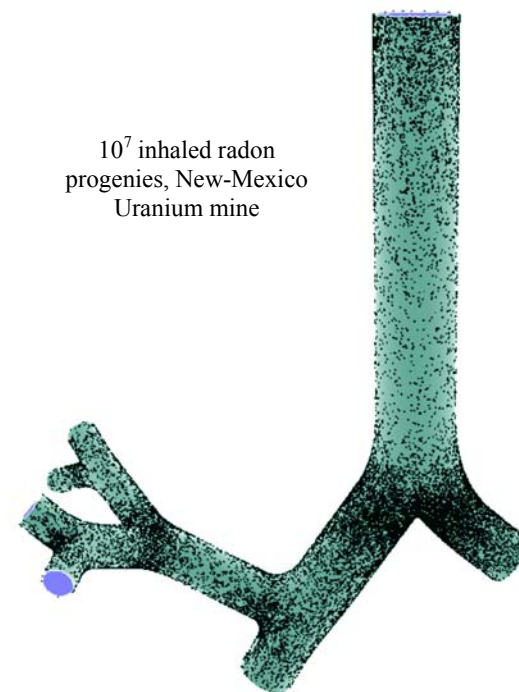

Figure 1. Deposition enhancement factor (EF) distribution of attached, 200 nm, and unattached, 1 nm, diameter inhaled radon progenies on a central airway bifurcation in airway generations 4-5 during

Figure 2. Distribution of cell nuclei hit with alpha particles in the epithelium of airway generations 1-5, leading to the right upper lobe.

Jani P., Nagy A., & Czitrovszky A. (1999). *SPIE* Vol. 3749, 458-459.

Parametric study of the ionizer induced Thoron progeny concentration depletion

M. Joshi, P. Kothalkar, A. Khan, R. Mishra, B.K. Sapra and Y.S. Mayya

Radiological Physics and Advisory Division, Bhabha Atomic Research Centre, Mumbai – 400085. India

Keywords: radon decay products, unattached fraction, deposition velocity, ionizer

It is well known that the negative ions emitted from the negative ion generator (NIG) help in charging the airborne particles, thereby removing them by electromigration in space charge-induced electric fields (Mayya *et al.,* 2004). The NIGs have also been used to reduce activity concentration of radon/thoron decay products (Sheets and Thomson 1995). The physical arguments suggest different reasons for the activity reduction namely; 1) direct plate-out of freshly formed, charged fine fraction of progeny through drift in the electric field and 2) removal of the coarse fraction, thereby increasing the highly mobile fine fraction and its consequent plate-out. To investigate these aspects, measurements of various parameters like activity concentrations, deposition velocity, aerosol number concentration and the unattached fraction in presence of NIG; a systematic study has been carried out in a room environment wherein a thorium nitrate powder was placed as a source of thoron progeny. The overall decrease in the progeny concentration with NIG is depicted in Fig. 1.
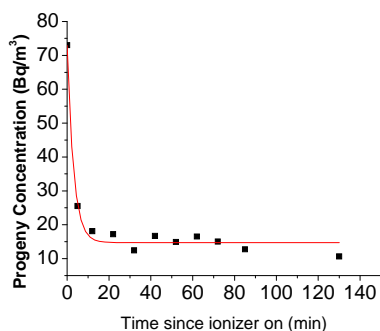
observations strongly point at the possibility of argument (2) cited above as the mechanism of activity reduction.

The particle concentration, measured using GRIMM 5.403 Scanning Mobility Particle Sizer (SMPS) in the size range of 9.8 nm to 875 nm, showed a 3-fold decrease after switching on the ionizer. The attachment rate, X, of the progeny to the ambient aerosols (concentration, Z /cc) can be estimated using the relationship: $X= \beta(d)Z$, where $\beta(d)$ is the size dependent attachment coefficient (cc/s). This is plotted in Fig. 2 and a decrease in the attachment rate is seen when the ionizer is switched on. Also, the activity median diameter was found to shift to larger sizes (94 nm to 150 nm). The lowered attachment rate also points at the increase in the unattached fraction as observed by wire-mesh filter paper sampling techniques. However, the implication of the reduction in activity concentration might not necessarily lead to a reduction in the lung dose and this requires a careful investigation.
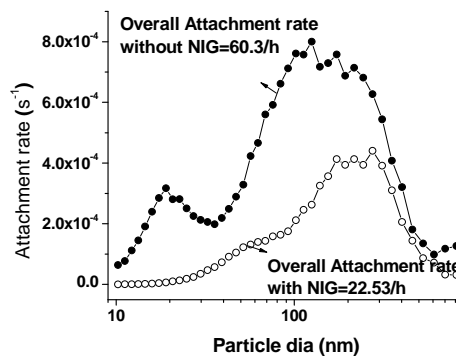

Figure 1: The decrease in the progeny concentration with the ionizer switched on.

Figure 2: Effect of ionizer on the attachment rate under ambient aerosol conditions

Deposition velocity of the progeny was measured using passive direct progeny sensors, which are deposition based absorber mounted LR115 detectors. It was observed that the deposition velocity increased from ~0.06 mh^{-1} to 0.3 mh^{-1} in presence of negative ions. The unattached fraction, estimated by wire-mesh and filter-paper sampling followed by Alpha counting, was also found to increase from 2% to 6.5%. Additionally, the activity deposited in the vicinity of the needles of the NIG showed negligible increase with NIG switched on. All these

References:
Sheets R. W. and Thompson C.C. (1995), *J. Radioanalytical and nuclear chemistry*, 193,301-308.
Mayya Y.S., Sapra B.K., Khan Arshad, Faby Sunny (2004), *J Aerosol Sci.,*35, 923-941.
Mishra R., Mayya Y.S., Kushwaha H.S. (2009), *J. Aerosol Sci.* , 40, 1-15.
Cheng Y.S. and Yeh H.C. (1980), *J Aerosol Sci.*, 11, 313-320.

Determination of loss factors of aerosol particles in the sampling systems of nuclear power plants

R.F.W.Jonas[1] and G.F.Lindenthal[2]

[1]TÜV Nord SysTec GmbH & Co. KG, Große Bahnstr. 31, D-22525 Hamburg , Germany,
[2]Ingenieurbüro für Partikeltechnologie und Umweltmesstechnik, Steinweg 8, D-34314 Espenau Germany

Aerosol measurement, particle deposition, radioactive particles, nuclear sampling systems

According to the German nuclear technical rule KTA 1503.1 the sampling system of a nuclear power plant must be able to collect aerosols with aerodynamic diameters between 0.1 μm and 20 μm with pipe retention factors below 3.

As with all measured quantities the stack emission of radioactive material of a nuclear power plant with exhaust air includes an uncertainty. This is caused by the statistical error and additionally by the non-representative sampling and the deposition of aerosols in the sampling systems. The non-representative sampling results from the insufficient mixing of the air (inhomogenous concentration) and from the non-isokinetic flow in reaching the inlet of the screen of the sampling system. The deposition depends on the particle diameter and is caused by molecular diffusion, impaction and sedimentation. The ratio of the mass concentrations in front of the screen and at the end of the sampling system is called the pipe retention factor.

Pipe retention factors and loss factors (without consideration of non representative sampling) are investigated for sampling systems of different nuclear power plants in Germany using three methods of determination:

1) Dispersing of test aerosols directly into probes of the screen of the sampling system and comparing the aerosol concentrations with those at the end of the sampling system

2) Generation of a defined quantity of aerosol particles at the bottom of the chimney and measuring the particle concentrations by using aerosol collectors or aerosol monitors at the end of the sampling system

3) Measuring the size distribution by number of the ambient aerosol in the chimney in front of the screen and at the end of the sampling system with optical particle counters.

The experimental results are in compliance with theoretical estimations. The measured loss factors and pipe retention factors lie below 3. The transfer properties of the sampling systems for larger particles (aerodynamic diameters up to 3 mm) also have been investigated. The results show that the sampling systems are suitable even in these cases. The presentation gives a survey of the measured pipe retention factors. The results of the three methods of determination are compared indicating advantages and disadvantages based on our experiences.

The solubility and leaching of aerosol particles – radionuclide carriers – collected on filters in the ventilation system of the Ignalina Nuclear Power Plant

R. Jasiulionis and A. Rožkov

Ignalina radioecological monitoring station, Institute of Physics, LT-02300 Vilnius, Lithuania

Nuclear power plants are permanent emission sources of fission (^{137}Cs, ^{134}Cs) and activation (^{60}Co, ^{54}Mn) radionuclides, attached to aerosol particles, into the air.

The Ignalina Nuclear Power Plant (NPP) has two RBMK graphite-moderated channel-type 1500 MW reactors: the power generation at the Unit 1 reactor was stopped in 2005, the Unit 2 reactor is in the operation till 2010. Being formed in the active zone of the reactor, radionuclides circulate with coolant in the closed circuit and undergo physical and chemical changes on their way. Only fine hydrated ionic compounds, carriers of radionuclides, overcome the water and vapor boundary and can participate in the aerosol particle formation and growth. Relatively long-lived ^{137}Cs ($t_{1/2} = 30.08$ year), ^{134}Cs ($t_{1/2} = 2.07$ year), ^{60}Co ($t_{1/2} = 5.27$ year) and ^{54}Mn ($t_{1/2} = 0.855$ year) radionuclides, which are registered in the emissions of the stopped reactor, pass to ventilation system by longer indirect pathways.

The dissolution of aerosol particles, carrier of ^{137}Cs and ^{60}Co, sampled on filters was studied by means of a leaching test with distilled water. Samples were collected from technological gas cleaning systems of the operating Ignalina NPP Unit 2 (before carbon adsorbers, before ventilation stack, and in the ventilations stack), in the environment in the vicinity of the Ignalina NPP and in the ventilation stack of the stopped Ignalina NPP Unit 1 in 2005-2007 (Table 1).

Table 1. Result of leaching of ^{137}Cs and ^{60}Co from aerosol particles sampled on filters

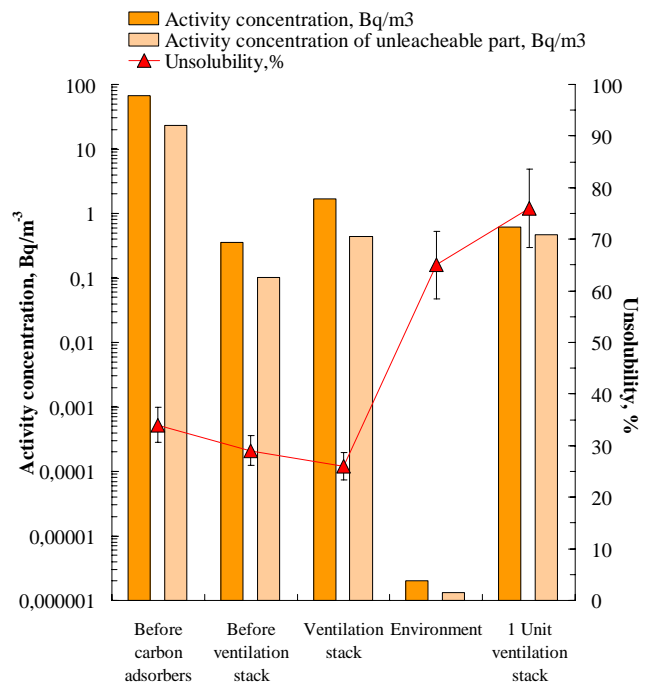| Sampling point	^{137}Cs			^{60}Co		
	C, Bq m^{-3}		W, %	C, Bq m^{-3}		W, %
	total	unleach.		total	unleach	
1	2	3	4	5	6	7
Unit 2 before adsorbers	68	23	34 ± 2	< 5	< 5	–
Before ventilation stack	0.35	0.10	29 ± 1	0.34	0.10	29 ± 6
Ventilation stack	1.69	0.44	26 ± 8	1.26	0.42	33 ± 8
Environment	3.29	2.14	65 ± 18	1.32	1.00	76 ± 22
Unit 1 (stopped) ventilation stack	0.62	0.47	76 ± 10	0.64	0.51	80 ± 15

Figure 1. Activity concentration of ^{137}Cs in aerosol particles, collected in operating Ignalina NPP Unit 2, in the environment in the vicinity of the Ignalina NPP and in the ventilation stack of the stopped Ignalina NPP Unit 1. Activity concentrations of ^{137}Cs in the unleached part of aerosol particles and the unsolubility of aerosol particles are given.

The insolubility in water of radionuclides attached to aerosol particles sampled on filters, collected in the operating Unit 2 reactor effluents, is clearly lower than the insolubility in water of radionuclides attached to aerosol particles sampled on filters, collected in the ground-level air and in the effluents of the stopped Unit 1 reactor (Figure 1).

Jasiulionis, R., Rožkov, A. (2008). *Applied Radiation and Isotopes*, 66 (12), 1992-1998.

Jasiulionis, R., Rožkov, A. (2008). European Aerosol Conference 2008 Abstract T06A181P.

Felmy, A., LeGore, V., Hartley, S. (2003). U.S. Nuclear Regulatory Commission Report NUREG/CR-6821.

Aerosol release from Silver Indium Cadmium control rod

T. Lind[1], A. Pintér Csordás[2] and J. Stuckert[3]

[1]Paul Scherrer Institut, Villigen, Switzerland
[2]HAS KFKI Atomic Energy Research Institute, Budapest, Hungary
[3]Forschungszentrum Karlsruhe, Karlsruhe, Germany

Keywords: nuclear aerosols, nuclear reactor, control rod, SIC

In nuclear reactor severe accident, radioactive fission products as well as structural materials are released from the core by evaporation, and the released gases form particles by nucleation and condensation. In addition, aerosol particles may be generated by droplet formation and fragmentation of the core. In pressurized water reactors (PWR), a commonly used control rod material is silver-indium-cadmium (SIC) covered with stainless steel cladding. The control rod elements, Cd, In and Ag, have relatively low melting temperatures, and especially Cd has also a very low boiling point (about 1040 K). Therefore, control rods are likely to fail early on in the accident affecting fuel rod degradation as well as aerosol source term to the environment in the event of containment failure (Petti, 1989; Haste and Plumecocq, 2003).

The QUENCH experimental program at Forschungszentrum Karlsruhe investigates phenomena associated with reflood of a degrading core under postulated severe accident conditions but where the geometry is still mainly rod-like and degradation is still at an early phase. QUENCH-13 test was the first in this program to include a SIC control rod of prototypic PWR design (Birchley et al., 2008). The effects of the control rod on degradation and reflood behaviour were examined under integral conditions, and for the first time the release of SIC aerosols following control rod rupture was measured.

To characterize the extent of aerosol release during the control rod failure, aerosol particle size distribution and concentration measurements in the off-gas pipe of the QUENCH facility were carried out. The aerosol concentration and size distribution released from the core were determined using Electrical Low-Pressure Impactor (ELPI), and Berner Low-Pressure Impactors (BLPI). The sampling system was isolated from the facility before core cooling by quench. A second aerosol sampling system with 10 impactors was used also during the quench phase of the test.

Two aerosol particle modes were generated, fine mode with D_{ae} = 0.1 – 2 μm generated by vaporization and subsequent nucleation, condensation and coagulation, and coarse particle mode with D_{ae} > 3 μm generated by droplet release and fragmentation. These findings indicate that the commonly used modeling of aerosol formation from control rod rupture by evaporation from molten material surface would need to be refined to include aerosol generation by mechanical processes, such as droplet formation and fragment entrainment.

The aerosol generation during QUENCH-13 test can be divided into five phases: 1) Transient phase: A small but steady aerosol concentration increase presumably due to release of Sn from the Zircaloy. 2) First significant aerosol release at peak bundle temperature 1560 K is thought to have been caused by a small crack in the control rod cladding. The particles contained mainly Cd as an oxide. 3) A very large, but short aerosol burst presumably due to a massive failure of the control rod contained particles rich in Cd and In, with some Ag in the fine mode particles. 4) Steady aerosol release followed the large burst at bundle peak temperature increase from 1650 to 1800 K. The particles were rich in Cd and In, and the amount of Ag increased with time. At this stage, molten control rod material was relocated downwards, and aerosol was released from molten material surface. 5) Particles released during bundle cooling by quench were mainly irregular, coarse particles containing Zr, Sn and W, along with varying amounts of Cd and In. Ag and Fe were present in some distinct particles.. The particles were presumably generated from the molten material, and by fragmentation of the Zircaloy cladding and heater elements due to thermal shocks.

Birchley, J., Austregesilo, H., Bals, C., Dubourg, R., Haste, T., Lamy, J.-S., Lind, T., Maliverney, B., Marchetto, C., Pinter, A., Steinbrück, M., Stuckert, J., Trambauer, K. Proc. of Nuclear Energy for New Europe, Sept. 8-11, 2008, Portoroz, Slovenia.

Haste, T., Plumecocq, W. (2003) 9th International QUENCH Workshop, FZK, Oct 13-15, 2003.

Petti, D.A. (1989) *Nucl. Technol.* 84, 128.

Stuckert, J., Sepold, L., Grosse, M., Stegmaier, U., Steinbrück, M., Birchley, J., Haste, T., Lind, T., Nagy, I., Vimi, A. (2008) SARNET 4th Ann. Review Meeting, 21-25 January, 2008, Bled, Slovenia.

Experimental determination of correction factors for assessment of the activity discharges of radionuclides bound to aerosol particles from nuclear facilities

K. Vogl[1]

[1]Federal Office of Radiation Protection, 85764 Oberschleißheim, Germany

From the stacks of nuclear facilities radionuclides bound to aerosol particles - beside radionuclides in gaseous form like noble gases, tritiated water vapour or C-14 containing carbon dioxide – are discharged into the environment. For the assessment of the discharged activities of these radionuclides a part of the effluent air stream is extracted by means of a rake of extraction probes and conducted by primary and secondary sampling tubes to the sampling devices equipped with particulate filters. The discharged activities are calculated using the measured activities of the radionuclides on the deposited particles and the measured volumes of the effluent air stream and the air steam through the particulate filters.

Through the following effects the activity concentrations at the upstream side of the particulate filters are generally lower than those in the free effluent air stream:

– anrepresentative extraction due to uneven distribution of air velocity and activity concentration in the effluent air stream over the diameter of the stack;
– changes of size distribution for activity and particle number due to anisokinetic extraction;
– losses of aerosol particles and activities of the bound radionuclides in the sampling tubes, generally due to turbulent deposition and impaction. The losses of aerosol particles with aerodynamic diameters lager than 3 µm are considerable. The losses of the activities of the aerosol particle bound radionuclides depend on the aerosol particle losses and the activity size distribution, which is a logarithmic standard deviation with a geometric mean diameter of about 1 µm in general; the values of these losses are in the range of some percent up to 40 percent. (Vogl, 1994).

Therefore, for the assessment of the true activity discharges correction factors have to be used.. The so-called tube factor takes into account only the losses of activity in the sampling tubes and is defined as the activity concentration at the inlet of the extraction probes to the activity concentration at the upstream side of the particulate filters. The so-called total correction factor considers all the above mentioned effects and is defined as the mean activity concentration in the effluent air stream to the activity concentration at the upstream side of the particulate filters.

For the experimental determination of both correction factors test aerosol particles may be used which differ from the aerosol particles in the effluent air by being radioactive, by the chemical composition or by a much higher mass concentration. In all cases the activity size distribution or the mass size distribution of the test aerosol particle collective must be similar to the activity size distribution of the radionuclides carrying aerosol particles in the effluent air stream. For most experimental determinations powders like titanium dioxide are dispersed.

For the experimental determination of the tube factor a known amount, e. g. activity or mass, of these test aerosol particles are injected into the inlets of the extraction probes. In case of the total correction factor, these test aerosol particles are injected into the air stream at several locations upstream of the extraction rake.

The amount of the test particles deposited on the particulate filter may be determined gravimetrically or by other methods, e. g. XFA.

The value of the tube factor is the ratio of the injected amount of the test aerosol particles and the amount of the test particles on the particulate filter. The value of the total correction factor is the mean value of the ratios of the injected amounts of the test aerosol particles and the amounts of the test particles on the particulate filters.

For 12 investigated nuclear facilities in Germany the values of both correction factors are in the range between 1,1 and 1,6.

Vogl, K. (1994) *Aerosol particle losses in the sampling lines of nuclear facilities: Assessment and experimental determination J. Aerosol Science, Suppl.. 1, S265 - S266*

Resuspension of particles inside packages containing radioactive powders

F. Gensdarmes[1], H.E. Thyebault[1], J. Vendel[1], B. Eckert[2] and S. Fourgeaud[2]

[1] Aerosol Physics and Metrology Laboratory, IRSN, 91192, Gif-sur-Yvette, France
[2] Safety Assessment Section for Transports, IRSN, 92260 Fontenay-aux-Roses, France

In the field of transport of radioactive materials, the products, like UO_2, PuO_2 or MOX (Mixed OXyde Fuel) powders are confined in packaging which should, in normal or accidental conditions of transport, assure a leakage rate compatible with the release regulatory criteria (IAEA, 2005). The above mentioned conditions are characterized by a drop test up to respectively 1.2 m and 9 m high. In the safety demonstrations, the hypotheses usually taken into account by the French applicants are concentrations of aerosols in the cavity of the package equal to:

- in normal conditions of transport: 10^{-3} g.m^{-3},
- in accidental conditions of transport: 9 g.m^{-3} for the first thirty minutes after the drop, and then to 0.1 g.m^{-3} for one week.

The current study aims at discussing the relevance of these hypotheses on the basis of a review of the most recent studies available in the literature (Curren & Bond, 1980; Sandoval *et al.* 1985; Barlow *et al.* 1995; Martens *et al.* 2005) on the one hand and on the other hand of new laboratory experiments with surrogate powders. The objective of these experiments is to evaluate the amount of airborne particles inside a container of powder falling on an unyielding target.

Three alumina powders are used as surrogates for these laboratory experiments. The corresponding particle size distributions measured with the Coulter technique (based on the equivalent volume diameter) are presented in table 1.

Table 1. Characteristics of the particle size distributions of the alumina powders.

Powders	Mass median diameter (µm)	Geometric standard deviation
G1	4.6	1.4
G2	17	1.3
G3	27	1.5

The container, half filled with powder, is dropped from 1 m height. The particles in suspension are sampled in real-time with an optical particle counter (OPC, Grimm 1.108) using a flexible line which is in vertical position after the drop. The total mass of aerosols is determined by weighing the OPC sampling filter. Figure 1 shows the experimental set-up.

Table 2 gives the results obtained for the three powders and two bulk density (packed and non packed). The results are corrected to take into account the particles settling during the sampling period.
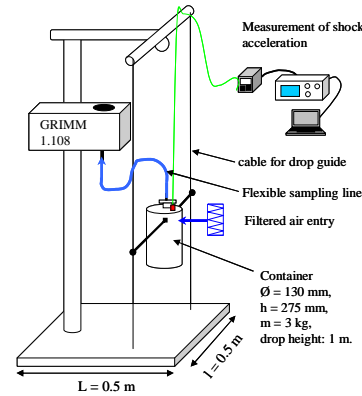

Figure 1. Experimental set-up.

Table 2. Characteristics of the airborne particles after the shock of the container filled with different powders.

Powder	Airborne particles mass (mg)	Initial aerosol concentration (g.m^{-3})
G1 non packed	20.3	8.07
G1 packed	12.4	4.05
G2 non packed	2.90	1.03
G2 packed	0.30	0.10
G3 non packed	0.78	0.26
G3 packed	0.18	0.06

The results obtained show the effects of the particle size distribution and of the powder bulk density on the particles resuspension.

Nevertheless, as the surrogate criterion used in this experiment was limited to the particle diameter, further experiments are necessary to evaluate, in particular, the impact on the results of the cohesive properties of the radioactive powders and of the high density of plutonium or uranium oxide particles.

IAEA (2005). *Regulations for the Safe Transport of Radioactive Material, 2005 Edition Safety Requirements*. Safety Standards Series No. TS-R-1.

Curren, W.D. and Bond, R.D. (1980). *Proc. 6th Int. Symp. on Packaging and Transportation of Radioactive Material:* West Berlin, nov 10-14.

Martens, R., Lange, F., Koch, W. and Nolte, O. (2005). *Forum EUROSAFE*, Brussels, nov 7-8.

Barlow S.V., Donelan P., Tso C.F. (1995). *Proc. 9th Int. Symp. on Packaging and Transportation of Radioactive Material.* Las Vegas, dec 3-8.

Sandoval R.P., Apple M.A., Grandjean N.R. (1985). *Sandia National Laboratories Report : SAND-84-2645;TTC-0537-* 1985 May 01.

A Miniature Collector for the Concentrated Collection of Fine Airborne Particles

S. V. Hering[1] and G. S. Lewis[1]

[1]Aerosol Dynamics Inc., 935 Grayson Street, Berkeley, CA 94710, USA

Over the last decade several types of real-time instruments have evolved that provide in-situ chemical characterization of ambient aerosols, yet because of their cost and operational demands, these instruments have not replaced the filter sampling for routine monitoring. Measurements in multiple locations, especially in remote regions, require small, low-cost, low-power instruments. Similarly micro-environmental and personal sampling demand small, light-weight, low-cost monitors. We seek here to develop a method that provides a concentrated, ready-to-analyze aerosol sample that takes advantage of low detection limits of many analytical methods, and yet has few operational demands.

As a first step in the development of such a monitor, we present here a miniature collector that provides a concentrated particulate sample. As in the water-based condensation particle counters (Hering and Stolzenburg, 2005), ambient particles are enlarged through water condensation using a laminar, thermally diffusive flow. Once enlarged the droplets are collected by impaction onto a solid surface, or into a small water reservoir.

This miniature collector, shown in Figure 1, utilizes a single, wet-walled tube, 4 mm ID, with an active length of 120mm. An annular thermal electric device mounted between the preconditioner and condenser acts as a heat pump to create a region of supersaturation for condensational growth. Cooling fins equipped with small fans are used to regulate the temperature of the condenser region. Typically, the system is operated with a preconditioner temperature of 5°-10°C, a condenser temperature of 30°-37°C and an air sampling rate of 0.4 L/min.

The droplets formed from this system are uniformly sized at approximately 2 µm in diameter, independent of the input particle size, as shown by measurements with an aerodynamic particle sizer in Figure 2. Once enlarged, the particles are deposited within a 300-µm spot by means of impaction. We

Figure 1. Miniature particle collector

120 mm

find that the water coating eliminates particle rebound, and indeed tests with 1.4 µm PSL showed that it is possible to form a "stack" of particles twice as high as it is wide. Ambient particles can also be collected into <80 µL volume of water.

Size dependent collection efficiencies are shown in Figure 3 for two types of aerosols, ammonium sulfate and oleic acid. We find high collection efficiency for all particles at sizes above 10 nm in diameter. This was found for both hygroscopic and hydrophilic particles. The efficiency was also tested as a function of particle concentrations. For this system, which was explicitly designed to minimize concentration effects, the collection efficiency remained high at the highest concentration tested of $10^5 cm^{-3}$.
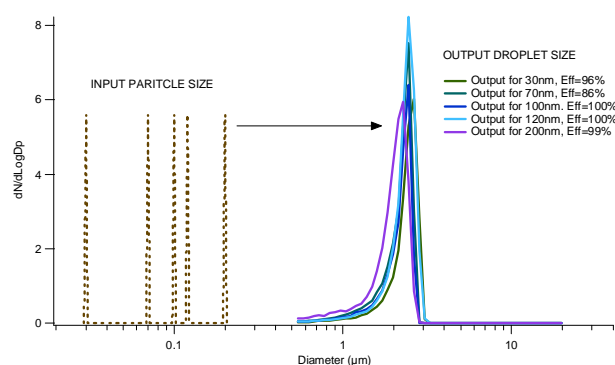

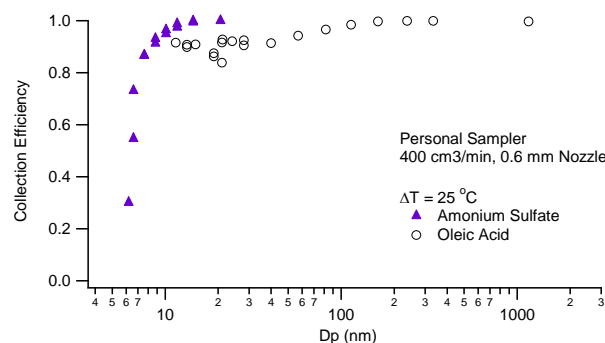Figure 2. Size distribution of droplets formed for varying input particle sizes.

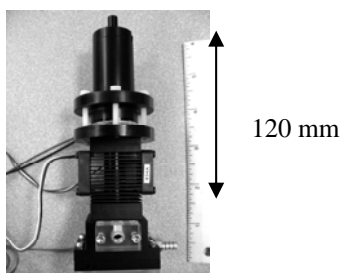Figure 3. Size-dependent collection efficiency.

Hering, S. V., Stolzenburg, M. R. (2005), *Aerosol Science and Technology*, 39: 428-436

Emission of submicron aerosol particles during the operation of a laser beam printer

Jeong Hoon Byeon[1], Sang Yoon Kim[2], Yong Kim[3], Dae Young Lee[1], and Jungho Hwang[2]

[1]Digital Printing Division, Samsung Electronics Co., Ltd., Suwon, 443-742, Republic of Korea
[2]School of Mechanical Engineering, Yonsei University, Seoul, 120-749, Republic of Korea
[3]Petrochemicals & Polymers Division, LG Chem, Ltd., Yeosu, 550-200, Republic of Korea

Keywords: Aerosol emission, Indoor sources, Number concentration, Submicron particles.

Laser beam printers for home or office use have attracted recent attention as a source of indoor submicron particles (He et al., 2007; Schripp et al., 2008; Géhin et al., 2008). Laser beam printers (LBPs) release not only volatile organic compounds but can also generate a considerable amount of submicron particles during the printing process (Kagi et al., 2007). The emission of particles from LBPs varies according to several parameters including the type of printer, cartridge, paper and toner.

The present study examined particle emissions from a commercial LBP under various operating conditions. The size distribution and number concentration of particles were measured using a scanning mobility particle sizer (SMPS). The particles generated from the printer ranged in size from 20 to 200 nm in equivalent mobility diameter, regardless of the operating conditions. Particles with a peak concentration of approximately 10^5 particles/cm^3 were detected when the fuser system was operated by fuser controller without development and the temperature of the heating roller was 190 °C. The peak particle concentrations for 0% covered white paper and 5% covered black paper were 1.5 x 10^5 particles/cm^3 and 3.3 x 10^5 particles/cm^3, respectively. This suggests that the rubber in the heating roller, paper and toner are the sources of the submicron particles.
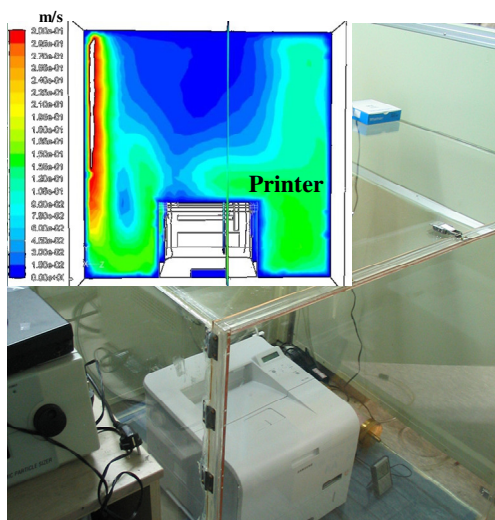

Figure 1. Photograph of experimental setup and velocity contour (inset) of the chamber inside.
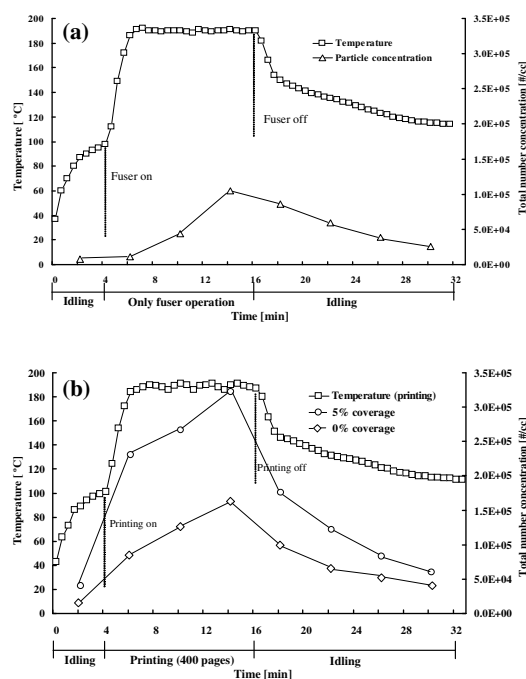

Figure 2. Particle number concentrations for only fusing (a) and printing (b) modes.

Fig. 2 shows results of particle number concentrations for only fusing (Fig. 2a) and printing (Fig. 2b) modes. The particle concentration increased with increasing fusing temperature. For the printing, the concentration at 5% coverage was remarkably higher than that in 0%.

He, C., Morawska, L., & Taplin, L. (2007). *Environ. Sci. Technol.*, 41, 6039-6045.

Schripp, T., Wensing, M., Uhde, E., Salthammer, T., He, C., & Morawska, L. (2008). *Environ. Sci. Technol.*, 42, 4338-4343.

Géhin, E., Ramalho, O., & Kirchner, S. (2008). *Atmos. Environ.*, 42, 8341-8352.

Kagi, N., Fujii, S., Horiba, Y., Namiki, N., Ohtani, Y., Emi, H., Tamura, H., & Kim, Y.S. (2007). *Build. Environ.*, 42, 1949-1954.

Wind direction versus sampling point: a real case study

M. Filice[1], P. De Luca[1]

[1]Department of Pianificazione Territoriale, University of Calabria, Rende, 87036, Cosenza, Italy

There is a wide range of parameters that play a central role in urban pollution, such as source apportionment, meteorological influence, and soil contribution. In this respect, the assessment of urban pollution may lead to significantly different results whether or not environmental conditions (e.g., meteorology, source properties) are taken into account. Several studies showed the role of meteorology on pollutants dispersion (De Gaetano & Doherty, 2004; Venkatram & Cimorelli,2007), mainly focusing on the temperature, wind action (Rigby *et al.*, 2006) pressure and rainy influences. The aim of this work is to observe the action of wind direction on particulate matter sampling. We focused on wind direction versus two variables: sampling point and pollutant sources.

11-h sampling was carried out during September 2008 nearby a road junction in a university area (University of Calabria). The sampling was separated into samples referring to two consecutive hours, alternating with 1-hour sampler cooling. The concentration was determined using a gravimetric method. The sampler was located north-east of road junction with an average traffic flow about 12 vehicles/min. Figure 1 compares the wind direction versus frequency classes, showing a bimodal distribution.
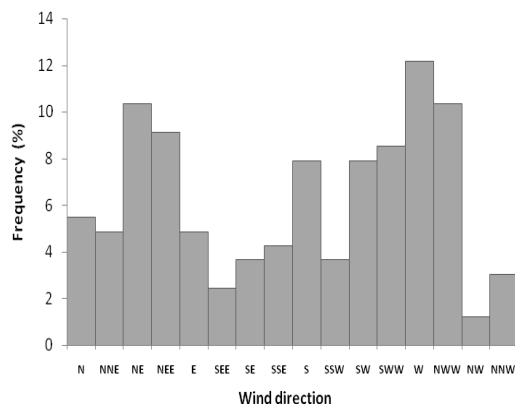

Figure 1. Wind direction frequency classes in September 2008, University of Calabria

Comparing PM10 concentration and traffic flows put evidence on the role of wind direction versus sampler position. We identified two conditions:

1. Adverse Condition (AC), i.e., the wind blows from the sampling point to the source;

2. Favorable Condition (FC), i.e., the wind blows from the source to the sampling point.

Wind direction was shown to have influence on the source contribution. In particular, we observed a roughly linear relation between PM concentration and traffic flow in FC status (Fig. 2(a)). By contrast, we observed a weak relation in AC status (fig. 2(b)).
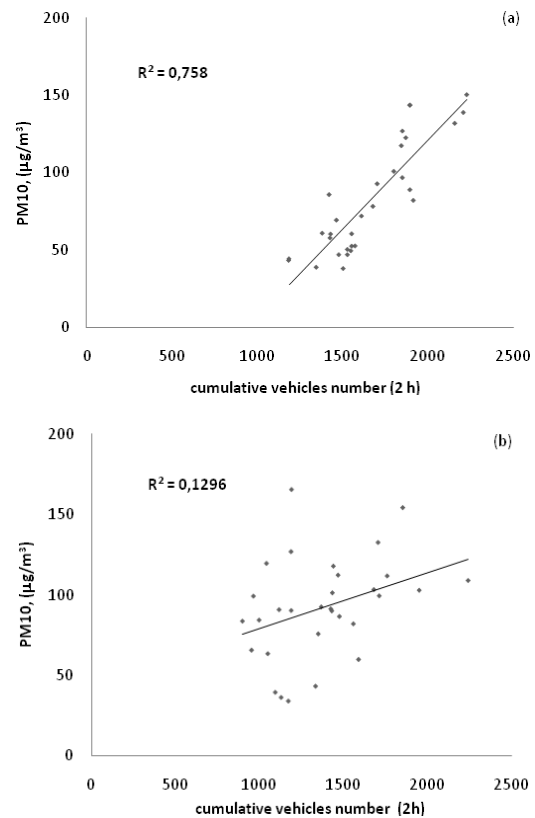

Figure2. Relation between PM10 concentration and traffic flow. Favorable condition of wind direction (a), adverse condition of wind direction (b).

This suggests that the "variable wind" should be considered with all its properties (intensity, direction). The wind direction can affect the measurement efficiency by altering the evaluation of real urban pollution.

De Gaetano A.T., Doherty O.M (2004). *Atmospheric Environment*, 38, 1547-1558

Rigby M., Timmis R., Toumi R (2006). *Atmospheric Environment*, 40, 5112-5124

Venkatram A., Cimorelli A.L., (2007). *Atmospheric Environment*, 41, 692-704

Biodiesel (soy-bean FAME) effect on particulate and gaseous pollutants from a passenger car

G. Fontaras, T. Tzamkiozis, L. Ntziachristos, and Z. Samaras

Laboratory of Applied Thermodynamics, Aristotle University of Thessaloniki, GR54124, Thessaloniki, Greece

Diesel vehicles are an important source of pollutant emissions, some of which potentially toxic. Biodiesel (fatty acid methyl esters – FAME) use as an automotive fuel is expanding around the world and this calls for better characterization of its impact on diesel combustion, emissions, air quality and ultimately on human health (Kousoulidou, Fontaras et al. 2007).

In this study a neat soybean-oil derived biodiesel (B100) and its 50% vol. blend with petroleum diesel (B50) were used on a Euro 2 diesel passenger car. The aim was to investigate biodiesel effect on regulated and non regulated pollutants such as carbonyl compounds (aldehydes and ketones), particle number and size distribution. Additionally, exhaust particle samples were collected for toxicological analysis. Measurements were conducted over the (cold-start) NEDC and the Artemis cycles on a chassis dynamometer.

Emissions of CO and HC increased up to 50% over the certification test, particularly with the B100 fuel. NOx increased by up to 10%, only with the B100 blend. Fuel consumption also increased by 9% (B50) and 17% (B100) over the legislated cycle and by 4.5% and 10% over Artemis respectively.

Despite some evidence which reports reduction of particulate matter (PM) with use of biodiesel, our measurements showed that PM more than doubled with B100 over the cold-start NEDC. The reduced volatility of biodiesel and engine-fuel interactions are important parameters with regard to the cold-start engine emission performance. The presence of biodiesel only led to significant reductions of PM emissions over the (hot) Artemis cycles.

In all cases solid particle number emissions decreased with the use of biodiesel. The reduction in solid particle number is mainly linked to the oxygen content in the biodiesel and, as a result, the lower C-atom proportion in its composition than petrodiesel. On the other hand, the total particle number (including volatiles) was increased. In addition, nucleation mode particles appeared more often than with petrodiesel. This effect was stronger at higher biodiesel blending ratios (Fig, 1). The formation of nucleation mode particles should be linked to the higher semi-volatile emissions and the lower soot mode of biodiesel, which promotes homogeneous nucleation that condensation. A negative effect (increase in emissions) was also observed for certain carbonyl compound emissions.

The results of this study showed that biodiesel at high blending ratios may strongly impact emissions from passenger cars, in a rather non-uniform manner, with the actual effect being dependant on driving conditions and blending ratio. The fact that certain results of this study are not in line with the general trends reported in literature (Lapuerta, Armas et al. 2008) indicates that biodiesel use under certain conditions and from different feedstocks may have different impacts, some of which strongly relate to health issues. Therefore, the detailed characterisation of emissions with use of biodiesels is required to thoroughly assess their environmental and health effects.
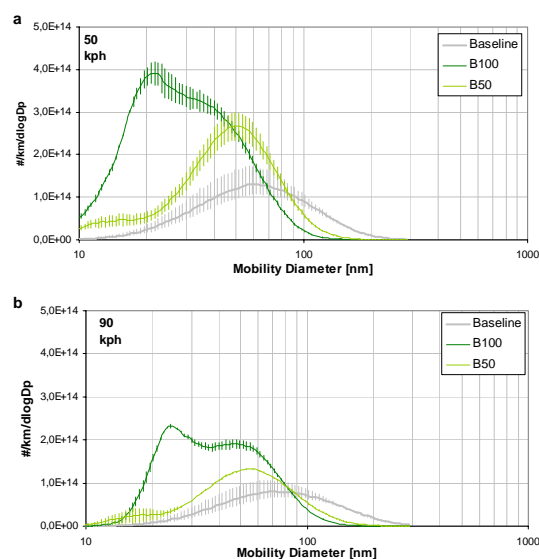

Figure 1 Particle mobility size distribution with use of petrodiesel (Baseline), neat biodiesel (B100), and a 50% blend (B50). (a) 50 km/h, and (b) 90 km/h.

Kousoulidou, M., G. Fontaras, et al. (2007). " Effect of biodiesel and bioethanol on exhaust emissions." ETC/ACC Technical Paper 2008/5.
Lapuerta, M., O. Armas, et al. (2008). "Effect of biodiesel fuels on diesel engine emissions." Progress in Energy and Combustion Science **34**: 198-223.

CHEMKAR PM$_{10}$: The extended results of a yearlong chemical characterisation of PM$_{10}$ at six sites in Flanders (Belgium)

J. Vercauteren[1], C. Matheeussen[1], E. Roekens[1], B. Geypens[2], R. Van Grieken[3] and W. Maenhaut[4]

[1] Flemish Environment Agency (VMM), Kronenburgstraat 45, 2000 Antwerpen, Belgium
[2] Institute for Reference Materials and Measurements, Retieseweg 111, 2440 Geel, Belgium
[3] Micro- and Trace Analysis Centre (MiTAC), Universiteitsplein 1, 2610 Wilrijk, Belgium
[4] Institute for Nuclear Sciences, Ghent University, Proeftuinstraat 86, 9000 Gent, Belgium

Keywords: PM10, PM and source apportionment, Aerosol characterisation, Sea salt, PAH(s),

In September 2006 the Flemish Environment Agency (VMM) started "*Chemkar PM$_{10}$*": the first large scale chemical characterization project for PM$_{10}$ in Flanders (Belgium). During one full year on every 6th day, PM$_{10}$ was sampled simultaneously at six monitoring sites: Houtem (HO, rural background near the sea), Zelzate (ZE, industrial), Borgerhout-Antwerp (BO, urban traffic), Mechelen (ME, urban background with traffic and industrial influence) Aarschot (AA, near city background), Hasselt (HA, urban background with traffic and industrial influence).

Sampling was done for 24h with two Leckel SEQ 47/50 instruments at 2.3 m^3/h on both pre-fired Whatman QM-A filters and Pall Teflo filters. The quartz fibre filters were used for the analysis of elementary and organic carbon (TOT), carbon and nitrogen stable isotope ratios (IR-MS) and water soluble ions (ion chromatography). The teflon filters were used to determine a whole range of elements (ED-XRF).

On three locations (BO, ZE, AA) additional samples were taken for genotoxicological tests and PAH determination. This was done with high volume samplers (Digitel DHA80 at 30 m^3/h) and a new method for PAHs that uses sorption on polydimethylsiloxane (PDMS).

The average blank-subtracted concentrations for PM$_{10}$ on the quartz fibre filters varied from 27 μg/m^3 (HO) to 36 μg/m^3 (BO). The mass on the teflon filters was on average 7% lower.
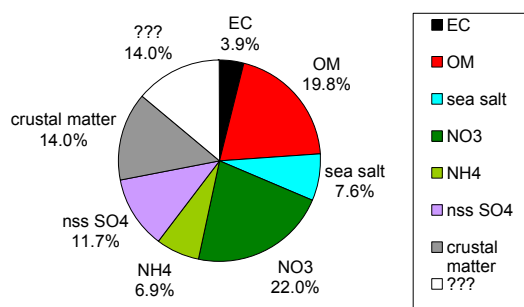
Table 1: Average concentrations of the main fractions for the six sites

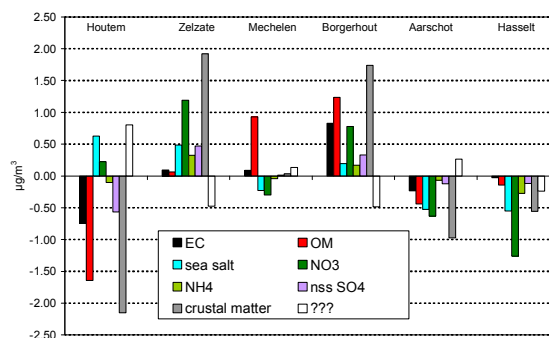| Av. (μg/m^3)	EC	OM	sea salt	NO$_3^-$	NH$_4^+$	SO$_4^{2-}$ (nss)	crustal matter	???	PM$_{10}$ (Q)
Houtem	0.47	4.49	2.98	7.04	2.04	3.07	2.17	5.13	27.4
Zelzate	1.31	6.20	2.84	8.00	2.47	4.11	6.24	3.85	35.0
Mechelen	1.30	7.06	2.12	6.51	2.10	3.65	4.35	4.46	31.6
Borgerhout	2.04	7.37	2.54	7.59	2.31	3.97	6.06	3.84	35.7
Aarschot	0.98	5.70	1.83	6.18	2.08	3.51	3.35	4.59	28.2
Hasselt	1.18	5.99	1.80	5.55	1.87	3.52	3.77	4.09	27.8
All stations	**1.21**	**6.14**	**2.35**	**6.81**	**2.14**	**3.63**	**4.32**	**4.33**	**30.9**

Fig 2: Local variations in average composition at the six Chemkar sites.

In addition to the basic results (Table 1, Fig 1 & Fig2) several advanced calculations were carried out. More information will be presented on:

- crustal enrichment factors of various elements
- factor analysis
- chloride depletion in the sea salt fraction
- the influence of sea salt on exceedances of the PM$_{10}$ limit values
- correlations between V an Ni and the effect of oil burning in Dunquerke
- additional characterisation of tunnel samples
- the loss of NH$_4$NO$_3$ in automatic samplers (TEOM, β-attenuation)
- the variations in C and N isotopic ratios
- PAH concentrations and the correlation with traffic tracers

Fig 1: Average composition of PM$_{10}$ at the six Chemkar sites.

Background concentrations of PAH:s in precipitation and air in Finland

M. Vestenius, H. Hellen and H. Hakola

Finnish Meteorological Institute, P.O. BOX 503
FI-00101 HELSINKI, FINLAND

Keywords: PAH, PM_{10}, precipitation, air quality.

The atmosphere contains large amounts of organic compounds, which originate from both natural and anthropogenic emissions.

Polycyclic aromatic hydrocarbons (PAH-compounds) are particularly harmful compounds due to their carcinogenic effect on humans. PAH-compounds are formed during incomplete burning of organic material and are emitted into the atmosphere from several natural and anthropogenic emission sources. Natural sources include for example emissions from volcanic activities and forest fires, whereas mainly anthropogenic sources consist of fuel burning in energy and electricity production, traffic and biomass burning (Ravindra et al.,2008).[1] Wood combustion, especially in house warming is a significant PAH-source, particularly in the Northern Europe (*Hellen et al.,* 2008).[2]

In this study, PAH-compounds from particulate matter in air (PM_{10} samples) and precipitation samples were collected at two background stations, Kuhmo and Virolahti, in Finland. The Kuhmo sampling station is situated in the eastern, and Virolahti in the south-eastern Finland. Both places are located in a rural district, near Russian border.

Daily PM_{10}-samples were collected with a low volume sampler ($38 \ 1 \ min^{-1}$) onto teflon filters. Current data covers samples from Virolahti from 2007 and 2008. Occasional samples were also collected during spring 2008 at Kuhmo (Hakola et al., 2008)[3]. Monthly precipitation samples were collected first into teflon bags in standard rainwater samplers, in Kuhmo from April 2007 to March 2008. Monthly precipitation PUF-sampling started at Virolahti on spring 2008.

Figure 1 shows the monthly mean concentrations of PAH-compounds in PM_{10} fraction together with temperature and Figure 2 shows the monthly mean concentrations in precipitation samples.
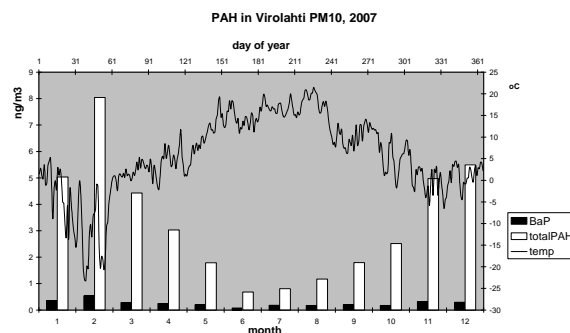

Fig.1. Monthly average total PAH and *Benzo(a)Pyrene (BaP)* concentrations [ng/m^2] in PM_{10}, and daily mean temperatures at Virolahti, in 2007.
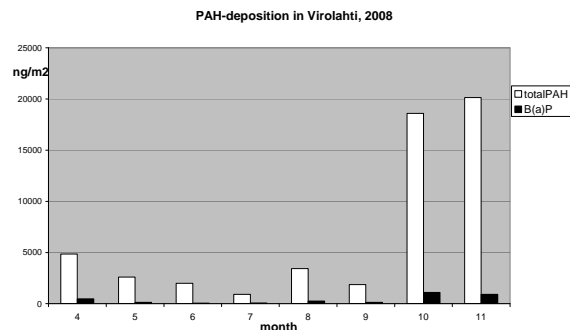

Fig.2. Monthly total PAH and B(a)P –concentrations [ng/m2] in precipitation at Virolahti, in 2008.

The results show that average concentrations of PAH-compounds in precipitation and PM_{10}-fraction are highest in winter. During winter, there are more PAH-sources due to heating. PAH-concentrations in PM_{10} are approximately inversely proportional to outdoor temperature. PAH-compounds decompose in photochemical reactions. These reactions are slower in wintertime, when there is less light, compared to summertime. The average monthly PAH-deposition in 2007 at Kuhmo and in 2008 at Virolahti were 3300 and 6800 ng m^{-2}, respectively. The spring mean PAH-concentration in PM_{10}-fraction in 2007 at Kuhmo and Virolahti were 1.1 and 4.1 ng m^{-3}. At Virolahti, mean weekly PAH-concentrations in spring 2007 and 2008 were 4.1 and 3.6 ng m^{-3}, respectively. Higher concentrations at Virolahti are expected since it is located only about 200 km from St Petersburg. In generally, PAH-concentrations in particulate matter in Finnish background areas are low.

[1] Ravindra, K., Sokhi, R., Van Grieken, R., Review: *Atmospheric polycyclic aromatic hydrocarbons: Source attribution, emission factors and regulation,* Atmospheric Environment 42 (2008), p.2895-2921.

[2] Hellen, H., Hakola, H., Haaparanta, S., Pietarila, S. and Kauhaniemi, M., *Influence of residential wood combustion on local air quality,* Science of the total environment 393(2008), p.283-290.

[3] Hakola, H, Vestenius, M., Hellen, H. and Paatero, J. *Polycyclic aromatic hydrocarbons (PAH) in air and in precipitation in Kainuu border area,* Final report, Euregio Karelia Neighbourhood programme, Kuhmo 2008, p.14-19.

Indoor versus outdoor air quality measurements: number, mass concentrations and chemical composition of PM at the University of Perugia, Italy

S. Ortu[1], L. Barcherini[1], D. Cappelletti[1], F. Marmottini[1], F. Scardazza[1], B. Moroni[2], B. Sebastiani[3]

[1]Dipartimento di Ingegneria Civile ed Ambientale
[2]Dipartimento di Scienze della Terra
[3]Dipartimento di Specialità Medico-Chirurgiche e Sanità Pubblica
Università degli Studi di Perugia, Perugia, Italy

Keywords: Indoor, mass concentration, chemical composition

According to recent reports, people living in urban areas in Central Europe spend 80% to 90% of their time indoors. In these contexts indoor concentrations of pollutants are frequently higher than outdoor. Many aerosol chemical compounds cause respiratory irritations and can provoke discomfort and other symptoms, typical of the "Sick Building Syndrome". Studies conducted in different countries on people working inside indoor public buildings, evidenced that 15 to 50% of them suffer from some discomfort.

Based on these general observations, we evaluated the air quality in some rooms at the University of Perugia and compared it with measurements carried out outdoor in the university campus. The sample campaign started in October 2006 and is still in progress. Since then, more than 250 samples have been collected. Single stage low volume (38 l/min) samplers combined with selective inlets for PM_{10}, $PM_{2,5}$ and PM_1, high volume 7 stages cascade impactors (0,57 m^3/min) and optical particle counters were employed and the samples collected on PTFE and PC filters, both indoor and outdoor. Samples on PTFE filters underwent chemical analysis by atomic emission spectroscopy (ICP-AES), UV-VIS spectroscopy, ionic chromatography (IC) and gas chromatography/mass spectrometry (GC-MS). Samples collected on PC filters underwent morphochemical analysis of the constituent phases by scanning electronic microscopy (SEM) coupled with EDS microanalysis.

Indoor annual mean values of PM_{10} and $PM_{2,5}$ were slightly higher than those outdoors (+8%), while the PM_1 values are practically the same. The number concentration of the particles showed a higher values on weekdays and lower values on weekends (fig. 1). In addition a clear difference in the indoor/outdoor ratio of mass concentrations was evidenced between weekdays compared to weekends when the activity is reduced to minimum. The mass concentration have higher values in the fine fraction <0,39 µm (approximately 35-40% of the mass) and show a higher difference in the 4,2-10µm class (weekends days).

The presence of heavy metals (Pb, Zn, Ni), is constant in the various size ranges, and represent globally in average 0,4% in mass. Elements of probable natural crustal origin (Al, Fe, Ca, Mg, Na) contributes for 13,7% to the mass of PM_{10}, and for 6,4% to the mass of PM_1. A distinguishing but not clear feature of PM_1 is the presence of Al and Zn in higher concentration (5-6 times) in indoor classrooms than outdoor. This could be perhaps related to some indoor source. For the heavier fractions of PM these ratios are inverted. Otherwise, the indoor presence in the PM_1 fraction of K, a typical element associated with fire burning which has been found in larger concentration outdoor, is a sign of a contribution from outside sources. The contribution of nitrates, sulphates, fluorides, and chlorides is lower indoor than outdoor, while ammonium is higher indoors.

Outdoor, anthropogenic sources mostly contribute to the organic fraction (PAHs, n-alkanes), whilst in the samples measured indoor the biogenic contribution is more evident, (fig. 2).
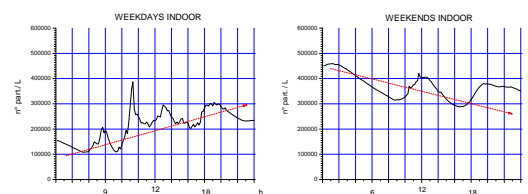

Figure 1. Indoor daily trend of particle number concentration (weekend- weekdays).
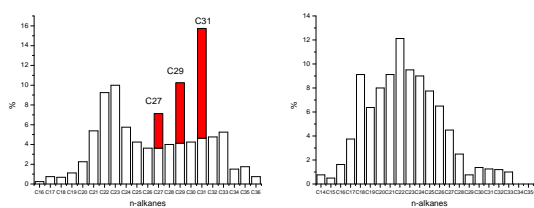

Figure 2. Comparison of n-alkanes distribution in PM_1 INDOOR (left) and PM_{10} OUTDOOR (right).

Characterization of fine aerosol particle (PM1) and trace element concentrations: assessment of the contribution of local sources and long-range transport

R. Caggiano[1], M. Macchiato[2], S. Sabia[1], G.A. Scardaccione[1] and S. Trippetta[1]

[1]Istituto di Metodologie per l'Analisi Ambientale, CNR, C.da Santa Loja-Zona Idustriale, 85050, Tito Scalo (PZ), Italy
[2]DSF, Dipartimento di Scienze Fisiche, CNISM, Università Federico II, Via Cintia, 80126, Napoli, Italy

Fine aerosol particles (such as PM2.5 and PM1, aerosol particles with aerodynamic diameter less than 2.5 μm and 1μm, respectively) have been found to have an impact on human health, ecosystems and atmospheric processes including the cloud formation, visibility, solar radiation and precipitation (Karar and Gupta, 2007). Due to the importance of these impacts, in the last few years a great deal of studies have been focused on aerosol levels, their elemental composition and the identification of their sources (related both to local or long-range transport). All this is very important not only for the development of air quality control strategies but also for better understanding the different phenomena which could significantly affect the atmospheric aerosol behaviour (Querol et al., 2007).

In this context, daily observations of PM1 were performed in the industrial area of Tito Scalo (40° 36' N, 15° 44' E, 760 m a.s.l., Basilicata region, southern Italy) from April 2006 to March 2007. PM1 concentrations were measured by means of a low-volume gravimetric sampler and each PM1 sample was analyzed by means of Inductively Coupled Plasma Optical Emission Spectrometry (ICP-OES) or Atomic Absorption Spectrometry (GFAAS and FAAS) techniques in order to determine its content in fourteen trace elements (Al, Ca, Cd, Cr, Cu, Fe, K, Mg, Mn, Na, Ni, Pb, Ti and Zn).

In the examined period, PM1 daily concentrations range between 0.3 $\mu g\ m^{-3}$ and 55 $\mu g\ m^{-3}$ with a mean value of 8±7 $\mu g\ m^{-3}$ and a median value of 6 $\mu g\ m^{-3}$. As far as the PM1 chemical composition is concerned, the trace element concentration mean values decrease in the following order: Ca>Fe>Al>Na>K>Cr>Mg>Pb>Ni≈Ti≈Zn>Cd≈Cu> Mn.

Principal Component Analysis (PCA) allows to identify four source profiles for the fourteen trace elements determined in the PM1 samples: a natural source profile, an anthropogenic/traffic source profile, an anthropogenic/industrial profile and a mixed industrial/natural profile.

Finally, the application of a procedure consisting of a combined use of analytical back trajectories, statistical analysis and the trace element concentration data allows to study the potential long-range transport contribution to the PM1 chemical composition. The results show that the long-range transport impact is difficult to quantify both because of the smallness of the aerosol particles and the strong influence of local emissions on the PM1 chemical composition.

Karar, K., & Gupta, A.K., (2007). *Atmospheric Research*, 84, 30–41.

Querol, X., Minguillón, M.C., Alastuey, A., Monfort, E., Mantilla, E., Sanz, M.J., Sanz, F., Roig, A., Renau, A., Felis, C., Miró, J.V., & Artíñano, B., (2007). *Atmospheric Environment*, 41, 1026–1040.

Analysis of ROS generated by PM_{10} sampled at a rural and urban location in North Rhine Westphalia

B. Hellack[1], U. Quass[2], T.A.J. Kuhlbusch [2], C. Albrecht[1], R.P.F. Schins [1]

[1] IUF gGmbH, Institut für umweltmedizinische Forschung, Auf´m Hennekamp 50, 40225 Düsseldorf, Germany
[2] IUTA e. V., Air Quality & Sustainable Nanotechnology Unit, Bliersheimer Str. 60, 47229 Duisburg, Germany

Keywords: ElectronSpinResonance (ESR), hydroxyl-radicals, PM_{10}/PM_1, Reactive Oxygen Species (ROS)

The formation of reactive oxygen species (ROS) and subsequent induction of oxidative stress in cells are nowadays considered to be the dominant factors responsible for the pulmonary toxicity of PM_{10} (Donaldson et al., 2004). Especially, a compound- and particle upon load-dependent hydroxyl-radical generation via Fenton-type reactions has been demonstrated. Electron Spin Resonance spectroscopy is a sophisticated technique for detecting ROS, predominantly hydroxyl-radicals, in cell free systems. In the present study a simplified filter preparation method was tested and used to point out potential differences between the hydroxyl-radical-generation potential of sampled air at a rural versus an urban location.

Measurements of PM_{10}- and PM_1-elicited ROS-activity on quartz fibre filters are carried out for more than one year (February 2008-March 2009) at a rural (Eifel, mountainous area) and an urban location (Styrum, Ruhr area), respectively (c.f. Quass et al., 2009, abstract T113A03). Samples are taken every other day on preheated quartz fibre filters (Munktell MK 360). For verifying the ROS-activity a simplified method is tested. Instead of preparing a particle suspension from the PM loaded filters by sonication, as usually described in literature (Shi et al., 2003), the filters are put directly into the reaction mixture containing H_2O_2 and the spin trap compound (DMPO), followed by the common preparation steps. This cost and time saving procedure is possible if no subsequent toxicity assessment is planned.

Tab. 1 method comparison exemplary for one selected loaded PM_1 quartz fibre filter from the rural location (a.u. = arbitrary unit); coefficient of variance (3 replications) <5%

technique	sonication t[min.]	ESR-signal a.u.
Shi et al., 2003	5	1049
	10	2274
	15	2094
this study	--	5565

First measurements confirm the applicability of the quartz fibre filters and the modified method for detecting the ROS-activity of PM loaded filters, shown in Tab. 1. No significant filter blank signals are detectable (not shown) and in comparison to the commonly applied method using particle suspensions the reactivity approximately doubles (see table 1).

The differences between the hydroxyl-radical generation at rural and urban locations are shown in Fig. 1.
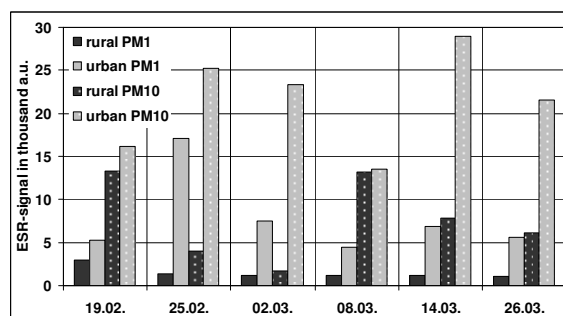

Fig. 1 hydroxyl-radical generation of PM_{10} and PM_1 loaded filters from a rural (black) and urban (grey) location (a.u. = arbitrary unit).

For both particle size-fractions a higher activity of samples collected at the urban site is apparent (ratio± SD rural/urban: PM_1 24± 17%; PM_{10} 43± 37%). Compared to PM_{10} samples, PM_1 reactivity is always less (ratio± SD PM_1/PM_{10}: rural 28± 22%; urban 36± 16%). This indicates a pronounced influence of the coarse particle fraction. For both sample types no correlation between ROS-activity and mass concentration was found. The variability of the values could probably be caused by differences in compounds and chemistry mixture and will be investigated by additional chemistry and mass measurements. In the end, based on the whole one-year dataset analysis, we will elucidate on the determination of location-dependent particulate ROS-activity as a marker for health risk.

Donaldson, K., Born, P.J.A., Stone, V., Jimenez, L.A., Gilmour, P.S., Schins, R.P.F., Shi, T., Rahman, I., Faux, A.P., Macnee, W. (2004), in Vallyathan V. (Ed.) 187, 257-288.

Quass, U., Sperber, O., Romazanowa, O., Luther, F. Caspari, A., Beyer, M., Pfeffer, U., Zang, T., Bruckmann, P., Kuhlbusch, T.A.J. (2009), Abstract T113A03, EAC 2009.

Shi, T., Schins, R.P.F., Knaapen, A.M., Kuhlbusch, T., Pitz, M., Heinrich, J., Born, P.J.A. (2003), J. Environ. Monit. 5, 550–556.

Influence of a Saharan dust outbreak on PM2.5 observations at a Mediterranean sampling site

S. Trippetta[1], R. Caggiano[1] and M. Macchiato[2]

[1]Istituto di Metodologie per l'Analisi Ambientale, CNR, C.da Santa Loja Zona Idustriale, 85050, Tito Scalo (PZ), Italy
[2]DSF, Dipartimento di Scienze Fisiche, CNISM, Università Federico II, Via Cintia, 80126, Napoli, Italy

Keywords: PM, trace elements, Saharan dust.

Atmospheric aerosols, originated from both natural and anthropogenic sources, play a crucial role in changes of global and regional climate as well as environmental pollution (Colette et al., 2008; IPCC, 2007). Atmospheric aerosols are characterized by high variability in terms of sources, chemical-physical composition, spatial and temporal distribution and they can be transported over long distance (IPCC, 2007). In particular, during the spring/summer seasons, large amounts of dust coming from Africa are transported over the Mediterranean basin (Rodrıguez et al., 2001; Escudero et al., 2006; Balis et al.,2006; Gobbi et al., 2007) affecting concentrations and chemical composition of aerosols at ground level in areas often very far from the dust source region.

In this context, we present a case study of a Saharan dust outbreak occurred over an experimental site located in the Mediterranean basin (Tito Scalo: 40° 36' N, 15° 44' E, 760 m a.s.l., Basilicata region, southern Italy) in the period 26-30 June, 2006. During this period, measurements of PM2.5 (aerosol particles with aerodynamic diameter less than 2.5 μm) and its content in Al, Ca, Cd, Cr, Cu, Fe, K, Mg, Mn, Na, Ni, Pb, Ti and Zn were carried out at Tito Scalo. The study was performed integrating in-situ measurements with satellite data and model forecasts. In particular, the combined analysis of OMI (Ozone Monitoring Instrument) aerosol index (AI) maps, SeaWIFS (Sea-viewing Wide Field of view Sensor) true color images and back-trajectories allowed the identification of a dust plume extending from Western Sahara toward Italy during the study period.

We observe an increase of the PM2.5 levels and Al, Fe, K, Mg and Ti concentrations, which are chemical elements generally considered as tracers of Saharan dust impact at ground level. Results highlight that, even if levels and chemical composition of aerosols at ground level are mostly influenced by local anthropic emissions, special events, such as Saharan dust outbreaks, may exert a strong influence on them.

Balis, D.S., Amiridis, V., Kazadzis, S., Papayannis, A., Tsaknakis, G., Tzortzakis, S., Kalivitis, M., Vrekoussis, M., Kanakidou, M., Mihalopoulos, N., Chourdakis, G., Nickovic, S., Perez, C., Baldasano, J., & Drakakis, M., (2006). *Annales Geophysicae*, 24, 807-821.

Colette, A., Menut, L., Haeffelin, M., & Morille, Y., (2008). *Atmospheric Environment*, 42, 390-402.

Escudero, M., Stein, A., Draxler, R.R., Querol, X., Alastuey, A., Castillo, S., and Avila, A., (2006). *Journal of Geophysical Research*, 111, D06210, doi:10.1029/2005JD006395.

Gobbi, G.P., Barnaba, F., & Ammannato, L., (2007). *Atmospheric Environment*, 41, 261–275.

IPCC, (2007). *Climate Change 2007: The Physical Science Basis. Contribution of Working Group I to the Fourth Assessment Report of the Intergovernmental Panel on Climate Change.* Cambridge, United Kingdom and New York, NY, USA: Cambridge University Press.

Rodriguez, S., Querol, X., Alastuey, A., Kallos, G., & Kakaliagou, O., (2001). *Atmospheric Environment*, 35, 2433- 2447.

Assessing the contribution of steel works to PM10 at nearby monitoring station using magnetic particles as tracers

E. Petrovský[1], A. Kapička[1], B. Kotlík[2], R. Zbořil[3], J. Novák[4] and H. Fialová[1]

[1]Institute of Geophysics ASCR, Boční II/1401, 141 31 Praha 4, Czech Republic
[2]National Institute of Public Health, Šrobárova 48, 100 42 Praha 10, Czech Republic
[3] Center for Nanomaterial Research, Palacký University, Šlechtitelů 11, 783 71 Olomouc, Czech Republic
[4] Czech Hydrometeorological Institute, Na Šabatce 17, 143 06 Praha 4, Czech Republic

Keywords: Industrial PM10, monitoring, PM10 and source aportionment, magnetic properties, Fe-oxides.

Several studies showed that PM10 contains significant portion of magnetic particles, typically spherules of anthropogenic origin, composed mainly of (metal-substituted) magnetite and/or maghemite (e.g., Flanders, 1994; Sagnotti *et al.*, 2006). These particles can be detected and characterized with very high sensitivity. Furthermore, depending on the pollution sources and sampling site, concentration of these particles may show significant correlation with the total PM10 concentration and several heavy metals (e.g., Muxworthy *et al.*, 2003; Sagnotti *et al.*, 2006).

In this contribution, we will show how highly sensitive magnetic measurements, reflecting concentration of ferrimagnetic iron oxides, vary due to meteorological conditions and may be interpreted in terms of significance of nearby steel works.

Our results (Fig. 1) show daily variations in PM10 concentration at industrial site, located less than 1 km from major steel works, normalized to weekly average. Variations in PM10 mimic very well changes in magnetic parameters, reflecting concentration of iron oxides. However, while PM10 concentrations vary within ±25% with respect to the weekly average, magnetic particles show much larger variations, from some 10% up to almost 300% of the weekly average.

Using the wind diagrams, related to the PM10 sampling periods, magnetic data can be interpreted in terms of meteorological control of the contribution of industrial PM10, emitted by the steel works. While concentration of magnetic particles reached their maximum during the days with prevailing weak wind (no more than 2-3 m/s) blowing from the steel works (Aug. 20), they were at the minimum level during the days with wind blowing towards the steel works (Aug. 17-18). Even winds from the steel works, if moderate to strong (> 4 m/s) caused decrease in concentration of magnetic particles, most probably due to "overshooting" effect (Aug. 16). Similar results were obtained for December 2007 campaign.

We suggest that magnetic measurements can help in assessing the relative contribution of steel works to total PM10 concentration at nearby sites. In this particular case, although PM10 concentrations are in general high (this site is classified as site with the most polluted atmosphere within the whole of Czech Republic), the steel works dominate this situation only during periods with specific meteorological conditions.
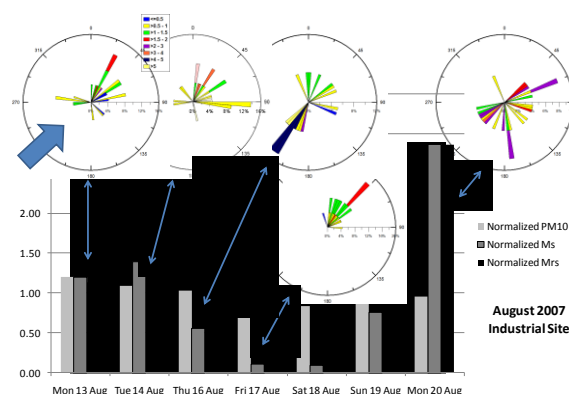

Figure 1. Concentration of PM10 and ferrimagnetic particles in samples collected over one week in summer campaign 2007 at industrial site, less than 1 km from big steel works, normalized with respect to weekly average. Ms and Mrs are saturation magnetization and saturation remanent magnetization, respectively, both reflecting concentration of ferrimagnetic iron oxides. Thick blue arrow indicates direction from the steel works.

Flanders, P.J., (1994). *J. Appl. Phys.*, 75, 5931-5936.

Muxworthy, A. R., Matzka, J., Davila A. F., & Petersen, N. (2003). *Atmos. Environ.*, 37, 4163-4169.

Sagnotti, L., Macri, P., Egli, R., & Mondino, M. (2006). *J. Geophys. Res.*, 111, B12S22, doi:10.1029/2006JB004508.

Week daily variation of PM$_{10}$ depending on air mass origin at German lowlands (Melpitz site) – a four year study

G. Spindler[1], E. Brüggemann[1], Th. Gnauk[1], A. Grüner[1], H. Herrmann[1],
K. Müller[1], M. Wallasch[2]

[1]Leibniz-Institut für Troposphärenforschung e.V., Permoserstrasse 15, 04318 Leipzig, Germany
[2]Umweltbundesamt, Wörlitzer Platz 1, 06844 Dessau-Roßlau, Germany

Keywords: PM$_{10}$, TEOM®, long-range transport, tropospheric Aerosol, trajectory

PM$_{10}$ concentration measurements were performed at the IfT-research station Melpitz (12°56' E, 51°32' N, 86 m asl.). This grassland site is located about 50 km northeast of Leipzig near the city of Torgau in a representative rural region in the German low-lands (Spindler et al., 2004). The distance to the Polish border in the East is about 120 km. The Melpitz site is an EMEP level 3 station (Co-operative Programme for Monitoring and Evaluation of the Long-Range Transmission of Air Pollutants in Europe) and provides results of complex scientific evaluation of measurements (EMEP, 2007). For this study quasi continuous half-hourly PM$_{10}$ mass-concentration measurements provided by a TEOM® (Type 1400a, Rupprecht & Patashnick Co., Inc., USA) over four years are used. The TEOM® was operated at 50 °C collecting particles on an oscillating microbalance. This operating temperature is necessary to avoid the condensation of water vapour (positive artefact) but can also generate systematic errors by evaporating volatile compounds (negative artefacts). Therefore the mean mass for 24 hours was corrected by a daily comparison with the mean PM$_{10}$ mass, detected gravimetrically from quartz fibre filters (Munktell, S). This daily PM$_{10}$ filter samples were collected using a high volume samplers (DHA-80, DIGITEL Electronic AG, CH).

The corrected half-hourly means were sorted for the seven weekdays and additionally separated for two mean air mass transport pattern. Under the dominating wind direction Southwest to Northwest (W) air masses from the Atlantic Ocean with integrated showers are transported to Meloitz, often during low pressure situations with relatively high wind velocities. They pass large parts of Germany. The second main wind direction is East (E). Then dry air masses are transported with moderate wind velocity during high pressure situations over long distances to Melpitz. The main sources regions for these continental air masses are in Russia, Poland, Belarus, Ukraine, and the North of Czech Republic. For identifying air mass source regions 96 hours backward trajectories (www.arl.noa.gov) were used.

In Figure 1 the week daily mean PM$_{10}$ concentrations are shown for all data (100 % of time) and for the days with air mass transport from E and W (about 19 % and 66 % of time, respectively).

The concentration course for all data shows a typical increase of PM$_{10}$ influenced by anthropogenic caused emissions from Monday to Friday, with lowest concentrations on Sunday. The mean PM$_{10}$ concentration pattern for air mass transport from W is similar to that but 5 to 8 µg/m³ lower. The PM$_{10}$ concentration for air mass transport from E is about 13 µgm^{-3} higher as for W. The concentration course shows a time shift of three days (minimum concentration for W at Sunday and for E at Wednesday). This is a hint for long range transport of anthropogenically emitted fine particles and precursor gases (particle mass formation during transport) in Eastern Europe. For a mean wind velocity range from E of 1.0 to 2.5 ms^{-1} these anthropogenic emissions are 250 to 650 km away from Melpitz. The results are in agreement with former findings of higher parts of sulphate, organic and black carbon during air mass transport from E in particles of different size range at Melpitz site (EMEP 2007).
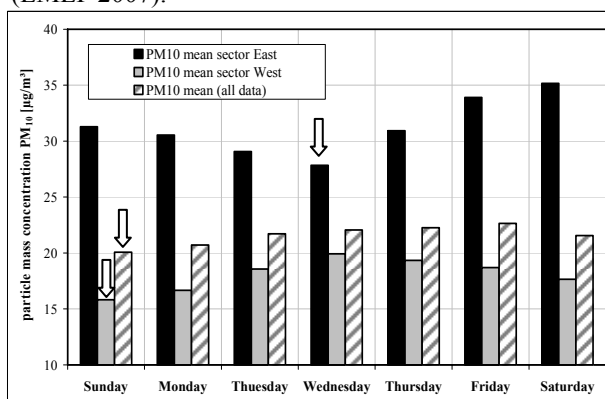

Figure 1. Week daily means for PM$_{10}$ based on half hourly PM$_{10}$ concentration measurements by a TEOM® (May 2004 until April 2008), hatching bars mean of all data, black bars and grey bars mean of data for days with air mass transport from East (E) and West (W), respectively. Minimum concentrations are marked by arrows.

EMEP (2007) Transboundary particulate matter in Europe. Status report 4/2007 Ed.: Yttri, K.-E., Aas, W., Tarrason, L., Vestreng, V., Tsyro, S., Simpson, D., Putaud, J.,P., Cavalli, F., NILU reference O-98134, ISSN: 1504-6109 (http://www.emep.int/publ/common_publications.html).

Spindler, G., Müller, K., Brüggemann, E., Gnauk, T., Herrmann, H. (2004). Long-term size-segregated characterization of PM$_{10}$, PM$_{2.5}$ and PM$_1$ at the IfT research station Melpitz downwind of Leipzig (Germany). Atmos. Environ., 38, 5333-5347.

Approaches to determine the contribution of natural sources to PM$_{10}$ concentrations in North-West Germany

U. Quass[1], O. Sperber[1], O. Romazanowa[1], F. Luther[1], A. Caspari[1], M. Beyer[1]
U. Pfeffer[2], T. Zang[2], P. Bruckmann[2], T.A.J. Kuhlbusch[1]
[1]IUTA e. V., Air Quality & Sustainable Nanotechnology Unit, Bliersheimer Straße 60,
D- 45229 Duisburg, Germany
[2]North Rhine-Westphalia State Agency for Nature, Environment and Consumer Protection
(LANUV NRW), D-45133 Essen, Germany

Keywords: sea salt, Saharan dust, back-trajectories

The 1st EU daughter directive on air quality [Council 1999] includes an exemption from the obligations to draw up action plans if exceedence of the PM$_{10}$ limit value is due to non-anthropogenic influence of natural sources. Moreover, the revised directive [Directive 2008] allow the reporting of contributions by natural sources to PM$_{10}$ concentrations. The reported values will be taken into account if limit values are exceeded. In North-West Germany such influence can predominantly be expected from sea salt advection, soil resuspension and Saharan dust events [see also Bruckmann *et al.*, 2008].

Measurements of PM$_{10}$ and PM$_1$ concentrations and their chemical composition are carried out for more than one year (Feb 2008-March 2009) at two locations in the regional background (site a, mountainous area, ca. 570 m asl) and in urban background, (site b, ca. 40 m asl), respectively. Samples are taken every second day. PM$_{2.5}$ is sampled additionally every third day. Preheated quartz fiber filters (Munktell MK 360) are used, PM$_{10}$ is also sampled on cellulose ester filters (Sartorius) to allow for silicon analyses. To characterise transport effects, back-trajectories based on the NOAA Hysplit model are used [Air Resources Laboratory, 2008].

First measurements and analyses results are directed towards the identification of sea salt contributions. NaCl concentrations and PM$_{10}$ levels are shown in Fig. 1. Characteristic meteorological parameters derived from back-trajectories are presented in table 1.
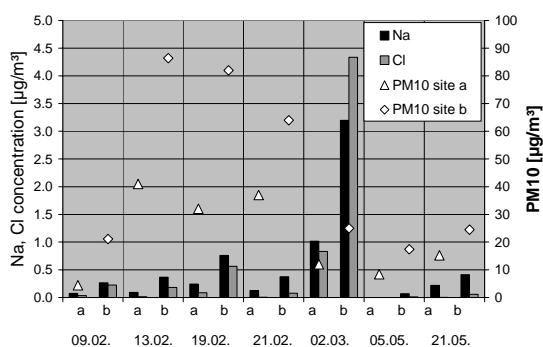
Table 1 Meteorological indicators obtained from back-trajectories (evaluated period: -24 h to -48 h)

	site	wind direction [degrees] a	wind direction [degrees] b	mean velocity [km/h] a	mean velocity [km/h] b	mean height of air mass [m agl] a	mean height of air mass [m agl] b	Land index a	Land index b
09.02.		66	74	32	30	1608	1540	0.90	0.92
13.02.		76	74	16	19	771	1395	1.00	0.98
19.02.		307	307	19	46	492	921	0.47	0.22
21.02.		255	256	18	17	603	584	0.78	0.63
02.03.		272	272	53	64	275	745	0.00	0.00
05.05.		64	61	20	21	1056	1208	0.85	0.79
21.05.		53	40	19	21	390	780	0.82	0.76

Sea salt concentrations do not correlate with PM$_{10}$ and were mostly low, except for the 02.03.08. This corresponds well with the meteorological indicators: low sea salt concentrations are observed at easterly wind directions, low wind speeds and high land index, while on 02.03. westerly wind with high wind speed and 100% residence over sea (zero land index) led to high sea salt concentration. With all samples analysed we will demonstrate the use of a multivariate model connecting trajectory-derived indicators with sea salt concentrations. Further, a method to attribute Saharan dust events will be shown. For this task, various approaches will be needed as recently demonstrated [Bruckmann et al., 2008].

Air Resources Laboratory, HYSPLIT 4.8 (Feb. 2008) http://www.arl.noaa.gov/HYSPLIT.php

Bruckmann, P.; Birmili, W.; Straub, W.; Pitz, M.; Gladtke, D.; Pfeffer, U.; Hebbinghaus, H.; Wurzler, S.; Olschewski, A. *Gefahrstoffe-Reinhaltung der Luft* 11/12-2008, 490-498

Council Directive 1999/30/EC of 22nd April 1999 to limit values for sulphur, nitrogen dioxide and oxides of nitrogen, particulate matter and lead in ambient air. *Official Journal* L 136 from 29.06.1999, p. 41-60.

Directive 2008/50/EC of the European Parliament and of the Council of 21 May 2008 on ambient air quality and cleaner air for Europe. *Official Journal* L152 from 11/06/2008

Fig. 1 Concentration of Na, Cl (left y-axis) and PM$_{10}$ (right y-axis), site a: regional b: urban background

Is PM2.5 the best descriptor of the atmospheric fine fraction aerosol?

M. Manigrasso[1], A. Febo[2], F. Guglielmi[2], V. Ciambottini[3], P. Avino[1]

[1]DIPIA ISPESL, via Urbana 167, 00184, Rome, Italy
[2] IIA-CNR, Area della Ricerca del C.N.R. di Roma, 00016, Monterotondo Scalo, Italy
[3]FAI Instruments S.r.l. via Aurora 15, 00013 Fonte Nuova, Rome, Italy

Keywords: Aerosol size distribution, fine aerosol, Radon decay products.

The work presented wants to highlight the importance of the study of aerosol size distribution both for health reasons and as a support to source apportionment studies. From the health stand point atmospheric Particulate Matter (PM) is regulated on mass basis through PM10 and PM2.5 conventions by the Directive 2008/50/EC. The Directive recognizes the negative impact on human health due to fine PM (PM2.5) and points out how the approach to be pursued should aim at a general reduction of PM2.5 concentrations in urban background. On the other hand, many studies have provided evidence that some particles become more toxic per unit mass as their size decreases and consequently have drawn the attention on particle surface area or number rather than mass, emphasizing the role of submicrometer particles, in particular of ultrafine particles. On this ground relies the importance of measuring size resolved aerosol number concentrations.

PM10, PM2.5 and PM1 measurements were performed in the northern periphery of Rome on November-December 2008, both as mass concentrations by β attenuation technique (SWAM 5a Dual Channel Monitor, FAI) and as size resolved number concentrations (APS 3321, TSI). β-radioactivity of short-lived decay products of Radon, with one hour time-resolution was measured (PBL Mixing Monitor. FAI) to obtain information about the pollutant vertical mass transport in the Planetary Boundary Layer (PBL).

The aerosol pollution was characterized by periods dominated mainly by local anthropic sources as on the days from December 7th to 9th, when the 0.58 μm fraction, assumed as representative of the fine fraction, (figure 1-a) followed the same modulation as the natural radioactivity (figure 1-b). Other periods were characterized by the advection of air masses transporting coarse PM, as in the period from December 14th to 16th, when the 3.79 μm fraction, assumed as representative of the coarse fraction increased (figure 1-a), while the levels of natural radioactivity decreased (figure 1-b), indicating the mixing of surface aerosol with upper air masses. The origin of such air masses from Saharan regions was indicated by the DREAM dust maps and the HYSPLIT backward trajectories. In the period studied, PM1, expressed as mass concentration, represented from about 20% to about 90% of PM2.5 while, as number concentration PM1

constituted more than 90% of PM2.5, when pollution was dominated by local sources (figure 2). The occurrence of air mass transport from Saharan regions, determined a reduction of PM1/PM2.5 ratio (figure 2). The greater relevance for human health of number concentration of submicrometric particles, together with the consideration that great part of PM2.5 number concentration is expressed by PM1 and finally taking into account, as shown by the aerosol size-spectra, that PM2.5 may be to some extent affected by the coarse fraction of PM, raise the question whether PM2.5 is the best choice to describe fine atmospheric aerosol rather than PM1.
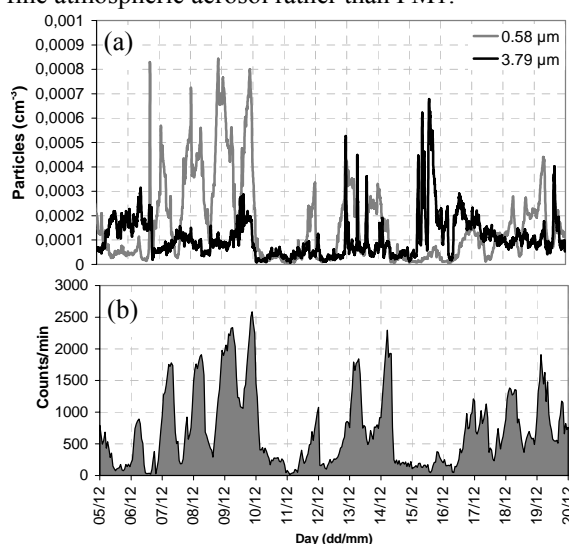

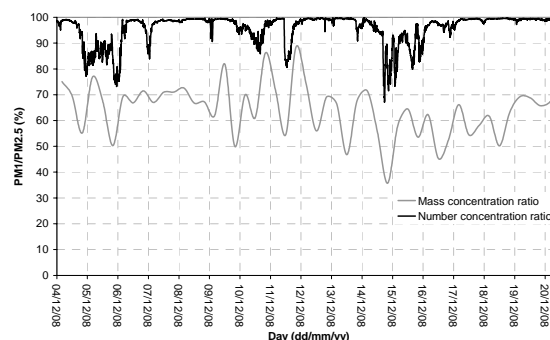Figure 1. Daily trends of fine (0.58 μm), coarse (3.79 μm) fractions (a) and of natural radioactivity (b).

Figure 2. Daily trends of mass and number PM1/PM2.5 ratios.

Sea salt concentrations in the Netherlands from a European perspective

A.M.M. Manders, M. Jozwiecka and M. Schaap

TNO, Unit Environment, Health and Safety, PO Box 80015, 3508 TA Utrecht, The Netherlands

Keywords: Sea salt, PM10, regional modelling, measurements

Introduction

It is known that particulate matter (PM) causes adverse health effects. Therefore, legislation for PM10 and PM2.5 becomes more and more stringent in Europe. Sea salt does contribute to the total concentration of PM. However, it cannot be influenced by measures and it is unlikely to cause adverse health effects. These are arguments that are used to subtract the sea salt contribution from total PM when the exceedance of the limit values for PM occur. EU legislation allows this.

In The Netherlands, sea salt contributes significantly to the PM concentrations on some days. The Dutch government has implemented a derogation guideline for sea salt. Here, we present an overview of recent sea salt observations, completed with model results. In our presentation, we compare the Dutch situation to other European countries and will discuss the implications of the newest findings for the derogation guideline.

Methodology

There is a fairly limited but growing set of sea salt concentration observations. We will present the first extensive compilation of measurements of sea salt over Europe, originating from several countries and campaigns. The compilation is based on sodium observations. Both annual mean concentrations and time variability were investigated to give an overview that is as complete as possible.

To further complete the picture, sea salt concentrations were modelled with the LOTOS-EUROS model (Schaap et al 2008). The modelled concentrations were compared to the observations and showed good agreement, with a good time correlation but with a structural overestimation for the PM10 fraction. The overestimation is within the uncertainties of the parameterizations of the sea salt source function. When a scaling factor is used, based on the measurements, the model results can be used to describe the concentrations over Europe.

Results

The results (Figure 1) show that sea salt concentrations in the Netherland are comparable with other coastal areas (Denmark, Northern Germany, Belgium). Annual mean concentrations are about 4 $\mu g/m^3$ close to the coast (Rotterdam area) to 2 $\mu g/m^3$ at 200 km land inward.
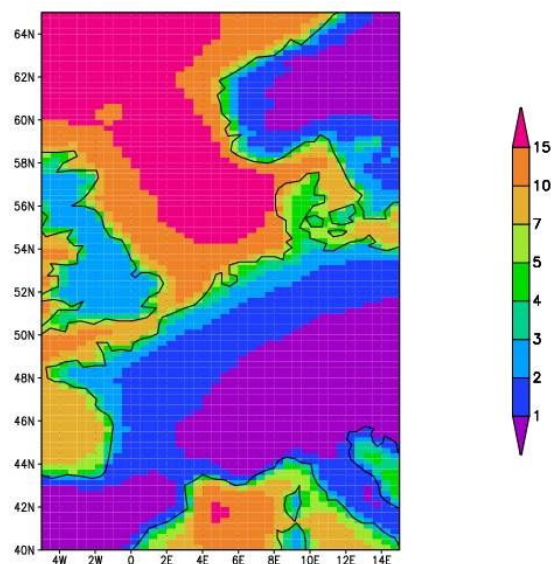

Figure 1 Scaled modelled annual mean sea salt aerosol concentration in PM10 in $\mu g/m^3$

The sea salt concentrations are highly variable. On individual days, concentrations near the coast may be up to 16 $\mu g/m^3$ (Rotterdam) to 10 $\mu g/m^3$ land inward. These high concentrations occur for strong winds from the sea, bringing relatively clean air. In contrast, in cases for which PM10 threshold levels are exceeded, winds are generally from over land. Therefore, the sea salt concentrations are in general negatively correlated with total PM10 and the contribution to PM10 limit value exceedances is very small.

References

Schaap, M. et al. (2008) Int. J. Environment and Pollution, Vol. 32, No.2

Evaluation of the contribution of ship traffic to PM2.5, PM0 concentration in the Venice harbour area

D. Contini[1], A. Gambaro[2], A. Donateo[1], F. Belosi[3], G. Santachiara[3], D. Cesari[1], S. De Pieri[2], F. Prodi[3]

[1]Istituto di Scienze dell'Atmosfera e del Clima, ISAC-CNR, Str. Lecce-Monteroni km 1.2, 73100, Lecce, Italy
[2]Environmental Sciences Department, Ca' Foscari University of Venice, 30123 Venice, Italy
[3]Istituto di Scienze dell'Atmosfera e del Clima, ISAC-CNR, Via Gobetti 101, 40129, Bologna, Italy

Emissions of ships near harbour areas could be a concern in several towns Isakson et al (2001). Specifically, in the Venice area, the assessments of the inventory emissions from the Environmental Regional Protection Agency (ARPAV) are roughly 21000 tons/year for NOx, 23000 tons/year for SOx and 1200 tons/year for PM10. The emissions from passenger ships are estimated in 1000 tons/year of NOx , 1100 tons/year of SO_2 and 170 tons/year of PM10. Therefore, in coastal areas, there is an increasing concern regarding the possible contribution that marine vessels make to poor air quality especially in cases in which the harbours are located nearby densely populated areas like in Venice. The goal of this work is to evaluate the contribution to fine (PM2.5) and coarse (PM10) aerosol due to ships in the inner part of the Venice harbour and to compare the results with the emission inventories on a local level. Some of the SO_2 and NOx emitted transforms into secondary inorganic aerosols (i.e. particulate matter). This is a relatively slow process and the secondary particles are transported tens to several hundreds of kilometres from where it was emitted. Such secondary particles were therefore not considered relevant to how ships in harbours pollute the nearby surroundings (Saxe, 2004). The measurements were made in three sites including the centre of the harbour area where it is present a relevant traffic of ferries, cruise ships and minor vessels. The main site is Sacca San Biagio (SSB) where it has been performed the high temporal (1Hz) resolution measurement of PM2.5, with a Mie pDR-1200 optical detector. The SSB site was operative in the summer 2007 period. The second site is Capitaneria di Porto (CDP), located along the path of ships coming and leaving the Venice passenger harbour. The site was equipped with PM2.5 and PM10 optical detectors (DustTrack®) operating at high temporal resolution (20s). The site was operated in the period between March and October 2007. The third site was Tronchetto (TRO) located on the roof of a building (about 15m tall) inside the harbour itself. Results indicate that daily concentration were not sufficient to extract information about the contribution of ships traffic to atmospheric aerosol. Therefore a method based on hourly concentrations has been developed. It is based on the simultaneous analysis of the wind directions and the database of effective passages of ships furnished by the Harbour Authority of Venice. The difference between concentrations associated to hours with ship passages and concentrations associated to the other hours in a specific wind direction sector (in which the site is downwind of the emissions) are calculated. The differences weighed with the frequency of passages allow to evaluate the contribution of ship emissions to the average aerosol concentration. Our results shows that the ship contribution to PM2.5 and to PM10 is basically the same.

Table 1. Comparison between theoretical predictions and experimental measurements.

Site	Period	Contribution
SSB	Summer	7-8%
	Annual (modulation)	5%
CDP	Summer	4%
	March-October	1-2%
	Annual (modulation)	2-3%
TRO	Summer	2-3%
	March-October	1%
	Annual (modulation)	1-2%

A three years statistics of monthly tonnages of ship traffic has been used to develop a modulation curve that has been used to evaluate the average annual contribution starting from the one calculated in the period of maximum traffic (summer). Result obtained are summarised in Table 1. The contribution of ship traffic is significantly different from site to site as a consequence of meteorological and micrometeorological effects. In particular the site TRO is very near the emissions that are relatively high above the ground and transported at high distances downwind. Instead SSB site is mainly influenced in nocturnal hours characterised by a shallow boundary-layer able to entrap pollution. CDP is mainly influenced by ship traffic in diurnal hours mainly in well mixed condition.

Isakson J., Persson T. A., Lindgren E. S., 2001. *Atmospheric Environment* 25, 3659-3666.
Saxe H., Larsen T., 2004. *Atmospheric Environment*, 38, 4057- 4067.

Integrated approach in the monitoring of particulate matter: relevant parameters for high pollution events

M. Amodio, E. Andriani, M. Caselli, B.E. Daresta, G. de Gennaro, A. Di Gilio, P. Ielpo, C.M. Placentino, M. Tutino

Department of Chemistry, University of Bari, via Orabona, 4, 70126, Bari, Italy

Keywords: PM, particle size distribution, boundary layer, meteorology.

PM consists of a mixture of many species with a large physical and chemical variability, deriving from different sources. As PM is characterized by several properties, its study needs a multivariate approach. Moreover, in atmosphere PM becomes subject to processes which control their transport, mixing and transformation. Identifying the main factors influencing PM concentrations in the investigated area is a useful tool to understand and control the phenomenon.

The results obtained by applying an integrated approach in the monitoring of PM using several typologies of instrumentations will be shown. The prototype, located close to Department of Chemistry in Bari town, is formed by a Swam dual-channel sampler, an OPC Monitor, a sonic anemometer, and a PBL Mixing monitor.

The analysis of data from October 2007 to January 2009 has demonstrated that atmospheric dispersion and mechanical advection are the main factors influencing the concentration levels of PM (Vardoulakis & Kassomenos, 2008; Vecchi *et al.,* 2007). Moreover, high PM concentrations were occasionally found due to long-range transport events. In particular, in September 2008 two high PM2.5 and PM10 episodes occurred (7th-9th, 12th-13th September 2008), as showed in figure 1. For these days the OPC data point out a considerable increase of particles which diameter ranging between 1 and 1.54 um in the first episode, while there was an increasing of all size fractions in the second one. In addition, on 7th-9th September the increase of particles was greater in diurnal than in nocturnal hours. This behaviour is typical for events of an air mass intrusion. Data obtained from satellites (Modis), remote sensing (Aeronet), and models such as Hysplit and Dream confirmed an outbreak from Saharan in the southern regions of Italy. On the contrary, on 12th-13th September high values of natural radioactivity (monitored by PBL mixing monitor) were detected. This means a high atmospheric stability that may favour the local formation of new particles. It was supported by the high ozone concentrations observed in the second event of high PM.

A next phase of work consists in designing, developing and testing on field the prototype for the determination of the contributions of a single source ('fugitive emission') on the fine PM concentrations.

It requires the individuation of three positions around the source (such as industrial site, town, etc…). Each position will have a prototype assembled with the instrumentations before described. The aim is to triangulate the area of the examined source on the basis of the prevalent directions of the wind. The investigation can be completed by chemical-physical characterization of PM2.5 and PM10 samples collected by the prototype in order to have additional information about the possible emissive sources. The analysis of data allows a detailed study of the impact of the local emissive source on the neighboring areas. Moreover, the prototype consents to identify and distinguish long range transport, regional and other local contributions on the fine PM concentrations.

The investigated site chosen for the "fugitive emission" application of prototype will be the iron and steel pole of Taranto. The great interest for Taranto is due to the presence of several activities of high impact as very wide industrial area close to the town and the numerous maritime and military activities in the harbour area (Amodio *et al.,* 2007).
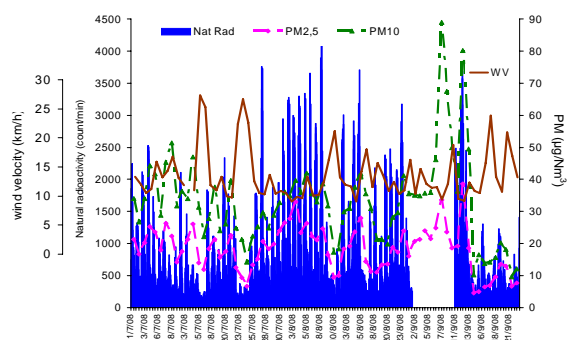

Figure 1. Hourly trend of natural radioactivity, daily trends of PM2.5, PM10, and wind velocity during July-September 2008.

Vardoulakis, S., & Kassomenos, P. (2008). *Atmospheric Environment*, 42(17), 3949-3963.

Vecchi, R., Marcazzan, G., & Valli G. (2007). *Atmospheric Environment*, 41(10), 2136-2144.

Amodio, M., et al. (2007). in *Proc. Ecomondo 2007*, Rimini (Maggioli, Rimini), 445-449.

Seasonal variation in trace elemental concentrations in PM$_{2.5}$ particles in Nairobi, Kenya

J. Boman[1], M.J. Gatari[2], S.M. Gaita[1], X. Zhang[1], B. Xue[1] and A. Wagner[1]

[1]Department of chemistry, University of Gothenburg, SE-412 96, Göteborg, Sweden
[2]Institute of Nuclear Science and Technology, University of Nairobi, P. O. Box 30197-00100, Nairobi, Kenya

Keywords: ambient PM, elemental content, EDXRF, air quality.

A better knowledge of the chemical and physical constituents of local aerosol particles is essential to assess their impact on the environment, the human health as well as identifying pollution sources. The air quality in many major cities of Africa is declining since regulations and control policies remains inadequate due to insufficient knowledge of pollutant levels and their sources. Previous measurement campaigns in Nairobi were on short time basis (for example van Vliet & Kinney 2007, Gatari and Boman 2003, Gatari et al. 2005) but the current campaign started early 2008 and will continue until the end of 2009

Aerosol samples were collected at an urban background site in Nairobi, Kenya, during a measurement campaign for the whole year 2008. A cyclone was used to collect fine aerosol particles (PM$_{2.5}$) over a period of 48 h per sample. PM$_{2.5}$ refers to particles with an equivalent aerodynamic diameter < 2.5 µm. The particles were collected on polycarbonate filters and were analyzed for particulate mass, black carbon (BC) and several trace elements ranging from Si to Pb.

The sampled integrated particle mass was determined gravimetrically with a Mettler Toledo TM5 microbalance. A photometer and an Energy Dispersive X-Ray Fluorescence (EDXRF) spectrometer were used to analyze BC and trace elements, respectively. The EDXRF spectrometer uses a Siemens diffraction x-ray tube and Mo secondary target. The target is a 1 mm thick Mo plate of 99.99 % purity. The fluoresced secondary x-rays propagate through two Ag collimators giving near monochromatic Mo characteristic x-rays for sample excitation. The spectrometer is laboratory built in an optimized three axial geometry that gives good signal to noise ratios for the analyzed elements.

Nairobi is the capital city of Kenya with a population estimated to more than 3 million inhabitants. The city's growth has been rapid through influx of citizens from rural Kenya. It is located just south of the equator at 1700 m above sea level. This high altitude gives Nairobi a moderate climate. There are two dry seasons that together with the "long rain" and "short rain" seasons characterizes the climate in Nairobi and its surroundings.

The local weather information was obtained from the Department of Meteorology, Government of Kenya, Nairobi. Evaluation of particulate mass and analyzed trace element concentrations with respect to local weather parameters and back trajectory calculations will elucidate seasonal variations.

The influence of natural and anthropogenic sources on air quality in Nairobi as a large African city will be discussed. The results will be compared to other large cities with air quality problems as well as to national air quality standards and WHO guideline limits.

Acknowledgements

References

Gatari M.J., Boman J. (2003) *Atmos Environ*, **37,** 1149-1154.

Gatari M., Wagner A. &, Boman J. (2005) *Sci Total Environ,* **341**, 241-249.

van Vliet, E. D. S. & Kinney, P. L. (2007). Environ Res Lett, doi:10.1088/1748-9326/2/4/045028

WHO Report, (2006). Fighting disease Fostering development, WHO, Geneva, Switzerland

Diurnal variations in the particle size distribution in Ouagadougou, Burkina Faso

J. Boman[1], B. Xue[1], X. Zhang[1] and S. Thorsson[2]

[1]Department of chemistry, atmospheric science, University of Gothenburg, SE-412 96, Göteborg, Sweden
[2]Department of earth science, urban climate group, University of Gothenburg, Box 460, SE-405 30, Göteborg, Sweden

Keywords: Particle size distribution, Saharan dust, urban aerosols.

Ouagadougou is the capital city of Burkina Faso. Currently there are approximately 1.1 million inhabitants in the city, but the number is increasing rapidly here just like in many developing countries. Burkina Faso is one of the poorest countries in Africa with an increasing transportation need. Most of the human transport is carried out with two wheelers that are using bad quality fuel and no maintenance scheme for the vehicles is required by the authorities. Taken all together the high number of people, the bad vehicle fleet and the use of fuel wood for cooking and heating makes the air quality in Ouagadougou very low.

Ouagadougou is located 12°20' N, 1°40' W in the Sahel region where the climate is hot arid steppe like, Figure 1.

There are two main seasons in Ouagadougou, one wet season from May to September, and a dry season from October to March. There are transition periods between these two seasons. The daily temperatures are normally between 27 and 37 degrees Celsius and during the wet period an average of 700 mm of rain falls, although the onset of the rainy season can vary (DMN 2007, Offerle et al., 2005)). During the dry period the air is dry and the particulate matter content is high, mainly depending on the so called Harmattan wind blowing from the Sahara desert in the northern part of Burkina Faso.

For 14 days in December 2007 a dust monitor optical particle counter from Grimm Aerosol Technik, Germany, was placed at roof top level (10 m above ground) in the central business district of Ouagadougou. The dust monitor measures the aerosol particle number in real time in 15 size ranges from 300 nm to 20 µm. Sampling frequency was set to 10 samples per minute. The aim was to determine a diurnal pattern in aerosol particle size distribution under different stability conditions.

The weather in Ouagadougou during the measurements was dominated by high pressure with variable cloudiness and no precipitation. The temperature varied between 19 - 38 °C and wind speeds were generally low. It reached a maximum of 6 m/s during daytime while the evenings and nights were calmer ($\leq$ 3 m/s) with more stable atmospheric conditions. During the campaign two types of weather stability prevailed. Most of the days the weather conditions were very stable, but during a short period in the middle of the campaign when the conditions were less stable.

The result of the analysis of the particle size data shows distinct diurnal variations in the particle distribution and a tendency of different distributions for different stability conditions.
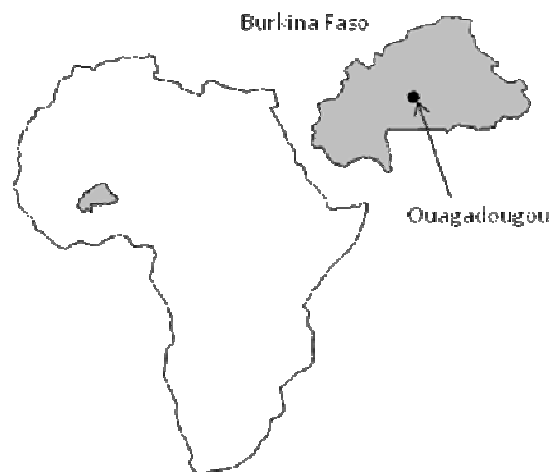

Figure 1. The African continent with Burkina Faso outlined and the location of its capital city Ouagadougou indicated.

Acknowledgements

References
Direction de la Météorologie National. DMN (2007) http://aochycos.ird.ne/HTMLF/PARTNAT/METEOBF/OHRAOC.HTM. [10 September 2007.]
Offerle B, Jonsson P, Eliasson, Grimmond CSB., J. of Climate, 2005. 18, 3983.

Emissions of PM$_1$ from silent surface road cover in Gothenburg, Sweden.

J. Boman[1], S. Janhäll[2] and E. Björkman[1]

[1]Department of chemistry, atmospheric science, University of Gothenburg, SE-412 96, Gothenburg, Sweden
[2]Department of Biogeochemistry, Max Planck Institute for Chemistry, D-55128, Mainz, Germany

Keywords: road dust, EDXRF, traffic emissions, PM$_1$.

As the traffic in many big cities around the world continuously increases, apart from the air quality problem, also the noise from the roads is becoming a big issue. The noise is a threat to the human health because it acts as a stress factor which eventually can lead to cardiovascular diseases.

In most cases the biggest source of the noise is the interaction between tires and surface. In an attempt to reduce the traffic noise, the focus has changed from measures like noise-reducing fences to the actual asphalt, or road cover. Several Swedish companies have therefore produced a new product called "silent surface". The surface reduces the noise with 8-10 dB(A) but has shown to be less resistant to wear. This could result in larger particle emissions affecting the air quality.

For seven weeks during the spring 2009, the PM$_1$ concentration along the road Högsboleden in Gothenburg, Sweden, covered with "silent surface" asphalt, was measured at curb side. A reference site along the same road was obtained 900 meters from the first measurement site. The road cover on the second location was normal asphalt. Gothenburg is the second largest city in Sweden with more than 0.5 million inhabitants and located on the Swedish west coast. Högsboleden is a busy commuter road in the western parts of the city with a high traffic density of personal cars and buses. The heavy vehicle traffic is less dense due to restrictions on heavy traffic in the city.

At both measurement sites the aerosol was pumped by a vacuum pump into a cyclone separating out the PM$_1$ particles from the air stream and collecting them on polycarbonate filters. Filters were changed at noon every day. The particles were analyzed for particulate mass, black carbon (BC) and trace elements ranging from Si to Pb.

The sampled integrated particle mass was determined gravimetrically with a Mettler Toledo TM5 microbalance. A photometer and an Energy Dispersive X-Ray Fluorescence (EDXRF) spectrometer were used to analyze BC and trace elements, respectively. The EDXRF spectrometer uses a diffraction x-ray tube and Mo secondary target. The target is a 1 mm thick Mo plate of 99.99 % purity. The fluoresced secondary x-rays propagate through two Ag collimators giving near monochromatic Mo characteristic x-rays for sample excitation. The tube was operated with a 55 kV voltage and a tube current of 20 mA. The spectrometer is laboratory built in an optimized three axial geometry that gives good signal to noise ratios for the analyzed elements (Gatari et al., 2005).

For a limited period a dust monitor optical particle counter from Grimm Aerosol Technik, Germany, was used to determine the particle size distribution. The dust monitor measures the aerosol particle number in real time in 15 size ranges from 300 nm to 20 µm. Sampling frequency was set to 10 samples per minute. The aim was to determine a more accurate size difference between the two measurement sites.

The local weather information was obtained from the Gothenburg city environmental protection office. Weather parameters were measured on one of the measurement sites as well, in an attempt to determine possible weather differences between the sites and the official weather data obtained at an urban background site in the city centre.

Evaluation of particulate mass and analyzed trace element concentrations with respect to local weather parameters and back trajectory calculations will reveal differences between the two measurement sites that can be attributed to the differences in road surface material. The results will be compared to experiments conducted under laboratory conditions (Skanska et al., 2007).
    T

References
Gatari M., Wagner A. &, Boman J. (2005) *Sci Total Environ,* **341**, 241-249.
Skanska, SBUF, Vägverket, VTI, SLB Analys (2007) Bullerreducerande beläggningars betydelse för partikelhalterna, slutrapport FUD 3066, SBUF 11748/11858.
    www.sbuf.se/projectdocuments/info/11748/SBUF%2011748%20Slutrapport.pdf [2009-01-20]

A summertime study of PM_{10} and $PM_{2.5}$ mass concentrations in urban and industrialized cities in Turkey

Eftade O. GAGA [1], **Akif ARI** [1], **Justin ARGANTE** [2], **Kees MELIEFSTE** [3], ,
Ozan Devrim YAY [1], **Gülçin DEMİREL**[1], **Sermin ÖRNEKTEKİN** [4], **Tuncay DÖĞEROĞLU** [1],
Wim van DOORN [5]

[1] Anadolu Üniversity, Faculty of Engineering and Architecture, Department of Environmental Engineering, Eskişehir, Turkey
[2] HAS Deb Bosch, Department of Environmental Technology, Hertogenbosch, Netherlands
[3] Institute for Risk Assessment Sciences (IRAS), Division Environmental Epidemiology, Utrecth, Netherlands
[4] Mustafa Kemal Üniversity, Faculty of Science and Literature, Chemistry Department, Hatay, Turkey
[5] Royal Haskoning, Nijmegen, Netherlands

Keywords: particulate matter, air quality, cyclone, impactor, PM2.5, PM10

Particulate matter (PM) is of great concern because of its adverse health effects. Epidemiological studies suggest a link between ambient PM concentrations and increased human morbitity and mortality. In this work, $PM_{2.5}$ and PM_{10} mass concentrations were measured in İskenderun and Eskişehir cities in Turkey as a part of the MATRA project "Together towards clean air in Eskisehir and Iskenderun". Two 2-weeks sampling campaigns were carried out and four stations (2 urban sites, 2 urban background sites) were established in each cities in the early summer of 2008. Sampling station locations were carefully choosen after an exploration of ambient air quality by a passive sampling campaign.

İskenderun is an industrialized city situated at the southern part of Turkey and it is one of the hot spots of the country because of the heavy metal industries and busy harbor. Eskişehir is situated at the Anatolian plateu of Turkey and it is not as much industrialized as İskenderun. High volume samplers, PUF samplers and dichotomous samplers were also set up in 2 of the 4 stations in each cities, to measure trace metals, semivolatile organic compounds and some other toxic species. However, only mass concentrations of PM were presented here.

Two low volume PM samplers were collocated at the sampling stations to collect 24 hours $PM_{2.5}$ nad PM_{10} samples. $PM_{2.5}$ samples were collected on 37 mm Teflon® filters using a small pump and KTL-cyclone (BGI Instruments, USA). A 3.5 L min^{-1} air flowrate was used for $PM_{2.5}$ sampling. PM_{10} samples were collected on same type filters by using an PEM-impactor type sampler (BGI Instruments, USA), with a 4 L min^{-1} air flowrate. All filters were pre and post weighted in very stable humidity and temperature conditions, in the weighting laboratory of Institute for Risk Assessment Sciences (IRAS), University Utrecht, Netherlands.

Daily PM_{10} and $PM_{2.5}$ mass concentrations showed variations depending on the meteorological conditions and source characteristics. PM_{10} and $PM_{2.5}$ concentrations were found to be higher in urban sampling locations in both cities.

The average concentrations of $PM_{2.5}$ and PM_{10} were found to be 24.0 and 60.0 μg/m^3 in urban background stations in İskenderun and 19.3 and 67.2 μg/m^3 in Eskişehir respectively. Urban site $PM_{2.5}$ and PM_{10} concentrations were found to be 27.6 and 136.4 μg/m^3 in İskenderun and 27.9 and 93.7 μg/m^3 in Eskişehir respectively. Highest average PM_{10} concentrations were measured in industrial polluted urban sites of İskenderun.

As, Cd, Cr, Cu, Ni and Pb in PM$_{2.5}$ in Gothenburg, Sweden

A. Wagner[1], J. Boman[1] and M.J. Gatari[2]

[1]Department of chemistry, University of Gothenburg, SE-412 96, Göteborg, Sweden
[2]Institute of Nuclear Science and Technology, University of Nairobi, P. O. Box 30197-00100, Nairobi, Kenya

Keywords: air quality, elemental composition, AAS, PM$_{2.5}$.

Ambient particles smaller than 2.5 µm (PM$_{2.5}$) are getting more and more attention worldwide (WHO, 2006). While legal focus is on sample mass, the composition of the particles is an important research field gaining increased interest. The interest is not only connected to possible health effects of the elemental content of the particles, but the elemental determination can also add valuable information to source apportionment.

Samples were collected during 20 days in November 2007 at the campus of the chemistry department, University of Gothenburg, approximately 2 kilometers south of the city centre of Gothenburg, Sweden. Gothenburg, located on the Swedish west coast, is the second largest city in Sweden with more than 500 000 inhabitants. The main local source of PM$_{2.5}$ at the measurement site is the 8000 cars/day on the street passing the measurement site.

At the measurement site the particles were collected using a cyclone separating out the PM$_{2.5}$ particles from the air stream and collecting them on polycarbonate filters. The air flow was controlled by a critical orifice. Filters were changed at early afternoon every day. The particles were analyzed for particulate mass, black carbon (BC) and the elements As, Cd, Cr, Cu, Ni and Pb.

In the present study, a well-established and sensitive analytical technique, graphite furnace atomic absorption spectroscopy (GF-AAS), has been used for the determination of trace elements in the particles. The Perkin Elmer SIMAA 6000 GF-AAS is capable of simultaneous analysis of up to six elements. A Mettler Toledo TM5 microbalance was used for gravimetric determination of the sampled integrated particle mass. A photometer was used to analyze black carbon.

The results show a large variation in sample mass, BC concentration as well as in the concentrations of the analyzed elements. The variation of the different constituents does not show the same pattern. This adds to the picture of different sources for different pollutants. The highest As concentration is noted on a day when the air masses were determined to come from the south east, i.e. Poland and some other eastern Europe countries, as illustrated by the back trajectory in red in figure 1. Table 1 shows the concentration range of the different components during the measurement period.

Table 1. The concentration range of the different components.

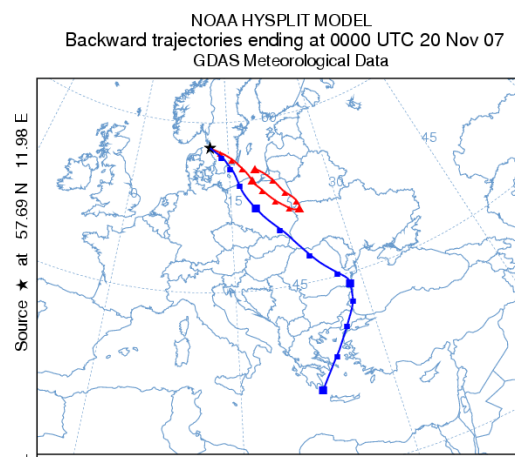| Parameter	Range (ng/m^3)
Particle mass (µg/m^3)	0.77 — 13
Black carbon (µg/m^3)	<DL – 0.82
As	<0.40 – 19
Cd	<0.076 – 0.13
Cr	2.2 – 25
Cu	2.3 – 98
Ni	1.4 – 99
Pb	<0.90 – 4.5

Figure 1. HYSPLIT back trajectory for November 20, 2007. The red line is a trajectory at 100 meters height upon arrival in Gothenburg while the blue was chosen to 500 m.

Acknowledgements

References
WHO Report, (2006). Air Quality Guidelines. Global update 2005, WHO, Geneva, Switzerland. http://www.euro.who.int/Document/E90038.pdf

Use of several receptor models - CMB, APCS and PMF - - as a tool to interpret air quality data

M. Amodio, E. Andriani, M. Caselli, B.E. Daresta, G. de Gennaro, A. Di Gilio,
P. Ielpo, C.M. Placentino, M. Tutino, L. Trizio

Department of Chemistry, University of Bari, via Orabona, 4, 70126, Bari, Italy

Keywords: PM, receptor model, source apportionment, PMF.

Particulate matter has been linked with negative cardiovascular and respiratory health outcomes, including effects leading to premature mortality. In addition, PM contributes to visibility impairment and acid deposition.

It is important to understand which emission sources contribute to the elevated daily PM levels for developing effective control strategies. Therefore a particular attention must be paid to a correct daily source apportionment; in fact, epidemiologic studies suggest that such sources have different health outcomes.

Receptor models, which attribute observed concentrations to sources through statistical and/or meteorological interpretation of data, often provide useful insights on aerosol sources.

Receptor modeling can be categorized into different types based on whether PM chemical characteristics from emission sources are required to be known before the source apportionment. On one hand, Chemical Mass Balance (CMB) requires 'a priori' knowledge of major sources and their emission characteristics in the area under investigation; on the other hand, models as factor analysis and Absolute Principal Component Scores (APCS) require ambient measurement data only to perform source apportionment. Positive Matrix Factorization (PMF), in addition, imposes the constraints that sources contributions and profiles cannot be negative.

CMB consists of a least squares solution to a set of linear equations that express each chemical concentration as a linear sum of products of source profiles and source contributions. The model needs two files as input data, species concentrations at receptor site and source profiles for sources taken into consideration (with relative uncertainties). The performance of CMB run is controlled by some statistical parameters as, for example, chi-square (the weighted sum of squares of the differences between the calculated and measured species concentrations ≤ 4) and R^2 value (the fraction of the variance in the measured concentrations explained by the regression ≥ 0.8).

The problem with CMB is that source patterns suitable for a particular receptor position are often incompletely known.

In APCS model, data matrix is decomposed into the product of two matrices containing source's patterns and contributions. These latent matrices are then rescaled using linear regression to produce real contributions and patterns having physical meaning.

PMF, leaving from random positive values for matrices having the same dimensions as contributes (F) and profiles ones (A), minimizes the difference between data matrix and the product of FxA by an iterative process. The goodness of the apportion procedures is both for APCS and PMF the best reconstruction of the data matrix.

As example, in Fig.1 percent composition of five sources obtained by PMF on a data set collected in Lecce (Apulia Region) is shown.

The aim of this work is to apply models above mentioned to PM samples collected in some sampling sites of Apulia Region and to compare obtained results.
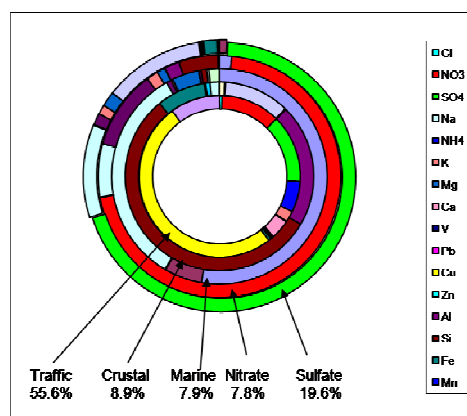

Figure 1. PMF percent contribution of five sources to PM_{10} samples collected in Lecce (Apulia Region).

Metzger, K.B, et al. (2004). *Epidemiology*, 15(1), 46-56.

Chow, J.C., et al. (2004). *Chemosphere*, 54(2), 185-208.

Viana, M., et al. (2008). *Atmospheric Environment*, 42(16), 3820-3832.

Evaluation of the characteristics of PM$_{10}$ time series in relation to the type of air monitoring station

M.A. Barrero[1], M. Cabello[2], J.A.G. Orza[2], L. Cantón[1]

[1]Department of Applied Chemistry, University of the Basque Country, 20018, San Sebastián, Spain
[2]SCOLAb, Física Aplicada, Universidad Miguel Hernández, 03202, Elche, Spain

Air Quality Monitoring Networks are often composed by a number of monitoring stations covering urban, suburban and industrial areas and some remote, background sites. These monitoring sites are typically classified as urban (traffic, industrial, background), suburban (traffic, industrial) and rural (background) stations, according to the location and the influence of the immediate surroundings.

Pollutants such as nitrogen dioxide, sulphur dioxide, carbon monoxide, PM10, PM2.5 and ozone are most commonly registered for air quality assessment, as there are specific limit values for them. The recordings of these pollutants contain usually enough information to decide *a posteriori* whether a particular station has been properly labelled.

We have studied the differences between monitoring stations by focussing solely on the PM10 dynamics. For this purpose, data from different types of station, in a number of locations in the Iberian Peninsula have been collected, processed and analysed.
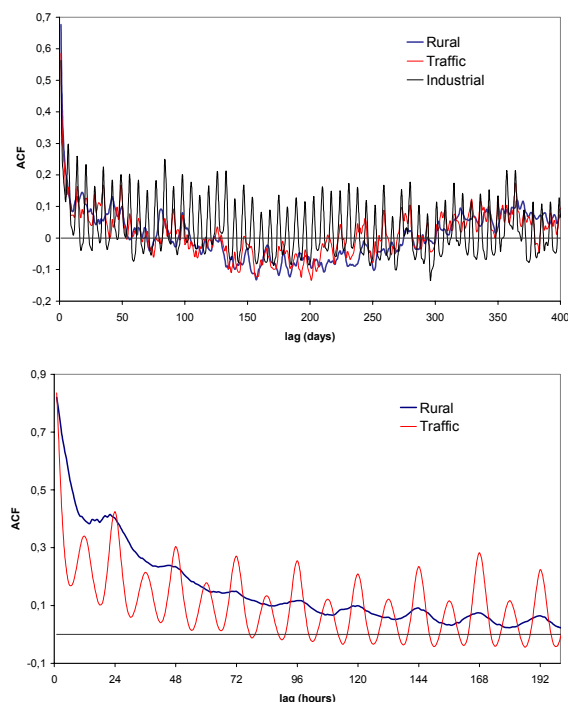
The autocorrelation function of the hourly and daily PM10 time series, the diurnal evolution of the average concentration both in summer and wintertime as well as the average values on working days and weekends were analyzed. The relative strength of periodicities related to anthropogenic and natural factors allow for a revision of station types and a deeper understanding of the particulate load in the study areas.

Some well-defined patterns were detected (Figs. 1 and 2). Correlations at 12-h lag are present at the traffic and industrial stations as secondary peaks with respect to those for 24-h. All stations but the rural ones show higher correlation at 7-day lag than at 6- or 8-day. Time and heights of the peaks (if any) in the evolution of the diurnal average concentrations are dependent on the type of monitoring site.

With all the gathered information, a "quick characterization method" was developed using the characteristics of the time series.
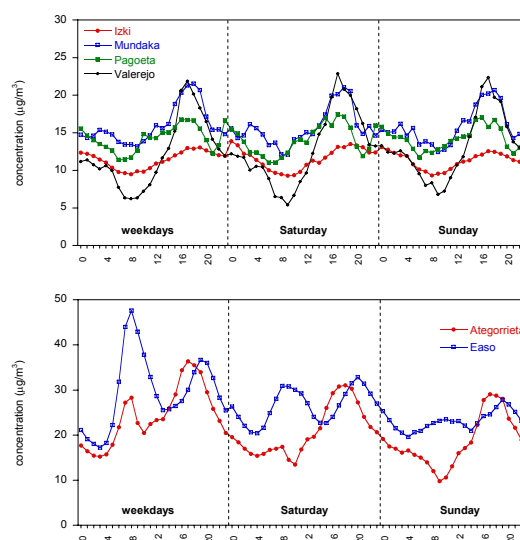

Figure 1. Autocorrelation functions of daily (up) and hourly (down) PM$_{10}$ levels at sites of different type in the Basque Country.

Figure 2. Evolution of average PM$_{10}$ hourly concentrations in rural background (up) and traffic (down) sites in the Basque Country.

Measurements Of Hydroxy And Nitro PAHs In Atmospheric Urban Aerosols.

A.I. Barrado Olmedo, S. García Alonso, R. Pérez Pastor, O. Pindado Jiménez.

Chemistry División, Department of Technology, CIEMAT, Avenue Complutense 22, 28040 Madrid, Spain. Tel. 913466523 / 913466539. Fax: 913466121. e-mail: anaisabel.barrado@ciemat.es, susana.garcia@ciemat.es, rosa.perez@ciemat.es, oscar.pindado@ciemat.es

Keywords: Atmospheric Urban Aerosol, NitroPAHs and HydroxyPAHs

The unsubstituted PAHs lead to the formation of intermediates and adducts, which can originate DNA-damage through metabolic and conversion reactions. Hence, the concern to study substituted polycyclic aromatic hydrocarbons (PAHs) such as hydroxylated and nitro derivatives is fosed on their genotoxicity and carcinogenicity (1).

Analytical methods include HPLC whit flourescence detection, which is a selective and sensible technique for the determination of this compounds. The aim of this work was the optimization of analytical methods to determine two hydroxylated PAHs and six nitro PAHs in ambient air and their identification in several samples of an open urban area at sourronding of Madrid.

1.- Regarding hydroxylated PAHs, few literature exist to measure these compounds in ambient air samples, and in particular, HPLC measurements with flourescence detection is rarely applied (2). The proposed method was focused on the optimizatoin of 2-hydroxy phenanthrene and 1-hydroxy pyrene determination and the possible identification on both the particulate and the gas phases of air samples.

Table 1 shows minimum, maximum and mean values of concentrations of OH-PAH's and their parents PAH's.

	2-OHPH	1-OHPYR	PHEN	PYR
Mean values pg/m^3	15.5	30.4	41.7	84.1
Min-Max pg/m^3	2.5-53.1	27.8-34.5	6.0-109.0	24.7-458.5

The preliminary results show that the concentration of 1-OHPYR has been kept constant in the sampling period, meanwhile the concentration of 2-OHPH shows an increment in a few days of March 2008. This similar variation was obtained for particles concentration (Fig. 3), so this would be consistent with the particle dependence of 1-OHPYR, but not 2-OHPH. In this sense, more concentration data is required to complete these observations and make a correlation study between selected OH-PAH's, and particle concetration.
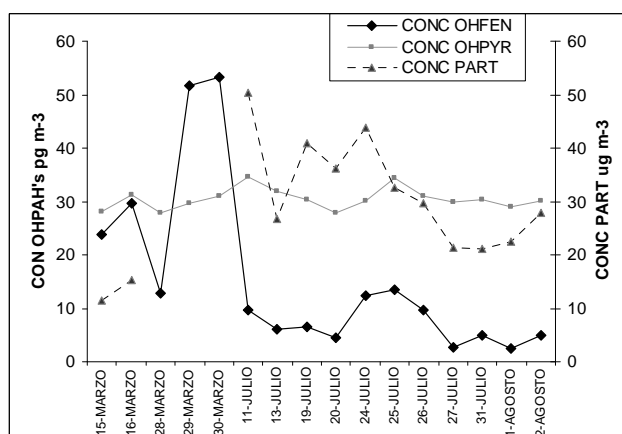

Figure 3. Concentration of OHPAH's and Particles.

2.- In relation to nitro PAHs, the conversion to nitro group to fluorescence species by reduction into amino grouo is the critical step and it must be carefully checked. In orden to achieve this, three methods for the determination of 1-nitro naphthalene, 1,3- dinitro naphthalene, 9-nitro phenanthrene, 3-nitro fluoranthene, 1-nitro pyrene and 1,3-nitro pyrene has been compared. In particular, the reduction reaction was accomplished by (3):

1. Sodium tetrahydroborate with copper (II) chloride.
2. Aqueous sodium hydrosulfide.
3. Zinc powder in hydrochloric acid.

The methods were applied to analyse aerosol an gas phases of air samples.

Thesis "Analysis of PAHs and their transformation products in contaminated soil and remedial processes". *2003, Department of Chemistry, Environmental Chemistry. Umeä. SWEDEN. ISBN 91-7305-452-6.*

N. Kishikawa, S. Morita, M. Wada, Y. Ohba, K. Nakashima and N, kuroda.   *"Analytical Science". 2004, 20, 129-132.*

J. Cvacka, J. Barek, A.G. Fogg, J.C. Moreira and J. Zima. *Analist. 1998, 123, 9R-18R.*

The use of air quality indices to evaluate atmospheric pollution in urban areas

A. Di Menno di Bucchianico, G. Cattani, R. Aceto, S. Bartoletti, A. Gaeta and A.M. Caricchia

ISPRA – Institute for Environmental Protection and Research, Via Brancati 48, 00144, Rome, Italy

Keywords: Urban pollution, PM_{10}, ozone, air quality indices, public communication.

In recent years atmospheric pollution indices have been widely used to describe the air quality status in urban areas and to inform citizens on potential risks or health effects caused by the air they breathe.

Communication to the public is reported using the Internet or other traditional media and daily air pollution levels are often presented on a scale of quality from good to bad (or from excellent to hazardous).

Aspiring to summarize at best the status of ambient air, a number of different quality indices have been developed in various countries.

In general, these indices are based on a series of sub-indices associated to a single pollutant and the actual AQ index is obtained combining in different ways the previously calculated sub-indices.

The aim of this work was to investigate the effective aptitude of different AQ indices for representing the real status of ambient air in a urban area.

Firstly a review of different national air quality indices was presented; secondly, examining their different approach and applying them to pollutant concentration data registered in the city of Rome, similarities and differences were exposed.

Then a proposal of a new synthetic AQ index was suggested and compared with the others.

This study showed that the commonly chosen method of considering the levels of only a pollutant at time was strongly disadvantageous and offered, sometimes, scarcely representative results.
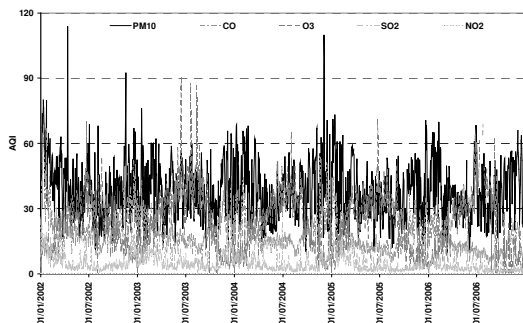
Attempting, for example, to apply the EPA Air Quality Index to our data this gave results strongly affected by the registered PM_{10} levels (see the EPA-AQI sub-indices trend in Figure 1).

This is the foreseeable product of a 'dominant pollutant' methodology. But, although PM_{10} is without doubt the most critical pollutant that presents generally the highest number of exceedances of European limit values, urban monitoring networks register frequently high concentration levels of other substances (such as ozone, nitrogen oxides and carbon monoxide).

On the contrary, the suggested new synthetic index tried to consider at the same time 5 of the most important air pollutants: PM_{10}, NO_2, SO_2, CO, O_3, and the compared results showed interesting seasonal differences (see Figure 2) and strong discrepancies during dust intrusion episodes.
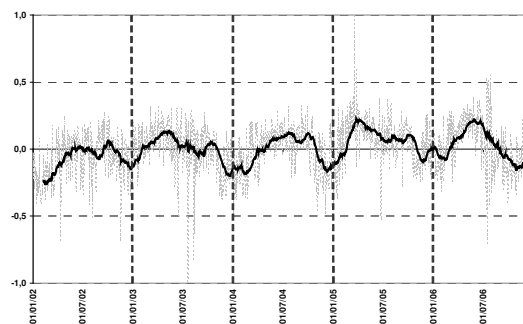
Figure 2. Seasonal differences between EPA–AQI and the proposed synthetic index.

Bruno, F., Cocchi, D. (2002). *Environmetrics*, 13, 243–261.

Cheng, W. L., Kuo, Y. C., Lin, P. L., Chang, K. H., Chen, Y. S., Lin, T. M., Huang, R. (2004). *Atmospheric Environment*, 38, 383–391.

Di Menno di Bucchianico, A., Cattani, G., Bartoletti, S., Aceto, R., Gaeta, A., Gangolfo, G., Caricchia, A.M. (2008). In *Proc. 3rd Nat. Conf. on Particulate Matter – PM2008*, Bari (SCI-IAS), 48.

US-EPA (2006). *Guideline for the reporting of daily air quality - Air Quality Index AQI*. http://airnow.gov/index.cfm?action=static.public ations.

Van den Elshout, S., Léger, K., Nussio, F. (2008). *Environment International*, 34, 720–726.

Figure 1. EPA–AQI sub-indices calculated from concentration data registered in Rome (2002-2006).

T12 Radioactive aerosols

Ten-year measurements of Radon's decay products to study the role of atmospheric dispersion on PM levels

R. Vecchi[1], G. Valli[1], V. Bernardoni[1], and A. Franchin[1]

[1]Department of Physics, University of Milan, and INFN, via Celoria 16, 20133, Milan, Italy

Keywords: radon decay products, dispersion, PM

The measurement of the concentration and temporal behaviour of radioactive aerosol in atmosphere can provide information on atmospheric thermodynamic conditions as well as on atmospheric processes that involve aerosols such as transport, dispersion, removal rates and residence time.

Since 1997 our group has been measured the concentration of Radon's short-lived decay products routinely and continuously in Milan (Italy) with hourly resolution (Marcazzan et al., 1995; Sesana et al., 2003; Vecchi et al., 2004).

Radon activity concentration outdoor is detected through the collection of its short-lived decay products attached to aerosol particles and the spectroscopic evaluation of their alpha activity by a home-made instrument with high sensitivity (detection limit = 0.2 Bq m^{-3}).

Long-term Radon measurements (Kataoka et al., 1998; Perrino et al., 2001; Sesana et al., 2003) show that the temporal variation of its concentration can give immediate information on the evolution of the stability conditions in the boundary layer. The stability conditions of the lower atmospheric layers, on a local scale, are very important as influence pollutants concentration on different time scales. Indeed, the dilution of pollutants in the mixing layer must be ascribed to thermal and dynamic turbulence, whilst the horizontal transport of pollutants is due to the wind field. In the Milan area and in the whole Po valley ventilation is scarce (despite sporadic advection episodes, typically Föhn events) and vertical dispersion plays the main role.

From long-term measurements performed in Milan by our group a typical daily pattern in Radon concentrations can be singled out: it is generally characterised by a minimum in late afternoon and a maximum in the early morning. This pattern is observed on sunny days with clear sky (both during day and night) and low ventilation rate and it occurs very frequently in Milan during both winter and summer months. The nocturnal accumulation of Radon is due to the low mixing layer generally caused by a low-height or ground-based temperature inversion of radiative origin. The variation of Radon concentration observed between the minimum in the afternoon and the maximum in the following day is a good indicator of the nocturnal mixing layer depth. When the sun rises in the morning and heats the ground the inversion is destroyed so that the re-mixing of Radon takes place in layers of increasing heights causing a decrease of its concentration levels. The minimum concentration is registered during the afternoon when the mixing layer reaches its maximum depth. The variation between maximum and minimum Radon concentration in the same day is an index of the maximum height of the mixing layer, which has been evaluated by means of a box model suitably set up (Pacifico, 2005).

The analyses performed on our long-term dataset have been singled out a significant correlation between PM10 and ^{222}Rn daytime concentrations evidencing the dominant role of atmospheric dispersion in determining the temporal variation of PM10 levels. Whenever ^{222}Rn concentrations accumulate during the night (indicating the formation of a nocturnal atmospheric stability), PM10 concentrations show higher values than those registered during the daytime before, despite a nocturnal decrease in emissions from active sources. On the contrary, when ^{222}Rn concentrations do not accumulate during night hours, PM10 levels are lower than those measured the daytime before. It is worth noting that in both cases the aerosols residence time plays a role and has to be taken into account.

Moreover, an analysis of the relationship between PM and atmospheric dispersion over the ten-year data set will be presented.

Kataoka, T., Yunoki, E., Shimizu, M., Mori, T., Tsukamoto, O., Ohhashi, Y., Sahashi, K., Maitani, T., Miyashita, K., Fujikawa, Y., Kudo, A. (1998). *Boundary-Layer Meteor.*, 89, 225–250

Marcazzan G.M., Mantegazza F., Astesani R. (1995). *Life Chemistry Reports* 13, 151-158.

Perrino, C., Pietrodangelo, A., Febo, A. (2001). *Atmos. Environ.*, 35, 5235-5244

Sesana, L., Caprioli, E., Marcazzan, G.M. (2003). *J. Environ. Radioact.*, 65, 147-160

Vecchi, R., Marcazzan, G., Valli, G., Ceriani, M., Antoniazzi, C. (2004). *Atmos. Environ.*, 38, 4437-4446

FACTORS CONTROLLING ^{7}Be AND ^{210}Pb ATMOSPHERIC DEPOSITION AT MALAGA (SPAIN)

C. Dueñas, M.C. Fernández, S. Cañete, E. Gordo and M. Pérez

Department of Applied Physics I, Faculty of Sciences, University of Málaga. 29071 Málaga (SPAIN)

E-mail: mcduenas@uma.es

Keywords: atmospheric aerosol, deposition, ^{7}Be, ^{210}Pb, precipitation

ABSTRACT.-Bulk atmospheric deposition of ^{7}Be and ^{210}Pb has been measured at Málaga (4º 28′ 80″ W; 36º 43′ 40″ N) a coastal Mediterranean station in the south of Spain, from January 2005 through April 2008 for monthly periods. The fluxes of ^{7}Be and ^{210}Pb were mainly correlated with rainfall and correlated one with the other .Concentrations of ^{210}Pb and Ca^{++} in rain were correlated with transport time of air masses over the continent

INTRODUCTION Berylium-7 is one of the radionuclide produced by spallation reactions of cosmic rays with light atmospheric nuclei. ^{7}Be rapidly associates primarily with submicron-sized aerosol particles. Lead-210 which is one of the natural radionuclide of the ^{238}U decay series is widely used as a tracer. ^{210}Pb depositional pattern gave us information on continental aerosols in lower troposphere. These two radionuclides with their different sources and therefore are useful to understand the mechanisms of aerosol removal from the atmosphere. These radionuclides have measured routinely in many places of the word in order to study the description of environmental processes such as aerosol transit and residence times in the troposphere, aerosol deposition velocities and aerosol trapping by ground vegetation.

MATERIAL AND METHODS.- The sampling site is one of the environmental radioactivity monitoring network stations operate by the Spanish Nuclear Security Council (CSN). The sampling point was located above the ground, on the roof of the Faculty of Sciences, University of Málaga. Monthly precipitation and dry fallout samples were routinely collected using a steel tray 1m^{2} in area as a collecting system and polyethylene vessels of 50 l capacity for rainwater samples reservoirs. Measurements by gamma spectrometry were performed to determine the ^{7}Be and ^{210}Pb activities of the samples using an intrinsic REGe detector. The peak analysis of ^{7}Be (I= 10.52 %, 477.7 KeV) and ^{210}Pb (I = 4%, 45 KeV) was done using SPECTRAN AT peak analysis software. The counting time was 172800s
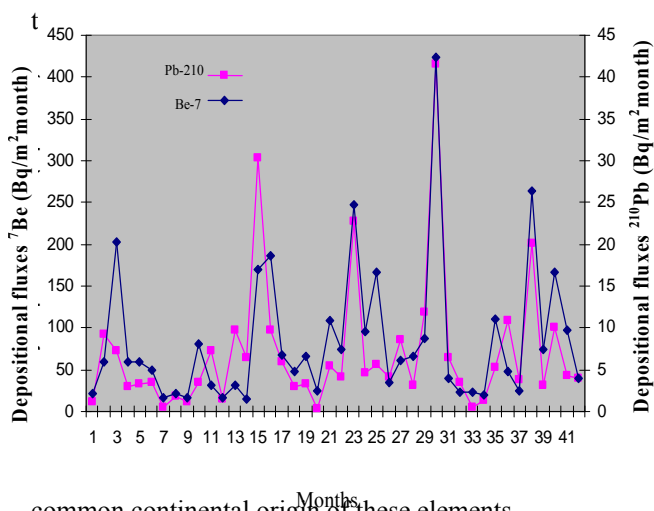
RESULTS The results from depositions of ^{7}Be and ^{210}Pb were correlated with four parameters: rainfall amount, rainfall duration, number of dry days and number of wet days. Table 1 provides the correlation coefficients between the fluxes of and the mentioned parameters.

Table 1. Linear correlations coefficients between fluxes of ^{7}Be and 210Pb and some parameters

	^{7}Be		^{210}Pb	
	r	p	r	p
Rainfall amount	0.80	99	0.70	99
Rainfall duration	0.44	99	0.36	95
Number of dry days	-0.72	99	-0.68	99
Number of wet days	0.74	99	0.71	99

The depositions of ^{7}Be and ^{210}Pb were well correlated with the amount of rainfall . Such relations have been commonly observed and explained by the fact that rainfall constitutes the major depositional pathway of these radionuclides. As previously observed, correlation of rainfall with ^{7}Be seems better than with ^{210}Pb (Caillet el al., 2001) likely due to a relatively greater contribution of ^{210}Pb from dry deposition.

The fluxes of ^{7}Be and ^{210}Pb are correlated one with the other (r = 0.83; p >99 %) . Figure shows the monthly results for period of measurements. There is a relationship between air mass trajectories and the concentrations of ^{210}Pb and Ca $^{++}$ illustrates t

common continental origin of these elements.

Caillet, S., P. Arpagaus, F. Monna and J. Dominik (2001). Factors controlling ^{7}Be and ^{210}Pb atmospheric deposition as revealed by sampling individual rain events in the region of Geneva, Switzerland.J. Environ. Radioactivity 53, 241-256.

DEPOSITION VELOCITIES AND WASHOUT RATIOS ON A COASTAL SITE CALCULATED FROM GROSS ALPHA AND GROSS BETA MEASUREMENTS

C. Dueñas, M.C. Fernández, E. Gordo, S. Cañete, and M. Pérez

Department of Applied Physics I, Faculty of Sciences, University of Málaga. 29071 Málaga (SPAIN)

E-mail: mcduenas@uma.es

Keywords: atmospheric aerosol, deposition velocity, precipitation, washout ratio

INTRODUCTION-The gross-alpha and gross beta activities in aerosols and bulk deposition samples were measured in Málaga, Southeastern Spain (36º43´40´´N; 4º28´8´´W). At the same sampling point, aerosols were colleted weekly on filters and monthly precipitation sampling was carried out to study depositions. Levels of particulate matter fraction were also monitorized in Málaga. Using the gross alpha and beta activities in air and their depositional fluxes, the deposition velocities of aerosols and washout ratios are calculated .The minimum and maximum value of alpha and beta deposition velocities are 0.42 - 7.69 cms^{-1} and 0.09 - 2,12 cms^{-1} respectively and the corresponding washout ratios are 449-6980 and 93-3760 respectively.

MATERIAL AND METHODS

The gross alpha activity was measured by a solid ZnS (Ag) scintillation counter. The gross beta activity was measured with a gas flow proportional counter of the low-background multiple detector type with four sample detectors (Camberra HT-1000) and PM10 concentrations were measured for the beta attenuation method.

RESULTS AND DISCUSSION The dates used in the analysis are means monthly   values of concentrations in surface air. The period of measurements was performed from October 2005 to September 2007. The dates were analyzed to derive the statistical estimates characterizing the distribution. Studies of the frequency distribution show lognormal distribution is significant at the 0.01 level assuming these types of distribution, the geometric mean should be used to characterize average values.

Table1 provides the statistical parameters from the measurements of alpha and beta deposition velocities ($V_{d\alpha}$ and $V_{d\beta}$) of aerosols and washout ratios($W_{R\alpha}$ and $W_{R\beta}$).

Variable	$V_{d\alpha}$ (cm/s)	$V_{d\beta}$ (cm/s)	$W_{R\alpha}$	$W_{R\beta}$
Geometric mean	1,26	0,48	2004,6	788,2
Dispersion factor	2,26	2,29	2,24	2,63

Table1. Statistical parameters.

Table 2 shows the correlation coefficients and associated probabilities between and some parameters. Since the p-values are less that 0.01, there is statistically significant relationship between deposition velocities of gross alpha and gross beta activities and the rainfall.

The maximum value of deposition velocities alpha and beta correspond with maximum value of rainfall

Parameters	Vd α (cm/s)	Vd β (cm/s)
Rainfall	0.76(0.01)	0.67(0.01)
PM10	-0.31(0.10)	-0.38(0.10)

Table2. Linear correlations coefficients of Vd and some parameters.

Figure 1 shows the negative correlation of rainfall with the variations of washout ratios alpha and beta. In the figure 2 is reflected in a positive correlation of alpha and beta washout ratios with PM10. The maximum washout ratios values of alpha and beta correspond with a minimum value of rainfall and an increase of the PM10.
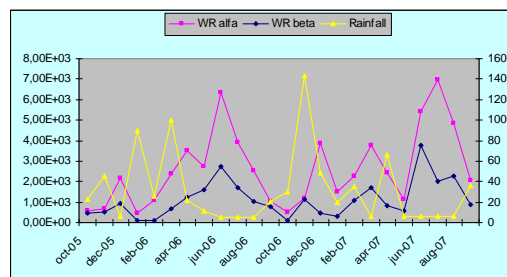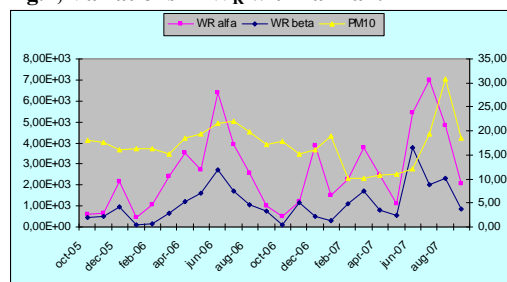

Fig.1, Variations in W_R with rainfall.

Fig.2 Variations in W_R with PM-10.

REFERENCES-.MCNEARY, D. and BASKARAN, M. Depositional characteristics of ^{7}Be and ^{210}Pb in southeastern Michigan. J. Geophys. Res. 108, D7, 4210-4225, 2003.

Assesment of air mass transport of Chernobyl originated radionuclides using clustering approach

G. Lujanienė[1], S. Byčenkienė[2], V. Aninkevičius[3]

[1]Nuclear and Environmental Radioactivity Research Laboratory, Institute of Physics,
Savanorių 231, LT-02300 Vilnius, Lithuania

[2]Environmental Physics and Chemistry Laboratory, Institute of Physics,
Savanorių 231, LT-02300 Vilnius, Lithuania

[3]Semiconductor Physics Institute, A. Goštauto 11, LT-01108 Vilnius, Lithuania

The Chernobyl accident caused the release of a great amount of radioactive substances into the atmosphere. Variations in ratio, concentrations and speciation of radionuclides observed after the accident were explained by different proportion of condensed and fuel particles in the Chernobyl fallout. The radioactive aerosols were detected at many locations in Europe more than 1000 km away from the source. Consequences of the Chernobyl accident have been intensively studied in the last two decades. Low activities of the Chernobyl originated radionuclides that are still present in the environment can be used to study the long distance transport of contaminants.

In order to evaluate the contribution of the transport of air masses to the ^{137}Cs air activity concentration, the time series of ^{137}Cs variation in aerosol samples from 1993 to 1999 and 2005-2006 were analysed. The three-dimensional 10-day air mass backward trajectory method was applied to determine possible transport pathways of ^{137}Cs. The relevant air masses were identified by using a filter and Ward's hierarchical clustering algorithm in combination with Euclidean distance (Ward, 1963) was performed on air mass backward trajectories. In this paper, we focus on the study domain, which covers the 30 km Chernobyl zone. The 10-day air mass backward trajectories were clustered and grouped according to season, travelled way, and height over the surface before arrival. The analysis of air mass pathway has indicated the transport of ^{137}Cs from the Chernobyl restricted zone and surrounding areas. A positive correlation was found between the frequency of air masses and the activity concentrations of ^{137}Cs during study periods (1997-1999 and 2005-2006).

The release of plutonium isotopes into the environment after the Chernobyl accident was insignificant: mean (0.224) and median (0.204) ^{240}Pu/^{239}Pu ratio values determined in 1995-2003 were close to those of the global fallout (Lujanienė et al., 2009). The exponential decrease in the ^{240}Pu/^{239}Pu atom ratio from 0.40 to 0.19 was observed (Fig. 1). It can be interpreted as a result of decrease in the amount of the Chernobyl originated plutonium in the environment due to deposition and mixing with plutonium isotopes derived from the global fallout. The mean and median data were fitted by the first order kinetic equation and the residence time of the Chernobyl derived plutonium in the environment was obtained to be about 1.6 -0.4 years.
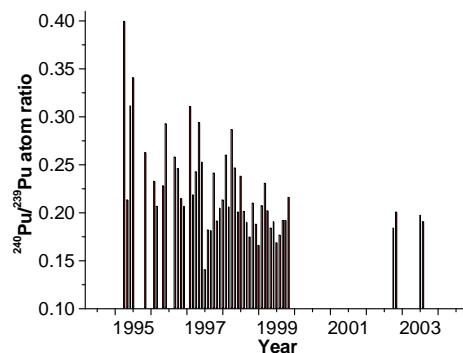

Figure 1. ^{240}Pu/^{239}Pu atom ratio in aerosol samples.

The activity concentrations of plutonium measured in monthly aerosol samples could not be traced back via backward trajectories precisely, however, its transport from contaminated territories can be expected. The comparative correlation analyses of mean monthly and daily activity concentrations of ^{137}Cs as well as ^{240}Pu/^{239}Pu atom ratio with the frequency of air masses was performed in order to approximately estimate the possible transport of the Chernobyl originated plutonium. Preliminary results indicated the identical correlation for the ^{137}Cs mean monthly activity concentrations in comparison with daily ones, while no positive correlation for the plutonium transport from the highly contaminated after the Chernobyl accident region was found in 1997-1999. Data analyses are in progress.

Ward, J. H., (1963). Hierarchical Grouping to Optimize an Objective Function. *Journal of the American Statistical Association*, 58, 236-244.

Lujanienė, G., et al. (2009) *J. of Environ. Radioactivity,* 100, 108-119.

Monitoring of ^{7}Be and heavy metals at the Basic Environmental Observatory "MOUSSALA"

I.Penev, J.Stamenov, M.Drenska, B.Damyanov and Ch.Angelov

Institute for Nuclear Research and Nuclear Energy,
Bulgarian Academy of Sciences, 72 Tscarigradsko shosse, 1784, Sofia, Bulgaria

Keywords: aerosol sampling, radioactive particles, natural radioactivity, man-made radioactivity.

The Basic Environmental Observatory is situated in the vicinity of peak of Moussala, 2971m., the highest point in Balkanian Peninsula. The peak is in the frame of reserve Central Rila, part of the National Park Rila. The observatory has been established by Institute for Nuclear Research and Nuclear Energy of Bulgaria Academy of Sciences. Here, in spite of very harsh conditions a wide spectrum of physical investigations are in full progress – meteo, atmosphere investigations, precipitations, monitoring of space and Earth radiations, different components of cosmic particles and etc., see http://beo-db.inrne.bas.bg/moussala/

A big sampler with capacity 1500-1800m^3/h has been mounted according to the program of aerosols investigations on BEO-"Moussala".The sampler is shown on figure 1.

Figure 1 Basic Environmental Observatory, on the roof is house for sampling

The air, ~ 15000m^3, is passing through fibber filter with high efficiency. After sampling the filter is pressed to the pill size: diameter 56mm and thickness 13-15mm. The pills are measured by H.P.Ge spectrometer with 30% relative efficiency. More detail description of the device and method are given in Uzunov at al., 2007 and Penev at al., 2007. For 2008 more then 160 samples were analyzed for natural and man made radioactivity. Special attention is paid to the behavior of the ^{7}Be and heavy metals isotopes. The fluctuation of the volume concentration of these isotopes is informative in exchange for the big air mass between different atmosphere strata.

The interval of the above mentioned fluctuations of ^{7}Be at the altitude ~3000m vary in size more then 15 times, see figure 2.
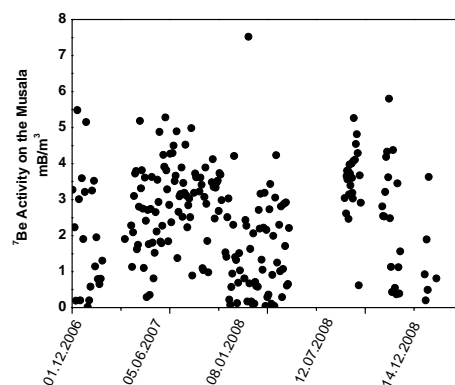

Figure 2. The data ^{7}Be for 2007-2008y at BEO-Moussala

The intensive interchange of very big air mass at Moussala, (wind velocity is in the frame 5 –50m/s) with aerosols with different origin, together with big sampling is a splendid opportunity to control the air quality. The minimal detectable activity of the method is from 10^5 to 10^6 times lower, and then max permissible according to the IAAE standards for man-made radioactivity.

It is planned to make an analysis of the aerosols for heavy metals and other elements in the near future. Remoteness of BEO from all kind urban activity gives good opportunity for such investigations.

Some correlations between ^{7}Be and cosmic rays including neutron component is under progress.

This work is done in the frame of BEOBAL EU project.

Uzunov, N., Janminchev, V., Penev, I., Drenska, M., Damyanov, B., Damyanova, A. (2007). in Annual of Constantin Preslavski University, Shumen vol.XVII B2

Penev, I., Stamenov, J., Drenska M., Damyanov, B., Valova, Tsc., Uzunov, N., Arhangelova, N. (2007), *Ecology and Future,* v.VI, n.3, 27-31.

Key issues in radionuclide labeled aerosol monitoring for resuspension studies and short to long-term post-accident characterizations
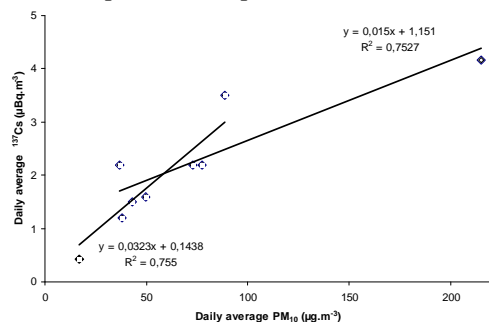
O. Masson[1], D. Piga[1], L. Bourcier[2]

[1] Institute of Radioprotection and Nuclear Safety, IRSN-Cadarache, 13115 Saint Paul lez Durance, France
[2] Laboratory of Physical Meteorology (LaMP), Blaise Pascal University, 24 Av[e] des Landais, 63177 Aubière, France

The French radioactive aerosol monitoring network (OPERA) celebrates its fiftieth anniversary this year. This monitoring was gradually updated both in terms of aerosol sampling (up to 700 m^3/h) and radioactivity measurement in order to determine current airborne levels as low as 0,2 µBq/m^3 for ^{137}Cs. One of the key issues in monitoring is linked to understanding the environmental transfer processes. These processes affect radioactive aerosols inside the atmospheric compartment (rainout, washout, dry deposition and impaction). Radioactive aerosol are also emitted from others compartments of the biosphere that received radionuclide fallout (via resuspension or biomass burnings). The least soil particle resuspension that has ^{137}Cs concentration of some hundreds to tens thousands Bq/m^2 (like in France) is enough to increase airborne levels temporarily. This is especially true during Saharan dust events because of high dust flux, even if the Saharan soil particle activity is lower. About a dozen Saharan events are count every year especially in the southern half of France. During Saharan dust outbreaks the daily airborne activity levels is correlated with PM10 evolution (fig. 1). Moreover the activity levels in deposited dust collected in France are quite concentrated when compared to the Saharan soils. This enrichment is due to the coarse particule segregation loss that have less affinity with ^{137}Cs than fine particles. Our findings show that yearly averaged activity levels are twice to ten times higher for altitude locations (mountainous). The cruising altitude of Saharan plumes is responsible of this.

Fires also lead to redistribution of formerly deposited radionuclides, mainly due to the burning of radionuclide-enriched forest litter even over long distances. During winter, temperature inversion in the lower atmospheric layers coupled with wood burning for domestic purposes may also lead to temporary increases in airborne artificial radionuclide levels. Except for these extreme events, routine and local resuspension, regular in time and mainly dependant on season also contributes to the background level. Local resuspension effect can also be found in the better relationship with ^{137}Cs airborne activity when considering coarse particles (PM_{10}) that don't travel far from their emission area, instead of fine particles ($PM_{2.5}$). In France a six year long study shows that oceanic air flux is correlated to a light positive longitudinal airborne activity gradient from west to east whereas there is no background PM_{10} gradient (15 µg.m^{-3}). Thus, the activity gradient can be explained by the soil activity related to the longitudinal Chernobyl fallout distribution. During eastern winds a remote contribution is added from areas more impacted by Chernobyl fallout. This added contribution results in quite the same averaged gradient but with 3 times more pronounced values at both France boundaries and a 4 times enhanced variability. At the scale of France and for the last 8 years, local and remote resuspension can explain about 1/3 of ^{137}Cs rising levels; biomass burnings 1/3 too. The last third corresponds to winter temperature inversion coupled with domestic wood burning emissions. Enhancing knowledge about these mechanisms is useful to mapping territorial radioecological sensitivity and to explain long term post-accident persistence of airborne radionuclides at trace levels. Current needs are concerning the radionuclide aerosol size segregation.

Fig.1: Relationship between ^{137}Cs activity level and PM_{10} of mineral origin from Sahara

Radiation burden of the up clearing deeply deposited radon progenies in the central airways

I. Balásházy[1,2] and G. Kudela[2]

[1]Health and Environmental Physics Department, Hungarian Academy of Sciences KFKI Atomic Energy Research Institute, Konkoly Thege M. út 29-33, 1121 Budapest, Hungary
[2]Aerohealth Scientific Research Development and Servicing Ltd., 2090 Remeteszőlős, Csillag sétány 7, Hungary

Keywords: radon decay products, health effects of aerosols, lung deposition, Monte Carlo simulations, clearance

Most of the lung cancers of former uranium miners developed in the large central airways and near 90% of the neoplastic lesions have been found in airway generations 2-5. Current computational fluid dynamics calculations indicate high primary deposition density values in the peaks of the central airways. However, the cellular burden of the radon progenies deposited in the deep regions of the bronchial and acinar sections of the lung and clears up by the mucociliary escalator may contribute to the health effects found in airway generations 2-5. The surface of the airways highly increases and the deposition efficiency does not decrease remarkably with generation number, thus, it looks a reasonable supposition that the dose contribution of the up clearing radon progenies may contribute to the health effects in the large airways.

In the present work, the primary deposition distributions of inhaled radon progenies were computed in the whole respiratory system by the stochastic lung deposition model at different breathing conditions. In addition, a new bronchial clearance model has been elaborated to simulate the up cleared fractions of attached and unattached radon progenies in each of the bronchial airway generations. Finally, the ratio of the up cleared and primarily deposited fractions has been calculated at airway generation level at two different breathing patterns and at two mucus velocities.

The main input data of the clearance model are the deposition data, the velocity of the mucus in a generation, the length of the airways and the half life of radon progenies.

Based on the results, in the central airways, the radiation burden of the up clearing, more deeply deposited, radon progenies can be significantly higher than the burden of the primarily deposited fraction in these airways both at resting and light physical activity breathing conditions in case of unattached and attached radon progenies. The dose contribution of the deeply deposited ^{218}Po and ^{214}Pb isotopes in the large airways are higher than that of ^{214}Bi. The radiation burden of the more deeply deposited ^{214}Po in the central airways is practically zero because of its short half life. The results demonstrate that one of the reasons of radon induced lung cancer may be the dose contributions,

in the central airways, of the up clearing, more deeply deposited, radon progenies.

The computed deposition distributions of inhaled particles in bronchial airways have been validated by A. Kerekes et al. (2009).

Figure 1. Primary deposition fractions of unattached ^{218}Po at light physical activity breathing condition and cleared up fractions at 15 and 5.5 mm/min mucus velocities.
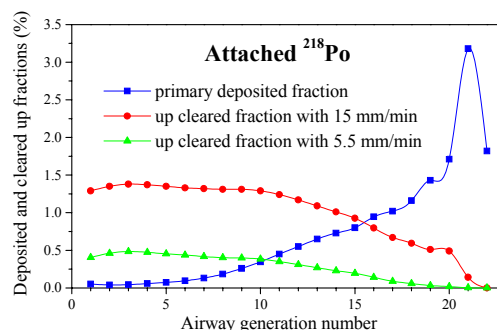

Figure 2. Primary deposition fractions of attached ^{218}Po at light physical activity breathing condition and cleared up fractions at 15 and 5.5 mm/min mucus velocities.

A. Kerekes, A. Nagy and A. Czitrovszky (2009) Experimental flow and deposition studies with hollow bronchial airway models. *17th ISAM Congress 2009*, Montery, California, USA. May 10-14 2009.

Airway deposition and health effects of inhaled radon progenies

I. Balásházy, Á. Farkas and I. Szőke

Health and Environmental Physics Department, Hungarian Academy of Sciences KFKI Atomic Energy Research
Institute, Konkoly Thege M. út 29-33, 1121 Budapest, Hungary

Keywords: radon decay products, health effects of aerosols, lung deposition, CFD, deposition efficiency

Inhaled radon progenies provide more than the half of natural radiation exposure. There is increasing evidence that the cellular distribution of radiation burden is an important factor regarding the biological response to ionisation radiation, thus, one of our tasks was the characterisation of the distribution of cellular exposure.

Histological studies of former uranium miners presented strong correlation between primer deposition hot spots and neoplastic lesions. Most of these lesions were located along the carinal regions of the large bronchial airways. In the present work, computational fluid dynamics (CFD) approaches have been applied to simulate the deposition distribution of inhaled radon progenies along central human airways. The geometry and the cellular structure of epithelial lung tissue were numerically reconstructed based on anatomical and histological data. Single and multiple alpha-hit and cellular dose distributions have been computed applying Monte Carlo modelling techniques at different breathing conditions.

light physical activity breathing condition. Size of scanning surface element is a 45μm side triangle.

Values of local per average deposition densities, that is, enhancement factors (Figure 1), hit probabilities (Figure 2) and doses may be up to two-three orders of magnitude higher in the deposition hot spots than the average values. Dose calculations revealed that some cell clusters may receive high doses even at low exposure conditions.

Applying the model to different radiation exposure conditions useful relations can be received regarding the linear-nonthreshold hypothesis.

Ultrafine deposition distributions can be experimentally validated by the measurement technique of Jani et al. 1999.

10^7 inhaled radon progenies, New-Mexico Uranium mine

Figure 1. Deposition enhancement factor (EF) distribution of attached, 200 nm, and unattached, 1 nm, diameter inhaled radon progenies on a central airway bifurcation in airway generations 4-5 during

Figure 2. Distribution of cell nuclei hit with alpha particles in the epithelium of airway generations 1-5, leading to the right upper lobe.

Jani P., Nagy A., & Czitrovszky A. (1999). *SPIE* Vol. 3749, 458-459.

Parametric study of the ionizer induced Thoron progeny concentration depletion

M. Joshi, P. Kothalkar, A. Khan, R. Mishra, B.K. Sapra and Y.S. Mayya

Radiological Physics and Advisory Division, Bhabha Atomic Research Centre, Mumbai – 400085. India

Keywords: radon decay products, unattached fraction, deposition velocity, ionizer

It is well known that the negative ions emitted from the negative ion generator (NIG) help in charging the airborne particles, thereby removing them by electromigration in space charge-induced electric fields (Mayya *et al.,* 2004). The NIGs have also been used to reduce activity concentration of radon/thoron decay products (Sheets and Thomson 1995). The physical arguments suggest different reasons for the activity reduction namely; 1) direct plate-out of freshly formed, charged fine fraction of progeny through drift in the electric field and 2) removal of the coarse fraction, thereby increasing the highly mobile fine fraction and its consequent plate-out. To investigate these aspects, measurements of various parameters like activity concentrations, deposition velocity, aerosol number concentration and the unattached fraction in presence of NIG; a systematic study has been carried out in a room environment wherein a thorium nitrate powder was placed as a source of thoron progeny. The overall decrease in the progeny concentration with NIG is depicted in Fig. 1.

observations strongly point at the possibility of argument (2) cited above as the mechanism of activity reduction.

The particle concentration, measured using GRIMM 5.403 Scanning Mobility Particle Sizer (SMPS) in the size range of 9.8 nm to 875 nm, showed a 3-fold decrease after switching on the ionizer. The attachment rate, X, of the progeny to the ambient aerosols (concentration, Z /cc) can be estimated using the relationship: $X = \beta(d)Z$, where $\beta(d)$ is the size dependent attachment coefficient (cc/s). This is plotted in Fig. 2 and a decrease in the attachment rate is seen when the ionizer is switched on. Also, the activity median diameter was found to shift to larger sizes (94 nm to 150 nm). The lowered attachment rate also points at the increase in the unattached fraction as observed by wire-mesh filter paper sampling techniques. However, the implication of the reduction in activity concentration might not necessarily lead to a reduction in the lung dose and this requires a careful investigation.
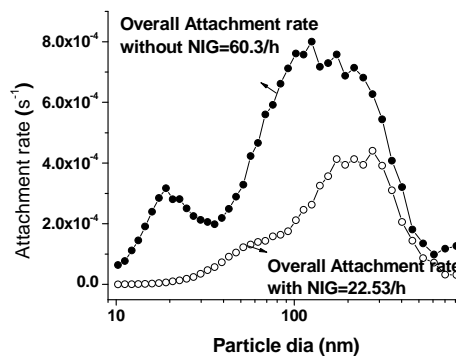

Figure 1: The decrease in the progeny concentration with the ionizer switched on.

Figure 2: Effect of ionizer on the attachment rate under ambient aerosol conditions

Deposition velocity of the progeny was measured using passive direct progeny sensors, which are deposition based absorber mounted LR115 detectors. It was observed that the deposition velocity increased from ~0.06 mh^{-1} to 0.3 mh^{-1} in presence of negative ions. The unattached fraction, estimated by wire-mesh and filter-paper sampling followed by Alpha counting, was also found to increase from 2% to 6.5%. Additionally, the activity deposited in the vicinity of the needles of the NIG showed negligible increase with NIG switched on. All these

References:

Sheets R. W. and Thompson C.C. (1995), *J. Radioanalytical and nuclear chemistry*, 193,301-308.

Mayya Y.S., Sapra B.K., Khan Arshad, Faby Sunny (2004), *J Aerosol Sci.,*35, 923-941.

Mishra R., Mayya Y.S., Kushwaha H.S. (2009), *J. Aerosol Sci.* , 40, 1-15.

Cheng Y.S. and Yeh H.C. (1980), *J Aerosol Sci.*, 11, 313-320.

Determination of loss factors of aerosol particles in the sampling systems of nuclear power plants

R.F.W.Jonas[1] and G.F.Lindenthal[2]

[1]TÜV Nord SysTec GmbH & Co. KG, Große Bahnstr. 31, D-22525 Hamburg , Germany,
[2]Ingenieurbüro für Partikeltechnologie und Umweltmesstechnik, Steinweg 8, D-34314 Espenau Germany

Aerosol measurement, particle deposition, radioactive particles, nuclear sampling systems

According to the German nuclear technical rule KTA 1503.1 the sampling system of a nuclear power plant must be able to collect aerosols with aerodynamic diameters between 0.1 µm and 20 µm with pipe retention factors below 3.

As with all measured quantities the stack emission of radioactive material of a nuclear power plant with exhaust air includes an uncertainty. This is caused by the statistical error and additionally by the non-representative sampling and the deposition of aerosols in the sampling systems. The non-representative sampling results from the insufficient mixing of the air (inhomogenous concentration) and from the non-isokinetic flow in reaching the inlet of the screen of the sampling system. The deposition depends on the particle diameter and is caused by molecular diffusion, impaction and sedimentation. The ratio of the mass concentrations in front of the screen and at the end of the sampling system is called the pipe retention factor.

Pipe retention factors and loss factors (without consideration of non representative sampling) are investigated for sampling systems of different nuclear power plants in Germany using three methods of determination:

1) Dispersing of test aerosols directly into probes of the screen of the sampling system and comparing the aerosol concentrations with those at the end of the sampling system

2) Generation of a defined quantity of aerosol particles at the bottom of the chimney and measuring the particle concentrations by using aerosol collectors or aerosol monitors at the end of the sampling system

3) Measuring the size distribution by number of the ambient aerosol in the chimney in front of the screen and at the end of the sampling system with optical particle counters.

The experimental results are in compliance with theoretical estimations. The measured loss factors and pipe retention factors lie below 3. The transfer properties of the sampling systems for larger particles (aerodynamic diameters up to 3 mm) also have been investigated. The results show that the sampling systems are suitable even in these cases. The presentation gives a survey of the measured pipe retention factors. The results of the three methods of determination are compared indicating advantages and disadvantages based on our experiences.

The solubility and leaching of aerosol particles – radionuclide carriers – collected on filters in the ventilation system of the Ignalina Nuclear Power Plant

R. Jasiulionis and A. Rožkov

Ignalina radioecological monitoring station, Institute of Physics, LT-02300 Vilnius, Lithuania

Nuclear power plants are permanent emission sources of fission (^{137}Cs, ^{134}Cs) and activation (^{60}Co, ^{54}Mn) radionuclides, attached to aerosol particles, into the air.

The Ignalina Nuclear Power Plant (NPP) has two RBMK graphite-moderated channel-type 1500 MW reactors: the power generation at the Unit 1 reactor was stopped in 2005, the Unit 2 reactor is in the operation till 2010. Being formed in the active zone of the reactor, radionuclides circulate with coolant in the closed circuit and undergo physical and chemical changes on their way. Only fine hydrated ionic compounds, carriers of radionuclides, overcome the water and vapor boundary and can participate in the aerosol particle formation and growth. Relatively long-lived ^{137}Cs ($t_{1/2}$ = 30.08 year), ^{134}Cs ($t_{1/2}$ = 2.07 year), ^{60}Co ($t_{1/2}$ = 5.27 year) and ^{54}Mn ($t_{1/2}$ = 0.855 year) radionuclides, which are registered in the emissions of the stopped reactor, pass to ventilation system by longer indirect pathways.

The dissolution of aerosol particles, carrier of ^{137}Cs and ^{60}Co, sampled on filters was studied by means of a leaching test with distilled water. Samples were collected from technological gas cleaning systems of the operating Ignalina NPP Unit 2 (before carbon adsorbers, before ventilation stack, and in the ventilations stack), in the environment in the vicinity of the Ignalina NPP and in the ventilation stack of the stopped Ignalina NPP Unit 1 in 2005-2007 (Table 1).

Table 1. Result of leaching of ^{137}Cs and ^{60}Co from aerosol particles sampled on filters

Sampling point	^{137}Cs			^{60}Co		
	C, Bq m^{-3}		W, %	C, Bq m^{-3}		W, %
	total	unleach.		total	unleach	
1	2	3	4	5	6	7
Unit 2 before adsorbers	68	23	34 ± 2	< 5	< 5	–
Before ventilation stack	0.35	0.10	29 ± 1	0.34	0.10	29 ± 6
Ventilation stack	1.69	0.44	26 ± 8	1.26	0.42	33 ± 8
Environment	3.29	2.14	65 ± 18	1.32	1.00	76 ± 22
Unit 1 (stopped) ventilation stack	0.62	0.47	76 ± 10	0.64	0.51	80 ± 15

Figure 1. Activity concentration of ^{137}Cs in aerosol particles, collected in operating Ignalina NPP Unit 2, in the environment in the vicinity of the Ignalina NPP and in the ventilation stack of the stopped Ignalina NPP Unit 1. Activity concentrations of ^{137}Cs in the unleached part of aerosol particles and the unsolubility of aerosol particles are given.

The insolubility in water of radionuclides attached to aerosol particles sampled on filters, collected in the operating Unit 2 reactor effluents, is clearly lower than the insolubility in water of radionuclides attached to aerosol particles sampled on filters, collected in the ground-level air and in the effluents of the stopped Unit 1 reactor (Figure 1).

Jasiulionis, R., Rožkov, A. (2008). *Applied Radiation and Isotopes*, 66 (12), 1992-1998.

Jasiulionis, R., Rožkov, A. (2008). European Aerosol Conference 2008 Abstract T06A181P.

Felmy, A., LeGore, V., Hartley, S. (2003). U.S. Nuclear Regulatory Commission Report NUREG/CR-6821.

Aerosol release from Silver Indium Cadmium control rod

T. Lind[1], A. Pintér Csordás[2] and J. Stuckert[3]

[1]Paul Scherrer Institut, Villigen, Switzerland
[2]HAS KFKI Atomic Energy Research Institute, Budapest, Hungary
[3]Forschungszentrum Karlsruhe, Karlsruhe, Germany

Keywords: nuclear aerosols, nuclear reactor, control rod, SIC

In nuclear reactor severe accident, radioactive fission products as well as structural materials are released from the core by evaporation, and the released gases form particles by nucleation and condensation. In addition, aerosol particles may be generated by droplet formation and fragmentation of the core. In pressurized water reactors (PWR), a commonly used control rod material is silver-indium-cadmium (SIC) covered with stainless steel cladding. The control rod elements, Cd, In and Ag, have relatively low melting temperatures, and especially Cd has also a very low boiling point (about 1040 K). Therefore, control rods are likely to fail early on in the accident affecting fuel rod degradation as well as aerosol source term to the environment in the event of containment failure (Petti, 1989; Haste and Plumecocq, 2003).

The QUENCH experimental program at Forschungszentrum Karlsruhe investigates phenomena associated with reflood of a degrading core under postulated severe accident conditions but where the geometry is still mainly rod-like and degradation is still at an early phase. QUENCH-13 test was the first in this program to include a SIC control rod of prototypic PWR design (Birchley et al., 2008). The effects of the control rod on degradation and reflood behaviour were examined under integral conditions, and for the first time the release of SIC aerosols following control rod rupture was measured.

To characterize the extent of aerosol release during the control rod failure, aerosol particle size distribution and concentration measurements in the off-gas pipe of the QUENCH facility were carried out. The aerosol concentration and size distribution released from the core were determined using Electrical Low-Pressure Impactor (ELPI), and Berner Low-Pressure Impactors (BLPI). The sampling system was isolated from the facility before core cooling by quench. A second aerosol sampling system with 10 impactors was used also during the quench phase of the test.

Two aerosol particle modes were generated, fine mode with $D_{ae} = 0.1 – 2$ µm generated by vaporization and subsequent nucleation, condensation and coagulation, and coarse particle mode with $D_{ae} > 3$ µm generated by droplet release and fragmentation. These findings indicate that the commonly used modeling of aerosol formation from control rod rupture by evaporation from molten material surface would need to be refined to include aerosol generation by mechanical processes, such as droplet formation and fragment entrainment.

The aerosol generation during QUENCH-13 test can be divided into five phases: 1) Transient phase: A small but steady aerosol concentration increase presumably due to release of Sn from the Zircaloy. 2) First significant aerosol release at peak bundle temperature 1560 K is thought to have been caused by a small crack in the control rod cladding. The particles contained mainly Cd as an oxide. 3) A very large, but short aerosol burst presumably due to a massive failure of the control rod contained particles rich in Cd and In, with some Ag in the fine mode particles. 4) Steady aerosol release followed the large burst at bundle peak temperature increase from 1650 to 1800 K. The particles were rich in Cd and In, and the amount of Ag increased with time. At this stage, molten control rod material was relocated downwards, and aerosol was released from molten material surface. 5) Particles released during bundle cooling by quench were mainly irregular, coarse particles containing Zr, Sn and W, along with varying amounts of Cd and In. Ag and Fe were present in some distinct particles.. The particles were presumably generated from the molten material, and by fragmentation of the Zircaloy cladding and heater elements due to thermal shocks.

Birchley, J., Austregesilo, H., Bals, C., Dubourg, R., Haste, T., Lamy, J.-S., Lind, T., Maliverney, B., Marchetto, C., Pinter, A., Steinbrück, M., Stuckert, J., Trambauer, K. Proc. of Nuclear Energy for New Europe, Sept. 8-11, 2008, Portoroz, Slovenia.

Haste, T., Plumecocq, W. (2003) 9th International QUENCH Workshop, FZK, Oct 13-15, 2003.

Petti, D.A. (1989) *Nucl. Technol.* 84, 128.

Stuckert, J., Sepold, L., Grosse, M., Stegmaier, U., Steinbrück, M., Birchley, J., Haste, T., Lind, T., Nagy, I., Vimi, A. (2008) SARNET 4th Ann. Review Meeting, 21-25 January, 2008, Bled, Slovenia.

Experimental determination of correction factors for assessment of the activity discharges of radionuclides bound to aerosol particles from nuclear facilities

K. Vogl[1]

[1]Federal Office of Radiation Protection, 85764 Oberschleißheim, Germany

From the stacks of nuclear facilities radionuclides bound to aerosol particles - beside radionuclides in gaseous form like noble gases, tritiated water vapour or C-14 containing carbon dioxide – are discharged into the environment. For the assessment of the discharged activities of these radionuclides a part of the effluent air stream is extracted by means of a rake of extraction probes and conducted by primary and secondary sampling tubes to the sampling devices equipped with particulate filters. The discharged activities are calculated using the measured activities of the radionuclides on the deposited particles and the measured volumes of the effluent air stream and the air steam through the particulate filters.

Through the following effects the activity concentrations at the upstream side of the particulate filters are generally lower than those in the free effluent air stream:
– anrepresentative extraction due to uneven distribution of air velocity and activity concentration in the effluent air stream over the diameter of the stack;
– changes of size distribution for activity and particle number due to anisokinetic extraction;
– losses of aerosol particles and activities of the bound radionuclides in the sampling tubes, generally due to turbulent deposition and impaction. The losses of aerosol particles with aerodynamic diameters lager than 3 μm are considerable. The losses of the activities of the aerosol particle bound radionuclides depend on the aerosol particle losses and the activity size distribution, which is a logarithmic standard deviation with a geometric mean diameter of about 1 μm in general; the values of these losses are in the range of some percent up to 40 percent. (Vogl, 1994).

Therefore, for the assessment of the true activity discharges correction factors have to be used.. The so-called tube factor takes into account only the losses of activity in the sampling tubes and is defined as the activity concentration at the inlet of the extraction probes to the activity concentration at the upstream side of the particulate filters. The so-called total correction factor considers all the above mentioned effects and is defined as the mean activity concentration in the effluent air stream to the activity concentration at the upstream side of the particulate filters.

For the experimental determination of both correction factors test aerosol particles may be used which differ from the aerosol particles in the effluent air by being radioactive, by the chemical composition or by a much higher mass concentration. In all cases the activity size distribution or the mass size distribution of the test aerosol particle collective must be similar to the activity size distribution of the radionuclides carrying aerosol particles in the effluent air stream. For most experimental determinations powders like titanium dioxide are dispersed.

For the experimental determination of the tube factor a known amount, e. g. activity or mass, of these test aerosol particles are injected into the inlets of the extraction probes. In case of the total correction factor, these test aerosol particles are injected into the air stream at several locations upstream of the extraction rake.

The amount of the test particles deposited on the particulate filter may be determined gravimetrically or by other methods, e. g. XFA.

The value of the tube factor is the ratio of the injected amount of the test aerosol particles and the amount of the test particles on the particulate filter. The value of the total correction factor is the mean value of the ratios of the injected amounts of the test aerosol particles and the amounts of the test particles on the particulate filters.

For 12 investigated nuclear facilities in Germany the values of both correction factors are in the range between 1,1 and 1,6.

Vogl, K. (1994) *Aerosol particle losses in the sampling lines of nuclear facilities: Assessment and experimental determination J. Aerosol Science, Suppl.. 1, S265 - S266*

Resuspension of particles inside packages containing radioactive powders

F. Gensdarmes[1], H.E. Thyebault[1], J. Vendel[1], B. Eckert[2] and S. Fourgeaud[2]

[1]Aerosol Physics and Metrology Laboratory, IRSN, 91192, Gif-sur-Yvette, France
[2] Safety Assessment Section for Transports, IRSN, 92260 Fontenay-aux-Roses, France

Keywords: aerosol generation, resuspension, powder, radioactive particle

In the field of transport of radioactive materials, the products, like UO_2, PuO_2 or MOX (Mixed OXyde Fuel) powders are confined in packaging which should, in normal or accidental conditions of transport, assure a leakage rate compatible with the release regulatory criteria (IAEA, 2005). The above mentioned conditions are characterized by a drop test up to respectively 1.2 m and 9 m high. In the safety demonstrations, the hypotheses usually taken into account by the French applicants are concentrations of aerosols in the cavity of the package equal to:

- in normal conditions of transport: 10^{-3} g.m^{-3},
- in accidental conditions of transport: 9 g.m^{-3} for the first thirty minutes after the drop, and then to 0.1 g.m^{-3} for one week.

The current study aims at discussing the relevance of these hypotheses on the basis of a review of the most recent studies available in the literature (Curren & Bond, 1980; Sandoval *et al.* 1985; Barlow *et al.* 1995; Martens *et al.* 2005) on the one hand and on the other hand of new laboratory experiments with surrogate powders. The objective of these experiments is to evaluate the amount of airborne particles inside a container of powder falling on an unyielding target.

Three alumina powders are used as surrogates for these laboratory experiments. The corresponding particle size distributions measured with the Coulter technique (based on the equivalent volume diameter) are presented in table 1.

Table 1. Characteristics of the particle size distributions of the alumina powders.

Powders	Mass median diameter (µm)	Geometric standard deviation
G1	4.6	1.4
G2	17	1.3
G3	27	1.5

The container, half filled with powder, is dropped from 1 m height. The particles in suspension are sampled in real-time with an optical particle counter (OPC, Grimm 1.108) using a flexible line which is in vertical position after the drop. The total mass of aerosols is determined by weighing the OPC sampling filter. Figure 1 shows the experimental set-up.

Table 2 gives the results obtained for the three powders and two bulk density (packed and non packed). The results are corrected to take into account the particles settling during the sampling period.

Figure 1. Experimental set-up.

Table 2. Characteristics of the airborne particles after the shock of the container filled with different powders.

Powder	Airborne particles mass (mg)	Initial aerosol concentration (g.m^{-3})
G1 non packed	20.3	8.07
G1 packed	12.4	4.05
G2 non packed	2.90	1.03
G2 packed	0.30	0.10
G3 non packed	0.78	0.26
G3 packed	0.18	0.06

The results obtained show the effects of the particle size distribution and of the powder bulk density on the particles resuspension.

Nevertheless, as the surrogate criterion used in this experiment was limited to the particle diameter, further experiments are necessary to evaluate, in particular, the impact on the results of the cohesive properties of the radioactive powders and of the high density of plutonium or uranium oxide particles.

IAEA (2005). *Regulations for the Safe Transport of Radioactive Material, 2005 Edition Safety Requirements.* Safety Standards Series No. TS-R-1.

Curren, W.D. and Bond, R.D. (1980). *Proc. 6th Int. Symp. on Packaging and Transportation of Radioactive Material:* West Berlin, nov 10-14.

Martens, R., Lange, F., Koch, W. and Nolte, O. (2005). *Forum EUROSAFE*, Brussels, nov 7-8.

Barlow S.V., Donelan P., Tso C.F. (1995). *Proc. 9th Int. Symp. on Packaging and Transportation of Radioactive Material.* Las Vegas, dec 3-8.

Sandoval R.P., Apple M.A., Grandjean N.R. (1985). *Sandia National Laboratories Report : SAND-84-2645;TTC-0537-* 1985 May 01.

T13 Special Session 1

Measurements using broadband cavity-enhanced absorption spectroscopy of the sum of NO₃ and N₂O₅ during REPARTEE II and associated model studies

A.K. Benton[1], J.M. Langridge[1], O. Dessens[1], S.M. Ball[2] and R.L. Jones[1]

[1]Centre for Atmospheric Science, Department of Chemistry, University of Cambridge, CB2 1EW, Cambridge, U.K.
[2]Department of Chemistry, University of Leicester, LE1 7RH, Leicester, U.K.

Keywords: Cavity enhanced absorption spectroscopy, Boundary Layer, Trace Gases, Urban Areas.

Cavity-enhanced absorption spectroscopy enables the unambiguous determination of gas concentrations at trace levels in both laboratory and field atmospheric studies. The versatility of this method has here been applied to the measurement of the nitrate radical (NO_3) absorption band centred at 662nm, corresponding to its $B^2E'-X^2A_2$ electronic transition using broadband cavity-enhanced absorption spectroscopy (BBCEAS) (Ball *et al* 2004; Langridge *et al*, 2006). A heated inlet was used to shift the equilibrium between NO_3 and dinitrogen pentoxide (N_2O_5) to convert all ambient N_2O_5 to NO_3 to allow the sum of these species to be measured. The nitrate radical is rapidly photolysed during the day and generally only builds to appreciable concentrations at night, except for under extremely high O_3 concentrations. NO_3 is the predominant night-time oxidiser of volatile organic compounds and other species. Conversion of NO_3 and N_2O_5 to HNO_3 is also an important NO_y removal mechanism as can be seen in figure 1.
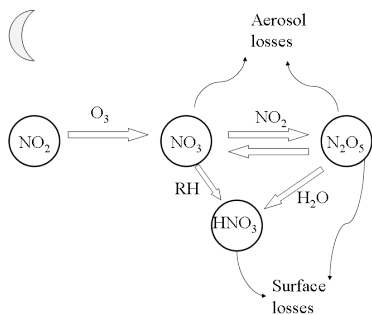
Figure 1 – A simplified schematic of night-time nitrate chemistry and the equilibrium between NO_3 and N_2O_5.

Measurements were made in an urban area at an altitude of 189m on balcony of the 35th Floor of the British Telecommunications (BT) Tower, London, during October and November 2007 as part of the second phase of the Regent's Park and Tower Campaign (REPARTEE II). A BBCEAS instrument, using a ~665nm LED light-source was deployed during this campaign. Calibration of the mirror reflectivity as a function of wavelength was required on a daily basis to account for build up of particulates on the high finesse mirrors although they were purged with nitrogen to reduce this effect. Mirror reflectivity, $R(\lambda)$, was derived from the phase-shift between the cavity output and the modulated LED source. Beer-Lambert retrieval over a range of wavelengths was used to retrieve absorber concentrations in every 10s sample from an absorption spectrum as shown in figure 2.
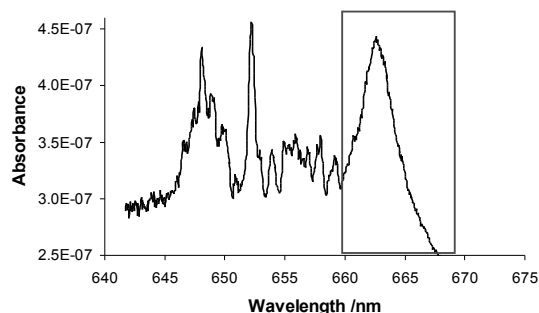
Figure 2 – An example absorbance spectrum from REPARTEE II depicting 4n+d polyad bands of H_2O and the NO_3 absorption band (boxed).

Ancillary measurements of nitrogen dioxide, pressure and temperature were used to infer the NO_3:N_2O_5 ratio. Wall losses have been determined for similar laboratory experiments to be ~20%. The data collated shows large variation in night-time concentrations of the sum of NO_3 and N_2O_5, (the vast majority of this being N_2O_5,) with some very high concentrations measured, often peaking at 1-2ppb with one night (30-31/10/2007) at ~8ppb. These measurements have important implications for the oxidative processes of the night-time boundary layer. Large-scale chemical models such as pTOMCAT currently reproduce the diurnal variability of NO_3 and N_2O_5 concentrations but predict very small concentrations (~2ppt maximum). Box-model studies were used to investigate the chemical scenarios developing such high N_2O_5 concentrations.

Ball, S. M., Langridge, J. M., & Jones, R.L. (2004). *Chem. Phys. Lett.,* 398, 68–74.
Langridge, J. M., Ball, S. M., & Jones, R.L. (2006). *Analyst,* 131, 8, 916-922.

Chemically-speciated aerosol fluxes above three UK cities

G.J. Phillips[1], E. Nemitz[1], R. Thomas[1,2], D. Famulari[1], P. Williams[2], J. Allan2, C. Di Marco[1], H. Coe[2], R.M. Harrison[3] and D. Fowler[1]

[1]Centre for Ecology and Hydrology, Bush Estate, Penicuik, EH26 0QB, UK
[2]School for Earth, Atmospheric and Environmental Sciences (SEAES), University of Manchester, UK.
[3]Division of Environmental Health and Risk Management, School of Geography, Earth and Environmental Sciences, University of Birmingham, UK.

Keywords: aerosol mass spectrometry, eddy covariance fluxes, organic aerosol, urban aerosol, traffic emission.

There is considerable uncertainty regarding the processes controlling the formation and transformation of organic aerosol (OA) in the atmosphere. Regional aerosol, advected into the city, mixes with the primary urban emissions of particles and VOCs to create an environment where particle composition is controlled by a number of factors, not least chemistry and complex urban meteorology. Measurements of chemically-speciated particle fluxes above urban areas can give us insight into exchanges between urban centres and the free troposphere, as well as the chemical and physical processing which occurs during transport.

We present chemically-speciated aerosol fluxes and concentrations measured three contrasting cities in the United Kingdom. An aerodyne quadropole-AMS was deployed on a tall building in the three urban centers; the Nelson Monument in Edinburgh, the Portland Tower in Manchester and the BT Tower in London. We use the coupled eddy covariance-AMS system as described in Nemitz *et al*., 2008 to measure the flux of non-refractory (NR) PM1 above the three cities. Supporting measurements of CO and CO_2 fluxes made by eddy covariance are also presented and emission factors relative to these pollution tracers have been calculated.

The organic aerosol component of the NR-PM1 mass has been further analysed using statistical techniques to ascertain the contribution to the OA flux and concentration of so-called hydrocarbon-like organic aerosol (HOA) and oxygenated organic aerosol (OOA). OA dominates the mass of PM1 in all three cities with nitrate the next major component of the mass in Edinburgh and Manchester and sulfate the next major component in London. HOA dominates the OA mass in Edinburgh and for some time periods in Manchester, in contrast to the finding of Zhang *et al*., for urban areas and situation in London where OOA was the larger proportion of the OA mass.

At all locations, HOA has a large relative emission flux relative to OOA. The HOA fluxes are generally are generally upward and show diurnal trend. Average flux densities of hydrocarbon-like organic aerosol (HOA) range from 63 ng m^{-2} s^{-1} in Edinburgh to 440 ng m^{-2} s^{-1} in London. Excellent correlation was found between emission fluxes of CO and CO_2. However, HOA fluxes show a much weaker correlation with these gases. Changes in the relative emission strengths of HOA and CO_2 are likely related to changes in the fuel mix, vehicle fleet and the changing contribution of building heating. However, the relatively constant CO/CO_2 flux ratio suggests that i) these changes were not pronounced and ii) was without a significant biogenic component; implying the CO_2 emission flux was due mainly to combustion. Assuming that both HOA and CO_2 (and CO) originate from similar sources, the measurements suggest that HOA undergoes considerable processing between emission and measurement of the flux high above the urban centre. The fraction of HOA that is evaporated and/or chemically processed is likely to depend on measurement height, temperature, radiation, photochemistry, and transport time-scale. Nevertheless, as the transport time-scale during these measurements is on the order of minutes to tens of minutes, the flux ratio HOA/CO_2 is likely to be more representative than emission ratios derived from urban concentration ratios, which accumulate over tens of minutes to hours. Emission ratios range from 0.24 to 1.37 g (kg C)$^{-1}$.

Nemitz, E.; Jimenez, J.L.; Huffman, J.A.; Canagaratna, M.R.; Worsnop, D.R.; Guenther, A.B. (2008). *Aerosol Science and Technology*, **42** (8). 636-657.

Zhang et al., (2007). *Geophysical Research Letters*, **34**, L13801, doi:10.1029/2007GL029979

Attribution of Organic Aerosols in UK Cities

J.D. Allan[1], P.I. Williams[1], J. Crosier[1], M.W. Gallagher[2] and H. Coe[2]

[1]National Centre for Atmospheric Science, University of Manchester, Manchester M13 9PL, UK
[2]School of Earth, Atmospheric and Environmental Sciences, University of Manchester, Manchester M13 9PL, UK

Organic matter represents a major fraction of particulates in urban environments, however attempts to quantitatively predict their loadings remains elusive (*Volkamer et al.*, 2006). Part of the problem is that we still lack effective ways of comprehensively and unambiguously characterising the fraction in terms of the compounds present, the functionality and the sources. Recently the technique of positive matrix factorisation (PMF) has been employed for source apportionment of aerosols and this has been shown to be highly useful when used with organic data from the Aerodyne Aerosol Mass Spectrometer (AMS) (*Lanz et al.*, 2007).

Traditionally, organic AMS data in polluted environments has been split into hydrocarbon-like and oxygenated organic aerosols (HOA and OOA) which in turn has been ascribed to primary and secondary organic aerosols respectively (*Zhang et al.*, 2005). The use of PMF, which can deliver many factors, has shown that many more fractions can be identified and quantified. The technique has also benefited from the use of time-of-flight mass spectrometers through the increase in signal-to-noise they provide (*Drewnick et al.*, 2005).

It is known that the importance of various sources and processes vary according to geographical location and meteorology. It is therefore important to characterise the organic aerosols as extensively as possible, using data from multiple measurement campaigns. To this end, this paper presents the analysis from a number of recent studies using time-of-flight AMS instruments, including the REPARTEE experiments in London and CityFlux in Manchester during 2006 and 2007. These data were collected in conjunction with measurements of aerosol number, size distribution, equivalent black carbon mass and single particle composition (using an ATOFMS). Locations used included roadside measurements on a busy bus corridor, roof level in the city centre and urban parkland.

Several differences and similarities were noted between the different datasets. Notably, in addition to the usual HOA, OOA1 and OOA2 factors normally associated with combustion and secondary organic aerosols, an additional factor was isolated that could be associated with cooking, based on diurnal profile and similarity of its mass spectra to previously reported cooking spectra. The fractional contribution of this during the REPARTEE 1 study was comparable to that of the primary organics from the transport sector (figure 1).

The primary factors could also be compared with measurements of carbon monoxide and black carbon to derive emission ratios representative of the sources (using roadside measurements) and the grid-scale cohort emissions (using roof-level measurements).

In common with most urban studies, large contributions from secondary organics were noted. In addition, potential biomass burning signatures were seen in Manchester, possibly coming from sources outside of the city.
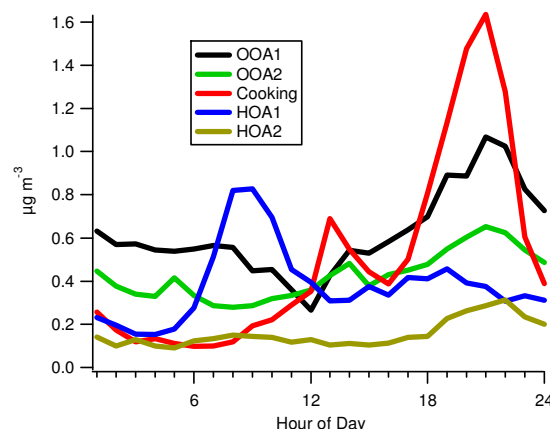

Figure 1: Median diurnal profiles from a 5-factor analysis of the REPARTEE 1 dataset in London.

Drewnick, F., et al. (2005), *Aerosol Sci. Technol.*, *39*, 637-658.
Lanz, V. A., et al. (2007), *Atmos. Chem. Phys.*, *7*(6), 1503-1522.
Volkamer, R., et al. (2006), *Geophys. Res. Lett.*, *33*(17), 4.
Zhang, Q., et al. (2005), *Environ. Sci. Technol.*, *39*(13), 4938-4952.

Real time chemical characterisation of aerosols via ATOFMS and ToF-AMS during REPARTEE I

M. Dall'Osto[1,2], Roy M. Harrison[1], J. Allan[3], P. Williams[3], H. Coe[3] and Eiko Nemitz[4]

[1]National Centre for Atmospheric Science, University of Birmingham, Birmingham, UK
[2]Centre for Climate & Air Pollution Studies National University of Ireland, Galway, Galway Ireland
[3]National Centre for Atmospheric Science, The University of Manchester, Manchester, UK
[4] Centre for Ecology & Hydrology (CEH), Edinburgh, UK

Keywords: Aerosol Mass Spectrometry, On Line Measurements, AMS, Aerosol Chemistry, Mixing State

The advent of techniques of particle mass spectrometry offers great insights into the source apportionment and atmospheric chemistry of aerosols. The aerosol time-of-flight mass spectrometer (ATOFMS) offered by TSI provides information on a polydisperse aerosol, acquiring precise aerodynamic diameter (±1%) within the range 0.3 to 3 micrometres and individual particle positive and negative mass spectral data in real time. The AMS (Aerodyne Research, Inc.) provides online, real time measurements of the mass of non-refractory components of aerosol particles as function of their size. ATOFMS is capable of single particle analysis, whilst AMS requires the collection of an ensemble of particles to obtain sufficient sample for analysis. However, the AMS can quantify the size resolved organic carbon, sulphate, ammonium and nitrate mass loadings of aerosol in the size range between 60 and 600 nm. The data shown herein were collected at Regents Park (London-October 2006) during the REPARTEE I project. The general overview of the findings of the two particle mass spectrometers will be presented elsewhere. Herein, three main key findings will be presented.

1. The ATOFMS classified two types of nitrate-containing particles; one being formed locally, the other regionally transported from continental Europe. Local nitrate was formed at nighttime. AMS nitrate mass loading and ATOFMS total nitrate containing particles showed a very good correlation. The ATOFMS showed that the LRT nitrate particle type exhibits a diurnal temporal variation, evaporating during the day due to the higher temperature. However, the core of the LRT nitrate containing particles is still detected during the day and is composed mainly of elemental carbon and sulphate with a size distributions shifted towards smaller particles.

2. A fog event was monitored with state-of-the art real-time aerosol mass spectrometers in an urban background location in London (England) during the REPARTEE-I experiment. Specific particle types rich in hydroxymethanesulphonate (HMS) were found only during the fog event. Formation of inorganic and organic secondary aerosol was observed as soon as fog was detected and two different mechanisms are suggested to be responsible for the production of two different types of aerosol. Nitrate aerosol is produced in the liquid phase within fog droplets. Contrary to previous studies, the formation of HULIS was observed on interstitial particles but not in evaporated fog droplets, suggesting heterogeneous formation mechanisms depending on parameters other than the water content and not fully understood. Not only are secondary aerosol constituents produced during the fog event, but the primary aerosol is observed to be processed by the fog event, dramatically changing its chemical properties.

3. The application of the ART-2a neural network algorithm to the ATOFMS data characterized a specific particle type (rich in secondary organic aerosol and polycyclic aromatic compounds; SOA-PAH). The temporal trend of this particle type presented a strong weekday-weekend variation, suggesting a strong link with traffic emissions. Comparisons with several other measurements taken during the REPARTEE-I (including positive matrix factorization (PMF) analysis of the AMS data) excluded local primary anthropogenic sources. ATOFMS single particle mass spectra revealed a strong component of oxidized organic carbon, associated with PAH signals and flavonoids. This particle type was internally mixed with strong acidic sulphate species, but not with nitrate. Moreover, this particle type was found peaking only during the warmest part of the day (11.00-14.00) and is therefore thought to be influenced by photochemical reactions in the particle phase. The SOA-PAH particle type, rich in flavonoids, could suggest a mechanism for production of secondary organic aerosol from gas-phase reactions of PAH.

ACKNOWLEDGEMENTS

The effect of boundary layer dynamics on the aerosol size distributions over London

M. Dall'Osto[1,2], J. F. Barlow[3], Roy. M. Harrison[1], D. Beddows[1] and T. Dunbar[3]

[1]National Centre for Atmospheric Science, University of Birmingham, Birmingham, UK
[2]Centre for Climate & Air Pollution Studies National University of Ireland, Galway, Galway Ireland
[3]Department of Meteorology, University of Reading, Reading, UK

Keywords: Lidar, SMPS, Aerosol Size Distributions, Urban Aerosols, Boundary Layer

Urban air pollution is one of the environmental problems of major concern and will, due to growing urbanization, probably become more and more important in the future. So much that air pollution is a typically urban problem, so little is known concerning the flow and dispersion characteristics over urban surfaces. Lidar permits the detection of the BL top with a vertical resolution of a few meters and a temporal resolution in the range of seconds to minutes.

The lidar instrument used on the REPARTEE II campaign was a Halo Photonics 1.5 micron scanning Doppler lidar (provided by UFAM and operated by the University of Salford). It was installed in the car park of the University of Westminster building on the Marylebone Road and was running continuously for three weeks between the 24th of October and the 14th November 2007. Due to the proximity and height of the neighbouring buildings, the lidar was restricted to making only vertical stare measurements i.e. directly upwards. During this study the lidar had a vertical resolution of 30 metres, with 66 gates measuring up to 2 km into the atmosphere. The lidar returns a measurement every about 4 s consisting of 20,000 'integrations', or accumulated signals and it was restricted to vertically pointing measurements. However, different measurements were possible, including aerosol layer top, boundary layer top, convective mixing layer height, turbulent mixing layer height

Moreover, during the REPARTEE-II, 3 SMSP systems were used simultaneously at the road, park and tower sites. The SMPS systems were deployed concurrently at the three locations measuring particles with diameters over the size range 15.1 to 661 nm. The same SMPS models were used in Regents Park and on the BT tower (namely, DMA TSI 3080 and CPC TSI 3022A), which were different to that used at the Marylebone Road (namely, DMA TSI 3080 and CPC TSI 3776). The 3 different systems were inter-compared and particle losses due to different sampling lines were obtained and data were corrected accordingly. Measurements were made concurrently at the 3 different sites at similar time resolution (5 minutes interval at RP and BT; 10 minutes interval at MR).

The field study was conducted between 17-10-07 and 09-11-07, and approximately 7000 SMPS size distributions were measured. These size distributions were averaged over 6 hour intervals (00-06, 06-12, 12-18, 18-00) reducing their number from 20,000 to 259, which were subsequently normalised by their vector-length and cluster analysed. The Dunn-Index for the results of the K-means cluster analysis for different cluster numbers showed a clear maximum for 15 clusters, some of which belonged only to specific sampling sites and to specific time of the day. The intensive observations of aerosols, trace gases and boundary layer dynamics were used to quantify the variability in urban aerosols due to both chemical and meteorological processes. The 15 clusters were composed of unique particle size distributions, and they were analyzed along with the urban boundary layer (UBL) dynamics obtained with the lidar.

Different case studies are presented including:

1. A higher particle number concentrations of nano particles (<50nm) was observed at the tower (170m above the city of London) during days affected by higher turbulence, implying a clear transport of freshly emitted traffic related particles from the ground to the upper part of the UBL.

2. A more uniform particle size distributions along the 3 sites were observed during shallow UBL conditions, implying that the urban aerosols were mixed along the shallow UBL and so the tower site was more affected by local aerosol emissions.

3. Clear conditions of UBL decoupling between the ground sites and the tower site caused the particle size distributions between being different between the 2 conditions. The tower site was characterised by long range transport particle size distributions, whilst the ground sites one by more urban-like ones.

Remarkable dynamics of nanoparticle in the urban atmosphere

M. Dall'Osto[1,2], Roy M. Harrison[1], A. Thorpe[1], P. Williams[3] and H. Coe[3]

[1]National Centre for Atmospheric Science, University of Birmingham, Birmingham, B15 2TT, UK
[2]Centre for Climate & Air Pollution Studies National University of Ireland, Galway University Road Galway Ireland
[3]School of Earth, Atmospheric & Environmental Sciences, The University of Manchester, Manchester, M13 9PL, UK

Keywords: Urban Aerosol, Aerosol Size Distribution, Aerosol Evolution, SMPS, Ultrafine Aerosols

Nanoparticles emitted from road traffic are the largest source of respiratory exposure for the general public living in urban areas. It has been suggested that adverse health effects of airborne particles may scale with airborne particle number, which if correct, focuses attention on the nanoparticle (less than 100 nanometre) size range which dominate the number count in urban areas.

During the REPARTEE field campaigns held in London each for four weeks in October 2006 and September 2007, measurements of particle number concentrations were made using condensation particle counters, and number size distributions using Scanning Mobility Particle Sizers at sampling sites located in the centre of Regents Park (of the order of 700 metres from major highways), and at a height of 170 metres above ground level on the BT Tower (1.2 km horizontally from the Regents Park site). Additionally, information collected at the urban central background site at London, North Kensington, and the roadside sampling site of London Marylebone Road which has traffic flows of around 70,000 vehicles per day and provides the main southern boundary to Regents Park and runs between Regents Park and the BT Tower were used.

The average diurnal pattern of particle number count at all four sites clearly showed a gradient in number concentrations from Marylebone Road, peaking at around 100 x 10^3 cm^{-3} to Regents Park (around 38 x 10^3 cm^{-3}), London, North Kensington (25 x 10^3 cm^{-3}) and the BT Tower (9 x 10^3 cm^{-3}). The high ratio in particle number concentrations between the ground-based sites and the BT Tower could not be explained by dispersion processes alone.

Further evidence on this phenomenon were derived from a comparison of particle size distributions at three sites (Figure 1).
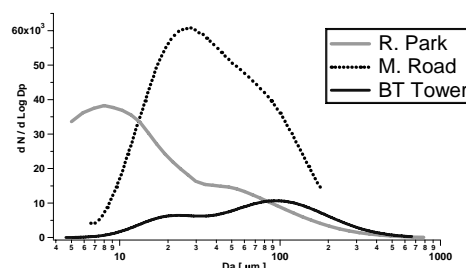
Figure 1. Average particle size distributions (mobility diameter, nm) at Marylebone Road, Regents Park and BT Tower.

The size distribution measured at Marylebone Road was typical of roadside and on-road number size distributions, peaking between 20 and 30 nm diameter. In contrast, data from the Regents Park site showed a mode which had shifted downwards to below 10 nm diameter together with some overall loss of area under the curve representing a loss of total particle number.

When a curve-fitting programme was used to disaggregate these size distributions into a number of log-normal distributions, the results suggested that even within the urban atmosphere, on distance scales of the order of 1 km and travel times of around 5 minutes upon moving away from major emissions sources very significant loss of the nanoparticle fraction is observed which manifests itself in a shift to smaller sizes within Regents Park and an almost complete loss of the sub-30 nanometre mode at the BT Tower site.

ACKNOWLEDGEMENTS

REPARTEE-I and REPARTEE-II
(Regent's Park and Tower Environmental Experiment)

Roy M. Harrison[1], M. Dall'Osto[1,12], M. Gallagher[2], P. Williams[2], H. Coe[2], J. Allan[2], E. Nemitz[3], G. Phillips[3], R. Jones[4], J. Barlow[5], A. Thorpe[1], W. Bloss[1], A. Benton[4], C. Di Marco[3], S. Ball[11], C. Martin[2], A. Lewis[6], D. Martin[7], F. Davies[8], R. Kinnersley[9], D. Green[10]

[1]National Centre for Atmospheric Science, University of Birmingham, Birmingham UK
[2]National Centre for Atmospheric Science, The University of Manchester; UK
[3]CEH Edinburgh; UK
[4]University of Cambridge; UK
[5]University of Reading; UK
[6]University of York; UK
[7]University of Bristol; UK
[8]University of Salford; UK
[9]Environment Agency; UK
[10]King's College; UK
[11]University of Leicester, UK
[12]NUI Galway, Ireland

Keywords: (Urban Aerosol, Aerosol Chemistry, Aerosol Evolution, Air Quality, Airborne Particles)

This project brought together NCAS (National Centre for Atmospheric Science) scientists to study atmospheric chemical processes, and particularly those affecting atmospheric aerosol, in London by using the following sampling platforms:

- the BT tower at an elevation of 170 metres above ground level.
- adjacent Regents Park where ground level measurements were made.
- Marylebone Road at roadside in the street canyon.

Two air sampling campaigns were carried out throughout the months of October 2006 and October/November 2007. The objectives of the two campaigns were:

1. To understand the fate of traffic-generated nano-particles in the urban atmosphere
2. To determine fluxes of trace gases and particles above central London
3. To use the vertical and horizontal separation of sampling sites to study the evolution of chemical composition and physical properties of particles
4. To study the chemical properties and formation mechanisms of major components of airborne particles (especially nitrogen-containing)

A wide range of measurements were taken including:

REPARTEE I (2006)

- Particle and gas fluxes were measured at the elevated site (AMS, CPC, GRAEGOR, O3, SO2, NOx, CO, CO2)
- Real time chemical composition of aerosol by particle mass spectrometry at the park (AMS, ATOFMS).

- 24-hours size resolved PM chemical composition with MOUDI and Partisol at the park and at the tower.
- Size distribution of particulate matter with SMPS and APS in order to describe the evolution of the traffic component vertically and horizontally at the 3 sites.
- Fluorocarbon tracer sampler release from the park

REPARTEE II (2007)

The REPARTEE I results added some more objectives, addressed with additional instrumentation deployed during the REPARTEE II:

- LIDAR, deployed near the road site in order to to describe the atmospheric boundary-layer (ABL) structure.
- NO3/N2O5 CEAS system at the tower in order to elucidate the nitrate chemistry.
- Nano-SMPS at the tower in order to monitor the fate of the nano particles.

An overview of the 3 monitoring sites, including instrumentation used, method of aerosol sampling will be presented together with an overview of results.

ACKNOWLEDGEMENTS

Physico-Chemical Aerosol Dispersion in Urban Environments

Tay, B.K.[1], McFiggans, G.M. [1], Gallagher, M.W.[1], Martin, C.[1], Flynn, M.J. [1], Harris, P. [2], Lindley, S. [2], Agius, R.[3], Harrison, R.M. [3].

[1]Centre for Atmospheric Science, SEAES, University of Manchester, Manchester, M13 9PL, UK.
[2]School of Gography, University of Manchester, Oxford Road, Manchester, M13 9PL, UK.
[3]School of Occupational & Environmental Health, University of Manchester, Manchester, M13 9PL, UK.
[4]University of Birmingham, Birmingham, UK.

Keywords: Aerosol Dynamics, Air Pollution, CFD, Chemical properties, Fluxes

The spatial heterogeneity of urban street canyons and the complex interplay of chemically, spatially and temporally varying ultrafine particle emission sources as a function of micrometeorological and meteorological factors represents a challenge to both computational fluid dynamical modelling approaches and field observations. Intensive measurement campaigns or networks generally have insufficient spatial resolution or temporal resolution respectively to adequately represent the entire vertical or horizontal spatial structure of aerosol and these must be informed by numerical dispersion modeling combined with realistic aerosol physico-chemical descriptions to be of benefit to epidemiological studies. Predictions of vertical and horizontal structure of aerosols in street canyons are therefore required to inform future directives regarding recommended sampling and monitoring protocols.

Here we compare first-order eddy viscosity turbulence closure CFD predictions with recent measurement results demonstrating the impact of different relative contributions of convective and turbulent diffusivities on aerosol distribution profiles at different locations within street canyons.

We describe preliminary results with a CFD model where we have incorporated more realistic aerosol processes such as condensation and coagulation by oxidation and condensation of hydrocarbon species. We examine how these processes influence the vertical and horizontal distributions of aerosol parameters.

From the dynamical perspective we investigate the different factors that influence the aerosol exchange velocity between street canyons and the urban boundary layer above. Both vertical turbulent fluxes as well as the fluxes due to mean flow are shown to contribute to the overall ventilation characteristics of a street canyon.

We then compare emission velocity structure within and above the canyon and compare these with observations, e.g. Longley et al. (2004). We then discuss these in context with tower based micrometeorological flux measurements that were obtained from the CITYFLUX and REPARTEE studies, Martin et al. (2009).

Whilst undoubtedly crude these comparisons may be used as a starting point for linking street level concentrations to those measured above the urban roughness layer e.g. on large scale micrometeorological flux measurement towers as used in REPARTEE and CITYFLUX with potential for validating high resolution regional scale air quality models.

How such approaches can be used to facilitate parameterizations suitable for other modelling platforms such as those that are more appropriate to the epidemiological study domain still remains a challenge. Again as a starting point we discuss potential linkages with ultrafine aerosol affinity zones, Harris et al. (2009), which can be derived using Geographical Information Science tools (GISc) model techniques. These zones require city specific validation. While this can be achieved partly by traditional sampling networks coupled with intensive micrometeorological canyon flux observations, these are expensive. There is potential cost benefit therefore to using area averaged flux footprint databases, determined by long term large tower based micrometeorological measurement systems, to inform many of these modeling approaches.

Harris, P., et al. (2009). Identification and verification of ultrafine particle affinity zones in urban neighbourhoods. NERC Environment and Human Health ProgrammeAnnual Science Day Conference & Workshop, Univ. Birmingham, February 2009

Longley, I.D., Gallagher, M.W., Dorsey, J.R, Flynn, M. (2004). A case-study of fine particle concentrations and fluxes measured in a busy street canyon in Manchester, Atmospheric Environment, 38 (22):3595-3603.

Martin, C., et al. (2009). Ultrafine particle fluxes above four major European cities. Atmospheric Environment (In Press ATMENV-D-08-00249R1).

Lidar data analysis from REPARTEE II campaign

T. M. Dunbar[1], J. F. Barlow[1] and C. R.Wood[1]

[1]Department of Meteorology, University of Reading, United Kingdom, RG

Keywords: aerosol dynamics, meteorology, mixing layer, lidar, urban areas

The atmospheric boundary layer is multi-structured, and the presence of an urban surface below makes this structure more complex. The varying surface types present within an urban landscape can cause the formation of internal layers with differing turbulence regimes within. These different layers can have significant effects upon the vertical mixing of aerosol throughout the lower atmosphere both in terms of height and velocity. Doppler lidars are the ideal instrument for examining the structure of the boundary layer, as they give us information on both the location of aerosols within the layer and the turbulent motion taking place. A doppler lidar was deployed during the REPARTEE II campaign and the data gathered has been analysed in terms of the dynamics of the boundary layer, concentrating in particular upon the identification of different layers within the boundary layer and the effect these have upon transport of aerosols.

The REPARTEE project aimed to compare aerosol measurements made at the surface at Regent's Park, to measurements from the top of the BT Tower (at 190m), and thereby study the transport and transformation of aerosols within the layer. As part of the experiment, the UFAM doppler lidar operated continuously for three weeks between the 24th of October and the 14th of November 2007. It was positioned on the Marylebone road near to Regent's Park, London .

Figure 1. below shows a time-height plot of lidar backscatter on a typical convective day during the REPARTEE campaign. Plotted on top of this are the mixing layer height, determined from meaurements of the vertical velocity variance, and the heights of two different aerosol layers, determined from the backscatter. During the daytime, from 0900 to 1700, the mixing layer grows from the surface to the top of the boundary layer, indicating the depth of vertical mixing present due to convective turbulence. After 1700, the lack of surface heating causes the mixing layer depth to return to the surface. During the preceding night, from 0000 to 0900, although there is little convective mixing present, there is a distinct layer of aerosol adjacent to the surface, indicating a stably stratified nocturnal layer, with some mixing present due to shear turbulence.

The lidar measurements have also been compared to those taken by the sonic anemometer at the top of the BT Tower. At night-time, discrepancies between the levels of turbulence at this height can be interpreted as the presence of a stable layer forming over Regents Park. This decoupling of the turbulence between the surface and aloft can be linked to the differing evolution of aerosol species measured at the two heights.
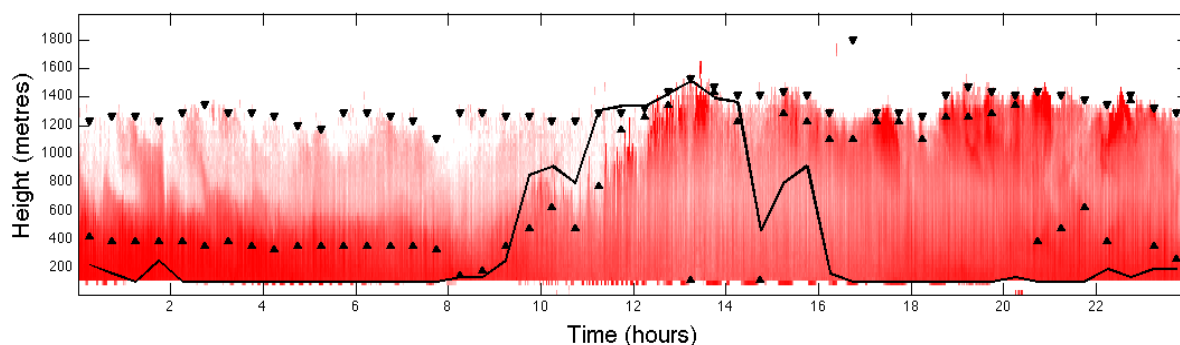

Figure 1: The backscatter detected by the lidar on the 6th of November, 2007 during the REPARTEE II campaign. Plotted on top are the heights of different aerosol layers as detected using the lidar measurements of backscatter (upward and downward pointing triangles) and the mixing layer height measured using the variance of the vertical velocity (solid line).

Nitrate Dynamics in UK Urban Environments

E. Nemitz[1], G.J. Phillips[1], R. Thomas[1,2], C.F. Di Marco[1], S. Tang[1], H. Coe[2], J. Allan[2], R.M. Harrison[3] and D. Fowler[1]

[1]Centre for Ecology and Hydrology, Penicuik, EH26 0QB, UK
[2]School for Earth, Atmospheric and Environmental Sciences (SEAES), University of Manchester, UK.
[3]Division of Environmental Health and Risk Management, School of Geography, Earth and Environmental Sciences, University of Birmingham, UK.

Nitrate makes a significant contribution to the concentration of $PM_{2.5}$ and PM_{10} with important implications for human health and regional climate forcing. This is particularly true for NW Europe, where large emissions of NH_3 and NO_x combine with comparably low temperatures and high relative humidities to create conditions that favour the production of NH_4NO_3. Despite its importance, most atmospheric chemistry models are still not modelling NH_4NO_3 very well, indicating that dynamics are still not represented correctly. In addition, due to its changing equilibrium, there are processes which operated at a sub-grid scale and are therefore difficult to simulate.

In this presentation we review new evidence on nitrate dynamics in urban environments, drawing on data from recent urban field studies, mainly, but not exclusively, in the UK. This new look is enabled through the use of new measurement technology such as Aerosol Mass Spectrometry (AMS), urban eddy-covariance flux measurements of aerosol chemical compounds and long-term nitrate measurements.

We quantify the relative contribution NH_4NO_3 to the UK aerosol, reviewing the existing UK AMS database and data from UK and European denuder/filter-pack networks.

Paired long-term measurements of aerosol concentrations in and outside of two UK urban areas (London & Edinburgh; Tang *et al*., 2008), have provided information on the urban NO_3^- increment. The measurements indicate that, on average:

$$NO_3^-(\text{urban}) = 1.13 \times NO_3^-(\text{rural}) + 0.58 \ \mu g \ m^{-3},$$

with somewhat larger increments during the winter months than during summer.

Measurements of the size-distributions of sub-micron non-refractory NO_3^- by aerosol mass spectrometry frequently show periods of a NO_3^- size mode in the range 100 to 300 nm, in addition to the accumulation mode at 300 to 800 nm. This suggests that NO_3^- is formed by condensation on the combustion mode which is prevalent near traffic sources. The fine NO_3^- mode is sporadically observed, and appears to correlate with cold, humid conditions and atmospheric inversions.

The role of urban areas in producing NH_4NO_3 is further supported by the growing database of aerosol chemical compounds above urban areas, by aerosol mass spectrometry (e.g. Nemitz et al., 2008), which suggests emission of NO_3^- from most cities, which is nevertheless highly variable between days (unlike the emission of organic aerosol).

Vertical gradient measurements above the city centre of London during the REPARTEE campaign (comparing measurements on the Telecom tower at 165 m with ground-based urban background measurements) show higher NO_3^- concentrations on the tower, possibly due to colder temperatures at higher heights shifting the gas/aerosol equilibrium towards the aerosol phase.

We also present evidence that the fate of NH_4NO_3 is affected by its dissociation potential. In warm conditions, NH_4NO_3 volatilises during the deposition process to semi-natural vegetation near the ground, where temperatures are raised and concentrations of NH_3 and HNO_3 lowered due to deposition. This greatly increases the effective deposition rate of NH_4NO_3 aerosol and greatly decreases its atmospheric lifetime. Since this volatilisation near the ground cannot be resolved by current CTMs, it is suggested that effective deposition rates need to be incorporated into models to account for this effect.

Nemitz, E.; Jimenez, J.L.; Huffman, J.A.; Canagaratna, M.R.; Worsnop, D.R.; Guenther, A.B. (2008). *Aerosol Science and Technology*, **42** (8). 636-657.

Tang, Y. S.; Sutton, M. A.; Simmons, I.; Love, L.; Vogt, E.; van Dijk, N.; Cape, J. N.; Smith, R. I.; Armas-Sanchez, E.; Lawrence, H.; Hayman, G. (2007). Monitoring of nitric acid, particulate nitrate and other species in the UK-2006. Interim report under the UK Acid Deposition Monitoring Network to NETCEN/DEFRA. Edinburgh, Centre for Ecology and Hydrology, 26pp.

T15 Special Session 3

Evaporative loss of accumulated semi-volatile liquid aerosol from fibrous filter

B. Sutter[1,2], J.C. Appert-Collin[2], D. Bémer[1] and D. Thomas[2]

[1]INRS, Rue du Morvan, CS 60027, 54519 Vandoeuvre Cedex, France
[2]LSGC-CNRS, University of Nancy, 1 rue Grandville BP 20451, 54001, Nancy Cedex, France

Keywords: Aerosol filtration, Fibrous filter, SVOC, Evaporation, Droplets.

The evaporative loss of Semi-Volatile Organic Compounds (SVOC) is well known by the scientific community of the atmosphere (Furuuchi *et al.*, 2001). Regarding the occupational field, to prevent the exposure of employees and to assess the atmospheric concentrations of semi-volatile liquid aerosols like metalworking fluids (Raynor & Leith, 1999) or pesticides, filtration on fibrous filters is commonly used. The collected aerosol can evaporate while the filtration is in progress. As a consequence, workers are exposed to vapours produced by the clogged filter, and the assessment samples results have a strong negative artefact.

This study aims to provide experimental data to better understand and to model the behaviour of a semi-volatile liquid aerosol collected on fibrous filters.

The evaporation behaviour of semi-volatile models aerosols composed by pure and mixed heavy alkanes (from C_{14} to C_{16}) is investigated with different masses and sizes of aerosols. Tested aerosols are collected on Whatman quartz fibrous filters QM-A before clean air is forced to pass through the clogged filters. The vapours produced by the clogged filters are adsorbed on activated charcoal sample tubes and then desorbed for quantification by a gaseous phase chromatography with a FID detector. This analytical method gives us the vapour concentration at time t of each component initially present in the collected aerosol. The results are compared and confronted with the theoretical model based on thermodynamics laws and the model of Furuuchi *et al.* (2001).

Results in figure 1 show that evaporation occurs in three steps whatever the initial mass of aerosol or the diameter of the droplets collected are. Models from the literature do not correctly predict the behaviour of tested aerosols. Some differences, between theoretical assumptions of the models and MEB observations (figure 2) on the shape of drops deposited on fibres, are assumed to be the major effect that causes the discrepancy.

However, the evaporation of aerosols composed by a mix of three alkanes are in great agreement with thermodynamics models (UNIFAC) for the first step of evaporation (results not plotted here). It is not the case for the two last steps.

This study will carry on the identification of the governing parameters of the evaporation and the development of theoretical model in accordance with the experimental results.
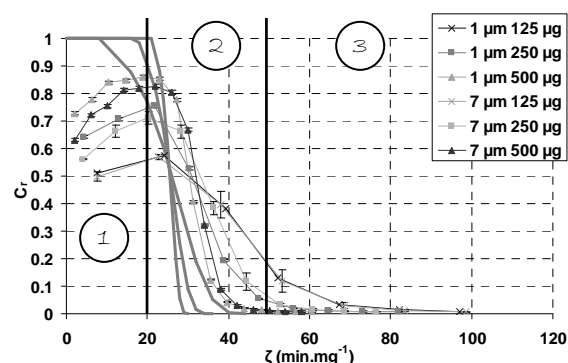

Figure 1. Evaporation of n-hexadecane aerosol collected on a Whatman QM-A filter for different initial masses and diameters. C_r = Vapours concentration (t) / Saturation vapours concentration. ζ = time [min] / Initial mass of aerosol deposed [mg].
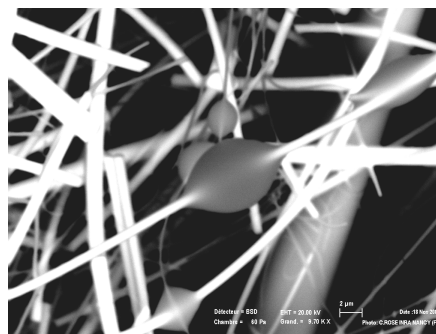

Figure 2. MEB observation of n-hexadecane droplets deposited on quartz fibres of a Whatman QM-A filter.

Furuuchi, M., Fissan, H., Horodecki, J. (2001), *Evaporation behavior of volatile particles on fibrous filter flushed with particle-free dry air*, Powder Technology, 118, pp. 171-179.

Raynor, C., & Leith, D. (1999). *Evaporation of Accumulated Multicomponent Liquids from Fibrous Filters*, Ann. Occup. Hyg., Vol 43, N°3, pp. 181-192.

Role of nitrogen-containing organics in secondary aerosol formation – identification of methylamine in ambient 31 nm – particles by ion trap TDCIMS

A. Held[1,2], G.J. Rathbone[2] and J.N Smith[2]

[1]Institute for Tropospheric Research, Leipzig, Germany
[2]Atmospheric Chemistry Division, National Center for Atmospheric Research, Boulder, 80303 CO, USA

Many reaction mechanisms and chemical species in secondary aerosol formation are still unknown. Nitrogen-containing organic compounds may play a key role in secondary aerosol formation events. For example, Barsanti et al. (2008) suggest that amines may be an important contributor to particle growth through the formation of organic salts, while one would not expect a contribution of low-molecular weight amines to condensational growth.

The ability to characterize the molecular constituents in freshly nucleated particles is one of the greatest challenges to improve our understanding of new particle formation and growth. However, rapid timescales for aerosol growth require measurements to be made at temporal resolutions as small as 10 minutes. Due to the small size of nucleation particles, samples of only a few ng or pg are collected. These small sample amounts require highly sensitive analytical techniques, and minimum exposure to potential contamination sources.

Thermal desorption chemical ionization mass spectrometry (TDCIMS) has been designed specifically to meet the requirements of nucleation particle characterization. Previously, TDCIMS has been applied successfully to measure chemical compounds of atmospheric particles in the 6 – 20 nm diameter range (Smith et al., 2004). Here, we report first experimental results of the chemical characterization of ambient 31 nm – particles with a new thermal desorption chemical ionization ion trap mass spectrometer (Held et al., 2009).

Atmospheric particles are size-classified and collected using a unipolar charger, a radial differential mobility analyzer and an electrostatic precipitator, and analyzed after thermal desorption and chemical ionization using an ion trap mass spectrometer. The ion trap mass spectrometer allows fast scans of the entire mass spectrum every 0.5 s and bears the potential to identify unknown organic compounds by tandem mass spectrometry. Particle collection efficiencies range from 90–100% for particles 25 nm in diameter and smaller to about 50% for 40 nm particles. In the current configuration, the absolute sensitivity of the instrument with regard to ammonium is in the range of 10–100 pg NH_4^+.

In ambient samples collected in the Colorado Front Range in December 2007, NH_4^+ was the major signal peak in the positive ion spectrum. In addition, minor signals and signal patterns of organic compounds were found including methylamine, dimethylamine and trimethylamine.

Another remarkable feature of the observed mass spectra was a wave pattern of signal strength in the mass range above m/z = 100. A closer investigation of these signals revealed a distance of 14 amu between the peaks and valleys, thus indicating a pattern of organic compounds varying in their number of CH_2 groups.

These findings add to recent studies indicating that organics contribute to the growth of newly formed particles, and likely include nitrogen-containing compounds such as amines.

Barsanti, K.C., McMurry, P.H., Smith, J.N. (2008) The potential contribution of organic salts to new particle growth. Atmos. Chem. Phys. Discuss. 8, 20723-20748.

Held, A., Rathbone, G.J., Smith, J.N. (2009) A thermal desorption chemical ionization ion trap mass spectrometer for the chemical characterization of ultrafine aerosol particles. Aerosol Sci. Technol. 43, 264 – 272.

Smith, J.N., Moore, K.F., McMurry, P.H., and Eisele, F.L. (2004) Atmospheric measurements of sub-20 nm diameter particle chemical composition by thermal desorption chemical ionization mass spectrometry. *Aerosol Sci. Technol.* 38, 100-110.

Comparison of 4 temperature protocols for differentiating between OC and EC in thermal-optical transmission analysis of aerosol samples collected on quartz fibre filters

W. Maenhaut, X. Chi and S. Dunphy

Dept. of Anal. Chem., Inst. for Nuclear Sci., Ghent University, Proeftuinstraat 86, BE-9000 Gent, Belgium

Keywords: carbonaceous particles, organic carbon, elemental carbon, urban aerosols, biomass burning.

It is well-known by now that the results for organic carbon (OC) and elemental carbon (EC) in aerosol samples depend upon the technique used and that for the same technique, such as the thermal-optical transmission (TOT) technique, they are dependent upon the operational parameters, and in particular on the analysis temperature program (Schauer *et al.*, 2003). In 2003-2004 we examined the EC/OC split of three different temperature programs for samples from widely different origin, thereby using two different TOT instruments from Sunset Lab (Maenhaut *et al.*, 2004). The three analysis temperature programs were (1) our "standard" program (ST), which is the program that we used in the aerosol carbon round robin (Schmid *et al.*, 2001), (2) a program called NIOSH2 (N2), which is very similar to the ACE-Asia base case program of Schauer *et al.* (2003), and (3) a program called ACE-Asia alternate3 (A3), which is identical to the one used by Schauer *et al.* (2003) and is a proxy for the IMPROVE program. The maximum temperatures during the first stage (in pure He) of the analysis for the three different programs are 900, 870, and 550°C, respectively, and the durations of the three programs, including the CH_4 internal calibration phase, are 620, 775, and 780 s, respectively. Currently, work is being done within Europe and within the EU project "European Supersites for Atmospheric Aerosol Research" to arrive at an improved protocol, and a protocol EUSAAR 2 (E2) has been defined. The maximum temperature during the first stage of the analysis in E2 is 650°C and the total duration of this program (including internal calibration) is 1170 s. We examined the performance of this E2 protocol for a subset of the samples of our earlier study, again for our two TOT instruments. The subset of samples consisted of PM2.5 samples from a 2003 winter campaign in Ghent, TSP samples collected during 2003 in Beijing, TSP samples from southern Austria taken in 1999, and PM2.5 samples from a 2003 summer campaign at K-puszta, Hungary, and from a pasture site in Amazonia taken in 2002 during the dry (biomass burning) season. All samples had been collected on quartz fibre filters (pre-fired Pall filters in the case of the PM2.5 samples). A summary of the various data obtained with our instrument B for the sample subset mentioned above is given in Table 1. For the urban samples from Ghent, rather similar EC/TC ratios were obtained with programs ST and N2, whereas A3 and E2 provided substantially larger ratios. For the rural samples from Austria and K-puszta and the biomass burning impacted samples from Amazonia, low EC/TC ratios were observed with the program ST. For the Austrian samples, there was less difference between the EC/TC ratios from the various protocols than was the case for the urban samples from Ghent and Beijing, whereas for samples from K-puszta, the differences in EC/TC ratios of the various protocols were fairly similar to the differences observed for the urban samples. The largest differences in EC/TC ratios between the four protocols were observed for the biomass burning impacted samples from Amazonia, which exhibited the lowest EC/TC ratios with our protocol ST. For each of the 5 sample sets there is clearly an inverse relationship between the EC/TC ratio and the maximum temperature in stage 1, with ST providing the lowest EC/TC ratio and A3 giving the largest.

Maenhaut, W., Dong, S., & Chi, X. (2004). *Eighth Int. Conf. on Carbonaceous Particles in the Atmosphere*, Vienna, Austria, Abstr. Book, p. 80.

Schauer, J.J., et al. (2003). *Environ. Science & Technol.* 37, 993-1001.

Schmid, H., et al. (2001). *Atmos. Environ.* 35, 2111-2121.

Table 1. Ranges for TC and for EC/TC, obtained with our program ST, and mean ratios (and assoc. st. dev.) to program ST for EC/TC for programs N2, A3, and E2 for 5 series of aerosol filter samples and instrument B. The ratios to ST for EC/TC were calculated per sample and then averaged over all samples of the same series.

Sample series	no. of samples	Range TC ($\mu g/cm^2$)		Range EC/TC		Mean ratios to program ST for EC/TC					
						N2		A3		E2	
Ghent	26	15 – 110	0.084		–0.35	1.04	±0.14	1.72	±0.26	1.70	±0.41
Beijing	5	71 – 240	0.15		–0.24	1.15	±0.05	2.02	±0.45	1.72	±0.20
Austria	16	18 – 40	0.076		–0.13			1.53	±0.24	1.21	±0.25
K-puszta	5	16 – 25	0.038		–0.056	1.38	±0.02	1.92	±0.15	1.51	±0.15
Amazon	5	57 – 98	0.021		–0.031	1.35	±0.07	2.90	±0.31	2.67	±0.43

Energy saving and pollution reduction of industrial boiler by using methanol- and isopropanol-contained wastewater emulsified heavy fuel-oil

Sheng-Lun Lin and Wen-Jhy Lee[*]

[*]Department of Environmental Engineering
National Cheng Kung University, Tainan 70101, TAIWAN
wjlee@mail.ncku.edu.tw

Keywords: emulsion, boiler, fuel oil, PM, wastewater.

With the increasing consumption of petroleum fuel, air pollutant emission was considered as a major problem. Boiler is commonly used (over 6000 sets) as a heating device in Taiwan. Three major fuel of boiler are coal, heavy fuel-oil (HFO), and natural gas when HFO is more recently considered in petroleum crisis. The annual HFO consumption in Taiwan during 1991 to 2008 is over 15 mega kiloliter (kL). Unfortunately, the annual carbon dioxide (CO_2) emission, the most considerable green house gas (GHG), from industrial HFO consumption is about 44.3 mega metric ton predicted by CO_2 emission factor of HFO (2.95 metric ton kL^{-1}-HOF) (Shih, 2001). Pollutant emission always comes along with the incompletely combustion. Improving the characteristics of fuel was the most relatively efficient and straight solution than others (optimizing combustion parameters and setting up air pollution control devices, APCDs) to drive more completely combustion and to decrease air pollutant emission. In subsequent years numerous studies were carried out on the water-in-oil (W/O) emulsification been used as an alternative fuel for combustion equipment to approach better fuel economy and less pollutants produced, such as CO, NO_x, SO_x and PM at the same time. Besides, lower combustion peak temperature caused by water quenching phenomenon also reduces the formation of NO_x (Ballester et al., 1996).

Micro-explosion phenomenon plays the most important role of emulsion spry combustion. For the purpose of breaking through the limit of combustion efficiency (9% improvement for general emulsified fuel), this study focuses on the kind and concentration of content in disperse phase of emulsified heavy fuel oil (EHFO) which had little been literature published. An10 metric tons industrial steam boilers which consume billions litter of heavy fuel-oil (HFO) in Taiwan were the testing unit in this study when methanol- and isopropanol-contained (about 3.5 and 6 %, respectively) wastewater produced by a chemical factory was used as disperse phase to produce wastewater emulsified heavy fuel-oil (WWEHFO). Tap water emulsified heavy fuel-oil (WEHFO) and crude HFO were also tested for comparison. The addition ratio of wastewater was optimized by three temperatures preheating centrifugal stability test. After test, 20% is the feasible ratio for wastewater additive. The emulsion was produced as 20% methanol-contained wastewater emulsified heavy fuel-oil (WWEHFO). Subsequently, 14-days stability test was held and the W/O droplet size was observed. The results show that WWEHFO has more stable state and smaller W/O droplet size. Finally, the testing fuel (HFO, WEHFO, WWEHFO) were combusted in a 10 metric ton per hour steam capacity industrial boiler as figure 1 shows to test the combustion efficiency.

As the results of boiler test, WWEHFO had a breakthrough energy efficiency improvement about 20% higher than HFO when WEHFO just increased 7%. PM, CO, NO_x and SO_x emission concentration by using WWHFO decreased 70, 80, 15 and 20%, respectively. The above results were even better than using WEHFO not only in energy efficiency improvement, but also pollutants emission reduction. Consequently, there are several advantages of using WWEHFO as boiler fuel: (1) significantly increasing of boiler efficiency and less fuel consumption; (2) more completely combustion leads to less pollutant, such as PM, CO emission and less sediment in combustion chamber; (3) fuel SO_x emission was reduced by the ratio of (waste) water addition when NOx was reduced by quenching phenomenon of water content; (4) reuse of wastewater to expand cleaner production and save wastewater treatment cost. Thus, methanol- and isopropanol-contained wastewater emulsified heavy fuel-oil was feasible for industrial boilers.
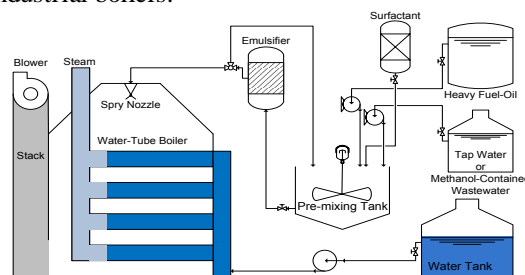

Figure 1. The boiler systems used in this study.

Ballester, J., Fueyo, N., Daopazo, C. (1996), Combustion characteristics of heavy oil-water emulsions. *Fuel*, 75, 695-705.

Nian-Ching Shih (2001), The characteristic analysis of energy consumption and SO_x、NO_x、CO_2 road transportation sector in Taiwan, *Master Degree Thesis*, Department of Environmental Engineering, National Cheng Kung University, R.O.C.

Monitoring of Particles PM10 and PM2.5 in the Mitrovica Urban Atmosphere

Afrim Syla[1*], Agron Veliu[2], Mexhit Musa[2], Bajram Kafexholli[2]

[1]MESP – Ministry of Environment and Spatial Planning of Kosova , 10000 Prishtina, KOSOVA
*Universitet of Prishtina, Faculty of Technology and Environment, Mitrovica 40000 Mitrovica
[2]University of Prishtina, Faculty of Mining and Metallurgy in Mitrovica, 40000 Mitrovica Kosova

Keywords: heavy metals, particulate matter

Abstract: The city of Mitrovica, approximately 40 km north of Prishtina, was the site of one the largest lead smelters in Europe. The present environmental situation in Mitrovica, put as in front of the responsibility to act more rationally towards nature and to be more responsible towards the protection of the environment for future generations. The lack of protection of the environment during the last ten years, as well as the conflict in Kosova is the origin of huge problems regarding present environmental situation in Mitrovica (Kosova). Mitrovica has its air divided in two kinds, speaking in quality terms: air above rural and mountainous zones, which is clean, air above city urban of the center and nearby different plants, which is more polluted. Urban air contains dust particles and gases, added on it is as results of normal activity of the city and industries in them. Now Mitrovica can be cited as one of the capitals of Europe with worst air pollution. Exposure to airborne particulates PM10 and PM2.5 containing low concentrations of heavy metals, such as Pb, Cd and Zn, may have serious health effects. However, little is known about the specification and particle size of these airborne metals. Fine and PM10 particles size with heavy metals in aerosol samples from the Mitrovica urban area were examined in detail to investigate metal concentrations and speciation. The crystal structures of the particles containing Pb, Cd and Zn were determined from their electron diffraction patterns by XRF methods.

Atmospheric particles aerosols are some of the key components of the atmosphere. They influence the energy balance of the Earth's surface, visibility, climate, human health and environment as a whole. According to World Health Organization (WHO), ozone, particulate matter, heavy metals and some hydrocarbons present the priority pollutants in the troposphere. The results of the long-term studies confirm that the adverse health effects are mainly due to particulate matter, especially small particles–less than 10 microns in diameter (PM10). According to the 1999/30/EC Directive, the countries-members are obligated to reduce the emission of the particles in urban areas by some 50% over the existing levels in order to meet the health-based limit values by 2005 and 2010. The majority of particles of industrial origin contain significant quantities of some potentially dangerous trace elements. As the result of condensation and adsorption processes, the elements as As, Cd, Mn, Ni, Pb and Zn can be found on the particle surface.

Sampling of suspended particulate matter, PM10 and PM2.5 started in July April 2003 and are still in progress at three sites in the very urban area of Mitrovica: roof of the FXM building MIP, roof of the elementary school "Bedri Gjina" at about 4m height; 40m far from heavy-traffic streets; on the platforms above entrance stairs to the faculty of Mining at the height above 3m from the ground. Suspended particles were collected on Pure Teflon filters, Whatman (37 mm diameter, 2µm pore size) and Pure Quartz, Whatman (37 mm diameter) filter paper, using the low volume air sampler Mini-Vol Airmetrics Co, Inc. (5 l min^{-1} flow rate). The duration of each sampling period was 24 hours. The filter samples were sealed in plastic bags and kept in portable refrigerators, in horizontal position during transport back to the laboratory. Particle mass was gravimetrically determined by weighting loaded and unloaded filters, after 48 hours conditioning in a desiccator's, in clean room class at the temperature T=20 ˚C and constant relative humidity RH around 50%.

For a quality assurance procedure, the quality of sample collection was determined by collecting blank samples in the field and by three control filters. During the sampling, conventional meteorological parameters were regularly recorded at the Meteorological Station of the Hydrometeorological Institute of Kosova located inside central urban area.

MoLa – A new mobile laboratory for atmospheric aerosol research

F. Drewnick[1], S.-L. von der Weiden[1,2], J. Schneider[1], S. R. Zorn[1,2], S. Borrmann[1,2]

[1]Particle Chemistry Dept., Max Planck Institute for Chemistry, Joh.-J.-Becherweg 27, 55128 Mainz, Germany
[2]Institute for Atmospheric Physics, University Mainz, Joh.-J.-Becherweg 21, 55128 Mainz, Germany

In recent years, significant improvements in the development of aerosol measurement instruments have been made, especially regarding on-line methods. A major limitation in analysing ambient aerosols is the large effort associated with the deployment of modern aerosol measurement technology in the field. Due to this issue, sampling is often performed at non-representative locations or under non-ideal conditions. In addition, traditional, fixed sampling setups do not allow measurements performed at changing locations, in order to determine the local variability of aerosol parameters.

Here we present a new aerosol research platform, which was developed at the Max Planck Institute for Chemistry in Mainz, Germany: the Mobile Aerosol Research Laboratory (MoLa). The Mobile Laboratory is equipped with state-of-the-art instrumentation for physical and chemical aerosol characterization as well as for the measurement of standard trace gas concentrations (Table 1).

Scientific applications of the Mobile Laboratory are mainly mobile measurements of the ambient aerosol for investigation of the spatial distribution of pollution parameters (e.g., area mapping), or for probing of individual mobile sources (e.g,. car chasing), but also stationary measurements under well-known sampling conditions (Figure 1).

The Mobile Laboratory is built on the basis of a Ford Transit F350. The vehicle is refitted with an air conditioning unit and two electrical generators, attached to the vehicle's engine. They generate a total of 10 kW of electrical power, of which 7 kW are UPS buffered and can be used for instrumentation. Intelligent power distribution selects the power source (internal or external power) according to a priority list, and feeds it into the three on-board power circuits.

Large effort in the development of MoLa was put into representativeness of the measurement setup. The aerosol inlet system has been optimized for minimum particle loss, especially for the size range relevant for the individual instruments (Figure 1). Using a recently developed software tool and additional characterization measurements, the particle losses in the inlet system were determined for all instruments (von der Weiden, 2008).
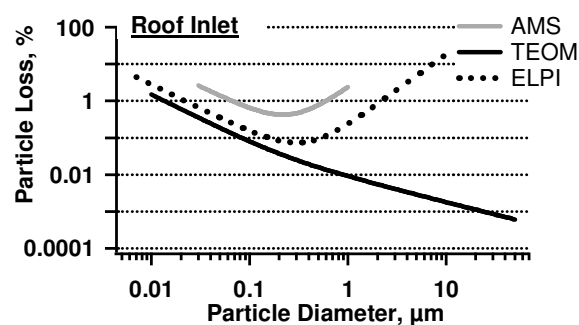
Figure 1: Calculated inlet losses for three of the instruments on MoLa

Three inlets are available: one inlet on the roof for stationary measurements, one inlet at the upper front for mobile measurements (e.g., area mapping), and one inlet at the lower front for car chasing measurements. The weather station is located at the top of a mast, which can be extended up to 10 m above ground level for stationary measurements.

In addition to a detailed description of the Mobile Laboratory, its instrumentation and its inlet setup and characterisation, we present first results from mobile and stationary measurements.

von der Weiden, S.-L. (2008), *Diploma Thesis,* University of Mainz.

Table 1. Instrumentation of MoLa.

Measured Quantity	Instrument	Time Resolution
Number conc.	CPC	1 s
$PM_{1/2.5/10}$	TEOM	15 min
Size distribution	FMPS (5-500 nm)	1 s
	OPC (0.2-32 µm)	6 s
	APS (0.5-10 µm)	1 s
	ELPI (0.03-10 µm)	1 s
Aeros. PAH	PAS2000 (<1 µm)	10 s
Soot	MAAP (<1 µm)	1 min
Size-resolved aerosol composition	HR-ToF-AMS (40 nm – 1 µm)	Few seconds
Trace gases (O_3, SO_2, NO_x, CO, CO_2)	AIRPOINTER LICOR 840	1 min 1 s
Meteorology	Vaisala WXT510	1 min

"Particle Loss Calculator" – A new software tool for the assessment of sampling and transport efficiencies of aerosol inlet systems

S.-L. von der Weiden[1,2], F. Drewnick[2] and S. Borrmann[1,2]

[1]Institute for Atmospheric Physics, University Mainz, Joh.-J.-Becher-Weg 21, 55128, Mainz, Germany
[2]Particle Chemistry Dept., Max Planck Institute for Chemistry, Joh.-J.-Becher-Weg 27, 55128, Mainz, Germany

In an ideal aerosol inlet system, the sampling and transport do not change the characteristics of the original aerosol. In real inlet systems, the sampling is non-ideal, and transport losses are often not negligible. Therefore, the optimization of the inlet and the quantitative determination of its influence on the measured aerosol properties are indispensable.

Here we introduce the new multifunctional software tool "*Particle Loss Calculator*" for the assessment of sampling and penetration efficiencies of aerosol inlet systems. It is applicable for the development and optimization of new inlet systems as well as for the determination of the characteristics of existing systems. The "*Particle Loss Calculator*" was already applied to the development and characterization of the aerosol inlet system of the Mobile Laboratory "*MoLa*" of the Max Planck Institute for Chemistry in Mainz (von der Weiden, 2008). Furthermore, the inlet characterization of a modified condensation particle counter was performed with this software (Saghafifar *et al.*, 2008).

The "*Particle Loss Calculator*" is based on simple empirical and theoretically derived relationships presented in the established literature. We compared the available equations for each process to ascertain the suitable relationships for the implementation into this software. The "*Particle Loss Calculator*" accounts for all relevant sampling and transport effects occurring under ambient aerosol measurements: non-isoaxial and non-isokinetic sampling, diffusion, sedimentation, turbulent inertial deposition and inertial deposition in bends and contractions.

We separated the calculation of the total inlet efficiency into the calculation of the sampling efficiency of the probe and the calculation of the transport efficiency of the tubing. Furthermore, the inlet system is separated into simple tube sections and the transport efficiency is determined for each section and each mechanism individually. All calculations are performed for each particle size in a user selectable size range to achieve a size-resolved quantity.

Furthermore, the user can choose either some or all of the mechanisms to be included in the calculation. With the software the occurring losses (or efficiencies) of the sampling and transport process (one process or the combination of both), as well as an array of curves of one tube section while varying one of the tubing parameters can be calculated.

In order to validate the "*Particle Loss Calculator*" we compared experimentally determined particle losses and those calculated with the software of eight simple test tube systems mainly designed for inertial deposition in bends, sedimentation and diffusion. One example of these validation experiments designed mainly for inertial effects (1/4 inch-tube, total angle of curvature: 720°), is shown in Figure 1.
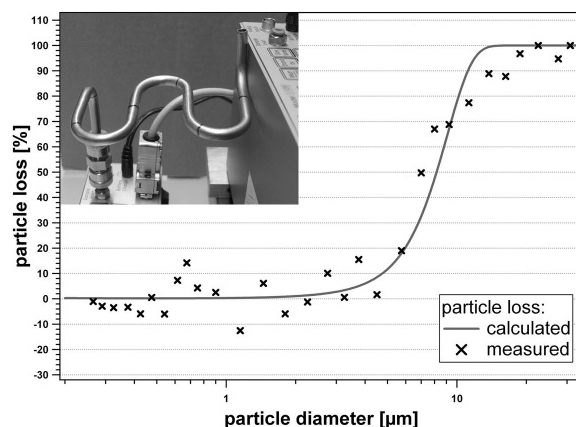

Figure 1. Measured and calculated particle loss in a test tube designed for mainly inertial effects.

As long as the tube geometries are not too extreme, the comparisons showed a satisfying agreement like in the given example.

Here, we give an overview of the mechanisms influencing aerosol sampling and transport, the theoretical basement of the software including the scope of the underlying parameterizations, and the basic working principle of the software. Part of the presentation is a discussion of the validation experiment results and the limitations of the software. Furthermore, we present various application examples of the "*Particle Loss Calculator*".

Saghafifar et al. (2008). submitted to *Aerosol Science & Technology.*

von der Weiden, S.-L. (2008), *Diploma Thesis,* University of Mainz

Development and first application of an Aerosol Collection Module (ACM) for quasi online compound specific aerosol measurements

T. Hohaus[1], A. Kiendler-Scharr[1], D. Trimborn[2], J. Jayne[2], and D. Worsnop[2]

[1]ICG-2: Troposphäre, Forschungszentrum Jülich, 52425 Jülich, Germany
[2]Aerodyne Research, Inc., Billerica, MA 01821, USA

Keywords: Aerosol sampling, Instrument development, GC-MS, Chemical composition, SOA

Atmospheric aerosols influence climate and human health on regional and global scales (IPCC, 2007). In many environments organics are a major fraction of the aerosol influencing its properties. Due to the huge variety of organic compounds present in atmospheric aerosol current measurement techniques are far from providing a full speciation of organic aerosol (Hallquist *et al.*, 2009). The development of new techniques for compound specific measurements with high time resolution is a timely issue in organic aerosol research.

Here we present first laboratory characterisations of an aerosol collection module (ACM) which was developed to allow for the sampling and transfer of atmospheric PM1 aerosol. The system consists of an aerodynamic lens system focussing particles on a beam. This beam is directed to a 3.4 mm in diameter surface which is cooled to -30 °C with liquid nitrogen. After collection the aerosol sample can be evaporated from the surface by heating it to up to 270 °C. The sample is transferred through a 60cm long line with a carrier gas.

In order to test the ACM for linearity and sensitivity we combined it with a GC-MS (Fisons GC 8060 – MD 800) system. The tests were performed with octadecane aerosol. The aerosol was generated with a TSI constant output aerosol generator (3076) and size selected with a DMA set to 250 nm mobility diameter. The aerosol flow was split to be characterized simultaneously with the ACM-GC-MS and a SMPS (TSI 3934) system.

Figure 1 shows the octadecane mass as measured with the ACM-GC-MS versus the mass as calculated from the SMPS derived total volume. The data correlate well (R^2 0.99, slope of linear fit 1.1) indicating 100 % collection efficiency. From 150 °C to 270 °C no effect of desorption temperature on transfer efficiency could be observed. As can be seen the ACM-GC-MS system was proven to be linear over the mass range 2-100 ng and has a detection limit of ~ 2 ng.

First experiments applying the ACM-GC-MS system were conducted at the Jülich Aerosol Chamber. Secondary organic aerosol (SOA) was formed from ozonolysis of 600 ppbv of b-pinene. The major oxidation product nopinone was detected in the aerosol and could be shown to decrease from 2 % of the total aerosol to 0.5 % of the aerosol over the 48 hours of experiment course (see figure 2).

The SOA was simultaneously characterized by an aerosol mass spectrometer (AMS). The ACM-GC-MS results will be compared with PMF analysis of the AMS organic aerosol. The correlation of specific compounds with PMF factors will be discussed together with future applications of the ACM-GC-MS system for ambient aerosol measurements.
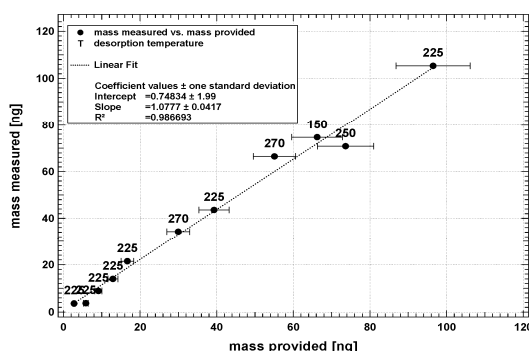

Figure 1. Calibration curve of the ACM- GC-MS system for octadecane aerosol.
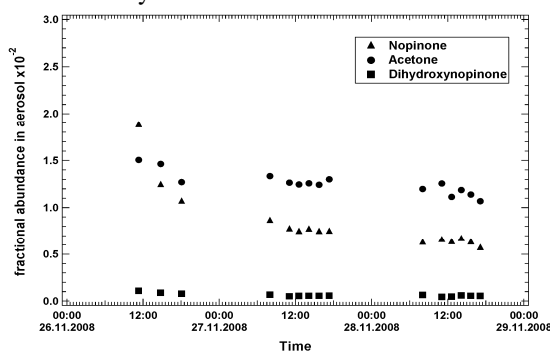

Figure 2: Time evolution of the fractional contributions of nopinone, acetone and dihydroxynopinone to the total SOA as obtained from combined ACM-GC-MS and SMPS measurements.

Intergovernmental Panel on Climate Change (IPCC): *Climate Change 2007*, Cambridge University Press, UK, 2007

Hallquist et al., *Atmos. Chem. Phys. Discuss.*, Vol.9, pp. 3555-3762, 2009

Stable carbon isotopic composition of PM2.5 in Taiwan

A. Kiendler-Scharr[1], G. Engling[2], R. Fisseha[1], W. Laumer[1], I. Gensch[1], Y. C. Wu[2], and Y. T. Chen[2]

[1]ICG-2: Troposphäre, Forschungszentrum Jülich, Jülich, Germany

[2]Research Centre for Environmental Changes, Academia Sinica, Taipei, Taiwan

Keywords: Carbonaceous aerosol, Stable carbon isotope, Source identification

Atmospheric aerosols influence climate and human health on regional and global scales. In many environments organics are a major fraction of the aerosol influencing its properties such as hygroscopicity, optical properties, and toxicity. Typically only a small fraction of the hundreds of organic compounds can be measured by state of the art analytical methods. The complexity of the organic aerosol component often hinders source apportionment. A new approach for organic aerosol source characterization and atmospheric chemistry studies is the use of stable carbon isotope measurements (Huang et al., 2006; Goldstein and Shaw, 2003).

Here we present results from a comparative study at two sites in Taiwan. The $\delta^{13}C$ of the total carbon is presented together with organic speciation data and compound specific $\delta^{13}C$ analysis.

Aerosol samples were collected at two sites in Taiwan: an urban site (Taipei, 25° 02' 31.2" N, 121° 37' 0.3" E, 22 m asl) and a remote site in central Taiwan (Mt. Lulin, 23° 28' 07" N, 120° 52' 25" E, 2860 m asl). Collection of the PM2.5 samples was carried out with Ecotech Hi-vol air samplers with nominal flow rates of 1130 L/min. and typical collection times of 12 hours (Taipei) or 24 hours (Mt. Lulin).

The stable carbon isotopic composition of the total carbon in the aerosol samples was analyzed using an elemental analyzer (Euro Vector, Germany) coupled to a GV-Optima isotope ratio mass spectrometer. As shown in figure 1 the isotopic composition of the total carbon was found to vary between -27 and -24 ‰ compared to VPDB standards for the Taipei sampling site. Generally the $\delta^{13}C$ was larger the larger the total carbon mass concentration was. At Mt. Lulin the total carbon isotopic composition was observed to be less variable with an average $\delta^{13}C$ of -24.1 ± 0.7 ‰.

The data will be discussed with respect to seasonality and aerosol sources, making use of organic speciation data, including ambient anhydrosugar and polyol concentrations, obtained by high-performance anion exchange chromatography (HPAEC). Furthermore, selected results from compound specific $\delta^{13}C$ analysis with a GC-IRMS system (Fisseha *et al.*, 2009) will be presented.

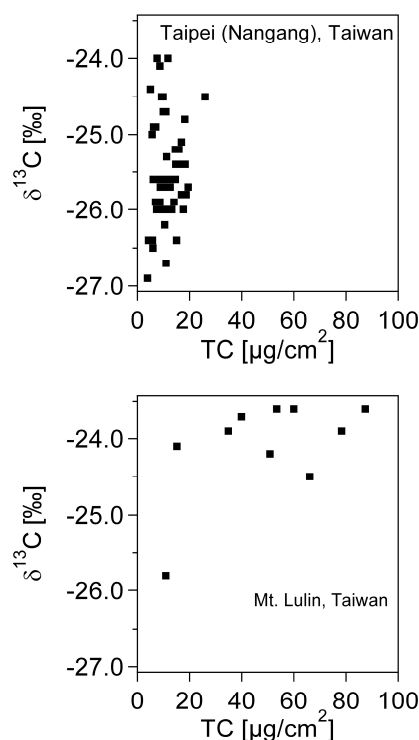Figure 1. Comparison of the dependence of $\delta^{13}C$ on the total carbon concentration per sample for Taipei (upper panel) and Mt. Lulin (lower panel).

R. Fisseha et al., *J. Geophys. Res. Atmospheres*; 2009. 114, D02304, doi:10.1029/2008JD011326

A. Goldstein and S. L. Shaw, *Chem. Rev.*, 103, 5025-5048, 2003

L. Huang et al., *Atmospheric Environment* 40, 2690-2705, 2006

AMS aerosols characterization at Seiffen (Germany)

L. Poulain, Y. Iinuma and H. Herrmann

Leibniz Institute for Tropospheric Research, Permoserstr. 15, 04318, Leipzig, Germany

Keywords: AMS, Aerosol characterization, Biomass Burning, PM_1.

Biomass burning aerosol characterization was performed at the village of Seiffen (Germany) during winter 2007-2008. The sampling place is located in a mountain area (640 m a.s.l.) at around 50km south-west of Dresden. The place is famous for its Christmas wood decoration production and wood combustion represents the most important source of domestic heating. During this campaign, an Aerodyne High Resolution Time of Flight Aerosol Mass Spectrometer (HR-ToF-AMS, DeCarlos *et al*, 2006) was deployed from the 10th of January to the 2nd of February 2008 with a time resolution of 5 min.

Time series of the main aerosol components showed periods with high and low aerosol concentration (Figure 1). Mass fraction of the major aerosols components showed that aerosols are mainly made of organics > sulphate > nitrate > ammonium and chloride.
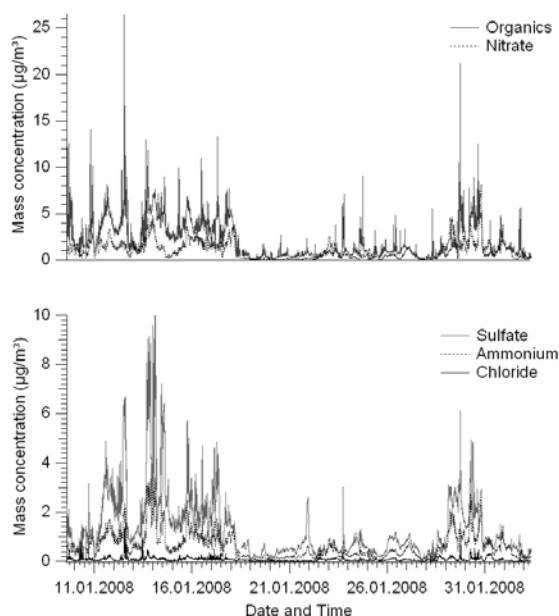
Figure 1: Time series of the main aerosol components.

In parallel to AMS, daily samples from a PM_1 high volume aerosol sampler (Digitel, Switzerland) were performed. From these samples, main anions were analysed by ion chromatography, PAH were analysed by Curie Point Pyrolysis Gas Chromatography Mass Spectrometry (CPP-GC-MS). Levoglucosan which is known to be an important tracer of biomass burning particles was analysed by High Performance Anion Exchange Chromatography coupled to Pulse Amperometric Detector (HPAEC-PAD). Moreover, Biomass Burning Organic Aerosol (BBOA) and more specifically levoglucosan can also be detected by AMS as two specific fragments m/z 60 ($C_2H_4O_2^+$) and m/z 73 ($C_3H_5O_2^+$), (Schneider *et al*, 2006). A similar ratio $C_2H_4O_2^+$ to $C_3H_5O_2^+$ from field and lab measurements of pure levoglucosan particles was obtained for most of time. This ratio validates that this two fragments are mainly coming from levoglucosan in our measurements. Comparisons between the different filters results (*i.e.* levoglucosan, PAH and potassium) and daily average AMS measurements showed a good agreements.

In addition, diurnal patterns of organics, BBOA, PAH and potassium showed similar time dependences: concentrations increase early in the morning and present maximum at the evening which is corresponding to the period of high heating activity in the village.

DeCarlo, P. F, Kimmel, J. R., Trimborn, A., Northway, M. J., Jayne, J. T., Aiken, A. C., Gonin, M., Fuhrer, K., Horvath, T., Docherty, K. S., Worsnop, D. R. & Jimenez, J. L. (2006), *Anal. Chem.* 78 (24), 8281-8289.

Schneider, J., Weimer, S., Drewnick, F., Borrmann, S., Helas, G., Gwaze, P., Schmid, O., Andreae, M. O., Kirchner, U. (2006), *Int. J. Mass. Spect.*, 258 (1-3), 37-49.

Studies of PM$_{2.5}$ elemental composition in Venice Lagoon area

A.M. Stortini[a], A. Freda[b], D. Cesari[c], S. De Pieri,[b], W. Cairns[a], D. Contini[c] and A. Gambaro[b, a]

a Institute for the Dynamics of Environmental Processes (CNR-IDPA), S. Marta 2137, 30123 Venice, Italy.
b Department of Environmental Sciences, University Ca' Foscari of Venice, S. Marta 2137, 30123 Venice, Italy.
c Institute of Atmospheric Sciences and Climate (CNR-ISAC), Str. Lecce-Monteroni km 1.2, 73100 Lecce, Italy.

Keywords: elemental composition, PM$_{2.5}$, PCA, anthropogenic sources, ICP-QMS.

On global scale, PM emissions reach 3400 Tons/year (IPCC, 1996), and anthropogenic sources contribute for only 10% of total PM amount, whereas the natural primary PM emissions reach 85% (2900 Tons/year). These values may drastically change according the local scenario, the rate and the kind of anthropic activities, and the particle cut-off prevailing.

The Venice lagoon area comprises the inland part and the insular part (historical nucleus). The emission sources of the inland part comprises vehicular traffic, industrial thermoelectric power plant, petrochemical plant, incinerator plant, domestic heating; while naval traffic (public transport, touristic and merchandise activities), glass factories, airport, domestic heating, etc., represent the typically anthropogenic sources of the Insular part. Venice area is characterised by atmosphere stability which lets horizontal and air stagnation episodes. Moreover, as well known, meteorological conditions like winds, temperature, humidity and precipitation events, strongly influence the PM distribution.

A monitoring campaign for PM$_{2.5}$ was performed in the central part of Venice Lagoon from spring to autumn in 2007. Studies about concentration and elemental composition (Na, Al, K, Ti, Mn, Fe, V, Ni, Zn, As, Pb, Se, Cd, Co) has been done by ICP-QMS measurements. In table 1 is reported the monthly average concentration. Besides comparisons between our PM$_{2.5}$ data and PM$_{10}$ data from local environmental regional agency (ARPAV, 2006), from Gambaro *et* al. (2003) and meteorological records have been done.

Table 1. Monthly average concentration and number of sampling days for PM$_{2.5}$ in 2007.

Month	Average (μg m^{-3})	N. days
March	24.9	3
April	27.3	21
May	18.6	27
June	12.1	27
July	12.7	29
August	13.7	31
September	10.9	23
October	22.3	30
November	23.0	4
TOTAL	16.9	195

The enrichment ratios (EF) for the elements detected was obtained taking into account the Mn like crustal element and upper crust values, both according Wedepohl (1995), and according Bini *et* al. (1999). Results are reported in figure 1.
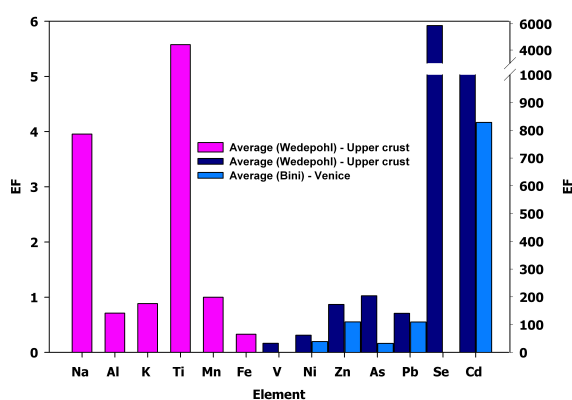

Figure 1. Enrichment factors (EF) calculated with Wedepohl (1995) upper crust values and Bini (1999) upper crust Venice values.

Principal component analysis has been applied on data obtained to associate groups of elements to emissions sources. From the loading plots obtained by the comparison of the principal components is possible to individualise four groups of elements that could be associated with different emission sources that are: 1) As, Se, Cd; 2) V, Co; 3) Mn, Fe, K; and 4) Pb. Data Elaboration with Positive Matrix Factorization (EPA PMF 3.0) is in progress.

Annual report about air quality. (2006). *Municipality of Venice and regional agency for the environmental protection of Veneto* (ARPAV).

Bini, C., Giandon P. & Vinci, I. (1999). *Proceedings. V-ICOBTE*, Wien, 1, 102-103.

Gambaro, A., Manodori, L., Toscano, G., Cairns, W., Stortini, A. M., Piazza, R., Moret, I. & Capodaglio, G. (2003). *Scientific research and safeguarding of Venice-CORILA*, Venice, III, 267-282.

IPCC. (1996). Second Assessment Report: Climate Change 1995.

Wedepohl, K. H. (1995). *Geochimica et Cosmochimica Acta*, 59, 1217-1232.

Calculating particle concentration fields for steady and unsteady aerosol sampling

A.K. Gilfanov[1], D.V. Maklakov[2], S.K. Zaripov[3]

[1]Institute of Mathematics and Mechanics, Kazan State University, Prof. Nuzina 1, 420008, Kazan, Russia
[2]Kazan State University of Architecture and Engineering, Zelenaya 1, 420043, Kazan, Russia
[3]Kazan State University, Faculty of Geography and Ecology, Kremlevskaja 18, 420008, Kazan, Russia

Keywords: aerosol sampling, particle concentration, aerosol modelling, CFD

The aspiration efficiency introduced in the aerosol sampling theory allows one to take into account the difference between the average value of particle concentration inside the measuring device and that in the undisturbed aerosol flow. To extend the knowledge of the sampling process it is important to study the space distribution of particle concentration outside and inside the sampler. The aerosol probes can be sampled from the aerosol streams with nonuniform space profiles of particle concentration which can affect the accuracy of measurements. Hence, mathematical models that allow one to calculate particle concentration fields are necessary.

We solve the problem of aerosol sampling into a thin-walled tube facing the moving air by making use of the potential and viscous flow models of incompressible fluid. By neglecting the influence of particles on the carrier phase due to the small concentration, the fluid velocity fields are obtained by the Boundary Element Method for potential flow and by using the CFD code FLUENT to solve numerically the Navier-Stokes equations for viscous flow. The equations of particle motion are supplemented with new equations which makes it possible to calculate the particle concentration along the trajectories. The used method of finding the particle concentration has been proposed by Osiptsov (1998) and has been applied recently to the problem of aerosol sampling into a slot by Gilfanov&Zaripov (2008).

The distributions of particle concentration outside and inside the sampler for various values of ratio R_a of wind and aspiration velocities and Stokes number St are numerically investigated. (St=$U_0\tau/D_t$, U_0 is the wind velocity, τ is the particle relaxation time, D_t is the tube diameter). The potential and viscous flow models give the same distributions of particle concentration outside the tube. The particle concentration increases as particles move to the sampler. But the calculations within the viscous flow approximation show that the zones with the particle concentration less than particle concentration in undisturbed aerosol flow appear inside the tube.

The particle concentration profiles in several cross-sections of the tube for two values of R_a at St=1 are presented in fig.1. The curves I-III corresponds to the cross-sections located at various nondimensional distances from the tube entrance. The particle concentration calculated within viscous flow model achieves a maximum at a certain value of the distance r from the axis of symmetry. This means that there exists an accumulation of particles trajectories near the edge of the aerosol jet inside the sampler. The nonuniformity of the profiles of particle concentration inside the tube can be high. This fact should be taken into account in calculating the collection efficiency of aerosol particles on the next measuring stages. The calculations show that the deviations of concentration profiles from uniform far from the sampler can considerably affect the aspiration efficiency for small values of R_a and large values of St.
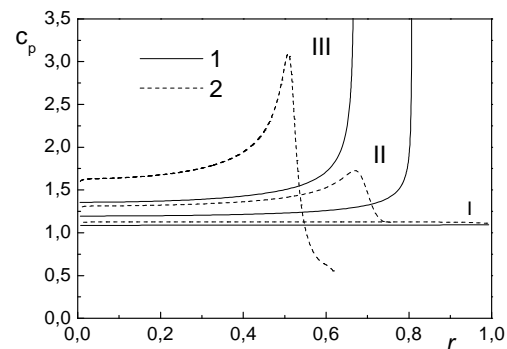

Fig.1. The particle concentration profiles for R_a=0.2 at St=1: 1 is the potential flow model, 2 is the viscous flow model; I-III – x=0, 0.5,1

The developed model is also used to construct the concentration fields for unsteady sampling case when a periodic suction flow simulates the human breathing process. The corresponding results will be presented on the conference.

Gilfanov, A. K., Zaripov S. K. (2008) Fluids dynamics, 43, 4, 563-572.
Osiptsov, A. N. (1998) in *Proc.3d Intern. Conf. on Multiphase Flow*, ICMF'98, Lyons, CD, 1-8.

Numerical study of thin-walled sampler performance for aerosols in low windspeed environments

S.K. Zaripov[1], A.K. Gilfanov[2], D.V. Maklakov[3]

[1]Kazan State University, Faculty of Geography and Ecology, Kremlevskaja 18, 420008, Kazan, Russia
[2]Institute of Mathematics and Mechanics, Kazan State University, Prof. Nuzina 1, 420008, Kazan, Russia
[3]Kazan State University of Architecture and Engineering, Zelenaya 1, 420043, Kazan, Russia

The low wind velocity regime, intermediate between the moving and calm air cases, is important for practical indoor aerosol sampling. But there is a gap in knowledge of the performances of samplers operating in such conditions. Only the case of tube sampler facing vertically upwards for air flow moving vertically downwards has been investigated by Grinshpun *et al.*, (1990). In indoor environments the air flow velocity is about 0.1-0.2 m/s and the settling velocity V_s of coarse particles can reach close values (for particles with size 80 μm V_s~0.17 m/s (Schmees *et al.*, 2008). This means that the particle velocity can be comparable with V_s and the gravity force will affect the aspiration efficiency.

In this work a mathematical model of aerosol sampling into a thin-walled tube facing horizontally in the slow moving air is developed. The fluid velocity field is obtained by BEM method for potential flow approximation and using FLUENT program for viscous flow model. In these fields the aspiration efficiency is studied in the range of small values of the ratio R_a of the wind and aspiration velocities. The aspiration coefficient is calculated without and with possible bounce of particles from the outer wall of the tube. The fair agreement of calculated dependencies $A(R_a)$ with known experimental data and the approximate formulas of Davies (1968) and Medvedev (2002) for small values of R_a is observed.

In the presence of gravity the particle motion can be defined by two nondimensional parameters: the Stokes number $St=U_s\tau/D_t$ (U_s is the sampling velocity, τ is the particle relaxation time, D_t is the tube diameter) and Froude number $Fr=U_s^2/gD_t$. The cross-sectional area of limiting particle trajectory surface changes its shape from circular for large R_a to noncircular for small R_a (fig.1, St=1, Fr=10).
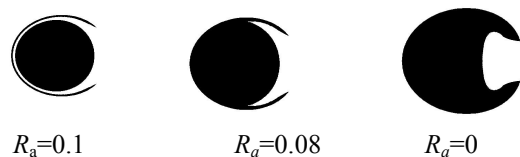
R_a=0.1 R_a=0.08 R_a=0
Fig.1. The cross-sectional area of limiting particle trajectory surface at various R_a

The values of the aspiration efficiency calculated with gravity influence are less than the values of A without gravity (fig.2). As R_a decreases up to zero the calculated aspiration efficiency tends to the values that correspond to the calm air sampling. Our results at R_a=0 are in agreement with the approximate formula for aspiration efficiency of thin-walled tube oriented horizontally in calm air (Vincent, 2007). The curves $A(R_a)$ in the case of acting gravity can be approximated by formula (1) that is the combination of the aspiration efficiencies A_0 for calm air sampling (Vincent, 2007) and A_m for moving air (Medvedev, 2002)

$$A=\begin{cases} A_0 +R_a(A_{mc}-A_0)/R_c, & R_a<R_c \\ A=A_m, & R_a>R_c \end{cases} \quad (1)$$
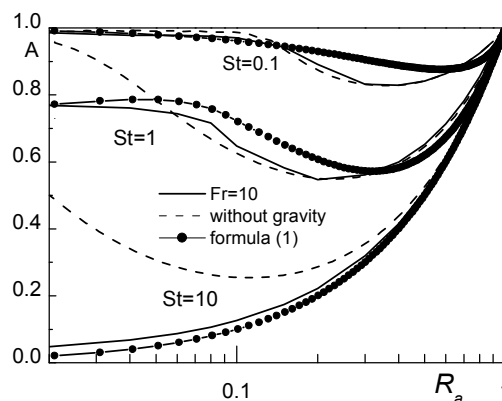
where R_c= St / Fr, $A_{mc}=A_m(R_c)$.

Fig.2. The dependence $A(R_a)$ calculated with and without gravity action

Davies, C.N. (1968) British Journal of Applied Physics, 25, 921-932.
Grinshpun, S., Lipatov, G.N., Sutugin, A.G. (1990) J. of Aerosol Science, 12, 716–740.
Medvedev, A.A. (2002) Atmospheric and Oceanic Optics, 15, 8, 663-666.
Schmees, D.K., Wu, Y.-H., Vincent, J.H. (2008) J. Environ. Monit., 10. 1426-1436.
Vincent, J. (2007) Aerosol sampling: science, standarts, instrumentation and applications, John Wiley&Sons.

Analysis of Oligomeric Glyoxal using HPLC-ESI-MS – Challenges and Possibilities

C.J. Kampf[1], T. Hoffmann[1]

[1]Institut of Inorganic and Analytical Chemistry, Johannes Gutenberg-University, Duesbergweg 10-14, 55128, Mainz, Germany

Keywords: Electrospray, LC/MS, mass spectrometry, water soluble organic compounds

Atmospheric aerosols both have a direct and indirect impact on earth's global climate due to their ability of scattering and reflecting sunlight back to space on the one hand and to act as cloud condensation nuclei (CCN) on the other hand. Adverse effects of a high aerosol burden on the human health are also subject of ongoing research. In recent years much effort has been put into the analysis of so called secondary organic aerosols (SOA). SOA is produced through gas phase oxidation of volatile organic compounds (VOC's) by atmospheric oxidants like OH- or NO_3-radicals or ozone with subsequent gas-particle partitioning of the low volatility products. VOC's are emitted by both biogenic and anthropogenic sources in large amounts into the atmosphere. However, it was found that gas-particle partitioning alone can not explain the complete amount of SOA produced in the atmosphere. It was therefore proposed that heterogeneous reactions on the particle surface or in the particles themselves could lead to the formation of additional SOA mass from semi-volatile compounds such as the reactive dialdehydes glyoxal and methyl glyoxal [1].

Global glyoxal emissions are estimated to be 45 Tg a^{-1} and the oxidation of biogenic isoprene contributes 47% of glyoxal [2]. Because of its high solubility in water, due to hydration of its aldehyde functions, glyoxal has a high potential to form SOA via heterogeneous reactions in the particle phase although its volatility is relatively high. Several studies propose oligomerisation reactions as a possible reason [1,3,4].

The chromatographic behaviour of glyoxal oligomers was investigated when separation with high performance liquid chromatography (HPLC) and mass spectrometric detection was used. Different chromatographic techniques were applied, such as reversed phase (RP) and size exclusion (SE) chromatography. Therefore, aqueous standard solutions with different glyoxal concentrations were prepared and measured with an Agilent HPLC system (1100er series) coupled to a Bruker Daltonics electrospray (ESI) ion trap (IT) mass spectrometer (MS) (HCT+) using either a reversed phase column (Pursuit XRs 3 C8, Varian) or a size exclusion column (PL Aquagel-OH 20, Polymerlabs) for separation.

Results of high concentration experiments with size exclusion chromatography indicate a dynamic equilibrium of the oligomerisation reaction of glyoxal since the oligomers do not completely follow the expected elution sequence. It is therefore likely that the state of oligomerisation changes over the course of separation, which complicates analysis of these oligomers in atmospheric samples using this technique, however, may on the other hand be a possibility to learn something about the reaction rate of the oligomerisation reactions in the liquid phase.

Reversed phase chromatography offers a faster but less efficient separation of glyoxal oligomers and therefore the effect discussed above is not visible using this technique. However, it seems to be more suited for the analysis of atmospheric samples and presents other interesting insights into the formation mechanisms of glyoxal oligomers. Mass spectra in the respective chromatograms show co-elution of oligomers which masses differ by 134 u corresponding to two units of glyoxal and one unit of water. An addition of this structural unit obviously does not change the overall polarity of the oligomer while additions of single units of water or glyoxal change the polarity and therefore the retention time of the molecule.

Kalberer, M., et al. (2004). *Science*, 303 (5664), 1659-1662.

Fu, T.-M., et al. (2008). *Journal of Geophysical Research*, 113, D15303.

Hastings, W. P., et al. (2005). *Environmental Science and Technology*, 39, 8728-8735.

Iinuma, Y., et al. (2004). *Atmospheric Environment* 38(5), 761-773.

Artifacts in size distributions from low time-resolution mobility sizers in varying particle concentrations.

M. D. Wright[1] and D. L. Henshaw[1].

[1] H. H. Wills Laboratory, University of Bristol, Tyndall Avenue, Bristol, BS8 1TL, U.K.

Keywords: SMPS, size distribution, measurement errors, concentration variability, traffic emissions

Devices for obtaining size distributions, such as Sequential/Scanning Mobility Particle Sizers (MPS), often require a period of several minutes to obtain a distribution. During this time, if the actual particle concentration changes, the distribution is distorted and is inaccurate. Ideally, high temporal resolution is required for the study of emissions from individual vehicles at roadside sites. Such systems have recently become commercially available. However, in order to prolong the use of low time-resolution systems, it is beneficial to determine under what circumstances they can reliably be used. This was a topic of studies by Yao et al. (2006a, b) who concluded that even at 6 s resolution, significant size distribution distortion could occur at roadsides. Clearly the characteristic timescale of variability in concentration, as well as concentration itself, is a key factor in determining the suitability and accuracy of SMPS operation.

In this study, two SMPS systems (SMPS+C, Grimm Aerosol Technik, GmbH) were used at fixed voltage to measure the concentration of particles of a range of diameters at a time resolution of 1 s, at a roadside site in central Bristol, UK during a weekday afternoon (Figure 1). These data were then used to define an 'influx event' of the form shown in Figure 2, for 5 concentrations at times during SMPS cycles corresponding to specific particle sizes. Parameters were chosen based on typical events observed experimentally. The influx was applied to a unimodal simulated count distribution (mean size 100 nm, GSD 2.0), prior to calculating the number particle distribution (NPD), to determine its effect on the resultant NPD. Results for three sizes are presented in Figure 3 (other sizes omitted for clarity).

For influx events at large particle size a high concentration is required to give a noticeable effect on the NPD. However at smaller sizes even low-concentration events, which regularly occur in measurements, give rise to artifacts. The mean particle diameter is shifted and distributions could be misclassified as bimodal. At small sizes, infrequent high concentration events lead to artifacts which could distort long-term averages of size distributions.

Particle production and dispersion mechanisms govern concentration and its variability, and therefore the suitability of low time-resolution measurements, at roadsides. Thus the form and timescale shown in Figure 2 is likely to be measurement-specific, but can be chosen so as to fit any particular influx event.

The poster will present further results from additional measurement sites, and simulations for both different initial distributions and 'influx event' forms, corresponding to experimental data and from data reported in the literature.
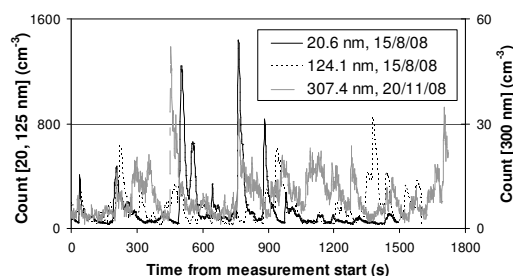

Figure 1. Data showing variability in particle counts at specific diameters at a roadside site.
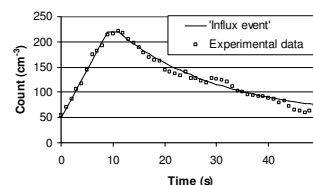

Figure 2. One 'influx event' (linear rise, plateau and exponential decay) fitted to experimental data.
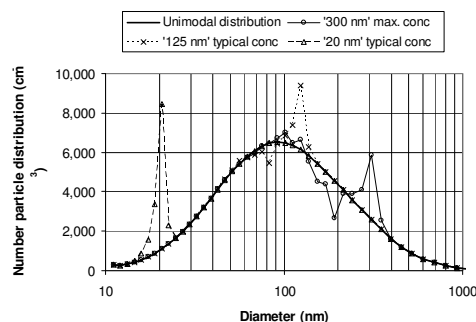

Figure 3. Distortion of size distributions with influx events at times corresponding to 20, 125 and 300 nm size measurements for typical/maximum concentrations observed in roadside measurements.

Yao, X., Chan, C. K., Lau, N. T., Lau, P. S. and Fang M. (2006a). *Aerosol Sci. Tech.* 40, 1080-1089.
Yao, X., Lau, N. T., Fang, M. and Chan, C. K. (2006b). *Atmos. Chem. Phys.* 6, 4801-4807.

Source apportionment and partitioning of persistent organic pollutants in rural site of Turkey

S. Yenisoy-Karakaş[1], M. Öz[1], E. O. Gaga[2] and A. Arı[2]

[1]Department of Chemistry, Abant Izzet Baysal University, Gölköy Campus, 14280, Bolu, Turkey
[2]Department of Environmental Engineering, Anadolu University, Iki Eylül Campus, 26555, Eskişehir, Turkey

Keywords: POPs, monitoring, determination of sources, meteorological parameters.

Samples of particulate matter were collected on glass fiber filters (GFF) and gas phase samples on polyurethane foam (PUF) by using PUF sampler which was set up on the roof of the presidency building in the campus of Abant Izzet Baysal University in Bolu. Daily samples were collected during four months period, being 2 months in winter time and 2 months in summer time. Developed and modified methods were validated to determine 15 polychlorinated biphenlys (PCBs), 18 organochlorine pesticides (OCPs) and 16 polyaromatic hydrocarbons (PAHs).

The concentrations of the most of the pesticide compounds other than beta BHC showed considerable increase in winter season. Concentrations of the pesticide compounds had higher concentrations in particulate phase except for beta BHC, 4,4 DDE and heptachloroepoxide. Generally, the concentrations of pesticides were found to be higher when the wind blown from the south, the south-east and the south-west. These wind directions are dominant ones and also there are heavy agricultural activities carried out in these directions. The concentrations of beta BHC and endrin were significantly higher than the concentrations that were found in other agricultural and rural areas of the world except for Izmir city which is urban and agricultural area of Turkey. Endosulfansulfate is a transformation product of endosulfan I and endosulfan II, therefore; its high concentrations are as a result of long term applications not due to fresh endosulfan inputs. The concentrations of endrin were 30-50 times higher than the literature values. Although its usage was banned in 1979 in Turkey, it seemed that it has been still in usage.

Back trajectory models showed that the sources of pesticides were generally local. Factor analysis explained 84.2% of the total variation with two factors. The compounds (endosulfan II, endosulfan I, endrin, endrin aldehyde, methoxychlor) under the factor 1 had higher concentrations at the directions of south-east, east-south-east, south-east, south-south-east. The second factor that affected the concentrations of the compounds was found to be at the directions of south, south-west and west. The factor loadings of the compounds 4,4 DDD, endosulfan sulfate and endrin aldehyde were high under the second factor.

Atmospheric concentrations of 15 PAHs were also determined in summer and winter seasons. The winter time concentrations were considerable higher than the summer time concentrations. Winter to summer concentration ratios of total PAHs was calculated as 14. The compounds of phenanthrene (Phe), fluoranthene (Flt), fluorene (Flu) and pyrene (Pyr) made the most significant contributions to total concentrations of PAHs as shown in Figure 1.
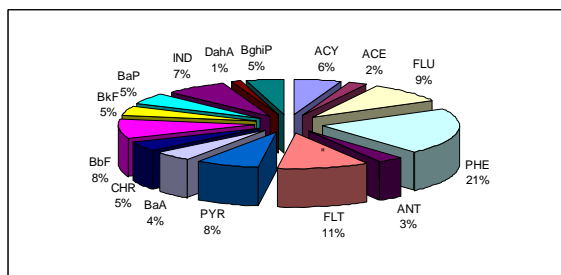

Figure 1. Percent distribution of total PAH concentrations.

Concentrations measured in winter season were found to be higher than the concentrations in rural areas while summer concentrations were in consisted with the literature values. Use of factor analysis together with PAH diagnostic ratios indicated coal combustion as a predominant source of PAHs in winter time. However, it was found that, summer PAH concentrations was affected mainly from traffic and stubble burning. The concentrations of PAHs in the sampling point were generally affected from the local sources.

Airborne Fungi Concentrations in Trains

Y.F. Wang[1*], L.C. Wang[2],
C. H. Tsai[3] and H.H. Yang[4]

[1]Department of Bioenvironmental Engineering, Chung Yuan Christian University, 320, Taiwan.
[2]Department of Chemical and Materials Engineering, Cheng-Shiu University, 833, Kaohsiung, Taiwan
[3]Department of Chemical and Material Engineering, National Kaohsiung University of Applied Sciences, 415 Chien-Kung Road, Kaohsiung 807, Taiwan
[4]Department of Environmental Engineering and Management, Chaoyang University of Technology, Taichung 413, Taiwan

Keywords: bioaerosols, fungi, size distribution

1 Introduction

Public transportation was common in urban city. Commuters regularly spent fixed time in the closed system and probably exposed to some potentially risky environment. Additionally, the circulation was not good in indoors, especially in these public transportation even there was air conditioners. Most studies were focused on some elevated levels of several pollutants (such as CO, VOCs, PAHs et al.,) and limited information was found on in-vehicle airborne microbes. These bioaerosols became an emerging topic for their pathogenesis in recent years; especially airborne fungi were always related with asthma and allergy.

2 Materials/Methods

Aerobiological studies in commuter trains in Taiwan were carried out from August, 2007 until July, 2008. A six-stage (>7μm, 4.7~7μm, 3.3~4.7μm, 2.1~3.3μm, 1.1~2.1μm, 0.65~1.1μm) Anderson sampler of 400 orifices attached to malt extract agar (MEA) plates with chloramphenicol addition was used to collect viable fungi. CO, CO_2, temperature and humidity in buses were also recorded during sampling. After field sampling, the MEA plates were incubated at 25℃ for five days. Fungi concentrations were calculated as colony forming units per cubic meter of air and expressed as CFU/m^3.

3 Results

Fungi concentrations ranged from 45 to 1905 CFU/m^3 and averaged 415 CFU/m^3. The lowest fungi concentration was happened in winter. Defining the fraction of fungi concentration: it's the fungi concentration in a specific stage divided by total fungi concentrations. The results showed that the highest fraction occurred in the fifth stage (1.1~2.1μm) for most sampling months except November and December (Figure 1). The result was a little different with that of our previous study in buses. (Wang et al., 2008) It's interesting to find the fraction of the fifth stage is always over 20% and the highest fraction happened in May (42%). Figure 2 showed the relationship of the fungi fraction with

seasons. The fraction of the fifth stage decreased from spring to winter, however, the fraction of the fourth stage increased from spring to fall and decreased in winter. The microbes in the fifth stage were easily deposited in the terminal bronchi and perhaps caused more serious health effect. The identification of these microbes warrant further investigation in the future

4 Recommendations

The IAQ regulations in Taiwan were just issued in 2008. It's more useful to provide identification information of these airborne microbes to evaluate the health risk, especially for those sensitive groups.
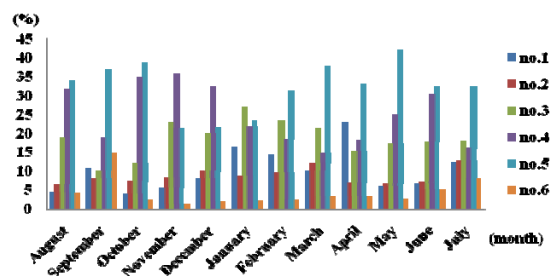

Figure 1. The relationship of airborne fungi fraction and sampling months
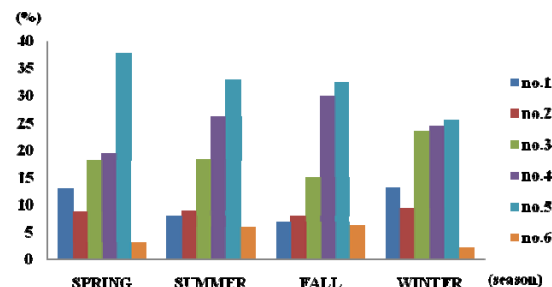

Figure 2. The relationship of airborne fungi fraction and sampling seasons

Wang, Y. F., Chao, H. R. Yang, H. H. and Hsieh, L. T. (2008) *The European Aerosol Conference*, Aug. 24-29, Thessaloniki, Greece.

Towards reference-free quantitation in multielemental TXRF analysis of nanoparticles – Effects of particle dimensions and load

J. Osán[1], F. Reinhardt[2], B. Beckhoff[2], A. Pap[3] and S. Török[1]

[1] Hungarian Academy of Sciences KFKI Atomic Energy Research Institute, P.O. Box 49, H-1525 Budapest, Hungary

[2] Physikalisch-Technische Bundesanstalt, Abbestr. 2-12, D-10587 Berlin, Germany

[3] Hungarian Academy of Sciences, Research Institute for Technical Physics and Materials Science, P.O. Box 49, H-1525 Budapest, Hungary

Keywords: aerosol measurement, cascade impactor, nanoparticles characterization, ultrafine particles, XRF

Air quality issues of large cities are becoming more and more important due to the dynamic growth of surface and air traffic. The sources of fine particulate matter ($PM_{2.5}$) have large temporal and spatial variation. In order to correlate the elemental composition of fine particulate matter in different size fractions to sources, special instrumentation and analytical technique need to be used. A novel combination of cascade impactor sampling and total reflection X-ray fluorescence (TXRF) analysis employing synchrotron radiation allows the determination of ultra-trace amounts (pg m^{-3}) of most elements from samples collected for less than 20 min, while retaining the full size resolution of the impactor (Groma et al., 2008). TXRF allows for non-destructive analysis of nano- and microparticles located on semiconductor surfaces (Beckhoff et al., 2007). In combination with X-ray absorption spectrometry, the technique is able to contribute to the speciation of the atmospherically important elements (Osán et al., 2006). However, to obtain quantitative results in elemental analysis of nanoparticles, fundamental research is necessary on particles of known dimensions and compositions.

In TXRF geometry, an X-ray standing wave field (XSW) results from the superposition of incident and reflected beam. Different particle dimensions and loads have a different impact on the XSW and therefore, on reference-free quantitation of TXRF and speciation capabilities of X-ray absorption fine structure measured in fluorescence detection mode (TXRF-XAFS). In this experiment the influence of deposited particles on the angular dependence of the XSW has been examined by tuning the angle of incident radiation.

For methodological investigations (a) artificial structures (pads) and (b) particles of known composition, deposited on silicon wafer surfaces using a cascade impactor, have been measured. The artificial structures were deposited on silicon wafer surfaces using the lift-off technique, containing Ni(34%)Fe(66%) alloy as well as Cr pads of 2.7 µm diameter with different heights in the range of 10 nm to 100 nm. Sub-micrometer copper sulphate particles were deposited on Si wafer surfaces through a May-type cascade impactor also used for sampling of atmospheric aerosols. The samples containing $CuSO_4$ particles were prepared in four size fractions in the 250 nm to 4 µm range.

Measurements in the soft X-ray range, i.e. the energy regime between 78 eV and 1860 eV, were performed at the PGM beamline for undulator radiation in the laboratory of the PTB at the electron storage ring BESSY II. The medium to hard X-ray regime between 1.75 keV and 10.5 keV is accessible at the FCM beamline for bending magnet radiation in the same laboratory. All instrumentation used is characterized and calibrated with respect to geometry factors as well as responses and efficiencies of the detectors employed (Beckhoff, 2008). Initial results indicate the high potential of this methodological approach to further contribute to reliable TXRF quantitation.

In the hard X-ray range, the angular scans recorded on the Si wafers containing $CuSO_4$ particles showed an angular dependence expected for particulate type deposition. The Cu-Kα and S-Kα intensities were doubled below the critical angle, with a plateau in a wide angular range. This behavior is due to the relatively wide size distribution of the particles, averaging out the contribution of the XSW effect on different particle sizes. The artificial metallic pads are, however, monodisperse, showing much more pronounced angular dependence of the X-ray intensities. The measured angular scans are to be interpreted by modeling the XSW field intensity in dependence of the height above the Si wafer surfaces.

Beckhoff, B., Fliegauf, R., Kolbe, M., Müller, M., Weser, J., & Ulm, G. (2007). *Anal. Chem.* 79, 7873.

Beckhoff, B. (2008). *J. Anal. At. Spectrom.* 23, 845.

Groma, V., Osán, J., Török, S., Meirer, F., Streli, C., Wobrauschek, P., & Falkenberg, G. (2008). *Időjárás* 112, 83-97.

Osán, J., Török, S., Beckhoff, B., Ulm, G., Hwang, H, Ro, C.-U., Abete, C., & Fuoco, R. (2006) *Atmos. Environ.* 40, 4691-4702.

Atmospheric pollution and particulate matter concentration at petrol station in semi-urban site

A. Akachat

Laboratoire LMMC, pollution atmosphèrique, Université M'Hamed Bougara Boumerdes,
Avenue de l'indépendance, Boumerdes 35000, Algérie
a.akachat@yahoo.fr

Keywords: air quality, atmospheric pollution, petrol station, particulate matter

The road traffic is the major source of air pollution in the agglomeration of Algiers. As part of the assessment and management of the ambient air quality, we have studied the impact of a petrol station located in a semi-urban site west of Algiers, a weighting of the frequency, the non-detection and the severity of the impact on air quality has been determined. The petrol stations were chosen for their wide setting up throughout the national territory, the proximity service they represent and the nature of services they provide (storage and distribution). The survey has enabled to identify six significant environmental aspects including a major emission of VOC known to be precursors of ozone in the presence of NOX we concluded that the petrol stations could be sites creating oxidant smog. A qualitative analysis by taking of dust by filter sampling system is in agreement with the obtained environmental weighting.

Particulate Matter Deposition Monitoring in the Surroundings of the Port of Koper

G. Jereb[1,7], B. Poljšak[1], B. Marzi[2], F. Cepak[2], G. Dražič[3], N. Ogrinc[4], M. Bizjak[1,5] and S. A. Katz[6,7]

[1] University of Ljubljana, College of Health Studies, Poljanska 26 a, 1000 Ljubljana, Slovenia
[2] Port of Koper, Vojkovo Nabrežje 38, 6000 Koper, Slovenia
[3] Department for Nanostructured Materials, Jožef Stefan Institute, Jamova 39, 1000 Ljubljana, Slovenia
[4] Department of Environmental Sciences, Jožef Stefan Institute, Jamova 39, 1000 Ljubljana, Slovenia
[5] Environmental Agency of the Republic of Slovenia, Vojkova 1b, 1000 Ljubljana, Slovenia
[6] Rutgers University, Department of Chemistry, Camden, NJ 08102-1411, USA
[7] University of Nova Gorica, School of Environmental Sciences, Vipavska 13, Nova Gorica, Slovenia

Among the activities performed in the Port of Koper are cargo handling and warehousing. At the European Energy Terminal (EET) in the Port of Koper, large amounts of coal and iron ore are handled and warehoused. The storage capacity of the landfill is 450,000 t for coal and 350,000 t for iron ore. The area covered by the coal and iron ore is 108,500 m^2. The impact of dust pollution from coal and iron ore handling will be presented.

The study included 10 sampling sites in the area of Ankaran, Koper and its surroundings. The collection of particulate matter deposition was conducted with the standard Bergerhoff precipitators according to Reinhaltung der Luft im VDI und DIN Guideline VDI 2119 part 2 (1996) - Measurement of Particulate Precipitations Determination of dust precipitation with collecting pots made of glass.

Samples were collected and analyzed (gravimetrically) on the 1st and 15th day of each month for a one year period from December 2007 to December 2008.

Gravimetric analyses was performed according to VDI 2119 part 2 (1996) guidelines. During the sampling period the total amount of particulate matter deposition at all sampling sites in the area of the municipality of Ankaran, Koper and surroundings never exceeded the recommended emission value of 350 mg/m^2 day (Figure 1).
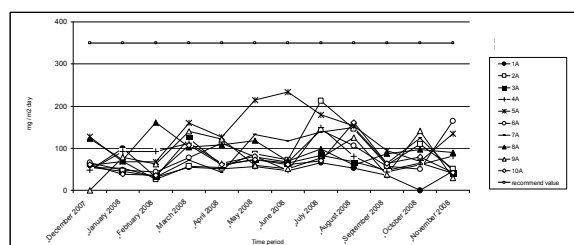

Figure 1: Particulate matter deposition (mg/m^{2}day)

The shape and size of the particles collected over a 12-month period and some of the elements they contained were determined by electron microscopy coupled with energy–dispersive x–ray fluorescence spectrometry.

According to the previous studies (Poljšak *et al*., 2006; ARSO, 2005) the quantity of particulate matter depositions depends mostly on weather conditions, especially the strength and direction of the wind and also the quantity of rainfall, which determined the dryness of the terrain and also dryness of coal and iron ore. For that reason a possible correlation between particulate matter deposition, weather conditions and cargo manipulation was analysed. Additionally the $^{13}C/^{12}C$ ratio in samples was also analysed to determine the sources of particulate organic matter.

For many years the inhabitants of Ankaran (distance from the iron ore and coal storage sites is approximately 1800 m) and its surroundings (the closest residential area is 1000 m from the storage sites) have complained about the pollution of their residential area with emissions from the terminal EET in the Port of Koper. Particulate matter depositions are visibly perceived on their yards, places of residence, linen and vegetables. For that reason the study described in this presentation was conducted to collect and analyze the particulate matter deposition around the Port of Koper, to determine the shape and size of particles and to identify the origin of dust deposition.

Clean air is one of the necessities for healthy life now and in the future. In order to achieve this goal the active participation of legislators, experts from various fields and all those who burden the air with their activities is required.

References

VDI und DIN Guideline VDI 2119 part 2 (1996) - *Measurement of Particulate Precipitations – Determination of dust precipitation with collecting pots made of glass.*

Poljšak B., Jereb G. and Cepak F (2006). *Measurement of particulate matter deposition in Ankaran and its surroundings in period from 15.10.2005 to 15.10.2006 – study report.*

ARSO (Environmental agency of the Republic of Slovenia) (2005). *Air pollution measurement in Ankaran city from 28th of June till 11th of September 2005 - study report.*

Investigation of a denuder-filter sampling technique for the determination of carbonyl compounds from monoterpene oxidation

A. Kahnt, Y. Iinuma, O. Böge and H. Herrmann

Leibniz-Institut für Troposphärenforschung, Permoserstr. 15, Leipzig D-04318, Germany

Keywords: Aerosol sampling, Chemical analysis, SOA

The atmospheric degradation of biogenic and anthropogenic volatile organic compounds (VOCs) produces a number of multifunctional oxidation products. Depending on their physical and chemical properties, these products partition into the gas- and particle phases, leading to the formation of secondary organic aerosol (SOA). Biogenic VOCs like isoprene, monoterpenes and sesquiterpenes are considered to be major SOA precursors due to their higher emission rates. Many of the species detected in laboratory generated SOA are early generation oxidation products, which are formed in the gas-phase and have condensed onto the particle-phase. The knowledge of the gas/particle partitioning of these products is essential towards better understanding of specific oxidation processed and products which lead to SOA formation.

For the determination of gaseous products, the application of a diffusion denuder prior to particle sampling is known to be an effective tool (e.g. Gundel *et al.,* 1995). In addition, in-situ derivatisation of selective target compounds has been tested to improve collection efficiency of denuders, particularly for polar volatile compounds such as carbonyl compounds. For example, these techniques use 2,4-dinitrophenylhydrazine (DNPH) coated denuders (Possanzini and Di Palo, 1999) or combine XAD-4 and O-(2,3,4,5,6-pentafluorobenzyl) hydroxylamine (PFBHA) (Temime *et al.,* 2007) to derivatise carbonyl compounds directly on the surface of the denuders.

In the present study, the results are shown from the evaluation of a denuder/PTFE filter sampling technique and the results from their application on selected monoterpene oxidation studies (α-pinene/OH and β-pinene/OH). XAD-4 and DNPH coated denuders were used to perform in-situ derivatisation of gas-phase carbonyl compounds. For the evaluation of the denuder operation parameters, selected carbonyl compounds were injected into a chamber at known concentrations. The gas-phase samples were collected using serially connected denuders. After sampling, the denuders were extracted with acetonitrile and the extract was purified using a solid phase extraction cartridge (SPE). Afterwards the samples were analysed with HPLC/ESI-TOFMS. First results from the evaluation of the denuder performance are summarised in Table 1, which includes the total sample preparation procedure. The absolute recoveries (i.e.

detected/expected) showed higher values for a higher flow rate with a larger sampling volume. On the other hand, no significant difference was found for breakthrough values (i.e. amount found in the first denuder/sum of first and second denuders) except for nopinone which showed a better breakthrough value at a lower flow rate and sampling volume.

Table 1. List of the 2,4-DNPH derivatives of oxidation products and the performance parameters of the denuders including the sample procedure in this study.

	30 l/min, 1.8m³		10 l/min, 0.6m³	
	Recovery [%]	Breakthrough [%]	Recovery [%]	Breakthrough [%]
Campholenic aldehyde	41	4	13	15
Nopinone	47	29	31	0
Pinon-aldehyde	43	12	21	15

The results show that the denuder operation parameters, such as the flow rate, are important for maximising the performance of denuders for sampling of these first generation oxidation products. The denuders which are characterised for their performance were used for the determination of the yields of pinonaldehyde and nopinone in the gas- and particle-phases from the OH oxidation of α-pinene and β-pinene (Table 2). These numbers agree well with previously reported yields (e.g. Aschmann *et al.*, 2002 and Wisthaler *et al.*, 2001).

Table 2. Yields of first generation products from α-pinene/OH and β-pinene/OH oxidation with $(NH_4)HSO_4$ seed particles in gas- and particle-phase determined in this study.

α-pinene/OH reaction	Gas-phase	Particle-phase
Pinonaldehyde	0.27	0.03

β-pinene/OH reaction	Gas-phase	Particle-phase
Nopinone	0.23	trace

References
Aschmann, S. M., et al. (2002), *Journal of Geophysical Research-Atmospheres*, *107*.
Gundel, L. A., et al. (1995), *Atmospheric Environment*, *29*, 1719-1733.
Possanzini, M., and V. Di Palo (1999), *Chromatographia*, *49*, 161-165.
Temime, B., et al. (2007), *Environmental Science & Technology*, *41*, 6514-6520.
Wisthaler, A., et al. (2001), *Atmospheric Environment*, *35*, 6181-6191.

A Photoacoustic Aerosol Absorption Spectrometer Working from 420 nm to 2200 nm

C. Haisch, P. Menzenbach, and R. Niessner

Chair for Analytical Chemistry, Technische Universität München, D-81377, Munich, Germany

Keywords: photoacoustic, optical properties, particle characterization.

Optical properties of aerosols are highly important for atmospheric research, as they significantly influence the global radiation balance. Optical absorption of the particles is usually measured after sampling on a filter, which may result in artefacts. Online measurements, where the particles remain dispersed in the carrier gas, are generally based on optical transmission measurements. Consequently, the results are extinction values, i.e. the sum of light scattering and absorption. Photoacoustic (PA) spectroscopy is nearly the only technique, which directly quantifies optical absorption. It is based on the conversion of absorbed light energy to heat on the particle's surface. The heat which is transferred to the surrounding gas leads to local expansion. When the light source is modulated or pulsed, the local expansion is modulated as well, which means that a sound wave is generated. This sound signal is proportional to the incident light intensity and the local absorption and can be detected by means of a microphone.

Several extremely sensitive PA-based systems are described in literature, which are able to measure concentrations down to tenth of ng m^{-3} (e.g. Arnott et al.) Nearly all these instruments employ a fixed set of up to four wavelengths. We developed a PA-based instrument for absorption measurement for the complete visible and Near Infrared (NIR) spectrum, operating from 420 nm to 2200 nm.
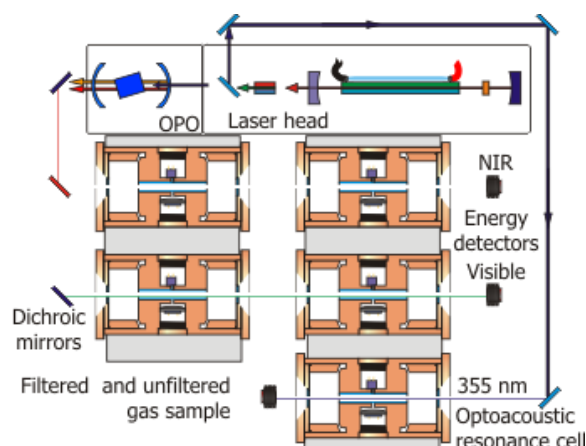
Figure 1   Schematic set-up of the PA aerosol spectrometer.

In contrast to most PA instruments, the system employs a pulsed laser source, because only pulsed lasers offer a tuning range over such wide spectral range. We use an OPO (Optical Parametrical Oscillator), pumped by a frequency-tripled Nd:YAG laser (355 nm). The OPO emits two beams, one in the visible spectral range and one in the NIR. Spectra are measured by stepwise changing the OPO wavelength. Each beam passes through two cells, one containing the sample and the other the gas after filtration. The absorption signal from the particles is the difference of the signal from the two cells. This approach is necessary as particularly in the NIR there is significant background absorption from gaseous compounds, e.g. water vapor. Through a fifth cell, the pump beam (355 nm) is guided. As the measurement of a full spectrum can take many minutes up to hours, depending on the number of laser pulses averaged and on the chosen wavelength step width, it has to be ensured that the particle concentration does not vary during the measurement, which would lead to artifacts. Assuming that the particles' optical properties remain constant during the measurement, we use the signal at 355 nm is used to correct for fluctuations of the particle concentration.
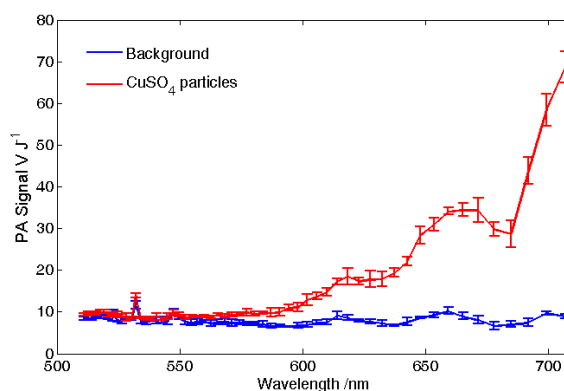

Figure 2   Absorption spectrum of CuSO$_4$ aerosol, measured with the PA spectrometer.

After calibration with water vapor, we use the system to measure absorption spectra of many different particle systems. As a typical result, the absorption of CuSO$_4$ aerosol is shown in Fig. 2. The signals are given in V J^{-1}, as each measurement is normalized on the corresponding laser pulse energy, which is measured parallel to the PA measurements. In combination with a particle counter, we can measure specific absorptions per particle number.

Arnott, W. P. et al. (2005) *Environ. Sci. & Technol.*, 39, 5398-5406.

Indoor and Outdoor Carbon Composition of $PM_{2.5}$ Aerosol in Mumbai, India

Abba Elizabeth Joseph[1], Seema Unnikrishnan [1] Rakesh Kumar[2]

[1] Department of Environment Management, National Institute of Industrial Engineering,
Vihar Lake Mumbai-400087, India
2 National Environmental Engineering Research Institute, Mumbai Zonal Laboratory,
Mumbai -400018, India

Key words: $PM_{2.5}$, Indoor/Outdoor, Elemental Carbon, Organic Carbon

Background: $PM_{2.5}$ aerosol cause adverse human health effects and climate change. In the US, Committee on Research Priorities for Airborne Particulate Matter, National Research Council identified that there is gap in understanding personal exposure since exposures to particles generated by outdoor sources take place not only outside but also in indoor environments, where the particles penetrate. The sources of fine, combustion-derived pollutants are less well understood for the indoor environment, prompting studies of relationships between outdoor sources and indoor air quality *(Fischer et al., 2000)*. In India, limited information is available on $PM_{2.5}$ aerosol hence there is need to understand and also correlate with Indoor levels so that it helps in setting ambient air quality standards and exposure studies. In the present study indoor and outdoor $PM_{2.5}$ was measured simultaneously at two sites residential (Khar) and industrial (Mahul) in Mumbai city, India during summer, post -monsoon and winter season for a week during year 2007-2008. $PM_{2.5}$ was monitored using Air metrics Minivol and DRI thermal optical analyzer was used for measuring Organic carbon (OC), Elemental carbon (EC) and Total Carbon (TC).

Results & Discussion: Average $PM_{2.5}$ and carbon levels for threes season is given in the **Table 1**. The Indoor/Outdoor (I/O) ratio for $PM_{2.5}$ was 0.8 and 0.78 at the respective sites. Pearson Correlation Coefficient among Indoor and Outdoor Pollutants was estimated. At 'R' site excellent correlation among $PM_{2.5}$, with EC and OC outdoors (r=0.85 and 0.67, p<0.01) is due to common combustion sources like vehicles which contributes to mass and carbonaceous fraction.   At residential site good correlation between $PM_{2.5}$ and EC indoors with EC outdoors (r=0.52 and 0.53, p<0.05) indicates penetration of outdoor air affecting inside air quality as the site is close to freeway. Previous study by *(Baxter et al., 2008)* observed that a large portion of the outdoor EC penetrates indoors and therefore people living in close proximity to freeways are exposed to increase indoor EC levels. At 'I' site had maximum outdoor mass levels and minimum carbon levels indoors as the household was in a high rise apartment. As indicated by *(Jo and Lee, 2006)* air quality in a high rise apartment is better than in low-rise apartment. India does not have standard for $PM_{2.5}$, compared ambient outdoor levels with the US- EPA standard at both sites during all season exceeded indicating bad air quality. The OC/EC ratio outdoors at R and I site was > 2 with average ratio of 5.31 and 3.99 implying that secondary organic aerosol is formed in Mumbai city

Table 1: Average Indoor & Outdoor Concentration of $PM_{2.5}$, EC & OC during 2007-2008

	$PM_{2.5}$	OC	EC	TC
R.	88.89 ± 39.12	32.76 ± 15.09	7.76 ± 5.17	40.94 ± 19.53
I.	96.84 ± 24.53	29.09 ± 16.32	7.61 ± 3.79	36.70 ± 18.97
R.	69.75 ± 27.02	24.50 ± 8.58	6.60 ± 5.38	31.39 ± 12.93
I.	76.58 ± 28.05	19.29 ± 9.5	3.61 ± 2.95	22.90 ± 12.43

Conclusions: Present study helped in removing the gap of understanding relationship between indoor and outdoor air pollutants. *(Wallace, 1996)* predicted that in absence of Indoor air sources the I/O ratio is (0.4-0.6), none of sites in the present study had such ratio indicating presence of indoor sources. This was a preliminary study, further research in understanding composition of fine particles w.r.t metals; ions and marker compounds in different season will improve scientific understanding of sources.

References:
Fischer, P.H., Hoek, G., vanReeuwijk, H., Briggs, D.J., Lebret, E., vanWijnen, J.H., Kingham, S., Elliott, P.E., (2000), *Amos. Environment,* 34, 3713–3722.
Baxter, L.K.,, Barzyk, T.M., Vette, A.F., Croghan, C., Williams, W.R., (2008), *Atmos. Environment* 42, 9080-9086.
Jo, W.K., Lee, J.Y., (2006) *Atmos. Environment* 40, 6067-6076.
Wallace, L., (1996). J.The Air and Waste Management Association, 46, 98-126

Molecular characterisation of biogenic secondary organic aerosols using ion mobility spectrometry - quadrupole time-of-flight mass spectrometry

Yoshiteru Iinuma and Hartmut Herrmann

Leibniz-Institut für Troposphärenforschung, Permoserstr. 15, Leipzig D-04318, Germany

Keywords: LC/MS, Mass spectrometry, Ion mobility, SOA, Organic compounds.

Molecular characterisation of unknown organic compounds is challenging, in particular the molecular identification of secondary organic aerosol constituents is extremely demanding due to their low quantities and high complexity of the sample matrix. The presence of multiple structural isomers and their complex structures often make the synthesis of reference compounds very difficult, hindering a positive identification of these compounds.

Traditionally, chromatographic separation is coupled to mass spectrometry for the structural elucidation of unknown compounds in atmospheric aerosol samples. While chromatographic separation provides information on the volatility or polarity of the unknowns, mass spectrometry provides their structural and/or molecular mass information. In particular, the applications of derivatisation GC/MS and HPLC/ESI-TOFMS techniques in recent years brought significant advances in our understanding of SOA constituent structures, leading to the identification of methyltetrols from isoprene oxidation (Claeys *et al.*, 2004), tricarboxylic acid from α-pinene oxidation (Szmigielski *et al.*, 2007), and structural proposals for various organosulphates (Iinuma *et al.*, 2007ab; Surratt *et al.,* 2007, 2008; Gómez-González *et al.*, 2008)

Ion mobility spectrometry coupled to mass spectrometry (IMS-MS) is a new analytical tool which offers a rapid separation of molecules by their mobility in the gas phase, hence their size/conformation. The drift time of molecules in the IMS is linearly related to the mobility. The mobility (K) of a gas phase ion is defined as $K = \upsilon_D/E$ where υ_D and E are the drift velocity and the electric field, respectively. The mobility can be calculated as follows:

$$K = \frac{\sqrt{18\pi}}{16} \sqrt{\frac{1}{m} + \frac{1}{m_B}} \frac{q}{\sqrt{\kappa T}} \frac{1}{N\Omega}$$

where m is the ion mass, m_B is the mass of buffer gas atom, q is the ion charge, κ is the Boltzmann constant, T is the temperature, N is the gas number density and Ω is the collision cross section of the ion. For isobaric isomers, differences in the collision cross section, hence their size and shape of the ions in the gas phase differentiate the drifting times/mobility values. Therefore, an ion with a smaller collision cross section has higher mobility, thus a shorter drifting time. Figure 1 shows an application of the IMS-MS to the analysis the *m/z*

249 compounds from α-pinene and β-pinene organosulphates. As can be seen, a larger β-pinene organosulphate with a sulphate group at a primary carbon atom (left above) shows a shorter drifting time than a smaller β-pinene organosulphate with a sulphate group at a tertiary carbon atom (left bottom). The same trend is observed for α-pinene organosulphates (right). The result presented here demonstrates a potential of the IMS-MS technique for structural elucidation of unknown SOA constituents.
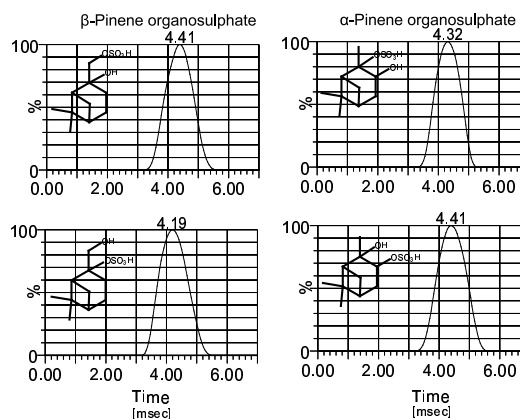

Figure 1. Drifting time obtained from the IMS analysis for α-pinene organosulphates (right) and β-pinene organosulphates (left).

M. Claeys *et al.* (2004). *Science*, 303, 1173-1176.

Y. Gómez-González *et al.* (2008). J Mass Spectrom, 43, 371-382.

Y. Iinuma *et al.* (2007a). Environ. Sci. Technol., 41, 6678-6683.

Y. Iinuma *et al.* (2007b). Atmos. Environ., 41, 5571-5583.

J. D. Surratt *et al.* (2007), Environ. Sci. Technol., 41, 517-527.

J. D. Surratt *et al.* (2008). J Phys Chem A, 112, 8345-8378, 10.1021/jp802310p

R. Szmigielski *et al.* (2007). Geophys. Res. Lett., 34, doi:10.1029/2007GL031338.

Assessment of fossil and non-fossil primary and secondary organic aerosol

A.S.H. Prévôt[1], S. Szidat[2], N. Perron[1,2], V. Lanz[1], M.R. Alfarra[1,3], P. DeCarlo[1], C. Mohr[1], and U. Baltensperger[1]

[1]Laboratory of Atmospheric Chemistry, Paul Scherrer Institut, Villigen, Switzerland
[2]Department of Chemistry and Biochemistry, University of Berne, Berne, Switzerland
[3]Atmospheric and Environmental Sciences, University of Manchester, Manchester, United Kingdom

Keywords: Aerosol mass spectrometer, AMS, ^{14}C, Source apportionment

A new approach of combining two in the last years developed measurement and data analysis techniques will be presented. The use of positive matrix factorization (PMF) of Aerodyne Aerosol mass spectrometer often allows the distinction of the contribution of biomass burning, hydrocarbon-like organic aerosol, and oxygenated organic aerosol (OOA) to organic mass (Lanz et al., 2007; Ulbrich et al., 2008). The hydrocarbon-like aerosol is interpreted to come from the combustion of fossil fuel (often mostly from traffic) and OOA is thought to consist of secondary organic aerosol which is supported by high correlations of OOA with ammonium sulfate and/or ammonium nitrate.

The measurements of $^{14}C/^{12}C$ ratios in organic carbon (OC) allows the calculation of fossil and non-fossil contributions to (OC) (Szidat et al., 2004, 2008). The PMF results of the AMS data can be combined with the radiocarbon measurements to distinguish the fossil and non-fossil contributions to the carbon of both the primary and secondary organic carbon. Necessary assumptions include OM/OC ratios of biomass burning, hydrocarbon-like organic aerosol and secondary organic aerosol.

Results of such combined analyses will be presented at different sites in urban and rural areas as well as close to highways and Alpine valleys. Not all results are finalized yet but results so far suggest that in most cases, secondary organic aerosol is mostly non-fossil both in winter and summer in Switzerland. We will discuss uncertainties due to necessary assumptions.

Lanz, V.A., M.R. Alfarra, U. Baltensperger, B. Buchmann, C. Hueglin, & A.S.H. Prevot (2007), *Atmos. Chem. Phys.*, 7, 1503-1522.

Szidat, S., T.M. Jenk, H.W. Gäggeler, H.-A. Synal, R. Fisseha, U. Baltensperger, M. Kalberer, V. Samburova, S. Reimann, A. Kasper-Giebl & I. Hajdas (2004) Atmos. Environ., 38, 4035-4044.

Szidat, S., A.S.H. Prevot, J. Sandradewi, M.R. Alfarra, H.-A. Synal, L. Wacker & U. Baltensperger (2007), *Geophys. Res. Lett.*, 34, L05820, doi:10.1029/2006GL028325.

Ulbrich, I.M., M.R. Canagaratna, Q. Zhang, D.R. Worsnop & J.L. Jimenez (2008), *Atmos. Chem. Phys. Discuss.*, 8, 6729-6791.

Tuning of Sunset EC/OC field instruments to obtain more than comparable data

J. Schwarz, P. Vodička

Institute of Chemical Process Fundamentals AS CR, Rozvojová 135, CZ-16502, Prague, Czech Republic

Keywords: Thermal optical transmission, OC/EC analysis.

Thermal optical transmission method (TOT) used to analyse organic and elemental carbon is, beside thermal optical reflectance (TOR) method, the most wide spread method of OC/EC analysis. The method itself gives very good agreement when it is compared based on total carbon (TC) data and quite good for organic carbon (OC) data. The comparison of elemental carbon data is much more difficult due to mostly lower EC concentration comparing to OC and its dependence on the temperature protocol used. The comparison of separate OC peaks (OC_1, OC_2, ...) that arise from separate temperature steps in He phase and so called pyrolitic carbon (PC) is possible for the same temperature protocol only and their real meaning is not completely clear yet. Our group installed 2 pieces of new version of Sunset labs field OC/EC analyser that enables PM10 sampling and analysis recently. To be able to compare the results of the two instruments, our first task was to get comparable results for the same PM fraction and a temperature protocol. The results we obtained are the main topic of this paper.

The temperature protocol EUSAAR II is now being tested in the frame of EUSAAR project at many rural background sites with an ambition to become European standard for OC/EC analysis. Therefore, we started our comparison using this protocol. This protocol is suggested for laboratory version of Sunset instrument and it has to be adopted to be used in the field version. Comparison of results (hourly data) we obtained for our two instruments in the beginning is depicted in Fig. 1.
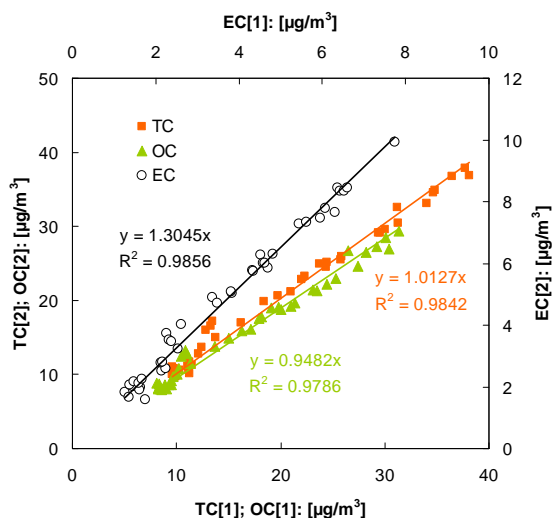
Fig. 1: Comparison of two instruments using adopted EUSAAR II protocol settings at both instruments.

From the figure it is clear that while TC comparability is very good, EC had systematic deviation that is non-negligible. There are two basic instrument parameters that influence the processes on the filter during the analysis: the real temperature of the filter, and the time spent at given temperature. We suppose that the errors in gas flow rates are negligible in comparison with the two previous parameters. Based on previous rationale and the producer's advice we started to change the temperature steps within the protocol so that we fixed the temperature steps in instrument 1 and we were changing the temperatures in the instrument 2 to get more comparable results, not only from EC point of view but also for separate peaks OC1 to OC4 and PC. Besides the temperature changes in the instrument 2, we also changed the lengths of individual time steps to decrease the influence of temperature regulation dynamics. These changes were done on both instruments. The best results we obtained for a comparable dataset are shown in Fig 2.
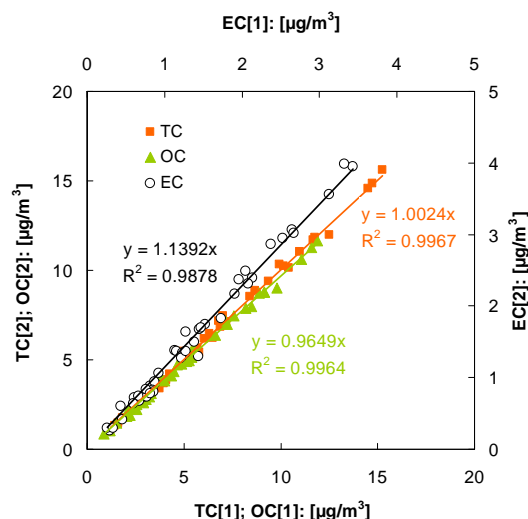

Fig. 2: Current state of comparison of the two field instruments. Font colors correspond to series color.

Although there is still some deviation in the EC, the main difference was obtained for PC. The slope went from 2 to 1.15 for the last dataset. The final results that we will have got will be shown at our poster.

A novel particle sampling system for toxicological characterization of emissions

J. Ruusunen[1], H. Lamberg[1], M. Tapanainen[3], K. Hytönen[1], O. Sippula[1], J. Tissari[1], M. Ihalainen[1], T. Karhunen[1], A.S. Pennanen[3], P. Willman[1], M-R. Hirvonen[3], R.O. Salonen[3] and J. Jokiniemi[1,2]

[1]University of Kuopio, Department of Environmental Science, Fine Particle and Aerosol Technology Laboratory, P.O. Box 1627, FI-70211 Kuopio, Finland.
[2]VTT Technical Research Centre of Finland, Fine Particles, P.O. Box 1602, 02044 VTT, Espoo, Finland.
[3]National Institute for Health and Welfare, Department of Environmental Health, P.O. Box 95, FI-70701 Kuopio, Finland

Keywords: aerosol sampling, cascade impactor, PM_1, chemical composition, toxicology

Several studies have shown that combustion-derived fine particles cause adverse health effects. Previous toxicity studies on combustion-derived fine particles have rarely involved multiple endpoints and a thorough analysis of chemical composition. Comprehensive toxicological characterization of the emission particles needs relatively large amount of sample mass (tens of milligrams). Thus, the samples have been previously collected with large equipments to reach sufficiently high flow rates. To get representative particle samples, the sample flow of flue gas is first diluted and cooled down to obtain semivolatile components in the particle phase. In this study, we have developed a new compact system to sample emission particles for toxicological analyses.

Two laboratory measurement campaigns were conducted to compare a modified Harvard high-volume cascade impactor (HVCI – 850 litres/min) (Sillanpää et al. 2003) with a new system that consists of a porous tube diluter, Dekati Gravimetric Impactor (DGI - 70 litres/min; Dekati Ltd.) and flow control. In the first campaign, the differences between the impactors were tested by drawing particle samples from a dilution tunnel with dilution ratio (DR) around 100. In the second campaign, the sample for DGI was diluted using a porous tube diluter with DR 10-20. The combustion sources used in the campaigns were a light-duty diesel engine, a pellet boiler and a conventional masonry heater. In addition, Dekati Low-Pressure Impactor (DLPI, Dekati Ltd) was used to measure a more detailed particle mass size distribution. To determine PM_1 emissions, polyurethane foam and PTFE backup filter were used as impaction substrates in the HVCI, while PTFE filters were used in the DGI. None of the substrates were greased, since it interferes with toxicological analyses.

The composition of emitted particles varied between the sources. PM_1 from diesel exhaust contained a lot of soot, and those from pellet boiler and masonry heater contained large amounts of alkali metal compounds and organic material, respectively.

There was a relatively good agreement on PM_1 concentration between the HVCI and DGI in the dilution tunnel. In contrast, the PM_1 emissions differed from each other, when the DGI was operated with the porous tube diluter. This may be due to different gas-to-particle conversion of organic vapours. The contributions of organic carbon in conventional masonry heater were between 8.5% and 16.9% to the DGI-PM_1 and between 7.1% and 10.6% to the HVCI-PM_1.
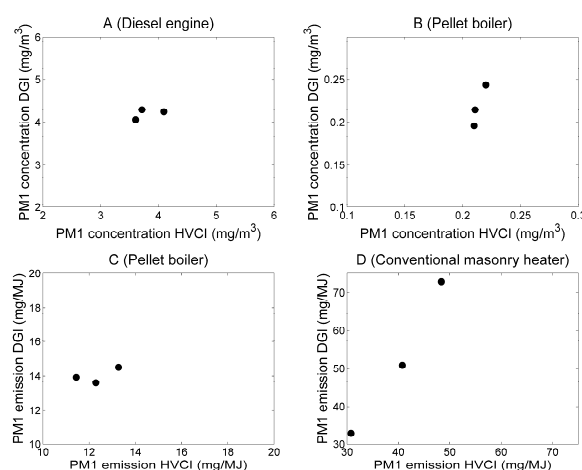

Figure 1. PM_1 emissions as measured using the DGI and HCVI. Panels A and B: All samples collected from dilution tunnel. Panels C and D: Samples for DGI collected using porous tube diluter.

The HVCI dilution tunnel method was found to result in a slightly lower PM_1 emission than the DGI porous tube diluter method. The differences in the measured PM_1 emission were likely connected to particulate organics. With the HVCI method, the DR was higher, which is known to give a lower fraction of emitted particulate organics (Lipsky et al., 2006).

Lipsky, E. M., & Robinson, A. L. (2006). *Environ. Sci. Technol.*, 40, 155-162.

Sillanpää, M. *et al.* (2003). *J. Aerosol. Sci.* 34:485-500.

T16 Special Session 4

Surface-atmosphere exchange of aerosol particles in the high Arctic – Results from ASCOS

A. Held[1,2], D. Orsini[1] and C. Leck[2]

[1] Institute for Tropospheric Research, Leipzig, Germany
[2] Department of Meteorology, Stockholm University, Stockholm, Sweden

Keywords: Arctic aerosols, Deposition, Fluxes

The Arctic Summer Cloud Ocean Study (ASCOS, www.ascos.se) investigates the physical and chemical processes leading to cloud formation in the high Arctic Ocean. This work examined a potential contribution of particles emitted from open leads to the Arctic aerosol using flux and gradient measurements made from an ice floe in the Arctic pack ice.

The Arctic sea-ice has been identified as an important tipping element in the Earth's climate system (e.g. Lenton et al., 2008) with potentially large implications for Europe and the rest of the world. However, current regional and global climate models lack many relevant cloud-ice-ocean feedback mechanisms. From earlier observations, a local natural biogenic source of aerosol particles from bursting bubbles at the water-air interface has been suggested in the Arctic region north of 80° N (e.g. Leck et al., 2004; Leck and Bigg, 2005a, 2005b). It may link marine biological activity, clouds and climate through the ejection of organic microcolloids from the surface microlayer of open leads into the atmosphere. Once airborne, some of these particles may act directly as CCN, while others are activated after condensational growth. In order to improve our understanding of the Arctic aerosol-cloud-climate relationship, the strength of this previously unaccounted source and its contribution to the atmospheric aerosol burden should be quantified.

During the ice-breaker borne ASCOS expedition in 2008, direct eddy covariance measurements of aerosol number fluxes were carried out with a sonic anemometer and a condensation particle counter from the edge of an ice floe drifting in the central Arctic Ocean between 87° – 87.5° N latitude and 2° – 10° W longitude. In addition, gradients of temperature and aerosol number concentration were measured in the lowest 2 m of the boundary layer over the open lead and over the ice surface using a levered pole. Applying simple flux-profile relationships, emission or deposition fluxes were derived from the gradient measurements and compared with eddy covariance fluxes.

On five out of nine days, particle number concentration gradient measurements could be evaluated assuming a logarithmic concentration profile. The transfer velocities derived from the concentration gradients ranged from -0.9 mm/s (emission) to +0.4 mm/s (deposition) while the corresponding transfer velocities calculated directly from eddy covariance ranged from -0.2 mm/s (emission) to +0.6 mm/s (deposition). These values are in agreement with previous particle flux estimates over snow surfaces and in the Arctic pack ice.

Our measurements over the open lead suggest time periods of particle emission, while the snow behaves primarily as a deposition surface. This indicates that open leads may play a role as particle sources especially when other particle sources such as advection from the open sea are not effective. This contribution is non-negligible especially in the summer months when the high Arctic is effectively separated from anthropogenic emissions due to atmospheric circulation patterns. Unfortunately, the total number flux data does not allow for reliable mass flux estimates or information about the size of emitted particles. Nevertheless, melting of sea ice will further increase the fraction of open leads in the Arctic pack ice, and potentially increase the relevance of the open lead particle source.

Leck, C., Tjernström, M., Matrai, P., Swietlicki, E., and Bigg, K. (2004) Can marine micro-organisms influence melting of the Arctic pack ice? *Eos Trans.* 85, 25-36.

Leck, C. and Bigg, E.K. (2005a) Biogenic particles in the surface microlayer and overlaying atmosphere in the central Arctic Ocean during summer. *Tellus* 57B, 305-316.

Leck, C. and Bigg, E.K. (2005b) Evolution of the marine aerosol - a new perspective. *Geophys. Res. Lett.* 32, L19803, doi:10.1029/2005GL023651.

Lenton, T.M., Held, H., Kriegler, E., Hall, J.W., Lucht, W., Rahmstorf, S. and Schellnhuber, H.J. (2008) Tipping elements in the Earth's climate system. *PNAS* 105, 1786-1793.

Effects of relative humidity on aerosol light scattering in the Arctic region

P. Zieger[1], R. Schmidhauser[1], E. Weingartner[1], J. Ström[2], and U. Baltensperger[1]

[1]Laboratory of Atmospheric Chemistry, Paul Scherrer Institut, 5253, Villigen, Switzerland
[2]Department of Applied Environmental Science, Stockholm University, 10691, Stockholm, Sweden

Keywords: arctic aerosols, light scattering, relative humidity, field measurements, aerosol modeling

The goal of this study is to investigate the effects of relative humidity on aerosol optical properties under maritime and arctic conditions. For this, we installed a newly developed humidified nephelometer (WetNeph, Schmidhauser et al. 2008), an aethalometer (AE31), a scanning mobility particle sizer (SMPS) and an optical particle counter (OPC) for three months from July to October 2008 at the Zeppelin station in Ny-Ålesund, Spitsbergen. The WetNeph, as our main instrument, measured the aerosol scattering coefficient at controlled relative humidity (RH). This instrument allows the determination of the scattering enhancement factor f(RH), which is defined as the scattering coefficient at a certain RH divided by the dry scattering coefficient measured by a second nephelometer running synchronously at low RH. The aethalometer measured the aerosol absorption coefficient at seven wavelengths, while the SMPS and OPC measured the aerosol size distribution between 15 nm and 22.5 μm.

These measurements are needed for the verification and improvement of our aerosol modeling activities. Here, the light scattering and absorption coefficients are modeled (as a function of relative humidity) with an advanced model using Mie theory. The results can then be used to recalculate long-term time series of light scattering and absorption coefficients, which are generally performed under dry conditions (RH<40%), to ambient (real) conditions. A continuous time series of dry nephelometer measurements exists at the Zeppelin station since 2001. The knowledge of the RH dependence is of eminent importance e.g. for climate models and for the comparison of ground based observations with satellite retrievals and aerosol parameters retrieved from lidar and sun photometers.

The WetNeph was set to measure humidograms: In the first hour, the RH was increased from ~35% RH to ~ 85% RH, to measure the lower branch of the hysteresis curve (humidifying the aerosol). In the second hour, the aerosol was exposed in the nephelometer to high RH (>80%) in the humidifier and then dried to a lower RH. This allows measuring the upper branch of the hysteresis curve. The nephelometer measured the light scattering and backscattering coefficients at the wavelengths of 450, 550, and 700 nm.

A typical humidogram of the scattering coefficient is seen in Figure 1. Compared to the dry conditions the scattering is enhanced at 85% RH by a factor of ~2.5. If one bears in mind that the mean RH in the instruments in the laboratory is typically below 10% and the mean RH in ambient air during August is ~85%, one can see how large the underestimation - here a factor of 2.5 - of the actual scattering is for that day. There is no hysteresis observed for most of the measuring period, meaning that the particles were always wet. At the end, with a higher sea salt content, hysteresis was partially observed.

Here, we will present the results of our comprehensive field campaign. In addition, we will present a procedure to recalculate the measured scattering coefficients to ambient conditions for the case of summer and fall months.
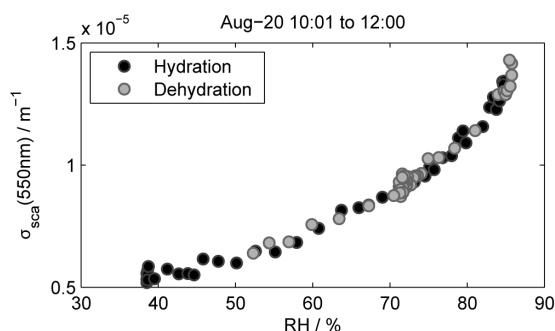

Figure 1. A typical humidogram of the scattering coefficient (at 550nm) measured on August 20th, 2008. The relative humidity (RH) was increased from ~38% to ~85% (hydration) and than decreased back to ~55% (dehydration).

Schmidhauser, R., Zieger, P., Wehrle, G., Jefferson, A., Ogren, J.A., Baltensperger, U. and Weingartner, E., *Characterization of a new humidified nephelometer – Instrument description and first application*, submitted to Environ. Sci. Technol., 2008.

Measurements of concentrations and deposition velocity of ultrafine aerosol over the Nansen Ice Sheet (Antarctica)

A.Donateo[1], D.Contini[1], F.Belosi[2] , F.M.Grasso[1], G.Santachiara[1] and F.Prodi[2]

[1]Institute of Atmospheric Science and Climate (ISAC-CNR), 73100, Lecce, Italy
[2] Institute of Atmospheric Science and Climate (ISAC-CNR), 40129, Bologna, Italy

Keywords: Antarctic aerosols, deposition velocity, nanoparticles, eddy covariance fluxes, deliquescence.

Antarctica, although not meteorologically isolated from the rest of the planet, is still one of the cleanest places on the Earth. Over the years Antarctic aerosol have been investigated in terms of its chemical composition, the total number and mass concentrations in different sites. In this work turbulent vertical particles number fluxes of nanoparticles (down to 10 nm in diameter) and the relative deposition velocity (vd) have been studied by eddy correlation (EC) technique in a remote site over the Nansen Ice Sheet (74° 30.0' S, 163° 27.5' E at 84 m a.s.l.).

Measurements were made between 8 and 31 December during Austral summer 2006. Particle number concentration has been measured using a CPC (Grimm model 5.403) with a time response of about 1.3s placed inside a glassfiber igloo. This instruments has been coupled for eddy correlation configuration with a sonic anemometer (Gill, R3) at the top of a meteorological tower (12m), by means of an aluminium inlet. A Rotronic (MP100A) thermo hygrometer, a fast response hygrometer (Campbell, model KH20) and a net radiometer were also installed to measure other micrometeorological and meteorological parameters. A DMA (Grimm, 5.500) was operated for a few days sampling at 2m height. In CPC data it has been observed a contamination from local sources that appeared as sharp peaks over relatively low and smooth concentrations. The period of these peaks are characterised by positive vertical turbulent fluxes compatible with ground-level sources. The contamination occurred when the wind was blowing from the direction of the unleaded gasoline generator (S-SE) used in the site for electrical supply. The wind directions from the sector NW-N were uncontaminated and often characterised by strong katabatic winds. The analysis of this sector of wind direction allowed to evaluate the deposition on the ice surface. During contamination the size distribution is significantly different from the one of uncontaminated aerosol (Fig.1) showing a marked unresolved peak around 12 nm. The average total particle number concentration, after removing the contamination peaks, varied between 830 and 450 particles/cm^3. The deposition velocities were corrected for the effect of density fluctuations (Webb et al, 1980) that usually accounted for less than 2%. Another correction is due to the attenuation of fluxes related to the slow CPC time-response. We used the

formulation in Horst (1997), that gives a correction of about 50% on average. This because the boundary-layer is generally characterised by stable conditions. However we are implementing a new correction based on the co-spectra actually measured in the site that could be more appropriate. Also correction to measured aerosol turbulent fluxes for hygroscopic growth of particles (deliquescence) is necessary (Kowalski, 2001). This because the energy fluxes in Antarctica during strong katabatic winds are characterised by negative sensible heat fluxes and relatively large positive latent heat fluxes due to ice sublimation that is favoured at high wind speed. In these particular flow conditions the apparent deposition velocity, due to deliquescence, is generally negative (apparent fluxes upward) and it can be as high as several mm/s. Therefore it is a relevant contribution to the measured deposition velocities for uncontaminated air masses that ranges between 1 and 15 mm/s and it has to be taken into account. Results indicate that deposition velocity increases with wind velocity and with friction velocity u*.
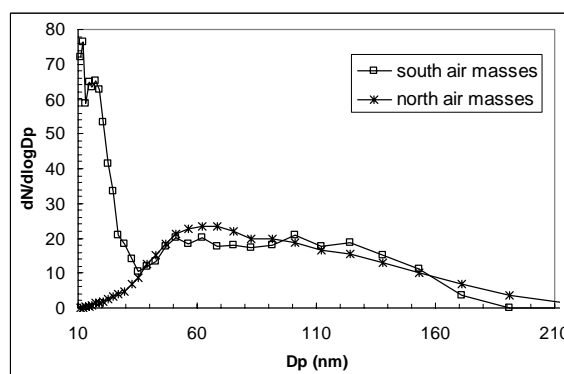

Figure 1. Size distribution for wind from S sector with polluted air and from N sector (16/12/2006).

Horst T.W. (1997). Boundary Layer Meteorology, 82, 219-233.
Kowalski A. (2001). Atmospheric Environment, 35, 4843-4851.
Webb E., Pearman G., Leuning R. (1980). Q.J.R. Meteorol Soc., 106, 85-100.

Impact of marine aerosol on Arctic Haze

T. Petelski[1], A. Rozwadowska[1], T. Zielinski[1], Maria Stock[2], Roland Neuber[2], Renate Treffeisen[2]

[1] Institute of Oceanology, PAS, Poland
[2] Alfred Wegener Institute, Germany

Keywords: Arctic, marine aerosol, optical properties.

Intensive measurement periods within the ASTAR Project were carried out in springs 2004 and 2007. Spring is the season in the Arctic when the so-called Arctic Haze phenomenon occurs. The ASTAR 2007 measurement campaign lasted from 28 March to 16 April. During the campaign the following instruments were used at the station in Hornsund: laser particle counter, sunphotometers, radiometers and pyranometers. Such instrumentation set-up facilitated the determination of the aerosol optical thickness, aerosol concentration and size distribution, upward and downward radiation fluxes. The results of the measurements indicate the cleaning role of marine aerosols in the Arctic conditions.

During the 2007 ASTAR campaign the Arctic Haze conditions were observed during only one day in the southern Spitsbergen area. Such small representation of Arctic Haze conditions can be related to higher up north shift of frozen sea surface areas.

The days with higher AOT values in Hornsund were under the influence of air masses advected directly from the north. Only in those cases air mass trajectories did not run over the open sea.

The ASTAR data indicate that the Arctic Haze phenomenon is weakened due to decrease of ice coverage in the Arctic. In order to confirm this thesis all AOT data collected in Koldeway station by the AWI team over a period of time 1995-2008 have been analyzed and compared with the ice coverage of the sea in the Spitsbergen region.

Significant correlation has been obtained between sea surface area free of ice in March and average AOT value in April (R=0.7). There is also correlation between free of ice sea surface area and the minimum, monthly AOT in April recorded in Ny-Alesund. There is no correlation between the maximum AOT values and ice sea coverage. The maximum AOT values are connected with the advection of air masses from remote areas and/or are related to events such as: forest fires, exceptionally high industrial input, volcano eruptions.
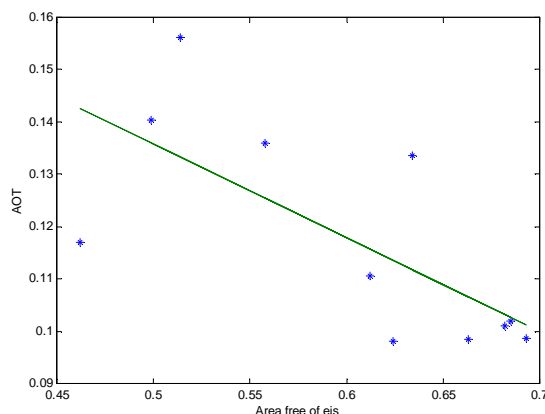
Petelski T., Piskozub J., (2006). *Vertical coarse aerosol fluxes in the atmospheric surface layer over the North Polar Waters of the Atlantic.* Journal of Geophysical Research. Vol. 11, C06039, doi: 10.1029/2005JC003295.

Rozwadowska A., (2004). *Optical thickness of stratiform clouds over the Baltic inferred from on-board irradiance measurements.* Atmospheric Research, 72: 129-147

Tomasi C., Vitale V., Lupi A., Di Carmine C., Campanelli M., Herber A., Treffeisen R., Stone R. S., Andrews E., Sharma S., Radionov V., von Hoyningen-Huene W., Stebel K., Hansen G. H., Myhre C. L., Wehrli C., Aaltonen V., Lihavainen H., Virkkula A., Hillamo R., Strom J., Toledano C., Cachorro V. E., Ortiz P., de Frutos A. M., Blindheim S., Frioud M., Gausa M., Zielinski T., Petelski T., Yamanouchi T., (2007). *Aerosols in polar regions: A historical overview based on optical depth and in situ observations.* Journal of Geophysical Research, 112, D16205, doi:10.1029/2007JD008432

Impact of air mass history on aerosol optical thickness at Hornsund station, Spitsbergen

A. Rozwadowska[1], T. Petelski[1], P. Sobolewski[2] and T. Zieliński[1]

[1] Institute of Oceanology, Polish Academy of Sciences, Powstancow Warszawy 55, 81-712, Sopot, Poland
[2] Institute of Geophysics, Polish Academy of Sciences, Ksiecia Janusza 64, 01-452 Warsaw, Poland

Keywords: AOD, Arctic aerosols, back trajectories

Hornsund has been a station of the Aerosol Robotic Network (AERONET) since 2005. The P.I. of the station is Brent Holben. In the present paper, data from Hornsund station from the period 2005-2008 were employed to study the impact of air mass history on aerosol optical thickness AOT in the southern part of Spitsbergen. Backward trajectories computed by the means of NOAA HYSPLIT model (Draxler & Rolph, 2003) were used to trace the air mass history. The trajectories were calculated for three atmospheric layers: 1 km, 2.5 km and 5 km a.s.l. In the Arctic, aerosol regimes in spring (March, April, May) and summer (mid June to mid September) differ considerably from each other (e.g. Herber et al., 2002, Tomasi et al., 2007). Therefore our analysis was performed for each season separately. Days with low daily mean of AOT(500) (*i.e.* days with $<AOT(500)>_{day} < q_{25}$, where q_{25} is the first quartile of $<AOT(500)>_{day}$ distribution for a given season) and cases with high AOT (*i.e.* days with $<AOT(500)>_{day} > q_{75}$, where q_{75} is the third quartile of the distribution) were selected. In spring, the period of Arctic Haze, the mean aerosol optical thickness for days with low and high AOT equal 0.068 ±0.005 and 0.171 ±0.007, respectively. In summer these means amount to 0.031 ±0.008 and 0.079 ±0.007. The mean of 25% lowest values of $<AOT>_d$ can be treated as the optical thickness of the background aerosol for the respective seasons. The eight-day back trajectories reveal that regardless of the season, in majority of low AOT cases the air had spent at least 7-8 days over the Arctic Ocean, Greenland, Nordic Seas and/or northern Canada before it reached Hornsund. In spring, the high AOT cases can be explained with advections of polluted air, mainly from Eurasia. Typically the air spent only 2-3 days over the Arctic Ocean or Nordic Seas prior to reaching Hornsund. In summer the mean AOT (500) for high AOT cases are much lower than that in spring and is comparable to the spring background value. Advections of polluted air from Eurasia are infrequent then and slightly elevated AOT (when compared to the background) can be caused mainly by local sources and higher humidity.

Draxler, R.R. and Rolph, G.D. (2003). *HYSPLIT (HYbrid Single-Particle Lagrangian Integrated Trajectory) Model access via NOAA ARL READY Website* http://www.arl.noaa.gov/ready/hysplit4.html

NOAA Air Resources Laboratory, Silver Spring, MD.

Herber, A., Thomason, L.W., Gernandt, H., Leiterer, U., Nagel, D., Schulz, K.H., Kaptur, J., Albrecht, T. and Notholt, J. (2002). *J. Geophys. Res.*, 107, D10, 4097, 10.1029/2001JD000536.

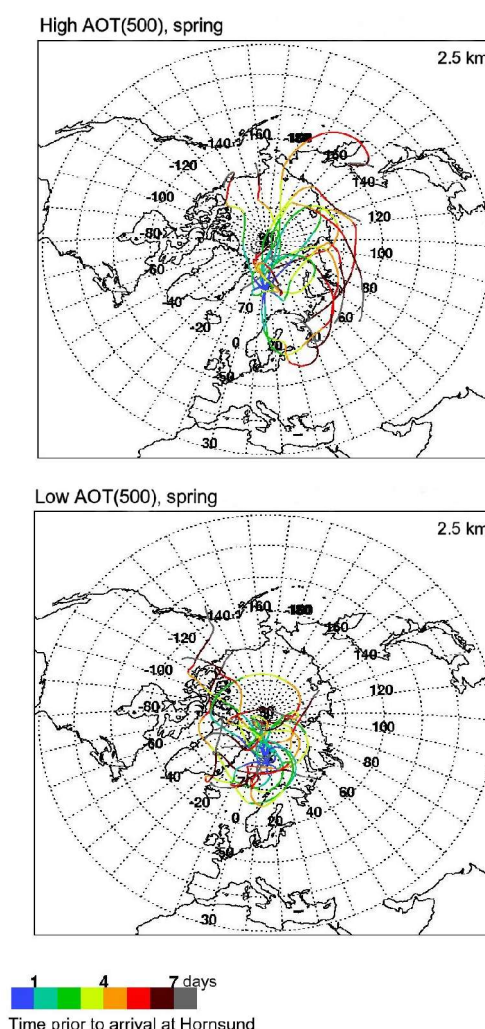Tomasi C., *et. al.* (2007), *J. Geophys. Res.*, 112, D16205, doi:10.1029/2007JD008432

Figure 1. Back trajectories of air which arrived at Hornsund station (2.5 km a.s.l.) during AOT measurements for cases of low ($<AOT(500)>_{day}$ <0.08) and high AOT ($<AOT(500)>_{day}$ >0.12), spring months.

Geochemical characterization of mineral aerosol at Dome Concordia
East Antarctic Plateau (Station Concordia project)

F. Marino[1], E. Castellano[1], S. Nava[2], M. Chiari[2], G. Calzolai[3], S. Becagli[1], F. Rugi[1], M. Severi[1], R. Traversi[1], F. Lucarelli[3], R. Udisti[1], D. Gaiero[4] and S. Gassò[5]

[1]Dept. of Chemistry, University of Florence. Via della Lastruccia, 3. I-50019, Sesto Fiorentino (FI) - Italy.
[2]INFN. Via G Sansone, 1. I-50019, Sesto Fiorentino (FI) - Italy.
[3]Dept. of Physics and INFN, University of Florence. Via G. Sansone, 1. I-50019, Sesto Fiorentino (FI) - Italy.
[4] CIGeS/CICTERRA/CONICET,Universidad Nacional de Córdoba, Córdoba - Argentina.
[5]NASA/GSFC Greenbelt, MD 20771 – USA.

Mineral dust is one of the more studied paleo-climatic and paleo-environmental proxies among those that can be recovered from ice cores collected in Polar Regions (Lambert *et al.*, 2008). Dust particles arrive in the remote polar areas after long-range transport from desertic and semi-desertic continental areas located at lower latitudes, such as the Asian deserts in the Northern Hemisphere and Australia and Southern South America in the Southern Hemisphere (Ruth *et al.*, 2007; Delmonte *et al*., 2008). Many characters of dust in the ice are measured and studied by glaciologists, because of their potential to provide different kind of paleo-climatic information: (1) the dust mass to infer past atmospheric dustiness, aridity at the dust continental sources and scavenging processes en-route from the source to the sink; (2) the dust particle size to study past atmospheric transport processes and pathways (e.g. Delmonte *et al.*, 2002); (3) the dust isotopic composition (Nd, Sr and Pb) to reconstruct the location of past dust sources (e.g. Delmonte *et al*., 2008); (4) finally the major and trace (such as Rare Earth Elements) geochemical composition and the mineralogy of dust to infer dust source locations and to study the geochemical evolution, in turn linked to paleo-environmental conditions, of dust at the source (Marino *et al*., 2008)

To date, published results from ice cores mainly regarded dust deposited in glacial periods, when atmospheric concentrations were higher; the isotopic and geochemical composition of dust deposited during glacial stages suggests a predominant role of Southern South America as dust source for the whole East Antarctic Plateau (Delmonte *et al*., 2008; Marino *et al*., 2008). On the other hand, the problem of interglacial dust characterization is far to be assessed and was only recently faced by few papers (e.g. Revel-Rolland *et al*., 2006; Delmonte *et al*., 2008; Marino *et al*., 2008), pointing out the possible additional role of the Australian source as dust supplier, as well as possible geographical differences among sites located in different areas of the Antarctic continent. Conversely, interglacial (and present day) dust characterization is far to be assessed.

At this purpose, in the framework of the Concordia Station Project, we set up a system for the all-year-round aerosol sampling able to collect a sufficient mass of mineral dust and a protocol of aerosol samples treatment and analysis for the determination of the mineral dust geochemical composition with monthly resolution. This system has been used to collect monthly aerosol samples during the 2006 and 2007 winter-over Antarctic Campaigns at Concordia Station, in the framework of a comprehensive program of aerosol monitoring, including several higher-resolution samplings of size-selected aerosol fractions.

Here we describe the experimental set up used at Dome Concordia for dust collection and in the laboratories of the Department of Chemistry and of LABEC (INFN and University of Florence – Italy) for sample handling and dust analysis. Preliminary results about dust particles geochemical composition and the estimation of the seasonal variability of atmospheric dust budget at Dome Concordia are presented.

Lambert, F., Delmonte B., Petit J.R., Bigler M., Kaufmann P.R., Hutterli M.A., Stocker T.F., Ruth U., Steffensen J.P. and Maggi V. (2008). *Nature,* 452, doi:10.1038/nature06763.

Ruth, U., *et al*. (2007). *Geophys. Res. Lett*., 34, L03706, doi:10.1029/2006GL027876.

Delmonte, B., *et al*. (2008). *Geophys. Res. Lett.*, 35, doi:10.1029/2008GL033382.

Delmonte, B., Petit J.R, Maggi V. (2002). *Clim. Dyn.,* 18(8), 647-660, 10.1007/s00382-001-0193-9.

Marino, F., *et al*. (2008). *Geochem. Geophys. Geosyst.*, 9, Q10018, doi:10.1029/2008GC002023.

Revel-Rolland, M., De Deckker P., Delmonte P., Hesse P.P., Magee J.W., Basile-Doelsch I., Grousset F., and Bosch D. (2006), *Earth Planet. Sci. Lett.*, 249, 1–13.

Results of a pilot study on the climate relevant particle burden on Greenland

E. Schultz[1], S. Norra[1], N. Schleicher[1], V. Dietze[2], M. Fricker[2], U. Kaminski[2], C.H. Pedersen[3] and B. Sittler[4]

[1]Universität Karlsruhe, Institute of Mineralogy and Geochemistry, 76128 Karlsruhe, Germany
[2] Deutscher Wetterdienst, Department of Human Biometeorology, 79104 Freiburg, Germany
[3]Danmarks Meteorologiske Institut/SRI International Kellyville, 3910 Kangerlussuaq, Greenland
[4]Universität Freiburg, Institute for Landscape Management, 79085 Freiburg, Germany

Keywords: Arctic aerosols, climate change, source identification, size distribution, passive sampler.

Within a biological monitoring project, particle concentration has been measured on Traill Island/NE-Greenland in summer months since 1991. For particle sampling the passive sampling technique Sigma-2 (VDI 2119-4, 1997) was used. Collected samples were analysed by automated light microscopy. Single particle analysis provided the size distribution of transparent mineral and black, typically elemental carbon containing particles between 3 µm to 100 µm particle diameter.

The time series of these data shows a striking reduction of black particles between 1991 and 1996. This trend was explained by the decline of industrial emissions of the former Eastern Bloc (Schultz et al., 2008). Since 2000 the level of anthropogenic particles is slowly rising again. Already since the end of the 90's a rising natural particle burden was detected. These results from passive particle sampling obviously are not only displaying the impact of local sources but also that of far distant emissions.

These findings reasoned the start of a Danish-German pilot study on Greenland in 2008 focussing on trends of the atmospheric particle burden. An increase of natural particles is supposed to be induced by the ongoing climate change and corresponding changes in land use on Greenland. The corresponding particle deposition is suspected to affect the albedo of the ice cap and to accelerate the ice melting by this. For an investigation of this effect the sampling of coarse (> 2.5m) and fine particles (PM2.5) was included in the pilot study. The sampling was started in July 2008 near Kangerlussuaq/West-Greenland in co-operation with the Danish Meteorological Institute. In parallel the sampling of only coarse particles was started by the Danish Polar Centre at Zackenberg and was continued on Traill Island, both sites are located at NE-Greenland.

First data from summer 2008 revealed a remote PM2.5 level of less than 2 µg/m³, ranging by factor three below German background conditions. The coarse particle concentration of 8.5 µg/m³, in contrast is ranging only little below the background of about 10 µg/m³ (Schauinsland, Hohenpeißenberg) in Germany. The quite high level of this mainly natural burden can be explained by the enhanced mobilisation of soil particles, under dry summer conditions.

The natural origin was microscopically confirmed by the high amount of soil particles in the collected samples and their mass size distribution peaking between 10 and 20 µm, typical for resuspended particles (Fig. 1).
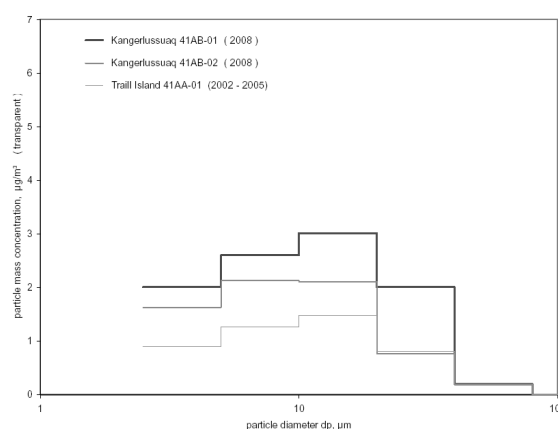

Figure 1. Size distribution of the mineral particles collected at KellyVille/Kangerlussuaq in 2008 and on Traill Island between 2002 and 2008. (Size intervals: 2.5 to 5, 5 to 10, 10 to 20, 20 to 40, 40 to 80 µm)

The increase of the natural particle load corresponds with the growth of highly erosive surfaces, which are set free by melting glaciers and which are more intensively exposed to wind due to longer snow free conditions.

The melting of the arctic sea ice and the Greenland ice cap seems to be underestimated by today's climate models (Zickfeld et al., 2007). One reason is the still unsatisfying data base of the arctic particle burden. In an international follow-up study, it is planned to set-up a sampling net-work around Greenland equipped with the described samplers. Comparability and transferability of the collected data will be assured by a collocated measuring with standard techniques at representative locations. The intended co-operation with modelers shall make sure that the provided data fulfill their needs to further improve numerical models.

Schultz, E., Dietze, V., Kaminski, U., Sittler, B. and Norra, S. (2008). In *Proc. 23. Int. Polartagg.* Münster, 65

Zickfeld, K., Levermann, A., Morgan, M. G., Kuhlbrodt, T., Rahmstorf, St. and Keith, D. W. (2007). Climatic Change 82, 235–265

Investigation of aerosol microphysical and chemical composition over White and Kara Seas

S.A.Terpugova[1], V.V. Polkin[1], M.V. Panchenko[1], L.P. Golobokova[2], T.V. Khodzher[2],
U.G. Filippova[2], V.S. Kozlov[1], V.P. Shmargunov[1], V.P. Shevchenko[3], and A.P. Lisitzin[3]

[1]V.E. Zuev Institute of Atmospheric Optics, 1, Ak. Zuev square, 634021, Tomsk, Russia
[2]Limnological Institute, 3, Ulan-Batorskaya str., 664033, Irkutsk, Russia
[3]P.P. Shirshov Institute of Oceanology, 36, Nakhimovskii ave., 117851, Moscow, Russia

Keywords: Arctic aerosols, marine aerosols, size distribution, chemical composition

The results are presented of five-year-long (2003–2007) study of the spatial - temporal variability of the near-water aerosol over White and Kara Seas (55, 64, 71 and 80-th cruises of RV "Professor Shtockman"; 53 and 54-th cruises of RV "Akademik Mstislav Keldysh").

Measurements of aerosol microphysical characteristics were carried out by means of the automated mobile aerosol complex consisting of nephelometer, photoelectric particle counter and aethalometer. About 1500 series of measurements were carried out in White Sea, and 1400 series in Kara Sea.

Aerosol chemical composition was determined from probes sampled on fiber filters (92 probes were sampled in White Sea and 48 in Kara Sea). Further, samples were analyzed under laboratory conditions. The H^+, Na^+, K^+, Ca^{2+}, Mg^{2+}, NH_4^+, Cl^-, NO_3^-, HCO_3^-, SO_4^{2-} ions were under examination.

The aerosol volume size distributions obtained were approximated by the sum of two lognormal fractions, submicron and coarse. The mean volume size distribution of submicron fraction in White Sea is fitted by the distribution with the variance of the radius logarithm $\sigma_s = 0.6$ and median radius $R_{s0} = 0.096$ μm, and the total volume concentration $V_s = 37.6$ μm^{3}cm^{-3}. Corresponding parameters of the coarse fraction are $\sigma_c = 1.19$, $R_{c0} = 2.15$ μm and $V_c = 19.7$ μm^{3}cm^{-3}. The distribution of submicron particles in the central part of Kara Sea is approximated by lognormal function with parameters $\sigma_s = 0.443$, $R_{s0} = 0.215$ μm and $V_s = 1.01$ μm^{3}cm^{-3}, while parameters of the coarse fraction are $\sigma_c = 0.825$, $R_c = 2.04$ μm and $V_c = 3.29$ μm^{3}cm^{-3}.

The main differences in the size spectra in White and Kara Seas are observed in the submicron radius range $R < 1$ μm. The higher values of the concentration of particles in this range are explained by the fact that White Sea, on the contrary to Kara Sea, is internal sea. So, near-water aerosol undergoes the effect of continental sources, which can have anthropogenic origin and generate great amount of submicron aerosol, which is transported to long distances.

Comparison of ion composition of aerosol over White and Kara Seas has shown that the concentrations of practically all ions, on average, are greater in the region of White Sea. The enhancement of ions of marine origin (Cl^-, Na^+, Mg^{2+}) is from 1.4 to 1.7 times. This ratio for "continental" ions (Ca^{2+}, SO_4^{2-}, NO_3^-, NH_4^+) reach 2.3÷3.7 times. The exception is K^+ ion, the concentration of which in Kara Sea is 1.4 times greater than in White Sea.

To estimate the contribution of continental and marine sources into formation of the chemical composition of near-water aerosol, the technique was applied using the factors V_{cont} and V_{ocean} representing the fraction of ions of continental and marine origin, respectively. Depending on the hydrometeorological conditions, V_{cont} varies in wide range ($\sim 0.1 \div 1$), and its mean value in White Sea is 0.38 (respectively, $V_{ocean} = 0.62$). That means, the contribution of continental sources is appreciable, although the role of marine sources prevails on average. The mean value of V_{cont} in central regions of Kara Sea is 0.3, but this factor in the regions adjacent to the continent can reach the values of 0.6÷0.8.

The obtained long-term data on the aerosol microphysical characteristics and chemical composition are convincing evidence of the fact that significant parts of the water area of White Sea undergo anthropogenic pollution through the atmospheric channels and are under permanent anthropogenic loading. They are coastal regions of Dvina Gulf and river Severnaya Dvina mouth, Kandalaksha Bay (near to the river Kandalaksha mouth), as well as coastal regions of Kola Peninsula.

Study of atmospheric aerosol and columnar water vapor in Antarctic region during 53 Russian Antarctic expedition in 2007-2008

S.A.Terpugova[1], V.V. Polkin[1], S.M. Sakerin[1], D.M. Kabanov[1],
B.N. Holben[2], I.A. Slutsker[2], A.V. Smirnov[2] and V.F. Radionov[3]

[1]V.E. Zuev Institute of Atmospheric Optics, 1, Ak. Zuev square, 634021, Tomsk, Russia
[2]Goddard Space Flight Center, NASA, Greenbelt, USA
[3]Arctic and Antarctic Research Institute, 38, Bering str., 199397, St. Petersburg, Russia

Keywords: Antarctic aerosols, optical depth, mass concentration

Regular monitoring of the atmosphere over the most clean background regions of the planet is especially significant under conditions of enhanced attention to the problem of climate change. Such region for atmospheric aerosol is Antarctica, which is the most far from main sources of natural and anthropogenic aerosol.

In this paper we present the results of measurements of the aerosol parameters, carried out in 53 Russian Antarctic Expedition (53 RAE) from November 2007 till May 2008 onboard the research vessel "Akademik Fedorov". The following parameters were measured: aerosol optical depth (τ^a) in the wavelength range 440 to 870 nm; columnar water vapour content W, aerosol mass concentration M_A, mass concentration of black carbon M_S, aerosol number concentration N in the particle's diameter range $0.4 - 10\ \mu m$, and particle size distribution function.

The route of the vessel was Saint-Petersburg – Cape Town (through Atlantic Ocean) – Russian Antarctic stations Molodezhnaya, Progress, Mirnyj – Melbourne – Antarctic stations Leningradskaya, Russkaya, Bellinsghausen – Cape Town – Antarctic stations Novolazarevskaya, Molodezhnaya, Progress, Mirnyj – Cape Town – Saint Petersburg. The characteristic feature of 53 RAE was circumnavigation around Antarctica with approaches to ports Melbourne and Cape Town, as well as to Antarctic stations.

Statistical characteristics of the measured aerosol parameters were analyzed. The range of variations of the aerosol mass concentration near Antarctica is from 0.36 to 5.5 $\mu g/m^3$ with the mean value of $1.69\pm1.01\ \mu g/m^3$. The mass concentration of black carbon varied within $0.001 - 0.1\ \mu g/m^3$ with mean value $0.012 \pm 0.007\ \mu g/m^3$.

Latitudinal dependences of the aerosol and water vapour parameters over Atlantic Ocean are obtained, as well as their longitudinal dependences around Antarctica.

Model description of the spatial distribution of τ^a over South Atlantic is proposed in the form of the linear dependence on the latitude φ:

$$\tau^a\ (550\ \text{nm}) = 0.161 - 1.96 \cdot 10^{-3}\text{°}\varphi.$$

Figure 1 shows temporal behaviour of the aerosol mass and number concentrations in the near-water layer, as well as the aerosol optical depth observed obtained during the expedition. It is seen that when moving from Europe to Antarctica, the aerosol concentration decreases by approximately one order of magnitude. Abrupt increase of all aerosol parameters is observed when passing through the area of emission of the Saharan dust (Dark Sea), and when approaching to ports Melbourne and Cape Town.
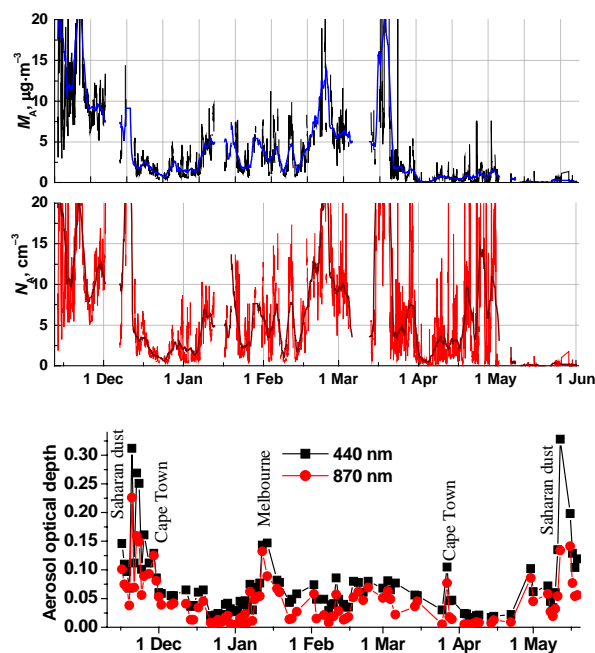

Figure 1. Temporal behavior of aerosol mass concentration (a), number concentration (b), and optical depth (c).

Central Arctic atmosphere pollution by smelter generated SO$_2$: Airborne detection and implications for Arctic Haze and clouds

F. Arnold[1,2], R. Nau[2], T. Jurkat[1], H. Schlager[1], A. Minikin[1], A. Dörnbrack[1], L. Pirjola[3,4], and A.Stohl[5]

[1]Atmospheric Physics Division, Max Planck Institute for Nuclear Physics (MPIK), P.O. Box 103980, D-69029 Heidelberg, Germany
[2]Institut für Physik der Atmosphere, Deutsches Zentrum für Luft- und Raumfahrt (DLR), Oberpfaffenhofen, 82234 Wessling, Germany
[3]Department of Physics, University of Helsinki, P.O. Box 64, FIN-00014 Helsinki, Finland
[4]Department of Technology, Metropolia University of Applied Sciences, P.O. Box 4000, 00180 Helsinki, Finland
[5]Norwegion Institute for Air Research (NILU), 2027 Kjeller, Norway

Keywords: arctic aerosols, particle formation and growth, CCN, sulphur dioxide, long-range transport.

Arctic Haze represents a dramatic manifestation of anthropogenic pollution of a remote and previously pristine atmospheric environment, which presently experiences faster climate warming than any other region on the planet. Arctic Haze influences visibility, ecosystems, and may contribute to Arctic climate warming. In spring, Arctic Haze occupies large parts of the Arctic lower troposphere, the so called Arctic Dome. The most abundant Arctic Haze component is sulphate, which was previously thought to stem preferably from extra-Arctic anthropogenic pollution sources. However, recent model simulations suggest that sulphate particle transport into the Arctic Dome is severely hindered. During the recent "Arctic Research Year", in 2007, we have made the first central Arctic SO$_2$ measurements with high vertical and horizontal resolution and detected SO$_2$ rich pollution plumes in the entire troposphere height range up to 9000 m. Below 2000 m, inside the Arctic Dome, these plumes were most pronounced and stemmed preferably from a giant Ni-Cu smelter complex, located in the Siberian sector of the Arctic Dome, near the city Norilsk, at a distance of 2100 km from our measurement region. Our measurements and accompanying model simulations indicate that SO$_2$ emitted by that smelter complex represents a major if not the dominant precursor of Arctic Dome cloud condensation nuclei and haze particles.

Along with SO$_2$, were measured aerosol particles and additional trace gases including also gas-phase NO$_y$ (sum of reactive nitrogen gases). Importantly, the abundance ratio R=SO$_2$/NO$_y$ is quite different for different SO$_2$ source types (about 1-2 for fossil fuel combustion, $<$ 0.1 for biomass burning, and about 40 for Ni/Cu smelting) and therefore serves as an SO$_2$-source marker. In addition to our air craft measurements, we have made accompanying model simulations of pollutant transport and aerosol formation and growth.

Our air craft measurements were part of the ASTAR 2007 (ASTAR=Arctic Study of Tropospheric Aerosols, Clouds, and Radiation) campaign and took place in March/April 2007 (during the recent "International Polar Research Year") aboard the German research air craft FALCON, mostly in the vicinity of Spitsbergen about 2100 km away from Norilsk. Atmospheric SO$_2$ was measured on 7 central Arctic FALCON flights at altitudes up to 10000 m in the geographic region between approximately 74-83 degrees North and 10-20 degrees East.

On the FALCON flights, Arctic Haze was often observed as a dark coloured band against the horizon (Fig. 1). During each of the 7 Central Arctic FALCON flights, stratified SO$_2$ rich pollution plumes, with elevated SO$_2$ mole fractions of 300-6000 ppt, have been detected below 2000 m. In comparison, measured atmospheric background SO$_2$ mole fractions were usually below about 40 ppt. In addition, numerous SO$_2$ rich pollution plumes were detected in almost the entire altitude range covered.

Figure 1. Arctic haze layer over Svalbard observed from the cokpit of the research air craft FALCON

Physicochemical characterics of marine aerosols of Western Arctic

A.V. Syroeshkin[1], M.A. Chichaeva[1]

[1]Laboratory of applied hydrochemistry and analytical chemistry, State Oceanographic Institute, Kropotkinsky line, 6, 119634, Moscow, Russia

Keywords: marine aerosols, Arctic aerosols, heavy metals.

Pollutants in sea water concentrate on the water-bottom and water-air borders. Enrichment of sea surface microlayer (SML) by hazardous substances results in achievement of pollutants on 2-3 orders higher than in column water. The marine aerosols formed from SML during wind-wave interactions and other processes lead to enrichment with a multicomponent mixture of toxic compounds (Pletenev, 2005).

During the investigations in Western Arctic (2004-2008, White, Barents and Kara seas) our group measured concentration of heavy metals, concentration and size spectra of marine aerosols. Measuring of chemical composition and physical characteristics of marine aerosols progressed synchronously with a number of the methods described earlier (Kolesnikov *et al*, 2005): aerosols counter, sample aerosols with filter AFA, graphite Zeeman assay of heavy metals. We studied availability of correlation between chemical composition and physical characteristics of marine aerosols. There are the correlations depended on geographical allocation (fig. 1). There are the groups of data points belongs to White sea region, the group appeared in Kara sea, the groups of insular (Frantz Josef Land) points the groups of data belongs to coastal regions of Kara sea. In mentioned geographical regions correlation coefficient reaches value of 0,95 and number of assays are 32.
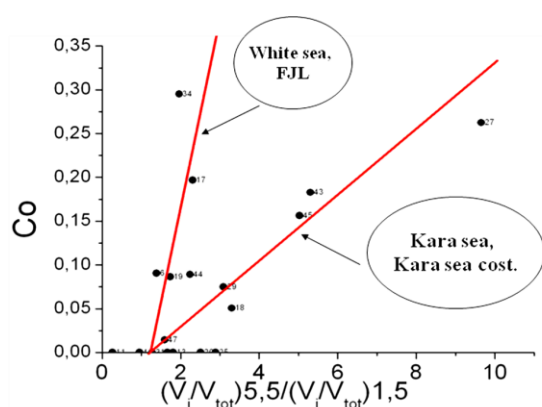
probe (per aerosols filter). The results are shown in table 1. Pair correlations indicate the combined emissions of these two elements with marine aerosols generated by sea surface.

Table 1. Paired correlation between concentrations of heavy metals in arctic marine aerosols ($p>0.9$, $n=54$).

Elements	Cu	Zn	As	Pb	Cd
Cr	-	-	+	+	-
Mn	-	-	-	-	+
Fe	+	+	-	-	-
Ni	-	-	-	+	-
Co	-	+	-	-	-
Pb	-	-	-	-	+

Low levels of concentration of heavy metals are in a good agreement with other authors (for example, *Lisitzin et al*, 2002). Comparison with EMEP and AMAP data let to consider the such levels of concentration of heavy metals as background levels. Existence of pair correlation between chemical composition and physical characteristics of marine aerosols gives an opportunity to determine chemical composition based on physical characteristics of aerosols.

Pletenev S.S., Lapshin V.B., Goncharuk V.V., Kolesnikov M.V., Smirnov A.N. & Syroeshkin A.V.(2005). Proceedings book. Clean Black sea working group. Varna: BAS, P. 45-46. http://www.igic.bas.bg/clean_black_sea

M.V. Kolesnikov, I.S. Matveeva, V.B. Lapshin, S.S. Pletenev, A.V. Grigoryev, A.N. Smirnov, A.V. Balyshev, P.I. Popov, A.V. Ignatchenko & A.V. Syroeshkin. Oceanology. –2005. V. 45. – Suppl. 1. P. S102-S111.

Lisitzin A.P. Sea-ice and Iceberg Sedimentation in the Ocean: Recent and Past. Berlin, Heidelberg: Springer-Verlag, 2002. 563 p.

Figure 1. Interdependency between concentration of Co (ng per m^3) in marine aerosols and ratio of volume concentrations of particles sizes 5.5 μ and 1.5 μ.

Another line of research was devoted to reconnaissance of pair correlation between concentrations of heavy metals within one aerosol

Organic hydroxyl and organosulfate groups in atmospheric particles during ICEALOT 2008

L.M. Russell[1], P.M. Shaw[1], A. Frossard[1], J.H. Kroll[2], P.K. Quinn[3] and T.S. Bates[3]

[1]Scripps Institution of Oceanography, University of California San Diego, La Jolla, CA 92093, USA
[2]Department of Civil and Environmental Engineering, Massachussetts Institute of Technology, Cambridge, MA 02139, USA
[3]National Oceanic and Atmospheric Administration, Pacific Marine Environmental Laboratory, Seattle, WA 98115, USA

Keywords: organic aerosols, Arctic aerosols, chemical composition, particle growth, single particle analysis.

Submicron organic aerosol functional groups were measured by Fourier Transform Infrared spectroscopy (FTIR) and Scanning Transmission X-ray Microscopy Near-Edge X-ray Absorption Fine Structure (STXM-NEXAFS) on samples collected during the International Chemistry Experiment in the Arctic LOwer Troposphere (ICEALOT), using the methods of Russell *et al.* (2009) and Takahama *et al.* (2007). The experiment included measurements of aerosol particles and reactive gases on board the *R/V* Knorr during March and April of 2009. In this work we consider the climate impacts of particles in the North Atlantic and Arctic regions.

The ICEALOT research cruise traveled from Woodshole, Massachussetts, to Tromso, Norway, continuing north of Svalbard past 80N, then returning southward to Iceland. Figure 1 shows the cruise track and daily back trajectories divided by air mass sectors.

Figure 1. ICEALOT research cruise track for R/V Knorr (gray) with back trajectories for Long Island Local Air Quality Study (green), North American outflow (yellow), North Atlantic (blue), European (pink), and Arctic (orange).

Organic particles may have unique direct and indirect impacts on the climate of the North Pole, especially during springtime Arctic haze. The composition and physical properties of this aerosol fraction are largely unknown, so there are few constraints available for including them in global climate models. Here we use organic functional groups to identify particle sources and properties.

The organic functional group composition of particles during ICEALOT overall has shown two unique features of the aerosol: (1) a larger fraction of organic hydroxyl (including polyol and other alcohol) groups than measured in North America and (2) a frequent signal of substantial organosulfate groups in the eastern North Atlantic, primarily from European air masses. Figure 2 shows time series of the chemical composition during the cruise.
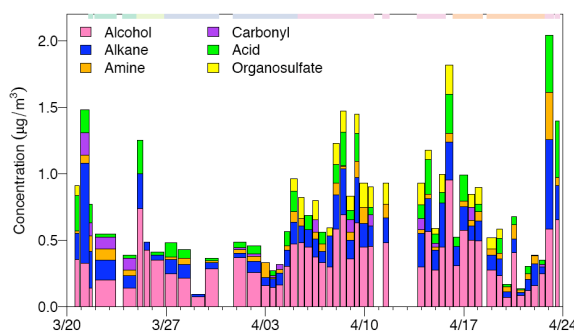

Figure 2. Concentrations of organic functional groups in equivalent mass of alcohol (including polyols and other organic hydroxyl groups), alkane, amine, carbonyl, carboxylic acid, and organosulfate groups. Color bars along the top indicate air mass sectors with the color code given in Figure 1.

The organic mass measured by FTIR was comparable to results from two aerosol mass spectrometers. The oxygen to carbon ratios retrieved by each technique were also compared

Russell, L.M., Takahama, S., Liu, S., Hawkins, L.N., Covert, D.S., Quinn, P.K., and Bates, T.S. *J. Geophys. Res.*, in press (http://www.agu.org/contents/journals/ViewPapersInPress.do?journalCode =JD#id2008JD011275).

Takahama, S., Gilardoni, S., Russell, L.M., and Kilcoyne, A.L.D. *Atmospheric Environment,* 41: 9435-9451, 2007.

Volatility of Nuclei Mode Arctic Aerosol Particles During Summer

G. Biskos[1,2], S. Vratolis[3] J. Ondráček[4], A.A. Karanasiou[3], K. Eleftheriadis[3]

[1]University of the Aegean, Department of Environmental Studies, Mytilene, Greece
[2]Delft University of Technology, Department of Chemical Technology, Delft, The Netherlands
[3]Institute of Nuclear Technology and Radiation Protection, Environmental Radioactivity Laboratory, National Centre of Scientific Research "Demokritos", 15310 Ag. Paraskevi, Attiki, Greece
[4]Laboratory of Aerosol Chemistry & Physics, I.C.P.F., ASCR, Rozvojová 135, Prague 6, 16502, Czech Republic

Aerosol characterization in the remote troposphere is of high importance due to the direct and indirect effects aerosol parameters have on climate. The physicochemical mechanisms governing new particle formation are only partly understood. New particle formation should be extensively investigated due to its strong variability, non linear dependence on anthropogenic or natural precursors and the potential effect on climate in a regional and global scale. It has also recently emerged that at certain areas part of newly formed particles is not volatile at temperatures between 250-300 ^{0}C At these temperature range particles consisting of sulphuric acid or sulphate should be fully volatile. Certain generalized schemes of chemical composition and respective size distribution of dry fine aerosol fraction exist for a variety of environments. However, such data are rare for the high Arctic. In order to test the above described hypotheses measurements of the volatility of sub-200-nm ambient particles were conducted in the Arctic background lower troposphere. The work was performed at the Ny Aalesund Zeppelin GAW site, due to its unique background aerosol properties and the high level of aerosol data and long term monitoring equipment already operating at the station. Nyeki et al., (2005) have presented results for the semi volatile and refractory aerosol fractions at Ny Aalesund. A volatility tandem DMA (VTDMA) system was set-up and installed at the Ny-Alesund Zeppelin monitoring station and operated during a period of three months. The system included two custom-made DMAs with recirculating sheath flows, a controlled thermal denuder, and a Condensation Particle Counter (TSI, Model 3022). Thermal processing at three temperatures 30, 110 and 280°C by an improved low flow volatility tube (Fierz et al., 2007) gave real-time information on the relative concentrations of i) H_2SO_4, ii) $(NH_4)_2SO_4/NH_4HSO_4$ and iii) refractory aerosol (NaCl, soot, mineral dust). The system monitored the volatility of particles having nominal mobility diameters (i.e., diameters dialled by the first DMA in the systme) of 18, 40, 150 and 200 nm in a continuous mode. The reproducibility of the system was checked using laboratory-generated particles.

Reproducibility is especially important for these measurements because particle number concentrations in the ambient air of the high arctic are relatively low. Preliminary results during the summer time period in 2008 were selected in order to examine the thermal behaviour of the nucleation mode particles. This mode was assumed to be adequately represented by particles having 18 nm nominal diameter. At least two occasions of increased nucleation mode particles were detected during the 8-day period shown in Figure 1. The appearance of these particles is characterized by the absence of equivalent increase in the Aitken and accumulation mode particle number concentration. It is observed that particle numbers of the nuclei mode particles plummet at the high temperature. This is an indication that the particles consist of ammonium sulphate or bisulphate.
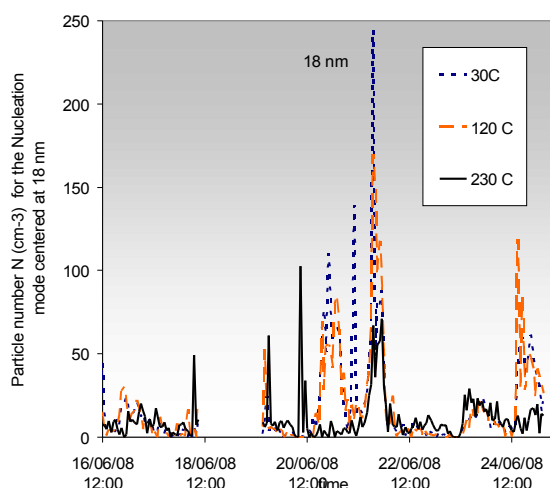

Figure 1. Time series of the number concentration of the nucleation mode processed at 3 different temperatures

S. Nyeki, G. Coulson, I. Colbeck, K. Eleftheriadis, U. Baltensperger, H. J. Beine (2005) "Overview of Aerosol Microphysics during Arctic Sunrise: Measurements during the NICE Renoxification Study", *Tellus* B 57 (1), 40-50

Fierz M. et al., (2007), An Improved low-flow thermodenuder, *J. of Aerosol Sci.* 38 (11), pp. 1163-1168

Analyses of laboratory-grown frost flowers, brine and the resultant sea-salt aerosol

A. V. Jackson[1], S. J. Walker[1], J. J. N. Lingard[1], B. J. Brooks[1],
R. Obbard[2], H. Roscoe[2] and M. H. Smith[1]

[1]Institute for Climate and Atmospheric Science, School of the Earth and Environment, University of Leeds, Leeds, LS2 9JT, United Kingdom
[2]British Antarctic Survey, Madingley Road, Cambridge, CB3 0ET, United Kingdom

Keywords: aerosol size spectra, ozone, sea salt, tropospheric particles.

Active halogen atom chemistry in the boundary layer can result in almost complete destruction of tropospheric ozone during polar springtime. Emission of halogen-containing material from snow and ice covered regions can therefore lead to significant perturbation of the overlying atmosphere. The surface of young sea ice provides sites for the formation of brine and saline ice crystals (known as frost flowers). However, it is not understood if it is the frost flowers themselves, the associated brine, or aerosol produced over the sea ice, that is the ultimate source of atmospheric bromine in Polar Regions. Further to this, polar ice cores contribute a powerful record of past climate changes provided they can be interpreted accurately. Contrary to the traditional view of the origin of sea-salt aerosol in these regions, it is now believed to be generated mostly from the sea-ice surface within the ice-pack, including from frost flowers, rather than from open water. This has consequences for interpretation of ice core records. Our understanding of these complex processes is therefore vital if we are to fully account for past and future polar environmental changes.

Laboratory measurements of frost flowers, brine and their associated aerosol were therefore undertaken to estimate the atmospheric impact of regions of polar sea ice. Synthetic frost flowers were grown on salt water ice at -40 to -20 °C in an environmental chamber to simulate polar conditions. Figure 1 shows regions where frost flowers were observed.

Frost flower and brine salinities were measured as a function of temperature, initial salt water salinity, relative humidity and wind speed. Compositional analyses of the frost flowers and brine were carried out by ion chromatography. The production, size distribution and composition of the accompanying aerosol associated with the frost flowers described in Figure 1 have been investigated. Particles of diameters from 0.1 to 45 µm were measured using a forward scattering spectrometer probe (FSSP), an optical particle counter (OPC) and an active scattering aerosol spectrometer probe (ASASP).
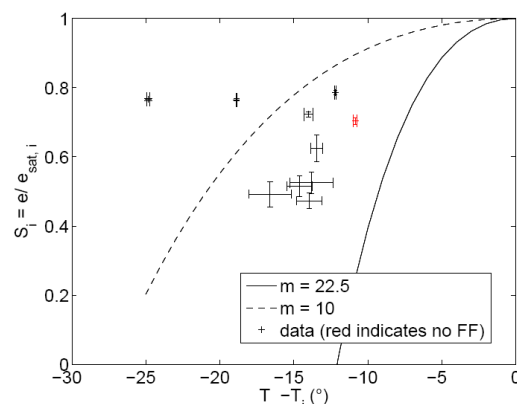

Figure 1. Relative humidity with respect to ice (S_i) as a function of the temperature difference ($T_\infty - T_i$) between the atmosphere and ice surface, showing regions where frost flowers form (in black) and are not observed (in red) with error bars indicating 1 standard deviation. Solid and dashed curves indicate $S_i > (1+m\tau)e^{-m\tau}$ where $m = ML/RT_\infty = 22.5$ and 10 respectively (the molar mass of water, M, the latent heat of vaporization per unit mass, L and the gas constant, R) and $\tau = (T_\infty - T_i)/T_\infty$ [based on a plot by Style and Worster, Geophys. Res. Lett., 2008 (submitted)].

Absorption properties of atmospheric aerosols in the ALOMAR station (summer 2008)

E. Montilla-Rosero[1], S. Mogo[1,2], J. F López[3], V. E. Cachorro[1], R. Rodrigo[1], A. De Frutos[1]

[1]Atmospheric Optics Group, University of Valladolid, Prado de la Magdalena s/n, 47011, Valladolid, Spain
[2]Department of Physics, Univesity of Beira Interior, 6201-001, Covilhã, Portugal
[3]Instituto Nacional de Técnica Aeroespacial: ESAt - El Arenosillo, 21130, Huelva, Spain

Keywords: light absorption, artic aerosol, aerosol photometer method, single scattering albedo

The atmospheric aerosols are known to influence the propagation of solar radiation in the atmosphere and to introduce one of the largest uncertainties in the radiative forcing of climate (IPCC, 2007; Bergstrom *et al*, 2007). A substantial fraction of that uncertainty has been associated with the optical properties of aerosols in cloud-free conditions, mainly the absorption of solar radiation. The single scattering albedo (SSA), defined as $\sigma_s/\sigma_s+\sigma_a$, is a key parameter in assessing the climate effect of aerosols (Lee *et al*, 2007).

In situ measurements of aerosol optical properties were made in summer 2008 at ALOMAR (69ºN, 16ºE), a rural site about 300 km north of the Arctic Circle. This work is the result of the participation of Atmospheric Optics Group in the POLARCAT project, lead by the Norwegian Institute for Air Research, and included in the International Polar Year. Several instruments for aerosol characterization were put together simultaneously. For this work we use a cascade impactor with four stages (DEKATI PM-10) for granulometry and absorption coefficient determination (σ_a) with a filter based technique (integrating sphere photometer), a particle soot absorption photometer (PSAP, Radiance Research), and an integrating nephelometer (model 3563, TSI) for measuring scattering coefficient (σ_s).

The PSAP measures in three wavelengths (470, 522 and 660 nm) with air flow set to 1.5 l/min; the integrating sphere photometer measures continuous spectra from UV until visible (Mogo   *et al*, 2006). Both methods are filter-based and derive absorption from the change in light transmision through a filter on wich particles have been collected (Bond *et al*, 2006). The nephelometer measures in three wavelengths (450, 550 and 700 nm) with flow of 46 l/min (Anderson *et al*, 1996). All the instruments have the same inlet system. The sample air is heated when necessary to achieve a low relative humidity of 40% prior to entering the instruments. Airflow through the sampling line is divided into several separate flows and is directed to individual instruments.

The daily time series of light absorption coefficient are shown in Figure 1. The ALOMAR station is very suitable for in situ and troposfaric measurements due to the absence of large local and regional pollution sources, thus, the specific impact is most likely enhanced in this high latitude region.

Absorption, scattering and SSA data are available from 13th June to 25th August 2008, and they are the first obtained in this subartic station. The preliminary results show good agreement between the two methods used for determination of the absorption coefficients. The σ_a does not exceed 12 Mm^{-1} in the hourly average, even during the events with stronger presence of absorbing aerosols, and the SSA values are in the expected range for this season and region (Tomasi *et al*, 2007). Backtrajectories of air masses are analyzed for most relevant events and these findings give tentative evidence about predominant sources of aerosol particles.
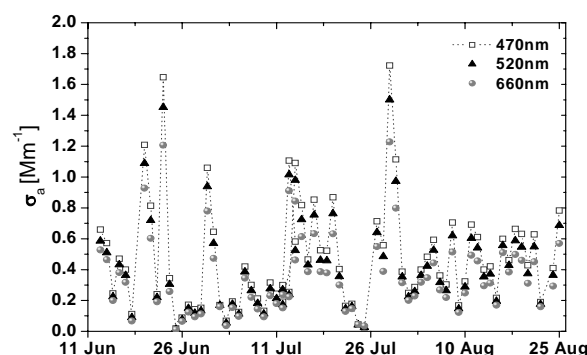

Figure 1. Daily time series measured with PSAP

Anderson T., *et al* (1996). *J. Atmos. Oceanic Technol.* 13(5), 967-986.

Bergstrom R., *et al* (2007). *Atmos. Chem. Phys.* 7, 5937-5943.

Bond, T. C., and, Bergstrom R. W. (2006). *Aerosol Science & Technology* 40: 27-67.

IPCC (2007). *Climate Change 2007: Impacts, Adaptation and Vulnerability.* UK, 7-22., Cambridge University Press.

Lee, K., *et al* (2007). *J. Geophys. Res.* 12, D22S15 doi:10.1029/2007JD009077

Mogo S., *et al* (2005). *Geophys. Res. Lett* 32, L13811. doi:10.1029/2005GL022938

Tomasi C., et al (2007). *J. Geophys. Res.*, 112(doi:10.1029/2007JD008432).

Aerosol type comparison among three sub-arctic sites: ALOMAR-Andenes, Abisko and Sodankylä in late spring and summer 2007

E. Rodríguez[1], C. Toledano[1], V. Cachorro[1], A. De Frutos[1], A. Berjón[1], B. Torres, M. Gausa[2], G. de Leeuw[3]

[1]GOA-Group of Atmospheric Optics, University of Valladolid, P. de la Magdalena s/n, 47071, Valladolid, Spain
[2]Artic Lidar Observatory for Middle Atmosphere Research-ALOMAR, Andenes, Norway
[3] Climate Change Unit, Atmos. Modeling and Observations, Finnish Meteorological Institute, Helsinki, Finland

Keywords: arctic aerosols, optical properties, CIMEL, Alpha Ångström coefficient

We have carried out a comparison of aerosol optical properties, the Aerosol Optical Depth (AOD) and the Ångström Exponent (AE), as elements that define the aerosol type. Three different sub-arctic locations in Europe are considered in this study: ALOMAR-Andenes (Norway), Abisko (Sweden) and Sodankylä (Finland). We will show data obtained in 2007 during the GOA-UVA summer campaign that is included in the activities of the group within the International Polar Year, and was partially supported by AERONET. The results give some insight about aerosol characteristics and the spatial variability in the European sub-arctic region.

The data from Sodankylä station are included in AERONET database at level 2.0 (Holben et al 1998). Most of the data of ALOMAR are also included at AERONET, the site called 'Andenes'. To process the data that are not included in AERONET and the data from Abisko, we are using the processing algorithm developed by the GOA-UVA, which follows the AERONET process. (Ortiz de Galisteo et al., 2008)

The sub-Arctic station ALOMAR (Arctic Lidar Observatory for Middle Atmosphere Research, 69N, 16E, 380m) is located about 300 km north of the Arctic Circle, on the Andøya Island in the Norwegian Atlantic coast. The climate is strongly influenced by the Gulf Stream, which provides mild temperatures during the entire year, with average temperature of -2ºC in January and 11ºC in July. Abisko station (68.35N, 18.81E, 385m) is situated about 200 km north of the Arctic Circle, on the southern shore of Lake Torneträsk. The average annual temperature is approximately −1.0°C. July is the warmest month (+11°C) and January the coldest (−12°C). In Sodankylä station (67.37N, 26.63E, 179m), the head quarters of the research centre is located at Sodankylä, in Finland Lapland, about 100 km north of the Arctic Circle. Due to the warming effect of the Gulf Stream the area is included in the boreal region.

Table 1 shows the mean value of AOD and AE with the standard deviation of each station for the analysed period based on daily mean data. The AOD levels are very low in all sites, where very clean days with background aerosol alternate with aerosol loaded air masses transported mainly from Europe. The AE is lower at ALOMAR, in agreement with the values expected on a coastal location affected by marine aerosols. The AE in Abisko and Sodankylä is larger, according to the continental conditions of the sites.

Table 1. Mean AOD and AE at the three locations

Stations	Mean AOD (STD)	Mean AE (STD)
ALOMAR	0.10 (0.05)	0.90 (0.35)
Abisko	0.06 (0.02)	1.12 (0.21)
Sodankylä	0.07 (0.02)	1.43 (0.25)

The analysis of aerosol types is made according to the threshold values in AOD and AE defined with the AERONET climatology (Holben et al., 2001) and the OPAC model (Hess et al., 1998). The first group has AOD below 0.16 and AE larger than 1.04. These aerosols can be classified as continental aerosol. The second group is the marine aerosol, with AOD below 0.16 and AE lower than 1.04. The third group has AOD above 0.16 and AE larger than 1.04 and correspond to the events of transported anthropogenic aerosol. The last one has AOD above 0.16 with low AE below 1.04, which corresponds with some few cases of transported coarse particles (desert dust).

Table 2. Aerosol type predominance at the three sites

Sites	Aerosol Type
ALOMAR	Predominant Maritime with 61%, 33% continental
Abisko	Mixture between maritime and continental, 43% maritime and 57% continental
Sodankylä	Continental aerosol the 95% and 2.7% maritime.

Bibliography

Hess, M. Koepke, P. and Shult, I. Bulletin of the American Meteorological Society, vol 79, 5. 831-844, 1988.

Holben B., et al Remote Sens. Environ., 66,1-16, 1998 (http://aeronet.gsfc.nasa.gov/).

Holben B., et *al J. Geophys. Res*., 106, 12067–12097, 2001.

Ortiz de Galisteo, P., et al, *Adv. Sci. Res*., 2, 5–8, 2008.

Possible rôle of internally mixed crustal materials in the enrichments in sulphur of supermicrometric Antarctic coastal aerosol particles

P. Mittner, D. Biancato, D. Ceccato, F. Chiminello

Dipartimento di Fisica "G. Galilei" Università di Padova, Italy

Keywords: antarctic aerosols, coastal particles, enrichment factor, single particles analysis, sulphur

The interactions of gaseous sulphur compounds with supermicrometric sea-salt particles may play an important rôle (1, 2) in the fluxes of such compounds out of the atmosphere at the Antarctic coastal site Baia Terra Nova (Lat. 74º42'43"S, Long. 164º06'58"E). Indirect evidences suggest a possible rôle of internally mixed crustal materials in those interactions (1,2). Here we try to face this last problem by means of microPIXE single particle analysis of three size-segregated coastal aerosol samples, collected (2002/03 campaign) at BTN, in the framework of a multiannual experiment. An SDI 12-stage impactor was used; bulk PIXE analysis covered the full SDI size range, whereas microPIXE concerned only the first four SDI stages (12. > $\varnothing_{aer}$ > 1.6 μm). The elemental masses (fg) of up to 9 elements (Na, Mg, Al, Si, S, Cl, K, Ca, Fe) were measured in 2800 particles. Elements Na and Cl were detected in (virtually) all particles; Si in roughly 60% and S in 90% of the particles. The results of a Principal Component Analysis, "PCA", of the multielemental data, concerning separately each size-segregated subsample and several distinct groups of elements, were published elsewhere (3). Depending on the particular group of considered elements (and on the corresponding set of particles), only one Principal Component, "PC", (interpreted as "sea-salt"), or, alternatively, two PC's ("sea-salt" and "crustal") satisfactorily explain the data. Elements Na and Si are convenient quantitative signatures of the two PC's. An "Internal Mixing", "IM", of crustal and sea-salt materials is present in those particles containing, at least, Si. Element S doesn't fit the PCA framework.

We can now face the initially mentioned problems by considering only the behaviour of elements Na, S, Si. We characterize each particle i by means of: $m_{Na}^i, m_S^i, m_{Si}^i$, respectively its Na, S, Si masses; $R_S^i = (m_S^i/m_{Na}^i)$, its S vs Na mass ratio; $E^i = (R_S^i/R_{sw})$, its "S-enrichment factor", R_{sw} being the sea-water S/Na density ratio; $e^i = (E^i-1)$, its relative "S-excess", which corresponds to the individual nssS/ssS (non-sea-salt/sea-salt) ratio. m_S^i vs m_{Na}^i scatterplots conveniently describe the situation for each size-segregated subsample jk of sample k. It is found that: almost always $e^i \geq 0$, (an indication of the overall quality of the results); the values of e^i are widely dispersed (thus explaining the impossibility of fitting PCA). The quantity

$$\varepsilon_{jk} = \left[\left(\sum_i m_S^i / \sum_i m_{Na}^i\right)/R_{SW} - 1\right] = (nssS/ssS)_{jk}$$

is the overall relative S-excess of subsample jk. Furthermore, we evaluate the individual relative amount of crustal materials by means of R_{Si}^i, the Si/Na mass ratio, and subdivide the particles into distinct sets, depending on whether their R_{Si}^i value is larger ("very crustal set") or smaller ("little crustal set") than a convenient cut value (the same for all subsamples). A further set, "general set", contains all the particles. We can thus evaluate for each subsample jk, three distinct values of ε_{jk}, corresponding respectively to the "little crustal set", the "general" set and the "very crustal set", in an order of increasing relative amounts of crustal materials. The figure displays the situation for sample 07. $<\varnothing_{aer} (μm)>$ is the geometric mean value of the aerodynamic diameter of each SDI stage. The values of ε_{jk} corresponding to the "very crustal" set are found to be much larger than the others. The other samples display similar results. The above is evidence that large mass fractions of crustal materials in the particles favour increased gas-particle interactions. More convenient sets, based on the presence, or the absence, of Si, are going to be used soon.
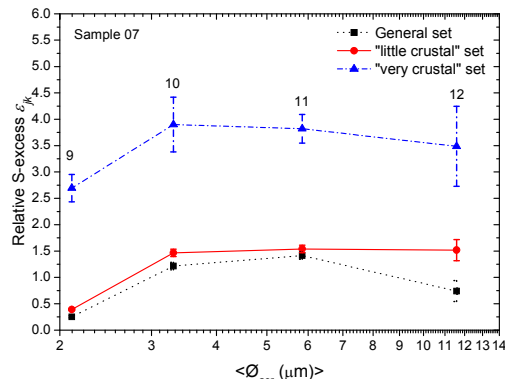
References
1. R. Hillamo et al., Int. J. Environ. Anal. Chem. 7, 353, (1998),
2. F. Chiminello, P. Mittner, A. Trevisiol, D. Ceccato Proc. 16th Int. Conf. on Nucleation and Atmospheric Aerosols (ICNAA), Kyoto, 649-652, (2004)
3. D. Biancato, D. Ceccato, F. Chiminello,. P. Mittner, Nucl. Instr. and Meth. in Physics Research B, 249, 561-565 (2006).

T17 Special Session 5

One-year climatology of the aerosol hygroscopicity at the High Alpine Research Station Jungfraujoch (3580 m asl.)

L. Kammermann[1], M. Gysel[1], E. Weingartner[1], U. Baltensperger[1]

[1]Laboratory of Atmospheric Chemistry, Paul Scherrer Institut, CH-5232, Villigen PSI, Switzerland

Keywords: H-TDMA, Hygroscopicity, Tropospheric aerosols, CLACE, Climatology

Hygroscopic aerosol particles are able to absorb water at high relative humidity (RH). The hygroscopic growth factor (GF) is defined as the ratio of the particle diameter at humidified and dry conditions. Hygroscopic growth influences both the aerosol direct and indirect effects on climate, therefore being highly relevant for climate models: Particles that have grown to larger diameters due to water uptake scatter the incident sunlight to a greater extent and are more likely to act as cloud condensation nuclei (IPCC, 2007).

The diameter-dependent water uptake of aerosol particles is typically measured by a HTDMA (Hygroscopicity Tandem Differential Mobility Analyzer). The instrument selects particles of a specific mobility diameter in the first DMA (Differential Mobility Analyzer) after having dried and neutralized the particles. The selected size class is then humidified, typically to 90% RH. The size distribution after the humidification is finally obtained by the second DMA and a CPC (Condensation Particle Counter). The HTDMA used in this study is based on the setup presented by Weingartner *et al.* (2002), and data are inverted according to Gysel *et al.* (2009).

The aerosol at the remote High Alpine Research Station Jungfraujoch (altitude 3580 m asl.) is representative of the aerosol found in the lower free troposphere. In summer, diurnal variations are found in most aerosol variables due to the injection of the planetary boundary layer (PBL) air, while in winter the site is in the undisturbed free troposphere

most of the time. GF data from previous intense campaigns in different years and seasons at the site are summarized in (Sjogren *et al.,* 2008). Here we present the first extended data set comprising hygroscopicity measurements of different particle dry sizes (D_0) at the Jungfraujoch, lasting from Mai 2008 to April 2009. Such long-term data sets are scarce to date (Swietlicki *et al.,* 2008).

Preliminary results confirm that in summer diurnal variations of the GF are found with minima at night (GF~1.45) for particles with $D_0 = 265$ nm during the selected period (Figure 1). In the afternoon, GFs up to GF~1.62 are found for this size class, giving evidence to the site being influenced by injection of PBL air. Smaller particles show a similar behaviour while GFs are in general lower. This large dataset is currently being analysed in more detail.

Gysel, M., et al. (2009). *J. Aerosol. Sci.*, *40*(2), 134-151.

IPCC (2007), *Climate Change 2007: The Physical Science Basis.* Cambridge, U.K.: Cambridge University Press.

Sjogren, S., et al. (2008). *Atmos. Chem. Phys.*, *8*(18), 5715-5729.

Swietlicki, E., et al. (2008). *Tellus Ser. B-Chem. Phys. Meteorol.*, *60*(3), 432-469.

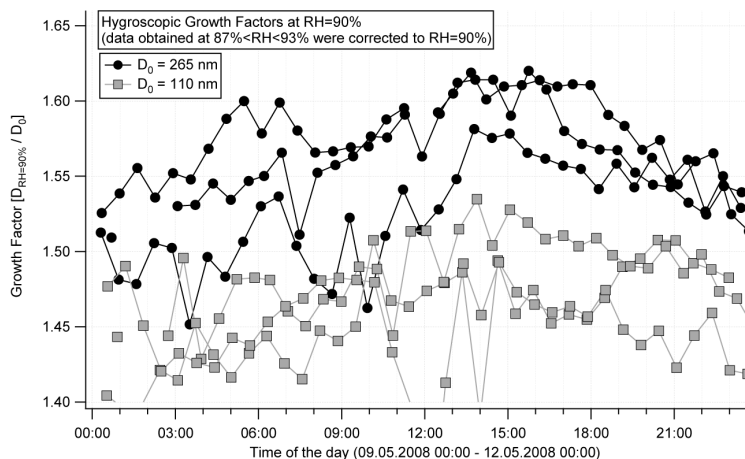Weingartner, E., et al. (2002). *Environ. Sci. Technol.*, *36*(1), 55-62.

Figure 1. Diurnal variations of the hygroscopic growth factors of two particle dry sizes measured at 90% RH.

The European Integrated project on Aerosol Cloud Climate and Air Quality Interactions - EUCAARI – Progress in 2007-2008

Ari Asmi[1], Markku Kulmala[1], Hanna Lappalainen[1] and EUCAARI team

[1]EUCAARI Project office, Department of Physics, University of Helsinki, FI-00014, Helsinki, Finland

Keywords: Climate effect, Clouds, Air quality, Measurements, Modelling.

Quantifying the effect of aerosols on the planet's radiative balance is one of the most urgent tasks in our efforts to understand future climate change. The contributions of the various aerosol sources, the role of long-range transport, and the contribution of primary and secondary particulate matter to the ambient aerosol concentrations over Europe are still largely unknown.

The objectives of EUCAARI are (Kulmala *et al.*, 2007)

(1)   Reduction of the current uncertainty of the impact of aerosol particles on climate by 50% and quantification of the relationship between anthropogenic aerosol particles and regional air quality, and

(2)   Quantification of the side effects of European air quality directives on global and regional climate, and provide tools for future quantifications for different stakeholders.

EUCAARI also contributes to technological developments in the aerosol measurements, enhancing future experiments and air-quality monitoring networks. The project is organised into four scientific elements designed to maximize the integration of methodologies, scales and ultimately our understanding of air quality and climate.

The main achievements during the first 24 months of EUCAARI are ranking from observations of neutral clusters to establishment of global measuring networks.

New instruments capable of detecting and estimating the number concentrations of neutral clusters in different atmospheric environments have been developed. Homogeneous nucleation experiments were conducted. A summary on the use of quantum chemical methods in studies of sulphuric acid-related nucleation mechanisms (mainly, binary sulphuric acid–water and ternary sulphuric acid–water–ammonia nucleation) was created.

A plant chamber system is used to investigate the formation of biogenic secondary organic aerosols. A kinetic model framework for aerosol surface chemistry and gas particle interactions has been established. The measurements are used and compared with simulations using the near-explicit Master Chemical Mechanism (MCM).

An anthropogenic particle number emission inventory and a method for parameterizing the effect of sub-grid scale aerosol dynamics on aerosol number emission rates have been established. A new European inventory of EC and OC for 2005 has been made.

The second year of EUCAARI has been extremely active in terms of data acquisition from both aircraft-based and ground based platforms. The year (April/May 2008- May 2009) has been a year of observation throughout Europe. Three instrumented aircrafts (BAe-146 FAAM, ATR-42 SAFIRE and DLR Falcon 20) with complementary instrumentation and performance formed a core of the operations for the scientific flights in EUCAARI with additional support from nationally funded aircraft. The airborne IOP took place in May 2008 and it was divided into two concurrent campaigns LONGREX and IMPACT. A great challenge to all researchers involved in EUCAARI and will be to compile all information available at the European scale. EUCAARI has also refined the methods for source apportionment of organic aerosol.

Cloud Condensation Nuclei (CCN) activation experiments have been performed for a variety of aerosol systems. The satellite retrieval work has focused on providing data contributing to the EUCAARI field campaigns LONGREX and IMPACT. Four measurement sites in developing countries have been selected and developed.

The EUCAARI database for observations is building on previous developments at NILU and the project utilises the EMEP database.

Model developments using new information gained from the project results are underway. Two benchmark tests have been developed in a pilot part of the project. These tests have been applied to the first simulations from the EUCAARI models and old model simulations being held in the AeroCom database. To make best use of the forthcoming EUCAARI model simulations a set of standard model diagnostics, which need to be respected by modellers who wish to make use of the benchmark tests, are being developed.

Kulmala, M., Asmi A. and Lappalainen H. (eds). *EUCAARI - description of work.* , Helsinki, 2007. ISBN: 978-952-10-3679

Aerosol regional background in Developing Countries

E. Vignati, S. Gilardoni and F. Cavalli

Joint Research Centre, Institute of Environment and Sustainability, Ispra, Italy

Keywords: regional background, aerosol modelling, aerosol measurements, EUCAARI

The atmospheric aerosol and its impact at regional and global scales are less investigated and understood in rapidly developing countries than in Europe or North America, countries where emerging economies are combined with serious air quality problems including particulate air pollution.

Regions in Brazil, India, China and South Africa were selected for intensive studies in the framework of the IP EUCAARI to fill the gap of knowledge about chemical and physical aerosol properties in those areas. To supplement these data existing datasets from ongoing and past projects and campaigns have been collected to help characterising the aerosol regional background in these regions, and also for model evaluation.

In this study the aerosol regional background for the four regions of interest is studied making use of the collected measurements and applying a global model. The observations give an estimation of the concentrations in the area surrounding the measuring site, and the model maps the levels over the whole continent.

The evaluation of the regional background is done for carbonaceous and inorganic species. Preliminary analysis is shown here for black carbon (BC).

To understand the impact of the sources in the regions the Chemistry Transport Model TM5 has been applied. TM5 is an off-line global model (Krol et al., 2005) that uses the meteorological data calculated by the ECMWF model. It has a spatial global resolution of $6° \times 4°$ and a two-way zooming algorithm that allows resolving regions with a finer resolution of $1° \times 1°$. Surface processes are globally treated on a resolution of $1° \times 1°$.

Figure 1 shows the comparison between observed and modelled BC concentrations for some of the stations where experimental data are available. The observed levels are quite high in Asia and South America. There is a large variability in the measured concentrations in continental Asia (Zhenbeitai, Goa, Changdao) compared to Africa and South America, and the lowest values are for marine sites. The comparison with the model results shows that in South America and Africa the concentrations are clearly underestimated by the model. This can be due to low estimation of black carbon emissions, used as input to the model, or to an overestimation of the wet removal. Stations, such as Cuiaba and Alta Foresta, where the measurements cover both dry and wet

season show the same behaviour for both, pointing to low emissions.
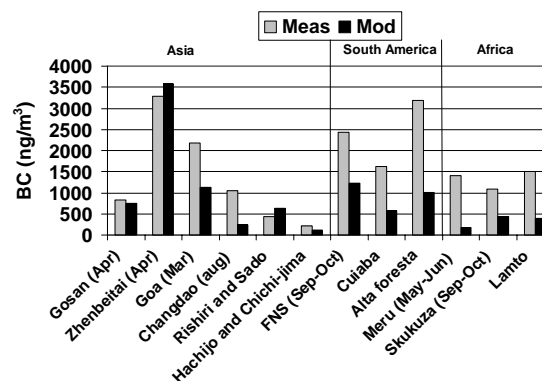

Figure 1. Comparison of modelled and observed black carbon for Asia, South America and Africa sites.

The annual average concentrations of modelled BC (Fig. 2) have the highest values in Asia where the model not always captures the observed values, while in Africa and South America the regional background is underestimated.
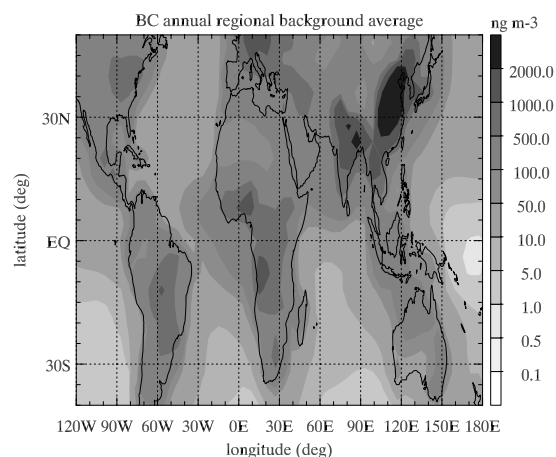

Figure 2. Concentration map of modelled black carbon

Krol, M., et al. (2005). Atmos. Chem. Phys., 5, 417–432.

SOA formation from stress induced BVOC emissions

E. Kleist[1], M. dal Maso[1], A. Kiendler-Scharr[1], T. Hoffmann[2], T. Hohaus[1], N. Lang-Yona[3] T. F. Mentel[1], C. Reinnig[2], Y. Rudich[3], R. Tillmann[1], R. Uerlings[1], J. Warnke[2], J. Wildt[1]

(1) Institut für Chemie und Dynamik der Geosphäre (ICG), Forschungszentrum Jülich, Germany
(2) Johannes Gutenberg University of Mainz, Mainz, Germany
(3) Dept. of Environmental Science, Weizmann Institute, Rehovot, Israel

Keywords: Particle formation and growth, SOA formation potential, Biogenic VOCs,

Formation of secondary organic aerosols (SOA) from biogenic volatile organic compounds (BVOC) was investigated in laboratory experiments with tree seedlings as BVOC sources. The main aim of this study was to determine how plants react on stress situations and to quantify the influence of stress on the SOA formation potential.

Plants were stored under well defined conditions in a continuously stirred tank reactor and their BVOC emissions were measured at the outlet of this plant chamber (gas chromatography mass spectrometry). A fraction of the air leaving the plant chamber was fed into a reaction chamber where SOA formation was induced by photochemical degradation of the BVOC. To quantify the SOA formation potential of a respective BVOC mix we used the maximum particle volume measured during the SOA formation events. Plots of these maximum particle volumes versus the carbon fed to the reaction chamber led to linear relationships as already described by Mentel et al. (2009).

During stress situations for the plants both, the amount and pattern of emitted BVOC changed. In the cases of spruce (*Picea abies* L.) we observed a shift from sesquiterpene (C_{15}) to monoterpene (C_{10}) dominated emissions when applying heat stress to the plant. However, plotting the maximum particle volume versus ppbC no deviation from the linear behaviour was found (Figure 1).

From this observation we conclude that the SOA formation potential of the BVOC mix emitted from spruce is independent of the exact contribution of mono- and sesquiterpenes to the mix. Only the number of carbon atoms in the emitted BVOC has to be considered.

Besides mono- and sesquiterpenes plants may emit large amounts of BVOC produced within the octadecanoid pathway (LOX products). These LOX products mainly consist of short chained C_6-aldehydes and C_6-alcohols and the emissions are a general consequence of lipid peroxidation (e.g. Heiden et al., 2003). In an experiment with some boreal tree species together (spruce, birch and beech seedlings) drought stress was applied to the plants. This stress application resulted in a decrease of monoterpene emissions and strong emissions of LOX products. In particular when the contribution of LOX products to the BVOC mixture was large, the maximum observed particle volume was lower than predicted by the linear behaviour observed for mono- and sesquiterpenes alone. From this we conclude that the potential of LOX products to grow SOA is lower than that of mono- and sesquiterpenes.

During plant louse attack on spruce (*Cinara pilicornis*) emissions of several volatile compounds containing 17 carbon atoms were found. Related to the amount of carbon the SOA formation potential of the mixture including the C_{17} compounds was much higher than that of only mono- and sesquiterpenes.

In summary, we show that stress to plants alters the BVOC emissions from these plants and therewith also the SOA formation potential of these emissions. The main quantity that has to be taken into account to model stress impacts for SOA formation is the amount of emitted carbon. Dependent on the species and type of stress, also the specific composition of emitted BVOC is important to assess the SOA formation potential.
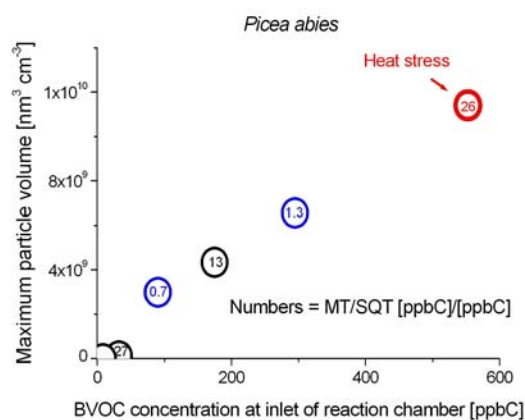

Figure 1: Relationship between maximum particle volume and amount of carbon fed into the reaction chamber. Blue circles: strong sesquiterpene (SQT) emissions, black or red circles: dominant mono-terpene (MT) emissions.

Mentel, T. et al. (2009) *Atmos. Chem. Phys. Discuss.*, 9, 3041-3094
Heiden, A., et al. (2003) *J. Atmos. Chem.* 45, 143–172

Chemical characterization of fine and coarse aerosols in a pristine rainforest site during EUCAARI

Stefania Gilardoni[1], Elisabetta Vignati[1], Ana Loureiro[2], Paulo Artaxo[2], Vorne Gianelle[3]

[1]Climate Change Unit, Institute for Environment and Sustainability, JRC, via E. Fermi 2749, Ispra, Italy
[2]Instituto de Fisica, Universidade de Sao Paulo, Rua do Matao, Sao Paulo, Brazil
[3]ARPA Lombardia, via Juvara 22, Milano, Italy

Keywords: atmospheric aerosol, organic carbon, biogenic particles, EUCAARI.

The characterization of atmospheric aerosol in developing countries is one of the objectives of the EUCAARI project, and derives from the scarcity of continuous measurements in these regions. This work reports the results of chemical characterization of fine and coarse aerosols in Manaus, Brazil.

The sampling site was located in a mostly pristine rain forest site, 60 km north of Manaus, in the Central Amazonia. The climate in Central Amazonia is characterized by a wet period from January to June and a dry period from July to December.

Here we present results from the analysis of fine and coarse aerosol samples, integrated over 72 hours, and collected continuously. Aerosol masses were obtained from gravimetric analysis (relative humidity 20%). Water soluble ion concentrations (chloride, sulfate, nitrate, ammonium, sodium, calcium, potassium, and magnesium) were measured by ion chromatography. Elemental carbon (EC) and organic carbon (OC) were characterized using an EC/OC thermo-optical analyzer (Sunset Laboratory) (Birch and Cary, 1996). Equivalent black carbon (EBC) was measured with a Smoke Stain Reflectometer (Diffusion System) (Andreae et al. 1984) that quantifies EBC deposited on filters from the reflectance of broad-band visible light.
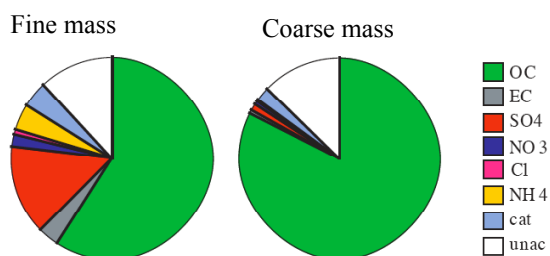

Figure 1. Average composition of fine and coarse aerosol mass; cat is the sum of water soluble inorganic cations, while unacc is the unaccounted mass.

The average composition of fine and coarse aerosol during the wet season is reported in Figure 1; fine and coarse mass averaged 2.6 ± 1.3 µg m^{-3} and 7.9 ± 3.0 µg m^{-3}, respectively.

OC represented more than 50% of the fine mass and more than 75% of the coarse mass. The source of OC was most biogenic as confirmed by results of principal component analysis applied to the EC/OC thermo-optical data. The biogenic character of OC fraction was further investigated with scanning electron microscopy – energy dispersive X-ray spectroscopy (SEM-EDX); figure 2 shows fine aerosol particles collected during the wet season on quartz filter. According to their morphological features they are classified as biological particles; the EDX spectrum shows the presence of a Si peak (due to the quartz filter), in addition to potassium and phosphorous, that are markers of biogenic material (Winiwarter et al. 2009, Lawson and Winchester 1979).
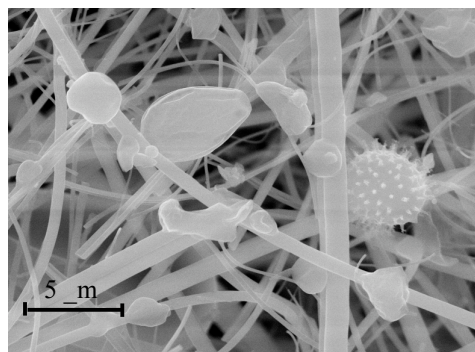

Figure 2. SEM image of biogenic particles.

Sulfate, nitrate, and ammonium concentrations in the fine aerosol averaged 0.33 µg m^{-3}, 0.13 µg m^{-3}, and 0.17 µg m^{-3}, respectively. Together these ions represented 20% of the fine mass and less than 5% of the coarse mass. Ammonium concentration was usually enough to fully neutralize sulfate and nitrate.

Andreae M. O., et al. (1984), *Science of the Total Environment*, *36*, 73-80.

Birch, M. E., and R. A. Cary (1996), *Aerosol Science and Technology*, *25*(3), 221-241.

Lawson and Winchester, *Journal of Geophysical Research*, 84(C7), 3723-3727.

Winiwarter et al. *Atmospheric Environment*, 43(7), 1403-1409.

AMS measurements of aerosol composition at Cabauw tower during IMPACT 2008

A. A. Mensah[1], A. Kiendler-Scharr[1], H. M. ten Brink[2], J. S. Henzing[3], R. Holzinger[4], Th. F. Mentel[1], M. Moerman[3], R. P. Otjes[2], and G.-J. van Zadelhoff[5]

[1] Forschungszentrum Jülich, Institut für Chemie und Dynamik der Geosphäre, Jülich, Germany
[2] Energy Research Centre of the Netherlands (ECN), 1755 ZG Petten, The Netherlands
[3] TNO - Built Environment and Geosciences Airquality & Climate, Utrecht, The Netherlands
[4] Institute of Marin and Atmospheric research Utrecht (IMAU), University of Utrecht, Utrecht, The Netherlands
[5] Royal Netherlands Meteorological Institute (KNMI), De Bilt, The Netherlands

Keywords: Aerosol mass spectrometry, Atmospheric aerosols, Chemical composition.

We present aerosol mass spectrometric measurements with an Aerodyne High-Resolution Time of Flight Aerosol Mass Spectrometer (HR-ToF AMS, (DeCarlo, P. F. *et al.*, 2006, Jayne, J. T. *et al.*, 2000)) from a field campaign at Cabauw Tower, The Netherlands. The Intensive Measurement Period at Cabauw Tower (IMPACT) campaign, was part of the EUCAARI Intensive Observation Period (IOP). Data was acquired from 28th of April to 30th of May 2008.

Three different meteorological conditions were observed during IMPACT 2008. Air masses originating from Central and Eastern Europe and moderate aerosol particle mass loadings of 4 µg/m³ to 10 µg/m³ were characteristic for the dominant meteorological situation (regional background). The origin of air masses changed to the North Sea for one week during mid of May. Precipitation scavenging and low aerosol particle mass loadings, down to 2 µg/m³ were characteristic for this period (scavenged background). High aerosol particle mass loadings of up to 30 µg/m³ and air masses probably origination from North Africa dominated the third meteorological situation at the end of May (Sahara dust event).

The HR-ToF AMS detects all non-refractory components (ammonium, nitrate, sulphate, chloride and organics) of aerosol particles. Additionally, high resolution data allow further insights to the actual composition especially of the organic fraction.

We present basic analysis such as time series of the major components, and the fractional aerosol particle composition. Furthermore, we use high resolution analysis to gain insights to different behaviour patterns of oxygenated and non-oxygenated organic species (Figure 1). Similar to the findings of Zhang (Zhang, Q. *et al.*, 2005), we find early morning (rush hour) peaks of non-oxygenated organic components associated with primary emissions from fossil fuel combustion.

We take advantage of the broad instrumentation at Cabauw tower during IMPACT 2008 and present several inter-instrumental comparisons. The aerosol particle mass measured by the AMS and the particle mass derived from Scanning Mobility Particle Sizer (SMPS) measurements agree well to each other. Up to 40% of the particulate phase consist of nitrate. Particulate nitrate, measured by a modified Proton Reaction Transfer Mass Spectrometer (PTR-MS, (Holzinger, R. *et al.*, 2008)) correlate good with AMS nitrate results. The comparison of results from the Monitor for Aerosol and Gases in Ambient Air (MARGA) and the enhanced MARGA-Sizer (ten Brink, H. *et al.*, 2007) show very good agreement.

Furthermore, we will compare the May 2008 results to measurements from the European Measurement and Observation Program (EMEP) campaign at the same location from March 2009. We will determine comparableness, discrepancies, and variations.
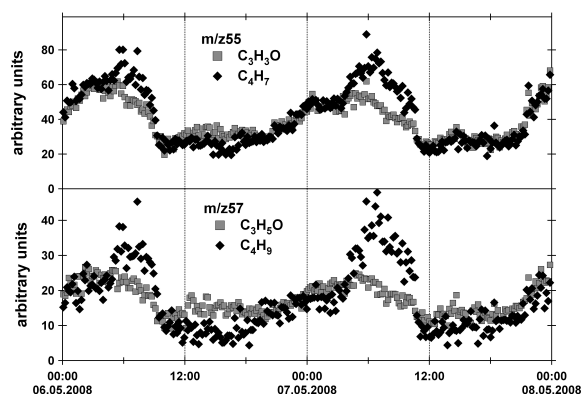

Figure 1. Time series of oxygenated and non-oxygenated organic species at m/z 55 and m/z 57.

DeCarlo, P. F., J. R. Kimmel, *et al.*, (2006). *Anal. Chem.*

Holzinger, R., S. V. Hering, *et al.*, 2008. *EGU General Assembly*, Vienna, Austria.

Jayne, J. T., D. C. Leard, *et al.*, (2000). *Aerosol Science and Technology*, 33, 49-70.

ten Brink, H., R. Otjes, *et al.*, (2007). *Atmospheric Environment*, 41, 2768-2779.

Zhang, Q., D. R. Worsnop, *et al.*, (2005). *Atmospheric Chemistry and Physics*, 5, 3289-3311.

Global model simulations of particle concentrations over Europe during the EUCAARI Intensive Observation Period

C. L. Reddington[1], M. G. Frontoso[1], K. S. Carslaw[1], D. V. Spracklen[1],
A. Minikin[2], T. Hamburger[2], H. Coe[3] and J. Trembath[3]

[1]Institute for Climate & Atmospheric Science, University of Leeds, LS2 9JT, U.K.
[2]Institut für Physik der Atmosphäre, Deutsches Zentrum für Luft- und Raumfahrt, Oberpfaffenhofen, Germany
[3]School of Earth, Atmospheric & Environmental Sciences, University of Manchester, M13 9PL, U.K.

Keywords: EUCAARI, aerosol modelling, number concentration, nucleation.

The alteration of the Earth's radiative balance by atmospheric aerosols is a major uncertainty in assessments and predictions of climate change on both global and regional scales (Forster *et al.*, 2007). In order to understand the impact of aerosols on climate we must understand how anthropogenic emissions alter the size and number distributions of atmospheric aerosol. Within the European Integrated Project on Aerosol Cloud Climate and Air Quality Interactions (EUCAARI) we aim to improve global model simulations of particle number and size distributions and to quantify the relative contributions of nucleation and primary emissions to total particle concentrations. Here we use observations from the EUCAARI LONGREX and IMPACT field campaigns to test the Global Model of Aerosol Processes (GLOMAP) (Spracklen *et al.*, 2005) over the European domain.

The GLOMAP model simulates the evolution of size and composition resolved aerosols, including their interaction with trace gases and clouds. The host model for GLOMAP is the TOMCAT global Eulerian grid-point chemical transport model (Chipperfield, 2006). The aerosol particle types included in GLOMAP are sea spray, sulphate aerosol, black and organic carbon, and a simple scheme for secondary organic material based on monoterpene oxidation products. The aerosol size distribution is described using a two-moment sectional bin scheme with 20 bins spanning 3nm to 25μm. New particle formation in the free troposphere is treated using the binary homogeneous H_2SO_4-H_2O nucleation scheme of Kulmala *et al.* (1998). Nucleation in the boundary layer is simulated assuming that the formation rate of 1 nm clusters (j_1) is proportional to the gas phase concentration of sulphuric acid (Kulmala *et al.*, 2006): $j_1=A[H_2SO_4]$; $A=2x10^{-6}\ s^{-1}$.

During the EUCAARI Intensive Observation Period (IOP) in May 2008, GLOMAP was setup to provide output every hour over a regional (European) domain. All the results in the present work have a horizontal resolution of 2.8°x2.8° and 20 vertical levels from surface to 10 km. The model is compared with particle number concentrations measured by the CPSA instrument onboard the DLR Falcon research aircraft. Due to the large number of vertical profiles performed by the Falcon at different locations we are able to map how the budget of particle number varies regionally and vertically over Europe.

Initial comparisons between the GLOMAP model output and observed number concentrations of Aitken-mode aerosol (particle diameter > 10nm), have revealed a large model discrepancy at low altitudes, particularly in the boundary layer. At an altitude of 600m the number concentration of particles > 10nm is under predicted in GLOMAP on average by a factor of ~ 5 when compared to vertical profiles of particle number from the Falcon aircraft. Further work is needed to determine the nature of this discrepancy in the model and how the spatial pattern of the discrepancy varies over Europe. These initial comparisons suggest the model performance is improved in areas with low aerosol loading.

Number concentrations of aerosols down to nucleation-mode particle sizes ($\geq$ 3nm) measured by the water-based CPC onboard the FAAM BAe-146 along with data from the DLR Falcon have been used to test the boundary layer nucleation scheme implemented in GLOMAP. Initial results suggest that nucleation is unlikely to explain the high particle concentrations observed.

To study primary aerosol emissions we have used non-volatile particle number (particle diameter > 14nm), measured onboard the Falcon, to compare with black carbon number from GLOMAP.

Further model comparisons with particle number concentration data from EUSAAR ground stations operated during the EUCAARI IOP will be performed to produce a more complete map of European aerosol number for this period.

Chipperfield, M. (2006). *Q. J. R. Meteorol. Soc.*, 132, 1179-1203.

Forster, P., Ramaswamy, V., *et al.* (2007). *Climate Change 2007: The Physical Science Basis.* Cambridge, U.K.: Cambridge University Press.

Kulmala, M., Laaksonen, A. & Pirjola, L. (1998). *J. Geophys. Res.-Atmos.*, 103, 8301-8307.

Kulmala, M., Lehtinen, K.E.J. & Laaksonen, A. (2006). *Atmos. Chem. Phys.*, 6, 787-793.

Spracklen, D. V., Pringle, K. J., *et al.* (2005). *Atmos. Chem. Phys.*, 5, 2227-2252.

Black carbon ageing over Europe during LONGREX-EUCAARI campaign

M.G. Frontoso[1], K. S. Carslaw[1], G. W. Mann[1] and D.V. Spracklen[1]
D. Liu [2], G. McMeeking[2], H. Coe[2], A. Stohl[3]

[1]Institute for Climate and Atmospheric Science, School of Earth and Environment, University of Leeds, Leeds, United Kingdom
[2]School of Earth, Atmospheric and Environmental Sciences, University of Manchester, United Kingdom
[3]Department of Regional and Global Pollution Issues, Norwegian Institute for Air Research, Kjeller, Norway

Keywords: black carbon, ageing, ADIENT, EUCAARI.

Black Carbon (BC), a byproduct of incomplete combustion of fossil fuels and biomass, is a strong absorber of solar radiation and is considered to make important contributions to the radiative forcing of the atmosphere. BC particles may exist as either insoluble particles, or in mixtures that are considered partly soluble. BC in a soluble mixture is more efficiently removed by dry and wet deposition processes, and has a shorter atmospheric residence time (Zuberi et al., 2005). Following emissions, BC is subject to atmospheric processes, which include oxidation, condensation and coagulation. These processes, termed the ageing processes, act to change the solubility of the BC aerosol. Therefore, parameterization of the BC ageing processes in global models is a key issue to the determination of the atmospheric abundance of this aerosol.

Also the radiative properties of BC depend strongly on the mixing state (Bond et al., 2006). Currently in most large-scale models, primary BC particles are emitted as separate particles and are assumed to transfer into the internally mixed mode dependent on the amount of secondary products that have condensed. Jacobson (2000) conducted a model simulation and reported that the radiative forcing of BC is $+0.27 W/m2$ when it is externally mixed, but this is enhanced to $+0.54 W/m2$ when internally mixed.

The GLObal Model of Aerosol Processes (GLOMAP, Spracklen et al., 2005) is a global model that combines a complete tropospheric chemistry scheme with an advanced aerosol microphysics module. It has a comprehensive sectional scheme (20 bins ranging from 1 nm to 25 micron) and includes sea spray, sulphate, elemental and organic carbon, dust and a simple scheme for secondary organic carbon into two distributions (soluble and insoluble). Aerosol can be transferred from the insoluble to the soluble distribution via "ageing" through coagulation and condensation of sulphuric acid on the insoluble aerosol when coated by 1 molecule of sulphuric acid (monolayer).

The focus of this study is on the conversion of insoluble BC to soluble/mixed BC. This conversion is crucial since soluble particles can act as cloud condensation or ice nuclei.

The analysed period occurred in May 2008 during the ADIENT/EUCAARI-LONGREX intensive aircraft field campaign where high aerosol loading was sampled during air mass transport over Europe. Size distribution, mass concentration and the mixing state of BC were measured using a single-particle soot photometer (SP2) flown on board the UK FAAM aircraft. The age of BC was estimated through the time series of the BC agespectrum, a product of the Lagrangian particle dispersion model FLEXPART (Stohl et al., 1998), used to determine the origin of aerosols. Backward simulations were done along the flight-path with a time resolution less than 1 minute. For each backward simulation, the relative contribution of the BC mass in 20 age bins (ranging from 1 day to 10 days) is calculated and then "fresh" and "aged" BC is estimated by a statistical analysis.

Comparisons with observations show that the parameterization of the ageing in GLOMAP is too fast (underestimation of the model in case of "aged" BC). Therefore, sensitivity runs with 10 molecules have been done (10 layer runs) and showed a better agreement with observations. A new model setup was also done to track the amount of sulfate in the soluble distribution.

Since aerosol optical properties like the single scattering albedo (SSA) strongly depend on the representation of the mixing state, the dependence of SSA on the BC ageing is also investigated.

Spracklen, D. V., Pringle K., Carslaw K. S., Chipperfield M. P. and G. W. Mann, (2005). *Atmos. Chem. Phys.,* 5, 2227-2252.

Bond, T. C., Habib G., and R. W. Bergstrom, (2006). *Aerosol. Sci. Technol.,* 40, 27-67, doi:10.1080/02786820500421521.

Jacobson, M. Z., (2000), *Geophys. Res. Lett.,* 27, 217-220, doi: 10.1029/1999GL010968.

Stohl, A. M., Hittenberger K., and G. Wotawa, (1998). *Atmos. Environ.,* 32, 4245-4246.

Zuberi, B., Johnson K. S., Aleks G. K., Molina L. T. and M. J. Molina, (2005). *Geophys. Res. Lett.,* 32, L01 807, doi: 10.1029/2004GL021496.

Meeting the challenge of multi-scale integration in EUCAARI:
sectional bin versus modal aerosol scheme for large scale modelling

M.G. Frontoso[1], K. S. Carslaw[1], G. W. Mann[1] and D.V. Spracklen[1]

[1]Institute for Climate and Atmospheric Science, School of Earth and Environmental, University of Leeds, LS2 9JT, Leeds, United Kingdom

Keywords: aerosol sectional scheme, aerosol modal scheme, EUCAARI.

Atmospheric aerosols play an important role in the global climate system. They modify the global radiation budget directly, by scattering and absorption (Mc Cormic and Ludwig, 1967) and indirectly, by their interaction with clouds (Twomey 1974). The quantitative evaluation of the aerosol effects is still uncertain (Kinne et al., 2005) both for the complexity of the global aerosol system and the short aerosol lifetime which causes large spatiotemporal inhomogeneities. Though in situ observations represent the most detailed insight into the aerosol system, they have limited spatial and temporal scales. Remote sensing data from ground-based instruments provide important information but they have sampling limitations as well. Then, satellite data only provide integral aerosol properties and retrievals rely on a priori information about the aerosol system and internal aerosol models. Global aerosol models can help to increase the understanding of the complex aerosol system for past, present and future conditions.

Due to the complexity of aerosol microphysics, global climate models generally only simulate aerosol mass and assume size distributions for the aerosol depending upon the composition. Sectional schemes resolving the size distribution of aerosol are often computationally expensive and therefore not suitable for inclusion within global circulation model (GCM). Aerosol can be represented by log-normal distribution scheme with a reduced computational time but with a priori assumption on the size distribution.

The GLObal Model of Aerosol Process (GLOMAP, Spracklen et al., 2005) has the unique advantage of having two aerosol schemes: a sectional bin scheme (GLOMAP-bin, 20 bins ranging from 1 nm to 25 um, carrying both number and mass) and a log-normal modal scheme (GLOMAP-mode, 7 lognormal modes defined in terms of number and masses of each chemical component), developed for use in the UK Met Office Unified Model (UM). For these reasons, GLOMAP is a useful tool to test how well a less computationally expensive modal scheme is able to represent aerosol compared with a bin scheme and meet the challenge of multi-scale integration in EUCAARI (European Integrated project on Aerosol Cloud Climate and Air Quality Interactions), designed to bridge the scales through connected activities ranging from molecular scale to regional and global scale.

GLOMAP-bin and GLOMAP-mode use identical emissions and comparable process descriptions, although the implementation is changed where necessary. The key difference is the representation of the aerosol size distribution.

Extensive evaluation of GLOMAP mass and size distributions have been made against measurements from several previous campaigns. However, the advantage of the intensive field campaign during EUCAARI project is that there are a lot of simultaneous measurements (mass concentration, size distribution, optical properties, hygroscopicity, mixing state, etc…), which avoid compensation error.

Results are very encouraging since they show a very good agreement between GLOMAP-bin and GLOMAP-mode at the surface for species mass concentration (sulphate, organic carbon, black carbon). Inter-model differences (slope ranging from 0.98 to 1.04, correlation factor ranging from 0.96 to 0.99) are found to be lower than model-observation differences (slope ranging from 0.5 to 1.9, correlation factor from 0.76 to 0.79). At higher altitudes (3 - 5km) since aerosols are driven by processes rather than by emissions, the agreement between the two models and the observations is less good. In particular, both models underestimate (factor 4) the organic aerosol mass from mass spectrometer measurements. Results suggest that GLOMAP well captures the Oxidised Organic Aerosol type 1 (OOA1), but not the Oxidised Organic Aerosol type 2 (OOA2) which is more volatile and is partitioning more into the aerosol at low temperature.

Kinne, S., and coauthors, (2005). *Atmos. Chem. Phys. Discuss,* 5, 81-114.

Lanz, S., and coauthors, (2007). *Atmos. Chem. Phys.,* 7, 1503-2007.

Mc Cormic, R. A. and J. H. Ludwig, (1967). *Science.,* 156, 1358-1359.

Spracklen, D. V., Pringle K., Carslaw K. S., Chipperfield M. P. and G. W. Mann, (2005). *Atmos. Chem. Phys.,* 5, 2227-2252.

Twomey S. (1974). *Atmos. Environ.,* 8, 1251-1256.

Origin, composition and volatility of aerosol in the Mediterranean during the EUCAARI intensive campaigns: The Finokalia Aerosol Measurement Experiments

Lea Hildebrandt[*1], Evangelia Kostenidou[2], Byong-Hyoek Lee[1], Gabriella J. Engelhart[1], Claudia Mohr[3], Katerina Bougiatioti[4], Peter F. DeCarlo[3], Andre S.H. Prevot[3], Urs Baltensperger[3], Nikos Mihalopoulos[4], Neil M. Donahue[1], Spyros N. Pandis[1,2]

[1] Carnegie Mellon University, Center for Atmospheric Particle Studies, Pittsburgh, PA 15213, USA
[2] University of Patras, Institute of Chemical Engineering and High Temperature Chemical Processes (ICE-HT), Foundation of Research and Technology (FORTH), Patra, Greece
[3] Paul Scherrer Institute, Laboratory of Atmospheric Chemistry, CH-5232 Villigen, Switzerland
[4] University of Crete, Department of Chemical Engineering, Heraklion, Greece

The Finokalia Aerosol Measurement Experiments (FAME) are part of the EUCAARI intensive measurement campaigns in late spring 2008 and winter of 2009. Finokalia is a remote site located in the Northeast of Crete, Greece with minimal nearby sources of pollution. This remote site allows the study of aged aerosol from different source regions: marine, continental and desert aerosol, as confirmed by the FLEXPART model (Stohl *et al*., 1998).

We measured the size-resolved composition of the aerosol using a Quadrupole Aerosol Mass Spectrometer (Q-AMS, Aerodyne Research, Inc) (Jayne *et al*., 2000; Jimenez *et al*., 2003), particle volume and number using a scanning mobility particle sizer (SMPS), and volatility using a thermodenuder system built based on the design of An *et al*. (2007). A suite of other measurements was performed during this campaign, including gas-phase and meteorological measurements, traditional filter sampling, measurements of aerosol optical properties, etc.

Results of FAME-2008 (spring) suggest that the non-refractory PM_1 (particulate matter less than 1μm in diameter) was mostly ammonium sulfate and bisulfate, with a 28 % contribution from organics on average, and very small amounts of nitrate. The organic aerosol from all source regions was highly oxidized: In the AMS, the fraction of organic aerosol due to fragments at m/z = 44 (% 44) was 18%. Thermodenuder measurements suggest that the volatility of the organic aerosol was low, consistent with the high extent of oxidation. The concentration and composition of the aerosol did not exhibit significant diurnal cycles. The extent of oxidation (% 44) of the organic aerosol showed a noticeable but modest diurnal cycle, suggesting that oxidation is ongoing but may be slow when the aerosol reaches the sampling site.

The analysis by source region suggests that most of the sulfate (and therefore most of the aerosol mass) sampled at Finokalia is due to sulfur emissions in Greece and the Balkans. Organic aerosol showed much less variation with source region than sulfate. This suggests that the sources of organic aerosol are of a more regional nature than the sources of sulfate. As expected, we observed lower organic PM_1 in the marine and desert than in continental air masses. The organic aerosol was most oxidized in the marine air mass (highly aged) and least oxidized in the air masses from Greece (fresher).

A further result with important implications to AMS and thermodenuder measurements in general is that the AMS collection efficiency (CE) of the particles sampled during FAME-2008 was between ~ 0.7 and 1 (higher than the commonly assumed value of 0.5), and that CE was lower after the aerosol had passed through the thermodenuder.

This work has shown that the Balkans are an important source of sulfate and, given their effect on total aerosol concentrations in the Mediterranean, this region should receive more attention in future modeling efforts. The constancy observed in the organic spectrum during FAME-2008 (only moderate changes in %44 for very different source regions) suggests that the organic aerosol reaches a stable oxidation state in the ~ 1-3 days of transport to the field site under strongly oxidizing conditions. Variation with source region and time-of-day is expected to be higher under more moderate oxidizing conditions (in the winter). Results from FAME-2009 (during the EUCAARI intensive winter campaign) will also be discussed.

An, W. J. *et al*. Journal of Aerosol Science, 38, 305-314, 2007.

Jayne, J. T. *et al.* Aerosol Science And Technology, 33, 49-70, 2000.

Jimenez, J. L. *et al.* Journal Of Geophysical Research-Atmospheres, 108, 8425-8437, 2003.

Stohl, A., Hittenberger, M., and Wotawa, G. Atmospheric Environment, 32, 4245-4264, 1998.

Measurements of the Volatility Distribution and Density of Ambient Organic Aerosols during the Finokalia Aerosol Measurement Experiment – 2008

E. Kostenidou[1,2], L. Hildebrant[3], G. J. Engelhart[3], B. Lee[3], C. Mohr[4], A. Bougiatioti[5], U. Baltensperger[4], N. Mihalopoulos[5] and S. N. Pandis[1,2,3]

[1]Institute of Chemical Engineering and High Temperature Chemical Processes, ICE-HT, Patras, Greece
[2]Department of Chemical Engineering, University of Patras, Patras, Greece
[3]Department of Chemical Engineering, Carnegie Mellon University, Pittsburgh, Pennsylvania, USA
[4]Paul Scherrer Institut, Laboratory of Atmospheric Chemistry,Villigen, Switzerland
[5] Department of Chemistry, University of Crete, Heraklion, Greece

Keywords: AMS, SMPS, thermodenuder, collection efficiency, organic density.

During the Finokalia Aerosol Measurement Experiment - 2008 (FAME–2008) a thermodenuder (An et al., 2007) coupled with an Aerosol Mass Spectrometer (AMS) and a Scanning Mobility Particle Sizer (SMPS) were operated for a period of one month. The temperature in the thermodenuder ranged between 100-140°C and the residence time was 6.5 seconds. The SMPS measured the volume distributions of the ambient aerosol after passing through the thermodenuder and the AMS the corresponding mass distributions. Filter samples and a steam sampler were also used to measure the aerosol composition.

The Finokalia aerosols, as seen by the AMS, consist of ammonium, sulphate, organics and water. The organic aerosol is quite aged and oxygenated and well mixed with the other aerosol components in the submicrometer size range. The mass distributions reviled that the particle density in not constant for all sizes. In order to estimate the organic density we apply the Kostenidou et al. (2007) algorithm including additionally the water content. This method combines the volume distributions calculated by the SMPS and the mass distributions provided by the AMS, This algorithm can also provide the collection efficiency (CE) of the AMS.

We applied this optimization algorithm both for the ambient and the thermodednuded data. The average ambient organic density was 1.37 g m^{-3} (ranging between 1.15 and 1.8 g m^{-3}). The average density of the organic aerosol that remained after passing through the thermodenuder (roughly half of the organics) was also 1.37 g m^{-3} (ranging between 0.9 and 1.78 g m^{-3}). In cases where the ratio of sulphate to water in the thermodenuder was similar to the ambient ratio of sulphate to water, the two organic densities were in the same range. At high temperatures in the thermodenuder, where most of the water evaporated, the thermodenuded density was distinguishingly higher.

The calculated average ambient AMS collection efficiency (CE) was 1.1 (ranging between 0.9 and 1.4) based on the algorithm matching the SMPS and AMS distributions. Using these CE values, the concentrations measured by the AMS for the ambient particles were in good agreement with the other independent concentration measurements (filters, steam sampler).

The CE for the particles after they passed through the thermodenuder was significantly lower by 10-20% during most of the study. The highest reductions were observed at the highest temperatures in the thermodenuder (where most of the aerosol water evaporated). Our results suggest that the evaporation of the water in the thermodenuder, increases the probability of particle bounce in the AMS and therefore decreases the CE. This change needs to be accounted in the calculation of the remaining mass fraction of the organic aerosol in the thermodenuder, otherwise the organic aerosol volatility will be overestimated.

The ratio of the organic mass after the aerosol passed through the thermodenuder and the ambient organic aerosol mass at different temperatures and residence times were used to calculate the ambient organic aerosol volatility distribution using the volatility basis set. Results suggest the organic aerosol volatility in Finokalia was 1-2 orders of magnitude lower than that of the fresh secondary organic investigated in smog chambers.

An, J. W., Pathak, K. R., Lee, B., & Pandis N. S (2007). *Aerosol volatility measurement using an improved thermodenuder: Application to secondary organic aerosol. J. Aerosol Science, 38, 3, 305-314.*

Kostenidou, E., Pathak, K. R & Pandis N. S (2007). *An algorithm for the calculation of secondary organic aerosol density combining AMS and SMPS data. Aerosl Science and Technology, 41, 1002-1010.*

Inside an air pollution plume – first results from EUCAARI-station in South Africa

L. Laakso[1,2], A. Virkkula[1], H. Laakso[1], V. Vakkari[1], P. Beukes[2], P. Van Zyl[2], J.J. Pienaar[2], K. Chiloane[3], G. Fourie[4], S. Piketh[5], K Ferguson[5], T. Tuch[6], A. Wiedensohler[6] and M. Kulmala[1]

[1]Department of Physics, University of Helsinki, Finland
[2]School of Physical and Chemical Sciences, North-West University, Potchefstroom, Republic of South Africa
[3]ESKOM, Sustainability and Innovation, Environmental Sciences Department, Republic of South Africa
[4]SASOL Technology R&D, Sasolburg, Republic of South Africa
[5]Climatology Research Group, University of the Witwatersrand, Johannesburg, Republic of South Africa
[6]Leibniz Institute for Tropospheric Research, Leipzig, Germany

Keywords: air pollution, aerosol optics, tropospheric aerosols, scattering coefficient, absorption, EUCAARI

In the framework of European Union-funded project EUCAARI (Kulmala et al., 2008) we have started extensive measurements on four locations outside Europe. These stations are located in Brazil (Manaus), India (New Delhi), China (Beijing) and South Africa (Elandsfontein). These locations are all in regions with high air pollution concentrations with potential impact on regional and global climate.

At Elandsfontein the current operational instrumentation include a SMPS-system (10-870 nm), 3-wavelength nephelometer, MAAP, PSAP, basic gases (SO_2, H_2S, NO_x and O_3) and basic meteorology (WD, WS, T, RH, solar radiation, precipitation and temperature gradient)

In the near future the measurements will be extended with a Partisol aerosol sampler for chemical analysis of the particles and an aerosol LIDAR.

The instrumentation at the station has been operational for a short time, thus only results from one specific plume episode on 8 February 2009 is shown here. During the late afternoon and evening (15:30 – 21:40) the measurement site was surrounded by a pollution plume due to technical problems at a petrochemical plant approximately 70 km upwind from the station (Dan Hlanyane, personal communication, 2009). The visibility inside the plume decreased to approximately one kilometre. Figure 1 show the aerosol scattering data for three different wave lengths at 700nm, 520nm and 450 nm.

Figure 2 show the aerosol number size distribution measured during the same period, while Figure 3 represent black carbon concentrations.

Hlanyane, Dan; personal communication, 10 February 2009

Kulmala, M., Asmi, A., Lappalainen, H. K., Carslaw, K. S., Pöschl, U., Baltensperger, U., Hov, Ø., Brenquier, J.-L., Pandis, S. N., Facchini, M. C., Hansson, H.-C., Wiedensohler, A., and O'Dowd, C. D.: Introduction: European Integrated project on Aerosol Cloud Climate and Air Quality interactions (EUCAARI) – integrating aerosol research from nano to global scales , ACP-D, 8, 19415-19455, 2008
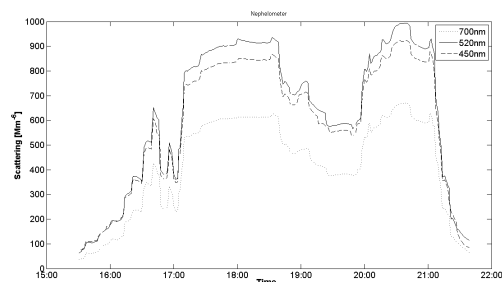
Figure 1: Aerosol scattering data measured with Ecotech Aurora 3000 nephelometer inside the plume on 8 February 2009.
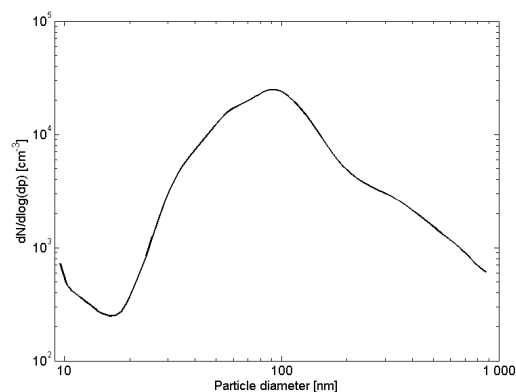

Figure 2: Mean aerosol size distribution (15:30-21:40) inside the plume on 8 February 2009.
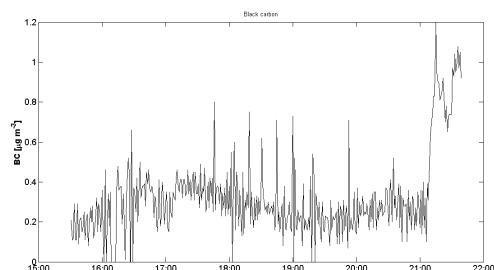

Figure 3: Black carbon concentration measured by a MAAP inside the plume on 8 February 2009.

Mass Spectrometric Investigations on OH-Radical Induced Ageing of Biogenic Secondary Organic Aerosol

L. Müller[1], M.-C. Reinnig[1], Th. F. Mentel[2], R. Tillmann[2], E. Schlosser[2], A. Wahner[2], H. Saathoff[3], N.H. Donahue[4] and T. Hoffmann[1]

[1]Department of inorganic chemistry and analytical chemistry, Johannes Gutenberg-University, Duesbergweg 10-14, 55128 Mainz, Germany
[2]Institute for Chemistry and Dynamic of the Geosphere II: Troposphere; Forschungszentrum Juelich, 52425 Juelich, Germany
[3]Institute for Meteorology and Climate Research, Forschungszentrum Karlsruhe Hermann-von-Helmholtz-Platz 1, 76344 Karlsruhe, Germany
[4]Department of Chemical Engineering and Chemistry, Carnegie Mellon University, 5000 Forbes Avenue, Pittsburgh PA 15213-3890, USA

Tropospheric aerosol is formed by various processes. Primary aerosol is directly emitted into the atmosphere (e.g. dessert dust, sea spray, bio mass burning). Secondary aerosol is formed in the atmosphere by the reaction of volatile organic and inorganic substances (e.g. unsaturated hydrocarbons, terpenes, SO_3) with atmospheric oxidants (e.g. ozone, OH-radicals, NO_3-radicals). The low volatile products can nucleate to new sub-micrometer particles or condense on pre-existing particulate matter. Among the secondary aerosol especially the biogenic secondary organic aerosol (SOA) attracts special attention because of the large amounts of VOC-precursors (e.g. terpenes, sesquiterpenes) emitted by terrestrial vegetation. Condensable organic material has a strong influence on aerosol composition and properties.

However, once in the atmosphere the aerosol composition can change by the influence of oxidative processes (e.g. OH-radicals) known as ageing. The chemical ageing (Rudich et al. 2007) of secondary organic aerosol (SOA) was investigated in two series of experiments using on-line mass spectrometry and off-line high performance liquid chromatography mass spectrometry (HPLC-MS).In a set of photochemical experiments, performed in the large outdoor reaction chamber SAPHIR (Jülich,Germany), SOA was generated from a boreal mixture including mono- and sesquiterpenes (-pinene, -pinene,3-carene, limonene, caryophyllene). During a long time experiment (30h) the generated SOA was exposed to OH-radicals and the chemical composition was analyzed on-line using atmospheric pressure ionization mass spectrometry (API-MS). The on-line method provides highly time resolved chemical information and therefore a direct insight into the temporal changes of SOA-composition. In parallel, filter samples analysed by HPLC-MS allow the enrichment of trace compounds and finally an unambiguous identification of individual substances. In addition, filter samples allow a direct comparison to samples from field studies. The ageing experiments showed a clear change in SOA composition. The compounds observed can be divided into two groups: A group of first generation SOA-compounds, generated by the OH oxidation of the terpenes and a group of second generation compounds, generated by the reaction of OH with SOA compounds. Among the second generation products, especially a tricarboxylic acid (3-methyl-1,2,3-butanetricarboxylic acid, m/z 203) (Szmigielski et al. 2007) was observed to be a good marker compound for BSOA ageing. A further set of experiments was carried out in another large aerosol chamber facility, the AIDA chamber of the Research Centre Karlsruhe. In this dark chamber, the experiments focused on the OH-induced ageing of a-pinene SOA and the influence of temperature. The results clearly show that the tricarboxylic acid is a distinctive marker for OH radical induced BSOA ageing and identify cis-pinonic acid as its precursor. To connect the results of the laboratory measurements with the ambient atmosphere, this paper also compares filter samples taken at the Finnish Forest Research Station in Hyytiälä to the filter samples obtained from SAPHIR/AIDA experiments.

Rudich, et al. (2007) Annual Review of Physical Chemistry 58: 321-352
Szmigielski, et al. (2007) Geophysical Research Letters 34(24)

The Mace Head EUCAARI intensive campaign

M. Dall'Osto[1], C. O'Dowd[1], D. Ceburnis[1], J. Bialek[1], R. Dupuy[1], D. Worsnop[3], R. Healy[2], J. Wenger[2]

[1]Centre for Climate & Air Pollution Studies
Environmental Change Institute, National University of Ireland, Galway, Ireland
[2]Department of Chemistry and Environmental Research Institute
University College Cork, Cork, Ireland
[3]Aerodyne Research, Inc., Billerica, MA 08121, USA

Located on the west coast of Ireland, the Atmospheric Research Station at Mace Head is unique in Europe, offering westerly exposure to the North Atlantic ocean (clean sector, 180 degrees through west to 300 degrees) and the opportunity to study atmospheric composition under Northern Hemispheric background conditions as well as European continental emissions when the winds favour transport from that region. The EUCAARI campaign took part between the 10th of May 2008 and the 15th of June 2008. A range of other on-line aerosol instruments was deployed to measure different physical characteristics of the ambient aerosols sampled such as size resolved particle number concentrations (5nm-10µm), Aethalometer, Nephelometer, Hygroscopicity Tandem Differential Mobility Analyzer (HTDMA), cloud condensation nuclei (CCN) and also two particle mass spectrometers (Aerosol Mass Spectrometer HR-ToF-AMS and Aerosol Time of flight Mass Spectrometer ATOFMS). During the 35 days of the intensive field study, two broad periods were clearly identified: the former heavily influenced by long range transport of pollutants from the European continent (10th-31st May), the latter characterized by a much lower aerosol loading with more marine, arctic and south east air masses (1st-15th June). Furthermore, a continuous clean marine period - with Black Carbon always lower than 50nm/m^3 - was identified between 3rd and 7th of June as well as a period characterized by air masses originated in the south west tropics (9th-10th June).
Moreover, several short term events were identified, including 18 coastal nucleation events, five local biomass events (19th and 26th May, 3rd, 7th and 9th of June), four events of high nitrate-containing aerosols regionally transported (16th, 18th, 23rd and 24th of May).
The ATOFMS dataset were analysed with the powerful ART-2a tool, an artificial intelligence algorithm that sorts single particle mass spectra into specific particle type or clusters. About 30 different particle types were identified by the ATOFMS, including for example sea salt, dust, Elemental carbon, biomass, Nitrate-rich and many others. Moreover, the technique of positive matrix factorisation (PMF) was employed for source apportionment of aerosols and this showed to be highly useful when used with organic data from the Aerodyne Aerosol Mass Spectrometer (AMS), identifying specific factors describing unique particle types belonging to specific sources, including marine ones. Moreover, a specific factor linked with nucleation events was found.
The overall measurements of aerosol size distributions, chemical composition, hygroscopic properties and CCN concentrations associated with the remote sensing ones will elucidate the rule of aerosol on the modification of cloud micro-physics and its radiative properties.

Evaporation of organic and inorganic/organic particles

A.A. Zardini[1], I. Riipinen[2], I.K. Koponen[3], M. Kulmala[2] and M. Bilde[1]

[1]Department of Chemistry, University of Copenhagen, DK-2100, Denmark
[2]Department of Physical Science, University of Helsinki, 00014, Finland
[3]National Research Centre for the Working Environment, DK-2100 ,Copenhagen, Denmark

Biogenic sources as well as human activities contribute large amounts of volatile organic compounds to the atmosphere. Upon oxidation, polyfunctional molecules such as dicarboxylic acids are formed. These molecules generally have lower vapor pressures than the parent molecules and are able to condense on existing particles or maybe even participate in formation of new particles in the atmosphere. Current knowledge about the thermodynamic properties governing this partitioning as well as the influence of the organic molecules on properties of aqueous solution droplets is poor .

We have therefore developed a method based on the HTDMA technique (Hygroscopicity Tandem Differential Mobility Analyzer, see Fig.1) for determining the sub-cooled liquid state vapor pressure as well as other thermodynamic properties of secondary organic aerosol components.
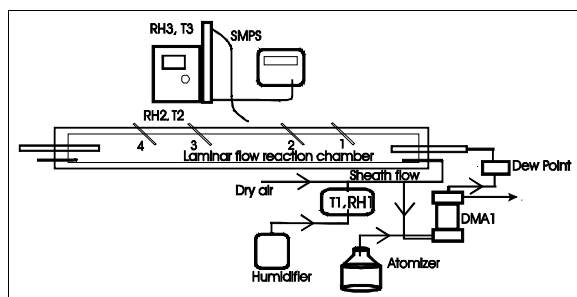
Figure 1. Our TDMA setup consists of three interconnected components: a particle generation system where a narrow size range of particles is selected in the first DMA; a laminar flow reactor where particles are allowed to evaporate at constant relative humidity and temperature; and a second DMA with a particle counter (SMPS) to measure the size of the particles at the sampling ports (1 to 4).

We have already measured evaporation rates of droplets containing one dicarboxylic acid (C3- to C5) and water (Koponen et al., 2007; Riipinen et al., 2006; Zardini et al., 2006). In this work we investigate more complex, multicomponent aqueous solution aerosol particles made of evaporating and non evaporating organic components together with inorganic salts.

The temporal evolution of the particles chemical composition is monitored by an Aerosol Mass Spectrometer operating in parallel with the HTDMA. The integrated results of evaporation and chemical composition changes are then compared to predictions from thermodynamic equilibrium models.

Koponen, I. K. et al. (2007). *Thermodynamic properties of malonic, succinic, and glutaric acids: Evaporation rates and saturation vapor pressures.* Environmental Science & Technology, 41(11), 3926-3933, 2007.

Riipinen, I. et al. (2006). *A method for determining thermophysical properties of organic material in aqueous solutions: Succinic acid.* Atmospheric Research, 82(3-4), 579-590, 2006.

Zardini A. A. et al. (2006). *White light Mie resonance spectroscopy used to measure very low vapor pressures of substances in aqueous solution aerosol particles.* Optics Express 14, 6951-6962, 2006.

Size dependency of ice nucleating properties of various mineral dust samples

O. Stetzer, A. Welti, F. Lüönd, and U. Lohmann

Institute for Atmospheric and Climate Science, ETH Zurich, 8092 Zurich, Switzerland

Keywords: Aerosol Cloud Interaction, Desert Dust, Heterogeneous Ice Nucleation, Ice Nuclei, Mineral Dust.

Airborne mineral dust particles are known to be one of the most efficient aerosol particle classes that form ice in mixed phase and cold clouds in the atmosphere. They are mainly emitted from desert regions like e.g. the Sahara. However, their chemical composition and mineral structures vary significantly and as a result their efficiency to nucleate ice. It is also known that size has an important impact on this particular property of a given particle.

In this study, several generic mineral dusts and a real dust sample have been used to study the activation of ice as a function of temperature and supersaturation. Aerosols from these dust samples have been dryly dispersed with a fluidized bed generator and size selected subsequently with a differential mobility analyzer. The monodispersed aerosol flow has then been split into two portions. These flows were then directed to a condensation particle counter and the Zurich Ice Nucleation Chamber (ZINC) respectively.

ZINC is a continuous flow diffusion chamber (CFDC) as described in Rogers (1988). However, instead of concentric cylinders it has a flat parallel plate geometry (Stetzer et al. 2008). The chamber consists of two ice-covered walls which are held at different temperatures. Diffusion of heat and water vapour leads to linear gradients in temperature and the water vapour concentration. As a result of the exponential dependence of the saturation vapour pressure with temperature, a supersaturation develops which can be tuned by the temperature difference between the walls. A sample flow layered between two sheath flows is then directed through the chamber such that the sample is exposed to the maximum in supersaturation.

Aerosols can activate as ice nuclei and the resulting crystals are grown to sizes which are detectable by means of an optical particle counter. The activated fraction of a sample is then recorded as a function of the supersaturation at a given temperature. Such activation spectra were then recorded for several temperatures in the range -55° to -20°C for each sample and for a selected size of 100, 200 400, and 800 nm, respectively. The aerosols we studied were in particular: montmorillonite, kaolinite, illite, and arizona test dust (ATD).

Deposition nucleation was only found below -35° to -30°C. A comparison of the threshold supersaturation for activation of 1% of all particles shows a clear size effect of a given dust sample. Larger particles required generally a lower supersaturation to activate. In particular, the difference between 100 and 200 nm particles is striking and was in the order of 10% RHi. Minimum RHi for 1% activation were 105% for illite, kaolinite and montmorillonite at -40° C, respectively 110% for ATD at -45° C.

In addition, a possible parameterization for the measured activation spectra is proposed, which could be used in modeling studies. It has as sigmosoidal shape and asymptotically reaches 100% activation for large supersaturations. The obtained functions are also compared to the parameterization from Möhler et al. (2006).
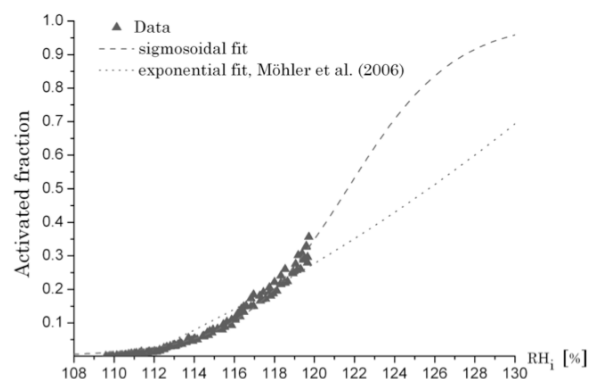

Figure 1. Measured activation spectrum at -55∘ C for 400 nm illite particles is shown with triangles. The least square fit of a sigmosoidal shaped curve is depicted as dashed line. The least square fit of an exponential parameterisation according to Möhler et al. (2006) is shown as dotted line.

Möhler, O., Field, P., Connolly, P., Benz, S., Saathoff, M., Wagner, R., Cotton, R., Krämer, M., Mangold, A., and Heymsfield, A. (2006). *Atmos. Chem. Phys.*, 6, 3007–3021.

Rogers, D. C. (1988). *Atmospheric Research*, 22, 149–181.

Stetzer, O., Baschek, B., Lueoend, F., & Lohmann, U. (2008). *Aerosol Sci. Tech.*, 42, 64–74.

The EUCAARI LONG- RANGE Experiment (LONGREX)

H. Coe[1], W. T. Morgan[1], G. McMeeking[1], P.I. Williams[2], J. D. Allan[2], M. J. Northway[3], C. McConnell E. J. Highwood[3], J. Haywood[4], S Osborne[4], R. Krecji[5], T. Hamburger[6], A. Minnikin[6], M. Frontoso[7], C. Reddington[7], K. S. Carslaw[7]

[1]School of Earth, Atmospheric and Environmental Sciences, University of Manchester, Manchester M13 9PL, UK
[2]National Centre for Atmospheric Science, University of Manchester, Manchester M13 9PL, UK
[3]Department of Meteorology, University of Reading, Reading, RG6 6BB, UK
[4]Met Office, Fitzroy Road, Exeter, EX1 3PB, UK
[5]Atmospheric Science Unit, Stockholm University, S 106 91, Stockholm, Sweden
[6]DLR, Munchner Strasse 20, 82234, Wessling, Germany
7SEE, University of Leeds, Leeds, UK

Keywords: aerosol mass spectrometry, ammonium nitrate, black carbon, organic aerosols, radiative properties

EUCAARI-LONGREX was an aircraft field campaign conducted between 6th May and 23rd May 2008.The experiment was part of **EUCAARI**, the European integrated project on Aerosol Cloud Climate and Air Quality Interactions. LONGREX stands for "LONG Range EXperiment".

The EUCAARI-LONGREX aircraft experiment was based in Oberpfaffenhofen, and involved two extensively equipped research aircraft: the DLR Falcon 20 and the FAAM BAe-146. The aircraft mainly flew West-East and North-South transects across Europe in order to follow the evolution of aerosol properties during air mass transport over Europe.

During the experimental period western Europe was greatly influenced by a large and relatively static anticyclonic system. Figure 1 shows the position of the anticyclone on 6th May 2008 but the pressure field was typical of much of the first 10 days of the experiment. During this time The DLR Falcon 20 flew mainly in the free troposphere and delivered information on aerosol microphysics across Europe during this time. It carried an aerosol LIDAR which delivered information on optical properties of the aerosol across Europe and its vertical structure. It also acted as a pathfinder for the BAe-146 which mainly performed in situ sampling at low level. Aerosol sources from the Poland-eastern Germany-Czech Republic area were dominated by sulphate and organic material. As these aerosol advected westwards towards the mouth of the Rhine and into the North Sea significant ammonium nitrate was observed to be present (Figure 1 shows an example of this). This greatly enhanced the water uptake of the aerosol and led to enhancements in the regional PM2.5, enhanced CCN concentration and the optical depth of the atmosphere in these regions during this period.

During these transport events the organic fraction was also observed to change significantly. Positive Matrix Factorization was performed on the organic mass fragment patterns obtained from an Aerodyne Aerosol Mass Spectrometer (see Lanz et al., 2007). This showed that the organic fraction shows appreciable ageing during transport across Europe. Measurements of black carbon mass on a particle by particle basis using a Single Particle Soot Photometer (SP-2), show increasing coatings of black carbon away from source and offer an assessment of the budget of black carbon.

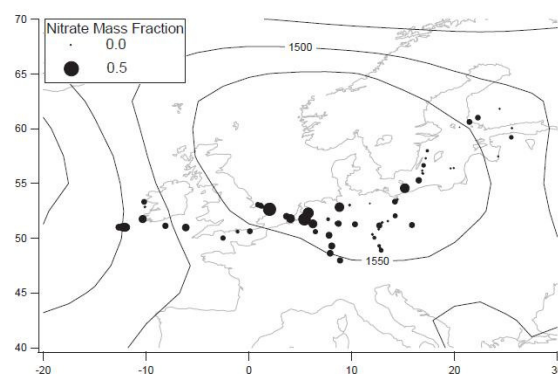The main highlights of these results will be presented.

Figure 1: The circles indicate the nitrate mass fraction in submicron aerosol as measured by an Aerodyne Aerosol Mass Spectrometer. Each circle represents the average of a single straight and level run. The data shown are for the whole of the anticyclonic period. Also shown is the ECMWF 850 hPa geopotential height field for 12 UTC on 6th May 2008. These conditions were representative of the first 10 days of the experiments.

Lanz, V. A., et al. (2007), *Atmos. Chem. Phys.*, *7*(6), 1503-1522.
Schwarz J. P. et al. (2006), *JGR*, *111 D16207*, 10.129/2006JD007076.

A diluter for a PSAP at a EUCAARI-station in South Africa

A. Virkkula[1], L. Laakso[1,2], H. Laakso[1], V. Vakkari[1], P. Beukes[2], P. Van Zyl[2], K. Pienaar[2], K. Chiloane[3], G. Fourier[4], S. Piketh[5], T. Tuch[6], A. Wiedensohler[6] and M. Kulmala[1]

[1]Department of Physics, University of Helsinki, Finland
[2]School of Physical and Chemical Sciences, North-West University, Potchefstroom, Republic of South Africa
[3]ESKOM, Environmental Sciences, Resources & Strategy Division, Rosherville, Republic of South Africa
[4]SASOL Technology Research & Development, Sasolburg, Republic of South Africa
[5] Climatology Research Group, University of Witwatersrand, Republic of South Africa
[6]Leibniz Institute for Tropospheric Research, Leipzig, Germany

One of the four EUCAARI (Kulmala et al., 2008) stations outside Europe is located in Elandsfontein, South Africa (Elandsfontein). An overview of these measurements is given by Laakso et al. (this issue). At the station light absorption by particles is measured with a Multi-Angle Absorption Photometer (MAAP) (Petzold and Schönlinner 2004). The MAAP measures light absorption at one wavelength only. ,Therefore, a 3-wavelength Particle Soot Absorption Photometer (3wl PSAP) (Virkkula et al. 2005) was also added to the setup in order to get information on the wavelength dependency of the light absorption, and also to provide wavelength dependent absorption data for comparisons for the scattering data provided by the 3-wavelenght nephelometer.

The PSAP is a filter-based method with a manual filter change. This creates problems at a station visited only weekly or even every 2 weeks. In order to prolong the filter changing period, the sample flow is diluted (Figure 1) approximately at the ratio of 1:10. The dilution is analogous to the closed-loop arrangement generally used in a DMPS or SMPS. Dilution is arranged by mixing the sample air flow with clean, filtered air. The flow makes a loop from a Thomas membrane pump through a flow fluctuation dampening chamber to an absolute filter, from where it goes to a mixing tube and back to the pump. The dilution flow is monitored by a differential pressure measurement (dP sensor). If there are no leaks in the system, the loop is closed and the flow to the PSAP (Q_{PSAP}) equals the sample flow (Q_S) from the inlet to the diluter tube.

The experiences gained from the first 6 months of the dilution system will be presented.

Kulmala, M., Asmi, A., Lappalainen, H. K., Carslaw, K. S., Pöschl, U., Baltensperger, U., Hov, Ø., Brenquier, J.-L., Pandis, S. N., Facchini, M. C., Hansson, H.-C., Wiedensohler, A., and O'Dowd, C. D.: Introduction: European Integrated project on Aerosol Cloud Climate and Air Quality interactions (EUCAARI) – integrating aerosol research from nano to global scales , ACP-D, 8, 19415-19455, 2008

Petzold, A., and Schönlinner,M. (2004). Multi-Angle Absorption Photometry —A New Method for the Measurement of Aerosol Light Absorption and Atmospheric Black Carbon, J. Aerosol Sci. 35:421–441.

Virkkula A., Ahlquist N.C., Covert D.S., Arnott W.P., Sheridan P.J., Quinn P.K., and Coffman D.J. (2005) Modification, calibration and a field test of an instrument for measuring light absorption by particles. Aerosol Sci. Technol., 39, 68 – 83.
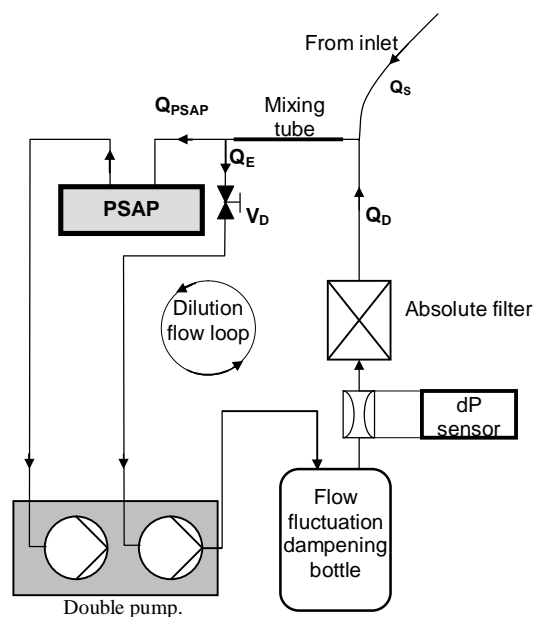
Figure 1. Flows of the PSAP dilution system at Elandsfontein, RSA.

Aerosol classification by airborne in-situ and high spectral resolution lidar measurements during EUCAARI

F. Abicht[1], M. Esselborn[1], T. Hamburger[1], B. Y. Liu[1, 2], A. Minikin[1], and A. Petzold[1]

[1] Institut für Physik der Atmosphäre, DLR, Oberpfaffenhofen, 82234 Wessling, Germany
[2] Ocean Remote Sensing Institute, Ocean University of China (OUC), Qingdao, 266003, China

Keywords: optical properties, extinction, optical depth, lidar, lidar ratio.

In the framework of the EUCAARI-LONGREX (European integrated project on Aerosol Cloud Climate and Air Quality Interactions - LONG Range EXperiment) fight campaign high spectral resolution lidar (HSRL; Esselborn et al., 2008) measurements were performed over several regions of Europe. Based on the HSRL measurements aerosol-specific quantities at $\lambda = 532$ nm were deduced including the aerosol backscatter coefficient, aerosol extinction coefficient, aerosol optical depth, the lidar ratio and aerosol depolarisation ratio.

Simultaneous to the HSRL measurements, airborne in-situ aerosol measurements were performed, including aerosol number size distribution, aerosol absorption, and aerosol volatility analyses. For selected aerosol layers, in situ data were used to deduce characteristic aerosol microphysical properties and link them to HSRL aerosol properties like lidar ratio and depolarisation.

Figure 2. Lidar properties for different aerosol types measured during EUCAARI-LONGREX and SAMUM (desert dust, biomass burning).
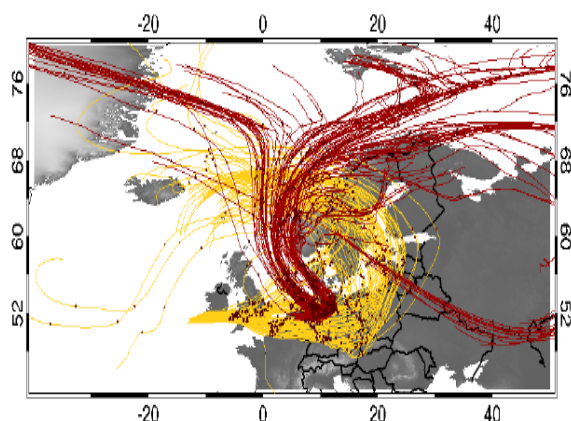

Figure 1. Air mass back trajectories for two key days during EUCAARI-LONGREX: 14 May 2008 (yellow) and 21 May 2008 (brown).

Figure 1 shows examples of back-trajectories for air mass which were probed in-situ and by HSRL: On 14 May 2008 air masses were probed which circulated for several days over Central Europe during a stagnant high pressure system situation, collecting anthropogenic pollution from various source regions. On 21 May, air masses were probed which moved into Central Europe across the North Sea, being considered as relatively clean compared to the previous weather situation.
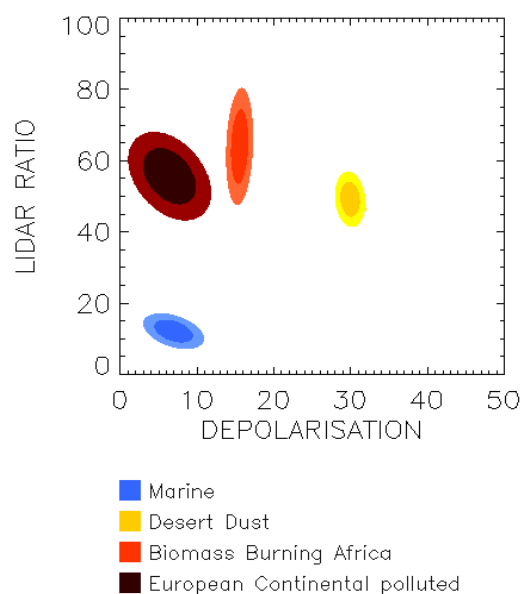
Aerosol properties accessible by HSRL cluster in characteristic patterns for different aerosol classes as shown in Figure 2. Aerosol in-situ microphysical data will be used to further investigate the HSRL aerosol classification capabilities and limitations. The favourable synoptic situation during the first part (06 – 14 May) of EUCAARI-LONGREX with an almost stationary anticyclone over Europe enables us to study aerosol transformation and aging over an anthropogenic source region from in-situ observations collocated with active remote sensing studies of the same aerosol.

The presented results serve as an important first step towards the assessment of future spaceborne active remote sensing instruments for the large-scale monitoring of the tropospheric aerosol.

Esselborn, M., M. Wirth, A. Fix, M. Tesche, and G. Ehret (2008). *Applied Optics*, 47, 346-358.

Aerosol microphysics during anticyclonic conditions over Europe during EUCAARI-LONGREX

T. Hamburger[1], A. Minikin[1], A. Dörnbrack[1], A. Petzold[1], H. Rüba[1], H. Schlager[1], M. Scheibe[1], A. Ibrahim[1], H. Coe[2], G. McMeeking[2], W. T. Morgan[2], A. Stohl[3]

[1] DLR, Institut für Physik der Atmosphäre, Oberpfaffenhofen, 82234 Wessling, Germany
[2] School of Earth, Atmospheric and Environmental Sciences, University of Manchester, Manchester M13 9PL, UK
[3] Norwegian Institute for Air Research (NILU), P.O. Box 100, 2027 Kjeller, Norway

Keywords: Aerosol characterization, Aerosol evolution, Aerosol measurement, European pollution, Meteorology.

Airborne measurements of tropospheric aerosol properties over Europe were conducted in May 2008 during the EUCAARI-LONGREX campaign, where LONGREX stands for "LONG Range EXperiment". 15 research flights were performed with the DLR Falcon 20, of which most flights were coordinated with research flights performed by the FAAM BAe-146. Both aircrafts operated from Oberpfaffenhofen (48.08° N, 11.28° E). The flights of the FAAM BAe-146 were mainly conducted in the boundary layer and lower free troposphere, whereas the flights of the DLR Falcon 20 focussed on the free troposphere up to the tropopause level and on obtaining an extensive set of vertical profiles. The vertical profiles performed by the DLR Falcon 20 cover a large part of Central Europe. In-situ measurements of aerosol properties were also performed in the vertical tropospheric column over EUSAAR ground sites like Melpitz and Cabauw.

DLR Falcon 20 aerosol data used for the analysis were measured by a set of Condensation Particle Counters (CPC), a thermodenuder at 250° C, two aerosol spectrometers by Grimm, two further optical particle counters, the Passive Cavity Aerosol Spectrometer Probe (PCASP-100X) and the Forward Scattering Spectrometer Probe (FSSP-300) and one Particle Soot Absorption Photometer (PSAP). More detailed information about the instrumentation can be found in Petzold *et al.*, 2007.

During the first part of the campaign a blocking anticyclone occurred over Central Europe with its core mainly situated over Denmark. This stable synoptic situation leads to accumulation of anthropogenic emissions in the continental boundary layer and westward transport of air masses across Northern Germany and South of England towards the Atlantic. Aerosol microphysical properties were measured in almost unpolluted air masses over the Baltic Sea advected from Scandinavia as well as in air masses within the anticyclone over Central Europe and the Atlantic.

Most measurements of accumulated and transported emissions showed a high fraction of non volatile particles within the total particle number concentration, up to almost 100 % in the boundary layer and lower troposphere. In contrast to this, the volatile fraction of the total volume of PM2.5 reaches 95 % as shown in Figure 1. This indicates an internally mixed aerosol with a high load of condensed and accumulated volatile material with a non volatile core.
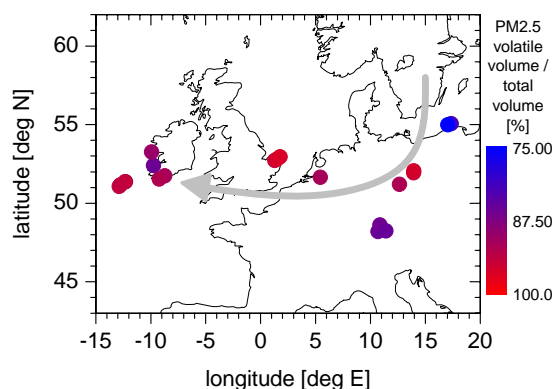

Figure 1. Aerosol properties during the May 2008 anticyclone. The colour indicates the volume fraction of volatile material of PM2.5 aerosol. The main transport direction is shown by the grey arrow.

The extensive data set obtained during EUCAARI-LONGREX within the stable synoptic situation over Europe combined with an analysis of the meteorological situation during air mass transport allows studies of aerosol microphysical properties during transformation and aging of anthropogenic emissions. These studies will also provide an important input to aerosol models. The main highlights of this analysis will be presented on the EAC 2009.

Petzold, A., et al. (2007). *Atmos. Chem. Phys.*, 7, 5105-5127.

Characterization of the sources of organic aerosol collected at K-Puszta

A. Hoffer[1], G. Kiss[1], C. Alves[2], C. Pio[2], A. Vicente[2], E. Finessi[3], S. Decesari[3], J. Genberg[4], K. Stenström[4], E. Swietlicki[4]

[1]Air Chemistry Group of the Hungarian Academy of Sciences, University of Pannonia, 8200 Veszpém, Hungary
[2]CESAM and Department of Environment and Planning, University of Aveiro, 3810 193 Aveiro, Portugal
[3]Instituto di Scienze dell Atmosfera e del Clima, Consiglio Nazionale delle Ricerche, 40129, Bologna, Italy
[4]Department of Physics, Lund University, S-221 00 Lund, Sweden

Keywords: carbonaceous aerosol, GC-MS, source apportionment.

Although it has been recognized that organic aerosol plays an increasingly important role in inadvertent climate modification, its origin in the boundary layer as well as in the free troposphere is virtually unknown. Knowing the origin of the organic aerosol is of utmost importance in predicting how future changes in human activities will affect the global distribution and properties of organic aerosol and thus how they will modify global climate.

During the European Integrated project on Aerosol Cloud Climate and Air Quality Interactions (EUCAARI) the anthropogenic, natural as well as primary and secondary aerosol components were studied in samples collected at different sampling sites in Europe. This information will help to determine the concentration of aerosols due to long range transport as well as the influence on AQ/PM of transnational transport within Europe.

In this work we present the results of tracer compound analyses and ^{14}C measurements of the samples collected at the Central European sampling site K-Puszta. The site is a rural measurement site located on the Great Hungarian Plain, 15 km northwest from the nearest town Kecskemét, and 80 km southeast from Budapest. The surroundings of the measurement site are dominated by mixed forest. Ten samples were collected in summer 2008 under the umbrella of the EUCAARI project by a high volume sampler.

The characterization of the bulk carbonaceous compounds was performed by a thermal optical method. The concentration of the elemental and organic carbon was measured and based on their concentration ratio conclusions were drawn about the importance and influence of the anthropogenic sources. In order to further characterize the carbonaceous components of the aerosol ^{14}C measurements and H-NMR analyses were also performed on the filters. These results were combined by the results of gas-chromatography-mass spectrometry. With this technique the concentration of biogenic and anthropogenic tracer compounds were determined. Due to the complex nature of the samples, prior the gas-chromatographic analysis the compounds were separated based on their polarity by flash chromatography (Alves et al., 2007). Thus, the polar and less polar compounds were measured separately. The concentrations of the less polar compounds were measured directly, whereas those of the more polar compounds were determined after derivatisation by BSTFA.

Based on the results we concluded on the importance of the primary and secondary aerosol sources as well as the contribution of anthropogenic and biogenic sources.

It can be established based on the results of the gas-chromatography-mass spectrometric measurements, that the n-alkanes show odd carbon number preference. These compounds are characteristic to the contribution of the waxes of the terrestrial higher plants. We have also measured the amount of the unresolved complex mixture of branched and cyclic hydrocarbon compounds, which give further information about the importance of the anthropogenic sources of the atmospheric aerosol at K-Puszta. However, PAH's can be found both in the gas and the aerosol phase, thus their concentration is highly dependent on the sampling conditions, from their presence in the samples we can conclude on ongoing fossil fuel and other burning processes. The n-alcohols showed even carbon number preference with the C_{26} compound being the most abundant substance. These compounds are attributable to terrestrial higher plants. The contribution of the biomass burning processes to the aerosol composition was followed by the measurement of the amount of levoglucosan, mannosan and galactosan as well as the aromatic compounds. The fatty acids showed even carbon number predominance, which indicates the contribution of higher plants to the aerosol composition at K-Puszta.

Alves, C., Oliveira, T., Pio, C., Silvestre, A.J.D., Fialho, P., Barata F., Legrand, M. (2007). *Characterization of carbonaceous aerosols from the Azorean Island of Terceira.* Atmospheric Environment 41, 1359–1373.

Photosensitized transformation of dicarboxylic acid in aerosols

A. Rouvière[1], P.F. DeCarlo[2], A. Schlierf[1], O. Favez[3], B. D'Anna[3], C. George[3], A. Prévôt[2] and M. Ammann[1]

[1] Laboratory for Radiochemistry and Environmental Chemistry, Paul Scherrer Institut, 5232 Villigen, Switzerland
[2] Laboratory of Atmospheric Chemistry, Paul Scherrer Institute, 5232 Villigen, Switzerland
[3] Université de Lyon, Lyon, F-69626, France ; CNRS, UMR5256, IRCELYON

Keywords: aerosol chemistry, dicarboxylic acids, organic aerosols, organic acids, photochemical processes.

Ultraviolet or visible light absorbing organic constituents of atmospheric aerosols may act as photosensitizers for a number of processes. Photosensitizers may be primary organics from combustion sources or be formed in situ during oxidation in the atmosphere. The significance of photosensitized processes has been demonstrated by showing enhanced uptake of atmospheric oxidants to organic films or aerosol particles (George *et al.*, 2005, Stemmler et al., 2006, 2007). In this work, we focus on photosensitized reaction of organic aerosol constituents.

The aerosols were produced by nebulizing a solution containing ammonium sulfate, a dicarboxylic acid and benzophenone. The aerosol flow passed through a photoreactor with about 9 min. residence time, which was coupled to either a chemical ionization mass spectrometer (CIMS) in proton transfer mode or a High Resolution Time of Flight Aerosol Mass Spectrometer (AMS) and two Scanning Mobility Particle Sizer (SMPS). Separate experiments were performed in bulk aqueous solution using laser photolysis allowing monitoring the decay kinetics of the photosensitizer excited state. The decay of the triplet state of benzophenone was followed at 525nm.

Fig. 1 shows results from the bulk solution experiments, indicating that the benzophenone triplet is quenched in presence of both succinic and adipic acid.
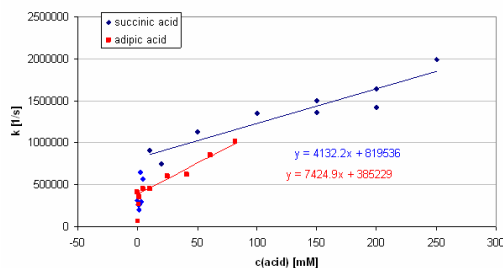

Figure 1. Benzophone triplet quenching kinetics in succinic and adipic acid solutions

Using the CIMS coupled to the aerosol photoreactor and with adipic acid aerosol present, we observed the characteristic fragmentation and an efficient ionization of the analyte. Adipic acid is seen mostly at m/z=147 and m/z=129. The peak m/z=129 indicates the loss of water, m/z=165 likely results from an additional attached water molecule. The presence of light between 300 and 400nm led to a reduction of adipic acid peaks.

Using the AMS, we observed changes to the ratio of m/z 44 to 43, with the changes being more pronounced in the case of succinic acid than in the case of adipic acid. This change in the 44 to 43 mass ratio is typically associated with the loss of carboxylic acid groups. A detailed analysis of the available data will allow extracting more information on potential products of the light induced reaction.

Overall, the results are a strong indication that the presence of a photosensitizer leads to light induced reactions of simple dicarboxylic acids.
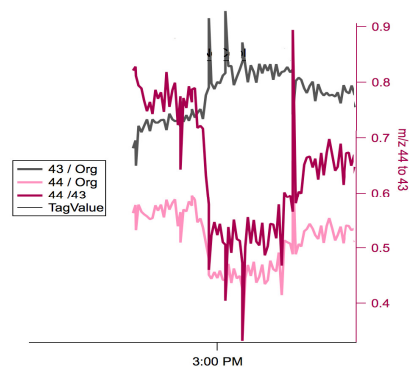

Figure 2. Result from the AMS measurements of the effect of light (switched on shortly before 3 pm) on m/z 44 and 43, both normalized to the total amount of organics, and on the ratio of m/z 44 to 43 (black line), for an aerosol containing succinic acid and a small amount of benzophenone.

References
George, C. et al., (2005). Faraday Discuss., 130, 195-210.
Stemmler, K. et al., (2006). Nature, 440, 195-198.
Stemmler, K. et al., (2007). Atmos. Chem. Phys., 7, 4237-4248.

Terpenes as potential precursors of humic-like substances in the atmosphere?

N. Törő[1], V. Domján[1], A. Hoffer[2], G. Kiss[2], R. Fisseha[3], A. Kiendler-Scharr[3], T. Brauers[3] and T.F. Mentel[3]

[1]University of Pannonia, Dept. Earth and Environmental Sciences, Egyetem 10, 8201 Veszprém, Hungary
[2]Air Chemistry Group of Hung. Acad. Sci. at University of Pannonia, Egyetem 10, 8200 Veszprém, Hungary
[3]Forschungszentrum Jülich, D-52425 Jülich, Germany

Keywords: SOA formation, terpenes, humic-like substances

Secondary aerosol formation from 5 monoterpenes (Ocimene, α-Pinene, β-Pinene, Limonene, Δ3-Carene) and 2 sesquiterpenes (β-Caryophyllene, α-Farnesene) under various conditions was studied in a series of experiments performed in the SAPHIR chamber at Forschungszentrum Jülich in June 2008. In these simulation experiments terpene species and their concentration were varied while in most cases ozone concentration was kept at 50 ppb. Light conditions in the outdoor chamber followed the weather situation. Aerosol microphysical characterization as well as aerosol mass spectrometry were performed on-line but filter sampling was also carried out for more detailed off-line chemical characterization. In most cases filter samples were collected on the first day of reaction then the aerosol particles aged in the chamber and filter samples were collected again on the second day. Reaction products were analyzed at University of Pannonia by electrospray ionization (ESI) mass spectrometry either directly or following HPLC separation. In some cases identification of oxidation products was supported by GC-MS as well.

Extracts of the filters were analyzed by reversed phase HPLC coupled to negative electrospray ionization MS. A number of intense ions were detected in the chromatograms as shown in Figure 1.
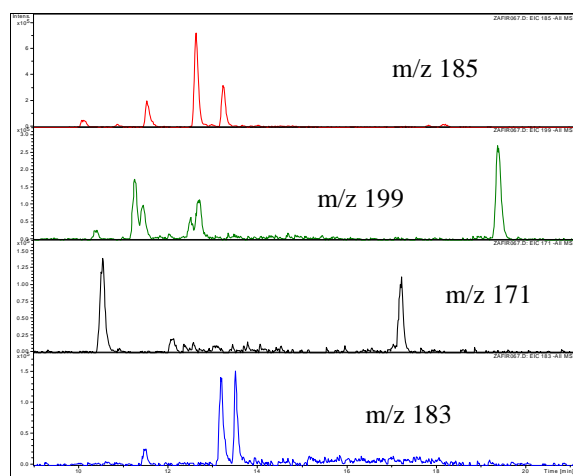

Figure 1 RP-HPLC ion chromatograms detected with ESI⁻-MS from 9 to 21 min. Peaks with the same m/z value indicates the formation of isomers: e.g. m/z=185 can be pinic acid, caric acid or norlimonic acid.

In the mass spectra of individual peaks very often the difference between m/z values equaled 44 that is characteristic for the CO_2 loss of carboxylate ions. Furthermore, the formation of cluster ions with Na^+ revealed the number of carboxylic groups within the molecules. Thus, numerous dicarboxylic acids were found among the terpene oxidation products. The drawback of HPLC-MS is that the sample is diluted in the chromatographic eluent and, consequently, less intense ions can be lost. Furthermore, irreversibly retained compounds will not elute from the column and therefore no information can be obtained about them. In order to avoid these problems direct injection MS was also applied to get information on the overall undiluted sample. A mass spectrum obtained with this technique is shown in Figure 2.
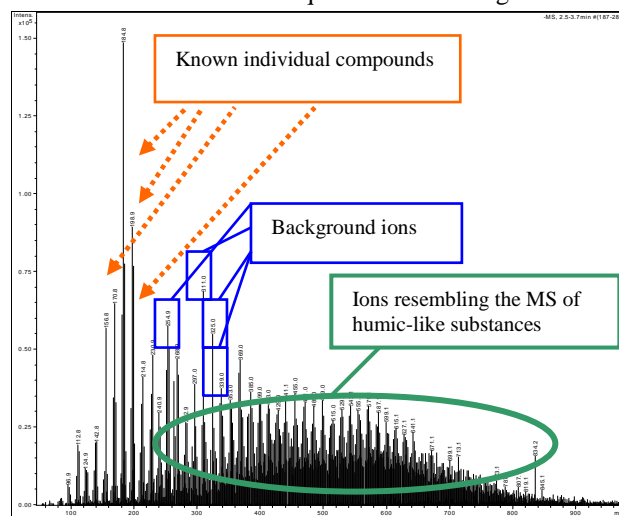

Figure 2 Direct injection ESI⁻-MS spectrum of a filter extract recorded from m/z 50 to 1000.

Most of the known monoterpene oxidation products form ions below m/z 200 while sesquiterpene oxidation products can be detected in the m/z 200-300 range. However, periodic spectral lines (Δm/z=14) were detected from approximately m/z 300 to 800 with maximum intensity around m/z 550. The periodicity and the wide range of ions resembled those of humic-like substances found in rural aerosol although the maximum in ambient samples was around m/z 250-300.

T19 Special Session 7

Synthesis and characterization of titanium dioxide particles for toxicity tests

A. J. Koivisto[1], H. Alenius[1], J. Joutsensaari[2], H. Norppa[1], M. Miettinen[2], P. Pasanen[2], L. Pylkkänen[1], E. Rossi[1], T. Tuomi[1], M. Vippola[1], J. Jokiniemi[2,3] and K. Hämeri[4]

[1]Finnish Institute of Occupational Health, Topeliuksenkatu 41 a A, 00250, Helsinki, Finland
[2]Department of Environmental Science, University of Kuopio, Yliopistonranta 1 E, 70210, Kuopio, Finland
[3]VTT Technical Research Centre of Finland, Vuorimiehentie 3, 02044, Espoo, Finland
[4]Department of physics, University of Helsinki, Gustaf Hällströmin katu 2, 00014, Helsinki, Finland

Keywords: TiO$_2$ nanoparticles, Nanoparticle production, Nanoparticles, characterization, Health effects of aerosols, Morphology.

Nanotechnology is controlling matter by adjusting dimensions of particles at roughly from 1 to 100 nanometers. In this size range the bulk material properties start to change, because number of surface atoms is increasing and quantum mechanical properties are changing. This change in properties may also affect to the matter toxicity and thus nanoparticles should not be treated as a bulk material. Here we introduce an inhalation exposure setup with laminar flow reactor, and present the results of titanium dioxide (TiO$_2$) particle production.

The experimental setup is shown in Figure 1. It consists of particle generator, humidifier and diluter, inhalation chamber, fabric filter and aerosol characterization instruments. The setup operates in atmospheric pressure where the produced aerosol is diluted and humidified to be suitable for mice experiments.
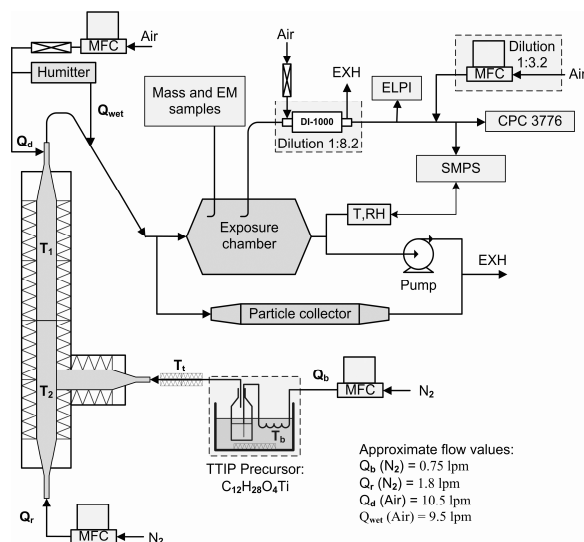

Figure 1. Scheme of the experimental setup with typical operation parameters.

Nano-sized TiO$_2$ particles were produced by thermal decomposition of titanium tetraisopropoxide (TTIP) (Ti(OC$_3$H$_7$)$_4$) vapour in the tubular flow reactor (Okuyama et al. 1986; Ahonen et al. 2001). Nitrogen carrier gas, with flow rate of Q$_b$, was saturated with the TTIP vapour. Inside the reactor TTIP is thermally decomposed: Ti(OC$_3$H$_7$)$_4$ → TiO$_2$ + 4C$_3$H$_6$ + 2H$_2$O.

TiO$_2$ molecules start to nucleate, and condensate to the seed particles, forming primary particles. Primary particles are further agglomerated by Brownian coagulation.

The experiments were done with aerosol mass concentrations of 0.8, 7.2, 10.0 and 28.5 mg/m^3. The aerosol size distributions were measured with scanning mobility particle sizer and electronic low pressure impactor. Aerosol particle concentration was measured with condensation particle counter.

Composition and shape of the particles were defined from grid samples with transmission electron microscopy (TEM). The fabric filter was used to collect particles for further analysis and experiments. Specific surface area of produced titanium dioxide was defined with Brunauer-Emmet-Teller method to be 61m^2/g. The crystalline structure of the particles was defined with X-ray diffraction method to be 74% anatase and 26% of brookite with crystalline size of 41 and 6 nm. In figure 2 is presented aerosol size distribution and figure of collected particles for aerosol with mass concentration of 10 mg/m^3.
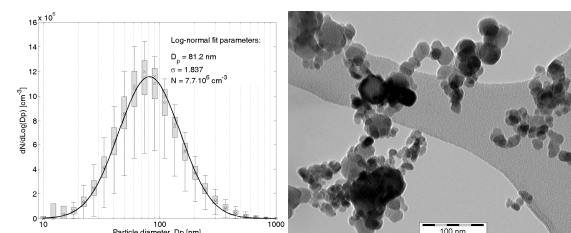

Figure 2. On the left is particle mobility size distribution. Fit is done for averaged values (○) of experiments. Symbols are median (x), standard deviation (box), and 5% and 95% percentiles (bars). On the right is TEM figure of collected particles.

Okuyama, K., Kousaka, Y., Tohge, N., Yamamoto, S., Wu, J. J., Flagan, R. C. and Seinfeld, J. H. (1986). AICHE Journal, 32, 2010-2019.
Ahonen, P. P., Moisala, A., Tapper, U., Brown, D. P., Jokiniemi, J. K., Kauppinen, E. I. (2001). Journal of Nanoparticle Research, 4, 43-52.

Characterization of polychlorinated dibenzo-p-dioxin/dibenzofuran emissions from joss paper burned in a furnace

M.T. Hu[1], S.J. Chen[1*], K.L. Huang[1], Y.C. Lin[2], G.P. Chang-Chien[3,4] and J.H. Tsai[1]

[1] Department of Environmental Engineering and Science, National Pingtung University of Science and Technology, 91201, Taiwan.
[2] Institute of Environmental Engineering, National Sun Yat-Sen University, Kaohsiung, 804, Taiwan.
[3] Department of Chemical and Materials Engineering, Cheng Shiu University, Kaohsiung County, 833, Taiwan.
[4] Super Micro Mass Research & Technology Center, Cheng Shiu University, Kaohsiung County, 833, Taiwan.

Keywords: joss paper burning, PCDD/Fs, emissions.

Burning joss paper in temples is popular in some Asian countries (e.g., China and Taiwan) where Buddhism and Taoism are practiced. During temple activities, those praying and visiting are usually exposed to toxic compounds emitted by burning joss paper. Several studies have measured PCDD/F emissions from burning wood (Bumb *et al.*, 1980; Choudhry & Hutzinger, 1983; Lemieux. *et al.*, 2004). The chlorine ions (Cl⁻) inside wood enhance formation of PCDD/Fs (Bumb *et al*., 1980; Choudhry & Hutzinger, 1983). Joss paper is primarily made of recycled paper, bamboo, furniture manufacturing waste, or architectural waste. Hence, PCDD/Fs may form when joss paper is burned in temple furnaces.

The joss paper in this study is widely used in Taiwanese temples—Taiwan has over ten kinds of joss paper in different shapes/sizes. The chlorine content (Cl⁻) in unburned and burned joss paper (B-ash) was 0.093 and 1.71 mg g^{-1}, respectively (Table 1). The theoretically calculated Cl⁻ content in burned joss paper was 1.98 (= 0.093×100/4.69) mg g^{-1}. In other words, about 10% of Cl⁻ content in joss paper was possibly associated with the formation of PCDD/Fs. The ash content in burned joss paper (B-ash) was high (84.6%). Hence, we infer that incomplete combustion and Cl⁻ release are related to PCDD/F emissions from combustion of joss paper in the furnace.

Table 1. Compositions of the selected joss paper and bottom ash (B-ash) of burned joss paper.

Proximate Analysis (%)	Joss papers	B-ash	Analytical Method
Combustible	87.2	15.1	NIEA R205.01C
Ash	4.69	84.6	NIEA R205.01C
Moisture	8.08	0.32	NIEA R203.01T
Ultimate Analysis(mg/g)			
Chlorine (Cl⁻)	0.093	1.71[1] 1.52[2] 1.54[3]	NIEA R205.01C / NIEA W415.52B

[1] B-ash of burned joss paper obtained from the temple furnace
[2] ash of re-burned B-ash obtained in lab
[3] ash of burned joss paper obtained in lab

Table 2 lists the mean PCDD/F content and relative standard deviation (RSD) in unburned joss paper and ash from burned joss paper. Notably, ratios >1.0 for PCDDs/PCDFs and their I-TEQ (11.4 and 1.24, respectively) indicate that the predominant PCDD/Fs in unburned joss paper were PCDDs, not PCDFs, and their toxic contribution was PCDDs > PCDFs. Gullett and Touati (2003) reported that PCDD/F content in ash from burning wheat and rice straw stubble was 0.5 ng I-TEQ kg^{-1}, significantly lower than that from burning joss paper. Additives such as dyes and paint in joss paper are likely responsible for differences in PCDD/F content. The TEQ of total PCDD/Fs in ash in this study was in the range of 1.62–5.23 ng I-TEQ kg^{-1} (mean = 3.42 ng I-TEQ kg^{-1}) higher than that for bottom ashes obtained from municipal solid waste incinerators in Taiwan (Chen *et al.*, 2006). Therefore, joss paper combustion is a significant source of PCDD/F emissions.

Table 2. Mean PCDD/F content in the joss paper and B-ash of burned joss paper (n = 6)

PCDD/Fs species	Joss paper		B-Ash	
	Mean (ng kg^{-1})	RSD (%)	Mean (ng kg^{-1})	RSD (%)
Total PCDDs	178	13.2	7.79	7.01
Total PCDFs	15.6	5.67	10.7	6.59
PCDDs/PCDFs	11.4	14.6	0.726	2.84
Total PCDD/Fs	193	12.1	18.5	6.62
	ng I-TEQ kg^{-1}	%	ng I-TEQ kg^{-1}	%
Total PCDDs	0.355	16.0	0.449	7.01
Total PCDFs	0.290	14.1	1.47	6.01
PCDDs/PCDFs	1.24	19.5	0.305	2.87
Total PCDD/Fs	0.645	11.9	1.92	6.14

Bumb, R.R., Crummett, W.B., Cutie, S.S., Gledhill, J.R., Hummel, R.H., Kagel, R.O., Lamparski, L.L., Luoma, E.V., Miller, D.L., Nestrick, T.J., ShadoD, L.A., Stehl, R.H., & Woods, J.S. (1980). *Science*, 210, 385–90.

Chen, C.K., Lin, C., Wang, L.C., & Chang-Chien, G.P. (2006). *Chemosphere*, 65, 514–520.

Choudhry, G.G., & Hutzinger, O. (1983). *Mechanistic aspects of the thermal formation of halogenated organic compounds including polychlorinated dibenzo-p-dioxins*. New York: Gordon and Breach.

Gullett, B., & Touati, A. (2003). *Atmospheric Environment*, 37, 4893–4899.

Lemieux, P.M., Lutes, C.C., & Santoianni, D.A. (2004). *Progress in energy and combustion science*, 30, 1-32.

Human type B synoviocytes, as a cellular model for a better knowledge of the pro-inflammatory effects of environmental PM

F. Cetta[1], F. Laghi Pasini[2], E. Selvi[2], A. Dhamo[1], M. Natale[2], R. Zangari[1], P. Laviano[1], L. Cantarini[2], E. Bolzacchini[3], M. Camatini[3], M. Galeazzi[2].

[1] Department of Surgery, Research Doctorate in Oncology and Genetics and [2] Department of Clinical Medicine and Immunology, University of Siena, Nuovo Policlinico "Le Scotte", viale Bracci,16, I-53100 Siena, Italy
[3] Department of Environmental Sciences, University of Milano-Bicocca, Piazza dell'Ateneo Nuovo, 1,20126 Milan, Italy

Human type B synoviocytes are involved in cartilage damage in chronic inflammatory joint diseases, particularly in rheumatic diseases, by producing inflammatory mediators such as interleukin 6 (IL-6). The increased level of purine and pyrimidine nucleotides in the synovial fluid of rheumatoid arthritis (RA) patients could activate the large family of purinergic P2 receptors. An interesting member of the P2X subfamily is the P2X7 receptor (P 2X7R), - expressed on inflammatory cells and human primary fibroblasts, - coupled to ion fluxes, microvescicle formation, and IL release (Caporali, 2008). Health effects from environmental particulate material (PM), in particular clinically evident diseases related to long-term exposure (asthma, COPD, pulmonary fibrosis etc), show striking similarities with autoinflammatory and autoimmune rheumatic diseases. In particular, epidemiological studies show that only a minority of the general population, namely predisposed people, are those mainly affected by adverse effects, whereas in the vast majority of the general population, clinically evident diseases usually do not occur, even after exposure to high peaks of environmental pollution (Cetta, 2007, 2009). The final clinical outcome is usually determined by common mechanisms such as ROS generation, oxidative stress, activation of pathways, such as NFKB, increased production of proinflammatory cytochines, such as interleukin (IL) 6, IL8, and tumor necrosis factor α (TNF α), similarly to what occurs in chronic inflammatory joint diseases. The aim of the present study has been to assess the "in vitro" effects of variable concentration (1-10-50 μg/cm^2) of various types of PM (PM 10,2.5,0.1) when incubated with human synoviocytes, to evaluate the occurrence of proinflammatory effects.

Daily levels of PM_{10} and $PM_{2.5}$ and PM_1 (diameter <10 μm, 2.5 μm, 1 μm, respectively) were measured by PM detection units, both outside and inside 2 schools for children and 2 hospices for retired people in Milan, Italy. Both OPC detectors (GRIMM) and low volume gravimetric detectors (Tecora, Milan, Italy) were used. Usually Teflon filters (47 mmØ, 2 μm, Pall Gilman, USA) were stored. Samples from these filters were used after sonication in sterile phosphate buffer saline (PBS). Aliquots of these samples at a concentration of 10/50/75μg/ml were incubated for 4 or 6 hours at 37°C with human type B synoviocytes.

Preliminary data showed both an increased production of interleukin IL-6, IL-8, and the functional activation of P2X7 receptors. In particular, biological PM - host interaction was mediated by cytosolic Ca^{2+} increase, triggering the NFKβ pathway, whereas various components of PM (PM10,2.5 and 0.1) interacted different with host cells and tissue, generating a wide variety of reactions involving microvescicle formation, phagocytosis, membrane alterations (cellular membrane holes).

Clinical and laboratory evidences show that the occurrence and the severity of evident diseases is not simply related to intrinsic toxicity of the various pollutants, which should be homogeneous in the various hosts, but host-particle interactions generate health end-points, which greatly depend not only on individual susceptibility, but also on the type of the response and on the entity or grade of the reaction. In particular, our working hypothesis is that PM-related diseases are not simply determined by an inflammatory mechanism, mediated by oxidative stress, but more complex responses are generated, namely those typical of autoinflammatory and/autoimmune diseases, which occur only in predisposed subjects.

Caporali, F., Natale, M., Selvi, E., Galeazzi, M., Laghi Pasini, F., et al., (2008). *J Mol Med.*, 86,937-949.
Cetta, F., Dhamo A., Schiraldi, G., Camatini, M., (2007). *Eur Respir J,* 10,805-806.
Cetta F., Dhamo A., Moltoni L., Bolzacchini E. (2009). *Environ Health Perspect.* In press.

Intrinsic toxicity and inflammatory potency and/or health damage of Particulate Material (PM) in physiologic and pathologic conditions

R. Zangari[1], F. Cetta[1], M. Sala[2], A. Dhamo [1], P. Laviano[1], F. Cisternino[1], G. Malagnino[1], G. Schiraldi[3], E. Bolzacchini[4]

[1] Department of Surgery, Research Doctorate in Oncology and Genetics, University of Siena, Nuovo Policlinico "Le Scotte", viale Bracci, 16, I-53100 Siena, Italy
[2]Department. of Pediatrics and [3]Toracopulmonary and Cardiovascular Department, University of Milan,Via Festa del Perdono,7,20122,Milan, Italy
[4] Department of Environmental Sciences, University of Milano-Bicocca, Piazza dell'Ateneo Nuovo, 1,20126 Milan, Italy

Once Particulate Material (PM) introduced by inhalation has reached pulmonary interstitial sites, uptake into the blood circulation, in addition to lymphatic pathways, can occur, depending on particle size, favouring nanoparticles. In particular, particle size, surface chemistry and possibly charge, govern translocation across epithelial and endothelial cell layers.

Depending on particle surface chemistry, nanoparticles have been shown to transcytose across alveolar type I epithelial cells and capillary endothelial cells, but not via cellular tight junctions in the healthy state. However, in a compromised or disease state, translocation across wide and tight junctions occurs as well, because of functional cell membrane damage due to sepsis.

Within the frameshift of the Milan Prolife Project, during the last 2 years (2007-2008), a 360° research on health effects of PM has been performed, with particular attention to host particle interactions.

In particular, cross sectional and panel longitudinal studies have been performed, both in children and in old patients. Clinical, laboratory (respiratory exhalate) and instrumental data (spirometry), BAL (bronchioloalveolar lavage) and in some cases tissue biopsy, BAL culture and pH analysis, were compared with seasonal PM concentration and speciation and in vitro studies on cell lines, incubated with the same PM (PM $_{10}$, PM$_{2,5}$, PM$_1$), that was collected in the same site and period as data collection for clinical study.

Namely, cross sectional studies included the comparison of pedriatic acute respiratory admissions to the main pediatric referral center. They were divided into upper airways, lower tract and asthmatic diseases and grouped as seasonal admissions and of old people acute admissions for respiratory or cardiovascular diseases to the entire network of Milan hospitals, with daily and seasonal PM concentration, monitored by fixed monitors. Longitudinal panel studies included: 1) the seasonal comparison of two groups of subjects 100 children (actual n completing the study=113) attending a school close to busy motorways and 100 (actual = 108) attending school far from vehicle traffic; 2) 100 subjects older than 65 living in hospices for old patients located close (n=89) or far (n= 90) from main motorways. Measures were made during two-week campaigns - both in winter and summer time - with direct measure of PM both outdoor and indoor by optical and gravimetric samplers.

Preliminary data showed that the most severe features and complications during PM peaks occurred in patients with previous long-lasting infections asthma, or COPD pulmonary.

Overall data suggest that, in addition to individual susceptibility, due to genetic variability, which greatly affects health effects of host particle interactions, in the presence of the same PM concentration and exposure, the occurrence and severity of symptoms greatly varies among subjects with physiologic or pathologic airway conditions.

Detection of pathogenetic mechanisms such as oxidative stress, - which could act as a common mechanistic pathway of PM related health damage - is useful, but oversimplification of complex interactions, such as host-particle interaction, could cause understatement or missing of other concomitant mechanistic pathways such as concomitant air tract infection or exposure to endotoxin which also play a major role in the occurrence of clinically evident diseases after PM exposure.

Previous personal history and pathophysiological conditions of each subject are major determinants of observed adverse effects of air pollutants.

Redox balance of Thiols in the exhaled breath condensate (BEC) in two populations with different exposure to traffic related pollutants.

F. Cetta[1], R. Accinni[2], G. Schiraldi[3], M. Sala[4], R. Zangari[1], P. Laviano[1], M. Guinea Montalvo[2], G. Giussani[2], C. Dellanoce[2], F. Minardi[5] , L.Allegra[3]

[1]Department of Surgery, University of Siena, Nuovo Policlinico "Le Scotte", 53100 Siena, Italy
[2]CNR Institute of Clinical Physiology, Niguarda Cà Granda Hospital, 20162, Milan, Italy
[3]Toracopulmonary and Cardiovascular Department and [4]Department. of Pediatrics and [5]Monzino Cardiologic Center, University of Milan,Via Festa del Perdono,7,20122,Milan, Italy

Keywords: air pollution, traffic emissions, field measurements, health effects of aereosols

Thiols such as cysteine (Cys), cysteinilglycine (Cysgly), homocysteine (Hcy) and glutathion (GSH) are widely distributed in humans and play an important role in biological systems. Normal levels of thiols in physiologic fluids are considered as markers of good homeostatic equilibrium (Bloemen, 2007) On the contrary, their alteration has been associated with various diseases (asthma, COPB), usually related with increased production of reactive oxygen species (ROS). Therefore, levels of reduced and oxidized forms of thiols in plasma, in red cells and, more in general in all biological fluids - including exhaled breath condensate (EBC)- is considered a good marker of ROS activation and an early marker of related diseases (Kharitonov, 2006). Two groups of patients (older than 65 years), living in "hospices for retired peoples" have been recruited and compared, (n= 38, age 82 ± 9y) with the aim of evaluating cardiovascular and respiratory adverse-effects of environmental pollution, namely of pollutants related to urban traffic. In particular, one Hospice was located within 200m from high traffic crossroads, whereas the other was sited in a park , far from the main crossroads, and this group of subjects was compared with 35 subjects (age 70±8y) living in Aprica, a remote alpine site (1118 m. a.s.l.). EBC samples were collected and HPLC analysis was performed for the evaluation of thiol levels. In addition, oxidative stress state was also evaluated by isoprostane (8-iso-PGF2alfa), a lipid peroxidation index, by LC-MS/MS method. No differences in 8-iso-PGF2alfa were found between the two groups as the levels were under the detection limits (150µM). In the EBC of 35 subjects from Aprica the presence of various molecules, showing SH groups, was found, in particular in the oxidized form (fig.). Retention time of eluted peaks did not correspond to known thiols. Therefore, an accurate qualitative and quantitative analysis of the various thiols was not possible, only using HPLC. However, there was a striking individual variability of the various chromatographic peaks, which corresponded to fluorescent adducts detected by fluorimetric detector. Since the method is highly specific for S containing groups, it is presumed that observed peaks mainly correspond to low molecular weight molecules with active SH groups (fig.). Since no signal concerning reduced species was detected, two possible hypotheses can be envisaged : 1) reduced species could be present in small amounts below the lowest treshold for detection; 2) the absence of reduced species could be due to the pro-oxidant environment of the breath exhaled condensate. In the latter evenience, total thiols, obtained by reduction of all thiols by a specific compound, such as tris (2carboxiethil) phosphine, only included oxidized thiols
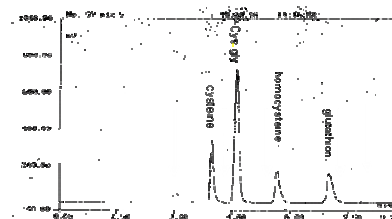
The number of samples from Milan, due to the very old age of patients living in public hospices, and then the difficulty of obtaining good quality samples, was not sufficient to permit a significant comparison between the 2 groups of subjects. More sensitive and specific detection instruments, such as mass LC, will provide a more precise detection of observed components with SH groups. However, present findings provide for the first time a method to analyze thiols in the exhaled breath condensate and then the possibility of using EBC thiols as an early marker of altered redox balance in the respiratory tract, in order to evaluate initial local damage from environmental pollution.

Bloemen, K., Lissens, G., Desagerb, K., et al., (2007). *Respiratory Medicine*,101,1331-1337.
Kharitonov, S.A., & Barnes, P.J., (2006). *Chest,*130,154

The possible impact of "sequential co-exposure" on ozone associated adverse health effects. Preliminary data from cumulative cross sectional and prospective studies in Milan.

F. Cetta[1], M. Sala[2], G. Schiraldi[3], E. Bolzacchini[4], A. Dhamo[1], L. Moltoni[1], G. Gerosa[5], A. Ballarin-Denti[5], L. Allegra[3]

[1] Department of Surgery, Research Doctorate in Oncology and Genetics, University of Siena,53100,Siena, Italy
[2] Department of Pediatrics, and [3]Thoraco pulmonary and Cardiovascular Dept, University of Milan ,Milan, Italy
[4] Department of Environmental Sciences, University of Milano-Bicocca,Milan, Italy
[5] Department of Mathematics and Physics, University "Cattolica del Sacro Cuore", Milan,Italy.

Keywords: air pollution, traffic emissions, exposure and health effects of aereosols

Aim of the study: The aim of this study has been to report on preliminary data concerning the possible impact of ozone as a single pollutant or together with other pollutants in the occurring of clinically relevant diseases.

Methods: Two monitoring campaigns (July-September 2008) (December-January 2009) covering the entire City area were performed in Milan, Italy. In particular, gaseous pollutants, - O_3, NO_2, CH6H6 - were monitored using passive samples (PASSAM, CH) in 50 different urban sites. Recorded values were processed by a GIS based geostatistical software to give the concentration profiles for the 3 selected pollutants. Fine particulate matter (PM_{10}) concentrations were measured in 5 urban sites representative of different areas of the City by gravimetric samplers. The heavy metal composition was analyzed by XRF techniques, during a 30-day-period.

Results: Benzene and NO_2 were representative of traffic emission, in particular during the Summer period. Both NO_2 and benzene (representative of traffic emission) showed elevated values in sites with intense vehicular traffic, as in the highly congested city centre and along the heavy- traffic roads. Ozone showed an opposite behaviour, being higher where NOx and benzene were lower.
In particular, Ozone values were higher inside the city gardens and parks. In fact, in vegetation-rich areas, the absence of traffic scavenging is summed up to the vegetation-released ozone precursors. Ozone average concentrations seldom reached values of more than $90\mu g/m^3$ (Fig. 1).
The greatest exposure was found in the City park, where ozone precursors were abundant and traffic related scavengers were relatively scarce. Close to City edge, exposures were lower, due to the reduced quantity of precursors and the increased quantity of traffic related scavengers. City center had an intense vehicular traffic, the emission of which contributed to the local ozone consumption. Interestingly, there was a reduction in ozone concentration during the first 3 weeks of August, in concomitance with the population reduction, because of Summer holidays, and a subsequent increase in September (Fig.1).
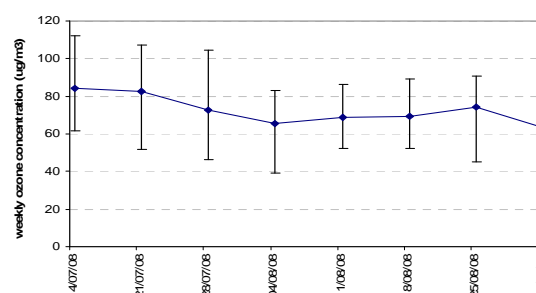

Figure 1. Weekly means of ozone concentration recorded by passive samplers at 50 different sites within the city of Milan in the summer 2008.

Conclusions: Clinical effects from environmental pollution can be considered as the end result of a complex mixture, including variable concentrations of various pollutants. In the occurrence of the health outcome not only PM $_{2,5}$ and/or PM $_{10}$, but also gaseous pollutants (ozone, NO_x, SO_2) and biological components cooperate together through concomitant or sequential co-exposure. A "sound" possibility for ozone to be dangerous is to be responsible for "sequential coexposure", i.e. to fill the gap, to make damage even during "the summer window", which could otherwise permit logical and physiological repair of previous damages, the ones that have been accumulated in the various cells, epithelia , because of other pollutants, the effect of which is more prevalent in Winter, or during Spring or Autumn. In this way, Ozone provides a continuous damage to human tissues, that will have no time left for re-epithelization, cell or tissue repair, due to the uninterrupted activity of multiple pollutants, each one having a preferred season, but also all acting together and in ordered sequence to guarantee a continuous damage. In this respect, not only concomitant co-exposure with SO_2 and other pollutants from combustion sources, but also sequential exposure, after damage caused by PM_{10}, $PM_{2,5}$, pollen and bacteria, could offer a "sound" pathophysiological working hypothesis for a causative role of ozone in the occurrence of pollution related adverse effects.

Comprehensive characterisation of manufactured nanoscaled powders following soft dispersion

K. Wittmaack[1, 2]

[1]Grimm Aerosol Technik GmbH, 83404 Ainring, Germany
[2]Helmholtz Zentrum München, Institute of Radiation Protection, 85758 Neuherberg, Germany

Concern has been raised that exposure to manufactured nanoparticles (NPs) may impose a significant risk to human health. The arguments largely originated from the adverse health effects that have previously been associated with the inhalation of ultrafine aerosol particles. But convincing evidence supporting this association has not yet been presented. A problem with the potential risk of engineered NPs is that commercially available powders are often assumed to be composed of primary particles with sizes < 100 nm. The purpose of this study was to characterise the size distribution and morphology of NP powders produced by a variety of different techniques.

Figure 1. (a) Size distribution of particles dispersed from an Fe_3O_4 powder. (b) Calculated mass distribution assuming spherical particles.

Briefly, dispersion was accomplished by directing a jet of dry nitrogen at the powder deposited in a small vessel. Particles transferred into the gas phase were carried to the analyser by a flow of filtered air. Size analysis was achieved using (i) a differential mobility analyser (DMA) coupled to a condensation particle counter and (ii) an optical counter. Pressure pulses of only 10-100 hPa were required to achieve efficient dispersion. Quite surprisingly, the fraction of dispersed primary particles contained in the spectra of nanopowders was found to be very small, as illustrated in Fig. 1, which constitutes a representative example for the general features observed with all powders studied (Fe_2O_3, Fe_3O_4, CeO_2, Co, ZnO, TiO_2, Si and Printex-90). Particularly important is a shoulder extending into the micrometer size range. The aggregates generating this shoulder, see Fig. 2(a) and (b), comprise more than 99% of the total dispersed mass. Clearly, discussing the toxic potential of nano-structured matter, these features must be considered.
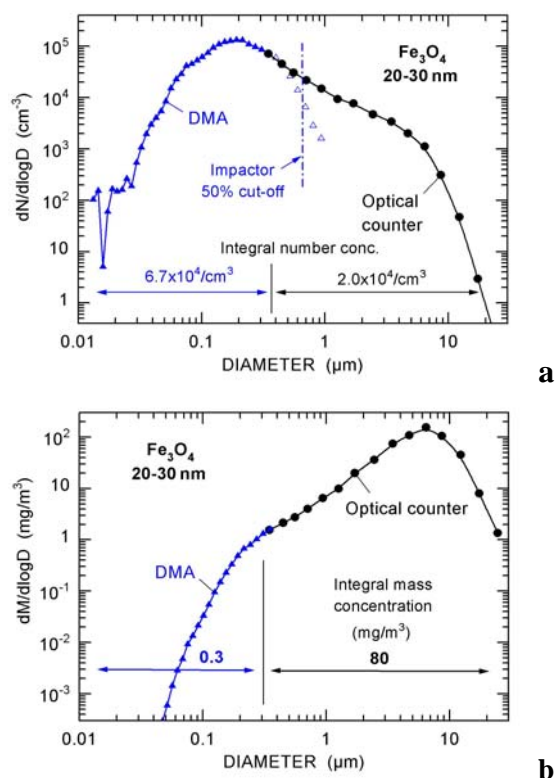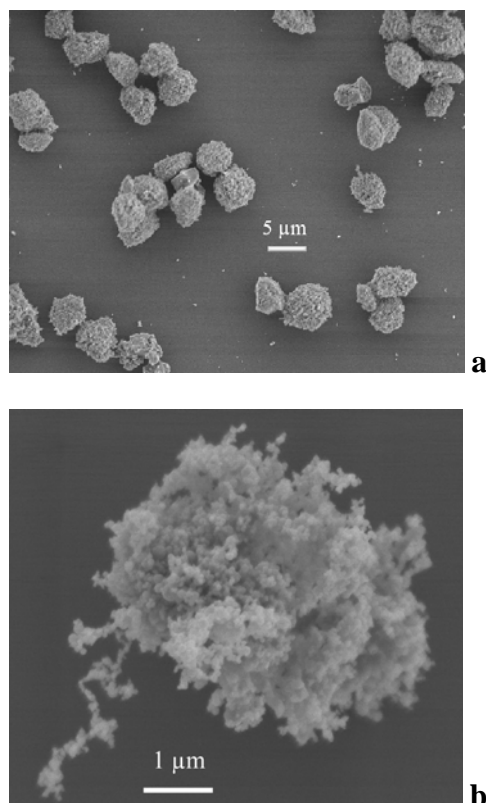

Figure 2. Examples of NP aggregates collected in a 5-stage impactor, (a) Fe_2O_3, (b) TiO_2.

A new exposure system for an efficient and controlled deposition of aerosol particles onto cell cultures

M. Kalberer[1], M. Geiser[2], M. Savi[2], D. Lang[2], A. Gaschen[2], M Ryser[3], J. Ricka[3], M. Fierz[4]

[1] Centre for Atmospheric Sciences, Department of Chemistry, University of Cambridge, Cambridge CB2 1EW, UK
[2] Institute of Anatomy, University of Bern, Bern, Switzerland
[3] Institute of Applied Physics, University of Bern, Bern, Switzerland
[4] Institute for Aerosol and Sensor Technology, University of Applied Sciences, Northwestern Switzerland, Windisch, Switzerland

Keywords: Aerosol instrumentation, Deposition, Health effects of aerosols, Lung/particle interaction

Epidemiologic studies have shown correlations between morbidity and particles smaller than 2.5μm generated from pollution processes. The increased use of nanoparticles in manufacturing processes is also a source of concern. The interaction of particles with the lung, the main pathway of undesired particle uptake, is poorly understood. In most studies investigating these interactions in vitro, particle deposition differs greatly from the in vivo situation, causing controversial results.

We present a novel nanoparticle deposition chamber designed to expose lung cells under conditions closely mimicking the particle deposition conditions in the lung (Savi *et al.*, 2008). In this deposition chamber, particles are deposited very efficiently, reproducibly, and uniformly onto the cell culture, a key aspect if cell responses are quantified in respect to the deposited particle number.

Particles are deposited onto the cells directly out of a conditioned air-flow, simulating accurately the physiological conditions in the lung, i.e., the aerosol is humidified to about 90% relative humidity, the CO_2 concentration is increased to 5% v/v and the aerosol is heated to 37°C. This assures that all cellular reactions are due to particle deposition and not due to other stress factors.

The key feature of the chamber is the electrostatic particle deposition. After passing a bipolar charger (Kr-85 source) particles are efficiently deposited by an alternating electrical field. To avoid accumulation of particles with one polarity on the cells, the polarity of the electrical field alternates (Fig. 1). For on-line monitoring of the state of the cell culture, the chamber is equipped with a device detecting the mucociliary activity, whose most conspicuous signature is the ciliary beat frequency. A fiber optic probe detects the vertical movement of the mucus induced by the beating cilia (Fig. 1). These in situ analyses of the lung cells are complemented by off-line biochemical, physiological, and morphological cell analyses.

The particle deposition chamber was extensively characterized to assure that particles are evenly and efficiently deposited on the cell culture. The distribution of the particles on the filter was determined by counting deposited particles off-line with a microscope on randomly selected locations along the filter insert radius and with modeling results. Particle deposition efficiency was tested with monodisperse polystyrene particles. 15–30% of all particles (50-600nm) are deposited, which is 5-45 times more efficient that existing particle deposition systems.

In a first series of experiments secondary organic aerosols were deposited in the chamber onto various lung cell culture types (Baltensperger *et al.*, 2008) and moderate inflammation reactions were observed.
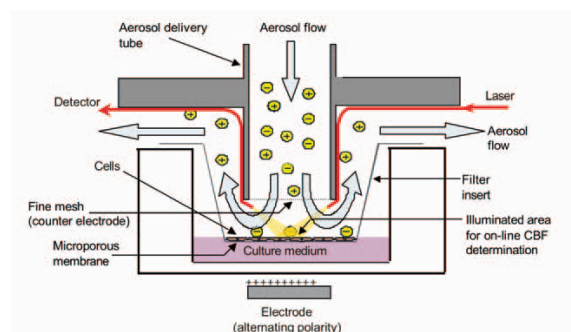

Fig. 1. Details of the particle deposition chamber showing the particle deposition on a cell culture filter insert inside the chamber. 12 cell cultures are simultaneously and individually exposed to particles. Particles are deposited in an electrical field between the particle delivery tube and the electrode. A separate electrode is placed directly beneath each filter insert.

Baltensperger, U. *et al.,* (2008). *J Aerosol Med Pulm Drug Deliv*. 21:145-154.
Savi, M. *et al.*, (2008). *Environ Sci Technol,* 42:5667-5674.

Trace Element Analyses of Spark Discharge Particles

E. Karg, B. Lentner, W.G. Kreyling and O. Schmid

Institute for Inhalation Biology, Helmholtz Zentrum München, D-85758 Neuherberg / Munich, Germany

Keywords: Generation of nanoparticles, nanoparticle characterization, elemental composition, spark discharge.

Aggregated carbonaceous particles as an experimental surrogate for Diesel exhaust particles are frequently produced by the spark discharge method (Kim *et al.*, 2006) and have been used for numerous exposure studies (Evans *et al.*, 2003; Alessandrini *et al.*, 2008). In our lab, a commercially available generator (model GFG1000, Palas, Karlsruhe, Germany) was used to produce particles in an inert carrier gas stream (Argon, quality better than 99.999 %) by controlled electric spark discharge between pure carbon electrodes.

In this study, elemental composition analyses were carried out from particle samples which were taken directly at the generator outlet. They are compared with analyses of the carbon electrodes and the carrier gas, available at the suppliers. Metal trace elements were analyzed by atomic emission spectroscopy (ICP-AES), C, O, H and N by pyrolytic methods. The results of the particle analyses as well as the corresponding electrode and gas analyses of the suppliers are listed in the table.

Table 1. Trace element concentrations.

particles[1]				electrodes[2]		carrier gas[3]	
ppm			%		ppm		ppm
Ca	35	C	82.3	Ca	0.2		
Cu	30	O	14.4	Cu	0.1	O_2	<2
Fe	75	H	1.4	Fe	0.2	H_2O	<3
Mg	6	N	0.65	Mg	0.05	N_2	<5
Si	2200			Si	0.5	HC	<0.2

[1] the mass concentration of particles in the aerosol output was 4.7 ppm for the standard operating conditions (6.5 lpm Argon flow rate and 220 s^{-1} spark frequency, 3.2 mg h^{-1} particle output). Gravimetry of the electrodes before and after operation showed that 42% of the eroded mass appears as particles at the outlet.
[2] data from PALAS, Karlsruhe, Germany for the electrode RW0
[3] data from Linde, Germany for Argon 5.0 (99.999%)

For the trace metals, the particle-to-electrode-ratio ranges from 120 to 4400. A constant ratio for all metals would explain the metal enrichment by oxidation of the carbon matrix. However, as the ratio is not found to be constant for the different metals, sources must be assumed in chamber walls and connectors which are stressed by the high energetic UV radiation produced during the spark discharge.

Desorption experiments with the particles (Matuschek *et al.*, 2007) showed a considerable loss of mass (about 14 %) during thermal treatment up to 800 °C. Analyses of the evolved gas phase showed low amounts of hydrocarbons (HC) but a significant release of the inorganic gases carbon monoxide (CO), carbon dioxide (CO_2) and and water (H_2O).

In this study, an oxygen mass concentration of 14 % is found in the particles. It may result from the adsorption of gaseous components on the particles' active surface sites from the ambient atmosphere during sample handling and preparation, but also from the impurities in the carrier gas. The carrier gas impurities are of similar mass concentration as the particles in the aerosol (see table foot notes). Even if we assume a 58 % loss of particles during transport in spark chamber and tubing (see table foot notes), the trace gas concentration of oxygen in the carrier gas is sufficient for about 15 % of oxygen in the particles.

The water vapour content of the carrier gas is taken as a hydrogen source as no data for the hydrogen trace gas content are available. From hydrolysis of H_2O in the spark discharge plasma, < 0.3 ppm H_2 and < 4.7 ppm O_2 can be expected. Therefrom, a hydrogen content up to 2.9 % is possible in the particles. The additional O_2 would be sufficient for up to 30 % of oxygen in the particles.

The nitrogen content of the carrier gas is sufficient for at most 31 % N in the particles. The measured content of 0.65 % shows nitrogen to be relatively inert during the discharge process.

We conclude that − during the spark discharge process − interaction takes place between the elemental carbon vaporized from the electrodes and trace elements available from the surrounding. The trace gas content in the carrier is sufficient to account for the impurities found. Sources for the trace metals must be assumed in the spark chamber walls. However, the adsorption of ambient gas components during sample preparation and handling as an additional source should also be considered.

Cellular responses after exposure of lung cell cultures to secondary organic aerosols

M. Geiser[1], M. Kalberer[2, 3], A. Gaschen[1], D. Lang[1], M. Savi[1], T. Geiser[4], A. Gazdhar[4], C.M. Lehr[5], M. Bur[5], J. Dommen[2] and U. Baltensperger[2]

[1] Institute of Anatomy, University of Bern, 3000 Bern 9, Switzerland
[2] Laboratory of Atmospheric Chemistry, Paul Scherrer Institut (PSI), 5232 Villigen, Switzerland
[3] Centre for Atmospheric Sciences, Department of Chemistry, University of Cambridge, Cambridge CB2 1EW, UK
[4] Division of Pulmonary Medicine, University Hospital, 3010 Bern, Switzerland
[5] Department for Biopharmaceutics and Pharmaceutical Technology, University of Saarland, 66123 Saarbrücken, Germany

Keywords: Aerosol instrumentation, Health effects of aerosols, Lung/particle interaction, SOA

Ambient fine and ultrafine particles have a variety of adverse health effects. The chemical and physical properties of aerosol particles causing these effects remain unclear. A major fraction of the ambient aerosol particle mass is composed of secondary organic aerosol (SOA). Within the interdisciplinary POLYSOA project (Baltensperger *et al.* 2008) this work aimed to examine in vitro the response of target lung cells to SOA particles with the goal to eventually identify particle components that are responsible for cell responses.

SOA particles were deposited on the air-liquid interface of cultured porcine and human lung epithelial cells (micro-dissected tracheal epithelium, primary cultures and cell lines) and lung surface macrophages in a recently constructed particle deposition chamber (Savi *et al.* 2008). Particles were applied under realistic ambient air and physiological conditions occurring when particles are inhaled by mammals.

Cellular responses were examined within 24 hrs after exposure to SOA. Ultrastructural changes of cells were assessed by transmission electron microscopy. Necrotic cell death was tested by measuring lactate dehydrogenase release. Phagocytic activity of macrophages was tested by post-exposure treatment with 6-μm polystyrene particles. Inflammatory responses were assessed by measuring TNF-α, IL-6 and IL-8 release. In addition, epithelial repair function was tested by measuring the closure of mechanically wounded alveolar epithelial cell monolayers using a computerized imaging technique (Geiser *et al.*, 2000).

Analyses of the lung cells indicate that a short time exposure to realistic concentrations of SOA does not induce cytotoxicity but leads to subtle changes in cell function that are essential for lung homoeostasis. We found decreased phagocytic activity in macrophages (Fig. 1) and cell type specific increases in IL-8 release. The alveolar epithelial wound repair was affected mainly due to alterations of cell spreading and cell migration at the edge of the wound.
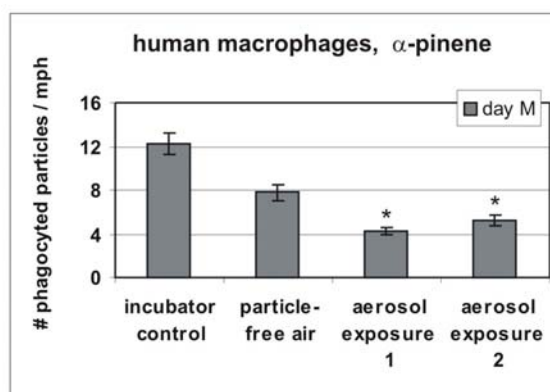

Figure 1. The phagocytic activity of human macrophages, i.e. the number of phagocytosed particles per macrophage (mph), was significantly decreased (*$p<0.05$) after exposure to SOA from α-pinene (2 experiments) as compared to untreated cells (incubator control) and cells exposed to particle-free air.

These analyses of cellular responses induced by organic aerosols will greatly help to understand the particle properties as well as the cellular mechanisms responsible for biological effects.

Baltensperger, U. *et al.,* (2008). *J Aerosol Med Pulm Drug Deliv,* 21:145-154.
Geiser, T. *et al.*, (2000). *Am J Physiol Lung Cell Mol Physiol,* 279:L1184-1190.
Savi, M. *et al.*, (2008). *Environ Sci Technol,* 42:5667-5674.

Minimal analytical characterisation of engineered nanomaterials need for hazard assessment in biological matrices

Hans Bouwmeester[1], Iseult Lynch[2], Michael Riediker[3] and Flemming R. Cassee[4]

[1] RIKILT-Institute of Food Safety, Wageningen UR, P.O. Box 230, 6700 AE Wageningen, The Netherlands
[2] University College Dublin, Centre for BioNanoInteractions, Belfield, Dublin 4, Ireland
[3] Institute for Work and Health, Rue du Bugnon 21, CH-1011 Lausanne, Switzerland
[4] National Institute for Public Health and the Environment, Bilthoven, The Netherlands
Keywords: engineered nanomaterials, hazard assessment, biological matrices, characterisation.

The safe and responsible development of engineered nanomaterials (ENM), nanotechnology-based materials and products, together with the definition of regulatory measures and implementation of "nano"-legislation in Europe require a widely supported scientific basis and sufficient high quality data upon which to base decisions. At the very core of such a scientific basis is a general agreement on key issues related to risk assessment of ENMs which encompass the key parameters to characterise ENMs, appropriate methods of analysis and best approach to express the effect of ENMs in widely accepted dose response toxicity tests.

The following major conclusions were drawn:
Due to high batch variability of ENMs characteristics of commercially available and to a lesser degree laboratory made ENMs it is not possible to make general statements regarding the toxicity resulting from exposure to ENMs.

- Concomitant with using the OECD priority list of ENMs, other criteria for selection of ENMs like relevance for mechanistic (scientific) studies or risk assessment-based studies, widespread availability (and thus high expected volumes of use) or consumer concern (route of consumer exposure depending on application) could be helpful. The OECD priority list is focussing on validity of OECD tests. Therefore source material will be first in scope for testing. However for risk assessment it is much more relevant to have toxicity data from material as present in products/matrices to which men and environment are be exposed.
- For most, if not all characteristics of ENMs, standardized methods analytical methods, though not necessarily validated, are available. Generally these methods are only able to determine one single characteristic and some of them can be rather expensive. Practically, it is currently not feasible to fully characterise ENMs.

Many techniques that are available to measure the same nanomaterial characteristic produce contrasting results (e.g. reported sizes of ENMs). It was recommended that at least two complementary techniques should be employed to determine a metric of ENMs.

The first great challenge is to prioritise metrics which are relevant in the assessment of biological dose response relations and to develop analytical methods for characterising ENMs in biological matrices.

It was generally agreed that one metric is not sufficient to describe fully ENMs.
- Characterisation of ENMs in biological matrices starts with sample preparation. It was concluded that there currently is no standard approach/protocol for sample preparation to control agglomeration/aggregation and (re)dispersion. It was recommended harmonization should be initiated and that exchange of protocols should take place. The precise methods used to disperse ENMs should be specifically, yet succinctly described within the experimental section of a publication.
- ENMs need to be characterised in the matrix as it is presented to the test system (in vitro/ in vivo).
- Alternative approaches (e.g. biological or in silico systems) for the characterisation of ENMS are simply not possible with the current knowledge.

Contributors: Iseult Lynch, Hans Marvin, Kenneth Dawson, Markus Berges, Diane Braguer, Hugh J. Byrne, Alan Casey, Gordon Chambers, Martin Clift, Giuliano Elia1, Teresa F. Fernandes, Lise Fjellsbø, Peter Hatto, Lucienne Juillerat, Christoph Klein, Wolfgang Kreyling, Carmen Nickel1, and Vicki Stone.

T20 Special Session 8

PM gravimetric measurements and blank filters

D. de Jonge[1] and J.H. Visser[1]

[1]Department of Air quality, Municipal Health Service Amsterdam,
Nieuwe Achtergracht 100, 1000 CE Amsterdam, The Netherlands

A significant weight increase of the quartz (Whatman QMA 47mm) field blank filters (FB) of around 140 µg has been found during gravimetrical PM10 measurements in 2006. Two types of samplers (single without- and sequential samplers with a temperature controlled storage) showed about the same results (table 1). Since the weight increase of the FB filters did not comply with EN 14907 demands, further research has been done. The manufacturer (Whatman) heats the quartz filters to 500°C in order to obtain the required purity. Short after the heating process the filters are packed and hermetically sealed. Our hypothesis is that adsorption of water vapour from ambient air could be the root cause of a significant mass increase. Also seasonal effects on the weight increase of FB filters have been observed. Possibly adsorption of volatile organic compounds also plays a part in the mass increase of quartz filters.

Table 1. Weight increase of 47mm quartz fibre filters

Device	Average weight increase FB (n, sd) µg
Derenda single filter holder	133 (32, 15µg)
Derenda sequential sampler	146 (32, 17µg)

In the Netherlands all air quality laboratories agreed to use one type and brand quartz fibre filters for PM2.5 measurements according to the EN 14907. EN 14907 is the European gravimetrical reference method on determination of the PM2.5 mass fraction of suspended particulate matter. This standard prescribes the use of FB filters and laboratory reference blank filters (RB). The mass change of a RB filter between two consecutive weighing sessions as well as the mass change of a FB filter should be less than 40 µg. One of the RB filters in the weighing room of Municipal Health Service Amsterdam has been in use for approximately 1800 days. This specific filter has always complied to the EN 14907 demand of 40 µg mass change at most over two consecutive weighing sessions. However the filter showed a slowly increasing mass of almost 500 µg over the first 1500 days (0,3 µg/day). We believe a mass increase of filters could be caused by adsorption of water vapour. Estimated, from these observations, Whatman QMA 47 mm quartz fibre filters kept at 20°C and 50% RH will be completely saturated with water after about 1500 days. (figure 1).

Additional to the EN 14907 weighing procedures, a pre treatment of the dry quartz filters has been added to our standard operational procedures. From January 2007 all filters have been stored for at least a month in opened packages in a with water vapour saturated environment at 20°C. The weight increase of three of these filters has been measured over 80 days. The weight increase was 5,1 µg/day, probably due to water adsorption. Compared to the RB filters the saturation process became almost 7 times faster, so complete saturation should be reached after about 3 months.

Figure 1. Weight increase of a RB

Weight increase laboratory blank
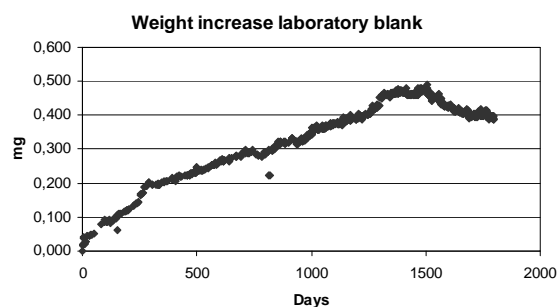
Before implementation of this procedure (2006) FB filters gained 140µg (n=64, sd=11 µg) on average. Whereas after implementation in 2007 FB filters gained only 55µg (n=384, sd=3 µg) on average.

EN 14907 (2005). *Standard gravimetric measurement method for the determination of the PM2,5 mass fraction of suspended particulate matter*. CEN/TC 264.

Semivolatile behaviour of dicarboxylic acids during summer campaigns at K-puszta

W. Maenhaut, W. Wang, L. Copolovici and X. Chi

Dept. of Anal. Chem., Inst. for Nuclear Sci., Ghent University, Proeftuinstraat 86, BE-9000 Gent, Belgium

Keywords: carbonaceous particles, filter sampling artifacts, dicarboxylic acids, PM2.5.

It is well-known that the collection of carbonaceous aerosols on quartz fibre filters is prone to both positive and negative artifacts (e.g., Turpin *et al.*, 2000). In studies on these artifacts, one normally concentrates on organic carbon (OC) as a whole or occasionally on water-soluble OC (WSOC). It is rare that studies are carried on individual organic species. One example of the latter type of study is that by Limbeck *et al.* (2001), who used a tandem filter set-up at a rural background site in South Africa and measured dicarboxylic acids (DCAs) and other polar organic species on the front and back filters. Substantial amounts were found on the back filter. The authors' interpretation was that the DCA concentrations on the back filters were caused by the adsorption of gaseous organic species and that DCAs have a semivolatile behaviour. Low-volume TSP samplers were used in that study, the face velocity across the filter was about 22 cm/s, and the collection time per sample was around one week.

We conducted a similar study as that of Limbeck *et al.* (2001), but there were also substantial differences. The samplings for our study took place during summer campaigns in 2003 and 2006 at K-puszta, Hungary; we used a high-volume dichotomous sampler (HVDS), which provides separate fine (PM2.5) and coarse size fractions, the face velocity through the PM2.5 filters was 80 cm/s, and the collection time per sample was around 12 hours. Pre-fired Gelman Pall quartz fibre filters were used for both size fractions. During the 2003 campaign it was consistently warm and dry, but the 2006 campaign was divided in separate cold and warm periods (Maenhaut *et al.*, 2008). The front and back filters for the PM2.5 size fraction of all samples were analyzed for OC, elemental carbon (EC), and total carbon (TC) with a thermal-optical transmission technique (Birch & Cary, 1996), for WSOC as described by Viana *et al.* (2006), and for water-soluble organic and inorganic anionic species by suppressed ion chromatography with conductometric detection. The median front filter concentrations for a number of components and the interquartile ranges of the back/front filter concentration ratios (both for PM2.5) are given in Table 1. The front/back filter ratios, as derived from the data of Limbeck *et al.* (2001), are included for comparison. Our back/front ratios for oxalic and succinic are low and clearly lower than those obtained by Limbeck *et al.* (2001); malonic was not present on the back filter in the earlier study, whereas we found larger back/front ratios than for oxalic and succinic; of the 4 DCAs studied by us, glutaric has the largest back/front ratio, but Limbeck *et al.* (2001) found an even greater back/front ratio for this species. It is clear that results from one site and sampler cannot be generalised to all sites and sampler types. Therefore, similar studies as the present one are being carried out for other sites in Europe.

Birch, M. E., & Cary, R. A. (1996). *Aerosol Sci. Technol.* 25, 221-241.

Limbeck, A., Puxbaum, H., Otter, L., & Scholes, M. C. (2001). *Atmos. Environ.* 35, 1853-1862.

Maenhaut, W., Raes, N., Chi, X., Cafmeyer, J., & Wang, W. (2008). *X-Ray Spectrom.* 37, 193-197.

Turpin, B. J., Saxena, P., & Andrews, E. (2000). *Atmos. Environ.* 34, 2983-3013.

Viana, M., et al. (2006). *Atmos. Environ.* 40, 2180-2193.

Table 1. Front filter median concentrations and interquartile ranges for the back/front filter concentration ratio (both for PM2.5 of the HVDS) at K-puszta. Comparison with data of Limbeck *et al.* (2001).

Species	Cold period 2006 Median front conc. (ng/m^3)	Cold period 2006 Interq. range for back/front ratio	Warm period 2006 Median front conc. (ng/m^3)	Warm period 2006 Interq. range for back/front ratio	2003 Median front conc. (ng/m^3)	2003 Interq. range for back/front ratio	Limbeck *et al.* (2001) Mean back/ front ratio
TC	2100	0.09 – 0.17	4600	0.12 – 0.16	4400	0.10 – 0.13	0.12
WSOC	970	0.17 – 0.26	2900	0.13 – 0.19	2600	0.15 – 0.19	
SO$_4^{2-}$	1790	0.00 – 0.00	3600	0.00 – 0.00	3500	0.00 – 0.01	
MSA	29	0.01 – 0.13	29	0.01 – 0.08			
Oxalic	73	0.01 – 0.02	210	0.01 – 0.03	196	0.01 – 0.03	0.14
Malonic	33	0.03 – 0.13	65	0.01 – 0.13			0.00
Succinic	32	0.02 – 0.08	142	0.01 – 0.05	41	0.01 – 0.03	0.26
Glutaric	7.1	0.17 – 0.35			7.8	0.15 – 0.22	0.38

Determination of vertical distribution of air pollution over Budapest by aircraft based measurements

B. Alföldy[1], V. Groma[1], E. Börcsök[1], A. Nagy[2], A. Czitrovszky[2], S. Török[1]

[1]KFKI Atomic Energy Research Institute, Konkoly-Th. M. u. 29-33., 1121, Budapest, Hungary
[2]Research Institute for Solid State Physics and Optics, Konkoly-Th. M. u. 29-33., 1121, Budapest, Hungary

Keywords: air pollution, mixing layer, Saharan dust, size distribution, trajectory.

Budapest (Bp) is the capital of Hungary, at the same time the largest city of the country. The air pollution of the city is principally determined by traffic related emissions however, contribution of industrial sources as well as pollution transport cannot be neglected.

Aircraft based measurement is an effective way to observe horizontal as well as vertical distribution of air pollution. Investigation of pollutant's vertical profile can provide additional information on the origin of the pollutants that helps the evaluation of urban air quality.

The aims of this work were (i) to study the homogeneity of the pollution in the mixing layer over the city; or (ii) find hot spots that can be associated to any specific emission source on the ground; (iii) to analyse the vertical profile of size fractioned aerosol concentration over downtown and suburban areas, in the mixing as well as the residual layer.

With this object fifteen flights were performed over Budapest and the surrounding area in June and September 2008, and January 2009. Aerosol count concentration and size distribution was measured by a Grimm 1.108 aerosol spectrometer. Black carbon concentration was measured by a Magee Scientific aethalometer. In addition, O_3 and CO concentrations were measured by Horiba gas monitors. The air pressure, temperature and relative humidity was registered by a compact meteorological sensor, while the geographical position was controlled and logged by GPS.

In the first figure concentration time series of two aerosol size fractions with particle diameter of 250nm and 700nm are presented together with the graph of the flying altitude on September 11, 2008. It is seen that until 15:30, while the flying altitude was varying around 400m AMSL the concentration of the two particle size fraction was correlated. After 15:30 the flying altitude increased. At 1400m AMSL, when the aircraft left the mixing layer the concentration of 250nm particles suddenly decreased, while concentration of 700nm particles increased. There was a significant drop in the O_3 concentration as well. These experimental facts together with the analysis of backward trajectories of air masses denote that Sahara originated air mass was sampled over the mixing layer.

Figure 2 shows results of air mass backward trajectory calculation by HYSPLIT model. It is seen

that air masses sampled under 1200m came from over the Atlantic Ocean, while air mass sampled at 1400m passed over the west part of Sahara before it reached European area. The air mass here picked up desert sand and transported into Europe.
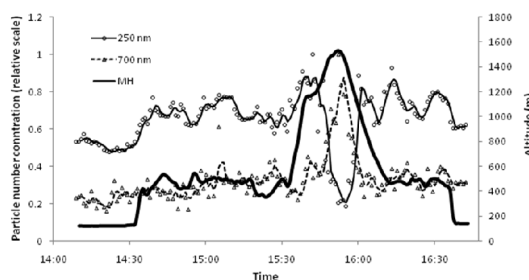

Figure 1. Count aerosol concentration of particles having 250 and 700nm diameter and flying altitude.
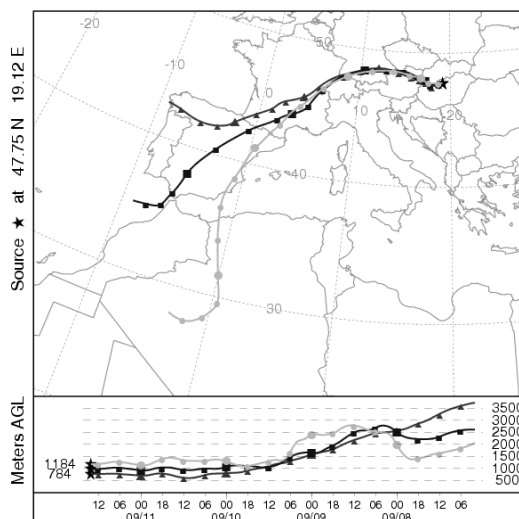

Figure 2. Backward trajectories of air masses sampled at 1000, 1200, 1400m AMSL over Bp.

It must be noted that over the mixing layer the calculated PM_{10} concentration was low (around $7\mu g/m^3$) comparing to the urban pollution concentration. The Saharan dust pass was able to be identified alone over the mixing layer, where the background concentration is negligible. The results reveal the importance of transported pollution in the forming of urban background. Especially naturally generated aerosols can have significant contribution to the PM level in Europe that is not limited to intensive episodes only like Saharan dust events.

The effect of season and microenvironment type on measurement bias of a photometer DustTrak

M. Braniš

Charles University in Prague, Institute for Environmental Studies, Albertov 6, 128 43 Prague 2, Czech Republic

In the last decade, light scattering devices (or photometers) have been widely used for continuous recording of particulate matter concentrations in exposure assessment studies. The principal advantage of these instruments is that they can be used not only for static but also for personal monitoring since they are portable and can operate on batteries which sustain usually longer than 24 hours. One of the most widely used devices is the DustTrak nephelometer (TSI, Model 8520). It is a real time photometer suitable for determination of aerosol mass concentrations between 0.001 and 100mg/m^3 for particles ranging in size from 0.1 to 10μm. As the instrument is calibrated by the manufacturer for Arizona dust (ISO 12103-1, A1 test dust) the values obtained from measurements performed in various types of indoor and outdoor microenvironments where the particles differ substantially are not actual gravimetric values. In previous studies using this type of device several attempts have been made to establish a recalculation/correction factor according to which the DustTrak data can be transformed into "real" gravimetric values (Chung et al., 2001; He et al., 2004; Heal et al., 2000; Jenkins et al., 2004; Lehocky a Williams, 1996; Levy et al., 2003; Moosmüller et al., 2001; Morawska et al., 2003; Ramachandran et al., 2003; Yanoski et al., 2002 and others). We present here the results of a long term collocation of Dustrak ($PM_{2.5}$) and a cascade impactor (PCIS). Our results showed that the correlation coefficients between the DustTRak and PCIS $PM_{2.5}$ concentrations were reasonably high, 0.922 and 0.936 for the outdoor and indoor microenvironments respectively.
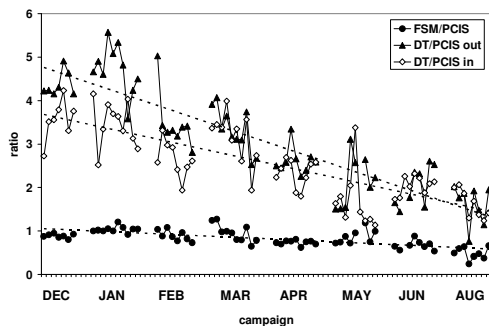

Figure 1: Ratio between $PM_{2.5}$ measured during different seasons in indoor and outdoor microenvironments by DustTrak and two other methods (PCIS and β-attenuation).

However, the 24-hour DustTrak values were in all cases higher than the PCIS ones (Fig. 1). The photometer gave values ranging from about less than 2 to over 5 times higher than the reference method. Higher DT/PCIS ratios were found in winter and in situations when smaller particles were abundant in the measured aerosol mixture.

Together with other authors we conclude that DustTrak is a good device for recording relative changes in aerosol concentrations but cannot be used for estimation of real PM mass concentration. However, with parallel gravimetric measurements a correction factor can be obtained and used in short term exposure assessment studies. When no simultaneous reference measurements are available, recalculations of DustTrak readings to gravimetrical values cannot be simply made on the basis of the existing literature data. Seasonal (temperature and relative humidity), specific microenvironmental characteristics (indoor, outdoor) and type of aerosol sources should be taken into account.

Chung, A., Chang, D.P.Y., Kleeman, M.J., Perry, K., Cahill, T.A., Dutcher, D., McDougal, E.M., Stroud, K. (2001), *J. Air Waste Manage. Assoc.* 51:109-120.

He, C., Morawska, L., Hitchins, J., Gilbert, D. (2004), *Atmos. Environ.* 38:3405-3415.

Heal, M.R., Beverland, I.J., McCabe, M., Hepburn, W., Agius, R.M. (2000), *J. Environ. Monit.* 2:455-461.

Jenkins, R.A., Ilgner, R.H., Tomkins, B.A. (2004), *J. Air Waste Manage. Assoc.* 54: 229-241.

Lehocky, A.H., Williams, P.L. (1996), *Am. Ind. Hyg. Assoc. J.* 57(11): 1013-1018.

Levy, J.I., Bennett, D.H., Melly, S.J., Spengler, J.D. (2003), *J. Exp. Anal. Environ. Epidemiol.* 13:364-371.

Moosmüller, H., Arnott, W.P., Rogers, C.F., Bowen, J.L., Gilles, J.A., Pierson, W.R., Collins, J.F., Durbin, T.D., Norbeck, J.M. (2001), *Environ. Sci. Technol.* 35:781-787.

Morawska, L., Congrong, H.E., Hitchins, J., Mengersen, K., Gilbert, D., (2003), *Atmos. Environ.* 37:4195-4203.

Ramachandran, G., Adgate, J.L., Pratt, G.C., Sexton, K. (2003), *Aerosol Sci. Technol.* 37:33-45.

Yanoski, J.D., Williams, P.L., MacIntosh, D.L. (2002), *Atmos. Environ.* 36:107-113.

Novel approach to identifying size dependent losses of semivolatile compounds during room temperature storage of sampled aerosol matter

K. Wittmaack

Helmholtz Zentrum München, Institute of Radiation Protection, 85758 Neuherberg, Germany

Keywords: Aerosol sampling, aerosol size distribution, cascade impactor, semivolatile, salt aerosol.

In recent studies we have discussed negative artefacts associated with the loss of semivolatile compounds of aerosol matter. It is well known – but not often fully appreciated – that the processes leading to such artefacts during sampling are in most cases quite significant (Wittmaack and Keck, 2004; Keck and Wittmack, 2005). Less well studied are losses that can occur during subsequent storage of aerosol matter on filters or on collection plates of impactors. Unpublished data suggest that even after several years of storage the losses might not be complete.

This study was performed to explore a novel 'soft' approach to identifying the total amount of matter that can be lost due to volatilisation during sample storage. In order to determine the size dependence of the effect, sampling was performed in impactors. Two essentially identical 8-stage cascade impactors (Berner type) were operated in parallel at flow rates of 30 L/min. PM2.5, PM10 and TSP mass concentrations were also determined by filter sampling. Particle size distributions in the range above 0.3 µm were recorded using an optical counter (Grimm model 1108). The results discussed here relate to 24-h sampling in late winter with temperatures around 0°C.

The collected masses were first determined by gravimetry. Thereafter one set of impactor samples was transferred into a vacuum chamber and stored at $< 10^{-6}$ hPa. The mass losses that occurred in vacuum were determined at storage times between 18 h and three weeks, at which point the losses had stabilized.

The water soluble fractions of the impactor deposits were carefully extracted and analysed by ion chromatography. Size distributions of SO_4^{2-} and NH_4^+, measured with as-sampled and vacuum treated impactor deposits, are presented in Figs. 1(a) and (b). Within experimental uncertainty the results for SO_4^{2-} are the same, indicating that this component did not suffer from any losses in vacuum. By contrast, NH_4^+ was lost very significantly throughout the whole spectrum, with possible exceptions at the lower and upper end of the spectra. Large losses were also observed with NO_3^-, see Fig. 1(c) and, to a lesser extent, for Cl^- (not shown).

Interpretation of the results was assisted by measuring the time dependence of mass losses in vacuum for the pure salts NH_4NO_3 and NH_4Cl.
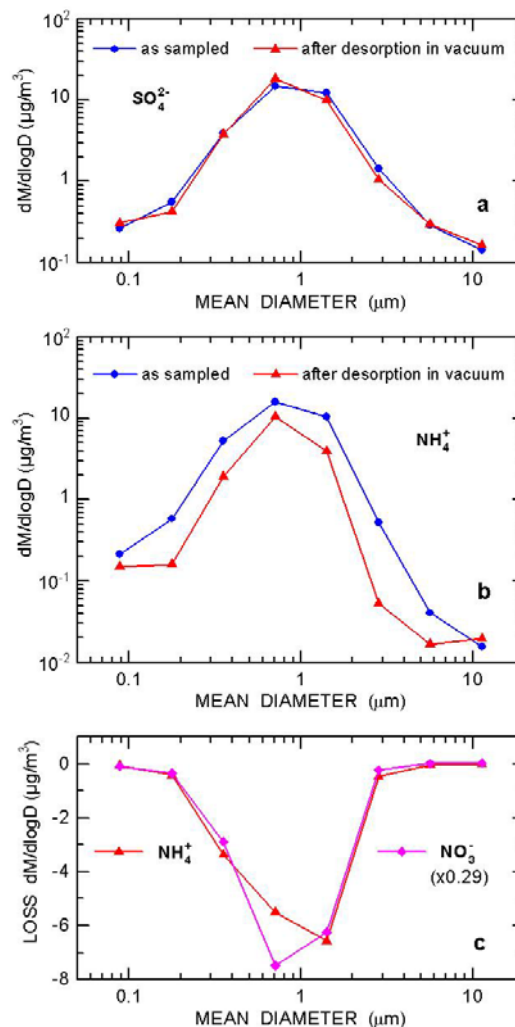

Figure 1. Comparison of the mass spectra of (a) SO_4 and (b) NH_4 ions in impactor deposits without and with long-term storage in vacuum. (c) Comparison of mass losses for NH_4 and NO_3.

Wittmaack, K., & Keck, L. (2004). *Atmos.Environ.*, 38, 5205-5215.
Keck, L. & Wittmaack, K. (2005). *Atmos. Environ.*, 39, 4093-4100.

What's up with the European PM reference methods?

J. Vercauteren, C. Matheeussen, R. De Lathouwer, V. Keppens, E. Roekens

Flemish Environment Agency (VMM), Kronenburgstraat 45, 2000 Antwerpen, Belgium

Quite recently it has become clear that the European reference methods for measuring **PM$_{10}$ (EN12341) and PM$_{2.5}$ (EN14907) can lead to much larger ranges of results than what was first assumed**. It turns out that certain artefacts were underestimated or even unknown when the standards were created. In the last couple of years the Flemish Environment Agency has carried out a range of experiments and tests in order to investigate some of the issues, and to put them on the agenda of CEN TC264 WG15 (which created both standards).

Some 5 years ago various types and brands of 47-mm filters were used in parallel in several field campaigns. To our surprise the differences between the different variations of the reference method were sometimes as high as 25% (as campaign averages). Of the two filters that were used the most, the **Whatman QM-A** (which contains 5% borosilicate and is pre-fired in the factory) **gave results that were on average 14% higher than Macherey-Nagel QF10** (a 100% pure quartz fiber filter). Tests with the standard EMERY 3004 aerosol (a poly alpha olefin) showed that the observed differences were not due to variations in physical separation efficiency, as all filters scored better than 99.9%.

In a more recent project ("Chemchar PM$_{10}$" a chemical characterisation project) the Whatman QM-A filters (which were extra pre-fired to obtain lower OC blanks) captured on average 7% more mass than teflon filters (Pall Teflo) that were sampled in parallel. Part of this difference was due to the higher blanks for the QM-As (112 µg absolute resulting in ± 2 µg/m^3) than for the teflon filters (56 µg absolute resulting in ± 1 µg/m^3).

A 3-step experiment with 5 filter types (Table 1) was done to investigate both the effects of pre-firing and the use of the 'Amsterdam' approach (= 'pre-conditioning' the blank filters by exposing them to 100% humidity for some weeks, before weighing and sampling). Each set of a filter type consisted of 3 new, identical filters.

In the first step of the experiments types 3 and 5 were fired (by Ghent University) for 24 h at 550 °C. This lead to a mass loss of 10 mg for the QF10s and 2 mg for the QM-As.

Table 1: Filter types used in 3-step experiment.

1. Pall Teflo	teflon
2. Macherey-Nagel QF10	100% quartz
3. Macherey-Nagel QF10*	100% quartz
4. Whatman QM-A	95% quartz + 5% glass
5. Whatman QM-A*	95% quartz + 5% glass

*to be fired in step 1

In the second step all 5 sets of filters were exposed to 100% relative humidity (RH) for 9 weeks (Fig 1). All quartz filters showed a rapid increase in the first couple of days and did not stabilise within the 9 weeks. Similar profiles, but in a lower mass range, had already been obtained at 50% RH and for field blanks.
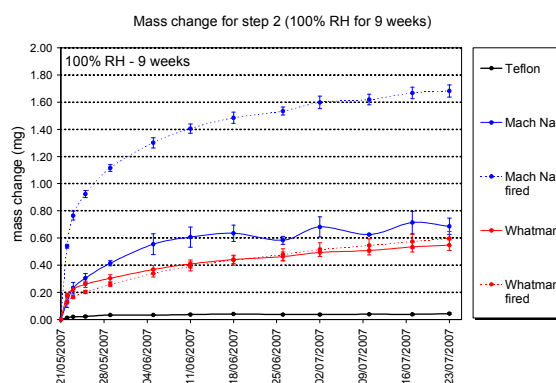

Figure 1: Mass change for step 2, at 100% RH.

In the third step all the filters were exposed to 50% humidity for 30 weeks. The results of the first 4 weeks are presented in Fig 2 and show that 3 of the 4 types of quartz filters reach an equilibrium weight within 48 h. For these 3 types this weight turned out to be the same as the weight they had after exactly 3 weeks in step 2 (at 100% RH**) indicating that at least 3 weeks of 'pre-conditioning' is desirable**. The 4th quartz type, the pre-fired QM-A showed only a small loss in mass and even started gaining weight again after 3 days. After the full 30 weeks this type had gained about 100 µg compared to the start of step 3. For the other types the mass was constant or less than 50 mg from the equilibrium weight.
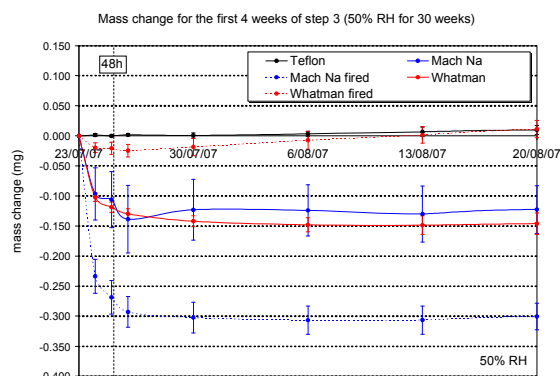

Figure 2: Mass change for step 3, at 50% RH.

Organic Carbon in Whatman-QMA field-blanks

H.M. ten Brink[1] and Frits van Arkel[2]

[1]Energy Research Centre of the Netherlands (ECN), Petten, the Netherlands
[2]National Institute for Public Health and the Environment (RIVM), Bilthoven, the Netherlands

Keywords: filter-blanks, OC, artefact

Guideline EN-12341 prescribes the use of quartz fibre filters in the reference sampling of PM10. It is well-known that quartz fibre filters exhibit artefacts. They take up volatile OC during sampling and may lose semi-volatile OC (Turpin et al. 2000). Adsorption is in general the most important artefact.

A large number of samples has been taken by now in EU counties with quartz fibre filters over the years and the OC-artefact must have lead to an appreciable artificial increase in the amount of PM10. However, searching for information we could not find data on the importance of this artefact.

A minimum value for the adsorption artefact may be provided by the so-called field blanks. These are filters that are put in the sample holders without being loaded. The filters take up OC via diffusion.

The networks in the US report field blanks that are large in comparison with the actual OC-data. Only some scattered data are available in Europe (e.g., Vecchi et al. 2009).

Filters as received from the manufacturer often contain OC and they are therefore cleaned by pre-firing in scientific studies. The commonly used Whatman-QMA filters are pre-fired in the factory, according to information form the manufacturer.

In order to assess the current uncertainties around field blanks and lot-blanks in the PM-studies in the Netherlands we performed a dedicated study on the two types of blanks with Whatman-QMA filters as used in the national reference sampling for PM10.

Field blanks

The study was part of a one-year investigation to assess the composition of PM in the Netherlands at regional and urban/kerb sites. Filter sampling was performed with automated reference samplers (KFG-Leckel) on 47 mm Whatman-QMA filters. Field blanks were filters that were in the Leckel filter carousels.

There are two carousels, one with the fresh filters from which every day a new filter is shifted into the filter holder. After sampling the filter is moved to a second carousel. 150 field blanks were taken evenly distributed between the two carousels and over the stations.

Analysis of the set of field blanks showed quite a variation in the OC-values. The average was 68 ug with an SD of 31 ug. The mentioned value for a total filter corresponds to a concentration of OC of **1.3** ug m-3. This translates into a value of Organic Matter (OM) of close to 2 ug m-3.

There was no systematic difference in the blanks from the urban sites versus those from the three regional sites, which seems to indicate that the filters are saturated with OC. This could imply that the field blanks can serve as a proxy for the adsorption artefact during sampling.

Lot blanks

In addition to the field blank we made a study of the "lot"-blanks, i.e., Whatman-QMA as received from the factory. These "lot"-blanks were taken from batches hat were unsealed immediately before analysis. Filters from three batches were analysed.

It was consistently observed that filters from the top of a stack contained high OC values. These values were higher than the average field blank.

Further down the stack of filters the values rapidly decreased. In to of the batches these were still appreciable with an average value of 25 ug, but in one batch the values were at the detection limit of 3 ug.

The bottom filters had (again) higher values.

Addendum: blanks for NO_3, SO_4 and NH_4

The average value in the (150) field blanks was resp. 1.1%, 2.1% and 0.7% of the average value in the actual samples.

Acknowledgement

Turpin et al., (2000). *Measuring and simulating particulate organics in the atmosphere: problems and prospects*. Atmos. Environ. 34, 2983-3013

Vecchi et al. (2009). *Organic and inorganic sampling artefacts assessment*. Atmos. Environ. 43, 1713-1720

Water uptake and retention by filter material used for PM sampling

T. Torzicky and R. Hitzenberger

University of Vienna
Faculty of Physics, Aerosol, Bio- and Environmental Physics, Boltzmanng. 5, A-1090 Vienna, Austria

Water uptake by atmospheric aerosol particles under conditions of elevated relative humidity is a well known phenomenon. Several models exist to predict the amount of water associated with the particles from their chemical composition. For PM measurements, weighing protocols have been developed that specify equilibration of filters at 50% humidity and 20°C for 24 hours before weighing. Under these conditions, most of the water should have evaporated from the particles. Recently, equilibration at 35% relative humidity has been suggested.

The question whether the filter material itself adsorbs water has been mentioned several times, but very few actual measurements (e.g. Demuynck, 1975; Hänninen et al., 2002) can be found in the open literature. If sampling was performed at elevated humidities and the filter material retains appreciable amounts of water vapor at the specified humidity for weighing even after the required equlilbration time, measured PM mass concentrations will be overestimated. As filter masses are much higher than deposit masses, even mass increases below the percent range will add a substantial bias to the measured deposit mass.

In this study, we investigate the changes in filter mass for different filter types (e.g. Quartz fibre, cellulose ester, glass fibre, polycarbonate filters) after 24 hr exposure to different humidities. We used the humidity chamber developed at the University of Vienna (Hitzenberger et al., 1997, current design: see Lehtinen et al., 2003). In this chamber (Figure 1), samples are put on an aluminum tray which is connected through a sealed opening to a semi-microbalance (Mettler AT 201, accuracy ± 10μg) mounted above the chamber. Humidity is controlled by using aqueous solutions of salts (in this study, we used $MgCl_2*6H_2O$) of different concentrations.
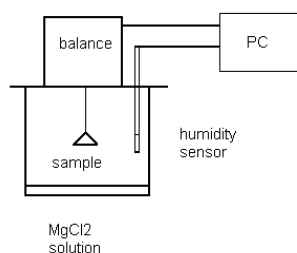
Measurements started at ambient humidity in the laboratory (usually around 50%), when the balance is tared so the mass readings during th emeasurement cycle directly correspond to the mass of water taken up by or lost from the filters. Mass, temperature and humidity are recorded automatically. In a typical measurement, filters are first exposed to a nominal humidity of 30% (in some cases 40%) and subsequently to 50%, 90%, 50% and 30% (or 40%)40%. Exposure time at each of these humidities was > 24 hrs.

First results showed that during the periods at high humidities, filters can take up appreciable amounts of water. For 5 different 47 mm diameter Quartz fiber filters (Pallflex Tissuequartz 2500 QAT-UP), masses increased on average by 6.13 mg when humidities were increased from 43 to 87%. Most of this mass is lost again, but at 53 % the average mass increase is still 1.4 mg (compared to the initial 43%). The filters do not reach their initial mass when humidities are reduced back to 43%, but still retain 0.54 mg on average. In terms of filter mass, this mass increase is negligible (average mass of filters: 130.5 mg), but in terms of deposit mass, this mass retention could lead to large errors at low mass deposits.

Demuynck, M. (1975). *Atmos. Environ.* 9, 523 – 528.
Hänninen, O., Koistinen, K. J., Kousa, A., Keski-Karhu, J. & Jantunen, M. J. (2002). *J. Air Waste Manage. Assoc.* 52, 134 – 139.
Hitzenberger, R., Dusek, U., Berner, A., & Alabashi, R. (1997). *Aerosol Sci. Technol.* 27, 116-130.
Lehtinen, K. E. J., Kulmala, M., Ctyroky, P., Futschek, T., Hitzenberger, R. (2003). *J. Phys. Chem. A* 107, 346-350.

Figure 1 schematic set-up of the humidity chamber

Level of uncertainty on $PM_{2.5}$ mass concentrations introduced by inorganic sampling artifacts

L. Rondo, K. Eleftheriadis

Institute of Nuclear Technology and Radiation Protection, Environmental Radioactivity Laboratory, National Centre of Scientific Research "Demokritos", 15310 Ag. Paraskevi, Attiki, Greece

Keywords: annular denuder; inorganic artifacts, filter pack, $PM_{2.5}$, "Demokritos" urban site

Inorganic aerosol compounds such as reactive acidic (SO_2, HNO_2 and HNO_3) and basic gases (NH_3) contribute to positive and negative artefacts significantly affecting $PM_{2.5}$ mass concentrations. The evaporative loss of the semi-volatile ammonium nitrate from the aerosol phase (negative artefact) or adsorption of nitric acid and sulphur dioxide gases (positive artefact) can occur during or after sampling. This work presents results obtained during a campaign for the assessment of sampling artefacts on the gravimetrically determined $PM_{2.5}$ mass concentration during winter.

The field campaign was carried out at the "Demokritos" urban background site in the periphery of the Athens Metropolitan area, Greece. An annular denuder system (ADS) and a filter pack (FP) were deployed in parallel for the evaluation of mass concentrations. A cyclone inlet preceded the annular denuder/filter pack system in order to remove coarse particles, while gases and fine particles are quantitatively transferred into the annular denuder and filter pack components. SO_2, HNO_2 and HNO_3 vapours are trapped by a Na_2CO_3 – coated annular denuder. A second Na_2CO_3 – coated annular denuder is used to retain excess nitrate and nitrite. The third denuder was coated with citric acid for trapping NH_3. The filter pack after the denuders contained a Teflon filter where the particulate matter was collected, a KOH coated cellulose filter where the gases evaporating due to the disequilibrium between gas and particulate phase were collected and a citric acid coated cellulose filter where the evaporating NH_3 was collected. The annular denuders and the triple filter pack together comprised the annular denuder sampling system (ADS). An identical triple filter pack equipped with a cyclone inlet was also sampling in parallel. Samples were collected at 24h intervals, where the sampling flow rate was set at 10 lt/min and values of ambient temperature, R.H. and pressure were monitored. After sampling, the aerosol mass concentration was determined gravimetrically on the Teflon filters from the ADS and FP systems. Filters were conditioned in a 20 0C and 50 % R.H. weighing room for 24h before and after sampling. Weighing was performed on a 10^{-5} gr resolution Sartorius Balance.

A control experiment was performed comparing the mass concentrations on Teflon filters obtained by an un-denuded ADS system and the filter pack, when sampling in parallel. Mass concentrations displayed an excellent correlation ($R^2 = 0.99$) and a ratio of 0.8 for the FP concentration over the ADS concentration. Results of the equivalent mass concentrations measured by the ADS and FP during the winter period (February – March – April) are shown in Fig 1.
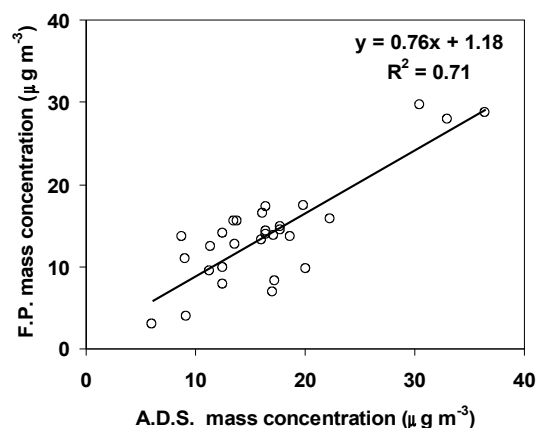

Figure 1. Relationship between denuder and filter pack system concentration in PM2.5 samples

Preliminary conclusions from the current results indicate that increased scatter in the data is apparent when the ADS and FP ratios are compared to the control experiment data. This is due to the variability in positive/negative artifact due to the disequilibrium between gas/particle phases at variable conditions. Below the effect of increasing RH is demonstrated to lead to FP/ADS ratio closer to unity as the particulate phase is favoured.
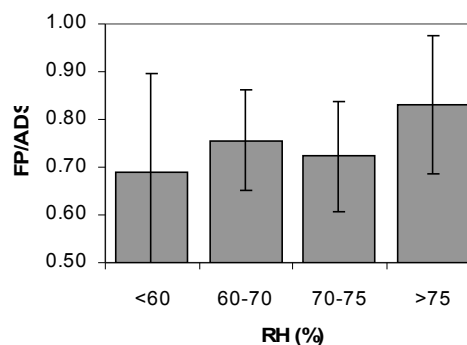

Figure 2.FP/ADS ratios with respect to ambient RH